TARGETED CANCER THERAPIES, FROM SMALL MOLECULES TO ANTIBODIES

EDITED BY: Zhe-Sheng Chen, Jian-ye Zhang, Yunkai Zhang and Yan-yan Yan
PUBLISHED IN: Frontiers in Oncology and Frontiers in Pharmacology

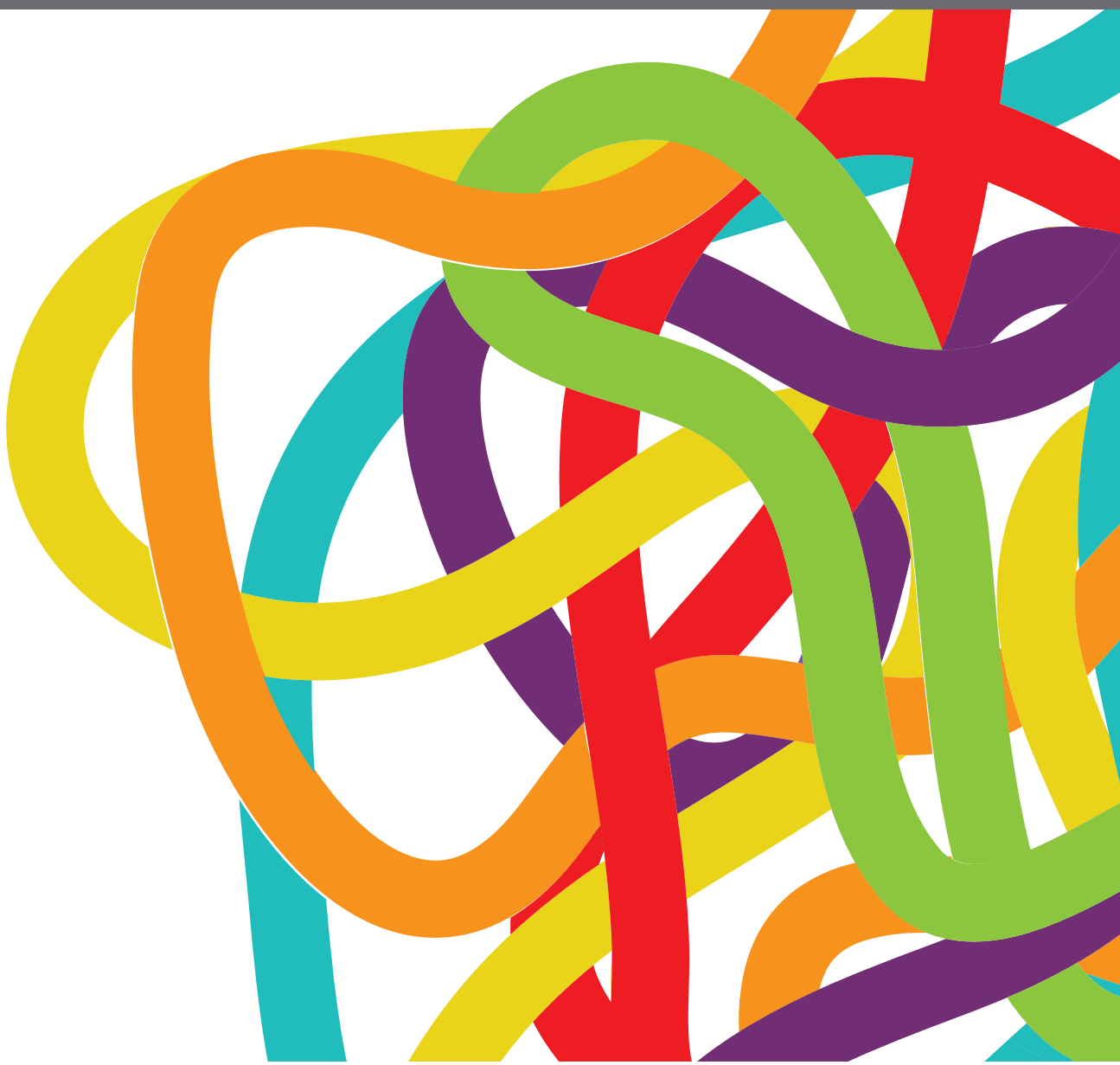

frontiers Research Topics

frontiers

ISSN 1664-8714
ISBN 978-2-88963-884-0
DOI 10.3389/978-2-88963-884-0

About Frontiers

Frontiers is more than just an open-access publisher of scholarly articles: it is a pioneering approach to the world of academia, radically improving the way scholarly research is managed. The grand vision of Frontiers is a world where all people have an equal opportunity to seek, share and generate knowledge. Frontiers provides immediate and permanent online open access to all its publications, but this alone is not enough to realize our grand goals.

Frontiers Journal Series

The Frontiers Journal Series is a multi-tier and interdisciplinary set of open-access, online journals, promising a paradigm shift from the current review, selection and dissemination processes in academic publishing. All Frontiers journals are driven by researchers for researchers; therefore, they constitute a service to the scholarly community. At the same time, the Frontiers Journal Series operates on a revolutionary invention, the tiered publishing system, initially addressing specific communities of scholars, and gradually climbing up to broader public understanding, thus serving the interests of the lay society, too.

Dedication to Quality

Each Frontiers article is a landmark of the highest quality, thanks to genuinely collaborative interactions between authors and review editors, who include some of the world's best academicians. Research must be certified by peers before entering a stream of knowledge that may eventually reach the public - and shape society; therefore, Frontiers only applies the most rigorous and unbiased reviews.
Frontiers revolutionizes research publishing by freely delivering the most outstanding research, evaluated with no bias from both the academic and social point of view. By applying the most advanced information technologies, Frontiers is catapulting scholarly publishing into a new generation.

What are Frontiers Research Topics?

Frontiers Research Topics are very popular trademarks of the Frontiers Journals Series: they are collections of at least ten articles, all centered on a particular subject. With their unique mix of varied contributions from Original Research to Review Articles, Frontiers Research Topics unify the most influential researchers, the latest key findings and historical advances in a hot research area! Find out more on how to host your own Frontiers Research Topic or contribute to one as an author by contacting the Frontiers Editorial Office: researchtopics@frontiersin.org

TARGETED CANCER THERAPIES, FROM SMALL MOLECULES TO ANTIBODIES

Topic Editors:
Zhe-Sheng Chen, St. John's University, United States
Jian-ye Zhang, Guangzhou Medical University, China
Yunkai Zhang, Vanderbilt University Medical Center, United States
Yan-yan YAN, Shanxi Datong University, China

Citation: Chen, Z.-S., Zhang, J.-Y., Zhang, Y., Yan, Y.-Y., eds. (2020). Targeted Cancer Therapies, From Small Molecules to Antibodies. Lausanne: Frontiers Media SA. doi: 10.3389/978-2-88963-884-0

Table of Contents

frontiers in Pharmacology

ORIGINAL RESEARCH
published: 12 September 2018
doi: 10.3389/fphar.2018.01042

CD13 Inhibition Enhances Cytotoxic Effect of Chemotherapy Agents

Jian Zhang[1†], Chunyan Fang[1†], Meihua Qu[1], Huina Wu[1], Xuejuan Wang[1], Hongan Zhang[1], Hui Ma[1], Zhaolin Zhang[2], Yongxue Huang[2], Lihong Shi[1], Shujuan Liang[3], Zhiqin Gao[4], Weiguo Song[1] and Xuejian Wang[1]**

[1] School of Pharmacy, Weifang Medical University, Weifang, China, [2] Weifang Bochuang International Biological Medicinal Institute, Weifang, China, [3] School of Clinical Medicine, Weifang Medical University, Weifang, China, [4] School of Bioscience and Technology, Weifang Medical University, Weifang, China

OPEN ACCESS

Edited by:
Zhe-Sheng Chen,
St. John's University, United States

Reviewed by:
Fabrizio Martelli,
Istituto Superiore di Sanità (ISS), Italy
Qi Xie,
University of California, San Diego, United States
Junjiang Chen,
Hong Kong Polytechnic University, Hong Kong

***Correspondence:**
Weiguo Song
songwg@139.com
Xuejian Wang
wangxuejian@wfmc.edu.cn;
wxj2901@126.com

[†]These authors have contributed equally to this work

Specialty section:
This article was submitted to Cancer Molecular Targets and Therapeutics, a section of the journal Frontiers in Pharmacology

Received: *07 July 2018*
Accepted: *27 August 2018*
Published: *12 September 2018*

Citation:
Zhang J, Fang C, Qu M, Wu H, Wang X, Zhang H, Ma H, Zhang Z, Huang Y, Shi L, Liang S, Gao Z, Song W and Wang X (2018) CD13 Inhibition Enhances Cytotoxic Effect of Chemotherapy Agents. Front. Pharmacol. 9:1042. doi: 10.3389/fphar.2018.01042

Multidrug resistance (MDR) of hepatocellular carcinoma is a serious problem. Although CD13 is a biomarker in human liver cancer stem cells, the relationship between CD13 and MDR remains uncertain. This study uses liver cancer cell model to understand the role of CD13 in enhancing the cytotoxic effect of chemotherapy agents. Cytotoxic agents can induce CD13 expression. CD13 inhibitor, bestatin, enhances the antitumor effect of cytotoxic agents. Meanwhile, CD13-targeting siRNA and neutralizing antibody can enhance the cytotoxic effect of 5-fluorouracil (5FU). CD13 overexpression increases cell survival upon cytotoxic agents treatment, while the knockdown of CD13 causes hypersensitivity of cells to cytotoxic agents treatment. Mechanistically, the inhibition of CD13 leads to the increase of cellular reactive oxygen species (ROS). BC-02 is a novel mutual prodrug (hybrid drug) of bestatin and 5FU. Notably, BC-02 can inhibit cellular activity in both parental and drug-resistant cells, accompanied with significantly increased ROS level. Moreover, the survival time of Kunming mice bearing H22 cells under BC-02 treatment is comparable to the capecitabine treatment at maximum dosage. These data implicate a therapeutic method to reverse MDR by targeting CD13, and indicate that BC-02 is a potent antitumor compound.

Keywords: CD13, MDR, bestatin, BC-02, 5FU

INTRODUCTION

Hepatocellular carcinoma (HCC) is the fifth most common cancer type and the third leading cause of cancer-related deaths worldwide (Mlynarsky et al., 2015). Prognosis remains poor due to the low percentage of patients with HCC eligible for surgery (9–29%) (Tsurusaki and Murakami, 2015), high tumor recurrence rates after resection (60%) (Cheng et al., 2005), and limited benefit of conventional chemotherapy (Cao et al., 2012; Deng et al., 2015). The resistance of cancer cells to structurally and mechanistically unrelated classes of anticancer drugs is known as multidrug resistance (MDR) (Gottesman et al., 2002). And MDR is one of the major causes of chemotherapeutic failure in HCC therapy. Therefore, exploring more effective therapeutic strategies for patients with HCC is urgently needed. Increasing clinical trials have proposed that combination therapy may provide new strategy for chemo-resistance in patients with advanced HCC (Alves et al., 2011; Cervello et al., 2012; Shin and Chung, 2013).

Aminopeptidase N (APN, EC 3.4.11.2), which is also known as CD13, is a type 2 transmembrane Zn-dependent metallopeptidase of the gluzincin superfamily. APN forms a non-covalent bond homodimer on the cellular membrane. It hydrolyzes oligopeptides and releases neutral amino acids from the N-terminal end of small peptides. In human non-small cell lung cancer, pancreatic carcinoma, and prostate cancer, CD13 expression is associated with poor prognosis, and CD13 expression is involved in cancer invasion and metastasis (Tokuhara et al., 2006; Su et al., 2012). CD13 is also a marker for semi-quiescent cancer stem cells (CSCs) in human liver cancer cell lines and clinical liver cancer samples (Haraguchi et al., 2010). CSCs or tumor-initiating cells are responsible for drug resistance and tumor recurrence. CSCs express high level of ATP-binding cassette (ABC) transporters. Suppression of Pim-3 kinase expression by targeting CD13 can reverse MDR in HCC cells. Therefore, ABC transporters and Pim-3 may contribute to CD13 mediated HCC MDR (Guo et al., 2017).

Bestatin, which is a [(2S,3R)-3-amino-2-hydroxy-4-phenylbutanoyl] leucine obtained from the culture filtrates of *Streptomyces olivoreticuli*, is a dipeptide with low molecular mass. It is also a potent competitive inhibitor of CD13 with antitumor activity. Bestatin synergistically enhances the antitumor effects of anticancer drugs in HCC cell lines, and the effects of bestatin are due to the increased intracellular reactive oxygen species (ROS) levels (Yamashita et al., 2016). Our previous data indicated that CD13 inhibitor 4cc synergizes the antitumor effects of 5-fluorouracil (5FU) on human liver cancer cells in a ROS-dependent manner. CD13-neutralizing antibody (clone WM15, CD13 Ab) can also significantly induce ROS production compared with control (Sun et al., 2015).

In the current study, we aim to understand the role of CD13 in MDR and evaluate the antitumor effect of BC-02, a novel mutual prodrug (hybrid drug) of bestatin and 5FU, which can be degraded into bestatin and 5FU (Dou et al., 2017), on drug-resistant tumor cells. CD13 inhibitor bestatin and neutralizing antibody can enhance the sensitivity of tumor cells to cytotoxic agents. CD13 overexpression or knockdown affects the sensitivity of cells to cytotoxic agents. Compound BC-02 can inhibit both parental and drug-resistance tumor cell proliferation more markedly than single treatment of bestatin, 5FU, or a combination of 5FU and bestatin. All together, this study may bring new strategy to reverse MDR in HCC cancer.

MATERIALS AND METHODS

Cell Culture and Reagents

Human hepatocarcinoma cell line PLC/PRF/5, Huh7, H7402, HepG2, and human colon cancer cell HCT116 were maintained in RPMI-1640 supplemented with 10% fetal calf serum (FCS). Human alveolar epithelial cell line A549 was grown in Dulbecco modified Eagle medium supplemented with 10% FCS. The cells were incubated at 37°C in a humidified atmosphere containing 5% CO_2. Lipofection 2000 was purchased from Invitrogen (Cat. 11668-019). siRNA was synthesized by Shanghai GenePharma. Bestatin (Cat. B8385), 5FU (Cat. F6627), and cisplatin (cis-DDP, Cat. P4394) were purchased from Sigma. Gemcitabine (GEM, Cat. G8970), Paclitaxel (PTX, Cat. SP8020), and doxorubicin (DOX, Cat. D8740) were purchased from Solarbio. BC-02 (12a) was synthesized by conjugating bestatin and 5FU as previously described (Jiang et al., 2018).

PLC/PRF/5-5FU Cell Culture

Low dose of 5FU was added into the medium of PLC/PRF/5. When cells need digest and passage, 5FU was also added after cell attachment. For a long time of incubation, higher concentration of 5FU was added. Then cells could survive at 40 μM 5FU.

Flow Cytometry

Determination of CD13 expression by FACS was described previously (Wang et al., 2011). 1×10^5 cells were washed with cold PBS and incubated with PE-conjugated monoclonal antibody targeting CD13 (BD Pharmingen, CD13mAb clone: WM15) for 60 min on ice. Then, the cells were analyzed on FACScan (FACSAria II; Becton-Dickinson). For ROS assay, cells were seeded and exposed to different drug samples. After 5 h incubation, cells were isolated and incubated at 37°C for 30 min with 10 μM 2,7-dichlorofluorescein diacetate (DCFH-DA) in the dark. Then the samples were washed and analyzed on a FACSCan.

Cell Viability Assays

2×10^3 cells/well were seeded in 96-well plate and allowed to grow for 4 h and the drugs were added to the wells at various concentrations. After 48 h, cells were incubated with 1% of 0.5 mg/ml MTT reagent for an additional 4 h. After that, the culture was removed, and the cells were lysed with 100 μl dimethyl sulfoxide (DMSO). The optical density of 570/630 nm was read on a plate reader (M5, MD) to calculate the inhibition rate. The inhibition rate of compounds was calculated by (ODcontrol-ODtested)/ODcontrol × 100%, where OD is the mean value of three replicate wells. The IC_{50} values were determined using ORIGIN 8 software (OriginLab Corporation, Northampton, MA, United States).

Transfection Assay

Cells were seeded on a 96-well plate and transfected with siRNA targeting the sequence of CCGAAATGCCACACTGGTCAA of the human ANPEP (CD13) sequence (NM_001150) (Lai et al., 2012). Non-specific scrambled siRNA duplex was also purchased from GenePharma (Shanghai, China). The transfection protocol was according to the lipofection 2000 instruction.

Lentivirus Infection

Lentivirus particles was supplied by GeneChem. The target of shRNA lentivirus was CCGAAATGCCACACTGGTCAA of the human ANPEP (CD13) sequence (NM_001150). The human ANPEP (CD13) sequence (NM_001150) was inserted into the vector of overexpression lentivirus. CD13 overexpression and knockdown lentivirus all overexpress green fluorescent protein. The procedure was according to the instruction. In brief, lentivirus particles was added into the medium of cells. Twelve hours later, the medium was replaced with completed culture

medium. Then puromycin treatment help to get the stably overexpression or knockdown cells.

Clone Formation Assay

Cells were plated in 6 or 48-well plates for overnight. Then cells were treated with different compounds for about 7–10 days. When the cells grew to visible colonies (>50 cells) the medium was discarded, and the cells were fiand with paraformaldehyde and stained with 0.1% crystal violet. Then clones were counted under an optical microscope.

Western Blot

Either 20 or 30 μg of total protein of each lysate were subjected to 10 or 12% SDS–PAGE and electrotransferred onto PVDF membranes (Cat. IPVH00010, Millipore). Membrane was blocked with BSA and then incubated with primary antibodies. After washing, HRP-conjugated secondary antibodies were incubated. Washed with TBST, the bound antibodies were visualized by enhanced chemiluminescence (ECL, Cat. WBKLS0050, Millipore).

In vivo Anti-tumor Assay

3×10^6 H22 cells were injected to enterocoelia of Kunming mice. And mice were divided into different groups randomly and treated with agents. The survival period was recorded. For drug-resistant cell assay, H22-bearing KM mice were given 86 mg/kg/day capecitabine. After 2 weeks, tumor tissues were dissected from mice and triturated into single cell suspension. Then cells were implanted subcutaneously in KM mouse. Then mice randomized into vehicle and treatment groups, and mice were treated with BC-02 (130 mg/kg/day, ig) and capecitabine (370 mg/kg/day, ig). The mice body weight was monitored. After 2 weeks, all mice were sacrificed and dissected to weigh the tumor tissues. Animal experiment was approved by the Guidelines of the Animal Care and Use Committee of Weifang Medical University. The protocol was approved by the Animal Care and Use Committee of Weifang Medical University.

Statistical Analysis

Data was presented as the mean ± SD, and analyzed by Student's two-tailed *t*-test. The limit of statistical significance was $P < 0.05$. Statistical analysis was done with SPSS/Win11.0 software (SPSS Inc., Chicago, IL, United States).

RESULTS

Cytotoxic Agent Results in Upregulation of CD13 Expression

As shown in **Figure 1A**, after the 5FU treatment, CD13 expression was upregulated in hepatoma tumor cells, such as

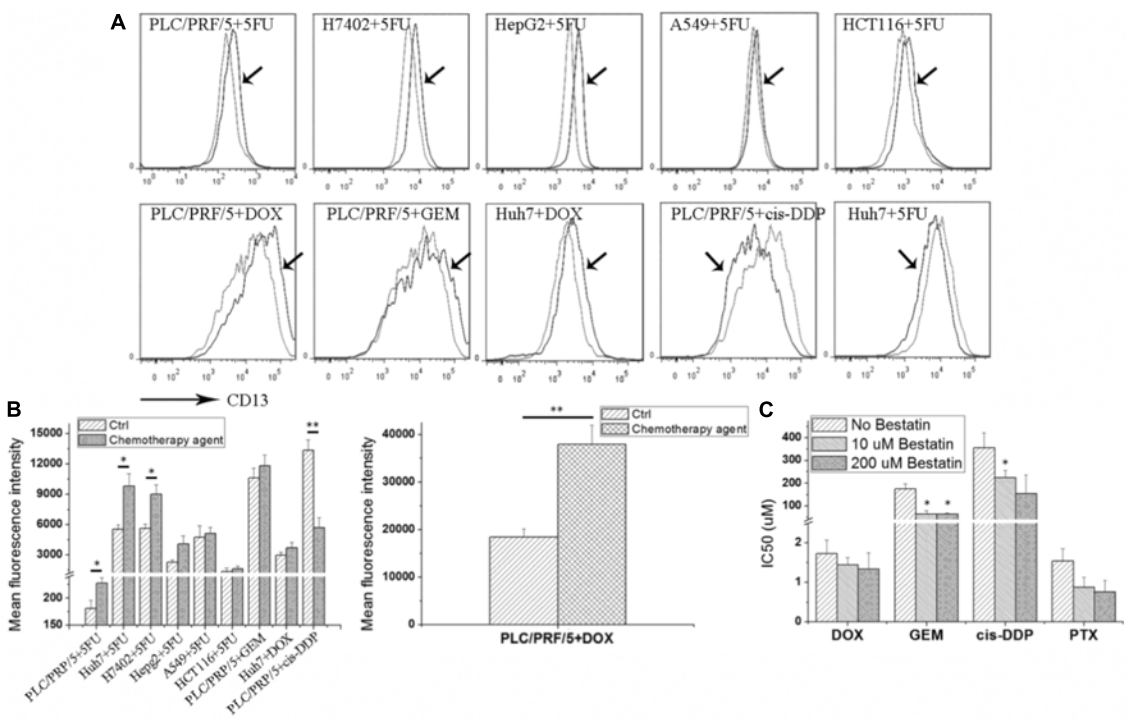

FIGURE 1 | Cytotoxic agents increase CD13 expression, and CD13 inhibitor bestatin enhances the antitumor effect of cytotoxic agents. Different tumor cells were incubated with low cytotoxic agent dosage for 3 days, and CD13 expression was detected **(A)**. Geometric mean fluorescence intensity was shown **(B)**. MTT assay was employed to detect the viability inhibition after cytotoxic agent treatments combined with different bestatin concentrations **(C)**. Data represent mean ± SD ($n = 3$). $^*P < 0.05$ and $^{**}P < 0.01$ vs. Ctrl.

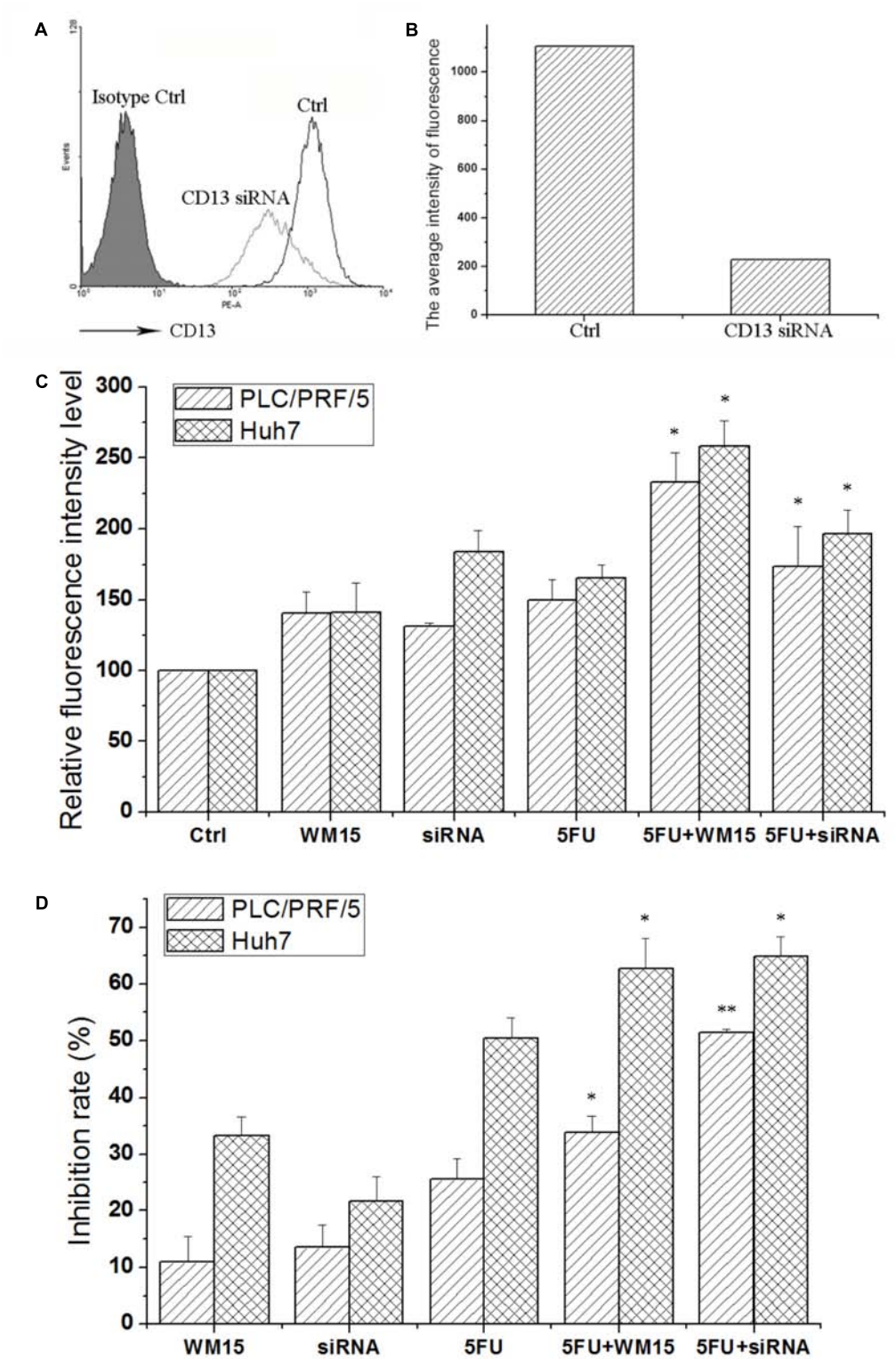

FIGURE 2 | CD13 inhibition enhances the cytotoxic effect of 5FU. PLC/PRF/5 cells were transfected with CD13-targeting siRNA. FCS was used to detect CD13 expression **(A)**. **(B)** The average intensity of fluorescence of one experiment. The results were from a representative of at least three repeated experiments. PLC/PRF/5 and Huh7 cells were treated with CD13-neutralizing antibody, CD13-targeting siRNA, 5FU, a combination of neutralizing antibody and 5FU, and a combination of siRNA and 5FU. Then, ROS level **(C)** and cell viability **(D)** were detected. Data represent mean ± SD ($n = 3$). *$P < 0.05$ vs. 5FU, **$P < 0.01$ vs. 5FU. The transfection protocol was performed according to the instructions of lipofection 2000.

PLC/PRF/5, Huh7, H7402, and HepG2. 5FU could also increase CD13 expression in human alveolar epithelial cell line A549 and human colon cancer cell HCT116. Other cytotoxic agents, such as DOX and GEM, could also increase CD13 expression in PLC/PRF/5 and Huh7 cells. Meanwhile, cis-DDP could decrease CD13 expression of in PLC/PRF/5 cells.

CD13 upregulation induced by cytotoxic agent treatments demonstrated that CD13 may contribute to cell resistance to anticancer drugs. We supposed that CD13 inhibitor should enhance the cytotoxic effect of these agents. Our data indicated that CD13 inhibitor bestatin could enhance the cytotoxic effect of DOX, GEM, cis-DDP, and PTX (**Figure 1B**). Combination of bestatin and cytotoxic agents remarkably inhibited the cell viability of PLC/PRF/5 cells, compared with single treatment of cytotoxic agents (**Figure 1C**). Thus, the increased CD13 expression may protect cells from cytotoxic agents, and CD13 inhibitor bestatin enhances the cytotoxic effect of anticancer drugs.

CD13-Targeting siRNA and Neutralizing Antibody Increase the ROS Level and Inhibit Cell Viability

Although bestatin could enhance the cytotoxic effect of anticancer drugs, off-target effect for small molecular compound was observed. To certify the role of CD13 in protecting cells resistant to cytotoxic agent, CD13-targeting siRNA and neutralizing antibody were employed to suppress CD13. CD13-targeting siRNA could remarkably decrease CD13 expression (**Figures 2A,B**). siRNA and neutralizing antibody could also increase the ROS level in PLC/PRF/5 and Huh7 cells (**Figure 2C**). Compared with single 5FU, a combination of siRNA and neutralizing antibody with 5FU could remarkably increase the ROS level (**Figure 2C**). We also obtained similar result in MTT assay. Compared with single 5FU, siRNA and neutralizing antibody could remarkably enhance the inhibitory effect of 5FU on proliferation (**Figure 2D**). These data prove the importance of

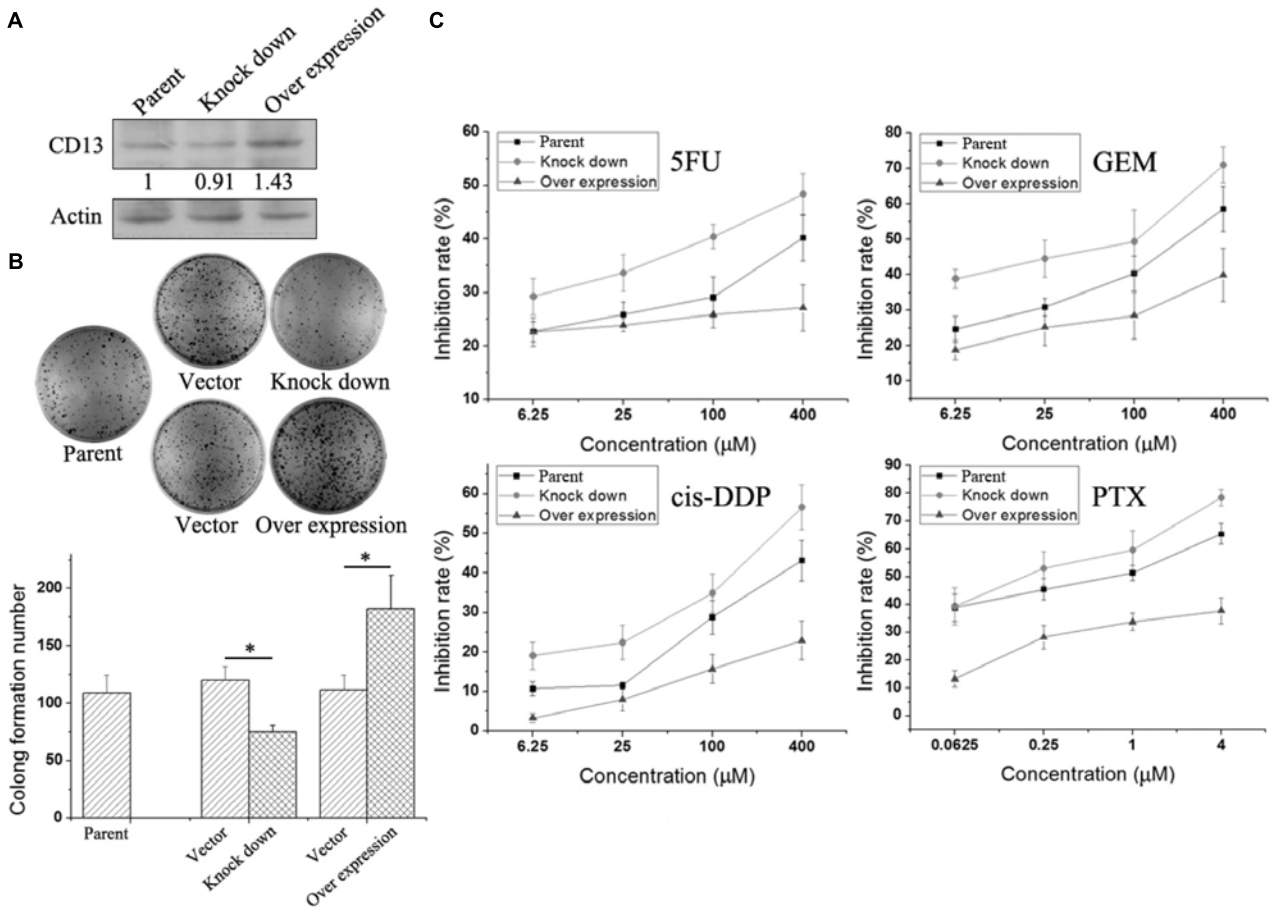

FIGURE 3 | Effect of CD13 expression on drug resistance. PLC/PRF/5 cells were infected with lentivirus. After puromycin screening, PLC/PRF/5 cells with stable CD13 overexpression or knockdown were obtained **(A)**. A representative immunoblot from three independent experiments giving similar results is shown for each western blot experiment. Densitometry for western blot was performed using AlphaEaseFC-v4.0.0 program. 1×10^3 PLC/PRF/5 cells, vector control, stable CD13 overexpression or knockdown PLC/PRF/5 cells were seeded in 6-well plates. Approximately 1 week later, cells were dyed with 0.1% crystal violet, and then photographs were taken **(B)**. The inhibition rate of different cytotoxic agents on overexpressed or knocked down cells were determined **(C)**. Data represent mean ± SD ($n = 3$). *$P < 0.05$.

CD13 in tumor cell proliferation through the modulation of ROS generation.

CD13 Overexpression Induces Cell Resistant to Cytotoxic Agent and CD13 Knockdown Leads to Sensitivity to Cytotoxic Agent

To further verify the relationship between CD13 expression and drug resistance, we used a lentiviral vector to overexpress or knockdown CD13 expression. PLC/PRF/5 cells with stable CD13 overexpression or knockdown were obtained (**Figure 3A**). CD13 overexpression or knockdown could promote or inhibit cell colony formation (**Figure 3B**). Then, we detected the sensitivity of cells to cytotoxic agents. Compared with parental cells, CD13 overexpression induced cell resistance to 5FU, GEM, cis-DDP, and PTX (**Figure 3C**). In addition, CD13 knockdown sensitized cells to cytotoxic agents (**Figure 3C**).

BC-02 Induces Higher ROS Generation Than 5FU and Inhibits Cell Viability

Compound BC-02 can be degraded into bestatin and 5FU (Dou et al., 2017). And BC-02 could inhibit the viability of PLC/PRF/5 and Huh7 cells more effectively, compared with single treatment of bestatin, 5FU, or a combination of 5FU and bestatin (**Figures 4A,B**). Clone formation assay also indicated that BC-02 could potently inhibit the clone formation of PLC/PRF/5 and Huh7 cells compared with 5FU and 1:1 combination group (**Figure 4C**). To verify specificity, we used CD13-neutralizing antibody, which could inhibit clone formation. Meanwhile, a combination of neutralizing antibody and 5FU could markedly inhibit clone formation compared

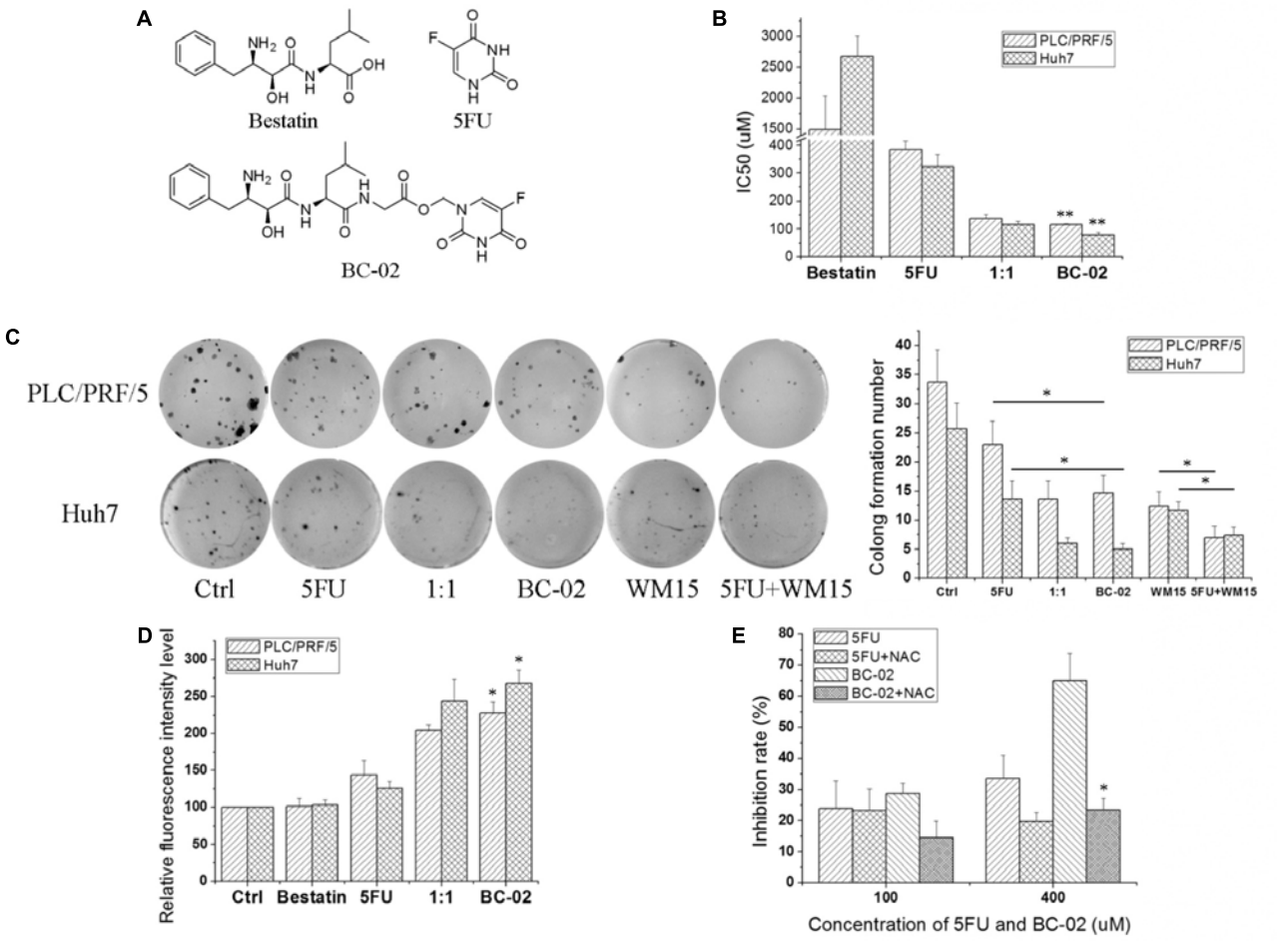

FIGURE 4 | BC-02 increases ROS level and inhibits cell viability. **(A)** The chemical structure of compounds. PLC/PRF/5 and Huh7 cells were treated with bestatin, 5FU, equal bestatin and 5FU molars (1:1), and BC-02 for 48 h. Inhibition rate was determined using MTT assay, and IC50 value was calculated **(B)**. **(C)** 250 PLC/PRF/5 or Huh7 cells were seeded in 48-well plates. After 8 h, 2 μM drugs or 1 μg/ml neutralizing antibody were added. Approximately 1 week later, cells were dyed with 0.1% crystal violet, and then photographs were taken. **(D)** PLC/PRF/5 and Huh7 cells were treated with different drugs for 5 h, and ROS level was detected. **(E)** MTT assay was used to detect the inhibition rate of 5FU, 5FU+500 μM NAC, BC-02, and BC-02+500 μM NAC by using PLC/PRF/5 cells. Data represent mean ± SD ($n = 3$). $^{*}P < 0.05$, $^{**}P < 0.01$.

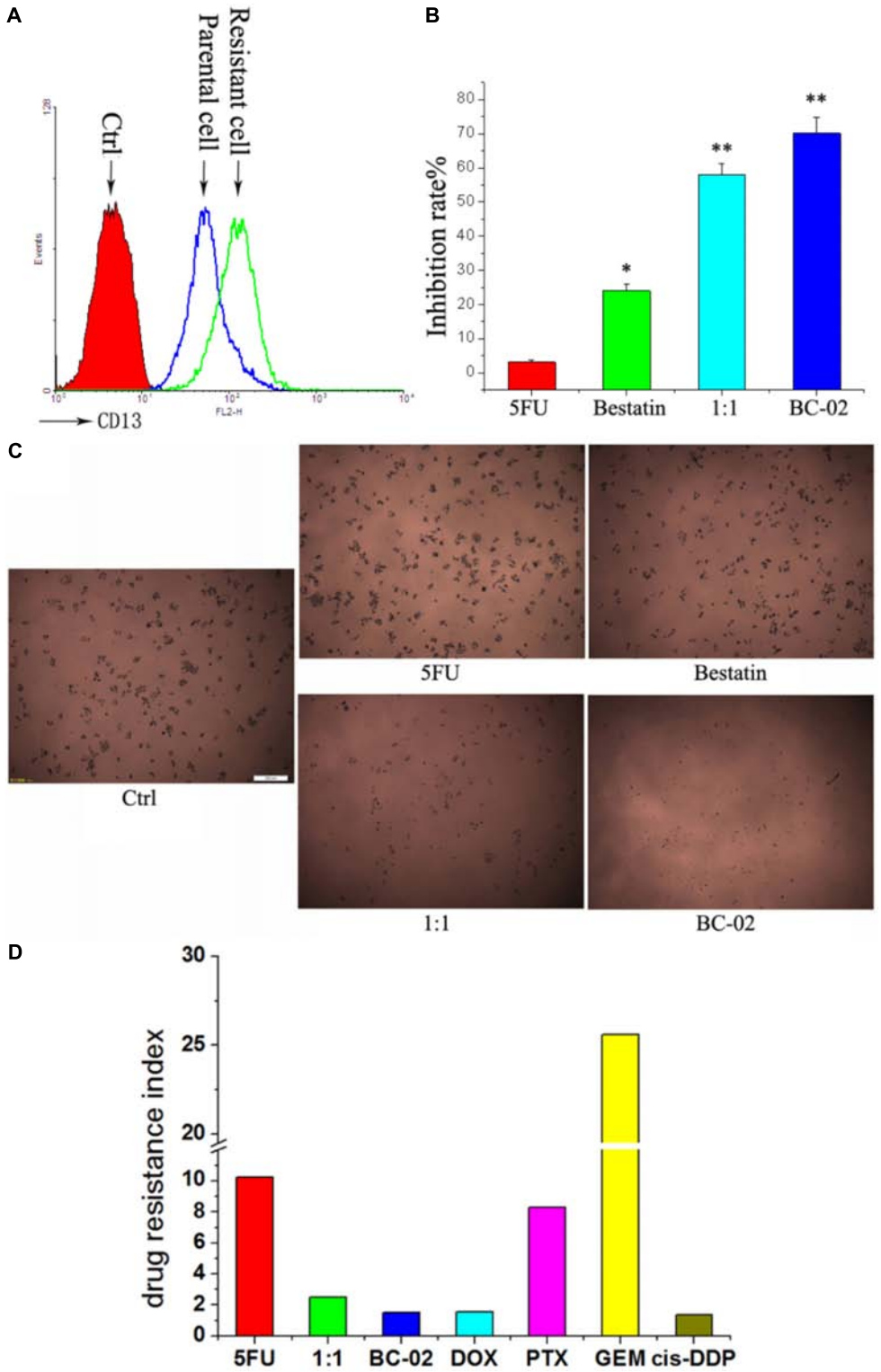

FIGURE 5 | BC-02 inhibits the viability of 5FU-resistant cells. After long period of 5FU incubation, 5FU-resistance PLC/PRF/5 cells (PLC/PRF/5-5FU) can survive at 40 μM 5FU. CD13 expression was detected by FCS **(A)**. The inhibition rate of different drugs at a concentration 100 μM on PLC/PRF/5-5FU cells were determined **(B)**. After MTT was added for 2 h, photographs of cells were taken **(C)**. The IC50 values of different cytotoxic agents on PLC/PRF/5 and PLC/PRF/5-5FU cells were determined using MTT assay. In addition, drug resistance index was calculated using the IC50 value of PLC/PRF/5-5FU cells versus the IC50 value of PLC/PRF/5 cells **(D)**. Data represent mean ± SD ($n = 3$). *$P < 0.05$, **$P < 0.01$ vs. 5FU.

with neutralizing antibody or 5FU alone (**Figure 4C**). Moreover, cellular ROS was detected by FCS. These data indicated that BC-02 could induce significantly higher level of ROS in PLC/PRF/5 and Huh7 cells more effectively, compared with single treatment of bestatin, 5FU, or a combination of 5FU and bestatin (**Figure 4D**). Moreover, ROS scavenger *N*-acetyl-L-cysteine (NAC) could protect cells from the cytotoxic effects of 5FU and BC-02 (**Figure 4E**). All these data together indicated that cell growth was inhibited through CD13 inhibition due to ROS generation.

5FU-Resistant Cancer Cells With Upregulated CD13 Expression Are More Sensitive to BC-02 Than 5FU

It is common to meet chemo-resistance for patients with HCC. Whether the chemo-resistant cells overexpress CD13 and remain sensitive to BC-02? To uncover this problem, we established 5FU-resistant PLC/PRF/5 cells (PLC/PRF/5-5FU) through low dose of 5FU incubation. After a long duration time of incubation with 5FU, PLC/PRF/5-5FU cells could survive at a concentration of 40 μM 5FU. FCS data confirmed that CD13 expression was upregulated in PLC/PRF/5-5FU chemo-resistant cells (**Figure 5A**). Moreover, PLC/PRF/5-5FU cells were resistant to 5FU but sensitive to BC-02 after being treated with 100 μM of either 5FU, bestatin, 5FU+bestatin (1:1), or BC-02 (**Figure 5B**). Photographs were also taken after MTT was added (**Figure 5C**). Almost no cells were observed in the BC-02 group. MTT assay further confirmed that almost no 5FU resistant cancer cells could survive after BC-02 treatment. The IC50 values of different cytotoxic agents to PLC/PRF/5 and PLC/PRF/5-5FU cells were determined, and drug resistance index was calculated using the IC50 value of PLC/PRF/5-5FU cells versus the IC50 value of PLC/PRF/5 cells. PLC/PRF/5-5FU cells were resistant to 5FU, PTX, and GEM, which were sensitive to BC-02, DOX, and cis-DDP, respectively (**Figure 5D**). All these data indicated that both parental and 5FU resistant cancer cells remain sensitive to BC-02.

BC-02 Inhibits H22 Tumor Growth *in vivo*

Capecitabine, a prodrug of 5FU, is used as a first- and second-line drugs for HCC treatment by several clinical trials (Murer et al., 2016; Casadei Gardini et al., 2017). The *in vivo* antitumor activity of capecitabine was stronger than that of 5FU in H22 cell-bearing Kunming (KM) mice transplant model (data not shown). Therefore, capecitabine was chosen as the positive control for our study in antitumor activity evaluation *in vivo*. In lifespan extension assay, H22 cell-bearing KM mice were treated with capecitabine (1 mmol/kg/day, iv), BC-02(①) (0.15 mmol/kg/day, iv), BC-02(②) (0.075 mmol/kg, bid, iv), or BC-02(③) (0.1125 mmol/kg, bid, iv). Both BC-02 and

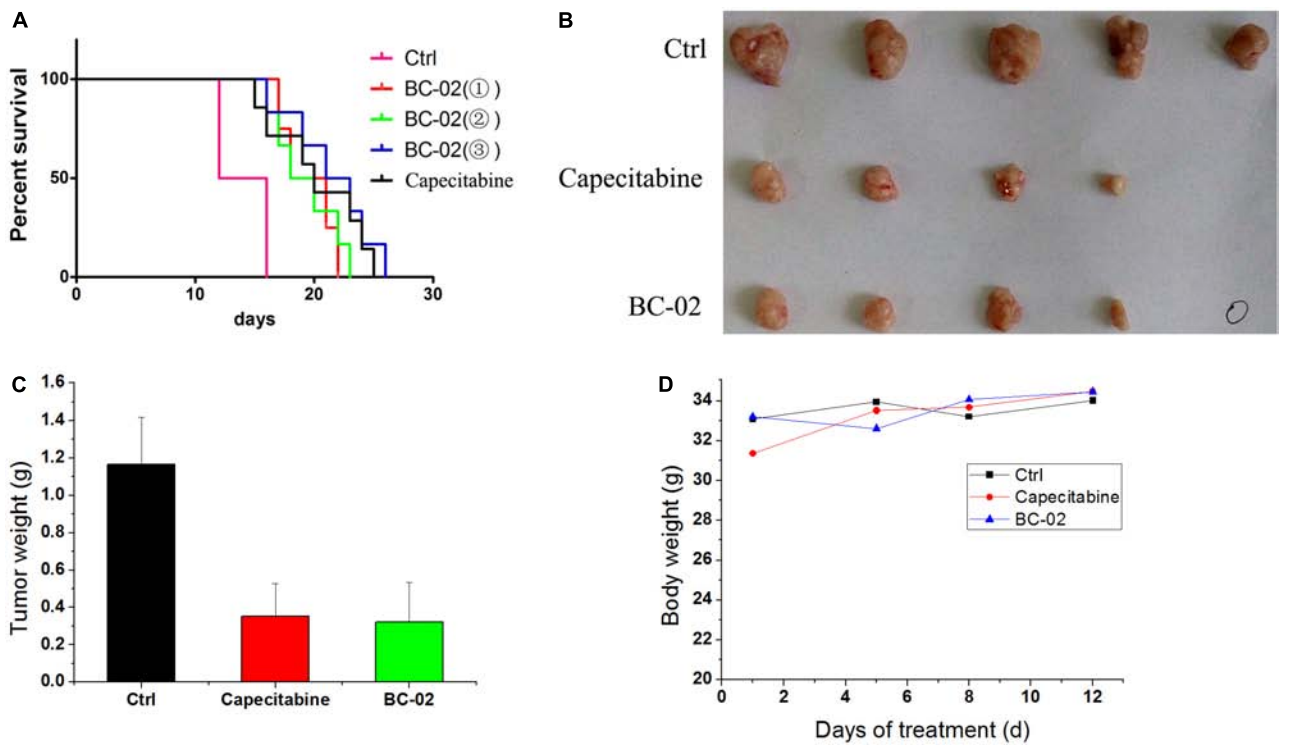

FIGURE 6 | Antitumor activities of BC-02 *in vivo*. 3×10^6 H22 cells were injected to the enterocoelia of Kunming mice. Then, mice were divided into different groups and treated with BC-02 and capecitabine, and survival period was recorded **(A)**. Capecitabine-resistant H22 cells was inoculated subcutaneously in KM mice, and they were treated with BC-02 and capecitabine. Then, mice body weight was monitored **(D)**. After 2 weeks, all mice were sacrificed and dissected to weigh tumor tissues **(B,C)**. "○" means no tumor was found.

capecitabine could extend the lifespan of mice, while BC-02(③) (0.1125 mmol/kg, bid, iv) was more potent than capecitabine (**Figure 6A**).

We also detected whether BC-02 inhibit the growth of capecitabine-resistant H22 cell. As described in the method section, capecitabine-resistant H22 cells were implanted subcutaneously in KM mice, and they were treated with BC-02 (130 mg/kg/day, ig) or capecitabine (370 mg/kg/day, ig). Both BC-02 and capecitabine could inhibit tumor growth (**Figures 6B,C**). No decrease in body weight was observed indicating the safety of BC-02 (**Figure 6D**). All together, BC-02 showed potent anti-tumor activity comparable to capecitabine *in vivo*.

DISCUSSION

HCC accounts for 85–90% of all liver cancer (El-Serag, 2011; Chacko and Samanta, 2016). Only a small portion of patients with HCC are available for surgery due to delayed diagnosis (Diaz-Gonzalez et al., 2016; Grandhi et al., 2016; Llovet et al., 2016; Mazzanti et al., 2016; Mazzoccoli et al., 2016). Because of low response rate and high toxicity, many chemotherapy agents have limited usage and can only provide minimal benefit to the survival time of patients with HCC (Simonetti et al., 1997; Connell et al., 2016). In this study, we found that CD13 was a therapeutic target which can reverse tumor cell MDR. Through the inhibition of CD13 activity, bestatin could enhance the cytotoxic effects of 5FU and other chemotherapy agents. Therefore, bestatin can be used as a good strategy for tumor therapy.

CD13 is a biomarker in human liver CSCs (Haraguchi et al., 2010), which are related to cancer MDR, recurrence, and metastasis. Therefore, we detected the relationship between CD13 and MDR. The results showed that CD13 inhibitor bestatin, CD13-neutralizing antibody, and CD13-targeting siRNA all could enhance the cytotoxic effect of 5FU and other chemotherapy agents. CD13 overexpression in PLC/PRF/5 cells could cause resistance to chemotherapy agents, while knocking down of CD13 could make PLC/PRF/5 cells to became sensitive to chemotherapy agents. All of these data together indicated that CD13 is a good therapeutic target to reverse MDR.

CD13-neutralizing antibody and bestatin can increase the ROS level in $CD13^{+}CD90^{-}$ PLC/PRF/5 and $CD13^{+}CD133^{+}$ Huh7 CSCs (Haraguchi et al., 2010). Excess of ROS induces cytotoxicity and apoptosis of cancer cells. Our previous work also indicated that BC-02 impaires the properties of liver CSCs by targeting CD13 and upregulating the intracellular ROS and ROS-induced DNA damage (Dou et al., 2017). APN inhibitor 4cc also synergizes the antitumor effects of 5FU in human liver cancer cells via ROS-mediated drug resistance inhibition and concurrent activation of the mitochondrial pathways of apoptosis (Sun et al., 2015). Therefore, we detected the relationship between CD13 inhibition and ROS. FCS data indicated that CD13 inhibitor bestatin, CD13-neutralizing antibody, and CD13 targeting-siRNA all could enhance the ROS upregulation effect of 5FU in tumor cells. Therefore, through CD13 inhibition, tumor cells cannot resist the ROS upregulation effect of 5FU, thereby leading to proliferation inhibition. Gclm participates in ROS scavenger pathway and encodes the glutamate-cysteine ligase which catalyzes the rate-limiting synthesis step of glutathione (GSH). GSH works as a critical cellular anti-oxidant and reducing agent. Gclm is overexpressed in the $CD13^{+}CD90^{-}$ fraction in PLC/PRF/5 cells (Haraguchi et al., 2010). Therefore, CD13 may protect cells from excessive ROS through up-regulation of Gclm.

Capecitabine has been tested as first- and second-line treatments for HCC by some studies (Murer et al., 2016; Casadei Gardini et al., 2017), and its antitumor activity was higher than that of 5FU in the mice transplant model. In the present assay, the capecitabine dosage was the maximum endurable dosage, while BC-02 was used at a much lower dosage. When treated with equal dosage, BC-02 performed better than capecitabine (data not shown). Moreover, BC-02 (0.1125 mmol/kg, bid, iv) was also more potent than the maximum endurable capecitabine dosage in lifespan assay. Furthermore, BC-02 was also sensitive in capecitabine-resistant H22 model. BC-02 achieved its antitumor activity through ROS upregulation. Silver nanoparticles also increased ROS level and lead to cell apoptosis (Wei et al., 2015). If BC-02 can be made into silver nanoparticles, its antitumor activity will be strengthened.

Li et al. (2015) reports that combining 5FU and bestatin could enhance the anticancer activity of 5FU in human tumor-derived cell lines and an H22 tumor-bearing mouse model. The authors mainly focused on normal tumor cells. In this study, we further indicated that the inhibition of CD13 could reverse the resistance of HCC cells to 5FU. ROS up-regulation is involved in the CD13 suppression induced cell death. However, we didn't detect the ROS generation and elimination molecular. Therefore, the underlying molecular mechanism is still unclear and needs further research.

CONCLUSION

Our study revealed CD13 as a promising target to reverse MDR. Through CD13 inhibition, the cytotoxic effect of chemo-agents will be enhanced via ROS upregulation. By the release of bestatin and 5FU, BC-02 remained sensitive to resistant cells. Taken together, BC-02 can be developed as a potent chemotherapeutic agent for human liver cancer.

AUTHOR CONTRIBUTIONS

JZ and CF participated in most of the experiments, such as cell biology and molecular biology experiments. MQ, HW, and XjuW performed the FCS assay. HZ and HM performed the MTT assay. ZZ and YH performed the mice assay. LS performed the colon assay. SL and ZG directed the data analysis. XjiW and WS designed the project.

FUNDING

This work was supported by National Natural Science Foundation of China (81503108, 31671208, and 81272319), the Project of Shandong Province Higher Educational Science and Technology Program (J15LM58), and Weifang Medical University Doctoral Scientific Research Foundation (2017BSQD12 and 2017BSQD33).

REFERENCES

Alves, R. C., Alves, D., Guz, B., Matos, C., Viana, M., Harriz, M., et al. (2011). Advanced hepatocellular carcinoma. Review of targeted molecular drugs. *Ann. Hepatol.* 10, 21–27.

Cao, H., Phan, H., and Yang, L. X. (2012). Improved chemotherapy for hepatocellular carcinoma. *Anticancer Res.* 32, 1379–1386.

Casadei Gardini, A., Foca, F., Scartozzi, M., Silvestris, N., Tamburini, E., Faloppi, L., et al. (2017). Metronomic capecitabine versus best supportive care as second-line treatment in hepatocellular carcinoma: a retrospective study. *Sci. Rep.* 7:42499. doi: 10.1038/srep42499srep42499

Cervello, M., McCubrey, J. A., Cusimano, A., Lampiasi, N., Azzolina, A., and Montalto, G. (2012). Targeted therapy for hepatocellular carcinoma: novel agents on the horizon. *Oncotarget* 3, 236–260. doi: 10.18632/oncotarget.466

Chacko, S., and Samanta, S. (2016). Hepatocellular carcinoma: a life-threatening disease. *Biomed. Pharmacother.* 84, 1679–1688. doi: 10.1016/j.biopha.2016.10.078

Cheng, H. Y., Wang, X., Chen, D., Xu, A. M., and Jia, Y. C. (2005). The value and limitation of transcatheter arterial chemoembolization in preventing recurrence of resected hepatocellular carcinoma. *World J. Gastroenterol.* 11, 3644–3646. doi: 10.3748/wjg.v11.i23.3644

Connell, L. C., Harding, J. J., and Abou-Alfa, G. K. (2016). Advanced hepatocellular cancer: the current state of future research. *Curr. Treat. Options Oncol.* 17:43. doi: 10.1007/s11864-016-0415-310.1007/s11864-016-0415-3

Deng, G. L., Zeng, S., and Shen, H. (2015). Chemotherapy and target therapy for hepatocellular carcinoma: new advances and challenges. *World J. Hepatol.* 7, 787–798. doi: 10.4254/wjh.v7.i5.787

Diaz-Gonzalez, A., Reig, M., and Bruix, J. (2016). Treatment of hepatocellular carcinoma. *Dig. Dis.* 34, 597–602. doi: 10.1159/000445275000445275

Dou, C., Fang, C., Zhao, Y., Fu, X., Zhang, Y., Zhu, D., et al. (2017). BC-02 eradicates liver cancer stem cells by upregulating the ROS-dependent DNA damage. *Int. J. Oncol.* 51, 1775–1784. doi: 10.3892/ijo.2017.4159

El-Serag, H. B. (2011). Hepatocellular carcinoma. *N. Engl. J. Med.* 365, 1118–1127. doi: 10.1056/NEJMra1001683

Gottesman, M. M., Fojo, T., and Bates, S. E. (2002). Multidrug resistance in cancer: role of ATP-dependent transporters. *Nat. Rev. Cancer* 2, 48–58. doi: 10.1038/nrc706

Grandhi, M. S., Kim, A. K., Ronnekleiv-Kelly, S. M., Kamel, I. R., Ghasebeh, M. A., and Pawlik, T. M. (2016). Hepatocellular carcinoma: from diagnosis to treatment. *Surg. Oncol.* 25, 74–85. doi: 10.1016/j.suronc.2016.03.002S0960-7404(16)30001-9

Guo, Q., Sui, Z. G., Xu, W., Quan, X. H., Sun, J. L., Li, X., et al. (2017). Ubenimex suppresses Pim-3 kinase expression by targeting CD13 to reverse MDR in HCC cells. *Oncotarget* 8, 72652–72665. doi: 10.18632/oncotarget.2019420194

Haraguchi, N., Ishii, H., Mimori, K., Tanaka, F., Ohkuma, M., Kim, H. M., et al. (2010). CD13 is a therapeutic target in human liver cancer stem cells. *J. Clin. Invest.* 120, 3326–3339. doi: 10.1172/JCI4255042550

Jiang, Y., Li, X., Hou, J., Huang, Y., Wang, X., Jia, Y., et al. (2018). Synthesis and biological characterization of ubenimex-fluorouracil conjugates for anti-cancer therapy. *Eur. J. Med. Chem.* 143, 334–347. doi: 10.1016/j.ejmech.2017.11.074

Lai, A., Ghaffari, A., Li, Y., and Ghahary, A. (2012). Microarray-based identification of aminopeptidase N target genes in keratinocyte conditioned medium-stimulated dermal fibroblasts. *J. Cell. Biochem.* 113, 1061–1068. doi: 10.1002/jcb.23438.

Li, J., Wang, X., Hou, J., Huang, Y., Zhang, Y., and Xu, W. (2015). Enhanced anticancer activity of 5-FU in combination with Bestatin: evidence in human tumor-derived cell lines and an H22 tumor-bearing mouse. *Drug Discov. Ther.* 9, 45–52. doi: 10.5582/ddt.2015.01006.

Llovet, J. M., Zucman-Rossi, J., Pikarsky, E., Sangro, B., Schwartz, M., Sherman, M., et al. (2016). Hepatocellular carcinoma. *Nat. Rev. Dis. Primers* 2:16018. doi: 10.1038/nrdp.2016.18

Mazzanti, R., Arena, U., and Tassi, R. (2016). Hepatocellular carcinoma: where are we? *World J. Exp. Med.* 6, 21–36. doi: 10.5493/wjem.v6.i1.21

Mazzoccoli, G., Miele, L., Oben, J., Grieco, A., and Vinciguerra, M. (2016). Biology, epidemiology, clinical aspects of hepatocellular carcinoma and the role of sorafenib. *Curr. Drug Targets* 17, 783–799. doi: 10.2174/1389450117666151209120831

Mlynarsky, L., Menachem, Y., and Shibolet, O. (2015). Treatment of hepatocellular carcinoma: steps forward but still a long way to go. *World J. Hepatol.* 7, 566–574 doi: 10.4254/wjh.v7.i3.566

Murer, F., Pozzan, C., Peserico, G., and Farinati, F. (2016). Capecitabine in advanced hepatocellular carcinoma. *Dig. Liver Dis.* 48, 1260–1261. doi: 10.1016/j.dld.2016.06.037S1590-8658(16)30516-3

Shin, J. W., and Chung, Y. H. (2013). Molecular targeted therapy for hepatocellular carcinoma: current and future. *World J. Gastroenterol.* 19, 6144–6155. doi: 10.3748/wjg.v19.i37.6144

Simonetti, R. G., Liberati, A., Angiolini, C., and Pagliaro, L. (1997). Treatment of hepatocellular carcinoma: a systematic review of randomized controlled trials. *Ann. Oncol.* 8, 117–136. doi: 10.1023/A:1008285123736

Su, L., Cao, J., Jia, Y., Zhang, X., Fang, H., and Xu, W. (2012). Development of synthetic aminopeptidase N/CD13 inhibitors to overcome cancer metastasis and angiogenesis. *ACS Med. Chem. Lett.* 3, 959–964. doi: 10.1021/ml3000758

Sun, Z. P., Zhang, J., Shi, L. H., Zhang, X. R., Duan, Y., Xu, W. F., et al. (2015). Aminopeptidase N inhibitor 4cc synergizes antitumor effects of 5-fluorouracil on human liver cancer cells through ROS-dependent CD13 inhibition. *Biomed. Pharmacother.* 76, 65–72. doi: 10.1016/j.biopha.2015.10.023S0753-3322(15)00241-3

Tokuhara, T., Hattori, N., Ishida, H., Hirai, T., Higashiyama, M., Kodama, K., et al. (2006). Clinical significance of aminopeptidase N in non-small cell lung cancer. *Clin. Cancer Res.* 12, 3971–3978. doi: 10.1158/1078-0432.CCR-06-0338

Tsurusaki, M., and Murakami, T. (2015). Surgical and locoregional therapy of HCC: tace. *Liver Cancer* 4, 165–175. doi: 10.1159/000367739lic-0004-0165

Wang, X., Jing, F., Zhu, H., Fang, H., Zhang, J., and Xu, W. (2011). Activity screening and structure-activity relationship of the hit compounds targeting APN/CD13. *Fundam. Clin. Pharmacol.* 25, 217–228. doi: 10.1111/j.1472-8206.2010.00844.xFCP844

Wei, L., Lu, J., Xu, H., Patel, A., Chen, Z. S., and Chen, G. (2015). Silver nanoparticles: synthesis, properties, and therapeutic applications. *Drug Discov. Today* 20, 595–601. doi: 10.1016/j.drudis.2014.11.014

Yamashita, M., Wada, H., Eguchi, H., Ogawa, H., Yamada, D., Noda, T., et al. (2016). A CD13 inhibitor, ubenimex, synergistically enhances the effects of anticancer drugs in hepatocellular carcinoma. *Int. J. Oncol.* 49, 89–98. doi: 10.3892/ijo.2016.3496

Conflict of Interest Statement: The authors declare that the research was conducted in the absence of any commercial or financial relationships that could be construed as a potential conflict of interest.

frontiers in Pharmacology

RESEARCH SNAPSHOT
published: 11 October 2018
doi: 10.3389/fphar.2018.01160

A Cell Model Suitable for a High-Throughput Screening of Inhibitors of the Wnt/β-Catenin Pathway

*Marina Grimaldi[1,2,3,4], Abdelhay Boulahtouf[1,2,3,4], Corinne Prévostel[1,2,3,4], Alain Thierry[1,2,3,4], Patrick Balaguer[1,2,3,4] and Philippe Blache[1,2,3,4]**

[1] Institut de Recherche en Cancérologie de Montpellier, Montpellier, France, [2] INSERM, U1194, Montpellier, France, [3] Université de Montpellier, Montpellier, France, [4] Institut Régional du Cancer de Montpellier, Montpellier, France

OPEN ACCESS

Edited by:
Yunkai Zhang,
Vanderbilt University Medical Center, United States

Reviewed by:
Zhenfang Du,
Vanderbilt University Medical Center, United States
Mao Wang,
St. John's University, United States

***Correspondence:**
Philippe Blache
philippe.blache@inserm.fr

Specialty section:
This article was submitted to Experimental Pharmacology and Drug Discovery, a section of the journal Frontiers in Pharmacology

Received: *14 August 2018*
Accepted: *24 September 2018*
Published: *11 October 2018*

Citation:
Grimaldi M, Boulahtouf A, Prévostel C, Thierry A, Balaguer P and Blache P (2018) A Cell Model Suitable for a High-Throughput Screening of Inhibitors of the Wnt/β-Catenin Pathway. Front. Pharmacol. 9:1160. doi: 10.3389/fphar.2018.01160

A constitutive activation of the Wnt/β-catenin pathway is an initiating event in colon carcinogenesis. We developed colon cancer cells models that highlight the non-selectivity of previously described inhibitors of the Wnt pathway and we propose our model as a suitable screening system for inhibitors of the pathway.

Keywords: cell models, Wnt/β-catenin pathway, inhibitors, high-throughput screening, colorectal cancer

RESULTS

A constitutive activation of the Wnt/β-catenin signaling pathway is admitted as an initiating event of carcinogenesis in at least 90% of colorectal cancers (Giles et al., 2003). This constitutive activity is mostly due to mutations of the APC tumor suppressor that result in the accumulation of β-catenin in the nucleus where β-catenin interacts with TCFs transcription factors to activate the transcription of target genes like c-myc (Sansom et al., 2007). To date, very few molecules targeting the Wnt pathway have been discovered and none has been yet approved for clinical practice (Kahn, 2014). Therefore, there is a great interest in identifying new inhibitors of Wnt signaling for clinical use.

Luciferase-based reporter assays are widely used for studying gene expression at the transcriptional level. Here, we use such a system to set up a high-throughput screening assay for inhibitors of the Wnt/β-catenin signaling pathway by using DLD-1 cells stably transfected with a luciferase TCF reporter plasmid (Veeman et al., 2003). The choice of a good control was critical given that a previous work dedicated to screen new Wnt inhibitors had recently been retracted due to a non-selective inhibition of the firefly luciferase activity (Li et al., 2017). Besides, a reporter system based on mutated TCF binding sites is available, but has a very low basal luciferase activity and is rather a control for a non-specific activation of the Wnt pathway. Here, we developed a genetically modified DLD-1 cell line model expressing the firefly luciferase under the control of the E2F1 promoter, an independent promoter of the WNT pathway.

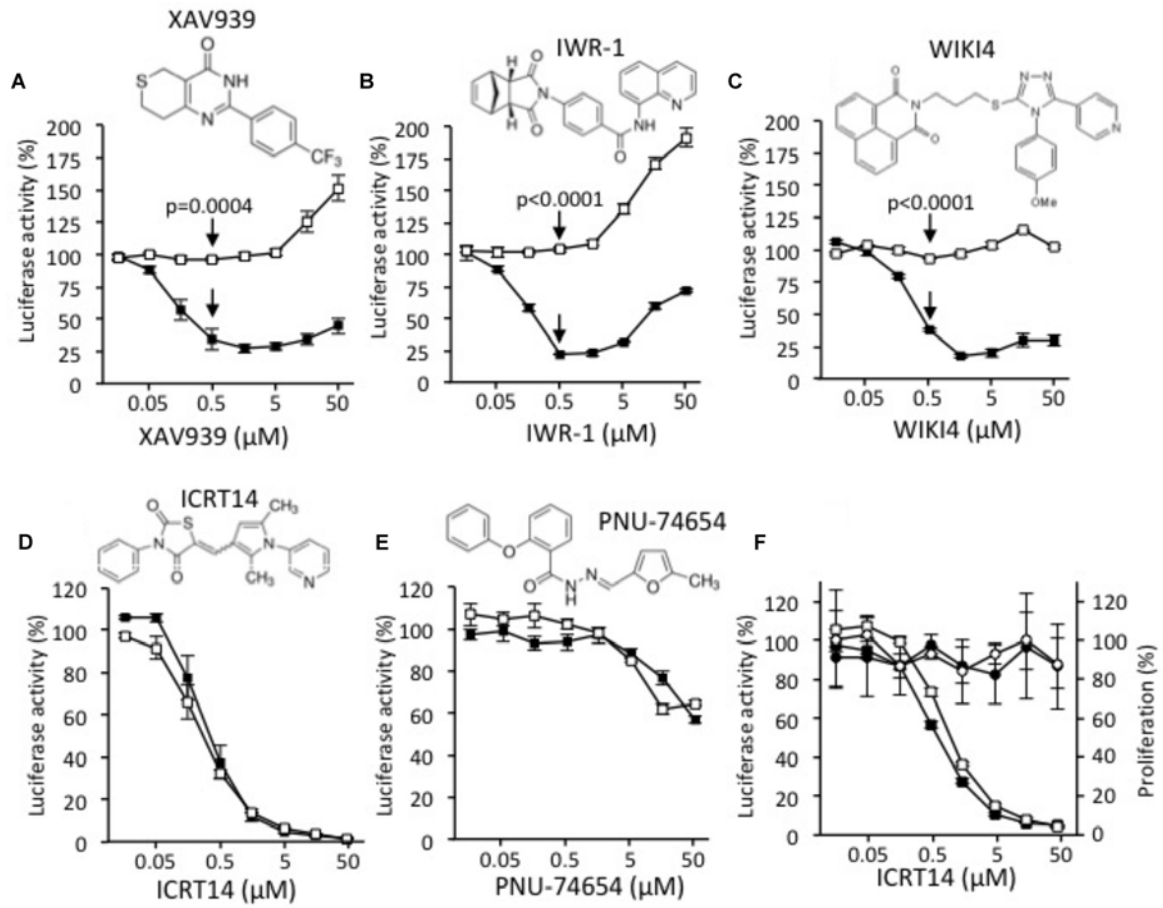

FIGURE 1 | Effects of XAV939 **(A)**, IWR-1 **(B)**, WIKI4 **(C)**, ICRT14 **(D)**, and PNU-74654 **(E)** on luciferase activity of DLD1-Wnt-luc cells (black squares) and of DLD1-luc control cells (white squares). **(F)** MTT assay was performed in presence of ICRT14 on DLD1-Wnt-luc cells (black circles) and on DLD1-luc control cells (white circles). In parallel, luciferase activity of DLD1-Wnt-luc cells (black squares) and of DLD1-luc control cells (white squares) was measured. The Student's *t*-test was performed for doses of 0.5 μM and the probability of error (*p*-value) is indicated by arrows.

Two types of available Wnt inhibitors were used in order to validate the model: the tankyrase (TNKS) inhibitors XAV939 (Huang et al., 2009), IWR-1 (Chen et al., 2009) and WIKI4 (James et al., 2012), and the destabilizers of the TCF/β-catenin complex ICRT14 (Gonsalves et al., 2011) and PNU-74654 (Trosset et al., 2006). TNKS acts as an activator of the Wnt/β-catenin signaling by mediating poly-adenosine diphosphate (ADP) ribosylation of AXIN-1 and -2, two key components of the β-catenin destruction complex whose inhibition enhances β-catenin degradation and consequently inhibits the Wnt/β-catenin signaling (Yamada and Masuda, 2017).

XAV939 (**Figure 1A**), IWR-1 (**Figure 1B**), and WIKI4 (**Figure 1C**) specifically inhibited the activity of the Wnt/β-catenin signaling, with and IC50 of 0.13, 0.21 and 0.28 μM, respectively. However, a side activating effect was observed at doses higher than 1 μM as evidenced by the increase of the luciferase activity observed in the control conditions. Besides, both ICRT14 (**Figure 1D**) and PNU-74654 (**Figure 1E**) behaved as non-selective inhibitors as evidenced by the inhibition of both Wnt dependent and independent luciferase activities. In addition, PNU-74654 was poorly efficient. To further determine whether the apparent inhibitory effect of ICRT14 on the Wnt independent luciferase activity was due to a toxicity, or not, we evaluated the impact of ICRT14 on cells viability by using the MTT system in parallel with measurement of the luciferase activity. As shown in **Figure 1F**, ICRT14 again decreased both Wnt dependent and independent luciferase activities in a dose dependent manner but had no significant effect on cells viability.

MATERIALS AND METHODS

Luciferase and MTT assays were done as we previously described (Molina-Molina et al., 2008). More details about the methods are available in the **Supplementary Material**.

DISCUSSION

With respects to the use of inhibitors previously reported as specific, studies have concluded that biological activities were

regulated by the Wnt/β-catenin pathway. In the present study, we demonstrate that the destabilizers of the TCF/β-catenin complex ICRT14 and PNU-74654 are unspecific inhibitors of the Wnt/β-catenin pathway. Therefore, to test the implication of the Wnt pathway in a biological mechanism, it seems more rationable to use at least one of the specific inhibitors confirmed here. Compared with the original reference system dedicated to test the impact of compounds on the activity of the Wnt/β-catenin signaling pathway, our method was set-up with an adequate control that lowers the number of false positives resulting from a non-specific inhibition of the luciferase enzymatic activity. For example, using our method points out ICRT14 as a non-specific inhibitor of the Wnt/β-catenin signaling pathway. Besides, true positives will have to be dose-dependent tested, and their ability to decrease the proliferation of colon cancer cells will have to be evaluated for further potential therapeutic purposes.

AUTHOR CONTRIBUTIONS

CP, PhB, and PaB designed the study. CP, PhB, and AT drafted the manuscript. MG, AB, and PhB performed the experimental work.

FUNDING

INSERM, the Institut du Cancer de Montpellier, and Lilly France financially supported this work.

SUPPLEMENTARY MATERIAL

The Supplementary Material for this article can be found online at: https://www.frontiersin.org/articles/10.3389/fphar.2018.01160/full#supplementary-material

REFERENCES

Chen, B., Dodge, M. E., Tang, W., Lu, J., Ma, Z., Fan, C.-W., et al. (2009). Small molecule-mediated disruption of Wnt-dependent signaling in tissue regeneration and cancer. *Nat. Chem. Biol.* 5, 100–107. doi: 10.1038/nchembio.137

Giles, R. H., van Es, J. H., and Clevers, H. (2003). Caught up in a Wnt storm: Wnt signaling in cancer. *Biochem. Biophys. Acta* 1653, 1–24.

Gonsalves, F. C., Klein, K., Carson, B. B., Katz, S., Ekas, L. A., Evans, S., et al. (2011). An RNAi-based chemical genetic screen identifies three small-molecule inhibitors of the Wnt/wingless signaling pathway. *Proc. Natl. Acad. Sci. U.S.A.* 108, 5954–5963. doi: 10.1073/pnas.1017496108

Huang, S.-M. A., Mishina, Y. M., Liu, S., Cheung, A., Stegmeier, F., Michaud, G. A., et al. (2009). Tankyrase inhibition stabilizes axin and antagonizes Wnt signalling. *Nature* 461, 614–620. doi: 10.1038/nature08356

James, R. G., Davidson, K. C., Bosch, K. A., Biechele, T. L., Robin, N. C., Taylor, R. J., et al. (2012). WIKI4, a novel inhibitor of tankyrase and Wnt/ß-catenin signaling. *PLoS One* 7:e50457. doi: 10.1371/journal.pone.0050457

Kahn, M. (2014). Can we safely target the WNT pathway? *Nat. Rev. Drug Discov.* 13, 513–532. doi: 10.1038/nrd4233

Li, Y., Oliver, P. G., Lu, W., Pathak, V., Sridharan, S., Augelli-Szafran, C. E., et al. (2017). SRI36160 is a specific inhibitor of Wnt/β-catenin signaling in human pancreatic and colorectal cancer cells. *Cancer Lett.* 389, 41–48. doi: 10.1016/j.canlet.2016.12.030

Molina-Molina, J.-M., Escande, A., Pillon, A., Gomez, E., Pakdel, F., Cavaillès, V., et al. (2008). Profiling of benzophenone derivatives using fish and human estrogen receptor-specific in vitro bioassays. *Toxicol. Appl. Pharmacol.* 232, 384–395. doi: 10.1016/j.taap.2008.07.017

Sansom, O. J., Meniel, V. S., Muncan, V., Phesse, T. J., Wilkins, J. A., Reed, K. R., et al. (2007). Myc deletion rescues Apc deficiency in the small intestine. *Nature* 446, 676–679. doi: 10.1038/nature05674

Trosset, J.-Y., Dalvit, C., Knapp, S., Fasolini, M., Veronesi, M., Mantegani, S., et al. (2006). Inhibition of protein-protein interactions: the discovery of druglike beta-catenin inhibitors by combining virtual and biophysical screening. *Proteins* 64, 60–67. doi: 10.1002/prot.20955

Veeman, M. T., Slusarski, D. C., Kaykas, A., Louie, S. H., and Moon, R. T. (2003). Zebrafish prickle, a modulator of noncanonical Wnt/Fz signaling, regulates gastrulation movements. *Curr. Biol.* 13, 680–685. doi: 10.1016/S0960-9822(03)00240-9

Yamada, T., and Masuda, M. (2017). Emergence of TNIK inhibitors in cancer therapeutics. *Cancer Sci.* 108, 818–823. doi: 10.1111/cas.13203

Conflict of Interest Statement: The authors declare that the research was conducted in the absence of any commercial or financial relationships that could be construed as a potential conflict of interest.

The reviewer ZD and handling Editor declared their shared affiliation.

frontiers in Oncology

REVIEW
published: 02 November 2018
doi: 10.3389/fonc.2018.00507

Targeted p53 on Small-Molecules-Induced Ferroptosis in Cancers

*Weifen Zhang[1], Chengcheng Gai[2], Dejun Ding[1], Fang Wang[3] and Wentong Li[2]**

[1] Department of Pharmacology, Weifang Medical University, Weifang, China, [2] Department of Pathology, Weifang Medical University, Weifang, China, [3] School of Clinical Medicine, Weifang Medical University, Weifang, China

OPEN ACCESS

Edited by:
Zhe-Sheng Chen,
St. John's University, United States

Reviewed by:
Wenjun Wu,
University of Chicago, United States
Pranav Gupta,
Massachusetts General Hospital, Harvard Medical School, United States
De-shen Wang,
Sun Yat-sen University Cancer Center (SYSUCC), China

***Correspondence:**
Wentong Li
liwentong11@163.com

Specialty section:
This article was submitted to Cancer Molecular Targets and Therapeutics, a section of the journal Frontiers in Oncology

Received: *23 September 2018*
Accepted: *16 October 2018*
Published: *02 November 2018*

Citation:
Zhang W, Gai C, Ding D, Wang F and Li W (2018) Targeted p53 on Small-Molecules-Induced Ferroptosis in Cancers. Front. Oncol. 8:507. doi: 10.3389/fonc.2018.00507

Ferroptosis is a type of programmed cell death characterized by the accumulation of lipid reactive oxygen species (L-ROS) driven by the oxidative degeneration of lipids in an iron-dependent manner. The mechanism by which lipid oxidative degradation drives ROS-ferroptosis involves metabolic dysfunctions that result in impaired intracellular metabolic processes and ROS production. Recent studies have found that p53 acts as a positive regulator of ferroptosis by promoting ROS production. p53 directly regulates the metabolic versatility of cells by favoring mitochondrial respiration, leading to ROS-mediated ferroptosis. In mild stress, p53 protects cell survival via eliminating ROS; additionally, in human colorectal cancer, p53 antagonizes ferroptosis by formation of the DPP4–p53 complex. In short, the mechanisms of p53-mediated ROS production underlying cellular response are poorly understood. In the context of recent research results, the indistinct roles of p53 on ROS-mediated ferroptosis are scrutinized to understand the mechanism underlying p53-mediated tumor suppression.

Keywords: p53, ferroptosis, reactive oxygen species, tumor suppression, metabolic gene

INTRODUCTION

Ferroptosis, a new form of cell death, was first described in a high-throughput screening of molecules for selectively inducing cell death in RAS mutant isoform cancer cells (1). As a novel subtype of programmed cell death, ferroptosis is primarily characterized by increased mitochondrial membrane density and volume shrinkage with distinct morphological, biochemical, and genetic differences from other types of cell death, including apoptosis, necrosis, necroptosis, and autophagy; for instance, the typical characteristics of apoptosis, including activated caspases, chromatin condensation, and DNA fragmentation, are absent in ferroptosis (1, 2), the distinctive morphological feature of erastin-treated cells involved smaller mitochondria with increased membrane density (3). In addition, loss of the plasma membrane integrity of necrotic morphological features and formation of double membrane-layered autophagic vacuoles during autophagy are not observed in ferroptosis.

Small molecules belonging to class I and class II ferroptosis-inducing agents trigger ferroptosis via inhibiting cystine-glutamate exchange transporter (*system* X_c^-) and glutathione peroxidase 4 (GPX4), respectively (4). Class I ferroptosis inducers, such as erastin, sorafenib, sulfasalazine and the neurotransmitter glutamate, *system* X_c^-, class II ferroptosis inducers, such as RSL3, FIN56 (5), or altretamine (6) are shown to induce ferroptosis via inhibition of GPX4.

Recent studies have reported that p53 activation is essential for ferroptosis in certain cancers. Since the discovery of p53, its role on tumor suppression in tumorigenesis and cancer therapy has attracted considerable attention. Loss of p53 is a vital event in the tumorigenesis of many human cancers (7, 8). In general, the tumor suppression activity of p53 in response to cellular stress relies on its capability to elicit cell-cycle arrest, apoptosis, and senescence. Nevertheless, recent efforts indicate that other unconventional activities of p53 are also crucial for tumor suppression (9, 10).

Novel roles of p53 on tumor suppression have come to light when a synthetic mutant of p53, incapable of transactivating the majority of known p53 target genes, displays antitumor activities in unstressed organisms and some cancer-prone mouse models (10, 11). A mutant p53 that loses acetylation at some definite residues of the DNA binding domain is disabled to evoke growth arrest, senescence, and apoptosis, thereby inhibiting spontaneous tumor development through sensitizing cells to ferroptosis (12, 13). Given that p53 is a main regulatory factor of critically important cellular biological processes, elucidating the mechanism by which p53 responds to stress may clarify the upstream signaling of ferroptosis. In the context of recent insights, the indistinct roles of p53 signaling in reactive oxygen species (ROS)-mediated ferroptosis via the transcriptional and non-transcriptional regulation of metabolic targets are scrutinized (**Table 1**).

ACTIVATION OF P53 SENSITIZES CELLS TO ROS AND TRIGGERS FERROPTOSIS

Increased accumulation of lipid reactive oxygen species (L-ROS) in an iron-dependent manner is a fundamental characteristic of ferroptosis (14, 27). Metabolic dysfunctions contribute to ferroptosis by elevating the production of ROS independent of mitochondria (5). Thus, several investigations have been devoted to elucidate the regulatory roles of p53 on metabolic targets in ROS production for regulating ferroptosis.

p53 participates in various cellular processes by acting as a DNA binding transcription factor that selectively modulates the expression of target genes. For example, wild-type p53 regulates the transactivation of cytochrome c oxidase 2 (SCO2), favoring mitochondrial respiration over glycolysis (28). In addition, p53 plays a negative regulatory role on glycolysis via transcriptionally modulating glucose transporter (GLUT)1, GLUT4 (24), TP53-induced glycolysis and apoptosis regulator (TIGAR), and glutaminase 2 (GLS2) (15, 29) (**Figure 1**). p53 could also suppress glucose metabolism directly by binding and inhibiting glucose-6-phosphate dehydrogenase (30). Clearly, p53 directly adjusts the metabolic polyfunctionality of cells by supporting mitochodial respiration, leading to ROS-mediated ferroptosis.

MODULATION OF P53 ON THE EXPRESSION OF SLC7A11 TO MEDIATE FERROPTOSIS

p53 Represses SLC7A11 Expression

SLC7A11 (xCT) is a light-chain subunit of the membrane Na^+-dependent *system* X_c^-, which is a disulfide-linked heterodimer composed of SLC7A11 and a heavy-chain subunit (SLC3A2) (31). Previous experiments showed the inconformity in the p53 activation and expression of SLC7A11, which could directly affect ferroptosis in mouse embryonic fibroblast (MEF) cells (32). *System* X_c^- transfers intracellular glutamate to the extracellular space and extracellular cystine into cells (33). Cystine is then converted into cysteine for synthesizing glutathione (GSH), which protects cells from oxidative stress. Inhibition of *system* X_c^- reduces intracellular GSH, resulting in an iron-dependent ferroptosis mediated by the accumulation of L-ROS (23).

Activation of p53 by nutlin-3 markedly decreases SLC7A11 expression in HT-1080 cells with basal *system* X_c^- activity (34). Knockdown of p53 completely abrogates the inhibition of SLC7A11 (35), and *system* X_c^- function and SLC7A11 expression in $p53^{KO}$ cells are insensitive to nutlin-3 (36). Furthermore, microarray analysis confirmed that SLC7A11 is a novel target gene of p53 in a tetracycline-controlled p53-inducible cell line (13). A previous study identified a p53-binding sequence at the 5′ flanking region of the SLC7A11 gene and subsequently confirmed the formation of a p53–DNA complex at the promoter region (13). The transcriptional repression of p53 on SLC7A11 leads to the destruction of cystine import, resulting in declined glutathione production and enhanced ROS-mediated ferroptosis (**Figure 2**).

p53-Dependent Repression of SLC7A11 Is Independent of p53 Mutation

The molecular cascade whereby p53 restrains cystine transfer by suppressing SLC7A11 expression to induce ferroptosis may be conducive to the oncosuppressive roles of p53 (13). Although an acetylation-absent $p53^{3KR}$ (K117/161/162R) variant at certain lysine residues cannot transcriptionally activate gene expression involved in pro-apoptotic and cell cycle arrest, knock-in mice expressing $p53^{3KR}$ are not tumor prone and exhibit similar overall survival with the wild-type mice (12). Similarly, studies on $p53^{25,26}$, a transactivation-compromised mutant variant of p53, displayed intact tumor suppression of $p53^{3KR}$ in the absence of the most downstream genes of p53 (10). Reduced levels of SLC7A11 expression caused by the $p53^{3KR}$ variant in xenograft tumor models lead to an apparent depression of tumor growth (13). This finding indicates that the intact p53-SLC7A11 axis, reserved in the $p53^{3KR}$ variant, promotes the inhibition

TABLE 1 | The mechanisms of transcriptional and post-translational regulation on metabolic genes involving in ferroptosis.

Active style	Targets	Function	References
Transcriptional regulation	GLUT1, GLUT4	Negatively regulates glycolysis by transcriptional repression	(14)
	TIGAR	Negatively regulates glycolysis by transactivation	(15–17)
	GLS2	Favoring aerobic glycolysis over oxidative phosphorylation and contributing to Warburg metabolism	(11, 18–20)
	SCO2	Coupling p53 to mitochondrial respiration provides a possible interpretation for the Warburg phenomenon	(13, 21)
	SLC7A11	Repression of SLC7A11 leads to destruction of cystine import, resulting in declined glutathione production and enhanced ROS-mediated ferroptosis	(9, 15)
	RRAD	Negatively regulates glycolysis	(17)
	SAT1	lipid peroxidation and ROS-induced ferroptosis	(22)
	p21	Slower depletion of intracellular glutathione and a reduced accumulation of toxic L-ROS	(23)
Post-translational regulation	G6PDH	Suppress glucose metabolism directly via binding and inhibiting with G6PDH	(24)
	DPP4	Dismantling of DPP4-p53 complex	(25)
	SOSC1	The regulation of SAT1 by p53 was SOCS1-dependent, stabilizating p53	(26)

of tumorigenesis independent of the conventional tumor suppression mechanisms of p53. Thus, ferroptosis can ensue from the transcriptional repression of SLC7A11 in a p53-dependent mechanism in response to stress, irrespective of p53 mutational status (37).

However, whether cell ferroptosis upon ROS-induced by $p53^{3KR}$ in human cancer cells is similar to that of wild-type p53 remains unclear. In addition, whether cyclophilin D could be a downstream responder of p53 activation has yet to be clarified (38).

Acetylation Is Crucial for p53-Mediated Ferroptosis

p53 activity is controlled by a complex fine-tuning network that includes protein stability, recruitment of co-inhibitor or activator, and various post-translational modifications, such as acetylation, ubiquitination, phosphorylation, and methylation (25, 39). In particular, acetylation of p53 serves a vital role in regulating downstream targets in a promoter-specific activation during stress responses. Acetylation of p53 at K120 by Tip60/MOF is crucial for p53-induced apoptosis (40). Nevertheless, p53-mediated cell cycle arrest is involved in the combinative acetylation of K120 by Tip60/MOF and K164 by CBP/p300 (41). The $p53^{3KR}$ mouse expressing acetylation-deficient p53, similar to the K120/164R mutations in human, displays intact p53-dependent metabolic regulation but lacks p53 functions in pro-apoptosis activity and growth arrest (12).

A recent study has found that p53 is acetylated at lysine residue K98 by acetyltransferase CBP. Acetylation of p53 at K98 lysine residue in mouse does not interfere with the steady-state, DNA-binding abilities and transcriptional activity of p53. However, combinatorial absence of K117/161/162 acetylation and K98 acetylation abrogates p53-mediated transcriptional regulation on SLC7A11, TIGAR, and GLS2 (32).

Binding of p53 With DPP4 Limits Ferroptosis by Regulating SLC7A11

Although p53 induces ferroptosis in a transcription-dependent manner in various cancers, in human colorectal cancer (CRC), it unusually functions in the regulation of erastin-mediated ferroptosis. p53-deficiency contributes to the increased lipid oxidation and GSH downregulation in CRC cells treated with erastin (42). Interestingly, the aforementioned alterations in malondialdehyde and GSH were recovered after transfecting p53 cDNA into $p53^{-/-}$ CRC cells (42).

Depletion of p53 contributing to ferroptosis is involved with interdicting dipeptidyl-peptidase-4 (DPP4) activity in a transcription-independent mechanism. DPP4, a membrane-bound dimeric peptidase, is widely expressed in different cell types and can cleave and degrade various bioactive peptides biologically (43, 44). The function of DPP4 in tumorigenicity has been studied in many tumors (45). Deviant expression of DPP4 is associated with tumor aggressiveness in different cancers (18, 46). Paradoxically, some advanced malignancies, including lung squamous cell carcinoma and endometrial carcinoma, show the absence of DPP4 (22). Thus, DPP4 may play different roles in different backgrounds or cancers, and further studies are needed to elucidate the exact mechanism of DPP4 in cancer.

DPP4 has been related to increased proportion of cancer stem cells and worse prognosis of CRC patients (16). Loss of p53 restrains the nuclear localization of DPP4 and boosts plasma-membrane-associated DPP4-dependent lipid peroxidation in CRC cells; then, the DPP4–NOX complex is formed and facilitates lipid peroxidation-induced ferroptosis. p53 antagonizes ferroptosis in CRC cells by facilitating DPP4 into nuclear to form the DPP4–p53 complex; dismantling of the DPP4–p53 complex can recover the ferroptosis sensitivity of CRC cells to erastin (**Figure 3**). This mechanism differs from the previously recognized role of p53 as a positive regulator of ferroptosis in non-CRC cells (13, 32, 47, 48). Thus, the

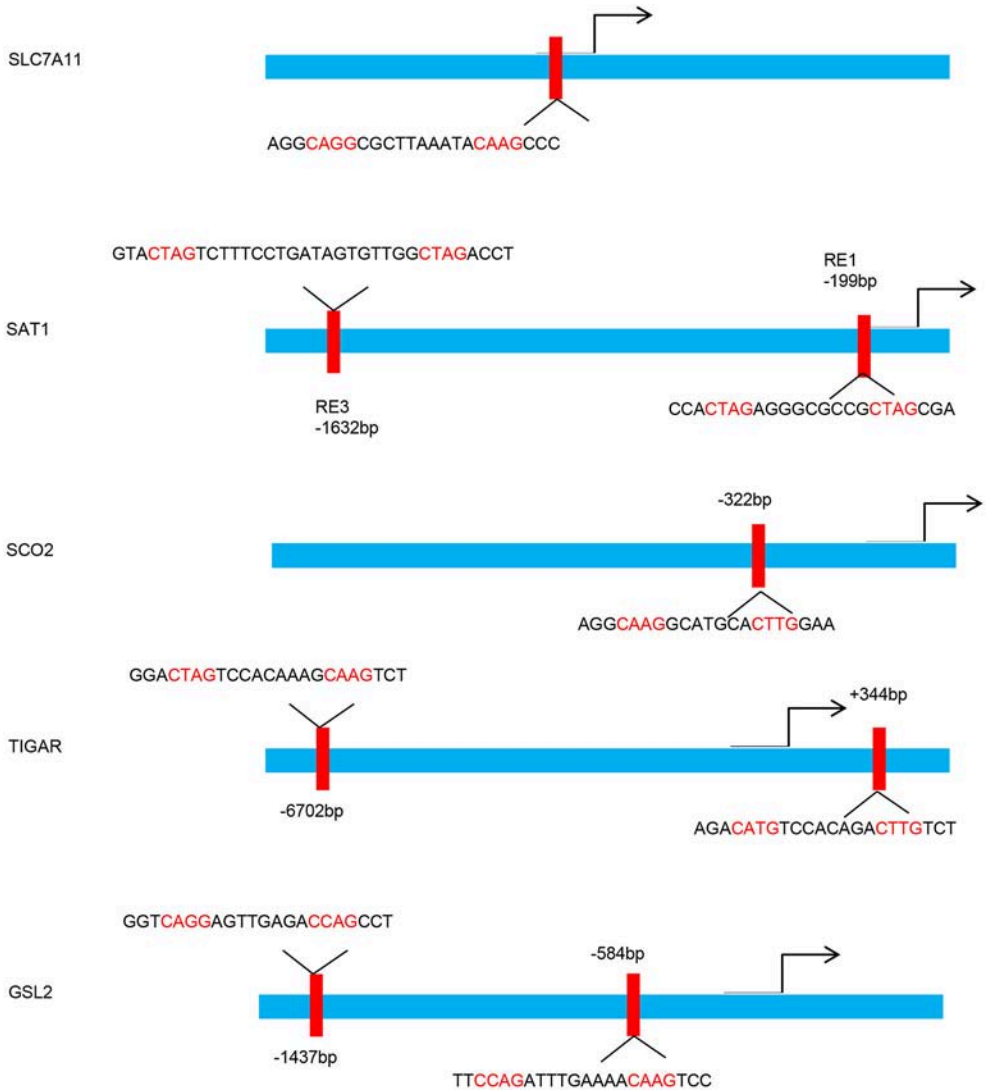

FIGURE 1 | p53 binding sites within the upstream regulatory region of the target gene promoters. Schematic diagram indicates the p53 binding sites within the upstream regulatory region of the SLC7A11, SAT1, SCO2, TIGAR, and GSL2 promoters.

bidirectional regulation of ferroptosis by p53 in a transcription-dependent and transcription-independent manner is dependent on tumor types and background.

However, many vital questions need to be elucidated. First, only two types of CRC cell lines are used in Xie's experiment (42), which is insufficient to prove the role of p53 and DPP4 on ferroptosis in CRC. Second, DPP4 is ubiquitously expressed in various cell types, including different tumors, whereas mutations and deletions of p53 are also common in malignant tumors. Further studies are needed to reveal the mechanism underlying the different roles of the DPP4–p53 complex on the regulation of SLC7A11 in CRC and other types of malignant tumors. Third, whether that p53 favors the localization of DPP4 into nuclear to form the DPP4–p53 complex could be affected by the mutation of p53 or modification of p53, such as acetylation, should be illuminated, and this may provide an answer to the opposite effects of p53 in different cellular context.

P53 REPRESSES THE TIGAR, GLS2, SCO2, AND SAT1 GENES TO MEDIATE FERROPTOSIS

TIGAR Plays an Antioxidant Functions in a p53-Dependent Manner

As a target of p53, TIGAR is prefigured to participate in tumor suppression and plays a role in antioxidant functions, which is in line with its functions in preventing cells from the acquirement of injury (49) (**Figure 2**). Nevertheless, in mouse models, the absence of TIGAR reduces capabilities to regenerate injured intestinal epithelium and represses tumor development with

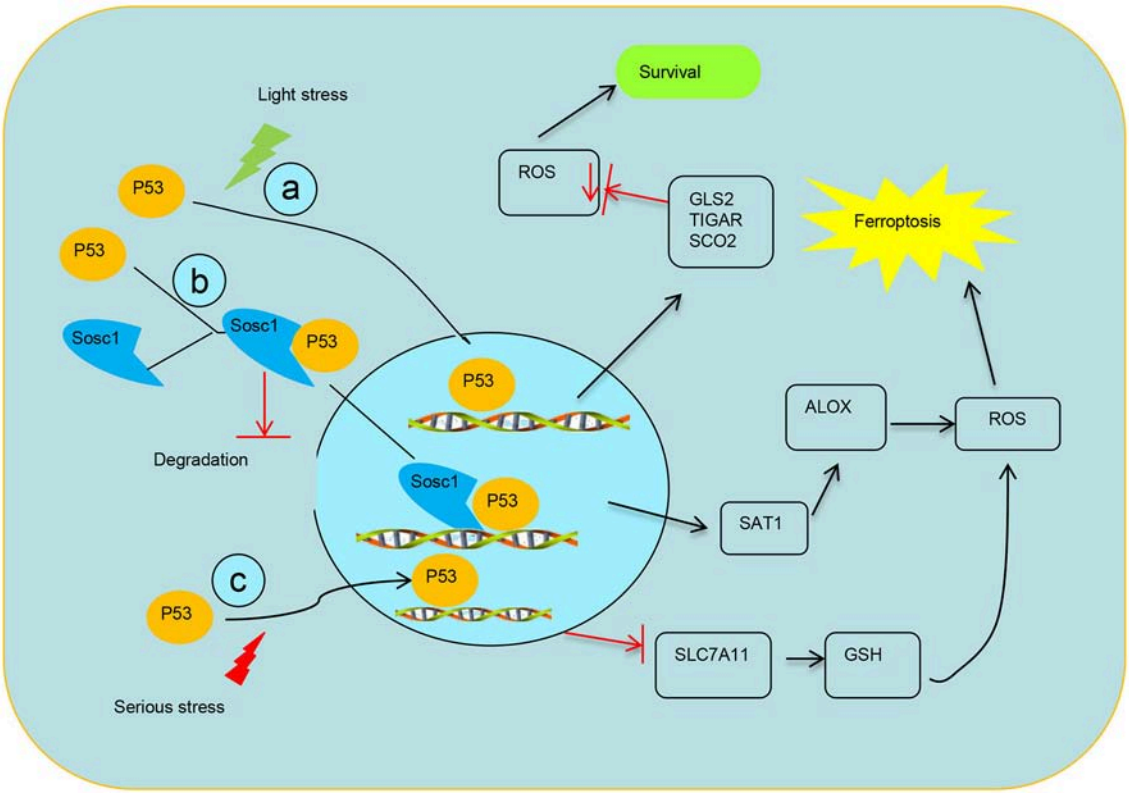

FIGURE 2 | Schematic diagram of transcriptional regulation of p53 on targets. **(a)** p53 transcriptionally represses the expression TIGAR, GLS2, and SCO2 to mediate ferroptosis. **(b)** SOCS1 is required for p53 modulating some target genes and SOCS1–p53 complex preserves a pool of preactive p53 via preventing p53 degradation. **(c)** Modulation of p53 on the expression of SLC7A11 system X_c^- activity to mediate ferroptosis.

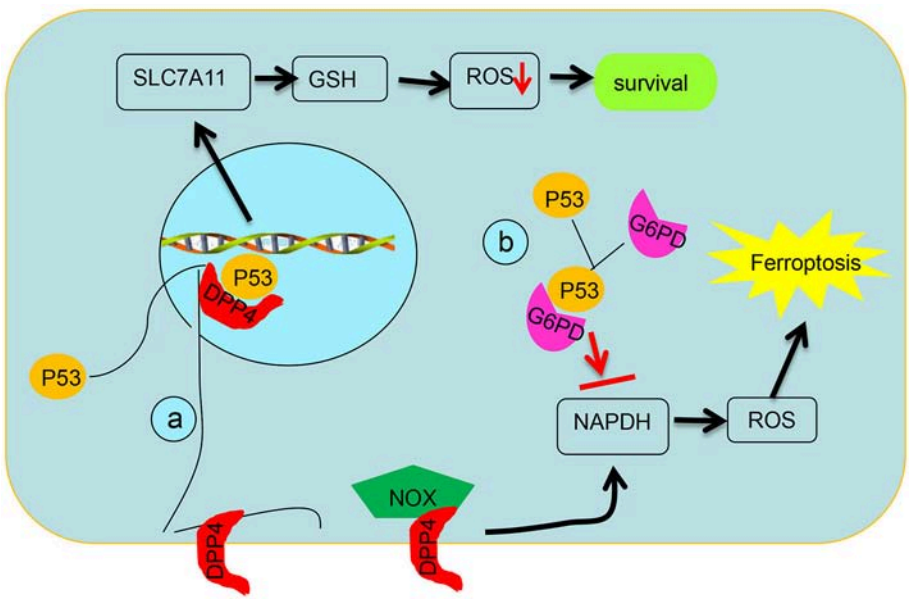

FIGURE 3 | Schematic diagram of post-translational regulation of p53 on targets. **(a)** p53 antagonizes ferroptosis by favoring DPP4 into a nuclear to form of the DPP4–p53 complex and impeding formation of the DPP4–NOX complex, which is required for lipid peroxidation in ferroptosis. **(b)** p53 suppresses glucose metabolism and production of NADPH via inhibiting glucose-6-phosphate dehydrogenase directly.

ROS restriction (50). TIGAR is upregulated in some cancer models and tumor types via a pattern that may be independent on the maintenance of p53 (51, 52). Furthermore, TIGAR expression negatively correlates with p53 expression in human breast cancer (53). p53-independent expression of TIGAR is poorly understood, although some transcription factors, such as SP1, CREB, and other members of the p53 family (p63 and p73), have been implicated in the regulation of p53 (17, 19, 54). In brief, these results highlight that TIGAR functions as a tumor suppressor in response to p53 but might also participate in cancer development when TIGAR expression is deregulated and uncoupled from p53 (20).

GLS2 Plays an Antioxidant Functions in a p53-Dependent Manner

Glutaminolysis plays crucial roles in ferroptosis (27). Glutaminolysis refers to the switch of glutamine into glutamate under the catalysis of GLS1 and GLS2. Although both enzymes are similar in structure and enzyme catalysis, GLS2 is required for ferroptosis (27). Human GLS2 gene is located on chromosome 12q13 and contains two potential p53 binding sites (BS). Adenovirus-mediated expression of p53 binds to both BS1 and BS2, but only BS2 is associated with endogenous p53. These data show that p53, once activated, can directly combine with BS2 in the GLS2 promoter and augment the mRNA expression of GLS2 (21). Upregulation of GLS2 contributes to p53-dependent ferroptosis by favoring aerobic glycolysis over oxidative phosphorylation and contributing to Warburg effect (27, 47, 55, 56) (**Figure 2**).

p53-Mediate Metabolisms via Repressing the SCO2

Synthesis of SCO2 is essential for regulating the cytochrome c oxidase complex, which is the main site of oxygen utilization in eukaryotic cells. The balance between the utilization of respiratory and glycolytic pathways is modulated by SCO2, which is a downstream target of p53 (57) (**Figure 2**). The source of energy from cellular respiration to glycolysis caused by the loss of p53 function resembles metabolic switch toward glycolysis in cancer cells with wild-type p53 when the SCO2 gene is depleted. SCO2 coupling p53 to mitochondrial respiration provides a possible interpretation for the Warburg phenomenon and supplies new ideas as to how p53 influences metabolism and ferroptosis (28).

P53-MEDIATED ACTIVATION OF SAT1 ENGAGES IN FERROPTOSIS

The polyamines, amino acid-derived polycationic alkylamines, are basic for the growth and survival of eukaryotic cells (58). Polyamine metabolism is frequently dysregulated in cancers (59). Spermidine/spermine N1-acetyltransferase 1 (SAT1), a rate-limiting enzyme, catalyzes the acetylation of spermidine and spermine into N1-acetylspermidine and N1-acetylspermine (60).

SAT1 could be highly induced by p53 (48). It is a p53-regulated target in wild-type p53 melanoma cells treated with Nutlin using RNA sequencing and two p53-binding sites have been found on the promoter region of SAT1. SAT1 transcriptionally activated in a p53-dependented manner is critical for lipid peroxidation and ROS-induced ferroptosis, and decreased expression of SAT1 significantly abrogates p53-induced ferroptosis. Elevation of prostaglandin-endoperoxide synthase 2 (PTGS2), a ferroptosis inducer, was identified in high-SAT1-expression xenograft tumors. Ferroptosis induced by SAT1 is arachidonate 15-lipoxygenase (ALOX15) dependent (**Figure 2**). ALOX15 is a lipoxygenase that catalyzes the peroxidation of arachidonic acid, and inhibition of ALOX15 can entirely rescue SAT1-induced ferroptosis. These results are consistent with the previous finding that ALOX15 is a main adjuster with which oxidative stress is transformed into lipid peroxidation and cell death (61). Nevertheless, whether that SAT1 plays a role in tumor suppression remains largely unknown.

SOCS1 REGULATES FERROPTOSIS BY ACTIVATING P53 VIA PHOSPHORYLATION AND STABILIZATION

Suppressor of cytokine signaling (SOCS) family proteins have been implicated as negative feedback regulators of cytokine signaling pathways mediated by JAK-STAT (62). SOCS is involved in tumor development by regulating STATs in the background of aberrant activation of the JAK/STAT5 pathway. In particular, SOCS1 is thought to act as a pivotal tumor suppressor through negative regulation of JAKs and plays vital roles in tumor progression. Downregulated SOCS1 expression in various human cancers has been associated with dysregulation of cytokine receptor signaling pathways (63), whereas upregulated SOCS1 expression is associated with earlier tumor stages and better clinical outcomes in breast cancer (64).

A significant correlation exists between the expression of SOCS1 and the SOCS1-dependent p53 target genes in human fibroblasts, and SOCS1 is required for p53 activation (26, 65). SOCS1-regulated genes overlap with a set of genes induced by oxidized phospholipids, which has been recently linked to ferroptosis (66). The regulation of SAT1 by p53 is SOCS1-dependent, suggesting a role for SOCS1 in ferroptosis. Aside from influencing p53 target gene expression, SOCS1 also plays a general role in senescence by stabilizing the interactions of p53 with protein complexes at DNA damage foci (**Figure 2**). This function of SOCS1 allows the maintenance of a pool of preactive p53 that could be slowly released and contribute to generate a lasting chronic p53 response (67). SOCS1 activates the functions of p53 via facilitating the serine 15 phosphorylation of p53 and stabilizing p53 by interfering with KAP1 (67).

DELAYED FERROPTOSIS ONSET REQUIRES P21

CDKN1A (encoding p21) is a well-characterized target of p53 and key mediator of p53-dependent cell-cycle progression. p21 upregulation could cause a coordinated p53-mediated response that normally decreases cystine import to match the lower

metabolic demands of growth-arrested cells. The impact of p21 on GSH metabolism renders it a reasonable target for inducing ferroptosis in the context of p53 (68). Stabilization of p53 and activation of the p53–p21 axis make many cancer cells insensitive to ferroptosis induced by *system* X_c^- inhibition or direct cystine deprivation. p21-dependent suppression of CDKs may be required to preserve GSH by regulating CDK-regulated metabolic enzymes and inhibit ferroptosis by inducing a complete cell-cycle arrest (69). However, the mechanism through which the p53–p21 axis reduces cellular reliance on *system* X_c^--mediated cystine import and ongoing *de novo* GSH synthesis is unclear (36). Thus, the p53–p21 axis may help cancer cell survive metabolic stress, such as cystine deprivation, by suppressing the onset of ferroptosis, indicating that the p53–p21 transcriptional axis negatively regulates ferroptosis in cancer cells.

S47 POLYMORPHISM OF P53 DECREASES FERROPTOSIS

Aside from mutations that impair p53 activity, single-nucleotide polymorphisms of p53 also alter cancer risk and clinical outcome significantly by impairing p53 signaling. About 20 years earlier, a naturally occurring polymorphism in p53 was discovered in Africans and African Americans; this polymorphism transforms the proline residue adjacent to Ser46 to a serine in human p53 (70). In particular, the Pro47Ser polymorphism (S47) impairs p53 apoptotic and transcriptional functions through reducing phosphorylation on serine 46 (47, 55). The defect in p53 function is traced to a restriction in downstream gene regulation that reduces cell ferroptosis in response to stress (70).

Profound cell death is induced in wild-type MEFs cells treated with erastin. However, cell viability assays certified that S47 MEFs and heterozygote S47/wild-type MEFs are resistant to erastin, especially S47 MEFs (47). Interestingly, treatment with erastin remarkably upregulates GLS2 expression in wild-type cells but not S47 cells, and depletion of GLS2 in wild-type MEFs recapitulates the cell death defect that is exhibited in S47 cells treated with erastin (47). The defective capacity of S47 to transactivate GLS2 might annotate the ferroptosis defect and tumor-prone characteristics of S47 mice (55).

In brief, elucidating the relevancy between p53 and ferroptosis has shown the other features of p53 biology and provided insights into the tumor suppression roles of p53. Clarification of the mechanism provides further insights into exploiting feasible therapeutic means through inducing ferroptosis defined by the occurrence of ROS in p53-retaining tumors. Nevertheless, the roles of p53 in ferroptosis remain formally demonstrated in different contexts due to the appearance of opposite effects in various cancer cells. Moreover, p53 could protect cells from slight stress damage via eliminating ROS, but p53-mediated ferroptosis owing to serious stress in cancer cells relies on the accumulation of ROS. Nevertheless, the mechanism of p53-mediated ROS production underlying cellular response is poorly understood.

AUTHOR CONTRIBUTIONS

WZ and CG took part in the writing of the article. DD and FW participated in the data arrangement and drawing. WL examined and verified the article.

FUNDING

This work was supported by grants from the National Natural Science Foundation of China (81774125, 81572578).

REFERENCES

1. Dixon SJ, Lemberg KM, Lamprecht MR, Skouta R, Zaitsev EM, Gleason CE, et al. Ferroptosis: an iron-dependent form of nonapoptotic cell death. *Cell* (2012) 149:1060–72. doi: 10.1016/j.cell.2012.03.042
2. Xie Y, Hou W, Song X, Yu Y, Huang J, Sun X, et al. Ferroptosis: process and function. *Cell Death Differ.* (2016) 23:369–79. doi: 10.1038/cdd.2015.158
3. Yagoda N, von Rechenberg M, Zaganjor E, Bauer AJ, Yang WS, Fridman DJ, Wolpaw AJ, et al. RAS-RAF-MEK-dependent oxidative cell death involving voltage-dependent anion channels. *Nature* (2007) 447:864–8. doi: 10.1038/nature05859
4. Conrad M, Angeli JP, Vandenabeele P, Stockwell BR. Regulated necrosis: disease relevance and therapeutic opportunities. *Nat Rev Drug Discov.* (2016) 15:348–66. doi: 10.1038/nrd.2015.6
5. Yang WS, SriRamaratnam R, Welsch ME, Shimada K, Skouta R, Viswanathan VS, et al. Regulation of ferroptotic cancer cell death by GPX4. *Cell* (2014) 156:317–31. doi: 10.1016/j.cell.2013.12.010
6. Woo JH, Shimoni Y, Yang WS, Subramaniam P, Iyer A, Nicoletti P, et al. Elucidating compound mechanism of action by network perturbation analysis. *Cell* (2015) 162:441–51. doi: 10.1016/j.cell.2015.05.056
7. Jackson JG, Lozano G. The mutant p53 mouse as a pre-clinical model. *Oncogene* (2013) 32:4325–30. doi: 10.1038/onc.2012.610
8. Wang SJ, Gu W. To be, or not to be: functional dilemma of p53 metabolic regulation. *Curr Opin Oncol.* (2014) 26:78–85. doi: 10.1097/CCO.0000000000000024
9. Junttila MR, Evan GI. p53–a Jack of all trades but master of none. *Nat Rev Cancer* (2009) 9:821–9. doi: 10.1038/nrc2728
10. Brady CA, Jiang D, Mello SS, Johnson TM, Jarvis LA, Kozak MM, et al. Distinct p53 transcriptional programs dictate acute DNA-damage responses and tumor suppression. *Cell* (2011) 145:571–83. doi: 10.1016/j.cell.2011.03.035
11. Jiang D, Brady CA, Johnson TM, Lee EY, Park EJ, Scott MP, et al. Full p53 transcriptional activation potential is dispensable for tumor suppression in diverse lineages. *Proc Natl Acad Sci USA.* (2011) 108:17123–8. doi: 10.1073/pnas.1111245108
12. Li T, Kon N, Jiang L, Tan M, Ludwig T, Zhao Y, et al. Tumor suppression in the absence of p53-mediated cell-cycle arrest, apoptosis, and senescence. *Cell* (2012) 149:1269–83. doi: 10.1016/j.cell.2012.04.026
13. Jiang L, Kon N, Li T, Wang SJ, Su T, Hibshoosh H, et al. Ferroptosis as a p53-mediated activity during tumour suppression. *Nature* (2015) 520:57–62. doi: 10.1038/nature14344
14. Torii S, Shintoku R, Kubota C, Yaegashi M, Torii R, Sasaki M, et al. An essential role for functional lysosomes in ferroptosis of cancer cells. *Biochem J.* (2016) 473:769–77. doi: 10.1042/BJ20150658
15. Hu W, Zhang C, Wu R, Sun Y, Levine A, Feng Z. Glutaminase 2, a novel p53 target gene regulating energy metabolism and antioxidant function. *Proc Natl Acad Sci USA.* (2010) 107:7455–60. doi: 10.1073/pnas.1001006107
16. Pang R, Law WL, Chu AC, Poon JT, Lam CS, Chow AK, et al. A subpopulation of CD26+ cancer stem cells with metastatic capacity in human colorectal cancer. *Cell Stem Cell* (2010) 6:603–15. doi: 10.1016/j.stem.2010.04.001

17. Zou S, Gu Z, Ni P, Liu X, Wang J, Fan Q. SP1 plays a pivotal role for basal activity of TIGAR promoter in liver cancer cell lines. *Mol Cell Biochem.* (2012) 359:17–23. doi: 10.1007/s11010-011-0993-0
18. Yamaguchi U, Nakayama R, Honda K, Ichikawa H, Hasegawa T, Shitashige M, et al. Distinct gene expression-defined classes of gastrointestinal stromal tumor. *J Clin Oncol.* (2008) 26:4100–8. doi: 10.1200/JCO.2007.14.2331
19. Lee P, Hock AK, Vousden KH, Cheung EC. p53- and p73-independent activation of TIGAR expression *in vivo*. *Cell Death Dis.* (2015) 6:e1842. doi: 10.1038/cddis.2015.205
20. Gnanapradeepan K, Basu S, Barnoud T, Budina-Kolomets A, Kung CP, Murphy ME. The p53 tumor suppressor in the control of metabolism and ferroptosis. *Front Endocrinol.* (2018) 9:124. doi: 10.3389/fendo.2018.00124
21. Suzuki S, Tanaka T, Poyurovsky MV, Nagano H, Mayama T, Ohkubo S, et al. Phosphate-activated glutaminase (GLS2), a p53-inducible regulator of glutamine metabolism and reactive oxygen species. *Proc Natl Acad Sci USA.* (2010) 107:7461–6. doi: 10.1073/pnas.1002459107
22. Kajiyama H, Kikkawa F, Ino K, Shibata K, Mizutani S. Expression of CD26/dipeptidyl peptidase IV in endometrial adenocarcinoma and its negative correlation with tumor grade. *Adv Exp Med Biol.* (2003) 524:245–8. doi: 10.1007/0-306-47920-6_29
23. Lo M, Ling V, Wang YZ, Gout PW. The xc- cystine/glutamate antiporter: a mediator of pancreatic cancer growth with a role in drug resistance. *Br J Cancer* (2008) 99:464–72. doi: 10.1038/sj.bjc.6604485
24. Schwartzenberg-Bar-Yoseph F, Armoni M, Karnieli E. The tumor suppressor p53 down-regulates glucose transporters GLUT1 and GLUT4 gene expression. *Cancer Res.* (2004) 64:2627–33. doi: 10.1158/0008-5472.CAN-03-0846
25. Kruse JP, Gu W. Modes of p53 regulation. *Cell* (2009) 137:609–22. doi: 10.1016/j.cell.2009.04.050
26. Mallette FA, Calabrese V, Ilangumaran S, Ferbeyre G. SOCS1, a novel interaction partner of p53 controlling oncogene-induced senescence. *Aging* (2010) 2:445–52. doi: 10.18632/aging.100163
27. Gao M, Monian P, Quadri N, Ramasamy R, Jiang X. Glutaminolysis and transferrin regulate ferroptosis. *Mol Cell* (2015) 59:298–308. doi: 10.1016/j.molcel.2015.06.011
28. Matoba S, Kang JG, Patino WD, Wragg A, Boehm M, Gavrilova O, et al. p53 regulates mitochondrial respiration. *Science* (2006) 312:1650–3. doi: 10.1126/science.1126863
29. Bensaad K, Tsuruta A, Selak MA, Vidal MN, Nakano K, Bartrons R, et al. TIGAR, a p53-inducible regulator of glycolysis and apoptosis. *Cell* (2006) 126:107–20. doi: 10.1016/j.cell.2006.05.036
30. Jiang P, Du W, Wang X, Mancuso A, Gao X, Wu M, et al. p53 regulates biosynthesis through direct inactivation of glucose-6-phosphate dehydrogenase. *Nat Cell Biol.* (2011) 13:310–6. doi: 10.1038/ncb2172
31. Conrad M, Sato H. The oxidative stress-inducible cystine/glutamate antiporter, system x (c) (-) : cystine supplier and beyond. *Amino Acids* (2012) 42:231–46. doi: 10.1007/s00726-011-0867-5
32. Wang SJ, Li D, Ou Y, Jiang L, Chen Y, Zhao Y, et al. Acetylation is crucial for p53-mediated ferroptosis and tumor suppression. *Cell Rep.* (2016) 17:366–73. doi: 10.1016/j.celrep.2016.09.022
33. Bridges RJ, Natale NR, Patel SA. System xc(-) cystine/glutamate antiporter: an update on molecular pharmacology and roles within the CNS. *Br J Pharmacol.* (2012) 165:20–34. doi: 10.1111/j.1476-5381.2011.01480.x
34. Dixon SJ, Patel DN, Welsch M, Skouta R, Lee ED, Hayano M, et al. Pharmacological inhibition of cystine-glutamate exchange induces endoplasmic reticulum stress and ferroptosis. *Elife* (2014) 3:e02523. doi: 10.7554/eLife.02523
35. Gupta AK, Bharadwaj M, Kumar A, Mehrotra R. Spiro-oxindoles as a promising class of small molecule inhibitors of p53-MDM2 interaction useful in targeted cancer therapy. *Top Curr Chem.* (2017) 375:3. doi: 10.1007/s41061-016-0089-0
36. Tarangelo A, Magtanong L, Bieging-Rolett KT, Li Y, Ye J, Attardi LD, et al. p53 suppresses metabolic stress-induced ferroptosis in cancer cells. *Cell Rep.* (2018) 22:569–75. doi: 10.1016/j.celrep.2017.12.077
37. Galluzzi L, Bravo-San Pedro JM, Kroemer G. Ferroptosis in p53-dependent oncosuppression and organismal homeostasis. *Cell Death Differ.* (2015) 22:1237–8. doi: 10.1038/cdd.2015.54
38. Ying Y, Padanilam BJ. Regulation of necrotic cell death: p53, PARP1 and cyclophilin D-overlapping pathways of regulated necrosis? *Cell Mol Life Sci.* (2016) 73:2309–24. doi: 10.1007/s00018-016-2202-5
39. Eischen CM, Lozano G. The Mdm network and its regulation of p53 activities: a rheostat of cancer risk. *Hum Mutat.* (2014) 35:728–37. doi: 10.1002/humu.22524
40. Sykes SM, Mellert HS, Holbert MA, Li K, Marmorstein R, Lane WS, et al. Acetylation of the p53 DNA-binding domain regulates apoptosis induction. *Mol Cell* (2006) 24:841–51. doi: 10.1016/j.molcel.2006.11.026
41. Tang Y, Zhao W, Chen Y, Zhao Y, Gu W. Acetylation is indispensable for p53 activation. *Cell* (2008) 133:612–26. doi: 10.1016/j.cell.2008.03.025
42. Xie Y, Zhu S, Song X, Sun X, Fan Y, Liu J, et al. The tumor suppressor p53 limits ferroptosis by blocking DPP4 activity. *Cell Rep.* (2017) 20:1692–704. doi: 10.1016/j.celrep.2017.07.055
43. Liang PI, Yeh BW, Li WM, Chan TC, Chang IW, Huang CN, et al. DPP4/CD26 overexpression in urothelial carcinoma confers an independent prognostic impact and correlates with intrinsic biological aggressiveness. *Oncotarget* (2017) 8:2995–3008. doi: 10.18632/oncotarget.13820
44. Carl-McGrath S, Lendeckel U, Ebert M, Rocken C. Ectopeptidases in tumour biology: a review. *Histol Histopathol.* (2006) 21:1339–53. doi: 10.14670/HH-21.1339
45. Cordero OJ, Salgado FJ, Nogueira M. On the origin of serum CD26 and its altered concentration in cancer patients. *Cancer Immunol Immunother.* (2009) 58:1723–47. doi: 10.1007/s00262-009-0728-1
46. Stremenova J, Krepela E, Mares V, Trim J, Dbaly V, Marek J, et al. Expression and enzymatic activity of dipeptidyl peptidase-IV in human astrocytic tumours are associated with tumour grade. *Int J Oncol.* (2007) 31:785–92. doi: 10.3892/ijo.31.4.785
47. Jennis M, Kung CP, Basu S, Budina-Kolomets A, Leu JI, Khaku S, et al. An African-specific polymorphism in the TP53 gene impairs p53 tumor suppressor function in a mouse model. *Genes Dev.* (2016) 30:918–30. doi: 10.1101/gad.275891.115
48. Ou Y, Wang SJ, Li D, Chu B, Gu W. Activation of SAT1 engages polyamine metabolism with p53-mediated ferroptotic responses. *Proc Natl Acad Sci USA.* (2016) 113:E6806–12. doi: 10.1073/pnas.1607152113
49. Rajendran R, Garva R, Ashour H, Leung T, Stratford I, Krstic-Demonacos M, et al. Acetylation mediated by the p300/CBP-associated factor determines cellular energy metabolic pathways in cancer. *Int J Oncol.* (2013) 42:1961–72. doi: 10.3892/ijo.2013.1907
50. Cheung EC, Athineos D, Lee P, Ridgway RA, Lambie W, Nixon C, et al. TIGAR is required for efficient intestinal regeneration and tumorigenesis. *Dev Cell* (2013) 25:463–77. doi: 10.1016/j.devcel.2013.05.001
51. Li B, Wang Z, Xie JM, Wang G, Qian LQ, Guan XM, et al. TIGAR knockdown enhanced the anticancer effect of aescin via regulating autophagy and apoptosis in colorectal cancer cells. *Acta Pharmacol Sin.* (2018). doi: 10.1038/s41401-018-0001-2. [Epub ahead of print].
52. Shen M, Zhao X, Zhao L, Shi L, An S, Huang G, et al. Met is involved in TIGAR-regulated metastasis of non-small-cell lung cancer. *Mol Cancer* (2018) 17:88. doi: 10.1186/s12943-018-0839-4
53. Won KY, Lim SJ, Kim GY, Kim YW, Han SA, Song JY, et al. Regulatory role of p53 in cancer metabolism via SCO2 and TIGAR in human breast cancer. *Hum Pathol.* (2012) 43:221–8. doi: 10.1016/j.humpath.2011.04.021
54. Zou S, Wang X, Deng L, Wang Y, Huang B, Zhang N, et al. CREB, another culprit for TIGAR promoter activity and expression. *Biochem Biophys Res Commun.* (2013) 439:481–6. doi: 10.1016/j.bbrc.2013.08.098
55. Basu S, Barnoud T, Kung CP, Reiss M, Murphy ME. The African-specific S47 polymorphism of p53 alters chemosensitivity. *Cell Cycle* (2016) 15:2557–60. doi: 10.1080/15384101.2016.1215390
56. Zhang C, Liu J, Liang Y, Wu R, Zhao Y, Hong X, et al. Tumour-associated mutant p53 drives the Warburg effect. *Nat Commun.* (2013) 4:2935. doi: 10.1038/ncomms3935
57. Qi Z, He J, Su Y, He Q, Liu J, Yu L, et al. Physical exercise regulates p53 activity targeting SCO2 and increases mitochondrial COX biogenesis in cardiac muscle with age. *PLoS ONE* (2011) 6:e21140. doi: 10.1371/journal.pone.0021140
58. Gerner EW, Meyskens FL Jr. Polyamines and cancer: old molecules, new understanding. *Nat Rev Cancer* (2004) 4:781–92. doi: 10.1038/nrc1454

59. Casero RA Jr, Marton LJ. Targeting polyamine metabolism and function in cancer and other hyperproliferative diseases. *Nat Rev Drug Discov.* (2007) 6:373–90. doi: 10.1038/nrd2243
60. Pegg AE. Spermidine/spermine-N(1)-acetyltransferase: a key metabolic regulator. *Am J Physiol Endocrinol Metab.* (2008) 294:E995–1010. doi: 10.1152/ajpendo.90217.2008
61. Shintoku R, Takigawa Y, Yamada K, Kubota C, Yoshimoto Y, Takeuchi T, et al. Lipoxygenase-mediated generation of lipid peroxides enhances ferroptosis induced by erastin and RSL3. *Cancer Sci.* (2017) 108:2187–94. doi: 10.1111/cas.13380
62. Slattery ML, Lundgreen A, Kadlubar SA, Bondurant KL, Wolff RK. JAK/STAT/SOCS-signaling pathway and colon and rectal cancer. *Mol Carcinogen.* (2013) 52:155–66. doi: 10.1002/mc.21841
63. Jiang M, Zhang WW, Liu P, Yu W, Liu T, Yu J. Dysregulation of SOCS-mediated negative feedback of cytokine signaling in carcinogenesis and its significance in cancer treatment. *Front Immunol.* (2017) 8:70. doi: 10.3389/fimmu.2017.00070
64. Sasi W, Jiang WG, Sharma A, Mokbel K. Higher expression levels of SOCS 1,3,4,7 are associated with earlier tumour stage and better clinical outcome in human breast cancer. *BMC Cancer* (2010) 10:178. doi: 10.1186/1471-2407-10-178
65. Calabrese V, Mallette FA, Deschenes-Simard X, Ramanathan S, Gagnon J, Moores A, et al. SOCS1 links cytokine signaling to p53 and senescence. *Mol Cell* (2009) 36:754–67. doi: 10.1016/j.molcel.2009.09.044
66. Kagan VE, Mao G, Qu F, Angeli JP, Doll S, Croix CS, et al. Oxidized arachidonic and adrenic PEs navigate cells to ferroptosis. *Nat Chem Biol.* (2017) 13:81–90. doi: 10.1038/nchembio.2238
67. Saint-Germain E, Mignacca L, Vernier M, Bobbala D, Ilangumaran S, Ferbeyre G. SOCS1 regulates senescence and ferroptosis by modulating the expression of p53 target genes. *Aging* (2017) 9:2137–62. doi: 10.18632/aging.101306
68. Maddocks OD, Berkers CR, Mason SM, Zheng L, Blyth K, Gottlieb E, et al. Serine starvation induces stress and p53-dependent metabolic remodelling in cancer cells. *Nature* (2013) 493:542–6. doi: 10.1038/nature11743
69. Ewald JC, Kuehne A, Zamboni N, Skotheim JM. The yeast cyclin-dependent kinase routes carbon fluxes to fuel cell cycle progression. *Mol Cell* (2016) 62:532–45. doi: 10.1016/j.molcel.2016.02.017
70. Lane D. p53: out of Africa. *Genes Dev.* (2016) 30:876–77. doi: 10.1101/gad.281733.116

Conflict of Interest Statement: The authors declare that the research was conducted in the absence of any commercial or financial relationships that could be construed as a potential conflict of interest.

frontiers in Pharmacology

MINI REVIEW
published: 19 November 2018
doi: 10.3389/fphar.2018.01323

Applications of Ruthenium Complex in Tumor Diagnosis and Therapy

Ke Lin[1], Zi-Zhuo Zhao[2], Hua-Ben Bo[1], Xiao-Juan Hao[3] and Jin-Quan Wang[1]**

[1] School of Bioscience and Biopharmaceutics, Guangdong Province Key Laboratory for Biotechnology Drug Candidates, Guangdong Pharmaceutical University, Guangzhou, China, [2] Department of Ultrasound, Sun Yat-sen Memorial Hospital, Sun Yat-sen University, Guangzhou, China, [3] Manufacturing, Commonwealth Scientific and Industrial Research Organisation, Clayton, VIC, Australia

Ruthenium complexes are a new generation of metal antitumor drugs that are currently of great interest in multidisciplinary research. In this review article, we introduce the applications of ruthenium complexes in the diagnosis and therapy of tumors. We focus on the actions of ruthenium complexes on DNA, mitochondria, and endoplasmic reticulum of cells, as well as signaling pathways that induce tumor cell apoptosis, autophagy, and inhibition of angiogenesis. Furthermore, we highlight the use of ruthenium complexes as specific tumor cell probes to dynamically monitor the active biological component of the microenvironment and as excellent photosensitizer, catalyst, and bioimaging agents for phototherapies that significantly enhance the diagnosis and therapeutic effect on tumors. Finally, the combinational use of ruthenium complexes with existing clinical antitumor drugs to synergistically treat tumors is discussed.

Keywords: ruthenium complexes, antitumor, diagnosis and therapy, drug combinations, synergistic effect

OPEN ACCESS

Edited by:
Zhe-Sheng Chen,
St. John's University, United States

Reviewed by:
Leli Zeng,
Shenzhen University, China
Qingbin Cui,
Guangzhou Medical University, China
Lili Liu,
Guangdong Provincial Occupational Disease Prevention Hospital, China

****Correspondence:***
Xiao-Juan Hao
xiaojuan.hao@csiro.au
Jin-Quan Wang
wangjinquan@gdpu.edu.cn

Specialty section:
This article was submitted to Cancer Molecular Targets and Therapeutics, a section of the journal Frontiers in Pharmacology

Received: *27 September 2018*
Accepted: *29 October 2018*
Published: *19 November 2018*

Citation:
Lin K, Zhao Z-Z, Bo H-B, Hao X-J and Wang J-Q (2018) Applications of Ruthenium Complex in Tumor Diagnosis and Therapy. Front. Pharmacol. 9:1323. doi: 10.3389/fphar.2018.01323

INTRODUCTION

Chemotherapy is an important modality for cancer treatment. Since the introduction of metal chemotherapeutics represented by cisplatinum (**Figure 1A**), numerous metal agents have been developed as antitumor drugs, and platinum-based drugs have become the focus of metal-based antitumor drug research (Harper et al., 2010; Burger et al., 2011; Wang X. et al., 2015). In recent years, the platinum-based drugs have become the first line of anti-cancer drugs because of their significant antitumor efficacy (Jakupec et al., 2008; Gasser et al., 2011; Wang and Guo, 2013). However, there are increasing reports that platinum-based anticancer drugs have severe side effects including myelotoxicity, peripheral neuropathy et al. (Galanski, 2006; Samimi et al., 2007). Therefore, researchers have turned their attention to other potential metal antitumor drugs. Ruthenium complexes have shown remarkable antitumor activity among the numerous metal compounds studied; they possess various advantages over platinum drugs, such as potent efficacy, low toxicity, less drug resistance, and are expected to become a new generation of clinical metal antitumor drugs (Abid et al., 2016; Thota, 2016; Southam et al., 2017).

There are three main oxidation states of ruthenium compounds. The high oxidation state of Ru(IV) compound is unstable, which limited its further development (Duan et al., 2009). Ru(III) complexes have good stability of thermodynamics and kinetics, and can be used as prodrugs under biological circumstances of hypoxia, acidic pH and high level glutathione, showing antitumor effect by reducing to corresponding Ru(II) counterparts *in vivo* (Minchinton and Tannock, 2006; Antonarakis and Emadi, 2010). Ru(II) can directly kill tumor cells *via* multiple

mechanisms (Zeng et al., 2015). Ru(II) complexes have great photophysical and chemical properties as well as multiple exchanging ligands. Combining with their applicability as nanomaterials and they have demonstrated significant antitumor efficacy (Poynton et al., 2017). Generally, the thermodynamic and kinetic stability of Ru(II) compounds are higher than Ru(III) due to their lower oxidation states (Duan et al., 2009). In addition, the nature and net charge of the ligands play important roles in the kinetics of Ru(II) compounds hydration (Abid et al., 2016). Many Ru(II) compounds showed better antitumor activities than their corresponding Ru(III) counterpart *in vivo* (Minchinton and Tannock, 2006; Hartinger et al., 2013). Generally speaking, the following options are viable in improving the water solubility of ruthenium compounds. (i) modifying the ligand structures; (ii) constructing the supramolecular ruthenium compounds; (iii) encapsulating ruthenium compounds into nanomaterial systems. (Suss-Fink, 2010; Jiang et al., 2012; Schmitt et al., 2012).

All the following ruthenium complexes that have progressed to clinical studies, NAMI-A {ImH[*trans*-$RuCl_4$(dmso)(imidazole)]} (**Figure 1B**), KP1019 {indazolium *trans*-[tetrachlorobis(1H-indazole)ruthenate(III)]} (**Figure 1C**), and KP1339, are Ru(III) complexes (Webb et al., 2013). NAMI-A showed potent inhibitory efficacy on tumor metastasis. However, the phase II clinical studies revealed that it caused severe side effects in patients and, therefore, further investigations were not undertaken (Bergamo et al., 2003; Alessio et al., 2004). KP1019 had also failed to be investigated because of its poor water solubility, severe side effects and unsatisfactory efficacy for clinical study, (Hartinger et al., 2006, 2008). To improve the low water solubility of KP1019, researchers designed a more soluble sodium salt complex, KP1339 [Na(*trans*-$RuCl_4$ $(Ind)_2$)] (**Figure 1D**), which is currently used in clinical studies (Heffeter et al., 2010). Using the potent photophysical and chemical properties of Ru(II) complex, researchers have synthesized a photosensitizer TLD1443 (**Figure 1E**), which has immensely enhanced photodynamic therapy (Zeng et al., 2017a). It has a significant therapeutic efficacy on bladder cancer and is currently in phase II clinical trials (Smithen et al., 2017).

Based on the characteristics of ruthenium compound, optimizing its structure with relevant modification is a good strategy to improve its targeting capability and antitumor activity (Blanck et al., 2012). Researchers designed a series of lipophilic ruthenium complexes that effectively increase the uptake efficiency of tumor cells (Svensson et al., 2010; Matson et al., 2011). They found that the difference in the length of alkyl ether chains contributed to the different organelle-targeting properties of ruthenium complexes. Coupling of targeted polypeptides with ruthenium complexes is another effective way to enhance their targeting capability (Chakrabortty et al., 2017). In addition, encapsulating ruthenium complexes into nanomaterials can improve their targeting capability through the enhanced permeation and retention (EPR) effect (Frasconi et al., 2013; Wei et al., 2015). Capitalizing the properties of Ru(II) complexes, researchers have designed a series of nanoruthenium complexes including, Ru(II)-selenium nanoparticles (Sun et al., 2013), Ru(II)-gold nanocomplexes (Rogers et al., 2014), Ru(II)-silicon nanocomplexes (Frasconi et al., 2013), Ru(II)-carbon nanotubes (Wang N. et al., 2015), and some organic and biometallic nanoruthenium complexes (Chakrabortty et al., 2017) with direct antitumor effects. These nanoruthenium complexes can also be used as a good catalyst, photosensitizer and tracer to enhance the therapeutic effect (Chakrabortty et al., 2017).

ANTITUMOR TARGETS AND MECHANISMS OF RUTHENIUM COMPLEXES

Ruthenium complexes show multiple targets and diverse mechanisms for its antitumor properties (**Figure 2**). Some ruthenium complexes act on telomere DNA, some interfere with replication and transcription of DNA, and others inhibit related enzymes (Kurzwernhart et al., 2012; Jain et al., 2018). Furthermore, ruthenium complexes can block the cell cycle (Kou et al., 2012; Wang et al., 2016; De Carvalho et al., 2018) and induce the formation of DNA photocrosslinking products to prevent RNA polymerization enzymes or exonucleases from binding to DNA, thereby causing tumor cell apoptosis (Le Gac et al., 2009; Rickling et al., 2010). Studies have found that some dinuclear and polynuclear Ru(II) polypyridyl complexes bind stably to the G-quadruplex (G4-DNA) structure of telomere DNA (Hiyama et al., 1995; Ambrus et al., 2006), inhibiting telomerase activity and blocking the function of DNA replication, thus, preventing normal cells from developing into immortalized tumor cells (Rajput et al., 2006; Shi et al., 2008). Ruthenium complexes have good topoisomerase (Topo) inhibitory activity (Kurzwernhart et al., 2012); however, some studies have found that inhibition of one type of Topo increases the activity of others (Crump et al., 1999; Vey et al., 1999). To solve this problem, studies have been conducted to synthesize a ruthenium complex with dual inhibitory property on Topo I and Topo II, which significantly inhibits tumor cell proliferation (Du et al., 2011; Zhang et al., 2013). Researchers have also designed a ruthenium complex with dual inhibitory effects on G4-DNA and Topo (Liao et al., 2015), achieving multitarget synergy with strong apoptosis promoting effects on tumor cells. In addition, Hurley and co-workers reported a ruthenium complex with dual stabilizing effects on Topo and G4-DNA, which also inhibited some drug resistant tumor cells (Kim et al., 2003).

In addition, it was found that ruthenium complexes accumulate more in organelles, such as mitochondria, endoplasmic reticulum, and lysosome, than in nucleus (Puckett and Barton, 2007; Groessl et al., 2011). A number of studies have revealed that mitochondria is a key target of ruthenium complexes (Wang et al., 2014; Liu et al., 2015; Wan et al., 2017), because ruthenium complexes can quickly decrease the membrane potential of mitochondria, leading to mitochondrial dysfunction or activating mitochondrial apoptosis pathways. Furthermore, this effect promoted the expression of pro-apoptotic members of the B-cell lymphoma-2 (Bcl-2) family, releasing cytochrome c (Cyto C), and activating cascade reactions of the caspase family members to induce tumor cell apoptosis. The endoplasmic reticulum is a key participant in tumor cell

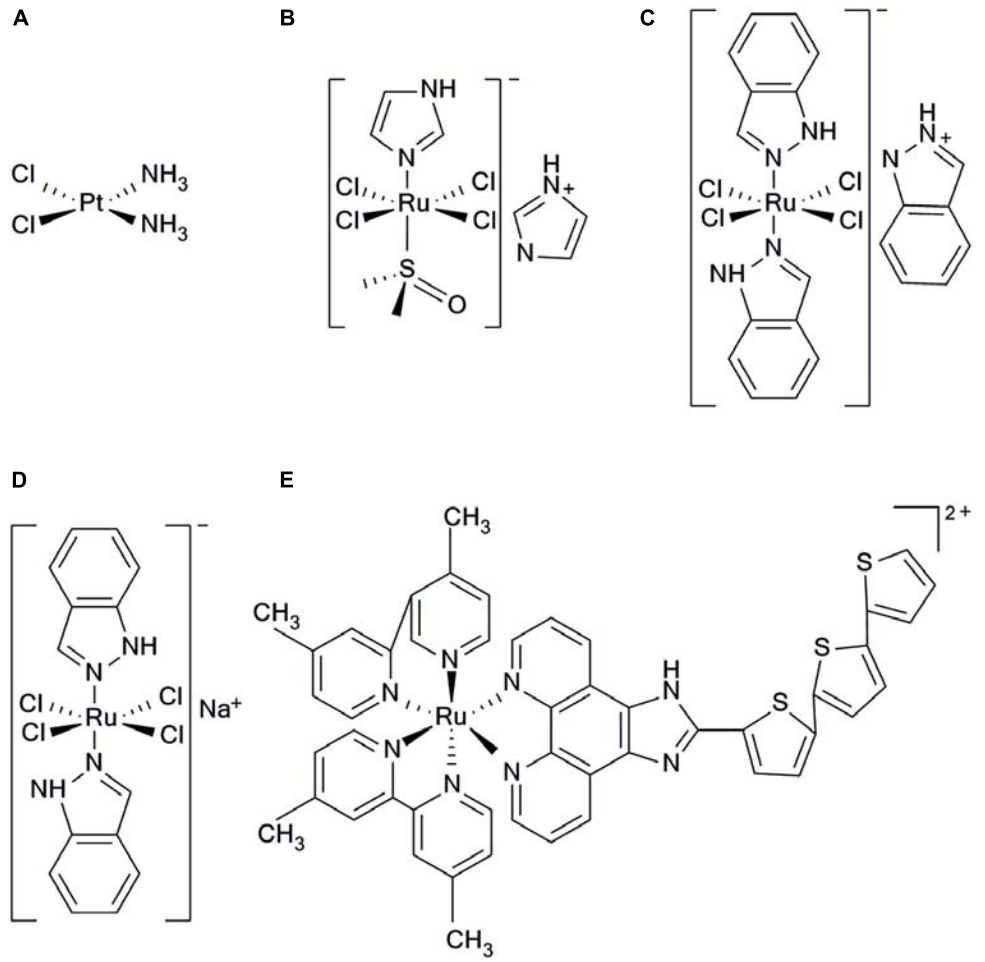

FIGURE 1 | Structure of five clinical complexes; **(A)** Cisplatinum, **(B)** NAMI-A, **(C)** KP1019, **(D)** KP1339, and **(E)** TLD1443.

apoptosis, autophagy, and drug resistance and, thus, is a target in antitumor research (Sano et al., 2012; Fernandez et al., 2015). Ruthenium complexes can target the endoplasmic reticulum, cause oxidative stress or endoplasmic reticulum stress (ERS), and induce tumor cell apoptosis by activating caspase family members (Gill et al., 2013; Sano and Reed, 2013). In addition, ruthenium complexes can target another significant participant in autophagy, the lysosomes, inducing autolysosome production and hydrolase release (Tan et al., 2010; Castonguay et al., 2012; Chen et al., 2016). Thereby, they increase apoptosis of tumor cells (Yuan et al., 2015).

A very important feature of ruthenium complexes is that it is effective against many platinum resistant tumors. Gasser et al. found that $[Ru(dppz)_2(CppH)]^{2+}$ (CppH = 2-(20-pyridyl)-pyrimidine-4-carboxylic acid)] accumulated in the mitochondria. Moreover, this Ru(II) complex showed more cytotoxic effect in cisplatin-resistant A2780/CP70 cells than cisplatin and less cytotoxic than cisplatin in normal MRC-5 cells (Pierroz et al., 2012). Dyson and co-workers also designed some ruthenium complexes which contained ethacrynic acid (EA) ligands that inhibited cisplatin resistant A2780cisR cells (Ang et al., 2007). Moreover, Chao's and Chen's group designed a series of mitochondria-targeted Ru(II) complexes, based on a 2-phenylimidazo[4,5-f] [1,10]phenanthroline (PIP) Ru(II) polypyridyl complexes. These complexes induced apoptosis *via* a mitochondrial pathway and were effective against cisplatin resistant tumor cells (Li et al., 2012c; Wang et al., 2014; Yu et al., 2014).

The membrane structure as a "protective barrier" not only regulates the entry of drug molecules into cells, but also acts as a direct target of drug molecules, effectively killing tumor cells. A number of studies have confirmed that ruthenium complexes directly act on cell membrane, changing its permeability to allow cellular content to flow out of cells and induce cell apoptosis (Deng et al., 2017). Using the photophysical properties of Ru(II) complexes, researchers designed a Ru(II) polypyridine complex that accumulates on mitochondrial membrane and tumor surface membrane. These complexes emit red phosphorescence and produce a large amount of $^1O_2$, thereby causing cytotoxicity and inducing cell apoptosis (Hess et al., 2017; Pal et al., 2018). Chao and colleagues synthesized Ru(II) pyridine complexes with two-photon performance and $^1O_2$ yield, which could serve as a

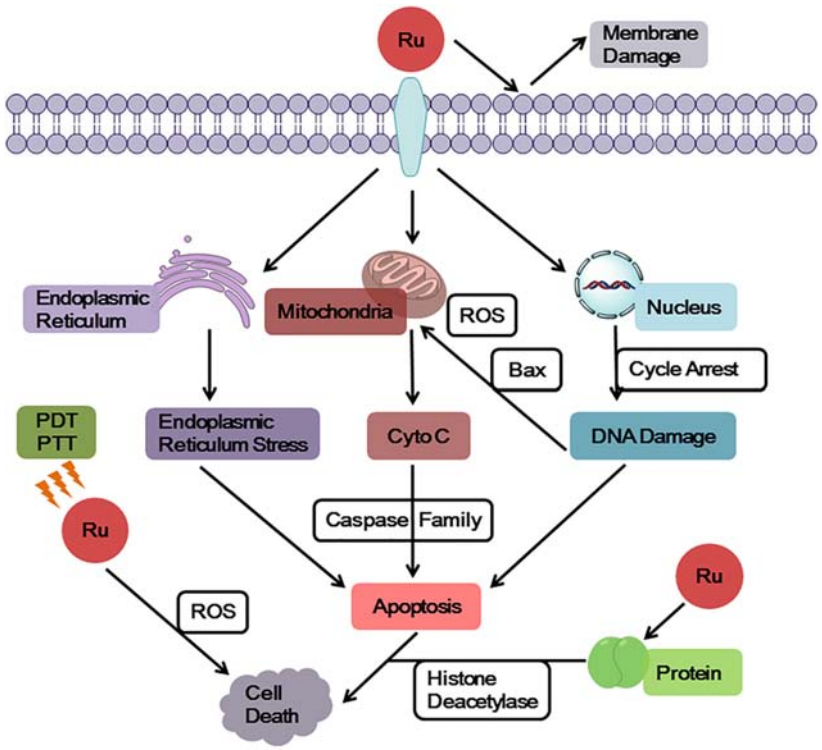

FIGURE 2 | General targets and mechanisms of anticancer action of ruthenium complexes.

photosensitizer to simultaneously target surface membrane and mitochondrial membrane of human cervical carcinoma (HeLa) cells, achieving a dual killing effect (Qiu et al., 2017).

THE USE OF RUTHENIUM COMPLEXES IN DIAGNOSIS AND TREATMENT OF TUMORS

The effective diagnosis and treatment of tumors is a major clinical challenge. Ruthenium complexes have shown promising application prospects to this difficulty. The combination of development and applications of subcellular targeting probes and bio-imaging technologies with the understanding of the occurrence and physiological development of tumors, is expected to facilitate the achievement of tumor-specific diagnosis and therapy. Ru(II) complexes have the advantages of considerable photothermal stability, large stokes shift, long luminescence lifetime, and low toxicity (Gill et al., 2009). They are ideal photosensitizers, catalysts, and imaging agents in phototherapy, and could serve as excellent probes and tracers for subcellular structure localization. Thomas and colleagues reported a lipophilic Ru(II) complex that can be used as a fluorescent probe, targeting the mitochondria and endoplasmic reticulum of human breast cancer cell (MCF-7), and it showed comparable cytotoxicity to that of cisplatin (Gill et al., 2013). In addition to targeting and imaging tumor subcellular structures, ruthenium complexes can also detect and specifically recognize biological components of the microenvironment. As a significant active ingredient in organisms, the level of thiol in tumor tissues can change rapidly. Specific recognition of the thiol level is important for tumor diagnosis and therapy (Dirican et al., 2016; Inal et al., 2017). The Ru(II)-gold nanocomplex synthesized by Chao and co-workers could be used as a specific two-photon probe for thiol level, as it detected biothiol levels in living HeLa cells and mouse hippocampus using two-photon microscopy, which provides a potent tool for molecular biology research in tumors (Zhang et al., 2014). The oxygen allotrope O_2 is an indispensable source of metabolic energy and could be specifically identified and used to monitor the local metabolites of tumor cells, which would facilitate tumor diagnosis and therapy. Keyes and colleagues found that a peptide-bridged dinuclear Ru(II) complex as the mitochondrial fluorescent probe can monitor the dynamic changes of O_2 concentration in mitochondria of HeLa cell, which could be used to monitor the malignant proliferation of tumor cells (Martin et al., 2014). The non-oxygen-dependent Ru(II) complex has been used as a photosensitizer in treating hypoxic tumors. This complex overcomes the limitations of low-depth-effect and low cell killing efficiency of phototherapy, significantly increasing $^1O_2$ production and fluorescence efficiency, thus, enhancing cytotoxicity of ruthenium complex and showing potent therapeutic effects (Volker et al., 2014; Sadhu et al., 2015; Cuello-Garibo et al., 2017).

The development of DNA structure recognition and imaging probes enables us to understand the pathogenesis of cancer at the genetic level, which has enhanced the study of antitumor

drugs. Using the optical switch effect of Ru(II) complex to DNA (Augustyn et al., 2007), a Ru(II) polypyridine complex as a DNA secondary structure recognition probe was designed. The Barton research team reported a selective Ru(II) complex for DNA mismatch detection and fluorescence localization, which effectively reduces the risk of carcinogenesis caused by base mismatches (McConnell et al., 2012). DNA bulge structures are caused by the DNA recombination process, which is likely to cause a frameshift mutation in DNA replication. This structure binds more tightly to DNA repair proteins than it does to normal double-stranded DNA, making the bulge structures a potential binding site for therapeutic drugs (Pieniazek et al., 2011). Keene and colleagues synthesized a series of binuclear Ru(II) complexes that selectively recognize and bind to DNA bulge structures *via* electrostatic interaction and zonal action, and have DNA-targeted repair function (Mulyana et al., 2011; Li et al., 2012a). Z-DNA induces gene deletion, translocation, and other instability (Dumat et al., 2016). Tridentate complexes, $[Ru(tpy)(ptn)]^{2+}$ and $[Ru(dmtpy)(ptn)]^{2+}$, were designed to induce Z-DNA transforms into a stable B-DNA dominant conformation, which effectively decreased the risk of mutations (Li et al., 2012b).

In addition to DNA imaging, some complexes were synthesized by coupling fluorescent Ru(II) complexes with histone deacetylase inhibitors (HDACIs). These complexes specifically recognize and image proteins (Kurzwernhart et al., 2012). Further investigation has found that it not only images and inhibits HDACs, but also produces a large amount of reactive oxygen species (ROS) under light irradiation, showing comparable cytotoxicity to that of cisplatin. Thus, it induces apoptosis of some tumor cells. Photoacoustic imaging (PA) is a novel imaging technique for tissue imaging based on optical absorption coefficients under the action of an imaging agent (Levi et al., 2014). Liu and co-workers used poly(nisopropylacrylamide) as a thermal response switch and $[Ru(bpy)_2(tip)]^{2+}$ as a photosensitizer in combination with gold nanomaterials to synthesize the Ru(II) complex pRu-pNIPAM@RBT (Chen et al., 2017). Under optical stimulation, this complex produces high heat and large amounts of ROS in tumor tissues, and it showed synergistic action in photothermal therapy (PTT) and photodynamic therapy (PDT) against tumors. Ruthenium complexes are good imaging agents for PA. Combination of infrared thermal imaging quantitative analysis and PA data, can be effectively used to distinguish healthy and tumor tissues, which has significantly improved the accuracy and efficiency of tumor therapy (Su et al., 2010).

At the organizational level, tumor cell proliferation and metastasis depend on adequate nutrient supply and angiogenesis. Therefore, blocking tumor angiogenesis is also a key strategy to inhibit tumor growth and migration (Gau et al., 2017). Studies have found that some ruthenium complexes have good antiangiogenic effects and effectively inhibit tumor growth (Silva Sousa et al., 2016). Liu and colleagues designed a fluorescent Ru(II)-selenium nanoparticles (Ru-SeNPs) that significantly inhibited the proliferation of liver carcinoma HepG2 cells. *In vivo* experiments in tumor bearing mice revealed that NAMI-A potently inhibited tumor angiogenesis and migration (Vacca et al., 2002). In another study, the nitric oxide synthase (NOS) pathway was found to play an important role in tumor angiogenesis (Chakraborty and Ain, 2017). Increasing NO levels is positively correlated with tumor growth and migration. Drugs that interfere with the NOS pathway can inhibit tumor angiogenesis. It has been observed that NAMI-A inhibits vascular endothelial growth factor (VEGF)-mediated angiogenesis in tumor tissues by scavenging NO (Morbidelli et al., 2003).

SYNERGISTIC EFFECT OF RUTHENIUM COMPLEXES

Drug combinations are common therapeutic strategies in clinical practices. Combinational drug molecules act on multiple targets and pathways simultaneously, which could enhance their synergistic effects, reduce dosage and side effects, and reduce the risk of drug resistance (Lehar et al., 2009). A ruthenium complex was combined with a second-line antitumor agent ketoconazole (KTZ) in hormone-refractory cancer therapy to form a $RuCl_2(KTZ)_2$ complex, which showed a favorable synergistic effect (Bozic et al., 2013). The combination of these two agents in a C8161 melanoma cell line significantly enhanced the expression of caspase-3 and promoted tumor cell apoptosis. Mechanistic studies have shown that $RuCl_2(KTZ)_2$ has mitochondrial targeting effects, releasing mitochondrial cytochrome c and activating superoxide dismutase (Mn-SOD), thereby facilitating apoptosis. In the melanoma (WM164) cell line, $RuCl_2(KTZ)_2$ displayed a stronger inhibitory effect on tumor cell growth than cisplatin, and induced apoptosis by activating poly-ADP ribose polymerase (PARP) fragmentation and the proapoptotic factor Bcl-2-associated X protein (Bax) expression. $RuCl_2(KTZ)_2$ acts on the P53 signaling pathway to effectively inhibit the proliferation of a variety of adherent tumor cells, and synergizes the anti-epidermal growth factor receptor (EGFR) inhibitor C225MAb to kill resistant spheroids (Gelfo et al., 2016).

Berger and colleagues studied the combinations of ruthenium complexes and first-line anticancer drugs. They found that the clinical drug, ruthenium complex KP1339 combined with multi-kinase inhibitor sorafenib was more effective in the therapy of hepatoma (Hep3B) than KP1339 or sorafenib alone (Heffeter et al., 2013). Specifically, the mean survival of patients was extended by 3.9-fold by the combination, whereas KP1339 and sorafenib alone extended it by 2.4-and 1.9-fold, respectively. The combination of both agents effectively inhibited sorafenib-resistant tumor cells. In-depth investigations have found that the combination substantially increased their intracellular accumulation and, thereby, interfered with the DNA synthesis process, rendering the cells unable to perform effective mitosis, and enhancing apoptosis induction.

In clinical studies, NAMI-A combined with gemcitabine, better inhibited the activity of non-small cell lung cancer cells and reduced tolerance compared with the use of gemcitabine alone, but the combination of both had significant side effects such as neutropenia, anemia, and renal impairment (Leijen et al., 2015). Sava and co-workers identified promising drug combinations with synergistic potential using high-throughput screening (Bergamo et al., 2015). NAMI-A and doxorubicin

were shown to have a potent synergistic antitumor efficacy. NAMI-A effectively increased the accumulation of doxorubicin in breast carcinoma. In *in vivo* studies of mouse MCa mammary carcinoma, this combination increased inhibition of tumor metastasis by 70%, compared to the use of doxorubicin alone. In a lung metastasis preclinical tumor model in mice, both agents demonstrated promising synergistic effects (Marien et al., 2017). However, there were noticeable side effects when the maximum doses were used.

The tumor vasculature is poorly organized, resulting in extravascular permeation of drug molecules (Pries et al., 2010). In addition, the decreased blood flow and oxygen supply affects drug uptake, which is also a major obstacle to effective tumor therapy (Siemann and Horsman, 2015). Studies on the combination of ovarian carcinoma chemotherapeutic doxorubicin and a ruthenium complex RAPTA-C have demonstrated that this combination significantly promoted the apoptosis of A2780 ovarian carcinoma cells compared with either single drug alone (Weiss et al., 2015). Normalization of tumor vasculature induced by apoptosis reduces vascular extravasation, and provides adequate oxygen for oxygen-dependent phototherapy, achieving synergism (Goel et al., 2011). These studies provide valid evidence for the interaction between anti-angiogenesis and antitumor effects.

CONCLUSION AND PERSPECTIVES

Investigation of the antitumor activity of ruthenium complexes has led to gratifying achievements and the identification of some promising antitumor compounds (Chen et al., 2016; Alves de Souza et al., 2017; Zeng et al., 2017b; Zhao et al., 2018). The ruthenium complex showed more potent activities than platinum drugs, and has a significant inhibitory effect on platinum-resistant tumor (Zeng et al., 2016). The peculiarity of ruthenium compounds suggests that the research methods used for investigating platinum-based drugs may not fully be applied in these agents, because the cytotoxic mechanisms of cisplatin and ruthenium are different. The primary target of cisplatin is DNA, but the target of some ruthenium complexes is mitochondria or endoplasmic reticulum. Although they can both regulate cell apoptosis and cell cycle, cisplatin induces a large number of genes related to DNA damage, P53 and apoptosis, while some ruthenium complexes facilitate the expression of oxidative stress and ER stress (Licona et al., 2017).

The existing research achievements should be combined with molecular biology and nanomaterials, applying the advantage of existing tools and methods to develop antitumor drugs with better therapeutic effects, based on these complexes. This prospect is extremely enlightening, and antitumor drugs with better efficacy than that of existing chemotherapeutic drugs, which are ineffective in treating certain tumors, could be developed. Furthermore, the prospective agents could be effective against tumors that have developed drug resistance for their potent efficacy (Wang N. et al., 2015; Purushothaman et al., 2018). The results of clinical studies should be reflectively considered in determining the reasons for the failure of the clinical investigations of NAMI-A and KP1019, which could lead to design drugs with less side effects, greater selectivity, and higher bioavailability. For example, KP1339, the sodium salt of KP1019, which is currently in clinical studies, has better water solubility and transmembrane absorption efficiency than KP1019 (Bytzek et al., 2016). The Ru(II) complex TLD1443, as a promising photosensitizer, significantly enhanced the efficacy of phototherapy and produced less toxicity *in vitro* and *in vivo* (Smithen et al., 2017).

Numerous breakthroughs have been made in the diagnosis and therapy of tumors using ruthenium complexes (Thota et al., 2018). As a probe, the ruthenium complex could be used for target localization and imaging of DNA, the mitochondria, endoplasmic reticulum, and lysosomes, achieving specific identification and dynamic monitoring of thiol and O_2 in tumors (Martin et al., 2014; Zhang et al., 2014). As a tracer, it enhances the understanding of the physiological development of tumors at the genetic level (Wilson et al., 2016; Xu et al., 2016). As photosensitizers and catalysts, these complexes have significant synergistic effects with phototherapies such as PDT, PTT, and photoactivated chemotherapy (PACT) (Chen et al., 2017). The combination of ruthenium complexes and PA imaging technology has significantly improved the accuracy and effectiveness of tumor diagnosis and therapy (Chen et al., 2014). In the therapy of tumors using drug combinations, ruthenium complexes have shown favorable efficacy. The Ru(II) complex combined with KTZ significantly inhibited the proliferation of C8161 melanoma cells and directly killed cisplatin-resistant spheroids (Bozic et al., 2013). KP1339 combined with the first-line anticancer drug sorafenib for hepatic carcinoma, demonstrated a remarkable therapeutic effect (Heffeter et al., 2013). Furthermore, NAMI-A combined with gemcitabine enhanced the inhibitory effect on non-small cell lung cancer while NAMI-A combined with doxorubicin showed potent inhibitory effects on lung metastasis *in vivo* (Bergamo et al., 2015). RAPTA-C and doxorubicin showed synergistically enhanced therapeutic effects on ovarian cancer and some solid tumors (Weiss et al., 2015). However, studies on the synergistic effect of ruthenium complexes are rare, because there are some uncertain factors such as the mechanism of drug synergy and how to choose drugs that cooperate with ruthenium complexes (Zhao et al., 2013; Madani Tonekaboni et al., 2018).

In conclusion, the results of the investigations on drugs combinations with ruthenium complexes are currently unsatisfactory. Perhaps the development and use of high-throughput screening technology and algorithm analysis tools are a viable strategy to promote the study of drug synergistic effects (Aviolat et al., 2018).

Presently, the mechanism of action of ruthenium complexes is unclear, and further research is still needed. Before the ruthenium complex can be used clinically, numerous problems need to be addressed, including strategies to improve the hydrolysis of ruthenium complexes to achieve effective absorption and better metabolism, as well as enhance their cellular penetration to achieve targeted tumor cell death. Furthermore, methods to avoid and alleviate the side effects of ruthenium complexes, enhance their efficacy *via* synergism, and overcome drug resistance are

imperative. The solution to these problems would provide a promising direction for the design and screening of ruthenium complexes, which are of great significance for their use in clinical diagnosis and therapy of tumors.

AUTHOR CONTRIBUTIONS

KL and Z-ZZ drafted and wrote the manuscript. J-QW conceived the idea for the manuscript. H-BB and X-JH provided critical analysis and language editing. All authors contributed to the writing and final approval of the manuscript.

FUNDING

This work was supported by the National Science Foundation of China (No. 21771042) and Natural Science Foundation of Guangdong Province (No. 2016A030310298).

REFERENCES

Abid, M., Shamsi, F., and Azam, A. (2016). Ruthenium complexes: an emerging ground to the development of metallopharmaceuticals for cancer therapy. *Mini Rev. Med. Chem.* 16, 772–786. doi: 10.2174/1389557515666151001142012

Alessio, E., Mestroni, G., Bergamo, A., and Sava, G. (2004). Ruthenium antimetastatic agents. *Curr. Top. Med. Chem.* 4, 1525–1535. doi: 10.2174/1568026043387421

Alves de Souza, C. E., Alves, de Souza, H. M., Stipp, M. C., Corso, C. R., Galindo, C. M., et al. (2017). Ruthenium complex exerts antineoplastic effects that are mediated by oxidative stress without inducing toxicity in Walker-256 tumor-bearing rats. *Free Radic. Biol. Med.* 110, 228–239. doi: 10.1016/j.freeradbiomed.2017.06.011

Ambrus, A., Chen, D., Dai, J., Bialis, T., Jones, R. A., and Yang, D. (2006). Human telomeric sequence forms a hybrid-type intramolecular G-quadruplex structure with mixed parallel/antiparallel strands in potassium solution. *Nucleic Acids Res.* 34, 2723–2735. doi: 10.1093/nar/gkl348

Ang, W. H., De Luca, A., Chapuis-Bernasconi, C., Juillerat-Jeanneret, L., Lo Bello, M., and Dyson, P. J. (2007). Organometallic ruthenium inhibitors of glutathione-S-transferase P1-1 as anticancer drugs. *Chem. Med. Chem.* 2, 1799–1806. doi: 10.1002/cmdc.200700209

Antonarakis, E. S., and Emadi, A. (2010). Ruthenium-based chemotherapeutics: are they ready for prime time? *Cancer Chemother. Pharmacol.* 66, 1–9. doi: 10.1007/s00280-010-1293-1

Augustyn, K. E., Stemp, E. D., and Barton, J. K. (2007). Charge separation in a ruthenium-quencher conjugate bound to DNA. *Inorg. Chem.* 46, 9337–9350. doi: 10.1021/ic701276t

Aviolat, H., Nomine, Y., Gioria, S., Bonhoure, A., Hoffmann, D., Ruhlmann, C., et al. (2018). SynAggreg: a multifunctional high-throughput technology for precision study of amyloid aggregation and systematic discovery of synergistic inhibitor compounds. *J. Mol. Biol.* doi: 10.1016/j.jmb.2018.09.009 [Epub ahead of print].

Bergamo, A., Messori, L., Piccioli, F., Cocchietto, M., and Sava, G. (2003). Biological role of adduct formation of the ruthenium(III) complex NAMI-A with serum albumin and serum transferrin. *Invest. New Drugs* 21, 401–411. doi: 10.1023/A:1026243000320

Bergamo, A., Riedel, T., Dyson, P. J., and Sava, G. (2015). Preclinical combination therapy of the investigational drug NAMI-A^{+} with doxorubicin for mammary cancer. *Invest. New Drugs* 33, 53–63. doi: 10.1007/s10637-014-0175-5

Blanck, S., Maksimoska, J., Baumeister, J., Harms, K., Marmorstein, R., and Meggers, E. (2012). The art of filling protein pockets efficiently with octahedral metal complexes. *Angew. Chem. Int. Ed. Engl.* 51, 5244–5246. doi: 10.1002/anie.201108865

Bozic, I., Reiter, J. G., Allen, B., Antal, T., Chatterjee, K., Shah, P., et al. (2013). Evolutionary dynamics of cancer in response to targeted combination therapy. *eLife* 2:e00747. doi: 10.7554/eLife.00747

Burger, H., Loos, W. J., Eechoute, K., Verweij, J., Mathijssen, R. H., and Wiemer, E. A. (2011). Drug transporters of platinum-based anticancer agents and their clinical significance. *Drug Resist. Updat.* 14, 22–34. doi: 10.1016/j.drup.2010.12.002

Bytzek, A. K., Koellensperger, G., Keppler, B. K., and G Hartinger, C. (2016). Biodistribution of the novel anticancer drug sodium trans-[tetrachloridobis(1H-indazole)ruthenate(III)] KP-1339/IT139 in nude BALB/c mice and implications on its mode of action. *J. Inorg. Biochem.* 160, 250–255. doi: 10.1016/j.jinorgbio.2016.02.037

Castonguay, A., Doucet, C., Juhas, M., and Maysinger, D. (2012). New ruthenium(II)–letrozole complexes as anticancer therapeutics. *J. Med. Chem.* 55, 8799–8806. doi: 10.1021/jm301103y

Chakrabortty, S., Agrawalla, B. K., Stumper, A., Vegi, N. M., Fischer, S., Reichardt, C., et al. (2017). Mitochondria targeted protein-ruthenium photosensitizer for efficient photodynamic applications. *J. Am. Chem. Soc.* 139, 2512–2519. doi: 10.1021/jacs.6b13399

Chakraborty, S., and Ain, R. (2017). Nitric-oxide synthase trafficking inducer is a pleiotropic regulator of endothelial cell function and signaling. *J. Biol. Chem.* 292, 6600–6620. doi: 10.1074/jbc.M116.742627

Chen, G., Xu, M., Zhao, S., Sun, J., Yu, Q., and Liu, J. (2017). Pompon-like RuNPs-Based theranostic nanocarrier system with stable photoacoustic imaging characteristic for accurate tumor detection and efficient phototherapy guidance. *ACS Appl. Mater. Interfaces* 9, 33645–33659. doi: 10.1021/acsami.7b10553

Chen, L., Li, G., Peng, F., Jie, X., Dongye, G., Cai, K., et al. (2016). The induction of autophagy against mitochondria-mediated apoptosis in lung cancer cells by a ruthenium (II) imidazole complex. *Oncotarget* 7, 80716–80734. doi: 10.18632/oncotarget.13032

Chen, Y., Lei, W., Jiang, G., Hou, Y., Li, C., Zhang, B., et al. (2014). Fusion of photodynamic therapy and photoactivated chemotherapy: a novel Ru(II) arene complex with dual activities of photobinding and photocleavage toward DNA. *Dalton Trans.* 43, 15375–15384. doi: 10.1039/c4dt01755b

Crump, M., Lipton, J., Hedley, D., Sutton, D., Shepherd, F., Minden, M., et al. (1999). Phase I trial of sequential topotecan followed by etoposide in adults with myeloid leukemia: a national cancer Institute of Canada clinical trials group study. *Leukemia* 13, 343–347. doi: 10.1038/sj.leu.2401308

Cuello-Garibo, J. A., Meijer, M. S., and Bonnet, S. (2017). To cage or to be caged? The cytotoxic species in ruthenium-based photoactivated chemotherapy is not always the metal. *Chem. Commun.* 53, 6768–6771. doi: 10.1039/c7cc03469e

De Carvalho, N. C., Neves, S. P., Dias, R. B., Valverde, L. F., Sales, C. B. S., Rocha, C. A. G., et al. (2018). A novel ruthenium complex with xanthoxylin induces S-phase arrest and causes ERK1/2-mediated apoptosis in HepG2 cells through a p53-independent pathway. *Cell Death Dis.* 9:79. doi: 10.1038/s41419-017-0104-6

Deng, Z., Gao, P., Yu, L., Ma, B., You, Y., Chan, L., et al. (2017). Ruthenium complexes with phenylterpyridine derivatives target cell membrane and trigger death receptors-mediated apoptosis in cancer cells. *Biomaterials* 129, 111–126. doi: 10.1016/j.biomaterials.2017.03.017

Dirican, N., Dirican, A., Sen, O., Aynali, A., Atalay, S., Bircan, H. A., et al. (2016). Thiol/disulfide homeostasis: a prognostic biomarker for patients with advanced non-small cell lung cancer? *Redox. Rep.* 21, 197–203. doi: 10.1179/1351000215y.0000000027

Du, K. J., Wang, J. Q., Kou, J. F., Li, G. Y., Wang, L. L., Chao, H., et al. (2011). Synthesis, DNA-binding and topoisomerase inhibitory activity of ruthenium(II) polypyridyl complexes. *Eur. J. Med. Chem.* 46, 1056–1065. doi: 10.1016/j.ejmech.2011.01.019

Duan, L., Fischer, A., Xu, Y., and Sun, L. (2009). Isolated seven-coordinate Ru(IV) dimer complex with [HOHOH]- bridging ligand as an intermediate for catalytic water oxidation. *J. Am. Chem. Soc.* 131, 10397–10399. doi: 10.1021/ja9034686

Dumat, B., Larsen, A. F., and Wilhelmsson, L. M. (2016). Studying Z-DNA and B- to Z-DNA transitions using a cytosine analogue FRET-pair. *Nucleic Acids Res.* 44:e101. doi: 10.1093/nar/gkw114

Fernandez, A., Ordonez, R., Reiter, R. J., Gonzalez-Gallego, J., and Mauriz, J. L. (2015). Melatonin and endoplasmic reticulum stress: relation to autophagy and apoptosis. *J. Pineal. Res.* 59, 292–307. doi: 10.1111/jpi.12264

Frasconi, M., Liu, Z., Lei, J., Wu, Y., Strekalova, E., Malin, D., et al. (2013). Photoexpulsion of surface-grafted ruthenium complexes and subsequent release of cytotoxic cargos to cancer cells from mesoporous silica nanoparticles. *J. Am. Chem. Soc.* 135, 11603–11613. doi: 10.1021/ja405058y

Galanski, M. (2006). Recent developments in the field of anticancer platinum complexes. *Recent Pat. Anticancer Drug Discov.* 1, 285–295. doi: 10.2174/157489206777442287

Gasser, G., Sosniak, A. M., and Metzler-Nolte, N. (2011). Metal-containing peptide nucleic acid conjugates. *Dalton Trans.* 40, 7061–7076. doi: 10.1039/c0dt01706j

Gau, D., Veon, W., Capasso, T. L., Bottcher, R., Shroff, S., Roman, B. L., et al. (2017). Pharmacological intervention of MKL/SRF signaling by CCG-1423 impedes endothelial cell migration and angiogenesis. *Angiogenesis* 20, 663–672. doi: 10.1007/s10456-017-9560-y

Gelfo, V., Rodia, M. T., Pucci, M., Dall'Ora, M., Santi, S., Solmi, R., et al. (2016). A module of inflammatory cytokines defines resistance of colorectal cancer to EGFR inhibitors. *Oncotarget* 7, 72167–72183. doi: 10.18632/oncotarget.12354

Gill, M. R., Cecchin, D., Walker, M. G., Mulla, R. S., Battaglia, G., Smythe, C., et al. (2013). Targeting the endoplasmic reticulum with a membrane-interactive luminescent ruthenium(ii) polypyridyl complexdagger Electronic supplementary information (ESI) available: experimental details, characterization of 2 and Fig. S1-S6. See doi: 10.1039/c3sc51725jClick here for additional data file. *Chem. Sci.* 4, 4512–4519. doi: 10.1039/c3sc51725j

Gill, M. R., Garcia-Lara, J., Foster, S. J., Smythe, C., Battaglia, G., and Thomas, J. A. (2009). A ruthenium(II) polypyridyl complex for direct imaging of DNA structure in living cells. *Nat. Chem.* 1, 662–667. doi: 10.1038/nchem.406

Goel, S., Duda, D. G., Xu, L., Munn, L. L., Boucher, Y., Fukumura, D., et al. (2011). Normalization of the vasculature for treatment of cancer and other diseases. *Physiol. Rev.* 91, 1071–1121. doi: 10.1152/physrev.00038.2010

Groessl, M., Zava, O., and Dyson, P. J. (2011). Cellular uptake and subcellular distribution of ruthenium-based metallodrugs under clinical investigation versus cisplatin. *Metallomics* 3, 591–599. doi: 10.1039/c0mt00101e

Harper, B. W., Krause-Heuer, A. M., Grant, M. P., Manohar, M., Garbutcheon-Singh, K. B., and Aldrich-Wright, J. R. (2010). Advances in platinum chemotherapeutics. *Chemistry* 16, 7064–7077. doi: 10.1002/chem.201000148

Hartinger, C. G., Groessl, M., Meier, S. M., Casini, A., and Dyson, P. J. (2013). Application of mass spectrometric techniques to delineate the modes-of-action of anticancer metallodrugs. *Chem. Soc. Rev.* 42, 6186–6199. doi: 10.1039/c3cs35532b

Hartinger, C. G., Jakupec, M. A., Zorbas-Seifried, S., Groessl, M., Egger, A., Berger, W., et al. (2008). KP1019, a new redox-active anticancer agent–preclinical development and results of a clinical phase I study in tumor patients. *Chem. Biodivers.* 5, 2140–2155. doi: 10.1002/cbdv.200890195

Hartinger, C. G., Zorbas-Seifried, S., Jakupec, M. A., Kynast, B., Zorbas, H., and Keppler, B. K. (2006). From bench to bedside–preclinical and early clinical development of the anticancer agent indazolium trans-[tetrachlorobis(1H-indazole)ruthenate(III)] (KP1019 or FFC14A). *J. Inorg. Biochem.* 100, 891–904. doi: 10.1016/j.jinorgbio.2006.02.013

Heffeter, P., Atil, B., Kryeziu, K., Groza, D., Koellensperger, G., Korner, W., et al. (2013). The ruthenium compound KP1339 potentiates the anticancer activity of sorafenib in vitro and in vivo. *Eur. J. Cancer* 49, 3366–3375. doi: 10.1016/j.ejca.2013.05.018

Heffeter, P., Bock, K., Atil, B., Reza Hoda, M. A., Korner, W., Bartel, C., et al. (2010). Intracellular protein binding patterns of the anticancer ruthenium drugs KP1019 and KP1339. *J. Biol. Inorg. Chem.* 15, 737–748. doi: 10.1007/s00775-010-0642-1

Hess, J., Huang, H., Kaiser, A., Pierroz, V., Blacque, O., Chao, H., et al. (2017). Evaluation of the medicinal potential of two ruthenium(II) polypyridine complexes as one- and two-photon photodynamic therapy photosensitizers. *Chemistry* 23, 9888–9896. doi: 10.1002/chem.201701392

Hiyama, E., Hiyama, K., Yokoyama, T., Matsuura, Y., Piatyszek, M. A., and Shay, J. W. (1995). Correlating telomerase activity levels with human neuroblastoma outcomes. *Nat. Med.* 1, 249–255. doi: 10.1038/nm0395-249

Inal, B. B., Emre, H. O., Baran, O., Ahmedov, M., Ozdemir, A. F., Kemerdere, R., et al. (2017). Dynamic thiol-disulphide homeostasis in low-grade gliomas: preliminary results in serum. *Clin. Neurol. Neurosurg.* 161, 17–21. doi: 10.1016/j.clineuro.2017.08.002

Jain, S. S., Anderson, C. M., Sapse, I. A., Lundgren, S. H., Freer, A. K., Hoang, H., et al. (2018). A ruthenium-platinum metal complex that binds to sarcin ricin loop RNA and lowers mRNA expression. *Chem. Commun.* 54, 8987–8990. doi: 10.1039/c8cc02131g

Jakupec, M. A., Galanski, M., Arion, V. B., Hartinger, C. G., and Keppler, B. K. (2008). Antitumour metal compounds: more than theme and variations. *Dalton Trans.* 183–194. doi: 10.1039/b712656p

Jiang, Q., Song, C., Nangreave, J., Liu, X., Lin, L., Qiu, D., et al. (2012). DNA origami as a carrier for circumvention of drug resistance. *J. Am. Chem. Soc.* 134, 13396–13403. doi: 10.1021/ja304263n

Kim, M. Y., Duan, W., Gleason-Guzman, M., and Hurley, L. H. (2003). Design, synthesis, and biological evaluation of a series of fluoroquinoanthroxazines with contrasting dual mechanisms of action against topoisomerase II and G-quadruplexes. *J. Med. Chem.* 46, 571–583. doi: 10.1021/jm0203377

Kou, J. F., Qian, C., Wang, J. Q., Chen, X., Wang, L. L., Chao, H., et al. (2012). Chiral ruthenium(II) anthraquinone complexes as dual inhibitors of topoisomerases I and II. *J. Biol. Inorg. Chem.* 17, 81–96. doi: 10.1007/s00775-011-08316

Kurzwernhart, A., Kandioller, W., Bartel, C., Bachler, S., Trondl, R., Muhlgassner, G., et al. (2012). Targeting the DNA-topoisomerase complex in a double-strike approach with a topoisomerase inhibiting moiety and covalent DNA binder. *Chem. Commun.* 48, 4839–4841. doi: 10.1039/c2cc31040f

Le Gac, S., Rickling, S., Gerbaux, P., Defrancq, E., Moucheron, C., and Kirsch-De Mesmaeker, A. (2009). A photoreactive ruthenium(II) complex tethered to a guanine-containing oligonucleotide: a biomolecular tool that behaves as a "seppuku molecule". *Angew. Chem. Int. Ed. Engl.* 48, 1122–1125. doi: 10.1002/anie.200804503

Lehar, J., Krueger, A. S., Avery, W., Heilbut, A. M., Johansen, L. M., Price, E. R., et al. (2009). Synergistic drug combinations tend to improve therapeutically relevant selectivity. *Nat. Biotechnol.* 27, 659–666. doi: 10.1038/nbt.1549

Leijen, S., Burgers, S. A., Baas, P., Pluim, D., Tibben, M., van Werkhoven, E., et al. (2015). Phase I/II study with ruthenium compound NAMI-A and gemcitabine in patients with non-small cell lung cancer after first line therapy. *Invest. New Drugs* 33, 201–214. doi: 10.1007/s10637-014-0179-1

Levi, J., Sathirachinda, A., and Gambhir, S. S. (2014). A high-affinity, high-stability photoacoustic agent for imaging gastrin-releasing peptide receptor in prostate cancer. *Clin. Cancer Res.* 20, 3721–3729. doi: 10.1158/1078-0432.ccr-13-3405

Li, F., Weber, D. K., Morgan, J. L., Collins, J. G., and Keene, F. R. (2012a). An approach to therapeutic agents through selective targeting of destabilised nucleic acid duplex sequences. *Dalton Trans.* 41, 6528–6535. doi: 10.1039/c2dt12146h

Li, L. Y., Jia, H. N., Yu, H. J., Du, K. J., Lin, Q. T., Qiu, K. Q., et al. (2012b). Synthesis, characterization, and DNA-binding studies of ruthenium complexes $[Ru(tpy)(ptn)]^{2+}$ and $Ru(dmtpy)(ptn)]^{2+}$. *J. Inorg. Biochem.* 113, 31–39. doi: 10.1016/j.jinorgbio.2012.03.008

Li, L., Wong, Y. S., Chen, T., Fan, C., and Zheng, W. (2012c). Ruthenium complexes containing bis-benzimidazole derivatives as a new class of apoptosis inducers. *Dalton Trans.* 41, 1138–1141. doi: 10.1039/c1dt11950h

Liao, G., Chen, X., Wu, J., Qian, C., Wang, Y., Ji, L., et al. (2015). Ruthenium(II) polypyridyl complexes as dual inhibitors of telomerase and topoisomerase. *Dalton Trans.* 44, 15145–15156. doi: 10.1039/c4dt03585b

Licona, C., Spaety, M. E., Capuozzo, A., Ali, M., Santamaria, R., Armant, O., et al. (2017). A ruthenium anticancer compound interacts with histones and impacts differently on epigenetic and death pathways compared to cisplatin. *Oncotarget* 8, 2568–2584. doi: 10.18632/oncotarget.13711

Liu, J., Chen, Y., Li, G., Zhang, P., Jin, C., Zeng, L., et al. (2015). Ruthenium(II) polypyridyl complexes as mitochondria-targeted two-photon photodynamic anticancer agents. *Biomaterials* 56, 140–153. doi: 10.1016/j.biomaterials.2015.04.002

Madani Tonekaboni, S. A., Soltan Ghoraie, L., Manem, V. S. K., and Haibe-Kains, B. (2018). Predictive approaches for drug combination discovery in cancer. *Brief Bioinform.* 19, 263–276. doi: 10.1093/bib/bbw104

Marien, E., Hillen, A., Vanderhoydonc, F., Swinnen, J. V., and Vande Velde, G. (2017). Longitudinal microcomputed tomography-derived biomarkers for lung metastasis detection in a syngeneic mouse model: added value to bioluminescence imaging. *Lab. Invest.* 97, 24–33. doi: 10.1038/labinvest.2016.114

Martin, A., Byrne, A., Burke, C. S., Forster, R. J., and Keyes, T. E. (2014). Peptide-bridged dinuclear Ru(II) complex for mitochondrial targeted monitoring of dynamic changes to oxygen concentration and ROS generation in live mammalian cells. *J. Am. Chem. Soc.* 136, 15300–15309. doi: 10.1021/ja508043q

Matson, M., Svensson, F. R., Norden, B., and Lincoln, P. (2011). Correlation between cellular localization and binding preference to RNA, DNA, and phospholipid membrane for luminescent ruthenium(II) complexes. *J. Phys. Chem. B* 115, 1706–1711. doi: 10.1021/jp109530f

McConnell, A. J., Lim, M. H., Olmon, E. D., Song, H., Dervan, E. E., and Barton, J. K. (2012). Luminescent properties of ruthenium(II) complexes with sterically expansive ligands bound to DNA defects. *Inorg. Chem.* 51, 12511–12520. doi: 10.1021/ic3019524

Minchinton, A. I., and Tannock, I. F. (2006). Drug penetration in solid tumours. *Nat. Rev. Cancer* 6, 583–592. doi: 10.1038/nrc1893

Morbidelli, L., Donnini, S., Filippi, S., Messori, L., Piccioli, F., Orioli, P., et al. (2003). Antiangiogenic properties of selected ruthenium(III) complexes that are nitric oxide scavengers. *Br. J. Cancer* 88, 1484–1491. doi: 10.1038/sj.bjc.6600906

Mulyana, Y., Weber, D. K., Buck, D. P., Motti, C. A., Collins, J. G., and Keene, F. R. (2011). Oligonuclear polypyridylruthenium(II) complexes incorporating flexible polar and non-polar bridges: synthesis, DNA-binding and cytotoxicity. *Dalton Trans.* 40, 1510–1523. doi: 10.1039/c0dt01250e

Pal, M., Nandi, U., and Mukherjee, D. (2018). Detailed account on activation mechanisms of ruthenium coordination complexes and their role as antineoplastic agents. *Eur. J. Med. Chem.* 150, 419–445. doi: 10.1016/j.ejmech.2018.03.015

Pieniazek, S. N., Hingorani, M. M., and Beveridge, D. L. (2011). Dynamical allosterism in the mechanism of action of DNA mismatch repair protein MutS. *Biophys. J.* 101, 1730–1739. doi: 10.1016/j.bpj.2011.08.039

Pierroz, V., Joshi, T., Leonidova, A., Mari, C., Schur, J., Ott, I., et al. (2012). Molecular and cellular characterization of the biological effects of ruthenium(II) complexes incorporating 2-pyridyl-2-pyrimidine-4-carboxylic acid. *J. Am. Chem. Soc.* 134, 20376–20387. doi: 10.1021/ja307288s

Poynton, F. E., Bright, S. A., Blasco, S., Williams, D. C., Kelly, J. M., and Gunnlaugsson, T. (2017). The development of ruthenium(ii) polypyridyl complexes and conjugates for in vitro cellular and in vivo applications. *Chem. Soc. Rev.* 4, 7706–7756. doi: 10.1039/c7cs00680b

Pries, A. R., Hopfner, M., le Noble, F., Dewhirst, M. W., and Secomb, T. W. (2010). The shunt problem: control of functional shunting in normal and tumour vasculature. *Nat. Rev. Cancer* 10, 587–593. doi: 10.1038/nrc2895

Puckett, C. A., and Barton, J. K. (2007). Methods to explore cellular uptake of ruthenium complexes. *J. Am. Chem. Soc.* 129, 46–47. doi: 10.1021/ja0677564

Purushothaman, B., Arumugam, P., Ju, H., Kulsi, G., Samson, A. A. S., and Song, J. M. (2018). Novel ruthenium(II) triazine complex $[Ru(bdpta)(tpy)]^{2+}$ co-targeting drug resistant GRP78 and subcellular organelles in cancer stem cells. *Eur. J. Med. Chem.* 156, 747–759. doi: 10.1016/j.ejmech.2018.07.048

Qiu, K., Wang, J., Song, C., Wang, L., Zhu, H., Huang, H., et al. (2017). Crossfire for two-pphoton photodynamic therapy with fluorinated ruthenium (II) photosensitizers. *ACS Appl. Mater. Interfaces* 9, 18482–18492. doi: 10.1021/acsami.7b02977

Rajput, C., Rutkaite, R., Swanson, L., Haq, I., and Thomas, J. A. (2006). Dinuclear monointercalating RuII complexes that display high affinity binding to duplex and quadruplex DNA. *Chemistry* 12, 4611–4619. doi: 10.1002/chem.200501349

Rickling, S., Ghisdavu, L., Pierard, F., Gerbaux, P., Surin, M., Murat, P., et al. (2010). A rigid dinuclear ruthenium(II) complex as an efficient photoactive agent for bridging two guanine bases of a duplex or quadruplex oligonucleotide. *Chemistry* 16, 3951–3961. doi: 10.1002/chem.200902817

Rogers, N. J., Claire, S., Harris, R. M., Farabi, S., Zikeli, G., Styles, I. B., et al. (2014). High coating of Ru(II) complexes on gold nanoparticles for single particle luminescence imaging in cells. *Chem. Commun.* 50, 617–619. doi: 10.1039/c3cc47606e

Sadhu, K. K., Lindberg, E., and Winssinger, N. (2015). In cellulo protein labelling with Ru-conjugate for luminescence imaging and bioorthogonal photocatalysis. *Chem. Commun.* 51, 16664–16666. doi: 10.1039/c5cc05405b

Samimi, G., Kishimoto, S., Manorek, G., Breaux, J. K., and Howell, S. B. (2007). Novel mechanisms of platinum drug resistance identified in cells selected for resistance to JM118 the active metabolite of satraplatin. *Cancer Chemother. Pharmacol.* 59, 301–312. doi: 10.1007/s00280-006-0271-0

Sano, R., Hou, Y. C., Hedvat, M., Correa, R. G., Shu, C. W., Krajewska, M., et al. (2012). Endoplasmic reticulum protein BI-1 regulates Ca^{2+}-mediated bioenergetics to promote autophagy. *Genes Dev.* 26, 1041–1054. doi: 10.1101/gad.184325.111

Sano, R., and Reed, J. C. (2013). ER stress-induced cell death mechanisms. *Biochim. Biophys. Acta* 1833, 3460–3470. doi: 10.1016/j.bbamcr.2013.06.028

Schmitt, F., Freudenreich, J., Barry, N. P., Juillerat-Jeanneret, L., Suss-Fink, G., and Therrien, B. (2012). Organometallic cages as vehicles for intracellular release of photosensitizers. *J. Am. Chem. Soc.* 134, 754–757. doi: 10.1021/ja207784t

Shi, S., Liu, J., Yao, T., Geng, X., Jiang, L., Yang, Q., et al. (2008). Promoting the formation and stabilization of G-quadruplex by dinuclear RuII complex $Ru_2(obip)L_4$. *Inorg. Chem.* 47, 2910–2912. doi: 10.1021/ic7021209

Siemann, D. W., and Horsman, M. R. (2015). Modulation of the tumor vasculature and oxygenation to improve therapy. *Pharmacol. Ther.* 153, 107–124. doi: 10.1016/j.pharmthera.2015.06.006

Silva Sousa, E. H., Ridnour, L. A., Gouveia, F. S. Jr., Silva da Silva, C. D., Wink, D. A., de Franca Lopes, L. G., et al. (2016). Thiol-activated HNO release from a ruthenium antiangiogenesis complex and HIF-1alpha inhibition for cancer therapy. *ACS Chem. Biol.* 11, 2057–2065. doi: 10.1021/acschembio.6b00222

Smithen, D. A., Yin, H., Beh, M. H., Hetu, M., Cameron, T. S., McFarland, S. A., et al. (2017). Synthesis and photobiological activity of Ru(II) dyads derived from pyrrole-2-carboxylate thionoesters. *Inorg. Chem.* 56, 4121–4132. doi: 10.1021/acs.inorgchem.7b00072

Southam, H. M., Butler, J. A., Chapman, J. A., and Poole, R. K. (2017). The microbiology of ruthenium complexes. *Adv. Microb. Physiol.* 71, 1–96. doi: 10.1016/bs.ampbs.2017.03.001

Su, J. L., Wang, B., Wilson, K. E., Bayer, C. L., Chen, Y. S., Kim, S., et al. (2010). Advances in clinical and biomedical applications of photoacoustic imaging. *Expert Opin. Med. Diagn.* 4, 497–510. doi: 10.1517/17530059.2010.529127

Sun, D., Liu, Y., Yu, Q., Zhou, Y., Zhang, R., Chen, X., et al. (2013). The effects of luminescent ruthenium(II) polypyridyl functionalized selenium nanoparticles on bFGF-induced angiogenesis and AKT/ERK signaling. *Biomaterials* 34, 171–180. doi: 10.1016/j.biomaterials.2012.09.031

Suss-Fink, G. (2010). Arene ruthenium complexes as anticancer agents. *Dalton Trans.* 39, 1673–1688. doi: 10.1039/b916860p

Svensson, F. R., Matson, M., Li, M., and Lincoln, P. (2010). Lipophilic ruthenium complexes with tuned cell membrane affinity and photoactivated uptake. *Biophys. Chem.* 149, 102–106. doi: 10.1016/j.bpc.2010.04.006

Tan, C., Lai, S., Wu, S., Hu, S., Zhou, L., Chen, Y., et al. (2010). Nuclear permeable ruthenium(II) beta-carboline complexes induce autophagy to antagonize mitochondrial-mediated apoptosis. *J. Med. Chem.* 53, 7613–7624. doi: 10.1021/jm1009296

Thota, S. (2016). Editorial: anticancer ruthenium complexes in drug discovery and medicinal chemistry. *Mini Rev. Med. Chem.* 16:771. doi: 10.2174/1389557516101605030034 05

Thota, S., Rodrigues, D. A., Crans, D. C., and Barreiro, E. J. (2018). Ru(II) compounds: next-generation anticancer metallotherapeutics? *J. Med. Chem.* 61, 5805–5821. doi: 10.1021/acs.jmedchem.7b01689

Vacca, A., Bruno, M., Boccarelli, A., Coluccia, M., Ribatti, D., Bergamo, A., et al. (2002). Inhibition of endothelial cell functions and of angiogenesis by the metastasis inhibitor NAMI-A. *Br. J. Cancer* 86, 993–998. doi: 10.1038/sj.bjc.6600176

Vey, N., Kantarjian, H., Beran, M., O'Brien, S., Cortes, J., Koller, C., et al. (1999). Combination of topotecan with cytarabine or etoposide in patients with refractory or relapsed acute myeloid leukemia: results of a randomized phase I/II study. *Invest. New Drugs* 17, 89–95. doi: 10.1023/A:1006271618635

Volker, T., Dempwolff, F., Graumann, P. L., and Meggers, E. (2014). Progress towards bioorthogonal catalysis with organometallic compounds. *Angew. Chem. Int. Ed. Engl.* 53, 10536–10540. doi: 10.1002/anie.201404547

Wan, D., Tang, B., Wang, Y. J., Guo, B. H., Yin, H., Yi, Q. Y., et al. (2017). Synthesis and anticancer properties of ruthenium (II) complexes as potent apoptosis

inducers through mitochondrial disruption. *Eur. J. Med. Chem.* 139, 180–190. doi: 10.1016/j.ejmech.2017.07.066

Wang, J. Q., Zhang, P. Y., Qian, C., Hou, X. J., Ji, L. N., and Chao, H. (2014). Mitochondria are the primary target in the induction of apoptosis by chiral ruthenium(II) polypyridyl complexes in cancer cells. *J. Biol. Inorg. Chem.* 19, 335–348. doi: 10.1007/s00775-013-1069-2

Wang, J.-Q., Zhao, Z.-Z., Bo, H.-B., and Chen, Q.-Z. (2016). Synthesis, characterization, and antitumor properties of ruthenium(II) anthraquinone complexes. *J. Coord. Chem.* 69, 177–189. doi: 10.1080/00958972.2015.1120291

Wang, N., Feng, Y., Zeng, L., Zhao, Z., and Chen, T. (2015). Functionalized multiwalled carbon nanotubes as carriers of ruthenium complexes to antagonize cancer multidrug resistance and radioresistance. *ACS Appl. Mater. Interfaces* 7, 14933–14945. doi: 10.1021/acsami.5b03739

Wang, X., Wang, X., and Guo, Z. (2015). Functionalization of platinum complexes for biomedical applications. *Acc Chem. Res.* 48, 2622–2631. doi: 10.1021/acs.accounts.5b00203

Wang, X., and Guo, Z. (2013). Targeting and delivery of platinum-based anticancer drugs. *Chem. Soc. Rev.* 42, 202–224. doi: 10.1039/c2cs35259a

Webb, M. I., Wu, B., Jang, T., Chard, R. A., Wong, E. W., Wong, M. Q., et al. (2013). Increasing the bioavailability of Ru(III) anticancer complexes through hydrophobic albumin interactions. *Chemistry* 19, 17031–17042. doi: 10.1002/chem.201302671

Wei, L., Lu, J., Xu, H., Patel, A., Chen, Z. S., and Chen, G. (2015). Silver nanoparticles: synthesis, properties, and therapeutic applications. *Drug Discov. Today* 20, 595–601. doi: 10.1016/j.drudis.2014.11.014

Weiss, A., Bonvin, D., Berndsen, R. H., Scherrer, E., Wong, T. J., Dyson, P. J., et al. (2015). Angiostatic treatment prior to chemo- or photodynamic therapy improves anti-tumor efficacy. *Sci. Rep.* 5:8990. doi: 10.1038/srep08990

Wilson, R., Espinosa-Diez, C., Kanner, N., Chatterjee, N., Ruhl, R., Hipfinger, C., et al. (2016). MicroRNA regulation of endothelial TREX1 reprograms the tumour microenvironment. *Nat. Commun.* 7:13597. doi: 10.1038/ncomms13597

Xu, L., Liu, Y. Y., Chen, L. M., Xie, Y. Y., Liang, J. X., and Chao, H. (2016). Mitochondria-targeted ruthenium (II) polypyridyl complexes with benzofuran group for live cell imaging. *J. Inorg. Biochem.* 159, 82–88. doi: 10.1016/j.jinorgbio.2016.02.028

Yu, Q., Liu, Y., Xu, L., Zheng, C., Le, F., Qin, X., et al. (2014). Ruthenium(II) polypyridyl complexes: cellular uptake, cell image and apoptosis of HeLa cancer cells induced by double targets. *Eur. J. Med. Chem.* 82, 82–95. doi: 10.1016/j.ejmech.2014.05.040

Yuan, J., Lei, Z., Wang, X., Zhu, F., and Chen, D. (2015). Ruthenium complex Lambda-WH0402 induces hepatocellular carcinoma LM6 (HCCLM6) cell death by triggering the Beclin-1-dependent autophagy pathway. *Metallomics* 7, 896–907. doi: 10.1039/c5mt00010f

Zeng, L., Chen, Y., Huang, H., Wang, J., Zhao, D., Ji, L., et al. (2015). Cyclometalated ruthenium(II) anthraquinone complexes exhibit strong anticancer activity in hypoxic tumor cells. *Chemistry* 21, 15308–15319. doi: 10.1002/chem.201502154

Zeng, L., Chen, Y., Liu, J., Huang, H., Guan, R., Ji, L., et al. (2016). Ruthenium(II) complexes with 2-phenylimidazo[4,5-f][1,10]phenanthroline derivatives that strongly combat cisplatin-resistant tumor cells. *Sci. Rep.* 6:19449. doi: 10.1038/srep19449

Zeng, L., Gupta, P., Chen, Y., Wang, E., Ji, L., Chao, H., et al. (2017a). The development of anticancer ruthenium(ii) complexes: from single molecule compounds to nanomaterials. *Chem. Soc. Rev.* 46, 5771–5804. doi: 10.1039/c7cs00195a

Zeng, L., Kuang, S., Li, G., Jin, C., Ji, L., and Chao, H. (2017b). A GSH-activatable ruthenium(ii)-azo photosensitizer for two-photon photodynamic therapy. *Chem. Commun.* 53, 1977–1980. doi: 10.1039/c6cc10330h

Zhang, P., Wang, J., Huang, H., Chen, H., Guan, R., Chen, Y., et al. (2014). RuNH2@AuNPs as two-photon luminescent probes for thiols in living cells and tissues. *Biomaterials* 35, 9003–9011. doi: 10.1016/j.biomaterials.2014.07.021

Zhang, P., Wang, J., Huang, H., Qiao, L., Ji, L., and Chao, H. (2013). Chiral ruthenium(II) complexes with phenolic hydroxyl groups as dual poisons of topoisomerases I and IIalpha. *Dalton Trans.* 42, 8907–8917. doi: 10.1039/c3dt50472g

Zhao, S., Nishimura, T., Chen, Y., Azeloglu, E. U., Gottesman, O., Giannarelli, C., et al. (2013). Systems pharmacology of adverse event mitigation by drug combinations. *Sci. Transl. Med.* 5:206ra140. doi: 10.1126/scitranslmed.3006548

Zhao, X., Li, M., Sun, W., Fan, J., Du, J., and Peng, X. (2018). An estrogen receptor targeted ruthenium complex as a two-photon photodynamic therapy agent for breast cancer cells. *Chem. Commun.* 54, 7038–7041. doi: 10.1039/c8cc03786h

Conflict of Interest Statement: The authors declare that the research was conducted in the absence of any commercial or financial relationships that could be construed as a potential conflict of interest.

frontiers in Pharmacology

ORIGINAL RESEARCH
published: 27 November 2018
doi: 10.3389/fphar.2018.01392

Osthole Synergizes With HER2 Inhibitor, Trastuzumab in HER2-Overexpressed N87 Gastric Cancer by Inducing Apoptosis and Inhibition of AKT-MAPK Pathway

Yun Yang[1,2,3], Feng Ren[1], Ziyin Tian[1], Wei Song[4], Binfeng Cheng[5] and Zhiwei Feng[1]**

[1] School of Basic Medical Sciences, Xinxiang Medical University, Xinxiang, China, [2] State Key Laboratory of Antibody Medicine and Targeted Therapy, Shanghai, China, [3] Henan Collaborative Innovation Center of Molecular Diagnosis and Laboratory Medicine, Xinxiang, China, [4] College of Life Science and Engineering, Henan University of Urban Construction, Pingdingshan, China, [5] School of Life Sciences and Technology, Xinxiang Medical University, Xinxiang, China

OPEN ACCESS

Edited by:
Zhe-Sheng Chen,
St. John's University, United States

Reviewed by:
Zhijun Liu,
Weifang Medical University, China
Ru Li,
Stony Brook University, United States
Pranav Gupta,
Harvard Medical School, United States

***Correspondence:**
Yun Yang
jamesyangyun1@126.com
Zhiwei Feng
123066@xxmu.edu.cn

Specialty section:
This article was submitted to Cancer Molecular Targets and Therapeutics, a section of the journal Frontiers in Pharmacology

Received: *17 October 2018*
Accepted: *12 November 2018*
Published: *27 November 2018*

Citation:
Yang Y, Ren F, Tian Z, Song W, Cheng B and Feng Z (2018) Osthole Synergizes With HER2 Inhibitor, Trastuzumab in HER2-Overexpressed N87 Gastric Cancer by Inducing Apoptosis and Inhibition of AKT-MAPK Pathway. Front. Pharmacol. 9:1392. doi: 10.3389/fphar.2018.01392

Background and Purpose: Although trastuzumab has shown considerable activity in the treatment of HER2-positive breast and gastric cancers, a significant proportion of patients do not respond to trastuzumab. Recent studies revealed that osthole, an active coumarin isolated from *Cnidium monnieri* (L.) Cusson possesses potent anti-tumor activity. Here, we for the first time investigated the anti-tumor activity of trastuzumab in combination with osthole in HER2-overexpressing cancers.

Materials and Methods: N87 and SK-BR-3 cell lines, which were HER2-overexpressing cancer cells were used in our study. Cell Counting Kit-8 (CCK-8) assay was utilized to test the inhibitory effects of trastuzumab plus osthole. Combination index (CI) values were calculated using the Chou-Talalay method. Fluorescence-Activated Cell Sorter (FACS) assay was used to examine the cell cycle change and apoptosis upon combinatorial treatment. N87 tumor xenografts were established to evaluate *in vivo* effects of trastuzumab plus osthole. In addition, molecular mechanisms were analyzed by Western blot *in vitro and in vivo*.

Results: As shown in our study, osthole alone exhibited effective anti-tumor activity against HER2-overexpressed N87 gastric cancer cells and SK-BR-3 breast cancer cells, which may be attributed to cell cycle arrest on G2/M phase and apoptosis. More importantly, our data demonstrated that trastuzumab plus osthole was much more potent than either agent alone in inhibiting the growth of N87 cancer cells *in vitro* and *in vivo*, which may be partly explained by the enhanced apoptosis upon the combinatorial treatment. Besides these, we also observed a significant decrease on the phosphorylation of AKT and MAPK in N87 cells when treated with trastuzumab plus osthole compared to either agent alone. Further data from N87 tumor xenografts

revealed that trastuzumab plus osthole exerted their synergistic effects mainly on AKT signaling pathway.

Conclusion: Collectively, these results support the clinical development of combination osthole with trastuzumab for the treatment of HER2-overexpressed gastric cancer.

Keywords: trastuzumab, osthole, gastric cancer, apoptosis, AKT

INTRODUCTION

Amplification of human epidermal growth factor receptor-2 (HER2), an important member of the ErbB family, is found in many solid tumors such as breast cancer and gastric cancer (Han et al., 2014; Yang et al., 2017). HER2 activation is dependent on HER2 homodimers or heterodimers with other ErbB family members, which could stimulate constitutive phosphorylation of HER2 and initiate the key downstream PI3K/AKT pathway or MAPK pathway that results in tumor growth and progression (Agus et al., 2002; Baselga and Swain, 2009; Wang et al., 2017). Trastuzumab is a well-known HER2-targeted humanized antibody that binds to the extracellular domain IV of HER2 and then causes inhibition of activation of downstream pathway (Wang et al., 2012; Li et al., 2013). It was approved by the US Food and Drug Administration (FDA) for clinical use for patients with HER2-overexpressing metastatic breast cancer in 1998, and for HER2-positive metastatic gastric cancer in 2010 (Baselga and Swain, 2009; Zheng et al., 2014). Despite the effectiveness, the majority of trastuzumab-responsive patients developed resistance within 1 year of treatment (Han et al., 2014; Zheng et al., 2014; Yang et al., 2017). Increased levels of membrane-bound EGFR and HER3 or sustained PI3K-AKT pathway activation has been implicated in the resistance to trastuzumab (Baselga and Swain, 2009). Collectively, there is an urgent need to enhance the efficacy of trastuzumab therapy.

Osthole is a natural coumarin, which was first derived from *Cnidium monnieri* (L.) Cusson (Zhang et al., 2015). As we know, osthole has been used in Traditional Chinese Medicine (TCM) for the treatment of cutaneous pruritus, eczema, trichomonas vaginalis infection, and sexual dysfunction for a long time (You et al., 2009; Zhang et al., 2012). Studies also revealed that osthole exhibited many pharmacological and biological activities, including anti-oxidation, anti-osteoporosis, and anti-inflammation (Liao et al., 2010; Chen et al., 2011). Recently, osthole was found to potently inhibit the growth of several types of cancer (Yang et al., 2003; Ye et al., 2013; Wang et al., 2015). However, its molecular mechanism has not been comprehensively elucidated although osthole has shown potent anti-tumor effects. Xu et al. (2011) revealed that osthole treatment caused G2/M arrest and apoptosis via modulating PI3K/Akt signaling pathway in lung cancer A549 cells. Besides, osthole was found to inhibit invasion and metastasis through down-regulation of MMP-5 and MMP-9 level in human lung adenocarcinoma cells (Kao et al., 2012). Moreover, studies revealed that osthole exerted anti-tumor effects on HER2-overexpressed breast cancer through inhibiting the c-Met/Akt/mTOR pathway (Lin et al., 2010; Hung et al., 2011). However, the anti-tumor activity of trastuzumab plus osthole in HER2-overexpressed cancers has not yet been reported.

Herein, we first investigated the anti-tumor effects of osthole alone in HER2-overexpressed N87 gastric cancer cells and SK-BR-3 breast cancer cells. Results revealed that osthole caused G2/M arrest and apoptosis in the two types of cancer cells, especially in SK-BR-3 cells. As we know, trastuzumab was an established anti-tumor therapeutic in treating HER2-positive breast cancer and gastric cancer (Baselga and Swain, 2009; Zheng et al., 2014). Next, we examined the anti-tumor activity of trastuzumab in combination with osthole against N87 and SK-BR-3 cells. Surprisingly, our results for the first time showed that osthole synergistically enhanced the growth-inhibitory effect of trastuzumab against N87 cancer cells *in vitro* and *in vivo*. Moreover, we found that the combination was more potent in inducing apoptosis and reducing the phosphorylation of AKT and MAPK than either agent alone in N87 cells, which may explain the synergistic effect. To conclude, these results shown in our study suggested that the effective regimen by combing trastuzumab with osthole has a great potential to treat HER2-overexpressed gastric cancer in clinics.

MATERIALS AND METHODS

Cell Lines

The human breast cancer cell line SK-BR-3 and gastric cancer cell line N87 were purchased from the American Type Culture Collection (ATCC).

Agents

Osthole was purchased from Shanghai Macklin Biochemical Co., Ltd. (Shanghai, China). It is over 99% pure determined by HPLC. The stock solution of osthole was prepared by dissolving in DMEM with 0.25% ethanol and 0.25% dimethyl sulfoxide (DMSO).

Animals

All experimental protocols were approved by the Animal Experimentation Ethics Committee of Xinxiang Medical University and all efforts were made to minimize animal suffering and reduce the number of animals used. All experiments were performed in accordance with the guideline of the Animal Care and Use Committee of Xinxiang Medical University. Five-week-old female BALB/c nude mice were obtained from the Beijing Vital River Laboratory Animal Technology Co., Ltd. (Beijing, China).

In vitro Cytotoxicity Assays

Cells were plated at a density of 5×10^3 per well and incubated with increasing concentrations of osthole, trastuzumab or the combination. Two days later, cell proliferation was determined using CCK-8 kit (Dojindo, Japan). The percentage of surviving cells was calculated using the following formula: [(A450 of experiment – A450 of background)/(A450 of untreated control – A450 of background)] × 100. Combination index (CI) values were calculated using the Chou-Talalay method by Compusyn software (Han et al., 2014). Drug synergy, addition, and antagonism are defined by C.I. values less than 1.0, equal to 1.0, or greater than 1.0, respectively.

In vivo Therapy Study

N87 cells (1×10^7 per mouse) were inoculated subcutaneously into the right flank of female BALB/c nude mice. When tumor volumes reached an average of about 150 mm^3 on day 8 after inoculation, the mice were randomly divided into four groups of six mice each. Mice were intraperitoneally injected with control IgG (15 mg/kg for two times every week), trastuzumab (15 mg/kg for two times every week), osthole (100 mg/kg once daily) or the combination of trastuzumab (15 mg/kg for two times every week), and osthole (100 mg/kg once daily) for 2 weeks. Tumors were measured with digital calipers, and tumor volumes were calculated by the formula: Volume = Length × $(\text{Width})^2/2$.

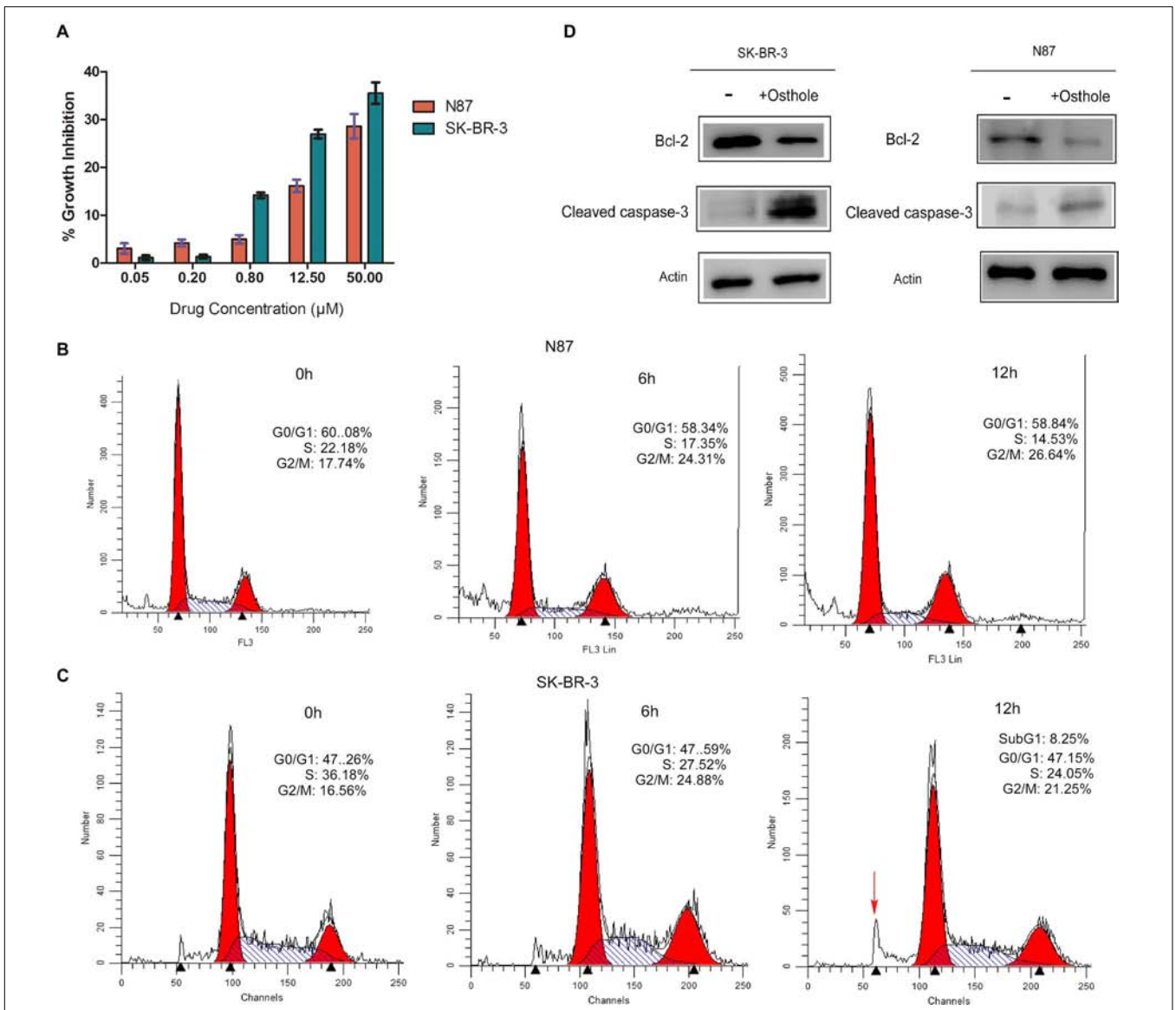

FIGURE 1 | Osthole inhibited the growth of N87 and SK-BR-3 cells and induced cell cycle arrest and apoptosis. **(A)** CCK-8 assay evaluating cell growth of N87 and SK-BR-3 cells upon treatment with increasing concentration of osthole for 48 h. **(B)** Cell cycle analysis of N87 cells following 40 μM osthole treatment for 0, 6, and 12 h by flow cytometry. **(C)** Effects of osthole on cell cycle of SK-BR-3 cells. **(D)** N87 and SK-BR-3 cells were treated with 40 μM osthole for 30 h and cleaved Caspase-3 and Bcl-2 were examined by Western blot.

Immunoblotting

Western blot was performed using established procedures.(Yang et al., 2017) Cells were lysed in lysis buffer (Beijing Dingguo Biotechnology Co., Ltd.), incubated on ice for 30 min and centrifuged for 20 min to remove cell debris. Total cell lysates were subjected to SDS–polyacrylamide and immunoblotted with primary antibodies and HRP-conjugated secondary antibody. After another wash of the membrane, the bands were detected using a super-sensitive ECL solution (Boster Biological Technology Co., Ltd., China), and visualized using an Amersham imager 600 (GE Healthcare Life Sciences, Fairfield, CT, United States).

Cell Cycle Analysis

This assay was performed according to previous report.(Kovtun et al., 2010) Cells (1×10^5/mL) were incubated with osthole for 0, 6, or 12 h at 37° C. Cells were then fixed with 1 mL of 70% ethanol, and DNA content was determined after staining with propidium iodide by flow cytometry. Flow cytometric data were analyzed using FlowJo 7.6 software.

Apoptosis Analysis

Apoptosis analysis was performed by flow cytometry using established procedures (Zhang et al., 2012). For flow cytometry analysis, N87 cells (5×10^6/well) were plated in 6-well plate and treated with osthole (40 μM), trastuzumab (10 μg/mL), or osthole (40 μM) in combination with trastuzumab (10 μg/mL) for 30 h at 37°C. The cells were then labeled with Annexin V and Propidium Iodide (PI; Beijing Dingguo Biotechnology Co., Ltd, Beijing). Apoptotic rates were determined by FACSCalibur flow cytometer (BD Biosciences, Franklin Lakes, NJ, United States) and analyzed by Flowjo software. The percentage of the early apoptosis was calculated by Annexin V (+) and PI (−), while the percentage of the late apoptosis was calculated by Annexin V (+) and PI (+).

Statistical Analysis

Statistical analysis was performed by Student's unpaired t test to identify significant differences unless otherwise indicated. Differences were considered significant at $p < 0.05$.

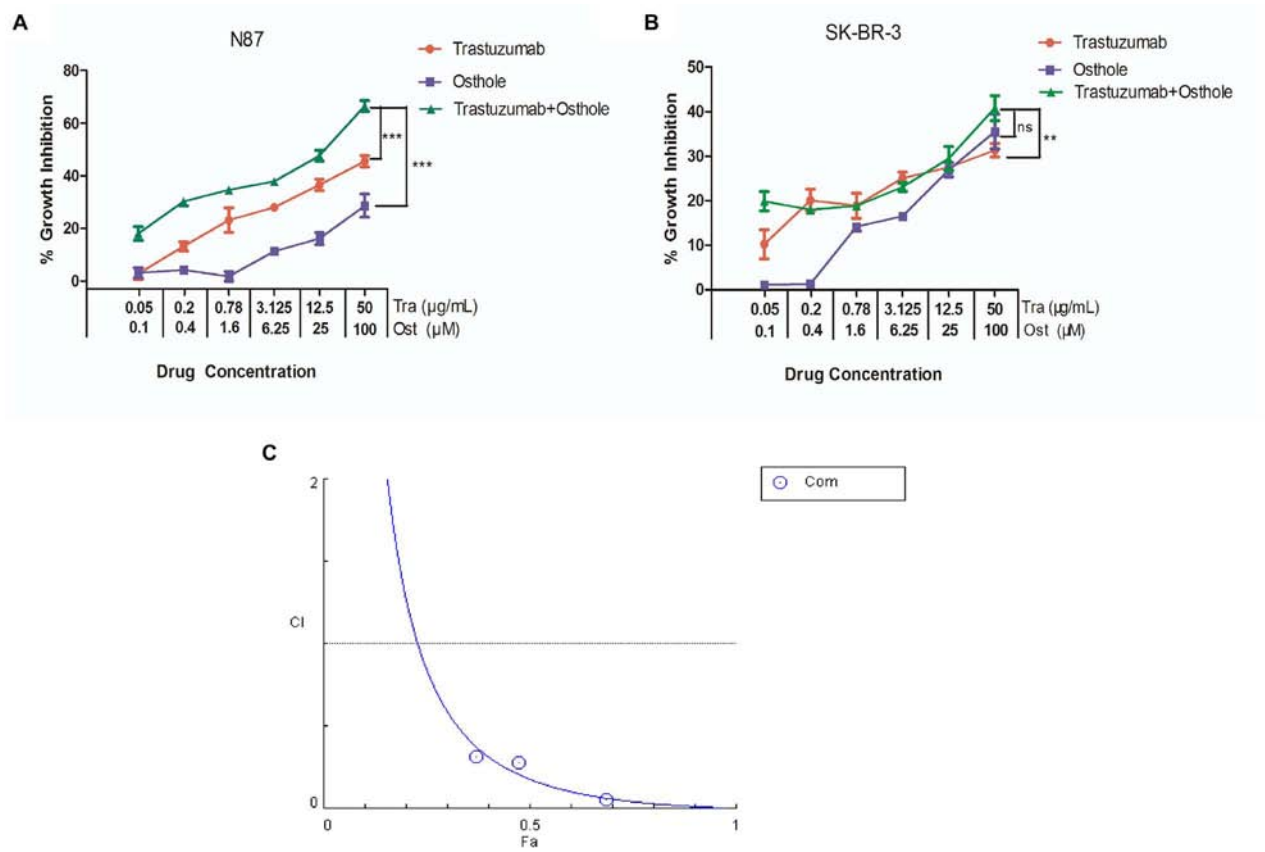

FIGURE 2 | Osthole and trastuzumab synergistically inhibited the *in vitro* growth of N87 cells. **(A)** The inhibitory effects of osthole and trastuzumab combinatorial treatment against N87 cells for 48 h. **(B)** The inhibitory effects of osthole and trastuzumab combinatorial treatment against SK-BR-3 cells for 48 h. **(C)** The synergistic effect of trastuzumab in combination with osthole on the growth of N87 cell line. Combination index (CI) values were calculated at the drug concentration of trastuzumab (3.125 μg/mL) plus osthole (6.25 μM), trastuzumab (12.5 μg/mL) plus osthole (25 μM), trastuzumab (50 μg/mL) plus osthole (100 μM) using the Chou-Talalay method. Drug synergy, addition, and antagonism are defined by C.I. values less than 1.0, equal to 1.0, or greater than 1.0, respectively. Data show the mean ± SD (three independent experiments); *$p < 0.05$; **$p < 0.01$; ***$p < 0.001$. ns, no significant difference.

RESULTS

Osthole Exhibits Growth-Inhibitory Activity Against HER2-Overexpressed N87 and SK-BR-3 Cancer Cells Through Cell Cycle Arrest and Apoptosis

We first examined the inhibitory effects of osthole alone on N87 and SK-BR-3 cell lines. As shown in **Figure 1A**, osthole inhibited the growth of N87 and SK-BR-3 cancer cells in a dose-dependent manner. Additionally, we found that SK-BR-3 cell line responded more sensitively to osthole compared with N87 cell line.

Furthermore, we investigated the effect of osthole on cell cycle arrest and apoptosis in N87 and SK-BR-3 cells. FACS assay showing that osthole significantly elevated the percentage of G2/M phase in both N87 and SK-BR-3 cells when treated for 6 and 12 h compared to control (**Figures 1B,C**). More importantly, elevated sub-G1 population in SK-BR-3 cells was observed after treatment for 12 h. As we know, Bcl-2 was an important anti-apoptotic protein that regulates a late step in the apoptosis pathway (Srinivas et al., 2000; Willis et al., 2007). And Caspase-3 is an important member in Caspase family, which is critical for cytochrome c-dependent apoptosis (Zou et al., 1997). In our study, we found that Bcl-2 was down-regulated and cleaved Caspase-3 was up-regulated after treatment with osthole for 30 h, suggesting apoptosis may be induced following cell cycle arrest in response to osthole treatment in SK-BR-3 and N87 cells (**Figure 1D** and **Supplementary Figure S1**). Taken together, osthole may exert its anti-tumor effects in SK-BR-3 and N87 cells through inducing cell cycle arrest and apoptosis.

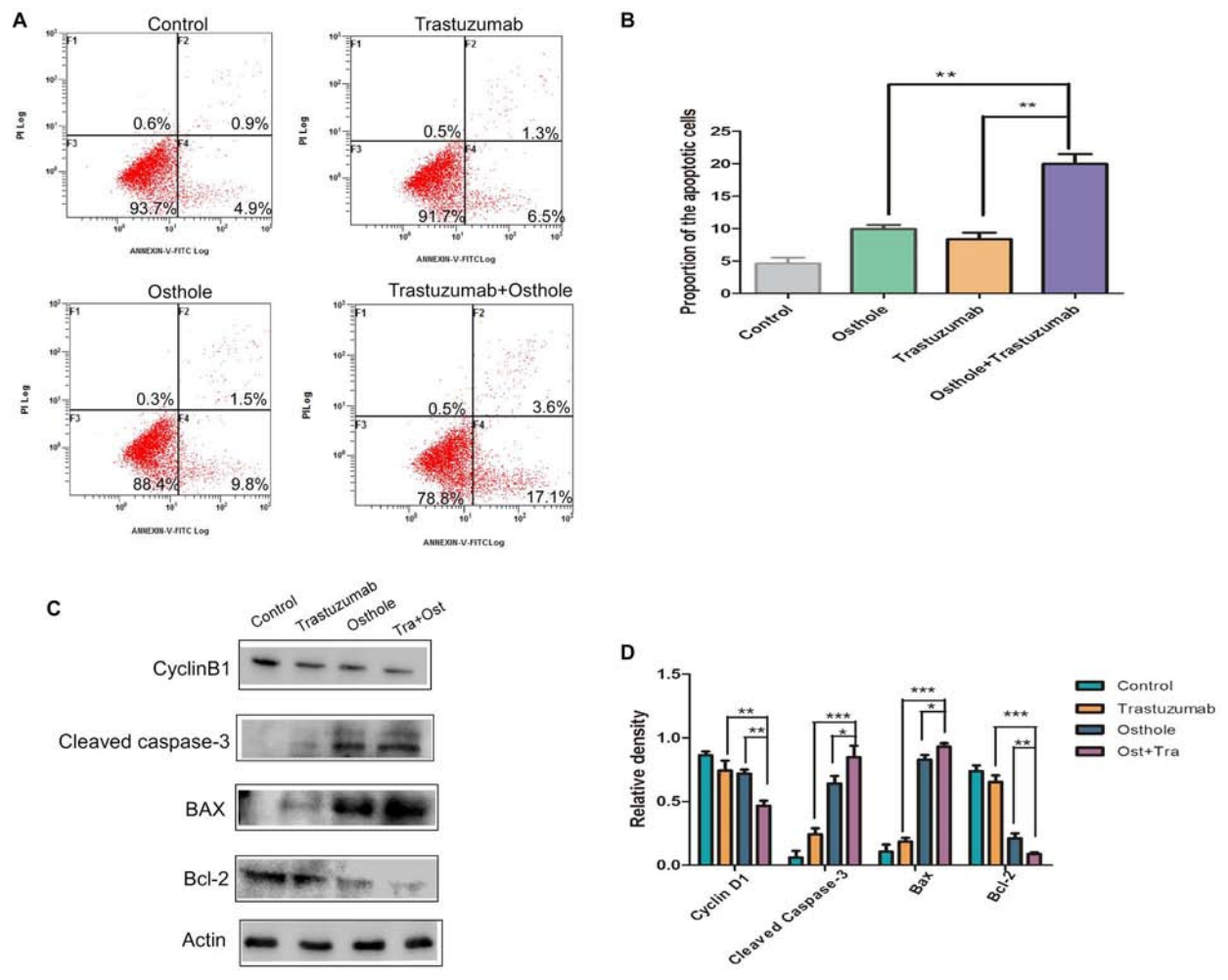

FIGURE 3 | Trastuzumab enhanced osthole-induced apoptosis, which may partly explained the synergistic anti-tumor effect of trastuzumab in combination with osthole. **(A)** Induction of apoptosis of N87 cells after control IgG (10 μg/mL), osthole (40 μM), trastuzumab (10 μg/mL) or the combinatorial treatment for 30 h. Apoptosis was measured by flow cytometry. **(B)** Statistical analysis of the percentages of the apoptotic cells. Data was shown with mean ± SD. **(C)** Cell cycle and apoptosis related protein (CyclinB1, cleaved Caspase-3, Bax or Bcl-2) was examined in N87 cells when treated with control IgG (10 μg/mL), osthole (40 μM), trastuzumab (10 μg/mL), or the combination for 30 h. **(D)** Quantification of Western blot signal intensity analysis is expressed relative to the β-actin loading control by using Image J software. Data show the mean ± SD (three independent experiments); $^{*}p < 0.05$; $^{**}p < 0.01$; $^{***}p < 0.001$.

Trastuzumab and Osthole Act Synergistically on N87 Gastric Cancer Cells *in vitro*

Next, we examined the inhibitory effects of trastuzumab in combination with osthole on N87 and SK-BR-3 cell lines. As shown in **Figures 2A,B**, trastuzumab plus osthole exhibited a significantly greater inhibitory activity than either agent alone in N87 cells, while no marked synergistic effect was found in SK-BR-3 cells.

To further examine whether the combination of trastuzumab with osthole is synergistic, we treated N87 cells with combination of trastuzumab and osthole at various concentrations. Data were analyzed using the method of Chou and Talalay to establish drug C.I. values (Han et al., 2014). Synergy is defined as C.I. values of <1.0, antagonism as C.I. values >1.0, and additivity as CI values equal to 1.0. Our results showed that trastuzumab and osthole synergistically inhibited the growth of N87 cells (**Figure 2C**).

Trastuzumab in Combination With Osthole Synergistically Induced Apoptosis

Furthermore, we investigated whether the co-treatment of trastuzumab with osthole may synergistically induce apoptosis in N87 cells. First, the apoptotic cell percentage was analyzed by flow cytometry following Annexin V and PI staining. Results showed that the percentage of apoptotic cells was significantly increased in the trastuzumab plus osthole treated cells compared to either agent mono-treated cells (**Figures 3A,B**).

And we further assessed the cell extracts for expression of apoptotic markers including cleaved Caspase-3, Bcl-2, and Bax. Compared to treatment with either agent alone, combinatorial treatment significantly up-regulated the level of cleaved Caspase-3 (**Figures 3C,D**). In addition, Bcl-2 was markedly down-regulated, while Bax that was a protein favoring induction of apoptosis was up-regulated in trastuzumab plus osthole treated cells. Besides these, the expression of cell cycle-related molecule, CyclinB1 was significantly decreased in N87 cells upon combinatorial treatment. Taken together, these results suggested the addition of trastuzumab markedly enhanced osthole-induced apoptosis, which may partly explain the superiority of combinatorial treatment.

Effect of Trastuzumab Plus Osthole on AKT and MAPK Signaling Pathway

To further investigate the mechanism that may explain the synergistic effect, we examined the level of AKT, phosphorylated AKT, MAPK, and phosphorylated MAPK in N87 cells treated with trastuzumab in combination with osthole. Compared to trastuzumab or osthole treatment alone, trastuzumab plus osthole more significantly inhibited the phosphorylation of both AKT and MAPK in N87 cell lines (**Figures 4A,B**). Notably, combinatorial treatment resulted in a more effective inhibition on phospho-AKT level than on phospho-MAPK level, whereas there was no substantially decrease in total AKT and MAPK protein levels. Therefore, our results suggested that trastuzumab in combination with osthole may exert their synergistic effect on inhibiting AKT and MAPK pathway, mainly inhibiting the phosphorylation of AKT, which also further explained the superior effects of trastuzumab plus osthole.

Trastuzumab in Combination With Osthole Potently Suppresses the *in vivo* Growth of N87 Cancer Xenografts

To assess the synergistic effect *in vivo*, we examined the therapeutic efficacy of trastuzumab plus osthole for nude mice bearing established N87 tumor xenografts. As shown in **Figures 5A,B** and **Supplementary Figure S2**, our *in vivo*

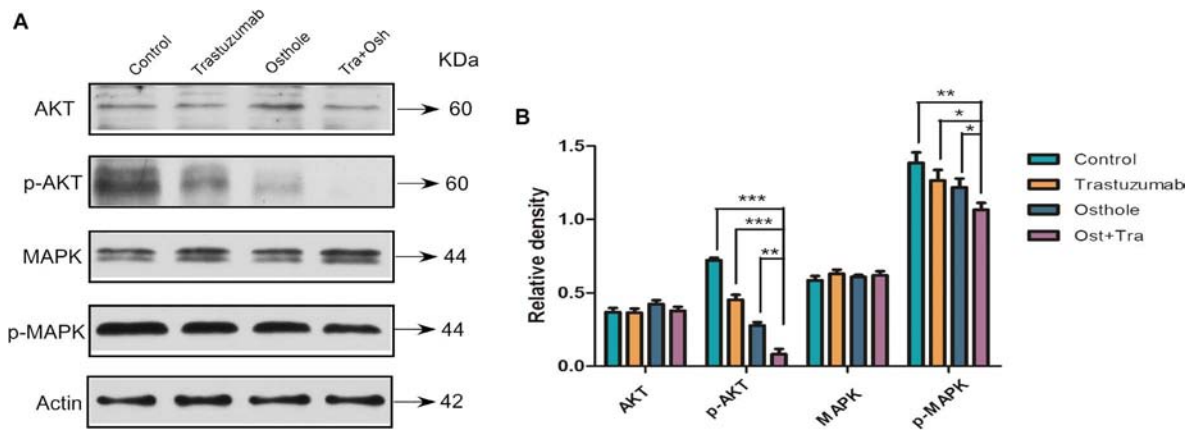

FIGURE 4 | Trastuzumab in combination with osthole blocked AKT pathway in a synergistic manner. **(A)** Immunoblots assessing AKT and MAPK signaling in the N87 cell lines upon treatment with control IgG (10 μg/mL), trastuzumab (10 μg/mL), osthole (40 μM), or trastuzumab (10 μg/mL) plus osthole (40 μM) for 30 h. Data are representative of three independent experiments. **(B)** Quantification of Western blot signal intensity analysis is expressed relative to the β-actin loading control by using Image J software. Data show the mean ± SD (three independent experiments); $^{*}p < 0.05$; $^{**}p < 0.01$; $^{***}p < 0.001$.

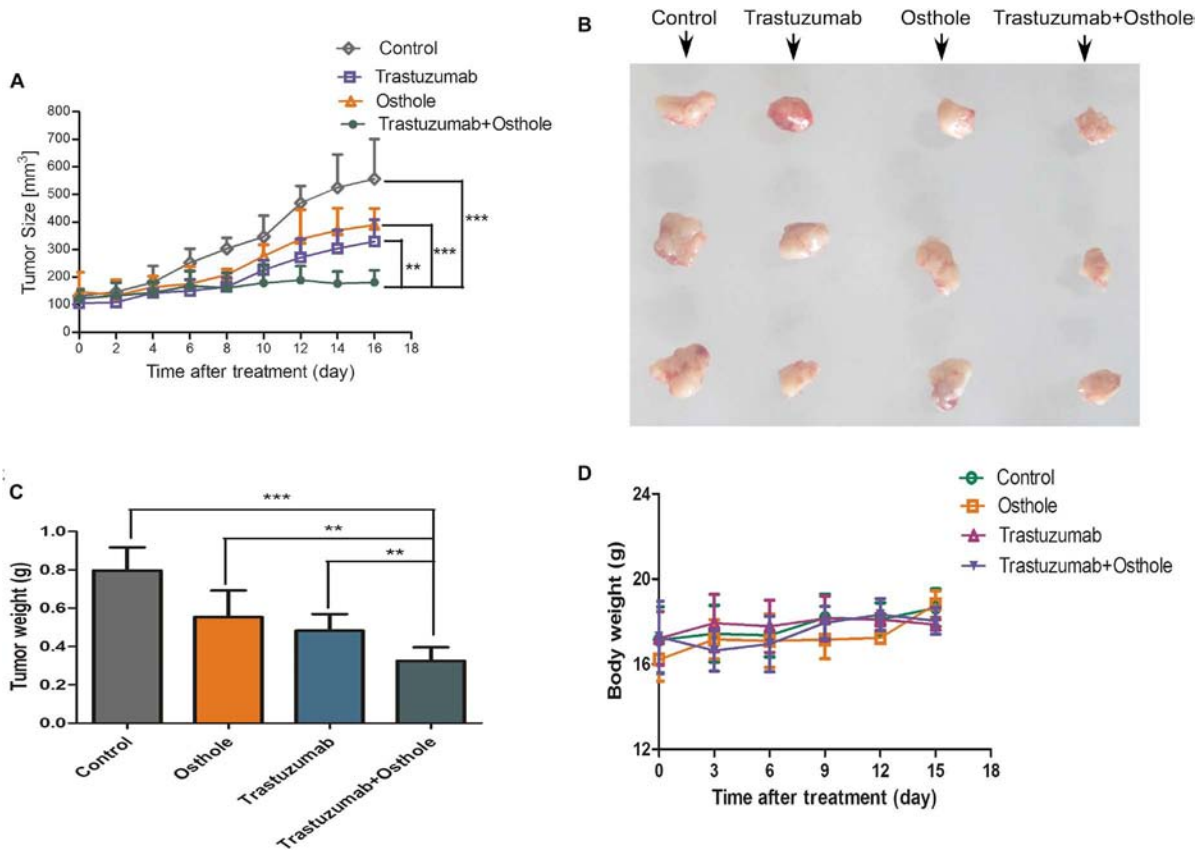

FIGURE 5 | Trastuzumab plus osthole combinatorial treatment inhibits the growth of N87 cancer cells *in vivo*. **(A)** Tumor volume of N87 xenografts after injection with control IgG (15 mg/kg), Trastuzumab (15 mg/kg), Osthole (100 mg/kg), or Trastuzumab (15 mg/kg) plus Osthole (100 mg/kg). **(B)** On day 16 post first injection, xenograft tumors from each group were removed and photographed. Representative tumors in each group were shown. **(C)** After xenograft tumors were removed, these tumors were weighted. **(D)** Effects of agents on tumor-bearing mice body weight were determined using N87 tumor-bearing nude mice. Mice were weighed at regular intervals during the whole period to monitor unspecific toxicity. Data are shown as mean ± SD. (n = 6 mice, each group); $^{**}p < 0.01$; $^{***}p < 0.001$.

experiments showed that the combinatorial therapy of trastuzumab with osthole significantly reduced tumor growth compared to either agent treatment alone. Compared to the control IgG, the treatment with trastuzumab and osthole combination resulted in a 50 % reduction in tumor weight (**Figure 5C**). Consistent with the observations *in vitro*, combinatorial treatment of trastuzumab with osthole resulted in a significant benefit over either agent alone in the N87 xenograft model. Moreover, we also preliminarily evaluated the unspecific-toxicity in these xenografts. As shown in **Figure 5D**, No marked weight loss was observed in trastuzumab plus osthole treated mice compared with that of in the control IgG treated group (p = 0.1934). Thus, our results showed that trastuzumab in combination with osthole exhibited potent inhibitory effects and good tolerance on N87 tumor xenografts.

Trastuzumab in Combination With Osthole Inhibited AKT Signaling Pathway *in vivo*

To further determine if combinatorial treatment caused inhibition of intracellular signaling cascade *in vivo*, we examined tumor samples from treated animals using western blot assay to evaluate the degree to which MAPK or AKT signaling was inhibited. As expected, the level of pAKT in tumors of combinatorial treatment group was more effectively regressed compared to that of in trastuzumab or osthole treatment group while the level of pMAPK was not substantially reduced in tumors from trastuzumab plus osthole treated mice (**Figures 6A,B**). Collectively, these results above may also suggest that trastuzumab plus osthole exerted their synergistic effects mainly on AKT signaling pathway in N87 tumor xenografts.

DISCUSSION

In our study, we for the first time reported the anti-tumor effects of trastuzumab in combination with osthole, a natural coumarin derivative extracted from Traditional Chinese Medicine on N87 gastric cancer cells and investigated the underlying mechanism involved. We first examined the inhibitory effects of osthole on HER2-amplified N87 and SK-BR-3 cells. Results revealed that osthole exhibited potent anti-tumor activity on the two cell lines, especially on SK-BR-3 cells. Previous studies suggested

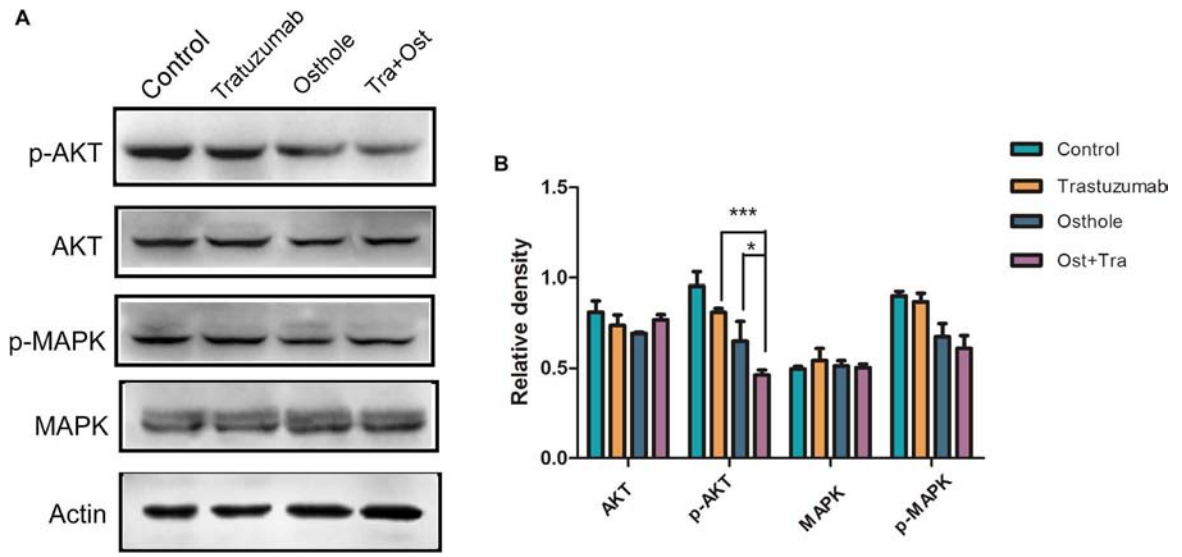

FIGURE 6 | Trastuzumab in combination with osthole inhibited AKT signaling pathway *in vivo*. **(A)** Tumor tissues isolated from N87 xenografts upon treatment with control IgG (15 mg/kg), Trastuzumab (15 mg/kg), Osthole (100 mg/kg), Sor Trastuzumab (15 mg/kg) plus Osthole (100 mg/kg) were then subjected to Western blot to detect the expression of AKT, p-AKT, MAPK and p-AMPK. Data are representative of three independent experiments. **(B)** Quantification of Western blot signal intensity analysis is expressed relative to the -actin loading control by using Image J software. Data show the mean ± SD (three independent experiments); $^{*}p < 0.05$; $^{**}p < 0.01$; $^{***}p < 0.001$.

that osthole could induce G2/M arrest and apoptosis in lung cancer A549 cells and hepatocellular carcinoma HepG2 cells (Xu et al., 2011; Chao et al., 2014). In consistent with these studies, we also found that osthole induced G2/M arrest and apoptosis in HER2-amplified N87 and SK-BR-3 cells. As we know, trastuzumab is a FDA-approved antibody therapeutic that has shown clinical efficacy in treating breast and gastric cancers (Hudis, 2007; Rose and Bekaii-Saab, 2011). Despite the effectiveness, numbers of patients with HER2-positive cancer treated with trastuzumab monotherapy exhibited *de novo* resistance unfortunately (Zhang et al., 2011). Thus, novel therapeutic regimens are urgently needed to enhance the efficacy of trastuzumab-therapy. Surprisingly, we found that osthole could synergistically enhance the inhibitory effect of trastuzumab against HER2-overexpressed N87 cells both *in vitro* and *in vivo*. However, the synergistic effect were not been observed in SK-BR-3 cells, which was the other trastuzumab-sensitive breast cancer cell line. The underlying mechanism explaining the different responses to trastuzumab plus osthole in the two HER2-overexpressed cancer cell lines will be further explored in our following research.

As previously reported, trastuzumab may exert its anti-tumor activity on HER2-overexpressed cancers through inducing apoptosis (Cuello et al., 2001; Milella et al., 2004). And osthole also caused cell cycle arrest and apoptosis in several types of cancer (Xu et al., 2011; Chao et al., 2014; Wang et al., 2016). In our present study, the hypothesis was investigated that if trastuzumab plus osthole may synergistically enhance the effect of apoptosis in N87 cells. As expectedly, our data revealed that trastuzumab in combination with osthole more effectively promoted apoptosis compared to either agent treatment alone.

As we know, studies have demonstrated that PI3K-AKT pathway activity is directly linked to the proliferation and growth of HER2-overexpressing cancer cells and trastuzumab mainly exerted its anti-tumor in inhibiting the HER2-PI3K-AKT pathway (Pal and Mandal, 2012; Li et al., 2013; Han et al., 2014). Recently, Lin et al. (2014) indicated that osthole inhibited IGF-1-induced EMT by blocking PI3K-Akt pathway in brain cancer cells. In our study, we also observed AKT and MAPK phosphorylation were regressed in N87 cells when treated with trastuzumab plus osthole. Especially, AKT phosphorylation was more markedly inhibited in the combinatorial treatment compared to either agent treatment alone, which was also verified in tumor samples from N87 tumor xenografts. Generally speaking, our study partly explained the molecular mechanism involved in the synergistic effects of trastuzumab in combination with osthole on HER2-overexpressed gastric cancer, which may provide a reference for other researchers. In our following study, we will explore if other AKT involved signaling pathway like c-Met/Akt/mTOR pathway may be related to the synergistic anti-tumor effects.

Taken together, our results suggested that osthole, a promising lead compound from traditional Chinese medicine could effectively inhibit N87 and SK-BR-3 cells with HER2-overexpression by causing cell cycle arrest and inducing apoptosis. More importantly, we found that combination of trastuzumab with osthole showed synergistic inhibitory effects on the growth of N87 cells, which may be partly attributed to the enhanced apoptosis. Phosphorylation of AKT were effectively inhibited *in vitro* and *in vivo* when treated with trastuzumab plus

osthole may also contribute to the synergistic effect. Therefore, combination of trastuzumab with osthole provides a new strategy for targeting HER2-overexpressed gastric cancer, which will contribute to enhancing the therapeutic effect of trastuzumab. Based on these results, our study also suggested that osthole can be developed into an adjuvant drug for HER2-targeted therapy in treating HER2-overexpressed gastric cancer. In addition, a novel antibody-drug conjugate may also be designed by conjugating osthole to trastuzumab, which may represent a new therapeutic approach.

CONCLUSION

Our results indicated that osthole alone exhibited effective anti-tumor activity against HER2-overexpressed N87 gastric cancer cells and SK-BR-3 breast cancer cells. Furthermore, osthole could synergistically enhance the inhibitory effect of trastuzumab against HER2-overexpressed N87 cells both *in vitro* and *in vivo*. Moreover, we explored the molecular mechanism involved in the synergistic effects, which may be attributed to the enhanced apoptosis effects and AKT-MAPK signaling pathway blockade. Collectively, these results support the clinical development of osthole plus trastuzumab for the treatment of HER2-overexpressed gastric cancer. Besides, our study may also provide a strategy for testing combinations of HER2-targeting agents with other bioactive constituents isolated from food in clinical studies.

DATA AVAILABILITY STATEMENT

Data arising from this study are contained within the manuscript.

ETHICS STATEMENT

This study was carried out in accordance with the Principle of Laboratory Animal Care (NIH Publication No. 85-23, revised 1985). The protocol was approved by the Animal Ethics Committee of Xinxiang Medical University.

AUTHOR CONTRIBUTIONS

YY and ZF designed the experiments and wrote the manuscript. YY, FR, ZT, WS, and BC carried out the experiments. ZF supervised and corrected the manuscript.

FUNDING

This work was supported by grants from the Natural Science Foundation of China (81703054, 81671226, and 81403161), National Major Scientific and Technological Special Project for "Significant New Drugs Development"(2018ZX09301002001), Key Scientific Research Project of Higher Education of Henan Province, China (17A350012 and 19A310004), Key Science and Technology Program of Henan Province, China (172102310614 and 182102310259), Key Science and Technology Program of Shanghai (16431904700, 16DZ1910400, 16431904100, and 17431901800), and Doctoral Foundation of Xinxiang Medical University (XYBSKYZZ201506).

SUPPLEMENTARY MATERIAL

The Supplementary Material for this article can be found online at: https://www.frontiersin.org/articles/10.3389/fphar.2018.01392/full#supplementary-material

REFERENCES

Agus, D. B., Akita, R. W., Fox, W. D., Lewis, G. D., Higgins, B., Pisacane, P. I., et al. (2002). Targeting ligand-activated ErbB2 signaling inhibits breast and prostate tumor growth. *Cancer Cell* 2, 127–137. doi: 10.1016/S1535-6108(02)00097-1

Baselga, J., and Swain, S. M. (2009). Novel anticancer targets: revisiting ERBB2 and discovering ERBB3. *Nat. Rev. Cancer* 9, 463–475. doi: 10.1038/nrc2656

Chao, X., Zhou, X., Zheng, G., Dong, C., Zhang, W., Song, X., et al. (2014). Osthole induces G2/M cell cycle arrest and apoptosis in human hepatocellular carcinoma HepG2 cells. *Pharm. Biol.* 52, 544–550. doi: 10.3109/13880209.2013.850517

Chen, T., Liu, W., Chao, X., Qu, Y., Zhang, L., Luo, P., et al. (2011). Neuroprotective effect of osthole against oxygen and glucose deprivation in rat cortical neurons: involvement of mitogen-activated protein kinase pathway. *Neuroscience* 183, 203–211. doi: 10.1016/j.neuroscience.2011.03.038

Cuello, M., Ettenberg, S. A., Clark, A. S., Keane, M. M., Posner, R. H., Nau, M. M., et al. (2001). Down-regulation of the erbB-2 receptor by trastuzumab (herceptin) enhances tumor necrosis factor-related apoptosis-inducing ligand-mediated apoptosis in breast and ovarian cancer cell lines that overexpress erbB-2. *Cancer Res.* 61, 4892–4900.

Han, S., Meng, Y., Tong, Q., Li, G., Zhang, X., Chen, Y., et al. (2014). The ErbB2-targeting antibody trastuzumab and the small-molecule SRC inhibitor saracatinib synergistically inhibit ErbB2-overexpressing gastric cancer. *MAbs* 6, 403–408. doi: 10.4161/mabs.27443

Hudis, C. A. (2007). Trastuzumab–mechanism of action and use in clinical practice. *N. Engl. J. Med.* 357, 39–51. doi: 10.1056/NEJMra043186

Hung, C. M., Kuo, D. H., Chou, C. H., Su, Y. C., Ho, C. T., and Way, T. D. (2011). Osthole suppresses hepatocyte growth factor (HGF)-induced epithelial-mesenchymal transition via repression of the c-Met/Akt/mTOR pathway in human breast cancer cells. *J. Agric. Food Chem.* 59, 9683–9690. doi: 10.1021/jf2021489

Kao, S. J., Su, J. L., Chen, C. K., Yu, M. C., Bai, K. J., Chang, J. H., et al. (2012). Osthole inhibits the invasive ability of human lung adenocarcinoma cells via suppression of NF-kappaB-mediated matrix metalloproteinase-9 expression. *Toxicol. Appl. Pharmacol.* 261, 105–115. doi: 10.1016/j.taap.2012.03.020

Kovtun, Y. V., Audette, C. A., Mayo, M. F., Jones, G. E., Doherty, H., Maloney, E. K., et al. (2010). Antibody-maytansinoid conjugates designed to bypass multidrug resistance. *Cancer Res.* 70, 2528–2537. doi: 10.1158/0008-5472.CAN-09-3546

Li, B., Meng, Y., Zheng, L., Zhang, X., Tong, Q., Tan, W., et al. (2013). Bispecific antibody to ErbB2 overcomes trastuzumab resistance through comprehensive blockade of ErbB2 heterodimerization. *Cancer Res.* 73, 6471–6483. doi: 10.1158/0008-5472.CAN-13-0657

Liao, P. C., Chien, S. C., Ho, C. L., Wang, E. I., Lee, S. C., Kuo, Y. H., et al. (2010). Osthole regulates inflammatory mediator expression through modulating NF-kappaB, mitogen-activated protein kinases, protein kinase C, and reactive oxygen species. *J. Agric. Food Chem.* 58, 10445–10451. doi: 10.1021/jf102812t

Lin, V. C., Chou, C. H., Lin, Y. C., Lin, J. N., Yu, C. C., Tang, C. H., et al. (2010). Osthole suppresses fatty acid synthase expression in HER2-overexpressing breast cancer cells through modulating Akt/mTOR pathway. *J. Agric. Food Chem.* 58, 4786–4793. doi: 10.1021/jf100352c

Lin, Y. C., Lin, J. C., Hung, C. M., Chen, Y., Liu, L. C., Chang, T. C., et al. (2014). Osthole inhibits insulin-like growth factor-1-induced epithelial to mesenchymal transition via the inhibition of PI3K/Akt signaling pathway in human brain cancer cells. *J. Agric. Food Chem.* 62, 5061–5071. doi: 10.1021/jf501047g

Milella, M., Trisciuoglio, D., Bruno, T., Ciuffreda, L., Mottolese, M., Cianciulli, A., et al. (2004). Trastuzumab down-regulates Bcl-2 expression and potentiates apoptosis induction by Bcl-2/Bcl-XL bispecific antisense oligonucleotides in HER-2 gene–amplified breast cancer cells. *Clin. Cancer Res.* 10, 7747–7756. doi: 10.1158/1078-0432.CCR-04-0908

Pal, I., and Mandal, M. (2012). PI3K and Akt as molecular targets for cancer therapy: current clinical outcomes. *Acta Pharmacol. Sin.* 33, 1441–1458. doi: 10.1038/aps.2012.72

Rose, J. S., and Bekaii-Saab, T. S. (2011). New developments in the treatment of metastatic gastric cancer: focus on trastuzumab. *Oncol. Targets Ther.* 4, 21–26. doi: 10.2147/OTT.S10188

Srinivas, G., Kusumakumary, P., Nair, M. K., Panicker, K. R., and Pillai, M. R. (2000). Mutant p53 protein, Bcl-2/Bax ratios and apoptosis in paediatric acute lymphoblastic leukaemia. *J. Cancer Res. Clin. Oncol.* 126, 62–67. doi: 10.1007/s004320050010

Wang, L., Peng, Y., Shi, K., Wang, H., Lu, J., Li, Y., et al. (2015). Osthole inhibits proliferation of human breast cancer cells by inducing cell cycle arrest and apoptosis. *J. Biomed. Res.* 29, 132–138. doi: 10.7555/JBR.27.20120115

Wang, L., Yang, L., Lu, Y., Chen, Y., Liu, T., Peng, Y., et al. (2016). Osthole induces cell cycle arrest and inhibits migration and invasion via pten/akt pathways in osteosarcoma. *Cell Physiol. Biochem.* 38, 2173–2182. doi: 10.1159/000445573

Wang, L., Yu, X., Wang, C., Pan, S., Liang, B., Zhang, Y., et al. (2017). The anti-ErbB2 antibody H2-18 and the pan-PI3K inhibitor GDC-0941 effectively inhibit trastuzumab-resistant ErbB2-overexpressing breast cancer. *Oncotarget* 8, 52877–52888. doi: 10.18632/oncotarget.17907

Wang, S., Chen, C., Meng, Y., Hu, S., Zheng, L., Song, J., et al. (2012). Effective suppression of breast tumor growth by an anti-EGFR/ErbB2 bispecific antibody. *Cancer Lett.* 325, 214–219. doi: 10.1016/j.canlet.2012.07.007

Willis, S. N., Fletcher, J. I., Kaufmann, T., van Delft, M. F., Chen, L., Czabotar, P. E., et al. (2007). Apoptosis initiated when BH3 ligands engage multiple Bcl-2 homologs, not Bax or Bak. *Science* 315, 856–859. doi: 10.1126/science.1133289

Xu, X., Zhang, Y., Qu, D., Jiang, T., and Li, S. (2011). Osthole induces G2/M arrest and apoptosis in lung cancer A549 cells by modulating PI3K/Akt pathway. *J. Exp. Clin. Cancer Res.* 30:33. doi: 10.1186/1756-9966-30-33

Yang, L. L., Wang, M. C., Chen, L. G., and Wang, C. C. (2003). Cytotoxic activity of coumarins from the fruits of Cnidium monnieri on leukemia cell lines. *Planta Med.* 69, 1091–1095. doi: 10.1055/s-2003-45188

Yang, Y., Guo, R., Tian, X., Zhang, Z., Zhang, P., Li, C., et al. (2017). Synergistic anti-tumor activity of nimotuzumab in combination with trastuzumab in HER2-positive breast cancer. *Biochem. Biophys. Res. Commun.* 489, 523–527. doi: 10.1016/j.bbrc.2017.06.001

Ye, Y., Han, X., Guo, B., Sun, Z., and Liu, S. (2013). Combination treatment with platycodin D and osthole inhibits cell proliferation and invasion in mammary carcinoma cell lines. *Environ. Toxicol. Pharmacol.* 36, 115–124. doi: 10.1016/j.etap.2013.03.012

You, L., Feng, S., An, R., and Wang, X. (2009). Osthole: a promising lead compound for drug discovery from a traditional Chinese medicine (TCM). *Nat. Prod. Commun.* 4, 297–302.

Zhang, L., Jiang, G., Yao, F., He, Y., Liang, G., Zhang, Y., et al. (2012). Growth inhibition and apoptosis induced by osthole, a natural coumarin, in hepatocellular carcinoma. *PLoS One* 7:e37865. doi: 10.1371/journal.pone.0037865

Zhang, S., Huang, W. C., Li, P., Guo, H., Poh, S. B., Brady, S. W., et al. (2011). Combating trastuzumab resistance by targeting SRC, a common node downstream of multiple resistance pathways. *Nat. Med.* 17, 461–469. doi: 10.1038/nm.2309

Zhang, Z. R., Leung, W. N., Cheung, H. Y., and Chan, C. W. (2015). Osthole: a review on its bioactivities, pharmacological properties, and potential as alternative medicine. *Evid Based Complement. Alternat. Med.* 2015:919616. doi: 10.1155/2015/919616

Zheng, L., Tan, W., Zhang, J., Yuan, D., Yang, J., and Liu, H. (2014). Combining trastuzumab and cetuximab combats trastuzumab-resistant gastric cancer by effective inhibition of EGFR/ErbB2 heterodimerization and signaling. *Cancer Immunol. Immunother.* 63, 581–586. doi: 10.1007/s00262-014-1541-z

Zou, H., Henzel, W. J., Liu, X., Lutschg, A., and Wang, X. (1997). Apaf-1, a human protein homologous to *C. elegans* CED-4, participates in cytochrome c-dependent activation of caspase-3. *Cell* 90, 405–413. doi: 10.1016/S0092-8674(00)80501-2

Conflict of Interest Statement: The authors declare that the research was conducted in the absence of any commercial or financial relationships that could be construed as a potential conflict of interest.

frontiers in Oncology

REVIEW
published: 28 November 2018
doi: 10.3389/fonc.2018.00563

Progresses and Perspectives of Anti-PD-1/PD-L1 Antibody Therapy in Head and Neck Cancers

Bo Yang[1,2], *Tingjun Liu*[1,2], *Yang Qu*[1,2], *Hangbo Liu*[1,2], *Song Guo Zheng*[3], *Bin Cheng*[1,2]* and *Jianbo Sun*[1,2]*

[1] Guanghua School of Stomatology, Hospital of Stomatology, Sun Yat-sen University, Guangzhou, China, [2] Guangdong Provincial Key Laboratory of Stomatology, Sun Yat-sen University, Guangzhou, China, [3] Division of Rheumatology, Penn State Health Milton S. Hershey Medical Center, Hershey, PA, United States

Head and neck cancer is the 6th most common malignancy worldwide and urgently requires novel therapy methods to change the situation of low 5-years survival rate and poor prognosis. Targeted therapy provides more precision, higher efficiency while lower adverse effects than traditional treatments like surgery, radiotherapy, and chemotherapy. Blockade of PD-1 pathway with antibodies against PD-1 or PD-L1 is such a typical targeted therapy which reconstitutes anti-tumor activity of T cell in treatments of cancers, especially those highly expressing PD-L1, including head and neck cancers. There are many clinical trials all over the world and FDA has approved anti-PD-1/PD-L1 drugs for head and neck cancers. However, with the time going, the dark side of this therapy has emerged, including some serious side effects and drug resistance. Novel materials like nanoparticles and combination therapy have been developed to improve the efficacy. At the same time, standards for evaluation of activity and safety are to be established for this new therapy. Here we provide a systematic review with comprehensive depth on the application of anti-PD1/PD-L1 antibodies in head and neck cancer treatment: mechanism, drugs, clinical studies, influencing factors, adverse effects and managements, and the potential future developments.

Keywords: PD-1, PD-L1, immune checkpoint inhibitor, head and neck cancer, immunotherapy, adverse effects

OPEN ACCESS

Edited by:
Jian-ye Zhang,
Guangzhou Medical University, China

Reviewed by:
Alexandre Corthay,
Department of Pathology, Oslo University Hospital, Norway
Karishma Rajani,
Mayo Clinic, United States

***Correspondence:**
Bin Cheng
chengbin@mail.sysu.edu.cn
Jianbo Sun
sunjb3@mail.sysu.edu.cn

Specialty section:
This article was submitted to Cancer Molecular Targets and Therapeutics, a section of the journal Frontiers in Oncology

Received: *23 August 2018*
Accepted: *12 November 2018*
Published: *28 November 2018*

Citation:
Yang B, Liu T, Qu Y, Liu H, Zheng SG, Cheng B and Sun J (2018) Progresses and Perspectives of Anti-PD-1/PD-L1 Antibody Therapy in Head and Neck Cancers. Front. Oncol. 8:563. doi: 10.3389/fonc.2018.00563

INTRODUCTION OF HEAD AND NECK CANCERS

Head and neck cancers are composed of various kinds of epithelial malignant tumors, including oral cancers, maxillofacial cancers, larynx cancers, and many others, almost all of which are head and neck squamous cell carcinoma (HNSCC). Although, there are other pathological types such as verrucous carcinoma, basaloid squamous cell carcinoma, papillary squamous cell carcinoma, they only make up a small percentage (1). HNSCC is the 6th most common malignancy worldwide, with number of 650,000 new cases a year and 350,000 deaths (2). Around 2/3 of patients present with advanced disease, often with regional lymph node involvement, while 10% present with distant metastases (3). According to epidemiological survey, the 5-years survival rate of HNSCC in all stages was about 60%, and the survival rate was even worse for specific primary sites such as hypopharynx. The main causes of head and neck cancers are tobacco and alcohol consumption (1, 4–8). Chewing betel quid is also well-recognized as a risk factor for the cancer of oral cavity (9). And human papillomavirus (HPV) and p53 mutation are related to certain subsets of head

and neck cancers (10–12). About 25% of HNSCC contain HPV genomic DNA (13). However, HPV positivity is a favorable prognostic factor in HNSCC (14). Patients with HPV^+ HNSCC show better responsiveness to radiation, chemotherapy, or both, and might be more susceptive to immunosurveillance of tumor-specific antigens (14).

COMMON TREATMENT STRATEGIES FOR HEAD AND NECK CANCERS

The location of the cancers makes it necessary to take the spiritual and plastic factors into consideration. Primary tumor site, stage, and resectability are also treatment concerns as well as the patient factors such as swallowing, airway, organ preservation, and comorbid illnesses. For plan making, doctors are needed and organized from different departments which include head and neck surgeons, plastic surgeons, medical oncologists, radiation oncologists, radiologists, and dentists (2).

Common treatment strategies for head and neck cancers include surgery, radiotherapy, and chemotherapy. At present, surgery is still the standard therapy for HNSCC. However, surgical operations are limited, owing to the complexity of structures and the need for organ preservation. Most surgeons agree that the carotid artery, the base of the skull, and the invasion of the pre-vertebral muscle tissue are unresectable (2). Moreover, when the tumor is too extensive or there are multiple distant metastases, patients are generally not suitable for surgical treatment. Radiotherapy alone can improve the cure rate of early glottis, tongue, and tonsil cancers (15). However, prolonged interruption of radiotherapy or delayed post-operative radiotherapy may impair the patient's prognosis, which may be due to the proliferation of cancer cells (16). Delivery of radiation remains to be improved with continuous technological progress, and customization of radiation dose and volume (17). Chemotherapy is the core component of local advanced HNSCC treatment (18). Platinum compounds Cisplatin is a standard reagent for combination with radiotherapy or other drugs. Huperzine compounds are active and have been tested in locally advanced HNSCC chemotherapy (19, 20). Concurrent chemotherapy with normo-fractionated radiotherapy (2 Gy/day, 5 days/week, for 5–7 weeks) is used most in current practice (21).

Traditional therapy can result in serious complications, from pain to malnutrition, risk of infection, and psychological distress (21). In order to ameliorate these drawbacks, comprehensive treatments are currently preferred for the advanced tumors. Comprehensive treatments must be well-designed and planned according to the patient's general condition and the stage of tumor development. At present, the treatment of oral and maxillofacial malignant tumors emphasizes the comprehensive treatment based on surgery, especially the triple therapy, which combines surgery with radiotherapy and chemotherapy.

Modern research has been keen on identifying specific molecular targets involved in the occurrence and progression of head and neck cancers. EGFR and VEGF are two main targets which are overexpressed in majority of both precancerous oral lesions and HNSCC (22–24). EGFR can bind to and be activated by different ligands, including the epidermal growth factor (EGF) and transforming growth factor-α (TGF-α) (25). EGFR activation initiates subsequent signaling pathways, eventually resulting in tumor cell resistance to apoptosis and promoting angiogenesis, tumor cell migration, and tumor cell proliferation (**Figure 1**) (25, 26). Current EGFR-targeted therapies include monoclonal antibodies (mAbs) and tyrosine kinase inhibitors (TKIs). Antibodies target the extracellular domain of EGFR while TKIs hinder downstream signaling pathways by binding to the cytoplasmic region of EGFR (27). To date, Cetuximab remains the only FDA-approved EGFR-targeted mAb for the treatment of recurrent/metastatic (R/M) HNSCC. Cetuximab in combination with radiotherapy is a standard treatment option for locally or regionally advanced HNSCC (28). VEGF, is a key regulator of physiological angiogenesis during embryogenesis, skeletal growth, and reproductive functions (29). The biological effects of VEGF, mediated by two receptor tyrosine kinases (RTKs), VEGFR-1 and VEGFR-2, cause receptor TK activation and downstream signaling to stimulate endothelial cell proliferation, vessel permeability, and migration (27). Bevacizumab, a humanized monoclonal antibody targeting VEGF-A, was approved by the FDA for treatment of advanced cancer types. Bevacizumab could increase the sensitivity of HNSCC to radiotherapy in preclinical trials. Bevacizumab was evaluated in phase I and II clinical trials in combination with Erlotinib, an EGFR inhibitor, in patients with R/M HNSCC (30, 31) and the combined treatments increased the complete response rate by ∼15% and median survival by 7.1 months (30). The phase II trial on the combination of Bevacizumab with chemotherapy, radiotherapy or EGFR inhibitors are ongoing.

IMMUNOLOGICAL TARGETED THERAPY

Immunotherapies stimulate host antitumor immune system and can elicit endurable responses in subsets of patients across different types of tumors (**Figure 1**) (32). Immune checkpoints, like cytotoxic T-lymphocyte-associated antigen-4 (CTLA-4) and programmed cell death-1 (PD-1), work as inhibitory pathways, playing an important role in self-tolerance under healthy conditions. Checkpoint inhibitors are part of immunotherapies that enhance antitumor T cell activity by hindering initiation of suppressive signaling pathways of activated T cells. The 2018 Nobel Prize in Physiology or Medicine was recently given to James P. Allison and Tasuku Honjo for their discovery and contribution in cancer immunotherapy correlated with CTLA-4

Abbreviations: APC, antigen presenting cell; ATF, activating transcription factor; CRC, colorectal cancer; GEM, chemotherapy drug gemcitabine; GOx, glucose oxidase; HNSCC, head and neck squamous cell carcinoma; IGF, insulin-like growth factor; NFAT, nuclear factor of activated T cells; NSCLC, non-small cell lung cancer; ORR, objective response rate; OS, overall survival; PIP, phosphatidylinositol; PLGF, placental growth factor; RCC, renal cell carcinoma; ROS, reactive oxygen species; RTK, receptor tyrosine kinases; SAEs, severe adverse events; sPD-1/sPD-L1, soluble PD-1/ soluble PD-L1; TCR, T cell receptors; TGF, transforming growth factor; TILs, tumor-infiltrating lymphocytes; TKIs, tyrosine kinase inhibitors; TNF, tumor necrosis factor; T-NHL, T-cell non-Hodgkin's lymphoma; trAEs, treatment-related adverse events.

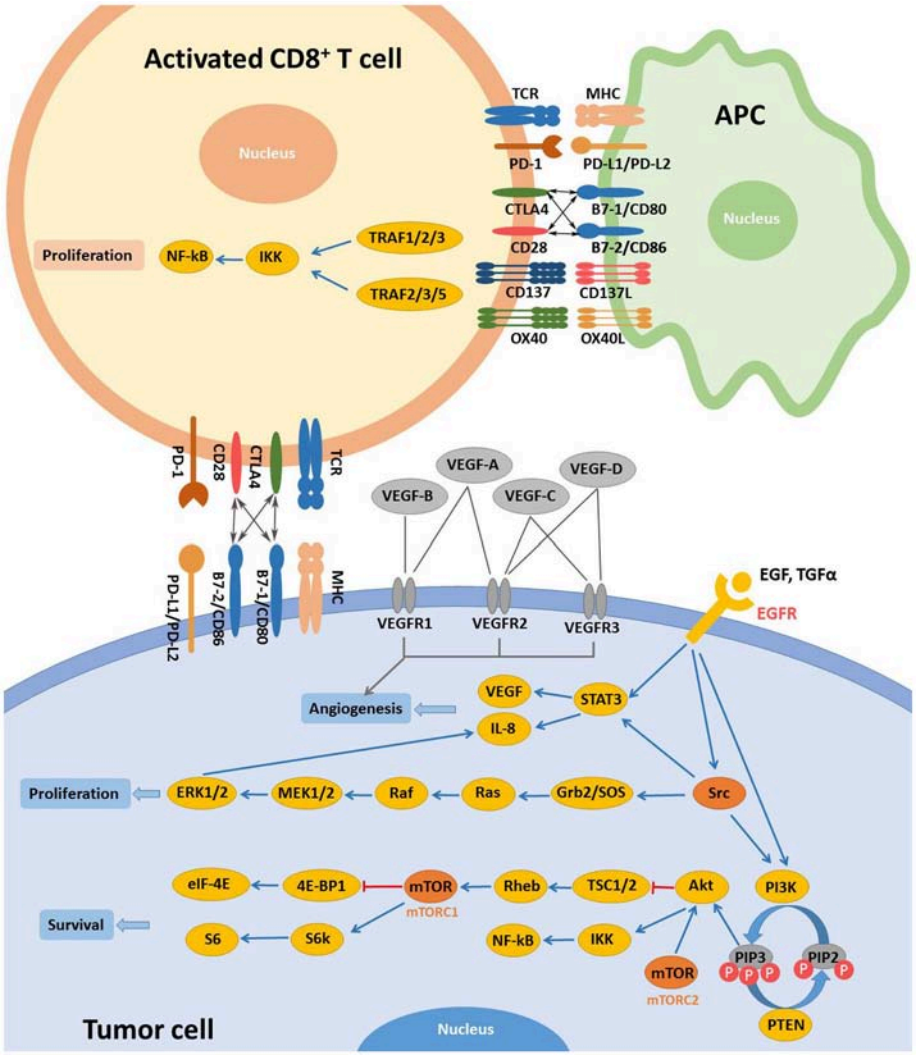

FIGURE 1 | Main targets and related signaling pathways involved in the targeted therapy for R/M HNSCC. Activation of EGFR by extracellular ligands initiates activation of Src, STAT3, and PI3K. Activated Src promotes cell proliferation mainly via RAS/RAF/MAPK pathway. In the PI3K/Akt pathway, phosphorylation of PIP2 is mediated by PI3K while dephosphorylation of PIP3 is controlled by PTEN. Akt could be activated independently by mTORC2 activation. Activation of Akt and mTORC1 inhibit TSC1/2/Rheb and 4E-BP1/eIF-4E downstream signaling, respectively while IKK/NF-kB and S6/S6k pathways are initiated, promoting tumor cell survival. Once activated, other targets, including VEGFR and c-MET, expressed on tumor cells share similar downstream signaling with EGFR. CD137L and OX40L activate CD137 and OX40, respectively. And proliferation of activated T cells is achieved via TRAF/IKK/NF-κB downstream signaling. CTLA-4 and its ligands are also demonstrated. Some pathways were simplified for clearer demonstration.

and PD-1. Other targets such as CD137 and OX40, unlike CTLA-4 and PD-1, work as immune activators and are as well under active investigation for cancer therapy (**Table 1**) (37, 38).

CTLA-4

Cytotoxic T lymphocyte-associated antigen-4 (CTLA-4; also known as CD152) is the first clinically targeted immune checkpoint receptor. CTLA-4, expressed on activated $CD8^+$ effector T cells, mainly regulates the early stage of T cell activation, enhances the activity of effector $CD4^+$ T cell, and inhibits Treg cell-dependent immunosuppression (39, 40). CD28 and CTLA-4 have the same ligands B7-1 (also known as CD80) and B7-2 (also known as CD86); and CTLA-4, compared to CD28, has a much higher affinity for B7-1 (41). CTLA-4 has been proved to be a negative regulator of T cell activation in an effort to prevent autoimmunity, antagonizing the CD28-B7 co-stimulatory signals. Research showed that the blockade of CTLA-4 results in enhanced antitumor immunity (42). Clinical studies using anti-CTLA-4 antibodies demonstrated activity in melanoma. Ipilimumab, an anti-CTLA-4 antibody, was the first targeted immunotherapy to prove a survival advantage for patients with metastatic melanoma. Hence, it was approved by FDA for the treatment of advanced melanoma in 2010 (43). In HNSCC, Yu et al. showed that CTLA4

TABLE 1 | Immunological targeted therapies approved or under investigation for the treatment of head and neck cancers.

Drug	Target	Modality	Status	References
MEDI0562	OX40	Antibody	Phase I Phase Ib Phase IPhase I	NCT03336606 NCT02315066
Urelumab	CD137	Antibody	Phase IPhase I	NCT02110082
PF-05082566	CD137	Antibody	Phase IPhase I	NCT02315066
Ipilimumab	CTLA-4	Antibody	Phase II Phase IPhase I Phase IPhase I	NCT03620123 NCT03098160 NCT02812524
Tremelimumab	CTLA-4	Antibody	Phase III Phase III Phase II Phase II Phase IPhase I-2	NCT02369874 NCT02551159 NCT03624231 NCT03292250 NCT03019003
Pembrolizumab	PD-1	Antibody	Approved	(33, 34)
Nivolumab	PD-1	Antibody	Approved	(35, 36)
Darvalumab	PD-L1	Antibody	Phase III Phase II Phase IPhase I	NCT02551159 NCT02207530 NCT02997332
Avelumab	PD-L1	Antibody	Phase III Phase IPhase I	NCT02952586 NCT02938273
INCB024360	PD-L1	Antibody	Phase IPhase I/2	NCT02318277

PD-1, programmed cell death protein 1; PD-L1, programmed death ligand 1; CTLA-4, cytotoxic T lymphocyte-associated antigen-4.

was upregulated in the tumor-infiltrating lymphocyte (TIL) of HNSCC and the high $CD8^+$/CTLA4 ratio was associated with improved prognosis (44). Further, Jie et al. found that intratumoral Tregs, compared to circulating Tregs, induced higher expression of CTLA-4 in HNSCC (45). Currently, clinical trials of Ipilimumab (NCT02551159, NCT03212469), alone or in combination with other treatments, for HNSCC are in progress (40).

CD137

CD137, a member of TNF receptor superfamily, is widely induced on activated $CD4^+$ T cells, $CD8^+$ T cells, B cells, NK cells, monocytes, and DC. The engagement of CD137 could promote the proliferation of T cells. The introduction of Urelumab, the fully human CD137-agonist mAb, has enabled modulation of CD137 function in immune-oncology, including application in combination with tumor targeting mAb (46). Srivastava et al. (38) confirmed that Cetuximab combined with CD137 agonist was effective in the treatment of HNC. CD137 has provided a new mechanism for the enhancement of Cetuximab (38).

OX40

OX40 is a member of the TNF receptor family and mediates an effective co-stimulation pathway which can enhance T cell memory, proliferation, and antitumor activity in patients with metastatic cancers (47, 48). Overexpression of OX40 in the TIL of patients with HNSCC has been identified (49). Furthermore, Montler et al. have noted co-expression of OX40 with PD-1 and CTLA-4 in a majority of tumor specimens, especially within the Treg population (49). The preclinical model showed the synergistic effects of anti-OX40 and anti-PD1, anti-OX40 and anti-CTLA-4, as well as anti-OX40 and anti-PDL1 (49). Anti-OX40 is currently being tested in early clinical trials of HNSCC, both as monotherapy and in combination with other immunotherapies (37).

ANTI-PD-1/PD-L1 THERAPY

T cells express the inhibitory receptor known as PD-1 on their surfaces to guard our body (50). When bound by its ligands PD-L1 or PD-L2, PD-1 transduces a signal into T cells to attenuate downstream signaling through the PI3K and PKCθ pathways (50, 51), which results in inhibition of T cell activation and proliferation. This protective mechanism is also utilized by tumor cells to escape immune attack through expressing high abundance of PD-L1 ligands on their surfaces.

Anti-PD-1/PD-L1 therapy has been a routine treatment to patients with PD-L1 highly expressing tumor (52). This kind of

immunotherapy could target tumors more precisely. Meanwhile, as anti-PD-1/PD-L1 therapy has been applied to more and more patients, the side effects and the factors hindering the therapeutic effects have been noticed. Thus, combined treatments and better administrating methods have been raised to improve the treatment.

Mechanism of PD-1/PD-L1 Inhibitors

Tumor infiltrating lymphocytes, especially $CD8^+$ T cells, exhibit high levels of PD-1 in HPV^+ HNSCC (12). When PD-1 binds to PD-L1 on tumor cells, T cell proliferation is suppressed and tumor cells are able to evade immune attack more effectively in the tumor microenvironment (12). Since tumors expressing PD-L1, compared to PD-L1–negative tumors, showed improved response to Nivolumab (a PD-1 inhibitor) (53), it is important to investigate the level of PD-L1 expression in tumor microenvironment. One study suggested that patients with HPV^- HNSCC expressed high levels of PD-1 in T cells and PD-L1 in a majority of tumor cells (54). Despite primary tumor sites, PD-L1 has been spotted on metastatic lesions (55). In summary, more than 29% of HPV^- and around 70% of HPV^+ HNSCC express PD-L1, suggesting that the majority of these cancers have potential for responding to PD-1 inhibitors (56). PD-L1 and PD-1 interaction is among the signals beneficial for tumor cells, which also include EGFR signaling, CD 28 stimulation and many others. And there are plenty of downstream pathways as well, which are composed of SHP2, RAS, ZAP70, P13K, and so on (**Figure 2**).

When bond by PD-1 ligands, PD-1 is able to recruit phosphatases including SHP2 toinhibit T cell functions by countering the positive signaling events mediated by the T cell receptors (TCR) and CD28 (50). For instance, they restrain ZAP70 and PI3K–AKT and RAS signaling pathways (50). In conclusion, this lowers down the activation of transcription factors such as AP-1, NFAT, and NF-κB, which are important for T cell activation, proliferation, growth, and survival. Besides, PD-1 is able to inhibit T cell functions by improving the expression of BATF transcription factor to inhibit the effector transcriptional programs. EGFR is an important target for mediating tumor metastasis and adhesion. After combining with epidermal growth factor (EGF), EGFR can deliver positive signaling events downstream. For example, it activates PI3K–AKT and RAS signaling pathways to promote tumor cells proliferation and migration (50). Successful anti-PD-1/PD-L1 therapy requires adequate amount of specific T cells in tumor microenvironment and competent ability of T cells to get enough nutrients (57). Studies have shown aerobic glycolysis is essential for T cells to secrete IFN-γand attack tumor cells. PD-1/PD-L1 inhibitors may help T cells compete for glucose in tumor microenvironment, promoting T cell glycolysis and IFN-γ secretion (57, 58).

Daste et al. reported a case that a 64-years-old patient with HNSCC developed local tumor flare-up under immunotherapy, and a dramatic response was achieved in the following chemotherapy (59). Owing to the "loco-regional phenomena" described in their case study, they suggested that although clinical efficacy was not achieved in this case, immunotherapy might enhance response sensitivity to chemotherapy in patients with HNSCC (59).

Overview of FDA-Approved PD-1 Inhibitors for Head and Neck Cancers

Pembrolizumab

Pembrolizumab was the first anti-PD-1 antibody approved by FDA to treat patients with unresectable or metastatic melanoma who progress after Ipilimumab treatment. It is also approved for the treatment for melanoma patients harboring a *BRAF V600E* mutation, following treatment with a BRAF inhibitor. Pembrolizumab has also been legal for the treatment of non-small-cell lung cancer (NSCLC) without EGFR mutation and ALK rearrangement but with disease progression or following platinum-based chemotherapy (60). In August 2016, FDA approved the use of Pembrolizumab in R/M HNSCC that has progressed on or after platinum-containing chemotherapy (33, 34).

Nivolumab

Nivolumab, a PD-1 inhibitor, has been approved by FDA to treat Hodgkin lymphoma, renal cell carcinoma, NSCLC, and melanoma. Recent breakthrough in the application of Nivolumab in patients with processed HNSCC during chemotherapy or R/M HNSCC after chemotherapy with platinum-based drugs has made Nivolumab second to the Pembrolizumab approved by FDA in HNSCC treatment (35, 36).

CLINICAL STUDIES OF PD-1/PD- L1 INHIBITORS

Inhibiting either PD-1 or PD-L1 function can block the PD-1 pathway. A number of PD-1/PD-L1 inhibitors are being investigated clinically and described in more details below (**Table 2**).

PD-1

Pembrolizumab (MK-3475, Previously Known as Lambrolizumab)

Preclinical anti-tumor effects were demonstrated in animals bearing multiple tumors. The first phase I clinical trial was carried out in patients with advanced solid tumors (61). Results suggested that Pembrolizumab was well-tolerated and associated with durable antitumor activity in multiple solid tumors (61). Two mg/kg per 3 weeks is considered a safe and effective minimum dose of antitumor activity (61). KEYNOTE-012 trial was a multicenter, open-label, phase Ib trial that included patients with R/M HNSCC in one of the cohorts. The objective response rate (ORR) was ∼20% and overall survival (OS) was better in HPV^+ patients (33). Then a larger HNSCC expansion cohort of KEYNOTE-012 reported an ORR of 18.2%, and response rates were similar in HPV^+ and HPV^- patients (62). In a recent single-arm, phase II KEYNOTE-055 study conducted in patients with R/M HNSCC, ORR was 16% and response rates were similar in HPV^+ and HPV^- patients, providing rationale for treatment with Pembrolizumab (NCT02255097) (63).

Monotherapy with Pembrolizumab is being carried out in patients with NSCLC (NCT01840579), advanced solid tumors

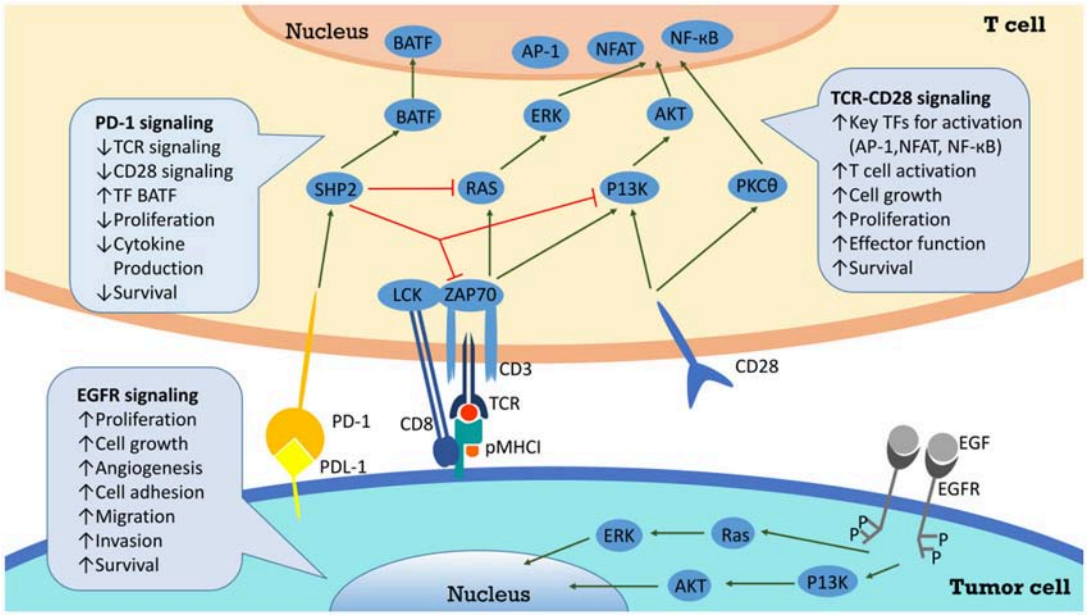

FIGURE 2 | PD-L1/PD-1 signaling pathway and the correlated network. Interaction between PD-L1 and PD-1 on T cells results in inhibition of Zap70 phosphorylation and PI3K activation, and finally attenuates TCR signaling, CD28 mediated co-stimulation, NF-κB, and AP-1 activation, and IL2 production. Through inhibition of T cell via overexpression of PD-L1, cancer cells evade the host immune system.

(NCT01295827) and hematologic malignancies (NCT01953692). Clinical trials of Pembrolizumab focusing on HNSCC are ongoing in comparison to chemotherapy (NCT02358031), in combination with radiotherapy (NCT02707588), and in combination with cisplatin and radiation (NCT02586207).

Nivolumab (MDX-1106, BMS-936558, ONO-4538)

The first phase I clinical trial was conducted in patients with treatment-refractory solid tumors such as advanced metastatic melanoma, colorectal cancer, castrate-resistant prostate cancer, NSCLC, and renal cell carcinoma (64). The study exhibited good tolerance and meaningful antitumor activity of PD-1 inhibitors, and the early results from a follow-up trial (NCT00730639) further confirmed this. It appeared that the PD-1 antibody was well-tolerated and demonstrated anti-tumor activity in many patients whose previous treatment failed (65). In a recent randomized, open-label, phase III clinical trial conducted in patients with R/M HNSCC, the ORR was 26.1% for Nivolumab, demonstrating a survival advantage compared with conventional treatments with ORR of 0% for investigators' choices of therapy (NCT02105636) (66). Ongoing clinical trials focusing on HNSCC include comparison to Cetuximab, Methotrexate or Docetaxel (NCT02105636), combination with Cisplatin, Cetuximab, or IMRT (NCT02764593), and monotherapy (NCT03132038, NCT03012581).

PD-L1

Durvalumab (MEDI4736)

In a phase I/II clinical trial that included a group of HNSCC patients, ORR was 17%, especially higher (25%) in PD-L1^{high} patients. The disease control rate in PD-L1 high subgroup was 44.9%, much greater than that in PD-L1 low or negative subgroup (21.5%) (67). These data support continued clinical development of Durvalumab in HNSCC. Durvalumab is being tested as monotherapy (NCT02207530), in combination with Docetaxel plus Displatin and 5-FU (NCT02997332), and in comparison to Durvalumab plus Tremelimumab (NCT02551159).

Avelumab

Avelumab is an anti-PD-L1 antibody. Studies of Avelumab targeting HNSCC has been scarce. It's currently assessed in combination with Cetuximab and radiotherapy in a phase I trial (NCT02938273), and in combination with standard care in a phase III trial (NCT02952586).

FACTORS INFLUENCING ANTI-PD-1/PD-L1 THERAPY

Gut Microbiota

It has been lately reported that gut microbiome plays important roles in many diseases, including influenza (68), multiple sclerosis (69, 70), diabetes (71), colorectal cancer (68, 72), and many others in various preclinical models, among which gut microbiome may modulate PD-1/PD-L1-based immunotherapy (73–76). Many kinds of bacteria have been proved to facilitate PD-1/PD-L1 blockades, meanwhile, there are bacteria that hamper the treatment (**Table 3**). It is reported that oral gavage of *Bifidobacterium* could achieve the same effects as anti-PD-L1 treatment, and combinational therapy almost eliminated tumor outgrowth, in which enhanced dendritic cell function led to more priming and accumulation of CD8$^+$ T cells in the tumor microenvironment (76). On one hand, *Akkermansia*

TABLE 2 | Clinical Trials on anti-PD-1/PD-L1 in head and neck cancers.

Immune checkpoint	Inhibitor	Other names	NCT-nummer	Phase	Arms	N of pts	Primary endpoint	Recruitment status
PD-1	pembrolizumab	Lambrolizumab/MK-3475 /Keytruda	NCT02586207	Phase I	Pembrolizumab + Cisplatin + Radiation	58	AE	recruiting
			NCT02358031	Phase III	Pembrolizumab vs. Pembrolizumab+Platinum+5-FU vs. Cetuximab+Platinum+5-FU	825	PFS, OS	Active, not recruiting
			NCT02707588	Phase II	Pembrolizumab+radiotherapy vs. Cetuximab+radiotherapy	133	LRC	Active, not recruiting
	nivolumab	Opdivo/BMS-936558/MDX-1106/NIVO/ONO-4538	NCT02764593	Phase I	Nivolumab+Cisplatin vs. Nivolumab+High-dose Cisplatin vs. Nivolumab+Cetuximab vs. Nivolumab+IMRT	40	DLT	Active, not recruiting
			NCT03132038	Phase II	Nivolumab	92	non-progression rate	recruiting
			NCT03012581	Phase II	Nivolumab	300	ORR	recruiting
			NCT02105636	Phase III	Nivolumab vs. Cetuximab/Methotrexate/ Docetaxel	506	OS	Active, not recruiting
PD-L1	Durvalumab	Imfinzi/MEDI4736	NCT02207530	Phase II	Durvalumab	112	ORR	Active, not recruiting
			NCT02997332	Phase I	Durvalumab+Docetaxel+ Cisplatin+5-FU	36	RP2D, DLT	recruiting
			NCT02551159	Phase III	Durvalumab vs. Durvalumab+Tremelimumab vs. SOC	823	OS	Active, not recruiting
	Avelumab	Bavencio	NCT02952586	Phase III	Avelumab+SOC CRT vs. Placebo+SOC CRT	640	PFS	recruiting
			NCT02938273	Phase I	Avelumab+cetuximab+ Radiation therapy	10	toxicity	recruiting
	INCB024360		NCT02318277	Phase I/ II	MEDI4736 + INCB024360	42	DLT, AE, ORR	Active, not recruiting

PD-L1, programmed death-1 ligand; FU, fluorouracil; HNSCC, head and neck squamous cell carcinoma; AE, adverse event; LRC, locoregional control; DLT, dose limiting toxicity; ORR, overall response rate; OS, overall survival; PFS, progression-free survival; SOC, standard of care; CRT, chemoradiation therapy; IMRT, intensity-modulated radiation therapy; RP2D, recommended phase II dose.

muciniphila was screened out to affect the anti-PD-1-based therapy in epithelial tumors in an IL-12 dependent fashion by enhancing the recruitment of $CCR9^+CXCR3^+CD4^+$ T cells (75). Further study in patients also revealed that responding patients had more diverse and abundant bacteria of the *Ruminococcaceae* family, enhanced systemic and antitumor immunity, functioning better in anabolic pathways as well (74). On the other hand, the recent study by Matson V reported *Blautia obeum* and *Roseburia intestinalis* with compromised efficacy of PD-1 blockade (77). These results provide important information for cancer therapy with immune checkpoint inhibitors.

Molecules Regulating PD-1/PD- L1

Some tumors respond more sensitively to anti-PD-1/PD-L1 therapy, while others do not. The mechanisms regulating anti-PD-1/PD-L1 therapy sensitivity have arisen wide attention. Recently, two molecules, CMTM6 and CMTM4, have been reported as PD-L1 protein regulators. CMTM6 could prevent the degradation of PD-L1, maintaining the stability of PD-L1 and facilitating the immune escape of tumors. Interfering either CMTM6 or CMTM4 would hamper the expression of PD-L1. They function through reducing the ubiquitination of PD-L1, prolonging its half-life period. This provides a new target for immunotherapy to enhance the anti-PD-1/PD-L1 treatment (78, 79).

ADVERSE EVENTS OF FDA-APPROVED PD-1 INHIBITORS AND THE RELEVANT MANAGEMENTS FOR HEAD AND NECK CANCERS

The fact that PD-1/PD-L1 axis contributes to the maintenance of self-tolerance implies that immune checkpoint blockade might disturb the balance of immune systems, resulting in treatment-related adverse events (trAEs) (80) (**Table 4**). TrAEs are frequent and occur in up to 80% of patients treated with an PD-1/PD-L1 antibody (81, 82). In the KEYNOTE-012 trial and the KEYNOTE-055 trial, trAEs occured in 63%-65% HNSCC patients treated with Pembrolizumab (33, 63). The most

TABLE 3 | Gut microbiome affecting efficacy of PD-1/PD-L1 treatment.

Effects	Bacteria	Models	Other effects on immune systems	Author/year	References
Enhanced efficacy	*Akkermansiacea muciniphila*	Human/mouse	Upregulating T_{CM}, CD4/Foxp3 ratio in tumor sites and IL-12 production; Increasing IFN- γ production	Bertrand Routy 2018	(75)
	Alistipes indistinctus	Human/mouse	/	Bertrand Routy 2018	(75)
	Bifidobacterium adolescentis	Human	Decreasing peripherally derived Tregs	Matson V 2018	(77)
	Bifidobacterium breve	Mouse	Stimulating DCs directly, inducing DCs maturation and cytokine secretion	Ayelet Sivan 2015	(76)
	Bifidobacterium longum	Mouse	Promoting DCs maturation and inducing cytokine production	Ayelet Sivan 2015	(76)
	Bifidobacterium longum	Human	/	Matson V 2018	(77)
	Collinsella aerofaciens	Human	Decreasing peripherally derived Tregs	Matson V 2018	(77)
	Enterococcus faecium	Human	Decreasing peripherally derived Tregs	Matson V 2018	(77)
	Enterococcus hirae	Human/mouse	Upregulating T_{CM}, CD4/Foxp3 ratio in tumor sites and IL-12 production; Increasing IFN- γ production	Bertrand Routy 2018	(75)
	Klebsiella pneumonia	Human	/	Matson V 2018	(77)
	Parabacteroides merdae	Human	Decreasing peripherally derived Tregs	Matson V 2018	(77)
	Ruminococcaceae	Human/mouse	Increasing effector T cells in peripheral blood and tumors	Gopalakrishnan V 2018	(74)
	Veillonella parvula	Human	/	Matson V 2018	(77)
Compromised efficacy	*Blautia obeum*	Human	/	Matson V 2018	(77)
	Roseburia intestinalis	Human	/	Matson V 2018	(77)

T_{CM} central memory T cell; Treg regulatory T cell; DC dendritic cell.

commonly observed trAEs were fatigue, decreased appetite, rash, hypothyroidism, nausea and diarrhea (63). Grade 3–4 trAEs occurred in around 9–14% of patients who had PD-1 inhibitors treatment. Three deaths were reported due to pulmonary toxicity (53, 82).

By comparing the various organs involved, grade 1–2 trAEs mainly influence the skin and the gut, while grade 3–4 events mainly affect the digestive tract. Data suggest that trAEs usually occur within 3–6 months after the PD-1/PD-L1 blockade treatment (83). Accumulative toxic effects with prolonged treatment of anti-PD-1 were not observed (65).

For T cell tumors, like T-cell non-Hodgkin's lymphoma (T-NHL), anti-PD-1/PD-L1 therapy could render the tumors better proliferative. The reason is in this kind of tumors, T cells don't play the role to attack the tumors, instead, they are the major part of the tumor. It highlights a dangerous possible adverse event of anti-PD-1 treatment (84).

Nivolumab

A randomized, open-label, phase III study was designed to investigate efficacy and safety of Nivolumab for patients with recurrent HNSCC that progressed within 6 months post platinum-based chemotherapy (36). In this trial, the primary end point was OS. Although rates of trAEs of any grade were similar between two groups, fewer events of grade 3 or 4 were observed in the Nivolumab treatment group when treated with Nivolumab than the standard therapy group. Fatigue, nausea, rash, decreased appetite, and pruritus were the most commonly reported trAEs of any grade in patients receiving Nivolumab. Two treatment-related deaths owing to pneumonitis and hypercalcemia were reported in the Nivolumab treatment group (36). Daste et al. (59) reported a case of a patient with HNSCC developed tumor flare-up after therapy with Nivolumab (59).

Pembrolizumab

TrAEs of any grade occurred within an average of 9 weeks after the initiation of Pembrolizumab (85, 86). In the KEYNOTE-012 trial, trAEs of any grade were observed in 63% of patients. The most frequently observed trAEs were fatigue, pruritus, nausea, decreased appetite and rash. Grade 3–4 trAEs were reported in 10 of 60 patients (17%), including increased ALT and AST, hyponatremia, atrial fibrillation and congestive heart failure (33). In the expansion cohort, 62% of patients had trAEs of any grade. The most common trAEs were fatigue, hypothyroidism and decreased appetite. Grade 3–4 trAEs were observed in around 9% of patients, including lowered appetite, facial swelling and

TABLE 4 | Incidents of treatment-related adverse events occurring in patients with head and neck cancers.

	Pembrolizumab 10 mg/kg every 2 weeks Ib/n 60 (33)		Pembrolizumab 200 mg every 2 weeks Ib/n 132 (62)		Pembrolizumab 200 mg every 2 weeks II/n 171 (63)		Nivolumab 3 mg/kg every 2 weeks III/n 236(GLOBAL) (36)		Nivolumab 3 mg/kg every 2 weeks III/n 23(ASIAN) (66)	
Adverse Events	Grade 1–2	Grade 3–4	Grade 1–2	Grade 3–4	Any Grade	Grade 3–5	Any Grade	Grade 3–4	Any Grade	Grade 3–4
Fatigue	20.00%	2.00%	21.00%	0	18.00%	1.00%	14.00%	2.10%	17.40%	0
Decreased appetite	0	0	7.00%	2.00%	5.00%	0	7.20%	0	21.70%	0
Rash	5.00%	2.00%	0	0	2.00%	1.00%	7.60%	0	17.40%	0
Nausea	0	0	5.00%	1.00%	6.00%	0	8.50%	0	8.70%	0
Hypothyroidism	0	0	11.00%	0	9.00%	0	0	0	0	0
Pruritus	12.00%	0	0	0	0	0	7.20%	0	17.40%	0
Diarrhea	2.00%	2.00%	0	0	6.00%	1.00%	6.80%	0	4.30%	0
Abdominal pain	0	0	1.00%	1.00%	0	0	0	0	0	0
Stomatitis	0	0	1.00%	1.00%	0	0	2.10%	0.40%	0	0
Colitis	0	0	0	1.00%	0	0	0	0	0	0
Lymphopenia	0	2.00%	0	0	0	0	0	0	0	0
Atrial fibrillation	0	2.00%	0	0	0	0	0	0	0	0
Congestive cardiac failure	0	2.00%	0	0	0	0	0	0	0	0
Neck abscess	0	2.00%	0	0	0	0	0	0	0	0
Alanine aminotransferase increase	0	3.00%	0	0	4.00%	0	0	0	0	0
Hyponatremia	0	3.00%	0	0	2.00%	1%%	0	0	0	0
Anemia	0	0	0	0	4.00%	2.00%	5.10%	1.30%	0	0
Musculoskeletal pain	2.00%	2.00%	0	0	0	0	1.30%	0	0	0
Immune thrombocytopenic purpura	0	0	0	1.00%	0	0	0	0	0	0
Dysphagia	0	0	1.00%	1.00%	0	0	0	0	0	0
Dehydration	0	0		1.00%	0	0	0	0	0	0
Facial swelling	0	0	2.00%	3.00%	0	0	0	0	0	0
Pneumonitis	0	0	2.00%	2.00%	4.00%	1.00%	0	0	0	0
Hyperglycemia	0	0	1.00%	1.00%	0	0	0	0	0	0
Asthenia	0	0	0	0	0	0	4.20%	0.40%	0	0

pneumonitis (62). In the KEYNOTE-055 trial, around 64% of patients exhibited trAEs. Grade 3–5 trAEs were reported in 15% of patients. One death owing to treatment-related pneumonitis was reported (63).

Severe Immune-Related Adverse Events in Crucial Organs

Myocarditis

Accounting for <0.3% of patients, myocarditis is a rare but severe immune-related adverse event that frequently results in rapid dyspnea and acute heart failure (87). More and more cases of patients with anti-PD-1/PD-L1 treatment-related heart diseases have been reported in recent 3 years (88). Semper et al. (89) reported a case of a patient, diagnosed with squamous cell carcinoma of the lung, developing Nivolumab-induced myocarditis. Three days post the 9th cycle of Nivolumab therapy, the patient with tumor remission developed acute chest pain and severe dyspnea, which was later confirmed to be immunotherapy-related (89). Johnson et al. (87) reported two more cases of patients, diagnosed with metastatic melanoma, developing lethal myocarditis induced by Nivolumab and Ipilimumab combined (87). Läubli et al. (90) reported a case of Pembrolizumab-induced myocarditis. A 73-years-old female patient with metastatic uveal melanoma developed severe Pembrolizumab-induced myocarditis which resulted in potentially life-threatening acute heart failure (90). In 2018, Frigeri et al. (91) reported the patients achieved complete remission of recurrent metastatic pulmonary adenocarcinoma after 7 cycles of Nivolumab administration. Unfortunately, she experienced rapid cardiogenic shock afterwards (91). A fatal case was reported by Matson et al. (92). One patient with NSCLC receiving Nivolumab developed acute heart failure (92). Moslehi et al. (88) have identified altogether 101 cases of severe immune checkpoint inhibitors-induced (ICIs-induced) myocarditis, 46% of which resulted in patients' deaths (88). A more conclusive mechanism of anti-PD-1-induced myocarditis is under investigation (87). Studies revealed that PD-L1 could be found on endothelium. Interaction between PD-1 and its ligands on endothelium is important in limiting T cell responses in the heart and thus controlling immune-mediated cardiac injury (93, 94). One suspected mechanism is that PD-L1 is expressed on the surface of various types of cells and tissues, including tumor cells and cardiac muscle cells. When patients receive anti-PD-1/PD-L1 treatment, owing to the distribution of drugs, T cell responses in cardiac muscles might be disturbed and enhanced, leading to the occurrence of lethal immune-related myocarditis (87, 95).

Pneumonitis

Incidence of pneumonitis of all grades during anti-PD-1 therapy was 2.7% and the incidence of pneumonitis for grade 3 or higher was around 0.8% (96). Patients diagnosed with lung cancers, compared to patients with other types of cancers had higher incidence of treatment-related pneumonitis, with incidence of grade 3 or higher being 1.8% and incidence of deaths being 0.4% (96, 97). In a randomized, open-label, phase II/III study on efficacy and safety of Pembrolizumab for patients with advanced NSCLC, three cases of deaths resulting from treatment-related pneumonitis were reported (85). As in clinical trial of PD-1 blockade treating HNSCC, two treatment-related deaths owing to pneumonitis and hypercalcemia were reported in the Nivolumab group of a randomized, open-label, phase III trial (NCT02105636) (36). In a phase II study, Bauml et al. evaluated efficacy of Pembrolizumab in patients with previously treated refractory head and neck cancers (KEYNOTE-055) and one death owing to immune-related pneumonitis was observed (63).

One patient with NSCLC, after receiving 2 cycles of anti–PD-1 therapy, developed symptoms of pneumonitis and received proper treatment. However, symptoms relapsed; treatments with corticosteroids displayed less efficacy and the patient died. Another case of a female patient with small-cell lung cancer (SCLC), treated with an anti-CTLA-4/PD-1 combination therapy, was reported. The patient showed responsiveness to corticosteroid treatment; with discontinuation of current immunotherapy, the patient recovered from pneumonitis and started next line of anti-tumor therapy (98).

Hepatitis

The incidence of immune-related hepatitis of all grades was around 3.1% and the incidence of grade 3 or higher was 0.5–0.6% (99). For a clinical trial with Pembrolizumab in patients with previously treated NSCLC (KEYNOTE-010), three cases of immune-related hepatitis were reported (97).

Management of Adverse Events

Before confirming the occurrence of immune-related adverse events, specialist should rule out all other possible diagnoses, including but not limited to infection and tumor progression (83). **Figure 3** gives a glimpse of main adverse events in patients receiving anti-PD-1/PD-L1 therapy. The general principle for managing trAEs are suggested as followed: patients with grade 1 adverse events are provided with supportive care; patients with grade 2 events are advised on treatment with topical or systemic steroids (0.5–1 mg/kg/day); patients with grade 3 or 4 events require hospitalization, treatment of steroids, 1–2 mg/kg/day, or discontinuation of the current immunotherapy, depending on specialists' assessments (97, 100). **Table 5** shows the management of some commonly observed trAEs. Most trAEs are manageable with steroids, which should be provided at a sufficient dose and gradually withdrawn. But there are some cases where trAEs may be permanent, and in those scenarios, adverse events can be treated with hormone instead (83, 100).

THE PERSPECTIVES OF ANTI-PD-1/PD-L1 THERAPY IN HEAD AND NECK CANCERS

Figure 4 shows the perspectives of anti-PD-1/PD-L1 therapy.

Criteria to Monitor the Immune-Checkpoint Blockade

Scientists brought up the importance of monitoring immune-checkpoint blockade. As it is a novel therapy for cancers, the response evaluation and biomarkers should be different. Immune-related response criteria is an important concept to evaluate the immunotherapy and is the first step of precision immunotherapy (101). There are many biomarkers of immunotherapy response including PD-L1, other immune-checkpoint molecules, tumor-infiltrating lymphocytes (TILs), IFN-γ (102–104), mutational burden, neoantigens, microsatellite instability, serum markers, radiographic markers, and the "immunoscore" (105) which evaluates the distribution of TILs in the core and in the invasive margin of tumors. A recent study showed that the frequency of $CD14^{+}CD16^{-}HLA^{-}DR^{hi}$ monocytes had strong correlation with progression-free and OS in response to therapy with anti-PD-1. The researchers used single-cell mass cytometry to analyze the immune cell subpopulations in the peripheral blood of patients with stage IV melanoma before and after anti-PD-1 therapy. It is an effective predictive biomarkers of a clinical response (106). Similarly, more predictive biomarkers are expected to be found and used in the near future.

Novel Materials Advancing the Effect

Nanoscale materials have potential as drug delivery systems that assist or advance the treatment in cancers. Some could even respond intelligently to molecular triggers (107, 108). A recent research reported that an autonomous DNA robot was programmed to transport blood coagulation protease thrombin within tubular nanorobot while DNA outside of the nanorobot as both a targeting domain and a molecular trigger. It could target the nucleolin specifically expressed in tumor blood vessels and caused tumor necrosis. Animal experiments with this DNA robot showed promising results (109). As it could carry the blood coagulation protease thrombin that is a type of protein, it would also be able to transport the anti-PD-1/PD-L1 antibody to specific areas with certain DNA targeting domains.

A microneedle, made by hyaluronic acid and pH-sensitive dextran nanoparticles, is developed to encapsulate anti-PD-1 antibody and glucose oxidase. Glucose oxidase can turn blood glucose into gluconic acid and generate an acidic environment in tumors to drive the self-dissociation of nanoparticles and finally substantially release anti-PD-1 antibodies. This newly developed tool with immunotherapy induced more robust immune response in melanoma. And the microneedle could carry more than one antitumor therapeutics like combination of anti-PD-1 and anti-CTLA-4 antibodies to enhance the treatment effect (110).

Years ago, Sun et al. utilized bacterial magnetosomes as drug carriers transporting doxorubicin to treat hepatocellular carcinoma and got a better result compared with the sole

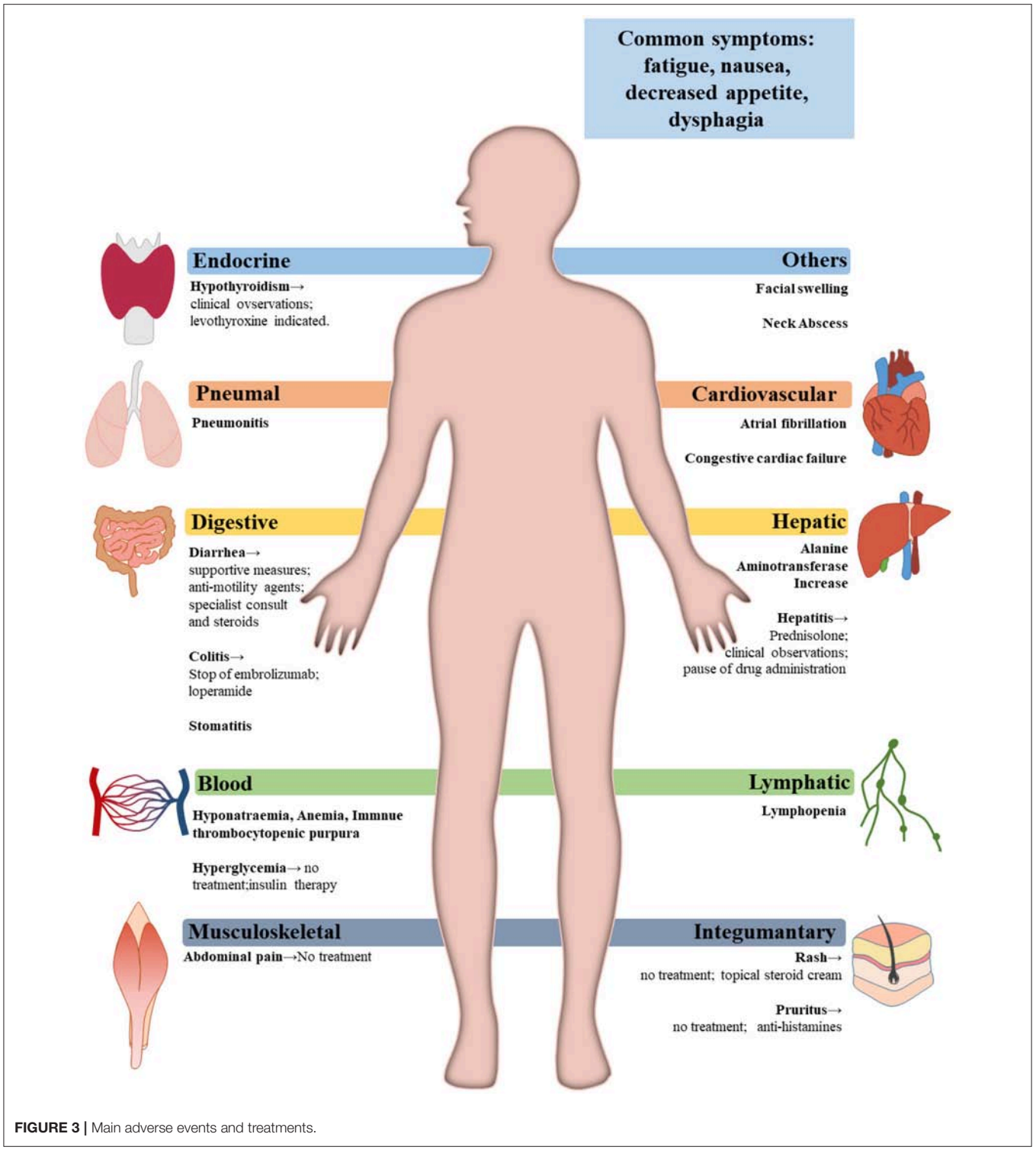

FIGURE 3 | Main adverse events and treatments.

doxorubicin group (111). Immobilization of anti-PD-1/PD-L1 antibodies on magnetic nanoparticles may also provide an efficient local delivery strategy of the drugs for malignant solid tumors. Local magnetic delivery of these immobilized antibodies would increase local concentration while reduce the administration times, total usage and peripheral distribution of the antibodies, reducing the adverse effects. It would be very easy to immobilize antibodies on either biosynthesized or chemical synthesized magnetic nanoparticles since there are a lot of linking methods available (112).

TABLE 5 | Management of treatment-related rash, pneumonitis, thyroid dysfunction and diarrhea (100).

Adverse events	Grade 1–2	Grade 3–4
Rash	≤30% BSA: anti-histamines for pruritus and topical steroid cream for rash.	>30% BSA:skin biopsy is needed and steroids with 1 mg/kg of prednisolone until BSA≤30%.If life-threatening, permanently discontinue drug administration.
Pneumonitis	Clinical or diagnostic observations; delay drug administration; daily monitoring.	Oxygen is needed; stop drug administration; hospitalization; high dose steroids with methylprednisolone; intensive care support.
Thyroid dysfunction	Clinical or diagnostic observations; daily monitoring; for hypothyroidism, levothyroxine indicated; for hyperthyroidism, propranolol is needed.	Hospitalization; specialist consult; clinical observation
Diarrhea	≤6 bowel actions/day: supportive measures; anti-motility agents when needed.	>7 bowel actions/day: hospitalization; specialist consult; clinical observation; steroids with 1–2mg/kg prednisolone.

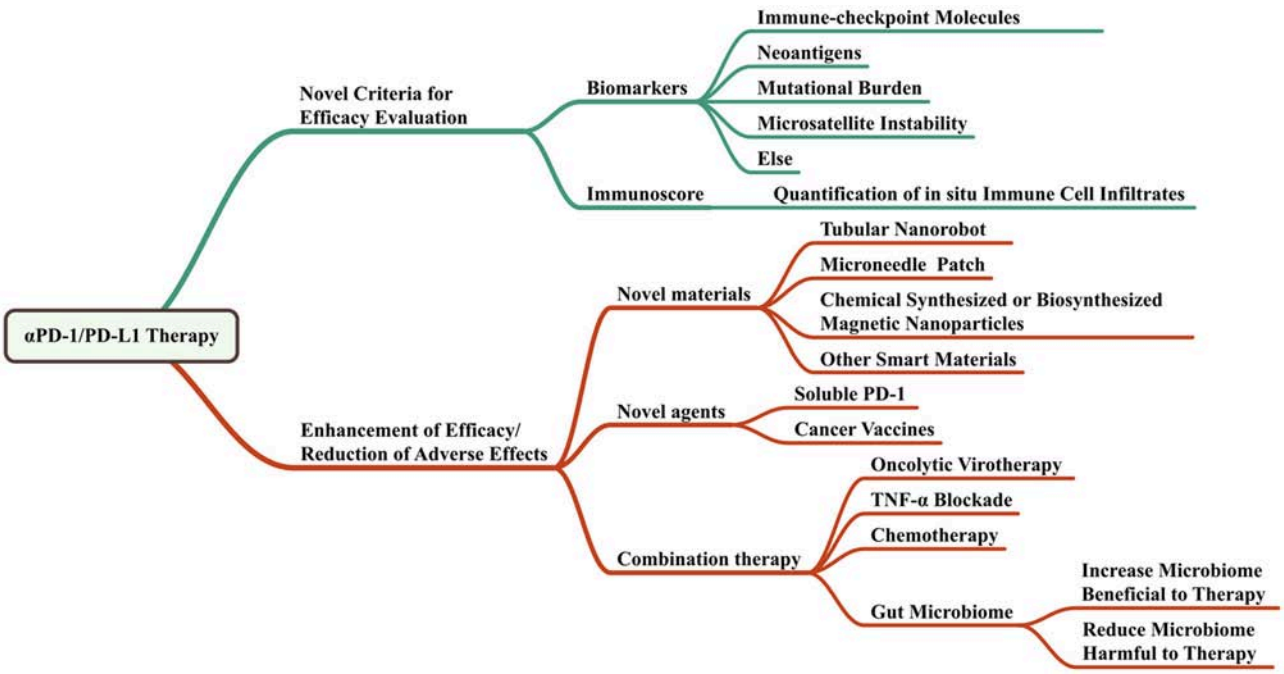

FIGURE 4 | Perspectives of anti-PD-1/PD-L1 therapy.

Novel Agents Providing Similar Blockade Effects of Anti-PD-1/PD-L1 Antibodies

Despite the anti-PD-1/PD-L1 antibodies, soluble PD-1 (sPD-1) peptides may provide similar inhibition effect of PD-1 pathway by competitively binding to PD-L1 expressed on tumor cells. The plasmids expressing sPD-1 peptides could also be developed as gene therapy drugs which turn tumor cells as producers of sPD-1.

Soluble Immune Checkpoint Molecules

In addition to membrane bound form, there are sPD-1 and soluble PD-L1 (sPD-L1). Currently, sPD-1 is thought to be the translational product of the PD-1Δex3 mRNA transcript, and sPD-L1 may be derived from the cleavage of membrane bound PD-L1 by matrix metalloproteinases.

sPD-1 and sPD-L1 can also bind to ligands, thus blocking the PD-1/PD-L1 signaling pathway, resulting in potent peripheral T-cell anti-tumor responses. It's reported that the PD-1 extracellular domain was transfected into tumors by adenoviral vectors and could antagonize the negative regulation of T cells by PD-1/PD-L1 pathway, thus inhibiting tumor growth and prolong survival of mice (113).

Compared with membranous molecules, soluble molecules can not only affect neighboring cells in the tumor microenvironment, but also affect the body farther through the blood circulation, having a wider range of biological effects.

The production and function of the sPD-1 and sPD-L1 require further investigation. sPD-1 and sPD-L1 can be used in immunomodulatory therapy in combination with other antitumor therapy, such as HSP70 vaccine, to enhance the anti-tumor efficacy of tumor vaccine (114). In addition, the soluble forms may be used as an additional biomarker to the membrane bound forms, helping more accurately determine the patient's immune status and predict efficacy (115).

Cancer Vaccines

Up to now, preclinical and recent clinical studies have indicated that combining PD-1 or PD-L1 checkpoint inhibitors with cancer vaccines improves antitumor activity compared with anti-PD-1 or PD-L1 antibody monotherapy alone (116). However, satisfactory results about vaccines targeting PD-1 or PD-L1 checkpoint molecular are few. The DNA vaccines under active study work well but safety is hard to guarantee. In contrast, protein vaccines are low in cost and high in safety. It provides a promising research direction for the future development of cancer treatment. A study using genetic engineering to prepare a Cholera Toxin B based vaccine that targets both mouse MUC1 and mouse PD-1 showed that this fused protein vaccine can produce a stronger immune response (117).

Combination Therapy

Luo et al. (118) developed a nano-vaccine by simply mixing an antigen with a synthesized polymeric nanoparticle, PC7A NP. It delivered tumor antigens to APCs in draining lymph nodes, increasing surface presentation and simultaneously activating type I interferon-triggered genes through STING pathway. Combination of PC7A nano-vaccine with anti-PD-1 antibodies demonstrated increased survival rate in animal tumor models. Tumor growth was completely inhibited when these vaccinated animals were rechallenged with tumor cells, suggesting generation of antitumor memory (118). Researchers found that exploiting the individual tumor mutations as neo-epitopes and utilizing them as vaccines could enhance the immune response to tumors. Some patients even completely responsed to vaccination during combinational therapy with anti-PD-1 (119, 120).

Oncolytic virotherapy has demonstrated promise, however, it only had efficacy in a small fraction of tumor patients. As the virus could upregulate PD-L1 expression on tumor cells, combination of oncolytic virus, and anti-PD-1/PD-L1 therapy could synergistically promote the treatment of cancers. This was tested in colon and ovarian cancer models, but was believed to own wider indications (121).

Recent study revealed that TNF-α blockade prevents death of tumor infiltrating T lymphocyte induced by anti-PD-1 as well as PD-L1 and TIM-3 expression. It is strongly rationalized to develop a combinational therapy with anti-PD-1/PD-L1 and anti-TNF-α in cancer patients (122).

Chemotherapy drug gemcitabine (GEM) and anti-PD-L1 antibodies could be released locally when an engineered reactive oxygen species (ROS)-degradable hydrogel was injected and formed in tumor microenvironment, which contained abundant ROS. Anti-PD-L1-GEM scaffold promoted an tumor regression in the tumor-bearing mice and prevention of tumor recurrence after primary resection (123). In this research, a novel material together with the combination therapy reinforced the effect and reduced side effects of the treatment.

The trends of anti-PD-1/PD-L1 therapy are to enhance the therapy effects while reduce the side effects. It would benefit from the combination of anti-PD-1/PD-L1 antibodies with other checkpoint inhibitors, other suppressor inhibitors, cytokine inhibitors or chemotherapy drugs. Emerging novel materials and delivery strategies like nanorobots, microneedle patches, and magnetic immobilization could help the therapeutics work better in the way of localizing them in the cancer sites or carrying other biomarkers like DNAs or proteins to target better.

AUTHOR CONTRIBUTIONS

BY, TL, YQ, and HL summarized the literature, wrote the manuscript, and prepared figures. SZ and BC provided critical comments and wrote part of the manuscript. JS supervised all the work and wrote the manuscript.

ACKNOWLEDGMENTS

This work was supported by Natural Science Foundation of Guangdong Province (2018A030313563) to JS; Program for Guangdong Introducing Innovative and Entrepreneurial Teams (2016ZT06S252) to JS; Science and Technology Program of Guangzhou (201704020063) to BC; and Special Grant for Precision Medicine from Sun Yat-sen University to BC.

REFERENCES

1. Argiris A, Eng C. Epidemiology, staging, and screening of head and neck cancer. *Cancer Treat Res*. (2003) 114:15–60. doi: 10.1007/0-306-48060-3_2
2. Argiris A, Karamouzis MV, Raben D, Ferris RL. Head and neck cancer. *Lancet* (2008) 371:1695–709. doi: 10.1016/S0140-6736(08)60728-X
3. Albers AE, Strauss L, Liao T, Hoffmann TK, Kaufmann AM. T cell-tumor interaction directs the development of immunotherapies in head and neck cancer. *Clin Dev Immunol*. (2010) 2010:236378. doi: 10.1155/2010/236378
4. Vineis P, Alavanja M, Buffler P, Fontham E, Franceschi S, Gao YT, et al. Tobacco and cancer: recent epidemiological evidence. *J Natl Cancer Inst*. (2004) 96:99–106. doi: 10.1093/jnci/djh014
5. Blot WJ, McLaughlin JK, Winn DM, Austin DF, Greenberg RS, Preston-Martin S, et al. Smoking and drinking in relation to oral and pharyngeal cancer. *Cancer Res*. (1988) 48:3282–87.
6. Tuyns AJ, Esteve J, Raymond L, Berrino F, Benhamou E, Blanchet F, et al., Cancer of the larynx/hypopharynx, tobacco and alcohol: IARC international case-control study in Turin and Varese (Italy), Zaragoza and Navarra (Spain), Geneva (Switzerland) and Calvados (France). *Int J Cancer* (1988) 41:483–91. doi: 10.1002/ijc.2910410403
7. Hashibe M, Boffetta P, Zaridze D, Shangina O, Szeszenia-Dabrowska N, Mates D, et al. Evidence for an important role of alcohol- and aldehyde-metabolizing genes in cancers of the upper aerodigestive tract. *Cancer Epidemiol Biomarkers Prev*. (2006) 15:696–703. doi: 10.1158/1055-9965.EPI-05-0710
8. Sturgis EM, Wei Q. Genetic susceptibility–molecular epidemiology of head and neck cancer. *Curr Opin Oncol*. (2002) 14:310–17. doi: 10.1097/00001622-200205000-00010
9. Warnakulasuriya S. Areca nut use following migration and its consequences. *Addict Biol*. (2002) 7:127–32. doi: 10.1080/13556210120091491
10. D'Souza G, Kreimer AR, Viscidi R, Pawlita M, Fakhry C, Koch WM, et al. Case-control study of human papillomavirus and oropharyngeal cancer. *N Engl J Med*. (2007) 356:1944–56. doi: 10.1056/NEJMoa 065497

11. Chan PK, Chor JS, Vlantis AC, Chow TL, Fung SC, Lau CH, et al. Smoking, human papillomavirus infection, and p53 mutation as risk factors in oropharyngeal cancer: a case-control study. *Hong Kong Med J*. (2017) 23 (Suppl. 5):12–16.
12. Lyford-Pike S, Peng S, Young GD, Taube JM, Westra WH, Akpeng B, et al. Evidence for a role of the PD-1:PD-L1 pathway in immune resistance of HPV-associated head and neck squamous cell carcinoma. *Cancer Res.* (2013) 73:1733–41. doi: 10.1158/0008-5472.CAN-12-2384
13. Kreimer AR, Clifford GM, Boyle P, Franceschi S. Human papillomavirus types in head and neck squamous cell carcinomas worldwide: a systematic review. *Cancer Epidemiol Biomarkers Prev*. (2005) 14:467–75. doi: 10.1158/1055-9965.EPI-04-0551
14. Licitra L, Perrone F, Bossi P, Suardi S, Mariani L, Artusi R, et al. High-risk human papillomavirus affects prognosis in patients with surgically treated oropharyngeal squamous cell carcinoma. *J Clin Oncol*. (2006) 24:5630–6. doi: 10.1200/JCO.2005.04.6136
15. Eisbruch A, Marsh LH, Dawson LA, Bradford CR, Teknos TN, Chepeha DB, et al. Recurrences near base of skull after IMRT for head-and-neck cancer: implications for target delineation in high neck and for parotid gland sparing. *Int J Radiat Oncol Biol Phys*. (2004) 59:28–42. doi: 10.1016/j.ijrobp.2003.10.032
16. Bentzen SM. Repopulation in radiation oncology: perspectives of clinical research. *Int J Radiation Biol*. (2003) 79:581–5. doi: 10.1080/09553000310001597002
17. Lin A. Radiation therapy for oral cavity and oropharyngeal cancers. *Dent Clin N Am*. (2018) 62:99–109. doi: 10.1016/j.cden.2017.08.007
18. Cohen EE, Lingen MW, Vokes EE. The expanding role of systemic therapy in head and neck cancer. *J Clin Oncol*. (2004) 22:1743–52. doi: 10.1200/JCO.2004.06.147
19. Argiris A. Induction chemotherapy for head and neck cancer: will history repeat itself? *J Natl Comprehen Cancer Netw*. (2005) 3:393–403. doi: 10.6004/jnccn.2005.0020
20. De Andres L, Brunet J, Lopez-Pousa A, Burgues J, Vega M, Tabernero JM, et al. Randomized trial of neoadjuvant cisplatin and fluorouracil versus carboplatin and fluorouracil in patients with stage IV-M0 head and neck cancer. *J Clin Oncol*. (1995) 13:1493–500. doi: 10.1200/JCO.1995.13.6.1493
21. Epstein JB, Thariat J, Bensadoun RJ, Barasch A, Murphy BA, Kolnick L, et al. Oral complications of cancer and cancer therapy: from cancer treatment to survivorship. *CA Cancer J Clin.* (2012) 62:400–22. doi: 10.3322/caac.21157
22. Young M, Neville B, Chi AC, Lathers D, Boyd-Gillespie M, Day T. Oral premalignant lesions induce immune reactivity to both premalignant oral lesions and head and neck squamous cell carcinoma. *Cancer Immunol Immunother.* (2007) 56:1077–86. doi: 10.1007/s00262-006-0242-7
23. Grandis JR, Tweardy DJ. Elevated levels of transforming growth factor alpha and epidermal growth factor receptor messenger RNA are early markers of carcinogenesis in head and neck cancer. *Cancer Res.* (1993) 53:3579.
24. Minchenko A, Bauer T, Salceda S, Caro J. Hypoxic stimulation of vascular endothelial growth factor expression *in vitro* and *in vivo*. *Lab Investig*. (1994) 71:374–9.
25. Pancari P, Mehra R. Systemic therapy for squamous cell carcinoma of the head and neck. *Surg Oncol Clin N Am*. (2015) 24:437–54. doi: 10.1016/j.soc.2015.03.004
26. Rubin GJ, Melhem MF, Gooding WE, Day R, Holst VA, Wagener MM, et al. Levels of TGF-alpha and EGFR protein in head and neck squamous cell carcinoma and patient survival. *J Natl Cancer Inst*. (1998) 90:824.
27. Ferreira MB, Lima JP, Cohen EE. Novel targeted therapies in head and neck cancer. *Expert Opin Investig Drugs* (2012) 21:281–95. doi: 10.1517/13543784.2012.651455
28. Bonner JA, Harari PM, Giralt J, Azarnia N, Shin DM, Cohen RB, et al. Radiotherapy plus cetuximab for squamous-cell carcinoma of the head and neck. *N Eng J Med.* (2006) 354:567–78. doi: 10.1056/NEJMoa053422
29. Yancopoulos GD, Davis S, Gale NW, Rudge JS, Wiegand SJ, Holash J. Vascular-specific growth factors and blood vessel formation. *Nature* (2000) 407:242–8. doi: 10.1038/35025215
30. Cohen EE, Davis DW, Karrison TG, Seiwert TY, Wong SJ, Nattam S, et al. Erlotinib and bevacizumab in patients with recurrent or metastatic squamous-cell carcinoma of the head and neck: a phase I/II study. *Lancet Oncol*. (2009) 10:247–57. doi: 10.1016/S1470-2045(09)70002-6
31. Burtness B. Commentary: bevacizumab and erlotinib with chemoradiation for head and neck cancer. *Cancer J.* (2011) 17:273–5. doi: 10.1097/PPO.0b013e3182326944
32. Hughes PE, Caenepeel S, Wu LC. Targeted therapy and checkpoint immunotherapy combinations for the treatment of cancer. Trends Immunol. (2016) 37:462–76. doi: 10.1016/j.it.2016.04.010
33. Seiwert TY, Burtness B, Mehra R, Weiss J, Berger R, Eder JP, et al. Safety and clinical activity of pembrolizumab for treatment of recurrent or metastatic squamous cell carcinoma of the head and neck (KEYNOTE-012): an open-label, multicentre, phase Iphase Ib trial, *Lancet Oncol*. (2016) 17:956–65. doi: 10.1016/S1470-2045(16)30066-3
34. Mulvey A. "*FDA Approves Pembrolizumab (Keytruda®), a PD-1 Antibody, for Head And Neck Cancer*". Cancer Research Institute (2016). Available online at: https://www.cancerresearch.org/blog/august-2016/fda-approves-pembrolizumab-keytruda-pd-1-antibody
35. Staff N. "*FDA Approves Nivolumab for Head and Neck Cancer was originally published by the National Cancer Institute*". National Cancer Institute (2016). Available online at: https://www.cancer.gov/news-events/cancer-currents-blog/2016/fda-nivolumab-scchn
36. Ferris RL, Blumenschein G Jr, Fayette J, Guigay J, Colevas AD, Licitra L, et al. Nivolumab for recurrent squamous-cell carcinoma of the head and neck. *N Eng J Med*. (2016) 375:1856–67. doi: 10.1056/NEJMoa1602252
37. Bell RB, Leidner RS, Crittenden MR, Curti BD, Feng Z, Montler R, et al. OX40 signaling in head and neck squamous cell carcinoma: overcoming immunosuppression in the tumor microenvironment. *Oral Oncol.* (2016) 52:1–10. doi: 10.1016/j.oraloncology.2015.11.009
38. Srivastava RM, Trivedi S, Concha-Benavente F, Gibson SP, Reeder C, Ferrone S, et al. CD137 stimulation enhances cetuximab-induced natural killer: dendritic cell priming of antitumor T-cell immunity in patients with head and neck cancer. *Clin Cancer Res*. (2017) 23:707–16. doi: 10.1158/1078-0432.CCR-16-0879
39. Schwartz RH. Costimulation of T lymphocytes: the role of CD28, CTLA-4, and B7/BB1 in interleukin-2 production and immunotherapy. *Cell* (1992) 71:1065–8. doi: 10.1016/S0092-8674(05)80055-8
40. Deng WW, Wu L, Sun ZJ. Co-inhibitory immune checkpoints in head and neck squamous cell carcinoma. *Oral Dis.* (2018) 24:120–3. doi: 10.1111/odi.12746
41. Collins AV, Brodie DW, R.Gilbert JC, Iaboni A, Manso-Sancho R, Walse B, et al. The interaction properties of costimulatory molecules revisited. *Immunity* (2002) 17:201–10. doi: 10.1016/S1074-7613(02)00362-X
42. Leach DR, Krummel MF, Allison JP. Enhancement of antitumor immunity by CTLA-4 blockade. *Science* (1996) 271:1734–36.
43. Pardoll DM. The blockade of immune checkpoints in cancer immunotherapy. *Nat Rev Cancer* (2012) 12:252–64. doi: 10.1038/nrc3239
44. Yu GT, Bu LL, Zhao YY, Mao L, Deng WW, Wu TF, et al. CTLA4 blockade reduces immature myeloid cells in head and neck squamous cell carcinoma. *Oncoimmunology* (2016) 5:e1151594. doi: 10.1080/2162402X.2016.1151594
45. Jie HB, Gildener-Leapman N, Li J, Srivastava RM, Gibson SP, Whiteside TL et al. Intratumoral regulatory T cells upregulate immunosuppressive molecules in head and neck cancer patients. *Br J Cancer* (2013) 109:2629–35. doi: 10.1038/bjc.2013.645
46. Ascierto PA, Kalos M, Schaer DA, Callahan MK, Wolchok JD. Biomarkers for immunostimulatory monoclonal antibodies in combination strategies for melanoma and other tumor types. *Clin Cancer Res*. (2013) 19:1009–20. doi: 10.1158/1078-0432.CCR-12-2982
47. Kjaergaard J, Peng L, Cohen PA, Drazba JA, Weinberg AD, Shu S. Augmentation versus inhibition: effects of conjunctional OX-40 receptor monoclonal antibody and IL-2 treatment on adoptive immunotherapy of advanced tumor. *J Immunol*. (2001) 167:6669–77. doi: 10.4049/jimmunol.167.11.6669
48. Gough MJ, Ruby CE, Redmond WL, Dhungel B, Brown A, Weinberg AD. OX40 agonist therapy enhances CD8 infiltration and decreases immune suppression in the tumor. *Cancer Res.* (2008) 68:5206–15. doi: 10.1158/0008-5472.CAN-07-6484
49. Montler R, Bell RB, Thalhofer C, Leidner R, Feng Z, Fox BA, et al. OX40, PD-1 and CTLA-4 are selectively expressed on tumor-infiltrating T cells in head and neck cancer. *Clin Transl Immunol*. (2016) 5:e70. doi: 10.1038/cti.2016.16

50. Sharpe AH, Pauken KE. The diverse functions of the PD1 inhibitory pathway, Nature reviews. *Immunology* (2018) 18:153–67. doi: 10.1038/nri.2017.108
51. Navarro MN, Cantrell DA. Serine-threonine kinases in TCR signaling. *Nat Immunol*. (2014) 15:808–14. doi: 10.1038/ni.2941
52. Ludin A, Zon LI. Cancer immunotherapy: the dark side of PD-1 receptor inhibition. *Nature* (2017) 552:41–42. doi: 10.1038/nature24759
53. Topalian SL, Hodi FS, Brahmer JR, Gettinger SN, Smith DC, McDermott DF, et al. Safety, activity, and immune correlates of anti-PD-1 antibody in cancer. *N Eng J Med*. (2012) 366:2443–54. doi: 10.1056/NEJMoa1200690
54. Malm IJ, Bruno TC, Fu J, Zeng Q, Taube JM, Westra W, et al. Expression profile and *in vitro* blockade of programmed death-1 in human papillomavirus-negative head and neck squamous cell carcinoma. *Head Neck* (2015) 37:1088–95. doi: 10.1002/hed.23706
55. Brahmer J, Reckamp KL, Baas P, Crinò LW, Eberhardt EE, Poddubskaya E, et al. Nivolumab versus docetaxel in advanced squamous-cell non–small-cell lung cancer. *N Eng J Med*. (2015) 373:123–35. doi: 10.1056/NEJMoa1504627
56. Swanson MS, Sinha UK. Rationale for combined blockade of PD-1 and CTLA-4 in advanced head and neck squamous cell cancer-review of current data. *Oral Oncol.* (2015) 51:12–15. doi: 10.1016/j.oraloncology.2014.10.010
57. Sukumar M, Kishton RJ, Restifo NP. Metabolic reprograming of anti-tumor immunity. *Curr Opin Immunol*. (2017) 46:14–22. doi: 10.1016/j.coi.2017.03.011
58. Gerriets VA, Kishton RJ, Nichols AG, Macintyre AN, Inoue M, Ilkayeva O, et al. Metabolic programming and PDHK1 control $CD4^+$ T cell subsets and inflammation. *J Clin Investig*. (2015) 125:194–207. doi: 10.1172/JCI76012
59. Daste A, de Mones E, Digue L, Francois L, Domblides C, Dupin C, et al. Immunotherapy in head and neck cancer: need for a new strategy? Rapid progression with nivolumab then unexpected response with next treatment. *Oral Oncol*. (2017) 64:e1–3. doi: 10.1016/j.oraloncology.2016.10.020
60. Khoja L, Butler MO, Kang SP, Ebbinghaus S, Joshua AM. Pembrolizumab. *J Immunother Cancer* (2015) 3:36. doi: 10.1186/s40425-015-0078-9
61. Patnaik A, Kang SP, Rasco D, Papadopoulos KP, Elassaiss-Schaap J, Beeram M, et al. Phase I study of pembrolizumab (MK-3475; Anti-PD-1 Monoclonal Antibody) in patients with advanced solid tumors. *Clin Cancer Res*. (2015) 21:4286–93. doi: 10.1158/1078-0432.CCR-14-2607
62. Chow LQM, Haddad R, Gupta S, Mahipal A, Mehra R, Tahara M, et al. Antitumor activity of pembrolizumab in biomarker-unselected patients with recurrent and/or metastatic head and neck squamous cell carcinoma: results from the phase Ib KEYNOTE-012 expansion cohort. *J Clin Oncol.* (2016) 34:3838–45. doi: 10.1200/JCO.2016.68.1478
63. Bauml J, Seiwert TY, Pfister DG, Worden F, Liu SV, Gilbert J, et al. Pembrolizumab for platinum- and cetuximab-refractory head and neck cancer: results from a single-arm, phase ii study. *J Clin Oncol*. (2017) 35:1542–9. doi: 10.1200/JCO.2016.70.1524
64. Brahmer JR, Drake CG, Wollner I, Powderly JD, Picus J, Sharfman WH, et al. Phase I study of single-agent anti-programmed death-1 (MDX-1106) in refractory solid tumors: safety, clinical activity, pharmacodynamics, and immunologic correlates. *J Clin Oncol*. (2010) 28:3167–75. doi: 10.1200/JCO.2009.26.7609
65. Topalian SL, Sznol M, McDermott DF, Kluger HM, Carvajal RD, Sharfman WH, et al. Survival, durable tumor remission, and long-term safety in patients with advanced melanoma receiving nivolumab. *J Clin Oncol.* (2014) 32:1020–30. doi: 10.1200/JCO.2013.53.0105
66. Kiyota N, Hasegawa Y, Takahashi S, Yokota T, Yen CJ, Iwae S, et al. A randomized, open-label, Phase III clinical trial of nivolumab vs. therapy of investigator's choice in recurrent squamous cell carcinoma of the head and neck: a subanalysis of Asian patients versus the global population in checkmate 141. *Oral Oncol.* (2017) 73:138–46. doi: 10.1016/j.oraloncology.2017.07.023
67. Powles T, O'Donnell PH, Massard C, Arkenau HT, Friedlander TW, Hoimes CJ, et al. Efficacy and safety of durvalumab in locally advanced or metastatic urothelial carcinoma: updated results from a Phase I Phase I/2 open-label study. *JAMA Oncol.* (2017) 3:e172411. doi: 10.1001/jamaoncol.2017.2411
68. Rosshart SP, Vassallo BG, Angeletti D, Hutchinson DS, Morgan AP, Takeda K, et al. Wild mouse gut microbiota promotes host fitness and improves disease resistance. *Cell* (2017) 171:1015–28 e1013. doi: 10.1016/j.cell.2017.09.016
69. Cekanaviciute E, Yoo BB, Runia TF, Debelius JW, Singh S, Nelson CA, et al. Gut bacteria from multiple sclerosis patients modulate human T cells and exacerbate symptoms in mouse models. *Proc Natl Acad Sci USA*. (2017) 114:10713–18. doi: 10.1073/pnas.1711235114
70. Berer K, Gerdes LA, Cekanaviciute E, Jia X, Xiao L, Xia Z, et al. Gut microbiota from multiple sclerosis patients enables spontaneous autoimmune encephalomyelitis in mice. *Proc Natl Acad Sci USA*. (2017) 114:10719–24. doi: 10.1073/pnas.1711233114
71. Yu H, Gagliani N, Ishigame H, Huber S, Zhu S, Esplugues E, et al. Intestinal type 1 regulatory T cells migrate to periphery to suppress diabetogenic T cells and prevent diabetes development. *Proc Natl Acad Sci USA*. (2017) 114:10443–8. doi: 10.1073/pnas.1705599114
72. Wong SH, Zhao L, Zhang X, Nakatsu G, Han J, Xu W, et al. Gavage of fecal samples from patients with colorectal cancer promotes intestinal carcinogenesis in germ-free and conventional mice. *Gastroenterology* (2017) 153:1621–33 e1626. doi: 10.1053/j.gastro.2017.08.022
73. Yi M, Yu S, Qin S, Liu Q, Xu H, Zhao W, et al. Gut microbiome modulates efficacy of immune checkpoint inhibitors. *J Hematol Oncol*. (2018) 11:47. doi: 10.1186/s13045-018-0592-6
74. Gopalakrishnan V, Spencer CN, Nezi L, Reuben A, Andrews MC, Karpinets TV, et al. Gut microbiome modulates response to anti-PD-1 immunotherapy in melanoma patients. *Science* (2018) 359:97–103. doi: 10.1126/science.aan4236
75. Routy B, Le Chatelier E, Derosa LC, Duong PM, Alou MT, Daillere R, et al. Gut microbiome influences efficacy of PD-1-based immunotherapy against epithelial tumors. Science (2018) 359:91–97. doi: 10.1126/science.aan3706
76. Sivan A, Corrales L, Hubert N, Williams JB, Aquino-Michaels K, Earley ZM, et al. Commensal *Bifidobacterium* promotes antitumor immunity and facilitates anti-PD-L1 efficacy. *Science* (2015) 350:1084–9. doi: 10.1126/science.aac4255
77. Matson V, Fessler J, Bao R, Chongsuwat T, Zha YY, Alegre ML, et al. The commensal microbiome is associated with anti-PD-1 efficacy in metastatic melanoma patients. *Science* (2018) 359:104–8. doi: 10.1126/science.aao3290
78. Mezzadra R, Sun C, Jae LT, Gomez-Eerland R, de Vries E, Wu W, et al. Identification of CMTM6 and CMTM4 as PD-L1 protein regulators. *Nature* (2017) 549:106–10. doi: 10.1038/nature23669
79. Burr ML, Sparbier CE, Chan YC, Williamson JC, Woods K, Beavis PA, et al. CMTM6 maintains the expression of PD-L1 and regulates anti-tumour immunity. *Nature* (2017) 549:101–5. doi: 10.1038/nature23643
80. Boussiotis VA. Molecular and biochemical aspects of the PD-1 checkpoint pathway. *N Eng J Med*. (2016) 375:1767–78. doi: 10.1056/NEJMra1514296
81. Boutros C, Tarhini A, Routier E, Lambotte O, Ladurie FL, Carbonnel F, et al. Safety profiles of anti-CTLA-4 and anti-PD-1 antibodies alone and in combination. *Nat Rev*. (2016) 13:473–86. doi: 10.1038/nrclinonc.2016.58
82. Brahmer JR, Tykodi SS, Chow QM, Hwu J, Topalian SL, Hwu P, et al. Safety and activity of anti–PD-L1 antibody in patients with advanced cancer. *N Eng J Med*. (2012) 366:2455–65. doi: 10.1056/NEJMoa1200694
83. Michot JM, Bigenwald C, Champiat S, Collins M, Carbonnel F, Postel-Vinay S, et al. Immune-related adverse events with immune checkpoint blockade: a comprehensive review. *Eur J Cancer* (2016) 54:139–48. doi: 10.1016/j.ejca.2015.11.016
84. Wartewig T, Kurgyis Z, Keppler S, Pechloff K, Hameister E, Ollinger R, et al. PD-1 is a haploinsufficient suppressor of T cell lymphomagenesis. *Nature* (2017) 552:121–5. doi: 10.1038/nature24649
85. Herbst RS, Baas P, Kim DW, Felip E, Perez-Gracia JL, Han JY, et al. Pembrolizumab versus docetaxel for previously treated, PD-L1-positive, advanced non-small-cell lung cancer (KEYNOTE-010): a randomised controlled trial. *Lancet* (2016) 387:1540–50. doi: 10.1016/S0140-6736(15)01281-7
86. Robert C, Schachter J, Long GV, Arance A, Grob JJ, Mortier L, et al. Pembrolizumab versus Ipilimumab in advanced melanoma. *N Eng J Med*. (2015) 372:2521–2. doi: 10.1056/NEJMoa1503093
87. Johnson DB, Balko JM, Compton ML, Chalkias S, Gorham J, Xu Y, et al. Fulminant myocarditis with combination immune checkpoint blockade. *N Eng J Med*. (2016) 375:1749–55. doi: 10.1056/NEJMoa1609214
88. Moslehi JJ, Salem JE, Sosman JA, Lebrun-Vignes B, Johnson DB. Increased reporting of fatal immune checkpoint inhibitor-associated myocarditis. *Lancet* (2018) 391:933. doi: 10.1016/S0140-6736(18)30533-6

89. Semper H, Muehlberg F, Schulz-Menger J, Allewelt M, Grohe C. Drug-induced myocarditis after nivolumab treatment in a patient with PDL1-negative squamous cell carcinoma of the lung. *Lung Cancer* (2016) 99:117–19. doi: 10.1016/j.lungcan.2016.06.025
90. Laubli H, Balmelli C, Bossard M, Pfister O, Glatz K, Zippelius A. Acute heart failure due to autoimmune myocarditis under pembrolizumab treatment for metastatic melanoma. *J Immunother Cancer* (2015) 3:11. doi: 10.1186/s40425-015-0057-1
91. Frigeri M, Meyer P, Banfi C, Giraud R, Hachulla AL, Spoerl D, et al. Immune checkpoint inhibitor-associated myocarditis: a new challenge for cardiologists. *Can J Cardiol*. (2018) 34:92.e91–2.e3. doi: 10.1016/j.cjca.2017.09.025
92. Matson DR, Accola MA, Rehrauer WM, Corliss RF. Fatal myocarditis following treatment with the PD-1 inhibitor nivolumab. *J Foren Sci*. (2017) 63:954–7. doi: 10.1111/1556-4029.13633
93. Tarrio ML, Grabie N, Bu DX, Sharpe AH, Lichtman AH. PD-1 protects against inflammation and myocyte damage in T cell-mediated myocarditis. *J Immunol*. (2012) 188:4876–84. doi: 10.4049/jimmunol.1200389
94. Grabie N, Gotsman I, DaCosta R, Pang H, Stavrakis G, Butte MJ, et al. Endothelial programmed death-1 ligand 1 (PD-L1) regulates $CD8^+$ T-cell mediated injury in the heart. *Circulation* (2007) 116:2062–71. doi: 10.1161/CIRCULATIONAHA.107.709360
95. Cheng F, Loscalzo J. Autoimmune cardiotoxicity of cancer immunotherapy. *Trends Immunol*. (2017) 38:77–8. doi: 10.1016/j.it.2016.11.007
96. Nishino M, Giobbie-Hurder A, Hatabu H, Ramaiya NH, Hodi FS. Incidence of programmed cell death 1 inhibitor-related pneumonitis in patients with advanced cancer: a systematic review and meta-analysis. *JAMA Oncol*. (2016) 2:1607–16. doi: 10.1001/jamaoncol.2016.2453
97. O'Kane GM, Labbe C, Doherty MK, Young K, Albaba H, Leighl NB. Monitoring and management of immune-related adverse events associated with programmed cell death protein-1 axis inhibitors in lung cancer. *Oncologist* (2017) 22:70–80. doi: 10.1634/theoncologist.2016-0164
98. Balaji A, Verde F, Suresh K, Naidoo J. Pneumonitis from anti-PD-1/ PD-L1 therapy. *Oncology* (2017) 31 739–46.
99. Zhang X, Ran Y, Wang K, Zhu Y, Li J. Incidence and risk of hepatic toxicities with PD-1 inhibitors in cancer patients: a meta-analysis. *Drug Design Dev Ther*. (2016) 10:3153–61. doi: 10.2147/DDDT.S115493
100. Spain L, Diem S, Larkin J. Management of toxicities of immune checkpoint inhibitors. *Cancer Treat Rev*. (2016) 44:51–60. doi: 10.1016/j.ctrv.2016.02.001
101. Nishino M, Ramaiya NH, Hatabu H, Hodi FS. Monitoring immune-checkpoint blockade: response evaluation and biomarker development. *Nat Rev Clin Oncol*. (2017) 14:655–68. doi: 10.1038/nrclinonc.2017.88
102. Gao J, Shi LZ, Zhao H, Chen J, Xiong L, He Q, et al. Loss of IFN-gamma pathway genes in tumor cells as a mechanism of resistance to anti-CTLA-4 therapy. *Cell* (2016) 167:397–404 e399. doi: 10.1016/j.cell.2016.08.069
103. Overacre-Delgoffe AE, Chikina M, Dadey RE, Yano H, Brunazzi EA, Shayan G, et al. Interferon-gamma drives treg fragility to promote anti-tumor immunity. *Cell* (2017) 169:1130–41 e1111. doi: 10.1016/j.cell.2017.05.005
104. Bifulco CB, Urba WJ. Unmasking PD-1 resistance by next-generation sequencing. *N Eng J Med*. (2016) 375:888–9. doi: 10.1056/NEJMe1606042
105. Galon J, Mlecnik B, Bindea G, Angell HK, Berger A, Lagorce C, et al. Towards the introduction of the 'Immunoscore' in the classification of malignant tumours. *J Pathol*. (2014) 232:199–209. doi: 10.1002/path.4287
106. Krieg C, Nowicka M, Guglietta S, Schindler S, Hartmann FJ, Weber LM, et al. High-dimensional single-cell analysis predicts response to anti-PD-1 immunotherapy. *Nat Med*. (2018) 24:144–53. doi: 10.1038/nm.4466
107. Douglas SM, Bachelet I, Church GM. A logic-gated nanorobot for targeted transport of molecular payloads. *Science* (2012) 335:831–4. doi: 10.1126/science.1214081
108. Modi S, Nizak C, Surana S, Halder S, Krishnan Y. Two DNA nanomachines map pH changes along intersecting endocytic pathways inside the same cell. *Nat Nanotechnol*. (2013) 8:459–67. doi: 10.1038/nnano.2013.92
109. Li S, Jiang Q, Liu S, Zhang Y, Tian Y, Song C, et al. A DNA nanorobot functions as a cancer therapeutic in response to a molecular trigger *in vivo*. *Nat Biotechnol*. (2018) 36:258–64. doi: 10.1038/nbt.4071
110. Wang C, Ye Y, Hochu GM, Sadeghifar H, Gu Z. Enhanced cancer immunotherapy by microneedle patch-assisted delivery of anti-PD1 antibody. *Nano Lett*. (2016) 16:2334–40. doi: 10.1021/acs.nanolett.5b05030
111. Sun JB, Duan JH, Dai SL, Ren J, Zhang YD, Tian JS, et al. *In vitro* and *in vivo* antitumor effects of doxorubicin loaded with bacterial magnetosomes (DBMs) on H22 cells: the magnetic bio-nanoparticles as drug carriers. *Cancer Lett*. (2007) 258:109–17. doi: 10.1016/j.canlet.2007.08.018
112. Sun J, Li Y, Liang XJ, Wang PC. Bacterial magnetosome: a novel biogenetic magnetic targeted drug carrier with potential multifunctions. *J Nanomater*. (2011) 2011:469031–43. doi: 10.1155/2011/469031
113. Elhag OA, Hu XJ, Wen-Ying Z, Li X, Yuan YZ, Deng LF, et al. Reconstructed adeno-associated virus with the extracellular domain of murine PD-1 induces antitumor immunity. *Asian Pacific J Cancer Prev*. (2012) 13:4031–6. doi: 10.7314/APJCP.2012.13.8.4031
114. Wang XH, Zhang GM, He YF, Zhang H, Feng ZH. [Soluble PD-1 can augment anti-tumor immunity induced by HSP70-peptide complex in tumor-bearing mice]. *Chin J Cell Mol Immunol*. (2004) 20:655–8. doi: 10.1007/s11670-004-0048-0
115. Liu C, Jiang J, Gao L, Wang X, Hu X, Wu M, et al. Soluble PD-1 aggravates progression of collagen-induced arthritis through Th1 and Th17 pathways. *Arthritis Res Ther*. (2015) 17:340. doi: 10.1186/s13075-015-0859-z
116. Soares KC, Rucki AA, Wu AA, Olino K, Xiao Q, Chai Y, et al. PD-1/PD-L1 blockade together with vaccine therapy facilitates effector T cell infiltration into pancreatic tumors. *J Immunother*. (2015) 38:1–11. doi: 10.1097/CJI.0000000000000062
117. Qiu L, Lu W, Lin Z, Cai H, Li R. Construction and Humoral Immunological analysis of a fusion protein vaccine that targets MUC1 and PD-1. *Genom Appl Biol*. (2016) 35:513–9. doi: 10.13417/j.gab.035.000513
118. Luo M, Wang H, Wang Z, Cai H, Lu Z, Li Y, et al. A STING-activating nanovaccine for cancer immunotherapy. *Nat Nanotechnol*. (2017) 12:648–54. doi: 10.1038/nnano.2017.52
119. Sahin U, Derhovanessian E, Miller M, Kloke BP, Simon P, Lower M, et al. Personalized RNA mutanome vaccines mobilize poly-specific therapeutic immunity against cancer. *Nature* (2017) 547:222–26. doi: 10.1038/nature23003
120. Ott PA, Hu Z, Keskin DB, Shukla SA, Sun J, Bozym DJ, et al. An immunogenic personal neoantigen vaccine for patients with melanoma. *Nature* (2017) 547:217–21. doi: 10.1038/nature22991
121. Liu Z, Ravindranathan R, Kalinski P, Guo ZS, Bartlett DL. Rational combination of oncolytic vaccinia virus and PD-L1 blockade works synergistically to enhance therapeutic efficacy. *Nat Commun*. (2017) 8:14754. doi: 10.1038/ncomms14754
122. Bertrand F, Montfort A, Marcheteau E, Imbert C, Gilhodes J, Filleron T, et al. TNF alpha blockade overcomes resistance to anti-PD-1 in experimental melanoma. *Nat Commun*. (2017) 8:2256. doi: 10.1038/s41467-017-02358-7
123. Wang C, Wang J, Zhang X, Yu S, Wen D, Hu Q, et al. *In situ* formed reactive oxygen species-responsive scaffold with gemcitabine and checkpoint inhibitor for combination therapy. *Sci Transl Med*. (2018) 10:eaan3682. doi: 10.1126/scitranslmed.aan3682

Conflict of Interest Statement: The authors declare that the research was conducted in the absence of any commercial or financial relationships that could be construed as a potential conflict of interest.

frontiers in Oncology

ORIGINAL RESEARCH
published: 05 December 2018
doi: 10.3389/fonc.2018.00573

Comparative Transcriptomics Unravels Prodigiosin's Potential Cancer-Specific Activity Between Human Small Airway Epithelial Cells and Lung Adenocarcinoma Cells

Bala Davient[1,2], *Jessica Pei Zhen Ng*[1,2], *Qiang Xiao*[3]*, *Liang Li*[4,2]* and *Liang Yang*[1,2,5]*

[1] Singapore Centre for Environmental Life Sciences Engineering, Nanyang Technological University, Singapore, Singapore, [2] School of Biological Sciences, Nanyang Technological University, Singapore, Singapore, [3] Respiratory Medicine, Shunde Hospital, Southern Medical University, The First People's Hospital of Shunde Foshan, Foshan, China, [4] Shenzhen Institute of Advance Technology, Chinese Academy of Sciences, Shenzhen, China, [5] School of Medicine, Southern University of Science and Technology, Shenzhen, China

OPEN ACCESS

Edited by:
Yunkai Zhang,
Vanderbilt University Medical Center, United States

Reviewed by:
Junyi Li,
University of Pittsburgh, United States
Zhenfang Du,
Vanderbilt University Medical Center, United States

***Correspondence:**
Qiang Xiao
xiaoq@mail2.sysu.edu.cn
Liang Li
liang.li@siat.ac.cn
Liang Yang
yangl@sustc.edu.cn

Specialty section:
This article was submitted to Cancer Molecular Targets and Therapeutics, a section of the journal Frontiers in Oncology

Received: *25 September 2018*
Accepted: *15 November 2018*
Published: *05 December 2018*

Citation:
Davient B, Ng JPZ, Xiao Q, Li L and Yang L (2018) Comparative Transcriptomics Unravels Prodigiosin's Potential Cancer-Specific Activity Between Human Small Airway Epithelial Cells and Lung Adenocarcinoma Cells. Front. Oncol. 8:573. doi: 10.3389/fonc.2018.00573

Objective: Non-Small Cell Lung Cancer (NSCLC) is extremely lethal upon metastasis and requires safe and effective systemic therapies to improve a patient's prognosis. Prodigiosin (PG) appears to selectively and effectively target cancer but not healthy cells. However, PG's cancer-specific activity has remained elusive until recently.

Methods: PG's cancer-specific performance was compared to Docetaxel (DTX), Paclitaxel (PTX), and Doxorubicin (DOX) against human lung adenocarcinoma (A549) and human small airway epithelial cells (HSAEC). Combination of PG with DTX, PTX, or DOX in a 1:1 ED50 ratio was also evaluated. MTT assay was used to determine the post-treatment cell viability. RNA-sequencing was used for comparative transcriptomics analysis between A549 and HSAEC treated with 1.0 μM PG for 24 h.

Results: PG reduced A549 cell viability by four-folds greater than HSAEC. In comparison to DTX, PTX and DOX, PG was ~1.7 times more toxic toward A549, and 2.5 times more protective toward HSAEC. Combination of PG in a 1:1 ED50 ratio with DTX, PTX, or DOX failed to exhibit synergistic toxicity toward A549 or protection toward HSAEC. In A549, genes associated in DNA replication were downregulated, while genes directly or indirectly associated in lipid and cholesterol biogenesis were upregulated. In HSAEC, co-upregulation of oncogenic and tumor-suppressive genes was observed.

Conclusion: An overactive lipid and cholesterol biogenesis could have caused A549's autophagy, while a balancing-act between genes of oncogenic and tumor-suppressive nature could have conferred HSAEC heightened survival. Overall, PG appears to be a smart chemotherapeutic agent that may be both safe and effective for NSCLC patients.

Keywords: prodigiosin, small molecule, chemotherapy, lung cancer, selective, RNA-sequencing

INTRODUCTION

Cancer represents a major disease burden to mankind (1–4), and it accounts for almost one out of six deaths worldwide (5). Out of the 8.8 million cancer deaths in 2015, 1.69 million was due to lung cancer (5). The high mortality in patients with lung cancer is often associated with an advanced metastatic disease state (6, 7). In such cases, effective systemic therapies are vital to improve a

patient's prognosis. Targeted therapy, immunotherapy and chemotherapy are all systemic therapies, each with their own strengths and weaknesses.

Targeted therapies can mitigate most side-effects commonly seen in chemotherapy by working on specific mutations unique to cancer cells (8), but their highly specific nature excludes patients whom do not harbor these mutations (9). Almost 80% of all lung cancers are Non-Small Cell Lung Cancer (NSCLC). The most studied target for NSCLC is the Epidermal Growth Factor Receptor (EGFR). There exist three classes of activating EGFR mutations that sensitizes NSCLCs to EGFR Tyrosine Kinase Inhibitors (TKIs). These activating EGFR mutations have been well summarized in the literature (10). Gefitinib, Erlotinib, Afatinib, Osimertinib, and Dacomitinib are a few prominent and promising EGFR TKIs used in NSCLC patients harboring specific activating EGFR mutations. Gefitinib and Erlotinib are inhibitors of a few specific EGFR mutations found in some NSCLC patients and have demonstrated enduring progression free survival for responders (11–13). Although effective, Gefitinib, Erlotinib, and the other EGFR TKIs are beneficial to only a small population of patients as only about 15% of Caucasian and 50% of Asian lung adenocarcinoma patients harbor EGFR mutations (14, 15).

Immunotherapy exploits the patient's own immune system against cancers (16), but its success depends on the cancer's ability to display its unique neoantigens on its outer cell membrane (17–19) to be identified and destroyed by immune cells (20). Cancers can evade immune destruction by expressing Programmed Death (PD) Ligand 1 (PD-L1), which binds to PD-1 receptors on CD8+ T-cells, inhibiting cytotoxic elimination (21). Nivolumab and Pembrolizumab are antibodies against PD-1. Their prevention of interaction with PD-1 allows CD8+ T-cells to eliminate cancer cells such as NSCLCs (22, 23). Anti-PD-1 effectiveness against NSCLC has been reported to positively correlate with the cancer cell's mutation burden, as a high mutation load generates unique neoantigens for T-cell recognition (24). However, response rates of anti-PD-1 in NSCLC patients appears to be low at ∼19% (22, 23, 25).

In contrast to targeted and immunotherapy, chemotherapy offers broader patient coverage and is still the mainstream cancer therapy available for the majority of cancer patients (26). Platinum-based doublet chemotherapies have been indicated as the first-line against NSCLC with response rates ranging from 25 to 35% (27, 28). However, despite better response rates, their inability to distinguish rapidly diving cancer cells from healthy cells could lead to debilitating side-effects such as anemia, nausea, and neurotoxicity (29).

NSCLC urgently require therapies that are effective, have wide coverage, and harbor fewer side effects. Many studies are ongoing to improve systemic therapies for metastatic NSCLC. In terms of chemotherapies, the search for newer and safer treatments, alone or in combination, persists (30–33).

Nature provides a rich source of anti-cancer agents suitable for chemotherapy. Docetaxel (DTX), Paclitaxel (PTX), and Doxorubicin (DOX) are natural compounds that have been used against NSCLC (34, 35). Recently, Prodigiosin (PG), a secondary metabolite from *Serratia marcescens*, was observed to inhibit NSCLC proliferation (36). Interestingly, PG has been reported to exhibit high cancer-specificity (37–39). This means that PG could potentially mitigate common side-effects associated with chemotherapies, making it a smart chemotherapy candidate.

The current understanding of PG's anti-cancer mechanisms of action encompasses cytoplasmic acidification through modulation of H^+/Cl^- symporters, DNA damage through copper-mediated oxidative cleavage, inhibition of topoisomerases, and ATP synthesis reduction through disruption of the mitochondrial proton gradient (40). At the molecular level, PG has been described to initiate autophagy through mTOR deactivation (39) and apoptosis through the disruption of BCL-2 family pro-survival members (39, 41) or downregulation of pro-survival Survivin (40, 42), a member of the inhibitor of apoptosis. In addition, common to many cancers is the dysregulation of p53, a protein that dictates cell survival or cell death upon cell stress. In most cancers, p53 activity is lost and cells attain a permanent survival status. In some reports, PG was able to induce cancer cell apoptosis in a p53-independent manner (43, 44). This reveals that PG could trigger alternative apoptosis pathways.

Altogether, PG appears to be a promising chemotherapeutic agent which warrants further research into its mechanisms of action. At present, there exists limited data on PG's mechanisms of action to draw meaningful links between studies. Here, we add value to the current knowledge by unveiling PG's potential cancer-specific activity through comparative transcriptomics analysis between Human Lung Adenocarcinoma (A549) and Human Small Airway Epithelial Cells (HSAEC), with Human Colorectal Carcinoma Cells (HCT116) as a cancer control. In addition, we also report on PG's *in vitro* effectiveness and safety, based on the degree of cancer cytotoxicity and selectivity, respectively, in comparison to DTX, PTX and DOX.

MATERIALS AND METHODS

Materials

Docetaxel purum (DTX), doxorubicin hydrochloride (DOX), paclitaxel from *Taxus brevifolia* (PTX), prodigiosin hydrochloride from *Serratia marcescens* (PG), and dimethyl sulfoxide (DMSO) were purchased from Sigma (St. Louis, MO, USA). 3-(4,5-Dimethylthiazol-2-yl)-2,5-diphenyltetrazolium bromide (MTT) was purchased from Bio Basic (Amherst, NY, USA). Proteinase K, RNase-Free DNase I and the RNAprotect Cell Reagent were purchased from Qiagen (Hilden, Germany). TURBO™ DNase, Qubit™ dsDNA HS, and RNA HS Assay Kits were purchased from Invitrogen (Waltham, MA, USA). Angencourt RNAClean XP Kit was purchased from Beckman Coulter (Bera, CA, USA). RNA ScreenTape was purchased from Agilent (Santa Clara, CA, USA).

Cell Culture

Primary Small Airway Epithelial Cells; Normal, Human (HSAEC) (ATCC® PCS301-010™), A549 (ATCC® CCL-185™), HCT116 (ATCC® CCL-247™), and the Airway Epithelial Cell Basal Medium (AECBM) with associated growth factors were purchased from the American Type Culture Collection (ATCC) (Manassas, VA, USA). Phosphate Buffered

Saline (PBS) without calcium and magnesium, high glucose Dulbecco's Modified Eagles Media (DMEM) with added L-glutamine, sodium pyruvate, and phenol red, were purchased from GE Healthcare Life Sciences (Logan, UT, USA). Heat-inactivated Fetal Bovine Serum (FBS) of South American origin and Trypsin-EDTA (0.25%) with phenol red were purchased from Gibco (Waltham, MA, USA). HSAEC cells were cultured with 8 mL AECBM while both A549 and HCT116 cells were cultured with 8 mL DMEM supplemented with 10% FBS, which henceforth will be referred to as complete media, in a 75 cm^2 culture flask. All culture flasks were incubated in a humidified atmosphere at 37°C with 5% CO_2. All incubations mentioned henceforth will be referring to these conditions. No *Mycoplasma* testing was performed.

Cell Viability Assay

DTX, PTX, DOX, and PG were reconstituted with DMSO to a stock concentration of 50, 50, 80, and 2 mM, respectively. Drugs were diluted in pre-warmed AECBM or complete media of 37°C. For each drug concentration tested, an equivalent DMSO concentration was created as control (**Supplementary Figure S1**).

At ∼90% cell confluency, cells were split into 96-well flat-bottomed plates at a seed density and final volume of 7,000 cells and 100 μL per well. Cultures were incubated overnight for 24 h. At ∼80% confluency, the spent media was replaced with either the treatment or control media to a final volume of 100 μL per well. The culture plates were incubated for another 48 h.

The MTT shipped in the powdered state was reconstituted with PBS to a final concentration of 5 mg/mL and sterile filtered with a 0.2 μm Acrodisk Syringe Filter (PALL, Port Washington, NY, USA). This was mixed at a 1:1 ratio with serum-free DMEM or AECBM to create the MTT mix. After the 48 h of treatment, the spent drug media was replaced with 100 μL of the MTT mix. The cultures were incubated for an additional 3 h before being homogenized with 150 μL of DMSO. Cell viability was measured with the Infinite® M200 Pro (Tecan, Männedorf, Zürich, Switzerland) microplate reader at 590 nm.

Drug Cytotoxicity Screening

HSAEC and A549 cells, both at passage P6, were split into three 25 cm^2 culture flasks. These cultures were propagated further for two more passages, and at P8, each cell line was considered to have three biological replicates of $n = 3$ (45). The cells were thereafter cultured in 96-well plates as technical duplicates per biological replicate.

DTX, PTX, DOX, and PG's ED50 were pre-determined with A549 cells (**Supplementary Figure S2**). The ED50 for DTX, PTX, DOX, and PG were 0.1, 0.1, 1, and 0.3 μM, respectively. For the combination therapies with PG, drugs were mixed in a 1:1 ED50 ratio. All treatments were first created as eight-fold stock concentrations and were serially diluted by two-folds (i.e., 8:8 to 4:4 till 0.25:0.25). All other steps conducted have been described under the "Cell Viability Assay" section.

RNA Extraction and Quality Controls

HSAEC, A549, and HCT116 at passage number P8 were cultured as technical triplicates in 25 cm^2 culture flasks, and after two more passages, each cell line was considered to have biological triplicates of $n = 3$ (45). At 90% confluency, HSAEC and A549 cells were split at a seed density of 3.0×10^4 cells/cm^2 while HCT116 cells were split at 6.0×10^4 cells/cm^2 into 6-well plates. After 24 h of incubation in 3 mL of AECBM or complete media, the spent media was replaced with 3 mL of either 1.0 μM PG (treatment) or 0.05% DMSO (control). Cells were incubated for another 24 h and thereafter, the media was replaced with 1 mL of RNAprotect Cell Reagent.

Cells were gently agitated on an orbital shaker at 80 revolutions per minute for 10 min. A lysis cocktail comprised of 10 μL 1% β-mercaptoethanol, 20 μL proteinase K, and 800 μL RLT buffer, which was a component from the RNeasy Mini Kit (Qiagen), was homogenized with cells in each well. The RNA extraction was conducted according to instructions found in the RNeasy Mini Kit.

A 30 min on-column DNase I treatment was performed. DNA contamination was further minimized with TURBO™ DNase treatment. Once RNA was purified with the Angencourt RNAClean XP Kit, RNA integrity was verified using the RNA ScreenTape with analysis on the Agilent 2200 TapeStation (Agilent). Using the Qubit™ dsDNA HS and RNA HS Assay Kits, total RNA was quantified fluorometrically via the Qubit™ Fluorometer 2.0 (Invitrogen).

RNA Sequencing and Data Processing

RNA library preparation and sequencing were conducted by an in-house facility at Singapore Centre for Environmental Life Science Engineering (SCELSE). Briefly, library preparation was executed with the Illumina® TruSeq® Stranded messenger RNA Sample Prep Kit (Illumina, San Diego, CA, USA). The output which was cDNA fragments were paired-end sequenced at read lengths of 100 nucleotides via the Illumina® HiSeq 2500 (Illumina) platform.

All samples had a sequencing depth of more than 24 million reads. These reads were processed using the CLC Genomics Workbench Version 11.0.1 (CLC Bio, Aarhus, Denmark). The default settings were used unless otherwise stated. All reads were trimmed with a quality score of 0.05. Using the "RNA-Seq Analysis" function, the trimmed reads were mapped onto the human genome GRCh38 downloaded from the Ensemble database. The maximum number of hits for a read was set to 1. Gene hits were annotated with GRCh38.92 acquired from the Ensemble database. Gene expression was measured as total counts, where each paired-read was considered as 1. A negative binomial test was performed using the workbench's "Differential Expression for RNA-Seq" tool to establish the differentially expressed genes (DEGs). All raw and processed sequence files may be acquired from Gene Expression Omnibus (Accession number: GSE118448).

Functional Analysis

DEG datasets were exported from CLC into the Ingenuity® Pathway Analysis (IPA; Qiagen) Version 44691306 software. A

Log2 Fold-change (Log2FC) of ±1 with a false discovery rate (FDR) adjusted p-value of < 0.05 was applied to the datasets. With these cut-off values, HSAEC had 2,222, A549 had 2,004, and HCT116 had 2,199 DEGs out of 37,258 successfully annotated gene identifiers.

Statistical Analysis

The Welch two-tailed t-test available in GraphPad Prism 8 was applied onto the drug cytotoxicity screening assay datasets. This statistical test considers the data to have been sampled from a Gaussian population but does not presume that the two populations under scrutiny have the same standard deviation. The null hypothesis is defined as the two populations tested having equal means. When $p > 0.05$, the null hypothesis is not rejected, and the interpretation would be that the evidence is not convincing enough to claim that the means of the two populations tested are different.

RESULTS

PG Demonstrated Selective Toxicity Toward A549 but not HSAEC

PG has been known to induce cancer cell death while preserving healthy cell's viability (37–39). Here, we evaluated PG's cancer-specific toxicity with cancer cell line A549 and immortalized human lung small airway epithelial cells (HSAEC; **Figure 1**). At PG's ED50 of 0.3 μM, cell viability of A549 was reduced by 67.7 ± 5.3%, while HSAEC was reduced by 15.6 ± 2.8%. As A549 is a cancer cell line while HSAEC is an immortalized healthy cell line, with both dividing rapidly, the greater reduction in A549 cell viability demonstrates PG's selective toxicity. PG concentrations >0.3 μM exhibited neither enhanced cancer toxicity nor healthy cell protection.

PG Outperformed DTX, PTX, and DOX in Terms of Cancer-Specificity

Here, we define performance as the agent's ability to protect normal cells while being toxic to cancer cells. In other words, the degree of cancer-specificity. Evaluation of DTX, PTX, DOX, and PG's ED50 of 0.1, 0.1, 1.0, and 0.3 μM, respectively, against A549 and HSAEC, revealed PG's superior performance as a cancer-specific agent. At these concentrations, PG preserved HSAEC viability by 2.8, 2.4, and 2.5 times more than DTX, PTX, and DOX, respectively (**Figure 1**). Moreover, PG reduced A549 cell viability at an average of 1.7 times greater than the other agents.

PG Exhibited Poor Performance in Combination With DTX, PTX, or DOX

DTX, PTX, or DOX in a 1:1 ED50 ratio with PG failed to exhibit anti-cancer synergism and were almost equally toxic, if not worst, toward HSAEC as compared to A549. 0.3 μM PG with 0.1 μM DTX reduced HSAEC viability by 63.0 ± 2.6% and A549 by 67.2 ± 3.7% (**Figure 1A**). 0.3 μM PG with 0.1 μM PTX reduced HSAEC viability by 66.4 ± 7.5% and A549 by 63.9 ± 4.3% (**Figure 1B**). 0.3 μM PG with 1.0 μM DOX reduced HSAEC viability by 71.4 ± 2.7% and A549 by 40.4 ± 10.4% (**Figure 1C**). PG in combination with DTX, PTX, or DOX, at 4:4, 2:2, 1:1, 0.5:0.5 or 0.25:0.25 ED50 ratio, failed to exhibit improved toxicity toward A549 with enhanced protection to HSAEC in comparison to 0.3 μM PG alone.

PG Altered Both A549 and HCT116 Cancer Cells' Morphology

To determine if PG's anti-cancer activity can be observed beyond lung adenocarcinoma cells, in addition to A549 cells, we treated HCT116 cells, another cancer type which could serve as a cancer control, with 1.0 μM PG for 24 h prior microscopic visualization. A549 cells were found in low numbers, elongated, shriveled, with a deformed nucleus and non-homogenous cytoplasm (**Figure 1Da**). HCT116 cells appeared rounded-up, detached from culture surfaces, but still adhered to neighboring cells (**Figure 1Db**). Overall, PG demonstrated substantial morphological alterations in both A549 and HCT116 cancer cell lines.

PG's Toxicity Possibly Mitigated Through a "Balancing Act" in HSAEC

To understand how PG protects healthy cells yet kills cancer cells, we conducted an RNA-sequencing experiment with HSAEC, A549 and HCT116 cells treated with 1.0 μM PG for 24 h. Using the top 50 up- and down-regulated genes per cell line, we were able to identify 84 DEGs specifically perturbed in HSAEC. These DEGs had an FDR p-value $< 4.0 \times 10^{-15}$ (**Figure 2**). For comparison validity, these 84 HSAEC-specific DEGs were filtered under two conditions. Firstly, the corresponding DEGs in A549 and HCT116 were required to have an FDR p-value < 0.05, and secondly, the difference in expression in terms of Log2FC with HSAEC had to be $> \pm 1.5$. Under these conditions, 21 DEGs were identified as fit for comparison (**Table 1**).

The 21 DEGs revealed a "balancing act" in HSAEC between genes of oncogenic and tumor-suppressive nature. Oncogenic genes such as *PDK4, RRAGD, HEY1, TSPAN15,* and *SERPINB9* were found overexpressed. At the same time, tumor-suppressive genes such as *MT1G, MT1M, CDKN1C,* and *DCN* were overexpressed. On the other hand, genes of oncogenic nature such as *SHCBP1, CPA4, KRT19, KRT15, and DSG3* were found downregulated. DEGs such as *BMP6, GULP1, AC106865.1, CNTN3, GDAP1, C1orf116, and SDSL* were uncategorizable due to their lack of information.

PG Possibly Induced DNA Replication Inhibition and Metabolic Rewiring in A549 and HCT116

To identify other possible anti-cancer mechanisms associated with PG, we performed a comparative transcriptomics analysis between A549, HCT116 and HSAEC cells treated with 1.0 μM PG for 24 h. A total of 18 DEGs were considered fit for comparison (**Table 2**) based on two conditions. Firstly, the DEGs commonly perturbed between A549 and HCT116 had to be upregulated by at least >2 Log2FC and downregulated by <-1.5 Log2FC. Secondly, the difference between A549 and HSAEC gene expression had to be $> \pm 1.5$ (**Figure 2**).

All commonly downregulated genes between A549 and HCT116 were found associated with DNA replication. These were *MCM10, H2AFX, DSCC1, MCM4,* and *RFC5* (**Table 2**).

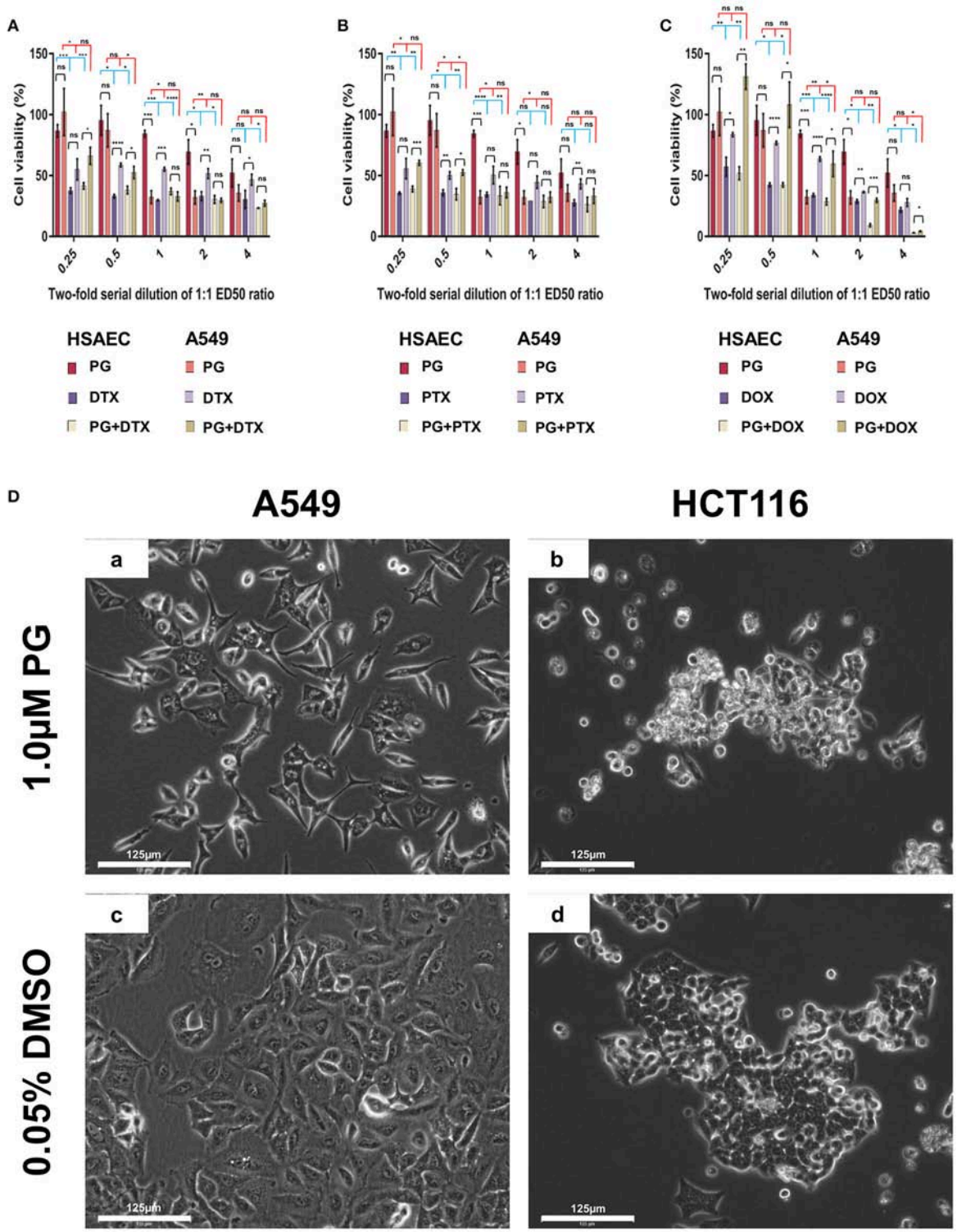

FIGURE 1 | Cell viability of HSAEC and A549 cell measured by the MTT assay after 48-h of PG treatment **(A–C)**. Effects of 1.0 μM PG on A549 and HCT116 cell morphology after 24 h treatment **(Da–Dd)**. **(A)** PG, DTX, and PG+DTX. **(B)** PG, PTX, and PG+PTX. **(C)** PG, DOX, and PG+DOX. Bar graphs represent mean cell viability from biological triplicates ($n = 3$) while the black vertical lines on the bar tops represent standard deviation (SD). A Welch *t*-test was applied to the datasets; black horizontal lines compare drug effects between HSAEC and A549, blue lines compare within HSAEC, and red lines compare within A549 (*$p < 0.05$, **$p < 0.01$, ***$p < 0.001$, ****$p < 0.0001$, and "ns" is not significant). **(Da)** A549 and **(Db)** HCT116 were treated with 1.0 μM PG. **(Dc)** A549 and **(Dd)** HCT116 were treated with 0.05% DMSO as a negative control. Phase-contrast images were acquired at 20X magnification with the EVOS FL Auto 2 microscope. Images have not been enhanced. Scale bars represent 125 μm.

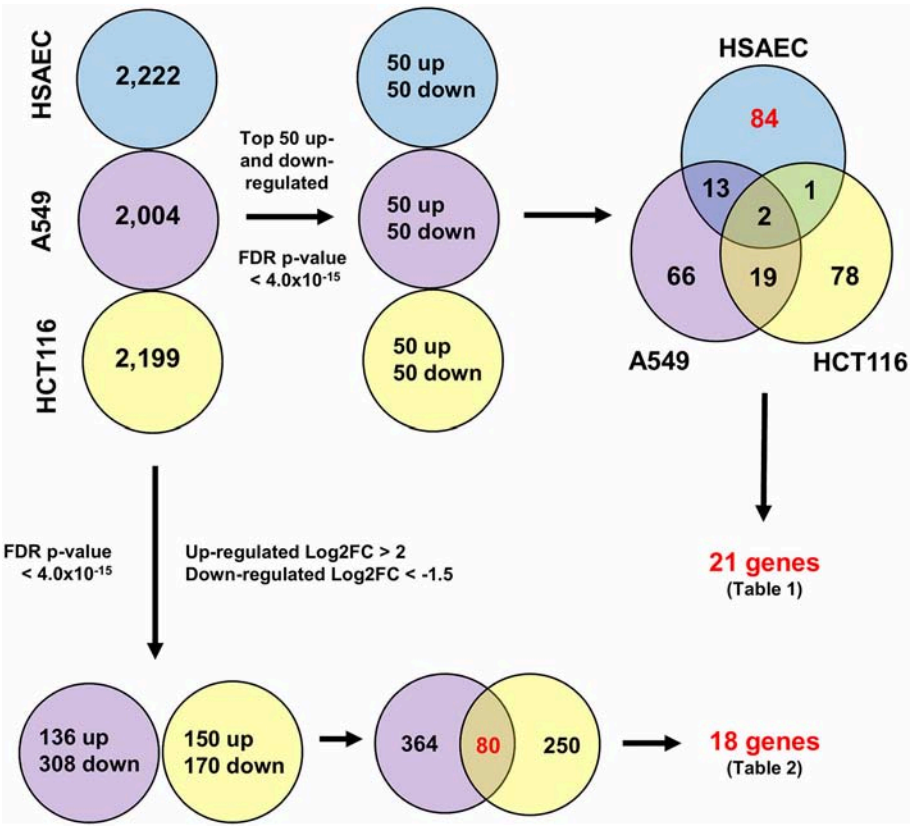

FIGURE 2 | Differentially expressed genes from CLC Workbench for HSAEC, A549 and HCT116 after 24 h treatment with 1.0 μM PG. Blue circles represents HSAEC, purple as A549 and yellow as HCT116. Twenty one genes for **Table 1** were derived from filtering 84 HSAEC-specific genes on the condition that corresponding genes in A549 and HCT116 had an FDR *p*-value < 0.05, and secondly, the difference of A549 and HCT116 gene expression in terms of Log2FC with HSAEC had to be > ± 1.5. Eighteen genes for **Table 2** were derived from filtering 80 genes common to A549 and HCT116 on the condition that corresponding genes in A549 with HSAEC had an FDR *p*-value < 0.05, and secondly, the difference of A549 and HSAEC gene expression in terms of Log2FC with HSAEC had to be > ± 1.5.

Surprisingly, *MCM10* and *DSCC1* expression were severely repressed in HSAEC than in A549 and HCT116. On the other hand, multiple genes associated with lipid and cholesterol metabolism, either directly or indirectly, were found commonly overexpressed between A549 and HCT116. These were *ALDOC, NDRG1, WIPI1, PCSK9, LIPG, MSMO1, MVD, IDI1,* and *ANGPTL4* (**Table 2**). The other genes that were overexpressed yet did not closely associate with the two main categories described here were *MIR210HG, CCNG2, P4HA1,* and *PPM1K* (**Table 2**). Confirmatory repeat experimental data for RNA sequencing result of A549 and HCT116 can be found in **Tables S1,S2**. Further pathway analysis also revealed different upstream regulator activities in PG-treated HSAEC, A549, and HCT116 cells (**Tables S3–S5**).

Based on pathway analysis, and in relation to DNA replication, the "Role of BRCA1 in DNA Damage Response" and the "Mitotic Roles of Polo-Like Kinase" pathways were seen perturbed in all three cell lines but were predicted to be inactivated (**Table 3**). In terms of DNA damage, the "Cell Cycle: G2/M DNA Damage Checkpoint Regulation" pathway was predicted to be activated (**Table 3**). In relation to metabolic rewiring, the "Superpathway of Cholesterol Biosynthesis," the "Cholesterol Biosynthesis III (via Desmosterol)," the "Cholesterol Biosynthesis II (via 24,25-dihydrolanosterol)," and the "Cholesterol Biosynthesis I" pathways were significantly perturbed and predicted to be highly activated (**Table 3**). Furthermore, these cholesterol pathways were not perturbed in HSAEC following PG treatment.

With experimental data, the IPA's Molecule Activity Prediction (MAP) algorithm managed to predict PG-induced mechanistic differences between HSAEC and A549 cells in terms of "Cell Cycle Progression," "Apoptosis," "Cell Survival," "Mitochondrial Respiration," "Glycolysis," "Autophagy," and "Senescence" (**Figure 3**). The overall prediction landscape seems to suggest PG-induced pro-survival in HSAEC but pro-death in A549. Interestingly, "DNA Repair" mechanism was predicted to be inhibited in both cell lines (**Figure 3**).

DISCUSSION

Metastatic lung cancers are extremely lethal and requires effective systemic therapies to improve clinical outcomes for patients (46). PG has demonstrated immense potential as a smart chemotherapeutic candidate. Its most promising feature is its ability to selectively eliminate cancer cells yet protect healthy

TABLE 1 | HSAEC-specific DEGs in comparison with A549 and HCT116 cells after 24 h treatment with 1.0 μM PG.

Gene name	Gene symbol	ENSEMBL ID	Log2FC		
			HSAEC	A549	HCT116
ONCOGENIC NATURED GENES					
Pyruvate Dehydrogenase Kinase 4	PDK4	ENSG00000004799	6.87	1.25	1.62
Ras Related GTP Binding D	RRAGD	ENSG00000025039	4.92	2.03	0.68
Hes Related Family BHLH Transcription Factor with YRPW Motif 1	HEY1	ENSG00000164683	4.54	0.93	1.41
Tetraspanin 15	TSPAN15	ENSG00000099282	4.19	-0.61	1.28
Serpin Family B Member 9	SERPINB9	ENSG00000170542	3.69	-0.78	0.72
SHC Binding and Spindle Associated 1	SHCBP1	ENSG00000171241	-3.73	-2.18	-1.14
Carboxypeptidase A4	CPA4	ENSG00000128510	-3.68	0.49	0.67
Keratin 19	KRT19	ENSG00000171345	-3.48	1.97	0.76
Keratin 15	KRT15	ENSG00000171346	-3.28	1.13	2.00
Desmoglein 3	DSG3	ENSG00000134757	-2.86	–	–
TUMOR-SUPPRESSIVE NATURED GENES					
Metallothionein 1G	MT1G	ENSG00000125144	5.80	–	–
Metallothionein 1M	MT1M	ENSG00000205364	5.64	–	–
Cyclin Dependent Kinase Inhibitor 1C	CDKN1C	ENSG00000129757	4.74	2.84	2.43
Decorin	DCN	ENSG00000011465	3.81	–	–
UNCATEGORIZABLE GENES					
Bone Morphogenetic Protein 6	BMP6	ENSG00000153162	5.49	2.18	-1.41
GULP, Engulfment Adaptor PTB Domain Containing 1	GULP1	ENSG00000144366	4.11	0.78	1.41
–	AC106865.1	ENSG00000250771	4.88	–	–
Contactin 3	CNTN3	ENSG00000113805	4.51	–	–
Ganglioside Induced Differentiation Associated Protein 1	GDAP1	ENSG00000104381	-3.93	-1.12	-0.63
Chromosome 1 Open Reading Frame 116	C1orf116	ENSG00000182795	-3.57	-1.47	1.23
Serine Dehydratase Like	SDSL	ENSG00000139410	-2.88	-0.68	-0.72

Upregulated genes are represented in red, downregulated in blue, and those with no detectable changes with the symbol "-". All genes curated had an FDR p-value $< 4.0 \times 10^{-15}$ *except the following; A549's CDKN1C (0.01) and HEY1 (0.04), HCT116's BMP6 (0.05). Experiments were conducted in biological triplicates of n = 3. Confirmatory repeat experimental data can be found in* ***Supplementary Table S1****.*

cells (37–39). Here, we were able to demonstrate PG's selective elimination of NSCLC by four-folds (**Figures 1A–C**). Beyond lung adenocarcinoma cells, we also showed that PG could cause substantial morphological alterations to colorectal carcinoma cells (**Figure 1D**). When compared to other naturally derived anti-cancer agents such as DTX, PTX, or DOX, PG exhibited heightened protection toward HSAEC while being more toxic to A549. Indeed, PG established itself as a promising cancer-specific agent. However, the random combination with other anti-cancer agents could ameliorate PG's cancer-specific activity and yield an undesirable outcome to healthy cells (**Figures 1A–C**). A rational drug combination approach could increase synergism, hence, greater success in combinatorial chemotherapies. To permit a rational combination of PG with other anti-cancer agents, we require a deeper understanding of the agent's molecular functions.

Previously, a microarray analysis for 1,176 genes was performed on human breast cancer cells treated with PG (44). Out of the 37 significantly perturbed genes (44), there were no similarities found with our study (**Table 2**). The lack of similarities was not unexpected as this could be due to the inherent limitation of the microarray technology (47), or simply because a different cell line was used. Nevertheless, using RNA-sequencing, a genome-wide transcriptomics approach, we were able to identify at least 2,000 significantly perturbed genes per cell line. With broader coverage, we were confident that employing such a technology would permit a more comprehensive analysis.

The comparative transcriptomics analysis between A549 and HCT116 revealed 18 genes that were significantly perturbed by PG (**Table 2**). These genes revealed the possibility of DNA replication inhibition and metabolic rewiring toward enhanced lipid and cholesterol biogenesis. In the study with breast cancer cells, PG was reported to perturb genes related to transcriptional regulation, cell adhesion, cell cycle, and apoptosis (44). Although we have not found perturbations in genes associated with transcriptional regulation or cell adhesion, based on experimental data, we have predicted cell cycle inhibition (**Table 3** and **Figure 3**) and reduced survival fitness in line with apoptosis (**Figure 3**) in A549 cells.

The gene products of *MCM10, MCM4, H2AFX, DSCC1,* and *RFC5* are necessary for DNA replication. However, they were found downregulated in both A549 and HCT116 after PG treatment (**Table 2**). MCM10 plays a crucial role in allowing

TABLE 2 | Common DEGs in both A549 and HCT116 cells after 24 h treatment with 1.0 μM PG.

Gene name	Gene symbol	ENSEMBL ID	Log2FC		
			HSAEC	A549	HCT116
DNA-REPLICATION ASSOCIATED GENES					
Minichromosome Maintenance 10 Replication Initiation Factor	MCM10	ENSG00000065328	-4.67	-3.09	-1.87
H2A Histone Family Member X	H2AFX	ENSG00000188486	-0.96	-2.70	-1.57
DNA Replication and Sister Chromatid Cohesion 1	DSCC1	ENSG00000136982	-3.93	-2.35	-1.55
Minichromosome Maintenance Complex Component 4	MCM4	ENSG00000104738	-0.33	-2.22	-1.87
Replication Factor C Subunit 5	RFC5	ENSG00000111445	-0.51	-2.11	-1.62
LIPID AND CHOLESTEROL METABOLISM ASSOCIATED GENES					
Aldolase, Fructose-Bisphosphate C	ALDOC	ENSG00000109107	1.74	5.36	4.71
N-Myc Downstream Regulated 1	NDRG1	ENSG00000104419	1.08	3.80	2.81
WD Repeat Domain, Phosphoinositide Interacting 1	WIPI1	ENSG00000070540	1.53	3.39	2.50
Proprotein Convertase Subtilisin/Kexin Type 9	PCSK9	ENSG00000169174	1.65	3.27	2.85
Lipase G, Endothelial Type	LIPG	ENSG00000101670	-0.27	2.82	3.35
Methylsterol Monooxygenase 1	MSMO1	ENSG00000052802	0.51	2.76	3.32
Mevalonate Diphosphate Decarboxylase	MVD	ENSG00000167508	0.52	2.48	2.76
Isopentenyl-Diphosphate Delta Isomerase 1	IDI1	ENSG00000067064	0.59	2.34	2.98
Angiopoietin Like 4	ANGPTL4	ENSG00000167772	-1.34	2.19	3.66
OTHER PATHWAYS ASSOCIATED GENES					
MIR210 (MicroRNA 210) Host Gene	MIR210HG	ENSG00000247095	1.00	4.57	3.60
Cyclin G2	CCNG2	ENSG00000138764	0.78	3.15	3.74
Prolyl 4-Hydroxylase Subunit Alpha 1	P4HA1	ENSG00000122884	0.30	2.40	2.68
Protein Phosphatase, Mg2+/Mn2+ Dependent 1K	PPM1K	ENSG00000163644	0.57	2.32	2.15

Upregulated genes are represented in red and downregulated in blue. All genes curated had an FDR p-value $< 4.0 \times 10^{-15}$ *except the following; HSAEC's MIR210HG* (4.09×10^{-15}), *LIPG* (7.17×10^{-3}), *MSMO1* (2.15×10^{-12}), *MVD* (5.92×10^{-10}), *P4HA1* (4.41×10^{-4}), *IDI1* (3.13×10^{-10}), *PPM1K* (8.86×10^{-3}), *MCM10* (3.26×10^{-7}), *H2AFX* (4.09×10^{-15}), *DSCC1* (8.96×10^{-4}), *MCM4* (2.54×10^{-3}), *and RCF5 (0.02). Experiments were conducted as biological triplicates of n = 3. Confirmatory repeat experimental data can be found in* ***Supplementary Table S2***.

CDC45:MCM2-7:GINS helicase to unwind DNA double-strand for replication initiation (48). After DNA has been unwounded, DNA replication requires DSCC1 and RFC5 complexed with other proteins to load Proliferating Cell Nuclear Antigen (PCNA) onto the DNA (49). PCNA is required to clamp DNA polymerase epsilon onto the DNA for replication (50). After DNA synthesis, to maintain genomic integrity, H2AFX serves as a sensor for DNA damage and recruits DNA repair complexes to the area of lesion (51). PG has been reported to cause genotoxicity directly through copper-mediated oxidative cleavage (52), or indirectly through inhibition of topoisomerases (53). One potential mechanism stemming from the downregulation of *H2AFX* is the loss of genomic integrity, induction of cell cycle arrest [*CCNG2* overexpression (**Table 2**) and predicted G2/M DNA damage checkpoint arrest activation (**Table 3**)] and therefore, DNA replication stand-still (54, 55). By throwing the DNA repair mechanisms off-balance [predicted BRCA pathway shutdown (**Table 3**)], genotoxic agents such as PG might increase sensitivity and effectiveness against cancer cells (56, 57).

Metabolic rewiring has been described as an emerging hallmark of cancer (58, 59), and there have been reports of lipid and cholesterol metabolism being drivers of tumorigenesis and progression (60–62). In fact, it has been mentioned that "highly proliferative cancer cells show a strong lipid and cholesterol avidity, which they satisfy by either increasing the uptake of exogenous (or dietary) lipids and lipoproteins or overactivating their endogenous synthesis (that is, lipogenesis and cholesterol synthesis, respectively)" (60). Interestingly, these overactivations were observed only after PG treatment (**Table 2**). ALDOC, MVD, and IDI1 are metabolic enzymes that support lipid and cholesterol biosynthesis. Their gene overexpression could potentially hint at an overactive endogenous lipid and cholesterol biogenesis. *ANGPTL4*, a lipoprotein lipase inhibitor, had a Log2FC difference of 3.53 between healthy HSAEC and cancerous A549 cells. *ANGPTL4* upregulation in A549 cells may have been in response to the overexpression of other lipogenic genes (63). On the flip side, upregulation of *PCKS9* hints at a potential supply cut-off of low-density lipoproteins (LDL) from exogenous sources by reducing LDL receptors (64, 65). As a compensatory mechanism to reduced LDL uptake, *NDRG1* and *LIPG* may have been upregulated to acquire LDL and fatty acids, respectively, from the cell's surroundings (66, 67). *CXCL8*, otherwise known as interleukin-8, has been implicated as a cancer growth factor (68, 69), as well as a molecule that promotes cholesterol accumulation (70). *MSMO1* is also believed to be involved in cholesterol metabolism and cancer (71, 72). Altogether, there may be a possibility that the blockade of exogenous LDL import, compounded with the rampant endogenous demand for lipid and cholesterol biogenesis to support rapidly dividing cancer cells, induced a suicidal metabolic rewiring that eventually led to autophagy (73).

TABLE 3 | Top 10 canonical pathways in A549 and HCT116 cells after 24 h of 1.0 μM PG treatment.

Top 10 Canonical pathways	-log(*p*-value)			Activation z-score		
	HSAEC	A549	HCT116	HSAEC	A549	HCT116
	0.0	15.1		-3.0	4.4	
Superpathway of Cholesterol Biosynthesis						
Cell Cycle Control of Chromosomal Replication				Not predictable		
Cholesterol Biosynthesis III (via Desmosterol)						
Cholesterol Biosynthesis II (via 24,25-dihydrolanosterol)						
Cholesterol Biosynthesis I						
Role of BRCA1 in DNA Damage Response						
Mitotic Roles of Polo-Like Kinase						
Hereditary Breast Cancer Signaling				Not predictable		
Mismatch Repair in Eukaryotes				Not predictable		
Cell Cycle: G2/M DNA Damage Checkpoint Regulation						

Pathways were ranked in descending order of decreasing -log(p-value) of the Fisher's exact test. Dark purple heat-map blocks represent high -log(p-value). Activation z-scores were calculated based on the IPA's pathway activity prediction algorithm. Dark orange heat-map blocks represent the possibility of a highly active pathway, whereas dark blue blocks represent inhibition.

Autophagy is a form of cellular self-cannibalization of cytoplasmic content via lysosomal compartments to recycle cell materials and provide substrates for cellular homeostasis under metabolic stress (74). However, autophagy can be a double-edged sword when it comes to cancers. It could either be pro-tumorigenic or anti-tumorigenic (75, 76). PG is known to bind and inhibit mTORC1 and mTORC2, initiating autophagy in cancer cells (39, 77, 78). We found *WIPI1*, a marker and an important player in autophagy (79, 80), markedly upregulated (**Table 2**). It is unclear if the lipid and cholesterol biosynthesis genes were upregulated to support the *de novo* biogenesis of autophagosomes.

How PG protects healthy cells yet eliminates cancer cells has been a mystery thus far. For the first time, we attempted to unravel PG's cancer-specific mechanisms of action through comparative transcriptomics analysis. Firstly, unlike in A549 and HCT116, there were little to no upregulation in lipid and cholesterol biosynthetic genes and pathways in HSAEC

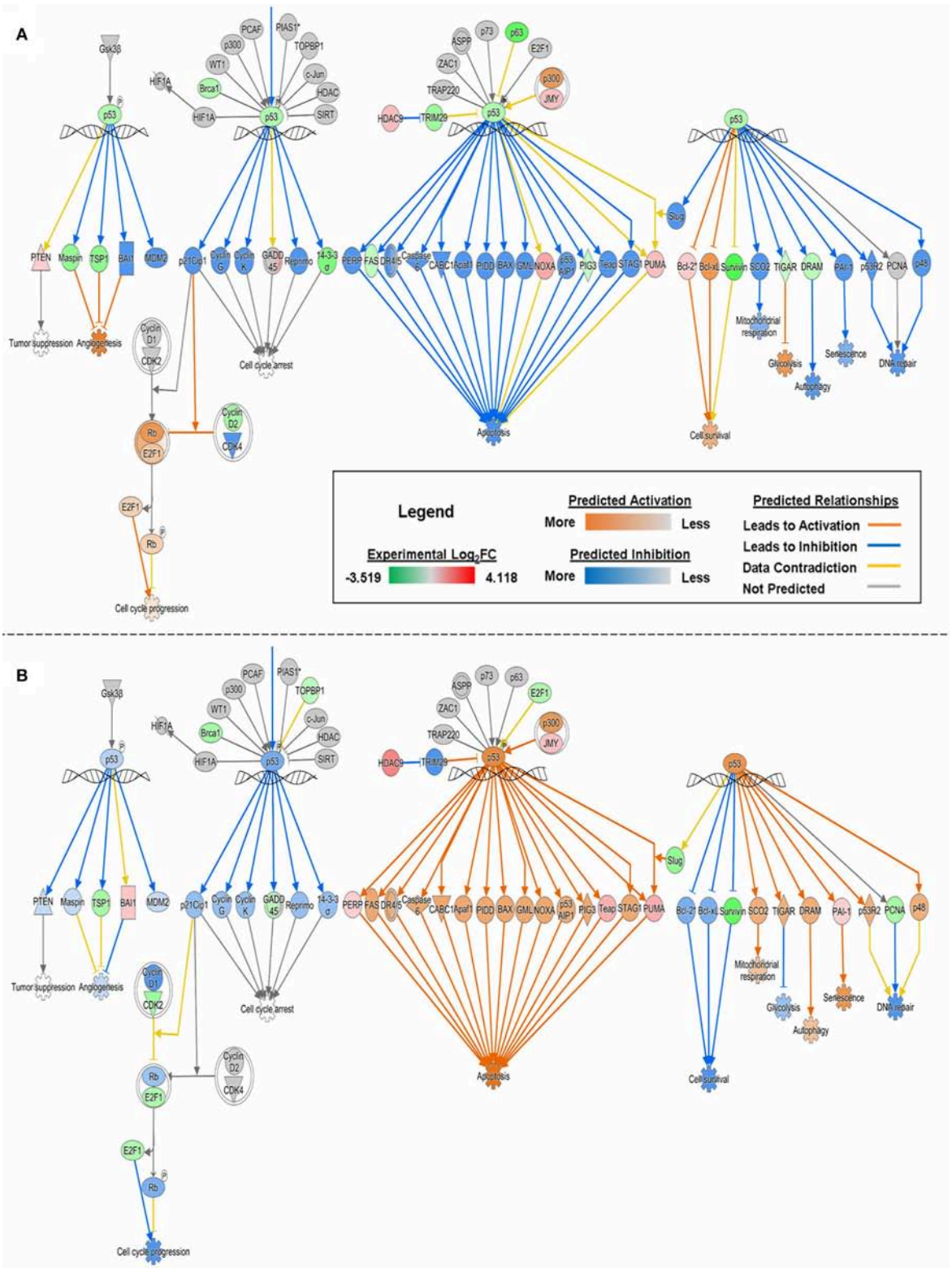

FIGURE 3 | MAP of "p53 Signaling" pathway in **(A)** HSAEC and **(B)** A549 cells treated with 1 μM PG over 24 h. Predictions were calculated based upon DEGs from the experimental dataset overlaid onto the Ingenuity Knowledge Base in IPA. Orange, blue, yellow, and gray lines corresponds to predicted activation, inhibition, contradiction, and the inability to predict an outcome, respectively. Red or green color intensities within shapes reflect the level of upregulation or downregulation, respectively, based upon the experimental Log2FC values. Orange or blue color intensities within shapes reflect the level of predicted activation or inhibition, respectively, based on upon IPA's predictions.

(**Tables 2**, **3**). In fact, the downregulation of *ANGPTL4* suggests an active catabolism of lipoproteins. Secondly, although *WIPI1* was upregulated, it was much lesser than A549, possibly reflecting a weaker autophagic status in HSAEC. Thirdly, the near-normal expression of *H2AFX* suggests that HSAEC may be able to overcome PG's genotoxic stress. However, how this could be possible despite *BRCA1* downregulation (**Figure 3**) and potential BRCA1 pathway inactivation (**Table 3**) is unclear. Fourth, a deep analysis of HSAEC-specific genes perturbed by PG revealed a "balancing act" expression of pro-cancer and anti-cancer genes (**Table 1**). This could potentially assist in HSAEC's viability under PG treatment. Lastly, and surprisingly, *MCM10* and *DSCC1* were found severely downregulated in HSAEC. As PG could inhibit topoisomerases (53), another potential means of PG genotoxicity could be mitigated here as the loss of MCM10 does not permit DNA to unwind for replication (48). Altogether, we suspect that HSAEC may have been conferred protection to PG through DNA replication inhibition, BRCA1-independent DNA repair availability and autophagic resistance.

PG's upregulation of cholesterol pathways in cancer cells and its ability to potentially inhibit DNA replication brings about two immediate concerns that should be addressed in future studies. Firstly, the degree of which PG could inhibit DNA replication in HSAEC should be monitored with cell growth rate compared to A549 and other rapidly dividing cells. This would elucidate the potential clinical benefits PG has over other conventional chemotherapeutics that falls short in protecting rapidly dividing healthy cells. Secondly, the impact of PG treatment with regards to hypercholesterolemia should be assessed *in vivo*. On the other hand, further studies on *MIR210HG,* the second most differentially expressed gene in both A549 and HCT116 (**Table 2**) could potentially highlight novel insights with regards to PG's cancer-specific mechanisms of action. To further improve PG's cancer specificity, chemical modifications may be explored to acquire novel PG analogs or develop targeted drug delivery strategies which studies have already begun (81, 82).

CONCLUSION

Numerous decades of cancer research, drug discovery, and development have led to major improvements in patients' quality of life. Research into systemic therapies for metastatic cancers continues at two major fronts, namely, safety and efficacy. PG appears to be a promising smart chemotherapeutic agent against NSCLC. PG not only demonstrated heightened anti-cancer activity against A549, but this activity was also cancer-specific. Understanding how such an agent differentiates cancerous from healthy cells has been unclear until recently. With RNA-sequencing, a next-generation tool for transcriptomics, we managed to unravel PG's potential cancer-specific mechanisms of action. Through an exogenous cholesterol supply cut-off and an internal overactivation of cholesterol synthesis, PG might have induced cancer cell autophagy to a point whereby self-cannibalization led to cell death. At the same time, through balancing the overexpression of oncogenic and tumor-suppressive genes, healthy cells might have been conferred a heightened survival status by PG. By exposing A549 transcriptome landscape perturbed by PG, we can now conduct further experiments with single or multiplexed knock-outs and knock-downs using CRISPR to yield definitive targets which could aid the development of precision medicine against NSCLC.

AUTHOR CONTRIBUTIONS

BD performed the cell cultures, cytotoxicity assays, RNA extraction, RNA purification, RNA-sequencing data processing in CLC Workbench, and the data analysis in IPA. JN repeated the RNA extraction throughout data analysis in IPA and reproduced the data. LL, QX, and LY conceptualized the study idea and provided material and technical support. BD and LL wrote the manuscript. BD, JN, QX, LL, and LY revised the manuscript.

FUNDING

This work was supported by the National Research Foundation and Ministry of Education Singapore under its Research Centre of Excellence Program (SCELSE), AcRF Tier 2 (MOE2016-T2-1-010) from the Ministry of Education, Singapore and The Marine Science Research and Development Programme (MSRDP-P34) from National Research Foundation, Singapore.

SUPPLEMENTARY MATERIAL

The Supplementary Material for this article can be found online at: https://www.frontiersin.org/articles/10.3389/fonc.2018.00573/full#supplementary-material

REFERENCES

1. Ma X, Yu H. Global burden of cancer. *Yale J Biol Med.* (2006) 79:85–94.
2. Rahib L, Smith BD, Aizenberg R, Rosenzweig AB, Fleshman JM, Matrisian LM. Projecting cancer incidence and deaths to 2030: the unexpected burden of thyroid, liver, and pancreas cancers in the United States. *Cancer Res* (2014) 74:2913–21. doi: 10.1158/0008-5472.Can-14-0155
3. Fidler MM, Bray F, Soerjomataram I. The global cancer burden and human development: a review. *Scand J Public Health* (2018) 46:27–36. doi: 10.1177/1403494817715400
4. Global Burden of Disease Cancer Collaboration. Global, regional, and national cancer incidence, mortality, years of life lost, years lived with disability, and disability-adjusted life-years for 32 cancer groups, 1990 to 2015: a systematic analysis for the global burden of disease study. *JAMA Oncol.* (2017) 3:524–48. doi: 10.1001/jamaoncol.2016.5688
5. World Health Organization. *Cancer key facts [Online]*. (2018). Available online at: http://www.who.int/news-room/fact-sheets/detail/cancer (Accessed 24 May 2018).
6. Herbst RS, Heymach JV, Lippman SM. Lung cancer. *N Engl J Med.* (2008) 359:1367–80. doi: 10.1056/NEJMra0802714
7. Morgensztern D, Ng SH, Gao F, Govindan R. Trends in stage distribution for patients with non-small cell lung cancer: a national cancer database survey. *J Thoracic Oncol.* (2010) 5:29–33. doi: 10.1097/JTO.0b013e3181c5920c
8. Baudino TA. Targeted cancer therapy: the next generation of cancer treatment. *Curr Drug Discov Technol* (2015) 12:3–20. doi: 10.2174/1570163812666150602144310

9. Huang M, Shen A, Ding J, Geng M. Molecularly targeted cancer therapy: some lessons from the past decade. *Trends Pharmacol Sci.* (2014) 35:41–50. doi: 10.1016/j.tips.2013.11.004
10. Kumar A, Petri ET, Halmos B, Boggon TJ. Structure and clinical relevance of the epidermal growth factor receptor in human cancer. *J Clin Oncol.* (2008) 26:1742–51. doi: 10.1200/JCO.2007.12.1178
11. Lynch TJ, Bell DW, Sordella R, Gurubhagavatula S, Okimoto RA, Brannigan BW, et al. Activating mutations in the epidermal growth factor receptor underlying responsiveness of non-small-cell lung cancer to gefitinib. *N Engl J Med.* (2004) 350:2129–39. doi: 10.1056/NEJMoa040938
12. Maemondo M, Inoue A, Kobayashi K, Sugawara S, Oizumi S, Isobe H, et al. Gefitinib or chemotherapy for non–small-cell lung cancer with mutated EGFR. *N Engl J Med.* (2010) 362:2380–8. doi: 10.1056/NEJMoa0909530
13. Morgillo F, Della Corte CM, Fasano M, Ciardiello F. Mechanisms of resistance to EGFR-targeted drugs: lung cancer. *ESMO Open* (2016) 1:e000060. doi: 10.1136/esmoopen-2016-000060
14. Rosell R, Moran T, Queralt C, Porta R, Cardenal F, Camps C, et al. Screening for epidermal growth factor receptor mutations in lung cancer. *N Engl J Med.* (2009) 361:958–67. doi: 10.1056/NEJMoa0904554
15. Shi Y, Au JS-K, Thongprasert S, Srinivasan S, Tsai C-M, Khoa MT, et al. A prospective, molecular epidemiology study of EGFR mutations in asian patients with advanced non-small-cell lung cancer of adenocarcinoma histology (PIONEER). *J Thoracic Oncol.* (2014) 9:154–62. doi: 10.1097/JTO.0000000000000033
16. Farkona S, Diamandis EP, Blasutig IM. Cancer immunotherapy: the beginning of the end of cancer? *BMC Med.* (2016) 14:73. doi: 10.1186/s12916-016-0623-5
17. Restifo NP, Marincola FM, Kawakami Y, Taubenberger J, Yannelli JR, Rosenberg SA. Loss of functional beta 2-microglobulin in metastatic melanomas from five patients receiving immunotherapy. *J Natl Cancer Inst.* (1996) 88:100–8.
18. Shukla SA, Rooney MS, Rajasagi M, Tiao G, Dixon PM, Lawrence MS, et al. Comprehensive analysis of cancer-associated somatic mutations in class I HLA genes. *Nat Biotechnol.* (2015) 33:1152–8. doi: 10.1038/nbt.3344
19. Anagnostou V, Smith KN, Forde PM, Niknafs N, Bhattacharya R, White J, et al. Evolution of neoantigen landscape during immune checkpoint blockade in non-small cell lung cancer. *Cancer Discov.* (2017) 7:264–76. doi: 10.1158/2159-8290.Cd-16-0828
20. Finn, O. J. (2012). Immuno-oncology: understanding the function and dysfunction of the immune system in cancer. *Ann Oncol.* 23(suppl_8):viii6–9. doi: 10.1093/annonc/mds256
21. Juneja VR, McGuire KA, Manguso RT, LaFleur MW, Collins N, Haining WN, et al. PD-L1 on tumor cells is sufficient for immune evasion in immunogenic tumors and inhibits CD8 T cell cytotoxicity. *J Exp Med.* (2017) 214:895–904. doi: 10.1084/jem.20160801
22. Borghaei H, Paz-Ares L, Horn L, Spigel DR, Steins M, Ready NE, et al. Nivolumab versus docetaxel in advanced nonsquamous non–small-cell lung cancer. *N Engl J Med.* (2015) 373:1627–39. doi: 10.1056/NEJMoa1507643
23. Garon EB, Rizvi NA, Hui R, Leighl N, Balmanoukian AS, Eder JP, et al. Pembrolizumab for the treatment of non–small-cell lung cancer. *N Engl J Med.* (2015) 372:2018–28. doi: 10.1056/NEJMoa1501824
24. Rizvi NA, Hellmann MD, Snyder A, Kvistborg P, Makarov V, Havel JJ, et al. Mutational landscape determines sensitivity to PD-1 blockade in non–small cell lung cancer. *Science* (2015) 348:124–8. doi: 10.1126/science.aaa1348
25. Topalian SL, Hodi FS, Brahmer JR, Gettinger SN, Smith DC, McDermott DF, et al. Safety, activity, and immune correlates of anti-PD-1 antibody in cancer. *N Engl J Med.* (2012) 366:2443–54. doi: 10.1056/NEJMoa1200690
26. American Cancer Society. *"Cancer Treatment & Survivorship Facts & Figures 2016-2017".* Atlanta, GA: American Cancer Society (2016). Available online at: https://www.cancer.org/research/cancer-facts-statistics/survivor-facts-figures.html
27. Socinski MA, Bondarenko I, Karaseva NA, Makhson AM, Vynnychenko I, Okamoto I, et al. Weekly nab-paclitaxel in combination with carboplatin versus solvent-based paclitaxel plus carboplatin as first-line therapy in patients with advanced non–small-cell lung cancer: final results of a phase III trial. *J Clin Oncol.* (2012) 30:2055–62. doi: 10.1200/JCO.2011.39.5848
28. Patel JD, Socinski MA, Garon EB, Reynolds CH, Spigel DR, Olsen MR, et al. PointBreak: a randomized phase III study of pemetrexed plus carboplatin and bevacizumab followed by maintenance pemetrexed and bevacizumab versus paclitaxel plus carboplatin and bevacizumab followed by maintenance bevacizumab in patients with stage IIIB or IV nonsquamous non–small-cell lung cancer. *J Clin Oncol.* (2013) 31:4349–57. doi: 10.1200/JCO.2012.47.9626
29. Rajeswaran A, Trojan A, Burnand B, Giannelli M. Efficacy and side effects of cisplatin- and carboplatin-based doublet chemotherapeutic regimens versus non-platinum-based doublet chemotherapeutic regimens as first line treatment of metastatic non-small cell lung carcinoma: a systematic review of randomized controlled trials. *Lung Cancer* (2008) 59:1–11. doi: 10.1016/j.lungcan.2007.07.012
30. Feng L-X, Li M, Liu Y-J, Yang S-M, Zhang N. Synergistic enhancement of cancer therapy using a combination of ceramide and docetaxel. *Int J Mol Sci.* (2014) 15:4201–20. doi: 10.3390/ijms15034201
31. Garon EB, Neidhart JD, Gabrail NY, de Oliveira MR, Balkissoon J, Kabbinavar F. A randomized Phase II trial of the tumor vascular disrupting agent CA4P (fosbretabulin tromethamine) with carboplatin, paclitaxel, and bevacizumab in advanced nonsquamous non-small-cell lung cancer. *OncoTargets Ther.* (2016) 9:7275–83. doi: 10.2147/OTT.S109186
32. Yan X, Ge H, Huang T, Hindra, Yang, D., Teng, Q., et al. (2016). Strain prioritization and genome mining for enediyne natural products. *MBio* 7:6. doi: 10.1128/mBio.02104-16
33. Wang S, Gao A, Liu J, Sun Y. First-line therapy for advanced non-small cell lung cancer with activating EGFR mutation: is combined EGFR-TKIs and chemotherapy a better choice? *Cancer Chemother Pharmacol.* (2018) 81:443–53. doi: 10.1007/s00280-017-3516-1
34. Schiller JH. Current standards of care in small-cell and non-small-cell lung cancer. *Oncology* (2001) 61(Suppl 1):3–13. doi: 10.1159/000055386
35. Huang CY, Ju DT, Chang CF, Muralidhar Reddy P, Velmurugan BK. A review on the effects of current chemotherapy drugs and natural agents in treating non-small cell lung cancer. *Biomedicine* (2017) 7:23. doi: 10.1051/bmdcn/2017070423
36. Hsieh H-Y, Shieh J-J, Chen C-J, Pan M-Y, Yang S-Y, Lin S-C, et al. Prodigiosin down-regulates SKP2 to induce p27(KIP1) stabilization and antiproliferation in human lung adenocarcinoma cells. *Br J Pharmacol.* (2012) 166:2095–108. doi: 10.1111/j.1476-5381.2012.01921.x
37. Montaner B, Pérez-Tomás R. Prodigiosin-induced apoptosis in human colon cancer cells. *Life Sci.* (2001) 68:2025–36. doi: 10.1016/S0024-3205(01)01002-5
38. Hassankhani R, Sam MR, Esmaeilou M, Ahangar P. Prodigiosin isolated from cell wall of Serratia marcescens alters expression of apoptosis-related genes and increases apoptosis in colorectal cancer cells. *Med Oncol.* (2015) 32:366. doi: 10.1007/s12032-014-0366-0
39. Cheng MF, Lin CS, Chen YH, Sung PJ, Lin SR, Tong YW, et al. Inhibitory growth of oral squamous cell carcinoma cancer via bacterial prodigiosin. *Mar Drugs* (2017) 15:7. doi: 10.3390/md15070224
40. Yenkejeh RA, Sam MR, Esmaeillou M. Targeting survivin with prodigiosin isolated from cell wall of Serratia marcescens induces apoptosis in hepatocellular carcinoma cells. *Hum Exp Toxicol.* (2017) 36:402–11. doi: 10.1177/0960327116651122
41. Soto-Cerrato V, Llagostera E, Montaner B, Scheffer GL, Perez-Tomas R. Mitochondria-mediated apoptosis operating irrespective of multidrug resistance in breast cancer cells by the anticancer agent prodigiosin. *Biochem Pharmacol.* (2004) 68:1345–52. doi: 10.1016/j.bcp.2004.05.056
42. Sam MR, Pourpak RS. Regulation of p53 and survivin by prodigiosin compound derived from Serratia marcescens contribute to caspase-3-dependent apoptosis in acute lymphoblastic leukemia cells. *Hum Exp Toxicol.* (2017) 2017:960327117718052. doi: 10.1177/0960327117718052
43. Montaner B, Navarro S, Pique M, Vilaseca M, Martinell M, Giralt E, et al. Prodigiosin from the supernatant of Serratia marcescens induces apoptosis in haematopoietic cancer cell lines. *Br J Pharmacol.* (2000) 131:585–93. doi: 10.1038/sj.bjp.0703614
44. Soto-Cerrato V, Vinals F, Lambert JR, Kelly JA, Perez-Tomas R. Prodigiosin induces the proapoptotic gene NAG-1 via glycogen synthase kinase-3beta activity in human breast cancer cells. *Mol Cancer Ther.* (2007) 6:362–9. doi: 10.1158/1535-7163.Mct-06-0266
45. Cumming G, Fidler F, Vaux DL. Error bars in experimental biology. *J Cell Biol.* (2007) 177:7. doi: 10.1083/jcb.200611141
46. Herbst RS, Morgensztern D, Boshoff C. The biology and management of non-small cell lung cancer. *Nature* (2018) 553:446. doi: 10.1038/nature25183

47. Zhao S, Fung-Leung W-P, Bittner A, Ngo K, Liu X. Comparison of RNA-Seq and microarray in transcriptome profiling of activated T cells. *PLoS ONE* (2014) 9:e78644. doi: 10.1371/journal.pone.0078644
48. Thu YM, Bielinsky A-K. MCM10: one tool for all—integrity, maintenance and damage control. *Semin Cell Dev Biol.* (2014) 30:121–30. doi: 10.1016/j.semcdb.2014.03.017
49. Bermudez VP, Maniwa Y, Tappin I, Ozato K, Yokomori K, Hurwitz J. The alternative Ctf18-Dcc1-Ctf8-replication factor C complex required for sister chromatid cohesion loads proliferating cell nuclear antigen onto DNA. *Proc Natl Acad Sci.* (2003) 100:10237–42. doi: 10.1073/pnas.1434308100
50. Bowman GD, O'Donnell M, Kuriyan J. Structural analysis of a eukaryotic sliding DNA clamp–clamp loader complex. *Nature* (2004) 429:724. doi: 10.1038/nature02585
51. Srivastava N, Gochhait S, de Boer P, Bamezai RNK. Role of H2AX in DNA damage response and human cancers. *Mutat Res Rev.* (2009) 681:180–8. doi: 10.1016/j.mrrev.2008.08.003
52. Melvin MS, Tomlinson JT, Saluta GR, Kucera GL, Lindquist N, Manderville RA. Double-strand DNA cleavage by copper·prodigiosin. *J Am Chem Soc.* (2000) 122:6333–4. doi: 10.1021/ja0000798
53. Montaner B, Castillo-Avila W, Martinell M, Ollinger R, Aymami J, Giralt E, et al. DNA interaction and dual topoisomerase I and II inhibition properties of the anti-tumor drug prodigiosin. *Toxicol Sci.* (2005) 85:870–9. doi: 10.1093/toxsci/kfi149
54. Hakem R. DNA-damage repair; the good, the bad, and the ugly. *Embo J.* (2008) 27:589–605. doi: 10.1038/emboj.2008.15
55. Lal A, Pan Y, Navarro F, Dykxhoorn DM, Moreau L, Meire E, et al. miR-24-mediated down-regulation of H2AX suppresses DNA repair in terminally differentiated blood cells. *Nat Struct Mol Biol.* (2009) 16:492–8. doi: 10.1038/nsmb.1589
56. Atsumi Y, Inase A, Osawa T, Sugihara E, Sakasai R, Fujimori H, et al. The Arf/p53 protein module, which induces apoptosis, down-regulates histone H2AX to allow normal cells to survive in the presence of anti-cancer drugs. *J Biol Chem.* (2013) 288:13269–77. doi: 10.1074/jbc.M112.402560
57. Jongen JMJ, van der Waals LM, Trumpi K, Laoukili J, Peters NA, Schenning-van Schelven SJ, et al. Downregulation of DNA repair proteins and increased DNA damage in hypoxic colon cancer cells is a therapeutically exploitable vulnerability. *Oncotarget* (2017) 8:86296–311. doi: 10.18632/oncotarget.21145
58. Ward PS, Thompson CB. Metabolic reprogramming: a cancer hallmark even warburg did not anticipate. *Cancer Cell* (2012) 21:297–308. doi: 10.1016/j.ccr.2012.02.014
59. Pavlova NN, Thompson CB. The emerging hallmarks of cancer metabolism. *Cell Metab.* (2016) 23:27–47. doi: 10.1016/j.cmet.2015.12.006
60. Beloribi-Djefaflia S, Vasseur S, Guillaumond F. Lipid metabolic reprogramming in cancer cells. *Oncogenesis* (2016) 5:e189. doi: 10.1038/oncsis.2015.49
61. Liu Q, Luo Q, Halim A, Song G. Targeting lipid metabolism of cancer cells: a promising therapeutic strategy for cancer. *Cancer Lett.* (2017) 401:39–45. doi: 10.1016/j.canlet.2017.05.002
62. Luo X, Cheng C, Tan Z, Li N, Tang M, Yang L, et al. Emerging roles of lipid metabolism in cancer metastasis. *Molecular Cancer* (2017) 16:76. doi: 10.1186/s12943-017-0646-3
63. Lim H, Lim Y-M, Kim KH, Jeon YE, Park K, Kim J, et al. A novel autophagy enhancer as a therapeutic agent against metabolic syndrome and diabetes. *Nat Commun.* (2018) 9:1438. doi: 10.1038/s41467-018-03939-w
64. Nassoury N, Blasiole DA, Tebon Oler A, Benjannet S, Hamelin J, Poupon V, et al. The cellular *traffic*king of the secretory proprotein convertase PCSK9 and its dependence on the LDLR. *Traffic* (2007) 8:718–32. doi: 10.1111/j.1600-0854.2007.00562.x
65. Zhang DW, Lagace TA, Garuti R, Zhao Z, McDonald M, Horton JD, et al. Binding of proprotein convertase subtilisin/kexin type 9 to epidermal growth factor-like repeat A of low density lipoprotein receptor decreases receptor recycling and increases degradation. *J Biol Chem.* (2007) 282:18602–12. doi: 10.1074/jbc.M702027200
66. Pietiainen V, Vassilev B, Blom T, Wang W, Nelson J, Bittman R, et al. NDRG1 functions in LDL receptor trafficking by regulating endosomal recycling and degradation. *J Cell Sci.* (2013) 126(Pt 17):3961–71. doi: 10.1242/jcs.128132
67. Olivecrona G. Role of lipoprotein lipase in lipid metabolism. *Curr Opin Lipidol.* (2016) 27:233–41. doi: 10.1097/mol.0000000000000297
68. Zhu YM, Webster SJ, Flower D, Woll PJ. Interleukin-8/CXCL8 is a growth factor for human lung cancer cells. *Br J Cancer* (2004) 91:1970. doi: 10.1038/sj.bjc.6602227
69. Liu Q, Li A, Tian Y, Wu JD, Liu Y, Li T, et al. The CXCL8-CXCR1/2 pathways in cancer. *Cytokine Growth Factor Rev.* (2016) 31:61–71. doi: 10.1016/j.cytogfr.2016.08.002
70. He M, Zhang W, Dong Y, Wang L, Fang T, Tang W, et al. Pro-inflammation NF-κB signaling triggers a positive feedback via enhancing cholesterol accumulation in liver cancer cells. *J Exp Clin Cancer Res.* (2017) 36:15. doi: 10.1186/s13046-017-0490-8
71. Yang Y-F, Jan Y-H, Liu Y-P, Yang C-J, Su C-Y, Chang Y-C, et al. Squalene synthase induces tumor necrosis factor receptor 1 enrichment in lipid rafts to promote lung cancer metastasis. *Am J Resp Critic Care Med.* (2014) 190:675–87. doi: 10.1164/rccm.201404-0714OC
72. Simigdala N, Gao Q, Pancholi S, Roberg-Larsen H, Zvelebil M, Ribas R, et al. Cholesterol biosynthesis pathway as a novel mechanism of resistance to estrogen deprivation in estrogen receptor-positive breast cancer. *Breast Cancer Res.* (2016) 18:58. doi: 10.1186/s13058-016-0713-5
73. Selwan EM, Finicle BT, Kim SM, Edinger AL. Attacking the supply wagons to starve cancer cells to death. *FEBS Lett.* (2016) 590:885–907. doi: 10.1002/1873-3468.12121
74. Mathew R, Karantza-Wadsworth V, White E. Role of autophagy in cancer. *Nat Rev Cancer* (2007) 7:961. doi: 10.1038/nrc2254
75. Proikas-Cezanne T, Waddell S, Gaugel A, Frickey T, Lupas A, Nordheim A. WIPI-1alpha (WIPI49), a member of the novel 7-bladed WIPI protein family, is aberrantly expressed in human cancer and is linked to starvation-induced autophagy. *Oncogene* (2004) 23:9314–25. doi: 10.1038/sj.onc.1208331
76. Choi KS. Autophagy and cancer. *Exp Mol Med.* (2012) 44:109. doi: 10.3858/emm.2012.44.2.033
77. Espona-Fiedler M, Soto-Cerrato V, Hosseini A, Lizcano JM, Guallar V, Quesada R, et al. Identification of dual mTORC1 and mTORC2 inhibitors in melanoma cells: prodigiosin vs. obatoclax. *Biochem Pharmacol.* (2012) 83:489–96. doi: 10.1016/j.bcp.2011.11.027
78. Cheng S-Y, Chen N-F, Kuo H-M, Yang S-N, Sung C-S, Sung P-J, et al. Prodigiosin stimulates endoplasmic reticulum stress and induces autophagic cell death in glioblastoma cells. *Apoptosis* (2018) 23:314–28. doi: 10.1007/s10495-018-1456-9
79. Tsuyuki S, Takabayashi M, Kawazu M, Kudo K, Watanabe A, Nagata Y, et al. Detection of WIPI1 mRNA as an indicator of autophagosome formation. *Autophagy* (2014) 10:497–513. doi: 10.4161/auto.27419
80. Proikas-Cezanne T, Takacs Z, Donnes P, Kohlbacher O. WIPI proteins: essential PtdIns3P effectors at the nascent autophagosome. *J Cell Sci.* (2015) 128:207–17. doi: 10.1242/jcs.146258
81. Dozie-Nwachukwu SO, Danyuo Y, Obayemi JD, Odusanya OS, Malatesta K, Soboyejo WO. Extraction and encapsulation of prodigiosin in chitosan microspheres for targeted drug delivery. *Mater Sci Eng C Mater Biol Appl.* (2017) 71:268–78. doi: 10.1016/j.msec.2016.09.078
82. Dozie-Nwachukwu SO, Obayemi JD, Danyuo Y, Anuku N, Odusanya OS, Malatesta K, et al. A comparative study of the adhesion of biosynthesized gold and conjugated gold/prodigiosin nanoparticles to triple negative breast cancer cells. *J Mater Sci Mater Med.* (2017) 28:143. doi: 10.1007/s10856-017-5943-2

Conflict of Interest Statement: The authors declare that the research was conducted in the absence of any commercial or financial relationships that could be construed as a potential conflict of interest.

frontiers in Oncology

MINI REVIEW
published: 07 December 2018
doi: 10.3389/fonc.2018.00598

Curaxin CBL0137 Exerts Anticancer Activity via Diverse Mechanisms

Ming-Zhu Jin[1†], *Bai-Rong Xia*[2†], *Yu Xu*[1] *and Wei-Lin Jin*[3,4,5*]

[1] Shanghai Jiao Tong University School of Medicine, Shanghai, China, [2] Department of Gynecology, The Affiliated Tumor Hospital, Harbin Medical University, Harbin, China, [3] Key Laboratory for Thin Film and Microfabrication Technology of Ministry of Education, Department of Instrument Science and Engineering, Shanghai Engineering Center for Intelligent Diagnosis and Treatment Instrument, School of Electronic Information and Electronic Engineering, Institute of Nano Biomedicine and Engineering, Shanghai Jiao Tong University, Shanghai, China, [4] National Center for Translational Medicine, Collaborative Innovational Center for System Biology, Shanghai Jiao Tong University, Shanghai, China, [5] Shaanxi Key Laboratory of Brain Disorders and Institute of Basic and Translational Medicine, Xi'an Medical University, Xi'an, China

Chemotherapy with or without radiation remains the first choice for most cancers. However, intolerant side effects and conventional drug resistance restrict actual clinical efficacy. Curaxin CBL0137 is designed to regulate p53 and nuclear factor-κB simultaneously and to prevent the resistance caused by a single target. Functionally, CBL0137 exhibits an antitumor activity in multiple cancers, including glioblastoma, renal cell carcinoma, melanoma, neuroblastoma, and small cell lung cancer (SCLC). Mechanistically, CBL0137 is originally identified to act by facilitates chromatin transcription (FACT) complex. Further investigations reveal that several pathways, such as NOTCH1 and heat shock factor 1 (HSF1), are involved in the process. CBL0137 has been reported to target cancer stem cells (CSCs) and enhance chemotherapy/monotherapy efficacy. The translational advance of CBL0137 into clinical practice is expected to provide a promising future for cancer treatment.

Keywords: cancer stem cells, CBL0137, chemotherapy, facilitates chromatin transcription, p53

OPEN ACCESS

Edited by:
Zhe-Sheng Chen,
St. John's University, United States

Reviewed by:
Ho Sup Yoon,
Nanyang Technological University, Singapore
Jihong Zhang,
Kunming University of Science and Technology, China
Chao Yan,
Nanjing University, China

***Correspondence:**
Wei-Lin Jin
weilinjin@yahoo.com;
weilinjin@sjtu.edu.cn

[†]*These authors have contributed equally to this work*

Specialty section:
This article was submitted to Cancer Molecular Targets and Therapeutics, a section of the journal Frontiers in Oncology

Received: *24 September 2018*
Accepted: *26 November 2018*
Published: *07 December 2018*

Citation:
Jin M-Z, Xia B-R, Xu Y and Jin W-L (2018) Curaxin CBL0137 Exerts Anticancer Activity via Diverse Mechanisms. Front. Oncol. 8:598. doi: 10.3389/fonc.2018.00598

INTRODUCTION

Cancer harbors several characteristics, including high heterogeneity, diverse gene mutation, or rapid progression; consequently, treating cancer is difficult, and it easily relapses. Remarkable achievements have been observed in treatment approaches, including surgery, radiotherapy, chemotherapy, immunotherapy, and targeted therapy. In particular, targeted therapies, such as HER2 inhibitor lapatinib, EGFR inhibitor erlotinib, BRAF inhibitor dabrafenib, promote treatment (1). However, we have failed to treat cancer. Malignancies, such as glioblastoma, are quite invasive and cannot be entirely removed by surgery. Chemotherapy is hindered by innate and acquired chemoresistance.

Originally, antimalarial agents, including quinacrine, can activate p53 and inhibit nuclear factor-κB (NF-κB) simultaneously (2, 3). These drugs have been used as a reference of curaxins, undergoing some structural changes but maintaining similar functions (2, 4). As a second-generation curaxin, CBL0137 satisfies the requirements for a drug design, that is, full efficacy while inducing the least adverse effects. Further research suggested that CBL0137 exerts an antitumor activity through multiple targets, including facilitates chromatin transcription (FACT), NOTCH1, and heat shock factor 1 (HSF1), in various cancers (**Table 1**). At present, CBL0137 in patients with hematological malignancies (ClinicalTrials.gov Identifier: NCT02931110) and solid tumors are under phase I clinical trials (ClinicalTrials.gov Identifier: NCT01905228). In this review, we

summarized the design of CBL0137, highlighted its antitumor mechanisms through multiple targets, and proposed its potential for clinical applications, especially as a combination drug.

CBL0137: A SECOND-GENERATION CURAXIN

Small molecular inhibitor CBL0137 [1,1′-(9-(2-(isopropylamino)ethyl)-9H-carbazole-3,6-diyl)bis(ethan-1-one) (IUPAC/chemical name)] is a second-generation curaxin. Dermawan et al. (12) found that quinacrine (CBLC-102), a first-generation curaxin, can overcome erlotinib resistance through preconceived mechanisms in non-small cell lung cancer (12). Similar results are also observed in ovarian (13) and breast (14) cancers. Second-generation curaxins, such as CBLC-000, CBLC-100, and CBLC-137 (CBL0137), have more exact targets than first-generation curaxins, such as quinacrine (CBLC-102). In particular, CBL0137 is water soluble because of its chemical structure and better tolerated in mice than other members of curaxins, showing great potential for cancer treatment (2). In addition to the two targets, namely, p53 and NF-κB, CBL0137 can intercalate DNA through FACT without causing any DNA damage or genotoxicity (2, 7, 15), and more targets are under investigation.

FACT: A CORE TARGET FOR CBL0137

FACT, a histone chaperone, contains two subunits of the suppressor of Ty 16 (SPT16) and structure-specific recognition protein 1 (SSRP1), which participates in DNA replication, transcription, repair, mitosis, and cell fate reprogramming (16–18). SPT16 remodels the histone structure after transcription, and SSRP1 recognizes nucleosomes with its high-mobility group (HMG)-1 domain (19, 20). SSRP1 is considered more like a target since it's more amplified in cancers at mRNA and protein levels. FACT is involved in the poor prognosis, malignant transformation, tumorigenesis, and aggressiveness of cancers (9, 16, 21–23). It can recognize the formation of alternative DNA structures and promote the activation of p53 to prevent DNA damage (24); thus FACT is regarded as a sensor for genome instability and mutation, which is one of the ten hallmarks of cancer treatment (24, 25) (**Figure 1**). It is highly expressed in cancer including glioblastoma (GBM) (6), breast cancer (16), and hepatocellular carcinoma (21), but is poor expressed in normal tissues or well-differentiated cells (26).

CBL0137, chemotherapeutic agents, UV radiation, oxygen-free radicals, and hypoxia stress can affect p53 activation (7, 27, 28). With Western Blot analysis, Gasparian et al. (7) have revealed that CBL0137 activates p53 through posttranslational modifications at serine 392 (Ser^{392}) rather than serine 15 (Ser^{15}), which involves casein kinase 2 (CK2) inhibition (7). Previous studies showed that CK2-induced p53 phosphorylation involves FACT. FACT, SPT16, and SSRP1 subunits, can bind to CK2 after CBL0137 is administered, and the SPT16-SSRP1-CK2 complex phosphorylates p53 at Ser^{392} and promotes p53 activation (2, 27) (**Figure 1**). Activated p53 induces apoptosis, promotes DNA repair, and inhibits tumor growth. Extensive evidence has also demonstrated that FACT can promote tumor growth, inhibit apoptosis or cell differentiation and induce cell proliferations through the regulation of multiple genes including TP53, MYC, NF-κB, OCT1, and HSF1 (23) (**Figure 1**).

FACT has recently been reported to correlate with the expression of cancer stem cell (CSC) markers, such as SOX2, OCT4, OLIG2, and NANOG in an adult GBM model. The transcriptional knockdown of FACT or its inhibition with a small molecule (CBL0137) reduces the expression of these genes (5).

CBL0137 EXERTS ANTITUMOR ACTIVITY BY INCREASING P53 AND DECREASING NF-κB SIMULTANEOUSLY

p53 is a classic tumor suppressor protein responsible for the prevention of oncogenic mutation accumulation, tumorigenesis and tumor progression (29). p53 mutation or inactivation is quite common in many cancers (30). p53 activities are regulated by diverse post-translational modifications such as Ser^{15} and Ser^{392} phosphorylation or lysine 382 acetylation and methylation (7, 31). NF-κB is a critical transcription factor in antiapoptosis and cell proliferation, which is activated in inflammation and cancers (32). CBL0137 is originally designed to activate p53 and inhibit NF-κB simultaneously to achieve an enhanced efficacy with modest toxicity (7).

The *in vitro* and *in vivo* experiments of CBL0137 have confirmed the issue. For example, a research on renal cell carcinoma has suggested that CBL0137 intercalates DNA and traps FACT, thereby leading to NF-κB inhibition. FACT binds to CK2 to form a complex, which further induces Ser^{392} phosphorylation of p53; otherwise, p53 is degraded by MDM2 (2, 7, 33) (**Figure 1**). Meanwhile, NF-κB is inhibited by the complex (6). Similar results have been shown in GBM research, temozolomide (TMZ)-resistant A1207, TMZ-responsive U87MG cell lines, and orthotopic model. CBL0137 prolongs the survival of orthotopic A1207 and U87MG models, though it is less effective than TMZ in the latter. Furthermore, 0.6 and 2.0 μM CBL0137 can increase p53 significantly in cell lines. These studies have exhibited the antitumor activity of CBL0137 by targeting p53 and NF-κB, which are the two most common transcription factors in oncogenic and tumor suppressor pathways.

CBL0137 INHIBITS THE SELF-RENEWAL OF CANCER STEM CELLS/TUMOR-INITIATING CELLS THROUGH NOTCH1 ACTIVATION

Therapeutic resistance is a complex phenomenon in cancer treatment, though many mechanisms have been proposed. "The bad seed" CSCs can explain the consequence to some degree (34). Conventional therapies that do not target CSCs may encounter cancer recurrence because CSCs can undergo self-renewal and differentiation (35). Dermawan et al. investigated CBL0137 in GBM and focused on cancer stem-like cells by using CD133 as

TABLE 1 | Targets and induced effects of CBL0137 reported in cancer research.

Indications	Targets	Effects	Experiment models	References
Glioblastoma	SSRP1↓ SOX2↓ OCT4↓ NANOG↓ OLIG2↓ CD133↓	Inhibited proliferation of patient-derived tumor cells	Cell lines Orthotopic mouse models	(5)
Glioblastoma (2)	FACT↓ p53↑ NF-κB↓	Induced Apoptosis and inhibited proliferation Increased survival of TMZ-responsive and -resistant GBM	Cell lines Orthotopic mouse models	(6)
Renal cell carcinoma	p53↑ NF-κB↓	Induced death of tumor cells through FACT with no DNA damage	Cell lines PDX mouse models	(7)
Melanoma	p53↑ NF-κB↓ HSF1↓	Enhanced anti-tumor activity by inhibiting heat shock responses of tumor cells	Cell lines Orthotopic mouse models	(8)
Neuroblastoma	MYCN↓	Reduced tumor initiation and progression	Cell lines TH-MYCN transgenic mouse models	(9)
Neuroblastoma (2)	SSRP1↓ SPT16↓ MYCN↓	Inhibited neuroblastoma cell growth	MYCN transgenic zebrafish	(10)
Small cell lung cancer	NOTCH1↑	Reduced the tumor cell growth Preferentially kills tumor-initiating cells	Cell lines PDX mouse models	(11)

PDX, patient-derived xenograft.

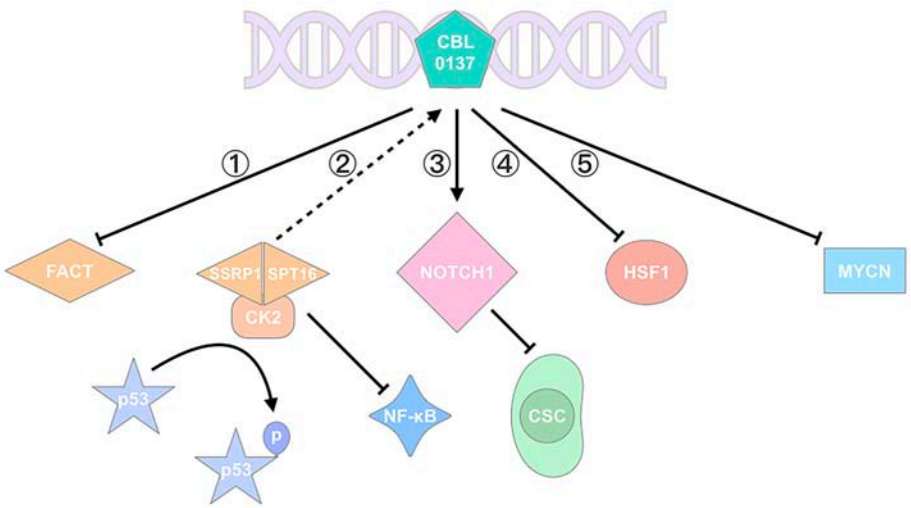

FIGURE 1 | CBL0137 exhibits its antitumor activity via multiple pathways. (1) CBL0137 can target SPT16 and SSRP1, the two subunits of FACT; (2) CBL0137 can induce p53 activation by phosphorylation and NF-κB inhibition, depending on the formation of SPT16-SSRP1-CK2 complex; (3) CBL0137 can reduce the self-renewal of CSCs through NOTCH1 signaling pathway activation; (4) CBL0137 can decrease HSF1 transcription level; (5) CBL0137 can downregulate MYCN expression.

a marker (5). CBL0137 accumulates in brain tissues in orthotopic mouse models, suggesting that it can penetrate the blood brain barrier; oral intake *ad libitum* can also achieve its efficacy. CBL0137 prefers to inhibit CD133+ tumor cell growth with the help of FACT, which is higher in CSCs than non-stem tumor cells. CBL0137 treatment decreases the expression of CD133 and the self-renewal of CSCs, increases asymmetric cell division, prevents tumor initiation and prolongs the survival of tumor-bearing animals (5). A similar consequence has been demonstrated in small cell lung cancer (SCLC) and pancreatic cancer (11, 36). Tumor-initiating cells (TICs) represent those with stemness. CBL0137 preferentially reduces $CD133^{high}$ and $CD44^{high}$ cells (TICs) over $CD133^{low}$ and $CD44^{low}$ (non-TICs) and attenuate the self-renewal of TICs (11).

The stemness of CSCs is well-modulated by stem-cell factors including p53, NF-κB, Sox2, Bmi1, c-Myc, and NOTCH1 (35, 37). Therefore, drugs should target CSCs and CSC-related factors. NOTCH signaling pathway plays a role in oncogenesis, angiogenesis and CSC maintenance (38). It exhibits oncogenic and suppressive roles in different cancers (11). NOTCH1, as a member of the NOTCH family, increases apoptosis and inhibits cell proliferation in SCLC (11). CBL0137 treatment in SCLC prevents SP3 binding to the NOTCH1 promoter, decreases achaete-scute homolog-1 (ASCL1) expression, increases the mRNA expression of NOTCH1, and inhibits CSC renewal. The expression levels of ASCL1 and SP3 are higher in TICs than non-TICs, negatively modulating NOTCH1. Therefore, the tendency of CBL0137 killing TICs may be a result of FACT and NOTCH1, though whether CBL0137 targeting NOTCH1 acts through FACT is unclear in this research (11). CBL0137 can activate NOTCH1 and inhibit the self-renewal of CSCs/TICs (5, 11, 36), thereby facilitating the enhanced prevention of therapeutic resistance and tumor progression.

HSF1 IS INVOLVED IN THE ANTIMELANOMA EFFECT OF CBL0137

Regional chemotherapy via isolated limb perfusion (ILP) is recommended for patients with in-transit extremity melanoma in which mild hyperthermia (42°C compared with 37°C) is adopted, thereby improving drug uptake by tumor cells (8). CBL0137 was then tested for potential use as a regional chemotherapeutic agent on B16 melanoma cell line and tumor-bearing mice. CBL0137 treatment by ILP reduces SSRP1 expression, suppresses HSF1/hsp70 transcription, and causes tumor cell death, and its efficacy can be improved by hyperthermia. Conversely, CBL0137 can downregulate HSF1 to inhibit heat shock responses brought by hyperthermia, thereby increasing tumor cell apoptosis. However, treatment of traditional melphalan had no statistically significant differences between 42 and 37°C. Moreover, the linkage of the ILP drug melphalan can be highly toxic and cause death. By contrast, even 0.1 mg of CBL0137 establishes a strong antitumor activity, suggesting its leakage causes minimal side effects (8). These results explain the antitumor mechanism of CBL0137 from the perspective of hyperthermia and HSF1, suggesting that CBL0137 can be considered as a promising candidate for ILP drug to treat melanoma.

MYCN IN NEUROBLASTOMA: A POTENTIAL INDICATOR OF CBL0137 SENSITIVITY

Approximately 20% of patients with neuroblastoma encounter MYCN amplification, which is a predictor of poor prognosis (9, 39). Considering that the expression of FACT and MYCN is closely related and high in precancerous TH-MYCN$^{+/+}$ neuroblasts, Carter et al. (9) treated TH-MYCN$^{+/+}$ and TH-MYCN$^{+/-}$ mice with CBL0137, which is regarded as the inhibitor of FACT. CBL0137 can downregulate FACT and MYCN expression and inhibit MYCN-driven tumor initiation and progression in MYCN mice and xenografts. In tumor-bearing zebrafish, CBL0137 elicits an inhibitory effect on neuroblastoma (10). Moreover, high-MYCN-expressing cell lines, such as SH-SY5Y and BE(2)C, require a lower IC_{50} of CBL0137 than those expressing normal or relatively low MYCN, suggesting that MYCN expression may be applied to evaluate CBL0137 sensitivity, though further investigation is needed (9).

COMBINATION APPROACH OF CBL0137: THE WAY TO GO

The initial goal of scientists from Clevel and BioLabs Inc. in designing curaxins is to regulate p53 and NF-κB (2). After the "target multiplier" FACT is introduced, the understanding of curaxins has improved. CBL0137 can reduce CSC populations and their stemness (5, 11, 36), which show its promising clinical prospect combined with standard treatment strategies.

The cisplatin resistance of SCLC is likely caused by CSCs. In this research, the combination of CBL0137 and cisplatin at a 1:1 molar ratio remarkably inhibits SCLC tumor growth in H82 xenograft (11). Drug combination delays tumor growth for 30 days and prolongs tumor-bearing mice survival for more than 10 days (11). FACT plays an important role in DNA repair; thus, researchers believed that these results may be due to FACT and its ability to inhibit DNA repair, though this hypothesis has yet to be further investigated (11). However, this hypothesis is partially confirmed in neuroblastoma. Combined with cisplatin, cyclophosphamide, etoposide, or vincristine, CBL0137 can inhibit DNA repair after a double-strand break occurs without genotoxicity. DNA damage markers remarkably increase after etoposide and CBL0137 are administered. The results showed that the effects of CBL0137 are observed in DNA synthesis inhibitors, such as hydroxyurea, rather than microtubule poisons, such as hydroxyurea (9). Another research has shown that the combination of CBL0137 and TMZ does not significantly affect GBM. Combination therapy surpasses CBL0137 monotherapy but not that of TMZ (6). These results are not satisfactory for GBM, but they provide insights into CBL0137 combined with chemotherapy. Further research should be conducted on this area.

Early studies revealed the crosstalk between NF-κB and epidermal growth factor receptor (EGFR), describing them as "partners in cancer" (31, 40–44). In a GBM research, EGFR inhibitor lapatinib and CBL0137 are combined at a 10:1 molar ratio. Lapatinib seldom inhibits CSC growth, which partially explains why it fails to achieve a satisfactory clinical efficacy in GBM treatment (5). The combination of lapatinib and CBL0137 confirms Shostak and Chariot's outlook and presents possibilities for CBL0137 to be applied with targeted therapy.

CONCLUSIONS AND FURTHER DIRECTIONS

Various small molecules, including PRIMA-1, COTI-2, ReACp53, ZMC1, PK7088 (45–51), and CBL0137, target

p53 and have been at preclinical and clinical stages. CBL0137 has a broad antitumor activity in a wide range of cancers, other than targeting p53 (7). CBL0137 can be considered as a candidate for monotherapy and applied to enhance the effectiveness of chemotherapy and targeted therapy, giving it more potential and clinical significance.

However, some concerns still exist. Tumor suppressor protein p53 is important in the oncogenic pathway, and almost 50% of cancers possess mutated or depleted p53; thus, resistance likely exists when one path is blocked. *In vitro* data have also shown that p53-wild type cells are slightly more susceptible to curaxins, including CBL0137-induced cell death, than p53-null cells (7). Discovering how CBL0137 works on those cancers is quite important; in addition, the effect of CBL0137 on the immune system is unknown, and further data support should be obtained to determine whether CBL0137 can synergize with immunotherapy to provide an enhanced efficacy. Further studies on these areas may lead to an in-depth understanding of the mechanism and application of CBL0137.

AUTHOR CONTRIBUTIONS

M-ZJ and B-RX conceived, wrote the manuscript, and completed the figure/table. YX contributed to the writing. W-LJ conceived, organized, and edited the text.

ACKNOWLEDGMENTS

We apologize to those colleagues whose important work could not be cited due to space constraints. This work was in part supported by the 12th undergraduate training programs for innovation of Shanghai Jiao Tong University School of Medicine (No. 1218201), National Natural Science Foundation of China (No. 81872430), the National Key Research and Development Program of China (No. 2017FYA0205302).

REFERENCES

1. Hughes PE, Caenepeel S, Wu LC. Targeted therapy and checkpoint immunotherapy combinations for the treatment of cancer. *Trends Immunol*. (2016) 37:462–76. doi: 10.1016/j.it.2016.04.010
2. Di Bussolo V, Minutolo F. Curaxins: a new family of non-genotoxic multitargeted anticancer agents. *ChemMedChem* (2011) 6:2133–6. doi: 10.1002/cmdc.201100476
3. Maluchenko NV, Chang HW, Kozinova MT, Valieva ME, Gerasimova NS, Kitashov AV, et al. Inhibiting the pro-tumor and transcription factor FACT: Mechanisms. *Mol Biol.* (2016) 50:599–610. doi: 10.1134/S0026893316040087
4. Gurova KV, Hill JE, Guo C, Prokvolit A, Burdelya LG, Samoylova E, et al. Small molecules that reactivate p53 in renal cell carcinoma reveal a NF-kappaB-dependent mechanism of p53 suppression in tumors. *Proc Natl Acad Sci USA*. (2005) 102:17448–53. doi: 10.1073/pnas.0508888102
5. Dermawan JK, Hitomi M, Silver DJ, Wu Q, Sandlesh P, Sloan AE, et al. Pharmacological targeting of the histone chaperone complex FACT preferentially eliminates glioblastoma stem cells and prolongs survival in preclinical models. *Cancer Res*. (2016) 76:2432–42. doi: 10.1158/0008-5472.CAN-15-2162
6. Barone TA, Burkhart CA, Safina A, Haderski G, Gurova KV, Purmal AA, et al. Anticancer drug candidate CBL0137, which inhibits histone chaperone FACT, is efficacious in preclinical orthotopic models of temozolomide-responsive and -resistant glioblastoma. *Neuro Oncol*. (2017) 19:186–96. doi: 10.1093/neuonc/now141
7. Gasparian AV, Burkhart CA, Purmal AA, Brodsky L, Pal M, Saranadasa M, et al. Curaxins: anticancer compounds that simultaneously suppress NF-kappaB and activate p53 by targeting FACT. *Sci Transl Med*. (2011) 3:95ra74. doi: 10.1126/scitranslmed.3002530
8. Kim M, Neznanov N, Wilfong CD, Fleyshman DI, Purmal AA, Haderski G, et al. Preclinical validation of a single-treatment infusion modality that can eradicate extremity melanomas. *Cancer Res*. (2016) 76:6620–30. doi: 10.1158/0008-5472.CAN-15-2764
9. Carter DR, Murray J, Cheung BB, Gamble L, Koach J, Tsang J, et al. Therapeutic targeting of the MYC signal by inhibition of histone chaperone FACT in neuroblastoma. *Sci Transl Med*. (2015) 7:312ra176. doi: 10.1126/scitranslmed.aab1803
10. Zhang X, Dong Z, Zhang C, Ung CY, He S, Tao T, et al. Critical role for GAB2 in neuroblastoma pathogenesis through the promotion of SHP2/MYCN cooperation. *Cell Rep*. (2017) 18:2932–42. doi: 10.1016/j.celrep.2017.02.065
11. De S, Lindner DJ, Coleman CJ, Wildey G, Dowlati A, Stark GR. The FACT inhibitor CBL0137 synergizes with cisplatin in small-cell lung cancer by increasing NOTCH1 expression and targeting tumor-initiating cells. *Cancer Res*. (2018) 78:2396–406. doi: 10.1158/0008-5472.CAN-17-1920
12. Dermawan JK, Gurova K, Pink J, Dowlati A, De S, Narla G, et al. Quinacrine overcomes resistance to erlotinib by inhibiting FACT, NF-kappaB, and cell-cycle progression in non-small cell lung cancer. *Mol Cancer Ther*. (2014) 13:2203–14. doi: 10.1158/1535-7163.MCT-14-0013
13. Khurana A, Roy D, Kalogera E, Mondal S, Wen X, He X, et al. Quinacrine promotes autophagic cell death and chemosensitivity in ovarian cancer and attenuates tumor growth. *Oncotarget* (2015) 6:36354–69. doi: 10.18632/oncotarget.5632
14. Preet R, Mohapatra P, Mohanty S, Sahu SK, Choudhuri T, Wyatt MD, et al. Quinacrine has anticancer activity in breast cancer cells through inhibition of topoisomerase activity. *Int J Cancer* (2012) 130:1660–70. doi: 10.1002/ijc.26158
15. Nesher E, Safina A, Aljahdali I, Portwood S, Wang ES, Koman I, et al. Role of chromatin damage and chromatin trapping of FACT in mediating the anticancer cytotoxicity of DNA-binding small-molecule drugs. *Cancer Res*. (2018) 78:1431–43. doi: 10.1158/0008-5472.CAN-17-2690
16. Fleyshman D, Prendergast L, Safina A, Paszkiewicz G, Commane M, Morgan K, et al. Level of FACT defines the transcriptional landscape and aggressive phenotype of breast cancer cells. *Oncotarget* (2017) 8:20525–42. doi: 10.18632/oncotarget.15656
17. Belotserkovskaya R, Saunders A, Lis JT, Reinberg D. Transcription through chromatin: understanding a complex FACT. *Biochim Biophys Acta* (2004) 1677:87–99. doi: 10.1016/j.bbaexp.2003.09.017
18. Kolundzic E, Ofenbauer A, Bulut SI, Uyar B, Baytek G, Sommermeier A, et al. FACT sets a barrier for cell fate reprogramming in caenorhabditis elegans and human cells. *Dev Cell* (2018) 46:611–26.e12. doi: 10.1016/j.devcel.2018.07.006
19. Draetta GF, Depinho RA. Cancer drug discovery faces the FACT. *Sci Transl Med*. (2011) 3:95ps34. doi: 10.1126/scitranslmed.3002822
20. Bondarenko MT, Maluchenko NV, Valieva ME, Gerasimova NS, Kulaeva OI, Georgiev PG, et al. Structure and function of histone chaperone FACT. *Mol Biol*. (2015) 49:891–904. doi: 10.1134/S0026893315060023
21. Ding Q, He K, Luo T, Deng Y, Wang H, Liu H, et al. SSRP1 contributes to the malignancy of hepatocellular carcinoma and is negatively regulated by miR-497. *Mol Ther*. (2016) 24:903–14. doi: 10.1038/mt.2016.9
22. Koman IE, Commane M, Paszkiewicz G, Hoonjan B, Pal S, Safina A, et al. Targeting FACT complex suppresses mammary tumorigenesis in Her2/neu transgenic mice. *Cancer Prev Res.* (2012) 5:1025–35. doi: 10.1158/1940-6207.CAPR-11-0529
23. Garcia H, Miecznikowski JC, Safina A, Commane M, Ruusulehto A, Kilpinen S, et al. Facilitates chromatin transcription complex is an "accelerator" of tumor transformation and potential marker and target of aggressive cancers. *Cell Rep*. (2013) 4:159–73. doi: 10.1016/j.celrep.2013.06.013

24. Hanahan D, Weinberg RA. Hallmarks of cancer: the next generation. *Cell* (2011) 144:646–74. doi: 10.1016/j.cell.2011.02.013
25. Safina A, Cheney P, Pal M, Brodsky L, Ivanov A, Kirsanov K, et al. FACT is a sensor of DNA torsional stress in eukaryotic cells. *Nucleic Acids Res*. (2017) 45:1925–45. doi: 10.1093/nar/gkw1366
26. Garcia H, Fleyshman D, Kolesnikova K, Safina A, Commane M, Paszkiewicz G, et al. Expression of FACT in mammalian tissues suggests its role in maintaining of undifferentiated state of cells. *Oncotarget* (2011) 2:783–96. doi: 10.18632/oncotarget.340
27. Keller DM, Lu H. p53 serine 392 phosphorylation increases after UV through induction of the assembly of the CK2.hSPT16.SSRP1 complex. *J Biol Chem*. (2002) 277:50206–13. doi: 10.1074/jbc.M209820200
28. Keller DM, Zeng X, Wang Y, Zhang QH, Kapoor M, Shu H, et al. A DNA damage-induced p53 serine 392 kinase complex contains CK2, hSpt16, and SSRP1. *Mol Cell* (2001) 7:283–92. doi: 10.1016/S1097-2765(01)00176-9
29. Kastenhuber ER, Lowe SW. Putting p53 in context. *Cell* (2017) 170:1062–78. doi: 10.1016/j.cell.2017.08.028
30. Cancer Genome Atlas Research N. Comprehensive genomic characterization defines human glioblastoma genes and core pathways. *Nature* (2008) 455:1061–8. doi: 10.1038/nature07385
31. Shi X, Kachirskaia I, Yamaguchi H, West LE, Wen H, Wang EW, et al. Modulation of p53 function by SET8-mediated methylation at lysine 382. *Mol Cell* (2007) 27:636–46. doi: 10.1016/j.molcel.2007.07.012
32. Perkins ND. The diverse and complex roles of NF-kappaB subunits in cancer. *Nat Rev Cancer* (2012) 12:121–32. doi: 10.1038/nrc3204
33. Bykov VJN, Eriksson SE, Bianchi J, Wiman KG. Targeting mutant p53 for efficient cancer therapy. *Nat Rev Cancer* (2018) 18:89–102. doi: 10.1038/nrc.2017.109
34. Colak S, Medema JP. Cancer stem cells–important players in tumor therapy resistance. *FEBS J*. (2014) 281:4779–91. doi: 10.1111/febs.13023
35. Qiu GZ, Sun W, Jin MZ, Lin J, Lu PG, Jin WL. The bad seed gardener: deubiquitinases in the cancer stem-cell signaling network and therapeutic resistance. *Pharmacol Ther*. (2017) 172:127–38. doi: 10.1016/j.pharmthera.2016.12.003
36. Burkhart C, Fleyshman D, Kohrn R, Commane M, Garrigan J, Kurbatov V, et al. Curaxin CBL0137 eradicates drug resistant cancer stem cells and potentiates efficacy of gemcitabine in preclinical models of pancreatic cancer. *Oncotarget* (2014) 5:11038–53. doi: 10.18632/oncotarget.2701
37. Shetzer Y, Solomon H, Koifman G, Molchadsky A, Horesh S, Rotter V. The paradigm of mutant p53-expressing cancer stem cells and drug resistance. *Carcinogenesis* (2014) 35:1196–208. doi: 10.1093/carcin/bgu073
38. Takebe N, Nguyen D, Yang SX. Targeting notch signaling pathway in cancer: clinical development advances and challenges. *Pharmacol Ther*. (2014) 141:140–9. doi: 10.1016/j.pharmthera.2013.09.005
39. Danovi S. Neuroblastoma: as a matter of FACT. *Nat Rev Cancer* (2016) 16:2. doi: 10.1038/nrc.2015.11
40. Shostak K, Chariot A. EGFR and NF-kappaB: partners in cancer. *Trends Mol Med*. (2015) 21:385–93. doi: 10.1016/j.molmed.2015.04.001
41. Yang W, Xia Y, Cao Y, Zheng Y, Bu W, Zhang L, et al. EGFR-induced and PKCepsilon monoubiquitylation-dependent NF-kappaB activation upregulates PKM2 expression and promotes tumorigenesis. *Mol Cell* (2012) 48:771–84. doi: 10.1016/j.molcel.2012.09.028
42. Le Page C, Koumakpayi IH, Lessard L, Mes-Masson AM, Saad F. EGFR and Her-2 regulate the constitutive activation of NF-kappaB in PC-3 prostate cancer cells. *Prostate* (2005) 65:130–40. doi: 10.1002/pros.20234
43. Biswas DK, Cruz AP, Gansberger E, Pardee AB. Epidermal growth factor-induced nuclear factor kappa B activation: a major pathway of cell-cycle progression in estrogen-receptor negative breast cancer cells. *Proc Natl Acad Sci USA*. (2000) 97:8542–7. doi: 10.1073/pnas.97.15.8542
44. Sun L, Carpenter G. Epidermal growth factor activation of NF-kappaB is mediated through IkappaBalpha degradation and intracellular free calcium. *Oncogene* (1998) 16:2095–102. doi: 10.1038/sj.onc.1201731
45. Bykov VJ, Issaeva N, Shilov A, Hultcrantz M, Pugacheva E, Chumakov P, et al. Restoration of the tumor suppressor function to mutant p53 by a low-molecular-weight compound. *Nat Med*. (2002).8:282–8. doi: 10.1038/nm0302-282
46. Salim KY, MalekiVareki S, Danter WR, Koropatnick J. COTI-2, a novel small molecule that is active against multiple human cancer cell lines *in vitro* and *in vivo*. *Oncotarget* (2016) 7:41363–79. doi: 10.18632/oncotarget.9133
47. Soragni A, Janzen DM, Johnson LM, Lindgren AG, Thai-Quynh Nguyen A, Tiourin E, et al. A designed inhibitor of p53 aggregation rescues p53 tumor suppression in ovarian carcinomas. *Cancer Cell* (2016). 29:90–103. doi: 10.1016/j.ccell.2015.12.002
48. Yu X, Vazquez A, Levine AJ, Carpizo DR. Allele-specific p53 mutant reactivation. *Cancer Cell* (2012) 21:614–25. doi: 10.1016/j.ccr.2012.03.042
49. Liu X, Wilcken R, Joerger AC, Chuckowree IS, Amin J, Spencer J, et al. Small molecule induced reactivation of mutant p53 in cancer cells. *Nucleic Acids Res*. (2013). 41:6034–44. doi: 10.1093/nar/gkt305
50. Duffy MJ, Synnott NC, Crown J. Mutant p53 as a target for cancer treatment. *Eur J Cancer* (2017) 83:258–65. doi: 10.1016/j.ejca.2017.06.023
51. Levine AJ. Targeting therapies for the p53 protein in cancer treatments. *Ann Rev Cancer Biol*. (2019) 3:1. doi: 10.1146/annurev-cancerbio-030518-055455

Conflict of Interest Statement: The authors declare that the research was conducted in the absence of any commercial or financial relationships that could be construed as a potential conflict of interest.

frontiers in Oncology

REVIEW
published: 12 December 2018
doi: 10.3389/fonc.2018.00608

CDK 4/6 Inhibitors as Single Agent in Advanced Solid Tumors

Francesco Schettini[1†], Irene De Santo[1†], Carmen G. Rea[1], Pietro De Placido[1], Luigi Formisano[1], Mario Giuliano[1,2], Grazia Arpino[1], Michelino De Laurentiis[3], Fabio Puglisi[4,5], Sabino De Placido[1‡] and Lucia Del Mastro[6,7‡]*

[1] University of Naples Federico II, Naples, Italy, [2] Baylor College of Medicine, Houston, TX, United States, [3] Istituto Nazionale Tumori Fondazione G. Pascale, Naples, Italy, [4] Department of Medicine, University of Udine, Udine, Italy, [5] IRCCS Centro di Riferimento Oncologico Aviano, Aviano, Italy, [6] Policlinico San Martino-IST, Genova, Italy, [7] University of Genova, Genova, Italy

Cyclin-dependent kinases (CDK) 4/6 inhibitors, namely abemaciclib, palbociclib, and ribociclib, interfere with cell cycle progression, induce cell senescence and might promote cancer cell disruption by a cytotoxic T cells-mediated effect. Phase III randomized clinical trials have proven that CDK4/6 inhibitors (CDK4/6i) in combination with several endocrine agents improve treatment efficacy over endocrine agents alone for hormone receptor positive (HR+) HER2 negative (HER2–) metastatic breast cancer (MBC). Based on such results, these combinations have been approved for clinical use. Preclinical studies in cell cultures and mouse models proved that CDK4/6i are active against a broad spectrum of solid tumors other than breast cancer, including liposarcoma, rhabdomyosarcoma, non-small cell lung cancer, glioblastoma multiforme, esophageal cancer, and melanoma. The role of CDK4/6i in monotherapy in several solid tumors is currently under evaluation in phase I, II, and III trials. Nowadays, abemaciclib is the only of the three inhibitors that has received approval as single agent therapy for pretreated HR+ HER2– MBC. Here we review biological, preclinical and clinical data on the role of CDK4/6 inhibitors as single agents in advanced solid tumors.

Keywords: solid tumors, cyclin-dependent kinases, palbociclib, ribociclib, abemaciclib, cell cycle

OPEN ACCESS

Edited by:
Yunkai Zhang,
Vanderbilt University Medical Center, United States

Reviewed by:
Mao Wang,
Memorial Sloan Kettering Cancer Center, United States
Zhenfang Du,
Vanderbilt University Medical Center, United States
Junyi Li,
University of Pittsburgh, United States

***Correspondence:**
Francesco Schettini
francescoschettini1987@gmail.com

†These authors have contributed equally to this work

‡These authors share co-last authorship

Specialty section:
This article was submitted to Cancer Molecular Targets and Therapeutics, a section of the journal Frontiers in Oncology

Received: *26 October 2018*
Accepted: *28 November 2018*
Published: *12 December 2018*

Citation:
Schettini F, De Santo I, Rea CG, De Placido P, Formisano L, Giuliano M, Arpino G, De Laurentiis M, Puglisi F, De Placido S and Del Mastro L (2018) CDK 4/6 Inhibitors as Single Agent in Advanced Solid Tumors. Front. Oncol. 8:608. doi: 10.3389/fonc.2018.00608

INTRODUCTION

The key role of cyclin-dependent kinases (CDK) and D-type Cyclins (CCND) in cell cycle progression from G1 to S phase was discovered more than 20 years ago (1). Since then, it has been demonstrated that several solid tumors present direct modifications of genes codifying for several proteins involved in CCND-CDK activity and regulation (2). As a result, in recent years, small molecule inhibitors which target this mitogenic pathway have been developed. Three of them are currently available for the treatment of metastatic breast cancer (MBC) in combination with aromatase inhibitors or fulvestrant. This review focuses on the role of CCND-CDK in normal cells, on how this pathway is altered in solid tumors and on the activity of CDK4/6 inhibitors (CDK4/6i), as single agents in the treatment of advanced solid tumors in adult patients.

THE ROLE OF CDK IN CELL CYCLE AND SOLID TUMORS

CCND interact with several CDK, including CDK 4/6, forming functional complexes that phosphorylate and inactivate retinoblastoma protein (pRb) (1). This protein operates a negative control on E2F transcription factors, resulting in an inhibition of cell cycle progression. Indeed, E2F modulates the expression of a broad variety of genes implied in cell cycle S1 phase and mitosis. On the opposite, functional CCND-CDK4/6 complexes allow E2F to be released from pRb control and promote the transition from the G1 to the S phase of the cell cycle (**Figure 1**) (1). Cyclin D is important in growth factor signaling and, more in general, is a common downstream pathway for several mitogenic signaling, including phosphatidylinositol 3-kinase (PI3K)/AKT/mammalian target of rapamycin (mTOR), mitogen-activated protein kinase (MAPK), wnt/beta-catenin, janus kinase (JAK)-signal transducer and activator of transcription (STAT), nuclear factor kappa-light-chain-enhancer of activated B cells (NF-kB), and steroid hormone signaling pathways (e.g., estrogen, progesterone, and androgen) (**Figure 1**) (2). CDK 4/6 activity is regulated by the INK4 family of proteins. Among them, $p16^{INK4A}$ appears to be the most relevant, in terms of tumor suppression activity. Several other factors, including $p21^{CIP1}$ and $p27^{KIP1}$ modulate CCND-CDK4/6 complexes' activity in a context-dependent manner (2). Finally, the SMARCB1/INI1/SNF5 tumor suppressor gene directly represses the transcription of the Cyclin-D coding gene CCND1 and increases the expression of CCND-CDK4/6 negative regulators $p16^{INK4A}$ and $p21^{CIP1}$ (2).

In solid tumors, an hyperactivation of the CCND-CDK4/6 activity can occur through: (1) increased activity of upstream mitogenic signaling pathways; (2) aberrant activity of the components of the pathway or their regulators. This latter may depend on various molecular mechanisms, i.e., point mutations, translocations or amplification of CDK4/6, amplification of D-type cyclins, deletions that cause the loss of $p16^{INK4A}$ or pRb expression, epigenetic modifications and downregulation of microRNAs (miRNAs) that target CDK4/6. Alterations of the expression of CCND-CDK4/6-INK4-Rb pathway components or of their direct regulators result in cell cycle progression and cell proliferation and represent a key mechanism of tumorigenesis (2). The solid tumors for which the CCND-CDK4/6-INK4-Rb pathway is more frequently deregulated through direct genetic, epigenetic or transcriptional modifications are breast, head and neck, lung, pancreatic, ovarian and bladder cancer, melanoma, endometrial carcinoma, liposarcoma, neuroblastoma, and malignant rabdoid tumors (3–25). Because of their central role in tumorigenesis and progression, CDK4 and 6 might represent a valid therapeutic target for cancer treatment in a broad spectrum of solid tumors.

Abbreviations: CDK4/6, cyclin-dependent kynases 4 and 6; CDK4/6i, CDK4/6 inhibitors; CCND, cyclin D; PI3K, phosphatidylinositol 3-kinase; mTOR, mammalian target of rapamycin; MAPK, mitogen-activated protein kinase; JAK, janus kinase; STAT, signal transducer and activator of transcription; NF-kB, nuclear factor kappa-light-chain-enhancer of activated B cells; miRNAs, microRNAs; pRb, retinoblastoma protein; ET, endocrine therapy; ER+, estrogen receptor positive; HR+, hormone receptor positive; HER2–, human epidermal growth factor receptor 2 negative; MBC, metastatic breast cancer; BC, breast cancer; GBM, glioblastoma multiforme; WD/DDLS, well-differentiated/dedifferentiated liposarcoma; NSCLC, non-small cell lung cancer; SCLC, small cell lung cancer; GIST, gastrointestinal stromal tumors; PDA, pancreatic ductal adenocarcinoma; EAC, esophageal adenocarcinoma; BBB, blood-brain barrier; ORR, overall response rate; PFS, progression-free survival; mPFS, median progression-free survival; TTP, time to progression; DCR, disease control rate; CBR, clinical benefit rate; DLT, dose-limiting toxicity; MTD, maximum tolerated dose; RP2D, recommended phase II dose; ADRs, adverse reactions; SD, stable disease; PR, partial response; CR, complete response; CI, confidence interval; HR, hazard ratio.

CDK 4/6 INHIBITORS: AN OVERVIEW

Mechanism of Action and Toxicities

After the discovery of CDK 4/6 role in tumorigenesis, several CDK inhibitors have been developed for clinical use. The most recent are selective for CDK4 and CDK6, preventing inhibition of other CDKs activity (1). Three CDK4/6i are currently approved in clinical practice, namely: palbociclib, ribociclib, and abemaciclib. Their mechanism of action is based on the binding to CDK 4 and 6 ATP pocket, which leads to a substantial inactivation of CCND-CDK4/6 complexes, with a subsequent increase in the activity of pRb. The logic consequence is a G1 phase arrest (**Figure 2**). The interference with cell cycle progression results in an increased apoptosis phenomena in tumor cells (1, 2).

Palbociclib and ribociclib are similar in chemical structure, while abemaciclib differs and has a higher CDK4/6 binding power than the other two CDK4/6i. More specifically, abemaciclib shows higher selectivity for the complex CDK4/cyclin D1 compared to the other two compounds, and is 14 times more potent against CDK4 than CDK6 (2, 26). Cell cycle arrest and subsequent apoptosis are sought to be the most relevant mechanism of action of CDK4/6i. However, a very recent study based on mouse models of breast cancer and other solid tumors and on a confirmatory trascriptomic analysis of serial biopsies from a clinical trial involving CDK4/6i in breast cancer, showed that CDK4/6 inhibition might also induce a broad spectrum of immunologic events. More precisely, they seem to increase the antigen presenting capability of tumor cells, while concurrently reducing the immunosuppressive population of T regulator lymphocytes. This could in turn enhance the activation of cytotoxic T cells, which ultimately kill tumor cells (27). However, immunologic effects of CDK4/6i are still object of debate and need further validation/confirmation. Despite a very similar mechanism of action, dose limiting toxicities (DLTs) observed in phase I trials differed, with neutropenia being the DLT for palbociclib, diarrhea and fatigue for abemaciclib, and neutropenia, mucositis, asymptomatic thrombocytopenia, pulmonary embolism, increased creatinine, hyponatriemia, and QTcF prolongation for ribociclib (2, 28). Some of the latter toxicities (such as creatinine increase or thromboembolic events) were also reported for abemaciclib however they did not represent formal DLTs in phase I trials. The most common CDK4/6i toxicities of any grade observed in pivotal phase III trials were neutropenia, leukopenia, fatigue and

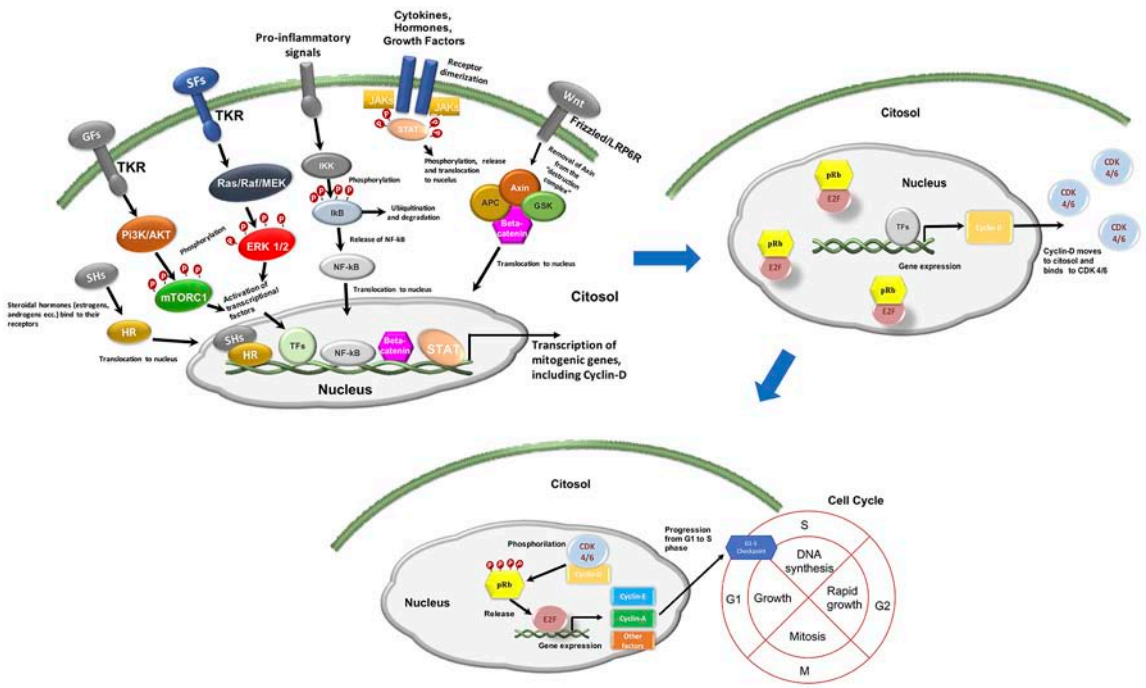

FIGURE 1 | Mitogenic signaling and cell cycle progression. GFs, growth factors; TKR, tyrosine kinase receptor; SFs, survival factors; HR, hormone receptor; SHs, steroidal hormones (i.e., estrogens, androgens); TFs, transcriptional factors.

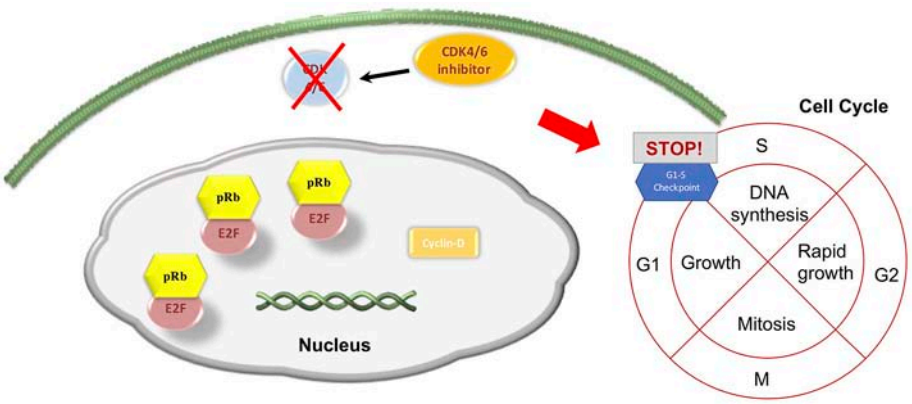

FIGURE 2 | CDK4/6 inhibitors' main effect on cell cycle progression.

nausea for palbociclib (29, 30), neutropenia, nausea, infections, fatigue and diarrhea for ribociclib (31, 32), creatinine increase, diarrhea, fatigue, and neutropenia for abemaciclib (33, 34). The pathophysiology of such toxicities has mostly to be linked to CDK4/6i mechanism of action. Additionally, abemaciclib-induced creatinine increase, might be due to its competitive inhibition of efflux transporters of creatinine (26). A comparison between main pharmacokinetic and pharmacodynamic properties among the three molecules is reported in **Table 1**. All of the three molecules are orally administered and are metabolized by the liver. Palbociclib and ribociclib, due to longer half-life than abemaciclib, can be administered once daily, while abemaciclib needs twice daily administration.

Current Indications

The three inhibitors are currently available for the treatment of hormone receptor positive (HR+) Human Epidermal Growth Factor Receptor 2 negative (HER2–) MBC in combination with an aromatase inhibitor (AI) as first-line endocrine therapy or in combination with fulvestrant in pretreated patients. All of these combinations substantially doubled the comparator in terms of median progression-free survival (PFS) (29–34). Moreover, ribociclib was also studied in combination with tamoxifen or AIs

TABLE 1 | CDK 4/6 inhibitors' pharmacological characteristics.

Drug properties	CDK 4/6 inhibitors		
	Palbociclib	**Ribociclib**	**Abemaciclib**
Bioavailability (35)	46%	Unknown	45%
Protein binding (35)	85%	∼70%	96.3%
Metabolism (35)	Liver	Liver	Liver
Elimination half-life (35)	29 (±5) h	32.0 (29.7–54.7) h	18.3 h
Excretion (35)	74% feces, 18% urine	69% feces, 23% urine	81% feces, 3% urine
IC50 (nM) (2)			
➢ CDK4-cyclin D1	11	10	2
➢ CDK6-cyclin D1-2-3	15	39	10
➢ CDK1-cyclin B	>10,000	113,000	1,627
➢ CDK2-cyclin A-E	>10,000	76,000	504
➢ CDK9-cyclin T	NR	NR	57
MTDs (2)	125 mg	900 mg	200 mg every 12 h
DLTs (2)	Neutropenia	Neutropenia, Mucositis, Asymptomatic thrombocytopenia, Pulmonary embolism, Increased creatinine, Hyponatriemia, QTcF prolongation (>500 ms)	Fatigue
Recommended dose (35)	125 mg/die on a 21-on-28-days schedule	600 mg/die on a 21-on-28-days schedule	200 mg twice daily
Administration (35)	Oral	Oral	Oral

and a GnRH analog (GnRHa) in pre-/perimenopausal setting in the context of the MONALEESA 7 phase III trial (36), which enrolled HR+ HER2– MBC in first line setting and results were in line with those published in the other CDK4/6i pivotal trials. Results and characteristics of the pivotal trials, namely PALOMA 2 and 3, MONALEESA 2, 3, and 7, and MONARCH 2 and 3 are reported in **Table 2**.

SINGLE AGENTS CDK4/6I: CURRENT EVIDENCE

As previously reported, the CCND-CDK4/6-INK4-Rb pathway is frequently deregulated through direct genetic, epigenetic or transcriptional modifications in a broad variety of neoplasms (3–25). Indeed, apart from their use in combination with ET for the treatment of HR+ HER2– MBC, CDK4/6i are also under study as single agent in breast cancer (BC) and other solid tumors. The following paragraphs will resume the current preclinical and clinical evidence supporting this experimental treatment strategy.

Preclinical Evidence

Single agent CDK4/6i have shown consistent activity in preclinical models (38–56). In brief, the most relevant results were observed in *in vivo* and/or *in vitro* models of colon cancer (palbociclib, abemaciclib), glioblastoma (palbociclib, abemaciclib), breast cancer (palbociclib, ribociclib, abemaciclib), prostate carcinoma (palbociclib), sarcomas (palbociclib and ribociclib), pancreatic ductal adenocarcinoma (palbociclib), melanoma (palbociclib, ribociclib, abemaciclib), non-small cell lung cancer (palbociclib, abemaciclib), and esophageal adenocarcinoma (abemaciclib).

Palbociclib

A study demonstrated a potent antitumor activity in different mice models, bearing colon cancer, glioblastoma, breast, and prostate carcinoma xenografts. Palbociclib, given as continuous treatment, was able to arrest growth and induce regression of tumor xenografts. A modest activity was also observed in non-small cell lung cancer (NSCLC) models (38). Palbociclib was also able to arrest the growth of estrogen receptor-positive (ER+) BC cell lines (39). A potent antitumor activity was also demonstrated in an *ex vivo* model of human breast tumors (40). Palbociclib activity was demonstrated on cell lines and intracranial xenografts of glioblastoma multiforme (GBM) (41). In the latter case, the proneural subtype appeared to be the most sensitive to palbociclib activity (42). In ovarian cancer cell lines, Palbociclib induces G0/G1 cell cycle arrest by reducing pRb phosphorylation (43). Palbociclib is also effective in arresting cell cycle progression and blocking proliferation in synovial sarcomas cell lines (44). Another study demonstrated that palbociclib may inhibit cellular growth and induce senescence in liposarcoma cell lines and mice xenografts (45) and in sarcoma cell lines (46). An antiproliferative effect was observed also in rhabdomyosarcoma-derived cell cultures (47). Palbociclib was also studied in immunocompromised mice with subcutaneous and intrasplenic injections of pancreatic ductal adenocarcinoma (PDA) cell lines derived from patients' specimens. The CDK 4/6i significantly disrupted extracellular matrix organization and increased quiescence and apoptosis, decreased invasion, metastatic spread and tumor progression (48).

Ribociclib

Ribociclib as single agent is effective in inhibiting cell growth in liposarcoma cell lines. Moreover, the administration to mice bearing human liposarcoma xenografts resulted in tumor growth inhibition and/or tumor regression. A similar effect was noted in preclinical models of breast cancers with intact estrogen receptor and/or activating aberrations of PIK3CA/HER2 (49). In preclinical models, ribociclib also showed some activity in melanomas with activating mutations of BRAF or NRAS (50).

Abemaciclib

Abemaciclib is effective in inducing cell cycle arrest and tumor growth inhibition in colon cancer and breast cancer cell lines and in mice bearing human melanoma and colon cancer xenografts (51, 52). Abemaciclib, similarly to temozolamide, increased survival in a rat xenograft model of glioblastoma

TABLE 2 | Characteristics of pivotal trials concerning CDK4/6 inhibitors approved for clinical practice.

Characteristics	Pivotal trials						
	Paloma 2 (29)	**Paloma 3 (30)**	**Monaleesa 2 (31)**	**Monaleesa 7 (36)**	**Monaleesa 3 (32)**	**Monarch-3 (33)**	**Monarch-2 (34)**
Combination	Palbociclib + letrozole vs. letrozole	Palbociclib + fulvestrant vs. fulvestrant	Ribociclib + letrozole vs. letrozole	Ribociclib + tamoxifen or AI + GnRHa vs. tamoxifen or AI + GnRHa	Ribociclib + fulvestrant vs. fulvestrant	Abemaciclib + NSAI vs. NSAI	Abemaciclib + fulvestrant vs. fulvestrant
Menopausal status	Post-menopausal (iatrogenic or physiologic)	Post-menopausal (iatrogenic or physiologic)	Post-menopausal	Pre- and perimenopausal	Post-menopausal	Post-menopausal (iatrogenic or physiologic)	Post-menopausal (iatrogenic or physiologic)
Setting	1st line HR+ HER2– MBC	≥1st line HR+ HER2– MBC	1st line HR+ HER2– MBC	1st line HR+ HER2– MBC	≥1st line HR+ HER2– MBC	1st line HR+ HER2– MBC	1st line HR+ HER2– MBC
Median PFS (months)	24.8 vs. 14.5	9.5 vs. 4.6	NR vs. 14.7	23.8 vs. 13.0	20.5 vs. 12.8	NR vs. 14.7	16.4 vs. 9.3
PFS HR (95% Cis); *p*-value*	0.58 (0.46–0.72); $p < 0.001$	0.46 (0.36–0.59); $p < 0.0001$	0.56 (0.43–0.72); $p = 3.29 \times 10^{-6}$	0.553 (0.441–0.694); $p < 0.0001$	0.59 (0.48–0.73); $p = 4.10 \times 10^{-7}$	0.543 (0.409–0.723); $p = 0.000021$	0.553 (0.449–0.681); $p = 0.000021$
ORR	42.1 vs. 34.7%	25 vs. 11%	40.7 vs. 27.5%	51 vs. 36%	41 vs. 9%	59.2 vs. 43.8%	48.1 vs. 21.3%
Trial phase	III	III	III	III	III	III	III
FDA/EMA status	A/A	A/A	A/A	A/NA	A/NA	A/A	A/A

**OS data not mature, yet, except for palbociclib + fulvestrant vs. fulvestrant [HR 0.81 (0.64–1.03); p = 0.043] (37).*
NSAI, non-steroidal aromatase inhibitor; AI, aromatase inhibitor; GnRHa, gonadotropin releasing hormone analog; HR+, ER and/or PgR positive; HER2–, human epidermal growth factor receptor 2 negative; A, approved; NA, not yet approved.

(53), thus suggesting a significant capability to cross the blood-brain barrier (BBB). It was also effective on NSCLC tumor xenografts (54). Abemaciclib was also able to inhibit growth of melanoma tumor xenografts and delay tumor recurrence in combination with vemurafenib. Furthermore, abemaciclib yielded tumor growth regression in a vemurafenib-resistant model, and induced apoptotic cell death in a concentration-dependent manner, suggesting that this drug might be a viable therapeutic option to overcome MAPK-mediated resistance to B-RAF inhibitors in B-RAF V600E melanoma (55). Abemaciclib was also evaluated in preclinical models of esophageal adenocarcinoma (EAC): in tumor cell lines it appeared to increased apoptosis and decrease proliferation while in mice models, it was able to decrease of more than 20% tumor volume (56).

Clinical Evidence

The preclinical data reviewed above offered a solid rationale to test single agent CDK4/6i in clinical trials.

Palbociclib: Completed Trials

Palbociclib was tested in a cohort of 41 patients affected by several solid tumors in the context of a phase I dose escalating study. Tumors had been screened for the presence of pRb. In this trial the maximum tolerated dose (MTD) and recommended phase II dose (RP2D) of single-agent palbociclib was 125 mg/day on a 21-of-28 days schedule. The most frequent G3/4 toxicities were neutropenia, leucopenia and anemia with the first present in 20% of cases, the second in 10% and the latter in 7% of cases. Albeit being a phase I trial, clinical activity was also reported. Among 37 evaluable patients, 27% achieved stable disease (SD) for at least 4 cycles and 16% for at least 10 cycles (57).

Several phase II studies tested palbociclib monotherapy in a broad variety of solid tumors, namely well-differentiated or dedifferentiated liposarcoma (WD/DDLS) (58, 59), NSCLC (60), gastric and esophageal cancer (61), urothelial carcinoma (62), epithelial ovarian cancer (63), HR+ and triple negative (TN) BC (64, 65). The best results were observed in WD/DDLS, ovarian and BC, counterbalanced by overall disappointing results in the other neoplasms. The most frequent grade (G)3/4 adverse reactions (ADRs) were hematologic.

More in details, a phase II study explored the activity and safety of palbociclib on a 200 mg/day on a 14-of-21-days schedule in patients with advanced CDK4-amplified WD/DDLS. The trial enrolled 30 patients. The estimated 12-weeks PFS rate was 66%, far exceeding the expected rate of 40% for an active agent. There was only one partial response (PR) and 19 SD at 12 weeks. Median PFS (mPFS) was 17.9 weeks. The most frequent G3/4 ADRs were neutropenia (50%), leukopenia (47%), thrombocytopenia (30%), lymphopenia (27%), and anemia (17%) (58). In a subsequent study, patients affected by advanced WD/DDLS were treated with standard palbociclib 125 mg for 21 days in 28 days-schedule. The trial results showed a successful PFS at 12 weeks of 57.2% [95% Confidence Interval (CI): 42.4–68.8%]. The median PFS was 17.9 weeks (95% CI: 11.9–24.0 weeks). One complete response (CR) was observed. G3/4 ADRs were primarily hematologic and included neutropenia (33%), without neutropenic fever (59). A clinical trial in previously-treated patients with recurrent or metastatic NSCLC was prematurely halted due to lack of objective tumor responses. Half

of evaluable patients achieved SD. The mPFS was 12.5 weeks. One patient experienced G3 transaminitis and unexpected G4 rhabdomyolysis, supposedly due to concomitant use of high-dose simvastatin. Some patients developed G3 or 4 neutropenia, and G3 thrombocytopenia (60). Single agent palbociclib was also not effective in advanced gastric and esophageal tumors, even if the patients had been selected for Rb expression and despite 19/38 tumors showed amplification of CCND1. The median duration of treatment was of 1.7 months, with a maximum of 5.5 months. No objective responses were observed (61). Similarly, palbociclib was not effective in a phase II trial conducted in patients affected by metastatic urothelial carcinoma with both p16 loss and pRb expression (62). A single arm phase II trial in patients with heavily pretreated epithelial ovarian cancer showed a discreet activity and efficacy for palbociclib as single agent. Thirty percent of patients were progression-free at 6 months, with a median PFS of 3.7 months (95% CI: 1.2–6.2). A 4% of PR and a 65% of SD were observed. The toxicity was minimal. Predictive biomarker analyses are ongoing (63). A phase II study of palbociclib as single agent was conducted in patients with metastatic pRb positive BC. The clinical benefit rate (CBR) at 6 months, composed of all complete responses (CR), PR and SD observed as best responses, was 21%, the median PFS were of 4.1 months (95% CI 2.3–7.7) for patients with ER+ HER2– BC, 18.8 months (95% CI: 5.1—NE) for ER+ HER2+ patients and 1.8 months (95% CI: 0.9—NE) for patients with triple negative (TN) tumors, respectively. Neutropenia (50%) and thrombocytopenia (21%) were the most frequent G3/4 toxicities (64). The TREND study, an Italian multicentre open-label phase II trial, compared single agent palbociclib with palbociclib combined with the same ET received prior to disease progression in post-menopausal women with HR+ HER2– MBC. The trial enrolled 115 patients, the primary endpoint was CBR. In both arms, 67% of pts had the study treatment as second line, 33% as third line, and about 1/3 of pts also had received 1 prior chemotherapy for MBC. The CBR was similar in both arms, 54% (95% CI: 42–67%) observed in the combination one, and 60% (95% CI: 48–73%) with palbociclib alone. The Overall Response Rates (ORR), composed of all CR and PR observed as best responses, were 11% (95% CI: 3–19%) and 7% (95% CI: 0.4–13%) with the combination therapy and palbociclib alone, respectively. The trial was not powered to estimate survival endpoints, however exploratory analyses were performed, with no significant differences observed in PFS ($p = 0.13$) and a longer median duration of clinical benefit for the combination than for the single agent [11.5 months, 95% CI: 8.6–17.8 vs. 6 months, 95% CI: 3.9–9.9; Hazard Ratio (HR): 0.31, 95% CI: 0.1–0.7, p-value 0.001]. Overall, however, the primary endpoint did not differ significantly between the 2 study arms, thereby lending support to the potential use of palbociclib as single agent in pretreated patients with HR+ HER2– MBC (65).

Palbociclib: Ongoing Trials

A number of trials are currently ongoing with single agent palbociclib in several advanced solid tumors.

Results are awaited from the NCT03219554 single arm phase II trial that is evaluating the efficacy of single agent palbociclib in patients with recurrent or metastatic advanced thymic epithelial tumors pretreated with one or more cytotoxic chemotherapy. The primary endpoint is PFS (66). The activity and efficacy of single agent palbociclib will be also evaluated in the Lung-MAP trial, a phase II/III biomarker-driven study for second line therapy of squamous cell lung cancer (SCLC). More specifically, single agent palbociclib will be studied in the context of a sub-study that includes all patients that harbored genetic alterations involving cell-cycle genes. The accrual has been completed and results are awaited (67). A phase II study, the NCT01907607—CYCLIGIST, has also already completed accrual and will evaluate the efficacy of single agent palbociclib in patients with gastrointestinal stromal tumors (GIST) refractory to imatinib and sunitinib. The primary endpoint is the non-progression rate at 4 months (68). Results are also awaited for the NCT01356628. This multicenter single arm phase II trial is exploring the efficacy of single agent palbociclib in advanced hepatocellular carcinoma pretreated with standard therapies. The primary endpoint is the time to disease progression (TTP) (69). Another phase II trial, the NCT02806648—PALBONET, is ongoing to demonstrate the safety and activity of palbociclib in subject affected by pNET with overexpression of CDK4, RB1, and CCND1. Results are awaited (70).

Several trials are currently recruiting participants. The NCT02530320 phase II study is ongoing in patients with oligodendroglioma or recurrent anaplastic oligoastrocytoma with preserved pRb activity. The primary end point is the PFS rate at 6 months (71). Another ongoing single arm phase II study (NCT03242382) will evaluate the efficacy of second-line palbociclib in patients with advanced soft tissue sarcomas with CDK4 overexpression. The primary endpoint is the PFS at 6 months (72). The NCT01037790 phase II clinical trial is studying activity, safety and tolerability of single agent palbociclib in preatreated refractory solid tumors, including metastatic colorectal cancer that harbors the Kras or BRAF mutation, metastatic breast cancer, advanced or metastatic esophageal and/or gastric cancer, cisplatin-refractory, unresectable germ cell tumors and any tumor type if tissue tests positive for CCND1 amplification, CDK4/6 mutation, CCND2 amplification or any other functional alteration at the G1/S checkpoint. Co-primary endpoints are the response rates and the safety and tolerability profile. The trial is currently recruiting participants (73).

Finally, a single arm phase II trial (NCT03454919) in acral melanoma bearing alterations in cell cycle pathways, including CDK4 amplification and/or CCND1 amplification and/or P16 (CDKN2A) loss, is going to start but not yet recruiting patients. The primary end point is PFS (74).

Ribociclib: Completed and Ongoing Trials

The initial phase I dose escalation study of single-agent ribociclib enrolled 128 patients with pRb positive advanced solid tumors and lymphomas. The MTD and RP2D were established as 900 and 600 mg/day, respectively, on a 21-of-28-days schedule. The most relevant G3/4 ADRs were neutropenia (27%), leukopenia (17%), fatigue (2%), and nausea (2%). An asymptomatic QTcF prolongation was observable, but mostly with doses ≥600 mg/day (9% of patients at 600 mg/day; 33% at doses >600 mg/day). Response rates were evaluable for 110 patients, though this was

a phase I trial. There were 3 PR and 43 SD as best response; eight patients were progression-free for more than 6 months (75). Results are awaited for an ongoing phase I study (NCT02345824) that will assess tumor pharmacokinetics and efficacy of ribociclib in patients with recurrent glioblastoma or anaplastic glioma (76).

Several phase II trials of single agent ribociclib are currently ongoing. More specifically, the NCT02571829 trial is assessing the efficacy and safety of ribociclib in patients with advanced WD/DDLS. Patients' recruitment has been completed (77). Another trial is ongoing in patients with advanced neuroendocrine tumors of foregut origin progressed after prior systemic therapy. The primary endpoint is the objective response rate (78). The NCT02300987 randomized study is ongoing in patients with relapsed, refractory, incurable teratoma with recent progression from at least 1 prior line of chemotherapy and for which no additional standard surgical or medical therapy exists. This trial will compare ribociclib to placebo. The primary endpoint is PFS. Recruitment has been completed and results are awaited (79). Another phase II single arm study (NCT03096912) assessing efficacy and safety of ribociclib in patients with advanced WD/DDLS is currently recruiting patients. The primary endpoint is the response to therapy after 36 months, as evaluated by RECIST and Choi criteria (80).

Abemaciclib: Completed Trials

Abemaciclib as single agent was investigated in a multicentre phase I study conducted by Patnaik and colleagues. In this study, the 225 enrolled patients were affected by NSCLC, BC, melanoma, colorectal cancer and GBM. The MTD was 200 mg twice daily and the DLT was G3 fatigue. The most relevant G3 ADRs were diarrhea (5%), nausea (4%), fatigue (7%), vomiting (2%), and neutropenia (7%). Activity data were also reported. Fifteen patients experienced SD for at least 4 cycles, with 3 patients achieving SD for 8, 16, and 26 cycles, respectively. One patient with ovarian cancer had a durable and relevant CA125 response. One patient with KRAS mutant NSCLC had a PR. One patient with NRAS mutant melanoma had a confirmed PR. The ORR was 31% for HR+ BC. Moreover, when also considering patients who achieved SD as a best response, 61% of the overall subjects obtained a clinical response lasting at least 6 months (81, 82). A focus on 49 NSCLC patients was also published. The most relevant G3 ADRs were diarrhea (2%), nausea (4%), fatigue (2%), vomiting (2%), and anemia (2%); there were no G4 events. Activity results were also shown. The disease control rate (DCR = CR + PR + SD) was 51% with 1 confirmed PR. The median duration of SD was 5.6 months and the median PFS was 2.1 months. Twenty patients reached at least 4 cycles and 13 reached at least 6 cycles. Among those 49 patients, 19 were affected by KRAS wildtype tumors, 26 by KRAS mutant tumors and 4 with unknown KRAS status. The DCR was 37% for KRAS wildtype and 54% for KRAS mutant NSCLC, consistently with what observed in xenograft studies. The MTD was 200 mg twice daily (83). A randomized phase III study JUNIPER, has compared abemaciclib plus best supportive care to erlotinib plus best supportive care in patients with metastatic NSCLC with a detectable KRAS mutation who have progressed after platinum-based chemotherapy. The primary endpoint was OS and the study failed to show a significant benefit. Moreover, researchers reported a higher-than-expected OS rate in the control group based on historical data (84, 85).

At present, the most relevant trial involving abemaciclib in monotherapy is the MONARCH-1. Such study was a single arm phase II trial in which the efficacy and safety profile of abemaciclib as a single agent were investigated in HR+ HER2– MBC. The 132 enrolled patients had to be progressed on or after prior ET and must have received at least two prior chemotherapy regimens, at least one but no more than two in the metastatic setting. Abemaciclib was administrated at the dose of 200 mg every 12 h on a continuous schedule. The ORR (primary endpoint) was 19.7% (95% CI, 13.3–27.5), the CBR was 42.4%, mPFS was 6 months (95% CI 4.2–7.5) and median overall survival (OS) was 17.7 months (95% CI, 16 to not reached). In this study the most common ADRs were diarrhea, fatigue, nausea, neutropenia, leukopenia, anemia and increased serum creatinine (86). This trial led to the FDA approval of abemaciclib as single therapy in pretreated patients with HR+ HER2– MBC.

Finally, preliminary results from a Simon 2-stage single arm phase II trial in patients affected by HR+ HER2– MBC, NSCLC or melanoma with brain metastases showed a number of brain partial responses that met the predefined threshold for expanding the trial to stage 2. For each patient cerebrospinal fluid concentration of unbound abemaciclib were comparable and consistent with those in the plasma and tumor tissue (87). This trial provided evidence that abemaciclib is able to cross the BBB in human, coherently with preclinical evidence on mice xenografts (53). The second stage is ongoing.

Abemaciclib: Ongoing Trials

Several ongoing trials with single agent abemaciclib have completed patients' recruitment. An asian phase I study (NCT02014129) is evaluating the safety and toxicities of abemaciclib in advanced solid tumors and lymphomas in Japanese participants (88). Abemaciclib is also currently investigated in GBM at first relapse in the NCT02981940 phase II trial. Tumors must be pRb wild type and carry inactivation of CDKN2A/B or C in the tumor by homozygous deletion. The coprimary endpoint are the intratumoral abemaciclib concentration and the 6-months PFS (89). Another phase II trial (active but no more recruiting), the NCT02450539, is evaluating the efficacy of abemaciclib compared to docetaxel in patients with metastatic squamous NSCLC previously treated with platinum-based chemotherapy. The primary endpoint is PFS (90). A phase II ongoing study (NCT02308020), currently recruiting participants, is evaluating the activity and efficacy of abemaciclib in patients with brain metastases secondary to HR+ breast cancer, NSCLC or melanoma. The primary endpoint is the objective intracranial response rate. Preliminary results have been reported in a previous section of this review (87). Other ongoing trials are currently enrolling participants. More specifically, the NCT02919696 phase I trial is studying abemaciclib in native chinese patients with advanced and/or metastatic cancers (91). A phase II trial (NCT03130439) is also investigating the efficacy and activity of abemaciclib in metastatic triple negative breast cancer expressing pRb. The primary endpoint is the ORR

TABLE 3 | Currently ongoing trials on CDK 4/6 inhibitors as single agent in solid tumors.

	CDK4/6 inhibitor	*N*	Phase and setting	Primary endpoint(s)
NCT03123744	Palbociclib	200	Non-randomized Phase II study of palbociclib in adult subjects with recurrent or refractory advanced cancers with aberration(s) in cyclin (CCN/CDK) signaling.	Response rates in subjects with advanced cancer and aberrations of cyclin pathway gene(s) who are treated with palbociclib
NCT02530320	Palbociclib	40	Phase II pilot, prospective, open label, multicenter clinical trial, to evaluate the safety and efficacy of palbociclib, in patients with oligodendroglioma or recurrent oligoastrocytoma anaplastic with the activity of the protein rb preserved	PFS, PFS6m
NCT03454919	Palbociclib	60	Phase II clinical study on efficacy of palbociclib in advanced acral melanoma with cell cycle gene aberrations	ORR, Complete response and partial response
NCT 03242382	Palbociclib	38	Phase II multicenter trial of palbociclib in second line of advanced sarcomas with CDK4 overexpression.	PFS rate
NCT03219554	Palbociclib	33	Phase II single center, open-label, single arm study of palbociclib treatment in patients with recurrent or metastatic advanced thymic epithelial tumor (TET) after failure of one or more cytotoxic chemotherapy regimens	PFS
NCT01907607	Palbociclib	63	Multicentre single-arm phase II study evaluating the efficacy and safety of orally Palbociclib, 125 mg/day, 21 days on/7 days off, in patients with documented disease progression while on therapy with second line sunitinib for unresectable and/or metastatic GIST.	Efficacy, assessed based on 4-months non-progression
NCT01356628	Palbociclib	23	Phase II study of Palbociclib in the treatment of patients with advanced hepatocellular carcinoma (HCC), a type of adenocarcinoma and the most common type of liver tumor.	Time to disease progression
NCT02806648	Palbociclib	21	Phase II trial to assess the activity and safety of Palbociclib in patients with well and moderately differentiated metastatic pancreatic neuroendocrine tumors (pNET)	Response rates
NCT01037790	Palbociclib	205	Phase II trial is studying the side effects and how well PD 0332991 works in treating patients with refractory solid tumors.	Response rates
NCT02345824	Ribociclib	3	Early-phase study to assess tumor pharmacokinetics and efficacy of the cdk4/6 inhibitor Ribociclib in patients with recurrent glioblastoma or anaplastic glioma	Inhibition of CDK4/CDK6 signaling pathway in cell proliferation
NCT03096912	Ribociclib	30	Phase II single arm study assessing efficacy and safety of Ribociclib in patients with advanced well-differentiated or dedifferentiated liposarcoma	Response to therapy as evaluated by RECIST 1.1 Response to therapy as evaluated by Choi [Time Frame: 36 months]
NCT02571829	Ribociclib	30	Phase II single arm study assessing efficacy and safety of Ribociclib in patients with advanced well-differentiated or dedifferentiated liposarcoma	Response to therapy as evaluated by RECIST 1.1 and Choi [Time Frame: 36 months (24 months accrual period and 12 months follow up period)]
NCT02300987	Ribociclib	10	Randomized, blinded, placebo-controlled, phase II trial of LEE011 in patients with relapsed, refractory, incurable teratoma with recent progression.	Progression free survival (PFS) [Time Frame: at 4 months]
NCT02919696	Abemaciclib	20	Phase I study of Abemaciclib in native Chinese patients with advanced and/or metastatic cancers.	Number of Participants with One or More Drug Related Adverse Events Number of participants with one or more drug related adverse events
NCT02014129	Abemaciclib	12	Phase I study of Abemaciclib in Japanese patients with advanced cancer	Number of Participants with LY2835219 Dose-Limiting Toxicities (DLT)
NCT02981940	Abemaciclib	36	Phase II study of Abemaciclib in recurrent glioblastoma	Intratumoral abemaciclib concentration [Time Frame: 2 years] PFS6m
NCT03130439	Abemaciclib	37	Phase II study of Abemaciclib for patients with retinoblastoma-positive, triple negative metastatic breast cancer.	Objective Response Rate [Time Frame: 2 years] ORR as confirmed Complete Response (CR) or Partial Response (PR) per Response Evaluation Criteria in Solid Tumors (RECIST)
NCT02846987	Abemaciclib	30	Phase II study of Abemaciclib in dedifferentiated liposarcoma	PFS [Time Frame: 12 weeks]
NCT03356587	Abemaciclib	32	Biomarker-driven, open label, single arm, multicentre phase II study of Abemaciclib in patients with recurrent or metastatic head and neck squamous cell carcinoma who failed to platinum-based therapy	Response rate [Time Frame: 24 months]

(Continued)

TABLE 3 | Continued

	CDK4/6 inhibitor	*N*	Phase and setting	Primary endpoint(s)
NCT03356223	Abemaciclib	25	Phase II trial aiming to evaluate the clinical interest of Abemaciclib monotherapy in patients with locally advanced/metastatic head and neck cancer after failure of platinum and Cetuximab or anti-EGFR-based therapy and harboring an homozygous deletion of cdkn2a, and/or an amplification of CCND1 and/or of CDK6	The 8-weeks non-progression rate defined as the rate of patients with complete response (CR), partial response (PR) or stable disease (SD) lasting at least 8 weeks, according to RECIST v1.1 [Time Frame: 8 weeks after start of treatment]
NCT02450539	Abemaciclib	150	Randomized phase II study of Abemaciclib vs. docetaxel in patients with stage iv squamous non-small cell lung cancer previously treated with platinum-based chemotherapy.	PFS
NCT02308020	Abemaciclib	247	Phase 2 study of Abemaciclib in patients with brain metastases secondary to hormone receptor positive breast cancer, non-small cell lung cancer, or melanoma.	Percentage of Participants Achieving Complete Response (CR) or Partial Response (PR): Objective Intracranial Response Rate (OIRR)
NCT03310879	Abemaciclib	38	Phase II study of the cdk4/6 inhibitor Abemaciclib in patients with solid tumors harboring genetic alterations in genes encoding D-type cyclins or amplification of CDK4 or 6.	Progression-free rate

(92). The NCT02846987 phase II trial is currently recruiting patients affected by not surgically resectable locally advanced or recurrent dedifferentiated liposarcoma with any number of prior therapies (including none). The primary endpoint is PFS (93). A biomarker-driven phase II study (NCT03356587) of abemaciclib in patients with recurrent or metastatic head and neck squamous cell carcinoma who failed to platinum-based therapy is also currently recruiting participants. Primary endpoint is response rate (94). Another phase II trial in (NCT03356223) patients with locally advanced/metastatic head and neck cancer is currently evaluating abemaciclib monotherapy after failure of platinum and cetuximab or anti-EGFR-based therapy, but only in tumors harboring a homozygous deletion of CDKN2A, and/or amplification of CCND1 and/or of CDK6. The primary endpoint is the 8-weeks non-progression rate (95). Finally, the NCT03310879 phase II study is testing abemaciclib in patients with solid tumors of non-breast origin harboring genetic alterations in genes encoding D-type Cyclins or amplification of CDK4/6 without therapeutic alternative. The progression-free rate at 4 months is the primary endpoint (96).

Ongoing trials for palbociclib, ribociclib, and abemaciclib are resumed in **Table 3**.

CONCLUSIONS

Albeit it is unquestionable, at present, that CDK 4/6i treatment proved to be more efficacious in combination strategies (e.g., in HR+ HER2– MBC is in combination with endocrine agents), the MONARCH 1 trial results (86) led to the FDA approval of abemaciclib as monotherapy for the treatment of adult patients with HR+ HER2– MBC with disease progression after prior ET and CT received in metastatic setting. This study opened up a new scenario for CDK4/6i, making them suitable as single agent treatment in heavily pretreated MBC. In this perspective, the TREND trial provided some evidence for some activity of palbociclib as single agent in pretreated patients with HR+HER2– MBC (65). A cross-trial comparison of response rate from the MONARCH-1 and TREND trial suggests that abemaciclib might be more effective than palbociclib in the same disease setting. However, this hint should be taken as hypothesis only, given the lack of direct comparisons between the two CDK4/6i. Additionally, there is a strong need for biomarkers predictive of response and resistance to better define which patients could benefit most from these drugs. In fact, mechanisms of resistance to CDK4/6i therapy have yet to be clearly identified. Laboratory evidences suggest that markers of intrinsic resistance might be the pRb loss and subsequent increase in $p16^{INK4A}$, deregulation of cyclin E expression, E2F family members amplification and TP53 mutations (97). Interestingly, a study recently published from Condorelli et al. showed for the first time in human patients that acquired mutations leading to functional loss of pRb encoding gene (RB1) might emerge under treatment with palbociclib and ribociclib, maybe due to selective pressure from the CDK4/6i and might potentially confer therapeutic resistance (98). Results from ongoing trials in solid tumors will surely shed a light on CDK4/6i future development as single agents. It is likely that eventual new treatment indications might be acquired by the three inhibitors in the next future, especially in tumors where few therapeutic options are available, such as sarcomas.

AUTHOR CONTRIBUTIONS

All authors conceived the review. FS, ID, CR, and PD performed the literature search. FS drew the figures. FS, ID, and LD wrote the first draft of the manuscript. All authors revised and approved the final version of the manuscript.

REFERENCES

1. Musgrove EA, Caldon CE, Barraclough J, Stone A, Sutherland RL. Cyclin D as a therapeutic target in cancer. *Nat Rev Cancer* (2011) 45:558–72. doi: 10.1038/nrc3090
2. Hamilton E, Infante JR. Targeting CDK4/6 in patients with cancer. *Cancer Treat Rev.* (2016) 45:129–38. doi: 10.1016/j.ctrv.2016.03.002
3. Cassier P, Trédan O, Seigne C, Lavergne E, Fayette J, Desseigne F, et al. Identifying actionable targets in advanced cancer patients: preliminary results from the Profiler program. *J Clin Oncol.* (2014) 32(5_Suppl.):2621. doi: 10.1200/jco.2014.32.15_suppl.2621
4. Cancer Genome Atlas Network. Comprehensive molecular portraits of human breast tumors. Nature (2012) 490:61–70. doi: 10.1038/nature11412
5. Geradts J, Wilson PA. High frequency of aberrant p16(INK4A) expression in human breast cancer. *Am J Pathol.* (1996) 149:15–20.
6. Lim JT, Mansukhani M, Weinstein IB. Cyclin-dependent kinase 6 associates with the androgen receptor and enhances its transcriptional activity in prostate cancer cells. *Proc Natl Acad Sci USA*. (2005) 102:5156–61. doi: 10.1073/pnas.0501203102
7. Young RJ, Waldeck K, Martin C, Foo JH, Cameron DP, Kirby L, et al. Loss of CDKN2A expression is a frequent event in primary invasive melanoma and correlates with sensitivity to the CDK4/6 inhibitor PD0332991 in melanoma cell lines. *Pigment Cell Melanoma Res.* (2014) 27:590–600. doi: 10.1111/pcmr.12228
8. Reed AL, Califano J, Cairns P, Westra WH, Jones RM, Koch W, et al. High frequency of p16 (CDKN2/MTS-1/INK4A) inactivation in head and neck squamous cell carcinoma. *Cancer Res.* (1996) 56:3630–3.
9. Molenaar JJ, Ebus ME, Koster J, van Sluis P, van Noesel CJ, Versteeg R, et al. Cyclin D1 and CDK4 activity contribute to the undifferentiated phenotype in neuroblastoma. *Cancer Res.* (2008) 68:2599–609. doi: 10.1158/0008-5472.CAN-07-5032
10. Crago AM, Singer S. Clinical and molecular approaches to well differentiated and dedifferentiated liposarcoma. *Curr Opin Oncol.* (2011) 23:373–8. doi: 10.1097/CCO.0b013e32834796e6
11. Singer S, Socci ND, Ambrosini G, Sambol E, Decarolis P, Wu Y, et al. Gene expression profiling of liposarcoma identifies distinct biological types/subtypes and potential therapeutic targets in well-differentiated and dedifferentiated liposarcoma. *Cancer Res.* (2007) 67:6626–36. doi: 10.1158/0008-5472.CAN-07-0584
12. Louis-Brennetot C, Coindre JM, Ferreira C, Pérot G, Terrier P, Aurias A. The CDKN2A/CDKN2B/CDK4/CCND1 pathway is pivotal in well-differentiated and dedifferentiated liposarcoma oncogenesis: an analysis of 104 tumors. *Genes Chromosomes Cancer* (2011) 50:896–907. doi: 10.1002/gcc.20909
13. Zuo L, Weger J, Yang Q, Goldstein AM, Tucker MA, Walker GJ, et al. Germline mutations in the p16INK4a binding domain of CDK4 in familial melanoma. *Nat Genet.* (1996) 12:97–9. doi: 10.1038/ng0196-97
14. Hodis E, Watson IR, Kryukov GV, Arold ST, Imielinski M, Theurillat JP, et al. A landscape of driver mutations in melanoma. *Cell* (2012) 150:251–63. doi: 10.1016/j.cell.2012.06.024
15. Haluska FG, Hodi FS. Molecular genetics of familial cutaneous melanoma. *J Clin Oncol.* (1998) 16:670–82. doi: 10.1200/JCO.1998.16.2.670
16. Potrony M, Puig-Butillé JA, Aguilera P, Badenas C, Carrera C, Malvehy J, et al. Increased prevalence of lung, breast, and pancreatic cancers in addition to melanoma risk in families bearing the cyclin-dependent kinase inhibitor 2A mutation: Implications for genetic counseling. *J Am Acad Dermatol.* (2014) 71:888–95. doi: 10.1016/j.jaad.2014.06.036
17. Dreyling M, Kluin-Nelemans HC, Beà S, Hartmann E, Salaverria I, Hutter G, et al. Update on the molecular pathogenesis and clinical treatment of mantle cell lymphoma: report of the 10th annual conference of the European Mantle Cell Lymphoma Network. *Leuk Lymphoma* (2011) 52:2226–36. doi: 10.3109/10428194.2011.600488
18. Pérez-Galán P, Dreyling M, Wiestner A. Mantle cell lymphoma: biology, pathogenesis, and the molecular basis of treatment in the genomic era. *Blood* (2011) 117:26–38. doi: 10.1182/blood-2010-04-189977
19. Fernandez V, Hartmann E, Ott G, Campo E, Rosenwald A. Pathogenesis of mantle-cell lymphoma: all oncogenic roads lead to dysregulation of cell cycle and DNA damage response pathways. *J Clin Oncol.* (2005) 23:6364–9. doi: 10.1200/JCO.2005.05.019
20. Abou-Zeid AA, Azzam AZ, Kamel NA. Methylation status of the gene promoter of cyclin-dependent kinase inhibitor 2A (CDKN2A) in ovarian cancer. *Scand J Clin Lab Invest.* (2011) 71:542–7. doi: 10.3109/00365513.2011.590224
21. Jackson EM, Sievert AJ, Gai X, Hakonarson H, Judkins AR, Tooke L, et al. Genomic analysis using high-density single nucleotide polymorphism-based oligonucleotide arrays and multiplex ligation-dependent probe amplification provides a comprehensive analysis of INI1/SMARCB1 in malignant rhabdoid tumors. *Clin Cancer Res.* (2009) 15:1923–30. doi: 10.1158/1078-0432.CCR-08-2091
22. Kuwahara Y, Charboneau A, Knudsen ES, Weissman BE. Reexpression of hSNF5 in malignant rhabdoid tumor cell lines causes cell cycle arrest through a p21 (CIP1/WAF1)-dependent mechanism. *Cancer Res.* (2010) 70:1854–65. doi: 10.1158/0008-5472.CAN-09-1922
23. Zhang ZK, Davies KP, Allen J, Zhu L, Pestell RG, Zagzag D, et al. Cell cycle arrest and repression of cyclin D1 transcription by INI1/hSNF5. *Mol Cell Biol.* (2002) 22:5975–88. doi: 10.1128/MCB.22.16.5975-5988.2002
24. Wang X, Wu J, Lin Y, Zhu Y, Xu X, Xu X, et al. MicroRNA-320c inhibits tumorous behaviors of bladder cancer by targeting Cyclin-dependent kinase 6. *J Exp Clin Cancer Res.* (2014) 33:69. doi: 10.1186/s13046-014-0069-6
25. Lin Y, Wu J, Chen H, Mao Y, Liu Y, Mao Q, et al. Cyclin-dependent kinase 4 is a novel target in micoRNA-195-mediated cell cycle arrest in bladder cancer cells. *FEBS Lett.* (2012) 586:442–7. doi: 10.1016/j.febslet.2012.01.027
26. Corona SP, Generali D. Abemaciclib: a CDK4/6 inhibitor for the treatment of HR+/HeR2– advanced breast cancer. *Drug Design Dev Ther.* (2018) 12:321–30. doi: 10.2147/DDDT.S137783
27. Goel S, DeCristo MJ, Watt AC, BrinJones H, Sceneay J, Li BB, et al. CDK4/6 inhibition triggers anti-tumor immunity. *Nature* (2017) 548:471–5. doi: 10.1038/nature23465
28. Knudsen ES, Hutcheson J, Vail P, Witkiewicz AK. Biological specificity of CDK4/6 inhibitors: dose response relationship, *in vivo* signaling, and composite response signature. *Oncotarget* (2017) 8:43678–91. doi: 10.18632/oncotarget.18435
29. Finn RS, Martin M, Rugo HS, Jones S, Im SA, Gelmon K, et al. Palbociclib and letrozole in advanced breast cancer. *N Engl J Med.* (2016) 375:1925–36. doi: 10.1056/NEJMoa1607303
30. Cristofanilli M, Turner NC, Bondarenko I, Ro J, Im SA, Masuda N, et al. Fulvestrant plus palbociclib versus fulvestrant plus placebo for treatment of hormone-receptor-positive, HER2-negative metastatic breast cancer that progressed on previous endocrine therapy (PALOMA-3): final analysis of the multicentre, double-blind, phase 3 randomised controlled trial. *Lancet Oncol.* (2016) 17:425–39. doi: 10.1016/S1470-2045(15)00613-0
31. Hortobagyi GN, Stemmer SM, Burris HA, Yap YS, Sonke GS, Paluch-Shimon S, et al. Ribociclib as first-line therapy for HR-positive, advanced breast cancer. *N Engl J Med.* (2016) 375:1738–48. doi: 10.1056/NEJMoa1609709
32. Slamon DJ, Neven P, Chia S, Fasching PA, De Laurentiis M, Im SA, et al. Phase III randomized study of ribociclib and fulvestrant in hormone receptor–positive, human epidermal growth factor receptor 2–negative advanced breast cancer: MONALEESA-3. *J Clin Oncol.* (2018) 36:2465–72. doi: 10.1200/JCO.2018.78.9909
33. Goetz MP, Toi M, Campone M, Sohn J, Paluch-Shimon S, Huober J, et al. MONARCH 3: abemaciclib as initial therapy for advanced breast cancer. *J Clin Oncol.* (2017) 35:3638–46. doi: 10.1200/JCO.2017.75.6155
34. Sledge GW Jr., Toi M, Neven P, Sohn J, Inoue K, Pivot X, et al. MONARCH 2: abemaciclib in combination with fulvestrant in women with HR+/HER2– advanced breast cancer who had progressed while receiving endocrine therapy. *J Clin Oncol.* (2017) 35:2875–84. doi: 10.1200/JCO.2017.73.7585
35. *Prescription Drug Information, Interactions & Side Effects* (2018). Available online at: https://www.drugs.com
36. Tripathy D, Im SA, Colleoni M, Franke F, Bardia A, Harbeck N, et al. Ribociclib plus endocrine therapy for premenopausal women with hormone-receptor-positive, advanced breast cancer (MONALEESA-7): a randomized phase 3 trial. *Lancet Oncol.* (2018) 19:904–15. doi: 10.1016/S1470-2045(18)30292-4
37. Turner NC, Slamon DJ, Ro J, Bondarenko I, Im SA, Masuda N, et al. Overall survival with palbociclib and fulvestrant in advanced breast cancer. *N Engl J Med.* (2018). doi: 10.1056/NEJMoa1810527

38. Fry DW, Harvey PJ, Keller PR, Elliott WL, Meade M, Trachet E, et al. Specific inhibition of cyclin-dependent kinase 4/6 by PD 0332991 and associated antitumor activity in human tumor xenografts. *Mol Cancer Ther.* (2004) 3:1427–38.
39. Finn RS, Dering J, Conklin D, Kalous O, Cohen DJ, Desai AJ, et al. PD 0332991, a selective cyclin D kinase 4/6 inhibitor, preferentially inhibits proliferation of luminal estrogen receptor-positive human breast cancer cell lines *in vitro*. *Breast Cancer Res.* (2009) 11:R77. doi: 10.1186/bcr2419
40. Dean JL, McClendon AK, Hickey TE, Butler LM, Tilley WD, Witkiewicz AK, et al. Therapeutic response to CDK4/6 inhibition in breast cancer defined by *ex vivo* analyses of human tumors. *Cell Cycle* (2012) 11:2756–61. doi: 10.4161/cc.21195
41. Michaud K, Solomon DA, Oermann E, Kim JS, Zhong WZ, Prados MD, et al. Pharmacologic inhibition of cyclin-dependent kinases 4 and 6 arrests the growth of glioblastoma multiforme intracranial xenografts. *Cancer Res.* (2010) 70:3228–38. doi: 10.1158/0008-5472.CAN-09-4559
42. Wiedemeyer WR, Dunn IF, Quayle SN, Zhang J, Chheda MG, Dunn GP, et al. Pattern of retinoblastoma pathway inactivation dictates response to CDK4/6 inhibition in GBM. *Proc Natl Acad Sci USA.* (2010) 107:11501–6. doi: 10.1073/pnas.1001613107
43. Konecny GE, Winterhoff B, Kolarova T, Qi J, Manivong K, Dering J, et al. Expression of p16 and retinoblastoma deter- mines response to CDK4/6 inhibition in ovarian cancer. *Clin Cancer Res.* (2011) 17:1591–602. doi: 10.1158/1078-0432.CCR-10-2307
44. Vlenterie M, Hillebrandt-Roeffen MH, Schaars EW, Flucke UE, Fleuren ED, Navis AC, et al. Targeting cyclin-dependent kinases in synovial sarcoma: palbociclib as a potential treatment for synovial sarcoma patients. *Ann Surg Oncol.* (2016) 23:2745–52. doi: 10.1245/s10434-016-5341-x
45. Barretina J, Taylor BS, Banerji S, Ramos AH, Lagos-Quintana M, Decarolis PL, et al. Subtype-specific genomic alterations define new targets for soft-tissue sarcoma therapy. *Nat Genet.* (2010) 42:715–21. doi: 10.1038/ng.619
46. Perez M, Muñoz-Galván S, Jiménez-García MP, Marín JJ, Carnero A. Efficacy of CDK4 inhibition against sarcomas depends on their levels of CDK4 and p16ink4 mRNA. *Oncotarget* (2015) 6:40557–74. doi: 10.18632/oncotarget.5829
47. Saab R, Bills JL, Miceli AP, Anderson CM, Khoury JD, Fry DW, et al. Pharmacologic inhibition of cyclin-dependent kinase 4/6 activity arrests proliferation in myoblasts and rhabdomyosarcoma-derived cells. *Mol Cancer Ther.* (2006) 5:1299–308. doi: 10.1158/1535-7163.MCT-05-0383
48. Chou A, Froio D, Nagrial AM, Parkin A, Murphy KJ, Chin VT, et al. Tailored first-line and second-line CDK4-targeting treatment combinations in mouse models of pancreatic cancer. *Gut* (2018) 67:2142–55. doi: 10.1136/gutjnl-2017-315144
49. Zhang YX, Sicinska E, Czaplinski JT, Remillard SP, Moss S, Wang Y, et al. Antiproliferative effects of CDK4/6 inhibition in CDK4-amplified human liposarcoma *in vitro* and *in vivo*. *Mol Cancer Ther.* (2014) 13:2184–93. doi: 10.1158/1535-7163.MCT-14-0387
50. Kim S, et al. LEE011: an orally bioavailable, selective small molecule inhibitor of CDK4/6–reactivating Rb in cancer. *Mol Cancer Ther.* (2014) 12(11_Supplement):PR02. doi: 10.1158/1535-7163.TARG-13-PR02
51. Tate SC, Cai S, Ajamie RT, Burke T, Beckmann RP, Chan EM, et al. Semi mechanistic pharmacokinetic/pharmacodynamic modeling of the antitumor activity of LY2835219, a new cyclin-dependent kinase 4/6 inhibitor, in mice bearing human tumor xenografts. *Clin Cancer Res.* (2014) 20:3763–74. doi: 10.1158/1078-0432.CCR-13-2846
52. Gelbert LM, Cai S, Lin X, Sanchez-Martinez C, Del Prado M, Lallena MJ, et al. Preclinical characterization of the CDK4/6 inhibitor LY2835219: *in-vivo* cell cycle-dependent/independent anti-tumor activities alone/in combination with gemcitabine. *Invest New Drugs* (2014) 32:825–37. doi: 10.1007/s10637-014-0120-7
53. Raub TJ, Wishart GN, Kulanthaivel P, Staton BA, Ajamie RT, Sawada GA, et al. Brain exposure of two selective dual CDK4 and CDK6 inhibitors and the antitumor activity of CDK4 and 6 inhibition in combination with temozolomide in an intracranial glioblastoma xenograft. *Drug Metab Dispos.* (2015) 43:9:1360–71. doi: 10.1124/dmd.114.062745
54. Dempsey JA, Chan EM, Burke TF, Beckmann RP. LY2835219, a selective inhibitor of CDK4 and CDK6, inhibits growth in preclinical models of human cancer. *Cancer Res.* (2013) 73(8_Suppl.):LB-122. doi: 10.1158/1538-7445.AM2013-LB-122
55. Yadav V, Burke TF, Huber L, Van Horn RD, Zhang Y, Buchanan SG, et al. The CDK4/6 inhibitor LY2835219 overcomes vemurafenib resistance resulting from MAPK reactivation and cyclin D1 upregulation. *Mol Cancer Ther.* (2014) 13:2253–63. doi: 10.1158/1535-7163.MCT-14-0257
56. Kosovec JE, Zaidi AH, Omstead AN, Matsui D, Biedka MJ, Cox EJ, et al. CDK4/6 dual inhibitor abemaciclib demonstrates compelling preclinical activity against esophageal adenocarcinoma: a novel therapeutic option for a deadly disease. *Oncotarget* (2017) 8:100421–32. doi: 10.18632/oncotarget.22244
57. Flaherty KT, Lorusso PM, Demichele A, Abramson VG, Courtney R, Randolph SS, et al. Phase I, dose-escalation trial of the oral cyclin-dependent kinase 4/6 inhibitor PD 0332991, administered using a 21-day schedule in patients with advanced cancer. *Clin Cancer Res.* (2012) 18:568–76. doi: 10.1158/1078-0432.CCR-11-0509
58. Dickson MA, Tap WD, Keohan ML, D'Angelo SP, Gounder MM, Antonescu CR, et al. Phase II trial of the CDK4 inhibitor PD0332991 in patients with advanced CDK4-amplified well-differentiated or dedifferentiated liposarcoma. *J Clin Oncol.* (2013) 31:2024–8. doi: 10.1200/JCO.2012.46.5476
59. Dickson MA, Schwartz GK, Keohan ML, D'Angelo SP, Gounder MM, Chi P, et al. Progression-free survival among patients with well-differentiated or dedifferentiated liposarcoma treated with CDK4 inhibitor palbociclib: a phase II clinical trial. *JAMA Oncol.* (2016) 2:937–40. doi: 10.1001/jamaoncol.2016.0264
60. Gopalan PK, Pinder MC, Chiappori A, Ivey AM, Villegas AG, Kaye FJ, et al. A phase II clinical trial of the CDK 4/6 inhibitor palbociclib (PD 0332991) in previously treated, advanced non-small cell lung cancer (NSCLC) patients with inactivated CDKN2A. *J Clin Oncol.* (2014) 32(5_Suppl.):8077. doi: 10.1200/jco.2014.32.15_suppl.8077
61. Karasic TB, O'Hara MH, Teitelbaum UR, Damjanov N, Giantonio BJ, d'Entremont TS, et al. Phase II trial of palbociclib in patients with advanced esophageal or gastric cancer. *J Clin Oncol.* (2018) 36(4_Suppl.):68. doi: 10.1200/JCO.2018.36.4_suppl.68
62. US National Library of Medicine. ClinicalTrials.gov (2018). Available online at: https://clinicaltrials.gov/ct2/show/NCT02334527?term=palbociclib&draw=2&rank=16
63. Konecny GE, Hendrickson AEW, Jatoi A, Burton JK, Paroly J, Glaspy JA, et al. A multicenter open-label phase II study of the efficacy and safety of palbociclib a cyclin-dependent kinases 4 and 6 inhibitor in patients with recurrent ovarian cancer. *J Clin Oncol.* (2016) 34(15_Suppl.):5557. doi: 10.1200/JCO.2016.34.15_suppl.5557
64. DeMichele A, Clark AS, Tan KS, Heitjan DF, Gramlich K, Gallagher M, et al. A phase II trial of an oral CDK 4/6 inhibitor, PD0332991, in advanced breast cancer. *J Clin Oncol.* (2013) 31(15_Suppl.):519. doi: 10.1200/jco.2013.31.15_suppl.519
65. Malorni L, Curigliano G, Minisini AM, Cinieri S, Tondini CA, D'Hollander K, et al. Palbociclib as single agent or in combination with the endocrine therapy received before disease progression for estrogen receptor-positive, HER2-negative metastatic breast cancer: TREnd trial. *Ann Oncol.* (2018) 29:1748–54. doi: 10.1093/annonc/mdy214
66. US National Library of Medicine. ClinicalTrials.gov (2018). Available online at: https://clinicaltrials.gov/ct2/show/NCT03219554?term=palbociclib&draw=7&rank=65
67. Steuer CE, Papadimitrakopoulou V, Herbst RS, Redman MW, Hirsch FR, Mack PC, et al. Innovative clinical trials: the LUNG-MAP study. *Clin Pharmacol Ther.* (2015) 97:488–91. doi: 10.1002/cpt.88
68. US National Library of Medicine. ClinicalTrials.gov (2018). Available online at: https://clinicaltrials.gov/ct2/show/NCT01907607
69. US National Library of Medicine. ClinicalTrials.gov (2018). Available online at: https://clinicaltrials.gov/ct2/show/NCT01356628?term=palbociclib&draw=11&rank=101
70. US National Library of Medicine. ClinicalTrials.gov (2018). Available online at: https://clinicaltrials.gov/ct2/show/NCT02806648
71. US National Library of Medicine. ClinicalTrials.gov (2018). Available online at: https://clinicaltrials.gov/ct2/show/NCT02530320?term=palbociclib&rank=8

72. US National Library of Medicine. ClinicalTrials.gov (2018). Available online at: https://clinicaltrials.gov/ct2/show/NCT03242382?term=palbociclib&draw=4&rank=37
73. US National Library of Medicine. ClinicalTrials.gov (2018). Available online at: https://clinicaltrials.gov/ct2/show/NCT01037790?term=palbociclib&draw=15&rank=145
74. US National Library of Medicine. ClinicalTrials.gov (2018). Available online at: https://clinicaltrials.gov/ct2/show/NCT03454919?term=palbociclib&draw=2&rank=12
75. Infante JR, Cassier PA, Gerecitano JF, Witteveen PO, Chugh R, Ribrag V, et al. A phase I study of the cyclin-dependent kinase 4/6 inhibitor ribociclib (LEE011) in patients with advanced solid tumors and lymphomas. *Clin Cancer Res*. (2016) 22:5696–705. doi: 10.1158/1078-0432.CCR-16-1248
76. US National Library of Medicine. ClinicalTrials.gov (2018). Available online at: https://clinicaltrials.gov/ct2/show/NCT02345824?term=ribociclib&draw=2&rank=4
77. US National Library of Medicine. ClinicalTrials.gov (2018). Available online at: https://clinicaltrials.gov/ct2/show/NCT02571829?term=ribociclib&draw=3&rank=12
78. US National Library of Medicine. ClinicalTrials.gov (2018). Available online at: https://clinicaltrials.gov/ct2/show/NCT02420691?term=ribociclib&draw=5&rank=32
79. US National Library of Medicine. ClinicalTrials.gov (2018). Available online at: https://clinicaltrials.gov/ct2/show/NCT02300987?term=ribociclib&draw=7&rank=60
80. US National Library of Medicine. ClinicalTrials.gov (2018). Available online at: https://clinicaltrials.gov/ct2/show/NCT03096912?term=ribociclib&draw=2&rank=2
81. Patnaik A, Rosen LS, Tolaney SM, Tolcher AW, Goldman JW, Gandhi L, et al. Efficacy and safety of abemaciclib, an inhibitor of CDK4 and CDK6, for patients with breast cancer, non–small cell lung cancer, and other solid tumors. *Cancer Discov*. (2016) 6:740–53. doi: 10.1158/2159-8290.CD-16-0095
82. Shapiro G, Rosen LS, Tolcher AW, Goldman JW, Gandhi L, Papadopoulos KP, et al. A first-in-human phase I study of the CDK4/6 inhibitor, LY2835219, for patients with advanced cancer. *J Clin Oncol*. (2013) 31(15_Suppl.):2500. doi: 10.1200/jco.2013.31.15_suppl.2500
83. Goldman JW, Gandhi L, Patnaik A, Rosen LS, Hilton JF, Papadopoulos KP, et al. Clinical activity of LY2835219, a novel cell cycle inhibitor selective for CDK4 and CDK6, in patients with non-small cell lung cancer. *J Clin Oncol*. (2014) 32(15_Suppl.):8026. doi: 10.1200/jco.2014.32.15_suppl.8026
84. The ASCO Post. *Results From the Phase III JUNIPER Trial Evaluating Abemaciclib in* KRAS-*Mutated, Advanced NSCLC*. The ASCO Post (2017). Available online at: http://www.ascopost.com/News/58135
85. US National Library of Medicine. ClinicalTrials.gov (2018). Available online at: https://clinicaltrials.gov/ct2/show/NCT02152631?term=Abemaciclib&draw=3&rank=19
86. Dickler MN, Tolaney SM, Rugo HS, Cortés J, Diéras V, Patt D, et al. MONARCH 1, a phase II study of abemaciclib, a CDK4 and CDK6 inhibitor, as a single agent, in patients with refractory HR(+)/HER2(−) metastatic breast cancer. *Clin Cancer Res*. (2017) 23:5218–24. doi: 10.1158/1078-0432.CCR-17-0754
87. Tolaney SM, Lin NU, Thornton D, Klise S, Costigan TM, Turner PK, et al. Abemaciclib for the treatment of brain metastases (BM) secondary to hormone receptor positive (HR+), HER2 negative breast cancer. *J Clin Oncol*. (2017) 35:1019. doi: 10.1200/JCO.2017.35.15_suppl.1019
88. US National Library of Medicine. ClinicalTrials.gov (2018). Available online at: https://clinicaltrials.gov/ct2/show/NCT02014129?term=abemaciclib&draw=3&rank=42
89. US National Library of Medicine. ClinicalTrials.gov (2018). Available online at: https://clinicaltrials.gov/ct2/show/NCT02981940?term=Abemaciclib&draw=2&rank=2
90. US National Library of Medicine. ClinicalTrials.gov (2018). Available online at: https://clinicaltrials.gov/ct2/show/NCT02450539?term=Abemaciclib&draw=3&rank=18
91. US National Library of Medicine. ClinicalTrials.gov (2018). Available online at: https://clinicaltrials.gov/ct2/show/NCT02919696?term=Abemaciclib&draw=2&rank=6
92. US National Library of Medicine. ClinicalTrials.gov (2018). Available online at: https://clinicaltrials.gov/ct2/show/NCT03130439?term=Abemaciclib&draw=2&rank=4
93. US National Library of Medicine. ClinicalTrials.gov (2018). Available online at: https://clinicaltrials.gov/ct2/show/NCT02846987?term=Abemaciclib&draw=2&rank=5
94. US National Library of Medicine. ClinicalTrials.gov (2018). Available online at: https://clinicaltrials.gov/ct2/show/NCT03356587?term=Abemaciclib&draw=2&rank=9
95. US National Library of Medicine. ClinicalTrials.gov (2018). Available online at: https://clinicaltrials.gov/ct2/show/NCT03356223?term=Abemaciclib&draw=3&rank=14
96. US National Library of Medicine. ClinicalTrials.gov (2018). Available online at: https://clinicaltrials.gov/ct2/show/NCT03310879?term=Abemaciclib&draw=3&rank=13
97. Condorelli R, Spring L, O'Shaughnessy J, Lacroix L, Bailleux C, Scott V, et al. Polyclonal RB1 mutations and acquired resistance to CDK4/6i in patients with metastatic breast cancer. *Ann Oncol*. (2017) 0:1–6. doi: 10.1093/annonc/mdx784
98. Knudsen ES, Witkiewicz AK. The strange case of CDK4/6 inhibitors: mechanisms, resistance, and combination strategies. *Trends Cancer* (2017) 3:39–55. doi: 10.1016/j.trecan.2016.11.006

Conflict of Interest Statement: The authors declare that the research was conducted in the absence of any commercial or financial relationships that could be construed as a potential conflict of interest.

frontiers in Oncology

ORIGINAL RESEARCH
published: 17 December 2018
doi: 10.3389/fonc.2018.00625

Phage Ligands for Identification of Mesenchymal-Like Breast Cancer Cells and Cancer-Associated Fibroblasts

*Kelvin M. Jones[1], Balasubramanyam Karanam[2], Jacqueline Jones-Triche[3], Maninder Sandey[4], Henry J. Henderson[1], Rajeev S. Samant[5], Samuel Temesgen[6], Clayton Yates[2] and Deepa Bedi[1]**

[1] Department of Biomedical Sciences, College of Veterinary Medicine, Tuskegee University, Tuskegee, AL, United States, [2] Department of Biology, Center for Cancer Research, Tuskegee University, Tuskegee, AL, United States, [3] Department of Biology and Environmental Sciences, Troy University, Troy, AL, United States, [4] Department of Pathobiology, Auburn University, Auburn, AL, United States, [5] Department of Pathobiology, The University of Alabama at Birmingham, Birmingham, AL, United States, [6] Department of Pathobiology, College of Veterinary Medicine, Tuskegee University, Tuskegee, AL, United States

OPEN ACCESS

Edited by:
Zhe-Sheng Chen,
St. John's University, United States

Reviewed by:
Dongmei Zhang,
Jinan University, China
Ning Ji,
Tianjin Medical University, China

***Correspondence:**
Deepa Bedi
dbedi@tuskegee.edu

Specialty section:
This article was submitted to Cancer Molecular Targets and Therapeutics, a section of the journal Frontiers in Oncology

Received: *08 July 2018*
Accepted: *03 December 2018*
Published: *17 December 2018*

Citation:
Jones KM, Karanam B, Jones-Triche J, Sandey M, Henderson HJ, Samant RS, Temesgen S, Yates C and Bedi D (2018) Phage Ligands for Identification of Mesenchymal-Like Breast Cancer Cells and Cancer-Associated Fibroblasts. Front. Oncol. 8:625. doi: 10.3389/fonc.2018.00625

Epithelial to mesenchymal transition (EMT) is believed to be crucial for primary tumors to escape their original residence and invade and metastasize. To properly define EMT, there is a need for ligands that can identify this phenomenon in tumor tissue and *invivo*. A phage-display selection screening was performed to select novel binding phage peptides for identification of EMT in breast cancer. Epithelial breast cancer cell line, MCF-7 was transformed to mesenchymal phenotype by TGF-β treatment and was used for selection. Breast fibroblasts were used for subtractive depletion and breast cancer metastatic cell lines MDA-MB-231, T47D-shNMI were used for specificity assay. The binding peptides were identified, and their binding capacities were confirmed by phage capture assay, phage-based ELISA, immunofluorescence microscopy. The phage peptide bearing the 7-amino acid sequence, LGLRGSL, demonstrated selective binding to EMT phenotypic cells (MCF-7/TGF-β and MDA-MB-231) as compared to epithelial subtype, MCF-7, T47D and breast fibroblasts (Hs578T). The selected phage was also able to identify metastatic breast cancer tumor in breast cancer tissue microarray (TMA). These studies suggest that the selected phage peptide LGLRGSL identified by phage-display library, showed significant ability to bind to mesenchymal-like breast cancer cells/ tissues and can serve as a novel probe/ligand for metastatic breast cancer diagnostic and imaging.

Keywords: Phage display, breast cancer, fibroblasts, EMT, cancer-associated fibroblasts

INTRODUCTION

Breast cancer is the most common cancer in women and the second leading causes of death due to cancer (1). The cause of death in breast cancer is often due metastasis to distant sites, resulting in organ failure accounting for a 5-year survival rate of 23%. Evidences support the observation that metastasis is an early event in breast cancer progression (2), with possibly up to 90% of patients already having metastasis at the time of diagnosis. Studies have shown that dissemination of cancer cells and metastasis into distant organs is often preceded by an epithelial to mesenchymal transition

(EMT) of cancer cells (3), which allows cancer cells to dedifferentiate, acquire mesenchymal including fibroblast-like morphology, enhanced migratory and invasive properties, enabling them to invade through the stroma and migrate and seed to distant organs (4, 5). The concept of EMT in breast cancer has been well demonstrated in numerous *invitro* studies in different normal, malignant mammary epithelial cells and in mouse models of mammary cancers (6, 7). It has been suggested that tumor microenvironment (8) and growth factors such as transforming growth factor-β (TGFβ), epidermal growth factor (EGF), platelet-derived growth factor (PDGF) has a dramatic effect on epithelial phenotype and in promoting motility and invasiveness via the induction of EMT (9, 10). TGFβ treatment changes epithelial cells from cubodial shape to more elongated ones with concomitant loss of epithelial markers and increased expression of mesenchymal markers vimentin, fibronectin and α-smooth muscle actin (11). These EMT markers are also present in activated cancer-associated fibroblasts (CAF's), which contributes to the pathogenesis of tumor progression and invasiveness (12). Several studies support a physiologic role of EMT during tumor progression (13–15) by monitoring EMT progression by the cadherin switch, E-cadherin to N-cadherin, which is normally also present in mesenchymal cells, fibroblasts, neural tissue (16). Similarly, vimentin is also often used to define cancer cells undergoing EMT, is also present in fibroblasts, endothelial cells, cells of the hematopoietic lineages, and glial cells (17, 18). There is a lack of specific ligands that can recognize mesenchymal-like cancer cells and define EMT in tumor and in cancer-associated fibroblasts.

Phage display offers great advantage as a high throughput profiling technology based on peptide libraries present on the surface of bacteriophage. Selective binding of phages from a library with billions of diversified peptides can make a clear distinction between two morphological same but functionally different targets and thus offers a complementary approach for comparative screening. Usually peptides can be displayed on the N-terminus of pIII protein coat protein (pIII phage display), which is displayed at one end of the filamentous phage in 3–5 copies (19) or can be displayed on the N-terminus of all copies of pVIII major coat protein (20). Diversity of pIII or pVIII combinatorial phage library has been exploited extensively to explore the cell surface repertoire of various cancer cells such as colon (21), prostate (22, 23), pancreatic (24), breast (25, 26) and to select many cell surface or cell internalizing peptides. Some of these highly specific and high affinity ligands have been used as diagnostic (24), molecular and targeting agents (27–30). Additionally, lamba (T7) phage display has been used to identify vascular zip codes (31) and markers for angiogenesis (32). These studies and more define the power of using combinatorial phage display to identify molecular differences and interactive regions of the proteins without knowing the nature of interaction.

In this study, we propose a novel and innovative study to use phage display libraries for identification of phages that can specifically and selectively bind to the mesenchymal breast cancer cells *invitro*. Since TGFβ is a known inducer of EMT, we have used a model of TGFβ induced EMT in MCF-7 breast cancer cells, (MCF-7/TGFβ) for selection of EMT-specific phages. CX7C PhD phage library was used for selection of phages binding to MCF-7/TGFβ cells after subtractive depletion from breast fibroblasts. These selected phages were then tested on breast cancer cells that exhibited EMT phenotype (MDA-MB-231 and T47D-shNMI) and breast cancer TMA of primary and metastatic site. The phage peptide LGLRGSL displayed specific binding to the EMT breast cancer cells as well recognized tumor in TMA's at primary as well as metastatic site.

MATERIALS AND METHODS

Materials

PhD CX7C phage library was purchased from New England Biolabs (NEB). Fetal calf serum (FCS) and cell culture media (Dulbecco's modified Eagle's medium, DMEM) was purchased from Sigma (USA). The phage display library contains random peptides constructed at the N terminus of the minor coat protein (cpIII) of M13 phage. The library contains a mixture of 3.1×10^9 individual clones, representing repertoire of phages with 7-mer peptide sequences, which expresses random 7-amino-acid sequences. The *Escherichia coli* host strain ER2738 (F+ strain, New England Biolabs) was used for M13 phage propagation. The human breast cancer cell lines MDA-MB-231, MCF-7 and breast fibroblasts (Hs 578T) were purchased from the American Type Culture Collection. MCF-7 cells were treated 1ng/mL of TGFβ for 16 days. MCF-7, MDA-MB-231, MCF-7/TGFβ, breast cancer cells, and SW620, colon cancer cells, were maintained in DMEM supplemented with 10% fetal bovine serum (Sigma) at 37°C. PC3, prostate cancer cells, were cultured in RPMI1640 media supplemented with 10% FBS at 37°C.Breast fibroblasts (Hs578T) were maintained in special hybricare medium supplemented with 15% FBS (ATCC).

Validation of EMT Marker in MCF7/TGFβ Cells by Western Blot

MCF-7 and MCF-7/TGFβ cells were grown in 25 cm^2 flask to 75–80% confluency. Confluent cells were lysed in ice-cold complete 1x RIPA buffer (PMSF solution, sodium orthovanadate solution, protease inhibitor cocktail solution, and 1x lysis buffer) (Santa Cruz Biotechnology, Santa Cruz, CA, United States). The protein concentration in the samples was quantified using the BCA Protein Assay Kit (Pierce Biotechnology, Rockford, IL, United States). Thirty microgram of protein from each sample was separated by a 4–12% SDS-PAGE gel and then transferred to a 0.2 μm polyvinylidene difluoride (PVDF) membrane. Membranes were blocked with 5% nonfat dry milk in PBS-T for 45 min and then incubated with the E-cad herin (Abcam, UK) or N-cadherin (Abcam, UK) primary antibody (1:1,000) overnight at 4°C. After washing, membranes were incubated with horseradish peroxidase (HRP)-conjugated secondary antibody (1:2,000). Subsequently, membranes were washed and blots were visualized using enhanced chemiluminescence. The membrane was stripped with mild stripping buffer and reprobed with β-actin (Cell Signaling, Danvers, MA, United States) to verify that equal

amount of protein was loaded. The relative quantification was normalized against β-actin using image J image analysis software.

In vitro Phage Selection

Biased protocol for selection of phages was employed as described (26) with some modifications. The PhD phage library (Cx7C) was depleted against a cell culture flask and breast fibroblasts (Hs578T). Unbound phages recovered from the depletion were incubated with confluent MCF-7/TGFβ cells at room temperature for 1 h. Unbound phages were washed away and cell-associated phages were eluted with elution buffer (200 mM glycine-HCl, 1 mg/ml BSA, 0.1 mg/ml phenol red, pH 2.2) for 10 min on ice. The eluate was neutralized with 376 μl of 1 M Tris (pH 9.1). Internalized phages were recovered with lysis buffer [2% CHAPS, 10 mM Tris, 2 mM EDTA (pH 8.0)] after further washing and propagated in bacteria to determine their titer as described previously (29). The results were expressed as a percentage of a ratio of output to input phage. The eluted phage and cell-internalized phage were amplified separately in bacteria and used in the second and third round of selection using the same protocol of depletion of the amplified phages (lysate and eluate) against breast fibroblasts and incubating MCF-7/TGFβ cells with unbound phages recovered from depletion. Sixty phages from the third round of selection were randomly picked and were propagated in the ER2738 bacteria. DNA was isolated form these 60 propagated clones using DNA isolation kit (QIAGEN GmbH, Hilden, Germany) and individual phage DNA sequences were identified. A sequencing primer used was 5′-CCC TCA TAG TTA GCG TAA CG-3′ (−96 gIII sequencing primer, provided in the Ph.D.-CX7C Phage display peptide library kit (NEB, MA).

Cell-Based ELISA and Phage Capture Assay

Selected phage clones were characterized for their selectivity toward EMT cells, MCF-7/TGFβ and MDA-MB-231 breast cancer cells in comparison with epithelial breast cancer cells, MCF-7, T47D, and breast fibroblasts using phage capture assay (29) and cell-based ELISA.

Briefly, in phage capture assay, target cells MCF-7/TGFβ, MDA-MB-231, MCF-7, T47D, T47D-shNMI, breast fibroblasts (Hs578T), PC3 (metastatic prostate cancer cells) and SW620 (metastatic colon cancer cells) were cultured in triplicate to confluence in separate wells of 12-well cell culture plates. Cells were incubated with phage (1×10^{10} pfu) at RT for 1.5 h. Cells were washed with 100 μl washing buffer for 5 min eight times to remove non-specifically interacting unbound phages. Cells were lysed with 50 μl lysis buffer (2.5% CHAPS) for 10 min on a rocker and the lysate containing phages was titered in *E. coli* ER2738 bacterial cells. Phage titer was calculated as a ratio of output to input phage.

ELISA:

Confluent monolayers of MCF-7/TGFβ, MDA-MB-231, MCF-7, T47D, T47D-shNMI and breast fibroblasts (Hs578T) cells were incubated at room temperature with individual phage clones (10^{10} PFU), for 1.5 h at RT. Subsequently, cells were washed with PBS containing 0.1% Tween-20, incubated with primary anti-M13-biotin antibody (1:1,000), for 1 h, at RT. Cells were washed again with PBS containing 0.1% Tween-20, incubated with secondary antibody streptavidin-HRP (1:2,000, 45 min, RT), developed with tetra methyl benzidine and read at absorbance 650 with microplate reader (BioTek).

Phage Capture Assay of Phage Binding to Cancer-Conditioned Media Activated Fibroblasts

Breast fibroblasts (Hs578T) were plated in a 12.5 cm^2 flask cultured until approximately 70% confluent. Once properly confluent, fibroblasts were then cultured in MDA-MB-231 conditioned media or normal fibroblasts media for 72 h. Thereafter, they were exposed to E11 phage (10^8 pfu) for 2 h and analyzed for binding in phage capture assay as described above.

Immunofluorescence Study of Selected Phages

MCF-7, MCF-7/TGFβ, MDA-MB-231 and Hs578T (breast fibroblasts) cells were seeded in 4-well chamber overnight. On next day, cells were fed with fresh medium. Phage LGLRGSL (E11) (10^8 pfu) was added in fresh medium and incubated at RT for 1 h. After removing the unbound phages, cells were washed with wash buffer (0.1% tween-20 in PBS) three times and fixed with 4% formaldehyde for 15 min at 37°C. Thereafter, cells were permeabilized with 0.2% Triton X-100 at RT for 10 min. Then, cells were washed with TBS 3 times. Before incubation with anti-phage antibody, cells were treated with blocking buffer for 30 min at RT. Cells were incubated with M13-pIII monoclonal antibody for 1 h at RT, washed and incubated with the secondary goat anti-mouse IgG antibody labeled with Alexa Flour® 488 (Molecular Probes) (1:500 in PBS containing 1% BSA) for 45 min at RT. Subsequently, cells were washed three times and stained with TOTO-3 for nucleus staining. Prolong Gold Anti-fade Reagents was used on the cells which were then covered with cover slides. Pictures were taken by using the NIKON eclipse TE 2000-E confocal microscope. The fluorescence intensity of the images was quantified using image J software.

Phage Binding to Breast Cancer Tissue Microarrays

The breast tissue microarrays were purchased from Novus Biological (Littleton, CO). TMA included 40 breast cancer infiltrating ductal carcinoma, 10 metastatic lymph node and 9 adjacent normal breast tissues. Clinico-histopathologic characteristics of the subjects in the tissue microarray study included grade, age, hormone status and clinical stage, according to information provided by the suppliers. Tissues were de-paraffinized in xylene, rehydrated in graded alcohols and endogenous peroxidase activity was quenched with 3% hydrogen peroxide for 5 min. Slides were treated with LGLRGSL phage (10^{10} pfu) overnight. Slides were subsequently washed and blocked by 3% goat serum at RT for 1 h in humidity chambers. Slides were then treated with M13-pIII phage monoclonal

antibody (NEB, MA) or Vimentin antibody (Cell Siganling, Danvers, MA, United States) (1:100) and then subsequently with HRP conjugated goat anti-mouse secondary antibody (Jackson Immunoresearch Laboratories Inc., West Grove, PA, United States) for 40 min. The antigen-antibody reaction was visualized after applying diaminobenzidine (Sigma-Aldrich, MO, United States) for 7 min. The slides were counterstained with hematoxylin (Sigma-Aldrich, MO, United States) for 1 min. Slides were dehydrated in alcohols and cleared in xylene baths before being mounted with Permount media.

Statistics

The significance of difference between two variables was assessed by the Student's *t*-test. The difference was considered significant if the *p*-value was <0.05. Data from all experiments are expressed as mean ± standard error (SD). All statistical calculations were performed using GraphPad Prism and Microsoft Excel.

RESULTS

Selection of Phages Binding to Breast Cancer Cells That Have Undergone EMT

MCF-7 (epithelial-luminal subtype) breast cancer cells were transformed into mesenchymal phenotype by long-term treatment with TGFβ (1 ng/mL for 16 days). **Figure 1A** shows the change of MCF-7 breast cancer cells change in morphology upon TGFβ treatment. Since reduction in E-cadherin and upregulation of mesenchyme markers, is a hallmark of metasatatic carcinoma's

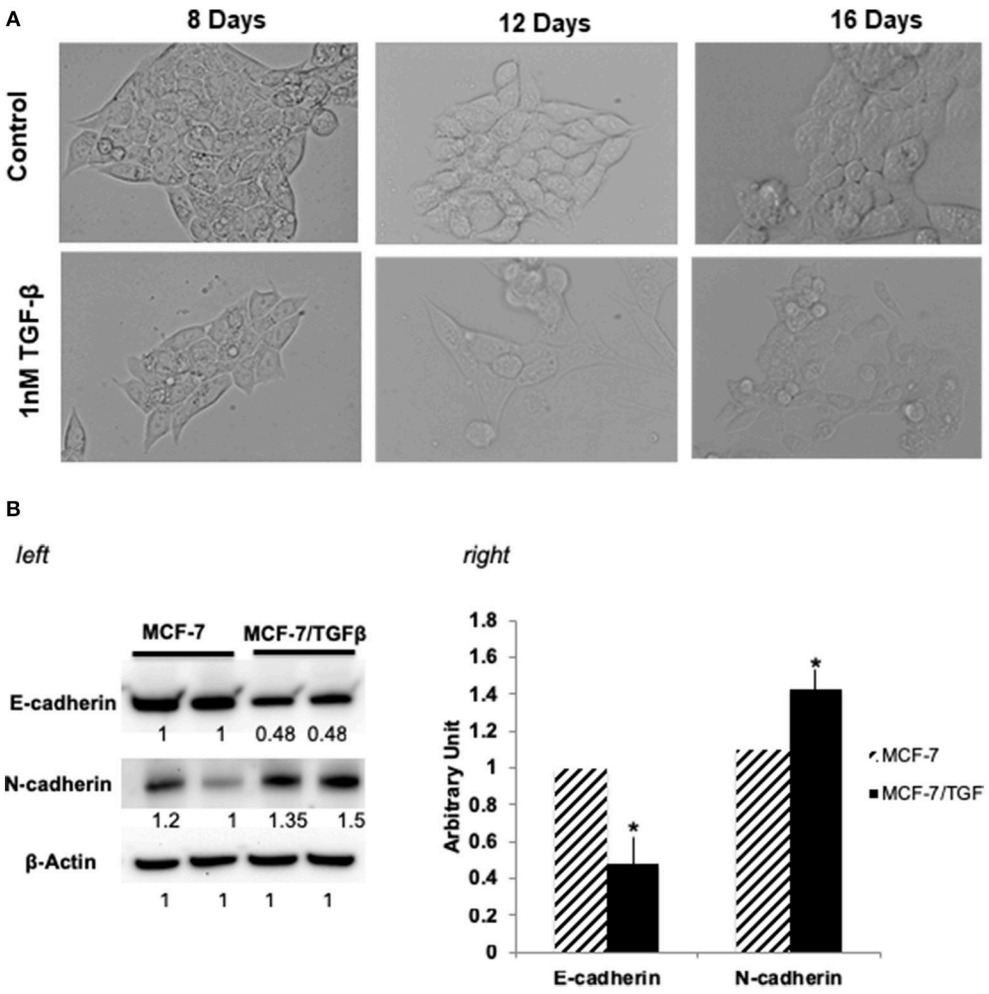

FIGURE 1 | (A) Morphological change in MCF-7 cells during TGFβ –induced EMT. Images of cells treated long term (16 days) with TGFβ showing spindle-shaped morphology as compared with control. Images were acquired by phase contrast microscopy using a 20 × objective. **(B) (left)** Immunoblot analysis of expression of EMT-related proteins. Protein expression levels of E-cadherin in TGFβ-treated MCF-7 cells were markedly decreased, whereas expression levels of N-cadherin and vimentin (mesenchymal markers) were dramatically increased. Numbers below each panel indicate the relative integrated density of the protein band in that lane. **(right)** Quantification analysis of the Western blot data showing the change in EMT markers (E-cadherin and N- cadherin) in MCF-7/TGFβ cells vs. MCF-7 breast cancer cells. The relative quantification was normalized against β-actin using image J image analysis software. All data represent the mean± S.D of three different experiments. *p <0.05, student-*t*-test.

and indication of EMT (33, 34), following treatment MCF-7/TGFβ cells were validated for EMT transition by looking at the protein expression of E-cadherin and N-cadherin (mesenchymal marker) (35). Consistent with literature that (33) demonstrated that TGFβ treatment downregulates E-cadherin expression in MCF-7 cells, our Western blot data confirmed these observations. **Figure 1B** showed downregulation of E-cadherin and upregulation of N-cadherin protein expression in MCF-7/TGFβ cells as compared to MCF-7 cells.

CX7C PhD phage library (NEB) was used to find phage clones that bind with high specificity and selectivity to MCF-7/TGFβ cells. Extensive depletion of the phage library against plastic, breast fibroblasts before enrichment of phage that interact with MCF-7-TGFβ breast cancer cells was employed for a robust selection of phage clones specific for cancer cells. This negative selection step was also performed after each round of panning on the MCF-7-TGFβ cells. Three such rounds of biopanning were performed on and in every round, phage library and sub-library was depleted against breast fibroblasts to preferentially select for phages that did not bind to normal fibroblasts. Phages associated with cells were eluted sequentially with acid and detergents. Titer of the phage increased from one round to another indicating successful enrichment for phage clones that bind to the target MCF-7-TGFβ cells (**Figure 2**). After the third round of selection, 100 phage clones were randomly picked after titering of the eluate and lysate fractions. Their DNA was isolated, sequenced and translated to reveal the sequence of the pIII fusion peptides. In total, 21 phage clones were isolated and classified based on their consensus foreign peptide motifs (**Table 1**).

Selectivity of Phages Toward Mesenchymal-Like Breast Cancer Cells

Phage clones obtained by screening of the CX7C phage library against MCF-7/TGFβ cancer cells were tested for their selective binding toward the target MCF-7/TGFβ, MDA-MB-231, T47D-shNMI cells and not to breast fibroblasts or epithelial subtype breast cancer cells MCF-7 and T47D in phage capture assay (**Figures 3A,B**) and phage based ELISA (**Figure 3C**).

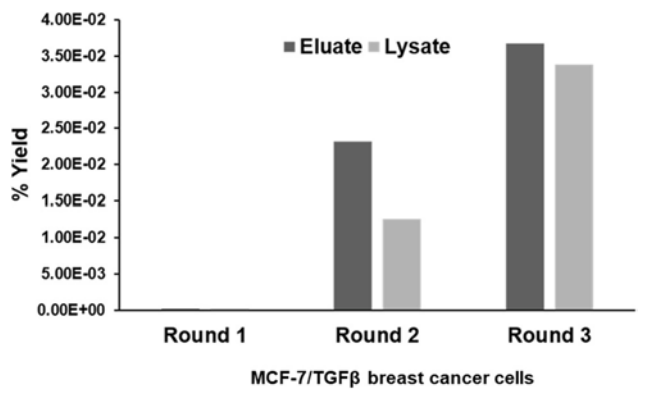

FIGURE 2 | Specific enrichment of eluate and lysate MCF-7/TGFβ cell-binding phage isolated from PhD CX7C library during three rounds of selection. The titer of recovered phages from each round was evaluated by blue plaque-forming assay on agar plates. The phage enrichment rate was calculated as yield (%), which is as output number/input number x100.

These cells lines MCF-7/TGFβ, MDA-MB-231, T47D-NMI exhibit mesenchymal phenotype or markers of EMT and are aggressive, are structurally similar to fibroblasts and expresses markers of EMT and thus are representation of EMT in breast cancer cells. MDA-MB-231 breast cancer cell line exhibit mesenchymal phenotype and are detonated EMT phenotype (36). T47D is an epithelial breast cancer cell line and was transitioned to EMT by silencing a gene, N-myc and STAT interactor (37).

In these assays, some phages demonstrated high selectivity toward EMT cells, while other phage showed selectivity for epithelial breast cancer cells as well as breast fibroblasts. Phages were considered selective if their relative binding to EMT phenotypic cells (MCF-7/TGFβ, MDA-MB-231, and T47D-shNMI) and were at least five times higher than those of epithelial breast cancer cells (MCF-7 and T47D) and breast fibroblasts. KGDYKLF (L42), phage selected from lysate fraction, showed high specificity toward MDA-MB-231 cells but not so selective toward MCF-7/TGFβ, MCF-7 and breast fibroblasts. Phages selected from eluate fraction, LGLRGSL (E11), GTFLFS (E32), and PNLPWVP (E45) were very selective for EMT phenotypic cells (MCF-7/TGFβ, MDA-MB-231, and T47D-shNMI) and

TABLE 1 | Displayed phage peptide sequences from isolated eluate and lysate phages from third round of selection against MCF/TGFβ breast cancer cells.

ELUATE PHAGE PEPTIDE SEQUENCES							
E9	I	L	N	C	M	R	N
E11	L	G	L	R	G	S	L
E12	A	R	K	T	N	P	L
E16	F	N	G	P	H	T	R
E20	T	K	F	H	F	S	G
E25	D	F	L	T	A	R	L
E29	N	T	F	S	W	H	T
E32	G	T	F	L	F	S	
E42	N	T	L	R	T	P	Y
E43	H	H	D	N	V	A	M
E45	P	N	L	P	W	V	P
E46	Y	E	H	H	P	R	I
E48	H	M	R	Q	G	M	A
LYSATE PHAGE PEPTIDE SEQUENCES							
L5	T	H	S	S	W	G	M
L9	N	M	W	E	S	V	P
L10	R	E	G	H	M	G	V
L24	K	D	S	H	E	P	W
L27	T	L	A	T	G	G	M
L30	P	Y	E	P	R	A	T
L42	K	G	D	Y	K	L	F
L45	S	I	L	S	K	N	H
L46	E	R	S	G	M	H	S
L47	H	W	P	A	K	H	I
L49	P	V	L	L	G	E	S

showed more than 10 times binding as compared to its binding to breast fibroblasts (Hs578T) and epithelial breast cancer cells (MCF-7 and T47D) in phage capture assay (**Figure 3A**). Phage E11 was confirmatory toward EMT cells in phage-based ELISA (**Figure 3B**) and thus was chosen for further characterization.

To determine if E11 could recognize EMT phenotype in other cell types of tumor microenvironment, E11 was screened against activated fibroblasts (fibroblasts converted to CAF's by treatment with cancer-conditioned media). E11 demonstrated higher binding (twice as much) to activated-fibroblasts than normal fibroblasts (**Figure 3C**). To see if E11 can recognize EMT on cancer other than breast, E11 was screened against other metastatic cancer cells, PC3 (prostate cancer) and SW620 (colon cancer) in phage capture assay. PC3 is a highly metastatic prostate cancer cell line and exhibits EMT phenotype (38, 39). SW620 are highly tumourigenic, metastatic and exhibit fibroblasts like morphology (40). E11 showed comparable binding to PC3 and SW620 like MDA-MB-231 (**Figure 3D**), which demonstrates that it is binding to a receptor common to metastatic phenotype.

Affirmation of Phages Binding to Target Cells *in vitro* Using Immunofluoresence Analysis

To further affirm the specificity of LGLRGSL (E11) toward breast cancer cells with an EMT phenotype, immunofluorescence microscopy of intact target mesenchymal phenotypic cells (MCF-7/TGF β and MDA-MB-231), control MCF-7 breast cancer cells and breast fibroblasts (Hs578T) was employed. All cells were treated with the phage (10^8 pfu) at RT for 1 h, and subsequently incubated with primary anti-pIII antibody and then stained with secondary anti-mouse Alexa fluor 488 secondary antibody. LGLRGSL (E11) showed almost no binding to breast fibroblasts (**Figure 4A**), some staining to MCF-7 cells (**Figure 4B**), while abundant binding to EMT cells, MCF-7/TGFβ (**Figure 4C**) and MDA-MB-231 (**Figure 4D**) as shown by green fluorescent phage staining and analysis (**Figure 4E**). We did not observe any background antibody as shown in the respective controls of cells treated with just primary and secondary antibodies.

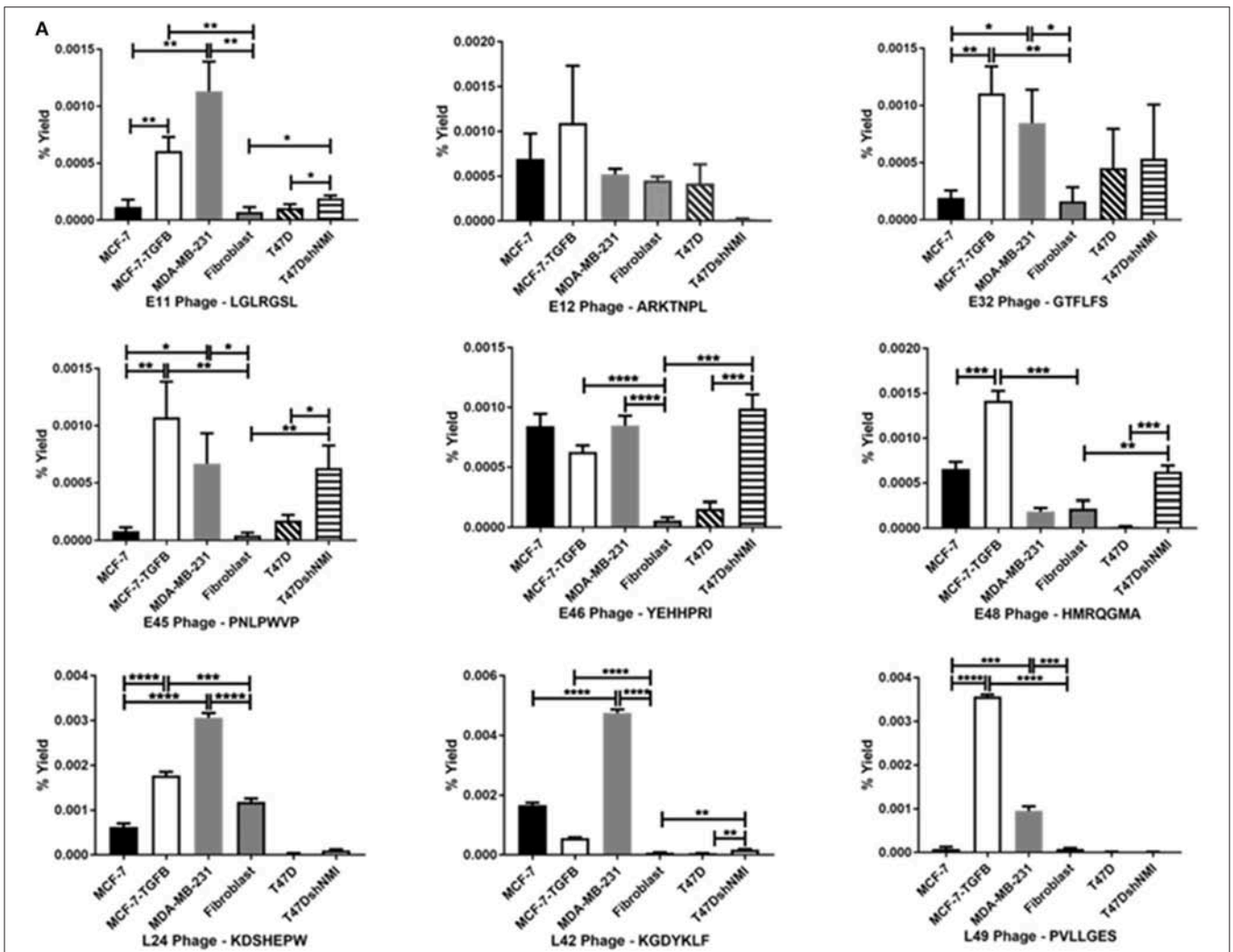

FIGURE 3 | continued

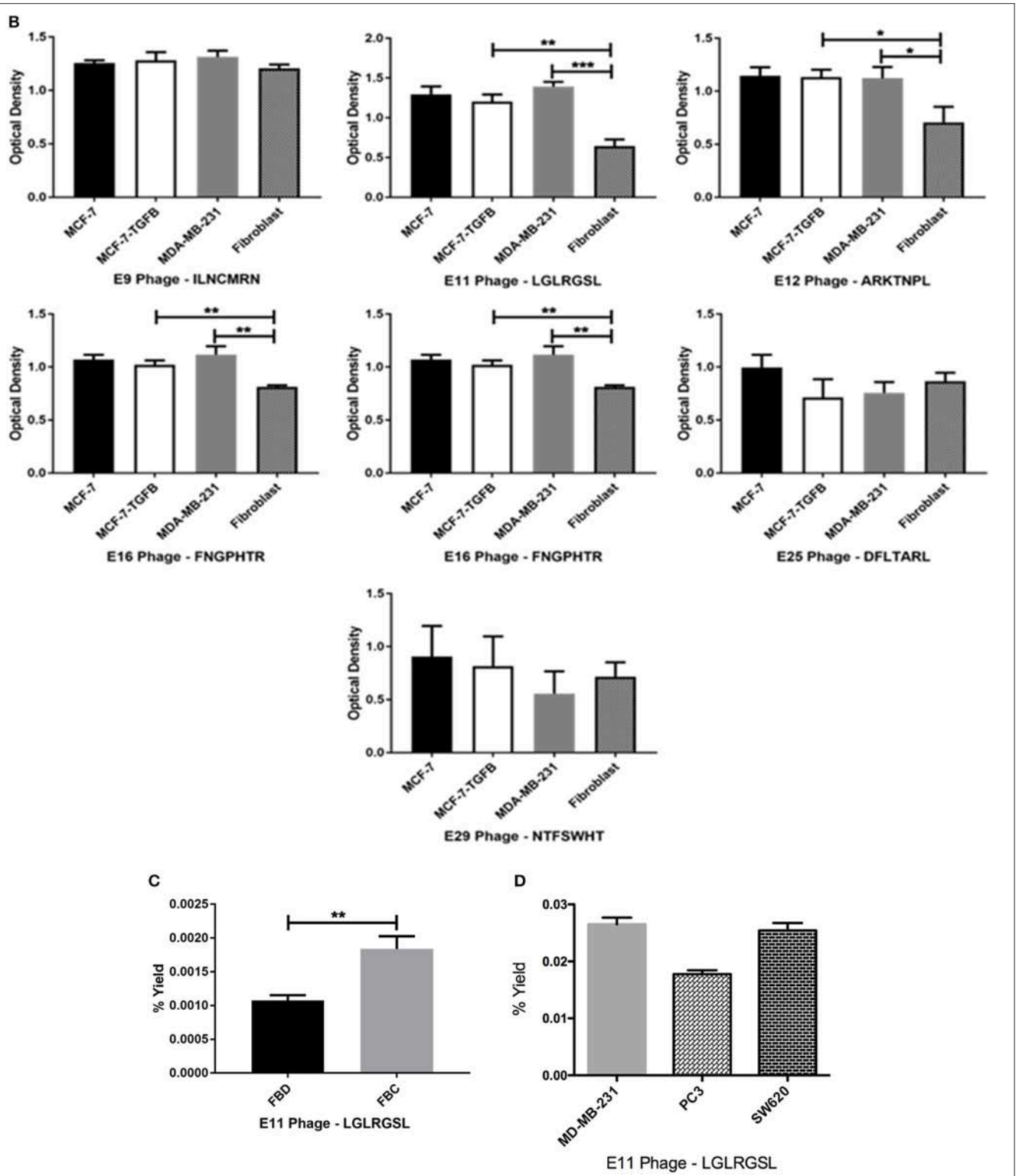

FIGURE 3 | Affinity selected eluate and lysate phage showed higher binding to MCF-7-TGFβ, MDA-MB-231, T47D-shNMI cells as compared to breast fibroblasts, T47D and MCF-7 cells in **(A)** phage capture assay; **(B)** in phage based-ELISA; **(C)** LGLRGSL (E11) was also highly reactive to activated fibroblasts. FBD denotes fibroblasts in normal fibroblast media and FBC denotes fibroblasts in MDA-MB-231 breast cancer cell conditioned media and **(D)** LGLRGSL showed comparable binding to PC3 and SW620 cancer cells as compared to MDA-MB-231 cancer cells. All data represent the mean± S.D. $^{*}p < 0.05$, $^{**}p \leq 0.01$, $^{***}p \leq 0.001$, and $^{****}p \leq 0.0001$.

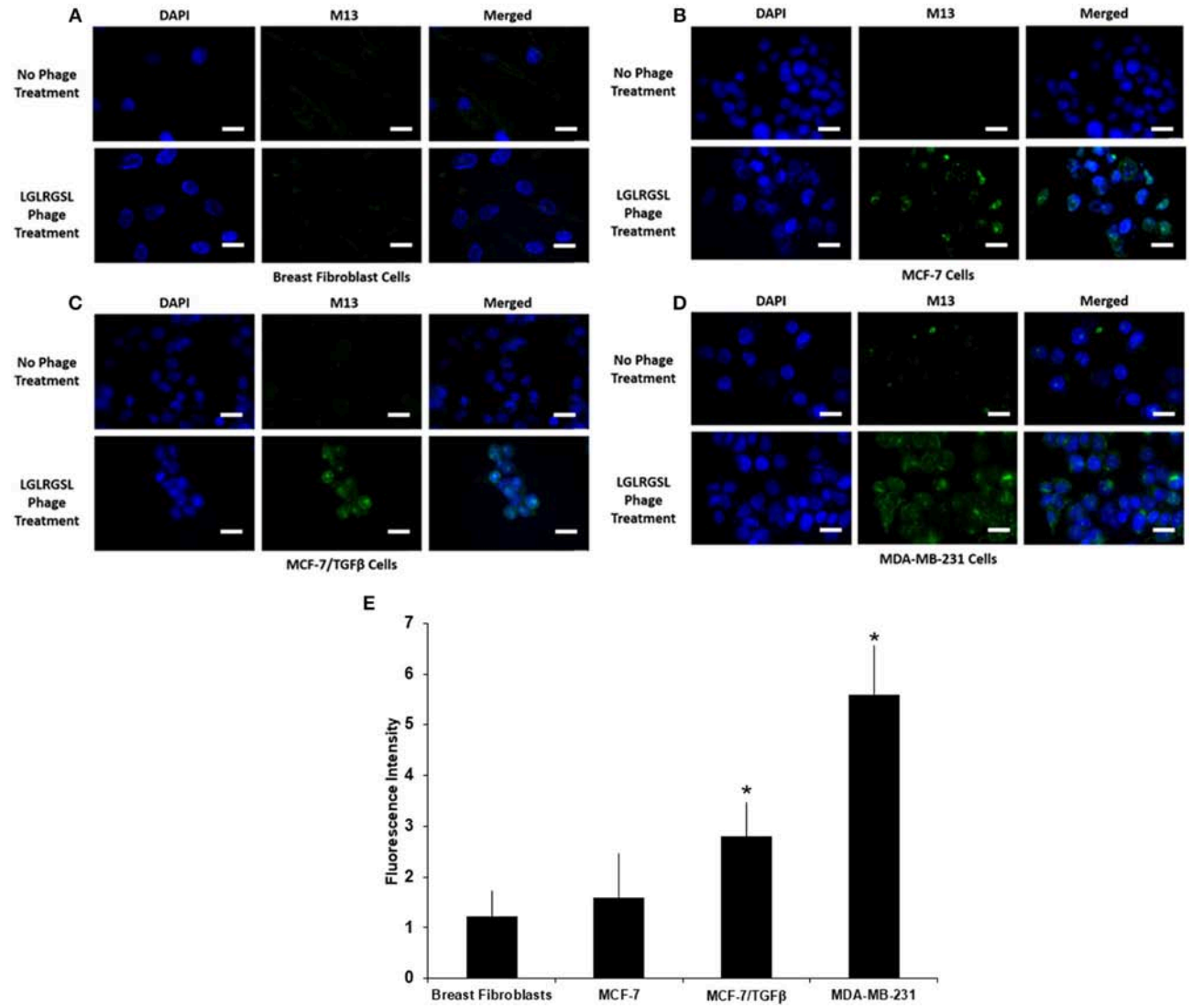

FIGURE 4 | A. Phage peptide LGLRGSL (E11) stained selective to EMT phenotypic cells in immunofluorescence microscopy analysis upper, **(A)** Breast Fibroblast, **(B)** MCF-7, **(C)** MCF-7/TGFβ, and **(D)** MDA-MB-231 cells without phage exposure; stained with DAPI and Alexa 488 secondary antibody, lower, **(A)** Breast Fibroblasts, **(B)**MCF-7, **(C)** MCF-7/TGF β, and **(D)**. MDA-MB-231 exposed to phage; stained with M13 primary antibody, DAPI and Alexa 488 secondary antibody. Scale bar is 20 μm. **(E)** Quantification data of the fluorescence intensity of the Breast fibroblasts, MCF-7, MCF-7/TGFβ, and MDA-MB-231 breast cancer cells. The fluorescence intensity of the images was quantified using Image J software. All data represent the mean± S.D of three different experiments. *p <0.05, student-t-test.

Validation of Phage Peptide Binding to Human Breast Cancer *Exvivo*

Next, we investigated the clinical relevance of these findings by assessing if LGLRGSL (E11) could be used to prospectively identify human invasive ductal carcinoma (IDC) breast tumors with a propensity to metastasize as metastatic cells undergo EMT before metastasizing (41). Immunostaining for phage in human breast cancer tissue indicated phage has substantial staining for invasive ductal breast cancer carcinoma (**Figures 5A–C**, left) and its staining intensity increased in tumors invading into adjacent lymph nodes (**Figure 5D**). Furthermore, we did not observe any binding in normal breast tissues (**Figure 5E**). Interestingly we observed that vimentin, a mesenchymal marker, within the same TMA (**Figures 5A–C**, right) demonstrated a different staining pattern than the LGLRGSL (E11) phage. While vimentin showed stromal staining, phage was immunoreactive to the tumor cells with robust staining around the invasive or leading edge of the tumor-stromal interaction.

DISCUSSION

There is accumulating evidence to show that epithelial cells can undergo transformation into migratory fibroblast-like mesenchymal cells in a process called EMT (Epithelial-to-Mesenchymal Transition). Normally, an embryo and organ development related phenomenon, EMT is believed to be crucial

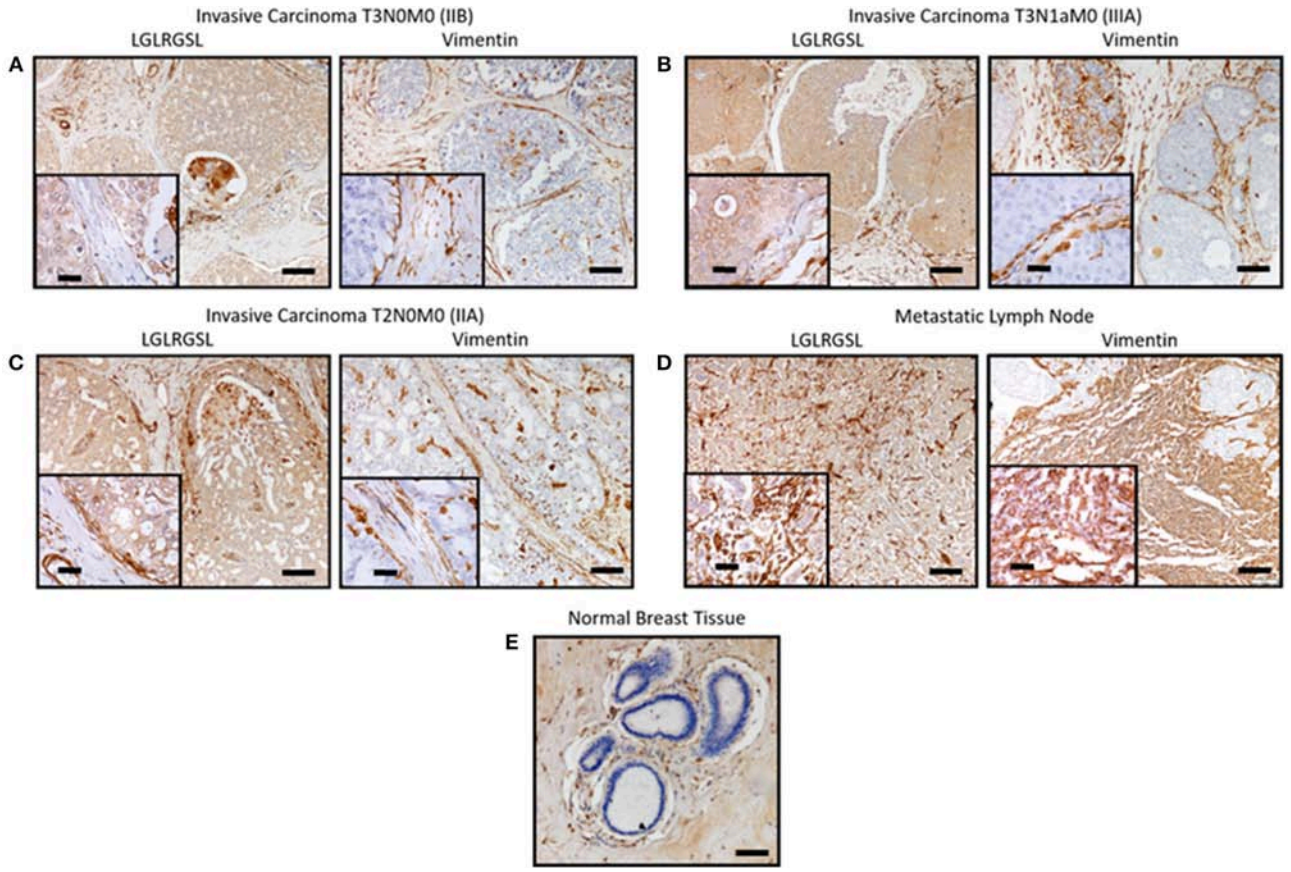

FIGURE 5 | *Ex vivo* phage binding to human breast cancer tissue microarray. Tissue microarray of invasive ductal carcinoma and adjacent normal tissues were incubated with 10^{10} pfu of LGLRGSL phage or Vimentin antibody and then subsequently with M13-pIII antibody for phage and secondary peroxidase antibody for phage and Vimentin, imaged with a digital light microscope. Strong brown staining of the phage and Vimentin was observed in invasive ductal carcinoma sections **(A–C)** and metastasis in lymph nodes, **(D)** while no staining was observed in normal breast tissue, **(E)** Scale Bar is 40 and 10 μm for the inserts.

for primary tumors to escape their original residence and invade and metastasize to other organs such as liver, lungs, bone and brain (42). Moreover, EMT is also a critical determinant of stemness and drug-related relapse (6, 41, 43). EMT of breast cancer cells is, in large part, dependent oncontingent on the tumor microenvironment (44). Because of the close cross-talk between the cancer cells and CAFs, it is evident that the development of cancer cannot be dissociated from its local microenvironment (45). Tumor cells signals stromal fibroblast cells and activate them into cancer-associated fibroblasts (CAFs) to undergo EMT through the stimulation of paracrine growth factors (46, 47) promotes EMT, cell survival (48) and progression (49) of cancer cells. To better understand the events involved from acquiring motility for invasion to seeding in distant organs, there is a need to develop probes that can selectively bind to invasive, metastatic and tumor-progressing CAF's (46). Such ligands can further ascertain the role of EMT in cancer metastasis and could enable the development of new approaches in the management of this disease.

In this study, we have successfully isolated phage ligands using CX7C phage library for EMT transformed breast cancer cells, MCF7/TGFβ and MDA-MB-231 by employing subtractive depletion of phages binding to breast fibroblasts. The optimizing procedures (several rounds of subtractive screening) were performed to improve the probability of successful selection, which is highly dependent on obtaining specific phages with high selectivity. The isolated clones were used in cell-ELISA and *invitro* phage capture assay to confirm their specificity to EMT phenotype cells, MCF-7/TGFβ, MDA-MB-231 and T47D-shNMI cells *in vitro* as compared to epithelial subtype cells, MCF-7, T47D and mesenchymal breast fibroblasts (Hs578T). Phage capture assay and ELISA demonstrated the selective affinity of various phages to EMT phenotype.

The best candidate, LGLRGSL (E11), was then selected for immunocytochemical assays. Immunofluorescence studies confirmed the selectivity of LGLRGSL (E11) to the target mesenchymal-like cells as there was minimal binding to the non-target epithelial breast cancer cells and mesenchymal breast fibroblasts. E11 also bound with great affinity to PC3, prostate cancer cells and SW620, colon cancer cells. It's binding to these other cancer cell type was as comparable as to MDA-MB-231 breast cancer cells. These findings suggest that LGLRGSL (E11) is

recognizing a receptor/antigen on mesenchymal-like cancer cells that are highly invasive and metastatic in nature and would be a useful probe to identify invasive front and metastatic tumor cells. Phage probing to the breast cancer tissue microarray identified tumor representing high grade and lymph node metastasis. When compared to Vimentin, a marker of mesenchymal-like cells metastasis, phage had more positive staining to the invasive front and lymph node metastasis.

More work is needed to characterize LGLRGSL (E11) as ligand binding to EMT marker of cancer origin. One such direction is the identification of the receptors responsible for LGLRGSL (E11) phage binding to the mesenchymal-like cells, that may allow for the discovery of novel cell surface molecules, which may yield future targets for drug design.

In conclusion, the 7-amino acid phage peptide, LGLRGSL, obtained by phage-display technology showed significant ability to bind to EMT breast cancer cells *in vitro* and tissues array *exvivo*. The phage peptide can be used for preparation of targeted devices for drug and gene delivery to metastatic cells; development of probes for molecular imaging of metastasis; and identification and isolation of cancer-specific receptors as potential components for development of therapeutic antibodies, anticancer vaccines and diagnostics.

AUTHOR CONTRIBUTIONS

KJ study design, performed experiments, data analysis and interpretation, and manuscript preparation. KJ, BK, JJ-T, HH and MS: performed experiments and data analysis. RS, ST, CY, and DB project supervision, study design, and manuscript preparation.

ACKNOWLEDGMENTS

This work was supported by SC2CA211028-03 (DB) (NIH/NCI/NIGMS) and U54-MD007585-26 (NIH/RCMI) [CY], U54 CA118623 (NIH/NCI) [CY], (NIH/NCI).

REFERENCES

1. Jemal A, Siegel R, Ward E, Hao Y, Xu J, Thun MJ. Cancer statistics, 2009. *Cancer J Clin.* (2009) 59:225–49. doi: 10.3322/caac.20006
2. Weng D, Penzner JH, Song B, Koido S, Calderwood SK, Gong J. Metastasis is an early event in mouse mammary carcinomas and is associated with cells bearing stem cell markers. *Breast Cancer Res.* (2012) 14:R18. doi: 10.1186/bcr3102
3. Tsai JH, Donaher JL, Murphy DA, Chau S, Yang J. Spatiotemporal regulation of epithelial-mesenchymal transition is essential for squamous cell carcinoma metastasis. *Cancer Cell* (2012) 22:725–36. doi: 10.1016/j.ccr.2012.09.022
4. Menezes ME, Devine DJ, Shevde LA, Samant RS. Dickkopf1: a tumor suppressor or metastasis promoter? *Int J Cancer* (2012) 130:1477–83. doi: 10.1002/ijc.26449
5. Quail DF, Joyce JA. Microenvironmental regulation of tumor progression and metastasis. *Nat Med.* (2013) 19:1423–37. doi: 10.1038/nm.3394
6. Wang Y, Zhou BP. Epithelial-mesenchymal transition in breast cancer progression and metastasis. *Chinese J Cancer* (2011) 30:603–11. doi: 10.5732/cjc.011.10226
7. Trimboli AJ, Fukino K, de Bruin A, Wei G, Shen L, Tanner SM, et al. Direct evidence for epithelial-mesenchymal transitions in breast cancer. *Cancer Res.* (2008) 68:937–45. doi: 10.1158/0008-5472.CAN-07-2148
8. Harris LG, Samant RS, Shevde LA. Hedgehog signaling: networking to nurture a promalignant tumor microenvironment. *Mol Cancer Res.* (2011) 9:1165–74. doi: 10.1158/1541-7786.MCR-11-0175
9. Barcellos-Hoff MH, Akhurst RJ. Transforming growth factor-beta in breast cancer: too much, too late. *Breast Cancer Res.* (2009) 11:202. doi: 10.1186/bcr2224
10. Gotzmann J, Fischer AN, Zojer M, Mikula M, Proell V, Huber H, et al. A crucial function of PDGF in TGF-β-mediated cancer progression of hepatocytes. *Oncogene* (2006) 25:3170–85. doi: 10.1038/sj.onc.1209083
11. Miettinen PJ, Ebner R, Lopez AR, Derynck R. TGF-beta induced transdifferentiation of mammary epithelial cells to mesenchymal cells: involvement of type I receptors. *J Cell Biol.* (1994) 127:2021–36. doi: 10.1083/jcb.127.6.2021
12. Li H, Fan X, Houghton J. Tumor microenvironment: the role of the tumor stroma in cancer. *J Cell Biochem.* (2007) 101:805–15. doi: 10.1002/jcb.21159
13. Mitra A, Menezes ME, Shevde LA. Samant RS, DNAJB6 induces degradation of beta-catenin and causes partial reversal of mesenchymal phenotype. *J Biol Chem.* (2010) 285:24686–94. doi: 10.1074/jbc.M109.094847
14. Moody SE, Perez D, Pan TC, Sarkisian CJ, Portocarrero CP, Sterner CJ, et al. The transcriptional repressor Snail promotes mammary tumor recurrence. *Cancer Cell* (2005) 8:197–209. doi: 10.1016/j.ccr.2005.07.009
15. Morrow KA, Das S, Metge BJ, Ye K, Mulekar MS, Tucker JA, et al. Loss of tumor suppressor Merlin in advanced breast cancer is due to post- translational regulation. *J Biol Chem.* (2011) 286:40376–85. doi: 10.1074/jbc.M111.250035
16. Zeisberg M, Neilson EG. Biomarkers for epithelial-mesenchymal transitions. *J Clin Invest.* (2009) 119:1429–37. doi: 10.1172/JCI36183
17. Franke WW, Schmid E, Osborn M, Weber K. Different intermediate-sized filaments distinguished by immunofluorescence microscopy. *Proc Natl Acad Sci USA.* (1978) 75:5034–8. doi: 10.1073/pnas.75.10.5034
18. Dellagi K, Vainchenker W, Vinci G, Paulin D, Brouet JC. Alteration of vimentin intermediate filament expression during differentiation of human hemopoietic cells. *EMBO J* (1983) 2:1509–14. doi: 10.1002/j.1460-2075.1983.tb01615.x
19. Smith GP, Petrenko VA. Phage Display. *Chem Rev.* (1997) 97:391–410. doi: 10.1021/cr960065d
20. Petrenko VA, Smith GP, Gong X, Quinn T. A library of organic landscapes on filamentous phage. *Protein Eng.* (1996) 9:797–801. doi: 10.1093/protein/9.9.797
21. Kelly KA, Jones DA. Isolation of a colon tumor specific binding peptide using phage display selection. *Neoplasia* (2003) 5:437–44. doi: 10.1016/S1476-5586(03)80046-5
22. Newton JR, Kelly KA, Mahmood U, Weissleder R, Deutscher SL. *In vivo* selection of phage for the optical imaging of PC-3 human prostate carcinoma in mice. *Neoplasia* (2006) 8:772–80. doi: 10.1593/neo.06331
23. Jayanna PK, Bedi D, Deinnocentes P, Bird RC, Petrenko VA. Landscape phage ligands for PC3 prostate carcinoma cells. *Protein Eng Design Select.* (2010) 23:423–30. doi: 10.1093/protein/gzq011
24. Kelly KA, Bardeesy N, Anbazhagan R, Gurumurthy S, Berger J, Alencar H, et al. Targeted nanoparticles for imaging incipient pancreatic ductal adenocarcinoma. *PLoS Med* (2008) 5:e85. doi: 10.1371/journal.pmed.0050085
25. Shukla GS, Krag DN. Cancer cell-specific internalizing ligands from phage displayed β-lactamase-peptide fusion libraries. *Protein Eng Design Select.* (2010) 23:431–40. doi: 10.1093/protein/gzq013
26. Fagbohun OA, Bedi D, Grabchenko NI, Deinnocentes PA, Bird RC, Petrenko VA. Landscape phages and their fusion proteins targeted to breast cancer cells. *Protein Eng Design Select.* (2012) 25:271–83. doi: 10.1093/protein/gzs013
27. Wang T, D'Souza GG, Bedi D, Fagbohun OA, Potturi LP, Papahadjopoulos-Sternberg B, et al. Enhanced binding and killing of target tumor cells by drug-loaded liposomes modified with tumor-specific phage fusion coat protein. *Nanomedicine* (2010) 5:563–74. doi: 10.2217/nnm.10.30
28. Bedi D, Musacchio T, Fagbohun OA, Gillespie JW, Deinnocentes P, Bird RC, et al. Delivery of siRNA into breast cancer cells via phage

fusion protein-targeted liposomes. *Nanomedicine* (2011) 7:315–23. doi: 10.1016/j.nano.2010.10.004
29. Jayanna PK, Bedi D, Gillespie JW, DeInnocentes P, Wang T, Torchilin VP, et al. Landscape Phage Fusion Protein-mediated Targeting of Nanomedicines Enhances their Prostate Tumor Cell Association and Cytotoxic Efficiency. *Nanomedicine* (2010) 6:538–46. doi: 10.1016/j.nano.2010.10.004
30. Rasmussen UB, Schreiber V, Schultz H, Mischler F, Schughart K. Tumor cell-targeting by phage-displayed peptides. *Cancer Gene Ther.* (2002) 9:606–12. doi: 10.1038/sj.cgt.7700476
31. Teesalu T, Sugahara KN, Ruoslahti E. Mapping of vascular ZIP codes by phage display. *Methods Enzymol.* (2012) 503:35–56. doi: 10.1016/B978-0-12-396962-0.00002-1
32. Li XB, Schluesener HJ, Xu SQ. Molecular addresses of tumors: selection by *in vivo* phage display. *Arch Immunol Ther Exp.* (2006) 54:177–81. doi: 10.1007/s00005-006-0026-y
33. Mahdi SH, Cheng H, Li J, Feng R. The effect of TGF-beta-induced epithelial-mesenchymal transition on the expression of intracellular calcium-handling proteins in T47D and MCF-7 human breast cancer cells. *Arch Biochem Biophys.* (2015) 583:18–26. doi: 10.1016/j.abb.2015.07.008
34. Lombaerts M, van Wezel T, Philippo K, Dierssen JWF, Zimmerman RME, Oosting J, et al. E-cadherin transcriptional downregulation by promoter methylation but not mutation is related to epithelial-to-mesenchymal transition in breast cancer cell lines. *Br J Cancer* (2006) 94:661–71. doi: 10.1038/sj.bjc.6602996
35. Nakajima S, Doi R, Toyoda E, Tsuji S, Wada M, Koizumi M, et al. N-cadherin expression and epithelial-mesenchymal transition in pancreatic carcinoma. *Clin Cancer Res.* (2004) 10:4125–33. doi: 10.1158/1078-0432.CCR-0578-03
36. D'Amato NC, Ostrander JH, Bowie ML, Sistrunk C, Borowsky A, Cardiff RD, et al. Evidence for phenotypic plasticity in aggressive triple-negative breast cancer: human biology is recapitulated by a novel model system. *PLoS ONE* (2012) 7:e45684. doi: 10.1371/journal.pone.0045684
37. Devine DJ, Rostas JW, Metge BJ, Das S, Mulekar MS, Tucker JA, et al. Loss of N-Myc interactor promotes epithelial-mesenchymal-transition by activation of TGF-β/SMAD signaling. *Oncogene* (2014) 33:2620–28. doi: 10.1038/onc.2013.215
38. Tai S, Sun Y, Squires JM, Zhang H, Oh WK, Liang CZ, et al. PC3 is a cell line characteristic of prostatic small cell carcinoma. *Prostate* (2011) 71:1668–79. doi: 10.1002/pros.21383
39. Ke XS, Qu Y, Goldfinger N, Rostad K, Hovland R, Akslen LA, et al. Epithelial to mesenchymal transition of a primary prostate cell line with switches of cell adhesion modules but without malignant transformation. *PLoS ONE* (2008) 3:e3368. doi: 10.1371/journal.pone.0003368
40. Hewitt RE, McMarlin A, Kleiner D, Wersto R, Martin P, Tsokos M, et al. Validation of a model of colon cancer progression. *J. Pathol.* (2000) 192:446–54. doi: 10.1002/1096-9896(2000)9999:9999<::AID-PATH775>3.0.CO;2-K
41. Heerboth S, Housman G, Leary M, Longacre M, Byler S, Lapinska K, et al. EMT and tumor metastasis. *Clin Transl Med.* (2015) 4:6. doi: 10.1186/s40169-015-0048-3
42. Seyfried TN, Huysentruyt LC. On the origin of cancer metastasis. *Crit Rev Oncogen.* (2013) 18:43–73. doi: 10.1615/CritRevOncog.v18.i1-2.40
43. Ayob AZ, Ramasamy TS. Cancer stem cells as key drivers of tumour progression. *J Biomed Sci.* (2018) 25:20. doi: 10.1186/s12929-018-0426-4
44. Schedin P, Borges V. Breaking down barriers: the importance of the stromal microenvironment in acquiring invasiveness in young women's breast cancer. *Breast Cancer Res.* (2009) 11:102. doi: 10.1186/bcr2235
45. Ishii G. Crosstalk Between Cancer Associated Fibroblasts and Cancer Cells in the Tumor Microenvironment After Radiotherapy. *EBioMedicine* (2017) 17:7-8. doi: 10.1016/j.ebiom.2017.03.004
46. Kalluri R, Zeisberg M. Fibroblasts in cancer. *Nature reviews. Cancer 6* (2006) 392–401. doi: 10.1038/nrc1877
47. Tejada ML, Yu L, Dong J, Jung K, Meng G, Peale FV, et al. Tumor-driven paracrine platelet-derived growth factor receptor alpha signaling is a key determinant of stromal cell recruitment in a model of human lung carcinoma. *Clin Cancer Res.* (2006) 12:2676–88. doi: 10.1158/1078-0432.CCR-05-1770
48. Martinez-Outschoorn UE, Trimmer C, Lin Z, Whitaker-Menezes D, Chiavarina B, Zhou J, et al. Autophagy in cancer associated fibroblasts promotes tumor cell survival: role of hypoxia, HIF1 induction and NFkappaB activation in the tumor stromal microenvironment. *Cell Cycle* (2010) 9:3515–33. doi: 10.4161/cc.9.17.12928
49. Giannoni E, Bianchini F, Masieri L, Serni S, Torre E, Calorini L, et al. Reciprocal activation of prostate cancer cells and cancer-associated fibroblasts stimulates epithelial-mesenchymal transition and cancer stemness. *Cancer Res.* (2010) 70:6945–56. doi: 10.1158/0008-5472.CAN-10-0785

Conflict of Interest Statement: The authors declare that the research was conducted in the absence of any commercial or financial relationships that could be construed as a potential conflict of interest.

frontiers in Pharmacology

REVIEW
published: 17 December 2018
doi: 10.3389/fphar.2018.01453

Therapeutic Potential of Nitrogen Mustard Based Hybrid Molecules

Yiming Chen[1†], Yuping Jia[2†], Weiguo Song[1] and Lei Zhang[1]*

[1] Department of Medicinal Chemistry, School of Pharmacy, Weifang Medical University, Weifang, China, [2] Shandong Academy of Pharmaceutical Science, Jinan, China

As medicine advances, cancer is still among one of the major health problems, posing significant threats to human health. New anticancer agents features with novel scaffolds and/or unique mechanisms of action are highly desirable for the treatment of cancers, especially those highly aggressive and drug-resistant ones. Nitrogen mustard has been widely used as an anticancer drug since the discovery of its antitumor effect in the 1942. However, the lack of selectivity to cancer cells restricts the wide usage of a mass of nitrogen mustard agents to achieve further clinical significance. Discovery of antitumor hybrids using nitrogen mustards as key functional groups has exhibited enormous potential in the drug development. Introduction of nitrogen mustards resulted in improvement in the activity, selectivity, targetability, safety, pharmacokinetics and pharmacodynamics properties of corresponding lead compounds or agents. Herein, the recently developed nitrogen mustard based hybrids have been introduced in the cancer therapy.

Keywords: antitumor, nitrogen mustard, hybrids, side effects, drug discovery

OPEN ACCESS

Edited by:
Zhe-Sheng Chen,
St. John's University, United States

Reviewed by:
Xiaozhuo Liu,
University at Buffalo, United States
Guannan Zhang,
University of Pennsylvania, United States

***Correspondence:**
Lei Zhang
leiqdu@foxmail.com

† These authors have contributed equally to this work

Specialty section:
This article was submitted to Experimental Pharmacology and Drug Discovery, a section of the journal Frontiers in Pharmacology

Received: *31 October 2018*
Accepted: *27 November 2018*
Published: *17 December 2018*

Citation:
Chen Y, Jia Y, Song W and Zhang L (2018) Therapeutic Potential of Nitrogen Mustard Based Hybrid Molecules. Front. Pharmacol. 9:1453. doi: 10.3389/fphar.2018.01453

INTRODUCTION

In recent years, malignant tumors have become a serious threat to human health due to their worldwide rising incidence and mortality. Second to cardiovascular diseases, cancer contributed the second most mortalities among all diseases (Torre et al., 2015; Ryerson et al., 2016; Lallukka et al., 2017). In recent decades, development of antitumor drugs has achieved significant progress in the treatment of cancer. Since nitrogen mustard, known as an alkylating agent, was proven effective in the treatment of malignant lymphoma in the 1940s, the usage of nitrogen mustard drugs in cancer chemotherapy has a history of over 70 years. At present, nitrogen mustard agents are still used clinically, and targeted modification of nitrogen mustards is an important strategy for the discovery of anticancer drugs. The development of nitrogen mustard derivatives originated from bis(2-chloroethyl) sulfide, which was used as a poison gas during World War II (Gilman, 1963; DeVita and Chu, 2008). After a terrible accident, it was found that bis(2-chloroethyl) sulfide exhibited therapeutic potential on leukemia. Because of its severe toxicity, bis(2-chloroethyl) sulfide was not applied as a antitumor drug for clinical use. However, nitrogen mustard antitumor drugs were developed based on the leukocyte killing effect of bis(2-chloroethyl) sulfide (**Figure 1**).

Nitrogen mustard is a kind of bio-alkylating agent, which can form active electron-deficient intermediates or other compounds with active electrophilic groups *in vivo*. The active intermediates can react electrophilically with some electron-rich groups in bio-macromolecules by forming covalent bonds, and results in activity inhibition of corresponding bio-macromolecules. The mechanism of nitrogen mustards includes DNA binding and cross-linking, thus preventing DNA

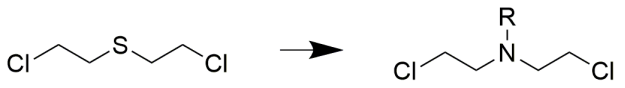

FIGURE 1 | Origin of nitrogen mustards.

replication and cell proliferation. Since its binding to the N7 nitrogen-atoms on DNA guanines with poor selectivity, nitrogen mustard agents are revealed to be toxic to normal cells (Kohn et al., 1987; Bank et al., 1989; Povirk and Shuker, 1994; Di Antonio et al., 2014).

Clinical application of nitrogen mustard compounds has a long history, but the present and future application of nitrogen mustards is limited by disadvantages including poor selectivity and severe adverse reactions (Frei et al., 1988; Sanderson and Shield, 1996; Schobert et al., 2009; Chen et al., 2014). Therefore, enormous effort has been made in the development of nitrogen mustard derivatives, aiming to obtain antitumor nitrogen mustard drugs with high activity and low toxicity (Zarytova et al., 1990). In recent years, the discovery of nitrogen mustard drugs and derivatives has become attractive field in the anticancer therapy. Development of nitrogen mustard based hybrid molecules by introducing druggable fragment, has been considered to be effective strategy in the antitumor drug discovery. Herein, recently development of nitrogen mustard based hybrids was reviewed and provided suggestions for the future study of bifunctional and multitargeted antitumor drugs.

NITROGEN MUSTARD DRUGS

According to different carriers, nitrogen mustard drugs can be classified into several classes, including fatty nitrogen mustard, aromatic nitrogen mustard, amide nitrogen mustard, amino acid and polypeptide nitrogen mustard, and heterocyclic nitrogen mustard.

Chlormethine **1** (**Figure 2**), a fatty nitrogen mustard, is now rarely used for clinic due to its poor selectivity and severe toxicity. The introduction of aromatic rings into nitrogen mustard causes the decrease of electrophilicity of the nitrogen atom. Consequently, aromatic nitrogen mustards are characterized with reduced reactivity and toxicity compared with fatty nitrogen mustard (Goodman and Wintrobe, 1946). Chlorambucil **2** (**Figure 2**) is used clinically for the treatment of ovarian cancer, Hodgkin's disease, chronic lymphocytic leukemia and lymphosarcoma (Galton et al., 1961). Clinical application of chlorambucil is also limited by adverse effects including nausea, vomiting, anemia, bone marrow suppression and neurotoxicity (Springer et al., 1990; Nicolle et al., 2004). Melphalan **3** (**Figure 2**), which takes phenylalanine as the carrier, has exhibited clinical effects on ovarian cancer, breast cancer, lymphoid sarcoma and multiple myeloma (Sarosy et al., 1988). Cyclophosphamide **4** (**Figure 2**), a heterocyclic amide nitrogen mustard, features a board spectrum of anti-malignancy activity, and is commonly utilized in the management of malignant lymphoma, acute lymphoblastic leukemia, multiple myeloma, lung cancer, neuroblastoma, breast cancer, ovarian cancer and nasopharyngeal cancer (Hughes et al., 2018). Moreover, cyclophosphamide has been discovered to be less toxicity than other types of nitrogen mustard drugs, due to the specific metabolic pathway.

NITROGEN MUSTARD BASED HYBRIDS

In recent years, it has been revealed that the conjugation of targeted antitumor drugs or natural molecules with nitrogen mustard drugs provides novel strategies for the discovery of antitumor molecules with improved antitumor effect, selectivity, and reduced toxicity.

Brefeldin A (BFA) **5** (**Figure 3**) is a 16-member macrolide antibiotic with a broad range of pharmacological activities, including antitumor, antiviral and antifungal effects (Rajamahanty et al., 2010; Moon et al., 2012; South et al., 2013; Toda et al., 2015; Grose and Klionsky, 2016; Huang et al., 2017). In the antiproliferative activity assay, BFA exhibited GI_{50} (half maximal growth inhibitory concentration) value of 40 nM against the national cancer institute NCI-60 cancer cell line (Anadu et al., 2006). Although BFA has great potentials to serve as a cancer chemotherapeutic drug, its development is still restricted by major limitations including severe undesirable effects and relatively low selectivity on tumor cells over normal ones (Kikuchi et al., 2003; Seehafer et al., 2013). Several novel BFA-nitrogen mustard conjugates were derived by introducing nitrogen mustards at 4-OH and/or 7-OH of BFA (Han et al., 2018). All the synthesized BFA-nitrogen mustard compounds **5a-i** (**Figure 3**) were assessed for their effectiveness against different tumor cell lines. Several hybrid molecules exhibited potent cytostatic activities and improved selectivity on malignant cells over normal ones. It is revealed that almost all the new BFA-nitrogen mustards showed stronger cytotoxic activities against one or more cell lines than nitrogen mustards and even 5-FU. Among all the tested compounds, molecule **5a** exhibited the most potent antiproliferative effects against various tumor cell lines (with IC_{50} (half maximal inhibitory concentration) values of 4.48, 9.37, 0.2, and 0.84 μM against human leukemia HL-60, human prostate PC-3, human hepatocellular carcinoma Bel-7402 and drug-resistant Bel-7402/5-FU cell lines), respectively. Molecule **5a** also displayed much lower cytotoxicity (IC_{50} < 0.001 μM) than BFA (IC_{50} = 9.74 μM) against normal human hepatic L-O2 cells. Therefore, introduction of nitrogen mustard to toxic natural products could be significant in the improvement the potency and safety of lead compounds.

Evodiamine **6** (**Figure 4**) is a natural quinolone alkaloid widely studied for the treatment of diverse human disorders including Alzheimer's disease, inflammation and especially cancer (Ogasawara et al., 2002; Yu et al., 2013; Lv et al., 2015; Shi L. et al., 2016; Wang et al., 2016; Wu et al., 2016; Fan et al., 2017; Shi et al., 2017). By targeting topoisomerase I and II, evodiamine has induced apoptosis and cell cycle arrest of a broad spectrum of tumor cell lines (Shyu et al., 2006). However, it is revealed that evodiamine is cytotoxic to human normal

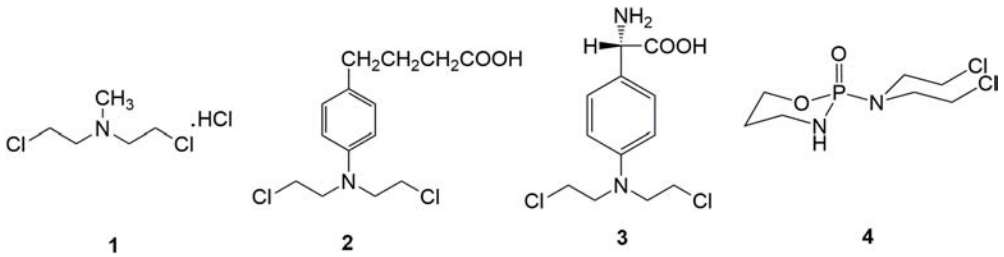

FIGURE 2 | Representative nitrogen mustard agents.

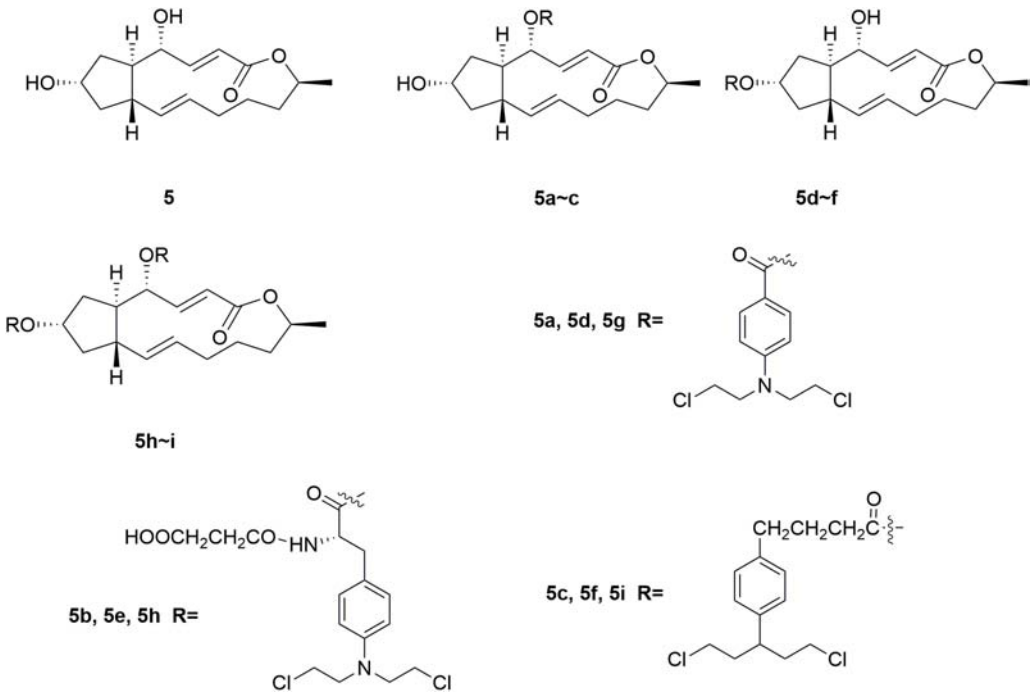

FIGURE 3 | Structures of Brefeldin A-nitrogen mustard hybrids.

cells, such as peripheral blood mononuclear cells (PBMC). In discovery of antitumor agent with improved potency and reduced adverse side effects, conjunct of evodiamine to nitrogen mustards was carried out by Li and coworkers (Hu et al., 2017). The synthesized nitrogen mustard-evodiamine hybrids were evaluated in the antitumor activity assay. Compared with evodiamine (IC_{50} values of 22.87 μM against PBMC cells), all the tested mustard-evodiamine hybrids **7a-d, 8a-d, 9a-d** (**Figure 4**) showed improved safety properties with IC_{50} values of more than 200 μM in inhibition the proliferation of PBMC cells. Remarkably, molecule **9c** revealed potent antiproliferative effects against human liver cancer HepG2, human leukemic THP-1 and HL-60 cell lines with IC_{50} value of 17.04 μM, 4.05 μM and 0.50 μM, respectively. The involved investigations indicated that further drug discovery based on **9c** is promising in the treatment of tumor, such as leukemia. Collectively, introduction of nitrogen mustard moiety has shown significance in the improvement of potency and safety, and the nitrogen mustard hybridation strategy could be productive for the optimization of lead compounds.

Oridonin **10** (**Figure 5**) is a kind of natural diterpenoids, which has a unique, safe, broad antitumor activity (Sun et al., 2006; Cui et al., 2007; Zhou et al., 2007; Bao et al., 2014; Li Y. et al., 2015; Ding et al., 2016; Dong et al., 2016; Shi M. et al., 2016; Liu et al., 2017). However, the utilization of oridonin in cancer chemotherapy was limited by its relatively low potency (Wang et al., 2012; Xu S.T. et al., 2014). Development of oridonin-nitrogen mustard conjugates used for antitumor application has been demonstrated to be promising in the drug discovery (Ding et al., 2013a,b). Several synthetic oridonin-nitrogen mustard conjugates **10a**∼**f** (**Figure 5**), and their anticancer activities evaluated in four human malignant cell lines (human leukemia K562 cells, human breast cancer MCF-7 cells, human hepatocellular carcinoma Bel-7402 cells, and human gastric cancer MCG-803 cells) were reported by Xu and coworkers (Xu S. et al., 2014). All the tested compounds exhibited better

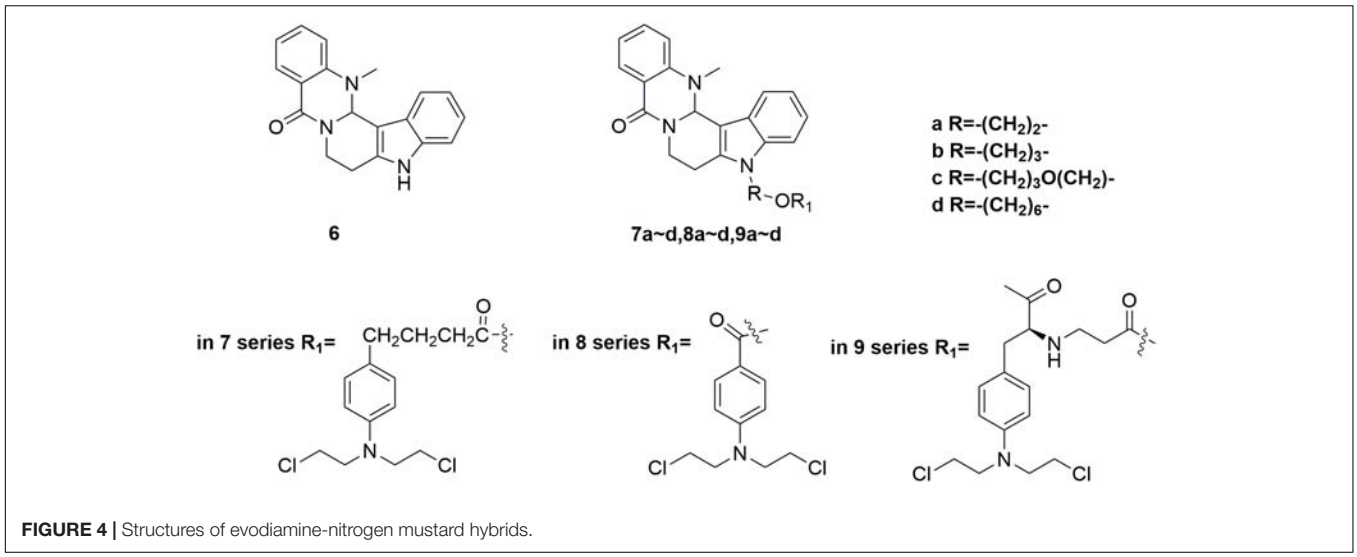

FIGURE 4 | Structures of evodiamine-nitrogen mustard hybrids.

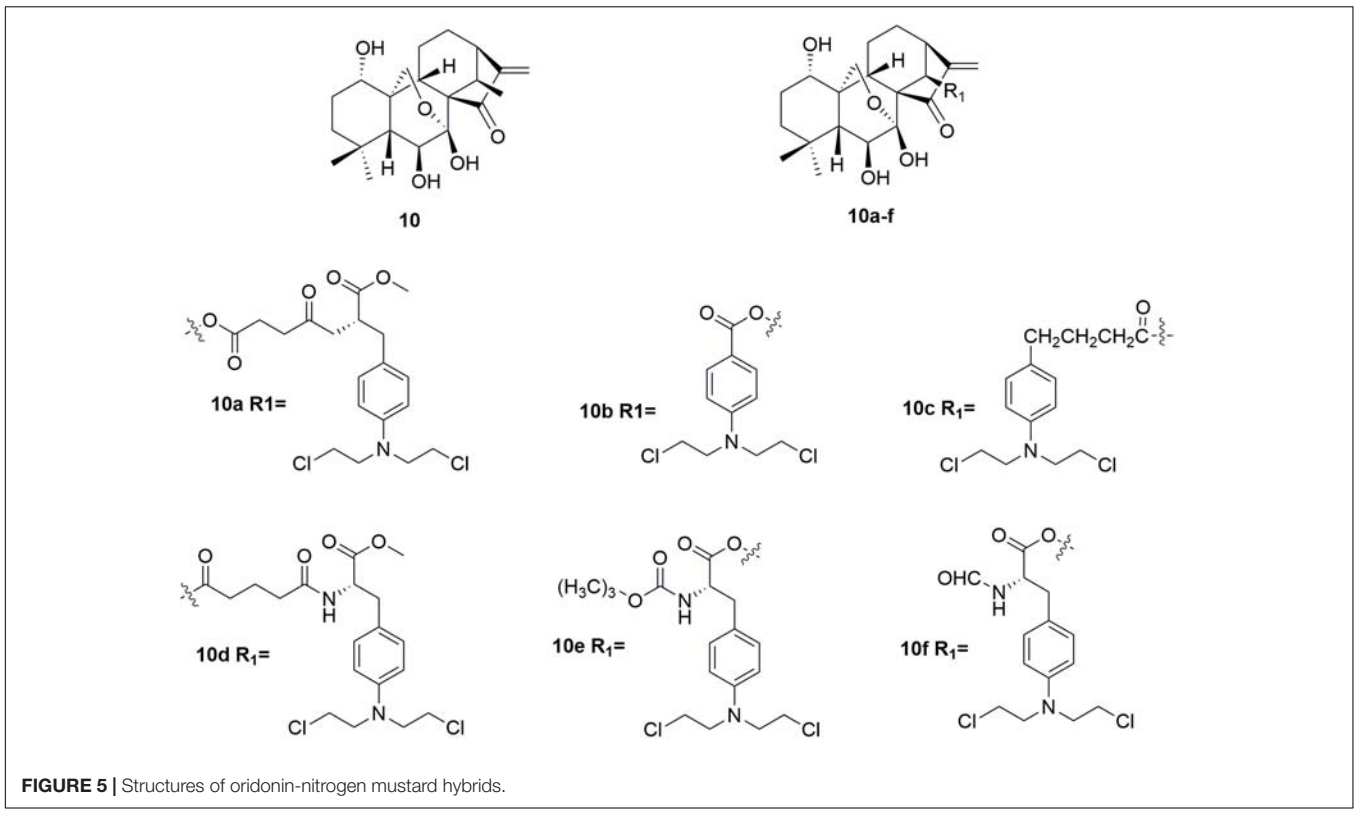

FIGURE 5 | Structures of oridonin-nitrogen mustard hybrids.

antiproliferative effects comparing to the positive control drugs, melphalan, chlorambucil and benzoic acid mustard. Among the synthetic oridonin mustards, compound **10b** was the most potent hybrid against MCF-7 and Bel-7402 cells with IC_{50} values of 0.68 μM and 0.50 μM, respectively. It is also revealed that **10b** and **10c** could inhibit the growth of drug-resistant cancer cells. Notably, molecule **10b** exhibits approximately eight-fold higher selectivity for cancer cells over normal cells, which is significantly higher than its parent oridonin compound and clinically available nitrogen mustard drugs. Collectively, the derived oridonin-nitrogen mustard conjugates exhibited improved activity and safety than the parent fragments, and introduction of nitrogen mustard make contributions to the potency and selectivity of oridonin based hybrids.

In addition to evodiamine, another alkaloid, sophoridine **11** (**Figure 6**) evaluated in detailed for its antitumor potency, was approved by the CFDA in 2005 for treatment several types of cancer, including liver, gastric and lung cancer (Sun et al., 2012; Liu and Liu, 2013; Wang et al., 2014). The sophoridine which could cause apoptotic cell death by inhibiting DNA

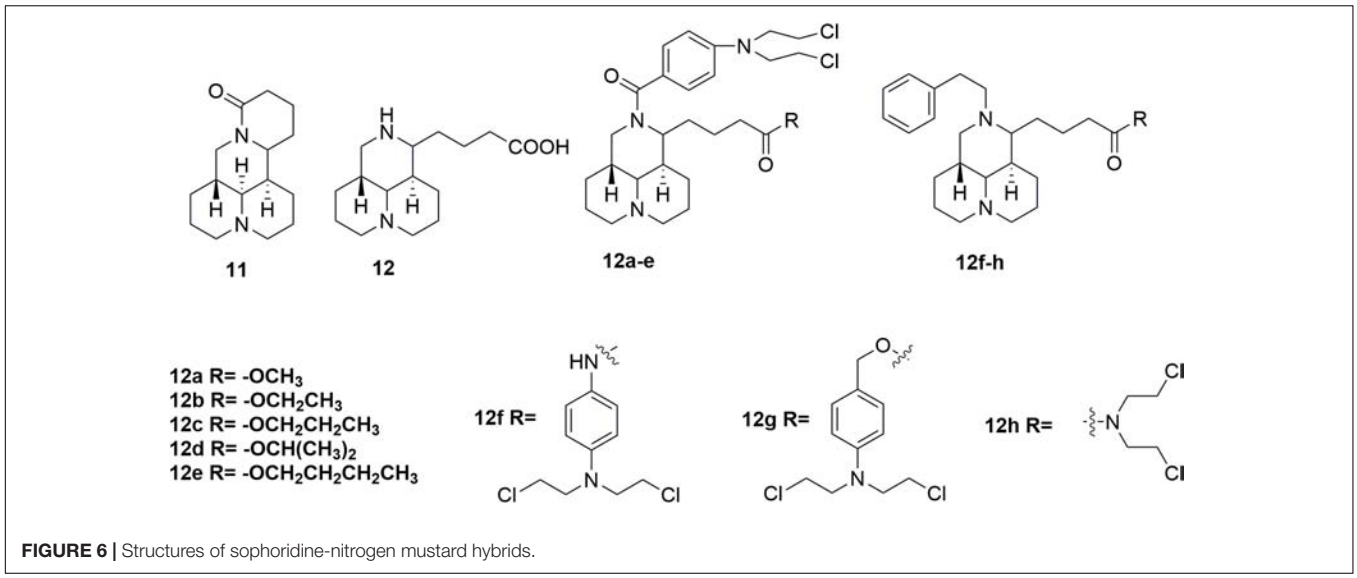

FIGURE 6 | Structures of sophoridine-nitrogen mustard hybrids.

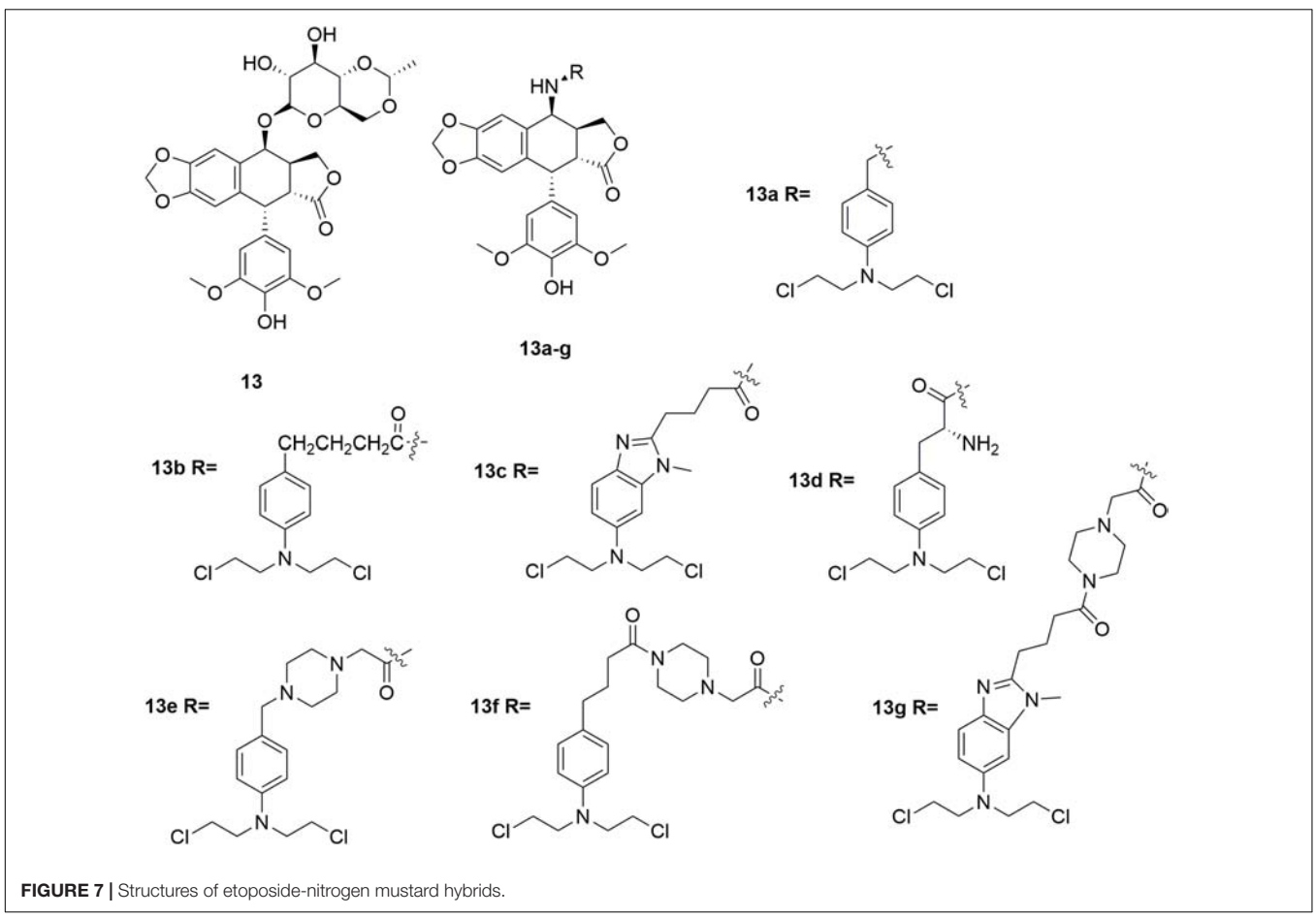

FIGURE 7 | Structures of etoposide-nitrogen mustard hybrids.

topoisomerase I activity and initiate cell cycle arrest at the G0/G1 phase, has high solubility and good safety profiles (Quo et al., 2013). However, the moderate anticancer activity of sophoridine limit its clinical application. Therefore, development of sophoridine derivatives was performed in discovery of more effective drug candidates. The D-ring of sophridine has been opened to generate sophoridinic acid **12** (**Figure 6**) for further structural modification. A series of sophoridinic acid-nitrogen mustard deivatives **12a-h** (**Figure 6**) were derived by modifying 12 nitrogen atom and carboxyl groups of **12** (Li D.D. et al., 2015).

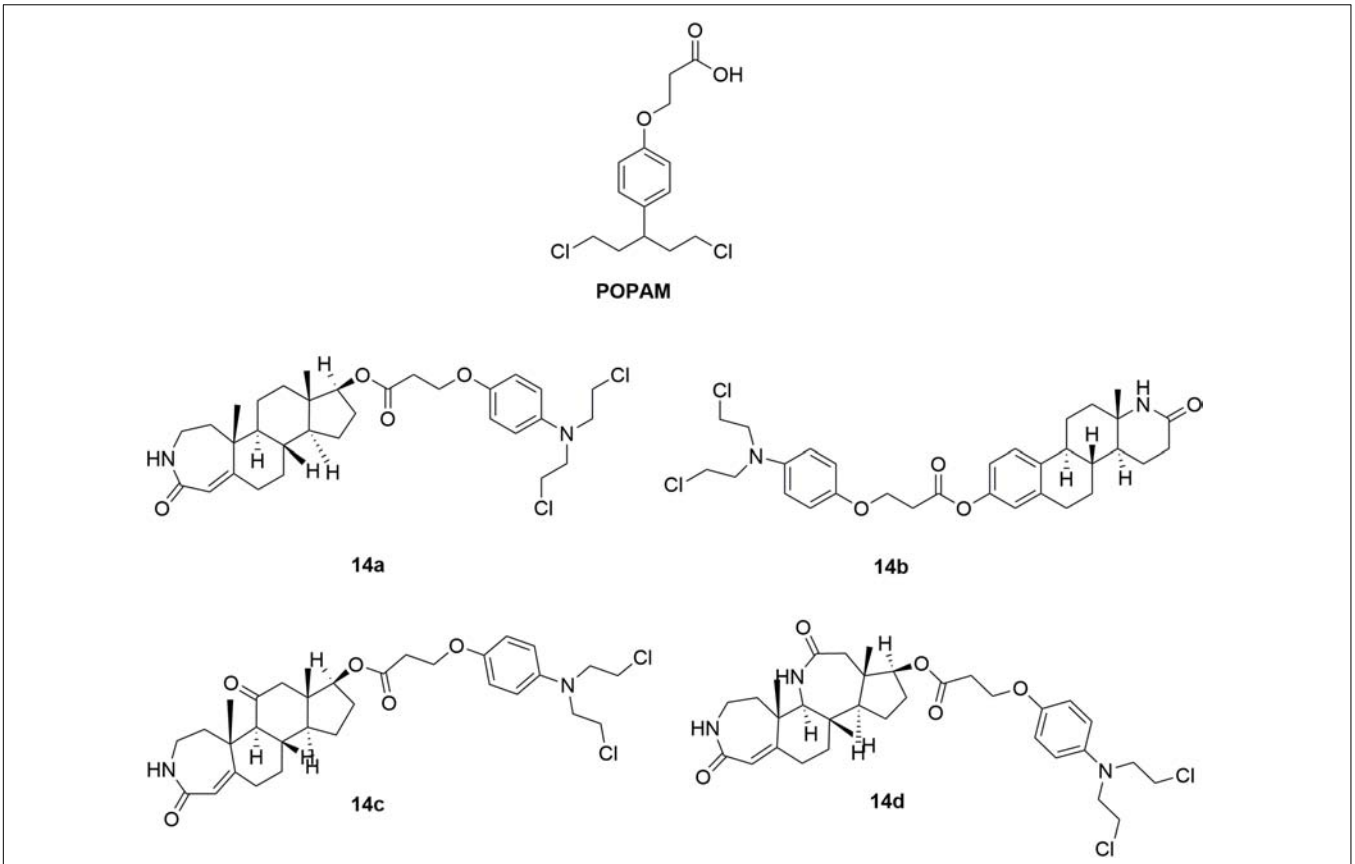

FIGURE 8 | Structures of steroid-nitrogen mustard hybrids.

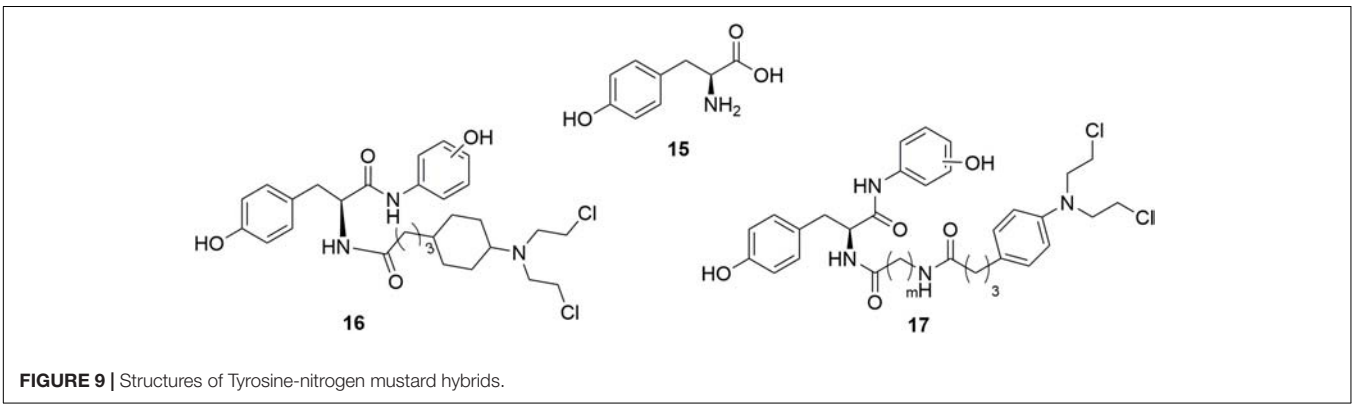

FIGURE 9 | Structures of Tyrosine-nitrogen mustard hybrids.

Compared with sophoridine (IC_{50} > 80 μM against human liver cancer HepG2 cells), several new synthesized hybrids showed improved antitumor activity. Especially compound **12f** showed IC_{50} value of 0.47 μM compared with melphalan (IC_{50} value of 0.41 μM) in the inhibition of HepG2 cells. SAR analysis indicated two promising substituents on the 12-nitrogen atom and carboxyl region, which were helpful for maintaining potent antitumor activity. Moreover, various decorating various substituents may be introduced to these two moieties, regulating the pharmacological effects of the compounds. Introduction of the cyclophosphamide metabolite (phosphamide mustard A) analogs also resulted in hybrids with significantly improved activities compared with sophoridine (Li D. et al., 2018). It is demonstrated that the introduction of nitrogen mustard on sophoridine could significantly improve interactions between sophoridine and DNA-Topo I, and subsequently increase the antitumor activity. Therefore, the study of nitrogen mustard as the parent drug is of great significance in the design and synthesis of antitumor drugs.

Etoposide **13** (**Figure 7**) is a topoisomerase II inhibitor effective in the treatments of various types of cancer including testicular cancer, lung cancer, lymphoma, leukemia,

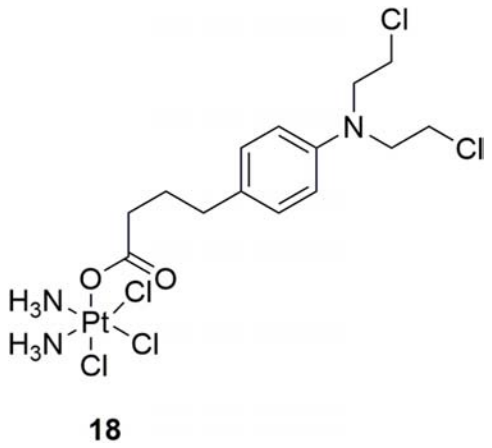

18

FIGURE 10 | Structure of Platinum-nitrogen mustard hybrid.

neuroblastoma, and ovarian cancer (Nitiss, 2009; Pommier and Marchand, 2011; Pommier, 2013). In discovery of etoposide analogs, glycoside moiety of etoposide was replaced by nitrogen mustard moiety designed to alkylate either protein residues on topoisomerase II, or the DNA bases on the DNA-topoisomeraseII complex (Deweese and Osheroff, 2009; Pommier et al., 2010; Wu et al., 2011). Seven N-mustard–epipodophyllotoxin hybrid compounds **13a-g** (**Figure 7**) were synthesized, and demonstrated to target topoisomerase II by kDNA decatenation assay, DNA cleavage assay, cellular ICE assay and the cell cycle analyses (Yadav et al., 2014). The derived molecules also exhibited nitrogen mustard-alike activity as it crosslinked DNA. In the *in vitro* antiproliferative assay, molecule **13e** exhibited the best antiproliferative activity with IC_{50} values of 0.27 μM and 0.85 μM against human leukemia K562 cells and etoposide-resistant K/VP.5 cells, and GI_{50} of 0.71 μM against NCI-60 cells in contrast to the control melphalan (IC_{50} values of 12 μM and 5.3 μM against K562 cells and K/VP.5 cells, and GI_{50} of 29 μM against NCI-60 cells) and etoposide (IC_{50} values of 0.29 μM and 4.9 μM against K562 cells and K/VP.5 cells, and GI_{50} of 12 μM against NCI-60 cells). The results suggested that hybridization of etoposide and nitrogen mustards is promising in the development of highly potent antitumor molecules both by topoisomerase II inhibition as well as DNA alkylation.

In order to decrease toxicity of nitrogen mustards, steroids have been tested as a vehicle to deliver the mustard drugs to a specific target tissue via interaction with steroid receptors (Wall et al., 1969; Catane, 1978). Such conjugates improved the lipophilicity and solubility of the resulting drugs. Development of steroidal alkylating agents has been reviewed by Bérubé and coworkers (Trafalis et al., 2016). Herein, the recently derived novel steroidal lactam derivatives and 3-(4-(bis(2-chloroethyl)amino)phenoxy)propanoic acid (POPAM) (**Figure 8**) conjunctions were described (Trafalis et al., 2016). Four new ester conjugates **14a-d** (**Figure 8**) of steroidal lactams with POPAM were synthesized and tested against human leukemia cell lines *in vitro*. Molecule **14c** was discovered to be the most potent hybrid with IC_{50} values of 90 μM, 65 μM, 80 μM, and 85 μM against human leukemia MOLT-4, CCRF-CEM, JURKAT and SUP-B15 cells compared with melphalan (IC_{50} > 100 μM against all the test cell lines) and POPAM (IC_{50} > 100 μM against all the test cell lines), respectively. In the *in vivo* antiproliferative assay, **14c** also exhibited improved antileukemic activity compared with their alkylating component alone (POPAM). Moreover, in the *in vivo* acute toxicity test, all the derived hybrids had significantly lower acute toxicity (LD_{10} (10% lethal dose) > 80 mg/kg), in contrast to the non-steroidal alkylators POPAM (LD_{10} = 14 mg/kg) and melphalan (LD_{10} = 15 mg/kg). Further investigation revealed that the chemical linkage between the nitrogen mustard and the lactam-steroids seems to both decreased the toxicities of the nitrogen mustards and improved the bioactivity and antitumor effects.

Tyrosine **15** (**Figure 9**), a natural amino acid, has been reported to share some structural similarities to that of the phenol group of estradiol (Anstead et al., 1997). Molecular modeling study indicated that the phenol group of tyrosine also interact with the estrogen receptor binding site in the same manner as the A-ring phenol of estradiol. Therefore, the tyrosine was modified to mimic the structure of estradiol (Muthyala et al., 2003; Descoteaux et al., 2012b). Tyrosinamide, combined tyrosine with hydroxyaniline, was proved to be structurally similar to estradiol. A series of tyrosinamide-nitrogen mustard derivatives were synthesized and tested by Bérubé and coworkers (Descoteaux et al., 2012a). It is revealed that all new compounds showed potent antitumor activities. Among the derived tyrosinamide-chlorambucil hybrids, compound ***m*-16** (**Figure 9**), showed IC_{50} values of 48.61 and 31.25 μM against human breast cancer MDA-MB-231 cells and MCF-7 cells compared with the parent compounds chloramucil (IC_{50} values of 136.85 and 130.36 μM against MDA-MB-231 cell and MCF-7 cells), respectively. Compared with chloramucil (IC_{50} values of 63.17, 66.11, 100.48 and 131.83 μM against human ovarian carcinoma A2780 cells, OVCAR-3 cells, human breast cancer ZR-75-1 cells and MDA-MB-468 cells, respectively), the ***m*-17** (**Figure 9**) showed potent antitumor activity with IC50 values of 31.79, 35.42, and 52.10 μM against OVCAR-3 cells, MDA-MB-468 cells and ZR-75-1 cells, respectively. It is found that all the synthesized tyrosinamide-chlrambucil molecules exhibited improved inhibitory activity in the inhibition of breast, ovarian and uterine cancer cells than the parental chlorambucil. Introduction of tyrosine entity to nitrogen mustards was considered to make contributes to the increased antitumor activity of the derived hybrid molecules.

Platinum-based antineoplastic drugs are usually considered as another class of alkylating agents with high antitumor potency (Jamieson and Lippard, 1999; Wang and Lippard, 2005). Notably, cisplatin is one of the most potent platinum(II) complexes used in cancer chemotherapy by binding to DNA and subsequently interfere with replication and transcription, eventually leading to cellular apoptosis (Abu-Surrah and Kettunen, 2006; Wheate et al., 2010). However, clinical application of cisplatin is limited by its severe adverse effects, including nephrotoxicity, hepatotoxicity, ototoxicity and neurotoxicity, etc. Acquired resistance is also a concern (Brabec et al., 2017). In discovery of more potent

and safe antitumor compounds, conjunction of two different types of DNA-damaging drugs by combining chlorambucil with platinum(IV) complexes was performed by Gou and coworkers (Qin et al., 2017). In the *in vitro* activity assay, molecule **18** (**Figure 10**), a hybrid of cisplatin and chlorambucil, displayed potent antiproliferative activities with IC_{50} values of 3.99 μM, 4.37 μM, 4.97 μM, 2.97 μM, and 4.23 μM against human breast cancer MCF-7, human colon cancer HCT-116, human liver cancer HepG-2, human gastric cancer SGC7901, and cisplatin-resistant SGC7901/CDDP cells, respectively. Compared with chlorambucil, cisplatin, and oxaliplatin, molecule **18** exhibited improved activity in the inhibition of cisplatin resistant SGC7901/CDDP cells. Further studies revealed that molecule **18** induced cell cycle arrest at S/G2 phases (distinct from those of cisplatin and chlorambucil), and revealed ability of overcome drug resistance. Collectively, hybridization of nitrogen mustards and platinum(IV) complexes resulted in conjunctions with improved antitumor potency, and with advantage of overcoming drug resistance of tumor cells.

Several highly potent 1,3,5-triazine scaffold-carrying cytostatic agents have been previously reported as inhibitors of cell proliferation-involved enzymes (Maeda et al., 2000; Riou et al., 2002; Gomez et al., 2003; Kaminski et al., 2004; Mandal et al., 2007; Paquin et al., 2008). Among them, ZSTK474 (**Figure 11**) was discovered to inhibit the growth of tumor cells in human cancer xenografts without toxic effects on critical organs by targeting PI3K (Di Francesco et al., 2000; Vedejs et al., 2003). In the structural modification of current melamine derivatives, a series of melamine-nitrogen mustard derivatives **19a-f** (**Figure 11**) were synthesized by introducing one or more 2-chloroethylamine groups (Kolesinska et al., 2012). It is revealed that all synthesized molecules showed potent antitumor activities. Compared with the positive control chlorambucil (IC_{50} value of 29.14 μM against human breast cancer MCF-7 cells), the obtained molecule **19f** showed potent antitumor activity with IC_{50} value of 18.70 μM against MCF-7 cells. Compound **19a** also exhibited potent antitumor activities with IC_{50} value of 0.62 μM, 0.99 μM, 1.40 μM, 2.06 μM and 3.45 μM against human leukemia Jurkat, human prostate adenocarcinoma LNCaP, human breast adenocarcinoma T47D, human lung adenocarcinoma A549 and human colorectal carcinoma SW707 cells, respectively. Further biological studies suggested that introducing nitrogen mustard into triazine is promising in the increase of antitumor activity by promoting alkylation.

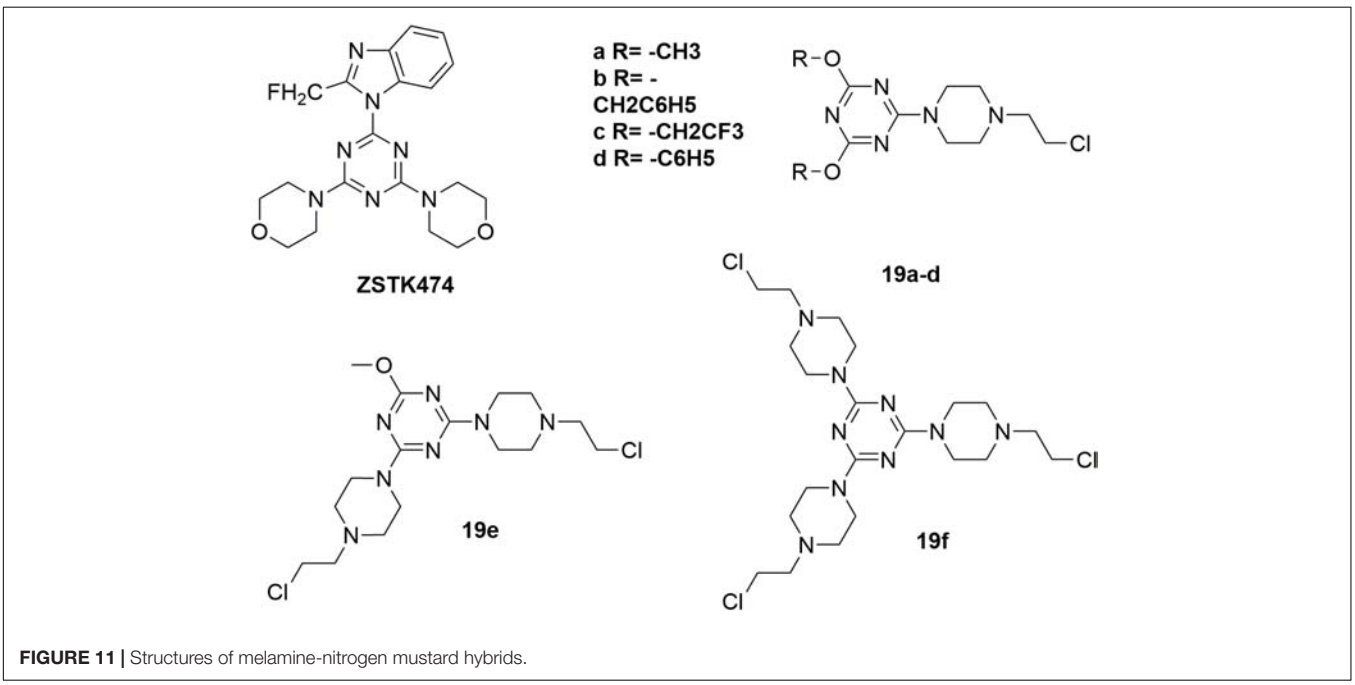

FIGURE 11 | Structures of melamine-nitrogen mustard hybrids.

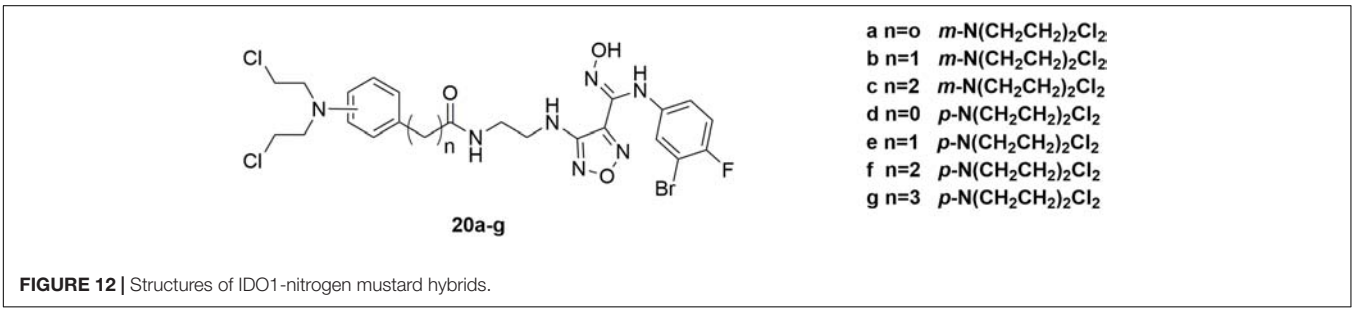

FIGURE 12 | Structures of IDO1-nitrogen mustard hybrids.

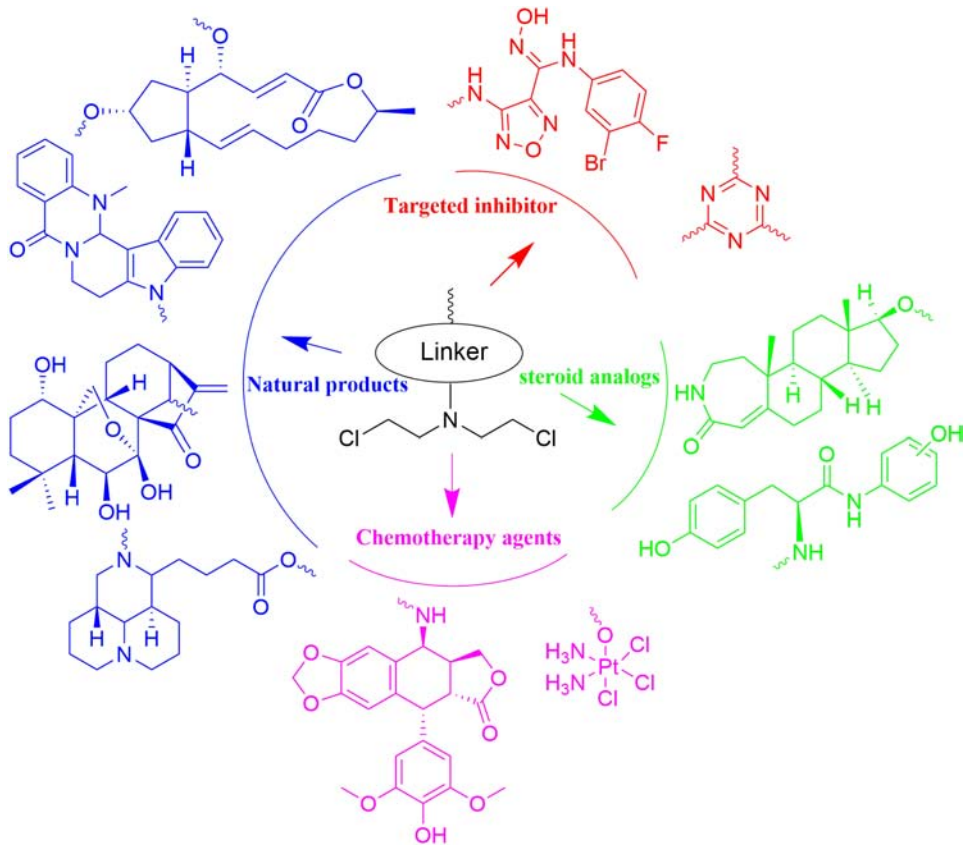

FIGURE 13 | Summary of the nitrogen mustard based hybridization strategy involved in the current article.

Accordingly, introduction of nitrogen mustard is regarded to make contribution to improve the selectivity, activity and lipophilicity of current drug-like cytotoxic derivatives.

IDO1, a heme-containing enzyme, plays an important role in carcinogenesis and its progression by converting Trp to Kyn (Jiang et al., 2015). Both Trp degradation and Kyn accumulation are associated with immune tolerance by affecting T cell activity and altering the tumor microenvironment (Moon et al., 2015). A number of studies showed that the combination of IDO1 inhibitors along with cytotoxic chemotherapeutic agents is an effective strategy in cancer treatment (Muller et al., 2005). However, such a simple combination will inevitably be limited by the severe adverse effects induced by the highly toxic cytotoxic agents and possible drug-drug interactions. Therefore, in discovery of potent antitumor molecules with reduced toxicity, a series of hybrid molecules **20a-g** (**Figure 12**) were synthesized by including the pharmacophores of both IDO1 inhibitors and nitrogen mustards (Fang et al., 2018). All the compounds showed potent antitumor activities compared with the positive drug chlorambucil in the inhibition of murine colorectal carcinoma CT-26, human lung adenocarcinoma A549, human colon cancer HCT116 and human colorectal adenocarcinoma HT-29 cells. Obviously, compound **20a** significantly inhibited IDO1 activity in tumor tissues and reduced Kyn level in plasma with IDO1 inhibitory IC_{50} value of 0.13 μM and antiproliferative EC_{50} (half maximal effect concentration) value of 0.27 μM aganist HeLa cells. Moreover, molecule **20a** exhibited high potent *in vivo* antitumor efficacy (tumor growth inhibition (TGI) = 58.2%) compared with clinical candidate IDO1 inhibitor epacadostat (TGI = 47.5%) in the allograft animal model with CT-26 without remarkable body weight loss or adverse effects. In conclusion, it is revealed that introduction of nitrogen mustard into pharmacophores of IDO1 inhibitors could significantly improve the antitumor activity and reduce toxicity of parent compound in the antitumor evaluation.

CONCLUSION AND PERSPECTIVE

Nitrogen mustards represent the earliest studied DNA cross-linking agents, and application of DNA alkylating agents has been widely utilized for the treatment of cancer for more than 70 years. In spite of their long history, several nitrogen mustard drugs, including cyclophosphamide, chlorambucil, and melphalan, still remained as first line antitumor agents in the management of various types of tumors. However, the clinical application of nitrogen mustards was restricted by their undesired adverse effects, relatively low efficacy compared with targeted antitumor drugs, and drug resistance caused by enhanced drug inactivation, decreased cellular uptake,

enhanced DNA repair and/or DNA damage tolerance. It is generally accepted that cancer has its pathological root in genetical mutations, affecting cell replication. Thus, targeting different proliferative mechanisms by the construction of hybrid anticancer drugs seem to be a promising strategy. Development of nitrogen mustard based hybrids has been revealed to be effective strategy in discovery of antitumor drugs with increased activity, reduced toxicity, and improved physicochemical properties such as the lipophilicity and the solubility.

With N,N-bis(2-chloroethyl)amine as functional group, nitrogen mustards has been hybridized with various drug-like fragments (**Figure 13**). Novel hybrids have been derived with improved potency, selectivity, safety, pharmacokinetics, pharmacodynamics properties and/or broader range of therapeutic activities. Current achievements make development of nitrogen mustard based conjunctions to be attractive area in the cancer treatment. Despite the reported advantages, unexpected side effects caused by introduction of nitrogen mustards also require careful attention in the drug design and biological evaluation. As questioned on the efficacy of twin drugs and prodrugs, it is also necessary to demonstrate advantages of the conjugates linked by ester bond or more stable bonds in comparison with the combined therapy with parental drugs.

AUTHOR CONTRIBUTIONS

YC and YJ participated in most of the literature retrieval and article writing. LZ and WS guided the review and revised the writing.

FUNDING

Some of the materials in this work were supported by National Natural Science Foundation of China (Youth Found, Grant No. 81803343).

REFERENCES

Abu-Surrah, A. S., and Kettunen, M. (2006). Platinum group antitumor chemistry: design and development of new anticancer drugs complementary to cisplatin. *Curr. Med. Chem.* 13, 1337–1357. doi: 10.2174/092986706776872970

Anadu, N. O., Davisson, V. J., and Cushman, M. (2006). Synthesis and anticancer activity of brefeldin A ester derivatives. *J. Med. Chem.* 49, 3897–3905. doi: 10.1021/jm0602817

Anstead, G. M., Carlson, K. E., and Katzenellenbogen, J. A. (1997). The estradiol pharmacophore: ligand structure-estrogen receptor binding affinity relationships and a model for the receptor binding site. *Steroids* 62, 268–303. doi: 10.1016/S0039-128X(96)00242-5

Bank, B. B., Kanganis, D., Liebes, L. F., and Silber, R. (1989). Chlorambucil pharmacokinetics and DNA binding in chronic lymphocytic leukemia lymphocytes. *Cancer Res.* 49, 554–559.

Bao, R. F., Shu, Y. J., Wu, X. S., Weng, H., Ding, Q., Cao, Y., et al. (2014). Oridonin induces apoptosis and cell cycle arrest of gallbladder cancer cells via the mitochondrial pathway. *BMC Cancer* 14:217. doi: 10.1186/1471-2407-14-217

Brabec, V., Hrabina, O., and Kasparkova, J. (2017). Cytotoxic platinum coordination compounds. DNA binding agents. *Coordin. Chem. Rev.* 351, 2–31. doi: 10.1016/j.ccr.2017.04.013

Catane, R. (1978). Clinical experience with estramustine phosphate and predinimustine, two steroidal alkylating agents compounds [proceedings]. *Cancer Treat. Rep.* 62, 1264–1265.

Chen, W. B., Balakrishnan, K., Kuang, Y. Y., Han, Y. Y., Fu, M., Gandhi, V., et al. (2014). Reactive Oxygen Species (ROS) inducible DNA cross-linking agents and their effect on cancer cells and normal lymphocytes. *J. Med. Chem.* 57, 4498–4510. doi: 10.1021/jm401349g

Cui, Q., Tashiro, S., Onodera, S., Minami, M., and Ikejima, T. (2007). Oridonin induced autophagy in human cervical carcinoma HeLa cells through Ras. JNK, and P38 regulation. *J. Pharmacol. Sci.* 105, 317–325. doi: 10.1254/jphs.FP0070336

Descoteaux, C., Brasseur, K., Leblanc, V., Parent, S., Asselin, E., and Berube, G. (2012a). Design of novel tyrosine-nitrogen mustard hybrid molecules active against uterine, ovarian and breast cancer cell lines. *Steroids* 77, 403–412. doi: 10.1016/j.steroids.2011.12.021

Descoteaux, C., Brasseur, K., Leblanc, V., Parent, S., Asselin, E., and Berube, G. (2012b). SAR study of tyrosine-chlorambucil hybrid regioisomers; synthesis and biological evaluation against breast cancer cell lines. *Amino Acids* 43, 923–935. doi: 10.1007/s00726-011-1152-3

DeVita, V. T. Jr., and Chu, E. (2008). A history of cancer chemotherapy. *Cancer Res.* 68, 8643–8653. doi: 10.1158/0008-5472.CAN-07-6611

Deweese, J. E., and Osheroff, N. (2009). The DNA cleavage reaction of topoisomerase II: wolf in sheep's clothing. *Nucleic Acids Res.* 37, 738–748. doi: 10.1093/nar/gkn937

Di Antonio, M., McLuckie, K. I. E., and Balasubramanian, S. (2014). Reprogramming the mechanism of action of chlorambucil by coupling to a G-Quadruplex ligand. *J. Am. Chem. Soc.* 136, 5860–5863. doi: 10.1021/ja5014344

Di Francesco, A. M., Hargreaves, R. H., Wallace, T. W., Mayalarp, S. P., Hazrati, A., Hartley, J. A., et al. (2000). The abnormal cytotoxicities of 2,5-diaziridinyl-1,4-benzoquinone-3-phenyl esters. *Anti Cancer Drug Des.* 15, 347–359.

Ding, C. Y., Zhang, Y. S., Chen, H. J., Yang, Z. D., Wild, C., Chu, L. L., et al. (2013a). Novel nitrogen-enriched oridonin analogues with thiazole-fused a-ring: protecting group-free synthesis, enhanced anticancer profile, and improved aqueous solubility. *J. Med. Chem.* 56, 5048–5058. doi: 10.1021/jm400367n

Ding, C. Y., Zhang, Y. S., Chen, H. J., Yang, Z. D., Wild, C., Ye, N., et al. (2013b). Oridonin ring a-based diverse constructions of enone functionality: identification of novel dienone analogues effective for highly aggressive breast cancer by inducing apoptosis. *J. Med. Chem.* 56, 8814–8825. doi: 10.1021/jm401248x

Ding, Y., Ding, C. Y., Ye, N., Liu, Z. Q., Wold, E. A., Chen, H. Y., et al. (2016). Discovery and development of natural product oridonin-inspired anticancer agents. *Eur. J. Med. Chem.* 122, 102–117. doi: 10.1016/j.ejmech.2016.06.015

Dong, X. J., Liu, F. Y., and Li, M. L. (2016). Inhibition of nuclear factor kappa B transcription activity drives a synergistic effect of cisplatin and oridonin on HepG2 human hepatocellular carcinoma cells. *Anticancer Drugs* 27, 286–299. doi: 10.1097/CAD.0000000000000329

Fan, X., Zhu, J. Y., Sun, Y., Luo, L., Yan, J., Yang, X., et al. (2017). Evodiamine inhibits Zymosan-induced inflammation in vitro and in vivo: inactivation of NF-kappa B by inhibiting I kappa B alpha phosphorylation. *Inflammation* 40, 1012–1027. doi: 10.1007/s10753-017-0546-0

Fang, K., Dong, G. Q., Wang, H. Y., He, S. P., Wu, S. C., Wang, W., et al. (2018). Improving the potency of cancer immunotherapy by dual targeting of IDO1 and DNA. *ChemMedChem* 13, 30–36. doi: 10.1002/cmdc.201700666

Frei, E. III, Teicher, B. A., Holden, S. A., Cathcart, K. N., and Wang, Y. Y. (1988). Preclinical studies and clinical correlation of the effect of alkylating dose. *Cancer Res.* 48, 6417–6423.

Galton, D. A., Wiltshaw, E., Szur, L., and Dacie, J. V. (1961). The use of chlorambucil and steroids in the treatment of chronic lymphocytic leukaemia. *Br. J. Haematol.* 7, 73–98. doi: 10.1111/j.1365-2141.1961.tb00321.x

Gilman, A. (1963). The initial clinical trial of nitrogen mustard. *Am. J. Surg.* 105, 574–578. doi: 10.1016/0002-9610(63)90232-0

Gomez, D., Aouali, N., Londono-Vallejo, A., Lacroix, L., Megnin-Chanet, F., Lemarteleur, T., et al. (2003). Resistance to the short term antiproliferative activity of the G-quadruplex ligand 12459 is associated with telomerase overexpression and telomere capping alteration. *J. Biol. Chem.* 278, 50554–50562. doi: 10.1074/jbc.M308440200

Goodman, L. S., and Wintrobe, M. M. (1946). Nitrogen mustard therapy; use of methyl-bis (beta-chloroethyl) amine hydrochloride and tris (beta-chloroethyl) amine hydrochloride for Hodgkin's disease, lymphosarcoma, leukemia and certain allied and miscellaneous disorders. *J. Am. Med. Assoc.* 132, 126–132. doi: 10.1001/jama.1946.02870380008004

Grose, C., and Klionsky, D. J. (2016). Alternative autophagy, brefeldin A and viral trafficking pathways. *Autophagy* 12, 1429–1430. doi: 10.1080/15548627.2016.1203489

Han, T., Tian, K. T., Pan, H. Q., Liu, Y. X., Xu, F. X., Li, Z. L., et al. (2018). Novel hybrids of brefeldin A and nitrogen mustards with improved antiproliferative selectivity: design, synthesis and antitumor biological evaluation. *Eur. J. Med. Chem.* 150, 53–63. doi: 10.1016/j.ejmech.2018.02.088

Hu, X., Wang, Y., Xue, J. J., Han, T., Jiao, R. W., Li, Z. L., et al. (2017). Design and synthesis of novel nitrogen mustard-evodiamine hybrids with selective antiproliferative activity. *Bioorg. Med. Chem. Lett.* 27, 4989–4993. doi: 10.1016/j.bmcl.2017.10.014

Huang, H. R., Liu, T., Guo, J. X., Yu, L., Wu, X. F., He, Y., et al. (2017). Brefeldin A enhances docetaxel-induced growth inhibition and apoptosis in prostate cancer cells in monolayer and 3D cultures. *Bioorg. Med. Chem. Lett.* 27, 2286–2291. doi: 10.1016/j.bmcl.2017.04.047

Hughes, E., Scurr, M., Campbell, E., Jones, E., Godkin, A., and Gallimore, A. (2018). T-cell modulation by cyclophosphamide for tumour therapy. *Immunology* 154, 62–68. doi: 10.1111/imm.12913

Jamieson, E. R., and Lippard, S. J. (1999). Structure, recognition, and processing of cisplatin-DNA adducts. *Chem. Rev.* 99, 2467–2498. doi: 10.1021/cr980421n

Jiang, T. Z., Sun, Y. Y., Yin, Z. C., Feng, S., Sun, L. P., and Li, Z. Y. (2015). Research progress of indoleamine 2,3-dioxygenase inhibitors. *Future Med. Chem.* 7, 185–201. doi: 10.4155/fmc.14.151

Kaminski, Z. J., Kolesinska, B., and Markowicz, S. W. (2004). Synthesis and cytostatic properties of monoterpene derivatives of cyanuric and isocyanuric acids. *Acta. Pol. Pharm.* 61(Suppl.), 29–32.

Kikuchi, S., Shinpo, K., Tsuji, S., Yabe, I., Niino, M., and Tashiro, K. (2003). Brefeldin A-induced neurotoxicity in cultured spinal cord neurons. *J. Neurosci. Res.* 71, 591–599. doi: 10.1002/jnr.10479

Kohn, K. W., Hartley, J. A., and Mattes, W. B. (1987). Mechanisms of DNA sequence selective alkylation of guanine-N7 positions by nitrogen mustards. *Nucleic Acids Res.* 15, 10531–10549. doi: 10.1093/nar/15.24.10531

Kolesinska, B., Barszcz, K., Kaminski, Z. J., Drozdowska, D., Wietrzyk, J., and Switalska, M. (2012). Synthesis and cytotoxicity studies of bifunctional hybrids of nitrogen mustards with potential enzymes inhibitors based on melamine framework. *J. Enzyme Inhib. Med. Chem.* 27, 619–627. doi: 10.3109/14756366.2011.604482

Lallukka, T., Millear, A., Pain, A., Cortinovis, M., and Giussani, G. (2017). GBD 2015 Mortality and Causes of Death Collaborators. Global, regional, and national life expectancy, all-cause mortality, and cause-specifi c mortality for 249 causes of death, 1980-2015: a systematic analysis for the Global Burden of Disease Study 2015 (vol 388, pg 1459, 2016). *Lancet* 389:E1.

Li, D., Dai, L., Zhao, X., Zhi, S., Shen, H., and Yang, Z. (2018). Novel sophoridine derivatives bearing phosphoramide mustard moiety exhibit potent antitumor activities in vitro and in vivo. *Molecules* 23:E1960. doi: 10.3390/molecules23081960

Li, D. D., Dai, L. L., Zhang, N., and Tao, Z. W. (2015). Synthesis, structure-activity relationship and biological evaluation of novel nitrogen mustard sophoridinic acid derivatives as potential anticancer agents. *Bioorg. Med. Chem. Lett.* 25, 4092–4096. doi: 10.1016/j.bmcl.2015.08.035

Li, Y., Wang, Y., Wang, S. H., Gao, Y. J., Zhang, X. F., and Lu, C. H. (2015). Oridonin phosphate-induced autophagy effectively enhances cell apoptosis of human breast cancer cells. *Med. Oncol.* 32:365. doi: 10.1007/s12032-014-0365-1

Liu, J. B., and Liu, Y. Q. (2013). Influence of Erbanxiao solution on inhibiting angiogenesis in stasis toxin stagnation of non-small cell lung cancer. *J. Tradit. Chin. Med.* 33, 303–306. doi: 10.1016/S0254-6272(13)60169-7

Liu, M., Wang, W. G., Sun, H. D., and Pu, J. X. (2017). Diterpenoids from Isodon species: an update. *Nat. Prod. Rep.* 34, 1090–1140. doi: 10.1039/c7np00027h

Lv, Q. L., Xue, Y., Li, G. D., Zou, L. F., Zhang, X., Ying, M. F., et al. (2015). Beneficial effects of evodiamine on P2X(4)-mediated inflammatory injury of human umbilical vein endothelial cells due to high glucose. *Int. Immunopharmacol.* 28, 1044–1049. doi: 10.1016/j.intimp.2015.08.020

Maeda, M., Ligo, M., Tsuda, H., Fujita, H., Yonemura, Y., Nakagawa, K., et al. (2000). Antimetastatic and antitumor effects of 2,4-diamino-6-(pyridine-4-yl)-1,3,5-triazine (4PyDAT) on the high lung metastatic colon 26 tumor in mice. *Anti Cancer Drug Des.* 15, 217–223.

Mandal, S., Berube, G., Asselin, E., Mohammad, I., Richardson, V. J., Gupta, A., et al. (2007). A novel series of potent cytotoxic agents targeting G2/M phase of the cell cycle and demonstrating cell killing by apoptosis in human breast cancer cells. *Bioorg. Med. Chem. Lett.* 17, 4955–4960. doi: 10.1016/j.bmcl.2007.06.033

Moon, J. L., Kim, S. Y., Shin, S. W., and Park, J. W. (2012). Regulation of brefeldin A-induced ER stress and apoptosis by mitochondrial NADP(+)-dependent isocitrate dehydrogenase. *Biochem. Bioph. Res. Commun.* 417, 760–764. doi: 10.1016/j.bbrc.2011.12.030

Moon, Y. W., Hajjar, J., Hwu, P., and Naing, A. (2015). Targeting the indoleamine 2,3-dioxygenase pathway in cancer. *J. Immunother. Cancer* 3:51. doi: 10.1186/s40425-015-0094-9

Muller, A. J., DuHadaway, J. B., Donover, P. S., Sutanto-Ward, E., and Prendergast, G. C. (2005). Inhibition of indoleamine 2,3-dioxygenase, an immunoregulatory target of the cancer suppression gene Bin1, potentiates cancer chemotherapy. *Nat. Med.* 11, 312–319. doi: 10.1038/nm1196

Muthyala, R. S., Carlson, K. E., and Katzenellenbogen, J. A. (2003). Exploration of the bicyclo[3.3.1]nonane system as a template for the development of new ligands for the estrogen receptor. *Bioorg. Med. Chem. Lett.* 13, 4485–4488. doi: 10.1016/j.bmcl.2003.08.061

Nicolle, A., Proctor, S. J., and Summerfield, G. P. (2004). High dose chlorambucil in the treatment of lymphoid malignancies. *Leuk. Lymphoma* 45, 271–275. doi: 10.1080/10428190310001595704

Nitiss, J. L. (2009). Targeting DNA topoisomerase II in cancer chemotherapy. *Nat. Rev. Cancer* 9, 338–350. doi: 10.1038/nrc2607

Ogasawara, M., Matsunaga, T., Takahashi, S., Saiki, I., and Suzuki, H. (2002). Anti-invasive and metastatic activities of evodiamine. *Biol. Pharm. Bull.* 25, 1491–1493. doi: 10.1248/bpb.25.1491

Paquin, I., Raeppel, S., Leit, S., Gaudette, F., Zhou, N., Moradei, O., et al. (2008). Design and synthesis of 4-[(s-triazin-2-ylamino)methyl]-N-(2-aminophenyl)-benzamides and their analogues as a novel class of histone deacetylase inhibitors. *Bioorg. Med. Chem. Lett.* 18, 1067–1071. doi: 10.1016/j.bmcl.2007.12.009

Pommier, Y. (2013). Drugging topoisomerases: lessons and challenges. *ACS Chem. Biol.* 8, 82–95. doi: 10.1021/cb300648v

Pommier, Y., Leo, E., Zhang, H., and Marchand, C. (2010). DNA topoisomerases and their poisoning by anticancer and antibacterial drugs. *Chem. Biol.* 17, 421–433. doi: 10.1016/j.chembiol.2010.04.012

Pommier, Y., and Marchand, C. (2011). Interfacial inhibitors: targeting macromolecular complexes. *Nat. Rev. Drug Discov.* 11, 25–36. doi: 10.1038/nrd3404

Povirk, L. F., and Shuker, D. E. (1994). DNA damage and mutagenesis induced by nitrogen mustards. *Mutat. Res.* 318, 205–226. doi: 10.1016/0165-1110(94)90015-9

Qin, X. D., Fang, L., Chen, F. H., and Gou, S. H. (2017). Conjugation of platinum(IV) complexes with chlorambucil to overcome cisplatin resistance via a "joint action" mode toward DNA. *Eur. J. Med. Chem.* 137, 167–175. doi: 10.1016/j.ejmech.2017.05.056

Quo, L., Xue, T. Y., Xu, W., and Gao, J. Z. (2013). Matrine promotes G(0)/G(1) arrest and down-regulates cyclin D1 expression in human rhabdomyosarcoma cells. *Panminerva Med.* 55, 291–296.

Rajamahanty, S., Alonzo, C., Aynehchi, S., Choudhury, M., and Konno, S. (2010). Growth inhibition of androgen-responsive prostate cancer cells with brefeldin A targeting cell cycle and androgen receptor. *J. Biomed. Sci.* 17:5. doi: 10.1186/1423-0127-17-5

Riou, J. F., Guittat, L., Mailliet, P., Laoui, A., Renou, E., Petitgenet, O., et al. (2002). Cell senescence and telomere shortening induced by a new series of specific G-quadruplex DNA ligands. *Proc. Natl. Acad. Sci. U.S.A.* 99, 2672–2677. doi: 10.1073/pnas.052698099

Ryerson, A. B., Eheman, C. R., Altekruse, S. F., Ward, J. W., Jemal, A., Sherman, R. L., et al. (2016). Annual report to the nation on the status of cancer, 1975-2012, featuring the increasing incidence of liver cancer. *Cancer* 122, 1312–1337. doi: 10.1002/cncr.29936

Sanderson, B. J., and Shield, A. J. (1996). Mutagenic damage to mammalian cells by therapeutic alkylating agents. *Mutat. Res.* 355, 41–57. doi: 10.1016/0027-5107(96)00021-8

Sarosy, G., Leyland-Jones, B., Soochan, P., and Cheson, B. D. (1988). The systemic administration of intravenous melphalan. *J. Clin. Oncol.* 6, 1768–1782. doi: 10.1200/JCO.1988.6.11.1768

Schobert, R., Biersack, B., Dietrich, A., Knauer, S., Zoldakova, M., Fruehauf, A., et al. (2009). Pt(II) complexes of a combretastatin A-4 analogous chalcone: effects of conjugation on cytotoxicity, tumor specificity, and long-term tumor growth suppression. *J. Med. Chem.* 52, 241–246. doi: 10.1021/jm801001d

Seehafer, K., Rominger, F., Helmchen, G., Langhans, M., Robinson, D. G., Ozata, B., et al. (2013). Synthesis and biological properties of novel brefeldin a analogues. *J. Med. Chem.* 56, 5872–5884. doi: 10.1021/jm400615g

Shi, C. S., Li, J. M., Chin, C. C., Kuo, Y. H., Lee, Y. R., and Huang, Y. C. (2017). Evodiamine induces cell growth arrest, apoptosis and suppresses tumorigenesis in human urothelial cell carcinoma cells. *Anticancer. Res.* 37, 1149–1159. doi: 10.21873/anticanres.11428

Shi, L., Yang, F., Luo, F., Liu, Y., Zhang, F., Zou, M. J., et al. (2016). Evodiamine exerts anti-tumor effects against hepatocellular carcinoma through inhibiting beta-catenin-mediated angiogenesis. *Tumor Biol.* 37, 12791–12803. doi: 10.1007/s13277-016-5251-3

Shi, M., Lu, X. J., Zhang, J., Diao, H., Li, G. M., Xu, L., et al. (2016). Oridonin, a novel lysine acetyltransferases inhibitor, inhibits proliferation and induces apoptosis in gastric cancer cells through p53-and caspase-3-mediated mechanisms. *Oncotarget* 7, 22623–22631. doi: 10.18632/oncotarget.8033

Shyu, K. G., Lin, S., Lee, C. C., Chen, E., Lin, L. C., Wang, B. W., et al. (2006). Evodiamine inhibits in vitro angiogenesis: implication for antitumorgenicity. *Life Sci.* 78, 2234–2243. doi: 10.1016/j.lfs.2005.09.027

South, P. F., Harmeyer, K. M., Serratore, N. D., and Briggs, S. D. (2013). H3K4 methyltransferase Set1 is involved in maintenance of ergosterol homeostasis and resistance to Brefeldin A. *Proc. Natl. Acad. Sci. U.S.A.* 110, E1016–E1025. doi: 10.1073/pnas.1215768110

Springer, C. J., Antoniw, P., Bagshawe, K. D., Searle, F., Bisset, G. M., and Jarman, M. (1990). Novel prodrugs which are activated to cytotoxic alkylating agents by carboxypeptidase G2. *J. Med. Chem.* 33, 677–681. doi: 10.1021/jm00164a034

Sun, H. D., Huang, S. X., and Han, Q. B. (2006). Diterpenoids from Isodon species and their biological activities. *Nat. Prod. Rep.* 23, 673–698. doi: 10.1039/b604174d

Sun, Q., Sattayakhom, A., Backs, J., Stremmel, W., and Chamulitrat, W. (2012). Role of myocyte enhancing factor 2B in epithelial myofibroblast transition of human gingival keratinocytes. *Exp. Biol. Med.* 237, 178–185. doi: 10.1258/ebm.2011.011261

Toda, T., Watanabe, M., Kawato, J., Kadin, M. E., Higashihara, M., Kunisada, T., et al. (2015). Brefeldin a exerts differential effects on anaplastic lymphoma kinase positive anaplastic large cell lymphoma and classical Hodgkin lymphoma cell lines. *Br. J. Haematol.* 170, 837–846. doi: 10.1111/bjh.13508

Torre, L. A., Bray, F., Siegel, R. L., Ferlay, J., Lortet-Tieulent, J., and Jemal, A. (2015). Global cancer statistics, 2012. *Cancer J. Clin.* 65, 87–108. doi: 10.3322/caac.21262

Trafalis, D., Geromichalou, E., Dalezis, P., Nikoleousakos, N., and Sarli, V. (2016). Synthesis and evaluation of new steroidal lactam conjugates with aniline mustards as potential antileukemic therapeutics. *Steroids* 115, 1–8. doi: 10.1016/j.steroids.2016.07.009

Vedejs, E., Naidu, B. N., Klapars, A., Warner, D. L., Li, V. S., Na, Y., et al. (2003). Synthetic enantiopure aziridinomitosenes: preparation, reactivity, and DNA alkylation studies. *J. Am. Chem. Soc.* 125, 15796–15806. doi: 10.1021/ja030452m

Wall, M. E., Abernethy, G. S. Jr., Carroll, F. I., and Taylor, D. J. (1969). The effects of some steroidal alkylating agents on experimental animal mammary tumor and leukemia systems. *J. Med. Chem.* 12, 810–818. doi: 10.1021/jm00305a021

Wang, C. Y., Bai, X. Y., and Wang, C. H. (2014). Traditional chinese medicine: a treasured natural resource of anticancer drug research and development. *Am. J. Chin. Med.* 42, 543–559. doi: 10.1142/S0192415X14500359

Wang, D., and Lippard, S. J. (2005). Cellular processing of platinum anticancer drugs. *Nat. Rev. Drug Discov.* 4, 307–320. doi: 10.1038/nrd1691

Wang, L., Li, D. H., Xu, S. T., Cai, H., Yao, H. Q., Zhang, Y. H., et al. (2012). The conversion of oridonin to spirolactone-type or enmein-type diterpenoid: synthesis and biological evaluation of ent-6,7-seco-oridonin derivatives as novel potential anticancer agents. *Eur. J. Med. Chem.* 52, 242–250. doi: 10.1016/j.ejmech.2012.03.024

Wang, Z. Y., Liu, J. G., Li, H., and Yang, H. M. (2016). Pharmacological effects of active components of chinese herbal medicine in the treatment of Alzheimer's disease: a review. *Am. J. Chin. Med.* 44, 1525–1541. doi: 10.1142/S0192415X16500853

Wheate, N. J., Walker, S., Craig, G. E., and Oun, R. (2010). The status of platinum anticancer drugs in the clinic and in clinical trials. *Dalton Trans.* 39, 8113–8127. doi: 10.1039/c0dt00292e

Wu, C. C., Li, T. K., Farh, L., Lin, L. Y., Lin, T. S., Yu, Y. J., et al. (2011). Structural basis of type II topoisomerase inhibition by the anticancer drug etoposide. *Science* 333, 459–462. doi: 10.1126/science.1204117

Wu, W. S., Chien, C. C., Chen, Y. C., and Chiu, W. T. (2016). Protein Kinase RNA-like endoplasmic reticulum kinase-mediated Bcl-2 protein phosphorylation contributes to evodiamine-induced apoptosis of human renal cell carcinoma cells. *PLoS One* 11:e0160484. doi: 10.1371/journal.pone.0160484

Xu, S., Pei, L. L., Wang, C. Q., Zhang, Y. K., Li, D. H., Yao, H. Q., et al. (2014). Novel hybrids of natural oridonin-bearing nitrogen mustards as potential anticancer drug candidates. *ACS Med. Chem. Lett.* 5, 797–808. doi: 10.1021/ml500141f

Xu, S. T., Pei, L. L., Li, D. H., Yao, H., Cai, H., Yao, H. Q., et al. (2014). Synthesis and antimycobacterial evaluation of natural oridonin and its enmein-type derivatives. *Fitoterapia* 99, 300–306. doi: 10.1016/j.fitote.2014.10.005

Yadav, A. A., Wu, X., Patel, D., Yalowich, J. C., and Hasinoff, B. B. (2014). Structure-based design, synthesis and biological testing of etoposide analog epipodophyllotoxin-N-mustard hybrid compounds designed to covalently bind to topoisomerase II and DNA. *Bioorg. Med. Chem.* 22, 5935–5949. doi: 10.1016/j.bmc.2014.09.014

Yu, H., Jin, H., Gong, W., Wang, Z., and Liang, H. (2013). Pharmacological actions of multi-target-directed evodiamine. *Molecules* 18, 1826–1843. doi: 10.3390/molecules18021826

Zarytova, V. F., Ivanova, E. M., and Chasovskikh, M. N. (1990). [Synthesis of steroid-containing oligonucleotides and their alkylating derivatives]. *Bioorg. Khim.* 16, 610–616.

Zhou, G. B., Kang, H., Wang, L., Gao, L., Liu, P., Xie, J., et al. (2007). Oridonin, a diterpenoid extracted from medicinal herbs, targets AML1-ETO fusion protein and shows potent antitumor activity with low adverse effects on t(8;21) leukemia in vitro and in vivo. *Blood* 109, 3441–3450. doi: 10.1182/blood-2006-06-032250

Conflict of Interest Statement: The authors declare that the research was conducted in the absence of any commercial or financial relationships that could be construed as a potential conflict of interest.

frontiers in Oncology

ORIGINAL RESEARCH
published: 18 December 2018
doi: 10.3389/fonc.2018.00631

Oxymatrine and Cisplatin Synergistically Enhance Anti-tumor Immunity of CD8$^+$ T Cells in Non-small Cell Lung Cancer

Jin Ye[1†], Man-Man Zou[2†], Pei Li[1], Xi-Jun Lin[1], Qi-Wei Jiang[3], Yang Yang[3], Jia-Rong Huang[3], Meng-Ling Yuan[3], Zi-Hao Xing[3], Meng-Ning Wei[3], Yao Li[3], Zhi Shi[3] and Hui Liu[2]**

[1] Department of Otolaryngology-Head and Neck Surgery, The Third Affiliated Hospital, Sun Yat-sen University, Guangzhou, China, [2] Division of Pulmonary and Critical Care, Department of Internal Medicine, The Third Affiliated Hospital, Sun Yat-sen University, Guangzhou, China, [3] Guangdong Provincial Key Laboratory of Bioengineering Medicine, Department of Cell Biology & Institute of Biomedicine, National Engineering Research Center of Genetic Medicine, College of Life Science and Technology, Jinan University, Guangzhou, China

OPEN ACCESS

Edited by:
Yan-yan Yan,
Shanxi Datong University, China

Reviewed by:
Hua Zhu,
The Ohio State University, United States
Xiao Qian Chen,
Huazhong University of Science and Technology, China

***Correspondence:**
Zhi Shi
tshizhi@jnu.edu.cn
Hui Liu
liuhui27@mail.sysu.edu.cn

†These authors have contributed equally to this work

Specialty section:
This article was submitted to Cancer Molecular Targets and Therapeutics, a section of the journal Frontiers in Oncology

Received: 12 November 2018
Accepted: 04 December 2018
Published: 18 December 2018

Citation:
Ye J, Zou M-M, Li P, Lin X-J, Jiang Q-W, Yang Y, Huang J-R, Yuan M-L, Xing Z-H, Wei M-N, Li Y, Shi Z and Liu H (2018) Oxymatrine and Cisplatin Synergistically Enhance Anti-tumor Immunity of CD8$^+$ T Cells in Non-small Cell Lung Cancer. Front. Oncol. 8:631. doi: 10.3389/fonc.2018.00631

Oxymatrine (OMT) has shown broad antitumor activities for the treatment of several types of cancers. However, little is known about its effect on anti-tumor immunity. Combination therapy is a potentially promising strategy of cancer to enhance anticancer activity, overcome drug resistance, and lower treatment failure rate. In the present study, we demonstrated that the combination of OMT with cisplatin (DDP) synergistically inhibited non-small cell lung cancer (NSCLC) cells growth when co-cultured with peripheral blood mononuclear cells *in vitro*. Furthermore, the combination of OMT with DDP significantly inhibited the growth of Lewis lung cancer (LLC) mouse xenograft tumors. Flow cytometry analysis revealed that OMT and DDP synergistically increase the CD8$^+$/ regulatory T cells ratio and enhanced more CD8$^+$ T cells secreted cytokines of IFN-γ, TNF-α, and IL-2 *in vivo*. Mechanistically, upregulation of *miR-155* and downregulation of suppressor of cytokine signaling-1 (*SOCS1*) were confirmed as a target signaling pathway to positively regulate the anti-tumor response of CD8$^+$ T cells. Overall, OMT in combination with DDP showed outstanding synergistic anti-tumor immunity, suggesting that this beneficial combination may offer a potential immunotherapy for NSCLC patients.

Keywords: oxymatrine, cisplatin, CD8$^+$ T cells, anti-tumor immunity, NSCLC

INTRODUCTION

Lung cancer is the leading cause of cancer-related death worldwide (1), and non-small cell lung cancer (NSCLC) accounts for approximately 85% of the whole lung cancer cases (2). Despite years of researches for early diagnosis and standard treatment, the prognosis for patients with lung cancer remains dismal, and 5-year survival rate remains <15% (3–6). T cell–mediated anti-tumor immunotherapy emerges as a promising treatment for human malignancies, in which CD8$^+$ T cells [cytotoxic T lymphocytes (CTLs)] represent a major of the cell-mediated anti-tumor response via providing host immune protection against intracellular pathogens and cancers (7, 8). However,

progressive tumors can escape immune recognition and attack by smartly establishing an immune tolerance involving immunosuppressive T lymphocytes (9, 10). In particular, regulatory T cells (T_{reg}) are proposed as key components of the immune suppressive tumor microenvironment with strong suppressive capacities toward $CD4^+$ and $CD8^+$ T lymphocytes, B cells, and dendritic cells etc. (11). Further, Baras et al. demonstrated that the $CD8^+/T_{reg}$ ratio in tumor infiltrating lymphocytes (TIL) densities rather than the two independent parameters was significantly associated with cisplatin-based neoadjuvant chemotherapy (12). MicroRNAs (miRNAs) have been confirmed as global regulators of gene expression programs that regulate specific target genes at the post-transcriptional level (13). Some of them have been identified as targets for anti-cancer therapeutics (14), and effects on tumor-infiltrating immune cells has become a hot spot besides their functions in cancer cells recent years (15). *miR-155* is an ancient regulator of the immune system (16). Elegant et al. demonstrated that *miR-155* was required for $CD8^+$ T cell responses in defending against infection and cancer by silencing suppressor of cytokine signaling-1 (*SOCS1*) (17, 18). Initial evidence has also unraveled the crucial role of *miR-155* in dendritic cells functions in multiple types of cancers (19, 20). Altogether, these studies suggested the pivotal functions of *miR-155* in various T cell subsets as they respond to solid tumors.

Cisplatin (DDP)-based doublet remains the foundation of treatment for the patients with NSCLC in the modern era (21). The resistance of NSCLC cells to DDP is also an emergent problem, therefore developing more effective strategies for the treatment of NSCLC is urgently required. Combination chemotherapy is identified as a potentially promising approach to enhance anticancer activity, overcome drug resistance, and lower treatment failure rate (22, 23). Oxymatrine (OMT) is a main alkaloid extracted from roots of Sophora species with a broad range of bioactivities. Especially, extensive researches have reported that OMT have anticancer effects by inducing cell cycle arrest, apoptosis and inhibition of angiogenesis in various cancer cells *in vitro* and *in vivo* (24). In the previous studies, immunoregulatory effects of OMT on hepatitis B of mice, rheumatoid arthritis in rats and mastitis in mice have been confirmed (25–27). Considering the extensive effects of OMT, we investigate the effect of OMT in combination with DDP on anti-tumor immunity in NSCLC and elucidate the potential mechanism.

MATERIALS AND METHODS

Cell Culture and Reagents

Human A549 NSCLC cell line and mouse Lewis lung cancer (LLC) cell line were cultured in Dulbecco' s modified Eagle's medium (DMEM) with 10% fetal bovine serum (FBS), penicillin (100 U/ml), and streptomycin (100 ng/ml) at 37°C with 5% CO_2 in a humidified incubator. OMT and DDP were ordered from Dalian Meilun Biotechnology and Qilu Pharmaceutical, respectively. OMT and DDP were dissolved in phosphate-buffered saline (PBS) on stock concentration (1 M and 10 mM, respectively) and stored at −20°C. Other reagents were purchased from Shanghai Sangon Biotech unless otherwise noted.

Cell Viability Assay

Freshly-isolated peripheral blood mononuclear cells (PBMCs) were suspended in DMED culture medium and seeded into a 96-well plate at a density of 1×10^4 cells/well and treated with various concentrations of drugs in three parallel wells for 72 h. CCK-8 (Dojindo Molecular Technologies, Shanghai, China) was then added to each well according to the protocol of the manufacture. The absorbance was measured at wavelengths of 450 nm after incubation with CCK-8 solution at 37°C for 4 h. Cells viability assay of A549 and LLC cells were measured using methylthiazolyldiphenyl-tetrazolium bromide (MTT) (28). Briefly, tumor cells were distributed (5,000 cells/well) into 96-well plates containing agents at different concentrations. After 3 days, MTT was added to each well at a final concentration of 0.5 mg/ml. After incubation for 4 h, the medium and MTT solution were removed from each well, and formazan crystals were dissolved in 100 μl of DMSO. Absorbance was measured at wavelengths of 570 nm. All absorbance was detected by Multiscan Spectrum (Thermo Fisher). The concentrations required to inhibit growth by 50% (IC_{50}) were calculated from survival curves using the Bliss method (29). Studies relative to human in this article were approved by the ethics committee of the Third Affiliated Hospital, Sun Yat-sen University (Approval No: [2014]2-17).

Tumor Cells/PBMCs Co-culture

After adherence of tumor cells into 6-well plates (target cells, 4×10^5 cells/well), a certain amount of PBMCs (effector cells) suspended in the appropriate DMEM pulsed with 10% FBS were added. Four ratios of effector cells to target cells, 0:1, 2:1, 4:1, and 6:1 were designed. After treated with OMT and DDP alone or combination, target cells (tumor cells) and effector cells (PBMCs) were co-cultured for 24 h at 37°C in 5% CO_2. The cellular remaining viable tumor cells were photographed under microscope (OLYMPUS IX71) and quantified, respectively.

Mice Xenograft Tumor Assay

Age-suitable C57BL/6 female mice were obtained from Vital River Laboratory Animal Technology (Beijing), and all mice have been maintained with sterilized food and water. All animal experimental procedures were approved by the Institutional Animal Care and Use Committee of Sun Yat-sen University (Approval No: IACUC-DB-17-0502). Briefly, female C57BL/6 mice within 6 weeks old and 20 g weight were used for each group. Each mouse was injected subcutaneously with LLC cells (2×10^6 in 100 μl of PBS) in right scapular region. When the subcutaneous tumors were approximately 0.3×0.3 cm^2 (two perpendicular diameters) in size, mice were randomized into four groups. Mice were injected intraperitoneally with vehicle alone (0.9% saline), OMT alone (100 mg/kg body weight per day), DDP alone (2 mg/kg body weight every 2 day), or a combination of OMT and DDP (administration method is as same as the relevant single drug group). The body weights of mice and the two perpendicular diameters (A and B) of tumors were recorded

TABLE 1 | The primer sequences for real time PCR (mouse).

miR-155 (RT)	5′-GTCGTATCCAGTGCAGGGTCCGAGGTATTCGCACTGGATACGACACCCCT-3′
miR-155 (F)	5′-GTCGTATCCAGTGCAGGGTCCGAGGTATTCGCACTGGATACGACACCCCT-3′
miR-155 (R)	5′-GTCGTATCCAGTGCAGGGTCCGAGGTATTCGCACTGGATACGACAAAATA-3′
U6 (RT)	5′-GTCGTATCCAGTGCAGGGTCCGAGGTATTCGCACTGGATACGACAAAATA-3
U6 (F)	5′-GCGCGTCGTGAAGCGTTC-3
U6 (R)	5′-GTGCAGGGTCCGAGGT-3
SOCS1 (F)	5′-CTGCGGCTTCTATTGGGGAC-3
SOCS1 (R)	5′-AAAAGGCAGTCGAAGGTCTCG-3
β-actin (F)	5′-CCTTCTTGGGTATGGAATCCTG-3
β-actin (R)	5′-CAATGCCTGGGTACATGGTG-3

every day. The tumor volumes (V) were calculated according to the formula:

$$V = \pi/6(1/2(A + B))^3$$

The mice were anesthetized after the experiment, and tumors were excised from the mice and weighted. Heparin anticoagulated peripheral blood, spleens and tumors were collected for further use. The rate of inhibition (IR) was calculated according to the formula below:

IR = 1-Mean tumor weight of experimental group/Mean tumor weight of control group × 100%.

Flow Cytometric Analysis

PBMCs and spleen lymphocytes were collected with Ficoll-diatrizoate (LTS1077, tbdscience, Tianjin) according to the protocol of the manufacture. For the separation of tumor infiltrating lymphocytes from LLC-bearing mice, xenograft tumors were mechanically disrupted into 1 mm^3 pieces and digested chemically in 7 ml of dissociation medium (DMEM medium plus with 10% FBS, collagenase type IV (5 mg/ml), DNase I (1 mg/ml), and hyaluronidase (1 mg/ml) for 30 min at 37°C followed by filtration through a 70 μm cell strainer (NEST Biotechnology, Wuxi). Dissociated tumor cells were washed twice by PBS. Erythrocytes were lysed by red blood cell lysing buffer (BD Pharmigen) if necessary. The following antibodies were used for staining: Fc block (anti-CD16/32, Cat: 553142), CD3 APC-A750 (Cat: 557596), CD8a BV510 (Cat: 563068), CD4a FITC (Cat: 553046), Foxp3 PE (Cat: 563101), CD45 Percp-cy5.5 (Cat: 550994), IFN-γ FITC (Cat: 554411), TNF-α (Cat: 554420), anti-IL-2 (eBioscience, Cat: 12-7021-81), PE Rat IgG2a, κ Isotype Control (Cat: 553930), FITC Rat IgG1, κ Isotype Control (Cat: 554684), APC Rat IgG1, κ Isotype Control (Cat: 554686), and Rat IgG2b kappa Isotype Control (eBioscience, Cat: 12-4031-82). As regards the concentrations of antibodies, 2 μl/test was used in PBMCs and spleen lymphocytes samples and 3 μl/test in TIL flow cytometry. All antibodies were purchased from BD Pharmigen unless otherwise noted. Briefly, all samples were block with anti-CD16/32 for 20 min on room temperature and then stained with appropriate antibodies for 30 min on ice. Anti-mouse FoxP3 staining (eBioscience, Cat: 00-5523) was used for intracellular staining according to the manufacturer's instructions. For intracellular staining of IFN-γ, TNF-α, and IL-2, single-cell suspensions were incubated at 37°C for 5 h in the presence of Cell Stimulation Cocktail (eBioscience, Cat: 85-00-4975-93) according to the manufacturer's protocol. Zombie Violet™ Fixable Viability Kit (Biolegend, Cat: 423113) was required to distinguish live/dead cells in tumor flow cytometry. Appropriate isotype control antibodies were used to determine the gating strategies.

$CD8^+$ T Cell Isolation

Freshly-separated single-cells of splenocytes were obtained according to the procedure above. For splenocytes $CD8^+$ T cells isolation, $CD8^+$ T cells were sorted by MACS (Miltenyi, Bergisch Gladbach, Germany) as described in the manufacturer's protocols. The purity of $CD8^+$ T cells was >95%, confirmed by flow cytometry.

Reverse Transcription Quantitative PCR

Total RNAs were extracted using RNeasy Mini Kit (Qiagen, Duesseldorf, Germany) in accordance with the manufacturer's instructions. We used 0.1 μg total RNAs as the template to synthesize cDNA via reverse transcription reaction through GoScript™ Reverse Transcription System kit (Promega) according to the manufacturer's instructions. For miRNA detection, equal RNA from each sample was reverse-transcribed to cDNA by means of specific miRNA stem-loop primers. Subsequently, quantitative real-time polymerase chain reactions were ran on Roche-LightCycler-480 by LightCycler 480 SYBR Green I Master. *β-actin* and *U6* were used as internal normalization controls. All assays were performed following the manufacturer's instructions. All sequences of primers listed in **Table 1** were synthesized by Sangon Biotech (Shanghai, China). The thermal cycling conditions include 5 min at 95°C, and 40 cycles of 10 s at 95°C and 20 s at 55°C. Samples were run in triplicate and differences in gene expression were calculated using the $2^{-\text{cycle threshold}}$ method (30, 31).

Statistical Analysis

All results were presented as mean ± standard deviation (SD). Comparisons between the treated and untreated groups were performed with Student's *t*-test. All data were analyzed using GraphPad Prism 5 and a values of $P < 0.05$ was set statistically significant.

RESULTS

OMT and DDP Synergistically Inhibit the Growth of NSCLC Cells Co-cultured With PBMCs *in vitro*

In the present study, we firstly investigate the effects of OMT and DDP on NSCLC cells and PBMCs. Cell survival was assessed by MTT assay. As shown in **Figures 1A,B**, the survival of all used cells was decreased in a dose-dependent manner *in vitro* after OMT or DDP treatment. OMT and DDP exhibited significant cytotoxicity against A549 and LLC cells, but weaker cytotoxicity against human and mice PBMCs. To assess the anti-tumor effects of OMT and DDP on growth of NSCLC cells in the presence of PBMCs, co-cultured NSCLC cells (target cells) with PBMCs (effect cells) at ratios of 1:0, 1:2, 1:4, and 1:6 were treated with OMT and DDP alone or combination. As showed in **Figure 1C**, after co-treatment with OMT and DDP, the survival of cancer cells were significantly reduced in comparison with OMT or DDP alone without PBMCs. Strikingly, the growth of tumor cells were more potently inhibited by OMT or (and) DDP administration when co-cultivated in combination with PBMCs at all target/effector cells ratio, and especially the ratio of target/effect cells at 1:6 exhibited most effective inhibition. These results suggest that OMT and DDP synergistically inhibit the growth of lung cancer cells when co-cultured with PBMCs *in vitro*.

OMT and DDP Synergistically Inhibit the NSCLC Xenografts Growth *in vivo*

To examine the synergistic anti-tumor effects of OMT and DDP *in vivo*, we generated the xenograft tumor models by transplanting LLC cells into C57BL/6 mice. As shown in **Figures 2A–C**, compared with OMT or DDP alone treatment, co-treatment OMT with DDP significantly inhibited the growth of subcutaneous tumors by diminishing the volume and weight of tumors. The inhibition rate of tumor growth in the co-treatment group reached 94.19%, which was obviously higher than that in either single treatment group (**Figure 2E**). In addition, mice body weights in DDP alone or co-treatment groups were lower than those of control group (**Figure 2D**). These data suggest that OMT and DDP can synergistically inhibit the NSCLC xenograft growth *in vivo*.

OMT and DDP Synergistically Increase the $CD8^+/T_{reg}$ Ratio *in vivo*

The interaction of immune system in malignant diseases is heralded as one of the most important advances in oncology. We speculated that heightened tumor regression after OMT and DDP treatments may be caused by strong anti-tumor immunity. The cytotoxic T lymphocytes (CTLs, also $CD8^+$ T cells, marked as $CD3^+CD8^+$ T cells) are pivotal immune cells directed against tumor cells susceptible to cell lysis, but $CD4^+Foxp3^+$ regulatory T cells (T_{reg}) disturb antitumor immunity by suppressing the activities of effector T cells. Our flow cytometry data revealed that compared with OMT or DDP alone treatment, co-treatment OMT with DDP significantly increased $CD8^+$ T cells percentage in PBMCs and spleen lymphocytes, and decreased T_{regs} cells percentage in PBMCs and tumor infiltrating lymphocytes (**Figures 3A–C**). Furthermore, compared with OMT or DDP alone treatment, co-treatment OMT with DDP significantly increased the $CD8^+/T_{reg}$ ratio in PBMCs, spleen lymphocytes and tumor infiltrating lymphocytes (**Figure 3D**). These results indicate that OMT and DDP can synergistically increase the $CD8^+/T_{reg}$ ratio *in vivo*.

OMT and DDP Synergistically Enhance $CD8^+$ T Cells Anti-tumor Immune Response

We further evaluated the immune status of $CD8^+$ T cells in mice bearing LLC, since $CD8^+$ T cells play a pivotal role in anti-tumor immunity. As shown in **Figures 4A,B**, compared with OMT or DDP alone treatment, co-treatment OMT with DDP significantly induced the increased intracellular IFN-γ and TNF-α and the decreased intracellular IL-2 in spleen lymphocytes, and the increased intracellular IFN-γ, TNF-α, and IL-2 in tumor infiltrating lymphocytes, suggesting that OMT and DDP synergistically enhance $CD8^+$ T cells anti-tumor immune response.

OMT and DDP Synergistically Upregulate *miR-155* and Downregulate *SOCS1* Expressions in Splenic $CD8^+$ T Cells

MiR-155 plays a key role in tumor immune response by targeting *SOCS1* (16). We detected *miR-155* and *SOCS1* expressions in splenic $CD8^+$ T cells. As shown in **Figure 5**, compared with OMT or DDP alone treatment, co-treatment with OMT and DDP significantly upregulated *miR-155* and downregulate *SOCS1* expressions in splenic $CD8^+$ T cells.

DISCUSSION

Natural products play an important role in the prevention and treatment of cancer and other disease in the world (32, 33). Our study clearly indicates that the combination of OMT and DDP synergistically enhanced NSCLC cells growth inhibition, $CD8^+/_{Treg}$ ratio and $CD8^+$ T cells anti-tumor immune response with the upregulation of *miR-155* and the silence of *SOCS1*. It has been reported that cancer immunotherapy has been a hot spot in the treatment of NSCLC (34). T_{reg} cells are highly immune suppressive cells and play central roles in the maintenance of self-tolerance and immune homeostasis (35). It can inhibit anti-tumor immunity in NSCLC by suppressing effector T cells directly by cell interaction or indirectly via the secretion of soluble factor-mediated suppression (36). We previously have reported that higher $T_{reg}/CD8^+$ ratio in tumor was an independent factor for poor response to platinum-based chemotherapy, but $CD8^+$ and T_{reg} tumor infiltrating lymphocytes was not correlated with any clinicopathological features in advanced NSCLC patients (37). Current findings on the model of mice bearing LLC have suggested that co-treatment OMT with DDP significantly enhanced the $CD8^+/T_{reg}$ ratio in comparison with single agent groups, which is also in agreement

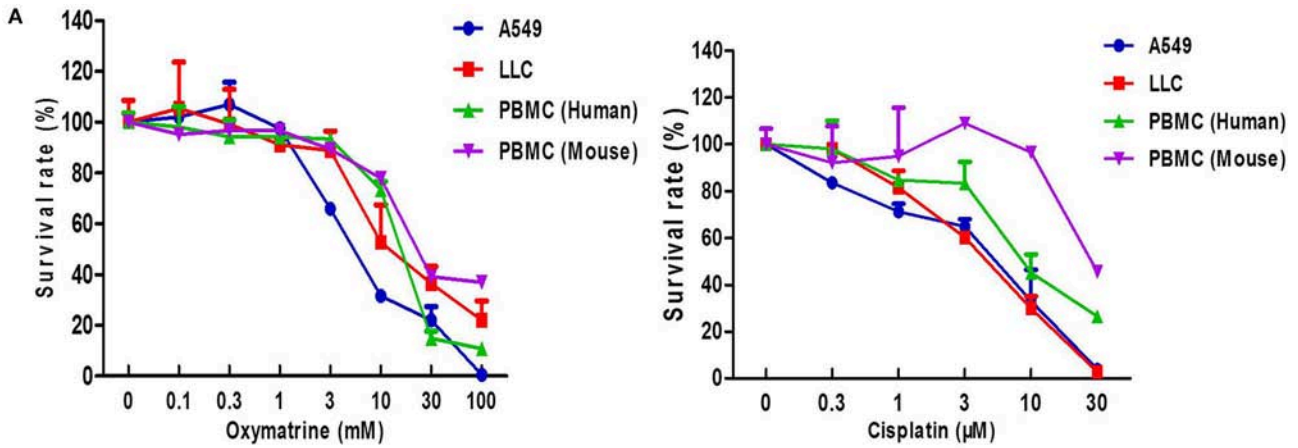

B

Summary of IC50 values of oxymatrine and cisplatin in the indicated cells.

Cell line	A549	LLC	PBMC (Human)	PBMC (Mouse)
Oxymatrine (mM)	5.35±1.24	12.54±0.99	18.09±0.16	23.27±1.58
Cisplatin (μM)	8.14±2.64	5.83±0.66	9.52±0.42	28.96±0.96

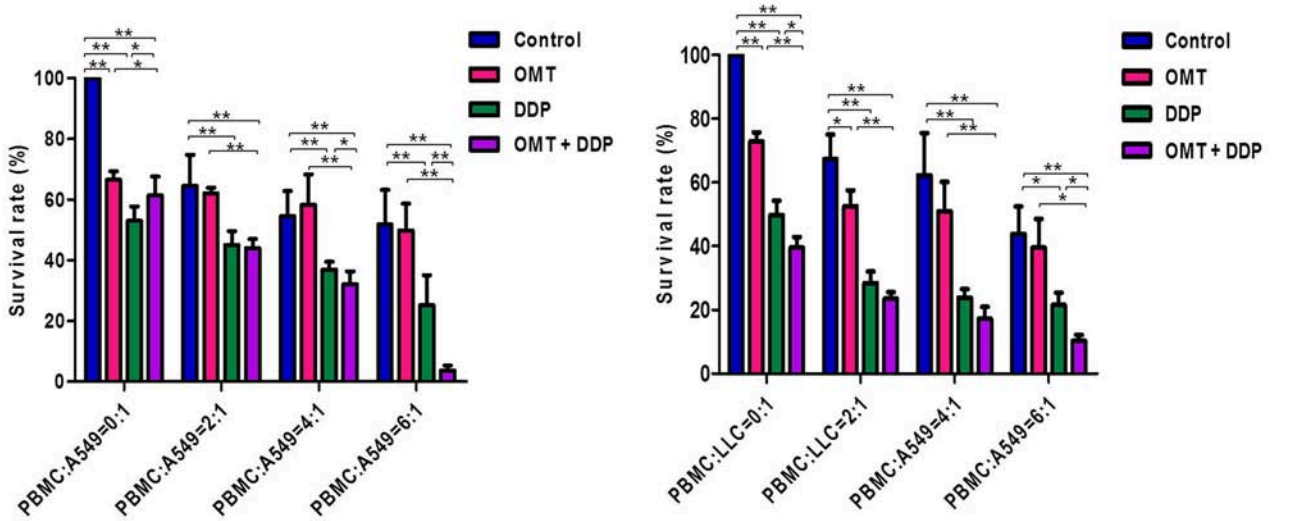

FIGURE 1 | OMT and DDP synergistically inhibit the growth of NSCLC cells co-cultured with PBMCs *in vitro*. Cells were treated with the indicated concentrations of OMT or DDP for 72 h, and cell survival was determined by MTT or CCK-8 assay and summary survival curves **(A)** and IC_{50} values in the indicated cells **(B)** were shown. Co-cultured NSCLC cells (target cells) with PBMCs (effect cells) at ratios of 1:0, 1:2, 1:4, and 1:6 were treated with OMT (3 mM) and DDP (2 μM) alone or combination for 24 h. Quantified results were shown in **(C).** The values presented are the means ± SD for each group. $^{*}P < 0.05$ and $^{**}P < 0.01$ *vs.* corresponding control.

with other clinical evidence that decreased $CD8^{+}/T_{reg}$ ratio among tumor infiltrating lymphocytes are correlated with poor prognosis in various types of human cancers (38–40). However, there are differences between the results of the present study and a report by Zhang et al. which demonstrated that higher ratio of $CD8^{+}/ T_{reg}$ was significantly associated with poor overall

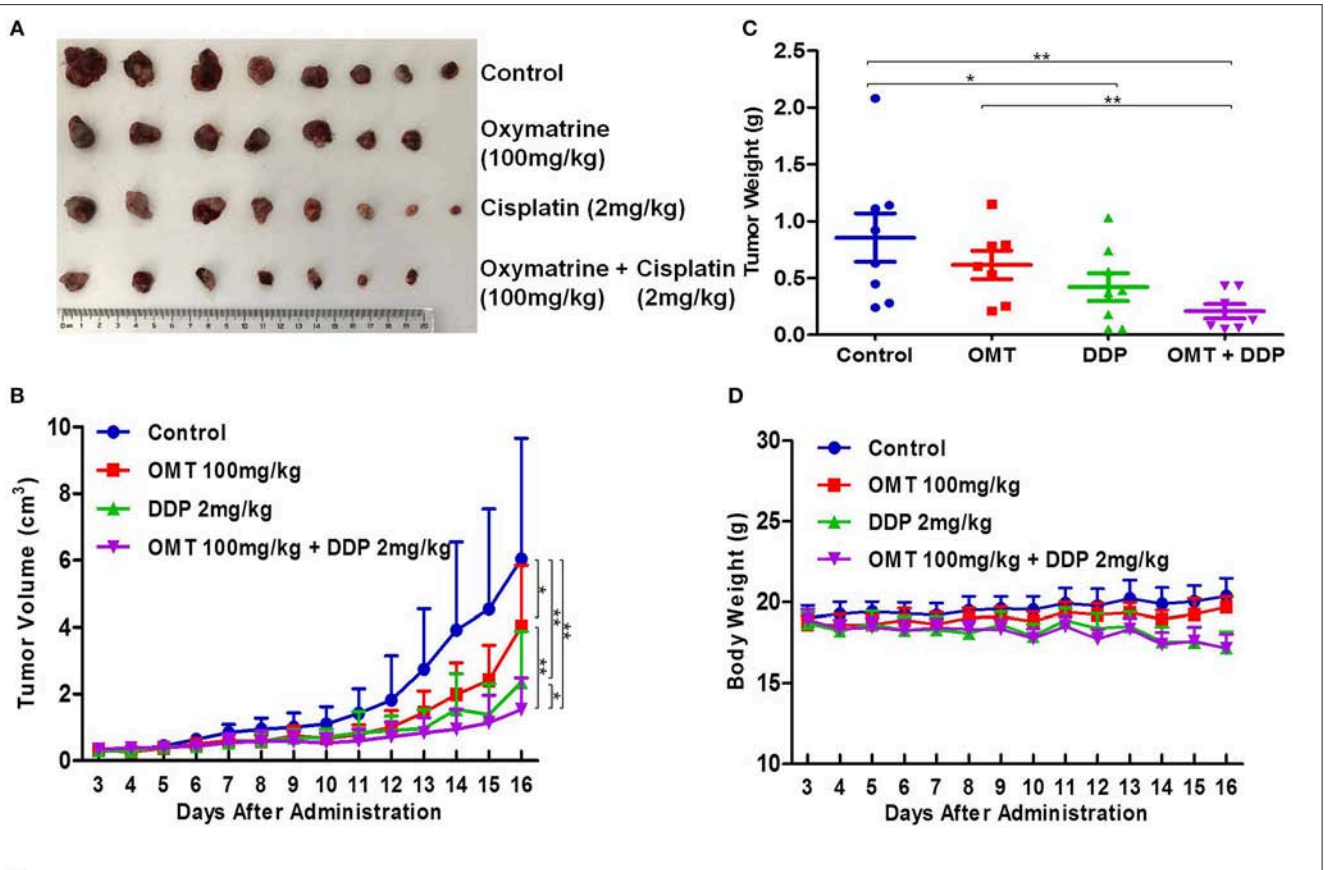

E

Summary of oxymatrine and cisplatin on the growth of LLC xenografts in C57BL/6 mice

Groups	Before Expriment		After Expriment		Weight of Tumor (g)	Inhibition(%)
	Mice (n)	Weight (g)	Mice (n)	Weight (g)		
Control	8	19.04±0.77	8	20.37±1.10	0.86±0.61	
Oxymatrine	7	18.64±0.52	7	19.69±0.66	0.55±0.36	52.32
Cisplatin	8	18.71±0.68	8	17.18±1.00	0.42±0.34*	67.44*
OMT + DDP	7	18.93±0.64	7	17.17±0.86	0.19±0.17**	94.19**

FIGURE 2 | OMT and DDP synergistically inhibit NSCLC xenografts growth *in vivo*. Each mouse was injected subcutaneously with LLC cells (2×10^6 in 100 μl of PBS) in right scapular region. When the subcutaneous tumors were approximately 0.3×0.3 cm^2 (two perpendicular diameters) in size, mice were randomized into four groups, and were injected intraperitoneally with vehicle alone (0.9% saline), OMT alone (100 mg/kg body weight per day), DDP alone (2 mg/kg body weight every 2 day), or a combination of OMT and DDP (administration method is as same as the relevant single drug group). The body weights and tumor volumes of mice were recorded. The mice were anesthetized after experiment, and tumors were excised from the mice and weighted. The original tumors **(A)**, tumor volumes **(B)**, tumor weights **(C)**, body weights **(D)**, and summary data **(E)** were shown. The values presented are the means ± SD for each group. $^*P < 0.05$ and $^{**}P < 0.01$ vs. corresponding control.

survival and progression-free survival in early nasopharyngeal carcinoma stage patients (41). Different chemotherapeutic regimens and tumor context may contribute to these differences.

It is well-known that $CD8^+$ effector T cells have a critical role in elimination of tumors. Previous studies showed that IFN-γ, TNF-α, and IL-2-expressing $CD8^+$ T cells are instrumental in anti-tumor immune response (42). IFN-γ-expressing T cells are essential in repressing tumor growth which promotes host responses to tumors. Moreover, IFN-γ can execute direct anti-proliferative, pro-apoptotic and anti-angiogenesis actions on various tumor cells (43). TNF-α is another multifunctional cytokine, which mediates anticancer adaptive immune response. In the report of Ando et al. TNF-α might be an effective therapy in some cases of NSCLC that have acquired resistance to gefitinib (44). IL-2 acts crossroads functions in activation and cell growth of T and NK cells and it can promote $CD8^+$ T cells and natural killer cells cytolytic activities in response to antigen (45). In lung

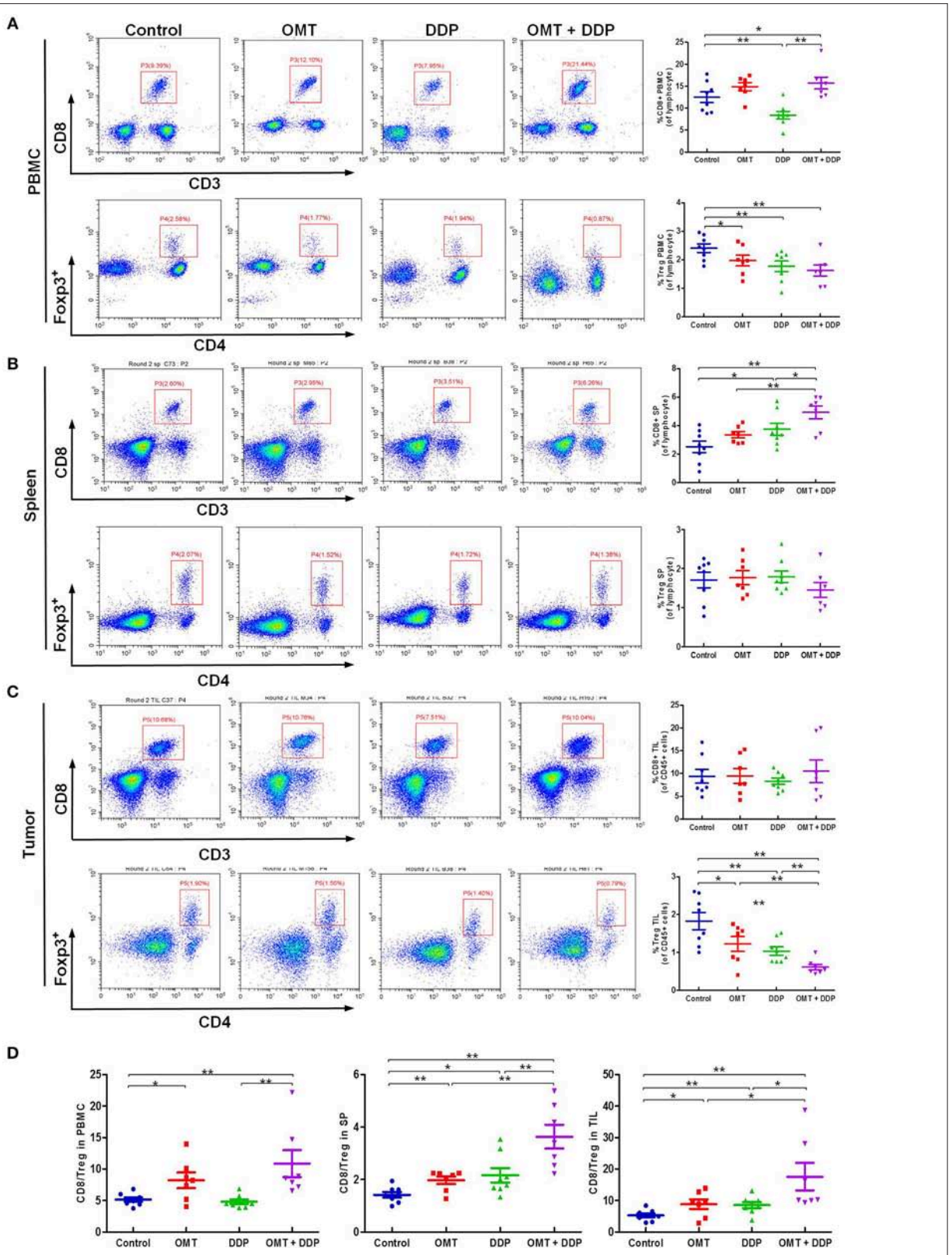

FIGURE 3 | OMT and DDP synergistically increase the $CD8^+/T_{reg}$ ratio *in vivo*. Isolated PBMCs, spleen lymphocytes and tumor infiltrating lymphocytes were stained with indicated antibodies and analyzed by flow cytometry. Representative flow plots and quantified results of $CD8^+$ T cells and T_{reg} cells in PBMCs **(A)**, spleen lymphocytes **(B),** and tumor infiltrating lymphocytes **(C)** were shown. The $CD8^+/T_{reg}$ ratios were quantified **(D)**. $^*P < 0.05$ and $^{**}P < 0.01$ vs. corresponding control.

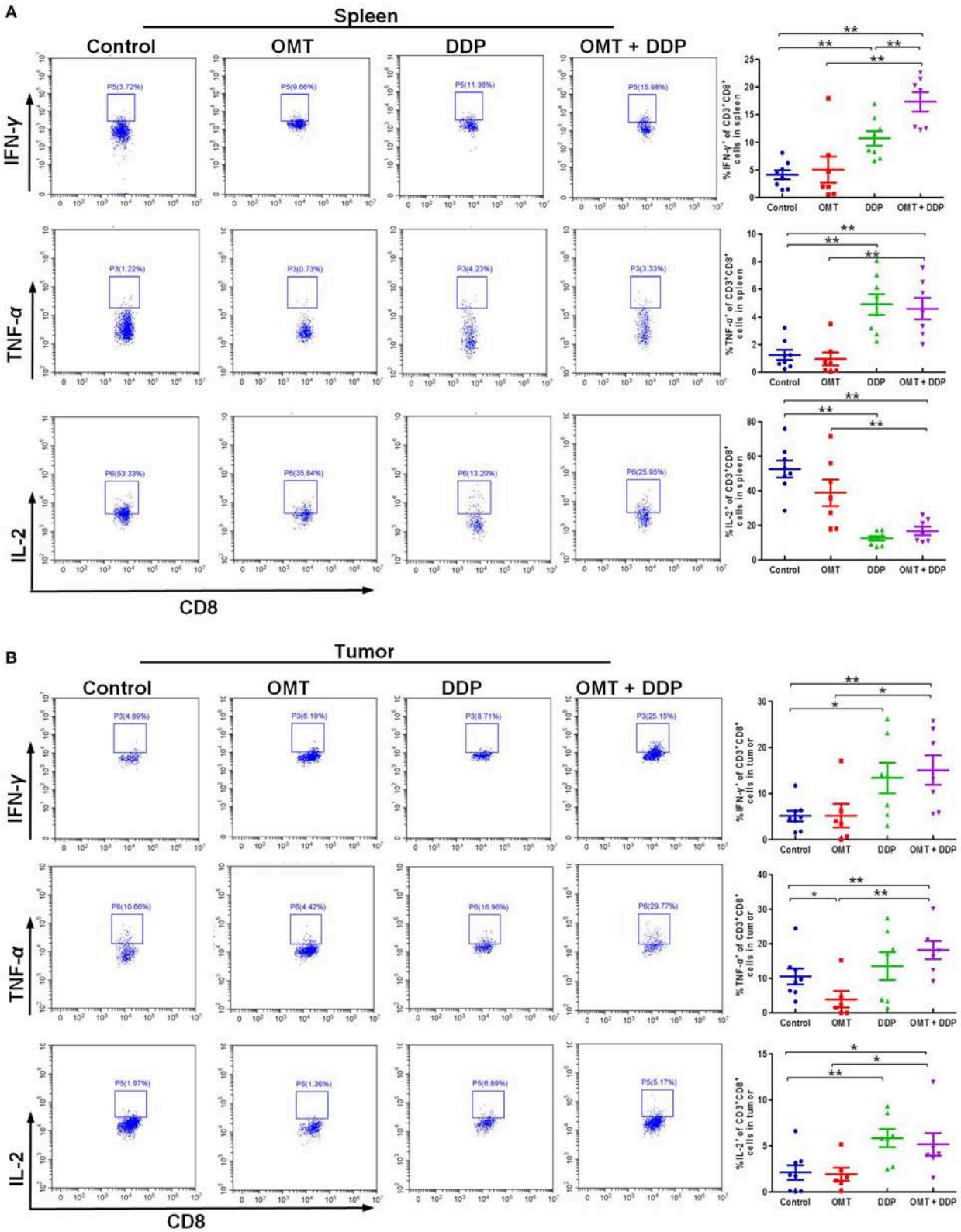

FIGURE 4 | OMT and DDP synergistically enhance $CD8^+$ T cells anti-tumor immune response. Spleen lymphocytes and tumor infiltrating lymphocytes were isolated, and intracellular IFN-γ, TNF-α, and IL-2 were determined by flow cytometry. Representative flow plots and quantified results of intracellular IFN-γ, TNF-α, and IL-2 expression in $CD8^+$ T cells of spleen lymphocytes **(A)** and tumor infiltrating lymphocytes **(B)** were shown. $^*P < 0.05$ and $^{**}P < 0.01$ vs. corresponding control.

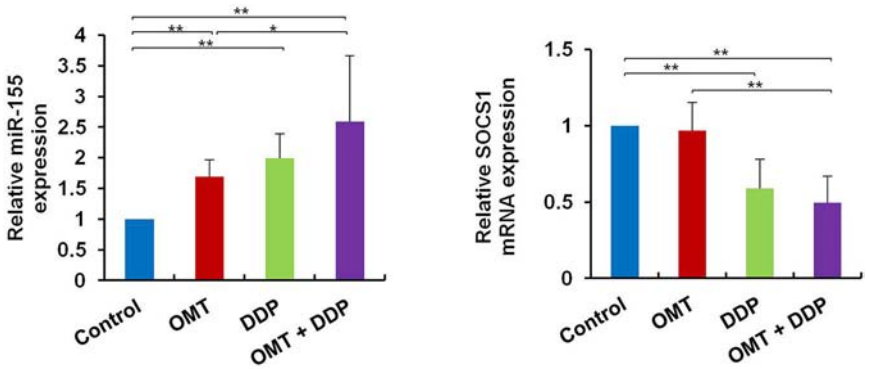

FIGURE 5 | OMT and DDP synergistically upregulate *miR-155* and downregulate *SOCS1* expressions in splenic CD8$^+$ T cells. Splenocytes CD8$^+$ T cells were separated by magnetic bead from MACS and the total RNAs were extracted immediately. Expression of *miR-155* and *SOCS1* in splenic CD8$^+$ T cells were determined by RT-qPCR. *U6* and β-actin were used as the normal controls. Data shown are representative of three independent experiments. *P <0.05 and **P < 0.01 vs. corresponding control.

cancer patients, IL-2 treatment reverses CD8$^+$ T cells exhaustion and markedly increases Granzyme B and IFN-γ in malignant pleural effusion. Our study indicated that OMT in combination with DDP significantly upregulated the production of IFN-γ and TNF-α in CD8$^+$ T cells compared with the single agent both in the splenocytes and tumor infiltrating lymphocytes. Nevertheless, expression of IL-2 is declined in splenocytes and increased in tumor infiltrating lymphocytes, inversely. These differences indicated the complexities of the effects of chemotherapeutic drugs in different immune organs. Since IL-2 is essential for the development and maintenance of T_{reg} (45), declined IL-2 secretion may be able to decrease the immune suppressive T_{reg}. This may be another manner to enhance CD8$^+$ T cells anti-tumor response to a certain extent.

One particular miRNA, *miR-155*, has emerged as a central regulator in immune homeostasis and antitumor immunity recent years (16, 46). *MiR-155* silencing promotes solid tumor growth through increasing the recruitment and functions of myeloid-derived suppressor cells in tumor microenvironment (47). Strikingly, *miR-155* can augments effector CD8$^+$ T-cell anti-tumor immunity against viruses and cancer (17, 18, 48, 49). In detail, *miR-155* overexpression and silence of its target *SOCS1* in CD8$^+$ T cells enhanced the antitumor response and augmented tumor destruction (17). According to Ji et al.'s report, *miR-155* restrained the expression of *SOCS1*, one of the negative regulators of signal transducer and activator of transcription 5 (*STAT5a*), and constitutively active *STAT5a* recapitulated the survival advantages conferred by miR-155 (18). In addition, it is reported that *miR-155* shapes cytokine signaling via downregulation of *SOCS1* in T_{reg} subsets. Consistently, these findings consider *miRNA-155* and its target *SOCS1* as key regulators of effector CD8$^+$ T cells that can be modulated to potentiate immunotherapies for cancers. In our study, increased *miR-155* and decreased *SOCS1* expressions in splenic CD8$^+$ T cells are much agreement with the aforementioned investigations, which demonstrated that co-treatment OMT with DDP can enhanced antitumor immunity via *miR-155-SOCS1* signaling pathway in mice bearing LLC tumor. Further researches need to elucidate the effects of "loss or gain" functions of *miR-155* gene in our mice NSCLC model when OMT co-treatment with DDP. Moreover, antitumor immunity is most complicated involved in effector and immunosuppressive networks in the tumor microenvironment. In addition to CD8$^+$ T cells and T_{regs}, dendritic cells, natural killer cells, suppressive dysfunctional dendritic cells and macrophagocytes, these are essential immunogenic elements to skew the balance of pro- and anti-tumor forces toward tumor-specific immunity (50). Their immunomodulated functions in our present study need to be further investigated.

Collectively, the present study offers the first evidence that OMT and DDP synergistically inhibit the growth of NSCLC cells when co-culture with PBMCs *in vitro*. Further *in vivo* studies provide strong evidence that combinational treatment OMT with DDP shows outstanding synergistic anticancer effect by tipping a favor anti-tumor immunity, suggesting this beneficial combination may offer a promising treatment option for NSCLC patients.

ETHICS STATEMENT

Studies relative to human in this article were approved by the ethics committee of the Third Affiliated Hospital, Sun Yat-sen University (Approval No: [2014]2-17). All animal experiments were performed strictly in accordance with the Guidelines for the Care and Use of Laboratory Animals (No. 55 issued by Ministry of Health, China on January 25, 1998), and experimental procedure were approved by the Institutional Animal Care and Use Committee of Sun Yat-sen University (Approval No: IACUC-DB-17-0502).

AUTHOR CONTRIBUTIONS

JY, M-MZ, ZS, and HL designed the experiments, performed the experiments, analyzed the data, and wrote the paper. PL, X-JL, Q-WJ, YY, J-RH, M-LY, Z-HX, M-NW, and YL performed the experiments. All authors read and approved the final manuscript.

FUNDING

This work was supported by funds from the National Key Research and Development Program of China No. 2017YFA0505104 (ZS), the National Natural Science Foundation of China Nos. 81772540 (ZS) and 81472760 (HL), the Guangdong Natural Science Funds for Distinguished Young Scholar No. 2014A030306001 (ZS), the Guangdong Special Support Program for Young Talent No. 2015TQ01R350 (ZS), the Science and Technology Program of Guangdong Nos. 2016A050502027 (ZS) and 2014A020212078 (HL), the Science and Technology Program of Guangzhou No. 201704030058 (ZS).

REFERENCES

1. Siegel R, Naishadham D, Jemal A. Cancer statistics, 2013. *CA Cancer J Clin*. (2013) 63:11–30. doi: 10.3322/caac.21166
2. Molina JR, Yang P, Cassivi SD, Schild SE, Adjei AA. Non-small cell lung cancer: epidemiology, risk factors, treatment, and survivorship. *Mayo Clin Proc*. (2008) 83:584–94. doi: 10.1016/S0025-6196(11)60735-0
3. Rosell R, Karachaliou N. Lung cancer in 2014: optimizing lung cancer treatment approaches. *Nat Rev Clin Oncol*. (2015) 12:75–6. doi: 10.1038/nrclinonc.2014.225
4. Thomas A, Liu SV, Subramaniam DS, Giaccone G. Refining the treatment of NSCLC according to histological and molecular subtypes. *Nat Rev Clin Oncol*. (2015) 12:511–26. doi: 10.1038/nrclinonc.2015.90
5. Bansal P, Osman D, Gan GN, Simon GR, Boumber Y. Recent advances in immunotherapy in metastatic NSCLC. *Front Oncol*. (2016) 6:239. doi: 10.3389/fonc.2016.00239
6. Blais N, Hirsh V. Chemotherapy in metastatic NSCLC - new regimens (pemetrexed, nab-paclitaxel). *Front Oncol*. (2014) 4:177. doi: 10.3389/fonc.2014.00177
7. Pluhar GE, Pennell CA, Olin MR. CD8(+) T Cell-independent immune-mediated mechanisms of anti-tumor activity. *Crit Rev Immunol*. (2015) 35:153–72. doi: 10.1615/CritRevImmunol.2015013607
8. Zhang N, Bevan MJ. CD8(+) T cells: foot soldiers of the immune system. *Immunity* (2011) 35:161–8. doi: 10.1016/j.immuni.2011.07.010
9. Berendt MJ. T-cell-mediated suppression of anti-tumor immunity. An explanation for progressive growth of an immunogenic tumor. *J Exp Med*. (1980) 151:69–80. doi: 10.1084/jem.151.1.69
10. Smyth MJ, Godfrey DI, Trapani JA. A fresh look at tumor immunosurveillance and immunotherapy. *Nat Immunol*. (2001) 2:293–9. doi: 10.1038/86297
11. Shevach EM. Mechanisms of foxp3+ T regulatory cell-mediated suppression. *Immunity* (2009) 30:636–45. doi: 10.1016/j.immuni.2009.04.010
12. Baras AS, Drake C, Liu JJ, Gandhi N, Kates M, Hoque MO, et al. The ratio of CD8 to Treg tumor-infiltrating lymphocytes is associated with response to cisplatin-based neoadjuvant chemotherapy in patients with muscle invasive urothelial carcinoma of the bladder. *Oncoimmunology* (2016) 5:e1134412. doi: 10.1080/2162402X.2015.1134412
13. Bartel DP. MicroRNAs: target recognition and regulatory functions. *Cell* (2009) 136:215–33. doi: 10.1016/j.cell.2009.01.002
14. Li Z, Rana TM. Therapeutic targeting of microRNAs: current status and future challenges. *Nat Rev Drug Discov*. (2014) 13:622–38. doi: 10.1038/nrd4359
15. Paladini L, Fabris L, Bottai G, Raschioni C, Calin GA, Santarpia L. Targeting microRNAs as key modulators of tumor immune response. *J Exp Clin Cancer Res*. (2016) 35:103. doi: 10.1186/s13046-016-0375-2
16. Vigorito E, Kohlhaas S, Lu D, Leyland R. miR-155: an ancient regulator of the immune system. *Immunol Rev*. (2013) 253:146–57. doi: 10.1111/imr.12057
17. Dudda JC, Salaun B, Ji Y, Palmer DC, Monnot GC, Merck E, et al. MicroRNA-155 is required for effector CD8+ T cell responses to virus infection and cancer. *Immunity* (2013) 38:742–53. doi: 10.1016/j.immuni.2012.12.006
18. Ji Y, Wrzesinski C, Yu ZY, Hu JH, Gautam S, Hawk NV, et al. miR-155 augments CD8(+) T-cell antitumor activity in lymphoreplete hosts by enhancing responsiveness to homeostatic gamma(c) cytokines. *Proc Natl Acad Sci USA*. (2015) 112:476–81. doi: 10.1073/pnas.1422916112
19. Dunand-Sauthier I, Santiago-Raber ML, Capponi L, Vejnar CE, Schaad O, Irla M, et al. Silencing of c-Fos expression by microRNA-155 is critical for dendritic cell maturation and function. *Blood* (2011) 117:4490–500. doi: 10.1182/blood-2010-09-308064
20. Wang J, Iwanowycz S, Yu F, Jia X, Leng S, Wang Y, et al. microRNA-155 deficiency impairs dendritic cell function in breast cancer. *Oncoimmunology* (2016) 5:e1232223. doi: 10.1080/2162402X.2016.1232223
21. Fennell DA, Summers Y, Cadranel J, Benepal T, Christoph DC, Lal R, et al. Cisplatin in the modern era: the backbone of first-line chemotherapy for non-small cell lung cancer. *Cancer Treat Rev*. (2016) 44:42–50. doi: 10.1016/j.ctrv.2016.01.003
22. Bozic I, Reiter JG, Allen B, Antal T, Chatterjee K, Shah P, et al. Evolutionary dynamics of cancer in response to targeted combination therapy. *Elife* (2013) 2:e00747. doi: 10.7554/eLife.00747
23. Diyabalanage HV, Granda ML, Hooker JM. Combination therapy: histone deacetylase inhibitors and platinum-based chemotherapeutics for cancer. *Cancer Lett*. (2013) 329:1–8. doi: 10.1016/j.canlet.2012.09.018
24. Liu Y, Xu Y, Ji W, Li X, Sun B, Gao Q, et al. Anti-tumor activities of matrine and oxymatrine: literature review. *Tumour Biol*. (2014) 35:5111–9. doi: 10.1007/s13277-014-1680-z
25. Sang X, Wang R, Han Y, Zhang C, Shen H, Yang Z, et al. T cell–associated immunoregulation and antiviral effect of oxymatrine in hydrodynamic injection HBV mouse model. *Acta Pharm Sin B* (2017) 7:311–8. doi: 10.1016/j.apsb.2017.02.005
26. Ma A, Yang Y, Wang Q, Wang Y, Wen J, Zhang Y. Antiinflammatory effects of oxymatrine on rheumatoid arthritis in rats via regulating the imbalance between Treg and Th17 cells. *Mol Med Rep*. (2017) 15:3615–22. doi: 10.3892/mmr.2017.6484
27. Yang Z, Yin R, Cong Y, Yang Z, Zhou E, Wei Z, et al. Oxymatrine lightened the inflammatory response of LPS-induced mastitis in mice through affecting NF-kappaB and MAPKs signaling pathways. *Inflammation* (2014) 37:2047–55. doi: 10.1007/s10753-014-9937-7
28. Lv G, Sun D, Zhang J, Xie X, Wu X, Fang W, et al. Lx2-32c, a novel semi-synthetic taxane, exerts antitumor activity against prostate cancer cells *in vitro* and *in vivo*. *Acta Pharm Sin B* (2017) 7:52–8. doi: 10.1016/j.apsb.2016.06.005
29. Li W-S, Yang Y, Liu J-J, Shen L, Shi Z, Wu J. Scaffold diversity-oriented synthesis of limonoid dimers: discovery of an axially chiral agent with *in vivo* anti-breast cancer activity. *Org Chem Front*. (2018) 5:1079–91. doi: 10.1039/C8QO00154E
30. Li P, Yang Y, Liu H, Yang AK, Di JM, Tan GM, et al. MiR-194 functions as a tumor suppressor in laryngeal squamous cell carcinoma by targeting Wee1. *J Hematol Oncol*. (2017) 10:32. doi: 10.1186/s13045-017-0402-6
31. Yang Y, Guan D, Lei L, Lu J, Liu JQ, Yang G, et al. H6, a novel hederagenin derivative, reverses multidrug resistance *in vitro* and *in vivo*. *Toxicol Appl Pharmacol*. (2018) 341:98–105. doi: 10.1016/j.taap.2018.01.015
32. Jiang QW, Cheng KJ, Mei XL, Qiu JG, Zhang WJ, Xue YQ, et al. Synergistic anticancer effects of triptolide and celastrol, two main compounds from thunder god vine. *Oncotarget* (2015) 6:32790–804. doi: 10.18632/oncotarget.5411
33. Jiang Q-W, Chen M-W, Cheng K-J, Yu P-Z, Wei X, Shi Z. Therapeutic potential of steroidal alkaloids in cancer and other diseases. *Med Res Rev*. (2016) 36:119–43. doi: 10.1002/med.21346
34. Anagnostou VK, Brahmer JR. Cancer immunotherapy: a future paradigm shift in the treatment of non-small cell lung cancer. *Clin Cancer Res*. (2015) 21:976–84. doi: 10.1158/1078-0432.CCR-14-1187
35. Takeuchi Y, Nishikawa H. Roles of regulatory T cells in cancer immunity. *Int Immunol*. (2016) 28:401–9. doi: 10.1093/intimm/dxw025
36. Zhang D, Chen Z, Wang DC, Wang X. Regulatory T cells and potential inmmunotherapeutic targets in lung cancer. *Cancer Metastasis Rev*. (2015) 34:277–90. doi: 10.1007/s10555-015-9566-0

37. Liu H, Zhang T, Ye J, Li H, Huang J, Li X, et al. Tumor-infiltrating lymphocytes predict response to chemotherapy in patients with advance non-small cell lung cancer. *Cancer Immunol Immunother* (2012) 61:1849–56. doi: 10.1007/s00262-012-1231-7
38. Shen Z, Zhou S, Wang Y, Li RL, Zhong C, Liang C, et al. Higher intratumoral infiltrated Foxp3+ Treg numbers and Foxp3+/CD8+ ratio are associated with adverse prognosis in resectable gastric cancer. *J Cancer Res Clin Oncol*. (2010) 136:1585–95. doi: 10.1007/s00432-010-0816-9
39. Sato E, Olson SH, Ahn J, Bundy B, Nishikawa H, Qian F, et al. Intraepithelial CD8+ tumor-infiltrating lymphocytes and a high CD8+/regulatory T cell ratio are associated with favorable prognosis in ovarian cancer. *Proc Natl Acad Sci USA*. (2005) 102:18538–43. doi: 10.1073/pnas.0509182102
40. Liu F, Lang R, Zhao J, Zhang X, Pringle GA, Fan Y, et al. CD8(+) cytotoxic T cell and FOXP3(+) regulatory T cell infiltration in relation to breast cancer survival and molecular subtypes. *Breast Cancer Res Treat*. (2011) 130:645–55. doi: 10.1007/s10549-011-1647-3
41. Zhang YL, Li J, Mo HY, Qiu F, Zheng LM, Qian CN, et al. Different subsets of tumor infiltrating lymphocytes correlate with NPC progression in different ways. *Mol Cancer* (2010) 9:4. doi: 10.1186/1476-4598-9-9
42. Yang J, Liu R, Deng Y, Qian J, Lu Z, Wang Y, et al. MiR-15a/16 deficiency enhances anti-tumor immunity of glioma-infiltrating CD8+ T cells through targeting mTOR. *Int J Cancer* (2017) 141:2082–92. doi: 10.1002/ijc.30912
43. Ikeda H, Old LJ, Schreiber RD. The roles of IFN gamma in protection against tumor development and cancer immunoediting. *Cytokine Growth Factor Rev*. (2002) 13:95–109. doi: 10.1016/S1359-6101(01)00038-7
44. Ando K, Ohmori T, Inoue F, Kadofuku T, Hosaka T, Ishida H, et al. Enhancement of sensitivity to tumor necrosis factor alpha in non-small cell lung cancer cells with acquired resistance to gefitinib. *Clin Cancer Res*. (2005) 11(24 Pt 1):8872–9. doi: 10.1158/1078-0432.CCR-05-0811
45. Liao W, Lin JX, Leonard WJ. Interleukin-2 at the crossroads of effector responses, tolerance, and immunotherapy. *Immunity* (2013) 38:13–25. doi: 10.1016/j.immuni.2013.01.004
46. Lind EF, Ohashi PS. Mir-155, a central modulator of T-cell responses. *Eur J Immunol.* (2014) 44:11–5. doi: 10.1002/eji.201343962
47. Wang J, Yu F, Jia X, Iwanowycz S, Wang Y, Huang S, et al. MicroRNA-155 deficiency enhances the recruitment and functions of myeloid-derived suppressor cells in tumor microenvironment and promotes solid tumor growth. *Int J Cancer* (2015) 136:E602–13. doi: 10.1002/ijc.29151
48. Huffaker TB, Lee SH, Tang WW, Wallace JA, Alexander M, Runtsch MC, et al. Antitumor immunity is defective in T cell-specific microRNA-155-deficient mice and is rescued by immune checkpoint blockade. *J Biol Chem*. (2017) 292:18530–41. doi: 10.1074/jbc.M117.808121
49. Huffaker TB, Hu R, Runtsch MC, Bake E, Chen X, Zhao J, et al. Epistasis between microRNAs 155 and 146a during T cell-mediated antitumor immunity. *Cell Rep*. (2012) 2:1697–709. doi: 10.1016/j.celrep.2012.10.025
50. Zou W. Immunosuppressive networks in the tumour environment and their therapeutic relevance. *Nature Rev Cancer* (2005) 5:263–74. doi: 10.1038/nrc1586

Conflict of Interest Statement: The authors declare that the research was conducted in the absence of any commercial or financial relationships that could be construed as a potential conflict of interest.

frontiers in Oncology

MINI REVIEW
published: 22 January 2019
doi: 10.3389/fonc.2019.00018

Salt-Inducible Kinase 2: An Oncogenic Signal Transmitter and Potential Target for Cancer Therapy

Fangyu Chen[1,2†], *Liuwei Chen*[2†], *Qin Qin*[1†] *and Xinchen Sun*[1*]

[1] Department of Radiation Oncology, The First Affiliated Hospital of Nanjing Medical University, Nanjing, China, [2] The First School of Clinical Medicine, Nanjing Medical University, Nanjing, China

Salt-inducible kinase (SIK), which belongs to the sucrose non-fermenting 1/AMP-activated protein kinase family, was first discovered in the adrenal cortex of a rat on a high-salt diet. As an isoform of the SIK family, SIK2 modulates various biological functions and acts as a signal transmitter in various pathways. Compared with that in adjacent normal tissues, the expression of SIK2 is significantly higher in multiple types of tumors, which indicates its pivotal effect in oncogenesis. Studies on SIK2 have recently underlined its role in several signaling pathways, including the PI3K-Akt-mTOR pathway, the Hippo-YAP pathway, the LKB1-HDAC axis, and the cAMP-PKA axis. Moreover, a few small-molecule SIK2 inhibitors have been found to be able to rescue the oncogenicity of SIK2 during tumor development and reverse its abnormal activation of downstream pathways. In this mini-review, we discuss the results of *in vivo* and *in vitro* studies regarding the SIK2 mechanism in different signaling pathways, particularly their regulation of cancer cells. This work may provide new ideas for targeting SIK2 as a novel therapeutic strategy in tumor therapy.

Keywords: salt-inducible kinase, SIK2, cancer, signaling pathway, target therapy

OPEN ACCESS

Edited by:
Zhe-Sheng Chen,
St. John's University, United States

Reviewed by:
Yun Dai,
Virginia Commonwealth University, United States
Luca Tamagnone,
Institute for Cancer Research and Treatment (IRCC), Italy
Xingxiang Pu,
Hunan Cancer Hospital, China

***Correspondence:**
Xinchen Sun
Sunxinchen2012@163.com

These authors have contributed equally to this work

Specialty section:
This article was submitted to Cancer Molecular Targets and Therapeutics, a section of the journal Frontiers in Oncology

Received: *09 October 2018*
Accepted: *07 January 2019*
Published: *22 January 2019*

Citation:
Chen F, Chen L, Qin Q and Sun X (2019) Salt-Inducible Kinase 2: An Oncogenic Signal Transmitter and Potential Target for Cancer Therapy. Front. Oncol. 9:18. doi: 10.3389/fonc.2019.00018

INTRODUCTION

Plasma ion balances regulate a wide range of cellular processes from cell proliferation to mitochondrial functions. The plasma concentrations of Na+ and K+ have been proven to play a vital role in the biosynthesis of aldosterone in the adrenal cortex. Studies have shown that changes in plasma ion concentration can target biomembrane ion channels, such as Na+-K+-ATPase to regulate extra- and intracellular ion balances (1, 2). As a major part of this ion modulation network, salt-inducible kinase (SIK) was first discovered in 1999 by Okamoto et al. in the adrenal cortex of a rat on a high-salt diet. SIK is a serine/threonine protein kinase that belongs to the sucrose non-fermenting 1/AMP-activated protein kinase (SNF1/AMPK) family. The SIK family comprises three isoforms, namely, SIK1, SIK2, and SIK3, all of which may act as metabolic transmitters. The SIK2 gene is located on chromosome 11 and encodes for the SIK2 protein, which has 926 amino acids and three domains (3, 4). The C-terminal domain of the SIK protein contains numerous unique sites that can be phosphorylated by different protein kinases and transmit various stimulation signals involved in different biological processes, including cell growth and apoptosis (4–8). In many malignant tumors, such as breast cancer, lung cancer, melanoma, primary liver

cancer, and ovarian cancer, SIK expression is significantly different from that in adjacent tissues (9–14).

Growing evidence has proven that the expression and action of SIK2 are tissue-specific. The cellular and subcellular distributions of SIK should be considered to determine its mechanism. Earlier investigations demonstrate that SIK2 maintains cell homeostasis via modulation of cAMP response element binding protein (CREB)-mediated gene transcription during starvation, which may be a possible mechanism for cancer cell survival under stress, such as chemoradiotherapy (15). SIK2 reduces glucose uptake in muscle cells and white adipocytes and downregulates lipogenesis and ketogenesis by phosphorylating the glucose-activated histone acetyltransferase coactivator p300 (16). SIK2 modulates several subtle cellular signaling pathways, and its abundant expression in melanoma and ovarian tumors is suggestive of its pivotal function in tumor development (13, 17). Thus, in this mini-review, we discuss the specific role and related signaling pathways of SIK2 in tumorigenesis. Our findings indicate the potential application of SIK2 as a therapeutic target for cancers.

SIK FAMILY AND THEIR FUNCTIONS

The structures of the SIK isoforms are shown in **Figure 1**. The three isoforms are similar to one another, particularly in three domains: a kinase domain near the N-terminal, a central SNF1 protein kinase homology (SNH) domain, and a phosphorylation domain near the C-terminal (3). SIK1 is a 776-amino acid protein with a kinase domain in the region of residues 27–278, an SNH domain in the region of residues 301–354, and a domain enriched with PKA-dependent phosphorylation sites in the region of residues 567–613. Similarly, SIK2 is a 931-amino acid protein with a kinase domain in the region of residues 20–271, an SNH domain in the region of residues 293–346, and a phosphorylation domain in the region of residues 577–623. Finally, SIK3 is a 1,263-amino acid protein with a kinase domain in the region of residues 8–259, an SNH domain in the region of residues 283–336, and a phosphorylation domain in the region of residues 486–518. Initial studies have found that SIK1 is most abundant in the adrenal cortex and an important regulator in the early phase of hormonal stimulation of the adrenal cortex (4, 18), adipose tissue (6), and neural tissue (19). It may overexpress in several non-adipose tissues, such as in the ovaries and lungs, and act as an oncogenic signal transmitter during the occurrence and progression of tumors in the aforementioned organs (18–20). Unlike SIK1, SIK2 modulates several subtle cellular signaling pathways, and the increased expression of SIK2 in adipose and neuronal tissues indicates its pivotal role in lipid metabolism and neural physiology. SIK2 promotes insulin resistance and diabetes by reducing glucose uptake in muscles and white adipose tissues and inhibiting gluconeogenesis (7). SIK2 is overexpressed in several cancer cell lines and boosts cancer cell tolerance to different stresses, such as deprivation of nutrients and taxol chemotherapy (21). It plays a proinflammatory role by repressing IL-10 secretion of regulatory macrophages (22). However, little is known about why the structural similarity of the SIK family leads to different biological functions.

SIK2 AND THE PI3K-Akt-mTOR PATHWAY

The expression level of SIK2 in cancers is significantly higher than that in adjacent and surrounding normal tissues, which suggests that SIK2 is critical in tumorigenesis and tumor development. Miranda et al. found that the loss of SIK2 reduces G1/S transition, delays mitotic progression, and decreases Akt phosphorylation levels (17). They also confirmed that SIK2 is overexpressed in adipocyte-rich metastatic deposits compared with ovarian primary lesions and that adipocytes activate SIK2 in ovarian cancer cells in a calcium-dependent manner. Following adipocyte-induced stimulation, the activated SIK2 alters metabolic effects in ovarian cancer cells by inhibiting acetyl-CoA carboxylase and promoting fatty acid oxidation. p85α, the regulatory subunit of the PI3K complex, was previously identified as a putative SIK2 substrate during chemical genetic screening. The identified p85α phosphorylation site (S154) resides in the known SIK2 phosphorylation consensus sequence L-x-[HKR]-[ST]-x-S-X(3)-L at L149–L158 (LYRTQSSSNL). Incubation of recombinant full-length SIK2 or its kinase domain with a peptide corresponding to L149–L158 of p85α confirmed that SIK2 catalyzes the phosphorylation of this sequence. More importantly, full-length SIK2, but not the kinase-inactive mutant, phosphorylated p85α was confirmed in isotopic labeling assay. Phosphopeptide mapping of p85α following incubation with SIK2 (kinase domain or full-length) revealed that the former was phosphorylated at S154 in the BH domain. The BH domain is thought to bind to proteins that modulate PI3K activity. Downstream S154 phosphorylation also appears to increase in an SIK2-dose-dependent manner. siRNA-mediated depletion or chemical inhibition confirms that SIK2 is required for p85α S154 phosphorylation. Moreover, p85α phosphorylation and concomitant Akt phosphorylation can be triggered by calcium-mediated SIK2 activation. Consistent with these observations, incubation of the PI3K complex with recombinant SIK2 leads to a profound increase in PI3K activity *in vitro* (up to 13.8-fold), while chemical inhibition of SIK2 induces a dose-dependent reduction in PI3K activity to its basal level. These data confirm that p85α is a direct catalytic substrate of SIK2 and that SIK2 S154 phosphorylation significantly increases the activity of the PI3K-Akt pathway in ovarian cancer cells.

While most reports suggest that SIK2 is an oncogenic marker, one study in Turkey claimed that SIK2 is a potential tumor suppressor in breast cancer (23); SIK2 expression was reportedly reduced in tumor tissues and breast cancer cell lines compared with that in normal counterparts. The researchers also found SIK2-mediated attenuation of proliferation and survival of breast cancer cells with parallel inhibition of the Ras-Erk and PI3K-Akt pathways. However, the mechanisms underlying the reduction of SIK2 levels in cancer tissues were not discussed. Thus, research into the mechanism of SIK2 loss will help future scholars better understand tumor transformation in breast tissue and design new treatment strategies.

SIK2 AND THE HIPPO-YAP PATHWAY

The Hippo pathway is a highly conserved growth regulatory signaling pathway that was first discovered in *Drosophila*. It can

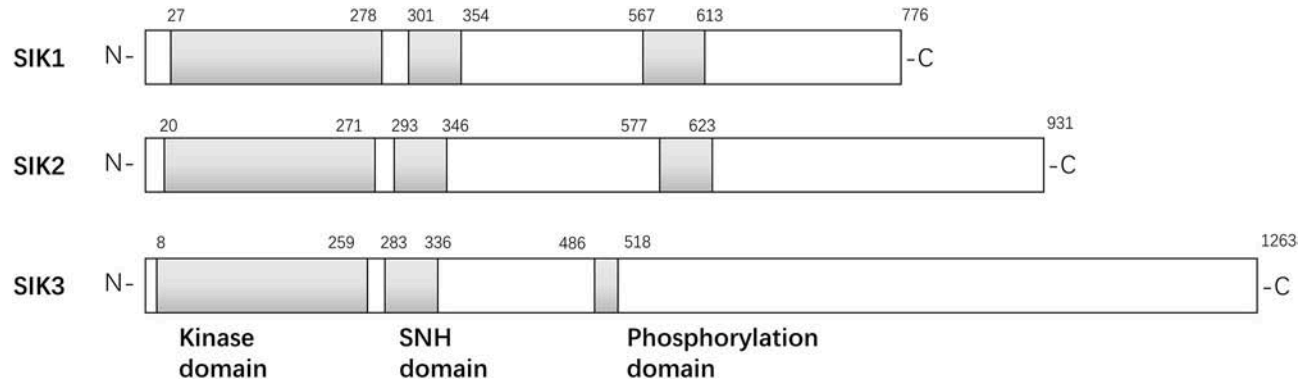

FIGURE 1 | Structures of isoforms in SIK family.

block the downstream pro-growth transcriptional co-activator Yorkie (Yki), which is homologous to mammalian Yes-associated protein (YAP), and exert its regulatory effects on organ size, cell proliferation, and apoptosis during organ development (24, 25). YAP has been shown to be highly expressed in various human tumors, such as endometrial carcinoma, primary liver cancer, and oral squamous cell carcinoma. Activation of YAP can remove tumor cell contact inhibition, leading to tumor metastasis (25–27). Tsujiura et al. immunohistochemically analyzed YAP in endometrial carcinoma tissue samples and found that the high expression of YAP in the nucleus is closely associated with higher tumor grading and staging, lymphatic/blood vessel invasion, increased recurrence, and metastasis. They then confirmed these results at the cellular level in knockdown and overexpression assays. Recent studies have demonstrated that YAP restricts the activity of the cell cycle checkpoints ATM and ChK2 to enable cancer cells to enter the cell cycle and mitosis after chemoradiotherapy despite unrepaired DNA damage, resulting in tumor growth, chemoradiotherapy resistance, and ongoing proliferation (28).

Wehr et al. characterized Drosophila salt-inducible kinase (sik2) as an upstream inhibitor of the Hippo pathway (29). sik2 has been identified as the ortholog of human SIK2. Activated sik2 phosphorylates Ser413 of the scaffold protein Salvador (Sav), a major part of the core kinase complex of the Hippo pathway, and subsequently abolishes the inhibition of the proto-oncogene Yki. In addition, sik2 directly induces the expression of Yki and facilitates Yki-dependent tissue overgrowth. Coincidentally, both SIK2 and YAP have been proven to be oncogenes in ovarian cancer. Research has confirmed a close interaction between the PI3K-Akt-mTOR and Hippo-YAP pathways via SIK2 (**Figure 2**). On the one hand, YAP directly activates PI3K-Akt-mTOR and alters cellular biological functions (30, 31). YAP also increases pAkt-S473 levels and suppresses apoptosis by induction of insulin-like growth factor 2 expression (28). On the other hand, mTOR complex 2 enhances the oncogenicity of YAP through phosphorylation of the Hippo pathway component AMOTL2 (32). These observations reveal that mutual activation between the PI3K-Akt-mTOR and Hippo-YAP pathways caused by SIK2 may be crucial in tumorigenesis. However, the precise role of SIK2 in these intersecting pathways is not well-understood, and future studies are still desperately needed to elucidate the related detailed mechanisms.

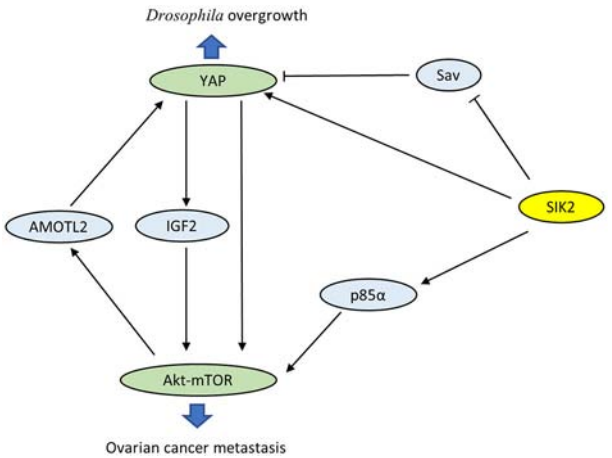

FIGURE 2 | Crosstalk between the PI3K-Akt-mTOR pathway and the Hippo-Yap pathway via SIK2.

SIK2 AND THE LKB1-HDAC SIGNALING AXIS

Epigenetic studies have confirmed that DNA acetylation modification is closely related to tumorigenesis, tumor invasion, and chemoradiotherapy resistance (33–35). The abnormal activation and overexpression of histone deacetylase (HDAC) down-regulates tumor suppressor genes and exhibits tumor-promoting effects. Using kinase domain-focused CRISPR techniques, researchers screened all dependent kinase in acute myeloid leukemia (AML), focusing subsequent experiments on SIK3, which scored strongly in MOLM-13 and MV4-11 AML cells and in a more intermediate fashion in other AML cell lines (36). Liver kinase B1 (LKB1) was also identified to show an AML-biased pattern of dependence. Since SIK3 is homologous to SIK1

and SIK2, further studies were conducted to determine whether a broader requirement exists for SIKs in cancer. By performing dual targeting of each SIK gene combination in 17 AML cell lines, researchers observed a broad AML-specific requirement for SIK2 + SIK3 resembling the pattern of LKB1 dependence with a bias for lines with mixed lineage leukemia fusions. In cDNA rescue assays, LKB1 was found to phosphorylate and activate SIK3 in AML. The SIK3 mutant was unable to maintain the proliferation of MOLM-13 cells, while a phosphomimetic allele of SIK3 rescued the proliferation arrest caused by inactivating LKB1. The reverse of SIK3 dependence for AML proliferation was observed during dual CRISPR targeting of HDAC4. Western blotting revealed reductions in HDAC4 phosphorylation upon genetic targeting of SIK3 or chemical inhibition of SIK. Taken together, these results indicate that the function of SIK3 is critical in AML and that inhibition of HDAC4 is one of the key functions of SIK3 in supporting AML proliferation.

Histone H3 lysine 27 acetylation (H3K27ac) is linked to the relevant downstream activity in the LKB1-SIK pathway, and ChIP-seq has confirmed that LKB1/SIK3-dependent H3K27ac coincides with sites of transcription factor MEF2C occupancy. While LKB1/SIK3 knockout or following SIK inhibitor HG-9-91-01 treatment did not change MEF2C protein expression, HG-9-91-01 exposure led to increased HDAC4 binding to MEF2C-bound sites. Epigenomic analysis suggests that LKB1-SIK signaling is critical in AML to prevent HDAC4 from inactivating the function of MEF2C on chromatin. These genetic experiments suggest that co-inhibition of SIK2 + SIK3 could be the ideal strategy to achieve potent MEF2C inhibition in AML. Since MEF2C is maladjusted in lymphoid malignancies, LKB1-SIK signaling is likely to be important in other hematopoietic cancers (37).

SIK2 AND THE cAMP-PKA SIGNALING AXIS

The G protein αs (GNAS) gene encodes the Gαs stimulatory subunit of G proteins, which mediate G-protein-coupled receptor signaling, a major mechanism that links multiple environmental stimuli with intracellular responses (38). The primary target is adenylyl cyclase, which generates the second messenger cAMP, which, in turn, activates downstream protein kinase A (PKA). In many tissues, GNAS–cAMP-PKA signaling is required during cell dormancy and cell growth (39–43). However, multiple types of human cancers show gain-of-function variations in this pathway (38). For example, loss of p53 promotes the advent of GNAS R201C mutations and induces malignant transformation in pancreatic benign tumors in the KGC mice model, which can rapidly develop cystic pancreatic tumors (44–47). Mutated GNAS R201C supports pancreatic tumor growth via cAMP-PKA signaling, which subsequently phosphorylates SIKs (SIK1, SIK2, and SIK3) and prevents them from phosphorylating downstream targets (48). Also, small molecule pan-SIK inhibitors (HG-9-91-01 and KIN-112) prevent the growth of KGC organoids after silencing GNAS, and their effects are directly proportional to the degree of SIK inhibition. Compared with wild-type SIK2, the SIK2-S4A mutant, which is resistant to cAMP-PKA activation, strongly inhibits the proliferation of KGC-like organs. In particular, SIK^{KO} rescues both organoid growth *in vitro* and subcutaneous tumor growth following GNAS R201C silencing, and these findings have been confirmed in human pancreatic ductal adenocarcinomas (PDA). Thus, the cAMP-PKA-SIK2 signaling pathway is a conserved tumorigenic mechanism in pancreatic tumor cells. The mutant GNAS drives downstream PKA-SIK2 axis and promotes lipid hydrolysis in addition to lipid synthesis and remodeling. While SIK2 is known to maintain cell homeostasis and energetic metabolism, particularly glucose and fatty acid oxidation (15), the suppression of SIK2 mediated by GNAS-PKA will inhibit the phosphorylation of its downstream CREB-regulated transcription co-activator (CRTC) and others (**Figure 3**). Then it will promote lipids absorption and synthesis, and the abundant lipids in tumor cells provide substrates for structural, signaling, and metabolic purposes, which explains why SIK2 act as a tumor suppressor in PDA.

While SIK2 is deemed to be a tumor promoter in most cases, in the context of GNAS mutated PDA, it is supposed to be a tumor suppressor, mainly because SIK2 plays different roles in different tissue and cells, similar to cAMP/PKA signaling. Given the context-dependent tumor-promoting and -suppressing roles of SIK2, administration of SIK2 inhibitors in GPCR-mutated or other overactive cAMP-PKA cancer types should be attempted with extremely caution to avoid potential pro-tumor effects. More investigations are necessary to clarify these issues and promote the use of SIK2 inhibitors in tumor therapy.

SIK2 IN CANCER THERAPY

Previous studies on SIK2 have reported its regulation of energetic metabolism, mostly based on its signaling pathways and the downstream role of LKB1 in adipocytes. Studies on SIK2 have recently underlined its role in several signaling pathways related to tumorigenesis. Clinical and pathological data indicate that

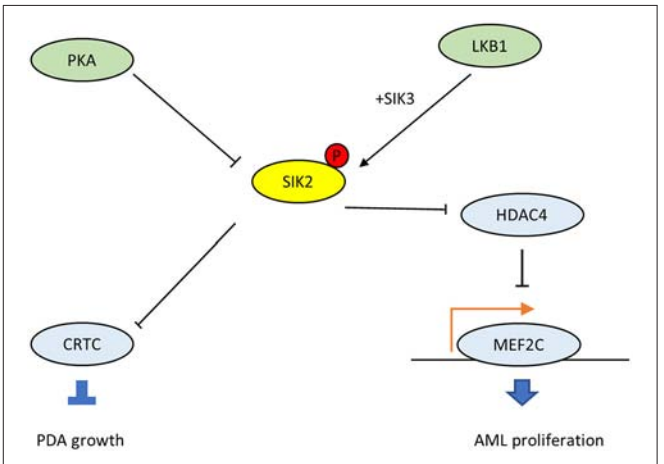

FIGURE 3 | The dichotomous oncogenic roles of SIK2 in the LKB1-HDAC axis and the cAMP-PKA axis.

SIK2 is a potential oncogenic marker in ovarian (17, 49), prostate (50), osteosarcoma (51), and colorectal (52) cancers by controlling different cellular mechanisms. Intriguingly, two studies report that SIK2 may act as a tumor suppressor in breast cancer and PDA. Since SIK2 plays a distinct role in different tissues and divergent pathways, its dysregulation may lead to conflicting phenotypes. Initial studies on SIK2 maily focused on its role in energetic metabolism, particularly in glucose, and lipids oxidation during starvation. The functions of SIK2 may be unique in cells that are involved in glycolipid metabolism, such as hepatocyte and pancreatic cells. As a consequence, SIK2 may act as both tumor promoter and suppressor due to the diversity of cancer cell types or different genetic background. The SIK2 inhibitors HG-9-91-01, ARN-3236, and KIN-112 have succeeded in cancer therapy approaches, validated in cultured cells and *in vivo* animal models (17, 36, 48), although additional optimization of these small molecules is required for therapeutic investigation. Further evaluation of these small molecules is necessary to achieve potent SIK2 inhibition in the uncontrolled signaling pathways of tumor cells while preserving the homeostatic and tumor-protective functions of SIK2 in other cell types.

CONCLUSION

In this mini-review, we discussed the role of the newly identified protein kinase, SIK2, in tumorigenesis, specifically focusing on different signaling pathways involving SIK2. SIKs present significant physiological functions, including novel roles in tumorigenesis and tumor progression. While most studies reveal SIK2 to be a tumor promoter, some claims indicate that SIK2 provides protection from cancer. Thus, the dichotomous function and mechanism between SIK2 and cancer must be further elucidated. As described earlier, SIK2 targeting may be applied as a novel strategy for treating multiple cancer types. Future studies to investigate the molecular mechanisms underlying the precise role of SIK2 in intersecting signaling pathways, as well as the therapeutic effects of SIK2 in preclinical and clinical trials, are recommended.

AUTHOR CONTRIBUTIONS

FC, LC, and QQ contributed to conception and manuscript writing. XS participated in its coordination and modification. All authors read and approved the final manuscript.

FUNDING

This work was supported by the National Natural Science Foundation of China (No. 81472809, No. 81502653, No. 81672983, No.81874217), A Project Funded by the Priority Academic Program Development of Jiangsu Higher Education Institutions (PAPD) (JX10231801), Young Medical Key Talents of Jiangsu Province (grant number QNRC2016572) and the Six Major Talent Peak Project of Jiangsu Province (No.2013-WSN-040).

REFERENCES

1. Muller J. Regulation of aldosterone biosynthesis. Physiological and clinical aspects. *Monogr Endocrinol.* (1987) 29:1–364.
2. Nussdorfer GG. Cytophysiology of the adrenal cortex. *Int Rev Cytol.* (1986) 98:1–405.
3. Katoh Y, Takemori H, Horike N, Doi J, Muraoka M, Min L, et al. Salt-inducible kinase (SIK) isoforms: their involvement in steroidogenesis and adipogenesis. *Mol Cell Endocrinol.* (2004) 217:109–12. doi: 10.1016/j.mce.2003.10.016
4. Wang Z, Takemori H, Halder SK, Nonaka Y, Okamoto M. Cloning of a novel kinase (SIK) of the SNF1/AMPK family from high salt diet-treated rat adrenal. *FEBS Lett.* (1999) 453:135–9. doi: 10.1016/S0014-5793(99)00708-5
5. Dentin R, Liu Y, Koo SH, Hedrick S, Vargas T, Heredia J, et al. Insulin modulates gluconeogenesis by inhibition of the coactivator TORC2. *Nature* (2007) 449:366–9. doi: 10.1038/nature06128
6. Horike N, Takemori H, Katoh Y, Doi J, Min L, Asano T, et al. Adipose-specific expression, phosphorylation of Ser794 in insulin receptor substrate-1, and activation in diabetic animals of salt-inducible kinase-2. *J Biol Chem.* (2003) 278:18440–7. doi: 10.1074/jbc.M211770200
7. Muraoka M, Fukushima A, Viengchareun S, Lombes M, Kishi F, Miyauchi A, et al. Involvement of SIK2/TORC2 signaling cascade in the regulation of insulin-induced PGC-1alpha and UCP-1 gene expression in brown adipocytes. *Am J Physiol Endocrinol Metab.* (2009) 296:E1430–9. doi: 10.1152/ajpendo.00024.2009
8. Wang Y, Li G, Goode J, Paz JC, Ouyang K, Screaton R, et al. Inositol-1,4,5-trisphosphate receptor regulates hepatic gluconeogenesis in fasting and diabetes. *Nature* (2012) 485:128–32. doi: 10.1038/nature10988
9. Ahmed AA, Lu Z, Jennings NB, Etemadmoghadam D, Capalbo L, Jacamo RO, et al. SIK2 is a centrosome kinase required for bipolar mitotic spindle formation that provides a potential target for therapy in ovarian cancer. *Cancer Cell* (2010) 18:109–21. doi: 10.1016/j.ccr.2010.06.018
10. Bricambert J, Miranda J, Benhamed F, Girard J, Postic C, Dentin R. Salt-inducible kinase 2 links transcriptional coactivator p300 phosphorylation to the prevention of ChREBP-dependent hepatic steatosis in mice. *J Clin Invest.* (2010) 120:4316–31. doi: 10.1172/JCI41624
11. Charoenfuprasert S, Yang YY, Lee YC, Chao KC, Chu PY, Lai CR, et al. Identification of salt-inducible kinase 3 as a novel tumor antigen associated with tumorigenesis of ovarian cancer. *Oncogene* (2011) 30:3570–84. doi: 10.1038/onc.2011.77
12. Cheng H, Liu P, Wang ZC, Zou L, Santiago S, Garbitt V, et al. SIK1 couples LKB1 to p53-dependent anoikis and suppresses metastasis. *Sci Signal.* (2009) 2:ra35. doi: 10.1126/scisignal.2000369
13. Horike N, Kumagai A, Shimono Y, Onishi T, Itoh Y, Sasaki T, et al. Downregulation of SIK2 expression promotes the melanogenic program in mice. *Pigment Cell Melanoma Res.* (2010) 23:809–19. doi: 10.1111/j.1755-148X.2010.00760.x
14. Imielinski M, Berger AH, Hammerman PS, Hernandez B, Pugh TJ, Hodis E, et al. Mapping the hallmarks of lung adenocarcinoma with massively parallel sequencing. *Cell* (2012) 150:1107–20. doi: 10.1016/j.cell.2012.08.029
15. Du J, Chen Q, Takemori H, Xu H. SIK2 can be activated by deprivation of nutrition and it inhibits expression of lipogenic genes in adipocytes. *Obesity* (2008) 16:531–8. doi: 10.1038/oby.2007.98
16. Zhang ZN, Gong L, Lv S, Li J, Tai X, Cao W, et al. SIK2 regulates fasting-induced PPAR alpha activity and ketogenesis through p300. *Sci Rep.* (2016) 6:23317. doi: 10.1038/srep23317
17. Miranda F, Mannion D, Liu S, Zheng Y, Mangala LS, Redondo C, et al. Salt-inducible kinase 2 couples ovarian cancer cell metabolism with survival at the adipocyte-rich metastatic niche. *Cancer Cell* (2016) 30:273–89. doi: 10.1016/j.ccell.2016.06.020
18. Lin X, Takemori H, Katoh Y, Doi J, Horike N, Makino A, et al. Salt-inducible kinase is involved in the ACTH/cAMP-dependent protein kinase signaling

in Y1 mouse adrenocortical tumor cells. *Mol Endocrinol.* (2001) 15:1264–76. doi: 10.1210/mend.15.8.0675
19. Feldman JD, Vician L, Crispino M, Hoe W, Baudry M, Herschman HR. The salt-inducible kinase, SIK, is induced by depolarization in brain. *J Neurochem.* (2000) 74:2227–38. doi: 10.1046/j.1471-4159.2000.0742227.x
20. Ruiz JC, Conlon FL, Robertson EJ. Identification of novel protein kinases expressed in the myocardium of the developing mouse heart. *Mech Dev.* (1994) 48:153–64. doi: 10.1016/0925-4773(94)90056-6
21. Du WQ, Zheng JN, Pei DS. The diverse oncogenic and tumor suppressor roles of salt-inducible kinase (SIK) in cancer. *Expert Opin Ther Targets* (2016) 20:477–85. doi: 10.1517/14728222.2016.1101452
22. MacKenzie KF, Clark K, Naqvi S, McGuire VA, Noehren G, Kristariyanto Y, et al. PGE(2) induces macrophage IL-10 production and a regulatory-like phenotype via a protein kinase A-SIK-CRTC3 pathway. *J Immunol.* (2013) 190:565–77. doi: 10.4049/jimmunol.1202462
23. Zohrap N, Saatci O, Ozes B, Coban I, Atay HM, Battaloglu E, et al. SIK2 attenuates proliferation and survival of breast cancer cells with simultaneous perturbation of MAPK and PI3K/Akt pathways. *Oncotarget* (2018) 9:21876–92. doi: 10.18632/oncotarget.25082
24. Gumbiner BM, Kim NG. The Hippo-YAP signaling pathway and contact inhibition of growth. *J Cell Sci.* (2014) 127 (Pt. 4):709–17. doi: 10.1242/jcs.140103
25. Zeng Q, Hong W. The emerging role of the hippo pathway in cell contact inhibition, organ size control, and cancer development in mammals. *Cancer Cell* (2008) 13:188–92. doi: 10.1016/j.ccr.2008.02.011
26. Fernandez LA, Kenney AM. The Hippo in the room: a new look at a key pathway in cell growth and transformation. *Cell Cycle* (2010) 9:2292–9. doi: 10.4161/cc.9.12.11919
27. Zhao B, Ye X, Yu J, Li L, Li W, Li S, et al. TEAD mediates YAP-dependent gene induction and growth control. *Genes Dev.* (2008) 22:1962–71. doi: 10.1101/gad.1664408
28. Fernandez LA, Squatrito M, Northcott P, Awan A, Holland EC, Taylor MD, et al. Oncogenic YAP promotes radioresistance and genomic instability in medulloblastoma through IGF2-mediated AKT activation. *Oncogene* (2012) 31:1923–37. doi: 10.1038/onc.2011.379
29. Wehr MC, Holder MV, Gailite I, Saunders RE, Maile TM, Ciirdaeva E, et al. Salt-inducible kinases regulate growth through the Hippo signalling pathway in Drosophila. *Nat Cell Biol.* (2013) 15:61–71. doi: 10.1038/ncb2658
30. Jiang J, Chang W, Fu Y, Gao Y, Zhao C, Zhang X, et al. SAV1 represses the development of human colorectal cancer by regulating the Akt-mTOR pathway in a YAP-dependent manner. *Cell Prolif.* (2017) 50:e12351. doi: 10.1111/cpr.12351
31. Zhang Y, Yuan J, Zhang X, Yan F, Huang M, Wang T, et al. Angiomotin promotes the malignant potential of colon cancer cells by activating the YAP-ERK/PI3K-AKT signaling pathway. *Oncol Rep.* (2016) 36:3619–26. doi: 10.3892/or.2016.5194
32. Artinian N, Cloninger C, Holmes B, Benavides-Serrato A, Bashir T, Gera J. Phosphorylation of the hippo pathway component AMOTL2 by the mTORC2 kinase promotes YAP signaling, resulting in enhanced glioblastoma growth and invasiveness. *J Biol Chem.* (2015) 290:19387–401. doi: 10.1074/jbc.M115.656587
33. Frame FM, Pellacani D, Collins AT, Simms MS, Mann VM, Jones GD, et al. HDAC inhibitor confers radiosensitivity to prostate stem-like cells. *Br J Cancer* (2013) 109:3023–33. doi: 10.1038/bjc.2013.691
34. Marampon F, Megiorni F, Camero S, Crescioli C, McDowell HP, Sferra R, et al. HDAC4 and HDAC6 sustain DNA double strand break repair and stem-like phenotype by promoting radioresistance in glioblastoma cells. *Cancer Lett.* (2017) 397:1–11. doi: 10.1016/j.canlet.2017.03.028
35. Roos WP, Krumm A. The multifaceted influence of histone deacetylases on DNA damage signalling and DNA repair. *Nucleic Acids Res.* (2016) 44:10017–30. doi: 10.1093/nar/gkw922
36. Tarumoto Y, Lu B, Somerville TDD, Huang YH, Milazzo JP, Wu XS, et al. LKB1, Salt-inducible kinases, and MEF2C are linked dependencies in acute myeloid leukemia. *Mol Cell* (2018) 69:1017–27 e6. doi: 10.1016/j.molcel.2018.02.011
37. Homminga I, Pieters R, Langerak AW, de Rooi JJ, Stubbs A, Verstegen M, et al. Integrated transcript and genome analyses reveal NKX2–1 and MEF2C as potential oncogenes in T cell acute lymphoblastic leukemia. *Cancer Cell* (2011) 19:484–97. doi: 10.1016/j.ccr.2011.02.008
38. O'Hayre M, Vazquez-Prado J, Kufareva I, Stawiski EW, Handel TM, Seshagiri S, et al. The emerging mutational landscape of G proteins and G-protein-coupled receptors in cancer. *Nat Rev Cancer* (2013) 13:412–24. doi: 10.1038/nrc3521
39. Drelon C, Berthon A, Sahut-Barnola I, Mathieu M, Dumontet T, Rodriguez S, et al. PKA inhibits WNT signalling in adrenal cortex zonation and prevents malignant tumour development. *Nat Commun.* (2016) 7:12751. doi: 10.1038/ncomms12751
40. He X, Zhang L, Chen Y, Remke M, Shih D, Lu F, et al. The G protein alpha subunit Galphas is a tumor suppressor in Sonic hedgehog-driven medulloblastoma. *Nat Med.* (2014) 20:1035–42. doi: 10.1038/nm.3666
41. Iglesias-Bartolome R, Torres D, Marone R, Feng X, Martin D, Simaan M, et al. Inactivation of a Galpha(s)-PKA tumour suppressor pathway in skin stem cells initiates basal-cell carcinogenesis. *Nat Cell Biol.* (2015) 17:793–803. doi: 10.1038/ncb3164
42. Pattabiraman DR, Bierie B, Kober KI, Thiru P, Krall JA, Zill C, et al. Activation of PKA leads to mesenchymal-to-epithelial transition and loss of tumor-initiating ability. *Science* (2016) 351:aad3680. doi: 10.1126/science.aad3680
43. Xing F, Luan Y, Cai J, Wu S, Mai J, Gu J, et al. The anti-warburg effect elicited by the cAMP-PGC1alpha pathway drives differentiation of glioblastoma cells into astrocytes. *Cell Rep.* (2017) 18:468–81. doi: 10.1016/j.celrep.2016.12.037
44. Amato E, Molin MD, Mafficini A, Yu J, Malleo G, Rusev B, et al. Targeted next-generation sequencing of cancer genes dissects the molecular profiles of intraductal papillary neoplasms of the pancreas. *J Pathol.* (2014) 233:217–27. doi: 10.1002/path.4344
45. Bailey P, Chang DK, Nones K, Johns AL, Patch AM, Gingras MC, et al. Genomic analyses identify molecular subtypes of pancreatic cancer. *Nature* (2016) 531:47–52. doi: 10.1038/nature16965
46. Zehir A, Benayed R, Shah RH, Syed A, Middha S, Kim HR, et al. Mutational landscape of metastatic cancer revealed from prospective clinical sequencing of 10,000 patients. *Nat Med.* (2017) 23:703–13. doi: 10.1038/nm.4333
47. Cancer Genome Atlas Research Network. Electronic address aadhe, Cancer Genome Atlas Research Network. Integrated Genomic Characterization of Pancreatic Ductal Adenocarcinoma. *Cancer Cell* (2017) 32:185–203 e13. doi: 10.1016/j.ccell.2017.07.007
48. Patra KC, Kato Y, Mizukami Y, Widholz S, Boukhali M, Revenco I, et al. Mutant GNAS drives pancreatic tumourigenesis by inducing PKA-mediated SIK suppression and reprogramming lipid metabolism. *Nat Cell Biol.* (2018) 20:811–22. doi: 10.1038/s41556-018-0122-3
49. Yang FC, Tan BC, Chen WH, Lin YH, Huang JY, Chang HY, et al. Reversible acetylation regulates salt-inducible kinase (SIK2) and its function in autophagy. *J Biol Chem.* (2013) 288:6227–37. doi: 10.1074/jbc.M112.431239
50. Bon H, Wadhwa K, Schreiner A, Osborne M, Carroll T, Ramos-Montoya A, et al. Salt-inducible kinase 2 regulates mitotic progression and transcription in prostate cancer. *Mol Cancer Res.* (2015) 13:620–35. doi: 10.1158/1541-7786.MCR-13-0182-T
51. Liu J, Zhu H, Zhong N, Jiang Z, Xu L, Deng Y, et al. Gene silencing of USP1 by lentivirus effectively inhibits proliferation and invasion of human osteosarcoma cells. *Int J Oncol.* (2016) 49:2549–57. doi: 10.3892/ijo.2016.3752
52. Liu Y, Gao S, Chen X, Liu M, Mao C, Fang X. Overexpression of miR-203 sensitizes paclitaxel (Taxol)-resistant colorectal cancer cells through targeting the salt-inducible kinase 2 (SIK2). *Tumour Biol.* (2016) 37:12231–9. doi: 10.1007/s13277-016-5066-2

Conflict of Interest Statement: The authors declare that the research was conducted in the absence of any commercial or financial relationships that could be construed as a potential conflict of interest.

frontiers in Pharmacology

ORIGINAL RESEARCH
published: 22 January 2019
doi: 10.3389/fphar.2019.00004

Liver-Targeted Combination Therapy Basing on Glycyrrhizic Acid-Modified DSPE-PEG-PEI Nanoparticles for Co-delivery of Doxorubicin and Bcl-2 siRNA

Guixiang Tian[1†], Ruiyan Pan[2†], Bo Zhang[2†], Meihua Qu[2], Bo Lian[1], Hong Jiang[1], Zhiqin Gao[1] and Jingliang Wu[1*]*

[1] School of Bioscience and Technology, Weifang Medical University, Weifang, China, [2] School of Pharmacy, Weifang Medical University, Weifang, China

OPEN ACCESS

Edited by:
Zhe-Sheng Chen,
St. John's University, United States

Reviewed by:
Yingfang Fan,
Zhujiang Hospital, Southern Medical University, China
Hua Zhu,
The Ohio State University, United States

***Correspondence:**
Zhiqin Gao
zhiqingao2013@163.com
Jingliang Wu
jlwu2008@163.com

† These authors have contributed equally to this work

Specialty section:
This article was submitted to Cancer Molecular Targets and Therapeutics, a section of the journal Frontiers in Pharmacology

Received: 20 November 2018
Accepted: 04 January 2019
Published: 22 January 2019

Citation:
Tian G, Pan R, Zhang B, Qu M, Lian B, Jiang H, Gao Z and Wu J (2019) Liver-Targeted Combination Therapy Basing on Glycyrrhizic Acid-Modified DSPE-PEG-PEI Nanoparticles for Co-delivery of Doxorubicin and Bcl-2 siRNA. Front. Pharmacol. 10:4. doi: 10.3389/fphar.2019.00004

Combination therapy based on nano-sized drug delivery system has been developed as a promising strategy by combining two or more anti-tumor mechanisms. Here, we prepared liver-targeted nanoparticles (GH-DPP) composed of 1,2-distearoyl-sn-glycero-3-phosphoethanolamine-polyethylene glycol-polyetherimide (DSPE-PEG-PEI) with Glycyrrhetinic acid-modified hyaluronic acid (GA-HA) for co-delivery of doxorubicin (DOX) and Bcl-2 siRNA. Particles size, zeta potential and morphology were determined for the drug-loaded GH-DPP nanoparticles (siRNA/DOX/GH-DPP). Cellular uptake and *in vitro* cytotoxicity were analyzed against HepG2 cells. *In vivo* bio-distribution and anti-tumor therapeutic effects of siRNA/DOX/GH-DPP were evaluated in H22-bearing mice. The results showed that siRNA/DOX/GH-DPP nanoparticles were nearly spherical and showed dose-dependent cytotoxicity against HepG2 cells. Compared to Glycyrrhetinic acid-free co-delivery system (siRNA/DOX/DPP) and GH-DPP nanoparticles for delivery of DOX or Bcl-2 siRNA alone, siRNA/DOX/GH-DPP nanoparticles could induce more cellular apoptosis, and showed higher anti-tumor effect. Herein GH-DPP nanoparticles could simultaneously deliver both chemotherapy drugs and siRNA into the tumor region, exhibiting great potential in anti-tumor therapy.

Keywords: combination therapy, nanoparticles, delivery, liver cancer, glycyrrhizic acid

INTRODUCTION

Liver cancer is one of prevalent cancers with high mortality rate around the world, and traditional chemotherapy is one effective approach used in anti-cancer therapy (Gravitz, 2014; Sia et al., 2017). However, many chemotherapeutic agents, such as DOX and paclitaxel, have many clinical limitations owing to severe system toxicity, non-specific targeting, and the development of multidrug resistance (MDR) (Zahreddine and Borden, 2013).

To improve selectivity toward liver cancer cells, an effective strategy is to design nano-sized carrier to realize liver-targeted delivery (Shamay et al., 2018). Recently, nanoparticles have been

proved to have the advantages in drug delivery with low system toxicity (Wei et al., 2015; Zeng et al., 2017; Arms et al., 2018). Many nano-sized drug delivery systems, such as natural and synthetic polymer nanoparticles, metal nanoparticles, and polymer-drug conjugates, have been investigated for delivery of anti-tumor drugs (Ekladious et al., 2018; Liu et al., 2018; Maeki et al., 2018). The nano-vehicles basing on phosphoethanolamine-polyethylene glycol polymers (PEG-PE) represent a promising nanoparticles delivery system owing to biocompatibility, prolonged circulation, and accumulation in tumors by the enhanced permeability and retention (EPR) effect (Perche et al., 2012; Kohay et al., 2017). In the past decade, many efforts have been made to prepare liver-targeting nano-carriers, which were modified by sugars, antibodies, and other ligands (Singh et al., 2016; Zhu et al., 2016; Yan et al., 2017; Wu J. et al., 2018). Glycyrrhetinic acid (GA), a metabolite of glycyrrhizin, has attracted growing interest in anti-hepatoma therapy (Wu J. et al., 2018). It has been reported that GA-modified nano-carriers could significantly improve liver-targeting efficiency and inhibit liver cancer development.

Moreover, development of MDR in cancer cells was a major cause of the failure in clinical chemotherapy. Bcl-2, an anti-apoptosis protein, is distributed on the endoplasmic reticulum, the outer membrane of nuclear and mitochondrion. Up-regulation of Bcl-2 expression was one of the mechanisms responsible for MDR, leading to the activation of anti-apoptotic pathways (Yin et al., 2014). The Bcl-2 siRNA, an antisense oligonucleotide sequence of Bcl-2, could silence the expression of Bcl-2 gene, resulting in cell apoptosis of liver cancer (Sun et al., 2018).

To overcome the limitations of traditional chemotherapy in clinical antitumor therapy, combination drug strategy has been applied as a novel anti-tumor therapy. It is based on co-delivery nanoparticles system for combination of chemotherapeutics with other treatment approaches like RNAi (Zuckerman and Davis, 2015). The nanoparticles can simultaneously co-deliver two or more drugs to tumor region and thus improve the cancer therapeutic effect by synergistic/combined therapy effect, and reverse the multi-drug resistance (MDR) (Zhang et al., 2016; Sun et al., 2018).

In previous study, we have prepared GA-modified hyaluronic acid micelles for DOX delivery (Wu et al., 2016). Hyaluronic acid (HA), a negatively charged polysaccharide, is present in the extracellular matrix and synovial fluids (Knopf-Marques et al., 2016). It can cover on the shell of positive nano-carriers, such as PEI-PE, chitosan, dendrimer, to decrease the uptake rate by reticuloendothelial systems (Nguyen and Alsberg, 2014; Zhao et al., 2016; Wickens et al., 2017; Parmar et al., 2018).

In this study, DSPE-PEG-PEI and GA-HA conjugates were synthesized, and GH-DPP nanoparticles were prepared for co-delivery of DOX and Bcl-2 siRNA (**Figure 1**). The characteristics of the drug-loaded nanoparticles were investigated using dynamic light scattering, transmission electron microscopy (TEM) and UV-Vis spectrophotometer. The *in vitro* cytotoxicity and cellular uptake of siRNA/DOX/GH-DPP were investigated against HepG2 cells. And the *in vivo* bio-distribution and anti-tumor effect were explored.

MATERIALS AND METHODS

Materials and Cell Lines

Branched poly(ethyleneimine) (PEI, Mw 1.8 kDa) was purchased from Sigma Aldrich (United States). DOX was purchased from Dalian Meilun Biology Technology Co., Ltd., (Dalian, China). 4-(4,6-dimethoxy-1,3,5-triazin-2-yl)-4-methylmorpholinium ch loride (DMT–MM) were purchased from Shanghai Medpep Co., Ltd., (Shanghai, China) 1,2-distearoyl-sn-glycero-3-phosphoethanolamine-N-[succinimidyl (polyethylene glycol) -2000] (DSPE-PEG-NHS) was purchased from Xi'an Rixi Technology Co., Ltd., (Xi'an, China). Bcl-2 siRNA and FITC-labeled siRNA were purchased from Guangzhou RiboBio Co., Ltd., (Guangzhou, China). 3-(4, 5-dimethylthiazol-2-yl)-2, 5-diphenyltetrazolium bromide (MTT) was purchased from Sigma Aldrich (United States). Fetal bovine serum and RPMI-1640 medium (RPMI) were purchased from Beijing Solarbio Co., Ltd., (Beijing, China). All other reagents were of commercial special grade and used without further purification.

Human hepatic cell line (HepG2), human lung adenocarcinoma cell line (A549) and murine HCC cells (H22) were obtained from the China Center for Type Culture Collection (Wuhan, China). Female BALB/c mice (weight: 18 ± 2 g) were supplied by the Experimental Animal Center of Weifang Medical University (Weifang, China), and approved by the WFMU Animal Research Ethics Committee.

Synthesis of HA-GA and DSPE-PEG-PEI Conjugates

GA-HA conjugate (GH) was synthesized using HA as a hydrophilic segment and GA as a hydrophobic segment (Wu et al., 2016). In brief, GA–NH_2 was obtained by adding ethylene diamine to the GA solution in the presence of DMT-MM. And the GA–HA conjugate was synthesized by the chemical modification of GA–NH_2 to HA chain.

Syntheses of DSPE-PEG-PEI (DPP) were conducted in one steps as shown in **Figure 2**. Briefly, PEI was dissolved in DMSO (10 mL) in a 25 mL glass flask, and then functional DSPE-PEG-NHS was added into the reaction solution under stirring. The reaction solution was stirred for 24 h at room temperature. The product was purified by dialysis against distilled water (MWCO 8000-14000 Da), lyophilized, and the chemical structure was confirmed by ^{1}H NMR (in D_2O, 300 MHz).

Preparation and Characteristics of Drug-Loaded GH-DPP Nanoparticles

siRNA/DOX/GH-DPP nanoparticles were prepared by three steps. Firstly, DOX was loaded into the core of DPP nanoparticles via a dialysis method. In brief, DOX • HCl was stirred with triethylamine (1.3-fold molar quantity of DOX) in DMF, and the DPP conjugates were dispersed in formamide. Then the DOX solution was added slowly to the DPP solution, followed by stirring overnight. The mixed system was dialyzed against deionized water. The solution in the dialysis bag was freeze-dried to obtain DOX-loaded DPP nanoparticles (DOX/DPP). Secondly, the DPP nanoparticles for co-delivery

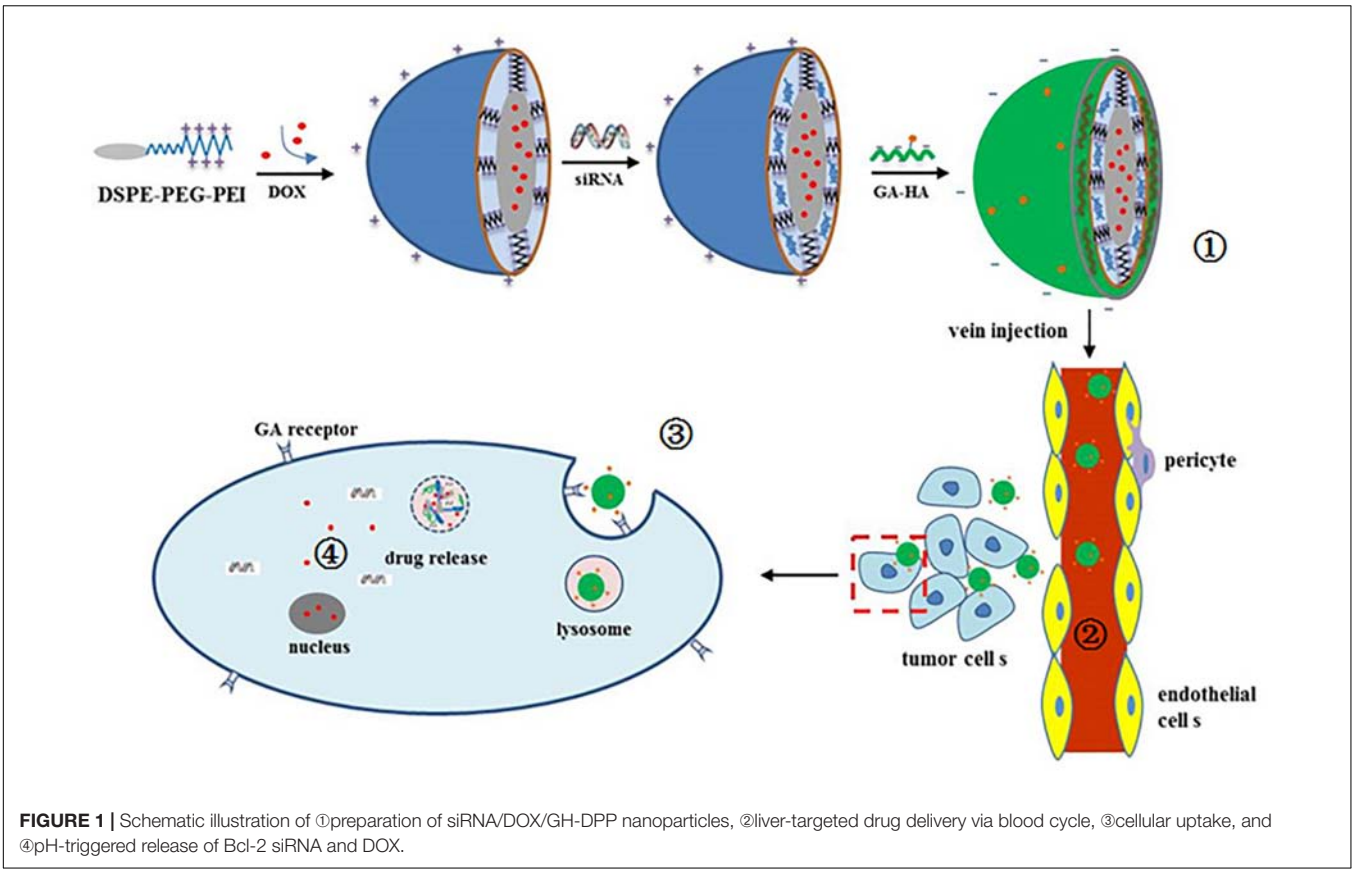

FIGURE 1 | Schematic illustration of ①preparation of siRNA/DOX/GH-DPP nanoparticles, ②liver-targeted drug delivery via blood cycle, ③cellular uptake, and ④pH-triggered release of Bcl-2 siRNA and DOX.

of DNA and siRNA were prepared by electrovalent interaction. The sequences of Bcl-2 siRNA were as follows: (sense) 5′ – GUACAUCCAUUAUAAGCUGUCdTdT-3′, (anti-sense) 5′ – GACAGCUUAUAAUGGAUGUACdTdT-3′. DOX/DPP nanoparticles were incubated with Bcl-2 siRNA in deionized water. In order to obtain the proper mass ratio of DPP to siRNA, the same amount of siRNA was incubated with different concentrations of DOX/DPP nanopaticles solutions for 1 h. The mass ratios of DOX/DPP to siRNA was set as 100:512, 100:256, 100:128, 100:64, 100:32, 100:16, and 100:8, respectively. The binding ability of DOX/DPP and siRNA was investigated by agarose gel retardation assay, followed by electrophoretic mobility shift assay via a UV gel imaging system. The proper mass ratio of DOX/DPP to siRNA was selected for preparation of siRNA/DOX/DPP nanoparticles. Thirdly, GA-HA conjugate was mixed with siRNA/DOX/DPP nanoparticles to prepare siRNA/DOX/GH-DPP by stirring slowly for 1 h. Then drug-loaded nanoparticles were freeze-dried, and the lyophilized power was stored at 4°C. The GH-DPP nanoparticles for delivery of DOX or siRNA alone were prepared as control.

The particle size and ζ potential of siRNA/DOX/GH-DPP nanoparticles were measured using a dynamic laser scattering method with a wavelength of 633 nm at 25°C. The detection angle was set to 90°. The polydispersingindex (PdI) was used to evaluate the size distribution. The concentration of siRNA/DOX/GH-DPP nanoparticles was kept 1 mg/mL, and all measurements were performed in triplicate. The morphology of siRNA/DOX/GH-DPP nanoparticles was observed by electron microscopy. One drop of drug-loaded nanoparticles solution were placed on a copper grid, and dried at room temperature. The sample was examined using a transmission electron microscope.

To evaluate the loading efficiency (LE) and encapsulation efficiency (EE) of GH/DPP nanoparticles, siRNA/DOX/GH-DPP nanoparticles were dissolved in formamide by gently heating, and measured using UV–Vis spectrophotometer at 480 nm. The concentration of DOX in the GH/DPP micelles was obtained using the standard curve. Then LE and EE were calculated using the following equation (1) and (2):

$$\mathrm{LE}(\%) = \mathrm{Ws}/\mathrm{Wt} \times 100\% \quad (1)$$

$$\mathrm{EE}(\%) = \mathrm{Ws}/\mathrm{Wa} \times 100\% \quad (2)$$

Ws = the amount of DOX measured in the GH/DPP nanoparticles; Wt = the total weight of siRNA/DOX/GH-DPP nanoparticles; and Wa = the initial amount of the DOX•HCl added.

In vitro Drug Release From GH-DPP Nanoparticles

The release of DOX and siRNA from GH-DPP nanoparticles was investigated in PBS buffer (pH 7.4 and 5.0) (Wang et al., 2016). 1 mg/mL siRNA/DOX/GH-DPP nanoparticles was dispersed in

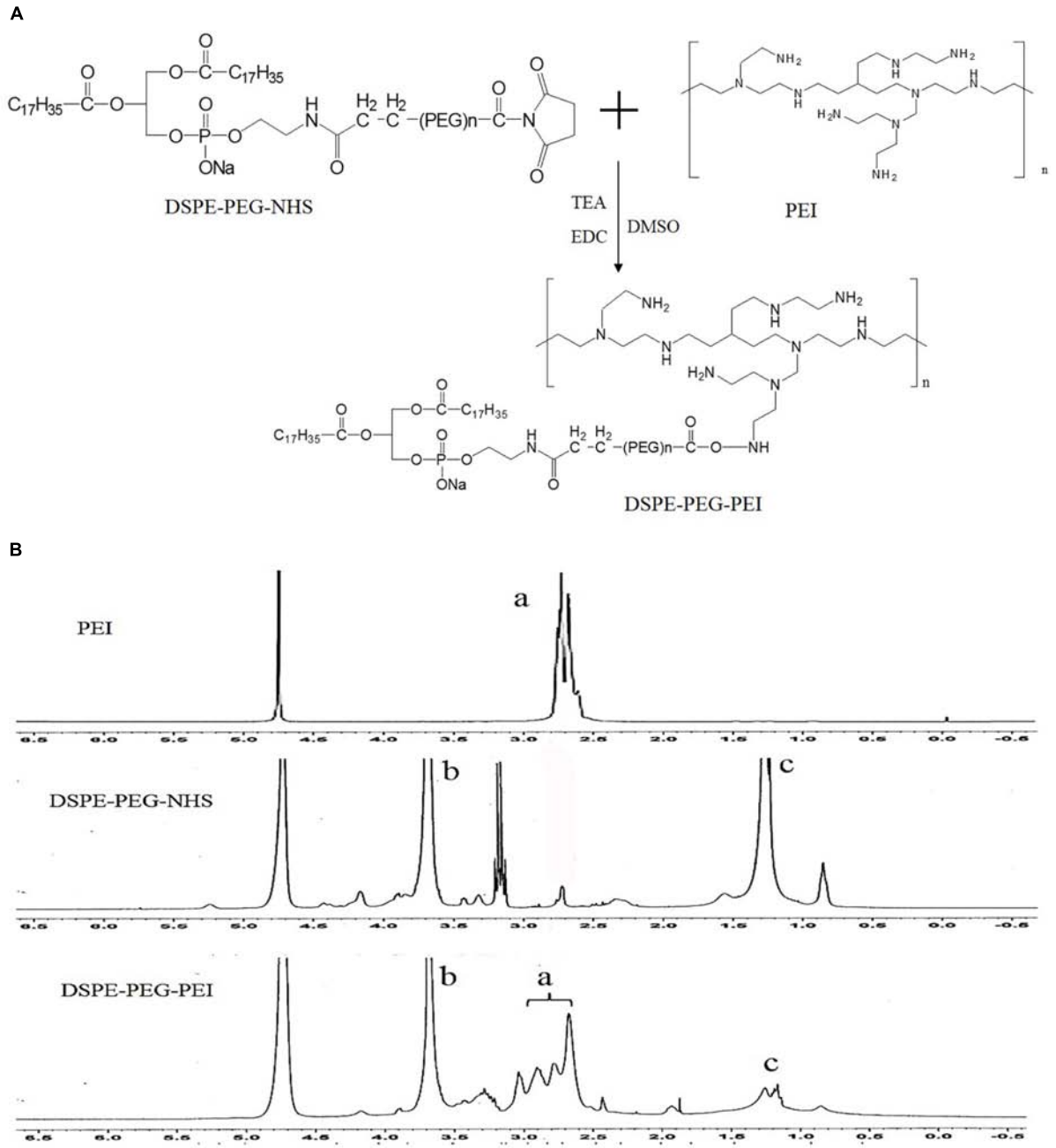

FIGURE 2 | Synthesis of DSPE-PEG-PEI conjugate. **(A)** Synthetic route of DSPE-PEG-PEI conjugate. **(B)** ^{1}H-NMR spectra of PEI, DSPE-PEG-NHS and DSPE-PEG-PEI (a: peaks of PEI; b and c: peaks of DSPE-PEG-NHS).

5 mL PBS, and the solution was placed in a dialysis bag (MWCO of 1000 and 20000 for DOX and siRNA, respectively). Then, the dialysis bag was placed in 20 mL of PBS buffer at 37°C under a shaking speed of 100 rpm. At predetermined time intervals, 1 mL of release media was taken out and 1 mL of fresh PBS buffer was added. The DOX and siRNA content was tested by UV-Vis spectroscopyat 480 and 260 nm, respectively. The release of DOX and siRNA was calculated by standard curve. The test was performed in triplicate.

Cytotoxicity Assay of siRNA/DOX/GH-DPP Nanoparticles

The cytotoxicity of blank DPP and GH-DPP nanoparticles against HepG2 and A549 cells was evaluated by MTT assay. Briefly, the tumor cells were seeded in 96-well plates (1×10^4 cells/well) and incubated for 48 h. Then, the cells were co-cultured with different concentrations (1, 10, 20, 50, and 100 μg/ml) of DPP or GH-DPP nanoparticles, respectively. After 48 h, 20 μL of MTT reagents (5 mg/mL) was added for another

4 h incubation at 37°C. The media were replaced with 200 μL of DMSO. The absorbance at 490 nm was measured using a Bio-Rad Microplate Reader (Model 680, Richmond, VA, United States).

The cytotoxicity of siRNA/DOX/GH-DPP nanoparticles was evaluated by MTT assay against HepG2 and A549 cells. The cells were incubated with the culture media containing free DOX, DOX/GH-DPP, siRNA/GH-DPP, siRNA/DOX/DPP and siRNA/DOX/GH-DPP nanoparticles at different DOX concentrations (0.01, 0.1, 0.5, 1, 2, and 5 μg/mL), respectively. The cytotoxicity of drug formulations was shown as a cell viability percentage with respect to the untreated tumor cells. All the experiments were repeated thrice.

Cellular Uptake Analysis

Cellular uptake of DOX and FITC-labeled siRNA was monitored by fluorescent microscopy (BX40, Olympus, Japan). HepG2 cells were seeded in a 12-well plate at a density of 1×10^5 cells/well at 37°C. After the cells reached 75% confluence, the media were replaced with fresh media containing free DOX and siRNA, siRNA/DOX/DPP, siRNA/DOX/GH-DPP nanoparticles, respectively. After 4 h, the cells were washed three times by cold PBS, and fixed with 4% paraformaldehyde solution. The intracellular localization of DOX was visualized by fluorescence microscope.

Western Blotting Analysis

Suppression of the BCL-2 protein was determined by Western blot using bicin-choninic acid protein assay kit (BCA, Invitrogen, United States). Sample proteins (30 μg) was subjected to electrophoresis in 10% sodium dodecyl sulfate polacrylamine gel. And the protein was transferred to polyvinylidene difluoride membranes, followed by incubation with non-fat milk for 1 h, and with antibody against BCL-2 and β-action (1:1000 dilution) for 12 h at 4°C. The membranes were washed thrice in TBST, and incubated with HRP conjugated goat anti-rabbit IgG (1:5000, Santa Cruz Biotech., United States) for 1 h. the complexes were visualized using chemiluminescence kit (KeyGEN, China).

In vivo Near-Infrared Fluorescence Imaging (NIFI)

In vivo biodistribution of the drug-loaded GH-DPP nanoparticles was monitored via near-infrared fluorescence imaging system. Preparation of DiR loaded GH-DPP nanoparticles was as followed: GH-DPP and DiR were dis-solved in methanol, and the solution was dripped to deionized water by a micro-syringe pump under magnetic stirring. The mixture system was dialyzed against deionized water for 48 h. The final concentration of DiR for tail vein injection was 40 μg/mL. The tumor-bearing mice model was established by subcutaneous inoculation of H22 cells in the flank of BALB/c female mice. When the volume of the tumor grew to approximately 100 mm^3, the mice were randomly divided into three groups. DiR was used as a fluorescence agent. DiR-loaded DPP and DiR-loaded GH-DPP nanoparticles were prepared, respectively. Free DiR, DiR-loaded DPP and DiR-loaded GH-DPP nanoparticles were administrated by intravenous injection. The *in vivo* near-infrared fluorescence imaging was performed at pre-determined times (2, 6, 12, and 24 h), using the Xenogen IVIS Spectrum from Caliper Life Sciences (Ex was 745 nm, Em was 835 nm).

Anti-tumor Effect Analysis

The therapeutic effects of drug-loaded GH-DPP nanoparticles were investigated through evaluation of their anti-tumor effects using H22 tumor-bearing mice as model. When the tumor size reached about 100 mm^3, H22-bearing mice was randomly divided into sever groups (five mice per group). The mice were administrated by physiological saline (control), blank GH-DPP nanoparticles, free DOX●HCl, siRNA/GH-DPP, DOX/GH-DPP, siRNA/DOX/DPP, and siRNA/DOX/GH-DPP nanoparticles, respectively. Drug treatment was set at a dose of 5 mg DOX/kg body weight every other day. The body weight and tumor volume was measured every day. Finally, all of the mice were sacrificed, and the tumors were harvested. The tumor volume was calculated by follow equation:

$$Vt = d^2 \times L/2$$

L is the longest diameter of tumor; d is the shortest diameter of tumor; and Vt is the tumor volume.

Statistical Analysis

All results are presented as mean ± S.D., $n = 3$ parallel samples. The data were analyzed by Student's *t*-test for comparison of two groups. A *p*-value less than 0.05 was considered to be significant.

Synthesis of DSPE-PEG-PEI Conjugates

Bi-functional DSPE-PEG-NHS was used to conjugate with PEI via the primary amine reactive NHS ester moiety at weakly basic pH, thus avoiding the conjugation and crosslinking of the maleimide groups to the amine functions of PEI, which occurs at higher pH (pH > 8). The structure of DSPE-PEG-NHS, PEI and resulting DSPE-PEG-PEI copolymer were verified by ^{1}H NMR. The peaks of PEG (3.6 ppm, -CH_2O-), DSPE (1.0–1.5 ppm, -CH_2-) and PEI (2.5–3.0 ppm, CH_2-N) were confirmed. The^{1}H-NMR spectrum of DSPE-PEG-PEI in D_2O exhibited characteristic peaks at 2.5–3.0 ppm (peaks of PEI), 3.6 ppm (peaks of PEG) and 1.0–1.5 ppm (peaks of DSPE), indicating that PEI was successfully introduced to the DSPE-PEG-NHS molecular.

Preparation and Physicochemical Characteristics of Drug-Loaded Nanoparticles

Doxorubicin and Bcl-2 siRNA were loaded in DPP or GH/DPP copolymers, named as siRNA/DOX/DPP and siRNA/DOX/GH-DPP, respectively. The characterization of DOX-loaded nanoparticles was shown in **Table 1**. The average particles size of siRNA/DOX/GH-DPP was bigger than that of siRNA/DOX/DPP, while the ζ potential was lower in siRNA/DOX/GH-DPP. The result was due to the coverage of GA-HA conjugate, resulting in bigger particles size and less ζ potential. LE and EE of DOX in siRNA/DOX/GH-DPP nanoparticles were measured by UV spectrophotometer. When the feed ratio of DOX to DPP was 10%, the EE and LE of DOX was 86.1 and 8.02%, respectively.

TABLE 1 | The particle size, polydispersity index (PDI) and zeta potential of siRNA/DOX/DPP and siRNA/DOX/GH-DPP (n = 3).

	Size (nm)	PDI	Zeta (mV)	EE[b](%)	DL[b](%)
siRNA/DOX/DPP	157.2 ± 5.7	0.272 ± 0.05	12.75 ± 2.19	87.4 ± 2.7	8.32 ± 1.4
siRNA/DOX/GH-DPP	185.4 ± 6.4[a]	0.294 ± 0.04	−2.64 ± 1.73[a]	86.1 ± 3.1	8.02 ± 1.6

[a]$P < 0.05$ siRNA/DOX/DPP vs siRNA/DOX/GH-DPP. [b]DOX loadeding.

To obtain the co-delivery system of DOX and siRNA, DOX/DPP and siRNA with different mass ratio were mixed and tested by gel retardation assay. **Figure 3A** showed that the fraction of free DNA disappeared at 100:16, suggesting that DOX/DPP could condense DNA efficaciously when the mass ratio of DPP to siRNA was over 100:16. The siRNA/DOX/DPP and siRNA/DOX/GH-DPP nanoparticles were well-separated with a rather narrow size distribution (**Figures 3B,C**). As shown in **Figures 3D,E**, the co-delivery system exhibited sphere in shape. Stability studies showed that drug-loaded GH-DPP nanoparticles were more stable than drug-loaded DPP nanoparticles under physiological conditions (**Supplementary Figure S1**).

DOX and siRNA Release From siRNA/DOX/GH-DPP Nanoparticles

The release of DOX and siRNA from siRNA/DOX/GH-DPP or siRNA/DOX/DPP nanoparticles was conducted in pH 7.4 and pH 5.0. The siRNA and DOX released from GA-DPP or DPP were time-dependent (**Figure 4**). Both GH-DPP and DPP nanoparticles showed a rapid release at pH 5.0. By contrast, the drug release was slower at pH 7.4. The possible explanation is that the electrostatic interaction between positive segments (PEI) and negative segments (siRNA, GA-HA) is weak at lower pH value, leading to rapid release of the drug from the nano-carriers (Sun et al., 2018). Compared to siRNA/DOX/GH-DPP nanoparticles, the siRNA/DOX/DPP released more drugs at the same time. This may due to the fact the coverage layer (GA-HA) could delay the release of DOX from GH-DPP nanoparticles (Manna et al., 2010).

In vitro Cytotoxicity of siRNA/DOX/GH-DPP Nanoparticls

The cytotoxicity of blank nano-carriers was determined using the MTT assay. The cytotoxicity of two blank nano-carriers was below 15% at the concentration of 10 to 100 μg/mL (**Figure 5A**). The results suggested that DPP and GH-DPP nanoparticles could be used in drug delivery materials due to their negligible toxicity.

The viability of A549 and HepG2 cells was evaluated after incubations with free DOX, DOX/GH-DPP, siRNA/GH-DPP, siRNA/DOX/DPP, and siRNA/DOX/GH-DPP nanoparticles for 48 h. **Figure 5B** showed that all of five drug formulations exhibited similar dose-dependent cytotoxic effects, and that the co-delivery nanoparticles groups (siRNA/DOX/DPP and siRNA/DOX/GH-DPP) showed higher cytotoxicity compared to free drug treatment groups. The half maximal inhibitory concentration (IC50 value) of siRNA/DOX/DPP and siRNA/DOX/GH-DPP nanoparticles against HepG2 cells was measured to be 1.02 and 0.76 DOX μg/mL, respectively, which were lower than that of free DOX (1.86 DOX μg/mL). The results suggested that co-delivery nanoparticles for DOX and Bcl-2 siRNA could enhanced inhibitory effect of DOX. This was due to the fact that sensitivity of HepG2 cells to DOX was enhanced owing to down-regulation of BCL-2 by RNA interference (Cao et al., 2011). As shown in **Figures 5C,D**, siRNA/DOX/GH-DPP nanoparticles exhibited higher toxicity against HepG2 cells than other DOX formulations, while, it was different at same treatment with A549 cells. The possible explanation was that GA-receptors were over-expressed on HepG2 cells, which enhanced cellular uptake of DOX and siRNA via GA receptor-mediated endocytosis. Whereas, the siRNA/DOX/GH-DPP nanoparticles against A549 cells showed lower cytotoxicity than siRNA/DOX/ DPP nanoparticles. The different cytotoxicity against HepG2 cells and A549 cells might due to different expressed level of GA-receptor on two tumor cells (Tian et al., 2010).

Cellular Uptake of siRNA/DOX/GH-DPP Nanoparticles and Suppression of BCL-2 Expression

The cellular uptake of siRNA/DOX/GH-DPP nanoparticles was investigated through fluorescence microscope. Green and red fluorescence signals indicate the uptake of siRNA and DOX, respectively, while blue fluorescence signals show the nuclei stained with DAPI. Overlays of three fluorescence picture revealed the distribution of DOX and siRNA in the cytoplasm. As shown in **Figure 6A**, there were obvious red fluorescence signals in cytoplasm of HepG2 cells incubating with three drug formulations, indicating that DOX was taken up by tumor cells. There was little green fluorescence signals in the group treated by mixture of free DOX and siRNA, indicating that little siRNA were taken up by tumor cells. Compared to drug-loaded DPP nanoparticles, stronger green fluorescence signals were found in HepG2 cells incubating with DOX/GH-DPP nanoparticles. This result was due to the coverage of GA-HA conjugate, which increase the amounts of drugs via GA-receptor-mediated endocytosis. The down-regulation of BCL-2 gene in HepG2 cells was assessed by western blot assays. After treated with siRNA/DOX/DPP and siRNA/DOX/GH-DPP nanoparticles, the expression of BCL-2 protein was inhibited obviously in comparison with the control group (**Figures 6B,C**), suggesting that the up-regulation of BCL-2 in HepG2 cells could be reversed by RNA interference basing on GH-DPP nanoparticles.

In vivo Biodistribution of GH-DPP Nanoparticles

DiR-loaded nanoparticles were prepared to investigate the biodistribution of GH-DPP *in vivo* (Frangioni, 2003). After injection of DiR formulations, fluorescence signals could be monitored in liver and tumor. As shown in **Figure 7**, there were strong fluorescence signals in the tumor for DiR-loaded nanoparticles compared to free DiR, indicating the nano-carrier

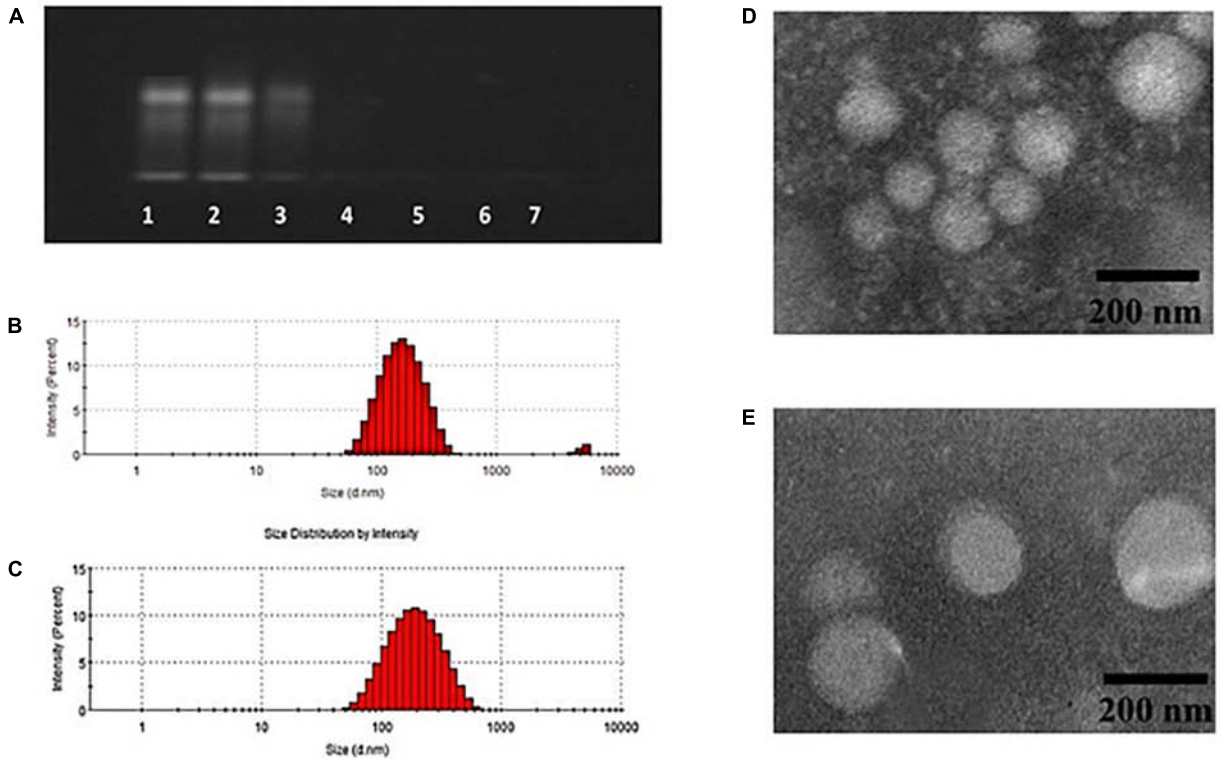

FIGURE 3 | Characteristics of siRNA/DOX-loaded GH-DPP nanoparticles. **(A)** The siRNA retardation assay of GH-DPP at the mass ratio of DPP to siRNA from 100:256 to 100:4 (1, 100:128; 2, 100:64; 3, 100:32; 4, 100:16; 5, 100:8; 6, 100:4). **(B–C)** Particle size distribution of siRNA/DOX/ DPP and siRNA/DOX/GH-DPP nanoparticles. **(D–E)** TEM image of siRNA/DOX/ DPP and siRNA/DOX/GH-DPP nanoparticles.

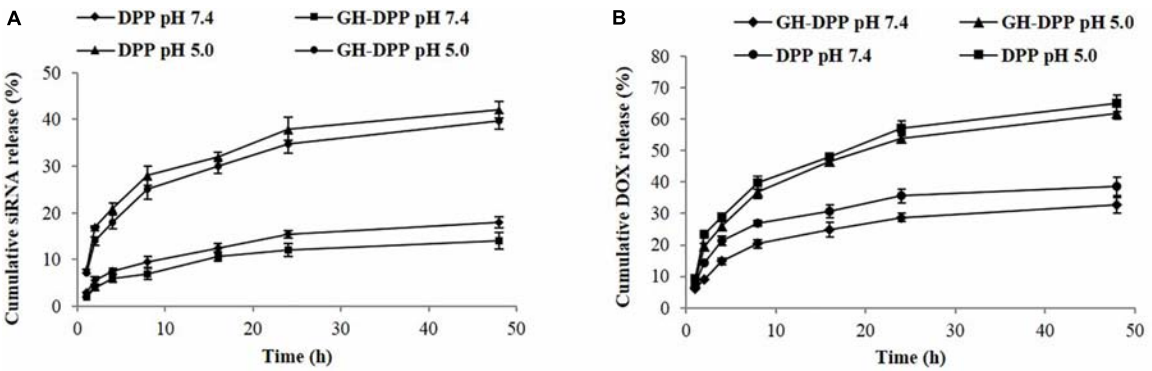

FIGURE 4 | Release profile of siRNA and DOX-loaded nanoparticles. **(A)** siRNA release from GH-DPP or DPP nanoparticles in pH 7.4 or 5.0, respectively. **(B)** DOX release from GH-DPP or DPP nanoparticles in pH 7.4 or 5.0, respectively.

could enhance drug accumulation in tumor region (Nichols and Bae, 2014). Moreover, the fluorescence intensity of DiR-loaded GH-DPP nanoparticles in the tumor was greater than that of DiR-loaded DPP nanoparticles. This may be due to the fact that GH-DPP nanoparticles increased accumulation in the liver cancer cells via liver-targeting delivery, and decreased the uptake by normal cells. After injection for 24 h, major organs and tumors were extracted for fluorescent intensity evaluation. Similar to DiR biodistribution in **Figure 7A**, the DiR-loaded GH-DPP treatment group show strongest fluorescent signals in tumor region (**Figure 7B**).

In vivo Anti-tumor Effect of siRNA/DOX/GH-DPP Nanoparticles

The combination of DOX and Bcl-2-siRNA was used in anti-hepatoma therapy. The anti-tumor effect of siRNA/DOX/GH-DPP nanoparticles was evaluated in the H22

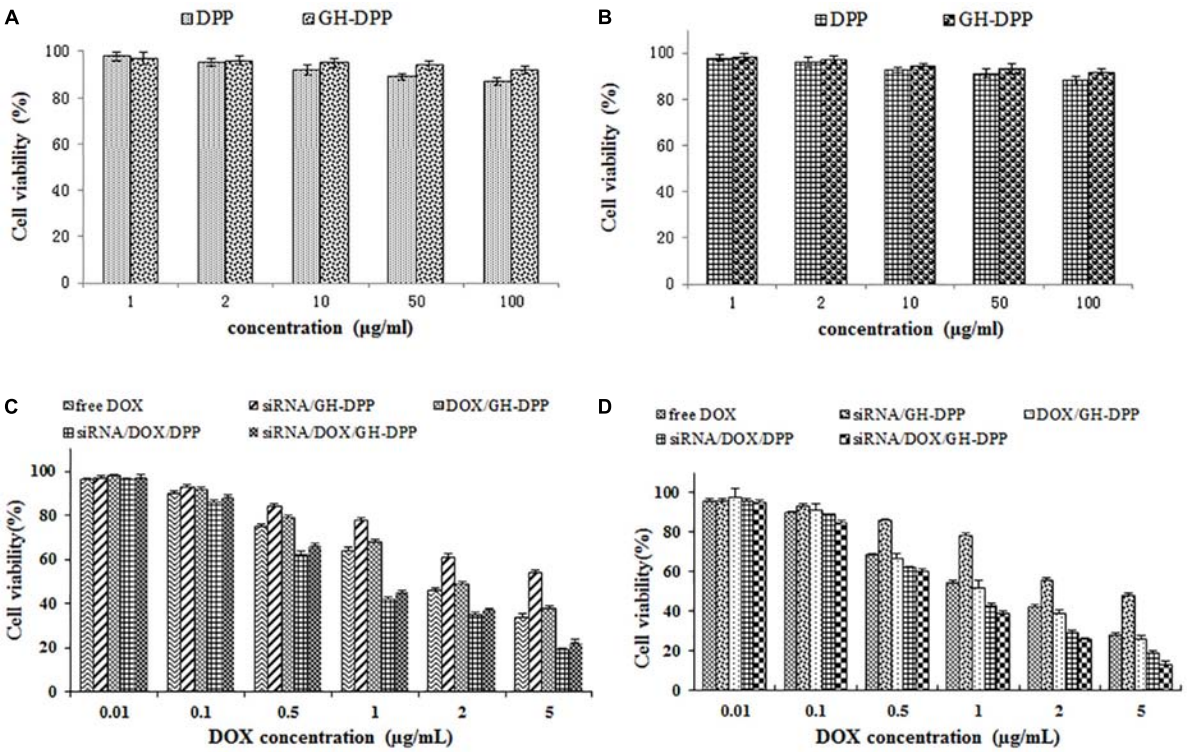

FIGURE 5 | The cell viability of blank nanoparticles against **(A)** A549 cells and **(B)** HepG2 cells for 48 h. The cell viability of drug formulations against **(C)** A549 cells and **(D)** HepG2 cells for 48 h.

tumor-bearing mice. As shown in **Figure 8**, the groups treated with saline and blank GH-DPP nanoparticles showed a rapid growth in tumor size, and no significant difference was observed between the blank GH-DPP group and the control group, indicating that the GH-DPP nanoparticles was biocompatible. In contrast, the groups treated with drug formulations showed obvious growth inhibition. *In vivo* tumor inhibition ratio (IR) of co-delivery nanoparticles for DOX and Bcl-2 siRNA was higher than GH-PDD nanoparticles for delivery of DOX or siRNA alone, indicating that combined therapy of DOX and Bcl-2 siRNA improved antitumor efficacy. Interestingly, siRNA/DOX/GH-DPP nanoparticles showed stronger anti-tumor effect than siRNA/DOX/DPP nanoparticles. This may be due to GA-HA conjugate promoting the accumulation of drug-loaded nanoparticles in tumor region, resulting in higher anti-hepatoma efficacy than siRNA/DOX/DPP nanoparticles.

Figure 8B showed that the body weight of mice treated with free DOX was lower than those treated with drug-loaded nanoparticles, indicating that GH-DPP nanoparticles decreased the systemic toxicity of DOX. As shown in **Figure 8E**, obvious intercellular vacuolation and dissolution of myocardial fibers were observed in the group of free DOX, indicating that the injection of free DOX induced significant cardiotoxicity. By contrast, there was no obvious degeneration of myocardial fibers in the groups which were injected by drug-loaded nanoparticles. These results showed that combined therapy basing on nano-carriers improved the anti-tumor effect and alleviated the systemic toxicity of DOX.

The tumors were extracted for H and E staining to evaluate the antitumor effect. As shown in **Figure 8F**, tumor cells treated with co-delivery system exhibited obvious karyolysis and pyknosis with more cytoplasmic vacuolation in comparison to single drug formulation, indicating that combination therapy exhibited higher antitumor effect. In comparison with siRNA/DOX/DPP nanoparticles, the siRNA/DOX/GH-DPP nanoparticles induced more shrunk nuclei and lower cellular density, suggesting that introduction of GA-HA promote the liver-targeting delivery of drugs, resulting in more effective treatment. The expression of BCL-2 protein was evaluated in the tumor by immunohistochemical assay. The high expression of BCL-2 protein was observed in the groups of free DOX and DOX/GH-DPP nanoparticles. By comparison, the group treated with co-delivery systems showed obvious suppression of BCL-2 expression (Cao et al., 2011).

DISCUSSION

Liver cancer has become one of the highest incidences of malignant tumor in the world. Conventional chemotherapy has severe system toxicity, and always fails in MDR (Perez-Herrero and Fernandez-Medarde, 2015). Some efforts have been focused on the combination of two or more therapeutic approaches

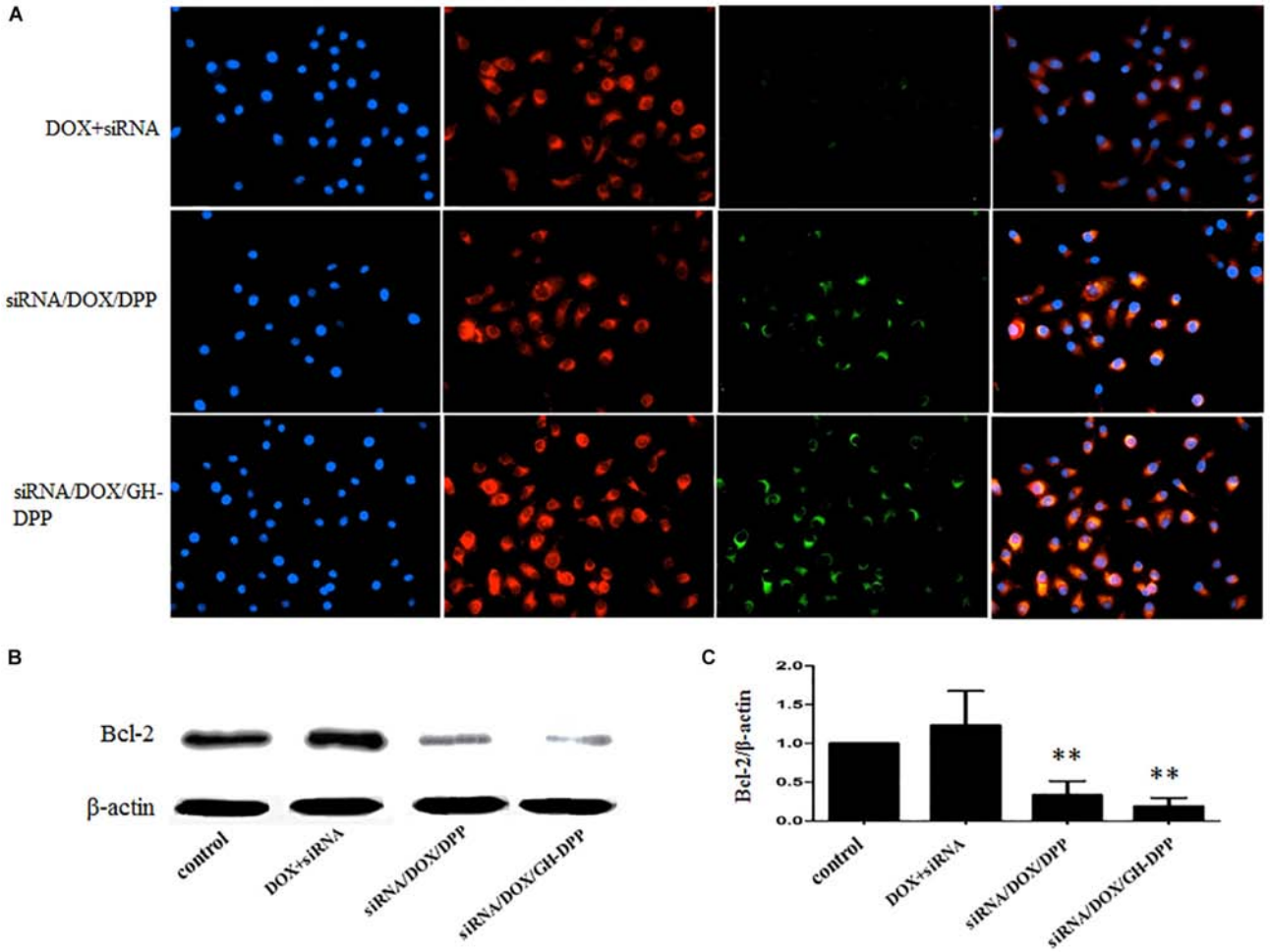

FIGURE 6 | Cellular uptake and western blot analyses. **(A)** The images of HepG2 cells treated with mixture of free DOX and FITC-labeled siRNA, siRNA/DOX/DPP or siRNA/DOX/GH-DPP nanoparticles for 4 h, respectively. FITC channel (green) for FITC-labeled siRNA, TRITC channel (red) for DOX, and DAPI channel (blue) for nucleus were presented simultaneously. **(B,C)** Protein expression of BCL-2 evaluated by western blot analysis with different treatments. $^{**}P < 0.01$ vs. control.

with different mechanisms. The combination of chemotherapy drugs and RNA interference has attracted more attention for the enhanced sensitivity of drugs against tumor cells due to the silence of oncogene (Li et al., 2018). Moreover, nanoparticles for drug delivery have been proven as the useful vehicles of anti-tumor drugs or gene for liver-targeting delivery. The nano-carriers could accumulate in tumor region via active-targeted manner when they are modified by liver-targeting moiety, resulting in loss of side effect from drugs (Chen et al., 2014).

In this study, we prepared the GH-DPP nanoparticles for co-delivery of DOX and Bcl-2 siRNA for liver cancer therapy. The siRNA/DOX/GH-DPP nanoparticles were spherical in shape, negative in zeta potential with an average particle size of 185.4 nm. There was an obvious difference in zeta potential between siRNA/DOX/GH-DPP (negative) and siRNA/DOX/DPP nanoparticles (positive). This was due to the introduction of the negatively charged GA-HA conjugate which induced the shift of surface charge of nano-carriers. The co-delivery system of DOX and Bcl-2 siRNA showed time-dependent sustained release *in vitro*. Compared to DPP nanoparticles, GH-DPP nanoparticles showed slower DOX release. This might due to the fact the coverage layer (GA-HA) delay the release of DOX from GH-DPP.

In vitro cytotoxicity test showed that siRNA/DOX/GH-DPP nanoparticles exhibited a better therapeutic effect than delivering DOX or Bcl-2 siRNA alone. This is due to that fact that co-delivery of DOX and Bcl-2 siRNA produce a synergistic anti-tumor effect in which sensitivity of HepG2 cells to DOX was enhanced owing to down-regulation of BCL-2 by RNA interference. Moreover, siRNA/DOX/GH-DPP nanoparticles exhibited higher cytotoxicity than siRNA/DOX/DPP nanoparticles against HepG2 cells (GA-receptor over-expressed). Interestingly, the cytotoxicity of siRNA/DOX/GH-DPP against A549 cells (no GA-receptor) was lower than that of siRNA/DOX/DPP. The possible explanation was that the introduction of GA-HA conjugate promotes the cellular uptake of drug-loaded GH-DPP nanoparticles by HepG2

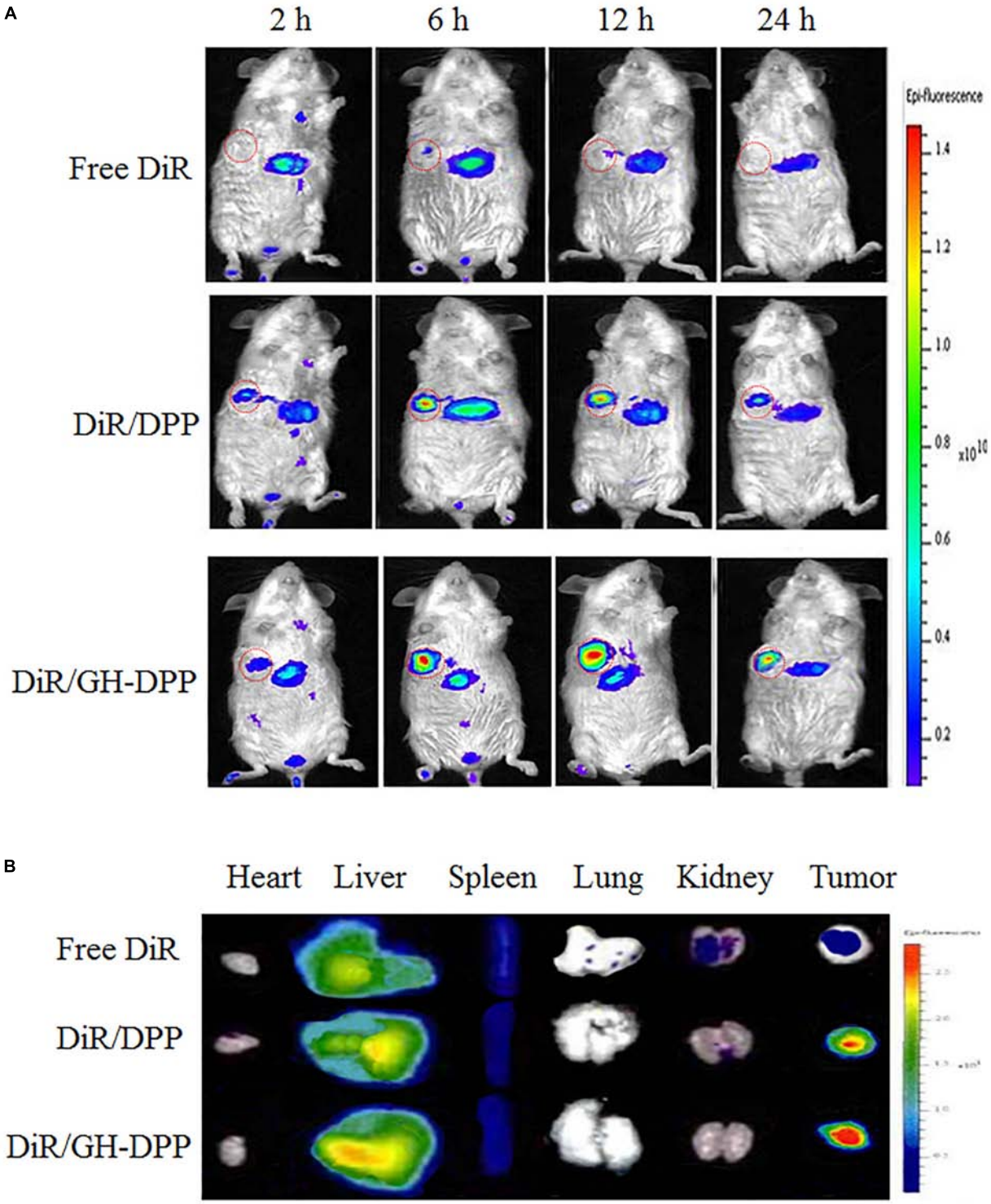

FIGURE 7 | (A) Real-time NIRF images of H22 tumors-bearing mice after tail vein injection of free DiR, DiR/DPP and DiR/GH-DPP nanoparticles for 24 h. The tumors are circled in red. **(B)** *Ex vivo* NIRF images of organs and tumors excised at 24 h.

cells via GA-receptor-mediated endocytosis, leading to higher cytotoxicity (Wu J. et al., 2018). However, there was no GA receptor on A549 cells, and drug-loaded DPP nanoparticles (positive charged) were easily taken up by tumor cells, resulting in higher cytotoxicity than drug-loaded GH-DPP nanoparticles (negative charged).

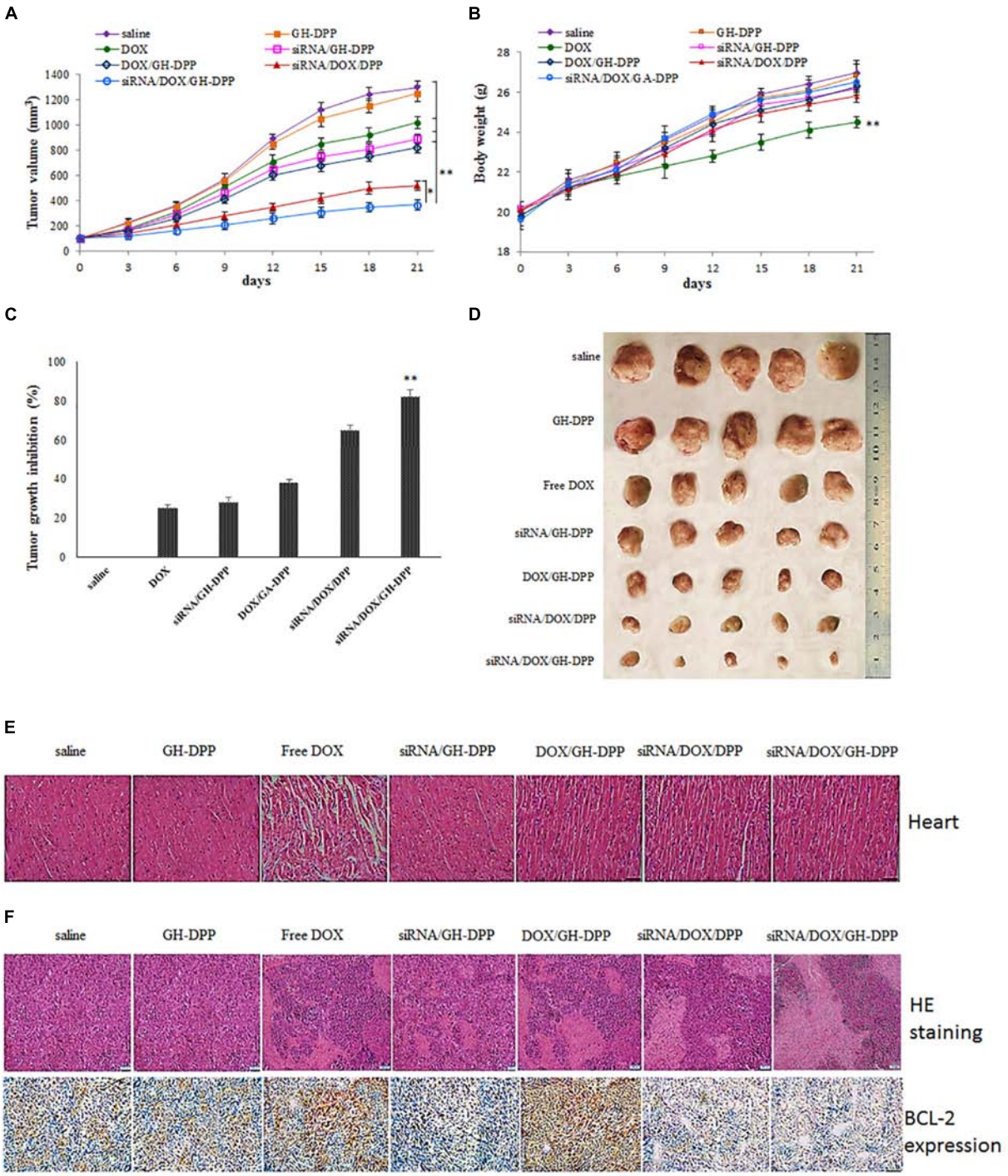

FIGURE 8 | Inhibition of tumor growth by injection of physiological saline (control), blank GH-DPP nanoparticles, free DOX, siRNA/DPP, DOX/DPP, siRNA/DOX/DPP or siRNA/DOX/GH-DPP nanoparticles, respectively. **(A)** Tumor growth curves; **(B)** Body weight changes; **(C)** The tumor growth inhibition rate; **(D)** excised tumors of each group; **(E)** Histological observation of heart for H22 tumor-bearing mice treated with different drug formulations; **(F)** The histological features of H22 subcutaneous tumor sections are characterized by H and E and BCL-2 immunohistochemical analysis. The data represent the mean of the tumor volume or body weight from five mice ± SD; $^{*}P < 0.05$ and $^{**}P < 0.01$.

Figure 6A showed that DOX or siRNA can be effectively taken up by HepG2 cells compared with mixture of free DOX and siRNA. There were stronger fluorescence signals in HepG2 cells incubated with drug-loaded GH-DPP than drug-loaded DPP nanoparticles. This result may be due to the coverage of GA-HA conjugate, which increase the amounts of cellular uptake

via GA-receptor-mediated endocytosis (Yan et al., 2018). *In vivo* near-infrared fluorescence imaging shows that the fluorescence intensity of DiR-loaded GH-DPP nanoparticles in the tumor was greater than that of DiR-loaded DPP nanoparticles. This may be due to the fact that DiR-loaded GH-DPP nanoparticles could be accumulated in the tumor tissue by liver-targeting delivery manner (Fan et al., 2015).

As shown in **Figure 8**, there was no significant difference in body weight and cardiotoxicity between the blank GH-DPP group and the control group. By contrast, the treatment of free DOX induced obvious intercellular vacuolation and dissolution of myocardial fibers, showing significant cardiotoxicity. This result suggested that the GH-DPP nanoparticles were biocompatible and useful for the delivery of chemotherapy drugs (Sun et al., 2018). Compared with nano-formulations for delivery DOX or siRNA alone, siRNA/DOX/GH-DPP nanoparticles showed stronger anti-tumor effect, indicating combination therapy could improve the anti-tumor efficiency by enhancing the sensitivity of cancer cells for chemotherapy drugs through inhibiting the expression of Bcl-2 protein (Chen et al., 2014). Compared to siRNA/DOX/DPP nanoparticles, siRNA/DOX/GH-DPP nanoparticles exhibit stronger antitumor effect. These results showed that the introduction of GA-HA conjugate was helpful to promote the accumulation of drug-loaded nanoparticles in tumor region, resulting in higher anti-hepatoma efficacy (Cai et al., 2016).

CONCLUSION

Doxorubicin-loaded DPP nanoparticles were self-assembled and then complexed successively with Bcl-2 siRNA and GA-HA conjugate to prepare a co-delivery system. The GH-DPP nanoparticles could simultaneously deliver siRNA and DOX into HepG2 cells, and GA-receptor-mediated internalization significantly increased the cellular uptake efficiency. *In vitro* and *in vivo* anti-tumor effects revealed that siRNA/DOX/GH-DPP nanoparticles could suppress the expression of Bcl-2 gene, enhanced cell apoptosis, and exhibited higher anti-tumor effect. The results showed that GH-DPP nanoparticles are efficient nano-carrier for co-delivery of siRNA and hydrophobic drug in combined therapy.

ETHICS STATEMENT

Animal studies were conducted according to the Regulation on Experimental Animals of Animal Research Ethics Committee of WeiFang Medical University.

AUTHOR CONTRIBUTIONS

JW, GT, and BZ designed the experiments. GT, BZ, and JW prepared the drug-loaded GH-DPP nanoparticles. GT, HJ, ZG, and RP performed *in vitro* anti-tumor analysis. BL, ZG, and RP made the anti-tumor effect *in vivo*. MQ, BZ, RP, and JW wrote the manuscript and contributed to data analyses.

FUNDING

This study was financially supported by National Science Foundation of China (8180346, 81871892, and 31671208), Natural Science Foundation of Shandong Province (ZR2018BH041 and ZR2017LC002), the Higher Education Science and Technology Project of Shandong Province (J17KA141), Medical and Health Technology Development Program in Shandong Province (2016WS0673) and Project of traditional Chinese Medicine Technology Development Program in Shandong Province (2017-212).

SUPPLEMENTARY MATERIAL

The Supplementary Material for this article can be found online at: https://www.frontiersin.org/articles/10.3389/fphar.2019.00004/full#supplementary-material

REFERENCES

Arms, L., Smith, D. W., Flynn, J., Palmer, W., Martin, A., Woldu, A., et al. (2018). Advantages and limitations of current techniques for analyzing the biodistribution of nanoparticles. *Front. Pharmacol.* 9:802. doi: 10.3389/fphar.2018.00802

Cai, Y., Xu, Y., Chan, H. F., Fang, X., He, C., and Chen, M. (2016). Glycyrrhetinic acid mediated drug delivery carriers for hepatocellular carcinoma therapy. *Mol. Pharm.* 13, 699–709. doi: 10.1021/acs.molpharmaceut.5b00677

Cao, N., Cheng, D., Zou, S., Ai, H., Gao, J., and Shuai, X. (2011). The synergistic effect of hierarchical assemblies of siRNA and chemotherapeutic drugs co-delivered into hepatic cancer cells. *Biomaterials* 32, 2222–2232. doi: 10.1016/j.biomaterials.2010.11.061

Chen, W., Yuan, Y., Cheng, D., Chen, J., Wang, L., and Shuai, X. (2014). Co-delivery of doxorubicin and siRNA with reduction and pH dually sensitive nanocarrier for synergistic cancer therapy. *Small* 10, 2678–2687. doi: 10.1002/smll.201303951

Ekladious, I., Colson, Y. L., and Grinstaff, M. W. (2018). Polymer-drug conjugate therapeutics: advances, insights and prospects. *Nat. Rev. Drug Discov.* doi: 10.1038/s41573-018-0005-0 [Epub ahead of print].

Fan, Y., Sahdev, P., Ochyl, L. J., Akerberg, J., and Moon, J. J. (2015). Cationic liposome-hyaluronic acid hybrid nanoparticles for intranasal vaccination with subunit antigens. *J. Control. Release* 208, 121–129. doi: 10.1016/j.jconrel.2015.04.010

Frangioni, J. V. (2003). In vivo near-infrared fluorescence imaging. *Curr. Opin. Chem. Biol.* 7, 626–634.

Gravitz, L. (2014). Liver cancer. *Nature* 516:S1. doi: 10.1038/516S1a

Knopf-Marques, H., Pravda, M., Wolfova, L., Velebny, V., Schaaf, P., Vrana, N. E., et al. (2016). Hyaluronic acid and its derivatives in coating and delivery systems: applications in tissue engineering, regenerative medicine and immunomodulation. *Adv. Healthc. Mater.* 5, 2841–2855. doi: 10.1002/adhm.201600316

Kohay, H., Sarisozen, C., Sawant, R., Jhaveri, A., Torchilin, V. P., and Mishael, Y. G. (2017). PEG-PE/clay composite carriers for doxorubicin: effect of composite

structure on release, cell interaction and cytotoxicity. *Acta Biomater.* 55, 443–454. doi: 10.1016/j.actbio.2017.04.008

Li, Y., Thambi, T., and Lee, D. S. (2018). Co-delivery of drugs and genes using polymeric nanoparticles for synergistic cancer therapeutic effects. *Adv. Healthc. Mater.* 7:1700886. doi: 10.1002/adhm.201700886

Liu, X. L., Chen, S., Zhang, H., Zhou, J., Fan, H. M., and Liang, X. J. (2018). Magnetic nanomaterials for advanced regenerative medicine: the promise and challenges. *Adv. Mater.* 30:e1804922. doi: 10.1002/adma.201804922

Maeki, M., Kimura, N., Sato, Y., Harashima, H., and Tokeshi, M. (2018). Advances in microfluidics for lipid nanoparticles and extracellular vesicles and applications in drug delivery systems. *Adv. Drug Deliv. Rev.* 128, 84–100. doi: 10.1016/j.addr.2018.03.008

Manna, U., Dhar, J., Nayak, R., and Patil, S. (2010). Multilayer single-component thin films and microcapsules via covalent bonded layer-by-layer self-assembly. *Chem. Commun.* 46, 2250–2252. doi: 10.1039/b924240f

Nguyen, M. K., and Alsberg, E. (2014). Bioactive factor delivery strategies from engineered polymer hydrogels for therapeutic medicine. *Prog. Polym. Sci.* 39, 1236–1265. doi: 10.1016/j.progpolymsci.2013.12.001

Nichols, J. W., and Bae, Y. H. (2014). EPR: evidence and fallacy. *J. Control Release* 190, 451–464. doi: 10.1016/j.jconrel.2014.03.057

Parmar, M. B., Meenakshi Sundaram, D. N., K C, R. B., Maranchuk, R., Montazeri Aliabadi, H., Hugh, J. C., et al. (2018). Combinational siRNA delivery using hyaluronic acid modified amphiphilic polyplexes against cell cycle and phosphatase proteins to inhibit growth and migration of triple-negative breast cancer cells. *Acta Biomater.* 66, 294–309. doi: 10.1016/j.actbio.2017.11.036

Perche, F., Patel, N. R., and Torchilin, V. P. (2012). Accumulation and toxicity of antibody-targeted doxorubicin-loaded PEG-PE micelles in ovarian cancer cell spheroid model. *J. Control Release* 164, 95–102. doi: 10.1016/j.jconrel.2012.09.003

Perez-Herrero, E., and Fernandez-Medarde, A. (2015). Advanced targeted therapies in cancer: drug nanocarriers, the future of chemotherapy. *Eur. J. Pharm. Biopharm.* 93, 52–79. doi: 10.1016/j.ejpb.2015.03.018

Shamay, Y., Shah, J., Isik, M., Mizrachi, A., Leibold, J., Tschaharganeh, D. F., et al. (2018). Quantitative self-assembly prediction yields targeted nanomedicines. *Nat. Mater.* 17, 361–368. doi: 10.1038/s41563-017-0007-z

Sia, D., Villanueva, A., Friedman, S. L., and Llovet, J. M. (2017). Liver cancer cell of origin, molecular class, and effects on patient prognosis. *Gastroenterology* 152, 745–761. doi: 10.1053/j.gastro.2016.11.048

Singh, B., Jang, Y., Maharjan, S., Kim, H. J., Lee, A. Y., Kim, S., et al. (2016). Combination therapy with doxorubicin-loaded galactosylated poly(ethyleneglycol)-lithocholic acid to suppress the tumor growth in an orthotopic mouse model of liver cancer. *Biomaterials* 116, 130–144. doi: 10.1016/j.biomaterials.11.040

Sun, W., Chen, X., Xie, C., Wang, Y., Lin, L., Zhu, K., et al. (2018). Co-delivery of doxorubicin and Anti-BCL-2 siRNA by pH-responsive polymeric vector to overcome drug resistance in *in vitro* and *in vivo* hepg2 hepatoma model. *Biomacromolecules* 19, 2248–2256. doi: 10.1021/acs.biomac.8b00272

Tian, Q., Zhang, C. N., Wang, X. H., Wang, W., Huang, W., Cha, R. T., et al. (2010). Glycyrrhetinic acid-modified chitosan/poly(ethylene glycol) nanoparticles for liver-targeted delivery. *Biomaterials* 31, 4748–4756. doi: 10.1016/j.biomaterials.2010.02.042

Wang, F. Z., Xing, L., Tang, Z. H., Lu, J. J., Cui, P. F., Qiao, J. B., et al. (2016). Codelivery of doxorubicin and shAkt1 by poly(ethylenimine)-glycyrrhetinic acid nanoparticles to induce autophagy-mediated liver cancer combination therapy. *Mol. Pharm.* 13, 1298–1307. doi: 10.1021/acs.molpharmaceut.5b00879

Wei, L., Lu, J., Xu, H., Patel, A., Chen, Z. S., and Chen, G. (2015). Silver nanoparticles: synthesis, properties, and therapeutic applications. *Drug Discov. Today* 20, 595–601. doi: 10.1016/j.drudis.2014.11.014

Wickens, J. M., Alsaab, H. O., Kesharwani, P., Bhise, K., Amin, M., Tekade, R. K., et al. (2017). Recent advances in hyaluronic acid-decorated nanocarriers for targeted cancer therapy. *Drug Discov. Today* 22, 665–680. doi: 10.1016/j.drudis.2016.12.009

Wu, F., Li, X., Jiang, B., Yan, J., Zhang, Z., Qin, J., et al. (2018). Glycyrrhetinic acid functionalized nanoparticles for drug delivery to liver cancer. *J. Biomed. Nanotechnol.* 14, 1837–1852. doi: 10.1166/jbn.2018.2638

Wu, J., Yuan, J., Ye, B., Wu, Y., Xu, Z., Chen, J., et al. (2018). Dual-responsive core crosslinking glycopolymer-drug conjugates nanoparticles for precise hepatocarcinoma therapy. *Front. Pharmacol.* 9:663. doi: 10.3389/fphar.2018.00663

Wu, J. L., Tian, G. X., Yu, W. J., Jia, G. T., Sun, T. Y., and Gao, Z. Q. (2016). pH-responsive hyaluronic acid-based mixed micelles for the hepatoma-targeting delivery of doxorubicin. *Int. J. Mol. Sci.* 17, 364. doi: 10.3390/ijms17040364

Yan, G., Wang, J., Hu, L., Wang, X., Yang, G., Fu, S., et al. (2017). Stepwise targeted drug delivery to liver cancer cells for enhanced therapeutic efficacy by galactose-grafted, ultra-pH-sensitive micelles. *Acta Biomater.* 51, 363–373. doi: 10.1016/j.actbio.2017.01.031

Yan, T., Cheng, J., Liu, Z., Cheng, F., Wei, X., Huang, Y., et al. (2018). Acid-sensitive polymeric vector targeting to hepatocarcinoma cells via glycyrrhetinic acid receptor-mediated endocytosis. *Mater. Sci. Eng. C Mater. Biol. Appl.* 87, 32–40. doi: 10.1016/j.msec.02.013

Yin, T., Wang, P., Li, J., Wang, Y., Zheng, B., Zheng, R., et al. (2014). Tumor-penetrating codelivery of siRNA and paclitaxel with ultrasound-responsive nanobubbles hetero-assembled from polymeric micelles and liposomes. *Biomaterials* 35, 5932–5943. doi: 10.1016/j.biomaterials.2014.03.072

Zahreddine, H., and Borden, K. L. (2013). Mechanisms and insights into drug resistance in cancer. *Front. Pharmacol.* 4:28. doi: 10.3389/fphar.2013.00028

Zeng, L., Gupta, P., Chen, Y., Wang, E., Ji, L., Chao, H., et al. (2017). The development of anticancer ruthenium(ii) complexes: from single molecule compounds to nanomaterials. *Chem. Soc. Rev.* 46, 5771–5804. doi: 10.1039/c7cs00195a

Zhang, X., Wang, Q., Qin, L., Fu, H., Fang, Y., Han, B., et al. (2016). EGF-modified mPEG-PLGA-PLL nanoparticle for delivering doxorubicin combined with Bcl-2 siRNA as a potential treatment strategy for lung cancer. *Drug Deliv.* 23, 2936–2945. doi: 10.3109/10717544.2015.1126769

Zhao, Y., Wang, W., Guo, S., Wang, Y., Miao, L., Xiong, Y., et al. (2016). PolyMetformin combines carrier and anticancer activities for in vivo siRNA delivery. *Nat. Commun.* 7:11822. doi: 10.1038/ncomms11822

Zhu, D., Tao, W., Zhang, H., Liu, G., Wang, T., Zhang, L., et al. (2016). Docetaxel (DTX)-loaded polydopamine-modified TPGS-PLA nanoparticles as a targeted drug delivery system for the treatment of liver cancer. *Acta Biomater.* 30, 144–154. doi: 10.1016/j.actbio.2015.11.031

Zuckerman, J. E., and Davis, M. E. (2015). Clinical experiences with systemically administered siRNA-based therapeutics in cancer. *Nat. Rev. Drug Discov.* 14, 843–856. doi: 10.1038/nrd4685

Conflict of Interest Statement: The authors declare that the research was conducted in the absence of any commercial or financial relationships that could be construed as a potential conflict of interest.

frontiers in Pharmacology

ORIGINAL RESEARCH
published: 23 January 2019
doi: 10.3389/fphar.2019.00001

Pathway Based Analysis of Mutation Data Is Efficient for Scoring Target Cancer Drugs

Marianna A. Zolotovskaia[1,2], Maxim I. Sorokin[3,4,5], Anna A. Emelianova[5], Nikolay M. Borisov[3,4], Denis V. Kuzmin[5], Pieter Borger[6], Andrew V. Garazha[4] and Anton A. Buzdin[1,3,5]*

[1] Oncobox Ltd., Moscow, Russia, [2] Department of Oncology, Hematology and Radiotherapy of Pediatric Faculty, Pirogov Russian National Research Medical University, Moscow, Russia, [3] The Laboratory of Clinical Bioinformatics, IM Sechenov First Moscow State Medical University, Moscow, Russia, [4] Omicsway Corp., Walnut, CA, United States, [5] Science-Educational Center Department, M. M. Shemyakin and Yu. A. Ovchinnikov Institute of Bioorganic Chemistry, Russian Academy of Sciences, Moscow, Russia, [6] Laboratory of the Swiss Hepato-Pancreato-Biliary, Department of Surgery, Transplantation Center, University Hospital Zurich, Zurich, Switzerland

Despite the significant achievements in chemotherapy, cancer remains one of the leading causes of death. Target therapy revolutionized this field, but efficiencies of target drugs show dramatic variation among individual patients. Personalization of target therapies remains, therefore, a challenge in oncology. Here, we proposed molecular pathway-based algorithm for scoring of target drugs using high throughput mutation data to personalize their clinical efficacies. This algorithm was validated on 3,800 exome mutation profiles from The Cancer Genome Atlas (TCGA) project for 128 target drugs. The output values termed Mutational Drug Scores (MDS) showed positive correlation with the published drug efficiencies in clinical trials. We also used MDS approach to simulate all known protein coding genes as the putative drug targets. The model used was built on the basis of 18,273 mutation profiles from COSMIC database for eight cancer types. We found that the MDS algorithm-predicted hits frequently coincide with those already used as targets of the existing cancer drugs, but several novel candidates can be considered promising for further developments. Our results evidence that the MDS is applicable to ranking of anticancer drugs and can be applied for the identification of novel molecular targets.

Keywords: cancer, DNA mutation, molecular pathways, biomarker, target drugs, tyrosine kinase inhibitors, nibs, mabs

OPEN ACCESS

Edited by:
Zhe-Sheng Chen,
St. John's University, United States

Reviewed by:
Honglin Jiang,
University of California, San Francisco, United States
Nelson Shu-Sang Yee,
Penn State Milton S. Hershey Medical Center, United States

****Correspondence:***
Marianna A. Zolotovskaia
zolotovskaya@oncobox.com

Specialty section:
This article was submitted to Cancer Molecular Targets and Therapeutics, a section of the journal Frontiers in Pharmacology

Received: *07 November 2018*
Accepted: *03 January 2019*
Published: *23 January 2019*

Citation:
Zolotovskaia MA, Sorokin MI, Emelianova AA, Borisov NM, Kuzmin DV, Borger P, Garazha AV and Buzdin AA (2019) Pathway Based Analysis of Mutation Data Is Efficient for Scoring Target Cancer Drugs. Front. Pharmacol. 10:1. doi: 10.3389/fphar.2019.00001

INTRODUCTION

Globally, cancer is one of the major causes of death (Centers for Disease Control and Prevention, 2017). For several decades, chemotherapy remains a key treatment for many cancers, often with impressive success rates. For example, its use in testicular cancer turned near complete mortality to >90% disease-specific survival (Hanna and Einhorn, 2014; Oldenburg et al., 2015). However, most of the advanced cancers remain incurable and/or unresponsive using standard chemotherapy approaches, frequently develop resistance to treatments and relapse (Vasey, 2003; Housman et al., 2014). More recently, a new generation of drugs has been developed that specifically target functional tumor marker molecules. These medicines termed *Target drugs* have one or a few

specific molecular targets in a cell (Druker et al., 2001a,b; Sawyers, 2004; Spirin et al., 2017). They have greater selectivity and generally lower toxicity than the conventional chemotherapy (Joo et al., 2013). Structurally, they can be either low molecular mass inhibitor molecules or monoclonal antibodies (Padma, 2015). The repertoire of their molecular targets is permanently growing and now includes receptor and intracellular tyrosine kinases (Baselga, 2006), vascular endothelial growth factor (Rini, 2009), immune checkpoint molecules such as PD1, PDL1, and CTLA4 (Azoury et al., 2015), poly(ADP-ribose) polymerase (Anders et al., 2010), mTOR inhibitors (Xie et al., 2016), hormone receptors (Ko and Balk, 2004), proteasomal components (Kisselev et al., 2012), ganglioside GD2 (Suzuki and Cheung, 2015), and cancer-specific fusion proteins (Giles et al., 2005). For many cancers, the emergence of target drugs was highly beneficial. For example, trastuzumab (anti-HER2 monoclonal antibody) and other related medications at least doubled median survival time in patients with metastatic HER2-positive breast cancer (Hudis, 2007; Nahta and Esteva, 2007). In melanoma, immune checkpoint inhibitors, and anti-BRAF target drugs like Vemurafenib and Dabrafenib dramatically increased the patient's chances to respond to treatment and to increase survival (Chapman et al., 2011; Prieto et al., 2012). Target drugs were also of a great advantage for inoperable kidney cancer, before almost uncurable (Ghidini et al., 2017).

The efficiencies of target drugs vary from patient to patient (Ma and Lu, 2011) and the results of clinical trials clearly evidence that the drugs considered inefficient for an overall cohort of a given cancer type, may be beneficial for a small fraction of the patients (Zappa and Mousa, 2016). For example, the anti-EGFR drugs gefitinib and erlotinib showed little advantage in the randomized trials on patients with non-small cell lung cancer. However, ∼10-15% of the patients responded to the treatment and had longer survival characteristics. It was further understood that these patients had activating mutations of *EGFR* gene and that these mutations, therefore, can predict response to the EGFR-targeting therapies (Gridelli et al., 2011). Interestingly, the same approach was ineffective in colorectal cancer, where EGFR-mutated status had no predictive power for the anti-EGFR drugs cetuximab and panitumumab. In the latter case, it is the wild-type status of *KRAS* gene (∼60% of all the cases) that is indicative of tumor response to these drugs (Grothey and Lenz, 2012).

The price for inefficient treatment is high as it is converted from decreased patient's survival characteristics and overall clinical expenses. There are currently more than 200 different anticancer target drugs approved in different countries, and this number grows every year (Law et al., 2014). However, the predictive molecular diagnostic tests are available for only a minor fraction of drugs, in a minor fraction of cancer types (Hornberger et al., 2005; Le Tourneau et al., 2014; Buzdin et al., 2018). This makes the clinician's decision on drug prescription a difficult task somewhat similar to finding needle in a haystack. The problem of choosing the right medication for the right patient is currently well understood, so US FDA(Food and Drug Administration) strongly recommends any new target drug emerging on the market to be supplied with the companion diagnostics test[1]. It is, therefore, of a great importance to identify robust predictive biomarkers of target drug efficacy, for as many cancer-drug combinations as possible. Recently, a new generation of molecular markers has been proposed involving gene combinations and even entire molecular pathways (Gu et al., 2011; Li et al., 2014; Toren and Zoubeidi, 2014). Here, the biomarkers used are not just a single gene or single locus-based mutation, expression or epigenetic features, but rather the aggregated combinations of those, crosslinking the physiologically relevant gene products (Diamandis, 2014; Sanchez-Vega et al., 2018; Zaim et al., 2018). The pathway-based approach has been better developed for the high throughput gene expression data (Khatri et al., 2012; Buzdin A. A. et al., 2017; Buzdin et al., 2018) where the *Pathway Activation Strength (PAS*) may be used as an aggregated biomarker (Buzdin et al., 2014). The formulas for *PAS* calculation may be different; they normally consider relative concentrations of gene products, internal molecular architecture of pathways and gene coexpression patterns (Ozerov et al., 2016; Aliper et al., 2017; Buzdin et al., 2018). *PAS* was shown to be more efficient as a biomarker than the individual gene expression data (Borisov et al., 2014, 2017), and *PAS* biomarkers were further generated for a plethora of normal and pathological conditions, including cancer response to treatments (Kurz et al., 2017; Petrov et al., 2017; Spirin et al., 2017; Wirsching et al., 2017; Sorokin et al., 2018).

Furthermore, a method for ranking of more than a 100 of target anticancer drugs has been recently published based on the *PAS* scoring and the pathway enrichments by the molecular targets of drugs (Artemov et al., 2015). This approach termed *Drug Scoring* was experimentally shown promising for drugs prescription to advanced solid tumor patients (Buzdin A. et al., 2017; Buzdin et al., 2018; Poddubskaya et al., 2018). However, good quality expression profiles required for *PAS*-based *Drug Scoring* frequently cannot be obtained due to apparent lack of biopsy biomaterials and RNA degradation. To our knowledge, so far there were no published reports on the application of gene mutation data for *Drug Scoring*.

In this study, for the first time we proposed and tested 10 alternative pathway-based *Drug Scoring* algorithms utilizing mutations data. These algorithms were used for the data from 3,800 published cancer mutation profiles representing eight tumor localizations and validated using the published clinical trials data. We showed that several mutation-based *Drug Scoring* methods can be used efficiently for predicting the effectiveness of target drugs. This has been evidenced by statistically significant positive correlations between *Drug Score* ratings of individual

Abbreviations: CDS length, Coding DNA Sequence Length; COSMIC, Catalog Of Somatic Mutations In Cancer; FDA, Food and Drug Administration; ICGC, International Cancer Genome Consortium; MDS, Mutational Drug Scores; MR, Mutation rate; nMR, Normalized mutation rate; NIH, The National Institutes of Health; PAS, Pathway Activation Strength; PI, Pathway instability; TCGA, The Cancer Genome Atlas; TC, Target Conversion.

[1]For Consumers - Personalized Medicine and Companion Diagnostics Go Hand-in-Hand Available at: https://www.fda.gov/ForConsumers/ucm407328.htm [Accessed October 15, 2018].

drugs and their therapeutic success reflected by the completed phases of clinical trials for the respective cancer types. We also used the best *Drug Scoring* algorithm to simulate all known protein coding genes as the potential drug targets. We found that the algorithm-predicted most efficient targets are highly congruent with the molecular targets already used by the real anticancer drugs.

MATERIALS AND METHODS

Mutation Data

The human mutation dataset was obtained from the Catalog Of Somatic Mutations In Cancer (COSMIC) (Forbes et al., 2017). COSMIC aggregates and annotates mutation data from various sources by providing lists of verified somatic mutations. We downloaded the data from COSMIC website, version 76. The complete dataset includes 6,651,236 somatic mutation records for 20,528 genes in 19,434 tumor samples of 37 primary localizations.

The Algorithm Validation Dataset

For the validation of drug scoring algorithms, we extracted mutation data only for the primary localizations containing at least 100 samples indexed in COSMIC and originally taken from The Cancer Genome Atlas (TCGA) project (Tomczak et al., 2015; Forbes et al., 2017) because of the uniform sequencing and data processing pipeline used there. For the algorithm validation dataset, we totally took 3,800 tumor mutation profiles from eight primary localizations: central nervous system, kidney, large intestine (including cecum, colon, and rectum), liver, lung, ovary, stomach, thyroid gland (**Table 1**).

The COSMIC data were processed with script written in R (version 3.4.3) to obtain mutation profile for each tumor[1]. The processed data is available as **Supplementary Data Sheet 1**.

The Dataset for Prediction of Potential Molecular Targets

We used the full COSMIC dataset to increase the statistical significance and to investigate the effectiveness of potential target drugs for a maximum range of cancer localizations. However, we excluded the samples related to cell cultures or tumor xenograft to standardize the analysis. We excluded records having the following marks in the "Sample source" field: organoid culture, short-term culture, cell-line, xenograft. Thus, the final dataset included 6,027,881 mutations records in 18,273 in tumor samples of 35 primary localizations. The COSMIC data were processed with script written in R (version 3.4.3) to return mutation rates for all genes[2]. The processed data is available as **Supplementary Data Sheet 2**.

TABLE 1 | The structure of algorithm validation dataset.

Localization (COSMIC nomenclature)	Number of samples	Disease, its abbreviation
Central nervous system	657	Gliomas, GL
Kidney	601	Kidney cancer, KC
Large intestine	620	Colorectal cancer, CRC
Liver	188	Hepatic cancer, HC
Lung	569	Non-small cell lung cancer, NSCLC
Ovary	474	Ovarian cancer, OVC
Stomach	288	Stomach cancer, STC
Thyroid	403	Thyroid cancer, THC

Clinical Trials Data

We extracted clinical trials data from the web sites of NIH (the National Institutes of Health)[3] and US FDA[4]. They were processed by manually curation of web data as of July 2017. The processed clinical trials data used for the correlation studies are shown on **Supplementary Table 1**.

Molecular Pathways Data

The gene contents data about 3,125 human molecular pathways used to calculate mutation drug scores were extracted from Reactome (Croft et al., 2014), NCI Pathway Interaction Database (Schaefer et al., 2009), Kyoto Encyclopedia of Genes and Genomes (Kanehisa and Goto, 2000), HumanCyc (Romero et al., 2004), Biocarta (Nishimura, 2001), Qiagen[5]. For drug scores calculation, we used only the 1,752 pathways including at least 10 gene products because of previously reported poor theoretical data aggregation effect for smaller pathways (Borisov et al., 2017). The information about molecular specificities of 128 anticancer target drugs were obtained from databases DrugBank (Law et al., 2014) and ConnectivityMap (Lamb et al., 2006).

Data Presentation

The results were visualized using package ggplot2 (Wickham, 2009).

RESULTS

In this study, we developed a molecular pathway-based method of target drug scoring using high throughput mutation data.

Algorithms of Mutation Drug Scoring

The principle of *Mutation Drug Scoring (MDS)* methods proposed here deals with quantization of mutation enrichment for the molecular pathways having molecular targets of a drug under investigation. Overall, they are based on the rationale that the greater is the mutation level of the respective pathways, the higher will be the expected drug efficiency. The mutation enrichment of a molecular pathway called pathway instability (*PI*) is calculated based on the relative *mutation rates* (*MR*) of its member genes. Under *mutations*, we meant here the changes in protein coding sequence understood as such in the Catalog of Somatic Mutations in Cancer (COSMIC) v.76 database (Forbes et al., 2016). COSMIC is the world's largest database of somatic

[2]Cosmic v76 processing Available at: https://gitlab.com/White_Knight/cosmic76_processing/tree/master [Accessed October 22, 2018].
[3]ClinicalTrials.gov Available at: https://clinicaltrials.gov/ [Accessed July 25, 2017]
[4]U S Food and Drug Administration Home Page Available at: https://www.fda.gov/ [Accessed July 25, 2017].
[5]QIAGEN - Sample to Insight Available at: https://www.qiagen.com/us/shop/genes-and-pathways/pathway-central/ [Accessed September 19, 2018].

mutations relating to human cancers. We used only Genome-wide Screen Data to estimate *MR* correctly. This part of COSMIC consists of peer reviewed large-scale genome screening data and data from the validated sources such as The Cancer Genome Atlas (TCGA) and International Cancer Genome Consortium (ICGC).

Mutation rate (*MR*) is calculated according to the formula:

$$MR_{n,g} = \frac{N\ mut(\ n,g)}{N\ samples\ (g)},$$

where $MR_{n,g}$ is *MR* of a gene *n* in a group of samples *g*; *N mut(n,g)* is the total number of mutations for gene *n* in a group of samples *g*; *N samples (g)* is the number of samples in a group *g*. The *MR* values strongly positively correlated with the lengths of gene coding DNA sequence (CDS; data not shown). In order to remove bias linked with the CDS length, we took for further consideration a normalized value termed *Normalized Mutation Rate* (*nMR*) expressed by the formula:

$$nMR_n = \frac{1000 * MR_n}{Length\ CDS\ (n)},$$

where nMR_n is the *nMR* of a gene *n*; MR_n is the *MR* of a gene *n*; *Length CDS(n)* is the length of CDS of gene *n* in nucleotides. Indeed, normalization of this metric enabled to terminate any CDS-linked bias (data not shown).

To determine if gene *n* is included in pathway *p*, we introduced a Boolean flag *pathway-gene indicator* $PG_{n,p}$ expressed by the formula:

$$PG_{n,p} = \begin{cases} 1, \text{ pathway } p \text{ includes gene } n, \\ 0, \text{ pathway } p \text{ doesn't include gene } n; \end{cases}$$

The *Pathway Instability* (*PI*) score is then calculated as follows:

$$PI_p = \sum\nolimits_n nMR_n PG_{n,p},$$

where PI_p is pathway instability score for a pathway *p*; nMR_n is the *normalized* mutation rate of a gene *n*, $PG_{n,p}$ is pathway-gene indicator for gene *n* and pathway *p*. *Pathway instability score* characterizes the mutation enrichment of a pathway (Pathway instability is an effective new mutation-based type of cancer biomarkers, 2018, in preparation). To formalize if gene *n* is molecular target of drug *d*, we introduced another Boolean flag *drug target index*, $DTI_{d,n}$:

$$\mathrm{DTI_{d,n}} = \begin{cases} 1, \text{ drug } d \text{ has target gene } n, \\ 0, \text{ drug } d \text{ doesn}'\text{t have target gene } n \end{cases}$$

To complete *DTI* database for this study, we used the data about molecular specificities of 128 target drugs extracted from the databases DrugBank (Law et al., 2014) and Connectivity Map (Lamb et al., 2006).

To link *PI* scores and estimated drug efficiencies, the following basic formula was proposed for the calculation of *Mutation Drug Score* (*MDS*):

$$\mathbf{MDS_d} = \sum\nolimits_{\mathbf{n}} \mathbf{DTI_{d,n}} \sum\nolimits_p PG_{n,p}\ PI_p, \quad (1)$$

where *d* is drug name; *n* is gene name; *p* is pathway name; MDS_d is *MDS* for drug *d*; $DTI_{d,n}$ is drug target index for drug *d* and gene *n*; PI_p is *Pathway Instability* of pathway *p*; $PG_{n,p}$ is pathway-gene indicator for gene *n* and pathway *p*.

The above basic formula (*1*) was modified to generate several alternative methods of drug scoring.

- *Pathway size-normalized*. Since molecular pathways include considerably different number of genes varying from dozens to hundreds, we proposed a modification of the calculation method (*1*) where normalization is performed for *MDS* on the respective number of genes for each *PI* member:

$$MDS\_N_d = \sum\nolimits_n \mathbf{DTI_{d,n}} \sum\nolimits_p PG_{n,p}\ PI_p/k_p, \quad (2)$$

where k_p is number of genes in pathway *p*.

- *Single count-normalized*. Impact of each gene participating in pathways targeted by drug *d* is counted only once:

$$\mathbf{MDS\_gene_d} = \sum\nolimits_n \mathbf{nMR}_n\ \mathbf{GII}_{d,n}, \quad (3)$$

where $GII_{d,n}$ – Boolean flag *gene involvement index*,

$$\mathrm{GII}_{d,n} = \begin{cases} 1, \text{ gene } n \text{ participates in at least one pathway targeted by drug } d \\ 0, \text{ gene } n \text{ doesn}'\text{t participate in pathways targeted by drug } d \end{cases}$$

- *Number of pathways-normalized*. *MDS* for drug *d* is normalized on the number of its targeted molecular pathways.

$$\mathbf{MDS\_m_d} = MDS_d/m_\mathbf{d}, \quad (4)$$

where m_d – number of pathways targeted by drug *d*.

- *Number of pathways-normalized*. *MDS_N* is additionally normalized on the number of pathways targeted by drug *d* (m_d).

$$\mathbf{MDS\_N\_m_d} = MDS\_N/m_d \quad (5)$$

- *Number of target genes-normalized*. MDS_b_d is additionally normalized on the number of target genes for drug *d*, (b_d).

$$\mathbf{MDS\_b_d} = MDS_d/b_d \quad (6)$$

- *Number of target genes-normalized MDS_N*. *MDS_N*, normalized on the number of target genes for drug *d*, (b_d).

$$\mathbf{MDS\_N\_b_d} = \mathbf{MDS\_N}/b_d \quad (7)$$

- *Number of target genes-normalized MDS_gene*. *MDS_gene*, normalized on the number of target genes for drug *d*, (b_d).

$$\mathbf{MDS\_gene\_b_d} = MDS\_gene/b_d \quad (8)$$

- *Target genes dependent only*. *MDS2* is calculated considering only mutation frequencies of target genes.

$$\mathbf{MDS2_d} = \sum\nolimits_p PG_{n,p} \sum\nolimits_n \mathbf{DTI_{d,n}} nMR_n \quad (9)$$

- *Single count-normalized, target genes dependent only. MDS2_gene* is calculated, considering each target gene for drug *d* only one time.

$$\mathbf{MDS2\_gene_d} = \sum\nolimits_n \mathbf{DTI_{d,n}}\ NMR_n\ \mathbf{GII}_{d,n} \qquad (10)$$

For these algorithms of mutation-based drug scoring, we next compared their congruences with the published clinical trials data.

Validation of Mutation Drug Scoring (MDS) Algorithms on Clinical Trials Data

We calculated different versions of *MDS* according to formulae (1–10) for 128 anticancer target drugs, for eight cancer types (**Supplementary Data Sheet 3**). We examined somatic mutation profiles for 3,800 samples of the following primary tumor localizations: large intestine (including cecum, colon and rectum), lung, kidney, stomach, ovarian, central nervous system, liver, thyroid (**Table 1**).

Mutation profiles were extracted from COSMIC v76 database (Forbes et al., 2016). To validate the *MDS* algorithms, we selected only tumor samples related to TCGA project because it was the largest source of biosamples profiled using a single deep sequencing and bionformatic pipeline (Tomczak et al., 2015). Molecular specificities of drugs were obtained from DrugBank (Law et al., 2014) and Connectivity Map (Lamb et al., 2006) databases. The information about clinical approval and the completion of phases of clinical trials for 128 target drugs for the above eight tumor localizations was taken from the web sites of NIH and US FDA. To measure completion of clinical investigations for a drug, we introduced the metric termed *Clinical Status*. These values are congruent with the apparent efficiencies of drugs for the given cancer types. The same drugs most frequently had different clinical statuses for the different cancer types.

The *Clinical Status* varied in a range from 0 to 1 proportional to the top phase of clinical trials passed by a drug for a given cancer type. The *Clinical Status* grows incrementally depending on the completion of the clinical trials phases 1–4, while the later phases have a greater specific weight, because they allow to more accurately determine clinical efficacy of a drug (**Table 2**).

TABLE 2 | Clinical Status of drug, according of the top passed phases of clinical trials.

Phase of clinical trials	Clinical status
Phase I ongoing	0.1
Phase I/II ongoing (Phase I completed)	0.2
Phase II ongoing	0.3
Phase II completed	0.4
Phase III ongoing	0.7
Phase III completed	0.85
Phase IV (drug approved and marketed)	1

The complete *Clinical Status* information for 128 drugs under investigation is shown on **Supplementary Table 1**. The major limitation of this approach is that only the drugs that had been already clinically investigated for the respective tumor type can be ranked in such a way.

To investigate the capacities of different versions of *Mutation Drug Scores* to successfully predicts clinical efficiencies of drugs, we analyzed how ranks of *MDS* values correlated with Clinical Status of drugs. We calculated correlations and compared distributions of the Spearman correlation coefficients. To calculate correlations, we took all cancer mutation profiles together without separation on cancer types (**Figure 1**).

Overall, the markedly better correlations were seen for the *MDS* and *MDS_N* types of drug scoring (**Figure 1**). We next analyzed the cancer type-specific distributions (**Figure 2**). It was seen that both *MDS* and *MDS_N* scores positively correlated with the drugs clinical efficiencies in all the localizations investigated, thus confirming their top status among the drug scoring algorithms. Among those, *MDS* showed best overall

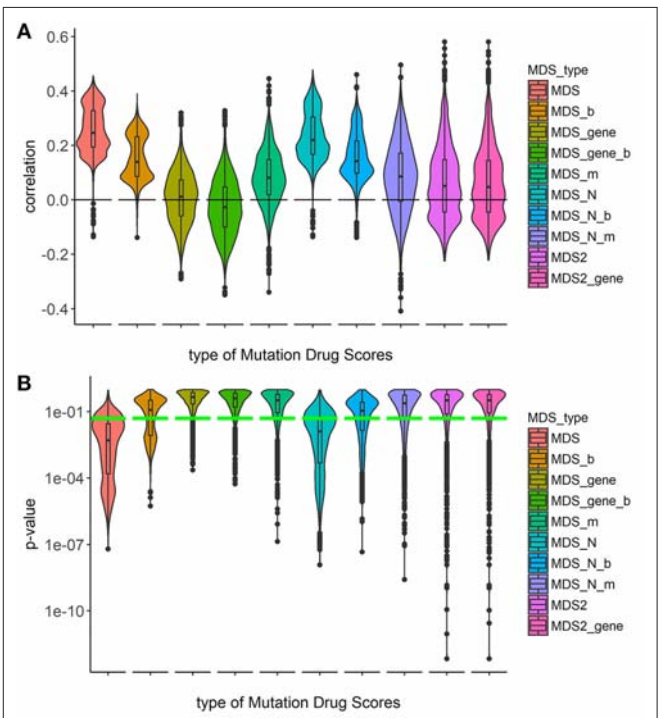

FIGURE 1 | Correlation between Clinical Status and MDS rank for 10 types of drug scoring in eight cancer types at once. **(A)** Distributions of Spearman correlation coefficients between Clinical Status and MDS rank for 128 target drugs in 3,800 tumor samples. MDS rank of a drug was calculated as the individual drug's position in the rating (from top to low) of all drugs under investigation. Ten violin plots distributed along X-axis, each represent a particular type of drug scoring. The Y-axis reflects density distributions of correlations between Clinical Status and MDS ranks. Boxes indicate the second and third quartiles of distribution, black dots indicate outliers. **(B)** The plot demonstrates the distributions of *p*-value for the correlation coefficients between Clinical Status and MDS rank for 128 target drugs in the same tumor samples. The horizontal green line corresponds to $p = 0.05$.

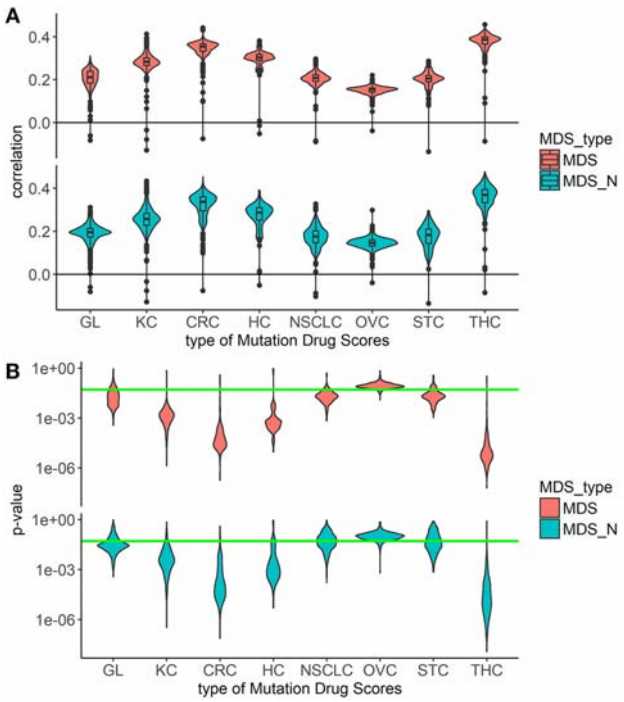

FIGURE 2 | Correlation between Clinical Status and MDS rank for two best types of drug scoring in eight cancer types separately. **(A)** Distributions of Spearman correlation coefficients between Clinical Status and MDS rank for 128 target drugs in eight tumor types. MDS rank of a drug was calculated as the drug's position in the rating (from top to low) of all drugs under study. The drug scoring methods are shown in horizontal lines, and the cancer types are placed vertically. The violin plots distributed along X-axis, each represent a particular cancer type. The Y-axis reflects density distributions of correlations between Clinical Status and MDS ranks. Boxes indicate the second and third quartiles of distribution, black dots indicate outliers. **(B)** The plot shows the distributions of *p*-value for the correlation coefficients between Clinical Status and MDS rank for 128 target drugs in the same tumor types. The horizontal green line corresponds to $p = 0.05$.

functional characteristics and was, therefore, used in further analyses.

Application of MDS for Identification of Possible Target Genes

We next tested the *MDS* algorithm for its capacity to identify potentially valuable drug targets. To this end, we modeled a situation when each gene specifically corresponds to one target drug. Those simulated, or virtual drugs, also were specific each to only one gene product. Using the database of 1,752 molecular pathways, we were able to calculate *MDS* for 8,736 *virtual drugs* specific to the same number of genes included in these pathways. For this analysis, we used 18,273 full-exome tumor mutation profiles from the COSMIC v76 database. Top 30 molecular targets with highest *MDS* values and already clinically approved cancer drugs specific for these molecular targets are listed on **Table 3**. The complete *MDS* calculation data are given in **Supplementary Table 2**.

We next ranked all the *virtual* drugs according to their *MDS* values and compared if the same molecular targets are already exploited by the *existing* 128 target cancer drugs (**Figure 3**).

TABLE 3 | Top 30 molecular targets sorted by MDS and clinically approved drugs using these molecular targets.

Potential molecular targets	MDS	Existing relevant drugs
PIK3CA	387.11	Idelalisib
PIK3R1	371.31	
MAPK1	354.75	
MAPK3	343.81	
HRAS	343.66	
PIK3CB	313.02	Idelalisib
AKT1	305.54	Perifosine
PIK3R2	302.74	
PIK3CD	293.15	Idelalisib
KRAS	291.42	
PIK3R3	290.07	
MAP2K1	288.80	Binimetinib, cobimetinib, selumetinib, trametinib
NRAS	287.90	
PIK3R5	279.34	
RAF1	271.72	Dabrafenib, regorafenib, sorafenib
MAPK8	267.73	
MAP2K2	257.33	Binimetinib, cobimetinib, selumetinib, trametinib
TP53	255.89	
GRB2	254.36	
SOS1	243.39	
RAC1	239.32	
MAPK9	233.01	
EGFR	232.80	Afatinib, brigatinib, cetuximab, erlotinib, flavopiridol, foretinib, gefitinib, lapatinib, masitinib, nimotuzumab, osimertinib, panitumumab, vandetanib, necitumumab
MAPK14	224.08	
MAPK10	222.51	
EGF	214.20	
RELA	212.43	
PRKCA	211.99	
NFKB1	211.63	Thalidomide
AKT2	205.38	Perifosine

To do this, we introduced an auxiliary value termed *Target Conversion* (*TC*). It reflects the percentage share of *known* molecular targets among *predicted* molecular targets.

$$\mathbf{TC} = \frac{\textbf{\textit{number of known}} \textbf{ molecular targets}}{\textbf{\textit{number of predicted}} \textbf{ molecular targets}} * \mathbf{100\%}$$

For the overall (complete) list of potential molecular targets, *TC* was 2.17%. However, there was an clear-cut incremental *TC* growth trend when the potential molecular targets were sorted in the ascending order of *MDS* value (**Figure 3A**, shown for deciles of the potential targets). The greater *TC* value exceeding 10% was

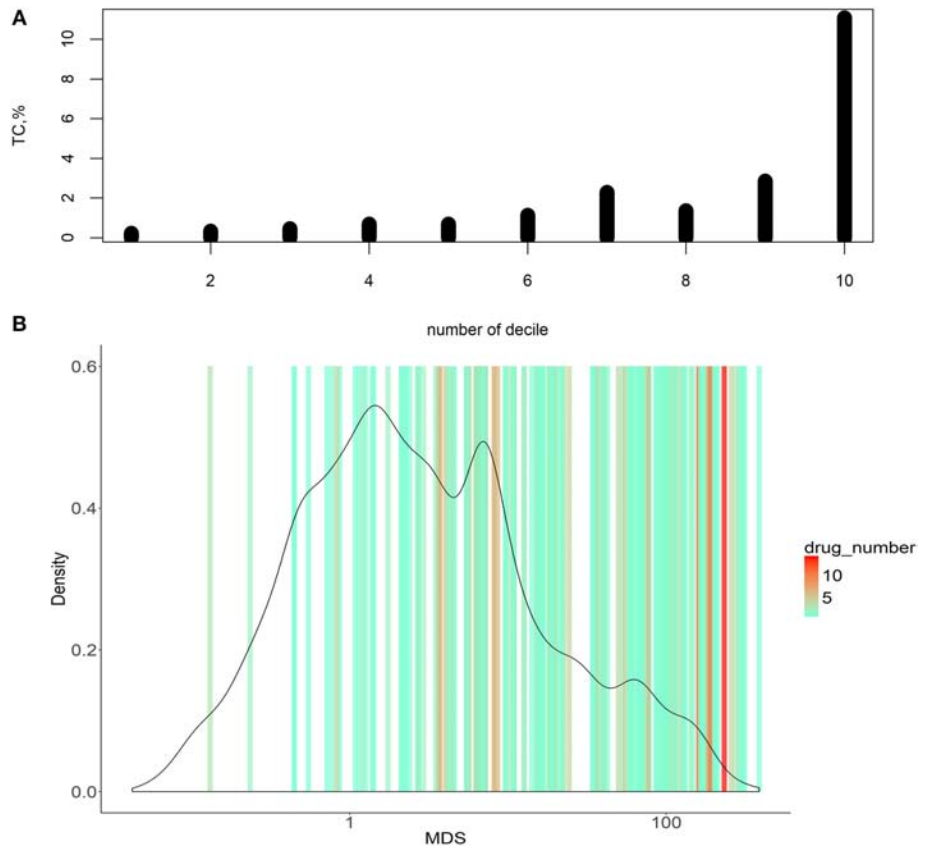

FIGURE 3 | Dependence of MDS and occurrence of molecular targets in approved cancer drugs. **(A)** Deciles of potential molecular targets sorted in ascending order according to MDS value. TC was calculated for each decile, shown on vertical axes. **(B)** Distribution of MDS values among the potential molecular drug targets. The color scale on the graph indicates densities of clinically approved cancer drugs exploiting the respective molecular targets.

observed for the decile of molecular targets having the highest *MDS* values.

Molecular targets with the highest *MDS* are clearly enriched by the existing clinically approved drugs compared to those with low *MDS* scores (**Figure 3A**). On the other hand, target genes with higher *MDS* are covered by a bigger number of approved drugs per target, as many drugs have common molecular specificities (**Figure 3B**).

The present algorithm for scoring potential drug targets considers a cumulative mutation enrichment of molecular pathways. For the example shown on **Figure 4** (Nectin adhesion pathway), most genes involved in a pathway are mutated in cancers, see the color scale. The mutation enrichment of a pathway may characterize its overall involvement in malignization. According to the present conception of drug scoring, the maximum efficiency of drug can be obtained by acting on the most strongly affected molecular pathways.

DISCUSSION

In this study, we report a new bioinformatic instrument of ranking target anticancer drugs using high throughput gene mutation data. We proposed here 10 different versions of molecular pathway-based *mutation drug scoring*. At least two types of this scoring could provide output data positively correlated with the clinical trials data for 128 drugs in all eight tumor localizations tested. We hope that the pathway-based mutation drug scoring approach has a potential of helping clinical oncologists to implement personalized selection of target drugs based on the individual, the patient's tumor-specific high throughput mutation profile.

We showed that the same approach can be applied to identify potentially efficient molecular targets in experimental oncology. The educated choice of new drug targets is one of the main tasks in pharmacology (Schenone et al., 2013). Experimental search for new efficient drug targets is still time consuming, laborious, and expensive (Haggarty et al., 2003), so since recently a credit is frequently given to computational predictive algorithms (Rifaioglu et al., 2018).

The history of computational prediction of drug targets began with prediction of druggability based on the structure of targets and biomedical text mining (Cheng et al., 2007; Zhu et al., 2007). Several methods have been also proposed based on known links between drugs and genes (Luo et al., 2017). Further development of bioinformatic methods allowed to apply for this task a set of systems approaches based on networks of molecular interactions (Mani et al., 2008).

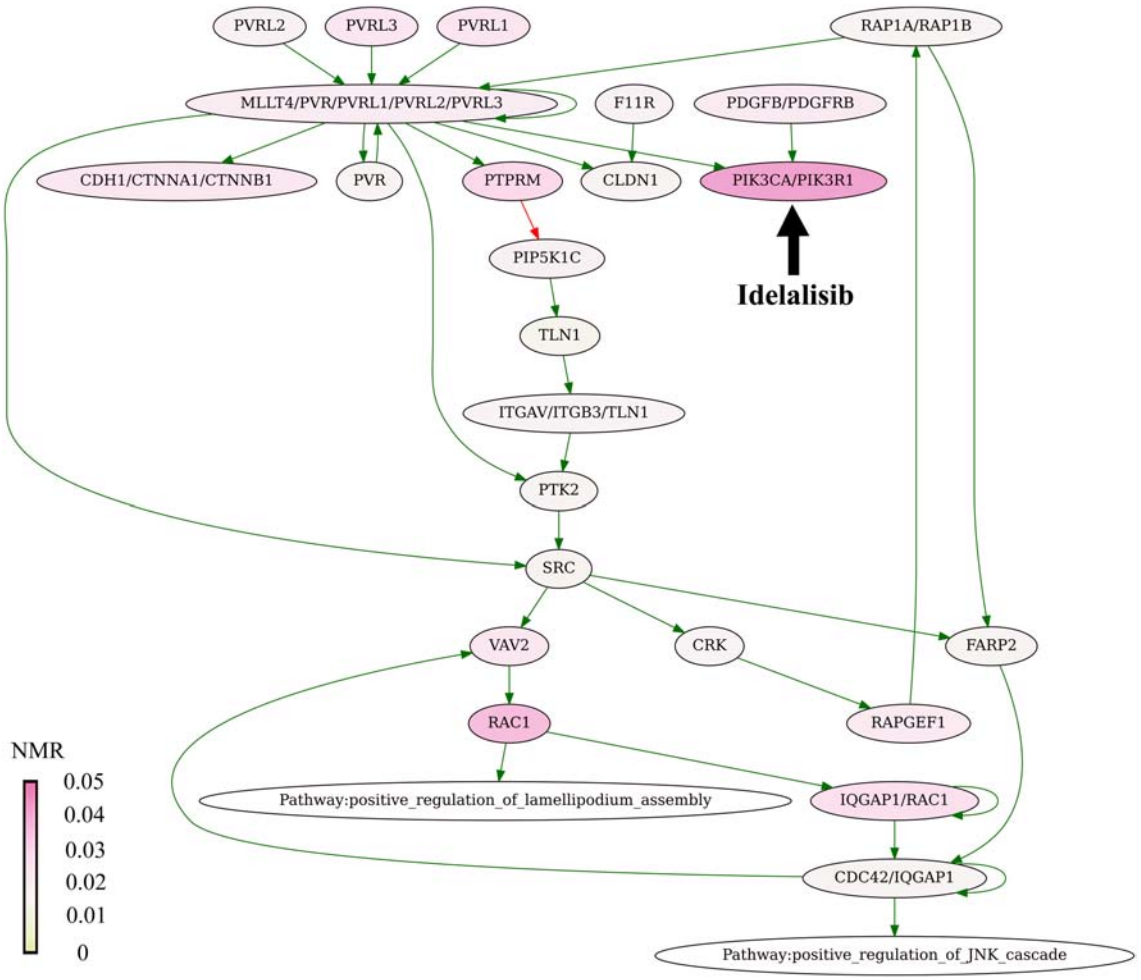

FIGURE 4 | Mutation enrichment of Nectin adhesion pathway. The pathway is targeted by Idelalisib. The pathway structure is taken from the NCI database (Schaefer et al., 2009). The mutation burden was visualized using Oncobox pathway plot tool. The color scale reflects mutation levels of the corresponding nodes on the pathway graph. The green arrows indicate activation, red arrow—inhibition, bold black arrow indicates molecular target of Idelalisib.

Our results provide principal evidence that the mutation drug scoring is applicable to ranking of anticancer drugs. On the other hand, our data suggest that these drug scoring algorithms can be applied for the identification of novel molecular targets for the prospective anticancer drugs. Although many genes with high *MDS* already serve as molecular targets of the approved cancer drugs, there is a number of top *MDS* genes that are not yet covered by the existing medications. This latter fraction of genes, therefore, can be considered a source of potential targets for new drug developments. For example, the following top 100 *MDS* genes can be mentioned that are not yet covered by approved or experimental cancer or antineoplastic drugs [according to DrugBank (Law et al., 2014), DGIdb (Cotto et al., 2018), FDA[6], HMDB (Wishart et al., 2018), Tocris[7], GeneCards (Safran et al., 2010) databases]: *GRB2, SOS1,SOS2, SHC1, GNB1, CREB1, GNG2, GNAQ, GNB5, GNAI2. Three* of them (*GRB2, GNG2, CREB1*) are the targets of approved non-oncological drugs (Pegademase bovine, Naloxone, Adenosine monophosphate, Citalopram, Halothane), thus illustrating *MDS* method potential in drug repurposing.

This study can be regarded as proof-of concept trial of *MDS* approach exemplified by bigger proportion of real cancer targets among the genes with higher *MDS* values. In this application, we assessed integral *MDS* for all cancer types. However, in further applications the same approach can be used for any specific tumor type or subtype to identify targets that may seem most promising for this particular disease. This could be valuable, for example, for drugs repurposing among the different tumor types and for more effectively identifying the patient cohorts in clinical trials

The present mutation drug scoring approach scores the molecular pathway instability caused by accumulation of mutations and ranks drugs according to a simple rationale—the higher is mutation burden of a pathway, the greater may be the efficiency of a drug targeting this pathway. We hope

[6]U S Food and Drug Administration Home Page Available at: https://www.fda.gov/ [Accessed July 25, 2017].

[7]Tocris Bioscience Available at: https://www.tocris.com/ [Accessed December 21, 2018].

these findings will be interesting to those working in the fields of oncology, drug discovery, systems biomedicine, high throughput mutation data analysis, personalized medicine and molecular diagnostics.

DATA AVAILABILITY STATEMENT

The datasets analyzed for this study can be found in the COSMIC repository (COSMICv76; CosmicGenomeScreensMutantExport.tsv.gz, https://cancer.sanger.ac.uk/cosmic/download).

AUTHOR CONTRIBUTIONS

MZ developed algorithms, did mutation drug scoring analyses, planned the research and wrote the manuscript. PB planned the research, extracted and filtered cancer mutation data. AG planned the research and developed algorithms. MS completed the molecular pathway database. DK completed and processed Clinical Status database. AE organized the information about molecular specificities of anticancer target drugs. NB developed algorithms, did statistical analyses, and planned the research. AB completed Clinical Status database, developed algorithms, planned the research, and wrote the manuscript.

FUNDING

This study was supported by the Oncobox research program in digital oncology, by the Russian Science Foundation grant no. 18-15-00061, by Amazon and Microsoft Azure grants for cloud-based computational facilities for this project.

SUPPLEMENTARY MATERIAL

The Supplementary Material for this article can be found online at: https://www.frontiersin.org/articles/10.3389/fphar.2019.00001/full#supplementary-material

Supplementary Data Sheet 1 | Mutation profiles for 3800 TCGA tumor samples obtained from COSMIC v76.

Supplementary Data Sheet 2 | Normalized mutation rate for genes that mutated in 18273 tumor samples from COSMIC v76.

Supplementary Data Sheet 3 | Mutation drug scores for 3800 TCGA tumor samples for 10 versions of drug scoring algorithm. The dataset contains 10 tables that match the 10 methods of drug scoring.

Supplementary Table 1 | The complete clinical status information for 128 target drugs in eight cancer localizations.

Supplementary Table 2 | Mutation Drug Scores for 8736 virtual drugs specific to the same number of genes.

REFERENCES

Aliper, A. M., Korzinkin, M. B., Kuzmina, N. B., Zenin, A. A., Venkova, L. S., Smirnov, P. Y., et al. (2017). Mathematical justification of expression-based pathway activation scoring (PAS). *Methods Mol. Biol.* 1613, 31–51. doi: 10.1007/978-1-4939-7027-8_3

Anders, C. K., Winer, E. P., Ford, J. M., Dent, R., Silver, D. P., Sledge, G. W., et al. (2010). Poly(ADP-Ribose) polymerase inhibition: andquot;targetedandquot; therapy for triple-negative breast cancer. *Clin. Cancer Res.* 16, 4702–4710. doi: 10.1158/1078-0432.CCR-10-0939

Artemov, A., Aliper, A., Korzinkin, M., Lezhnina, K., Jellen, L., Zhukov, N., et al. (2015). A method for predicting target drug efficiency in cancer based on the analysis of signaling pathway activation. *Oncotarget* 6, 29347–29356. doi: 10.18632/oncotarget.5119

Azoury, S. C., Straughan, D. M., and Shukla, V. (2015). Immune checkpoint inhibitors for cancer therapy: clinical efficacy and safety. *Curr. Cancer Drug Targets* 15, 452–462. doi: 10.2174/1568009615061508051 45120

Baselga, J. (2006). Targeting tyrosine kinases in cancer: the second wave. *Science* 312, 1175–1178. doi: 10.1126/science.1125951

Borisov, N., Suntsova, M., Sorokin, M., Garazha, A., Kovalchuk, O., Aliper, A., et al. (2017). Data aggregation at the level of molecular pathways improves stability of experimental transcriptomic and proteomic data. *Cell Cycle* 16, 1810–1823. doi: 10.1080/15384101.2017.1361068

Borisov, N. M., Terekhanova, N. V., Aliper, A. M., Venkova, L. S., Smirnov, P. Y., Roumiantsev, S., et al. (2014). Signaling pathways activation profiles make better markers of cancer than expression of individual genes. *Oncotarget* 5, 10198–10205. doi: 10.18632/oncotarget.2548

Buzdin, A., Sorokin, M., Garazha, A., Sekacheva, M., Kim, E., Zhukov, N., et al. (2018). Molecular pathway activation - new type of biomarkers for tumor morphology and personalized selection of target drugs. *Semin. Cancer Biol.* 53, 110–124. doi: 10.1016/j.semcancer.2018.06.003

Buzdin, A., Sorokin, M., Glusker, A., Garazha, A., Poddubskaya, E., Shirokorad, V., et al. (2017). Activation of intracellular signaling pathways as a new type of biomarkers for selection of target anticancer drugs. *J. Clin. Oncol.* 35:e23142. doi: 10.1200/JCO.2017.35.15_suppl.e23142

Buzdin, A. A., Prassolov, V., Zhavoronkov, A. A., and Borisov, N. M. (2017). Bioinformatics meets biomedicine: oncofinder, a quantitative approach for interrogating molecular pathways using gene expression data. *Methods Mol. Biol.* 1613, 53–83. doi: 10.1007/978-1-4939-7027-8_4

Buzdin, A. A., Zhavoronkov, A. A., Korzinkin, M. B., Venkova, L. S., Zenin, A. A., Smirnov, P. Y., et al. (2014). Oncofinder, a new method for the analysis of intracellular signaling pathway activation using transcriptomic data. *Front. Genet.* 5:55. doi: 10.3389/fgene.2014.00055

Centers for Disease Control and Prevention (2017). *Leading Causes of Death and Numbers of Deaths, by Sex, Race, and Hispanic Origin: United States, 1980 and 2016.*

Chapman, P. B., Hauschild, A., Robert, C., Haanen, J. B., Ascierto, P., Larkin, J., et al. (2011). Improved survival with vemurafenib in melanoma with BRAF V600E mutation. *N. Engl. J. Med.* 364, 2507–2516. doi: 10.1056/NEJMoa1103782

Cheng, A. C., Coleman, R. G., Smyth, K. T., Cao, Q., Soulard, P., Caffrey, D. R., et al. (2007). Structure-based maximal affinity model predicts small-molecule druggability. *Nat. Biotechnol.* 25, 71–75. doi: 10.1038/nbt1273

Cotto, K. C., Wagner, A. H., Feng, Y. Y., Kiwala, S., Coffman, A. C., Spies, G., et al. (2018). DGIdb 3.0: a redesign and expansion of the drug–gene interaction database. *Nucleic Acids Res.* 46, D1068–D1073. doi: 10.1093/nar/gkx1143

Croft, D., Mundo, A. F., Haw, R., Milacic, M., Weiser, J., Wu, G., et al. (2014). The reactome pathway knowledgebase. *Nucleic Acids Res.* 42, D472–D477. doi: 10.1093/nar/gkt1102

Diamandis, E. P. (2014). Towards identification of true cancer biomarkers. *BMC Med.* 12:156. doi: 10.1186/s12916-014-0156-8

Druker, B. J., Sawyers, C. L., Kantarjian, H., Resta, D. J., Reese, S. F., Ford, J. M., et al. (2001a). Activity of a specific inhibitor of the BCR-ABL tyrosine kinase in the blast crisis of chronic myeloid leukemia and acute lymphoblastic leukemia with the Philadelphia chromosome. *N. Engl. J. Med.* 344, 1038–1042. doi: 10.1056/NEJM200104053441402

Druker, B. J., Talpaz, M., Resta, D. J., Peng, B., Buchdunger, E., Ford, J. M., et al. (2001b). Efficacy and safety of a specific inhibitor of the BCR-ABL tyrosine kinase in chronic myeloid leukemia. *N. Engl. J. Med.* 344, 1031–1037. doi: 10.1056/NEJM200104053441401

Forbes, S. A., Beare, D., Bindal, N., Bamford, S., Ward, S., Cole, C. G., et al. (2016). COSMIC: high-resolution cancer genetics using the catalogue of somatic mutations in cancer. *Curr. Protoc. Hum. Genet.* 91, 10.11.1–10.11.37. doi: 10.1002/cphg.21

Forbes, S. A., Beare, D., Boutselakis, H., Bamford, S., Bindal, N., Tate, J., et al. (2017). COSMIC: somatic cancer genetics at high-resolution. *Nucleic Acids Res.* 45, D777–D783. doi: 10.1093/nar/gkw1121

Ghidini, M., Petrelli, F., Ghidini, A., Tomasello, G., Hahne, J. C., Passalacqua, R., et al. (2017). Clinical development of mTor inhibitors for renal cancer. *Expert Opin. Investig. Drugs* 26, 1229–1237. doi: 10.1080/13543784.2017.1384813

Giles, F. J., Cortes, J. E., and Kantarjian, H. M. (2005). Targeting the kinase activity of the BCR-ABL fusion protein in patients with chronic myeloid leukemia. *Curr. Mol. Med.* 5, 615–623. doi: 10.2174/156652405774641115

Gridelli, C., De Marinis, F., Di Maio, M., Cortinovis, D., Cappuzzo, F., and Mok, T. (2011). Gefitinib as first-line treatment for patients with advanced non-small-cell lung cancer with activating epidermal growth factor receptor mutation: review of the evidence. *Lung Cancer* 71, 249–257. doi: 10.1016/j.lungcan.2010.12.008

Grothey, A., and Lenz, H. J. (2012). Explaining the unexplainable: EGFR antibodies in colorectal cancer. *J. Clin. Oncol.* 30, 1735–1737. doi: 10.1200/JCO.2011.40.4194

Gu, Y., Zhao, W., Xia, J., Zhang, Y., Wu, R., Wang, C., et al. (2011). Analysis of pathway mutation profiles highlights collaboration between cancer-associated superpathways. *Hum. Mutat.* 32, 1028–1035. doi: 10.1002/humu.21541

Haggarty, S. J., Koeller, K. M., Wong, J. C., Butcher, R. A., and Schreiber, S. L. (2003). Multidimensional chemical genetic analysis of diversity-oriented synthesis-derived deacetylase inhibitors using cell-based assays. *Chem. Biol.* 10, 383–396. doi: 10.1016/S1074-5521(03)00095-4

Hanna, N., and Einhorn, L. H. (2014). Testicular cancer: a reflection on 50 years of discovery. *J. Clin. Oncol.* 32, 3085–3092. doi: 10.1200/JCO.2014.56.0896

Hornberger, J., Cosler, L. E., and Lyman, G. H. (2005). Economic analysis of targeting chemotherapy using a 21-gene RT-PCR assay in lymph-node-negative, estrogen-receptor-positive, early-stage breast cancer. *Am. J. Manag. Care* 11, 313–324.

Housman, G., Byler, S., Heerboth, S., Lapinska, K., Longacre, M., Snyder, N., et al. (2014). Drug resistance in cancer: an overview. *Cancers* 6, 1769–1792. doi: 10.3390/cancers6031769

Hudis, C. A. (2007). Trastuzumab — mechanism of action and use in clinical practice. *N. Engl. J. Med.* 357, 39–51. doi: 10.1056/NEJMra043186

Joo, W. D., Visintin, I., and Mor, G. (2013). Targeted cancer therapy–are the days of systemic chemotherapy numbered? *Maturitas* 76, 308–314. doi: 10.1016/j.maturitas.2013.09.008

Kanehisa, M., and Goto, S. (2000). KEGG: kyoto encyclopedia of genes and genomes. *Nucleic Acids Res.* 28, 27–30. doi: 10.1093/nar/28.1.27

Khatri, P., Sirota, M., and Butte, A. J. (2012). Ten years of pathway analysis: current approaches and outstanding challenges. *PLoS Comput. Biol.* 8:e1002375. doi: 10.1371/journal.pcbi.1002375

Kisselev, A. F., van der Linden, W. A., and Overkleeft, H. S. (2012). Proteasome inhibitors: an expanding army attacking a unique target. *Chem. Biol.* 19, 99–115. doi: 10.1016/j.chembiol.2012.01.003

Ko, Y. J., and Balk, S. P. (2004). Targeting steroid hormone receptor pathways in the treatment of hormone dependent cancers. *Curr. Pharm. Biotechnol.* 5, 459–470. doi: 10.2174/1389201043376616

Kurz, S., Thieme, R., Amberg, R., Groth, M., Jahnke, H. G., Pieroh, P., et al. (2017). The anti-tumorigenic activity of A2M-A lesson from the naked mole-rat. *PLoS ONE* 12:e0189514. doi: 10.1371/journal.pone.0189514

Lamb, J., Crawford, E. D., Peck, D., Modell, J. W., Blat, I. C., Wrobel, M. J., et al. (2006). The connectivity map: using gene-expression signatures to connect small molecules, genes, and disease. *Science* 313, 1929–1935. doi: 10.1126/science.1132939

Law, V., Knox, C., Djoumbou, Y., Jewison, T., Guo, A. C., Liu, Y., et al. (2014). DrugBank 4.0: shedding new light on drug metabolism. *Nucleic Acids Res.* 42, D1091–D1097. doi: 10.1093/nar/gkt1068

Le Tourneau, C., Paoletti, X., Servant, N., Bièche, I., Gentien, D., Rio Frio, T., et al. (2014). Randomised proof-of-concept phase II trial comparing targeted therapy based on tumour molecular profiling vs conventional therapy in patients with refractory cancer: results of the feasibility part of the SHIVA trial. *Br. J. Cancer* 111, 17–24. doi: 10.1038/bjc.2014.211

Li, H., Zeng, J., and Shen, K. (2014). PI3K/AKT/mTOR signaling pathway as a therapeutic target for ovarian cancer. *Arch. Gynecol. Obstet.* 290, 1067–1078. doi: 10.1007/s00404-014-3377-3

Luo, Y., Zhao, X., Zhou, J., Yang, J., Zhang, Y., Kuang, W., et al. (2017). A network integration approach for drug-target interaction prediction and computational drug repositioning from heterogeneous information. *Nat. Commun.* 8:573. doi: 10.1038/s41467-017-00680-8

Ma, Q., and Lu, A. Y. (2011). Pharmacogenetics, pharmacogenomics, and individualized medicine. *Pharmacol. Rev.* 63, 437–459. doi: 10.1124/pr.110.003533

Mani, K. M., Lefebvre, C., Wang, K., Lim, W. K., Basso, K., Dalla-Favera, R., et al. (2008). A systems biology approach to prediction of oncogenes and molecular perturbation targets in B-cell lymphomas. *Mol. Syst. Biol.* 4:169. doi: 10.1038/msb.2008.2

Nahta, R., and Esteva, F. J. (2007). Trastuzumab: triumphs and tribulations. *Oncogene* 26, 3637–3643. doi: 10.1038/sj.onc.1210379

Nishimura, D. (2001). BioCarta. *Biotech. Softw. Internet Rep.* 2, 117–120. doi: 10.1089/152791601750294344

Oldenburg, J., Aparicio, J., Beyer, J., Cohn-Cedermark, G., Cullen, M., Gilligan, T., et al. (2015). Personalizing, not patronizing: the case for patient autonomy by unbiased presentation of management options in stage I testicular cancer. *Ann. Oncol.* 26, 833–838. doi: 10.1093/annonc/mdu514

Ozerov, I. V., Lezhnina, K. V., Izumchenko, E., Artemov, A. V., Medintsev, S., Vanhaelen, Q., et al. (2016). *In silico* pathway activation network decomposition analysis (iPANDA) as a method for biomarker development. *Nat. Commun.* 7:13427. doi: 10.1038/ncomms13427

Padma, V. V. (2015). An overview of targeted cancer therapy. *BioMedicine* 5:19. doi: 10.7603/s40681-015-0019-4

Petrov, I., Suntsova, M., Ilnitskaya, E., Roumiantsev, S., Sorokin, M., Garazha, A., et al. (2017). Gene expression and molecular pathway activation signatures of MYCN-amplified neuroblastomas. *Oncotarget* 8, 83768–83780. doi: 10.18632/oncotarget.19662

Poddubskaya, E. V., Baranova, M. P., Allina, D. O., Smirnov, P. Y., Albert, E. A., Kirilchev, A. P., et al. (2018). Personalized prescription of tyrosine kinase inhibitors in unresectable metastatic cholangiocarcinoma. *Exp. Hematol. Oncol.* 7:21. doi: 10.1186/s40164-018-0113-x

Prieto, P. A., Yang, J. C., Sherry, R. M., Hughes, M. S., Kammula, U. S., White, D. E., et al. (2012). CTLA-4 blockade with ipilimumab: long-term follow-up of 177 patients with metastatic melanoma. *Clin. Cancer Res.* 18, 2039–2047. doi: 10.1158/1078-0432.CCR-11-1823

Rifaioglu, A. S., Atas, H., Martin, M. J., Cetin-Atalay, R., Atalay, V., and Dogan, T. (2018). Recent applications of deep learning and machine intelligence on in silico drug discovery: methods, tools and databases. *Brief. Bioinform.* doi: 10.1093/bib/bby061. [Epub ahead of print].

Rini, B. I. (2009). Vascular endothelial growth factor-targeted therapy in metastatic renal cell carcinoma. *Cancer* 115, 2306–2312. doi: 10.1002/cncr.24227

Romero, P., Wagg, J., Green, M. L., Kaiser, D., Krummenacker, M., and Karp, P. D. (2004). Computational prediction of human metabolic pathways from the complete human genome. *Genome Biol.* 6:R2. doi: 10.1186/gb-2004-6-1-r2

Safran, M., Dalah, I., Alexander, J., Rosen, N., Iny Stein, T., Shmoish, M., et al. (2010). GeneCards Version 3: the human gene integrator. *Database* 2010:baq020. doi: 10.1093/database/baq020

Sanchez-Vega, F., Mina, M., Armenia, J., Chatila, W. K., Luna, A., La, K. C., et al. (2018). Oncogenic signaling pathways in the cancer genome atlas. *Cell* 173, 321–337.e10. doi: 10.1016/j.cell.2018.03.035

Sawyers, C. (2004). Targeted cancer therapy. *Nature* 432, 294–297. doi: 10.1038/nature03095

Schaefer, C. F., Anthony, K., Krupa, S., Buchoff, J., Day, M., Hannay, T., et al. (2009). PID: the pathway interaction database. *Nucleic Acids Res.* 37, D674–D679. doi: 10.1093/nar/gkn653

Schenone, M., Dancík, V., Wagner, B. K., and Clemons, P. A. (2013). Target identification and mechanism of action in chemical biology and drug discovery. *Nat. Chem. Biol.* 9, 232–240. doi: 10.1038/nchembio.1199

Sorokin, M., Kholodenko, R., Grekhova, A., Suntsova, M., Pustovalova, M., Vorobyeva, N., et al. (2018). Acquired resistance to tyrosine kinase inhibitors

may be linked with the decreased sensitivity to X-ray irradiation. *Oncotarget* 9, 5111–5124. doi: 10.18632/oncotarget.23700

Spirin, P., Lebedev, T., Orlova, N., Morozov, A., Poymenova, N., Dmitriev, S. E., et al. (2017). Synergistic suppression of t(8;21)-positive leukemia cell growth by combining oridonin and MAPK1/ERK2 inhibitors. *Oncotarget* 8, 56991–57002. doi: 10.18632/oncotarget.18503

Suzuki, M., and Cheung, N. K. (2015). Disialoganglioside GD2 as a therapeutic target for human diseases. *Expert Opin. Ther. Targets* 19, 349–362. doi: 10.1517/14728222.2014.986459

Tomczak, K., Czerwinska, P., and Wiznerowicz, M. (2015). The cancer genome atlas (TCGA): an immeasurable source of knowledge. *Contemp. Oncol.* 19, A68–77. doi: 10.5114/wo.2014.47136

Toren, P., and Zoubeidi, A. (2014). Targeting the PI3K/Akt pathway in prostate cancer: challenges and opportunities (Review). *Int. J. Oncol.* 45, 1793–1801. doi: 10.3892/ijo.2014.2601

Vasey, P. A. (2003). Resistance to chemotherapy in advanced ovarian cancer: mechanisms and current strategies. *Br. J. Cancer* 89, S23–S28. doi: 10.1038/sj.bjc.6601497

Wickham, H. (2009). *Ggplot2 : Elegant Graphics for Data Analysis*. New York, NY: Springer-Verlag.

Wirsching, A., Melloul, E., Lezhnina, K., Buzdin, A. A., Ogunshola, O. O., Borger, P., et al. (2017). Temporary portal vein embolization is as efficient as permanent portal vein embolization in mice. *Surgery* 162, 68–81. doi: 10.1016/j.surg.2017.01.032

Wishart, D. S., Feunang, Y. D., Marcu, A., Guo, A. C., Liang, K., Vázquez-Fresno, R., et al. (2018). HMDB 4.0: the human metabolome database for 2018. *Nucleic Acids Res.* 46, D608–D617. doi: 10.1093/nar/gkx1089

Xie, J., Wang, X., and Proud, C. G. (2016). mTOR inhibitors in cancer therapy. *F1000Research* 5:F1000 Faculty Rev-2078. doi: 10.12688/f1000research.9207.1

Zaim, S. R., Li, Q., Schissler, A. G., and Lussier, Y. A. (2018). Emergence of pathway-level composite biomarkers from converging gene set signals of heterogeneous transcriptomic responses. *Pac. Symp. Biocomput.* 23, 484–495. doi: 10.1142/9789813235533_0044

Zappa, C., and Mousa, S. A. (2016). Non-small cell lung cancer: current treatment and future advances. *Transl. Lung Cancer Res.* 5, 288–300. doi: 10.21037/tlcr.2016.06.07

Zhu, S., Okuno, Y., Tsujimoto, G., and Mamitsuka, H. (2007). Application of a new probabilistic model for mining implicit associated cancer genes from OMIM and medline. *Cancer Inform.* 2, 361–371. doi: 10.1177/117693510600200025

Conflict of Interest Statement: MS, NB, AG were employed by company Omicsway Corp. MZ, AB were employed by company Oncobox Ltd.

The remaining authors declare that the research was conducted in the absence of any commercial or financial relationships that could be construed as a potential conflict of interest.

frontiers in Oncology

MINI REVIEW
published: 23 January 2019
doi: 10.3389/fonc.2019.00015

Progression on Citrullination of Proteins in Gastrointestinal Cancers

*Shuzheng Song and Yingyan Yu**

Department of Surgery, Ruijin Hospital, Shanghai Jiao Tong University School of Medicine, Shanghai Key Laboratory for Gastric Neoplasms, Shanghai, China

The citrullination modification (Cit) of proteins has received increasing attention in recent years. This kind of protein modification was first discovered in autoimmune diseases such as rheumatoid arthritis. The citrullination modification process is catalyzed by the peptidyl arginine deiminases (PADIs) family. A well-known citrullination of histone involves the key mechanism of neutrophil extracellular traps (NETs) of inflammation in the peripheral blood. Further studies revealed that citrullination modification of proteins also involves in carcinogenesis in human being. Citrullinated proteins disturbed the stability of proteins and caused DNA damages. There is increasing evidence that citrullinated proteins can be used as potential targets for cancer diagnosis or treatment. This review introduces the concept of citrullination modification of proteins, substrate proteins, examining methods and biological significances.

Keywords: citrullination, proteins, histone, PADIs, molecular targets

OPEN ACCESS

Edited by:
Zhe-Sheng Chen,
St. John's University, United States

Reviewed by:
Kathy Keqin LI,
Georgia State University, United States
Qingyuan Zhang,
Ningxia Medical University, China
Qi Liu,
Tongji University, China

****Correspondence:***
Yingyan Yu
yingyan3y@sjtu.edu.cn

Specialty section:
This article was submitted to Cancer Molecular Targets and Therapeutics, a section of the journal Frontiers in Oncology

Received: *18 November 2018*
Accepted: *04 January 2019*
Published: *23 January 2019*

Citation:
Song S and Yu Y (2019) Progression on Citrullination of Proteins in Gastrointestinal Cancers. Front. Oncol. 9:15. doi: 10.3389/fonc.2019.00015

INTRODUCTION

Proteins are the main executor of life activities. The epigenetics and post-translational modification of proteins, such as phosphorylation, acetylation, glycosylation, methylation, ubiquitination and citrullination have been found to play important roles on pathogenesis and carcinogenesis (1–3). Citrullination of proteins is a new kind of post-translational modification, which has been reported to be involved in large numbers of autoimmune diseases and cancers. This review focuses on the mechanisms, regulation, and the clinical significance of citrullinated proteins in the field of gastrointestinal diseases.

DEFINITION OF CITRULLINATED PROTEINS

Citrullination of protein refers to the process by which the peptidyl arginine residue is converted to citrulline by a catalytic enzyme (**Figure 1**). Since this process is accompanied by the removal of an amino group, it is also called a peptidyl arginine deamination reaction. This chemical reaction is accompanied by a change in electrostatic charge, which may affect the folding state and function of protein, especially on histones. To date, it has been confirmed that arginine residues of dozens of proteins can undergo citrullination modifications. The substrates could be enolase, vimentin, keratin, filaggrin, serine protease inhibitors, proteases and metabolic enzymes (4). Moreover, arginine residues of histones such as H3R2/R8/R17/R26, H4R3, H2A, and H1 could be citrullinated by peptidyl arginine deiminases (PADIs) (5–8).

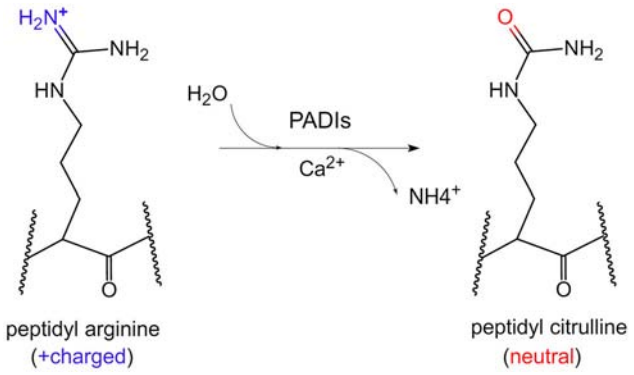

FIGURE 1 | The chemical conversion process of protein citrullination. In the presence of calcium ions, PADIs could catalyze the formation of peptidyl citrulline from peptidyl arginine, which removes an amino group, accompanied by the positive charge becoming electrically neutral.

Citrullination of proteins is catalyzed by PADIs, which include five isoenzymes (PADI1-4 and PADI6) in humans. The genes of these five isozymes are located on chromosome 1p36.13. The coding regions of PADIs are about 2k in size, and consist of three parts: the nitrogen end, middle part and catalytic groups of carbon end. Regarding the subcellular localization, the PADI4 is located in the nucleus with a nuclear localization signal, while others are mainly localized in the cytosol (9) (**Figure 2**). PADI2 had been shown to be undergoing nuclear translocation in some cells for modifying histones (10). Therefore, citrullinated modification of histones may catalyzed by PADI4 and PADI2. The citrullination of proteins occurs in various life processes, including regulation of gene expression, immune response and protein degradation (10, 11). The citrullination of proteins is also associated with carcinogenesis in the stomach (12, 13), the large intestine (13–15), the pancreas (16), the liver (13), and so on.

CITRULLINATION OF NON-HISTONE PROTEINS

Citrullination of proteins could be induced by chemical compounds. Qu et al. reported that the antiparasitic drug nitazoxanide could induce citrullination of protein β-catenin in colorectal cancer cells via up-regulation of PADI2 enzyme. Citrullination of β-catenin resulted in the instability of the protein, and then inhibited the Wnt signaling pathway. ING4, a tumor suppressor protein, was identified as a substrate of PADI4 enzyme. Citrullination of ING4 interfered with its interaction with p53, and then decreased the tumor suppressor function in colon cancer cells (17). On the other hand, some research indicated that DNA damage induced PADI4, and then increased the citrullination of NPM1 and lamine C, which inhibited cell growth through the p53 pathway in colon cancer cells (18). Cantarino and colleagues found that down-regulation of PADI2 is an early event in the pathogenesis of colorectal cancer and is associated with poor prognosis (14). Overexpression of PADI2 inhibited cell growth and was accompanied with an increase in citrullinated protein in colon cancer cells. Overexpression of PADI2 did not increase cell apoptosis, but arrested the cell cycle in G1 phase (15). The exact effect of citrullination of proteins on cancer should be studied further.

Citrullination of proteins is not only detected in *in vitro* experiments, but also in human blood. Ordóñez et al. (19) reported that up-regulation of citrullinated antithrombin in peripheral blood of patients with rheumatoid arthritis and colorectal cancer predicted higher risk of thrombosis. Yuzhalin et al. (20) found that PADI4 could be secreted into the extracellular matrix by colorectal cancer cells, catalyzing the citrullination of proteins, thereby promoting distant metastasis of cancer cells to liver. Increased PADI4 could be found in the peripheral blood of patients with various malignancies such as gastric cancer, lung cancer, hepatocellular carcinoma, esophageal squamous cell carcinoma and breast cancer (13, 21). Until now, multiple proteins have been found as substrates of citrullination, including NF-κB p65 (22), CXCL8 (23), CXCL12 (24), E2F-1 (25), GSK3β (26), MEK1 (27), VEGFR2 (28), and so on. Obviously, citrullination of proteins involve double-sided roles in promoting both inflammation and anti-inflammation, as well as cancer promotion and inhibition.

CITRULLINATION OF HISTONE PROTEINS

Citrullinated modification of histones is an epigenetic event. As introduced above, both PADI2 and PADI4 involve the citrullination process of histones in the nucleus. Recently, increased citrullinated histone H3 (H3Cit) has been considered a novel prognostic blood marker in patients with advanced cancer, due to its higher levels compared to healthy controls (29). PADI2 has been found playing an important role in mediating histone H3Cit modification, and promoting disease progression in some non-digestive cancers (30, 31). McNee et al. (32) found that PADI2 could up-regulate IL-6 expression by catalyzing H3R26Cit of bone marrow mesenchymal stem cells of multiple myeloma, which ultimately lead to chemo-resistance to bortezomib. PADI4 is another important enzyme in catalyzing the citrullination of histones. DNA damage could activate the PADI4-p53 network and catalyze histone chaperone protein, nucleophosmin (NPM1) (18). In addition, DNA damage could catalyze citrullination of the arginine 3 residue of histone H4 (H4R3cit) through the p53-PADI4 pathway in non-small cell lung cancer (33).

CITRULLINATION OF PROTEINS AND IMMUNE RESPONSE

The immune system is a major weapon against cancer. Citrullination of proteins exist widely in immune-related diseases and cancers. Makrygiannakis and colleagues examined biopsy tissues from rheumatoid arthritis, myositis, tonsillitis and inflammatory bowel disease via immunohistochemistry. They found that there is a significant increase in citrullinated proteins in inflammatory tissues, compared to corresponding normal controls (34). The immune system is composed of innate immunity and acquired immunity. Neutrophils are a member of

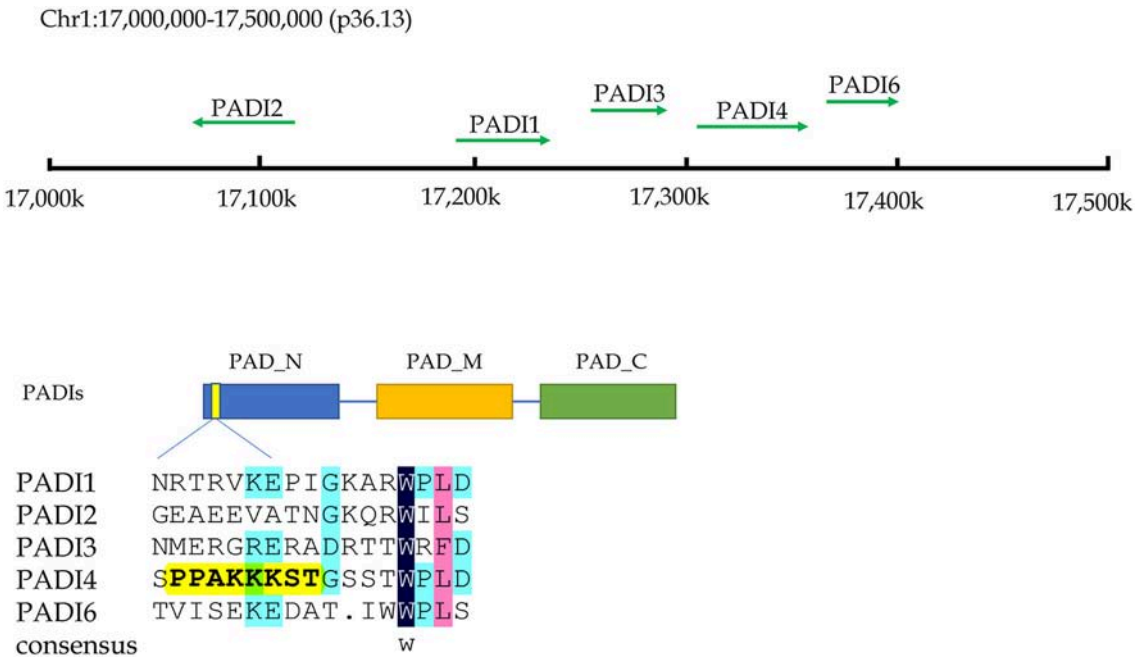

FIGURE 2 | The chromosome location and structural characteristics of PADIs family. Five PADIs genes (PADI 1, 2, 3, 4, and 6) are located in the p36.13 of chromosome 1 across a region of approximately 500 k bases. PADIs members have similar structural regions, which can be divided into three sections: nitrogen zone, middle zone, and carbon end catalytic zone. Only PADI4 contains a nuclear localization signal at the nitrogen end of sequence, implying that PADI4 may play a role in the cell nucleus.

the cells of innate immunity. In process of clearing bacteria, the neutrophils secrete cell DNA, histones, and intracellular proteins to the extracellular space or circulatory system, forming so-called neutrophil extracellular traps (NETs). The citrullination of histones is involved in the process of NETs. In this process, PADI4 mediates the citrullination of histones, and results in the unwinding of DNA and subsequently excreting into the extracellular space (35–37). NETs are a self-protective mechanism against harmful bacteria. Recently, Thalin et al. found that H3Cit was significantly increased in the peripheral blood of advanced cancer patients (29). The proportion of H3Cit-positive neutrophils was increased in more serious patients. The expression level of H3Cit of serum was strongly correlated with the neutrophil activation markers, such as neutrophil elastase, myeloperoxidase and NETs-induced factors IL-6, as well as IL-8. Therefore, H3Cit is considered a useful blood biomarker for evaluating inflammatory response and prognosis in advanced cancers. Up-regulation of NETs was also identified in pancreatic ductal adenocarcinoma. The histone modification of H3Cit was proposed as a marker of NETs (16). In the pancreas, stimulating factors such as pancreatic juice could induce NETs in pancreatic ducts. Excess in NETs blocks the pancreatic duct and eventually causes pancreatitis (38).

In the cancer immunity area, the new epitopes caused by post-translational modification of proteins may provide a novel target for cancer-specific immune therapy. The condition of the cancer microenvironment including nutrient deficiency, hypoxia, redox stress and DNA damage could irritate active expression of PADIs, and catalyze production of citrullinated peptides. Increased content of citrullinated peptides may be a good target for the immune system. The cancer-specific microenvironment could induce the immune response by citrullinated peptides, and this is non-toxic and safe to the host. Carbohydrate metabolizing enzyme α-enolase is a substrate of citrullinated modification. Cook et al. (39) found that citrullination significantly induced elevation of α-enolase in Th1 immune cells, while unmodified wild-type peptides of α-enolase did not show this efficacy. Citrullinated peptides of α-enolase also induced CD4+ T activation (40, 41). The results suggested that developing tumor vaccines against citrullinated peptides of α-enolase may be a useful strategy (39). The function of citrullinated protein epitope has revealed promising utility in anti-cancer immunity.

DETECTION AND BIOLOGICAL SIGNIFICANCE OF CITRULLINATION MODIFICATION

Citrullination modification of proteins has been reported in several fields of cancer research. Along with the progression of biomedical techniques, detection and identification of citrullinated proteins in complex biological systems becomes more feasible. Clinically, the detection of anti-cyclic citrulline antibody has been used as an assistive method for diagnosis and monitoring clinical rheumatoid arthritis (42, 43). Since the citrullination modification itself leads to 1Da mass change only,

detection of the change of low abundance is still a challenging work. Phenylglyoxal (PG) could be covalently bonded with citrullinated residues specifically, and used for specific probes of labeling citrullinated proteins. The reaction could be colored by coupling dyes such as rhodamine (Rh) or biotin, and then identified by ELISA or mass spectrometry (13, 21, 29, 42, 43). By means of this technology, more and more antigens with citrullinated modification could be found, which will provide new targets for diagnosis and treatment of cancers.

In an animal experiment, Mohamed and colleagues found that nanomaterials could induce production of citrullinated protein and auto-antibodies in mice. In their study, after injection of nickel nanowires into mice, the levels of citrullinated protein and PADIs enzymes were elevated in the spleen, kidney and lymph nodes of mice, implying a systemic response to environmental materials (44). Their results suggested that safety of the nanoparticles needs to be evaluated further. Citrullination modification of proteins may be an important event for the host to recognize foreign antigens. Citrullinated proteins may be recognized as new antigens, and are promising for targeted therapy or CAR-T/NK cell-specific recognition targets.

Inhibitors of PADIs demonstrated strong potential of anti-autoimmune and anti-cancer functions *in vitro* and *in vivo*. PADI4 is the only member of the PADI family containing a nuclear localization signal, and can citrullinate many substrates including histones. PADI4 functions as a corepressor of p53 and cooperates with a histone deacetylase HDAC2 to repress the expression of tumor suppressor genes. Chlor-amidine (Cl-amidine) is a pan-PADI inhibitor that shows inhibitory effects on several members of PADIs family. However, its higher IC50 (150–200 μM) limit its preclinical exploration in cancer study and treatment (44–47). Recently, Wang and colleagues found a lead compound, YW3-56, which could activate a cohort of p53 target genes, and realize inhibitory efficacy on the mTORC1 signaling pathway, thereby disturbing autophagy and inhibiting cancerous cell growth (45). However, since the feature of a pan-PADIs inhibitor, Cl-amidine, is still be used in experimental study (48), and many new small molecule inhibitors of PADI4 are being developed by pharmacologists (49).

In summary, compared to other modification of proteins, citrullination modification is relatively novel. The exact regulatory mechanisms and biological significance in carcinogenesis are largely unclear. As shown in **Figure 3**, many substrates of citrullination modification are very important in life processes and development of cancers. The accurate identification of citrullination sites may help researchers to elucidate the underlying molecular mechanisms of citrullination and designing drugs for related human diseases. Several groups made efforts to predict citrullination sites by bioinformatics. Ju and Wang (50) provided a user-friendly web-server for CKSAAP_CitrSite. Zhang et al. (51) published their pioneering work of maximum-relevance-minimum-redundancy to analyze citrullination sites, and constructed classifier by random forest algorithm. We believe that in citrullination research area, bioinformatics will provide some useful insights and assistance.

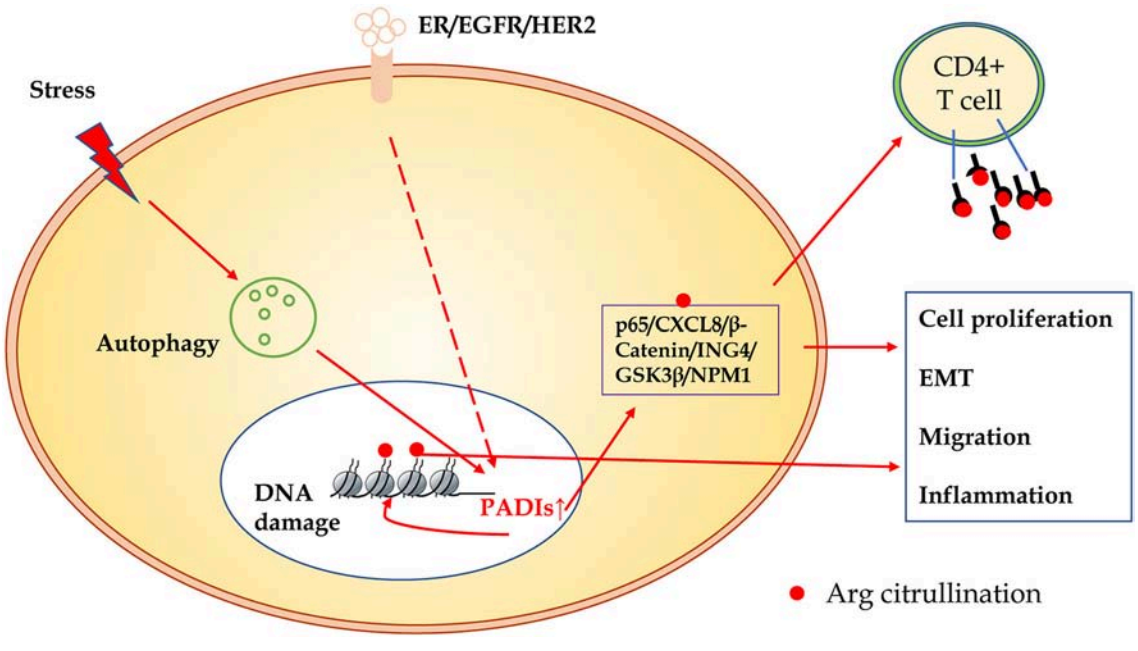

FIGURE 3 | The schematic presentation of citrullinated modification of proteins and its biological significance. PADIs enzymes are activated through receptors of ER/EGFR/HER2, oxidative stress, hypoxia, and other microenvironment factors, which initiate autophagy and DNA damage. Increased PADIs catalyze citrullination modification of histones and non-histone proteins, and result in cell proliferation, epithelial-mesenchymal transition, migration, and inflammation. Citrullinated proteins as a new antigen may activate immune response of T cells or induce specific antibodies.

AUTHOR CONTRIBUTIONS

SS and YY were involved in concept and design. All authors wrote, reviewed and revised the manuscript.

FUNDING

This project was supported by National Key R&D Program of China (2017YFC0908300, 2016YFC1303200), the National Natural Science Foundation of China (81772505), Shanghai Science and Technology Committee (18411953100), the Cross-Institute Research Fund of Shanghai Jiao Tong University (YG2017ZD01, YG2015MS62), Innovation Foundation of Translational Medicine of Shanghai Jiao Tong University School of Medicine (15ZH4001, TM201617, and TM201702), and Technology Transfer Project of Science & Technology Department Shanghai Jiao Tong University School of Medicine.

REFERENCES

1. Bettermann K, Benesch M, Weis S, Haybaeck J. SUMOylation in carcinogenesis. *Cancer Lett.* (2012) 316:113–25. doi: 10.1016/j.canlet.2011.10.036
2. Okudela K, Mitsui H, Suzuki T, Woo T, Tateishi Y, Umeda S, et al. Expression of HDAC9 in lung cancer–potential role in lung carcinogenesis. *Int J Clin Exp Pathol.* (2014) 7:213–20.
3. Chrun ES, Modolo F, Daniel FI. Histone modifications: a review about the presence of this epigenetic phenomenon in carcinogenesis. *Pathol Res Pract.* (2017) 213:1329–39. doi: 10.1016/j.prp.2017.06.013
4. Tilvawala R, Nguyen SH, Maurais AJ, Nemmara VV, Nagar M, Salinger AJ, et al. The rheumatoid arthritis-associated citrullinome. *Cell Chem Biol.* (2018) 25:691–704.e6. doi: 10.1016/j.chembiol.2018.03.002
5. Hagiwara T, Nakashima K, Hirano H, Senshu T, Yamada M. Deimination of arginine residues in nucleophosmin/B23 and histones in HL-60 granulocytes. *Biochem Biophys Res Commun.* (2002) 290:979–83. doi: 10.1006/bbrc.2001.6303
6. Arita K, Shimizu T, Hashimoto H, Hidaka Y, Yamada M, Sato M. Structural basis for histone N-terminal recognition by human peptidylarginine deiminase 4. *Proc Natl Acad Sci USA.* (2006) 103:5291–6. doi: 10.1073/pnas.0509639103
7. Saiki M, Watase M, Matsubayashi H, Hidaka Y. Recognition of the N-terminal histone H2A and H3 peptides by peptidylarginine deiminase IV. *Protein Pept Lett.* (2009) 16:1012–6. doi: 10.2174/092986609789055449
8. Christophorou MA, Castelo-Branco G, Halley-Stott RP, Oliveira CS, Loos R, Radzisheuskaya A, et al. Citrullination regulates pluripotency and histone H1 binding to chromatin. *Nature* (2014) 507:104–8. doi: 10.1038/nature12942
9. Nakashima K, Hagiwara T, Yamada M. Nuclear localization of peptidylarginine deiminase V and histone deimination in granulocytes. *J Biol Chem.* (2002) 277:49562–8. doi: 10.1074/jbc.M208795200
10. Amin B, Voelter W. Human deiminases: isoforms, substrate specificities, kinetics, and detection. *Prog Chem Org Nat Prod.* (2017) 106:203–40. doi: 10.1007/978-3-319-59542-9_2
11. Fert-Bober J, Giles JT, Holewinski RJ, Kirk JA, Uhrigshardt H, Crowgey EL, et al. Citrullination of myofilament proteins in heart failure. *Cardiovasc Res.* (2015) 108:232–42. doi: 10.1093/cvr/cvv185
12. Zheng Y, Zhao G, Xu B, Liu C, Li C, Zhang X, et al. PADI4 has genetic susceptibility to gastric carcinoma and upregulates CXCR2, KRT14 and TNF-alpha expression levels. *Oncotarget* (2016) 7:62159–76. doi: 10.18632/oncotarget.11398
13. Guo W, Zheng Y, Xu B, Ma F, Li C, Zhang X, et al. Investigating the expression, effect and tumorigenic pathway of PADI2 in tumors. *Onco Targets Ther.* (2017) 10:1475–85. doi: 10.2147/OTT.S92389
14. Cantariño N, Musulén E, Valero V, Peinado MA, Perucho M, Moreno V, et al. Downregulation of the deiminase PADI2 is an early event in colorectal carcinogenesis and indicates poor prognosis. *Mol Cancer Res.* (2016) 14:841–8. doi: 10.1158/1541-7786.MCR-16-0034
15. Funayama R, Taniguchi H, Mizuma M, Fujishima F, Kobayashi M, Ohnuma S, et al. Protein-arginine deiminase 2 suppresses proliferation of colon cancer cells through protein citrullination. *Cancer Sci.* (2017) 108:713–8. doi: 10.1111/cas.13179
16. Boone BA, Orlichenko L, Schapiro NE, Loughran P, Gianfrate GC, Ellis JT, et al. The receptor for advanced glycation end products (RAGE) enhances autophagy and neutrophil extracellular traps in pancreatic cancer. *Cancer Gene Ther.* (2015) 22:326–34. doi: 10.1038/cgt.2015.21
17. Guo Q, Fast W. Citrullination of inhibitor of growth 4 (ING4) by peptidylarginine deminase 4 (PAD4) disrupts the interaction between ING4 and p53. *J Biol Chem.* (2011) 286:17069–78. doi: 10.1074/jbc.M111.230961
18. Tanikawa C, Ueda K, Nakagawa H, Yoshida N, Nakamura Y, Matsuda K. Regulation of protein Citrullination through p53/PADI4 network in DNA damage response. *Cancer Res.* (2009) 69:8761–9. doi: 10.1158/0008-5472.CAN-09-2280
19. Ordóñez A, Yélamos J, Pedersen S, Miñano A, Conesa-Zamora P, Kristensen SR, et al. Increased levels of citrullinated antithrombin in plasma of patients with rheumatoid arthritis and colorectal adenocarcinoma determined by a newly developed ELISA using a specific monoclonal antibody. *Thromb Haemost.* (2010) 104:1143–9. doi: 10.1160/TH10-05-0297
20. Yuzhalin AE, Gordon-Weeks AN, Tognoli ML, Jones K, Markelc B, Konietzny R, et al. Colorectal cancer liver metastatic growth depends on PAD4-driven citrullination of the extracellular matrix. *Nat Commun.* (2018) 9:4783. doi: 10.1038/s41467-018-07306-7
21. Chang X, Han J, Pang L, Zhao Y, Yang Y, Shen Z. Increased PADI4 expression in blood and tissues of patients with malignant tumors. *BMC Cancer* (2009) 9:40. doi: 10.1186/1471-2407-9-40
22. Sun B, Dwivedi N, Bechtel TJ, Paulsen JL, Muth A, Bawadekar M, et al. Citrullination of NF-kappaB p65 promotes its nuclear localization and TLR-induced expression of IL-1beta and TNFalpha. *Sci Immunol.* (2017) 2:eaal3062. doi: 10.1126/sciimmunol.aal3062
23. Proost P, Loos T, Mortier A, Schutyser E, Gouwy M, Noppen S, et al. Citrullination of CXCL8 by peptidylarginine deiminase alters receptor usage, prevents proteolysis, and dampens tissue inflammation. *J Exp Med.* (2008) 205:2085–97. doi: 10.1084/jem.20080305
24. Struyf S, Noppen S, Loos T, Mortier A, Gouwy M, Verbeke H, et al. Citrullination of CXCL12 differentially reduces CXCR4 and CXCR7 binding with loss of inflammatory and anti-HIV-1 activity via CXCR4. *J Immunol.* (2009) 182:666–74. doi: 10.4049/jimmunol.182.1.666
25. Ghari F, Quirke AM, Munro S, Kawalkowska J, Picaud S, McGouran J, et al. Citrullination-acetylation interplay guides E2F-1 activity during the inflammatory response. *Sci Adv.* (2016) 2:e1501257. doi: 10.1126/sciadv.1501257
26. Stadler SC, Vincent CT, Fedorov VD, Patsialou A, Cherrington BD, Wakshlag JJ, et al. Dysregulation of PAD4-mediated citrullination of nuclear GSK3beta activates TGF-beta signaling and induces epithelial-to-mesenchymal transition in breast cancer cells. *Proc Natl Acad Sci USA.* (2013) 110:11851–6. doi: 10.1073/pnas.1308362110
27. Qin H, Liu X, Li F, Miao L, Li T, Xu B, et al. PAD1 promotes epithelial-mesenchymal transition and metastasis in triple-negative breast cancer cells by regulating MEK1-ERK1/2-MMP2 signaling. *Cancer Lett.* (2017) 409:30–41. doi: 10.1016/j.canlet.2017.08.019
28. Sase T, Arito M, Onodera H, Omoteyama K, Kurokawa MS, Kagami Y, et al. Hypoxia-induced production of peptidylarginine deiminases and citrullinated proteins in malignant glioma cells. *Biochem Biophys Res Commun.* (2017) 482:50–6. doi: 10.1016/j.bbrc.2016.10.154
29. Thålin C, Lundström S, Seignez C, Daleskog M, Lundström A, Henriksson P, et al. Citrullinated histone H3 as a novel prognostic blood marker in patients with advanced cancer. *PLoS ONE* (2018) 13:e0191231. doi: 10.1371/journal.pone.0191231

30. Wang L, Song G, Zhang X, Feng T, Pan J, Chen W, et al. PADI2-mediated citrullination promotes prostate cancer progression. *Cancer Res.* (2017) 77:5755–68. doi: 10.1158/0008-5472.CAN-17-0150
31. DeVore SB, Young CH, Li G, Sundararajan A, Ramaraj T, Mudge J, et al. Histone citrullination represses miRNA expression resulting in increased oncogene mRNAs in somatolactotrope cells. *Mol Cell Biol.* (2018) 38:e00084-18. doi: 10.1128/MCB.00084-18
32. McNee G, Eales KL, Wei W, Williams DS, Barkhuizen A, Bartlett DB, et al. Citrullination of histone H3 drives IL-6 production by bone marrow mesenchymal stem cells in MGUS and multiple myeloma. *Leukemia* (2017) 31:373–81. doi: 10.1038/leu.2016.187
33. Tanikawa C, Espinosa M, Suzuki A, Masuda K, Yamamoto K, Tsuchiya E, et al. Regulation of histone modification and chromatin structure by the p53-PADI4 pathway. *Nat Commun.* (2012) 3:676. doi: 10.1038/ncomms1676
34. Makrygiannakis D, af Klint E, Lundberg IE, Löfberg R, Ulfgren AK, Klareskog L, et al. Citrullination is an inflammation-dependent process. *Ann Rheum Dis.* (2006) 65:1219–22. doi: 10.1136/ard.2005.049403
35. Neeli I, Khan SN, Radic M. Histone deimination as a response to inflammatory stimuli in neutrophils. *J Immunol.* (2008) 180:1895–902. doi: 10.4049/jimmunol.180.3.1895
36. Wang Y, Li M, Stadler S, Correll S, Li P, Wang D, et al. Histone hypercitrullination mediates chromatin decondensation and neutrophil extracellular trap formation. *J Cell Biol.* (2009) 184:205–13. doi: 10.1083/jcb.200806072
37. Honda M, Kubes P. Neutrophils and neutrophil extracellular traps in the liver and gastrointestinal system. *Nat Rev Gastroenterol Hepatol.* (2018) 15:206–21. doi: 10.1038/nrgastro.2017.183
38. Leppkes M, Maueröder C, Hirth S, Nowecki S, Günther C, Billmeier U, et al. Externalized decondensed neutrophil chromatin occludes pancreatic ducts and drives pancreatitis. *Nat Commun.* (2016) 7:10973. doi: 10.1038/ncomms10973
39. Cook K, Daniels I, Symonds P, Pitt T, Gijon M, Xue W, et al. Citrullinated alpha-enolase is an effective target for anti-cancer immunity. *Oncoimmunology* (2018) 7:e1390642. doi: 10.1080/2162402X.2017.1390642
40. Brentville VA, Metheringham RL, Gunn B, Symonds P, Daniels I, Gijon M, et al. Citrullinated vimentin presented on MHC-II in tumor cells is a target for CD4+ T-cell-mediated antitumor immunity. *Cancer Res.* (2016) 76:548–60. doi: 10.1158/0008-5472.CAN-15-1085
41. Durrant LG, Metheringham RL, Brentville VA. Autophagy, citrullination and cancer. *Autophagy* (2016) 12:1055–6. doi: 10.1080/15548627.2016.1166326
42. Bicker KL, Subramanian V, Chumanevich AA, Hofseth LJ, Thompson PR. Seeing citrulline: development of a phenylglyoxal-based probe to visualize protein citrullination. *J Am Chem Soc.* (2012) 134:17015–8. doi: 10.1021/ja308871v
43. Lewallen DM, Bicker KL, Subramanian V, Clancy KW, Slade DJ, Martell J, et al. Chemical proteomic platform to identify citrullinated proteins. *ACS Chem Biol.* (2015) 10:2520–8. doi: 10.1021/acschembio.5b00438
44. Mohamed BM, Boyle NT, Schinwald A, Murer B, Ward R, Mahfoud OK, et al. Induction of protein citrullination and auto-antibodies production in murine exposed to nickel nanomaterials. *Sci Rep.* (2018) 8:679. doi: 10.1038/s41598-017-19068-1
45. Wang Y, Li P, Wang S, Hu J, Chen XA, Wu J, et al. Anticancer peptidylarginine deiminase (PAD) inhibitors regulate the autophagy flux and the mammalian target of rapamycin complex 1 activity. *J Biol Chem.* (2012) 287:25941–53. doi: 10.1074/jbc.M112.375725
46. Mondal S, Parelkar SS, Nagar M, Thompson PR. Photochemical control of protein arginine deiminase (PAD) activity. *ACS Chem Biol.* (2018) 13:1057–65. doi: 10.1021/acschembio.8b00053
47. Bozdag M, Dreker T, Henry C, Tosco P, Vallaro M, Fruttero R, et al. Novel small molecule protein arginine deiminase 4 (PAD4) inhibitors. *Bioorg Med Chem Lett.* (2013) 23:715–9. doi: 10.1016/j.bmcl.2012.11.102
48. Witalison EE, Cui X, Hofseth AB, Subramanian V, Causey CP, Thompson PR, et al. Inhibiting protein arginine deiminases has antioxidant consequences. *J Pharmacol Exp Ther.* (2015) 353:64–70. doi: 10.1124/jpet.115.222745
49. Witalison EE, Cui X, Causey CP, Thompson PR, Hofseth LJ. Molecular targeting of protein arginine deiminases to suppress colitis and prevent colon cancer. *Oncotarget* (2015) 6:36053–62. doi: 10.18632/oncotarget.5937
50. Ju Z, Wang SY. Prediction of citrullination sites by incorporating k-spaced amino acid pairs into Chou's general pseudo amino acid composition. *Gene* (2018) 664:78–83. doi: 10.1016/j.gene.2018.04.055
51. Zhang Q, Sun X, Feng K, Wang S, Zhang YH, Wang S, et al. Predicting citrullination sites in protein sequences using mRMR method and random forest algorithm. *Comb Chem High Throughput Screen.* (2017) 20:164–73. doi: 10.2174/1386207319666161227124350

Conflict of Interest Statement: The authors declare that the research was conducted in the absence of any commercial or financial relationships that could be construed as a potential conflict of interest.

frontiers in Pharmacology

ORIGINAL RESEARCH
published: 24 January 2019
doi: 10.3389/fphar.2019.00010

A Smart pH-Sensitive Delivery System for Enhanced Anticancer Efficacy via Paclitaxel Endosomal Escape

Yihua Yang[1,2], Zhe Wang[3], Ying Peng[1], Jinsong Ding[1] and Wenhu Zhou[1]**

[1] Xiangya School of Pharmaceutical Sciences, Central South University, Changsha, China, [2] Jiangsu Key Laboratory of New Drug Research and Clinical Pharmacy, School of Pharmaceutical Sciences, Xuzhou Medical University, Xuzhou, China, [3] Xiangya International Academy of Translational Medicine, Central South University, Changsha, China

Micelles are highly attractive nano-drug delivery systems for targeted cancer therapy. While they have been demonstrated to significantly alleviate the side-effects of their cargo drugs, the therapy outcomes are usually suboptimal partially due to ineffective drug release and endosome entrapment. Stimulus-responsive nanoparticles have allowed controlled drug release in a smart fashion, and we want to use this concept to design novel micelles. Herein, we reported pH-sensitive paclitaxel (PTX)-loaded poly (ethylene glycol)-phenylhydrazone-dilaurate (PEG-BHyd-dC_{12}) micelles (PEG-BHyd-dC_{12}/PTX). The micelles were spherical, with an average particle size of ∼135 nm and a uniform size distribution. The pH-responsive properties of the micelles were certified by both colloidal stability and drug release profile, where the particle size was strikingly increased accompanied by faster drug release as pH decreased from 7.4 to 5.5. As a result, the micelles exhibited much stronger cytotoxicity than the pH-insensitive counterpart micelles against various types of cancer cells due to the hydrolysis of the building block polymers and subsequent rapid PTX release. Overall, these results demonstrate that the PEG-BHyd-dC_{12} micelle is a promising drug delivery system for cancer therapy.

Keywords: pH-sensitive, micelles, cancer, paclitaxel, endosomal escape

OPEN ACCESS

Edited by:
Zhe-Sheng Chen,
St. John's University, United States

Reviewed by:
Lei Zhang,
Fujian Institute of Research on the Structure of Matter (CAS), China
Qi Liu,
Johns Hopkins Medicine, United States

****Correspondence:***
Jinsong Ding
dingjs0221@163.com
Wenhu Zhou
zhouwenhuyaoji@163.com

Specialty section:
This article was submitted to Cancer Molecular Targets and Therapeutics, a section of the journal Frontiers in Pharmacology

Received: *10 July 2018*
Accepted: *07 January 2019*
Published: *24 January 2019*

Citation:
Yang Y, Wang Z, Peng Y, Ding J and Zhou W (2019) A Smart pH-Sensitive Delivery System for Enhanced Anticancer Efficacy via Paclitaxel Endosomal Escape. Front. Pharmacol. 10:10. doi: 10.3389/fphar.2019.00010

INTRODUCTION

With the development of nanotechnology, various materials such as polymers, lipid, and metals (oxides), have been widely applied to design drug delivery system, especially for cancer therapy (Farokhzad and Langer, 2009). Nanoparticles based on the above materials have been demonstrated to realize controlled drug release and effectively targeting drug delivery (Wilczewska et al., 2012). To this end, micelles composed of amphipathic copolymers have received wide attention owing to their attractive features, such as small and uniform size, tumor targeting ability *via* the enhanced permeability and retention (EPR) effect, high stability in aqueous solution and excellent biocompatibility (Felber et al., 2012; Liu J. et al., 2014; Wang et al., 2018).

However, albeit with the extensive research efforts, the clinical translations of micelles from bench to bedsides are rather limited, partially due to their suboptimal therapy outcomes caused by

the inefficient drug release at the tumor site and the endosomal entrapment of micelles (Kanamala et al., 2016). Plain micelles exhibit relatively slow drug release rate, which may result in ineffective drug concentration inside targeted cells (Wu et al., 2013). To mitigate these issues, smarter micelles are desired to be equipped with endosomal escape and rapid drug release abilities, which could be able to provide sufficient drug concentration for effective killing of the tumor cells.

To achieve such goals, environmentally sensitive polymers that can respond to different stimuli to trigger drug release have been extensively investigated, such as light (Liu et al., 2012; Cao et al., 2013), temperature (Kim et al., 2010; Wang et al., 2014), ultrasound (Yin et al., 2013; Ahmed et al., 2015), magnetic field (Ao et al., 2014; Deng et al., 2015), pH (Liu Y. et al., 2014; Yuba et al., 2017), redox properties (Yin et al., 2015; Zhang et al., 2016), and enzyme activity (Rao and Khan, 2013; Harnoy et al., 2014). Among of them, the pH-sensitive polymeric micelle appears to be a highly appealing candidate due to the intrinsic differences between solid tumors and the surrounding normal tissues in terms of their relative acidity. The pH-sensitive polymer micelles were devised based on copolymers composed of hydrophobic and hydrophilic polymers linked *via* acid-liable bonds, including hydrazone (Mo et al., 2012), benzoic imine (Yuan et al., 2012), oxime (Liu B. et al., 2014), acetal (Li et al., 2016), ester (Gao et al., 2018) and orthoester (Tang et al., 2011). Hydrolysis of the acid-labile bonds leads to rapid drug release at an acidic pH.

Herein, we synthesized the amphiphilic polymer PEG-BHyd-dC_{12} via an acid-labile hydrazone bond and constructed pH-responsive micelles. The hydrophilic PEG segment on micelles surface affords high colloidal stability *in vitro* and long circulation time *in vivo*, while it is readily departed from micelles at the tumor site under acid conditions, which is beneficial for cellular uptake (Du et al., 2011). Paclitaxel (PTX), one of the most effective antitumor drugs, was encapsulated into micelles due to its hydrophobic nature, and released in a pH-responsive manner. For comparison, the pH-insensitive counterpart polymer of PEG-BAmi-dC_{12} was also synthesized for micelles preparation. The physicochemical characterization, colloidal stability, drug release, cellular uptake, and *in vitro* cytotoxicity of the micelles were evaluated.

MATERIALS AND METHODS

Chemicals and Reagents

Paclitaxel (PTX), 1-ethyl-3-[3-dimethylaminopropyl] carbodiimide hydrochloride (EDC), *N*-hydroxysulfosuccinimide (NHS), 4-dimethylaminopyridine (DMAP), lauroyl chloride, α-methoxy-x-amino-poly(ethylene glycol) (Mn = 2000) (MeO-PEG2000-NH_2) were purchased from Shanghai Aladdin Reagent Co. Ltd. (Shanghai, China). mPEG-hydrazide (Mn = 2000) was from Seebio Biotech, Inc. (Shanghai, China), and 3,5-dihydroxybenzaldehyde was from Bide Pharmatech Ltd. (Shanghai, China). 3,5-Dihydroxybenzoic acid was obtained from Saen Chemical Technology Co. Ltd. (Shanghai, China). Potassium hydroxide (KOH), tetrahydrofuran (THF), dimethyl sulfoxide (DMSO), petroleum ether, ethyl acetate were purchased from Sinopharm Chemical Reagent Co., Ltd. (Shanghai, China). 3-(4,5-dimethylthiazol-2-yl)-2,5-diphenyl tetrazolium bromide (MTT), coumarine (Cou-6) and 4′,6-diamidino-2-phenylindole (DAPI) were obtained from Sigma-Aldrich Co. (St. Louis, MO, United States). Lysotracker red was supplied from Beyotime Institute of Biotechnology (Jiangsu, China). Dulbecco's modified Eagle's medium (DMEM), RPMI 1640, penicillin, streptomycin, phosphate buffered saline (PBS), fetal bovine serum (FBS) were purchased from Gibco Life Technologies, Inc. (Carlsbad, CA, United States). Human lung cancer cells (A549), human breast cancer cells (MDA-MB-231), human ovarian cancer cells (A2780) were obtained from Xiangya cell center (Changsha, China). PTX-resistant human lung cancer cells (A549/T) was bought from Gefan Biotechnology Co., Ltd. (Shanghai, China).

Synthesis of the pH-Sensitive Copolymer PEG-BHyd-dC_{12}

3,5-Dihydroxybenzaldehyde was dissolved in THF, followed by the addition of KOH. Lauroyl chloride was added dropwise into the above mixture and vigorously stirred for 6 h to yield 3,5-dilaurate benzaldehyde. The purified 3,5-dilaurate benzaldehyde and mPEG-hydrazide were dissolved in ethyl alcohol and stirred for 24 h. After purification, the final amphiphilic polymer PEG-BHyd-dC_{12} was obtained.

Synthesis of the pH-Insensitive Copolymer PEG-BAmi-dC_{12}

First, lauroyl chloride was added dropwise to a mixture of 3,5-dihydroxybenzoic acid with KOH in anhydrous acetone at 0°C under stirring to obtain 3,5-dilaurate benzoic acid. Then, 3,5-dilaurate benzoic acid, EDC, DMAP and NHS were dissolved into DMSO and stirred at room temperature for 2 h, followed by the addition of MeO-PEG2000-NH_2. The resulting solution was dialyzed and subsequently lyophilized to obtain PEG-BAmi-dC_{12}.

Characterization of Copolymers

The ^{1}H-NMR spectra of PEG-BHyd-dC_{12} and PEG-BAmi-dC_{12} were recorded using a Bruker Avance 400 MHz NMR spectrometer (Varian, United States) with deuterated chloroform ($CDCl_3$) as the solvent. The self-assembly behavior of polymers was investigated by the fluorescence probe technique (Xiong et al., 2017). First, 100 μL of pyrene in acetone (2.9×10^{-2} mM) was evaporated to form a thin film on the flask bottom. Then, various concentrations of polymer solutions (from 0.1 μg/mL to 200 μg/mL) were added to the pyrene-coated vials and stored in the dark overnight. The fluorescence intensity ratio of I_{337}/I_{334} in the emission spectra of pyrene was calculated and plotted against the logarithm of the polymer concentrations. The CMC value was obtained based on the fluorescence excitation spectra of the mixed solution.

Preparation of Micelles

PTX-loaded micelles were prepared by a thin-film hydration method. In brief, PEG-BHyd-dC_{12} or PEG-BAmi-dC_{12} (20.0 mg) and PTX (1 mg) were dissolved in dichloromethane (4 mL).

The solution was evaporated under reduced pressure to form a uniform film. Deionized water (10 mL) was added and rotated for another 1 h. The obtained colloidal solution was then centrifuged at 3,000 rpm for 10 min and filtered through 0.45 μm pore size filter, followed by lyophilization. Blank micelles were prepared in a similar way in the absence of PTX.

Characterization of Micelles

The particle size, PDI, and zeta potential measurement were determined by dynamic light scattering (DLS) method using a Malvern Zeta Sizer Nano series (Nano ZS, Malvern Instruments, United Kingdom) at 25°C. The morphologies of the micelles were observed using transmission electron microscopy (TEM) (Titan G2-F20, FEI, United States).

The determination of PTX was carried out using a high-performance liquid chromatography (HPLC) system (LC-2010, Shimadzu, Tokyo, Japan). The chromatographic column was an ODS C_{18} (250 × 4.6 mm, 5 μm, Diamonsil, Beijing, China). The mobile phase consisted of mixtures of acetonitrile and water (55:45, v/v). The flow rate was 1 $mL{\cdot}min^{-1}$, and the detection wavelength was 227 nm. Micelles were centrifuged in an ultrafiltration tube (MWCO 10 kDa) at 5,000 rpm for 10 min and filtered through 0.22 μm filter to remove the unloaded PTX. PTX-loaded micelles were disrupted by methanol. The PTX loading content (LC) and encapsulated efficiency (EE) were calculated using the following formulae:

$$\text{EE (\%)} = \text{Amount of PTX in micelles/Amount of PTX fed initially} \times 100\%$$

$$\text{LC (\%)} = \text{Amount of PTX in micelles/Amount of PTX-loaded micelles} \times 100\%$$

Colloidal Stability

Micelles were incubated with 10% FBS or 10 mM phosphate buffer solutions (pH 7.4, 6.5, and 5.5) at 37°C for 72 h, and the size was measured by DLS at different intervals.

In vitro Drug Release

The release study was assessed by the dialysis method. The release media was PBS solutions containing 0.5% Tween-80 with different pH values (5.5, 6.5, and 7.4). Typically, 2 mL of PTX-loaded micelles was placed in a dialysis bag (MWCO 3500) and dialyzed against 25 mL of buffer medium under mechanical shaking (100 rpm) at 37°C. At predetermined time intervals, 2 mL of release medium was withdrawn and replenished with an equal volume of fresh medium. The released PTX was detected by HPLC.

Cell Culture

A549 and A549/T cells were maintained in RPMI 1640 medium supplemented with 10% FBS, penicillin (50 U/mL) and streptomycin (50 U/mL) in a 5% CO_2 atmosphere at 37°C. MDA-MB-231 and A2780 were maintained in DMEM medium supplemented with 10% FBS, penicillin (50 U/mL) and streptomycin (50 U/mL) in a 5% CO_2 atmosphere at 37°C.

Intracellular Distribution

Cou-6 loaded micelles were constructed according to the above method, except the drug was replaced with Cou-6. A549 cells were seeded on glass coverslips in the 24-well plates at a density of 4×10^4 per well. After culturing for 24 h, Cou-6 loaded micelles ([Cou-6] = 200 ng/mL) were added and incubated for 1 h. Alternatively, the cells were incubated with Cou-6 loaded micelles for 1 h, then washed and cultured in fresh media for another 3 h. Then, the medium was replaced with 70 nM lysotracker red and incubated for another 1 h. Afterward, the cells were fixed with 4% formaldehyde for 20 min at room temperature and visualized using a CLSM (LSM 780, Carl Zeiss, Jena, German).

Cellular Uptake

A549 cells were seeded in 6-well plates with a density of 3×10^5 cells per well and incubated overnight, and then, the medium was replaced with Cou-6 loaded micelles at final Cou-6 concentration of 200 ng/mL. After 1 h or 4 h of incubation, the cells were harvested and quantified by flow cytometry (FACSVerse, BD, United States).

Cytotoxicity Assay

The cytotoxicity of micelles with or without an anticancer drug was determined by MTT assay. The cells were seeded in a 96-well plate at a density of 6,000 cells per well and maintained for 24 h. The medium was then replaced with the micelles and further incubated for 72 h. Then, 20 μL of MTT solution (5 mg/mL) was added to each well of the plate for another 4 h. Subsequently, 100 μL of DMSO was added to dissolve the formazan crystals, and the absorbance was measured at 570 nm by a microplate reader (ELX800, Bio-Tek, United States). The untreated cells were used as controls.

Hemolysis Tests

The hemocompatibility of micelles was evaluated by hemolysis assay (Yang et al., 2016). First, fresh rabbit blood was extracted from the heart of a rabbit. Subsequently, erythrocytes were obtained by centrifugation at 3,000 rpm for 15 min and washed with normal saline (NS). Serial dilutions of micelles were then added to the 2% erythrocytes (v/v) and incubated for 2 h at 37°C in a thermostatic water bath. Finally, the mixtures were centrifuged at 3,500 rpm for 15 min, and the supernatant of all samples was measured for UV absorbance (A) at 540 nm. NS and 0.5% Triton X-100 were regarded as the negative and positive controls, respectively. The hemolysis ratio was calculated as follows:

$$\text{Hemolysis (\%)} = (A_{\text{sample}} - A_{\text{control}(-)})/(A_{\text{control}(+)} - A_{\text{control}(-)})$$

Statistical Analysis

The data were expressed as the mean ± standard deviation (SD). Statistical analysis was performed using a two-tailed Student's *t*-test and analysis of variance (ANOVA) with the aid of SPSS 23.0 software. Differences were considered statistically significant when *p*-values were less than 0.05.

RESULTS AND DISCUSSION

Synthesis and Characterizations of Copolymers

The synthesis schemes of PEG-BHyd-dC_{12} and PEG-BAmi-dC_{12} were illustrated in **Figures 1A,B**. To synthesize the PEG-BHyd-dC_{12} di-block amphiphilic polymer, the hydrophobic fragment of 3,5-dilaurate benzaldehyde was conjugated with the hydrophilic fragment of PEG through the linkage of hydrazone. The 3,5-dihydroxybenzaldehyde was first reacted with lauroyl chloride to form a 3,5-dilaurate benzaldehyde intermediate with a yield of 90%, and then the aldehyde group on 3,5-dilaurate benzaldehyde reacted with the hydrazine groups on mPEG-hydrazide to give PEG-BHyd-dC_{12} with a final yield was 69%. All of the synthetic compounds were characterized by ^{1}H-NMR spectra (**Figures 1C,D**), which were in good agreement with their depicted structures as described in the following:

^{1}H NMR of intermediate compound 3,5-dilaurate benzaldehyde: ^{1}H NMR (400 MHz, $CDCl_3$) δ (ppm) 0.91 (6H, t, -CH_3), 1.21–1.45 (32H, m, -$(CH_2)_n$), 1.75 (4H, m, CO-βH), 2,59 (4H, t, CO-αH), 7.20 (1H, t, 4-ArH), 7.52 (2H, d, 2,6-ArH), 9.98 (1H, s, -CHO).

^{1}H NMR of PEG-BHyd-dC_{12}: ^{1}H NMR (400 MHz, $CDCl_3$) δ (ppm) 0.89 (6H, t, -CH_3), 1.22–1.45 (32H, m, -$(CH_2)_n$), 1.74 (4H, m, CO-βH), 2,54 (4H, t, CO-αH), 3.39 (3H, s, -OCH_3 from PEG), 3.50–3.84 ((-OCH_2CH_2-)$_n$), 4.19 (2H, s, CO-αH, from PEG), 6.94 (1H, t, 4-ArH), 7.41 (2H, d, 2,6-ArH), 8.24 (1H, s, -NH), 10.5 (1H, s, -CH = N).

As for PEG-BHyd-dC_{12}, the characteristic peaks at 3.5–3.84 ppm were from PEG, and the proton peak at 10.5 ppm indicated the formation of the hydrazone bond. In addition, the absence of proton peak of aldehyde (9.98 ppm) suggested that free 3,5-dilaurate benzaldehyde was removed in the purified PEG-BHyd-dC_{12}.

^{1}H NMR of intermediate compound 3,5-dilaurate benzoic acid: ^{1}H NMR (400 MHz, $CDCl_3$) δ (ppm) 0.90 (6H, t, -CH_3), 1.21–1.44 (32H, m, -$(CH_2)_n$), 1.71 (4H, m, CO-βH), 2,61 (4H, t, CO-αH), 7.20 (1H, t, 4-ArH), 7.72 (2H, d, 2,6-ArH).

^{1}H NMR of PEG-BAmi-dC_{12}: ^{1}H NMR (400 MHz, $CDCl_3$) δ (ppm) 0.90 (6H, t, -CH_3), 1.22–1.45 (32H, m, -$(CH_2)_n$), 1.75 (4H, m, CO-βH), 2,58 (4H, t, CO-αH), 3.40 (3H, s, -OCH_3 from PEG), 3.50–3.84 ((-OCH_2CH_2-)$_n$), 7.06 (1H, t, 4-ArH), 7.45 (2H, d, 2, 6-ArH), 7.79 (1H, d, -CONH).

The characteristic peaks of PEG (3.50–3.84 ppm) were obvious, and the peak of new amide bond can be seen at 7.79 ppm for PEG-BAmi-dC_{12}.

CMC Measurement

As amphiphilic materials, a key parameter for their applications as a nanocarrier is their CMC. Micelles can be formed at concentrations above the CMC. The CMC values of PEG-BHyd-dC_{12} and PEG-BAmi-dC_{12} were determined by a well-established method using pyrene as a fluorescence probe, resulting in

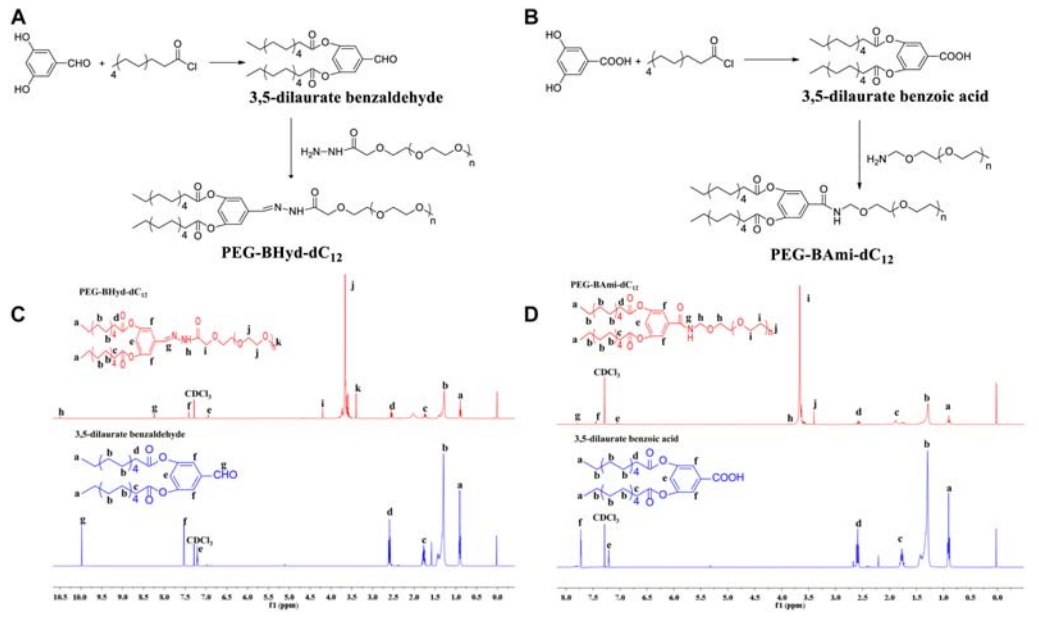

FIGURE 1 | Synthesis and characterization of PEG-BHyd-dC_{12} **(A,C)** and PEG-BAmi-dC_{12} **(B,D)**. The synthesis of PEG-BHyd-dC_{12} **(A)** and PEG-BAmi-dC_{12} **(B)**, H1-NMR spectrum of PEG-BHyd-dC_{12} **(C)**, and PEG-BAmi-dC_{12} **(D)**.

7.5 μg/mL for PEG-BHyd-dC$_{12}$ and 5.6 μg/mL for PEG-BAmi-dC$_{12}$ (**Figure 2**). These CMC values were within the typical concentration range for most polymeric micelle CMCs, which can be directly applied *in vivo* (Maysinger et al., 2007; Diezi et al., 2010; Owen et al., 2012). It is reasonable that these two polymers have comparable CMC values, as their structures are nearly identical; they only differed at the junction between the hydrophobic and hydrophilic blocks (one with a hydrazone bond and the other with an amide bond). Therefore, PEG-BAmi-dC$_{12}$ is an excellent control to study the pH-responsive property of PEG-BHyd-dC$_{12}$ for drug delivery.

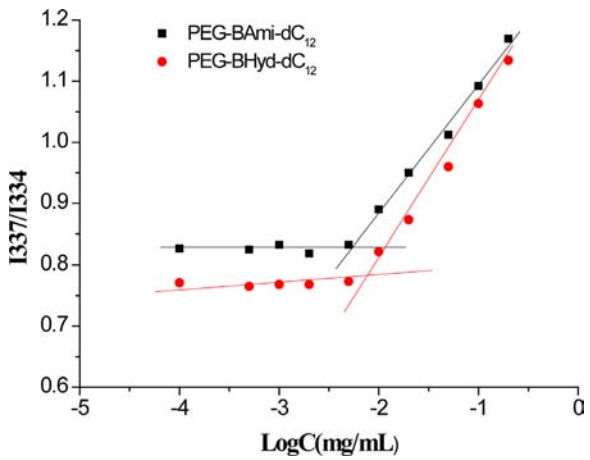

FIGURE 2 | The CMC curve of PEG-BHyd-dC$_{12}$ and PEG-BAmi-dC$_{12}$.

Preparation and Characterization of Micelles

From the above experiments, we have demonstrated that both PEG-BHyd-dC$_{12}$ and PEG-BAmi-dC$_{12}$ were able to self-assemble into micelles at very low concentrations, implying their applicability for the development of a nano-drug delivery system. We next used these polymers to prepare micelles, and the hydrophobic PTX was used a model to encapsulate into the hydrophobic core of the micelles (**Figure 3A**). The pH-sensitive micelles (PEG-BHyd-dC$_{12}$/PTX) were prepared using a standard thin-film hydration method. After removing the organic solvents, the solution appeared to be semi-transparent with light-blue opalescence (Inset in **Figure 3B**, left), suggesting the successful preparation of nano-sized micelles. The particle size was approximately 135 nm as determined by DLS (**Figure 3B**, left); this size is suitable for passive accumulation in the tumor tissue through the EPR effect (Danhier et al., 2010). From TEM, the micelles were well dispersed with spherical morphology (Inset in **Figure 3B**, left). The LC efficiency of PEG-BHyd-dC$_{12}$/PTX was 3% (**Figure 3C**), which was comparable to many other PTX-loading micelles reported previously, and was sufficient for subsequent *in vitro*/*in vivo* therapeutic applications (Lee et al., 2003; Zhu et al., 2010; Mei et al., 2015).

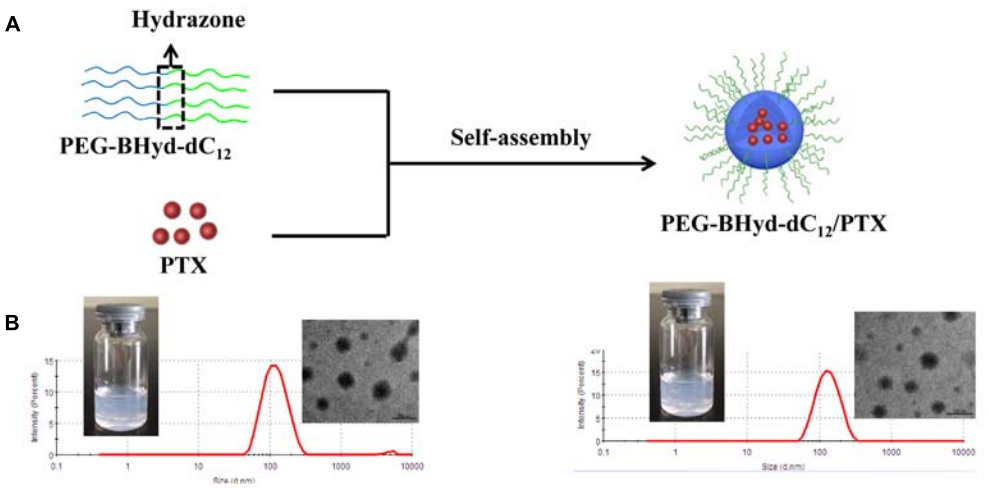

C

	Size (nm)	PDI	EE (%)	LC (%)
PEG-BHyd-dC$_{12}$/PTX	135.50±0.24	0.25±0.019	65.53±3.11	3.2±1.12
PEG-BAmi-dC$_{12}$/PTX	127.30±0.28	0.23±0.017	67.65±2.98	3.1±1.09

FIGURE 3 | Preparation and characterization of micelles. Schematic preparation **(A)**, appearance, size distribution, and TEM images (**B**, left presents PEG-BHyd-dC$_{12}$/PTX, right presents PEG-BAmi-dC$_{12}$/PTX), characterization **(C)**. Data were presented as mean ± standard deviation (SD; n = 3).

By using the same method, the pH-insensitive PEG-BAmi-dC$_{12}$/PTX micelles were also prepared and characterized (**Figure 3B**, right; **Figure 3C**). Interestingly, these two types of micelles displayed quite similar properties in terms of appearance, particle size, morphology and drug loading efficiency. Therefore, a parallel comparison between these micelles can be made for their *in vitro/in vivo* biological performance, which can be rationalized by the pH-responsive bond linkage.

Colloidal Stability

The colloidal stability of the micelles was first studied under different buffer solutions. Interestingly, with pH decrease from 7.4 to 6.5 and 5.5, the particle size of PEG-BHyd-dC$_{12}$/PTX markedly increased, while it remained unchanged for PEG-BAmi-dC$_{12}$/PTX (**Figure 4A**). This can be rationalized by the pH-responsive property of the PEG-BHyd-dC$_{12}$/PTX, which could swell and then collapse at lower pH (Li et al., 2016; Qiu et al., 2017). We also challenged the micelles with 10% FBS, and both types of micelles were quite stable even after 72 h incubation (**Figure 4B**). Therefore, the pH-sensitive micelles were stable in blood circulation and can rapidly collapse to release the payload under acidic conditions.

In vitro Drug Release

The release behavior of PTX from polymeric micelles was evaluated under various conditions at 37°C. Different buffer solutions were employed to simulate the micro-environment of the blood circulation (pH 7.4), tumor tissue (pH 6.5), and endosome (pH 5.5). We first studied the performance of pH-sensitive PEG-BHyd-dC$_{12}$/PTX micelles. At pH 7.4, almost no PTX was released in the initial 4 h, which was followed by a sustained release phase with only 38% PTX release after 48 h (**Figure 5A**, black trace). Therefore, the micelles can stably encapsulate PTX for a long time, which is important for decreasing the side effects and increasing the drug accumulation in tumor sites. By lowering the pH to 6.5, a notable increase in drug release was observed at each time point (**Figure 5A**, blue trace). With further decrease of the pH to 5.5, the micelles showed an even higher rate of drug release (**Figure 5A**, red trace). After 48 h, the cumulative drug release was 50% and 65%, respectively, significantly higher than that at pH 7.4 (∼40%), indicating a good pH-responsive capability. This pH-responsive drug release profile can be ascribed to the hydrazone bond between the hydrophilic and hydrophobic chains of the polymer. As the pH decreases, the hydrazone bond tends to hydrolyse

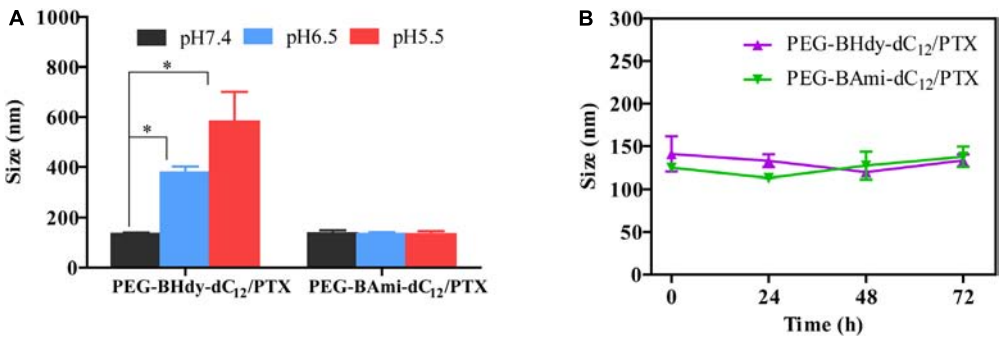

FIGURE 4 | Colloidal stability of micelles. Size change of PEG-BHyd-dC$_{12}$/PTX micelles and PEG-BAmi-dC12/PTX micelles in phosphate buffers with different pH values **(A)** and 10% FBS **(B)** at 37°C for 72 h. The pHs were buffered by disodium hydrogen phosphate and sodium dihydrogen phosphate with total phosphate concentration of 10 mM. Data were shown as mean ± SD (n = 3). $^*p < 0.05$.

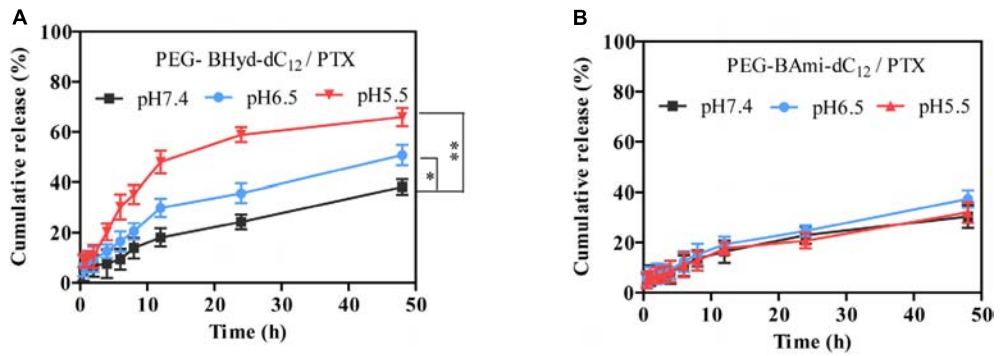

FIGURE 5 | Release profiles of PEG-BHyd-dC$_{12}$/PTX micelles **(A)** and PEG-BAmi-dC12/PTX micelles **(B)** at different pHs at 37°C. The pHs were buffered by disodium hydrogen phosphate and sodium dihydrogen phosphate with total phosphate concentration of 10 mM. Data were shown as mean ± SD (n = 3). $^*p < 0.05$, $^{**}p < 0.01$.

and thus the micelles collapse, resulting in burst drug release.

As a control, we also performed the drug release experiment with pH-insensitive PEG-BAmi-dC_{12}/PTX micelles. In this case, slow and sustained drug release was seen under different conditions, and pH had little effect on the rate of drug release, giving a cumulative drug release of less than 40% after 48 h (**Figure 5B**). Considering the structural difference

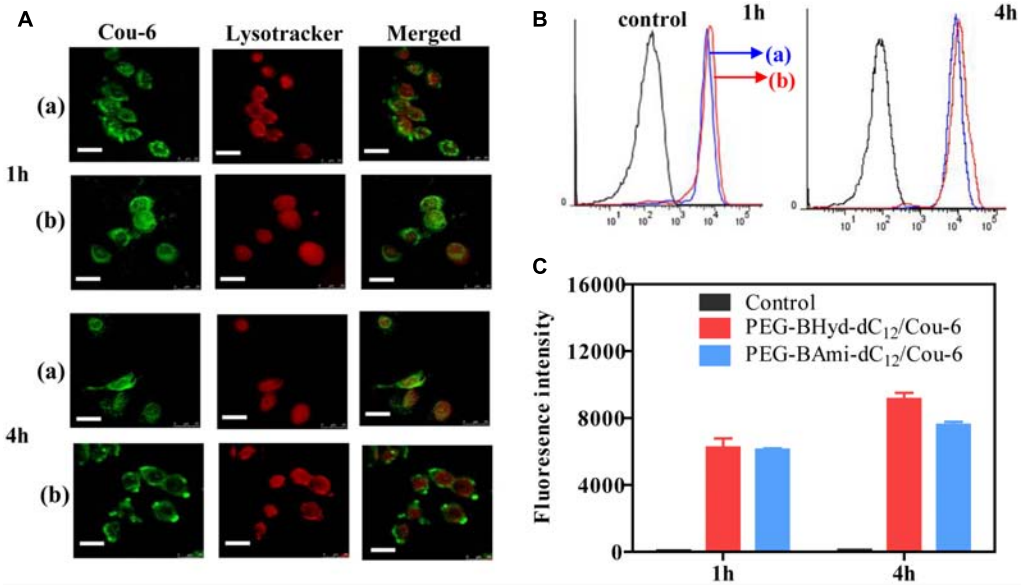

FIGURE 6 | Cellular uptake studies of PEG-BHyd-dC_{12}/Cou-6 and PEG-BAmi-dC_{12}/Cou-6 in A549 cells by using CLSM **(A)**, flow cytometry **(B)**, fluorescence intensities quantified from **B (C)**. The (a) indicated PEG-BAmi-dC12/Cou-6 while the (b) represented PEG-BHyd-dC_{12}/Cou-6. The scale bar is 25 μm.

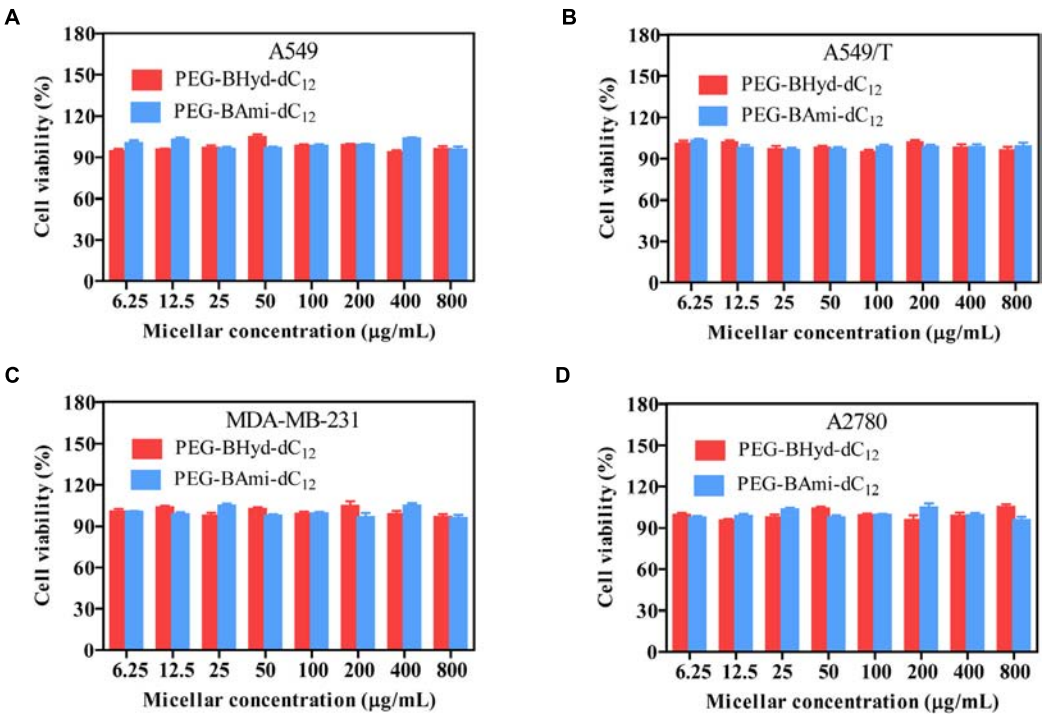

FIGURE 7 | Cell viability of blank micelles after incubating with A549 **(A)**, A549/T **(B)**, MDA-MB-231 **(C)**, and A2780 **(D)** cells for 72 h. Data were shown as mean ± SD (n = 4).

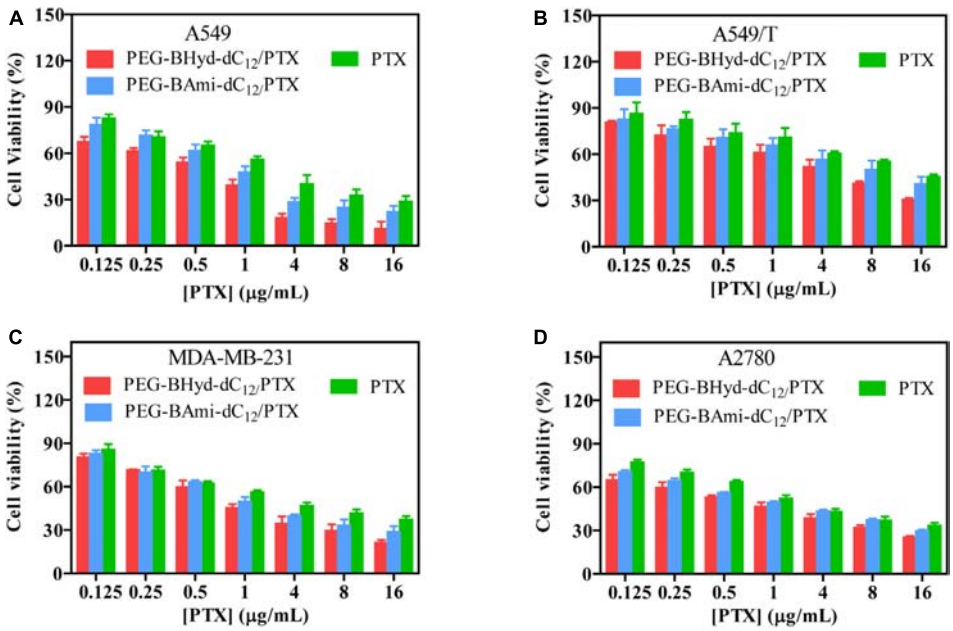

FIGURE 8 | Cell viability of PTX-loaded micelles and free PTX after incubating with A549 **(A)**, A549/T **(B)**, MDA-MB-231 **(C)**, and A2780 **(D)** cells for 72 h. Data were shown as mean ± SD (n = 4).

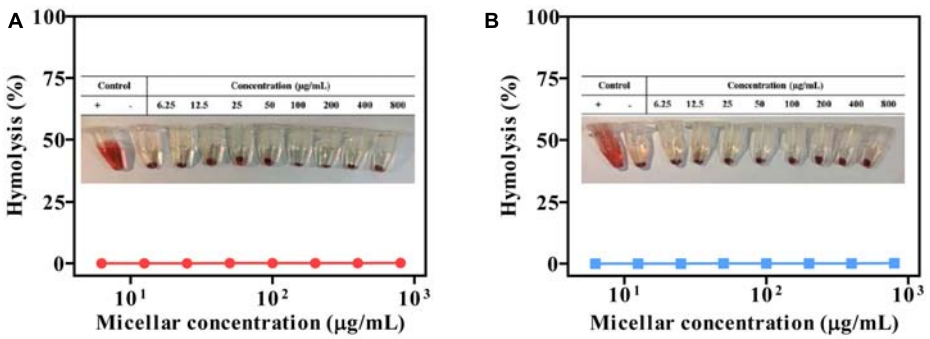

FIGURE 9 | Compatibility studies of micelles (pH 7.4). PEG-BHyd-dC12 **(A)** and PEG-BAmi-dC12 **(B)**. "+" represents positive control by using 0.5% Triton X-100, and "–" represents negative control of non-treatment.

TABLE 1 | IC_{50} value of the micelles and free PTX to A549, A549/T, MDA-MB-231, and A2780 cells for 72 h incubation (mean ± SD, n = 4).

	IC_{50} (μg/mL)			
	A549	**A549/T**	**MDB-MA-231**	**A2780**
PTX	1.87 ± 0.08	11.17 ± 1.15	2.99 ± 0.37	2.01 ± 0.04
PEG-BHyd-dC_{12}/PTX	0.57 ± 0.16*▲	3.04 ± 1.13*▲	1.16 ± 0.06*▲	0.75 ± 0.08**▲
PEG-BAmi-dC_{12}/PTX	1.10 ± 0.06#	6.77 ± 0.30#	1.64 ± 0.13#	1.33 ± 0.13#

*PTX vs. PEG-BHyd-dC_{12}/PTX, *$p < 0.05$, **$p < 0.01$; PTX vs. PEG-BAmi-dC_{12}/PTX, #$p < 0.05$; PEG-BHyd-dC_{12}/PTX vs. PEG-BAmi-dC_{12}/PTX, ▲$p < 0.05$.*

between PEG-BHyd-dC_{12}/PTX and PEG-BAmi-dC_{12}/PTX, these results further demonstrated critical role of the hydrazone bond for the pH-sensitive property of the PEG-BHyd-dC_{12}/PTX micelles.

Intracellular Uptake Study

Having demonstrated the pH-responsive property of the PEG-BAmi-dC_{12}/PTX micelles, we next studied the performance of the micelles inside cells. To conveniently track the micelles inside cells, Cou-6 (a hydrophobic green fluorophore) instead of PTX was encapsulated into micelles, and the acidic organelles (i.e., lysosomes and endosomes) were stained by Lysotracker red. A549 cancer cell line was used as a model since PTX has been widely used in clinic for lung cancer therapy (Singla et al., 2002). From confocal laser scanning microscopy (CLSM), substantial green fluorescence was observed for both types of micelles after 1 h incubation (**Figure 6A**), indicating a high level of cellular

internalization. To visualize the co-localization of micelles and endo/lysosomes, we merged the green and red channels, and the emergence of orange spots indicated the localization of micelles in the endo/lysosomes. Both PEG-BHyd-dC_{12}/Cou-6 and PEG-BAmi-dC_{12}/Cou-6 micelles showed obvious spots after 1 h of incubation, consistent with the endocytosis pathway of the micelles (Zhang et al., 2017).

We next studied the intracellular performance of the micelles. To do this, the cells were washed and cultured in fresh media so that further internalization of micelles was avoided. After 4 h incubation, the pH-insensitive micelles were still largely entrapped into the endo/lysosomes. In contrast, the orange spots of pH-sensitive micelles were weakened, and green color was evenly distributed throughout the cytoplasm, which showed minimal co-localization with the red fluorescence of the endo/lysosomes. The micelles detached from endosome due to hydrolysis of copolymer under acidic organelles, which facilitated efficient release of drug. Therefore, successful endo/lysosomal escape of pH-sensitive micelles was indicated. It is known that the successful escape of a nano-delivery system from the intracellular endosome/lysosome for drug release is a key issue in determining their therapeutic efficiency (Qiu et al., 2017). After cellular uptake, micelles were first entrapped into endosome/lysosome (Chou et al., 2011; Varkouhi et al., 2011). Once entering the endo/lysosomes, the pH-sensitive micelles were disassembled because of pH-triggered hydrolysis of the acid-labile chemical linkage, and the drug rapidly escaped from the endosome/lysosome, resulting in pH-triggered intracellular burst release (Fang et al., 2016).

To have a quantitative understanding, we next performed flow cytometry experiments to study the uptake of micelles by A549 cells (**Figures 6B,C**). After 1 h incubation, there was no difference in intensity between pH-sensitive and pH-insensitive micelles. Interestingly, after 4 h, the fluorescence from pH-responsive micelles was considerably higher than that of pH-insensitive micelles (**Figure 6C**), in agreement with a previous report (Qiu et al., 2017). While the pH-responsiveness of micelles has little effect on cell uptake process, the relative lower fluorescence for PEG-BAmi-dC_{12}/PTX was likely due to the efflux of the micelles from cells to medium. As has been demonstrated, the endo/lysosome entrapped micelles can be pumped out by ATP-binding cassette protein B1 (ABCB1) transporter (Sakai-Kato et al., 2012). Since the pH-responsive micelles collapse faster in endo/lysosome, relatively less micelles were cleared from cells by this pump-out process, resulting in stronger fluorescence inside cells.

Cytotoxicity Assay

Cytotoxicity studies were performed by incubating micelles with different types of cells for 72 h, and cell viability was measured by MTT assay. The cytotoxicity of the polymers was tested by incubating the cells with blank micelles (without PTX loading), and all types of cells remained >90% viability with concentration up to 800 μg/mL, indicating high biocompatibility (**Figure 7**). As for A549, at the highest PTX concentration (16 μg/mL), the viabilities of cells incubated with PEG-BHyd-dC_{12}/PTX, PEG-BAmi-dC_{12}/PTX and free PTX dropped to 11%, 22%, and 28%, respectively, showing high toxicity to cancer cells (**Figure 8A**). The anti-cancer capability was quantified by measuring the half-maximal inhibitory concentration (IC_{50}), which was in order of PEG-BHyd-dC_{12}/PTX (0.57 μg/mL) < PEG-BAmi-dC_{12}/PTX (1.1 μg/mL) < free PTX (1.87 μg/mL) (**Table 1**). Therefore, PEG-BHyd-dC_{12}/PTX exhibited the highest activity, which was attributable to the pH-responsive property for rapid endo/lysosome drug escape to enhance the antitumor effect.

To test the generality, we further performed the anti-tumor assay by using MDA-MB-231 and A2780 cells, and analogous results were observed (**Figures 8C,D**). The PEG-BHyd-dC_{12}/PTX displayed the best anti-cancer activity, followed by PEG-BAmi-dC_{12}/PTX and then free PTX. Therefore, such micelles can be implemented for different types of cancer therapy. As one limitation of PTX for long-term cancer treatment is the acquired drug resistance by cancer cells (Yusuf et al., 2003), we also tested whether the nano-systems could reverse drug resistance by using PTX-resistant A549/T cells as a proof-of-concept. The cytotoxicity of PTX and micelles was also dose dependent (**Figure 8B**), while the overall IC_{50} value was much higher due to the drug resistance (**Table 1**). Notably, cytotoxicity of PEG-BHyd-dC_{12}/PTX was 3.7-fold higher than that of free PTX, which may be useful to reverse drug resistance.

Hemolysis Assay

The biocompatibility of polymeric micelles is the prerequisite for biomedical application. We studied this property by using hemolysis assay. Typically, the micelles were incubated with erythrocytes, and the release of hemoglobin was measured to quantify the erythrocyte-damaging properties (Nogueira et al., 2013). The positive control of 0.5% Triton X-100 showed obvious hemolysis, as high as 100%, while the micelles produced less than 2% at different concentration (**Figure 9**). Therefore, the micelles were highly biocompatible and can be directly administrated by intravenous injection.

CONCLUSION

In this work, pH-sensitive PTX-loaded PEG-BHyd-dC_{12} micelles were constructed and characterized. These nanoparticles exhibited pH-dependent drug release profile and endosomal escape ability after intracellular delivery, and displayed enhanced anti-tumor activity compared with the pH-insensitive counterpart micelles and the free PTX. All of these results suggested that the PEG-BHyd-dC_{12} micelles-based drug delivery system is a promising drug carrier for targeted cancer treatment.

AUTHOR CONTRIBUTIONS

YY performed the cell experiments and wrote the manuscript. ZW performed the synthesis and characterization. YP performed drug release. JD and WZ designed the experiments.

FUNDING

Thanks to the supported of the Innovation-Driven Project of Central South University (Grant No. 20170030010004), National Natural Science Foundation of China (Grant Nos. 81573374 and 81502997), Key Laboratory Breeding Base of Hunan Oriented Fundamental and Applied Research in Innovative Pharmaceutics (Grant No. 2016TP1029), Hunan Engineering Research Center for Optimization of Drug Formulation and Early Clinical Evaluation (Grant No. 2015TP2005), and Director Fund of Jiangsu Key Laboratory of New Drug Research and Clinical Pharmacy (Grant No. ZR-XY201406).

REFERENCES

Ahmed, S. E., Martins, A. M., and Husseini, G. A. (2015). The use of ultrasound to release chemotherapeutic drugs from micelles and liposomes. *J. Drug Target.* 23, 16–42. doi: 10.3109/1061186X.2014.954119

Ao, L., Wang, B., Liu, P., Huang, L., Yue, C., Gao, D., et al. (2014). A folate-integrated magnetic polymer micelle for MRI and dual targeted drug delivery. *Nanoscale* 6, 10710–10716. doi: 10.1039/c4nr02484b

Cao, J., Huang, S., Chen, Y., Li, S., Li, X., Deng, D., et al. (2013). Near-infrared light-triggered micelles for fast controlled drug release in deep tissue. *Biomaterials* 34, 6272–6283. doi: 10.1016/j.biomaterials.2013.05.008

Chou, L. Y., Ming, K., and Chan, W. C. (2011). Strategies for the intracellular delivery of nanoparticles. *Chem. Soc. Rev.* 40, 233–245. doi: 10.1039/c0cs00003e

Danhier, F., Feron O., and Préat, V. (2010). To exploit the tumor microenvironment: passive and active tumor targeting of nanocarriers for anti-cancer drug delivery. *J. Control. Release* 148, 135–146. doi: 10.1016/j.jconrel.2010.08.027

Deng, L., Ren, J., Li, J., Leng, J., Qu, Y., Lin, C., et al. (2015). Magnetothermally responsive star-block copolymeric micelles for controlled drug delivery and enhanced thermo-chemotherapy. *Nanoscale* 7, 9655–9663. doi: 10.1039/c5nr00642b

Diezi, T. A., Bae, Y., and Kwon, G. S. (2010). Enhanced stability of PEG-block-poly(N-hexyl stearate l-aspartamide) micelles in the presence of serum proteins. *Mol. Pharm.* 7, 1355–1360. doi: 10.1021/mp100069p

Du, J. Z., Du, X. J., Mao, C. Q., and Wang, J. (2011). Tailor-made dual pH-sensitive polymer-doxorubicin nanoparticles for efficient anticancer drug delivery. *J. Am. Chem. Soc.* 133, 17560–17563. doi: 10.1021/ja207150n

Fang, X. B., Zhang, J. M., Xie, X., Liu, D., He, C. W., Wan, J. B., et al. (2016). pH-sensitive micelles based on acid-labile pluronic F68-curcumin conjugates for improved tumor intracellular drug delivery. *Int. J. Pharm.* 502, 28–37. doi: 10.1016/j.ijpharm.2016.01.029

Farokhzad, O. C., and Langer, R. (2009). Impact of nanotechnology on drug delivery. *ACS Nano* 3, 16–20. doi: 10.1021/nn900002m

Felber, A. E., Dufresne, M. H., and Leroux, J. C. (2012). pH-sensitive vesicles, polymeric micelles, and nanospheres prepared with polycarboxylates. *Adv. Drug Deliv. Rev.* 64, 979–992. doi: 10.1016/j.addr.2011.09.006

Gao, Y., Xiao, Y., Liu, S., and Yu, J. (2018). Camptothecin prodrug nanomicelle based on a boronate ester-linked diblock copolymer as the carrier of doxorubicin with enhanced cellular uptake. *J. Biomater. Sci. Polym. Ed.* 29, 160–180. doi: 10.1080/09205063.2017.1406632

Harnoy, A. J., Rosenbaum, I., Tirosh, E., Ebenstein, Y., Shaharabani, R., Beck, R., et al. (2014). Enzyme-responsive amphiphilic PEG-dendron hybrids and their assembly into smart micellar nanocarriers. *J. Am. Chem. Soc.* 136, 7531–7534. doi: 10.1021/ja413036q

Kanamala, M., Wilson, W. R., Yang, M., Palmer, B. D., and Wu, Z. (2016). Mechanisms and biomaterials in pH-responsive tumour targeted drug delivery: a review. *Biomaterials* 85, 152–167. doi: 10.1016/j.biomaterials.2016.01.061

Kim, T. H., Chen, Y., Mount, C. W., Gombotz, W. R., Li, X., and Pun, S. H. (2010). Evaluation of temperature-sensitive, indocyanine green-encapsulating micelles for noninvasive near-infrared tumor imaging. *Pharm. Res.* 27, 1900–1913. doi: 10.1007/s11095-010-0190-y

Lee, S. C., Kim, C., Kwon, I. C., Chung, H., and Jeong, S. Y. (2003). Polymeric micelles of poly(2-ethyl-2-oxazoline)-block-poly(epsilon-caprolactone) copolymer as a carrier for paclitaxel. *J. Control. Release* 89, 437–446. doi: 10.1016/S0168-3659(03)00162-7

Li, M., Gao, M., Fu, Y., Chen, C., Meng, X., Fan, A., et al. (2016). Acetal-linked polymeric prodrug micelles for enhanced curcumin delivery. *Colloids Surf. B Biointerfaces* 140, 11–18. doi: 10.1016/j.colsurfb.2015.12.025

Liu, B., Chen, H., Li, X., Zhao, C., Liu, Y., Zhu, L., et al. (2014). pH-responsive flower-like micelles constructed via oxime linkage for anticancer drug delivery. *RSC Adv.* 4, 48943–48951. doi: 10.1039/c4ra08719d

Liu, G., Chen, C., Li, D., Wang, S., and Ji, J. (2012). Near-infrared light-sensitive micelles for enhanced intracellular drug delivery. *J. Mater. Chem.* 22, 16865–16871. doi: 10.1039/c2jm00045h

Liu, J., Huang, Y., Kumar, A., Tan, A., Jin, S., Mozhi, A., et al. (2014). pH-sensitive nano-systems for drug delivery in cancer therapy. *Biotechnol. Adv.* 32, 693–710. doi: 10.1016/j.biotechadv.2013.11.009

Liu, Y., Feng, L., Liu, T., Zhang, L., Yao, Y., Yu, D., et al. (2014). Multifunctional pH-sensitive polymeric nanoparticles for theranostics evaluated experimentally in cancer. *Nanoscale* 6, 3231–3242. doi: 10.1039/c3nr05647c

Maysinger, D., Lovrić, J., Eisenberg, A., and Savić, R. (2007). Fate of micelles and quantum dots in cells. *Eur. J. Pharm. Biopharm.* 65, 270–281. doi: 10.1016/j.ejpb.2006.08.011

Mei, D., Lin, Z., Fu, J., He, B., Gao, W., Ma, L., et al. (2015). The use of α-conotoxin ImI to actualize the targeted delivery of paclitaxel micelles to α7 nAChR-overexpressing breast cancer. *Biomaterials* 42, 52–65. doi: 10.1016/j.biomaterials.2014.11.044

Mo, G., Hu, X., Liu, S., Yue, J., Wang, R., Huang, Y., et al. (2012). Influence of coupling bonds on the anti-tumor activity of polymer-pirarubicin conjugates. *Eur. J. Pharm. Sci.* 46, 329–335. doi: 10.1016/j.ejps.2012.02.013

Nogueira, D. R., Tavano, L., Mitjans, M., Perez, L., Infante, M. R., and Vinardell, M. P. (2013). *In vitro* antitumor activity of methotrexate via pH-sensitive chitosan nanoparticles. *Biomaterials* 34, 2758–2772. doi: 10.1016/j.biomaterials.2013.01.005

Owen, S. C., Chan, D. P., and Shoichet, M. S. (2012). Polymeric micelle stability. *Nano Today* 7, 53–65. doi: 10.1016/j.nantod.2012.01.002

Qiu, L., Zhu, M., Gong, K., Peng, H., Ge, L., Zhao, L., et al. (2017). pH-triggered degradable polymeric micelles for targeted anti-tumor drug delivery. *Mater. Sci. Eng. C Mater. Biol. Appl.* 78, 912–922. doi: 10.1016/j.msec.2017.04.137

Rao, J., and Khan, A. (2013). Enzyme sensitive synthetic polymer micelles based on the azobenzene motif. *J. Am. Chem. Soc.* 135, 14056–14059. doi: 10.1021/ja407514z

Sakai-Kato, K., Ishikura, K., Oshima, Y., Tada, M., Suzuki, T., Ishii-Watabe, A., et al. (2012). Evaluation of intracellular trafficking and clearance from HeLa cells of doxorubicin-bound block copolymers. *Int. J. Pharm.* 423, 401–409. doi: 10.1016/j.ijpharm.2011.12.022

Singla, A. K., Garg, A., and Aggarwal, D. (2002). Paclitaxel and its formulations. *Int. J. Pharm.* 235, 179–192. doi: 10.1016/S0378-5173(01)00986-3

Tang, R., Ji, W., Panus, D., Palumbo, R. N., and Wang, C. (2011). Block copolymer micelles with acid-labile ortho ester side-chains: synthesis, characterization, and enhanced drug delivery to human glioma cells. *J. Control. Release* 151, 18–27. doi: 10.1016/j.jconrel.2010.12.005

Varkouhi, A. K., Scholte, M., Storm, G., and Haisma, H. J. (2011). Endosomal escape pathways for delivery of biologicals. *J. Control. Release* 151, 220–228. doi: 10.1016/j.jconrel.2010.11.004

Wang, X., Li, S., Wan, Z., Quan, Z., and Tan, Q. (2014). Investigation of thermo-sensitive amphiphilic micelles as drug carriers for chemotherapy in cholangiocarcinoma in vitro and in vivo. *Int. J. Pharm.* 463, 81–88. doi: 10.1016/j.ijpharm.2013.12.046

Wang, Z., Deng, X., Ding, J., Zhou, W., Zheng, X., and Tang, G. (2018). Mechanisms of drug release in pH-sensitive micelles for tumour targeted drug delivery system: a review. *Int. J. Pharm.* 535, 253–260. doi: 10.1016/j.ijpharm.2017.11.003

Wilczewska, A. Z., Niemirowicz, K., Markiewicz, K. H., and Car, H. (2012). Nanoparticles as drug delivery systems. *Pharmacol. Rep.* 64, 1020–1037. doi: 10.1016/s1734-1140(12)70901-5

Wu, H., Zhu, L., and Torchilin, V. P. (2013). pH-sensitive poly(histidine)-PEG/DSPE-PEG co-polymer micelles for cytosolic drug delivery. *Biomaterials* 34, 1213–1222. doi: 10.1016/j.biomaterials.2012.08.072

Xiong, D., Zhang, X., Peng, S., Gu, H., and Zhang, L. (2017). Smart pH-sensitive micelles based on redox degradable polymers as DOX/GNPs carriers for controlled drug release and CT imaging. *Colloids Surf. B Biointerfaces* 163, 29–40. doi: 10.1016/j.colsurfb.2017.12.008

Yang, M., Ding, J., Zhang, Y., Chang, F., Wang, J., Gao, Z., et al. (2016). Activated macrophage-targeted dextran–methotrexate/folate conjugate prevents deterioration of collagen-induced arthritis in mice. *J. Mater. Chem. B* 4, 2102–2113. doi: 10.1039/c5tb02479j

Yin, T., Wang, L., Yin, L., Zhou, J., and Huo, M. (2015). Co-delivery of hydrophobic paclitaxel and hydrophilic AURKA specific siRNA by redox-sensitive micelles for effective treatment of breast cancer. *Biomaterials* 61, 10–25. doi: 10.1016/j.biomaterials.2015.05.022

Yin, T., Wang, P., Li, J., Zheng, R., Zheng, B., Cheng, D., et al. (2013). Ultrasound-sensitive siRNA-loaded nanobubbles formed by hetero-assembly of polymeric micelles and liposomes and their therapeutic effect in gliomas. *Biomaterials* 34, 4532–4543. doi: 10.1016/j.biomaterials.2013.02.067

Yuan, Z., Que, Z., Cheng, S., Zhuo, R., and Li, F. (2012). pH-triggered blooming of 'nano-flowers' for tumor intracellular drug delivery. *Chem. Commun.* 48, 8129–8131. doi: 10.1039/c2cc34225a

Yuba, E., Yamaguchi, A., Yoshizaki, Y., Harada, A., and Kono, K. (2017). Bioactive polysaccharide-based pH-sensitive polymers for cytoplasmic delivery of antigen and activation of antigen-specific immunity. *Biomaterials* 120, 32–45. doi: 10.1016/j.biomaterials.2016.12.021

Yusuf, R. Z., Duan, Z., Lamendola, D. E., Penson, R. T., and Seiden, M. V. (2003). Paclitaxel resistance: molecular mechanisms and pharmacologic manipulation. *Curr. Cancer Drug Targets* 3, 1–19. doi: 10.2174/1568009033333754

Zhang, J., Zhao, X., Chen, Q., Yin, X., Xin, X., Li, K., et al. (2017). Systematic evaluation of multifunctional paclitaxel-loaded polymeric mixed micelles as a potential anticancer remedy to overcome multidrug resistance. *Acta Biomater.* 50, 381–395. doi: 10.1016/j.actbio.2016.12.021

Zhang, P., Zhang, H., He, W., Zhao, D., Song, A., and Luan, Y. (2016). Disulfide-linked amphiphilic polymer-docetaxel conjugates assembled redox-sensitive micelles for efficient antitumor drug delivery. *Biomacromolecules* 17, 1621–1632. doi: 10.1021/acs.biomac.5b01758

Zhu, C., Jung, S., Luo, S., Meng, F., Zhu, X., Park, T. G., et al. (2010). Co-delivery of siRNA and paclitaxel into cancer cells by biodegradable cationic micelles based on PDMAEMA-PCL-PDMAEMA triblock copolymers. *Biomaterials* 31, 2408–2416. doi: 10.1016/j.biomaterials.2009.11.077

Conflict of Interest Statement: The authors declare that the research was conducted in the absence of any commercial or financial relationships that could be construed as a potential conflict of interest.

frontiers in Oncology

ORIGINAL RESEARCH
published: 25 January 2019
doi: 10.3389/fonc.2019.00025

Molecular, Biological and Structural Features of V_L CDR-1 Rb44 Peptide, Which Targets the Microtubule Network in Melanoma Cells

*Natalia Girola[1], Pedro T. Resende-Lara[2], Carlos R. Figueiredo[1,3], Mariana H. Massaoka[4], Ricardo A. Azevedo[1], Rodrigo L. O. R. Cunha[5], Luciano Polonelli[6] and Luiz R. Travassos[1,7]**

[1] Department of Microbiology, Immunology and Parasitology, Experimental Oncology Unit, Federal University of São Paulo, São Paulo, Brazil, [2] Computational Biology and Bioinformatics Laboratory, Federal University of ABC, Santo André, Brazil, [3] Department of Molecular and Clinical Cancer Medicine, University of Liverpool, Liverpool, United Kingdom, [4] Cancer Focus, São Paulo, Brazil, [5] Chemical Biology Laboratory, Natural and Human Sciences Center, Federal University of ABC, Santo André, Brazil, [6] Unit of Biomedical, Biotechnological and Translational Sciences, Department of Medicine and Surgery, Universitá degli Studi di Parma, Parma, Italy, [7] Recepta Biopharma, São Paulo, Brazil

OPEN ACCESS

Edited by:
Jian-ye Zhang, Guangzhou Medical University, China

Reviewed by:
Chakrabhavi Dhananjaya Mohan, University of Mysore, India
César de la Fuente, Massachusetts Institute of Technology, United States

***Correspondence:**
Luiz R. Travassos
luiztravassos@gmail.com

Specialty section:
This article was submitted to Cancer Molecular Targets and Therapeutics, a section of the journal Frontiers in Oncology

Received: *21 August 2018*
Accepted: *08 January 2019*
Published: *25 January 2019*

Citation:
Girola N, Resende-Lara PT, Figueiredo CR, Massaoka MH, Azevedo RA, Cunha RLOR, Polonelli L and Travassos LR (2019) Molecular, Biological and Structural Features of V_L CDR-1 Rb44 Peptide, Which Targets the Microtubule Network in Melanoma Cells. Front. Oncol. 9:25. doi: 10.3389/fonc.2019.00025

Microtubules are important drug targets in tumor cells, owing to their role in supporting and determining the cell shape, organelle movement and cell division. The complementarity-determining regions (CDRs) of immunoglobulins have been reported to be a source of anti-tumor peptide sequences, independently of the original antibody specificity for a given antigen. We found that, the anti-Lewis B mAb light-chain CDR1 synthetic peptide Rb44, interacted with microtubules and induced depolymerization, with subsequent degradation of actin filaments, leading to depolarization of mitochondrial membrane-potential, increase of ROS, cell cycle arrest at G2/M, cleavage of caspase-9, caspase-3 and PARP, upregulation of Bax and downregulation of Bcl-2, altogether resulting in intrinsic apoptosis of melanoma cells. The *in vitro* inhibition of angiogenesis was also an Rb44 effect. Peritumoral injection of Rb44L1 delayed growth of subcutaneously grafted melanoma cells in a syngeneic mouse model. L1-CDRs from immunoglobulins and their interactions with tubulin-dimers were explored to interpret effects on microtubule stability. The opening motion of tubulin monomers allowed for efficient L1-CDR docking, impairment of dimer formation and microtubule dissociation. We conclude that Rb44 V_L-CDR1 is a novel peptide that acts on melanoma microtubule network causing cell apoptosis *in vitro* and melanoma growth inhibition *in vivo*.

Keywords: metastatic melanoma, microtubule, tubulin, peptide, complementarity-determining region, apoptosis

INTRODUCTION

The polymerization dynamics of cytoskeleton molecules is crucial to the survival and to the energetic and mechanistic properties of cells and organisms. As important polymers in the mitotic process, microtubules are targets of anticancer drugs, with several compounds already being studied (1, 2).

Microtubule targeting agents (MTAs) exert inhibitory effects on cell proliferation, with cell cycle arrest at G2-M and induction of apoptosis (3). They may act as vascular-targeting drugs, disrupting microtubules in endothelial cells, which affects the blood supply in the tumor tissue (4). Microtubules also induce maturation and migration of dendritic cells, which are essential to the immune response (5).

MTAs can be divided into mechanistic acting categories as they either stabilize or destabilize microtubules (6). Microtubule-stabilizing agents such as paclitaxel and docetaxel bind to the taxane-binding site on β-tubulin, inhibiting microtubule depolymerization and intensifying its polymerization. Recently, Taxol/Paclitaxel has been described as first billion-dollar anticancer drug (7). Microtubule-destabilizing agents including colchicine and vinca alkaloid, typically bind to sites located at the intra-dimer interface and near the GTP binding site on β-tubulin, respectively. Such interactions induce inhibition of microtubule polymerization and promote depolymerization (8, 9). Although these agents are widely used in medicine, particularly paclitaxel and vinca alkaloids, drug resistance and side effects such as neurotoxicity, are significant limitations to MTAs clinical success (10, 11).

In the last decade, peptides displaying anticancer properties have been studied as promising alternative agents for cancer therapy (12, 13). Peptides are mostly non-genotoxic, have high affinity and selectivity for molecular targets on cancer cells, low cost production with feasible synthesis of derivatives, exhibiting low antigenicity and good tissue penetration (14, 15). Peptides can also be conjugated to large molecules to improve pharmacokinetics (16). Peptides can be displayed on the phage surface giving rise to specific sequences targeting different tissues or be developed from internal regions of transcription factors (17). Peptides and derivatives from natural sources such as marine animals and insects have been described with preferential antitumor activity without affecting normal cells (18, 19). Complementarity-determining regions (CDRs) of immunoglobulins (Igs) have been found to exhibit with high frequency, antiinfective, immunomodulatory, and antitumor activities (20–22).

Synthetic peptides corresponding to the Ig hypervariable CDRs, may display antitumor activities *in vivo*, as well as cytotoxic effects *in vitro* including cell cycle arrest, inhibition of tumor cell migration and invasion, induction of apoptosis, disruption of cytoskeleton dynamics (22–28), and many others.

We have previously described a novel bioactive mAb V_L CDR 1 peptide (C36L1), displaying *in vitro* and *in vivo* anti-tumor activities. Depolymerization of microtubules, leading to cytotoxic and cytostatic effects mediated by Rho-GTPase, PTEN, and PI3K/Akt signaling, have been characterized (26).

Presently, we investigated a V_L CDR1-derived synthetic peptide, Rb44, expressed in a anti-Lewis B monoclonal antibody, focusing on structural, biological and molecular docking properties, in comparison with two other V_L CDR1 peptides (Rb29L1 and C36L1), to understand the mechanism of action of Ig-CDR derived, apoptotic peptides targeting microtubules. Rb44L1 exerted both *in vitro* and *in vivo* anti-melanoma activities and inhibited endothelial cell sprouting *in vitro*.

MATERIALS AND METHODS

Peptides

The L1 CDR amino acid sequences were obtained from the anti-Lewis B mAb antibody, V_L Rb44L1 (RSSQTITHGNGNTYLY-$_{NH2}$), and from the anti-A34 mAb, V_L Rb29L1 (RSSTSLLHGNGNTYLT-$_{NH2}$) according to Kabat et al. (29) CDR definition. The peptide sequences were purchased from Peptide 2.0 (Chantilly, VA) at 95–98% purity. All peptides were amidated at the C-terminus. Peptides were diluted in 1% DMSO-RPMI medium. In some experiments a scrambled Rb44L1 (Scr44) peptide was used (SIGTYSTRNYQHNLTG-$_{NH2}$). The previously described C36L1 (KSSQSVFYSSNNKNYLA-$_{NH2}$) was comparatively studied for molecular modeling.

Tumor Cell Lines and Cell Culture

B16F10-Nex2 subline of murine melanoma cells was isolated at the Experimental Oncology Unit (UNONEX) of Federal University of São Paulo (UNIFESP) and registered in the Banco de Células do Rio de Janeiro (BCRJ), no. 0342. The original B16F10 cell line was obtained from the Ludwig Institute for Cancer Research (LICR), São Paulo Branch. Human melanoma cell line A2058; human carcinoma cell lines of colon, HCT-8; uterine cervix, SiHa; and breast, MCF-7; murine fibroblasts, 3T3-NIH; and human fibroblasts, GM637, were provided by the Ludwig Institute for Cancer Research and were a gift from Dr. Luiz F. Lima Reis (Hospital Sírio-Libanez, São Paulo). Human umbilical vein endothelial cells (HUVEC) were kindly provided by the Department of Immunology, Institute of Biomedical Sciences (University of São Paulo). Both cell lines were cultured at 37°C, under humid atmosphere and 5% CO_2, in RPMI-1640 medium for tumorigenic cell lines and DMEM for non-tumorigenic ones, in both cases supplemented with 10 mM N-2-hydroxyethylpiperazine-N2 ethane sulfonic acid (HEPES), 24 mM sodium bicarbonate, 40 mg/L gentamicin, pH 7.2 and 10% fetal bovine serum (FBS).

Cell Viability Assay

For IC_{50} determination, 1×10^4 tumorigenic and non-tumorigenic cell lines were seeded in 96-well plates and treated at different concentrations ranging from 0 to 1 mM of Rb44L1 and Rb29L1 peptides for 24 h. Viable cells were quantified using the MTT (3-[4,5-dimethylthiazol-2-yl]-2,5-diphenyltetrazolium bromide) (Sigma-Aldrich, St. Louis, MO) assay. After incubation, 5 μL of MTT solution (5 mg/ml) was added to the cells, followed by incubation for 3 h at 37°C. Absorbance was measured in a microplate reader at 570 nm (SpectraMax-M2, Molecular Devices Software Pro 5.4, Sunnyvale, CA). IC_{50} was calculated using GraFit 5 data analysis software (Version 5.0.13).

Chromatin Condensation and DNA Fragmentation Assays

Apoptotic melanoma cells treated with Rb44L1 peptide were examined by TUNEL staining, using the *in situ* Cell Death Detection Kit according with the manufacture's instruction (Roche Applied Science, Madison, WI). B16F10-Nex2 melanoma cells (1×10^4) were seeded on 96-well clear-bottom black

polystyrene microplate and incubated with 0, 130 and 260 μM of Rb44L1 peptide for 18 h. After incubation, cells were fixed in formaldehyde 2% for 20 min at room temperature, washed in PBS, and incubated with Hoechst 33342 (Invitrogen, Eugene, OR), at 10 μg/mL final concentration in the reaction buffer and TUNEL enzymatic substrate. Cells were washed and images were acquired and analyzed in a Cytell Cell image cytometer (GE Healthcare, Little Chalfont, UK).

Annexin V and Propidium Iodide Labeling

B16F10-Nex2 cells (5×10^5) were cultured in 6-well plates and further incubated with Rb44L1 at 0, 80 and 100 μM for 18 h at 37°C. After incubation, the Annexin V-FITC Apoptosis Detection Kit (Sigma-Aldrich, St. Louis, MO) was used and cells labeled with propidium iodide (PI) and FITC annexin V (AV) were analyzed by flow cytometry (BD Bioscience FACSCanto II equipment, Franklin Lakes, NJ), using FlowJo software (TreeStar Inc., Ashland, OR).

Cell Cycle Analysis

B16F10-Nex2 (5×10^5) cells were seeded in conical centrifugation tubes and incubated with 65 μM Rb44L1 peptide for 16 h in suspension. After incubation, the cells were washed with PBS and fixed in ethanol 70% for 1 h at 4°C. Cells were then washed again with PBS and stained with propidium iodide (PI) solution (50 μg/ml PI, 0.1 mg/ml RNAse A) for 20 min at 4°C in the dark. DNA fluorescence staining was acquired by FACSCalibur flow cytometer (Becton Dickinson, San Jose, CA). FlowJo software (Tree Star Inc., Ashland, OR) was used for post-acquisition analysis (20.000 events per sample). The microtubule depolymerizing CA4 (combretastatin A4, Sigma-Adrich, St. Louis, MO) was used at 75 μM as positive control of G2/M cell cycle arrest.

Transmission Electron Microscopy

B16F10-Nex2 cells (1×10^6) were seeded in 6-well plates. Cells were then incubated with peptide Rb44L1 at 260 μM for 18 h at 37°C. Fixation, dehydration and staining of the samples were performed as previously described (23). Jeol 1200 EXII electron microscope (Tokyo, Japan) was used for image acquisition.

Mitochondrial Membrane Potential ($\Delta\psi m$)

B16F10-Nex2 cells (1×10^4) were pre-incubated with the cationic lipophilic dye tetramethylrhodamine ethyl ester (TMRE) at 20 nM for 30 min, and then with peptide Rb44L1 at 0, 130, and 260 μM for 6 h. After the incubation period, images of living cells were acquired and analyzed by Cytell Cell Imaging System (GE Healthcare, Little Chalfont, UK).

Superoxide Anion Measurement

Superoxide anion production was measured by dihydroethidium (DHE) assay. Briefly, 1×10^4 cells cultivated on 96-well clear-bottom black plate were pre-incubated with DHE for 30 min at 37°C. Rb44L1 was added at 130 and 260 μM concentrations and fluorescence units were quantified after 16 h in a microplate reader (Molecular Devices M2, Sunnyvale, CA) adjusted for excitation at 370 nm and emission at 420 nm. As positive control, cells were treated with 5 mM of H_2O_2 at 37°C for 20 min, and the negative control run with no peptide.

Cell Lysate Extracts and Western Blotting

B16F10-Nex2 cells (10^6) were incubated with 0 and 130 μM of Rb44L1 peptide for different times (1, 3, 6, 8, and 24 h). After incubation, cells were washed in PBS and lysed with 300 μL of SDS sample buffer (62.5 mM Tris-HCl, pH 6.8 at 25°C, 2% w/v SDS, 10% glycerol, 50 mM DTT, 0.01% w/v bromophenol blue). Proteins from whole cell extracts were analyzed by Western blotting as previously described (20). The following primary, highly specific monoclonal antibodies, were used: rabbit anti-Bcl-2, -Bcl-xl, -Bax, -caspase-9 and cleaved caspase-9, -caspase-3 and cleaved caspase-3, -Parp and cleaved Parp, and -GAPDH (for total protein loading control), with secondary anti-rabbit IgG conjugated with horseradish peroxidase (HRP). All antibodies were purchased from Cell Signaling Technology (Beverly, MA) except for anti-GAPDH, acquired from Sigma-Aldrich (St. Louis, MO). Immunoreaction was revealed using the Luminata™ Forte solution (Millipore, Billerica, MA) and images were acquired using Uvitec Cambridge (Cambridge, UK). The molecular mass of each protein was estimated based on a pre-stained protein standard (Spectra Multicolor, ThermoScientific, Waltham, MA). Full-length Western blotting membranes are displayed in **Figure S1**.

In vitro Angiogenesis Assay

The basement matrix Geltrex™ (Invitrogen, Eugene, OR) was added (30 μl/well) to coat a 96-well plate and allowed to polymerize for 40 min at 37°C. HUVEC cells (5×10^3) suspended in RPMI medium supplemented with 0.2% of fetal calf serum were plated alone (control) or mixed with 5 μM of Rb44L1 peptide. The cells were incubated at 37°C for 6 h and images were captured with a microscope digital camera (Olympus, Tokyo, Japan). The numbers of pro-angiogenic structures (typically closed compartments or rings formed after endothelial cell sprouting) were counted from 3 different wells.

Ethics Statement

The present study is part of Project 2010/51423-0 granted by the São Paulo State Research Support Foundation (FAPESP), Brazil. The protocols used for animal experiments were carried out in accordance with the Ethics Committee of Federal University of São Paulo, Brazil and have been approved via document CEP 1234/2011.

Mice and Subcutaneous Melanoma Model

Eight-week-old male C57Bl/6 mice were acquired from the Center for Development of Experimental Models (CEDEME) at Federal University of São Paulo (UNIFESP), Brazil. The Ethics Committee for Animal Experimentation (UNIFESP) approved protocols of animal experiments. In the subcutaneous (s.c.) melanoma model, male C57Bl/6 mice (five per group) were subcutaneously grafted in the right flank with 1×10^5 syngeneic B16F10-Nex2 melanoma cells. Animals were subjected to 5 peritumoral daily doses of 300 μg (total 10 mg/kg) of Rb44L1. DMSO (1%) in PBS, was the vehicle control. Treatment started

after the tumor size reached 80 mm^3 as measured with a caliper. The tumor volume (V) was calculated by the formula $V = 0.52 \times d^2 \times D$, where d and D are short and long diameters of the tumor, respectively, measured every other day. Mice were euthanized at the end of experiments or when the tumor size reached the maximum allowed volume of 3,000 mm^3.

Live-Cell Imaging of Microtubule Dynamics

Real-time fluorescence microscopy of living B16F10-Nex2 melanoma cells previously modified by viral transduction for the expression of green fluorescent tubulin (CellLight® Reagents −2.0 BacMam, Life Technologies), was used to investigate the peptide interaction with microtubules. Viable green fluorescence protein (GFP) tubulin-expressing cells (1×10^4) were incubated with Rb44L1 and Rb29L1 at 260 μM and fluorescent images were taken at 10-min intervals during 2 h using the time-lapse BioStation fluorescence microscope (Nikon Instruments, Inc, Melville, NY). For instance, humidity, temperature (37°C) and CO_2 (5%) were carefully controlled. Fluorescence analysis and quantification were performed with the ImageJ software and the video was processed with the NIS-Elements analysis software (Nikon, Tokyo) and Adobe After Effects software.

Fluorescence Staining of F-Actin

B16F10-Nex2 cells (5×10^4) were seeded in 24-well microplates and incubated with different concentrations of Rb44L1 (0, 130 and 260 μM) for 30 min and 3 h. After incubation, cells were fixed in 3.7% of formaldehyde for 20 min at 4°C, blocked (1% BSA, 5% SFB, 0.1% Triton in 1X PBS) for 30 min at room temperature and stained with Hoechst 33342 (Invitrogen, Eugene, OR) and anti-phalloidin conjugated with FITC for 1 h at 37°C. Images were acquired and analyzed by Cytell Cell Imaging System (GE healthcare, Little Chalfont, UK).

System Preparation and Molecular Dynamics

De novo peptide structure prediction was made by Pep-Fold3 webserver (30). We obtained the tubulin structure from PDB 4TV9 (31) (chains A and B). Protonation analysis was made by PROPKA3 (32). Energy minimization was carried out on GROMACS 5.1 (33) using CHARMM36 force field (34). Systems were built by CHARMM-GUI webserver (35, 36) with TIP3P water molecules (37) and counter ions, when charge balancing was required. Simulations consisted of 5,000 steps of steepest descent energy minimization, followed by 25 ps of NVT equilibration dynamics for L1-CDR peptides and 10 ns for tubulin. A NPT production molecular dynamics of 100 ns was carried out on GROMACS 5.1 using CHARMM36 force field for each system. Secondary structure assignment and hydrogen bonds (H-bonds) were analyzed by using VMD (38) plugins. H-bonds distance cut-off was set up at 3.0 Å with angle cut-off of 20°. All further MD analyses were made by GROMACS 5.1.

Normal Mode Calculations and Generation of Low-Energy Conformations

Normal mode analysis (NMA) was performed using CHARMM c41b1 (39) and CHARMM36 force filed using DIMB (40) module and excluding CMAP (41). A distance dependent dielectric constant was employed to treat the electrostatic shielding by the solvent as described by Philot et al. (42). We used the mode 08 (open/close of tubulin monomers) as directional constraint to generate low-energy conformers along the mode trajectory using the VMOD algorithm in CHARMM as depicted by Louet et al. (43). The restraints were applied only on Cα atoms and the energy was computed for all atoms. The structures were displaced from 0.0 Å to +6.0 Å (open direction) using steps of 1.0 Å, resulting in 7 intermediate low-energy structures along the mode.

Molecular Docking

In order to obtain different structures to perform molecular docking, we clustered the MD trajectory of each peptide. All MD frames were fitted to the reference structure and clustered with GROMOS method by using GROMACS 5.1, with a backbone RMSD cutoff of 2.0 Å for Rb29 and Rb44 and 5.0 Å for C36 (since the last is very flexible) resulting in 3, 11, and 8 different clusters, respectively. The center structure of each peptide cluster was then used in docking simulations, performed with Hex 8.0 (44). Hex depicts proteins as rigid bodies and makes a blind search through protein surface while it evaluates the interaction correlation by using the fast Fourier transformation algorithm. As described in Meissner et al. (45), solvation and desolvation effects were treated as surface phenomena, since the Hex algorithm models the interaction, excluding volume and complementarity of form. Approximately 350 solutions were found for each combination. We used BINANA 1.2 (46) as a rescore method to investigate the specific molecular basis guiding the interaction between tubulin and peptides.

Chemiluminescent Dot-Blotting

Peptide Rb44L1 binding to microtubule structures was determined by chemiluminescent (CL) dot-blotting as described elsewhere (26) with some modifications. Peptides C36L1 (positive control), Rb44L1, scrambled-Rb44L1 (Scr44) at 10 μg/10 μL each, or vehicle (1% DMSO in milli-Q water), were applied on nitrocellulose membranes. They were blocked with 5% BSA in 0.05% PBS-Tween 20. B16F10-Nex2 cell protein lysate (50 μg/ml), prepared with non-denaturing protein extraction buffer according to the manufacturer's instructions (Cell Signaling, Beverly, MA), was applied onto the nitrocellulose membranes and incubated overnight at 4°C. After washing, membranes were incubated with anti-alpha tubulin antibody (Sigma-Aldrich, St. Louis, MO) for 1 h at 37°C followed by anti-rabbit IgG-HRP antibody for 1 h at 37°C. Immunoreactivity was determined using the Luminata™ Forte solution (Millipore, Billerica, MA). Images were acquired by Uvitec Cambridge (Cambridge, UK) with 1-min membrane exposure time. No reactivity with the control peptide was observed. To investigate the influence of GTP and Mn^{2+} on the peptide binding with α-tubulin, the membranes coated with 10 μg Rb44L1 or scrambled (Scr44) peptide were blotted with or without 1 mM GTP (Cytoskeleton, Denver, CO) and/or 1 mM $Mn_2SO_4H_2O$ (Sigma-Aldrich, St. Louis, MO) added to the cell lysate (50 μg/ml), for 2 h at 37°C. Chemiluminescence was detected as described above but with short membrane exposure time (20 s).

Tubulin Polymerization Assay

Microtubule polymerization was evaluated using the Tubulin Polymerization Assay kit (Cytoskeleton, Inc., Denver, CO). Rb44L1 (130 μM) or Scr44 (130 μM); colchicine (50 μM); Rb44L1 (130 μM) + colchicine (50 μM), diluted with 1% DMSO in distilled water were added to 50 μl of the tubulin reaction mix with optimized volumes for inhibitor detection containing 2 mg/ml or 1 mg/ml of tubulin in 80 mM PIPES (piperazine-N-N'-bis [2- ethane sulfonic acid] sodium salt), pH 6.9, 2 mM $MgCl_2$, 0.5 mM EGTA (ethylene glycol-bis N,N,N',N'- tetra acetic acid), 60% v/v glycerol, 1 mM GTP, and 10 μM of the fluorescent reporter. The black, flat bottom, half area 96-well plate, with the samples, was examined in a fluorescence microplate reader (SpectraMax-M2e, Molecular Devices, Sunnyvale, CA) every 1 min at 340 nm of excitation and 410 nm of emission for 40 or 180 min. To monitor the tubulin polymerization in the same condition as of the dot blotting assay, the reaction was prepared as described above with 2 mg/ml of purified tubulin in 0.1% of BSA in PBS and 3.4% of cell lysis buffer, without cell lysate.

Statistical Analysis

The software GraphPad Prism 5.0 (San Diego, CA) was utilized for all tests. Statistical differences between groups were compared by Student's *t*-test. Differences in survival time and rate were evaluated by the Kaplan-Meier survival curves. *P*-values are indicated as $^{*}p < 0.05$, $^{**}p < 0.01$ and, $^{***}p < 0.001$.

RESULTS

L1-CDR Peptides Differ in Dynamic Features

Peptides Rb44L1 and Rb29L1 were studied in comparison with peptide (C36L1), which exerts cytotoxicity by depolymerization of microtubules and displays antitumor activities, as previously investigated (26).

In spite of the sequence similarity, the dynamics of L1-CDRs were very different from each other. Rb29L1 assumed a stable β-hairpin conformation, with residues ^{5}SLL and ^{13}TYL forming the β-sheet (**Figures 1A,B**). In turn, Rb44L1 showed only an intermittent β-bridge between residues ^{5}TI and ^{14}YL (**Figures 1C,D**). C36L1, however, did not assume any ordered structure (**Figures 1E,F**). Root-mean-squared deviation (RMSD) of backbone heavy atoms and Cα root-mean-squared fluctuation (RMSF) calculations were performed to evaluate structure stability along the molecular dynamics (MD). Results confirmed the stability of Rb29L1, while C36L1 showed several conformational shifts (**Figure 1G**). Flexibility analysis confirmed this profile (**Figure 1H**). H-bonds formation during the dynamics could address these structural differences among the peptides. Rb29L1 showed more internal H-bonds than the other peptides, therefore it is more rigid. **Table 1** summarizes these interactions. The trajectories of each peptide MD were clustered, according to RMSD, onto representative conformations to perform docking simulations (**Figure S2**).

In vitro Cytotoxicity of CDR Peptides

We investigated the anti-tumor potential of two L1-CDR-derived peptides: Rb44L1 from anti-Lewis B mAb and Rb29L1 from anti-A34 mAb. The IC_{50} values were determined for the Rb44L1 and Rb29L1 against different tumorigenic and non-tumorigenic cell lines (**Table 2**). Peptide Rb44L1 showed the lowest IC_{50} values as compared to Rb29L1. The concentrations of 130 μM (IC_{50}) and 260 μM (IC_{100}), respectively, were therefore used in the subsequent experiments with B16F10-Nex2 melanoma cells. Rb44L1, was less active against non-tumorigenic cells, including murine and human fibroblasts, 3T3-NIH and GM637 cell lines. In the concentration range of 0 to 0.140 mM, no cytotoxicity was observed in these cells. Rb29L1 IC_{50} values were 3- to 10-fold higher than those of Rb44L1 in tumorigenic cell lines.

Rb44L1 Induces Apoptosis

Changes in the dynamics of the cytoskeleton have been implicated in the induction of apoptosis. Here, we show that Rb44L1 induced morphological alterations typical of apoptotic cell death such as cellular shrinkage, membrane blebs and cell rounding-up with pseudopodia retraction in B16F10-Nex2 melanoma cells when incubated with peptide at IC_{50} (130 μM) and IC_{100} (260 μM) for 18 h (**Figure 2A**). Chromatin condensation was observed in 95% and 98% of tumor cells treated with Rb44L1 at 130 and 260 μM, respectively, for 18 h. DNA fragmentation was determined by green positive TUNEL staining in B16F10-Nex2 cells treated with 130 and 260 μM of Rb44L1 (**Figures 2B,C**). Both DNA condensation and fragmentation were significantly higher in Rb44L1-treated cells as compared with the negative control (for chromatin condensation, $^{**}p < 0.01$ at 130 μM, $^{***}p < 0.001$ at 260 μM; and for DNA fragmentation, $^{***}p < 0.001$ at both concentrations). Additionally, we observed that Rb44L1 could significantly enhance the translocation of phosphatidylserine (PS) to the outer leaflet of the plasma membrane, indicating early apoptosis. We observed a significant increase in the number of early apoptotic events in cells treated with Rb44L1 at 80 and 100 μM, in comparison with untreated control cells (**Figure 2D**). Finally, Rb44L1 inhibited cell proliferation with cell cycle arrest, at 65 μM (**Figure 2E**). The S-phase area decreased from 22.3 to 13.4%, with increase of the G2/M phase (from 21.8 to 33.5%). Microtubule depolymerizing combretastatin-A4 was used as positive control.

Morphological and Functional Alterations in Mitochondria and ROS Production

Transmission electron microscopy (TEM) of Rb44L1-treated B16F10-Nex2 cells, at 260 μM for 18 h, showed condensed chromatin, nuclear membrane detachment, enlarged, and vacuolated mitochondria with damaged cristae surrounded by heavily injured cytoplasmic organelles compared to untreated cells (**Figure 3A**). The collapse of the mitochondria transmembrane potential ($\Delta\psi m$) was observed on early incubation with Rb44L1 (0, 130, and 260 μM). After 6 h, reduction of TMRE fluorescence (53 and 94% reduction in cells treated with 130 and 260 μM, respectively; $^{**}p < 0.01$ and $^{***}p < 0.001$ in relation to untreated cells) was observed indicating mitochondrial damage in these cells (**Figure 3B**).

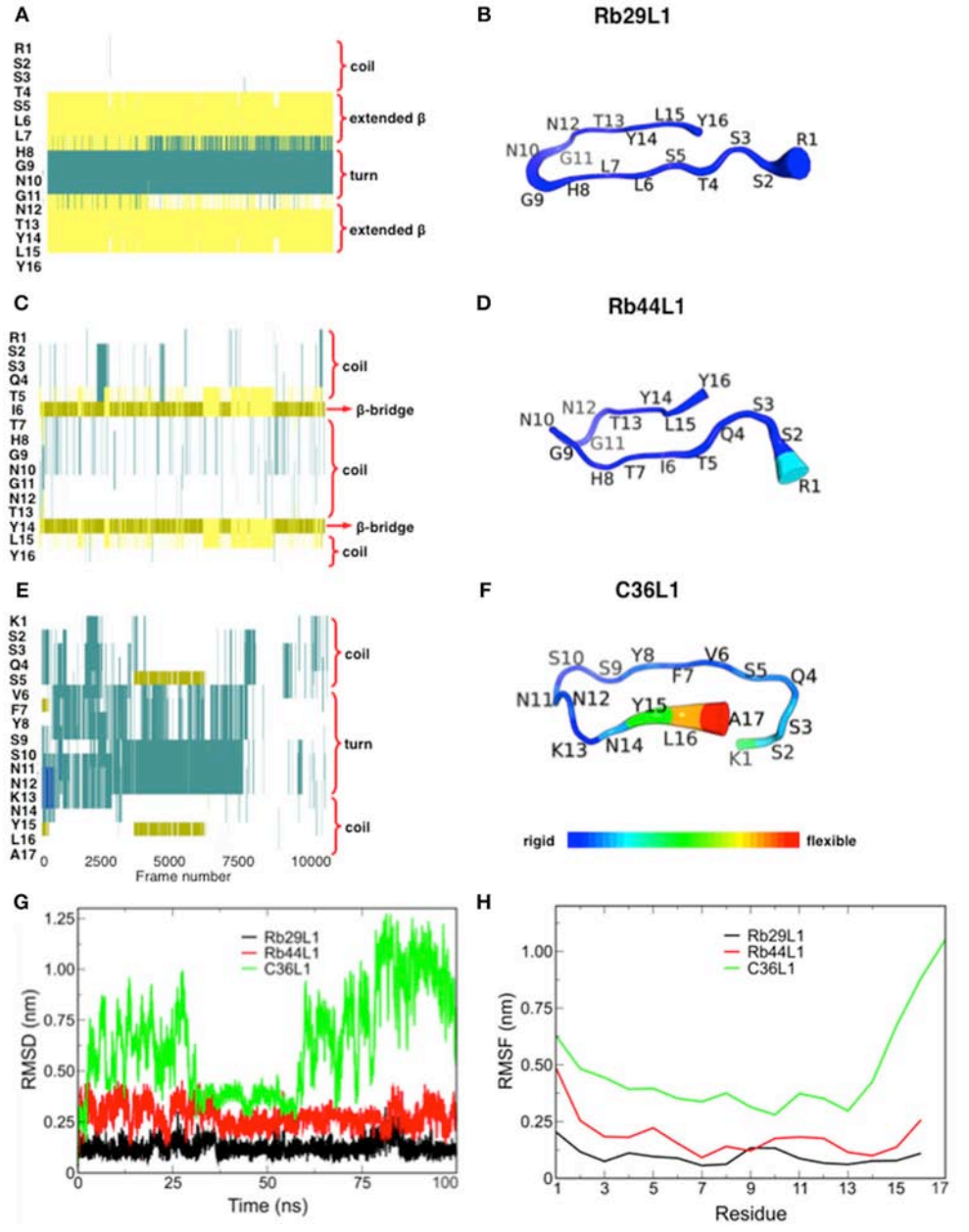

FIGURE 1 | Secondary structure assignment during molecular dynamics and structural analysis of L1-CDRs. **(A,B)** Rb29L1 assumes a stable β-hairpin conformation during MD, showing a well established β-sheet between residues ^{5}SLL and ^{13}TYL; **(C,D)** Rb44L1 shows a recurrent β-bridge between residues ^{5}TI and ^{14}YL; **(E,F)** C36L1 presents the most flexible conformation, in its majority composed by turn and coil. Secondary structure color code: turn, in green; extended conformation (β-sheet), in yellow; isolated bridge, in gold; 3-10 helix, in blue; coil, in white; **(G)** root-mean-squared deviation of backbone atoms of Rb29L1, Rb44L1, and C36L1. Rb29L1 remains nearly at the same conformation during all MD, an effect also seen for Rb44L1, although with less intensity. C36L1, nonetheless, presented a great conformational variation; **(H)** root-mean-squared fluctuations of Cα atoms of Rb29L1, Rb44L1 and C36L1. Cα fluctuation, or flexibility, follows RMSD pattern. Rb29L1 presents a rigid structure while Rb44L1 and C36L1 are more flexible, the latter more pronounced.

Tumor cells were incubated with Rb44L1 at 130 and 260 μM for 16 h and ROS levels were detected using DHE dye measured by fluorimetry. Hydrogen peroxide (H_2O_2) was used as positive control (Control +) at 5 mM. Accumulation of ROS (59% in relation to untreated cells; $^{***}p < 0.001$) was observed in cells treated with Rb44L1 at both concentrations (**Figure 3C**).

Rb44L1 Elicited Caspase Activation

Different pro- and anti-apoptotic proteins in total cell lysates were evaluated by Western blotting in Rb44L1-treated B16F10-Nex2 cells at 130 μM and different incubation periods. We observed that Rb44L1 induced early increase of pro-apoptotic Bax protein, followed by the cleavage of caspase-9, caspase-3 and

TABLE 1 | Hydrogen bonds formation during molecular dynamics of L1-CDR peptides*.

Hydrogen bonds	Occupancy (%)
Rb29L1	
ARG1-Side-NH1 – TYR16-Side-OT1	34.94
ARG1-Side-NH1 – TYR16-Side-OT2	17.56
ARG1-Side-NH2 – TYR16-Side-OT1	17.78
ARG1-Side-NH2 – TYR16-Side-OT2	37.64
SER3-Side-OG – TYR16-Side-OT1	27.63
SER3-Side-OG – TYR16-Side-OT2	18.97
THR4-Main-N – TYR16-Side-OT1	11.7
THR4-Main-N – TYR16-Side-OT2	27.13
LEU6-Main-N – TYR14-Main-O	42.05
HIS8-Main-N – ASN12-Main-O	43.21
TYR14-Main-N – LEU6-Main-O	36.03
TYR16-Main-N – THR4-Main-O	43.64
TYR16-Side-OH – HIS8-Side-NE2	17.83
Rb44L1	
THR7-Main-N – THR13-Main-O	36.35
LEU15-Main-N – THR5-Main-O	54.47
C36L1	
ALA17-Main-N – GLN4-Main-O	11.51

Only interactions with ≥ 10% occupancy are shown.

TABLE 2 | IC_{50} values of the bioactive peptide Rb44L1 and control Rb29L1 against tumorigenic and non-tumorigenic lineages after 16 h of incubation.

Cell lineages	IC_{50} (μM) ± SD	
	Rb44L1	Rb29L1
B16F10-Nex2	130 ± 5.8	465 ± 67
A2058	66 ± 2.0	265 ± 16
MCF-7	134 ± 2.4	858 ± 53
SIHA	51 ± 6.6	773 ± 61
HCT-8	81 ± 1.5	821 ± 57
3T3-NIH*	>140	>140
GM637*	>140	>140

*Non-tumorigenic cell lines.

PARP, together with downregulation of anti-apoptotic protein Bcl-2 (**Figure 3D**). GAPDH was used as loading control.

Rb44L1 Inhibited Angiogenesis *in vitro*

The cytotoxicity of Rb44L1 at different concentrations was assayed in the HUVEC lineage (**Figure 4A**). A non-cytotoxic concentration was used for the inhibition of endothelial cell (HUVEC) sprouting in Geltrex™ Matrix. Rb44L1 at 5 μM for 6 h, significantly inhibited 90% of endothelial cell sprouting, with the number of compartments built by intercellular connections being compared to that of the control ($^{**}p < 0.01$; **Figures 4B,C**).

Antitumor Activity *in vivo* Against Subcutaneous Melanoma

The *in vivo* antitumor activity was also investigated in a subcutaneously grafted, syngeneic murine melanoma model. Peritumoral injections of Rb44L1 at 15 mg/Kg significantly delayed tumor volume progression ($^{**}p < 0.01$), and also prolonged mice survival ($^{**}p < 0.01$) (**Figures 4D,E**). Mice were euthanized at the scheduled end of experiments, or before, should the tumors ulcerate or reach the maximum allowed volume of 3,000 mm^3.

Rb44L1 Interacts With Microtubules and Induces Cytoskeleton Disruption in Melanoma Cells

Disruption of the microtubule integrity in B16F10-Nex2 cells was monitored during the incubation with Rb44L1 and Rb29L1. Microtubules were assessed by live-cell imaging using B16F10-Nex2 cells previously transduced with a genetic modified insect virus (baculovirus) containing a tubulin-green fluorescent fusion-protein construct (CellLight®, Life Technologies). The fluorescence of live murine melanoma cells was monitored and quantified for 2 h during incubation with 260 μM of Rb44L1 and Rb29L1. The Rb44L1 peptide drastically reduced microtubule fluorescence compared to the negative control (**Figures 5A,B**), indicating that the microtubule network was depolymerized during the incubation with Rb44L1, whereas no depolymerization was seen in Rb29L1 treated cells. A representative video showing the kinetics of microtubule depolymerization in B16F10-Nex2 cells during the incubation with Rb44L1 and Rb29L1 is available in **Video S1**.

In addition to investigating whether Rb44L1 would also affect the integrity of F-actin, the reaction was assessed simultaneously using a phalloidin-FITC probe, as described in methods. We observed that F-actin integrity was completely lost after 3 h of incubation with Rb44L1 at 260 and 130 μM (**Figure 5C**). Actin degradation occurred after the microtubule disruption process, as evidenced in the cytoskeleton integrity quantification analysis (**Figure 5D**), suggesting that actin filaments were disrupted as a consequence of microtubule depolymerization ($^{*}p < 0.05$ comparing microtubule and actin disruption). Less than 55 or 65% of cytotoxicity was seen when testing both concentrations of Rb44L1 at 260 and 130 μM, respectively, in the first hours of incubation (**Figure S3**).

Normal Modes Expose Nonexchangeable Nucleotide and Colchicine Binding Sites

Normal mode analysis (NMA) was employed to investigate the opening motion of tubulin monomers. We hypothesized that this opening motion would be required to expose the nucleotide binding site located at α-tubulin (N-site) and dimer interface. Such exposition could favor the efficient docking of L1-CDR peptides and impair the tubulin dimer assembly, finally leading to microtubule dissociation. This motion was verified as the normal mode 8 (**Figures 6A,B**). Using the VMOD routine implemented on CHARMM, we performed a mass-weighted displacement of tubulin structure along mode 8, to produce energy-relaxed structures with gradually exposed nucleotide site. Tubulin residues originally in contact with GTP (contacts within 4.5 Å) showed a solvent-accessible surface area (SASA) of 511

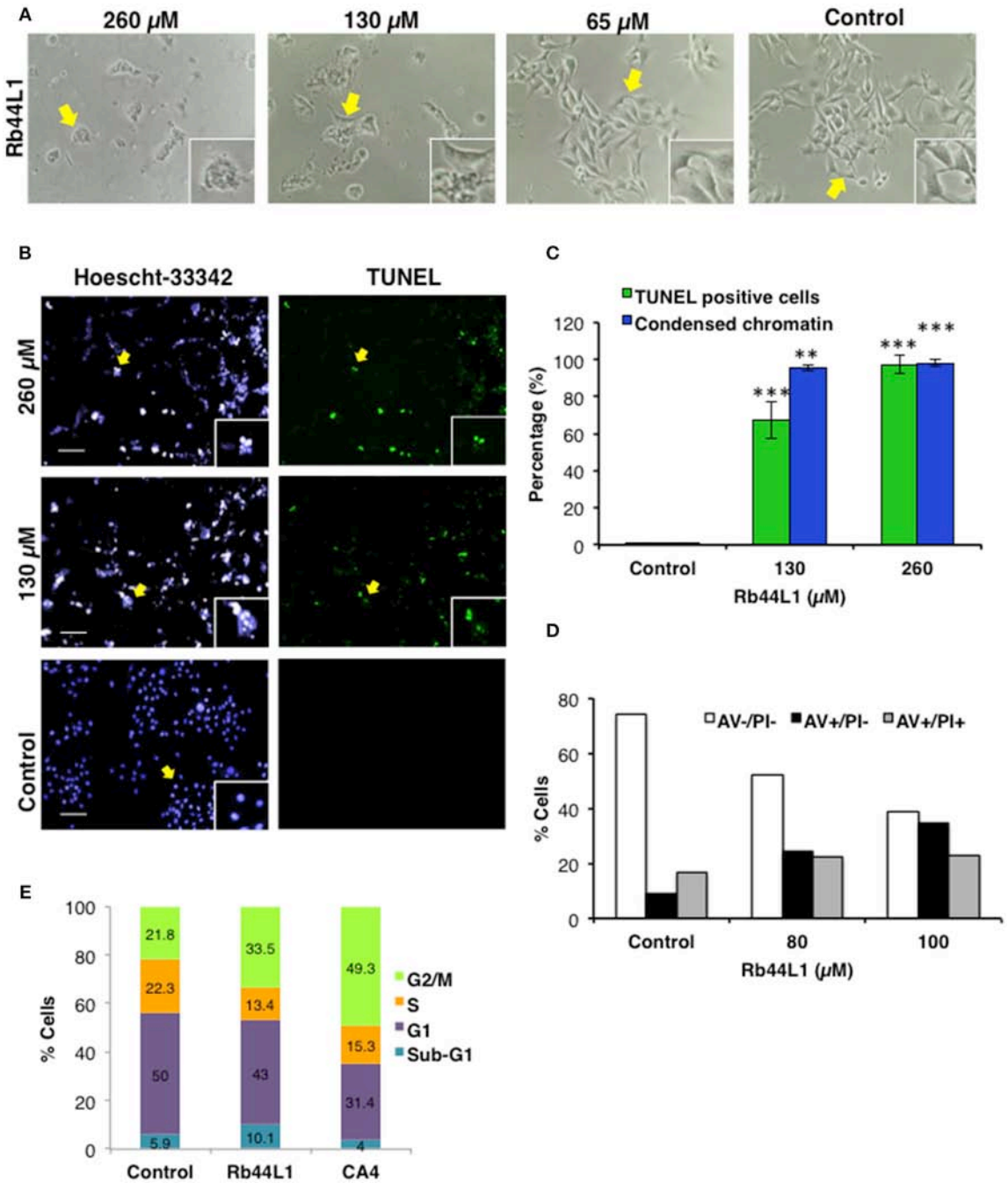

FIGURE 2 | Rb44L1 induces apoptosis in melanoma cells. **(A)** morphological changes were analyzed by light microscopy. Representative images of cells treated with different doses of Rb44L1 or untreated cells (control). Arrows indicate inserts (x200, magnification); **(B)** representative images of chromatin condensation (Hoescht 33342, blue) and DNA fragmentation (TUNEL, green) of tumor cells treated with different concentrations of Rb44L1 for 18 h. Scale bar represents 50 μm; **(C)** percentage of TUNEL positive cells and condensed nuclei. $^{**}p < 0.01$ and $^{***}p < 0.001$ in comparison to untreated cells; **(D)** percentage of apoptotic cells determined by the externalization of phosphatidylserine; **(E)** cell cycle of B16F10-Nex2 cells after incubation with Rb44L1 at 65 μM for 16 h. Percent tumor cells at Sub-G1, G1, S, and G2/M phases are indicated. CA4 was used as positive control.

Å² at the crystallographic structure (PDB 4TV9), while the same residues were more exposed after a displacement of 6 Å, presenting a SASA of 588 Å² (**Figures 6C,D**). The same occurred for the colchicine site, which presented a SASA of 225 Å² before the displacement and 236 Å² after mass-weighted displacement of 6 Å.

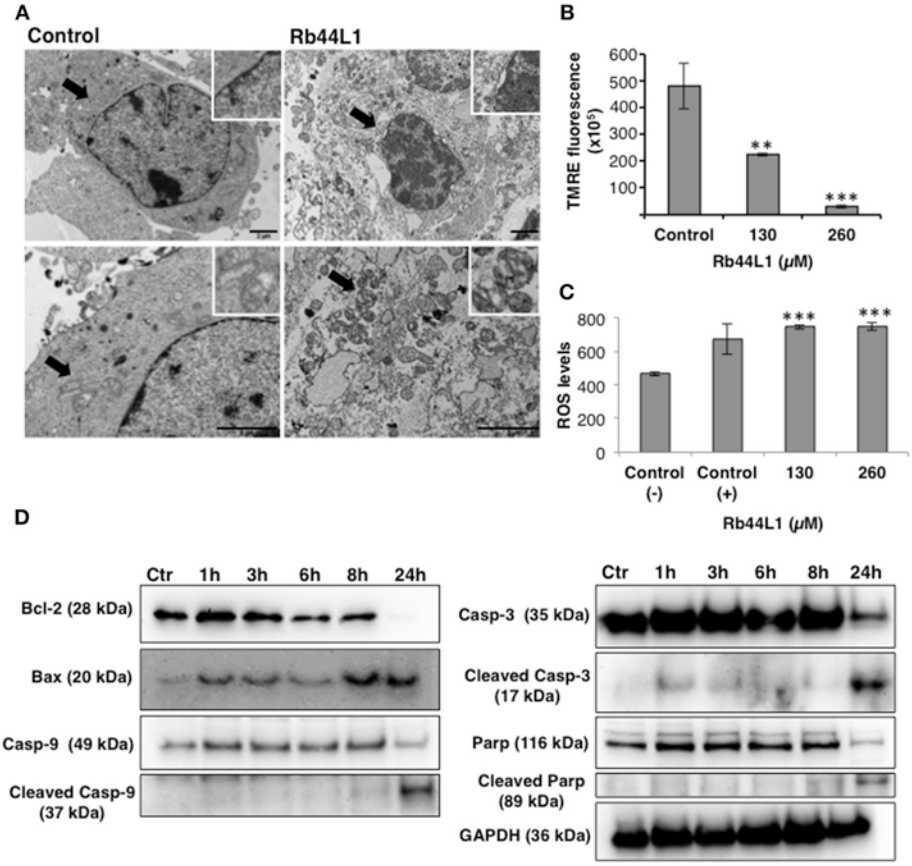

FIGURE 3 | Rb44L1 induces morphological alterations in mitochondria. **(A)** B16F10-Nex2 cells were treated with 260 μM of Rb44L1 for 18 h and examined by transmission electron microscopy. Representative micrographs of untreated cells (control) and Rb44L1 treated cells. Arrows indicate mitochondrial ultrastructure in the inserts; scale bar represents 2 μm; **(B)** loss of mitochondrial transmembrane potential in B16F10-Nex2 cells treated with 130 and 260 μM of Rb44L1 for 6 h, probed with red TMRE. $^{**}p < 0.01$ and $^{***}p < 0.001$ in comparison to the control; **(C)** enhanced superoxide anion production observed by DHE staining in B16F10-Nex2 cells treated with different concentrations of Rb44L1 for 16 h, vehicle control (Control −) and 5 mM H_2O_2 as positive control (Control +). The conversion of DHE to ethidium by oxidation was acquired at 370 nm (excitation) and 420 nm (emission). $^{***}p < 0.001$ in relation to control (−); **(D)** levels of apoptosis related proteins in Rb44L1-treated melanoma cells. Time-dependent effect on cell signaling of B16F10-Nex2 incubated with Rb44L1 at 130 μM. Levels of total and cleaved caspase-3,−9, cleaved PARP, Bax, Bcl-2, and Bcl-xl during Rb44-induced apoptosis are shown by Western blotting. GAPDH was used as loading control. A single cell-lysate sample was used in the same experiment and the Western blotting membranes were processed in parallel for antibody reactivity. Uncropped, full-length blottings are shown in **Figure S1**.

Docking Studies Reveal the Importance of Electrostatic Interactions

Docking calculations were performed using 7 tubulin structures generated from NMA displacement against the central structure of each L1-CDR peptide cluster (3 for Rb29L1, 11 for Rb44L1, and 8 for C36L1). In every docking round, an average of 350 different solutions was calculated. We then evaluated the best solution from Hex with BINANA to better understand the key binding characteristics governing the interaction.

Results indicated less favorable interactions for Rb29L1 than C36L1 and Rb44L1 in almost all displacements (as summarized in **Table 3**, detailed in **Table S1**, respectively), according to experimental results. At the best pose for Rb44L1 (docked with tubulin displaced by 2 Å) the ^{1}R side-chain is buried in the cavity formed between tubulin monomers, participating in 3 of 6 H-bonds and 2 salt-bridges (**Figures 7A,C,E,G**). In fact, interactions involving ^{1}R were observed in all displacements except at 3 Å and 4 Å. This indicates the putative importance of this residue to maintain the interaction with tubulin. When the ^{1}R is replaced by alanine, the results showed a systematic worsening of energy values (as summarized in **Table 3**, detailed in **Table S1**). Biological assays confirmed this prediction since the R1A substitution in Rb44L1 was not cytotoxic to B16F10-Nex2 cells, in the 0 to 500 μM range (data not shown). C36L1 pose analysis also indicated the involvement of a basic residue governing the interaction with tubulin. The ^{13}K was present participating of H-bond, salt-bridge or cation-pi interactions in all tubulin displacements but at 5 Å. At the best pose–docked with tubulin displaced by 4 Å, ^{13}K appeared in two H-bonds and in a salt-bridge (**Figures 7B,D,F,H**). Moreover, its side-chain was also buried in a cavity between tubulin monomers. On the other hand, although Rb29L1 had a greater number of H-bonds, the lack of

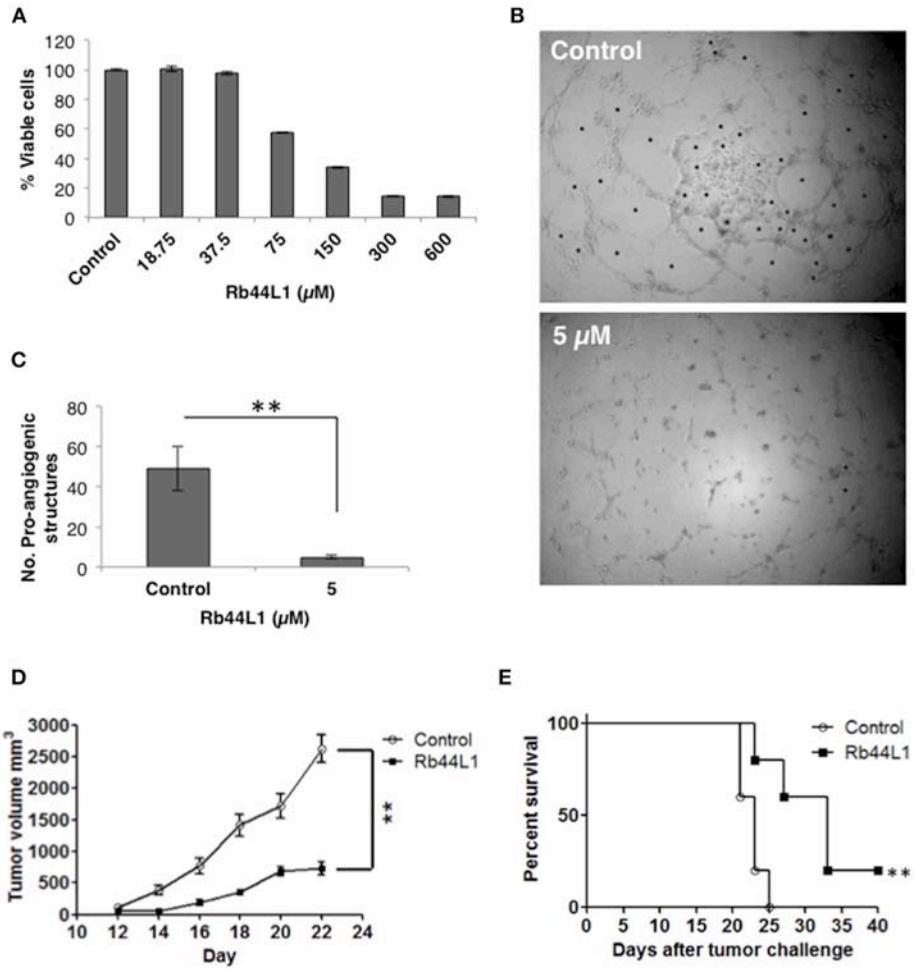

FIGURE 4 | Rb44L1 inhibits HUVEC sprouting on Geltrex^{TM} Matrix. **(A)** dose-response curve of Rb44L1 on HUVEC cells; **(B,C)** Inhibition by Rb44L1 (5 μM) on HUVEC sprouting on Geltrex^{TM} Matrix to form closed proangiogenic structures; $^{**}p < 0.01$ compared to untreated control. Rb44L1 prevents tumor progression. **(D)** 1×10^5 syngeneic B16F10-Nex2 cells were subcutaneously injected in C57Bl/6 mice. Peritumoral daily doses of 300 μg of Rb44L1 peptide were administered during five consecutive days. Tumor volume was measured and documented during the treatment period. $^{**}p < 0.01$ in comparison with control group treated with PBS; **(E)** survival of C57Bl/6 challenged mice after treatment with Rb44L1 or PBS (control). $^{**}p < 0.01$ in relation to control group.

charged residues would contribute to predicted energies higher than the other peptides.

Docking Studies Showed the L1-CDR Interactions Preferentially at the Nonexchangeable Nucleotide-Binding Site

We evaluated the best docking pose for both Rb44L1 and C36L1 in relation to the exposed nucleotide and colchicine binding sites. Rb44L1 interacted with three residues of the N-site (^{11}Q, ^{69}D, and ^{71}E) and with one residue of the colchicine site (^{252}K). The ^{1}R participated in all interactions. C36L1, however, interacted with different residues of the N- site (^{71}E, ^{11}Q, ^{224}Y, ^{206}N, ^{177}V) and one residue of colchicine site (^{179}T). These interactions depended on ^{13}K and ^{11}N residues of the C36L1 peptide (**Figures 8A,B**). Rb29L1 showed interactions with tubulin similarly with those of C36L1 (^{177}V, ^{179}T, ^{206}N, and ^{224}Y). In contrast, there were interactions shared with Rb44L1 and C36L1 (^{11}Q and ^{71}E), which were absent in Rb29L1 (**Figure 8C**). Taken together, these results showed that tubulin-opening motion corresponded to a decrease of summed electrostatic energy values of the displaced structures (**Figure 8D**).

Both Rb44L1 and C36L1 interacted with the region of helices α2, α3 and α8 of α-tubulin subunit, and showed differences in relation to β-tubulin monomer. While Rb44L1 interacts with loops α1β1 and α7α8, C36L1 interacts with loop β9α11 and helix α11. The overlapping of C36L1 and Rb44L1 best poses showed residues ^{13}K and ^{1}R occupying the same region at the tubulin dimer interface, that is blocked by residues ^{70}LEPT of α-tubulin and ^{243}PGQL of β-tubulin in a minimized structure (**Figure 8E**). Rb44L1 interaction with α-tubulin subunit was further confirmed using a chemiluminescence dot-blotting assay. We observed that Rb44L1 significantly bound to α-tubulin present in B16F10-Nex2 cell extract, as compared to the negative

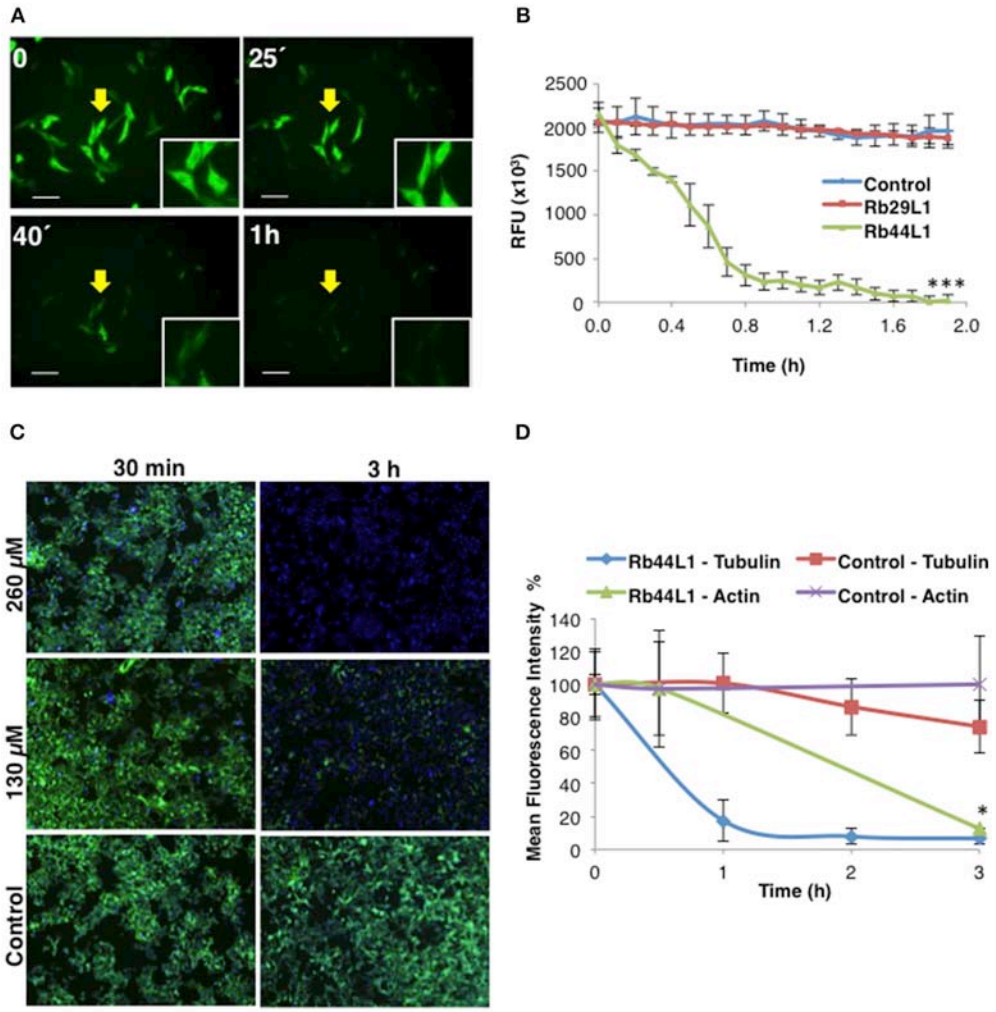

FIGURE 5 | Rb44L1 targets microtubules and disrupts tubulin assembly. **(A)** B16F10-Nex2 cells expressing baculovirus-transduced fluorescent tubulin were incubated with Rb44L1 at 260 μM; representative image of microtubule integrity is shown. Scale bar represents 50 μm; **(B)** microtubule dissociation was quantified in Rb44L1 and Rb29L1 treated cells and expressed as fluorescence decreased intensity and complete dispersion. ***$p < 0.001$ in comparison to untreated cells; **(C)** representative images of B16F10-Nex2 cells treated for different times with 130 and 260 μM of Rb44L1. Merged images of phalloidin-FITC and Hoescht 33342 staining are shown; **(D)** loss of actin and tubulin assembly integrity in Rb44L1 treated cells was quantified and compared. Results are expressed by fluorescence intensity. *$p <$ 0.05 comparing microtubules and actin disruption.

control and the scrambled peptide (Scr44), which was inactive. The C36L1 peptide was used as a positive control (**Figure 8F**). Different concentrations of the coated peptide Rb44L1 were tested and we found 10 μg/10 μl to give the best resolution in the dot-blotting (**Figure S4**). Interaction with β-actin was also evaluated and no reaction was seen (data not shown). As the docking studies revealed that the Rb44L1 interacted preferentially close to the N-site, we investigated the influence of additional GTP and Mn^{2+} on the peptide binding to α-tubulin in a dot-blotting assay with fixed peptide and melanoma cell lysate as a source of α-tubulin (monomeric, modified, dimeric). The peptide binding was enhanced in the presence of both GTP and Mn^{2+}, but not with these agents added separately (**Figure S5**). Since the GTP N-site is nonexchangeable and non-catalytic, most likely the addition of GTP and Mn^{2+} triggered tubulin assembly by interacting on the E-site. Oligomeric tubulin bound to the peptide explains the increased reactivity with anti-α-tubulin antibody used to reveal the dot-blotting assay.

Rb44L1 Inhibits Purified Tubulin Assembly

The microtubule destabilization effect of Rb44L1 was also evaluated using a fluorescence recombinant tubulin polymerization assay kit (Cystoskeleton, Inc., Denver, CO). In this setting and starting with 2 mg/ml tubulin, 0.2 mg/ml of Rb44L1 delayed tubulin assembly and reduced approximately 1/4 of the total assembly capacity compared to the control (***$p < 0.001$) and the scrambled peptide, Scr44 (**Figures 9A,B**). This effect was significantly more evident at half the tubulin concentration (1 mg/ml) and 0.2 mg/ml of Rb44L1 (***$p < 0.001$

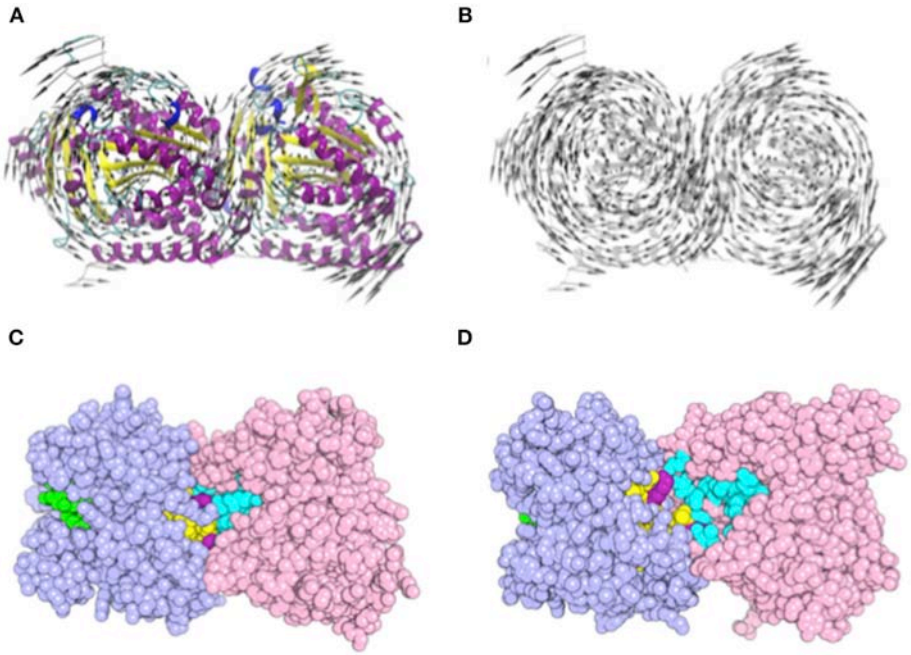

FIGURE 6 | Motion representation of normal mode 8 and nucleotide/colchicine site exposition as a result of α/β-tubulin displacement. **(A)** cartoon representation of α/β-tubulin normal mode 8. The circular motion in opposite directions of each tubulin monomer promotes the exposition of a nucleotide and colchicine binding sites; **(B)** highlight of vector directions. Vectors are placed into Cα atoms of each residue. Secondary structure color code: turn in green; β-sheet in yellow; β-bridge in gold; α-helix in purple; G, 3-10 helix in blue; and C, Coil in white. **(C,D)** α/β-tubulin crystallographic structure (PDB 4TV9) where atoms are represented as spheres. **(C)** comparison of GTP N-site (cyan), colchicine (yellow), and GTP E-site (green) site exposition between **(C)** α/β-tubulin crystallographic structure (PDB 4TV9); and **(D)** α/β-tubulin displaced by 6 Å along normal mode 8. Atoms are represented as spheres and residues present in both colchicine, and GTP N-site are colored in purple. α-Tubulin is represented in light-pink and β-tubulin in light-blue.

compared to the control). Polymerization was inhibited in 3/4 followed by depolymerization, after approximately 150 min incubation (**Figures 9C,D**). Since colchicine is a well-known microtubule inhibitor and has a binding-site mostly on β-tubulin, we assayed the effect of simultaneous addition of colchicine and Rb44L1. Increased inhibition of tubulin assembly was observed with this combination, suggesting independent interaction sites of Rb44L1 and colchicine, $^{***}p < 0.001$ compared to the colchicine alone (**Figure 9E**). It should be pointed out that single drugs such as the MT- depolymerizing colchicine and the MT-polymerizing paclitaxel when used in combination, the depolymerization effect has predominated (47).

DISCUSSION

The microtubules together with various stabilizing and destabilizing molecules display many important physiological functions. Due to their indispensability in the mitotic cell division, microtubules have been selected as preferred anticancer targets. Indeed, microtubule directed drugs are among the most commonly prescribed agents in cancer chemotherapy (2). Recently, anti-tumor peptides targeting microtubules (26) have been studied as tubulin interacting ligands that may evolve to be used in cancer therapy.

Novel anti-tumor peptides may have advantages over mAbs and tyrosine-kinase inhibitors, such as low cost, high specificity and potency due to their compatibility with targeted proteins, ability to penetrate the cell membrane, reduced immunogenicity, and improved safety (48). For example, the ADH-1 (Exherin), is an anticancer peptide distributed by Adhex Technologies®, which targets N-cadherin and induced partial and complete protective responses in patients with metastatic melanoma (49).

The microtubule destabilizing Ig V_L CDR1 peptide (C36L1) triggered cytotoxic and cytostatic effects on melanoma cells *in vitro* (23). Besides C36L1, we found that another CDR-L1 derived peptide, from anti-Lewis B mAb, exhibited similar cytotoxic mechanisms, targeting microtubules (MT). In the present work, we studied the molecular structure and biological effects of different L1-CDR-derived peptides: C36L1, Rb44L1 and Rb29L1 on microtubules. We analyzed the structure of L1-CDR-destabilizing MT peptides C36L1 and Rb44L1, as compared to the inactive one, Rb29L1. The latter demonstrated the most stable and rigid structure, assuming a β-hairpin conformation with several high occupancy H-bonds. Rb44L1 showed less rigidity as compared to Rb29L1, with a stable β-bridge conformation, while C36L1 was the most flexible peptide among them.

The biological effects of the peptides were examined and Rb44L1 showed the highest cytotoxic activity, selectively in different cancer cell lines with no significant effects on non-tumorigenic cell lines (**Table 2**).

Morphological and biochemical changes during tumor cells incubation with cytotoxic concentrations of Rb44L1 were

TABLE 3 | Key binding characteristics governing tubulin and L1-CDR interaction.

	Displacement (Å)						
	0	**1**	**2**	**3**	**4**	**5**	**6**
Rb29L1							
Energy*	434.76	751.84	383.90	−60.19	800.12	**−101.62**	−37.13
H-bonds	2	3	5	4	8	**1**	8
Salt-bridges	–	1	–	–	–	–	–
Cation-pi	–	–	1	–	–	–	–
T-stacking	–	–	–	–	–	–	1
Hydrophobic contacts	27	69	33	45	57	**60**	58
C36L1							
Energy*	−41.64	−186.92	15.15	−59.66	**−287.46**	195.54	−271.06
H-bonds	7	2	2	2	**6**	–	4
Salt-bridges	1	1	1	1	**1**	–	–
Cation-pi	–	–	1	–	–	–	1
T-stacking	–	–	–	–	–	–	–
Hydrophobic contacts	60	67	56	45	**42**	59	87
Rb44L1							
Energy*	216.31	−169.17	**−300.48**	45.49	−70.64	−30.10	−165.28
H-bonds	4	2	**6**	3	1	3	3
Salt-bridges	1	–	**2**	–	–	–	–
Cation-pi	–	–	–	–	–	–	–
T-stacking	–	–	–	–	–	–	–
Hydrophobic contacts	51	57	**61**	47	47	56	64
Rb44L1-R1A							
Energy*	253.99	45.25	−52.26	35.38	−37.68	−78.29	**−125.58**
H-bonds	2	3	3	–	2	3	**4**
Salt-bridges	–	–	–	–	–	–	–
Cation-pi	–	–	–	–	–	–	–
T-stacking	–	–	–	–	–	–	–
Hydrophobic contacts	41	53	51	46	47	56	**64**

*Best poses are highlighted in bold (energy values in kJ/mol).*Predicted summed electrostatic energy by atom-type pair according to Gasteiger partial charges.*

observed. Apoptosis was recognized by the remarkable shrinkage of the cytoplasm, roundup cells with pseudopodia retraction and shriveling without cell lysis, genomic DNA condensation and fragmentation, and exposure of phosphatidylserine at the surface of peptide-treated cells (50). The intrinsic pathway involves the functional deregulation of mitochondria, which may culminate in activation of caspases and the cascade of events that drives to cell death (51, 52). Early disruption of mitochondrial membrane potential, as evidenced by time-lapse fluorescence microscopy and TEM, together with later production of ROS, cleavage of caspase-9, caspase-3, the PARP, upregulation of Bax and downregulation of Bcl-2 were effects induced by Rb44L1, and they are all consistent with the intrinsic pathway of apoptosis (53, 54), strongly suggesting that this is the main *in vitro* cytotoxic mechanism of the peptide in melanoma cells.

P53 is activated in response to different stresses leading tumor cells to apoptosis and growth arrest (55). In this regard, accumulation of active p53 may also be attributed to disintegration of the cytoskeleton. Microtubule targeted-drugs are one of the main stimuli able to increase levels and activate p53 (56).

The main mechanism that seems to be involved in the intrinsic apoptosis by Rb44L1 peptide is the early disruption of the microtubules in melanoma cells. Rb44L1 destabilized labeled microtubules during early stages of incubation, as observed by fluorescence microscopy. In contrast, Rb29L1 did not affect the microtubule dynamics, under the same conditions.

The actin cytoskeleton integrity was also evaluated, as observed by fluorescence microscopy. Rb44L1 induced the degradation of actin filaments in melanoma cells to a maximum effect after 3 h of tumor cell treatment with this peptide. Alterations of actin dynamics are sufficient to induce apoptosis. They involve changes in F-actin levels, in the flux of actin through the filament pool, or both (57). In addition, F-actin depolymerization has been implicated in reduced MMP and elevated ROS production, together with shortening of cell lifespan (58), as observed in melanoma cells treated with Rb44L1. The peptide, however, did not directly interact with F-actin to induce depolymerization as suggested by a late kinetics, which follows microtubule depolymerization. In fact, the actin cytoskeleton integrity has been shown to be highly dependent on the microtubule dynamics (59, 60), which is crucial in tumor cells constantly entering the mitotic program as compared to non-tumorigenic cells (2). Cellular functions depend on the crosstalk between microtubules and actin filaments, in which specific proteins bind to microtubules and actin filaments simultaneously, promoting co-organization and coupled growth of both networks (61). Both cytoskeleton constituents are intrinsically related and rearranged during the progress of apoptosis. Important events are regulated by ROCK kinases that actively regulate the actomyosin contractile ring, a process facilitated by the early disruption of microtubules. Protrusions of the plasma membrane also called apoptotic bodies or blebs, are formed, with subsequent depolymerization of actin filaments (62).

Rb44L1 interaction with microtubules and induction of their depolymerization with subsequent degradation of actin filaments increased the number of tumor cells in the G2/M phase leading to a mitotic catastrophe. Such effects, coupled to inhibited angiogenesis as observed *in vitro,* are consistent with the described effects of other microtubule targeting drugs (2, 63). A schematic illustration of the effects induced by Rb44L1 on melanoma cells is detailed in the **Figure 10**.

Most importantly, this peptide showed a promising antitumor protective effect against subcutaneously grafted melanoma, with no systemic toxicity being observed.

Once proteins exist in equilibrium of multiple conformations in solution, we used a theoretical approach that mixed analyses of molecular dynamics and normal modes, to sample distinct structural states of α/β-tubulin dimer. This hybrid methodology allowed for the assignment of both local and collective motions of the system, that are essential dynamic features related to conformational selection and induced fit, respectively (64–66).

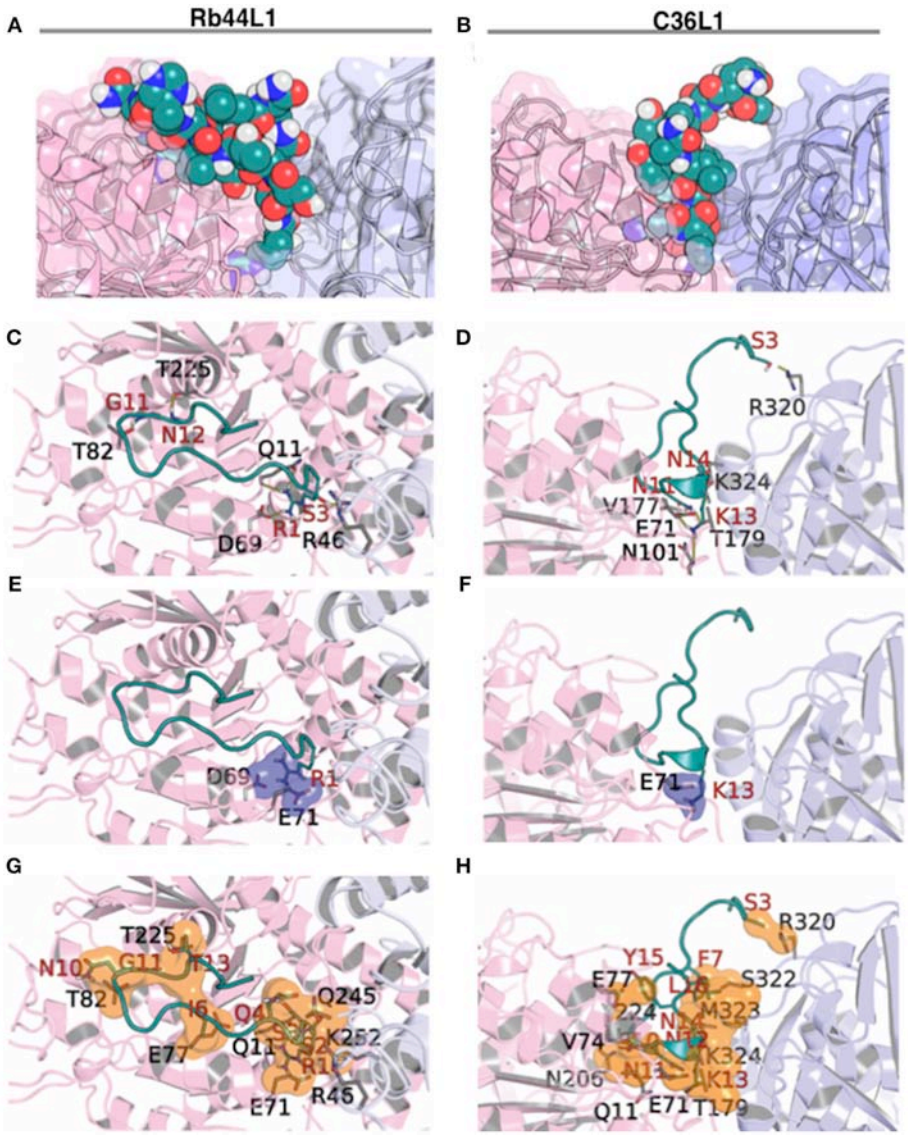

FIGURE 7 | Rb44L1 and C36L1 interactions with α/β-tubulin displaced by 2 Å and 4 Å, respectively. **(A,B)** surface complementarity; **(C,D)** hydrogen bonds formed; **(E,F)** salt bridges form a tiny pocket demonstrated in navy blue surface; **(G,H)** hydrophobic contacts form pockets represented by orange surface. α-Tubulin is represented in light-pink and β-tubulin in light-blue.

Microtubules are dynamic cellular structures that switch between growing and pruning cycles both *in vivo* and *in vitro*. Stabilization or destabilization of microtubule dynamics is promoted by a number of endogenous and exogenous compounds that regulate the process in different ways, either by competition with GTP (67), structural modification of the protein-protein interface between α and β monomers (8, 31, 68) or by allosteric mechanisms (69). One of the most frequently described mechanisms is the ligand binding at the colchicine site on β-tubulin, which is spatially next to an α-tubulin nucleotide binding site, with nonexchangeable, noncatalytic characteristics, known as N-site. Therefore, we explored the exposition of both binding sites as a molecular docking strategy, since their coupling might trigger the structural destabilization of tubulin dimer exerted by some L1-CDR peptides.

The tubulin heterodimer has two guanine binding sites: at the exchangeable, catalytic site (E-site) on the β chain, GTP is hydrolyzed to GDP during microtubule assembly; the nonexchangeable, noncatalytic site (N-site), on the α chain, is always occupied by GTP, suggesting that it may function as a structural cofactor of tubulin (70). Divalent cations have high affinity for both sites and their binding is associated to the structural stability of tubulin dimer (71). Mg^{2+} is a well-established ion required for microtubule assembly and stability, and contributes to strong GTP binding to the E-site (72). Q-band EPR and electron spin echo envelope modulation spectroscopy

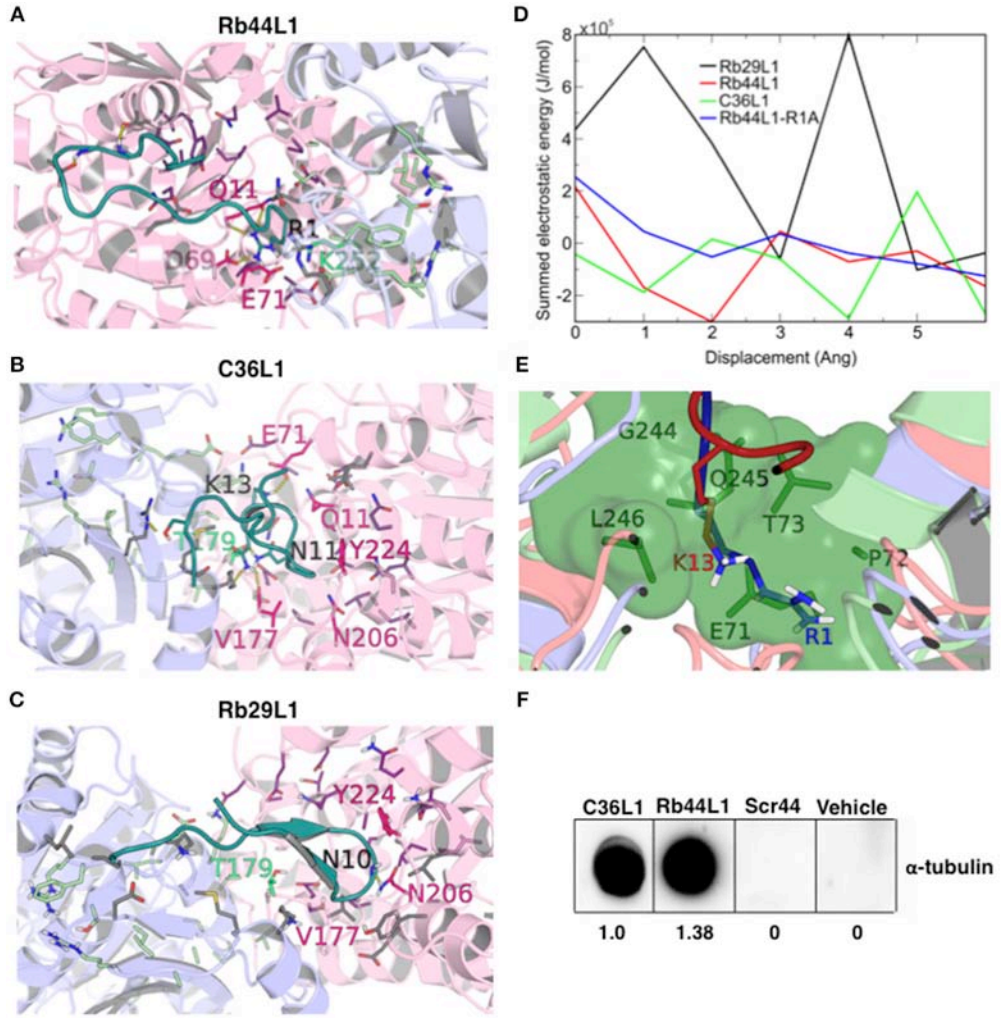

FIGURE 8 | CDR-L1 docking poses in relation to α/β-tubulin N-site and colchicine binding sites and energy re-score of docked complexes. **(A)** Rb44L1; **(B)** C36L1; **(C)** Rb29L1 best docking pose highlighting their position in relation to residues at N-site and colchicine binding sites. α-Tubulin is represented in light-pink and β-tubulin in light-blue. N-site and colchicine binding site residues are represented as purple and pale green, respectively, whereas those that interact with the CDRs are hot pink and lime green for nucleotide and colchicine binding site, respectively. The camera was inverted 170° on the y-axis and 80° on the x-axis for better visualization of the C36L1 and Rb29L1 interactions; **(D)** summed electrostatic energy of Rb29L1, Rb44L1, C36L1 and Rb44L1-R1A complexed with α/β-tubulin at different displacements; **(E)** overlapping of Rb44L1 and C36L1 docked complexes. Residues ^{1}R and ^{13}K of Rb44L1 (blue) and C36L1 (red), respectively, occupy the same region at the tubulin dimer interface, that is blocked by residues ^{70}LEPT of α-tubulin and ^{243}PGQL of β-tubulin at minimized structure (green surface); **(F)** Rb44L1 binds to tubulin present in the lysate of B16F10-Nex2 cells. Dot-blottings were performed by coating the nitrocellulose membranes with 10 μg of C36L1, Rb44L1, scrambled-Rb44L1 (Scr44), and vehicle (1% DMSO in milli-Q water). Experimental and control dot-blottings were performed as described in methods. Quantitation of dots was performed using ImageJ, and are represented as arbitrary units.

showed that Mn^{2+} at both N and E-sites directly coordinated to the triphosphate of GTP, proving that the divalent cation at both sites directly interacts with GTP (73). Mn^{2+} slowly exchanged for Mg^{2+} at the N-site and other divalent and trivalent cations may also exchange at this site and play a role in the assembly of microtubules (74, 75). Chelation of divalent cations in general, inhibits the assembly of tubulin dimers.

L1-CDR peptides bound at the nucleotide/colchicine binding site at the dimer interface, but most of the interactions were made at the N-site. The best solution of Rb44L1 peptide was in an α/β-tubulin semi-open state. We observed that the ^{1}R is a key residue for interaction with tubulin dimer. The mutation of this residue for alanine, weakened the interaction, increasing the free energy. This result was further corroborated by experimental assays. Interestingly, the ^{13}K of C36L1 used the same tubulin cavity as that of ^{1}R of Rb44L1, although C36L1 best docking pose was observed in an open conformation. This polar pocket may play an important role in tubulin depolymerization induced by L1-CDR peptides since the inactive Rb29L1 did not present a favorable interaction on this region.

The inactivity of Rb29L1 peptide is noteworthy, since its sequence is quite similar to Rb44L1 except between residues 4

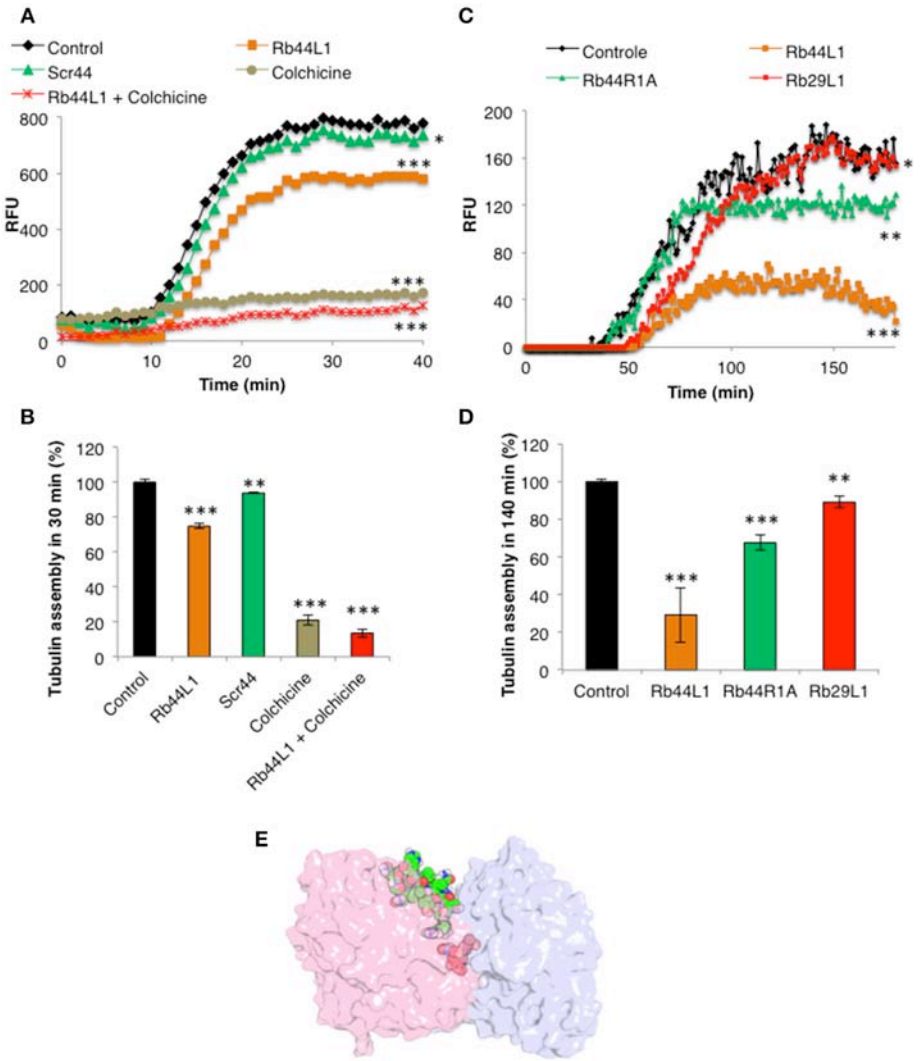

FIGURE 9 | Effects of Rb44L1 on microtubule assembly. **(A)** Polymerization kinetics in presence of Rb44L1 and Scr44 (130 μM) with purified fluorescent tubulin at 2 mg/ml. Inhibition by colchicine (50 μM) was assayed alone or in combination with Rb44L1. **(B)** bar graph represents the percentage of tubulin assembly measured at 30 min from kinetic curve demonstrated in **(A)**. **(C)** Rb44L1, Rb29L1, and Rb44R1A were incubated with tubulin at 1 mg/ml and polymerization/destabilization was measured. **(D)** bar graph represents the percentage of tubulin assembly measured at 140 min from kinetic curve demonstrated in **(C)**. $^{*}p < 0.05$, $^{**}p < 0.01$, and $^{***}p < 0.001$ in comparison to the control **(E)** structural alignment between the best pose from molecular docking and PDB 4O2B (chains A and B) illustrating the possibility of Rb44L1 (green) and colchicine (red) interact concomitantly with α/β-tubulin at its interface. PDB4O2B was firstly aligned with PDB4TV9, and then the comparison was made. α-Tubulin is represented in light-pink and β-tubulin in light-blue.

and 7, which is TSLL in the former peptide and QTIT in the latter. Interestingly, the most favorable docking poses showed a different interaction pattern with tubulin, since Rb44L1 QTIT residues were less solvent exposed than Rb29L1 TSLL residues, which are 70 $Å^2$ more exposed to solvent. This is a direct consequence of the observed R interaction pattern with buried tubulin residues (^{69}D and ^{11}Q) in the N-site, and could be related to the observed activity differences.

A dot-blotting assay showed that in the presence of both GTP and Mn^{2+}, but not with these agents added separately, the Rb44L1 peptide bound with increased affinity to the tubulin α-chains of monomeric, modified or dimeric substrates from a tumor cell lysate. This may have occurred by the GTP-E site induced oligomerization of tubulin dimers present in the cell lysate during incubation, indicating that under the conditions used, the dot-blotting assay with fixed peptide did not impair tubulin assembly on the latter (**Figure S6**).

In contrast, what is the possible mechanism triggering Rb44L1 depolymerization of tubulin? We found that the surface overlapping of the docked conformation of the peptide and the closed α/β-tubulin revealed that the peptide represents a steric constraint to the protein in this conformation. The effect noticed in the overlapping regions of ^{1}R, ^{3}S, and ^{12}N residues, and the peptide size

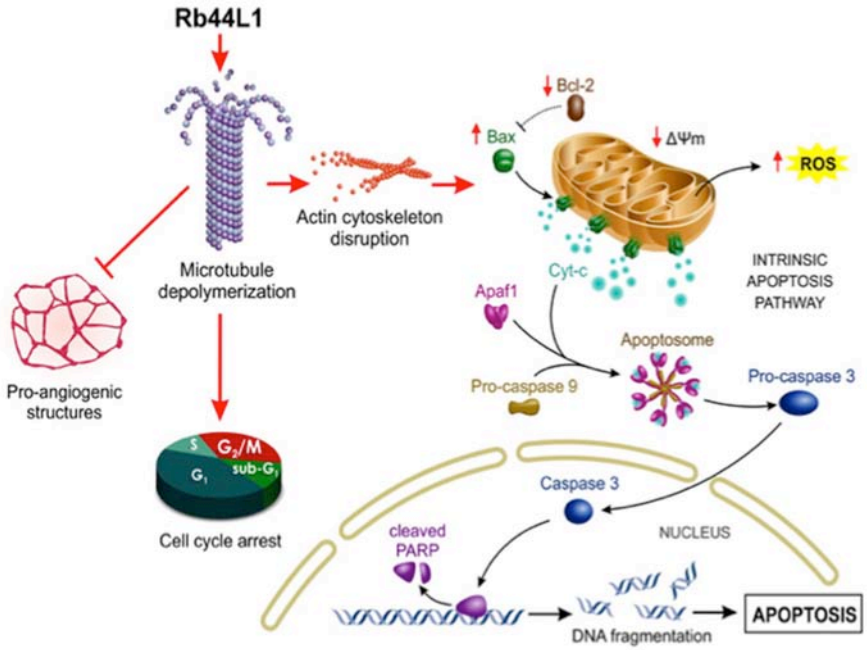

FIGURE 10 | Schematic illustration of proposed Rb44L1 effects on melanoma cells. Rb44L1 peptide interacts at the tubulin monomers' interface in microtubules promoting depolymerization. Alteration of microtubule dynamics led to actin filaments degradation, disrupting the cytoskeleton integrity. In response to changes in the environment, mitochondria produce high amounts of ROS and release co-factors that trigger intrinsic apoptosis. Upon activation by binding to and neutralization of Bcl-2, insertion of Bax into mitochondrial outer membrane form pores to allow the passage of proteins from the intermembrane space to the cytosol. It involves the disruption of mitochondrial membrane potential ($\Delta\psi m$) followed by release of cytochrome c in the cytosol that binds to Apaf-1, ATP, and pro-caspase 9 to form an oligomeric apoptosome, which results in the caspase cascade initiation. Activation of caspase 3 by caspase 9 is responsible for the proteolytic cleavage of the nuclear enzyme Parp-1, which abolishes its DNA repair ability and induces DNA fragmentation in cells undergoing apoptosis. In addition, Rb44L1 inhibited pro-angiogenic structure formation *in vitro* and induced cell cycle arrest at G2/M. Abbreviations: Apaf-1, Apoptotic protease activating factor 1; Cyt-c, Cytochrome-c; ROS, Reactive oxygen species; $\Delta\psi m$, Mitochondrial membrane potential; Bcl-2, B-cell lymphoma 2; Bax, Bcl-2 associated X protein; Parp-1, Poly [ADP-ribose] polymerase 1. The illustration was designed by Carolina de Amat.

of 1675.0 $Å^3$, which preclude the α/β-tubulin return to a closed conformation, is a source of structure destabilization (**Video S2**).

Taken together, we propose that Rb44L1 peptide is a novel candidate to be developed as a drug, acting on the microtubule network of tumor cells. Molecular docking on tubulin monomers in opening motion, and the possible mechanisms of action leading to microtubule depolymerization were explored in comparison with other Ig CDR-L1 derived peptides, all tested against *in vitro* models of melanoma cells.

DATA AVAILABILITY STATEMENT

Datasets are available on request. The raw data supporting the conclusions of this manuscript will be made available by the authors, without undue reservation, to any qualified researcher.

ETHICS STATEMENT

This study was carried out in accordance with the recommendations of the Ethics Committee of Federal University of São Paulo, Brazil for animal manipulation and experimental procedures. Animals were provided by Centro de desenvolvimento de modelos experimentais para medicina e biologia (CEDEME), of Federal University of São Paulo. The protocol was approved by the Ethics Committee of Federal University of São Paulo, Brazil via document CEP 1234/2011.

AUTHOR CONTRIBUTIONS

NG and CF performed the biological experiments, analyzed data, and designed the figures. MM carried out annexin V and propidium iodide labeling analysis and designed **Figure 2D**. RA carried out the cell cycle analysis and designed **Figure 2E**. PR-L and RC carried out all the chemical analysis. NG wrote the manuscript and LP and LT designed the research project. All authors reviewed and approved the manuscript.

FUNDING

This work was supported by Fundação de Amparo a Pesquisa do Estado de São Paulo (Fapesp), grant 10/51423-0 and by the National Council for Scientific and Technological Development (CNPq).

ACKNOWLEDGMENTS

The authors acknowledge Carolina de Amat for the illustration of Rb44L1 effects.

SUPPLEMENTARY MATERIAL

The Supplementary Material for this article can be found online at: https://www.frontiersin.org/articles/10.3389/fonc.2019.00025/full#supplementary-material

REFERENCES

1. Stanton RA, Gernert KM, Nettles JH, Aneja R. Drugs that target dynamic microtubules: a new molecular perspective. *Med Res Rev.* (2011) 31:443–81. doi: 10.1002/med.20242
2. Jordan MA, Wilson L. Microtubules as a target for anticancer drugs. *Nat Rev Cancer* (2004) 4:253–65. doi: 10.1038/nrc1317
3. Jordan A, Hadfield JA, Lawrence NJ, McGown AT. Tubulin as a target for anticancer drugs: agents which interact with the mitotic spindle. *Med Res Rev.* (1998) 18:259–96. doi: 10.1002/(SICI)1098-1128(199807)18:43.3.CO;2-T
4. Tozer GM, Kanthou C, Parkins CS, Hill SA. The biology of the combretastatins as tumour vascular targeting agents. *Int J Exp Pathol.* (2002) 83:21–38. doi: 10.1046/j.1365-2613.2002.00211.x
5. Mizumoto N, Gao J, Matsushima H, Ogawa Y, Tanaka H, Takashima A. Discovery of novel immunostimulants by dendritic-cell-based functional screening. *Blood* (2005) 106:3082–9. doi: 10.1182/blood-2005-03-1161
6. Dumontet C, Jordan MA. Microtubule-binding agents: a dynamic field of cancer therapeutics. *Nat Rev Drug Discov.* (2010) 9:790–803. doi: 10.1038/nrd3253
7. Uzma F, Mohan CD, Hashem A, Konappa NM, Rangappa S, Kamath PV, et al. Endophytic fungi-alternative sources of cytotoxic compounds: a review. *Front Pharmacol.* (2018) 9:309. doi: 10.3389/fphar.2018.00309
8. Prota AE, Danel F, Bachmann F, Bargsten K, Buey RM, Pohlmann J, et al. The novel microtubule-destabilizing drug BAL27862 binds to the colchicine site of tubulin with distinct effects on microtubule organization. *J Mol Biol.* (2014) 426:1848–60. doi: 10.1016/j.jmb.2014.02.005
9. Prota AE, Bargsten K, Zurwerra D, Field JJ, Diaz JF, Altmann KH, et al. Molecular mechanism of action of microtubule-stabilizing anticancer agents. *Science* (2013) 339:587–90. doi: 10.1126/science.1230582
10. Fojo T, Menefee M. Mechanisms of multidrug resistance: the potential role of microtubule-stabilizing agents. *Ann Oncol.* (2007) 18 (Suppl. 5):v3–8. doi: 10.1093/annonc/mdm172
11. Quasthoff S, Hartung HP. Chemotherapy-induced peripheral neuropathy. *J Neurol.* (2002) 249:9–17. doi: 10.1007/PL00007853
12. Xiao YF, Jie MM, Li BS, Hu CJ, Xie R, Tang B, et al. Peptide-based treatment: a promising cancer therapy. *J Immunol Res.* (2015) 2015:1–13. doi: 10.1155/2015/761820
13. Thundimadathil J. Cancer treatment using peptides: current therapies future prospects. *J Amino Acids* (2012) 2012:967347. doi: 10.1155/2012/967347
14. Fosgerau K, Hoffmann T. Peptide therapeutics: current status future directions. *Drug Discov Today* (2015) 20:122–8. doi: 10.1016/j.drudis.2014.10.003
15. Bhutia SK, Maiti TK. Targeting tumors with peptides from natural sources. *Trends Biotechnol.* (2008) 26:210–7. doi: 10.1016/j.tibtech.2008.01.002
16. Srivatsan A, Ethirajan M, Pey SK, Dubey S, Zheng X, Liu TH, et al. Conjugation of cRGD peptide to chlorophyll a based photosensitizer (HPPH) alters its pharmacokinetics with enhanced tumor-imaging photosensitizing (PDT) efficacy. *Mol Pharm.* (2011) 8:1186–97. doi: 10.1021/mp200018y
17. Massaoka MH, Matsuo AL, Figueiredo CR, Girola N, Farias CF, Pasqualoto K, et al. A subtraction tolerization method of immunization allowed for Wilms' tumor protein-1 (WT1) identification in melanoma discovery of an antitumor peptide sequence. *J Immunol Methods* (2014) 414:11–9. doi: 10.1016/j.jim.2014.08.003
18. Suarez-Jimenez GM, Burgos-Hernez A, Ezquerra-Brauer JM. Bioactive peptides depsipeptides with anticancer potential: sources from marine animals. *Mar Drugs* (2012) 10:963–86. doi: 10.3390/md10050963
19. Torres MDT, Andrade GP, Sato RH, Pedron CN, Manieri TM, Cerchiaro G, et al. Natural redesigned wasp venom peptides with selective antitumoral activity. *Beilstein J Org Chem.* (2018) 14:1693–703. doi: 10.3762/bjoc.14.144
20. Gabrielli E, Pericolini E, Cenci E, Ortelli F, Magliani W, Ciociola T, et al. Antibody complementarity-determining regions (CDRs): a bridge between adaptive innate immunity. *PLoS ONE* (2009) 4:e8187. doi: 10.1371/journal.pone.0008187
21. Polonelli L, Ciociola T, Magliani W, Zanello PP, D'Adda T, Galati S, et al. Peptides of the constant region of antibodies display fungicidal activity. *PLoS ONE* (2012) 7:e34105. doi: 10.1371/journal.pone.0034105
22. Polonelli L, Ponton J, Elguezabal N, Moragues MD, Casoli C, Pilotti E, et al. Antibody complementarity-determining regions (CDRs) can display differential antimicrobial, antiviral antitumor activities. *PLoS ONE* (2008) 3:e2371. doi: 10.1371/journal.pone.0002371
23. Dobroff AS, Rodrigues EG, Juliano MA, Friaca DM, Nakayasu ES, Almeida IC, et al. Differential antitumor effects of IgG IgM monoclonal antibodies their synthetic complementarity-determining regions directed to new targets of B16F10-Nex2 melanoma cells. *Transl Oncol.* (2010) 3:204–17. doi: 10.1593/tlo.09316
24. Arruda DC, Santos LC, Melo FM, Pereira FV, Figueiredo CR, Matsuo AL, et al. Travassos: beta-Actin-binding complementarity-determining region 2 of variable heavy chain from monoclonal antibody C7 induces apoptosis in several human tumor cells is protective against metastatic melanoma. *J Biol Chem.* (2012) 287:14912–22. doi: 10.1074/jbc.M111.322362
25. Figueiredo CR, Matsuo AL, Massaoka MH, Polonelli L, Travassos LR. Anti-tumor activities of peptides corresponding to conserved complementary determining regions from different immunoglobulins. *Peptides* (2014) 59:14–9. doi: 10.1016/j.peptides.2014.06.007
26. Figueiredo CR, Matsuo AL, Azevedo RA, Massaoka MH, Girola N, Polonelli L, et al. A novel microtubule de-stabilizing complementarity-determining region C36L1 peptide displays antitumor activity against melanoma *in vitro in vivo*. *Sci Rep.* (2015) 5:14310. doi: 10.1038/srep14310
27. Girola N, Matsuo AL, Figueiredo CR, Massaoka MH, Farias CF, Arruda DC, et al. The Ig VH complementarity-determining region 3-containing Rb9 peptide, inhibits melanoma cells migration invasion by interactions with Hsp90 an adhesion G-protein coupled receptor. *Peptides* (2016) 85:1–15. doi: 10.1016/j.peptides.2016.08.006
28. Rabaça AN, Arruda DC, Figueiredo CR, Massaoka MH, Farias CF, Tada DB, et al. AC-1001 H3 CDR peptide induces apoptosis signs of autophagy *in vitro* exhibits antimetastatic activity in a syngeneic melanoma model. *FEBS Open Bio.* (2016) 6:885–901. doi: 10.1002/2211-5463.12080
29. Kabat EA, Wu TT, Bilofsky H. Unusual distributions of amino acids in complementarity-determining (hypervariable) segments of heavy light chains of immunoglobulins their possible roles in specificity of antibody-combining sites. *J Biol Chem.* (1977) 252:6609–16.
30. Lamiable A, Thevenet P, Rey J, Vavrusa M, Derreumaux P, Tuffery P. PEP-FOLD3: faster *de novo* structure prediction for linear peptides in solution in complex. *Nucleic Acids Res.* (2016) 44:W449–54. doi: 10.1093/nar/gkw329
31. Prota AE, Bargsten K, Diaz JF, Marsh M, Cuevas C, Liniger M, et al. A new tubulin-binding site pharmacophore for microtubule-destabilizing anticancer drugs. *Proc Natl Acad Sci USA.* (2014) 111:13817–21. doi: 10.1073/pnas.1408124111
32. Olsson MH, Sondergaard CR, Rostkowski M, Jensen JH. PROPKA3: consistent treatment of internal surface residues in empirical pKa predictions. *J Chem Theory Comput.* (2011) 7:525–37. doi: 10.1021/ct100578z
33. Van Der Spoel D, Lindahl E, Hess B, Groenhof G, Mark AE, Berendsen HJ. GROMACS: fast, flexible, free. *J Comput Chem.* (2005) 26:1701–18. doi: 10.1002/jcc.20291
34. Huang J, MacKerell ADJr. CHARMM36 all-atom additive protein force field: validation based on comparison to NMR data. *J Comput Chem.* (2013) 34:2135–45. doi: 10.1002/jcc.23354
35. Jo S, Kim T, Iyer VG, Im W. CHARMM-GUI: a web-based graphical user interface for CHARMM. *J Comput Chem.* (2008) 29:1859–65. doi: 10.1002/jcc.20945

36. Lee J, Cheng X, Swails JM, Yeom MS, Eastman PK, Lemkul JA, et al. CHARMM-GUI input generator for NAMD, GROMACS, AMBER, OpenMM, CHARMM/OpenMM simulations using the CHARMM36 additive force field. *J Chem Theory Comput.* (2016) 12:405–13. doi: 10.1021/acs.jctc.5b00935
37. Boonstra S, Onck PR, Giessen E. CHARMM TIP3P water model suppresses peptide folding by solvating the unfolded state. *J Phys Chem B* (2016) 120:3692–8. doi: 10.1021/acs.jpcb.6b01316
38. Humphrey W, Dalke A, Schulten K. VMD: visual molecular dynamics. *J Mol Graph.* (1996) 14:33–8, 27–8. doi: 10.1016/0263-7855(96)00018-5
39. Brooks BR, Brooks CL III, Mackerell ADJr, Nilsson L, Petrella RJ, Roux B, et al. CHARMM: the biomolecular simulation program. *J Comput Chem.* (2009) 30:1545–614. doi: 10.1002/jcc.21287
40. Perahia D, Mouawad L. Computation of low-frequency normal modes in macromolecules: improvements to the method of diagonalization in a mixed basis application to hemoglobin. *Comput Chem.* (1995) 19:241–6. doi: 10.1016/0097-8485(95)00011-G
41. Buck M, Bouguet-Bonnet S, Pastor RW, MacKerell ADJr. Importance of the CMAP correction to the CHARMM22 protein force field: dynamics of hen lysozyme. *Biophys J.* (2006) 90:L36–8. doi: 10.1529/biophysj.105.078154
42. Philot EA, Perahia D, Braz AS, Costa MG, Scott LP. Binding sites hydrophobic pockets in human thioredoxin 1 determined by normal mode analysis. *J Struct Biol.* (2013) 184:293–300. doi: 10.1016/j.jsb.2013.09.002
43. Louet M, Perahia D, Martinez J, Floquet N. A concerted mechanism for opening the GDP binding pocket release of the nucleotide in hetero-trimeric G-proteins. *J Mol Biol.* (2011) 411:298–312. doi: 10.1016/j.jmb.2011.05.034
44. Ritchie DW, Venkatraman V. Ultra-fast FFT protein docking on graphics processors. *Bioinformatics* (2010) 26:2398–405. doi: 10.1093/bioinformatics/btq444
45. Meissner GO, de Resende Lara PT, Scott LP, Braz AS, Chaves-Moreira D, Matsubara FH, et al. Molecular cloning *in silico* characterization of knottin peptide, U2-SCRTX-Lit2:from brown spider (Loxosceles intermedia) venom glands. *J Mol Model.* (2016) 22:196. doi: 10.1007/s00894-016-3067-0
46. Durrant JD, McCammon JA. BINANA: a novel algorithm for lig-binding characterization. *J Mol Graph Model.* (2011) 29:888–93. doi: 10.1016/j.jmgm.2011.01.004
47. Bombuwala K, Kinstle T, Popik V, Uppal SO, Olesen JB, Vina J, et al. Colchitaxel, a coupled compound made from microtubule inhibitors colchicine paclitaxel. *Beilstein J Org Chem.* (2006) 2:13. doi: 10.1186/1860-5397-2-13
48. Miller MJ, Foy KC, Kaumaya PT. Cancer immunotherapy: present status, future perspective, a new paradigm of peptide immunotherapeutics. *Discov Med.* (2013) 15:166–76.
49. Augustine CK, Yoshimoto Y, Gupta M, Zipfel PA, Selim MA, Febbo P, et al. Targeting N-cadherin enhances antitumor activity of cytotoxic therapies in melanoma treatment. *Cancer Res.* (2008) 68:3777–84. doi: 10.1158/0008-5472.CAN-07-5949
50. Galluzzi L, Vitale I, Abrams JM, Alnemri ES, Baehrecke EH, Blagosklonny MV, et al. Molecular definitions of cell death subroutines: recommendations of the nomenclature committee on cell death 2012. *Cell Death Differ.* (2012) 19:107–20. doi: 10.1038/cdd.2011.96
51. Elmore S. Apoptosis: a review of programmed cell death. *Toxicol Pathol.* (2007) 35:495–516. doi: 10.1080/01926230701320337
52. Thornberry NA, Lazebnik Y. Caspases: enemies within. *Science* (1998) 281:1312–6. doi: 10.1126/science.281.5381.1312
53. Kroemer G, Galluzzi L, Brenner C. Mitochondrial membrane permeabilization in cell death. *Physiol Rev.* (2007) 87:99–163. doi: 10.1152/physrev.00013.2006
54. Desouza M, Gunning PW, Stehn JR. The actin cytoskeleton as a sensor mediator of apoptosis. *Bioarchitecture* (2012) 2:75–87. doi: 10.4161/bioa.20975
55. Jimenez GS, Khan SH, Stommel JM, Wahl GM. p53 regulation by post-translational modification nuclear retention in response to diverse stresses. *Oncogene* (1999) 18:7656–65. doi: 10.1038/sj.onc.1203013
56. Giannakakou P, Nakano M, Nicolaou KC, O'Brate A, Yu J, Blagosklonny MV, et al. Enhanced microtubule-dependent trafficking p53 nuclear accumulation by suppression of microtubule dynamics. *Proc Natl Acad Sci USA*. (2002) 99:10855–60. doi: 10.1073/pnas.132275599
57. Franklin-Tong VE, Gourlay CW. A role for actin in regulating apoptosis/programmed cell death: evidence spanning yeast, plants animals. *Biochem J.* (2008) 413:389–404. doi: 10.1042/BJ20080320
58. Boldogh IR, Pon LA. Interactions of mitochondria with the actin cytoskeleton. *Biochim Biophys Acta* (2006) 1763:450–62. doi: 10.1016/j.bbamcr.2006.02.014
59. Akhshi TK, Wernike D, Piekny A. Microtubules actin crosstalk in cell migration division. *Cytoskeleton* (2014) 71:1–23. doi: 10.1002/cm.21150
60. Rodriguez OC, Schaefer AW, Mato CA, Forscher P, Bement WM, Waterman-Storer CM. Conserved microtubule-actin interactions in cell movement morphogenesis. *Nat Cell Biol.* (2003) 5:599–609. doi: 10.1038/ncb0703-599
61. Elie A, Prezel E, Guerin C, Denarier E, Ramirez-Rios S, Serre L, et al. Tau co-organizes dynamic microtubule actin networks. *Sci Rep*. (2015) 5:9964. doi: 10.1038/srep09964
62. Ávila MO, Vega AF, Maraver JG, Paz MV, Lavera I, Mata M, et al. The apoptotic microtubule network during the execution phase of apoptosis. In: Ntuli T, editor. *Cell Death - Autophagy, Apoptosis and Necrosis*. London: INTECH (2015). 299–329.
63. Rapino F, Naumann I, Fulda S. Bortezomib antagonizes microtubule-interfering drug-induced apoptosis by inhibiting G2/M transition MCL-1 degradation. *Cell Death Dis*. (2013) 4:e925. doi: 10.1038/cddis.2013.440
64. Csermely P, Palotai R, Nussinov R. Induced fit, conformational selection independent dynamic segments: an extended view of binding events. *Trends Biochem Sci*. (2010) 35:539–46. doi: 10.1016/j.tibs.2010.04.009
65. Nussinov R, Ma B, Tsai CJ. Multiple conformational selection induced fit events take place in allosteric propagation. *Biophys Chem*. (2014) 186:22–30. doi: 10.1016/j.bpc.2013.10.002
66. Tobi D, Bahar I. Structural changes involved in protein binding correlate with intrinsic motions of proteins in the unbound state. *Proc Natl Acad Sci USA*. (2005) 102:18908–13. doi: 10.1073/pnas.0507603102
67. Winder BS, Strgaard CS, Miller MG. The role of GTP Binding microtubule-associated proteins in the inhibition of microtubule assembly by carbendazim. *Toxicol Sci*. (2001) 59:138–46. doi: 10.1093/toxsci/59.1.138
68. Ravelli RB, Gigant B, Curmi PA, Jourdain I, Lachkar S, Sobel A, et al. Insight into tubulin regulation from a complex with colchicine a stathmin-like domain. *Nature* (2004) 428:198–202. doi: 10.1038/nature02393
69. Brindisi M, Maramai S, Brogi S, Fanigliulo E, Butini S, Guarino E, et al. Development of novel cyclic peptides as pro-apoptotic agents. *Eur J Med Chem*. (2016) 117:301–20. doi: 10.1016/j.ejmech.2016.04.001
70. Spiegelman BM, Penningroth SM, Kirschner MW. Turnover of tubulin the N site GTP in Chinese hamster ovary cells. *Cell* (1977) 12:587–600. doi: 10.1016/0092-8674(77)90259-8
71. Menendez M, Rivas G, Diaz JF, Andreu JM. Control of the structural stability of the tubulin dimer by one high affinity bound magnesium ion at nucleotide N-site. *J Biol Chem*. (1998) 273:167–76. doi: 10.1074/jbc.273.1.167
72. Croom HB, Correia JJ, Baty LT, Williams RCJr. Release of exchangeably bound guanine nucleotides from tubulin in a magnesium-free buffer. *Biochemistry* (1985) 24:768–75.
73. Correia JJ. Effects of antimitotic agents on tubulin-nucleotide interactions. *Pharmacol Ther*. (1991) 52:127–47.
74. Correia JJ, Beth AH, Williams RCJr. Tubulin exchanges divalent cations at both guanine nucleotide-binding sites. *J Biol Chem*. (1988) 263:10681–6.
75. Buttlaire DH, Czuba BA, Stevens TH, Lee YC, Himes RH. Manganous ion binding to tubulin. *J Biol Chem*. (1980) 255:2164–8.

Conflict of Interest Statement: The authors declare that the research was conducted in the absence of any commercial or financial relationships that could be construed as a potential conflict of interest.

frontiers in Oncology

ORIGINAL RESEARCH
published: 28 January 2019
doi: 10.3389/fonc.2019.00002

Celastrol Inhibits the Growth of Ovarian Cancer Cells *in vitro* and *in vivo*

Li-Na Xu[1†], Na Zhao[1†], Jin-Yan Chen[2†], Piao-Piao Ye[1], Xing-Wei Nan[1], Hai-Hong Zhou[1], Qi-Wei Jiang[3], Yang Yang[3], Jia-Rong Huang[3], Meng-Ling Yuan[3], Zi-Hao Xing[3], Meng-Ning Wei[3], Yao Li[3], Zhi Shi[3] and Xiao-Jian Yan[1,4*]*

[1] Department of Gynecology, The First Affiliated Hospital of Wenzhou Medical University, Wenzhou, China, [2] Department of Gynecology, The Second Affiliated Hospital of Zhejiang University School of Medicine, Hangzhou, China, [3] Department of Cell Biology and Institute of Biomedicine, National Engineering Research Center of Genetic Medicine, Guangdong Provincial Key Laboratory of Bioengineering Medicine, College of Life Science and Technology, Jinan University, Guangzhou, China, [4] Center for Uterine Cancer Diagnosis & Therapy Research of Zhejiang Province, Women's Hospital and Institute of Translational Medicine, Zhejiang University School of Medicine, Zhejiang, China

OPEN ACCESS

Edited by:
Yan-Yan Yan,
Shanxi Datong University, China

Reviewed by:
Changliang Shan,
Nankai University, China
Nana Zhang,
Chinese Academy of Medical Sciences, China

***Correspondence:**
Zhi Shi
tshizhi@jnu.edu.cn
Xiao-Jian Yan
yxjbetter@126.com

[†]These authors have contributed equally to this work

Specialty section:
This article was submitted to Cancer Molecular Targets and Therapeutics, a section of the journal Frontiers in Oncology

Received: 06 December 2018
Accepted: 02 January 2019
Published: 28 January 2019

Citation:
Xu L-N, Zhao N, Chen J-Y, Ye P-P, Nan X-W, Zhou H-H, Jiang Q-W, Yang Y, Huang J-R, Yuan M-L, Xing Z-H, Wei M-N, Li Y, Shi Z and Yan X-J (2019) Celastrol Inhibits the Growth of Ovarian Cancer Cells in vitro and in vivo. Front. Oncol. 9:2. doi: 10.3389/fonc.2019.00002

Celastrol is a natural triterpene isolated from the Chinese plant Thunder God Vine with potent antitumor activity. However, the effect of celastrol on the growth of ovarian cancer cells *in vitro* and *in vivo* is still unclear. In this study, we found that celastrol induced cell growth inhibition, cell cycle arrest in G2/M phase and apoptosis with the increased intracellular reactive oxygen species (ROS) accumulation in ovarian cancer cells. Pretreatment with ROS scavenger N-acetyl-cysteine totally blocked the apoptosis induced by celastrol. Additionally, celastrol inhibited the growth of ovarian cancer xenografts in nude mice. Altogether, these findings suggest celastrol is a potential therapeutic agent for treating ovarian cancer.

Keywords: celastrol, reactive oxygen species, N-acetyl-cysteine, apoptosis, ovarian cancer

INTRODUCTION

Ovarian cancer is the most lethal gynecologic cancer and the fifth leading cause of female cancer-related deaths in the United States in 2018 (1). Because of the late stage diagnoses, the prognosis of ovarian cancer remains poor, despite advances in aggressive surgery and combination chemotherapy (2–4). Current treatments for ovarian cancer are far from satisfactory, therefore it is of considerable interest to develop novel therapeutic agents to improve the outcomes of ovarian cancer.

Celastrol is a natural triterpene isolated from the Chinese plant Thunder God Vine (*Tripterygium wilfordii*),which has been reported with a wide range of bioactivities, such as antitumor (5), anti-inflammatory (6), antidiabetic activities (7) and antihypertensive (8). Celastrol has shown the potent antitumor activity in various cancers including prostate, breast, liver, colon, and lung (9–13). Although celastrol is able to induce apoptosis and inhibit proliferation, migration and invasion in ovarian cancer cells *in vitro* (14–16), the effect of celastrol on the growth of ovarian cancer cells *in vivo* is still unknown. Here, we have comprehensively investigated the antitumor activity of celastrol in ovarian cancer cells *in vitro* and *in vivo*.

MATERIALS AND METHODS

Cells Lines and Reagents

The human ovarian cancer lines A2780 and SKOV3 were cultured in Dulbecco's modified Eagle's medium (DMEM) supplemented with 10% fetal bovine serum (FBS), penicillin (100 U/ml) and

streptomycin (100 ng/ml) at 37°C with 5% CO2 in a humidified incubator. Celastrol was purchased from Shanghai Tauto Biotechnology. N-acetyl-L-cysteine (NAC) and dihydroethidium (DHE) were purchased from Sigma-Aldrich. Methythiazolyldiphenyl-tetrazolium bromide (MTT), propidium iodide (PI) and other chemicals were purchased from Shanghai Sangon Biotech. Anti-p27 (610241), Anti-Cyclin B1 (554177), and Anti-Cyclin E (51-1459GR) antibodies were from BD Biosciences. Anti-RAF1 (SC-133) antibodies were from Santa Cruz Biotechnology. Anti-PARP (9542), Anti-AKT (4691), Anti-pAKT S473 (4060), Anti-ERK (4695), Anti-pERK T202/T204 (4370), Anti-JNK (9252), Anti-pJNK T183/Y185 (4668), Anti-p38 (9212), Anti-pp38 T180/Y182 (4511) antibodies were from Cell Signaling Technologies. Anti-GAPDH (LK9002T) antibodies were from Tianjin Sungene Biotech.

MTT Assay

Cells were seeded into a 96-well plate at a density of 0.5 $\times 10^4$ cells/well. Then, different concentrations of celastrol (10 μL/well) were added to designated wells. After 72 h, 10 μL of MTT was added to each well at a final concentration of 0.5 mg/ml, and the plate was further incubated for 4 h, allowing viable cells to change the yellow MTT into dark-blue formazan crystals. Subsequently, the medium was discarded and 50 μL of dimethylsulfoxide (DMSO) was added to each well to dissolve the formazan crystals. The absorbance in individual well was determined at 570 nm by multidetection microplate reader 680 (BioRad, PA, USA). The concentrations required to inhibit growth by 50% (IC_{50}) were calculated from survival curves using the Bliss method (17).

Cell Cycle Analysis

Cells were harvested and washed twice with cold PBS and then fixed with 70% ice-cold ethanol at 4°C for 30 min. After centrifugation at 200 × g for 10 min, cells were washed twice with PBS, resuspended with 0.5 mL PBS containing PI (50 μg/mL), Triton X-100(0.1%, v/v), 0.1% sodium citrate, and DNase-free RNase (100 μg/mL), and detected by flow cytometry (FCM) after 15 min incubation in the dark at room temperature. Fluorescence was measured at an excitation wave length of 480 nm through a FL-2 filter. Data were analyzed using ModFit LT 3.0 software (Becton Dickinson) (18, 19).

Apoptosis Analysis

Cell apoptosis was evaluated with FCM assay. Briefly, cells were harvested and washed twice with cold PBS, then stained with Annexin V-FITC and PI in the binding buffer, and detected by FACSCalibur FCM (BD, CA, USA) after 15 min incubation in

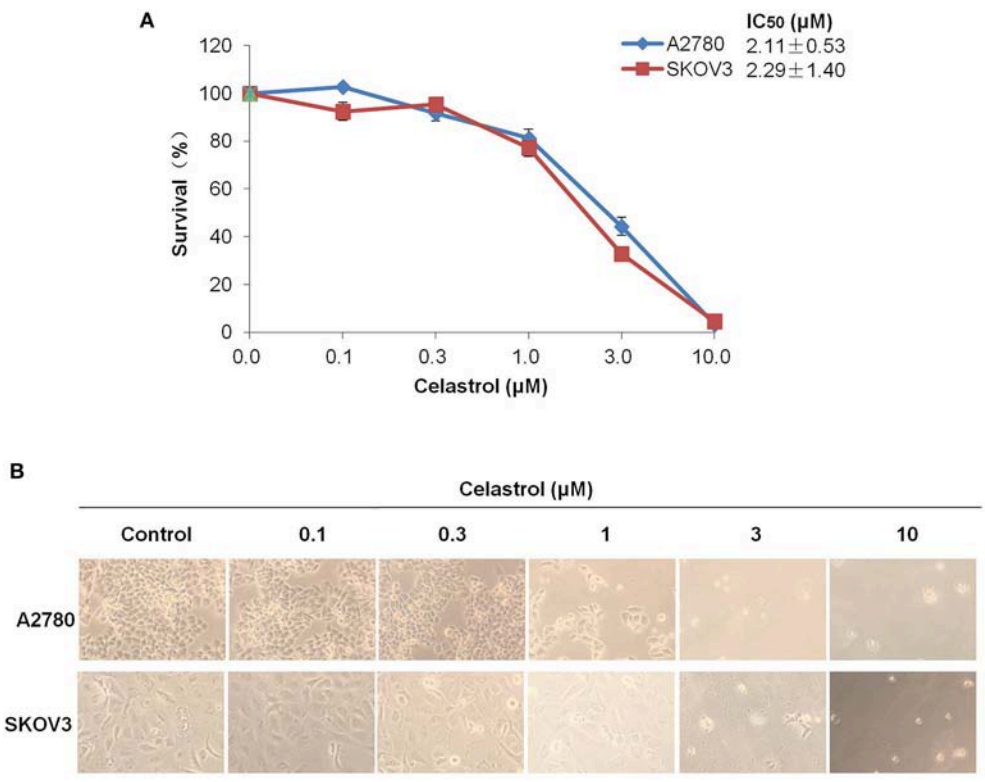

FIGURE 1 | Celastrol inhibited the growth of ovarian cancer cells *in vitro*. **(A)** The growth curves, IC_{50} values and **(B)** phase-contrast images of A2780 and SKOV3 cells treated with the indicated concentrations of celastrol (0, 0.1, 0.3, 1, 3, and 10 μM) for 72 h. Cell survival was measured by MTT assay, and the IC_{50} values of celastrol in each cell lines were calculated.

the dark at room temperature. Fluorescence was measured at an excitation wave length of 480 nm through FL-1 (530 nm) and FL-2 (585 nm) filters. The early apoptotic cells (Annexin V positive only) and late apoptotic cells (Annexin V and PI positive) were quantified (20).

Western Blot Analysis

Cells were harvested and washed twice with cold PBS and then resuspended and lysed in RIPA buffer (1% NP-40, 0.5% sodium deoxycholate, 0.1% SDS, 10 ng/mL PMSF, 0.03% aprotinin, and 1 μM sodium orthovanadate) at 4°C for 30 min.

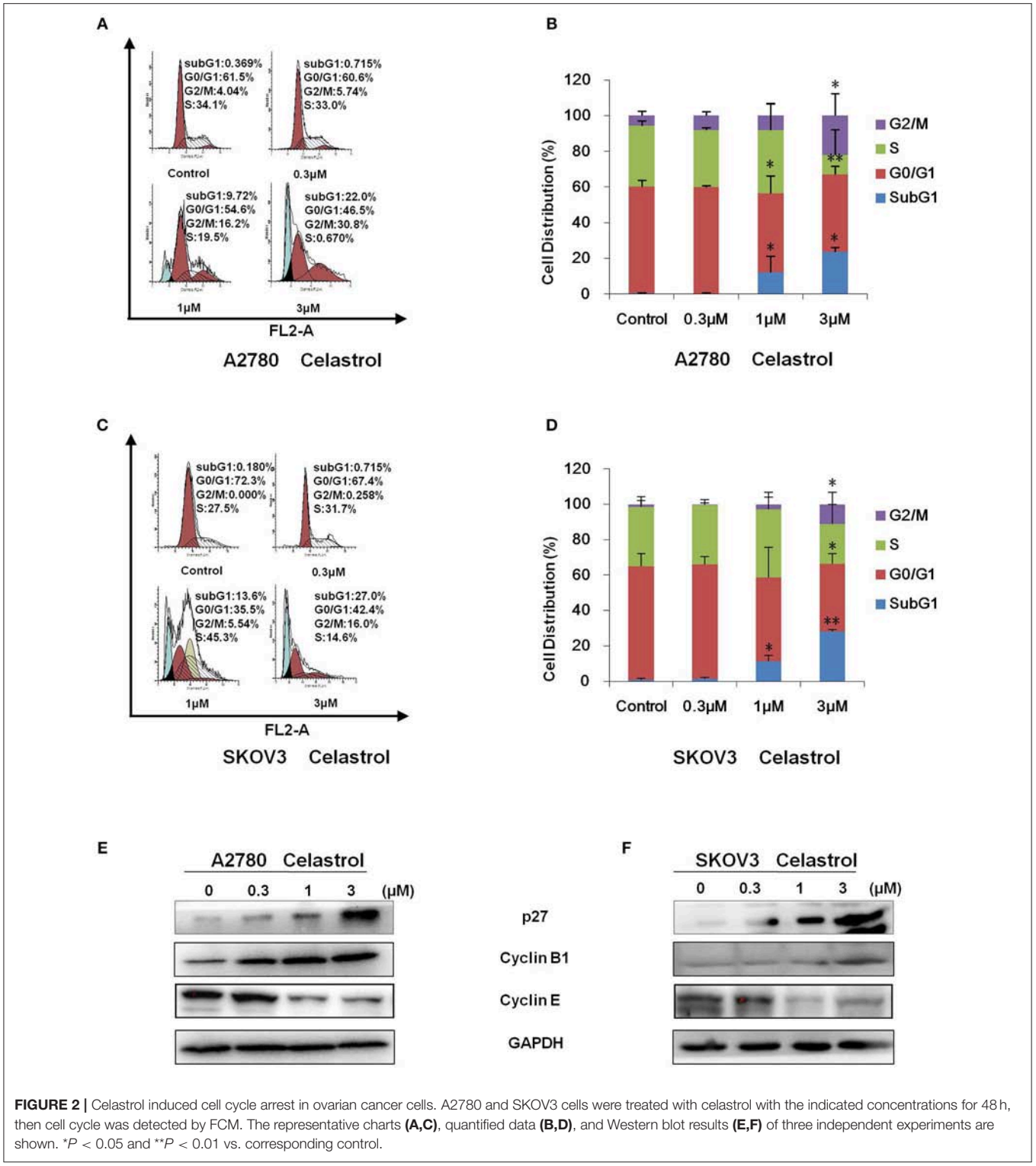

FIGURE 2 | Celastrol induced cell cycle arrest in ovarian cancer cells. A2780 and SKOV3 cells were treated with celastrol with the indicated concentrations for 48 h, then cell cycle was detected by FCM. The representative charts **(A,C)**, quantified data **(B,D)**, and Western blot results **(E,F)** of three independent experiments are shown. *$P < 0.05$ and **$P < 0.01$ vs. corresponding control.

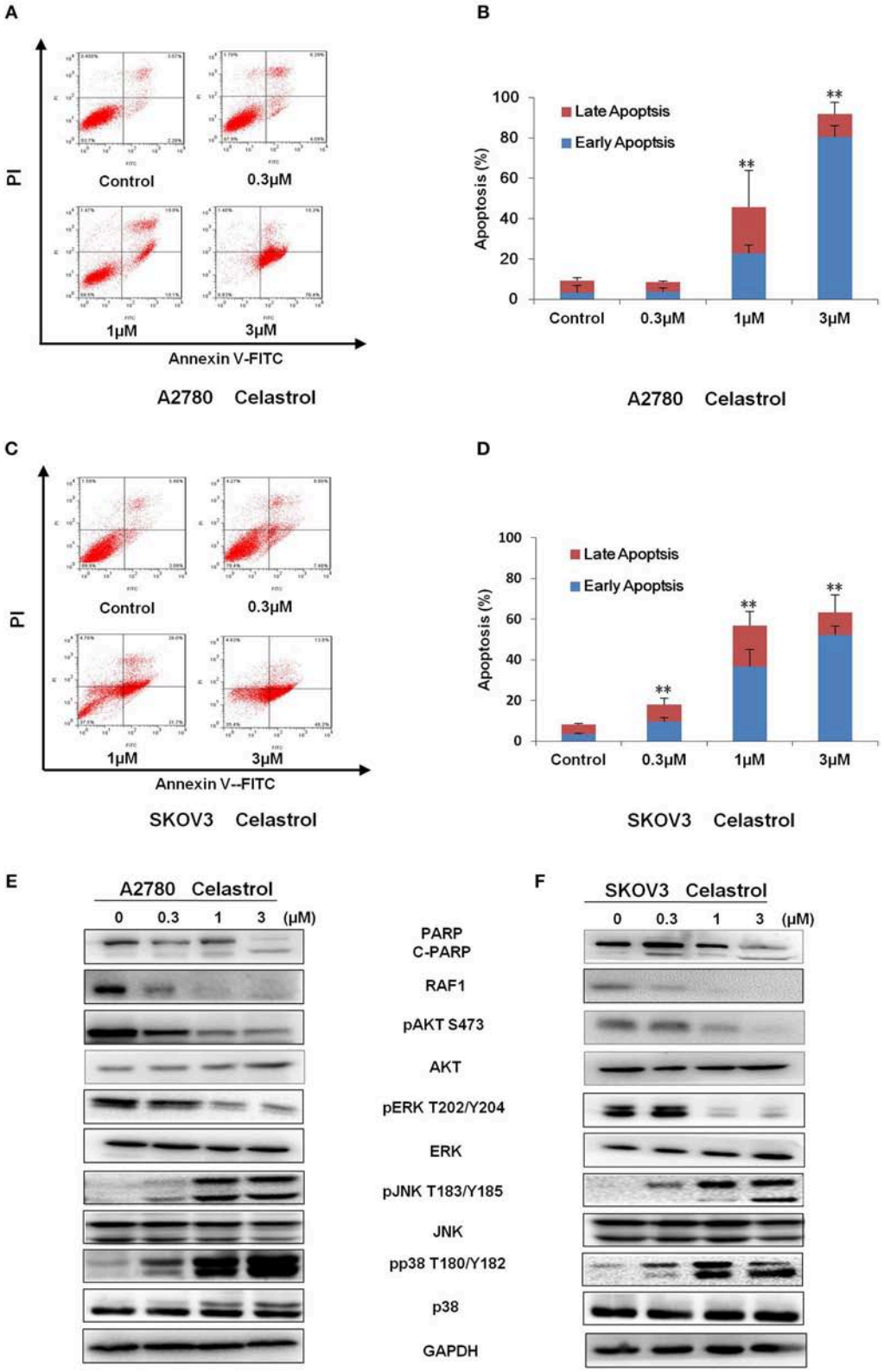

FIGURE 3 | Celastrol induced apoptosis in ovarian cancer cells. A2780 and SKOV3 cells were treated with celastrol with the indicated concentrations for 48 h, then cell apoptosis was detected by FCM. The representative charts **(A,C)**, quantified data **(B,D)**, and Western blot results **(E,F)** of three independent experiments are shown. The same GAPDH image of **Figure 2** has been used as loading control. $^{**}P < 0.01$ vs. corresponding control.

Lysates were centrifuged at 14,000 × g for 10 min and supernatants were collected. Proteins were separated on 12% SDS-PAGE gels and transferred to polyvinylidene difluoride membranes. Membranes were blocked with 5% BSA and incubated with the indicated primary antibodies. Corresponding horseradish peroxidase-conjugated secondary antibodies were used against each primary antibody. Proteins were detected using the chemiluminescent detection reagents and films (21, 22).

Reactive Oxygen Species Assay

Cells were incubated with 10 μM of DHE at 37°C for 30 min, washed twice with PBS, and microphotographed under a conventional fluorescent microscope (Olympus, Japan) immediately. For each well, 5 fields were taken randomly. Then, cells were rapidly digested, harvested and washed twice with cold PBS, and detected by FCM. The DHE Fluorescence intensity was measured and quantified at an excitation wave length of 518 nm through PE filters (23, 24).

Nude Mice Xenograft Assay

Balb/c nude mice were obtained from the Guangdong Medical Laboratory Animal Center and maintained with sterilized food and water. This study was carried out in accordance with the recommendations of the Guidelines for the Care and Use of Laboratory Animals, and the protocol were approved by the Institutional Animal Care and Use Committee of Jinan University. Four female nude mice with 4–5 weeks old and 20–22 g weight were used for each group. Each mouse was injected subcutaneously with A2780 cells (4×10^6 in 100 μl of medium) under the left and right shoulders. Mice were randomized into two groups, when the subcutaneous tumors were approximately 0.3×0.3 cm^2 (two perpendicular diameters) in size, and were injected intraperitoneally with vehicle alone (0.5% methylcellulose) and celastrol (2 mg/kg) every day. The body weights of mice and the two perpendicular diameters (A and B) of tumors were recorded every day. The tumor volume (V) was calculated as:

$$V = \pi/6\ (1/2(A + B))^3$$

The mice were anaesthetized after experiment, and tumor tissue was excised from the mice and weighted. The rate of inhibition (IR) was calculated according to the formula:

IR=1-Mean tumor weight of experimental group/Mean tumor weight of control group × 100% (25)

Statistical Analysis

A student's *t*-test was used to compare individual data points between two groups. A *P*-value of < 0.05 was set as the criterion for statistical significance.

RESULTS

Celastrol Inhibited the Growth of Ovarian Cancer Cells *in vitro*

To access the effect of celastrol on ovarian cancer cells, we treated two ovarian cancer cell lines A2780 and SKOV3 with the increasing concentrations of celastrol range from 0.1 to 10 μM for 72 h. As shown in **Figures 1A,B**, the results of MTT assay revealed that the growth of two ovarian cancer cell lines was similarly inhibited by celastrol in a dose-dependent manner with the IC_{50} values were 2.11 and 2.29 μM in A2780 and SKOV3 respectively. These data suggested that celastrol inhibits the growth of ovarian cancer cells.

Celastrol Induced Cell Cycle Arrest in Ovarian Cancer Cells

To determine whether celastrol is able to induce cell cycle arrest, cell cycle distribution was examined after celastrol treatment. A2780 and SKOV3 cells were treated with 0.3, 1 and 3 μM of celastrol for 48 h, then stained with PI and examined by FCM. As shown in **Figures 2A–D**, celastrol induced the accumulation in Sub G1 and G2/M phase and reduction in G0/G1 and S phase in two ovarian cancer cell lines. Next, the cell cycle related proteins were detected by Western Blot. As shown in **Figures 2E,F**, increased p27 and Cyclin B1 and decreased Cyclin E proteins were detected in celastrol-treated A2780 and SKOV3 cells. Together, these results indicated that celastrol induces cell cycle arrest in ovarian cancer cells.

Celastrol Induced Apoptosis in Ovarian Cancer Cells

To determine whether celastrol could induce cell apoptosis, A2780 and SKOV3 cells were treated with indicated concentrations of celastrol for 48 h, apoptosis was assessed by FCM with Annexin V/PI staining. As shown in **Figures 3A–D**, celastrol dose-dependently induced early stage of apoptosis (Annexin V+/PI–) and late stage of apoptosis (Annexin V+/PI+) in both cells. Treatment of celastrol upregulated the protein expressions of cleaved-PARP, pp38 T180/Y182 and pJNK T183/Y185 but downregulated the protein expressions of pERK T202/Y204, pAKT S473 and RAF1 (**Figures 3E,F**). Consequently, these results suggest that celastrol induces cell apoptosis in ovarian cancer cells.

ROS Generation Was Critical for Celastrol-Induced Apoptosis in Ovarian Cancer Cells

Numerous antitumor agents demonstrate antitumor activity via ROS-dependent activation of apoptotic cell death (26, 27). It has previously been reported that the elevated intracellular ROS mediated celastrol-induced apoptosis in several human cancer cells (28). Thus, we surmised that celastrol caused apoptosis in ovarian cancer cells was due to excessive ROS generation. Firstly, the cellular ROS was tagged by DHE fluorescence staining in celastrol-treated cells. As shown in **Figure 4**, celastrol enhanced the detectable red fluorescent signals of DHE in both A2780 and SKOV3 cells, suggesting the intracellular ROS levels were increased after celastrol treatment. Then we pre-treated A2780 and SKOV3 cells with NAC (a specific ROS scavenger), Celastrol-induced cell apoptosis were totally attenuated by NAC in both ovarian cancer cells

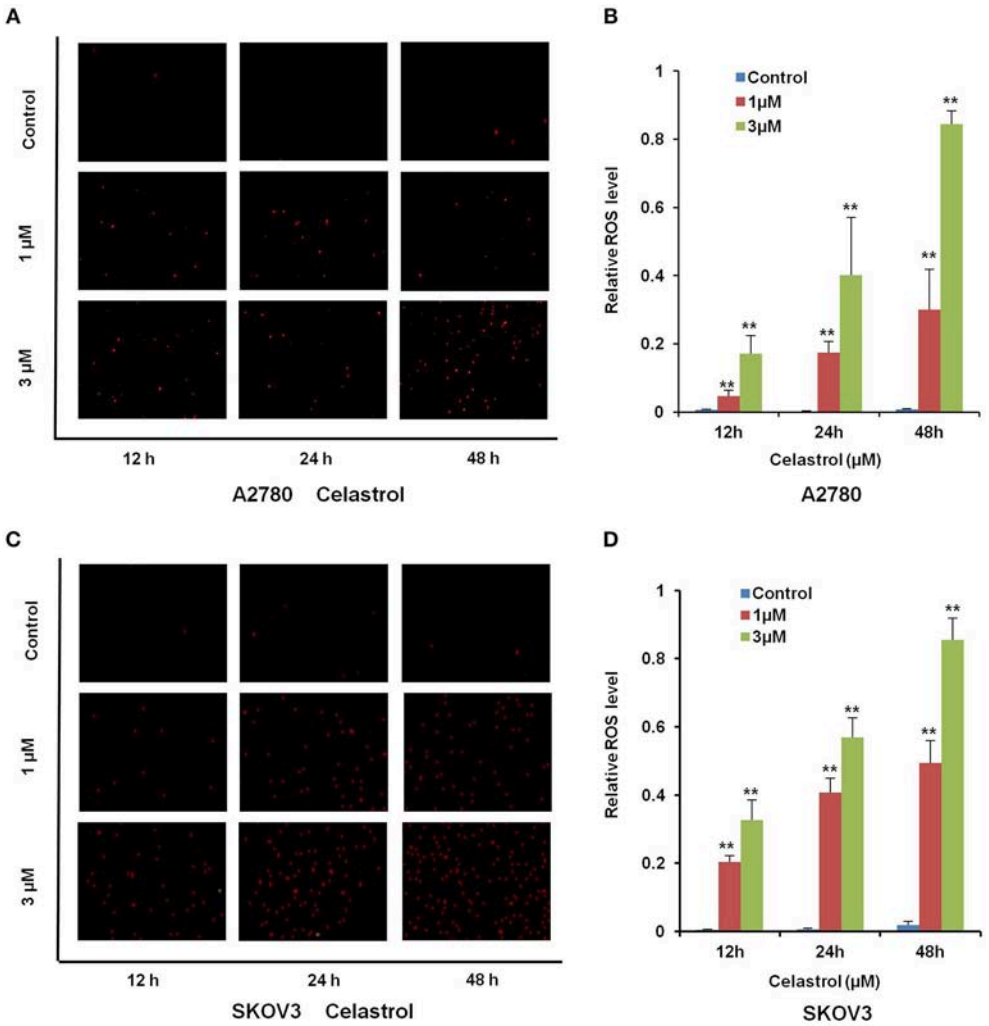

FIGURE 4 | Celastrol enhanced the intracellular ROS levels in ovarian cancer cells. A2780 and SKOV3 cells were treated with celastrol with indicated times and concentrations, stained with DHE, photographed and quantified respectively under fluorescent microscope and FCM. The representative micrographs **(A,C)** and quantified results **(B,D)** were shown. $^{**}P < 0.01$ vs. corresponding control.

(**Figure 5**). Collectively, these results suggest that ROS generation was critical for celastrol-induced apoptosis in ovarian cancer cells.

Celastrol Inhibited the Tumor Growth of Ovarian Cancer in Nude Mice

To confirm the antitumor effects of celastrol *in vivo*, A2780 subcutaneous xenograft tumors were generated in the nude mice. As shown in **Figures 6A–E**, treatment of celastrol did inhibit the growth of A2780 xenograft tumors with the inhibition ratio of 28.60% by diminishing the tumor volumes and weights. Furthermore, mice body weight in celastrol group was close to that of control group, suggesting that celastrol at the indicated dose did not cause toxicity in mice (**Figure 6C**).

DISCUSSION

Natural products attract more and more attention in the prevention and treatment of cancer in recent years. Products from the plant *Tripterygium wilfordii*, including celastrol and triptolide, are of special attention because of its superior anti-tumor activities against a variety of cancer types, and therefore are the traditional herb medicines considered to have the most potential in modern cancer therapy. For the treatment of ovarian cancer, triptolide has been shown to inhibit the proliferation, migration and invasion of ovarian cancer in multiple pathways (29–31) and demonstrated to exert efficacy in preclinical models (32). Celastrol has also been reported to induce apoptosis and inhibit proliferation, migration and invasion in ovarian cancer cells *in vitro* (14, 16), but the mechanism for its anti-tumor effect and the effect of celastrol on the growth of ovarian cancer cells *in vivo* are not fully understood. In our present study,

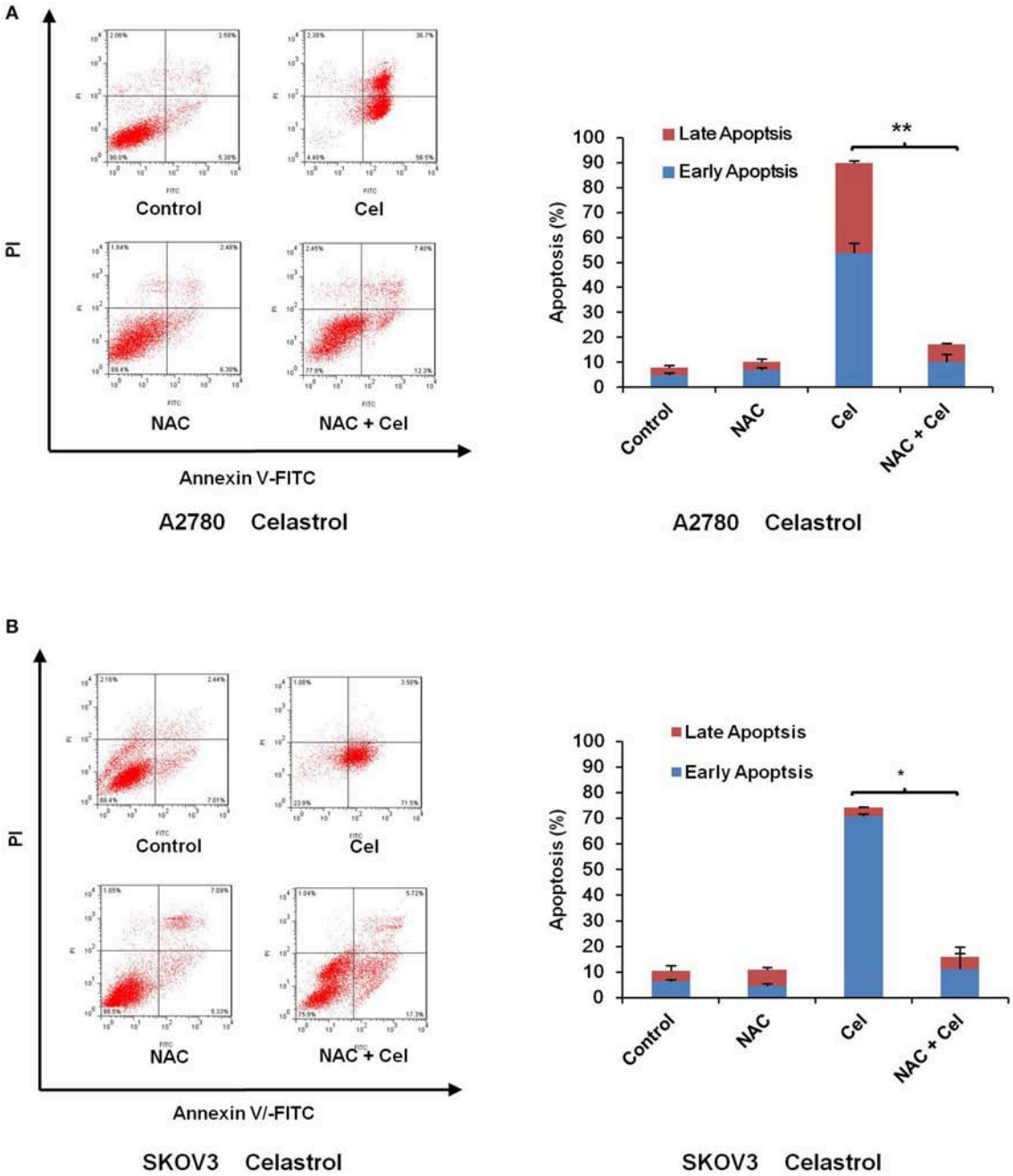

FIGURE 5 | NAC impeded celastrol-induced cell apoptosis. A2780 and SKOV3 cells were treated with 3 μM celastrol for 48 h in the presence or absence of 5 mM NAC pretreated for 1 h. The apoptosis was detected by FCM. The apoptosis charts and quantified data **(A,B)** were shown. *$P < 0.05$ and **$P < 0.01$ vs. corresponding control.

we have demonstrated that celastrol mediated dose-dependent anti-growth effects on human ovarian cancer cell lines SKOV3 and A2780. The IC_{50} value after 72 h treatment with celastrol ranged from 2 to 3 μM in these two human ovarian cancer cell lines, similarly to the IC_{50} value of celastrol of ovarian cancer in other articles (15, 16). We have also shown that celastrol induced both the early and late stage of apoptosis and cell cycle arrest in G2/M phase with obvious up-regulation of cleaved-PARP, pp38 T180/Y182, pJNK T183/Y185, p27 and Cyclin B1 and down-regulation of pERK T202/Y204, pAKT S473, RAF1 and Cyclin E in a dose-dependent manner. Similar with our results, celastrol can induce the activation of JNK and inactivation of AKT in multiple myeloma cells RPMI-8226 (33), activation of p38 in ovarian cancer cells OVCAR-8 and colorectal cancer

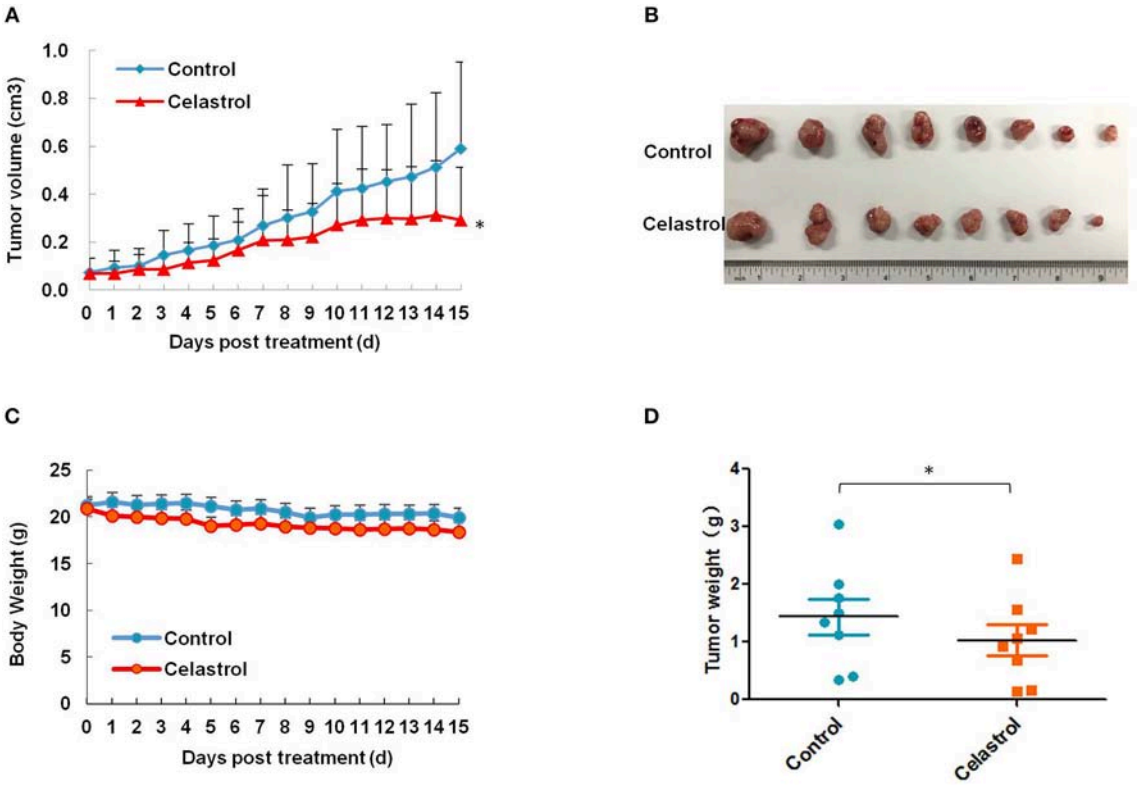

E

Cell	Groups	Before Experiment		After Experiment		Weight of	Inhibition(%)
		Mice	Weight(g)	Mice	Weight(g)	Tumors(g)	
A2780	Control	4	21.19±1.03	4	19.95±0.60	1.44±0.88	
	Celastrol	4	20.91±0.80	4	18.40±1.48	1.03±0.75	28.60*

FIGURE 6 | Celastrol inhibited the tumor growth of ovarian cancer in nude mice. Each mouse was injected subcutaneously with A2780 cells (4×10^6 in 100 μl of medium) under the left and right shoulders. When the subcutaneous tumors were approximately 0.3 × 0.3 cm in size, mice were randomized into two groups, and received intraperitoneal injection of vehicle alone (0.5% methylcellulose) or celastrol (2 mg/kg) every day. The body weight and tumor volume were recorded every day. After experiment, the mice were anesthetized, and tumor tissue was excised from the mice and weighted. The tumor volume **(A)**, original tumors **(B)**, body weight **(C)**, tumor weight **(D)**, and summary data **(E)** were shown. *$P < 0.05$ vs. corresponding control.

cells SW620 cells (34) and inactivation of ERK in hepatoma cells Hep3B (35). Furthermore, celastrol inhibited the growth of A2780 ovarian cancer subcutaneous xenograft tumors in nude mice by diminishing the tumor volumes and weights, and mice body weight in celastrol group was close to that of control group. These *in vitro* and *in vivo* data strongly indicate that celastrol may be a appropriate candidate for treating ovarian cancer.

Biological roles of ROS were intricate and important in cancer cells (36). The intracellular ROS plays a significant role in regulating multifarious cell physiological process such as growth, differentiation, death and so on (37). ROS changes the cellular redox condition, induces DNA damage and influences the activities of tumor suppressor or oncogene, thereby involving in the initiation and progression of cancer (38, 39). Lots of studies have shown that cancer cells normally produce more ROS than normal cells (40). Interestingly, accumulating evidence suggests that cancer cells are more vulnerable to ROS-induced death because they are under the increased oxidative stress (41). A variety of agents like YM155, dinaciclib and triptolide may be selectively toxic to tumor cells because they enhanced intracellular oxidant stress and push these already stressed cells beyond their limitation (24, 38, 42, 43). In addition, previous studies have demonstrated that ROS plays a pivotal role in celastrol-induced apoptosis in multiple cancers, such as colon cancer, liver cancer, osteosarcoma, etc. (9, 28, 44). In this study, we have found that the intracellular ROS levels were increased after celastrol treatment, and pre-treated with ROS scavenger NAC totally attenuated celastrol-induced cell apoptosis in ovarian cancer cells. It has been reported that celastrol enhanced the intracellular ROS to induce apoptosis by inhibiting mitochondrial respiratory chain

complex I activity in lung cancer H1299 cells (45). Whether celastrol induces ROS accumulation to trigger apoptosis in the same way in ovarian cancer cells need to be further investigated.

In summary, our data have shown that celastrol induced cell growth inhibition, cell cycle arrest in G2/M phase and apoptosis with the increased intracellular ROS accumulation in ovarian cancer cells *in vitro* and *in vivo*. Pretreatment with NAC totally blocked the apoptosis induced by celastrol. Altogether, these findings suggest celastrol is a potential therapeutic agent for treating ovarian cancer.

AUTHOR CONTRIBUTIONS

L-NX, NZ, J-YC, ZS, and X-JY designed the experiments, performed the experiments, analyzed the data, and wrote the paper. X-WN, H-HZ, P-PY, Q-WJ, YY, J-RH, M-LY, Z-HX, M-NW, and YL performed the experiments. All authors read and approved the final manuscript.

FUNDING

This work was supported by funds from the National Key Research and Development Program of China (No. 2017YFA0505104 to ZS), the National Natural Science Foundation of China (No. 81772540 to ZS and No. 81503293 to X-JY), the Guangdong Natural Science Funds for Distinguished Young Scholar (No. 2014A030306001 to ZS), the Guangdong Special Support Program for Young Talent (No. 2015TQ01R350 to ZS), the Science and Technology Program of Guangdong (No. 2016A050502027 to ZS) and the Science and Technology Program of Guangzhou (No. 201704030058 to ZS), the Zhejiang major disease diagnosis and treatment technology research center (No. JBZX-201803 to X-JY).

REFERENCES

1. Siegel RL, Miller KD, Jemal A. Cancer statistics, 2018. *CA Cancer J Clin* (2018) 68:7–30. doi: 10.3322/caac.21442
2. Torre LA, Trabert B, DeSantis CE, Miller KD, Samimi G, Runowicz CD, et al. Ovarian cancer statistics, 2018. *CA Cancer J Clin.* (2018) 68:284–96. doi: 10.3322/caac.21456
3. Fields EC, McGuire WP, Lin L, Temkin SM. Radiation treatment in women with Ovarian cancer: past, present, and future. *Front Oncol.* (2017) 7:177. doi: 10.3389/fonc.2017.00177
4. Ohman AW, Hasan N, Dinulescu DM. Advances in tumor screening, imaging, and avatar technologies for high-grade serous ovarian cancer. *Front Oncol.* (2014) 4:322. doi: 10.3389/fonc.2014.00322
5. Uttarkar S, Dasse E, Coulibaly A, Steinmann S, Jakobs A, Schomburg C, et al. Targeting acute myeloid leukemia with a small molecule inhibitor of the Myb/p300 interaction. *Blood* (2016) 127:1173–82. doi: 10.1182/blood-2015-09-668632
6. Lin L, Sun Y, Wang D, Zheng S, Zhang J, Zheng C. Celastrol ameliorates ulcerative colitis-related colorectal cancer in mice via suppressing inflammatory responses and epithelial-mesenchymal transition. *Front Pharmacol.* (2015) 6:320. doi: 10.3389/fphar.2015.00320
7. Liu J, Lee J, Salazar Hernandez MA, Mazitschek R, Ozcan U. Treatment of obesity with celastrol. *Cell* (2015) 161:999–1011. doi: 10.1016/j.cell.2015.05.011
8. Wong KF, Yuan Y, Luk JM. *Tripterygium wilfordii* bioactive compounds as anticancer and anti-inflammatory agents. *Clin Exp Pharmacol Physiol.* (2012) 39:311–20. doi: 10.1111/j.1440-1681.2011.05586.x
9. Jiang QW, Cheng KJ, Mei XL, Qiu JG, Zhang WJ, Xue YQ, et al. Synergistic anticancer effects of triptolide and celastrol, two main compounds from thunder god vine. *Oncotarget* (2015) 6:32790–804. doi: 10.18632/oncotarget.5411
10. Jang SY, Jang SW, Ko J. Celastrol inhibits the growth of estrogen positive human breast cancer cells through modulation of estrogen receptor alpha. *Cancer Lett.* (2011) 300:57–65. doi: 10.1016/j.canlet.2010.09.006S0304-3835(10)00429-5
11. Yang H, Chen D, Cui QC, Yuan X, Dou QP. Celastrol, a triterpene extracted from the Chinese "Thunder of God Vine," is a potent proteasome inhibitor and suppresses human prostate cancer growth in nude mice. *Cancer Res.* (2006) 66:4758–65. doi: 10.1158/0008-5472.CAN-05-4529
12. Li YJ, Sun YX, Hao RM, Wu P, Zhang LJ, Ma X, et al. miR-33a-5p enhances the sensitivity of lung adenocarcinoma cells to celastrol by regulating mTOR signaling. *Int J Oncol.* (2018) 52:1328–38. doi: 10.3892/ijo.2018.4276
13. Jannuzzi AT, Kara M, Alpertunga B. Celastrol ameliorates acetaminophen-induced oxidative stress and cytotoxicity in HepG2 cells. *Hum Exp Toxicol.* (2018) 37:742–51. doi: 10.1177/0960327117734622
14. Li X, Wang H, Ding J, Nie S, Wang L, Zhang L, et al. Celastrol strongly inhibits proliferation, migration and cancer stem cell properties through suppression of Pin1 in ovarian cancer cells. *Eur J Pharmacol.* (2018) 842:146–56. doi: 10.1016/j.ejphar.2018.10.043
15. Wang Z, Zhai Z, Du X. Celastrol inhibits migration and invasion through blocking the NF-kappaB pathway in ovarian cancer cells. *Exp Ther Med.* (2017) 14:819–24. doi: 10.3892/etm.2017.4568ETM-0-0-4568
16. Zhang H, Li J, Li G, Wang S. Effects of celastrol on enhancing apoptosis of ovarian cancer cells via the downregulation of microRNA21 and the suppression of the PI3K/AktNFkappaB signaling pathway in an *in vitro* model of ovarian carcinoma. *Mol Med Rep.* (2016) 14:5363-8. doi: 10.3892/mmr.2016.5894
17. Shi Z, Liang YJ, Chen ZS, Wang XW, Wang XH, Ding Y, et al. Reversal of MDR1/P-glycoprotein-mediated multidrug resistance by vector-based RNA interference *in vitro* and *in vivo*. *Cancer Biol Ther.* (2006) 5:39–47.
18. Chen X, Gong L, Ou R, Zheng Z, Chen J, Xie F, et al. Sequential combination therapy of ovarian cancer with cisplatin and gamma-secretase inhibitor MK-0752. *Gynecol Oncol.* (2016) 140:537–44. doi: 10.1016/j.ygyno.2015.12.011
19. Lv M, Qiu JG, Zhang WJ, Jiang QW, Qin WM, Yang Y, et al. Wallichinine reverses ABCB1-mediated cancer multidrug resistance. *Am J Transl Res* (2016) 8:2969–80.
20. Shi Z, Park HR, Du Y, Li Z, Cheng K, Sun SY, et al. Cables1 complex couples survival signaling to the cell death machinery. *Cancer Res.* (2015) 75:147–58. doi: 10.1158/0008-5472.CAN-14-0036
21. Zheng DW, Xue YQ, Li Y, Di JM, Qiu JG, Zhang WJ, et al. Volasertib suppresses the growth of human hepatocellular carcinoma *in vitro* and *in vivo*. *Am J Cancer Res* (2016) 6:2476–88.
22. Yang Y, Qiu JG, Li Y, Di JM, Zhang WJ, Jiang QW, et al. Targeting ABCB1-mediated tumor multidrug resistance by CRISPR/Cas9-based genome editing. *Am J Transl Res* (2016) 8:3986-94.
23. Xie FF, Pan SS, Ou RY, Zheng ZZ, Huang XX, Jian MT, et al. Volasertib suppresses tumor growth and potentiates the activity of cisplatin in cervical cancer. *Am J Cancer Res.* (2015) 5:3548–59.
24. Hou LJ, Huang XX, Xu LN, Zhang YY, Zhao N, Ou RY, et al. YM155 enhances docetaxel efficacy in ovarian cancer. *Am J Transl Res.* (2018) 10:696–708.
25. Yuan ML, Li P, Xing ZH, Di JM, Liu H, Yang AK, et al. Inhibition of WEE1 suppresses the tumor growth in laryngeal squamous cell carcinoma. *Front Pharmacol.* (2018) 9:1041. doi: 10.3389/fphar.2018.01041
26. Gong LH, Chen XX, Wang H, Jiang QW, Pan SS, Qiu JG, et al. Piperlongumine induces apoptosis and synergizes with cisplatin or paclitaxel

in human ovarian cancer cells. *Oxid Med Cell Longev*. (2014) 2014:906804. doi: 10.1155/2014/906804
27. Geng YD, Zhang C, Lei JL, Yu P, Xia YZ, Zhang H, et al. Walsuronoid B induces mitochondrial and lysosomal dysfunction leading to apoptotic rather than autophagic cell death via ROS/p53 signaling pathways in liver cancer. *Biochem Pharmacol*. (2017) 142:71–86. doi: 10.1016/j.bcp.2017.06.134
28. Li HY, Zhang J, Sun LL, Li BH, Gao HL, Xie T, et al. Celastrol induces apoptosis and autophagy via the ROS/JNK signaling pathway in human osteosarcoma cells: an *in vitro* and *in vivo* study. *Cell Death Dis* (2015) 6:e1604. doi: 10.1038/cddis.2014.543
29. Zhao H, Yang Z, Wang X, Zhang X, Wang M, Wang Y, et al. Triptolide inhibits ovarian cancer cell invasion by repression of matrix metalloproteinase 7 and 19 and upregulation of E-cadherin. *Exp Mol Med* (2012) 44:633–41. doi: 10.3858/emm.2012.44.11.072
30. Wang Y, Liu T, Li H. Enhancement of triptolide-loaded micelles on tumorigenicity inhibition of human ovarian cancer. *J Biomater Sci Polym Ed*. (2016) 27:545–56. doi: 10.1080/09205063.2015.1131667
31. Hu H, Huang G, Wang H, Li X, Wang X, Feng Y, et al. Inhibition effect of triptolide on human epithelial ovarian cancer via adjusting cellular immunity and angiogenesis. *Oncol Rep* (2018) 39:1191–6. doi: 10.3892/or.2017.6158
32. Patil S, Lis LG, Schumacher RJ, Norris BJ, Morgan ML, Cuellar RA, et al. Phosphonooxymethyl Prodrug of Triptolide: Synthesis, Physicochemical Characterization, and Efficacy in Human Colon Adenocarcinoma and Ovarian Cancer Xenografts. *J Med Chem*. (2015) 58:9334–44. doi: 10.1021/acs.jmedchem.5b01329
33. Kannaiyan R, Manu KA, Chen L, Li F, Rajendran P, Subramaniam A, et al. Celastrol inhibits tumor cell proliferation and promotes apoptosis through the activation of c-Jun N-terminal kinase and suppression of PI3 K/Akt signaling pathways. *Apoptosis* (2011) 16:1028–41. doi: 10.1007/s10495-011-0629-6
34. Zhu H, Liu XW, Ding WJ, Xu DQ, Zhao YC, Lu W, et al. Up-regulation of death receptor 4 and 5 by celastrol enhances the anti-cancer activity of TRAIL/Apo-2L. *Cancer Lett*. (2010) 297:155–64. doi: 10.1016/j.canlet.2010.04.030S0304-3835(10)00260-0
35. Ma J, Han LZ, Liang H, Mi C, Shi H, Lee JJ, et al. Celastrol inhibits the HIF-1alpha pathway by inhibition of mTOR/p70S6K/eIF4E and ERK1/2 phosphorylation in human hepatoma cells. *Oncol Rep*. (2014) 32:235–42. doi: 10.3892/or.2014.3211
36. Halliwell B. The antioxidant paradox: less paradoxical now? *Br J Clin Pharmacol*. (2013) 75:637–44. doi: 10.1111/j.1365-2125.2012.04272.x
37. Murphy MP, Holmgren A, Larsson NG, Halliwell B, Chang CJ, Kalyanaraman B, et al. Unraveling the biological roles of reactive oxygen species. *Cell Metab*. (2011) 13:361–6. doi: 10.1016/j.cmet.2011.03.010
38. Chen XX, Xie FF, Zhu XJ, Lin F, Pan SS, Gong LH, et al. Cyclin-dependent kinase inhibitor dinaciclib potently synergizes with cisplatin in preclinical models of ovarian cancer. *Oncotarget* (2015) 6:14926–39. doi: 10.18632/oncotarget.3717
39. Sabharwal SS, Schumacker PT. Mitochondrial ROS in cancer: initiators, amplifiers or an Achilles' heel? *Nat Rev Cancer* (2014) 14:709–21. doi: 10.1038/nrc3803
40. Szatrowski TP, Nathan CF. Production of large amounts of hydrogen peroxide by human tumor cells. *Cancer Res* (1991) 51:794–8.
41. Schumacker PT. Reactive oxygen species in cancer cells: live by the sword, die by the sword. *Cancer Cell* (2006) 10:175–6. doi: 10.1016/j.ccr.2006.08.015
42. Li R, Jia Z, Trush MA. Defining ROS in biology and medicine. *React Oxyg Species (Apex)* (2016) 1:9–21. doi: 10.20455/ros.2016.803
43. Tan BJ, Chiu GN. Role of oxidative stress, endoplasmic reticulum stress and ERK activation in triptolide-induced apoptosis. *Int J Oncol*. (2013) 42:1605–12. doi: 10.3892/ijo.2013.1843.
44. Liu X, Gao RW, Li M, Si CF, He YP, Wang M, et al. The ROS derived mitochondrial respirstion not from NADPH oxidase plays key role in Celastrol against angiotensin II-mediated HepG2 cell proliferation. *Apoptosis* (2016) 21:1315–26. doi: 10.1007/s10495-016-1294-6
45. Chen G, Zhang X, Zhao M, Wang Y, Cheng X, Wang D, et al. Celastrol targets mitochondrial respiratory chain complex I to induce reactive oxygen species-dependent cytotoxicity in tumor cells. *BMC Cancer* (2011) 11:170. doi: 10.1186/1471-2407-11-170

Conflict of Interest Statement: The authors declare that the research was conducted in the absence of any commercial or financial relationships that could be construed as a potential conflict of interest.

frontiers in Oncology

ORIGINAL RESEARCH
published: 30 January 2019
doi: 10.3389/fonc.2019.00022

Inhibition of FAK Signaling Elicits Lamin A/C-Associated Nuclear Deformity and Cellular Senescence

*Hsiang-Hao Chuang[1], Pei-Hui Wang[1], Sheng-Wen Niu[2], Yen-Yi Zhen[2], Ming-Shyan Huang[3], Michael Hsiao[4,5] and Chih-Jen Yang[1,6,7]**

[1] Division of Pulmonary and Critical Care Medicine, Department of Internal Medicine, Kaohsiung Medical University Hospital, Kaohsiung Medical University, Kaohsiung, Taiwan, [2] Division of Nephrology, Department of Internal Medicine, Kaohsiung Medical University Hospital, Kaohsiung Medical University, Kaohsiung, Taiwan, [3] Department of Internal Medicine, E-Da Cancer Hospital, School of Medicine, I-Shou University, Kaohsiung, Taiwan, [4] Genomics Research Center, Academia Sinica, Taipei, Taiwan, [5] Department of Biochemistry, College of Medicine, Kaohsiung Medical University, Kaohsiung, Taiwan, [6] Department of Internal Medicine, Kaohsiung Municipal Ta-Tung Hospital, Kaohsiung Medical University, Kaohsiung, Taiwan, [7] Department of Respiratory Therapy, College of Medicine, Kaohsiung Medical University, Kaohsiung, Taiwan*

Focal adhesion kinase (FAK) is a non-receptor kinase that facilitates tumor aggressiveness. The effects of FAK inhibition include arresting proliferation, limiting metastasis, and inhibiting angiogenesis. PF-573228 is an ATP-competitive inhibitor of FAK. Treating lung cancer cells with PF-573228 resulted in FAK inactivation and changes in the expressions of lamin A/C and nuclear deformity. Since lamin A/C downregulation or deficiency was associated with cellular senescence, the senescence-associated β-galactosidase (SA-β-gal) assay was used to investigate whether PF-573228 treatment drove cellular senescence, which showed more SA-β-gal-positive cells in culture. p53 is known to play a pivotal role in mediating the progression of cellular senescence, and the PF-573228-treated lung cancer cells resulted in a higher p53 expression level. Subsequently, the FAK depletion in lung cancer cells was employed to confirm the role of FAK inhibition on cellular senescence. FAK depletion and pharmacological inhibition of lung cancer cells elicited similar patterns of cellular senescence, lamin A/C downregulation, and p53 upregulation, implying that FAK signaling is associated with the expression of p53 and the maintenance of lamin A/C levels to shape regular nuclear morphology and manage anti-senescence. Conversely, FAK inactivation led to p53 upregulation, disorganization of the nuclear matrix, and consequently cellular senescence. Our data suggest a new FAK signaling pathway, in that abolishing FAK signaling can activate the senescence program in cells. Triggering cellular senescence could be a new therapeutic approach to limit tumor growth.

Keywords: non-small cell lung cancer, senescence, focal adhesion kinase, nuclear deformity, lamin A/C

OPEN ACCESS

Edited by:
Zhe-Sheng Chen,
St. John's University, United States

Reviewed by:
Shiv K. Gupta,
Mayo Clinic, United States
Ji-Ye Yin,
Central South University, China

****Correspondence:***
Chih-Jen Yang
chjeya@cc.kmu.edu.tw

Specialty section:
This article was submitted to Cancer Molecular Targets and Therapeutics, a section of the journal Frontiers in Oncology

Received: *24 October 2018*
Accepted: *08 January 2019*
Published: *30 January 2019*

Citation:
Chuang H-H, Wang P-H, Niu S-W, Zhen Y-Y, Huang M-S, Hsiao M and Yang C-J (2019) Inhibition of FAK Signaling Elicits Lamin A/C-Associated Nuclear Deformity and Cellular Senescence. Front. Oncol. 9:22. doi: 10.3389/fonc.2019.00022

INTRODUCTION

Focal adhesion kinase (FAK) is a multifunctional non-receptor tyrosine kinase that participates in a variety of signaling axes (1–5). In response to extracellular stimuli, FAK translocates to the focal adhesion complex, and mediates molecular signaling for cellular events (6–9). In focal adhesion, FAK cascades signal the focal adhesion complex to promote cell proliferation and migration

(4, 9, 10). In addition to the focal adhesion complex and cytoplasm, FAK is also present in the cell nucleus (3, 11). Nuclear FAK acts as a cotranscriptional factor in gene transcription and is involved in p53 degradation, in contrast to its enzymatic function in protein phosphorylation (3, 11, 12). Whereas, FAK in the focal adhesion complex affects the expressions of cyclin B1 and cyclin D1 to program tumor cell proliferation (6, 13, 14), nuclear FAK elicits p53 degradation to drive cell cycle progression (11, 12).

The biological roles of FAK in cell migration and proliferation have also been implicated in pathological progression and in the development of cancer. There are several lines of evidence suggesting that FAK activity can manipulate tumor phenotypes, leading to uncontrolled proliferation, neovascularization, and metastasis (5, 15, 16), and the FAK signaling to tumor cell propagation represents tumorigenic capacity (5, 11). Given the crucial roles of FAK in these malignant processes, FAK is regarded to be a potential target for anti-cancer therapy (17, 18). Experiments have shown that FAK depletion results in silencing of cancer-promoting gene expressions in human hepatocellular carcinoma (HCC) xenotransplants in nude and severe combined immunodeficiency (SCID) mice (19). Moreover, the enzymatic function of FAK involves in proliferation and metastasis (9, 15, 20). Suppressing the catalytic activity of FAK or sequestering FAK in the cytoplasm has been reported to potentially perturb FAK signaling, which implies that chemical inhibitors of the enzymatic activity of FAK may be a pharmacological strategy to limit cancer growth and metastasis (6, 7, 21, 22).

Triggering cell apoptosis and arresting cell cycle progression with pharmacological regimens are common strategies to limit tumor cell growth. FAK inhibition represents an anti-cancer therapeutic strategy, as FAK inhibitors have effects on anti-angiogenesis, anti-proliferation, and anti-invasion effects (5, 15, 23). Besides, inducing cellular senescence in tumor cells could be a new therapeutic approach to limit tumor cell growth (24). Although therapy-induced senescence (TIS) in cancer cells may result from deficient apoptosis (25), driving cancer cells to cellular senescence could be a way to limit tumor propagation (26). In general, chemotherapy-induced DNA damage, telomere shortening, and oncogenic stress are the three main pathological causes of senescence (24, 27–32), and the induction of cellular senescence with these drug regimens is a side effect. Cases of β-gal-positive lung cancer biopsies in response to chemotherapy have been reported (24, 29, 33). Inducing cellular senescence could be a new approach to limit cancer growth based on phenotypic aging without DNA damage or genomic instability (31, 34). Chromatin or nuclear skeleton disorganization could be a cause of cellular senescence instead of oncogenic stress and replicative failure (8, 26).

Recent pharmacological advances in cancer therapy have led to an increased focus on developing chemical compounds that are able to target specific molecules in tumor cells to both improve efficacy and lower toxicity (4, 35). PF-573228, which competes with ATP binding to abolish the catalytic function of FAK, can inhibit the phosphorylation of FAK at tyrosine 576/577 and FAK kinase function (36, 37). Consequently, PF-573228 efficiently suppresses both the growth and metastasis of epithelial carcinoma (4, 36). The pharmacological effects of PF-573228 have been characterized based on the inhibition of FAK catalytic activity (36). In this study, we hypothesized that inhibiting the enzymatic function of FAK would stop lung cancer cell growth and invasion. Interestingly, the enzymatic inactivation of FAK resulted in nuclear deformity. When we investigated the cause and effect of nuclear deformity by PF-573228, we observed that p53 upregulation, lamin A/C downregulation, and cellular senescence in the lung cancer cells exposed to PF-573228. Strikingly, perturbation of FAK signaling led to downregulation of lamin A/C and cellular senescence rather than proliferative arrest, and halted migration of the lung cancer cells. These results showed that treatment with a FAK inhibitor could be a therapeutic approach to abrogate tumor growth. In addition, these findings revealed the crucial role of FAK signaling in anti-senescence, and that inhibition of FAK resulted in the progression of senescence.

MATERIALS AND METHODS

Materials

Detailed information on the materials is listed in **Supplementary Table S1**.

Cell Culture and Drug Treatment

A549 cells, H1299 cells, and H460 cells were purchased from ATCC. The cells were cultured in RPMI 1640 medium supplemented with 10% fetal bovine serum (FBS) at 37°C in a humidified atmosphere at 5% CO_2, and treated with PF-573228 (TOCRIS, Bristol, UK) at concentrations of 0, 0.1, 1, or 10 μM.

Western Blot Analysis

The cells were harvested and lysed in 1x RIPA buffer (Merck, Darmstadt, Germany) containing protease and phosphatase inhibitors. The protein concentration was determined using a Bio-Rad DC protein assay kit (Bio-Rad, California, USA). For Western blot analysis, 30 μg of total protein was applied to SDS-PAGE and transferred to a PVDF membrane. The membranes were blocked in 5% skim milk for 2 h in TBST buffer (20 mM Tris-Cl, 150 mM NaCl, 0.1% Tween 20, pH 7.4). After blocking, the membranes were probed with the primary antibody overnight. Antibodies against FAK, p-FAK, cyclin B1, p53, and lamin A/C were used in immunoblotting. The given protein bands were identified by horseradish peroxidase-conjugated secondary antibodies and developed with an enhanced chemiluminescence solution.

Flow Cytometry Cell Cycle Analysis

The cells were harvested and washed with PBS buffer, and then fixed in 70% (v/v) ethanol. The fixed cells were stained with propidium iodide solution and injected into an Attune NxT Flow Cytometer (Life Tech, California, USA) to analyze the cell cycle profile.

Immunofluorescent Staining and Immunofluorescent Microscopic Imaging

A Leica DMi8S epifluorescence microscope (Wetzlars, Germany) equipped with an X-Cite XCT10A (Lumen Dynamics,

Wiesbaden, Germany) light source, filters and objectives (10x, 20x, 40x, and 63x) was used to observe fluorescent signals in the cells. In addition to epifluorescence, confocal images were captured using an OLYMPUS FV1000 confocal laser scanning microscope equipped with a light source, filters and objectives (10x, 20x, 40x, 63x, and 100x). Cells were seeded on 12-mm coverslips in a 24-well culture plate. The cells were harvested and fixed in 4% paraformaldehyde in PBS for 10 min, and permeabilized in 0.5% Triton in PBS for 5 min. After fixation, the cells were subjected to immunofluorescent staining with antibodies recognizing FAK and emerin. Phalloidin-TRITC was used as an additional reagent. Cell nuclei were stained with 0.2 μg/mL 4′, 6-diamidino-2-phenylindole (DAPI).

Senescence-Associated β-Galactosidase Staining

The cells were fixed with 4% paraformaldehyde for 15 min. After fixation, acidic β-galactosidase (SA-β-gal) was assayed in senescence assay buffer (1 mg/mL 5-bromo-4-chloro-3-indolyl β D-galactopyranoside (X-gal), 5 mM $K_3Fe(CN)_6$, 5 mM $K_4Fe(CN)_6$, 2 mM $MgCl_2$, 150 mM NaCl, 40 mM citric acid, and 40 mM Na_2HPO_4 at pH 6.0) in the dark at 37°C for 16 h. SA-β-gal activity was detected based on SA-β-gal-hydrolyzed X-gal, which produces a blue color. All chemical reagents were purchased from Sigma-Aldrich.

Cell Growth Assay

The cells were trypsinized, resuspended in 1xPBS, and stained with trypan blue (Sigma-Aldrich). The number of cells was counted with a hemocytometer.

Lentiviral Production and Infection

Lentivirus-associated plasmids encoding luciferase, and FAK short hairpin RNA (shRNA) were obtained from the National RNAi Core Facility of Academia Sinica, Taiwan. The production and infection of lentiviruses were performed according to the guidelines of the National RNAi Core Facility.

Statistical Analysis

The experimental data were digitized and analyzed. Data are presented as the mean ± the standard error of the mean (SEM). One-way ANOVA was used to compare digitized data and measurements from independent experiments in two or more groups, and the Student's *T*-test was used to compare two independent samples. A $p < 0.05$ was considered to indicate a statistically significant difference.

RESULTS

PF-573228 Causes Cessation of the Propagation of Lung Cancer Cells

Focal adhesion signaling is involved in cell proliferation, and FAK plays a key role in the focal adhesion complex that relays focal adhesion signals to the cell proliferation program (9, 15). Given the role of FAK signaling in tumor growth and metastasis, we hypothesized that inhibiting the catalytic activity of FAK may disrupt FAK signaling and blunt tumor cell proliferation. Therefore, we treated three distinct non-small cell lung cancer cell lines (A549 lung adenocarcinoma cells and H460 and H1299 large cell carcinoma cells) with PF-573228, an enzymatic inhibitor of FAK. PF-573228 was administered to the lung cancer cells for 4 days at three doses: 0.1, 1, or 10 μM. The growth curves showed that 10 μM PF-573228 effectively induced cessation of cell growth (**Figures 1A–C**).

We then examined the expression level of the cell cycle regulator cyclin B1, which has been reported to be a downstream effector of FAK signaling. Western blot analysis showed that cyclin B1 expression levels were much lower after the cells were exposed to 10 μM PF-573228 (**Figures 1D–F**). To further characterize the effect of PF-573228 treatment on cell cycle progression, we analyzed the cell cycle distribution using flow cytometry analysis. The results showed that a low PF-573228 concentration had little influence on cell cycle progression (**Figures 1G–I**), whereas a high PF-573228 concentration (10 μM) halted cell cycle progression at the G2/M transition (**Figures 1J,K**). This showed that PF-573228 treatment effectively suppressed multiplication of lung cancer cells.

PF-573228 Administration Inactivates FAK

Since phosphorylation of FAK at Tyr-576 and Tyr-577 (p-FAK) represents enzymatic activation of FAK (37), an antibody against p-FAK was used to confirm the kinase activity of FAK and verify the effect of PF-573228 on FAK inactivation. FAK activity was practically blocked by 10 μM PF-573228 in A549 cells (**Figures 2A,C**). To further confirm the inactivation of FAK by PF-573228 treatment, we also examined the phosphorylation of tyrosine 397 in FAK (pTyr-397). The results showed that the intensity of pTyr-397 was decreased after PF-573228 treatment (**Figure S1**). FAK is a key regulator of integrin signaling for focal adhesion assembly (38, 39). In addition to FAK inhibition, PF-573228 has been shown to perturb integrin-based signaling for focal adhesion maturation (36).

Treatment of the lung cancer cells with PF-573228 resulted in failure of FAK activation, and translocation to focal adhesion was observed in immunofluorescent imaging (**Figure 2B**). When the cells were cultured in PF-573228-free medium, more FAK translocated to focal adhesions, which appeared as plaque-like patterns in the cell periphery that formed at the tips of stress fibers, as visualized in cells stained with phalloidin-labeled F-actin and an antibody against FAK (**Figure 2B**). By contrast, in the A549 cells treated with PF-573228, only a few FAK molecules translocated to focal adhesions, and tiny FAK-based focal adhesions formed at the tips of F-actin bundles, indicating failure of focal adhesion maturation (**Figure 2B**). The sizes of focal adhesions were measured and the areas of FAK at the tips of the actin stress fibers were digitized using Image Pro software. The sizes of focal adhesions ranged from 12 to 28 μm^2 in the cells without PF-573228 treatment, whereas the extent of FAK-based focal adhesion was approximately 3–12 μm^2 after PF-573228 treatment (**Figure 2D**).

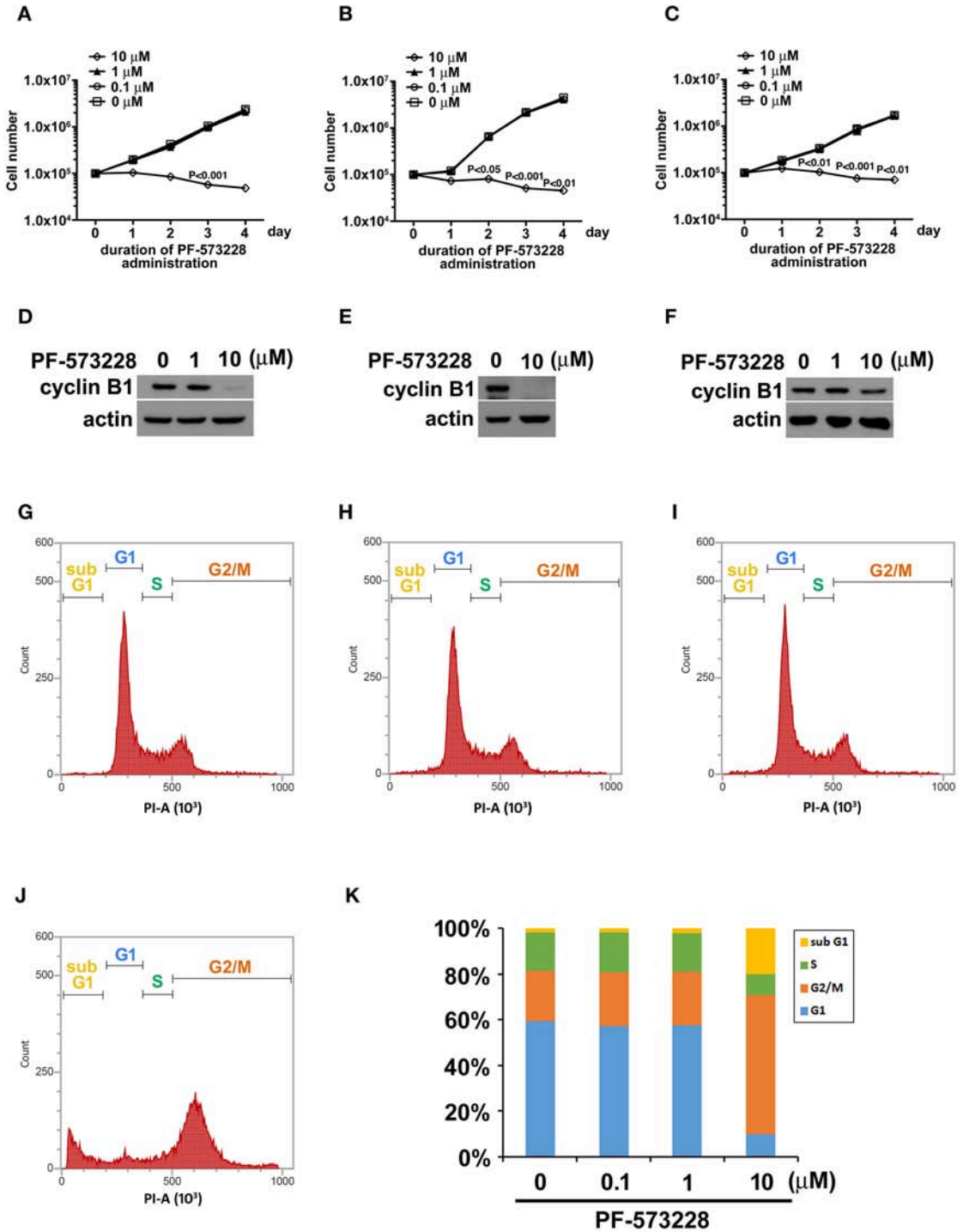

FIGURE 1 | PF-573228 inhibited lung cancer cell growth. Three different types of lung cancer cells, **(A)** A549 lung adenocarcinoma and **(B)** H460, and **(C)** H1299 large cell carcinoma, were selected for the PF-573228 administration regimen. Cell growth curves of the three lung cancer cell lines treated with various doses of PF-573228 for 4 days were established. The administration of PF-573228 at 10 μM to the lung cancer cells effectively suppressed cell growth *in vitro*, as proliferative activity totally ceased in the cells exposed to 10 μM PF-573228. **(D)** On the third day, PF-573228-treated cells were harvested and subjected to Western blot analysis for cyclin B1. Cyclin B1 levels were much higher in A549 cells with 1 μM PF-573228 or without PF-573228 treatment than in the cells treated with higher concentrations of PF-573228. **(E)** After 10 μM PF-573228 treatment, cyclin B1 levels declined markedly in H460 cells. **(F)** PF-573228 administration slightly reduced cyclin B1 levels in H1299 cells. A549 cells were harvested and subjected to flow cytometry analysis for cell cycle profiling after PF-573228 treatment for 3 days. The concentrations of PF-573228 were 0 μM **(G)**, 0.1 μM **(H)**, 1 μM **(I)** and 10 μM **(J)**, respectively, **(K)** After 10 μM PF-573228 treatment, the G2/M ratio was significantly extended. The apoptotic ratio was also increased in A549 cells with 10 μM PF-573228 treatment.

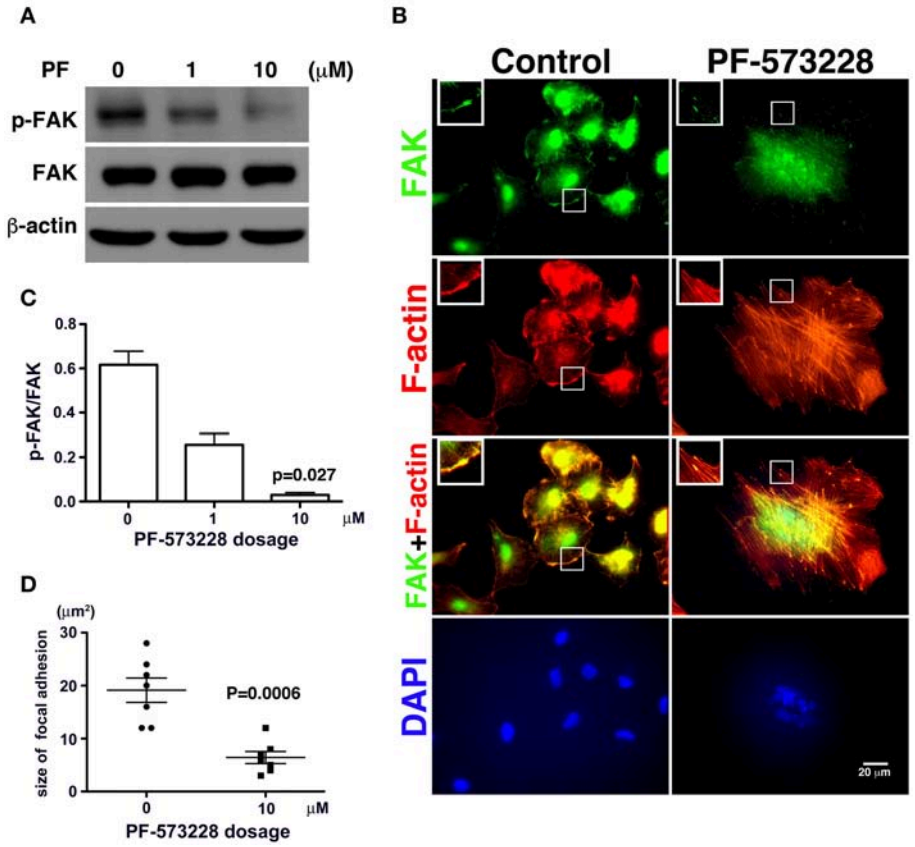

FIGURE 2 | PF-573228 as a catalytic inhibitor inactivated the kinase function of FAK. **(A)** FAK expression levels and FAK activity, as measured by the phosphorylation of FAK at tyrosine 576 and 577, were quantified by Western blot analysis after treatment of lung cancer cells with PF-573228 for 3 days. **(B)** The cells were stained with phalloidin to visualize F-actin (red) and a FAK antibody to visualize the FAK distribution (green). In cells without PF-573228 administration, FAK translocated to focal adhesions at the tips of actin stress fibers, and the focal adhesions were relatively large. When cells were exposed to 10 μM PF-573228, FAK translocation to focal adhesions was reduced, and the sizes of the focal adhesions were smaller. Nuclei in cells treated with PF-573228 were deformed, as visualized with DAPI staining, whereas most nuclei in cells without PF-573228 treatment were oval shaped. **(C)** The p-FAK/FAK ratios in the cells with exposure to 1 μM and 10 μM PF-573228 were reduced to less than half and one tenth compared with the cells without PF-573228 treatment, respectively. **(D)** The sizes of FAK-based focal adhesions were 19 μm^2 on average in the cells without PF-573228 treatment and 6.4 μm^2 on average in the cells without PF-573228 treatment.

Aberrant Nuclear Appearance and Lamin A/C Downregulation Occur Concurrently in the Lung Cancer Cells Exposed to PF-573228

In the absence of PF-573228, most cells contained oval or round nuclei, as visualized by DAPI staining (**Figure 2B**). Interestingly, a distorted nuclear morphology was observed in the A549 cells treated with PF-573228 (**Figure 2B**). As DAPI staining was insufficient to clearly visualize the nuclear appearance in detail, an antibody against emerin (40), a nuclear inner membrane protein, was used to visualize the nuclear shape in the PF-573228-treated A549 cells. Emerin staining revealed that the cells without PF-573228 treatment harbored oval-like nuclei. By contrast, most nuclei were larger and had irregular shapes with invagination in the cells upon exposure to 10 μM PF-573228 (**Figure 3A**).

Lamin A/C is the nuclear skeleton responsible for maintaining and stabilizing the nuclear architecture (41–44). Because interrupting FAK signaling resulted in nuclear deformity (**Figure 2B**), changes in lamin A/C expression levels were assessed. The effects of FAK signaling on the expressions of lamin A/C and other nuclear skeletal proteins inferred that the nuclear deformity caused by PF-573228 was attributable to changes in lamin A/C expression.

To investigate changes in lamin A/C expressions in cells exposed to PF-573228, PF-573228-treated cells were harvested and subjected to Western blot analysis. Inhibition of FAK activity led to lower p-FAK levels (**Figures 3B,C**) and deformed nuclei in the lung cancer cells (**Figure 3A**). To quantify the expressions of lamin A and C, the intensities of their protein bands were normalized to β-actin (**Figure 3B**). The expressions of lamin A and C were much lower in the A549, H460, and H1299 cells treated with PF-573228 compared to those without PF-573228 treatment (**Figure 3B** and **Figures S2A,B**). The lamin A and C band intensities were quantified and plotted in bar charts. The ratios of lamin A/β-actin and lamin C/β-actin in A549 cells exposed to PF-573228 were reduced by one third and one half, respectively, compared to A549 cells without PF-573228

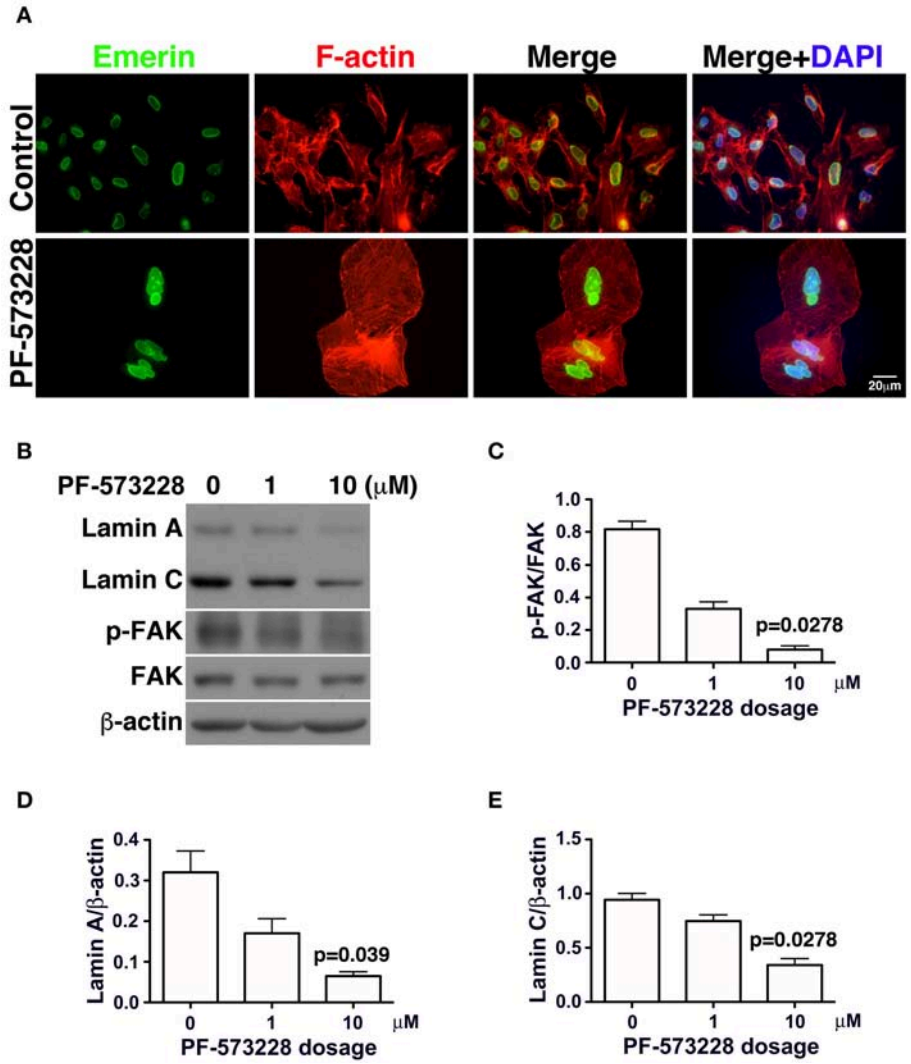

FIGURE 3 | Downregulation of lamin A and lamin C and nuclear deformity in A549 cells exposed to PF-573228. **(A)** After PF-573228 treatment of A549 cells, the cells were fixed and stained with phalloidin to label F-actin (red) and an antibody against emerin (green) to outline the nuclear shape. Cells treated with PF-573228 were extremely large and had deformed nuclei, whereas mostly oval-like nuclei were present in the cells without PF-573228 treatment. **(B)** The cells treated with 10 μM PF-573228 exhibited a decrease in p-FAK levels. Lamin A and lamin C expression levels were much lower in A549 cells exposed to 10 μM PF-573228. **(C)** The p-FAK/FAK ratios in A549 cells exposed to 1 μM and 10 μM PF-573228 were less than half and one tenth of those in A549 cells without PF-573228 treatment, respectively. **(D,E)** Decreased lamin A and lamin C levels appeared in A549 cells treated with PF-573228.

treatment (**Figures 3D,E**). Similar trends of downregulation of lamin A and lamin C by PF-573228 treatment were also detected in the two other lung cancer cell lines (**Figures S2A,B**).

Lung Cancer Cells Are Destined to Senescence After Inhibition of FAK Enzymatic Function

Mutant LMNA, mutations that affect lamin A/C expression, and lamin A/C depletion in cells have been associated with premature aging and cellular senescence (8, 30, 32, 42, 45). Based on the concurrent lamin A/C downregulation and nuclear deformity observed in lung cancer cells exposed to PF-573228 (**Figures 3A,B**), we examined the development of cellular senescence in lung cancer cells treated with PF-573228. The SA-β-gal activity in cells was assayed by *in situ* staining using the chromogenic substrate X-gal, which colored SA-β-gal-positive cells blue. As noted in **Figure 4A**, blue cells were clearly visible in the cells treated with PF-573228 (**Figure 4A**), whereas a sporadic distribution of blue-colored cells was observed in the cells without PF-573228 treatment (**Figure 4A**). The bar chart in **Figure 4B** shows that nearly 90% of the cells exposed to a higher dose of PF-573228 were positive for SA-β-gal, compared to ∼20% of the cells exposed to a lower dose of PF-573228, and ∼1% of the cells without PF-573228 treatment.

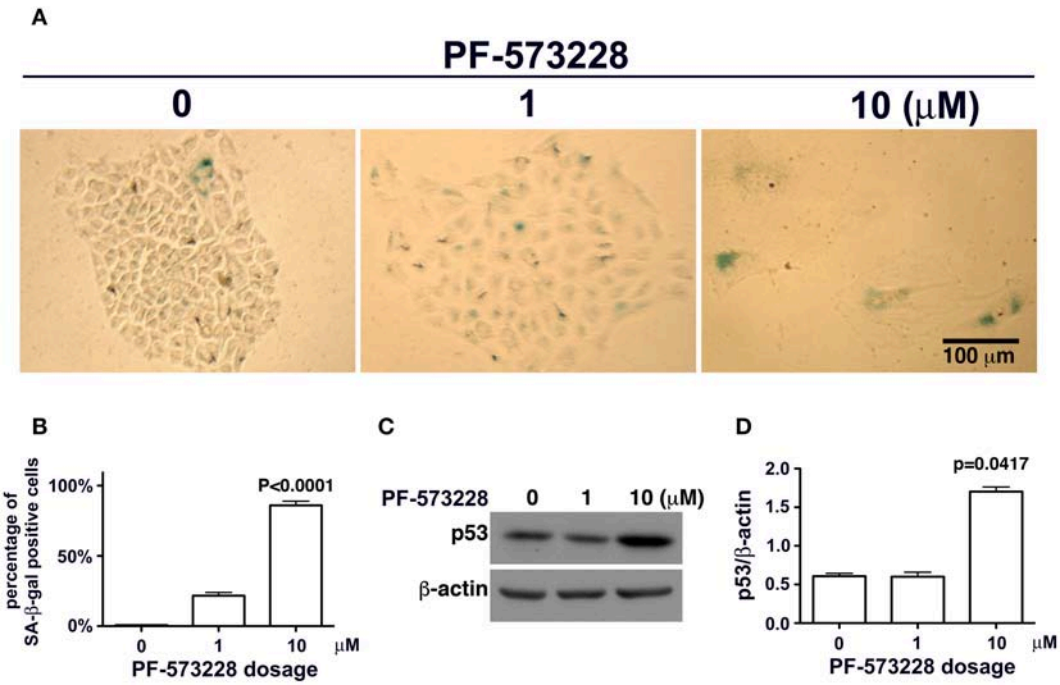

FIGURE 4 | Cellular senescence occurred in lung cancer cells after FAK inhibition. **(A)** A549 cells were exposed to 0, 1 μM, or 10 μM PF-573228 for 7 days. SA-β-gal-positive cells appeared sporadically in cells without PF-573228 treatment. The cells treated with 1 μM PF-573228 were slightly enlarged, with few β-gal-positive cells. The cells treated with 10 μM PF-573228 were quite large, and most were β-gal positive. **(B)** The ratio of SA-β-gal-positive cells to the total population was calculated and plotted in a bar chart. SA-β-gal-positive cells represented <1% of the total A549 cell population without PF-573228 treatment, ∼21% in the 1 μM PF-573228-treated A549 cell population, and more than 80% in the 10 μM PF-573228-treated A549 cell population. **(C)** A549 cells were treated with 0, 1, or 10 μM PF-573228 for 4 days. p53 was not obviously increased in 1 μM PF-573228 treated-A549 cells and was significantly elevated in 10 μM PF-573228-treated A549 cells. **(D)** p53 levels approximately tripled in A549 cells exposed to 10 μM PF-573228 compared to cells with or without 1 μM PF-573228 treatment.

Upregulation of p53 in Cells Exposed to PF-573228

Disruption of FAK signaling by PF-573228 caused cellular senescence. However, the mechanisms by which inhibition of FAK signaling affects senescence programming remain unclear. Cellular senescence in chemotherapy-affected cancer cells has been observed in several studies (24, 29, 46). In addition, clinical studies have reported that p53 plays a role in the development of cellular senescence in chemotherapy-affected cancer cells (46, 47). p53 is known to be a transcription factor in programed senescence and cell cycle arrest (48), and it may play a similar role in the cellular senescence program in lung cancer cells exposed to PF-573228 as in cells in which FAK signaling is interrupted.

To investigate whether or not p53 plays a role in PF-573228-induced cellular senescence, p53 expression levels were examined in PF-573228-treated cells. Western blot analysis showed that p53 expression levels increased significantly by more than 3-fold compared to cells without PF-573228 treatment and cells treated with a low concentration of PF-573228 (**Figures 4C,D**, and **Figure S3**).

Engagement of FAK Signaling With Nuclear Integrity and p53 Expression

FAK is not the only molecule targeted by PF-573228 (36). Although FAK enzymatic activity was blocked by PF-573228 administration, off-target effects could also have turned off other kinases, for example, cyclin-dependent kinases. Therefore, signaling perturbations of other kinases may have caused the pathogenic senescence in the lung cancer cells.

If FAK has an anti-senescence effect, FAK depletion would cause anti-senescence to fail and escalate senescence programing. To clarify the role of loss of FAK signaling in the development of cellular senescence and nuclear deformity with changes in lamin A and lamin C expressions, we used an shRNA targeting FAK to deplete the expression of FAK in lung cancer cells. After introducing shFAK into lung cancer cells, cells harboring shFAK were selected. To assess FAK knockdown, two shFAK clones were selected for Western blot analysis and senescence assays, which showed that shFAK successfully caused FAK depletion in A549, H460, and H1299 cells (**Figure 5A** and **Figure S4A**). In addition, the impact of FAK depletion on the downregulation of lamin C and cyclin B1 and upregulation of p53 was validated (**Figure 5A** and **Figure S4A**). We also assessed nuclear appearance using emerin staining, which revealed that A549 cells without FAK depletion harbored oval-like nuclei. By contrast, the ratio of nuclei harboring slightly larger and irregular shapes was increased in the cells with FAK depletion (**Figure 5B**). Similar results were obtained in the H460 and H1299 cells (**Figures S4B,C**). In addition, lung cancer cells harboring shLuc or shFAK were subjected to senescence assays, which revealed

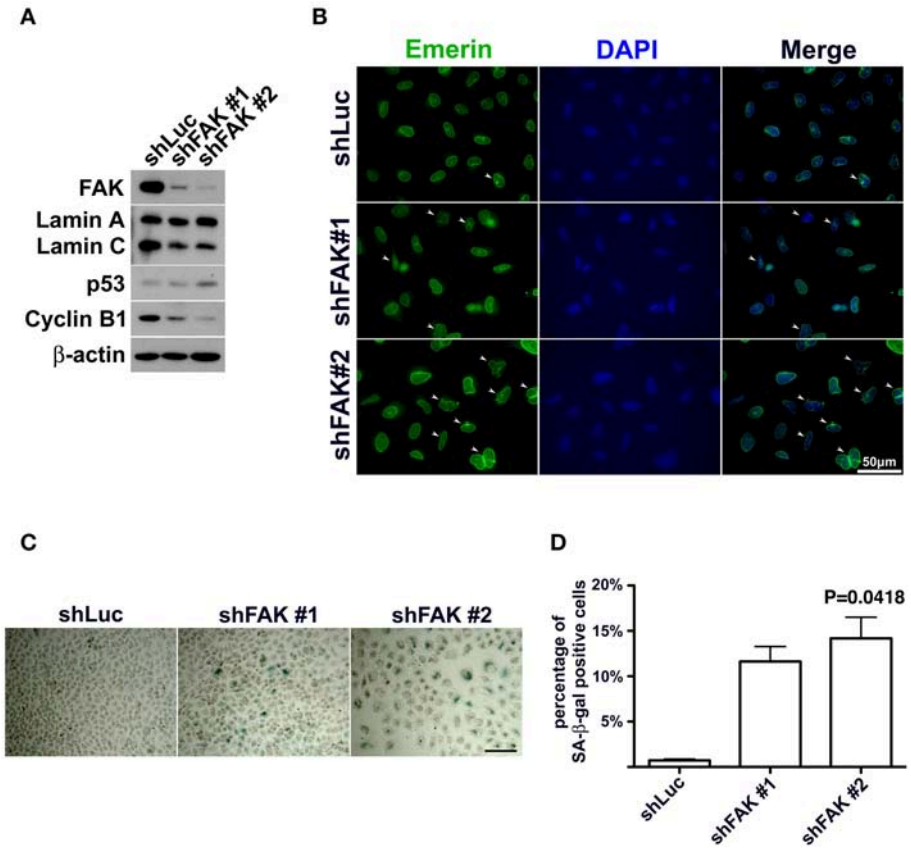

FIGURE 5 | FAK depletion resulted in nuclear deformity and cellular senescence. **(A)** A549 cells with FAK depletion by shRNA were seeded and incubated for 7 days. Western blot analysis revealed low FAK levels in the cells with shFAK and higher levels in the cells with shLuc. Upon FAK depletion, lamin C and cyclin B1 levels decreased, and p53 expression levels increased. **(B)** The cells were fixed and stained with an antibody against emerin (green) to outline the nuclear shape. Cells with FAK depletion were slightly larger, with a higher proportion of deformed nuclei (arrowhead), whereas mostly oval-like nuclei were present in cells without FAK depletion. (Scale bar, 50 μm) **(C)** SA-β-gal-positive cells were sporadically visible in A549 cells with shLuc. By contrast, more SA-β-gal-positive cells were observed among cells with shFAK. (Scale bar, 100 μm) **(D)** The bar chart shows that <1% of the cells in the shLuc population were SA-β-gal-positive, whereas more than 10% of the shFAK cell population was SA-β-gal positive.

more SA-β-gal-positive A549 cells harboring shFAK (**Figure 5C**). By contrast, few SA-β-gal-positive cells were visible in those harboring shLuc. The SA-β-gal-positive cells represented ∼0.7% of the shLuc A549 population. In the two shFAK cell clones, SA-β-gal-positive cells represented ∼11 and 15%, respectively (**Figure 5D**). Similar results were observed in H460 and H1299 cells (**Figures S4D–F**). However, H460 cells grew in single and multiple layers (**Figure S4D**), and it was difficult to measure the ratio of SA-β-gal-positive cells.

Senescent Cells Reactivate Their Proliferative Activity After PF-573228 Withdrawal From Cell Culture

Aging and cellular senescence are often present in replicative failure, oncogenic induction, and telomere shortening (8, 34, 49). In clinical cases, chemotherapy or radiation has been shown to induce cellular senescence, and DNA damage or genomic instability is thought to be the pathological cause. Therapy-induced senescence can be classified as replicative senescence (24, 27, 33, 48), and replicative senescence is able to cease tumor growth (47, 50). However, this cellular senescence is reversible (31, 51, 52). Senescent cells expressing low levels of p16 have been shown to reversibly exit senescence when p53 expression levels fall (52).

In this study, FAK signaling downregulated the expression of p53, and inhibition of FAK signaling upregulated the expression of p53 in A549 cells (**Figures 4C,D**, **5A**). The A549 cells that entered senescence due to PF-573228 administration exhibited regrowth and return to a non-senescent state after withdrawal of PF-573228 from the culture (**Figures 6A–C**). The proliferative activity of A549 cells was based on cyclin B1 expression after the cells were incubated in PF-573228-free medium (**Figure 6D**).

Restoration of Lamin a and Lamin C Expressions in Senescent Lung Cancer Cells After PF-573228 Withdrawal

We then tested whether senescence in lung cancer cells with FAK inhibition was reversible or irreversible. The three lung

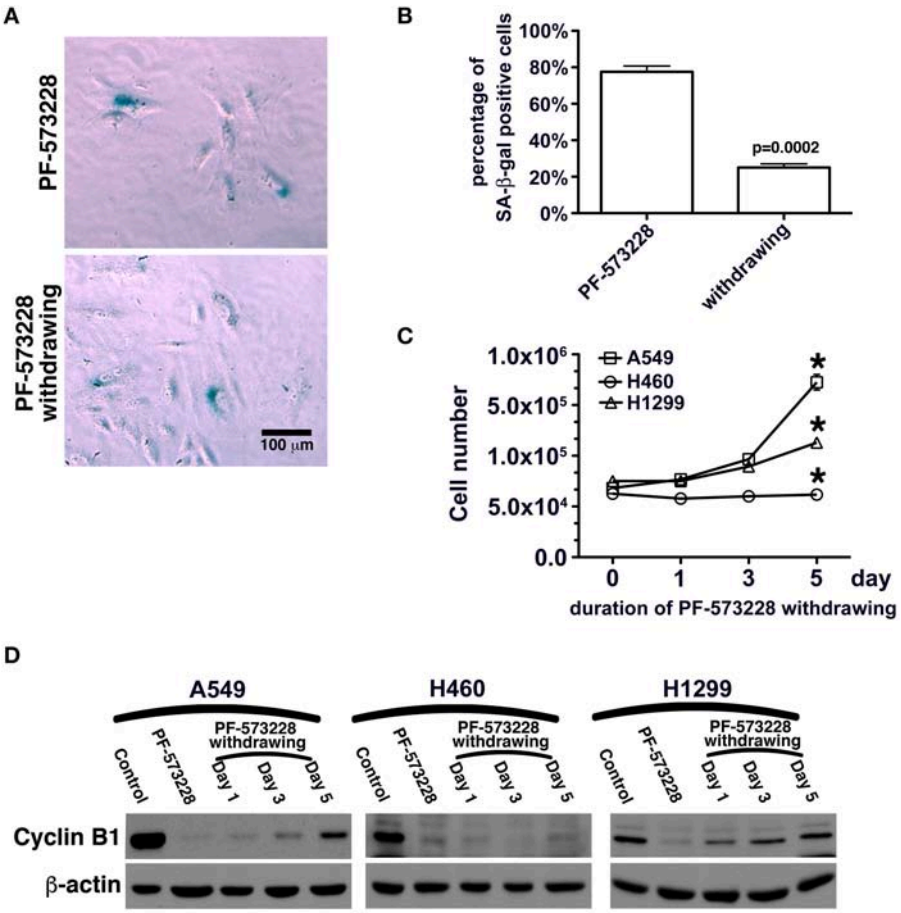

FIGURE 6 | Recovery of the proliferative activity of lung cancer cells after PF-573228 withdrawal. **(A)** The population of SA-β-gal-positive A549 cells declined after the cells were released from PF-573228 inhibition. **(B)** The proportion of SA-β-gal-positive A549 cells was ~80% when cells were exposed to PF-573228, and only 25% after PF-573228 withdrawal. **(C)** Initially, the cells were senescent, and proliferation ceased in the three lung cancer cell lines with PF-573228 treatment. After PF-573228 withdrawal, the A549 cells grew exponentially, H1299 cells grew linearly, and H460 cells continued to exhibit cessation of division. **(D)** When cells were exposed to PF-573228, cyclin B1 expression level was extremely low. After the cells were released from PF-573228 inhibition, cyclin B1 levels gradually increased in A549 cells and H1299 cells. However, cyclin B1 remained at low levels in H460 cells after PF-573228 withdrawal. *$P < 0.05$.

cancer cells lines were cultured in medium containing 10 μM PF-573228 to induce cell senescence in a 5-day induction course, after which the expressions of lamin A and lamin C decreased (**Figure 7A**). After the induction of senescence, PF-573228 withdrawal was scheduled over 6 days. Lamin A and lamin C expressions in A549 cells and H1299 cells gradually recovered after PF-573228 withdrawal (**Figures 7A,B**). By contrast, lamin A and lamin C levels in H460 cells remained lower when senescent H460 cells were incubated in PF-573228-free medium (**Figures 7A,B**). After PF-573228 withdrawal, senescent A549 cells escaped from senescence, as the SA-β-gal-positive A549 cell population declined to nearly half by the fifth day of PF-73228 withdrawal (**Figure 8A**).

DISCUSSION

FAK is a signaling mediator of integrin-based signaling and is associated with epidermal growth factor receptor (EGFR) signaling (23, 53). FAK-associated cross-talk between EGFR and integrin pathways have been shown to lead to tumor growth and metastasis in lung cancer (39, 53–55). Phosphorylation at tyrosine 576/577 (p-FAK) has been reported to result in catalytic activity and to be involved in tumor cell proliferation and metastasis (2, 12, 15, 16). Therefore, inhibition of the enzymatic function of FAK has been proposed to be a therapeutic strategy to limit tumor growth, angiogenesis, and metastasis (5, 7, 16, 23). In the present study, we tested the pharmacological effect of PF-573228 on inhibiting FAK activity and limiting lung cancer cell growth. When lung cancer cells were treated with PF-573228, an abnormal nuclear shape was observed. A similar cytological phenomenon has been reported in previous studies (56), however the molecular mechanism has not been clearly elucidated. In addition, nuclear lobulation and distorted nuclear morphology have been reported in cells with the LNMA mutation or lamin A/C downregulation (41–43). The LNMA mutation or lamin A/C downregulation has been shown to result in nuclear distortion

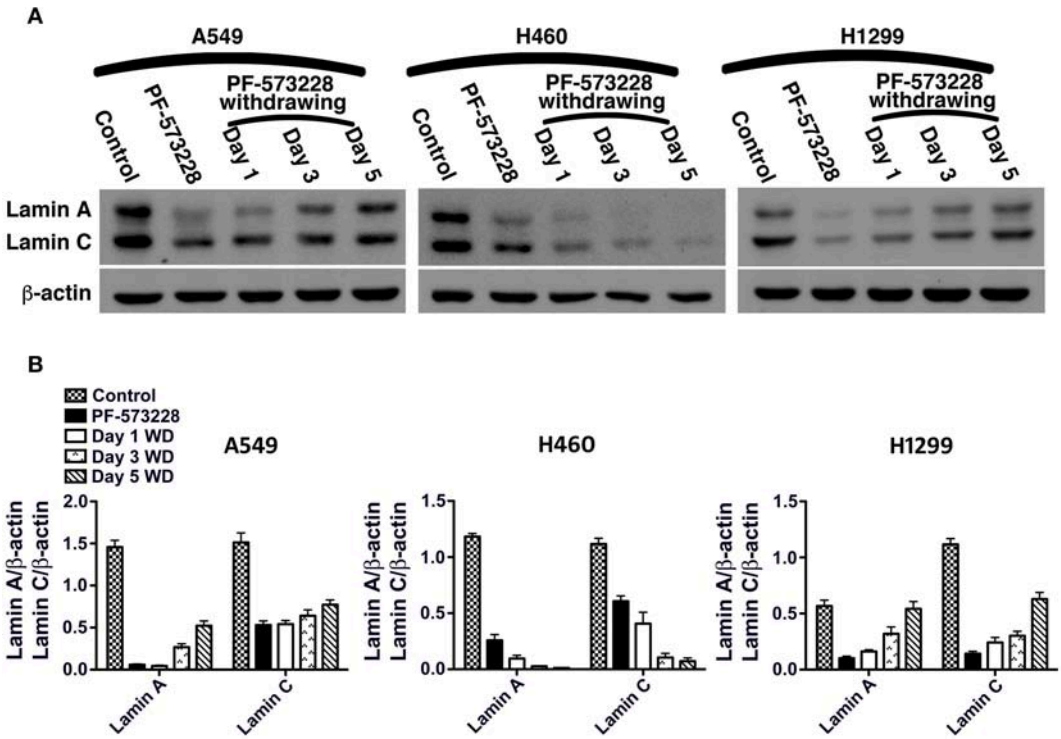

FIGURE 7 | Restoration of lamin A and lamin C expressions in lung cancer cells after PF-573228 withdrawal (WD). **(A)** The senescent cells were released from PF-573228 inhibition for the indicated period. Western blot analysis revealed that the expression levels of lamin A and lamin C were gradually restored in A549 cells and H1299 cells. However, the lamin A and lamin C levels remained lower in H460 cells when senescent H460 cells were incubated in PF-573228-free medium. **(B)** The expression levels of lamin A and lamin C in A549 cells increased after the cells were released from PF-573228 inhibition. However, H460 cells expressed lower levels of lamin A and lamin C when exposed to PF-573228, and lamin A and lamin C expression in H460 cells remained lower when PF-573228-treated cells were cultured in PF-573228-free medium. Lamin A and lamin C levels in H1299 cells decreased when cells were exposed to PF-573228. After PF-573228 withdrawal, the expression levels of lamin A and lamin C gradually increased in H1299 cells previously treated with PF-573228.

with a pathogenic tendency to develop aging and senescence (8, 30, 42, 57). The nuclear deformity in PF-573228-treated lung cancer cells (**Figures 2B**, **3A–C**) supports a pathophysiological impact from the inactivation of FAK signaling to downregulate lamin A/C.

In this study, we examined the expressions of lamin A/C and assayed SA-β-gal activity in lung cancer cells exposed to PF-573228. Our experimental results demonstrated that FAK inhibition and FAK depletion elicited similar downregulation of lamin A/C, upregulation of p53, and cellular senescence (**Figures 4A,C,D**, **5A,C**). These results imply that FAK signaling regulates the expression of lamin A/C to maintain a regular nuclear shape and activate anti-senescence programs (**Figure 8B**). The finding that FAK signaling affects lamin A/C expressions and influences the cellular context in which lamin A/C organizes the nuclear architecture is an important biological theme. The degradation of lamin A/C has recently been reported to be regulated by Akt1 or cdk5 signaling (30, 58). Akt signaling was shown to slightly alter the amount of lamin A/C in cells, but this small change in lamin A/C expressions did not seem to have a notable effect on nuclear shape. On the other hand, nuclear FAK has also been shown to act as a transactivator to regulate gene expressions and stem cell differentiation rather than stem cell renewal (59). In addition, nuclear FAK and Oct-4 have been shown to coordinate gene expression programming with the expression of Oct-4 in stem cell renewal. However, the role of nuclear FAK in gene expression programming does not seem to be associated with changes in lamin A/C expressions. Furthermore, we found that PF-573228 treatment does not dramatically affect nuclear translocation of FAK in A549 cells (**Figure S5**). This implied that FAK-mediated signaling to maintain lamin A/C expression may not be through transcriptional regulation. By contrast, inactivation of FAK signaling or nestin silencing (30) has been shown to significantly downregulate lamin A/C and cause round or oval nuclei to become lobulated or irregular in shape. Our results indicated that FAK-mediated signaling is crucial to maintain nuclear shape and, potentially, for chromatin reorganization.

In addition to the downregulation of lamin A/C, this study showed that FAK inhibition-mediated p53 upregulation also played a crucial role in cellular senescence, and that p53 was increased during FAK inhibition either by a small compound or shRNA-mediated downregulation. Lim et al. demonstrated that nuclear FAK could promote p53 downregulation via enhanced Mdm2-dependent p53 ubiquitination in a kinase-independent manner (11). However, in our study, both the amount of

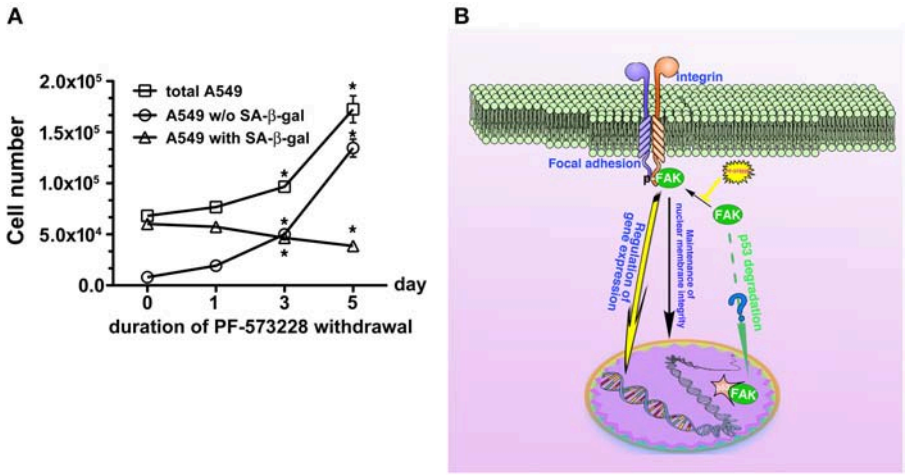

FIGURE 8 | Disruption of FAK signaling with cellular senescence. Reactivation of FAK signaling was observed in A549 cells in which senescence was induced by 5 days of PF-573228 treatment after PF-573228 withdrawal. **(A)** The proportion of SA-β-gal-positive A549 cells declined to half when the senescent cells were cultured in PF-573228-free medium. In addition, A549 cells grew exponentially after A549 cells were released from inhibition by 10 μM PF-573228. *$P < 0.05$. **(B)** The proposed scheme shows that integrin-based signaling activates FAK to trigger cell proliferation, to manage lamin A/C expression to maintain nuclear shape and program anti-senescence. Blockade of FAK signaling by PF-573228 induced cell cycle arrest and senescence.

FAK protein and its enzymatic function affected the expression level of p53. PF-573228 treatment suppressed the enzymatic activity of FAK but did not significantly affect its abundance. However, an obvious effect on cell senescence was observed in the inhibitor treatment group. This result implies an important role of FAK enzymatic function in suppressing senescence. Downstream signaling such as the PI3K/Akt axis may play a critical role in modulating Mdm2 function and p53 regulation, and p53 activation may suppress cell proliferation and further trigger senescence. However, FAK inhibition also repressed the proliferation of p53 null cancer cells such as H1299 cells and induced senescence. FAK inhibition also reduced lamin A/C expressions in H1299 cells, with changes in chromatin integrity followed by the induction of senescence. These observations indicate that the induction of cellular senescence by perturbations in lamin A/C-mediated chromatin alterations is independent of p53 (30, 34, 60).

Downregulation or degradation of lamin A/C and upregulation of p53 by PF-573228 treatment or FAK depletion are the main causes of cellular senescence. Baell et al. reported that inhibition of histone acetyltransferase could induce cellular senescence (26), and that the pharmacological effects of VM-8014 and VM-1119 on chromatin remodeling caused cellular senescence (26). The induction of senescence by PF-573228, VM-8014, and VM-1119 may also be due to defective chromatin remolding. Because FAK and lamin A/C are also involved in chromatin remodeling (43, 55, 61), this cellular senescence is likely to be reversible (**Figures 6A–C**, **8A**). Therefore, when the enzymatic activity of FAK is restored, lamin A/C and cyclin B1 expression levels recover (**Figures 7A,B**, **6D**).

Inhibition of FAK signaling may have a therapeutic role in limiting cancer cell growth. In the present study, we demonstrated that disruption of the FAK signaling pathway led to cellular senescence in lung cancer cells. We also tested the sensitivity of human normal lung epithelial cells, BEAS-2B, to PF-573228 treatment. It appeared that a high concentration of PF-573228 could attenuate the propagation of BEAS-2B cells. However, the BEAS-2B cells cultured in medium containing serum still underwent cell cycle progression with a low proliferative rate (**Figure S6A**). This implies that oncogene addiction occurs in lung cancer cells for FAK signaling (54). We also evaluated whether FAK inhibition causes cellular senescence in BEAS-2B cells. The results showed that a high dose of PF-573228 treatment promoted cellular senescence in BEAS-2B cells (**Figures S6B,C**). However, the ratio of SA-β-gal positive cells was <3% (**Figure S6C**). This implies that normal cells are more insensitive to high concentrations of PF-573228 than lung cancer cells and FAK inhibitors have a therapeutic potential for cancer treatment. However, there was no evidence showing that FAK signaling can result in anti-senescence and convert senescent cells to non-senescent cells upon FAK inhibitor withdrawal in A549 cells (**Figures 8A,B**). We calculated the ratios of SA-β-gal-positive and SA-β-gal-negative A549 cells after PF-573228 withdrawal and plotted curves with the timing of PF-573228 withdrawal. The slope of the curve for SA-β-gal-negative cells over 5 days indicated a reduction of 5,402 cells per day in the linear variation of SA-β-gal-negative cell numbers (**Figure 8A**). SA-β-gal-negative cells increased exponentially after PF-573228 withdrawal in A549 cells, and the curves of the SA-β-gal-negative cell growth were convergent with the growth curve of total A549 cells (**Figure 8A**). These results may be due to reversion of some of the senescent cells to non-senescent cells, as described in the schematic representation of FAK signaling in anti-senescence and PF-573228 treatment signaling cellular senescence (**Figure 8B**).

Previously, therapeutic outcomes were measured in terms of anti-angiogenesis, anti-proliferation, and anti-invasion

(16, 39, 62). In this study, FAK inhibition limited lung cancer cell propagation by inducing cellular senescence (**Figure 8B**). Driving cell senescence programing is a new trend for the treatment of tumor diseases (26), as this therapeutic approach does not chemically elicit genomic evolution in cancer cells and does not severely damage non-cancer cells (63). Although cellular senescence does not kill tumor cells, limiting cancer growth could eliminate cancer cell malignancy. However, cellular senescence is an inducer of autophagy (64) and increases susceptibility to cell-mediated cytotoxicity by activated killer cells (65). Furthermore, FAK inhibition also increases immune surveillance (66). Consequently, FAK appears to be an attractive target for pharmacological strategies for cancer therapy. Our data reveal a signaling pathway for senescence and support a therapeutic strategy for cancer.

AUTHOR CONTRIBUTIONS

H-HC, Y-YZ, and C-JY conceptualized and designed this study. P-HW devised the methodology. H-HC, P-HW, and Y-YZ performed the experiments. S-WN and Y-YZ performed formal analysis. M-SH and MH provided the resources. H-HC and Y-YZ wrote the draft. M-SH, MH, and C-JY reviewed and edited the manuscript. All authors reviewed the manuscript.

FUNDING

This work was supported by the Ministry of Science and Technology [MOST 102-2314-B-037-028-MY3] to C-JY; Kaohsiung Municipal Ta-Tung Hospital [grant number KMTTH-106-006]. This research was also supported by Academia Sinica and Ministry of Science and Technology [MOST 106-0210-01-15-02, MOST 107-0210-01-19-01] to MH.

ACKNOWLEDGMENTS

We thank Dr. Lee, Che-Hsin for technical assistance for the flow cytometry analysis.

SUPPLEMENTARY MATERIAL

The Supplementary Material for this article can be found online at: https://www.frontiersin.org/articles/10.3389/fonc.2019.00022/full#supplementary-material

REFERENCES

1. Oktay M, Wary KK, Dans M, Birge RB, Giancotti FG. Integrin-mediated activation of focal adhesion kinase is required for signaling to Jun NH2-terminal kinase and progression through the G1 phase of the cell cycle. *J Cell Biol*. (1999) 145:1461–9. doi: 10.1083/jcb.145.7.1461
2. Schaller MD, Parsons JT. Focal adhesion kinase: an integrin-linked protein tyrosine kinase. *Trends Cell Biol*. (1993) 3:258–62. doi: 10.1016/0962-8924(93)90053-4
3. Lim ST. Nuclear FAK: a new mode of gene regulation from cellular adhesions. *Mol Cells* (2013) 36:1–6. doi: 10.1007/s10059-013-0139-1
4. Kleinschmidt EG, Schlaepfer DD. Focal adhesion kinase signaling in unexpected places. *Curr Opin Cell Biol*. (2017) 45:24–30. doi: 10.1016/j.ceb.2017.01.003
5. Sulzmaier FJ, Jean C, Schlaepfer DD. FAK in cancer: mechanistic findings and clinical applications. *Nat Rev Cancer* (2014) 14:598–610. doi: 10.1038/nrc3792
6. Zhao J, Bian ZC, Yee K, Chen BP, Chien S, Guan JL. Identification of transcription factor KLF8 as a downstream target of focal adhesion kinase in its regulation of cyclin D1 and cell cycle progression. *Mol Cell* (2003) 11:1503–15. doi: 10.1016/S1097-2765(03)00179-5
7. Zhao JH, Reiske H, Guan JL. Regulation of the cell cycle by focal adhesion kinase. *J Cell Biol*. (1998) 143:1997–2008.
8. Cao K, Blair CD, Faddah DA, Kieckhaefer JE, Olive M, Erdos MR, et al. Progerin and telomere dysfunction collaborate to trigger cellular senescence in normal human fibroblasts. *J Clin Invest*. (2011) 121:2833–44. doi: 10.1172/JCI43578
9. Lee FY, Zhen YY, Yuen CM, Fan R, Chen YT, Sheu JJ, et al. The mTOR-FAK mechanotransduction signaling axis for focal adhesion maturation and cell proliferation. *Am J Transl Res*. (2017) 9:1603–17.
10. Ruest PJ, Roy S, Shi E, Mernaugh RL, Hanks SK. Phosphospecific antibodies reveal focal adhesion kinase activation loop phosphorylation in nascent and mature focal adhesions and requirement for the autophosphorylation site. *Cell Growth Differ*. (2000) 11:41–8.
11. Lim ST, Chen XL, Lim Y, Hanson DA, Vo TT, Howerton K, et al. Nuclear FAK promotes cell proliferation and survival through FERM-enhanced p53 degradation. *Mol Cell* (2008) 29:9–22. doi: 10.1016/j.molcel.2007.11.031
12. Canel M, Byron A, Sims AH, Cartier J, Patel H, Frame MC, et al. Nuclear FAK and runx1 cooperate to regulate IGFBP3, cell-cycle progression, and tumor growth. *Cancer Res*. (2017) 77:5301–12. doi: 10.1158/0008-5472.CAN-17-0418
13. Ding Q, Grammer JR, Nelson MA, Guan JL, Stewart JE, Jr. Gladson CL. p27Kip1 and cyclin D1 are necessary for focal adhesion kinase regulation of cell cycle progression in glioblastoma cells propagated *in vitro* and *in vivo* in the scid mouse brain. *J Biol Chem*. (2005) 280:6802–15. doi: 10.1074/jbc.M409180200
14. Liu TJ, LaFortune T, Honda T, Ohmori O, Hatakeyama S, Meyer T, et al. Inhibition of both focal adhesion kinase and insulin-like growth factor-I receptor kinase suppresses glioma proliferation *in vitro* and *in vivo*. *Mol Cancer Ther*. (2007) 6:1357–67. doi: 10.1158/1535-7163.MCT-06-0476
15. Pirone DM, Liu WF, Ruiz SA, Gao L, Raghavan S, Lemmon CA, et al. An inhibitory role for FAK in regulating proliferation: a link between limited adhesion and RhoA-ROCK signaling. *J Cell Biol*. (2006) 174:277–88. doi: 10.1083/jcb.200510062
16. Parsons JT, Slack-Davis J, Tilghman R, Roberts WG. Focal adhesion kinase: targeting adhesion signaling pathways for therapeutic intervention. *Clin Cancer Res*. (2008) 14:627–32. doi: 10.1158/1078-0432.CCR-07-2220
17. Cance WG, Kurenova E, Marlowe T, Golubovskaya V. Disrupting the scaffold to improve focal adhesion kinase-targeted cancer therapeutics. *Sci Signal*. (2013) 6:pe10. doi: 10.1126/scisignal.2004021
18. Carter BZ, Mak PY, Wang X, Yang H, Garcia-Manero G, Mak DH, et al. Focal adhesion kinase as a potential target in AML and MDS. *Mol Cancer Ther*. (2017) 16:1133–44. doi: 10.1158/1535-7163.MCT-16-0719
19. Gnani D, Romito I, Artuso S, Chierici M, De Stefanis C, Panera N, et al. Focal adhesion kinase depletion reduces human hepatocellular carcinoma growth by repressing enhancer of zeste homolog 2. *Cell Death Differ*. (2017) 24:889–902. doi: 10.1038/cdd.2017.34
20. Schwartz MA, Assoian RK. Integrins and cell proliferation: regulation of cyclin-dependent kinases via cytoplasmic signaling pathways. *J Cell Sci*. (2001) 114:2553–60.
21. Zhang HM, Keledjian KM, Rao JN, Zou T, Liu L, Marasa BS, et al. Induced focal adhesion kinase expression suppresses apoptosis by activating NF-kappaB signaling in intestinal epithelial cells. *Am J Physiol Cell Physiol*. (2006) 290:C1310–20. doi: 10.1152/ajpcell.00450.2005

22. Livshits G, Kobielak A, Fuchs E. Governing epidermal homeostasis by coupling cell-cell adhesion to integrin and growth factor signaling, proliferation, and apoptosis. *Proc Natl Acad Sci USA* (2012) 109:4886–91. doi: 10.1073/pnas.1202120109
23. Fan H, Guan JL. Compensatory function of Pyk2 protein in the promotion of focal adhesion kinase (FAK)-null mammary cancer stem cell tumorigenicity and metastatic activity. *J Biol Chem*. (2011) 286:18573–82. doi: 10.1074/jbc.M110.200717
24. Ewald JA, Desotelle JA, Wilding G, Jarrard DF. Therapy-induced senescence in cancer. *J Natl Cancer Inst*. (2010) 102:1536–46. doi: 10.1093/jnci/djq364
25. Schosserer M, Grillari J, Breitenbach M. The dual role of cellular senescence in developing tumors and their response to cancer therapy. *Front Oncol*. (2017) 7:278. doi: 10.3389/fonc.2017.00278
26. Baell JB, Leaver DJ, Hermans SJ, Kelly GL, Brennan MS, Downer NL, et al. Inhibitors of histone acetyltransferases KAT6A/B induce senescence and arrest tumour growth. *Nature* (2018) 560:253–7. doi: 10.1038/s41586-018-0387-5
27. Ewald JA, Jarrard DF. Decreased skp2 expression is necessary but not sufficient for therapy-induced senescence in prostate cancer. *Transl Oncol*. (2012) 5:278–87. doi: 10.1593/tlo.12181
28. Gibadulinova A, Pastorek M, Filipcik P, Radvak P, Csaderova L, Vojtesek B, et al. Cancer-associated S100P protein binds and inactivates p53, permits therapy-induced senescence and supports chemoresistance. *Oncotarget* (2016) 7:22508–22. doi: 10.18632/oncotarget.7999
29. Roberson RS, Kussick SJ, Vallieres E, Chen SY, Wu DY. Escape from therapy-induced accelerated cellular senescence in p53-null lung cancer cells and in human lung cancers. *Cancer Res*. (2005) 65:2795–803. doi: 10.1158/0008-5472.CAN-04-1270
30. Zhang Y, Wang J, Huang W, Cai J, Ba J, Wang Y, et al. Nuclear Nestin deficiency drives tumor senescence via lamin A/C-dependent nuclear deformation. *Nat Commun*. (2018) 9:3613. doi: 10.1038/s41467-018-05808-y
31. Wright WE, Pereira-Smith OM, Shay JW. Reversible cellular senescence: implications for immortalization of normal human diploid fibroblasts. *Mol Cell Biol*. (1989) 9:3088–92. doi: 10.1128/MCB.9.7.3088
32. Lenain C, Gusyatiner O, Douma S, van den Broek B, Peeper DS. Autophagy-mediated degradation of nuclear envelope proteins during oncogene-induced senescence. *Carcinogenesis* (2015) 36:1263–74. doi: 10.1093/carcin/bgv124
33. Demaria M, O'Leary MN, Chang J, Shao L, Liu S, Alimirah F, et al. Cellular senescence promotes adverse effects of chemotherapy and cancer relapse. *Cancer Discov*. (2017) 7:165–76. doi: 10.1158/2159-8290.CD-16-0241
34. Prieur A, Besnard E, Babled A, Lemaitre JM. p53 and p16(INK4A) independent induction of senescence by chromatin-dependent alteration of S-phase progression. *Nat Commun*. (2011) 2:473. doi: 10.1038/ncomms1473
35. Singh Y, Palombo M, Sinko PJ. Recent trends in targeted anticancer prodrug and conjugate design. *Curr Med Chem*. (2008) 15:1802–26. doi: 10.2174/092986708785132997
36. Slack-Davis JK, Martin KH, Tilghman RW, Iwanicki M, Ung EJ, Autry C, et al. Cellular characterization of a novel focal adhesion kinase inhibitor. *J Biol Chem*. (2007) 282:14845–52. doi: 10.1074/jbc.M606695200
37. Lietha D, Cai X, Ceccarelli DF, Li Y, Schaller MD, Eck MJ. Structural basis for the autoinhibition of focal adhesion kinase. *Cell* (2007) 129:1177–87. doi: 10.1016/j.cell.2007.05.041
38. Eke I, Deuse Y, Hehlgans S, Gurtner K, Krause M, Baumann M, et al. beta(1)Integrin/FAK/cortactin signaling is essential for human head and neck cancer resistance to radiotherapy. *J Clin Invest*. (2012) 122:1529–40. doi: 10.1172/JCI61350
39. Shibue T, Weinberg RA. Integrin beta1-focal adhesion kinase signaling directs the proliferation of metastatic cancer cells disseminated in the lungs. *Proc Natl Acad Sci USA* (2009) 106:10290–5. doi: 10.1073/pnas.0904227106
40. Shimojima M, Yuasa S, Motoda C, Yozu G, Nagai T, Ito S, et al. Emerin plays a crucial role in nuclear invagination and in the nuclear calcium transient. *Sci Rep*. (2017) 7:44312. doi: 10.1038/srep44312
41. Piekarowicz K, Machowska M, Dratkiewicz E, Lorek D, Madej-Pilarczyk A, Rzepecki R. The effect of the lamin A and its mutants on nuclear structure, cell proliferation, protein stability, and mobility in embryonic cells. *Chromosoma* (2017) 126:501–17. doi: 10.1007/s00412-016-0610-9
42. Goldman RD, Shumaker DK, Erdos MR, Eriksson M, Goldman AE, Gordon LB, et al. Accumulation of mutant lamin A causes progressive changes in nuclear architecture in Hutchinson-Gilford progeria syndrome. *Proc Natl Acad Sci USA* (2004)101:8963–8. doi: 10.1073/pnas.0402943101
43. Dechat T, Pfleghaar K, Sengupta K, Shimi T, Shumaker DK, Solimando L, et al. Nuclear lamins: major factors in the structural organization and function of the nucleus and chromatin. *Genes Dev*. (2008) 22:832–53. doi: 10.1101/gad.1652708
44. Goldman RD, Gruenbaum Y, Moir RD, Shumaker DK, Spann TP. Nuclear lamins: building blocks of nuclear architecture. *Genes Dev*. (2002) 16:533–47. doi: 10.1101/gad.960502
45. Liao CY, Anderson SS, Chicoine NH, Mayfield JR, Academia EC, Wilson JA, et al. Rapamycin reverses metabolic deficits in lamin A/C-deficient mice. *Cell Rep*. (2016) 17:2542–52. doi: 10.1016/j.celrep.2016.10.040
46. Schmitt CA, Fridman JS, Yang M, Lee S, Baranov E, Hoffman RM, et al. A senescence program controlled by p53 and p16INK4a contributes to the outcome of cancer therapy. *Cell* (2002) 109:335–46. doi: 10.1016/S0092-8674(02)00734-1
47. Rufini A, Tucci P, Celardo I, Melino G. Senescence and aging: the critical roles of p53. *Oncogene* (2013) 32:5129–43. doi: 10.1038/onc.2012.640
48. Jackson JG, Pant V, Li Q, Chang LL, Quintas-Cardama A, Garza D, et al. p53-mediated senescence impairs the apoptotic response to chemotherapy and clinical outcome in breast cancer. *Cancer Cell* (2012) 21:793–806. doi: 10.1016/j.ccr.2012.04.027
49. Shay JW, Wright WE. Senescence and immortalization: role of telomeres and telomerase. *Carcinogenesis* (2005) 26:867–74. doi: 10.1093/carcin/bgh296
50. Lidzbarsky G, Gutman D, Shekhidem HA, Sharvit L, Atzmon G. Genomic instabilities, cellular senescence, and aging: *in vitro*, *in vivo* and aging-like human syndromes. *Front Med*. (2018) 5:104. doi: 10.3389/fmed.2018.00104
51. Martinez-Zamudio RI, Robinson L, Roux PF, Bischof O. SnapShot: cellular senescence pathways. *Cell* (2017) 170:816. e1. doi: 10.1016/j.cell.2017.07.049
52. Beausejour CM, Krtolica A, Galimi F, Narita M, Lowe SW, Yaswen P, et al. Reversal of human cellular senescence: roles of the p53 and p16 pathways. *EMBO J*. (2003) 22:4212–22. doi: 10.1093/emboj/cdg417
53. Weinstein B. Relevance of the concept of oncogene addiction to hormonal carcinogenesis and molecular targeting in cancer prevention and therapy. *Adv Exp Med Biol*. (2008) 617:3–13. doi: 10.1007/978-0-387-69080-3_1
54. Weinstein IB, Joe A. Oncogene addiction. *Cancer Res*. (2008) 68:3077–80. discussion. 3080. doi: 10.1158/0008-5472.CAN-07-3293
55. Luo SW, Zhang C, Zhang B, Kim CH, Qiu YZ, Du QS, et al. Regulation of heterochromatin remodelling and myogenin expression during muscle differentiation by FAK interaction with MBD2. *EMBO J*. (2009) 28:2568–82. doi: 10.1038/emboj.2009.178
56. Rao L, Perez D, White E. Lamin proteolysis facilitates nuclear events during apoptosis. *J Cell Biol*. (1996) 135:1441–55. doi: 10.1083/jcb.135.6.1441
57. DiLoreto R, Murphy CT. The cell biology of aging. *Mol Biol Cell* (2015) 26:4524–31. doi: 10.1091/mbc.E14-06-1084
58. Naeem AS, Zhu Y, Di WL, Marmiroli S, O'Shaughnessy RF. AKT1-mediated Lamin A/C degradation is required for nuclear degradation and normal epidermal terminal differentiation. *Cell Death Differ*. (2015) 22:2123–32. doi: 10.1038/cdd.2015.62
59. Villa-Diaz LG, Kim JK, Laperle A, Palecek SP, Krebsbach PH. Inhibition of focal adhesion kinase signaling by integrin alpha6beta1 supports human pluripotent stem cell self-renewal. *Stem Cells* (2016) 34:1753–64. doi: 10.1002/stem.2349
60. Moiseeva O, Lessard F, Acevedo-Aquino M, Vernier M, Tsantrizos YS, Ferbeyre G. Mutant lamin A links prophase to a p53 independent senescence program. *Cell Cycle* (2015) 14:2408–21. doi: 10.1080/15384101.2015.1053671
61. Mei L, Xiong WC. FAK interaction with MBD2: a link from cell adhesion to nuclear chromatin remodeling? *Cell Adh Migr*. (2010) 4:77–80. doi: 10.4161/cam.4.1.10343
62. Xu B, Lefringhouse J, Liu Z, West D, Baldwin LA, Ou C, et al. Inhibition of the integrin/FAK signaling axis and c-Myc synergistically disrupts ovarian cancer malignancy. *Oncogenesis* (2017) 6:e295. doi: 10.1038/oncsis.2016.86
63. Yates LR, Desmedt C. Translational genomics: practical applications of the genomic revolution in breast cancer. *Clin Cancer Res*. (2017) 23:2630–9. doi: 10.1158/1078-0432.CCR-16-2548
64. Gerland LM, Peyrol S, Lallemand C, Branche R, Magaud JP, Ffrench M. Association of increased autophagic inclusions labeled for

beta-galactosidase with fibroblastic aging. *Exp Gerontol*. (2003) 38:887–95. doi: 10.1016/S0531-5565(03)00132-3

65. Petti C, Molla A, Vegetti C, Ferrone S, Anichini A, Sensi M. Coexpression of NRASQ61R and BRAFV600E in human melanoma cells activates senescence and increases susceptibility to cell-mediated cytotoxicity. *Cancer Res*. (2006) 66:6503–11. doi: 10.1158/0008-5472.CAN-05-4671
66. Jiang H, Hegde S, Knolhoff BL, Zhu Y, Herndon JM, Meyer MA, et al. Targeting focal adhesion kinase renders pancreatic cancers responsive to checkpoint immunotherapy. *Nat Med*. (2016) 22:851–60. doi: 10.1038/nm.4123

Conflict of Interest Statement: The authors declare that the research was conducted in the absence of any commercial or financial relationships that could be construed as a potential conflict of interest.

frontiers in Oncology

SYSTEMATIC REVIEW
published: 01 February 2019
doi: 10.3389/fonc.2019.00030

Molecular Targeted Therapy in the Treatment of Chordoma: A Systematic Review

Tong Meng[1,2,3†], *Jiali Jin*[4†], *Cong Jiang*[5], *Runzhi Huang*[1], *Huabin Yin*[2,3*], *Dianwen Song*[2,3*] *and Liming Cheng*[1,6*]

[1] Division of Spine, Department of Orthopedics, Tongji Hospital Affiliated to Tongji University School of Medicine, Shanghai, China, [2] Shanghai Bone Tumor Institution, Shanghai, China, [3] Department of Orthopedics, Shanghai General Hospital, School of Medicine, Shanghai Jiaotong University, Shanghai, China, [4] Department of Central Laboratory, Shanghai Tenth People's Hospital of Tongji University, School of Medicine, School of Life Sciences and Technology, Tongji University, Shanghai, China, [5] Beth Israel Deaconess Medical Center, BIDMC Cancer Center, Harvard Medical School, Cancer Research Institute, Boston, MA, United States, [6] Key Laboratory of Spine and Spinal Cord Injury Repair and Regeneration, Ministry of Education, Tongji University, Shanghai, China

Objectives: Chordoma is a rare bone malignancy that affects the spine and skull base. Treatment dilemma leads to a high rate of local relapse and distant metastases. Molecular targeted therapy (MTT) is an option for advanced chordoma, but its therapeutic efficacy and safety have not been investigated systematically. Therefore, a systematic review was conducted on studies reporting MTT regimens for chordoma.

Methods: Clinical trials, case series and case reports on chordoma MTT were identified using MEDLINE, Cochrane library and EMBASE, and systematically reviewed. Data on clinical outcomes, such as median overall survival, progression-free survival, response rate and adverse events (AEs) were extracted and analyzed.

Results: Thirty-three eligible studies were selected for the systematic review, which indicated that imatinib and erlotinib were the most frequently used molecular targeted inhibitors (MTIs) for chordoma. For PDGFR-positive and/or EGFR-positive chordoma, clinical benefits were achieved with acceptable AEs. Monotherapy is preferred as the first-line of treatment, and combined drug therapy as the second-line treatment. In addition, the brachyury vaccine has shown promising results.

Conclusions: The selection of MTIs for patients with advanced or relapsed chordoma should be based on gene mutation screening and immunohistochemistry (IHC). Monotherapy of TKIs is recommended as the first-line management, and combination therapy (two TKIs or TKI plus mTOR inhibitor) may be the choice for drug-resistant chordoma. Brachyury vaccine is a promising therapeutic strategy and requires more clinical trials to evaluate its safety and efficacy.

Keywords: molecular targeted therapy, bone tumor, chordoma, systematic review, imatinib, erlotinib

OPEN ACCESS

Edited by:
Jian-ye Zhang,
Guangzhou Medical University, China

Reviewed by:
Claudia Palena,
National Cancer Institute (NCI), United States
Victor C. Kok,
Asia University, Taiwan

***Correspondence:**
Huabin Yin
yinhuabin@aliyun.com
Dianwen Song
osongdianwen@126.com
Liming Cheng
limingcheng@tongji.edu.cn

[†]These authors have contributed equally to this work and share first authorship

Specialty section:
This article was submitted to Cancer Molecular Targets and Therapeutics, a section of the journal Frontiers in Oncology

Received: *05 November 2018*
Accepted: *10 January 2019*
Published: *01 February 2019*

Citation:
Meng T, Jin J, Jiang C, Huang R, Yin H, Song D and Cheng L (2019) Molecular Targeted Therapy in the Treatment of Chordoma: A Systematic Review. Front. Oncol. 9:30. doi: 10.3389/fonc.2019.00030

INTRODUCTION

Chordoma is a relatively rare malignant bone tumor with an incidence of 0.08 per 100,000 (1). It accounts for 1–4% of all bone malignancies, and ∼20% of primary spine tumors (2). Although it can occur at any segment of the spine, the predominant site of chordoma are fused segments like clivus and sacrococcyx (3). It is an indolent malignancy that progresses slowly, but exhibits strong local aggressiveness and often grows into huge masses that compress vital nerves and blood vessels (4). In addition, since chordoma is usually unresponsive to the conventional radiotherapy and cytotoxic chemotherapy, surgery is the primary therapeutic option (1, 5). Large case series including our previous one have shown that a total resection of the tumor, with the goal of negative microscopic margins, is crucial for long-term positive outcomes (6). However, the complex anatomy of the spine and the relatively large tumor volume make a clean resection technically challenging, leading to a high rate of local relapse and distant metastases (7). Regarding to this advanced setting, conventional therapeutic methods were shown to be not highly effective (1). Therefore, novel therapeutic strategies are needed to prolong patients' survival and improve the quality of life.

Pathologically, chordoma arises from residual notochord cells within the vertebral body (8), as verified on the basis of genetic and immuno-phenotypic biomarkers (9). New insights into the molecular mechanism underlying chordoma have also identified novel therapeutic targets (5). Molecular targeted therapy (MTT) in chordoma includes (1) imatinib and dasatinib against platelet-derived growth factor receptors (PDGFR) and stem cell factor receptor (KIT) (10, 11); (2) erlotinib, lapatinib, gefitinib, and cetuximab against epidermal growth factor receptor (EGFR) and erbB-2/human epidermal growth factor receptor 2 (HER2/neu) (12, 13); (3) sorafenib, pazopanib, and sunitinib that target angiogenic factors like vascular endothelial growth factor receptor (VEGFR) (14–16); and (4) temsirolimus and sirolimus that target the phosphoinositide 3-kinase (PI3K)/AKT/mammalian target of rapamycin (mTOR) pathway (17).

The indications for MTTs in chordoma patients are largely based on a few prospective clinical trials, small retrospective studies, and even case reports (10–17). However, the efficacy and safety of MTT regimens in chordoma patients, as well as the underlying molecular mechanisms, lack systematic investigation. Therefore, we conducted a systematic review on MTT regimens in chordoma patients to determine the clinical outcomes and underlying molecular mechanisms.

MATERIALS AND METHODS

Search Strategy

For this systematic review, we used standard procedures from PRISMA guidelines (18). A comprehensive, systematic search was performed using MEDLINE (via PubMed), Cochrane Library and EMBASE. To find appropriate studies in MEDLINE, we used a combination of terms related to the MeSH terms "Chordoma/drug therapy" OR the free-text searching "Chordoma" AND ("targeted therapy OR inhibitor OR inhibit OR inhibition"). This search was further modified as appropriate for Cochrane Library and EMBASE. Initial search was performed on January 17, 2018 and repeated on July 1, 2018.

Eligibility Criteria

Studies were deemed eligible for the assessment of MTTs in patients with chordoma, irrespective of previous and subsequent other treatment. Only English language publications were included. For clinical trials, case series and case reports published exclusively in abstract or news form, only those containing new data were analyzed. For literature reviews, new personal unpublished data is also included. Reference lists of selected studies and previous reviews associated with similar topics were screened manually. New clinical trials for chordoma were found from Chordoma Foundation, ClinicalTrials.gov, EU Clinical Trials Register and WHO International Clinical Trials Registry Platform. Although gray literature (such as unpublished reports, conference abstracts and dissertations) might provide some negative results and decrease the publication bias, we did not access them, because they were usually not peer reviewed and might be later published in peer-reviewed journals.

Data Extraction and Synthesis

After removal of duplicates, titles and abstracts of all identified publications were systematically screened by two independent reviewers (MT and YHB). Discrepancies between reviewers were resolved by discussion. When eligibility criteria seemed to be met, the two reviewers (MT and YHB) independently assessed retrieved full texts and extracted information. If disagreements were still remained, the third reviewer (SDW) helped to reach an agreement. We contacted with the Chordoma Foundation in order to get helpful information. Additionally, we corresponded with researchers clarify study eligibility if the published study was unclear, although responses were poor. Extracted data were study characteristics (study design, first author, year of publication), patient characteristics (total number, history of treatment) and tumor characteristics (gene mutation and immunohistochemistry), MTT information (type of agents, dosage, course of treatment and adverse events), evaluation criteria (Choi's criteria, the response evaluation criteria in solid tumor (RECIST), clinical and radiological or metabolic response), and survival (duration of follow-up, progression-free survival and overall survival).

RESULTS

Search Results

The flow-chart for the selection and exclusion of relevant publications is shown in **Figure 1**. We identified 293 studies in the initial screening, and after removing duplicates and papers based on their titles and abstracts, selected 64 publications for full-text assessment. Twenty-seven studies met our inclusion criteria, and six more were included—three from manually searching the reference list of the selected articles, two from repeated search and one with the help of the Chordoma

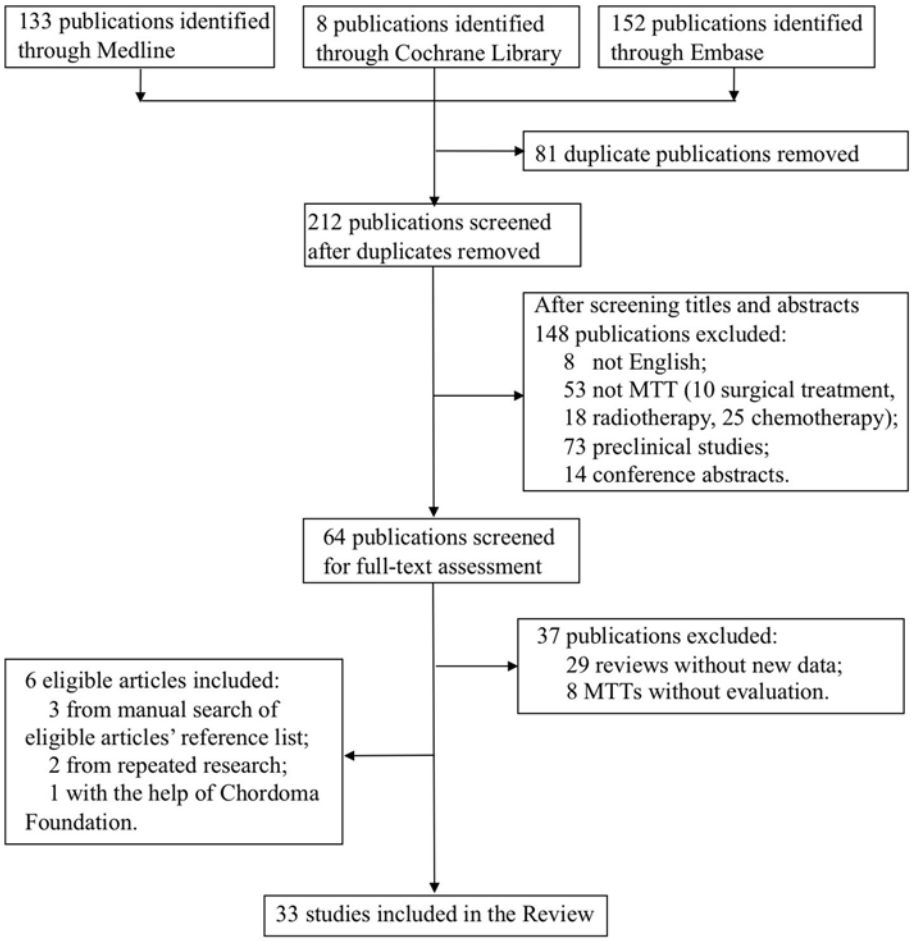

FIGURE 1 | PRISMA flow diagram of the study selection process.

Foundation. Finally, 33 studies were included in this systematic review.

Study Characteristics

Among 33 studies, nine studies were clinical trials (10–12, 14, 15, 19–22), with eight retrospective case series (16, 17, 23–28), and 16 case reports (13, 29–43). Imatinib was assessed in 18 studies with a total of 221 patients (10, 16, 17, 19, 23–28, 32, 34–36, 38, 39, 41, 42), erlotinib in 10 studies with 16 patients (13, 17, 22, 33, 35, 38, 40–42), cetuximab in five studies (seven patients) (13, 30, 31, 33, 41), sorafenib in four studies (65 patients) (15, 17, 21, 37), pazopanib in four studies with seven patients (16, 28, 41, 43) and sunitinib in three studies with 11 patients (14, 17, 28). Sirolimus, thalidomide, bevacizumab, gefitinib, linsitinib, and everolimus were accessed in two studies each (13, 22, 25, 28–31, 33, 34, 40–42), whereas dasatinib (32 patients) (11), lapatinib (18 patients) (12), rapamycin (one patients) (34), temosirolimus (one patients) (17) and yeast-brachyury (GI-6301) vaccine (11 patients) (20) were only analyzed in one study each (**Figures 2** and **3**). Monotherapy of MTTs was reported in 24 studies (10–12, 14–17, 20, 21, 23, 24, 26–28, 32, 34–39, 41, 43, 44) with combination therapy in 13 studies (13, 19, 22, 25, 28–31, 33, 39–42).

RECIST evaluation criteria was used in 19 studies (10–15, 17, 19, 20, 22, 25–28, 32, 40, 42, 43, 45) and Choi's criteria is applied in three studies (11, 12, 25). Twenty-one studies were evaluated by clinical/radiological or metabolic responses (16, 23–27, 29–43). Adverse events (AEs) were reported in 25 studies, including hematological anomalies like anemia, thrombocytopenia, as well as non-hematological AEs like fatigue, fever, anorexia, QTc prolongation, abnormal liver function, nausea, and vomiting (10–15, 19, 22, 23, 26–38, 40, 43, 45).

Efficacy and Safety of MTT Regimens in Chordoma Patients

PDGFR Inhibitors (Table 1)

Imatinib mesylate (IM), a specific tyrosine kinase inhibitor (TKI) targeting PDGFR and KIT (10, 46), was the most frequently-used MTT in chordoma patients. Eighteen studies investigated the therapeutic efficacy of IM on 221 patients (10, 16, 17, 19, 23–28, 32, 34–36, 38, 39, 41, 42), including three clinical trials (10, 19,

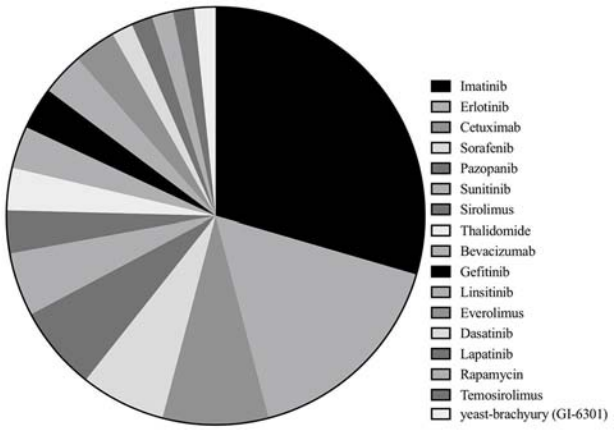

FIGURE 2 | Of the included studies, the proportion of studies reporting each molecular targeted inhibitor.

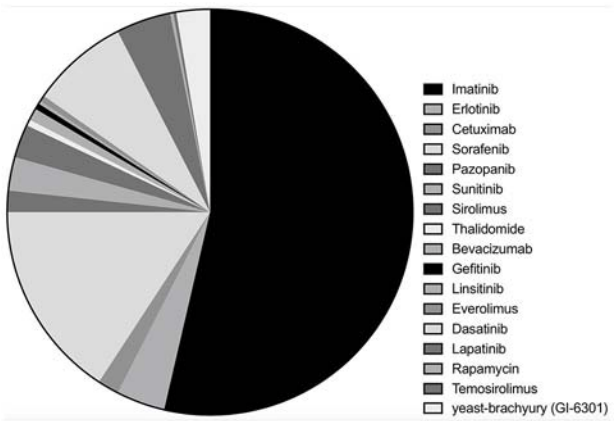

FIGURE 3 | Of the included chordoma patients, the proportion of patients received each molecular targeted inhibitor.

28), seven retrospective case series (16, 17, 23–27), and eight case reports (32, 34–36, 38, 39, 41, 42). Fourteen studies (204 patients) analyzed the efficacy of imatinib as monotherapy (10, 16, 17, 23, 24, 26–28, 32, 34–36, 39, 41), of which four studies (181 patients) used RECIST and 3 were focused on PDGFRβ-expressing chordoma. In these four studies, four patients achieved partial response (PR) (2.2%), 133 cases sustained stable disease (SD) (73.5%) and 44 cases experienced progressive disease (PD) (24.3%) (10, 17, 26, 27, 32). Clinical/radiological or metabolic responses were evaluated in 13 studies (85 patients), with 33 patients achieving PR (38.8%), 23 patients sustaining SD (27.1%) and 29 patients experiencing PD (34.1%) (16, 23, 24, 26–28, 32, 34–36, 38, 39, 41). Five of the above studies (73 patients) focused on PDGFRβ-expressing chordoma, with 45.2% PR, 31.5% SD, and 23.3% PD cases (23, 24, 26, 27, 36), and eight studies included 12 patients that experienced PD within a short period of time.

Progression-free survival (PFS) and overall survival (OS) are important indices of clinical outcome, and they were reported in two large case-studies (10, 27). Stacchiotti et al. conducted a phase II trial in 56 patients with chordoma, and the median PFS and OS were 9 and 35 months, respectively (10). A retrospective study on 46 chordoma patients reported a median PFS of 9.9 months (27).

AEs were reported in eight studies (10, 23, 27, 32, 34, 36), with skin rash being the most common, followed by oedema, chronic anemia, fatigue and fluid retention (10, 26). Subacute intraventricular hemorrhage was seen in one case of clivus chordoma treated with imatinib (36).

Dasatinib, an inhibitor of PDGFR and Src, was evaluated in a phase II study (NCT00464620) (11) on 32 patients. The median PFS and 6 months PFS rate were 6.3 months and 54%, respectively. The 2- and 5-years OS rate were 43 and 18%, respectively. Six patients had an objective response (OR) according to Choi criteria and one for RECIST. Fatigue, fever, anorexia, nausea, and vomiting occurred in more than 5% of the patients.

EGFR Inhibitors (Table 2)

Erlotinib was the most commonly used anti-EGFR agent and was analyzed in 10 studies (16 patients) for the treatment of chordoma (13, 17, 22, 32, 33, 35, 38, 40–42), including one clinical trials (22), one retrospective case study (17) and eight case reports (13, 17, 22, 32, 33, 35, 38, 40–42). Monotherapy with erlotinib was used in five studies (nine patients) (17, 32, 35, 38, 42), three (seven patients) of which were evaluated by RECIST (17, 32, 42), reporting PR in two patients and SD in five patients. Three case reports were evaluated by clinical/radiological or metabolic responses (32, 35, 38). All achieved PR and significant tumor bulk reduction was seen in two patients (70 and 46%, respectively). Skin rashes were commonly seen in the erlotinib-treated patients.

Lapatinib monotherapy was evaluated in a phase II clinical trial on 18 patients with EGFR-positive chordoma (12). Six patients achieved PR and seven sustained SD, with the median PFS of 6 months according to the Choi criteria. In contrast, all patients had SD by RECIST criteria with the median PFS of 8 months. Most patients experienced G $\geq$ 2 AEs.

Combined therapy with EGFR inhibitors was used in seven studies (eight patients) (13, 22, 30, 31, 33, 40, 41). Erlotinib was also the most common agents used in the combined MTT regimens (five studies, seven patients) (13, 22, 33, 40, 41).

Linsitinib, an inhibitor of IGF-1R/insulin receptor (INSR), was evaluated in a phase I study in combination with erlotinib (NCT00739453) (22). One patient with chordoma achieved PR for 18 months according to RECIST, with a PFS of 5 years. AEs included QTc prolongation, abnormal liver function, hyperglycemia and anorexia (22, 40).

The anti-EGFR monoclonal antibody (mAb) cetuximab was applied in combination with erlotinib in one patient with EGFR-positive chordoma, and he had a SD for 6 months (41). However, four patients with EGFR-negative chordoma experienced PD after receiving the same regimen. The treatment failure prompted a switch to bevacizumab, an anti-VEGF mAb (13, 33). Following this change, two patients achieved PR and another two presented SD. Treatment-related fatigue was observed in one patient (13, 33). Combined regimen of cetuximab and gefitinib was also effective in two cases of EGFR-positive chordoma (30, 31), where

TABLE 1 | Molecular targeted therapy of chordomas with PDGFR inhibitors (imatinib, dasatinib).

References	Study design	Levels of evidence	Sample size	Conditions	IHC positive	Drug (dosage)	Median treatment time (months)	AEs	Outcomes			Median follow-up (months)	Median PFS (months)	Median OS (months)
									Choi's criteria	RECIS	TRMR			
Stacchiotti et al. (10)	Phase II	IV	56	Advanced chordoma	PDGFRB/ PDGFB	Imatinib (800 mg/day)	9.1	Grade 3 toxicity: 72%	—	PR: 2%; SD: 70%; PD: 28%	—	26.4	9.2	35
Casali et al. (23)	Case series	IV	6	Advanced chordoma	PDGFRB	Imatinib (800 mg/day)	—	Toxicity: 33.3%	—	—	PR: 66.6%; SD: 16.7%; PD: 16.7%	—	—	—
Hindiet al. (27)	Case series	IV	46	Advanced chordoma	PDGFB/ PDGFRB	Imatinib (800 mg/day)	—	Toxicity: 87.5%	—	PR: 0; SD: 74%; PD: 26%	PR: 40%; SD: 28%; PD: 32%	24.5	9.9	30
Geoerger et al. (24)	Case series	IV	3	Chordoma	PDGFB/ PDGFRB/KIT	Imatinib (800 mg/day)	—	—	—	—	PR: 67%; SD: 33%	—	—	—
Ferraresi et al. (26)	Case series	IV	17	Advanced chordoma	PDGFRB	Imatinib (800 mg/day)	—	—	—	SD	PR: 54%; SD + PD: 46%	—	—	—
Launay et al. (35)	Case report	V	1	Advanced chordoma	EGFR	Imatinib (600 mg/day)	—	None	—	—	PD	—	—	—
Singhal et al. (32)	Case report	V	1	Recurrent chordoma	EMA/ cytokeratins	Imatinib (600 mg/day)	—	Grade 2 skin rash	—	—	PD	—	—	—
Trapani et al. (42)	Case report	V	1	Recurrent chordoma	PDGFRB, EGFR, pS6	Imatinib (400 mg/day) + everolimus	—	—	—	PD	—	—	—	—
Stacchiotti et al. (25)	Case series	IV	10	Advanced chordoma	mTOR effectors (AKT, S6) PDGFR	Imatinib (400 mg/day) + sirolimus (2 mg/day)	9	Grade 3 toxicity 30%	PR: 78%; SD: 11%; PD: 11%	PR: 11%; SD: 78%; PD: 11%	PR: 78%	—	—	—
Lebellec et al. (17)	Case series	IV	62	Advanced chordoma	—	Imatinib	—	—	—	PR: 5%; SD: 69%; PD: 26%	—	—	—	—
Adenis et al. (19)	Phase I	IV	7	Chordoma	—	MC (50 mg two times daily) + imatinib (400 mg/day)	—	Anemia, Nausea, vomiting, Fatigue	—	Long-lasting SD, PD at last	—	—	10.2	—
Lipplaa et al. (28)	Case series	IV	2	Metastatic chordoma	VEGFR	Imatinib	9		—	—	PD	—	—	—
Lipplaa et al. (28)	Case series	IV	1	Metastatic chordoma	VEGFR	Imatinib + sirolimus	—	Grade 2 fatigue, intermittent diarrhea	—	—	PD	—	—	—
Mercier et al. (36)	Case report	V	1	Recurrent chordoma	PDGFRB	Imatinib (400–800 mg/day)	2.25	Intracranial hemorrhage	—	—	PD	—	—	—

(Continued)

TABLE 1 | Continued

References	Study design	Levels of evidence	Sample size	Conditions	IHC positive	Drug (dosage)	Median treatment time (months)	AEs	Outcomes			Median follow-up (months)	Median PFS (months)	Median OS (months)
									Choi's criteria	RECIS	TRMR			
Chay et al. (34)	Case report	V	1	Recurrent chordoma	–	Imatinib	1.25	Persistent vomiting	–	–	PD	–	–	–
Houessinon et al. (38)	Case report	V	1	Recurrent chordoma	–	Imatinib (400–800 mg/day)	5	–	–	–	PD	–	–	–
Rohatgi et al. (39)	Case report	V	2	Metastatic chordoma	–	Imatinib (800 mg/day)	–	–	–	–	PR	–	60	–
Migliorini et al. (41)	Case report	V	2	Recurrent chordoma	Brachyury, EGFR, p53	Imatinib	–	–	–	–	PD	–	–	–
Jagersberg et al. (16)	Case series	V	2	Recurrent chordoma	–	Imatinib	–	–	–	–	PD	–	9	–
Schuetze et al. (11)	Phase II	IV	32	Incurable chordoma by conventional treatments	Src family of kinases, PDGFR, KIT, ephrin	Dasatinib (50–100 mg twice daily)	4	Grade 3 toxicity: 39.7%; Grade 4 toxicity: 6.9%	OR: 18.75%	OR: 3.125%	–	–	6.3	–

IHC, immunohistochemistry; AEs, adverse events; RMR, radiological or metabolic response; PR, partial response; SD, stable disease; PD, progressive disease; TVR, tumor volume regression; MC, metronomic cyclophosphamide.

one achieved a PR for 9 months and the other had a 44% reduction in tumor bulk. Pronounced AEs, such as rash, acne, diarrhea, and skin defects, were reported in both cases (30, 31).

VEGFR Inhibitors (Table 3)

Sorafenib, a TKI against VEGFR and PDGFR, was assessed in four studies (15, 17, 21, 37). A phase II trial was conducted on 27 patients with chordomas (NCT00874874) (15), and OR was observed in one patient as per RECIST. The 12 months PFS and OS rates were 73.0 and 86.5%, respectively. In a study on 11 patients treated with sorafenib, PR was obtained in one patient, with SD in nine patients and PD in one patient according to RECIST (17). Another study assessing sorafenib reported a PFS of 12 months (37). However, sorafenib was limited by severe AEs like thrombocytopenia and diarrhea, and the rates of grade 3 and 4 toxicity were 77.8 and 14.8%, respectively.

Sunitinib, a multi-targeting TKI against VEGFR and PDGFR, was assessed in three studies (14, 17, 28). A phase II trial on sunitinib was conducted on nine patients (14), four of which achieved SD according to RECIST, concurrent to a qualitative decrease in tumor density, along with a median PFS of 12 months (14). Two patients treated with sunitinib had at least SD according to RECIST (17, 28), and one achieved a PR after a 27 months SD (28). The major toxicities were of grade 1 or 2 (14).

Pazopanib, another VEGFR inhibitor, was analyzed in seven patients (16, 28, 41, 43), of which four sustained SD with the median PFS of 15 months and the remaining three experienced PD. Thalidomide, an inhibitor of VEGF, was used as a second-line treatment for chordoma after failure of imatinib, rapamycin and other chemotherapy (29, 34). While one patient achieved a 50% tumor reduction, another experienced a PD (29, 34). In addition, severe toxicities of grade 3 and 4 were reported in both cases.

Other Molecular Targeted Inhibitors (MTIs) (Table 4)

Monotherapy with the mTOR inhibitors rapamycin and everolimus were ineffective in chordoma patients (34, 41). The combined MTT regimen of everolimus and imatinib resulted in sustained SD in one patient, with a PFS of 16 months (42). In addition, IM plus sirolimus was used in 10 patients with IM-refractory chordoma and activated mTOR (25). Nine patients were assessed, of which one achieved PR, seven sustained SD and one experienced PD according to RECIST. According to Choi criteria, seven patients achieved PR, and one sustained SD and one experienced PD. The same MTT regimen was also used against IM- and sunitinib-refractory chordoma but was not effective due to short of the mTOR expression (28). A phase I trial evaluated the effect of IM plus metronomic cyclophosphamide (MC)-based chemotherapy on 7 IM- and sunitinib-refractory chordoma patients (19). The median PFS was 10.2 months, and the 12 months PFS and OS rates were 42.9 and 85.7%, respectively according to RECIST. No dose-limiting toxicity and drug pharmacokinetic interactions were observed.

Brachyury Vaccine (Table 4)

A phase I dose-escalation trial using a recombinant *Saccharomyces cerevisiae* (yeast) vaccine encoding brachyury (GI-6301) was conducted on 11 patients (20), and 10 evaluable

TABLE 2 | Molecular targeted therapy of chordomas with EGFR inhibitors (erlotinib, linsitinib, cetuximab, lapatinib, gefitinib).

References	Study design	Levels of evidence	Sample size	Conditions	IHC positive	Drug (dosage)	Median treatment time (months)	AEs	Outcomes			Median follow-up (months)	Median PFS (months)	Median OS (months)
									Choi's criteria	RECIST	RMR			
Launay et al. (35)	Case report	V	1	Advanced chordoma	EGFR	Erlotinib (150 mg/day)	40	None	—	—	TVR (70%)	40	12	40
Singhal et al. (32)	Case report	V	1	Recurrent chordoma	EMA, cytokeratins	Erlotinib (150 mg/day)	18	Grade 2 skin rash	—	PR	TVR (46%)	18	11	18
Trapani et al. (42)	Case report	V	1	Recurrent chordoma	PDGFR-β, EGFR, pS6	Erlotinib (150 mg/day)	—	—	—	PD (4 months), SD (16 months)	—	—	—	—
Asklund et al. (13)	Case report	V	3	Recurrent chordoma	—	Erlotinib (100–150 mg/day) + cetuximab;	—	Infection	—	—	—	—	—	—
Asklund et al. (13)	Case report	V	3	Recurrent chordoma	—	Erlotinib 100–150 mg/day + bevacizumab 10 mg/kg*week	—	Infection	—	PR: 33%, SD: 67%	—	—	—	—
Aleksic et al. (40)	Case report	V	1	Recurrent chordoma	brachyury, EGFR, IGF-1R	Erlotinib (100 mg/day) + linsitinib (50 mg/day)	61	Toxicity ≤ grade 2	—	PR	TVR	69	60	69
Lebellec et al. (17)	Case series	IV	5	Advanced chordoma	—	Erlotinib	—	—	—	PR: 20%, SD: 80%	—	—	4	—
Macaulay et al. (22)	Phase I	V	1	Advanced chordoma	—	Erlotinib + linsitinib	—	—	—	—	—	—	—	—
Migliorini et al. (41)	Case report	V	1	Recurrent and metastatic chordoma	Brachyury, EGFR, p53	Erlotinib + cetuximab	—	—	—	—	SD	—	—	—
Asklund et al. (33)	Case report	V	1	Advanced chordoma	—	Erlotinib + cetuximab	—	—	—	—	PD	—	—	—
Asklund et al. (33)	Case report	V	1	Advanced chordoma	—	Erlotinib + bevacizumab	—	—	—	—	TVR	—	—	—
Houessinon et al. (38)	Case report	V	1	Recurrent chordoma	—	Erlotinib (150 mg/day)	28	A moderate rash and diarrhea	—	—	PR	—	28	—
Stacchiotti et al. (12)	Phase II	V	18	Advanced chordoma	EGFR and HER2/neu	Lapatinib (1,500 mg/day)	—	G ≥ 2 toxicity	PR: 33%, SD: 39%, PD: 28%	PR: 40%, SD: 50%, PD: 10%	—	10.5	6 (Choi); 8 (RECIST)	25

(Continued)

TABLE 2 | Continued

References	Study design	Levels of evidence	Sample size	Conditions	IHC positive	Drug (dosage)	Median treatment time (months)	AEs	Outcomes			Median follow-up (months)	Median PFS (months)	Median OS (months)
									Choi's criteria	RECIST	RMR			
Lindén et al. (31)	Case report	V	1	Recurrent and metastatic chordoma	—	Cetuximab 500 mg/week + gefitinib 250 mg/day	4	Facial acne	—	—	TVR (44%)	4	4	4
Hof et al. (30)	Case report	V	1	Recurrent and metastatic chordoma	EGFR	Cetuximab 500 mg/week + gefitinib 250 mg/day	12	Facial acne, diarrhea and skin defects	—	—	TVR	12	12	12

IHC, immunohistochemistry; AEs, adverse events; RMR, radiological or metabolic response; PR, partial response; SD, stable disease; PD, progressive disease; TVR, tumor volume regression.

patients showed a median PFS of 8.3 months. One patient achieved PR, with eight sustaining SD and one experiencing PD at 3 months according to RECIST. Seven patients had no evidence of PD, giving a clinical benefit rate of 70% at 5 months. The most common AEs were injection site reactions.

Ongoing and planned clinical trials on chordoma MTT are listed in **Table 5**.

DISCUSSION

Novel therapeutic strategies against chordoma are urgently needed to prolong the overall survival and relieve symptoms. Elucidation of the underlying molecular mechanisms of chordoma have helped identify numerous potential therapeutic targets (47, 48), and several anti-chordoma agents are currently being tested in animal models and clinical trials. This systematic review is focused on the pharmacological management of chordoma patients and the clinical outcomes. Furthermore, the molecular mechanisms of MTT action have also been assessed.

Molecular Targets

Chordoma is a genetically heterogeneous tumor with frequent imbalances of large chromosomal regions. Somatic duplications of the notochordal transcription factor brachyury (47, 48), chromosomal copy loss of phosphatase and tensin homolog (PTEN) (49), tuberous sclerosis complex (TSC) (50), cyclin-dependent kinase inhibitor 2A and 2B (CDKN2A and CDKN2B) (51), SMARCB1 (49), and PIK3CA (9) mutations are key aspects of chordoma pathogenesis, and therefore potential targets.

RTKs are the key players in the development and progression of chordoma, and their mutated forms can activate signaling cascades resulting in dysregulation of many essential proteins. Therefore, mutational analyses and IHC can greatly assist oncologists to determine the optimal inhibitors (52–56). It needs to be emphasized that mutations in the molecular targets are clinically more relevant than their immunoreactivity, since target overexpression is not always driven by the activation of the corresponding signaling pathway. For example, high levels of EGFR in the chordoma cell line JHC7 was not accompanied by activated EGFR signaling (57).

Indications and Evaluation Criteria for MTTs

MTTs are not the first treatment options for chordoma, and only recommended for advanced or recurrent chordoma that are unresponsive to either surgical resection or radiotherapy.

The outcomes of MTTs is often difficult to evaluate in chordoma. Choi's criteria is based on changes in tumor size and density following contrast administration in CT or MRI (58). A radiological PR is defined as $\geq$10% decrease in tumor size or $\geq$15% decrease in tumor density/contrast enhancement in CT/MRI. RECIST defines PR as $\geq$20% decrease in tumor growth, which occurs later than that required for Choi criteria. Therefore, RECIST is not fully adequate to evaluate the clinical response in chordoma (59). Clinical/radiological and metabolic responses include symptom relief, anti-tumor effects (such as liquefaction) and changes in tumor density in the CT scan,

TABLE 3 | Molecular targeted therapy with VEGF and VEGFR inhibitors (sorafenib, sunitinib, thalidomide, pazopanib).

References	Study design	Levels of evidence	Sample size	Conditions	IHC positive	Drug (dosage)	Median treatment time (months)	AEs	Outcomes			Median follow-up (months)	Median PFS (months)	Median OS (months)
									Choi's criteria	RECIS	TRMR			
Bompas et al. (15)	Phase II	IV	27	Locally advanced and metastatic chordoma	—	Sorafenib (800 mg/day)	8.7	Grade 3 (77.8%); grade 4 (14.8%)	—	OR: 4%; PR: 4%; SD + PD: 92%	—	—	PFS rates: 6 m (85.3%), 9 m (73.0%), 12 m (73.0%)	OS rates: 6 m (100%), 9 m (86.5%), 12 m (86.5%)
Lebellec et al. (21)	Phase II	IV	26	Advanced chordoma	—	Sorafenib	—	—	—	—	—	—	—	—
Lebellec et al. (17)	Case series	IV	11	Advanced chordoma	—	Sorafenib	—	—	—	PR: 9%; SD: 82%; PD: 9%	—	—	—	—
Svoboda et al. (37)	Case report	IV	1	Recurrent and metastatic chordoma	—	Sorafenib (200 mg/day)	—	Thrombocytopenia; diarrhea		—	SD	—	12	—
George et al. (14)	Phase II	IV	9	Advanced chordoma	VEGFR, PDGFRB	Sunitinib (37.5 mg/day)	—	Grade 1 or 2 (fatigue, diarrhea, hypertension)	—	SD: 44%; PD: 56%	—	—	—	—
Lipplaa et al. (28)	Case series	IV	1	Metastatic chordoma	VEGFR	Sunitinib (37.5–50 mg/day)	—	Grade 2 nausea, fatigue	—	PR	TVR	—	27	—
Lebellec et al. (17)	Case series	IV	1	Advanced chordoma	—	Sunitinib	—	—	—	—	—	—	—	—
Schonegger et al. (29)	Case report	V	1	Recurrent and metastatic chordoma	—	Thalidomide	12	—	—	—	PD	—	—	—
Chay et al. (34)	Case report	V	1	Recurrent chordoma	—	Thalidomide (100–300 mg/day)	23+	—	—	—	TVR (more than 50%)	—	21	—
Lipplaa et al. (28)	Case series	IV	4	Unresectable or metastatic chordoma	VEGFR	Pazopanib (600–800 mg/day)	—	Grade 2 diarrhea, fatigue	—	SD: 50%; PD: 50%	—	—	8.5	—
Ribeiro et al. (43)	Case report	V	1	Recurrent chordoma	Cytokeratins, EMA and vimentin	Pazopanib (800 mg/day)	—	Grade 3 neutropenia	—	SD	TVR (23.1%)	—	15	—
Migliorini et al. (41)	Case report	V	1	Recurrent chordoma	Brachyury, EGFR, p53	Pazopanib	6	—	—	—	PD	—	—	—
Jagersberg et al. (16)	Case series	IV	1	Recurrent chordoma	—	Pazopanib	—	—	—	—	PR	—	24	—

IHC, immunohistochemistry; AEs, adverse events; RMR, radiological or metabolic response; OR, objective response; PR, partial response; SD, stable disease; PD, progressive disease; TVR, tumor volume regression.

TABLE 4 | Molecular targeted therapy of chordomas with other inhibitors (rapamycin, temsirolimus, yeast brachyury vaccine).

References	Study design	Levels of evidence	Sample size	Conditions	IHC positive	Drug (dosage)	Median treatment time (months)	AEs	Outcomes		Median follow-up (months)	Median PFS (months)	Median OS (months)
									Choi's criteria	RECIS	TRMR			
Chay et al. (34)	Case report	V	1	Recurrent chordoma	–	Rapamycin	2	–	–	–	PD	–	–	–
Migliorini et al. (41)	Case report	V	1	Recurrent and metastatic chordoma	Brachyury, EGFR, p53	Everolimus	–	–	–	–	PD	–	–	–
Lebellec et al. (17)	Case series	IV	1	Advanced chordoma	–	Temsirolimus	–	–	–	–	SD	–	–	–
Migliorini et al. (41)	Case report	V	1	Recurrent chordoma	Brachyury	Pembrolizumab	6	–	–	–	TVR	–	6	–
Heery et al. (20)	Phase I	IV	11	Advanced chordoma	–	Yeast-brachyury (GI-6301) vaccine (40-80 YU)	–	–	–	PR: 10%; SD: 80%; PD: 10%	–	–	8.3	–

IHC, immunohistochemistry; AEs, adverse events; RMR, radiological or metabolic response; PR, partial response; SD, stable disease; PD, progressive disease; TVR, tumor volume regression.

reduction in contrast enhancement in MR, and maximum standardized uptake (SUVmax) in PET (23). However, typical tumor tissue characteristics like component and scirrhosity may also affect tumor-related symptoms, even in the absence of any changes in tumor size, resulting in incorrect readings.

MTTs for Chordoma

Imatinib was the first effective agent tested against chordoma, and is currently the most commonly used MTIs (23). Most patients with PDGFRβ-positive chordoma benefited from imatinib treatment and avoided rapid PD, likely due to tumor necrosis and intra-tumoral subacute bleeding that manifest as liquefaction (36). A dosage of 800 mg/day is recommended, except in cases of high toxicity. The major AEs associated with imatinib include oedema, chronic anemia, fatigue and even subacute intraventricular hemorrhage (36).

Several trials have also reported the ineffectiveness of imatinib in chordoma (19, 28, 32, 35, 38, 42). In such cases, EGFR inhibitor is the second line of treatment, since PDGFRβ activation can also stimulate EGFR, given an EGFR gene copy number gain (CNG) or strong intra-tumoral EGFR staining is detected. Around 40% of chordoma patients show CNG of the chromosome band 7p12, where EGFR is located. Erlotinib has shown a good clinical effect EGFR-positive chordoma, and could serve as the second choice for imatinib-refractory chordoma (32, 35). The combination of gefitinib and cetuximab, two other inhibitors of EGFR, showed improved clinical benefits and decreased AEs (30, 31).

HER2/neu is involved in EGFR dimer formation, and the possibility of heterodimerization increases the sensitivity of EGFR-positive chordoma to 54% (60). Lapatinib, a bi-specific inhibitor blocking both EGFR and HER2/neu, achieved 33.3% PR and 38.9% SD as per Choi criteria and 100% SD according to RECIST in EGFR-positive chordoma (12). Afatinib, another bi-specific inhibitor of EGFR and HER2/neu, was the only agent which showed cytotoxic effects across multiple chordoma cell lines in a drug sensitivity assessment (57). On this basis, a new clinical trial on the effects of afatinib is currently enrolling patients (NCT03083678).

IGF signaling is also important in chordoma tumorigenesis, since IGF-1 and IGF-1R have been detected in 92 and 76% of chordoma tissues (61), and are absent in benign notochordal cell tumor and fetal notochord (52). Linsitinib, an IGF-1R inhibitor, was assessed in two studies (22, 40), and effectively controlled chordoma progression in combination with erlotinib (22, 40).

VEGF levels are significantly higher in chordoma tissues and associated with angiogenesis (62). Five VEGFR or VEGF inhibitors (sorafenib, sunitinib, pazopanib, thalidomide, bevacizumab) were evaluated in this systematic review. Although occasional severe AEs were observed occasionally, sorafenib, sunitinib, and pazopanib monotherapy resulted in substantial clinical effects. Although thalidomide was effective against drug-resistant chordomas, severe toxicities limit its clinical application. Bevacizumab can be used as a supplement for erlotinib in drug-resistant chordomas, and their combination showed good clinical effect and high tolerance. A new phase II trial evaluating the efficacy and safety of regorafenib, a

TABLE 5 | Clinical trials programs of chordomas in progress.

Official title	Trial registration number	Type	Medical condition:	Interventions	Mechanism	Sites	Status
Nilotinib with radiation for high risk chordoma	NCT01407198	Phase I	Histologically confirmed chordoma	Nilotinib (daily 200–400 mg BID) Radiation therapy	A Bcr-Abl kinase inhibitor	USA	Active, not recruiting
Study of Imatinib, a platelet-derived growth factor receptor inhibitor, and LBH589, a histone deacetylase inhibitor, in the treatment of newly diagnosed and recurrent chordoma	NCT01175109	Phase I	Histologically confirmed chordoma	Imatinib + LBH589	Imatinib: a PDGFR inhibitor LBH589: a HDAC inhibitor	USA	Unknown
CDK4/6 inhibition in locally advanced/metastatic chordoma	NCT03110744 EUDRACT 2016-004660-19	Phase II	Locally advanced or metastatic chordoma refractory to tyrosine kinase inhibitors	Palbociclib	A CDK4/6 inhibitor	Germany	Recruiting
Afatinib in locally advanced and metastatic chordoma	NCT03083678	Phase II	Locally advanced or metastatic, pathologically proven, EGFR expressing chordoma	Afatinib (40 mg/day)	A Her2 and EGFR kinases inhibitor	Italy, Netherlands, UK	Not yet recruiting
Phase I safety study of stereotactic radiosurgery with concurrent and adjuvant PD-1 antibody nivolumab in subjects with recurrent or advanced chordoma	NCT02989636	Phase I	Histologically confirmed chordoma	Nivolumab Stereotactic Radiosurgery	Nivolumab: a PD-1 Antibody	USA	Recruiting
A randomized, double-blind, phase 2 trial of GI-6301 (Yeast-Brachyury Vaccine) vs. placebo in combination with standard of care definitive radiotherapy in locally advanced, unresectable, chordoma	NCT02383498	Phase II	Histologically confirmed chordoma	GI-6301 Vaccine (Yeast-Brachyury) GI-6301 Placebo Radiotherapy	A heat-killed, recombinant yeast-based vaccine engineered to express the transcription factor, Brachyury	USA	Recruiting
Phase II trial of the immune checkpoint inhibitor nivolumab in patients with select rare CNS cancers	NCT03173950	Phase II	Primary brain sarcoma including chordoma	Nivolumab	A PD-1 Antibody	USA	Recruiting
A phase II trial of dasatinib in advanced sarcomas	NCT00464620	Phase II	Unresectable, recurrent, or metastatic soft tissue or bone sarcoma including chordoma	Dasatinib (70 mg, twice daily)	An inhibitor of Src family of kinases, PDGFR, KIT, ephrin	USA	Active, not recruiting
DART: dual anti-CTLA-4 and anti-PD-1 blockade in rare tumors	NCT02834013	Phase II	Rare tumors including chordoma	Ipilimumab Nivolumab	Ipilimumab: a CTLA-4 inhibitor Nivolumab: a PD-1 inhibitor	USA	Recruiting
A phase II, multicenter study of the EZH2 inhibitor tazemetostat in adult subjects with INI1-negative tumors or relapsed/refractory synovial sarcoma	NCT02601950 EUDRACT 2015-002469-41	Phase II	Poorly differentiated chordoma (or other chordoma with sponsor approval)	Tazemetostat (800 mg BID)	An EZH2 Inhibitor	USA, Australia, Belgium, Canada, France, Germany, Italy, Taiwan, UK	Recruiting
A phase 1 study of the EZH2 inhibitor tazemetostat in pediatric subjects with relapsed or refractory INI1-negative tumors or synovial sarcoma	NCT02601937 EUDRACT 2015-002468-18	Phase I	INI1-negative tumors including chordoma	Tazemetostat	An EZH2 Inhibitor	USA, Australia, Canada, Denmark, France, Germany, Italy, Netherlands, UK	Active, not recruiting

(Continued)

TABLE 5 | Continued

Official title	Trial registration number	Type	Medical condition:	Interventions	Mechanism	Sites	Status
A phase II multi-arm study to test the efficacy of immunotherapeutic agents in multiple sarcoma subtypes	NCT02815995	Phase II	Advanced and/or metastatic sarcoma including chordoma	Durvalumab Tremelimumab	Durvalumab: a PD-L1 inhibitor; Tremelimumab: a CTLA-4 inhibitor	USA	Recruiting
A randomized phase II study of Durvalumab (MEDI4736) and Tremelimumab compared to doxorubicin in patients with advanced or metastatic soft tissue sarcoma.	EUDRACT 2016-004750-15	Phase II	Advanced or metastatic soft tissue sarcoma including chordoma	Durvalumab Tremelimumab	Durvalumab: a PD-L1 inhibitor; Tremelimumab: a CTLA-4 inhibitor	Germany	Ongoing
A phase I, open-label, multiple-ascending dose trial to investigate the safety, tolerability, pharmacokinetics, biological and clinical activity of MSB0011359C in subjects with metastatic or locally advanced solid tumors and expansion to selected indications	NCT02517398	Phase I	Solid tumors including chordoma	MSB0011359C (M7824)	A PD-L1 inhibitor	USA	Recruiting
An open-label phase 1 trial to evaluate the safety and tolerability of a Modified Vaccinia Ankara (MVA) priming followed by fowlpox booster vaccines modified to express brachyury and T-cell costimulatory molecules (MVA-BN-Brachyury/FPV-Brachyury)	NCT03349983	Phase I	Metastatic or unresectable locally advanced malignant solid tumors including chordoma	MVA-BN-Brachyury FPV-Brachyury	A brachyury vaccine	USA	Recruiting
An open phase I clinical study assessing safety and tolerability of MVX-ONCO-1 in patients with solid tumor who are not/not any longer amenable to standard therapy	NCT02193503	Phase I	—	MVX-ONCO-1	An autologous tumor vaccine	Switzerland	Recruiting
Secured access to pembrolizumab for adult patients with selected rare cancer types	NCT03012620 EUDRACT 2016-002260-14	Phase II	Unresectable, recurrent, or metastatic soft tissue or bone sarcoma including chordoma	Pembrolizumab	A PD-L1 inhibitor	France	Recruiting
A randomized phase II, placebo-controlled, multicenter study evaluating efficacy and safety of regorafenib in patients with metastatic bone sarcomas	NCT02389244	Phase II	Advanced metastatic cancer in progression including chordoma	Regorafenib Placebo	A multi-kinase inhibitor; angiogenesis inhibitor	France	Recruiting
Phase 2 study on imatinib in combination with RAD001 in advanced chordoma	EUDRACT 2010-021755-34	Phase II	PDGFRB and mTOR (or S6 or 4BP1) positive advanced chordoma	Imatinib Everolimus	Imatinib: a PDGFRB inhibitor Everolimus: a mTOR inhibitor	Italy	Ongoing
A phase 2, single arm, European multi-center trial evaluating the efficacy of afatinib as first-line or later-line treatment in advanced chordoma.	EUDRACT 2016-002766-31	Phase II	Metastatic or unresectable chordoma	Afatinib	A Her2 and EGFR kinases inhibitor	Netherlands	Ongoing
Phase II study of lapatinib in EGFR/HER2NEU positive advanced chordoma	EUDRACT 2009-014456-29	Phase II	Advanced EGFR/Her2Neu positive chordoma	Lapatinib	EGFR/Her2Neu inhibitor	Germany	Ongoing

PDGFR, platelet-derived growth factor receptor; HDAC, histone deacetylase; Her2, human epidermal growth factor receptor 2; EGFR, epidermal growth factor receptor; PD-1, programmed cell death protein 1; CTLA4, cytotoxic T lymphocyte antigen 4.

multi-kinase inhibitor of VEGFR, is ongoing in France for metastatic bone sarcoma (NCT02389244).

Chordomas with indication of anti-RTK agents may also relapse or progress early. In TKI-resistant chordomas, p-AKT is a relative reliable indicator and its persistent expression following tyrphostin treatment resulted in relapse and progression (54). AKT is activated by mTOR, its downstream molecules (RPS6 and eIF4E), and Stat3. The combination of the antagonists of upstream RTKs and downstream mTOR/PI3K/MAPK/Stat not only synergistically reduced chordoma growth by avoiding the negative feedback loop (63) and PI3K-dependent feedback loop (64), but also significantly decreased the cytotoxicity of either agent (65). For example, monotherapy of rapamycin or everolimus was ineffective against tumor progression (34, 41), while combining imatinib with everolimus or sirolimus induced good clinical effects in 3 studies (12 patients) (25, 28, 42). Therefore, the combined therapy can be considered for drug-resistant chordoma.

Mutations in the downstream effectors of RTKs, like PTEN and PIK3CA, also impair TKI response (66, 67). PTEN deficient chordoma cell lines exhibit increased proliferation, reduced apoptosis and enhanced migration in chordoma cell lines (68). Reintroduction of PTEN in tumor cells increased their therapeutic sensitivity to PDGFR inhibitors, and the combination of histone deacetylase (HDAC) and PDGFR inhibitors effectively reduced the growth and invasion of chordoma cells, irrespective of PTEN status (69). On this basis, a new phase I trial of Imatinib and LBH589 (a HDAC inhibitor) is ongoing in chordoma patients (NCT01175109).

Chordomas frequently show deletions in the SMARCB1 locus (49). SMARCB1 directly antagonizes the histone methyltransferase EZH2 and regulates the cell-cycle by activating CDKN2A (45). A phase I trial on the EZH2 inhibitor tazemetostat, confirmed complete or partial responses were observed in two children with chordoma according to RECIST (NCT02601937) (45). Therefore, another phase II clinical trial on tazemetostat is ongoing in patients with SMARCB1/INI1 deleted chordoma (NCT02601950).

The loss of chromosome 9 or 9p region, which contains CDKN2A, has been reported in some chordoma patients (51). The inactivation of CDKN2A universally activates the CDK4/6 and Rb pathways (70), which are highly expressed in the chordoma tissues (71). The CDK4/6 inhibitors palbociclib and LY2835219 inhibited chordoma cell growth and proliferation *in vitro* efficiently (72, 73). A phase II clinical trial on palbociclib is currently enrolling patients with chordoma (NCT031 10744).

Somatic duplications of the notochordal transcription factor brachyury was demonstrated in chordoma, and enhanced tumor growth by activating YAP (9, 47, 48). Preclinical studies have shown that a recombinant *Saccharomyces cerevisiae* (yeast) vaccine encoding brachyury (GI-6301) activates human T cells *in vitro*. A phase II GI-6301 dose-escalation trial showed a 70% clinical benefit rate in chordoma patients (20). A phase II clinical trial on the combination of GI-6301 and radiotherapy is currently enrolling chordoma patients in the United States (NCT02383498). Additionally, a phase I trial of a Modified Vaccinia Ankara (MVA)-brachyury and a fowlpox (FPV)-brachyury vaccines is currently ongoing in patients with solid tumors, including chordoma (NCT03349983).

Limitations

In order to decrease the selection bias, this systematic review screened all published studies enrolling chordoma patients treated with MTT, including clinical trials, case series and even case reports, and provides the most detailed information. However, there were some limitations that need to be addressed. We included case reports on account of the rarity of chordoma and the paucity of available studies. However, a case report might overemphasize the final results due to lack of strong results. In addition, we only included English language publications which can also increase the selection bias. Furthermore, the baseline conditions of the patients and the evaluation criteria were not consistent across studies which is another factor contributing to selection bias. Therefore, large prospective randomized clinical trials are warranted to help clinicians determine the optimum treatment modality for chordoma patients.

CONCLUSIONS

The selection of MTIs for patients with advanced or relapsed chordoma should be based on gene mutation screening and immunohistochemistry (IHC). Monotherapy of TKIs is recommended as the first-line treatment. Combined therapy (two TKIs or TKI plus mTOR inhibitor) may be the choice for drug-resistant chordoma. Brachyury vaccine is a promising therapeutic strategy and requires more clinical trials to evaluate its safety and efficacy.

AUTHOR CONTRIBUTIONS

TM did the literature search, data and data analysis, and led the writing of the review. HY, JJ, and RH contributed to the design, data collection, and analysis. HY, DS, and LC contributed their experience of clinical practice in chordoma to ensure the relevance of findings. JJ and CJ contributed their experience in the discussion of the molecular mechanism underlying chordoma and drug interaction.

FUNDING

This work was supported in part by the National Natural Science Foundation of China [grant numbers 81702659, 81772856] and National Key R&D Program of China [grant numbers 2016YFA0100800].

ACKNOWLEDGMENTS

We acknowledge the contributions of Josh Sommer of the Chordoma Foundation, who assisted with the revision of concept and the final manuscript.

REFERENCES

1. Walcott BP, Nahed BV, Mohyeldin A, Coumans JV, Kahle KT, Ferreira MJ. Chordoma: current concepts, management, and future directions. *Lancet Oncol.* (2012) 13:e69–76. doi: 10.1016/S1470-2045(11)70337-0
2. Mcmaster ML, Goldstein AM, Bromley CM, Ishibe N, Parry DM. Chordoma: incidence and survival patterns in the United States, 1973–1995. *Cancer Causes Control.* (2001) 12:1–11. doi: 10.1023/A:1008947301735
3. Chugh R, Tawbi H, Lucas DR, Biermann JS, Schuetze SM, Baker LH. Chordoma: the nonsarcoma primary bone tumor. *Oncologist* (2007) 12:1344–50. doi: 10.1634/theoncologist.12-11-1344
4. Casali PG, Stacchiotti S, Sangalli C, Olmi P, Gronchi A. Chordoma. *Curr Opin Oncol.* (2007) 19:367–70. doi: 10.1097/CCO.0b013e3281214448
5. Stacchiotti S, Sommer J. Building a global consensus approach to chordoma: a position paper from the medical and patient community. *Lancet Oncol.* (2015) 16:e71–83. doi: 10.1016/S1470-2045(14)71190-8
6. Meng T, Yin H, Li B, Li Z, Xu W, Zhou W, et al. Clinical features and prognostic factors of patients with chordoma in the spine: a retrospective analysis of 153 patients in a single center. *Neuro Oncol.* (2015) 17:725–32. doi: 10.1093/neuonc/nou331
7. Stacchiotti S, Casali PG, Lo Vullo S, Mariani L, Palassini E, Mercuri M, et al. Chordoma of the mobile spine and sacrum: a retrospective analysis of a series of patients surgically treated at two referral centers. *Ann Surg Oncol.* (2010) 17:211–9. doi: 10.1245/s10434-009-0740-x
8. Arain A, Hornicek FJ, Schwab JH, Chebib I, Damron TA. Chordoma arising from benign multifocal notochordal tumors. *Skeletal Radiol.* (2017) 46:1745–52. doi: 10.1007/s00256-017-2727-1
9. Tarpey PS, Behjati S, Young MD, Martincorena I, Alexandrov LB, Farndon SJ, et al. The driver landscape of sporadic chordoma. *Nat Commun.* (2017) 8:890. doi: 10.1038/s41467-017-01026-0
10. Stacchiotti S, Longhi A, Ferraresi V, Grignani G, Comandone A, Stupp R, et al. Phase II study of imatinib in advanced chordoma. *J Clin Oncol.* (2012) 30:914–20. doi: 10.1200/JCO.2011.35.3656
11. Schuetze SM, Bolejack V, Choy E, Ganjoo KN, Staddon AP, Chow WA, et al. Phase 2 study of dasatinib in patients with alveolar soft part sarcoma, chondrosarcoma, chordoma, epithelioid sarcoma, or solitary fibrous tumor. *Cancer* (2017) 123:90–7. doi: 10.1002/cncr.30379
12. Stacchiotti S, Tamborini E, Lo Vullo S, Bozzi F, Messina A, Morosi C, et al. Phase II study on lapatinib in advanced EGFR-positive chordoma. *Ann Oncol.* (2013) 24:1931–6. doi: 10.1093/annonc/mdt117
13. Asklund T, Sandstrom M, Shahidi S, Riklund K, Henriksson R. Durable stabilization of three chordoma cases by bevacizumab and erlotinib. *Acta Oncol.* (2014) 53:980–4. doi: 10.3109/0284186X.2013.878472
14. George S, Merriam P, Maki RG, Van Den Abbeele AD, Yap JT, Akhurst T, et al. Multicenter phase II trial of sunitinib in the treatment of nongastrointestinal stromal tumor sarcomas. *J Clin Oncol.* (2009) 27:3154–60. doi: 10.1200/JCO.2008.20.9890
15. Bompas E, Le Cesne A, Tresch-Bruneel E, Lebellec L, Laurence V, Collard O, et al. Sorafenib in patients with locally advanced and metastatic chordomas: a phase II trial of the French Sarcoma Group (GSF/GETO). *Ann Oncol.* (2015) 26:2168–73. doi: 10.1093/annonc/mdv300
16. Jagersberg M, El Rahal A, Dammann P, Merkler D, Weber DC, Schaller K. Clival chordoma: a single-centre outcome analysis. *Acta Neurochir (Wien).* (2017) 159:1815–23. doi: 10.1007/s00701-017-3163-7
17. Lebellec L, Chauffert B, Blay JY, Le Cesne A, Chevreau C, Bompas E, et al. Advanced chordoma treated by first-line molecular targeted therapies: outcomes and prognostic factors. A retrospective study of the French Sarcoma Group (GSF/GETO) and the Association des Neuro-Oncologues d'Expression Francaise (ANOCEF). *Eur J Cancer* (2017) 79:119–28. doi: 10.1016/j.ejca.2017.03.037
18. Liberati A, Altman DG, Tetzlaff J, Mulrow C, Gotzsche PC, Ioannidis JP, et al. The PRISMA statement for reporting systematic reviews and meta-analyses of studies that evaluate healthcare interventions: explanation and elaboration. *BMJ* (2009) 339:b2700. doi: 10.1136/bmj.b2700
19. Adenis A, Ray-Coquard I, Italiano A, Chauzit E, Bui-Nguyen B, Blay JY, et al. A dose-escalating phase I of imatinib mesylate with fixed dose of metronomic cyclophosphamide in targeted solid tumours. *Br J Cancer* (2013) 109:2574–8. doi: 10.1038/bjc.2013.648
20. Heery CR, Singh BH, Rauckhorst M, Marte JL, Donahue RN, Grenga I, et al. Phase I trial of a yeast-based therapeutic cancer vaccine (GI-6301) targeting the transcription factor brachyury. *Cancer Immunol Res.* (2015) 3:1248–56. doi: 10.1158/2326-6066.CIR-15-0119
21. Lebellec L, Bertucci F, Tresch-Bruneel E, Bompas E, Toiron Y, Camoin L, et al. Circulating vascular endothelial growth factor (VEGF) as predictive factor of progression-free survival in patients with advanced chordoma receiving sorafenib: an analysis from a phase II trial of the french sarcoma group (GSF/GETO). *Oncotarget* (2016) 7:73984–94. doi: 10.18632/oncotarget.12172
22. Macaulay VM, Middleton MR, Eckhardt SG, Rudin CM, Juergens RA, Gedrich R, et al. Phase I dose-escalation study of linsitinib (OSI-906) and erlotinib in patients with advanced solid tumors. *Clin Cancer Res.* (2016) 22:2897–907. doi: 10.1158/1078-0432.CCR-15-2218
23. Casali PG, Messina A, Stacchiotti S, Tamborini E, Crippa F, Gronchi A, et al. Imatinib mesylate in chordoma. *Cancer* (2004) 101:2086–97. doi: 10.1002/cncr.20618
24. Geoerger B, Morland B, Ndiaye A, Doz F, Kalifa G, Geoffray A, et al. Target-driven exploratory study of imatinib mesylate in children with solid malignancies by the Innovative Therapies for Children with Cancer (ITCC) European Consortium. *Eur J Cancer* (2009) 45:2342–51. doi: 10.1016/j.ejca.2009.03.007
25. Stacchiotti S, Marrari A, Tamborini E, Palassini E, Virdis E, Messina A, et al. Response to imatinib plus sirolimus in advanced chordoma. *Ann Oncol.* (2009) 20:1886–94. doi: 10.1093/annonc/mdp210
26. Ferraresi V, Nuzzo C, Zoccali C, Marandino F, Vidiri A, Salducca N, et al. Chordoma: clinical characteristics, management and prognosis of a case series of 25 patients. *BMC Cancer* (2010) 10:22. doi: 10.1186/1471-2407-10-22
27. Hindi N, Casali PG, Morosi C, Messina A, Palassini E, Pilotti S, et al. Imatinib in advanced chordoma: a retrospective case series analysis. *Eur J Cancer* (2015) 51:2609–14. doi: 10.1016/j.ejca.2015.07.038
28. Lipplaa A, Dijkstra S, Gelderblom H. Efficacy of pazopanib and sunitinib in advanced axial chordoma: a single reference centre case series. *Clin Sarcoma Res.* (2016) 6:19. doi: 10.1186/s13569-016-0059-x
29. Schonegger K, Gelpi E, Prayer D, Dieckmann K, Matula C, Hassler M, et al. Recurrent and metastatic clivus chordoma: systemic palliative therapy retards disease progression. *Anticancer Drugs* (2005) 16:1139–43. doi: 10.1097/00001813-200511000-00015
30. Hof H, Welzel T, Debus J. Effectiveness of cetuximab/gefitinib in the therapy of a sacral chordoma. *Onkologie* (2006) 29:572–4. doi: 10.1159/000096283
31. Linden O, Stenberg L, Kjellen E. Regression of cervical spinal cord compression in a patient with chordoma following treatment with cetuximab and gefitinib. *Acta Oncol.* (2009) 48:158–9. doi: 10.1080/02841860802266672
32. Singhal N, Kotasek D, Parnis FX. Response to erlotinib in a patient with treatment refractory chordoma. *Anticancer Drugs* (2009) 20:953–5. doi: 10.1097/CAD.0b013e328330c7f0
33. Asklund T, Danfors T, Henriksson R. PET response and tumor stabilization under erlotinib and bevacizumab treatment of an intracranial lesion non-invasively diagnosed as likely chordoma. *Clin Neuropathol.* (2011) 30:242–6. doi: 10.5414/NP300371
34. Chay WY, Teo M, Sittampalam K, Toh HC. Effective use of thalidomide in the treatment of recurrent metastatic chordoma. *J Clin Oncol.* (2011) 29:e477–80. doi: 10.1200/JCO.2010.34.2139
35. Launay SG, Chetaille B, Medina F, Perrot D, Nazarian S, Guiramand J, et al. Efficacy of epidermal growth factor receptor targeting in advanced chordoma: case report and literature review. *BMC Cancer* (2011) 11:423. doi: 10.1186/1471-2407-11-423

36. Mercier F, Guiot MC, Bojanowski MW. Treatment of chordoma with imatinib complicated by intracranial hemorrhage: a case showing dissociation between biological effect and therapeutic outcome. *J Neurooncol.* (2012) 107:435–7. doi: 10.1007/s11060-011-0767-2
37. Svoboda RM, Mackay D, Welsch MJ, Anderson BE. Multiple cutaneous metastatic chordomas from the sacrum. *J Am Acad Dermatol.* (2012) 66:e246–7. doi: 10.1016/j.jaad.2011.07.037
38. Houessinon A, Boone M, Constans JM, Toussaint P, Chauffert B. Sustained response of a clivus chordoma to erlotinib after imatinib failure. *Case Rep Oncol.* (2015) 8:25–9. doi: 10.1159/000371843
39. Rohatgi S, Ramaiya NH, Jagannathan JP, Howard SA, Shinagare AB, Krajewski KM. Metastatic chordoma: report of the two cases and review of the literature. *Eurasian J Med.* (2015) 47:151–4. doi: 10.5152/eurasianjmed.2015.52
40. Aleksic T, Browning L, Woodward M, Phillips R, Page S, Henderson S, et al. Durable response of spinal chordoma to combined inhibition of IGF-1R and EGFR. *Front Oncol.* (2016) 6:98. doi: 10.3389/fonc.2016.00098
41. Migliorini D, Mach N, Aguiar D, Vernet R, Landis BN, Becker M, et al. First report of clinical responses to immunotherapy in 3 relapsing cases of chordoma after failure of standard therapies. *Oncoimmunology* (2017) 6:e1338235. doi: 10.1080/2162402X.2017.1338235
42. Trapani D, Conforti F, De Pas T. EGFR Inhibition in a pretreated sacral chordoma: a role for erlotinib? Case Report and a Brief Review of Literature. *Transl Med UniSa* (2017) 16:30–3.
43. Ribeiro M, De Sousa MC, Hanna SA, Maldaun MVC, Kurimori CO, De Lima L, et al. Tumor reduction with pazopanib in a patient with recurrent lumbar chordoma. *Case Rep Oncol Med.* (2018) 2018:4290131. doi: 10.1155/2018/4290131
44. Mcpherson CM, Suki D, Mccutcheon IE, Gokaslan ZL, Rhines LD, Mendel E. Metastatic disease from spinal chordoma: a 10-year experience. *J Neurosurg Spine* (2006) 5:277–80. doi: 10.3171/spi.2006.5.4.277
45. Chi S, Fouladi M, Shukla N, Bourdeaut F, Margol A, Makin G, et al. Phase 1 study of the EZH2 inhibitor, tazemetostat, in children with relapsed or refractory INI1-negative tumors including rhabdoid tumors, epithelioid sarcoma, chordoma, and synovial sarcoma. *Mol Cancer Ther.* (2018) 17:1. doi: 10.1158/1535-7163
46. Tamborini E, Miselli F, Negri T, Lagonigro MS, Staurengo S, Dagrada GP, et al. Molecular and biochemical analyses of platelet-derived growth factor receptor (PDGFR) B, PDGFRA, and KIT receptors in chordomas. *Clin Cancer Res.* (2006) 12:6920–8. doi: 10.1158/1078-0432.CCR-06-1584
47. Presneau N, Shalaby A, Ye H, Pillay N, Halai D, Idowu B, et al. Role of the transcription factor T (brachyury) in the pathogenesis of sporadic chordoma: a genetic and functional-based study. *J Pathol.* (2011) 223:327–35. doi: 10.1002/path.2816
48. Shah SR, David JM, Tippens ND, Mohyeldin A, Martinez-Gutierrez JC, Ganaha S, et al. Brachyury-YAP regulatory axis drives stemness and growth in cancer. *Cell Rep.* (2017) 21:495–507. doi: 10.1016/j.celrep.2017.09.057
49. Choy E, Macconaill LE, Cote GM, Le LP, Shen JK, Nielsen GP, et al. Genotyping cancer-associated genes in chordoma identifies mutations in oncogenes and areas of chromosomal loss involving CDKN2A, PTEN, and SMARCB1. *PLoS ONE* (2014) 9:e101283. doi: 10.1371/journal.pone.0101283
50. Lee-Jones L, Aligianis I, Davies PA, Puga A, Farndon PA, Stemmer-Rachamimov A, et al. Sacrococcygeal chordomas in patients with tuberous sclerosis complex show somatic loss of TSC1 or TSC2. *Genes Chromosomes Cancer* (2004) 41:80–5. doi: 10.1002/gcc.20052
51. Hallor KH, Staaf J, Jonsson G, Heidenblad M, Vult Von Steyern F, Bauer HC, et al. Frequent deletion of the CDKN2A locus in chordoma: analysis of chromosomal imbalances using array comparative genomic hybridisation. *Br J Cancer* (2008) 98:434–42. doi: 10.1038/sj.bjc.6604130
52. Sommer J, Itani DM, Homlar KC, Keedy VL, Halpern JL, Holt GE, et al. Methylthioadenosine phosphorylase and activated insulin-like growth factor-1 receptor/insulin receptor: potential therapeutic targets in chordoma. *J Pathol.* (2010) 220:608–17. doi: 10.1002/path.2679
53. Tamborini E, Virdis E, Negri T, Orsenigo M, Brich S, Conca E, et al. Analysis of receptor tyrosine kinases (RTKs) and downstream pathways in chordomas. *Neuro Oncol.* (2010) 12:776–89. doi: 10.1093/neuonc/noq003
54. De Castro CV, Guimaraes G, Aguiar S Jr, Lopes A, Baiocchi G, Da Cunha IW, et al. Tyrosine kinase receptor expression in chordomas: phosphorylated AKT correlates inversely with outcome. *Hum Pathol.* (2013) 44:1747–55. doi: 10.1016/j.humpath.2012.11.024
55. Akhavan-Sigari R, Gaab MR, Rohde V, Abili M, Ostertag H. Prognostic significance of immunohistochemical expression of VEGFR2 and iNOS in spinal chordoma. *Eur Spine J.* (2014) 23:2416–22. doi: 10.1007/s00586-014-3417-5
56. Hu Y, Mintz A, Shah SR, Quinones-Hinojosa A, Hsu W. The FGFR/MEK/ERK/brachyury pathway is critical for chordoma cell growth and survival. *Carcinogenesis* (2014) 35:1491–9. doi: 10.1093/carcin/bgu014
57. Magnaghi P, Salom B, Cozzi L, Amboldi N, Ballinari D, Tamborini E, et al. Afatinib is a new therapeutic approach in chordoma with a unique ability to target EGFR and brachyury. *Mol Cancer Ther.* (2018) 17:603–13. doi: 10.1158/1535-7163.MCT-17-0324
58. Choi H, Charnsangavej C, Faria SC, Macapinlac HA, Burgess MA, Patel SR, et al. Correlation of computed tomography and positron emission tomography in patients with metastatic gastrointestinal stromal tumor treated at a single institution with imatinib mesylate: proposal of new computed tomography response criteria. *J Clin Oncol.* (2007) 25:1753–9. doi: 10.1200/JCO.2006.07.3049
59. Eisenhauer EA, Therasse P, Bogaerts J, Schwartz LH, Sargent D, Ford R, et al. New response evaluation criteria in solid tumours: revised RECIST guideline (version 1.1). *Eur J Cancer* (2009) 45:228–47. doi: 10.1016/j.ejca.2008.10.026
60. Stommel JM, Kimmelman AC, Ying H, Nabioullin R, Ponugoti AH, Wiedemeyer R, et al. Coactivation of receptor tyrosine kinases affects the response of tumor cells to targeted therapies. *Science* (2007) 318:287–90. doi: 10.1126/science.1142946
61. Scheipl S, Froehlich EV, Leithner A, Beham A, Quehenberger F, Mokry M, et al. Does insulin-like growth factor 1 receptor (IGF-1R) targeting provide new treatment options for chordomas? A retrospective clinical and immunohistochemical study. *Histopathology* (2012) 60:999–1003. doi: 10.1111/j.1365-2559.2012.04186.x
62. Akhavan-Sigari R, Gaab MR, Rohde V, Brandis A, Tezval H, Abili M, et al. Expression of vascular endothelial growth factor receptor 2 (VEGFR-2), inducible nitric oxide synthase (iNOS), and Ki-M1P in skull base chordoma: a series of 145 tumors. *Neurosurg Rev.* (2014) 37:79–88. doi: 10.1007/s10143-013-0495-5
63. Roux PP, Shahbazian D, Vu H, Holz MK, Cohen MS, Taunton J, et al. RAS/ERK signaling promotes site-specific ribosomal protein S6 phosphorylation via RSK and stimulates cap-dependent translation. *J Biol Chem.* (2007) 282:14056–64. doi: 10.1074/jbc.M700906200
64. Carracedo A, Ma L, Teruya-Feldstein J, Rojo F, Salmena L, Alimonti A, et al. Inhibition of mTORC1 leads to MAPK pathway activation through a PI3K-dependent feedback loop in human cancer. *J Clin Invest.* (2008) 118:3065–74. doi: 10.1172/JCI34739
65. Yang C, Schwab JH, Schoenfeld AJ, Hornicek FJ, Wood KB, Nielsen GP, et al. A novel target for treatment of chordoma: signal transducers and activators of transcription 3. *Mol Cancer Ther.* (2009) 8:2597–605. doi: 10.1158/1535-7163.MCT-09-0504
66. Ohashi K, Maruvka YE, Michor F, Pao W. Epidermal growth factor receptor tyrosine kinase inhibitor-resistant disease. *J Clin Oncol.* (2013) 31:1070–80. doi: 10.1200/JCO.2012.43.3912
67. Chen K, Mo J, Zhou M, Wang G, Wu G, Chen H, et al. Expression of PTEN and mTOR in sacral chordoma and association with poor prognosis. *Med Oncol.* (2014) 31:886. doi: 10.1007/s12032-014-0886-7
68. Han S, Polizzano C, Nielsen GP, Hornicek FJ, Rosenberg AE, Ramesh V. Aberrant hyperactivation of akt and Mammalian target of rapamycin complex 1 signaling in sporadic chordomas. *Clin Cancer Res.* (2009) 15:1940–6. doi: 10.1158/1078-0432.CCR-08-2364
69. Lee DH, Zhang Y, Kassam AB, Park MJ, Gardner P, Prevedello D, et al. Combined PDGFR and HDAC inhibition overcomes PTEN disruption in chordoma. *PLoS ONE* (2015) 10:e0134426. doi: 10.1371/journal.pone.0134426
70. Wang L, Zehir A, Nafa K, Zhou N, Berger MF, Casanova J, et al. Genomic aberrations frequently alter chromatin regulatory genes in chordoma. *Genes Chromosomes Cancer* (2016) 55:591–600. doi: 10.1002/gcc.22362

71. Bosotti R, Magnaghi P, Di Bella S, Cozzi L, Cusi C, Bozzi F, et al. Establishment and genomic characterization of the new chordoma cell line Chor-IN-1. *Sci Rep*. (2017) 7:9226. doi: 10.1038/s41598-017-10044-3
72. Liu T, Shen JK, Choy E, Zhang Y, Mankin HJ, Hornicek FJ, et al. CDK4 Expression in chordoma: a potential therapeutic target running title: CDK4 expression in chordoma. *J Orthop Res*. (2018) 36:1581–9. doi: 10.1002/jor.23819
73. Levy J. *Chordoma Foundation In Vivo Drug Screening Program*. Chordoma Foundation (2018). Available online at: https://figshare.com/projects/Chordoma_Foundation_In_Vivo_Drug_Screening_Program/25948 (accessed January 25, 2018).

Conflict of Interest Statement: The authors declare that the research was conducted in the absence of any commercial or financial relationships that could be construed as a potential conflict of interest.

frontiers in Pharmacology

REVIEW
published: 01 February 2019
doi: 10.3389/fphar.2019.00065

PD-1/PD-L1 Inhibitors in Cervical Cancer

Yuncong Liu[1,2†], Li Wu[2†], Ruizhan Tong[1], Feiyue Yang[2], Limei Yin[1,3], Mengqian Li[1,3], Liting You[1,3], Jianxin Xue[1,3] and You Lu[1,3*]*

[1] West China School of Medicine, Sichuan University, Chengdu, China, [2] Department of Gynaecological Oncology, Guizhou Provincial People's Hospital, Guiyang, China, [3] Department of Thoracic Oncology, Cancer Center, West China Hospital, Sichuan University, Chengdu, China

Cervical cancer is one of the most common gynecological tumors, and the majority of early-stage cervical cancer patients achieve good recovery through surgical treatment and concurrent chemoradiotherapy (CCRT). However, for patients with recurrent, persistent, metastatic cervical cancer, effective treatment is rare, except for bevacizumab combined with chemotherapy. Programmed cell death-1/programmed cell death-ligand 1 (PD-1/PD-L1) inhibitors might be a novel choice to improve the clinical outcomes of these patients. Thus far, some pivotal trials, including Keynote 028, Keynote 158 and Checkmate 358, have indicated established clinical benefit of PD-1/PD-L1 inhibitors in cervical cancer. In light of these data, the FDA has approved pembrolizumab for patients with recurrent or metastatic cervical cancer with disease progression during or after chemotherapy. There are also some ongoing studies that may provide more evidence for the PD-1/PD-L1 pathway as a therapeutic target in cervical cancer. In this review, we have summarized the status and application of PD-1/PD-L1 inhibitors in clinical trials for the treatment of cervical cancer and suggested some future directions in this field.

Keywords: cervical cancer, programmed cell death-1/programmed cell death-ligand 1 (PD-1/PD-L1), immune checkpoint inhibitors, immunotherapy, human papillomavirus (HPV)

OPEN ACCESS

Edited by:
Yan-Yan Yan,
Shanxi Datong University, China

Reviewed by:
Daniel Olive,
Aix-Marseille Université, France
Jingying Zhou,
The Chinese University of Hong Kong, China

****Correspondence:***
Jianxin Xue
radjianxin@163.com
You Lu
radyoulu@hotmail.com

† These authors have contributed equally to this work

Specialty section:
This article was submitted to Cancer Molecular Targets and Therapeutics, a section of the journal Frontiers in Pharmacology

Received: *27 November 2018*
Accepted: *18 January 2019*
Published: *01 February 2019*

Citation:
Liu Y, Wu L, Tong R, Yang F, Yin L, Li M, You L, Xue J and Lu Y (2019) PD-1/PD-L1 Inhibitors in Cervical Cancer. Front. Pharmacol. 10:65. doi: 10.3389/fphar.2019.00065

INTRODUCTION

Cervical cancer is one of the most common gynecological tumors. More than 569,847 women are diagnosed with cervical cancer annually worldwide, resulting in over 311,365 deaths (Bray et al., 2018). Although the incidence of cervical cancer has been greatly reduced by the use of HPV vaccines and cervical cancer screening (Goodman, 2015), cervical cancer is second in terms of morbidity among gynecological tumors in developing countries (Sahasrabuddhe et al., 2012). Over 70% of cervical cancer cases diagnosed in developing countries are locally invasive or metastatic, contributing to the high mortality rate of cervical cancer. The 5-year OS rate of local cervical cancer can achieve approximately 75–85% through effective treatments such as surgery CCRT, etc. (Chen et al., 2015). Nevertheless, the 5-year OS of recurrent, persistent, metastatic cervical cancer is only approximately 15%. The poor prognosis is mainly due to limited therapeutic options (Guitarte et al., 2014). The majority of these patients can only be treated with palliative

Abbreviations: AE, adverse event; APCs, antigen-presenting cells; CCRT, concurrent chemoradiotherapy; CRs, complete responses; CRT, chemoradiotherapy; CTLA-4, cytotoxic T-lymphocyte-associated protein-4; hfRT, hyperfraction radiotherapy; HNSCC, head and neck squamous cell carcinoma; HPV, human papillomavirus; mAb, monoclonal antibody; NSCLC, non-small cell lung cancer; ORR, objective response rate; OS, overall survival rate; PD-1/PD-L1, programmed cell death-1/programmed cell death-ligand 1; PFS, progression-free survival; PRs, partial responses; SCCs, squamous cell cancers; TILs, tumor infiltrating lymphocytes; uPRs, unconfirmed partial responses.

chemotherapy (Boussios et al., 2016), in which platinum-based chemotherapies were the prior choice (Monk et al., 2009). In 2014, the GOG 240 trial indicated that when bevacizumab was added to the chemotherapy, the ORR was improved from 36 to 48% (Tewari et al., 2014), and the OS could be prolonged from 13 to 17 months for recurrent, persistent, metastatic cervical cancer, thus laying the foundation for the first-line choice of combining bevacizumab with chemotherapy for this population (Tewari et al., 2017). However, for those who progress during the first-line treatment, the lack of effective second-line treatment remains to be the main reason for the high mortality rate (Minion and Tewari, 2018). Currently, immune checkpoint inhibitors (Schumacher and Schreiber, 2015), especially PD-1/PD-L1 inhibitors (Constantinidou et al., 2018), have achieved favorable efficacy in treating multiple solid tumors (Gettinger et al., 2018), including cervical cancer (Borcoman and Le Tourneau, 2017). Accumulating evidence has demonstrated that PD-1/PD-L1 inhibitors may be a promising approach for cervical cancer treatment.

IMMUNE CHECKPOINT INHIBITORS

Numerous immunomodulatory therapies are being investigated in clinical trials with diverse potential targets, including PD-1/PD-L1, CTLA-4, Tim-3, ICOS, 4-1BB, and OX-40. Among these novel targets, ICOS (Amatore et al., 2018), 4-1BB (Compte et al., 2018), and OX-40 (Polesso et al., 2018) are costimulatory receptors, while PD-1/PD-L1 (Raedler, 2015), CTLA-4 (Lheureux et al., 2018), and Tim-3 (Gorris et al., 2018) are negative immune regulators of T cells. Currently, only CTLA-4 inhibitors (Hodi et al., 2010) and PD-1/PD-L1 inhibitors (Bagcchi, 2014) have been approved by the FDA. CTLA-4 integrates with the costimulatory molecules CD80 (B7-1) and CD86 (B7-2) that express on the surfaces of APCs (Fife and Bluestone, 2008), while PD-L1 is expressed on a wide variety of cell types, including tumor-associated fibroblasts, tumor cells, APCs, etc. (Boussiotis, 2016). As a result, CTLA-4 inhibits T cell activation within secondary lymphoid organs (Kurup et al., 2017), but PD-1/PD-L1 chiefly regulates T cell function within peripheral tissues and the tumor microenvironment (Pardoll, 2012). Therefore, PD-1/PD-L1 signaling is more specific to tumor than CTLA-4 signaling, and inhibitors of PD-1/PD-L1 may cause less damage to healthy tissue (Boussiotis, 2016; Minion and Tewari, 2018) (**Figure 1**).

Based on the above mechanism, ipilimumab (monoclonal anti-CTLA-4), the first immune checkpoint inhibitor, approved for melanoma, had little clinical benefit until the emergence of pembrolizumab, and the combination of the two drugs further improved treatment efficacy in malignant melanoma (Wang et al., 2017). To date, another mAb for CTLA-4, tremelimumab, has not been approved for the treatment in any type of cancer. However, mAbs targeting PD-1 [pembrolizumab (Paz-Ares et al., 2018), nivolumab (Long et al., 2018), and cemiplimab (Sidaway, 2018)] and PD-L1 [atezolizumab (Hsu et al., 2018), durvalumab (Siu et al., 2018), and avelumab (Le Tourneau et al., 2018)] have presented clinical advantages in malignant melanoma, advanced NSCLC, urothelial cancer (Zhang and Li, 2018) and other tumors (Lim et al., 2018) (**Table 1**). In addition, extensive research has been carried out on gynecological tumors, such as ovarian cancer (Liu and Zamarin, 2018) and breast cancer (Julia et al., 2018), and clinical researches on cervical cancer are ongoing. At present, some initial results have been achieved.

THEORETICAL BASIS FOR PD-1/PD-L1 INHIBITORS IN CERVICAL CANCER

The PD-1/PD-L1 axis is one of the most well-known immune-checkpoint pathways with a mechanism of immune evasion for cancer cells and thus inhibiting the immune response in various kinds of solid tumors, including cervical cancer Cancer Genome Atlas Research Network et al. (2017). In brief, PD-L1 expresses on the surface of cervical tumor cells, APCs and TILs, while the PD-1-positive cells were mostly identified as T cells in the stroma of cervical tumors. For the expression of PD-1 in the tumor stroma of cervical cancer, Meng et al. (2018) reported that 60.82% (59/97) of the patients exhibited PD-1 expression, while another study showed PD-1 expression in 46.97% (31/66) of the patients (Feng et al., 2018).

To date, numerous studies have investigated the expression of PD-L1 in cervical cancer (Yang et al., 2013; Chen et al., 2016). The expression of PD-L1 has been reported in 34.4–96% of cervical carcinoma tissues, while expression of PD-L1 in histologically normal cervical tissues was rarely found (Enwere et al., 2017). Opal Reddy et al. (2017) showed that PD-L1 expression was positive in 32 of 93 (34.4%) cervical carcinoma samples, subcategorically in 28 of 74 (37.8%) SCCs, 2 of 7 (28.6%) adenosquamous carcinomas, and 2 of 12 (16.7%) endocervical adenocarcinomas. In another study, PD-L1 expression was found in 96% of the samples (Enwere et al., 2017). Specifically, for cervical SCC, PD-L1 expression was found in 80% (56/70) cases (Mezache et al., 2015). In the TCGA database for cervical SCCs, the amplification or gain of PD-L1 was found in 28 of 129 (22%) cases (Dijkstra et al., 2016). In addition, PD-L1 can also be expressed on TILs, which plays a role in antitumor response inhibition. A study found that for cervical SCCs samples, the expression rates of PD-L1 on cancer cells and TILs were 59.1 and 47.0%, respectively (Feng et al., 2018). Collectively, these data suggest that both PD-L1 and PD-1 are widely expressed in cervical cancer tumor cells and stroma, providing potential therapeutic targets for PD-1/PD-L1 inhibitors.

Notoriously, persistent HPV infection is involved in the pathogenesis of cervical cancer and is related to its prognosis. Several teams have interrogated whether HPV infection could affect PD-L1 expression in cervical cancer and found that HPV positivity was positively correlated with increased PD-L1 expression (Mezache et al., 2015; Liu et al., 2017).

Considerable effort has been made to dissect the underlying mechanism of the association between HPV status and PD-L1 expression in HPV-related solid tumors, mainly HNSCC and cervical cancer. In HPV-HNSCCs, membranous expression of PD-L1 and significant increased levels of mRNA of IFN-γ were found in the tonsillar crypts, As tonsillar crypts witnesses the initial HPV infection, and IFN-γ induces PD-L1 expression, this

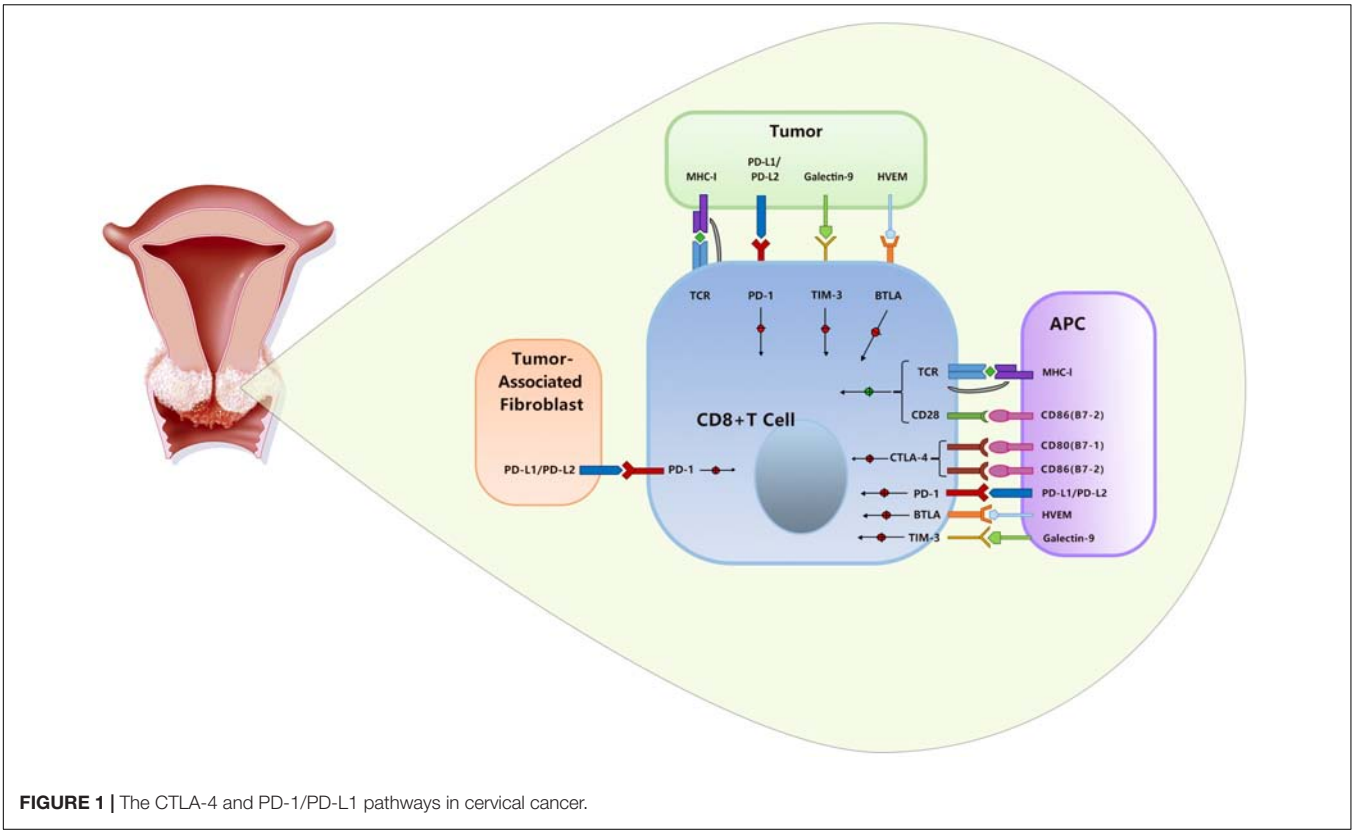

FIGURE 1 | The CTLA-4 and PD-1/PD-L1 pathways in cervical cancer.

evidence might support the role of the PD-1/PD-L1 interaction in creating an "immune-privileged" site for initial viral infection and subsequent adaptive immune resistance (Franzen et al., 2018). In another study, DNA methylation of PD-L1 was inversely correlated with PD-L1 mRNA expression ($p \leq 0.002$) and was further significantly associated with HPV infection in the TCGA cohort, indicating that DNA methylation of PD-L1 is associated with transcriptional silencing and HPV infection in HNSCCs (Balermpas et al., 2017). In cervical cancer, Qin et al. (2017) indicated that HPV-induced somatic mutations and a multitude of neoantigens, which played a crucial role in the inhibitory tumor microenvironment and could lead to notable alterations among checkpoint-related genes such as CTLA-4, PD-1, and PD-L1. Specifically, PD-L1 showed a positive correlation with ENO1, PRDM1, OVOL1, and MNT, all of which are related master regulators of HPV16 E6 and E7 (Qin et al., 2017). Of

TABLE 1 | The characteristics of the clinical application of monoclonal antibodies (mAbs) of immune checkpoint inhibitors in cervical cancer.

Target	Drug (trade name)	Antibody type	Formerly name	Manufacturer	Time to market (FDA)	Indications
CTLA-4	Ipilumumab (Yervoy)	IgG1	–	BMS	March, 2011	Melanoma, colorectal cancer, renal cell carcinoma
	Tremelimumab	IgG2	Ticilimumb, CP-675,206	Pfizer	–	Undergoing human trials has not attained approval for any
PD-1	Pembrolizumab (Keytruda)	IgG4	MK-3475 Lambrolizumab	MSD	September, 2014	Advanced melanoma, non-small cell lung cancer, Hodgkin's lymphoma, and head and neck SCC[1]
	Nivolumab (Opdivo)	IgG4	BMS-9365580 NO-4538	BMS	December, 2014	Metastatic melanoma, squamous non-small cell lung cancer, renal cell carcinoma
	Cemiplimab (REGN2810)	IgG4	–	Sanofi	September, 2018 (EMA[2])	squamous cell skin cancer (EMPOWER-CSCC 1)
PD-L1	Durvalumab (Imfiniz)	IgGlK	–	AstraZeneca	May, 2017	Bladder cancer, NSCLC[3]
	Atezolizumab (Tecentriq)	IgGl	–	Roche	April, 2016	Lung cancer, bladder cancer, advanced triple negative breast cancer

[1]SCC, squamous cell cancers; [2]EMA, European Medicines Agency; [3]NSCLC, non-small cell lung cancer.

TABLE 2 | Clinical research outcomes on PD-1/PD-L1 inhibitors in cervical cancer.

Study	Author	Study population (n)	Phase	Treatment arm(s)	Principal results	Toxicity	Significance
REGN2810	Papadopoulos et al., 2016	Advanced solid tumors	I	Cemiplimab	62.8% patients had disease control	No dose-limiting toxicities	Higher response rate when combined with radiation suggesting abscopal responses
Keynote 028	Frenel et al., 2017	Recurrent cervical cancer with PD-L1 positive tumors (24)	Ib	Pembrolizumab 10 mg/kg q2w	ORR[1] 17% (95% CI: 5–37%)	Grade=3 AE[2] including rash and proteinuria	Well-tolerated and active in cervical cancer
Keynote 158	Schellens et al., 2017	Recurrent cervical cancer with progression or intolerance to standard therapy (82)	II	Pembrolizumab 200 mg/kg q2w	Preliminary results: ORR[1] 17% (95% CI: 8–31%); patients with >27 weeks of follow up, ORR 27% (95% CI: 8–55%)	Grades 3–4 AE[2] included AST/ALT[3] elevation and pyrexia	Demonstrates activity in cervical cancer and increasing response with a longer duration of follow-up
Checkmate 358	Hollebecque et al., 2017	Recurrent or metastatic HPV[4]-related cancers (19)	I–II	Nivolumab 240 mg q2w	Preliminary results: ORR[1] 26% (95% CI: 9.1–51.2%) in cervical cancer patients	Grade 3–4 AE[2] included hyponatremia, syncope, diarrhea and hepatocellular injury	Durable responses demonstrated in cervical cancer patients, with at least 6 months duration

[1]ORR, objective response rate; [2]AE, adverse event; [3]AST/ALT, aspartate transaminase/alanine transaminase; [4]HPV, human papillomavirus.

note, a single-arm, phase II study investigated durvalumab in patients with recurrent/metastatic HNSCCs (n = 112) and found that HPV-positive patients had a higher response rate and better survival than that of the HPV-negative patients (Zandberg et al., 2018). Nevertheless, for cervical cancer, the association of HPV status and the efficacy of PD-1/PD-L1 inhibitors is not yet certain due to the paucity of available data.

Several studies have probed the role of PD-L1 expression in the prognosis and therapeutic efficacy of cervical cancer. These results separately proved that an increase in PD-L1 expression was positively associated with tumor metastasis (Yang et al., 2017), tumor progression (Hsu et al., 2018) and poor prognosis in cervical cancer (Heeren et al., 2016). In this regard, the negative relationship between HPV infection and the clinical outcomes of cervical cancer may be partially attributed to the PD-L1 expression induced by HPV infection (Yang et al., 2017). For patients with locally advanced cervical adenocarcinoma and adenosquamous carcinoma treated with CRT, the underexpression of PD-L1 was a prognostic factor for tumor relapse (p = 0.041), indicating that PD-L1 expression might be a novel biomarker for CRT outcome (Lai et al., 2017).

CLINICAL RESEARCH OUTCOMES OF PD-1/PD-L1 INHIBITORS IN CERVICAL CANCER

Since 2015, multiple clinical trials have been conducted to explore the application of PD-1/PD-L1 antibodies in cervical cancer. To date, four studies have yielded preliminary results (**Table 2**). Keynote 028 (a phase Ib study) and Keynote 158 (a phase II study) evaluated pembrolizumab at the dose of 10 mg/kg and 200 mg/kg, respectively, in recurrent, metastatic cervical cancer. In Keynote 028 (Frenel et al., 2017), 24 patients were enrolled, and the overall response rate (RECIST v1.1) was 17% (95% CI: 5 to 37%). In terms of toxicity, 5 patients experienced grade 3 AEs (NCI-CTCAE 3.0), while no grade 4 AEs was observed. In Keynote 158 (Schellens et al., 2017), 98 patients with recurrent or metastatic cervical cancer were enrolled. With a median follow-up time of 11.7 months, the ORR in 77 patients was 14.3% (95% CI: 7.4 to 24.1%), including 2.6% of the patients with CRs and 11.7% of patients with PRs, whereas no response was observed in patients without PD-L1 expression in tumor cells. The most frequent serious adverse reactions included anemia (7%), fistula (4.1%), hemorrhage (4.1%), and infection (4.1%). Based on Keynote 158, the FDA approved pembrolizumab on June 12, 2018, for advanced cervical cancer with disease progression during or after chemotherapy[1]. Checkmate 358 (Hollebecque et al., 2017) (phases I–II studies) adopted nivolumab (200 mg/kg q2w) for the treatment of recurrent, metastatic cervical cancer and resulted in an ORR of 26.3%. The disease control rate was 70.8%. The related grades 3–4 toxic effects included hyponatremia, syncope, diarrhea, and hepatocellular injury. From these three studies, pembrolizumab and nivolumab showed promising antitumor effects and were well-tolerated in patients with recurrent or metastatic cervical cancer. However, due to a limited follow-up time, PFS and OS were not reported. Additionally, the REGN2810 study (Papadopoulos et al., 2016), a phase I multicenter study, assessed REGN2810 (a PD-1 mAb) as a monotherapy and in combination with hfRT, in combination with cyclophosphamide (CTX) or with CTX + hfRT in patients with advanced solid tumors, including cervical cancer. This study adopted a dose escalation design, and as of February 2016, no dose-limiting

[1]https://www.fda.gov/Drugs/InformationOnDrugs/ApprovedDrugs/ucm610572.htm

TABLE 3 | Ongoing clinical research on PD-1/PD-L1 in cervical cancer.

Clinical trial code	Study	Study population (n)	Phase	Treatment arm(s)	Primary outcome measures	Secondary outcome measures
NCT02257528	Nivolumab in Treating Patients with Persistent, Recurrent, or Metastatic Cervical Cancer (NRG-GYO-02)	Recurrent or metastatic cervical cancer (25)	II	Nivolumab	ORR[1] [5 y]; AE[2] [100 d]	PFS[3] [5 y], OS[4] [5 y]
NCT03298893	Nivolumab in Association with Radiotherapy and Cisplatin in Locally Advanced Cervical Cancers Followed by Adjuvant Nivolumab for up to 6 Months (NiCOL)	Locally advanced cervical cancer (21)	III	Nivolumab	DLT[5] [11 w]	ORR[1] [2 m], PFS[3] [2 y], DFS[6] [2 y], SAE[7] [100 d], AE[2] [100 d], etc.
NCT03257267	Study of REGN2810 in Adults with Cervical Cancer (GOG 3016/ENGOT-cx9) (EMPOWER-Cervical)	Recurrent or metastatic platinum-refractory cervical cancer (436)	III	Cemiplimab (REGN2810)	OS[4] [32 m]	PFS[3] [32 m], ORR[1] [32 m], DOR[8] [32 m], Quality of life (QOL) [100 w]
NCT03104699	Phase 1/2 Study of AGEN2034 in Advanced Tumors and Cervical Cancer	Advanced cervical cancer (75)	I–II	AGEN2034	DLTs[5] [3 w], MTD[9] [1 y], BOR[10] [1 y]	Cmax[11] [1 y], AUC[12] [1 y], PFS[3] [1 y], DOR[8] [1 y], OS[4] [1 y]
NCT03518606	Metronomic Oral Vinorelbine Plus Anti-PD-L1/Anti-CTLA4 ImmunothErapy in Patients with Advanced Solid Tumors (MOVIE)	Advanced solid tumors (150) including cervical cancer	I–II	Durvalumab +Tremelimumab +metronomic Vinorelbine	Phase I: MTD[9] and RP2D[13] [9 m] Phase II: CBR[14] [24 m]	None
NCT03556839	Platinum Chemotherapy Plus Paclitaxel with Bevacizumab and Atezolizumab in Metastatic Carcinoma of the Cervix	Carcinoma of the cervix, stage IVB (404)	III	Atezolizumab	OS[4] [48 m]	PFS[3] [48 m], ORR[1] [48 m], DOR[8] [48 m], AE[2] [48 m], etc.
NCT01975831	A Phase 1 Study to Evaluate MEDI4736 in Combination with Tremelimumab	Solid tumors (106) including cervical cancer	I	MEDI4736 (Durvalumab)+Trem elimumab	AE[2] [1 y]	AUC[12], Cmax[11] [15 m], PFS[3] [15 m], OS[4] [15 m], etc.
NCT02914470	Pilot Study of Durvalumab and Vigil in Advanced Women's Cancers (PROLOG)	Solid tumors (12) including cervical cancer	I	Durvalumab and Vigil	Toxicity [30 d]	ORR[1] [120 m]
NCT02725489	Pilot Study of Durvalumab and Vigil in Advanced Women's Cancers	Solid tumors (15) including cervical cancer	II	Vigil+durvalumab	AEs[2] [90 d]	ORR[1] [12 m], Disease status [12 m], IFNγ-ELISPOT conversion rate [12 w]
NCT02921269	Atezolizumab and Bevacizumab in Treating Patients with Recurrent, Persistent, or Metastatic Cervical Cancer	Recurrent, persistent, or metastatic cervical cancer (22)	II	Atezolizumab +Bevac izumab	ORR[1] [2 y]	PFS[3] [2 y], OS[4] [2 y] AE[2] [30 d], PD-L1, etc.
NCT03635567	Efficacy and Safety Study of First-line Treatment with Pembrolizumab (MK-3475) Plus Chemotherapy Versus Placebo Plus Chemotherapy in Women with Persistent, Recurrent, or Metastati Cervical Cancer (MK-3475-826/KEYNOTE-826)	Cervical cancer (600) c	I–II	Pembrolizumab	PFS[3] [2y] OS[4] [2 y]	ORR[1] [2 y], DOR[8] [2 y], etc.
NCT03144466	A Study of Pembrolizumab And Platinum with Radiotherapy in Cervix Cancer (PAPAYA)	Cervical cancer (26)	I	Pembrolizum	MTD[9] [2 y] ab Efficacy [2 y]	OS[4] [2 y], PFS[3] [2 y], etc.
NCT03255252	Assessment Study to Evaluate Specific Immune Response in Locally Advanced Cervix Cancer After Radio-chemotherapy (IMMUVIX)	Cervical cancer (100)	II	Cisplatin	Expression of CD8+CD39+PD1+	Effect on 1-year DFS[6] of other putative biomarkers (CD73, CD39, PD1 and Tim3)
NCT03559803	A Prospective Study of Monitoring Immune Response in Locally Advanced Cervix Cancer(GHR002)	Cervical cancer(50)	Not appli cable	Cisplatin	PD-L1 [3w, 2 m]	PD1+CD4+T [3w, 2 m], PD1+CD8+T [3w, 2 m], TCR[3w, 2 m]

[1]ORR, objective response rate; [2]AE, adverse event; [3]PFS, progression-free survival; [4]OS, overall survival rate; [5]DLT, dose limiting toxicity; [6]DFS, disease-free survival; [7]SAE, serious adverse event; [8]DOR, duration of response; [9]MTD, maximum tolerated dose; [10]BOR, best overall response; [11]Cmax, maximum plasma concentration; [12]AUC, area under curve; [13]RP2D, phase II recommended dose; [14]CBR, clinical benefit response.

toxicity (DLT) was observed. The most common treatment-related AEs were fatigue (n = 14, 24.1%), arthralgia (n = 7, 12.1%), and nausea (n = 6, 10.3%). Additionally, 4 patients experienced grade $\geq$ 3 AEs. For 9/22 (40.9%) patients who received REGN2810 + hfRT and 2/21 (9.5%) patients who received REGN2810 monotherapy, they were determined to have partial/uPRs, suggesting that the treatment response was augmented by the addition of hfRT.

ONGOING CLINICAL RESEARCH ON PD-1/PD-L1 IN CERVICAL CANCER

As of September 2018, 11 clinical trials have been conducted, mainly in patients with persistent, recurrent, or metastatic cervical cancer, with only three studies on patients with locally advanced cervical cancer. Twenty to thirty cases were intended to be included in the majority of these studies, while there were only three studies (Keynote 826, GOG 3016/ENGOT-cx9, and NCT03556839) in which more than 200 cases were intended to be included. Except for the two studies (IMMUVIX, GHR002) aimed at exploring the immune status of PD-1/PD-L1 in patients with locally advanced cervical cancer, the remaining 12 studies all looked into the applicability of PD-1/PD-L1 inhibitors in cervical cancer. Of these 12 studies, there are 2 studies on nivolumab, 2 on pembrolizumab, 4 on durvalumab, 2 on atezolizumab, 1 on cemiplimab (REGN2810) and 1 on AGEN2034. For PD-1 inhibitors, the difference between the 2 studies on nivolumab is the study population. NRG-GYO-02 was conducted in patients with persistent, recurrent, or metastatic cervical cancer, while the NiCOL study enrolled more patients with locally advanced cervical cancer. The main difference between the two studies on pembrolizumab is that KEYNOTE-826 adopted pembrolizumab in combination with chemotherapy versus placebo, while PAPAYA mainly adopted pembrolizumab in combination with platinum and radiotherapy. The GOG 3016/ENGOT-cx9 (EMPOWER-Cervical) study is an important phase III clinical study to advance the clinical application of cemiplimab (REGN2810) in advanced cervical cancer. NCT03104699 is a phase I/II clinical study on AGEN2034, another PD-1 inhibitor, in advanced solid tumors that includes 75 cases of cervical cancer. In terms of treatment combinations, tremelimumab (a fully human mAb against CTLA-4), Vigil vaccine for cervical cancer, bevacizumab, and chemotherapy were paired with PD-1/PD-L1 inhibitors throughout these studies (**Table 3**).

CONCLUSION

Although there are a few studies suggesting the potential feasibility of PD-1/PD-L1 inhibitors for the treatment of cervical cancer, a consideration should be made for the clinical application of PD-1/PD-L1 inhibitors. The inadequate number of cases included and the insufficient follow-up time are the main defects of all the studies, leading to the unavailability of data regarding OS, PFS, AEs, drug resistance and the treatment mechanism as well. These data are very pivotal not only for obtaining a more convincing result, but also for guiding physicians to select the appropriate patients for PD-1/PD-L1 inhibitors.

Currently, most of these studies, including ongoing studies, are mostly limited to recurrent, persistent, metastatic cervical cancer, which accounts for only a minor portion of patients with cervical cancer. There are several future directions that can be given more attention. First, the latest evidence suggests a clinical benefit of PD-1/PD-L1 inhibitors as neoadjuvant therapy in lung cancer (Lommatzsch et al., 2018). For patients with early-stage cervical cancer, studies in a small sample size can be conducted to investigate PD-1/PD-L1 inhibitors with attempted surgical treatment or to prevent post-operative recurrence. Second, for patients with locally advanced cervical cancer who are not sensitive to CCRT or who relapse in the short term after initial treatment, PD-1/PD-L1 inhibitors may be a useful treatment, and we are looking forward to the research targeting this population. Third, for locally advanced cervical cancer patients, whether PD-1/PD-L1 inhibitors can achieve better therapeutic efficacy in tumors with higher PD-L1 expression before CCRT begins will provide a better understanding of the effects of these inhibitors. Finally, since PD-L1 expression is correlated with HPV status, more studies are warranted to provide further insights into the association of HPV status and the efficacy of PD-1/PD-L1 inhibitors in patients with cervical cancer. Combining the level of HPV DNA with the expression of PD-L1 may also provide a novel predictive biomarker of the efficacy of PD-1/PD-L1 inhibitors and the prognosis of patients with cervical cancer.

AUTHOR CONTRIBUTIONS

JX and YoL conceived the review. YuL and LYi searched the literature. YuL, LYi, LW, FY, ML, LY, and RT critically appraised the literature and wrote and all authors approved the final version of the manuscript.

FUNDING

This work was supported by National Natural Science Foundation of China (grants 81672982 and 81602670) and Sichuan Provincial Research Foundation for Basic Research (No. 18YYJC1284).

REFERENCES

Amatore, F., Gorvel, L., and Olive, D. (2018). Inducible co-stimulator (ICOS) as a potential therapeutic target for anti-cancer therapy. *Expert. Opin. Ther. Targets* 22, 343–351. doi: 10.1080/14728222.2018.1444753

Bagcchi, S. (2014). Pembrolizumab for treatment of refractory melanoma. *Lancet Oncol.* 15:e419. doi: 10.1016/S1470-2045(14)70348-1

Balermpas, P., Martin, D., Wieland, U., Rave-Frank, M., Strebhardt, K., Rodel, C., et al. (2017). Human papilloma virus load and PD-1/PD-L1, CD8(+) and FOXP3 in anal cancer patients treated with chemoradiotherapy: rationale for

immunotherapy. *Oncoimmunology* 6:e1288331. doi: 10.1080/2162402X.2017.1288331

Borcoman, E., and Le Tourneau, C. (2017). Pembrolizumab in cervical cancer: latest evidence and clinical usefulness. *Ther. Adv. Med. Oncol.* 9, 431–439. doi: 10.1177/1758834017708742

Boussios, S., Seraj, E., Zarkavelis, G., Petrakis, D., Kollas, A., Kafantari, A., et al. (2016). Management of patients with recurrent/advanced cervical cancer beyond first line platinum regimens: where do we stand? A literature review. *Crit. Rev. Oncol. Hematol.* 108, 164–174. doi: 10.1016/j.critrevonc.2016.11.006

Boussiotis, V. A. (2016). Molecular and biochemical aspects of the PD-1 checkpoint pathway. *N. Engl. J. Med.* 375, 1767–1778. doi: 10.1056/NEJMra1514296

Bray, F., Ferlay, J., Soerjomataram, I., Siegel, R. L., Torre, L. A., and Jemal, A. (2018). Global cancer statistics 2018: globocan estimates of incidence and mortality worldwide for 36 cancers in 185 countries. *CA Cancer J. Clin.* 68, 394–424. doi: 10.3322/caac.21492

Cancer Genome Atlas Research Network, Albert Einstein College of Medicine, Analytical Biological Services, Barretos Cancer Hospital, Baylor College of Medicine, Beckman Research Institute of City of Hope, et al. (2017). Integrated genomic and molecular characterization of cervical cancer. *Nature* 543, 378–384. doi: 10.1038/nature21386

Chen, J., Gu, W., Yang, L., Chen, C., Shao, R., Xu, K., et al. (2015). Nanotechnology in the management of cervical cancer. *Rev. Med. Virol.* 25(Suppl. 1), 72–83. doi: 10.1002/rmv.1825

Chen, Z., Pang, N., Du, R., Zhu, Y., Fan, L., Cai, D., et al. (2016). Elevated expression of programmed death-1 and programmed death ligand-1 negatively regulates immune response against cervical cancer cells. *Med. Inflamm.* 2016:6891482. doi: 10.1155/2016/6891482

Compte, M., Harwood, S. L., Munoz, I. G., Navarro, R., Zonca, M., Perez-Chacon, G., et al. (2018). A tumor-targeted trimeric 4-1BB-agonistic antibody induces potent anti-tumor immunity without systemic toxicity. *Nat. Commun.* 9:4809. doi: 10.1038/s41467-018-07195-w

Constantinidou, A., Alifieris, C., and Trafalis, D. T. (2018). Targeting programmed cell death -1 (PD-1) and ligand (PD-L1): a new era in cancer active immunotherapy. *Pharmacol. Ther.* 18, 30173–30176. doi: 10.1016/j.pharmthera.2018.09.008

Dijkstra, K. K., Voabil, P., Schumacher, T. N., and Voest, E. E. (2016). Genomics- and transcriptomics-based patient selection for cancer treatment with immune checkpoint inhibitors: a review. *JAMA Oncol.* 2, 1490–1495. doi: 10.1001/jamaoncol.2016.2214

Enwere, E. K., Kornaga, E. N., Dean, M., Koulis, T. A., Phan, T., Kalantarian, M., et al. (2017). Expression of PD-L1 and presence of CD8-positive T cells in pre-treatment specimens of locally advanced cervical cancer. *Mod. Pathol.* 30, 577–586. doi: 10.1038/modpathol.2016.221

Feng, Y. C., Ji, W. L., Yue, N., Huang, Y. C., and Ma, X. M. (2018). The relationship between the PD-1/PD-L1 pathway and DNA mismatch repair in cervical cancer and its clinical significance. *Cancer Manag. Res.* 10, 105–113. doi: 10.2147/CMAR.S152232

Fife, B. T., and Bluestone, J. A. (2008). Control of peripheral T-cell tolerance and autoimmunity via the CTLA-4 and PD-1 pathways. *Immunol. Rev.* 224, 166–182. doi: 10.1111/j.1600-065X.2008.00662.x

Franzen, A., Vogt, T. J., Muller, T., Dietrich, J., Schrock, A., Golletz, C., et al. (2018). PD-L1 (CD274) and PD-L2 (PDCD1LG2) promoter methylation is associated with HPV infection and transcriptional repression in head and neck squamous cell carcinomas. *Oncotarget* 9, 641–650. doi: 10.18632/oncotarget.23080

Frenel, J. S., Le Tourneau, C., O'neil, B., Ott, P. A., Piha-Paul, S. A., Gomez-Roca, C., et al. (2017). Safety and efficacy of pembrolizumab in advanced, programmed death ligand 1-positive cervical cancer: results from the phase Ib KEYNOTE-028 trial. *J. Clin. Oncol.* 35, 4035–4041. doi: 10.1200/JCO.2017.74.5471

Gettinger, S., Horn, L., Jackman, D., Spigel, D., Antonia, S., Hellmann, M., et al. (2018). Five-year follow-up of nivolumab in previously treated advanced non-small-cell lung cancer: results from the CA209-003 study. *J. Clin. Oncol.* 36, 1675–1684. doi: 10.1200/JCO.2017.77.0412

Goodman, A. (2015). HPV testing as a screen for cervical cancer. *BMJ* 350:h2372. doi: 10.1136/bmj.h2372

Gorris, M. A. J., Halilovic, A., and Rabold, K. (2018). Eight-color multiplex immunohistochemistry for simultaneous detection of multiple immune checkpoint molecules within the tumor microenvironment. *J. Immunol.* 200, 347–354. doi: 10.4049/jimmunol.1701262

Guitarte, C., Alagkiozidis, I., Mize, B., Stevens, E., Salame, G., and Lee, Y. C. (2014). Glassy cell carcinoma of the cervix: a systematic review and meta-analysis. *Gynecol. Oncol.* 133, 186–191. doi: 10.1016/j.ygyno.2014.01.048

Heeren, A. M., Punt, S., Bleeker, M. C., Gaarenstroom, K. N., Van Der Velden, J., Kenter, G. G., et al. (2016). Prognostic effect of different PD-L1 expression patterns in squamous cell carcinoma and adenocarcinoma of the cervix. *Mod. Pathol.* 29, 753–763. doi: 10.1038/modpathol.2016.64

Hodi, F. S., O'day, S. J., Mcdermott, D. F., Weber, R. W., Sosman, J. A., Haanen, J. B., et al. (2010). Improved survival with ipilimumab in patients with metastatic melanoma. *N. Engl. J. Med.* 363, 711–723. doi: 10.1056/NEJMoa1003466

Hollebecque, A., Meyer, T., Moore, K. N., Machiels, J.-P. H., De Greve, J., López-Picazo, J. M., et al. (2017). An open-label, multicohort, phase I/II study of nivolumab in patients with virus-associated tumors (CheckMate 358): efficacy and safety in recurrent or metastatic (R/M) cervical, vaginal, and vulvar cancers. *J. Clin. Oncol.* 35:5504. doi: 10.1200/JCO.2017.35.15_suppl.5504

Hsu, P. C., Li, S. H., and Yang, C. T. (2018). Recurrent pneumonitis induced by atezolizumab (anti-programmed death ligand 1) in NSCLC patients who previously experienced anti-programmed death 1 immunotherapy-related pneumonitis. *J. Thorac. Oncol.* 13, e227–e230. doi: 10.1016/j.jtho.2018.06.022

Julia, E. P., Amante, A., Pampena, M. B., Mordoh, J., and Levy, E. M. (2018). Avelumab, an IgG1 anti-PD-L1 immune checkpoint inhibitor, triggers NK cell-mediated cytotoxicity and cytokine production against triple negative breast cancer cells. *Front. Immunol.* 9:2140. doi: 10.3389/fimmu.2018.02140

Kurup, S. P., Obeng-Adjei, N., Anthony, S. M., Traore, B., Doumbo, O. K., Butler, N. S., et al. (2017). Regulatory T cells impede acute and long-term immunity to blood-stage malaria through CTLA-4. *Nat. Med.* 23, 1220–1225. doi: 10.1038/nm.4395

Lai, Y. L., Chen, L. C., Huang, C. Y., Chiang, S. F., Liang, J. A., Chao, K. S. C., et al. (2017). PD-L1 as the prognostic immune biomarker for predicting the relapse of locally advanced cervical adenocarcinoma and adenosquamous carcinoma treated with definitive chemoradiation therapy. *Int. J. Radiat. Oncol. Biol. Phys.* 99, E299–E300. doi: 10.1016/j.ijrobp.2017.06.1318

Le Tourneau, C., Hoimes, C., Zarwan, C., Wong, D. J., Bauer, S., Claus, R., et al. (2018). Avelumab in patients with previously treated metastatic adrenocortical carcinoma: phase 1b results from the JAVELIN solid tumor trial. *J. Immunother. Cancer* 6:111. doi: 10.1186/s40425-018-0424-9

Lheureux, S., Butler, M. O., Clarke, B., Cristea, M. C., Martin, L. P., Tonkin, K., et al. (2018). Association of ipilimumab with safety and antitumor activity in women with metastatic or recurrent human papillomavirus-related cervical carcinoma. *JAMA Oncol.* 4:e173776. doi: 10.1001/jamaoncol.2017.3776

Lim, M., Xia, Y., Bettegowda, C., and Weller, M. (2018). Current state of immunotherapy for glioblastoma. *Nat. Rev. Clin. Oncol.* 15, 422–442. doi: 10.1038/s41571-018-0003-5

Liu, C., Lu, J., Tian, H., Du, W., Zhao, L., Feng, J., et al. (2017). Increased expression of PDL1 by the human papillomavirus 16 E7 oncoprotein inhibits anticancer immunity. *Mol. Med. Rep.* 15, 1063–1070. doi: 10.3892/mmr.2017.6102

Liu, Y. L., and Zamarin, D. (2018). Combination immune checkpoint blockade strategies to maximize immune response in gynecological cancers. *Curr. Oncol. Rep.* 20:94. doi: 10.1007/s11912-018-0740-8

Lommatzsch, M., Bratke, K., and Stoll, P. (2018). Neoadjuvant PD-1 blockade in resectable lung cancer. *N. Engl. J. Med.* 379:e14. doi: 10.1056/NEJMc1808251

Long, G. V., Tykodi, S. S., Schneider, J. G., Garbe, C., Gravis, G., Rashford, M., et al. (2018). Assessment of nivolumab exposure and clinical safety of 480 mg every 4 weeks flat-dosing schedule in patients with cancer. *Ann. Oncol.* 29, 2208–2213. doi: 10.1093/annonc/mdy408

Meng, Y., Liang, H., Hu, J., Liu, S., Hao, X., Wong, M. S. K., et al. (2018). PD-L1 Expression correlates with tumor infiltrating lymphocytes and response to neoadjuvant chemotherapy in cervical cancer. *J. Cancer* 9, 2938–2945. doi: 10.7150/jca.22532

Mezache, L., Paniccia, B., Nyinawabera, A., and Nuovo, G. J. (2015). Enhanced expression of PD L1 in cervical intraepithelial neoplasia and cervical cancers. *Mod. Pathol.* 28, 1594–1602. doi: 10.1038/modpathol.2015.108

Minion, L. E., and Tewari, K. S. (2018). Cervical cancer - state of the science: from angiogenesis blockade to checkpoint inhibition. *Gynecol. Oncol.* 148, 609–621. doi: 10.1016/j.ygyno.2018.01.009

Monk, B. J., Sill, M. W., Mcmeekin, D. S., Cohn, D. E., Ramondetta, L. M., Boardman, C. H., et al. (2009). Phase III trial of four cisplatin-containing doublet combinations in stage IVB, recurrent, or persistent cervical carcinoma: a gynecologic oncology group study. *J. Clin. Oncol.* 27, 4649–4655. doi: 10.1200/JCO.2009.21.8909

Papadopoulos, K. P., Crittenden, M. R., Johnson, M. L., Lockhart, A. C., Moore, K. N., and Falchook, G. S. (2016). A first-in-human study of REGN2810, a monoclonal, fully human antibody to programmed death-1 (PD-1), in combination with immunomodulators including hypofractionaed radiotherapy (hfRT). *J. Clin. Oncol.* 34:3024. doi: 10.1200/JCO.2016.34.15_suppl.3024

Pardoll, D. M. (2012). The blockade of immune checkpoints in cancer immunotherapy. *Nat. Rev. Cancer* 12, 252–264. doi: 10.1038/nrc3239

Paz-Ares, L., Luft, A., Vicente, D., Tafreshi, A., Gumus, M., Mazieres, J., et al. (2018). Pembrolizumab plus chemotherapy for squamous non-small-cell lung cancer. *N. Engl. J. Med.* 379, 2040–2051. doi: 10.1056/NEJMoa1810865

Polesso, F., Weinberg, A., and Moran, A. E. (2018). Late stage tumor regression after PD-L1 blockade with a concurrent OX40 agonist. *Cancer Immunol. Res.* doi: 10.1158/2326-6066.CIR-18-0222 [Epub ahead of print].

Qin, Y., Ekmekcioglu, S., Forget, M. A., Szekvolgyi, L., Hwu, P., Grimm, E. A., et al. (2017). Cervical cancer neoantigen landscape and immune activity is associated with human papillomavirus master regulators. *Front. Immunol.* 8:689. doi: 10.3389/fimmu.2017.00689

Raedler, L. A. (2015). Opdivo (Nivolumab): second PD-1 inhibitor receives FDA approval for unresectable or metastatic melanoma. *Am. Health Drug Benefits* 8, 180–183.

Reddy, O. L., Shintaku, P. I., and Moatamed, N. A. (2017). Programmed death-ligand 1 (PD-L1) is expressed in a significant number of the uterine cervical carcinomas. *Diagn. Pathol.* 12:45. doi: 10.1186/s13000-017-0631-6

Sahasrabuddhe, V. V., Parham, G. P., Mwanahamuntu, M. H., and Vermund, S. H. (2012). Cervical cancer prevention in low- and middle-income countries: feasible, affordable, essential. *Cancer Prevent. Res.* 5, 11–17. doi: 10.1158/1940-6207.CAPR-11-0540

Schellens, J. H. M., Marabelle, A., Zeigenfuss, S., Ding, J., Pruitt, S. K., and Chung, H. C. (2017). Pembrolizumab for previously treated advanced cervical squamous cell cancer:preliminary results from the phase 2 KEYNOTE-158 study. *J. Clin. Oncol.* 35:5514. doi: 10.1200/JCO.2017.35.15_suppl.5514

Schumacher, T. N., and Schreiber, R. D. (2015). Neoantigens in cancer immunotherapy. *Science* 348, 69–74. doi: 10.1126/science.aaa4971

Sidaway, P. (2018). Cemiplimab effective in cutaneous SCC. *Nat. Rev. Clin. Oncol.* 15:472. doi: 10.1038/s41571-018-0056-5

Siu, L. L., Even, C., Mesia, R., Remenar, E., Daste, A., Delord, J. P., et al. (2018). Safety and efficacy of durvalumab with or without tremelimumab in patients with PD-L1-low/negative recurrent or metastatic HNSCC: the phase 2 CONDOR randomized clinical trial. *JAMA Oncol.* doi: 10.1001/jamaoncol.2018.4628[Epub ahead of print].

Tewari, K. S., Sill, M. W., Long, H. J. III, Penson, R. T., Huang, H., Ramondetta, L. M., et al. (2014). Improved survival with bevacizumab in advanced cervical cancer. *N. Engl. J. Med.* 370, 734–743. doi: 10.1056/NEJMoa1309748

Tewari, K. S., Sill, M. W., Penson, R. T., Huang, H., Ramondetta, L. M., Landrum, L. M., et al. (2017). Bevacizumab for advanced cervical cancer: final overall survival and adverse event analysis of a randomised, controlled, open-label, phase 3 trial (gynecologic oncology group 240). *Lancet* 390, 1654–1663. doi: 10.1016/S0140-6736(17)31607-0

Wang, J., Chmielowski, B., Pellissier, J., Xu, R., Stevinson, K., and Liu, F. X. (2017). Cost-Effectiveness of pembrolizumab versus ipilimumab in ipilimumab-naive patients with advanced melanoma in the United States. *J. Manag. Care Spec. Pharm.* 23, 184–194. doi: 10.18553/jmcp.2017.23.2.184

Yang, W., Lu, Y. P., Yang, Y. Z., Kang, J. R., Jin, Y. D., and Wang, H. W. (2017). Expressions of programmed death (PD)-1 and PD-1 ligand (PD-L1) in cervical intraepithelial neoplasia and cervical squamous cell carcinomas are of prognostic value and associated with human papillomavirus status. *J. Obstet. Gynaecol. Res.* 43, 1602–1612. doi: 10.1111/jog.13411

Yang, W., Song, Y., Lu, Y. L., Sun, J. Z., and Wang, H. W. (2013). Increased expression of programmed death (PD)-1 and its ligand PD-L1 correlates with impaired cell-mediated immunity in high-risk human papillomavirus-related cervical intraepithelial neoplasia. *Immunology* 139, 513–522. doi: 10.1111/imm.12101

Zandberg, D. P., Algazi, A. P., Jimeno, A., Good, J. S., Fayette, J., Bouganim, N., et al. (2018). Durvalumab for recurrent or metastatic head and neck squamous cell carcinoma: results from a single-arm, phase II study in patients with > / = 25% tumour cell PD-L1 expression who have progressed on platinum-based chemotherapy. *Eur. J. Cancer* 107, 142–152. doi: 10.1016/j.ejca.2018.11.015

Zhang, S., and Li, W. (2018). The effort in exploration of a definitive predictive factor from PD-1/PD-L1 blockade in advanced or metastatic urothelial cancer. *J. Clin. Oncol.* 36, 3056–3057. doi: 10.1200/JCO.2018.79.1400

Conflict of Interest Statement: The authors declare that the research was conducted in the absence of any commercial or financial relationships that could be construed as a potential conflict of interest.

frontiers in Oncology

MINI REVIEW
published: 06 February 2019
doi: 10.3389/fonc.2019.00040

The CXCL8-CXCR1/2 Axis as a Therapeutic Target in Breast Cancer Stem-Like Cells

*Pier Adelchi Ruffini**

Research and Development Department, Dompé farmaceutici S.p.A., Milan, Italy

Cancer stem-like cells (CSC) have been targeted by different strategies over the last decade. This mini review focuses on preclinical and clinical results obtained by interfering with chemokine receptors CXCR1 and CXCR2 in breast cancer. This strategy is currently being tested in a randomized, double blind phase 2 clinical trial.

Keywords: CXCR1, CXCL8, cancer stem-like cells, reparixin, breast cancer

OPEN ACCESS

Edited by:
Zhe-Sheng Chen,
St. John's University, United States

Reviewed by:
Vijay Pandey,
National University of Singapore, Singapore
Fabrizio Martelli,
Istituto Superiore di Sanità (ISS), Italy

***Correspondence:**
Pier Adelchi Ruffini
pieradelchi.ruffini@dompe.com

Specialty section:
This article was submitted to Cancer Molecular Targets and Therapeutics, a section of the journal Frontiers in Oncology

Received: *30 October 2018*
Accepted: *15 January 2019*
Published: *06 February 2019*

Citation:
Ruffini PA (2019) The CXCL8-CXCR1/2 Axis as a Therapeutic Target in Breast Cancer Stem-Like Cells. Front. Oncol. 9:40. doi: 10.3389/fonc.2019.00040

Cancer stem-like cells (CSC) have been the focus of several clinical investigations testing different strategies for a more effective anticancer treatment through inhibition of this unique cell population (1). Targeting the CXCL8-CXCR1/2 axis is one such strategy that has moved from preclinical models to an ongoing randomized phase 2 clinical trial in breast cancer.

CXCL8 (formerly IL-8) is a chemokine whose biological effects are mediated by two G-protein-coupled receptors: **CXCR1** and **CXCR2** (2). CXCL8 has been reported to play multiple roles in cancer, such as increasing proliferation, angiogenesis, invasion, and metastases (3). In **breast cancer**, recent evidence points to this chemokine as a key regulator of CSC activity (4).

PRECLINICAL EVIDENCE IN BREAST CANCER

In breast cancer, tumor cells capable of forming tumors in immunocompromised mice (i.e., CSC by a functional definition) are identified by the expression of either the enzyme aldehyde dehydrogenase (ALDH) (5) and/or the $CD24^{-}/CD44^{+}$ phenotype (6), representing two largely non-overlapping cell populations. CXCR1 was identified as a druggable target on breast cancer CSC identified by the expression of ALDH, while its expression was almost undetectable on bulk (i.e., non-CSC) tumor cells (7). In keeping, breast cancer CSC were shown to proliferate *in vitro* in response to the addition of exogenous CXCL8 while a small molecular weight antagonist of CXCR1/2 (**reparixin**) (8) or a blocking anti-CXCR1 (but not anti-CXCR2) monoclonal antibody were both able to deplete CSC *in vitro* (9). A FAS-FASL mediated bystander effect killed the vast majority of bulk tumor cells *in vitro*, suggesting the possibility of synergistic effects with chemotherapy (9). In human breast cancer cell lines or breast cancer patient-derived xenografts orthotopically implanted in mice, the combination of weekly docetaxel and reparixin for 4 weeks was more effective than either treatment alone in reducing tumor size (9). However, in tumors recovered from mice that had been treated with reparixin, either alone or in combination with chemotherapy, CSC proportion was far lower than in tumors recovered from mice receiving chemotherapy alone (9). These results were framed in a model where, following administration of chemotherapy, CXCL8 and FASL are released by dying bulk tumor cells. Engagement of CXCR1 on the surface of CSC by CXCL8 shelters CSC from apoptotic signals delivered by FASL. To the contrary, when CXCR1 signaling on CSC is blocked by reparixin these cells undergo FASL-mediated apoptosis. Evidence provided later by independent laboratories supports this model. First, as originally reported by Ginestier and coworkers, tumor cells exposed to taxane

in vitro release CXCL8 (10). Also, Triple-Negative Breast Cancer (TNBC) tumor cells recovered from immunocompromised mice following two doses of paclitaxel displayed a marked and dose-dependent increase in mammosphere forming efficiency as compared with untreated mice (10). Furthermore, and again in line with the original report by Ginestier, administration of a CXCR1 inhibitor reduced CSC percentage *in vitro*. Consistent findings were later reported by an independent group (11). Second, in breast cancer patients with pleural effusions and/or ascites CXCL8 levels were measured and tumor cells recovered and cultured *in vitro* (4). A direct correlation was observed between CXCL8 levels and CSC activity by means of mammosphere formation (4). Surface CXCR1 was detected on the majority of mammosphere cells, and the effects of exogenous CXCL8 on mammosphere formation were blocked by a CXCR1/2 inhibitor, SCH563705 (4).

The relative contribution of CXCR1 inhibition and paclitaxel in this model were further investigated in CSC-enriched mammospheres from the human TNBC cell line MDA-MB231. The combination treatment displayed a synergistic effect on mammosphere number and an additive effect on mammosphere volume as compared with either treatment alone (12). Different than paclitaxel, which increased the number of dead cells, reparixin increased the number of non-proliferating cells, and the combination treatment exerted both effects (12). In keeping with previous reports (9), also in MDA-MB231-derived tumorspheres reparixin activity was mediated by inhibition of the FAK/AKT pathway which is unaffected by paclitaxel. When the effects on cell cycle were investigated, a shift of tumor cells in S phase or a block in G2 phase were observed upon paclitaxel and combination treatment, respectively. In keeping, cyclin B1, which is responsible for the cell cycle progression from G2 to S phase, was also inhibited by the combination treatment (12). Furthermore, paclitaxel + reparixin treatment induced "cell senescence by decreasing PI3K-Akt activation paralleled by a decrease of the cytosolic p-FOXO3A (inactive) and by an increase of p27" (12). The effects on cell cycle, cyclin B1 and p-FAK levels recorded upon exposure to reparixin were reproduced using neutralizing anti-CXCR1 and anti-CXCL8 monoclonal antibodies, thus providing indirect evidence of the ability of reparixin to downregulate CXCL8-CXCR1signaling pathway (12).

Another set of experiments aimed at testing the hypothesis that inhibition of CSC would reduce metastatic spread. First, it was shown that reparixin administration reduced metastasis formation in mice following injection of luciferase-transfected human breast cancer cells into the bloodstream (9). Second, the suppressive activity of CXCR1 inhibition on the metastatic process was tested in a mouse model of brain metastases by the TNBC cell line MDA-MB231. In the absence of brain metastases, reparixin does not cross the blood brain barrier (BBB). However, in the presence of brain metastases and an allegedly damaged BBB, reparixin can be found in the central nervous system (12). When treatment was started on the same day when tumor cells were injected, a significant decrease of both the number and the volume of brain metastases was observed following single agent (i.e., reparixin or paclitaxel) as well as the combination treatment. When treatment was started at day 7 following tumor cell injection and continued until day 21, a significant reduction of the number of brain metastases was observed only following combination treatment, which also showed a trend toward an inhibitory effect on metastases volume (12).

PRECLINICAL EVIDENCE IN TUMORS OTHER THAN BREAST CANCER

Anti-tumor and anti CSC activity of reparixin has been demonstrated in human epithelial thyroid cancer *in vitro* and *in vivo* (13). Reparixin ability to inhibit stemness (evaluated by stemness marker expression and tumorsphere formation) and epithelial-mesenchymal transition (EMT) (evaluated at both the biochemical and functional level) of thyroid cancer was shown to be dependent, different than in breast cancer (9), on its activity on both CXCR1 and CXCR2 (13).

In malignant melanoma, CXCR1/2 inhibition reduced the percentage of ALDH+ cells in human tumors growing in nude athymic mice (14).

In pancreatic cancer (15) a positive correlation was found between CXCR1 and both CD44 and CD133 stemness marker expression. Exogenous CXCL8 added to pancreatic cancer cells *in vitro* increased their invasion ability, tumorsphere formation, and CSC population and addition of a CXCR1-blocking monoclonal antibody was able to revert all these effects (15).

CLINICAL TRIALS IN BREAST CANCER

In a phase Ib study (NCT02001974) (16), patients with HER-2 negative metastatic breast cancer not known to be refractory to paclitaxel who had received no more than three lines of cytotoxic chemotherapy in the metastatic setting were enrolled in cohorts of 3–6 patients to receive escalating doses of the CXCR1/2 inhibitor reparixin oral tablets three times per day (t.i.d.) from day 1 to 21 in combination with a fixed dose of weekly paclitaxel (80 mg/m^2) on days 1, 8, and 15 of a 28-days cycle, for as long as clinical benefit was observed. Primary objectives were the assessment of the safety of the combination and the pharmacokinetic (PK) profile of oral reparixin. Expansion of the highest dose cohort was foreseen to gain additional PK and safety data. Cohorts 1–3 received reparixin 400, 800, and 1,200 mg t.i.d. respectively. In cycle 1 only, patients received a 3 days course of reparixin alone (day −3 to −1) at the assigned dose for the cohort, for purpose of obtaining single agent PK data.

Thirty-three patients were enrolled in the study. Eighty-three percent of patients had visceral disease, and the majority had two or more sites of metastasis. 20/33 patients had received prior (neo)adjuvant chemotherapy, and 16 of these patients had received a taxane in the (neo)adjuvant setting. 19/33 had received chemotherapy in the metastatic setting, with 11 having one prior metastatic regimen and eight having two or more chemotherapy regimens. Thirty patients were evaluated for safety. There were no dose limiting toxicities in any cohort. Most adverse reactions (ADR) were of grade 1 (79.8%), with only 2.7% grade 3 ADR. There was no apparent dose effect of increasing reparixin dose

on the incidence, severity or profile of treatment emergent adverse events (TEAE) experienced by the treatment groups, and there were no clinically significant differences between the treatment groups with regards to laboratory measurements, vital signs, ECG, and physical examination assessments. Twenty-seven patients were evaluated for antitumor activity. In total, 8/27 patients had a confirmed RECIST response. Of responding patients, all but one were from cohort 3. Median time to progression (TTP) (95% C.I.) for the 3 cohorts were 58 days (44-infinity) for cohort 1, 67 days (58–82) for cohort 2 and 162 days (60–229) for cohort 3. Remarkably, there were long term remissions among patients treated (16). In this trial, it was not possible to obtain optional serial biopsies of tumor tissue at study entry and during treatment from any patient. However, blood-based biomarkers of CSC were explored. The circulating biomarkers included Circulating Tumor Cell (CTC) enumeration, evaluation of ALDEFLUOR, and EMT transcription factors in peripheral blood, and serum cytokine measurements. Unfortunately, no clear pattern of change in any of these markers was observed. This is likely related to multiple issues, including but not limited to small sample size, low CTC number in the enrolled patient population leading to limited tumor material for testing, and high baseline heterogeneity in the measurements.

Operable breast cancer is a more suitable clinical setting to evaluate the ability of a novel agent to reduce the number of CSC following treatment, as they can be measured on readily available tumor tissue. Thus, after reviewing safety data from the second cohort of the above trial, a window-of-opportunity, pilot trial (NCT01861054) of single agent reparixin was started (17).

Patients with previously untreated HER-2 negative operable breast cancer not eligible for neo(adjuvant) treatment were divided into two cohorts, i.e., group A: histologically proven ER^+ and/or PgR^+ and group B: ER^-/PgR^- breast cancer (i.e., TNBC). This design allowed potential to identify the cohort of patients who might benefit the most from this treatment in later stage clinical trials. Oral reparixin was administered at 1,000 mg t.i.d. for 21 consecutive days before curative surgery. Core biopsies were taken at baseline (day −14 to 0) and at the completion of therapy (day 21). The primary objectives of this study were to evaluate the effects of orally administered reparixin on CSC in the primary tumor and the tumor microenvironment and to evaluate the safety of oral reparixin. Signal of activity was defined as a ≥20% reduction of CSC (defined by either the $ALDH^+$ or $CD24^-/CD44^+$ phenotype) in tumor tissue from baseline values as measured by flow cytometry accompanied by a consistent reduction of the same cell population by immunohistochemistry (IHC).

A total of 20 patients were enrolled, 18 of whom in group A. Signal of activity was detected by flow cytometry in the majority of patients (18), but the very low numbers of CSC hindered the possibility to confirm flow cytometry results by IHC. However, the later published evidence that the two breast cancer CSC populations (i.e., $ALDH^+$ and $CD24^-/CD44^+$) investigated reside in different areas of primary breast tumors and can transition from one phenotype to the other (19) might affect the reliability of CSC counts in this patient population. More in general, the clinical relevance of a ≥20% reduction of CSC following a single 21-day course of reparixin in this patient population is unknown and was beyond the scope of this trial.

From a safety standpoint, also in this trial reparixin appeared to be well-tolerated with 10/20 patients experiencing one or more ADR, all of which of grade ≤2. Neither TEAE leading to treatment discontinuation nor delays in surgery due to TEAE were recorded.

CONCLUSIONS

Evidence for a CXCL8-CXCR1/2 axis in CSC has been reported by independent laboratories and offers a potential therapeutic target. Clinical trials aimed at testing the effective targeting of CSC through this axis have been conducted in breast cancer, where the most information is available from preclinical research. Reparixin appeared to be well-tolerated, however, such trials were faced with several issues for efficacy evaluation, e.g., the very low numbers of CSC in primary operable breast cancer. To circumvent this limitation, circulating markers for monitoring the effect of anti-CSC agents were explored but these assays turned out to be inadequate.

Future prospects for CSC targeting agents include the development of reliable assays to measure stem cell number and/or activity (20) in serial biopsies from accessible tumors (e.g., window-of-opportunity trials), and alternative endpoints in clinical trials in the metastatic setting. One possible endpoint is the development of metastases at new sites (21), which can have also clinical significance (22). In keeping with preclinical findings (9, 12), it is hypothesized that an effective anti-CSC treatment will impact on development of new metastases while progression of pre-existing metastases is more consistent with proliferation of non-CSC, bulk tumor cells that should be addressed by chemotherapy.

As concerns CXCR1/2 inhibition, a randomized, placebo-controlled clinical trial (NCT02370238) of weekly paclitaxel with and without reparixin in front line treatment of metastatic TNBC has completed enrolment. Identification of clinical (e.g., disease sensitivity to chemotherapy) and/or cellular/molecular biomarkers of patients most likely to benefit from treatment represents a future direction of research, while analysis of time to new metastasis may fuel development of this strategy in the (neo)adjuvant setting, also leveraging on safety data generated in metastatic patients.

AUTHOR CONTRIBUTIONS

The author confirms being the sole contributor of this work and has approved it for publication.

ACKNOWLEDGMENTS

The author is grateful to Sonia Amicarella (Dompé farmaceutici S.p.A.) for assistance with formatting the manuscript.

REFERENCES

1. Ramos EK, Hoffmann AD, Gerson SL, Liu H. New opportunities and challenges to defeat cancer stem cells. *Trends Cancer* (2017) 3:780–96. doi: 10.1016/j.trecan.2017.08.007
2. Zlotnik A, Yoshie O. The chemokine superfamily revisited. *Immunity* (2012) 36:705–16. doi: 10.1016/j.immuni.2012.05.008
3. Waugh DJ, Wilson C. The interleukin-8 pathway in cancer. *Clin Cancer Res.* (2008) 14:6735–41. doi: 10.1158/1078-0432.ccr-07-4843
4. Singh JK, Farnie G, Bundred NJ, Simoes BM, Shergill A, Landberg G, et al. Targeting CXCR1/2 significantly reduces breast cancer stem cell activity and increases the efficacy of inhibiting HER2 via HER2-dependent and -independent mechanisms. *Clin Cancer Res.* (2013) 19:643–56. doi: 10.1158/1078-0432.ccr-12-1063
5. Ginestier C, Hur MH, Charafe-Jauffret E, Monville F, Dutcher J, Brown M, et al. ALDH1 is a marker of normal and malignant human mammary stem cells and a predictor of poor clinical outcome. *Cell Stem Cell* (2007) 1:555–67. doi: 10.1016/j.stem.2007.08.014
6. Al-Hajj M, Wicha MS, Benito-Hernandez A, Morrison SJ, Clarke MF. Prospective identification of tumorigenic breast cancer cells. *Proc Natl Acad Sci USA.* (2003) 100:3983–8. doi: 10.1073/pnas.0530291100
7. Charafe-Jauffret E, Ginestier C, Iovino F, Wicinski J, Cervera N, Finetti P, et al. Breast cancer cell lines contain functional cancer stem cells with metastatic capacity and a distinct molecular signature. *Cancer Res.* (2009) 69:1302–13. doi: 10.1158/0008-5472.can-08-2741
8. Bertini R, Allegretti M, Bizzarri C, Moriconi A, Locati M, Zampella G, et al. Noncompetitive allosteric inhibitors of the inflammatory chemokine receptors CXCR1 and CXCR2: prevention of reperfusion injury. *Proc Natl Acad Sci USA.* (2004) 101:11791–6. doi: 10.1073/pnas.0402090101
9. Ginestier C, Liu S, Diebel ME, Korkaya H, Luo M, Brown M, et al. CXCR1 blockade selectively targets human breast cancer stem cells *in vitro* and in xenografts. *J Clin Invest.* (2010) 120:485–97. doi: 10.1172/jci39397
10. Bhola NE, Balko JM, Dugger TC, Kuba MG, Sanchez V, Sanders M, et al. TGF-beta inhibition enhances chemotherapy action against triple-negative breast cancer. *J Clin Invest.* (2013) 123:1348–58. doi: 10.1172/jci65416
11. Samanta D, Gilkes DM, Chaturvedi P, Xiang L, Semenza GL. Hypoxia-inducible factors are required for chemotherapy resistance of breast cancer stem cells. *Proc Natl Acad Sci USA.* (2014) 111:E5429–38. doi: 10.1073/pnas.1421438111
12. Brandolini L, Cristiano L, Fidoamore A, De Pizzol M, Di Giacomo E, Florio TM, et al. Targeting CXCR1 on breast cancer stem cells: signaling pathways and clinical application modelling. *Oncotarget* (2015) 6:43375–94. doi: 10.18632/oncotarget.6234
13. Liotti F, De Pizzol M, Allegretti M, Prevete N, Melillo RM. Multiple anti-tumor effects of Reparixin on thyroid cancer. *Oncotarget* (2017) 8:35946–61. doi: 10.18632/oncotarget.16412
14. Kemp DM, Pidich A, Larijani M, Jonas R, Lash E, Sato T, et al. Ladarixin, a dual CXCR1/2 inhibitor, attenuates experimental melanomas harboring different molecular defects by affecting malignant cells and tumor microenvironment. *Oncotarget* (2017) 8:14428–42. doi: 10.18632/oncotarget.14803
15. Chen L, Fan J, Chen H, Meng Z, Chen Z, Wang P, et al. The IL-8/CXCR1 axis is associated with cancer stem cell-like properties and correlates with clinical prognosis in human pancreatic cancer cases. *Sci Rep.* (2014) 4:5911. doi: 10.1038/srep05911
16. Schott AF, Goldstein LJ, Cristofanilli M, Ruffini PA, McCanna S, Reuben JM, et al. Phase Ib pilot study to evaluate reparixin in combination with weekly paclitaxel in patients with HER-2-negative metastatic breast cancer. *Clin Cancer Res.* (2017) 23:5358–65. doi: 10.1158/1078-0432.ccr-16-2748
17. Goldstein L, Sparano J, Perez R, Vito C, Reuben J, Landis M, et al. Abstract OT2-6-03: a single arm, preoperative, pilot study to evaluate the safety and biological effects of orally administered reparixin in early breast cancer patients who are candidates for surgery. *Cancer Res.* (2013) 73(24 Suppl.):OT2-6-03-OT02-06-03. doi: 10.1158/0008-5472.sabcs13-ot2-6-03
18. Goldstein LJ, Perez RP, Yardley DA, Han LK, Reuben JM, McCanna S, et al. Abstract CT057: a single-arm, preoperative, pilot study to evaluate the safety and biological effects of orally administered reparixin in early breast cancer patients who are candidates for surgery. *Cancer Res.* (2016) 76(14 Suppl.):CT057-CT057. doi: 10.1158/1538-7445.am2016-ct057
19. Liu S, Cong Y, Wang D, Sun Y, Deng L, Liu Y, et al. Breast cancer stem cells transition between epithelial and mesenchymal states reflective of their normal counterparts. *Stem Cell Rep.* (2014) 2:78–91. doi: 10.1016/j.stemcr.2013.11.009
20. Saygin C, Matei D, Majeti R, Reizes O, Lathia JD. Targeting cancer stemness in the clinic: from hype to hope. *Cell Stem Cell* (2019) 24:25–40. doi: 10.1016/j.stem.2018.11.017
21. Giuliano M, Giordano A, Jackson S, De Giorgi U, Mego M, Cohen EN, et al. Circulating tumor cells as early predictors of metastatic spread in breast cancer patients with limited metastatic dissemination. *Breast Cancer Res.* (2014) 16:440. doi: 10.1186/s13058-014-0440-8
22. Twelves C, Cortes J, Kaufman PA, Yelle L, Awada A, Binder TA, et al. "New" metastases are associated with a poorer prognosis than growth of pre-existing metastases in patients with metastatic breast cancer treated with chemotherapy. *Breast Cancer Res.* (2015) 17:150. doi: 10.1186/s13058-015-0657-1

Conflict of Interest Statement: PAR is a full time employee of Dompé farmaceutici S.p.A.

frontiers in Pharmacology

ORIGINAL RESEARCH
published: 06 February 2019
doi: 10.3389/fphar.2019.00075

Iron-Chelated Polydopamine Decorated Doxorubicin-Loaded Nanodevices for Reactive Oxygen Species Enhanced Cancer Combination Therapy

*Xu-Jing Li[1†], Wen-Tong Li[1,2†], Zi-Hao-Ran Li[1], Li-Ping Zhang[3], Cheng-Cheng Gai[1], Wei-Fen Zhang[2,3] and De-Jun Ding[2,3]**

[1] Department of Pathology, Weifang Medical University, Weifang, China, [2] Collaborative Innovation Center for Target Drug Delivery System, Weifang Medical University, Weifang, China, [3] College of Pharmacy, Weifang Medical University, Weifang, China

OPEN ACCESS

Edited by:
Zhe-Sheng Chen,
St. John's University, United States

Reviewed by:
Xuan Zhou,
George Washington University, United States
Jiwei Cui,
Shandong University, China

***Correspondence:**
De-Jun Ding
dejunding@wfmc.edu.cn

† These authors have contributed equally to this work

Specialty section:
This article was submitted to Cancer Molecular Targets and Therapeutics, a section of the journal Frontiers in Pharmacology

Received: *11 December 2018*
Accepted: *21 January 2019*
Published: *06 February 2019*

Citation:
Li X-J, Li W-T, Li Z-H-R, Zhang L-P, Gai C-C, Zhang W-F and Ding D-J (2019) Iron-Chelated Polydopamine Decorated Doxorubicin-Loaded Nanodevices for Reactive Oxygen Species Enhanced Cancer Combination Therapy. Front. Pharmacol. 10:75. doi: 10.3389/fphar.2019.00075

Combination therapy which enhances efficacy and reduces toxicity, has been increasingly applied as a promising strategy for cancer therapy. Here, a reactive oxygen species (ROS) that enhanced combination chemotherapy nanodevices was fabricated based on the Fe-chelated polydopamine (PDA) nanoparticles (NPs). The structure was characterized by dynamic light scattering-autosizer, transmission electron microscopy, energy dispersive spectroscopy, and Fourier-transform infrared (FT-IR) spectrophotometer. The *in vitro* drug release profile triggered by low intracellular pH indicated that the system demonstrated controlled therapeutic activity. *In vitro* cell uptake studies showed that doxorubicin (DOX)-loaded Fe-PDA/ folic acid (FA)-polyethylene glycol (DOX@Fe-PDA/FA-PEG) had a strong uptake capacity and can be rapidly internalized by MCF-7 cells. The *in vitro* experiments demonstrated that DOX@Fe-PDA/FA-PEG triggered the intracellular ROS overproduction, thereby enhancing its therapeutic effect on breast cancer. In summary, this experiment demonstrated the novel DOX-loaded composite NPs used as a potential targeted nanocarrier for breast cancer treatment, which could be a promising therapeutic strategy against breast cancer.

Keywords: polydopamine, combination therapy, reactive oxygen species, doxorubicin, breast cancer

INTRODUCTION

As one of the most common malignant tumors among women, breast cancer is the second and common cause of cancer-related death in women (Wood et al., 2017; Bray et al., 2018). Chemotherapy has become one of the most mature and common treatment option for breast cancer (Fisher et al., 1998; Miller et al., 2016; Spiegel and Koontz, 2018). Doxorubicin (DOX) is an anthracycline non-specific broad-spectrum anticancer drug that is widely used to treat breast cancer. Doxorubicin can exert its effects by elevating reactive oxygen species (ROS) thereby activating of caspase and ultimately leading to apoptosis (Russell and Cotter, 2015; Chakravarti et al., 2016). However, serious side effects, such as myelosuppression, cardiotoxicity, and drug resistance, are the major clinical chemotherapeutic drawbacks of DOX.

It has been proposed that combination therapeutics plays a synergistic effect and can enhance efficacy and reduce the toxicity of chemotherapy (Xu et al., 2015; Camacho et al., 2016; Kemp et al., 2016; Seo et al., 2017). Dayton et al. (2011) reported that the use of HO-3867, which is a synthetic curcumin analog, combined with DOX, in low doses to achieve enhanced cell death and reduced myocardial toxicity. And the increased generation of ROS, thereby resulting in oxidative damage to the cellular constituents, is widely exploited for therapeutic benefits on cancer (Matés and Sánchez-Jiménez, 2000; Schumacker Paul, 2015; Zhou et al., 2016). Fe, which plays a role in several types of cell death, has long been associated with toxicity because it induces hydroxyl radical (OH·), which is a ROS formed via Fenton reaction (Dixon and Stockwell, 2013; Shen et al., 2018; Zhang et al., 2018). Using ROS-producing agents could enhance the anticancer activity of DOX in cancer therapy through ROS-mediated apoptosis (Xia et al., 2017; Wu et al., 2017), autophagy (Fong et al., 2012), and ferroptosis (Zheng et al., 2017). Fan et al. (2014) identified the synergistic effect of DOX/ selenocystine sensitized to DOX by through ROS overproduction. Dai et al. (2018) fabricated assembled metal-phenolic network Nps as a novel ROS promoted synergistic nanomedicine platform for cancer therapy. This observation inspires us to import an iron-supply system in combination with DOX to elicit a synergistic effect on the cancer therapy.

Recently, researchers attempted to build some drug carrier systems to load and transport DOX overcoming the low bioavailability, poor absorption, and high toxicity of DOX (Xu et al., 2015; Kemp et al., 2016; Indermun et al., 2018). Particularly, polydopamine (PDA), which is a natural-inspired polymer, is an appealing material as drug carrier due to its good biocompatibility (Lynge et al., 2015; Indermun et al., 2018; Ryu et al., 2018). Considering its abundant aromatic rings, PDA NPs could be an efficient platform for loading DOX through π–π stacking and hydrogen-bonding interactiron. Meanwhile, the existence of phenolic hydroxyl groups on the surface makes it suitable for further modification with PEG, which could endow nanoparticles excellent physiological stability of NPs (Liu et al., 2014). More attractively, the phenolic surface have excellent chelating ability with metal ions such as Mn (Miao et al., 2015; Xi et al., 2017), Cu (Ge et al., 2017), and Fe (Li et al., 2016).

Keep all the issues in mind, we hypothesized that the Fe-chelated PDA nanoparticles with DOX loading could act as an Fe-supply system used for Fe and DOX combined cancer theranostics, as shown in **Figure 1**. The designed DOX@Fe-PDA/folic acid (FA)-PEG could be provided with several advantages, as follows: (Wood et al., 2017) Combination therapy. The chemotherapy drug DOX undergoes redox cycles to generate and increase H_2O_2 in living cells. The released Fe from PDA further reacts with H_2O_2 to generate hydroxyl radical via Fenton reaction and induces cell death. In combination with Fe, DOX was prone to kill cancer cells efficiently (Bray et al., 2018). Biocompatibility and safety. PDA, which is a natural biopolymer, possesses biocompatibility. The coated PEG and chelated Fe of PDA Nps were metabolic. Meanwhile, the pH-triggered release performance of PDA in tumor microenvironment, avoids damage to surrounding tissues. The PEG-coating can help Nps to ameliorate long-term circulation (Fisher et al., 1998). Tumor targeted. Considering folate receptor overexpression on the surface of breast cancer cells, the FA conjugated NPs may improve cell uptake via receptor mediated endocytosis. In summary, the DOX@Fe-PDA/FA-PEG system could be used as potential combination chemotherapy nanodevice for breast cancer treatment.

MATERIALS AND METHODS

NPs Synthesis

The synthesis of NPs was modified based on the previously introduced procedure (Li et al., 2016). In brief, 4.08 mg $FeCl_3$ and 15 mg dopamine plus 10 mL of water were mixed and stirred at room temperature for 1 h. Then 500 mg Tris was added, and the mixture was stirred at room temperature for 1.5 h. The mixture was centrifuged at 12000 rpm for 15 min to obtain Fe-PDA NPs. A total of 3.85 mL Fe-PDA NPs (5.2 mg/mL) were mixed with 20 mg FA-PEG-SH, 4.7 mg Tris, and 100 μL *tris*(2-carboxyethyl)phosphine (8 mg/mL). The mixture was vigorously stirred for 1 h at room temperature. Then, the FA-PEG modified NPs (Fe-PDA/PEG-FA) were purified via centrifugation and washed with deionized water.

Drug Loading

A total of 2 mg adriamycin hydrochloride were added into 300 μL of dimethyl sulfoxide and 8.2 μL of triethylamine was added. The mixture was stirred in dark at room temperature for 12 h to desalinate hydrochloride. Then, the neutral DOX (2 mg) above-mentioned was added dropwise to 1 mL of Fe-PDA/FA-PEG NPs (10 mg/mL). Afterward, Tris (2.42 mg) was added and volume of 3 mL was obtained by adding distilled water. After vigorous stirring for 24 h in the dark, free DOX was removed via centrifugation at 12000 rpm for 10 min, then washed with phosphate buffer solution (PBS) and stored at 4°C in the dark. The DOX loading capacity of NPs was determined by UV-Vis spectrophotometer at the wavelength of 480 nm. The encapsulation efficiency (EE) of DOX was calculated by the following equation: EE = (initial amount of feeding drugs – free drugs)/initial amount of feeding drugs.

NPs Characterization

The size and Zeta potential of the prepared NPs were measured by dynamic light scattering-autosizer (DLS) on Zetasizer Nano ZS90 (Malvern Instruments, Malvern, United Kingdom). The liquid sample was sonicated before measurement. Three independent test results were recorded. The shape and surface morphology of the NPs were imaged by a transmission electron microscope (TEM, JEM-1230; JEOL, Tokyo, Japan). TEM, energy dispersive X-ray spectroscopy (EDS) and corresponding EDS-mapping were adopted for morphology and elemental distribution analyses on the JEM-1230 electron microscope operated at 200 kV. The chemical composition and structural changes of NPs were analyzed by Fourier transform infrared (FT-IR) spectroscopy (VERTEX 70; Bruker, Bremen, Germany). The IR spectra

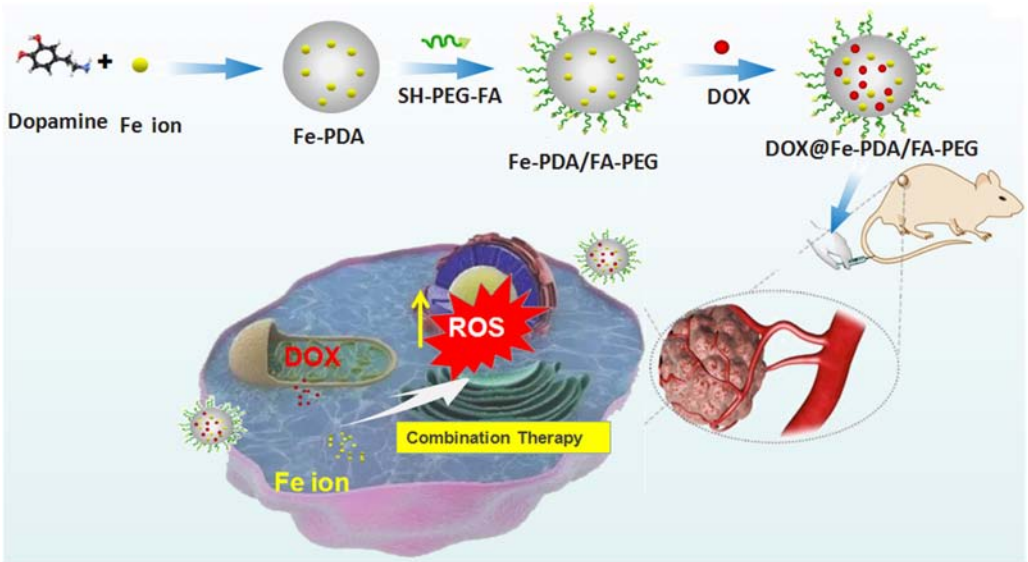

FIGURE 1 | Schematic representation of DOX@Fe-PDA/PEG-FA synthesis, targeted cell uptake and intracellular drug release and combination therapy.

of the samples were obtained in the range of 4000 and 500 cm^{-1}.

In vitro Drug Release Profiles

The *in vitro* DOX release behavior of DOX@Fe-PDA/FA-PEG was tested as reported previously (Liu et al., 2014). Briefly, DOX@Fe-PDA/FA-PEG was dispersed in 2 mL PBS with the pH of either 7.2 or 5.5. The tube was shaken at 37°C with 100 rpm in dark. At appropriate time points, the full release buffer was collected via centrifugation at 12000 rpm for 10 min, and replaced with 2 mL of fresh PBS. The amount of released drug DOX was quantified by a UV spectrophotometer at the wavelength of 480 nm. The correlation between the accumulative DOX released from NPs and time was plotted.

Cell Culture

The *in vitro* cell cytotoxicity cellular uptake and ROS measurement were assessed on human breast cancer cell line MCF-7, which was purchased from American Type Culture Collection. Cells were incubated at 37°C with modified Eagle's medium (MEM) containing 10% fetal bovine serum (FBS), 100 U/mL penicillin, and 100 mg/mL streptomycin in a 5% CO_2 atmosphere.

Cellular Uptake Study

A total of 2×10^5 cells/well MCF-7 cells were seeded in 6-well plates for 24 h. Then, the samples (free DOX, DOX@Fe-PDA/FA-PEG) were added to each well (equivalent DOX concentration of 10 μg/mL) and the cells were incubated at 37°C for an appropriate time at an additional of 24 h. Afterward, the cells were washed with PBS and stained by Hoechst 33342 (Sangon Biotech, Shanghai, China). Confocal laser scanning microscopy (CLSM) imaging was performed on LSM 410 fluorescence microscope (Zeiss, Jena, Germany). The fluorescence signal of DOX was excited at 488 nm and measured at 610 nm. The fluorescence signal stained by Hoechst 33342 was excited at 405 nm and detected at 490 nm.

In vitro Cytotoxicity by Using MTT Assay

MCF-7 cells were seeded in 96-well plates at a density of 5000 cells per well and incubated in 100 mL of medium for 24 h to allow attachment. Then, the cells were incubated with free DOX and DOX@Fe-PDA/FA-PEG (DOX concentration of 0.1093, 0.2187, 04375, 0.875, 1.75, and 3.5 μg/mL) for 24 and 48 h, respectively. A total of 20 μL MTT solution (5 mg/mL) were added to each well and incubated for 4 h. The crystals were dissolved by adding DMSO. The optical density value of each well was measured at 490 nm by an iMark plate reader (Bio-Rad, Berkeley, CA, United States). All data were obtained in quadruplicate.

Intracellular ROS Content Measurement

MCF-7 cells were seeded on 6-well plates at a density of 2×10^5 cells per well. Then the cells were incubated with free DOX and DOX@Fe-PDA/FA-PEG (equivalent DOX concentration of 10 μg/mL) for 8 h at 37°C. Afterward, diluted 2′,7′-dichlorofluorescein diacetate (DCFH-DA; Solarbio, Beijing, China), which is a cell-permeable fluorescent probe, were added. Then, the cells were placed in a 6-well plate at 37°C and incubated for another 30 min. The cells were washed for three times with serum-free medium to remove DCFH-DA completely and finally observed using fluorescence microscope.

Data Analysis Methodology

All experiments were performed at least three times unless otherwise stated. All experimental data were expressed as

mean ± SD and both were treated with SPSS 18.0 (SPSS, Chicago, IL, United States).

RESULTS AND DISCUSSION

DOX@ Fe-PDA/FA-PEG Synthesis and Characterization

The design and synthetic strategy of DOX@Fe-PDA/FA-PEG is shown in **Figure 1**. First, the Fe-PDA was synthesized using an oxidative self-polymerization method according to previously literature (Li et al., 2016). In addition, folic acid conjugated PEG was introduced to modify the PDA in enhancing the targeting effect and improving the stability of the NPs. Finally, DOX was loaded via diffusion in an aqueous media. The mean hydrodynamic sizes of DOX@PDA/FA-PEG, DOX@Fe-PDA/FA-PEG and the unloaded Fe-PDA/FA-PEG were 239.5 ± 28.82, 267.7 ± 34.16, and 283.22 ± 21.6 nm, respectively, with a narrow size distribution as demonstrated in **Figure 2A**. This particle size is theoretically suitable for cellular uptake and tumor cell permeation duo to EPR effect (Maeda, 2015). Zeta potential plays a key role in the stability and penetration through cell membranes for Nps (Bhattacharjee, 2016). Considering the presence of the carboxyl group of FA, the zeta potentials of all NPs are negative (**Supplementary Figure 1**), thereby indicating that these Nps were stable *in vivo* by electrostatic repulsion, which is the basis of drug delivery (Wu et al., 2011). The zeta potential of Fe-PDA/FA-PEG (−30 mV) is slightly lower than that of Fe-PDA/FA-PEG loaded with DOX (−27.2 mV) (**Supplementary Figure 1**), thereby suggesting that the positively charged amino groups on DOX partially neutralized the negative charge.

The morphologies of Fe-PDA/FA-PEG (wihout DOX loaded), DOX@PDA/FA-PEG (without Fe chelated), DOX@Fe-PDA/FA-PEG were observed by TEM. The results revealed that the DOX-loaded PDA/FA-PEG exhibited a spherical and uniform morphology (**Figure 2B**). The particle size observed by TEM was substantially the same as the particle size measured by DLS. Scanning electron microscopy used to perform accurate elemental analysis of Nps. Using dark field image (DFI) characterization, electron energy loss spectroscopy (EELS), energy dispersive spectroscopy (EDS), and corresponding element mapping (EDS mapping) (**Figure 3**) clearly show the morphological structure of the nanoparticles and distribution of four elements (C, N, O, Fe). The results showed that the coexistence of C, N, O, and Fe signals coexisted in the EDS spectra of Fe-PDA and Fe-PDA/FA-PEG. The uniform distribution of C, N, O, and Fe was confirmed by EDS element mapping. This result indicated the success and dispersion loads of Fe, PDA, and PEG in the DOX-loaded Fe-PDA/FA-PEG and unloaded Fe-PDA/FA-PEG. However, in the EDS element mapping of PDA, only C, N, and O signals coexisted and were distributed, thereby indicating the success and dispersion load of PDA and PEG in the DOX-loaded PDA/FA-PEG. Further, the FR-IR was performed to evaluat the surface characterization. As shown in **Supplementary Figure 2**, the, the characteristic peaks of N-H bending vibration appearing at 1512, 1589, and 3250 cm^{-1}. The peaks at 1493 and 1445 cm^{-1} can be ascribed to the existence of FA. Compared with PDA, the peaks of PEG at 1128 cm^{-1} (C-O-C stretching) were observed.

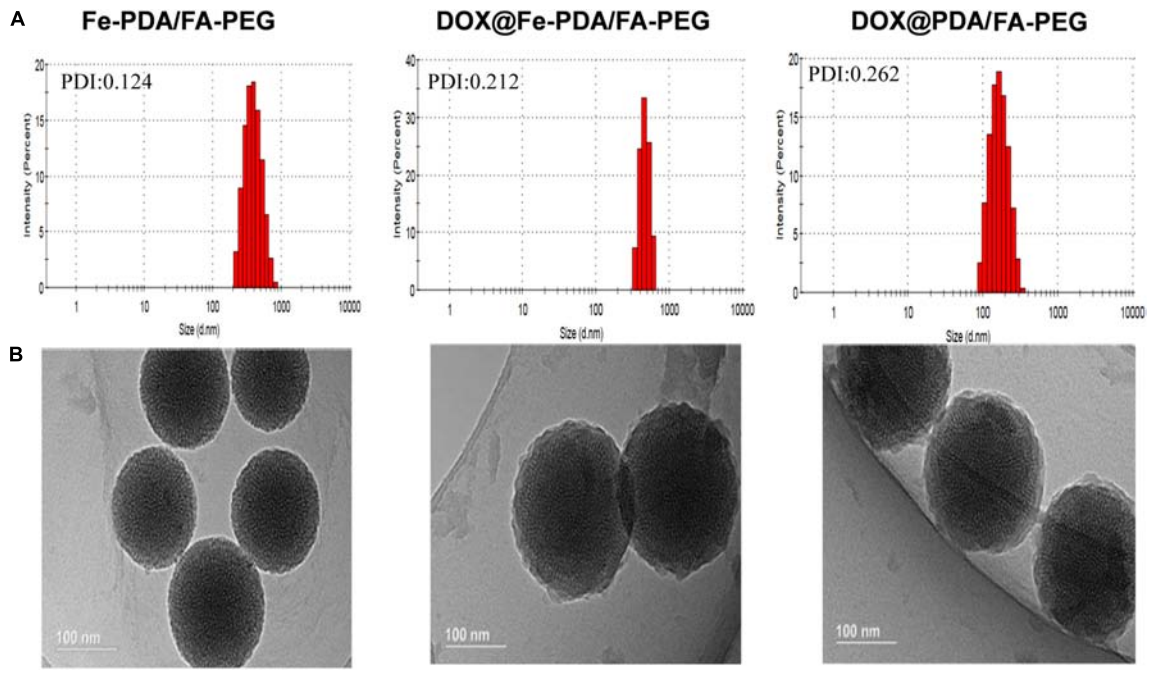

FIGURE 2 | The characterization of different nanoparticl nanoparticles. **(A)** Size distributions of Fe-PDA/FA-PEG, DOX@Fe-PDA/FA-PEG, DOX@PDA/FA-PEG. **(B)** TEM image of PDA/FA-PEG, DOX@Fe-PDA/FA-PEG, DOX@PDA/FA-PEG. Scale bar: 100 nm.

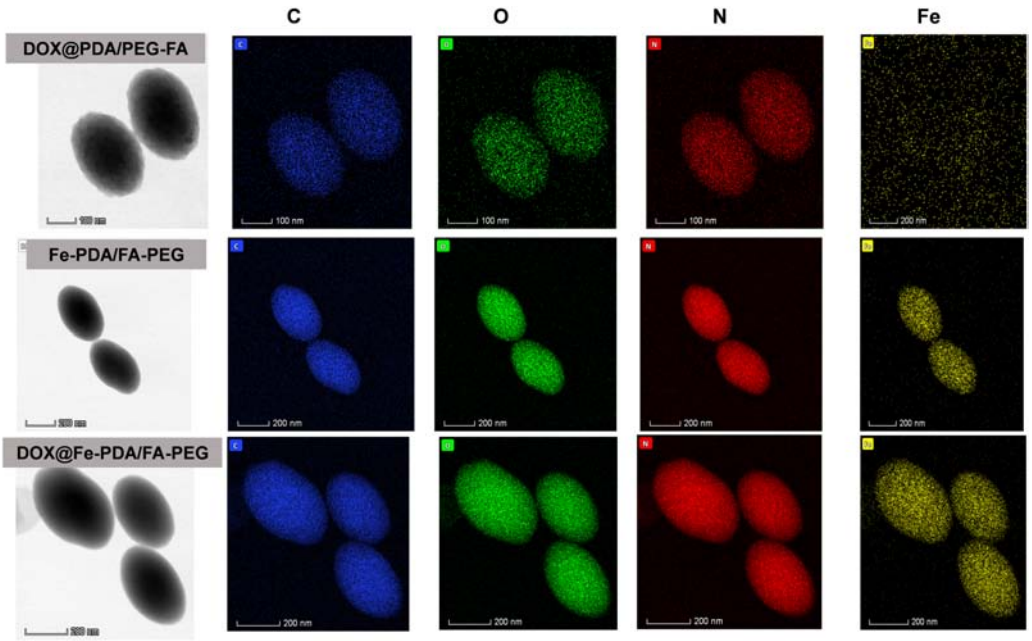

FIGURE 3 | Dark-field image, and corresponding area-elemental mappings of PDA/FA-PEG, DOX@Fe-PDA/FA-PEG, DOX@PDA/FA-PEG. Scale bar: 50 nm.

In vitro pH-Stimuli Release Study

At a drug to Fe-PDA/FA-PEG feeding ratio of 1:5 in weight, the encapsulation efficiency of DOX in the Fe-PDA/FA-PEG was 76.6 ± 5.2% determined by UV-Vis absorption spectrophotometer. As PDA NPs exist abundant aromatic rings and phenolic hydroxyl groups, the DOX was loaded through π−π stacking and hydrogen-bonding interaction. Subsequently, the pH dependent release capability of DOX@Fe-PDA/FA-PEG was investigated at 37°C under the pH levels of 7.2 and 5.5. The accumulative drug release kinetics curves are shown in **Figure 4**. The drug release of both the DOX-loaded Fe-PDA/FA-PEG was significantly pH-dependent. As shown in **Figure 4**, the release of the drug was as low as 25.5% at the of pH 7.2 within 36 h, and even 30.1% within 48 h. However, under acidic conditions, the release amount reached 34.6% within 8 h at the pH of 5.5, and the release rate at 48 h was 47.2%. This indicated that the drug-loaded Nps can cause the drug release under acidic condition, mainly due to the extremely high pH responsiveness of the PDA-modified NPs. This phenomenon allowed the rapid drug release at low pH. Considering the acidic microenvironment of the tumor and intracellular acidic endosomes and lysosomes, drugs are released only after being phagocytized by lysosomes in tumor cells, thereby effectively reducing drug waste and enhancing the antitumor effects by rapidly increasing the lysosome concentration (Duo et al., 2017).

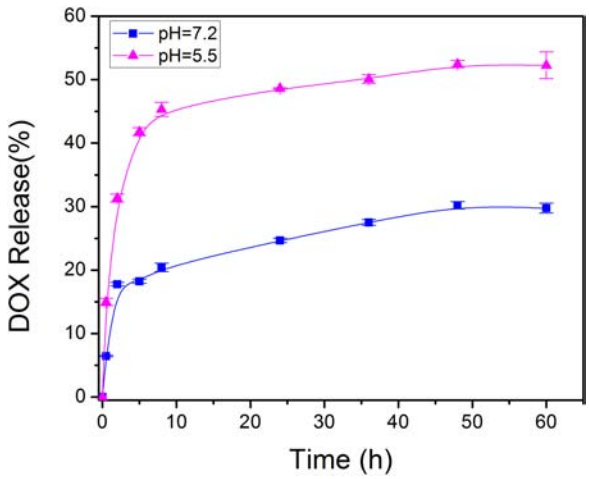

FIGURE 4 | *In vitro* drug release profile of DOX@Fe-PDA/FA-PEG in media with different pH value (pH 7.2 and 5.5).

Cellular Uptake

To study the cellular uptake and the intracellular distribution, we investigated the intracellular delivery of free DOX by using a confocal microscopy. **Figure 5A** shows the fluorescence of DOX distrubuted in the cytoplasm and cell nuclei after incubation with free DOX for 1 h. However the red flourescence with NPS observed in nucleus was not obvious. Based on the different intracellular fates of DOX, it was indicated that the NPs were internalized into cell mainly via endocytic pathway. And then we continued to incubate for another 9 h and observed under a fluorescence microscope as shown in **Figure 5B**. Apparently, the uptake intensities of DOX-loaded NPs was higher than that of free DOX, and it was contributed by the targeting effect of folate receptor. Moreover, the cell uptake intensities of DOX-loaded NPs were positive correlation with incubation time. While the fluorescence intensity of free DOX

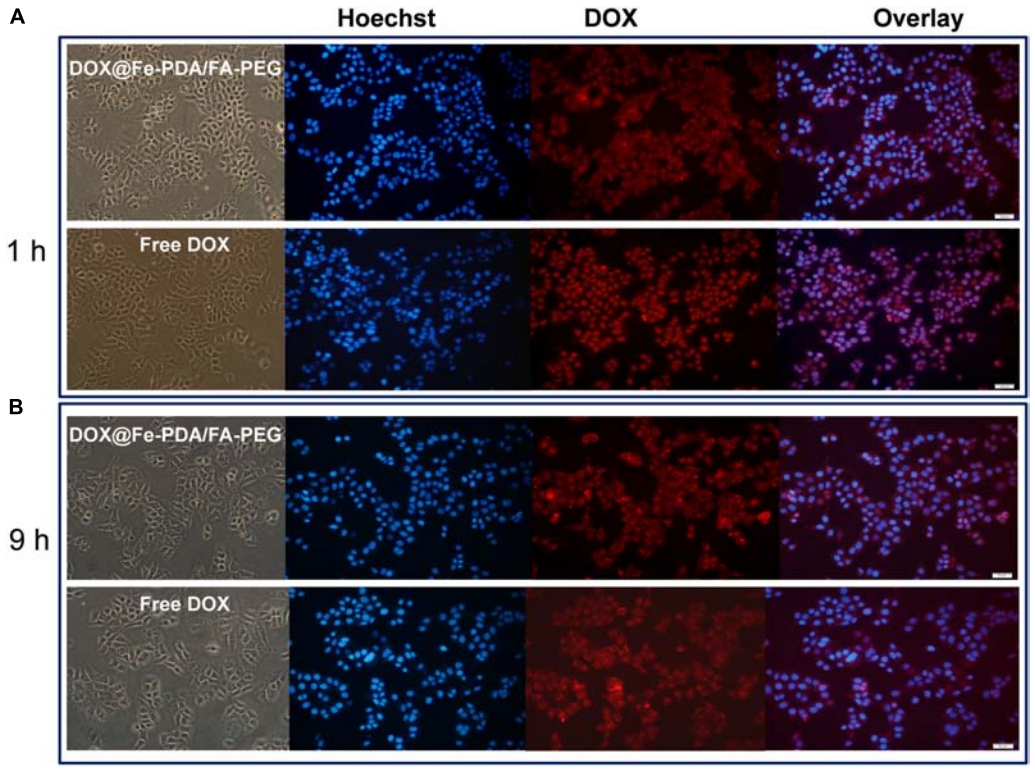

FIGURE 5 | Confocal laser scanning microscopy (CLSM) images of MCF-7 cells after incubation with free DOX, DOX-@ Fe-PDA/FA-PEG for 1 h **(A)**, and 9 h **(B)**. The cells were stained by Hoechst (blue) and drug DOX was red.

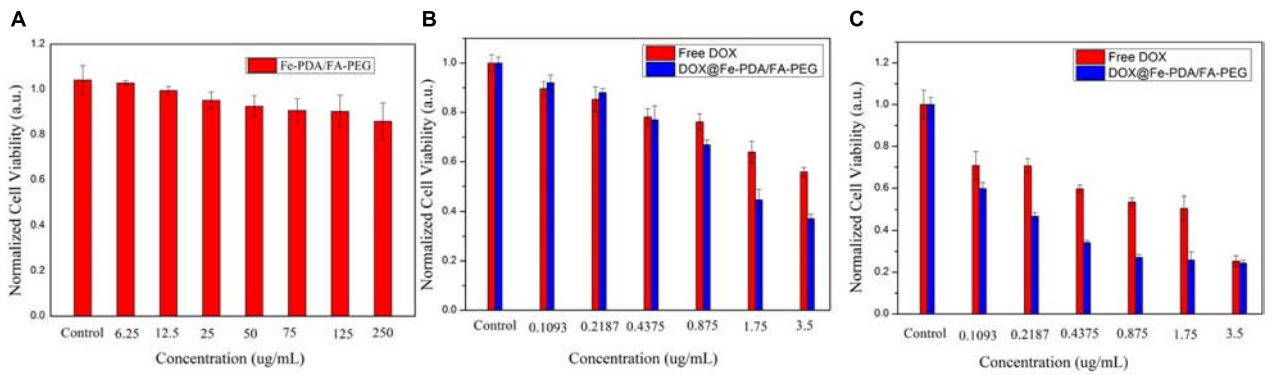

FIGURE 6 | Relative viabilities of MCF-7 cells after incubated with PDA/FA-PEG for 48 h **(A)** and free DOX and DOX@Fe-PDA/FA-PEG at different concentrations 24 h **(B)** and 48 h **(C)**.

in the cells is weaker than that of the doxorubicin-loaded NPs, indicating that the intracellular free DOX decays with time. According to the *in vitro* drug release profiles, this phenomenon proves that the DOX-loaded Nps have a sustained release effect, which may help to enhance the cytotoxicity of DOX.

Cytotoxicity of DOX-Loaded NPs

To assess the cytotoxicity of DOX@Fe-PDA/FA-PEG, we performed the MTT assays. In order to confirm the high biocompatibility and safety of the NPs, we incubated the Fe-PDA/FA-PEG NPs with MCF-7 cells. As shown in **Figure 6A**, the Fe-PDA/FA-PEG NPs without drug-loading exhibited a negligible cytotoxicity the concentration ranging from 0 to 250 μg/mL for 48 h. This result suggested that the prepared material possessed high biocompatibility and low cell cytotoxicity. Then, we compared the results of cytotoxicity of free DOX and DOX-loaded Nps at 24 and 48 h. **Figures 6B,C** shows the cytotoxicity of DOX on MCF-7 was time and dose-dependent. As the DOX concentration and incubation time prolonged, the

greater the toxicity of the drug to MCF-7 cell. Apparently, the cytotoxicity of DOX-loaded Fe-PDA/FA-PEG NPs was greater than that free DOX, thereby demonstrating that Fe enhanced the killing effect of DOX on the MCF-7 cells. And it was found that the 48 h of incubation exhibited a considerable killing effect on MCF-7 cells than 24 h. This result further confirmed the sustained release of NPs.

ROS Detection

Reactive oxygen species -induced cell death has been a widely uesed strategy for tumor therapy (Matés and Sánchez-Jiménez, 2000; Dixon and Stockwell, 2013; Schumacker Paul, 2015; Zhou et al., 2016). As we know, DOX could activate nicotinamide adenine dinucleotide phosphate oxidases, and further produce ROS, which contribute to anticancer drug-induced toxicity (Chakravarti et al., 2016; Seo et al., 2017). Recently, synergistic approaches by using ROS-producing agents with DOX have attracted considerable attention (Xia et al., 2017). Intriguingly, the presence of Fe (II and III) contributes to the enhanced chemotherapy efficacy by converting the accumulated H_2O_2 to the hydroxyl radical via Fenton reactions (Dixon and Stockwell, 2013). To explore the underlying mechanism of enhanced antiproliferating effects of DOX@Fe-PDA/FA-PEG further, we quantified the intracellular ROS by using 2′-7′-dichlorofuorescin diacetate. Compared with the control group, green fluorescence was observed after incubation with DOX and DOX@Fe-PDA/FA-PEG (**Figure 7**). In addition, cells treated with DOX-loaded Fe-PDA/FA-PEG had the highest fluorescence intensity, thereby indicating the highest ROS production. The results showed that the cells treated with DOX loaded Fe-PDA/FA-PEG can synergistically produce ROS to kill tumor cells. DOX used to undergo redox cycles to generate high H_2O_2 levels inside the cancer cells. After endocytosis by tumor cells, the DOX@Fe-PDA/FA-PEG was decomposed by the acidic microenvironment. The elevated H_2O_2 of DOX can be further catalyzed by Fe ions via Fenton reaction to generate abundant highly toxic resulting in enhancing anticancer effects of DOX through oxidative damage to DNA, protein, and lipid (Matés and Sánchez-Jiménez, 2000; Schumacker Paul, 2015; Zhou et al., 2016). Previous investigations have developed iron-based nanomaterials, including iron nanometallic glasses and iron oxide, have been employed to upregulation of ROS by using the situ Fenton reaction (Zhang et al., 2016; Liu et al., 2018; Tang et al., 2018). However, current iron-based nanomaterials is far from satisfactory. Some of the nanomaterials such as Fe^0 nanoparticles (Zhang et al., 2016) and iron oxide nanoplatform (Liu et al., 2018), are difficult to fabricate and the synthetic conditions generally are harsh and complicated. In this work, we synthesized the iron-chelated PDA NPs via a one-pot reaction and the FA-PEG as the surface ligand for tumor homing with a low cost and biocompable biocompatibility. And the pH-stimuli release profiles included being highly selective and logical, and amenable to activation by endogenous stimuli. This strategy present an approach for synergistic combination of ROS and chemotherapy to enhance the anticancer efficacy.

CONCLUSION

In this study, we successfully fabricated a novel nanocarrier on the basis of Fe-chelated PDA nanoparticles used for Fe and DOX combined cancer theranostics through ROS over-generation. The obtained DOX@Fe-PDA/FA-PEG Nps had a hydrodynamic size of about 250 nm, and the structure was characterized by DLS, TEM, EDS, and FT-IR. The *in vitro* drug release profile triggered by low intracellular pH indicated that the system demonstrated controlled therapeutic activity. Further, *in vitro* cell uptake studies indicate that DOX-loaded Fe-PDA /FA-PEG can be internalized by MCF-7 cells and exhibited high targeting efficiency due to specific recognition. The *in vitro* experiments demonstrated that DOX@Fe-PDA/FA-PEG trigged the intracellular ROS overproduction, thereby enhancing the therapeutic effect on breast cancer. Taken together, this study provides a strategy to harness Fe-PAD nanocarrier for Fe and DOX combined cancer theranostics.

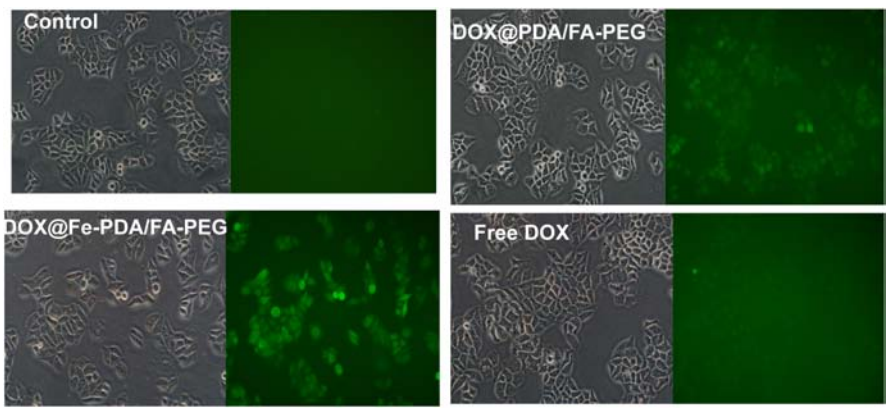

FIGURE 7 | The intracellular ROS stained with DCFH-DA in MCF-7 cells after incubation with free DOX, DOX@Fe-PDA/FA-PEG, DOX@PDA/FA-PEG for 8 h were measured by fluorescence microscopic.

AUTHOR CONTRIBUTIONS

X-JL and W-TL performed the experiments and drafted the manuscript. Z-H-RL and L-PZ prepared and characterized the NPs. C-CG and performed the statistical design of the experiments. W-FZ and D-JD conceived the initial idea. All authors helped to correct and polish the manuscript and read and approved the final manuscript.

FUNDING

The authors are grateful for the generous financial support of the Project of Shandong Province Higher Educational Science and Technology Program (Grant No. J18KA279), National Natural Science Foundation of China (Grant No. 81774125), Project of Collaborative Innovation Center for Target Drug Delivery System of Weifang Medical University (2017), and College Students' Technology Innovation Project of Weifang Medical University (Grant No. KX2017045).

ACKNOWLEDGMENTS

We appreciate the experimental assistance of bachelor students Ling-Yan Liao, Ruo-Bing Liu, Yajing Ji, and Yanan Li.

SUPPLEMENTARY MATERIAL

The Supplementary Material for this article can be found online at: https://www.frontiersin.org/articles/10.3389/fphar.2019.00075/full#supplementary-material

REFERENCES

Bhattacharjee, S. (2016). DLS and zeta potential – what they are and what they are not? *J. Controll. Release* 235, 337–351. doi: 10.1016/j.jconrel.2016.06.017

Bray, F., Ferlay, J., Soerjomataram, I., Siegel, R. L., Torre, L. A., and Jemal, A. (2018). Global cancer statistics 2018: GLOBOCAN estimates of incidence and mortality worldwide for 36 cancers in 185 countries. *CA Cancer J. Clin.* 68, 394–424. doi: 10.3322/caac.21492

Camacho, K. M., Menegatti, S., Vogus, D. R., Pusuluri, A., Fuchs, Z., Jarvis, M., et al. (2016). DAFODIL: a novel liposome-encapsulated synergistic combination of doxorubicin and 5FU for low dose chemotherapy. *J. Controll. Release* 229, 154–162. doi: 10.1016/j.jconrel.2016.03.027

Chakravarti, B., Yang, J., Luo, Z., and Ahlers, K. E. (2016). Contribution of NADPH oxidase (Nox)-derived reactive oxygen species (ROS) to doxorubicin-induced cardiomyopathy mediated by regulator of g protein signaling 6 (RGS6). *FASEB J.* 30:939.3. doi: 10.1096/fasebj.30.1_supplement.939.3

Dai, Y., Yang, Z., Cheng, S., Wang, Z., Zhang, R., Zhu, G., et al. (2018). Toxic reactive oxygen species enhanced synergistic combination therapy by self-assembled metal-phenolic network nanoparticles. *Adv. Mat.* 30:1704877. doi: 10.1002/adma.201704877

Dayton, A., Selvendiran, K., Meduru, S., Khan, M., Kuppusamy, M. L., Naidu, S., et al. (2011). Amelioration of doxorubicin-induced cardiotoxicity by an anticancer-antioxidant dual-function compound, HO-3867. *J. Pharmacol. Exp. Ther.* 339:350. doi: 10.1124/jpet.111.183681

Dixon, S. J., and Stockwell, B. R. (2013). The role of iron and reactive oxygen species in cell death. *Nat. Chem. Biol.* 10:9. doi: 10.1038/nchembio.1416

Duo, Y., Li, Y., Chen, C., Liu, B., Wang, X., Zeng, X., et al. (2017). DOX-loaded pH-sensitive mesoporous silica nanoparticles coated with PDA and PEG induce pro-death autophagy in breast cancer. *RSC Adv.* 7, 39641–39650. doi: 10.1039/C7RA05135B

Fan, C., Zheng, W., Fu, X., Li, X., Wong, Y.-S., and Chen, T. (2014). Strategy to enhance the therapeutic effect of doxorubicin in human hepatocellular carcinoma by selenocystine, a synergistic agent that regulates the ROS-mediated signaling. *Oncotarget* 5, 2853–2863. doi: 10.18632/oncotarget.1854

Fisher, B., Bryant, J., Wolmark, N., Mamounas, E., Brown, A., Fisher, E. R., et al. (1998). Effect of preoperative chemotherapy on the outcome of women with operable breast cancer. *J. Clin. Oncol.* 16, 2672–2685. doi: 10.1200/jco.1998.16.8.2672

Fong, M. Y., Jin, S., Rane, M., Singh, R. K., Gupta, R., and Kakar, S. S. (2012). Withaferin a synergizes the therapeutic effect of doxorubicin through ROS-mediated autophagy in ovarian cancer. *PLoS One* 7:e42265. doi: 10.1371/journal.pone.0042265

Ge, R., Lin, M., Li, X., Liu, S., Wang, W., Li, S., et al. (2017). Cu2+-loaded polydopamine nanoparticles for magnetic resonance imaging-guided pH- and near-infrared-light-stimulated thermochemotherapy. *ACS Appl. Mat. Interfaces* 9, 19706–19716. doi: 10.1021/acsami.7b05583

Indermun, S., Govender, M., Kumar, P., Choonara, Y. E., and Pillay, V. (2018). "2 - Stimuli-responsive polymers as smart drug delivery systems: classifications based on carrier type and triggered-release mechanism," in *Stimuli Responsive Polymeric Nanocarriers for Drug Delivery Applications*, Vol. 1, eds A. S. H. Makhlouf and N. Y. Abu-Thabit (Sawston: Woodhead Publishing), 43–58. doi: 10.1016/B978-0-08-101997-9.00002-3

Kemp, J. A., Shim, M. S., Heo, C. Y., and Kwon, Y. J. (2016). "Combo" nanomedicine: co-delivery of multi-modal therapeutics for efficient, targeted, and safe cancer therapy. *Adv. Drug Deliv. Rev.* 98, 3–18. doi: 10.1016/j.addr.2015.10.019

Li, Y., Xie, Y., Wang, Z., Zang, N., Carniato, F., Huang, Y., et al. (2016). Structure and function of iron-loaded synthetic melanin. *ACS Nano* 10, 10186–10194. doi: 10.1021/acsnano.6b05502

Liu, Y., Ai, K., and Lu, L. (2014). Polydopamine and its derivative materials: synthesis and promising applications in energy, environmental, and biomedical fields. *Chem. Rev.* 114, 5057–5115. doi: 10.1021/cr400407a

Liu, Y., Ji, X., Tong, W. W. L., Askhatova, D., Yang, T., Cheng, H., et al. (2018). Engineering multifunctional RNAi nanomedicine to concurrently target cancer hallmarks for combinatorial therapy. *Angew. Chem. Int. Ed.* 57, 1510–1513. doi: 10.1002/anie.201710144

Lynge, M. E., Schattling, P., and Städler, B. (2015). Recent developments in poly(dopamine)-based coatings for biomedical applications. *Nanomedicine* 10, 2725–2742. doi: 10.2217/nnm.15.89

Maeda, H. (2015). Toward a full understanding of the EPR effect in primary and metastatic tumors as well as issues related to its heterogeneity. *Adv. Drug Deliv. Rev.* 91, 3–6. doi: 10.1016/j.addr.2015.01.002

Matés, J. M., and Sánchez-Jiménez, F. M. (2000). Role of reactive oxygen species in apoptosis: implications for cancer therapy. *Int. J. Biochem. Cell Biol.* 32, 157–170. doi: 10.1016/S1357-2725(99)00088-6

Miao, Z.-H., Wang, H., Yang, H., Li, Z.-L., Zhen, L., and Xu, C.-Y. (2015). Intrinsically Mn2+-chelated polydopamine nanoparticles for simultaneous magnetic resonance imaging and photothermal ablation of cancer cells. *ACS Appl. Mat. Interfaces* 7, 16946–16952. doi: 10.1021/acsami.5b06265

Miller, K. D., Siegel, R. L., Lin, C. C., Mariotto, A. B., Kramer, J. L., Rowland, J. H., et al. (2016). Cancer treatment and survivorship statistics, 2016. *CA Cancer J. Clin.* 66, 271–289. doi: 10.3322/caac.21349

Russell, E. G., and Cotter, T. G. (2015). "Chapter six - new insight into the role of reactive oxygen species (ROS) in cellular signal-transduction processes," in *International Review of Cell and Molecular Biology*, Vol. 319, ed. K. W. Jeon (Cambridge, MA: Academic Press), 221–254.

Ryu, J. H., Messersmith, P. B., and Lee, H. (2018). Polydopamine surface chemistry: a decade of discovery. *ACS Appl. Mat. Interfaces* 10, 7523–7540. doi: 10.1021/acsami.7b19865

Schumacker Paul, T. (2015). Reactive oxygen species in cancer: a dance with the devil. *Cancer Cell* 27, 156–157. doi: 10.1016/j.ccell.2015.01.007

Seo, S. U., Kim, T. H., Kim, D. E., Min, K.-J., and Kwon, T. K. (2017). NOX4-mediated ROS production induces apoptotic cell death via down-regulation of c-FLIP and Mcl-1 expression in combined treatment with thioridazine and curcumin. *Redox Biol.* 13, 608–622. doi: 10.1016/j.redox.2017.07.017

Shen, Z., Song, J., Yung, B. C., Zhou, Z., Wu, A., and Chen, X. (2018). Cancer therapy: emerging strategies of cancer therapy based on ferroptosis. *Adv. Mat.* 30:1870084. doi: 10.1002/adma.201870084

Spiegel, D. Y., and Koontz, B. F. (2018). Meeting the needs of long-term survivors: a testament to success in the care of patients with cancer. *Cancer* 124, 2488–2490. doi: 10.1002/cncr.31381

Tang, Z., Liu, Y., He, M., and Bu, W. (2018). Chemodynamic therapy: tumour microenvironment-mediated fenton and fenton-like reactions. *Angew. Chem. Int. Ed.* 58, 946–956. doi: 10.1002/anie.201805664

Wood, R., Mitra, D., de Courcy, J., and Iyer, S. (2017). Patient-reported quality of life and treatment satisfaction in patients With HR+/HER2-advanced/metastatic breast cancer. *Clin. Ther.* 39, 1719–1728. doi: 10.1016/j.clinthera.2017.07.009

Wu, H., Liu, S., Gong, J., Liu, J., Zhang, Q., Leng, X., et al. (2017). VCPA, a novel synthetic derivative of α-tocopheryl succinate, sensitizes human gastric cancer to doxorubicin-induced apoptosis via ROS-dependent mitochondrial dysfunction. *Cancer Lett.* 393, 22–32. doi: 10.1016/j.canlet.2017.02.007

Wu, L., Zhang, J., and Watanabe, W. (2011). Physical and chemical stability of drug nanoparticles. *Adv. Drug Deliv. Rev.* 63, 456–469. doi: 10.1016/j.addr.2011.02.001

Xi, J., Da, L., Yang, C., Chen, R., Gao, L., Fan, L., et al. (2017). Mn2+-coordinated PDA@DOX/PLGA nanoparticles as a smart theranostic agent for synergistic chemo-photothermal tumor therapy. *Int. J. Nanomed.* 2017, 3331–3345. doi: 10.2147/IJN.S132270

Xia, J., Inagaki, Y., Gao, J., Qi, F., Song, P., Han, G., et al. (2017). Combination of cinobufacini and doxorubicin increases apoptosis of hepatocellular carcinoma cells through the Fas- and mitochondria-mediated pathways. *Am. J. Chin. Med.* 45, 1537–1556. doi: 10.1142/s0192415x17500835

Xu, X., Ho, W., Zhang, X., Bertrand, N., and Farokhzad, O. (2015). Cancer nanomedicine: from targeted delivery to combination therapy. *Trends Mol. Med.* 21, 223–232. doi: 10.1016/j.molmed.2015.01.001

Zhang, C., Bu, W., Ni, D., Zhang, S., Li, Q., Yao, Z., et al. (2016). Synthesis of iron nanometallic glasses and their application in cancer therapy by a localized fenton reaction. *Angew. Chem. Int. Ed.* 55, 2101–2106. doi: 10.1002/anie.201510031

Zhang, W., Gai, C., Ding, D., Wang, F., and Li, W. (2018). Targeted p53 on small-molecules-induced ferroptosis in cancers. *Front. Oncol.* 8:507. doi: 10.3389/fonc.2018.00507

Zheng, D.-W., Lei, Q., Zhu, J.-Y., Fan, J.-X., Li, C.-X., Li, C., et al. (2017). Switching apoptosis to ferroptosis: metal–organic network for high-efficiency anticancer therapy. *Nano Lett.* 17, 284–291. doi: 10.1021/acs.nanolett.6b04060

Zhou, Z., Song, J., Nie, L., and Chen, X. (2016). Reactive oxygen species generating systems meeting challenges of photodynamic cancer therapy. *Chem. Soc. Rev.* 45, 6597–6626. doi: 10.1039/C6CS00271D

Conflict of Interest Statement: The authors declare that the research was conducted in the absence of any commercial or financial relationships that could be construed as a potential conflict of interest.

frontiers in Oncology

CASE REPORT
published: 07 February 2019
doi: 10.3389/fonc.2019.00055

Bevacizumab Combined With Oxaliplatin/Capecitabine in Patient With Refractory and Recurrent Mucinous Adenocarcinoma of the Appendix: A Case Report

Wenzhi Liu[1†], Lili Liu[2†], Ruoyu Wang[1†], Guanyu Gong[1,3], Xinjia Ding[4], Bin Yang[3,5], Yun Bao[1], Zhiqiang Wang[1], Bo Zhang[4], Dewei Zhao[1], Fei Wu[1] and Yan Ding[1,5*]*

[1] The Institute for Translational Medicine, The Affiliated Zhongshan Hospital of Dalian University, Dalian, China, [2] Department of Oncology, The Second Affiliated Hospital of Dalian Medical University, Dalian, China, [3] Genomic Future Inc., Lexington, MA, United States, [4] Department of Neurosurgery, The Second Affiliated Hospital of Dalian Medical University, Dalian, China, [5] Department of Pediatrics, Children's Hospital of Boston, Harvard Medical School, Boston, MA, United States

OPEN ACCESS

Edited by:
Yunkai Zhang,
Vanderbilt University Medical Center,
United States

Reviewed by:
Antonio Rozzi,
INI, Istituto Neurotraumatologico Italiano, Italy
Daekyu Sun,
University of Arizona, United States

***Correspondence:**
Fei Wu
wufei0348@126.com
Yan Ding
yan.ding@childrens.harvard.edu

[†] These authors have contributed equally to this work

Specialty section:
This article was submitted to Cancer Molecular Targets and Therapeutics, a section of the journal Frontiers in Oncology

Received: 30 November 2018
Accepted: 21 January 2019
Published: 07 February 2019

Citation:
Liu W, Liu L, Wang R, Gong G, Ding X, Yang B, Bao Y, Wang Z, Zhang B, Zhao D, Wu F and Ding Y (2019) Bevacizumab Combined With Oxaliplatin/Capecitabine in Patient With Refractory and Recurrent Mucinous Adenocarcinoma of the Appendix: A Case Report. Front. Oncol. 9:55. doi: 10.3389/fonc.2019.00055

Primary appendiceal adenocarcinoma with peritoneal pseudomyxoma (PPM) has a high recurrence rate and refractory to medical interventions such as repetitive debulking surgery and systemic chemotherapy. Genome-based targeted therapy for such cases has not been well-documented. Here we present a 63-years-old women, who was diagnosed with recurrent mucinous adenocarcinoma of the appendix with local invasions and peritoneal carcinomatosis, was refractory to systemic chemotherapy after surgery. We used a regime developed using whole exome sequencing. Somatic mutations in the genes encoding VEGFR2, FGFR1, FGFR2, FGFR3, and KRAS were identified in the patient's tumor tissue. The patient was then treated with bevacizumab plus oxaliplatin. After 4 months of treatment, pelvic CT showed dramatic reduction of pseudomyoma and a decline of CA199 level from 5436.7 to 1121.4 U/ml. Continual treatment with bevacizumab-capecitabine remained effective and the patient's CA199 level further decreased to 401.26 U/ml according to the follow-up examination on Aug 15th, 2018. Results from this study show the evidence of gene mutations involving VEGF signal activation in the recurrence of appendiceal adenocarcinoma. Our results also suggest the association of these mutations with the effectiveness of anti-VEGF treatment using bevacizumab. Therefore, the screening of gene mutations involved in VEGF signaling and targeted therapy with anti-VEGF drugs may provide a new option to manage refractory/recurrent advanced-stage appendiceal adenocarcinoma.

Keywords: appendiceal adenocarcinoma, peritoneal carcinomatosis, next generation sequencing, bevacizumab, targeted therapy

BACKGROUND

Primary adenocarcinoma of the appendix is a rare malignancy and accounts for 0.4% of gastrointestinal tumors, according to a report of national cancer institute (NCI) (1). Mucinous adenocarcinoma is the most common histological subtype (37%), followed by colonic and carcinoid subtypes (2). The clinical presentations of appendiceal cancer are vague until advanced stage. As a

result, early diagnosis of appendiceal cancer is often difficult. Common complications of late stage disease include rupture and acute appendicitis (accounting for ∼1% appendectomy cases) (3), local invasion and peritoneal carcinomatosis (PC)/peritoneal pseudomyxoma (PPM) (4, 5). The advanced stage has a poor overall survival rate with median survival time of 5.2–12.6 months (5). Currently there is no standard medical care for the disseminated late-stage appendiceal cancer with PC/PPM. It has been generally recommended to perform cytoreductive surgery (CRS) combined with perioperative hyperthermic intraperitoneal chemotherapy (HIPEC) or postoperative intraperitoneal chemotherapy (EPIC) with mitomycin C, cisplatin, 5-FU, or a combination (5, 6). Unfortunately, most appendiceal cancer patients with PC/PPM experience recurrent and refractory to treatment, and fail to repetitive surgery and systemic chemotherapy (6).

Targeted therapy has been successfully used to treat many types of cancers including colorectal cancer. However, to the best of our knowledge, genome-based targeted therapy for the appendiceal cancer has never been reported. In the present case, a patient was diagnosed with mucinous adenocarcinoma of the appendix with peritoneal carcinomatosis and multiple local invasions. The patient received routine treatments by CRS-HEPIC-EPIC but relapsed after 1 year. Then the patient's condition deteriorated continuously and experienced recurrent and refractory to the treatment. Using whole exome sequencing and targeted medicine, optimal therapeutical efficacy was achieved with a gradual remission and remains progression-free until now.

CASE PRESENTATION

A 63-years-old Chinese female presented with asymptomatic palpable abdominal mass, increased carbohydrate antigen 19-9 (CA-199) level and pelvic mass on CT scan. An opening surgery observed an appendiceal mass involving the entire layer of the appendix, rupture, invasion of bilateral ovaries, wide-spreading nodular implantations with pseudomyxoma in peritoneal cavity, greater omentum, small intestine mesentery and hepatic and splenic regions. Debulking surgery with peritoneal nodule ablation and mucus reduction was performed in Beijing 301 Hospital. Postoperative pathology confirmed mucinous adenocarcinoma of the appendix T4NxM1, stage IV with peritoneal carcinomatosis (**Figure 1**). After surgery, the patient received one time standard perioperative hyperthermic intraperitoneal chemotherapy (HIPEC) with mitomycin C. Because of the excessive peritoneal carcinomatosis, the patient was given three cycles of postoperative intraperitoneal chemotherapy (EPIC) with 5-FU plus mitomycin C. The patient remained symptom free for 1 year until she developed progressive abdominal distension, loss of appetite and worsening nourishment. The patient failed to response to further systemic chemotherapy, and a large number of PPM (**Figures 2A,B**). Then a second surgery was performed, intestinal obstruction by mucous cavities was observed, and a colostomy was given. Shortly after operation, cetuximab, a monoclonal antibody binding to and inhibiting EGFR, was given to the patient for 20 days (yet without gene testing) at a local hospital, but failed to show any improvement. By then the patient had tried all available approved options and became refractory to the treatments.

TABLE 1 | Mutated genes identified in the present case of mucinous adenocarcinoma.

AKT1	ATM	CSFIR	ERBB2	FGFR1	FGFR2	FGFR3	FLT3
GNA11	JAK3	KDR	KIT	KRAS	NOTCH1	PIK3CA	PET
SMARCB1	SMO	STK11	TP53				

At the time when the patient visited us, she was severely wasted, with progressive abdominal distension and elevated CA-199 level at 5436.7 U/ml. Considering her weak constitution and failure of previous interventions, alternative treatment strategies, especially a rationally designed targeted therapy, emerged to be the last-ditch option to the patient. Targeted therapy is usually based on a patient's genomic profile by genetic testing. In order to find the accurate target, we decided to use the paraffin-embedded surgical tumor tissue from the patient, and detect gene mutations using the TruSeq Rapid Capture Exome Kit for whole exome sequencing (WES) on the Illumina NextSeq500 sequencing platform. The WES data was then analyzed using OncoDecoder™ (Genomic Future, Inc. USA). Several key gene mutations were identified including a missense mutation p.Gln472His (exon 11) in KDR/VEGFR-2, a missense mutation p.Arg281Gln (exon 8) in FGFR1, a missense mutation p.Lys296Arg (exon 7) in FGFR2, a missense mutation p.Thr654Ser (exon 14) in FGFR3 and a missense mutation p.Gly12Asp (exon 2) in KRAS. Additional 38 gene mutations including TP53, ERBB2, KIT, GNA11, and JAK3 were also detected (**Table 1**).

Although no NCCN-guided targeted therapy regime for appendiceal mucinous adenocarcinoma is documented as of to-date, there are two approved drugs for colorectal cancer may be considered as potential candidates: bevacizumab and cetuximab. Bevacizumab is a monoclonal antibody blocking the VEGF ligand, and bevacizumab in combination with standard chemotherapy has been approved by FDA as first line treatment for metastatic colorectal cancer (7, 8). We predicted that bevacizumab may be a suitable targeted drug candidate for our case based on the following three reasons: Firstly, the gene testing results showed several mutations involving KDR/VEGFR-2, FGFR1, FGFR2, and FGFR3. Although these mutations are currently classified as variation of uncertain significance (VUS), hyperactive VEGF pathway is a common event in colorectal cancer and contributes to tumor metastatic activity (9). A recent study from the MD Anderson cancer center showed improved average overall survival and progression-free survival by providing anti-VEGF treatment to patients diagnosed with unresectable appendiceal epithelial neoplasm (yet no gene

Abbreviations: CT, computed tomography; PC, peritoneal carcinomatosis; PPM, peritoneal pseudomyxoma; CRS, cytoreductive surgery; HIPEC, hyperthermic intraperitoneal chemotherapy; EPIC, intraperitoneal chemotherapy; VEGFR, Vascular endothelial growth factor receptor; FGFR, Fibroblast growth factor receptor.

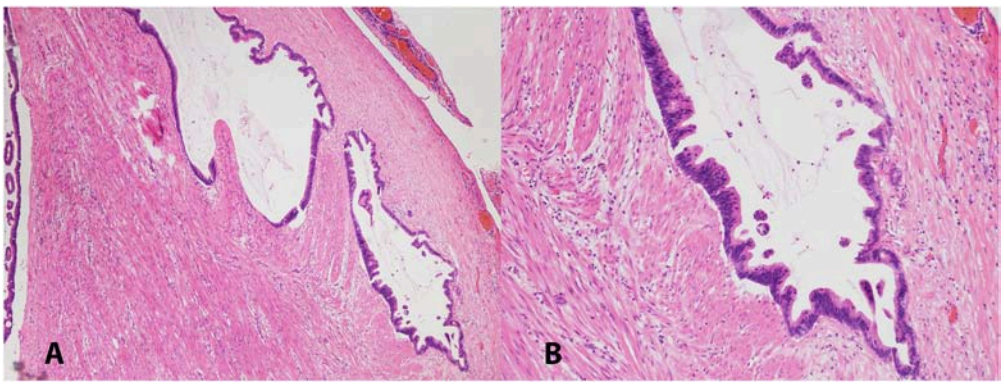

FIGURE 1 | Low (**A**, 40X) and high (**B**, 100X) magnification pictures of appendiceal mucinous adenocarcinoma. H&E stained.

testing was performed) (10). This finding suggests that VEGF hyperactivity could be a common event in appendiceal cancer, and bevacizumab could be a promising targeted drug. Next, it has been known that the efficacy of certain EGFR monoclonal antibody drugs, including cetuximab and panitumumab, could be affected by KRAS mutation (6). Indeed, in the present case, we identified KRAS p.Gly12Asp missense mutation, which could cause inefficient response to cetuximab (11). However, the efficacy of bevacizumab for colorectal cancer treatment has been testified to be independent from KRAS mutation (8). Thirdly, there was no contraindication of bevacizumab usage to the patient. The common risk factors include low WBC count, high blood pressure, impaired heart function and poor renal function.

Under our advice, the patient received treatment of bevacizumab (7.5 mg/Kg, in total 450 mg, IV-GTT) plus oxaliplatin (130 mg/m^2, in total 200 mg IV-GTT) on day 1 every 3 weeks for 6 cycles since August, 2016. Follow-up examination after treatment showed significant improvement of the patient's condition, and CT scan imaging results showed dramatic reduction of her peritoneal mucus (as shown in **Figures 2C,D**). In addition, the patient's CA-199 level decreased from 5,436.7 U/ml (before treatment) to 1121.4 U/ml (after treatment). Afterwards, the patient received continuous maintenance treatment using bevacizumab (7.5 mg/Kg, in total 450 mg, IV-GTT on day 1 each 3 weeks) plus capecitabine (1,500 mg, oral, twice a day) for days 1 to 14 until now. The patient has been followed up routinely to evaluate the treatment efficacy and to monitor the adverse effects. The main adverse effects were numbness in the hands and feet, dry nose and epistaxis, dry throat, fatigue, loss of appetite. The patient has been progression-free as of recent follow-up on September 26th, 2018 with the most recent CA-199 being 401.26 U/ml on August 15th, 2018.

DISCUSSION

Primary adenocarcinoma of the appendix is a rare neoplasm with an incidence of 1.2 cases per 100,000 people each year (12). The prognosis of appendiceal adenocarcinoma varies depending on the histology types, including colonic-type adenocarcinoma, typical carcinoid, mucinous adenocarcinoma, and singlet ring cell adenocarcinoma (3). The mucinous adenocarcinoma is similar to the ovarian adenocarcinoma, and peritoneal dissemination is a frequent metastatic route (12). Like most colorectal cancers, the appendiceal adenocarcinoma presents with non-specific symptoms and is difficult to be diagnosed preoperatively (4, 5). As a result, it is often found at an advanced stage in which the disease has already spread within abdomen (5). Appendiceal adenocarcinoma-derived peritoneal carcinomatosis (PC) or peritoneal pseudomyxoma (PPM) is a very poor prognostic factor with average life expectancy between half and 1 year (5). In the present case, the patient presented with asymptomatic abdominal mass, local invasions to greater omentum and fallopian tubes and peritoneal carcinomatosis with multiple pseudomyxoma cavities at the initial visit.

The management of mucinous appendiceal adenocarcinoma varies depending on the stages and does not have standard guideline. Right hemicolectomy remains the treatment of choice for the early stage local or regional appendiceal adenocarcinoma (5, 6). CRS-HIPEC or EPIC is usually recommended for the appendiceal or colonic-type carcinoma with confined peritoneal metastasis (5). However, there is no standardized protocol for HIPEC or EPIC (5), and it only achieved complete response in some patients (5, 6). In our case, the patient received CRS-HIPEC-EPIC regime but relapse of peritoneal carcinomatosis occurred 1 year later. Systemic 5-fluorouracil-based chemotherapy was barely beneficial.

Recently, genome-based precision medicine has made great progress to treat a variety of cancers, including colorectal cancer (13). Targeted drugs feature high efficiency and low toxicity. To the best of our knowledge, genome-based targeted therapy for metastatic appendiceal adenocarcinoma has not yet been reported. In order to seek for appropriate targeted therapy for the patient with recurrent and refractory appendiceal cancer, we performed whole exome sequencing with the patient surgical pathology tissue at our genetic testing lab. Several

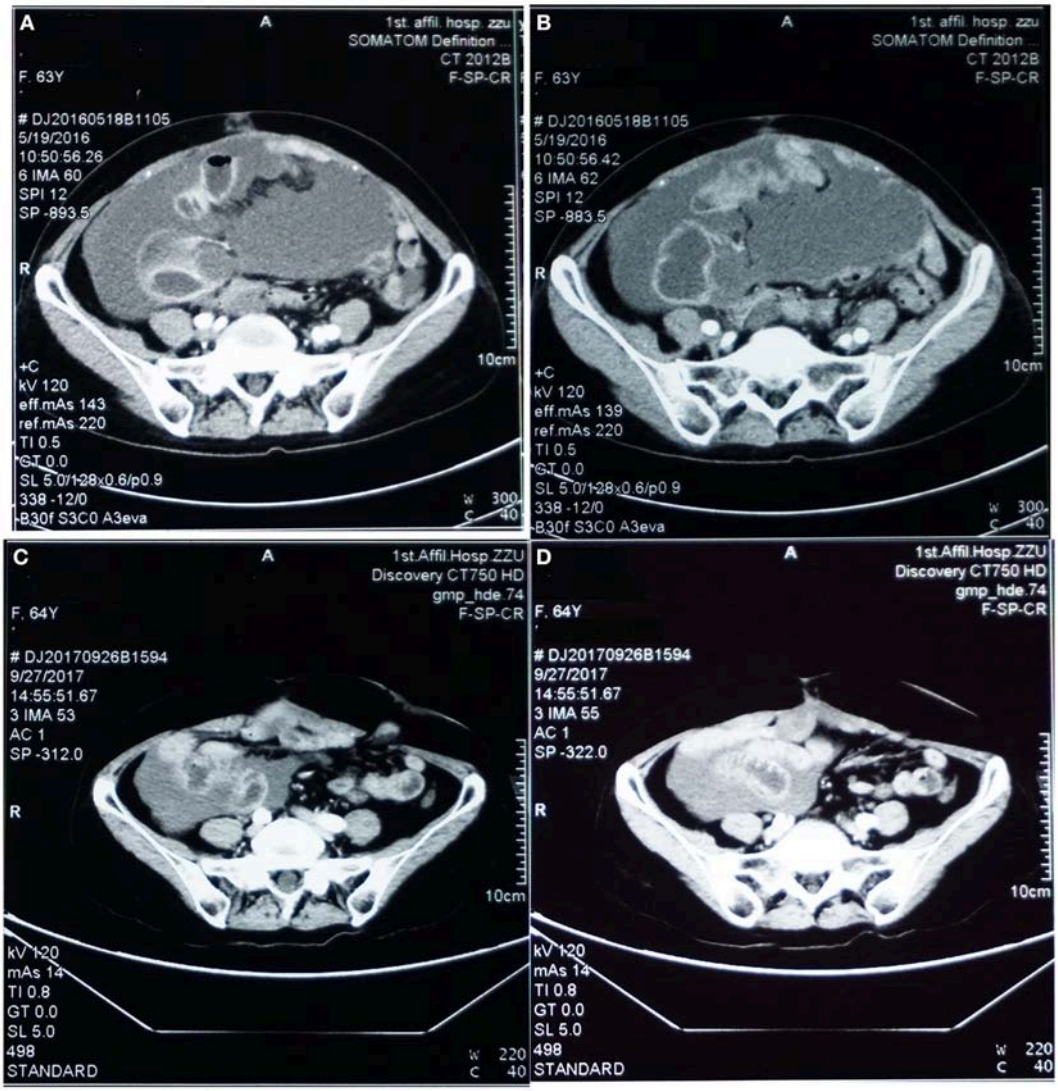

FIGURE 2 | Pelvic CT images before **(A,B)** vs. after **(C,D)** targeted therapy. **(A,B)** Prior to targeted therapy, images showed intraperitoneal multiple nodules, and a large number of peritoneal cavities filled up with mucus. **(C,D)** After targeted therapy using bevacizumab and oxaliplatin, image on the same sections showed significantly reduced peritoneal nodules and mucous cavities, suggesting stabilization of disease progression and partial response.

candidate target gene mutations involved in the angiogenesis pathway including KDR/VEGFR-2 and FGFR1, FGFR2, FGFR3 were identified. Both VEGF and FGF pathways function as angiogenetic mediators to promote metastasis of many neoplasms (9). Based on the gene mutation profile, the patient received the bevacizumab-oxaliplatin regime and then the bevacizumab-capecitabine as maintenance treatment. The results showed great effectiveness of the treatment and the patient remains progression-free and continuous decrease of CA-199 level as of to-date. The use of bevacizumab for metastatic appendiceal cancer treatment has been reported in a recent study (10). However, the treatment achieved therapeutical benefits in some patients but not the others, owing to the fact that no gene testing was performed before treatment (10). Therefore, our case report is the first study demonstrating evidence-based therapy for metastatic mucinous appendiceal adenocarcinoma. Indeed, we argue that certain level of cost-effective gene testing may be necessary prior to administration of targeted drugs in order to avoid the abuse of targeted medicines. A good example could be found in our case that the blind usage of anti-EGFR drug cetuximab without prior detection of KRAS mutation from the patient pathology tissue failed to achieve any treatment benefit.

In conclusion, accurate detection of gene mutation can help clinicians to make the optimal choice of individualized targeted drugs, and improve the prognosis and life quality of patients. The present report is one case and limited and waits for more cases to be filled in to expand our knowledge

about the genome mutations and personalized medicine of appendiceal cancer.

ETHICS STATEMENT

The patient of this case report agreed and provided written informed consent in accordance with the Declaration of Helsinki. Written informed consent was obtained from the patient for the purpose of publication of the present case report and any relevant images.

AUTHOR CONTRIBUTIONS

All authors listed have made a substantial, direct and intellectual contribution to the work, and approved it for publication.

REFERENCES

1. Hesketh KT. The management of primary adenocarcinoma of the vermiform appendix. *Gut* (1963) 4:158. doi: 10.1136/gut.4.2.158
2. Turaga KK, Pappas SG, Gamblin T. Importance of histologic subtype in the staging of appendiceal tumors. *Ann Surg Oncol.* (2012) 19:1379–85. doi: 10.1245/s10434-012-2238-1
3. Connor SJ, Hanna GB, Frizelle FA. Appendiceal tumors: retrospective clinicopathologic analysis of appendiceal tumors from 7,970 appendectomies. *Dis Colon Rectum* (1998) 41:75–80. doi: 10.1007/BF02236899
4. Ruoff C, Hanna L, Zhi W, Shahzad G, Gotlieb V, Salf MW. Cancers of the appendix: review of the literatures. *ISRN Oncol.* (2011) 2011:728579. doi: 10.5402/2011/728579
5. Winder T, Lenz HJ. Mucinous adenocarcinomas with intra-abdominal dissemination: a review of current therapy. *Oncologist* (2010) 15:836–44. doi: 10.1634/theoncologist.2010-0052
6. Pietrantonio F, Maggi C, Fanetti G, Iacovelli R, Di Bartolomeo M, Ricchini F, et al. FOLFOX-4 chemotherapy for patients with unresectable or relapsed peritoneal pseudomyxoma. *Oncologist* (2014) 19:845–50. doi: 10.1634/theoncologist.2014-0106
7. Saltz LB, Clarke S, Díaz-Rubio E, Scheithauer W, Figer A, Wong R, et al. Bevacizumab in combination with oxaliplatin-based chemotherapy as first-line therapy in metastatic colorectal cancer: a randomized phase III study. *J Clin Oncol.* (2008) 26:2013–9. doi: 10.1200/JCO.2007.14.9930.
8. Bencsikova B, Bortlicek Z, Halamkova J, Ostrizkova L, Kiss I, Melichar B, et al. Efficacy of bevacizumab and chemotherapy in the first-line treatment of metastatic colorectal cancer: broadening KRAS-focused clinical view. *BMC Gastroenterol.* (2015) 15:37. doi: 10.1186/s12876-015-0266-6
9. Ellis LM, Takahashi Y, Liu W, Shaheen RM. Vascular endothelial growth factor in human colon cancer: biology and therapeutic implications. *Oncologist.* (2000) 5 (Suppl. 1):11–5. doi: 10.1634/theoncologist.5-suppl_1-11
10. Choe JH, Overman MJ, Fournier KF, Royal RE, Ohinata A, Rafeeq S, et al. Improved survival with anti-VEGF therapy in the treatment of unresectable appendiceal epithelial neoplasms. *Ann Surg Oncol.* (2015) 22:2578–84. doi: 10.1245/s10434-014-4335-9
11. Karapetis CS, Khambata-Ford S, Jonker DJ, O'Callaghan CJ, Tu D, Tebbutt NC, et al. K-ras mutations and benefit from cetuximab in advanced colorectal cancer. *N Engl J Med.* (2008) 359:1757–65. doi: 10.1056/NEJMoa0804385
12. Arellano ML, Gonzalez-Dominguez Y, Molina-Ortiz F, Garceau MAH, Cantero R, Rodriguez-Montes JA. Primary adenocarcinoma of the appendix: experience at La Paz University Hospital of Madrid (1967-2014). *Int J Surg Open* (2016) 4:23–6. doi: 10.1016/j.ijso.2016.06.003
13. Linnekamp JF, Wang X, Medema JP, Vermeulen L. Colorectal cancer heterogeneity and targeted therapy: a case for molecular disease subtypes. *Cancer Res.* (2015) 75:245–9. doi: 10.1158/0008-5472.CAN-14-2240

Conflict of Interest Statement: The authors declare that the research was conducted in the absence of any commercial or financial relationships that could be construed as a potential conflict of interest.

frontiers in Pharmacology

REVIEW
published: 14 February 2019
doi: 10.3389/fphar.2019.00009

A Natural Isoquinoline Alkaloid With Antitumor Activity: Studies of the Biological Activities of Berberine

Da Liu[1,2], Xue Meng[1,2], Donglu Wu[1,2], Zhidong Qiu[1,2] and Haoming Luo[1,2]**

[1] Department of Pharmacy, Changchun University of Chinese Medicine, Changchun, China, [2] Key Laboratory of Effective Components of Traditional Chinese Medicine, Changchun University of Chinese Medicine, Changchun, China

Coptis, a traditional medicinal plant, has been used widely in the field of traditional Chinese medicine for many years. More recently, the chemical composition and bioactivity of Coptis have been studied worldwide. Berberine is a main component of Rhizoma Coptidis. Modern medicine has confirmed that berberine has pharmacological activities, such as anti-inflammatory, analgesic, antimicrobial, hypolipidemic, and blood pressure-lowering effects. Importantly, the active ingredient of berberine has clear inhibitory effects on various cancers, including colorectal cancer, lung cancer, ovarian cancer, prostate cancer, liver cancer, and cervical cancer. Cancer, ranked as one of the world's five major incurable diseases by WHO, is a serious threat to the quality of human life. Here, we try to outline how berberine exerts antitumor effects through the regulation of different molecular pathways. In addition, the berberine-mediated regulation of epigenetic mechanisms that may be associated with the prevention of malignant tumors is described. Thus, this review provides a theoretical basis for the biological functions of berberine and its further use in the clinical treatment of cancer.

Keywords: berberine, biological activities, antitumor, autophagy, epigenetic effects

OPEN ACCESS

Edited by:
Zhe-Sheng Chen,
St. John's University, United States

Reviewed by:
Di Wang,
Jilin University, China
Min Ye,
Peking University, China

****Correspondence:***
Zhidong Qiu
Qiuzd@ccucm.edu.cn
Haoming Luo
luo.haoming@163.com

Specialty section:
This article was submitted to Cancer Molecular Targets and Therapeutics, a section of the journal Frontiers in Pharmacology

Received: *21 November 2018*
Accepted: *07 January 2019*
Published: *14 February 2019*

Citation:
Liu D, Meng X, Wu D, Qiu Z and Luo H (2019) A Natural Isoquinoline Alkaloid With Antitumor Activity: Studies of the Biological Activities of Berberine. Front. Pharmacol. 10:9. doi: 10.3389/fphar.2019.00009

INTRODUCTION

Natural medicine plays a very important role in novel drug discovery (Zhang et al., 2013; Zhang L. et al., 2017). In recent years, many natural products have been confirmed to play an important role in cancer prevention and therapy (Tao et al., 2015; Zhang et al., 2015, 2016; Meng et al., 2018). Coptis chinensis is a valuable Chinese medicine used commonly in China. The medicinal parts are the dried rhizome of *Coptis chinensis* Franch., *Coptis deltoidea* C.Y.Cheng, and P.K.Hsiao, or *Coptis teeta* Wall (Wang et al., 2015b). It has been reported that Coptis exerts antibacterial, immune-enhancing, anti-ulcer, hypoglycemic, detoxifying, antitumor, and other pharmacological

Abbreviations: AP-1, activating protein 1; AMPK, AMP-activated protein kinase; BTG2, B-cell translocation gene 2; Bax, BCL2 associated X; BBC3, BCL2-binding component 3; CCNB, cyclin B; CCND, cyclin D; CCNE, cyclin E; CDK, cyclin-dependent kinases; CDKN1A/p21, cyclin-dependent kinase inhibitor; COX2, cyclooxygenase-2; DNMT, DNA methyltransferase; EGFR, epidermal growth factor receptor; GMCSF, granulocyte-macrophage colony-stimulating factor; GADD45, growth arrest and DNA damage-inducible 45; HCC, hepatocellular carcinoma cells; HAT, histone acetyltransferase; HDAC, histone deacetylase; HIF1α, hypoxia-induced factor α; INOS, inducible NO synthase; IL-8, interleukin-8; MMPs, matrix metalloproteinases; NSCLC, non-small cell lung cancer cells; NF-κB, nuclear factor kappa B; PARP, poly-ADP ribose polymerase; PGE2, prostaglandin E2; STAT3, signal transducer and activator of transcription 3; SIRT, sirtuins; Bcl-2, the B cell lymphoma-2; TNF, tumor necrosis factor; uPA, urokinase-type plasminogen activator; VEGF, vascular endothelial growth factor.

effects (Imenshahidi and Hosseinzadeh, 2016). Coptis is mainly used for the adjuvant treatment of depression, coronary heart disease, diabetes, liver cancer, and other malignant tumors. There are several active ingredients of Coptis chinensis, such as berberine (BBR), palmatine, coptisine, jatrorrhizine, worenine, columbamine, cedarone, obakunone, obakulactone, magnoflorine, and ferulic acid; berberine is the main bioactive component of Coptis chinensis and is present at a content of 5.20–7.69%. Consequently, it has become one of the natural small-molecule drugs used commonly in the clinical setting treatment for chronic disease such like diabetes (Cicero and Baggioni, 2016; Tabeshpour et al., 2017).

Berberine hydrochloride, the more commonly available salt form of berberine, is a quaternary ammonium isoquinoline alkaloid with the chemical formula $C_{20}H_{18}ClNO_4$ (**Figure 1**) that forms yellow needle-like crystals (Neag et al., 2018). Berberine was originally used as a broad-spectrum antibacterial drug. Extensive research revealed a wide range of pharmacological activities, including antibacterial, anti-inflammatory, antihypertensive, hypolipidemic, and antidiarrheal effects. In addition, berberine exhibits inhibitory effects on a variety of tumors (Xu et al., 2017), such as esophageal cancer. Many studies (Kumar et al., 2015; Foroutan F. et al., 2018; Foroutan T. et al., 2018; Mirhadi et al., 2018) have confirmed that berberine affects the development of tumor cells through the inhibition of tumor cell growth and the induction of apoptosis and cell cycle arrest (Iizuka et al., 2000; Kong et al., 2004; Tang and Feng, 2009; Xue et al., 2013; Signorelli et al., 2017).

It is reported that 8.2 million people die of cancer every year globally and that this number is continuously rising; according to the American Cancer Society, cancer is the cause of more than 600,000 deaths every year in the United States, a mortality rate second only to heart disease (Khalil et al., 2016; Walker et al., 2017). Owing to the seriousness of this situation, scientific approaches to the prevention and control of cancer have become a major public health issue (Gu et al., 2015; Viegas et al., 2017).

It has long been believed that the occurrence and development of tumors are attributable to only genetic abnormalities, which include gene mutations, translocations, and chromatin insertions (Dupont et al., 2009; Li et al., 2018). However, in recent years, the emergence and progress of genome sequencing technology have led to the rapid development of epigenetics and many researchers have determined that epigenetics plays an important role in the regulation of tumors. Epigenetic changes are reversible, heritable changes in gene expression and protein function in which the genomic DNA sequence remains unchanged (Biswas and Rao, 2018). Epigenetic changes can regulate gene expression at multiple levels, for example, at the DNA level through DNA methylation, at the RNA level through non-coding RNA regulation, at the protein level through histone modification, and at the chromatin level through chromatin remodeling. The continuous presence of these mechanisms in cell division allows cells to retain their respective characteristics, respond to intrinsic cellular signals, and participate in cell evolution and adaptation to environmental changes. Many research studies have confirmed that epigenetic mechanisms are implicated in tumorigenesis through the regulation of oncogene activation and tumor suppressor gene inactivation. For example, DNA methylation can inactivate tumor suppressor genes, abnormal histone acetylation can change tumor-associated gene expression, and non-coding microRNAs can result in dysregulation of tumor suppressor genes (Blandino et al., 2014; Wong and Chim, 2015). It is of note that different epigenetic modifications in cells often interact with each other in a synergistic manner to maintain body's homeostasis through the regulation of the expression of key genes, and that when abnormal changes occur, they may cause a variety of diseases, including tumors (Vijayaraghavalu et al., 2013). Recent evidence has suggested that epigenetic modifications may be involved in the processes tumor cells use to shape a microenvironment suitable for their own growth (Honda et al., 2006). There are a large number of active substances, such as growth factors, inflammatory factors, and proteases, in the tumor microenvironment and these participate in the various processes of tumorigenesis through their own functional properties or mediated signaling pathways (Booth and Gutierrez-Hartmann, 2015). Epigenetic modifications are involved in the regulation of the secretory processes of these biomolecules or their mediated signaling pathways (Li et al., 2018). From the perspective of the tumor development process, the regulation of epigenetic modification in the tumor microenvironment occurs at various stages of tumorigenesis, progression, and metastasis, and is one of the important tools for diversifying between tumor cells and the tumor microenvironment. That is to say, tumors may have specific epigenetic modification characteristics that may lead to changes in cell biological characteristics and malignant transformation. Therefore, an exploration the mechanism of tumor biology from the perspective of epigenetics is of great significance.

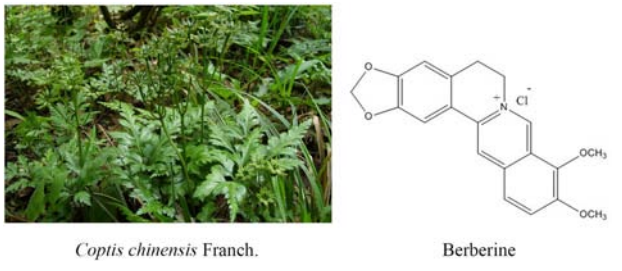

FIGURE 1 | *Coptis chinensis* Franch. and chemical structure of berberine.

THE BIOLOGICAL EFFICACY OF BERBERINE

Berberine Inhibits the Migration and Invasion of Tumor Cells

Migration and invasion are the basic characteristics of tumor cells. Therefore, it is valuable to study whether berberine can affect the migration and invasion ability of tumor cells. It is well known that E-cadherin and *N*-Cadherin proteins are closely

related to cell migration and invasion. Moreover, E-cadherin is not only an important mediator that regulates cell-cell adhesion, but also an important molecule in the maintenance of the morphology and structural integrity of epithelial cells (Qi et al., 2014; Shi et al., 2017). There is a large amount of experimental evidence suggesting that berberine can inhibit the migration and invasion of tumor cells. In human lung cancer A549 cells, berberine increased the expression of E-cadherin protein in a concentration- and time-dependent manner (Li et al., 2018), and significantly downregulated the expression of *N*-cadherin; these changes inhibited invasion and metastasis. MMPs are a class of important proteins that are involved in that the degradation of the extracellular matrix barrier, which is the first step in tumor cell metastasis (Hao et al., 2017). Studies have shown that berberine inhibits the expression of MMP2 and MMP9 in a time- and concentration-dependent manner. Simultaneously, berberine also regulates the expression of MMPs through the inhibition of the transfer of p-STAT3 to the nucleus, which affects its activity. Wang X et al. found that berberine was an effective inhibitor of the invasion and migration of HCC cells. Berberine treatment of HCC cells downregulated the expression of cox-2, NF-κB, uPA, and MMP9 in a dose-dependent manner (Sengupta et al., 2017). In summary, the data strongly suggest that berberine has an important role in the regulation of cadherin- and MMP-mediated pathways, which leads to inhibitory effects on cancer migration and invasion (**Table 1**).

Furthermore, Jin Y. et al. (2017) showed that the effect of berberine on the metastatic potential of cancer cells may be mediated by the activation of the AMPK signaling pathway, which reduces the activity of ERK and the expression of COX-2, thereby inhibiting the adhesion, migration, and invasion of tumor cells. Moreover, berberine inhibited tumor cells through signaling pathways, including the NF-κB and AMPK pathways. Studies have demonstrated that berberine prevents tumor cells from producing IL-8 and blocks NF-κb signaling pathway, ultimately inhibiting endometrial cancer metastasis, and that colon cancer cell migration was inhibited by targeting AMPK signaling (Li et al., 2014).

Vascular endothelial growth factor, the most important angiogenic factor secreted from tumor cells, stimulates tumor neovascularization through an increase in the mitogenic and survival properties of vascular endothelial cells. Berberine not only reduces the expression of SC-M1 cells with normal oxygen content and low oxygen content. VEGF also directly inhibits the proliferation and migration of umbilical vein epithelial cells. Berberine treatment in B16F-10 melanoma cells reduced the expression of VEGF mRNA and inhibited angiogenesis. Inflammation plays an important role in tumor angiogenesis, which is mainly manifested through the activation of NF-κB to regulate VEGF, and results have shown that berberine treatment of tumor cells significantly inhibited NF-κB and ultimately decreased the expression of VEGF and IL-8 in tumor cells (Hamsa and Kuttan, 2011; Siveen and Kuttan, 2011). In addition, berberine significantly inhibited the VEGF-induced migration and invasion of human umbilical vein endothelial cells HUVEC in a dose-dependent manner, and significantly reduced the expression of COX-2, Inos, and VEGF mRNA and downregulated pro-angiogenic factors to inhibit angiogenesis (Naveen et al., 2016; Wang et al., 2018). These results indicated the critical effects of berberine on the HIF1α/VEGF pathway.

Angiogenesis plays an important role in tumor growth, as progression and metastasis are prerequisites for solid tumor growth. The angiogenic process is therefore a target for the inhibition of tumor growth and metastasis (Ma et al., 2008) Studies have shown that berberine can reduce the levels of IL-1β, IL-6, TNF, and GMCSF in the serum of tumor-inoculated animals and inhibit the elevation of NO and TNF-α, inflammatory mediators involved in angiogenesis. Wang Y et al. inferred that berberine suppressed the growth and metastasis of endometrial cancer cells via miR-101/COX2, and berberine is also known to inhibit tumors via the COX-2/PGE2 signaling pathway. The transcription of miR-101 is up-regulated by berberine through AP-1 to regulate the transcription of COX-2 in EC cells (Wu et al., 2012). The high expression of p-STAT3 in malignant tumor cells and the expression level of p-STAT3 in tumor tissues, the more obvious the proliferation and metastasis of tumor cells (Munir et al., 2000).

Berberine Inhibits Tumor Cell Proliferation (Autophagy, Apoptosis)

Apoptosis is an ideal form of cell death in cancer therapy because it generally does not cause an inflammatory response. Thus, the induction of apoptosis is one of the various mechanisms that inhibit the growth of tumor cells (Yakata et al., 2007). It has also been reported that berberine significantly inhibited the proliferation of human prostate cancer PC3 cells (Huang et al., 2015). In recent years, studies have shown that the proliferation of renal cell cancer cells can be effectively inhibited by berberine; when a certain concentration of berberine is treated to renal cell cancer cells, the effects continue for some time. The inhibitory effect of berberine on the tumor cells gradually increased, and it was found that the effect of inhibitory effect was greatest for treatment times of up to 48 h. In addition, the total apoptotic rate of renal tumor cells detected by a double staining method showed that after treatment of renal cell cancer cell lines A498 and 786-0 with different concentrations of berberine, the rate of total apoptosis in cells gradually increased as the concentration of the drug increased (Wang et al., 2015a; Liu et al., 2017a,b, 2018).

Berberine induces apoptosis in tumor cells, mainly through upregulation of pro-apoptotic genes and downregulation of apoptosis-inhibiting genes. For example, berberine can upregulate the expression of the pro-apoptotic protein BAD in HL-60 cells and downregulate the expression of anti-apoptotic protein Bcl-2 to achieve regulation of tumor cell apoptosis. In addition, apoptosis can be induced by the mitochondrial/caspase pathway, DNA cleavage induces tumor cell apoptosis, tumor cell apoptosis is induced by inflammatory factors, and tumor cell apoptosis is induced by cyclooxygenase. For example, berberine treatment of liver cancer cells revealed that DNA fragments, caspase-3, and caspase-8 were activated, which was followed by the activation of PARP, and the release of cytochrome c to inhibit tumor metastasis (Mistry et al., 2017).

Studies have showed that berberine can regulate apoptosis-associated proteins. Caspase cleavage is a typical phenomenon in apoptosis cells. Thus, numerous reports have used the detection of this cleavage to clarify the role of berberine in the induction of apoptosis. For example, berberine decreased the expression of Bcl-2 and survivin and, conversely, increased the expression of the pro-apoptotic genes Bax and cleaved caspase-3 in a dose-dependent manner in human ovarian cancer SKOV3 cells (Su et al., 2015). Moreover, the treatment of berberine to treat human colorectal adenocarcinoma (HCT-15) cells significantly increased the expression of spliced caspase-3 and the mitochondrial apoptosis-related protein Bax, and significantly decreased the expression of Bcl-2 and survivin, finally inducing apoptosis (Agnarelli et al., 2018). Berberine inhibited the proliferation of human cervical cancer Ca Ski cells through alteration of the ratio of p53 and Bax/Bcl-2 proteins, upregulation of ROS, and enhancement of caspase-3 activity to induce apoptosis (Kalaiarasi et al., 2016). In addition, berberine induced the proliferation of BIU-87 and T24 cells through the inhibition of protein expression, the induction of G1 cell cycle arrest, and the induction of apoptosis via the caspase-3 and caspase-9 pathways (Lu et al., 2015). Agnarelli A et al. treated U343 cells and MIA PaCa-2 cells with 50 μM berberine for 48 h, and found that the activity of caspase-3 was decreased in U343 cells and increased in MIA PaCa-2 cells. Therefore, they concluded that berberine promoted the apoptosis of tumor cells (Katona et al., 2014). It has been reported that berberine induces Bax activation in human lung cancer A549 cells, enables p53 pathway-mediated cytochrome c release, and leads to the activation of caspase signaling ultimately causing apoptosis (Shi et al., 2013). The reported data also showed that berberine induced cancer cell apoptosis mainly through the regulation of the expression of caspases and Bcl-2; this results in the release of cytochrome c and the activation of the mitochondria-dependent apoptotic pathway to promote apoptosis in PC3 cells (Wang et al., 2017).

Autophagy is one type of cellular self-protection mechanism, consisting mainly of the degradation of macromolecular material and damaged organelles in cytoplasm after autophagosome formation with lysosomes. The products of degradation are used to restore cell homeostasis. There are three forms of cell autophagy: macro-autophagy, micro-autophagy, and autophagy, which are mediated by different molecular chaperones. Autophagy is involved in many of the physiological and pathological processes of cells, and there is a close relationship between autophagy and tumorigenesis. The effects of autophagy vary in different cell lines and maybe inhibitory or stimulatory. In addition, the occurrence of autophagy is regulated by various signal pathways. Recent experimental studies have shown that berberine inhibits the proliferation of colon cancer cells through the downregulation of the expression of EGFR and that it activates autophagy and apoptosis through the p38 signaling pathway to inhibit the proliferation of HCT-15 cells. Similarly, in berberine-treated HCT-15 cells, the autophagy marker proteins ATG5 and LC3 were upregulated in a time-dependent manner (Zhang L. et al., 2017), indicating that berberine induced autophagy in HCT-15 cells. These data demostrate a role of Berberin in regulating cancer cell proliferation (**Tables 1**, **2**).

Berberine Arrests Tumor Cell Cycle

Many studies have shown that low concentrations of berberine arrest human osteosarcoma U20S cells in the G1 phase through the induction of DNA double-strand breaks that activate the p53-p21 pathway. In contrast to low concentrations of berberine, high concentrations induce arrest in the G2/M phase, but do not depend on the p53-p21 pathway (Yang et al., 2015; Li et al., 2017). Other studies demonstrated that berberine significantly inhibited human ovarian cancer cells (HEY and SKOV3 cells) in a time- and dose-dependent manner. It is demonstrated that that berberine exerts a significant inhibitory effect on human gastric cancer MGC 80 3 cells in a dose-dependent manner. Using laser confocal microscopy, the nucleus condenses, and apoptotic bodies are seen, which indicate that berberine can inhibit the proliferation of MGC 80 3 cells and arrest cells in the G0/G1 phase to inhibit the proliferation of tumor cells *in vitro*.

B-cell translocation gene 2 is a transient early-response gene induced by p53. It is a member of the gene family that regulates cell proliferation and is an important bridge molecule that links

TABLE 1 | Inhibitory effects of berberine on tumor migration and invasion.

Cell lines	Mechanism	Reference
Human non-small cell lung cancer (A549)	N-Cadherin↓ E-cadherin↑	Li et al., 2018
Hepatocellular carcinoma (HCC) cells	COX-2↓,NF-κB↓ UPA,MMP-9↓	Sengupta et al., 2017
Endothelial canjcer colon cells	IL-8↓, NF-κB↓ AMPK↑	Li et al., 2014
Mouse melanoma cell (B16F-10)	VEGF mRNA↓	Siveen and Kuttan, 2011; Hamsa and Kuttan, 2011
Human umbilical vein endothelial cells (HUVEC)	COX-2↓, iNOS↓, VEGF mRNA↓	Ma et al., 2008
Human endometrial cancer cell lines(AN3 CA and HEC-1-A)	COX-2↓ PEG-2↓	Wu et al., 2012

TABLE 2 | Inhibitory effects of berberine on tumor cell proliferation.

Cell Lines	Mechanism	Reference
Liver cancer cells	Caspase-3↑, Caspase-8↑,PARP↑	Mistry et al., 2017
Human ovarian cancer cell (SKOV3)	Bcl-2↓ Bax↑, Cleaved-Caspase-3↑,	Su et al., 2015
Colorectal adenocarcinoma cell line (HCT-15)	EGFR↓, Bcl-2↓, Survivin↓ ATG5↑, Bax↑, LC3↑	Agnarelli et al., 2018
Human cervical cancer cell (CaSki)	p53↑, Bax/Bcl-2↑ ROS↑, Caspase-3↑	Kalaiarasi et al., 2016
Human bladder cancer cell (BIU-87, T24)	Caspase-3↑, Caspase-9↑	Lu et al., 2015
Human pancreatic carcinoma cell (MIA PaCa-2)	Caspase-3↑ P53↓	Katona et al., 2014

p53, pRB, the cell cycle, cell proliferation, and differentiation. The current body of evidence indicates that berberine can promote the cell cycle arrest of human hepatoma HEPG2 cells in the G1 phase through the upregulation of BTG2 and the downregulation of cyclin D1, consequently inhibiting the proliferation of hepatoma cells and inducing apoptosis.

Cyclin is one of the target proteins that regulate the G1 phase. As a proto-oncogene, it is involved in the regulation of the cell cycle, and its overexpression is closely related to the occurrence and development of tumors. Berberine has a variety of effects on the cell cycle; for example, it can arrest the G2/M phase in the cell growth cycle through a reduction in the expression of cyclin B1 and increase in the expression of Wee1, which stops the tumor cells in the early stage of DNA synthesis (G1) and late DNA synthesis (G2). The induction of tumor cell apoptosis through the downregulation of cyclin E expression and upregulation of p21 expression, which causes G1 arrest in HEY and SKOV3 cells and downregulates Bcl-2 protein expression and upregulates Bax protein expression. Berberine treatment of MDA-MB-231 and MCF-7 human breast cancer cells dose-dependently caused G0/G1 arrest, which was possibly associated with a decrease in the cell cycle regulation protein cyclin B1. Furthermore, it increased the expression of CDC4 and cyclin B1 through an increase in the expression of CDC2 and caspase-3 in human hepatoma HepG2 cells, causing arrest in the S and G2/M phases, and activating the AMPK signaling pathway to induce the apoptosis of HepG2 cells (Chidambaram et al., 2012; Murthy et al., 2012; Balestrieri et al., 2018). Li et al. demonstrated that berberine regulates the PI3K-AKT and MAPK signaling pathways in PTC (the most common subtype) and ATC (the most malignant and aggressive subtype), leading to mitochondrial apoptosis, G0/G1 cell cycle arrest, increased Bax/Bcl-2, cleaved caspase-3, p21, and decreased cyclin E1, CDK2, and vimentin were verified by western blotting (Waterbeemd et al., 2013). The combination of drugs upregulated the expression of the cell cycle-dependent kinase inhibitory proteins p27 and p21, and downregulated the expression of cyclin D1, CDK2, and CDK4-cyclin.

In addition, studies have reported that berberine can bind to topoisomerase (TOP1), which hinders the synthesis of S phase cells and prevents cell proliferation.

Effects of Berberine in Compatibility

With the identification of numerous anti-tumor drugs, research of cancer therapy has gradually shifted from a focus on monotherapy to combined therapy. More and more reports have demonstrated that berberine combined with radio-therapy or chemotherapy drugs can achieve better anti-tumor effect. For instance, berberine combined with gamma-radiation enhance the anti-cancer effects, including inducing apoptosis and ROS generation (Jung-Mu et al., 2009). Also, berberine sensitizes lung cancer cells to radiation via autophagy both *in vitro* and *in vivo* (Peng et al., 2008). Indicated an adjuvant role in radio-therapy of cancer. Another major anti-cancer therapy is chemotherapy, several novel chemotherapy drugs such like doxorubicin, rapamycin were texted combined with berberine, and showed a more effective result. It is reported that berberine sensitizes mutliple human cancer cells to the anticancer effects of doxorubicin (Tong et al., 2012). More details and drugs were summarized in **Table 3**, which clarified that berberine synergistic work with chemotherapy drugs in anti-tumor proliferation through inducing cell cycle arrest, apoptosis, as well as autophagy. These data have laid theoretical foundation for the combined therapy in clinic trial.

EPIGENETIC EFFECTS OF BERBERINE ON TUMORS

For many years, researchers have been studying and developing drugs for cancer prevention and treatment. Chinese medicines, such as berberine, are commonly used as drugs. As an active ingredient of Coptis, berberine is inevitably closely related to the occurrence and development of tumors (Wang-Johanning et al., 2008; Coward et al., 2014; Delga-docruzata et al., 2015; Dkhil et al., 2015). Extensive research has led scholars to conclude that, ultimately, the antitumor effect of berberine may be related to epigenetic effects. The following is a brief description of the methods through which berberine regulates tumor cells, including migration, proliferation, and apoptosis, through epigenetic mechanisms.

DNA Methylation

DNA methylation refers to the covalent attachment of the fifth carbon atom of cytosine on the CpG dinucleotide to the methyl group through the action of DNMT, which is modified to 5-methylcytosine. DNA methylation is a potential epigenetic mechanism involving a variety of biological processes. The DNMT family consists of three main members: DNMT1, DNMT3A, and DNMT3B. DNMT1 mainly maintains DNA methylation status and DNMT3A and DNMT3B catalyze new DNA methylations (Kalinkova et al., 2018; Li et al., 2018; Puneet et al., 2018). Human CpG exists mainly in two forms: one is dispersed in genomic DNA; the other is highly aggregated to form CpG islands, which are present in the promoter region or the first exon region of various genes. In the human genome, the CpG site is usually in an unmethylated state in the CpG islands, but in a methylated outside the CpG islands. When tumors occur, the degree of unmethylation of CpG sites outside CpG islands increases, whereas the CpG sites in CpG islands are highly methylated, causing a decrease in the overall methylation level of the genome, as well as certain gene CpG islands. Local methylation levels are abnormally elevated, leading to genomic instabilities, such as chromosomal instability, the activation of proto-oncogenes, and the silencing of tumor suppressor genes (Qing et al., 2014; Crawford et al., 2018; Lee and Gang, 2018; Sanna et al., 2018). DNA methylation abnormalities are mainly divided into the hypomethylation state of proto-oncogenes and the hypermethylation state of tumor suppressor genes. The most studied of these is the hypermethylation of tumor suppressor genes. It is of interest that berberine has been found to inhibit the expression of human DNA methyltransferases DNMT1 and DNMT3B in multiple myeloma U266 cells. For example, berberine can alter the CpG methylation of p53

TABLE 3 | Berberine combined with chemotherapy drugs.

Combined With	Cells	Mechnisms/Effect	Reference
2-deoxy-D-glucose	Human lymphoblastoid TK6 cells	BBR combined with the glucose analog 2-deoxy-D-glucose (2-dG) synergistic inducing the apoptosis of human lymphoblastoid TK6 cells	Halicka et al., 2017
5-Fluorouracil	Gastric cancer cells AGS	BBR sensitized gastric cancer cells to 5-FU, the combination shows a synergistic inhibition of surviving and STAT3 level	Pandey et al., 2015
Cinnamaldehyde	Lung carcinogenesis A549 cell	BBR combined with cinnamaldehyde prevented A549 cell substance permeability via AMPK-reduced AQP-1 expression	Meng et al., 2017
Cisplatin	Breast cancer MCF-7	BBR sensitized MCF-7 cells to cisplatin through inducing DNA breaks and caspase-3-dependent apoptosis	Zhao et al., 2016
D-limonene	Human gastric carcinoma cell line MGC803	BBR in combination with d-limonene showed synergistic anticancer effects on MGC803 cells through inducing cell-cycle arrest, ROS production, and apoptosis via the mitochondria-mediated intrinsic pathway	Zhang et al., 2014
Doxorubicin	Murine melanoma B16F10 cells	BBR combined with Doxorubicin inhibit melanoma tumor growth through casepase-3 dependtent apoptosis	Mittal et al., 2014
	Lung cancer cell lines	BBR sensitizes lung cancer cells to Doxorubicin by promoting STAT3 degradation, inhibiting doxorubicin mediated STAT3 activation.	Zhu et al., 2015
Evodiamine	Breast cancer MCF-7	BBR in combination with evodiamine inducing cell cycle arrest and apoptosis, further inhibit MCF-7 prolieration	Du et al., 2017
Hsp90 inhibitor NVP-AUY922	Colorectal cancer	BBR combined with NVP-AUY922 inhibit proliferation of colorectal cancer via mutiple pathways	Su et al., 2015
Metformin	NSCLC	BBR combined with metformin synergistic induced cell cycle arrest, as well as reduced migration and invasion of NSCLC cells	Zheng et al., 2018
Rapamycin	Human hepatoma cell SMMC7721 cells	BBR combined with rapamycin can improve HCC therapy through inhibiting the mTOR signaling pathway	Guo et al., 2014
S-allyl-cysteine (SAC)	Human liver cancer HepG2 cells	BBR combined with SAC effectively reduced Rb-phosphorylation resulting insignificant nuclear E2F presence, further inhibiting cancer cell proliferation	Sengupta et al., 2017
	DEN+CCl4 induced hepatocarcinoma	BBR in combination with SAC inhibited Akt mediated cell proliferation, and inducing PP2A/JNK mediated apoptosis.	Sengupta et al., 2014
Sorafenib	Human liver cancer SMMC-7721 and HepG2 cells	berberine combined with sorafenib inhibited the proliferation of liver cancer cells by inducing cancer cell apoptosis.	Huang Y. et al., 2018
Tamoxifen	Breast cancer MCF-7	BBR sensitized MCF-7 cells to tamoxifen via inducing the G1 phase arrest and activating apoptosis.	Wen et al., 2016
Tetrahydropalmatine	MDA-MB-231 breast cancer cells	BBR combined with tetrahydropalmatine synergistic inhibited the proliferation of MDA-MB-231	Zhao et al., 2014
TPD7	T-cell acute lymphoblastic leukemia cell	BBR combined with TPD7 induced G1 -phase cell-cycle arrest of T-cell acute lymphoblastic leukemia cell.	Ma et al., 2017

DNA, affect the mRNA expression of key apoptosis-related proteins, and increases apoptosis in U266 cells, and thereby leads to cell cycle arrest. Although the hypomethylation of the p53 promoter can regulate apoptosis-related genes, such as GADD45, Bax, PMAIP1, BBC3, CCNB1, CCND3, and CCNE1. Specifically, in the p53 pathway, CDKN1A, GADD45B, Bax, PMAIP1, and BBC3 were upregulated, and CCNB1, CCND3, and CCNE1 were downregulated, which suggested that berberine activated the p53 signaling pathway through the impairment of U266 cells. In addition, results have shown that treatment of colorectal cancer cells with berberine results in a significant increase in the expression of DNMT1 and DNMT3A in the presence of TGF-β1; this hypermethylation in the promoter CpG island leads to further silencing of TSG, which results in tumor cell proliferation (Riaz et al., 2015; Asadi et al., 2018; Nardi et al., 2018).

Histone Modification

Histones play an important role in gene expression and tumorigenesis and development. The nucleosome is the basic constituent unit of chromatin. A nucleosome is an octamer composed of histones H2A, H2B, H3, and H4 and DNA entangled on the outside of the 147 base pairs. Histones not only protect the DNA structure and genetic information, but also participate in the regulation of gene expression. The extracellular amino terminus of histones can be modified by a variety of

TABLE 4 | Epigenetic regulation of berberine on tumor.

Type of Regulation	Cell Lines	Mechanism	Reference
DNA methylation	Multiple myeloma	DNMT1↓, DNMT3B↓ CDKN1A↑, GADD45B↑ Bax↑, PMAIP1↑	Asadi et al., 2018; Riaz et al., 2015; Nardi et al., 2018
	U266 cells	CCNB1↓, CCND3↓, CCNE1↓	
Histone Modification	Human non small cell lung cancer A549	HDAC↓MMP2↓ MMP9↓	Huang et al., 2017
	U266 cells	CBP/P300↑ SIRT3↑	Sun et al., 2017
MicroRNA	Human U266 multiple myeloma cells	miRNA21, Bcl-2↓	Hashiguchi et al., 2017
	Colon cancer	miR-152↓; miR-429↓ miR-29a↓	Hu et al., 2013

enzymes to form specific "histone codes" that alter the "open" or "closed" state of the local chromatin structure, or determine which proteins bind to specific DNA regions. Consequently, they regulate the various functions of DNA, including transcription and damage repair. Histone acetylation is highly dynamic and is coordinated by HATs and HDACs, and occurs at the amino-specific lysine residues of histones (Stevens et al., 1984; Yan et al., 2001; Bhat et al., 2018; Georgoff et al., 2018; Liu et al., 2018; Rahnamoun et al., 2018). Histone modification is a major determinant of the epigenetic silencing of genes and the regulation of cellular processes. Histone modifications often occur at the amino terminus of histones, and modifications of various chemical groups are acceptable due to exposure to chromatin (Oliver et al., 2013; Bennetzen and Wang, 2014; Hoen and Bureau, 2015; Yamada et al., 2015; Zhang et al., 2015; Li and Zhao, 2016; Rayan et al., 2016; Jiang et al., 2018; Salimian et al., 2018; Shang et al., 2018; Yan et al., 2018; Sahebi et al., 2018; Zhang L. et al., 2018; Zhang S. et al., 2018). The most widely studied are the acetylation and methylation of lysine K on histone H3 and H4. Histone acetylation plays an important role in the epigenetic theory proposed in recent years. Histone acetylation can affect the chromatin structure in cells, and thus participate in the transcriptional regulation of genes at specific sites, playing an important role in cell growth and differentiation. With a deeper understanding of the mechanism of histone acetylation in gene transcriptional regulation, the role of HDAC inhibitors in tumor therapy has received increasing attention (Sun et al., 2017).

CBP and p300 proteins with acetylase activity are transcriptional coactivators and hematopoietic tumor suppressors. Studies have shown that berberine can upregulate the expression of CBP/P300 and SIRT3 in U266 cells, and downregulate the expression of HDAC8; however, in HL-60/ADR and KG1-α cells, CBP/P300 and SIRT3 were also upregulated, but HDAC8 did not change significantly. Histone acetylation maintains its balance through HAT and HDAC. Berberine downregulated HDAC in human lung cancer A549 cells, which resulted in decreased expression of the metalloproteinases MMP-2 and MMP-9 mRNA and protein, inhibiting cell migration and invasion (Huang et al., 2017). Simultaneously, another study has shown that berberine treatment of A549 cells significantly reduced the expression of class I, II-a, II-b, and IV mRNA, histone H3, and H4 hyperacetylation.

MicroRNA

MicroRNAs (miRNAs) are short-chain non-coding RNAs of 19–22 nucleotides in length that bind to the 3′UTR in target mRNAs, thereby degrading or blocking the translation of target mRNAs. It plays an important role in the growth, differentiation, apoptosis, and tumor cell development. miRNAs can regulate the expression of multiple tumor-associated genes. In accordance with the function of miRNAs, they can be divided into two types: oncogenes or tumor suppressor genes (Hu et al., 2013). Not only can it act directly as a proto-oncogene or a tumor suppressor gene, but also regulate the expression of other proto-oncogenes or tumor suppressor genes. miRNAs play a central role in many cellular biology processes, and their dysregulation is a ubiquitous feature in tumors. Epigenetic effects have been shown to be a major cause of miRNA dysregulation in tumors (Hashiguchi et al., 2017). In the TGF-β1-induced colorectal cancer model, berberine significantly decreased the expression of miR-152

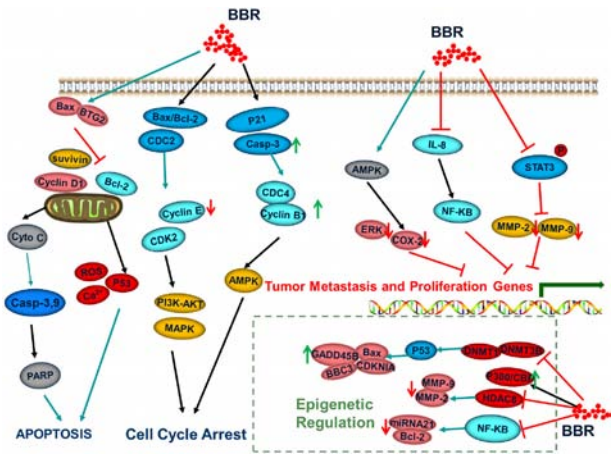

FIGURE 2 | Signaling pathways regulated by berberine.

(targeting DNMT1), miR-429 (targeting DNMT3A), and miR-29a (targeting DNMT3A/3B), which suggested that berberine inactivates some tumor suppressor factors, including DNMT1 and DNMT3A/3B, through the regulation of the expression of the above miRNAs during colon cancer development. Furthermore, other evidence has suggested that berberine treatment of human U266 multiple myeloma cells led to the inhibition of NF-κB nuclear translocation via Set9-mediated lysine methylation, which resulted in decreased miRNA21 and Bcl-2 expression, inducing the cells to produce ROS and promoting cell apoptosis. Berberine treatment of colorectal cancer cells increased the expression of miR-200a-5p and decreased the expression of miR-429. These epigenetic regulation affected by Berberine was briefly summarized in **Table 4**.

SUMMARY AND FUTURE PERSPECTIVES

The importance of epigenetic regulation in the occurrence and development of tumors is now an established fact. An increasing body of research has been devoted to the exploration of epigenetic molecular markers for the early diagnosis, treatment, and prognosis of tumors. Simultaneously, epigenetic drugs provide a new direction for the treatment of tumors owing to the reversibility and ease of regulation of epigenetics. At present, the anticancer drugs that inhibit the proliferation of malignant tumor cells via induction of apoptosis or that regulate signal transduction are mostly multi-targeted (He et al., 2010). Berberine is a natural isoquinoline alkaloid that significantly contributed to the development of anticancer drugs (**Figure 2**). Given the continuous development in the field of medicine and the extension of research and development in the field of medicine, berberine has gained attention of researchers owing to the combination of multiple effects. Berberine is not irreplaceable with respect to its traditional pharmacological activities, such as antibacterial, anti-inflammatory, and antiviral effects (Huang S.X. et al., 2018). Moreover, the efficacy of the antihypertensive, antitumor, and hypolipidemic effects has also become a "hot topic" in contemporary research. Berberine regulates the molecular mechanisms that cause tumor cells through a variety of signaling pathways, confirming the potential therapeutic effects in a variety of tumor cells. However, there are few reports on the effects of berberine on the epigenetic functions of tumors. Epigenetics is also the main controlling factor of oncogenes in the development of cancer. Therefore, the application of epigenetic properties of berberine in the treatment of malignant tumors offers broad prospects for drug development. At the same time, extended research into epigenetics has provided a new strategy to understand the various characteristics of tumors, optimize the early diagnosis of tumors, and improve the prognosis of patients. In future, basic research and clinical transformations in the epigenetics of cancer will provide new strategies for the precise diagnosis and treatment of cancer.

AUTHOR CONTRIBUTIONS

DL contributed significantly to analysis and manuscript preparation. XM contributed significantly to manuscript preparation. DW helped to writing the manuscript. ZQ and HL contributed to the conception of the study.

FUNDING

This work was supported by the National Natural Science Foundation of China (Grant No. 81803680). Jilin Province Science and Technology Development Project in China (Grant Nos. 20170307031 and YY20180520050JH).

REFERENCES

Agnarelli, A., Natali, M., Garciagil, M., Pesi, R., Tozzi, M. G., Ippolito, C., et al. (2018). Cell-specific pattern of berberine pleiotropic effects on different human cell lines. *Sci. Rep.* 8:10599. doi: 10.1038/s41598-018-28952-3

Asadi, R., Omrani, M. D., Ghaedi, H., Mirfakhraie, R., Azargashb, E., Habibi, M., et al. (2018). Premutations of fmr1 cgg repeats are not related to idiopathic premature ovarian failure in iranian patients: a case control study. *Gene* 676, 189–194. doi: 10.1016/j.gene.2018.07.034

Balestrieri, E., Argaw-Denboba, A., Gambacurta, A., Cipriani, C., Bei, R., Serafino, A., et al. (2018). Human endogenous retrovirus k in the crosstalk between cancer cells microenvironment and plasticity: a new perspective for combination therapy. *Front. Microbiol.* 9:1448. doi: 10.3389/fmicb.2018.01448

Bennetzen, J. L., and Wang, H. (2014). The contributions of transposable elements to the structure, function, and evolution of plant genomes. *Annu. Rev. Plant Biol.* 65:505. doi: 10.1146/annurev-arplant-050213-035811

Bhat, A. V., Hora, S., Pal, A., Jha, S., and Taneja, R. (2018). Stressing the (epi) genome: dealing with reactive oxygen species in cancer. *Antioxid. Redox Signal.* 29, 1273–1292. doi: 10.1089/ars.2017.7158

Biswas, S., and Rao, C. M. (2018). Epigenetic tools (The Writers, the readers and the erasers) and their implications in cancer therapy. *Eur. J. Pharmacol.* 837, 8–24. doi: 10.1016/j.ejphar.2018.08.021

Blandino, G., Fazi, F., Donzelli, S., Kedmi, M., Saschen, A., Muti, P., et al. (2014). Tumor suppressor microrna: a novel non-coding alliance against cancer. *FEBS Lett.* 588, 2639–2652. doi: 10.1016/j.febslet.2014.03.033

Booth, A. K., and Gutierrez-Hartmann, A. (2015). Signaling pathways regulating pituitary lactotrope homeostasis and tumorigenesis. *Adv. Exp. Med. Biol.* 846, 37–59. doi: 10.1007/978-3-319-12114-7_2

Chidambaram, A., Fillmore, H. L., Van Meter, T. E., Dumur, C. I., Band roaddus, W. C., (2012). Novel report of expression and function of CD97 in malignant gliomas: correlation with Wilms tumor 1 expression and glioma cell invasiveness. *J. Neurosurg.* 116, 843–853. doi: 10.3171/2011.11.JNS111455

Cicero, A. F., and Baggioni, A. (2016). Berberine and its role in chronic disease. *Adv. Exp. Med. Biol.* 928:27. doi: 10.1007/978-3-319-41334-1_2

Coward, W. R., Feghalibostwick, C. A., Jenkins, G., Knox, A. J., and Pang, L. (2014). A central role for g9a and ezh2 in the epigenetic silencing of cyclooxygenase-2 in idiopathic pulmonary fibrosis. *FASEB J.* 28, 3183–3196. doi: 10.1096/fj.13-241760

Crawford, B., Craig, Z., Mansell, G., White, I., Spaull, S., Imm, J., et al. (2018). DNA methylation and inflammation marker profiles associated with a history of depression. *Hum. Mol. Genet.* 27, 2840–2850. doi: 10.1093/hmg/ddy199

Delga-docruzata, L., Zhang, W., Mcdonald, J. A., Tsai, W. Y., Valdovinos, C., Falci, L., et al. (2015). Dietary modifications, weight loss, and changes in

metabolic markers affect global dna methylation in hispanic, african american, and afro-caribbean breast cancer survivors. *J. Nutr.* 145:783. doi: 10.3945/jn.114.202853

Dkhil, M. A., Metwaly, M. S., Saleh, A. Q., Sherif, N. E., Denis, D., Omar, S. Y. A., et al. (2015). Anti-eimeria activity of berberine and identification of associated gene expression changes in the mouse jejunum infected with eimeria papillata. *Parasitol. Res.* 114, 1–13. doi: 10.1007/s00436-015-4344-z

Du, J., Sun, Y., Lu, Y. Y., Lau, E., Zhao, M., Zhou, Q. M., et al. (2017). Berberine and evodiamine act synergistically against human breast cancer mcf-7 cells by inducing cell cycle arrest and apoptosis. *Anticancer Res.* 37, 6141–6151.

Dupont, C., Armant, D. R., and Brenner, C. A. (2009). Epigenetics: definition, mechanisms and clinical perspective. *Semin. Reprod. Med.* 27, 351–357. doi: 10.1055/s-0029-1237423

Foroutan, F., Alba, A. C., Stein, M., Krakovsky, J., Chien, K. G. W., Chih, S., et al., (2018). Validation of the International Society for Heart and Lung Transplantation primary graft dysfunction instrument in heart transplantation. *J. Heart Lung Transplant.* doi: 10.1016/j.healun.2018.12.007 [Epub ahead of print].

Foroutan, T., Farhadi, A., Abroun, S., and Mohammad Soltani, B. (2018). Adipose derived stem cells affect miR-145 and p53 expressions of co-cultured hematopoietic stem cells. *Cell J.* 19, 654–659. doi: 10.22074/cellj.2018.4393

Georgoff, P. E., Nikolian, V. C., Higgins, G., Chtraklin, K., Eidy, H., Ghandour, M. H., et al. (2018). Valproic acid induces pro-survival transcriptomic changes in swine subjected to traumatic injury and hemorrhagic shock. *J. Trauma Acute Care Surg.* 84:1. doi: 10.1097/TA.0000000000001763

Gu, L., Frommel, S. C., Oakes, C. C., Simon, R., Grupp, K., Gerig, C. Y., et al. (2015). Baz2a (tip5) is involved in epigenetic alterations in prostate cancer and its overexpression predicts disease recurrence. *Nat. Genet.* 47:22. doi: 10.1038/ng.3165

Guo, N., Yan, A., Gao, X., Chen, Y., He, X., Hu, Z., et al. (2014). Berberine sensitizes rapamycin-mediated human hepatoma cell death in vitro. *Mol. Med. Rep.* 10, 3132–3138. doi: 10.3892/mmr.2014.2608

Halicka, H. D., Garcia, J., Li, J., Zhao, H., and Darzynkiewicz, Z. (2017). Synergy of 2-deoxy-d-glucose combined with berberine in inducing the lysosome/autophagy and transglutaminase activation-facilitated apoptosis. *Apoptosis* 22, 229–238. doi: 10.1007/s10495-016-1315-5

Hamsa, T. P., and Kuttan, G. (2011). Studies on anti-metastatic and anti-invasive effects of harmine using highly metastatic murine b16f-10 melanoma cells. *J. Environ. Pathol. Toxicol. Oncol.* 30:123. doi: 10.1615/JEnvironPatholToxicolOncol.v30.i2.40

Hao, D. C., He, C. N., and Shen, J. (2017). Anticancer chemodiversity of ranunculaceae medicinal plants molecular mechanisms and functions. *Curr. Genomics* 18, 39–59. doi: 10.2174/1389202917666160803151752

Hashiguchi, Y., Kawano, S., Goto, Y., Yasuda, K., Kaneko, N., Sakamoto, T., et al. (2017). Tumor-suppressive roles of Δnp63β-mir-205 axis in epithelial-mesenchymal transition of oral squamous cell carcinoma via targeting zeb1 and zeb2. *J. Cell. Physiol.* 233, 6565–6577. doi: 10.1002/jcp.26267

He, X. Y., Chen, J. X., Zhang, Z., Li, C. L., Peng, Q. L., and Peng, H. M. (2010). The let-7a microrna protects from growth of lung carcinoma by suppression of k-ras and c-myc in nude mice. *J. Cancer Res. Clin. Oncol.* 136, 1023–1028. doi: 10.1007/s00432-009-0747-5

Hoen, D. R., and Bureau, T. E. (2015). Discovery of novel genes derived from transposable elements using integrative genomic analysis. *Mol. Biol. Evol.* 32, 1487–1506. doi: 10.1093/molbev/msv042

Honda, H., Pazin, M. J., Ji, H., Wernyj, R. P., and Morin, P. J. (2006). Crucial roles of sp1 and epigenetic modifications in the regulation of the cldn4 promoter in ovarian cancer cells. *J. Biol. Chem.* 281:21433. doi: 10.1074/jbc.M603767200

Liu, H. C., Lämke, J., Lin, S. Y., Hung, M. J., Liu, K. M., Charng, Y. Y., et al. (2018). Distinct heat shock factors and chromatin modifications mediate the organ-autonomous transcriptional memory of heat stress. *Plant J.* 95, 401–413. doi: 10.1111/tpj.13958

Hu, H., Li, K., Wang, X., Liu, Y., Lu, Z. G., Dong, R. H., et al. (2013). Set9, NF-κB, and microRNA-21 mediate berberine-induced apoptosis of human multiple myeloma cells. *Acta Pharmacol. Sin.* 34:157. doi: 10.1038/aps.2012.161

Huang, C., Liu, H., Gong, X. L., Wu, L. Y., and Wen, B. (2017). Effect of evodiamine and berberine on the interaction between dnmts and target micrornas during malignant transformation of the colon by tgf-β1. *Oncol. Rep.* 37, 1637–1645. doi: 10.3892/or.2017.5379

Huang, S. X., Qiu, G., Cheng, F. R., Pei, Z., Yang, Z., Deng, X. H., et al. (2018). Berberine protects secondary injury in mice with traumatic brain injury through anti-oxidative and anti-inflammatory modulation. *Neurochem. Res.* 43, 1–12. doi: 10.1007/s11064-018-2597-5

Huang, Y., Wang, K., Gu, C., Yu, G., Zhao, D., Mai, W., et al. (2018). Berberine, a natural plant alkaloid, synergistically sensitizes human liver cancer cells to sorafenib. *Oncol. Rep.* 40, 1525–1532. doi: 10.3892/or.2018.6552

Huang, Z. H., Zheng, H. F., Wang, W. L., Wang, Y., Zhong, L. F., Wu, J. L., et al. (2015). Berberine targets epidermal growth factor receptor signaling to suppress prostate cancer proliferation in vitro. *Mol. Med. Rep.* 11:2125. doi: 10.3892/mmr.2014.2929

Iizuka, N., Miyamoto, K., Okita, K., Tangoku, A., Hayashi, H., Yosino, S., et al. (2000). Inhibitory effect of coptidis rhizoma and berberine on the proliferation of human esophageal cancer cell lines. *Cancer Lett.* 148, 19–25. doi: 10.1016/S0304-3835(99)00264-5

Imenshahidi, M., and Hosseinzadeh, H. (2016). Berberis vulgaris and berberine. *Phytother. Res.* 30, 1745–1764. doi: 10.1002/ptr.5693

Jiang, L., Xue, W., and Wang, Y. (2018). Inhibition of miR-31a-5p decreases inflammation by down-regulating IL-25 expression in human dermal fibroblast cells (CC-2511 cells) under hyperthermic stress via Wnt/β-catenin pathway. *Biomed. Pharmacother.* 107, 24–33. doi: 10.1016/j.biopha.2018.07.142

Jin, Y., Liu, S., Ma, Q., Xiao, D., and Chen, L. (2017). Berberine enhances the ampk activation and autophagy and mitigates high glucose-induced apoptosis of mouse podocytes. *Eur. J. Pharmacol* 794, 106–114. doi: 10.1016/j.ejphar.2016.11.037

Jung-Mu, H., Mee-Sun, H., Sang-Yong, L., Woo-Yiel, L., and Dongho, K. (2009). The combination of berberine and irradiation enhances anti-cancer effects via activation of p38 mapk pathway and ros generation in human hepatoma cells. *J. Cell. Biochem.* 107, 955–964. doi: 10.1002/jcb.22198

Kalaiarasi, A., Anusha, C., Sankar, R., Rajasekaran, S., John, M. J., Muthusamy, K., et al. (2016). Plant isoquinoline alkaloid berberine exhibits chromatin remodeling by modulation of histone deacetylase to induce growth arrest and apoptosis in the a549 cell line. *J. Agric. Food Chem.* 64:9542. doi: 10.1021/acs.jafc.6b04453

Kalinkova, L., Zmetakova, I., Smolkova, B., Minarik, G., Sedlackova, T., Kajabova, V. H., et al. (2018). Decreased methylation in the SNAI2 and ADAM23 genes associated with de-differentiation and haematogenous dissemination in breast cancers. *BMC Cancer* 18:875. doi: 10.1186/s12885-018-4783-x

Katona, B. W., Liu, Y., Ma, A., Jin, J., and Hua, X. (2014). Ezh2 inhibition enhances the efficacy of an egfr inhibitor in suppressing colon cancer cells. *Cancer Biol. Ther.* 15:11. doi: 10.4161/15384047.2014.972776

Khalil, I., Colombara, D. V., Forouzanfar, M. H., Troeger, C., Daoud, F., Moradi-Lakeh, M., et al. (2016). Burden of diarrhea in the eastern mediterranean region, 1990–2013: findings from the global burden of disease study 2013. *Am. J. Trop. Med. Hyg.* 95, 1319–1329. doi: 10.4269/ajtmh.16-0339

Kong, W., Wei, J., Abidi, P., Lin, M., Inaba, S., Li, C., et al. (2004). Berberine is a novel cholesterol-lowering drug working through a unique mechanism distinct from statins. *Nat. Med.* 7, 464–464. doi: 10.1016/S1567-5688(06)81865-9

Kumar, A., Ekavali, Chopra, K., Mukherjee, M., Pottabathini, R., and Dhull, D. K. (2015). Current knowledge and pharmacological profile of berberine: an update. *Eur. J. Pharmacol.* 761, 288–297. doi: 10.1016/j.ejphar.2015.05.068

Lee, C., and Gang, J. (2018). A label-free detection of ndei endonuclease activity by using dna-templated silver nanoclusters. *J. Nanosci. Nanotechnol.* 18:6339. doi: 10.1166/jnn.2018.15657

Li, B., Wang, Z., Wu, H., Xue, M., Lin, P., Wang, S., et al. (2018). Epigenetic regulation of cxcl12 plays a critical role in mediating tumor progression and the immune response in osteosarcoma. *Cancer Res.* 78:3938. doi: 10.1158/0008-5472.can-17-3801

Li, C. H., Wu, D. F., Ding, H., Zhao, Y., Zhou, K. Y., and Xu, D. F. (2014). Berberine hydrochloride impact on physiological processes and modulation of twist levels in nasopharyngeal carcinoma cne-1 cells. *Asian Pac. J. Cancer Prev.* 15, 1851–1857. doi: 10.7314/APJCP.2014.15.4.1851

Li, J., Liu, F., Jiang, S., Liu, J., Chen, X., Zhang, S., et al. (2018). Berberine hydrochloride inhibits cell proliferation and promotes apoptosis of non-small

cell lung cancer via the suppression of the mmp2 and bcl-2/bax signaling pathways. *Oncol. Lett.* 15:7409. doi: 10.3892/ol.2018.8249

Li, L., Wang, X., Sharvan, R., Gao, J., Qu, S., Li, L., et al. (2017). Berberine could inhibit thyroid carcinoma cells by inducing mitochondrial apoptosis, g0/g1 cell cycle arrest and suppressing migration via pi3k-akt and mapk signaling pathways. *Biomed. Pharmacother.* 95, 1225–1231. doi: 10.1016/j.biopha.2017.09.010

Li, L., and Zhao, G. (2016). Downregulation of microrna-218 relieves neuropathic pain by regulating suppressor of cytokine signaling 3. *Int. J. Mol. Med.* 37:851. doi: 10.3892/ijmm.2016.2455

Li, N., Xu, F., Cheng, J., Zhang, Y., Huang, G., Zhu, J., et al. (2018). Perfluorocarbon nanocapsules improve hypoxic microenvironment for the tumor ultrasound diagnosis and photodynamic therapy. *J. Biomed. Nanotechnol.* 14, 2162–2171. doi: 10.1166/jbn.2018.2656

Li, W., Li, Q., Kang, S., Same, M., Zhou, Y., Sun, C., et al. (2018). Cancerdetector: ultrasensitive and non-invasive cancer detection at the resolution of individual reads using cell-free dna methylation sequencing data. *Nucleic Acids Res.* 46:e89.

Liu, L., Chen, L., Jiang, C., Guo, J., Xie, Y., Kang, L., et al. (2017a). Berberine inhibits the lps-induced proliferation and inflammatory response of stromal cells of adenomyosis tissues mediated by the lps/tlr4 signaling pathway. *Exp. Therap. Med.* 14:6125. doi: 10.3892/etm.2017.5316

Liu, L., Luo, N., Guo, J., Xie, Y., Chen, L., and Cheng, Z. (2017b). Berberine inhibits growth and inflammatory invasive phenotypes of ectopic stromal cells: imply the possible treatment of adenomyosis. *J. Pharmacol. Sci.* 137, 5–11. doi: 10.1016/j.jphs.2017.12.001

Lu, W., Du, S., and Wang, J. (2015). Berberine inhibits the proliferation of prostate cancer cells and induces g0/g1 or g2/m phase arrest at different concentrations. *Mol. Med. Rep.* 11, 3920–3924. doi: 10.3892/mmr.2014.3139

Ma, C. Y., Shen, S. C., Huang, D. W., Chang, H. M., and Wu, J. S. B. (2008). Growth inhibition and induction of apoptosis in u937 cells by coptis chinensis extract. *J. Food Sci.* 73, H127–H133. doi: 10.1111/j.1750-3841.2008.00837.x

Ma, W., Zhu, M., Yang, L., Yang, T., and Zhang, Y., (2017). Synergistic effect of TPD7 and berberine against leukemia jurkat cell growth through regulating ephrin-B2 signaling. *Phytother. Res.* 31, 1392–1399.

Meng, F. C., Wu, Z. F., Yin, Z. Q., Lin, L. G., Wang, R., and Zhang, Q. W. (2018). Coptidis rhizoma and its main bioactive components: recent advances in chemical investigation, quality evaluation and pharmacological activity. *Chinese Med.* 13:13. doi: 10.1186/s13020-018-0171-3

Meng, M., Geng, S., Du, Z., Yao, J., Zheng, Y., Li, Z., et al. (2017). Berberine and cinnamaldehyde together prevent lung carcinogenesis. *Oncotarget* 8:76385. doi: 10.18632/oncotarget.20059

Mirhadi, E., Rezaee, M., and Malaekehnikouei, B. (2018). Nano strategies for berberine delivery, a natural alkaloid of berberis. *Biomed. Chromatogr. BMC* 1060:e4279. doi: 10.1002/bmc.4279

Mistry, B. M., Keum, Y. S., Pandurangan, M., Kim, D. H., Moon, S. H., Kadam, A. A., et al. (2017). Synthesis and evaluation of antioxidant and cytotoxicity of the n-mannich base of berberine bearing benzothiazole moieties. *Anti-cancer Agents Med. Chem.* 17, 1652–1660. doi: 10.2174/1871520617666170710180549

Mittal, A., Tabasum, S., and Singh, R. P. (2014). Berberine in combination with doxorubicin suppresses growth of murine melanoma b16f10 cells in culture and xenograft. *Phytomedicine* 21, 340–347. doi: 10.1016/j.phymed.2013.09.002

Munir, I., Fukunaga, K., Kanasaki, H., Miyazaki, K., Ohba, T., Okamura, H., et al. (2000). Expression of cyclooxygenase 2 by prostaglandin e2 in human endometrial adenocarcinoma cell line hec-1b1. *Biol. Reprod.* 63, 933–941. doi: 10.1095/biolreprod63.3.933

Murthy, K. N. C., Kim, J., Vikram, A., and Patil, B. S. (2012). Differential inhibition of human colon cancer cells by structurally similar flavonoids of citrus. *Food Chem.* 132, 27–34. doi: 10.1016/j.foodchem.2011.10.014

Nardi, I., Reno, T., Yun, X., Sztain, T., Wang, J., Dai, H., et al. (2018). Triptolide inhibits Wnt signaling in NSCLC through upregulation of multiple Wnt inhibitory factors via epigenetic modifications to Histone H3. *Int. J. Cancer* 143, 2470–2478. doi: 10.1002/ijc.31756

Naveen, C. R., Gaikwad, S., and Agrawalrajput, R. (2016). Berberine induces neuronal differentiation through inhibition of cancer stemness and epithelial-mesenchymal transition in neuroblastoma cells. *Phytomed. Int. J. Phytother. Phytopharmacol.* 23, 736–744. doi: 10.1016/j.phymed.2016.03.013

Neag, M. A., Mocan, A., Echeverría, J., Pop, R. M., Bocsan, C. I., Crişan, G., et al. (2018). Berberine: botanical occurrence, traditional uses, extraction methods, and relevance in cardiovascular, metabolic, hepatic, and renal disorders. *Front. Pharmacol.* 9:557. doi: 10.3389/fphar.2018.00557

Oliver, K. R., Mccomb, J. A., and Greene, W. K. (2013). Transposable elements: powerful contributors to angiosperm evolution and diversity. *Genome Biol. Evol.* 5, 1886–1901. doi: 10.1093/gbe/evt141

Pandey, A., Vishnoi, K., Mahata, S., Tripathi, S. C., Misra, S. P., Misra, V., et al. (2015). Berberine and curcumin target survivin and stat3 in gastric cancer cells and synergize actions of standard chemotherapeutic 5-fluorouracil. *Nutr. Cancer Int. J.* 67, 1293–1304. doi: 10.1080/01635581.2015.1085581

Peng, P. L., Kuo, W. H., Tseng, H. C., and Chou, F. P., (2008). Synergistic tumor-killing effect of radiation and berberine combined treatment in lung cancer: the contribution of autophagic cell death. *Int. J. Radiat. Oncol. Biol. Phys.* 70, 529–542. doi: 10.1016/j.ijrobp.2007.08.034

Puneet, Kazmi, H. R., Kumari, S., Tiwari, S., Khanna, A., and Narayan, G. (2018). Epigenetic mechanisms and events in gastric cancer-emerging novel biomarkers. *Pathol. Oncol. Res.* 2, 1–14. doi: 10.1007/s12253-018-0410-z

Qi, H. W., Xin, L. Y., Xu, X., Ji, X. X., and Fan, L. H. (2014). Epithelial-to-mesenchymal transition markers to predict response of berberine in suppressing lung cancer invasion and metastasis. *J. Trans. Med.* 12:22. doi: 10.1186/1479-5876-12-22

Qing, Y., Hu, H., Liu, Y., Feng, T., Meng, W., Jiang, L., et al. (2014). Berberine induces apoptosis in human multiple myeloma cell line u266 through hypomethylation of p53 promoter. *Cell Biol. Int.* 38, 563–570. doi: 10.1002/cbin.10206

Rahnamoun, H., Lee, J., Sun, Z., Lu, H., Ramsey, K. M., Komives, E. A., et al. (2018). RNAs interact with BRD4 to promote enhanced chromatin engagement and transcription activation. *Nat. Struct. Mol. Biol.* 25:687. doi: 10.1038/s41594-018-0102-0

Rayan, N. A., Rosario, R. C. H. D., and Prabhakar, S. (2016). Massive contribution of transposable elements to mammalian regulatory sequences. *Semin. Cell Dev. Biol.* 57, 51–56. doi: 10.1016/j.semcdb.2016.05.004

Riaz, S. K., Saeed, M., and Malik, M. F. (2015). Clinical and therapeutic implications of histone acetylation in breast cancer. *West Indian Med. J.* 65, 337–344. doi: 10.7727/wimj.2014.297

Sahebi, M., Hanafi, M. M., van Wijnen, A. J., Rice, D., Rafii, M. Y., Azizi, P., et al. (2018). Contribution of transposable elements in the plant's genome. *Gene* 665, 155–166. doi: 10.1016/j.gene.2018.04.050

Salimian, N., Peymani, M., Ghaedi, K., and Esfahani, M. (2018). Modulation in mir-200a/sirt1axis is associated with apoptosis in mpp+-induced sh-sy5y cells. *Gene* 674, 24–30. doi: 10.1016/j.gene.2018.06.061

Sanna, L., Marchesi, I., Melone, M. A. B., and Bagella, L. (2018). The role of enhancer of zeste homolog 2: from viral epigenetics to the carcinogenesis of hepatocellular carcinoma. *J. Cell. Physiol.* 233, 6508–6517. doi: 10.1002/jcp.26545

Sengupta, D., Chowdhury, K. D., Chatterjee, S., Sarkar, A., Paul, S., Sur, P. K., et al. (2017). Modulation of adenylate cyclase signaling in association with mkk3/6 stabilization under combination of sac and berberine to reduce hepg2 cell survivability. *Apoptosis* 22, 1–18. doi: 10.1007/s10495-017-1407-x

Sengupta, D., Chowdhury, K. D., Sarkar, A., Paul, S., and Sadhukhan, G. C., (2014). Berberine and S allyl cysteine mediated amelioration of DEN+ CCl4 induced hepatocarcinoma. *Biochim. Biophys. Acta (BBA)-Gen. Subjects* 1840, 219–244. doi: 10.1016/j.bbagen.2013.08.020

Shang, A., Bylipudi, S., and Bieszczad, K. M. (2018). Inhibition of histone deacetylase 3 via rgfp966 facilitates cortical plasticity underlying unusually accurate auditory associative cue memory for excitatory and inhibitory cue-reward associations. *Behav. Brain Res.* 356, 453–469. doi: 10.1016/j.bbr.2018.05.036

Shi, H. L., Wu, X. J., Liu, Y., and Xie, J. Q. (2013). Berberine counteracts enhanced il-8 expression of ags cells induced by evodiamine. *Life Sci.* 93, 830–839. doi: 10.1016/j.lfs.2013.09.010

Shi, Y., Zhao, Y., Shao, N., Ye, R., Lin, Y., Zhang, N., et al. (2017). Overexpression of microrna-96-5p inhibits autophagy and apoptosis and enhances the

proliferation, migration and invasiveness of human breast cancer cells. *Oncol. Lett.* 13, 4402–4412. doi: 10.3892/ol.2017.6025

Signorelli, C., Odone, A., Ciorba, V., Cella, P., Audisio, R. A., Lombardi, A., et al. (2017). Human papillomavirus 9-valent vaccine for cancer prevention: a systematic review of the available evidence. *Epidemiol. Infect.* 145:21. doi: 10.1017/s0950268817000747

Siveen, K. S., and Kuttan, G. (2011). Thujone inhibits lung metastasis induced by b16f-10 melanoma cells in c57bl/6 mice. *Can. J. Physiol. Pharmacol.* 89:691. doi: 10.1139/y11-067

Stevens, M. S., Aliabadi, Z., and Moore, M. R. (1984). Associated effects of sodium butyrate on histone acetylation and estrogen receptor in the human breast cancer cell line mcf-7. *Biochem. Biophys. Res. Commun.* 119, 132–138. doi: 10.1016/0006-291X(84)91628-0

Su, Y. H., Tang, W. C., Cheng, Y. W., Sia, P., Huang, C. C., Lee, Y. C., et al. (2015). Targeting of multiple oncogenic signaling pathways by hsp90 inhibitor alone or in combination with berberine for treatment of colorectal cancer. *BBA – Mol. Cell Res.* 1853, 2261–2272. doi: 10.1016/j.bbamcr.2015.05.012

Sun, W., Zhang, L., and Li, R. (2017). Overexpression of miR-206 ameliorates chronic constriction injury-induced neuropathic pain in rats via the MEK/ERK pathway by targeting brain-derived neurotrophic factor. *Neurosci. Lett.* 646, 68–74. doi: 10.1016/j.neulet.2016.12.047

Tabeshpour, J., Imenshahidi, M., and Hosseinzadeh, H. (2017). A review of the effects ofberberis vulgarisand its major component, berberine, in metabolic syndrome. *Iran. J. Basic Med. Sci.* 20, 557–568. doi: 10.22038/IJBMS.2017.8682

Tang, J., and Feng, Y. S. (2009). Berberine and coptidis rhizoma as novel antineoplastic agents: a review of traditional use and biomedical investigations. *J. Ethnopharmacol.* 126, 5–17. doi: 10.1016/j.jep.2009.08.009

Tao, Y., Lin, Y., She, Z., Lin, M., Chen, P., and Zhang, J. (2015). Anticancer activity and mechanism investigation of beauvericin isolated from secondary metabolites of the mangrove endophytic fungi. *Anti-Cancer Agents Med. Chem.* 15, 258–266. doi: 10.2174/1871520614666140825112255

Tong, N., Zhang, J., Chen, Y., Zhubo, L. I., Luo, Y., Zuo, H., et al. (2012). Berberine sensitizes mutliple human cancer cells to the anticancer effects of doxorubicin in vitro. *Oncol. Lett.* 3, 1263–1267. doi: 10.3892/ol.2012.644

Viegas, S., Ladeira, C., Costaveiga, A., Perelman, J., and Gajski, G. (2017). Forgotten public health impacts of cancer – An overview. *Arh. Hig. Rada. Toksikol.* 68:287. doi: 10.1515/aiht-2017-68-3005

Vijayaraghavalu, S., Dermawan, J. K., and Cheriyath, V. (2013). Highly synergistic effect of sequential treatment with epigenetic and;anticancer drugs to overcome drug resistance in breast cancer cells is;mediated via activation of p21 gene expression leading to g2/m cycle;arrest. *Mol. Pharm.* 10, 337–352. doi: 10.1021/mp3004622

Walker, D. K., Edwards, R. L., Bagcivan, G., and Bakitas, M. A. (2017). Cancer and palliative care in the united states, turkey, and malawi: developing global collaborations. *Asia-Pacific J. Oncol. Nurs.* 4, 209–219. doi: 10.4103/apjon.apjon_31_17

Wang, J., Kang, M., Wen, Q., Qin, Y. T., Wei, Z. X., Xiao, J. J., et al. (2017). Berberine sensitizes nasopharyngeal carcinoma cells to radiation through inhibition of sp1 and emt. *Oncol. Rep.* 37, 2425–2432. doi: 10.3892/or.2017.5499

Wang, N., Feng, Y., Cheung, F., Wang, X., Zhang, Z., and Feng, Y. (2015a). A chinese medicine formula gegen qinlian decoction suppresses expansion of human renal carcinoma with inhibition of matrix metalloproteinase-2. *Integr. Cancer Ther.* 14:75. doi: 10.1177/1534735414550036

Wang, N., Tan, H. Y., Li, L., Yuen, M. F., and Feng, Y. (2015b). Berberine and coptidis rhizoma as potential anticancer agents: recent updates and future perspectives. *J. Ethnopharmacol.* 176, 35–48. doi: 10.1016/j.jep.2015.10.028

Wang, S., Xiao, Z., Hong, Z., Jiao, H., Zhu, S., Zhao, Y., et al. (2018). FOXF1 promotes angiogenesis and accelerates bevacizumab resistance in colorectal cancer by transcriptionally activating VEGFA. *Cancer Lett.* 439, 78–90. doi: 10.1016/j.canlet.2018.09.026

Wang-Johanning, F., Radvanyi, L., Rycaj, K., Plummer, J. B., Yan, P., Sastry, K. J., et al. (2008). Human endogenous retrovirus k triggers an antigen-specific immune response in breast cancer patients. *Cancer Res.* 68, 5869–5877. doi: 10.1158/0008-5472.CAN-07-6838

Waterbeemd, B. V. D., Mommen, G. P. M., Pennings, J. L. A., Eppink, M. H., Wijffels, R. H., Pol, L. A. V. D., et al. (2013). Quantitative proteomics reveals distinct differences in the protein content of outer membrane vesicle vaccines. *J. Proteome Res.* 12, 1898–1908. doi: 10.1021/pr301208g

Wen, C., Wu, L., Fu, L., Zhang, X., and Zhou, H. (2016). Berberine enhances the anti-tumor activity of tamoxifen in drug-sensitive MCF-7 and drug-resistant MCF-7/TAM cells. *Mol. Med. Rep.* 14, 2250–2256. doi: 10.3892/mmr.2016.5490

Wong, K. Y., and Chim, C. S. (2015). DNA methylation of tumor suppressor protein-coding and non-coding genes in multiple myeloma. *Epigenomics* 7, 985–1001. doi: 10.2217/epi.15.57

Wu, Y. Q., Chen, X. S., and Chai, J. B. (2012). The involvement of the cd40-cd40l pathway in activated platelet-induced changes in huvec cox-2 and pparα expression. *Inflammation* 35, 1184–1190. doi: 10.1007/s10753-011-9427-0

Xu, Z., Feng, W., Shen, Q., Yu, N., Yu, K., Wang, S., et al. (2017). Rhizoma coptidis and berberine as a natural drug to combat aging and aging-related diseases via anti-oxidation and ampk activation. *Aging Dis.* 8, 760–777. doi: 10.14336/AD.2016.0620

Xue, M., Yang, M. X., Zhang, W., Li, X. M., Gao, D. H., Ou, Z. M., et al. (2013). Characterization, pharmacokinetics, and hypoglycemic effect of berberine loaded solid lipid nanoparticles. *Int. J. Nanomed.* 8(Issue 1), 4677–4687. doi: 10.2147/IJN.S51262

Yakata, Y., Nakayama, T., Yoshizaki, A., Kusaba, T., and Sekine, I. (2007). Expression of p-stat3 in human gastric carcinoma: significant correlation in tumour invasion and prognosis. *Int. J. Oncol.* 30, 437–442. doi: 10.3892/ijo.30.2.437

Yamada, K., Mizukoshi, E., Sunagozaka, H., Arai, K., Yamashita, T., Takeshita, Y., et al. (2015). Response to importance of confounding factors in assessing fatty acid compositions in patients with non-alcoholic steatohepatitis. *Liver Int.* 35, 1773–1773. doi: 10.1111/liv.12755

Yan, L., Yang, X., and Davidson, N. E. (2001). Role of dna methylation and histone acetylation in steroid receptor expression in breast cancer. *J. Mamm. Gland Biol. Neoplasia* 6, 183–192. doi: 10.1023/a:1011308707512

Yan, X. T., Zhao, Y., and Cheng, X. L. (2018). Inhibition of mir-200b/mir-429 contributes to neuropathic pain development through targeting zinc finger e box binding protein-1. *J. Cell Physiol.* 233, 4815–4824. doi: 10.1002/jcp.26284

Yang, M., Yang, Y., Cui, H., Guan, Z., Yang, Y., Zhang, H., et al. (2015). The natural compound gambogic acid radiosensitizes nasopharyngeal carcinoma cells under hypoxic conditions. *Tumori* 102:135. doi: 10.5301/tj.5000411

Zhang, J., Lai, Z., Huang, W., Ling, H., Lin, M., Tang, S., et al. (2017). Apicidin inhibited proliferation and invasion and induced apoptosis via mitochondrial pathway in non-small cell lung cancer glc-82 cells. *Anti-cancer Agents Med. Chem.* 17, 1374–1382. doi: 10.2174/1871520617666170419120044

Zhang, J., Yi, T., Liu, J., Zhao, Z., and Chen, H. (2013). Quercetin induces apoptosis via the mitochondrial pathway in kb and kbv200 cells. *J. Agric. Food Chem.* 61, 2188–2195. doi: 10.1021/jf305263r

Zhang, J., Zhang, H., and Zi, T. (2015). Overexpression of microrna-141 relieves chronic constriction injury-induced neuropathic pain via targeting high-mobility group box 1. *Int. J. Mol. Med.* 36:1433. doi: 10.3892/ijmm.2015.2342

Zhang, J. Y., Huang, W. J., Sun, H. M., Liu, Y., Zhao, X. Q., Tang, S. L., et al. (2017). Structure identification and in vitro anticancer activity of lathyrol-3-phenylacetate-5,15-diacetate. *Molecules* 22:1412. doi: 10.3390/molecules22091412

Zhang, J. Y., Lin, M. T., Tung, H. Y., Tang, S. L., Yi, T., Zhang, Y. Z., et al. (2016). Bruceine d induces apoptosis in human chronic myeloid leukemia k562 cells via mitochondrial pathway. *Am. J. Cancer Res.* 6:819.

Zhang, J. Y., Lin, M. T., Zhou, M. J., Yi, T., Tang, Y. N., Tang, S. L., et al. (2015). Combinational treatment of curcumin and quercetin against gastric cancer mgc-803 cells in vitro. *Molecules* 20, 11524–11534. doi: 10.3390/molecules200611524

Zhang, L., Fang, Y., Xu, X. F., and Jin, D. Y. (2017). Moscatilin induces apoptosis of pancreatic cancer cells via reactive oxygen species and the jnk/sapk pathway. *Mol. Med. Rep.* 15, 1195–1203. doi: 10.3892/mmr.2017.6144

Zhang, L., Wang, Y., Wang, L., Yin, G., Li, W., Xian, Y., et al. (2018). miR-23c suppresses tumor growth of human hepatocellular carcinoma by attenuating ERBB2IP. *Biomed. Pharmacother.* 107, 424–432. doi: 10.1016/j.biopha.2018.07.155

Zhang, S., Chang, M., Zhou, Z., Dai, X., and Xu, Z. (2018). Pdhs-elm: computational predictor for plant dnase i hypersensitive sites based on extreme learning machines. *Mol. Genet. Genomics* 293, 1035–1049. doi: 10.1007/s00438-018-1436-3

Zhang, X. Z., Wang, L., Liu, D. W., Tang, G. Y., Zhang, H. Y., et al. (2014). Synergistic inhibitory effect of berberine and d-limonene on human gastric carcinoma cell line MGC803. *J. Med. Food* 17, 955–962. doi: 10.1089/jmf.2013.2967

Zhao, Y., Gao, J. L., Ji, J. W., Gao, M., Yin, Q. S., Qiu, Q. L., et al. (2014). Cytotoxicity enhancement in MDA-MB-231 cells by the combination treatment of tetrahydropalmatine and berberine derived from *Corydalis yanhusuo* WT Wang. *J. Int. Ethnopharmacol.* 3:68. doi: 10.5455/jice.20140123040224

Zhao, Y., Jing, Z., Li, Y., and Mao, W., (2016). Berberine in combination with cisplatin suppresses breast cancer cell growth through induction of dna breaks and caspase-3-dependent apoptosis. *Oncol. Rep.* 36, 567–572. doi: 10.3892/or.2016.4785

Zheng, F., Wu, J., Tang, Q., Xiao, Q., Wu, W., Hann, S. S., et al. (2018). The enhancement of combination of berberine and metformin in inhibition of DNMT1 gene expression through interplay of SP1 and PDPK1. *J. Cell Mol. Med.* 22, 600–612. doi: 10.1111/jcmm.13347

Zhu, T., Li, L. L., Xiao, G. F., Luo, Q. Z., Liu, Q. Z., Yao, K. T., et al. (2015). Berberine increases doxorubicin sensitivity by suppressing stat3 in lung cancer. *Am. J. Chin. Med.* 43, 1487–1502. doi: 10.1142/S0192415X15500846

Conflict of Interest Statement: The authors declare that the research was conducted in the absence of any commercial or financial relationships that could be construed as a potential conflict of interest.

frontiers in Oncology

ORIGINAL RESEARCH
published: 21 February 2019
doi: 10.3389/fonc.2019.00100

Wheat Germ Agglutinin as a Potential Therapeutic Agent for Leukemia

Bradley Ryva[1], *Keman Zhang*[2], *Abhishek Asthana*[2], *Derek Wong*[1], *Yorleny Vicioso*[1] *and Reshmi Parameswaran*[1,2,3]*

[1] Department of Pathology, School of Medicine, Case Western Reserve University, Cleveland, OH, United States, [2] Division of Hematology/Oncology, Department of Medicine, School of Medicine, Case Western Reserve University, Cleveland, OH, United States, [3] The Case Comprehensive Cancer Center, Case Western Reserve University School of Medicine, Cleveland, OH, United States

Dietary lectins are carbohydrate-binding proteins found in food sources. We used a panel of seven dietary lectins to analyze cytotoxicity against hematological cancers. Wheat germ agglutinin (WGA), even at low doses, demonstrated maximum toxicity toward acute myeloid leukemia (AML) cells. Using AML cell lines, we show time- and dose-dependent killing by WGA. We also show that low doses of WGA kills primary patient AML cells, irrespective of subtype, with no significant toxicity to normal cells. WGA caused AML cell agglutination, but failed to agglutinate RBC's at this dose. WGA, primarily, binds to *N*-acetyl-D-glucosamine (GlcNAc) and is also reported to interact with sialic-acid-containing glycoconjugates and oligosaccharides. After neuraminidase pre-treatment, which catalyzes the hydrolysis of terminal sialic acid residues, AML cells were less sensitive to WGA-induced cell death. AML cells were also not sensitive to succinyl-WGA, which does not react with sialic acid. Incubation with LEL lectin, which recognizes GlcNAc or SNA, which binds preferentially to sialic acid attached to terminal galactose in α-2,6 and to a lesser degree α-2,3 linkage, did not alter AML cell viability. These data indicate that WGA-induced AML cell death is dependent on both GlcNAc binding and interaction with sialic acids. We did not observe any *in vitro or in vivo* toxicity of WGA toward normal cells at the concentrations tested. Finally, low doses of WGA injection demonstrated significant *in vivo* toxicity toward AML cells, using xenograft mouse model. Thus, WGA is a potential candidate for leukemia therapy.

Keywords: WGA, leukemia, therapy, lectin, GlcNAc

OPEN ACCESS

Edited by:
Zhe-Sheng Chen,
St. John's University, United States

Reviewed by:
Daekyu Sun,
University of Arizona, United States
Kajian Hou,
Guangzhou University of Chinese Medicine, China
Minfeng Chen,
Jinan University, China

***Correspondence:**
Reshmi Parameswaran
rxp278@case.edu

Specialty section:
This article was submitted to Cancer Molecular Targets and Therapeutics, a section of the journal Frontiers in Oncology

Received: *13 September 2018*
Accepted: *04 February 2019*
Published: *21 February 2019*

Citation:
Ryva B, Zhang K, Asthana A, Wong D, Vicioso Y and Parameswaran R (2019) Wheat Germ Agglutinin as a Potential Therapeutic Agent for Leukemia. Front. Oncol. 9:100. doi: 10.3389/fonc.2019.00100

INTRODUCTION

Lectins, carbohydrate-binding proteins, have been well characterized for more than 40 years (1). Because they are present in many of our major staple foods, such as wheat, potato, soy, and tomato, they play an important role for humans (2). Their true biological function is as a pesticide and anti-fungal, preventing disease from spreading and killing the plant or organism (3). Lectins, also present in animals and fungi, are classified by evolutionary origin, three-dimensional structure, and binding specificity (4, 5). In the last 10 years, with technological improvements in protein structural analysis, lectins have been organized into seven families. Most lectins are within the legume, chitin-binding (hevein domain), type 2 ribosome-inactivating, and monocot mannose-binding lectin families; but there are also jacalin-related, amaranthin, and Cucurbitacea phloem families (6).

Lectins have wide-ranging biological activity at cellular, tissue, and organism levels. *In vitro*, it has been demonstrated that incubation with lectin from red kidney bean lead to T cell proliferation and increased cytokine production (7). Haas et al. demonstrated that certain dietary lectins can cause IL-4 and IL-13 release from basophils (8), while Gong et al. demonstrated that plant lectins can activate NLRP3 inflammasome in macrophages, although at concentrations outside of normal physiological conditions (9). Recently it has been shown that certain lectins can activate toll-like receptors (TLRs) in a distinct, yet comparable, fashion to activation by pathogens. Specifically, the lectin ArtinM leads to TLR activation, resulting in increased pro-inflammatory cytokine release (10). Since their first isolations, lectins have been known to agglutinate cells, including red blood cells (11). When lectins are ingested, they have effects on tissues and organs, partially because they are not digested by gut enzymes (12) but pass through the gut wall and enter the circulation (13, 14). Lectins have also been shown to cause gut inflammation and have been potentially linked to autoimmune disease, such as rheumatoid arthritis (15). Besides this biological activity toward normal tissues, lectins have been shown to exhibit specific effects on cancer cells.

Many lectins have demonstrated cytotoxic and anti-proliferative effect on cancer cells. In the early 1980s, it was shown that lectin from *Griffonia simplicifolia* administered to mice *in vivo* was cytotoxic toward ascites tumor cells (16). Miyoshi et al. showed that rice bran agglutinin (RBA) caused apoptosis and cell cycle disruption on human U937 monoblastic leukemia cells (17). Lectins like *Concanavalin* A, *Griffonia simplicifolia* (GSA-1A4), and *Phaseolus vulgaris* were shown to be toxic toward melanoma cell lines (18). Finally, Wang et al. looked at various lectins and their effects on cancers of the liver, chorion, skin, and bone. They determined that lectins from mushroom, soybean, and potato had varying impacts on these cell lines (19). Of the lectins tested, wheat germ agglutinin (WGA) had the most profound cytotoxic effects against these cell lines.

WGA, the lectin derived from wheat germ, binds specifically to *N*-Acetyl-D-glucosamine (GlcNAc). It has been reported that WGA also binds *N*-acetyl-neuraminic (sialic) acid; however more recently it has been characterized as interacting with sialic acid residues on glyconjugates and oligosaccharides (20). WGA is one of the most characterized and studied lectins. While studying the effect of WGA on normal gut epithelium, it was determined that WGA can bind the apical side of gut-like cells and alter the cell membrane permeability (21). Pellegrina et al. also quantified whether the amount of wheat consumed in the normal diet is toxic. They concluded that in order to reach toxic levels more than 1 kilogram of uncooked pasta would need to be consumed in one meal (21). Despite the limited toxicity to normal tissues, it has been shown that WGA is toxic to pancreatic, liver, bone (osteosarcoma), and skin (melanoma) cancer in low doses (18, 19, 22). WGA causes killing via apoptosis and cell cycle arrest in melanoma and human monoblastic leukemia (14, 17). It may also work in a novel apoptotic fashion that is Fas-, caspase-3, Bax, and Bak independent (23). Recently, there is evidence that WGA can kill via a completely different pathway. It has been demonstrated that WGA induces paraptosis-like cell death in cervical carcinoma cells (24). These different modes of killing, dependent on target cells, makes WGA an intriguing protein to study.

Because lectins, specifically wheat germ agglutinin, have been shown to be cytotoxic toward pancreatic cancer, osteosarcoma, hepatoma, etc. (19, 22), we screened three hematological malignancies [acute myeloid leukemia (AML), acute lymphoblastic leukemia (ALL), and non-Hodgkin lymphoma (NHL)] against a panel of lectins. AML is a common childhood leukemia. In patients who acquire the malignancy in adulthood it has a low survival rate (25). ALL is the most common pediatric cancer. If relapse occurs, patients have an even lower survival rate (26). NHL is an umbrella term for many different malignancies that originate in the lymphoid system (27). Because of this broad category, NHL is one of the most common cancers in the United States and the American Cancer Society estimates that more than 70,000 cases will be diagnosed in 2018 (28). Because these three cancer types are very common impacting large numbers of people, we looked at the cytotoxic effects of various lectins on these cancer cells.

Abbreviations: WGA, Wheat germ agglutinin; AML, acute myeloid leukemia, ALL, acute lymphoid leukemia; NHL, non-Hodgkin Lymphoma; sWGA, Succinyl-WGA; LEL, *L. esculentum* lectin; SNA, *S. nigra*; *N*-acetyl-D-neuraminic (sialic) acid; GlcNAc, *N*-acetyl-D-glucosamine.

METHODS

Cell Culture

Human acute myeloid leukemia cell lines, OCI-AML3 and HL-60, obtained from DMSZ and American Type Culture collection, respectively, were cultured in sterile RPMI-1640 medium (R8758) with 10% Serum Plus II and 5% penicillin streptomycin. Human acute lymphoblastic leukemia cell lines, ALL-1 and ALL-2, were cultured in MEM medium (M4526) with 20% FBS. ALL-1 NSG cell line had been passaged through mice before freezing and usage. Human non-Hodgkin lymphoma cell lines, JVM2 and OCI-Ly10, were cultured in RPMI complete medium and in Iscove's DMEM (10-016CV) (20% SPII and 1% Glutamax), respectively. Non-cancerous control cells, HEK293 and OP9, were cultured in DMEM (sc-224478) and MEM, respectively. All cell lines were cultured at 37°C and 5% carbon dioxide. When cells reached confluency, they were passaged.

Patient Samples

Primary patient AML cells were ordered from the Hematopoietic Stem Cell Core Facility at Case Western Reserve University and cultured in RPMI-1640 complete medium (10% FBS). Peripheral blood mononuclear cells (PBMCs), isolated from blood, were obtained from the Hematopoietic Stem Cell Core Facility at Case Western and cultured in RPMI-1640 complete medium (10% Serum Plus II). Human blood was also obtained from Hematopoietic Stem Cell Core Facility at Case Western Reserve University.

Lectins

Lectins from: *Pisum sativum* (L5380), *Arachis hypogaea* (L0881), *Triticum vulgaris* (L9640), *Glycine max* (L1395), *Phaseolus vulgaris* (61764), *Agaricus bisprous* (L5640), *Lycopersicon esculentum* (L2886) were purchased from Sigma-Aldrich, dissolved in sterile phosphate-buffered saline (PBS), and stored at 4°C in a concentration of 1 mg/mL. Succinyl-WGA (W0110) and wheat germ agglutinin FITC-conjugate (L4895), were purchased at Vector Laboratories and Sigma-Aldrich, respectively. These variants were also dissolved in sterile phosphate-buffered saline (PBS) and stored at 4°C in a concentration of 1 mg/mL. Lectin from *Sambucus nigra* (ZB0106) was purchased from Vector Laboratories. Detailed information on each lectin is included in **Table 1** and obtained from Sigma-Aldrich product sheets.

Reagents

Neuraminidase (N7885) was purchased from Sigma-Aldrich and stored at 4°C. Propidium Iodide/RNAase staining kit (P40875) was obtained from Cell Signaling Technology. Annexin V Apoptosis Detection Kit with PI (640914) was purchased from BioLegend. Trypan blue (T8154) was purchase from Sigma-Aldrich. Alsever's Solution was prepared using Sally E. Grimes's protocol (29). Citric acid (1940) and Sodium chloride (BP-358-10) was purchased from Sigma-Aldrich, while Sodium citrate (S-4641) and D-glucose (G-5767) were purchased from Fisher Scientific.

Cell Death Assay

HL60 and OCI cells were seeded in 12-well plates at a concentration of 250,000 cells/mL (1 mL per well). Cells were treated with WGA at various concentrations on day 0, then again at 24 h intervals up until the final day of measurement. Two microliter PBS were added as a negative control. Cell count and cell viability were assessed using 1:1 trypan blue staining (Sigma-Aldrich) and an automated cell counter (Bio-Rad TC-20). Measurements were conducted in triplicate. Data was graphed and analyzed using GraphPad Prism 7.

Apoptosis Assay

Cells were treated with 2 μg/mL WGA for 24 h. Cells were centrifuged at 300 × *g* for 5 min and the supernatant was removed. The pellet was washed with PBS and resuspended in 100 μL Annexin V/ Propidium iodide (AV/PI) buffer. Samples and positive controls were incubated with 3 μL of Annexin V antibody and 10 μL of Propidium Iodide for 15 min at room temperature. The samples were run using fluorescence-activated cell sorting (FACS BD Accuri™C6). 20,000 events were recorded per sample. AV/PI kit from Biolegend, USA was used to perform apoptosis assay.

Cell Cycle Analysis

Cells were seeded at 250,000 cells per mL in 4 mL and treated with WGA. Cells were spun at 600 rpm for 5 min and washed with PBS twice. Pellet was resuspended in PBS and vortexed to make single cell suspension. While vortexing the sample, 1 mL of ice-cold 70% ethanol was added. Samples were incubated overnight in −20°C. Then, samples were pelleted, washed, resuspended in PBS, and incubated with 100 μL of Propidium Iodide at room temperature for 15 min. Samples were analyzed with FACS, counting 10,000 events. Events collected were gated on live cell populations, avoiding debris and aggregate populations.

For cell aggregation/agglutination assay, HL-60, OCI, and healthy human white blood cells (WBCs) were seeded in 12-well plates at a concentration of 250,000 cells/mL (1 mL per well). Cells were treated with either 2 μg/mL WGA or with 2 μL PBS as a negative control. After 20 h treatment, cells were assessed at 10x magnification using bright field microscopy (Leica DM IL LED) and captured using Leica LAS X imaging software.

WGA Binding

WGA-FITC working stock was made by diluting the 1 μg/mL stock solution. HL-60 AML cells were seeded at 250,000 cells per mL and treated with 0.5 μg/mL WGA-FITC at 37°C. At each time point, samples were washed with PBS and analyzed using FACS.

Sialic Acid-Based Treatments

Cells were treated with succinylated-WGA (sWGA) at 2 μg/mL at 37°C for 24 h. Samples were counted using trypan blue. For neuraminidase pre-treatment, the protocol described in Schwarz et al. where 4 million cells in 2 mL serum free media are incubated with 50 mU/mL neuraminidase for 1 h at 37°C was used (22). Samples were washed twice in complete media and seeded in wells at 250,000 cells/mL. Samples were treated with WGA in the same manner as described above. Cells were stained with Propidium iodide and cell viability was determined using flow cytometry.

E-670 Cell Proliferation Assays

OCI AML-3 and HL-60 cell lines were labeled with 1 mM cell proliferation Dye eFluor 670™ (Thermo Fisher Scientific) as per manufacturer's instructions. After staining cells were washed two times and cultured at 37°C in media alone or in the presence of 2.5 μg/mL WGA for the indicated times. Proliferation of live cells was assessed via flow cytometry (Accuri 6C).

In vitro Toxicity

Two AML patient samples were treated in the absence or presence of with 2 μg/mL WGA for 24 h at 37°C. The samples were analyzed for viability by flow cytometry. OP9 and HEK293 cells were plated and incubated for 24 h with doses of WGA. Confocal images were acquired using EVOS® XL Core Imaging System.

Hemagglutination (HA) Assay

The protocol designed by Virapur® was modified as follows (30). Acquired mouse blood was stored in prepared Alsever's solution. After three washes in PBS, 10% blood stock solution was made in PBS. A working stock (5%) solution was made using the 10% stock and PBS. A serial dilution of WGA (50 μg to 0.09 μg/mL) was prepared using a round-bottomed 96-well plate. 0.0 μg/mL WGA was used as a negative control. The plate was incubated for 30–60 min at room temperature and images were taken. The plates were analyzed by looking for "buttons" in each well. Diffuse blood in the well is analyzed as hemagglutination. Experiments were performed on human blood, as well, but the blood was

TABLE 1 | All lectins used and their name, source, molecular weight, and sugar specificities.

Lectin	Source[a]	Molecular weight[b] (kDa)	Sugar specificity[c]
Wheat germ agglutinin (WGA)	*T. vulgaris* (wheat)	36	$(GlcNAc)_2$ & NeuNAc
Succinyl-Wheat germ agglutinin (sWGA)	*T. vulgaris* (wheat)	36	$(GlcNAc)_2$
Pisum sativum agglutinin (PSA)	*P. sativum(pea)*	49	α-man
Peanut agglutinin (PNA)	*A. hypogaea* (peanut)	120	Gal-β(1→ 3)-GalNAc
Soybean agglutinin (SBA)	*Glycine max* (soy)	110	GalNAc
Phytohemagglutinin (PHA)	*P. vulgaris* (red kidney bean)	126/128	Oligosaccharide
Agaricus bisporus lectin (ABL)	*A. bisporus* (mushroom)	58.5	β-gal(1→ 3)GalNAc
Lycopersicon esculentum lectin (LEL)	*L. esculentum* (tomato)	71	$(GlcNAc)_3$
Sambucus nigra lectin (SNA)	*S. nigra* (elderberry)	140	αNeuNAc(2→ 6)gal & GalNAc

Information obtained from Sigma-Aldrich data sheets.
[a,b,c]All values and specificities from Sigma Aldrich product information sheet.

not stored in Alsever's solution because it already contains the anti-coagulant heparin.

In vivo Toxicity

Twelve-week-old C57BL mice were given WGA (2 mg/kg) by intraperitoneal injection on days 1, 4, and 8. Mouse weights were also taken throughout the time of administration. After WGA administration was completed, the mice were sacrificed and spleen, kidney, and liver were harvested and fixed in formalin. H&E staining was completed at the Immunohistochemistry Core Facility at CWRU. Blood was collected in EDTA-coated tubes and analyzed using HemaVet.

Xenograft *in vivo* Model

NSG mice were subcutaneously injected with 5×10^6 HL-60 cells to generate solid AML xenograft mice model, followed by three intra-tumor injection of WGA or PBS.

Statistical Analysis

Data were analyzed using unpaired Student's *t*-test. All experiments were done in triplicate ($n = 3$). *P*-values in figures correspond to: ns = non-significant (>0.05), $^*P < 0.05$, $^{**}P < 0.01$, $^{***}P < 0.001$. All graphs were made and statistical analyses were performed using GraphPad Prism program.

RESULTS

Lectins Demonstrate Variable Cytotoxic Activity Toward Different Cancers

In order to determine how WGA killing compares to other lectin treatment, we looked at a panel of varied lectins. Cytotoxic effects of seven different dietary lectins at 2.0 μg/mL were tested toward AML, ALL, and NHL. Two cell lines from each disease type were used. Wheat germ agglutinin (WGA) consistently showed significant cytotoxicity toward all five cancer cell lines, except OCI-Ly10. As shown in **Figure 1**, WGA-mediated cell killing of OCI-AML3 ($p = 0.0028$), HL60 ($p = 0.0005$), ALL-1 ($p = 0.0058$), ALL-2 ($p = 0.03$), and JVM2 ($p = 0.009$) were statistically significant (**Figures 1A–C**). All other lectins tested did not show significant cytotoxic activity toward these cancer cells. Binding specificities of all these lectins are detailed in **Table 1**.

WGA Binds and Kills Cancer Cells in a Dose- and Time-Dependent Manner

We were interested at which dose and time WGA would be most effective, so we looked at binding and killing at different doses and time points. We utilized a FITC-labeled WGA at 0.5 μg/mL, in order to analyze cellular binding using flow cytometry at a sub-lethal WGA dose. From the flow cytometry data, it is evident that within 45 min of incubation with WGA, the lectin is bound to the surface of the OCI-AML3 cells. This binding is present up to 24-h after incubation (**Figure 2A**). We also wanted to elucidate the relationship between binding and killing, so we looked at binding of WGA to OCI-Ly10 compared to HL-60 AML. We show that there is a significant reduction in WGA-binding to OCI-Ly10 (**Figure 2B**). This reduction in binding coincides with the absence of WGA-induced cell killing of OCI-Ly10 (**Figure 1C**).

Sensitivity of AML cells to WGA up to 4 days was calculated using OCI-AML3 and HL-60 cell lines, using four different doses. Significant killing for HL-60, occurred at 1.0, 2.0, and 4.0 μg/mL, starting from day 1 of WGA treatment (**Figure 2C**). We analyzed cell killing at day 1, 2, 3, and 4. At day 4, almost all cells were killed except for 0.5 μg/mL WGA treated wells. Viable cell count data shows that most of the cells were killed at day 1 itself. Dose kinetics of OCI-AML3 cells show significant killing at 2.0 and 4.0 μg/ml WGA (**Figure 2D**). HL-60 was more sensitive to WGA induced cell death, even at 1.0 μg/ml, while OCI-AML3 was sensitive to 2.0 μg/ml WGA.

WGA Kills Different Subtypes of Primary Patient AML Cells

In order to further evaluate our findings using AML cell lines, we tested if WGA has same effect on primary cells derived from AML patients. AML can be divided into eight different subclasses (M0-M7) based on the differentiation status, according to the French-American-British (FAB) classification (31). AML also can be divided into subtypes based on WHO classification of genetic abnormalities (32). Primary acute myeloid leukemia blood samples from two AML patients (subtype M1 and M5) were treated with 2 μg/mL WGA for 24 h and analyzed by flow cytometry. The flow cytometry count of viable cells (as determined by analyzing forward and side scatter) demonstrates very significant cell killing at this dose of WGA for both

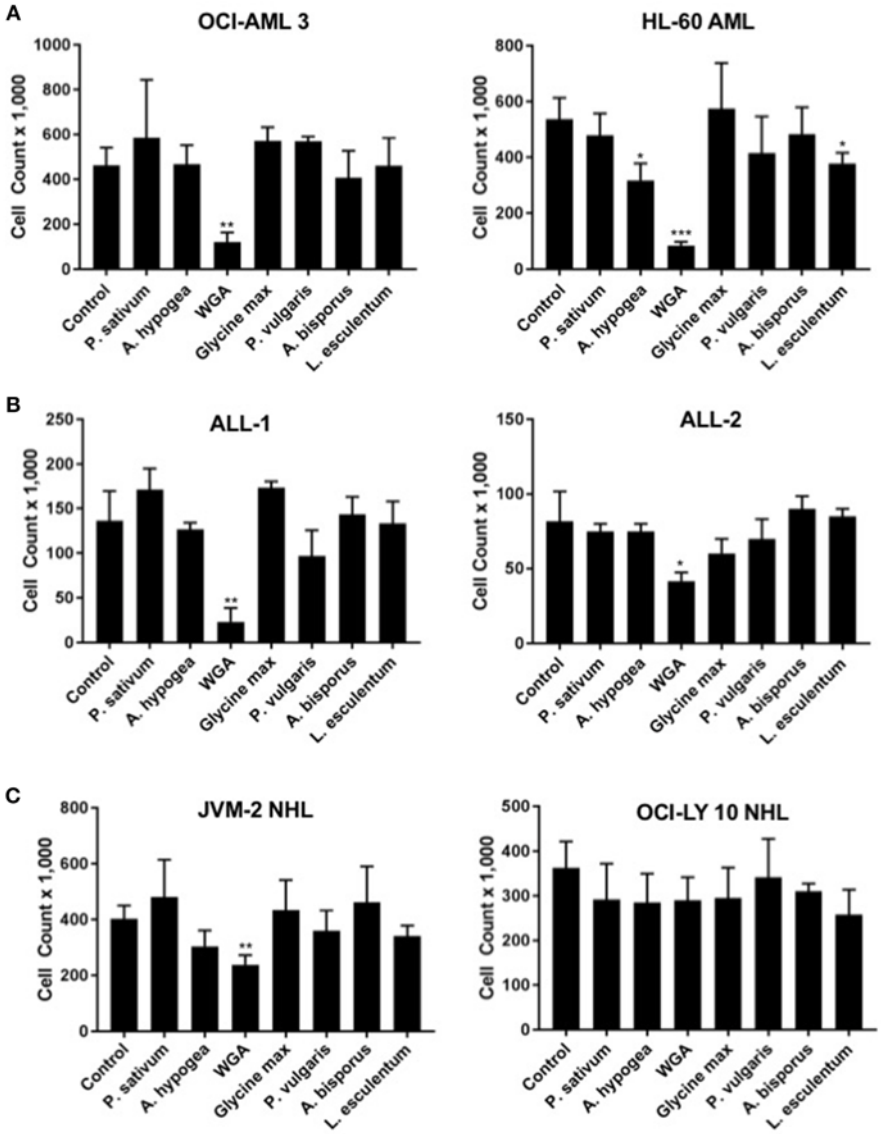

FIGURE 1 | Lectins demonstrate variable toxicities to cancer types. **(A)** Viable cell count of AML (OCI-AML3 and HL-60) cells treated with different dietary lectins as indicated. **(B)** Viable cell count of ALL (ALL-1 and ALL-2) cells treated with different dietary lectins as indicated. **(C)** Viable cell count of NHL (JVM2 and OCI-Ly10) cells treated with different dietary lectins as indicated. All seven lectins administered at 2 μg/mL for 24 h for all cell types. Un-labeled bars were non-significant compared to control. $^{*}p < 0.05$, $^{**}p < 0.01$, $^{***}p < 0.001$, and ns > 0.05.

patient samples ($p = 0.0001$) (**Figure 3A**). Further, we analyzed sensitivity of seven more different AML subtypes to WGA induced killing and found that all six subtypes except M2 subtype showed significant cell killing after exposure to 1.0 and 2.0 μg/ml WGA (**Figure 3B**). M2 subtype with MDS related changes showed maximum killing, even after exposure to 1.0 μg/ml WGA (**Figure 3B**).

After confirming WGA induced cell death in different AML cell lines and patient cells, we wanted to elucidate the specific method of cell killing that WGA utilizes toward AML cells by focusing on cell death and cell cycle. Annexin V (AV)/Propidium Iodide (PI) stain can be used to distinguish between necrotic and apoptotic cell death. AV staining works by binding to phosphatidylserine, which normally resides on the inner cell membrane. However, in early apoptosis, the cellular membrane undergoes changes where phosphatidylserine is present on the outer membrane. PI staining works due to cell membrane rupture, which allows the stain to enter the cell which are in late apoptotic phase or undergoing necrotic death. Flow cytometry scatter demonstrates that at 2 μg/mL there are AV+ and PI+ cells. There is a significant difference between AV–/PI–, AV+, and AV+/PI+ of control and treated HL-60 AML cells ($p = 0.0002$, $p = 0.0068$, $p = 0.0006$). However, there was no statistical difference between PI+ (alone) of control and treated

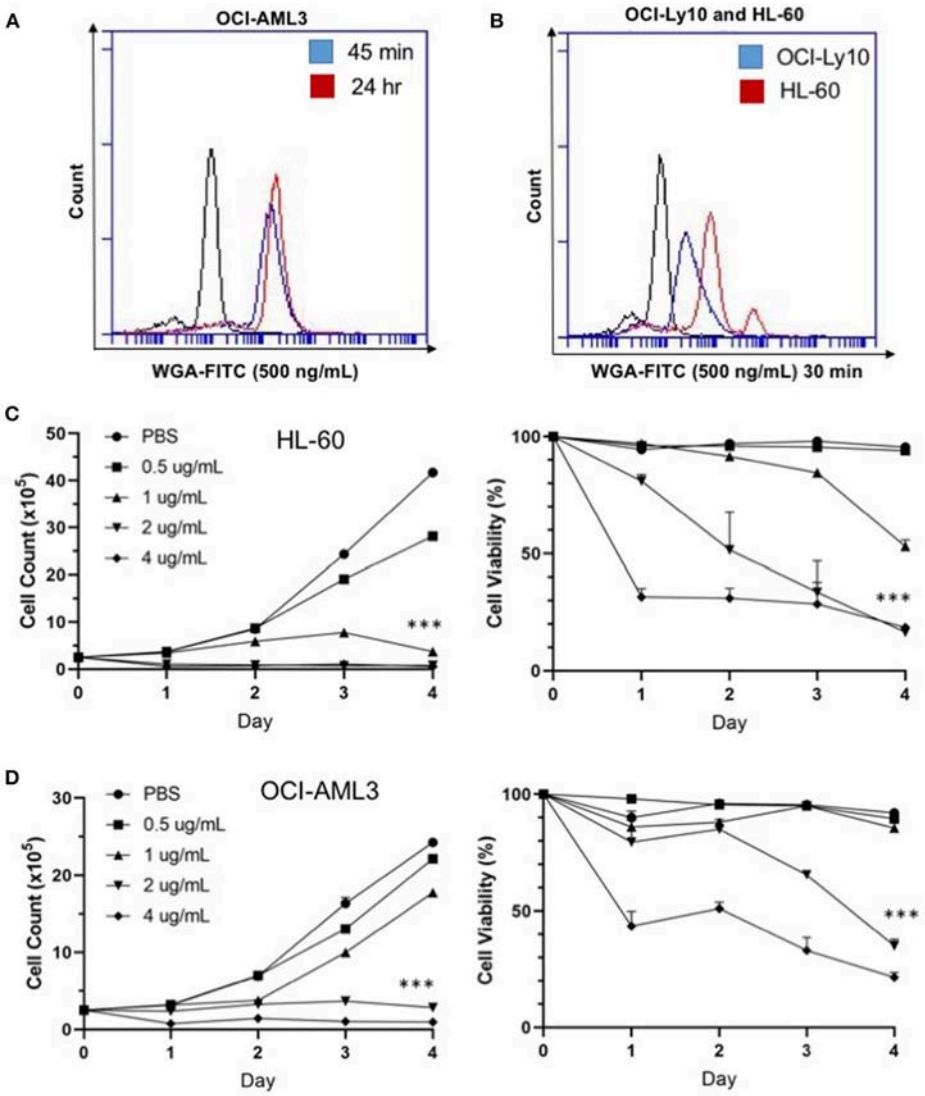

FIGURE 2 | WGA binds and kills in a dose- and time-dependent manner. **(A)** OCI-AML3 cells treated with WGA-FITC (500 ng/mL) and analyzed for binding using flow cytometry. Binding to cells at 45 min (blue peak) and 24 h (red peak) compared to control (black peak). **(B)** OCI-Ly10 and HL-60 cells treated with WGA-FITC (500 ng/mL) for 30 min and analyzed for binding using flow cytometry. **(C,D)** Viable cell count and percent viability of HL-60 **(C)** and **(D)** OCI-AML3 with WGA treatment (0.5, 1.0, 2.0, and 4.0 μg/mL) for 1–4 days, counted using trypan blue. ***$p < 0.001$.

(**Figure 3C**). There is also a significant difference between control and treated cells if all positively staining populations (AV+, AV+/PI+, PI+) are grouped together ($p = 0.0002$). Because it has been shown in the literature that WGA can disrupt cell cycle (14, 17), we tested AML cell cycle changes after being incubated with WGA. Fixing cells and staining with PI allows for the different phases of the cell cycle to be distinguished. Flow cytometry analysis shows that OCI-AML3 cells incubated with 2 μg/mL WGA for 24 h have non-significant changes to G_0/G_1, S, and G_2/M phases compared to untreated control cells (**Figure 3D**). In order to analyze the effect of WGA on cell proliferation, we performed E-670 cell proliferation analysis of OCI-AML3 and HL-60 cells before and after 16 and 24 h of WGA treatment (**Figure 3E**). We did not see any significant changes in staining of these cells. Since WGA induced AML cell killing is a rapid process happening within 24 h, we could not analyze further time points.

WGA Induced AML Cell Death Depends on Both Interaction With Sialic Acid and GlcNAc Binding

WGA binds primarily to GlcNAc and also interacts with sialic-acid containing glyconjugates and oligosaccharides. We tested which binding activity of WGA contributes to its cancer killing activity. Neuraminidase, also called sialidase, is an enzyme that

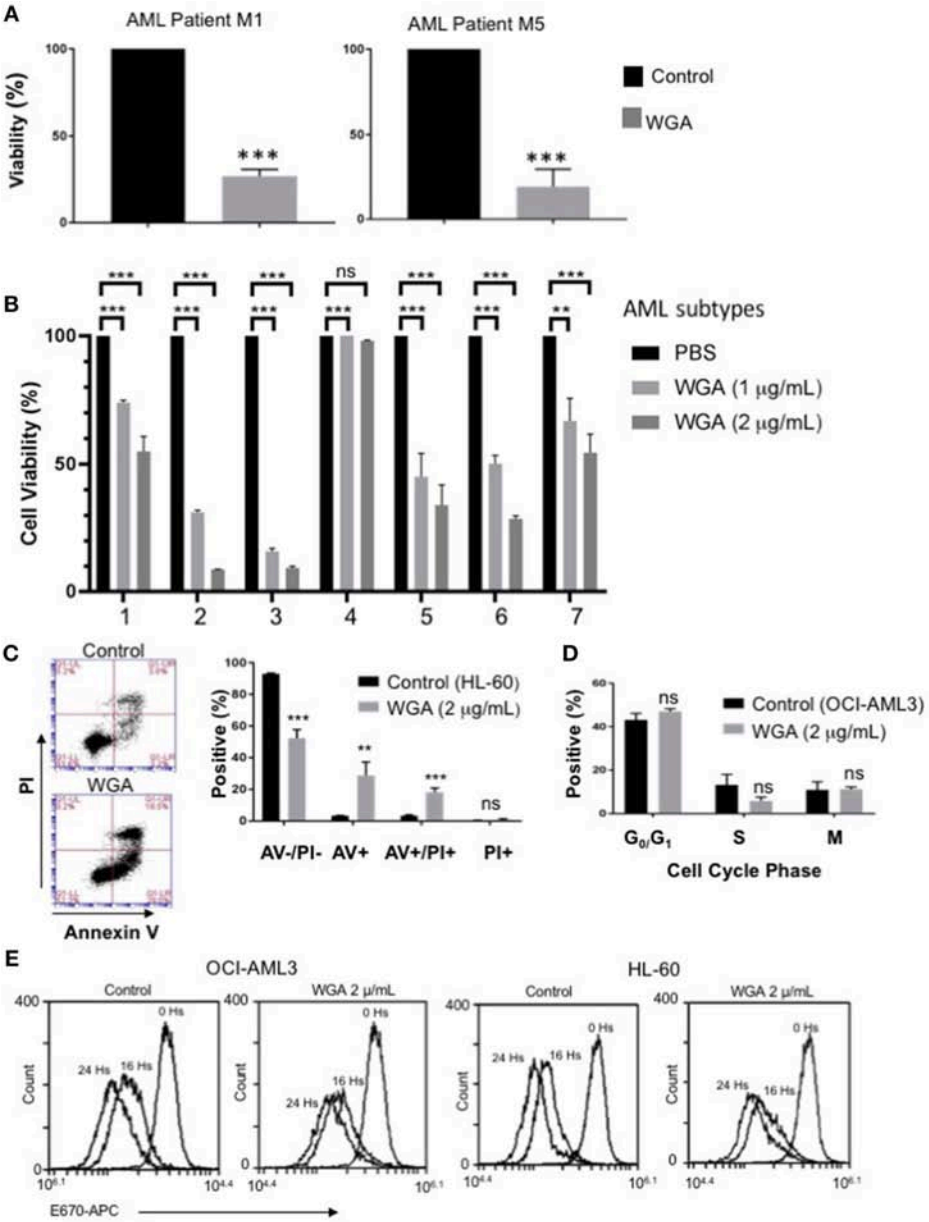

FIGURE 3 | WGA is toxic to primary patient cells and kills AML cells without altering cell cycle. **(A,B)** Percent viability calculated using FSC/SSC live gating of primary AML patient cells belonging to different subtypes **(A)** M1&M5 **(B)** M4Eo; inv16 (1), AML with MDS related changes (2), M2 with MDS-related changes (3), M2(4), CEBPA;c-Kit;TET2(5), NPM1;IDH1(6), IDH1;DNMT3a;FLT3-TKD;trisomy8(7) all treated with or without 2 μg/mL WGA for 24 h. Control was standardized to one hundred percent. **(C)** Annexin V/Propidium Iodide staining of HL-60 cells treated with WGA (2.0 μg/mL) for 24 h. **(D)** Cell cycle analysis of gated live OCI-AML3 cells treated with WGA (2 μg/mL) for 24 h. **(E)** E-670 cell proliferation assays using OCI-AML-3 and HL-60 cell lines in media alone or in the presence of 2.5 μg/mL WGA for the indicated times. Proliferation of live cells was assessed via flow cytometry (Accuri 6C). $^{**}p < 0.01$, $^{***}p < 0.001$, and ns > 0.05.

can catalyze the hydrolysis of sialic acid glycosidic linkages. After neuraminidase pre-treatment, the sialic acid should be cleaved off the cell membrane. Hence, to determine the role of sialic acid interaction with WGA in WGA-mediated cancer cytotoxicity, we pre-treated HL-60 cells with neuraminidase (50 mU/mL) for 2 h and then incubated with 4 μg/mL WGA for 4 h. After treatment, we stained the cells with Propidium iodide and analyzed using flow cytometry. There was a significant increase in PI staining in the WGA-treated groups with and without neuraminidase ($p = 0.0001$, $p = 0.0002$, respectively) (**Figure 4B**). However, when the cells were pre-treated with neuraminidase followed by WGA treatment, the amount of PI staining is significantly reduced compared to cells treated with WGA alone ($p = 0.0033$) (**Figure 4B**). We used FITC-labeled WGA at sub-toxic levels (500 ng/mL) analyzed with flow cytometry to confirm that neuraminidase reduced WGA binding.

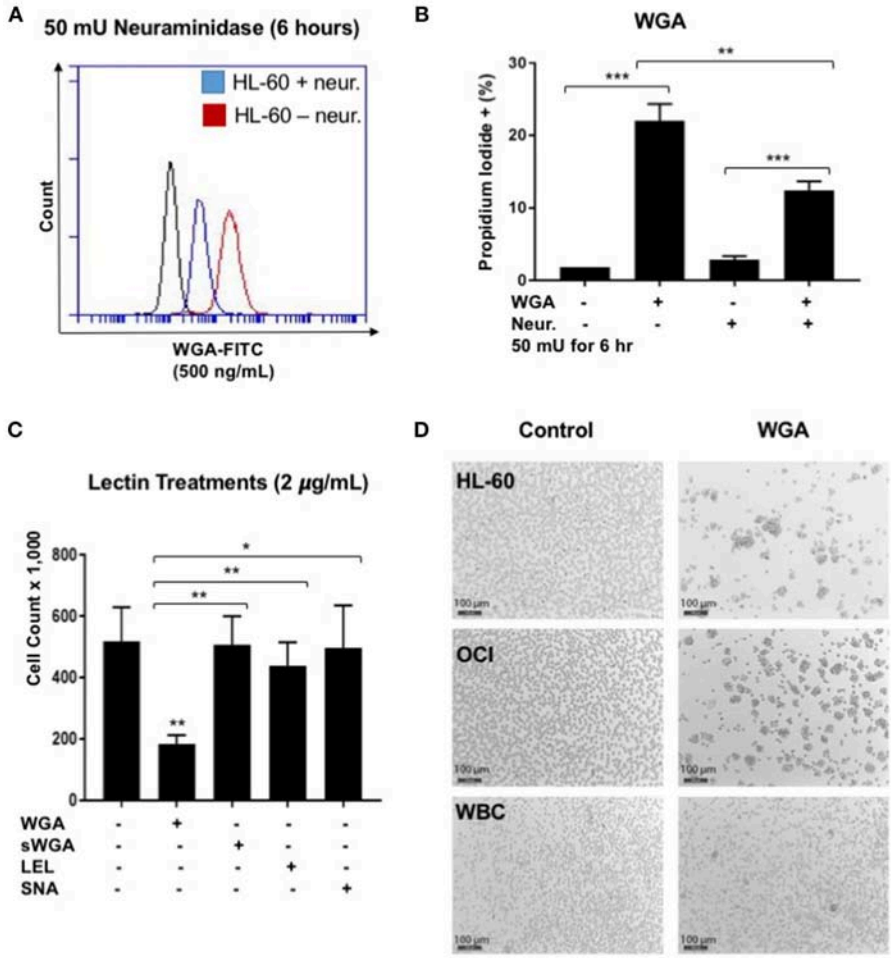

FIGURE 4 | WGA effect on AML is sialic acid dependent. **(A)** HL-60 cells treated with WGA-FITC (500 ng/mL) to analyze WGA binding using flow cytometry. Cells untreated with neuraminidase (red peak) were overlaid with cells treated with neuraminidase (50 mU/mL) for 6 h. **(B)** Percentage Propidium iodide positive HL-60 cells treated with WGA (4 μg/mL) for 4 h were analyzed with flow cytometry. HL-60 cells were either untreated or pre-treated with neuraminidase (50 mU/mL) for 2 h. **(C)** Viable cell count of OCI-AML3 cells treated with 2 μg/mL WGA, sWGA, LEL, and SNA for 24 h counted using trypan blue. **(D)** HL-60, OCI, and healthy human white blood cells (WBCs) treated with either 2 μg/mL WGA or with 2 μL PBS as a negative control and after 20 h treatment, cells were assessed at 10× magnification using bright field microscopy. Scale bar 100 μm shown. $^{*}p < 0.05$, $^{**}p < 0.01$, $^{***}p < 0.001$, and ns > 0.05.

At 6 h, there was a noticeable reduction in binding to HL-60 cells (**Figure 4A**).

We also wanted to look at other lectins, specific for the carbohydrate moieties WGA interacts with. Succinyl-WGA is a modified form of WGA that only binds GlcNAc. We used succinyl-WGA to determine the role of GlcNAc binding in WGA cytotoxicity. We found a significant difference between OCI-AML3 cells treated with succinylated-WGA and unmodified WGA ($p = 0.0237$) (**Figure 4C**), showing that the sialic acid interaction is important for WGA-induced killing. Cells treated with 2 μg/mL SNA lectin, which are specific for sialic acid attached to terminal galactose in α-2,6 and to a lesser degree α-2,3 linkage, are not affected compared to control (**Figure 4C**). OCI-AML3 cells treated with 2 μg/mL LEL, which binds GlcNAc, are also not affected compared to control (**Figure 4C**); however, HL-60 cells treated with LEL showed a significant decrease ($p = 0.0302$) (**Figure 1A**). We also observed cell aggregation/agglutination in HL-60 and OCI-AML3 cells preceding cell death (**Figure 4D**). WGA did not agglutinate normal white blood cells (WBC's) at this concentration and time point (**Figure 4D**).

WGA Exhibits Limited Toxicity to Normal Cells *in vitro* and *in vivo*

At this point, we had demonstrated WGA kills leukemia cells at 1.0–2.0 μg/mL, but we could not discount indiscriminate killing. Because of this concern, we tested various non-cancerous cells with WGA. Propidium iodide staining and flow cytometry analysis shows no significant changes between peripheral blood mononuclear cells treated without WGA and with 0.5, 1.0, and 2.0 μg/mL WGA (**Figure 5A**). OP9, a stromal cell line, was treated with 2.0 μg/mL WGA and no significant morphological changes were apparent microscopically. The cells were not detached from the plates and maintained normal shape

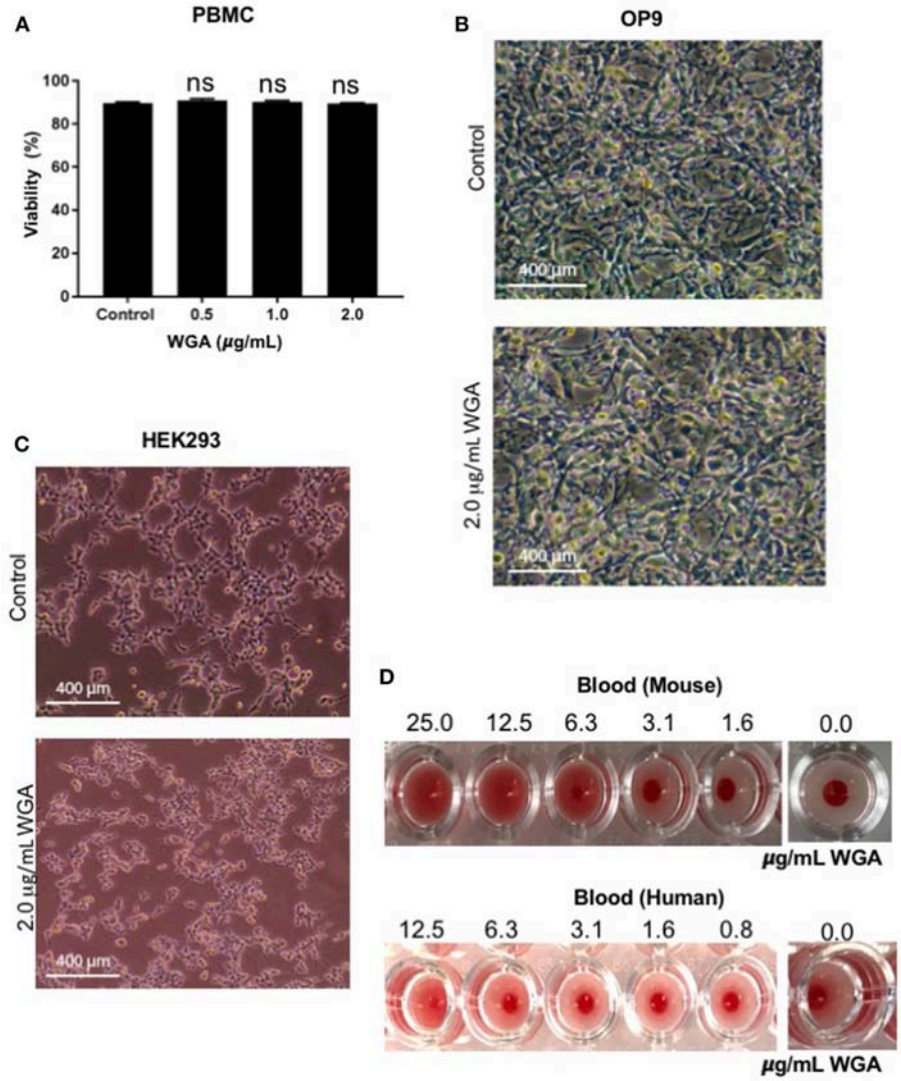

FIGURE 5 | WGA treatment exhibits little or no toxicity toward normal cells *in vitro*. **(A)** Viable peripheral blood mononuclear cells (PBMCs) treated with 0.5, 1.0, and 2.0 μg/mL WGA for 24 h were calculated by PI uptake using flow cytometry. **(B)** Light microscopy of OP9 stromal cells showing phenotype. Cells were treated with 2.0 μg/mL WGA for 24 h and imaged. Scale bar 400 mm shown. **(C)** Light microscopy of HEK293 cells showing phenotype. Cells were treated with 2.0 μg/mL WGA for 24 h and imaged. Scale bar 400 mm shown. **(D)** Hemagglutination assay on 96-well micro-plate of mouse and human blood using serial dilution of WGA (25 to 1.6 μg and 12.5 to 0.8 μg, respectively). Absence of lectin control (0.0 μg) for mouse and human blood are included. ns > 0.05.

(**Figure 5B**). HEK293 cells were also treated with 2.0 μg/mL WGA and imaged. There were no morphological changes after incubation (**Figure 5C**). All these data points to the different toxicity of WGA toward cancer cells and normal cells. Because WGA is known to cause red blood cell (RBC) agglutination (20), we wanted to test whether the WGA dose we are using for the cytotoxic assay causes agglutination in mouse and human RBCs. Hemagglutination assays of human and murine blood after exposure to WGA demonstrated lack of hemagglutination at the indicated doses used. This is evident by the button of blood settled to the bottom of the well. A positive hemagglutination result is diffuse blood in the well as shown in the higher doses imaged (**Figure 5D**).

Finally, because we had determined effect of WGA on normal cells *in vitro*, we tested whether WGA is toxic *in vivo*. We conducted a study to obtain information of WGA dose toxicity where WGA was injected (2 mg/kg) by IP to 2 C57BL/6 mice on days 1, 4, and 8. Mice were sacrificed on day 9 for further analysis (**Figure 6A**). Age and sex-matched, non-treated mice served as controls. The mortality and changes to body weight, clinical signs, gross observation, organ weight, and histopathology of principal organs (spleen, liver and kidney) were monitored. We found no mortalities, WGA treatment-related clinical signs, changes to the body and organ weights, or gross and histopathological findings (**Figures 6B,C**). Since some reports say WGA can cross blood brain barrier (BBB) (33), we analyzed

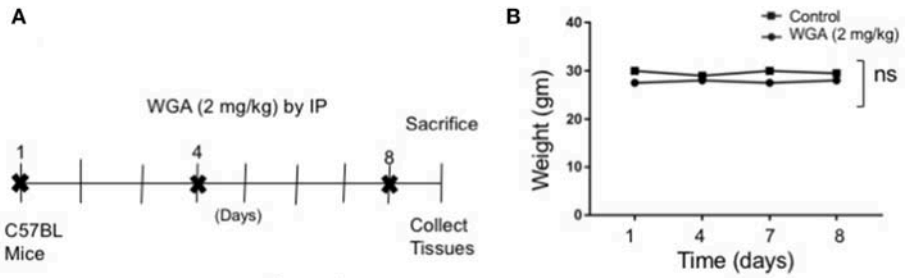

E

	Control	WGA (2 mg/kg)	NORMAL VALUES
WBC (K/µL)	9.91	7.21	1.8 – 10.7
NE	4.855	1.92	0.1 – 2.4
LY	3.965	4.93	0.9 – 9.3
MO	0.365	0.16	0.0 – 0.4
EO	.59	0.17	0.0 – 0.2
BA	.13	0.06	0.0 – 0.2
NE %	46.22	26.61	6.6 – 38.9
LY %	42.815	68.33	55.8 – 91.6
MO%	4.17	2.12	0.0 – 7.5
EO%	5.545	2.33	0.0 – 3.9
BA%	1.2145	0.63	0.0 – 2.0
RBC (M/µL)	6.585	4.725	6.36 – 9.42
Hb (g/dL)	9.55	6.95	11.0 – 15.1
HCT %	30.55	22.4	35.1 – 45.4

FIGURE 6 | WGA treatment demonstrated little toxicity to normal cells *in vivo*. **(A)** Treatment scheme where 2 mg/kg WGA was IP administered to two mice on days 1, 4, and 8. Mice were sacrificed on day 9. **(B)** Weights of mice treated with WGA during duration of treatment. **(C)** Histological analysis of WGA-treated tissues. Spleen, liver, and kidney stained with H&E and imaged by light microscopy at 10X magnification. Scale bar 400 µm shown **(D)** Histological analysis of Hematoxylin&Eosin stained brain tissues from PBS and WGA (5 mg/kg) injected mice. Scale bar 100 µm shown **(E)** HEMAVET blood toxicity analysis of treated mice after sacrifice compared to control mice and normal values. Normal values were given with HemaVet instructions. ns > 0.05.

brain tissue from WGA (5 mg/kg) and PBS injected C57BL/6 mice. Histochemical stainings of brain sections showed normal structures comparable to PBS injected mice, with no signs of toxicity (**Figure 6D**).

We also analyzed different blood cells using HEMAVET. WGA-treated mice displayed cell counts within normal ranges as shown in **Figure 6E**, except for slightly reduced red blood cell count values, such as RBC, hemoglobin, and hematocrit levels (**Figure 6E**). These suggest that WGA at this dose is safe to use *in vivo*.

WGA Induced AML Cell Killing in Xenograft Mouse Model

We further evaluated WGA killing of AML cells *in vivo* using a xenograft mouse model. Severely immunodeficient NSG mice were used for this study. HL-60 AML cells were injected subcutaneously (s.c.) into NSG mice and injected WGA intra-tumorally at days 6, 8, and 10 (**Figure 7A**). Mice tumor volume was measured every alternate day and WGA injected mice showed a very significant inhibition in tumor progression, compared to PBS injected mice (**Figures 7B,C**). We sacrificed

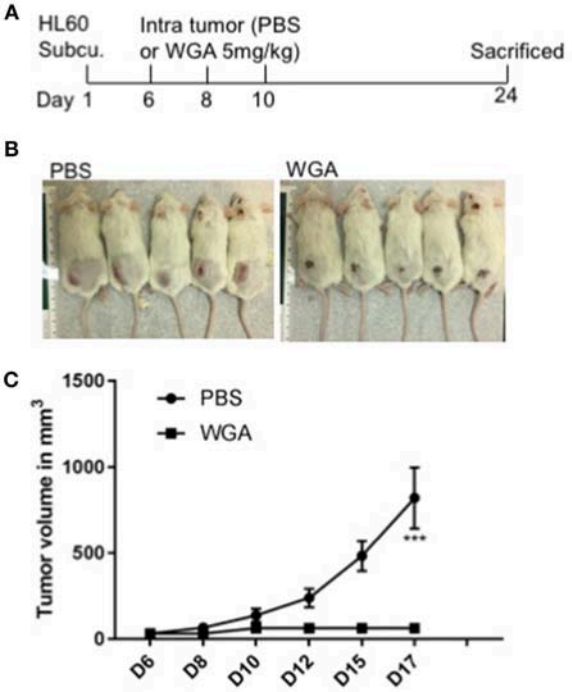

FIGURE 7 | WGA induced AML cell killing in xenograft mouse model. **(A)** Treatment scheme- HL-60 cells injected at day 1 and at day 6, 8 and 10 WGA 5mg/kg injected intratumorally and mice were sacrificed at day 24. **(B)** Pictures of mice treated with PBS or WGA **(C)** Graph showing tumor volume (mm^3) of PBS and WGA injected mice. ***$p < 0.001$.

these mice at day 24. Tumors in PBS injected mice reached volume upto 1,000 mm^3, while there were no measurable tumors in WGA injected mice. NSG mice lack mature lymphocytes including B cells, T cells and NK cells, so it is highly likely that AML cell killing by WGA lectin seen in this model is a direct anti-leukemic effect by WGA. Mice injected with WGA did not show any obvious signs of toxicity suggesting that this therapeutic strategy may be safe, and it is worthy of further development for AML, provided route of administration is optimized.

DISCUSSION

Dietary lectins, particularly wheat germ agglutinin, have been shown to have important anti-cancer properties (18, 19, 22). However, knowledge of lectins' impact on hematological malignancies, such as AML, ALL, and NHL, is lacking. Because these malignancies are in need of potential new treatments, exploring dietary lectins can be a valuable starting point. The panel of lectins chosen encompasses various carbohydrate binding specifities and sizes, as well as sources of origin. We demonstrated that lectins' effects on cancer is variable, with the vast majority of dietary lectins having no impact at all on cancer cell viability. WGA showed significant cell killing against five cell lines tested (out of six). WGA was ineffective against OCI-Ly10. Normal cells were also insensitive to doses of WGA, where it showed significant killing activity against cancer cells. High concentrations of WGA will kill normal cells as well, so choosing the right dose of WGA is key to the success of treatment. We demonstrate the dose specificity of WGA with AML cells showing a significant cytotoxic effect on AML cells but not with the normal cells. WGA killed all AML subtypes tested except M2, this has to be tested further using many M2 patient samples and if WGA fails to kill this particular subtype, it has to be studied further. The exact reasons for this specificity is not known. WGA binds to GlcNAc and it also interacts with sialic-acid containing glyconjugates and oligosaccharides. Since most of the cancer cells are hyper O-GlcNAcylated and hyper silalylated (34–39), we could speculate that it might be the differences in levels of GlcNAc expression and presence of sialylation on cell membrane in different cells which accounts for WGA's cell binding and toxicity specificity. At higher doses, the mechanism of cell killing may be agglutination of cell membrane.

Our data and the literature show the importance of both sialic acid and GlcNAc in the cytotoxicity of WGA. However, the role of each carbohydrate moiety in the lectin-induced death of cells might vary from cell to cell. Sialic acid-specific lectins and GlcNAc-specific lectins were not able to kill AML cells on their own, signifying both properties are necessary for cell killing. If sialic acid is removed using neuraminidase, there is a reduction in binding and killing. The dual interaction to both carbohydrate moieties might be required because of the different locations of the carbohydrates within the cells. The sialic acid interaction may occur outside the cell on the cell membrane, while the GlcNAc binding may occur within the cell after internalization as proposed by Schwarz et al. (22). However, this mechanism of action may be specific to the pancreatic cancer cells used in the study. Further studies are required to understand any AML cell specific mechanism. Sialic acid and GlcNAc interaction within the cell upon internalization may also be key to the cell killing effects. These cell specific differences could also be why the method of killing varies by cancer type. Mechanisms of cytotoxicity by WGA includes apoptosis, necrosis, paraptosis, and cell cycle arrest. Our data demonstrates WGA induces apoptosis and necrosis, but cell cycle analysis revealed no significant differences.

WGA injected into the tumor arrested tumor growth in an NSG xenograft AML model. PBS injected mice had large tumors as expected, which excludes the possibility that intratumoral injection procedure has any effect on tumor growth. Since we used severely immune-compromised mice which lacks a proper innate immune response, the AML killing effect observed might be solely from WGA's direct effect on AML. Studies in the past suggested the possibility that WGA has harmful effects, however, several recent studies have re-evaluated many of those assumptions and suggested that WGA dangers are either non-existent or have limited effects (40, 41). Importantly, the *in vitro* and *in vivo* concentrations of WGA used in this study is very low and no toxicity is reported using this low concentration. Interestingly, more recently dietary lectins including WGA have been associated with the beneficial effect on health, including reduced risks of type 2 diabetes, cardiovascular disease, some types of cancer and weight management (41). Chronic exposure

of high doses of WGA can lead to toxic effects like development of anti WGA antibodies, platelet aggregation or red blood cell (RBC) agglutination. We used low doses of WGA and short exposure timings, where these kind of toxicity is not a concern. WGA has been shown to elicit pro-inflammatory conditions, and its toxic effects could only be seen at a very high dose (of 7 g/kg body weight over a period of 10 days) in the normal gastrointestinal tract of rats, suggesting that WGA being non-toxic in a huge range (21, 40). A final word on toxicity or atoxicity of WGA is pending due to lack of *in vivo* studies, whereas microgram range of WGA used for targeting or carrier system is unlikely to provoke toxic effects (40).

The current therapies for treatment of AML include chemotherapy, radiation therapy, and stem cell transplant. These therapies rely on cell killing and differentiation which lead to cell death. AML treatment regimen can also change depending on the age and health of the patient. In a young patient, induction therapy of high doses of cytarabine and daunorubicin will be used to clear as much of the tumor burden as possible. Once the tumor is cleared, lower doses of these drugs will be used for maintenance. In older and unhealthy patients, these high doses are contraindicated because of their toxicity and potential life-threatening effects. In the AML M3 subtype acute promyelocytic leukemia (APL), ATRA and arsenic trioxide can be used (42). Common side effects of cytarabine include headache, nausea, vomiting, and low blood counts, while less common side effects include flu-like symptoms, loss of appetite, and pain in the hands, feet, and eyes (43). The side effects of daunorubicin's include nausea, vomiting, diarrhea, and hair loss (44). Because of the complexity of AML and its multiple subtypes, the treatment of AML has changed very little over the last few decades. Because of these factors, exploring WGA as a potential therapeutic is worthwhile. The side effects of WGA, such as adverse toxicity and hemagglutination, could be curtailed if administered at low doses.

We show that dietary lectins may be a unique therapeutic tool against hematological malignancies because of their cytotoxic potential and limited toxicity to normal cells and tissues. We characterized the effects on one subtype, OCI-AML3, leaving open the exploration of many other cancer types and conditions, such as drug-resistance and relapse. Characterization of WGA-killing may also lead to more information on novel cell killing pathways. Insights into WGA as a drug-delivery system (45, 46), might also be utilized in combination with our findings to develop potential targeted treatments for hematological malignancies.

ETHICS STATEMENT

Case Western Reserve University's Institution's Animal Care and Use Committee (IACUC) reviewed and approved the Animal Experimentation performed in this study and followed IACUC guide lines and protocol. Mice were maintained in ARC facility at Case Western Reserve University under a 12-h day-night cycle and had *ad libitum* access to food and water. Human samples from normal donors and leukemia patients were obtained from Hematopoietic Stem Cell Core Facility located in Case Western Reserve University. Discarded human blood samples were used in this study and informed consent documents were approved by the University Hospitals Case Medical Center Institutional Review Board.

AUTHOR CONTRIBUTIONS

BR: performed experiments, data analysis, and writing. KZ: performed *in vivo* xenograft experiment. AA: performed *in vivo* toxicity experiments. DW: performed some of the *in vitro* experiments. YV: performed some of the *in vitro* experiments. RP: conceived the idea, analyzed data, wrote and edited manuscript.

FUNDING

St. Baldrick's Foundation (RP), Mizutani foundation for Glycoscience (RP), The Andrew McDonough B+ Foundation (RP), Velosano Foundation (RP) grants and NIH 1R21CA201775-01A1 (RP).

ACKNOWLEDGMENTS

This research was supported by the Athymic Animal and Hemapoietic Biorepository and Cellular therapy core facilities, Shared Resources of the Case Comprehensive Cancer Center (P30CA043703) for their support and funding. We thank Dr. Distelhorst who gifted JVM2 and OCI-Ly10 and Sarah Groft who gifted SNA lectin.

REFERENCES

1. Sharon N, Lis H. Lectins: cell-agglutinating and sugar-specific proteins. *Science* (1972) 177:949–59. doi: 10.1126/science.177.4053.949
2. Etzler ME. Distribution and function of plant lectins. In: Liener IE, Sharon N, Goldstein IJ, editors. *The Lectins: Properties, Functions, and Applications in Biology and Medicine*. Orlando, FL: Academic Press. (1986). p. 371–91. doi: 10.1016/B978-0-12-449945-4.50011-7
3. Vandenborre G, Van Damme E, Smagghe G. Natural products: plant lectins as important tools in controlling pest insects. In: Rami Horowitz, A. editor. *Biorational Control of Arthropod Pests- Application and Resistance Management*. Springer Verlag (2009). p. 163–87.
4. Peumans WJ, Van Damme EJ. Lectins as plant defense proteins. *Plant Physiol*. (1995) 109:347–52. doi: 10.1104/pp.109.2.347
5. Fujimoto Z, Tateno H, Hirabayashi J. Lectin structures: classification based on the 3-D structures. *Methods Mol Biol*. (2014) 1200:579–606. doi: 10.1007/978-1-4939-1292-6_46
6. Damme EJMV, Peumans WJ, Barre A, Rougé P. Plant lectins: a composite of several distinct families of structurally and evolutionary related proteins with diverse biological roles. *Critic Rev Plant Sci*. (2010) 575–692. doi: 10.1080/07352689891304276
7. Hubbard SC, Kranz DM, Longmore GD, Sitkovsky MV, Eisen HN. Glycosylation of the T-cell antigen-specific receptor and its potential role in lectin-mediated cytotoxicity. *Proc Natl Acad Sci USA*. (1986) 83:1852–6. doi: 10.1073/pnas.83.6.1852

8. Haas H, Falcone FH, Schramm G, Haisch K, Gibbs BF, Klaucke J, et al. Dietary lectins can induce *in vitro* release of IL-4 and IL-13 from human basophils. *Eur J Immunol.* (1999) 29:918–27. doi: 10.1002/(SICI)1521-4141(199903)29:03<918::AID-IMMU918>3.0.CO;2-T
9. Gong T, Wang X, Yang Y, Yan Y, Yu C, Zhou R, et al. Plant lectins activate the NLRP3 inflammasome to promote inflammatory disorders. *J Immunol.* (2017) 198:2082–92. doi: 10.4049/jimmunol.1600145
10. Ricci-Azevedo R, Roque-Barreira MC, Gay NJ. Targeting and recognition of toll-like receptors by plant and pathogen lectins. *Front Immunol.* (2017) 8:1820. doi: 10.3389/fimmu.2017.01820
11. Goldstein IJ, Hayes CE. The lectins: carbohydrate-binding proteins of plants and animals. *Adv Carbohydr Chem Biochem.* (1978) 35:127–340. doi: 10.1016/S0065-2318(08)60220-6
12. Pusztai A, Grant G. Assessment of lectin inactivation by heat and digestion. *Methods Mol Med.* (1998) 9:505–14.
13. Kilpatrick DC, Pusztai A, Grant G, Graham C, Ewen SW. Tomato lectin resists digestion in the mammalian alimentary canal and binds to intestinal villi without deleterious effects. *FEBS Lett.* (1985) 185:299–305. doi: 10.1016/0014-5793(85)80927-3
14. Kim M, Rao MV, Tweardy DJ, Prakash M, Galili U, Gorelik E. Lectin-induced apoptosis of tumour cells. *Glycobiology* (1993) 3:447–53. doi: 10.1093/glycob/3.5.447
15. Vasconcelos IM, Oliveira JT. Antinutritional properties of plant lectins. *Toxicon* (2004) 44:385–403. doi: 10.1016/j.toxicon.2004.05.005
16. Eckhardt AE, Malone BN, Goldstein IJ. Inhibition of Ehrlich ascites tumor cell growth by Griffonia simplicifolia I lectin *in vivo*. *Cancer Res.* (1982) 42:2977–9.
17. Miyoshi N, Koyama Y, Katsuno Y, Hayakawa S, Mita T, Ohta T, et al. Apoptosis induction associated with cell cycle dysregulation by rice bran agglutinin. *J Biochem.* (2001) 130:799–805. doi: 10.1093/oxfordjournals.jbchem.a003051
18. Lorea P, Goldschmidt D, Darro F, Salmon I, Bovin N, Gabius HJ, et al. *In vitro* characterization of lectin-induced alterations on the proliferative activity of three human melanoma cell lines. *Melanoma Res.* (1997) 7:353–63. doi: 10.1097/00008390-199710000-00001
19. Wang H, Ng TB, Ooi VE, Liu WK. Effects of lectins with different carbohydrate-binding specificities on hepatoma, choriocarcinoma, melanoma and osteosarcoma cell lines. *Int J Biochem Cell Biol.* (2000) 32:365–72. doi: 10.1016/S1357-2725(99)00130-2
20. Van Damme JM. *Handbook of Plant Lectins: Properties and Biomedical Applications*. Chichester: John Wiley & Sons (1998).
21. Dalla Pellegrina C, Rizzi C, Mosconi S, Zoccatelli G, Peruffo A, Chignola R. Plant lectins as carriers for oral drugs: is wheat germ agglutinin a suitable candidate? *Toxicol Appl Pharmacol.* (2005) 207:170–8. doi: 10.1016/j.taap.2005.01.001
22. Schwarz RE, Wojciechowicz DC, Picon AI, Schwarz MA, Paty PB. Wheatgerm agglutinin-mediated toxicity in pancreatic cancer cells. *Br J Cancer* (1998) 80:1754–62. doi: 10.1038/sj.bjc.6690593
23. Gastman B, Wang K, Han J, Zhu ZY, Huang X, Wang GQ, et al. A novel apoptotic pathway as defined by lectin cellular initiation. *Biochem Biophys Res Commun.* (2004) 316:263–71. doi: 10.1016/j.bbrc.2004.02.043
24. Tsai TL, Wang HC, Hung CH, Lin PC, Lee YS, Chen HHW, et al. Wheat germ agglutinin-induced paraptosis-like cell death and protective autophagy is mediated by autophagy-linked FYVE inhibition. *Oncotarget* (2017) 8:91209–22. doi: 10.18632/oncotarget.20436
25. Brown CM, Larsen SR, Iland HJ, Joshua DE, Gibson J. Leukaemias into the 21st century: part 1: the acute leukaemias. *Intern Med J.* (2012) 42:1179–86. doi: 10.1111/j.1445-5994.2012.02938.x
26. Puckett Y, Chan O. *Cancer, Leukemia, Lymphocytic, Acute (ALL)*. Treasure Island, FL: StatPearls Publishing (2017).
27. Nogai H, Dorken B, Lenz G. Pathogenesis of non-Hodgkin's lymphoma. *J Clin Oncol.* (2011) 29:1803–11. doi: 10.1200/JCO.2010.33.3252
28. *Key Statistics for Non-Hodgkin Lymphoma.* (2018). Available online at: https://www.cancer.org/cancer/non-hodgkin-lymphoma/about/key-statistics.html
29. Grimes SE. *A Basic Laboratory Manual for Small Scale Production and Testing of I-2 Newcastle Disease Vaccine.* (2002). Available online at: http://www.fao.org/docrep/005/ac802e/ac802e00.htm
30. Assay Services. *VIRAPUR, LLC, Hemagglutination (HA) Assay Protocol.* (2018). Available online at: http://www.virapur.com/assay_services/assay_services.php
31. Bennett JM, Catovsky D, Daniel MT, Flandrin G, Galton DA, Gralnick HR, et al. Proposed revised criteria for the classification of acute myeloid leukemia. A report of the French-American-British Cooperative Group. *Ann Intern Med.* (1985) 103:620–5. doi: 10.7326/0003-4819-103-4-620
32. Döhner H, Estey E, Grimwade D, Amadori S, Appelbaum FR, Büchner T, et al. Diagnosis and management of AML in adults: 2017 ELN recommendations from an international expert panel. *Blood* (2017) 129:424–47. doi: 10.1182/blood-2016-08-733196
33. Villegas JC, Broadwell RD. Transcytosis of protein through the mammalian cerebral epithelium and endothelium. II Adsorptive-transcytosis of WGA-HRP and the blood-brain and brain-blood barriers. *J Neurocytol.* (1993) 22:67–80. doi: 10.1007/BF01181571
34. Zhang X, Qiao Y, Wu Q, Chen Y, Zou S, Liu X, et al. The essential role of YAP O-GlcNAcylation in high-glucose-stimulated liver tumorigenesis. *Nat Commun.* (2017) 8:15280. doi: 10.1038/ncomms15280
35. Fardini Y, Dehennaut V, Lefebvre T, Issad T. O-GlcNAcylation: A New Cancer Hallmark? *Front Endocrinol.* (2013) 4:99. doi: 10.3389/fendo.2013.00099
36. Shi Y, Tomic J, Wen F, Shaha S, Bahlo A, Harrison R, et al. Aberrant O-GlcNAcylation characterizes chronic lymphocytic leukemia. *Leukemia* (2010) 24:1588–98. doi: 10.1038/leu.2010.152
37. Asthana A, Ramakrishnan P, Vicioso Y, Zhang K, Parameswaran R. Hexosamine Biosynthetic Pathway (HBP) inhibition leads to AML cell differentiation and cell death. *Mol Cancer Ther.* (2018) 17:2226–37. doi: 10.1158/1535-7163.MCT-18-0426.
38. Bull C, Stoel MA, den Brok MH, Adema GJ. Sialic acids sweeten a tumor's life. *Cancer Res.* (2014) 74:3199–204. doi: 10.1158/0008-5472.CAN-14-0728
39. Pearce OM, Laubli H. Sialic acids in cancer biology and immunity. *Glycobiology* (2016) 26:111–28. doi: 10.1093/glycob/cwv097
40. Gabor F, Bogner E, Weissenboeck A, Wirth M. The lectin–cell interaction and its implications to intestinal lectin-mediated drug delivery. *Adv Drug Delivery Rev.* (2004) 56:459–80. doi: 10.1016/j.addr.2003.10.015
41. Van Buul VJ, Brouns FJPH. Health effects of wheat lectins: a review. *J Cereal Sci.* (2014) 59:112–7. doi: 10.1016/j.jcs.2014.01.010
42. *Treating Acute Myeloid Leukemia.* (2018). Available online at: https://www.cancer.org/cancer/acute-myeloid-leukemia/treating.html
43. Cancer CC. *Cytarabine - Drug Information – Chemocare.* (2018). Available online at: http://chemocare.com/chemotherapy/drug-info/cytarabine.aspx
44. Cancer CC. *Daunorubicin - Drug Information – Chemocare.* (2018). Available online at: http://chemocare.com/chemotherapy/drug-info/daunorubicin.aspx
45. Plattner VE, Wagner M, Ratzinger G, Gabor F, Wirth M. Targeted drug delivery: binding and uptake of plant lectins using human 5637 bladder cancer cells. *Eur J Pharm Biopharm.* (2008) 70:572–6. doi: 10.1016/j.ejpb.2008.06.004
46. Wang C, Ho PC, Lim LY. Wheat germ agglutinin-conjugated PLGA nanoparticles for enhanced intracellular delivery of paclitaxel to colon cancer cells. *Int J Pharm.* (2010) 400:201–10. doi: 10.1016/j.ijpharm.2010.08.023

Conflict of Interest Statement: The authors declare that the research was conducted in the absence of any commercial or financial relationships that could be construed as a potential conflict of interest.

frontiers in Pharmacology

ORIGINAL RESEARCH
published: 21 February 2019
doi: 10.3389/fphar.2019.00137

MiR-409-3p Inhibits Cell Proliferation and Invasion of Osteosarcoma by Targeting Zinc-Finger E-Box-Binding Homeobox-1

*Liang Wu†, Yiming Zhang†, Zhongyue Huang, Huijie Gu, Kaifeng Zhou, Xiaofan Yin and Jun Xu**

Minhang Hosptial, Fudan University, Shanghai, China

Osteosarcoma (OS) is the most common bone cancer worldwide. There is evidence that microRNA-409 (miR-409-3p) is involved in tumorigenesis and cancer progression, however, its possible role in OS requires clarification. In the present study, we evaluated the expression level, clinical significance, and mode of action of miR-409-3p in OS. The miR-409-3p levels were diminished in the OS cells and tissues compared with associated adjacent non-tumor tissues and a non-cancer osteoplastic cell line. Low miR-409-3p expression levels were associated with clinical stage and distant metastasis in patients with OS. Resumption of miR-409-3p expression attenuated OS cell proliferation and invasion. Additionally, based on informatics analyses, we predicted that zinc-finger E-box-binding homeobox-1 (ZEB1) is a possible target of miR-409-3p. This hypothesis was confirmed using luciferase reporter assays, reverse transcription-quantitative real-time polymerase chain reaction, and Western blot analyses. The findings of the current study indicated that ZEB1 was up-regulated in the OS tissues and cell lines, and that this up-regulation was inversely proportional to miR-409-3p expression levels. Furthermore, down-regulation of ZEB1 decreased OS cell invasion and proliferation, illustrating that the tumor suppressive role of miR-409-3p in OS cells may be exerted *via* negative regulation of ZEB1. Taken together, our observations highlight the potential role of miR-409-3p as a tumor suppressor in OS partially through down-regulation of ZEB1 and suggest that miR-409-3p has potential applications in OS treatment.

Keywords: osteosarcoma, microRNA-409, molecular mechanism, zinc-finger E-box-binding homeobox-1, invasion

OPEN ACCESS

Edited by:
Jian-ye Zhang,
Guangzhou Medical University, China

Reviewed by:
Jianmeng Wang,
First Affiliated Hospital of Jilin University, China
Jixue Wang,
Jilin University, China

***Correspondence:**
Jun Xu
Aline_Adam@126.com

†These authors have contributed equally to this work

Specialty section:
This article was submitted to Cancer Molecular Targets and Therapeutics, a section of the journal Frontiers in Pharmacology

Received: *22 October 2018*
Accepted: *06 February 2019*
Published: *21 February 2019*

Citation:
Wu L, Zhang Y, Huang Z, Gu H, Zhou K, Yin X and Xu J (2019) MiR-409-3p Inhibits Cell Proliferation and Invasion of Osteosarcoma by Targeting Zinc-Finger E-Box-Binding Homeobox-1. Front. Pharmacol. 10:137. doi: 10.3389/fphar.2019.00137

INTRODUCTION

Osteogenic sarcoma (osteosarcoma; OS) is among the most common forms of bone cancer globally. The incidence ranges from 4 to 5 cases per million among children and teenagers (Gill et al., 2013; Tang et al., 2014). The OS tumors are always located in the distal femur or proximal tibia, and tumors in these regions present a high tendency to destroy adjacent normal tissues (Cates, 2016; Righi et al., 2016). Despite considerable advances in treatment strategies such as surgery, radiotherapy, chemotherapy and new antineoplastic agent (Li et al., 2015), cases with metastatic or recurrent OS have an inferior prognosis, and the likelihood of long-term survival for patients

with advanced OS remains very low (Anderson, 2015; Isakoff et al., 2015). Genetic and epigenetic variations and potential environmental factors that block mesenchymal stem cell differentiation into osteoblasts contribute to OS tumorigenesis and tumor development (Sun et al., 2015; Li et al., 2018; Zhang et al., 2018), however, the detailed and complex molecular mechanisms underlying OS development remain largely unknown. Therefore, the molecular mechanisms underlying OS formation and progression require investigation to facilitate the development of novel therapeutic approaches for application in patients with OS.

MicroRNAs (miRNAs) are a subtype of endogenous, non-coding, single-stranded, short RNAs, with an approximate range in length of 19–25 nucleotides (Esteller, 2011). miRNAs can regulate the expression of protein-coding genes by binding to complementary sequences in the 3′-untranslated regions (3′ UTRs) of target genes, causing translational repression or mRNA cleavage (Bartel, 2004). miRNAs play key roles in various cellular processes, including apoptosis, cell proliferation, differentiation, angiogenesis, invasion, and metastasis (Gambari et al., 2016). Recently, the abnormal expression of miRNAs has been implicated in the etiology and development of various human cancers (Chen et al., 2016; Li and Wang, 2016; Wang et al., 2016). The potential biological roles of several miRNAs abnormally expressed in OS during its tumorigenesis have also been highlighted. For example, miR-422a expression is down-regulated in OS cell lines and tissues. Conversely, high levels of miR-422a expression can suppress OS cell invasion and proliferation, and improve paclitaxel and cisplatin-mediated apoptosis (Liu et al., 2016). Therefore, there is a need to explore the potential role of miRNA expression in OS and to unravel the underlying primary molecular mechanisms, which may provide information useful for designing new and efficient therapeutic strategies aimed at curing OS.

The effect of miR-409-3p has been investigated in various human malignancies, including breast (Ma et al., 2016), gastric (Zheng et al., 2012), colon (Tan et al., 2016), and prostate (Josson et al., 2015) cancers, however, its role of miR-409-3p in OS remains unclear. Latest study confirmed the interaction of miR-409-3p and ZEB1 played a role in the progression process of non-small cell lung cancer, indicating ZEB1 acted as a direct target of miR409-3p and could be modulated by miR-409-3p (Qu et al., 2018). Herein, we hypothesis there exists the miR-409-3p/ZEB1 axis in OS and report the first investigation of the expression levels, clinical significance, and biological functions of miR-409-3p in OS, as well as its underlying molecular mechanism.

MATERIALS AND METHODS

Ethics Statement

All study participants voluntarily provided written consent before entering the study. We obtained the approval of The Ethics Committee of the Minhang Hospital, Zhongshan Hospital, Fudan University for Disease Control and Prevention. The methodology used in this study completely conformed to the recommendations of CONSORT 2010.

Tissue Specimens

Forty-nine pairs of osteosarcoma tumor and adjacent non-tumor tissues were collected from patients with osteosarcoma at Minhang Hospital, Zhongshan Hospital, Fudan University. No participants underwent chemotherapy or radiotherapy before surgery. All tissues samples were directly transferred into liquid nitrogen and were stored at −80°C until RNA extraction.

Cell Lines

OS cell lines, including HOS (GDC76) and MG63 (GDC074) were obtained directly from the Chinese Academy of Medical Sciences (Beijing, China) Cell Resource Center. A non-cancer osteoblastic cell line (hFOB 1.19 CRL-11372) was obtained from the American Type Culture Collection (ATCC; Manassas, VA, United States). All cells were incubated in Dulbecco's modified Eagle medium (DMEM; Gibco, Invitrogen Life Technologies, Carlsbad, CA, United States) supplemented with 10% fetal bovine serum (FBS; Gibco, Invitrogen Life Technologies, Carlsbad, CA, United States). All experimental cells were maintained at 37°C in 5% (V/V) carbon dioxide (CO_2) and passaged every 2–3 days.

Cells were then seeded in 6-well plates at a density of 50–60% confluence for transfection. After overnight incubation, cells were transfected with miR-409-3p mimics, negative control miRNA mimics (miR-NC), ZEB1 siRNA, or scrambled siRNA (GenePharma, Shanghai, China), using Lipofectamine 2000 transfection reagent (Invitrogen, Carlsbad, CA, United States), according to the manufacturer's guidelines. Post-transfection (6 h), the culture medium was changed to DMEM containing 10% FBS.

Reverse Transcription-Quantitative Real-Time Polymerase Chain Reaction (RT–qPCR)

RNA was extracted using Trizol reagent (Invitrogen, Carlsbad, CA, United States), following the manufacturer's directions. A TaqMan Micro-RNA Reverse Transcription Kit (Applied Biosystems, Foster City, CA, United States) was used to reverse-transcribe miRNA, and qPCR performed using a TaqMan Micro-RNA PCR Kit (Applied Biosystems, Foster City, CA, United States). Reverse transcription of mRNA was performed using the M-MLV Reverse Transcription system (Promega Corporation, Madison, WI, United States). To determine *ZEB1* mRNA expression levels we used the primers: forward 5′-AGGCAATAGGTTTTGAGGGCCAT-3′ and reverse 5′-TGCACCTTCTGTCTCGGTTTCTT-3′ and SYBR Premix Ex Taq (TaKaRa, Dalian, China). Endogenous U6 small nuclear RNA (primers: forward, 5′-CTCGCTTCGGCAGCACA-3′; reverse, 5′-AACGCTTCACGAATTTGCGT-3′) was amplified as an internal control for miR-409-3p, and β-actin (primers: forward, 5′-AGCGAGCATCCCCCAAAGTT-3′; reverse, 5′-GGGCACGAAGGCTCATCATT-3′) was amplified as an internal control for *ZEB1* mRNA. All RT-qPCR experiments were conducted using an ABI7500 Real-time PCR system (Applied Biosystems, Carlsbad, CA, United States). Relative mRNA or miRNA expression levels were quantified using the $2^{-\Delta\Delta Ct}$ method (Livak and Schmittgen, 2001).

3-(4,5-Dimethylthiazol-2-yl)-2,5-Diphenyltetrazolium Bromide (MTT) Assay

Post-transfection (24 h), cells were re-seeded into 96-well plates at 3,000 per well. Cells were maintained at 37°C in 5% (*V*/*V*) CO_2 for 4 days. Then, cell proliferation was tested at the indicated times using the MTT assay (Sigma, St. Louis, MO, United States). In brief, 0.5 mg/mL MTT solution was added to cells, which were then incubated at 37°C for a further 4 h. Subsequently, we added 150.0 μL DMSO (Sigma, St. Louis, MO, United States) into each to dissolve the formazan crystals. Spectrometric absorbance was determined using a microplate reader (Bio-Rad Laboratories Inc., Hercules, CA, United States) at a wavelength of 490 nm.

Cell Invasion Assay

After 48 h transfection, cells were collected and suspended in FBS-free culture medium. Then, 5×10^4 cells were added into upper chambers of a 24-well Transwell Permeable Support device (8-μm pores, Costar; Corning Incorporated, Corning, NY, United States) coated with Matrigel (BD Biosciences, San Jose, CA, United States), while 500.0 μL culture medium containing 20% FBS was added to the lower chambers and cells incubated at 37°C in 5% CO_2 for 48 h. We removed cells in the upper chambers using cotton swabs, then invaded cells were fixed with methanol, stained with 0.5% crystal violet, washed, and dried in air. An inverted microscope (Olympus Corporation, Tokyo, Japan) (200 × magnification) was used to calculate the number of invading cells in five randomly selected fields.

Prediction of miR-409-3p Targets and Luciferase Reporter Assays

Two miRNA targeted-gene databases, TargetScan[1] and miRanda[2], were used to predict target genes of miR-409-3p. HEK293T cells (ATCC) were seeded into 24-well plates at 40–50% confluence. After 24 h, cells were transfected with miR-409-3p mimics or miR-NC and pmirGLO-ZEB1-3′UTR-mutant (Mut) (GenePharma) or pmirGLO-ZEB1-3′UTR-wild-type (Wt) using Lipofectamine 2000. Cells were maintained at 37°C in 5% (*V*/*V*) CO_2 for 48 h and luciferase reporter assays conducted using the Dual-Luciferase Reporter Assay System (Promega Corporation, Madison, WI, United States). Renilla luciferase was used as an internal control.

Western Blot Analyses

Cells were harvested after transfection for 72 h and lysed with RIPA Lysis Buffer (Beyotime Institute of Biotechnology, Haimen, China). Protein concentrations were determined using a BCA assay kit (Pierce™; Thermo Fisher Scientific, Inc.). Equal amounts of protein were separated by SDS-PAGE, transferred to polyvinylidene difluoride membranes (Millipore, MA, United States), blocked with 5% skimmed milk for 2 h at room temperature, then incubated overnight at 4°C with mouse anti-human GAPDH monoclonal antibody (sc-137179; 1:1000 dilution; Santa Cruz Biotechnology) or mouse anti-human ZEB1 monoclonal antibody (sc-81428; 1:1000 dilution; Santa Cruz Biotechnology, CA, United States). Membranes were then washed three times using Tris-buffered saline containing 0.1% Tween-20 and probed with horseradish peroxidase-conjugated secondary immunoglobulin G goat anti-mouse (catalog no, sc-2005; 1:10,000) for 2 h at room temperature. Protein bands were visualized using enhanced chemiluminescence reagents (Bio-Rad Laboratories Inc., Hercules, CA, United States) and band densities analyzed using AlphaEase FC software (version 4.0.1; ProteinSimple, San Jose, CA, United States).

Statistical Analyses

Data were presented as means ± S.D. or box plots. We used SPSS 17.0 software (SPSS Inc., Chicago, IL, United States) for data analyses. Differences among groups were evaluated using one-way ANOVA corrected for multiple comparisons or Student's *t*-tests. The χ^2-test was used to evaluate associations between miR-409-3p expression levels and clinicopathological factors. Spearman's correlation analysis was used to determine the correlation between miR-409-3p and *ZEB1* mRNA expression levels. All statistical tests were two-sided; $P < 0.05$ were considered statistically significant.

RESULTS

MiR-409-3p Was Downregulated in OS Tissues and Cell Lines

RT-qPCR was used to evaluate miR-409-3p expression levels in OS tumor and adjacent non-tumor tissues. Expression of miR-409-3p was lower in OS tissues than that in adjacent non-tumor and normal tissue controls (**Figure 1A**, $P < 0.05$). Moreover, remarkable low levels of MiR-409-3p expression were detected in two OS cell lines relative to those in a non-cancer osteoblastic cell line (hFOB 1.19) (**Figure 1B**, $P < 0.05$).

Relationship Between miR-409-3p Expression and OS Clinicopathological Factors

We also determined the relationship between miR-409-3p expression levels and OS clinicopathological factors. Our data showed that low miR-409-3p expression levels were significantly associated with advanced clinical stage ($P = 0.035$) and distant metastasis ($P = 0.030$), however, there were no significance associations with other clinicopathological factors, including sex ($P = 0.961$), age ($P = 0.804$), and tumor size ($P = 0.851$) (**Table 1**).

MiR-409-3p Reduces OS Cell Proliferation and Invasion

To investigate the role of miR-409-3p in OS, we transfected MG63 and HOS cells with miR-409-3p mimics, and used RT-qPCR to determine miR-409-3p expression levels (**Figure 2A**, $P < 0.05$). We investigated the role of miR-409-3p in OS cell proliferation using MTT assays conducted in MG63 and HOS cells transfected with miR-409-3p mimics or miR-NC. Expression

[1] http://www.targetscan.org/index.html

[2] http://www.microrna.org

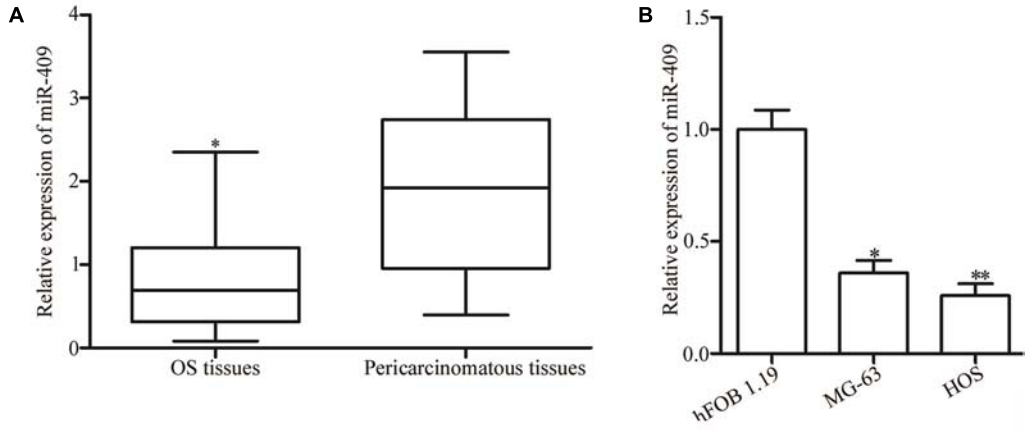

FIGURE 1 | Expression of miR-409-3p in OS tissues and cell lines. **(A)** Relative expression levels of miR-409-3p in 49 paired OS tumor and adjacent non-tumor tissues were evaluated by RT-qPCR. **(B)** Expression of miR-409-3p in OS cell lines compared with that in a non-cancer osteoblastic cell line (hFOB1.19). miR-409-3p, microRNA-409. OS, osteosarcoma. *$P < 0.05$, **$P < 0.01$ compared with the control group.

TABLE 1 | Correlation of microRNA-409 expression with clinicopathological feature of osteosarcoma.

Variables	Case number	microRNA-409 expression		*P*
		Low	High	
Sex				0.961
Male	31	17	14	
Female	18	10	8	
Age (years)				0.804
< 20*	21	12	9	
≥ 20	28	15	13	
Tumor size (cm)				0.851
< 8	26	14	12	
≥ 8	23	13	10	
Clinical stage				0.035*
I-II	23	9	14	
III-IV	26	18	8	
Distant metastasis				0.030*
Present	24	17	7	
Absent	25	10	15	

**These participants were above 16 years age. *P < 0.05.*

of miR-409-3p led to a significant decline in MG63 and HOS cell proliferation (**Figure 2B**, $P < 0.05$). Similarly, the invasion capacity of HOS and MG63 cells transfected with miR-NC or miR-409-3p mimics was estimated using a cell invasion assay. As illustrated in **Figure 2C**, the introduction of miR-409-3p mimics into HOS and MG63 cells resulted in a considerable decline of invasion ability relative to the miR-NC group ($P < 0.05$). These observations suggested that miR-409-3p has a crucial role in the suppression of OS growth and metastasis.

A Potential miR-409-3p Target in OS

We then investigated the molecular mechanisms underlying the tumor suppression caused by miR-409-3p in OS by predicting its potential targets using bioinformatics analysis. The 3′ UTR of *ZEB1* was predicted to contain an miR-409-3p seed match at position 1280-1286 and has previously been reported as extensively upregulated in OS and participates in the regulation of OS tumorigenesis and progression (Shen et al., 2012; Li et al., 2016; Liu and Lin, 2016); therefore, we primarily focused on ZEB1 (**Figure 3A**) in this study. To validate the prediction, we performed luciferase reporter assays in HEK293T cells transfected with plasmids containing Mut and Wt ZEB 3′ UTR, along with miR-409-3p mimics or miR-NC. Luciferase activity was markedly downregulated in cells transfected with Wt ZEB1-3′ UTR and miR-409-3p mimics (**Figure 3B**, $P < 0.01$), however, no significant difference was observed in cells transfected with mutated ZEB1-3′ UTR and miR-409-3p mimics, suggesting that miR-409-3p could directly target the 3′ UTR of *ZEB1*. Additionally, RT-qPCR data showed that restoration of miR-409-3p expression led to down-regulation of *ZEB1* mRNA expression in MG63 and HOS cells (**Figure 3C**, $P < 0.01$). Moreover, Western blot analysis demonstrated that miR-409-3p reduced ZEB1 protein expression in MG63 and HOS cells (**Figure 3D**, $P < 0.05$). *In vivo* assay showed the protein levels in tumor tissues were significantly lower than those in adjacent normal tissues (**Figure 3E**, $P < 0.01$). To summarize, Our data demonstratedthat ZEB1 is potentially a direct target gene of miR-409-3p in OS.

Upregulation of ZEB1 in OS Tissues and Negative Correlation of Its Expression With That of miR-409-3p

ZEB1 is recognized as a direct target gene of miR-409-3p in OS; therefore, we next investigated whether miR-409-3p expression levels were negatively correlated with those of *ZEB1* in OS. Therefore, we performed RT-qPCR to evaluate *ZEB1* mRNA expression levels and found that they were higher in OS specimens than adjacent non-tumor tissues (**Figure 4A**, $P < 0.05$). Moreover, Spearman's correlation analysis indicated an inverse relationship between miR-409-3p and *ZEB1* mRNA

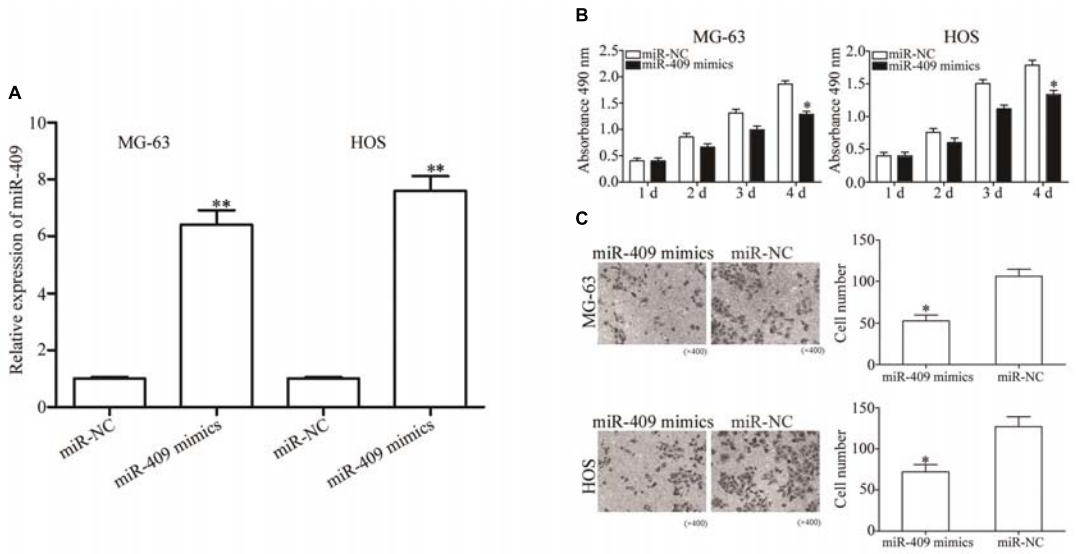

FIGURE 2 | The effects of miR-409-3p overexpression on cell proliferation and invasion in OS. **(A)** Relative expression of miR-409-3p in MG63 and HOS cells following transfection with miR-409-3p mimics or miR-NC. **(B)** MTT assays were performed to assess the effect of miR-409-3p overexpression on MG63 and HOS cells proliferation. **(C)** Cell invasion assays were conducted in MG63 and HOS cells following transfection with miR-409-3p mimics or miR-NC. miR-409, microRNA-409-3p (magnification, ×200). OS, osteosarcoma. miR-NC, negative control microRNA mimics. $^{*}P < 0.05$, $^{**}P < 0.01$ compared with the control group.

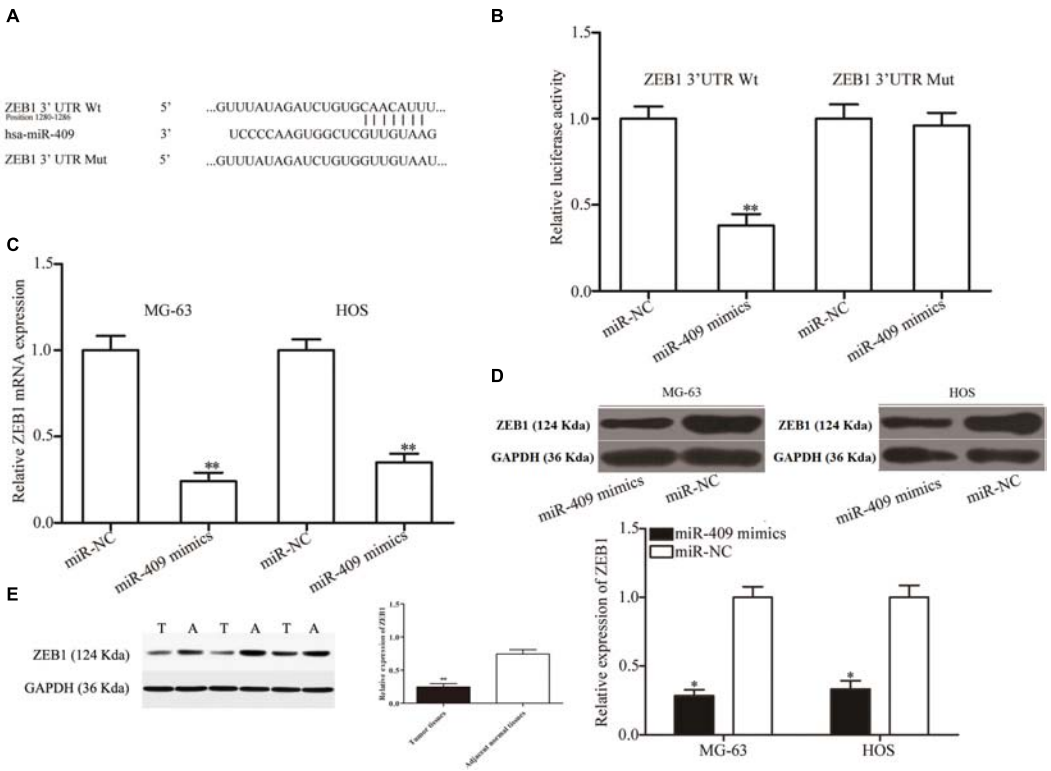

FIGURE 3 | ZEB1 is a direct target of miR-409-3p in OS. **(A)** *ZEB1* 3′ UTR sequences containing wild type and mutant miR-409-3p binding sites. **(B)** Luciferase reporter assays performed in HEK293T cells co-transfected with miR-409-3p mimics or miR-NC, and pmirGLO-ZEB1-3′UTR Wt or pmirGLO-ZEB1-3′UTR Mut. After transfection (48 h), cells were collected and luciferase activities measured. ZEB1 mRNA **(C)** and protein **(D)** were detected in MG63 and HOS cells transfected with miR-409-3p mimics or miR-NC. miR-409, microRNA-409-3p. **(E)** Protein levels of ZEB1 in tumor tissues and adjacent normal tissues. OS, osteosarcoma. miR-NC, negative control microRNA mimics. Wt, wild type. Mut, mutant. ZEB1, Zinc-finger E-box-binding Homeobox-1. $^{*}P < 0.05$, $^{**}P < 0.01$ compared with the control group.

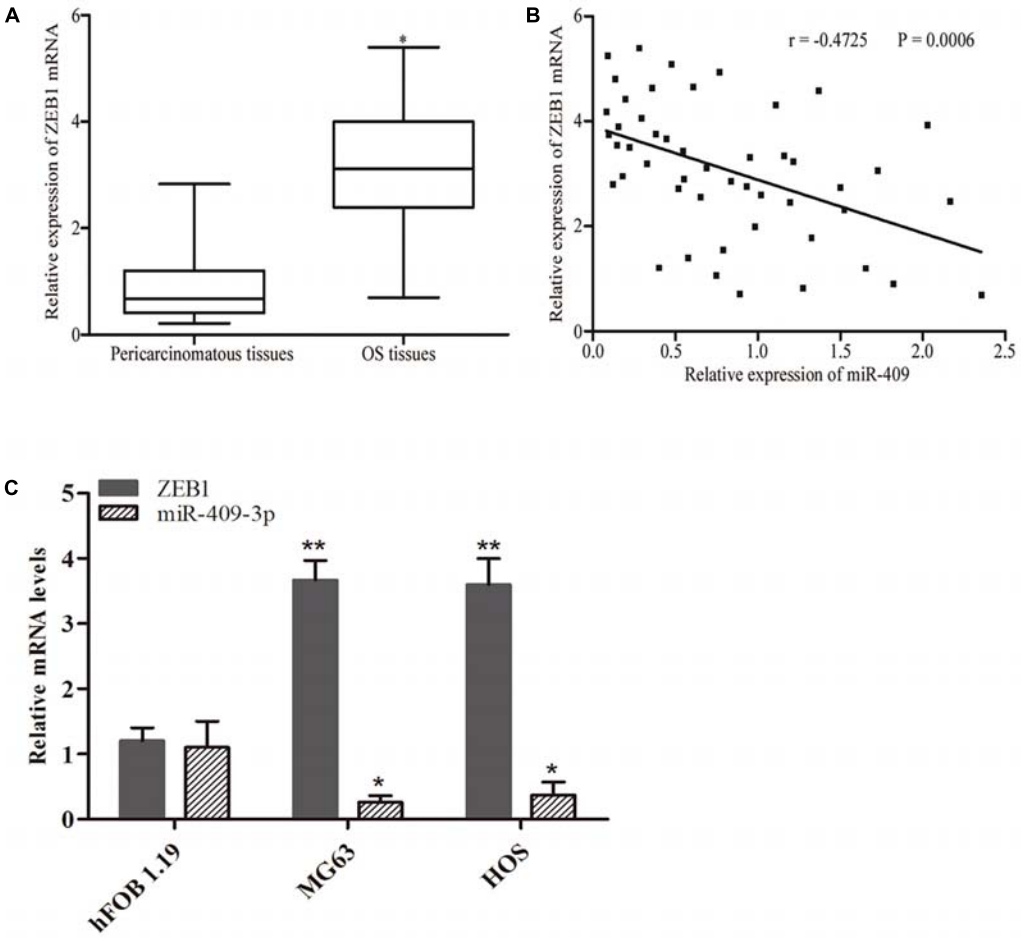

FIGURE 4 | Inverse correlation between miR-409-3p and *ZEB1* mRNA expression levels in OS tissues. **(A)** RT-qPCR analysis showing that *ZEB1* mRNA levels were increased in OS tissues. **(B)** Spearman's correlation analysis of the association between miR-409-3p and *ZEB1* mRNA in OS tissues. **(C)** Expressions of miR-409-3p and *ZEB1* mRNA in cell lines. miR-409, microRNA-409-3p. OS, osteosarcoma. ZEB1, Zinc-finger E-box-binding Homeobox-1. mRNA, message RNA. $^{*}P < 0.05$, $^{**}P < 0.01$ compared with the control group.

expression (**Figure 4B**, r = -0.4725, P = 0.0006) in OS tissue samples. As shown in **Figure 4C**, we observed higher expression of *ZEB1* mRNA and lower expression of miR-409-3p in tumor cell lines, when compared to normal cell line. Our results further confirm ZEB1 as a potential target of miR-409-3p in OS.

Inhibition of ZEB1 Has Similar Effects to Those of miR-409-3p Overexpression in OS Cells

To explore the biological roles of ZEB1 in response to miR-409-3p inhibition in OS, we investigated whether ZEB1 knockdown mimicked the effects of miR-409-3p overexpression in OS cells. ZEB1-targeting siRNA was used to knockdown ZEB1 expression in HOS and MG63 cells. As shown in **Figure 5A**, ZEB1 protein was successfully knocked down in HOS and MG63 cells transfected with ZEB1 siRNA ($P < 0.01$). MTT and cell invasion assays showed that knockdown of ZEB1 by the introduction of ZEB1 siRNA suppressed MG63 and HOS cell proliferation (**Figure 5B**, $P < 0.05$) and invasion (**Figure 5C**, $P < 0.05$), suggesting that negative regulation of ZEB1 may mediate the tumor suppressive effects of miR-409-3p in OS cells.

DISCUSSION

Dysregulation of miRNAs is a frequent event in various types of human cancer and has a pivotal role in the instigation of tumorigenesis and tumor progression where miRNAs can function as oncogenes or tumor suppressor genes (Fenger et al., 2014; Vanas et al., 2016). Furthermore, targeting miRNA with various types of chemically modified oligonucleotides has the potential to alter miRNA functions, providing a theoretical foundation for miRNA-based targeted therapy for specific human cancers (Trang et al., 2010; Imani et al., 2017; Tsai et al., 2017). Thus, research into the expression levels, biological roles, and fundamental molecular mechanisms of miRNAs has the potential to stimulate the development of novel approaches to

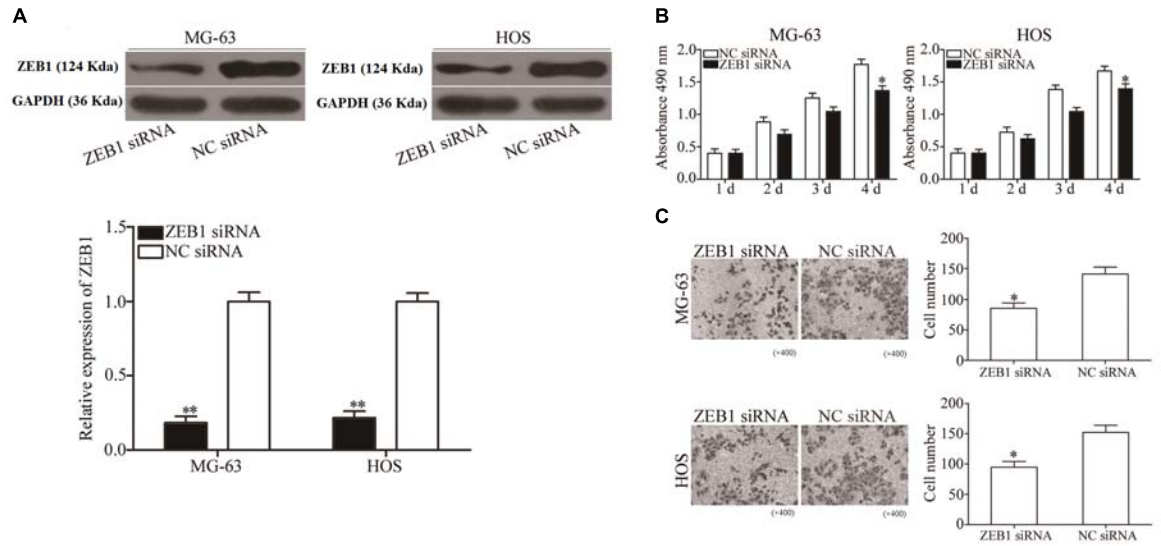

FIGURE 5 | ZEB1 under-expression has similar effects to miR-409-3p over-expression on OS cell proliferation and invasion. **(A)** ZEB1 protein expression was detected in MG63 and HOS cells transfected with ZEB1 siRNA or NC siRNA. MTT **(B)** and cell invasion **(C)** assays were conducted in MG63 and HOS cells transfected with ZEB1 siRNA or NC siRNA. miR-409, microRNA-409-3p (magnification, × 200). OS, osteosarcoma. ZEB1, Zinc-finger E-box-binding Homeobox-1. mRNA, message RNA. siRNA, small interfering RNA. NC, negative control. $^{*}P < 0.05$, $^{**}P < 0.01$ compared with the control group.

the treatment of different types of cancer. Our data demonstrated that miR-409-3p expression levels were significantly down-regulated in OS tissues and cells relative to adjacent non-tumor tissues and a non-cancer osteoblastic cell line, respectively. Our observations are consistent with the findings of Ma et al. in breast cancer tissues and cell lines (Zheng et al., 2012). Additionally, reduced miR-409-3p expression levels were associated with clinical stage and distant metastasis in patients with OS, and our results also demonstrate that expression of miR-409-3p suppressed proliferation and invasion of OS cells. Furthermore, our data suggest that ZEB1 is a functional target of miR-409-3p in OS.

Recently, several studies have reported roles for abnormal miR-409-3p expression in the initiation and progression of various human cancers. For example, Josson et al. found that miR-409-3p expression was elevated in prostate cancer and that its re-expression in normal prostate fibroblasts resulted in a cancer-associated stroma-like phenotype, and miR-409-3p was released in extracellular vesicles to induce cancer initiation and epithelial-to-mesenchymal transition both *in vitro* and *in vivo* (Josson et al., 2015). Zheng et al. (2012) showed that miR-409-3p expression levels were decreased in gastric cancer and that they were negatively associated with tumor-node-metastasis stage and lymph node metastasis in patients with gastric cancer. Upregulation of miR-409-3p attenuated gastric cancer cell motility *in vitro* and decreased their ability to induce distal pulmonary metastases and peritoneal diffusion *in vivo* (Zheng et al., 2012). Tan et al. (2016) found that miR-409-3p was expressed at low levels in colon tumors and that its expression was negatively correlated with resistance to oxaliplatin. Ectopic expression of miR-409-3p improved the chemosensitivity of oxaliplatin-sensitive and oxaliplatin-resistant colon cancer cells (Tan et al., 2016). Therefore, miR-409-3p is a strong candidate for a new therapeutic target for the treatment of cancer because of its essential roles in cancer initiation and progression.

MiR-409-3p target identification is essential for understanding its potential functions in OS and developing novel targeted therapies for improving OS treatment. Potential miR-409-3p target genes have been previously reported; for example, Beclin-1 in colon cancer (Tan et al., 2016), radixin in gastric cancer (Zheng et al., 2012), and Ras suppressor 1 and stromal antigen 2 in prostate cancer (Josson et al., 2015). In the current study, we identified ZEB1 as a novel direct target of miR-409-3p in OS. Based on bioinformatics analysis, we predicted that *ZEB1* contains a miR-409-3p seed match at position 1280–1286 of the *ZEB1* 3′ UTR. Luciferase reporter assays demonstrated that miR-409-3p directly targeted the 3′ UTR of *ZEB1*. Furthermore, Western blot and RT-qPCR analysis indicated that endogenous miR-409-3p has a negative regulatory effect on *ZEB1* mRNA and protein expression in OS cells. Moreover, ZEB1 expression was high in OS tissues and inversely associated with that of miR-409-3p expression and knockdown of ZEB1 led to decreased OS cell proliferation and invasion, similar to miR-409-3p overexpression.

ZEB1, a member of the deltaEF1 family of two-handed zinc-finger transcription factors, maps to the short arm of human chromosome 10 (Zhang et al., 2019). ZEB1 expression is abnormally upregulated in various types of human cancer, including thyroid (Zhang et al., 2016), cervical (Ma et al., 2015), gastric (Jia et al., 2012), endometrial (Feng et al., 2014), and prostate (Drake et al., 2009) cancers. Accumulating evidence shows that ZEB1 has crucial roles during cancer initiation and progression (Kenney et al., 2011; Jia et al., 2012; Liu et al., 2012). In OS, Shen et al. reported that ZEB1 is highly

expressed in tumor tissues and that its levels are significantly associated with lung metastasis. The signal network of ZEB1 involved in malignant transformation in various types of tumor is complicated. All of the upstream and downstream molecules participate in activating the signaling pathways in cell survival, senescence, chemosensitivity and immune escape, which may trigger the regulation of miR-409-3p. These findings suggest that inhibition of OS has the potential to be a novel and effective therapeutic target with the aim of curing this type of cancer. The limitations of this study include that we did not investigate the effects of ectopic ZEB1 over-expression on cell proliferation and invasion activity of miR-409-3p-expressing osteosarcoma cells and that the number of samples in this study is small thus multi-center trial is still needed.

CONCLUSION

In conclusion, here we establish for the first time that miR-409-3p expression is down-regulated in OS tissues and cell lines. Decreased miR-409-3p expression levels were associated with clinical stage and distant metastasis. MiR-409-3p targets ZEB1, which may be associated with OS carcinogenesis and progression, leading to inhibition of OS cell proliferation and invasion. Thus, the miR-409-3p/ZEB1 axis can be considered a novel therapeutic target for OS treatment. Further research is needed to explore whether the potential of miR-409-3p/ZEB1 can be realized to treat OS.

AUTHOR CONTRIBUTIONS

These studies were conceived of and designed by all authors. Experiments were performed by LW and YZ. Data analysis, data interpretation, manuscript preparations were done by ZH, HG, KZ, XY, and JX.

FUNDING

The work was supported by General Projects of Shanghai Health State Planning Commission (No. 201640219).

ACKNOWLEDGMENTS

We thank Australian Saqlain Abbas for helping us in editing our manuscript.

REFERENCES

Anderson, M. E. (2015). Update on survival in osteosarcoma. *Orthop. Clin. North Am.* 2016, 283–292. doi: 10.1016/j.ocl.2015.08.022

Bartel, D. P. (2004). MicroRNAs: genomics, biogenesis, mechanism, and function. *Cell* 116, 281–297. doi: 10.1016/S0092-8674(04)00045-5

Cates, J. M. (2016). Utility of examination of biopsy tracts in osteosarcoma resection specimens. *Am. J. Clin. Pathol.* 146, 324–327. doi: 10.1093/ajcp/aqw119

Chen, X., Chen, X. G., Hu, X., Song, T., Ou, X., Zhang, C., et al. (2016). MiR-34a and miR-203 inhibit survivin expression to control cell proliferation and survival in human osteosarcoma cells. *J. Cancer* 7, 1057–1065. doi: 10.7150/jca.15061

Drake, J. M., Strohbehn, G., Bair, T. B., Moreland, J. G., and Henry, M. D. (2009). ZEB1 enhances transendothelial migration and represses the epithelial phenotype of prostate cancer cells. *Mol. Biol. Cell* 20, 2207–2217. doi: 10.1091/mbc.E08-10-1076

Esteller, M. (2011). Non-coding RNAs in human disease. *Nat. Rev. Genet.* 12, 861–874. doi: 10.1038/nrg3074

Feng, G., Wang, X., Cao, X., Shen, L., and Zhu, J. (2014). ZEB1 expression in endometrial biopsy predicts lymph node metastases in patient with endometrial cancer. *Dis. Markers* 2014:680361. doi: 10.1155/2014/680361

Fenger, J. M., Bear, M. D., Volinia, S., Lin, T. Y., Harrington, B. K., London, C. A., et al. (2014). Overexpression of miR-9 in mast cells is associated with invasive behavior and spontaneous metastasis. *BMC Cancer* 14:84. doi: 10.1186/1471-2407-14-84

Gambari, R., Brognara, E., and Spandidos, D. A. (2016). Targeting oncomiRNAs and mimicking tumor suppressor miRNAs: new trends in the development of miRNA therapeutic strategies in oncology (Review). *Int. J. Oncol.* 49, 5–32. doi: 10.3892/ijo.2016.3503

Gill, J., Ahluwalia, M. K., Geller, D., and Gorlick, R. (2013). New targets and approaches in osteosarcoma. *Pharmacol. Ther.* 137, 89–99. doi: 10.1016/j.pharmthera.2012.09.003

Imani, S., Wei, C., Cheng, J., Khan, M. A., Fu, S., Yang, L., et al. (2017). MicroRNA-34a targets epithelial to mesenchymal transition-inducing transcription factors (EMT-TFs) and inhibits breast cancer cell migration and invasion. *Oncotarget* 8, 21362–21379. doi: 10.18632/oncotarget.15214

Isakoff, M. S., Bielack, S. S., and Meltzer, P. (2015). Osteosarcoma: current treatment and a collaborative pathway to success. *J. Clin. Oncol.* 33, 3029–3035. doi: 10.1200/JCO.2014.59.4895

Jia, B., Liu, H., Kong, Q., and Li, B. (2012). Overexpression of ZEB1 associated with metastasis and invasion in patients with gastric carcinoma. *Mol. Cell Biochem.* 366, 223–229. doi: 10.1007/s11010-012-1299-6

Josson, S., Gururajan, M., Sung, S. Y., Hu, P., Shao, C., Zhau, H. E., et al. (2015). Stromal fibroblast-derived miR-409 promotes epithelial-to-mesenchymal transition and prostate tumorigenesis. *Oncogene* 34, 2690–2699. doi: 10.1038/onc.2014.212

Kenney, P. A., Wszolek, M. F., Rieger-Christ, K. M., Neto, B. S., Gould, J. J., Harty, N. J., et al. (2011). Novel ZEB1 expression in bladder tumorigenesis. *BJU Int.* 107, 656–663. doi: 10.1111/j.1464-410X.2010.09489.x

Li, C., Xu, W., Ding, J., Zhang, Y., Wang, J., Zhuang, X., et al. (2015). Micellization of antineoplastic agent to significantly upregulate efficacy and security. *Macromol. Biosci.* 15, 328–341. doi: 10.1002/mabi.201400356

Li, R. Z., and Wang, L. M. (2016). Decreased microRNA-452 expression and its prognostic significance in human osteosarcoma. *World J. Surg. Oncol.* 14:150. doi: 10.1186/s12957-016-0900-y

Li, S., Zhang, T., Xu, W., Ding, J., Yin, F., Xu, J., et al. (2018). Sarcoma-targeting peptide-decorated polypeptide nanogel intracellularly delivers shikonin for upregulated osteosarcoma necroptosis and diminished pulmonary metastasis. *Theranostics* 8, 1361–1375. doi: 10.7150/thno.18299

Li, Y., Zeng, C., Tu, M., Jiang, W., Dai, Z., Hu, Y., et al. (2016). MicroRNA-200b acts as a tumor suppressor in osteosarcoma via targeting ZEB1. *Onco. Targets Ther.* 9, 3101–3111. doi: 10.2147/OTT.S96561

Liu, C., and Lin, J. (2016). Long noncoding RNA ZEB1-AS1 acts as an oncogene in osteosarcoma by epigenetically activating ZEB1. *Am. J. Transl. Res.* 8, 4095–4105.

Liu, M., Xiusheng, H., Xiao, X., and Wang, Y. (2016). Overexpression of miR-422a inhibits cell proliferation and invasion, and enhances chemosensitivity in osteosarcoma cells. *Oncol. Rep.* 36, 3371–3378. doi: 10.3892/or.2016.5182

Liu, Z., Sun, B., Qi, L., Li, H., Gao, J., and Leng, X. (2012). Zinc finger E-box binding homeobox 1 promotes vasculogenic mimicry in colorectal cancer through induction of epithelial-to-mesenchymal transition. *Cancer Sci.* 103, 813–820. doi: 10.1111/j.1349-7006.2011.02199.x

Livak, K. J., and Schmittgen, T. D. (2001). Analysis of relative gene expression data using real-time quantitative PCR and the 2(-Delta Delta C(T) Method. *Methods* 25, 402–408. doi: 10.1006/meth.2001.1262

Ma, Y., Zheng, X., Zhou, J., Zhang, Y., and Chen, K. (2015). ZEB1 promotes the progression and metastasis of cervical squamous cell carcinoma via the promotion of epithelial-mesenchymal transition. *Int. J. Clin. Exp. Pathol.* 8, 11258–11267.

Ma, Z., Li, Y., Xu, J., Ren, Q., Yao, J., and Tian, X. (2016). MicroRNA-409-3p regulates cell invasion and metastasis by targeting ZEB1 in breast cancer. *IUBMB Life* 68, 394–402. doi: 10.1002/iub.1494

Qu, R., Chen, X., and Zhang, C. (2018). LncRNA ZEB1-AS1/miR-409-3p/ZEB1 feedback loop is involved in the progression of non-small cell lung cancer. *Biochem. Biophys. Res. Commun.* 507, 450–456. doi: 10.1016/j.bbrc.2018.11.059

Righi, A., Gambarotti, M., Sbaraglia, M., Sisto, A., Ferrari, S., Tos, A. P., et al. (2016). p16 expression as a prognostic and predictive marker in high grade localized osteosarcoma of the extremities: an analysis of 357 cases. *Hum. Pathol.* 58, 15–23. doi: 10.1016/j.humpath.2016.07.023

Shen, A., Zhang, Y., and Yang, H. (2012). Overexpression of ZEB1 relates to metastasis and invasion in osteosarcoma. *J. Surg. Oncol.* 105, 830–834. doi: 10.1002/jso.23012

Sun, L., Li, Y., Zhang, J., Li, H., Li, B., and Ye, Z. (2015). Prognostic value of pathologic fracture in patients with high grade localized osteosarcoma: a systemic review and meta-analysis of cohort studies. *J. Orthop. Res.* 33, 131–139. doi: 10.1002/jor.22734

Tan, S., Shi, H., Ba, M., Lin, S., Tang, H., Zeng, X., et al. (2016). miR-409-3p sensitizes colon cancer cells to oxaliplatin by inhibiting Beclin-1-mediated autophagy. *Int. J. Mol. Med.* 37, 1030–1038. doi: 10.3892/ijmm.2016.2492

Tang, J., Shen, L., Yang, Q., and Zhang, C. (2014). Overexpression of metadherin mediates metastasis of osteosarcoma by regulating epithelial-mesenchymal transition. *Cell Prolif.* 47, 427–434. doi: 10.1111/cpr.12129

Trang, P., Medina, P. P., Wiggins, J. F., Ruffino, L., Kelnar, K., Omotola, M., et al. (2010). Regression of murine lung tumors by the let-7 microRNA. *Oncogene* 29, 1580–1587. doi: 10.1038/onc.2009.445

Tsai, S. C., Lin, C. C., Shih, T. C., Tseng, R. J., Yu, M. C., Lin, Y. J., et al. (2017). The miR-200b-ZEB1 circuit regulates diverse stemness of human hepatocellular carcinoma. *Mol. Carcinog.* 56, 2035–2047. doi: 10.1002/mc.22657

Vanas, V., Haigl, B., Stockhammer, V., and Sutterluty-Fall, H. (2016). MicroRNA-21 increases proliferation and cisplatin sensitivity of osteosarcoma-derived cells. *PLoS One* 11:e0161023. doi: 10.1371/journal.pone.0161023

Wang, G. C., He, Q. Y., Tong, D. K., Wang, C. F., Liu, K., Ding, C., et al. (2016). MiR-367 negatively regulates apoptosis induced by adriamycin in osteosarcoma cells by targeting KLF4. *J. Bone Oncol.* 5, 51–56. doi: 10.1016/j.jbo.2016.02.002

Zhang, Y., Liu, G., Wu, S., Jiang, F., Xie, J., and Wang, Y. (2016). Zinc finger E-box-binding homeobox 1: its clinical significance and functional role in human thyroid cancer. *Onco. Targets Ther.* 9, 1303–1310. doi: 10.2147/OTT.S96723

Zhang, Y., Wang, F., Li, M., Yu, Z., Qi, R., Ding, J., et al. (2018). Self-Stabilized hyaluronate nanogel for intracellular codelivery of doxorubicin and cisplatin to osteosarcoma. *Adv. Sci.* 5:1700821. doi: 10.1002/advs.201700821

Zhang, Y., Xu, L., and Li, A. (2019). The roles of ZEB1 in tumorigenic progression and epigenetic modifications. *Biomed. Pharmacother.* 110, 400–408. doi: 10.1016/j.biopha.2018.11.112

Zheng, B., Liang, L., Huang, S., Zha, R., Liu, L., Jia, D., et al. (2012). MicroRNA-409 suppresses tumour cell invasion and metastasis by directly targeting radixin in gastric cancers. *Oncogene* 31, 4509–4516. doi: 10.1038/onc.2011.581

Conflict of Interest Statement: The authors declare that the research was conducted in the absence of any commercial or financial relationships that could be construed as a potential conflict of interest.

frontiers in Oncology

ORIGINAL RESEARCH
published: 27 February 2019
doi: 10.3389/fonc.2019.00080

Targeting uPAR by CRISPR/Cas9 System Attenuates Cancer Malignancy and Multidrug Resistance

*Kun Wang†, Zi-Hao Xing†, Qi-Wei Jiang, Yang Yang, Jia-Rong Huang, Meng-Ling Yuan, Meng-Ning Wei, Yao Li, Sheng-Te Wang, Kun Liu and Zhi Shi**

Guangdong Provincial Key Laboratory of Bioengineering Medicine, Department of Cell Biology and Institute of Biomedicine, College of Life Science and Technology, Jinan University, National Engineering Research Center of Genetic Medicine, Guangzhou, China

Urokinase plasminogen activator receptor (uPAR), a member of the lymphocyte antigen 6 protein superfamily, is overexpressed in different types of cancers and plays an important role in tumorigenesis and development. In this study, we successfully targeted uPAR by CRISPR/Cas9 system in two human cancer cell lines with two individual sgRNAs. Knockout of uPAR inhibited cell proliferation, migration and invasion. Furthermore, knockout of uPAR decreases resistance to 5-FU, cisplatin, docetaxel, and doxorubicin in these cells. Although there are several limitations in the application of CRISPR/Cas9 system for cancer patients, our study offers valuable evidences for the role of uPAR in cancer malignancy and drug resistance.

Keywords: cancer, uPAR, CRISPR/Cas9, malignancy, drug resistance

OPEN ACCESS

Edited by:
Yan-yan Yan,
Shanxi Datong University, China

Reviewed by:
Zui Pan,
University of Texas at Arlington, United States
Hui Yang,
Second Affiliated Hospital of Guangzhou Medical University, China

***Correspondence:**
Zhi Shi
tshizhi@jnu.edu.cn

†These authors have contributed equally to this work

Specialty section:
This article was submitted to Cancer Molecular Targets and Therapeutics, a section of the journal Frontiers in Oncology

Received: *25 December 2018*
Accepted: *29 January 2019*
Published: *27 February 2019*

Citation:
Wang K, Xing Z-H, Jiang Q-W, Yang Y, Huang J-R, Yuan M-L, Wei M-N, Li Y, Wang S-T, Liu K and Shi Z (2019) Targeting uPAR by CRISPR/Cas9 System Attenuates Cancer Malignancy and Multidrug Resistance. Front. Oncol. 9:80. doi: 10.3389/fonc.2019.00080

INTRODUCTION

Urokinase plasminogen activator (uPA) receptor (uPAR), also known as CD87 and encoded by PLAUR gene, is a member of the lymphocyte antigen 6 protein superfamily (1). uPAR is a glycoprotein consisting of 313 amino acid residues with only the extracellular domain, no transmembrane and intracellular structures, and is attached to the cell membrane via glycosylphosphatidylinositol anchors (1). uPAR binds to and activates uPA to cleaving plasminogen to plasmin, thus triggering the remodeling of extracellular matrix and playing a key role in cell adhesion, migration, proliferation, and survival (2). Besides uPA, uPAR can interact with other proteins, including vitronectin, integrins, and EGFR, etc to regulate multiple signal pathways (2). Compared to normal tissues, uPAR is highly expressed in many human cancers including lung, breast, gastric, colorectal, pancreatic, bladder, and prostate cancers, etc (3). The expression of uPAR in these cancers promotes the proliferation, metastasis, and invasion of cancer cells (3). Therefore, uPAR may be an important biomarker and target for cancers. Indeed, many inhibitors of uPAR have been developed. The inhibitors blocks the interaction of uPAR with uPA, including: small molecules UK1 (4), WX-UK1 (5), WX-671 (6), etc; peptides Mupain-1 (7), AE105 (8), ATF (9), etc; and monoclonal antibody ATN-291 (10). In addition, there are inhibitors that inhibit the interaction of uPAR with integrins, including: peptides P25 (11), a325 (12), H245A (13), etc; and monoclonal antibody ATN-658 (14). However, the poor affinity and bioavailability limit the application of these inhibitors in clinic. Consequently, it is necessary to develop new approaches to target uPAR for treatment cancer and other diseases.

The RNA-guided clustered regularly interspaced short palindromic (CRISPR) in combination with a CRISPR-associated nuclease 9 (Cas9) nuclease system is a novel gene editing technology by delivering the Cas9 complexed with a synthetic guide RNA (gRNA) into a cell to cut the desired genome location, allowing existing genes to be removed and/or new ones added (15). Due to the advantages of faster, cheaper, more accurate, and efficient, CRISPR/Cas9 system has been widely used as a basic biology research tool, development of biotechnology products and potentially to treat diseases (16). In this study, we used CRISPR/Cas9 system targeting uPAR to verify the role of uPAR in cancers.

MATERIALS AND METHODS

Cells and Reagents

The two multidrug resistant cancer cell lines HCT8/T and KB_{V200} were cultured in Dulbecco's modified Eagle's medium (DMEM) with 10% FBS, penicillin (100 U/ml) and streptomycin (100 ng/ml) at 37°C in a humidified atmosphere of 5% CO_2. Restriction endonuclease BsmBI was from New England Biolabs. Polyetherimide (PEI) was from Ploysciences. Cisplatin was from Shandong Qilu Pharmaceutical. 5-FU, docetaxel, and doxorubicin were from LC Laboratories. Puromycin was from Selleck Chemicals. Methylthiazolyldiphenyl-tetrazolium bromide (MTT) was from ApexBio Technology. Anti-uPAR (D121140) antibody was from Shanghai sangon biotech. Anti-Vinculin antibody (BM1611) was from Wuhan Boster Biotech.

Vector Generation, Lentivirus Production, and Transduction

LentiCRISPRv2 vector (from Addgene #52961) was digested with BsmBI and ligated with annealed oligonucleotides (uPAR-sg1-F: 5′-CACCGGACCAACGGGGATTGCCGTG-3′, uPAR-sg1-R: 5′-AA-ACCACGGCAATCCCCGTTGGTCC-3′; uPAR-sg2-F: 5′-CACCGGGACCACGATCGTGCGCTTG-3′, uPAR-sg2-R: 5′-AAACCAAGCGCACGATCGTGGTCCC-3′). HEK293T were transfected using PEI at 70% confluency with recombinant vectors and packaging vectors pMD2G and psPAX2. Viral supernatant was harvested 96 h after transfection and stored at −80°C. HCT-8/T and KB_{V200} cells were transducted with viral supernatant containing 10 μg/ml polybrene, and were selected with 100 and 10 μg/ml puromycin respectively to establish the stable cell lines.

Genomic PCR and Sequencing Analysis

The genomic DNA of cells was extracted with the QuickExtract DNA extraction kit following the manufacturer's protocol and amplified with a pair of primers (Detection 1-F: 5′-GACAACGGACAGACTGGAA-3′, Detection 1-R: 5′-CCGAATCGCTCTAAGTGG-3′) designed for the target region of interest using a Pfu DNA polymerase. Followed by agarose gel electrophoresis and ethidium bromide staining, the purified PCR products were sequencing with an ABI 3131xl Genetic analyzer.

Western Blot Analysis

Cells were harvested and lysed in RIPA buffer (1% NP-40, 0.5% sodium deoxycholate, 0.1%SDS, 10 ng/ml PMSF, 0.03% aprotinin, 1 μM sodium orthovanadate) at 4°C for 30 min. Lysates were centrifuged for 10 min at 14,000×g and supernants were stored at −80°C as whole cell extracts. Protein concentration was quantified using with Bradford assay. Proteins were separated on 10% SDS-PAGE gels and transferred to polyvinylidene difluoride membranes. Membranes were blocked with 5% BSA and incubated with the indicated primary antibodies. Corresponding horseradish peroxidase-conjugated secondary antibodies were used against each primary antibody. Proteins were detected using the chemiluminescent detection reagents and films.

Cell Morphology Assay

Cells were seeded on glass cover slips for 24 h and then fixed in 4% paraformaldehyde for 20 min and permeabilized with 0.1% Triton X-100 for 15 min at room temperature. The coverslips were incubated in the dark with 100 nM rhodamine-phalloidin at room temperature for 30 min. Nuclei were counterstained with 100 nM DAPI. The coverslips were rinsed in PBS and inverted on a drop of anti-fade mounting media on a glass slide. Then, these slides were sealed with neutral balsam and viewed under the confocal microscope.

Cell Viability Assay

Cells were seeded into a 96-well plate at a density of 5,000 cells/well and treated with various concentrations of agents for 72 h. Then 10 μl MTT was added to each well at a final concentration of 0.5 mg/ml. After incubation for 4 h, formazan crystals were dissolved in 50 μl of DMSO, and absorbance at 570 nm was measured by plate reader. The concentrations required to inhibit growth by 50% (IC_{50}) were calculated from survival curves as previously described (17).

Sphere Formation Assay

Cells were trypsinized, suspended in medium containing 0.3% agar and 10% FBS and seeded at a density of 5×10^2 cells/well in a 12-well plate. The agar–cell mixture was plated onto a bottom layer with 0.5% agar. Then treated cells were incubated in a humidified incubator and fresh medium was added every 3 days. Two weeks later, colonies were analyzed microscopically.

Cell Migration Assay

Cells were seeded into a 6-well plate, and reached 80–90% confluence, the cell monolayer was wounded using a sterilized 10 μl pipette tip and washed with PBS two times. Cells were allowed to migrate for 12, 24, and 36 h in serum-free medium, and the wounds were observed and captured. The gap lengths were measured from the photomicrographs.

Cell Invasion Assay

Cell invasion assays were performed with a modified Boyden chamber (Corning) containing matrigel-coated polycarbonate membrane filter (6.5 mm diameter, 8 μm pore size). Cells were plated in the upper chamber and the lower chamber contained medium with 10% FBS, and incubated for 24 h

at 37°C in 5% CO_2. Non-migrated cells were scraped from the upper surface of the membrane, and migrated cells remaining on the bottom surface were photographed and counted.

Statistical Analysis

The experimental data of this paper are the results of three independent repetitions. The data obtained is presented in the form of an average and a standard deviation. Statistical analysis

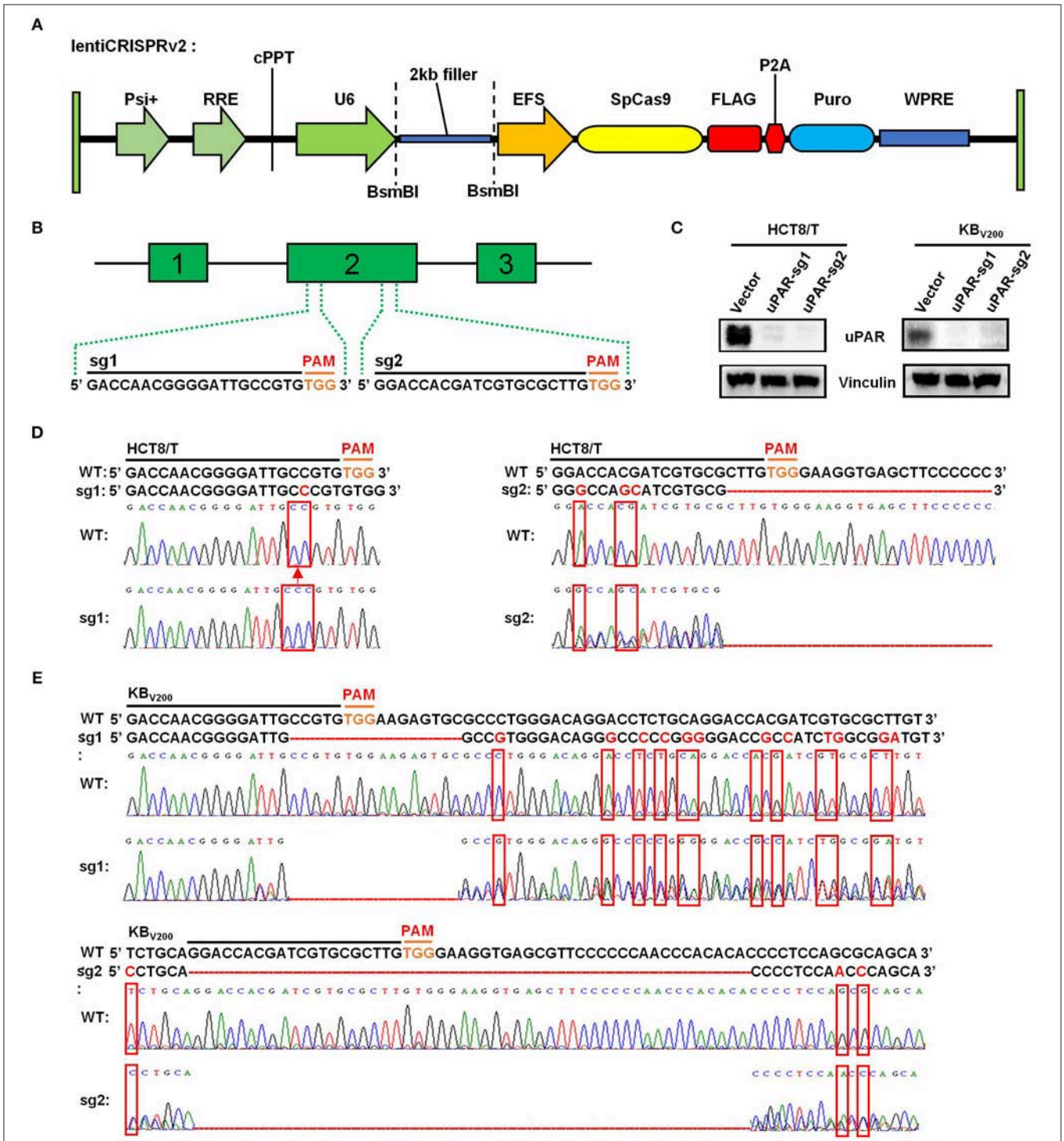

FIGURE 1 | Knockout of uPAR by CRISPR/Cas9 system. **(A)** The map of lentiCRISPRv2 vector. **(B)** The locations and sequences of two sgRNAs of uPAR. **(C)** The protein expression levels of uPAR were examined by Western blot, and vinculin was used as loading control. The genomic DNA of cells was amplified and sequenced by the designed primers. The sequencing comparison and original data of HCT8/T **(D)** and KB_{V200} **(E)** cells are shown.

of data differences using *t*-test method. A *P*-value of <0.05 was set as the criterion for statistical significance.

RESULTS

Knockout of uPAR by CRISPR/Cas9 System

To target uPAR with CRISPR/Cas9 system, we firstly used lentiCRISPRv2 vector which expresses both hSpCas9 and the chimeric guide RNA (**Figure 1A**) linked respectively, with two targeting sequences from exon 2 of human uPAR gene (PLAUR) end with a 5′NGG3′ PAM (protospacer adjacent motif) sequence (**Figure 1B**). Then, the two successfully generated vectors expressed sgRNA1 (sg1) or sgRNA2 (sg2) to target uPAR were identified by sequencing. To establish cell lines stably expressed sgRNA to target uPAR, HCT8/T, and KB_{V200} cells were selected with puromycin after transduction with LentiCRISPRv2 viral supernatant. As shown in **Figure 1C**, the protein levels of uPAR were undetectable by western blot in both HCT8/T and KB_{V200} cells stably expressed either sg1 or sg2. To further identify the genomic change of targeting uPAR by CRISPR/Cas9 system, the genomic DNA of cells was extracted and amplified using the designed primers by PCR reaction. The sequencing results of PCR productions showed that 1 base was inserted into the target position of HCT8/T uPAR-sg1 cells and 3 base mismatches and a large deletion in the target position of HCT8/T uPAR-sg2 cells (**Figure 1D**). There were 16 base deletions and 12 base mismatches in the target position of KB_{V200} uPAR-sg1 cells and 51 base deletions and 3 base mismatches in the target position of KB_{V200} uPAR-sg2 cells (**Figure 1E**). These data suggest that cells with stable knockout of uPAR by CRISPR/Cas9 system were successfully established.

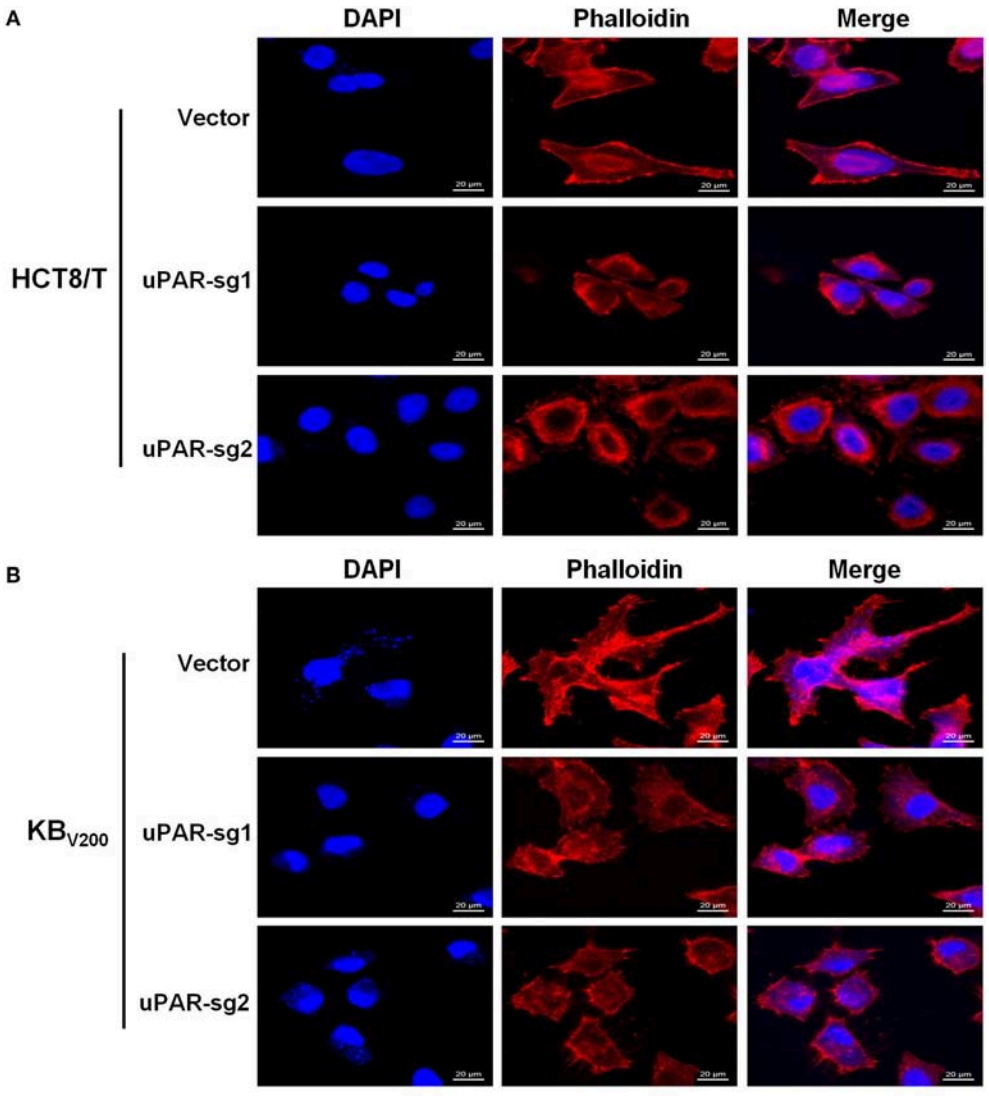

FIGURE 2 | Knockout of uPAR alters cell morphology. The morphology of HCT8/T **(A)** and KB_{V200} **(B)** cells was obtained with confocal microscope.

Knockout of uPAR Alters Cell Morphology

To explore the effect of knockout of uPAR on cell morphology, we stained cells with Rhodamine-labeled phalloidin and DAPI. The results showed that HCT8/T and KB_{V200} cells with uPAR knockout underwent morphologic changes from spindle-shaped phenotype to round phenotype (**Figures 2A,B**), indicating that knockout of uPAR alters cell morphology.

Knockout of uPAR Attenuates Cell Proliferation

To investigate the effect of knockout of uPAR on cell proliferation, we detected cell proliferation by MTT and sphere formation assays. As shown in **Figure 3A**, knockout of uPAR inhibited the growth of HCT8/T and KB_{V200} cells. Further sphere formation assay showed that knockout of uPAR reduced the sphere number and size of HCT8/T and KB_{V200} cells (**Figures 3B–E**). These results suggest that knockout of uPAR attenuates cell proliferation.

Knockout of uPAR Inhibits Cell Migration

To examine the effect of knockout of uPAR by CRISPR/Cas9 on cell migration, wound healing assay was used to detect cell migration. The results showed that cell migration was reduced in HCT8/T and KB_{V200} cells with uPAR knockout (**Figure 4**), indicating that knockout of uPAR inhibits cell migration.

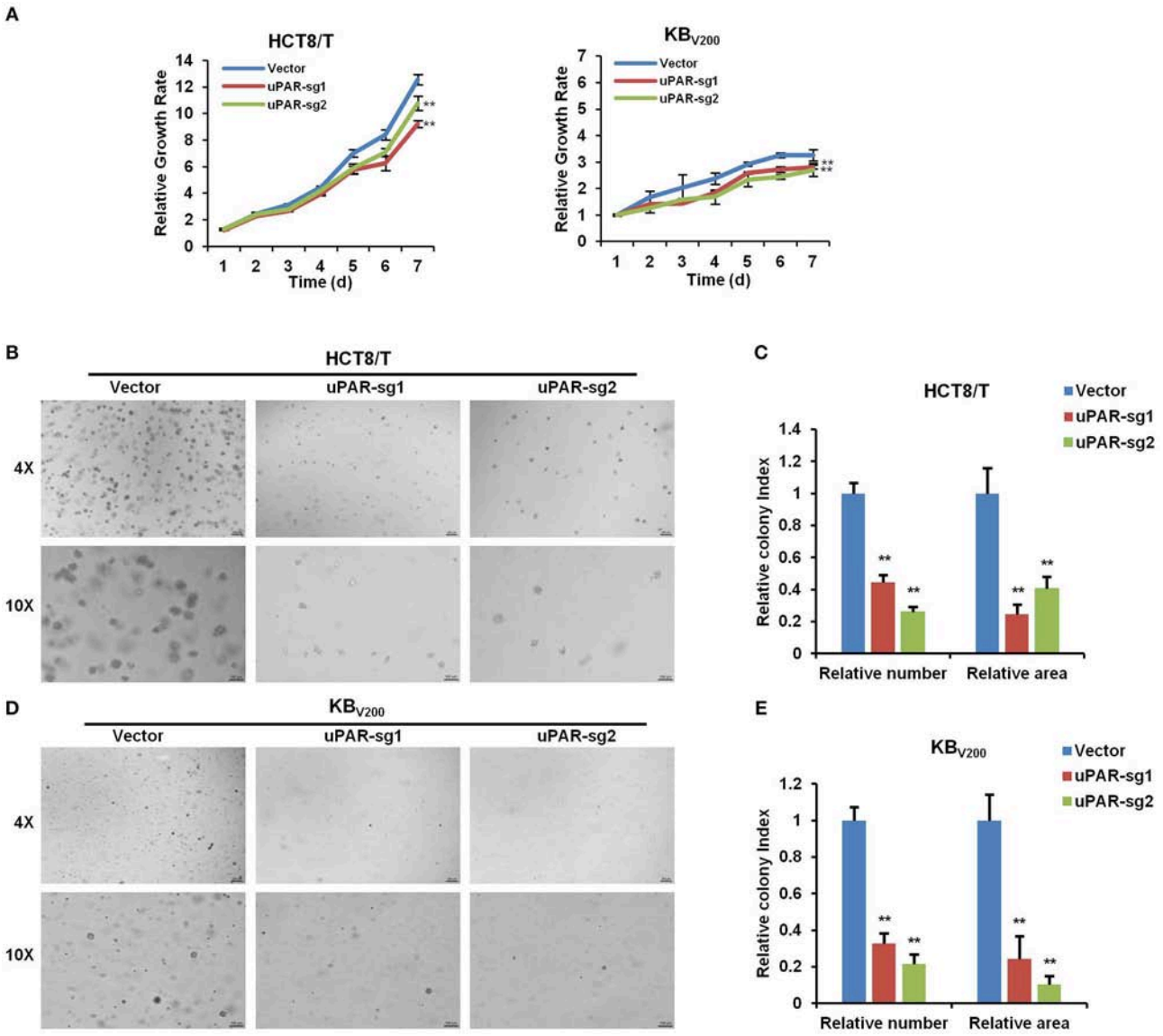

FIGURE 3 | Knockout of uPAR attenuates cell proliferation. **(A)** Cell proliferation was evaluated by MTT assay. Representative spheres images and quantification of HCT8/T **(B,C)** and KB_{V200} **(D,E)** cells were determined by sphere formation assay. $^{**}P < 0.01$ vs. corresponding control.

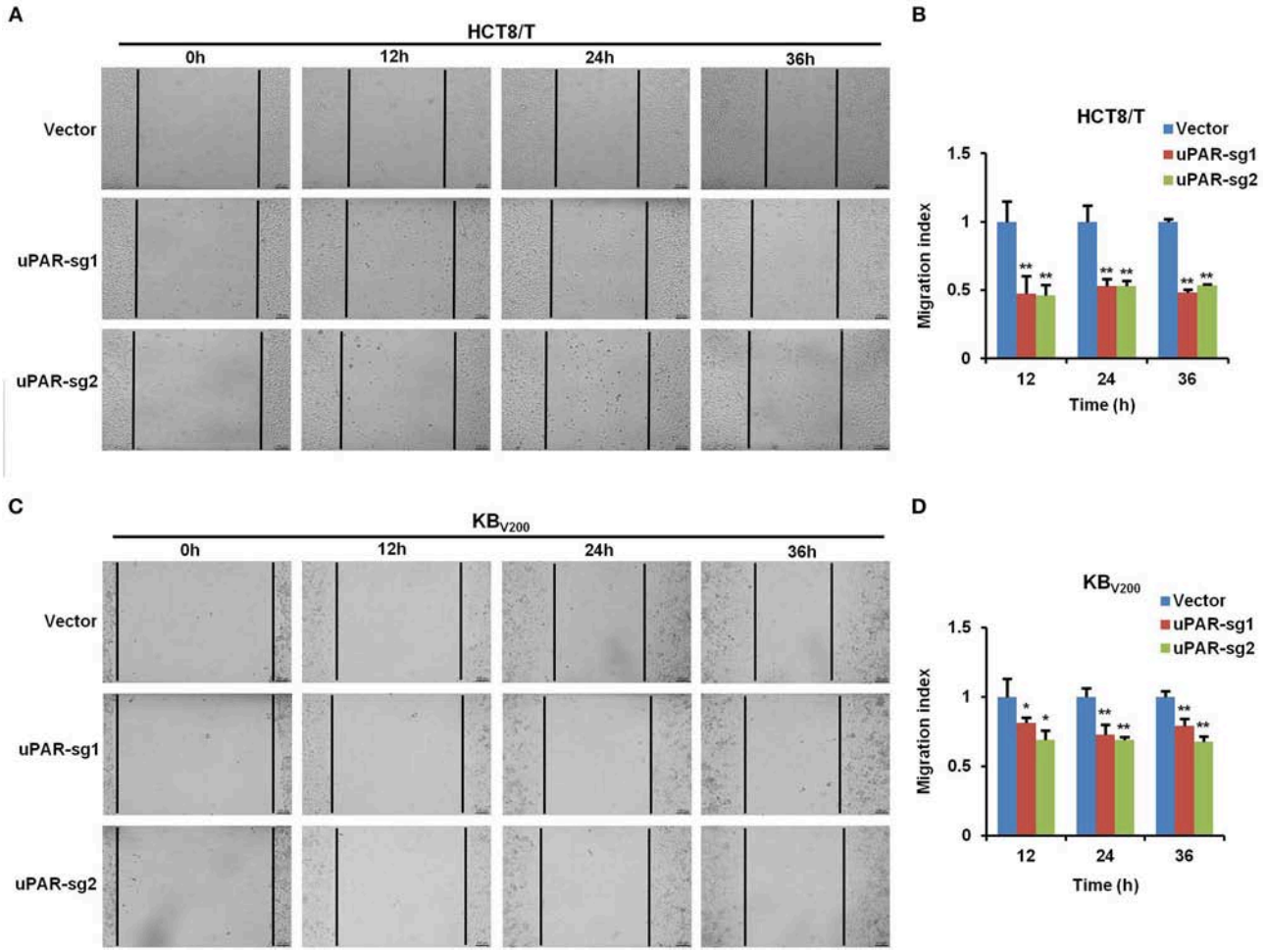

FIGURE 4 | Knockout of uPAR inhibits cell migration. Cell migration was determined with wound healing assay. Representative migration images and quantification of HCT8/T **(A,B)** and KB_{V200} **(C,D)** cells were shown. $^{*}P < 0.05$ and $^{**}P < 0.01$ vs. corresponding control.

Knockout of uPAR Inhibits Cell Invasion

To further evaluate the effect of knockout of uPAR by CRISPR/Cas9 on cell invasion, transwell assay was used to detect cell invasion. As shown in **Figure 5**, cell invasion was reduced in HCT8/T and KB_{V200} cells with uPAR knockout, suggesting that knockout of uPAR inhibits cell invasion.

Knockout of uPAR Decreases Multidrug Resistance

To study the effect of knockout of uPAR by CRISPR/Cas9 on multidrug resistance, four chemotherapeutical drugs 5-FU, cisplatin, docetaxel, and doxorubicin were used to treat cells, and cell survival was detected by MTT assays. As shown in **Figure 6**, the cell survival curves shifted to downward, and IC_{50} values of these four drugs were reduced in HCT8/T and KB_{V200} cells with uPAR knockout. These data indicate that knockout of uPAR suppresses multidrug resistance.

DISCUSSION

Recently, it has been demonstrated that knockout of uPAR using CRISPR/Cas9 system in mouse neuroblastoma Neuro 2A cells inhibit cell proliferation, reduce the number of Ki-67 positive cells, and down-regulate the mRNA expression level of TrkC receptor (18). In the current study, we successfully targeted uPAR in two cancer cell lines by CRISPR/Cas9 system with two individual sgRNAs. Knockout of uPAR suppresses cell proliferation, migration and invasion. Moreover, knockout of uPAR decreases resistance to 5-FU, cisplatin, docetaxel, and doxorubicin in these cells. Previous studies have shown that high expression of uPAR leads to small cell lung cancer, head and neck squamous cell carcinoma, and malignant pleural mesothelioma resistant to chemotherapy (19–21). uPAR promotes the resistance to tamoxifen in breast cancer by activated ERK1/2 activity (22), and confers the resistance to gefitinib in non-small-cell lung cancer through activated EGFR/pAKT/survivin signal pathway (23). Therefore, uPAR plays important roles not only in cancer malignancy but also in drug resistance.

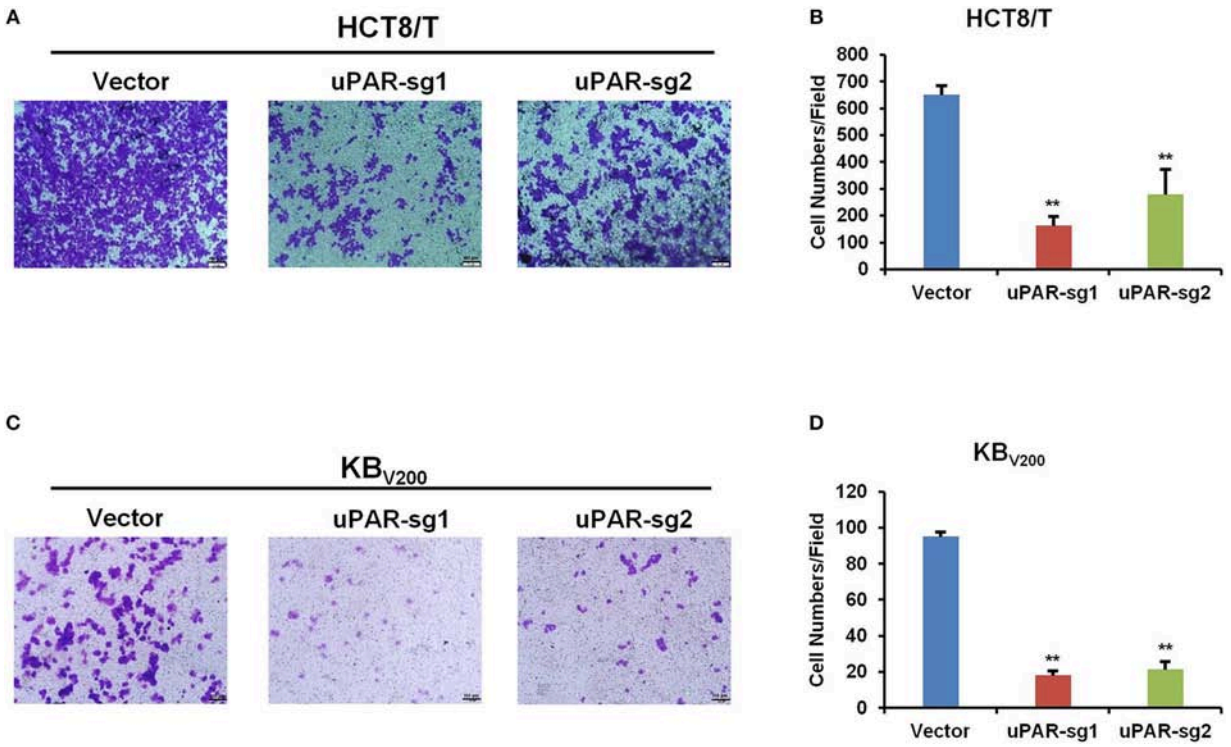

FIGURE 5 | Knockout of uPAR inhibits cell invasion. Cell invasion was determined with transwell assay. Representative invasion images and quantification of HCT8/T **(A,B)** and KB_{V200} **(C,D)** cells were shown. $^{**}P < 0.01$ vs. corresponding control.

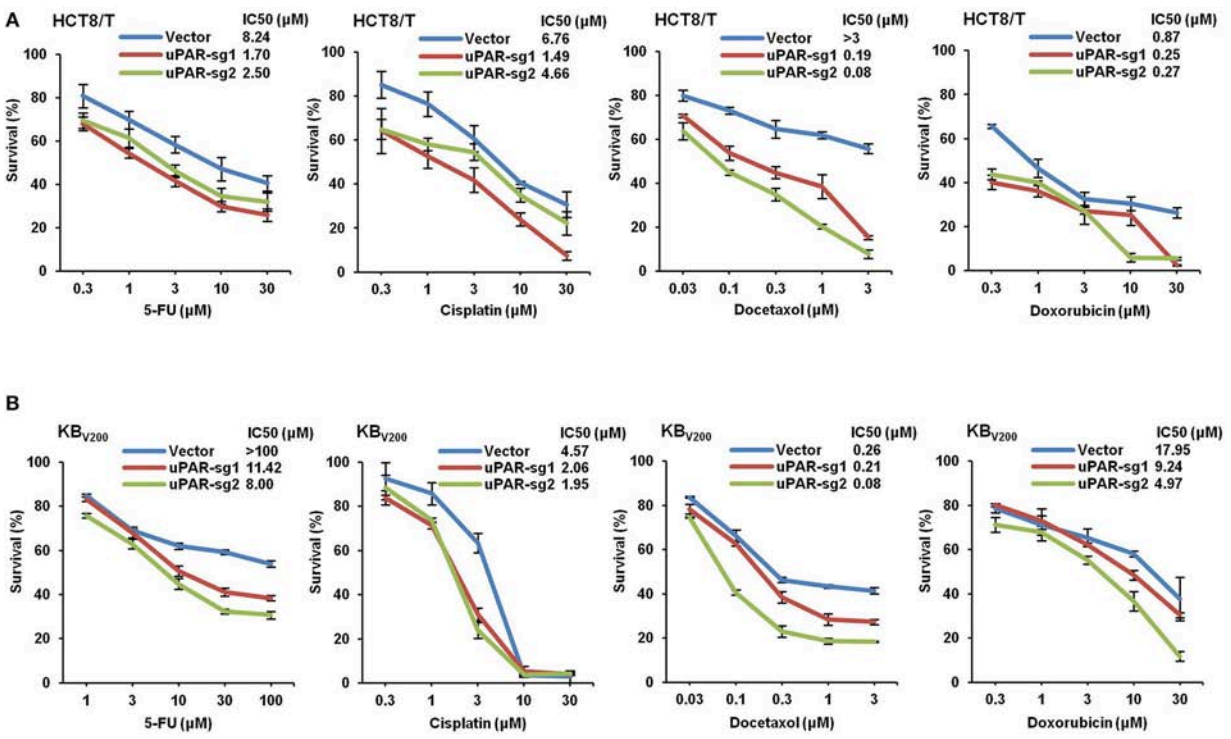

FIGURE 6 | Knockout of uPAR decreases multidrug resistance. Cells survival was measured by MTT assay. The representative growth curve of HCT8/T **(A)** and KB_{V200} **(B)** cells treated with the indicated concentrations of 5-FU, cisplatin, docetaxel, and doxorubicin for 72 h were shown.

CRISPR/Cas9 system has been widely applied in exploring the molecular mechanism of tumorigenesis, generating the models for cancer research and identifying the targets for cancer treatment, etc. A genome-wide CRISPR screen shows that loss-of-function mutations of some genes including NF2, PTEN, CDKN2A, TRIM72, FGA, miR-152, miR-345, and so on are able to drive tumor growth and metastasis in a mouse model (24). Using CRISPR/Cas9 technology to target MAN2A1-FER fusion gene inhibits tumor proliferation and metastasis in the mouse models of prostate and liver cancer (25). Colorectal cancer from normal human intestinal epithelium organoids are generated by introducing mutations in the tumor suppressor genes APC, SMAD4 and TP53, and oncogenes KRAS and/or PIK3CA with CRISPR/Cas9 system (26, 27). Liver tumors in mice are occurred by using hydrodynamic injection of CRISPR/Cas9 plasmids and sgRNAs that directly target the tumor suppressor genes PTEN and p53 (28). Mouse pancreatic ductal adenocarcinoma models are established by introducing 13 sgRNAs of different tumor suppressor genes into expression vectors and then transferred them to mouse pancreatic tissue (29). CDC25A is identifies as a determinant of sensitivity to ATR inhibitors by a genome-wide CRISPR screen (30). Deletion of genes such as NF1 and MED12 with CRISPR/Cas9 system is associated with resistance to vemurafenib (31). Moreover, the combination of CRISPR/Cas9 gene editing technology and immunotherapy, especially with CAR-T cell therapy, will have enormous therapeutic potential in leukemia, lymphoma, and some solid tumors (32, 33). Using CRISPR/Cas9 system can produce universal CAR-T cells by simultaneously targeting TCR and HLA-I (34) and enhanced CAR-T cells by deleting T cell inhibitory receptor or signaling molecule genes such as PD1 and CTLA4 (33, 35). We previously have demonstrated that targeting ABCB1 by CRISPR/Cas9-based genome editing reverses ABCB1-mediated multidrug resistance in cancer cells, resulting in the increase of the sensitivity and intracellular accumulation of the anti-cancer drugs (36). Although there are several limitations such as off-targets and delivery in the clinical application of CRISPR/Cas9 technology, it is believed that CRISPR/Cas9 system will benefit cancer patients in the near future.

In summary, our results have demonstrated that targeting uPAR by CRISPR/Cas9-based genome editing causes knockout of uPAR in human cancer cell lines, resulting in attenuation of cell proliferation, migration, invasion and multidrug resistance. Our study offers valuable evidences for the role of uPAR in cancer malignancy and drug resistance.

AUTHOR CONTRIBUTIONS

KW, Z-HX, and ZS designed the experiments, performed the experiments, analyzed the data, and wrote the paper. Q-WJ, YY, J-RH, M-LY, M-NW, YL, S-TW, and KL performed the experiments. All authors read and approved the final manuscript.

FUNDING

This work was supported by funds from the National Key Research and Development Program of China No. 2017YFA0505104 ZS, the National Natural Science Foundation of China No. 81772540 ZS, the Guangdong Natural Science Funds for Distinguished Young Scholar No. 2014A030306001 ZS, the Guangdong Special Support Program for Young Talent No. 2015TQ01R350 ZS, the Science and Technology Program of Guangdong No. 2016A050502027 ZS, the Science and Technology Program of Guangzhou No. 201704030058 ZS.

REFERENCES

1. Mahmood N, Mihalcioiu C, Rabbani SA. Multifaceted role of the urokinase-type plasminogen activator (uPA) and its receptor (uPAR): diagnostic, prognostic, and therapeutic applications. *Front Oncol.* (2018) 8:24. doi: 10.3389/fonc.2018.00024
2. Smith HW, Marshall CJ. Regulation of cell signalling by uPAR. *Nat Rev Mol Cell Biol.* (2010) 11:23–36. doi: 10.1038/nrm2821
3. Noh H, Hong S, Huang S. Role of urokinase receptor in tumor progression and development. *Theranostics.* (2013) 3:487–95. doi: 10.7150/thno.4218
4. Setyono-Han B, Sturzebecher J, Schmalix WA, Muehlenweg B, Sieuwerts AM, Timmermans M, et al. Suppression of rat breast cancer metastasis and reduction of primary tumour growth by the small synthetic urokinase inhibitor WX-UK1. *Thromb Haemost.* (2005) 93:779–86. doi: 10.1160/TH04-11-0712
5. Zhu M, Gokhale VM, Szabo L, Munoz RM, Baek H, Bashyam S, et al. Identification of a novel inhibitor of urokinase-type plasminogen activator. *Mol Cancer Ther.* (2007) 6:1348–56. doi: 10.1158/1535-7163.MCT-06-0520
6. Heinemann V, Ebert MP, Pinter T, Bevan P, Neville NG, Mala C. Randomized phase II trial with an uPA inhibitor (WX-671) in patients with locally advanced nonmetastatic pancreatic cancer. *J Clin Oncol.* (2010) 28:4060. doi: 10.1200/jco.2010.28.15_suppl.4060
7. Andersen LM, Wind T, Hansen HD, Andreasen PA. A cyclic peptidylic inhibitor of murine urokinase-type plasminogen activator: changing species specificity by substitution of a single residue. *Biochem J.* (2008) 412:447–57. doi: 10.1042/BJ20071646
8. Ploug M, Ostergaard S, Gardsvoll H, Kovalski K, Holst-Hansen C, Holm A, et al. Peptide-derived antagonists of the urokinase receptor. Affinity maturation by combinatorial chemistry, identification of functional epitopes, and inhibitory effect on cancer cell intravasation. *Biochemistry.* (2001) 40:12157–68. doi: 10.1021/bi010662g
9. Luparello C, Del Rosso M. *In vitro* anti-proliferative and anti-invasive role of aminoterminal fragment of urokinase-type plasminogen activator on 8701-BC breast cancer cells. *Eur J Cancer.* (1996) 32A:702–7. doi: 10.1016/0959-8049(95)00657-5
10. Mazar AP, Ahn RW, O'Halloran TV. Development of novel therapeutics targeting the urokinase plasminogen activator receptor (uPAR) and their translation toward the clinic. *Curr Pharm Des.* (2011) 17:1970–8. doi: 10.2174/138161211796718152
11. Ahmed N, Oliva K, Wang Y, Quinn M, Rice G. Downregulation of urokinase plasminogen activator receptor expression inhibits Erk signalling with concomitant suppression of invasiveness due to loss of uPAR-beta 1 integrin complex in colon cancer cells. *Brit J Cancer.* (2003) 89:374–84. doi: 10.1038/sj.bjc.6601098
12. Zhang F, Tom CC, Kugler MC, Ching TT, Kreidberg JA, Wei Y, et al. Distinct ligand binding sites in integrin alpha 3 beta 1 regulate matrix adhesion and cell-cell contact. *J Cell Biol.* (2003) 163:177–88. doi: 10.1083/jcb.200304065
13. Ghosh S, Johnson JJ, Sen R, Mukhopadhyay S, Liu Y, Zhang F, et al. Functional relevance of urinary-type plasminogen activator receptor-alpha3beta1 integrin association in proteinase regulatory pathways. *J Biol Chem.* (2006) 281:13021–9. doi: 10.1074/jbc.M508526200

14. Kenny HA, Leonhardt P, Ladanyi A, Yamada SD, Montag A, Im HK, et al. Targeting the urokinase plasminogen activator receptor inhibits ovarian cancer metastasis. *Clin Cancer Res.* (2011) 17:459–71. doi: 10.1158/1078-0432.CCR-10-2258
15. Barrangou R, Doudna JA. Applications of CRISPR technologies in research and beyond. *Nat Biotechnol.* (2016) 34:933–41. doi: 10.1038/nbt.3659
16. Fellmann C, Gowen BG, Lin PC, Doudna JA, Corn JE. Cornerstones of CRISPR-Cas in drug discovery and therapy. *Nat Rev Drug Discov.* (2017) 16:89–100. doi: 10.1038/nrd.2016.238
17. Yuan ML, Li P, Xing ZH, Di JM, Liu H, Yang AK, et al. Inhibition of WEE1 suppresses the tumor growth in laryngeal squamous cell carcinoma. *Front Pharmacol.* (2018) 9:1041. doi: 10.3389/fphar.2018.01041
18. Rysenkova KD, Semina EV, Karagyaur MN, Shmakova AA, Dyikanov DT, Vasiluev PA, et al. CRISPR/Cas9 nickase mediated targeting of urokinase receptor gene inhibits neuroblastoma cell proliferation. *Oncotarget.* (2018) 9:29414–30. doi: 10.18632/oncotarget.25647
19. Gutova M, Najbauer J, Gevorgyan A, Metz MZ, Weng Y, Shih CC, et al. Identification of uPAR-positive chemoresistant cells in small cell lung cancer. *PLoS ONE.* (2007) 2:e243. doi: 10.1371/journal.pone.0000243
20. Cortes-Dericks L, Carboni GL, Schmid RA, Karoubi G. Putative cancer stem cells in malignant pleural mesothelioma show resistance to cisplatin and pemetrexed. *Int J Oncol.* (2010) 37:437–44. doi: 10.3892/ijo-0000692
21. Huang Z, Wang L, Wang Y, Zhuo Y, Li H, Chen J, et al. Overexpression of CD147 contributes to the chemoresistance of head and neck squamous cell carcinoma cells. *J Oral Pathol Med.* (2013) 42:541–6. doi: 10.1111/jop.12046
22. Eastman BM, Jo M, Webb DL, Takimoto S, Gonias SL. A transformation in the mechanism by which the urokinase receptor signals provides a selection advantage for estrogen receptor-expressing breast cancer cells in the absence of estrogen. *Cell Signal.* (2012) 24:1847–55. doi: 10.1016/j.cellsig.2012.05.011
23. Zhou J, Kwak KJ, Wu Z, Yang D, Li J, Chang M, et al. PLAUR confers resistance to gefitinib through EGFR/P-AKT/Survivin signaling pathway. *Cell Physiol Biochem.* (2018) 47:1909–24. doi: 10.1159/000491071
24. Chen S, Sanjana NE, Zheng K, Shalem O, Lee K, Shi X, et al. Genome-wide CRISPR screen in a mouse model of tumor growth and metastasis. *Cell.* (2015) 160:1246–60. doi: 10.1016/j.cell.2015.02.038
25. Chen ZH, Yu YP, Zuo ZH, Nelson JB, Michalopoulos GK, Monga S, et al. Targeting genomic rearrangements in tumor cells through Cas9-mediated insertion of a suicide gene. *Nat Biotechnol.* (2017) 35:543–50. doi: 10.1038/nbt.3843
26. Matano M, Date S, Shimokawa M, Takano A, Fujii M, Ohta Y, et al. Modeling colorectal cancer using CRISPR-Cas9-mediated engineering of human intestinal organoids. *Nat Med.* (2015) 21:256–62. doi: 10.1038/nm.3802
27. Drost J, van Jaarsveld RH, Ponsioen B, Zimberlin C, van Boxtel R, Buijs A, et al. Sequential cancer mutations in cultured human intestinal stem cells. *Nature.* (2015) 521:43–7. doi: 10.1038/nature14415
28. Xue W, Chen S, Yin H, Tammela T, Papagiannakopoulos T, Joshi NS, et al. CRISPR-mediated direct mutation of cancer genes in the mouse liver. *Nature.* (2014) 514:380–4. doi: 10.1038/nature13589
29. Maresch R, Mueller S, Veltkamp C, Oellinger R, Friedrich M, Heid I, et al. Multiplexed pancreatic genome engineering and cancer induction by transfection-based CRISPR/Cas9 delivery in mice. *Nat Commun.* (2016) 7:10770. doi: 10.1038/ncomms10770
30. Ruiz S, Mayor-Ruiz C, Lafarga V, Murga M, Vega-Sendino M, Ortega S, et al. A genome-wide CRISPR screen identifies CDC25A as a determinant of sensitivity to ATR inhibitors. *Mol Cell.* (2016) 62:307–13. doi: 10.1016/j.molcel.2016.03.006
31. Shalem O, Sanjana NE, Hartenian E, Shi X, Scott DA, Mikkelsen TS, et al. Genome-Scale CRISPR-Cas9 knockout screening in human cells. *Science.* (2014) 343:84–7. doi: 10.1126/science.1247005
32. Maus MV, Grupp SA, Porter DL, June CH. Antibody-modified T cells: CARs take the front seat for hematologic malignancies. *Blood.* (2014) 123:2625–35. doi: 10.1182/blood-2013-11-492231
33. Ren JT, Zhao YB. Advancing chimeric antigen receptor T cell therapy with CRISPR/Cas9. *Protein Cell.* (2017) 8:634–43. doi: 10.1007/s13238-017-0410-x
34. Ren JT, Liu XJ, Fang CY, Jiang SG, June CH, Zhao YB. Multiplex genome editing to generate universal CAR T cells resistant to PD1 inhibition. *Clin Cancer Res.* (2017) 23:2255–66. doi: 10.1158/1078-0432.CCR-16-1300
35. Hoos A. Development of immuno-oncology drugs - from CTLA4 to PD1 to the next generations. *Nat Rev Drug Discov.* (2016) 15:235–47. doi: 10.1038/nrd.2015.35
36. Yang Y, Qiu JG, Li Y, Di JM, Zhang WJ, Jiang QW, et al. Targeting ABCB1-mediated tumor multidrug resistance by CRISPR/Cas9-based genome editing. *Am J Transl Res.* (2016) 8:3986–94.

Conflict of Interest Statement: The authors declare that the research was conducted in the absence of any commercial or financial relationships that could be construed as a potential conflict of interest.

frontiers in Pharmacology

ORIGINAL RESEARCH
published: 01 March 2019
doi: 10.3389/fphar.2019.00140

Integrated Bioinformatics Analysis the Function of RNA Binding Proteins (RBPs) and Their Prognostic Value in Breast Cancer

Ke Wang[1]†, Ling Li[2]†, Liang Fu[2], Yongqiang Yuan[2], Hongying Dai[2], Tianjin Zhu[2], Yuxi Zhou[3] and Fang Yuan[3]*

[1] Clinical Laboratory, Yongchuan People's Hospital of Chongqing, Chongqing, China, [2] Clinical Laboratory, Yongchuan Hospital of Chongqing Medical University, Chongqing, China, [3] Yidu Cloud (Beijing) Technology Co., Ltd., Beijing, China

Background and Purpose: Breast cancer is one of the leading causes of death among women. RNA binding proteins (RBPs) play a vital role in the progression of many cancers. Functional investigation of RBPs may contribute to elucidating the mechanisms underlying tumor initiation, progression, and invasion, therefore providing novel insights into future diagnosis, treatment, and prognosis.

Methods: We downloaded RNA sequencing data from the cancer genome atlas (TCGA) by UCSC Xena and identified relevant RBPs through an integrated bioinformatics analysis. We then analyzed biological processes of differentially expressed genes (DEGs) by DAVID, and established their interaction networks and performed pathway analysis through the STRING database to uncover potential biological effects of these RBPs. We also explored the relationship between these RBPs and the prognosis of breast cancer patients.

Results: In the present study, we obtained 1092 breast tumor samples and 113 normal controls. After data analysis, we identified 90 upregulated and 115 downregulated RBPs in breast cancer. GO and KEGG pathway analysis indicated that these significantly changed genes were mainly involved in RNA processing, splicing, localization and RNA silencing, DNA transposition regulation and methylation, alkylation, mitochondrial gene expression, and transcription regulation. In addition, some RBPs were related to histone H3K27 methylation, estrogen response, inflammatory mediators, and translation regulation. Our study also identified five RBPs associated with breast cancer prognosis. Survival analysis found that overexpression of DCAF13, EZR, and MRPL13 showed worse survival, but overexpression of APOBEC3C and EIF4E3 showed better survival.

Conclusion: In conclusion, we identified key RBPs of breast cancer through comprehensive bioinformatics analysis. These RBPs were involved in a variety of biological and molecular pathways in breast cancer. Furthermore, we identified five RBPs as a potential prognostic biomarker of breast cancer. Our study provided novel insights to understand breast cancer at a molecular level.

Keywords: breast cancer, RNA binding protein, integrated bioinformatics analysis, survival, prognosis

OPEN ACCESS

Edited by:
Jian-ye Zhang,
Guangzhou Medical University, China

Reviewed by:
Zhi Shi,
Jinan University, China
Changliang Shan,
Nankai University, China

****Correspondence:***
Ke Wang
wk125@126.com

† These authors have contributed equally to this work

Specialty section:
This article was submitted to Cancer Molecular Targets and Therapeutics, a section of the journal Frontiers in Pharmacology

Received: *12 November 2018*
Accepted: *06 February 2019*
Published: *01 March 2019*

Citation:
Wang K, Li L, Fu L, Yuan Y, Dai H, Zhu T, Zhou Y and Yuan F (2019) Integrated Bioinformatics Analysis the Function of RNA Binding Proteins (RBPs) and Their Prognostic Value in Breast Cancer. Front. Pharmacol. 10:140. doi: 10.3389/fphar.2019.00140

INTRODUCTION

Breast cancer is the most commonly diagnosed cancer and a main cause of cancer death among women. In 2018, there was an estimated 2.1 million newly diagnosed female breast cancer cases worldwide, accounting for about 25% of cancer cases among women (Bray et al., 2018). In recent years, with great progress in medical technology, the diagnosis incidence of breast cancer has increased year by year, and the age of onset or diagnosis has consequently become younger. Breast cancer is aggressive and has a high recurrence rate. Currently, the diagnosis of breast cancer mainly relies on pathological assessments, imaging tests, and tumor markers (McDonald et al., 2016), which creates difficulty for meeting clinical requirements. In order to reduce the recurrence rate and mortality of breast cancer patients, and to improve their quality of life, it is vital to increase ability in surveillance, early detection and diagnosis. Over the years there has been an increase of molecular research on early diagnosis, drug resistance and prognosis, and it is therefore valuable to find new molecular markers on the occurrence, progression, and prognosis, to further expand this research.

RNA-binding proteins (RBPs) are abundant and ubiquitously expressed in cells. They play a central and conserved role in gene regulation (Gerstberger et al., 2014b), and act as important participants and coordinators to maintain genome integrity (Nishida et al., 2017). RBPs have extensive capabilities including regulating stability, maturation, posttranscriptional regulation of mRNA stability, splicing, editing and translation, mRNA localization and polyadenylation, which ultimately impacts the expression of every gene in the cell (Campos-Melo et al., 2014; Gerstberger et al., 2014a). Although it is known that post-transcription contributes to tumor initiation and progression, the role of RBPs in cancer remain relatively unexplored (Wurth and Gebauer, 2015).

There is a large number of Human RBPs, but very few have been studied in depth, such as AGO2, Nova, PTB, HuR, AUF1, TTP, CUGBP2 which are known for their role in many regulation processes, including interacting with non-coding RNAs (Iadevaia and Gerber, 2015), controlling intracellular localization of non-coding RNAs (Glisovic et al., 2008), methylation (Harvey et al., 2017), forming the RNA induce silencing complex (Connerty et al., 2015), and alternative splicing (Paronetto et al., 2010). RBPs participate in comprehensive biological processes, such as reproductive development, tumorigenesis and apoptosis, and is therefore closely related to many human diseases. A systematic functional study of RBPs will be helpful to understand the function and mechanism of non-coding RNA, but will also have a significant applied value in studying the pathogenesis of diseases and in the screening of innovative drug targets.

Currently, genes and signaling pathways that participate in breast cancer tumorigenesis and progression remain to be further investigated. Exploring new genes and pathways associated with breast cancer may help to identify potential molecular mechanisms, diagnostic markers and therapeutic targets (Wang et al., 2018). High-throughput genomic analysis techniques can be applied to screening for differentially expressed genes (DEGs) and to understand the relevant pathways and protein interaction networks (Vogelstein et al., 2013). In this study, we downloaded breast cancer data from the cancer genome atlas (TCGA), and selected differential expressed RBPs to perform gene ontology (GO), KEGG pathways and an interaction network and survival analysis. The study identified a number of RBPs involved in breast cancer. Some of which might be used as potential prognostic biomarkers in the future.

RESULTS

Identification of Differently Expressed RBPs (DEGs)

The database analysis contained 1092 breast tumor samples and 113 no-tumor control samples. We conducted a deep analysis of 1912 RBPs and a total of 205 RBPs were identified, including 90 upregulated and 115 downregulated RBPs (**Supplementary Table S1**). We also constructed an expression heat map for all DEGs (**Figure 1**).

Functional and Pathway Enrichment Analysis of DEGs

To determine the function and mechanisms of these RBPs, all DEGs were divided into two groups (upregulated group and down-regulated group), and submitted to the David database for

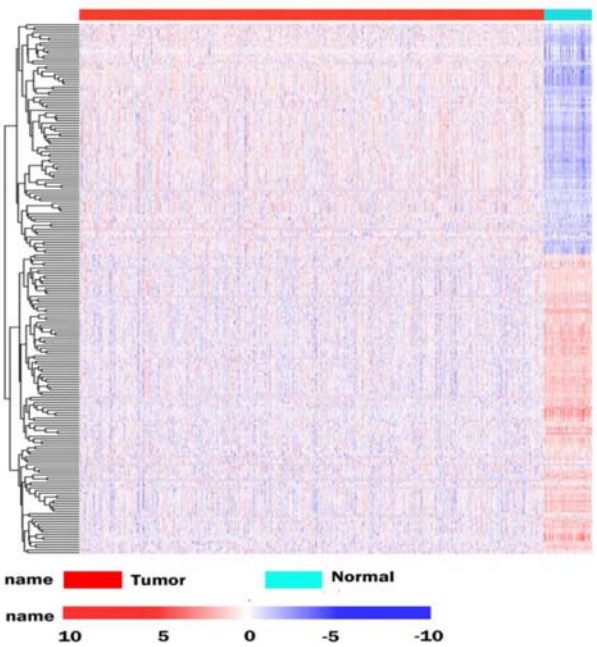

FIGURE 1 | Differentially expressed RBPs in BRCA cancer. Unsupervised clustering analysis was performed using the pheatmap function, using complete and Euclidean as metrics in R, based on log2-transformed FPKM values. The columns are samples and the rows are RBPs. The blue represents down-regulation, while red represents up-regulation.

GO analysis. We then conducted a KEGG pathway analysis for all DEGs. We found that upregulated DEGs were significantly enriched in RNA processing, RNA binding, mRNA binding, and located in the non-membrane-bounded organelle, intracellular non-membrane-bounded organelle, ribonucleoprotein complex, intracellular organelle lumen, organelle lumen, membrane-enclosed lumen, nuclear lumen, and the nucleolus (**Table 1**). The GO result of down-regulated DEGs were significantly enriched in the RNA processing, posttranscriptional regulation of gene expression, mRNA metabolic process, mRNA processing, regulation of translation and the RNA binding, and these genes mainly consisted of the chromatoid body, P granule, germ plasm, pole plasm, intracellular non-membrane-bounded organelle and the non-membrane-bounded organelle (**Table 1**).

TABLE 1 | GO enrichment analysis results of differentially up-regulated genes and down-regulated genes (DEGs).

	Term	*P* value	FDR
Up-regulated genes (DEGs)	RNA processing	3.23E-06	0.00478286
	Non-membrane-bounded organelle	4.53E-13	5.56E-10
	Intracellular non-membrane-bounded organelle	4.53E-13	5.56E-10
	Ribonucleoprotein complex	5.00E-11	6.15E-08
	Intracellular organelle lumen	1.81E-09	2.22E-06
	Organelle lumen	3.09E-09	3.80E-06
	Membrane-enclosed lumen	4.90E-09	6.02E-06
	Nuclear lumen	1.32E-06	0.00162684
	Nucleolus	1.59E-06	0.00194848
	RNA binding	5.78E-16	6.77E-13
	mRNA binding	2.37E-05	0.02904478
Down-regulated genes (DEGs)	RNA processing	1.41E-10	2.21E-07
	Posttranscriptional regulation of gene expression	2.29E-09	3.58E-06
	mRNA metabolic process	1.81E-08	2.82E-05
	mRNA processing	2.40E-07	3.74E-04
	Regulation of translation	1.05E-06	0.00164623
	Chromatoid body	2.05E-06	0.00250038
	P granule	3.57E-06	0.00436073
	Germ plasm	3.57E-06	0.00436073
	Pole plasm	3.57E-06	0.00436073
	Intracellular non-membrane-bounded organelle	1.94E-05	0.02370618
	Non-membrane-bounded organelle	1.94E-05	0.02370618
	RNA binding	1.46E-23	1.83E-20

TABLE 2 | The KEGG pathway analysis of all DEGs.

Term	*P* value
Dorso-ventral axis formation	4.18E-03
Fatty acid elongation in mitochondria	3.11E-02
Pathogenic *Escherichia coli* infection	2.06E-02

According to the KEGG pathway enrichment analysis, all DEGs mainly participated in Dorso-ventral axis formation, fatty acid elongation in mitochondria and pathogenic *Escherichia coli* infection (**Table 2**).

Protein-Protein Interaction Network Building and Interrelation Analysis Between Pathways

To better understand the role of these differentially expressed RBPS in breast cancer development, we constructed co-expression networks. All DEGs were submitted to STRING 10.5, we obtained 294 PPI nodes, 174 edges, and a *p*-value of PPI concentration <1.00–16, while also including the result of the GO and KEGG pathway. In the biological process, there was mainly enrichment in the regulation of transcription, translation level and epigenetics, and it also played an important role in histone modification, mitochondrial gene expression, cell metabolism, production of inflammatory mediators and estrogen response. The cellular components are significantly located in the ribosome, mitochondria, chromosomes, and the telomeres, etc. Molecular functions showed that they can bind to a variety of RNA and specific regions, and were closely related to regulated enzymes activity, including various metabolic and gene expressions, modification and regulation of enzymes, and also bound to steroid hormones and estrogen receptors. For KEGG pathway analysis, it was mainly enriched in Glycolysis/Gluconeogenesis, mRNA surveillance pathway, RNA degradation and pathogenic *E. coli* infection. Then, we constructed the PPI network of these DEGs using Cytoscape (**Figure 2A**). Two topological features, degree and betweenness, were calculated to identify candidate hub nodes. The higher the two quantitative values of a gene, the greater the importance within the network (Liu et al., 2018b). The co-expression network revealed that ELAVL2, VIM, MRPS12, HSPE1, EZH2, HIST1H4B, and MRPL13 played a vital role in the progression of breast cancer, and we further selected important modules of target genes through MCODE (**Figures 2B,C**). Finally, we used the ClueGO to externalize all biological processes (**Figures 3A,B**) and the interaction modes of molecular functions (**Figures 4A,B**).

Survival Analysis

The correlation between RBP expression and overall survival was assessed using both the Cox regression analysis and the Kaplan-Meier estimation method. Then, survival correlation $P < 0.05$ and key RBPs were selected to analyze their correlation with survival prognosis. After that we used both the Kaplan-Meier estimates and the log-rank test to assess the significant differences of the two-group survival curves. As shown in the **Figure 5**, the expression of selected target genes in tumor and normal tissues was significantly different. In addition, patients with highly expressed RBPs of EZR, DCAF13, and MRPL13 showed lower survival, but patients with highly expressed RBPs of APOBEC3C, EIF4E3 showed better survival (**Figure 5**). Therefore these genes could be potential biomarkers for breast cancer prognosis.

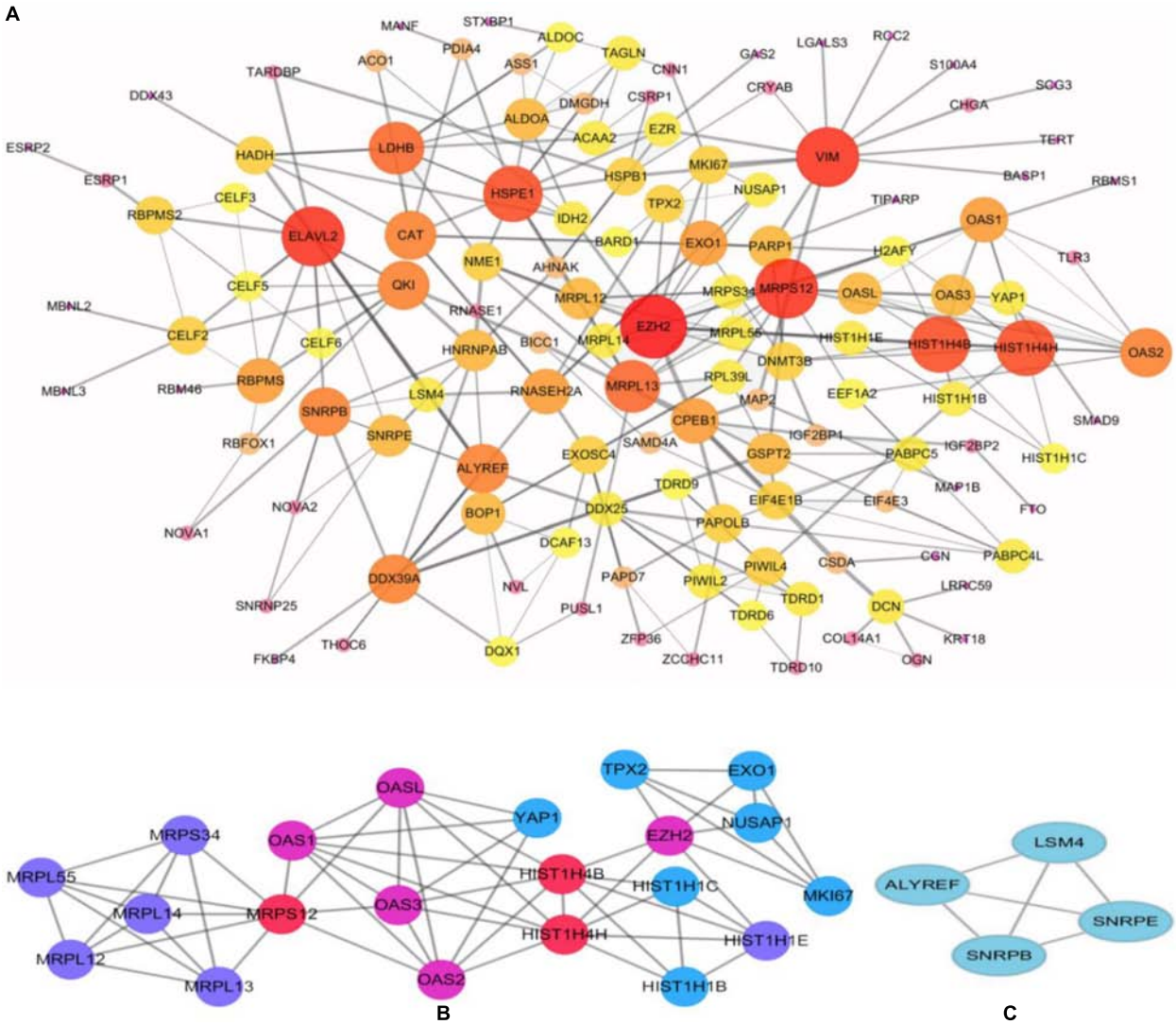

FIGURE 2 | Construction of protein-protein interaction (PPI) network. **(A)** Modules inferred from protein-protein interaction network. Elected important modules of target gene (**B**,**C**) MCODE score >4, nodes >4.

MATERIALS AND METHODS

Data Sources Analysis

The corresponding clinical data was downloaded from the following website http://gdac.broadinstitute.org/. Combined with the RNA-seq expression data set, 1075 patients had clinical information available including age, gender and disease stage. The details have been listed in **Supplementary Table S1**. We downloaded the RBPs expression data (TOIL RSEM expected count and FPKM) processed by the Toil pipeline (Vivian et al., 2017) based on RNA sequencing (RNA-Seq) for TCGA Pan-Cancer cohort from the website https://xena.ucsc.edu/. The data included the 60498 genes annotated by GENCODE version 23. We then used custom Perl script to extract the data from BRCA cancer, for subsequent analysis. We applied the Voom function (Law et al., 2014) in the Limma package, to estimate DEGs between tumor and normal tissues for BRCA cancer. Those with a fold change ≥ 1 and FDR < 0.05 were considered to have statistical significance. We further identified significantly dysregulated RBPs based on our RBP catalog. Unsupervised clustering of differentially expressed RBPs was performed based on log2-transformed FPKM values using the "pheatmap" package in R.

GO Functional and Pathway Enrichment Analysis

In order to comprehensively analyze the biological functions of these RBPS, we used the GO and kyoto encyclopedia of genes and genomes (KEGG) analysis by The database for annotation, visualization and integrated discovery (DAVID) version 6.7. The GO Term analysis included the

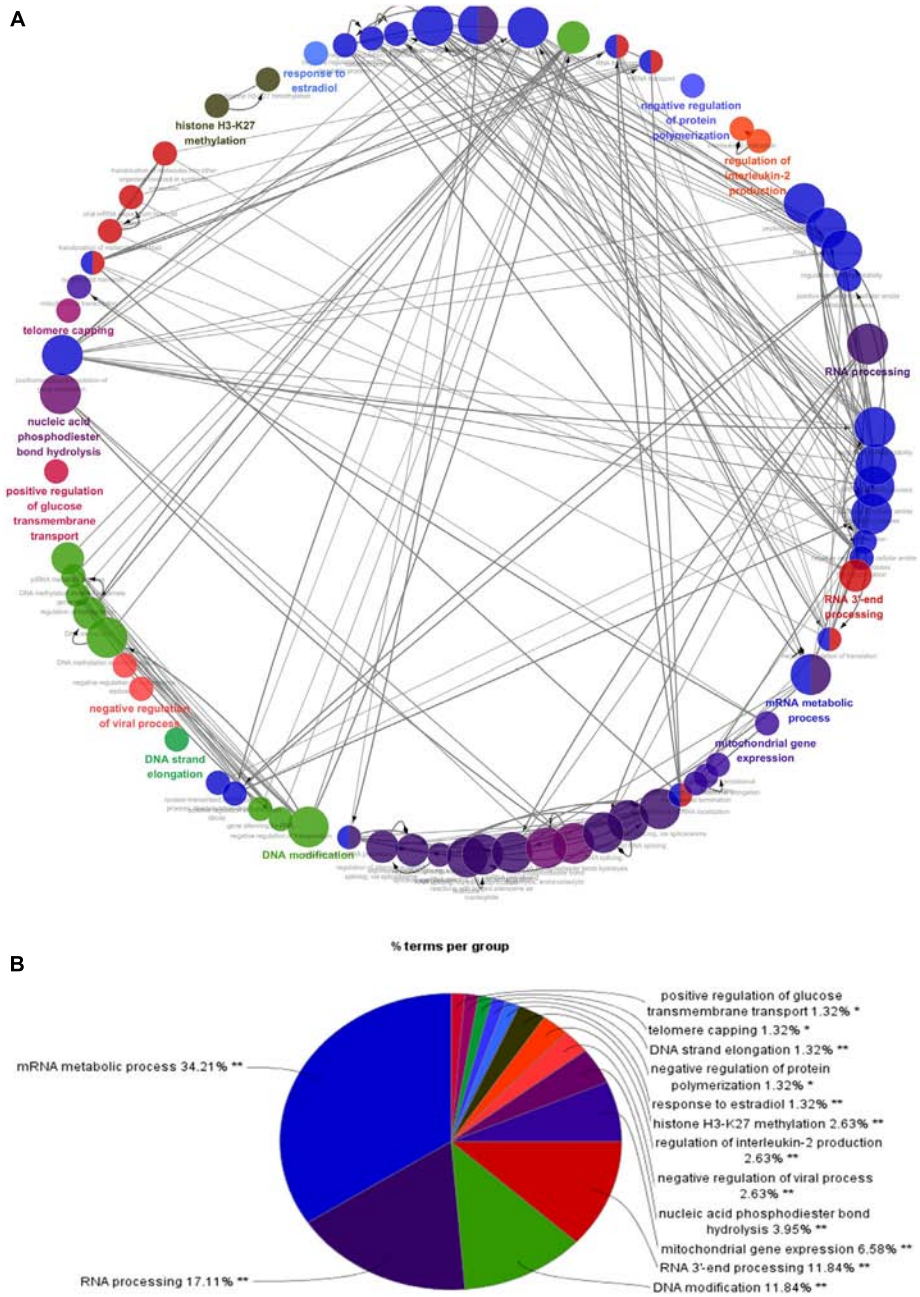

FIGURE 3 | Interrelation analysis between pathways (biological process). **(A)** Interrelation between biological process pathways. **(B)** The proportion of each pathway.

biological process, cellular component and the molecular function. Both $P < 0.05$ and FDR < 0.05 were considered statistically significant.

Protein Interaction Network (PPI) and Pathways Interaction Analysis Building

SRTING version 10.5 was used to evaluate the protein interaction information of all DEGs, and their biological functions were also obtained. Then, the interaction network of these proteins was visualized by Cytoscape3.6.0, and important modules both MCODE score and node number > 4 were selected by the MCODE plug in to Cytoscape version 3.6.0. Furthermore, the pathway enrichment of $P < 0.05$ was analyzed by the ClueGO plug to Cytoscape version 3.6.0.

Statistical Analysis

The correlation of RBP expression and overall survival was assessed using both the Cox regression analysis and the Kaplan-Meier estimation method, based on the "survival"

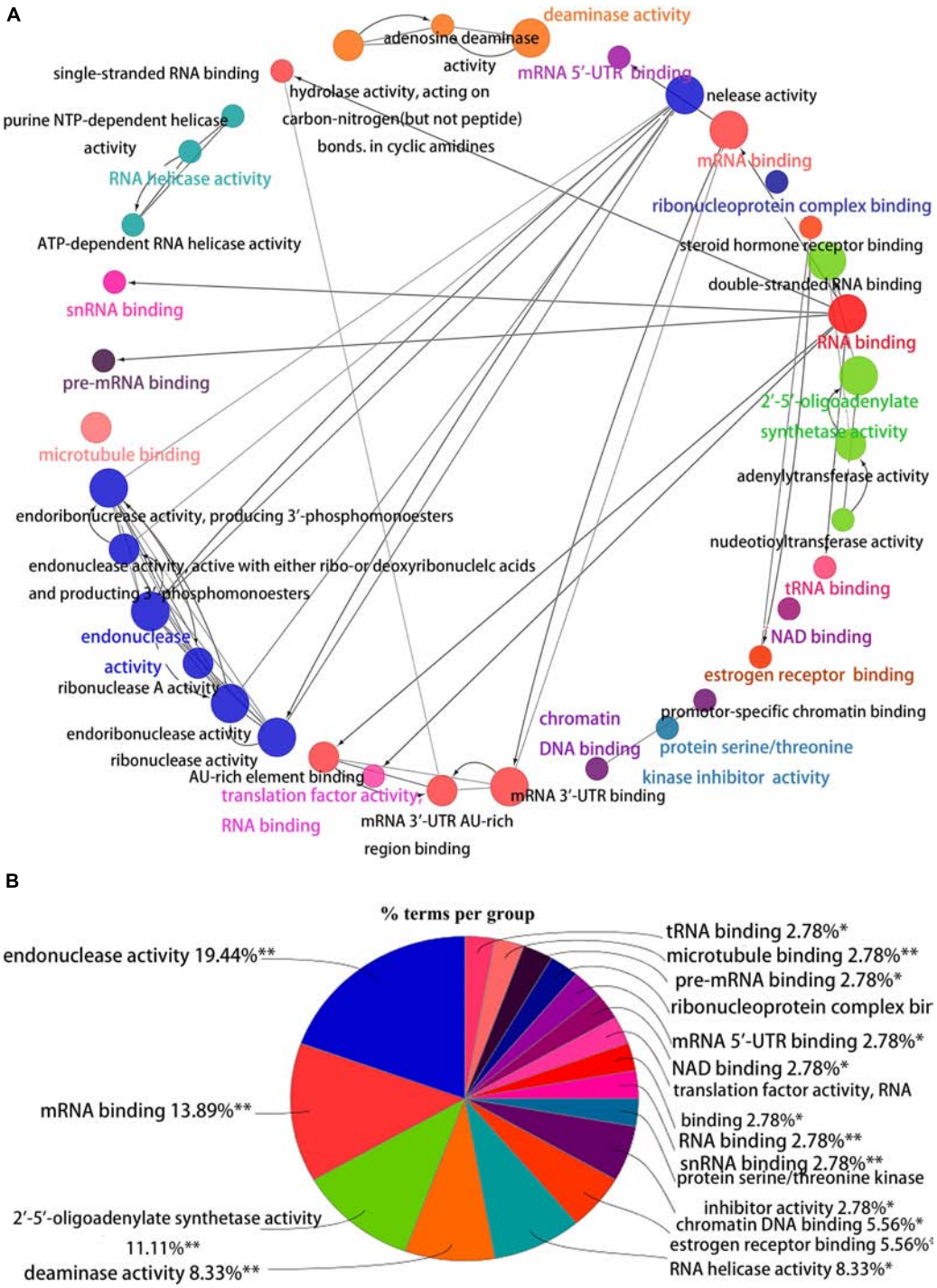

FIGURE 4 | Interrelation analysis between pathways molecular functions. **(A)** Interrelation between molecular functions pathways. **(B)** The proportion of each pathway.

package in R. For the Cox regression analysis, the RBP was evaluated as a continuous variable with age and gender as additional covariables. For the Kaplan-Meier estimates, we defined the high-expression group and low-expression group using the median RBP expression value as a cut-off point. A significant difference of two-group survival curves was assessed by a log-rank test. $P < 0.05$ was considered as statistically significant.

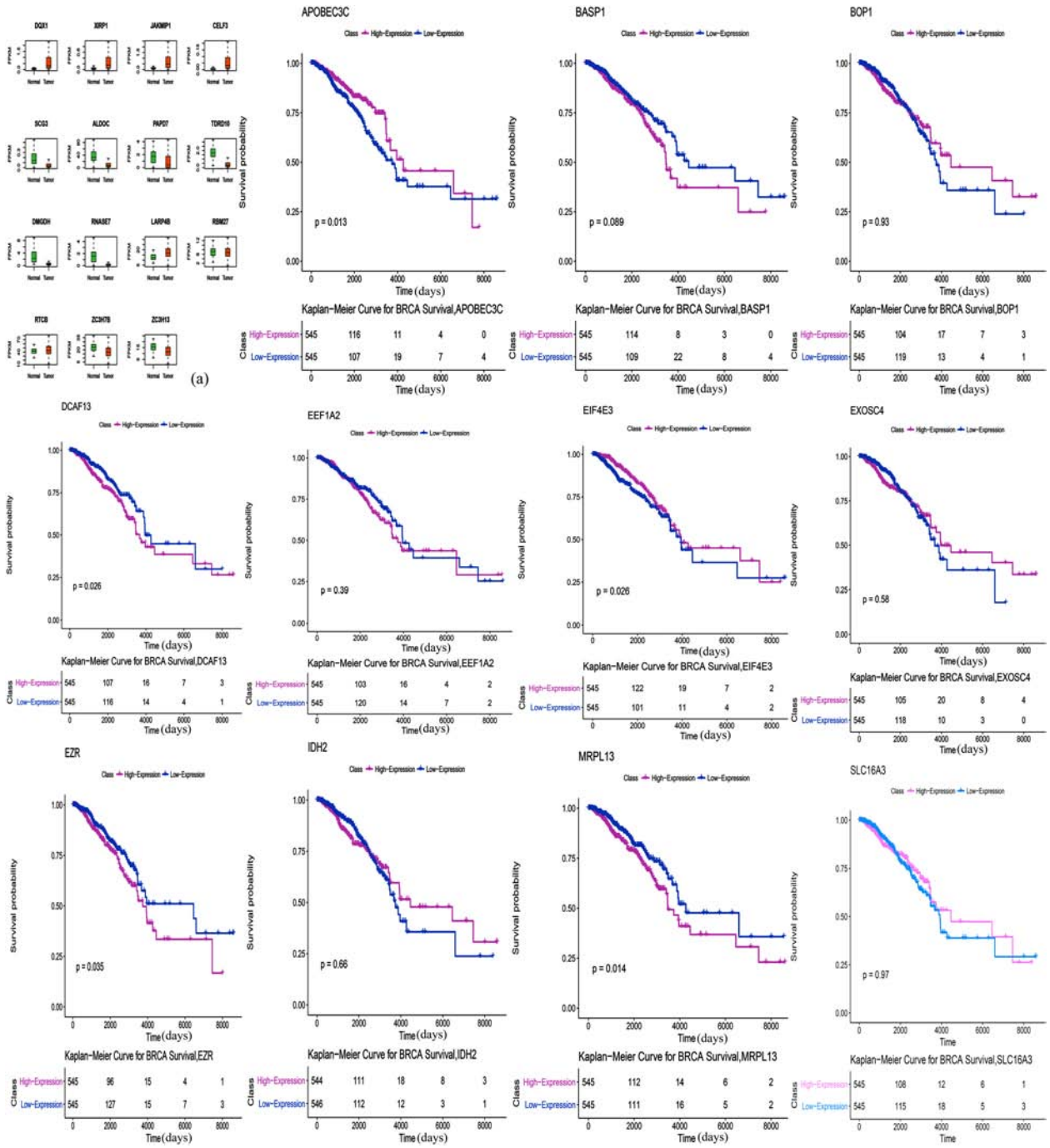

FIGURE 5 | Survival Kaplan-Meier Estimate (EZR $p = 0.035$, DCAF13 $p = 0.026$, MRPL13 $p = 0.014$, APOBEC3C $p = 0.013$, and EIF4E3 $p = 0.026$). Expression of selected target genes in tumor and normal tissues was significantly different.

DISCUSSION

Currently, cancer causes more death than coronary heart diseases or stroke does (Lin et al., 2017a). In recent years, although molecular targeted therapy has improved treatment effect, breast cancer is still the primary cause of death among women. During clinical practice, biomarkers that indicate the grade malignancy, metastasis and the prognosis of breast cancer are needed. Microarray and high-throughput sequencing technologies provide effective tools for deciphering key genetic or epigenetic changes in the occurrence of cancer, as well as promising biomarkers

for cancer diagnosis, treatment, and prognosis (Kulasingam and Diamandis, 2008; Cancer Genome Atlas Research and Network, 2014). Our study integrated TCGA RNA sequencing data, and identified DEGs between tumor and normal tissue. We analyzed relevant biological pathways, constructed protein interaction networks and performed survival analyses to explore biological functions and clinical application of these RBPs.

The biological functions of these DEGs were obtained using the GO and KEGG pathway analysis. Firstly, the enrichment of cell components is mainly located in the ribosome, exonuclease, endonuclease, spliceosome and the ribonuclease, which are important sites protecting the transmission of biological information. The ribosome is a key organelle that performs protein synthesis. The mutation of the ribosomal protein regulates the translation and activity of p53, finally resulting in diseases, and cancers (Goudarzi and Lindstrom, 2016). A number of RBPs exist in exonuclease, endonuclease and sites with DNA damage, which may participate in DNA damage repair (Goudarzi and Lindstrom, 2016). In addition, RBPs are widely present in spliceosome. Expression of eukaryotic genes is often accompanied by the RNA splicing process, especially in the alternative splicing of RNA, which could produce tissue and development specific mRNA. For example, Sam68 can result in drug resistance and poor prognosis by regulating the expression ratio of cyclinD1, an alternative splicing in breast cancer (Paronetto et al., 2010). Some RBPs also expressed in the telomere and telomerase and regulate their activity. Telomere play an important role in regulating cell growth and division. Some studies have found that telomerase activity was suppressed in normal tissues but was reactivated in tumors. Telomerase is overexpressed in 80–95% of cancers and is likely to participate in cell malignant transformation (Ruden and Puri, 2013). During the analysis of cellular components, we also found the occurrence of RBPs in the exosome, which could cause tumor invasion and metastasis, immune escape and therapeutic resistance. For example, SYNCRIP, as a component of the miRNA sorting mechanism, in hepatocyte exosomes, can directly bind to specific miRNA rich in exosomes, and regulates miRNA localization (Santangelo et al., 2016).

Secondly, in terms of molecular function, RPBs can bind to various RNAs such as pre-mRNA, Sn RNA, tRNA, mRNA and regulates the activity of various enzymes, such as hydrolytic enzyme, purine metabolic enzyme, and enzymes involved in DNA synthesis, repair, and RNA metabolism. Furthermore, some RBPs also bind to estrogen and steroid hormone receptors. For example, MSI2 is highly expressed in ER(+) breast cancer, and its expression is significantly correlated with ESR1 expression, which affects the growth of breast cancer cells, by changing the function of ESR1 (Kang et al., 2017).

Next, for the biological process, the function enrichment of differential RBPs mainly occurred in RNA processing, splicing, localization, transport, hydrolysis, and RNA silencing. It participates in transposition regulation, methylation, and alkylation of DNA. Some RBPs were also related to histone H3K27 methylation, inflammatory mediators, and translation regulation. Our findings are consistent with the consensus that multiple genes, multiple molecules, and multiple pathways are involved in breast cancer. Although the relationship with breast cancer remains unclear, some RBPs have been reported in other cancers. HuR can promote the growth of colorectal cancer cell by regulating mRNA expression (Lopez de Silanes et al., 2003). CRD-BP can regulate many mRNAs with coding for cancer-related genes, including Gli1, PTEN, PTEN, ptlcp1, MAPK4, MDR1, IGF2, H19, c-myc, etc. (Fakhraldeen et al., 2015). HNRNPA2B1 controls the replacement splicing for the pre-mRNA of cancer-related genes, and which is up-regulated in diverse cancers (Stockley et al., 2014). HuR can bind with DNMT3b and maintain its stability, thus affecting abnormal DNA methylation (Lopez de Silanes et al., 2009). Numerous studies reported that a change of mitochondrial function plays a key role in all kinds of cancers (Tao et al., 2015; Lin et al., 2017b; Zhang J.Y. et al., 2017; Zhang J. et al., 2017), and RBPs involved in the expression and transcription regulation of mitochondrial genes, such as LRPPRC, GRSF1, SLIRP, and other RBPs can interact with mt-RNA to affect the expression and metabolism of mitochondrial transcripts (Dong et al., 2017). The incidence of breast cancer and female estrogen levels are closely related. Some RBPs can respond with estrogen, for example, through Nova1, 17-b estradiol can regulate the replacement splicing of estrogen receptor b in the brain of aging female mice (Shults et al., 2018). Then, the results of the KEGG pathway analysis indicated that these RBPs may affect the occurrence and development of breast cancer through glycolysis, glycosylation, mRNA monitoring pathways, and RNA degradation regulation. RPBs have various basic biological functions, especially the function of RNA which has been studied widely. Other RBPs functions should therefore be studies further.

By constructing a protein network for DEGs, we found that breast cancer is associated with immune response, splicing, transcript regulation, and intercellular signaling transduction. HSPE1 is a member of the heat shock protein family (Hsp10) E, which usually acts as a chaperone to assist protein folding in the mitochondria, which is highly expressed in various cancers, such as lung cancer, pancreatic cancer and bladder cancer. Some studies reported that it may protect cancer cells from apoptosis, and facilitate the immune escape of cancer, by down-regulating the immune response (Rappa et al., 2016; Liu et al., 2018a). ELAVL2 is a neurospecific RNA binding protein, which is involved in splicing and transcript trafficking to regulate protein localization (Berto et al., 2016). Elevated methylation of ELAVL2 was shown in high Gleason scores of prostate tumors (Wu et al., 2016). VIM is expressed in a variety of cell types and is responsible for maintaining cell shape, cytoplasmic integrity, and stabilizing cytoskeletal. It is also involved in immune responses, attachment, migration, and cell signaling in tissues. Previous studies have shown that vimentin regulated Ras, Slug and TGF glows in cancer cells, which is necessary for EMT induction. It is also highly expressed in various tumors such as lung cancer, breast cancer and gastric cancer, and is

closely related to invasion, metastasis and the poor prognosis of tumors (Satelli and Li, 2011; Virtakoivu et al., 2015). High expressions of EZH2 is associated with malignancy and hyper-invasiveness in a variety of cancers. EZH2 can activate NF-κB targets and NOTCH1 in breast cancer cells, which has also been implicated in the transcriptional activation of gene expression in breast cancer. Research has shown that it induces the expression of genes that are regulated by the estrogen receptor (ER) and Wnt signaling transcription factors, by physically bridging between the ER and components of Wnt signaling (Kim and Roberts, 2016).

These RBPS may lead to breast cancer by regulating mitochondrial translation, splicing of pre-mRNA, activation of RNase L, and histone modifications through two modules selected from the PPI network. It has been reported that the upregulation of mitochondrial translation may meet the energy needs of cancer cells in human tumors, but the mechanism of its tumorigenesis remains unclear. There are many studies targeting the inhibition of mitochondrial translation in various cell types, to obliterate cancer stem cells. Currently, suppressing mitochondrial translation is considered a valuable therapeutic target (Kim et al., 2017). RNase L was activated through the synthesis of 2′, 5′ -oligoadenylic acid by OAS (OAS1, OAS2, and OAS3). It was found that the activated OAS-RNase L system can degrade virus and cell RNA, promote cell apoptosis, and inhibit protein synthesis (Bhosle et al., 2016). In addition, single nucleotide polymorphisms of OAS are associated with cancer, such as OAS1 SNP rs2660 AA (Mandal et al., 2011). However, no studies reported the exact role of OAS in breast cancer. As we know, epigenetic change is involved in the initiation and progression of cancer, which includes histone modifications and DNA methylation. Studies have shown that the regulation of histone is gene specific, but their function is diversified. Histone cluster 1 can interact with some regulatory factors, such as inhibiting p53-dependent chromatin transcription, and maintaining or establishing specific DNA methylation patterns (Perez-Magan et al., 2010). It has been demonstrated that the function of protecting DNA with histone may be an independent prognostic factor for better survival of cervical cancer patients (Li et al., 2017). Furthermore, splicing affects the expression of most genes, and eventually influences the levels of proteins. In the module, SNRPE, SNRPB, and ALYREF participate in the splicing of pre-mRNA. Knockdown SNRPE significantly reduces the expressed level of mTOR mRNA and protein, and is accompanied by the imbalance of the mTOR pathway, which activates abnormal mTOR signaling and which can result in the growth and metastasis of tumor cells (Quidville et al., 2013).

Finally, we performed a survival analysis and found five genes that are associated with survival in breast cancer patients. The overexpression of DCAF13, EZR, and MRPL13 in patients were associated with lower survival, which reveals that these genes might be associated with tumor invasion, progression and poor prognosis. Whereas, overexpression of APOBEC3C and EIF4E3 in patients were associated with better survival, suggesting their potential role as tumor suppressor genes. DCAF13 is amplified in all kinds of cancers. Studies have shown that overexpression of DCAF13 in hepatocellular carcinoma is significantly correlated with low survival and it may be involved in the regulation of cell cycle (Cao et al., 2017). It also reported that the E3 ligase formed by DCAF13, CUL4B and DDB1, could induce ubiquitination of tumor suppressor PTEN *in vivo* and *in vitro* (Chen et al., 2018). Mutated or inactivated PTEN was helpful to infiltrate and spread cancer cells. As a member of the ERM protein family, Ezrin has been linked to molecules that control the phosphatidylinositol-3-kinase, AKT, Erk1/2 MAPK and Rho pathways, which are functionally involved in regulating cell survival, proliferation and migration, and it is an indicator of poor prognosis of multiple cancers (Hunter, 2004). It has been shown that overexpressed EZR in a nude mice phantom of pancreatic cancer, can increase the number of metastasis and is closely related to the progression of malignant cancer (Meng et al., 2010). MRPL13 is a mitochondrial ribosomal protein. Loss of MRPL13 can lead to the loss of mitochondrial DNA, and eventually lead to the loss of the ability of mitochondrial coding proteins (Gruschke et al., 2010). In a study, reduced MRPL13 expression in hepatocellular carcinoma was a key factor in the regulation of mitochondrial ribosome and subsequent OXPHOS deficiency, which regulates the aggressive activity of liver cancer cells (Lee et al., 2017). APOBEC can mediate c-to-t mutagenesis in various cancers, while the APOBEC3 gene family is overexpressed in breast cancer and other cancer cells and tissues. Some studies suggest that it is regulated by estrogen in breast cancer (Long et al., 2013). At present, there are few studies about APOBEC3C in breast cancer, and some studies have found that it should play a positive role in the invasiveness and prognosis of hepatocellular carcinoma (Zhang et al., 2015). EIF4E3 belongs to the EIF4E family of translational initiation factors that interact with the 5-prime cap structure of mRNA. A study demonstrated that EIF4E3 relies on cap-binding activity to act as a tumor suppressor and compete with the growth-promoting functions of EIF4E. In fact, reduced EIF4E3 levels in high-expressed EIF4E cancers suggests that EIF4E3 underlies a clinically relevant inhibitory mechanism that is lost in some malignancies (Osborne et al., 2013). Other studies also found that EIF4E3 can impede oncogenic transformation (Volpon et al., 2013).

Over all, we identified key genes and related pathways through bioinformatics analysis of differential expressions of RBPs in breast cancer. These RBPs may be involved in the occurrence, development, invasion and metastasis of breast cancer. The survival analysis suggested that DCAF13, EZR, MRPL13, APOBEC3C, and EIF4E3 might have a prognostic value for breast cancer. Future *in vitro* and *in vivo* studies are needed to verify the functions of these genes.

DATA AVAILABILITY

Publicly available datasets were analyzed in this study. This data can be found here: https://xena.ucsc.edu/.

AUTHOR CONTRIBUTIONS

LL and KW conceived and designed the experiments. LF, YY, TZ, and HD analyzed the data. LL, YZ, and FY wrote the manuscript. All authors reviewed and approved the final manuscript.

FUNDING

This study was supported by the Natural Science Foundation Project of Yongchuan People's Hospital of Chongqing (Grant No. YCPH2019001). Chongqing Health and the Health Committee and Chongqing Science and Technology Commission (Grant No. 2018MSXM020) and the Natural Science Foundation Project of Yongchuan (Grant No. Ycstc.2017nc5020).

SUPPLEMENTARY MATERIAL

The Supplementary Material for this article can be found online at: https://www.frontiersin.org/articles/10.3389/fphar.2019.00140/full#supplementary-material

REFERENCES

Berto, S., Usui, N., Konopka, G., and Fogel, B. L. (2016). ELAVL2-regulated transcriptional and splicing networks in human neurons link neurodevelopment and autism. *Hum. Mol. Genet.* 25, 2451–2464. doi: 10.1093/hmg/ddw110

Bhosle, S. M., Hunt, A., and Chaudhary, J. (2016). A modified coupled spectrophotometric method to detect 2-5 oligoadenylate synthetase activity in prostate cell lines. *Biol. Proced. Online* 18:9. doi: 10.1186/s12575-016-0038-x

Bray, F., Ferlay, J., Soerjomataram, I., Siegel, R. L., Torre, L. A., and Jemal, A. (2018). Global cancer statistics 2018: GLOBOCAN estimates of incidence and mortality worldwide for 36 cancers in 185 countries. *CA Cancer. J. Clin.* 68, 394–424. doi: 10.3322/caac.21492

Campos-Melo, D., Droppelmann, C. A., Volkening, K., and Strong, M. J. (2014). RNA-binding proteins as molecular links between cancer and neurodegeneration. *Biogerontology* 15, 587–610. doi: 10.1007/s10522-014-9531-2

Cancer Genome Atlas Research and Network (2014). Comprehensive molecular characterization of gastric adenocarcinoma. *Nature* 513, 202–209. doi: 10.1038/nature13480

Cao, J., Hou, P., Chen, J., Wang, P., Wang, W., Liu, W., et al. (2017). The overexpression and prognostic role of DCAF13 in hepatocellular carcinoma. *Tumour Biol.* 39:1010428317705753. doi: 10.1177/1010428317705753

Chen, Z., Zhang, W., Jiang, K., Chen, B., Wang, K., Lao, L., et al. (2018). MicroRNA-300 regulates the ubiquitination of PTEN through the CRL4B(DCAF13) E3 ligase in osteosarcoma cells. *Mol. Ther. Nucleic Acids* 10, 254–268. doi: 10.1016/j.omtn.2017.12.010

Connerty, P., Ahadi, A., and Hutvagner, G. (2015). RNA Binding Proteins in the miRNA Pathway. *Int. J. Mol. Sci.* 17:31. doi: 10.3390/ijms17010031

Dong, Y., Yoshitomi, T., Hu, J. F., and Cui, J. (2017). Long noncoding RNAs coordinate functions between mitochondria and the nucleus. *Epigen. Chromatin* 10:41. doi: 10.1186/s13072-017-0149-x

Fakhraldeen, S. A., Clark, R. J., Roopra, A., Chin, E. N., Huang, W., Castorino, J., et al. (2015). Two isoforms of the RNA binding protein, coding region determinant-binding protein (CRD-BP/IGF2BP1), are expressed in breast epithelium and support clonogenic growth of breast tumor cells. *J. Biol. Chem.* 290, 13386–13400. doi: 10.1074/jbc.M115.655175

Gerstberger, S., Hafner, M., Ascano, M., and Tuschl, T. (2014a). Evolutionary conservation and expression of human RNA-binding proteins and their role in human genetic disease. *Adv. Exp. Med. Biol.* 825, 1–55. doi: 10.1007/978-1-4939-1221-6-1

Gerstberger, S., Hafner, M., and Tuschl, T. (2014b). A census of human RNA-binding proteins. *Nat. Rev. Genet.* 15, 829–845. doi: 10.1038/nrg3813

Glisovic, T., Bachorik, J. L., Yong, J., and Dreyfuss, G. (2008). RNA-binding proteins and post-transcriptional gene regulation. *FEBS Lett.* 582, 1977–1986. doi: 10.1016/j.febslet.2008.03.004

Goudarzi, K. M., and Lindstrom, M. S. (2016). Role of ribosomal protein mutations in tumor development. *Int. J. Oncol.* 48, 1313–1324. doi: 10.3892/ijo.2016.3387

Gruschke, S., Grone, K., Heublein, M., Holz, S., Israel, L., Imhof, A., et al. (2010). Proteins at the polypeptide tunnel exit of the yeast mitochondrial ribosome. *J. Biol. Chem.* 285, 19022–19028. doi: 10.1074/jbc.M110.113837

Harvey, R., Dezi, V., Pizzinga, M., and Willis, A. E. (2017). Post-transcriptional control of gene expression following stress: the role of RNA-binding proteins. *Biochem. Soc. Trans.* 45, 1007–1014. doi: 10.1042/BST20160364

Hunter, K. W. (2004). Ezrin, a key component in tumor metastasis. *Trends Mol. Med.* 10, 201–204. doi: 10.1016/j.molmed.2004.03.001

Iadevaia, V., and Gerber, A. P. (2015). Combinatorial control of mRNA fates by RNA-binding proteins and non-coding RNAs. *Biomolecules* 5, 2207–2222. doi: 10.3390/biom5042207

Kang, M. H., Jeong, K. J., Kim, W. Y., Lee, H. J., Gong, G., Suh, N., et al. (2017). Musashi RNA-binding protein 2 regulates estrogen receptor 1 function in breast cancer. *Oncogene* 36, 1745–1752. doi: 10.1038/onc.2016.327

Kim, H.-J., Maiti, P., and Barrientos, A. (2017). Mitochondrial ribosomes in cancer. *Semin. Cancer Biol.* 47, 67–81. doi: 10.1016/j.semcancer.2017.04.004

Kim, K. H., and Roberts, C. W. (2016). Targeting EZH2 in cancer. *Nat. Med.* 22, 128–134. doi: 10.1038/nm.4036

Kulasingam, V., and Diamandis, E. P. (2008). Strategies for discovering novel cancer biomarkers through utilization of emerging technologies. *Nat. Clin. Pract. Oncol.* 5, 588–599. doi: 10.1038/ncponc1187

Law, C. W., Chen, Y., Shi, W., and Smyth, G. K. (2014). Voom: precision weights unlock linear model analysis tools for RNA-seq read counts. *Genome Biol.* 15:R29. doi: 10.1186/gb-2014-15-2-r29

Lee, Y. K., Lim, J. J., Jeoun, U. W., Min, S., Lee, E. B., Kwon, S. M., et al. (2017). Lactate-mediated mitoribosomal defects impair mitochondrial oxidative phosphorylation and promote hepatoma cell invasiveness. *J. Biol. Chem.* 292, 20208–20217. doi: 10.1074/jbc.M117.809012

Li, X., Tian, R., Gao, H., Yang, Y., Williams, B. R. G., Gantier, M. P., et al. (2017). Identification of a histone family gene signature for predicting the prognosis of cervical cancer patients. *Sci. Rep.* 7:16495. doi: 10.1038/s41598-017-16472-5

Lin, M., Bi, H., Yan, Y., Huang, W., Zhang, G., Zhang, G., et al. (2017a). Parthenolide suppresses non-small cell lung cancer GLC-82 cells growth via B-Raf/MAPK/Erk pathway. *Oncotarget* 8, 23436–23447. doi: 10.18632/oncotarget.15584

Lin, M., Tang, S., Zhang, C., Chen, H., Huang, W., Liu, Y., et al. (2017b). Euphorbia factor L2 induces apoptosis in A549 cells through the mitochondrial pathway. *Acta Pharm. Sin. B* 7, 59–64. doi: 10.1016/j.apsb.2016.06.008

Liu, X., Weng, Y., Liu, P., Sui, Z., Zhou, L., Huang, Y., et al. (2018a). Identification of PGAM1 as a putative therapeutic target for pancreatic ductal adenocarcinoma metastasis using quantitative proteomics. *Onco Targets Ther.* 11, 3345–3357. doi: 10.2147/OTT.S162470

Liu, X., Wu, J., Zhang, D., Bing, Z., Tian, J., Ni, M., et al. (2018b). Identification of potential key genes associated with the pathogenesis and prognosis of gastric cancer based on integrated bioinformatics analysis. *Front. Genet.* 9:265. doi: 10.3389/fgene.2018.00265

Long, J., Delahanty, R. J., Li, G., Gao, Y. T., Lu, W., Cai, Q., et al. (2013). A common deletion in the APOBEC3 genes and breast cancer risk. *J. Natl. Cancer Inst.* 105, 573–579. doi: 10.1093/jnci/djt018

Lopez de Silanes, I., Fan, J., Yang, X., Zonderman, A. B., Potapova, O., Pizer, E. S., et al. (2003). Role of the RNA-binding protein HuR in colon carcinogenesis. *Oncogene* 22, 7146–7154. doi: 10.1038/sj.onc.1206862

Lopez de Silanes, I., Gorospe, M., Taniguchi, H., Abdelmohsen, K., Srikantan, S., Alaminos, M., et al. (2009). The RNA-binding protein HuR regulates DNA methylation through stabilization of DNMT3b mRNA. *Nucleic Acids Res.* 37, 2658–2671. doi: 10.1093/nar/gkp123

Mandal, S., Abebe, F., and Chaudhary, J. (2011). 2′-5′ oligoadenylate synthetase 1 polymorphism is associated with prostate cancer. *Cancer* 117, 5509–5518. doi: 10.1002/cncr.26219

McDonald, E. S., Clark, A. S., Tchou, J., Zhang, P., and Freedman, G. M. (2016). Clinical diagnosis and management of breast cancer. *J. Nucl. Med.* 57(Suppl. 1), 9S–16S. doi: 10.2967/jnumed.115.157834

Meng, Y., Lu, Z., Yu, S., Zhang, Q., Ma, Y., and Chen, J. (2010). Ezrin promotes invasion and metastasis of pancreatic cancer cells. *J. Transl. Med.* 8:61. doi: 10.1186/1479-5876-8-61

Nishida, K., Kuwano, Y., Nishikawa, T., Masuda, K., and Rokutan, K. (2017). RNA binding proteins and genome integrity. *Int. J. Mol. Sci.* 18:1341. doi: 10.3390/ijms18071341

Osborne, M. J., Volpon, L., Kornblatt, J. A., Culjkovic-Kraljacic, B., Baguet, A., and Borden, K. L. (2013). eIF4E3 acts as a tumor suppressor by utilizing an atypical mode of methyl-7-guanosine cap recognition. *Proc. Natl. Acad. Sci. U.S.A.* 110, 3877–3882. doi: 10.1073/pnas.1216862110

Paronetto, M. P., Cappellari, M., Busa, R., Pedrotti, S., Vitali, R., Comstock, C., et al. (2010). Alternative splicing of the cyclin D1 proto-oncogene is regulated by the RNA-binding protein Sam68. *Cancer Res.* 70, 229–239. doi: 10.1158/0008-5472.CAN-09-2788

Perez-Magan, E., Rodriguez de Lope, A., Ribalta, T., Ruano, Y., Campos-Martin, Y., Perez-Bautista, G., et al. (2010). Differential expression profiling analyses identifies downregulation of 1p, 6q, and 14q genes and overexpression of 6p histone cluster 1 genes as markers of recurrence in meningiomas. *Neuro Oncol.* 12, 1278–1290. doi: 10.1093/neuonc/noq081

Quidville, V., Alsafadi, S., Goubar, A., Commo, F., Scott, V., Pioche-Durieu, C., et al. (2013). Targeting the deregulated spliceosome core machinery in cancer cells triggers mTOR blockade and autophagy. *Cancer Res.* 73, 2247–2258. doi: 10.1158/0008-5472.Can-12-2501

Rappa, F., Pitruzzella, A., Marino Gammazza, A., Barone, R., Mocciaro, E., Tomasello, G., et al. (2016). Quantitative patterns of Hsps in tubular adenoma compared with normal and tumor tissues reveal the value of Hsp10 and Hsp60 in early diagnosis of large bowel cancer. *Cell Stress Chaperones* 21, 927–933. doi: 10.1007/s12192-016-0721-5

Ruden, M., and Puri, N. (2013). Novel anticancer therapeutics targeting telomerase. *Cancer Treat. Rev.* 39, 444–456. doi: 10.1016/j.ctrv.2012.06.007

Santangelo, L., Giurato, G., Cicchini, C., Montaldo, C., Mancone, C., Tarallo, R., et al. (2016). The RNA-binding protein SYNCRIP is a component of the hepatocyte exosomal machinery controlling microRNA sorting. *Cell Rep.* 17, 799–808. doi: 10.1016/j.celrep.2016.09.031

Satelli, A., and Li, S. (2011). Vimentin in cancer and its potential as a molecular target for cancer therapy. *Cell. Mol. Life Sci.* 68, 3033–3046. doi: 10.1007/s00018-011-0735-1

Shults, C. L., Dingwall, C. B., Kim, C. K., Pinceti, E., Rao, Y. S., and Pak, T. R. (2018). 17beta-estradiol regulates the RNA-binding protein Nova1, which then regulates the alternative splicing of estrogen receptor beta in the aging female rat brain. *Neurobiol. Aging* 61, 13–22. doi: 10.1016/j.neurobiolaging.2017.09.005

Stockley, J., Villasevil, M. E., Nixon, C., Ahmad, I., Leung, H. Y., and Rajan, P. (2014). The RNA-binding protein hnRNPA2 regulates beta-catenin protein expression and is overexpressed in prostate cancer. *RNA Biol.* 11, 755–765. doi: 10.4161/rna.28800

Tao, Y. W., Lin, Y. C., She, Z. G., Lin, M. T., Chen, P. X., and Zhang, J. Y. (2015). Anticancer activity and mechanism investigation of beauvericin isolated from secondary metabolites of the mangrove endophytic fungi. *Anticancer Agents Med. Chem.* 15, 258–266. doi: 10.2174/1871520614666140825112255

Virtakoivu, R., Mai, A., Mattila, E., De Franceschi, N., Imanishi, S. Y., Corthals, G., et al. (2015). Vimentin-ERK signaling uncouples slug gene regulatory function. *Cancer Res.* 75, 2349–2362. doi: 10.1158/0008-5472.CAN-14-2842

Vivian, J., Rao, A. A., Nothaft, F. A., Ketchum, C., Armstrong, J., Novak, A., et al. (2017). Toil enables reproducible, open source, big biomedical data analyses. *Nat. Biotechnol.* 35, 314–316. doi: 10.1038/nbt.3772

Vogelstein, B., Papadopoulos, N., Velculescu, V. E., Zhou, S., Diaz, L. A. Jr., and Kinzler, K. W. (2013). Cancer genome landscapes. *Science* 339, 1546–1558. doi: 10.1126/science.1235122

Volpon, L., Osborne, M. J., Culjkovic-Kraljacic, B., and Borden, K. L. (2013). eIF4E3, a new actor in mRNA metabolism and tumor suppression. *Cell Cycle* 12, 1159–1160. doi: 10.4161/cc.24566

Wang, Y., Zhang, Y., Huang, Q., and Li, C. (2018). Integrated bioinformatics analysis reveals key candidate genes and pathways in breast cancer. *Mol. Med. Rep.* 17, 8091–8100. doi: 10.3892/mmr.2018.8895

Wu, Y., Davison, J., Qu, X., Morrissey, C., Storer, B., Brown, L., et al. (2016). Methylation profiling identified novel differentially methylated markers including OPCML and FLRT2 in prostate cancer. *Epigenetics* 11, 247–258. doi: 10.1080/15592294.2016.1148867

Wurth, L., and Gebauer, F. (2015). RNA-binding proteins, multifaceted translational regulators in cancer. *Biochim. Biophys. Acta* 1849, 881–886. doi: 10.1016/j.bbagrm.2014.10.001

Zhang, J. Y., Huang, W. J., Sun, H. M., Liu, Y., Zhao, X. Q., Tang, S. L., et al. (2017). Structure identification and in vitro anticancer activity of lathyrol-3-phenylacetate-5,15-diacetate. *Molecules* 22:1412. doi: 10.3390/molecules22091412

Zhang, J., Lai, Z., Huang, W., Ling, H., Lin, M., Tang, S., et al. (2017). Apicidin inhibited proliferation and invasion and induced apoptosis via mitochondrial pathway in non-small cell lung cancer GLC-82 cells. *Anticancer Agents Med. Chem.* 17, 1374–1382. doi: 10.2174/1871520617666170419120044

Zhang, Y., Delahanty, R., Guo, X., Zheng, W., and Long, J. (2015). Integrative genomic analysis reveals functional diversification of APOBEC gene family in breast cancer. *Hum. Genomics* 9:34. doi: 10.1186/s40246-015-0056-9

Conflict of Interest Statement: YZ and FY were employed by company Yidu Cloud Technology Co.

The remaining authors declare that the research was conducted in the absence of any commercial or financial relationships that could be construed as a potential conflict of interest.

frontiers in Oncology

ORIGINAL RESEARCH
published: 01 March 2019
doi: 10.3389/fonc.2019.00120

MiR-1-3p Inhibits Lung Adenocarcinoma Cell Tumorigenesis via Targeting Protein Regulator of Cytokinesis 1

*Tao Li, Xiuxiu Wang, Lijun Jing and Yu Li**

Department of Respiratory Diseases, Qilu Hospital of Shandong University, Jinan, China

Lung adenocarcinoma (LUAD) is one of the most lethal malignancies, posing a threat to human health. However, the molecular mechanisms underlying LUAD development remain largely unknown. In this study, we found that miR-1-3p was significantly downregulated in human LUAD tissues and cell lines and played an inhibitory role in LUAD cell tumorigenesis, as evidenced by the significantly reduced viability, migration, and invasion of LUAD cells in response to miR-1-3p overexpression. Mechanistically, microRNA (miR)-1-3p physically interacted with the 3′-untranslated region (UTR) of protein regulator of cytokinesis 1 (PRC1) mRNA, leading to downregulation of PRC1. Overexpression of PRC1 reversed the inhibitory effects of miR-1-3p on LUAD cell tumorigenesis, suggesting that the miR-1-3p/PRC1 axis is majorly involved in suppressing LUAD development and progression. Consistently, PRC1 was dramatically induced in LUAD tissues and cell lines as well as associated with a poor prognosis in LUAD patients. Taken together, our study identified the miR-1-3p/PRC1 axis as an important regulatory mechanism contributing to LUAD inhibition and provided valuable clues for the future development of therapeutic strategies against LUAD.

Keywords: lung adenocarcinoma, miR-1-3p, protein regulator of cytokinesis 1, malignant behavior, mechanism

OPEN ACCESS

Edited by:
Jian-ye Zhang,
Guangzhou Medical University, China

Reviewed by:
Frank Arfuso,
Curtin University, Australia
Kuzhuvelil B. Harikumar,
Rajiv Gandhi Centre for Biotechnology, India

****Correspondence:***
Yu Li
qlliyures@163.com

Specialty section:
This article was submitted to Cancer Molecular Targets and Therapeutics, a section of the journal Frontiers in Oncology

Received: *13 November 2018*
Accepted: *11 February 2019*
Published: *01 March 2019*

Citation:
Li T, Wang X, Jing L and Li Y (2019) MiR-1-3p Inhibits Lung Adenocarcinoma Cell Tumorigenesis via Targeting Protein Regulator of Cytokinesis 1. Front. Oncol. 9:120. doi: 10.3389/fonc.2019.00120

INTRODUCTION

Lung adenocarcinoma (LUAD) is the most common subtype of non-small cell lung cancer (NSCLC), accounting for 80–85% of all lung cancers; worldwide, approximately 40% of all lung cancer patients are diagnosed with LUAD (1). Compared to other subtypes of NSCLC, LUAD has a higher incidence and a shorter survival time among patients, with a 5-year survival rate as low as 10–15% (2, 3); thus, LUAD poses a serious threat to human health. Currently, chemotherapy is a relatively effective therapeutic option for NSCLC (4). However, the existence and development of intrinsic or acquired chemoresistance greatly limit the application of chemotherapy in cancer treatment. Therefore, there is still an urgent need to develop novel therapeutic strategies against LUAD that are based on the mechanisms underlying the development and progression of LUAD.

MicroRNAs (miRNAs) are a class of small endogenous non-coding RNA molecules (∼22 nucleotides) found in animals and plants that are responsible for the degradation or translation repression of mRNAs by binding to the 3′-untranslated region (UTR) of target mRNAs (5). A variety of miRNAs have been identified as novel biomarkers or promising therapeutic targets of human malignant tumors. Among them, miR-1-3p plays an antitumor role in multiple cancer

types, including rhabdomyosarcoma as well as lung, thyroid, prostatic, bladder, colorectal, and hepatocellular carcinomas (6–11). However, the role of miR-1-3p in LUAD has not yet been investigated. In addition, the association between miR-1-3p and its target genes may deepen our understanding of the molecular mechanisms contributing to LUAD development, thus facilitating the discovery of improved therapies for LUAD.

The microtubule-associated protein regulator of cytokinesis 1 (PRC1) has been found to be majorly involved in the organization of antiparallel microtubules in the central spindle during cytokinesis. The human PRC1 gene, located on chromosome 15q26.1, encodes a 620-amino-acid protein with a molecular weight of 71 kDa (3). An abnormally high expression of PRC1 has been observed in breast cancer (12), bladder cancer (13), hepatocellular carcinoma (14), and pancreatic cancer (15), which suggests a promotive role of PRC1 in tumorigenesis. However, it remains largely unknown whether there is a functional association between miR-1-3p and the regulation of PRC1 in LUAD. In this study, we examined the role of miR-1-3p in LUAD growth and metastasis as well as the underlying mechanism.

MATERIALS AND METHODS

Tissue Samples From LUAD Patients

Human LUAD tissues were collected from LUAD patients undergoing pulmonary resection or bronchoscopy biopsy, and normal tissues adjacent to cancer were collected from LUAD patients undergoing pulmonary resection at Qilu Hospital between May and September 2018. None of the patients had received chemotherapy or radiotherapy prior to surgery. All the fresh samples were stored in RNAlater Stabilization Solution (Ambion) at −80°C until use. This study was approved by the Ethics Committee of Shandong University, and written informed consent was obtained from all patients prior to enrollment in the present study. The clinicopathological characteristics of the patients are shown in **Supplementary Table 1**.

Cell Culture

Three LUAD cell lines (A549, H1299, and H1975 cells) and a human alveolar epithelial cell line (HPAEpiC) were purchased from the Cell Bank of the Type Culture Collection of the Chinese Academy of Sciences (Shanghai, China). The cells were maintained in RPMI 1640 medium (Gibco, USA) containing 10% fetal bovine serum (Gibco, USA), 100 U/mL penicillin, and 100 μg/mL streptomycin in a humidified atmosphere of 5% CO_2 at 37°C. Cells in the exponential phase of growth were used for the following experiments.

Construction of the miR-1-3p Overexpression Cell Lines

The pre-miR-1-3p sequences were synthesized by Biosune Biotechnology Company (Shanghai, China) and cloned into the lentiviral vector pGIPZ. Lentivirus was produced in HEK293T cells using the packaging vectors psPAX2 and pMD2.G. The cells were infected with lentivirus for 24 h and then cultured for 1 week in medium containing 2 μg/mL puromycin (Merck Millipore, USA) for screening to acquire cells with stable expression of miR-1-3p.

Transient Transfection

The miR-1-3p mimic and its negative control (NC) were chemically synthesized by GenePharma Co., Ltd. (Shanghai, China). The cells were transiently transfected with 50 nM miR-1-3p mimic or 50 nM NC (Boshang, Inc., China) using Lipofectamine 2000 (Invitrogen; Thermo Fisher Scientific, Inc.), according to the manufacturer's protocol. The cells were harvested at 24 or 48 h after the transfection. The NC was a scrambled oligonucleotide that does not encode any known miRNA. The transfection efficiency was confirmed by detecting the miR-1-3p expression level using the SYBR green (Takara)-based real-time quantitative polymerase chain reaction (qPCR) system.

RNA Isolation and qPCR

Total RNA was extracted from the cells using Trizol reagents (Invitrogen; Thermo Fisher Scientific, Inc.), according to the manufacturer's instructions. The cDNA of miRNA was synthesized with the One Step PrimeScript miRNA cDNA Synthesis Kit (Takara Biotechnology, Co., Ltd., Dalian, China). qPCR was performed using the SYBR green Premix Ex Taq II (Takara Biotechnology, Co., Ltd.) with the Step One Plus Real-Time PCR System (Applied Biosystems; Thermo Fisher Scientific, Inc.). The expression of U6 was used as an internal control. The primers for miR-1-3p are indicated in **Supplementary Table 2**.

Western Blot Analysis

The cells were lysed in ice-cold RIPA lysis buffer, and the cell lysates were obtained by centrifugation at 12,000 rpm and 4°C for 10 min. The protein concentration was determined using the bicinchoninic acid method. The protein samples (5–10 μg) were separated by sodium dodecyl sulfate–polyacrylamide gel electrophoresis, followed by transfer to polyvinylidene difluoride membranes, and then immunoblotted with the indicated antibodies. After blocking with 5% nonfat milk, the membranes were incubated with the respective primary antibody overnight at 4°C, followed by incubation with the horseradish peroxidase-coupled secondary antibody for 1 h at room temperature. The protein bands were visualized using enhanced chemiluminescence reagents (PerkinElmer) with an ImageQuant LAS 4000 system (GE Healthcare Life Sciences). The following antibodies were used: anti-PRC1, anti-fibronectin, anti-N-cadherin, anti-vimentin, and anti-β-actin (Cell Signaling Technology).

3-(4,5-Dimethylthiazol-2-yl)-2,5-Diphenyltetrazolium Bromide (MTT) Assay

The cells were seeded into 96-well plates at a density of 2,000 cells/well and grown for 5 days. After the addition of 100 μL of 5 mg/mL MTT solution, the cells were incubated for an additional 4 h at 37°C, and then the supernatant was removed and dissolved in 100 μL of dimethyl sulfoxide (Sigma-Aldrich).

Cell viability was assessed on the 1st, 2nd, 3rd, 4th, and 5th day. The absorbance of each well was measured in triplicate using an iMark Microplate Absorbance Reader (Bio-Rad).

Luciferase Reporter Assay

Luciferase reporter constructs containing wild-type (WT) or mutant PRC1 3′-UTR (pmirGLO-PRC1-WT or pmirGLO-PRC1-mut, respectively) were generated by GenePharma Inc. (Shanghai, China). The cells were cotransfected with 25 ng of PRC1 3′-UTR reporter constructs and 20 nM miR-1-3p mimic using Lipofectamine 2,000 (Invitrogen) in 24-well plates. At 24 h after transfection, luciferase assays were performed using the Dual-Luciferase reporter assay system (Promega). *Renilla* luciferase activity was used to normalize the luciferase activity of the PRC1 3′-UTR reporter constructs.

In vivo Tumorigenicity Assays

Four-week-old male BALB/c nude mice were purchased from the Shanghai Laboratory Animal Center of the Chinese Academy of Sciences (Shanghai, China). The mice were randomly divided into two groups and injected subcutaneously with A549 cells (2×10^6 cells/mouse, $n = 5$ mice/group) that were infected with either control lentivirus or miR-1-3p-overexpressing lentivirus. Tumor growth was monitored by measuring the tumor diameter. Tumor

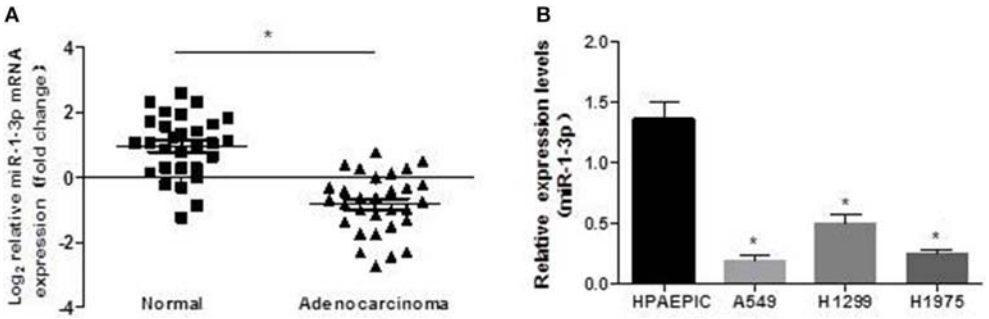

FIGURE 1 | Expression pattern of miR-1-3p in human LUAD tissues and cell lines. qPCR was performed to determine the expression levels of miR-1-3p in human LUAD tissues **(A)** and cell lines **(B)**, as indicated. *$P < 0.05$ in **(A)** ($n = 30$); *$P < 0.05$ vs. HPAEpiCs in **(B)** ($n = 3$).

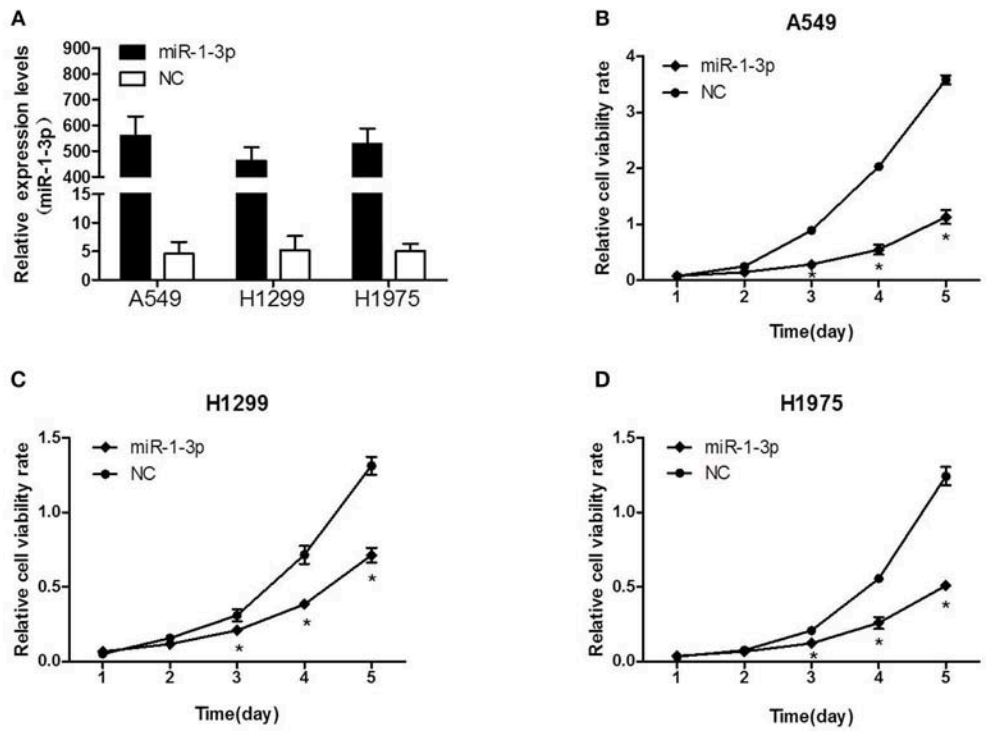

FIGURE 2 | The effect of miR-1-3p overexpression on LUAD cell viability. **(A)** qPCR was performed to validate the overexpression efficiency of miR-1-3p in A549, H1299, and H1975 cells. **(B–D)** The MTT assay was performed to measure the viability of miR-1-3p-overexpressing A549, H1299, and H1975 cells. *$P < 0.05$ vs. the corresponding negative control (NC) groups ($n = 3$).

volume was calculated according to the formula TV (cm^3) = a × b^2 × π/6, where a is the longest diameter and b is the shortest diameter. The mice were sacrificed after 3 weeks, and then the tumors were excised and weighed. All animal experiments were approved by the Shandong University Animal Care and Use Committee.

Bioinformatics Analyses

PRC1 genetic alterations and copy number variation in LUAD were retrieved from the cBioPortal for Cancer Genomics (http://www.cbioportal.org/) (16, 17). The Cancer Genome Atlas RNA expression data of LUAD tissues were processed and analyzed by the Cancer Genomics Browser (https://xena.ucsc.edu/welcome-to-ucsc-xena/) (18). The PRC1 expression levels and copy number variation were analyzed by Proteinatlas (https://www.proteinatlas.org/), Oncomine (www.oncomine.org) (19), and Gene Expression Profiling Interactive Analysis (http://gepia.cancer-pku.cn/) in LUAD and normal lung tissues via immunohistochemistry. Kaplan–Meier plots (http://kmplot.com/analysis/) (20) were used to analyze the overall survival of the LUAD patients.

Statistical Analysis

Statistical analysis was performed using GraphPad Prism 6.0 (GraphPad Software, La Jolla, CA, USA). Data are expressed as the mean ± standard deviation. Comparison between two groups was performed using the Student's *t*-test or the Mann-Whitney *U*-test. The correlation between the expression levels of miR-1 and PRC1 was analyzed using Pearson's correlation analysis. LUAD tissues with lower miR-1 and PRC1 expression than the median expression were assigned to the low-expression group, whereas those with higher miR-1 and PRC1 expression than the median expression were assigned to the high-expression group. Associations between the clinicopathological features and the expression levels of miR-1 and PRC1 were analyzed using the χ^2 test. Overall survival curves were determined according to the Kaplan–Meier method. A $p < 0.05$ was considered statistically significant.

RESULTS

MiR-1-3p Is Downregulated in Human LUAD Tissues and Cell Lines

To investigate the possible role of miR-1-3p in LUAD development, we first examined the expression levels of miR-1-3p in human LUAD tissues and cell lines. As shown in **Figure 1A**, miR-1-3p expression was significantly decreased in LUAD tissues, compared with the matched adjacent normal lung tissues. Similarly, marked downregulation of miR-1-3p was also observed in the human LUAD cell lines A549, H1299, and H1975,

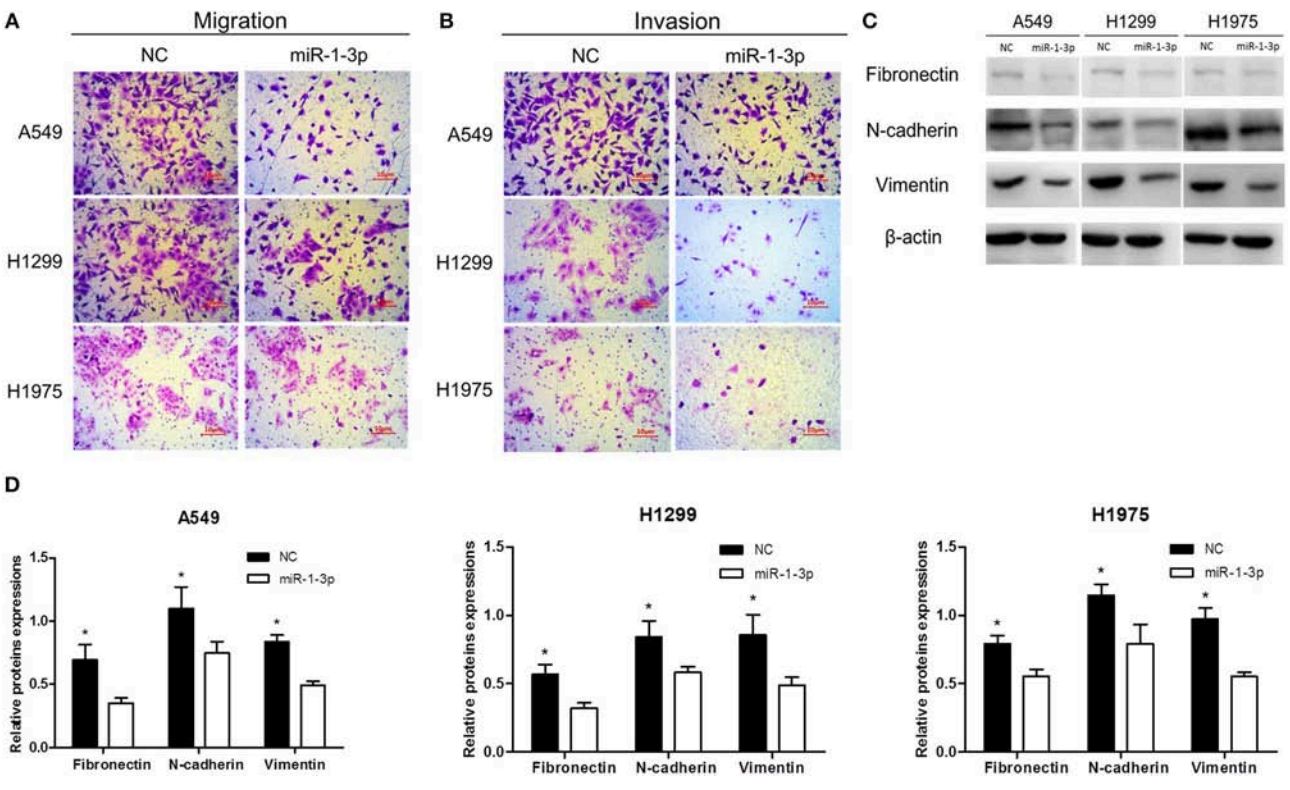

FIGURE 3 | The effect of miR-1-3p overexpression on LUAD cell migration and invasion as well as epithelial-mesenchymal transition. Transwell assays for migration **(A)** and invasion **(B)** of miR-1-3p-overexpressing LUAD cells. **(C)** Western blot assay for the expression of the indicated mesenchymal markers. β-Actin was used as an internal control. **(D)** Quantification of the western blot assay results shown in **(C)**. *$P < 0.05$ vs. miR-1-3p groups in **(C)** ($n = 3$).

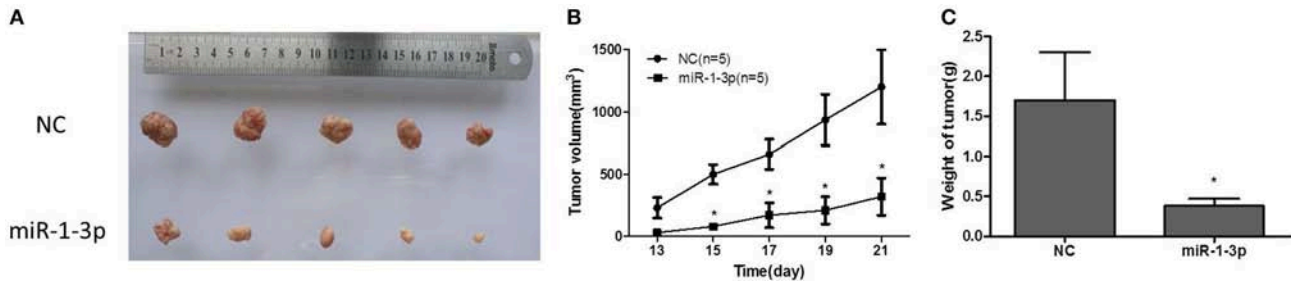

FIGURE 4 | The effect of miR-1-3p overexpression on tumorigenesis *in vivo*. **(A)** Overexpression of miR-1-3p reduced LUAD cell-derived tumor growth in a xenograft model. **(B)** Summary of the tumor growth data; the error bars indicate the standard deviation. **(C)** miR-1-3p overexpression results in a decline of tumor weight. $^*P < 0.05$.

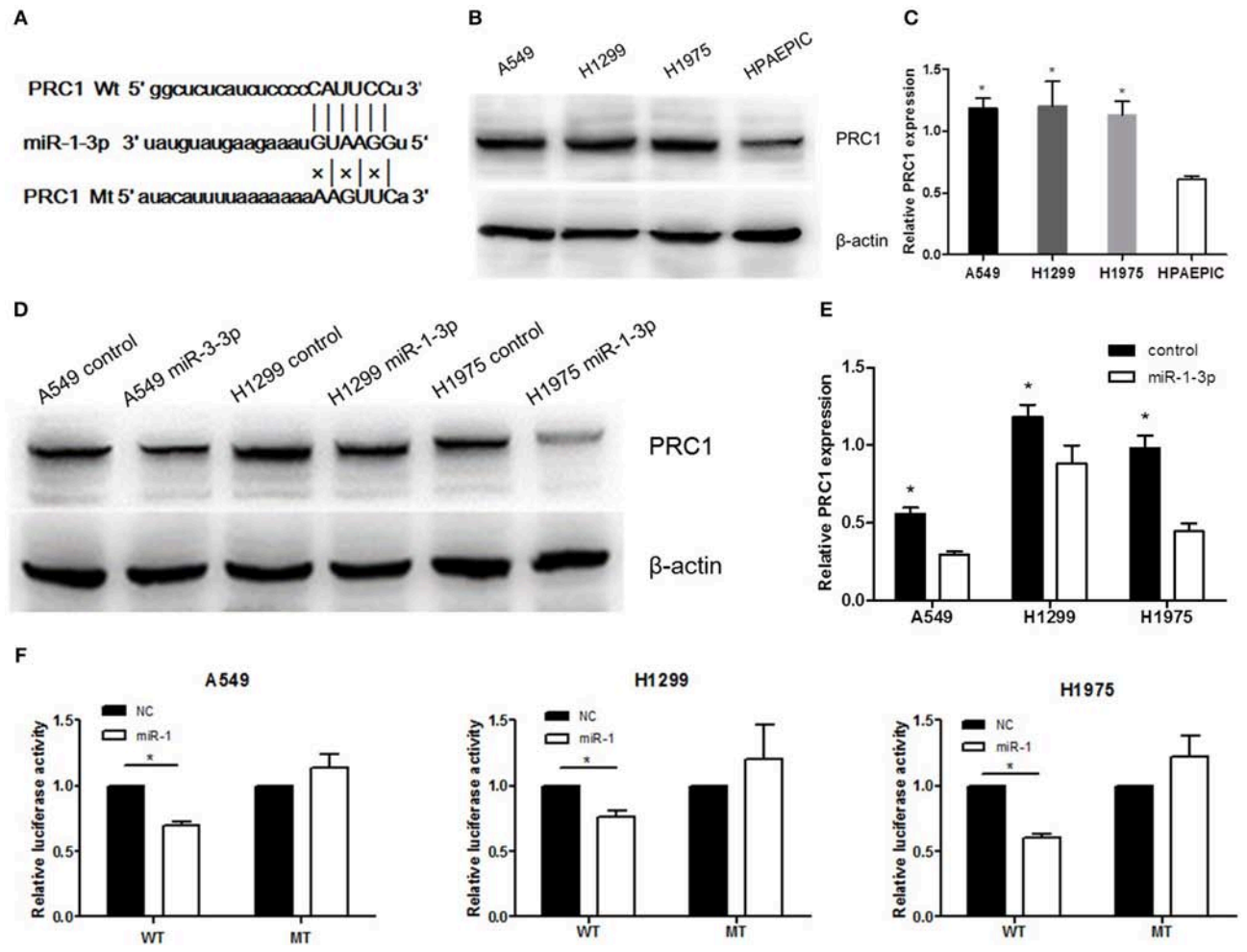

FIGURE 5 | PRC1 is a direct target of miR-1-3p in LUAD cells. **(A)** The putative miR-1-3p-binding sites in PRC1 3′-UTR and the mutated binding sites are shown. **(B,D)** Western blot analysis of PRC1 expression in the nontransfected negative control (NC)- or miR-1-3p-transfected LUAD cells. β-Actin was used as an internal control. **(C)** Quantification of the western blot assay results shown in **(B)**. $^*P < 0.05$ vs. HPAEpiCs ($n = 3$). **(E)** Quantification of the western blot assay results shown in **(D)**. $^*P < 0.05$ vs. the miR-1-3p groups ($n = 3$). **(F)** Luciferase reporter assay for LUAD cells transfected with wild-type (WT) or mutated (MT) pGL3-3′-UTR. The luciferase activity was normalized to *Renilla* luciferase activity. $^*P < 0.05$ ($n = 3$).

compared with the normal HPAEpiCs (**Figure 1B**). These *in vivo* and *in vitro* results suggest that miR-1-3p may play an inhibitory role in LUAD development.

Overexpression of miR-1-3p Suppresses LUAD Cell Viability *in vitro*

Next, we sought to investigate whether miR-1-3p indeed plays a role in suppressing LUAD development using a gain-of-function assay. As shown in **Figure 2A**, transfection of the miR-1-3p mimic led to a dramatic increase in miR-1-3p expression in the LUAD cell lines A549, H1299, and H1975. Importantly, overexpression of miR-1-3p significantly inhibited the viability of these three cell lines in a time-dependent manner, compared with the NC groups (**Figures 2B–D**). These results demonstrate that miR-1-3p is sufficient to suppress LUAD cell growth *in vitro*.

Overexpression of miR-1-3p Inhibits LUAD Cell Migration and Invasion *in vitro*

To further investigate whether miR-1-3p inhibits LUAD progression, Transwell assays were performed to examine the effects of miR-1-3p overexpression on LUAD cell migration and invasion. As shown in **Figures 3A,B**, overexpression of miR-1-3p resulted in a significant decrease in LUAD cell migration and invasion abilities, compared with the NC groups. Consistently, overexpression of miR-1-3p markedly suppressed epithelial-mesenchymal transition (EMT), a process contributing to tumor metastasis, as evidenced by downregulation of the mesenchymal markers fibronectin, N-cadherin, and vimentin (**Figures 3C,D**). These data suggest that miR-1-3p overexpression may suppress LUAD progression through reducing LUAD cell migration and invasion as well as inhibiting EMT in these cells.

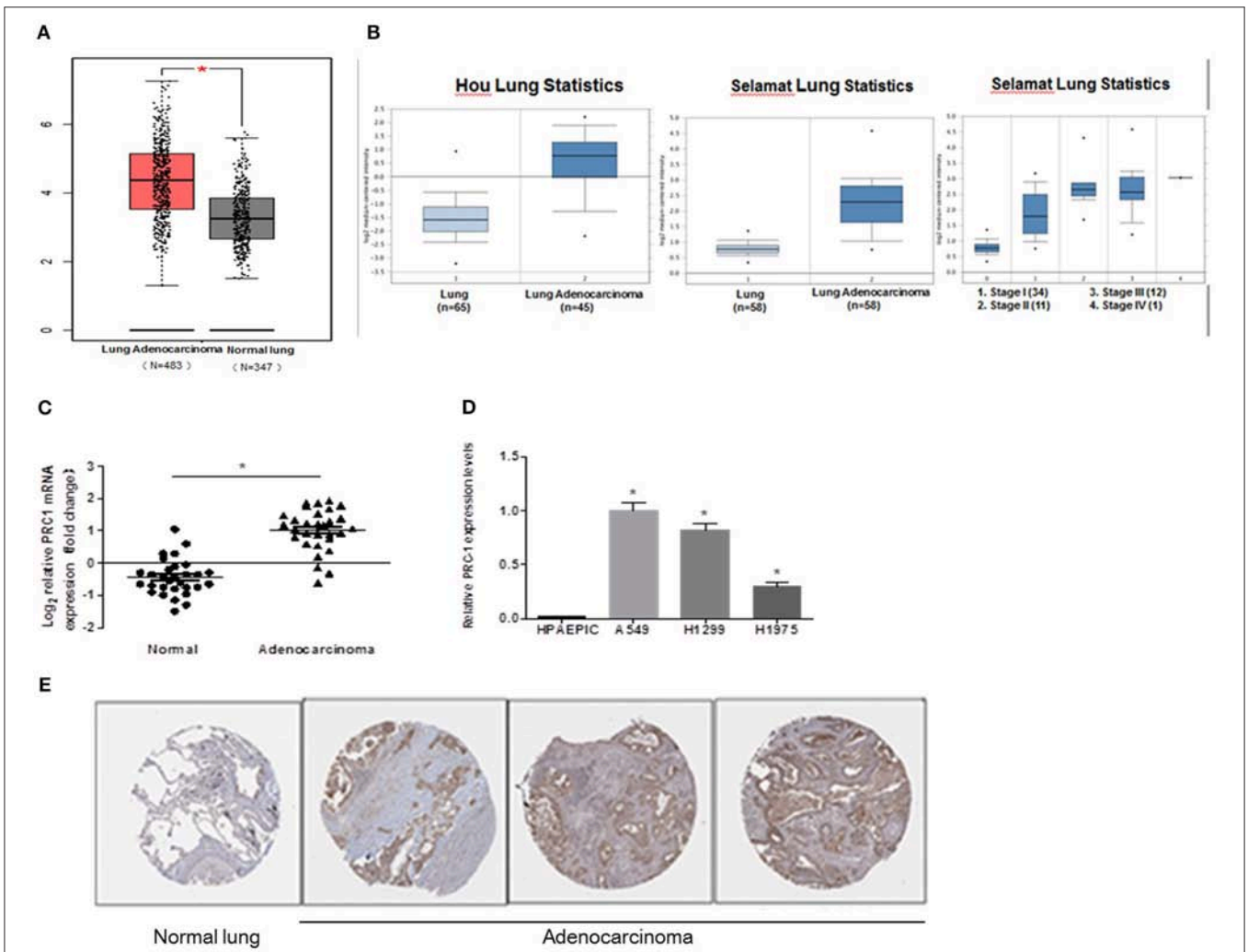

FIGURE 6 | Expression pattern of PRC1 in LUAD tissues and cell lines. **(A)** The data of copy number variation in LUAD from The Cancer Genome Atlas cohort. **(B)** The mRNA expression of PRC1 in different TNM staging groups in Oncomine. **(C)** qPCR analysis of PRC1 expression in LUAD tissues ($n = 30$). **(D)** qPCR analysis of PRC1 expression in LUAD cells and HPAEpiCs. **(E)** Representative images of the immunohistochemical staining of PRC1 from The Human Protein Atlas in LUAD and normal lung tissues. *$P < 0.05$ in **(C)** ($n = 30$); *$P < 0.05$ vs. HPAEpiCs in **(D)** ($n = 3$).

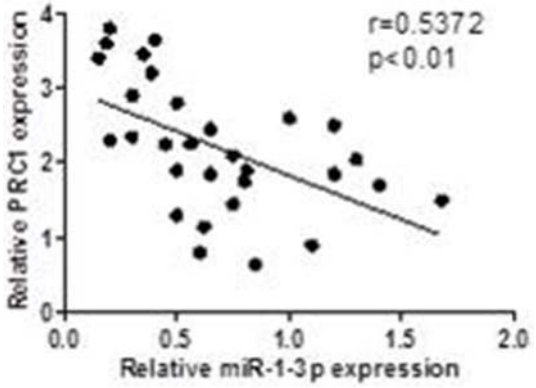

FIGURE 7 | Association between the miR-1-3p and PRC-1 levels in LUAD patients. The PRC1 and miR-1 levels were determined by qPCR in LUAD tissues and matched adjacent normal tissues ($n = 30$).

miR-1-3p Inhibits Xenograft Tumor Growth of LUAD Cells

To further explore whether miR-1-3p overexpression could suppress LUAD growth *in vivo*, human LUAD A549 cells with and without miR-1-3p overexpression were subcutaneously inoculated into nude mice. At 1 week after inoculation, all mice had developed detectable tumors. However, at 3 weeks after inoculation, the mice bearing tumors with miR-1-3p overexpression demonstrated a dramatic decrease in the tumor size and weight (**Figures 4A–C**), compared to the control groups. These results show that overexpression of miR-1-3p inhibits tumorigenesis *in vivo*.

PRC1 Is a Direct Target Gene of miR-1-3p

To further examine the mechanism underlying miR-1-3p-mediated suppression of LUAD development and progression, we employed the TargetScan computational algorithm to predict the target genes of miR-1-3p (21). The results indicated complementary base-pairing between miR-1-3p and the 3′-UTR of PRC1 (**Figure 5A**), suggesting that PRC1 may be a target gene of miR-1-3p. To verify this finding, we detected the expression of PRC1 in LUAD cells. As shown in **Figures 5B,C**, the protein expression of PRC1 was markedly induced in LUAD cells, compared with normal HPAEpiCs, consistent with the expression pattern of miR-1-3p in LUAD tissues and cells. Importantly, miR-1-3p overexpression led to downregulation of PRC1 in LUAD cells (**Figures 5D,E**), confirming that PRC1 is a downstream target of miR-1-3. To determine whether PRC1 is directly targeted by miR-1-3p, we performed a mutation assay through introducing a PRC1 3′-UTR mutation in the pmirGLO vector. The results demonstrated that the PRC1 3′-UTR mutation had no significant effect on the luciferase activity in miR-1-3p-transfected LUAD cells, compared with that in the NC-transfected cells (**Figure 5F**), suggesting that WT PRC1 3′-UTR is essential for the function of miR-1-3p. Taken together, our data show that PRC1 is a direct downstream target gene of miR-1-3p.

PRC1 Is Induced in LUAD Tissues and Cell Lines

To determine whether PRC1 contributes to LUAD development and progression, we examined the expression profile of PRC1 in LUAD tissues using the publicly accessible database Oncomine. As shown in **Figure 6A**, the mRNA expression levels of PRC1 were significantly enhanced in the LUAD tissues, compared with the normal lung tissues. In addition, we also analyzed the mRNA expression of PRC1 in LUAD tissues using two microarray datasets from the Hou and Selamat lung cancer groups, which were downloaded from Oncomine. The results demonstrated that the mRNA expression of PRC1 was significantly induced in the LUAD tissues of these groups and positively correlated with the tumor, lymph node, metastasis (TNM) staging of LUAD (**Figure 6B**). These findings were further confirmed by our mRNA expression data of PRC1 and the immunohistochemical staining of PRC1 in human LUAD tissues and matched adjacent normal lung tissues (**Figures 6C,E**). For the *in vitro* study, the mRNA levels of PRC1 were dramatically increased in the LUAD cell lines A549, H1299, and H1975, compared to those in normal HPAEpiCs (**Figure 6D**). Collectively, these results suggest that PRC1 may be involved in LUAD development and progression.

Correlation of miR-1-3p/PRC1 and Clinicopathological Characteristics of LUAD Patients

To investigate whether the miR-1-3p/PRC1 axis plays a role in LUAD development, we first analyzed the association between the miR-1-3p and PRC1 levels in LUAD tissues. The results revealed that the miR-1-3p levels were negatively correlated with the PRC1 mRNA expression ($r = -0.5858$; $P < 0.01$; **Figure 7**) in the LUAD tissues. Importantly, low levels of miR-1-3p and high levels of PRC1 were strongly associated with the TNM stage, lymph node metastasis, and distant metastasis (**Table 1**). These data suggest that LUAD development may be at least partially attributable to the miR-1-3p/PRC1 axis.

miR-1-3p Inhibits LUAD Cell Metastasis via PRC1

To determine whether miR-1-3p-mediated suppression of PRC1 expression is a major mechanism inhibiting LUAD development and progression, we cotransfected LUAD cells with miR-1-3p and a PRC1-overexpression plasmid for Transwell assays. The plasmid transfection efficacy of miR-1-3p and PRC1 was validated in **Figures 8A,B**. We found that miR-1-3p significantly inhibited the migration and invasion of three LUAD cell lines and that the inhibitory effects of miR-1-3p were markedly reversed by PRC1 overexpression (**Figures 8C–E**), suggesting that miR-1-3p inhibits LUAD cell metastasis in a PRC1-depedent manner and the miR-1-3p/PRC1 axis is majorly involved in LUAD development and progression.

Overexpression of PRC1 Is Associated With a Poor Prognosis in LUAD Patients

MiR-1-3p functions through suppressing PRC1 expression, suggesting a promotive role of PRC1 in LUAD development. To

TABLE 1 | The clinicopathological characteristics of 30 lung adenocarcinoma patients.

Clinicopathological features	*n*	Percent (%)	PRC1 expression		*p*	miR-1-3p expression		*p*
			Low ($n = 9$)	High ($n = 21$)		Low ($n = 18$)	High ($n = 12$)	
GENDER								
Male	19	63.33	7	12	0.419	11	9	0.694
Female	11	36.67	2	9	–	7	3	–
AGE (YEARS)								
≤60	13	43.33	6	7	0.123	8	5	1.000
>60	17	56.67	3	14	–	10	7	–
TUMOR SIZE								
T1 and T2	6	20.00	1	5	0.637	4	2	1.000
T3 and T4	24	80.00	8	16	–	14	10	–
TNM STAGE								
I and II	7	23.33	5	2	0.014	1	6	0.009
III and IV	23	76.67	4	19	–	17	6	–
LYMPHATIC METASTASIS								
Negative	12	40.00	8	4	0.001	2	10	0.000
Positive	18	60.00	1	17	–	16	2	–
DISTANT METASTASIS								
M0	12	40.00	7	5	0.013	3	9	0.002
M1	18	60.00	2	16	–	15	3	–

TNM, tumor, lymph node, metastasis stage.

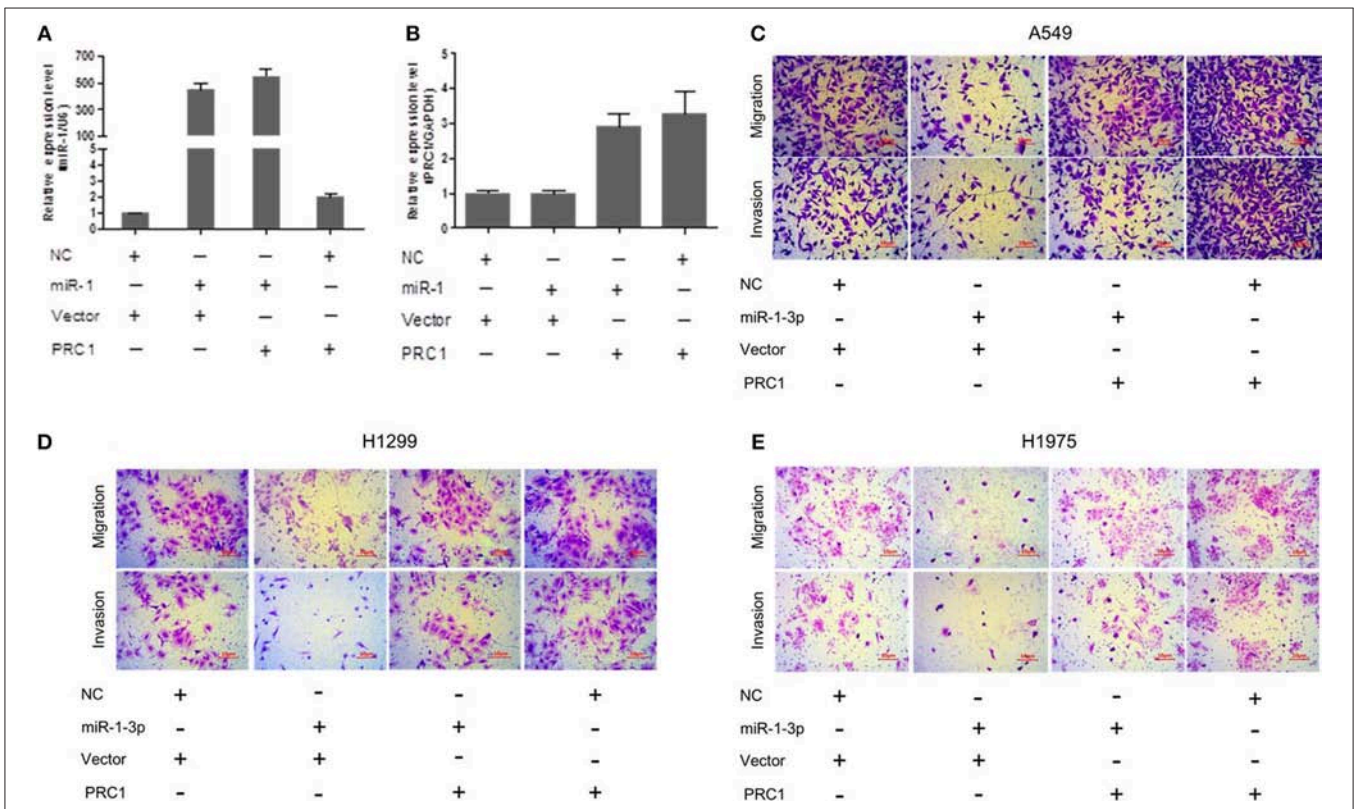

FIGURE 8 | miR-1-3p inhibits LUAD cell migration and invasion via PRC1. **(A,B)** qPCR analysis of the transfection efficiency of the miR-1-3p mimic and the PRC1-overexpression plasmid in LUAD cells. **(C–E)** Transwell assays for migration and invasion of LUAD cells transfected with the miR-1-3p mimic and/or the PRC1-overexpression plasmid.

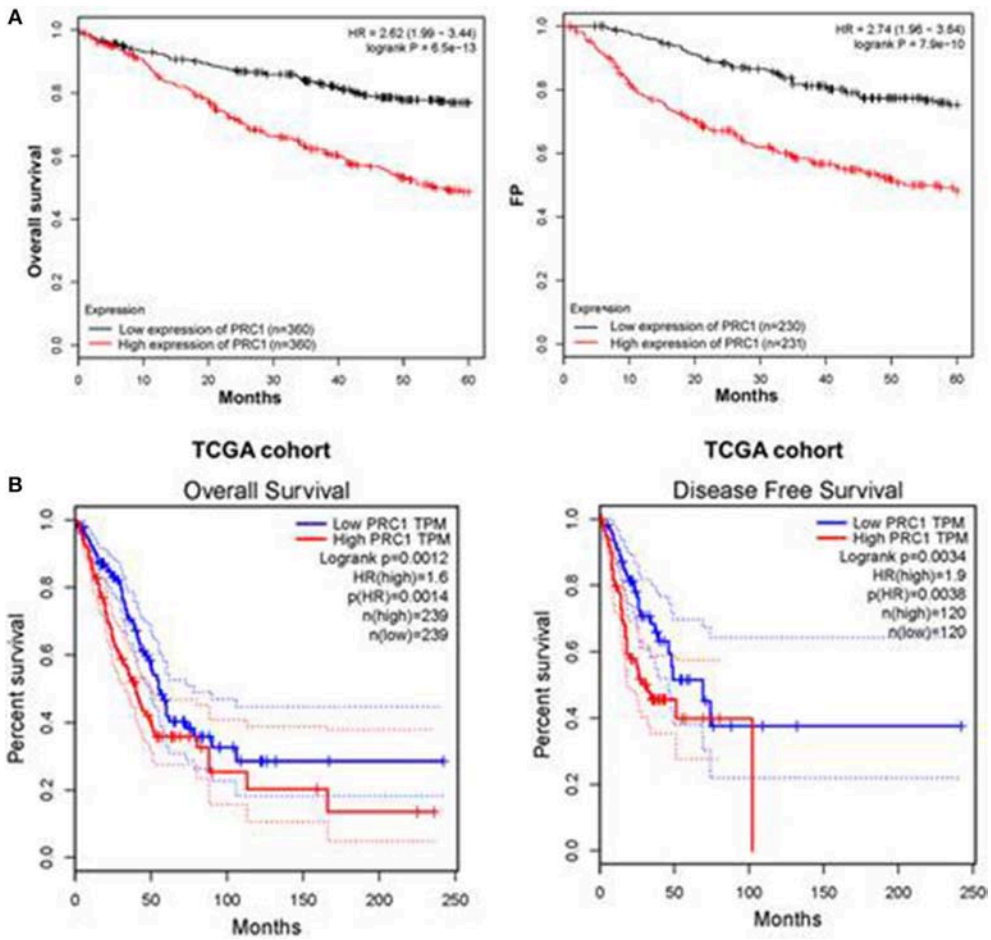

FIGURE 9 | Overexpression of PRC1 is associated with a poor prognosis in LUAD patients. **(A)** The prognostic effect of PRC1 in LUAD patients was evaluated using Kaplan–Meier plots. **(B)** The overall and disease-free survival rates in LUAD patients with different PRC1 expression patterns were evaluated for The Cancer Genome Atlas (TCGA) cohort.

confirm this, we examined the prognostic effect of PRC1 in LUAD patients from a public database by performing Kaplan–Meier analysis (http://www.kmplot.com). The results showed that the LUAD patients with a higher mRNA expression of PRC1 had shorter overall and disease-free survival times than those with a lower mRNA expression of PRC1 (**Figures 9A,B**). These data suggest that PRC1 overexpression may serve as a biomarker of a poor prognosis for LUAD patients, further supporting our findings that miR-1-3p plays a key role in inhibiting LUAD development through targeting PRC1.

DISCUSSION

Carcinogenesis of LUAD is a complex and multistage process involving the regulation of a wide range of genes by miRNAs (22–24). Among them, miR-1-3p, a muscle-specific miRNA, has been shown to play a key role in skeletal muscle differentiation and have inhibitory effects on the growth, migration, and invasion of LUAD (25). The present study revealed that miR-1-3p was significantly downregulated in LUAD tissues and cells. Lower levels of miR-1-3p were strongly associated with a higher TNM stage, earlier lymph node metastasis, and more distant metastasis. Therefore, miR-1-3p is suggested as a tumor suppressor in LUAD. The detection of miR-1-3p expression may be a valuable tool to evaluate the invasion and metastasis of LUAD.

There are hundreds of possible target genes of miR-1-3p, among which PRC1 is a critical protein in cytokinesis and characterized as a mitotic spindle-associated cyclin-dependent kinase substrate (26). Previous studies have provided evidence that PRC1 is involved in different types of cancer (27, 28). Loss of PRC1 leads to the accumulation of bi- and multi-nucleated cells in lung cancer, which further supports its role as the major central spindle organizer in cytokinesis (29). In view of our findings that miR-1-3p overexpression inhibits LUAD cell viability, there is a possibility that the function of PRC1 in apoptosis and senescence is due to induction of miR-1-3p. In this study, we demonstrated that the function of miR-1-3p could be suppressed by dysregulated expression of PRC1. In accordance with the above-mentioned studies, we confirmed that the overexpression of PRC1 significantly promoted the viability, invasion, and migration of LUAD cells. A higher PRC1

expression was also related to a worse outcome in patients with LUAD. Because Wnt/β-catenin signaling is dysregulated in lung cancer (30) and the overexpression of Wnt proteins (Wnt1 and Wnt5a) is significantly associated with adverse outcomes in lung cancer patients (31), we speculate that the miR-1-3p/PRC1 axis participates in dysregulation of Wnt/β-catenin signaling in LUAD development (32); however, this hypothesis requires further investigation. Although our study demonstrated that the miR-1-3p/PRC1 axis is a major mechanism underlying LUAD development, we do not exclude the possibility that other miRNAs or protein regulators besides miR-1-3p/PRC1 are also involved in LUAD pathogenesis. Therefore, more research is needed.

In summary, we identified miR-1-3p as a novel regulator of PRC1 in LUAD. A high PRC1 expression correlates with a poor prognosis in LUAD patients. Thus, targeting miR-1-3p/PRC1 may be a potential therapeutic intervention for the treatment of LUAD.

ETHICS STATEMENT

The Ethics Committee of Qilu Hospital at Shandong University approved this study [KYLL-2018 (KS)-156]. All participants in this study provided informed consent.

AUTHOR CONTRIBUTIONS

TL designed the questionnaire and drafted the manuscript. XW did the statistical analysis. TL and LJ did the relationship analysis and collected the data. YL conceived the study, supervised and reviewed the entire study, and edited the manuscript.

SUPPLEMENTARY MATERIAL

The Supplementary Material for this article can be found online at: https://www.frontiersin.org/articles/10.3389/fonc.2019.00120/full#supplementary-material

REFERENCES

1. Siegel RL, Miller KD, Jemal A. Cancer statistics. *CA Cancer J Clin.* (2017) 67:7–30. doi: 10.3322/caac.21387
2. Zhang W, Fan J, Chen Q, Lei C, Qiao B, Liu Q. SPP1 and AGER as potential prognostic biomarkers for lung adenocarcinoma. *Oncol Lett.* (2018) 15:7028–36. doi: 10.3892/ol.2018.8235
3. Jiang W, Jimenez G, Wells NJ, Hope TJ, Wahl GM, Hunter T, et al. PRC1: a human mitotic spindle-associated CDK substrate protein required for cytokinesis. *Mol Cell.* (1998) 2:877–85. doi: 10.1016/S1097-2765(00)80302-0
4. Peters S, Popat S, Reinmuth N, De Ruysscher D, Kerr KM, Peters S, et al. Metastatic non-small-cell lung cancer (NSCLC): ESMO clinical practice guidelines for diagnosis, treatment and follow-up. *Ann Oncol.* (2012) 23(Suppl. 7):vii56–64. doi: 10.1093/annonc/mds226
5. Leva GD, Croce CM. The role of microRNAs in the tumorigenesis of ovarian cancer. *Front Oncol.* (2013) 3:153. doi: 10.3389/fonc.2013.00153
6. Han C, Yu Z, Duan Z, Kan Q. Role of microRNA-1 in human cancer and its therapeutic potentials. *Biomed Res Int.* (2014) 2014:428371. doi: 10.1155/2014/428371
7. Li J, Guan J, Long X, Wang Y, Xiang X. mir-1-mediated paracrine effect of cancer-associated fibroblasts on lung cancer cell proliferation and chemoresistance. *Oncol Rep.* (2016) 35:3523–31. doi: 10.3892/or.2016.4714
8. Li SM, Wu HL, Yu X, Tang K, Wang SG, Ye ZQ, et al. The putative tumour suppressor miR-1–3p modulates prostate cancer cell aggressiveness by repressing E2F5 and PFTK1. *J Exp Clin Cancer Res.* (2018) 37:219. doi: 10.1186/s13046-018-0895-z
9. Diniz GP, Lino CA, Moreno CR, Senger N, Barreto-Chaves MLM. MicroRNA-1 overexpression blunts cardiomyocyte hypertrophy elicited by thyroid hormone. *J Cell Physiol.* (2017) 232:3360–8. doi: 10.1002/jcp.25781
10. Gao L, Yan P, Guo FF, Liu HJ, Zhao ZF. MiR-1–3p inhibits cell proliferation and invasion by regulating BDNF-TrkB signaling pathway in bladder cancer. *Neoplasma.* (2018) 65:89–96. doi: 10.4149/neo_2018_161128N594
11. Zhu D, Sun Y, Zhang D, Dong M, Jiang G, Zhang X, et al. miR1 inhibits the progression of colon cancer by regulating the expression of vascular endothelial growth factor. *Oncol Rep.* (2018) 40:589–98. doi: 10.3892/or.2018.6463
12. Shimo A, Nishidate T, Ohta T, Fukuda M, Nakamura Y, Katagiri T. Elevated expression of protein regulator of cytokinesis 1, involved in the growth of breast cancer cells. *Cancer Sci.* (2007) 98:174–81.doi: 10.1111/j.1349-7006.2006.00381.x
13. Kanehira M, Katagiri T, Shimo A, Takata R, Shuin T, Miki T, et al. Oncogenic role of MPHOSPH1, a cancer-testis antigen specific to human bladder cancer. *Cancer Res.* (2007) 67:3276–85. doi: 10.1158/0008-5472.CAN-06-3748
14. Chen J, Rajasekaran M, Xia H, Zhang X, Kong SN, Sekar K, et al. The microtubule-associated protein PRC1 promotes early recurrence of hepatocellular carcinoma in association with the Wnt/beta-catenin signalling pathway. *Gut.* (2016) 65:1522–34. doi: 10.1136/gutjnl-2015-310625
15. Nakamura T, Furukawa Y, Nakagawa H, Tsunoda T, Ohigashi H, Murata K, et al. Genome-wide cDNA microarray analysis of gene expression profiles in pancreatic cancers using populations of tumor cells and normal ductal epithelial cells selected for purity by laser microdissection. *Oncogene.* (2004) 23:2385–400. doi: 10.1038/sj.onc.1207392
16. Gao J, Aksoy BA, Dogrusoz U, Dresdner G, Gross B, Sumer SO, et al. Integrative analysis of complex cancer genomics and clinical profiles using the cBioPortal. *Sci Signal.* (2013) 6:pl1. doi: 10.1126/scisignal.2004088
17. Cerami E, Gao J, Dogrusoz U, Gross BE, Sumer SO, Aksoy BA, et al. The cBio cancer genomics portal: an open platform for exploring multidimensional cancer genomics data. *Cancer Discov.* (2012) 2:401–4. doi: 10.1158/2159-8290.CD-12-0095
18. Zhu J, Sanborn JZ, Benz S, Szeto C, Hsu F, Kuhn RM, et al. The UCSC cancer genomics browser. *Nat Methods.* (2009) 6:239–40. doi: 10.1038/nmeth0409-239
19. Rhodes DR, Yu J, Shanker K, Deshpande N, Varambally R, Ghosh D, et al. ONCOMINE: a cancer microarray database and integrated data-mining platform. *Neoplasia.* (2004) 6:1–6. doi: 10.1016/S1476-5586(04)80047-2
20. Gyorffy B, Surowiak P, Budczies J, Lánczky A. Online survival analysis software to assess the prognostic value of biomarkers using transcriptomic data in non-small-cell lung cancer. *PLoS ONE.* (2013) 8:e82241. doi: 10.1371/journal.pone.0082241
21. Jiao D, Chen J, Li Y, Tang X, Wang J, Xu W, et al. miR-1–3p and miR-206 sensitizes HGF-induced gefitinib-resistant human lung cancer cells through inhibition of c-Met signalling and EMT. *J Cell Mol Med.* (2018) 22:3526–36. doi: 10.1111/jcmm.13629
22. Nadal E, Chen G, Gallegos M, Lin L, Ferrer-Torres D, Truini A, et al. Epigenetic inactivation of microRNA-34b/c predicts poor disease-free survival in early-stage lung adenocarcinoma. *Clin Cancer Res.* (2013) 19:6842–52. doi: 10.1158/1078-0432.CCR-13-0736
23. Yu QQ, Wu H, Huang X, Shen H, Shu YQ, Zhang B, et al. MiR-1 targets PIK3CA and inhibits tumorigenic properties of A549 cells. *Biomed Pharmacother.* (2014) 68:155–61. doi: 10.1016/j.biopha.2014.01.005
24. Singh A, Happel C, Manna SK, Acquaah-Mensah G, Carrerero J, Kumar S, et al. Transcription factor NRF2 regulates miR-1 and miR-206 to drive tumorigenesis. *J Clin Invest.* (2013) 123:2921–34. doi: 10.1172/JCI 66353
25. Chiu KL, Lin YS, Kuo TT, Lo CC, Huang YK, Chang HF, et al. ADAM9 enhances CDCP1 by inhibiting miR-1 through EGFR signaling

activation in lung cancer metastasis. *Oncotarget*. (2017) 8:47365–78. doi: 10.18632/oncotarget.17648
26. Zhan P, Zhang B, Xi GM, Wu Y, Liu HB, Liu YF, et al. PRC1 contributes to tumorigenesis of lung adenocarcinoma in association with the Wnt/beta-catenin signaling pathway. *Mol Cancer*. (2017) 16:108. doi: 10.1186/s12943-017-0682-z
27. Brynychova V, Ehrlichova M, Hlavac V, Nemcova-Furstova V, Pecha V, Leva J, et al. Genetic and functional analyses do not explain the association of high PRC1 expression with poor survival of breast carcinoma patients. *Biomed Pharmacother.* (2016) 83:857–64. doi: 10.1016/j.biopha.2016.07.047
28. Hanselmann S, Wolter P, Malkmus J, Gaubatz S. The microtubule-associated protein PRC1 is a potential therapeutic target for lung cancer. *Oncotarget*. (2018) 9:4985–97. doi: 10.18632/oncotarget.23577
29. Glotzer M. The 3Ms of central spindle assembly: microtubules, motors and MAPs. *Nat Rev Mol Cell Biol*. (2009) 10:9–20. doi: 10.1038/nrm2609
30. Stewart DJ. Wnt signaling pathway in non-small cell lung cancer. *J Natl Cancer Inst*. (2014) 106:djt356. doi: 10.1093/jnci/djt356
31. Jin J, Zhan P, Qian H, Wang X, Katoh M, Phan K, et al. Prognostic value of wingless-type proteins in non-small cell lung cancer patients: a meta-analysis. *Transl Lung Cancer Res*. (2016) 5:436–42. doi: 10.21037/tlcr.2016.08.08
32. Anton R, Chatterjee SS, Simundza J, Cowin P, Dasgupta R. A systematic screen for micro-RNAs regulating the canonical Wnt pathway. *PLoS ONE*. (2011) 6:e26257. doi: 10.1371/journal.pone.0026257

Conflict of Interest Statement: The authors declare that the research was conducted in the absence of any commercial or financial relationships that could be construed as a potential conflict of interest.

frontiers in Pharmacology

MINI REVIEW
published: 05 March 2019
doi: 10.3389/fphar.2019.00208

Inhibitors of Human ABCG2: From Technical Background to Recent Updates With Clinical Implications

Yu Toyoda, Tappei Takada and Hiroshi Suzuki*

Department of Pharmacy, The University of Tokyo Hospital, Faculty of Medicine, The University of Tokyo, Tokyo, Japan

The ATP-binding cassette transporter G2 (ABCG2; also known as breast cancer resistance protein, BCRP) has been suggested to be involved in clinical multidrug resistance (MDR) in cancer like other ABC transporters such as ABCB1 (*P*-glycoprotein). As an efflux pump exhibiting a broad substrate specificity localized on cellular plasma membrane, ABCG2 excretes a variety of endogenous and exogenous substrates including chemotherapeutic agents, such as mitoxantrone and several tyrosine kinase inhibitors. Moreover, in the normal tissues, ABCG2 is expressed on the apical membranes and plays a pivotal role in tissue protection against various xenobiotics. For this reason, ABCG2 is recognized to be an important determinant of the pharmacokinetic characteristics of its substrate drugs. Although the clinical relevance of reversing the ABCG2-mediated MDR has been inconclusive, an appropriate modulation of ABCG2 function during chemotherapy should logically enhance the efficacy of anti-cancer agents by overcoming the MDR phenotype and/or improving their pharmacokinetics. To confirm this possibility, considerable efforts have been devoted to developing ABCG2 inhibitors, although there is no clinically available substance for this purpose. As a clue for addressing this issue, this mini-review provides integrated information covering the technical backgrounds necessary to evaluate the ABCG2 inhibitory effects on the target compounds and a current update on the ABCG2 inhibitors. This essentially includes our recent findings, as we serendipitously identified febuxostat, a well-used agent for hyperuricemia as a strong ABCG2 inhibitor, that possesses some promising potentials. We hope that an overview described here will add value to further studies involving in the multidrug transporters.

Keywords: BCRP, cancer chemotherapy, drug repurposing, febuxostat, Ko143, multidrug resistance, tumor lysis syndrome, vesicle transport

OPEN ACCESS

Edited by:
Yunkai Zhang,
Vanderbilt University Medical Center, United States

Reviewed by:
Tomohiro Terada,
Shiga University of Medical Science, Japan
Ning Ji,
Tianjin Medical University, China
Shinobu Ohnuma,
Tohoku University, Japan

****Correspondence:***
Tappei Takada
tappei-tky@umin.ac.jp

Specialty section:
This article was submitted to Experimental Pharmacology and Drug Discovery, a section of the journal Frontiers in Pharmacology

Received: *25 December 2018*
Accepted: *19 February 2019*
Published: *05 March 2019*

Citation:
Toyoda Y, Takada T and Suzuki H (2019) Inhibitors of Human ABCG2: From Technical Background to Recent Updates With Clinical Implications. Front. Pharmacol. 10:208. doi: 10.3389/fphar.2019.00208

INTRODUCTION

Two decades ago, the ABC transporter G2 (ABCG2) was discovered in drug-resistant cancer cells and human placenta (Allikmets et al., 1998; Doyle et al., 1998; Miyake et al., 1999). Thereafter, many studies were conducted to determine the role of ABCG2 in developing MDR in cancer. Moreover, in the first decade, *in vivo* studies using *Abcg2* knockout mice (Jonker et al., 2002)

Abbreviations: ABC, ATP-binding cassette; BBB, blood–brain barrier; CML, chronic myeloid leukemia; EC_{50}, half-maximal effective concentration; FTC, fumitremorgin C; IC_{50}, half-maximal inhibitory concentration; MDR, multidrug resistance; TKI, tyrosine kinase inhibitor, TLS, tumor lysis syndrome.

coupled with biochemical characterizations revealed the importance of ABCG2 in the biological defense mechanisms against xenobiotics (Vlaming et al., 2009). Indeed, ABCG2—a 655-amino acid protein working as a homodimer on cellular plasma membranes (Robey et al., 2009)—is expressed not only in cancer cells but also in several normal tissues, such as brush border membranes of epithelium in the intestine and of proximal tubules in the kidney, bile canalicular membranes of the hepatocytes in the liver, luminal membranes of the mammary gland epithelium, and blood-facing membranes of the endothelial cells forming the BBB. In these tissues ABCG2 plays a pivotal role in the extrusion of various endogenous and exogenous substrates including drugs (Mizuno et al., 2004, 2007; Adachi et al., 2005; Hirano et al., 2005; Jonker et al., 2005; Ando et al., 2007). Hence, this transporter is recognized as an important determinant of the pharmacokinetic characteristics profiles of various drugs (Giacomini et al., 2010).

In the next decade, after identifying ABCG2 as a physiologically important urate transporter, a positive relationship between ABCG2 dysfunction and increased risk of human diseases, such as gout and hyperuricemia was revealed (Matsuo et al., 2009; Woodward et al., 2009; Ichida et al., 2012; Higashino et al., 2017). In addition to the sulfate conjugates of endogenous steroids (Suzuki et al., 2003) and porphyrins (Zhou et al., 2005; Robey et al., 2009), phytoestrogen sulfate conjugates (van de Wetering and Sapthu, 2012) and a uremic toxin indoxyl sulfate (Takada et al., 2018) were added in the growing list of ABCG2 substrates. Contrary to these advances in understanding the pathophysiological importance of ABCG2, the clinical relevance of reversing ABCG2-mediated MDR has been inconclusive (Robey et al., 2018).

ABCG2 overexpression can render the cancer cells resistant to the ABCG2 substrate chemotherapy agents, such as mitoxantrone, doxorubicin, SN-38, and several TKIs. To the best of our knowledge, no published clinical trial has ever succeeded in reversing the ABCG2-mediated MDR. This is because, despite a lot of efforts in ABCG2 inhibitor development, chemical knock-out/down of ABCG2 in clinical situations has not been achieved yet due to the lack of an appropriate candidate molecule. We herein describe some well-used experimental systems to evaluate the ABCG2 inhibitory activity, followed by a recent update on the ABCG2 inhibitors that includes a potent substance, febuxostat.

TECHNICAL BACKGROUND FOR FUNCTIONAL VALIDATION

Various experimental models are available to examine the functions of the ABC transporters. Mainly focusing on ABCG2, with a current update this section introduces some *in vitro* and *in vivo* models that have been used in ABC transporter field. Broadly, the *in vitro* models are classified into two types, namely membrane-based systems and cell-based systems (**Figure 1**).

Plasma Membrane Vesicle-Based Methods

Preparation of Plasma Membrane Vesicles

In mammals, most of the ABC transporters are membrane proteins and work as an efflux pump involved in the transport of its substrates from the cytosol, either to the extracellular space or into organelles by an ATP-dependent manner. Therefore, isolation of the target ABC protein-enriched cell membrane is the first step for biochemical analyses. For ABCG2, sucrose density gradient ultracentrifugation for the isolation of plasma membrane fraction is generally employed to prepare plasma membrane vesicles from ABCG2-expressing cells (related notes are inscribed in the legend of **Figure 1**). For this purpose, not only mammalian cells but also insect cells [e.g., baculovirus-infected Sf9 cells (Saito et al., 2006)] could be used as host cells. Nonetheless, for easy and convenient preparation of ABCG2-expressing cells, we here recommend plasmid-based overexpression in non-polarized cells exhibiting high transfection efficiency, such as HEK293 cells (Miyata et al., 2016).

Vesicle Transport Assay

Vesicle transport assay is a well-established *in vitro* method employed to quantitatively evaluate ABC transporter function. The presence of ATP-dependent active transport across the cell membrane was directly proved using this method (Ishikawa, 1989). In this assay, ATP-regeneration components—enough amount of creatine phosphate and creatine kinase—are employed to maintain ATP levels in the reaction mixtures during prolonged incubation, and AMP is used as an alternative of ATP for the ATP-deficient controls. After incubation for the transport reaction, the plasma membrane vesicles are washed by filtration and then the intravesicularly accumulated substances are detected. To make this process more convenient and sensitive, radiolabeled or fluorescent substrates are usually used; alternatively, mass spectrometry is used (Toyoda et al., 2016; Takada et al., 2018). With ABCG2, [^{14}C]-urate (Miyata et al., 2016; Stiburkova et al., 2016; Higashino et al., 2017) and [^{3}H]-estrone sulfate (Suzuki et al., 2003) are well-used radiolabeled substrates that exhibit comparatively lower background signal for the quantitative detection due to their relatively hydrophilic properties. Additionally, non-radiolabeled experiments are conducted by the combined use of hematoporphyrin (a fluorescent ABCG2 substrate) and gel filtration techniques (Tamura et al., 2006).

ATPase Assay

Since ABC protein is driven by the free energy of ATP hydrolysis, ATPase activity is recognized as an indicator of the substrate transport. In this assay, the release of inorganic phosphate from ATP coupled with the transport of substrates is estimated using a colorimetric method, such as malachite green procedure (Baykov et al., 1988). This catalytic assay is relatively convenient for estimating the activity of some ABC proteins that prefer lipophilic compounds as their substrates because the non-specifically adsorbed substrates on the vesicles interfere with the measurement of direct transport. Considering that ABCB1 activity has been well

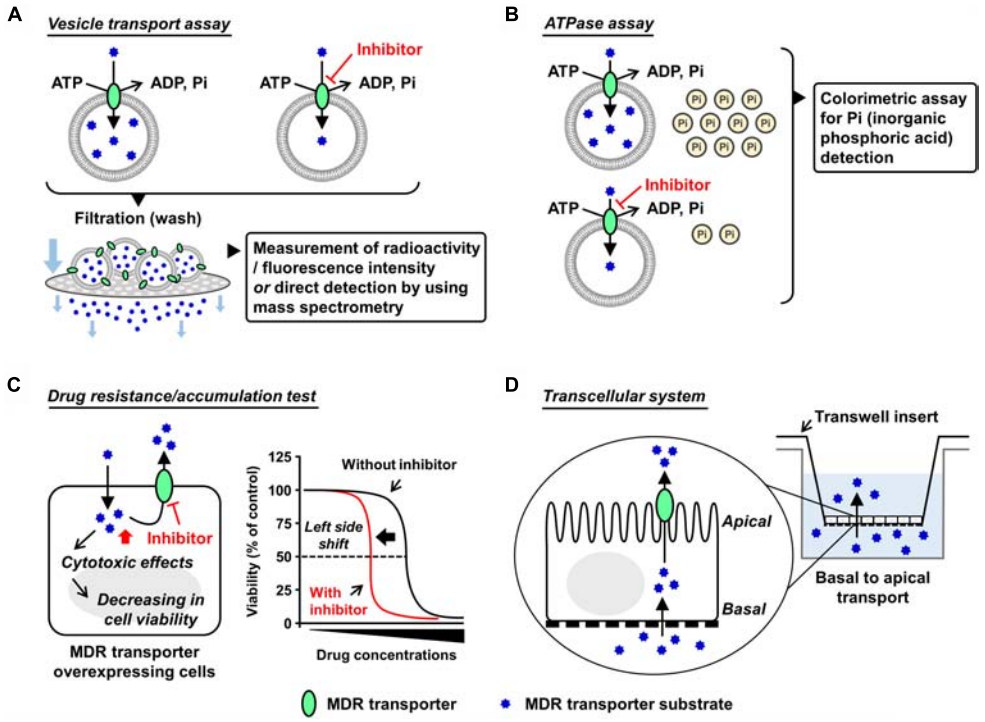

FIGURE 1 | Schematic illustrations of each *in vitro* assay. Generally used *in vitro* models which are classified into membrane-based systems and cell-based systems (Hegedus et al., 2009) are shown. In the former systems, investigators can use culture cell-derived plasma membrane vesicles or reconstituted proteoliposomes as described in the main text. In the latter systems, aside from a couple of exceptions using *Xenopus laevis* oocytes (Nakanishi et al., 2003; Woodward et al., 2009), mammalian cells expressing target ABC protein are generally used. **(A,B)** Plasma membrane vesicle- or proteoliposome-based methods: vesicle transport assay **(A)** and ATPase assay **(B)**. Both plasma membrane vesicles and reconstituted proteoliposomes are applicable to the vesicle transport assay and the ATPase assay. Of note, the final step of the vesicle preparation—gentle homogenization of isolated membrane fraction—is empirically important for the formation of inside-out plasma membrane vesicles, whose outer faces are the cytoplasmic aspects of the parent membranes. Although the resulting plasma membrane vesicles are the mixture of inside-out and right-side-out components, without any separation of the right-side-out vesicles they are generally stored at –80°C and subjected to further assays. This is because that in these *in vitro* assays, only ABC proteins embedded in the inside-out vesicles have their ABCs outside of the vesicles and can use ATP in the reaction mixture for their transport function. In other words, the ABC proteins in the right-side-out vesicles cannot work due to an inaccessibility of the ABCs with ATP. Additionally, ABCG2-enriched plasma membrane vesicles are used for a biochemical analysis to study interactions of candidate chemicals with ABCG2 at the substrate-binding sites, known as the photoaffinity labeling of ABCG2 with [^{125}I]-iodoarylazido-prazosin (Shukla et al., 2006). **(C,D)** Cell-based methods: drug resistance/accumulation test **(C)** and transcellular system **(D)**. MDR, multidrug resistance.

studied based on the ATPase assay, this method will be appropriate when investigators would need to compare the inhibitory effects of target compounds on ABCB1 and ABCG2 (Zhang et al., 2016; Guo et al., 2018). Nonetheless, since the ATPase assay does not evaluate the direct transport, regarding ABCG2, we recommend the vesicle transport assay for more precise evaluation.

Proteoliposome-Based Methods

An artificial lipid membrane system characterized by the reconstitution of purified ABC protein into proteoliposomes (Ambudkar et al., 1998; Jackson et al., 2018) is also a powerful technique. The ABC protein-contained proteoliposomes can be used as an alternative to the plasma membrane vesicles, and their detailed preparation methods are described previously (Geertsma et al., 2008). Additionally, this approach serves as the first choice in the functional studies involving the ABC proteins localized on the organelle membrane (Okamoto et al., 2018).

Cell-Based Methods

Drug Resistance/Accumulation Test

The cells overexpressing MDR machinery show lower sensitivity against its substrate drugs exhibiting cytotoxic or anti-proliferative effects compared to their parent cells, indicating that the ABC protein-expressing cells have higher half maximal effective concentration (EC_{50}) values for cytotoxic transporter substrates. In such situations, co-treatment of the transporter inhibitors with the substrate decreases the EC_{50} values, which is depicted as a left-side shift of cell viability curve in the cytotoxic assay. Additionally, if fluorescence transporter substrates are available, flow cytometry analyses addressing their intracellular accumulation will be useful for inhibitor screening (Murakami et al., 2017; Wu et al., 2017).

Transcellular System

To investigate the transcellular transport of substances, monolayer culture of polarized cells expressing target transporter(s) in Transwell® inserts system has been used (Hegedus et al.,

2009). For instance, using double-transfected Madin-Darby canine kidney II cells overexpressing both organic anion-transporting polypeptide 1B1 (OATP1B1, a basal uptake transporter) and ABCG2 (an apical efflux transporter), an earlier study has observed an enhanced vectorial transport of [^{3}H]estrone sulfate—an ABCG2 substrate that cannot passively penetrate the plasma membrane—from the basal to the apical side (Matsushima et al., 2005). A similar strategy employing ABCG2-expressing polarized cells was used for *in vitro* studies investigating the active secretion of drugs and toxins into milk via ABCG2 (Wassermann et al., 2013; Ito et al., 2015). Of note, in this transcellular system, endogenous transporters and metabolic reactions in the cells may affect apparent transport activities of target transporters.

In vivo Evaluation Methods

Xenograft Models

Athymic nude mice models with MDR-xenografts have been used to test whether co-administration of a potential MDR inhibitor with an anti-cancer agent can reverse the MDR phenotype (Tiwari et al., 2013; Zhang et al., 2017, 2018). In such models, the obtained results could be affected by the difference in the origin of the transplanted cancer cells. This concern might be important while xenograft models are studied.

Focusing on Pharmacokinetic Characteristics

To examine the *in vivo* effects of different chemicals on the target ABC transporter, its pharmacokinetic role has been focused (Robey et al., 2018). With ABCG2, the pharmacokinetic parameters related to the intestinal absorption or the brain distribution of ABCG2 substrate drugs will be good indicators for ABCG2 activity *in vivo*. For example, pre-dosing of enough quantity of ABCG2 inhibitors increased the bioavailability of sulphasalazine—an ABCG2 substrate—in wild-type mice. This was, however, not observed in *Abcg2*-knockout mice, suggesting the *in vivo* inhibition of Abcg2 (Kusuhara et al., 2012; Miyata et al., 2016). Interestingly, the utility of a combination of brain-specific firefly luciferase transgenic mice and D-luciferin, a chemiluminescent luciferase substrate transported by ABCG2 (Zhang et al., 2007) to investigate the *in vivo* inhibitory effects of test compounds on ABCG2 in the BBB was reported (Bakhsheshian et al., 2016). Further methodological progress will aid evaluation of *in vivo* ABCG2 function.

Structure-Based *in silico* Approaches

A main approach to abolish MDR is to discover specific inhibitors of the drug-efflux pump. For this purpose, quantitative structure-activity relationship (QSAR) analysis among the series of compounds can serve for the design of lead inhibitors (Nicolle et al., 2009; Ishikawa et al., 2012; Marighetti et al., 2013; Shukla et al., 2014). With ABCG2, since three-dimensional structures of this protein determined by cryo-electron microscopy (EM) were very recently presented (Taylor et al., 2017; Jackson et al., 2018), a deeper understanding of the chemicals–ABCG2 interactions will be achieved as described below.

HISTORY AND RECENT UPDATE OF THE ABCG2 INHIBITORS

As a MDR machinery in cancer cells and an important drug gatekeeper in tissues like the intestine and the brain, ABCG2 is involved in the efficacy of cancer chemotherapy in patients treated with ABCG2 substrate anti-cancer drugs. To achieve appropriate modulation of ABCG2 by small molecules, the inhibitory potency of various compounds against ABCG2 activity has been extensively evaluated. In this section, we highlight the history and recent update of ABCG2 inhibitors.

Overview of the History of ABCG2 Inhibitors

The first ABCG2 inhibitor reported was FTC, a mycotoxin produced by *Aspergillus fumigatus* (Rabindran et al., 1998, 2000). The *in vivo* use of FTC was unfortunately precluded due to its neurotoxicity. Among the FTC derivatives, Ko143 was identified as a highly potent ABCG2 inhibitor *in vivo* as it was less neurotoxic than the native FTC and was not overtly toxic to mice (Allen et al., 2002). Cell-based assays showed that the EC_{90} concentrations of Ko143 were 23 nM (Abcg2-mediated mitoxantrone resistance), 5.5 μM (ABCB1-mediated paclitaxel resistance) and >8 μM (ABCC1-mediated etoposide resistance), respectively; these results indicated that Ko143 inhibits ABCG2 stronger than ABCB1 and ABCC1, but is not selective to ABCG2 (Allen et al., 2002). Furthermore, from a series of ABCB1 inhibitors, some ABCG2 inhibitors, such as elacridar (GF120918) (Allen et al., 1999; Kruijtzer et al., 2002) and tariquidar (XR9576) (Robey et al., 2004) are frequently used in basic research as well as Ko143.

To date, the molecular bases relating to the chemical inhibition of ABCG2 are not fully understood. The cryo-EM structures of ABCG2 (Taylor et al., 2017) and ABCG2 bound to Ko143 derivatives or tariquidar (Jackson et al., 2018) will be an important to address this issue. Besides, another group of researchers has revealed the structural characteristics of ABCG2 protein critical for its function based on a molecular modeling approach combined with biochemical characterizations of ABCG2 mutants (Khunweeraphong et al., 2017). Previous studies employing the QSAR approaches predicted some structural requirements of compounds for interacting with ABCG2 as an inhibitor (Ishikawa et al., 2012; Mao and Unadkat, 2015); not being true for all ABCG2 inhibitors, the representative features are lipophilicity, planner structure, and amine bonded to one carbon of a heterocyclic ring. Furthermore, a virtual screening strategy employing a ligand-based *in silico* classification model to predict the inhibitory potential of drugs toward ABCG2 presented some favorable outcomes (Montanari et al., 2017). Integration of these findings will contribute to providing a basis for the design of new ABCG2 inhibitors.

Hitherto, many studies focusing on the chemicals–ABCG2 interactions identified a large number of ABCG2 inhibitors with diverse chemical structures (Mao and Unadkat, 2015; Wiese, 2015; Pena-Solorzano et al., 2017; Silbermann et al., 2019). An expanding list of the ABCG2 inhibitors, which include ABCG2

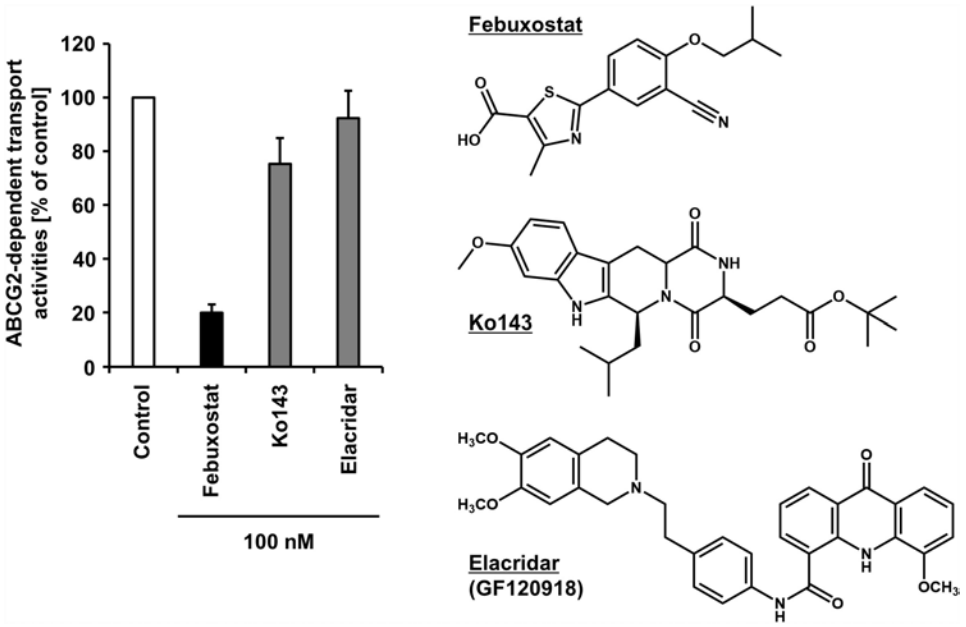

FIGURE 2 | Inhibitory effect of febuxostat against ABCG2 is stronger than that of Ko143 and elacridar, two well-used ABCG2 inhibitors. Febuxostat is known as an oral hypouricemic agent inhibiting xanthine oxidoreductase, a key enzyme for uric acid production. **(Left)** Effect of each compound on the transport activity of ABCG2 are shown. Data from our previous study under CC BY license (Miyata et al., 2016) are shown graphically, in which in the absence (vehicle control) or presence of 100 nM of each compound, the ATP-dependent urate transport activities of ABCG2 were measured using the vesicle transport assay. Data are expressed as the mean ± SD, $n = 3$. Of note, the half-maximal inhibitory concentration (IC_{50}) of febuxostat against the urate transport activity of ABCG2 was 27 nM in the previous study. **(Right)** Chemical structures of each compound are depicted.

substrates (competitive inhibitors), contains such drugs on the market as TKIs and anti-HIV drugs [some of them are often ABCG2 substrates (Polgar et al., 2008; Mao and Unadkat, 2015)] and such dietary phytochemicals as flavonoids and rotenoids. Nevertheless, to the best of our knowledge, the clinical use of such chemicals for ABCG2 inhibition has not yet been achieved probably due to concerns on safety and/or *in vivo* efficacy of them, which may have been common reasons responsible for the failure of the clinical development of ABCG2 inhibitors. Recent studies importantly showed that two potential anti-cancer compounds under clinical development could competitively inhibit both ABCG2 and ABCB1 (Ji et al., 2018a,b).

Febuxostat, a Highly Potent ABCG2 Inhibitor Applicable in Clinical Situations

Regarding the difficulty in the clinical applications of existing ABCG2 inhibitors, our recent study may open up further avenues, in which febuxostat—an approved agent for hyperuricemia globally used in clinical situations—was serendipitously identified as a strong ABCG2 inhibitor both *in vitro* and *in vivo* (Miyata et al., 2016). Using the vesicle transport assay, we revealed that febuxostat inhibits ABCG2 more strongly than Ko143 and elacridar (**Figure 2**). This indicates that febuxostat has a superior safety profile and better inhibitory ability against ABCG2 compared to these two compounds. Moreover, the study demonstrated that the IC_{50} of febuxostat against urate transport activity of ABCG2 (0.027 μM) was lower than its maximum plasma unbound concentrations reported in humans (0.09 μM), suggesting that febuxostat might inhibit human ABCG2 at a clinically used dose. Thus, febuxostat can be a promising candidate as a potential ABCG2 inhibitor in humans. The structural characteristics and molecular mechanisms of febuxostat as an ABCG2 inhibitor remain to be elucidated, as well as the effects of febuxostat on the function of other ABC transporters, including ABCB1.

Febuxostat will be used in cancer chemotherapy more frequently because recently this drug has been approved in Europe and Japan for the prophylaxis of TLS. TLS is a potentially life-threatening condition caused by an abrupt release of intracellular metabolites after tumor cell lysis in cancer patients on chemotherapy (Alakel et al., 2017). It is the most common treatment-related emergency in patients with hematologic malignancies and characterized by metabolic abnormalities including hyperuricemia that triggers several mechanisms resulting in acute kidney injury. Appropriate control of serum uric acid is therefore important in the prevention of TLS. Recent studies demonstrated that febuxostat—an oral hypouricemic agent—can successfully prevent TLS in cancer patients (Spina et al., 2015; Tamura et al., 2016). In such situations, since the patients will be treated with febuxostat before and during chemotherapy, there would be drug-drug interactions between febuxostat and ABCG2 substrate anti-cancer agents.

Importantly, ABCG2 is reportedly expressed on the malignant hematopoietic and the lymphoid cells frequently; its expression in several types of human leukemia has been investigated

(Jordanides et al., 2006; Eechoute et al., 2011; Stacy et al., 2013). Considering that initiating cells in CML arises from a multipotent hematopoietic stem cell (HSC), together with high expression of ABCG2 in human HSCs (Zhou et al., 2001; Scharenberg et al., 2002), overexpression of ABCG2 has been considered to confer drug resistance ability to the CML stem cell population (Brendel et al., 2007). However, the clinical relevance of ABCG2 inhibition in CML patients from the view point of reversing MDR remains to be clarified. Since several TKIs used for CML are ABCG2 substrates (Hira and Terada, 2018), the combination use of febuxostat may be a future research topic.

Additionally, ABCG2 expressed in tumor cells is reportedly involved in the efflux of photosensitizers in 5-aminolevulinic acid-based photodynamic therapy (Ishikawa et al., 2015). Hence, febuxostat might enhance the efficacy of this minimally invasive modality for treating solid cancers by accumulating photosensitizers in the target cells. The details are discussed in our previous report (Miyata et al., 2016).

CONCLUSION AND PERSPECTIVE

Here, we summarized some key experimental systems that will continuously contribute to generating novel ABCG2 inhibitors and described an overview of the current update of ABCG2 inhibitors. Among them, febuxostat will be one of the most promising candidates for clinical use. Considering that dysfunctional *ABCG2* genotypes, which are summarized in a recent review (Heyes et al., 2018), alter the pharmacokinetic characteristics of ABCG2 substrate drugs such as several TKIs (Hira and Terada, 2018) and rosuvastatin (Keskitalo et al., 2009), ABCG2 inhibitors will also exert similar effects in humans. As a beneficial application of this clinical possibility, we have proposed a novel concept named febuxostat-boosted therapy (Miyata et al., 2016), in which febuxostat is expected to enhance the bioavailability of ABCG2 substrate drugs. For a similar purpose, ritonavir and cobicistat are used as pharmacokinetic boosters inhibiting cytochrome P450 3A4, a major pathway of drug metabolism, to increase the plasma concentrations of certain drugs (Shah et al., 2013). No pharmacokinetic enhancer targeting transporter proteins has been, however, successfully evaluated in clinical trials. In this context, the potential benefits of the febuxostat-boosted therapy should be validated in the near future. Furthermore, this concept could also be applied to enhance the BBB penetration of ABCG2 substrate drugs for brain cancer chemotherapy. Despite the potential risks of adverse events in the combination therapy, further clinical studies to elucidate whether febuxostat is beneficial in enhancing the efficacy of pharmacotherapy via ABCG2 inhibition are warranted.

AUTHOR CONTRIBUTIONS

YT researched the data for the manuscript, provided substantial contributions to discussion of its content, and wrote the manuscript. TT contributed to the discussion and the writing of the manuscript. HS critiqued the manuscript and provided intellectual inputs. All the authors reviewed and edited the manuscript before submission and have made final approval of the manuscript.

FUNDING

This work and relating our findings were supported by the JSPS KAKENHI Grant Numbers 15H05610 to YT, 16H1808 and 18KK0247 to TT, 22136015 to HS; TT has received research grants from Gout Research Foundation, The Uehara Memorial Foundation, Mochida Memorial Foundation for Medical and Pharmaceutical Research, The Takeda Medical Foundation, and MSD Life Science Foundation, Public Interest Incorporated Foundation.

ACKNOWLEDGMENTS

The authors would like to acknowledge Drs. Hiroshi Miyata, Hirotaka Matsuo, and Kimiyoshi Ichida for their contribution to our studies highlighted in this mini-review article as well as Drs. Toshihisa Ishikawa and Yuichi Sugiyama for their previous mentorships and encouragements.

REFERENCES

Adachi, Y., Suzuki, H., Schinkel, A. H., and Sugiyama, Y. (2005). Role of breast cancer resistance protein (Bcrp1/Abcg2) in the extrusion of glucuronide and sulfate conjugates from enterocytes to intestinal lumen. *Mol. Pharmacol.* 67, 923–928. doi: 10.1124/mol.104.007393

Alakel, N., Middeke, J. M., Schetelig, J., and Bornhauser, M. (2017). Prevention and treatment of tumor lysis syndrome, and the efficacy and role of rasburicase. *Onco Targets Ther.* 10, 597–605. doi: 10.2147/OTT.S103864

Allen, J. D., Brinkhuis, R. F., Wijnholds, J., and Schinkel, A. H. (1999). The mouse Bcrp1/Mxr/Abcp gene: amplification and overexpression in cell lines selected for resistance to topotecan, mitoxantrone, or doxorubicin. *Cancer Res.* 59, 4237–4241.

Allen, J. D., Van Loevezijn, A., Lakhai, J. M., Van Der Valk, M., Van Tellingen, O., Reid, G., et al. (2002). Potent and specific inhibition of the breast cancer resistance protein multidrug transporter in vitro and in mouse intestine by a novel analogue of fumitremorgin C. *Mol. Cancer Ther.* 1, 417–425.

Allikmets, R., Schriml, L. M., Hutchinson, A., Romano-Spica, V., and Dean, M. (1998). A human placenta-specific ATP-binding cassette gene (ABCP) on chromosome 4q22 that is involved in multidrug resistance. *Cancer Res.* 58, 5337–5339.

Ambudkar, S. V., Lelong, I. H., Zhang, J., and Cardarelli, C. (1998). Purification and reconstitution of human P-glycoprotein. *Methods Enzymol.* 292, 492–504. doi: 10.1016/S0076-6879(98)92038-9

Ando, T., Kusuhara, H., Merino, G., Alvarez, A. I., Schinkel, A. H., and Sugiyama, Y. (2007). Involvement of breast cancer resistance protein (ABCG2) in the biliary excretion mechanism of fluoroquinolones. *Drug Metab. Dispos.* 35, 1873–1879. doi: 10.1124/dmd.107.014969

Bakhsheshian, J., Wei, B. R., Hall, M. D., Simpson, R. M., and Gottesman, M. M. (2016). In vivo bioluminescent imaging of ATP-binding cassette transporter-mediated efflux at the blood-brain barrier. *Methods Mol. Biol.* 1461, 227–239. doi: 10.1007/978-1-4939-3813-1_19

Baykov, A. A., Evtushenko, O. A., and Avaeva, S. M. (1988). A malachite green procedure for orthophosphate determination and its use in alkaline

phosphatase-based enzyme immunoassay. *Anal. Biochem.* 171, 266–270. doi: 10.1016/0003-2697(88)90484-8

Brendel, C., Scharenberg, C., Dohse, M., Robey, R. W., Bates, S. E., Shukla, S., et al. (2007). Imatinib mesylate and nilotinib (AMN107) exhibit high-affinity interaction with ABCG2 on primitive hematopoietic stem cells. *Leukemia* 21, 1267–1275. doi: 10.1038/sj.leu.2404638

Doyle, L. A., Yang, W., Abruzzo, L. V., Krogmann, T., Gao, Y., Rishi, A. K., et al. (1998). A multidrug resistance transporter from human MCF-7 breast cancer cells. *Proc. Natl. Acad. Sci. U.S.A.* 95, 15665–15670. doi: 10.1073/pnas.95.26.15665

Eechoute, K., Sparreboom, A., Burger, H., Franke, R. M., Schiavon, G., Verweij, J., et al. (2011). Drug transporters and imatinib treatment: implications for clinical practice. *Clin. Cancer Res.* 17, 406–415. doi: 10.1158/1078-0432.CCR-10-2250

Geertsma, E. R., Nik Mahmood, N. A., Schuurman-Wolters, G. K., and Poolman, B. (2008). Membrane reconstitution of ABC transporters and assays of translocator function. *Nat. Protoc.* 3, 256–266. doi: 10.1038/nprot.2007.519

Giacomini, K. M., Huang, S. M., Tweedie, D. J., Benet, L. Z., Brouwer, K. L., Chu, X., et al. (2010). Membrane transporters in drug development. *Nat. Rev. Drug Discov.* 9, 215–236. doi: 10.1038/nrd3028

Guo, C., Liu, F., Qi, J., Ma, J., Lin, S., Zhang, C., et al. (2018). A novel synthetic dihydroindeno[1,2-b] indole derivative (LS-2-3j) reverses ABCB1- and ABCG2-mediated multidrug resistance in cancer cells. *Molecules* 23:E3264. doi: 10.3390/molecules23123264

Hegedus, C., Szakacs, G., Homolya, L., Orban, T. I., Telbisz, A., Jani, M., et al. (2009). Ins and outs of the ABCG2 multidrug transporter: an update on in vitro functional assays. *Adv. Drug Deliv. Rev.* 61, 47–56. doi: 10.1016/j.addr.2008.09.007

Heyes, N., Kapoor, P., and Kerr, I. D. (2018). Polymorphisms of the multidrug Pump ABCG2: a systematic review of their effect on protein expression, function, and drug pharmacokinetics. *Drug Metab. Dispos.* 46, 1886–1899. doi: 10.1124/dmd.118.083030

Higashino, T., Takada, T., Nakaoka, H., Toyoda, Y., Stiburkova, B., Miyata, H., et al. (2017). Multiple common and rare variants of ABCG2 cause gout. *RMD Open* 3:e000464. doi: 10.1136/rmdopen-2017-000464

Hira, D., and Terada, T. (2018). BCRP/ABCG2 and high-alert medications: biochemical, pharmacokinetic, pharmacogenetic, and clinical implications. *Biochem. Pharmacol.* 147, 201–210. doi: 10.1016/j.bcp.2017.10.004

Hirano, M., Maeda, K., Matsushima, S., Nozaki, Y., Kusuhara, H., and Sugiyama, Y. (2005). Involvement of BCRP (ABCG2) in the biliary excretion of pitavastatin. *Mol. Pharmacol.* 68, 800–807. doi: 10.1124/mol.105.014019

Ichida, K., Matsuo, H., Takada, T., Nakayama, A., Murakami, K., Shimizu, T., et al. (2012). Decreased extra-renal urate excretion is a common cause of hyperuricemia. *Nat. Commun.* 3:764. doi: 10.1038/ncomms1756

Ishikawa, T. (1989). ATP/Mg2+-dependent cardiac transport system for glutathione S-conjugates. A study using rat heart sarcolemma vesicles. *J. Biol. Chem.* 264, 17343–17348.

Ishikawa, T., Kajimoto, Y., Inoue, Y., Ikegami, Y., and Kuroiwa, T. (2015). Critical role of ABCG2 in ALA-photodynamic diagnosis and therapy of human brain tumor. *Adv. Cancer Res.* 125, 197–216. doi: 10.1016/bs.acr.2014.11.008

Ishikawa, T., Saito, H., Hirano, H., Inoue, Y., and Ikegami, Y. (2012). Human ABC transporter ABCG2 in cancer chemotherapy: drug molecular design to circumvent multidrug resistance. *Methods Mol. Biol.* 910, 267–278. doi: 10.1007/978-1-61779-965-5_11

Ito, N., Ito, K., Ikebuchi, Y., Toyoda, Y., Takada, T., Hisaka, A., et al. (2015). Prediction of drug transfer into milk considering breast cancer resistance protein (BCRP)-mediated transport. *Pharm. Res.* 32, 2527–2537. doi: 10.1007/s11095-015-1641-2

Jackson, S. M., Manolaridis, I., Kowal, J., Zechner, M., Taylor, N. M. I., Bause, M., et al. (2018). Structural basis of small-molecule inhibition of human multidrug transporter ABCG2. *Nat. Struct. Mol. Biol.* 25, 333–340. doi: 10.1038/s41594-018-0049-1

Ji, N., Yang, Y., Cai, C. Y., Lei, Z. N., Wang, J. Q., Gupta, P., et al. (2018a). VS-4718 antagonizes multidrug resistance in ABCB1- and ABCG2-overexpressing cancer cells by inhibiting the efflux function of ABC transporters. *Front. Pharmacol.* 9:1236. doi: 10.3389/fphar.2018.01236

Ji, N., Yang, Y., Lei, Z. N., Cai, C. Y., Wang, J. Q., Gupta, P., et al. (2018b). Ulixertinib (BVD-523) antagonizes ABCB1- and ABCG2-mediated chemotherapeutic drug resistance. *Biochem. Pharmacol.* 158, 274–285. doi: 10.1016/j.bcp.2018.10.028

Jonker, J. W., Buitelaar, M., Wagenaar, E., Van Der Valk, M. A., Scheffer, G. L., Scheper, R. J., et al. (2002). The breast cancer resistance protein protects against a major chlorophyll-derived dietary phototoxin and protoporphyria. *Proc. Natl. Acad. Sci. U.S.A.* 99, 15649–15654. doi: 10.1073/pnas.202607599

Jonker, J. W., Merino, G., Musters, S., Van Herwaarden, A. E., Bolscher, E., Wagenaar, E., et al. (2005). The breast cancer resistance protein BCRP (ABCG2) concentrates drugs and carcinogenic xenotoxins into milk. *Nat. Med.* 11, 127–129. doi: 10.1038/nm1186

Jordanides, N. E., Jorgensen, H. G., Holyoake, T. L., and Mountford, J. C. (2006). Functional ABCG2 is overexpressed on primary CML CD34+ cells and is inhibited by imatinib mesylate. *Blood* 108, 1370–1373. doi: 10.1182/blood-2006-02-003145

Keskitalo, J. E., Zolk, O., Fromm, M. F., Kurkinen, K. J., Neuvonen, P. J., and Niemi, M. (2009). ABCG2 polymorphism markedly affects the pharmacokinetics of atorvastatin and rosuvastatin. *Clin. Pharmacol. Ther.* 86, 197–203. doi: 10.1038/clpt.2009.79

Khunweeraphong, N., Stockner, T., and Kuchler, K. (2017). The structure of the human ABC transporter ABCG2 reveals a novel mechanism for drug extrusion. *Sci. Rep.* 7:13767. doi: 10.1038/s41598-017-11794-w

Kruijtzer, C. M., Beijnen, J. H., Rosing, H., ten Bokkel Huinink, W. W., Schot, M., Jewell, R. C., et al. (2002). Increased oral bioavailability of topotecan in combination with the breast cancer resistance protein and P-glycoprotein inhibitor GF120918. *J. Clin. Oncol.* 20, 2943–2950. doi: 10.1200/JCO.2002.12.116

Kusuhara, H., Furuie, H., Inano, A., Sunagawa, A., Yamada, S., Wu, C., et al. (2012). Pharmacokinetic interaction study of sulphasalazine in healthy subjects and the impact of curcumin as an in vivo inhibitor of BCRP. *Br. J. Pharmacol.* 166, 1793–1803. doi: 10.1111/j.1476-5381.2012.01887.x

Mao, Q., and Unadkat, J. D. (2015). Role of the breast cancer resistance protein (BCRP/ABCG2) in drug transport–an update. *AAPS J.* 17, 65–82. doi: 10.1208/s12248-014-9668-6

Marighetti, F., Steggemann, K., Hanl, M., and Wiese, M. (2013). Synthesis and quantitative structure-activity relationships of selective BCRP inhibitors. *ChemMedChem* 8, 125–135. doi: 10.1002/cmdc.201200377

Matsuo, H., Takada, T., Ichida, K., Nakamura, T., Nakayama, A., Ikebuchi, Y., et al. (2009). Common defects of ABCG2, a high-capacity urate exporter, cause gout: a function-based genetic analysis in a Japanese population. *Sci. Transl. Med.* 1:5ra11. doi: 10.1126/scitranslmed.3000237

Matsushima, S., Maeda, K., Kondo, C., Hirano, M., Sasaki, M., Suzuki, H., et al. (2005). Identification of the hepatic efflux transporters of organic anions using double-transfected Madin-Darby canine kidney II cells expressing human organic anion-transporting polypeptide 1B1 (OATP1B1)/multidrug resistance-associated protein 2, OATP1B1/multidrug resistance 1, and OATP1B1/breast cancer resistance protein. *J. Pharmacol. Exp. Ther.* 314, 1059–1067. doi: 10.1124/jpet.105.085589

Miyake, K., Mickley, L., Litman, T., Zhan, Z., Robey, R., Cristensen, B., et al. (1999). Molecular cloning of cDNAs which are highly overexpressed in mitoxantrone-resistant cells: demonstration of homology to ABC transport genes. *Cancer Res.* 59, 8–13.

Miyata, H., Takada, T., Toyoda, Y., Matsuo, H., Ichida, K., and Suzuki, H. (2016). Identification of febuxostat as a new strong ABCG2 inhibitor: potential applications and risks in clinical situations. *Front. Pharmacol.* 7:518. doi: 10.3389/fphar.2016.00518

Mizuno, N., Suzuki, M., Kusuhara, H., Suzuki, H., Takeuchi, K., Niwa, T., et al. (2004). Impaired renal excretion of 6-hydroxy-5,7-dimethyl-2-methylamino-4-(3-pyridylmethyl) benzothiazole (E3040) sulfate in breast cancer resistance protein (BCRP1/ABCG2) knockout mice. *Drug Metab. Dispos.* 32, 898–901.

Mizuno, N., Takahashi, T., Kusuhara, H., Schuetz, J. D., Niwa, T., and Sugiyama, Y. (2007). Evaluation of the role of breast cancer resistance protein (BCRP/ABCG2) and multidrug resistance-associated protein 4 (MRP4/ABCC4) in the urinary excretion of sulfate and glucuronide metabolites of edaravone (MCI-186; 3-methyl-1-phenyl-2-pyrazolin-5-one). *Drug Metab. Dispos.* 35, 2045–2052. doi: 10.1124/dmd.107.016352

Montanari, F., Cseke, A., Wlcek, K., and Ecker, G. F. (2017). Virtual screening of DrugBank reveals two drugs as new BCRP inhibitors. *SLAS Discov.* 22, 86–93. doi: 10.1177/1087057116657513

Murakami, M., Ohnuma, S., Fukuda, M., Chufan, E. E., Kudoh, K., Kanehara, K., et al. (2017). Synthetic analogs of curcumin modulate the function of multidrug resistance-linked ATP-binding cassette transporter ABCG2. *Drug Metab. Dispos.* 45, 1166–1177. doi: 10.1124/dmd.117.076000

Nakanishi, T., Doyle, L. A., Hassel, B., Wei, Y., Bauer, K. S., Wu, S., et al. (2003). Functional characterization of human breast cancer resistance protein (BCRP, ABCG2) expressed in the oocytes of *Xenopus laevis*. *Mol. Pharmacol.* 64, 1452–1462. doi: 10.1124/mol.64.6.1452

Nicolle, E., Boumendjel, A., Macalou, S., Genoux, E., Ahmed-Belkacem, A., Carrupt, P. A., et al. (2009). QSAR analysis and molecular modeling of ABCG2-specific inhibitors. *Adv. Drug Deliv. Rev.* 61, 34–46. doi: 10.1016/j.addr.2008.10.004

Okamoto, T., Kawaguchi, K., Watanabe, S., Agustina, R., Ikejima, T., Ikeda, K., et al. (2018). Characterization of human ATP-binding cassette protein subfamily D reconstituted into proteoliposomes. *Biochem. Biophys. Res. Commun.* 496, 1122–1127. doi: 10.1016/j.bbrc.2018.01.153

Pena-Solorzano, D., Stark, S. A., Konig, B., Sierra, C. A., and Ochoa-Puentes, C. (2017). ABCG2/BCRP: specific and nonspecific modulators. *Med. Res. Rev.* 37, 987–1050. doi: 10.1002/med.21428

Polgar, O., Robey, R. W., and Bates, S. E. (2008). ABCG2: structure, function and role in drug response. *Expert Opin. Drug Metab. Toxicol.* 4, 1–15. doi: 10.1517/17425255.4.1.1

Rabindran, S. K., He, H., Singh, M., Brown, E., Collins, K. I., Annable, T., et al. (1998). Reversal of a novel multidrug resistance mechanism in human colon carcinoma cells by fumitremorgin C. *Cancer Res.* 58, 5850–5858.

Rabindran, S. K., Ross, D. D., Doyle, L. A., Yang, W., and Greenberger, L. M. (2000). Fumitremorgin C reverses multidrug resistance in cells transfected with the breast cancer resistance protein. *Cancer Res.* 60, 47–50.

Robey, R. W., Pluchino, K. M., Hall, M. D., Fojo, A. T., Bates, S. E., and Gottesman, M. M. (2018). Revisiting the role of ABC transporters in multidrug-resistant cancer. *Nat. Rev. Cancer* 18, 452–464. doi: 10.1038/s41568-018-0005-8

Robey, R. W., Steadman, K., Polgar, O., Morisaki, K., Blayney, M., Mistry, P., et al. (2004). Pheophorbide a is a specific probe for ABCG2 function and inhibition. *Cancer Res.* 64, 1242–1246. doi: 10.1158/0008-5472.CAN-03-3298

Robey, R. W., To, K. K., Polgar, O., Dohse, M., Fetsch, P., Dean, M., et al. (2009). ABCG2: a perspective. *Adv. Drug Deliv. Rev.* 61, 3–13. doi: 10.1016/j.addr.2008.11.003

Saito, H., Hirano, H., Nakagawa, H., Fukami, T., Oosumi, K., Murakami, K., et al. (2006). A new strategy of high-speed screening and quantitative structure-activity relationship analysis to evaluate human ATP-binding cassette transporter ABCG2-drug interactions. *J. Pharmacol. Exp. Ther.* 317, 1114–1124. doi: 10.1124/jpet.105.099036

Scharenberg, C. W., Harkey, M. A., and Torok-Storb, B. (2002). The ABCG2 transporter is an efficient Hoechst 33342 efflux pump and is preferentially expressed by immature human hematopoietic progenitors. *Blood* 99, 507–512. doi: 10.1182/blood.V99.2.507

Shah, B. M., Schafer, J. J., Priano, J., and Squires, K. E. (2013). Cobicistat: a new boost for the treatment of human immunodeficiency virus infection. *Pharmacotherapy* 33, 1107–1116. doi: 10.1002/phar.1237

Shukla, S., Kouanda, A., Silverton, L., Talele, T. T., and Ambudkar, S. V. (2014). Pharmacophore modeling of nilotinib as an inhibitor of ATP-binding cassette drug transporters and BCR-ABL kinase using a three-dimensional quantitative structure-activity relationship approach. *Mol. Pharm.* 11, 2313–2322. doi: 10.1021/mp400762h

Shukla, S., Robey, R. W., Bates, S. E., and Ambudkar, S. V. (2006). The calcium channel blockers, 1,4-dihydropyridines, are substrates of the multidrug resistance-linked ABC drug transporter, ABCG2. *Biochemistry* 45, 8940–8951. doi: 10.1021/bi060552f

Silbermann, K., Shah, C. P., Sahu, N. U., Juvale, K., Stefan, S. M., Kharkar, P. S., et al. (2019). Novel chalcone and flavone derivatives as selective and dual inhibitors of the transport proteins ABCB1 and ABCG2. *Eur. J. Med. Chem.* 164, 193–213. doi: 10.1016/j.ejmech.2018.12.019

Spina, M., Nagy, Z., Ribera, J. M., Federico, M., Aurer, I., Jordan, K., et al. (2015). FLORENCE: a randomized, double-blind, phase III pivotal study of febuxostat versus allopurinol for the prevention of tumor lysis syndrome (TLS) in patients with hematologic malignancies at intermediate to high TLS risk. *Ann. Oncol.* 26, 2155–2161. doi: 10.1093/annonc/mdv317

Stacy, A. E., Jansson, P. J., and Richardson, D. R. (2013). Molecular pharmacology of ABCG2 and its role in chemoresistance. *Mol. Pharmacol.* 84, 655–669. doi: 10.1124/mol.113.088609

Stiburkova, B., Miyata, H., Zavada, J., Tomcik, M., Pavelka, K., Storkanova, G., et al. (2016). Novel dysfunctional variant in ABCG2 as a cause of severe tophaceous gout: biochemical, molecular genetics and functional analysis. *Rheumatology* 55, 191–194. doi: 10.1093/rheumatology/kev350

Suzuki, M., Suzuki, H., Sugimoto, Y., and Sugiyama, Y. (2003). ABCG2 transports sulfated conjugates of steroids and xenobiotics. *J. Biol. Chem.* 278, 22644–22649. doi: 10.1074/jbc.M212399200

Takada, T., Yamamoto, T., Matsuo, H., Tan, J. K., Ooyama, K., Sakiyama, M., et al. (2018). Identification of ABCG2 as an exporter of uremic toxin indoxyl sulfate in mice and as a crucial factor influencing CKD progression. *Sci. Rep.* 8:11147. doi: 10.1038/s41598-018-29208-w

Tamura, A., Watanabe, M., Saito, H., Nakagawa, H., Kamachi, T., Okura, I., et al. (2006). Functional validation of the genetic polymorphisms of human ATP-binding cassette (ABC) transporter ABCG2: identification of alleles that are defective in porphyrin transport. *Mol. Pharmacol.* 70, 287–296.

Tamura, K., Kawai, Y., Kiguchi, T., Okamoto, M., Kaneko, M., Maemondo, M., et al. (2016). Efficacy and safety of febuxostat for prevention of tumor lysis syndrome in patients with malignant tumors receiving chemotherapy: a phase III, randomized, multi-center trial comparing febuxostat and allopurinol. *Int. J. Clin. Oncol.* 21, 996–1003. doi: 10.1007/s10147-016-0971-3

Taylor, N. M. I., Manolaridis, I., Jackson, S. M., Kowal, J., Stahlberg, H., and Locher, K. P. (2017). Structure of the human multidrug transporter ABCG2. *Nature* 546, 504–509. doi: 10.1038/nature22345

Tiwari, A. K., Sodani, K., Dai, C. L., Abuznait, A. H., Singh, S., Xiao, Z. J., et al. (2013). Nilotinib potentiates anticancer drug sensitivity in murine ABCB1-, ABCG2-, and ABCC10-multidrug resistance xenograft models. *Cancer Lett.* 328, 307–317. doi: 10.1016/j.canlet.2012.10.001

Toyoda, Y., Takada, T., and Suzuki, H. (2016). Halogenated hydrocarbon solvent-related cholangiocarcinoma risk: biliary excretion of glutathione conjugates of 1,2-dichloropropane evidenced by untargeted metabolomics analysis. *Sci. Rep.* 6:24586. doi: 10.1038/srep24586

van de Wetering, K., and Sapthu, S. (2012). ABCG2 functions as a general phytoestrogen sulfate transporter in vivo. *FASEB J.* 26, 4014–4024. doi: 10.1096/fj.12-210039

Vlaming, M. L., Lagas, J. S., and Schinkel, A. H. (2009). Physiological and pharmacological roles of ABCG2 (BCRP): recent findings in Abcg2 knockout mice. *Adv. Drug Deliv. Rev.* 61, 14–25. doi: 10.1016/j.addr.2008.08.007

Wassermann, L., Halwachs, S., Baumann, D., Schaefer, I., Seibel, P., and Honscha, W. (2013). Assessment of ABCG2-mediated transport of xenobiotics across the blood-milk barrier of dairy animals using a new MDCKII in vitro model. *Arch. Toxicol.* 87, 1671–1682. doi: 10.1007/s00204-013-1066-9

Wiese, M. (2015). BCRP/ABCG2 inhibitors: a patent review (2009-present). *Expert Opin. Ther. Pat.* 25, 1229–1237. doi: 10.1517/13543776.2015.1076796

Woodward, O. M., Kottgen, A., Coresh, J., Boerwinkle, E., Guggino, W. B., and Kottgen, M. (2009). Identification of a urate transporter, ABCG2, with a common functional polymorphism causing gout. *Proc. Natl. Acad. Sci. U.S.A.* 106, 10338–10342. doi: 10.1073/pnas.0901249106

Wu, C. P., Hsiao, S. H., Murakami, M., Lu, Y. J., Li, Y. Q., Huang, Y. H., et al. (2017). Alpha-mangostin reverses multidrug resistance by attenuating the function of the multidrug resistance-linked ABCG2 transporter. *Mol. Pharm.* 14, 2805–2814. doi: 10.1021/acs.molpharmaceut.7b00334

Zhang, G. N., Zhang, Y. K., Wang, Y. J., Gupta, P., Ashby, C. R. Jr., Alqahtani, S., et al. (2018). Epidermal growth factor receptor (EGFR) inhibitor PD153035 reverses ABCG2-mediated multidrug resistance in non-small cell lung cancer: in vitro and in vivo. *Cancer Lett.* 424, 19–29. doi: 10.1016/j.canlet.2018.02.040

Zhang, W., Chen, Z., Chen, L., Wang, F., Li, F., Wang, X., et al. (2017). ABCG2-overexpressing H460/MX20 cell xenografts in athymic nude mice maintained original biochemical and cytological characteristics. *Sci. Rep.* 7:40064. doi: 10.1038/srep40064

Zhang, Y., Bressler, J. P., Neal, J., Lal, B., Bhang, H. E., Laterra, J., et al. (2007). ABCG2/BCRP expression modulates D-Luciferin based bioluminescence imaging. *Cancer Res.* 67, 9389–9397. doi: 10.1158/0008-5472.CAN-07-0944

Zhang, Y. K., Zhang, G. N., Wang, Y. J., Patel, B. A., Talele, T. T., Yang, D. H., et al. (2016). Bafetinib (INNO-406) reverses multidrug resistance by inhibiting the efflux function of ABCB1 and ABCG2 transporters. *Sci. Rep.* 6:25694. doi: 10.1038/srep25694

Zhou, S., Schuetz, J. D., Bunting, K. D., Colapietro, A. M., Sampath, J., Morris, J. J., et al. (2001). The ABC transporter Bcrp1/ABCG2 is expressed in a wide variety of stem cells and is a molecular determinant of the side-population phenotype. *Nat. Med.* 7, 1028–1034. doi: 10.1038/nm0901-1028

Zhou, S., Zong, Y., Ney, P. A., Nair, G., Stewart, C. F., and Sorrentino, B. P. (2005). Increased expression of the Abcg2 transporter during erythroid maturation plays a role in decreasing cellular protoporphyrin IX levels. *Blood* 105, 2571–2576. doi: 10.1182/blood-2004-04-1566

Conflict of Interest Statement: TT and HS have a patent pending.

The remaining author declares that the research was conducted in the absence of any commercial or financial relationships that could be construed as a potential conflict of interest.

frontiers in Oncology

ORIGINAL RESEARCH
published: 12 March 2019
doi: 10.3389/fonc.2019.00137

Glucose-Regulated Protein 78 Signaling Regulates Hypoxia-Induced Epithelial–Mesenchymal Transition in A549 Cells

*Ling-Ling Sun, Chang-Ming Chen, Jue Zhang, Jing Wang, Cai-Zhi Yang and Li-Zhu Lin**

Integrative Cancer Centre, the First Affiliated Hospital of Guangzhou University of Chinese Medicine, Guangzhou, China

Objective: Metastasis and therapeutic resistance are the major determinants of lung cancer progression and high mortality. Epithelial–mesenchymal transition (EMT) plays a key role in the metastasis and therapeutic resistance. Highly expressed glucose-regulated protein 78 (GRP78) is a poor prognostic factor in lung cancer and possibly correlated with EMT. This study aims to examine whether the up-regulation of GRP78 is involved in EMT in lung adenocarcinoma and explore the underlying downstream molecular pathways.

Study Design: EMT was assessed by analysis of cell morphology and expression of EMT protein markers in A549 cells under normoxia, hypoxia and silencing GRP78 conditions. The expression levels of Smad2/3, Src, and MAPK (p38, ERK, and JNK) proteins were examined by Western blot analysis under hypoxia and treatments with phosphorylation inhibitors.

Results: Under hypoxic conditions, the EMT morphology significantly changed and the GRP78 expression was significantly up-regulated in A549 cells compared with those in normoxia control. The expression and phosphorylation levels of smad2/3, Src, p38, ERK, and JNK were also upregulated. When GRP78 was silenced, EMT was inhibited, and the levels of phospho-smad2/3, phospho-Src, phospho-p38, phospho-ERK, and phospho-JNK were suppressed. When the activation of Smad2/3, Src, p38, ERK, and JNK was inhibited, EMT was also inhibited. The inhibition effect on EMT by these phosphorylation inhibitors was found to be weaker than that of GRP78 knockdown.

Conclusions: Hypoxia-induced EMT in A549 cells is regulated by GRP78 signaling pathways. GRP78 promotes EMT by activating Smad2/3 and Src/MAPK pathways. Hence, GRP78 might be a potential target for treatment of lung adenocarcinoma.

Keywords: lung cancer, lung adenocarcinoma, epithelial mesenchymal transition, hypoxia, glucose-regulated protein 78, GRP78

OPEN ACCESS

Edited by:
Zhe-Sheng Chen,
St. John's University, United States

Reviewed by:
Qi Xie,
University of California, San Diego, United States
JiaXing Zhang,
Sun Yat-sen University, China

****Correspondence:***
Li-Zhu Lin
lizhulin26@yahoo.com

Specialty section:
This article was submitted to Cancer Molecular Targets and Therapeutics, a section of the journal Frontiers in Oncology

Received: *09 December 2018*
Accepted: *15 February 2019*
Published: *12 March 2019*

Citation:
Sun L-L, Chen C-M, Zhang J, Wang J, Yang C-Z and Lin L-Z (2019) Glucose-Regulated Protein 78 Signaling Regulates Hypoxia-Induced Epithelial–Mesenchymal Transition in A549 Cells. Front. Oncol. 9:137. doi: 10.3389/fonc.2019.00137

INTRODUCTION

Lung cancer is the leading cause of cancer death worldwide; according to the estimated data from GLOBOCAN in 2012, one of five cancer deaths is due to lung cancer (1.59 million deaths, 19.4% of the total cancer deaths) (1). Despite significant progress in the development of new therapies for lung cancer, metastasis and therapeutic resistance remain the major determinants of lung cancer progression and high mortality (2).

Mounting evidence demonstrated that epithelial–mesenchymal transition (EMT) is involved in the metastasis and therapeutic resistance of lung cancer. EMT refers to the biological process by which epithelial cells are transformed into mesenchymal phenotypes through specific procedures. EMT inhibits the expression of E-cadherin and cytokeratin in epithelial cells, upregulates the expression of N-cadherin and vimentin in mesenchymal cells and promotes the ability of cells to secrete matrix metalloproteinase and fibronectin. EMT can be induced by various factors, such as TGF-beta, which increases the expression of key nuclear transcription factors including Twist, Snail and ZEB (3) and causes phenotypic changes by activating intrinsic cellular signal molecules including Src, MAPK, Smad2/3, and other signals (4–6).

Hypoxia is a common hallmark of several human malignancies and an independent and unfavorable prognostic factor associated with the occurrence of EMT (7–9). Previous studies found that cAMP-dependent protein kinase, hypoxia factor Hif-1alpha(HIF1a) and unfolded protein response can potentiate EMT; moreover, treatment with insulin-like growth factor 1 receptor inhibitor reverses hypoxia-induced EMT (8–11), However, the mechanisms of hypoxia-induced EMT remain unknown. Understanding the biology of hypoxia-induced EMT and their implications in therapeutic relapse may provide new crucial approaches for development of improved therapeutic strategies.

The 78-kDa glucose-regulated protein (GRP78), also known as BiP and HSPA5, is highly expressed in many types of cancers, including lung, hepatocellular cancer, and breast cancer (12–15). It could inhibit apoptosis of cancer cells, and induce chemoresistance of cancer (16–18). What's more, it is closely related to EMT. Zhang et al. (19) reported that high expressed GRP78 induced EMT in hepatocellular carcinoma cell lines. Lizardo et al. (20) that up-regulation of GRP78 in metastatic cancer cells is necessary for lung metastasis in some highly metastatic cell line models, such as osteosarcomas and murine mammary adenocarcinoma. Zhang et al. (21) demonstrated that overexpressing GRP78 facilitated the expression and secretion of TGF-beta1, which further activated EMT. However, Chang et al. (22) stated that overexpressing GRP78 inhibited the metastasis of colon cancer through EMT biomarkers. Thus far, the relationship between GRP78 expression and EMT remains controversial. Whether GRP78 expression has causality link with EMT in lung cancer also remains unknown. Hence, the present study aims to examine the role of up-regulation of GRP78 in EMT in lung adenocarcinoma and explore the downstream molecular pathways involved.

METHODS

Cell Culture and Conditioning

Human lung adenocarcinoma A549 cells were purchased from the Cell Bank of the Chinese Academy of Sciences (Shanghai, China) and cultured in RPMI-1640 medium (Gibco, USA) supplied with 10% FBS (Gibco, USA) and 100 U/ml penicillin/streptomycin in 5% CO_2 incubator at 37°C. The medium was changed every 3 days. The cells were treated with normal O_2 as control.

A549 cells were cultured with 2% O_2 for hypoxia condition. The concentration of protein inhibitors for treatment of A549 cells were as follows: 550 nM SB505124 (phospho-Smad2/3 inhibitor), 25 nM KX2-391 (phospho-Src inhibitor), 100 nM JNK-IN-8 (phospho-JNK inhibitor), 2.5 μM SB203580 (phospho-p38 inhibitor), and 1.5 μM FR180204 (phospho-ERK). All of the inhibitors were purchased from Celleck Chemicals (USA).

Assessment of Cell Morphology

Morphological changes were examined using phase-contrast microscopy (Olympus, Japan).

Real-Time Quantitative Fluorescent PCR

Experiments were performed following the methods in our previous study. The cells were collected to extract total RNA using Trizol method. The cDNA was synthesized with Prime Script TMRT Master Mix (RR036A; Takara, Japan) through reverse transcription and used as template to amplify target genes with real-time quantitative fluorescent PCR with SYBR® Premix Ex TaqII (RR820A; Takara, Japan). The specific primers (Invitrogen, USA) of each transcription factor (Snail1, Snail2, Twist, ZEB1 and ZEB2) were also based on such study (23). The reaction condition was 95°C for 30 s, followed by 95°C for 5 s and 60°C for 30 s with 40 cycles. The amplified productions were quantitatively analyzed with 2-ΔΔCt method. All tests were repeated three times.

Western Blot Analysis

Experiments were performed following the methods in our previous study. The specific program and concentration of each antibody were also based on such study (23). Briefly, the protein was extracted with PIRA buffer and centrifuged at 12,000 g for 15 min at 4°C. Fifty microgram total proteins were separated with 10%SDS-PAGE. After electrophoresis, proteins were blotted to polyvinylidene fluoride (PVDF) membranes and then blocked with 5% skim milk powder with 0.1% Tween-20. The blots were then probed at 4°C overnight with the relevant primary antibodies respectively, and incubated in 4°C for overnight. The membranes were rinsed with TBST for 3 times, 10 min each time. Then secondary goat anti-rabbit or anti-mouse IgG-HRP antibodies were added for incubation in room temperature for 2 h. The membranes were rinsed with TBST for 3 times, and 10 min per time. Then the membranes were developed with ECL (Beijing Kangwei Biotech, China) and taken photos to analyze the relative expression of proteins with GAPDH as internal referral. All tests were repeated three times.

Immunofluorescence Staining

Cells were cultured on six-well chamber slides for immunofluorescent staining. The cells were fixed in 4% paraformaldehyde for 30 min at room temperature. After washing with PBS three times for 10 min each time, the cells were permeabilised with 0.1% Triton X-100 in PBS for 15 min. After three washes with PBS, the cells were blocked with 5%

BSA for 30 min at room temperature. The cells were incubated with the indicated GRP78 antibody (1:250) overnight at 4°C, washed three times with PBS and incubated with fluorescent secondary antibodies. Nuclear staining was performed in the dark with DAPI at room temperature. Phase contrast and fluorescent microscopy was performed using an NikonTi-U Inverted Fluorescence Microscope (Nikon, Japan).

Plasmid Transfection and Identification

GRP78 short hairpin RNA(GRP78shRNA) eukaryotic expression plasmid was designed and synthesized by Invitrogen, USA. Transfection and identification were conducted according to the protocol of Lipofectamine 3000. using previously published methods (24). Briefly, 7.5 μl Lipofectamine 3000 Reagent was diluted with 125 μl Opti-MEM media, then blended with a diluted plasmid DNA which diluted by 10 μl P3000 Reagent and 125 μl Opti-MEM media. After incubating for 5 min, the overall mixture was added into the culture cells and cultured for 72 h. The cells carrying green fluorescence are plasmids transfected successfully in inverted microscope. 20 μg/ml blasticidin was used to screen the cells and the maintenance concentration of blasticidin is 10 μg/ml. Blank shRNA was used as a control. The mRNA and protein expression levels of GRP78 decreased by 70 and 85.33%, respectively, suggesting successful transfection.

Statistical Analysis

Data were expressed as mean ± SD. Comparison between two groups was performed with *t*-test for independent samples. Comparison among multiple groups was performed with one-way ANOVA following LSD (equal variances) or Dunnett's *t*-test (unequal variances). $P<0.05$ was set as the significance level. All analyses were performed using SPSS 22.0 software.

RESULTS

Activation of EMT by Hypoxia in A549 Cells

A549 cells cultured under hypoxia condition for 72 h showed morphological changes, from oblate fusiform-shaped epithelial cells to elongated spindle-shaped mesenchymal cells (**Figure 1A**). The expression levels of EMT-related genes including Snail1, Snail2, Twist, ZEB1, and ZEB2 were increased by approximately three times under hypoxic condition compared with that in the control group. The Western blot analysis showed that the protein expression of E-cadherin (biomarker of epithelial phenotype) under hypoxia found to be approximately three times less than that in the control group. The expression levels of vimentin and fibronectin (biomarker of mesenchymal phenotype) were increased by 1.48 and 1.22 times, respectively, under hypoxia condition compared with that in the control group ($P < 0.05$ compared with Normoxia, **Figures 1B,C**).

Expression of GRP78 Under Normoxia and Hypoxia Conditions

The expression and location of the GRP78 protein in A549 cells under hypoxia and normoxia conditions were determined by immunofluorescence staining. Under normoxia condition, GRP78 (green fluorescence) showed weak staining intensity and was mainly distributed in the cytoplasm (**Figure 1A**). By contrast, under hypoxia, A549 cells showed an elongated spindle-shaped mesenchymal phenotype, and GRP78 showed strong staining intensity and was mainly distributed in the cytoplasm and cell membrane (**Figure 1A**). The Western blot analysis showed that the expression of GRP78 in A549 cells under hypoxia was found to be 1.36 times more than that under normoxia (**Figure 1B**).

Effect of GRP78 Knockdown on the Expression of EMT Markers

The expression of GRP78 in GRP78 knockdown A549 cells under hypoxia was reduced by 70% compared with that under hypoxia. In A549 cells transfected with GRP78 shRNA under hypoxia, the expression levels of vimentin and fibronectin significantly decreased by 52 and 60%, respectively. Meanwhile, the mRNA expression levels of transcription factors (Snail1, Snail2, Twist, ZEB1, and ZEB2) were significantly inhibited under hypoxia condition and decreased by approximately 70% compared with that in the normoxia group (**Figures 1B,C**). The significant change in the expression of EMT biomarkers and its transcription factor mRNAs after GRP78 knockdown indicated that GRP78 might play an important role in hypoxia-induced EMT.

Expression of Smad2/3, Src, p38, ERK and JNK in A549 Cells Under Hypoxia Condition

The expression levels of phosphorylated Smad2/3, p38, and JNK in A549 cells significantly increased by approximately 2.4 times under hypoxia condition compared with those under normoxia condition, whereas the levels of the phosphorylated Src and ERK increased by approximately 1.8 times (all $p < 0.05$, **Figure 2A**). Hence, these signaling pathways were activated under hypoxia condition.

The inhibitors of Smad2/3, Src, p38, ERK, and JNK were used to treat A549 cells under hypoxia condition to further verify the relationship between these signaling molecules with hypoxia-induced EMT. The expression levels of EMT protein markers and transcription factor mRNAs were also examined. The changes in EMT protein markers and transcription factor mRNAs in A549 cells were approximately similar to that in the group treated with Smad2/3 and Src inhibitors. The levels of vimentin, fibronectin and mRNAs decreased by approximately 50%, whereas that of E-cadherin increased by 2-fold compared with those in the cells under hypoxia. The change in the three other groups was found to be smaller than that in the group treated with Smad2/3 and Src inhibitors. The levels of vimentin, fibronectin and mRNAs were reduced by approximately 30%. Hence, EMT is inhibited in A549 cells when the activation of Smad2/3, Src, p38, ERK, and JNK proteins is inhibited under hypoxia (**Figure 2B**).

The changes in the expression of EMT protein markers were compared in A549 cells transfected by GRP78shRNA or treated by different protein inhibitors under hypoxia condition. The changes in the mRNA expression of EMT markers and signaling molecules were the most evident in GRP78 knockdown cells ($P < 0.05$ compared with the other groups, **Figures 3A,B**). Similar results were obtained on the protein expression of signaling molecules (Smad2/3, Src, p38, ERK, and JNK). After GRP78

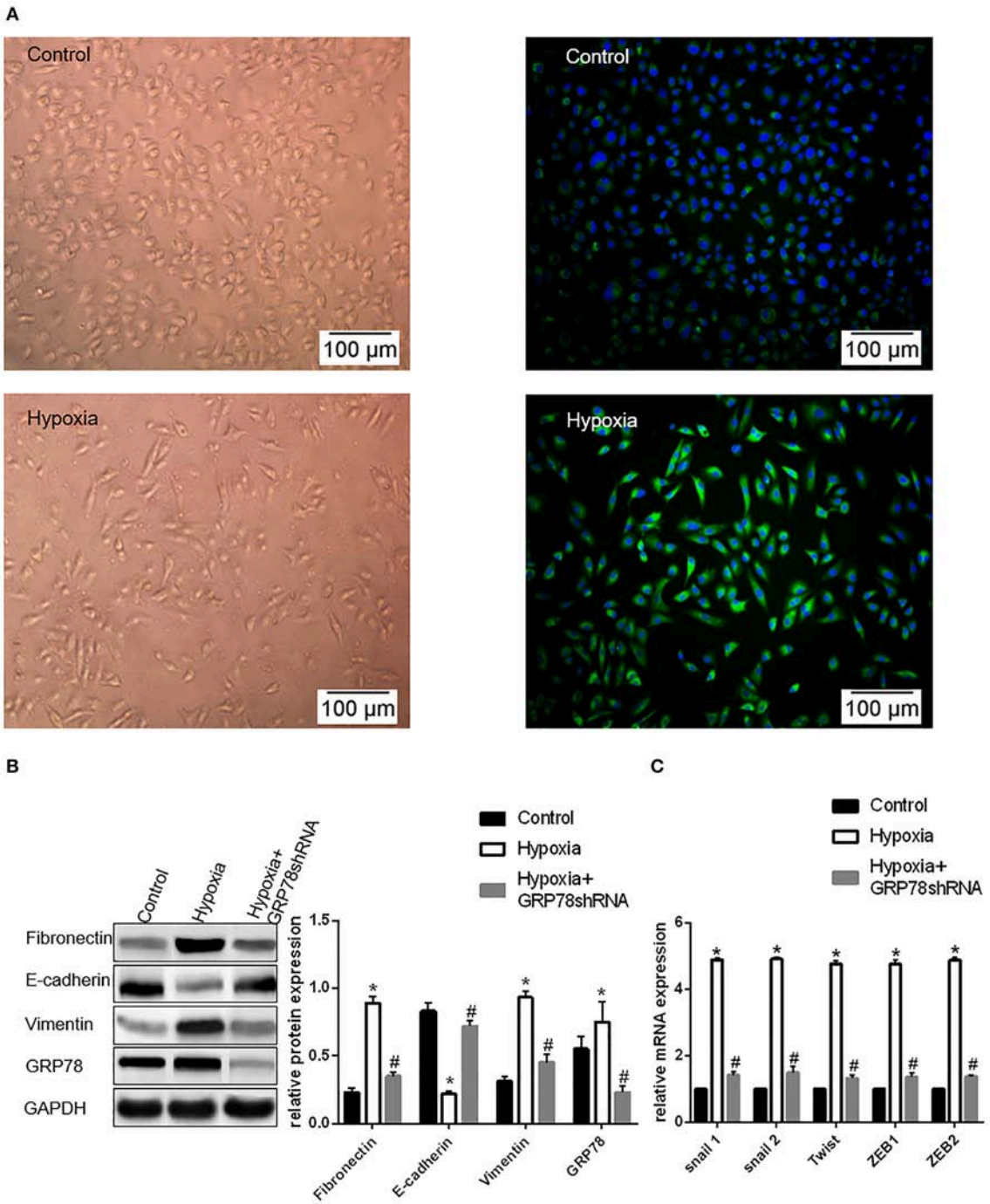

FIGURE 1 | Up-regulation of GRP78 plays an important role in hypoxia-induced EMT in A549 cells. **(A)** A549 cells acquire spindle-shaped mesenchymal morphology after 72 h of 2% O_2 hypoxia (left, 100×). GRP78 (green fluorescence) is highly expressed in A549 cells with spindle-shaped mesenchymal morphology (right, 100×). **(B)** EMT-related markers (E-cadherin, Vimentin and Fibronectin) and GRP78 were examined by Western blot analysis (left). GAPDH was used as internal control. The protein relative value (GAPDH) is plotted in the right panel (mean ± SD in three separate experiments). *$P < 0.05$, compared with A549 cells under the condition of normal oxygen, the expression of E-cadherin decreases, while those of Vimentin and Fibronectin increase in A549 cells under hypoxia (2% O_2 72 h). The expression of GRP78 also increases in A549 cells under hypoxia. #$P < 0.05$, compared with the A549 cells under the condition of hypoxia; the expression of E-cadherin increases, and those of Vimentin and Fibronectin decrease in GRP78 knockdown A549 cells under hypoxia. **(C)** EMT-related genes including Snail1, Snail2, Twist, ZEB1, and ZEB2 were examined by real-time quantitative PCR; mRNA expression relative value (control group) is plotted (mean ± SD in three separate experiments). *$P < 0.05$, compared with A549 cells in the control group, the mRNA expression levels of EMT-related genes including Snail1, Snail2, Twist, ZEB1, and ZEB2 increase under hypoxic condition (2% O_2 72 h); #$P < 0.05$, compared with A549 cells under the condition of hypoxia, the mRNA expression levels of EMT-related genes decrease in GRP78 knockdown A549 cells under hypoxia.

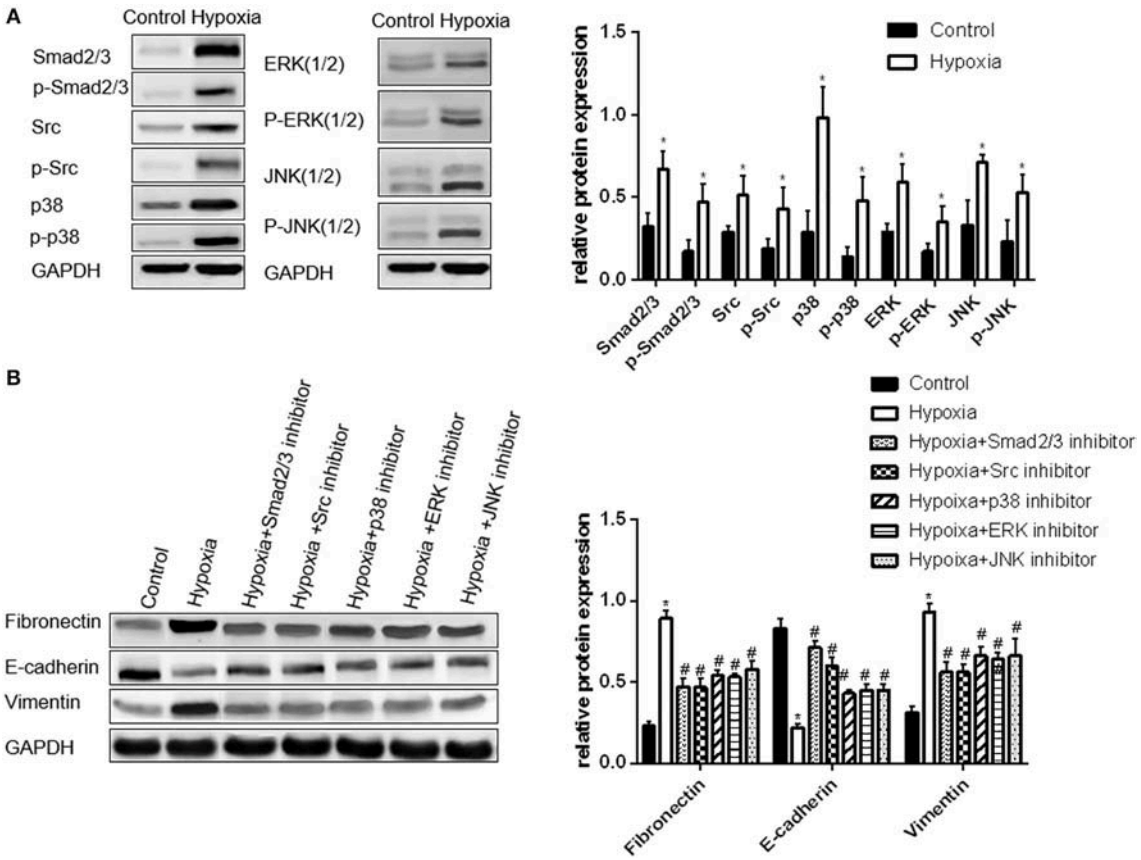

FIGURE 2 | Activation of Smad2/3, Src, p38, ERK, and JNK is important in hypoxia-induced EMT in A549 cells. **(A)** Smad2/3, Src, p38, ERK, JNK, and their phosphorylated forms were examined by Western blot analysis (left). GAPDH was used as internal control. The protein relative value (GAPDH) is plotted in the right panel (mean ± SD in three separate experiments). *$P < 0.05$, compared with A549 cells in the normal oxygen environments, the Smad2/3, Src, and MAPK proteins of A549 cells are highly regulated and activated in hypoxia environments. **(B)** EMT markers were examined by Western blot analysis (left). GAPDH was used as internal control. The protein relative value (GAPDH) is plotted in the right panel (mean ± SD in three separate experiments). *$P < 0.05$, compared with A549 cells in the normal oxygen environments, the EMT process of A549 cells under hypoxia is activated; #$P < 0.05$, compared with A549 cells in the hypoxia environments, the EMT process of A549 cells under hypoxia is inhibited separately by Smad2/3, Src, p38, ERK, and JNK inhibitors. The expression levels of Fibronectin and Vimentin decrease, and that of E-cadherin increases.

silencing, the expression of Smad2/3, Src, p38, ERK, and JNK and their phosphorylated proteins in hypoxia cells was significantly inhibited compared with that in the vehicle control under hypoxia ($P < 0.05$, **Figures 3C, 4A**).

Different effects were observed on the expression of the signaling molecules after inhibition of a particular pathway. After Smad2/3 inhibition, the expression of the four other signaling molecules did not significantly change ($P > 0.05$, **Figures 4A,B**). After inhibition of Src, JNK, ERK, and p38 pathways, the expression of Smad2/3 was not significantly changed (P>0.05, **Figures 4A,C**). After inhibiting Src, the activation of p38, ERK, and JNK (MAPK pathway) was also inhibited ($P < 0.05$, **Figures 4A,D**).

DISCUSSION

This study shows that GRP78 highly expressed under hypoxia condition is likely to play an essential role in hypoxia-induced EMT in A549 cells. This main finding is supported by the following observations: (1) the expression of GRP78 was significantly elevated under hypoxia condition and closely associated with the changes in the EMT markers; (2) GRP78 silencing significantly inhibited hypoxia-induced EMT markers; and (3) GRP78 silencing inhibited the expression of several signaling molecules, especially Smad2/3. This work is the first to demonstrate that GRP78 has a causal relationship with hypoxia-induced EMT in lung adenocarcinoma. Hence, targeted inhibition on GRP78 might could hamper EMT, which could further inhibit metastasis and overcome therapeutic resistance.

GRP78 was highly expressed in lung cancer cells under hypoxia condition; this finding is consistent with those reported by Song and Pi (25, 26). Chronic hypoxia induced GRP78 in human cancer cells possibly through the protein kinase C-epsilon/ERK/AP-1 signaling cascade (25).

A causal relationship between high GRP78 expression and EMT was confirmed by the GRP78 knock-down experiment. A very strong correlation was found between changes in the expression of GRP78 and EMT markers. Previous studies

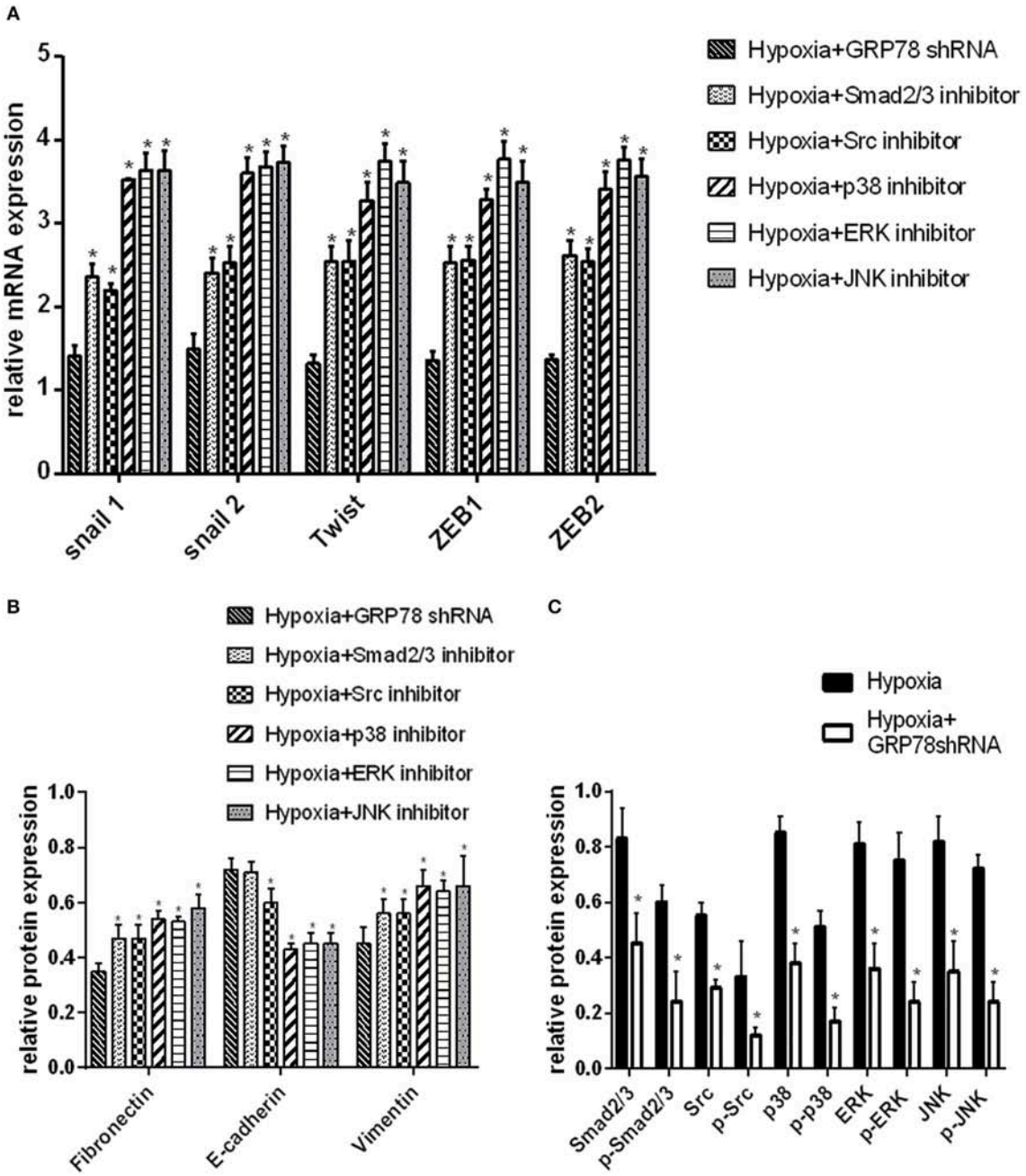

FIGURE 3 | GRP78 is the upper reaches of the Smad2/3, Src and MAPK pathways in hypoxia-induced EMT in A549 cells. **(A)** The mRNA relative value (control group) of EMT transcription factors is plotted (mean ± SD in three separate experiments). *$P < 0.05$, compared with EMT transcription factors in A549 cells under hypoxia condition separately inhibited by Smad2/3, Src, p38, ERK, and JNK inhibitors, the expression is higher than that in GRP78 knockdown A549 cells under hypoxia. **(B)** The protein relative value (GAPDH) of EMT markers was examined by Western blot analysis and plotted (mean ± SD in three separate experiments). *$P <$ 0.05, compared with EMT markers of A549 cells under hypoxia condition separately inhibited by Smad2/3, Src, p38, ERK, and JNK inhibitors, the expression is higher than that in GRP78 knockdown A549 cells in the hypoxia. **(A,B)** indicate that the inhibition effect of GRP78 silencing is more powerful than those of the five other inhibitors. **(C)** The protein relative values (GAPDH) of Smad2/3, Src, p38, ERK, JNK, and their phosphorylated forms were examined by Western blot analysis and plotted (mean ± SD in three separate experiments). *$P < 0.05$, compared with A549 cells under hypoxia, the expression levels of Smad2/3, Src, p38, ERK, JNK, and their activation forms decrease compared with those in GRP78 knockdown A549 cells under hypoxia. After GRP78 silencing, the expression and activation of these proteins are inhibited significantly.

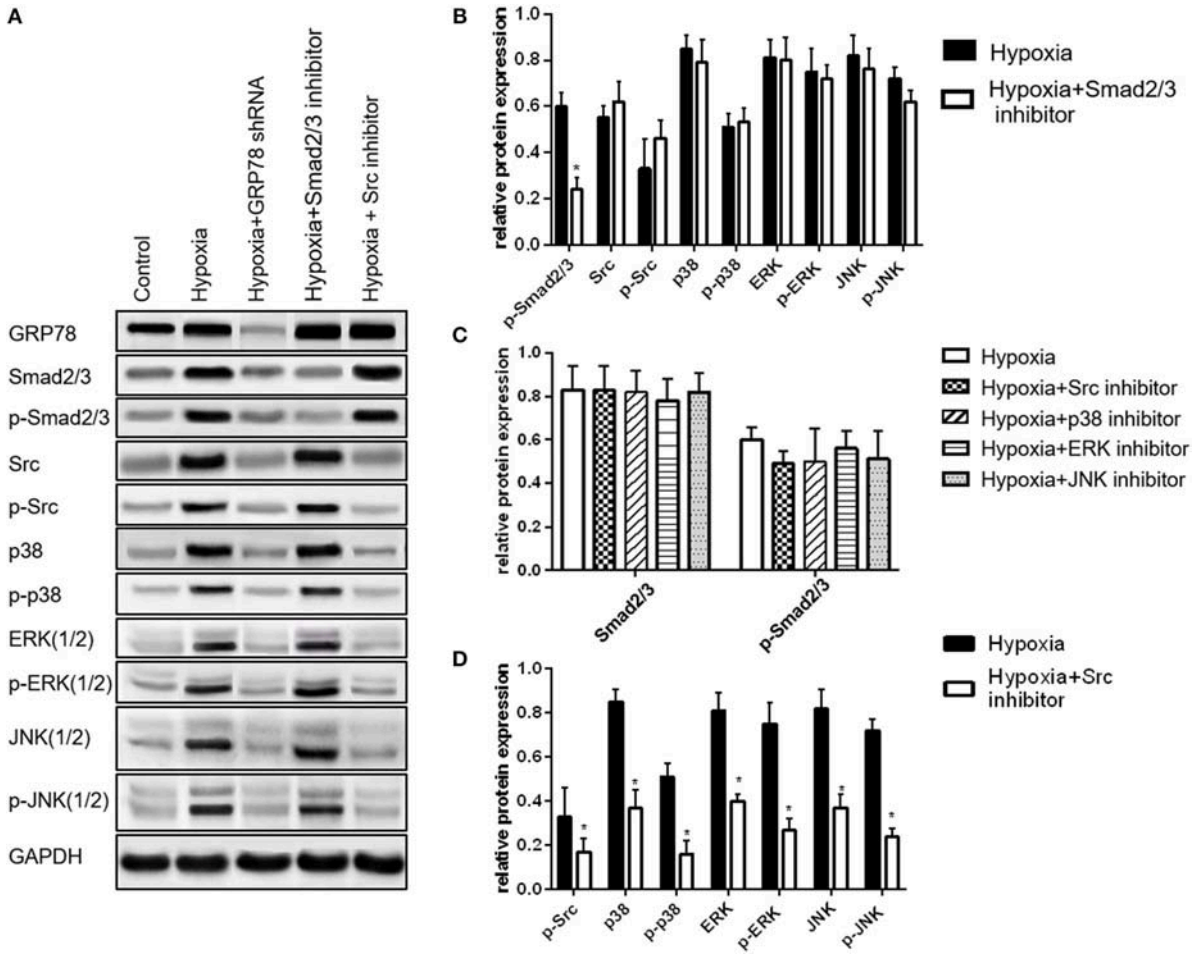

FIGURE 4 | Smad2/3 and Src/MAPK are two dependent signaling pathways in hypoxia-induced EMT in A549 cells. **(A)** Smad2/3, Src, p38, ERK, JNK, and their phosphorylated forms were examined by Western blot analysis. **(B)** Compared with the expression levels of Src, JNK, p38, ERK, and their activation forms in A549 cells under hypoxia, their expression levels do not change after inhibiting the activation of Smad2/3. **(C)** Compared with the expression levels of Smad2/3 and p-Smad2/3 in A549 cells under hypoxia, their expression does not change after inhibiting the activation of Src, JNK, ERK and p38. **(D)** $^*P < 0.05$, compared with the expression levels of p38, ERK, JNK (three forms of MAPK) and their activated forms in A549 cells under hypoxia, their expression levels decrease after inhibiting the activation of Src. MAPK is the downstream pathway of Src.

suggested that other methods for silencing GRP78 could inhibit EMT. For example, neutralization of endogenous GRP78 on the cell surface with the anti-GRP78 antibody inhibited the ability of adhesion and invasion of hepatocellular carcinoma cell lines Mahlavu and SMMC7721 (19). The mitigation of GRP78 up-regulation by using short hairpin RNA or treatment with the small molecule IT-139 inhibited metastatic growth in the lung microenvironment in four highly metastatic cell line models (three human osteosarcomas and one murine mammary adenocarcinoma) (20). However, no rational interpretation is available regarding the inconsistency on the relationship between GRP78 expression and EMT in colorectal cancer.

The mechanism of GRP78 downstream signaling for EMT promotion has been demonstrated. Cell surface GRP78 can accelerate breast cancer cell proliferation and migration by activating STAT3 (27). We found two key molecular pathways (Smad2/3 and Src/MAPK) of GRP78 that may play an important role in hypoxia-induced EMT by using multiple protein inhibitors. These findings were consistent with those of previous works. Li et al. reported that overexpressing or knocking down GRP78 induced the corresponding activation or inhibition of the Smad2/3 pathway in colon cancer cells (28). Zhao et al. reported that GRP78 interacted directly with Src, thereby promoting the phosphorylation of Src in hepatocellular cancer cells (29). Tanjore et al. also suggested that the combination of the Smad2/3 inhibitor (SB431542) and the Src kinase inhibitor (PP2) blocked the EMT of alveolar epithelial cells induced by ER stress inducer tunicamycin, which also induced high GRP78 expression (30). In the present study, the activation of the Smad2/3 and Src/MAPK pathways follows the same trend with the up-regulation of GRP78; moreover, knockdown of GRP78 inhibited the activation of Smad2/3 and Src, suggesting a causal link between GRP78

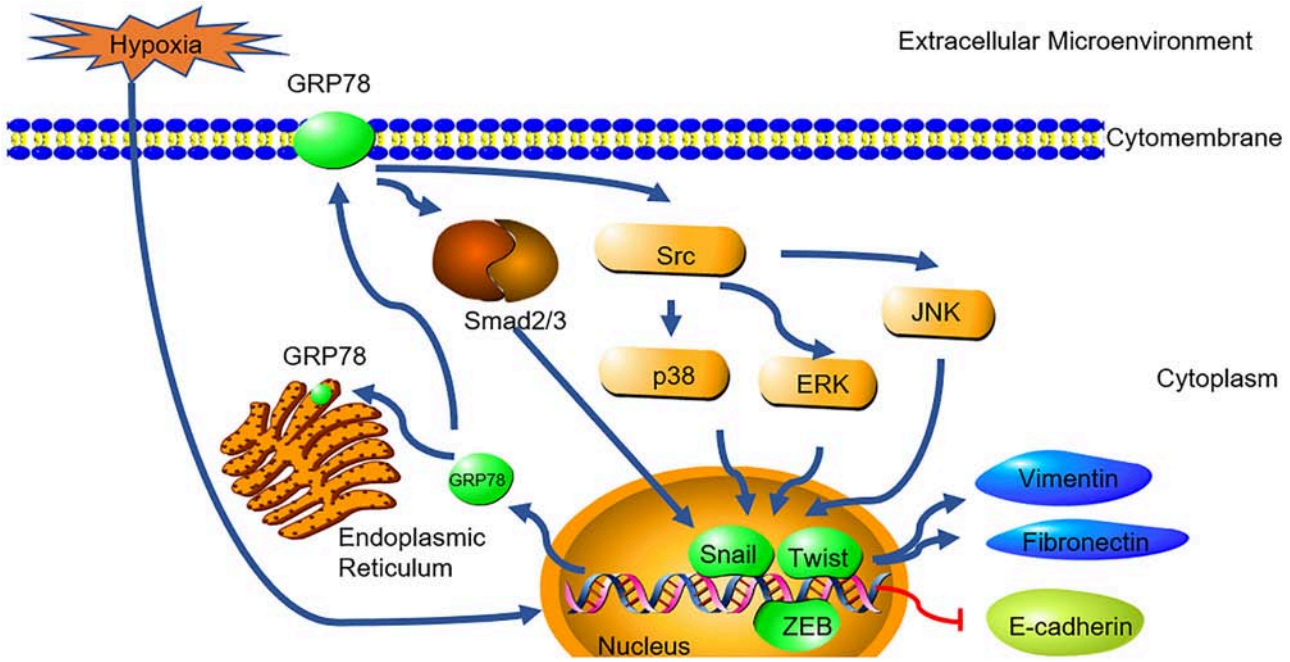

FIGURE 5 | GRP78 mediates hypoxia-induced EMT through smad2/3 and SRC/MAPK signaling. Hypoxia induced the high expression of GRP78. High expressed GRP78 activated the smad2/3 and Src/MAPK pathway. The pathway activated the expression of EMT transcription factor (snail, Twist and ZEB) and collaborated with them to induce the expression of Fibronectin, Vimentin and inhibit the expression of E-cadherin.

and activation of the two pathways in lung cancer. Smad2/3 inhibition did not interact with the inhibition of Src, p38, ERK, and JNK. By contrast, inhibiting the activation of Src was accompanied by the inhibition of p38, ERK, and JNK. Hence, the Smad2/3 and Src/MAPK pathways are two independent downstream signaling pathways of GRP78 during hypoxia-induced EMT in A549 cells. However, we did not perform the knockdown experiment of Smad2/3 and Src, and the co-immunoprecipitation experiment; as such, we cannot provide additional evidence for such link. And the control shRNA was not applied in the present study, which might limiting its evidence.

Other pitfall of the present study is that we have not explored the relationship between GRP78 and HIF1a, which is a key regulator on hypoxia induced EMT. But there are some evidences in other cell lines, that the expression of GRP78 is regulated by HIF1a (31). What's more, all the results in the study are limited to one cell line, limiting its evidence.

In summary, this study demonstrated the possible causal link between GRP78 and hypoxia-induced EMT in A549 cells (**Figure 5**). Together with its roles in anti-apoptosis and chemoresistance, it indicates that GRP78 might be a potential target for treatment of lung adenocarcinoma. Further, studies are needed to elucidate the exact mechanisms involved in the GRP78-EMT pathway in hypoxia and their relevant clinical significance.

DATA AVAILABILITY

All datasets generated for this study are included in the manuscript and/ or the supplementary files.

AUTHOR CONTRIBUTIONS

L-ZL and L-LS: designed the experiments. L-LS, C-MC, and JW: performed the experiments. JZ and C-ZY: analyzed the data. L-LS and C-ZY: prepared the figures. L-LS and JZ: wrote the main manuscript. All authors reviewed the manuscript.

FUNDING

This study was supported by grant from the National Natural Science Foundation of China (NSFC) (Nos. 81403227 to L-LS and 81573870 to L-ZL).

ACKNOWLEDGMENTS

We would like to thank the colleagues from First Affiliated Hospital of Guangzhou University of Chinese Medicine, China. We would also like to thank the support from Prof. Chunguang Li, Prof. Xiaoshu Zhu, Prof. Alan Bensussan from the Western Sydney University, Australia and Prof. Kevin Chang from New South Wales Association of Chinese Medicine, Australia.

REFERENCES

1. Ferlay J, Soerjomataram I, Dikshit R, Eser S, Mathers C, Rebelo M, et al. Cancer incidence and mortality worldwide: sources, methods and major patterns in GLOBOCAN 2012. *Int J Cancer*. (2015) 136:E359–86. doi: 10.1002/ijc.29210
2. Zhao Y, Adjei AA. New strategies to develop new medications for lung cancer and metastasis. *Cancer Metastasis Rev*. (2015) 34:265–75. doi: 10.1007/s10555-015-9553-5
3. Skovierova H, Okajcekova T, Strnadel J, Vidomanova E, Halasova E. Molecular regulation of epithelial-to-mesenchymal transition in tumorigenesis (Review). *Int J Mol Med*. (2018) 41:1187–200. doi: 10.3892/ijmm.2017.3320
4. Xu J, Lamouille S, Derynck R. TGF-beta-induced epithelial to mesenchymal transition. *Cell Res*. (2009) 19:156–72. doi: 10.1038/cr.2009.5
5. Patel A, Sabbineni H, Clarke A, Somanath PR. Novel roles of Src in cancer cell epithelial-to-mesenchymal transition, vascular permeability, microinvasion and metastasis. *Life Sci*. (2016) 157:52–61. doi: 10.1016/j.lfs.2016.05.036
6. Zhao L, Li X, Song N, Li A, Hou K, Qu X, et al. Src promotes EGF-induced epithelial-to-mesenchymal transition and migration in gastric cancer cells by upregulating ZEB1 and ZEB2 through AKT. *Cell Biol Int*. (2018) 42:294–302. doi: 10.1002/cbin.10894
7. Ruan J, Zhang L, Yan L, Liu Y, Yue Z, Chen L, et al. Inhibition of hypoxia-induced epithelial mesenchymal transition by luteolin in non-small cell lung cancer cells. *Mol Med Rep*. (2012) 6:232–8. doi: 10.3892/mmr.2012.884
8. Shaikh D, Zhou Q, Chen T, Ibe JC, Raj JU, Zhou G. cAMP-dependent protein kinase is essential for hypoxia-mediated epithelial-mesenchymal transition, migration, and invasion in lung cancer cells. *Cell Signal*. (2012) 24:2396–406. doi: 10.1016/j.cellsig.2012.08.007
9. Nurwidya F, Takahashi F, Kobayashi I, Murakami A, Kato M, Minakata K, et al. Treatment with insulin-like growth factor 1 receptor inhibitor reverses hypoxia-induced epithelial-mesenchymal transition in non-small cell lung cancer. *Biochem Biophys Res Commun*. (2014) 455:332–8. doi: 10.1016/j.bbrc.2014.11.014
10. Barriga EH, Maxwell PH, Reyes AE, Mayor R. The hypoxia factor Hif-1alpha controls neural crest chemotaxis and epithelial to mesenchymal transition. *J Cell Biol*. (2013) 201:759–76. doi: 10.1083/jcb.201212100
11. Shen X, Xue Y, Si Y, Wang Q, Wang Z, Yuan J, et al. The unfolded protein response potentiates epithelial-to-mesenchymal transition (EMT) of gastric cancer cells under severe hypoxic conditions. *Med Oncol*. (2015) 32:447. doi: 10.1007/s12032-014-0447-0
12. Su R, Li Z, Li H, Song H, Bao C, Wei J, et al. Grp78 promotes the invasion of hepatocellular carcinoma. *BMC Cancer*. (2010) 10:20. doi: 10.1186/1471-2407-10-20
13. Sun Q, Hua J, Wang Q, Xu W, Zhang J, Zhang J, et al. Expressions of GRP78 and Bax associate with differentiation, metastasis, and apoptosis in non-small cell lung cancer. *Mol Biol Rep*. (2012) 39:6753–61. doi: 10.1007/s11033-012-1500-8
14. Chang YW, Chen HA, Tseng CF, Hong CC, Ma JT, Hung MC, et al. De-acetylation and degradation of HSPA5 is critical for E1A metastasis suppression in breast cancer cells. *Oncotarget*. (2014) 5:10558–70. doi: 10.18632/oncotarget.2510
15. Chen HA, Chang YW, Tseng CF, Chiu CF, Hong CC, Wang W, et al. E1A-mediated inhibition of HSPA5 suppresses cell migration and invasion in triple-negative breast cancer. *Ann Surg Oncol*. (2015) 22:889–98. doi: 10.1245/s10434-014-4061-3
16. Roller C, Maddalo D. The molecular chaperone GRP78/BiP in the development of chemoresistance: mechanism and possible treatment. *Front Pharmacol*. (2013) 4:10. doi: 10.3389/fphar.2013.00010
17. Xie J, Tao ZH, Zhao J, Li T, Wu ZH, Zhang JF, et al. Glucose regulated protein 78 (GRP78) inhibits apoptosis and attentinutes chemosensitivity of gemcitabine in breast cancer cell via AKT/mitochondrial apoptotic pathway. *Biochem Biophys Res Commun*. (2016) 474:612–9. doi: 10.1016/j.bbrc.2016.03.002
18. Gifford JB, Hill R. GRP78 Influences Chemoresistance and Prognosis in Cancer. *Curr Drug Targets*. (2018) 19:701–8. doi: 10.2174/1389450118666170615100918
19. Zhang XX, Li HD, Zhao S, Zhao L, Song HJ, Wang G, et al. The cell surface GRP78 facilitates the invasion of hepatocellular carcinoma cells. *Biomed Res Int*. (2013) 2013:917296. doi: 10.1155/2013/917296
20. Lizardo MM, Morrow JJ, Miller TE, Hong ES, Ren L, Mendoza A, et al. Upregulation of glucose-regulated protein 78 in metastatic cancer cells is necessary for lung metastasis progression. *Neoplasia*. (2016) 18:699–710. doi: 10.1016/j.neo.2016.09.001
21. Zhang L, Li Z, Fan Y, Li H, Li Z, Li Y. Overexpressed GRP78 affects EMT and cell-matrix adhesion via autocrine TGF-beta/Smad2/3 signaling. *Int J Biochem Cell Biol*. (2015) 64:202–11. doi: 10.1016/j.biocel.2015.04.012
22. Chang YJ, Chen WY, Huang CY, Liu HH, Wei PL. Glucose-regulated protein 78 (GRP78) regulates colon cancer metastasis through EMT biomarkers and the NRF-2/HO-1 pathway. *Tumour Biol*. (2015) 36:1859–69. doi: 10.1007/s13277-014-2788-x
23. Chen CM, Sun LL, Fang RM, Lin LZ. YiQi ChuTan recipe inhibits epithelial mesenchymal transition of A549 cells under hypoxia. *Cell Mol Biol (Noisy-le-grand)*. (2016) 62:10–5. doi: 10.14715/cmb/2016.62.1.3
24. Chen C, Sun L, Lin L. Construction of eukaryotic expression vector for glucose regulated protein 78-shRNA and establishment of stably transfected A549 cell line. *Chi J Biologic*. (2016) 29:348–53. doi: 10.13200/j.cnki.cjb.001289
25. Song MS, Park YK, Lee JH, Park K. Induction of glucose-regulated protein 78 by chronic hypoxia in human gastric tumor cells through a protein kinase C-epsilon/ERK/AP-1 signaling cascade. *Cancer Res*.(2001) 61:8322–30. Available online at: http://cancerres.aacrjournals.org/content/61/22/8322
26. Pi L, Li X, Song Q, Shen Y, Lu X, Di B. Knockdown of glucose-regulated protein 78 abrogates chemoresistance of hypopharyngeal carcinoma cells to cisplatin induced by unfolded protein in response to severe hypoxia. *Oncol Lett*. (2014) 7:685–92. doi: 10.3892/ol.2013.1753
27. Yao X, Liu H, Zhang X, Zhang L, Li X, Wang C, et al. Cell surface GRP78 accelerated breast cancer cell proliferation and migration by activating STAT3. *PLoS ONE*. (2015) 10:e0125634. doi: 10.1371/journal.pone.0125634
28. Li Z, Zhang L, Zhao Y, Li H, Xiao H, Fu R, et al. Cell-surface GRP78 facilitates colorectal cancer cell migration and invasion. *Int J Biochem Cell Biol*. (2013) 45:987–94. doi: 10.1016/j.biocel.2013.02.002
29. Zhao S, Li H, Wang Q, Su C, Wang G, Song H, et al. The role of c-Src in the invasion and metastasis of hepatocellular carcinoma cells induced by association of cell surface GRP78 with activated alpha2M. *BMC Cancer*. (2015) 15:389. doi: 10.1186/s12885-015-1401-z
30. Tanjore H, Cheng DS, Degryse AL, Zoz DF, Abdolrasulnia R, Lawson WE, et al. Alveolar epithelial cells undergo epithelial-to-mesenchymal transition in response to endoplasmic reticulum stress. *J Biol Chem*. (2015) 290:3277. doi: 10.1074/jbc.A110.181164
31. Lee JH, Yoon YM, Lee SH. Hypoxic preconditioning promotes the bioactivities of mesenchymal stem cells via the HIF-1alpha-GRP78-Akt Axis. *Int J Mol Sci*. (2017) 18:E1320. doi: 10.3390/ijms18061320

Conflict of Interest Statement: The authors declare that the research was conducted in the absence of any commercial or financial relationships that could be construed as a potential conflict of interest.

frontiers in Oncology

ORIGINAL RESEARCH
published: 15 March 2019
doi: 10.3389/fonc.2019.00150

Targeting TF-AKT/ERK-EGFR Pathway Suppresses the Growth of Hepatocellular Carcinoma

Shan-Zhou Huang[1,2†], Meng-Ning Wei[3†], Jia-Rong Huang[3†], Zi-Jian Zhang[4], Wen-Ji Zhang[3], Qi-Wei Jiang[3], Yang Yang[3], Huan-Yu Wang[5], Hui-Lin Jin[1], Kun Wang[3], Zi-Hao Xing[3], Meng-Ling Yuan[3], Yao Li[3], Xiao-Shun He[2], Zhi Shi[2*] and Qi Zhou[1,6*]*

[1] Department of Hepatic Surgery, The First Affiliated Hospital, Sun Yat-sen University, Guangzhou, China, [2] Organ Transplant Center, The First Affiliated Hospital, Sun Yat-sen University, Guangzhou, China, [3] Guangdong Provincial Key Laboratory of Bioengineering Medicine, Department of Cell Biology and Institute of Biomedicine, National Engineering Research Center of Genetic Medicine, College of Life Science and Technology, Jinan University, Guangzhou, China, [4] Department of Hepatobiliary Surgery, The Seventh Affiliated Hospital of Sun Yat-sen University, Shenzhen, China, [5] Department of Thyroid and Breast Surgery, Nanshan District People's Hospital, Shenzhen, China, [6] Department of General Surgery, Hui Ya Hospital of The First Affiliated Hospital, Sun Yat-sen University, Huizhou, China

Tissue factor (TF) is a transmembrane glycoprotein to initiate blood coagulation and frequently overexpressed in a variety of tumors. Our previous study has showed that the expression of TF is upregulated and correlated with prognosis in hepatocellular carcinoma (HCC). However, the role and molecular mechanism of TF in the growth of HCC are still unclear. *In vitro* and *in vivo* functional experiments were performed to determine the effect of TF on the growth of HCC cells. A panel of biochemical assays was used to elucidate the underlying mechanisms. TF could promote the growth of HCC *in vitro* and *in vivo* by activating both ERK and AKT signaling pathways. TF induced EGFR upregualtion, and inhibition of EGFR suppressed TF-mediated HCC growth. In addition, TF protein expression was correlated with EGFR in HCC tissues. TF promotes HCC growth by upregulation of EGFR, and TF as well as EGFR may be potential therapeutic targets of HCC.

Keywords: hepatocellular carcinoma, tissue factor, epidermal growth factor receptor, AKT/ERK, tumor growth

OPEN ACCESS

Edited by:
Yunkai Zhang,
Vanderbilt University Medical Center, United States

Reviewed by:
Chuan Wang,
Auburn University, United States
Shujue Lan,
Institute of Biochemistry and Cell Biology, Shanghai Institutes for Biological Sciences (CAS), China
Jing Zhao,
Fourth Military Medical University, China

***Correspondence:**
Zhi Shi
tshizhi@jnu.edu.cn
Xiao-Shun He
gdtrc@163.com
Qi Zhou
zhouqi@mail.sysu.edu.cn

† These authors have contributed equally to this work

Specialty section:
This article was submitted to Cancer Molecular Targets and Therapeutics, a section of the journal Frontiers in Oncology

Received: *25 January 2019*
Accepted: *22 February 2019*
Published: *15 March 2019*

Citation:
Huang S-Z, Wei M-N, Huang J-R, Zhang Z-J, Zhang W-J, Jiang Q-W, Yang Y, Wang H-Y, Jin H-L, Wang K, Xing Z-H, Yuan M-L, Li Y, He X-S, Shi Z and Zhou Q (2019) Targeting TF-AKT/ERK-EGFR Pathway Suppresses the Growth of Hepatocellular Carcinoma. Front. Oncol. 9:150. doi: 10.3389/fonc.2019.00150

INTRODUCTION

Hepatocellular carcinoma (HCC) is the fifth most lethal cancers worldwide, while China accounted for more than half of all cases and deaths in 2012 (1). More than 400,000 people die from liver cancer and over 450,000 new cases are diagnosed in China each year (2). Though the treatments for HCC have been greatly advanced in recent years, the outcome of HCC is still unoptimistic. Postoperative recurrence, the main reason for poor survival of HCC patients, mainly owes to the tendency of the invasion and metastasis of HCC cells (3, 4). Therefore, understanding the mechanism of HCC tumorigenesis and progression is critical to improve the clinical outcome of HCC patients.

Tissue factor (TF, also known as platelet tissue factor, factor III, thromboplastin, or CD142, encoded by the F3 gene) is a 47 kD transmembrane glycoprotein that contains 263 amino acid residues totally including a 219 amino acid extracellular region, a 23 amino acid hydrophobic transmembrane region, and a 21 amino acids C-terminal intracellular tail (5). Originally, TF is found on the surface of intravascular cells, such as platelets, leukocytes, and endothelial cells and

functions as the principal initiator of the extrinsic coagulation cascade by binding with circulating factor VII or VIIα (FVII/VIIα) (6). Recently, TF is frequently overexpressed in a variety of tumors, including breast cancer, colorectal carcinoma, gastric cancer, non-small cell lung, and pancreatic ductal carcinoma, etc. (7). We and other groups have reported that the expression of TF is upregulated and correlated with prognosis in HCC (8–10). In the current study, we investigate the role and molecular mechanism of TF in the growth of HCC cells.

MATERIALS AND METHODS

Patients and Tissue Specimens

A total 144 HCC tissues were obtained from patients who underwent curative resection between Jan 2008 and Dec 2010 at the First Affiliated Hospital, Sun Yat-sen University. None of the patients received neoadjuvant radiotherapy or chemotherapy before surgery. Signed informed consents were obtained from all patients. The study was approved by the ethics committee of the First Affiliated Hospital, Sun Yat-sen University.

Cell Culture and Reagents

The human HCC cell lines HepG2, BEL-7402, SK-HEP1, SMMC-7721, and normal hepatic cell line LO2 were from China Center for Type Culture Collection and cultured in Dulbecco's modified Eagle's medium (DMEM) supplemented with 10% fetal bovine serum (FBS), penicillin (100 U/ml) and streptomycin (100 ng/ml) in a humidified incubator at 37°C with 5% CO_2 atmosphere. U0126, LY294002, and Gefitinib were from ApexBio. Anti-TF (ab17375) and Anti-Ki-67 (2724-1) were from Abcam. Anti-pAKT (4060), Anti-AKT (4691), Anti-pERK (4370), and Anti-ERK (4695) antibodies were from Cell Signaling Technologies. Anti-EGFR (SC-03) and Anti-c-Myc (SC-40) antibodies were from Santa Cruz Biotechnology. Anti-β-actin

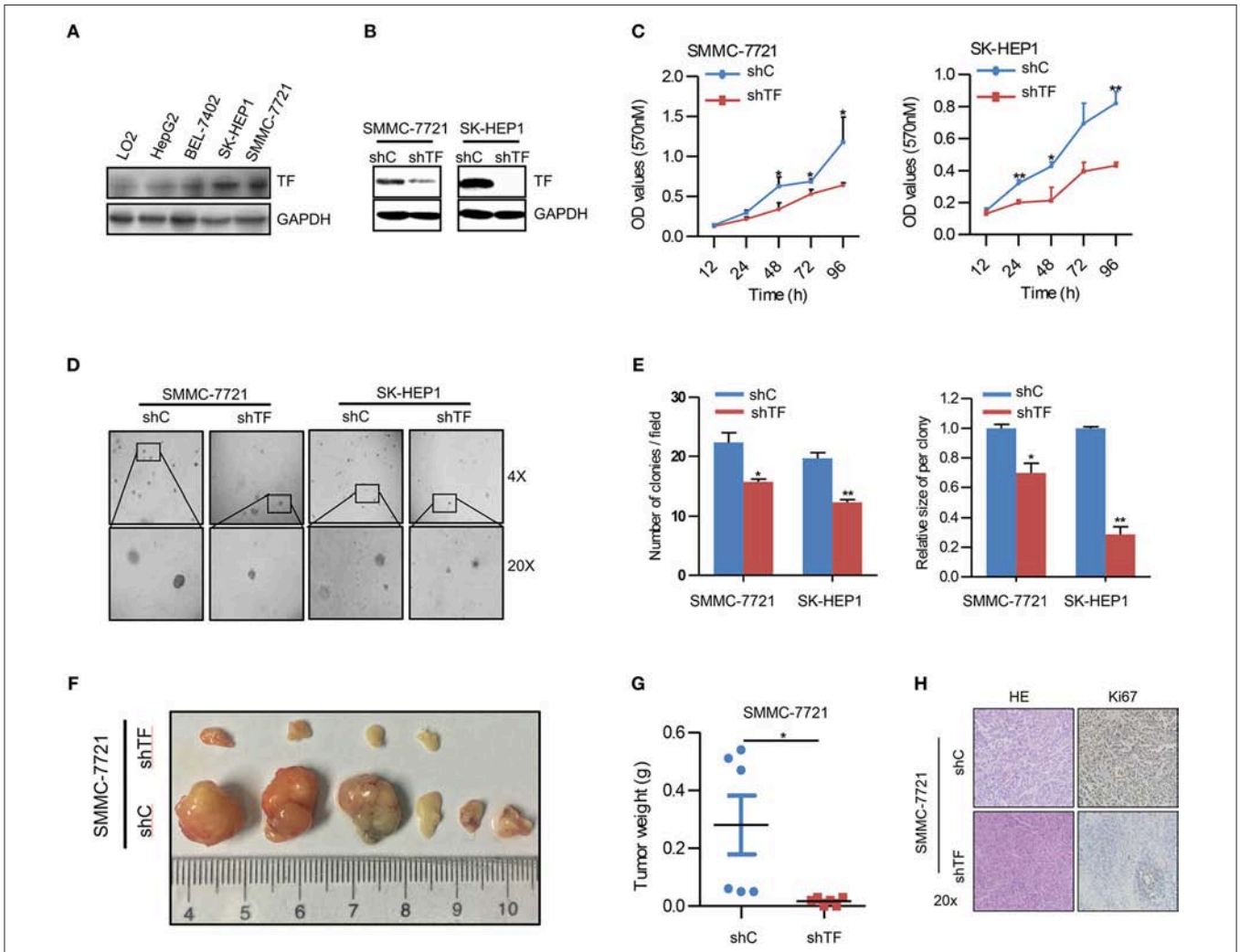

FIGURE 1 | Knockdown of TF inhibits the growth of HCC. **(A,B)** Western blot analysis of the protein expressions in the indicated cells. **(C)** Cell growth of the indicated cells as determined with MTT assay. **(D)** Representative images and **(E)** quantification of the indicated cells sphere as determined with sphere formation assay. **(F)** The indicated subcutaneous tumors and **(G)** tumor weight of nude mice were shown. **(H)** Representative images of H&E and Ki-67 staining in the indicated tumor sections as determined with IHC assay. Error bars, mean ± SD. *$p < 0.05$ and **$p < 0.01$ [two-tailed Student's *t*-test **(C,E,G)**].

(LK9001T) and Anti-GAPDH (LK9002T) antibodies were from Tianjin Sungene Biotech.

Plasmid Construction and Lentivirus Production

The human TF cDNA was cloned into pLVX-AcGFP1-N1 lentiviral vector, and shRNA targeting human TF mRNA (5′-GCGCUUCAGGCACUACAAA-3′) was cloned into pLKO.1 lentiviral vector. Lentivirus was packaged in HEK293T cells and collected from the medium supernatant. Stable cell lines were established by infecting lentivirus into cells, followed by puromycin selection (11, 12).

siRNA Transfection

The EGFR siRNA (sense sequences: 5′- CUGACUCCGUCCAGUAUUGAU−3′) and negative control siRNA were synthesized by Guangzhou Ribobio. Each siRNA solution was mixed gently with the respective volume of the X-tremeGENE siRNA Transfection Reagent and allowed to form transfection mixture for 20 min. Cells were cultured in 6-well plate with DMEM until 50% of confluence and added with the transfection mixture for 24 h before the next experiment (13, 14).

Western Blot

Cells were harvested and washed twice with cold PBS, then resuspended and lysed in RIPA buffer (1% NP-40, 0.5% sodium deoxycholate, 0.1% SDS, 10 ng/ml PMSF, 0.03% aprotinin, 1 μM sodium orthovanadate) at 4°C for 30 min. Lysates were centrifuged for 10 min at 14,000 × g and supernatants were stored at −80°C as whole cell extracts. Proteins were separated on 12% SDS-PAGE gels and transferred to polyvinylidene difluoride membranes. Membranes were blocked with 5% BSA and incubated with the indicated primary antibodies. Corresponding horseradish peroxidase-conjugated secondary antibodies were used against each primary antibody. Signals were detected using

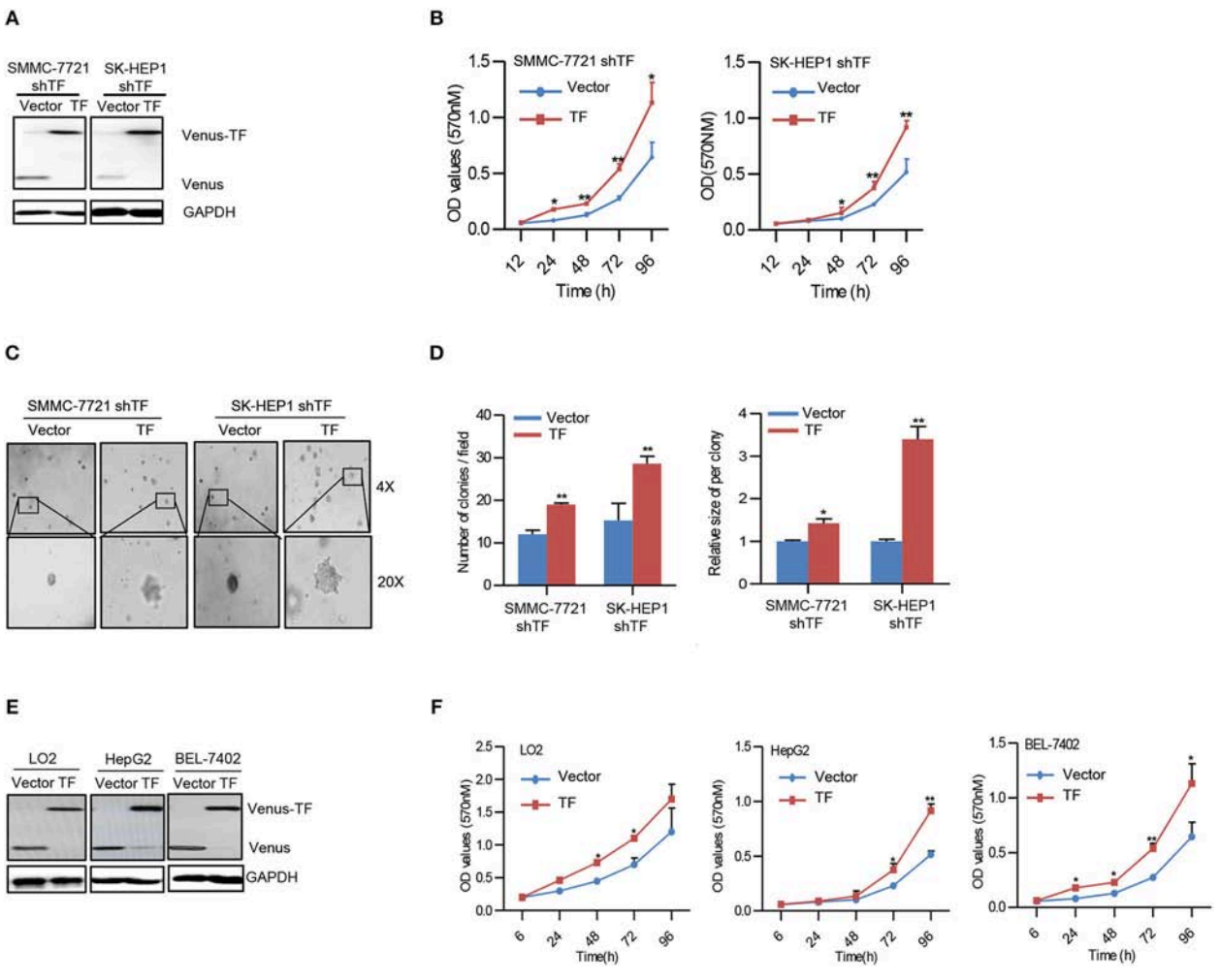

FIGURE 2 | Overexpression of TF promotes the growth of HCC. **(A,E)** Western blot analysis of the protein expressions in the indicated cells. **(B,F)** Cell growth of the indicated cells as determined with MTT assay. **(C)** Representative images and **(D)** quantification of the indicated cells sphere as determined with sphere formation assay. Error bars, mean ± SD. *$p < 0.05$ and **$p < 0.01$ [two-tailed Student's *t*-test **(B,D,F)**].

the ChemiDoc XRS chemiluminescent gel imaging system (Bio-RAD) (15, 16).

MTT Assay

Cells were seeded into a 96-well plate at a density of 0.5–1 × 10^4 cells/well and treated with various concentrations of agents. After 3 days, 3-(4, 5-dimethylthiazolyl-2)-2, 5-diphenyltetrazolium bromide (MTT) was added to each well at a final concentration of 0.5 mg/ml. After incubation for 4 h, the medium and MTT solution were removed from each well, and formazan crystals were dissolved in 100 μl of DMSO. Absorbance was measured at 570 nm by Multiscan Spectrum (Thermofisher) (17, 18).

Sphere Formation Assay

Cells were trypsinized, suspended in medium containing 0.3% agar and 10% FBS and seeded at a density of 5 × 10^2 cells/well in a 12-well plate. The agar–cell mixture was plated onto a bottom layer with 0.5% agar. Then treated cells were incubated in a humidified incubator and fresh medium was added every 3 days. Two weeks later, colonies were analyzed microscopically (19, 20).

Nude Mice Xenograft Tumor Assay

The female Balb/c nude mice with 5 weeks old and 16–18 g weight were obtained from the Shanghai SLAC Laboratory Animal Co and maintained with sterilized food and water. For xenograft tumor assay, 4 × 10^6 cells in 100 μl of DMEM were injected subcutaneously under the shoulder of six mice per group. The mice were anesthetized after experiment, and tumors or lungs were removed, weighed, and sectioned. All experimental procedures were approved by the Institutional Animal Care and Use Committee of Jinan University (21, 22).

Immunohistochemistry Assay

Immunohistochemistry (IHC) assay was performed with a microwave-enhanced avidin-biotin staining method. Formalin-fixed, paraffin embedded human HCC tissue array and subcutaneous tumors in mice were stained with antibodies, respectively, using a microwave-enhanced avidin-biotin staining method. To quantify the protein expression, the following formula was used: IHC score = percentage of positive cells × intensity score. The intensity was scored as follows: 0, negative (no staining); 1, weak (light yellow); 2, moderate (yellow brown); and 3, intense (brown) (23, 24).

Statistical Analysis

Statistical analyses were performed using SPSS 19.0 for Windows (SPSS) and Graph-Pad Prism 6. Data were expressed as the mean ± standard deviation (SD) from at least three independent experiments. Quantitative data between two groups were compared using the Student's *t*-test. Categorical data

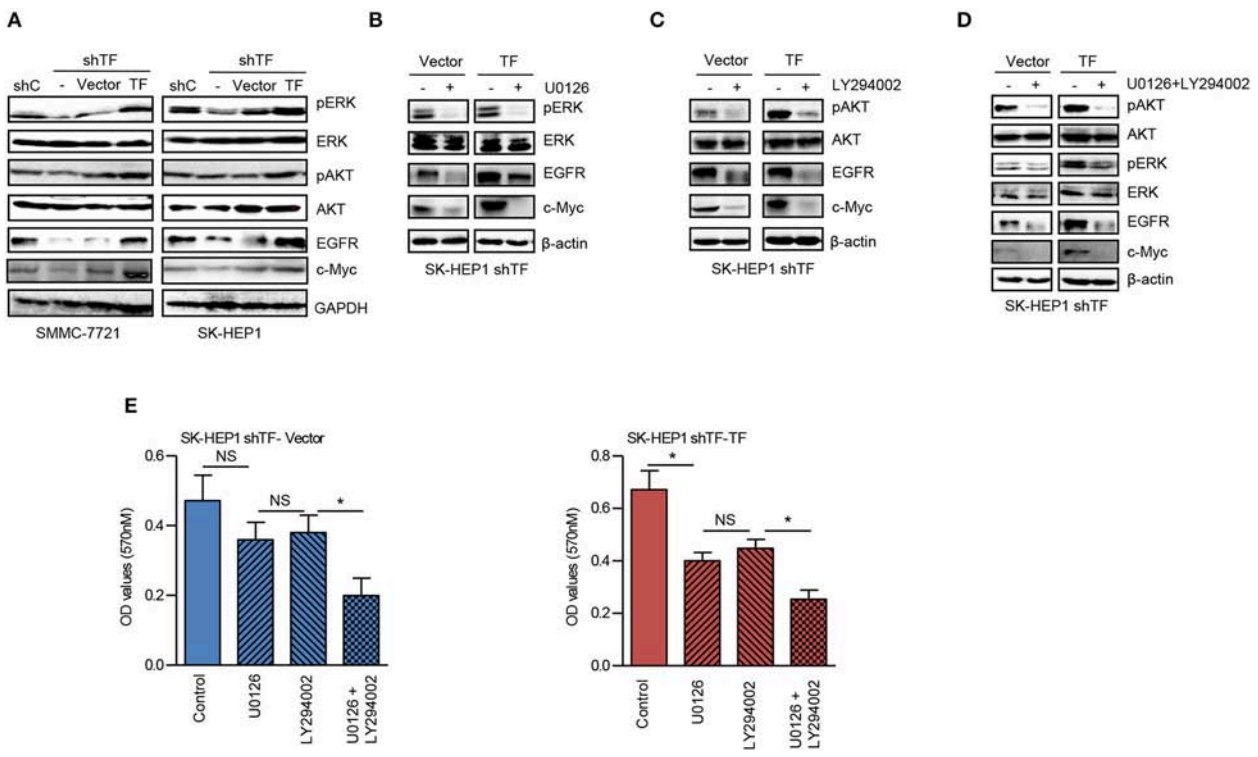

FIGURE 3 | TF promotes the growth of HCC by activating both ERK and AKT signaling pathways. **(A)** Western blot analysis of the protein expressions in the indicated cells. SK-HEP1 shTF-Vector and SK-HEP1 shTF-TF cells were treated with/without U0126 and LY294002 at the concentration of 10 μM for 24 h. **(B–D)** Western blot and **(E)** MTT assay analysis of the protein expressions and cell growth. Error bars, mean ± SD. *$p < 0.05$ (two-tailed Student's *t*-test **E**).

were analyzed by the χ^2 test or Fisher exact test. Correlations between different protein expressions level were determined using Spearman's rank analysis. The $p < 0.05$ was considered as statistical significance. $^{*}p < 0.05$; $^{**}p < 0.01$; NS: no statistical significance.

RESULTS

Knockdown of TF Inhibits the Growth of HCC

To explore the potential biological function of TF in HCC, we first examined the protein expression of TF in human HCC cell lines including HepG2, BEL-7402, SK-HEP1, SMMC-7721, and normal hepatic cell line LO2. Notably, all HCC cell lines displayed higher protein levels of TF than normal hepatic cell line, and SK-HEP1 and SMMC-7721 cells showed the highest protein levels of TF in all cells (**Figure 1A**). To further investigate the role of TF in HCC malignancy, we generated the cells with shRNA-mediated stable knockdown of endogenous TF in both SK-HEP1 and SMMC-7721 cells (**Figure 1B**). Knockdown of TF decreased the cell amounts, sphere numbers and sizes in both SK-HEP1 and SMMC-7721 cells as detected by MTT and sphere formation assays (**Figures 1C–E**). Additionally, the data of subcutaneous tumor models in nude mice showed that TF knockdown inhibited the growth of SMMC-7721 xenografts by decreasing the volumes and weights of tumors as well as the numbers of $Ki67^{+}$ proliferating cells (**Figures 1F–H**).

Overexpression of TF Promotes the Growth of HCC

To confirm the effect of TF on HCC growth, we performed rescue experiments by ectopic expression of TF in both TF-silenced SMMC-7721 and SK-HEP1 cells (**Figure 2A**). Ectopic expression of TF increased the cell amounts, sphere numbers, and sizes in both TF-silenced SMMC-7721 and SK-HEP1 cells (**Figures 2B–D**). Furthermore, overexpression of TF increased the cell amounts in LO2, HepG2, and BEL-7402 cells (**Figures 2E, F**). Taken together, these results suggest that TF can promote the growth of HCC.

TF Promotes the Growth of HCC by Activating Both ERK and AKT Signaling Pathways

To further explore the molecular mechanism of TF-promoted HCC growth, we detected the downstream signaling pathway of TF. As shown in **Figure 3A**, knockdown of TF decreased the protein levels of phosphorylated ERK (pERK), phosphorylated AKT (pAKT), and their downstream transcriptional factor c-Myc in both SMMC-7721 and SK-HEP1 cells. While ectopic expression of TF increased the protein levels of pERK, pAKT and c-Myc in both TF-silenced SMMC-7721 and SK-HEP1 cells. Interesting, the protein level of EGFR was downregulated in TF-silenced HCC cells and upregulated in TF-overexpressed HCC cells (**Figure 3A**). To define the roles of ERK and AKT in TF-mediated HCC growth, we examined the effects of MEK inhibitor U0126 and PI3K inhibitor LY294002 on the growth of both SK-HEP1 shTF-Vector and -TF cells. Treatment with U0126 or/and LY294002 decreased the protein levels of EGFR, c-Myc, pERK or/and pAKT in both SK-HEP1 shTF-Vector and -TF cells (**Figures 3B–D**). However, with U0126 or LY294002 alone inhibited the growth only in SK-HEP1 shTF-TF cells but not in SK-HEP1 shTF-Vector cells. After treating with the combination of U0126 and LY294002 significantly

TABLE 1 | The correlation between TF and EGFR protein expressions in HCC tissues.

		TF expression			*P*
		High	**Low**	**Total**	**r**
EGFR expression	High	82	9	91	< 0.001
	Low	23	30	53	0.668
		105	39	144	

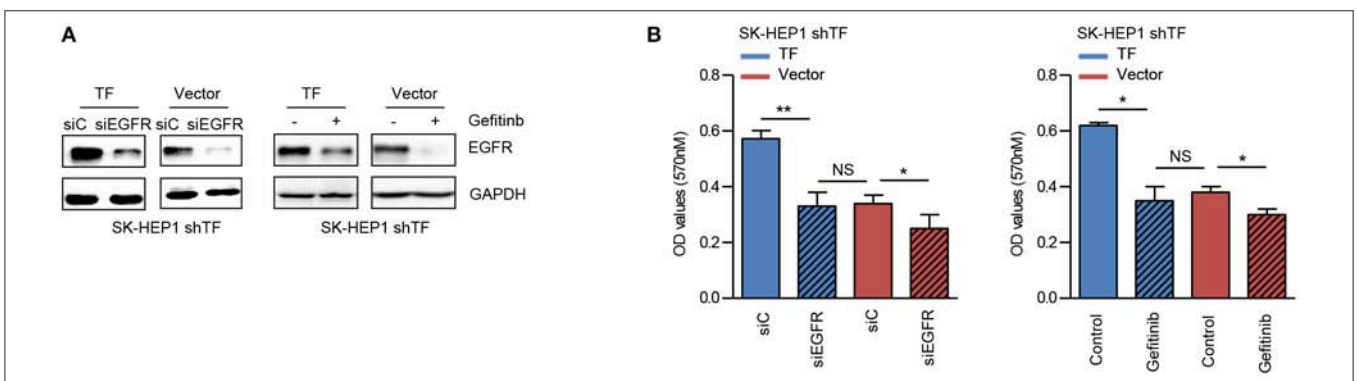

FIGURE 4 | Inhibition of EGFR suppresses TF-mediated HCC growth. SK-HEP1 shTF-Vector and SK-HEP1 shTF-TF cells were transfected with siControl or siEGFR or treated with/without gefinib at the concentration of 10 μM for 24 h. **(A)** Western blot and **(B)** MTT assay analysis of the protein expressions and cell growth. Error bars, mean ± SD. $^{*}p < 0.05$ and $^{**}p < 0.01$ (two-tailed Student's *t*-test **B**).

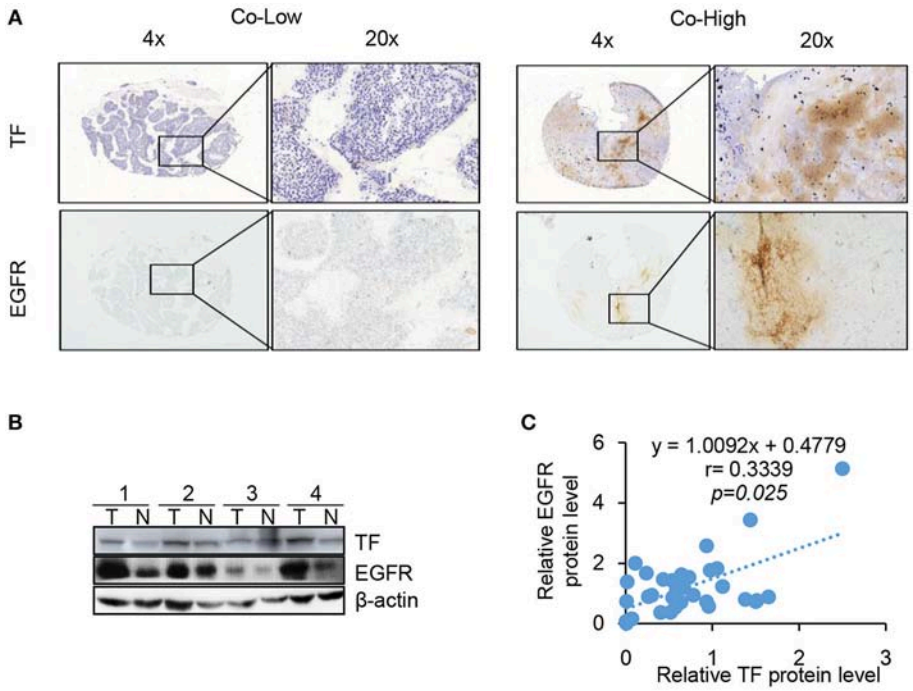

FIGURE 5 | TF protein expression is correlated with EGFR and poor HCC patient prognosis. TF and EGFR protein expressions in 144 HCC tissues were examined with IHC assay. **(A)** Representative images of positive and negative expression of both TF and EGFR were shown at 4 X and 20 X magnification. **(B)** Representative images of western blot analysis of TF and EGFR protein expression in the paired HCC tissues and adjacent normal tissues. **(C)** Spearman's rank correlation test showed the correlation between TF and EGFR protein expressions by Western blot.

inhibited the growth in both SK-HEP1 shTF-Vector and -TF cells (**Figure 3E**). In short, these data suggest that TF promotes the growth of HCC by activating both ERK and AKT signaling pathways.

Inhibition of EGFR Suppresses TF-Mediated HCC Growth

EGFR has been identified as a key player in the development of HCC (25). To verify the role of EGFR in TF-mediated HCC growth, we examined the effects of EGFR siRNA and EGFR inhibitor gefitinib on the growth of both SK-HEP1 shTF-Vector and -TF cells. EGFR siRNA or gefitinib decreased the protein levels of EGFR in both SK-HEP1 shTF-Vector and -TF cells (**Figure 4A**). Furthermore, EGFR siRNA or gefitinib inhibited the growth more significantly in SK-HEP1 shTF-TF cells than in SK-HEP1 shTF-Vector cells, indicating that inhibition of EGFR suppresses TF-mediated HCC growth (**Figure 4B**).

TF Protein Expression Is Correlated With EGFR in HCC Tissues

Our results clearly demonstrate that EGFR is regulated by TF in cell culture. To determine whether this is also the case in tumor tissues, we compared the protein levels of TF and EGFR in human 144 HCC tissues by IHC assay. High TF and EGFR staining were present in 105 (72.9%) and 91 (63.2%) out of 144 HCC tissues, respectively. Results of representative tissues with co-low or co-high staining of TF and EGFR were shown in **Figure 5A**. The expression of TF was highly correlated with the expression of EGFR in HCC tissues (**Table 1** and **Figures 5B, C**).

DISCUSSION

It has been demonstrated that TF-induced tumor progression need the activation of intracellular signaling pathways, where TF cytoplasmic domain couples to proteolytic activation of the protease activated receptor (PAR) 2 and subsequently activates ERK, AKT and other signaling pathways (26). For example, TF was involved in retinoblastoma cell proliferation via activating both ERK and AKT signaling pathways (27). Knockdown of TF suppressed human lung adenocarcinoma growth *in vitro* and *in vivo* through inhibiting both ERK and AKT signaling pathways (28). Similarly, our results showed that TF promoted the growth of HCC *in vitro* and *in vivo* by activating both ERK and AKT signaling pathways. Inhibition of ERK and AKT blocked TF-mediated growth of HCC. Therefore, activation of both ERK and AKT signaling pathways is indispensable for TF-promoted the growth of HCC.

EGFR is a member of ErbB/HER family of transmebrane receptor tyrosine kinases. It is activated by specific ligands resulting in the activation of multiple intracellular signaling pathways including ERK, AKT. Those signaling pathways is related to cell proliferation, migration and invasion (29–31). The gene expression of EGFR is regulated by the transcription factor c-Myc (32). In this study, we found that TF could enhance

the expression of c-Myc and EGFR, and inhibition of ERK and AKT could block TF-induced c-Myc and EGFR upregulation. Phosphorylation of serine 62 amino acid residues by ERK prevents c-Myc protein from degradation (33). AKT stabilizes c-Myc protein by phosphorylation and inactivation of GSK-3β which phosphorylated threonine 58 amino acid residues of c-Myc to promote c-Myc degradation (33).

Inhibition of EGFR with either small molecule inhibitors or specific antibodies has achieved promising results in the preclinical HCC models. In human HCC cells, gefitinib, erlotinib or cetuximab could induce growth inhibition, cell cycle arrest and apoptosis (34–36). In the orthotopic HCC models, gefitinib significantly inhibited the growth and metastasis of HCC tumors, and enhanced by the combination with cisplatin (37, 38). However, the outcome of targeting EGFR in HCC was modest in the clinical trials. When used as a single agent in HCC patients, erlotinib only acquired moderate effects (39, 40), and cetuximab showed no antitumor activity (41). Treatment failure with EGFR inhibitors in HCC patients may cause by many reasons, such as the levels and mutations of EGFR, EMT status of tumor cells, etc. (42–44). In the current study, we found that treatment with EGFR siRNA or gefitinib suppressed the growth more significantly in the TF highly expressed HCC cells, suggesting that the levels of TF in tumor cells may influence the effects of EGFR inhibitors. Furthermore, our IHC data showed that both positive ratios of TF and EGFR protein in the HCC tissue were 72.9% (105/144) and 63.2% (91/144), respectively. The expression of TF was highly correlated with the expression of EGFR in HCC tissues. Therefore, it may be valuable to investigate the relation of TF expressions and EGFR inhibitors effects in the future studies.

CONCLUSIONS

Our results provide proof-of-principle insights into a novel mechanism driven by TF on HCC growth and suggest that TF and EGFR may be potential therapeutic targets of HCC.

DATA AVAILABILITY

The datasets generated for this study are available on request to the corresponding author.

AUTHOR CONTRIBUTIONS

S-ZH, M-NW, J-RH, Z-JZ, W-JZ, Q-WJ, and YY performed experiments. H-YW, H-LJ, KW, Z-HX, M-LY, and YL collected and analyzed data. X-SH, ZS, and QZ prepared the manuscript.

FUNDING

This work was supported by funds from the National Natural Science Foundation of China Nos. 81661148049 and 81772540 (ZS), the Guangdong Natural Science Funds for Distinguished Young Scholar No. 2014A030306001 (ZS), the Guangdong Special Support Program for Young Talent No. 2015TQ01R350 (ZS), the Science and Technology Program of Guangdong Nos. 201300000187 (QZ) and 2016A050502027 (ZS), the Science and Technology Program of Guangzhou No. 201704030058 (ZS), the Science and Technology Program of Huizhou (170520181743174/2017Y229 and 180529101741637/2018Y305), and the Program Sci-tech Research Development of Guangdong Province 2014A020212717 (QZ).

REFERENCES

1. Torre LA, Bray F, Siegel RL, Ferlay J, Lortet-Tieulent J, Jemal A. Global cancer statistics, 2012. *CA Cancer J Clin.* (2015) 65:87–108. doi: 10.3322/caac.21262
2. Chen W, Zheng R, Baade PD, Zhang S, Zeng H, Bray F, et al. Cancer statistics in China, 2015. *CA Cancer J Clin.* (2016) 66:115–32. doi: 10.3322/caac.21338
3. Sun T, Liu H, Ming L. Multiple roles of autophagy in the sorafenib resistance of hepatocellular carcinoma. *Cell Physiol Biochem.* (2017) 44:716–27. doi: 10.1159/000485285
4. Li C, Chen J, Zhang K, Feng B, Wang R, Chen L. Progress and prospects of long noncoding RNAs (lncRNAs) in hepatocellular carcinoma. *Cell Physiol Biochem.* (2015) 36:423–34. doi: 10.1159/000430109
5. Versteeg HH, Spek CA, Peppelenbosch MP, Richel DJ. Tissue factor and cancer metastasis: the role of intracellular and extracellular signaling pathways. *Mol Med.* (2004) 10:6–11. doi: 10.2119/2003-00047.Versteeg
6. Mackman N. Role of tissue factor in hemostasis, thrombosis, and vascular development. *Arterioscler Thromb Vasc Biol.* (2004) 24:1015–22. doi: 10.1161/01.ATV.0000130465.23430.74
7. Ruf W. Tissue factor and cancer. *Thromb Res.* (2012) 130(Suppl. 1):S84–87. doi: 10.1016/j.thromres.2012.08.285
8. Zhou Q, Huang T, Wang YF, Zhou XB, Liang LJ, Peng BG. Role of tissue factor in hepatocellular carcinoma genesis, invasion and metastasis. *Chin Med J.* (2011) 124:3746–51.
9. Kaido T, Oe H, Yoshikawa A, Mori A, Arii S, Imamura M. Tissue factor is a useful prognostic factor of recurrence in hepatocellular carcinoma in 5-year survivors. *Hepatogastroenterology.* (2005) 52:1383–7.
10. Poon RT, Lau CP, Ho JW, Yu WC, Fan ST, Wong J. Tissue factor expression correlates with tumor angiogenesis and invasiveness in human hepatocellular carcinoma. *Clin Cancer Res.* (2003) 9:5339–45.
11. Yang Y, Qiu JG, Li Y, Di JM, Zhang WJ, Jiang QW, et al. Targeting ABCB1-mediated tumor multidrug resistance by CRISPR/Cas9-based genome editing. *Am J Transl Res.* (2016) 8:3986–94.
12. Shi Z, Li Z, Li ZJ, Cheng K, Du Y, Fu H, et al. Cables1 controls p21/Cip1 protein stability by antagonizing proteasome subunit alpha type 3. *Oncogene.* (2015) 34:2538–45. doi: 10.1038/onc.2014.171
13. Luo Y, Jiang QW, Wu JY, Qiu JG, Zhang WJ, Mei XL, et al. Regulation of migration and invasion by toll-like receptor-9 signaling network in prostate cancer. *Oncotarget.* (2015) 6:22564–74. doi: 10.18632/oncotarget.4197
14. Zhang WJ, Li Y, Wei MN, Chen Y, Qiu JG, Jiang QW, et al. Synergistic antitumor activity of regorafenib and lapatinib in preclinical models of human colorectal cancer. *Cancer Lett.* (2017) 386:100–9. doi: 10.1016/j.canlet.2016.11.011
15. Lv M, Qiu JG, Zhang WJ, Jiang QW, Qin WM, Yang Y, et al. Wallichinine reverses ABCB1-mediated cancer multidrug resistance. *Am J Transl Res.* (2016) 8:2969–80.
16. Chen X, Gong L, Ou R, Zheng Z, Chen J, Xie F, et al. Sequential combination therapy of ovarian cancer with cisplatin and gamma-secretase inhibitor MK-0752. *Gynecol Oncol.* (2016) 140:537–44. doi: 10.1016/j.ygyno.2015.12.011
17. Lin M, Bi H, Yan Y, Huang W, Zhang G, Tang S, et al. Parthenolide suppresses non-small cell lung cancer GLC-82 cells growth via B-Raf/MAPK/Erk pathway. *Oncotarget.* (2017) 8:23436–47. doi: 10.18632/oncotarget.15584
18. Gong LH, Chen XX, Wang H, Jiang QW, Pan SS, Qiu JG, et al. Piperlongumine induces apoptosis and synergizes with cisplatin or paclitaxel

in human ovarian cancer cells. *Oxid Med Cell Longev.* (2014) 2014:906804. doi: 10.1155/2014/906804
19. Li P, Yang Y, Liu H, Yang AK, Di JM, Tan GM, et al. MiR-194 functions as a tumor suppressor in laryngeal squamous cell carcinoma by targeting wee1. *J Hematol Oncol.* (2017) 10:32. doi: 10.1186/s13045-017-0402-6
20. Jiang QW, Cheng KJ, Mei XL, Qiu JG, Zhang WJ, Xue YQ, et al. Synergistic anticancer effects of triptolide and celastrol, two main compounds from thunder god vine. *Oncotarget.* (2015) 6:32790–804. doi: 10.18632/oncotarget.5411
21. Zheng DW, Xue YQ, Li Y, Di JM, Qiu JG, Zhang WJ, et al. Volasertib suppresses the growth of human hepatocellular carcinoma *in vitro* and *in vivo*. *Am J Cancer Res.* (2016) 6:2476–88.
22. Mei XL, Yang Y, Zhang YJ, Li Y, Zhao JM, Qiu JG, et al. Sildenafil inhibits the growth of human colorectal cancer *in vitro* and *in vivo*. *Am J Cancer Res.* (2015) 5:3311–24.
23. Shi Z, Park HR, Du Y, Li Z, Cheng K, Sun SY, et al. Cables1 complex couples survival signaling to the cell death machinery. *Cancer Res.* (2015) 75:147–58. doi: 10.1158/0008-5472.CAN-14-0036
24. Qiu JG, Zhang YJ, Li Y, Zhao JM, Zhang WJ, Jiang QW, et al. Trametinib modulates cancer multidrug resistance by targeting ABCB1 transporter. *Oncotarget.* (2015) 6:15494–509. doi: 10.18632/oncotarget.3820
25. Berasain C, Avila MA. The EGFR signalling system in the liver: from hepatoprotection to hepatocarcinogenesis. *J Gastroenterol.* (2014) 49:9–23. doi: 10.1007/s00535-013-0907-x
26. Han X, Guo B, Li Y, Zhu B. Tissue factor in tumor microenvironment: a systematic review. *J Hematol Oncol.* (2014) 7:54. doi: 10.1186/s13045-014-0054-8
27. Lee BJ, Kim JH, Woo SH, Kim DH, Yu YS. Tissue factor is involved in retinoblastoma cell proliferation via both the akt and extracellular signal-regulated kinase pathways. *Oncol Rep.* (2011) 26:665–70. doi: 10.3892/or.2011.1314
28. Xu C, Gui Q, Chen W, Wu L, Sun W, Zhang N, et al. Small interference RNA targeting tissue factor inhibits human lung adenocarcinoma growth *in vitro* and *in vivo*. *J Exp Clin Cancer Res.* (2011) 30:63. doi: 10.1186/1756-9966-30-63
29. Grant S, Qiao L, Dent P. Roles of ERBB family receptor tyrosine kinases, and downstream signaling pathways, in the control of cell growth and survival. *Front Biosci.* (2002) 7:d376–89. doi: 10.2741/grant
30. Normanno N, De Luca A, Bianco C, Strizzi L, Mancino M, Maiello MR, et al. Epidermal growth factor receptor (EGFR) signaling in cancer. *Gene.* (2006) 366:2–16. doi: 10.1016/j.gene.2005.10.018
31. Ma P, Fu Y, Chen M, Jing Y, Wu J, Li K, et al. Adaptive and acquired resistance to EGFR inhibitors converge on the MAPK pathway. *Theranostics.* (2016) 6:1232–43. doi: 10.7150/thno.14409
32. Perini G, Diolaiti D, Porro A, Della Valle G. *In vivo* transcriptional regulation of n-myc target genes is controlled by E-box methylation. *Proc Natl Acad Sci USA.* (2005) 102:12117–22. doi: 10.1073/pnas.0409097102
33. Sears R, Nuckolls F, Haura E, Taya Y, Tamai K, Nevins JR. Multiple ras-dependent phosphorylation pathways regulate Myc protein stability. *Genes Dev.* (2000) 14:2501–14. doi: 10.1101/gad.836800
34. Okano J, Matsumoto K, Nagahara T, Murawaki Y. Gefitinib and the modulation of the signaling pathways downstream of epidermal growth factor receptor in human liver cancer cells. *J Gastroenterol.* (2006) 41:166–76. doi: 10.1007/s00535-005-1736-3
35. Hopfner M, Sutter AP, Huether A, Schuppan D, Zeitz M, Scherubl H. Targeting the epidermal growth factor receptor by gefitinib for treatment of hepatocellular carcinoma. *J Hepatol.* (2004) 41:1008–16. doi: 10.1016/j.jhep.2004.08.024
36. Huether A, Hopfner M, Sutter AP, Schuppan D, Scherubl H. Erlotinib induces cell cycle arrest and apoptosis in hepatocellular cancer cells and enhances chemosensitivity towards cytostatics. *J Hepatol.* (2005) 43:661–9. doi: 10.1016/j.jhep.2005.02.040
37. Matsuo M, Sakurai H, Saiki I. ZD1839, a selective epidermal growth factor receptor tyrosine kinase inhibitor, shows antimetastatic activity using a hepatocellular carcinoma model. *Mol Cancer Ther.* (2003) 2:557–61.
38. Zhu BD, Yuan SJ, Zhao QC, Li X, Li Y, Lu QY. Antitumor effect of gefitinib, an epidermal growth factor receptor tyrosine kinase inhibitor, combined with cytotoxic agent on murine hepatocellular carcinoma. *World J Gastroenterol.* (2005) 11:1382–6. doi: 10.3748/wjg.v11.i9.1382
39. Philip PA, Mahoney MR, Allmer C, Thomas J, Pitot HC, Kim G, et al. Phase II study of erlotinib (OSI-774) in patients with advanced hepatocellular cancer. *J Clin Oncol.* (2005) 23:6657–63. doi: 10.1200/JCO.2005.14.696
40. Thomas MB, Chadha R, Glover K, Wang X, Morris J, Brown T, et al. Phase 2 study of erlotinib in patients with unresectable hepatocellular carcinoma. *Cancer.* (2007) 110:1059–67. doi: 10.1002/cncr.22886
41. Zhu AX, Stuart K, Blaszkowsky LS, Muzikansky A, Reitberg DP, Clark JW, et al. Phase 2 study of cetuximab in patients with advanced hepatocellular carcinoma. *Cancer.* (2007) 110:581–9. doi: 10.1002/cncr.22829
42. Lanaya H, Natarajan A, Komposch K, Li L, Amberg N, Chen L, et al. EGFR has a tumour-promoting role in liver macrophages during hepatocellular carcinoma formation. *Nat Cell Biol.* (2014) 16:972–7. doi: 10.1038/ncb3031
43. Su MC, Lien HC, Jeng YM. Absence of epidermal growth factor receptor exon 18-21 mutation in hepatocellular carcinoma. *Cancer Lett.* (2005) 224:117–21. doi: 10.1016/j.canlet.2004.10.010
44. Fuchs BC, Fujii T, Dorfman JD, Goodwin JM, Zhu AX, Lanuti M, et al. Epithelial-to-mesenchymal transition and integrin-linked kinase mediate sensitivity to epidermal growth factor receptor inhibition in human hepatoma cells. *Cancer Res.* (2008) 68:2391–9. doi: 10.1158/0008-5472.CAN-07-2460

Conflict of Interest Statement: The authors declare that the research was conducted in the absence of any commercial or financial relationships that could be construed as a potential conflict of interest.

frontiers in Oncology

ORIGINAL RESEARCH
published: 22 March 2019
doi: 10.3389/fonc.2019.00175

Schistosoma japonicum MiRNA-7-5p Inhibits the Growth and Migration of Hepatoma Cells via Cross-Species Regulation of S-Phase Kinase-Associated Protein 2

Chao Hu[1], *Shanli Zhu*[1], *Jing Wang*[1], *Yu Lin*[1], *Li Ma*[1], *Liufang Zhu*[1], *Pengyue Jiang*[1], *Zhengli Li*[1] *and Weiqing Pan*[1,2]*

[1] *Institute for Infectious Diseases and Vaccine Development, Tongji University School of Medicine, Shanghai, China,*
[2] *Department of Tropical Diseases, Second Military Medical University, Shanghai, China*

OPEN ACCESS

Edited by:
Yunkai Zhang,
Vanderbilt University Medical Center, United States

Reviewed by:
Yang Li,
University of Arizona, United States
Hui Wang,
Vanderbilt University, United States

***Correspondence:**
Weiqing Pan
wqpan0912@aliyun.com

Specialty section:
This article was submitted to Cancer Molecular Targets and Therapeutics, a section of the journal Frontiers in Oncology

Received: *24 October 2018*
Accepted: *28 February 2019*
Published: *22 March 2019*

Citation:
Hu C, Zhu S, Wang J, Lin Y, Ma L, Zhu L, Jiang P, Li Z and Pan W (2019) Schistosoma japonicum MiRNA-7-5p Inhibits the Growth and Migration of Hepatoma Cells via Cross-Species Regulation of S-Phase Kinase-Associated Protein 2. Front. Oncol. 9:175. doi: 10.3389/fonc.2019.00175

MicroRNAs (miRNAs) play important roles in human diseases, such as cancer. Human miRNA-7-5p is a tumor suppressor miRNA that inhibits tumor growth by regulating multiple oncogenic signal pathways. Recently, studies revealed that plant miRNAs could regulate mammalian gene expression in a cross-kingdom manner. *Schistosoma japonicum* miRNA-7-5p (designated as sja-miR-7-5p) is conserved between the parasites and mammals. Thus, we investigated whether sja-miR-7-5p has similar antitumor activity to its mammalian counterpart. We first showed that sja-miR-7-5p was detected in host hepatocytes during *S. japonicum* infection. The sja-miR-7-5p mimics significantly inhibited the growth, migration, and colony formation of mouse and human hepatoma cell lines *in vitro*, and induced G1/G0 cell cycle arrest. In a xenograft animal model, the tumor volume and weight were significantly reduced in mice inoculated with hepatoma cells transfected with sja-miR-7-5p mimics compared with those transfected with NC miRNAs. Furthermore, the antitumor activity of sja-miR-7-5p was suggested by cross-species downregulation of the S-phase kinase-associated protein 2 gene in the host. Thus, sja-miR-7-5p is translocated into hepatocytes and exerts its anti-cancer activities in mammals, implying that sja-miR-7-5p might strengthen host resistance to hepatocellular carcinoma during schistosome infection.

Keywords: *Schistosoma japonicum*, microRNA, hepatoma cell, SKP2, cross-species regulation

INTRODUCTION

The primary pathology of schistosomiasis caused by *S. japonicum* is egg-induced granuloma and fibrosis. The female adult worms living in the host mesenteric veins lay numerous eggs, and most of them are trapped in the liver tissues via the portal venous system, causing a granulomatous reaction and fibrosis. The parasite eggs in the granuloma are surrounded by host cells, including immunocytes, hepatic mesenchymal cells, and hepatocytes (1). Our previous studies indicated that *S. japonicum* secretes many microRNAs (miRNAs), including *Schistosoma*-specific and conserved miRNAs (2), and parasite miRNA-containing exosomes (2).

MiRNAs are a class of highly conserved, small non-coding RNAs, with a length of about 20–24 nucleotides (nt) that post-transcriptionally regulate gene expression through complete or incomplete binding to their target mRNAs (3). MiRNAs have extensive effects on not only physiological processes, but also on the progression of many human diseases, such as cancers (4, 5). Aberrant miRNA expression promotes the occurrence and development of various cancers (6–8); however, some miRNAs can exert therapeutic effects on multiple cancers through regulation of tumor-related genes, including those that control tumor cell growth or apoptosis (9, 10). Interestingly, miRNAs derived from plants can regulate the expression of their target genes in mammals in a cross-kingdom manner (11–13). For example, miR-159 derived from plants was detectable in human sera and inhibited breast cancer growth by targeting the human transcription factor 7 (*TCF7*) gene (13). Accumulating evidence indicates that heterogeneous miRNAs can modulate cell functions in mammals. However, it remains unclear how the plant miRNAs can survive the passage through the gastrointestinal tract following ingestion.

Unlike plant miRNAs, which need to pass through the gastrointestinal tract before release into the host serum or entering host cells, schistosomal miRNAs from eggs trapped in liver tissue may be directly transferred to the neighboring host cells. Thus, we hypothesized that parasite miRNAs from the eggs might be translocated into neighboring hepatocytes to exert various biological effects, including some that are beneficial to the host, for example, strengthening the resistance of the host to diseases such as cancer, as do plant-derived miRNAs (13). Human miRNA-7-5p (designated as hsa-miR-7-5p) is a tumor suppressor miRNA that regulates multiple oncogenic signal pathways and reverses drug resistance in certain cancers (14–17). Our previous study identified a *S. japonicum* miRNA-7-5p (designated as sja-miR-7-5p) that is conserved between the parasite and mammals, i.e., there is an identical seed sequence (2–8 nt at the 5′ region) in both parasites and mammalian miRNA-7-5p, despite there being 6 nt differences in the rest of the sequence. Thus, it would be interesting to investigate if sja-miR-7-5 secreted by *S. japonicum* has a similar antitumor activity to hsa-miR-7-5p. In the present study, we demonstrated that sja-miR-7-5p is present in hepatocytes during the *S. japonicum* infection and the sja-miR-7-5p exerts anticancer effects on multiple hepatoma cells (assessed using *in vitro* and *in vivo* models) by targeting the S-phase kinase-associated protein 2(*SKP2*) gene, which is a component of the SCF (Skp1-Cullin 1-F-box) E3 ubiquitin-ligase complex. Previous studies have shown that overexpression of the *SKP2* gene was observed in many cancers, such as in liver cancer (18), prostate cancer (19), lymphoma (20), melanoma (21), and breast cancer (22), which plays an important role in regulating cellular proliferation and cancer progression, mainly by targeting cell cycle regulators in an ubiquitin-dependent manner, followed by 26S proteasome degradation (23). In addition, the *SKP2* overexpression also enhanced tumor cell invasion (24), metastasis (25), and resistance to apoptosis (26), and was associated with tumor aggressiveness (27) and poor prognosis (28).

Abbreviations: *S. japonicum*, *Schistosoma japonicum*; HCC, hepatocellular cancer; SKP2, S-phase kinase associated protein 2; P27(also known as CDKN1B), cyclin dependent kinase inhibitor 1B; MMP9, matrix metallopeptidase 9; miRNA, microRNA; siRNA, small interfering RNA; NC, negative control; Mock, mock control.

MATERIALS AND METHODS

Infection of Mice With *S. japonicum* Cercariae

Animal experiments were performed in accordance with the Guide for the Care and Use of Laboratory Animals of the National Institutes of Health, and approved by the Internal Review Board of Tongji University School of Medicine. The animal surgeries were undertaken under sodium pentobarbital anesthesia. Cercariae of *S. japonicum* were provided by National Institute of Parasitic Disease, Chinese Center for Disease Control and Prevention (CDC). 36 six-week-old male C57BL/6J mice (18–20 g, 3 mice per group), purchased from experimental animal center of the Second Military Medical University and housed under specific pathogen-free conditions, were percutaneously infected with 50 or 100 cercariae of *S. japonicum* per mouse (50 for collection of infected hepatocytes and 100 for collection of early stage parasites). For collection of parasites, the hepatic schistosomula were isolated from the portal system and mesenteric veins of infected mice at 7, 14, and 42 days post-infection (dpi). In addition, 42 days male and female adult worms were manually separated under a light microscope. The eggs were isolated with a traditional method, as described by Cai et al. (29). All the freshly isolated parasites were washed three times with PBS (pH 7.4) and were immediately used for extraction of total RNA or frozen at −80°C until being subjected to further analysis.

Isolation of Primary Mouse Hepatocytes

The primary mouse hepatocytes were isolated by a two-step collagenase perfusion procedure, as described by He et al. (30) with minor modifications. Briefly, after infection, livers of the infected mice collected at various time points of 7, 9, 11, 14, 28, and 42 dpi ($n = 5$) along with the livers of uninfected mice were initially *in situ* digested with 0.03% collagenase type IV and then further digested with 0.08% collagenase type IV at 37°C in a shaking bath for 30 min. The single cell suspensions were harvested by filtration through 400-mesh sieves for removal of the remaining tissue debris and parasite eggs. Next, hepatocytes were isolated by centrifugation of the resulting cell suspensions at 50×g for 4 min and further purified by centrifugation at 50 × g for 4 min. Purified hepatocytes were resuspend in DMEM containing 20 μg/ml Ribonuclease A (Sigma-Aldrich, USA) at 37°C for 30 min to eliminate any miRNA that might be released by schistosome eggs. After washing with PBS for three times, the cell pellet was immediately used for extraction of total RNA or frozen at −80°C until used.

Cell Proliferation Assay

Cells (2×10^5) were seeded in a 6-well plate overnight, respectively. Then cells were transfected with sja-miR-7-5p

mimics or NC mimics, respectively, four replicates per group. And 24 h later, cells were digested and seeded in a 96-well plate (2×10^3) for 1, 2, 3, and 4 d. At each indicated time, 10 μL Cell Counting Kit-8(CCK-8, Dojindo, Japan) was added to each well and cells were incubated for 1 h at 37 °C, then, using the Microplate reader (Bio-Tek, USA) to measure the abosorbance at 450 nm.

Cell Cycle Analysis

Cells (1×10^5) were seeded in a 12-well plate overnight, respectively. Then, cells were transfected with sja-miR-7-5p mimics or NC mimics, respectively, three replicates per group. And 48 h later, cells were collected and fixed with ice-cold 75%(v/v) ethanol and stored at 4°C overnight, then, cells were washed and resuspended in 200 μL phosphate-buffered saline (PBS) contained with 0.05 mg/mL RNase A (Beyotime, China) and 25 mg/mL propidium iodide (PI) (Beyotime, China), cell cycle was determined by the FACSverse flow cytometer (BD Biosciences, USA).

Colony Formation Assay

Cells (2×10^5) were seeded in a 6-well plate overnight, then cells were transfected with sja-miR-7-5p mimics or NC mimics, respectively. And 24 h later, cells were digested and 200 cells in 500 μL complete medium were seeded in 24-well plate, three replicates per group. After incubation for 8 days, then cells were

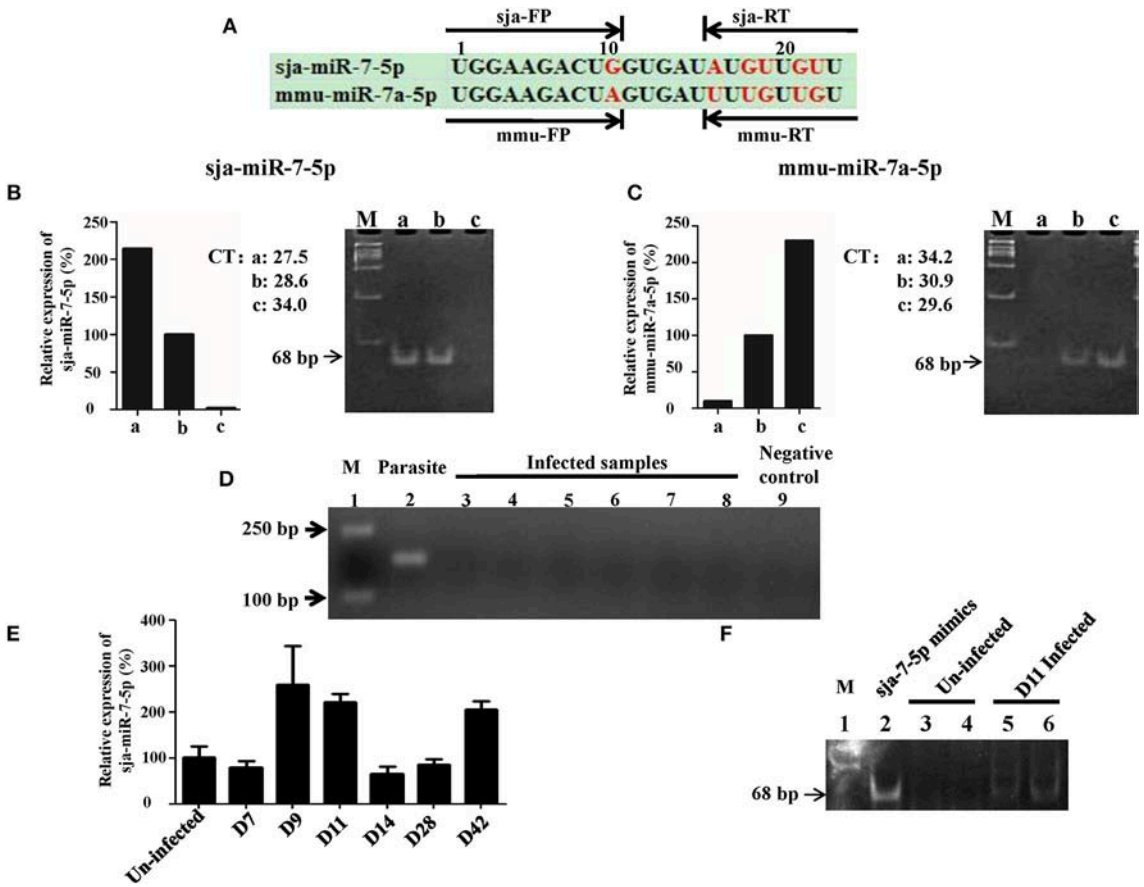

FIGURE 1 | Detection of sja-miR-7-5p in infected hepatocytes**. (A)** A schematic diagram represents two sets of primers of reverse transcription stem-loop primer (RT) and forward primer (FP) for sja-miR-7-5p or mmu-miR-7a-5p, respectively. **(B,C)** Preparation of RNA samples: a. 200 ng *Schistosoma japonicum* egg RNA; b. mixture of equal amount of *Schistosoma japonicum* egg RNA (100 ng) and Hepa1-6 cell RNA (100 ng); c. 200 ng Hepa1-6 cell RNA. The three RNA templates were transcribed into cDNA using the corresponding reverse transcription stem-loop primer, respectively, which were used for qRT-PCR by the corresponding forward primer and common reverse primer, respectively. The PCR products were separated by polyacrylamide gel electrophoresis (PAGE). As shown in B and C, the two sets of primers can effectively distinguished the sja-miR-7-5p and mmu-miR-7a-5p, e.g., the set of sja-miR-7-5p RT and forward primer FP amplified the sja-miR-7-5p [**(B)**, lane a and b] but not mmu-miR-7a-5p (lane c), while the set of mmu-miR-7a-5p RT and forward primer FP generated the mmu-miR-7a-5p but not the sja-miR-7-5p **(C)**. **(D)** Analysis of the RNA samples to ensure no contamination with parasite RNA: the RNA samples used for the above analysis were detected as described in Method by PCR for presence of the NADH gene of *S. japonicum*. Lane 1: marker. Lane 2: parasite positive control: RNA samples of *S. japonicum* eggs as described above. Lane 3–8: six samples of infected hepatocytes with RNase pre-incubation. Lane 9: negative control without the template. **(E)** qRT-PCR analysis of sja-miR-7-5p in the infected hepatocytes at various days after infection; **(F)** 12% PAGE analysis showing sja-miR-7-5p PCR product (68 bp) from the infected hepatocytes: Lane 1: marker; Lane 2: sja-miR-7-5p mimics positive control; Lanes 3 and 4: two uninfected hepatocyte samples with pre-incubation with RNase; Lanes 5 and 6: two infected hepatocyte samples at day 11 post-infection with the pre-incubation. Data are presented as the mean ± SD, $n = 3$.

fixed in methanol for 30 min, followed by staining in crystal violet for 15 min. The number of colonies containing > 50 cells was counted under a light microscope.

Tumor Xenograft Animal Model

Male athymic nude mice were housed and manipulated according to the protocols approved by the Shanghai Medical Experimental Animal Care Commission. Hepa1-6 cells or HepG2 cells were transfected with sja-miR-7-5p mimics or NC mimics, respectively. And 24 h later, for each mouse, 1×10^6 cells in 100 μL PBS after treated with sja-miR-7-5p mimics were injected subcutaneously to the left scapula, while cells after treated with NC mimics were injected subcutaneously to the right scapula, respectively. Tumor volume was measured at 2, 4, 6, and 7 d after injection, At day 7, the mice were sacrificed and tumors were separated to measure their weight and volume. Tumor volume was measured using the formula: $0.5 \times L \times S^2$, where L is the longest diameter of tumor and S is the shortest diameter of tumor. The content of sja-miR-7-5p mimics transfected into the tumor cells measured by quantitative real-time reverse transcription PCR (qRT-PCR), the protein level of SKP2 was determined by Western blotting. And also the expression of Ki67 in the tumor was measured by immunohistochemistry (IHC) as described under this section.

Immunohistochemistry

To determine Ki67 expression in xenograft tumor tissues from the athymic nude mice, immunohistochemistry (IHC) was performed as described previously (31), Antibody against Ki67 was used (1:50 dilution).

Statistical Analysis

All experiments were performed in triplicate and the results were presented as mean ± standard deviation (mean ± SD). All data were analyzed by one-way ANOVA using the software GraphPad Prism 5.0(GraphPad Software, Inc. La Jolla, CA, USA). A value of $P < 0.05$ was considered statistically significant.

RESULTS

Presence of sja-miR-7-5p in Infected Hepatocytes

We first investigated whether sja-miR-7-5p was present in the host liver cells during schistosome infection. For this purpose, we designed a set of two sets primers that could distinguish the sja-miR-7-5p from corresponding miRNA derived from mouse (mmu-miR-7-5p) and human (hsa-miR-7-5p). The sja-miR-7-5p has an identical seed sequence (2–8 nt at the 5' region), but

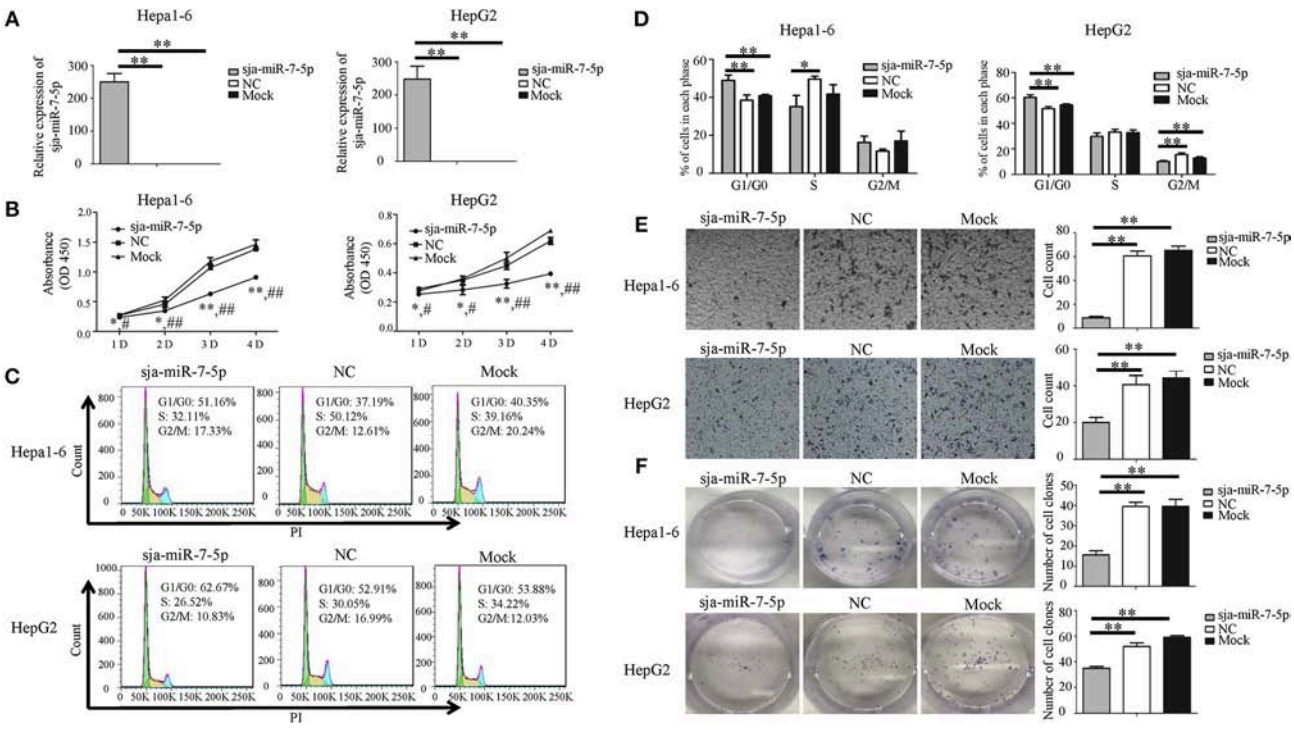

FIGURE 2 | Sja-miR-7-5p inhibits cell proliferation and migration of Hepa1-6 and HepG2 cells *in vitro*. **(A–F)** Hepa1-6 and HepG2 cells were transfected with sja-miR-7-5p mimics and NC (negative control) mimics, respectively, and 48 h later [except for the cell counting kit-8(CCK-8) assay, which was 24 h later], the expression of sja-miR-7-5p was determined using qRT-PCR (A). Cell proliferation was evaluated by CCK-8 assay at 1, 2, 3, and 4 days **(B)**, data are presented as the mean ± SD, $n = 3$, $^*p < 0.05$ or $^{**}p < 0.01$ indicates the comparison between the two groups of sja-miR-7-5p and NC; $\#p < 0.05$ or $\#\#p < 0.01$ indicates the comparison between the groups of sja-miR-7-5p and Mock. Cell cycle was determined by flow cytometry analysis **(C,D)**. Cell migration was evaluated using Transwell inserts without matrigel coating **(E)**. The ability to form cell clones was determined using a colony formation assay **(F)**. Data are presented as the mean ± SD, $n = 3$, $^*p < 0.05$, $^{**}p < 0.01$.

there are 6 nt differences in the rest of the sequence among the species (**Figure 1A**, and **Figure S1**), which allowed us to design sets of specific primers for the mmu-miR-7a-5p (mmu-FP/RT) and the sja-miR-7-5(sja- FP/RT). We first tested specificity of the primers using the RNA samples derived from *S. japonicum* eggs (a), mouse Hepa1-6 cell line (c), and mixture of equal amount of a and c (b). As shown in **Figures 1B,C**, the sja-FP/RT pair primers successfully generated the sja-miR-7a-5p from the samples of a and b, but not c (**Figure 1B**), while the mmu-FP/RT pair primers generated the mmu-miR-7a-5p from the sample b and c, but not a (**Figure 1C**). These data indicated that the two sets of primers can effectively distinguish the sja-miR-7-5p and mmu-miR-7a-5p, and no cross reaction between the mmu-FP/RT and sja-FP/RT primers. All the primers are listed in **Table S1**.

We next used the sja-FP/RT primers for detection of presence of sja-miR-7-5p in the liver cells of infected mice with *S. japonicum*. We prepared RNA samples from the infected liver cells, and carefully analyzed the samples to ensure no contamination with parasite RNA (**Figure 1D**). We showed that sja-miR-7-5p was detected by using qRT-PCR in the hepatocytes from infected mice at the early stage (i.e., days 9 and 11 post infection) and the late stage of infection (day 42) (**Figure 1E**). The presence of this parasite miRNA was further verified by PCR (**Figure 1F**) and cloning and sequencing of the PCR product showed identical sequence of sja-miR-7-5p (**Figure S2A**). In addition, we showed that sja-miR-7-5p was expressed at all these stages, and higher expression of sja-miR-7-5p was detected in adult males compared with that in adult females (**Figure S2B**). These findings indicated that this sja-miR-7-5p is present in the host liver cells during schistosome infection.

Inhibition of Proliferation and Migration of Hepatoma Cells by Sja-miR-7-5p

To investigated the effects of sja-miR-7-5p on the growth of hepatoma cells *in vitro,* both mouse and human hepatoma cells (e.g., Hepa1-6 cells and HepG2 cells) were transfected with the sja-miR-7-5p mimics, NC (a negative control mimics that has no target gene in mice and human) and Mock (transfection reagents only). As shown in **Figure 2A**, the sja-miR-7-5p mimics were effectively transfected into both cell lines. The schistosomal miRNA significantly suppressed the proliferation of both cell lines, as measured by the CCK-8 assay (**Figure 2B**), and substantially arrested the cell cycle at G1/G0 phase, as detected by flow cytometry (**Figures 2C,D**). We also showed that transfection of the sja-miR-7-5p mimics significantly suppressed cell migration, as assessed using the Transwell inserts without matrigel coating (**Figure 2E**) and by the wound-healing assay (**Figures S3B,C**) compared with the NC or Mock control cells. Colony formation assays showed that sja-miR-7-5p inhibited colony formation of hepatoma cells to a greater extent that those in the NC group or Mock group (**Figure 2F**). In addition, the Hepa1-6 cells transfected with sja-miR-7-5p mimics grew bigger and rounder compared with those in the NC or Mock control cells (**Figure S3A**). These data indicated that sja-miR-7-5p inhibited growth, migration, and colony formation of both mouse and human hepatoma cells and arrested their cell cycle

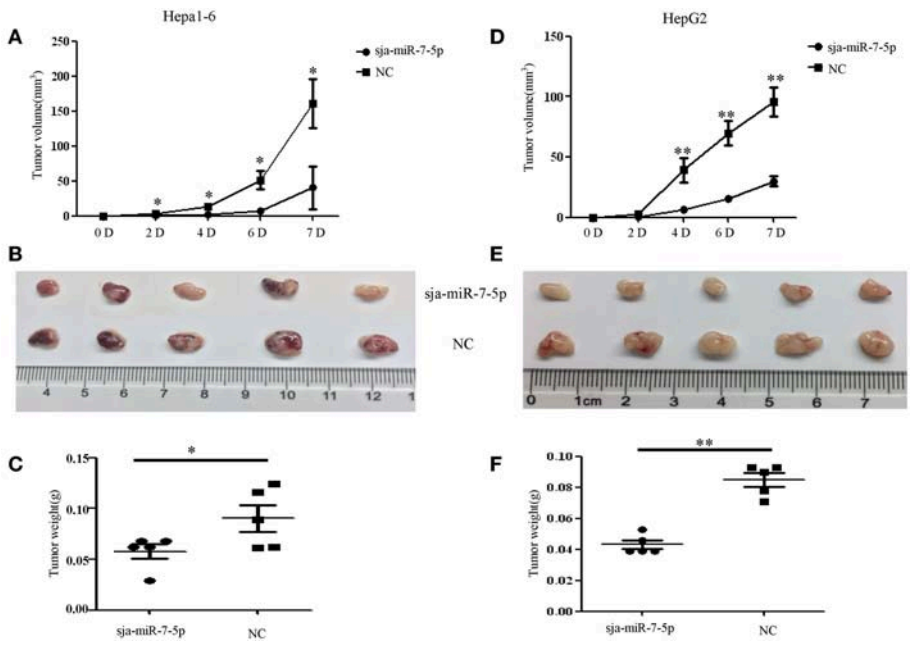

FIGURE 3 | Sja-miR-7-5p inhibits hepatoma cell growth *in vivo*. **(A–F)** Hepa1-6 and HepG2 cells were transfected with sja-miR-7-5p mimics or NC mimics, respectively, and then the sja-miR-7-5p-treated cells (1×10^6) were injected subcutaneously to the left scapula of athymic nude mice, and the NC-treated cells were injected subcutaneously into the right scapula ($n = 5$), respectively. Tumor volumes were measured at days 2, 4, 6, and 7 after injection. At day 7, the mice were sacrificed and tumors were separated to measure their weight and volume, **(A–C)** for Hepa1-6 cells, **(D–F)** for HepG2 cells. Data are presented as the mean ± SD, $n = 5$, $^*p < 0.05$, $^{**}p < 0.01$.

at G1/G0 phase *in vitro*, indicating that the schistosomal miRNA is also a tumor suppressor.

Sja-miR-7-5p-Mediated Inhibition of Hepatoma Cell Growth *in vivo*

To further investigate whether sja-miR-7-5p inhibits growth of liver cancer cells *in vivo*, both Hepa1-6 and HepG2 cells were transfected with sja-miR-7-5p mimics or NC mimics, and then injected subcutaneously to the left and right scapula of athymic nude mice to generate subcutaneous tumors. The tumor volume was measured at days 2, 4, 6, and 7 after injection. At day 7, mice were sacrificed and tumors were excised to measure their weight and volume. The results showed that both the tumor volume and weight were significantly reduced in the mice inoculated with Hepa1-6 cells transfected with sja-miR-7-5p mimics compared with those in mice receiving cells transfected with NC miRNAs (**Figures 3A–C**). Similar results were obtained with the human cell line of HepG2 (**Figures 3D–F**). These data indicated that sja-miR-7-5p suppressed tumor growth *in vivo*.

SKP2 Is a Direct Target of Sja-miR-7-5p

To determine the molecular mechanisms by which sja-miR-7-5p inhibits hepatoma cell growth, we used the online software miRDB (32) (http://www.mirdb.org/miRDB/index.html), MR-microT (33) (http://diana.imis.athena-innovation.gr/DianaTools/index.php?r=mrmicrot/index) and RNAhybrid (34) (http://bibiserv.techfak.uni-bielefeld.de/rnahybrid?id=rnahybrid_view_submission).

To search for potential targets of sja-miR-7-5p. We identified the gene encoding S-phase kinase-associated protein 2(*SKP2*) as a potential target for sja-miR-7-5p, because a binding site was located at the 3' UTR of the both murine and human *SKP2* gene that perfectly matched the seed sequence of sja-miR-7-5p. In addition, the *SKP2* gene in human has been characterized as an oncogene during tumorigenesis (21, 35–38).

To investigate the relationship between sja-miR-7-5p and *SKP2* gene in both human and mouse, first, we constructed two plasmids that contain the luciferase reporter gene: One was the pmirGLO-*SKP2*-WT construct in which the firefly luciferase gene is fused to the 3' UTR of *SKP2* gene; the other was the pmirGLO-*SKP2*-MT in which the seven nucleotides in the miRNA binding site were mutated (**Figure 4A**). The constructs were simultaneously transfected with sja-miR-7-5p mimics or NC mimics into both Hepa1-6 cells and HepG2 cells. As shown in **Figure 4B**, the luciferase activity was significantly decreased in the cells transfected with the pmirGLO-*SKP2*-WT but not with the pmirGLO-*SKP2*-MT, indicating that sja-miR-7-5p mimics could directly bind to the site in the 3′ UTR of the *SKP2* gene, while the mutations in the seed sequence abrogated the inhibitory effect.

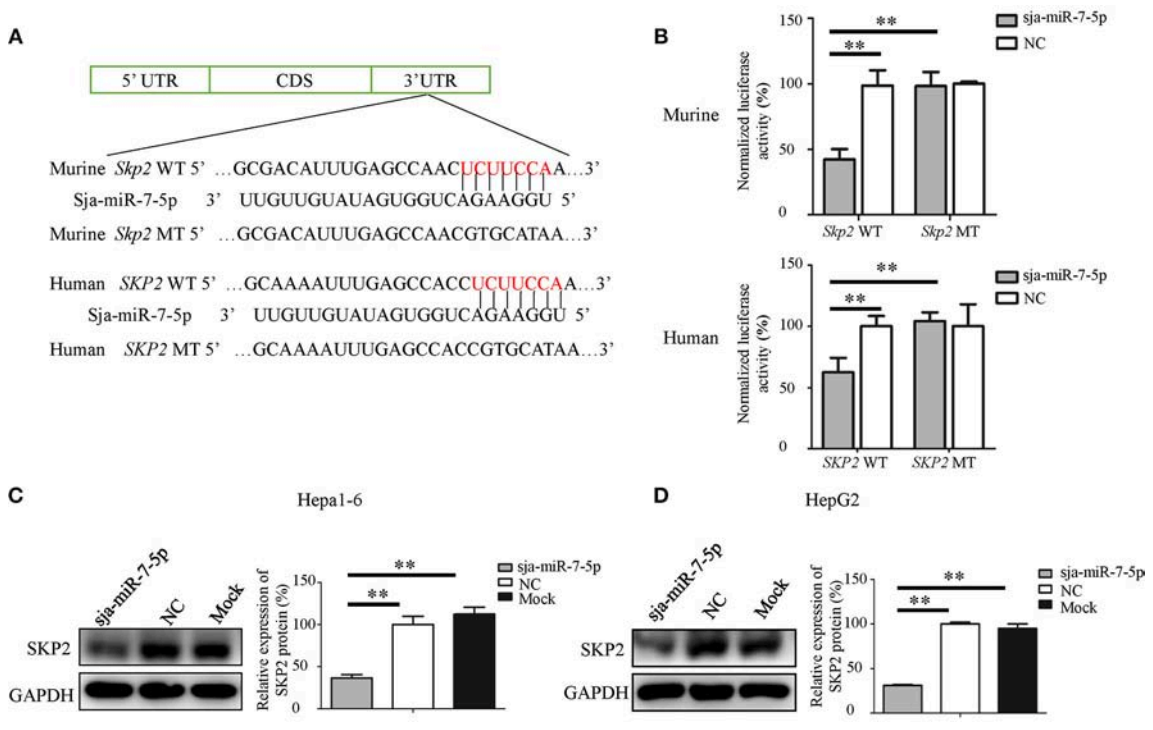

FIGURE 4 | *SKP2* (encoding S-phase kinase-associated protein 2) is a direct target of sja-miR-7-5p. **(A)** A schematic diagram representing the wild-type or mutant 3' untranslated region (UTR) sites of murine *Skp2* and human *SKP2* genes targeted by sja-miR-7-5p. **(B)** A dual-luciferase reporter assay was used to measure the activity of the reporter gene, and the firefly luciferase activity was normalized to renilla luciferase activity. **(C,D)** The protein levels of murine SKP2 **(C)** and human SKP2 **(D)** were measured using western blotting after transfection with sja-miR-7-5p mimics or NC mimics, respectively. Data are presented as the mean ± SD, $n = 3$, $^{**}p < 0.01$.

We then detected the level of the SKP2 protein in both Hepa1-6 or HepG2 cells transfected with sja-miR-7-5p mimics using Western blotting. We found that sja-miR-7-5p downregulated the levels of SKP2 in both Hepa1-6 cells and HepG2 cells compared with that in cells transfected with NC or Mock controls (**Figures 4C,D**).

Sja-miR-7-5p-Mediated Suppression of the Hepatoma Cell Growth Through Downregulation of SKP2 Expression

To investigate whether sja-miR-7-5p inhibits the growth of hepatoma cells through inhibition of SKP2 expression, both Hepa1-6 cells and HepG2 cells were transfected with the *SKP2* small interfering RNAs (siRNAs). We showed that both murine *Skp2* siRNA (SKP2-786) and human *SKP2* siRNA (SKP2-1291) significantly reduced the SKP2 expression in Hepa1-6 cells and HepG2 cells, respectively, at both transcriptional and translational levels detected by qRT-PCR and Western blotting (**Figure 5A**). Importantly, similar to the observations in the sja-miR-7-5p mimics-treated cells, the transfected Hepa1-6 cells and HepG2 cells with the siRNA showed cell cycle arrest at the G0/G1 phase (**Figures 5C,D**), and inhibition of cell proliferation (**Figure 5B**), cell migration (**Figure 5E**), and colony formation (**Figure 5F**), whereas these inhibitory effects were not observed in the cells treated with the NC siRNA. The phenotypes of the cells treated with *SKP2* siRNA were similar to those of sja-miR-7-5p mimics-treated cells, which suggested that the inhibitory effects of the schistosome miRNA on hepatoma cells function by downregulating SKP2 expression.

We also detected the expression of *SKP2* gene in the subcutaneous tumors generated by Hepa1-6 or HepG2 cells transfected with sja-miR-7-5p or NC mimics, respectively. As shown in **Figures 6A,B**, the transfected sja-miR-7-5p was detectable in the tumors on day 7 after injection. We then detected the SKP2 protein level using Western blotting, which showed that the level of SKP2 was significantly decreased in the tumors of both Hepa1-6 and HepG2 cells receiving sja-miR-7-5p compared with that in tumors from cells transfected with the NC control (**Figures 6C,D**). Meanwhile, we evaluated the proliferation of the tumor cells using immunohistochemistry (IHC) for Ki67, which showed that the protein level of Ki67 was also significantly decreased in tumor cells transfected with sja-miR-7-5p compared with that in cells transfected with the NC control (**Figure 6E**). These data further suggested that sja-miR-7-5p inhibited proliferation

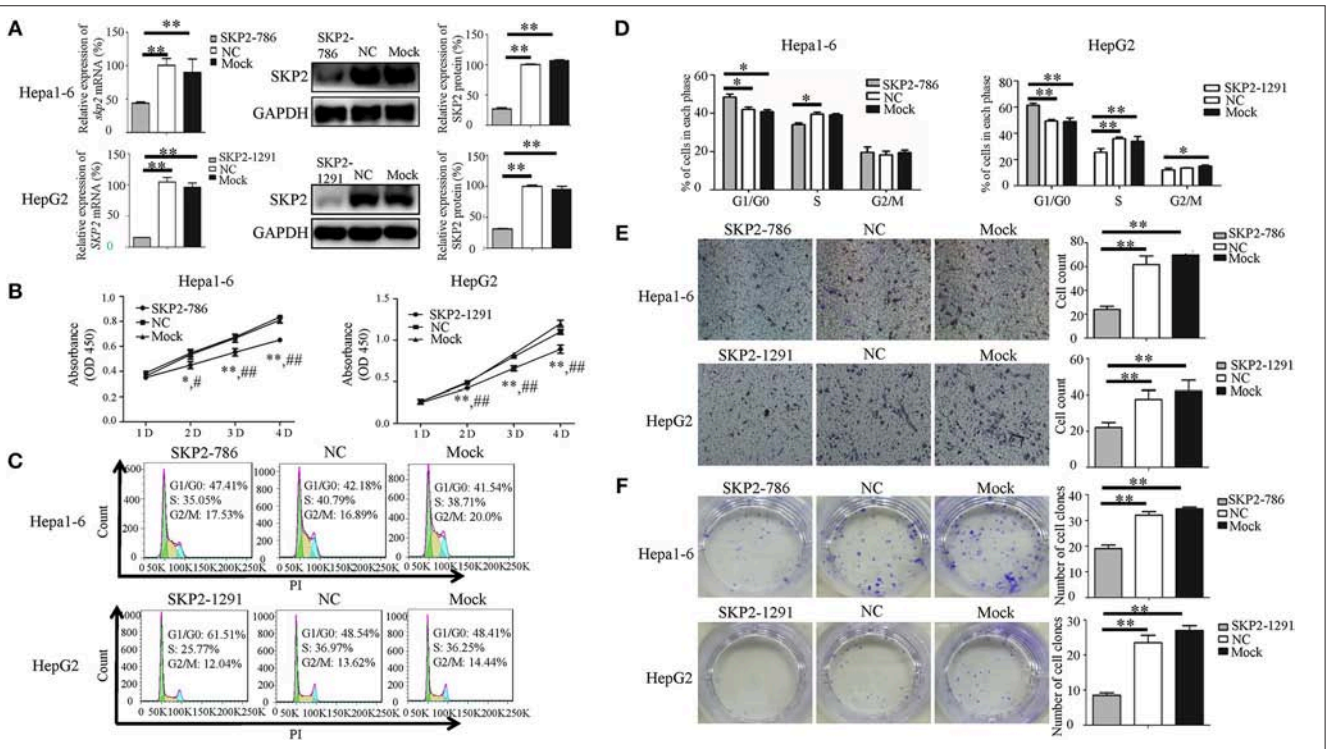

FIGURE 5 | Knockdown of *SKP2* inhibits cell proliferation and migration of Hepa1-6 and HepG2 cells *in vitro*. **(A–F)** Hepa1-6 and HepG2 cells were transfected with *SKP2* siRNA and negative control (NC) siRNA, respectively, and 48 h later (except for the cell counting kit-8(CCK-8) assay, which was 24 h later), the expression of *SKP2* was determined using qRT-PCR and western blotting **(A)**. Cell proliferation was evaluated using the CCK-8 assay at 1, 2, 3, and 4 d **(B)**, data are presented as the mean ± SD, $n = 3$, $^{*}p < 0.05$ or $^{**}p < 0.01$ indicates the comparison between the two groups of sja-miR-7-5p and NC; $\#p < 0.05$ or $\#\#p < 0.01$ indicates the comparison between the two groups of sja-miR-7-5p and Mock. Cell cycle was determined using flow cytometry analysis **(C,D)**. Cell migration was evaluated by using Transwell inserts without matrigel coating **(E)**. The ability to form cell clones was determined using a colony formation assay **(F)**. Data are presented as the mean ± SD, $n = 3$, $^{*}p < 0.05$, $^{**}p < 0.01$.

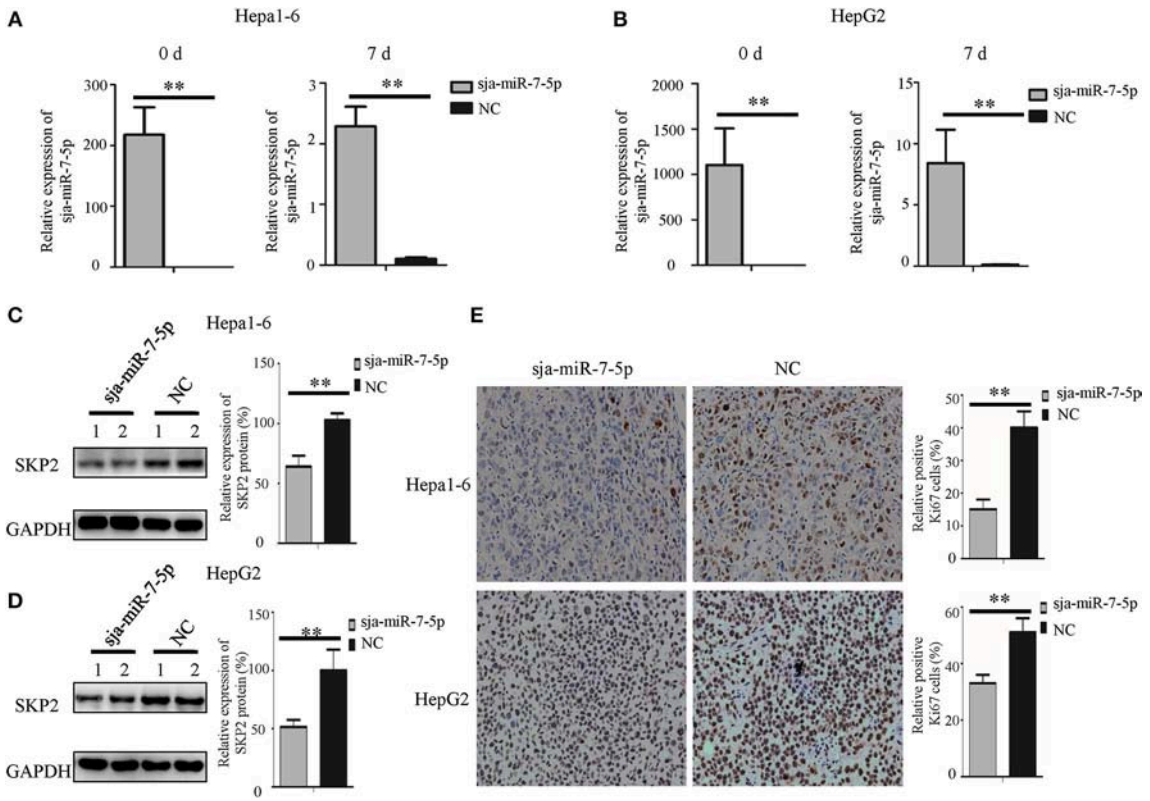

FIGURE 6 | Sja-miR-7-5p inhibits the expression of SKP2 and Ki67 within hepatoma cell tumors. **(A,B)**The content of sja-miR-7-5p mimics after transfection into tumor cells was measured using qRT-PCR before inoculation (0 d) and after sacrifice (7 d), with U6 as the internal control, **(A)** for Hepa1-6 cells, **(B)** for HepG2 cells. Data are presented as the mean ± SD, $n = 5$, $^{**}p < 0.01$. **(C,D)** The protein level of SKP2 was determined by Western blotting, with glyceraldehyde-3-phosphate (GAPDH) as the internal control, **(C)** for Hepa1-6 cells, **(D)** for HepG2 cells. **(E)** The level of Ki67 in tumors was determined using immunohistochemistry.

of both Hepa1-6 cells and HepG2 cells via downregulation of SKP2 expression.

To further explore the molecular mechanism by which sja-miR-7-5p exerts its antitumor activities, we detected the expression of two downstream nodes of SKP2, e.g., P27 [also known as cyclin dependent kinase inhibitor 1B (CDKN1B)] and matrix metalloproteinase 9(MMP9), using Western blotting. We found that sja-miR-7-5p downregulated the level of SKP2, which led to significantly increased levels of P27 and reduced levels of MMP9 in the cells receiving sja-miR-7-5p mimics compared with those in the cells receiving the NC mimics (**Figure 7A**). In addition, transfection of the hepatoma cells with the murine *Skp2* siRNA generated a similar outcome to that in cells transfected with sja-miR-7-5p mimics (**Figure 7B**). These data suggested that sja-miR-7-5p exerts its antitumor activity by targeting *SKP2* to elevate P27 levels, which led to suppression of tumor cell growth, and reducing MMP9 levels, resulting in inhibition of cell migration.

DISCUSSION

Hsa-miR-7-5p is well-characterized as a tumor suppressor miRNA that suppresses survival, proliferation, invasion, and migration of multiple cancer cells, as well as increasing the sensitivity of resistant tumor cells to therapeutics. The molecular mechanism underpinning its anticancer activities involves regulation of multiple signaling related genes such as *PI3K/Akt*, *FAK*, *KLF4*, and *REGγ* (10, 39–41). This miRNA has therapeutic potential for human cancers (42). Our previous studies identified a conserved miR-7-5p from *S. japonicum*, sja-miR-7-5p, that has an identical seed sequence to those of hsa-miR-7-5p and mouse mmu-miR-7-5p, although there are 6 nt differences in the rest of the sequence of the miRNA among species. In this study, we have demonstrated that the schistosome miRNA, sja-miR-7-5p, is present in host hepatocytes during schistosome infection, and the *in vitro* transfection of sja-miR-7-5p mimics into hepatoma cells led to cell cycle arrest and inhibition of cell proliferation, colony formation, and cell migration. Furthermore, we showed that sja-miR-7-5p suppressed the growth of both human and mouse hepatoma cells in a xenograft animal model. Analysis of the molecular mechanisms revealed that sja-miR-7-5p exerts its activities by targeting the *SKP2* gene, which is involved in regulation of cell viability and migration. Thus, the present data indicated that the schistosome sja-miR-7-5p is also a tumor suppressor miRNA that may have therapeutic potential for human cancers. In addition, both the presence of

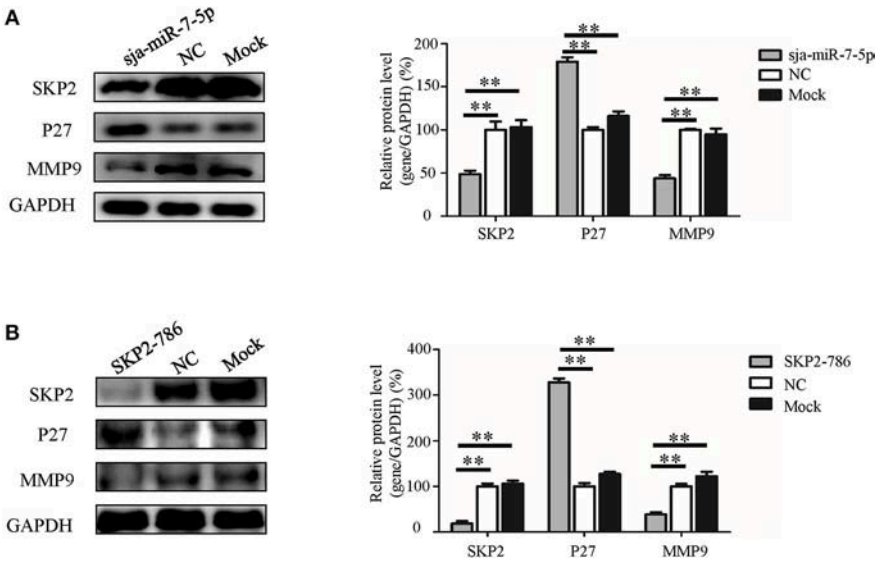

FIGURE 7 | The molecular mechanism whereby sja-miR-7-5p exerts its antitumor activity in hepatoma cells. **(A,B)** In Hepa1-6 cells, the protein levels of SKP2, P27, and MMP9 were measured by Western blotting after transfection with sja-miR-7-5p mimics **(A)** or *Skp2* siRNA **(B)** and their corresponding negative controls, with glyceraldehyde-3-phosphate (GAPDH) as the internal control. Data are presented as the mean ± SD, $n = 3$, $^{**}p < 0.01$.

this miRNA in host hepatocytes and its antitumor effects on human hepatoma cells suggest that schistosome non-small RNA-mediated anticarcinogenic effects might exist in the host liver during schistosome infection.

Infection with several parasites, such as *Opisthorchis viverrini* and *Clonorchis sinensis,* has been reported to be associated with cancer (43, 44). Schistosomiasis is a neglected tropical parasitic disease, affecting approximately 210 million people worldwide. Infection with *Schistosoma haematobium* is associated with bladder cancer (43, 44). However, for infection with *S. japonicum*, the association with hepatocellular carcinoma (HCC) is less evident, although a potential association with colorectal cancer was reported (45). The large retrospective epidemiological surveys conducted in highly endemic areas for schistosomiasis in China showed no correlation between HCC and *S. japonicum* infection (46). Although several other epidemiological and case–control studies proposed a potential association between HCC and *S. japonicum* infection, the evidences for the association remain a matter of debate because the schistosomiasis patients are highly associated with HBV and HCV infections, which are hepatic carcinogens (47). However, accumulating evidence indicates that chronic inflammation plays an important role in carcinogenesis (48). For *S. japonicum* infection, the liver-trapped eggs induce severe hepatic chronic inflammation and fibrosis that could be risk factors for HCC (49). These factors derived from *S. japonicum* infection should contribute to HCC, but this does not seem to happen in *S. japonicum* schistosomiasis. Therefore, we speculated that the *S. japonicum* eggs trapped in the liver might play a dual role in the HCC occurrence and development, i.e., carcinogenic and anticancer activities, similar to those reported for the protozoan *Trypanosoma cruzi*, which has carcinogenic and anticancer activities during infection (50). This study demonstrated that a non-coding small RNA secreted by *S. japonicum,* sja-miR-7-5p, perhaps together with other miRNAs derived from the parasite, could be translocated into liver cells during parasitic infection, and exerts anticancer activity, implying that the *S. japonicum*-producing non-coding small RNAs may, in part, contribute to the anticancer activities in the infected host.

As described above, mammalian miR-7-5p exerts its anticancer activities through regulation of multiple target genes such as *PI3K/Akt*, *FAK* and *KLF4*. To identify the target gene of the parasite sja-miR-7-5p, we first used three online software to search for its potential target genes. We found 5 target gene candidates (*Skp2, Psme3, Pik3cd, Klf4, and Hoxb5*) that were consistently predicted by the three software and involved in tumor-related signaling pathway. Three of them (i.e., *Pik3cd, Klf4, Hoxb5*) were excluded through analysis of their expression in hepatoma cells transfected with the sja-miR-7-5p mimics. Although both *Skp2* and *Psme3* genes were validated as target gene by luciferase reporter assay, our experimental data with *Skp2* and *Psme3* siRNA showed that only the hepatoma cell transfected with the *Skp2* siRNA produced similar phenotype to that of sja-miR-7-5p mimics-treated cells. Thus, *Skp2* gene has been identified as the target gene of sja-miR-7-5p.

SKP2, also known as P45, FBL1, FLB1, and FBXL1, is a component of the SCF (Skp1-Cullin 1-F-box) E3 ubiquitin-ligase complex. Many studies have reported that SKP2 is overexpressed in various cancers of different organs, including the liver (18), colon (51), breast (52), prostate (53), and stomach (54). *SKP2* is characterized as an oncogene, and is involved in modulation of the cell cycle, cell growth, and survival by regulation of

its downstream node molecules, such as P27, P16, P21, P57, E2F-1, and c-MYC in an ubiquitin-dependent manner, followed by 26S proteasome degradation (23). Previous studies showed that loss of *SKP2* reduced the migration and invasion abilities of oral squamous cell carcinoma cells by downregulating the expression of MMP2 and MMP9 (55). The best-known substrate of SKP2 is the cyclin dependent kinase (CDK) inhibitor, P27. Overexpression of SKP2 leads to reduction of P27, which is strongly associated with aggressive tumor behavior and poor clinical outcome (19, 36, 56), while knockdown of *SKP2* resulted in the accumulation of P27, causing cell cycle arrest at G1/G0 phase (57). However, the relationship between miR-7-5p and *SKP2* has not yet been reported in HCC. In the present study, we found that in liver cancer cells, including Hepa1-6 cells and HepG2 cells, sja-miR-7-5p inhibited the growth and migration of both mouse and human hepatoma cells by targeting *SKP2* to elevate the expression of P27 and decrease the expression of MMP9. These data were consistent with the results of experiments using the *SKP2* siRNA, and with the outcome of a study in which miRNA-7-5p could suppress cell proliferation of CHO cells partly by targeting *skp2* (58). Therefore, our data demonstrated that sja-miR-7-5p suppresses hepatoma cell growth and migration by downregulating *SKP2*.

The present study demonstrated that sja-miR-7-5p is present in infected hepatocytes, selectively affects the growth and migration of human and mouse tumor cells by targeting the *SKP2* gene, implying that sja-miR-7-5p might strengthen resistance of host to cancer during schistosome infection.

DATA AVAILABILITY

All datasets generated for this study are included in the manuscript and/or the **Supplementary Files**.

AUTHOR CONTRIBUTIONS

CH and WP conceived and designed the study. CH, SZ, JW, YL, LM, LZ, PJ, and ZL performed the experiments. CH, SZ, and WP analyzed the data. CH and WP wrote the manuscript. All authors read and approved the final manuscript.

FUNDING

This study was supported by the National Natural Science Foundation of China (81430051).

ACKNOWLEDGMENTS

We thank the staff of the National Institute of Parasitic Disease, Chinese Center for Disease Control and Prevention for their help with parasite infections.

SUPPLEMENTARY MATERIAL

The Supplementary Material for this article can be found online at: https://www.frontiersin.org/articles/10.3389/fonc.2019.00175/full#supplementary-material

REFERENCES

1. Colley DG, Bustinduy AL, Secor WE, King CH. Human schistosomiasis. *Lancet.* (2014) 383:2253–64. doi: 10.1016/S0140-6736(13)61949-2
2. Zhu SL, Wang S, Lin Y, Jiang PY, Cui XB, Wang XY, et al. Release of extracellular vesicles containing small RNAs from the eggs of *Schistosoma japonicum*. *Parasit Vectors.* (2016) 9:574. doi: 10.1186/s13071-016-1845-2
3. Bartel DP. MicroRNAs: Genomics, biogenesis, mechanism, and function. *Cell.* (2004) 116:281–97. doi: 10.1016/S0092-8674(04)00045-5
4. Calin GA, Croce CM. MicroRNA signatures in human cancers. *Nat Rev Cancer.* (2006) 6:857–66. doi: 10.1038/nrc1997
5. Berindan-Neagoe I, Monroig PD, Pasculli B, Calin GA. MicroRNAome genome: a treasure for cancer diagnosis and therapy. *Ca-a Cancer J Clini.* (2014) 64:311–36. doi: 10.3322/caac.21244
6. Mi Y, Zhang D, Jiang W, Weng J, Zhou C, Huang K, et al. miR-181a-5p promotes the progression of gastric cancer via RASSF6-mediated MAPK signalling activation. *Cancer Lett.* (2017) 389:11–22. doi: 10.1016/j.canlet.2016.12.033
7. Xue X, Fei X, Hou W, Zhang Y, Liu L, Hu R. miR-342-3p suppresses cell proliferation and migration by targeting AGR2 in non-small cell lung cancer. *Cancer Lett.* (2018) 412:170–8. doi: 10.1016/j.canlet.2017.10.024
8. Zhu Y, Gu J, Li Y, Peng C, Shi M, Wang X, et al. MiR-17-5p enhances pancreatic cancer proliferation by altering cell cycle profiles via disruption of RBL2/E2F4-repressing complexes. *Cancer Lett.* (2018) 412:59–68. doi: 10.1016/j.canlet.2017.09.044
9. Hatziapostolou M, Polytarchou C, Aggelidou E, Drakaki A, Poultsides GA, Jaeger SA, et al. An HNF4 alpha-miRNA inflammatory feedback circuit regulates hepatocellular oncogenesis. *Cell.* (2011) 147:1233–47. doi: 10.1016/j.cell.2011.10.043
10. Fang YX, Xue JL, Shen Q, Chen JZ, Tian L. MicroRNA-7 inhibits tumor growth and metastasis by targeting the phosphoinositide 3-kinase/Akt pathway in hepatocellular carcinoma. *Hepatology.* (2012) 55:1852–62. doi: 10.1002/hep.25576
11. Zhang L, Hou DX, Chen X, Li DH, Zhu LY, Zhang YJ, et al. Exogenous plant MIR168a specifically targets mammalian LDLRAP1: evidence of cross-kingdom regulation by microRNA. *Cell Res.* (2012) 22:107–26. doi: 10.1038/cr.2011.158
12. Zhou Z, Li XH, Liu JX, Dong L, Chen Q, Liu JL, et al. Honeysuckle-encoded atypical microRNA2911 directly targets influenza A viruses. *Cell Res.* (2015) 25:39–49. doi: 10.1038/cr.2014.130
13. Chin AR, Fong MY, Somlo G, Wu J, Swiderski P, Wu XW, et al. Cross-kingdom inhibition of breast cancer growth by plant miR159. *Cell Res.* (2016) 26:217–28. doi: 10.1038/cr.2016.13
14. Liu HX, Huang J, Peng J, Wu XX, Zhang Y, Zhu WL, et al. Upregulation of the inwardly rectifying potassium channel Kir2.1 (KCNJ2) modulates multidrug resistance of small-cell lung cancer under the regulation of miR-7 and the Ras/MAPK pathway. *Mol Cancer.* (2015) 14:59. doi: 10.1186/s12943-015-0298-0
15. Liu HX, Wu XX, Huang J, Peng J, Guo LL. miR-7 modulates chemoresistance of small cell lung cancer by repressing MRP1/ABCC1. *Int J Exp Pathol.* (2015) 96:240–7. doi: 10.1111/iep.12131
16. Suto T, Yokobori T, Yajima R, Morita H, Fujii T, Yamaguchi S, et al. MicroRNA-7 expression in colorectal cancer is associated with poor prognosis and regulates cetuximab sensitivity via EGFR regulation. *Carcinogenesis.* (2015) 36:338–45. doi: 10.1093/carcin/bgu242
17. Cheng MW, Shen ZT, Hu GY, Luo LG. Prognostic significance of microRNA-7 and its roles in the regulation of cisplatin resistance in lung

adenocarcinoma. *Cell Physiol Biochem.* (2017) 42:660–72. doi: 10.1159/000477884
18. Lee SW, Li CF, Jin G, Cai Z, Han F, Chan CH, et al. Skp2-dependent ubiquitination and activation of LKB1 is essential for cancer cell survival under energy stress. *Mol Cell.* (2015) 57:1022–33. doi: 10.1016/j.molcel.2015.01.015
19. Wang Z, Gao D, Fukushima H, Inuzuka H, Liu P, Wan L, et al. Skp2: a novel potential therapeutic target for prostate cancer. *Biochim Biophys Acta.* (2012) 1825:11–7. doi: 10.1016/j.bbcan.2011.09.002
20. Seki R, Okamura T, Koga H, Yakushiji K, Hashiguchi M, Yoshimoto K, et al. Prognostic significance of the F-box protein Skp2 expression in diffuse large B-cell lymphoma. *Am J Hematol.* (2003) 73:230–5. doi: 10.1002/ajh.10379
21. Rose AE, Wang G, Hanniford D, Monni S, Tu T, Shapiro RL, et al. Clinical relevance of SKP2 alterations in metastatic melanoma. *Pigment Cell Melanoma Res.* (2011) 24:197–206. doi: 10.1111/j.1755-148X.2010.00784.x
22. Radke S, Pirkmaier A, Germain D. Differential expression of the F-box proteins Skp2 and Skp2B in breast cancer. *Oncogene.* (2005) 24:3448–58. doi: 10.1038/sj.onc.1208328
23. Bochis OV, Irimie A, Pichler M, Berindan-Neagoe I. The Role of Skp2 and its Substrate CDKN1B (p27) in colorectal cancer. *J Gastrointes Liver Dis.* (2015) 24:225–34. doi: 10.15403/jgld.2014.1121.242.skp2
24. Hung WC, Tseng WL, Shiea J, Chang HC. Skp2 overexpression increases the expression of MMP-2 and MMP-9 and invasion of lung cancer cells. *Cancer Lett.* (2010) 288:156–61. doi: 10.1016/j.canlet.2009.06.032
25. Yokoi S, Yasui K, Mori M, Iizasa T, Fujisawa T, Inazawa J. Amplification and overexpression of SKP2 are associated with metastasis of non-small-cell lung cancers to lymph nodes. *Am J Pathol.* (2004) 165:175–80. doi: 10.1016/S0002-9440(10)63286-5
26. Shi C, Pan BQ, Shi F, Xie ZH, Jiang YY, Shang L, et al. Sequestosome 1 protects esophageal squamous carcinoma cells from apoptosis via stabilizing SKP2 under serum starvation condition. *Oncogene.* (2018) 37:3260–74. doi: 10.1038/s41388-018-0217-0
27. Osoegawa A, Yoshino I, Tanaka S, Sugio K, Kameyama T, Yamaguchi M, et al. Regulation of p27 by S-phase kinase-associated protein 2 is associated with aggressiveness in non-small-cell lung cancer. *J Clin Oncol.* (2004) 22:4165–73. doi: 10.1200/JCO.2004.01.035
28. Zhu CQ, Blackhall FH, Pintilie M, Iyengar P, Liu N, Ho J, et al. Skp2 gene copy number aberrations are common in non-small cell lung carcinoma, and its overexpression in tumors with ras mutation is a poor prognostic marker. *Clin Cancer Res.* (2004) 10:1984–91. doi: 10.1158/1078-0432.CCR-03-0470
29. Cai PF, Piao XY, Hao LL, Liu S, Hou N, Wang H, et al. A deep analysis of the small non-coding RNA population in *Schistosoma japonicum* eggs. *PLoS ONE.* (2013) 8:64003. doi: 10.1371/journal.pone.0064003
30. He X, Xie J, Zhang DM, Su Q, Sai X, Bai RP, et al. Recombinant adeno-associated virus-mediated inhibition of microRNA-21 protects mice against the lethal schistosome infection by repressing both IL-13 and transforming growth factor beta 1 pathways. *Hepatology.* (2015) 61:2008–17. doi: 10.1002/hep.27671
31. Yin XD, Xiang TX, Li LL, Su XW, Shu XS, Luo XR, et al. DACT1, an antagonist to Wnt/beta-catenin signaling, suppresses tumor cell growth and is frequently silenced in breast cancer. *Breast Cancer Res.* (2013) 15:R23. doi: 10.1186/bcr3399
32. Wong N, Wang XW. miRDB: an online resource for microRNA target prediction and functional annotations. *Nucl Acids Res.* (2015) 43:D146–52. doi: 10.1093/nar/gku1104
33. Reczko M, Maragkakis M, Alexiou P, Grosse I, Hatzigeorgiou AG. Functional microRNA targets in protein coding sequences. *Bioinformatics.* (2012) 28:771–6. doi: 10.1093/bioinformatics/bts043
34. Kruger J, Rehmsmeier M. RNAhybrid: microRNA target prediction easy, fast and flexible. *Nucl Acids Res.* (2006) 34:W451–4. doi: 10.1093/nar/gkl243
35. Lim MS, Adamson A, Lin ZS, Perez-Ordonez B, Jordan RCK, Tripp S, et al. Expression of Skp2, a p27(Kip1) ubliquitin ligase, in malignant lymphoma: correlation with p27(Kip1) and proliferation index. *Blood.* (2002) 100:2950–6. doi: 10.1182/blood.V100.8.2950
36. Shapira M, Ben-Izhak O, Linn S, Futerman B, Minkov I, Hershko DD. The prognostic impact of the ubiquitin ligase subunits Skp2 and Cks1 in colorectal carcinoma. *Cancer.* (2005) 103:1336–46. doi: 10.1002/cncr.20917
37. Hershko DD. Oncogenic properties and prognostic implications of the ubiquitin ligase Skp2 in cancer. *Cancer.* (2008) 112:1415–24. doi: 10.1002/cncr.23317
38. Schuler S, Diersch S, Hamacher R, Schmid RM, Saur D, Schneider G. SKP2 confers resistance of pancreatic cancer cells towards TRAIL-induced apoptosis. *Int J Oncol.* (2011) 38:219–25. doi: 10.3892/ijo_00000841
39. Kong XJ, Li GP, Yuan Y, He Y, Wu XL, Zhang WJ, et al. MicroRNA-7 Inhibits Epithelial-to-mesenchymal transition and metastasis of breast cancer cells via targeting FAK expression. *PLoS ONE.* (2012) 7:e41523. doi: 10.1371/journal.pone.0041523
40. Okuda H, Xing F, Pandey PR, Sharma S, Watabe M, Pai SK, et al. miR-7 suppresses brain metastasis of breast cancer stem-like cells by modulating KLF4. *Cancer Res.* (2013) 73:1434–44. doi: 10.1158/0008-5472.CAN-12-2037
41. Shi Y, Luo XR, Li P, Tan JX, Wang XY, Xiang TXS, et al. miR-7-5p suppresses cell proliferation and induces apoptosis of breast cancer cells mainly by targeting REG gamma. *Cancer Lett.* (2015) 358:27–36. doi: 10.1016/j.canlet.2014.12.014
42. Kalinowski FC, Brown RAM, Ganda C, Giles KM, Epis MR, Horsham J, et al. microRNA-7: a tumor suppressor miRNA with therapeutic potential. *Int J Biochem Cell Biol.* (2014) 54:312–7. doi: 10.1016/j.biocel.2014.05.040
43. Bouvard V, Baan R, Straif K, Grosse Y, Secretan B, El Ghissassi F, et al. A review of human carcinogens–Part B: biological agents. *Lancet Oncol.* (2009) 10:321–2. doi: 10.1016/S1470-2045(09)70096-8
44. IARC Working Group on the Evaluation of Carcinogenic Risks to Humans. Biological agents. Volume 100 B. A review of human carcinogens. *IARC Monogr Eval Carcinog Risks Hum.* (2012) 100:1–441.
45. Chen MG. Assessment of morbidity due to Schistosoma japonicum infection in China. *Infect Dis Poverty.* (2014) 3:6. doi: 10.1186/2049-9957-3-6
46. Liu BQ, Rong ZP, Sun XT, Wu YP, Gao RQ. Geographical correlation between colorectal cancer and schistosomiasis in China. *Zhongguo Yi Xue Ke Xue Yuan Xue Bao*. (1983) 5:173–7.
47. Arzumanyan A, Reis HM, Feitelson MA. Pathogenic mechanisms in HBV- and HCV-associated hepatocellular carcinoma. *Nat Rev Cancer.* (2013) 13:123–35. doi: 10.1038/nrc3449
48. Zhang R, Takahashi S, Orita S, Yoshida A, Maruyama H, Shirai T, et al. p53 gene mutations in rectal cancer associated with schistosomiasis japonica in Chinese patients. *Cancer Lett.* (1998) 131:215–21. doi: 10.1016/S0304-3835(98)00154-2
49. Takemura Y, Kikuchi S, Inaba Y. Epidemiologic study of the relationship between schistosomiasis due to *Schistosoma japonicum* and liver cancer/cirrhosis. *Am Journal Tropi Med Hygiene.* (1998) 59:551–6. doi: 10.4269/ajtmh.1998.59.551
50. van Tong H, Brindley PJ, Meyer CG, Velavan TP. Parasite infection, carcinogenesis and human malignancy. *EBioMedicine.* (2017) 15:12–23. doi: 10.1016/j.ebiom.2016.11.034
51. Fujita T, Liu WJ, Doihara H, Wan Y. Regulation of Skp2-p27 axis by the Cdh1/anaphase-promoting complex pathway in colorectal tumorigenesis. *Am J Pathol.* (2008) 173:217–28. doi: 10.2353/ajpath.2008.070957
52. Liu J, Wei XL, Huang WH, Chen CF, Bai JW, Zhang GJ. Cytoplasmic Skp2 expression is associated with p-Akt1 and predicts poor prognosis in human breast carcinomas. *PLoS ONE.* (2012) 7:e52675. doi: 10.1371/journal.pone.0052675
53. Moro L, Arbini AA, Marra E, Greco M. Up-regulation of Skp2 after prostate cancer cell adhesion to basement membranes results in BRCA2 degradation and cell proliferation. *J Biol Chem.* (2006) 281:22100–7. doi: 10.1074/jbc.M604636200
54. Ma XM, Liu Y, Guo JW, Liu JH, Zuo LF. Relation of overexpression of S phase kinase-associated protein 2 with reduced expression of p27 and PTEN in human gastric carcinoma. *World J Gastroenterol.* (2005) 11:6716–21. doi: 10.3748/wjg.v11.i42.6716
55. Yamada SI, Yanamoto S, Naruse T, Matsushita Y, Takahashi H, Umeda M, et al. Skp2 Regulates the Expression of MMP-2 and MMP-9, and enhances the invasion potential of oral squamous cell carcinoma. *Pathol Oncol Res.* (2016) 22:625–32. doi: 10.1007/s12253-016-0049-6

56. Wang Z, Fukushima H, Inuzuka H, Wan L, Liu P, Gao D, et al. Skp2 is a promising therapeutic target in breast cancer. *Front Oncol.* (2012) 1:18702. doi: 10.3389/fonc.2011.00057
57. Ding L, Li R, Han X, Zhou Y, Zhang H, Cui Y, et al. Inhibition of Skp2 suppresses the proliferation and invasion of osteosarcoma cells. *Oncol Rep.* (2017) 38:933–40. doi: 10.3892/or.2017.5713
58. Sanchez N, Gallagher M, Lao N, Gallagher C, Clarke C, Doolan P, et al. MiR-7 Triggers Cell Cycle Arrest at the G1/S Transition by Targeting Multiple Genes Including Skp2 and Psme3. *PLoS ONE.* (2013) 8:e65671. doi: 10.1371/journal.pone.0065671

Conflict of Interest Statement: The authors declare that the research was conducted in the absence of any commercial or financial relationships that could be construed as a potential conflict of interest.

frontiers in Oncology

MINI REVIEW
published: 29 March 2019
doi: 10.3389/fonc.2019.00194

Epigenetic Enzyme Mutations: Role in Tumorigenesis and Molecular Inhibitors

Mei Han†, Lina Jia†, Wencai Lv, Lihui Wang and Wei Cui**

Department of Pharmacology, Shenyang Pharmaceutical University, Shenyang, China

Epigenetic modifications, such as DNA methylation and histone modification, result in heritable changes in gene expression without changing the DNA sequence. Epigenetic regulatory enzymes such as DNA methyltransferases, histone methyltransferases, and histone deacetylases are involved in epigenetic modification. Studies have shown that the dysregulation caused by changes in the amino acid sequence of these enzymes is closely correlated with tumor onset and progression. In addition, certain amino acid changes in the metabolic enzyme isocitrate dehydrogenase (IDH) are linked to altered epigenetic modifications in tumors. Some small molecule inhibitors targeting these aberrant enzymes have shown promising anti-cancer efficacy in preclinical and clinical trials. For example, the small molecule inhibitor ivosidenib, which targets IDH1 with a mutation at R132, has been approved by the FDA for the clinical treatment of acute myeloid leukemia. In this review, we summarize the recurrent "hotspot" mutations in these enzymes in various tumors and their role in tumorigenesis. We also describe candidate inhibitors of the mutant enzymes which show potential therapeutic value. In addition, we introduce some previously unreported mutation sites in these enzymes, which may be related to tumor development and provide opportunities for future study.

Keywords: DNMT, mutation, small molecule inhibitors, tumor, histone modification enzyme

OPEN ACCESS

Edited by:
Zhe-Sheng Chen,
St. John's University, United States

Reviewed by:
Jing Tan,
Sun Yat-sen University, China
Maria Rosa Ciriolo,
University of Rome Tor Vergata, Italy

****Correspondence:***
Lihui Wang
lhwang@syphu.edu.cn
Wei Cui
cuiwei@syphu.edu.cn

† These authors have contributed equally to this work

Specialty section:
This article was submitted to Cancer Molecular Targets and Therapeutics, a section of the journal Frontiers in Oncology

Received: *25 December 2018*
Accepted: *06 March 2019*
Published: *29 March 2019*

Citation:
Han M, Jia L, Lv W, Wang L and Cui W (2019) Epigenetic Enzyme Mutations: Role in Tumorigenesis and Molecular Inhibitors. Front. Oncol. 9:194. doi: 10.3389/fonc.2019.00194

INTRODUCTION

The term "epigenetics" describes inheritable changes of gene expression with no alteration of the DNA sequence (1). As the field of epigenetics has expanded, the connection between epigenetic changes and the occurrence and development of tumors has received more attention (2). The structure of chromatin is the basis for modulating gene expression: euchromatin has an open structure that is typically associated with active transcription, while heterochromatin is tightly compacted and usually associated with transcriptional repression. Epigenetic modification such as DNA methylation and histone modification are important for regulating chromatin structure and therefore gene expression. These modifications are catalyzed by epigenetic regulatory enzymes, including DNA methyltransferases, histone methyltransferases and histone deacetylases.

Recent studies have shown that the dysregulation (e.g., overexpression) of these enzymes plays a crucial role in tumorigenesis. Some small molecule inhibitors targeting these aberrantly expressed epigenetic regulatory enzymes have been approved by the FDA for the treatment of certain cancers. For example, the small molecule inhibitor 5-azacytidine, which targets the DNA methyltransferase DNMT3A, has been approved for clinical treatment of patients with acute lymphoblastic leukemia (AML) (3), and belinostat, which targets histone deacetylases (HDACs)

in peripheral T-cell lymphoma (PTCL), was approved for use in 2014 (4). In addition, the inhibitor EPZ6438, which targets EZH2, a histone methyltransferase, has been approved for testing in the clinic (5).

In recent years, increasing evidence has shown that epigenetic regulatory enzymes are mutated in various types of cancer, and mutations of these enzymes are closely related to the malignant phenotype (6, 7). Hence, inhibitors that target these mutant enzymes have gradually entered preclinical and clinical research. In this review, we first summarize the epigenetic regulatory enzymes and their mutations in different types of tumors, and then we explain how the mutations are correlated with tumorigenesis. Finally, we present some small molecule inhibitors which target epigenetic regulatory enzymes, especially their mutated forms, and may have potential therapeutic value in the future.

DNMTS AND THEIR MUTATIONS IN CANCER

DNMTs in Cancer

DNA methylation, which is one of the major epigenetic regulatory mechanisms, plays a crucial role in many life processes (8). In eukaryotic cells, DNA methylation is a stable gene silencing modification that is copied during DNA replication (9). DNA methylation predominately occurs at cytosine residues in 5′-CpG-3′ dinucleotides, with S-adenosyl methionine (SAM) as the methyl donor (10). In mammals, DNA methylation is catalyzed by enzymes in the DNA methyltransferase (DNMT) family, mainly DNMT1, DNMT3A, and DNMT3B. DNMT1 maintains the methylation status of newly replicated (hemi-methylated) DNA, whereas DNMT3A and DNMT3B are responsible for *de novo* DNA methylation (11). The mechanism by which DNA methylation regulates gene expression involves blocking the binding of transcription factors to DNA and the recruitment of proteins containing a methylated CpG-binding domain to inhibit gene expression in tumor cells (12). The methylation profiles in different cells are not the same, and this has functional consequences. In normal cells, gene promoters containing CpG islands are usually unmethylated, which maintains the chromatin in an open structure, and hence enhances the transcription of the gene. However, in tumor cells, the CpG island-containing promoters of tumor suppressor genes are usually methylated, and thus the euchromatin is converted to compacted heterochromatin (13). These findings indicate that DNA methylation regulates tumorigenesis and progression by inhibiting the expression of tumor suppressor genes.

DNMT Mutations in Cancer

Recently, studies have shown that mutations of DNMT family, especially DNMT3A, are prominent features of many tumors and can lead to malignant transformation (14). DNMT3A is one of the most frequently mutated DNA methyltransferase in AML (6) and myelodysplastic syndromes (MDS) (15). Some reports have shown that mutations in DNMT3A are present in up to 20% of AML cases and are associated with poor prognosis (8, 16). Although a large number of mutations in the DNMT3A have been reported, ∼50% of the changes are in the catalytic domain at position R882 (most commonly R882H) (8, 17, 18). **Table 1** shows DNMT3A mutations, including hotspots and non-reported mutation sites, in various tumors. In addition, mutations in DNMT1 have been described in colorectal (29), prostate and hematological malignancies (30). The gene encoding DNMT3B was reported to be mutated in immunodeficiency syndrome, but mutations have rarely been reported in tumors (31). In addition, except DNMTs' mutations in various cancers, DNA hydroxymethylase TET2, which catalyzes the conversion of 5-methyl-cytosine to 5-hydroxymethyl-cytosine, has been reported in recent years for its mutations in various diseases, especially AML and MDS (32). The above results indicated that the mutations in DNMT and its related enzyme are frequent, which suggesting the potential role of them in tumorigenesis.

Function of DNMT Mutations

Mutations in DNMTs are closely correlated with the biological characteristics of malignant tumors and they increase the ability of cancer cells to undergo proliferation, migration, colony formation, and self-renewal. Recently, the relationship between the DNMT3A R882C mutation and the migration of tumor cells has been investigated *in vitro* (33). The results showed that the OCI-AML3 cell line, which carries the R882C mutation, had a greater migration ability than cell lines carrying wild-type (WT) DNMT3A, and infiltrated into the meninges of mice after intravenous infusion. This indicates that the DNMT3A R882 mutation contributes to the enhanced migration of malignant cells. It was also shown that the DNMT3A R882H mutation increases the proliferative capacity of hematopoietic cells and actively promotes the growth of monocytes and macrophages (33). Mechanistically, DNMT3A R882 mutant proteins interact with polycomb repressive complex 1 (PRC1) to block the differentiation of hematopoietic stem cells and lymphocytes by down-regulating differentiation-associated genes (34). Furthermore, cells with DNMT3A R882 mutations have a higher colony forming capacity than WT cells (34). In addition, it was reported that DNMT3A R882 mutations may induce chemotherapy resistance in AML patients. Guryanova et al. reported that the DNMT3A R882H mutation increases the risk of AML patients being resistant to anthracycline therapy by dysregulating nucleosome remodeling (35). Some reports have shown that the DNMT3A R882 mutation was negatively correlated with the prognosis of AML patients. The 5-year overall survival of AML patients with DNMT3A mutations was significantly shorter than AML patients without such mutations (36, 37). Accordingly, Delhommeau et al. reported that TET2 mutations are early events in patients with some MDS and secondary AML and confirmed the important role of TET2 in maintaining the balance between hematopoietic cell survival, growth and differentiation (38). Studies have shown that leukemia-associated missense mutations impair the enzymatic activity of TET2 and lead to a decrease in the genomic level of 5-hydroxymethyl-cytosine, which disrupts normal hematopoiesis and may accelerate leukemia formation (32). All of the above

TABLE 1 | Epigenetic regulatory enzymes mutation sites and their function in different types of cancer.

Enzyme	Gain-of-function mutation	Function of mutation	Non-reported mutation	Cancer type (references)	Inhibitor
DNMT3A	R882(H/C/P);	Migration;	Y735F, V716F, R729(Q/H/W), R803S, R736H, K829R, P718L, C497Y, D781G, G646V, A741V, F909C, M801V;	**Leukemia (6, 8, 16)**	5-azacytidine;
	R882C	Proliferation;	R792H, G26V, S708C, G412W, A254P, E629D, G293W, V763F, R771Q, Y533C, Q485H, K680R, S878P, E725V, R209P, P59L,	Lung cancer	Dichlone;
		Colony formation;	R379L, M864I, R326P, P804S, V258M, W327G, C494S, S312F, D781H, G413S, S669C, A116S, F909S, R458Q, R55H, Y724C,		SYC-52221;
		Blocking differentiation	V563M, D857V, W795C, P89R, D618N, Y735C, V560L, G570W, M78I, D279V, E392D, M224V, Q248R, V895M, V401L,		EPZ004777;
			G685V, C559Y, E854Q, G49R, G890C, E323K, P709L, Y359C, E213D, G746V, P58L, R885S, V687F, P425T		EPZ5676;
					(pan-inhibitors)
EZH2	Y641(S/H/F/N), A687V, A677G, Y646H;	Migration;	E740K, R679H, G159R, N670K, S271F, W113C, K660R, K660E, D185H, T53M, D183E, M701V, Y447H, V702G, C642S, T144I,	**Lymphoma (19–21)**	EPZ005687;
		Proliferation;	E636D, R685H, D659A, F672L;		GSK126;
	Y641(S/H/N/F), Y646(S/H);	Tumor growth;	S533L, R342Q, R216(Q/W), P132S, P219S, G2(D/S), D316G, R34P, P746S, S229L, S405L, T4(I/P), D142V, A226V, S228F,	**Melanoma (22)**	EPZ-6438;
		Poor prognosis;	P426S, R355G, C530W, G704S, G459E, R81S, P417Q, R456S, P535H, R382M, P262H, P631H, L338F, S474F, E391K, P527L,		CPI-1205;
			N366S, K510R, V675M, D511N, A590V, H521Y, I651T;		(pan-inhibitors)
	Y646H, A687V		K426Q, S652(C/F), P493A, I633M, T467P, S624C, K550T, I150V, E173Q, H129D, Q653E, K545T, L315V, Q648E, S647C;	Breast cancer	
			K510R, E374Q, Q548E, N310S, A340T, P262(L/T/I), R685G, E650Q, R308L, A715V, A622, R497Q, D233Y, R34L, E341K,	Lung cancer	
			R64M, D186N, K39E, H613Q, S647C, Q66R, R357L, E312K, Q94R, P481S, F667L, H502Q, R52I, G5R, S647F, R527W,S40C		
IDH1	R132(C/S/G/H/L);	Proliferation;	G339E, G161R;	**Glioma (7, 23)**	Ivosidenib (specific
	R132(C/H);	Migration;	V178I, G370D, S210N, R20Q;	**Lymphoma (24)**	targeting mutant
	R132(C/G/H);	Colony formation;	R119Q, E306D, T106M;	**Prostate cancer (25)**	IDH1 in R132);
	R132(C/S/G/L);	Blocking differentiation;	N349S;	**Cholangiocarcinoma (26)**	FT-2120 (specific
	R132(C/G/L);	Angiogenesis;	C297S, Q198P, N171T, M182V;	**Hepatic carcinoma (27)**	targeting mutant
	R132(C/H);	Inhibition of apoptosis	D160E, D79N, T327A, G263V, L88F, K217N, Y235C, R338T, K81N, K151N, A179D, I189V, E84Q;	Breast cancer	IDH1 in R132); IDH-305 (specific
	R132(C/L)		R49C, M290I, Q228R, E361K, E360K, S94P, A341V, G339W, G284V, A282V;	Melanoma	targeting mutant
			I102T, E28Q, R109K, D375Y, A179D, Y34C, I333V, V294L, I189F, A193S,	Lung cancer	IDH1);
			D299E, G175V, G221(L/V/W), L359F, E262Q, K406E		AGI-881 (pan-
			T302R, R119W, G310V, I380F, N961		inhibitor)
DH2	R172(S/K/G/W/M);	Proliferation;	G383V, K251N;	**Glioma (7, 28)**	Enasidenib
	R172(K/G/M/S);	Migration;	H430Y, R140(Q/L/G), D225N, N156I;	**Lymphoma (24)**	(specific targeting
	R172K;	Colony formation;	I62V, I61V;	**Prostate cancer (25)**	mutant IDH2);
	R172(K/S);	Blocking differentiation;	S301L, N156S, R60G, F270S, I419T;	**Hepatic carcinoma (27)**	AGI-881(pan-
	R172K	Angiogenesis;	R122(C/S), I139F, G137E, G387W, E68K, M248I, P198T, G176N, A321V,	Melanoma	inhibitor)
			M221I, R362W;	Lung cancer	
			R188W, H273D, Q267E, S249G, Q322K, I62M;	Breast cancer	
			I240V, F192L, T146S, E345K;		
HDAC2	–	–	Q354L, D175N, D231H, S118P, K466Q, N470I;	Leukemia	–
			M65V, G28R, A257T, P102A, R78(L/W), L42F, D456N, A120V, C101F, E109Q, A122S, D426Y	Lung cancer	

Publications reporting cancers with the indicated gain-of-function mutations are in bold. Non-reported mutations in the same proteins were identified from the cBioPortal website.

observations show that mutations in DNMT3A and TET2, to some extent, promote oncogenesis, and tumor progression.

HMTS AND THEIR MUTATIONS IN CANCER

HMTs in Cancer

Histone methylation is involved in the regulation of various biological processes such as gene expression, DNA repair, differentiation, replication and growth (39). Histone methyltransferases catalyze the transfer of the methyl group of SAM to histone arginine or lysine residues. A number of HMTs have been identified, including histone lysine methyltransferases (HKMTs) and histone arginine methyltransferases (HRMTs), which have specific substrates and residues. EZH2 belongs to the HKMT family and is frequently overexpressed in various cancerous tissue types such as breast, prostate and lung (19, 20, 40).

HMT Mutations in Cancer

EZH2 is a histone methyltransferase that catalyzes the trimethylation of arginine 27 in histone H3 (H3K27). Reports of EZH2 mutations in cancer have increased in recent years. Mutations in epigenetic regulatory enzymes are either gain-of-function or loss-of-function (3). EZH2 gain-of-function mutations were previously reported in lymphoma, and the probability of EZH2 mutation in melanoma was recently reported to be about 2%. Popov et al. found that 27% of follicular lymphoma cases had EZH2 mutations at 3 recurrent hotspots (Y646, A682, and A692) (24). Other gain-of-function hotspot mutations including Y641, A677, and A687 in the catalytic SET domain of EZH2 are prevalent, accounting for ∼10–24% of non-Hodgkin's lymphoma (26). In addition to these hotspot mutations, we have summarized some non-reported mutation sites that have yet to be studied, as shown in **Table 1**.

Function of HMT Mutations

The dysregulation of H3K27 trimethylation (H3K27me3) is important in human tumorigenesis (25), and some reports have shown that mutant EZH2 increases the level of H3K27me3 in follicular lymphoma, germinal center B-cell type diffuse large B-cell lymphomas (21, 24, 41) and metastatic skin melanoma (42). The level of H3K27 monomethylation and dimethylation in cancer cells and tumor tissues with heterozygous EZH2 mutations at Y641 and A677 is decreased, while the level of H3K27 trimethylation is increased, resulting from the changed substrate preference of the mutant enzymes (22, 41). Barsotti et al. revealed that cells with a gain-of-function EZH2 mutation at Y641 displayed enhanced motility compared to control cells, forming highly dynamic collective migrating chains under 3D culture conditions (42). The Y641 EZH2 gain-of-function mutant cells also had a significant growth advantage in melanoma xenografts. Others have reported that mutations in EZH2 can promote lymphocyte proliferation and maintain the enhanced histone methyltransferase activity *in vivo*, subsequently increasing tumorigenicity (26). Somatic mutations in EZH2 have been shown in many reports to correlate with poor prognosis in patients with AML and myeloproliferative neoplasms (6, 43). Thus, mutations in EZH2 may contribute to the enhancement of the malignant phenotype.

HMT-RELATED ENZYMES AND THEIR MUTATIONS IN CANCER

HMT-Related Enzymes in Cancer

Isocitrate dehydrogenase (IDH) plays a key role in the Kreb's cycle, catalyzing the conversion of isocitrate into α-ketoglutarate (α-KG). The two major human IDH proteins, IDH1 and IDH2, are not HMTs, but their mutant forms indirectly contribute to effects on histone methylation by catalyzing the conversion of α-KG to 2-hydroxyglutarate (2-HG). Accumulation of 2-HG can inhibit the activity of a broad range of histone demethylases, inducing hypermethylation which is observed in certain cancers such as gliomas (44). In addition, high levels of 2-HG can inhibit α-KG-dependent prolyl hydroxylase, which is important for the degradation of hypoxia-inducible factor (HIF)-1α, a regulator of histone demethylases (7, 23, 28). Mutated forms of IDH therefore mimic the effects of HMTs.

HMT-Related Enzyme Mutations in Cancer

As mentioned above, specific mutants of IDH can catalyze the conversion of α-KG to 2-HG, and 2-HG inhibits not only histone demethylases but also TET DNA demethylases. This can cause increased methylation of both DNA and histones (3). Therefore, mutant IDH may be an oncoprotein and 2-HG may be an "oncometabolite" (7). In recent years, hotspot mutations in IDH1/2 have been reported in various tumors (**Table 1**). It has been reported that mutations of IDH1 and IDH2 occur in the vast majority of low-grade gliomas and secondary high-grade gliomas, and also in some cases of AML (27). In addition, IDH mutations have been found in solid tumors such as cholangiocarcinoma and prostate cancer (45, 46). The hotspot mutation of IDH1 is located at R132, while the hotspot mutation of IDH2 is located at R172, which is homologous to R132 in IDH1. We also found that other mutations of IDH1, including G339(E/W), R49C, R119(Q/W), and V294L, may be hotspot mutations in various tumors (**Table 1**). In addition to mutations in the enzyme of IDH family in the Kreb's cycle, two other metabolic enzymes involved in epigenetic regulation, SDH and FH, have also been reported in recent years to mutate in germline frequently. Ciccarone et al. concluded that SDH mutations in germline are responsible for the formation of hereditary paragangliomas and adrenal gland pheochromocytoma, whereas FH mutations are typical of hereditary leiomyomatosis and renal cell cancer (HLRCC) (47).

Function of HMT-Related Enzyme Mutations

Several groups have investigated the effect of IDH hotspot mutations, which mimic the activity of HMTs, in cancer. Cohen et al. elucidated that mutant IDH can trigger tumorigenesis. In detail, they found that somatic mutations in IDH1 at R132 or IDH2 at R172 led to increased risk of glioma, hemangiomas and chondrosarcoma, and they demonstrated that the mutated IDH contributed to the increased cell proliferation, colony

formation, and inability to differentiate (7). In addition, Fu et al. showed that the IDH2 R172 mutation accelerated the migration and growth of C6 glioma cells by increasing the stability of HIF-1α (48). They also reported that IDH mutations promoted glioma cell metastasis and resistance to chemotherapy through up-regulation of the HIF-1α signaling pathway (49). IDH mutations also play an important role in blocking cell differentiation. Mutant IDH blocks hepatocyte differentiation by inhibiting the HNF-4α pathway (50). Other studies have shown that high levels of 2-HG caused by mutations in IDH can inhibit histone and DNA demethylases, resulting in hypermethylation of histones and DNA which eventually blocks cell differentiation (51, 52). Interestingly, there is no significant difference in the median overall survival rate of intrahepatic cholangiocarcinoma patients with mutant or WT IDH (53). In general, mutated IDH catalyzes the production of high levels of 2-HG, which has multiple effects including the inhibition of α-KG-dependent prolyl hydroxylase, which leads to the accumulation of HIF-1α in cells. This results in the induction of HIF-1α target genes that influence growth, migration, differentiation and angiogenesis as well as cell apoptosis (7), ultimately promoting tumor onset and progression (see **Figure 1**).

HDACS, HATS, AND THEIR MUTATIONS IN CANCER

Histone acetylation is an important epigenetic modification that mainly occurs in the N-terminal region of the histone tail. This modification weakens the binding between histones and DNA, which relaxes the chromatin and enhances gene expression (54). Histone acetyltransferases (HATs) mediate the acetylation in histones, whereas histone deacetylases (HDACs) catalyze the removal of acetyl groups from histones. The HATs are mainly divided into five major families, including GCN5/PCAF, MYST, TAFII250, CBP/p300, and SRC (55). The HDACs are divided into four classes. Class I HDACs include HDAC1, HDAC2, HDAC3, HDAC8; class II HDACs are further divided into two groups, class IIa (HDAC4, HDAC5, HDAC7, HDAC9) and class IIb (HDAC6, HDAC10); class III contains SIRT1-7; and class IV contains one enzyme, HDAC11 (56, 57). Class I, II, and IV HDACs are all Zn^{2+}-dependent enzymes, while class III HDACs do not show any sequence similarity to the other three classes and depend on NAD+ as a co-factor (56, 57). By reversing the histone acetylation status, HDACs mostly regulate the expression of tumor suppressor genes (4). The dysregulation of HATs and HDACs is correlated with the occurrence and development of various diseases, including cancer.

Mutations in genes encoding HDACs are associated with the progression of tumors, owing to the abnormal transcription of key genes that regulate important cellular functions such as cell proliferation, cell cycle regulation and apoptosis. Some studies have shown that HDACs are mutated in certain cancers. For example, somatic mutations of HDAC1 were detected in ∼8% of dedifferentiated human liposarcomas, and the dysfunction of HDAC2 expression caused by a frame-shift mutation was investigated in human epithelial cancers and in colorectal cancer (58). **Table 1** summarizes some of the mutated sites in HDAC2, which may correlate with the development and progression of tumors. However, most of the mutations in HDACs have not been studied and require further investigation. In addition to the discovery that HDACs are mutated in a variety of cancers, there have been many reports in recent years that the HAT CREBBP somatic mutations are more frequent in lymphomas, lung cancer, urothelial carcinoma, and other human tumor types. Jiang et al. reported that somatic mutations in CREBBP occur in 6.4–22.3% of patients with DLBCL and 30.8–68% of follicular lymphoma. Their findings suggest that CREBBP mutation can promote lymphomagenesis *in vivo* (59). Similarly, the results of Jia et al. showed that *CREBBP* acts as a tumor suppressor gene, and its inactivating mutations can promote tumorigenesis of pre-neoplastic neuroendocrine cells and accelerate small cell lung cancer in the autochthonous mouse model (60). The above results suggested that the mutations in HATs and HDACs, although relative low in frequency, might also be involved into the carcinogenesis in various tumors.

INHIBITORS TARGETING MUTATIONS OF EPIGENETIC REGULATORY ENZYMES

Inhibitors Targeting DNMT Mutants

The DNMT inhibitors 5-azacytidine and decitabine (5-aza-2′-deoxycytidine) have already been approved by the FDA (3). These inhibitors are nucleoside analogs which are incorporated into DNA and then covalently trap DNMTs. The results of research by Xu et al. showed that 5-azacytidine might be a suitable drug for the treatment of AML with DNMT3A mutations (8). In a study comparing small molecule inhibitors of DNMT3A R882H, compound 9 (dichlone) displayed superior efficacy, indicating its potential for targeting mutant DNMT3A (61). Interestingly, a recent study showed that targeting DOT1L, a histone lysine methyltransferase without a SET domain, also has an obvious antitumor effect in DNMT3A mutant leukemia. Rau et al. found that the DOT1L inhibitors SYC-52221 and EPZ004777 decreased tumor cell proliferation and induced cell apoptosis, cycle arrest and terminal differentiation in DNMT3A mutant cell lines in a dose- and time-dependent manner (62). Furthermore, they reported that the DOT1L inhibitor EPZ5676 showed promising efficacy in a nude mouse xenograft model of AML with mutant DNMT3A (62). Since pharmacological inhibitors of DOT1L have been tested in clinical trials, DOT1L may be an indirect therapeutic target for the treatment of AML with DNMT3A mutations. These results suggesting a novel approach for treating patients with DNMT3A mutations.

For the TET2, although inhibitors targeting TET2 mutations have not yet been developed, the results of Bejar et al. indicated that cells in MDS patients with TET2-deficient are more sensitive to azacitidine treatment, and this suggests that patients with MDS carrying the TET2 mutation can improve their response to hypomethylating agents (63). However, the detailed mechanisms mediating this process need further study.

Inhibitors Targeting EZH2 Mutants

Recently, studies have shown that small molecule inhibitors can effectively target tumors driven by EZH2 mutations.

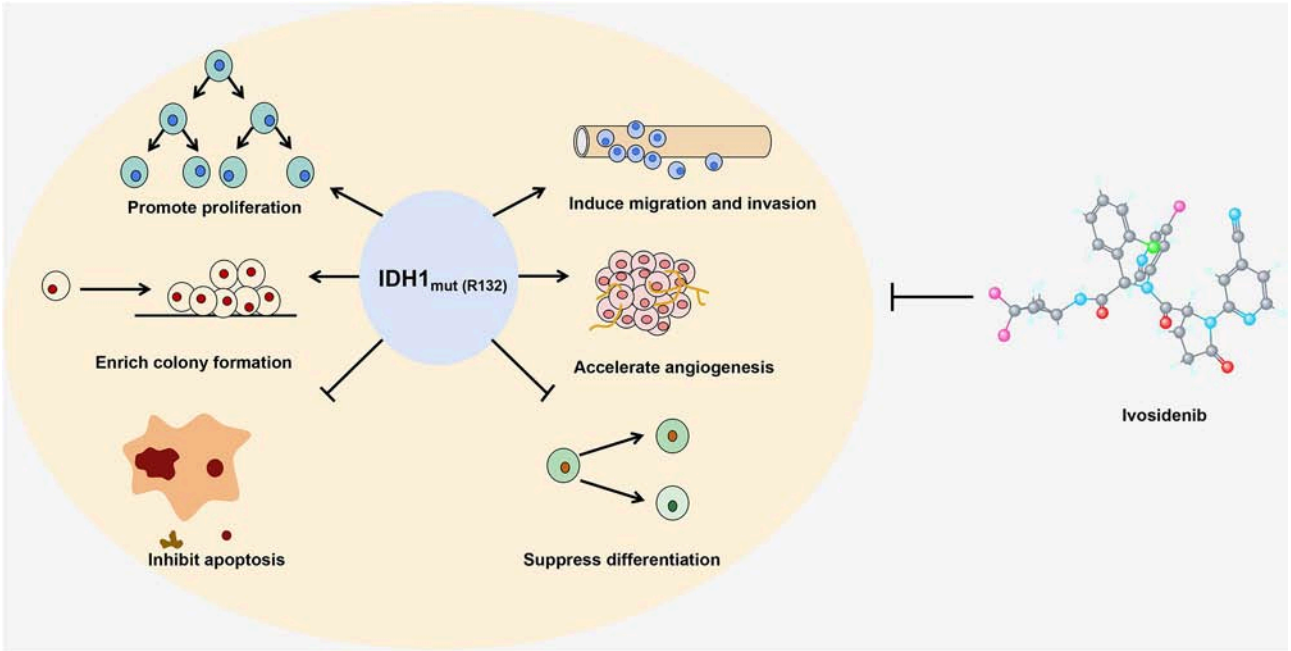

FIGURE 1 | The IDH1 R132 mutant is shown as an example to illustrate how a gain-of-function mutation in an epigenetic enzyme affects the growth and differentiation of cells. Ivosidenib, a specific inhibitor of the IDH1 R132 mutant, is shown at the right.

Knutson et al. have reported that the SAM-competitive EZH2 inhibitor EPZ005687, which is highly selective for EZH2 over other methyltransferases, significantly reduced the viability of lymphoma cell lines carrying the EZH2 Y641 and A677 mutations (64). McCabe et al. discovered that GSK126 is a SAM-competitive small molecule inhibitor of EZH2 methyltransferase activity that efficiently and selectively reduced H3K27me3 levels and reactivated the silenced target genes of polycomb repressive complex 2 (PRC2) (41). Their results also revealed that GSK126 effectively inhibited the proliferation of EZH2-mutant diffuse large B-cell lymphoma (DLBCL) cell lines and retarded the growth of EZH2-mutant DLBCL xenografts in mice (41). In addition, EPZ-6438, another selective inhibitor of EZH2, exerted potent antitumor activity against EZH2-mutant non-Hodgkin's lymphoma (65). Also, CPI-1205, an orally available selective inhibitor of EZH2, killed cells in both EZH2-WT and EZH2-mutant B-cell non-Hodgkin's lymphoma by altering PRC2 target gene expression in a dose- and time-dependent manner (5). All of the above inhibitors markedly reduced the high level of H3K27 trimethylation caused by EZH2 mutations, indicating that inhibition of EZH2 methyltransferase activity may be an effective way of treating EZH2 mutant lymphomas. EPZ005687 is currently in preclinical research, whereas GSK126, EPZ-6438 and CPI-1205 are under phase I/II investigation to assess their efficacy in patients with non-Hodgkin's lymphoma and certain solid tumors (5). In view of the high rate of EZH2 mutation in certain cancers, the application of these inhibitors in the clinic is expected to be successful in the future.

However, in addition to focusing on the effects of the EZH2 inhibitor itself on EZH2 mutant enzymes, we also need to consider the use of EZH2 inhibitors in synthetic lethality. Recently, targeting chromatin deficiency in cancer based on synthetic lethality has been used in cancer treatment. Synthetic lethality defines a relationship between two genes, where the loss of either gene is compatible with cell viability, but the loss of both genes causes cell death. Morel *et al.* summarized that the deficiency of SMARCB1, ARID1A, SMARCA4, and PBRM1, which constitute the chromatin remodeling complex SWI/SNF subunit, led to an EZH2 oncogenic dependence in tumor cells, and pharmacological EZH2 inhibitors such as tazemetostat induced dramatic tumor shrinkage in these subunits-deficient tumors (66). Therefore, synthetic lethality strategy may pave the way to potential epigenetic drugs targets.

Inhibitors Targeting IDH Mutants

Inhibitors targeting mutant IDH enzymes have also been widely investigated. In preclinical studies, it is reported that inhibitors targeting mutated forms of IDH1 and IDH2 can inhibit the growth of glioma cells and induce the differentiation of primary human IDH mutant AML cells *in vitro* (67). Encouragingly, clinical studies of inhibitors targeting mutated IDH have entered the phase I stage, and two inhibitors have been approved by the FDA for clinical use (68). For example, enasidenib (AG-221), a novel-specific small molecule inhibitor targeting mutant IDH2, was approved by the FDA in August 2017 for the treatment of relapsed AML (69). Another novel specific small molecule inhibitor, ivosidenib (AG-120), was approved by the FDA in July 2018 for clinical treatment of relapsed and refractory AML. Ivosidenib targets IDH1 with a mutation at the R132 site (see **Figure 1**) (70). Three other small molecule inhibitors, AGI-881,

IDH305, and FT-2102, are currently in phase I clinical trials. AGI-881 is a non-specific small molecule inhibitor which can target the mutant forms of both IDH1 and IDH2, whereas IDH-305 and FT-2102 target mutant IDH1 (68). These inhibitors prevent the reduction of α-KG to 2-HG by binding to the active site of the mutated IDH enzyme. High levels of 2-HG can inhibit DNA and histone demethylation, leading to hypermethylation. Borodovsky et al. have demonstrated that hypomethylating agents strongly induce differentiation, reduce colony formation ability, and suppress the growth of IDH mutant cells *in vivo* (71). Therefore, inhibitors targeting DNA and histone modifications may have potential therapeutic value. The DNA methyltransferase inhibitors decitabine (DAC) and 5-azacytidine have been approved by the FDA for clinical application and may have a therapeutic effect on tumors caused by IDH mutations (72). These findings also suggest that there is crosstalk among different epigenetic regulatory enzymes. In contrast to IDH mutation inhibitors, studies on inhibitors targeting SDH and FH mutations are currently lagging behind, which may lay the foundation for the development of new anti-tumor drugs.

CONCLUSION AND PERSPECTIVES

DNA methylation and histone modification are common epigenetic changes in eukaryotes, and the dysregulation of epigenetic regulatory enzymes is closely related to the onset and progression of various types of cancer. Mutations, especially gain-of-function mutations, may be responsible for some changes in epigenetic enzyme activity. Mutant epigenetic regulatory enzymes, and mutant forms of IDH that affect epigenetic changes, can enhance the ability of cancer cells to proliferate, migrate and form colonies. Therefore, these mutations are closely related to tumor onset and progression. Some inhibitors that specifically target the mutant forms of epigenetic regulatory enzymes and IDH have now entered clinical trials. The potential therapeutic effects of these inhibitors on tumors caused by mutations are summarized in **Figure 1**.

Many of the mechanisms by which mutations cause changes in the activity or function of epigenetic regulatory enzymes are not fully understood. Elucidation of these mechanisms may drive our understanding of the characteristics of different tumors. Further research into drugs that target these mutant enzymes will also accelerate the process of individualized treatment of tumors.

DATA AVAILABILITY

Publicly available datasets were analyzed in this study. This data can be found here: http://www.cbioportal.org.

AUTHOR CONTRIBUTIONS

MH contributes to draft manuscript and analysis the data. LJ contributes to draft manuscript. WL contributes to analysis the data. LW and WC contribute to design and draft the manuscript.

FUNDING

This work was financially supported by the National Natural Science Foundation of China (No. 81673652, 81572947, 81773780, 81773216), the Natural Science Foundation of Liaoning Province (No. 20170540841, 20180550076), the Scientific Research Fund of Liaoning Provincial Education Department (No. 2017LFW01) and the Science Foundation of Shenyang Pharmaceutical University (No. DFJJ2018210).

REFERENCES

1. Egger G, Liang G, Aparicio A, Jones PA. Epigenetics in human disease and prospects for epigenetic therapy. *Nature*. (2004) 429:457–63. doi: 10.1038/nature02625
2. Lund AH, Lohuizen MV. Epigenetics and cancer. *Genes Dev*. (2004) 18:2315–35. doi: 10.1101/gad.1232504
3. Carlberg C, Molnár F. Cancer epigenomics. *Hum Epigenomics*. (2018) 159–74. doi: 10.1007/978-981-10-7614-5_10
4. Mottamal M, Zheng S, Huang T, Wang G. Histone deacetylase inhibitors in clinical studies as templates for new anticancer agents. *Molecules*. (2015) 20:3898–941. doi: 10.3390/molecules20033898
5. Gulati N, Béguelin W, Giulino-Roth L. Enhancer of zeste homolog 2 (EZH2) inhibitors. *Leuk Lymphoma*. (2018) 59:1574–85. doi: 10.1080/10428194.2018.1430795
6. Tatton-Brown K, Seal S, Ruark E, Harmer J, Ramsay E, Rahman N, et al. Mutations in the DNA methyltransferase gene DNMT3A cause an overgrowth syndrome with intellectual disability. *Nat Genet*. (2014) 46:385–8. doi: 10.1038/ng.2917
7. Cohen AL, Holmen SL, Colman H. IDH1 and IDH2 mutations in gliomas. *Curr Neurol Neurosci Rep*. (2013) 13:345. doi: 10.1007/s11910-013-0345-4
8. Xu J, Wang YY, Dai YJ, Zhang W, Zhang WN, Xiong SM, et al. DNMT3A Arg882 mutation drives chronic myelomonocytic leukemia through disturbing gene expression/DNA methylation in hematopoietic cells. *Proc Natl Acad Sci USA*. (2014) 111:2620–5. doi: 10.1073/pnas.1400150111
9. Ballestar E. The impact of chromatin in human cancer: linking DNA methylation to gene silencing. *Carcinogenesis*. (2002) 23:1103–9. doi: 10.1093/carcin/23.7.1103
10. Singal R, Ginder GD. DNA methylation. *Blood*. (1999) 93:4059–70. doi: 10.1016/S0887-7963(99)80035-2
11. Chen QW, Zhu XY, Li YY, Meng ZQ. Epigenetic regulation and cancer. *Oncol Rep*. (2014) 31:523–32. doi: 10.3892/or.2013.2913
12. Boyes J, Bird A. DNA methylation inhibits transcription indirectly via a methyl-CpG binding protein. *Cell*. (1991) 64:1123–34. doi: 10.1016/0092-8674(91)90267-3
13. Costello JF, Frühwald MC, Smiraglia DJ, Rush LJ, Robertson GP, Gao X, et al. Aberrant CpG-island methylation has non-random and tumour-type–specific patterns. *Nat Genet*. (2000) 24:132–8. doi: 10.1038/72785
14. Baylin SB, Jones PA. A decade of exploring the cancer epigenome — biological and translational implications. *Nat Rev Cancer*. (2011) 11:726–34. doi: 10.1038/nrc3130
15. Yamashita Y, Yuan J, Suetake I, Suzuki H, Ishikawa Y, Choi YL, et al. Array-based genomic resequencing of human leukemia. *Oncogene*. (2010) 29:3723–31. doi: 10.1038/onc.2010.117
16. Elsayed GM, Fahmi AEA, Shafik NF, Elshimy RAA, Abd Elhakeem HK, Attea SA. Study of DNA methyl transferase 3A mutation in acute myeloid leukemic patients. *Egypt J Med Hum Genet*. (2018) 19:315–9. doi: 10.1016/j.ejmhg.2018.05.005
17. Russler-Germain DA, Spencer DH, Young MA, Lamprecht TL, Miller CA, Fulton R, et al. The R882H DNMT3A mutation associated with AML

dominantly inhibits wild-type DNMT3A by blocking its ability to form active tetramers. *Cancer Cell*. (2014) 25:442–54. doi: 10.1016/j.ccr.2014.02.010
18. Pløen GG, Nederby L, Guldberg P, Hansen M, Ebbesen LH, Jensen UB, et al. Persistence of DNMT3A mutations at long-term remission in adult patients with AML. *Br J Haematol*. (2014) 167:478–86. doi: 10.1111/bjh.13062
19. Varambally S, Dhanasekaran SM, Zhou M, Barrette TR, Kumar-Sinha C, Sanda MG, et al. The polycomb group protein EZH2 is involved in progression of prostate cancer. *Nature*. (2002) 419:624–9. doi: 10.1038/nature01075
20. Behrens C, Solis LM, Lin H, Yuan P, Tang X, Kadara H, et al. EZH2 Protein Expression Associates with the early pathogenesis, tumor progression, and prognosis of non-small cell lung carcinoma. *Clin Cancer Res*. (2013) 19:6556–65. doi: 10.1158/1078-0432.ccr-12-3946
21. Zhou Z, Gao J, Popovic R, Wolniak K, Parimi V, Winter JN, et al. Strong expression of EZH2 and accumulation of trimethylated H3K27 in diffuse large B-cell lymphoma independent of cell of origin and EZH2 codon 641 mutation. *Leuk Lymphoma*. (2015) 56:2895–901. doi: 10.3109/10428194.2015.1006220
22. Sneeringer CJ, Scott MP, Kuntz KW, Knutson SK, Pollock RM, Richon VM, et al. Coordinated activities of wild-type plus mutant EZH2 drive tumor-associated hypertrimethylation of lysine 27 on histone H3 (H3K27) in human B-cell lymphomas. *Proc Natl Acad Sci USA*. (2010) 107:20980–5. doi: 10.1073/pnas.1012525107
23. Kickingereder P, Sahm F, Radbruch A, Wick W, Heiland S, Deimling A, et al. Wiestler, B. (2015). IDH mutation status is associated with a distinct hypoxia/angiogenesis transcriptome signature which is non-invasively predictable with rCBV imaging in human glioma. *Sci Rep*. 5:16238. doi: 10.1038/srep16238
24. Bodor C, Grossmann V, Popov N, Okosun J, O'Riain C, Tan K, et al. EZH2 mutations are frequent and represent an early event in follicular lymphoma. *Blood*. (2013) 122:3165–8. doi: 10.1182/blood-2013-04-496893
25. Souroullas GP, Jeck WR, Parker JS, Simon JM, Liu J-Y, Paulk J, et al. An oncogenic Ezh2 mutation induces tumors through global redistribution of histone 3 lysine 27 trimethylation. *Nat Med*. (2016) 22:632–40. doi: 10.1038/nm.4092
26. Majer CR, Jin L, Scott MP, Knutson SK, Kuntz KW, Keilhack H, et al. A687V EZH2 is a gain-of-function mutation found in lymphoma patients. *FEBS Lett*. (2012) 586:3448–51. doi: 10.1016/j.febslet.2012.07.066
27. Dang L, Jin S, Su SM. IDH mutations in glioma and acute myeloid leukemia. *Trends Mol Med*. (2010) 16:387–97. doi: 10.1016/j.molmed.2010.07.002
28. Pollard PJ, Loenarz C, Mole DR, McDonough MA, Gleadle JM, Schofield CJ, et al. Regulation of Jumonji-domain-containing histone demethylases by hypoxia-inducible factor (HIF)-1α. *Bioch J*. (2008) 416:387–94. doi: 10.1042/bj20081238
29. Kanai Y, Ushijima S, Nakanishi Y, Sakamoto M, Hirohashi S. Mutation of the DNA methyltransferase (DNMT) 1 gene in human colorectal cancers. *Cancer Lett*. (2003) 192:75–82. doi: 10.1016/s0304-3835(02)00689-4
30. Yang L, Rau R, Goodell MA. DNMT3A in haematological malignancies. *Nat Rev Cancer*. (2015) 15:152–65. doi: 10.1038/nrc3895
31. Hansen RS, Wijmenga C, Luo P, Stanek AM, Canfield TK, Weemaes CMR, et al. The DNMT3B DNA methyltransferase gene is mutated in the ICF immunodeficiency syndrome. *Proc Natl Acad Sci USA*. (1999) 96:14412–7. doi: 10.1073/pnas.96.25.14412
32. Ko M, Bandukwala HS, An J, Lamperti ED, Thompson EC, Hastie R, et al. Ten-Eleven-Translocation 2 (TET2) negatively regulates homeostasis and differentiation of hematopoietic stem cells in mice. *Proc Natl Acad Sci USA*. (2011) 108:14566–71. doi: 10.1073/pnas.1112317108
33. Xu J, Zhang W, Yan XJ, Lin XQ, Li W, Mi JQ, et al. DNMT3A mutation leads to leukemic extramedullary infiltration mediated by TWIST1. *J Hematol Oncol*. (2016) 9:106. doi: 10.1186/s13045-016-0337-3
34. Koya J, Kataoka K, Sato T, Bando M, Kato Y, Tsuruta-Kishino T, et al. DNMT3A R882 mutants interact with polycomb proteins to block haematopoietic stem and leukaemic cell differentiation. *Nat Commun*. (2016) 7:10924. doi: 10.1038/ncomms10924
35. Guryanova OA, Shank K, Spitzer B, Luciani L, Koche RP, Garrett-Bakelman FE, et al. DNMT3A mutations promote anthracycline resistance in acute myeloid leukemia via impaired nucleosome remodeling. *Nat Med*. (2016) 22:1488–95. doi: 10.1038/nm.4210
36. Ley TJ, Ding L, Walter MJ, McLellan MD, Lamprecht T, Larson DE, et al. DNMT3A mutations in acute myeloid leukemia. *New Engl J Med*. (2010) 363:2424–33. doi: 10.1056/nejmoa1005143
37. Ferreira HJ, Heyn H, Vizoso M, Moutinho C, Vidal E, Gomez A, et al. DNMT3A mutations mediate the epigenetic reactivation of the leukemogenic factor MEIS1 in acute myeloid leukemia. *Oncogene*. (2015) 35:3079–82. doi: 10.1038/onc.2015.359
38. Delhommeau F, Dupont S, Valle VD, James C, Trannoy S, Massé A, et al. Mutation inTET2in Myeloid Cancers. *New Engl J Med*. (2009) 360:2289–301. doi: 10.1056/nejmoa0810069
39. Wei S, Li C, Yin Z, Wen J, Meng H, Xue L, et al. Histone methylation in DNA repair and clinical practice: new findings during the past 5-years. *J Cancer*. (2018) 9:2072–81. doi: 10.7150/jca.23427
40. Simon JA, Lange CA. Roles of the EZH2 histone methyltransferase in cancer epigenetics. *Mutat Res Fund Mol Mech Mutag*. (2008) 647:21–9. doi: 10.1016/j.mrfmmm.2008.07.010
41. McCabe MT, Ott HM, Ganji G, Korenchuk S, Thompson C, Van Aller GS, et al. EZH2 inhibition as a therapeutic strategy for lymphoma with EZH2-activating mutations. *Nature*. (2012) 492:108–12. doi: 10.1038/nature11606
42. Barsotti AM, Ryskin M, Zhong W, Zhang W-G, Giannakou A, Loreth C, et al. Epigenetic reprogramming by tumor-derived EZH2 gain-of-function mutations promotes aggressive 3D cell morphologies and enhances melanoma tumor growth. *Oncotarget*. (2015) 6:2928–38. doi: 10.18632/oncotarget.2758
43. Vannucchi AM, Lasho TL, Guglielmelli P, Biamonte F, Pardanani A, Pereira A, et al. Mutations and prognosis in primary myelofibrosis. *Leukemia*. (2013) 27:1861–9. doi: 10.1038/leu.2013.119
44. Saldanha SN, Tollefsbol TO. Epigenetic approaches to cancer therapy. *Epigenet Hum Dis*. (2018) 219–47. doi: 10.1016/b978-0-12-812215-0.00007-8
45. Kipp BR, Voss JS, Kerr SE, Barr Fritcher EG, Graham RP, Zhang L, et al. Isocitrate dehydrogenase 1 and 2 mutations in cholangiocarcinoma. *Hum Pathol*. (2012) 43:1552–8. doi: 10.1016/j.humpath.2011.12.007
46. Ghiam AF, Cairns RA, Thoms J, Dal Pra A, Ahmed O, Meng A, et al. IDH mutation status in prostate cancer. *Oncogene*. (2011) 31:3826. doi: 10.1038/onc.2011.546
47. Ciccarone F, Vegliante R, Di Leo L, Ciriolo MR. The TCA cycle as a bridge between oncometabolism and DNA transactions in cancer. *Sem Cancer Biol*. (2017) 47:50–6. doi: 10.1016/j.semcancer.2017.06.008
48. Fu Y, Zheng Y, Li K, Huang R, Zheng S, An N, et al. Mutations in isocitrate dehydrogenase 2 accelerate glioma cell migration via matrix metalloproteinase-2 and 9. *Biotechnol Lett*. (2011) 34:441–6. doi: 10.1007/s10529-011-0800-8
49. Fu Y, Zheng S, Zheng Y, Huang R, An N, Liang A, et al. Glioma derived isocitrate dehydrogenase-2 mutations induced up-regulation of HIF-1α and β-catenin signaling: Possible impact on glioma cell metastasis and chemo-resistance. *Int J Biochem Cell Biol*. (2012) 44:770–5. doi: 10.1016/j.biocel.2012.01.017
50. Saha SK, Parachoniak CA, Ghanta KS, Fitamant J, Ross KN, Najem MS, et al. Mutant IDH inhibits HNF-4α to block hepatocyte differentiation and promote biliary cancer. *Nature*. (2014) 513:110–4. doi: 10.1038/nature13441
51. Figueroa ME, Abdel-Wahab O, Lu C, Ward PS, Patel J, Shih A, et al. Leukemic IDH1 and IDH2 Mutations result in a hypermethylation phenotype, disrupt TET2 function, and impair hematopoietic differentiation. *Cancer Cell*. (2010) 18:553–67. doi: 10.1016/j.ccr.2010.11.015
52. Lu C, Ward PS, Kapoor GS, Rohle D, Turcan S, Abdel-Wahab O, et al. IDH mutation impairs histone demethylation and results in a block to cell differentiation. *Nature*. (2012) 483:474–8. doi: 10.1038/nature10860
53. Goyal L, Govindan A, Sheth RA, Nardi V, Blaszkowsky LS, Faris JE, et al. Prognosis and clinicopathologic features of patients with advanced stage Isocitrate Dehydrogenase (IDH) Mutant and IDH wild-type intrahepatic cholangiocarcinoma. *Oncologist*. (2015) 20:1019–27. doi: 10.1634/theoncologist.2015-0210
54. Kelly AD, Issa JPJ. The promise of epigenetic therapy: reprogramming the cancer epigenome. *Curr Opin Genet Dev*. (2017) 42:68–77. doi: 10.1016/j.gde.2017.03.015

55. Marmorstein R, Roth SY. Histone acetyltransferases: function, structure, and catalysis. *Curr Opin Genet Dev*. (2001) 11:155–61. doi: 10.1016/s0959-437x(00)00173-8
56. Yanginlar C, Logie C. HDAC11 is a regulator of diverse immune functions. *Biochim Biophys Acta Gene Regul Mech*. (2018) 1861:54–9. doi: 10.1016/j.bbagrm.2017.12.002
57. Wang L, Beier UH, Akimova T, Dahiya S, Han R, Samanta A, et al. Histone/protein deacetylase inhibitor therapy for enhancement of Foxp3+ T-regulatory cell function posttransplantation. *Am J Transpl*. (2018) 18:1596–603. doi: 10.1111/ajt.14749
58. Ropero S, Esteller M. The role of histone deacetylases (HDACs) in human cancer. *Mol Oncol*. (2007) 1:19–25. doi: 10.1016/j.molonc.2007.01.001
59. Jiang Y, Ortega-Molina A, Geng H, Ying H-Y, Hatzi K, Parsa S, et al. CREBBP inactivation promotes the development of HDAC3-dependent lymphomas. *Cancer Disc*. (2016) 7:38–53. doi: 10.1158/2159-8290.cd-16-0975
60. Jia D, Augert A, Kim DW, Eastwood E, Wu N, Ibrahim AH, et al. Crebbp loss drives small cell lung cancer and increases sensitivity to HDAC inhibition. *Cancer Disc*. (2018) 8:1422–37. doi: 10.1158/2159-8290.cd-18-0385
61. Emperle M, Rajavelu A, Kunert S, Arimondo PB, Reinhardt R, Jurkowska RZ, et al. The DNMT3A R882H mutant displays altered flanking sequence preferences. *Nucleic Acids Res*. (2018) 46:3130–9. doi: 10.1093/nar/gky168
62. Rau RE, Rodriguez BA, Luo M, Jeong M, Rosen A, Rogers JH, et al. DOT1L as a therapeutic target for the treatment of DNMT3A-mutant acute myeloid leukemia. *Blood*. (2016) 128:971–81. doi: 10.1182/blood-2015-11-684225
63. Bejar R, Lord A, Stevenson K, Bar-Natan M, Perez-Ladaga A, Zaneveld J, et al. TET2 mutations predict response to hypomethylating agents in myelodysplastic syndrome patients. *Blood*. (2014) 124:2705–12. doi: 10.1182/blood-2014-06-582809
64. Knutson SK, Wigle TJ, Warholic NM, Sneeringer CJ, Allain CJ, Klaus CR, et al. A selective inhibitor of EZH2 blocks H3K27 methylation and kills mutant lymphoma cells. *Nat Chem Biol*. (2012) 8:890–6. doi: 10.1038/nchembio.1084
65. Knutson SK, Kawano S, Minoshima Y, Warholic NM, Huang K-C, Xiao Y, et al. Selective inhibition of EZH2 by EPZ-6438 leads to potent antitumor activity in EZH2-mutant non-hodgkin lymphoma. *Mol Cancer Ther*. (2014) 13:842–54. doi: 10.1158/1535-7163.mct-13-0773
66. Morel D, Almouzni G, Soria JC, Postel-Vinay S. Targeting chromatin defects in selected solid tumors based on oncogene addiction, synthetic lethality and epigenetic antagonism. *Ann Oncol*. (2016) 28:254–69. doi: 10.1093/annonc/mdw552
67. Dang L, Yen K, Attar EC. IDH mutations in cancer and progress toward development of targeted therapeutics. *Ann Oncol*. (2016) 27:599–608. doi: 10.1093/annonc/mdw013
68. Montalban-Bravo G, DiNardo CD. The role of IDH mutations in acute myeloid leukemia. *Future Oncol*. (2018) 14:979–93. doi: 10.2217/fon-2017-0523
69. Kim ES. Enasidenib: first global approval. *Drugs*. (2017) 77:1705–11. doi: 10.1007/s40265-017-0813-2
70. Popovici-Muller J, Lemieux RM, Artin E, Saunders JO, Salituro FG, Travins J, et al. Discovery of AG-120 (Ivosidenib): a first-in-class mutant IDH1 inhibitor for the treatment of IDH1 mutant cancers. *ACS Med Chem Lett*. (2018) 9:300–5. doi: 10.1021/acsmedchemlett.7b00421
71. Borodovsky A, Salmasi V, Turcan S. 5-azacytidine reduces methylation, promotes differentiation and induces tumor regression in a patient-derived IDH1 mutant glioma xenograft. *Oncotarget*. (2013) 4:1737–47. doi: 10.18632/oncotarget.1408
72. Roy DM, Walsh LA, Chan TA. Driver mutations of cancer epigenomes. *Protein Cell*. (2014) 5:265–96. doi: 10.1007/s13238-014-0031-6

Conflict of Interest Statement: The authors declare that the research was conducted in the absence of any commercial or financial relationships that could be construed as a potential conflict of interest.

frontiers in Oncology

ORIGINAL RESEARCH
published: 02 April 2019
doi: 10.3389/fonc.2019.00185

CACNA2D3 Enhances the Chemosensitivity of Esophageal Squamous Cell Carcinoma to Cisplatin via Inducing Ca^{2+}-Mediated Apoptosis and Suppressing PI3K/Akt Pathways

Changjun Nie[1,2,3,4†], *Xiaohui Qin*[4†], *Xiaoyan Li*[1,2,3†], *Baoqing Tian*[1,2,3], *Ying Zhao*[1,2,3], *Yuan Jin*[1,2,3], *Yadan Li*[1,2,3], *Qiang Wang*[1,2,3], *Dingyuan Zeng*[4], *An Hong*[1,2,3*] *and Xiaojia Chen*[1,2,3*]

[1] Department of Cell Biology, Institute of Biomedicine, Jinan University, Guangzhou, China, [2] National Engineering Research Center of Genetic Medicine, Guangzhou, China, [3] Guangdong Provincial Key Laboratory of Bioengineering Medicine, Guangzhou, China, [4] Department of Medical Genetics, Liuzhou Maternal and Children Healthcare Hospital, Liuzhou, China

Resistance to platinum-based combination chemotherapy is the main cause of poor prognosis in patients with advanced esophageal squamous cell carcinoma (ESCC). Previously, we showed that CACNA2D3 (voltage-dependent subunit alpha 2 delta 3 of a calcium channel complex) was significantly downregulated and functioned as a tumor suppressor in ESCC, but its role in the chemosensitivity of ESCC to cisplatin remained unknown. Here, we found that the expression of CACNA2D3 was significantly associated with poor platinum response in ESCC patients from the Gene Expression Omnibus database. Overexpression of CACNA2D3 increased sensitivity to cisplatin in ESCC *in vitro*, whereas knockdown of CACNA2D3 increased cisplatin resistance. CACNA2D3 promoted cisplatin-induced apoptosis by modulating intracellular Ca^{2+} stores. *In vivo* experiments further showed that overexpression of CACNA2D3 enhanced cisplatin anti-tumor effects in a xenograft mouse model. CACNA2D3 overexpression also resulted in the attenuation of PI3K and Akt phosphorylation. Treatment with the PI3K/Akt inhibitor LY294002 restored the chemosensitivity of CACAN2D3-knockdown cells to cisplatin. In conclusion, the results of the current study indicate that CACAN2D3 enhances the chemosensitivity of ESCC to cisplatin via inducing Ca^{2+}-mediated apoptosis and suppressing PI3K/Akt pathways. Therefore, regulating the expression of CACNA2D3 is a potential new strategy to increase the efficacy of cisplatin in ESCC patients.

Keywords: CACNA2D3, chemosensitivity, ESCC, voltage-gated calcium channel, LY294002

OPEN ACCESS

Edited by:
Yunkai Zhang,
Vanderbilt University Medical Center, United States

Reviewed by:
Leyuan Liu,
Texas A&M University, United States
Zhenfang Du,
Vanderbilt University Medical Center, United States

***Correspondence:**
An Hong
tha@jnu.edu.cn
Xiaojia Chen
tchenxj@jnu.edu.cn;
carolcxj@qq.com

†These authors have contributed equally to this work

Specialty section:
This article was submitted to Cancer Molecular Targets and Therapeutics, a section of the journal Frontiers in Oncology

Received: *24 January 2019*
Accepted: *04 March 2019*
Published: *02 April 2019*

Citation:
Nie C, Qin X, Li X, Tian B, Zhao Y, Jin Y, Li Y, Wang Q, Zeng D, Hong A and Chen X (2019) CACNA2D3 Enhances the Chemosensitivity of Esophageal Squamous Cell Carcinoma to Cisplatin via Inducing Ca^{2+}-Mediated Apoptosis and Suppressing PI3K/Akt Pathways. Front. Oncol. 9:185. doi: 10.3389/fonc.2019.00185

INTRODUCTION

Esophageal cancer (EC) is a fatal digestive tract malignancy (1). EC is composed of two major histologic subtypes: adenocarcinoma and squamous cell carcinoma. Esophageal squamous cell carcinoma (ESCC) is more common in Southeast and Central Asia (2, 3). China is a high incidence area for ESCC, especially in Linzhou and Cixian of North China (4). Esophagectomy is the usual method for the treatment of early esophageal cancer. However, most ESCC patients are diagnosed at an advanced stage when surgery is no longer effective. Recently, the use of comprehensive perioperative therapies has dramatically improved the therapeutic efficacy of ESCC, particularly with respect to long-term survival (5–7). A cisplatin-based regimen is widely used as the first-line treatment in advanced ESCC (8–10). However, cisplatin chemotherapy is often limited by natural and acquired resistance. Consequently, it is critical to identify potential resistance mechanisms in order to restore tumor cell sensitivity to cisplatin.

The human *CACNA2D3* gene is located on the short arm of chromosome 3 at position 3p21.1, a common region of allelic deletion, and has been found to possess a potential tumor suppressor function in multiple tumor types, including gastric cancer (11–13), nasopharyngeal cancer (14), breast cancer (15), renal cell cancer neuroblastoma (16), lung cancer (17), and glioma (18). The promoter of CACNA2D3 was shown to be highly methylated in gastric cancer, and this was associated with a low survival rate (12). Similarly, suppression of CACNA2D3 by methylation was found to promote the metastatic phenotype of breast cancer (15). Another study showed that CACNA2D3 could increase intracellular Ca^{2+} levels and promote apoptosis in nasopharyngeal cancer and glioma, causing changes in the network of tumor-suppressive properties and inducing upregulation of Nemo-like kinase (NLK) through the non-canonical Wnt/Ca^{2+} signaling pathway (14, 18). In neuroblastomas with poor prognosis, the expression of CACNA2D3 is often downregulated (19, 20). Our previous study also identified CACNA2D3 as a tumor suppressor gene, and methylation of its promoter and allele deletion could inhibit its expression in ESCC (21). Recently, CACNA2D3 was implicated in the development of chemoresistance. The downregulation of CACNA2D3 was detected in five cytarabine-resistant leukemic cell lines compared with parental cells (22). However, the underlying mechanism by which CACNA2D3 might function in chemosensitivity has not been identified.

In this study, we aimed to investigate the function of CACNA2D3 in cisplatin-based chemotherapy of ESCC and discover its underlying mechanisms. We found that the expression of CACNA2D3 was significantly associated with poor platinum response in ESCC patients. Overexpression of CACNA2D3 significantly sensitized ESCC cell lines to cisplatin, while CACNA2D3 knockdown induced cellular resistance to cisplatin. Further research showed that CACNA2D3 overexpression enhanced cisplatin-induced apoptosis by modulating intracellular Ca^{2+}. Moreover, CACNA2D3 overexpression resulted in the attenuation of PI3K and Akt phosphorylation. LY294002 is a commonly used PI3K/AKT pathway inhibitor, and treatment with LY294002 could restore the chemosensitivity of CACAN2D3-knockdown cells to cisplatin.

MATERIALS AND METHODS

Cell Lines and Reagents

Six ESCC cell lines (KYSE30, KYSE140, KYSE180, KYSE410, KYSE510, and KYSE520) were purchased from DSMZ, the German Resource Centre for Biological Material (23). The short tandem repeat (STR) analysis technique was used to periodically identify all cell lines. Cell lines were cultured in RPMI1640 medium (Hyclone, Logan, UT, USA) supplemented with 10% fetal bovine serum and 1 × penicillin/streptomycin (100 units/mL, 100 μg/mL) (Gibco, NY, USA) at 37°C in a humidified incubator (5% CO_2/95% air). Cisplatin was acquired from Sigma. LY294002 was purchased from Selleck.

Plasmid Constructs and Stable Transfection

CACNA2D3 cDNA was amplified from normal human esophageal epithelial cells. The eukaryotic expression vector pcDNA3.1 (+) (Invitrogen, Carlsbad, CA, USA) was used for cloning the human CACNA2D3 gene. Then pcDNA3.1-CACNA2D3 was transfected into the ESCC cell line KYSE30 using Lipofectamine™ 3000 (Invitrogen, Carlsbad, CA, USA). The empty vector was used as a negative control. KYSE30 cells stably expressing CACNA2D3 were screened with 500 μg/ml G418.

RNA Interference

Small interfering RNA (siRNA) (SR310953) targeting CACNA2D3 and scrambled negative control siRNA (SR30004) were purchased from OriGene. After transfection for 48 h, the relative expression of CACNA2D3 was detected by quantitative real-time PCR (qRT-PCR) and western blotting.

Cell Viability Assay

A Cell Counting Kit-8 (CCK-8) assay (Dojindo, Kumamoto, Japan) was performed to measure cell viability. Cells were seeded at a density of 1×10^4 cells/well in 96-well plates and incubated with serial dilutions of cisplatin for 72 h. The CCK-8 reagent and RPMI-1640 were diluted in a 1:9 ratio and used to replace the original medium. After incubation at 37°C for 2.5 h, absorbance at a wavelength of 450 nm was measured using a microplate reader. Three independent experiments were conducted. Half maximal inhibitory concentration (IC50) was calculated to evaluate cell resistance to cisplatin using GraphPad Prism 5.0.

Colony Formation Assay

Cells were seeded at a density of 1.5×10^3 cells/well in six-well plates and treated with respective concentrations of cisplatin. After incubation for 10–14 days, the cell colonies were fixed with ethanol for 30 min and then stained with 0.1% crystal violet for 15 min. Colonies (≥50 cells) were counted. All assays were independently performed in triplicate.

Intracellular Calcium Assay

The fluorescent probe Fluo-3 AM assay (Beyotime, Haimen, China) was used to measure intracellular Ca^{2+} concentrations. Cells were washed twice with phosphate-buffered saline (PBS) and then loaded with Fluo-3 AM (1 μM) for 30 min in the dark at 37°C. When Fluo-3 AM penetrates the cellular membrane, it is hydrolyzed by cellular esterases to Fluo-3. Fluo-3 emits green fluorescence when combined with Ca^{2+}. The intracellular Ca^{2+} concentration was measured by flow cytometric analysis.

Apoptosis Assays

Apoptosis in ESCC cells treated with or without cisplatin were evaluated using an Annexin V-FITC/propidium iodide (PI) kit (Beyotime, Haimen, China). In brief, cells were digested, washed, and centrifuged twice with cold PBS. After fixing in 75% ethanol for 3 h, cells were stained with Annexin V-FITC and PI at room temperature for 30 min. Then, cells were measured by flow cytometry with FL-1 (530 nm) and FL-2 (585 nm) at an excitation wave length of 480 nm. The data were quantified using the FlowJo software.

Mitochondrial Membrane Potential Array

The mitochondrial membrane potential ($\Delta\Psi m$) was analyzed using a JC-1 assay kit (Beyotime, Haimen, China). JC-1 is a fluorescent probe for detecting mitochondrial membrane potential; it accumulates in the mitochondrial matrix and forms a red fluorescent polymer under high membrane potential. When the mitochondrial membrane potential is low, JC-1 exists as a monomer and produces green fluorescence. The cells were trypsinized and stained with JC-1 (10 mg/mL) at 37°C for 20 min. After being washed twice in PBS, cells were analyzed by flow cytometry using emission wavelengths of 590 and 525 nm.

Quantitative Real-Time PCR

Total RNA was extracted from ESCC cells using TRIzol reagent (Invitrogen, Carlsbad, CA, USA). First-strand cDNA was synthesized using the Reverse Transcription System (Promega, Wisconsin, USA), and mRNA expression levels were measured by qRT-PCR using a CFX96 Touch™ Real-Time PCR Detection System with SYBR Green Dye mixes (Applied Biosystems, Foster City, CA, USA). The PCR primers used for q-PCR were as follows. CACNA2D3: forward (5′-AGGGATTCACGG TTATGCCTT-3′), reverse (5′-GCCACACCTAAACCCTTT GTC-3′); β-Actin, forward (5′-GCTTGTCCAAGAGTGCAT GGT-3′), reverse (5′-CAGGGCTGGTTCTCGATGG-3′). The amplification parameters were: 5 min denaturation at 94°C, 40 cycles of denaturation 15 s at 94°C, 15 s annealing at 60°C, and 15 s elongation at 72°C, with final extension for 10 min at 72°C. The results were normalized to an internal standard with β-actin, and gene expression was analyzed using the $2^{-\Delta\Delta CT}$ method.

Tumor Xenograft Models

BALB/c nude mice (specific pathogen-free grade, 4–5 weeks old, and 15–20 g in weight) were purchased from Guangdong Medical Laboratory Animal Center (Guangzhou, China). The animals were raised at Jinan University Experimental Animal Management Center. KYSE30-CACNA2D3 cells and KYSE30-vector cells (6×10^6) were subcutaneously inoculated into the right armpit of each nude mouse. Tumor-bearing nude mice were randomly assigned to one of two groups of five mice: the treatment group mice received intraperitoneal injection cisplatin (2 mg/kg, twice per week for 4 weeks), and the control group mice were injected with PBS. Tumor volumes (mm^3) were calculated by the formula $V = 0.5 \times L \times W^2$. The mice were sacrificed and the tumors were isolated, weighed, and imaged. This study was carried out in accordance with the principles of the Basel Declaration and recommendations of the Guide for the Care and Use of Laboratory Animals, US National Institutes of Health (NIH Publication No. 85–23, revised 1996). The protocol was approved by the Laboratory Animal Ethics Committee of Jinan University.

Immunohistochemistry

Immunohistochemical staining was performed with primary antibodies against CACNA2D3 (Novus Biological, Littleton, CO, USA). Sections of xenografts from mice were deparaffinized with xylene and rehydrated in alcohol baths, then incubated in 3% hydrogen peroxide for 20 min to block endogenous peroxidase activity. Antigen retrieval was performed by microwave antigen retrieval in a citric acid buffer (pH 6.0). The slides were subsequently incubated with primary antibodies at 4°C overnight and then incubated with biotinylated secondary antibodies at room temperature for 30 min, followed by incubation with horseradish peroxidase (HRP)-streptavidin for 30 min. Finally, diaminobenzidine (DAB) staining and hematoxylin counterstaining were performed. All samples were observed through a high-power light microscope.

TUNEL Analysis

A colorimetric TUNEL apoptosis assay kit (Beyotime, Haimen, China) was used to identify apoptotic cells in the xenograft. Sections of xenograft from mice were deparaffinized, rehydrated, and incubated with proteinase K for 5 min at 37°C. Endogenous peroxidase was inactivated by treatment with 0.3% hydrogen peroxide for 20 min at room temperature. The sections were washed in PBS and incubated with a labeling buffer containing TdT at 37°C for 1 h, before being incubated with HRP-streptavidin for 30 min. Finally, the sections were incubated with DAB solution for coloration. All samples were observed through a high-power light microscope.

RNA Sequencing (RNA-seq) and Sequencing Analysis

Equal amounts of RNA samples were used to construct strand-specific RNA libraries, following the manufacturer's standard procedures. The libraries were sequenced on a HiSeq X Ten (Illumina, San Diego, CA, USA) platform in PE150 mode. The index of the reference genome was built using Bowtie v2.2.3 (24). Differentially expressed genes (DEGs) were identified using DESeq2 (25). The thresholds for DEGs were set as false discovery rate (FDR) ≤ 0.05 and $|\log_2$ fold change$| \geq 1$. Gene ontology (GO; http://www.geneontology.org) classification analysis was performed for DEGs, including molecular function,

cellular component, and biological process information (26). The Kyoto Encyclopedia of Genes and Genomes (KEGG; http://www.kegg.jp) was used for systematic analysis of the signaling pathways involving the DEGs (27), and related pathways were evaluated by gene set enrichment analysis (GSEA; http://software.broadinstitute.org/gsea/) (28).

Western Blot Assay

Western blot analysis was performed according to conventional methods. Antibodies against Akt, phosphor-Akt, PI3K, phosphor-PI3K, and GAPDH were from Cell Signaling Technology.

Statistical Analysis

Statistical analysis was performed using GraphPad Prism 5.0 and SPSS 19.0. Data were expressed as mean ± standard deviation (S.D.). Significant differences between two independent groups were identified by student's *t*-test and expressed as $^{*}p < 0.05$, $^{**}p < 0.01$, or $^{***}p < 0.001$.

RESULTS

Downregulation of CACNA2D3 Is Correlated With Chemoresistance in ESCC

To analyze the relationship between the expression of CACNA2D3 and chemoresistance in ESCC, we screened microarray data predicting the response of esophageal cancer patients to neoadjuvant chemotherapy from the Gene Expression Omnibus (GSE45670) (29). As shown in **Figure 1A**, the expression of CACNA2D3 in the neoadjuvant chemotherapy responder group was significantly higher than that in the non-responder group ($p < 0.05$). We further investigated the association of CACNA2D3 expression with chemotherapeutic response in ESCC cell lines by calculating the IC50 values of cisplatin during treatment. Six ESCC cell lines were treated with different concentrations of cisplatin. The IC50 dose was calculated in each cell, and qRT-PCR was used to determine the expression level of CACNA2D3. The results showed that the IC50 value of cisplatin was negatively correlated with CACNA2D3 expression in ESCC cell lines (**Figures 1B,C**). These observations indicated that CACNA2D3 might regulate chemosensitivity in ESCC.

CACNA2D3 Enhances Cisplatin Sensitivity in ESCC

To investigate the role of CACNA2D3 in regulating cisplatin sensitivity in ESCC cells, a KYSE30 cell line stably expressing CACNA2D3 (30-CAC) was constructed. Control cells were transfected with empty vector (30-Vec). The expression of CACNA2D3 was determined by western blotting and qRT-PCR (**Figure 2A**). CCK8 assays showed that overexpression of CACNA2D3 (30-CAC) could significantly increase the cells' chemosensitivity to cisplatin compared with controls (30-Vec) (**Figure 2B**). The sensitivity of 30-CAC cells to cisplatin was more than twice that of 30-Vec control cells, based on the IC50 value (**Figure 2C**). In colony formation experiments, we also found that overexpression of CACNA2D3 combined with cisplatin could inhibit the formation of clones more significantly (**Figure 2D**). We next examined whether knocking down CACNA2D3 would contribute to cisplatin resistance in ESCC. The results showed that specific siRNA against CACNA2D3 could significantly suppress the expression of CACNA2D3 up to 48 h after transfection in KYSE180 (**Figure 2E**). Knockdown of CACNA2D3 (180-siCAC) significantly induced cisplatin resistance compared with the scrambled siRNA (180-scr) (**Figure 2F**). The IC50 value of 180-siCAC was higher than that of 180-scr cells ($p < 0.001$) (**Figure 2G**). CACNA2D3 knockdown resulted in significantly higher colony formation efficiency in 180-siCAC cells than in control cells in the presence of cisplatin (**Figure 2H**). Taken together, the data showed that CACNA2D3 sensitized ESCC cells to cisplatin.

CACNA2D3 Enhances Cisplatin-Induced Apoptosis Through the Mitochondria-Dependent Pathway

CACNA2D3, as a regulatory subunit, has been reported to elevate the influx of extracellular Ca^{2+} into cells. In our study, Ca^{2+} levels were detected by Fluo-3 AM staining to evaluate their relationship with CACNA2D3 expression levels. CACNA2D3-overexpressing KYSE30 cells (30-CAC) showed significantly increased intracellular Ca^{2+} compared with the control cells (30-Vec), whereas knockdown of CACNA2D3 in KYSE180 cells (180-siCAC) caused a decrease in intracellular Ca^{2+} levels compared with control cells (180-scr) (**Figure 3A**). As Ca^{2+} can induce mitochondrial permeability changes and regulate the initiation phase of apoptosis, we performed an apoptosis assay to evaluate the effect of CACNA2D3 on the apoptosis of ESCC cells. Surprisingly, CACNA2D3 overexpression did not affect ESCC cell apoptosis, but promoted cisplatin-induced apoptosis. The percentage of apoptotic cells in 30-CAC cells increased by 24.8 ± 3.9% with cisplatin treatment, compared with 13.3 ± 1.7% in 30-Vec cells. In KYSE180 cells, cisplatin increased apoptosis by 14.2 ± 2.3% in 180-siCAC cells and by 32.3 ± 3.2% in 180-scr cells (**Figures 3B,C**). In addition, the JC-1 probe was used to assess changes in mitochondrial membrane potential in ESCC cells treated with cisplatin. As shown in **Figures 3D,E**, with cisplatin treatment, the membrane potential of 30-Vec cells decreased by 14.3 ± 2.5%, while that of 30-CAC cells decreased by 25.5 ± 1.6%. In KYSE180 cells, the membrane potential decreased by 24.2 ± 1.8% in 180-scr cells and by 9.6 ± 3.4% in 180-siCAC cells. Western blot analysis demonstrated that the ratios of cleaved Caspase9/Caspase9 and cleaved Caspase3/Caspase3 in CACNA2D3-overexpressing KYSE30 cells were higher than those in the control cells. Conversely, these ratios decreased in 180-siCAC cells treated with cisplatin compared with 180-scr cells (**Figure 3F**). Taken together, these results suggested that CACNA2D3 sensitized ESCC cells to cisplatin through enhancing mitochondria-mediated apoptosis.

CACNA2D3 Increases Cisplatin Sensitivity *in vivo*

In order to better understand the role of CACNA2D3 in cisplatin sensitivity *in vivo*, we established a subcutaneous

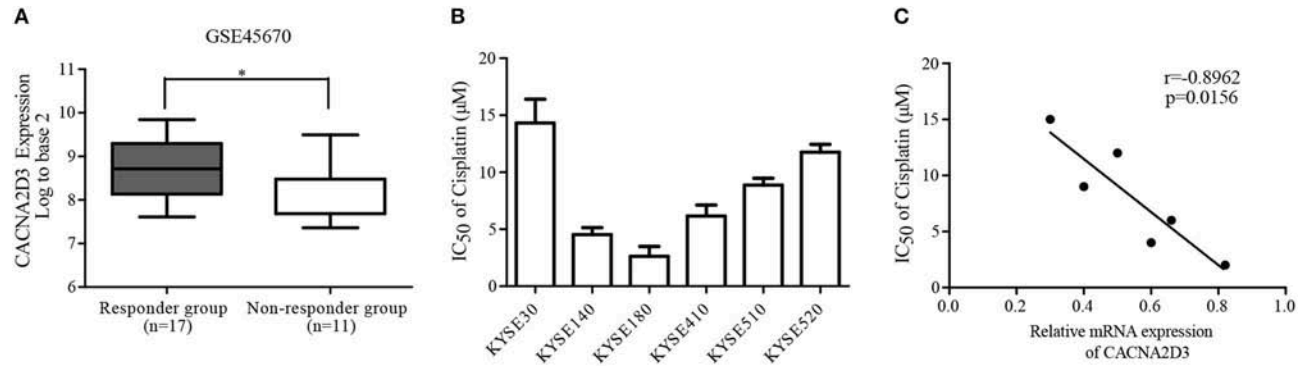

FIGURE 1 | Downregulation of CACNA2D3 is associated with poor chemotherapy response in ESCC. **(A)** Box and whisker plot of CACNA2D3 mRNA levels in neoadjuvant chemotherapy responder and non-responder groups (GSE45670). *$p < 0.05$. **(B)** IC50 values for cisplatin in six ESCC cell lines. Cells were treated with a range of concentrations of cisplatin for 72 h, and IC50 was calculated. Data are represented as the mean ± SD of three independent experiments. **(C)** Correlation of CACNA2D3 mRNA levels and IC50 values for cisplatin in six ESCC cell lines. r, Pearson correlation coefficient.

xenograft model by injecting CACNA2D3-overexpressing cells and control cells into BALB/c-nude mice. When the tumor volumes reached about 100 mm^3, 2 mg/kg cisplatin was injected intraperitoneally twice per week for 4 weeks, while the control group received PBS. As shown in **Figure 4A**, we found that overexpression of CACNA2D3 and cisplatin both inhibited the growth of xenografts. However, CACNA2D3 overexpression in combination with cisplatin could more significantly inhibit the tumorigenic ability of ESCC cells. The mean tumor size (**Figure 4B**) and weight (**Figure 4C**) in the CACNA2D3 overexpression group were significantly lower than those in the vector control group after cisplatin treatment. Moreover, immunohistochemical staining showed that the expression of CACNA2D3 was increased in the CACNA2D3-overexpressing tumors compared with the control tumors (**Figure 4D**). TUNEL analysis also revealed that the apoptosis rate of CACNA2D3 overexpression cells was significantly higher than that of the control cells after cisplatin treatment (**Figure 4E**). These results together indicated that CACNA2D3 increased cisplatin sensitivity *in vivo*.

CACANA2D3 Regulates the Sensitivity of ESCC to Cisplatin Through Inhibiting the PI3K/Akt Pathways

To better understand the molecular mechanism underlying CACNA2D3-enhanced ESCC cisplatin sensitivity, we compared the gene expression profiles of CACNA2D3 stably overexpressed KYSE30 cells with those of control cells using RNA-seq after cisplatin treatment, and identified 2439 DEGs (FDR < 0.05, $|\log_2$ fold change$| \geq 1$) between the two groups. A total of 1,137 genes were upregulated, and 1,302 genes were downregulated (**Figure 5A**). We further explored the biological functions of DEGs by GO, KEGG, and GSEA pathway enrichment analyses. Using the DAVID online GO database for comprehensive analysis, we found that CACNA2D3 was associated with multiple processes, including metabolic processes, biological regulation, regulation of biological processes, and response to stimulus (**Figure 5B**). KEGG database analysis revealed that multiple signaling pathway pathways were highly enriched, including "PI3K-Akt signaling pathway," "Pathways in cancer," "MAPK signaling pathway," and "ABC transporters" (**Figure 5C**). GSEA also showed that the CACNA2D3-regulated genes were enriched in the cell growth pathway and PI3K-Akt-mTOR signaling pathway (**Figure 5D**). Western blotting showed that CACNA2D3 dramatically suppressed the phosphorylation of PI3K and Akt, and the suppression persisted in the presence of cisplatin (**Figure 5E**). These results indicated that CACNA2D3 enhanced cisplatin sensitivity by inhibiting the PI3K/Akt pathway.

LY294002 Restores the Sensitivity of ESCC to Cisplatin in CACNA2D3-Knockdown Cells

For the rescue experiments, we treated CACNA2D3-knockdown cells with Akt inhibitor LY294002. Western blotting showed that LY294002 inhibited Akt activation in 180-siCAC cells and 180-scr cells (**Figure 6A**). The CACNA2D3-knockdown cells showed significantly higher sensitivity to cisplatin after treatment with LY294002 (**Figure 6B**). The effect of LY294002 on the IC50 reduction caused by cisplatin was significantly stronger in 180-siCAC cells than in 180-scr cells (**Figure 6C**). The colony formation assays also demonstrated that the combination of cisplatin and LY294002 suppressed colony formation more significantly in 180-siCAC cells than in control cells (**Figure 6D**). These results suggest that inhibition of the Akt signaling pathway can restore the chemosensitivity of CACNA2D3-knockdown cells to cisplatin.

DISCUSSION

ESCC is a cancer of the digestive system with high incidence in China. Although therapeutic strategies for ESCC have advanced considerably, its mortality rate remains high, and further efforts are needed to improve patient prognosis. Cisplatin is widely used

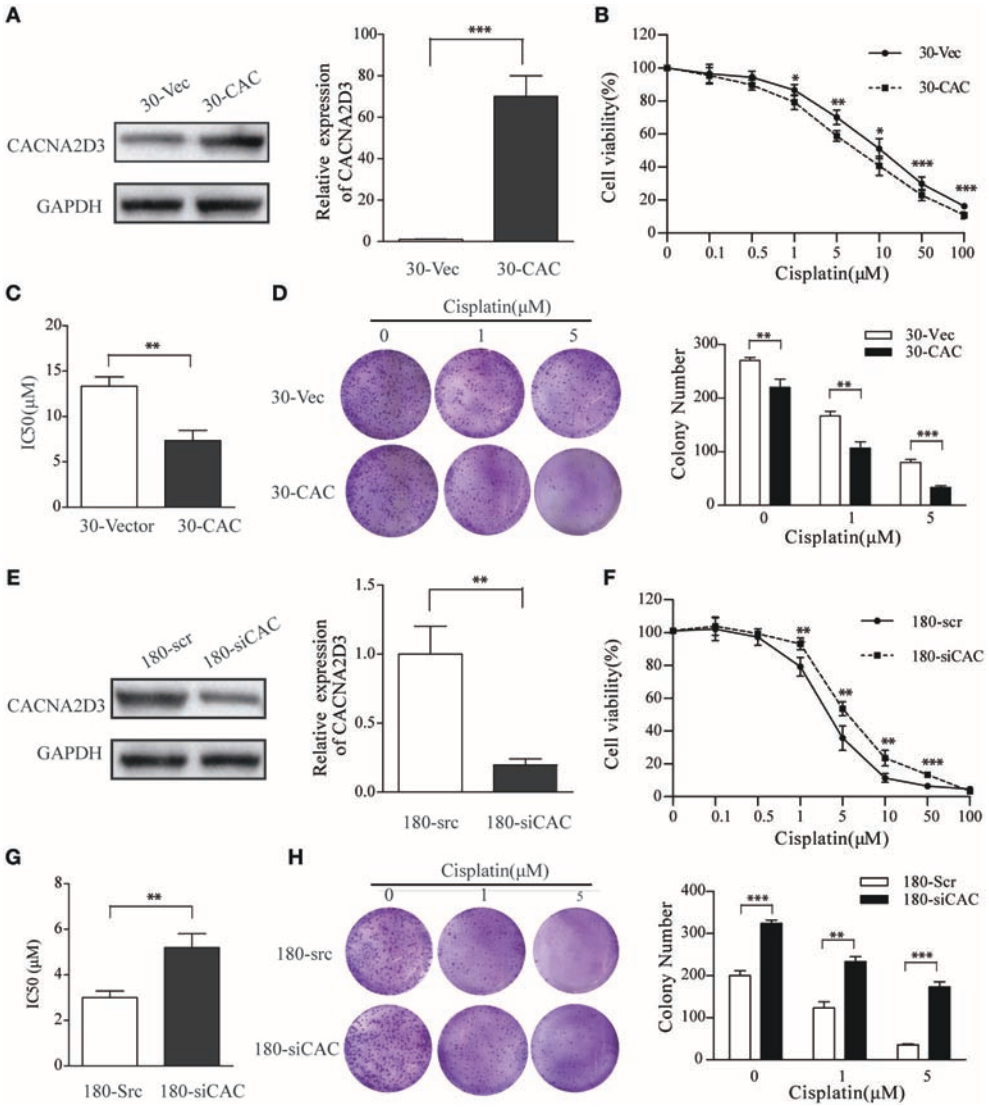

FIGURE 2 | CACNA2D3 promotes chemosensitivity to cisplatin *in vitro*. **(A,E)** Stable expression of CACNA2D3 in KYSE30 cells generated by pCDNA3.1-CACNA2D3 transfection and silencing of CACNA2D3 in KYSE180 cells by siRNA were examined by western blotting and qRT-PCR. GAPDH and β-Actin were employed as a loading control. **(B,F)** CACNA2D3-overexpressing KYSE30 cells and CACNA2D3-knockdown cells were treated with cisplatin at the indicated concentrations for 72 h. The number of viable cells was measured by CCK-8 assay. **(C,G)** IC50 values were calculated using linear or logarithmic regression ($R^2 > 0.9$). Values are presented as the mean ± SD of three wells. **(D,H)** Colony forming assays were used to determine colony forming ability after cisplatin treatment. Data are presented as the mean ± SD of three wells. $^{**}p < 0.01$, $^{***}p < 0.001$.

in the clinical chemotherapy of various types of human tumors, including esophageal, gastric, testicular, bladder, ovarian, and lung cancers (30–32). However, cisplatin resistance is often the biggest obstacle to the success of chemotherapy. Therefore, it is extremely important to be able to predict cisplatin response before chemotherapy, in order to select the most appropriate treatment strategy for patients.

Calcium ions (Ca^{2+}) are vital intracellular second messengers involved in multiple functions of cells, including proliferation, differentiation, fertilization, development, muscle contraction, cell death, learning, and memory (33–35). The voltage-gated calcium channel is a multi-subunit protein complex consisting of a channel-forming α1 subunit and three regulatory subunits, α2δ, β, and γ (36–38). CACNA2D3 encodes one of the α2δ subunits. Our previous study identified CACNA2D3 as a novel tumor suppressor gene for ESCC. Downregulation of CACNA2D3 predicted poor prognosis. Exogenous expression of CACNA2D3 can strongly inhibit cell growth, migration, and invasion, and induce apoptosis (21). In the current study, we first found that the expression of CACNA2D3 was higher in a platinum-based neoadjuvant chemotherapy responder group than in the non-responder group. Based on a serious of assays *in vitro* and *in vivo*, we confirmed the effect of CACNA2D3 on the chemosensitivity of cisplatin in ESCC cells.

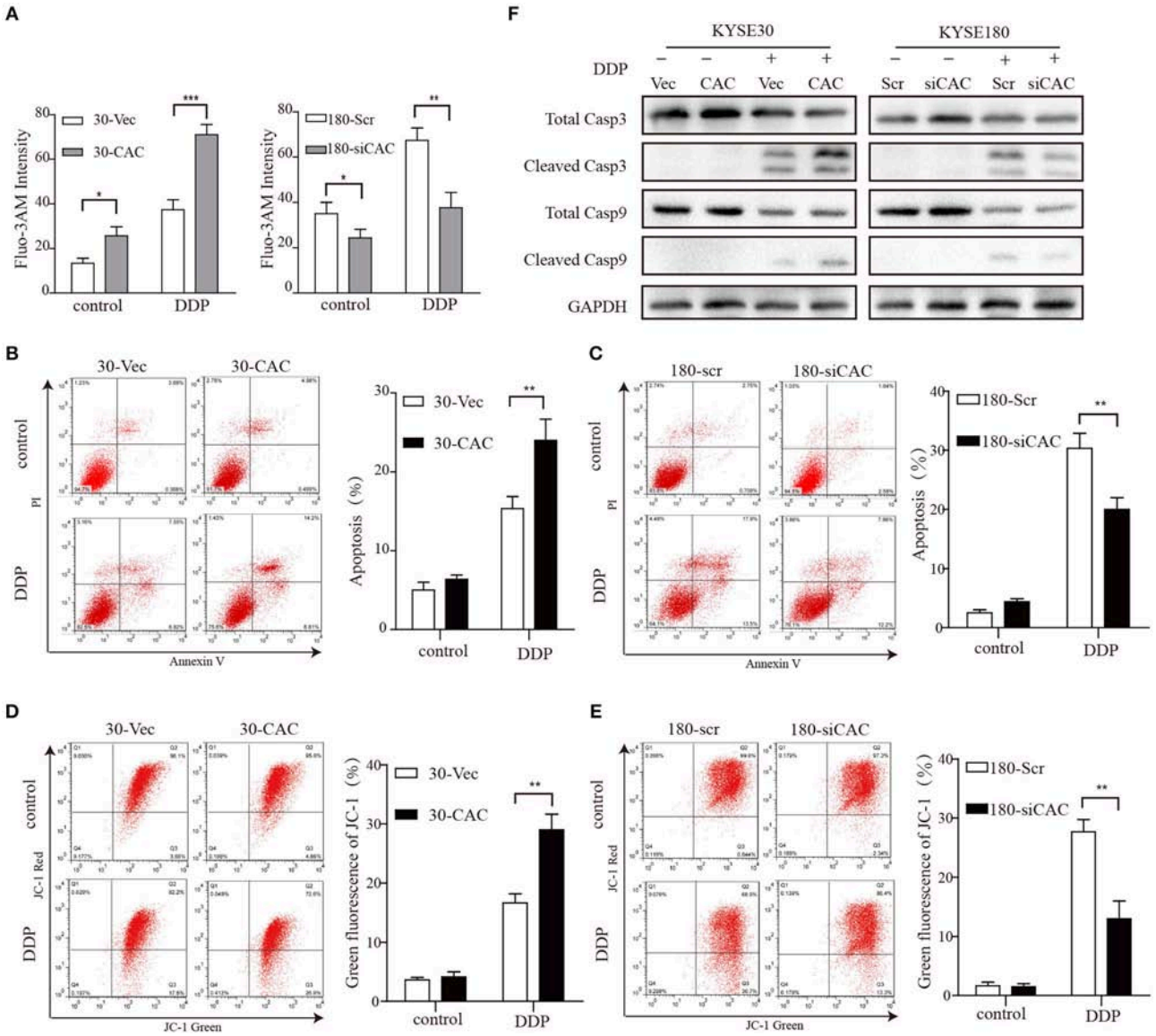

FIGURE 3 | CACNA2D3 enhances cisplatin-induced apoptosis through mitochondria-dependent pathway. **(A)** Intracellular Ca^{2+} levels were detected by fluorescence-activated cell sorting (FACS) with Fluo-3 AM. **(B,C)** Annexin V/PI staining in CACNA2D3 overexpression and knockdown cell lines treated with cisplatin for 48 h; apoptosis was analyzed by FACS. The percentages of apoptotic cells are presented as the mean ± SD of three independent experiments. **(D,E)** The mitochondrial membrane potential was measured using fluorescent dye JC-1 after treatment with cisplatin for 48 h. Percentages of green fluorescence from JC-1 in cells are presented as the mean ± SD of three independent experiments. **(F)** Levels of cleaved caspase-3, total caspase-3, cleaved caspase-9, and total caspase-9 proteins were analyzed by western blotting in CACNA2D3-overexpressing and knockdown cell lines treated with or without cisplatin. $^{*}p < 0.05$; $^{**}p < 0.01$; $^{***}p < 0.001$.

Cisplatin is a conventional chemotherapy drug. It is activated upon entering the cell, when its chloride atoms are replaced by water molecules. The resulting hydrolytic product is an effective electrophilic reagent, which can react with any nucleophile, including DNA, RNA, and proteins. DNA is the primary target of cisplatin. Cisplatin tends to bind to the N7 site of purine bases to form a DNA adduct, causing DNA damage in cancer cells, blocking cell division, and leading to apoptosis (39–41). Several mechanisms of cisplatin resistance have been discovered, including reduced intracellular drug accumulation, increased activity of efflux pumps, changed drug targets, lost mismatch-repair ability, and escape apoptosis (42–44). The voltage-dependent calcium channel α2δ subunits have been found to regulate extracellular Ca^{2+} influx (45). Our study consistently demonstrated that the overexpression of CACNA2D3 increased the uptake of intracellular free Ca^{2+} in ESCC. Apoptosis is closely related to increased intracellular Ca^{2+} concentration. Here, we found that CACNA2D3 overexpression

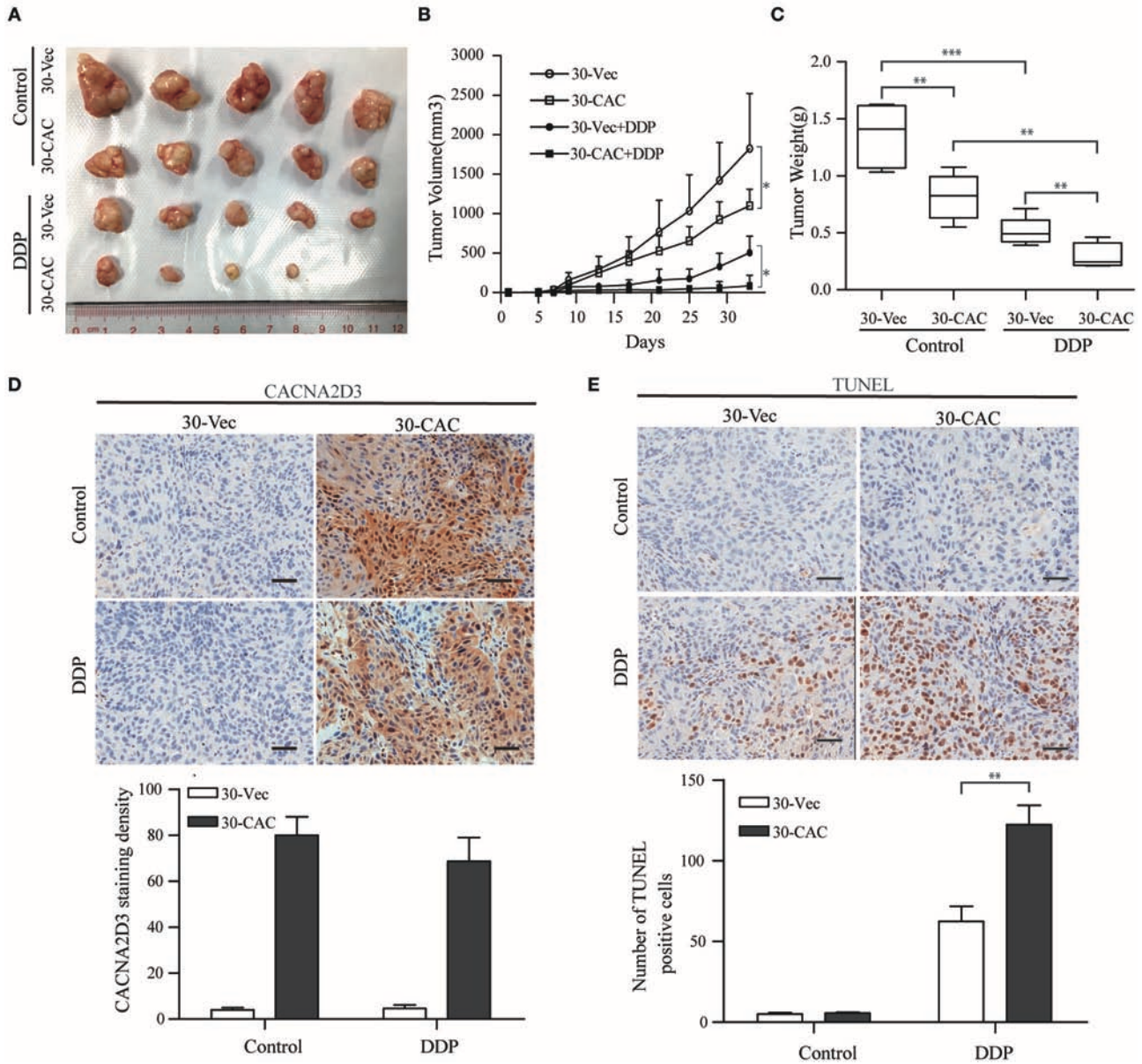

FIGURE 4 | CACNA2D3 increases chemosensitivity of ESCC cells to cisplatin *in vivo*. **(A)** Representative images of xenografted tumors derived from Balb/c-nu mice at day 33. **(B)** The mice in the treatment groups were intraperitoneally injected with 2 mg/kg every 3 days. Tumor volumes were measured at 4 days intervals. Data are presented as mean ± SD. **(C)** Tumor weights were measured after mice were sacrificed. **(D)** Detection of CACNA2D3 from tumor sections by immunohistochemical staining. Quantification was performed by calculating the percentage of the staining intensities using ImageJ. **(E)** TUNEL staining of tumor sections from each group; the number of TUNEL-positive cells was quantified by counting. $^{*}p < 0.05$; $^{**}p < 0.01$; $^{***}p < 0.001$.

did not in itself affect the apoptosis rate of ESCC cells; however, it significantly increased cisplatin-induced apoptosis. Mitochondria often have a decisive role in stimulus-induced apoptosis. Mitochondrial membrane destruction and infiltration are common phenomena related to apoptosis. Excessive Ca^{2+} accumulation inside mitochondria is thought to be a powerful apoptosis stimulator that induces mitochondrial membrane depolarization and activates downstream caspases and finally induces apoptosis (46, 47). We confirmed that ectopic expression of CACNA2D3 led to depolarization of the mitochondrial membrane potential after cisplatin treatment. Moreover, the immunoblotting results showed that CACNA2D3 overexpression activated caspase-3 and caspase-9 in ESCC cells. CACNA2D3 and cisplatin synergistically induce apoptosis by increasing Ca^{2+}-dependent collapse of mitochondrial membrane potential, indicating that CACNA2D3 enhances cisplatin-induced apoptosis by activating the mitochondrial pathway.

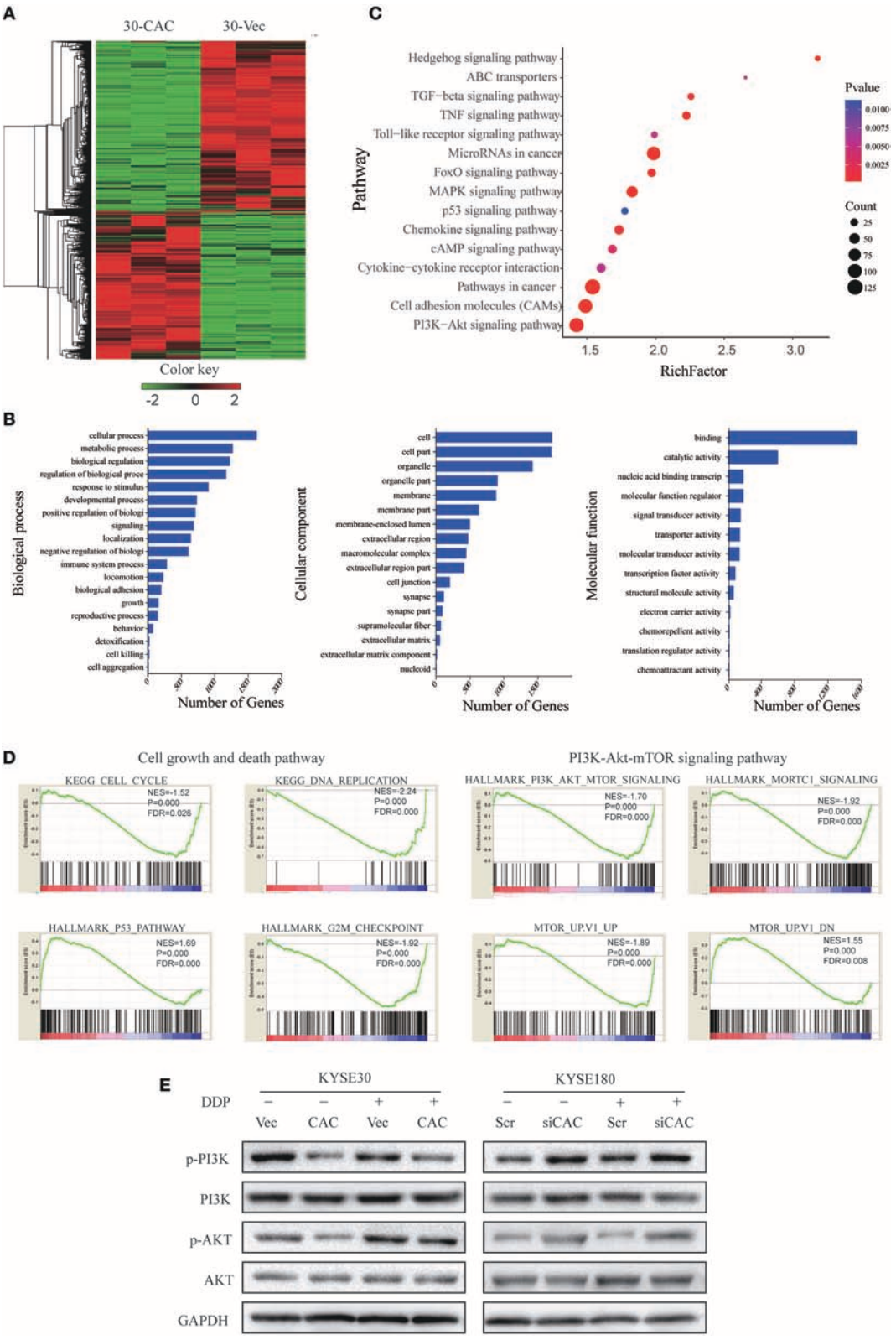

FIGURE 5 | CACANA2D3 regulated the sensitivity of ESCC to cisplatin through inhibiting the PI3K/Akt pathways. **(A)** DEG heatmap and hierarchical clustering results for CACNA2D3-overexpressing KYSE30 ESCC cells. Red and green indicate high and low gene expression, respectively. **(B)** GO enrichment analysis of the DEGs. The genes were divided into three categories: cellular component, biological process, and molecular function genes. **(C)** KEGG pathway enrichment analysis

(Continued)

FIGURE 5 | of differentially expressed pathways upon CACNA2D3 overexpression. The ordinates represent the enriched KEGG pathway. $p < 0.05$ was considered statistically significant. **(D)** GSEA analysis of differentially expressed pathways upon CACNA2D3 overexpression. NES, normalized enrichment score. **(E)** Levels of P-PI3K, PI3K, P-Akt, and Akt proteins were analyzed by western blotting in CACNA2D3-overexpressing and knockdown cell lines treated with or without cisplatin.

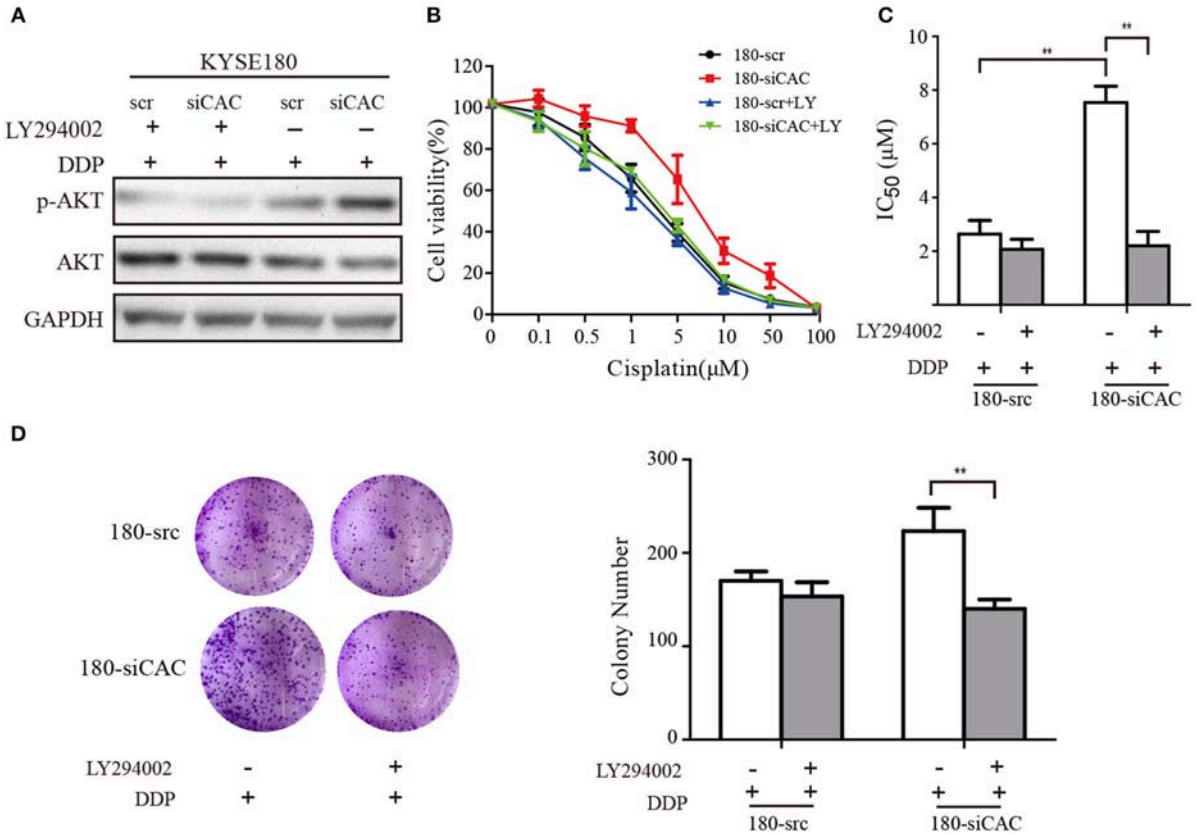

FIGURE 6 | LY294002 restores the sensitivity of ESCC to cisplatin in CACNA2D3-knockdown cells. **(A)** CACNA2D3-knockdown KYSE180 cells and control cells were treated with cisplatin at the indicated concentrations with or without LY294002 for 72 h. Levels of P-Akt and Akt proteins were analyzed by western blotting. **(B)** The number of viable cells was measured by CCK-8 assay. **(C)** IC50 values were calculated using linear or logarithmic regression (R2 > 0.9). Data are presented as the mean ± SD from triplicate wells. **(D)** Colony forming assays were used to determine the colony forming ability after cisplatin with or without LY294002 treatment. Data are presented as the mean ± SD from three wells. $^{**}p < 0.01$.

To systematically investigate the underlying molecular mechanism mediating CACNA2D3-induced ESCC cisplatin sensitivity, we compared the expression profiles of KYSE30 cells with and without CACNA2D3 overexpression after cisplatin treatment using RNA-seq. By pathway enrichment analyses, we found that CACNA2D3 could inhibit DNA replication and block ESCC cells in the G2/M phase by inhibiting the expression of p53, as shown in our previous study (21). We also found the PI3K/Akt pathway to be inactivated in CACNA2D3-overexpressing ESCC cells. The PI3K/Akt signaling pathway has important roles in promoting cell growth, proliferation, invasion, angiogenesis, and drug resistance. In-depth studies of the relationship between the PI3K/Akt signaling pathway and drug resistance have led to this pathway being considered as a new target for chemotherapy drug resistance therapy (48, 49). Here, we found that the phosphorylation of PI3K and Akt was blocked in CACNA2D3-overexpressing KYSE30 cells. Consistently, when CACNA2D3 was knocked down in KYSE180 cells, the phosphorylation level of Akt showed a significant increase. Interestingly, our data also showed that blockade of the PI3K/Akt pathway by LY294002 in CACNA2D3-knockdown cells could restore chemosensitivity to cisplatin.

In summary, in this work we first proved that the expression of CACNA2D3 was associated with chemosensitivity in ESCC patients treated with cisplatin-based therapy. Moreover, CACNA2D3 increased chemosensitivity to cisplatin in cell experiments and xenograft tumors, indicating that it could be used as a tumor marker to predict and improve patients' response to cisplatin. We further found that CACNA2D3 regulated cisplatin-induced apoptosis and decreased Akt phosphorylation. Detection of CACNA2D3 expression might be helpful for individualized treatment of ESCC patients.

AUTHOR CONTRIBUTIONS

CN, XC, and AH designed the study. CN, XQ, XL, YZ, YJ, YL, and QW performed the experiments. CN, XQ, XL, DZ, and BT analyzed the data. CN, XL, and XC wrote the paper.

FUNDING

This work was supported by grants from the National Natural Science Foundation of China (grants 81360365, 81472337, 81473131), the National Key Basic Research Program of China (973 Program) (grant 2015CB553706), the Science & Technology Program of Guangdong province (grant 2016A020217012), the Science &Technology Program of Guangzhou (grant 2016201604030039), and the Guangxi Natural Science Foundation of China (grant 2014GXNSFBA118205, 2017GXNSFAA198157). We thank Yuying Zhou and Shujun Guo from the Institute of Biomedicine of Jinan University for technical assistance.

REFERENCES

1. Ferlay J, Soerjomataram I, Dikshit R, Eser S, Mathers C, Rebelo M, et al. Cancer incidence and mortality worldwide: sources, methods and major patterns in GLOBOCAN 2012. *Int J Cancer*. (2015) 136:E359–86. doi: 10.1002/ijc.29210
2. Arnold M, Soerjomataram I, Ferlay J, Forman, D. Global incidence of oesophageal cancer by histological subtype in 2012. *Gut*. (2015) 64:381–7. doi: 10.1136/gutjnl-2014-308124
3. Zhang Y. Epidemiology of esophageal cancer. *World J Gastroenterol.* (2013) 19:5598–606. doi: 10.3748/wjg.v19.i34.5598
4. Lin Y, Totsuka Y, He Y, Kikuchi S, Qiao Y, Ueda J, et al. Epidemiology of esophageal cancer in Japan and China. *J epidemiol.* (2013) 233–42. doi: 10.2188/jea.JE20120162
5. Ando N, Iizuka T, Ide H, Ishida K, Shinoda M, Nishimaki T, et al. Surgery plus chemotherapy compared with surgery alone for localized squamous cell carcinoma of the thoracic esophagus: a Japan clinical oncology group study–JCOG9204. *J Clin Oncol.* (2003) 21:4592–6. doi: 10.1200/JCO.2003.12.095
6. Iinuma H, Fukushima R, Inaba T, Tamura J, Inoue T, Ogawa E, et al. Phase I clinical study of multiple epitope peptide vaccine combined with chemoradiation therapy in esophageal cancer patients. *J Transl Med.* (2014) 12:84. doi: 10.1186/1479-5876-12-84
7. Lyu X, Huang J, Mao Y, Liu Y, Feng Q, Shao K, et al. Adjuvant chemotherapy after esophagectomy: is there a role in the treatment of the lymph node positive thoracic esophageal squamous cell carcinoma? *J Surg Oncol.* (2014) 110:864–8. doi: 10.1002/jso.23716
8. Kato K, Muro K, Minashi K, Ohtsu A, Ishikura S, Boku N, et al. Phase II study of chemoradiotherapy with 5-fluorouracil and cisplatin for Stage II-III esophageal squamous cell carcinoma: JCOG trial (JCOG 9906). *Int J Rad Oncol Biol Phys.* (2011) 81: 684–90. doi: 10.1016/j.ijrobp.2010.06.033
9. Miyazaki T, Sohda M, Tanaka N, Suzuki S, Ieta K, Sakai M, et al. Phase I/II study of docetaxel, cisplatin, and 5-fluorouracil combination chemoradiotherapy in patients with advanced esophageal cancer. *Cancer Chemother Pharmacol.* (2015) 75:449–55. doi: 10.1007/s00280-014-2659-6
10. Hashimoto J, Kato K, Ito Y, Kojima T, Akimoto T, Daiko H, et al. Phase II feasibility study of preoperative concurrent chemoradiotherapy with cisplatin plus 5-fluorouracil and elective lymph node irradiation for clinical stage II/III esophageal squamous cell carcinoma. *Int J Clin Oncol.* (2018) 24:60–7. doi: 10.1007/s10147-018-1336-x
11. Yuasa Y, Nagasaki H, Akiyama Y, Hashimoto Y, Takizawa T, Kojima K, et al. DNA methylation status is inversely correlated with green tea intake and physical activity in gastric cancer patients. *Int J Cancer*. (2009) 124:2677–82. doi: 10.1002/ijc.24231
12. Wanajo A, Sasaki A, Nagasaki H, Shimada S, Otsubo T, Owaki S, et al. Methylation of the calcium channel-related gene, CACNA2D3, is frequent and a poor prognostic factor in gastric cancer. *Gastroenterology*. (2008) 135:580–90. doi: 10.1053/j.gastro.2008.05.041
13. Qu Y, Dang S, Hou P. Gene methylation in gastric cancer. *Clin Chim Acta*. (2013) 424:53–65. doi: 10.1016/j.cca.2013.05.002
14. Wong AM, Kong KL, Chen L, Liu M, Wong AM, Zhu C, et al. Characterization of CACNA2D3 as a putative tumor suppressor gene in the development and progression of nasopharyngeal carcinoma. *Int J Cancer*. (2013) 133:2284–95. doi: 10.1002/ijc.28252
15. Palmieri C, Rudraraju B, Monteverde M, Lattanzio L, Gojis O, Brizio R, et al. Methylation of the calcium channel regulatory subunit alpha2delta-3 (CACNA2D3) predicts site-specific relapse in oestrogen receptor-positive primary breast carcinomas. *Br J Cancer*. (2012) 107:375–81. doi: 10.1038/bjc.2012.231
16. Hanke S, Bugert P, Chudek J, Kovacs G. Cloning a calcium channel alpha2delta-3 subunit gene from a putative tumor suppressor gene region at chromosome 3p21.1 in conventional renal cell carcinoma. *Gene.* (2001) 264: 69–75. doi: 10.1016/S0378-1119(00)00600-4
17. Tai AL, Mak W, Ng PK, Chua DT, Ng MY, Fu L, et al. High-throughput loss-of-heterozygosity study of chromosome 3p in lung cancer using single-nucleotide polymorphism markers. *Cancer Res.* (2006) 66:4133–8. doi: 10.1158/0008-5472.CAN-05-2775
18. Jin Y, Cui D, Ren J, Wang K, Zeng T, Gao L. CACNA2D3 is downregulated in gliomas and functions as a tumor suppressor. *Mol Carcinogene.* (2017) 56: 945–59. doi: 10.1002/mc.22548
19. De Preter K, Vandesompele J, Heimann P, Yigit N, Beckman S, Schramm A, et al. Human fetal neuroblast and neuroblastoma transcriptome analysis confirms neuroblast origin and highlights neuroblastoma candidate genes. *Genome Biol.* (2006) 7:R84. doi: 10.1186/gb-2006-7-9-r84
20. Thorell K, Bergman A, Caren H, Nilsson S, Kogner P, Martinsson T, et al. Verification of genes differentially expressed in neuroblastoma tumours: a study of potential tumour suppressor genes. *BMC Med Genom.* (2009) 2:53. doi: 10.1186/1755-8794-2-53
21. Li Y, Zhu CL, Nie CJ, Li JC, Zeng TT, Zhou J, et al. Investigation of tumor suppressing function of CACNA2D3 in esophageal squamous cell carcinoma. *PLoS ONE.* (2013) 8:e60027. doi: 10.1371/journal.pone.0060027
22. Negoro E, Yamauchi T, Urasaki Y, Nishi R, Hori H, Ueda T. Characterization of cytarabine-resistant leukemic cell lines established from five different blood cell lineages using gene expression and proteomic analyses. *Int J Oncol.* (2011) 38:911–9. doi: 10.3892/ijo.2011.933
23. Shimada Y, Imamura M, Wagata T, Yamaguchi N, Tobe T. Characterization of 21 newly established esophageal cancer cell lines. *Cancer*. (1992) 69:277–84. doi: 10.1002/1097-0142(19920115)69:2<277::AID-CNCR2820690202>3.0.CO;2-C
24. Langmead B, Trapnell C, Pop M, Salzberg SL. Ultrafast and memory-efficient alignment of short DNA sequences to the human genome. *Genome Biol.* (2009) 10:R25. doi: 10.1186/gb-2009-10-3-r25
25. Love MI, Huber W, Anders S. Moderated estimation of fold change and dispersion for RNA-seq data with DESeq2. *Genome Biol.* (2014) 15:550. doi: 10.1186/s13059-014-0550-8
26. Ashburner M, Ball CA, Blake JA, Botstein D, Butler H, Cherry JM, et al. Gene ontology: tool for the unification of biology. The gene ontology consortium. *Nat Genet.* (2000) 25:25–9. doi: 10.1038/75556
27. Huang da W, Sherman BT, Lempicki RA. Systematic and integrative analysis of large gene lists using DAVID bioinformatics resources. *Nat Protocol*. (2009) 4: 44–57. doi: 10.1038/nprot.2008.211
28. Subramanian A, Tamayo P, Mootha VK, Mukherjee S, Ebert BL, Gillette MA, et al. Gene set enrichment analysis: a knowledge-based approach for interpreting genome-wide expression profiles. *Proc Natl Acad Sci USA*. (2005) 102:15545–50. doi: 10.1073/pnas.0506580102
29. Wen J, Yang H, Liu MZ, Luo KJ, Liu H, Hu Y, et al. Gene expression analysis of pretreatment biopsies predicts the pathological response of esophageal

squamous cell carcinomas to neo-chemoradiotherapy. *Ann Oncol.* (2014) 25:1769–74. doi: 10.1093/annonc/mdu201
30. Sersa G, Stabuc B, Cemazar M, Miklavcic D, Rudolf Z. Electrochemotherapy with cisplatin: clinical experience in malignant melanoma patients. *Clin Cancer Res.* (2000) 6:863–7.
31. Kelland L. The resurgence of platinum-based cancer chemotherapy. *Nat Rev Cancer.* (2007) 7:573–84. doi: 10.1038/nrc2167
32. Galluzzi L, Vitale I, Michels J, Brenner C, Szabadkai G, Harel-Bellan A, et al. Systems biology of cisplatin resistance: past, present and future. *Cell Death Dis.* (2014) 5: e1257. doi: 10.1038/cddis.2013.428
33. Berridge MJ, Bootman MD, and Lipp P. Calcium–a life and death signal. *Nature*. (1998) 395: 645–8. doi: 10.1038/27094
34. Webb SE, Miller AL. Calcium signalling during embryonic development. *Nat Rev Mol Cell Biol*. (2003) 4:539–51. doi: 10.1038/nrm1149
35. Monteith GR, McAndrew D, Faddy HM, Roberts-Thomson SJ. Calcium and cancer: targeting Ca^{2+} transport. *Nat Rev Cancer.* (2007) 7:519–30. doi: 10.1038/nrc2171
36. Gong HC, Hang J, Kohler W, Li L, Su TZ. Tissue-specific expression and gabapentin-binding properties of calcium channel alpha2delta subunit subtypes. *J Membr Biol.* (2001) 184:35–43. doi: 10.1007/s00232-001-0072-7
37. Davies A, Hendrich J, Van Minh AT, Wratten J, Douglas L, Dolphin AC. Functional biology of the alpha(2)delta subunits of voltage-gated calcium channels. *Trends Pharmacol Sci.* (2007) 28:220–8. doi: 10.1016/j.tips.2007.03.005
38. Qin N, Yagel S, Momplaisir ML, Codd EE, D'Andrea MR. Molecular cloning and characterization of the human voltage-gated calcium channel alpha(2)delta-4 subunit. *Mol Pharmacol.* (2002) 62: 485–96. doi: 10.1124/mol.62.3.485
39. Siddik ZH. Cisplatin: mode of cytotoxic action and molecular basis of resistance. Oncogene (2003) 22: 7265-79. doi: 10.1038/sj.onc.1206933
40. Wang D, Lippard SJ. Cellular processing of platinum anticancer drugs. *Nat Rev Drug Disc.* (2005) 4:307–20. doi: 10.1038/nrd1691
41. Johnstone TC, Suntharalingam K, Lippard SJ. The next generation of platinum drugs: targeted Pt(II) agents, nanoparticle delivery, and Pt(IV) prodrugs. *Chem Rev.* (2016) 116:3436–86. doi: 10.1021/acs.chemrev.5b00597
42. Hall MD, Okabe M, Shen DW, Liang XJ, Gottesman MM. The role of cellular accumulation in determining sensitivity to platinum-based chemotherapy. *Ann Rev Pharmacol Toxicol.* (2008) 48: 495–535. doi: 10.1146/annurev.pharmtox.48.080907.180426
43. Holohan C, Van Schaeybroeck S, Longley DB, Johnston PG. Cancer drug resistance: an evolving paradigm. *Nat Rev Cancer.* (2013) 13:714–26. doi: 10.1038/nrc3599
44. Ferreira JA, Peixoto A, Neves M, Gaiteiro C, Reis CA, Assaraf YG, et al. Mechanisms of cisplatin resistance and targeting of cancer stem cells: Adding glycosylation to the equation. *Drug Resist Updates*. (2016) 24:34–54. doi: 10.1016/j.drup.2015.11.003
45. Dolphin AC. The alpha2delta subunits of voltage-gated calcium channels. *Biochim Biophys Acta.* (2013) 1828:1541–9. doi: 10.1016/j.bbamem.2012.11.019
46. Wang X. The expanding role of mitochondria in apoptosis. *Genes Dev.* (2001) 15:2922–33.
47. Gogvadze V, Orrenius S, Zhivotovsky B. Multiple pathways of cytochrome c release from mitochondria in apoptosis. *Biochim Biophys Acta*. (2006) 1757: 639–47. doi: 10.1016/j.bbabio.2006.03.016
48. West KA, Castillo SS, Dennis PA Activation of the PI3K/Akt pathway and chemotherapeutic resistance. *Drug Resist Updates*. (2002) 5:234–48. doi: 10.1016/S1368-7646(02) 00120-6
49. Burris HA III. Overcoming acquired resistance to anticancer therapy: focus on the PI3K/AKT/mTOR pathway. *Cancer Chemother Pharmacol.* (2013) 71:829–42. doi: 10.1007/s00280-012-2043-3

Conflict of Interest Statement: The authors declare that the research was conducted in the absence of any commercial or financial relationships that could be construed as a potential conflict of interest.

frontiers in Pharmacology

ORIGINAL RESEARCH
published: 05 April 2019
doi: 10.3389/fphar.2019.00356

Copper Chaperone for Superoxide Dismutase Promotes Breast Cancer Cell Proliferation and Migration *via* ROS-Mediated MAPK/ERK Signaling

Yanping Li[1†], Ronghui Liang[1†], Xiaoya Zhang[1], Jiyan Wang[2], Changliang Shan[1,2], Shuangping Liu[3*], Leilei Li[1*] and Shuai Zhang[4*]*

[1]Biomedical Translational Research Institute, Jinan University, Guangzhou, China, [2]State Key Laboratory of Medicinal Chemical Biology, College of Pharmacy and Tianjin Key Laboratory of Molecular Drug Research, Nankai University, Tianjin, China, [3]Department of Pathology, Medical School, Dalian University, Dalian, China, [4]School of Integrative Medicine, Tianjin University of Traditional Chinese Medicine, Tianjin, China

Copper chaperone for superoxide dismutase (CCS) is a critical component of oxidation–reduction system and functions as a potential tumor promoter in several cancers. However, the function and clinical significance of CCS in breast cancer remain unclear. Here, we found CCS was highly expressed in breast cancer, where it promoted breast cancer cell proliferation and migration. Suppression of CCS expression was sufficient to attenuate the phosphorylation level of ERK1/2 and increase the accumulation of reactive oxygen species (ROS). Mechanistically, we found that knockdown of CCS decreases the activity of ERK1/2 mediated by the accumulation of ROS, which leads to the inhibition of cell proliferation and migration. In summary, these results indicated that CCS promotes the growth and migration of breast cancer cells *via* regulating the ERK1/2 activity mediated by ROS.

Keywords: breast cancer, CCS, ROS, MAPK/ERK, proliferation, migration

OPEN ACCESS

Edited by:
Jian-ye Zhang,
Guangzhou Medical University, China

Reviewed by:
Bolin Liu,
Louisiana State University, United States
Xinliang Mao,
Soochow University, China

***Correspondence:**
Changliang Shan
changliangshan@nankai.edu.cn
Shuangping Liu
liushuangping@dlu.edu.cn
Leilei Li
89509306@qq.com
Shuai Zhang
shuaizhang@tjutcm.edu.cn

[†]These authors have contributed equally to this work

Specialty section:
This article was submitted to Cancer Molecular Targets and Therapeutics, a section of the journal Frontiers in Pharmacology

Received: *12 January 2019*
Accepted: *21 March 2019*
Published: *05 April 2019*

Citation:
Li Y, Liang R, Zhang X, Wang J, Shan C, Liu S, Li L and Zhang S (2019) Copper Chaperone for Superoxide Dismutase Promotes Breast Cancer Cell Proliferation and Migration via ROS-Mediated MAPK/ERK Signaling. Front. Pharmacol. 10:356. doi: 10.3389/fphar.2019.00356

INTRODUCTION

Breast cancer is the leading cause of cancer-related deaths in women worldwide (Christofori, 2006; Bray et al., 2018). Breast cancer patients with metastases have an extremely poor prognosis (Gupta et al., 2005; Bacac and Stamenkovic, 2008; Thiery, 2009; Chaffer and Weinberg, 2011; Valastyan and Weinberg, 2011). Thus, exploring new targets for breast cancer treatment is important.

Copper, a redox-active transition metal essential for most living organisms, serves as a catalytic cofactor for enzymes that function in antioxidant defense, iron homeostasis, cellular respiration, and a variety of biochemical processes (Mandinov et al., 2003; Lowndes and Harris, 2005; Ashino et al., 2010; Xu et al., 2016; Sciegienka et al., 2017). The uncontrolled accumulation of copper could lead to increased oxidative stress and inappropriate binding to macromolecules. Copper chaperone for superoxide dismutase (CCS) delivers copper to specific cellular destinations and to superoxide dismutase (SOD1) (Kawamata and Manfredi, 2008; Ulloa, 2009). Mounting evidences

suggest that CCS plays a crucial role in oxidative metabolism (Kawamata and Manfredi, 2008; Leitch et al., 2009; Suzuki et al., 2013a; Wang et al., 2015). Blockade of the copper-trafficking chaperone CCS contributes to the increased cellular reactive oxygen species (ROS) level due to the overall accumulation of copper inside the cells and the decreased SOD1 activity (Ulloa, 2009). Wang et al reported that inhibiting CCS blocks lung cancer and leukemia cell growth (Wang et al., 2015). In addition, they show that blocking copper trafficking induces cellular oxidative stress and reduces cellular ATP levels. The reduced level of ATP results in activation of the AMP-activated protein kinase that leads to reduced lipogenesis. However, the mechanisms underlying the relationship between CCS and tumorigenesis are still largely unknown, although the positive correlation between CCS and redox homeostasis has been revealed (Wang et al., 2015). Therefore, this study aimed to explore the critical role and molecular mechanism of CCS in migration and proliferation of breast cancer.

In aforementioned study by Wang et al, a CCS inhibitor was developed and shown to have the same effect as knocking down CCS in cancer cells (Wang et al., 2015). However, the precise role of CCS in migration and proliferation of breast cancer cells is unknown. In the present study, we report that CCS is highly expressed in breast cancer tissues and invasive breast cancer cells and promotes cell proliferation and migration. Furthermore, we found that inhibition of CCS by shRNA or an inhibitor blocks breast cancer proliferation and migration by triggering ROS mediated ERK activity. These results suggest that metastasis-prone breast cancer cells reprogram oxidative metabolism to promote cell proliferation and migration. Targeting CCS may represent a promising approach for selectively causing cell proliferation and migration in breast cancer cells.

MATERIALS AND METHODS

Reagents and Antibodies

DC_AC50, a CCS inhibitor, was provided by the Shanghai Institute of Materia Medica of the Chinese Academy of Sciences. U0126-EtOH (catalog number: S1102) was purchased from Selleck. Antibody against phospho-p44/42 MAPK (Erk1/2) (Thr202/Tyr204) (1:1000 times dilution) (catalog number: 4370S), p44/42 MAPK (Erk1/2) (1:1000 times dilution) (catalog number: 4695S), phpspho-MEK1/2 (Ser217/221) (1:1000 times dilution) (catalog number: 9154S), MEK1/2 (1:1000 times dilution) (catalog number: 8727S), β-actin (1:1000 times dilution) (catalog number: 8457S), mouse IgG (1:3000 times dilution) (catalog number: 7076S), and rabbit IgG (1:3000 times dilution) (catalog number: 7074S) were from cell signaling technology. Anti-Superoxide Dismutase 4 (1:500 times dilution) (catalog number: ab167170) was from Abcam. Anti-Flag tag (1:1000 times dilution) (catalog number: 66008) was from proteintech. CCS shRNA was purchased from Open Biosystems, Huntsville, AL. The sequence of targeted CCS shRNA was as follows: 5′-CCGGCTGATTATTGATGAGGGAGAACTCGAGTTCTCCC TCATCAATA ATCAGTTTTTG-3′. Lipofectamine RNA iMAX was purchased from Invitrogen. The sequences of targeted CCS siRNA were as follows: sense: 5′-GUCUUGGUACACACCAC UCUA-3′; Antisense: 5′-UAGAGUGGUGUGUACCAAGAC-3′.

Abbreviations: AMP, Adenosine Monophosphate; ATP, Adenosine Triphosphate; CCS, Copper Chaperone for Superoxide Dismutase; ERK, Extracellular Regulated Protein Kinases; MAPK, Mitogen-Activated Protein Kinase; NAC, N-Acetyl-L-cysteine; ROS, Reactive Oxygen Species; PCR, Polymerase Chain Reaction; PEI, Polymine; PVDF, Polyvinylidene Fluoride; qRT-PCR, Real-time Quantitative Reverse Transcription-PCR; SDS-PAGE, Sodium Dodecyl Sulfate Polyacrylamide Gel Electropheresis; ShRNA, Short Hairpin RNA; SiRNA, Small Interfering RNA; SOD1, Superoxide Dismutase; TCGA, The Cancer Genome Atlas.

Cell Culture and Cell Lines

The human breast cancer cell lines MDA-MB-231, MCF-7, SUM159, and T47D were obtained from American Type Culture Collection (Manassas, USA). The human normal epithelial lung cell line BEAS-2B was gifted from Dr. Chenglai Xia (Guangzhou Medical University, Guangdong, China). MDA-MB-231, MCF-7, SUM159, and T47D cells were cultured in Dulbecco Modified Eagle Medium (DMEM) with 10% fetal bovine serum (FBS, ExCell Bio). BEAS-2B cells were cultured in RPMI 1640 medium with 10% FBS. For routine passages, cultures were split 1:3 when they reached 80–90% confluences. All experiments were performed on exponentially growing cells.

Plasmid Construction and Lentivirus Packaging

Exogenous human CCS CDS sequence was inserted into pLVX-3FLAG plasmid. Primer sequences were as follows: pLVX-3FLAG-CCS: 5′-CGGGATCCATGGCTTCGGATTCGG-3′ (forward) and 5′-CCCTCGAGTCAAAGGTGGGCAGG-3′ (reverse). Exogenous pCDH-HA-MEK plasmid was gifted from Dr. ShiZhi (JinanUniversity, Guangdong, China). For transient transfections, cells were grown to 80% confluency and transfected with plasmids using PEI Transfection Reagent (Invitrogen, USA) according to the manufacturer's protocol. Stable knockdown of endogenous CCS was achieved by using lentiviral vector harboring shRNA construct. 5′-CCGGCTGATTATTGATGAGG GAGAACTCGAGTTCTCCCTCATCAATAATCAGTTTTTG-3′. We generated CCS stable knockdown cell lines by infected lentiviral shRNA and selected by antibiotic puromycin. The knockdown effective was confirmed by western blot. PLKO.1 is the name of the lentiviral vector as a control.

Small Interference RNA Transfection

MDA-MB-231, MCF-7, and BEAS-2B cells (2×10^5) were seeded into 6-well plates and cultured in a humidified incubator at 37°C and 5% CO_2 for 24 h. Cells were transfected with a negative control siRNA (NC-siRNA) and siRNA targeting CCS by Lipofectamine RNA iMAX (Invitrogen corporation). Transfected cells were cultured for 48°C before being used for further experiments. The sequences of targeted CCS siRNA were 5′-GUCUUGGUACACACCACUCUA-3′. The sequences of negative control siRNA were 5′-UUCUCCGAACGUGUCACGUTT-3′(forward). All siRNA sequences were purchased from the Invitrogen Ribobio corporation of Guangzhou.

Real-Time Quantitative Reverse Transcription-PCR

Total cellular RNA was extracted using the Eastep & Super RNA Extract reagent Kit (Promega). cDNA was generated from purified RNA using PrimeSciptTM RT reagent Kit (Takara) according to the manufacturer's instructions. Gene expression levels and PCR efficiency, along with its standard error, were calculated using the Bio-Rad CFX Manager, version 3.1 (Bio-Rad), The efficiencies were nearly 100%, allowing the use of the $2^{-\triangle\triangle Ct}$ method for calculating the relative gene expression levels and reference gene normalization using β-actin. All PCR runs were performed in triplicate, and the data analyzed by CFX Manager software (Bio-Rad). Primer sequences were as following: CCS: 5′-CATCGAGG GAACTATTGACG-3′ (forward) and 5′-ATGCTCCATCAGGGT TAAAG-3′(reverse); β-actin:5′-ACGTGGACATCCGCAAAG-3′ (forward) and 5′-GACTCGTCATACTCCTGCTTG-3′ (reverse).

Cell Proliferation Assay

Cell proliferation assays were performed by seeding 5×10^4 cells in 6-well plates and culturing the cells at 37°C. Relative cell proliferation was determined by cell numbers recorded at 4 days after being seeded and normalized to that of each of the cell lines at the starting time (t = 0 h).

Western Blot Analysis

Cells were lysed with lysis buffer (1.5 M NaCl, 1 M HEPES [pH = 7.0], 1% NP40, 0.1 M $Na_4P_2O_7$, 0.1 M NaF, 0.1 M Na_3VO_4, protease inhibitor) on ice 30 min and then centrifuged at 12,000 rpm for 15 min at 4°C. Protein samples were separated by 12%.

SDS-PAGE and transferred onto PVDF membranes (Millipore). The membranes were blocked with 5% non-fat milk for 2 h and then incubated overnight at 4°C with the primary antibody and 1 h at room temperature with secondary antibody. Signals were detected using luminol substrate solution.

Transwell Migration Assay

For the Transwell (24-well insert, 8 mm pore size with polycarbonate membrane; Corning Costar, Lowell, MA, USA) migration assays, 600-mL media supplemented with 10% FBS was added to the lower chamber, and the cells resuspended in serum-free media were added to the upper insert after transfection. Transwell membranes were fixed and stained using crystal violet after specified time. The cells adhering to the lower surface of the membrane were counted under a light microscope (Olympus, Tokyo, Japan) at a magnification of 200.

Wound Healing Assay

To determine cell motility, cells were seeded into 6-well plates and grown to 90% confluence. A monolayer of the cells was then scratched with a sterile micropipette tip, followed by washing with PBS to remove cellular debris. The cell migration was observed and counted under a light microscope (Olympus, Tokyo, Japan) at a magnification of 200. The cells that migrated across the black lines were counted in three randomly chosen fields from each triplicate treatment.

Intracellular Reactive Oxygen Species (ROS) Production

The amount of intracellular ROS was measured by detecting dichlorodihydrofluorescein, which is the cleavage product of carboxy-H_2DCFDA (Invitrogen) by ROS. A total of 200,000 cells were seeded in 6-well plate. Twenty-four hours after seeding, cells were washed with PBS and loaded with 12.5 μM carboxy-H_2DCFDA for 60 min. The cells were harvested, resuspended in PBS, and analyzed using a FACS (BD Biosciences; excitation and emission at 490 and 530 nm, respectively).

Bioinformatics Analysis

The public Gene Expression Omnibus datasets (GSE9574 and GSE21422) and the TCGA (The Cancer Genome Atlas) dataset were used for bioinformatics analysis.

Statistical Analysis

The concentration of DC_AC50 required to reduce cell proliferation by 50% (IC50) was determined graphically using the Dose-response-Stimulation function in GraphPad Prism7 (San Diego, CA, United States). Statistical analyses of the significance of differences between groups were performed using Student's t-test with GraphPad Prism7. All data were obtained from three independent experiments performed in triplicate and were presented as the mean ± standard error. $p < 0.05$ was considered to indicate a statistically significant difference.

RESULTS

Higher CCS Gene Expression in Breast Cancer Patients

Bioinformatics analysis has been used to discover previously unknown function of genes associated with cancer. To determine the role of CCS in human breast cancer, we first examined the expression of CCS utilizing Gene Expression Omnibus (GEO) profiles; we found that the expression of CCS was higher in breast cancer tissue than in noncancerous tissue (**Figure 1A,** GSE9574). We also confirmed these finding using The Cancer Genome Atlas (TCGA) dataset. CCS expression was also significantly higher in breast cancer tissue than in noncancerous tissue in the Cancer Genome Atlas (TCGA) (**Figure 1B**). In addition, we also found that the expression of CCS was higher in invasive ductal carcinoma (IDC) than in ductal carcinoma (DCIS) (**Figure 1A,** GSE21422). To validate these findings, we checked CCS expression in various breast cancer cells lines. CCS was differentially expressed in several breast cancer cell lines, including MCF-7, T47D, MDA-MB-231, and SUM159. Of note, the expression of CCS was higher in T47D and MDA-MB-231 cell lines compared to MCF-7 and SUM159 cells (**Figure 1D**). All these findings indicate the potential role of CCS in tumor formation and progression.

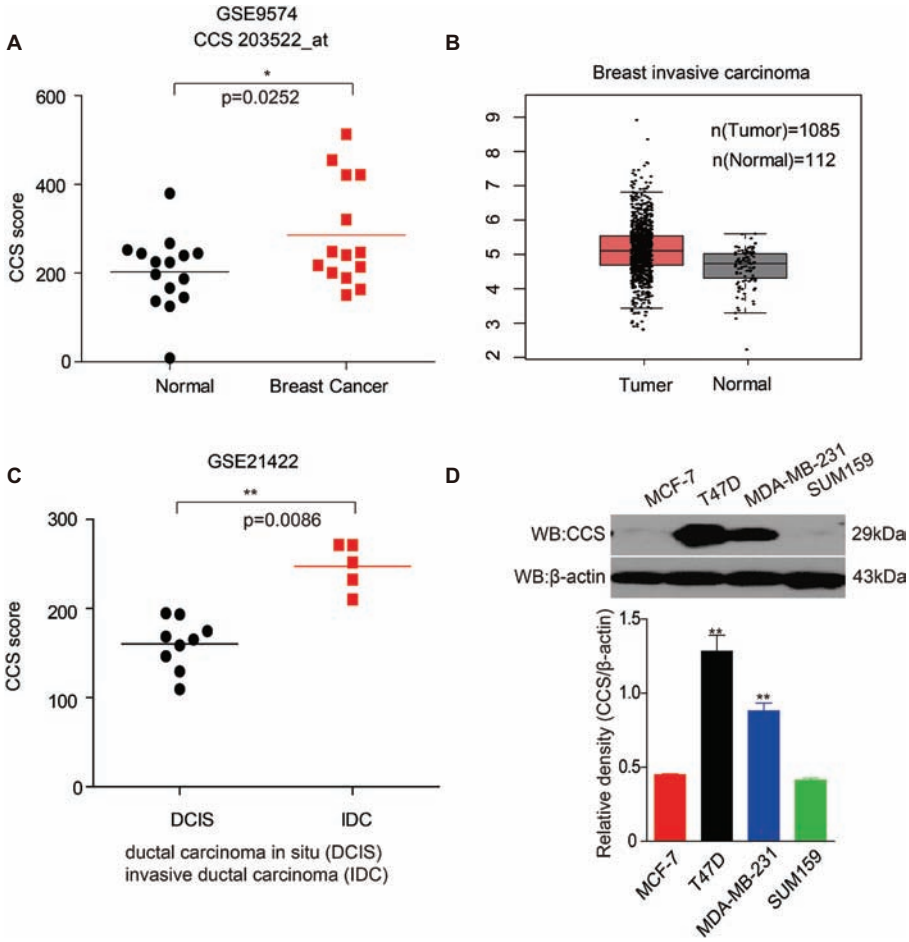

FIGURE 1 | Up-regulation of CCS is associated with cell proliferation and metastasis in human breast cancer. **(A)** CCS expression was analyzed in normal and breast cancer cells using Gene Expression Omnibus (GEO) profiles (GSE9574). **(B)** CCS expression was determined in normal and breast cancer cells in TCGA. **(C)** CCS expression was analyzed in ductal carcinoma in situ (DCIS) and invasion ductal carcinoma (IDC) using Gene Expression Omnibus (GEO) profiles (GSE21422). **(D)** CCS protein levels were analyzed in the majority of a spectrum of diverse human breast cancer cells, including MCF-7, MDA-MB-231, SUM159, and T47D by western blotting. *$p < 0.05$; **$p < 0.01$.

CCS Promotes Breast Cancer Cell Proliferation *in vitro*

We found that the expression of CCS was higher in breast cancer tissue than in noncancerous tissue, suggesting the potential role of CCS in breast cancer cell proliferation. To test our hypothesis, we generated stable cell lines in which CCS was knocked down in MDA-MB-231 cells (**Figure 2A** lower) and exogenously expressed in MCF-7 and SUM159 cells (**Figures 2B,C** lower). Cell number counting assays showed that knockdown of CCS reduced the proliferation of MDA-MB-231 cells (**Figure 2A** upper), while exogenous expression of CCS demonstrated the opposite effect (**Figures 2B,C** upper). To validate these findings, we knocked down the expression of CCS in MDA-MB-231, MCF-7, and BEAS-2B cells using siRNA. Cell number counting assays showed that knockdown of CCS significantly inhibited the proliferation of metastasis-prone breast cancer cell lines MDA-MB-231 but did not have any effect on the proliferation of breast cancer MCF-7 cells or normal BEAS-2B cells (**Figures 2D–F**). Real-time PCR was used to determine the knockdown efficiency of CCS by siRNA (**Figure 2G**). Next, we sought to explore the role DC_AC50, a potent and selective CCS inhibitor, in breast cancer. DC_AC50 has been shown to inhibit the proliferation of acute leukemia cells (Wang et al., 2015). We treated cells with DC_AC50 and found that MCF-7 cells exhibited significantly higher resistance to DC_AC50 than MDA-MB-231 cells (**Figure 2H**). Meanwhile, DC_AC50 treatment resulted in decreased cell proliferation of MDA-MB-231 cells in a time and dose-dependent manner (**Figure 2I**). These results imply that CCS plays an important role in breast cancer cell proliferation and suggests that CCS is a promising anti-cancer target.

CCS Promotes Breast Cancer Cells Migration

We found that the expression of CCS was higher in invasive ductal carcinoma than in ductal carcinoma (**Figure 1C**), suggesting the potential role of CCS in promoting breast cancer migration.

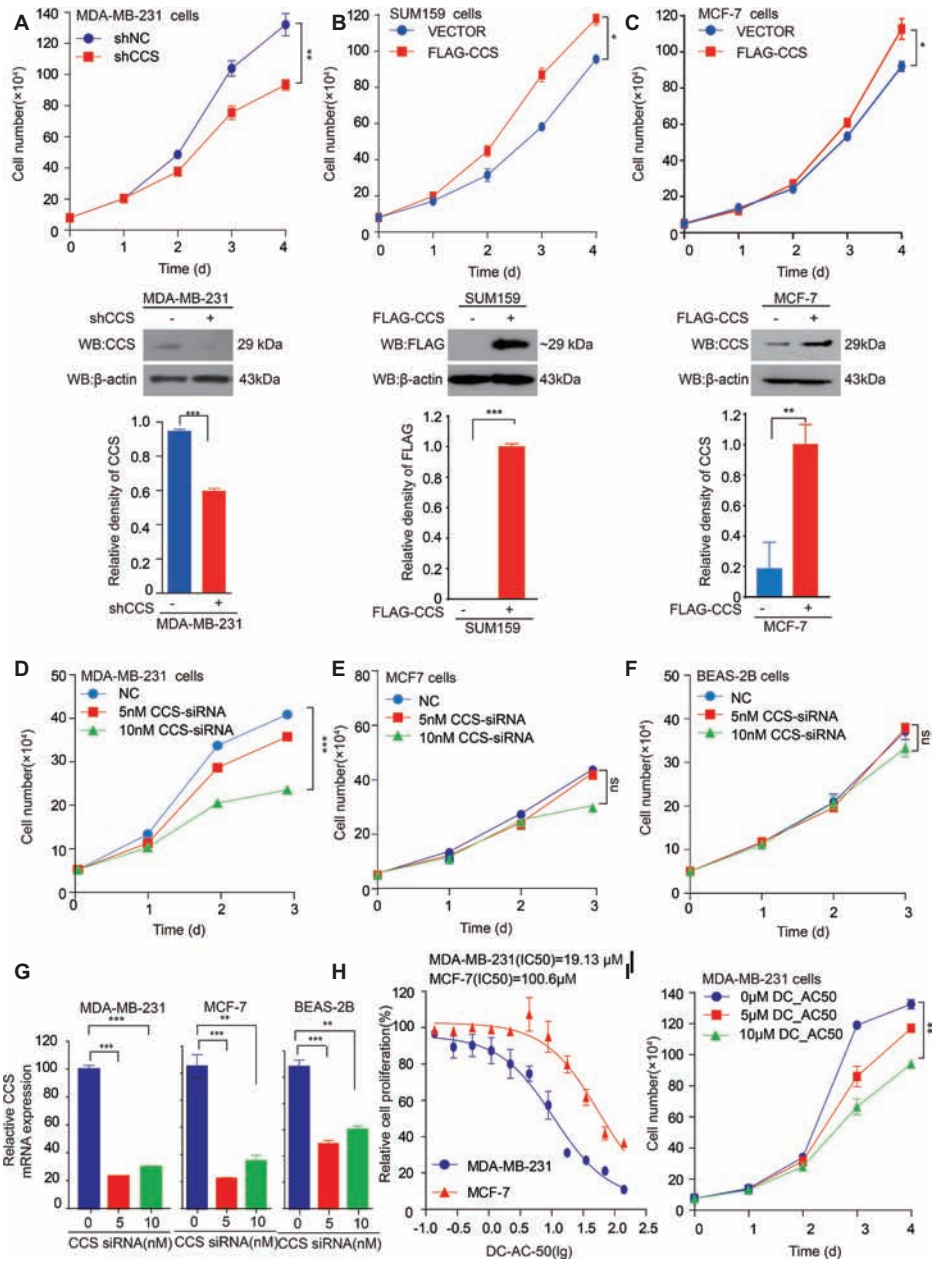

FIGURE 2 | CCS promotes breast cancer cell proliferation. **(A)** Cell proliferation was determined by cell number counting assays in CCS stable knockdown MDA-MB-231 cells, and the knockdown efficiency was determined by western blotting. **(B)** Cell proliferation was determined by cell number counting assays in CCS overexpressing SUM159 cells, and CCS expression was determined by western blotting. **(C)** Cell proliferation was determined by cell number counting assays in CCS overexpressing MCF-7 cells, and CCS expression was determined by western blotting. **(D–F)** Cell proliferation was determined by cell number counting assays in MDA-MB-231 cells **(D)**, MCF-7 cells **(E)**, and normal human BEAS-2B cells **(F)**, which were transiently transfected with increasing concentrations of CCS siRNA and control siRNA. **(G)** The relative CCS mRNA level was determined by q-PCR in MDA-MB-231, MCF-7and BEAS-2B cells, which were transiently transfected with increasing concentrations of CCS siRNA and control siRNA. **(H)** The sensitivities of MDA-MB-231 and MCF-7 cells to DC_AC50 were determined by cell number counting assays when the cells were treated with increasing concentrations of DC_AC50 for 48 h. **(I)** Cell proliferation was determined by cell count assays in MDA-MB-231 cells treated with increasing concentrations of DC_AC50. All results performed above are presented as mean ± SD from three independent experiments. $^{*}p < 0.05$; $^{**}p < 0.01$; $^{***}p < 0.001$, ns: not significant.

Next, we explore the role of CCS in the motility of the breast cancer cells. We performed a transwell migration assay that showed knockdown of CCS significantly inhibited breast cell migratory abilities in MDA-MB-231 (**Figure 3A**), while exogenous express CCS exhibited the opposite effects in MCF-7 and SUM159 cells (**Figures 3B,C**). To validate these finding, we treated MDA-MB-231 with CCS inhibitor, DC_AC50, and performed a transwell migration assay. We found that DC_AC50 blocked MDA-MB-231 cell migration in a dose-dependent manner (**Figure 3D**). In addition, we also assessed migration of MDA-MB-231 in a wound

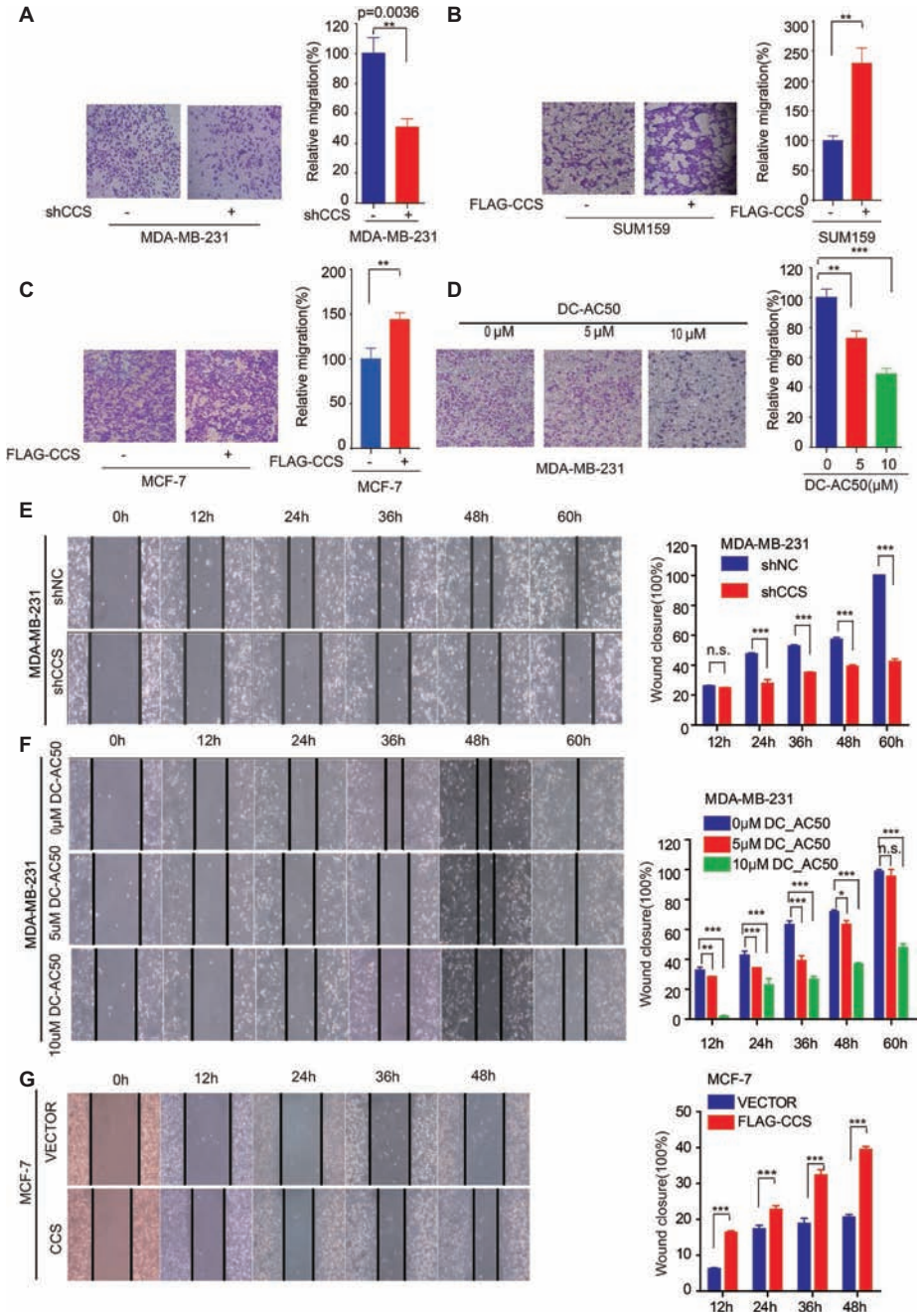

FIGURE 3 | CCS promotes breast cancer cell migration. **(A)** Cell migration in CCS knockdown and control MDA-MB-231 cells was determined by transwell migration assay (Boyden chamber assay). **(B)** Cell migration in CCS overexpressing and control SUM159 cells was determined by transwell migration assay. **(C)** Cell migration in CCS overexpressing and control MCF-7 cells was determined by transwell migration assay. **(D)** Cell migration in CCS overexpressing and control MDA-MB-231 cells with increasing concentrations of DC_AC50 was determined by transwell migration assay. **(E)** Cell migration in CCS knockdown and control MDA-MB-231 cells was also determined by wound healing assay. **(F)** Cell migration in MDA-MB-231 cells treated with increasing concentrations of DC_AC50 was determined by wound healing assay. **(G)** Cell migration in CCS overexpressing and control MCF-7 cells was determined by the wound healing assay. The modified migration assay was evaluated by calculating the ratio of the cell numbers through the chamber or wound closure after the wound healing assay. All results performed above are presented as mean ± SD from three independent experiments. $^{*}p < 0.05$; $^{**}p < 0.01$; $^{***}p < 0.001$, ns: not significant.

healing assay. We found that knockdown or inhibition of CCS dramatically suppressed MDA-MB-231 cell migratory abilities (**Figures 3E,F**). To consolidate our findings, we overexpressed FLAG tagged CCS in MCF-7 cells. As expected, overexpression of CCS accelerated breast cancer cell migration in a wound healing assay (**Figure 3G**). Taken together, our results suggest that CCS plays an important role in promoting breast cancer cells migration.

CCS Promotes Breast Cancer Migration *via* MAPK/ERK Signaling

Activation of survival signaling has been shown to play an essential role in tumor development (Baud and Karin, 2001). Several studies have demonstrated that the MAPK/ERK signaling pathway is activated in cancer cells to promote cancer cell proliferation, migration, and invasion (Rajalingam et al., 2005; El Touny et al., 2014). Therefore, we examined whether

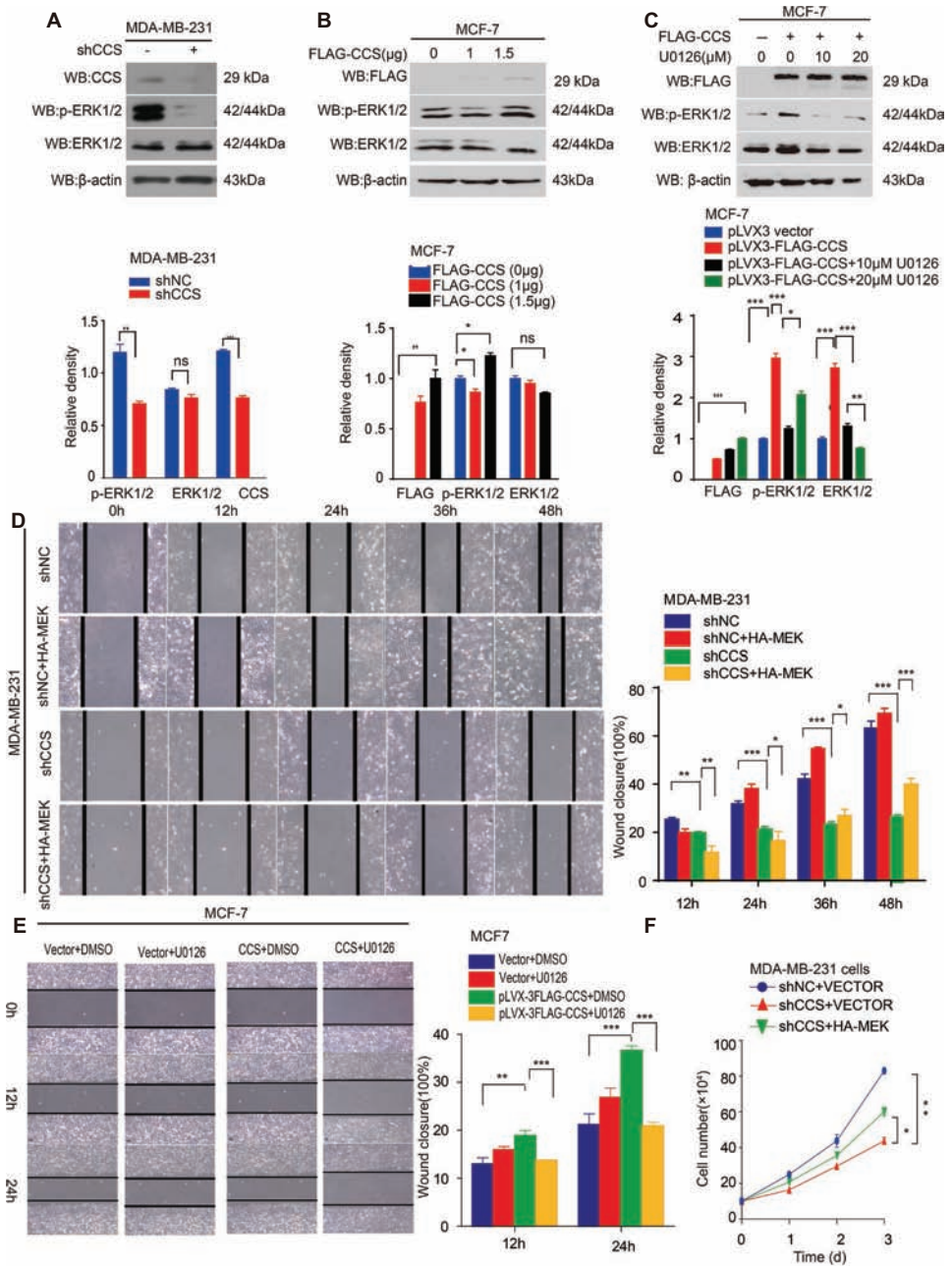

FIGURE 4 | CCS promotes breast cancer cell migration and cell proliferation *via* ERK1/2 activity. **(A)** Phosphorylated ERK1/2 and total ERK1/2 levels were determined in CCS knockdown MDA-MB-231 cells by western blotting. **(B)** Phosphorylated ERK1/2 and total ERK1/2 levels were determined in CCS overexpressing MCF-7 cells by western blotting. **(C)** Phosphorylated ERK1/2 and total ERK1/2 levels were determined in CCS overexpressing MCF-7 cells treated with increasing concentrations of U0126 for 12 h by western blotting. **(D)** Cell migration in CCS knockdown and control MDA-MB-231 cells as determined by wound healing assay when overexpressing exogenous HA-tagged MEK. **(E)** Cell migration in CCS overexpressing and control MCF-7 cells treated with U0126 was determined by wound healing assay. The modified migration assay was evaluated by calculating the ratio of the cell numbers through the chamber or wound closure after the wound healing assay. **(F)** Cell proliferation was determined by cell number counting assays in CCS stable knockdown MDA-MB-231 cells with overexpression of exogenous HA-tagged MEK. All results performed above are presented as mean ± SD from three independent experiments. $^{*}p < 0.05$; $^{**}p < 0.01$; $^{***}p < 0.001$, ns not significant.

MAPK/ERK signaling is involved in CCS mediated cell proliferation and migration. To test this hypothesis, we examined the ERK1/2 and MEK1/2 activity in CCS knockdown MDA-MB-231 cells. Western blotting shows that the activity of ERK1/2 was drastically decreased in CCS knockdown MDA-MB-231 cells (**Figure 4A**). Additionally, overexpression of FLAG tagged CCS increased the activity of ERK1/2 in MCF-7 cells (**Figure 4B**), but the increased activity of ERK1/2 was blocked in MCF-7 with ERK inhibitor U0126 (**Figure 4C**). To validate the role of MAPK signaling in the process of CCS-induced migration and proliferation in breast cancer cells, we first reactivated ERK by transfecting exogenous HA tagged MEK into MDA-MB-CCS-KD cells. As expect, the replenishment of MEK in MDA-MB-231-CCS-KD cells could partially rescue the capability of migration in MDA-MB-231-CCS-KD cells due to the reactivation of ERK1/2 (**Figure 4D**). Secondly, we demonstrated that inhibition of MEK with U0126 treatment inhibited CCS-induced cell migration (**Figure 4E**). Thirdly, overexpression of MEK in MDA-MB-231-CCS-KD cells partially rescues the decreased cell proliferation in CCS knockdown MDA-MB-231 cells (**Figure 4F**). These results suggest that activation of the MAPK/ERK pathway is essential for the CCS-promoted migration abilities and cell proliferation of breast cancer cells.

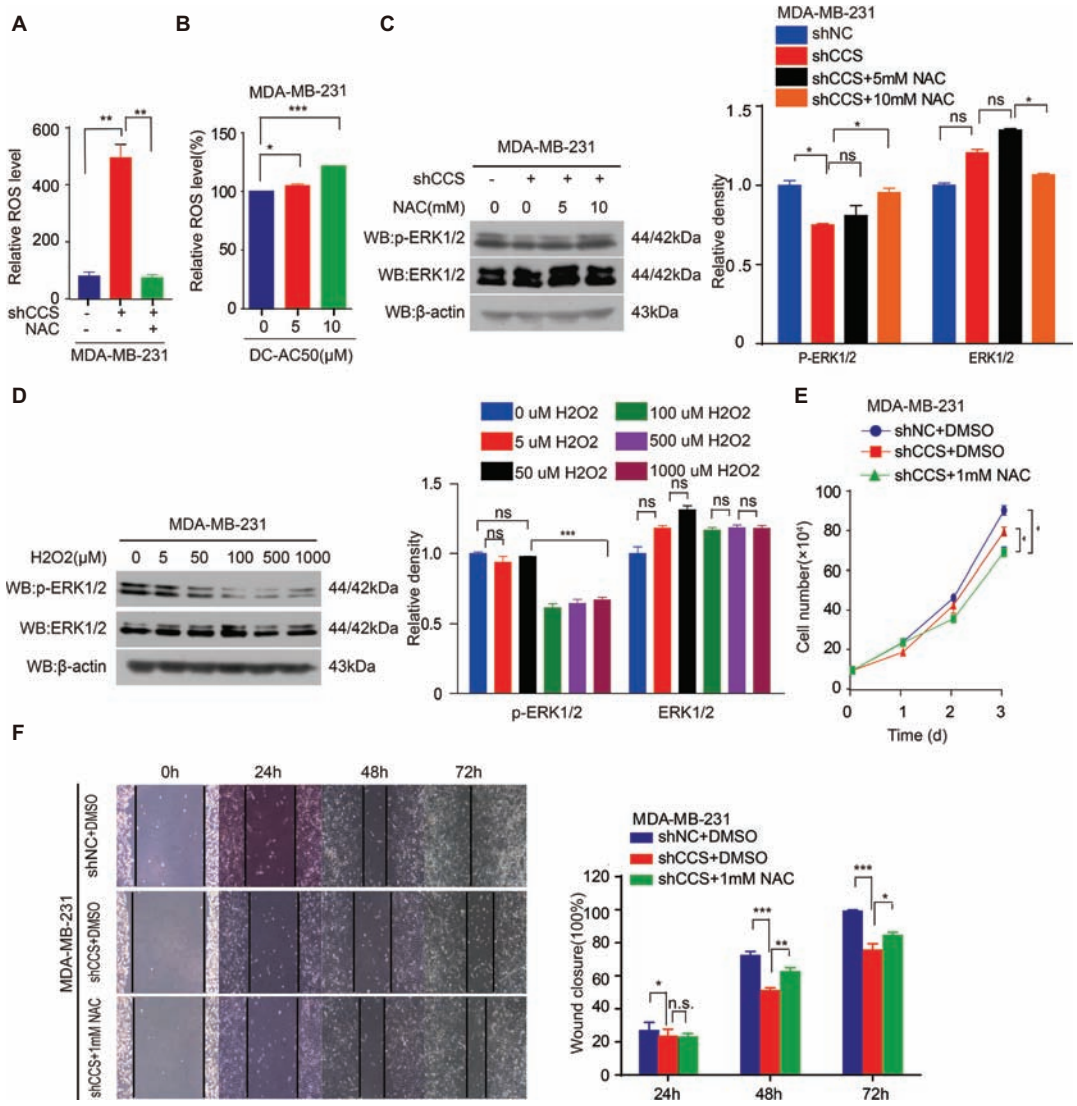

FIGURE 5 | CCS promotes breast cancer cell migration and cell proliferation via ERK1/2 activity mediated by ROS. **(A)** Knockdown of CCS increased ROS level in MDA-MB-231 cells, which was rescued by treatment with 1 mM NAC. **(B)** Treatment with DC_AC50 (5, 10 μM) induced ROS elevation in MDA-MB-231 cells. **(C)** Western blot analysis of total and phosphorylated ERK1/2 levels. β-actin was used as a loading control. Reduced ERK1/2 activity by CCS knockdown was rescued by treatment with NAC (5, 10 mM) for 12 h. **(D)** H_2O_2 significantly abolished ERK1/2 activity in MDA-MB-231cells after 12 h. **(E)** Cell proliferation assays showed that NAC (1 mM) treatment partially rescued the decreased cell proliferation in CCS knockdown MDA-MB-231 cells. **(F)** Wound healing assays showed that NAC (1 mM) treatment partially rescued the decreased cell migration in CCS knockdown MDA-MB-231 cells. All results performed above are presented as mean ± SD from three independent experiments. $^{*}p < 0.05$; $^{**}p < 0.01$; $^{***}p < 0.001$, ns: not significant.

CCS Activates MAPK/ERK Signaling *via* ROS

The inhibition of CCS leads to increased ROS levels. Thus, we hypothesized that CCS regulates the activity of ERK1/2 through ROS. To test this hypothesis, we examined ROS levels in MDA-MB-231 cells treated with CCS shRNA or DC_AC50. Indeed, we found that knockdown or inhibition of CCS significantly increases the cellular ROS levels (**Figures 5A,B**), while the increased ROS was blocked by treating cells with antioxidant N-Acetyl-L-cysteine (NAC; **Figure 5A**). In addition, we also observed that NAC abrogates the decreased activity of ERK1/2 in CCS knockdown MDA-MB-231 cells (**Figure 5C**). Consistently, we also found that H_2O_2 impaired phosphorylation of ERK1/2 in a dose-dependent manner but did not affect the total expression level of ERK1/2 (**Figure 5D**). Finally, we found that NAC could rescue the decreased cell proliferation and migration of MDA-MB-231 CCS knockdown cells (**Figures 5E,F**). These results further support the idea that inhibition of CCS induces a ROS overload, which impairs MAPK/ERK signaling to attenuate cancer cell proliferation. The combined results presented here also establish CCS as a viable anticancer target and copper trafficking as a new pathway for future therapeutic development.

DISCUSSION

Rapid cellular growth and migratory abilities play a crucial role in tumorigenesis and metastasis, which have been recognized to be associated with ROS levels (Aykin-Burns et al., 2009; Doskey et al., 2016). Those cells that survive oxidative stress stand a good chance to have acquired adaptive mechanisms to counteract the potential toxic effects of elevated ROS and to promote cell-survival pathways (Irmak et al., 2003). CCS, a co-enzyme of SOD1, is a critical component of the oxidation–reduction system in cancer, and its differential expression in different types of breast cancer suggests a relationship between CCS and cancer cell growth and migration (**Figure 6**). However, the link between CCS-activated ROS and the occurrence and development of tumors is still in its infancy.

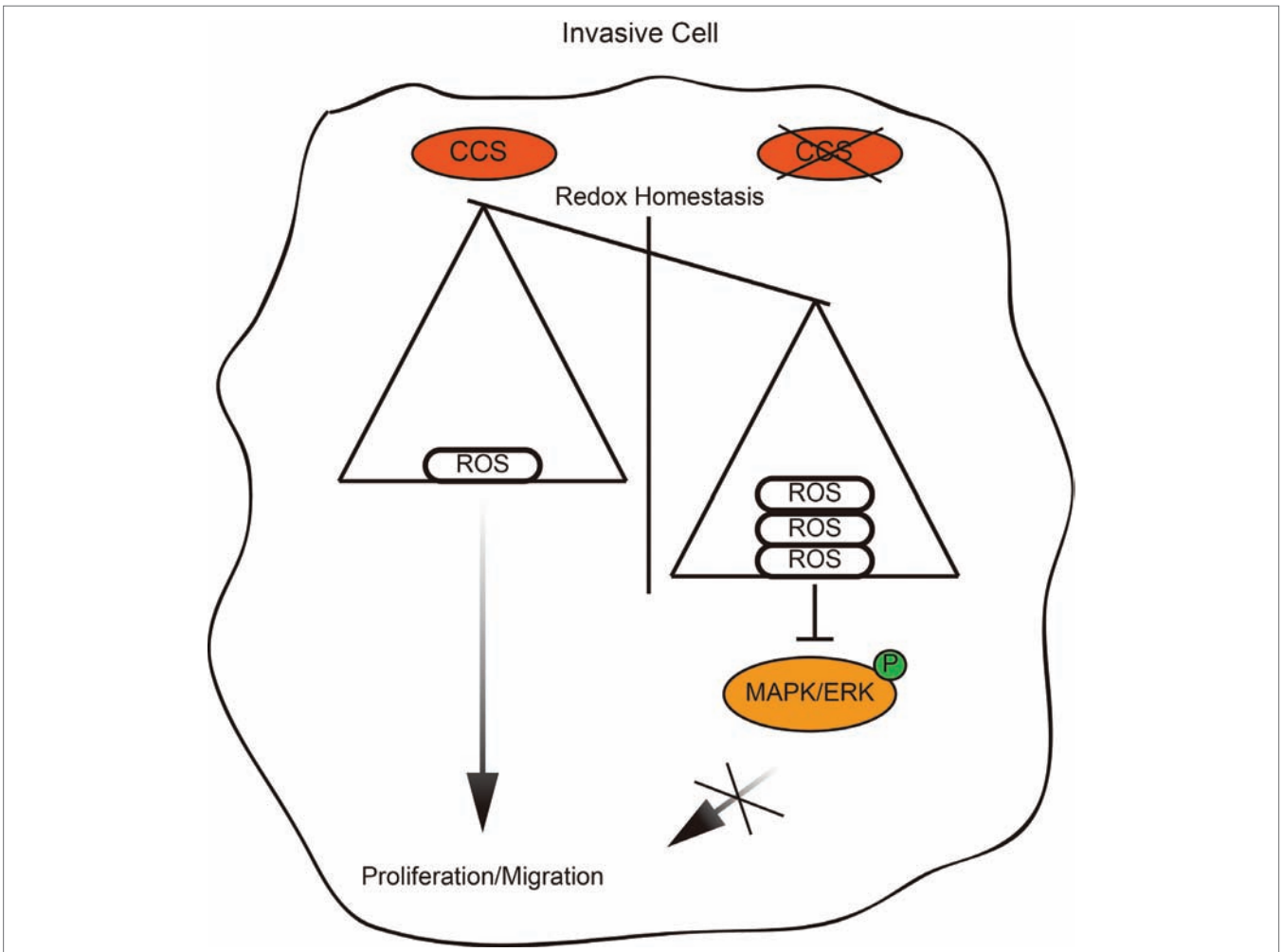

FIGURE 6 | Proposed working model. Schematic model shows that the role and mechanism of CCS in promoting breast cancer cell proliferation and migration.

In this study, we utilized MDA-MB-231 cells (triple-negative breast cancer) and MCF-7 cells (estrogen receptor positive breast cancer) as human cell line models and identified a novel function and mechanism of CCS in facilitating breast cancer cell proliferation and migration. This novel mechanism provides a link between oxidative metabolism and survival signaling. Wang et al. reported that inhibition of CCS leads to a selective suppression of cancer cell proliferation (Wang et al., 2015). Consistent with this, we found that knockdown of CCS significantly reduced cell proliferation in MDA-MB-231 cells but not MCF-7. Interestingly, we revealed a novel function of CCS in regulating migration of breast cancer cells by transwell and wound healing assays. In all, we show that CCS not only plays a vital role in cell proliferation, but it also drives breast cancer migration.

Previous evidence has shown that CCS serves as a co-enzyme of SOD1 to activate its catalytic activity, which is a critical component of oxidation–reduction system (Suzuki et al., 2013b). Since ROS associated oxidative stress has been proven to play important roles in several cancer types and served as promising target for therapy (Perše, 2013; Sosa et al., 2013), we hypothesized that dysregulated ROS levels provide a second signal for CCS-induced proliferation and migration in breast cancer cells. In our study, we showed that knockdown or inhibition of CCS led to increased total ROS levels in MDA-MB-231. ROS overload blocks the activation of the MAPK/ERK pathway, which plays a critical role in tumor formation and progression (Berger et al., 2017; Mayo et al., 2017). By mimicking oxidative stress with H_2O_2 treatment, we were able to suppress the phosphorylation level of ERK1/2, which could be reversed upon treatment with antioxidant NAC. Furthermore, we found that the activation of MAPK/ERK pathways was essential for CCS-induced cell proliferation and migration. Treatment of MCF-7 with U0126-EtOH, a highly selective ERK kinase inhibitor, diminished CCS-induced migration. Conversely, overexpression of MEK enhanced the phosphorylation level of ERK1/2 and partially rescued migration in CCS knockdown MDA-MB-231 cells.

In summary, CCS-mediated ROS decreases the activation of ERK1/2, resulting in attenuation of cell proliferation and migration. Thus, CCS may be a therapeutic strategy to suppress tumor growth and metastasis.

AUTHOR CONTRIBUTIONS

RL and YL performed and analyze all the experiments. XZ and JW drafted the work an provided intellectual content. LL and CS edited the language and figures. CS, SL and SZ designed the study and wrote the manuscript.

FUNDING

This work was supported by the Science and Technology Program of Guangzhou (Grant 201807010003), the Program from the Science and Technology Department of Guangdong Province of China (Grant 2017A030313890), and the National Nature Science Foundation of China (31560312, 81672781 and 81702746). This work was also supported by the China Postdoctoral Science Foundation (2017M612839), the Fundamental Research Funds for the Central Universities (21616323, 21617433), and the Program of Introducing Talents of Discipline to Universities (111 Project, No. B16021).

ACKNOWLEDGMENTS

We thank Dr. Shannon Elf (The University of Chicago) for critical review and edit of the manuscript.

REFERENCES

Ashino, T., Sudhahar, V., Urao, N., Oshikawa, J., Chen, G. F., Wang, H., et al. (2010). Unexpected role of the copper transporter ATP7A in PDGF-induced vascular smooth muscle cell migration. *Circ. Res.* 107, 787–799. doi: 10.1161/CIRCRESAHA.110.225334

Aykin-Burns, N., Ahmad, I. M., Zhu, Y., Oberley, L. W., and Spitz, D. R. (2009). Increased levels of superoxide and H_2O_2 mediate the differential susceptibility of cancer cells versus normal cells to glucose deprivation. *Biochem. J.* 418, 29–37. doi: 10.1042/BJ20081258

Bacac, M., and Stamenkovic, I. (2008). Metastatic cancer cell. *Annu. Rev. pathmechdis. Mech. Dis.* 3, 221–247. doi: 10.1146/annurev.pathmechdis.3.121806.151523

Baud, V., and Karin, M. (2001). Signal transduction by tumor necrosis factor and its relatives. *Trends Cell Biol.* 11, 372–377. doi: 10.1016/S0962-8924(01)02064-5

Berger, M. D., Stintzing, S., Heinemann, V., Yang, D., Cao, S., Sunakawa, Y., et al. (2017). Impact of genetic variations in the MAPK signaling pathway on outcome in metastatic colorectal cancer patients treated with first-line FOLFIRI and bevacizumab: data from FIRE-3 and TRIBE trials. *Ann. Oncol.* 28, 2780–2785. doi: 10.1093/annonc/mdx412

Bray, F., Ferlay, J., Soerjomataram, I., Siegel, R. L., Torre, L. A., and Jemal, A. (2018). Global cancer statistics 2018: GLOBOCAN estimates of incidence and mortality worldwide for 36 cancers in 185 countries. *CA Cancer J. Clin.* 68, 394–424. doi: 10.3322/caac.21492

Chaffer, C. L., and Weinberg, R. A. (2011). A perspective on cancer cell metastasis. *Science* 331, 1559–1564. doi: 10.1126/science.1203543

Christofori, G. (2006). New signals from the invasive front. *Nature* 441:444. doi: 10.1038/nature04872

Doskey, C. M., Buranasudja, V., Wagner, B. A., Wilkes, J. G., Du, J., Cullen, J. J., et al. (2016). Tumor cells have decreased ability to metabolize H_2O_2: implications for pharmacological ascorbate in cancer therapy. *Redox Biol.* 10, 274–284. doi: 10.1016/j.redox.2016.10.010

El Touny, L. H., Vieira, A., Mendoza, A., Khanna, C., Hoenerhoff, M. J., and Green, J. E. (2014). Combined SFK/MEK inhibition prevents metastatic outgrowth of dormant tumor cells. *J. Clin. Invest.* 124, 156–168. doi: 10.1172/JCI70259

Gupta, P. B., Mani, S., Yang, J., Hartwell, K., and Weinberg, R. A. (2005). The evolving portrait of cancer metastasis. *Cold Spring Harbor Symposia on Quantitative Biology* 70, 291–297. doi: 10.1101/sqb.2005.70.033

Irmak, M. B., Ince, G., Ozturk, M., and Cetin-Atalay, R. (2003). Acquired tolerance of hepatocellular carcinoma cells to selenium deficiency: a selective survival mechanism? *Cancer Res.* 63, 6707–6715. doi: 10.1016/S0165-4608(02)00795-1

Kawamata, H., and Manfredi, G. (2008). Different regulation of wild-type and mutant Cu, Zn superoxide dismutase localization in mammalian mitochondria. *Hum. Mol. Genet.* 17, 3303–3317. doi: 10.1093/hmg/ddn226

Leitch, J. M., Jensen, L. T., Bouldin, S. D., Outten, C. E., Hart, P. J., and Culotta, V. C. (2009). Activation of Cu, Zn-superoxide dismutase in the absence of oxygen and the copper chaperone CCS. *J. Biol. Chem.* 284, 21863–21871. doi: 10.1074/jbc.M109.000489

Lowndes, S. A., and Harris, A. L. (2005). The role of copper in tumour angiogenesis. *J. Mammary Gland Biol. Neoplasia* 10, 299–310. doi: 10.1007/s10911-006-9003-7

Mandinov, L., Mandinova, A., Kyurkchiev, S., Kyurkchiev, D., Kehayov, I., Kolev, V., et al. (2003). Copper chelation represses the vascular response to injury. *Proc. Natl. Acad. Sci.* 100, 6700–6705. doi: 10.1073/pnas.1231994100

Mayo, J. C., Hevia, D., Quiros-Gonzalez, I., Rodriguez-Garcia, A., Gonzalez-Menendez, P., Cepas, V., et al. (2017). IGFBP 3 and MAPK/ERK signaling mediates melatonin-induced antitumor activity in prostate cancer. *J. Pineal Res.* 62:e12373. doi: 10.1111/jpi.12373

Perše, M. (2013). Oxidative stress in the pathogenesis of colorectal cancer: cause or consequence? *Biomed. Res. Int.* 2013. doi: 10.1155/2013/725710

Rajalingam, K., Wunder, C., Brinkmann, V., Churin, Y., Hekman, M., Sievers, C., et al. (2005). Prohibitin is required for Ras-induced Raf–MEK–ERK activation and epithelial cell migration. *Nat. Cell Biol.* 7:837. doi: 10.1038/ncb1283

Sciegienka, S. J., Solst, S. R., Falls, K. C., Schoenfeld, J. D., Klinger, A. R., Ross, N. L., et al. (2017). D-penicillamine combined with inhibitors of hydroperoxide metabolism enhances lung and breast cancer cell responses to radiation and carboplatin via H_2O_2-mediated oxidative stress. *Free Radic. Biol. Med.* 108, 354–361. doi: 10.1016/j.freeradbiomed.2017.04.001

Sosa, V., Moliné, T., Somoza, R., Paciucci, R., Kondoh, H., and LLeonart, M. E. (2013). Oxidative stress and cancer: an overview. *Ageing Res. Rev.* 12, 376–390. doi: 10.1016/j.arr.2012.10.004

Suzuki, Y., Ali, M., Fischer, M., and Riemer, J. (2013a). Human copper chaperone for superoxide dismutase 1 mediates its own oxidation-dependent import into mitochondria. *Nat. Commun.* 4, 1–9. doi: 10.1038/ncomms3430

Suzuki, Y., Ali, M., Fischer, M., and Riemer, J. (2013b). Human copper chaperone for superoxide dismutase 1 mediates its own oxidation-dependent import into mitochondria. *Nat. Commun.* 4:2430. doi: 10.1038/ncomms3430

Thiery, J. P. (2009). Metastasis: alone or together? *Curr. Biol.* 19, R1121–R1123. doi: 10.1016/j.cub.2009.11.001

Ulloa, J. L. (2009). *The copper chaperone as a dual regulator of effects related to oxidative stress and chromatin remodeling*. (ProQuest Dissertations Publishing: The Johns Hopkins University), 3339899.

Valastyan, S., and Weinberg, R. A. (2011). Tumor metastasis: molecular insights and evolving paradigms. *Cell* 147, 275–292. doi: 10.1016/j.cell.2011.09.024

Wang, J., Luo, C., Shan, C., You, Q., Lu, J., Elf, S., et al. (2015). Inhibition of human copper trafficking by a small molecule significantly attenuates cancer cell proliferation. *Nat. Chem.* 7, 968–979. doi: 10.1038/nchem.2381

Xu, S., Hoshan, L., and Chen, H. (2016). Improving lactate metabolism in an intensified CHO culture process: productivity and product quality considerations. *Bioprocess Biosyst. Eng.* 39, 1689–1702. doi: 10.1007/s00449-016-1644-3

Conflict of Interest Statement: The authors declare that the research was conducted in the absence of any commercial or financial relationships that could be construed as a potential conflict of interest.

frontiers in Oncology

ORIGINAL RESEARCH
published: 10 April 2019
doi: 10.3389/fonc.2019.00258

A Novel Antibody-Toxin Conjugate to Treat Mantle Cell Lymphoma

*Gulam M. Rather[1], Siang-Yo Lin[1], Hongxia Lin[1], Zoltan Szekely[2] and Joseph R. Bertino[1]**

[1] Departments of Pharmacology and Medicine, Rutgers Cancer Institute of New Jersey, Rutgers, The State University of New Jersey, New Brunswick, NJ, United States, [2] Department of Pharmaceutics, Ernest Mario School of Pharmacy, Rutgers, The State University of New Jersey, Piscataway, NJ, United States

Matriptase is a transmembrane serine protease, synthesized as an inactive single-chain zymogen on the endoplasmic reticulum and transported to the plasma membrane. Matriptase is activated in different epithelial and some B-cell malignancies and changes its conformation and activity is inhibited mainly by its endogenous inhibitor HAI-1. Activated matriptase plays a key role in tumor initiation as well as tumor progression, including invasiveness, and metastasis. To target the anti-mitotic toxin (monomethyl auristatin-E) to activated matriptase, a novel antibody to activated matriptase was conjugated with this toxin via a valine-citrulline-PABA linker. In a previous study, this antibody-toxin conjugate was found to be effective against triple negative breast cancer cell lines and xenografts, alone, or in combination with cisplatin (1). In this study, we examined the anti-tumor effect of the antibody toxin conjugate (ADC) against activated matriptase positive mantle cell lymphoma cell lines (JeKo-1, Maver, Mino, and Z138). This ADC was cytotoxic to these cell lines with IC_{50}s between 5 and 14 μg/mL. The ADC also showed a dose dependent anti-tumor effect on the JeKo-1 xenograft in mice without toxicity.

Keywords: activated matriptase, antibody drug conjugate, monomethyl auristatin-E, mantle cell lymphoma, xenograft

OPEN ACCESS

Edited by:
Zhe-Sheng Chen,
St. John's University, United States

Reviewed by:
Lokesh Jain,
Merck, United States
Jianhua Yang,
Baylor College of Medicine, United States

***Correspondence:**
Joseph R. Bertino
bertinoj@cinj.rutgers.edu

Specialty section:
This article was submitted to Cancer Molecular Targets and Therapeutics, a section of the journal Frontiers in Oncology

Received: *15 August 2018*
Accepted: *21 March 2019*
Published: *10 April 2019*

Citation:
Rather GM, Lin S-Y, Lin H, Szekely Z and Bertino JR (2019) A Novel Antibody-Toxin Conjugate to Treat Mantle Cell Lymphoma. Front. Oncol. 9:258. doi: 10.3389/fonc.2019.00258

INTRODUCTION

Mantle Cell Lymphoma (MCL), represents 6- percent of all lymphoma cases, and currently the survival time is 4–5 years, shorter compared to other hematologic malignancies (2–4). MCL cells express CD20, aberrant expression of CD5, and due to a translocation t(11;14)(q13;q32), overexpression of cyclin-D1, encoded by the CCND1 gene located on chromosome 11, which mediates cell cycle progression through the G1 phase (5, 6). The currently used drugs to treat MCL patients include bortezomib, ibrutinib, rituximab, bendamustine, and combinations of these drugs.

Matriptase, a glycoprotein (80–90 kDa), is a member of type II transmembrane serine proteases. It is synthesized as a latent single-chain structure and with many regulatory mechanisms and functions (7, 8), and is activated through an auto-activation step resulting in a disulfide-linked-two-chain structure. Following activation, matriptase is rapidly inactivated by its endogenous inhibitor HAI-1. This activated matriptase-HAI-1 complex remains present in most epithelial carcinomas and some B-cell malignancies (9–11). Importantly, while matriptase is present in a latent form on epithelial cells and B-cells, activated matriptase expression is mainly restricted to the membranes of epithelial tumors, and some B-cell malignancies, in particular MCL (10–12).

Of importance, given the increase in reactive oxygen species (ROS) and the acidic environment of solid tumors (ROS), these environments activate the matriptase zymogen (13–21).

In this study we show that a novel anti-matriptase antibody toxin (Monomethyl auristatin-E, MMAE) conjugate potently inhibited growth of mantle cell lymphoma cell lines (JeKo-1, Maver, Mino and Z138) and caused significant growth inhibition of the JeKo-1 xenograft *in vivo*.

MATERIALS AND METHODS

Animals

NOD/SCID/IL2 receptor gamma chain null (NOD/SCID/IL2rg^{null}, NSG) mice were obtained from the Jackson Laboratory (Bar Harbor, ME).

Materials

For cell culture, RPMI 1640, and fetal bovine serum were from Invitrogen (Fisher Scientific).

Cell Culture

The MCL cells (JeKo-1, Mino, Maver, and Z138) were cultured in 1X RPMI Media 1,640 (Life Technologies) containing 10% fetal bovine serum (FBS) at 37°C and 5% carbon dioxide. All the cell lines were obtained from American Type Culture Collection (ATCC) and were checked for mycoplasma by MycoAlert™ mycoplasma detection kit (Lonza USA).

Western Blotting

The MCL cells were scraped into a micro centrifuge tube from petri-dishes after 75% confluency. After centrifugation, cell pellets were lysed in lysis buffer (20 mM Tris, pH 7.4) containing 1% triton-X100, a commercial protease inhibitor cocktail (Roche) and 1 mM 5,5′-dithio-bis(2-nitrobenzoic acid) (DTNB). Since, DTNB interferes with the Bradford reagent (Bio-Rad Laboratories), equal volume of protein samples was resolved by 10% SDS-PAGE, without any boiling and under non-reducing sample buffer conditions and transferred onto a nitrocellulose membrane (Bio-Rad Laboratories). After blocking the membrane with 5% non-fat dry milk prepared in Tris buffered saline with 0.1% Tween-20 (TBST), the membrane was incubated with the desired primary antibody M69 at 4°C overnight. The membrane was washed thrice in TBST and then incubated for 2 h at room temperature with the appropriate peroxidase-conjugated secondary antibody. Bands were visualized using an enhanced chemiluminescence kit (Pierce). Anti-glyceraldehyde 3-phosphate dehydrogenase (GAPDH) (from Millipore) and was used as a control. Anti-HAI-1, anti-Vinculin and anti-mouse secondary antibody were from Santa Cruz Biotechnologies. Anti-mouse secondary antibody was used to probe the ADC (mouse antibody recognizing human activated matriptase) and also to probe GAPDH, HAI-1, and Vinculin which are mouse generated.

Cytotoxicity Assay

Five thousand cells per well were plated in RPMI 1,640 media supplemented with 10% FBS. After overnight culture, media was removed and fresh media containing the ADC was added and incubated for different time periods. To assess cell viability, the MCL cell lines with or without drug treatment were collected and cell viability was determined using the Vi-CELL™ Series Cell Viability Analyzer (Beckman Coulter, Carlsbad, CA). The 50% inhibitory concentration (IC_{50}; the drug concentration required to obtain 50% cell kill compared to control) was determined using the non-linear regression curve fit of the graphs drawn by GraphPad Prism 4 software (GraphPad Software Inc., CA). All experiments were performed in triplicate, and all experiments were repeated at least three times.

Migration Assay

MCL (suspension cells) cells were treated with ADC (IC_{50}) for 48 h and washed twice with IX PBS. The cells were then serum starved for 1.5 h in FBS-free RPMI at 37°C and 5% carbon dioxide in presence of ADC. Three hundred microliters of FBS-free RPMI (8×10^5 cells) were added to the top chamber of a cell culture insert (24-well format) of eight-micron pore size (Corning). Cells were treated with ADC (IC_{50}) throughout the experiment (means ADC is present in FBS-free media in inserts as well as in the lower well of that insert). Inserts had been previously transferred to wells containing 700 mL of RPMI (containing 10% FBS) with or without ADC. After 24 h of incubation at 37°C and 5% carbon dioxide, cells were collected from both insert chamber and lower well (of 24-well plate) and checked for viability using the Vi-CELL™ Series Cell Viability Analyzer (Beckman Coulter, Carlsbad, CA). The percent viable cells migrated toward FBS (in lower well) of total viable cells added in insert, were plotted against ADC treatment. Each experiment was done at-least three times and in four replicates.

Animal Studies

The JeKo-1 cell line was used for anti-tumor studies. Cells ($10 \times 10^{6)}$ in 100 μL of PBS were injected subcutaneously into the right flank of 6-week-old NSG female mice. Once tumors were palpable, the mice were randomized to different groups. Mice were treated i.p. with the ADC, and treatment periods were indicated by arrows. Saline was used as a control treatment. Tumor size and body weights were measured twice a week and the tumor volume was calculated using the formula width^2 × (length/2). Results are presented as mean ± SEM.

Histologic Preparation and Immunohistochemistry Staining

Samples were fixed in 4% formalin and paraffin-embedded. Immunohistochemistry was performed on 4 μm sections with antibodies to Ki67 (Santa Cruz Biotechnologies, USA) and Cleaved caspase-3 (Cell Signaling Technology USA #9661). Sections were developed and stained with hematoxylin and eosin using standard methods. All histological preparations and immunostaining were conducted by the Rutgers Cancer Institute of New Jersey Biospecimen Repository and Histopathology Core.

Statistical Analysis

Statistical analysis was performed using Prism software (GraphPad). In all cases, ANOVA followed by two-tailed,

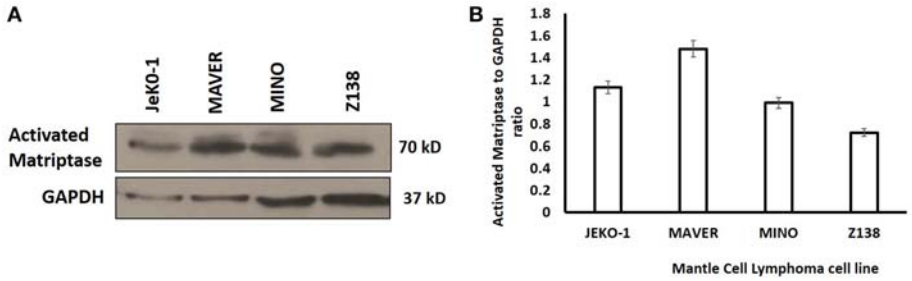

FIGURE 1 | (A) Western Blot analysis of activated matriptase expression in Mantle Cell Lymphoma cells (JeKo-1, MAVER, MINO, and ZI38). Equal volume of lysate was loaded in 10% SDS-PAGE (see methods). **(B)** Activated matriptase to GAPDH ratio for all the four mantle cell lymphoma cell lines.

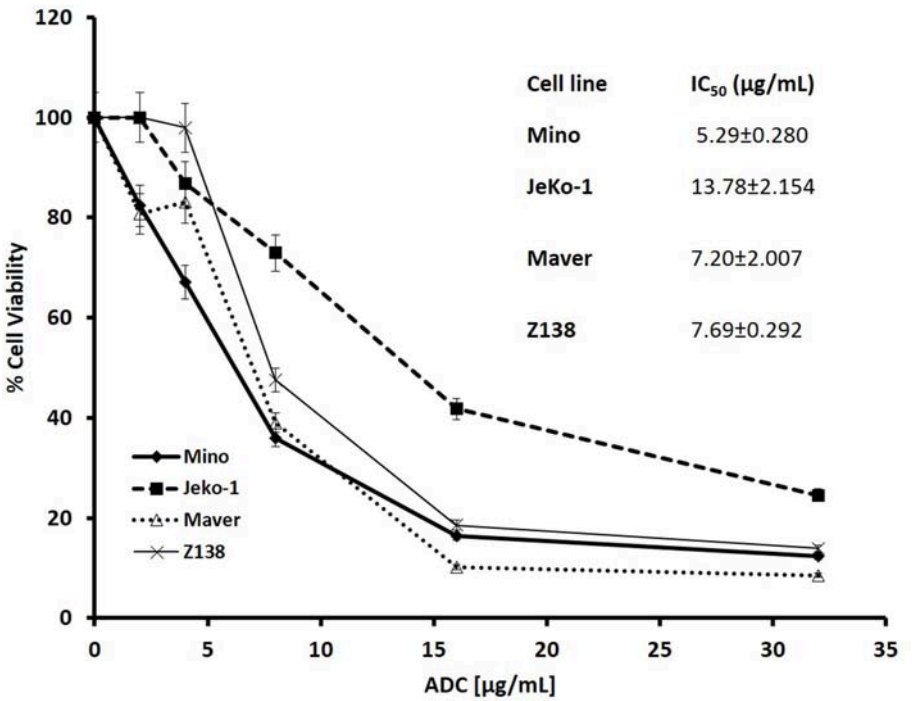

FIGURE 2 | Cytotoxicity of M69-MMAE conjugate (ADC) against different MCL cell lines. Five thousand cells/well were plated in a 96-well plate and the cells were treated the next day with the ADC for 72 h. Cytotoxicity of the ADC was measured by trypan blue dye exclusion method using a Vi-Cell XR© cell viability analyzer (Beckman Coulter). All the reading points were carried out in triplicates. The IC_{50} values (insert) are calculated using GraphPad Prism 4 software. Results are presented as mean ± SEM.

unpaired Student *t*-tests was performed to analyze statistical differences between groups. *P*-values of <0.05 were considered statistically significant.

Antibody-Toxin Conjugate Preparation and Characterization

The anti-matriptase antibody (M69) was generated against purified activated matriptase-HAI complex from human milk as described by Lin et al. (22). Seattle Genetics' valine-citrulline-PABA linker technology was used for conjugation of a potent tubulin-inhibitor, monomethyl auristatin-E (MMAE) to the M69 antibody. The valine-citrulline dipeptide based linker has been shown to be stable in circulation but cleavable by cathepsin B in the lysosome to generate free drug (23). Copper free click chemistry is used to load the toxin in a stoichiometrically controlled manner to M69 antibody under very mild conditions. The technology involves conjugating the linker-toxin with the lysine side chains on the antibody surface. The conjugation procedure does not affect the disulfide bridges between cysteines of the antibody, thus maintaining the structure of the antibody without any loss of antibody activity by misfolding or dissociation of antibody chains. Analysis by mass spectrometry (HR-MALDI-TOF) showed an increase of 7,000 Da average M.W. corresponding to an average of 3.5 toxin (MMAE) molecules linked to each mAb molecule (1).

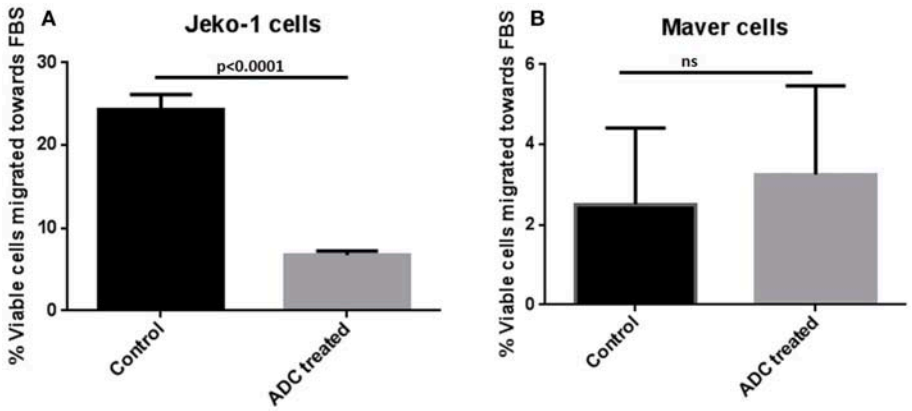

FIGURE 3 | Effect of ADC on migration of MCL cell lines *in vitro*. **(A)** JeKo-1 **(B)** Maver cells. Cells were treated with ADC for 48 h and washed twice with 1X PBS and starved for 1.5 h in FBS-free RPMI and then added in a cell culture insert having 8-micron pore size in 300 μl of FBS-free RPMI (with and without ADC). The insert was transferred to a well containing 700 μl of FBS-containing RPMI (with and without ADC) for 24 h at 37°C and 5% carbon dioxide. Cells were checked for viability from both insert and lower well using the Vi-CELL™ Series Cell Viability Analyzer (Beckman Coulter, Carlsbad, CA). The percent viable cells migrated toward the lower well (having FBS-RPMI) of total viable cells added in insert were plotted against ADC treatment. Each experiment was done at-least three times and in four replicates. Results are presented as mean ± SEM.

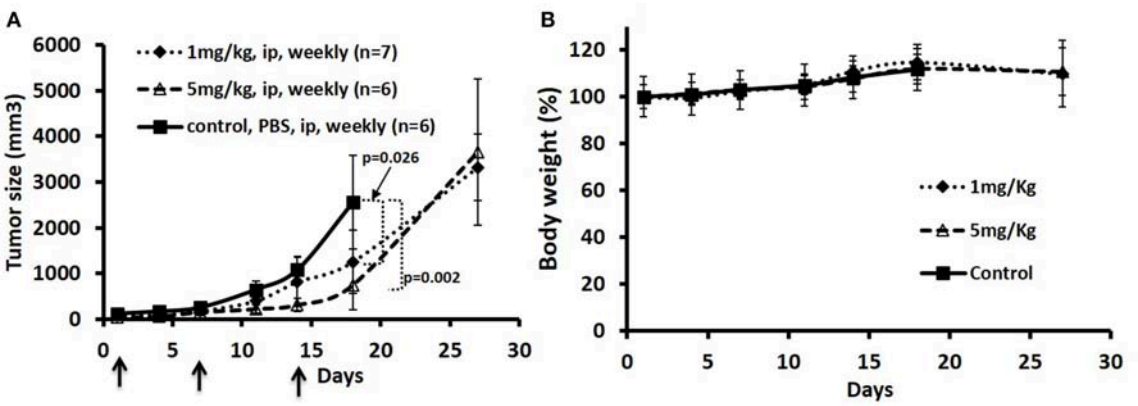

FIGURE 4 | Treatment of JeKo-1 xenografts in mice using different doses of matriptase-MMAE conjugate (ADC). **(A)** Xenograft studies with M69-MMAE. NOD/SCID mice were inoculated with 10×10^6 JeKo-1 cells in PBS in the right flanks. When the tumor was palpable (100–200 mm^3), mice ($n = 19$) were randomized into: control (antibody alone), 1 and 5 mg/kg M69-MMAE treatment groups. M69-MMAE was administrated by i.p. weekly x 2. Tumor volume was measured twice a week. Tumor volumes were calculated using the formula $width^2$ x (length/2). Results are presented as mean ± SEM **(B)** Mice body weight change in the control and treatment groups. Treatments are shown by arrows.

RESULTS

In vitro Cytotoxicity of M69-MMAE (ADC) Against Mantle Cell Lymphoma (MCL) Cell Lines

Activated matriptase expression was evaluated in different MCL cell lines (JeKo-1, Mino, Maver, and Z138) by Western blotting using the M-69 antibody that recognizes activated matriptase alone or in complex with HAI-1. The four cell lines showed increased levels of activated matriptase, although the level of expression varied (**Figure 1**). The expression level of hepatocyte growth factor activator inhibitor (HAI)-1 protein in mantle cells is shown in **Figure S1**.

Cytotoxicity studies showed that the ADC decreased the viability of all the cell lines (**Figure 2**) with IC_{50}s at single digit μg/ml of the conjugate. As 3.5 molecules of toxin are bound on the average to each antibody molecule, the IC_{50} values for the toxin ranged from 125 to 611 pM. Based on the IC_{50} values, Mino, Maver and Z138 cells were 1.8–2.6-fold more sensitive to ADC compared to JeKo-1. In order to check whether the ADC is stable in media, the ADC was incubated (37°C and 5% carbon dioxide) in complete media (RPMI with 10% FBS) for 48 h before used for cytotoxicity test and it was found that 48 h incubated ADC and fresh ADC are equally effective against Maver cell line as shown in **Figure S2**. In order to study the role of matriptase in metastasis and invasiveness, the ADC was found to inhibit the migration of JeKo-1 cells *in vitro*. Of interest, only a small percent of cell from the Maver cell line migrated as compared to the JeKo-1 cell line, and the ADC did not enhance migration (**Figure 3**).

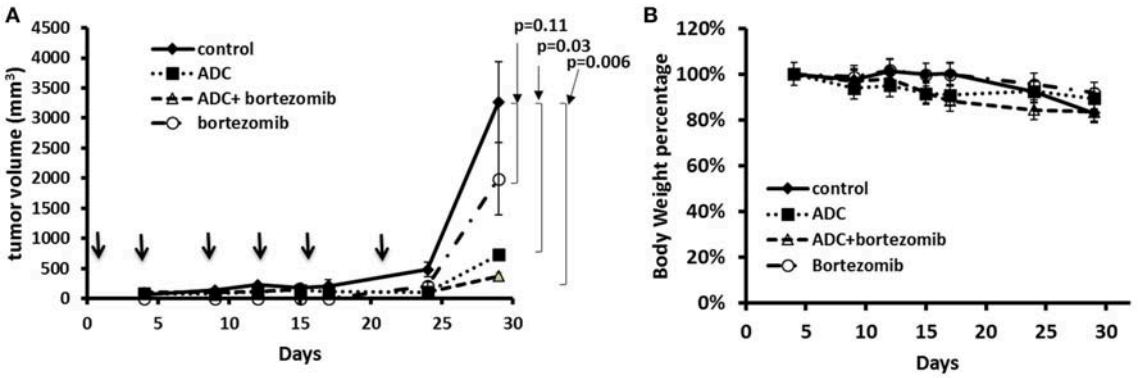

FIGURE 5 | Treatment of JeKo-1 xenografts in mice using the matriptase-MMAE conjugate (ADC) and bortezomib. **(A)** Xenograft studies with M69-MMAE and bortezomib. NOD/SCID mice were inoculated with 10 × 106 JeKo-1 cells in PBS in the right flank. When tumors were palpable, mice were randomized into control, bortezomib, M69-MMAE, and bortezomib plus M69-MMAE treatment groups. M69-MMAE (5 mg/kg) was administrated by i.p. twice weekly for 3 weeks. Bortezomib (0.75 mg/kg) was given i.p. weekly. Bortezomib and M69-MMAE were given together with the same dose schedule. Tumor volume was measured twice a week, and the tumor volume calculated using the formula width^2 x (length/2). Results are presented as mean ± SEM. **(B)** Mice body weight percentage during the treatment. Treatments are shown by arrows.

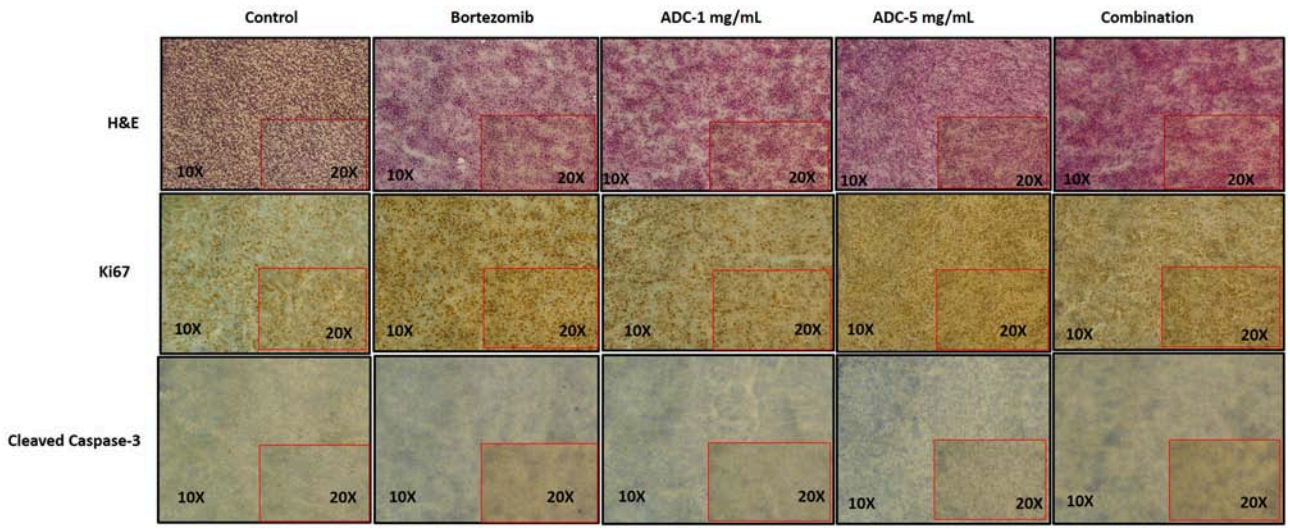

FIGURE 6 | Immunohistochemistry staining of JeKo-1 tumors extracted from mice in **Figures 4**, **5** against various biomarkers. The tumors were harvested from control, 1 and 5 mg/kg (i.p. weekly) M69-MMAE treatment groups from experiment four and Bortezomib and M69-MMAE combination (Bortezomib (0.75 mg/kg, i.p. weekly and M69-MMAE, 5mg/kg i.p. twice weekly) from experiment five. Ki67 staining showing proliferation of JeKo-1; and Cleaved caspase-3 showing the apoptotic cell death. The tonsil tissue was used as a positive control for various IHC staining.

JeKo-1 Xenograft Studies

To test the anti-tumor effects of the ADC in one of the MCL tumors in a mouse model, we elected to test the JeKo-1 cell line. We tested two dose schedules of the ADC: 1 vs. 5 mg/Kg administered i.p. weekly. The 5 mg/Kg weekly dose was more effective than the 1 mg/Kg dose. Even at the higher dose, there were no signs of toxicity as measured by observation and weight loss (**Figure 4**). Previous studies with the naked antibody showed that it had no anti-tumor activity *per se* (1).

As bortezomib is used to treat MCL, alone and in combination, we also tested the ADC in combination with bortezomib in a JeKo-1 xenograft study. Using a similar inoculum, this tumor grows rapidly in NOD-SCID-gamma mice, and the biweekly 5 mg/kg dose schedule, both bortezomib and the ADC caused marked tumor growth inhibition ($p = 0.006$). The combination of bortezomib and the ADC was more effective than either drug alone (**Figure 5**).

We harvested the tumors at the end of the experiment and then used immunohistochemistry to test for various biomarkers. **Figure 6** showed that there was no significant change in Ki-67 staining; however, cleaved caspase-3 staining (apoptosis) showed a significant increase in the combination group (ADC with bortezomib) compared to either drug alone.

DISCUSSION

Brentuximab vedotin (Adcetris), consisting of an antibody that targets CD30, conjugated with MMAE is approved for the treatment of Hodgkin disease, as well anaplastic large cell lymphoma (ALCL) (24). CAT-3888 (BL22), another immunotoxin, which targets the CD22 antigen on certain lymphoma cells, attached to a bacterial Pseudomonas exotoxin, PE38, has shown activity against hairy cell leukemia (HCL) in early clinical trials (25). CAT-8015 (moxetumomab pasudotox), an updated version of this drug, is now being studied for use against lymphomas (26).

Our novel antibody against activated matriptase, overexpressed in B-cell lymphoma and epithelial tumors and involved in tumorogenesis, invasiveness and metastasis (27–29), conjugated with the tubulin binding, mitotic inhibitor toxin, monomethyl auristatin E (MMAE), demonstrates that activated matriptase is a bonafide target for use with antibodies that recognize activated matriptase, armed with a toxin. The pre-incubated ADC was as potent as the non-incubated fresh ADC, indicating that the ADC was stable in FBS and media. The *in vitro* experiments also confirmed that this ADC showed significant inhibition of migration of JeKo-1 cells. No observable toxicity was found with this ADC, however, as this is a mouse antibody that recognizes human, but not mouse matriptase, other toxic effects of the ADC would not be noted. We currently have constructed a chimeric matriptase antibody, suitable for toxicity studies in a primate model and for Phase I trials in humans.

Future plans are to use this ADC alone and in combination with other chemotherapeutic drugs (bortezomib and ibrutinib) in primary MCL xenografts with the goal of generating additional sufficient preclinical data to allow for future clinical development.

ETHICS STATEMENT

All the cell line studies were performed through Rutgers Cancer Institute of New Jersey using protocols approved by the Rutgers Environmental Health and Safety (REHS). Animal experiments were conducted in accordance with Rutgers Cancer Institute of New Jersey Animal Care and Use Committee guidelines using an approved protocol number 15-040.

AUTHOR CONTRIBUTIONS

GR, S-YL, HL, ZS, and JRB conception and design, development of methodology, analysis and interpretation of data (e.g., statistical analysis, biostatistics, computational analysis), writing, review, and/or revision of the manuscript, and administrative, technical, or material support (i.e., reporting or organizing data, constructing databases). GR, S-YL, and HL acquisition of data (provided animals, acquired and managed patients, provided facilities, etc.). S-YL, ZS (for ADC conjugation study), and JRB (overall) study supervision.

ACKNOWLEDGMENTS

This work was supported in part by a Breast Cancer Research Foundation grant to JRB. The author acknowledges Dr. Lin CY and Dr. Johnson M (Georgetown Medical School, USA) for their generous M69-antibody gift. An abstract of this work was published [The American Society of Hematology annual meeting 2017 (Blood 2017 130:5159)].

SUPPLEMENTARY MATERIAL

The Supplementary Material for this article can be found online at: https://www.frontiersin.org/articles/10.3389/fonc.2019.00258/full#supplementary-material

Figure S1 | Western Blot analysis showing the hepatocyte growth factor activator inhibitor (HAI)-1 expression in Mantle Cell Lymphoma cells (Lane1: JEKO-1, Lane 2: MAVER). 10% SDS-PAGE was used.

Figure S2 | Cytotoxicity of M69-MMAE conjugate (ADC) after 48 h incubation in complete media against Maver cell line. Five thousand cells/well were plated in a 96-well plate and the cells were treated the next day with the ADC (fresh and 48 h incubated one) for 72 h. Cytotoxicity was measured using an MTS assay. All the reading points were carried out in triplicates. Results are presented as mean ± SEM.

REFERENCES

1. Rather GM, Lin SY, Lin H, Banach-Petrosky W, Hirshfield KM, Lin CY, et al. Activated matriptase as a target to treat breast cancer with a drug conjugate. *Oncotarget.* (2018) 9:25983–92. doi: 10.18632/oncotarget.25414
2. Shah BD, Martin P, Sotomayor EM. Mantle cell lymphoma: a clinically heterogeneous disease in need of tailored approaches. *Cancer Control.* (2012) 19:227–35. doi: 10.1177/107327481201900307
3. Vose JM. Mantle cell lymphoma: 2012 update on diagnosis, risk-stratification, and clinical management. *Am J Hematol.* (2012) 87:604–9. doi: 10.1002/ajh.23176
4. Dreyling M, Geisler C, Hermine O, Kluin-Nelemans HC, Le Gouill S, Rule S, et al. Newly diagnosed and relapsed mantle cell lymphoma: ESMO clinical practice guidelines for diagnosis, treatment and follow-up. *Ann Oncol.* (2014) 25 (Suppl. 3):iii83–92. doi: 10.1093/annonc/mdu264
5. Williams ME, Swerdlow SH. Cyclin D1 overexpression in non-Hodgkin's lymphoma with chromosome 11 bcl-1 rearrangement. *Ann Oncol.* (1994) 5 (Suppl. 1):71–3. doi: 10.1093/annonc/5.suppl_1.S71
6. Yin CC, Luthra R. Molecular detection of t(11;14)(q13;q32) in mantle cell lymphoma. *Methods Mol Biol.* (2013) 999:211–6. doi: 10.1007/978-1-62703-357-2_14
7. Uhland K. Matriptase and its putative role in cancer. *Cell Mol Life Sci.* (2006) 63:2968–78. doi: 10.1007/s00018-006-6298-x
8. List K, Bugge TH, Szabo R. Matriptase: potent proteolysis on the cell surface. *Mol Med.* (2006) 12:1–7. doi: 10.2119/2006-00022.List
9. Murai N, Miyake Y, Tsuzuki S, Inouye K, Fushiki T. Involvement of the cytoplasmic juxtamembrane region of matriptase in its exclusive localization to the basolateral membrane domain of Madin-Darby canine kidney epithelial cells. *Cytotechnology.* (2009) 59:169–76. doi: 10.1007/s10616-009-9205-0
10. Oberst M, Anders J, Xie B, Singh B, Ossandon M, Johnson M, et al. Matriptase and HAI-1 are expressed by normal and malignant epithelial cells *in vitro* and *in vivo*. *Am J Pathol.* (2001) 15:1301–11. doi: 10.1016/S0002-9440(10)64081-3
11. Benaud CM, Oberst M, Dickson RB, Lin C-Y. Deregulated activation of matriptase in breast cancer cells. *Clin Exp Metastasis.* (2002) 19:639–49. doi: 10.1023/A:1020985632550

12. Chou FP, Chen YW, Zhao XF, Xu-Monette ZY, Young KH, Gartenhaus RB, et al. Imbalanced matriptase pericellular proteolysis contributes to the pathogenesis of malignant B-Cell lymphomas. *Am J Pathol.* (2013) 183:1306–17. doi: 10.1016/j.ajpath.2013.06.024
13. Chen CJ, Wu BY, Tsao PI, Chen CY, Wu MH, Chan YLE, et al. Increased matriptase zymogen activation in inflammatory skin disorders. *Am J Physiol Cell Physiol.* (2011) 300:C406–15. doi: 10.1152/ajpcell.00403.2010
14. Tseng IC, Xu H, Chou FP, Li G, Vazzano AP, Kao JPY, et al. Matriptase activation, an early cellular response to acidosis. *J Biol Chem.* (2010) 285:3261–70. doi: 10.1074/jbc.M109.055640
15. Kato Y, Ozawa S, Miyamoto C, Maehata Y, Suzuki A, Maeda T, et al. Acidic extracellular microenvironment and cancer. *Cancer Cell Int.* (2013) 13:89. doi: 10.1186/1475-2867-13-89
16. Gupta SC, Singh R, Pochampally R, Watabe K, Mo Y-Y. Acidosis promotes invasiveness of breast cancer cells through ROS-AKT-NF-κB pathway. *Oncotarget.* (2014) 5:12070–82. doi: 10.18632/oncotarget.2514
17. Gatenby RA, Gillies RJ. Why do cancers have high aerobic glycolysis? *Nat Rev Cancer.* (2004) 4:891–9. doi: 10.1038/nrc1478
18. Bailey KM, Wojtkowiak JW, Hashim AI, Gillies RJ. Targeting the metabolic microenvironment of tumors. *Adv Pharmacol.* (2012) 65:63–107. doi: 10.1016/B978-0-12-397927-8.00004-X
19. Choi SYC, Collins CC, Gout PW, Wang Y. Cancer-generated lactic acid: a regulatory, immunosuppressive metabolite. *J Pathol.* (2013) 203:350–5. doi: 10.1002/path.4218
20. Gillies RJ, Verduzco D, Gatenby RA. Evolutionary dynamics of carcinogenesis and why targeted therapy does not work. *Nat Rev Cancer.* (2012) 12:487–93. doi: 10.1038/nrc3298
21. Wojtkowiak JW, Verduzco D, Schramm KJ, Gillies RJ. Drug resistance and cellular adaptation to tumor acidic pH microenvironment. *Mol Pharm.* (2011) 8:2032–8. doi: 10.1021/mp200292c
22. Lin CY, Anders J, Johnson M, Dickson RB. Purification and characterization of a complex containing matriptase and a Kunitz-type serine protease inhibitor from human milk. *J Biol Chem.* (1999) 274:18237–42. doi: 10.1074/jbc.274.26.18237
23. Sanderson RJ, Hering MA, James SF, Sun MM, Doronina SO, Siadak AW, et al. *In vivo* drug-linker stability of an anti-CD30 dipeptide-linked auristatin immunoconjugate. *Clin Cancer Res.* (2005) 11:843–52. Available online at: http://clincancerres.aacrjournals.org/content/11/2/843
24. Zhao B, Chen R, O'Connor OA, Gopal AK, Ramchandren R, Goy A, et al. Brentuximab vedotin, an antibody–drug conjugate, in patients with CD30-positive haematologic malignancies and hepatic or renal impairment. *Br J Clin Pharmacol.* (2016) 82:696–705. doi: 10.1111/bcp.12988
25. Kreitman RJ, Wilson WH, Stetler-Stevenson M, Noel P, FitzGerald DJ, Pastan I. Long term results of BL22 (CAT-3888) in multiply relapsed hairy cell leukemia. *Blood.* (2009) 114:3442. Available online at: http://www.bloodjournal.org/content/114/22/3442
26. Alderson RF, Kreitman RJ, Chen T, Yeung P, Herbst R, Fox JA, et al. CAT-8015: a second-generation pseudomonas exotoxin A-based immunotherapy targeting CD22 -expressing hematological malignancies. *Clin Cancer Res.* (2009) 15:832–9. doi: 10.1158/1078-0432.CCR-08-1456
27. Ko CJ, Huang CC, Lin HY, Juan CP, Lan SW, Shyu HY, et al. Androgen-induced TMPRSS2 activates matriptase and promotes extracellular matrix degradation, prostate cancer cell invasion, tumor growth, and metastasis. *Cancer Res.* (2015) 75:2949–60. doi: 10.1158/0008-5472.CAN-14-3297
28. Mukai S, Yorita K, Kawagoe Y, Katayama Y, Nakahara K, Kamibeppu T, et al. Matriptase and MET are prominently expressed at the site of bone metastasis in renal cell carcinoma: immunohistochemical analysis. *Hum Cell.* (2015) 28:44–50. doi: 10.1007/s13577-014-0101-3
29. Tsai CH, Teng CH, Tu YT, Cheng TS, Wu SR, Ko CJ, et al. HAI-2 suppresses the invasive growth and metastasis of prostate cancer through regulation of matriptase. *Oncogene.* (2014) 33:4643–52. doi: 10.1038/onc.2013.41

Conflict of Interest Statement: S-YL and JRB are founders of Xiconic, LLC. ZS is an officer of Xiconic, LLC.

The remaining authors declare that the research was conducted in the absence of any commercial or financial relationships that could be construed as a potential conflict of interest.

frontiers in Oncology

ORIGINAL RESEARCH
published: 10 April 2019
doi: 10.3389/fonc.2019.00250

Nanocarriers of Fe_3O_4 as a Novel Method for Delivery of the Antineoplastic Agent Doxorubicin Into HeLa Cells *in vitro*

Kun-kun Xia[1,2†], Yong Lyu[2†], Wei-tang Yuan[2], Gui-xian Wang[2], Harrison Stratton[3], Shui-jun Zhang[1] and Jie Wu[1,3]*

[1] Department of Hepatobiliary and Pancreatic Surgery, First Affiliated Hospital of Zhengzhou University, Zhengzhou, China, [2] Department of Colon and Rectal Surgery, First Affiliated Hospital of Zhengzhou University, Zhengzhou, China, [3] Department of Neurobiology, Barrow Neurological Institute, St. Joseph's Hospital and Medical Center, Phoenix, AZ, United States

Here we report the synthesis and *in vitro* characterization of a redox-sensitive, magnetically inducible nanoparticle carrier system based on the doxorubicin (DOX) drug delivery model. Each quantal nanocarrier unit consists of a magnetite Fe_3O_4 nanoparticle core that is further encapsulated in self-assembled micelles of the redox-responsive polyethylene glycol derivative, DSPE-SS-mPEG. The nanocarrier system was prepared using a combination of ultrasonication and dialysis to produce the microenvironment sensitive delivery system. The final synthesized and DOX-loaded magnetic nanocarriers had an average size of ∼150 nm when assembled with a 6.9% DOX payload. The release rate of DOX from these redox-responsive magnetic nanocarriers was shown to be accelerated *in vitro* when in the presence of glutathione (GSH). Furthermore, we demonstrated that more redox-responsive magnetic nanocarriers could be taken up by HeLa cells when a local magnetic field was applied. Once internalized within a cell, the micelles of the outer nanocarrier complex were broken down in the presence of higher concentrations of GSH, which accelerated the release of DOX. This produces a particle with dual operating characteristics that can be controlled via a specific cellular environment coupled with an exogenously applied signal in the form of a magnetic field triggering release.

Keywords: redox-responsive, Fe_3O_4, nanocarriers, drug delivery, HeLa cells

OPEN ACCESS

Edited by:
Yan-yan Yan,
Shanxi Datong University, China

Reviewed by:
Cheng Xiao,
Xuzhou Medical University, China
Yixian Wang,
California State University,
Los Angeles, United States

****Correspondence:***
Jie Wu
jie.wu@dignityhealth.org;
jiewubni@gmail.com

† These authors have contributed equally to this work

Specialty section:
This article was submitted to Cancer Molecular Targets and Therapeutics, a section of the journal Frontiers in Oncology

Received: *28 December 2018*
Accepted: *19 March 2019*
Published: *10 April 2019*

Citation:
Xia K, Lyu Y, Yuan W, Wang G, Stratton H, Zhang S and Wu J (2019) Nanocarriers of Fe_3O_4 as a Novel Method for Delivery of the Antineoplastic Agent Doxorubicin Into HeLa Cells in vitro. Front. Oncol. 9:250. doi: 10.3389/fonc.2019.00250

INTRODUCTION

Chemotherapy is the most commonly used approach to treating cancer. Traditionally, the chemotherapeutic agents (doxorubicin, paclitaxel, etc.) are systemically delivered through intravenous injection. While this is often an effective approach and can successfully eliminate malignant cell populations, treatment-associated morbidity is often significant (1). Quite frequently this is a result of unintended action of the therapeutic agent at non-specific cellular targets causing injury to healthy somatic cells in addition to the desired effect on malignant cells (2–6). Despite this large unintended effect on healthy cells of the patient, chemotherapy remains a pillar of cancer treatment due to its efficacy, particularly when used as part of a multimodal treatment plan. At the intersection of the potency of chemotherapy as a curative agent and the extensive side effect

profile causing wide-ranging cytotoxicity lays a rationale that suggests transport of the chemotherapeutic agent directly to the tumor site, which avoids systematic exposure, may alleviate unintentional cytotoxic effects on healthy tissue. This concept has existed in the medical literature for quite some time, but only recently has progress in functionalization of mesoscopic carrier particles led to significant progress in realizing this goal. There are now several readily available preparations for a medical oncology approach to cancer treatment that utilizes nanotechnology, in the form of nanoparticle assemblies, to facilitate the transport of highly potent cytotoxic compounds more selectively into tumor sites with restricted systemic circulating concentrations (7–9). These nanoparticles can be constructed such that they resist degradation or internalization except at the target tissue of interest where they are then able to deposit and release their payload at the site of the malignancy and not in healthy tissue (10–12). These particles can also be used to focus energy from external radiative sources into tumor masses acting to physically damage the cancerous cells in addition to the chemical damage affected by the pharmacological agent (13). This is an elegant solution to the problem of how to transport chemotherapeutic drugs to the tumor site without leakage and subsequently release a drug into the tumor-specific microenvironment is an important issue that needs to be solved in the treatment of cancer. The rise of nanotechnology has provided a new set of tools for use in solving this problem of targeted drug delivery (14–17).

The use of nanoparticles as a carrier vehicle for the targeted delivery of chemotherapeutic drugs has the potential to greatly reduce collateral damage to non-cancerous human tissues and organs (18, 19). For example, by modifying the surface of a nanoparticle with intelligent molecules, the nano drug carriers can stimulate drug release in response to the particular micro-environment of pathological tissues to reduce the incidence of healthy cell damage and selectively kill cancer cells (20–22). The study of nano drug carriers provides a new direction for the delivery of care in addition to the traditional cancer treatment approaches already in use and possesses significant potential for future clinical applications (20, 23, 24). In this study, we constructed spherical nanoparticle carriers containing doxorubicin (an antineoplastic drug) with a diameter of about 150 nm. We provide functional data to demonstrate that the entry of the drug carriers into HeLa cells can be enhanced in a magnetic field and the release of the drug can be facilitated by elevating the concentration of glutathione (GSH), resulting in the demise of HeLa cells. As several cancer cells have high intracellular GSH concentrations, using the constructed nanoparticle carriers may achieve satisfying efficacy in killing cancer cells, while causing only minor damage in normal tissue (25–27).

MATERIALS AND METHODS

Materials

The Fe_3O_4 nanoparticles were prepared using a thermal decomposition method described previously (28). DSPE-SS-mPEG 2000 was purchased from Xi'an Ruixi Biotechnology Co. (Xi'an, China), Doxorubicin hydrochloride (DOX·HCl) and GSH were purchased from Sigma-Aldrich (St. Louis, MO, USA), dimethyl sulfoxide (DMSO) and triethylamine (TEA) were obtained from Shanghai Chemical Co. (Shanghai, China) (29).

Human cervical adenocarcinoma (HeLa) cells were purchased from the China Center for Type Culture Collection (Wuhan University) and cultured in Dulbecco's modified Eagle's medium (DMEM, Gibco Life, Grand Island, NY, USA) supplemented with 10% fetal bovine serum (FBS, HyClone, Logan, UT), 2×10^{-3} M L-glutamine and 1% antibiotics mixture (10,000 U of penicillin and 10 mg of streptomycin) (Gibco). The cells were incubated in a humidified atmosphere containing 5% CO_2 at 37°C.

Preparation of Nanocarriers

DOX-loaded redox-responsive magnetic nanocarriers were prepared using an ultrasonication-dialysis method. Briefly, DOX·HCl (10 mg) was stirred in DMSO (5 mL) with twice the number of mole of TEA for 2 h to obtain the DOX base. 80 mg of DSPE-SS-mPEG was added to the solution, which was stirred at room temperature for another 2 h. Meanwhile, the Fe_3O_4 nanoparticles (20 mg) were dissolved in 10 mL of (tetrahydrofuran) THF. The above two solutions were mixed and added to ultrapure water (25 mL) with ultrasonication. The mixed solution was then transferred into a dialysis tube and dialyzed against ultrapure water for 48 h at room temperature. Similarly, DOX-free nanocarriers were prepared using the above mentioned protocol without the addition of DOX.

Characterization of Nanocarriers

The size of the nanocarriers in aqueous solution was measured using a Zetasizer analyzer (Malvern Zetasizer Nano, Zen 3690+MPT2, Malvern, UK). Ultrastructural features and surface geometry of the synthesized nanocarriers was observed by transmission electron microscopy (TEM) (Tecnai G2 F20 S-TWIN electron microscope, FEI company. the USA) at an accelerating voltage of 200 kV.

DOX-loaded nanocarriers were dissolved in DMSO to determine the total content of loaded drug. The DOX content in DMSO was determined by high-performance liquid chromatography (HPLC, Agilent) using a calibration curve obtained from DOX/DMSO solutions containing a known concentration of DOX.

For Fe_3O_4 content measurement, the weighed, freeze-dried nanocarriers were digested in a 1 M HCl solution. The resulting digestion product was then analyzed for atomic species using inductively coupled plasma-atomic emission spectroscopy (TCP-AES, Thermo Electron, USA).

Redox-Triggered Disassembly of Nanocarriers

The change in the size of redox-responsive magnetic nanocarriers in response to 20 mM GSH in PBS (0.01 M, pH 7.4) was measured using dynamic light scattering (DLS). Briefly, 20 mM GSH was added to 1.5 mL of PBS containing nanocarriers within a glass cell. The solution was then placed in a shaking water bath at 37°C, oscillating at 150 rpm. At varying intervals following agitation, the size of nanocarrier particles contained in solution was assessed using DLS.

In vitro Redox-Triggered Release of DOX From DOX-Loaded Nanocarriers

The *in vitro* release profile of nanocarriers was investigated using dialysis of DOX-loaded nanocarriers in two different media: PBS or PBS supplemented with 20 mM GSH. Each solution was diluted to 1.5 mg/mL and 5 mL of the solution was transferred into a membrane tubing. The tubing with the solution was immersed in a tube containing 50 mL of the buffer solution in a shaking water bath at 37°C to acquire the "sink" condition. At predetermined intervals, 20 mL of the external buffer was withdrawn and replaced with a fresh solution of the corresponding buffer. The amount of DOX released was determined using HPLC.

Cell TEM Imaging

For TEM imaging, HeLa cells were incubated with DOX-loaded nanocarriers at a final DOX concentration of 5 μg/mL in DMEM for 2 h at 37°C in the presence or absence of an externally applied magnetic field. The culture medium was removed and the cells were pre-fixed with 2.5% glutaraldehyde in PBS at 4°C for 2 h and post-fixed with 1% osmium tetroxide in PBS at 4°C for 2 h. The cells were then dehydrated using serially increasing concentrations of ethanol and flat embedded in Epon 812. After polymerization at 60°C for 48 h, ultrathin sections (60–80 nm) were trimmed and further stained with uranyl acetate and lead citrate. Micrographs of the stained samples were collected with an FEI Tecnaio G220 TWIN Transmission Electron Microscope.

Cell Viability Assay

To evaluate the anti-tumor activity of DOX-loaded nanocarriers, the cytotoxicity of DOX-loaded nanocarriers or free DOX against HeLa cells was evaluated *in vitro* using the MTT assay. HeLa cells were seeded into a 96-well plate at a density of 4.0×10^3 cells/well in 100 μL of complete DMEM. The cells were cultured for 24 h at 37°C in a 5% CO_2 atmosphere. Subsequently, the cells were incubated with DOX-loaded nanocarriers or free DOX for 24 h at 37°C with or without the presence of an external magnetic field. DOX-loaded nanocarriers or free DOX were diluted in complete DMEM to a final DOX concentration ranging from 0.4 to 40 μg/mL. After the incubation, 10 μL of MTT solution (5 mg/mL in PBS 7.4) was added to each well and incubated for 4 h. The media with MTT solution was removed and 200 μL of DMSO was added to dissolve the formazan crystals and further incubated for 15 min at 37°C. The absorbance readings were recorded using a microplate spectrophotometer (PowerWave XS2, BioTek Instruments, USA) at a wavelength of 540 nm. The cell viability was normalized to that of cells cultured in complete DMEM. The dose-effect curves were plotted and data are presented as the average ± SD ($n = 4$).

Confocal Laser Scanning Microscopy (CLSM) Observation

CLSM was used to examine the intracellular distribution of DOX. HeLa cells were seeded on coverslips in the wells of a 24-well plate at a density of 4.0×10^4 cells/well in 1 mL of complete DMEM. The cells were incubated for 24 h at 37°C in a 5% CO_2 atmosphere. The cells were incubated with DOX-loaded nanocarriers at a final DOX concentration of 5 μg/mL in DMEM for 2 h at 37°C with or without an external magnetic field. After removal of the medium, the cells were washed three times with cold PBS, fixed with 1 mL of 4% paraformaldehyde for 30 min at 4°C, and stained with 2-(4-amidinophenyl)-6-indolecarbamidine dihydrochloride (DAPI, Roche) for 10 min. Finally, the slides were mounted with 10% glycerol solution and viewed using a LeicaTCS SP8 (Leica Microscopy Systems Ltd., Germany).

TABLE 1 | Properties of DOX-free and DOX-loaded nanocarriers.

DOX-free nanocarriers			DOX-loaded nanocarriers			
Size (nm)	PDI	Fe content (wt%)	Size (nm)	PDI	Fe content (wt%)	PLC (wt%)
131	0.26	14.7	150	0.19	13.3	4.6

RESULTS AND DISCUSSION

Characterization of Nanocarriers

The particle size and polydispersity (PDI) of DOX-free or DOX-loaded nanocarriers were determined by DLS, as shown in **Table 1**. The prepared DOX-free nanocarriers and DOX-loaded nanocarriers (**Figure 1A**) were determined to be 131 or 150 nm respectively, with a narrow size distribution, thereby making them suitable as anticancer drug carriers. The morphology of the redox-responsive magnetic nanocarriers was observed using TEM. **Figure 1B** shows the morphology of the nanocarriers. Because DSPE-SS-mPEG does not significantly attenuate electron scattering under TEM, nanocarriers are largely present as isolated clusters of Fe_3O_4 nanoparticles with a spherical shape. The drug loading content values of DOX-loaded nanocarriers was 4.6% (**Table 1**). Whereas, the Fe content of DOX-free or DOX-loaded nanocarriers was 14.7 and 13.3%, respectively (**Table 1**).

The Redox-Responsive Stability of Nanocarriers

Disulfide linkages are known to be readily reduced into free thiols in the presence of reducing agents. To demonstrate the responsiveness, the size change of redox-responsive magnetic nanocarriers in response to 20 mM GSH in PBS was measured by DLS. **Figure 2** shows that the average size of the nanocarriers gradually increased within the first 15 min after the addition of GSH. The size increased from 131 to 340 nm in 15 min, indicating the detachment of hydrophilic PEG shells from the nanocarriers and the enhanced hydrophobic interaction of the inner core. After 1 h, two populations at 547 nm and 1,038 nm were observed, however, after 3 h, the complete destruction of the nanocarriers was observed, and no nanoparticles were detected in the solution.

In vitro Redox-Responsive DOX Release

The drug release behavior of the DOX-loaded nanocarriers was investigated in PBS at 37°C in the presence or absence of

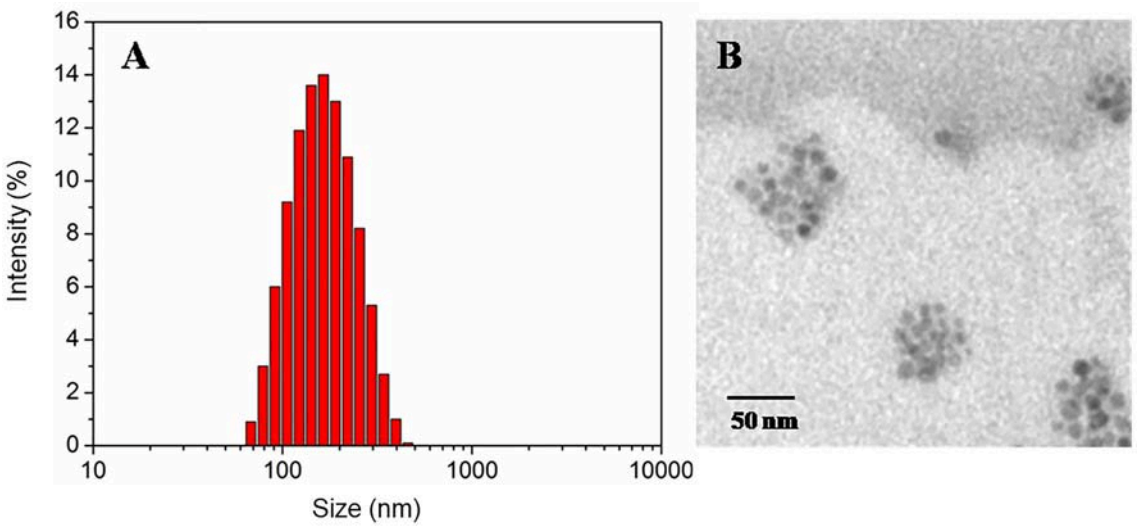

FIGURE 1 | The size distribution by DLS **(A)**, and TEM micrographs **(B)** of redox-responsive magnetic nanocarriers.

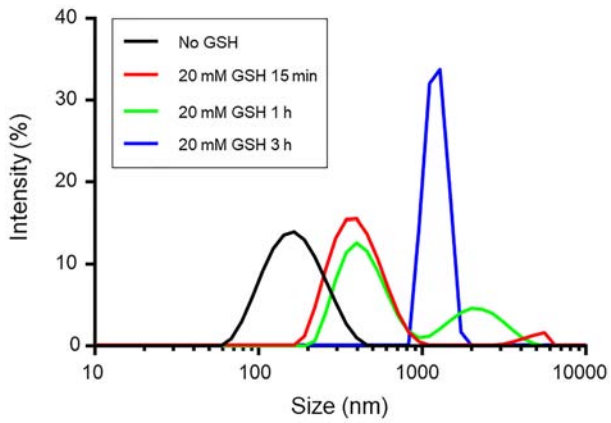

FIGURE 2 | The size change of redox-responsive magnetic nanocarriers in response to 20 mM GSH in PBS determined by DLS measurement.

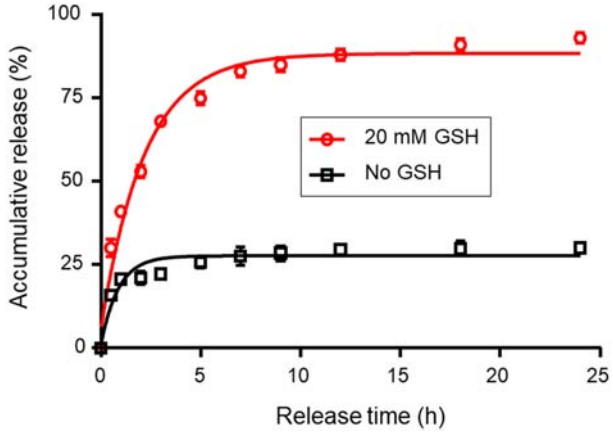

FIGURE 3 | Redox-triggered release of DOX from redox-responsive magnetic nanocarriers in PBS with or without 20 mM GSH. The standard deviation for each data point was averaged over three samples ($n = 3$).

GSH (20 mM). **Figure 3** shows the accumulative drug release profiles as a function of time. **Figure 3** demonstrates that the release of DOX from nanocarriers was markedly correlated with the presence or absence of GSH. The release of DOX from nanocarriers was accelerated by the addition of GSH to the media. In the presence of 20 mM GSH, nanocarriers rapidly released DOX, such that 93.8% of the DOX dose was released within 24 h. However, only 28.7% of DOX was released in the absence of GSH. This difference might be due to cleavage of disulfide bonds, thereby causing the destruction of the nanocarriers and the accelerated release of encapsulated DOX.

Cell TEM Imaging

The rapid accumulation of DOX-loaded nanocarriers was found to be magnetically inducible *in vitro* and was characterized using TEM. When HeLa cells were incubated for 2 h with DOX-loaded nanocarriers in either the presence or absence of a magnetic field, the accumulation of nanocarriers was found to be altered. TEM images demonstrating this observation are shown in **Figure 4**. The heavily electro-dense iron-containing nanoparticles are reproduced in the TEM images as a significantly darker region in contrast to the cellular environment, which facilitated identification of relative particle density between groups. The number of magnetic nanoparticles in cells significantly increased when a magnetic field was applied (**Figure 4B**), suggesting that the presence of a magnetic field enhanced the accumulation of nanocarriers in cells.

Cell Viability Assay

The *in vitro* cytotoxicity of DOX-loaded nanocarriers and free DOX was evaluated using the MTT assay. **Figure 5** shows the

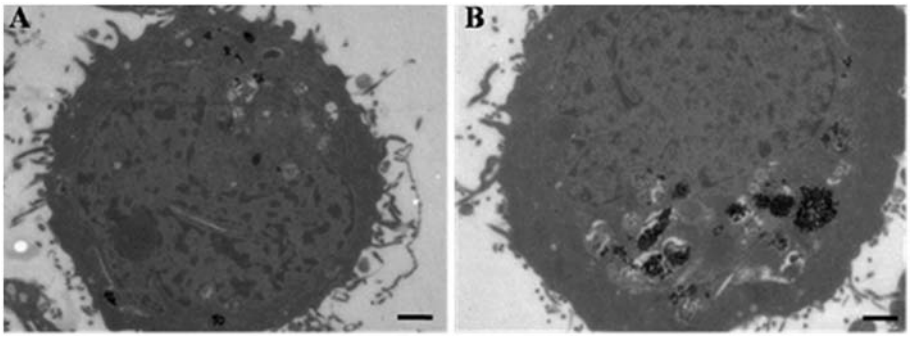

FIGURE 4 | TEM images of HeLa cells incubated with DOX-loaded nanocarriers in the absence **(A)** or presence **(B)** of a magnetic field. Scale bar is 1 μm.

resulting levels of observed cytotoxicity measured as a function of DOX concentration from 0.4 to 40 μg/mL. All test conditions exhibited a dose-dependent cytotoxic effect of the treatment on the population of viable and metabolically active HeLa cells. DOX-loaded nanocarriers exhibited lower cytotoxicity to HeLa cells with or without the magnetic field, as compared to free DOX at the same DOX dose (**Figure 5A**). As a control experiment, we performed a group of experiments using nanocarriers without DOX and examined cytotoxicity under magnetic and non-magnetic conditions, suggesting that the nanocarriers alone did not exhibit cytotoxicity (**Figure 5B**). Given that DOX is a small molecule, it can be quickly transported into cells and enter nuclei by passive diffusion. Furthermore, we found that the presence of a local magnetic field could significantly increase the cytotoxicity of DOX-loaded nanocarriers. This process may be due to the magnetic field increasing cellular uptake of nanocarriers, and once internalized, the redox-responsive nanocarriers are destroyed by high levels of GSH. The DOX is then rapidly released from the destroyed redox-responsive nanocarriers. Taken together these results indicate that the DOX-loaded nanocarriers can achieve both magnetic targeting and reduction-sensitive release simultaneously.

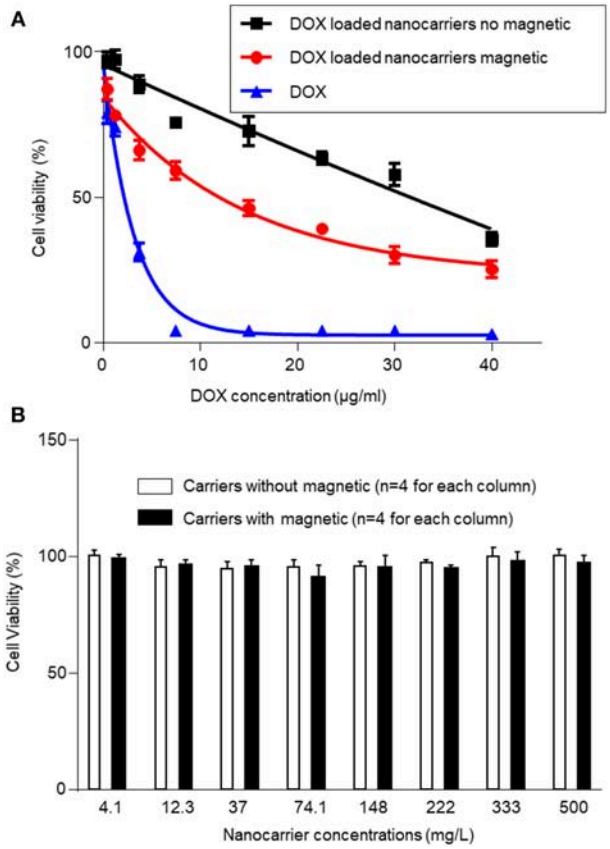

FIGURE 5 | Cytotoxicity of DOX-loaded magnetic nanocarriers and free DOX in HeLa cells with or without magnetic field after incubation for 24 h **(A)**. **(B)** In control experiments, we examined cytotoxicity using magnetic nanocarriers alone with or without magnetic field after incubation for 24 h, and found no cytotoxicity. The standard deviation for each data point was averaged over four samples ($n = 4$) for **(A,B)**.

In vitro Cellular Uptake of DOX-Loaded Nanocarriers

The cellular uptake of the nanocarriers and the intracellular location of the encapsulated DOX was monitored by CLSM in HeLa cells. The nuclei of HeLa cells were stained with DAPI, which presented blue fluorescence to distinguish from the red fluorescence of the labeled DOX. **Figure 6** shows CLSM images of HeLa cells incubated with DOX-loaded nanocarriers for 2 h with or without magnet field treatment. As shown in **Figure 6**, we found that cells incubated with DOX-loaded nanocarriers with applied magnetic field demonstrated stronger DOX fluorescence compared to no applied magnetic field. This phenomenon is primarily a result of the magnetic field increase in the cellular uptake of the DOX-loaded nanocarriers. Our results indicate that these nanocarriers are responsive to either magnetic or redox stimulated activation and are therefore suitable for application as anticancer drug carriers.

CONCLUSION

In this article, we use the amphiphilic copolymer DSPE-SS-mPEG, which is connected by disulfide bonds. Afterward, the

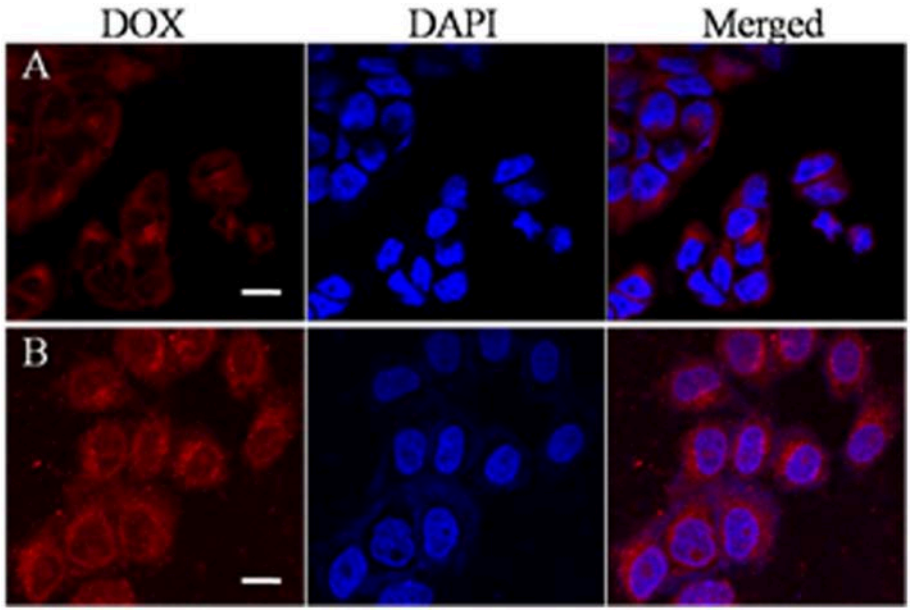

FIGURE 6 | CLSM images of HeLa cells after treatment with DOX-loaded magnetic nanocarriers for 2 h in the absence **(A)** or presence **(B)** of a magnetic field. Scale bar is 15 μm.

magnetic Fe_3O_4 nanoparticles and the hydrophobic drug are made by the self-assembly of the amphiphilic copolymer. DOX is encapsulated in the amphiphilic copolymer to form a magnetic nano drug controlled release system which is sensitive and responds to a reducing environment. This controlled release system can dissociate the disulfide bonds in the presence of dithiothreitol, thereby triggering the release system to disintegrate and expel the drug.

When the DOX-loaded nanocarrier is transported into the cell, intracellular GSH breaks the disulfide bonds, resulting in the disintegration of the transport system and the release of DOX. It is a well-designed enzyme-responsive magnetic-field controlled release system and provides a new foundation for building an efficient and safe nanoscale drug delivery system.

AUTHOR CONTRIBUTIONS

KX and YL equally contributed to this work, conducted the experiments, analyzed data, prepared original figures, and revised the manuscript. WY and GW participated in experimental design, analyzed the data, and revised the manuscript. HS analyzed the data and revised the manuscript. SZ designed the experiments and revised the manuscript. JW designed the experiments and analyzed the data, finalized the figures, and wrote the manuscript.

ACKNOWLEDGMENTS

This work was supported by the Science and Technology Department of Henan Province (Grant # 192102310411) and the Education Department of Henan Province (Grant # 19A320043).

REFERENCES

1. Yasui H. Safe handling of cancer chemotherapy drugs. *Gan to kagaku ryoho Cancer Chemother.* (2016) 43:503–8.
2. Paez JG, Jänne PA, Lee JC, Tracy S, Greulich H, Gabriel S, et al. EGFR mutations in lung cancer: correlation with clinical response to gefitinib therapy. *J Sci.* (2004) 304:1497–500. doi: 10.1126/science.1099314
3. Kerr JF, Winterford CM, Harmon BV. Apoptosis. Its significance in cancer and cancer therapy. *J Cancer.* (1994) 73:2013–26. doi: 10.1002/1097-0142(19940415)73:8<2013::AID-CNCR2820730802>3.0.CO;2-J
4. Wang CY, Mayo MW, Baldwin AS. TNF-and cancer therapy-induced apoptosis: potentiation by inhibition of NF-κB. *J Sci.* (1996) 274:784–7. doi: 10.1126/science.274.5288.784
5. Lowe SW, Bodis S, McClatchey A, Remington L, Ruley HE, Fisher DE, et al. p53 status and the efficacy of cancer therapy *in vivo*. *J Sci.* (1994) 266:807–10. doi: 10.1126/science.7973635
6. Brown JM, Giaccia AJ. The unique physiology of solid tumors: opportunities (and problems) for cancer therapy. *J Cancer Res.* (1998) 58:1408–16.
7. Anselmo AC, Mitragotri S. Nanoparticles in the clinic. *Bioeng Transl Med.* (2016) 1:10–29. doi: 10.1002/btm2.10003
8. Wicki A, Witzigmann D, Balasubramanian V, Huwyler J. Nanomedicine in cancer therapy: challenges, opportunities, and clinical applications. *J Control Release.* (2015) 200:138–57. doi: 10.1016/j.jconrel.2014.12.030
9. Mi Y, Wolfram J, Mu C, Liu X, Blanco E, Shen H, et al. Enzyme-responsive multistage vector for drug delivery to tumor tissue. *Pharmacol Res.* (2016) 113(Pt A):92–9. doi: 10.1016/j.phrs.2016.08.024
10. Bigall NC, Curcio A, Leal MP, Falqui A, Palumberi D, Di Corato R, et al. Magnetic nanocarriers with tunable pH dependence for controlled loading and release of cationic and anionic payloads. *Adv Mater.* (2011) 23:5645–50. doi: 10.1002/adma.201103505
11. Nagaoka H, Sato Y, Xie X, Hata H, Eguchi M, Sakurai N, et al. Coupling stimuli-responsive magnetic nanoparticles with antibody-antigen

detection in immunoassays. *Anal Chem.* (2011) 83:9197–200. doi: 10.1021/ac201814n
12. Ruan G, Vieira G, Henighan T, Chen A, Thakur D, Sooryakumar R, et al. Simultaneous magnetic manipulation and fluorescent tracking of multiple individual hybrid nanostructures. *Nano Lett.* (2010) 10:2220–4. doi: 10.1021/nl1011855
13. Jain S, Hirst DG, O'Sullivan JM. Gold nanoparticles as novel agents for cancer therapy. *Br J Radiol.* (2012) 85:101–13. doi: 10.1259/bjr/59448833
14. Ferrari M. Cancer nanotechnology: opportunities and challenges. *J. Nat Rev Cancer.* (2005) 5:161–71. doi: 10.1038/nrc1566
15. Farokhzad OC, Langer R. Nanomedicine: developing smarter therapeutic and diagnostic modalities. *J Adv Drug Del Rev.* (2006) 58:1456–9. doi: 10.1016/j.addr.2006.09.011
16. Riehemann K, Schneider SW, Luger TA, Godin B, Ferrari M, Fuchs H. Nanomedicine? challenge and perspectives. *J Angewandte Chemie Int Edn.* (2009) 48:872–97. doi: 10.1002/anie.200802585
17. Peer D, Karp JM, Hong S, Farokhzad OC, Margalit R, Langer R. Nanocarriers as an emerging platform for cancer therapy. *J Nat Nanotechnol.* (2007) 2:751–60. doi: 10.1038/nnano.2007.387
18. Xu R, Zhang G, Mai J, Deng X, Segura-Ibarra V, Wu S, et al. An injectable nanoparticle generator enhances delivery of cancer therapeutics. *Nat Biotechnol.* (2016) 34:414–8. doi: 10.1038/nbt.3506
19. Lucky SS, Idris NM, Huang K, Kim J, Li Z, Thong PS, et al. *In vivo* Biocompatibility, biodistribution and therapeutic efficiency of titania coated upconversion nanoparticles for photodynamic therapy of solid oral cancers. *Theranostics.* (2016) 6:1844–65. doi: 10.7150/thno.15088
20. von Maltzahn G, Park JH, Lin KY, Singh N, Schwoppe C, Mesters R, et al. Nanoparticles that communicate *in vivo* to amplify tumour targeting. *Nat Mater.* (2011) 10:545–52. doi: 10.1038/nmat3049
21. Sun S, Murray CB, Weller D, Folks L, Moser A. Monodisperse FePt nanoparticles and ferromagnetic FePt nanocrystal superlattices. *Science.* (2000) 287:1989–92. doi: 10.1126/science.287.5460.1989
22. Gao W, Kagan D, Pak OS, Clawson C, Campuzano S, Chuluun-Erdene E, et al. Cargo-towing fuel-free magnetic nanoswimmers for targeted drug delivery. *Small.* (2012) 8:460–7. doi: 10.1002/smll.201101909
23. Jain RK, Stylianopoulos T. Delivering nanomedicine to solid tumors. *J Nat Rev Clin Oncol.* (2010) 7:653–64. doi: 10.1038/nrclinonc.2010.139
24. Farokhzad OC, Langer R. Impact of nanotechnology on drug delivery. *J ACS Nano.* (2009) 3:16–20. doi: 10.1021/nn900002m
25. Hong R, Han G, Fernandez JM, Kim BJ, Forbes NS, Rotello VM. Glutathione-mediated delivery and release using monolayer protected nanoparticle carriers. *J Am Chem Soc.* (2006) 128:1078–9. doi: 10.1021/ja056726i
26. Chong SF, Chandrawati R, Stadler B, Park J, Cho J, Wang Y, et al. Stabilization of polymer-hydrogel capsules via thiol-disulfide exchange. *Small.* (2009) 5:2601–10. doi: 10.1002/smll.200900906
27. Jones DP, Carlson JL, Samiec PS, Sternberg P, Jr, Mody VC Jr, Reed RL, et al. Glutathione measurement in human plasma. Evaluation of sample collection, storage and derivatization conditions for analysis of dansyl derivatives by HPLC. *Clin Chim Acta.* (1998) 275:175–84.
28. Park J, An K, Hwang Y, Park JG, Noh HJ, Kim JY, et al. Ultra-large-scale syntheses of monodisperse nanocrystals. *J Nat Mater.* (2004) 3:891–5. doi: 10.1038/nmat1251
29. Xu ZC, Shen CM, Hou YL, Gao HJ, Sun SH. Oleylamine as both reducing agent and stabilizer in a facile synthesis of magnetite nanoparticles. *Chem Mater.* (2009) 21:1778–80. doi: 10.1021/cm802978z

Conflict of Interest Statement: The authors declare that the research was conducted in the absence of any commercial or financial relationships that could be construed as a potential conflict of interest.

frontiers in Oncology

PERSPECTIVE
published: 16 April 2019
doi: 10.3389/fonc.2019.00263

Identification of Genetic Mutations in Cancer: Challenge and Opportunity in the New Era of Targeted Therapy

Jing Jin[1†], Xu Wu[2,3†], Jianhua Yin[2,3], Mingxing Li[2,3], Jing Shen[2,3], Jing Li[4], Yueshui Zhao[2,3], Qijie Zhao[2,3], Jingbo Wu[1], Qinglian Wen[1], Chi Hin Cho[2,3], Tao Yi[5], Zhangang Xiao[2]* and Liping Qu[6]*

[1] Department of Oncology, The Affiliated Hospital of Southwest Medical University, Southwest Medical University, Luzhou, China, [2] Laboratory of Molecular Pharmacology, Department of Pharmacology, School of Pharmacy, Southwest Medical University, Luzhou, China, [3] South Sichuan Institute of Translational Medicine, Luzhou, China, [4] Department of Oncology and Hematology, Hospital (T.C.M) Affiliated to Southwest Medical University, Luzhou, China, [5] School of Chinese Medicine, Hong Kong Baptist University, Hong Kong, China, [6] College of Pharmacy, Chengdu University of Traditional Chinese Medicine, Chengdu, China

OPEN ACCESS

Edited by:
Yan-yan Yan,
Shanxi Datong University, China

Reviewed by:
Shengpeng Wang,
University of Macau, China
Maria Munoz Caffarel,
Biodonostia Health Research Institute, Spain
Tinghong Ye,
Sichuan University, China

***Correspondence:**
Tao Yi
yitao@hkbu.edu.hk
Zhangang Xiao
xzg555898@hotmail.com

[†]These authors have contributed equally to the work

Specialty section:
This article was submitted to Cancer Molecular Targets and Therapeutics, a section of the journal Frontiers in Oncology

Received: 25 January 2019
Accepted: 22 March 2019
Published: 16 April 2019

Citation:
Jin J, Wu X, Yin J, Li M, Shen J, Li J, Zhao Y, Zhao Q, Wu J, Wen Q, Cho CH, Yi T, Xiao Z and Qu L (2019) Identification of Genetic Mutations in Cancer: Challenge and Opportunity in the New Era of Targeted Therapy. Front. Oncol. 9:263. doi: 10.3389/fonc.2019.00263

The introduction of targeted therapy is the biggest success in the treatment of cancer in the past few decades. However, heterogeneous cancer is characterized by diverse molecular alterations as well as multiple clinical profiles. Specific genetic mutations in cancer therapy targets may increase drug sensitivity, or more frequently result in therapeutic resistance. In the past 3 years, several novel targeted therapies have been approved for cancer treatment, including drugs with new targets (i.e., anti-PD1/PDL1 therapies and CDK4/6 inhibitors), mutation targeting drugs (i.e., the EGFR T790M targeting osimertinib), drugs with multiple targets (i.e., the EGFR/HER2 dual inhibitor neratinib) and drug combinations (i.e., encorafenib/binimetinib and dabrafenib/trametinib). In this perspective, we focus on the most up-to-date knowledge of targeted therapy and describe how genetic mutations influence the sensitivity of targeted therapy, highlighting the challenges faced within this era of precision medicine. Moreover, the strategies that deal with mutation-driven resistance are further discussed. Advances in these areas would allow for more targeted and effective therapeutic options for cancer patients.

Keywords: targeted therapy, cyclin-dependent kinases 4/6, somatic mutation, resistance, EGFR, PD-1/PD-L1

INTRODUCTION

Targeted therapies usually present with high selectivity, target precisely to specific gene or protein, and exert a biological function with minimal side effects (1), which has distinguished them from most conventional non-specific chemotherapeutic drugs. Targeted therapy has thus been regarded as the biggest success in the treatment of cancer in the past few decades. Many novel promising agents have been experimentally designed and developed and are increasingly entering clinical evaluation. However, the frequently observed alterations in the drug targets have posed a big challenge to successful cancer treatment. Genetic mutations in cancer are resulted from both inherited and environmental factors. In a recent report, it is demonstrated that a large proportion of cancer-related mutations

are due to randomized DNA replication errors (2). Notably, the mutations in cancer therapy targets can greatly affect drug sensitivity. Mutation-driven drug resistance is very common in cancer. The efficacy of targeted therapy is thus largely dependent on the mutation profile of tumors in patients. Accurate molecular and genetic profiling of tumor cells is becoming a routine practice before the introduction of targeted therapy in patients.

In recent years, great progress has been made in targeted therapy discovery. Notably, many new drugs are designed primarily based on specific genetic background. For instance, nearly 40–50% of metastatic cutaneous melanoma possess v-raf murine sarcoma viral oncogene homolog B1 (BRAF) mutations (3), and ∼90% of these BRAF mutations are caused by substitution of glutamic acid for valine at codon 600 (V600E) (4). Two selective BRAF inhibitors vemurafenib and dabrafenib were approved for the treatment of patients with BRAF-V600E mutation, showing improved progression-free survival (5). In November 2018, the U.S. Food and Drug Administration (FDA) approved an inhibitor of tropomyosin receptor kinases (TRKs), larotrectinib, for treatment of any type of solid tumors with TRK gene fusion (6). This is the second targeted therapy approved not for specific cancer types but for any cancers with specific mutations. Targeted therapies are becoming more precise.

In this perspective, we focus on the updated knowledge of targeted therapy in the last 3 years and describe how genetic mutations influence sensitivity of targeted therapy, highlighting the challenges faced within this era of precision medicine. Moreover, the strategies dealing with mutation-driven resistance are further discussed.

INFLUENCE OF GENETIC MUTATION ON SENSITIVITY OF TARGETED THERAPY

It is well-acknowledged that mutations in therapeutic targets can increase or decrease drug sensitivity (**Table 1**). The main challenge of targeted therapy today is the identification of particular cancer mutations which affect efficacy of targeted therapies as well as the identification of a specific group of patients most likely or unlikely to respond to certain targeted therapies. Despite the great challenges, in the last 3 years, we have seen significant progress in targeted therapy (**Table 2**), largely owing to the rise of large-scale sequencing technology and big data analysis. Several novel targets, including the programmed death-1/programmed death-ligand 1 (PD1/PDL1) and cyclin-dependent kinases 4 and 6 (CDK4/6), have been validated, with several new targeted drugs being approved. Some newly approved drugs are directly designed to deal with some known activating mutations, such as the T790M mutation in epidermal growth factor receptor (EGFR). Moreover, many new findings have been added to our knowledge of how mutations influence targeted therapies [e.g., the inhibitors of human epidermal growth factor receptor 2 (HER2) and anaplastic lymphoma kinase (ALK)]. Here, based on the most updated research in the last 3 years, we summarize the recent advances of several targeted therapies.

Anti-PD1/PDL1 Therapies

So far, there are a total of 6 anti-PD1/PDL1 therapies that have been approved by the FDA. Notably, in 2017, a PD1 antibody pembrolizumab was approved for the treatment of any solid tumor with a mismatch repair deficiency or a microsatellite instability. Monotherapy of PD1/PDL1 blockade has received great success in many types of cancers (21, 22). However, there are certain patients that are gradually developing resistance after an initial response (23). Mutation-driven resistance of anti-PD1/PDL1 therapies has recently been studied in a small number of cancer patients. Zaretsky et al. reported that mutations of JAK1/JAK2 led to the desensitization of cancer cells to IFN-γ and contributed to an acquired resistance of pembrolizumab in patients with melanoma (23). Moreover, in one resistant patient, a frame-shift deletion in exon 1 of the β-2-microglobulin was detected, which may result in the loss of expression of surface the MHC class I (23). More studies are advocated to explore the acquired resistance of immune checkpoint inhibitors.

Resistance of CDK4/6 Inhibitors

Currently, three CDK 4/6 selective targeting inhibitors, palbociclib, ribociclib, and abemaciclib have been approved to treat breast cancer. CDK4/6 inhibitors are increasingly used in clinical settings, but patients eventually show disease progression and the major reasons remain unclear (24). Dysregulation of cyclin D1-CDK4/6-retinoblastoma (Rb) pathway has been implicated in hormone receptor positive (HR^+) breast cancer and in chemotherapeutic drug-resistance. Rb is usually intact in HR^+ breast cancer and is important for the efficacy of CDK4/6-inhibitors in the treatment of breast cancer (25). It is indicated that T47D cells that become resistant to CDK4/6 inhibitors, develop CCNE1 amplification or Rb1 loss (26). Moreover, the acquisition of multiple *de novo* somatic Rb1 mutations in metastatic breast cancer patients may result in the emergence of a resistance to CDK 4/6 inhibitors (24). Until now, there has been no report on CDK4/6 mutations in cancer patients and their effect on efficacy of CDK4/6 inhibitors.

EGFR and Different Generation of Tyrosine Kinase Inhibitors (TKIs)

EGFR is a prevalent target in several human cancers, such as lung, breast, colorectal, thyroid, and melanoma cancer. In lung cancer, several generations of small-molecular inhibitors have been developed to target the EGFR tyrosine kinases (27), such as inhibitors gefitinib, erlotinib, osimertinib, and necitumumab. The EGFR mutation in non-small cell lung cancer (NSCLC) was first identified in 2004, and the major missense and deletion mutation of EGFR in NSCLC occurs in the tyrosine kinase-coding domain in exons 18–21 (28). The L858R mutation in the exon 21 and exon-19 frame deletion are the most commonly detected mutation types of EGFR, representing 50 and 40% of tumor patients, respectively (7). These two types of mutations are sensitive to EGFR tyrosine kinase inhibitors (TKIs) in NSCLC. The first-generation TKIs, gefitinib and erlotinib,

TABLE 1 | Therapeutic response of targeted therapy in mutant cancers.

Drugs	Sensitivity	Target mutations	Cancer types	Reference
Gefitinib	+	EGFR-L858R	Lung cancer	(7)
Erlotinib	+	EGFR-L858R	Lung cancer	(7)
Gefitinib	–	EGFR-T789M	Lung cancer	(8)
Osimertinib	+	EGFR-T790M	Lung cancer	(9)
Osimertinib	–	EGFR-L718Q	Lung cancer	(10)
Trastuzumab	–	HER2-A859T, -G776L	Lung cancer	(11)
Afatinib	+	HER2-p.Tyr772_Ala775dup	Lung cancer	(12)
Neratinib	–	HER2-T798I, -L869R	Breast cancer	(13)
Lapatinib	–	HER2-T798M	Breast cancer	(14)
Trastuzumab	–	HER2-T798M	Breast cancer	(14)
Neratinib	+	HER2-S310, -L755, -V777, -G778_P780dup, and -Y772_A775dup	Breast, cervical and biliary cancers	(15)
Crizotinib	–	ALK-C1156Y, -L1196M	Lung cancer	(16, 17)
Lorlatinib	–	ALK-L1198F	Lung cancer	(18)
2,4-Pyrimidinediamine derivative	–	EML4-ALK-C1156Y, -L1196M	Lung cancer	(19)
TAE684	–	EML4-ALK-L1152R	Lung cancer	(20)
Dabrafenib	+	BRAF-V600E	Melanoma	(5)

TABLE 2 | Cancer targeted therapy approved by FDA in 2017 and 2018.

Drugs	Targets	Cancer types
Pembrolizumab (2017)	PD-1	Solid tumor with mismatch repair deficiency or microsatellite instability
Cemiplimab (2018)	PD-1	Squamous cell carcinoma
Durvalumab (2017)	PD-L1	Urothelial carcinoma
Avelumab (2017)	PD-L1	Merkel cell carcinoma, urothelial carcinoma
Brigatinib (2018)	ALK	ALK-positive NSCLC
Lorlatinib (2018)	ALK	ALK-positive NSCLC
Ribociclib (2017)	CDK4/6	Breast cancer
Abemaciclib (2017)	CDK4/6	Breast cancer
Niraparib (2017)	PARP	Ovarian cancer, peritoneal cancer
Dacomitinib (2018)	EGFR	NSCLC with EGFR exon 19 deletion or exon 21 L858R substitution mutations
Talazoparib (2018)	PARP	Breast cancer with germline BRCA mutations
Duvelisib (2018)	PI3Kδ, PI3Kγ	Chronic lymphocytic leukemia, small lymphocytic lymphoma
Larotrectinib (2018)	TRKs	Solid tumor with TRK gene fusion
Neratinib (2017)	EGFR/HER2	HER2-amplified breast cancer

have a high selective inhibitory activity against both wild-types and these sensitive mutant EGFR (29). Previous studies show that gefitinib and erlotinib are important for the first-line treatment of NSCLC patients with the sensitive EGFR mutations (30, 31). On the other hand, another mutation T790M, a secondary EGFR mutation emerging in NSCLC, can lead to the resistance of more than half of patients' TKIs treatment (32). Very recently, the third-generation TKI inhibitor osimertinib has been approved to effectively target to EGFR T790M mutation with a response rate of 61% in NSCLC, significantly extending the overall survival in patients with the T790M mutation (9). However, the further mutation of a residue in the P-loop (L718Q) has been found to cause resistance to osimertinib (10). Nevertheless, though diverse EGFR mutations are present, the overall survival of lung cancer patients is markedly improved with TKI therapy.

HER2 and Its Inhibitors

In breast cancer, the overall HER2 mutation rate is ∼1.6% (25 out of 1,499 patients). In a study by Bose et al., seven HER2 somatic mutations including G309A, D769H, D769Y, V777L, P780ins, V842I, and R896C, have been identified as activating mutations (33). Several patients with HER2 activating mutations are resistant to the reversible HER2 inhibitor lapatinib, but sensitive to the irreversible HER2 inhibitor neratinib. Neratinib as a dual inhibitor of HER2 and EGFR was approved by FDA in 2017. It has been shown that the HER2 L755S mutation results in an acquired resistance to lapatinib in breast cancer, which could be overcome by the neratinib (34). In another study, the HER2-T798I gatekeeper mutation in breast cancer patients with a AHER2-L869R mutation was identified as a mechanism of acquired resistance to neratinib (13). The trial of neratinib has also been conducted in colorectal cancer

(CRC) patients. The HER2 gene amplification and mutation in CRC can lead to the resistance of EGFR-targeted therapies cetuximab and panitumumab (35, 36). A negative effect of neratinib monotherapy has recently been confirmed in 12 CRC patients with different tumors harboring HER2 mutations (15). There were no positive therapeutic response and the median PFS was only 1.8 months, indicating that monotherapy with neratinib is ineffective. The underlying mechanisms still require further investigations.

ALK and Different Generation of ALK Inhibitors

ALK has long been identified as a therapeutic target in cancer. The first ALK inhibitor crizotinib was approved by the FDA in 2011 (37). Although most NSCLC patients respond to this drug, tumors become resistant after 1–2 years of treatment. Around 1/3 of crizotinib-resistant tumors harbor mutations within the ALK kinase domain. The most commonly observed mutations of L1196M and G1269A lead to a decreased affinity for crizotinib (38). Other ALK point mutations, such as L1152R, C1156Y, I1171T, F1174L, G1202R, and S1206Y, are also associated with crizotinib resistance (39). Another oncoprotein of fusion-type tyrosine kinase, the EML4-ALK, results from the inversion within the short arm of the human chromosome 2 in 4–5% of cases of NSCLC (40). Two mutations of EML4-ALK, C1156Y, and L1196M, confer a significant resistance to ALK inhibitors, such as crizotinib and PDD (2,4-pyrimidinediamine derivative) (19). The EML4-ALK C1156Y mutation can contribute to a higher resistance to PDD than those in the L1196M mutant form. It is reported that a candidate ALK inhibitor TAE684 can bind to these mutant kinases, which may have potency in overcoming the mutation-driven resistance (41). The new generation ALK inhibitors lorlatinib and brigatinib were approved in 2018 for the treatment of patients with ALK-rearranged NSCLC. Lorlatinib has been demonstrated to inhibit resistant ALK mutations, including ALK G1202R (16). However, Shaw et al. showed that an ALK L1198F mutation together with the C1156Y mutation results in the resistance of lorlatinib in a patient with metastatic ALK-rearranged NSCLC (18). However, the L1198F mutation re-sensitized crizotinib treatment of a resistant tumor. It was demonstrated that both lorlatinib and brigatinib can overcome crizotinib resistance in NSCLC patients (42, 43). Moreover, when brigatinib was combined with anti-EGFR antibody, it was effective against EGFR triple-mutant cells *in vitro* and *in vivo* (44).

STRATEGIES FOR OVERCOMING MUTATION-DRIVEN RESISTANCE

Mutations in cancer therapy targets usually result in the loss of functions and the accumulation of dysfunctional proteins in tumors (45). Moreover, many mutants have oncogenic gain-of-function (GOF) activities including increased tumor proliferation, metastasis and drug resistance (46). Notably, tumor cells that receive targeted therapy may lead to an overactivation of the by-pass signaling pathways to develop resistance. In most cases, multiple alterations are observed in a resistant tumor.

Recently, many strategies dealing with mutation-driven drug resistance have been proposed and evaluated both experimentally and clinically. The traditional chemotherapy concept of "one ligand to one receptor" for a biological response is inadequate. The treatment of a particular type of cancer with the prescriptive drugs involves many special genes, interacting with their respective targets and triggering a series of biological responses. The concept of using multi-drug therapy and seeking multifunctional compounds that can efficiently interact with various targets might be feasible (47). Currently, to overcome mutation-driven drug resistance, the main strategies include: (1) the design of new mutation-targeted compounds to restore wide-type protein activities, to delete mutants or to influence downstream targets; (2) the application of combinational therapy or new compounds for multiple targeting. Here, we give some examples of how to overcome mutation-driven resistance of targeted therapy.

Dacomitinib, an Irreversible Pan-ERBB Inhibitor, Targeting EGFR Activating Mutants

Recently, dacomitinib was approved to use for metastatic NSCLC with EGFR exon 19 deletion or exon 21 L858R substitution mutations. In a randomized, multicenter, open-label, phase III trial (ARCHER 1050), the patients with newly diagnosed advanced NSCLC and one EGFR mutation (exon 19 deletion or L858R) received a 45 mg/day dose of oral dacomitinib or a 250 mg/day gefitinib for 28 days. In the dacomitinib group, the progression-free survival (14.7 months, 95% CI 11.1–16.6) was significantly longer than that in the gefitinib group (9.2 months, 95% CI 9.1–11.0) (48). This investigation supports the dacomitinib as the first line therapy for EGFR-mutation NSCLC patients.

Dacomitinib is initially designed for irreversible pan-ERBB inhibition. As a small-molecule covalent binding inhibitor of enzymatically active HER family tyrosine kinases EGFR and HER2, it may act as a potent inhibitor of EGFR T790M mutation (49). Additionally, dacomitinib significantly inhibits both wild-type and the gefitinib-resistant ERBB2 mutation in lung cancer. Based on an in-depth investigation, dacomitinib is an effective drug that may treat NSCLC patients with a T790M-related acquired resistance to gefitinib or erlotinib (8). It has been indicated that dacomitinib significantly improves progression-free survival in EGFR-mutation NSCLC patients and is considered as a new treatment option for this population.

Encorafenib/Binimetinib and Dabrafenib/Trametinib for Dual Inhibition of BRAF and MEK

The FDA approved dabrafenib plus trametinib for the anaplastic thyroid cancer (ATC) with BRAF-V600E mutation in May 2018, as well as for the adjuvant treatment of BRAF V600E/K-mutated melanoma in April 2018. Previous studies revealed that dabrafenib plus trametinib have shown substantial antitumor activity in patients with previously treated BRAF-V600E mutated metastatic NSCLC and untreated BRAFV-600E mutated NSCLC (50, 51). Trametinib is an orally administered MEK1/MEK2

inhibitor that suppresses RAF-dependent MEK phosphorylation and persistently inhibits phosphorylated ERK (a substrate of MEK) (52). Dabrafenib is a reversible and high-efficiency ATP-competitive inhibitor of RAF kinases, especially the mutant BRAF (53). Subbiah et al. reported that the overall response rate of dabrafenib plus trametinib applied in BRAF V600E-mutated ATC (complete reaction plus partial reaction to the best overall response) is 69% (54). In contrast to BRAF inhibitor monotherapy, it has longer progression-free survival and overall survival. Overall, the most common adverse events include fatigue, pyrexia and nausea (54), consistent with previous reports in advanced or metastatic melanoma and NSCLC (50). Dabrafenib plus trametinib is the first regimen approved to have significant clinical efficacy in BRAF V600E-mutated ATC.

In June 2018, the FDA approved the combination of BRAF inhibitor encorafenib and the MEK inhibitor binimetinib for treatment of patients with unresectable or metastatic melanoma with a BRAF-V600E or -V600K mutation. It is the third BRAF/MEK inhibitor combination approved following the dabrafenib/trametinib and vemurafenib/cobimetinib combinations (55). The main adverse events for encorafenib plus binimetinib when applied to BRAF-V600 mutant melanoma are gastrointestinal reactions, including nausea, diarrhea and vomiting. Additionally, this combination has a lower calorific value and photosensitivity than other available BRAF-MEK inhibitor combinations do (56). Considerable evidence supports that the median progression-free survival was 14.9 months with encorafenib plus binimetinib, compared with 7.3 months with vemurafenib (57). Therefore, it is an effective therapeutic option in patients with unresectable or metastatic melanoma, with a BRAF V600E or V600K mutation.

CONCLUSIONS

In the new era of targeted therapy, treatment options are increasingly based on the precise molecular and genetic profiling of tumor cells (58). Currently, the main challenge for further novel drug development in targeted therapy is the clarification of specific molecular mechanisms underlying the varied forms of tumors in clinic. It has been acknowledged that cancer is caused by a set of driver mutations. In this regard, it is of great significance to: (1) identify and validate key mutant genes and proteins in cancers as new targets; (2) identify patients most likely and unlikely to benefit from certain targeted therapies; (3) evaluate the mechanism of mutation-driven drug resistance. In past decades, several key mutations which influence drug sensitivity have been identified in various cancers. In order to deal with mutation-driven drug resistance, new methods and drugs have been discovered and approved for clinical use (47). Even so, detailed individualized treatment strategies targeting specific tumorigenesis and drug resistant mechanisms are still required. Advances in these areas would allow for more targeted and effective therapeutic options for more cancer patients.

AUTHOR CONTRIBUTIONS

ML, JS, JL, YZ, JW, LQ, and QW were responsible for the review of the literature. JJ, JY, XW, QZ, CC, and ML wrote the manuscript. XW and LQ drew the Tables. XW, TY, and ZX designed the study and contributed with the valuable discussion and revision of the manuscript.

FUNDING

This work was supported by the National Natural Science Foundation of China (Grant nos. 81503093, 81602166, and 81672444) and the Joint Funds of the Southwest Medical University and Luzhou (2016LZXNYD-T01, 2017LZXNYD-Z05, and 2017LZXNYD-J09). The funding from National Natural Science Foundation of China (Grant nos. 81503093) will cover open access fee.

REFERENCES

1. Scotti L, Mendonca Junior FJ, Ishiki HM, Ribeiro FF, Singla RK, Barbosa Filho JM, et al. Docking studies for multi-target drugs. *Curr Drug Targ.* (2017) 18:592–604. doi: 10.2174/1389450116666150825111818
2. Tomasetti C, Li L, Vogelstein B. Stem cell divisions, somatic mutations, cancer etiology, and cancer prevention. *Science.* (2017) 355:1330–4. doi: 10.1126/science.aaf9011
3. Curtin JA, Fridlyand J, Kageshita T, Patel HN, Busam KJ, Kutzner H, et al. Distinct sets of genetic alterations in melanoma. *N Engl J Med.* (2005) 353:2135–47. doi: 10.1056/NEJMoa050092
4. Davies H, Bignell GR, Cox C, Stephens P, Edkins S, Clegg S, et al. Mutations of the BRAF gene in human cancer. *Nature.* (2002) 417:949–54. doi: 10.1038/nature00766
5. Hauschild A, Grob JJ, Demidov LV, Jouary T, Gutzmer R, Millward M, et al. Dabrafenib in BRAF-mutated metastatic melanoma: a multicentre, open-label, phase 3 randomised controlled trial. *Lancet.* (2012) 380:358–65. doi: 10.1016/s0140-6736(12)60868-x
6. Drilon A, Laetsch TW, Kummar S, DuBois SG, Lassen UN, Demetri GD, et al. Efficacy of larotrectinib in TRK fusion–positive cancers in adults and children. *N Engl J Med.* (2018) 378:731–9. doi: 10.1056/NEJMoa1714448
7. Shigematsu H, Lin L, Takahashi T, Nomura M, Suzuki M, Wistuba II, et al. Clinical and biological features associated with epidermal growth factor receptor gene mutations in lung cancers. *J Natl Cancer Inst.* (2005) 97:339–46. doi: 10.1093/jnci/dji055
8. Kobayashi S, Boggon TJ, Dayaram T, Janne PA, Kocher O, Meyerson M, et al. EGFR mutation and resistance of non-small-cell lung cancer to gefitinib. *N Engl J Med.* (2005) 352:786–92. doi: 10.1056/NEJMoa044238
9. Mok TS, Wu YL, Ahn MJ, Garassino MC, Kim HR, Ramalingam SS, et al. Osimertinib or platinum-pemetrexed in EGFR T790M-positive lung cancer. *N Engl J Med.* (2017) 376:629–40. doi: 10.1056/NEJMoa1612674
10. Callegari D, Ranaghan KE, Woods CJ, Minari R, Tiseo M, Mor M, et al. L718Q mutant EGFR escapes covalent inhibition by stabilizing a non-reactive conformation of the lung cancer drug osimertinib. *Chem Sci.* (2018) 9:2740–9. doi: 10.1039/c7sc04761d
11. Cappuzzo F, Bemis L, Varella-Garcia M. HER2 mutation and response to trastuzumab therapy in non-small-cell lung cancer. *N Engl J Med.* (2006) 354:2619–21. doi: 10.1056/NEJMc060020
12. De Greve J, Teugels E, Geers C, Decoster L, Galdermans D, De Mey J, et al. Clinical activity of afatinib (BIBW 2992) in patients with lung

adenocarcinoma with mutations in the kinase domain of HER2/neu. *Lung Cancer.* (2012) 76:123–7. doi: 10.1016/j.lungcan.2012.01.008
13. Hanker AB, Brewer MR, Sheehan JH, Koch JP, Sliwoski GR, Nagy R, et al. An acquired HER2(T798I) gatekeeper mutation induces resistance to neratinib in a patient with HER2 mutant-driven breast cancer. *Cancer Discov.* (2017) 7:575–85. doi: 10.1158/2159-8290.cd-16-1431
14. Rexer BN, Ghosh R, Narasanna A, Estrada MV, Chakrabarty A, Song Y, et al. Human breast cancer cells harboring a gatekeeper T798M mutation in HER2 overexpress EGFR ligands and are sensitive to dual inhibition of EGFR and HER2. *Clin Cancer Res.* (2013) 19:5390–401. doi: 10.1158/1078-0432.ccr-13-1038
15. Hyman DM, Piha-Paul SA, Won H, Rodon J, Saura C, Shapiro GI, et al. HER kinase inhibition in patients with HER2- and HER3-mutant cancers. *Nature.* (2018) 554:189–94. doi: 10.1038/nature25475
16. Katayama R, Lovly CM, Shaw AT. Therapeutic targeting of anaplastic lymphoma kinase in lung cancer: a paradigm for precision cancer medicine. *Clin Cancer Res.* (2015) 21:2227–35. doi: 10.1158/1078-0432.ccr-14-2791
17. Shaw AT, Kim DW, Mehra R, Tan DS, Felip E, Chow LQ, et al. Ceritinib in ALK-rearranged non-small-cell lung cancer. *N Engl J Med.* (2014) 370:1189–97. doi: 10.1056/NEJMoa1311107
18. Shaw AT, Friboulet L, Leshchiner I, Gainor JF, Bergqvist S, Brooun A, et al. Resensitization to crizotinib by the lorlatinib ALK resistance mutation L1198F. *N Engl J Med.* (2016) 374:54–61. doi: 10.1056/NEJMoa1508887
19. Choi YL, Soda M, Yamashita Y, Ueno T, Takashima J, Nakajima T, et al. EML4-ALK mutations in lung cancer that confer resistance to ALK inhibitors. *N Engl J Med.* (2010) 363:1734–9. doi: 10.1056/NEJMoa1007478
20. Sasaki T, Koivunen J, Ogino A, Yanagita M, Nikiforow S, Zheng W, et al. A novel ALK secondary mutation and EGFR signaling cause resistance to ALK kinase inhibitors. *Cancer Res.* (2011) 71:6051–60. doi: 10.1158/0008-5472.can-11-1340
21. Hamid O, Robert C, Daud A, Hodi FS, Hwu WJ, Kefford R, et al. Safety and tumor responses with lambrolizumab (anti-PD-1) in melanoma. *N Engl J Med.* (2013) 369:134–44. doi: 10.1056/NEJMoa1305133
22. Peters S, Kerr KM, Stahel R. PD-1 blockade in advanced NSCLC: a focus on pembrolizumab. *Cancer Treat Rev.* (2018) 62:39–49. doi: 10.1016/j.ctrv.2017.10.002
23. Zaretsky JM, Garcia-Diaz A, Shin DS, Escuin-Ordinas H, Hugo W, Hu-Lieskovan S, et al. Mutations associated with acquired resistance to PD-1 blockade in melanoma. *N Engl J Med.* (2016) 375:819–29. doi: 10.1056/NEJMoa1604958
24. Condorelli R, Spring L, O'Shaughnessy J, Lacroix L, Bailleux C, Scott V, et al. Polyclonal RB1 mutations and acquired resistance to CDK 4/6 inhibitors in patients with metastatic breast cancer. *Ann Oncol.* (2018) 29:640–5. doi: 10.1093/annonc/mdx784
25. Cancer Genome Atlas Network. (2012). Comprehensive molecular portraits of human breast tumours. *Nature.* 490, 61–70. doi: 10.1038/nature11412
26. Herrera-Abreu MT, Palafox M, Asghar U, Rivas MA, Cutts RJ, Garcia-Murillas I, et al. Early adaptation and acquired resistance to CDK4/6 inhibition in estrogen receptor-positive breast cancer. *Cancer Res.* (2016) 76:2301–13. doi: 10.1158/0008-5472.can-15-0728
27. Renhowe PA. Inhibitors of growth factor receptor kinase-dependent signaling pathways in anticancer chemotherapy–clinical progress. *Curr Opin Drug Discov Devel.* (2002) 5:214. doi: 10.2174/09298670246 06957
28. Pao W, Miller V, Zakowski M, Doherty J, Politi K, Sarkaria I, et al. EGF receptor gene mutations are common in lung cancers from "never smokers" and are associated with sensitivity of tumors to gefitinib and erlotinib. *Proc Natl Acad Sci USA.* (2004) 101:13306–11. doi: 10.1073/pnas.04052 20101
29. Morin MJ. From oncogene to drug: development of small molecule tyrosine kinase inhibitors as anti-tumor and anti-angiogenic agents. *Oncogene.* (2000) 19:6574–83. doi: 10.1038/sj.onc.1204102
30. Inoue A, Kobayashi K, Usui K, Maemondo M, Okinaga S, Mikami I, et al. First-line gefitinib for patients with advanced non-small-cell lung cancer harboring epidermal growth factor receptor mutations without indication for chemotherapy. *J Clin Oncol.* (2009) 27:1394–400. doi: 10.1200/JCO.2008.18.7658
31. Maemondo M, Inoue A, Kobayashi K, Sugawara S, Oizumi S, Isobe H, et al. Gefitinib or chemotherapy for non-small-cell lung cancer with mutated EGFR. *N Engl J Med.* (2010) 362:2380–8. doi: 10.1056/NEJMoa0909530
32. Bell DW, Gore I, Okimoto RA, Godin-Heymann N, Sordella R, Mulloy R, et al. Inherited susceptibility to lung cancer may be associated with the T790M drug resistance mutation in EGFR. *Nat Genet.* (2005) 37:1315–6. doi: 10.1038/ng1671
33. Bose R, Kavuri SM, Searleman AC, Shen W, Shen D, Koboldt DC, et al. Activating HER2 mutations in HER2 gene amplification negative breast cancer. *Cancer Discov.* (2013) 3:224–37. doi: 10.1158/2159-8290.cd-12-0349
34. Xu X, De Angelis C, Burke KA, Nardone A, Hu H, Qin L, et al. HER2 Reactivation through acquisition of the HER2 L755S mutation as a mechanism of acquired resistance to HER2-targeted therapy in HER2(+) breast cancer. *Clin Cancer Res.* (2017) 23:5123–34. doi: 10.1158/1078-0432.ccr-16-2191
35. Dienstmann R, Tabernero J. Spectrum of gene mutations in colorectal cancer: implications for treatment. *Cancer J.* (2016) 22:149–55. doi: 10.1097/ppo.0000000000000191
36. Ross JS, Fakih M, Ali SM, Elvin JA, Schrock AB, Suh J, et al. Targeting HER2 in colorectal cancer: the landscape of amplification and short variant mutations in ERBB2 and ERBB3. *Cancer.* (2018) 124:1358–73. doi: 10.1002/cncr.31125
37. Ou SH. Crizotinib: a novel and first-in-class multitargeted tyrosine kinase inhibitor for the treatment of anaplastic lymphoma kinase rearranged non-small cell lung cancer and beyond. *Drug Des Devel Ther.* (2011) 5:471–85. doi: 10.2147/dddt.s19045
38. Kimura AGM. Molecularly targeted therapy: past, present and future. *Chemotherapy* 1:105. doi: 10.4172/2167-7700.1000105
39. Zhang S, Wang F, Keats J, Zhu X, Ning Y, Wardwell SD, et al. Crizotinib-resistant mutants of EML4-ALK identified through an accelerated mutagenesis screen. *Chem Biol Drug Des.* (2011) 78:999–1005. doi: 10.1111/j.1747-0285.2011.01239.x
40. Soda M, Choi YL, Enomoto M, Takada S, Yamashita Y, Ishikawa S, et al. Identification of the transforming EML4-ALK fusion gene in non-small-cell lung cancer. *Nature.* (2007) 448:561–6. doi: 10.1038/nature05945
41. Heuckmann JM, Holzel M, Sos ML, Heynck S, Balke-Want H, Koker M, et al. ALK mutations conferring differential resistance to structurally diverse ALK inhibitors. *Clin Cancer Res.* (2011) 17:7394–74. doi: 10.1158/1078-0432.ccr-11-1648
42. Zhang S, Anjum R, Squillace R, Nadworny S, Zhou T, Keats J, et al. The potent ALK inhibitor brigatinib (AP26113) overcomes mechanisms of resistance to first- and second-generation ALK inhibitors in preclinical models. *Clin Cancer Res.* (2016) 22:5527–38. doi: 10.1158/1078-0432.ccr-16-0569
43. Shaw AT, Felip E, Bauer TM, Besse B, Navarro A, Postel-Vinay S, et al. Lorlatinib in non-small-cell lung cancer with ALK or ROS1 rearrangement: an international, multicentre, open-label, single-arm first-in-man phase 1 trial. *Lancet Oncol.* (2017) 18:1590–9. doi: 10.1016/s1470-2045(17)30680-0
44. Uchibori K, Inase N, Araki M, Kamada M, Sato S, Okuno Y, et al. Brigatinib combined with anti-EGFR antibody overcomes osimertinib resistance in EGFR-mutated non-small-cell lung cancer. *Nat Commun.* (2017) 8:14768. doi: 10.1038/ncomms14768
45. Iranzo J, Martincorena I, Koonin EV. Cancer-mutation network and the number and specificity of driver mutations. *Proc Natl Acad Sci USA.* (2018) 115:E6010–9. doi: 10.1073/pnas.1803155115
46. Yue X, Zhao Y, Xu Y, Zheng M, Feng Z, Hu W. Mutant p53 in cancer: accumulation, gain-of-function, and therapy. *J Mol Biol.* (2017) 429:1595–606. doi: 10.1016/j.jmb.2017.03.030
47. Wang L, Wang H, Song D, Xu M, Liebmen M. New strategies for targeting drug combinations to overcome mutation-driven drug resistance. *Semin Cancer Biol.* (2017) 42:44–51. doi: 10.1016/j.semcancer.2016.11.002
48. Wu YL, Cheng Y, Zhou X, Lee KH, Nakagawa K, Niho S, et al. Dacomitinib versus gefitinib as first-line treatment for patients with EGFR-mutation-positive non-small-cell lung cancer (ARCHER 1050): a randomised, open-label, phase 3 trial. *Lancet Oncol.* (2017) 18:1454–66. doi: 10.1016/s1470-2045(17)30608-3
49. Engelman JA, Zejnullahu K, Gale CM, Lifshits E, Gonzales AJ, Shimamura T, et al. PF00299804, an irreversible pan-ERBB inhibitor, is effective in lung cancer models with EGFR and ERBB2 mutations that are resistant to gefitinib. *Cancer Res.* (2007) 67:11924–32. doi: 10.1158/0008-5472.can-07-1885

50. Chen G, McQuade JL, Panka DJ, Hudgens CW, Amin-Mansour A, Mu XJ, et al. Clinical, molecular, and immune analysis of dabrafenib-trametinib combination treatment for BRAF inhibitor-refractory metastatic melanoma: a phase 2 clinical trial. *JAMA Oncol.* (2016) 2:1056–64. doi: 10.1001/jamaoncol.2016.0509
51. Planchard D, Smit EF, Groen HJM, Mazieres J, Besse B, Helland A, et al. Dabrafenib plus trametinib in patients with previously untreated BRAF(V600E)-mutant metastatic non-small-cell lung cancer: an open-label, phase 2 trial. *Lancet Oncol.* (2017) 18:1307–16. doi: 10.1016/s1470-2045(17)30679-4
52. Gilmartin AG, Bleam MR, Groy A, Moss KG, Minthorn EA, Kulkarni SG, et al. GSK1120212 (JTP-74057) is an inhibitor of MEK activity and activation with favorable pharmacokinetic properties for sustained *in vivo* pathway inhibition. *Clin Cancer Res.* (2011) 17:989–1000. doi: 10.1158/1078-0432.ccr-10-2200
53. Puszkiel A, Noe G, Bellesoeur A, Kramkimel N, Paludetto MN, Thomas-Schoemann A, et al. Clinical pharmacokinetics and pharmacodynamics of dabrafenib. *Clin Pharmacokinet.* (2019) 58:451–67. doi: 10.1007/s40262-018-0703-0
54. Subbiah V, Kreitman RJ, Wainberg ZA, Cho JY, Schellens JHM, Soria JC, et al. Dabrafenib and trametinib treatment in patients with locally advanced or metastatic BRAF V600-mutant anaplastic thyroid cancer. *J Clin Oncol.* (2018) 36:7–13. doi: 10.1200/jco.2017.73.6785
55. Dummer R, Ascierto PA, Gogas HJ, Arance A, Mandala M, Liszkay G, et al. Overall survival in patients with BRAF-mutant melanoma receiving encorafenib plus binimetinib versus vemurafenib orencorafenib (COLUMBUS): a multicentre, open-label, randomised, phase 3 trial. *Lancet Oncol.* (2018b) 19:1315–27. doi: 10.1016/s1470-2045(18)30497-2
56. Sullivan RJ, Weber JS, Patel SP, Dummer R, Miller WH, Cosgrove D, et al. A phase Ib/II study of BRAF inhibitor (BRAFi) encorafenib (ENCO) plus MEK inhibitor (MEKi) binimetinib (BINI) in cutaneous melanoma patients naive to BRAFi treatment. *J Clin Oncol.* (2015) 33:9007–9007. doi: 10.1200/jco.2015.33.15_suppl.9007
57. Dummer R, Ascierto PA, Gogas HJ, Arance A, Mandala M, Liszkay G, et al. Encorafenib plus binimetinib versus vemurafenib or encorafenib in patients with BRAF-mutant melanoma (COLUMBUS): a multicentre, open-label, randomised phase 3 trial. *Lancet Oncol.* (2018) 19:603–15. doi: 10.1016/s1470-2045(18)30142-6
58. Huang M, Shen A, Ding J, Geng M. Molecularly targeted cancer therapy: some lessons from the past decade. *Trends Pharmacol Sci.* (2014) 35:41–50. doi: 10.1016/j.tips.2013.11.004

Conflict of Interest Statement: The authors declare that the research was conducted in the absence of any commercial or financial relationships that could be construed as a potential conflict of interest.

frontiers in Oncology

ORIGINAL RESEARCH
published: 16 April 2019
doi: 10.3389/fonc.2019.00274

Synthesis and Anticancer Activity Evaluation of Novel Phenanthridine Derivatives

Minghui Wan†, Lei Zhang†, Yiming Chen, Qiang Li, Wenli Fan, Qingxia Xue, Fang Yan and Weiguo Song**

School of Pharmacy, Weifang Medical University, Weifang, China

Based on the structure of sanguinarine, fourteen phenanthridine derivatives were designed and synthesized in the current study. The cytotoxic activities of synthesized compounds were evaluated against five human cancer cell lines (MCF-7, PC3, Hela, A549, and HepG2 cell lines) via MTT assay. Among all the compounds tested, molecule **8a** exhibited significant cytotoxic activity against MCF-7 cells with a IC_{50} value of 0.28 μM. A following up enzymatic assay indicated that compound **8a** could inhibit the activity of DNA topoisomerase I/II. Further mechanistic studies performed in the MCF-7 cell line revealed that compound **8a** could arrest cell cycle in S phase and induce cell apoptosis via downregulation of Bcl-2 and upregulation of Bax. Collectively, a potent DNA topoisomerase inhibitor (**8a**) was discovered, which exhibited potential as a candidate chemotherapeutic agent for the management of tumors in the present study.

Keywords: phenanthridine, anticancer, topoisomerase, apoptosis, cell cycle arrest

OPEN ACCESS

Edited by:
Zhe-Sheng Chen,
St. John's University, United States

Reviewed by:
Xiangbao Meng,
Peking University, China
Pranav Gupta,
Harvard Medical School,
United States

****Correspondence:***
Fang Yan
yanfang303@163.com
Weiguo Song
songwg@139.com

†These authors have contributed equally to this work

Specialty section:
This article was submitted to Cancer Molecular Targets and Therapeutics, a section of the journal Frontiers in Oncology

Received: *24 February 2019*
Accepted: *25 March 2019*
Published: *16 April 2019*

Citation:
Wan M, Zhang L, Chen Y, Li Q, Fan W, Xue Q, Yan F and Song W (2019) Synthesis and Anticancer Activity Evaluation of Novel Phenanthridine Derivatives. Front. Oncol. 9:274. doi: 10.3389/fonc.2019.00274

INTRODUCTION

Sanguinarine (SA) belongs to the chrysene-skeleton-based heterocyclic benzo [c] phenanthridine alkaloids family (**Figure 1**), which are widely distributed in plants, such as *Sanguinaria canadensis* and *Papaveraceae* (1–3). Although SA was isolated in the late 1940s (4), extensive research focusing on the molecular mechanism of its anti-tumor effects has commenced only recently (5). SA has attracted extensive attention because of its significant biological activities, including anti-tumor (6, 7), anti-inflammatory, anti-angiogenesis, antiplatelet, antiviral, and anti-fungal effects (8–11). The flat polyaromatic structure of SA enabled it to directly interact with DNA (12). SA-induced cell cycle arrest and apoptosis was found to not only be caused by DNA damage, but also to be a combined result of targeting other cell structures, such as topoisomerases (Top) (13, 14), antiapoptotic protein (6, 15, 16), and mitochondrial membranes (17, 18).

Previous studies reported that SA might interfere with mitochondrial membranes and induce apoptosis in the CEM leukemia cell line HL-60 (18, 19) and KB carcinoma cell line (17). The potential mechanism was associated with nuclear factor (NF-κB) activation (1), mitochondria damage induced caspase activation (20), and increased expression of Bax/Bcl-2 (21, 22). The proapoptotic effects of SA have significant potential in the development of novel antitumor agents with SA as a lead compound. In addition, SA elicited G0/G1 cell cycle arrest (23), which can be associated with the translocation of cyclin D1 and Top II from nucleus to cytoplasm (24, 25). Additionally, NF-κB, AP-1, MMP-9, and STAT3 inhibition were also observed following SA treatment (26–28) and subsequently resulted in suppressed cancer cell metastasis. Moreover,

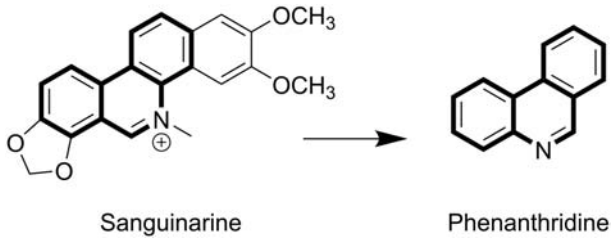

FIGURE 1 | The structures of SA and phenanthridine.

abolishment of VEGF-induced AKT activation was also proposed as another potential mechanism for the antiangiogenic activity of SA (29, 30), which was believed to contribute to its anti-tumor effects in the animal models of melanoma (31) and colorectal cancer (26).

SA exhibited significant potential in the development of new antitumor drugs, as indicated from the results of a wide range of *in vitro* and *in vivo* investigations. Due to the structure of multiple aromatic rings, further development of SA as antitumor agent is restricted by its low solubilities and severe side effects. To discover SA analogs with improved solubilities and activities, a series of phenanthridine derivatives with reduced aromaticities were designed and synthesized using phenanthridine as a core scaffold. All the derived compounds were identified with ^{13}C NMR, ^{1}H NMR, HRMS, and biologically evaluated against MCF-7 (human breast cancer), PC3 (human prostatic cancer), Hela (human cervical cancer), A549 (human lung cancer), and HepG2 (human hepatocellular carcinoma) cell lines. During further investigation of the underlying mechanism, molecular techniques such as flow cytometry, hoechst 33258 staining and western blotting were utilized with the representative compounds synthesized in the current study.

Chemistry

The synthetic pathway of phenanthridine derivatives is shown in **Scheme 1**. As illustrated, amino protection of starting material **1** was performed to afforded compound **2**. The following bromine substitution and deprotection of amino group were carried out to generate intermediate **4**. Preparation of intermediate **5** was performed by Suzuki coupling of 2-bromoaniline derivatives with corresponding phenylboronic acids. Treatment of intermediate **5** under acidic condition yielded compound **6**, and subsequent dehydration of compound **6** afforded 2-isocyanobiphenyls derivatives **7a**-**t**. In the presence of benzoyl peroxide, phenanthridine derivatives **8a**-**n** were derived by reacting of 2-isocyanobiphenyls derivatives with carbon tetrachloride (32).

Cytotoxicity Assay

The cytotoxicity of synthesized compounds was evaluated against five tumor cell lines (A549, PC3, MCF-7, HepG2, and Hela) via MTT assay. Initially, two doses of each compound (5 and 1 μmol/L) were evaluated. As shown in **Table 1**, compounds **8a**, **8b**, **8d**, **8e**, **8l**, **8m**, and **8n** exhibited significant inhibitory activities against MCF-7, PC3, and Hela cells at the dose of 5 μmol/L. However, when compared with the lead compound SA, molecule **8d**, **8l**, and **8n** exhibited lower inhibitory activity at the dose of 1 μmol/L.

Based on the data mentioned above, compounds **8a**, **8b**, **8e**, and **8m** were selected for further test with more doses against the tumor cell lines. The IC_{50} values of these compounds were summarized in **Table 2**, all the four compounds exhibited potent cytotoxicity against the five tumor cell lines tested compared with the positive control SA and clinically used antitumor drug Etoposide (VP 16). The results indicated that compounds **8a** and **8m** exhibited potent activities against all the tested cancer cell lines. Molecule **8a** ($IC_{50} = 0.28 \pm 0.08$) showed potency of over 6 times higher than SA ($IC_{50} = 1.77 \pm 0.06$) in the inhibition of MCF-7 cells, and molecule **8m** ($IC_{50} = 0.39 \pm 0.08$) exhibited 8.9 times of potency comparing to SA ($IC_{50} = 3.49 \pm 0.41$) in the inhibition of HepG2 cells. Therefore, **8a**, **8b**, **8e**, and **8m** were selected for further mechanistical studies.

Topoisomerase Inhibition Assay

To elucidate the target profiles of the cytotoxic compounds (**8a**, **8b**, **8e**, and **8m**), the inhibitory effects of these compounds were tested against human DNA Top I and IIα by relaxing assay using pBR322 DNA. 10-hydroxy camptothecin (OPT) and VP 16 were used as a positive control for Top I and IIα inhibition, respectively. The Top I/II were able to completely convert the supercoiled DNA to open circular form in the absence of inhibitors (**Figure 2,** lane B). In contrast, positive control (OPT/VP 16) and active compounds inhibited the activity of Top, which affected the unwinding of the supercoiled DNA, leading to a band pattern similar to the negative control (**Figure 2**). As shown in **Figure 2A**, positive control OPT and SA inhibited the activity of both Top I and Top IIα. Compound **8a** exhibited weak Top I inhibition, which was similar to OPT. In the Top IIα test, all the tested compounds exhibited potent DNA Top IIα inhibitory activities at the concentration of 100 μM (**Figure 2B**). Based on the above findings, molecule **8a** with most potent cytotoxicity and enzymatic inhibitory activities is chosen as a potential candidate for further investigation.

Cell Cycle Analysis

To elucidate the effects of molecule **8a** on cell cycle distributions, MCF-7 cells were treated with various doses of molecule **8a** (0, 0.15, 0.3, and 0.6 μM) for 24 h. As shown in **Figure 3**, compound **8a** treatment led to significant accumulation of MCF-7 cells at S phase (from 18.86 to 42.99%) dose-dependently. While reduced cells at the G2/M phase was detected from 23.46 to 10.45% (0.15 μM), 8.69% (0.3 μM), and 5.62% (0.6 μM) following treatment with compound **8a** dose-dependently. These results suggest that compound **8a** exhibited a significant antitumor effect and led to MCF-7 cell cycle arrest at the S phase in a dose-dependent manner.

Cell Apoptosis Assay

To further investigate the role of apoptosis in the antitumor effect of compound **8a**, Hoechst 33258 staining was performed to investigate the nuclear morphological changes following molecule **8a** treatment on MCF-7 cells. Hoechst 33258 is a

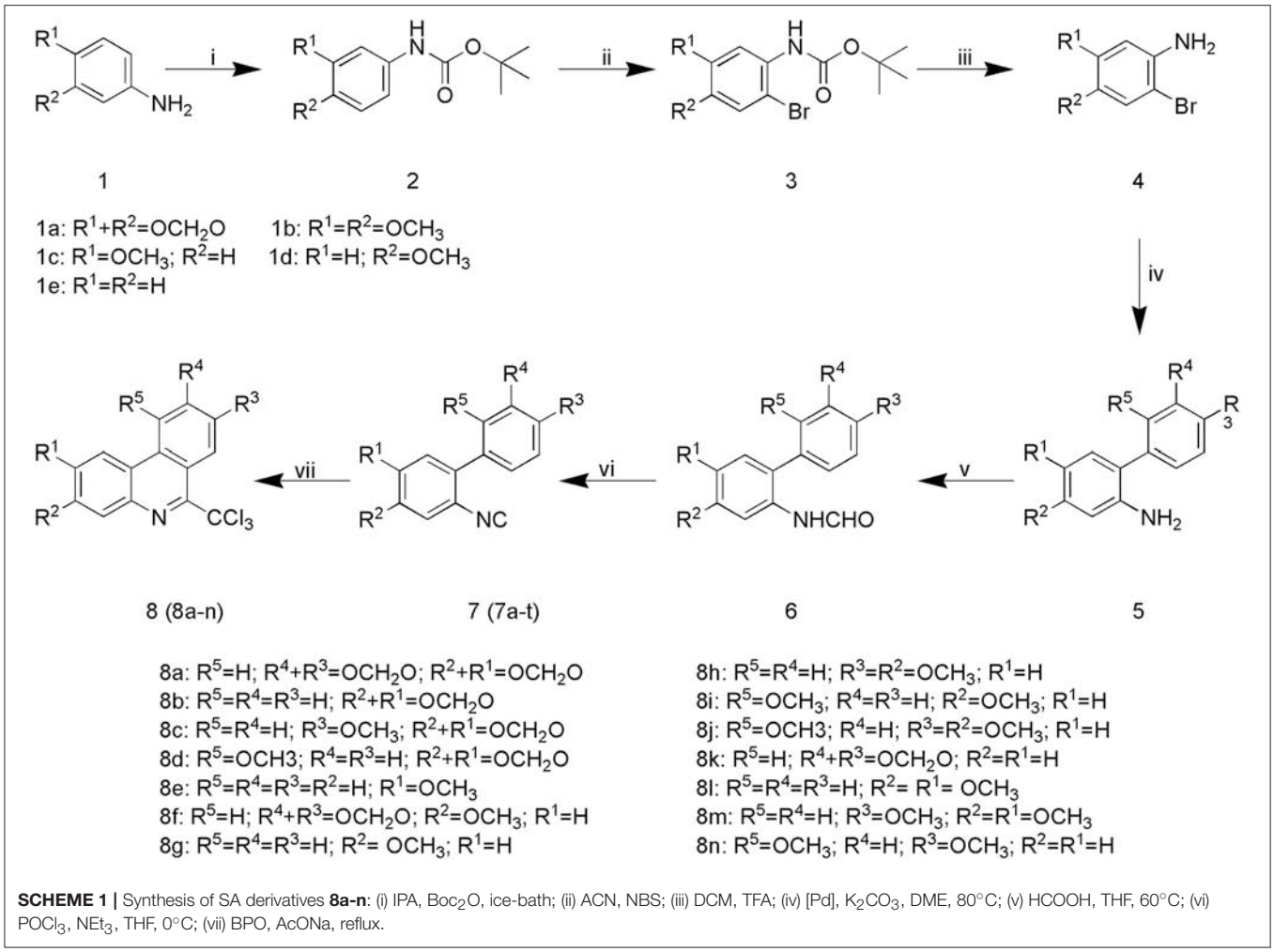

SCHEME 1 | Synthesis of SA derivatives **8a-n**: (i) IPA, Boc_2O, ice-bath; (ii) ACN, NBS; (iii) DCM, TFA; (iv) [Pd], K_2CO_3, DME, 80°C; (v) HCOOH, THF, 60°C; (vi) $POCl_3$, NEt_3, THF, 0°C; (vii) BPO, AcONa, reflux.

fluorescent stain used to label DNA; live cells nuclei will be stained with uniformly light blue and apoptotic cells nuclei will be stained with bright blue because of chromatin condensation. As shown in **Figure 4A**, higher levers of apoptotic cells with nuclear condensation, nuclear fragmentation and enhanced brightness were detected in the cells following treatment with various doses of molecule **8a** (0.15, 0.3, and 0.6 μM). To quantify the number of apoptotic cells and to distinguish early apoptosis and secondary necrosis, MCF-7 cells were stained with annexin V-FITC/PI. As shown in **Figure 4B**, after treatment with difference doses of compound **8a** (0, 0.15, 0.3, and 0.6 μM), the percentage of apoptotic cells were significantly increased from 11.16% of the control to 14.35, 22.79, and 28.98%, respectively, indicating that induction of cell apoptosis contributes to the antitumor effect of compound **8a**.

Protein Expressions of Bcl-2 and Bax

Apoptosis is a heavily regulated cell death process influenced by a series of regulatory molecules (33). The mitochondria-dependent pathway has been described as an important signaling pathway of cell apoptosis regulated by the Bcl-2 family including the pro- and anti-apoptotic proteins such as Bax (pro-apoptotic protein) and Bcl-2 (anti-apoptotic protein) (34–36). Moreover, the ratio of Bax/Bcl-2 is important for apoptosis induced by the mitochondrial pathway. Therefore, the effect of compound **8a** on the levels of Bax and Bcl-2 was evaluated in MCF-7 cells. The results indicated that compound **8a** could significantly downregulate Bcl-2 levels and upregulate Bax levels in MCF-7 cells, increasing the ratio of Bax/Bcl-2 in a dose-dependent manner (**Figure 5**). Collectively, these results suggest that compound **8a** induced apoptosis by regulating the expression of apoptosis-related proteins.

CONCLUSIONS

Based on the structure of sanguinarine, fourteen phenanthridine derivatives **8a**-**m** were synthesized and evaluated for their cytotoxic activity against five different human cancer cell lines. Among the evaluated compounds, **8a** exhibited a broad spectrum of anti-proliferative activities against all the tested cancer cell lines. Further mechanistic assay revealed that compound **8a** could inhibit the activity of both DNA Top I and Top II, as well as preventing cell transition

TABLE 1 | The inhibitory activity on tumor cell of phenanthridine derivatives[a].

Compound[b]	MCF-7 (%)		PC3 (%)		Hela (%)	
	5 μM	1 μM	5 μM	1 μM	5 μM	1 μM
8a	95.66	71.50	91.21	78.47	88.50	58.76
8b	93.66	58.29	89.77	64.16	84.90	54.01
8c	25.06	19.56	25.32	<5	19.66	16.00
8d	83.17	27.48	81.72	43.50	58.92	28.78
8e	95.36	60.07	88.65	73.04	83.80	23.52
8f	36.73	15.99	15.65	<5	16.26	<5
8g	18.23	23.76	<5	<5	<5	<5
8h	31.23	16.30	26.40	<5	15.74	8.61
8i	16.15	13.60	<5	<5	<5	<5
8j	62.18	14.00	64.62	<5	37.46	7.47
8k	19.74	32.60	12.81	<5	8.14	<5
8l	94.05	34.75	89.37	42.52	81.62	32.25
8m	97.83	89.34	95.26	88.75	87.57	80.26
8n	72.26	49.63	64.61	<5	30.69	9.72
SA	98.29	53.86	96.42	95.60	96.13	64.41
VP16	41.84	13.67	38.39	22.39	29.18	17.42

[a]*Values are average of three determinations and deviation of data results is <20%.*
[b]*All compounds were dissolved in DMSO for testing.*

TABLE 2 | The IC_{50}^{a} of phenanthridine derivatives.

Compound	IC_{50} (μM) [a]				
	MCF-7	PC3	Hela	A549	HepG2
8a	0.28 ± 0.08	0.30 ± 0.06	0.48 ± 0.07	0.89 ± 0.07	0.70 ± 0.09
8b	0.77 ± 0.04	0.76 ± 0.01	0.66 ± 0.12	0.85 ± 0.03	1.23 ± 0.08
8e	0.61 ± 0.03	0.45 ± 0.04	1.93 ± 0.02	0.89 ± 0.09	2.21 ± 0.14
8m	0.24 ± 0.08	0.22 ± 0.04	0.49 ± 0.02	0.85 ± 0.04	0.39 ± 0.08
SA	1.77 ± 0.06	1.67 ± 0.33	1.07 ± 0.06	2.68 ± 0.18	3.49 ± 0.41
VP16	>10	>10	>10	>10	>10

[a]*IC_{50} values are represented as mean ±SD (n = 3).*

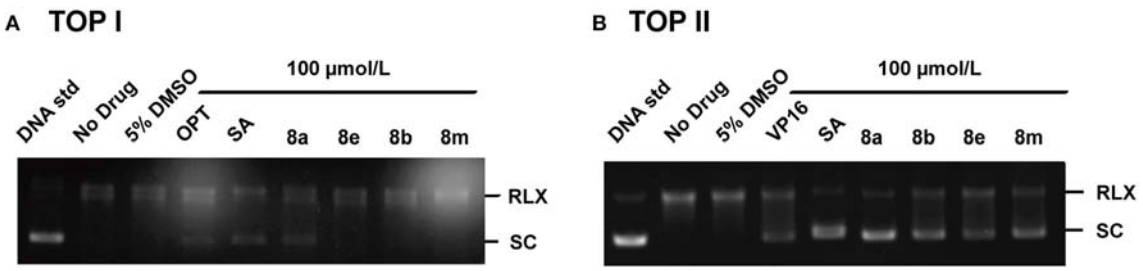

FIGURE 2 | Effects of phenanthridine derivatives and positive control on human Top I **(A)**/IIa **(B)**. Native superhelix pBR322 was incubated at 37°C for 30 min with 2 units of human Top I/IIα in the absence (lane 2) or presence of compound at concentration 100 μM. One hundred micromolar OPT, VP 16, and SA were used as positive controls, respectively. Negatively supercoiled pBR322 (SC) and relaxed DNA (RLX) were shown. DNA samples were run on agarose gel followed by Genecolour I TM staining.

from S to G2 phase dose-dependently. Apoptosis studies against MCF-7 cells indicated that downregulation of Bcl-2 and upregulation of Bax expression may contribute to the anti-proliferative activities. In summary, these findings suggest that molecule **8a** is a potent lead compound in the derived phenanthridine derivatives. Further molecule **8a** based structural

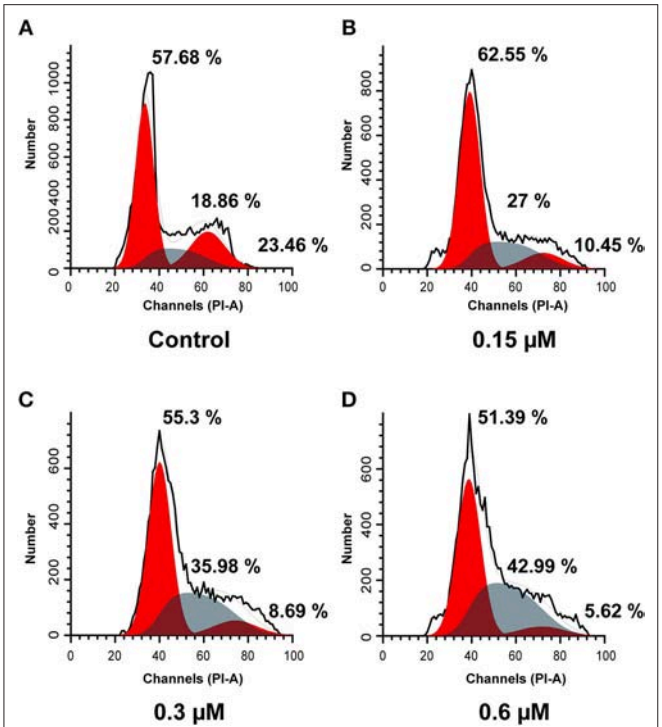

FIGURE 3 | Cell cycle analysis using PI staining of compound **8a** on MCF-7 cells. Cells were treated with compound **8a** at 0.15 **(B)**, 0.3 **(C)**, and 0.6 **(D)** μM for 24 h, compared with the control **(A)**. Cell cycle were detected by flow cytometry.

modification may be beneficial in the discovery of novel anticancer agents with improved antitumor activity and reduced side effects.

MATERIALS AND METHODS

Chemistry

All chemicals were obtained from commercial suppliers and used without further purification. Reactions progress was detected by thin layer chromatography (TLC) and visualized under UV light. Two hundred to three hundred mesh silica gel was used for column chromatography. All compounds were characterized by ^{13}C NMR, ^{1}H NMR, and HRMS. ^{1}H and ^{13}C NMR spectra were recorded on Mercury Plus-400 with internal standard used TMS and recorded in parts per million (ppm). Date were reported as s (singlet), br (broad), s (singlet), d (doublet), t (triplet), q (quartet), m (multiplet), and coupling constant (J) in hertz (Hz). Melting point was determined by MP 100 Automatic Melting Point Apparatus.

Representative Procedure for the Synthesis of Compounds 7a-t

To dissolve compound **6**, THF and NEt_3 was added, the solution was added to $POCl_3$ (11 mmol) until the solution was cooled to 0°C. The reaction was quenched by saturated Na_2CO_3 until complete consumption of starting material, monitored by TLC. The solution of the crude product was extracted with ethyl acetate, and organic layer was dried over Na_2SO_4 and evaporated to dryness. The residue was purified by column chromatography with silica gel (200–300 mesh).

2-isocyano-3′,4′-Methylenedioxy-4,5-methylenedioxy-1,1′-biphenyl (7a)

Yellowish -white solid, Yield 78%; Mp (154.4–156.1°C); ^{1}H NMR (400 MHz, $CDCl_3$) δ 6.90 (d, J = 8.9 Hz, 4H), 6.78 (s, 1H), 6.05 (s, 2H), 6.01 (s, 2H).

2-isocyano-4,5-methylenedioxy-1,1′-biphenyl (7b)

Brown solid, Yield 80%; Mp (90.1–90.3°C); ^{1}H NMR (400 MHz, $CDCl_3$) δ 7.54–7.30 (m, 5H), 6.91 (s, 1H), 6.82 (s, 1H), 6.05 (s, 2H).

2-isocyano-4,5-methylenedioxy-4′-methoxy-1,1′-biphenyl (7c)

White solid, Yield 81%; Mp (132–133.1°C);^{1}H NMR (400 MHz, $CDCl_3$) δ 7.39 (d, J = 8.7 Hz, 2H), 6.98 (d, J = 8.7 Hz, 2H), 6.90 (s, 1H), 6.80 (s, 1H), 6.05 (s, 2H), 3.85 (s, 3H).

2-isocyano-4,5-methylenedioxy-2′-methoxy-1,1′-biphenyl (7d)

Yellowish-white solid, Yield 82%; Mp (139.4–140.7°C); ^{1}H NMR (400 MHz, $CDCl_3$) δ 7.43–7.34 (m, 1H), 7.20 (dd, J = 7.5, 1.8 Hz, 1H), 7.07–6.96 (m, 2H), 6.90 (s, 1H), 6.79 (s, 1H), 6.05 (s, 2H), 3.83 (s, 3H).

2-isocyano-4,5-methylenedioxy-2′,4′-dimethoxy-1,1′-biphenyl (7e)

Brown solid, Yield 79%; Mp (161.4–161.9°C); ^{1}H NMR (400 MHz, $CDCl_3$) δ 7.10 (s, 1H), 6.88 (s, 1H), 6.77 (s, 1H), 6.56 (dt, J = 5.2, 2.5 Hz, 2H), 6.04 (s, 2H), 3.85 (s, 3H), 3.81 (s, 3H).

2-isocyano-3′,4′-methylenedioxy-5-methoxy-1,1′-biphenyl (7f)

Yellowish-white solid, Yield 81%; Mp (119.6–120.1°C); ^{1}H NMR (400 MHz, $CDCl_3$) δ 7.58 (d, J = 8.6 Hz, 1H), 7.12 (d, J = 1.7 Hz, 1H), 7.09–6.95 (m, 4H), 6.10 (s, 2H), 3.84 (s, 3H).

2-isocyano-5-methoxy-1,1′-biphenyl (7g)

Black oil, Yield 83%; ^{1}H NMR (400 MHz, $CDCl_3$) δ 7.62 (d, J = 8.7 Hz, 1H), 7.58–7.42 (m, 5H), 7.08–6.99 (m, 2H), 3.85 (s, 3H).

2'-isocyano-3,4-methylenedioxy-1,1′-biphenyl (7h)

Green solid, Yield 85%; Mp (71.6–73.9°C); ^{1}H NMR (400 MHz, $CDCl_3$) δ 6.02 (s, 2H), 7.02–6.94 (m, 2H), 6.94–6.87 (m, 1H), 7.46 (d, J = 9.3 Hz, 1H), 7.43–7.30 (m, 3H).

2'-isocyano-2,4-dimethoxy-1,1′-biphenyl (7i)

Yellowish-white solid, Yield 79%; Mp (90.1–90.5°C); ^{1}H NMR (400 MHz, $CDCl_3$) δ 7.41 (ddd, J = 8.9, 7.4, 1.8 Hz, 2H), 7.38–7.29 (m, 2H), 7.18–7.10 (m, 1H), 6.58 (dd, J = 5.7, 2.2 Hz, 2H), 3.86 (s, 3H), 3.81 (s, 3H).

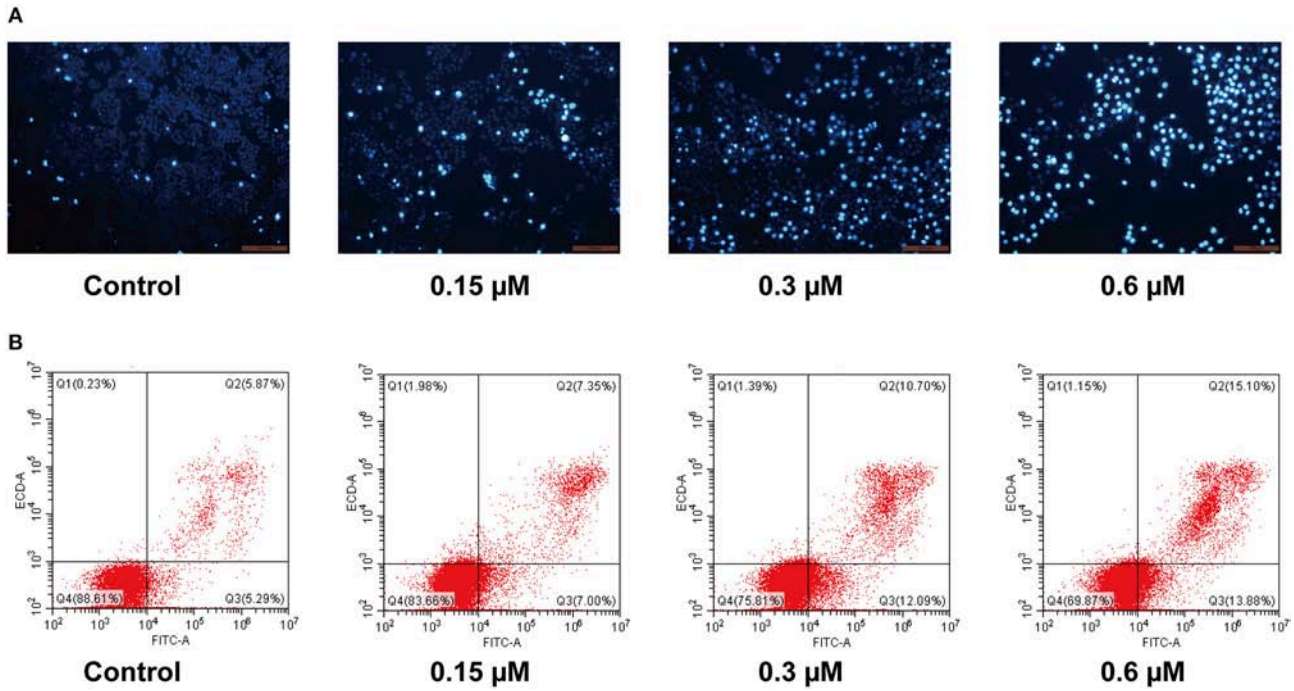

FIGURE 4 | Pro-apoptotic effect of compound **8a** on MCF-7 cells. **(A)** Apoptotic assay by Hoechst 33258. MCF-7 cells were treated with compound **8a** at 0.15, 0.3, and 0.6 μM for 24 h, and then cells were stained with Hoechst 33258 and visualized under a fluorescent microscope. **(B)** Apoptotic assay by flow cytometry. MCF-7 cells were treated with compound **8a** at 0.15, 0.3, and 0.6 μM for 24 h. Then cells were stained with Annexin V-FITC/PI and were detected by flow cytometry analysis.

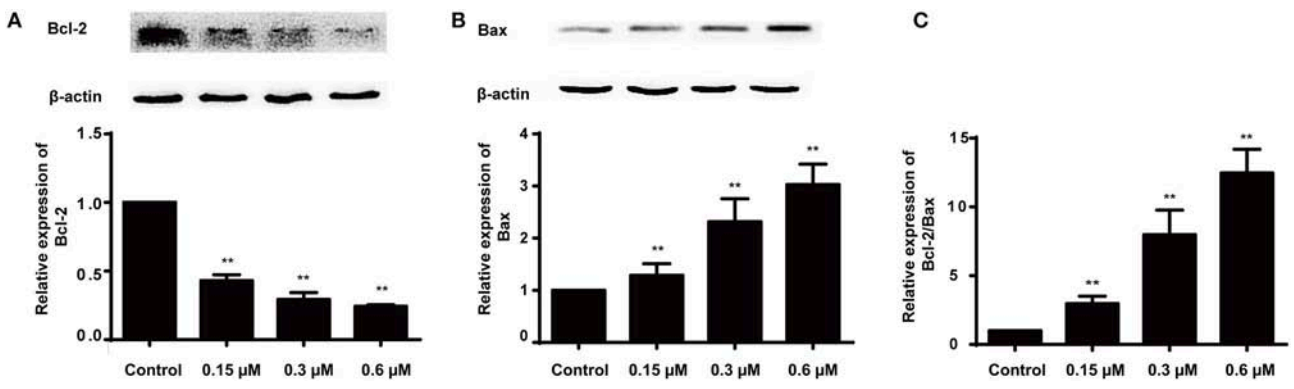

FIGURE 5 | Effects of **8a** on the expressions of Bcl-2 **(A)**, Bax **(B)** and the expression ratio **(C)** in MCF-7 cells. The cells were treated with different concentrations (0.15, 0.3, and 0.6 μM) for 24 h; β-actin served as an internal control. All date were represented as mean ± SD ($n = 3$). $^{**}p < 0.01$, compared with control group.

2′-isocyano-2,4,5′-trimethoxy-1,1′-biphenyl (7j)

Yellow solid, Yield 80%; Mp (104.6–104.9°C); ^{1}H NMR (400 MHz, $CDCl_3$) δ 7.35 (d, $J = 8.4$ Hz, 1H), 7.14 (d, $J = 8.9$ Hz, 1H), 6.88–6.79 (m, 2H), 6.58 (dd, $J = 5.4$, 2.3 Hz, 2H), 3.86 (s, 3H), 3.82 (s, 6H).

2-isocyano-3′,4′-methylenedioxy-4-methoxy-1,1′-biphenyl (7k)

Yellowish-white solid, Yield 75%; Mp (120.6–120.9°C); ^{1}H NMR (400 MHz, $CDCl_3$) δ 7.28 (d, $J = 8.4$ Hz, 1H), 7.02–6.86 (m, 5H), 6.02 (s, 2H), 3.85 (s, 3H).

2-isocyano-4-methoxy-1,1′-biphenyl (7l)

Yellow solid, Yield 78%; Mp (117.3–117.6°C); ^{1}H NMR (400 MHz, $CDCl_3$) δ 7.53–7.43 (m, 4H), 7.43–7.36 (m, 1H), 7.33 (d, $J = 9.0$ Hz, 1H), 7.05–6.97 (m, 2H), 3.86 (s, 3H).

2-isocyano-4,4′-dimethoxy-1,1′-biphenyl (7m)

Yellowish brown solid, Yield 83%; Mp (102.4–102.8°C); ^{1}H NMR (400 MHz, $CDCl_3$) δ 7.44–7.37 (m, 2H), 7.30 (d, $J = 9.0$ Hz, 1H), 6.99 (d, $J = 9.0$ Hz, 4H), 3.85 (d, $J = 4.0$ Hz, 6H).

2-isocyano-2′,4-dimethoxy-1,1′-biphenyl (7n)
White solid, Yield 82%; Mp (125.5–126°C); ^{1}H NMR (400 MHz, $CDCl_3$) δ 7.48–7.34 (m, 1H), 7.33–7.17 (m, 2H), 7.08–6.94 (m, 4H), 3.84 (d, J = 5.4 Hz, 6H).

2-isocyano-2′,4,4′-trimethoxy-1,1′-biphenyl (7o)
Yellowish-white solid, Yield 80%; Mp (105.9–107.3°C); ^{1}H NMR (400 MHz, $CDCl_3$) δ 7.26 (d, J = 1.7 Hz, 1H), 7.12 (d, J = 8.9 Hz, 1H), 7.01–6.93 (m, 2H), 6.61–6.53 (m, 2H), 3.90–3.79 (m, 9H).

2-isocyano-3′,4′-methylenedioxy-4,5-dimethoxy-1,1′-biphenyl (7p)
Brown solid, Yield 84%; Mp (171.7–172.3°C); ^{1}H NMR (400 MHz, $CDCl_3$) δ 6.99–6.86 (m, 4H), 6.80 (s, 1H), 6.02 (s, 2H), 3.91 (d, J = 2.5 Hz, 6H).

2-isocyano-4,5-dimethoxy-1,1′-biphenyl (7q)
Yellowish-white solid, Yield 82%; Mp (139.4–139.9°C); ^{1}H NMR (400 MHz, $CDCl_3$) δ 7.27 (s, 1H), 7.01 (s, 1H), 3.85 (d, J = 3.7 Hz, 5H), 7.58–7.47 (m, 3H), 7.47–7.39 (m, 1H).

2-isocyano-4,4′,5-trimethoxy-1,1′-biphenyl (7r)
Yellowish brown solid, Yield 84%; Mp (102.7–103.7°C); ^{1}H NMR (400 MHz, $CDCl_3$) δ 7.43 (d, J = 8.7 Hz, 2H), 7.00 (d, J = 8.7 Hz, 2H), 6.93 (s, 1H), 6.82 (s, 1H), 3.92 (d, J = 1.5 Hz, 6H), 3.86 (s, 3H).

2-isocyano-2′,4,5-trimethoxy-1,1′-biphenyl (7s)
Yellow solid, Yield 83%; Mp (103–103.6°C); ^{1}H NMR (400 MHz, $CDCl_3$) δ 7.44–7.35 (m, 1H), 7.28–7.20 (m, 1H), 7.09–6.98 (m, 2H), 6.94 (s, 1H), 6.82 (s, 1H), 3.94–3.82 (m, 9H).

2-isocyano-2′,4,4′,5-tetramethoxy-1,1′-biphenyl (7t)
Yellowish-white solid, Yield 82%; Mp (123.4–123.9°C); ^{1}H NMR (400 MHz, $CDCl_3$) δ 7.15 (d, J = 8.9 Hz, 1H), 6.92 (s, 1H), 6.79 (s, 1H), 6.57 (dq, J = 4.2, 2.4 Hz, 2H), 3.91 (s, 3H), 3.88 (s, 3H), 3.86 (s, 3H), 3.82 (s, 3H).

Representative Procedure for the Synthesis of Compounds 8a-8n

A mixture was produced of 2-isocyanobiphenyls derivatives (0.5 mmol), benzoyl peroxide (0.6 mmol), AcONa (1.0 mmol) in CCl_4 (2 mL) under an atmosphere of N_2. The reaction was stirred under reflux until complete consumption of starting material, monitored by TLC (about 16h). The solution of the crude product was extracted with ethyl acetate. The organic layers were washed with a saturated solution of $NaHCO_3$ and dried over Na_2SO_4 and evaporated to dryness. The residue was purified by column chromatography with silica gel (200–300 mesh) to afford the product 6-trichloromethylphenanthridine.

2,3-methylenedioxy-8,9-methylenedioxy-6-(trichloromethyl)phenanthridine (8a)
Yellow solid, Yield 40%; Mp (198.7–199.6°C); ^{1}H NMR (400 MHz, $CDCl_3$): δ 8.23 (s, 1H), 7.77 (s, 1H), 7.67 (s, 1H), 7.53 (s, 1H), 6.18 (d, J = 8.5 Hz, 4H); ^{13}C NMR(101 MHz, DMSO): δ 151.43, 150.27, 149.97, 149.09, 148.77, 147.57, 133.32, 129.68, 128.98, 115.89, 107.21, 104.01, 103.18, 102.90, 101.57, 100.33; HRMS (ESI) *m/z* 383.9592 (M+H).

2,3-methylenedioxy-6-(trichloromethyl)phenanthridine (8b)
Yellowish solid, Yield 39%; Mp (175.4–176.5°C); ^{1}H NMR(400 MHz, $CDCl_3$): δ 8.92 (d, J = 8.4 Hz, 1H), 8.49 (d, J = 8.2 Hz, 1H), 7.91–7.78 (m, 2H), 7.68 (t, J = 7.6 Hz, 1H), 7.60 (s, 1H), 6.19 (s, 2H); ^{13}C NMR(101 MHz, DMSO): δ 150.59, 150.37, 150.29, 137.46, 134.81, 131.31, 127.60, 127.04, 124.18, 121.88, 119.36, 107.77, 103.08, 100.50; HRMS (ESI) *m/z* 339.9696 (M+H).

2,3-methylenedioxy-8-methoxy-6-(trichloromethyl)phenanthridine (8c)
Brown solid, Yield 41%; Mp (93.8–95.0°C); ^{1}H NMR(400 MHz, $CDCl_3$) δ 8.12–8.05 (m, 8H), 7.80 (s, 1H), 7.67 (t, J = 7.5 Hz, 4H), 6.17 (s, 2H), 4.01 (s, 3H); ^{13}C NMR(101 MHz, DMSO) δ 167.67, 163.08, 162.77, 135.60, 134.08, 133.34, 131.07, 130.82, 129.93, 129.87, 129.78, 129.70, 129.31, 129.01, 128.45, 124.97; HRMS (ESI) *m/z* 369.9804 (M+H).

2,3-methylenedioxy-10-methoxy-6-(trichloromethyl)phenanthridine(8d)
Yellow solid; Yield 38%; Mp (219.7–222.3°C); ^{1}H NMR (400 MHz, DMSO) δ 7.95 (d, J = 6.3 Hz, 1H), 7.81 (t, J = 8.3 Hz, 1H), 7.59 (d, J = 3.6 Hz, 2H), 7.31 (t, J = 7.8 Hz, 1H), 6.32 (s, 2H), 3.69 (s, 3H); HRMS (ESI) *m/z* 369.9804 (M+H).

2-methoxy-6-(trichloromethyl)phenanthridine (8e)
Yellowish-white solid; Yield 37%; Mp (119–120.9°C); ^{1}H NMR (400 MHz, $CDCl_3$): δ 8.96 (d, J = 8.2 Hz, 1H), 8.65 (d, J = 8.4 Hz, 1H), 8.19 (d, J = 9.0 Hz, 1H), 7.94–7.83 (m, 2H), 7.80–7.71 (m, 1H), 7.42 (dd, J = 9.0, 2.7 Hz, 1H), 4.05 (s, 3H); ^{13}C NMR (101 MHz, DMSO): δ 160.62, 149.93, 135.31, 134.27, 132.51, 131.38, 128.05, 127.82, 126.70, 124.59, 120.53, 120.27, 104.00, 98.71, 56.46; HRMS (ESI) *m/z* 325.9901 (M+H).

8,9-methylenedioxy-3-methoxy-6-(trichloromethyl)phenanthridine (8f)
Brown solid; Yield 32%; Mp (197.5–197.8°C); ^{1}H NMR (400 MHz, $CDCl_3$) δ 8.36–8.19 (m, 2H), 7.91 (s, 1H), 7.59 (d, J = 2.7 Hz, 1H), 7.35 (dd, J = 9.1, 2.7 Hz, 1H), 6.20 (s, 2H), 4.00 (s, 3H); ^{13}C NMR (101 MHz, DMSO): δ 160.32, 151.87, 141.76, 133.80, 124.77, 120.86, 119.65, 115.39, 109.96, 108.77, 104.45, 103.88, 103.25, 101.29, 100.64, 56.08; HRMS (ESI) *m/z* 369.9798 (M+H).

3-methoxy-6-(trichloromethyl)phenanthridine (8g)
Yellow solid; Yield 26%; Mp (175.1–175.3°C); ^{1}H NMR (400 MHz, $CDCl_3$): δ 8.93 (d, J = 8.7 Hz, 1H), 8.62 (d, J = 8.4 Hz, 1H), 8.48 (d, J = 9.1 Hz, 1H), 7.90–7.81 (m, 1H), 7.72–7.63 (m, 2H), 7.44–7.36 (m, 1H), 4.02 (s, 3H). ^{13}C NMR (101 MHz, DMSO): δ 160.81, 152.92, 142.01, 135.11, 131.94, 127.91, 126.82, 124.58, 123.65, 120.95, 119.09,119.06, 110.67, 98.60, 56.13. HRMS (ESI) *m/z* 325.9899 (M+H).

3,8-dimethoxy-6-(trichloromethyl)phenanthridine (8h)
Yellow solid; Yield 40%; Mp (146.7–147.2°C); ^{1}H NMR (400 MHz, $CDCl_3$): δ 8.52 (d, J = 9.2 Hz, 1H), 8.39 (d, J = 9.1 Hz, 1H), 8.28 (d, J = 2.6 Hz, 1H), 7.63 (d, J = 2.7 Hz, 1H), 7.50 (dd, J = 9.2, 2.6 Hz, 1H), 7.38 (dd, J = 9.1, 2.7 Hz, 1H), 4.01 (d, J = 2.4 Hz, 6H); ^{13}C NMR (101 MHz, DMSO): δ 160.06, 157.07, 151.84, 141.12, 129.60, 125.46, 124.08, 122.20, 121.18, 120.32, 119.35, 110.40, 108.81, 56.07, 55.91; HRMS (ESI) *m/z* 356.0009 (M+H).

3,10-dimethoxy-6-(trichloromethyl)phenanthridine (8i)
Yellow solid; Yield 37%; Mp (149.9–150.9°C). ^{1}H NMR (400 MHz, $CDCl_3$): δ 9.46 (d, J = 9.5 Hz, 1H), 8.60 (d, J = 8.5 Hz, 1H), 7.72–7.56 (m, 2H), 7.41–7.29 (m, 2H), 4.16 (s, 3H), 4.02 (s, 3H); ^{13}C NMR (101 MHz, DMSO) δ 159.78, 157.90, 152.59, 142.64, 129.33, 127.12, 125.28, 120.88, 120.27, 120.03, 118.54, 113.19, 110.92, 56.63, 55.97; HRMS (ESI) *m/z* 356.0009 (M+H).

3,8,10-trimethoxy-6-(trichloromethyl)phenanthridine (8j)
Yellow solid; Yield 35%; Mp (97–97.3°C); ^{1}H NMR (400 MHz, $CDCl_3$): δ 7.98 (d, J = 2.3 Hz, 1H), 7.70–7.60 (m, 3H), 7.35 (dd, J = 9.5, 2.9 Hz, 1H), 4.12 (s, 3H), 4.01 (d, J = 2.9 Hz, 6H); ^{13}C NMR (101 MHz, DMSO): δ 162.77, 159.25, 159.09, 157.44, 135.58, 130.82, 129.78, 129.00, 128.38, 120.61, 120.42, 110.71, 103.67, 101.47, 56.84, 55.95, 55.92; HRMS (ESI) *m/z* 386.0112 (M+H).

8,9-methylenedioxy-6-(trichloromethyl)phenanthridine (8k)
Yellowish solid; Yield 32%; Mp (164.4–165°C); ^{1}H NMR (400 MHz, $CDCl_3$) δ 8.43–8.36 (m, 1H), 8.30 (s, 1H), 8.27–8.20 (m, 1H), 8.02 (s, 1H), 7.73 (tt, J = 7.1, 5.3 Hz, 2H), 6.24 (d, J = 16.4 Hz, 2H); ^{13}C NMR (101 MHz, DMSO) δ 151.82, 151.22, 148.15, 140.03, 133.36, 130.68, 129.57, 125.30, 123.39, 118.56, 116.49, 114.73, 104.69, 103.41, 101.84; HRMS (ESI) *m/z* 339.9697 (M+H).

2,3-dimethoxy-6-(trichloromethyl)phenanthridine (8l)
Yellow solid; Yield 43%; Mp (174.5–176.1°C); ^{1}H NMR (400 MHz, $CDCl_3$): δ 8.95 (d, J = 8.6 Hz, 1H), 8.58 (d, J = 8.4 Hz, 1H), 8.16–8.08 (m, 4H), 7.86 (s, 2H), 7.74–7.58 (m, 4H), 7.49 (t, J = 7.8 Hz, 4H), 4.16 (s, 3H), 4.11 (s, 3H); ^{13}C NMR (101 MHz, DMSO): δ 167.75, 151.93, 151.86, 133.29, 131.16, 129.69, 128.99, 127.70, 126.77, 124.17, 119.98, 119.33, 110.56, 102.99, 56.68, 56.30; HRMS (ESI) *m/z* 356.0010 (M+H).

2,3,8-trimethoxy-6-(trichloromethyl)phenanthridine (8m)
Yellow solid; Yield 39%; Mp (125.5–126.9°C); ^{1}H NMR (400 MHz, $CDCl_3$): δ 8.48 (d, J = 9.1 Hz, 1H), 8.29 (d, J = 2.5 Hz, 1H), 7.77 (s, 1H), 7.62 (s, 1H), 7.50 (dd, J = 9.2, 2.6 Hz, 1H), 4.14 (s, 3H), 4.09 (s, 3H), 4.02 (s, 3H); ^{13}C NMR (101 MHz, DMSO): δ 157.06, 152.00, 151.26, 149.05, 135.36, 129.09, 128.95, 126.01, 121.63, 120.63, 120.29, 110.36, 108.35, 102.47, 56.64, 56.23, 55.89; HRMS (ESI) *m/z* 386.0115 (M+H).

8,10-dimethoxy-6-(trichloromethyl) phenanthridine (8n)
Yellow solid; Yield 39%; Mp (161.3–162°C); ^{1}H NMR (400 MHz, $CDCl_3$): δ 9.45–9.38 (m, 1H), 8.28–8.21 (m, 1H), 8.01 (d, J = 2.3 Hz, 1H), 7.71 (dd, J = 6.5, 3.5 Hz, 2H), 7.00 (d, J = 2.4 Hz, 1H), 4.13 (s, 3H), 4.02 (s, 3H); ^{13}C NMR (101 MHz, DMSO): δ 160.02, 158.37, 151.25, 139.93, 130.95, 130.05, 128.51, 127.15, 124.74, 122.76, 119.71, 103.62, 101.98, 99.01, 56.93, 56.04; HRMS (ESI) *m/z* 356.0007 (M+H).

Pharmacology

Cell Culture

A549, PC3, MCF-7, HepG2 and Hela cell lines were obtained from the Chinese Academy of Sciences Cell Bank. A549, Hela and PC3 were cultured in RPMI-1640 medium supplemented with 10% FBS, MCF-7 cells were maintained in MEM medium supplemented with 10% FBS, HepG2 cells were cultured in DMEM medium supplemented with 10% FBS. All the cell lines were cultured at humidified atmosphere containing 5% CO_2 at 37°C. The stock solutions (20 mM) of phenanthridine derivatives were prepared in DMSO and added at desired concentrations to the cell culture. DMSO concentration did not exceed 1:1,000 in the final culture.

MTT Assay

Cytotoxic activities of the phenanthridine derivatives was evaluated by MTT assay. The stock solutions of phenanthridine derivatives were diluted with culture medium. The cells were seeded in 96-well plates at a density 5 × 10^3 cells per well and incubated until confluency 90–95%, then each well was treated with 100 μL medium containing the desired concentrations of phenanthridine derivatives and incubated for 48 h. 20 μL MTT working solution (5 mg/mL) was then added to each well and incubated for another 4 h. At the end of incubation, the medium was carefully removed, and 200 μL DMSO was added. The optical density at 490 nm and 630 nm were then measured with a microplate reader (MODEL). The percentage of cell growth inhibition was calculated with the following equation: % inhibition = [1–(Sample group OD_{490} - Sample group OD_{630})/(Control group OD_{490}-Control group OD_{630})] × 100%. The IC_{50} values were calculated with Origin 7.5 software, and standard deviations of the IC_{50} values were obtained from at least 3 independent experiments.

DNA Top I and IIα Relaxation Assay *In vitro*

The human Top I and IIα inhibitory activity was determined by agarose gel electrophoresis. Reaction mixture was prepared with 0.5 μg pBR322 supercoiled DNA (TaKaRa) and human Top I (TaKaRa) or IIα (TopoGEN) enzyme in the absence or presence of compound in the Top reaction buffer (Top I: DNA Top I buffer 2 μL, DNA Top I 1U, 0.1% BSA 2 μL and sterile water up to 20 μL; Top IIα: DNA Top IIα buffer A 2 μL, DNA Top IIα buffer B 2 μL, DNA Top IIα 1U and sterile water up to 20 μL). After 30 min of incubation at 37°C, the reaction mixture was electrophoresed on 0.8% agarose gel at 80 V for 50 min with TAE running buffer. The gel was then immersed in the Genecolour I TM staining solution for 45 min and photographed under UV light.

Cell Cycle Assay

MCF-7 cells in logarithmic growth phase were seeded in 6-well plates (6 × 10^5 cells/well) and incubated with different doses of compound **8a** (0, 0.15, 0.3, and 0.6 μM) for 24 h. Cells were then washed twice with cold PBS and fixed in 70% precooled ethanol at 4°C for 12 h. After the fixation, cells were washed again with PBS

and stained with PI/RNase A for 30 min at room temperature, and eventually subjected to flow cytometry (CytoFLEX, Beckman Coulter). for cell cycle distribution determination.

Hoechst 33258 Staining

MCF-7 cells in logarithmic growth phase were seeded in 6-well plates (4×10^5 cells/well) and incubated with different doses of compound **8a** (0, 0.15, 0.3, and 0.6 μM) for 24 h. Cells were then washed twice with PBS and stained with Hoechst 33258 working solution for 30 min at 37°C under 5% CO_2. The morphological changes of apoptotic cells were observed with a fluorescence microscope (Leica DMI 4000B) with blue filter.

Annexin V/PI Detection

MCF-7 cells in logarithmic growth phase were seeded in 6-well plates (4×10^5 cells/well) and incubated with different doses of compound **8a** (0, 0.15, 0.3, and 0.6 μM) for 24 h. After the incubation, cells were washed with PBS, collected, resuspended with binding buffer from the Annexin V-FITC kit (Thermo fisher Co., USA), and then added with 5 μl annexin V-FITC and mixed gently. After 10 min of incubation, 1 μl PI was added to each sample and mixed gently. After incubation at room temperature for another 20 min in the dark, cells were subjected to flow cytometer (CytoFLEX, Beckman Coulter).

Western Blotting

MCF-7 cells were incubated with different doses of compound **8a** (0, 0.15, 0.3, and 0.6 μM) for 24 h, and then total cell proteins were extracted with RIPA buffer supplemented with 1:100 protease inhibitor (info) and phosphatase inhibitor (info). Sample protein concentrations were determined with BCA assay (ComWin Biotech Co., Beijing, China), then equal amounts of protein (30 μg) were mixed with sampling buffer and denatured for 5 min at 100°C. Resulting samples were then subjected to Sodium dodecyl sulfate-polyacrylamide electrophoresis (SDS-PAGE). After electrophoresis, proteins were transferred to polyvinylidene difluoride (PVDF) membrane (Millipore) and blocked with 5% fat-free dry milk in 1×Tris-buffered saline (TBST) for 2 h at room temperature. Membranes were then probed with Bcl-2 (rabbit, 1:1,000, Santa Cruz, CA), Bax (rabbit, 1:1,000, Santa Cruz, CA) and β-actin antibodies at 4°C overnight. The membranes were then washed with TBST three times and incubated with anti-rabbit secondary antibody (Santa Cruz, CA) and visualized with ECL-detecting reagents (ComWin Biotech Co., Beijing, China). The images were obtained from 6000 pro (Clinx Science Instruments Co., Ltd., Shanghai, China) and analyzed with Image Studio Lite software.

Statistical Analysis

Results were expressed as mean ± standard deviation (SD) of three independent experiments performed in triplicates ($n = 3$). SPSS 19.0 software were used for statistical analysis and the means between two groups were compared by one way analysis of variance (ANOVA) with Dunnett's test, $P < 0.05$ was considered significant.

DATA AVAILABILITY

The raw data supporting the conclusions of this manuscript will be made available by the authors, without undue reservation, to any qualified researcher.

AUTHOR CONTRIBUTIONS

WS and FY designed the project. MW, YC, QL, and QX performed the experiments. MW and LZ analyzed the data and wrote the manuscript. All authors discussed the results and contributed to the manuscript.

FUNDING

This work was supported by National Natural Science Foundation of China (Youth Found, Grant No. 81803343).

REFERENCES

1. Chaturvedi MM, Kumar A, Darnay BG, Chainy GB, Agarwal S, Aggarwal BB. Sanguinarine (pseudochelerythrine) is a potent inhibitor of NF-kappaB activation, IkappaBalpha phosphorylation, and degradation. *J Biol Chem.* (1997) 272:30129–34. doi: 10.1074/jbc.272.48.30129
2. Croaker A, King GJ, Pyne JH, Anoopkumar-Dukie S, Liu L. *Sanguinaria canadensis*: traditional medicine, phytochemical composition, biological activities and current uses. *Int J Mol Sci.* (2016) 17:17091414. doi: 10.3390/ijms17091414
3. Achkar IW, Mraiche F, Mohammad RM, Uddin S. Anticancer potential of sanguinarine for various human malignancies. *Future Med Chem.* (2017) 9:933–50. doi: 10.4155/fmc-2017-0041
4. Sarkar SM. Isolation from argemone oil of dihydrosanguinarine and sanguinarine; toxicity of sanguinarine. *Nature.* (1948) 162:265. doi: 10.1038/162265a0
5. Kalogris C, Garulli C, Pietrella L, Gambini V, Pucciarelli S, Lucci C, et al. Sanguinarine suppresses basal-like breast cancer growth through dihydrofolate reductase inhibition. *Biochem Pharmacol.* (2014) 90:226–34. doi: 10.1016/j.bcp.2014.05.014
6. Slaninová I, Pěnčíková K, Urbanová J, Slanina J, Táborská E. Antitumour activities of sanguinarine and related alkaloids. *Phytochemistry Rev.* (2014) 13:51–68. doi: 10.1007/s11101-013-9290-8
7. Zhang R, Wang G, Zhang PF, Zhang J, Huang YX, Lu YM, et al. Sanguinarine inhibits growth and invasion of gastric cancer cells via regulation of the DUSP4/ERK pathway. *J Cell Mol Med.* (2017) 21:1117–27. doi: 10.1111/jcmm.13043
8. Eun JP, Koh GY. Suppression of angiogenesis by the plant alkaloid, sanguinarine. *Biochem Biophys Res Commun.* (2004) 317:618–24. doi: 10.1016/j.bbrc.2004.03.077
9. Miao F, Yang XJ, Zhou L, Hu HJ, Zheng F, Ding XD, et al. Structural modification of sanguinarine and chelerythrine and their antibacterial activity. *Nat Prod Res.* (2011) 25:863–75. doi: 10.1080/14786419.2010.482055
10. Yang XJ, Miao F, Yao Y, Cao FJ, Yang R, Ma YN, et al. *In vitro* antifungal activity of sanguinarine and chelerythrine derivatives against phytopathogenic fungi. *Molecules.* (2012) 17:13026–35. doi: 10.3390/molecules171113026
11. Cee VJ, Chavez FJr, Herberich B, Lanman BA, Pettus LH, Reed AB, et al. Discovery and optimization of macrocyclic quinoxaline-pyrrolo-dihydropiperidinones as potent pim-1/2 kinase inhibitors. *ACS Med Chem Lett.* (2016) 7:408–12. doi: 10.1021/acsmedchemlett.5b00403

12. Maiti M, Nandi R, Chaudhuri K. Sanguinarine: a monofunctional intercalating alkaloid *FEBS Lett.* (1982) 142:280–4.
13. Champoux JJ. DNA topoisomerases: structure, function, and mechanism. *Annu Rev Biochem.* (2001) 70:369–413. doi: 10.1146/annurev.biochem.70.1.369
14. Wang JC. Cellular roles of DNA topoisomerases: a molecular perspective. *Nat Rev Mol Cell Biol.* (2002) 3:430–40. doi: 10.1038/nrm831
15. Chen XM, Zhang M, Fan PL, Qin YH, Zhao HW. Chelerythrine chloride induces apoptosis in renal cancer HEK-293 and SW-839 cell lines. *Oncol Lett.* (2016) 11:3917–24. doi: 10.3892/ol.2016.4520
16. Wang X, Tanaka M, Krstin S, Peixoto HS, Wink M. The interference of selected cytotoxic alkaloids with the cytoskeleton: an insight into their modes of action. *Molecules.* (2016) 21:906. doi: 10.3390/molecules21070906
17. Chang MC, Chan CP, Wang YJ, Lee PH, Chen LI, Tsai YL, et al. Induction of necrosis and apoptosis to KB cancer cells by sanguinarine is associated with reactive oxygen species production and mitochondrial membrane depolarization. *Toxicol Appl Pharmacol.* (2007) 218:143–51. doi: 10.1016/j.taap.2006.10.025
18. Kaminskyy V, Kulachkovskyy O, Stoika R. A decisive role of mitochondria in defining rate and intensity of apoptosis induction by different alkaloids. *Toxicol Lett.* (2008) 177:168–81. doi: 10.1016/j.toxlet.2008.01.009
19. Vrba J, Dolezel P, Vicar J, Ulrichova J. Cytotoxic activity of sanguinarine and dihydrosanguinarine in human promyelocytic leukemia HL-60 cells. *Toxicol In Vitro.* (2009) 23:580–8. doi: 10.1016/j.tiv.2009.01.016
20. Adhami VM, Aziz MH, Mukhtar H, Ahmad N. Activation of prodeath Bcl-2 family proteins and mitochondrial apoptosis pathway by sanguinarine in immortalized human HaCaT keratinocytes. *Clin Cancer Res.* (2003) 9:3176–82.
21. Ahsan H, Reagan-Shaw S, Breur J, Ahmad N. Sanguinarine induces apoptosis of human pancreatic carcinoma AsPC-1 and BxPC-3 cells via modulations in Bcl-2 family proteins. *Cancer Lett.* (2007) 249:198–208. doi: 10.1016/j.canlet.2006.08.018
22. Liu Y, Jiao R, Ma ZG, Liu W, Wu QQ, Yang Z, et al. Sanguinarine inhibits angiotensin II-induced apoptosis in H9c2 cardiac cells via restoring reactive oxygen species-mediated decreases in the mitochondrial membrane potential. *Mol Med Rep.* (2015) 12:3400–8. doi: 10.3892/mmr.2015.3841
23. Lee B, Lee SJ, Park SS, Kim SK, Kim SR, Jung JH, et al. Sanguinarine-induced G1-phase arrest of the cell cycle results from increased p27KIP1 expression mediated via activation of the Ras/ERK signaling pathway in vascular smooth muscle cells. *Arch Biochem Biophys.* (2008) 471:224–31. doi: 10.1016/j.abb.2008.01.008
24. Holy J, Lamont G, Perkins E. Disruption of nucleocytoplasmic trafficking of cyclin D1 and topoisomerase II by sanguinarine. *BMC Cell Biol.* (2006) 7:13. doi: 10.1186/1471-2121-7-13
25. Xu JY, Meng QH, Chong Y, Jiao Y, Zhao L, Rosen EM, et al. Sanguinarine inhibits growth of human cervical cancer cells through the induction of apoptosis. *Oncol Rep.* (2012) 28:2264–70. doi: 10.3892/or.2012.2024
26. Pica F, Balestrieri E, Serafino A, Sorrentino R, Gaziano R, Moroni G, et al. Antitumor effects of the benzophenanthridine alkaloid sanguinarine in a rat syngeneic model of colorectal cancer. *Anticancer Drugs.* (2012) 23:32–42. doi: 10.1097/CAD.0b013e32834a0c8e
27. Sun M, Liu C, Nadiminty N, Lou W, Zhu Y, Yang J, et al. Inhibition of Stat3 activation by sanguinarine suppresses prostate cancer cell growth and invasion. *Prostate.* (2012) 72:82–9. doi: 10.1002/pros.21409
28. Park SY, Jin ML, Kim YH, Lee SJ, Park G. Sanguinarine inhibits invasiveness and the MMP-9 and COX-2 expression in TPA-induced breast cancer cells by inducing HO-1 expression. *Oncol Rep.* (2014) 31:497–504. doi: 10.3892/or.2013.2843
29. Basini G, Bussolati S, Santini SE, Grasselli F. Sanguinarine inhibits VEGF-induced angiogenesis in a fibrin gel matrix. *Biofactors.* (2007) 29:11–8. doi: 10.1002/biof.5520290102
30. Dong XZ, Zhang M, Wang K, Liu P, Guo DH, Zheng XL, et al. Sanguinarine inhibits vascular endothelial growth factor release by generation of reactive oxygen species in MCF-7 human mammary adenocarcinoma cells. *Biomed Res Int.* (2013) 2013:517698. doi: 10.1155/2013/517698
31. De Stefano I, Raspaglio G, Zannoni GF, Travaglia D, Prisco MG, Mosca M, et al. Antiproliferative and antiangiogenic effects of the benzophenanthridine alkaloid sanguinarine in melanoma. *Biochem Pharmacol.* (2009) 78:1374–81. doi: 10.1016/j.bcp.2009.07.011
32. Zhou Y, Wu C, Dong X, Qu J. Synthesis of 6-trichloromethylphenanthridines by transition metal-free radical cyclization of 2-isocyanobiphenyls. *J Org Chem.* (2016) 81:5202–8. doi: 10.1021/acs.joc.6b00885
33. Fuchs Y, Steller H. Programmed cell death in animal development and disease. *Cell.* (2011) 147:742–58. doi: 10.1016/j.cell.2011.10.033
34. Nunez G, Clarke MF. The Bcl-2 family of proteins: regulators of cell death and survival. *Trends Cell Biol.* (1994) 4:399–403. doi: 10.1016/0962-8924(94)90053-1
35. Boise LH, Gottschalk AR, Quintans J, Thompson CB. Bcl-2 and Bcl-2-related proteins in apoptosis regulation. *Curr Top Microbiol Immunol.* (1995) 200:107–21. doi: 10.1007/978-3-642-79437-7_8
36. Zhang H, Xu Q, Krajewski S, Krajewska M, Xie Z, Fuess S, et al. BAR: An apoptosis regulator at the intersection of caspases and Bcl-2 family proteins. *Proc Natl Acad Sci USA.* (2000) 97:2597–602. doi: 10.1073/pnas.97.6.2597

Conflict of Interest Statement: The authors declare that the research was conducted in the absence of any commercial or financial relationships that could be construed as a potential conflict of interest.

frontiers in Oncology

MINI REVIEW
published: 17 April 2019
doi: 10.3389/fonc.2019.00268

Diverse Mechanisms of BRAF Inhibitor Resistance in Melanoma Identified in Clinical and Preclinical Studies

Stephen A. Luebker and Scott A. Koepsell*

Department of Pathology and Microbiology, University of Nebraska Medical Center, Omaha, NE, United States

BRAF inhibitor therapy may provide profound initial tumor regression in metastatic melanoma with BRAF V600 mutations, but treatment resistance often leads to disease progression. A multi-center analysis of BRAF inhibitor resistant patient tissue samples detected genomic changes after disease progression including multiple secondary mutations in the MAPK/Erk signaling pathway, mutant BRAF copy number gains, and BRAF alternative splicing as the predominant putative mechanisms of resistance, but 41.7% of samples had no known resistance drivers. *In vitro* models of BRAF inhibitor resistance have been developed under a wide variety of experimental conditions to investigate unknown drivers of resistance. Several *in vitro* models developed genetic alterations observed in patient tissue, but others modulate the response to BRAF inhibitors through increased expression of receptor tyrosine kinases. Both secondary genetic alterations and expression changes in receptor tyrosine kinases may increase activation of MAPK/Erk signaling in the presence of BRAF inhibitors as well as activate PI3K/Akt signaling to support continued growth. Melanoma cells that develop resistance *in vitro* may have increased dependence on serine or glutamine metabolism and have increased cell motility and metastatic capacity. Future studies of BRAF inhibitor resistance *in vitro* would benefit from adhering to experimental parameters that reflect development of BRAF inhibitor resistance in patients through using multiple cell lines, fully characterizing the dosing strategy, and reporting the fold change in drug sensitivity.

Keywords: melanoma, BRAF inhibitor, vemurafenib, dabrafenib, cell line, drug resistance, metabolism, invasion

OPEN ACCESS

Edited by:
Zhe-Sheng Chen,
St. John's University, United States

Reviewed by:
Karishma Rajani,
Mayo Clinic, United States
Yun Dai,
Virginia Commonwealth University, United States

****Correspondence:***
Stephen A. Luebker
stephen.luebker@unmc.edu

Specialty section:
This article was submitted to Cancer Molecular Targets and Therapeutics, a section of the journal Frontiers in Oncology

Received: *19 December 2018*
Accepted: *25 March 2019*
Published: *17 April 2019*

Citation:
Luebker SA and Koepsell SA (2019) Diverse Mechanisms of BRAF Inhibitor Resistance in Melanoma Identified in Clinical and Preclinical Studies. Front. Oncol. 9:268. doi: 10.3389/fonc.2019.00268

INTRODUCTION

Melanoma makes up 6% of estimated new cancer cases in men and 4% in women, and incidence has been increasing since 1975 (1). BRAF mutations occur in more than 50% of cutaneous melanomas, and BRAF V600E occurs most frequently, which confers constitutive monomeric activation of BRAF kinase activity (2, 3). The identification of oncogenic BRAF signaling increased interest in targeted inhibitors toward mutant BRAF variants, and the FDA has approved two targeted BRAF inhibitors, vemurafenib in 2011 and dabrafenib in 2013, for treatment of non-resectable BRAF V600E/K mutant melanoma. Despite the rapid response and short-term increases in patient survival, resistance to BRAF inhibition persists. In 2017, combination therapy of dabrafenib plus the MEK inhibitor, trametinib was FDA approved for treatment of melanoma to forestall the development of BRAF inhibitor resistance. This review summarizes the potential events driving

BRAF inhibitor resistance detected in patient tissue and contrasts them with *in vitro* studies of BRAF inhibitor resistance through comparison of methods and results.

BRAF Inhibitor Resistance in Patients With Melanoma

Phase-3 clinical trials of vemurafenib treatment for BRAF V600E/K melanoma demonstrated improvements in median progression-free survival relative to dacarbazine (6.9 months vs. 1.6 months) and increased median overall survival (13.6 vs. 9.7 months) (4). Phase-3 clinical trials of dabrafenib treatment for BRAFV600E melanoma observed improvements in median progression free survival relative to dacarbazine (5.1 vs. 2.7 months) (5). Phase-3 clinical trials of dabrafenib and trametinib combination therapy vs. dabrafenib alone found increased median progression-free survival (11.1 vs. 8.8 months) and increased median overall survival (25.1 vs. 18.7 months) (6). Treatment with BRAF/MEK inhibitors often provides remarkable disease regression initially, but resistance to therapy frequently develops within 12 months as indicated by median progression-free survival.

BRAF inhibitor resistance in melanoma is supported through recovery of MAPK/Erk signaling or activation of PI3K/Akt signaling. These pathways may be activated through mutations, copy-number alterations, or changes in expression. A summary diagram including these signaling pathways and a breakdown of common alterations supporting BRAF inhibitor resistance are illustrated in **Figure 1**. A multi-center analysis of BRAF inhibitor resistance combining three comprehensive genome sequencing studies of pre-treatment and post-progression cases of melanoma identified resistance driving events in 58.3% (77/132) of samples obtained from 100 individuals, but failed to identify any known mechanism of resistance in the remaining 41.7% of samples (7). Johnson et al. provide a complete breakdown of the frequency of the resistance mechanisms within this combined data set. Multiple resistance mechanisms were observed within individual samples and unique resistance mechanisms were observed between samples from the same patient. BRAF amplification and alternative splicing were observed most frequently followed by NRAS mutations and MEK1/2 mutations. Mutations in the PI3K/Akt pathway are less frequently observed in patient samples. Despite increased median progression-free survival when treating patients with dabrafenib plus trametinib relative to dabrafenib alone, treatment resistance still develops. Patients treated with dabrafenib/trametinib combination therapy developed alterations in the same genes that support single-agent resistance including MEK1/2 mutations, BRAF amplification, BRAF alternative splicing, and NRAS mutations between pre-treatment and post-progression samples (8, 9). Clinical studies of BRAF inhibitor resistance leave an incomplete picture of the diverse set of mechanisms supporting BRAF inhibitor resistance. This review summarizes recent studies in which BRAF inhibitor resistance was induced stochastically in cell lines via prolonged exposure to a BRAF inhibitor. Major mechanisms identified in these studies are included in **Figure 1** and discussed in more detail in this review.

BRAF Inhibitor Resistance in Melanoma Cell Lines

Receptor Tyrosine Kinase Expression

Receptor tyrosine kinases may act as upstream activators of MAPK/Erk signaling, and increased expression in BRAF inhibitor resistant cells has been described in multiple studies. Shaffer et al. demonstrated that resistance to BRAF inhibitors in WM989 and WM983B cells occurs through non-heritable, transient expression of multiple resistance-associated genes including receptors like AXL receptor tyrosine kinase (AXL), epidermal growth factor receptor (EGFR), fibroblast growth factor receptor 1 (FGFR1), and platelet-derived growth factor receptor beta (PDGFRB) among others (10). Other studies have detected expression changes in these genes but do not point to a single pattern of expression change. Nazarian et al. demonstrated that increased expression of PDGFRB conferred resistance to M229 and M238 cells, but Jazirehi et al. found that resistant M238 cells had increased expression of EGFR and decreased expression of PDGFRB (11, 12). Shao et al. found resistant WM793 and M238 cells both had increased PDGFRB but decreased Insulin-like growth factor 1 receptor (IGF1R) expression (13). Increased PDGFRB expression has also been described in resistant A375 cells (14). In two other studies using A375 cells, increased expression of fibroblast growth factor receptor 3 (FGFR3) expression was associated with BRAF inhibitor resistance (15, 16). Resistant A375 cells have also been shown to increase expression of IGF1R while resistant SKMEL28 cells increased expression of PDGFRB (17). In a separate study, resistant SKMEL28 cells had increased expression of both EGFR and PDGFRB (18). Jazirehi et al. found that resistant M249 cells had increased expression of EGFR, KIT proto-oncogene receptor tyrosine kinase (KIT), MET proto-oncogene receptor tyrosine kinase (MET), and PDGFRB with decreased IGF1R (11). Resistance-associated gene expression may occur through loss of SOX10 expression and gain of JUN, AP-1, and TEAD transcription factor activity (10). EGFR expression may be regulated through MITF expression, but both increased and decreased MITF expression have been observed in BRAF inhibitor resistant cell lines (19, 20). Sun et al. demonstrated that miR-7 was significantly downregulated in resistant A375 and MEL-CV cells, and exogenous expression could reduce resistance with EGFR, IGF1R, CRAF, and AXL as potential targets (21). Overall, changes in growth factor expression are inconsistent between studies using the same cell lines. Increased expression of any growth factor receptor that activates MAPK/Erk may potentially drive resistance in melanoma.

Secondary MAPK/Erk Mutations

In addition to upstream activation of MAPK/Erk through receptor tyrosine kinases, increased MAPK/Erk signaling may be achieved through direct alteration to members of the RAS/RAF/MEK/Erk signaling cascade. Secondary BRAF mutations and alternative BRAF splicing have been shown to induce vemurafenib resistance in multiple cell lines (19, 22). In a patient derived xenograft model, increased BRAF V600E expression sustained resistance, and cells demonstrated

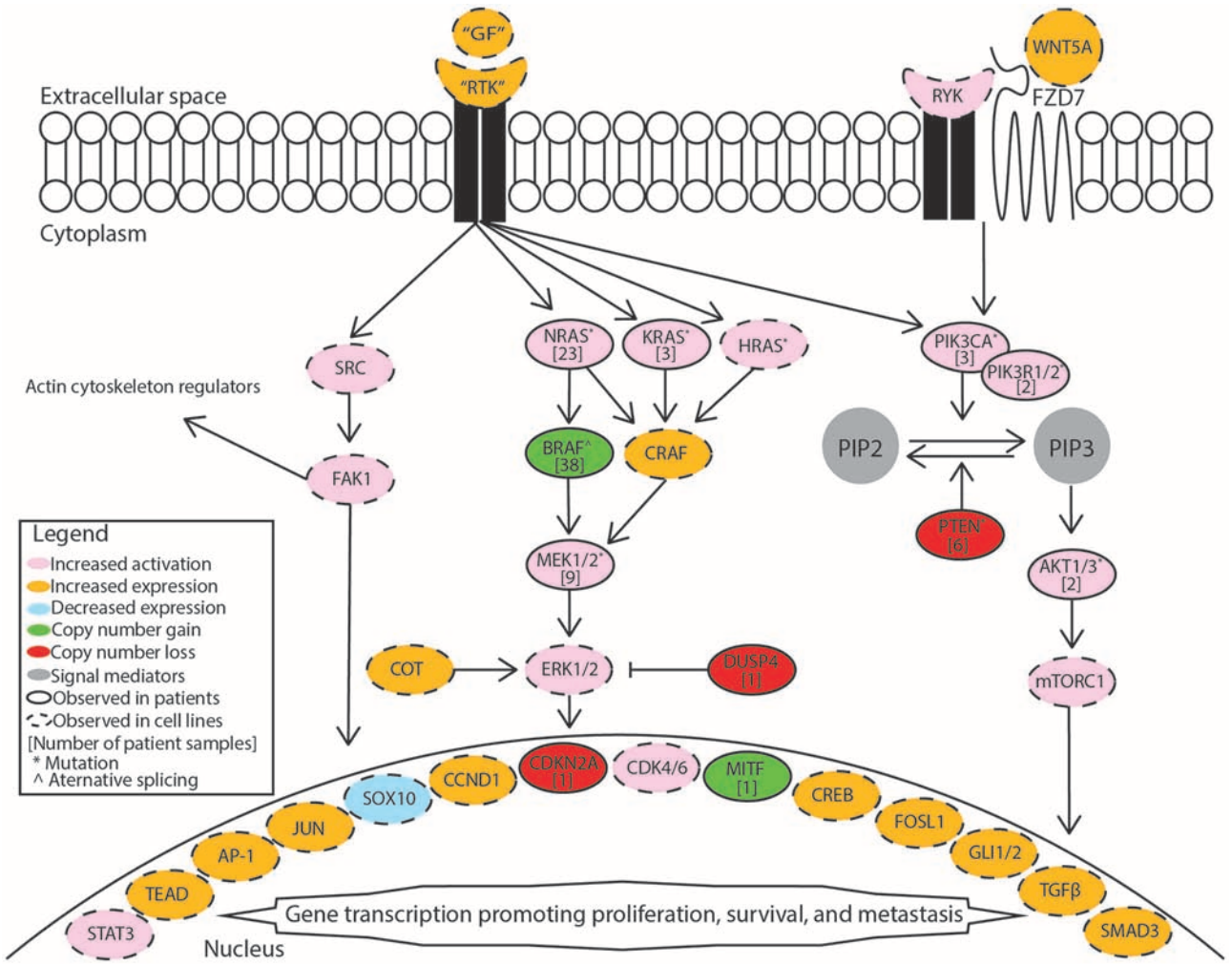

FIGURE 1 | Mechanisms supporting BRAF inhibitor resistance in melanoma. Receptor tyrosine kinases (RTK) include AXL receptor tyrosine kinase (AXL), epidermal growth factor receptor (EGFR), fibroblast growth factor receptor 1 (FGFR1), fibroblast growth factor receptor 3 (FGFR3), platelet-derived growth factor receptor beta (PDGFRB), MET proto-oncogene receptor tyrosine kinase (MET), and KIT proto-oncogene receptor tyrosine kinase (KIT). Growth factors (GF) correspond to the specific receptor tyrosine kinase. The MAPK/Erk pathway includes the Ras GTPases (N/K/HRAS), Serine/threonine-protein kinase B-raf (BRAF), RAF proto-oncogene serine/threonine-protein kinase (CRAF), mitogen-activated and extracellular signal-regulated kinase kinase 1 or 2 (MEK1/2), extracellular signal-regulated kinase 1 or 2 (ERK1/2), cancer Osaka thyroid (COT), and dual specificity protein phosphatase 4 (DUSP4). The PI3K/Akt pathway includes phosphatidylinositol-4,5-bisphosphate 3-kinase catalytic subunit alpha (PIK3CA), phosphatidylinositol 3-kinase regulatory subunit 1 or 2 (PIK3R1/2), phosphatidylinositol 4,5-bisphosphate (PIP2), phosphatidylinositol 3,4,5-trisphosphate (PIP3), phosphatase and tensin homolog (PTEN), AKT serine/threonine kinase 1 or 2 (AKT1/2), mammalian target of rapamycin complex 1 (mTORC1). Src signaling factors include SRC proto-oncogene non-receptor tyrosine kinase (SRC) and focal adhesion kinase 1 (FAK1). Transcription factors include signal transducer and activator of transcription 3 (STAT3), TEA domain transcription factor protein family (TEAD), activator protein 1 complex (AP-1), Jun proto-oncogene AP-1 transcription factor subunit (JUN), SRY-box 10 (SOX10), melanocyte inducing transcription factor (MITF), cyclic AMP responsive element binding protein family (CREB), FOS like 1 AP-1 transcription factor subunit (FOSL1), GLI family zinc finger 1 or 2 (GLI1/2), transforming growth factor beta (TGFβ), SMAD family member 3 (SMAD3). Cell cycle regulators included cyclin D1 (CCND1), cyclin dependent kinase 4 or 6 (CDK4/6). Non-canonical Wnt signaling mediators include receptor like tyrosine kinase (RYK), frizzled class receptor 7 (FZD7), and Wnt family member 5A (WNT5A).

drug-dependence for continued proliferation (23). Resistant tumors derived from 1205LU cells in a mouse xenograft model contained distinct alternative BRAF splicing events in two tumors and HRAS Q61K mutation in one tumor (24). Other alterations within RAS/RAF/MEK/Erk cascade have been observed in SKMEL28, A375, COLO829, and M249 cells, including COT overexpression and NRAS Q61K mutation (12, 17). Dabrafenib resistant A375 and MEL-RMU cells were found to have mutations in MEK1 and NRAS as previously described in vemurafenib resistant cells (25, 26). NRAS mutations may also make cell lines cross-resistant to MEK inhibitors due to elevated PI3K/Akt signaling (27). Resistant A375 cells were found to have an NRAS G13R mutation, high expression of CRAF, and increased Akt phosphorylation (28). Resistant A375 cells with a KRAS K117N also had elevated expression of CRAF and activation of Akt (29). Resistant M249 cells and M376 cells with secondary NRAS mutations had increased Akt activation (30). Resistant WM793 cells with

secondary NRAS Q61K mutation require CRAF expression and SHOC2 scaffold protein to re-activate MAPK/Erk (31). *In vitro* models of BRAF inhibitor resistance indicate that secondary mutations may support increased activation of MAPK/Erk in the presence of inhibitor or support sustained growth through activation of PI3K/Akt signaling.

Alternative Resistance Pathways

Downstream effectors of PI3K/Akt activation promote survival of resistant cells. PI3K/Akt activation upregulates AEBP1 through increased CREB binding, and increased AEBP1 leads to IκBα degradation and NF-κB activation (32). A375, SKMEL28, and WM239 cells resistant to either dabrafenib or vemurafenib all had increased expression of Mcl-1 relative to their pre-treatment counterparts, which promotes cell survival through inhibition of apoptosis, and Mcl-1 expression may be regulated by STAT, cAMP, and NF-κB binding sites (33). Growth factor receptors may also cross activate PI3K/Akt separately or in addition to MAPK/Erk activation. Resistance induced in SKMEL28 cells increased expression of EGFR and activated Akt (34). Resistant LM17 cells had increased IGF1R expression as well as increased Akt phosphorylation (35). Increased expression of WNT5A in A375 and MEL-264 was correlated with increased phosphorylation of Akt and activation of RYK and FZD7 receptors supporting non-canonical Wnt signaling (36). PI3K/Akt activation in multiple BRAF inhibitor resistant melanoma cell lines also up-regulates of FOSL1, which drives secretion of multiple factors from tumor cells that support surrounding tumor growth (37). Melanoma cells may support the resistance of surrounding cells in addition to other stromal cells. Hepatocyte growth factor (HGF) secretion by surrounding stromal cells in co-culture supports tumor growth in the presence of BRAF inhibitors through activation of the MET receptor tyrosine kinase and downstream MAPK/Erk activation (38). The adaptive resistance of melanoma cells may be supported through both neighboring cancer and non-cancer cells. MAPK/Erk signaling and/or PI3K/Akt signaling may be activated in BRAF inhibitor resistant cells frequently through common mechanisms.

Phenotypic Changes in BRAF Inhibitor Resistant Cell Lines

Increased Motility and Invasion

Resistant cell lines acquire a more invasive phenotype characterized by increased cell motility and metastatic capacity. Multiple studies have noted increased invasive capacity of BRAF inhibitor resistant melanoma cell lines, and recent proteomic studies of melanoma cell lines before and after developing BRAF inhibitor resistance have specifically characterized differences in kinase expression and changes in phosphorylation. Quantitative phosphoproteomics of vemurafenib resistant LM-MEL-28 cells demonstrated increased activation of MAPK/Erk signaling and de-phosphorylation of key cytoskeletal regulators (39). Activity-based protein profiling of kinases in WM164, WM793, A375, and 1205LU cells detected increased ATP uptake by FAK1, SLK, LYN, PRKDC, and KCC2D, but overall changes between cell lines showed differences in differential phosphorylation (40). Phospho-array analysis and quantitative phosphoproteomics identified increased EGFR phosphorylation in vemurafenib resistant A375 and COLO829 cell lines leading to Src family kinase phosphorylation and STAT3 activation, which was associated with increased invasion and phosphorylation of cytoskeletal proteins (41). The increase in cytoskeletal remodeling also has downstream effects in cell signaling. For example, actin remodeling has been shown to increase YAP/TAZ nuclear localization in BRAF inhibitor resistant melanoma cells, and YAP/TAZ nuclear localization increases expression of EGFR, AKT, and MYC (42). The expression of receptor tyrosine kinases is associated with the invasive behavior of melanoma cell lines through increased metalloprotease expression. EGFR signaling was found to drive resistance in SKMEL28 cells, and resistance was also associated with upregulation of MMP2 and downregulation of the MMP regulator, TIMP2 (43). Increased expression of EGFR in SKMEL28 cells was also correlated with increased activation of Non-canonical Hedgehog Signaling (GLI1, GLI2, TGFβ, and SMAD3), and inhibition of GLI1 and GLI2 increased vemurafenib sensitivity while decreasing invasiveness (44). Dabrafenib resistant A375 cells had increased expression of epithelial to mesenchymal transition markers including CD90 and decreased expression of E-cadherin with increased cell motility (45). A separate study of dabrafenib resistant A375 cells also detected increased secretion of VEGFA and MMP9, which was associated with increased invasiveness (46).

Metabolism

Alterations in the metabolism of BRAF inhibitor resistant cells have also been described, including increased dependence on serine or glutamine. Vemurafenib resistant SKMEL28 were dependent on serine metabolism, and knockout of PHGDH or depletion of serine in the media reduced viability of resistant cells (47). Additionally, vemurafenib resistant M229 and M249 cells or vemurafenib/selumetinib dual treatment resistant M249 cells had increased glutamine uptake and were dependent on glutamine for survival independently of the underlying mechanism of resistance (48). More complex metabolic reprogramming may occur during the development of BRAF inhibitor resistance. Gene set enrichment of KEGG pathways using quantitative phosphoproteomic analysis of vemurafenib resistant LM-MEL-28 cells detected enrichment in DNA replication and cell cycle but decreases in glycolysis/gluconeogenesis, fatty acid metabolism, valine/leucine/isoleucine degradation, pyruvate metabolism, and tryptophan metabolism (39).

Future Directions of *in vitro* Research

McDermott et al. have recently published a general review of important considerations for developing *in vitro* resistance to targeted inhibitors and chemotherapeutic agents in cancer cell lines (49). Important considerations for *in vitro* models of BRAF inhibitor resistance in melanoma cell lines include choice of cell line, dosing strategy, and resistant cell selection criteria. Examples of current methods that have been applied to A375 cells are summarized in **Table 1**. This review focuses on studies that

develop resistant cell lines through drug treatment and excludes studies of primary resistance or genetically induced resistance.

Selecting Cell Lines

The first major consideration in this type of model is the degree of heterogeneity between cells. There is a great deal of cell-to-cell heterogeneity in melanoma *in vivo* (51). Sub-clones may harbor mutations conferring primary resistance to BRAF inhibitors. Selection of single-cell derived clones may reduce the heterogeneity observed within a single cell line. Studies show that there are genetic differences between cell lines and tumors *in vivo*, and only a few cell lines are most frequently used (52–56). *In vitro* resistance studies would benefit from using multiple cell lines to compare resistance mechanisms and potential novel combination therapy outcomes. The use of multiple cell lines also helps verify findings by highlighting mechanisms observed across cells types as opposed to findings that are specific only to that clone or test system.

Treatment Strategy

The treatment strategy employed to induce resistance in cell lines *in vitro* may or may not represent how the drug is administered clinically. Vemurafenib is administered as 960 mg tablets twice daily and reaches an average maximum plasma concentration of 4.8 ± 3.34 μg/ml after 8 h and 61.4 ± 22.76 μg/ml after 168 h with a half-life of 34.1 ± 19.66 h (57). Dabrafenib is administered as 150 mg oral tablets twice daily and reaches an average maximum plasma concentration of 986 ng/ml in a median 2 h with a half-life of 5 h (58). Both dabrafenib and vemurafenib quickly reach a high plasma concentration and have long half-lives, which would be best represented by continuously treating cells to develop resistance. Fofaria et al. employed a pulsed treatment strategy, which includes a treatment window followed by a recovery period, to generate vemurafenib resistant cell lines (33). A pulsed treatment strategy does not reflect how the drug is administered clinically. However, it has been shown that lower vemurafenib plasma concentration was significantly associated with higher likelihood of tumor progression, and patients had high inter-individual variability in vemurafenib plasma concentration (13.0–109.8 μg/ml) (59). Others have noted that the melanoma cell lines may become dependent on the presence of the BRAF inhibitor for continued growth and continuous treatment is often required, which may potentially be mitigated through a pulsed treatment method (13, 28, 34, 60). Mechanisms regulating development of resistance in each type of model may be different, and clear distinctions should be made between which type of model was employed. Data obtained from studies that use drug exposure methods never observed in patients should be interpreted with caution.

Defining Resistance

There is no standard for defining when a cell line is drug resistant. The selection criteria used to define treatment resistance critically influences results. Ideally the fold change in drug sensitivity should be reported along with the duration of drug exposure. Treatment durations for studies of A375 cells range from 6 days to 1 year of treatment, and fold change in drug sensitivity

TABLE 1 | *In vitro* BRAF inhibitor resistance in A375 melanoma cells.

References	Drug details	Treatment strategy	Dose (μM)	Clonal selection	Time to resistance	IC50 (μM)	Resistance driver	Pathway reactivation
Cordaro et al. (45)	Dabrafenib	Increasing continuous	NA	None	4 weeks	0.0095–110.5	Undetermined	Undetermined
Greger et al. (25)	Dabrafenib	Increasing continuous	up to 1.6	Single cell derived clones	NA	0.028 to >10	MEK1 K59del	pErk
Caporali et al. (46)	Dabrafenib	Increasing continuous	0.001–1.5	None	4 months	0.001041 to >10	Undetermined	pErk and pAkt
Zeiderman et al. (50)	Vemurafenib	Continuous	1	None	1 year	NA	Undetermined	Undetermined
Smyth et al. (14)	Vemurafenib	Continuous	2	None	3 weeks	0.087 to > 10	Undetermined	Undetermined
Jameson et al. (17)	Vemurafenib	Continuous	1	Colonies by limiting dilution	4-6 weeks	0.287–13.47	PDGFRB overexpression	Undetermined
Graziani et al. (28)	Vemurafenib	Increasing continuous	up to 2.5	None	3 months	1.47–20.37	NRAS G13R and CRAF overexpression	pErk and pAkt
Anastas et al. (36)	Vemurafenib	Increasing continuous	2	None	10 weeks	NA	WNT5A overexpression	pAkt
Yadav et al. (15)	Vemurafenib	Increasing continuous	0.2–2	None	4 months	0.085–4.8	FGFR3 phosphorylation	pErk
Girotti et al. (41)	Vemurafenib	Increasing continuous	0.1–2	None	2 months	0.155–5.76	EGFR phosphorylation	pErk and pAkt
Ji et al. (19)	Vemurafenib	Increasing continuous	0.5–10	None	NA	> 10-fold	BRAF splicing	pErk and pAkt
Muller et al. (20)	Vemurafenib	Increasing continuous	up to 3	None	NA	NA	MITF loss	pErk
Sharma et al. (40)	Vemurafenib	Continuous	2.5	None	3 months	NA	Undetermined	Undetermined
Wang et al. (18)	Vemurafenib	Increasing continuous	up to 2.5	None	3 months	0.57–28.9	PDGFRB overexpression	pERK and pAKT
Sun et al. (21)	Vemurafenib	Increasing continuous	up to 2	None	6 months	NA	EGFR, IGF1R, and CRAF overexpression	pERK
Obenauf et al. (37)	Vemurafenib	Increasing continuous	1–3	Low density seeding colonies	8 weeks	NA	EGFR and MET overexpression	pERK
Su et al. (29)	Vemurafenib	Increasing continuous	NA	None	3 months	86–119-fold	KRAS K117N	pERK and pAKT
Fofaria et al. (33)	Vemurafenib	Pulsed	0.2–10	None	1 year	0.1–3	Undetermined	pERK

ranges from 3x to more than 100x (**Table 1**). Correlation to drug levels observed in patients should also be considered. Care must also be taken when reporting drug sensitivity since common colorimetric assays may not be accurate or reproducible due to variations in growth rate; a cell counting based method should be employed when possible (61, 62). Multiple studies have observed changes in cell line growth rate after developing treatment resistance, which may be dependent on the presence of drug (13, 34, 47, 60). Growth rate changes may confound the measurement of drug sensitivity between treatment resistant and pre-treatment cells.

CONCLUSION

Although treatment with BRAF inhibitors provides rapid response in most patients, treatment resistance persists. The few clinical studies of BRAF inhibitor resistance in patients indicate that genetic alterations that activate MAPK/Erk make up half of resistance mechanisms. Preclinical studies of BRAF inhibitor resistance in melanoma support the mechanisms observed in patients and indicate that the development of resistance is more complex than single mutations. *In vitro* models may be very helpful in studying mechanisms in the other half of patients with no known genetic driver of BRAF inhibitor resistance. Overall, BRAF inhibitor resistance depends on oncogenic signaling through reactivation of MAPK/Erk or activation of PI3K/Akt, which may be acquired by directly affecting genes in each pathway, by upregulation of receptor tyrosine kinases, or by affecting downstream signaling. BRAF inhibitor resistance increases invasiveness through changes in phosphorylation actin cytoskeleton regulators and increased extracellular matrix metalloprotease expression. Resistant cells have also been shown to undergo metabolic reprogramming characterized by increased glutamine or serine dependence. A375 cells have been used to model BRAF inhibitor resistance across multiple studies, but the methods and conclusions vary. To improve preclinical *in vitro* research, future studies of BRAF inhibitor resistance in melanoma should include multiple cell lines, consider a continuous-dose treatment strategy, and report drug sensitivity in order to facilitate better comparison across studies.

AUTHOR CONTRIBUTIONS

All authors listed have made a substantial, direct and intellectual contribution to the work, and approved it for publication.

FUNDING

This work was funded by the University of Nebraska Medical Center Chancellor's Program of Excellence Physician-Scientist Training Program.

REFERENCES

1. Siegel RL, Miller KD, Jemal A. Cancer statistics, 2018. *CA Cancer J Clin.* (2018) 68:7–30. doi: 10.3322/caac.21442
2. Zhang T, Dutton-Regester K, Brown KM, Hayward NK. The genomic landscape of cutaneous melanoma. *Pigment Cell Melanoma Res.* (2016) 29:266–83. doi: 10.1111/pcmr.12459
3. Menzies AM, Haydu LE, Visintin L, Carlino MS, Howle JR, Thompson JF, et al. Distinguishing clinicopathologic features of patients with V600E and V600K BRAF-mutant metastatic melanoma. *Clin Cancer Res.* (2012) 18:3242–9. doi: 10.1158/1078-0432.CCR-12-0052
4. McArthur GA, Chapman PB, Robert C, Larkin J, Haanen JB, Dummer R, et al. Safety and efficacy of vemurafenib in BRAF(V600E) and BRAF(V600K) mutation-positive melanoma (BRIM-3): extended follow-up of a phase 3, randomised, open-label study. *Lancet Oncol.* (2014) 15:323–32. doi: 10.1016/S1470-2045(14)70012-9
5. Hauschild A, Grob JJ, Demidov LV, Jouary T, Gutzmer R, Millward M, et al. Dabrafenib in BRAF-mutated metastatic melanoma: a multicentre, open-label, phase 3 randomised controlled trial. *Lancet.* (2012) 380:358–65. doi: 10.1016/S0140-6736(12)60868-X
6. Long GV, Stroyakovskiy D, Gogas H, Levchenko E, de Braud F, Larkin J, et al. Dabrafenib and trametinib versus dabrafenib and placebo for Val600 BRAF-mutant melanoma: a multicentre, double-blind, phase 3 randomised controlled trial. *Lancet.* (2015) 386:444–51. doi: 10.1016/S0140-6736(15)60898-4
7. Johnson DB, Menzies AM, Zimmer L, Eroglu Z, Ye F, Zhao S, et al. Acquired BRAF inhibitor resistance: a multicenter meta-analysis of the spectrum and frequencies, clinical behaviour, and phenotypic associations of resistance mechanisms. *Eur J Cancer.* (2015) 51:2792–9. doi: 10.1016/j.ejca.2015.08.022
8. Wagle N, Van Allen EM, Treacy DJ, Frederick DT, Cooper ZA, Taylor-Weiner A, et al. MAP kinase pathway alterations in BRAF-mutant melanoma patients with acquired resistance to combined RAF/MEK inhibition. *Cancer Discov.* (2014) 4:61–8. doi: 10.1158/2159-8290.CD-13-0631
9. Long GV, Fung C, Menzies AM, Pupo GM, Carlino MS, Hyman J, et al. Increased MAPK reactivation in early resistance to dabrafenib/trametinib combination therapy of BRAF-mutant metastatic melanoma. *Nat Commun.* (2014) 5:5694. doi: 10.1038/ncomms6694
10. Shaffer SM, Dunagin MC, Torborg SR, Torre EA, Emert B, Krepler C, et al. Rare cell variability and drug-induced reprogramming as a mode of cancer drug resistance. *Nature.* (2017) 546:431–5. doi: 10.1038/nature22794
11. Jazirehi AR, Nazarian R, Torres-Collado AX, Economou JS. Aberrant apoptotic machinery confers melanoma dual resistance to BRAF(V600E) inhibitor and immune effector cells: immunosensitization by a histone deacetylase inhibitor. *Am J Clin Exp Immunol.* (2014) 3:43–56.
12. Nazarian R, Shi H, Wang Q, Kong X, Koya RC, Lee H, et al. Melanomas acquire resistance to B-RAF(V600E) inhibition by RTK or N-RAS upregulation. *Nature.* (2010) 468:973–7. doi: 10.1038/nature09626
13. Shao Y, Aplin AE. BH3-only protein silencing contributes to acquired resistance to PLX4720 in human melanoma. *Cell Death Differ.* (2012) 19:2029–39. doi: 10.1038/cdd.2012.94
14. Smyth T, Paraiso KHT, Hearn K, Rodriguez-Lopez AM, Munck JM, Haarberg HE, et al. Inhibition of HSP90 by AT13387 delays the emergence of resistance to BRAF inhibitors and overcomes resistance to dual BRAF and MEK inhibition in melanoma models. *Mol Cancer Ther.* (2014) 13:2793–804. doi: 10.1158/1535-7163.MCT-14-0452
15. Yadav V, Zhang X, Liu J, Estrem S, Li S, Gong XQ, et al. Reactivation of mitogen-activated protein kinase (MAPK) pathway by FGF receptor 3 (FGFR3)/Ras mediates resistance to vemurafenib in human B-RAF V600E mutant melanoma. *J Biol Chem.* (2012) 287:28087–98. doi: 10.1074/jbc.M112.377218
16. Yadav V, Burke TF, Huber L, Van Horn RD, Zhang Y, Buchanan SG, et al. The CDK4/6 inhibitor LY2835219 overcomes vemurafenib resistance resulting from MAPK reactivation and cyclin D1 upregulation. *Mol Cancer Ther.* (2014) 13:2253–63. doi: 10.1158/1535-7163.MCT-14-0257

17. Jameson KL, Mazur PK, Zehnder AM, Zhang J, Zarnegar B, Sage J, et al. IQGAP1 scaffold-kinase interaction blockade selectively targets RAS-MAP kinase-driven tumors. *Nat Med.* (2013) 19:626–30. doi: 10.1038/nm.3165
18. Wang J, Chen J, Miller DD, Li W. Synergistic combination of novel tubulin inhibitor ABI-274 and vemurafenib overcome vemurafenib acquired resistance in BRAFV600E melanoma. *Mol Cancer Ther.* (2014) 13:16–26. doi: 10.1158/1535-7163.MCT-13-0212
19. Ji Z, Erin Chen Y, Kumar R, Taylor M, Jenny Njauw CN, Miao B, et al. MITF Modulates Therapeutic Resistance through EGFR Signaling. *J Invest Dermatol.* (2015) 135:1863–72. doi: 10.1038/jid.2015.105
20. Muller J, Krijgsman O, Tsoi J, Robert L, Hugo W, Song C, et al. Low MITF/AXL ratio predicts early resistance to multiple targeted drugs in melanoma. *Nat Commun.* (2014) 5:5712. doi: 10.1038/ncomms6712
21. Sun X, Li J, Sun Y, Zhang Y, Dong L, Shen C, et al. miR-7 reverses the resistance to BRAFi in melanoma by targeting EGFR/IGF-1R/CRAF and inhibiting the MAPK and PI3K/AKT signaling pathways. *Oncotarget.* (2016) 7:53558–70. doi: 10.18632/oncotarget.10669
22. Choi J, Landrette SF, Wang T, Evans P, Bacchiocchi A, Bjornson R, et al. Identification of PLX4032-resistance mechanisms and implications for novel RAF inhibitors. *Pigment Cell Melanoma Res.* (2014) 27:253–62. doi: 10.1111/pcmr.12197
23. Das Thakur M, Salangsang F, Landman AS, Sellers WR, Pryer NK, Levesque MP, et al. Modelling vemurafenib resistance in melanoma reveals a strategy to forestall drug resistance. *Nature.* (2013) 494:251–5. doi: 10.1038/nature11814
24. Basile KJ, Abel EV, Dadpey N, Hartsough EJ, Fortina P, Aplin AE. *In vivo* MAPK reporting reveals the heterogeneity in tumoral selection of resistance to RAF inhibitors. *Cancer Res.* (2013) 73:7101–10. doi: 10.1158/0008-5472.CAN-13-1628
25. Greger JG, Eastman SD, Zhang V, Bleam MR, Hughes AM, Smitheman KN, et al. Combinations of BRAF, MEK, and PI3K/mTOR inhibitors overcome acquired resistance to the BRAF inhibitor GSK2118436 dabrafenib, mediated by NRAS or MEK mutations. *Mol Cancer Ther.* (2012) 11:909–20. doi: 10.1158/1535-7163.MCT-11-0989
26. Gowrishankar K, Snoyman S, Pupo GM, Becker TM, Kefford RF, Rizos H. Acquired resistance to BRAF inhibition can confer cross-resistance to combined BRAF/MEK inhibition. *J Invest Dermatol.* (2012) 132:1850–9. doi: 10.1038/jid.2012.63
27. Atefi M, von Euw E, Attar N, Ng C, Chu C, Guo D, et al. Reversing melanoma cross-resistance to BRAF and MEK inhibitors by co-targeting the AKT/mTOR pathway. *PLoS ONE.* (2011) 6:e28973. doi: 10.1371/journal.pone.0028973
28. Graziani G, Artuso S, De Luca A, Muzi A, Rotili D, Scimeca M, et al. A new water soluble MAPK activator exerts antitumor activity in melanoma cells resistant to the BRAF inhibitor vemurafenib. *Biochem Pharmacol.* (2015) 95:16–27. doi: 10.1016/j.bcp.2015.03.004
29. Su F, Bradley WD, Wang Q, Yang H, Xu L, Higgins B, et al. Resistance to selective BRAF inhibition can be mediated by modest upstream pathway activation. *Cancer Res.* (2012) 72:969–78. doi: 10.1158/0008-5472.CAN-11-1875
30. Atefi M, Titz B, Tsoi J, Avramis E, Le A, Ng C, et al. CRAF R391W is a melanoma driver oncogene. *Sci Rep.* (2016) 6:27454. doi: 10.1038/srep27454
31. Kaplan FM, Kugel CH III, Dadpey N, Shao Y, Abel EV, Aplin AE. SHOC2 and CRAF mediate ERK1/2 reactivation in mutant NRAS-mediated resistance to RAF inhibitor. *J Biol Chem.* (2012) 287:41797–807. doi: 10.1074/jbc.M112.390906
32. Hu W, Jin L, Jiang CC, Long GV, Scolyer RA, Wu Q, et al. AEBP1 upregulation confers acquired resistance to BRAF (V600E) inhibition in melanoma. *Cell Death Dis.* (2013) 4:e914. doi: 10.1038/cddis.2013.441
33. Fofaria NM, Frederick DT, Sullivan RJ, Flaherty KT, Srivastava SK. Overexpression of Mcl-1 confers resistance to BRAFV600E inhibitors alone and in combination with MEK1/2 inhibitors in melanoma. *Oncotarget.* (2015) 6:40535–56. doi: 10.18632/oncotarget.5755
34. Thang ND, Nghia PT, Kumasaka MY, Yajima I, Kato M. Treatment of vemurafenib-resistant SKMEL-28 melanoma cells with paclitaxel. *Asian Pac J Cancer Prev.* (2015) 16:699–705. doi: 10.7314/APJCP.2015.16.2.699
35. Vergani E, Vallacchi V, Frigerio S, Deho P, Mondellini P, Perego P, et al. Identification of MET and SRC activation in melanoma cell lines showing primary resistance to PLX4032. *Neoplasia.* (2011) 13:1132–42. doi: 10.1593/neo.111102
36. Anastas JN, Kulikauskas RM, Tamir T, Rizos H, Long GV, von Euw EM, et al. WNT5A enhances resistance of melanoma cells to targeted BRAF inhibitors. *J Clin Invest.* (2014) 124:2877–90. doi: 10.1172/JCI70156
37. Obenauf AC, Zou Y, Ji AL, Vanharanta S, Shu W, Shi H, et al. Therapy-induced tumour secretomes promote resistance and tumour progression. *Nature.* (2015) 520:368–72. doi: 10.1038/nature14336
38. Straussman R, Morikawa T, Shee K, Barzily-Rokni M, Qian ZR, Du J, et al. Tumour micro-environment elicits innate resistance to RAF inhibitors through HGF secretion. *Nature.* (2012) 487:500–4. doi: 10.1038/nature11183
39. Parker R, Vella LJ, Xavier D, Amirkhani A, Parker J, Cebon J, et al. Phosphoproteomic analysis of cell-based resistance to BRAF inhibitor therapy in melanoma. *Front Oncol.* (2015) 5:95. doi: 10.3389/fonc.2015.00095
40. Sharma R, Fedorenko I, Spence PT, Sondak VK, Smalley KS, Koomen JM. Activity-based protein profiling shows heterogeneous signaling adaptations to BRAF inhibition. *J Proteome Res.* (2016) 15:4476–89. doi: 10.1021/acs.jproteome.6b00613
41. Girotti MR, Pedersen M, Sanchez-Laorden B, Viros A, Turajlic S, Niculescu-Duvaz D, et al. Inhibiting EGF receptor or SRC family kinase signaling overcomes BRAF inhibitor resistance in melanoma. *Cancer Discov.* (2013) 3:158–67. doi: 10.1158/2159-8290.CD-12-0386
42. Kim MH, Kim J, Hong H, Lee SH, Lee JK, Jung E, et al. Actin remodeling confers BRAF inhibitor resistance to melanoma cells through YAP/TAZ activation. *EMBO J.* (2016) 35:462–78. doi: 10.15252/embj.201592081
43. Sandri S, Faiao-Flores F, Tiago M, Pennacchi PC, Massaro RR, Alves-Fernandes DK, et al. Vemurafenib resistance increases melanoma invasiveness and modulates the tumor microenvironment by MMP-2 upregulation. *Pharmacol Res.* (2016) 111:523–33. doi: 10.1016/j.phrs.2016.07.017
44. Faiao-Flores F, Alves-Fernandes DK, Pennacchi PC, Sandri S, Vicente AL, Scapulatempo-Neto C, et al. Targeting the hedgehog transcription factors GLI1 and GLI2 restores sensitivity to vemurafenib-resistant human melanoma cells. *Oncogene.* (2017) 36:1849–61. doi: 10.1038/onc.2016.348
45. Cordaro FG, De Presbiteris AL, Camerlingo R, Mozzillo N, Pirozzi G, Cavalcanti E, et al. Phenotype characterization of human melanoma cells resistant to dabrafenib. *Oncol Rep.* (2017) 38:2741–51. doi: 10.3892/or.2017.5963
46. Caporali S, Alvino E, Lacal PM, Levati L, Giurato G, Memoli D, et al. Targeting the PI3K/AKT/mTOR pathway overcomes the stimulating effect of dabrafenib on the invasive behavior of melanoma cells with acquired resistance to the BRAF inhibitor. *Int J Oncol.* (2016) 49:1164–74. doi: 10.3892/ijo.2016.3594
47. Ross KC, Andrews AJ, Marion CD, Yen TJ, Bhattacharjee V. Identification of the serine biosynthesis pathway as a critical component of BRAF inhibitor resistance of melanoma, pancreatic, and non-small cell lung cancer cells. *Mol Cancer Ther.* (2017) 16:1596–609. doi: 10.1158/1535-7163.MCT-16-0798
48. Hernandez-Davies JE, Tran TQ, Reid MA, Rosales KR, Lowman XH, Pan M, et al. Vemurafenib resistance reprograms melanoma cells towards glutamine dependence. *J Transl Med.* (2015) 13:210,015-0581-2. doi: 10.1186/s12967-015-0581-2
49. McDermott M, Eustace AJ, Busschots S, Breen L, Crown J, Clynes M, et al. *in vitro* development of chemotherapy and targeted therapy drug-resistant cancer cell lines: a practical guide with case studies. *Front Oncol.* (2014) 4:40. doi: 10.3389/fonc.2014.00040
50. Zeiderman MR, Egger ME, Kimbrough CW, England CG, Dupre TV, McMasters KM, et al. Targeting of BRAF resistant melanoma via extracellular matrix metalloproteinase inducer receptor. *J Surg Res.* (2014) 190:111–8. doi: 10.1016/j.jss.2014.02.021
51. Tirosh I, Izar B, Prakadan SM, Wadsworth MH II, Treacy D, Trombetta JJ, et al. Dissecting the multicellular ecosystem of metastatic melanoma by single-cell RNA-seq. *Science.* (2016) 352:189–96. doi: 10.1126/science.aad0501
52. Domcke S, Sinha R, Levine DA, Sander C, Schultz N. Evaluating cell lines as tumour models by comparison of genomic profiles. *Nat Commun.* (2013) 4:2126. doi: 10.1038/ncomms3126
53. Jiang G, Zhang S, Yazdanparast A, Li M, Pawar AV, Liu Y, et al. Comprehensive comparison of molecular portraits between cell lines and tumors in breast cancer. *BMC Genomics.* (2016) 17(Suppl. 7):525,016-2911-z. doi: 10.1186/s12864-016-2911-z

54. Sinha R, Winer AG, Chevinsky M, Jakubowski C, Chen YB, Dong Y, et al. Analysis of renal cancer cell lines from two major resources enables genomics-guided cell line selection. *Nat Commun.* (2017) 8:15165. doi: 10.1038/ncomms15165
55. Vincent KM, Findlay SD, Postovit LM. Assessing breast cancer cell lines as tumour models by comparison of mRNA expression profiles. *Breast Cancer Res.* (2015) 17:114,015-0613-0. doi: 10.1186/s13058-015-0613-0
56. Vincent KM, Postovit LM. Investigating the utility of human melanoma cell lines as tumour models. *Oncotarget.* (2017) 8:10498–509. doi: 10.18632/oncotarget.14443
57. Grippo JF, Zhang W, Heinzmann D, Yang KH, Wong J, Joe AK, et al. A phase I, randomized, open-label study of the multiple-dose pharmacokinetics of vemurafenib in patients with BRAF V600E mutation-positive metastatic melanoma. *Cancer Chemother Pharmacol.* (2014) 73:103–11. doi: 10.1007/s00280-013-2324-5
58. Falchook GS, Long GV, Kurzrock R, Kim KB, Arkenau HT, Brown MP, et al. Dose selection, pharmacokinetics, and pharmacodynamics of BRAF inhibitor dabrafenib (GSK2118436). *Clin Cancer Res.* (2014) 20:4449–58. doi: 10.1158/1078-0432.CCR-14-0887
59. Funck-Brentano E, Alvarez JC, Longvert C, Abe E, Beauchet A, Funck-Brentano C, et al. Plasma vemurafenib concentrations in advanced BRAFV600mut melanoma patients: impact on tumour response and tolerance. *Ann Oncol.* (2015) 26:1470–5. doi: 10.1093/annonc/mdv189
60. Tap WD, Gong KW, Dering J, Tseng Y, Ginther C, Pauletti G, et al. Pharmacodynamic characterization of the efficacy signals due to selective BRAF inhibition with PLX4032 in malignant melanoma. *Neoplasia.* (2010) 12:637–49. doi: 10.1593/neo.10414
61. He Y, Zhu Q, Chen M, Huang Q, Wang W, Li Q, et al. The changing 50% inhibitory concentration (IC50) of cisplatin: a pilot study on the artifacts of the MTT assay and the precise measurement of density-dependent chemoresistance in ovarian cancer. *Oncotarget.* (2016) 7:70803–21. doi: 10.18632/oncotarget.12223
62. Clark NA, Hafner M, Kouril M, Williams EH, Muhlich JL, Pilarczyk M, et al. GRcalculator: an online tool for calculating and mining dose-response data. *BMC Cancer.* (2017) 17:3689–3. doi: 10.1186/s12885-017-3689-3

Conflict of Interest Statement: The authors declare that the research was conducted in the absence of any commercial or financial relationships that could be construed as a potential conflict of interest.

frontiers in Oncology

ORIGINAL RESEARCH
published: 18 April 2019
doi: 10.3389/fonc.2019.00304

A Novel Citrullinated Modification of Histone 3 and Its Regulatory Mechanisms Related to IPO-38 Antibody-Labeled Protein

*Shuzheng Song, Zhen Xiang, Jun Li, Jun Ji, Ranlin Yan, Zhenggang Zhu and Yingyan Yu**

Department of Surgery, Ruijin Hospital affiliated to Shanghai Jiao Tong University School of Medicine, Shanghai Key Laboratory for Gastric Neoplasms, Shanghai, China

IPO-38 is a potential biomarker for early diagnosis of gastric cancer that we recently identified. Although we characterized its chemical nature as a nucleosome histone, we suspected the existence of histone modification for the IPO-38 antibody-labeled protein. Here, we used a commercially available modified histone peptide array to identify the type and site of histone modification labeled by the IPO-38 monoclonal antibody. In protein array analysis, the citrulline modification of histone 3 on arginine 26 (H3R26Cit) yielded the strongest signal. Although peptidyl arginine deiminase-2 and -4 (PADI2 and PADI4, respectively) can catalyze the conversion of arginine to citrulline, we observed that only PADI4 expression correlated with the citrulline histone modification of H3R26Cit. Overexpression of PADI4, via transfection of a eukaryotic expression vector, and knockdown of PADI4 gene expression, by a PADI4 CRISPR/Cas9 vector, confirmed the crucial function of PADI4 on the increased level of H3R26Cit in gastric cancer cell lines. By immunoprecipitation and immunoblotting, we found an interaction between H3R26Cit and H3K27me3. Our study established the first link between the IPO-38 antigen and citrullinated histone 3, and clarified the upstream regulatory enzyme PADI4. The new findings suggest an important role for the citrullination modification of histone in gastric cancer biology, and should help us optimize the development of a sensitive and specific diagnostic reagent.

Keywords: IPO-38, histone modification, citrullination, PADI4, biomarker

OPEN ACCESS

Edited by:
Zhe-Sheng Chen,
St. John's University, United States

Reviewed by:
Ger J. M. Pruijn,
Radboud University Nijmegen, Netherlands
Qi Liu,
Tongji University, China
Qingyuan Zhang,
Ningxia Medical University, China

****Correspondence:***
Yingyan Yu
yingyan3y@sjtu.edu.cn

Specialty section:
This article was submitted to Cancer Molecular Targets and Therapeutics, a section of the journal Frontiers in Oncology

Received: *21 January 2019*
Accepted: *02 April 2019*
Published: *18 April 2019*

Citation:
Song S, Xiang Z, Li J, Ji J, Yan R, Zhu Z and Yu Y (2019) A Novel Citrullinated Modification of Histone 3 and Its Regulatory Mechanisms Related to IPO-38 Antibody-Labeled Protein. Front. Oncol. 9:304. doi: 10.3389/fonc.2019.00304

INTRODUCTION

Gastric cancer is a disease with high morbidity and mortality rates worldwide, especially in East Asia. Data from GLOBOCAN 2018 show there are 1,033,701 new cases and 782,685 death cases of gastric cancer all over the world (1). Currently, methods are limited for early diagnosis of gastric cancer. Patients are often diagnosed with gastric cancer at an advanced stage with poor prognosis. Therefore, early diagnosis is a key to improving the outcome of patients. Our group proposed a candidate biomarker IPO-38 for diagnosis of gastric cancer (2). Assaying IPO-38 provides significantly higher specificity and sensitivity (56.7 and 93.3%, respectively), over routinely used biomarkers CEA, CA199, and CA72-4. IPO-38 has long been used as a cell proliferation nuclear antigen (3, 4). Although we identified it as a member of the histone protein family based on mass spectrometry, we considered that the histone was modified chemically (2).

Protein function is specified by appropriately folded secondary structure and post-translational modifications, including acetylation, methylation, phosphorylation, and citrullination (5). Histone modification plays an important role in maintaining homeostasis. Disorders of histone modification associate with cancer, neurological diseases, as well as autoimmune diseases (6, 7). Histone modifications potentially alter the electrical charge between histones and DNA duplexes, impacting chromatin organization and transcription. Histone modifications also affect gene regulation by modulating binding with transcription factors (6–8). In addition, histone modifications are involved in the formation of neutrophil extracellular traps (NETs), a crucial process for microbe clearance (9), which also plays a role on cancer metastasis through protein citrullination in peripheral blood (10–12).

Specific antibody analysis and mass spectrometry are commonly used for detection of histone modifications. However, the number of histone-specific antibodies is limited, which has restricted progress in studying histone modifications and functions. Mass spectrometry potentially overcomes the defect of insufficient antibodies to some extent, but trypsin digestion in the sample pretreatment step often destroys many modification sites, and ultimately reduces sensitivity (13). In 2010, a new histone modified peptide array was developed, promoting research to understand the function, metabolism, and significance of histone modifications (14–16).

To clarify the histone modification characteristics and biological significance of the IPO-38 antigen, we used the modified peptide array to identify the IPO-38 monoclonal antibody-binding protein. We characterized the novel modified histone H3, and identified that PADI4 is a key enzyme catalyzing citrullination modification of histone 3.

MATERIALS AND METHODS

Modified Histone Peptide Array Analysis

MODified™ Histone Peptide Array from Active motif (Active Motif, California, USA) is a histone modified polypeptide chip of 59 single-site histone modifications and different permutations in 384 dot matrixes. Each chip is divided into left and right wings and repeating lattice arrangement. The chip was first blocked with 5% BSA (Sangon Biotech, Shanghai, China) for 1 h at room temperature, and then incubated with IPO-38 monoclonal antibody (1:1000, Thermo Fisher, Massachusetts, USA) overnight at 4°C. The next day, the chip was washed three times with 1×PBST [1×PBS with 0.1% (v/v) Tween-20], and then incubated with HRP-labeled goat anti-mouse IgM second antibody for 1 h at room temperature (1:5000, Sangon Biotech, Shanghai, China). After incubation, the chip was again washed with 1×PBST three times and the signal was detected using ECL luminescent reagent (Meilun, Shanghai China), in a chemiluminometer (Tanon, Shanghai, China). The histone modification sites and signal intensity analysis were conducted with the special software provided by Active Motif (https://www.activemotif.com/catalog/668).

Cell Culture

Gastric cancer cell lines, SGC7901, MKN45, HGC27, and BGC823, were purchased from the Cell Bank of the Chinese Academy of Sciences (Shanghai, China). Gastric cancer cell lines, Hs746T, AGS, and NCI-N87, were purchased from the American Type Culture Collection (ATCC, Maryland, USA), and the human gastric mucosal cells, GES1, and 293T cells were preserved in our laboratory. Cell lines were cultured in 37°C culture incubator with 5% carbon dioxide using RPMI 1640 or DMEM medium (Hyclone, Utah, USA) containing 10% FBS (Gibco, New York, USA) according to the manufacturer's instructions.

Construction of PADI2 and PADI4 Eukaryotic Expression Vectors and PADI4 CRISPR/Cas9 Vector

Primers were designed for the coding region sequences of the PADI2 (NM_007365.2), PADI4 (NM_012387.2), and the restriction sites for the eukaryotic expression vector pCDH-CMV-MCS-EF1-Puro (SBI, California, USA). The high-fidelity PCR enzyme KOD plus neo (Toyobo, Osaka, Japan) was used to amplify the coding region sequences of PADI2 and PADI4 from a 293T cell cDNA library. Agarose gel (1%) electrophoresis was used to confirm the PCR product size, and T4 ligase (NEB, Massachusetts, USA) was used to link the target fragment to the empty linear vector after digestion. Competent TNF5α cells (Tiangen, Shanghai, China) were transformed with the expression vectors, and three positive colonies were selected for sequencing to verify the plasmid.

CRISPR/Cas9 vector targeting PADI4 (NM_012387.2) was constructed using the lentiCRISPRv2 vector, which was a gift from the Feng Zhang lab at MIT. The online guide RNA design website (http://crispr.mit.edu) was used to design the target sequence near the transcription start site of PADI4. The top two scored sequences were selected as the gene editing sites for primers (gRNA1: 5′-GGGACGAGCTAGCCCGACGA-3′; gRNA2: 5′-TCACACGGATCAATGTCCCC-3′). In this study we adopted an all-in-one method. Primers designed according to the two gRNA sequences and the tracRNA-U6 vector sequences were used to produce a gRNA1-tracRNA-U6-gRNA2 fragment. Then the proper fragment was ligated into the lentiCRISPRv2 vector and verified by sequencing.

Lentiviral Packaging and Stable Cell Line Screening

The constructed eukaryotic expression vector and gene knockdown vector were transfected into the 293T cells with the packaging plasmids psPAX2 and pMD2.G using Lipofectamine 2000 (Thermo Fisher, Massachusetts, USA). The lentivirus was harvested 48 h after transfection, and the lentivirus supernatant was filtered using a 0.45 μm filter. One day prior to infection, the three cell lines (AGS, SGC7901, and MKN45) were plated at 2×10^5 cells per well in 6-well tissue culture plates. The lentivirus was added into the separate cell lines, and polybrene was added at a density of 6 ng/ul (Sigma, California, USA). After 24 h, the infection medium was removed and replaced

with normal culture medium. After 48 h, the cell lines were screened using 2 ng/μl puromycin (Sangon Biotech, Shanghai, China), and a stable cell line was formed after 1 week of continuous selection.

Western Blot

Whole cellular protein was extracted using RIPA lysis buffer (Beyotime, Shanghai, China) containing a protease inhibitor cocktail (Roche, Basel, Switzerland). The cytoplasmic and nuclear protein fractions were isolated using a Nuclear and Cytoplasmic Protein Extraction Kit (Beyotime, Shanghai, China) according to the manufacturer's instructions. Protein samples were separated by SDS-PAGE gel containing 10% acrylamide, electrophoresis and transferred to a 0.45 μm PVDF membrane (Millipore, Massachusetts, USA). The transferred membranes were blocked with 5% BSA for 1 h at room temperature. Then the membranes were incubated with the corresponding primary antibodies: mouse anti-human IPO-38 monoclonal antibody (1:1000, Thermo Fisher, Massachusetts, USA); rabbit anti-human H3K27ac polyclonal antibody, rabbit anti-human H3R26Cit/H3K27me3 monoclonal antibody, and mouse anti-human PADI4 monoclonal antibody (1:1000, Abcam, Cambridge, UK); rabbit anti-human EZH2 monoclonal antibody (1:1000, CST, Boston, Massachusetts USA), rabbit anti-human PADI2 polyclonal antibody, (1:1000, Proteintech, Chicago, Illinois, USA), and HRP-labeled mouse anti-human GAPDH monoclonal antibody (1:2000, Proteintech, Chicago, Illinois, USA), and mouse anti-human histone H3 monoclonal antibody (1:1000, Abcam, Cambridge, UK) as an internal reference antibody overnight at 4°C. The next day, 1×TBST buffer [10 mM Tris-HCl, pH 8.0, 150 mM NaCl, 0.1% (v/v) Tween-20] was used to wash the membranes 3 times for 10 min each time at RT. HRP-labeled goat anti-rabbit or mouse IgG secondary antibody (1:5000, Proteintech, Chicago, Illinois, USA) of the corresponding species was incubated for 1 h at RT. HRP-labeled goat anti-mouse IgM secondary antibody (Sangon Biotech, Shanghai, China) was used as the second antibody for the IPO-38 IgM monoclonal antibody. After the incubation of the secondary antibody, the membranes were washed 3 times for 10 min each time at RT with 1×TBST buffer, and then the signal was detected in the chemiluminometer using ECL luminescent solution (Meilun, Shanghai China).

Histone Immunoprecipitation

To reduce the interference of non-histone proteins and nucleotides, we used enzymatic digestion to obtain histones for further immunoprecipitation. After collecting the cell pellet, we used the hypotonic buffer [0.3 M sucrose, 60 mM KCl, 15 mM NaCl, 5 mM $MgCl_2$, 0.1 mM EGTA, 15 mM Tris-HCl pH 7.5, 5 mM sodium butyrate, 0.4% NP40, and Complete™ EDTA-free protease inhibitor mixture (Roche, Basel, Switzerland)] to rupture the cell membrane, and then collected the nuclear pellet. Nuclear deposition concentration was measured by nanodrop (Thermo Fisher, Massachusetts, USA), and 200 U/5 μg of micrococcal nuclease (NEB, Massachusetts, USA) was used to digest the nucleosome at 37°C for 6 min. EDTA (Sigma, California, USA) was added to stop the reaction. After centrifugation, the supernatant, which contains histone DNA complexes, namely nucleosomes, was collected, and concentration was measured. The appropriate amount of lysate was taken as input, and the remainder was divided into 3 groups, and 20 μl of protein A/G magnetic beads (Thermo Fisher, Massachusetts, United States), and 5 μg of anti-H3K27me3 antibody, anti-H3K27ac antibody, or normal rabbit IgG (CST, Boston, Massachusetts, USA) was added to each sample of lysate. After incubating overnight at 4°C on a shaker, the complexes were washed with RIPA buffer three times in the magnetic frame (Invitrogen, California, USA). Finally, the bound proteins were eluted into 1×SDS loading buffer (Beyotime, Shanghai, China). The subsequent steps followed the immunoblotting protocol described above, and the rabbit anti-human H3R26Cit polyclonal antibody was used to detect the corresponding histone modification.

Immunofluorescence

The MKN45 and SGC7901 cancer cell lines (5×10^3 cells per plate) were seeded on a fluorescence chamber culture plate. After the cells fully stretched and adhered to the plate 12 h later, they were fixed in 4% paraformaldehyde for 15 min at RT, and the cell and nuclear membranes were permeabilized in 0.5% Triton X-100 (Sangon Biotech, Shanghai, China) for 20 min at RT. The plate was washed 3 times for 5 min with 1×PBS. Goat serum (Sangon Biotech, Shanghai, China) was used for antigen blocking for 1 h at RT. After blocking, the samples were incubated with mouse anti-human PADI4 monoclonal antibody (1:100) and rabbit anti-human PADI2 polyclonal antibody (1:100) at 4°C overnight in a wet box. The plate was then washed with 1×PBST three times for 5 min each, and incubated with Alexa Fluor 488 goat anti-mouse red fluorescent secondary antibody and Alexa Fluor 555 goat anti-rabbit green fluorescent secondary antibody (1:250, Invitrogen, California, USA) at RT in the dark for 1 h. Nuclei were stained for 5 min at room temperature in the dark with DAPI (Sigma, California, USA). Finally, plates were washed 3 times for 5 min with 1×PBST. Fluorescence signal could be observed and the fluorescent images were taken with a fluorescence microscope (Nikon, Tokyo, Japan).

Real-Time PCR

Total mRNA was extracted from the cell lines using Trizol (Invitrogen, California, USA), according to the manufacturer's protocol. The obtained mRNA was reverse transcribed using the ReverTra Ace® qPCR RT Kit (Toyobo, Osaka, Japan). The mRNA levels of PADI2, PADI4, EZH2, KDM6A, KDM6B, and GAPDH were detected using the following specific primers: Primers for PADI2, forward: 5′- GCACCTACCTCTGGACC GAT-3′, reverse: 5′-ACACGTGTTCCGAGTGCTTC-3′, product length 81 bp; primers for PADI4, forward: 5′- GACCCCC AAGGACTTCTTCA-3′, reverse: 5′-GCTGCACTTGG AGGACAGTT-3′, product length 115 bp; primers for EZH2, forward: 5′-CATACGCTTTTCTGTAGGCGA-3′, reverse: 5′-TCCGCTTATAAGTGTTGGGTG-3′, product length 82

bp; primers for KDM6A, forward: 5′-TCTCCAAAAGTCCT TGGAAGC-3′, reverse: 5′-AAGGCATCCTGAACTTTCCC-3′, product length 96 bp; primers for KDM6B, forward: 5′-TACAGA CCCTCGAAATCCCA-3′, reverse: 5′-CAGGGTCTTGGTGG AGAAGA-3′, product length 88 bp; and primers for GAPDH, forward: 5′-ACGGATTTGGTCGTATTGGGCG-3′, reverse: 5′-CTCCTGGAAGATGGTGATGG-3′, product length 212 bp. The qPCR reaction was carried out in a Roche Light cycler 480 PCR machine (Roche, Basel, Switzerland) using SYBR Green PCR master mix (Life Technologies, California, USA).

Statistical Analysis

The mRNA expression data analysis was performed by Student's *t*-test using GraphPad Prism 8.0.1 software (GraphPad Software, San Diego, California, USA). Differences were considered statistically significant when $P < 0.05$.

RESULTS

Identification of Histone Modifications Marked by the IPO-38 Monoclonal Antibody

The IPO-38 monoclonal antibody detects proteins with a molecular weight around 15 kDa in total cellular protein lysates of human gastric epithelial cells (GES1) and gastric cancer cell lines (SGC7901 and NCI-N87) (**Figure 1A**). After incubating the modified histone peptide chip with the IPO-38 monoclonal antibody, 10 high intensity signals were obtained that corresponded to: H3R26Cit-K27me2, H3R26Cit-K27me1, H3R26Cit-K27me3, H3R26Cit, H3K27ac, H3R26me2a-K27ac, H3K12ac-K16ac-K20ac, H3R26me2s-K27ac, H3K16ac-K20ac, and H3K12ac-K16ac-K20me2 (**Figures 1B–D**). Results were duplicated on the left and right wings of the chip (**Figure 1B**), and signal intensities aligned well and showed good consistency (**Figure 1C**). Specific analysis of modified histone peptides revealed that the highest specificity of IPO-38 antibody-binding was for H3R26Cit, followed by the H3K27me2 modification (**Figure 1E**). We noticed that the signal intensity of H3R26Cit site was significantly enhanced when the adjacent site H3K27 was methylated. In particular, the presence of K27me2 modification resulted in 3-fold up-regulation of signaling intensity than that of R26Cit alone based on signaling intensity analysis. Immunoblotting using an antibody specific for H3R26Cit correlated well with protein levels detected using the IPO-38 antibody in the gastric cancer cell lysates (**Figure 1F**).

Expression Levels of H3R26Cit and Related Catalytic Enzyme PADIs

Since PADI2 or PADI4 catalyzes the conversion of arginine to citrulline in humans, we examined the protein levels of PADI2, PADI4, and H3R26Cit in several human gastric cancer cell lines. We observed that the basal expression level of H3R26Cit was higher in SGC7901 and MKN45 cells, and basal expression of PADI4 was also higher in those cancer cell lines. No significant difference of PADI2 was found in those cancer cell lines (**Figure 2A**). The mRNA expression level of PADI2 and PADI4 was lower in cancer cell lines, compared to GES1 control cells, by q-RT-PCR (**Figure 2B**), though PADI4 protein levels were higher in SGC7901 and MKN45 cells. There was discrepancy between the mRNA and protein levels of PADI2 and PADI4. By immunofluorescence microscopy, PADI2 was shown to localize in both the cytoplasm and nucleus, whereas PADI4 was found only in the nucleus (**Figure 2C**).

The Impact of PADI2 and PADI4 Overexpression and Knockdown on H3R26Cit Level

PADI2 and PADI4 eukaryotic expression vectors were packaged with lentivirus. Although PADI4 protein level was higher in SGC7901 and MKN45 cell lines (**Figure 2A**), but they took longer exposure time with ECL luminescence reagent (2 min). Then we chose a PADI4 low expression AGS cell line and a PADI4 moderate expression SGC7901 cell line for the overexpression study, and SGC7901 and MKN-45 cells were used for the knockdown study. After PADI2 and PADI4 were successfully expressed, we examined the expression level of H3R26Cit (**Figures 3A,B**). Overexpression of PADI4 significantly increased intracellular expression of H3R26Cit, compared to PADI2 overexpression, shown by both Western blot with shorter exposure time (2 s) (**Figure 3C**).

The "all-in-one" single plasmid dual target PADI4 gene knockdown system was constructed using CRISPR/Cas9 technology, which targeted a dual target near the PADI4 transcription start site (**Figure 3D**). The plasmid was packaged with lentivirus and SGC7901 and MKN45 cell lines were infected. The puromycin was used to select a stable cell line. The significant decrease in the expression level of PADI4 in experimental cells was accompanied by a decrease in the expression level of H3R26Cit (**Figure 3E**).

Analysis of Interaction Between H3R26Cit and Other Post-translational Modification

Since H3K27ac and H3K27me3 were also highlighted in the modified histone peptide array, we analyzed the interaction between H3R26Cit and other histone modifications. As shown in **Figure 4A**, overexpression of PADI4 resulted in a significant decrease of H3K27me3 levels in AGS and SGC7901 cells, but led to increased expression of H3K27ac. To clarify the potential crosstalk between H3R26Cit and H3K27me, we extracted nucleosomes from cell nucleus by means of the micrococcal nuclease method, and performed immunoprecipitations using H3K27me3 and H3K27ac antibodies. H3R26Cit was not detected in the H3K27me3 pull-down product, but co-precipitated with H3K27ac (**Figure 4B**), which supports an interaction between H3R26Cit and H3K27ac. We further examined expression levels of EZH2, an H3K27me3 methyltransferase, and KDM6A/KDM6B demethylases after PADI4 overexpression. The expression level of EZH2 was significantly decreased in SGC7901 and AGS cells ($P < 0.001$), while the expression level of KDM6A was significantly increased ($P = 0.037$; $P = 0.0046$, for SGC7901 and AGS cells, respectively). The expression

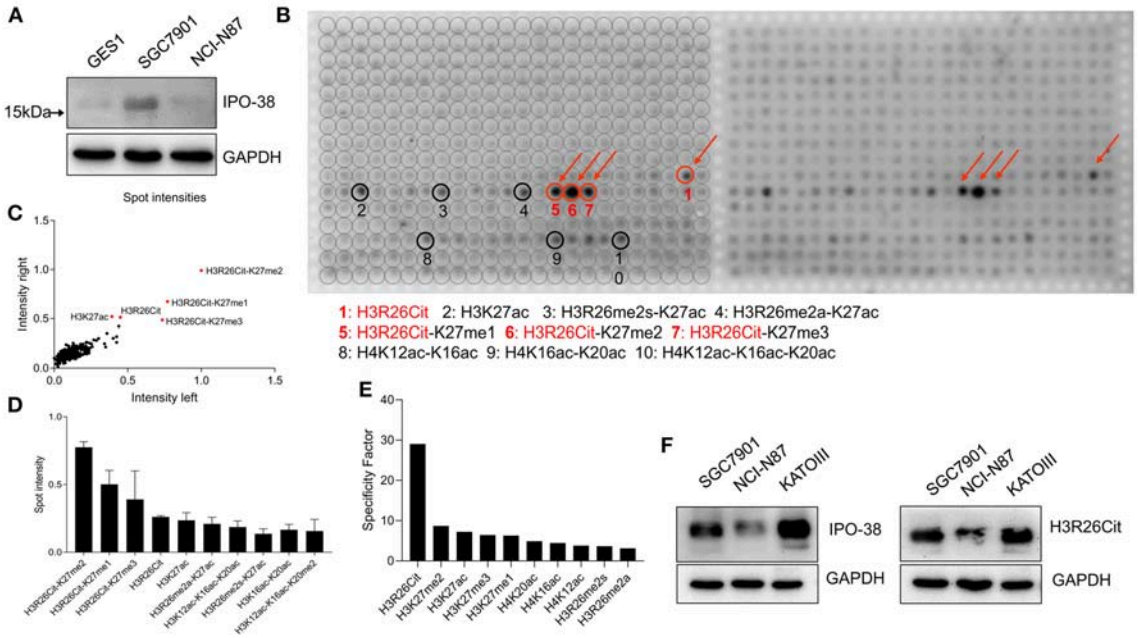

FIGURE 1 | Analysis of histone modification peptide array using IPO-38 monoclonal antibody. **(A)** The protein expression of IPO-38 in gastric mucosal cell GES-1 and gastric cancer cell lines. **(B)** Presentation of signal intensity on modified histone peptide array based on incubation with the IPO-38 monoclonal antibody. **(C)** The consistency assay of two repeated detections on the modified histone peptide array. **(D)** The top 10 histone modifications with the strongest binding to the IPO-38 monoclonal antibody. **(E)** The top 10 histone modification sites with the best specificity for IPO-38 monoclonal antibody binding. **(F)** Comparison of H3R26Cit and IPO-38 protein levels in three gastric cancer cell lines.

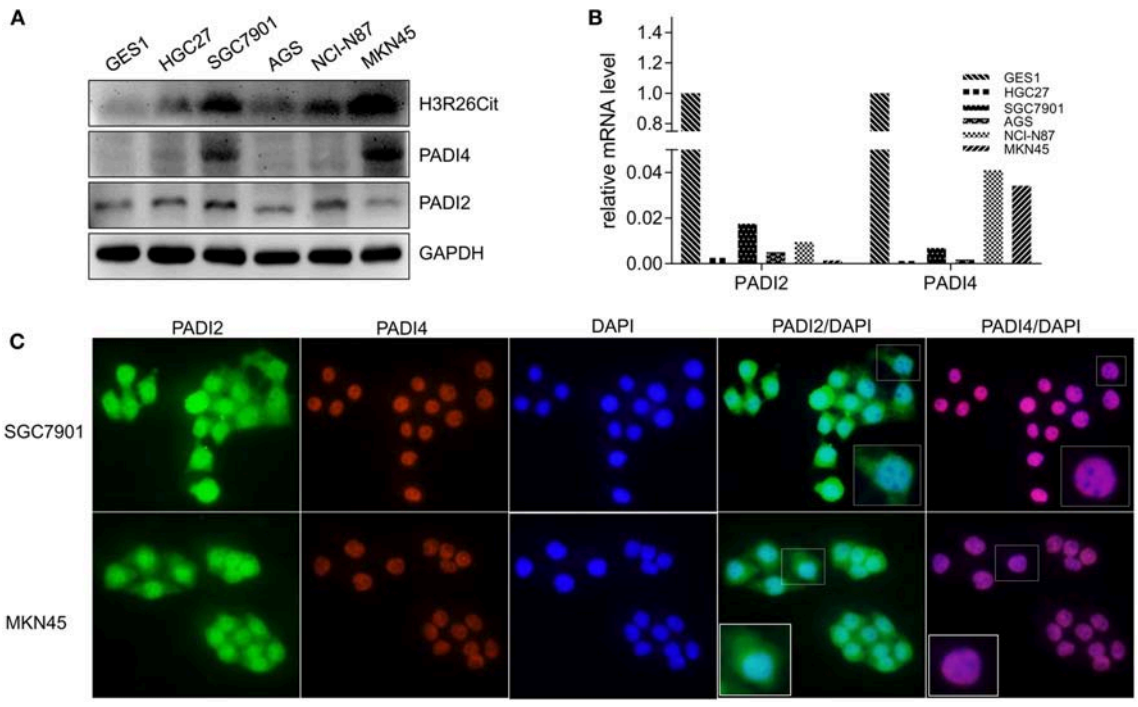

FIGURE 2 | Analysis of basal expression of H3R26Cit and its catalytic enzymes PADIs. **(A)** The protein expression of H3R26Cit, PADI2, and PADI4 in GES-1 gastric mucosa cells and several gastric cancer cell lines. **(B)** The expression of PADI2 and PADI4 mRNA in GES-1 gastric mucosa cells and several gastric cancer cell lines. **(C)** Subcellular localization of PADI2 and PADI4 proteins in SGC7901 and MKN45 gastric cancer cell lines.

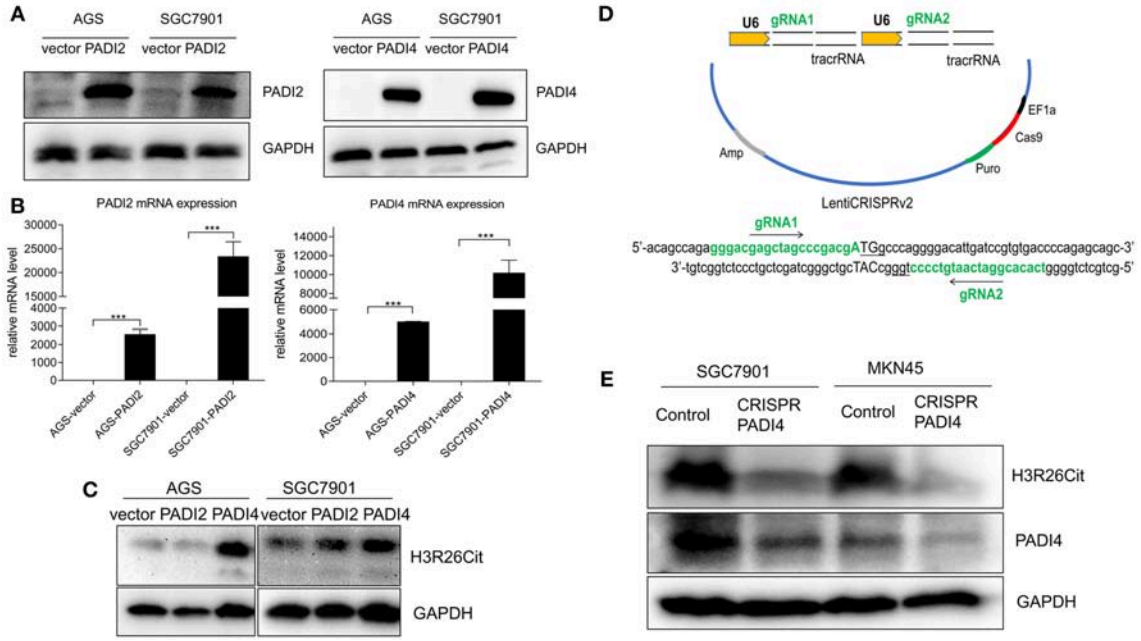

FIGURE 3 | The influence of PADI2 and PADI4 overexpression or knockdown on H3R26Cit. **(A)** Detection of protein level changes after overexpression of PADI2 and PADI4. **(B)** Detection of mRNA level changes after overexpression of PADI2 and PADI4 (*** indicates $P < 0.001$). **(C)** The protein level of H3R26Cit is significantly increased after enforcing PADI4 expression, compared to enforcing PADI2 expression. **(D)** Schematic diagram of the construction of CRISPR/Cas9 all-in-one plasmid system with a double target on the PADI4 gene. **(E)** The protein level of H3R26Cit is significantly decreased after knockdown of PADI4 in both SGC7901 and MKN45 gastric cancer cell lines.

level of KDM6B was increased to some extent ($P = 0.46$; $P = 0.012$) (**Figure 4C**). A significant down-regulation of EZH2 in the nucleus was found; as internal controls, GAPDH was only expressed in the cytoplasm and histone 3 was only expressed in nucleus (**Figure 4D**). The results suggest that PADI4 not only catalyzes H3R26Cit modification, but also influences the activities of EZH2, KDM6A, and KDM6B, as reflected in the decreased level of H3K27me3 in the nucleus (**Figure 4E**).

DISCUSSION

IPO-38 is a diagnostic biomarker for gastric cancer identified in our previous clinical proteome study. We proposed that the protein labeled by IPO-38 monoclonal antibody was a nucleosome histone and suspected it was a modified histone H2B (2). We could not, however, clarify the exact histone modification due to insufficient methods.

In recent years, the relationship between histone modification and tumorigenesis has attracted greater attention. Technologies for detecting and studying histone modifications have been developed and greatly improved. Using the self-developed chromatin immunoprecipitation-based microarray method (ChIP-chip) technology, Heintzman and coworkers demonstrated that cell-specific histone modifications bound to cell-specific enhancers affect cell-specific gene expression spectrum (17). Cejas et al. developed fixed-tissue chromatin immunoprecipitation sequencing, which enables reliable extraction of soluble chromatin from formalin-fixed paraffin-embedded tissues for accurate detection of histone marks. By using multiple histone marks, they generated chromatin state maps and identified cis-regulatory elements in clinical samples for various tumor types (18).

In the current study, a modified histone peptides array was used. This protein array covers 59 different combinations of post-translational modifications such as methylation, acetylation, phosphorylation, and citrullination in up to four different modifications per peptide (15, 16). This array is suitable for assessing the specificity of histone-modified antibodies and for analyzing interactions between different histone modification sites. The processing is straightforward, similar to Western blotting, and used in different molecular oncology laboratories (15, 16, 19). By means of this protein array, we characterized the antigen labeled by the IPO-38 antibody as H3R26Cit, which could interact with H3K27me and form a H3R26Cit-H3K27me complex. This new finding suggests that detection of H3K27me may be helpful to recognize H3R26Cit indirectly.

Previously, most studies on histone modifications focused on acetylation, methylation, and phosphorylation. The studies of histone citrullination are limited, especially for gastric cancer. Protein citrullination, also known as deamination, refers to a post-translational modification of arginine to citrulline (20, 21). Studies on the relationship between histone citrullination and tumors have mainly focused on histone H3. Thalin and coworkers reported that elevated H3Cit in peripheral blood predicted poor prognosis for advanced cancer

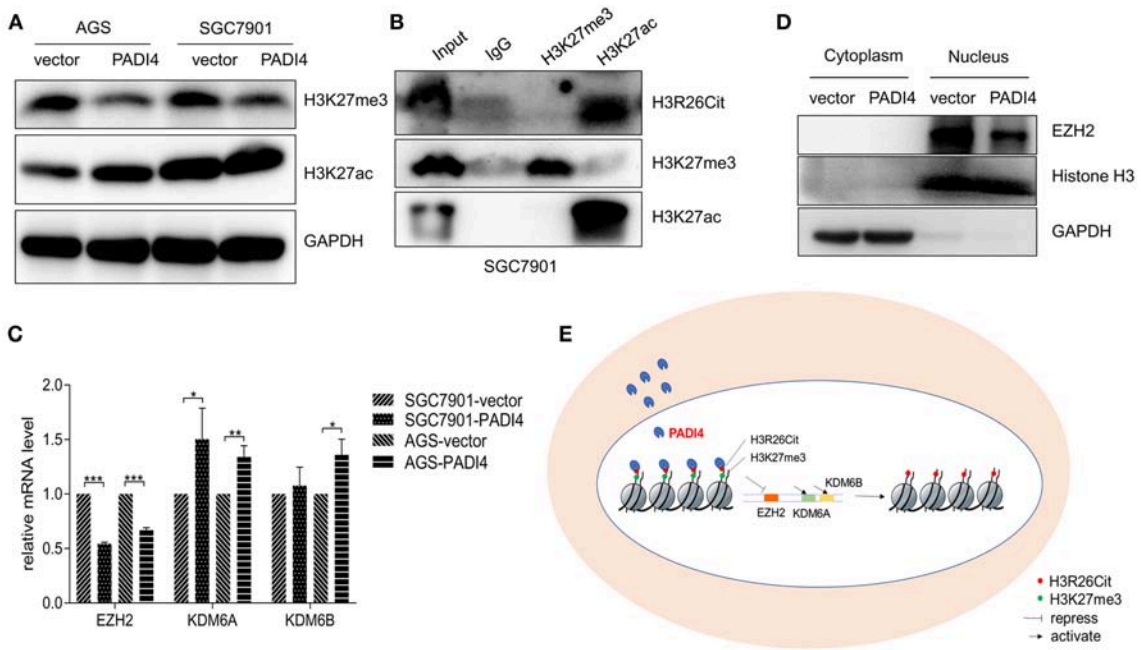

FIGURE 4 | Interaction assay of H3R26Cit and other post-translational modifications. **(A)** An increase in the level of H3K27ac protein and decreased H3K27me3 protein level were observed in both AGS and SGC7901 gastric cancer cell lines in which PADI4 was overexpressed. **(B)** Immunoprecipitation was performed by H3K27me3 and H3K27ac antibodies. H3R26Cit was not detected in the H3K27me3 pull-down product, but was found in the H3K27ac pull-down product. **(C)** Effect of PADI4 overexpression on mRNA expression of the H3K27 methyltransferase EZH2 and demethylases, KDM6A and KDM6B (*, **, and *** represent $P < 0.05$, $P < 0.01$, and $P < 0.001$, respectively) **(D)** EZH2 expression assay revealed that the protein was located in nucleus, and its expression level was decreased after PADI4 overexpression, with histone 3 and GAPDH serving as internal controls. **(E)** Schematic diagram of influences on histone modifications of H3R26Cit and H3K27me3 after PADI4 overexpression.

patients including colorectal cancer, gastric cancer, and breast cancer (10). Neutrophil extracellular traps (NETs) could be a source of citrullinated histones in the blood. PADI4 mediates histone citrullination in NETs formation (11, 22, 23). Protein citrullination also participates in the regulation of stem cell pluripotency, cancer-related genes, and immune responses (24–27). Although we characterized the antigen labeled by IPO-38 antibody, the exact clinical significance of citrullinated histone 3 needs further investigation.

The protein citrullination refers to a chemical conversion of arginine to citrulline, which is catalyzed by peptidylarginine deiminases (PADIs) in human beings (28). Among PADIs family, PADI4 carries a nuclear localization signal, and is mainly located in the nucleus (29). PADI2 might also undergo nuclear translocation in some cells to modify histones (26). Since both PADI4 and PADI2 might be involved in the citrullination of histones, we examined the expression levels of H3R26Cit, PADI4, and PADI2 synchronously and confirmed that PADI4, but not PADI2, regulates H3R26Cit formation. In addition, we found that the expression levels of mRNA and protein of PADI2 and PADI4 was inconsistent, which might be attributed to post-transcriptional modification of mRNA or post-translational modification of protein (30, 31).

In addition to intracellular histone citrullination, PADI4 in neutrophils can facilitate histone citrullination of NETs. This kind of extracellular histone modification facilitated ovarian cancer premetastatic niche formation in the omentum. Interfering NETs formation could inhibit cancer metastasis (32). Yuzhalin and colleagues indicated that extracellular histone modifications can promote liver metastasis of colorectal cancer (12). Therefore, protein citrullination of the extracellular matrix and microenvironment may play an important role on tumor progression. Higher levels of PADI4 have been reported in peripheral blood in several types of cancers (33).

Histone modification is a complex area. The precise correlation of H3R26Cit and H3K27me3 or H3K27ac is largely unknown. In this paper, we identified the crosstalk between H3R26Cit and H3K27me3, which was mentioned by other study before (34). According to our results, the binding ability of IPO-38 antibody to antigen might be affected by their crosstalk, but more experiments need to be done. EZH2 is an enzyme that mediates methylation of H3K27me3 (34). EZH2 was found up-regulated in melanoma, lymphoma, breast cancer, and prostate cancer, and related to promoting tumorigenesis, cell proliferation, and epithelial mesenchymal transition (35). KDM6A and KDM6B are enzymes involved in demethylation of H3K27me3 (36). Although we found that overexpression of PADI4 influences the expression levels of H3K27me3 and H3R26Cit, we did not find a confirm correlation between expression of PADI4 and methylation-related enzymes such as

EZH2, KDM6A, and KDM6B. Our study clarified that PADI4 is a main regulatory enzyme of histone citrullination, at least in gastric cancer. This discovery will be used to optimize the sensitivity and specificity of IPO-38 as a diagnostic reagent for gastric cancer.

Since the technical limitations, we did not analyze the clinical correlations. Next, we prepare to immunize mice with synthetic histone-modified polypeptide antigen to obtain specific monoclonal antibody, and then perform immunohistochemistry by new developed specific monoclonal antibody. We will establish a sandwich ELISA reagent to examine blood samples from patients.

AUTHOR CONTRIBUTIONS

SS and YY formulated the experimental concept and design. ZX, JL, JJ, and RY performed experiments. ZZ and YY supported the research. All authors wrote, reviewed, and revised the manuscript.

FUNDING

This project was supported by National Key R&D Program of China (2016YFC1303200, 2017YFC0908300), the National Natural Science Foundation of China (81772505), Shanghai Science and Technology Committee (18411953100), the Cross-Institute Research Fund of Shanghai Jiao Tong University (YG2017ZD01, YG2015MS62), Innovation Foundation of Translational Medicine of Shanghai Jiao Tong University School of Medicine (15ZH4001, TM201617, and TM 201702), Zhangjiang special development fund for key project (2017-05-HP-C1086-012), and Technology Transfer Project of Science & Technology Department of Shanghai Jiao Tong University School of Medicine.

REFERENCES

1. Bray F, Ferlay J, Soerjomataram I, Siegel RL, Torre LA, Jemal AJ. *Global Cancer Statistics 2018: GLOBOCAN Estimates of Incidence and Mortality Worldwide for 36 Cancers in 185 Countries*. (2018). 68:394–424. doi: 10.3322/caac.21492
2. Hao Y, Yu Y, Wang L, Yan M, Ji J, Qu Y, et al. IPO-38 is identified as a novel serum biomarker of gastric cancer based on clinical proteomics technology. *J Proteome Res*. (2008) 7:3668–77. doi: 10.1021/pr700638k
3. Sidorenko SP, Vetrova EP, Iurchenko OV, Shlapatskaia LN, Berdova AG, Elenskaia AM, et al. Monoclonal antibodies of the IPO series in studying and diagnosing malignant lymphoproliferative diseases. *Gematologiia i Transfuziologiia*. (1990) 35:19–22.
4. Thosaporn W, Iamaroon A, Pongsiriwet S, Ng KH. A comparative study of epithelial cell proliferation between the odontogenic keratocyst, orthokeratinized odontogenic cyst, dentigerous cyst, and ameloblastoma. *Oral Dis*. (2004) 10:22–6. doi: 10.1046/j.1354-523X.2003.00974.x
5. Tan MJ, Luo H, Lee S, Jin FL, Yang JS, Montellier E, et al. Identification of 67 histone marks and histone lysine crotonylation as a new type of histone modification. *Cell*. (2011) 146:1015–27. doi: 10.1016/j.cell.2011.08.008
6. Portela A, Esteller M. Epigenetic modifications and human disease. *Nat Biotechnol*. (2010) 28:1057–68. doi: 10.1038/nbt.1685
7. Audia JE, Campbell RM. Histone modifications and cancer. *Cold Spring Harb Perspect Biol*. (2016) 8:a019521. doi: 10.1101/cshperspect.a019521
8. Berger SL. Histone modifications in transcriptional regulation. *Curr Opin Genet Dev*. (2002) 12:142–8. doi: 10.1016/S0959-437X(02)00279-4
9. Dwivedi N, Radic M. Citrullination of autoantigens implicates NETosis in the induction of autoimmunity. *Ann Rheum Dis*. (2014) 73:483–91. doi: 10.1136/annrheumdis-2013-203844
10. Thalin C, Lundstrom S, Seignez C, Daleskog M, Lundstrom A, Henriksson P, et al. Citrullinated histone H3 as a novel prognostic blood marker in patients with advanced cancer. *PLoS ONE*. (2018) 13:e0191231. doi: 10.1371/journal.pone.0191231
11. Honda M, Kubes P. Neutrophils and neutrophil extracellular traps in the liver and gastrointestinal system. *Nat Rev Gastroenterol Hepatol*. (2018) 15:206–21. doi: 10.1038/nrgastro.2017.183
12. Yuzhalin AE, Gordon-Weeks AN, Tognoli ML, Jones K, Markelc B, Konietzny R, et al. Colorectal cancer liver metastatic growth depends on PAD4-driven citrullination of the extracellular matrix. *Nat Commun*. (2018) 9:4783. doi: 10.1038/s41467-018-07306-7
13. Yuan ZF, Arnaudo AM, Garcia BA. Mass spectrometric analysis of histone proteoforms. *Annu Rev Anal Chem*. (2014) 7:113–28. doi: 10.1146/annurev-anchem-071213-015959
14. Kungulovski G, Kycia I, Tamas R, Jurkowska RZ, Kudithipudi S, Henry C, et al. Application of histone modification-specific interaction domains as an alternative to antibodies. *Genome Res*. (2014) 24:1842–53. doi: 10.1101/gr.170985.113
15. Bock I, Dhayalan A, Kudithipudi S, Brandt O, Rathert P, Jeltsch A. Detailed specificity analysis of antibodies binding to modified histone tails with peptide arrays. *Epigenetics*. (2011) 6:256–63. doi: 10.4161/epi.6.2.13837
16. Bock I, Kudithipudi S, Tamas R, Kungulovski G, Dhayalan A, Jeltsch A. Application of Celluspots peptide arrays for the analysis of the binding specificity of epigenetic reading domains to modified histone tails. *BMC Biochem*. (2011) 12:48. doi: 10.1186/1471-2091-12-48
17. Heintzman ND, Hon GC, Hawkins RD, Kheradpour P, Stark A, Harp LF, et al. Histone modifications at human enhancers reflect global cell-type-specific gene expression. *Nature*. (2009) 459:108–12. doi: 10.1038/nature07829
18. Cejas P, Li L, O'Neill NK, Duarte M, Rao P, Bowden M, et al. Chromatin immunoprecipitation from fixed clinical tissues reveals tumor-specific enhancer profiles. *Nat Med*. (2016) 22:685–91. doi: 10.1038/nm.4085
19. Mann M, Cortez V, Vadlamudi R. PELP1 oncogenic functions involve CARM1 regulation. *Carcinogenesis*. (2013) 34:1468–75. doi: 10.1093/carcin/bgt091
20. Makrygiannakis D, Af Klint E, Lundberg IE, Lofberg R, Ulfgren AK, Klareskog L, et al. Citrullination is an inflammation-dependent process. *Ann Rheum Dis*. (2006) 65:1219–22. doi: 10.1136/ard.2005.049403
21. Ordonez A, Yelamos J, Pedersen S, Minano A, Conesa-Zamora P, Kristensen SR, et al. Increased levels of citrullinated antithrombin in plasma of patients with rheumatoid arthritis and colorectal adenocarcinoma determined by a newly developed ELISA using a specific monoclonal antibody. *Thromb Haemost*. (2010) 104:1143–9. doi: 10.1160/TH10-05-0297
22. Neeli I, Khan SN, Radic M. Histone deimination as a response to inflammatory stimuli in neutrophils. *J Immunol*. (2008) 180:1895–902. doi: 10.4049/jimmunol.180.3.1895
23. Wang Y, Li M, Stadler S, Correll S, Li P, Wang D, et al. Histone hypercitrullination mediates chromatin decondensation and neutrophil extracellular trap formation. *J Cell Biol*. (2009) 184:205–13. doi: 10.1083/jcb.200806072
24. McNee G, Eales KL, Wei W, Williams DS, Barkhuizen A, Bartlett DB, et al. Citrullination of histone H3 drives IL-6 production by bone marrow mesenchymal stem cells in MGUS and multiple myeloma. *Leukemia*. (2017) 31:373–81. doi: 10.1038/leu.2016.187
25. DeVore SB, Young CH, Li G, Sundararajan A, Ramaraj T, Mudge J, et al. Histone citrullination represses miRNA expression resulting in increased oncogene mRNAs in somatolactotrope cells. *Mol Cell Biol*. (2018) 38:e00084–18. doi: 10.1128/MCB.00084-18
26. Amin B, Voelter W. Human deiminases: isoforms, substrate specificities, kinetics, and detection. *Prog Chem Org Nat Prod*. (2017) 106:203–40. doi: 10.1007/978-3-319-59542-9_2

27. Fert-Bober J, Giles JT, Holewinski RJ, Kirk JA, Uhrigshardt H, Crowgey EL, et al. Citrullination of myofilament proteins in heart failure. *Cardiovasc Res*. (2015) 108:232–42. doi: 10.1093/cvr/cvv185
28. Bicker KL, Thompson PR. The protein arginine deiminases: structure, function, inhibition, and disease. *Biopolymers*. (2013) 99:155–63. doi: 10.1002/bip.22127
29. Nakashima K, Hagiwara T, Yamada M. Nuclear localization of peptidylarginine deiminase V and histone deimination in granulocytes. *J Biol Chem*. (2002) 277:49562–8. doi: 10.1074/jbc.M208795200
30. Pradet-Balade B, Boulme F, Beug H, Mullner EW, Garcia-Sanz JA. Translation control: bridging the gap between genomics and proteomics? *Trends Biochem Sci*. (2001) 26:225–9. doi: 10.1016/S0968-0004(00)01776-X
31. El Hajj P, Gilot D, Migault M, Theunis A, van Kempen LC, Sales F, et al. SNPs at miR-155 binding sites of TYRP1 explain discrepancy between mRNA and protein and refine TYRP1 prognostic value in melanoma. *Br J Cancer*. (2015) 113:91–8. doi: 10.1038/bjc.2015.194
32. Lee W, Ko SY, Mohamed MS, Kenny HA, Lengyel E, Naora H. Neutrophils facilitate ovarian cancer premetastatic niche formation in the omentum. *J Exp Med*. (2018) 216:176–94. doi: 10.1084/jem.20181170
33. Chang X, Han J, Pang L, Zhao Y, Yang Y, Shen Z. Increased PADI4 expression in blood and tissues of patients with malignant tumors. *BMC Cancer*. (2009) 9:40. doi: 10.1186/1471-2407-9-40
34. Clancy KW, Russell AM, Subramanian V, Nguyen H, Qian Y, Campbell RM, et al. Citrullination/methylation crosstalk on histone H3 regulates ER-target gene transcription. *ACS Chem Biol*. (2017) 12:1691–702. doi: 10.1021/acschembio.7b00241
35. Margueron R, Reinberg D. The Polycomb complex PRC2 and its mark in life. *Nature*. (2011) 469:343–9. doi: 10.1038/nature09784
36. Greer EL, Shi Y. Histone methylation: a dynamic mark in health, disease and inheritance. *Nat Rev Genet*. (2012) 13:343–57. doi: 10.1038/nrg3173

Conflict of Interest Statement: The authors declare that the research was conducted in the absence of any commercial or financial relationships that could be construed as a potential conflict of interest.

frontiers in Oncology

REVIEW
published: 24 April 2019
doi: 10.3389/fonc.2019.00297

Gene Therapy Leaves a Vicious Cycle

*Reena Goswami[1], Gayatri Subramanian[2], Liliya Silayeva[1], Isabelle Newkirk[1], Deborah Doctor[1], Karan Chawla[2], Saurabh Chattopadhyay[2], Dhyan Chandra[3], Nageswararao Chilukuri[1] and Venkaiah Betapudi[1,4]**

[1] Neuroscience Branch, Research Division, United States Army Medical Research Institute of Chemical Defense, Aberdeen, MD, United States, [2] Department of Medical Microbiology and Immunology, University of Toledo College of Medicine and Life Sciences, Toledo, OH, United States, [3] Roswell Park Comprehensive Cancer Center, Buffalo, NY, United States, [4] Department of Physiology and Biophysics, Case Western Reserve University, Cleveland, OH, United States

The human genetic code encrypted in thousands of genes holds the secret for synthesis of proteins that drive all biological processes necessary for normal life and death. Though the genetic ciphering remains unchanged through generations, some genes get disrupted, deleted and or mutated, manifesting diseases, and or disorders. Current treatment options—chemotherapy, protein therapy, radiotherapy, and surgery available for no more than 500 diseases—neither cure nor prevent genetic errors but often cause many side effects. However, gene therapy, colloquially called "living drug," provides a one-time treatment option by rewriting or fixing errors in the natural genetic ciphering. Since gene therapy is predominantly a viral vector-based medicine, it has met with a fair bit of skepticism from both the science fraternity and patients. Now, thanks to advancements in gene editing and recombinant viral vector development, the interest of clinicians and pharmaceutical industries has been rekindled. With the advent of more than 12 different gene therapy drugs for curing cancer, blindness, immune, and neuronal disorders, this emerging experimental medicine has yet again come in the limelight. The present review article delves into the popular viral vectors used in gene therapy, advances, challenges, and perspectives.

Keywords: gene therapy, viral vectors, modern medicines, diseases and disorders, clinical trials

OPEN ACCESS

Edited by:
Zhe-Sheng Chen,
St. John's University, United States

Reviewed by:
Paul B. Fisher,
Virginia Commonwealth University, United States
Rocco Savino,
Università degli studi Magna Græcia di Catanzaro, Italy

***Correspondence:**
Venkaiah Betapudi
Venkbetapudi@gmail.com

Specialty section:
This article was submitted to Cancer Molecular Targets and Therapeutics, a section of the journal Frontiers in Oncology

Received: *11 January 2019*
Accepted: *01 April 2019*
Published: *24 April 2019*

Citation:
Goswami R, Subramanian G, Silayeva L, Newkirk I, Doctor D, Chawla K, Chattopadhyay S, Chandra D, Chilukuri N and Betapudi V (2019) Gene Therapy Leaves a Vicious Cycle. Front. Oncol. 9:297. doi: 10.3389/fonc.2019.00297

INTRODUCTION

The human genome contains ~25,000 genes that encode a wide variety of proteins colloquially called the building blocks and workhorses of the cell to drive every biological process necessary for life and death (1–4). Though the genetic ciphering remains largely unchanged through generations, some genes go awry due to mutations, and disruptions or deletions (5). These underlying and inevitable genetic changes translate into altered protein functions affecting normal cell structures, functions, and their physiological roles manifesting into a serious disease or deficiency or disorder (6, 7). According to the Genetic and Rare Diseases Information Center (GARD) and Global Genes®, the leading rare disease patient advocacy organization in the world, dysfunctional genes account for 80% of the total 7,136 diseases reported to date. Nearly 30 million people in the United States alone and more than 300 million people in the rest of the world are affected by genetic diseases; unfortunately, half of them are estimated to be children. According to the National Center for Advancing Translational Sciences (NCATS), only 500 human diseases are treatable with an estimated 10,000 drugs available to date, underscoring the necessity to develop new drugs and treatment options.

Although a significant advancement has been made in developing modern medicine, including chemotherapy, radiation, and surgery, many drugs are synthetic chemicals designed to alter the body's chemistry and create dependency overtime, and offer only temporary relief by reducing disease symptoms and increasing lifespan. These issues are partly addressed by developing protein therapy based on transcription factors, signaling proteins, gene editing enzymes, growth factors, engineered protein scaffolds, hormones, blood factors, thrombolytes, antibodies, and antigens. Some of them, especially the monoclonal antibody-based drugs including Humira, Rituxan, Avastin, Herceptin, Remicade, Lucentis, Enbrel, Synazis, and several others, are being used to treat cancer, diabetes, autoimmune disorders, infectious diseases, and others (8). In fact, both protein and peptide-based drugs have emerged as a major class of therapeutics with nearly 380 marketed pharmaceuticals available in the world (9). However, these protein-based therapies are facing many challenges including low solubility and bioavailability, *in vivo* physicochemical instability, short circulating half-life, penetrability *in vivo*, biodistribution, and causing toxicity in large amounts (10–15). Another adverse effect of introducing therapeutic proteins into a patient's body is that it may result in severe immune responses, inflammation, and fever (16). To add to the woes, the production and manufacturing of high quality therapeutic proteins have become highly complex activity (17). In fact, more than 5,000 critical steps are involved in developing a single therapeutic protein (8). Therefore, the quotient of unpredictability is very high in developing both chemical and protein-based therapies. Gene therapy, on the other hand, leads to long-lasting production of the desired therapeutic protein and can localize protein expression to an area of the body, fixing the problem at its source (18). Also, prognosis for a large number of incurable diseases appears grim, which is why gene therapy presents itself as a breakthrough alternative with immense potential to provide a one-time treatment option for a complete cure as well as disease and disorder prevention. Gene therapy is an emerging experimental treatment that delivers functional genes into a patient's body to counter or replace malfunctioning ones, thus curing disease without pharmacological intervention, radiotherapy, or surgery. This modern approach has the potential to offer complete protection against lethal nerve gases (13, 19–22) and treat monogenic and cardiovascular diseases, immunodeficiency, cancer, and more (23–27). Apart from genetic defects, several other diseases that cannot be treated with drugs or antibodies can be cured with gene therapy. In addition, every prescribed and non-prescribed drug comes with unwanted side effects, ranging from minor discomfort to death. According to Drugwatch®, a non-profit drug information network and organization, an estimated four million patients in the USA alone visit doctors annually due to adverse effects of prescription drugs. Hence, gene therapy that aligns with the natural human genetic transcriptome has the potential to become an unquestionable choice for complete treatment of diseases, disorders, and infectious diseases.

Gene therapy appears simple in principle but involves identification of affected gene(s), cloning and loading of a wild type or recombinant healthy version in a suitable vector for optimal delivery and expression in the target cells or tissue and thus has seen its fair share of hurdles. Because it often uses repurposed viruses to deliver therapeutic genes, gene therapy has been caught in a vicious cycle for nearly two decades owing to immune response, insertional mutagenesis, viral tropism, off-target activity, unwanted clinical outcomes (ranging from illness to death of participants in clinical trials), and patchy regulations (23, 28–31). This led to a sharp decline in research funding for basic, preclinical development and vector production via individual investigators grants such as R01 and program grants. Thus, with limited information of preclinical data and vector production, the number of clinical trials conducted worldwide did not rise steadily from 1999 to 2015 (32). Furthermore, funding of the actual clinical trial was not guaranteed even vectors have been produced and certified for human use at significant cost. The American Society of Gene Therapy has taken lead in fixing this fragmented funding method by making many recommendations including the elimination of redundant regulatory processes and establishment of the National Gene Vector Laboratories (NGVL) to review vector production and toxicology. Now, with new technological advances in gene delivery and editing methods, increased enthusiasm of clinicians and drug companies, the advent of several viral-based drugs in the market, and the potential to provide a one-time treatment option without corrupting the genetic code, gene therapy is breaking free of this cycle. Undoubtedly, the resurgent interest in offering gene therapy-based treatments is one of the most defining developments in the pharmaceutical industry and is expected to have far-reaching implications on curing dangerous diseases in the future. With an estimated US $11 billion market in the next 10 years, both clinical trials and pharmaceutical industry are anticipated to benefit immensely from gene therapy. Here, we describe popular viral vectors used in gene therapy and gene therapy drugs available in the market.

GENE THERAPY AND ITS KINDS

While the idea of gene therapy has been around for the past 80 years, Professor William Szybalski's demonstration in 1962 on correcting a genetic defect by delivering foreign DNA into mammalian cells is regarded as its birth (33). The Food and Drug Administration (FDA) defines gene therapy as products that "mediate their effects by transcription and/or translation of transferred genetic material and/or by integrating into the host genome and that are administered as nucleic acids, viruses, or genetically engineered microorganisms," and the European Medicines Agency (EMA) describes gene therapy medicinal product (GTMP) as a "biological medicinal product that contains an active substance which contains or consists of a recombinant nucleic acid used in or administered to humans to regulate, repair, replace, add or delete genetic sequences and its therapeutic, prophylactic or diagnostic effect relates directly to the recombinant nucleic acid sequence it contains, or to the product of genetic expression of this sequence" (32, 34). Typically, DNA, mRNA, siRNA, miRNA, and anti-sense

oligonucleotides are the genetic materials used for therapeutic delivery into a defective target cell or tissue to restore a specific gene function or turn off a gene responsible for disease or disorder development (35). Other methods include swapping the mutated gene for a functional gene using homologous recombination, repairing the mutated gene using selective reverse mutation, and regulating the mutated gene (36). Gene therapy allows the delivery of therapeutic genetic material to any specific cell or tissue and or organs of the body for treatment.

Based on the type of cells or tissues targeted for gene delivery and treatment, gene therapy is divided into germ-line and somatic cell gene therapies. Germ-line gene therapy involves genetic manipulation of the reproductive cells sperm and egg to make heritable changes. The potential of germ line therapy was successfully demonstrated in mouse, rat, rabbit, sheep, cattle, goat, and pig (37–40) but not in humans because of a moratorium due to ethical reasons, lack of advanced tools, and societal consensus (41–46). However, with recent technological advances in genome editing and gene delivery methods, renewal of debates on revisiting germ line therapy appears not far from reality (47–50). Therefore, the present review is focused on somatic cell gene therapy.

SOMATIC CELL GENE THERAPY

In somatic cell gene therapy, every cell except sperm and egg is targeted for therapeutic treatment. It is considered safe because genetic changes remain in the patient and are not passed onto the offspring. However, the requirement of skill set and sophistication in delivering a therapeutic gene into the target cells or tissue of the patient elevates the quotient for an unpredictable clinical outcome. Therefore, many advanced methods are being developed to deliver therapeutic genetic materials, and they are broadly divided into *ex vivo*, *in situ,* and *in vivo* methods. *Ex vivo,* also called "outside the living body" method, involves isolating the cells to be treated from the patient, modifying them with a therapeutic gene, and re-introducing into the patient's body. Hepatocytes in the liver, retina photoreceptors in the eye, stem cells in the bone marrow, and T lymphocytes have been the focus of this method (43). Recently, the FDA has approved Kymriah™, a groundbreaking prescription cancer treatment that uses the patient's own white blood cells or T cells for inserting the CD19 gene *ex vivo* (51). After being re-introduced into the patient's blood, these genetically engineered T cells will have greater ability to target cancer cells. Less side effects than other methods, no risk of reaching germ-line cells, minimized immune response, and less renal clearance are other advantages of *ex vivo* method (52–54). Zalmoxis™ is another advanced somatic cell therapy product recently approved by the EMA for treating serious blood cancers such as certain types of leukemia and lymphomas. Zalmoxis™ consists of donor lymphocytes transfected with Herpes simplex virus-1 thymidine kinase (HSV-TK) and truncated low affinity nerve growth factor receptor (ΔLNGF). *In situ* delivery, or "in position" delivery, involves administration of the desired genetic material directly into the target cells or tissue. For example, Neovasculgen®, a plasmid vector carrying vascular endothelial growth factor (VEGF) gene, is directly injected into the target ischemic tissue to stimulate blood vessel growth (55–57). This method is being explored to cure cystic fibrosis, muscular dystrophy, and cancer but still requires more technological advancement in delivery methods for a successful clinical outcome (58–60). Though delivering genetic material by this method works well for localized conditions, it cannot be used for treating systemic disorders. The last and most important method of gene delivery is *in vivo*, or "in the living body." In this method, viral, or non-viral vectors are used to deliver the therapeutic material to the defective target cells or tissue in the body (**Figure 1**). A wide variety of physical and chemical methods including needles, gene guns, electroporation, sonoporation, photoporation, magnetofection, hydroporation, mechanical massage, lipid, calcium phosphate, silica, and gold nanoparticles are being used to deliver genetic material to target cells. However, none of them is more efficient than viruses in delivering therapeutic genetic materials to the target cells due to their inherent shortcomings and operational complexity. The present review article is focused on viral vectors only.

VIRUSES IN DELIVERING THERAPEUTIC GENES

There has been a quite bit of resentment in availing the benefits of viruses due to ignorance, bad rap, and skewed view. In fact, the human body offers shelter to viruses, fungi, protozoa, and worms by adopting appropriate mechanisms for mutual benefits in order to survive and thrive (61). For example, viruses offer immunity against bacterial pathogens and tumor cells, and modulate gut bacterial genes to improve host digestion (62). Though the word *virus* implies mortality and morbidity, viruses are considered nature's genetic engineers because of their ability to infect most kinds of organisms including bacteria, humans, animals, and plants. Also, viruses help certain plants to survive in extreme weather conditions (62). We have identified powerful viral promoters and enhancer elements that can be used to construct plasmid vectors for high level expression of foreign proteins (63, 64). They have an advantage over others by carrying several genes encoding structural and non-structural proteins to infect and propagate in host cells. Some viruses have the ability to transduce the cells they infect, i.e., stably express a gene along with the host's genome. They allow manipulation of their genome and removal of virulent genes without losing the ability to infect host cells. This makes them nearly dead or not alive, and the versatile biological entities, a pragmatic reason to accept them as sophisticated biological tools for delivering foreign genetic materials into eukaryotic cells. For example, we have manipulated and reconstituted Sendai viral envelopes containing only the fusion glycoprotein to deliver a reporter gene to liver *in vivo* (65). In fact, viral vectors were the first carriers of nucleic acids used in gene therapy (18).

Because of their abundance on the earth and difference in genetic makeup, many viruses are being used in preclinical and clinical investigations but each comes with its own unique

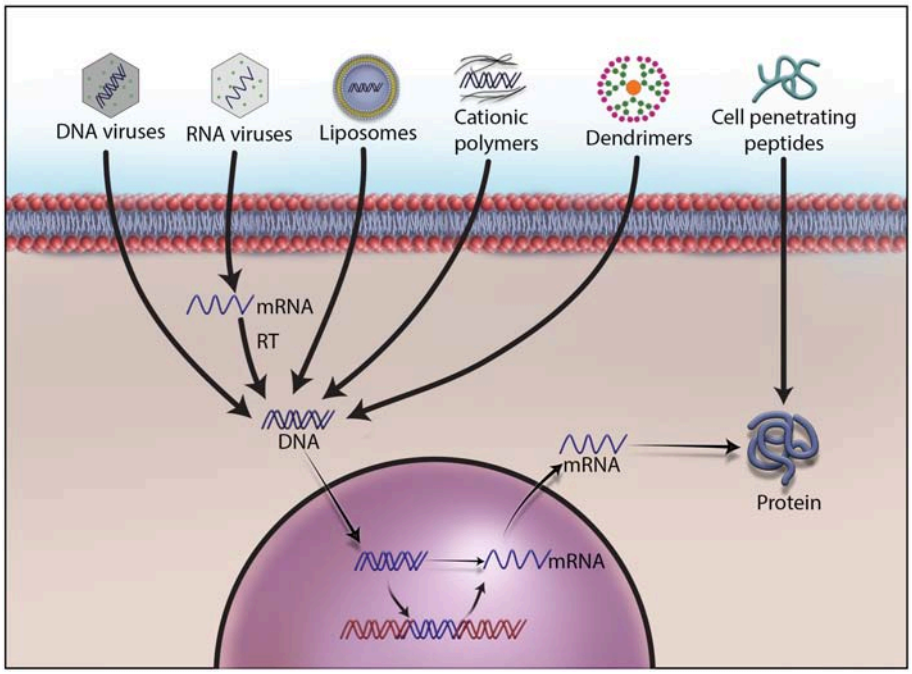

FIGURE 1 | Different methods to deliver therapeutic DNA and proteins to target cells. Non-viral gene delivery methods have many advantages over viral vectors in gene therapy. They do not cause immunogenicity and carcinogenicity, and can deliver a large size of therapeutic DNA efficiently with a low price tag. As no one-size-fits-all solution to therapeutic DNA delivery exits, development, and formulations remain the main focus of research on non-viral methods.

advantages and disadvantages. Therefore, finding a suitable vector to deliver therapeutic genetic material has become a challenge to make gene therapy a viable and better treatment option than conventional methods. Part of the challenge is therapeutic DNA's inability to pass through the cell membrane because of its large size and negative charge. Also, the therapeutic DNA needs to escape the cellular endonucleases and renal clearance. An ideal vector should have enough space to transport large therapeutic genes, high transduction efficiency, and the ability to provide long-term and stable expression, as well as target specific cells, avoid random insertion of the therapeutic gene into the host genome, and infect mitotic as well as post-mitotic cells. It should not be immunogenic or pathogenic, should not cause inflammation and should possess the ability to be manufactured on a large scale. Research on developing novel viral vectors is advancing steadily with a special focus on substituting pathogenic genes with therapeutic DNA (66). In fact, non-pathogenic, replication-defective, and human-friendly viral vectors are being used in more than 70% of the ongoing gene therapy clinical trials worldwide (67). One particularly popular use of viral vectors, such as adenovirus, Seneca Valley virus, poliovirus, vaccinia virus, herpes simplex virus, reovirus, Coxsackievirus, parvovirus, Newcastle disease virus, vesicular stomatitis virus, and measles virus, is in the form of oncolytic viruses (OV). In 2016 alone, more than 40 clinical trials using OV were conducted (68). OV destroy malignant cancer cells by specifically replicating in those cells to effectively lyse them as well as induce a robust antitumor immune response. OV selectively replicate in tumor cells through a variety of methods such as virus-specific receptors on the cells. They can be used to deliver anti-angiogenesis genes, suicide genes, immunostimulatory genes, and DNA encoding small nucleic acids. Apart from carrying immunostimulatory genes, OV can induce an immune response by releasing cell debris and viral antigens (68). Many other innovative approaches are being developed to use viral vectors for treating diseases and disorders. Since Edward Tatum's initial proposal to repurpose viruses for therapeutic gene delivery in 1966, gene therapy has come a long way from the construction of many types of viral vectors to their use in more than 3,000 clinical trials to date (32, 69, 70). However, during this incredible journey with obscure regulations, gene therapy has experienced a few undesired clinical outcomes due to off-target effects, cytotoxicity, viral transmissibility, impurity, and an immune response to the viral vector itself (68). Nonetheless, diseases for which a cure has been attempted include β-thalassemia, X-linked severe combined immunodeficiency (X-SCID), adenosine deaminase deficiency (ADA-SCID), cystic fibrosis, hemophilia, liver enzyme ornithine transcarbamylase (OTC) deficiency, head and neck cancer, metastatic melanoma, HIV, Leber's congenital amaurosis, Wiskott-Aldrich syndrome (WAS), metachromatic leukodystrophy (MLD), and severe lipoprotein lipase deficiency disorder (LPLD) (52, 71). In fact, the possibilities for gene therapy-mediated treatments are endless because virtually every cell in the human body is a potential target for genetic manipulation. Viruses display specificity in infecting cell types;

therefore, viral vectors can be selected based on the type of cell that needs gene delivery. Here, we describe some widely used viral vectors in gene therapy.

ADENOVIRUS (AV)

AV was the first viral vector developed for gene therapy and was approved for clinical trials in 1990. It was isolated from human adenoid tissue-derived cell cultures for the first time in 1953, hence the term adenovirus, and included in a diverse family of non-enveloped double-stranded DNA (dsDNA) viruses called *Adenoviridae* (72). According to the Centers for Disease Control and Prevention (CDC), AV rarely causes serious illness and death in healthy individuals but immuno-compromised individuals may develop a wide range of illnesses including the common cold, sore throat, bronchitis, pneumonia, diarrhea, conjunctivitis, fever, and neurologic disease. As of today, there are 57 human AV serotypes isolated and classified into seven categories based on their properties of agglutination (73, 74). AV carries a linear dsDNA ranging from 26 to 45 kb in a medium sized (∼100 nm) non-enveloped icosahedral viral particle composed of penton and hexon subunits. While the hexon subunits form a major part of the viral capsid coat and carry antigenic motifs, the penton subunits constitute fiber and knob domains required for infection (75). The fiber knob domain initiates AV infection by binding to a variety of proteins such as MHC-1 α2 subunit, CD46, sialic acid saccharides on glycoproteins, coxsackievirus, and AV receptor (CAR) expressed on cell surface (76). The interaction between arginine-glycine-aspartic acid (RGD) sequence of the fiber penton subunit and αν integrins on the cell surface drives endocytosis of viral particle and completion of viral infection (77–79). This creates broad tissue tropism and a nodal for AV transduction efficiency, giving an opportunity to manipulate binding sites for CAR and other ligands to de-target AV infection, an essential feature of popular viral vectors used in gene therapy. Therefore, since its discovery, AV has been repurposed through the deletion of its pathogenic genes.

Based on the expression of AV genes during infection and multiplication, its genome is organized into early (E1, E2a, E2b, E3, and E4), intermediate (IVA2 and IX), and late genes (L1, L2, L3, L4, and L5). Also, its genome carries non-coding inverted terminal repeat (ITR) sequences, ψ packaging sequences, and many viral RNAs (75, 80, 81). The genome of AV has been manipulated many times to develop safe and efficient vectors for gene therapy applications. The first-generation vectors with a partial deletion of E1 or E3 genes do not replicate or display oncogenicity but can deliver less than an 8 kb gene and display leaky expression of viral proteins, strong immune response, and contamination with replication-competent virus (82). To circumvent this, second-generation vectors were created by deleting E2A, E2B, and E4 from the genome of the first-generation AV vectors. However, their production has become complicated, and they do not prevent leaky expression of viral proteins and rapid loss of therapeutic gene expression, and thus have lost enthusiasm for their widespread use in gene therapy (83, 84). The third-generation vectors, otherwise known as gutless or helper-dependent AV vectors, lack all viral genes except the ψ and ITR sequences. They have received special attention because of their capacity to carry larger therapeutic genes (up to 37 kb in size), their ability to display long-term transgene expression, and lesser contamination with replicating virus particles. They are also less immunogenic than first- and second-generation vectors (85). The third-generation vectors were successfully used to express transgenes for about 2 years in animals with no adverse effects (86, 87). Co-transduction of these vectors with Sleeping Beauty transposon along with FLP recombinase was used to insert a FIX gene in the chromosome of dogs suffering from hemophilia B and expressed for up to 960 days (88, 89). Recently, they were successfully used for the long-term expression of a gene encoding an alanine-glyoxylate aminotransferase (AGT) in patients with primary hyperoxaluria type 1 (PH1), a rare kidney disorder that causes recurrent kidney stones (90).

Since AV vectors allow episomal or stable insertion of therapeutic genes, they carry advantages over vectors that integrate into cellular DNA. This provides clinicians an opportunity to offer appropriate treatment for patients with different diseases or disorders. For instance, AV is suitable for treating cancers and offering bioscavenger-mediated short-term protection against nerve gases and other chemical weapons. As depicted in **Figure 2**, we have demonstrated an AV-mediated episomal insertion of *PON1*, *BChE*, and *PD* bioscavenger genes in the liver to express and secrete proteins to detoxify the circulating lethal nerve gases for 10–15 days in mice (13, 20–22, 36). Since the immune system has the natural ability to detect and destroy abnormal cells in our body, new AV vectors that can induce immune response and destroy target cells have been developed. For example cancer cells can go undetected by reducing the expression of tumor antigens on their surfaces, inducing immune cell inactivation, and releasing substances in the microenvironment to promote their growth and survival. Therefore, new oncolytic adenoviruses that effectively induce immune response, and specifically target and lyse tumor cells are being created by replacing their native E1A promoter with tumor-specific promoters and genetically modified CAR, a highly expressed AV receptor in tumor cells (68, 91). For example, the CV706 and OBP-30 AV vectors carry the viral E1A gene under prostate cancer-specific antigen promoter and telomerase reverse transcriptase promoter, respectively (92). Other engineered oncolytic adenoviruses target the components of tumor cells and their microenvironment and inhibit their proliferation by expressing antibodies, relaxin, hyaluronidase, and inhibitors of metalloproteinases to hinder angiogenesis and proper function of the extracellular matrix (91, 93). Oncolytic adenoviral vectors that induce autophagy-related immunogenic cell death were also developed to treat cancer (94). A novel oncolytic AV vector expressing an interfering long non-coding RNA (lncRNA) to inhibit 12 oncogenic miRNAs has been constructed in order to perform selective killing of tumor cells (95). AV vectors carrying complementary sequences of liver-specific miRNA-122a incorporated into 3'-UTR of *E2A, E4,* or *pIX* to reduce the leaky expression of viral genes and hepatotoxicity were developed (96). In addition, AV vectors with *E1A* carrying mutations complementary to retinoblastoma (RB) or p53 gene mutations

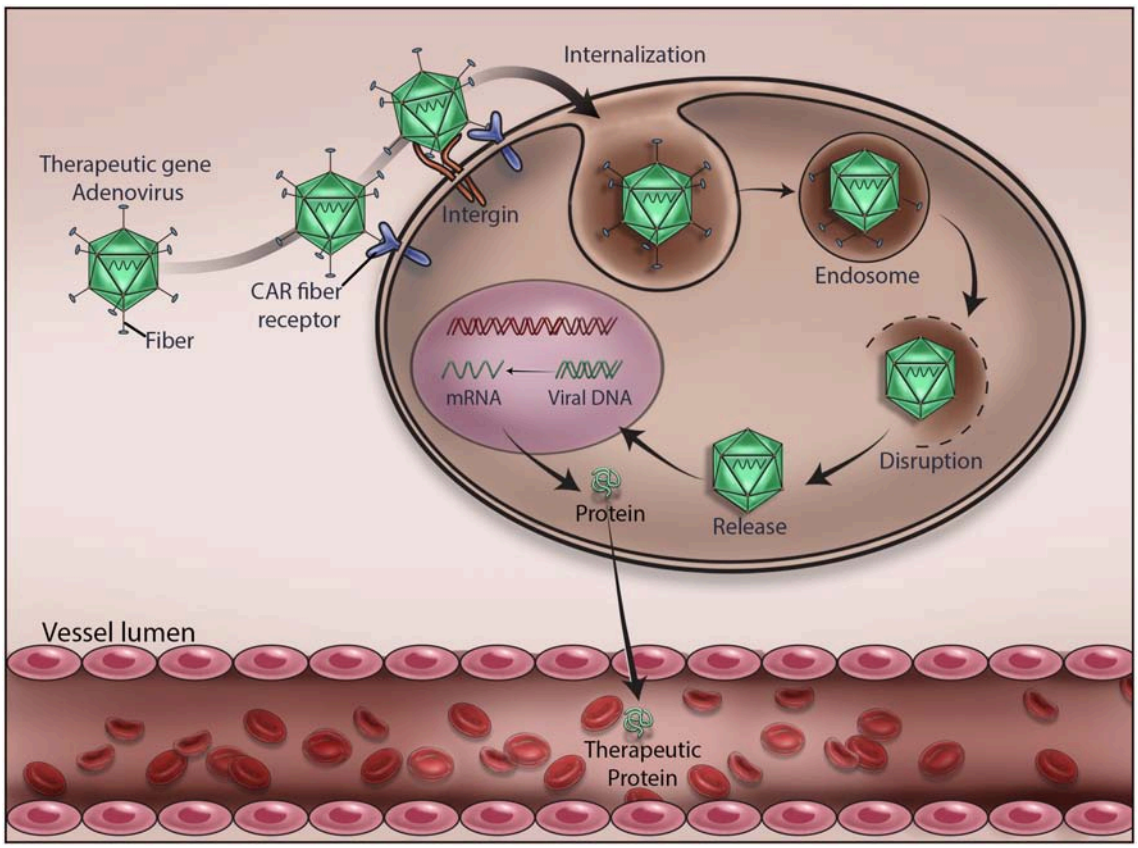

FIGURE 2 | Mechanism of adenovirus-mediated delivery of a therapeutic DNA. Upon infection, adenovirus delivers the encapsulated therapeutic DNA into the cytoplasm of the target cells. Various stages of viral gene delivery, *viz* cell attachment, internalization, endocytosis, uncoating, transcription and translation of the therapeutic protein, are shown.

in tumor cells that can specifically replicate and lyse tumor cells were created (92).

Despite many technological improvements made in vector design and production, there are still certain issues that have to be addressed for better clinical outcome. For example, infecting target cells with the optimal amount of highly purified AV particles is critical for the successful insertion of a therapeutic gene. Recently, it was shown that 10^{10}-10^{12} AV particles per patient are required for a successful Ebola vaccination (97). Production of such high titer virus with no or minimal empty vector contamination is still a formidable challenge. Also, high prevalence of anti-AV vector immunity in the human population and differential expression of CAR and other receptor proteins on target cells have been serious issues in clinical trials (98, 99). For example, the transduction efficiency of the widely used AV serotype 5 in gene therapy is dampened by the prevalence of neutralizing antibodies in the human population (100, 101). An estimated 80% of the human population is believed to carry antibodies against AV serotype 5, resulting in a significant transduction deficiency and stimulation of inflammatory shock (102). There has been a positive correlation between body fat and the presence of circulating antibodies against AV serotype 36 in humans (103). In addition, during systemic administration, the tendency of AV vectors to undergo sequestration in the liver has prevented efficient transgene transduction and displayed severe hepatotoxicity, even causing the death of a clinical trial participant (104, 105). This was due to the binding of blood coagulation factor FV and FX to the hyper variable region (HPV) of AV hexon subunit (106, 107). Therefore, mutating the HPV site in such a way that it neither activates complementary pathway nor interacts with FX could be an ideal way to resolve the liver sequestration issue. Attempts are being made to improve the safety of AV vectors by treating with chemicals and developing chimeric and hybrid vectors to minimize inflammation and immunogenicity (108, 109). For example, the chimeric AV serotype 5 vector carrying receptor-binding epitopes derived from other human AV serotype 3, serotype 35, and serotype 43 displayed low seroprevalence and low affinity for CAR (110, 111). Similarly, the chimeric human AV serotype 5/3, consisting of receptor epitopes derived from serotype 3 and 5, showed high binding affinity for CD46, an AV receptor commonly expressed on many solid tumors. It was thus found to be particularly useful in targeting solid tumors (112, 113). Another CD46-targeted chimeric AV vector derived from human serotype 5 and 35 has been shown to be suitable for transducing vascular smooth muscle cells, treating colorectal cancers, and ischemic wounds

as well as manipulating T-cells (114–117). Novel chimeric AV vectors developed from AV serotypes 5 and 11 and 3 and 11 were found very effective in exclusively targeting glioma and colon cancer cells, respectively (118, 119). Other types of chimeric vectors were also derived entirely from low prevalent human and non-human AV serotypes such as human AV serotype 26, canine AV serotype 2, and chimpanzee serotype 3. For example, the chimeric AV vector developed from human AV serotype 26 and chimpanzee AV serotype 5 has been used successfully for Ebola vaccination in animal models (120, 121). A novel hybrid vector developed from AV serotype 5 and alpha virus was found very useful for the expression of transgenes in malignant hematopoietic cells (122). Many laboratories have developed a library of AV vectors that carry random-peptides on their fiber knobs in order to overcome the paucity of cancer-specific ligands (123–125). This resulted in the generation of many AV vectors that are specific to prostate and pancreatic cancer as well as glioma (123, 125–128). One such vector carrying pancreatic cancer-targeting ligand has shown strong oncolytic effect in primary pancreatic neuroendocrine tumors and appears promising as a next-generation therapy (129). Given the advancements made in developing safe and efficient AV vectors, their choice for delivering therapeutic genes has become apparent in clinical trials.

ADENO-ASSOCIATED VIRUS (AAV)

AAV is yet another popular viral vector used in gene therapy. This small microbe was first isolated as a contaminant in the simian adenovirus preparation and then named adeno-associated virus (AAV) by the Bob Atchison group at Pittsburgh University and the Wallace Rowe group at the NIH (130, 131) and later found in a wide range of animal samples including human, non-human primates, avian, bovine, reptiles, pigs, sea lions, bats, and caprine samples. The 4.7-kb-long single-stranded DNA (ssDNA) packed inside a non-enveloped viral particle carries p5, p19, and p40 promoters as well as rep and cap genes flanked by two 145 nucleotide-long inverted terminal repeats (ITR) and no polymerase gene (132, 133). While ITRs having palindromic sequences base pair to allow synthesis of cDNA, both rep and cap genes undergo alternate splicing to express replication proteins (Rep78, Rep68, Rep52, and Rep40), capsid or virion proteins (VP1, VP2, and VP3), and an assembly activating protein (AAP), respectively (134). Being a non-structural protein, AAP assists virion proteins in capsid formation (135). VP1, VP2, and VP3 expressed from p40 promoter at a ratio of 1:1:10 form the outer capsid of the virion. These capsid proteins carry phospholipase domain to protect virions from the onslaught of intracellular protease system (136). Unlike other viruses, AAV requires a few other helper proteins, agents or viruses such as AV, herpes simplex virus type I/II, pseudorabies virus, cytomegalovirus, genotoxic agents, UV radiation, or hydroxyurea to infect cells and complete replication (137). AAV can also be generated by providing the missing genes E1a, E1b, E2a, E4orf6, and VA that are needed for viral infection. These genes are often cloned in pXX6 helper plasmid and used to co-transfect HEK293 cells along with AAV expression plasmid (rep-cap plasmid) to produce AAV (134, 138). Therapeutic genes are cloned in the AAV expression plasmid carrying ITR sequences, and their size can be increased by cotransfecting another plasmid carrying rep-cap genes or by generating virus in rep-cap stable cells. Since the formation of dsDNA from its ssDNA is the rate-limiting step of viral infection, gene delivery, and expression in the target cells, a self-complementary viral dsDNA (scAAV) is developed; however, it reduces the capacity of AAV vectors to deliver a therapeutic gene (139, 140). AAV inserts a therapeutic gene in the genome of target cells to provide long-term transgene expression. For instance, the gene expressing FIX blood coagulation factor in one individual of a cohort persisted for more than 10 years during a clinical trial (141). AAV inserts a therapeutic gene in the host genome at a specific location on the q arm of chromosome 19 (142, 143). Despite having no large homology regions, more than 70% of the transgene integration events occur within this site; however, the underlying mechanism remains unknown. But AAV lacking its rep-cap genes can deliver a therapeutic gene in the episomal form without inserting into the genome of the target cells. The therapeutic gene in the episomal form can develop into a chromatin-like structure and remain quiescent in cells for months to years without damaging the patient's body. Recently, we have used AAV vectors to make episomal insertion and expression of a bioscavenger gene in the liver cells for about 6 months (unpublished results). This allows clinicians to apply AAV-mediated gene therapy to treat a wide variety of diseases or disorders.

AAV displays broad tropism but requires the expression of heparin sulfate proteoglycan, $\alpha_v\beta_5$ integrin, $\alpha_5\beta_1$ integrin, fibroblast growth factor receptor 1, platelet-derived growth factor receptor, hepatocyte growth factor receptor, epidermal growth factor receptor, laminin receptor, and sialic acid moieties on the surface of target cells for efficient transduction and delivery of a therapeutic gene. Recently, AAVR has been identified as a universal host cell receptor for AAV infections (144). Although every serotype has the ability to infect cells, transport to nucleus, uncoat, and insert its genome into the host's chromosome or leave in the episomal form, not all 13 AAV serotypes isolated to date use the same receptor repertoire on host cell surface for infection (145, 146). This makes AAV a very useful system for a specific cell or tissue type transduction. For example, AAV1 displays high transduction efficiency of muscles, neurons, heart, and retinal pigment epithelium. AAV2 has been shown to infect many types of cancer cells, neurons, kidney, retinal pigment epithelium, and photoreceptor cells. AAV2 is the only serotype that can infect and delivery a therapeutic gene to kidney. AAV4 and AAV5 serotypes infect retina and retinal pigment epithelium, respectively. While AAV6 displays strong tropism for heart, AAV7 has some bias for liver (147). AAV6 is also effective in infecting airway epithelial cells (148). AAV8 and AAV9 have displayed successful infection of lymphoma and HPV tumors, respectively (149). AAV8 is the only serotype that infects pancreas, and it was extensively used to express a therapeutic *FIX* in the liver to treat hemophilia in clinical trials (150). AAV tropism was further refined by mixing the capsid proteins of one serotype with the genome of another serotype. For example, AAV2/5 serotype, which

transduces neurons more efficiently than the parental AAV2, was generated by packaging AAV2 genome in AAV5 capsid proteins. Another example, the pseudotyped AAV8 and AAV9, can cross the endothelial barrier of blood vessels to target muscles (66). For increasing transduction efficiency, hybrid AAV serotypes were also generated by mixing the capsid proteins of multiple serotypes with the genome of another serotype. For example, AAV-DJ serotype that consists of a hybrid capsid is generated by mixing the capsid proteins of eight different AAV serotypes. This made AAV-DJ to display higher transduction efficiency than any other wild type serotype *in vitro* and high infectivity of a broad range of tissue *in vivo*. Its mutant, AAV-DJ8 serotype, displays high infectivity of brain. AAVHSC, a new class of genetic vector isolated from hematopoietic stem cells, has been shown to be ideal for manipulating stem cells (151). Since more than 50% of the adult human population carries AAV neutralizing antibodies, a wide range of mosaic or hybrid vectors were generated by engineering and *de novo* shuffling of capsid proteins (152, 153). For example, the AAV2.5 hybrid vector generated by combining the muscle tropism determinants of AAV1 with parental AAV2 displays immune evasion of their neutralizing antibodies (154). The other hybrid vectors AAV6.2, AAV2i8, AAVrh10, and AAVrh32.33 were found beneficial for intravenous delivery, reduction of liver sequestration, and T-cell response in the clinic, respectively (138, 155–157). Since CpG motifs are responsible for immune response and failure of many clinical trials, AAV vectors were further refined by deleting CpG motifs, known ligands of Toll-like receptor 9 (TLR9), to reduce immune response for maximal expression of a transgene in clinical trials (158). Cre-recombination-based AAV variants are also developed to allow efficient transgene expression in the central nervous system, muscle, and liver (159, 160). Also, the AAV-CRISPR/Cas9 system has been developed to perform *in vivo* genome editing and broaden therapeutic horizons (161).

HERPES SIMPLEX VIRUS (HSV)

Herpes simplex viruses are believed to have tremendous potential as a preventative and therapeutic vaccine against cancer and other diseases because of their ability to evade the immune system and circulating anti-viral drugs, deliver multiple genes, infect a wide variety of cells, pose low risk of adverse health effects, and multiply specifically in tumor cells. They are large enveloped viruses that carry a linear dsDNA of 120–240 kb and infect reptiles, birds, fish, amphibians, and mammals. There are eight known human herpesviruses: herpes simplex virus-1 (HSV-1), herpes simplex virus-2 (HSV-2), human cytomegalovirus (HCMV), varicella-zoster virus (VZV), Epstein-Barr virus (EBV), Kaposi's sarcoma-associated herpesvirus (KSHV), and human herpesviruses 6 and 7 grouped under alpha, beta, and gamma genera. Though they share common virion structure and replication cycle, and many other biological properties, there is a significant difference in their tropism, infection, and clinical manifestations. Some of their genes show homology with regions of human chromosomes. Here, we delve into HSV that infects ∼60% of the human population worldwide and mainly transmits through contact, especially oral-oral contact (162). After infecting oral or genital epithelial cells, HSV enters neurons to establish lifelong latent infection and reactivates periodically causing fever, blisters, cold sores, genital herpes stromal keratitis, blindness, cancer, and encephalitis. Both HSV-1 and HSV-2 carry envelope and sub-envelope structures called tegument and a regular icosahedral capsid consisting of a relatively large dsDNA of 153 kb encoding ∼200 proteins (163). Nearly half of the total 84 genes present in the HSV genome encode proteins required for virus replication, and many were found unnecessary for delivering therapeutic genes. Several genes involved in virulence and immune evasion, and those considered non-essential for viral life cycle *in vivo* were also identified. HSV-1 is relatively less pathogenic than HSV-2 and is, therefore, ideal for vector development and gene therapy (164). HSV infects cells by using its envelope glycoprotein B, glycoprotein C, and glycoprotein D to bind cell surface particles and transmembrane receptors such as heparin sulfate, herpesvirus entry mediator (HVEM), nectin-1, and 3-O sulfated heparin sulfate. While the nectin receptors provide a strong point of viral interaction with the host cell, the other viral envelope proteins, especially glycoprotein B, glycoprotein D, glycoprotein H, glycoprotein L, and HVEM, create an entry pore for the viral capsid. The viral capsid enters through capsid pore and travels through the cytoplasm to the nucleus in order to inject its DNA content. HSV evades the immune system by secreting its immediate-early protein, ICP47, and inducing a transporter associated antigen processing (TAP) protein to block MHC class I antigen presentation on the cell surface. HSV-1 infects many types of mitotic and post-mitotic cells including neurons (36). After infection, HSV induces the expression of the virion host shutoff protein (VHS or UL41) to inhibit protein synthesis by degrading the host mRNA. This makes way for viral replication and lysis of the host cells.

The HSV genome carries immediate-early, early, and late genes for replication and allows creation of replication-competent, replication-incompetent, and helper-dependent vectors, or amplicon vectors, for preclinical and clinical studies. The replication-competent vectors have the capacity to deliver transgenes up to 50 kb in size or the entire locus since treatment of certain diseases requires huge therapeutic gene cassettes carrying complex regulatory elements. These vectors can replicate selectively in cancer cells and have less virulence because of deleted genes. They do not insert transgenes in the host chromosomes and are therefore used primarily as oncolytic viruses to treat glioma, melanoma and ovarian cancers and to stimulate an immune response (66). They are further refined by using tumor specific promoters to express viral genes and target tumor-specific receptors. These vectors with robust replication capacity are believed to enhance intramural vector distribution and lyse tumor cells very effectively. These vectors are generally constructed by homologous recombination in eukaryotic cells by co-transfecting the viral genome and a plasmid carrying the therapeutic gene flanked by the sequences homologous to the target locus on viral genome to undergo recombination. The replication-incompetent vectors are created by either mutating or deleting several immediate early genes including ICP4 and ICP27 that are essential for replication and, therefore, can grow

only in specifically designed cell lines complemented transiently. For example, Vero-7b cell line is capable of providing in trans the proteins encoded by deleted viral genes (165). They are safe and non-inflammatory advanced vector platforms known to persist and express in the nerve cells for life and therefore used to treat neuropathic, inflammatory, and cancer-associated pain (166–168). The helper-dependent HSV vectors, or amplicon vectors, carry deletions in one or more non-essential genes and retain the ability to replicate *in vitro* but are compromised *in vivo* in a context-dependent manner (169, 170). These viruses are the same as wild type HSV, with plasmids containing a packaging signal and the gene of interest. Amplicons have the ability to accommodate a very large therapeutic sequence up to 100 kb in size but have production and stability issues. The replication-incompetent vectors and amplicons have been used to express genes in the nervous system, muscle, heart, and liver.

RETROVIRUS (RV)

Retroviruses are spherical (∼100 nm in diameter) and enveloped microbes belonging to a *Retroviridae* family that comprises foamy virus, human immunodeficiency virus (HIV-1), simian immunodeficiency virus (SIV), bovine immunodeficiency virus, feline immunodeficiency virus, equine infectious anemia virus (EIAV), murine leukemia virus (MLV), bovine leukemia virus, Rous sarcoma virus (RSV), spleen necrosis virus (SNV), and mouse mammary tumor virus. Unlike all other RNA viruses, these viruses are capable of reverse transcribing their genetic blueprint of positive, single-stranded RNA into dsDNA, and inserting it into the host cell genome. RVs carry a non-covalently linked dimers (two copies) of RNA genetic material probably as a fail-safe mechanism for producing genomic DNA and increasing viral RNA diversity due to interstrand recombination (171). Thus, RNA dimerization has been viewed as a prerequisite for RV genome encapsidation and life cycle. With restricted vertebrate hosts, these viruses are divided into exogenous retroviruses (XRV) and endogenous retroviruses (ERV). While the XRVs transmit horizontally among hosts, the ERVs inherit vertically in the genome of their hosts (172). By scattering all over chromosomes and comprising nearly eight percent of the human genome, the ERVs are thought to be relics of ancient retroviral germline infections and believed to play a role of friend or foe in human life (173–175). The two most common types of retroviruses are gammaretrovirus and lentivirus, which are derived from MLV and HIV-1, respectively. The genome of gammaretrovirus has three essential genes, *gag, pol* and *env*, and is flanked on both sides by long terminal repeats (LTRs). *Gag* inserts viral genome mRNA into virions when assembling, *pol* is the reverse transcriptase, integrase, and protease encoding gene, and *env encodes the surface and the transmembrane glycoprotein*. Also, RV genome carries a cis-acting ψ packaging element that involves in regulating the essential process of packaging the RV mRNA into viral capsid during replication. In addition, RV genome carries RNA dimerization signal element. With U3, R, U5 elements, the LTRs display promoter/enhancer activity for gene transcriptional regulation. RVs use their envelope proteins to bind a variety of receptor molecules such as murine cationic amino acid transporter (mCAT), a sodium-dependent Pi transporter (PiT2), xenotropic and polytropic retrovirus receptor 1 (XPR1), CD4, CD46, CD150, and the RD114-and-D-type-retrovirus/alanine-serine-cysteine transporter 2 (RDR/ASCT2) expressed on different cell surfaces to initiate infection, a critical step in determining the target cell tropism of the virus. This leads to a conformational change in the envelope proteins, leading to the entry of virus into the cytoplasm via fusion or endocytosis. With the help of the host cell proteins, the endosome travels through cytoplasm to eject its RNA. After the RNA reverse transcription takes place, viral DNA is integrated into the host cell chromatin, transcribed into RNA with 5' Cap and 3' poly(A) tail, and translated into viral proteins that assemble and bud from the plasma membrane to complete the life cycle with extracellular maturation (171). The matured RVs can infect a wide variety of somatic cells including embryonic stem cells, hematopoietic and neural stem cells. With active nuclear elements, these vectors can transduce therapeutic genes into proliferating cells only and are, therefore, ideal for targeting specifically cancer cells. A downside to gammaretrovirus is that it has broad species specificity, leaving the possibility of transducing undesired cells, faulty reverse transcription, intracellular restriction factors, and risk of insertional mutagenesis. The major difference between gammaretrovirus and lentivirus is that lentivirus can infect post-mitotic cells. It requires four plasmids for production: the *gag* and *pol* plasmid, the *rev* plasmid to transport mRNA into the cytoplasm, VSV-G for membrane fusion and the gene of interest. Other retroviruses require three plasmids: the *gag* and *pol* plasmid, the VSV-G plasmid and the gene of interest. Transient or stable co-expression of all these plasmids in HEK293T packaging cell lines produces RV vector particles carrying no replication-competent virions that are essential for research and therapeutic purposes. Using these cell lines, methods to produce clinical grade RV particles at a concentration of 10^6 to10^7/ml are optimized (176). As *gag*/*pol* and *env* expression constructs carry no ψ packaging and RNA dimerization element, viral structural proteins only recognize the ψ-containing RV vector construct resulting in a preferential packaging of RV vector genomes into infectious particles. After entry of the particle into the host cell, only the RNA of the RV vector construct is reverse transcribed and stably integrated into the host genome. This method prevents generation of replication competent retroviral vector progeny during therapeutic viral particles production. Lentivirus has been used to treat X-SCID, cancers and monogenic diseases. For example, self-inactivating lentiviral vectors can engineer T cells with receptors to better target tumors when treating cancer. Recently, we have successfully used lentiviral vectors to deliver an anti-angiogenic Kininogen gene to budding blood vessels (177, 178). There have been no reports of significant adverse effects from the lentivirus (37).

Some advantages of using retroviruses are that they can accommodate a 9–12-kb-large insert size for the gene of interest and produce high titers. The most significant disadvantages are lack of cell specificity and the possibility of insertional mutagenesis (18). The enzyme "integrase" inserts copies of the retroviral genome into the host cell chromosomes but there

is a risk of inserting the genome copy into an unfavorable location such as a tumor suppressor gene or an oncogene, which would lead to uncontrolled cell division (36). It is critical to evaluate the risk of insertional mutagenesis for each retroviral vector. Gammaretroviral vectors have a tendency to integrate near gene regulatory regions, which can pose a significant risk. For example, patients in a cohort of 20 died due to leucosis development in a clinical trial (179). On the other hand, lentiviral vectors tend to integrate into the body of genes, leading to lower risk of genotoxicity (52). A possible step to address this issue would be to use self-inactivating retroviral vectors that are transcriptionally inactive. Since mature T cells are relatively resistant to oncogenic transformation by RV, developing T cell-based therapeutic approaches to treat cancer and other diseases would be another approach to avoid insertional mutagenesis. Recently, a non-integrating RV-based CRISPR/Cas9 vectors have been created for targeted gene knockout (180). Creating such vectors to target specific genes would help developing therapeutic approaches without insertional mutagenesis issue. Renal fibrosis was treated by using high-fidelity RV-based CRISPR/Cas9 vectors (181). Development of similar vectors would not only address insertional mutagenesis issue but also radically transform basic and applied biomedical research. Also, using AAV vector which inserts a therapeutic gene selectively into known chromosome 19 sequences would be another possibility. Using zinc finger nucleases or including certain sequences such as the β-globin locus control region to direct the site of integration to specific chromosomal sites is yet another way to minimize the risks. However, further studies are needed to address this issue by designing specific vectors and understanding the frequency of insertional mutagenesis, and role of other factors involved. Insertional mutagenesis is an issue that will likely be solved in the coming years. Until then, the use of retroviruses remains a concern. Nonetheless, over 500 gene therapy clinical trials have been conducted using retrovirus to date.

GENE THERAPY DRUGS IN THE MARKET

Despite many technological challenges and barriers, more than a dozen gene therapy-based drugs have entered the world pharmaceutical market to date (**Figure 3**). The first gene therapy drug, Gendicine™, was developed by Shenzhen SiBiono GeneTech for the treatment of patients with tumors carrying a mutated p53 gene, a common cause for more than 50% of all types of human cancers. The State Food Drug Administration of China approved Gendicine™ for the treatment of head and neck squamous cell carcinoma on October 16, 2003 (182, 183). However, the USFDA has turned down Introgen's Advexin, another AV-based viral drug that uses p53 due to concerns about the safety of the AV vectors after Jesse Gelsinger died in 1999 while participating in a clinical trial but no information is available about the submission of Gendicine™ clinical data for approval from the USFDA to date. Gendicine™, a replication defective AV loaded with wild-type p53 gene, is given to patients by less invasive intramural injections and or intracavity infusions. According to the manufacturer, a single dose of this viral drug, costing less than US $400, is given to patients once a week for 8 weeks as a cure. After injection, the therapeutic activity of p53 activated by target tissue cellular stress induces cell-cycle arrest, DNA repair, apoptosis, senescence, and autophagy to cause tumor growth regression. Gendicine™ has been given to more than 30,000 cancer patients, and it has displayed an exemplary safety record with no significant side effects to date (14). According to the manufacturer, Gendicine™ has shown a higher response rate when combined with chemotherapy and radiotherapy in comparison with standard therapies alone. Because Gendicine™ is injected directly into tumors and becomes useless for treating tumors neither detectable nor accessible, other advanced replication-defective AV-based drugs, such as Advexin and SCH-58500, that carry wild type p53 gene were developed to target all tumors in the patient's body in an intravenous injection; however, neither Advexin and SCH-58500 has entered the pharmaceutical market to date. However, Oncorine™, another replication defective AV-based drug that carries p53 gene to cure head and neck cancer, made it to the Chinese pharmaceutical market in 2005. According to the manufacturer, Shanghai Sunway Biotech Co., the curative effective of Oncorine™ combined with chemotherapy is superior to chemotherapy alone with a good safety profile. Since low transduction is a major issue with these approved replication defective AV drugs, more advanced tumor-specific p53-expressing conditionally replicating AV vectors such as ONYX 015, AdDelta24-p53, SG600-p53, H101, and OBP-702 have been developed but none of them is approved for cancer treatment to date. As many clinicians prefer cancer management rather than a cure due to the complex nature of the disease, the future of oncolytic viral therapy demands further advancement in vector design and discovery of appropriate therapeutic genes for better treatment.

The next advanced gene therapy drug, Rexin-G™, a chimeric retrovector loaded with a cytocidal dominant negative cyclin G1 gene to target and kill solid tumors, was approved by the Philippines FDA in 2005. Rexin-G™ developed by Epeius Biotechnologies Corporation was designated by the US FDA as an orphan drug for pancreatic cancer. After intravenous injection, this viral drug carrying a motif derived from von Willebrand coagulation factor (vWF) on its surface selectively binds receptors and collagenous proteins exposed heavily in tumor microenvironment in order to fuse, enter, uncoat, and insert its genetic material randomly in the chromosomes of the actively dividing tumor cells only (184). Recent clinical studies confirmed its safety, anti-tumor activity, and potential to increase survival time and survival rate of patients. Recently, another retrovirus-based drug, Strimvelis™, was approved in Europe to treat an ultra-rare immunodeficiency syndrome, ADA-SCID, or Bubble Boy Syndrome, a fatal and life-threatening disease due to lymphopenia, and recurrent and opportunistic infections. A bone marrow transplant from a young child donor with matched leukocyte antigen is the recommended treatment for ADA-SCID patients, but the availability of a suitable donor is challenging. Therefore, Strimvelis™ is designed and developed to offer *ex vivo* gene therapy and involves use of RV to insert copies of the ADA gene into the chromosomes of stem cells extracted from the

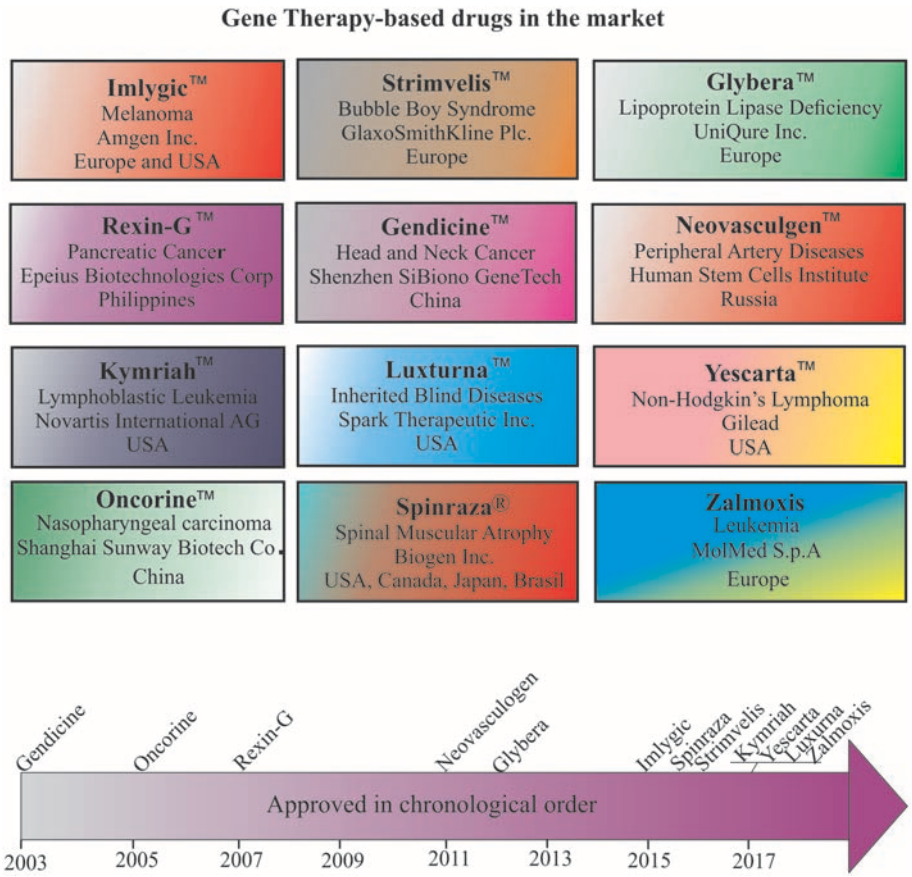

FIGURE 3 | Gene therapy drugs in the pharmaceutical market and a timeline of their approval.

bone marrow of patients. The stem cells carrying the ADA gene are then reintroduced into the patients whose bodies can express protein to repair their immune system on their own. This drug, with a list price of $714,000, is available for ADA-SCID patients without a donor that has matched human leukocyte antigen (HLA). Clinical studies revealed a 100% remission rate for Strimvelis™ (**Table 2**). Nonetheless, there is now a push toward using self-inactivating retroviral vectors that have less risk of insertional mutagenesis, especially self-inactivating HIV-1-based lentiviral vectors (185). A few months ago, the FDA approved Kymriah™, a lentivirus-based chimeric antigen receptor T cell (CAR-T) therapy for acute lymphoblastic leukemia (186). The underlying mechanism of this cancer type disease development still remains unknown, but patients carry abnormal lymphocytes in many of their body parts. Kymriah™ was developed by Novartis in collaboration with the University of Pennsylvania to treat patients with non-Hodgkin lymphoma (NHL) and B-cell acute lymphoblastic leukemia (ALL). Kymriah™ is a novel immunocellular therapy that uses a patient's own reprogrammed T cells with a transgene encoding CAR to identify and eliminate CD19-expressing malignant and non-malignant cells; overall remission rate with the therapy is 83% (**Table 2**). The autologous peripheral blood T cells are reprogrammed to carry intracellular 4-1BB and CD3-zeta costimulatory domains fused with a murine single-chain antibody fragment in its CAR to recognize CD19 increase, cellular expansion, and persistence. Yescarta™ is another retrovirus-based CAR-T cell immunotherapy developed by Kite, a Gilead company, and approved by the FDA in 2017. This breakthrough hematologic cancer drug is a customized treatment generated using an NHL patient's own T-cells to help fight lymphoma. The patient's T-cells are collected and genetically modified using a RV to generate a CAR consisting of anti-CD19 CAR-T cells linked to CD28 and CD3-zeta co-stimulatory domains. This drug is specifically designed to treat diffuse large B-cell lymphoma (DLBCL), a common aggressive NHL that accounts for three out of every five cases. According to the manufacturer, ∼7,500 patients with refractory DLBCL are qualified to receive Yescarta treatment in the USA alone. With a list price of $373,000 in the USA, Yescarta is believed to get approval for the European market in the near future. Zalmoxis is another T-cell based medicine designated an orphan drug and approved by the EMA for treating certain leukaemias and lymphomas. This is used as an add-on treatment in patients who received hematopoietic a stem cell transplant (HSCT) from a partially matched donor to restore the immune system. This is a somatic cell therapy product consisting of T-cells that

are genetically modified using a RV to express ΔNGFR and HSV-TK Mut2 suicide genes. This drug sometimes attacks the patient's body by causing graft-vs.-host disease, but the suicide gene makes these T cells become susceptible to ganciclovir or valganciclovir medicine commonly given to treat and prevent further disease development.

Neovasculgen™, a non-viral first-in-class gene therapy drug developed by the Russian Human Stem Cells Institute, has been available since 2012 for the treatment of atherosclerotic peripheral arterial disease (PAD) including critical limb ischemia. Intramuscular injection of a single dose of this drug, costing less than $50, delivers a plasmid DNA-carrying VEGF gene cloned under a CMV promoter and stimulates angiogenesis and blood supply to decrease the risk of amputation and death in patients suffering from PAD. A recent post-marketing surveillance study revealed a significant increase in pain-free walking distance by PAD patients and confirmed the therapeutic efficacy of this drug (56, 57). Recently, Spinraza® has become the first approved treatment for the rare and often fatal disease spinal muscular atrophy (SMA). SMA patients suffer muscle strength affecting their ability to sit, stand, and breathe. SMA is caused by widespread splicing defects due to mutations in survival motor neuron 1 (*SMN*1), a ubiquitously expressed cytoplasmic and nuclear protein involved in transcriptional regulation, biogenesis of small ribonucleoproteins, telomerase regeneration, and intracellular trafficking. Although the SMA patients carry its paralog *SMN*2, low-level expression due to alternative pre-mRNA splicing appears responsible for this disease development. Therefore, Spinraza carrying *SMN*2-directed antisense oligonucleotides is designed and developed to resurrect normal SMN2 protein expression in SMA patients. This non-viral drug developed by Biogen Inc. has received orphan drug status and was approved for treating all types of SMA in the USA, Canada, Japan, the European Union, Switzerland, Australia, South Korea, Chile, and Brazil. Spinraza solution upon intravenous and or intrathecal administration enters many cells in the body and induces SMN2 protein expression. According to the manufacturer, this medicine, with a list price of $125,000 per injection, costs $750,000 per year for the first year and hundreds of thousands of dollars every year for the rest of patient's life. An AAV-mediated drug designed to express SMN1 protein in patients was developed by a Novartis company, AveXis Inc., and may become available for the treatment of SMA in the near future.

The first AAV1-based drug, Alipogene tiparvovec, or Glybera™, was approved by the EMA to treat LPLD, a rare monogenic genetic disorder characterized by accumulation of triglycerides in plasma due to mutations in *LPL*. Glybera™ carrying correct copies of *LPL* was developed by UniQure Inc., and widely heralded as the "the first gene therapy" in the Western world (**Figure 3**). However, only one or two people in every one million are estimated to carry LPLD, and despite Glybera' s demonstrated potential in curing LPLD, it was withdrawn from the market due to low patient demand. Recently, another AAV-based drug has entered the pharmaceutical market to treat Leber congenital amaurosis, an inherited visual dysfunction characterized by pigmented retina, wandering nystagmus, and amaurotic pupils and caused by a mutation in the *RPE65* (187). Upon completion of the late-stage clinical trials, this AAV2-based voretigene neparvovec, Luxturna™, has been designated by the FDA as a breakthrough therapy and an orphan drug for the treatment of choroideremia. Clinical trials revealed a remarkable improvement in the patients' ability to see in dim light (188). According to the manufacturer, Spark Therapeutics, Inc., Philadelphia, USA, Luxturna™ has successfully cured one blind America's Got Talent semifinalist, Christian Guardino. Recently, Luxturna™ has become the first viral-based drug approved by the FDA to treat blindness. Luxturna™, loaded with wildtype *RPE65*, will be given to patients with confirmed biallelic *RPE65* mutation-associated retinal dystrophy to restore their vision within a few months. Since Luxturna™ comes with a record sticker price, the manufacturing company offers an outcome-based rebate arrangement with a long-term durability measure and payment option over multiple years. Another AAV-based drug is poised to enter the pharmaceutical market in the near future to treat choroideremia, an X-linked inherited retinal dystrophy that causes night blindness and a constricted visual field.

Recently, the USFDA approved an HSV-based drug called T-VEC (Imlygic™) Talimogene Laherparepvec, developed by BioVex Inc., and now acquired by Amgen for melanoma treatment. T-VEC directly kills metastatic melanoma cells and enhances the immune response against them. According to the manufacturer, this advanced oncolytic virus replicates in the tumor cells and synthesizes granulocyte-macrophage colony stimulating factor (GM-CSF), resulting in tumor-lysis and release of tumor antigen, which can then trigger an immune response. The target areas include cutaneous, subcutaneous and nodal lesions. Imlygic™ also serves as an *in-situ* vaccine (189). The T-VEC treatment course involves a series of HSV injections into the melanoma lesions for 6 months for a complete cure. T-VEC was approved also in Europe and Australia for melanoma treatment. G47Δ or DS-1647 is a third generation oncolytic HSV developed by Daiichi-Sankyo Ltd., Japan, and Professor Tomoki Todo at the University of Tokyo for the treatment of malignant glioma. This has shown excellent safety and efficacy in treating glioma in preclinical and clinical studies and has been designated as an orphan drug and "Sakigake," or ahead of the world, by the Ministry of Health, Labor and Welfare of Japan (190). However, this drug is not available for the treatment of cancer patients to date. In addition, a few more drugs are available in the market for treating different diseases (**Table 2**).

GENE THERAPY DRUGS IN CLINICAL TRIALS

The world's first gene therapy clinical study was conducted to test a viral-mediated drug at the NIH in 1989, and now 3704 gene therapy studies from 204 countries are listed in the US Government's clinical trials database to date (**Figure 4A**). More than 50% of them are being conducted in the USA alone. Recently, the US government has removed NIH special oversight rules on gene therapy studies, and the USFDA has

decided to consider gene therapy drugs like other medications for approval in order to make gene therapy a therapeutic reality for patients. These clinical studies are testing both viral and non-viral gene therapy drugs to find cures for a wide variety of human diseases, disorders, and infectious diseases. While the majority of these clinical studies are focused on treating cancer, and immune and digestive diseases, skin diseases are yet to receive momentum (**Figure 4B**). These ongoing gene therapy clinical studies are delivering a wide variety of therapeutic cytotoxic/suicide, tumor suppressor, vaccine antigen, cytokine, receptor, replication inhibitor, and anti-angiogenic genes. Some of the therapeutic genes, vectors, targeted diseases, and their manufacturers are mentioned in **Table 1**. A large number of non-viral vectors are being used to deliver these therapeutic genes, but viruses dominate as successful vectors in the ongoing clinical studies. The most popular viral vectors being used in clinical studies are AV, AAV, HSV, and RV.

AV-MEDIATED GENE THERAPIES IN CLINICAL TRIALS

Both AV and RV vectors are being used in more than 50% of the ongoing viral-mediated clinical studies (**Figure 4C**). The main focus of these are on vaccination and oncolytic therapies. For example, an AV-mediated Theragene (Ad5-yCD/mutTKSR39rep-ADP) delivers a double suicide gene to target stage III pancreatic cancer. AV is being used to deliver the p53 gene in phase II trials to treat recurrent ovarian epithelial, fallopian tube, and primary peritoneal cancer as well as hepatocellular carcinoma (NCT02435186). Also, AV vectors are being used to deliver anti-angiogenic and immunostimulatory genes to treat prostate cancer and malignant pleural mesothelioma (NCT02555397 and NCT01119664). A significant antitumor activity has been demonstrated in phase I-III clinical trials when an AV-based Onyx-015 that undergoes replication selectively in tumors was applied in combination with chemotherapy (14, 191). Vaccination using AV, along with other viruses such as the modified vaccinia Ankara virus (MVA), retrovirus, Sendai virus, and vaccinia virus, is being tested in many clinical trials. AV vectors are also being tested in delivering therapeutic genes for treating malaria, anthrax, HIV, influenza, hepatitis B and C, and severe hemophilia, as well as cardiovascular and many more diseases. AV vectors carrying site-specific endonucleases are being used to edit the CCR5 gene in hematopoietic stem or progenitor cells in AIDS clinical trials (192). The lack of functional dendritic cells in the brain has been attributed to the growth of one of the most aggressive and malignant tumors called gliomas. AV vectors are being used to empower the immune system by expressing the HSV-1 derived thymidine kinase (HSV-1 TK) and cytokine fms-like tyrosine kinase 3 ligand (Flt3L) in the brain. While HSV-1 TK converts ganciclovir into phospho-ganciclovir, a toxic compound to dividing glioma cells, Flt3L differentiates precursors into dendritic cells and acts as a chemokine for dendritic cells resulting into killing of glioma cells and release of tumor antigens in the tumor microenvironment. This follows release of HMGB1, a TLR2 agonist that activates dendritic cells and stimulates dendritic cells loaded with glioma antigens to migrate to the cervical lymph nodes to prime a systemic CD8+ T cytotoxic killing of glioma cells without causing brain toxicity and autoimmunity (193). The median survival of glioma patient is under 2 years and the ongoing clinical trials with DNX-2401, a replication-competent oncolytic AV capable of infecting and killing glioma cells by stimulating an anti-tumor immune response revealed favorable safety profile and prolonged survival of glioma patients (194, 195). Enadenotucirev, a non-natural chimeric oncolytic AV that can retain anti-tumor activity despite intravenous delivery, showed a predictable and manageable safety profile in several advanced cancer patients in phase I clinical studies (196). With encouraging clinical outcome being observed in a large number of ongoing clinical trials, especially in treating cancer, AV-mediated gene therapy is anticipated to make a significant impact on eradicating cancer in the near future.

Although the AV-mediated gene therapy carries a unique advantage over other systems, several concerns must be addressed to offer treatment without side effects. For instance, further improvement in vector development technologies is essential to avoid activation of the endogenous signal transduction pathways and production of cytokines due to anti-vector immune responses that can potentially complicate the clinical outcomes. The necessity of integrin and CAR protein expression on the surface of target cells or tissue to allow efficient infection of AV limits the prospects of treating many diseases. Therefore, generation of novel AV vectors that can infect and transduce target cell or tissue with high specificity, express transgenes up to the therapeutic requirement, induce low organ toxicity and inflammation, and can be detected easily *in vivo* is the need of the hour. Understanding the disease-specific biomarkers, designing and engineering novel AV capsids carrying cell or tissue-specific receptor binding epitopes can reduce the occurrence of unwanted clinical outcome. Since the presence of AV-neutralizing antibodies varies from patient to patient, designing and developing personalized patient-specific capsids can be a promising approach to cure diseases in the future. Development of AV particles that resist inactivation by serum proteins is necessary to promote intravenous administration of therapeutic particles during treatment. Development of strategies to avoid dose-associated toxicity is needed. In addition, contamination with replication-competent virus still remains a serious issue in large scale production of AV preparation for therapeutic purposes (197). Therefore, further advancement in the production of purified AV and AV-based gene delivery technologies is required for using gene therapy to its full potential.

AAV-MEDIATED GENE THERAPIES IN CLINICAL TRIALS

AAV vectors are being used in more than 200 ongoing clinical studies to treat a wide variety of diseases and disorders worldwide. After the approval of the AAV-based drugs Gendicine and Luxturna, another AAV-based drug is poised to enter the

TABLE 1 | Naked DNA and viral-mediated drugs in clinical trials.

Viral Drug/ Intervention	Company/Sponsor	Gene/Ab/Ligand	Disease/Disorder	Vector	Currentstatus	Clinical trial number
Theragene®	SNUBH	CD/TKrep	Cancer	AV	Phase I	NCT02894944
Ad5-Gag	BDHCMU	Gag	AIDS vaccine	AV	Phase I	NCT02762045
AdMA3	BCCA	MG1MA3	Solid tumor	AV	Phase I	NCT02285816
Ad/L523S	CCF	L523S	Lung Cancer	AV	Phase I	NCT00062907
AdAg85A	MUMC	Ag85A	Tuberculosis	AV	Phase I	NCT02337270
Ad35.CS.01	SUSM	CS.01	Malaria	AV	Phase I	NCT00371189
dAd5GNE	WCMC	GNE	Cocaine	AV	Phase I	NCT02455479
ChAd63-METRAP	CCVTM	METRAP	Malaria	AV	Phase I	NCT03084289
Ad5FGF-4	Angionetics	FGF	Angina	AV	Phase III	NCT02928094
AAV5-hFIX	UniQure	hFIX	Hemophilia B	AAV	Phase I/II	NCT02396342
AAV2-GDNF	NIH	GDNF	Parkinson's	AAV	Phase I	NCT01621581
AAV OPTIRPE65	MEH	OPTIRPE65	Eye Diseases	AAV	Phase I/II	NCT02946879
AAV2hAQP1	NIH	hAQP1	AADC	AAV	Phase I	NCT02852213
rAAV1-PG9DP	SCRC	PG9DP	HIV	AAV	Phase I	NCT01937455
scAVV9.CB.CLN6	NCH	CB.CLN6	Batten Disease	AAV	Phase I/II	NCT02725580
SPK-8011	Spark Thera.	FVII	Hemophilia A	AAV	Phase I/II	NCT03003533
scAAV9.U1ahSGSH	Abeona Thera.	SGSH	MPS III	AAV	Phase I/II	NCT02716246
LentiGlobin BB305	Bluebird Bio	HBB	β Thalassemia	LV	Phase III	NCT03207009
Sin-γ- RV-ADA	BCH	ADA	SCID-X1	γ-RV	Phase I/II	NCT01129544
Anti-MAGE-A3-DP4	NIH	TCR	Cancer	RV	Phase II	NCT02111850
Anti-EGFRvIII CAR PBL	NIH	CAR	Glioma	RV	Phase I/II	NCT01454596
Filgrastim	FHCRC	Filgrastim	FA	RV	Phase I	NCT01331018
MO32(NSC 733972)	UA	IL-12	Gliosarcoma	HSV-1	Phase I	NCT02062827
OrienX010	Oriengene Bio	GM-CSF	Melanoma	HSV-1	Phase I	NCT03048253
HSV1716	NCH	ICP34.5	Neuroblastoma	HSV	Phase I	NCT00931931
NP2	Diamyd Inc.	PENK	Cancer Pain	HSV-1	Phase I	NCT00804076
G207	UA	+ radiation	Brain tumor	HSV-1	Phase I	NCT02457845
SGT-94	SynerGene	RB94	Solid tumors	DNA	Phase I	NCT01517464
CYL2-02	InvivoGen	SST2+DCK	Cancer	DNA	Phase II	NCT02806687

SNUBH, Seoul National University Bundang Hospital; BDHCMU, Beijing Ditan Hospital of Capital Medical University; BCCA, Vancouver Cancer Centre Vancouver, British Columbia Canada; CCF, Cancer Center of Florida; MUMC, McMaster University Medical Center; SUSM, Stanford University School of Medicine; WCMC, Weill Medical College of Cornell University; CCVTM, Centre for Clinical Vaccinology and Tropical Medicine; MEH, Moorfield's Eye Hospital; AADC, Aromatic L-amino Acid Decarboxylase Deficiency; SCRC, Surrey Clinical Research Centre; NCH, Nationwide Children's Hospital; BCH, Boston Children's Hospital; TCR, T cell receptor; FHCRC, Fred Hutchinson Cancer Research Center; FA, Fanconi Anemia; UA, University of Alabama; Oriengene Bio, Oriengene Biotechnology Ltd; PENK, Preproenkephalin.

pharmaceutical market in the near future to treat Choroideremia, an X-linked inherited retinal dystrophy that causes night blindness and a constricted visual field. Mutations in *REP1* encoding Rab escort protein 1, a protein involved in lipid modification of Rab proteins, have been implicated in the development of Choroideremia. Patients that received AAV-REP1 therapy showed a significant increase in their visual acuity (198). The product of *CNGB3* provides instructions for making the β-subunit of the cone photoreceptor cyclic nucleotide-gated (CNG) channel, but mutations lead to a defective photoreceptor, decreased visual acuity, and total color blindness, or achromatopsia. In a phase I/II clinical trial sponsored by Applied Genetic Technologies Corporation, AAV was used to deliver *CNGB3* for the successful treatment of achromatopsia (187). AAV is being tested to cure another eye disease, Leber's hereditary optic neuropathy (LHON), a maternally transmitted common mitochondrial disorder caused by point mutations in mitochondrial DNA and impairment of ATP generation. The LHON disease is characterized by apoplectic, bilateral, and severe visual loss. In an ongoing phase I interventional clinical trial, scAAV2 is being used to deliver the P1ND4 gene to rescue visual loss in five legally blind patients (NCT02161380). P1ND4 is a synthetic nuclear encoding gene involved in mitochondrial oxidative phosphorylation. The initial results obtained from this study have showed an improved acuity in two of five patients with no serious adverse events (199). Since treating diseases of the central nervous system is challenging due to the blood brain barrier (BBB), many AAV vectors, especially AAV1, AAV2, AAV5, AAV8, and AAV9, are found to be very useful in transducing neurons (200), and therefore, many AAV-mediated treatments are being tested to cure lysosomal storage disorders, Alzheimer's disease, Parkinson's disease, amyotrophic lateral sclerosis (ALS), epilepsy, spinal muscular atrophy type 1, metachromatic leukodystrophy, aromatic L-amino acid

TABLE 2 | The cellular and gene therapy products available in the market.

Drug	Company	Therapeutic	Disease/Disorder	Remission
Luxturna™	Spark Therapeutics	*RPE65*	Inherited blindness	93%
Kymriah™	Novartis	CAR-T	Leukemia (ALL)	80%
Glybera®	uniQure	*LPL*	LPLD	NA
Gendicine®	Benda Pharmaceutical	*p53*	Head and neck cancer	67%
Strimvelis™	GlaxoSmithKline	HSC	ADA-SCID	100%
Oncorine™	Shanghai Sunway Biotech	*p53*	Head and neck cancer	NA
Neovasculogen™	Human Stem Cell Institute	*VEGF*	PAD and CLI	90%
SPRS-therapy®	Human Stem Cell Institute	Fibroblasts	Skin damage	75%
laViv™	Fibrocell Science	Fibroblasts	Nasolabial fold Wrinkles	57%
Provenge™	Valeant Pharmaceuticals	Dendritic cells	Prostate cancer	38%
Imlygic™	Biogen	ICP34.5 & GM-CSM	Melanoma	50%
Carticel™	Genzyme	Chondrocyte	Knee cartilage injury	92%
Rexin-G™	Epeius Biotechnologies	Cyclin G1	Breast cancer, Sarcoma	40%

CAR-T, Chimeric antigen receptor T- cell; ALL, Acute lymphoblastic leukemia; LPL, Lipoprotein lipase; LPLD, Lipoprotein lipase deficiency; ADA, SCID—Adenosine deaminase severe combined immunodeficiency; HSC, Hematopoietic stem cell; VEGF, Vascular endothelial growth factor; PAD, Peripheral arterial disease; CLI, Critical limb ischemia; ICP34.5, Infected cell protein 34.5; GM, CSF-Granulocyte-macrophage colony stimulating factor.

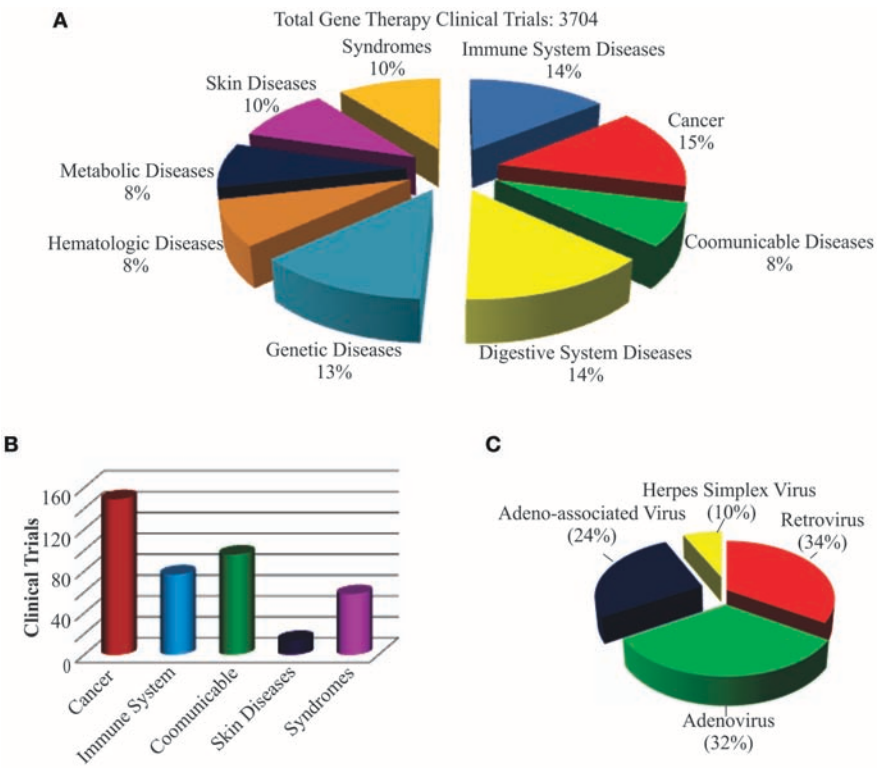

FIGURE 4 | Recent trends in gene therapy research and clinical trials. **(A)** Different diseases being treated by gene therapy in clinical trials. The clinical studies database was searched for the total number of gene therapies conducted in the world to treat different diseases to date. The main focus of the clinical trials was found to be treating cancer, immune, digestive, and genetic diseases. **(B)** Clinical trials actively recruiting patients for testing gene therapy-mediated medicines in curing diseases. This includes both viral and non-viral vector-mediated gene therapies. A relatively large number of clinical trials are recruiting cancer patients for testing different gene therapy-based medicines. **(C)** Different recombinant viral vectors being tested in gene therapy-based treatments.

decarboxylase (AADC) deficiency, and Batten disease. Like AV, AAV is yet another useful viral vector for cancer gene therapy. Several AAV vectors are being used to test the expression of anti-angiogenic, cytotoxic, cytokine, and tumor suppressor genes, small RNAs, antigens, and antibodies for cancer cures. A large number of preclinical studies revealed successful treatment with AAV-mediated gene therapy for improved tumor regression (201–206). AAV is considered a powerful vector in targeting

the liver for treating hematological diseases. Complete treatment of severe hemophilia B by delivering *FIX* in patients was described as the "holy grail" of gene therapy clinical application (207). In ongoing phase I/II clinical trials, *FVIII* and *FIX* are being delivered to hemophilia A and B patients, respectively (NCT03003533, NCT02484092).

Although AAV vectors are non-pathogenic and safe, and found among the commonly used platforms for gene delivery in preclinical and clinical studies, their potential application in gene therapy is limited by the inability to deliver a therapeutic gene more than 5.0 kb in size, immunogenicity of capsid proteins, difficulty in producing a large supply, requirement of large doses of highly purified vectors, broad tropism, and presence of an extensive anti-AAV immunity in human populations (208–211). Adding empty vectors of AAV to the final vector preparations to serve as a decoy and developing new vectors with high transduction and gene expression potential as well as better understanding of T-cell response to all AAV serotypes in clinical settings would reduce inflammation, immune response, and other viral particle-associated side effects because capsid is the primary interface with the target cell that defines pharmacological, immunological, and molecular properties (150, 207, 212, 213). Therefore, designing and developing more chimeric capsid proteins are critical to generate disease- and cell- or tissue-specific viral particles. For example, substitution of tyrosine to phenylalanine in the AAV capsid protein has enhanced the transduction efficiency with reduced toxicity (214). Better understanding of the underlying mechanisms of intracellular transportation of AAV particles in a disease-specific setting will help developing strategies to improve gene delivery efficacy. AAV vectors are commonly delivered to patients by systemic, intramural, central nervous system, cardiac, and pulmonary delivery but certain sites of the human body elicit no immune response to injection of antigens or viral particles because the BBB prevents the entry of antibodies or resting lymphocytes and the absence of traditional antigen-presenting cells. Therefore, applying AAV particles to patients through immune-privileged sites, such as the central nervous system, mucosal surfaces, eye, placenta, fetus, testicles, and articular cartilage, could be a better option to avoid T-cell response. For example, AAV vectors injected intraparenchymally into the central nervous system to treat Batten's, Canavan, and Parkinson's diseases showed little or no adaptive immune response in many clinical trials (155, 215–218). Monitoring T-cell response in patients by using advanced tools especially multicolor flow cytometry, mass cytometry, and enzyme-linked immunospot (ELISpot) assay will minimize the risk of the unexpected clinical outcome (209). Also, for reduced T-cell response and optimal expression of a therapeutic gene, intramuscular instead of systematic injection of AAV particles is recommended because healthy muscles express only low levels of MHC class I antigens (209, 219). Use of immunosuppressive drugs was found safe to maintain therapeutic gene expression in many clinical trials (150, 220, 221), and their use could be an option for better clinical outcome, but maintenance of transgene expression remains unpredictable. Although AAV offers the expression of a therapeutic gene for nearly 1 year without integrating into the host's chromosomes, applying CRISPR/Cas9 technology would resolve long-term expression and mutagenesis issues. Production of high titers of purified AAV particles by employing ionic iodixanol gradients and ion exchange chromatography instead of using the toxic CsCl is also important for the success of gene therapy (222, 223). Recent developments in the production of high quality AAV particles from transfection efficient HEK293 cell suspensions in shaker flasks and WAVE bioreactors free of all animal and human products will certainly improve the success of gene therapy application (224). This system was further improved by changing the NaCl concentration in the medium and optimizing conditions for Expi293F cell infection by helper herpes simplex virus (HSV) (225). However, contamination of the final AAV particle preparation with HSV cannot be ruled out. The AAV particles generated from the baculovirus expression system carry low levels of VP1 capsid protein, so high doses are used in clinical trials to increase transduction efficiency at the expense of immune response (226). No disease caused by AAV infection has been reported to date but repression of PPP1R12C gene promoter in host cells by the rep proteins of AAV2 is clearly a concern (227). Therefore, more efforts are necessary to smooth out the landscape surrounding AAV for its more pronounced clinical benefits in gene therapy.

HSV-MEDIATED GENE THERAPIES IN CLINICAL TRIALS

More than 90 gene therapy clinical trials have been conducted using HSV as a vector to deliver therapeutic genes for curing various diseases to date. They have been extensively used for tumor therapy and vaccine development. After the advent of HSV-based T-VEC drug for melanoma treatment, many HSV vectors are being used to deliver suicide genes to treat anaplastic thyroid cancer (228). Since immunotherapy is currently a hot topic in cancer research and gaining more attention; oncolytic viruses are often combined with immune checkpoint blockades such as T-VEC combined with anti-PD1 Pembrolizumab, anti-CTLA-4 Ipilimumab, and neoadjuvant to increase their therapeutic potential (68). Also, the oncolytic HSV-1 carrying four copies of miR-145 target sites combined with radiation has been shown to be more effective than radiation alone (122, 229). A current phase I clinical trial uses an engineered HSV rRp450 designed to kill cancer cells in order to treat liver metastases and primary liver tumors (NCT01071941). HSV is also used as a transneuronal tracer defining connections among neurons by virtue of traversing synapses (230). HSV has much potential in treating problems of the urinary system. A recent study reports HSV-1 as a vector for delivering poreless TRPV1 channels or protein phosphatase 1α to reduce bladder over-activity in rats (231). HSV-mediated treatment also alleviated bladder pain. These have the potential to offer treatment to cases of overactive bladder (OAB) and interstitial cystitis/bladder pain syndrome (IC/BPS). However, infectivity of solid tumors, leakage, off target viral replication, sequestration, and delivery methods are still hampering the progress of HSV-mediated oncolytic viral therapy.

Although the nervous system is the natural site for HSV latency, the full potential of HSV-mediated gene therapy in treating nerve diseases is yet to be discovered. Several studies treating chronic pain were successful in animal models but very few have reached clinical trials to date. HSV vectors have certainly promising perspectives in clinic trials but detailed understanding of virus-host interaction will minimize cytotoxicity and biohazards generation. Recently, strategies to develop transduction efficient, alternate vector entry and transcriptionally retargeted oncolytic HSV viruses were reviewed (232–234). The therapeutic potential of amplicons is still undermined by production and stability issues; therefore, focus needs to be on improving vector design, construction, and production technology. Developing new HSV vectors carrying genes that enhance tumor cell lysis will increase oncolytic therapeutic efficacy. While gliomas do not express miR-124, it is highly expressed in normal brain, and designing HSV vectors carrying the same could be a promising approach to treat glioma. The full potential of expression libraries created by using HSV vectors in regenerative medicine is yet to be seen in curing human diseases (235). Since oncolytic virus therapy is considered a major breakthrough in treating cancer after the success of radiation and immunotherapies, development of safe and tumor-selective new HSV vectors is necessary for its promising future. Optimizing vector delivery methods especially to solid tumors and in immune-compromised patients will certainly improve oncolytic viral therapy. Exploring their roles in gene editing and repair will expand the horizons of gene therapy.

RV-MEDIATED GENE THERAPIES IN CLINICAL TRIALS

RV vectors can be applied to cure a wide variety of diseases and disorders such as cancer, HIV, ADA-SCID, melanoma, WAS, and many others. Though the majority of retinal gene therapy trials use AAV, some use lentivirus because of its larger gene capacity. For example, Usher syndrome causes hearing loss, less vestibular function, and a pigmented retina (187). Currently, a phase II trial is underway to use lentivirus to deliver a 5.0-kb *MYO7A*. Additionally, a phase II trial that is projected to deliver *ABCA4* by lentivirus to treat Stargadt disease, an inherited macular degeneration that causes cell degeneration, is underway (187). Furthermore, lentivirus is a favorable vector to treat sickle cell anemia because of the advantages it offers, including a large transgene capacity, stable long-term expression, and safer integration (236). A single base substitution in the β-globin gene causes the erythrocyte sickling characteristic of sickle cell anemia. Treatments for sickle cell anemia are transitioning into self-inactivating lentivirus with a deletion in the U3 region of the 3' LTR, which has a safer integration profile (236). A clinical trial sponsored by Bluebird Bio used LentiGlobin BB305, which delivered β-globin T87Q. Clinical results showed 24% anti-sickling (NCT03207009). For treating immunodeficiency, there have been adverse effects reported in the past by gammaretroviral vectors. In the treatment of X-linked SCID, CD34+ hematopoietic stem cells were transduced with murine gammaretroviral vector, which led to an increase in immune function, but 5 patients developed T cell leukemia because of insertional mutagenesis into oncogenes (185). In the treatment of WAS, a gammaretroviral vector expressing *WAS* transgene delivered to patients caused 7 out of 10 to develop leukemia (185). Recently, self-inactivating lentivirus was used to treat five patients with X-linked SCID. Two patients had restoration of immune function even 2–3 years after treatment (237). A current phase I/II clinical trial is using a self-inactivating gammaretrovirus to treat SCID-X1 (NCT01129544). Other current clinical trials include a phase II trial using a retroviral vector to transfer ADA into hematopoietic stem cells to treat ADA-SCID (NCT00598481). A replicating Toca 511 RV vector is being used in a phase I trial to treat recurrent high-grade glioma (NCT02598011). RV is being used in a phase I/II trial to transduce white blood cells with the CAR-T cell receptor to target mesothelin for patients with metastatic cancer (NCT01583686). Donor T cells are being transduced with RV to express the caspase-9 suicide gene in a phase I trial to treat cancer (NCT01494103). Duchenne muscular dystrophy occurs when a lack of dystrophin expression causes muscle degeneration. In a proof-of-concept study, the full-length sequence of dystrophin was spread over two co-packaged RNA copies and delivered via a lentiviral vector. The vector integrated and gave long-term expression of dystrophin (238). Additionally, a RV vector expressing MazF endoribonuclease is being used to transduce CD4+ T cells to treat HIV in a phase I trial (NCT01787994). AIDS-related non-Hodgkin lymphoma is being treated in a phase I clinical trial that transduces stem cells with genes for HIV RNA using lentivirus in order to evoke an immune response (NCT01961063).

Since immunity is the primary barrier for the success of viral gene therapy, it is critical to design viral vectors that can subvert the complement system. The LTRs of RV serve as promoters, enhancers, binding sites for various nuclear proteins, chromatin modulators, and polyadenylation signals. Therefore, applying genetic engineering and CRISPR technology will avoid exacerbating the insertional mutagenesis issue. This issue can also be avoided by using non-integrating RV vectors or integrase inhibitors during treatment. The RV-mediated gene therapy will immensely benefit from developing technologies to guide and monitor transgene insertion in the host cell chromatin. Although RV vectors can deliver a transgene up to 10 kb in size, production of high titer virus, chromatin structure, and epigenetic modification near the insertion site still remain issues in clinical applications. Thus, better RV vectors are needed for future gene therapy applications. Since viral infection depends on the expression of target cell surface receptors and viral envelope protein, designing and constructing to produce efficient and cell-, tissue- and disease-specific recombinant RV vectors are necessary to obtain the expected clinical outcome. New RV vectors with optimized LTRs, created by replacing promoter/enhancer elements with cell- and tissue-specific promoters and enhancer sequences, will boost their use in curing many diseases with fewer or no side effects. Novel RV vectors are needed to transduce heart and other body organs for their wide spread use in gene therapy. Introduction of miRNA binding sites in the viral RNA has been suggested to control posttranscriptional regulation of

disease-causing genes (239). The use of advanced RV vectors carrying the woodchuck posttranscriptional regulatory element (wPRE) to increase transgene mRNA stability, export, and translatability will help to accomplish better clinical outcome (240). As delivering genetic information in the form of RNA is an increasingly popular method, RVs carrying no RT or integrase are poised to play a significant role in a gene editing, vaccination, tumor therapy, gene therapy, transdifferentiation, reprogramming, and other biotechnological applications in the near future (241).

RISKS ASSOCIATED WITH VIRAL VECTORS

Since an estimated 10^{31} virus-like particles exist on the Earth and they are present in the blood, nose, mouth, lung, vagina, gastrointestinal tract, conjunctiva, skin, and the mammalian genome, viruses appear to play a major role in human life (242, 243). The general concerns with viral vectors are the risks of an immune response, off-target effects, inflammation, and insertional mutagenesis. An immune response could make a viral treatment less efficient, or the resulting creation of antibodies could preclude a second dosage of the same virus (244–248). Inflammation was seen as a worst-case scenario in the 1999 death of Jesse Gelsinger caused by a very high dosage of adenovirus (249). Tailoring the viral dose to the patient, however, can better control this risk. Also, insertional mutagenesis is a major obstacle that the gene therapy field must overcome. The risk of inserting a gene into a tumor suppressor gene or activating an oncogene is present for the vectors that integrate into the unwanted locations of the genome, such as retrovirus. To counter this, vectors can be used that do not integrate readily into the genome. Additionally, self-inactivating vectors can be manufactured that do not contain their own promoter; rather, another internal promoter in the cell is used. This leads to less genotoxicity and is a safer alternative to traditional integrating vectors (52). Other concerns are that viral vectors are only relevant for monogenic disorders because of their limited DNA-carrying capability. However, HSV-1 is an example of a virus that has enough carrying capacity for multiple genes. Additionally, dual vector systems, such as dual vector adeno-associated virus, have larger transgene capacities. Also, finding the appropriate virus to infect the desired cells is often difficult, and there is the risk that the virus could cross the Weismann barrier and infect germ line cells. Furthermore, viruses are generally susceptible to genetic variations. Integration into undesirable sites such as regulatory, oncogenes or tumor-suppressor genes would be undesirable. Deletion of virulence genes may affect their ability to infect or integrate with the host chromosome, thus compromising their effectiveness as vectors. Additionally, a social stigma is associated with viral therapy. Most patients would be concerned about being infected by a live virus—a concern also held about viral vaccines. Since their ubiquitous presence is a reality, why shouldn't humankind start accepting them as wonderful molecular biological tools with which to build novel and powerful medicine?

CHALLENGES AND THE WAY FORWARD

Since its birth in the 1960s, gene therapy has come quite a long way by providing an alternate one-time treatment option for cancer, metabolic disorders, and neuronal, immune, and infectious diseases. Notably, it has been able to treat beta thalassemia, Leber's congenital amaurosis, severe immunodeficiency diseases such as ADA-SCID, and more. However, the full potential of gene therapy is yet to be witnessed in regenerative medicine, a branch of translational medicine where engineering or regenerating human cells, tissue or organs enables restoration or establishment of normal function. With recent impressive results observed in vaginal gene therapy in preclinical trials, gene therapy is poised to enter the clinical phase for treating infectious diseases in the near future (250). Both viral and non-viral vectors can be used to deliver DNA, each of which has its own advantages and disadvantages. Additionally, genome-editing technology is an up-and-coming method of delivering DNA to specific parts of the genome. With all of these breakthroughs have come hurdles, such as the death of Jesse Gelsinger in 1999 and the development of leukemia in patients who have been treated for WAS and ADA-SCID. The ethical concerns of patients must be heeded as well. However, these challenges do not reflect a flaw in the concept. Simply, more research is needed to avoid technical issues such as the production of viral particles in large scale, formulations for long-term storage stability, immune responses, and insertional mutagenesis. Loading of viral particles with a therapeutic gene during production is mostly done by transient transfections, a rate-limiting step in large scale production of viral particles. Alternate approaches such as stable cell lines expressing capsid proteins and insect cells based baculovirus expression systems would be useful for mass production of viral particles. This underdeveloped modern medicine needs discovery and engineering of better viral vectors to deliver therapeutic genes precisely to the target diseased cells or tissue.

Gene therapy is a rapidly expanding field, and it seems that scientists have only scratched the surface of its potential. The more that is discovered about how to optimize gene delivery vectors, the closer this field gets to delivering wide-scale solutions to modern medicine. The future of gene therapy moves toward engineering safer and more efficient vectors, combining multiple existing strategies such as viral vectors with genetic engineering technologies, and personalizing all characteristics of gene therapy treatments to the patient, as it has been shown that host genetic variants affect the efficacy of vector-mediated gene delivery (251). This includes understanding of the repertoire of receptors on a target cell in diseased conditions to help in designing appropriate capsid proteins for viral particles. Although the full panoply of gene therapy's might is yet be witnessed, it has enormous potential to shed light on human afflictions, add value to patients' lives, and contribute to future economic growth. Although gene therapy currently shares less than one percent of the total $1.2 trillion world annual pharmaceutical market, it is expected to create approximately a $12 billion market in the next 10 years. According to a market research and advisory

company, Allied Market Research, cancer gene therapy alone has created a $289 million market in 2016 but it is expected to reach $2,082 million by 2023. Gaining popularity among the global medicinal community, gene therapy has become an attractive market for companies and investors. However, the ethical acceptance and advancement in the technology to avoid unwanted clinical outcomes are critical for driving its market growth. Also, the translation of laboratory studies to animal studies and then to clinical trials is a long, tedious, and expensive process to ensure the safety of patients. As a result, if the USFDA, with its patchy regulations, continues its approval rate, providing gene therapies for all the genetic diseases will take many years to come. Therefore, a new perspective on creating a conducive atmosphere for improving this modern cutting-edge gene therapy technology is necessary to transform the lives of patients with severe genetic illnesses, infectious diseases, and disorders. As mentioned elsewhere, knowledge has no boundaries, and there exist unlimited methods to develop a novel invention; every bump in the investigating path can be considered an inspiration and source of energy to advance research, a never-ending learning process.

AUTHOR CONTRIBUTIONS

VB and RG conceived the concept and wrote the manuscript, and the other authors listed made substantial, direct intellectual contributions to the work, and approved it for publication.

FUNDING

Funding for this work was provided by Joint Science and Technology Office (JSTO), Defense Threat Reduction Agency (DTRA), Department of the Army, Department of Defense, United States of America.

ACKNOWLEDGMENTS

Authors thank Mr. Abraham A. James for his artwork and Ms. Neehar Mishra for her comments, and Dr. Manubhai Patel and the late Dr. Douglas M. Cerasoli for their unconditional support. Authors apologize to the scientists whose contributions to gene therapy could not be acknowledged because of space limitations.

REFERENCES

1. Avery OT, Macleod CM, McCarty M. Studies on the chemical nature of the substance inducing transformation of pneumococcal types : induction of transformation by a desoxyribonucleic acid fraction isolated from Pneumococcus Type Iii. *J Exp Med*. (1944) 79:137–58.
2. Crawford GE, Holt IE, Mullikin JC, Tai D, Blakesley R, Bouffard G, et al. Identifying gene regulatory elements by genome-wide recovery of DNase hypersensitive sites. *Proc Natl Acad Sci USA*. (2004) 101:992–7. doi: 10.1073/pnas.0307540100
3. Omenn GS, Lane L, Lundberg EK, Beavis RC, Overall CM, Deutsch EW. Metrics for the Human Proteome Project 2016: progress on identifying and characterizing the human proteome, including post-translational modifications. *J Proteome Res*. (2016) 15:3951–60. doi: 10.1021/acs.jproteome.6b00511
4. Thul PJ, Lindskog C. The human protein atlas: a spatial map of the human proteome. *Protein Sci*. (2018) 27:233–44. doi: 10.1002/pro.3307
5. Loewe L, Hill WG. The population genetics of mutations: good, bad and indifferent. *Philos Trans R Soc Lond B Biol Sci*. (2010) 365:1153–67. doi: 10.1098/rstb.2009.0317
6. Barney M. Mutations: The raw material for evolution? *Acts & Facts*. (2007) 36:10.
7. Joel CL. Mutations are the raw materials of evolution. *Nat Educ Knowledge*. (2011) 3:10.
8. Lagasse HA, Alexaki A, Simhadri VL, Katagiri NH, Jankowski W, Sauna ZE, et al. Recent advances in (therapeutic protein) drug development. *F1000Res*. (2017) 6:113. doi: 10.12688/f1000research.9970.1
9. Usmani SS, Bedi G, Samuel JS, Singh S, Kalra S, Kumar P, et al. THPdb: Database of FDA-approved peptide and protein therapeutics. *PLoS ONE*. (2017) 12:e0181748. doi: 10.1371/journal.pone.0181748
10. Mata DG, Rezk PE, Sabnekar P, Cerasoli DM, Chilukuri N. Investigation of evolved paraoxonase-1 variants for prevention of organophosphorous pesticide compound intoxication. *J Pharmacol Exp Ther*. (2014) 349:549–58. doi: 10.1124/jpet.114.213645
11. Chilukuri N, Parikh K, Sun W, Naik R, Tipparaju P, Doctor BP, et al. Polyethylene glycosylation prolongs the circulatory stability of recombinant human butyrylcholinesterase. *Chem Biol Interact*. (2005) 157–158:115–21. doi: 10.1016/j.cbi.2005.10.013
12. Chilukuri N, Sun W, Naik RS, Parikh K, Tang L, Doctor BP, et al. Effect of polyethylene glycol modification on the circulatory stability and immunogenicity of recombinant human butyrylcholinesterase. *Chem Biol Interact*. (2008) 175:255–60. doi: 10.1016/j.cbi.2008.05.020
13. Duysen EG, Parikh K, Aleti V, Manne V, Lockridge O, Chilukuri N. Adenovirus-mediated human paraoxonase1 gene transfer to provide protection against the toxicity of the organophosphorus pesticide toxicant diazoxon. *Gene Ther*. (2011) 18:250–7. doi: 10.1038/gt.2010.136
14. Zhang WW, Li L, Li D, Liu J, Li X, Li W, et al. The first approved gene therapy product for cancer Ad-p53 (Gendicine): 12 years in the clinic. *Hum Gene Ther*. (2018) 29:160–79. doi: 10.1089/hum.2017.218
15. Thakur A, Huang M, Lum LG. Bispecific antibody based therapeutics: strengths and challenges. *Blood Rev*. (2018) 32:339–47. doi: 10.1016/j.blre.2018.02.004
16. Spicer CD, Jumeaux C, Gupta B, Stevens MM. Peptide and protein nanoparticle conjugates: versatile platforms for biomedical applications. *Chem Soc Rev*. (2018) 47:3574–620. doi: 10.1039/c7cs00877e
17. Walsh G. Biopharmaceutical benchmarks 2014. *Nat Biotechnol*. (2014) 32:992–1000. doi: 10.1038/nbt.3040
18. Ibraheem D, Elaissari A, Fessi H. Gene therapy and DNA delivery systems. *Int J Pharm*. (2014) 459:70–83. doi: 10.1016/j.ijpharm.2013.11.041
19. Chilukuri N, Duysen EG, Parikh K, Sun W, Doctor BP, Lockridge O, et al. Adenovirus-mediated gene transfer of human butyrylcholinesterase results in persistent high-level transgene expression *in vivo*. *Chem Biol Interact*. (2008) 175:327–31. doi: 10.1016/j.cbi.2008.04.009
20. Chilukuri N, Duysen EG, Parikh K, diTargiani R, Doctor BP, Lockridge O, et al. Adenovirus-transduced human butyrylcholinesterase in mouse blood functions as a bioscavenger of chemical warfare nerve agents. *Mol Pharmacol*. (2009) 76:612–7. doi: 10.1124/mol.109.055665
21. Aleti V, Reddy GB, Parikh K, Arun P, Chilukuri N. Persistent and high-level expression of human liver prolidase *in vivo* in mice using adenovirus. *Chem Biol Interact*. (2013) 203:191–5. doi: 10.1016/j.cbi.2012.08.021
22. Mata DG, Sabnekar P, Watson CA, Rezk PE, Chilukuri N. Assessing the stoichiometric efficacy of mammalian expressed paraoxonase-1 variant I-F11 to afford protection against G-type nerve agents. *Chem Biol Interact*. (2016) 259:233–41. doi: 10.1016/j.cbi.2016.04.013
23. Dunbar CE, High KA, Joung JK, Kohn DB, Ozawa K, Sadelain M. Gene therapy comes of age. *Science*. (2018) 359:eaan4672.. doi: 10.1126/science.aan4672
24. Prondzynski M, Mearini G, Carrier L. Gene therapy strategies in the treatment of hypertrophic cardiomyopathy. *Pflugers Arch-Eur J Physiol*. (2018) P. 1–9. doi: 10.1007/s00424-018-2173-5.

25. Hidai C, Kitano H. Nonviral gene therapy for cancer: a review. *Diseases*. (2018) 6:E57. doi: 10.3390/diseases6030057
26. Esrick EB, Bauer DE. Genetic therapies for sickle cell disease. *Semin Hematol*. (2018) 55:76–86. doi: 10.1053/j.seminhematol.2018.04.014
27. Prakash V, Moore M, Yanez-Munoz RJ. Current progress in therapeutic gene editing for monogenic diseases. *Mol Ther*. (2016) 24:465–74. doi: 10.1038/mt.2016.5
28. Verma IM, Somia N. Gene therapy - promises, problems and prospects. *Nature*. (1997) 389:239. doi: 10.1038/38410
29. Cotrim AP, Baum BJ. Gene therapy: some history, applications, problems, and prospects. *Toxicol Pathol*. (2008) 36:97–103. doi: 10.1177/0192623307309925
30. Jafarlou M, Baradaran B, Saedi TA, Jafarlou V, Shanehbandi D, Maralani M, et al. An overview of the history, applications, advantages, disadvantages and prospects of gene therapy. *J Biol Regul Homeost Agents*. (2016) 30:315–21.
31. Giacca M. *Ethical and Social Problems OG Gene Therapy*. Milan:Springer (2010).
32. Hanna E, Remuzat C, Auquier P, Toumi M. Gene therapies development: slow progress and promising prospect. *J Mark Access Health Policy*. (2017) 5:1265293. doi: 10.1080/20016689.2017.1265293
33. Szybalska EH, Szybalski W. Genetics of human cess line. IV. DNA-mediated heritable transformation of a biochemical trait. *Proc Natl Acad Sci USA*. (1962) 48:2026–34.
34. Wirth T, Parker N, Yla-Herttuala S. History of gene therapy. *Gene*. (2013) 525:162–9. doi: 10.1016/j.gene.2013.03.137
35. Chen C, Yang Z, Tang X. Chemical modifications of nucleic acid drugs and their delivery systems for gene-based therapy. *Med Res Rev*. (2018) 38:829–69. doi: 10.1002/med.21479
36. Misra S. Human gene therapy: a brief overview of the genetic revolution. *J Assoc Physicians India*. (2013) 61:127–33.
37. Cartier-Lacave N, Ali R, Yla-Herttuala S, Kato K, Baetschi B, Lovell-Badge R, et al. Debate on Germline Gene Editing. *Hum Gene Ther Methods*. (2016) 27:135–42. doi: 10.1089/hgtb.2016.28999.deb
38. Wolf E, Schernthaner W, Zakhartchenko V, Prelle K, Stojkovic M, Brem G. Transgenic technology in farm animals–progress and perspectives. *Exp Physiol*. (2000) 85:615–25.
39. Jaenisch R. Transgenic animals. *Science*. (1988) 240:1468–74.
40. Gordon JW, Scangos GA, Plotkin DJ, Barbosa JA, Ruddle FH. Genetic transformation of mouse embryos by microinjection of purified DNA. *Proc Natl Acad Sci USA*. (1980) 77:7380–4.
41. McCarthy M. Scientists call for moratorium on clinical use of human germline editing. *BMJ*. (2015) 351:h6603. doi: 10.1136/bmj.h6603
42. Travis J. Genetic engineering. Germline editing dominates DNA summit. *Science*. (2015) 350:1299–300. doi: 10.1126/science.350.6266.1299
43. Naldini L. Gene therapy returns to centre stage. *Nature*. (2015) 526:351–60. doi: 10.1038/nature15818
44. Cohen IG, Adashi EY. Science and regulation. The FDA is prohibited from going germline. *Science*. (2016) 353:545–6. doi: 10.1126/science.aag2960
45. LaBarbera AR. Proceedings of the International Summit on Human Gene Editing: a global discussion-Washington, D.C., December 1-3, 2015. *J Assist Reprod Genet*. (2016) 33:1123–7. doi: 10.1007/s10815-016-0753-x
46. Hildt E. Human germline interventions-think first. *Front Genet*. (2016) 7:81. doi: 10.3389/fgene.2016.00081
47. Pergament E. The promise of gene therapy. *Curr Opin Obstet Gynecol*. (2016) 28:132–5. doi: 10.1097/GCO.0000000000000255
48. Vassena R, Heindryckx B, Peco R, Pennings G, Raya A, Sermon K, Veiga A. Genome engineering through CRISPR/Cas9 technology in the human germline and pluripotent stem cells. *Hum Reprod Update*. (2016) 22:411–9. doi: 10.1093/humupd/dmw005
49. Portin P. [New possibilities will open up in human gene therapy]. *Duodecim*. (2016) 132:26–32.
50. Calos MP. Genome editing techniques and their therapeutic applications. *Clin Pharmacol Ther*. (2017) 101:42–51. doi: 10.1002/cpt.542
51. Morrow T. Novartis's kymriah: harnessing immune system comes with worry about reining in costs. *Manag Care*. (2017) 26:28–30.
52. Kaufmann KB, Buning H, Galy A, Schambach A, Grez M. Gene therapy on the move. *EMBO Mol Med*. (2013) 5:1642–61. doi: 10.1002/emmm.201202287
53. Herrero MJ, Sabater L, Guenechea G, Sendra L, Montilla AI, Abargues R, et al. DNA delivery to *'ex vivo'* human liver segments. *Gene Ther*. (2012) 19:504–12. doi: 10.1038/gt.2011.144
54. Suhonen J, Ray J, Blomer U, Gage FH, Kaspar B. *Ex vivo* and *in vivo* gene delivery to the brain. *Curr Protoc Hum Genet*. (2006) Chapter 13:Unit 13 3. doi: 10.1002/0471142905.hg1303s51
55. Deev RV, Bozo IY, Mzhavanadze ND, Voronov DA, Gavrilenko AV, Chervyakov YV, et al. pCMV-vegf165 Intramuscular Gene Transfer is an Effective Method of Treatment for Patients With Chronic Lower Limb Ischemia. *J Cardiovasc Pharmacol Ther*. (2015) 20:473–82. doi: 10.1177/1074248415574336
56. Deev R, Plaksa I, Bozo I, Isaev A. Results of an International postmarketing surveillance study of pl-VEGF165 Safety and Efficacy in 210 Patients with Peripheral Arterial Disease. *Am J Cardiovasc Drugs*. (2017) 17:235–42. doi: 10.1007/s40256–016-0210–3
57. Deev R, Plaksa I, Bozo I, Mzhavanadze N, Suchkov I, Chervyakov Y, et al. Results of 5-year follow-up study in patients with peripheral artery disease treated with PL-VEGF165 for intermittent claudication. *Ther Adv Cardiovasc Dis*. (2018) 12:237–46. doi: 10.1177/1753944718786926
58. Manunta MD, Tagalakis AD, Attwood M, Aldossary AM, Barnes JL, Munye MM, et al. Delivery of ENaC siRNA to epithelial cells mediated by a targeted nanocomplex: a therapeutic strategy for cystic fibrosis. *Sci Rep*. (2017) 7:700. doi: 10.1038/s41598–017-00662–2
59. Nance ME, Hakim CH, Yang NN, Duan D. Nanotherapy for duchenne muscular dystrophy. *Wiley Interdiscip Rev Nanomed Nanobiotechnol*. (2017). 10:e1472. doi: 10.1002/wnan.1472
60. Guan X, Guo Z, Wang T, Lin L, Chen J, Tian H, et al. A pH-Responsive Detachable PEG shielding strategy for gene delivery system in cancer therapy. *Biomacromolecules*. (2017) 18:1342–9. doi: 10.1021/acs.biomac.7b00080
61. Roossinck MJ. Move over, bacteria! Viruses make their mark as mutualistic microbial symbionts. *J Virol*. (2015) 89:6532–5. doi: 10.1128/jvi.02974–14
62. Roossinck MJ, Bazan ER. Symbiosis: viruses as intimate partners. *Annu Rev Virol*. (2017) 4:123–39. doi: 10.1146/annurev-virology-110615–042323
63. Viswanathan P, Betapudi V, Kumar MS, Rasheedi S, Vrati S, Bashyam MD, Hasnain SE. The homologous region sequence (hr1) of Autographa californica multinucleocapsid polyhedrosis virus can enhance transcription from non-baculoviral promoters in mammalian cells. *J Biol Chem*. (2003) 278:52564–71. doi: 10.1074/jbc.M309351200
64. Betapudi V, Viswanathan P, Habib S, Hasnain SE. An additional copy of the homologous region (hr1) sequence in the Autographa californica multinucleocapsid polyhedrosis virus genome promotes hyperexpression of foreign genes. *Biochemistry*. (2004) 43:8143–51. doi: 10.1021/bi049953q
65. Ramani K, Hassan Q, Betapudi V, Hasnain SE, Sarkar DP. Site-specific gene delivery *in vivo* through engineered Sendai viral envelopes. *Proc Natl Acad Sci USA*. (1998) 95:11886–90.
66. Giacca M Zacchigna S. Virus-mediated gene delivery for human gene therapy. *J Control Release*. (2012) 161:377–88. doi: 10.1016/j.jconrel.2012.04.008
67. Yin H, Kanasty RL, Eltoukhy AA, Vegas AJ, Dorkin JR Anderson DG. Non-viral vectors for gene-based therapy. *Nat Rev Genet*. (2014) 15:541–55. doi: 10.1038/nrg3763
68. Lawler SE, Speranza MC, Cho CF, Chiocca EA. Oncolytic viruses in cancer treatment: a review. *JAMA Oncol*. (2017) 3:841–9. doi: 10.1001/jamaoncol.2016.2064
69. Tatum EL. Molecular biology, nucleic acids, and the future of medicine. *Perspect Biol Med*. (1966) 10:19–32.
70. Ginn SL, Alexander IE. Gene therapy: progress in childhood disease. *J Paediatr Child Health*. (2012) 48:466–71. doi: 10.1111/j.1440–1754.2011.02204.x
71. Ginn SL, Alexander IE, Edelstein ML, Abedi MR, Wixon J. Gene therapy clinical trials worldwide to 2012 - an update. *J Gene Med*. (2013) 15:65–77. doi: 10.1002/jgm.2698
72. Rowe WP, Huebner RJ, Gilmore LK, Parrott RH, Ward TG. Isolation of a cytopathogenic agent from human adenoids undergoing spontaneous degeneration in tissue culture. *Proc Soc Exp Biol Med*. (1953) 84:570–3.
73. Crystal RG. Adenovirus: the first effective *in vivo* gene delivery vector. *Hum Gene Ther*. (2014) 25:3–11. doi: 10.1089/hum.2013.2527

74. Rauschhuber C, Noske N, Ehrhardt A. New insights into stability of recombinant adenovirus vector genomes in mammalian cells. *Eur J Cell Biol*. (2012) 91:2–9. doi: 10.1016/j.ejcb.2011.01.006
75. Nemerow GR, Stewart PL, Reddy VS. Structure of human adenovirus. *Curr Opin Virol*. (2012) 2:115–21. doi: 10.1016/j.coviro.2011.12.008
76. Shayakhmetov DM, Lieber A. Dependence of adenovirus infectivity on length of the fiber shaft domain. *J Virol*. (2000) 74:10274–86.
77. Bai M, Harfe B, Freimuth P. Mutations that alter an Arg-Gly-Asp (RGD) sequence in the adenovirus type 2 penton base protein abolish its cell-rounding activity and delay virus reproduction in flat cells. *J Virol*. (1993) 67:5198–205.
78. Wickham TJ, Segal DM, Roelvink PW, Carrion ME, Lizonova A, Lee GM Kovesdi I. Targeted adenovirus gene transfer to endothelial and smooth muscle cells by using bispecific antibodies. *J Virol*. (1996) 70:6831–8.
79. Sharma P, Martis PC, Excoffon KJ. Adenovirus transduction: More complicated than receptor expression. *Virology*. (2017) 502:144–51. doi: 10.1016/j.virol.2016.12.020
80. Davison AJ, Benko M, Harrach B. Genetic content and evolution of adenoviruses. *J Gen Virol*. (2003) 84:2895–908. doi: 10.1099/vir.0.19497–0
81. Majhen D, Ambriovic-Ristov A. Adenoviral vectors–how to use them in cancer gene therapy? *Virus Res*. (2006) 119:121–33. doi: 10.1016/j.virusres.2006.02.001
82. Liu Q, Muruve DA. Molecular basis of the inflammatory response to adenovirus vectors. *Gene Ther*. (2003) 10:935–40. doi: 10.1038/sj.gt.3302036
83. Amalfitano A, Hauser MA, Hu H, Serra D, Begy CR, Chamberlain JS. Production and characterization of improved adenovirus vectors with the E1, E2b, and E3 genes deleted. *J Virol*. (1998) 72:926–33.
84. Wen S, Schneider DB, Driscoll RM, Vassalli G, Sassani AB, Dichek DA. Second-generation adenoviral vectors do not prevent rapid loss of transgene expression and vector DNA from the arterial wall. *Arterioscler Thromb Vasc Biol*. (2000) 20:1452–8.
85. Sakhuja K, Reddy PS, Ganesh S, Cantaniag F, Pattison S, Limbach P, et al. Optimization of the generation and propagation of gutless adenoviral vectors. *Hum Gene Ther*. (2003) 14:243–54. doi: 10.1089/10430340360535797
86. Alba R, Bosch A, Chillon M. Gutless adenovirus: last-generation adenovirus for gene therapy. *Gene Ther*. (2005) 12 (Suppl. 1):S18–27. doi: 10.1038/sj.gt.3302612
87. Vetrini F, Ng P. Gene therapy with helper-dependent adenoviral vectors: current advances and future perspectives. *Viruses*. (2010) 2:1886–917. doi: 10.3390/v2091886
88. Hausl MA, Zhang W, Muther N, Rauschhuber C, Franck HG, Merricks EP, et al. Hyperactive sleeping beauty transposase enables persistent phenotypic correction in mice and a canine model for hemophilia B. *Mol Ther*. (2010) 18:1896–906. doi: 10.1038/mt.2010.169
89. Hausl M, Zhang W, Voigtlander R, Muther N, Rauschhuber C, Ehrhardt A. Development of adenovirus hybrid vectors for Sleeping Beauty transposition in large mammals. *Curr Gene Ther*. (2011) 11:363–74.
90. Castello R, Borzone R, D'Aria S, Annunziata P, Piccolo P, Brunetti-Pierri N. Helper-dependent adenoviral vectors for liver-directed gene therapy of primary hyperoxaluria type 1. *Gene Ther*. (2016) 23:129–34. doi: 10.1038/gt.2015.107
91. Rosewell Shaw A, Suzuki M. Recent advances in oncolytic adenovirus therapies for cancer. *Curr Opin Virol*. (2016) 21:9–15. doi: 10.1016/j.coviro.2016.06.009
92. Russell SJ, Peng KW, Bell JC. Oncolytic virotherapy. *Nat Biotechnol*. (2012) 30:658–70. doi: 10.1038/nbt.2287
93. Dai B, Roife D, Kang Y, Gumin J, Rios Perez MV, Li X, et al. Preclinical Evaluation of Sequential Combination of Oncolytic Adenovirus Delta-24-RGD and phosphatidylserine-targeting antibody in pancreatic ductal adenocarcinoma. *Mol Cancer Ther*. (2017) 16:662–70. doi: 10.1158/1535–7163.MCT-16–0526
94. Tazawa H, Kuroda S, Hasei J, Kagawa S, Fujiwara T. Impact of autophagy in oncolytic adenoviral therapy for cancer. *Int J Mol Sci*. (2017) 18:E1479. doi: 10.3390/ijms18071479
95. Ji W, Sun B, Su C. Targeting MicroRNAs in cancer gene therapy. *Genes (Basel)*. (2017) 8:E21. doi: 10.3390/genes8010021
96. Shimizu K, Sakurai F, Tomita K, Nagamoto Y, Nakamura S, Katayama K, et al. Suppression of leaky expression of adenovirus genes by insertion of microRNA-targeted sequences in the replication-incompetent adenovirus vector genome. *Mol Ther Methods Clin Dev*. (2014) 1:14035. doi: 10.1038/mtm.2014.35
97. Ledgerwood JE, DeZure AD, Stanley DA, Coates EE, Novik L, Enama ME, et al. Chimpanzee Adenovirus Vector Ebola Vaccine. *N Engl J Med*. (2017) 376:928–38. doi: 10.1056/NEJMoa1410863
98. Capone S, D'Alise AM, Ammendola V, Colloca S, Cortese R, Nicosia A, et al. Development of chimpanzee adenoviruses as vaccine vectors: challenges and successes emerging from clinical trials. *Expert Rev Vaccines*. (2013) 12:379–93. doi: 10.1586/erv.13.15
99. Appaiahgari MB, Vrati S. Adenoviruses as gene/vaccine delivery vectors: promises and pitfalls. *Expert Opin Biol Ther*. (2015) 15:337–51. doi: 10.1517/14712598.2015.993374
100. Barouch DH, Kik SV, Weverling GJ, Dilan R, King SL, Maxfield LF, et al. International seroepidemiology of adenovirus serotypes 5, 26, 35, and 48 in pediatric and adult populations. *Vaccine*. (2011) 29:5203–9. doi: 10.1016/j.vaccine.2011.05.025
101. Wang X, Xing M, Zhang C, Yang Y, Chi Y, Tang X, et al. Neutralizing antibody responses to enterovirus and adenovirus in healthy adults in China. *Emerg Microbes Infect*. (2014) 3:e30. doi: 10.1038/emi.2014.30
102. Fausther-Bovendo H, Kobinger GP. Pre-existing immunity against Ad vectors: humoral, cellular, and innate response, what's important? *Hum Vaccin Immunother*. (2014) 10:2875–84. doi: 10.4161/hv.29594
103. Atkinson RL, Dhurandhar NV, Allison DB, Bowen RL, Israel BA, Albu JB, et al. Human adenovirus-36 is associated with increased body weight and paradoxical reduction of serum lipids. *Int J Obes (Lond)*. (2005) 29:281–6. doi: 10.1038/sj.ijo.0802830
104. Imperiale MJ. Keeping adenovirus away from the liver. *Cell Host Microbe*. (2008) 3:119–20. doi: 10.1016/j.chom.2008.02.007
105. Wilson JM. Lessons learned from the gene therapy trial for ornithine transcarbamylase deficiency. *Mol Genet Metab*. (2009) 96:151–7. doi: 10.1016/j.ymgme.2008.12.016
106. Kalyuzhniy O, Di Paolo NC, Silvestry M, Hofherr SE, Barry MA, Stewart PL, et al. Adenovirus serotype 5 hexon is critical for virus infection of hepatocytes *in vivo*. *Proc Natl Acad Sci USA*. (2008) 105:5483–8. doi: 10.1073/pnas.0711757105
107. Irons EE, Flatt JW, Doronin K, Fox TL, Acchione M, Stewart PL, et al. Coagulation factor binding orientation and dimerization may influence infectivity of adenovirus-coagulation factor complexes. *J Virol*. (2013) 87:9610–9. doi: 10.1128/jvi.01070–13
108. Yoon AR, Hong J, Kim SW, Yun CO. Redirecting adenovirus tropism by genetic, chemical, and mechanical modification of the adenovirus surface for cancer gene therapy. *Expert Opin Drug Deliv*. (2016) 13:843–58. doi: 10.1517/17425247.2016.1158707
109. Brunetti-Pierri N, Ng P. Gene therapy with helper-dependent adenoviral vectors: lessons from studies in large animal models. *Virus Genes*. (2017) 53:684–91. doi: 10.1007/s11262–017-1471-x
110. Abbink P, Lemckert AA, Ewald BA, Lynch DM, Denholtz M, Smits S, et al. Comparative seroprevalence and immunogenicity of six rare serotype recombinant adenovirus vaccine vectors from subgroups B and D. *J Virol*. (2007) 81:4654–63. doi: 10.1128/jvi.02696–06
111. Belousova N, Mikheeva G, Xiong C, Stagg LJ, Gagea M, Fox PS, et al. Native and engineered tropism of vectors derived from a rare species D adenovirus serotype 43. *Oncotarget*. (2016) 7:53414–29. doi: 10.18632/oncotarget.10800
112. Trinh HV, Lesage G, Chennamparampil V, Vollenweider B, Burckhardt CJ, Schauer S, et al. Avidity binding of human adenovirus serotypes 3 and 7 to the membrane cofactor CD46 triggers infection. *J Virol*. (2012) 86:1623–37. doi: 10.1128/jvi.06181–11
113. Tuve S, Wang H, Ware C, Liu Y, Gaggar A, Bernt K, et al. A new group B adenovirus receptor is expressed at high levels on human stem and tumor cells. *J Virol*. (2006) 80:12109–20. doi: 10.1128/jvi.01370–06
114. Parker AL, White KM, Lavery CA, Custers J, Waddington SN, Baker AH. Pseudotyping the adenovirus serotype 5 capsid with both the fibre and penton of serotype 35 enhances vascular smooth muscle cell transduction. *Gene Ther*. (2013) 20:1158–64. doi: 10.1038/gt.2013.44

115. Guo L, Li X, Yang S, Xu Y, Tao R, Wulan H, et al. A highly infectious chimeric adenovirus expressing basic fibroblast growth factor exerts potent targeted therapy for rabbit ear chronic ischemic wounds. *Plast Reconstr Surg*. (2014) 134:248e-56e. doi: 10.1097/prs.0000000000000364
116. Cho YS, Do MH, Kwon SY, Moon C, Kim K, Lee K, et al. Efficacy of CD46-targeting chimeric Ad5/35 adenoviral gene therapy for colorectal cancers. *Oncotarget*. (2016) 7:38210–23. doi: 10.18632/oncotarget.9427
117. Zhang WF, Shao HW, Wu FL, Xie X, Li ZM, Bo HB, et al. Influence of cell physiological state on gene delivery to T lymphocytes by chimeric adenovirus Ad5F35. *Sci Rep*. (2016) 6:22688. doi: 10.1038/srep22688
118. Pesonen S, Kangasniemi L, Hemminki A. Oncolytic adenoviruses for the treatment of human cancer: focus on translational and clinical data. *Mol Pharm*. (2011) 8:12–28. doi: 10.1021/mp100219n
119. Li X, Mao Q, Wang D, Xia H. A novel Ad5/11 chimeric oncolytic adenovirus for improved glioma therapy. *Int J Oncol*. (2012) 41:2159–65. doi: 10.3892/ijo.2012.1674
120. Sykes C, Reisman M. Ebola: working toward treatments and vaccines. *P T*. (2015) 40:521–5.
121. Tapia MD, Sow SO, Lyke KE, Haidara FC, Diallo F, Doumbia M, et al. Use of ChAd3-EBO-Z Ebola virus vaccine in Malian and US adults, and boosting of Malian adults with MVA-BN-Filo: a phase 1, single-blind, randomised trial, a phase 1b, open-label and double-blind, dose-escalation trial, and a nested, randomised, double-blind, placebo-controlled trial. *Lancet Infect Dis*. (2016) 16:31–42. doi: 10.1016/s1473–3099(15)00362-x
122. Yang Y, Xiao F, Lu Z, Li Z, Zuo H, Zhang Q, et al. Development of a novel adenovirus-alphavirus hybrid vector with RNA replicon features for malignant hematopoietic cell transduction. *Cancer Gene Ther*. (2013) 20:429–36. doi: 10.1038/cgt.2013.37
123. Miura Y, Yoshida K, Nishimoto T, Hatanaka K, Ohnami S, Asaka M, et al. Direct selection of targeted adenovirus vectors by random peptide display on the fiber knob. *Gene Ther*. (2007) 14:1448–60. doi: 10.1038/sj.gt.3303007
124. Lupold SE, Kudrolli TA, Chowdhury WH, Wu P, Rodriguez R. A novel method for generating and screening peptides and libraries displayed on adenovirus fiber. *Nucleic Acids Res*. (2007) 35:e138. doi: 10.1093/nar/gkm914
125. Miura Y, Yamasaki S, Davydova J, Brown E, Aoki K, Vickers S, et al. Infectivity-selective oncolytic adenovirus developed by high-throughput screening of adenovirus-formatted library. *Mol Ther*. (2013) 21:139–48. doi: 10.1038/mt.2012.205
126. Nishimoto T, Yamamoto Y, Yoshida K, Goto N, Ohnami S, Aoki K. Development of peritoneal tumor-targeting vector by *in vivo* screening with a random peptide-displaying adenovirus library. *PLoS ONE*. (2012) 7:e45550. doi: 10.1371/journal.pone.0045550
127. Nishimoto T, Yoshida K, Miura Y, Kobayashi A, Hara H, Ohnami S, et al. Oncolytic virus therapy for pancreatic cancer using the adenovirus library displaying random peptides on the fiber knob. *Gene Ther*. (2009) 16:669–80. doi: 10.1038/gt.2009.1
128. Wu P, Kudrolli TA, Chowdhury WH, Liu MM, Rodriguez R, Lupold SE. Adenovirus targeting to prostate-specific membrane antigen through virus-displayed, semirandom peptide library screening. *Cancer Res*. (2010) 70:9549–53. doi: 10.1158/0008–5472.can-10–1760
129. Yamamoto Y, Nagasato M, Rin Y, Henmi M, Ino Y, Yachida S, et al. Strong antitumor efficacy of a pancreatic tumor-targeting oncolytic adenovirus for neuroendocrine tumors. *Cancer Med*. (2017) 6:2385–97. doi: 10.1002/cam4.1185
130. Atchison RW, Casto BC, Hammon WM. Adenovirus-associated defective virus particles. *Science*. (1965) 149:754–6.
131. Hoggan MD, Blacklow NR, Rowe WP. Studies of small DNA viruses found in various adenovirus preparations: physical, biological, and immunological characteristics. *Proc Natl Acad Sci USA*. (1966) 55:1467–74.
132. Laughlin CA, Westphal H, Carter BJ. Spliced adenovirus-associated virus RNA. *Proc Natl Acad Sci USA*. (1979) 76:5567–71.
133. Marcus CJ, Laughlin CA, Carter BJ. Adeno-associated virus RNA transcription *in vivo*. *Eur J Biochem*. (1981) 121:147–54.
134. Grieger JC, Samulski RJ. Adeno-associated virus vectorology, manufacturing, and clinical applications. *Methods Enzymol*. (2012) 507:229–54. doi: 10.1016/B978–0-12–386509-0.00012–0
135. Sonntag F, Schmidt K, Kleinschmidt JA. A viral assembly factor promotes AAV2 capsid formation in the nucleolus. *Proc Natl Acad Sci USA*. (2010) 107:10220–5. doi: 10.1073/pnas.1001673107
136. Jay FT, Laughlin CA, Carter BJ. Eukaryotic translational control: adeno-associated virus protein synthesis is affected by a mutation in the adenovirus DNA-binding protein. *Proc Natl Acad Sci USA*. (1981) 78:2927–31.
137. Carter BJ. Adeno-associated virus and the development of adeno-associated virus vectors: a historical perspective. *Mol Ther*. (2004) 10:981–9. doi: 10.1016/j.ymthe.2004.09.011
138. Vandenberghe LH, Breous E, Nam HJ, Gao G, Xiao R, Sandhu A, et al. Naturally occurring singleton residues in AAV capsid impact vector performance and illustrate structural constraints. *Gene Ther*. (2009) 16:1416–28. doi: 10.1038/gt.2009.101
139. McCarty DM, Monahan PE, Samulski RJ. Self-complementary recombinant adeno-associated virus (scAAV) vectors promote efficient transduction independently of DNA synthesis. *Gene Ther*. (2001) 8:1248–54. doi: 10.1038/sj.gt.3301514
140. McCarty DM, Fu H, Monahan PE, Toulson CE, Naik P, Samulski RJ. Adeno-associated virus terminal repeat (TR) mutant generates self-complementary vectors to overcome the rate-limiting step to transduction *in vivo*. *Gene Ther*. (2003) 10:2112–8. doi: 10.1038/sj.gt.3302134
141. Buchlis G, Podsakoff GM, Radu A, Hawk SM, Flake AW, Mingozzi F, et al. Factor IX expression in skeletal muscle of a severe hemophilia B patient 10 years after AAV-mediated gene transfer. *Blood*. (2012) 119:3038–41. doi: 10.1182/blood-2011–09-382317
142. Kotin RM, Siniscalco M, Samulski RJ, Zhu XD, Hunter L, Laughlin CA, et al. Site-specific integration by adeno-associated virus. *Proc Natl Acad Sci USA*. (1990) 87:2211–5.
143. Samulski RJ, Zhu X, Xiao X, Brook JD, Housman DE, Epstein N, et al. Targeted integration of adeno-associated virus (AAV) into human chromosome 19. *Embo J*. (1991) 10:3941–50.
144. Pillay S, Meyer NL, Puschnik AS, Davulcu O, Diep J, Ishikawa Y, et al. An essential receptor for adeno-associated virus infection. *Nature*. (2016) 530:108–12. doi: 10.1038/nature16465
145. Gao G, Vandenberghe LH, Alvira MR, Lu Y, Calcedo R, Zhou X, et al. Clades of Adeno-associated viruses are widely disseminated in human tissues. *J Virol*. (2004) 78:6381–8. doi: 10.1128/jvi.78.12.6381–6388.2004
146. Weitzman MD, Linden RM. Adeno-associated virus biology. *Methods Mol Biol*. (2011) 807:1–23. doi: 10.1007/978–1-61779–370-7_1
147. Zincarelli C, Soltys S, Rengo G, Rabinowitz JE. Analysis of AAV serotypes 1–9 mediated gene expression and tropism in mice after systemic injection. *Mol Ther*. (2008) 16:1073–80. doi: 10.1038/mt.2008.76
148. Strobel B, Duechs MJ, Schmid R, Stierstorfer BE, Bucher H, Quast K, et al. Modeling pulmonary disease pathways using recombinant adeno-associated virus 6.2. *Am J Respir Cell Mol Biol*. (2015) 53:291–302. doi: 10.1165/rcmb.2014–0338MA
149. Luo H, Chen Y, Ye Z, Sun X, Shi Y, Luo Q, et al. Evaluation of the Association Between Common Genetic Variants Near the ABCA1 Gene and Primary Angle Closure Glaucoma in a Han Chinese Population. *Invest Ophthalmol Vis Sci*. (2015) 56:6248–54. doi: 10.1167/iovs.15–16741
150. Nathwani AC, Nienhuis AW, Davidoff AM. Our journey to successful gene therapy for hemophilia B. *Hum Gene Ther*. (2014) 25:923–6. doi: 10.1089/hum.2014.2540
151. Smith LJ, Ul-Hasan T, Carvaines SK, Van Vliet K, Yang E, Wong KK Jr, et al. Gene transfer properties and structural modeling of human stem cell-derived AAV. *Mol Ther*. (2014) 22:1625–34. doi: 10.1038/mt.2014.107
152. Murphy SL, Li H, Zhou S, Schlachterman A, High KA. Prolonged susceptibility to antibody-mediated neutralization for adeno-associated vectors targeted to the liver. *Mol Ther*. (2008) 16:138–45. doi: 10.1038/sj.mt.6300334
153. Zinn E, Pacouret S, Khaychuk V, Turunen HT, Carvalho LS, Andres-Mateos E, et al. *In silico* reconstruction of the viral evolutionary lineage yields a potent gene therapy vector. *Cell Rep*. (2015) 12:1056–68. doi: 10.1016/j.celrep.2015.07.019
154. Bowles DE, McPhee SW, Li C, Gray SJ, Samulski JJ, Camp AS, et al. Phase 1 gene therapy for Duchenne muscular dystrophy using

a translational optimized AAV vector. *Mol Ther*. (2012) 20:443–55. doi: 10.1038/mt.2011.237
155. Worgall S, Sondhi D, Hackett NR, Kosofsky B, Kekatpure MV, Neyzi N, et al. Treatment of late infantile neuronal ceroid lipofuscinosis by CNS administration of a serotype 2 adeno-associated virus expressing CLN2 cDNA. *Hum Gene Ther*. (2008) 19:463–74. doi: 10.1089/hum.2008.022
156. Mays LE, Vandenberghe LH, Xiao R, Bell P, Nam HJ, Agbandje-McKenna M, et al. Adeno-associated virus capsid structure drives CD4-dependent CD8+ T cell response to vector encoded proteins. *J Immunol*. (2009) 182:6051–60. doi: 10.4049/jimmunol.0803965
157. Lin SW, Hensley SE, Tatsis N, Lasaro MO, Ertl HC. Recombinant adeno-associated virus vectors induce functionally impaired transgene product-specific CD8+ T cells in mice. *J Clin Invest*. (2007) 117:3958–70. doi: 10.1172/jci33138
158. Faust SM, Bell P, Cutler BJ, Ashley SN, Zhu Y, Rabinowitz JE, et al. CpG-depleted adeno-associated virus vectors evade immune detection. *J Clin Invest*. (2013) 123:2994–3001. doi: 10.1172/jci68205
159. Deverman BE, Pravdo PL, Simpson BP, Kumar SR, Chan KY, Banerjee A, et al. Cre-dependent selection yields AAV variants for widespread gene transfer to the adult brain. *Nat Biotechnol*. (2016) 34:204–9. doi: 10.1038/nbt.3440
160. Choudhury SR, Fitzpatrick Z, Harris AF, Maitland SA, Ferreira JS, Zhang Y, et al. *In vivo* selection yields AAV-B1 capsid for central nervous system and muscle gene therapy. *Mol Ther*. (2016) 24:1247–57. doi: 10.1038/mt.2016.84
161. Ran FA, Cong L, Yan WX, Scott DA, Gootenberg JS, Kriz AJ, et al. *in vivo* genome editing using Staphylococcus aureus Cas9. *Nature*. (2015) 520:186–91. doi: 10.1038/nature14299
162. Lin C, Li H, Hao M, Xiong D, Luo Y, Huang C, et al. Increasing the efficiency of CRISPR/Cas9-mediated precise genome editing of HSV-1 virus in human cells. *Sci Rep*. (2016) 6:34531. doi: 10.1038/srep34531
163. Marconi P, Fraefel C, Epstein AL. Herpes simplex virus type 1 (HSV-1)-derived recombinant vectors for gene transfer and gene therapy. *Methods Mol Biol*. (2015) 1254:269–93. doi: 10.1007/978–1-4939–2152-2_20
164. Goins WF, Huang S, Cohen JB, Glorioso JC. Engineering HSV-1 vectors for gene therapy. *Methods Mol Biol*. (2014) 1144:63–79. doi: 10.1007/978–1-4939–0428-0_5
165. Krisky DM, Wolfe D, Goins WF, Marconi PC, Ramakrishnan R, Mata M, et al. Deletion of multiple immediate-early genes from herpes simplex virus reduces cytotoxicity and permits long-term gene expression in neurons. *Gene Ther*. (1998) 5:1593–603. doi: 10.1038/sj.gt.3300766
166. Wolfe D, Mata M, Fink DJ. A human trial of HSV-mediated gene transfer for the treatment of chronic pain. *Gene Ther*. (2009) 16:455–60. doi: 10.1038/gt.2009.17
167. Goss JR, Cascio M, Goins WF, Huang S, Krisky DM, Clarke RJ, et al. HSV delivery of a ligand-regulated endogenous ion channel gene to sensory neurons results in pain control following channel activation. *Mol Ther*. (2011) 19:500–6. doi: 10.1038/mt.2010.246
168. Artusi S, Miyagawa Y, Goins WF, Cohen JB, Glorioso JC. Herpes simplex virus vectors for gene transfer to the central nervous system. *Diseases*. (2018) 6:E74. doi: 10.3390/diseases6030074
169. Advani SJ, Weichselbaum RR, Whitley RJ, Roizman B. Friendly fire: redirecting herpes simplex virus-1 for therapeutic applications. *Clin Microbiol Infect*. (2002) 8:551–63. doi: 10.1046/j.1469-0691.2002.00432.x
170. Argnani R, Lufino M, Manservigi M, Manservigi R. Replication-competent herpes simplex vectors: design and applications. *Gene Ther*. (2005) 12 (Suppl.1):S170–7. doi: 10.1038/sj.gt.3302622
171. Maetzig T, Galla M, Baum C, Schambach A. Gammaretroviral vectors: biology, technology and application. *Viruses*. (2011) 3:677–713. doi: 10.3390/v3060677
172. Hayward A. Origin of the retroviruses: when, where, and how? *Curr Opin Virol*. (2017) 25:23–7. doi: 10.1016/j.coviro.2017.06.006
173. Kassiotis G, Stoye JP. Making a virtue of necessity: the pleiotropic role of human endogenous retroviruses in cancer. *Philos Trans R Soc Lond B Biol Sci*. (2017) 372:20160277. doi: 10.1098/rstb.2016.0277
174. Meyer TJ, Rosenkrantz JL, Carbone L, Chavez SL. Endogenous retroviruses: with us and against Us. *Front Chem*. (2017) 5:23. doi: 10.3389/fchem.2017.00023
175. Buzdin AA, Prassolov V, Garazha AV. Friends-enemies: endogenous retroviruses are major transcriptional regulators of human DNA. *Front Chem*. (2017) 5:35. doi: 10.3389/fchem.2017.00035
176. Schambach A, Swaney WP, van der Loo JC. Design and production of retro- and lentiviral vectors for gene expression in hematopoietic cells. *Methods Mol Biol*. (2009) 506:191–205. doi: 10.1007/978–1-59745–409-4_14
177. Betapudi V, Shukla M, Alluri R, Merkulov S, McCrae KR. Novel role for p56/Lck in regulation of endothelial cell survival and angiogenesis. *Faseb J*. (2016) 30:3515–26. doi: 10.1096/fj.201500040
178. Shukla M, Betapudi V, Alluri RK, Merkulov S, Hale J, Lathia J, et al. Regulation of the tumor microenvironment by high molecular weight kininogen. *Blood*. (2016) 128:1394
179. Hacein-Bey-Abina S, Garrigue A, Wang GP, Soulier J, Lim A, Morillon E, et al. Insertional oncogenesis in 4 patients after retrovirus-mediated gene therapy of SCID-X1. *J Clin Invest*. (2008) 118:3132–42. doi: 10.1172/jci35700
180. Knopp Y, Geis FK, Heckl D, Horn S, Neumann T, Kuehle J, et al. Transient retrovirus-based CRISPR/Cas9 all-in-one particles for efficient, targeted gene knockout. *Mol Ther Nucleic Acids*. (2018) 13:256–74. doi: 10.1016/j.omtn.2018.09.006
181. Xu X, Tan X, Tampe B, Wilhelmi T, Hulshoff MS, Saito S, et al. High-fidelity CRISPR/Cas9- based gene-specific hydroxymethylation rescues gene expression and attenuates renal fibrosis. *Nat Commun*. (2018) 9:3509. doi: 10.1038/s41467–018-05766–5
182. Pearson S, Jia H, Kandachi K. China approves first gene therapy. *Nat Biotechnol*. (2004) 22:3–4. doi: 10.1038/nbt0104–3
183. Garber K. China approves world's first oncolytic virus therapy for cancer treatment. *J Natl Cancer Inst*. (2006) 98:298–300. doi: 10.1093/jnci/djj111
184. Kim S, Federman N, Gordon EM, Hall FL, Chawla SP. Rexin-G((R)), a tumor-targeted retrovector for malignant peripheral nerve sheath tumor: a case report. *Mol Clin Oncol*. (2017) 6:861–5. doi: 10.3892/mco.2017.1231
185. Kuo CY, Kohn DB. Gene therapy for the treatment of primary immune deficiencies. *Curr Allergy Asthma Rep*. (2016) 16:39. doi: 10.1007/s11882–016-0615–8
186. Ruella M, Kenderian SS. Next-generation chimeric antigen receptor t-cell therapy: going off the shelf. *BioDrugs*. (2017) 31:473–81. doi: 10.1007/s40259–017-0247–0
187. Sengillo JD, Justus S, Cabral T, Tsang SH. Correction of monogenic and common retinal disorders with gene therapy. *Genes (Basel)*. (2017) 8:E53. doi: 10.3390/genes8020053
188. MacLaren RE, Groppe M, Barnard AR, Cottriall CL, Tolmachova T, Seymour L, et al. Retinal gene therapy in patients with choroideremia: initial findings from a phase 1/2 clinical trial. *Lancet*. (2014) 383:1129–37. doi: 10.1016/S0140–6736(13)62117–0
189. Breitbach CJ, Lichty BD, Bell JC. Oncolytic viruses: therapeutics with an identity crisis. *EBioMedicine*. (2016) 9:31–6. doi: 10.1016/j.ebiom.2016.06.046
190. Fukuhara H, Ino Y, Todo T. Oncolytic virus therapy: A new era of cancer treatment at dawn. *Cancer Sci*. (2016) 107:1373–9. doi: 10.1111/cas.13027
191. Kirn D. Clinical research results with dl1520 (Onyx-015), a replication-selective adenovirus for the treatment of cancer: what have we learned? *Gene Ther*. (2001) 8:89–98. doi: 10.1038/sj.gt.3301377
192. Saydaminova K, Ye X, Wang H, Richter M, Ho M, Chen H, et al. Efficient genome editing in hematopoietic stem cells with helper-dependent Ad5/35 vectors expressing site-specific endonucleases under microRNA regulation. *Mol Ther Methods Clin Dev*. (2015) 1:14057. doi: 10.1038/mtm.2014.57
193. Lowenstein PR, Castro MG. Evolutionary basis of a new gene- and immune-therapeutic approach for the treatment of malignant brain tumors: from mice to clinical trials for glioma patients. *Clin Immunol*. (2018) 189:43–51. doi: 10.1016/j.clim.2017.07.006
194. Tejada S, Diez-Valle R, Dominguez PD, Patino-Garcia A, Gonzalez-Huarriz M, Fueyo J, et al. DNX-2401, an oncolytic virus, for the treatment of newly diagnosed diffuse intrinsic pontine gliomas: a case report. *Front Oncol*. (2018) 8:61. doi: 10.3389/fonc.2018.00061
195. Stepanenko AA, Chekhonin VP. Recent advances in oncolytic virotherapy and immunotherapy for glioblastoma: a glimmer of hope in the search for an effective therapy? *Cancers (Basel)*. (2018) 10 E492. doi: 10.3390/cancers10120492

196. Machiels JP, Salazar R, Rottey S, Duran I, Dirix L, Geboes K, et al. A phase 1 dose escalation study of the oncolytic adenovirus enadenotucirev, administered intravenously to patients with epithelial solid tumors (EVOLVE). *J Immunother Cancer*. (2019) 7:20. doi: 10.1186/s40425–019-0510–7
197. Kallel H, Kamen AA. Large-scale adenovirus and poxvirus-vectored vaccine manufacturing to enable clinical trials. *Biotechnol J*. (2015) 10:741–7. doi: 10.1002/biot.201400390
198. Edwards TL, Jolly JK, Groppe M, Barnard AR, Cottriall CL, Tolmachova T, et al. Visual Acuity after Retinal Gene Therapy for Choroideremia. *N Engl J Med*. (2016) 374:1996–8. doi: 10.1056/NEJMc1509501
199. Feuer WJ, Schiffman JC, Davis JL, Porciatti V, Gonzalez P, Koilkonda RD, et al. Gene therapy for leber hereditary optic neuropathy: initial results. *Ophthalmology*. (2016) 123:558–70. doi: 10.1016/j.ophtha.2015.10.025
200. Hocquemiller M, Giersch L, Audrain M, Parker S, Cartier N. Adeno-associated virus-based gene therapy for CNS diseases. *Hum Gene Ther*. (2016) 27:478–96. doi: 10.1089/hum.2016.087
201. Mahendra G, Kumar S, Isayeva T, Mahasreshti PJ, Curiel DT, Stockardt CR, et al. Antiangiogenic cancer gene therapy by adeno-associated virus 2-mediated stable expression of the soluble FMS-like tyrosine kinase-1 receptor. *Cancer Gene Ther*. (2005) 12:26–34. doi: 10.1038/sj.cgt.7700754
202. Li ZB, Chen YX, Zhao JY, Lu J. Effects of pharmacological concentrations of estrogens on growth of 3AO human ovarian cancer cells. *Yi Chuan Xue Bao*. (2006) 33:782–92. doi: 10.1016/s0379–4172(06)60111-x
203. Ma H, Liu Y, Liu S, Kung HF, Sun X, Zheng D, et al. Recombinant adeno-associated virus-mediated TRAIL gene therapy suppresses liver metastatic tumors. *Int J Cancer*. (2005) 116:314–21. doi: 10.1002/ijc.20982
204. Tu SP, Cui JT, Liston P, Huajiang X, Xu R, Lin MC, et al. Gene therapy for colon cancer by adeno-associated viral vector-mediated transfer of survivin Cys84Ala mutant. *Gastroenterology*. (2005) 128:361–75.
205. Wu S, Meng L, Wang S, Wang W, Xi L, Tian X, et al. Reversal of the malignant phenotype of cervical cancer CaSki cells through adeno-associated virus-mediated delivery of HPV16 E7 antisense RNA. *Clin Cancer Res*. (2006) 12:2032–7. doi: 10.1158/1078–0432.ccr-05–2567
206. Ho DT, Wykoff-Clary S, Gross CS, Schneider D, Jin F, Kretschmer PJ, et al. Growth inhibition of an established A431 xenograft tumor by a full-length anti-EGFR antibody following gene delivery by AAV. *Cancer Gene Ther*. (2009) 16:184–94. doi: 10.1038/cgt.2008.68
207. Nathwani AC, Reiss UM, Tuddenham EG, Rosales C, Chowdary P, McIntosh J, et al. Long-term safety and efficacy of factor IX gene therapy in hemophilia B. *N Engl J Med*. (2014) 371:1994–2004. doi: 10.1056/NEJMoa1407309
208. Mingozzi F, Maus MV, Hui DJ, Sabatino DE, Murphy SL, Rasko JE, et al. CD8(+) T-cell responses to adeno-associated virus capsid in humans. *Nat Med*. (2007) 13:419–22. doi: 10.1038/nm1549
209. Ertl HCJ, High KA. Impact of AAV capsid-specific T-cell responses on design and outcome of clinical gene transfer trials with recombinant adeno-associated viral vectors: an evolving controversy. *Hum Gene Ther*. (2017) 28:328–37. doi: 10.1089/hum.2016.172
210. Calcedo R, Vandenberghe LH, Gao G, Lin J, Wilson JM. Worldwide epidemiology of neutralizing antibodies to adeno-associated viruses. *J Infect Dis*. (2009) 199:381–90. doi: 10.1086/595830
211. Boutin S, Monteilhet V, Veron P, Leborgne C, Benveniste O, Montus MF, et al. Prevalence of serum IgG and neutralizing factors against adeno-associated virus (AAV) types 1, 2, 5, 6, 8, and 9 in the healthy population: implications for gene therapy using AAV vectors. *Hum Gene Ther*. (2010) 21:704–12. doi: 10.1089/hum.2009.182
212. Vandenberghe LH, Wang L, Somanathan S, Zhi Y, Figueredo J, Calcedo R, et al. Heparin binding directs activation of T cells against adeno-associated virus serotype 2 capsid. *Nat Med*. (2006) 12:967–71. doi: 10.1038/nm1445
213. Mingozzi F, Anguela XM, Pavani G, Chen Y, Davidson RJ, Hui DJ, et al. Overcoming preexisting humoral immunity to AAV using capsid decoys. *Sci Transl Med*. (2013) 5:194ra92. doi: 10.1126/scitranslmed.3005795
214. Zhong L, Li B, Jayandharan G, Mah CS, Govindasamy L, Agbandje-McKenna M, et al. Tyrosine-phosphorylation of AAV2 vectors and its consequences on viral intracellular trafficking and transgene expression. *Virology*. (2008) 381:194–202. doi: 10.1016/j.virol.2008.08.027
215. McPhee SW, Janson CG, Li C, Samulski RJ, Camp AS, Francis J, et al. Immune responses to AAV in a phase I study for Canavan disease. *J Gene Med*. (2006) 8:577–88. doi: 10.1002/jgm.885
216. Davidson BL, Stein CS, Heth JA, Martins I, Kotin RM, Derksen TA, et al. Recombinant adeno-associated virus type 2, 4, and 5 vectors: transduction of variant cell types and regions in the mammalian central nervous system. *Proc Natl Acad Sci USA*. (2000) 97:3428–32. doi: 10.1073/pnas.050581197
217. Eberling JL, Jagust WJ, Christine CW, Starr P, Larson P, Bankiewicz KS, et al. Results from a phase I safety trial of hAADC gene therapy for Parkinson disease. *Neurology*. (2008) 70:1980–3. doi: 10.1212/01.wnl.0000312381.29287.ff
218. LeWitt PA, Rezai AR, Leehey MA, Ojemann SG, Flaherty AW, Eskandar EN, et al. AAV2-GAD gene therapy for advanced Parkinson's disease: a double-blind, sham-surgery controlled, randomised trial. *Lancet Neurol*. (2011) 10:309–19. doi: 10.1016/s1474–4422(11)70039–4
219. Daar AS, Fuggle SV, Fabre JW, Ting A, Morris PJ. The detailed distribution of HLA-A, B, C antigens in normal human organs. *Transplantation*. (1984) 38:287–92.
220. Nathwani AC, Tuddenham EG, Rangarajan S, Rosales C, McIntosh J, Linch DC, et al. Adenovirus-associated virus vector-mediated gene transfer in hemophilia B. *N Engl J Med*. (2011) 365:2357–65. doi: 10.1056/NEJMoa1108046
221. Ferreira V, Twisk J, Kwikkers K, Aronica E, Brisson D, Methot J, et al. Immune responses to intramuscular administration of alipogene tiparvovec (AAV1-LPL(S447X)) in a phase II clinical trial of lipoprotein lipase deficiency gene therapy. *Hum Gene Ther*. (2014) 25:180–8. doi: 10.1089/hum.2013.169
222. Zolotukhin S, Byrne BJ, Mason E, Zolotukhin I, Potter M, Chesnut K, et al. Recombinant adeno-associated virus purification using novel methods improves infectious titer and yield. *Gene Ther*. (1999) 6:973–85. doi: 10.1038/sj.gt.3300938
223. Grieger JC, Choi VW, Samulski RJ. Production and characterization of adeno-associated viral vectors. *Nat Protoc*. (2006) 1:1412–28. doi: 10.1038/nprot.2006.207
224. Grieger JC, Soltys SM, Samulski RJ. Production of recombinant adeno-associated virus vectors using suspension HEK293 cells and continuous harvest of vector from the culture media for GMP FIX and FLT1 clinical vector. *Mol Ther*. (2016) 24:287–97. doi: 10.1038/mt.2015.187
225. Adamson-Small L, Potter M, Byrne BJ, Clement N. Sodium chloride enhances recombinant adeno-associated virus production in a serum-free suspension manufacturing platform using the herpes simplex virus system. *Hum Gene Ther Methods*. (2017) 28:1–14. doi: 10.1089/hgtb.2016.151
226. Smith RH, Levy JR, Kotin RM. A simplified baculovirus-AAV expression vector system coupled with one-step affinity purification yields high-titer rAAV stocks from insect cells. *Mol Ther*. (2009) 17:1888–96. doi: 10.1038/mt.2009.128
227. Dutheil N, Smith SC, Agundez L, Vincent-Mistiaen ZI, Escalante CR, Linden RM, et al. Adeno-associated virus Rep represses the human integration site promoter by two pathways that are similar to those required for the regulation of the viral p5 promoter. *J Virol*. (2014) 88:8227–41. doi: 10.1128/jvi.00412–14
228. Kalimuthu S, Oh JM, Gangadaran P, Zhu L, Lee HW, Jeon YH, et al. Genetically engineered suicide gene in mesenchymal stem cells using a Tet-On system for anaplastic thyroid cancer. *PLoS ONE*. (2017) 12:e0181318. doi: 10.1371/journal.pone.0181318
229. Li JM, Kao KC, Li LF, Yang TM, Wu CP, Horng YM, et al. MicroRNA-145 regulates oncolytic herpes simplex virus-1 for selective killing of human non-small cell lung cancer cells. *Virol J*. (2013) 10:241. doi: 10.1186/1743–422x-10–241
230. Norgren RB Jr. Lehman MN. Herpes simplex virus as a transneuronal tracer. *Neurosci Biobehav Rev*. (1998) 22:695–708.
231. Majima T, Funahashi Y, Takai S, Goins WF, Gotoh M, Tyagi P, et al. Herpes simplex virus vector-mediated gene delivery of poreless TRPV1 channels reduces bladder overactivity and nociception in rats. *Hum Gene Ther*. (2015) 26:734–42. doi: 10.1089/hum.2015.026

232. Campadelli-Fiume G, Petrovic B, Leoni V, Gianni T, Avitabile E, Casiraghi C, et al. Retargeting strategies for oncolytic herpes simplex viruses. *Viruses*. (2016) 8:63. doi: 10.3390/v8030063
233. Lou W, Ji F, Fu J, Han Z, Di W, Zhang N. Transcriptional retargeting of herpes simplex virus for cell-specific replication to control cancer. *J Cancer Res Clin Oncol*. (2018) 144:2107. doi: 10.1007/s00432–017-2566–4
234. Uchida H, Hamada H, Nakano K, Kwon H, Tahara H, Cohen JB, et al. Oncolytic herpes simplex virus vectors fully retargeted to tumor-associated antigens. *Curr Cancer Drug Targets*. (2018) 18:162–70. doi: 10.2174/1568009617666170206105855
235. Wolfe D, Craft AM, Cohen JB, Glorioso JC. A herpes simplex virus vector system for expression of complex cellular cDNA libraries. *J Virol*. (2010) 84:7360–8. doi: 10.1128/jvi.02388–09
236. Hoban MD, Orkin SH, Bauer DE. Genetic treatment of a molecular disorder: gene therapy approaches to sickle cell disease. *Blood*. (2016) 127:839–48. doi: 10.1182/blood-2015–09-618587
237. De Ravin SS, Wu X, Moir S, Anaya-O'Brien S, Kwatemaa N, Littel P, et al. Lentiviral hematopoietic stem cell gene therapy for X-linked severe combined immunodeficiency. *Sci Transl Med*. (2016) 8:335ra57. doi: 10.1126/scitranslmed.aad8856
238. Counsell JR, Asgarian Z, Meng J, Ferrer V, Vink CA, Howe SJ, et al. Lentiviral vectors can be used for full-length dystrophin gene therapy. *Sci Rep*. (2017) 7:44775. doi: 10.1038/srep44775
239. Brown BD, Venneri MA, Zingale A, Sergi Sergi L, Naldini L. Endogenous microRNA regulation suppresses transgene expression in hematopoietic lineages and enables stable gene transfer. *Nat Med*. (2006) 12:585–91. doi: 10.1038/nm1398
240. Schambach A, Bohne J, Baum C, Hermann FG, Egerer L, von Laer D, et al. Woodchuck hepatitis virus post-transcriptional regulatory element deleted from X protein and promoter sequences enhances retroviral vector titer and expression. *Gene Ther*. (2006) 13:641–5. doi: 10.1038/sj.gt.3302698
241. Schott JW, Morgan M, Galla M, Schambach A. Viral and Synthetic RNA vector technologies and applications. *Mol Ther*. (2016) 24:1513–27. doi: 10.1038/mt.2016.143
242. Breitbart M, Rohwer F. Here a virus, there a virus, everywhere the same virus? *Trends Microbiol*. (2005) 13:278–84. doi: 10.1016/j.tim.2005.04.003
243. Carding SR, Davis N, Hoyles L. Review article: the human intestinal virome in health and disease. *Aliment Pharmacol Ther*. (2017) 46:800–15. doi: 10.1111/apt.14280
244. Chattopadhyay S, Sen GC. Tyrosine phosphorylation in Toll-like receptor signaling. *Cytokine Growth Factor Rev*. (2014) 25:533–41. doi: 10.1016/j.cytogfr.2014.06.002
245. Chattopadhyay S, Sen GC. RIG-I-like receptor-induced IRF3 mediated pathway of apoptosis (RIPA): a new antiviral pathway. *Protein Cell*. (2017) 8:165–8. doi: 10.1007/s13238–016-0334-x
246. Chattopadhyay S, Sen GC. dsRNA-activation of TLR3 and RLR signaling: gene induction-dependent and independent effects. *J Interferon Cytokine Res*. (2014) 34:427–36. doi: 10.1089/jir.2014.0034
247. Fensterl V, Chattopadhyay S, Sen GC. No love lost between viruses and interferons. *Annu Rev Virol*. (2015) 2:549–72. doi: 10.1146/annurev-virology-100114–055249
248. Subramanian G, Kuzmanovic T, Zhang Y, Peter CB, Veleeparambil M, Chakravarti R, et al. A new mechanism of interferon's antiviral action: Induction of autophagy, essential for paramyxovirus replication, is inhibited by the interferon stimulated gene, TDRD7. *PLoS Pathog*. (2018) 14:e1006877. doi: 10.1371/journal.ppat.1006877
249. Stolberg SG. The biotech death of Jesse Gelsinger. *N Y Times Mag*. (1999):136–40, 49–50.
250. Rodriguez-Gascon A, Del Pozo-Rodriguez A, Isla A, Solinis MA. Vaginal gene therapy. *Adv Drug Deliv Rev*. (2015) 92:71–83. doi: 10.1016/j.addr.2015.07.002
251. Suwanmanee T, Ferris MT, Hu P, Gui T, Montgomery SA, Pardo-Manuel de Villena F, et al. Toward Personalized Gene Therapy: Characterizing the Host Genetic Control of Lentiviral-vector-mediated hepatic gene delivery. *Mol Ther Methods Clin Dev*. (2017) 5:83–92. doi: 10.1016/j.omtm.2017.03.009

Disclaimer: The views expressed in this review article are those of the author(s) and do not reflect the official policy of the Department of Army, Department of Defense, or the U.S. Government.

Conflict of Interest Statement: The authors declare that that they have no affiliations with or involvement in any organization or entity with any financial interest (such as honoraria; educational grants; participation in speakers' bureaus; membership, employment, consultancies, stock ownership, or other equity interest; and expert testimony or patent-licensing arrangements), or non-financial interest (such as personal or professional relationships, affiliations, knowledge or beliefs) in the subject matter or materials discussed in this manuscript.

frontiers in Pharmacology

REVIEW
published: 24 April 2019
doi: 10.3389/fphar.2019.00373

The Analysis of Key Factors Related to ADCs Structural Design

Haichao Tang[1,2], Yan Liu[3], Zhaojin Yu[1,2], Mingli Sun[1,2], Lu Lin[1,2], Wensi Liu[1,2], Qiang Han[1,2], Minjie Wei[1,2] and Ying Jin[3]**

[1] Department of Pharmacology, School of Pharmacy, China Medical University, Shenyang, China, [2] Liaoning Engineering Technology Research Center for the Research, Development and Industrialization of Innovative Peptide Drugs, China Medical University, Shenyang, China, [3] Liaoning Research Institute of Family Planning, Shenyang, China

Antibody–drug conjugates (ADCs) have developed rapidly in recent decades. However, it is complicated to map out a perfect ADC that requires optimization of multiple parameters including antigens, antibodies, linkers, payloads, and the payload-linker linkage. The therapeutic targets of the ADCs are expected to express only on the surface of the corresponding target tumor cells. On the contrary, many antigens usually express on normal tissues to some extent, which could disturb the specificity of ADCs and limit their clinical application, not to mention the antibody is also difficult to choose. It requires to not only target and have affinity with the corresponding antigen, but it also needs to have a linkage site with the linker to load the payloads. In addition, the linker and payload are indispensable in the efficacy of ADCs. The linker is required to stabilize the ADC in the circulatory system and is brittle to release free payload while the antibody combines with antigen. Also, it is a premise that the dose of ADCs will not kill normal tissues and the released payloads are able to fulfill the killing potency in tumor cells at the same time. In this review, we mainly focus on the latest development of key factors affecting ADCs progress, including the selection of antibodies and antigens, the optimization of payload, the modification of linker, payload-linker linkage, and some other relevant parameters of ADCs.

Keywords: antibody–drug conjugates, precision choice antibody and antigen, elaborate modification linkers, proper payloads, optimized linker-payload linkage

OPEN ACCESS

Edited by:
Zhe-Sheng Chen,
St. John's University, United States

Reviewed by:
Xiaolan Deng,
Beckman Research Institute of City of Hope, United States
Liwu Fu,
Sun Yat-sen University, China
Zhaoqian Liu,
Xiangya Hospital, Central South University, China

****Correspondence:***
Minjie Wei
weiminjiecmu@163.com
Ying Jin
13998830123@139.com

Specialty section:
This article was submitted to Cancer Molecular Targets and Therapeutics, a section of the journal Frontiers in Pharmacology

Received: *17 January 2019*
Accepted: *26 March 2019*
Published: *24 April 2019*

Citation:
Tang H, Liu Y, Yu Z, Sun M, Lin L, Liu W, Han Q, Wei M and Jin Y (2019) The Analysis of Key Factors Related to ADCs Structural Design. Front. Pharmacol. 10:373. doi: 10.3389/fphar.2019.00373

INTRODUCTION

In traditional tumor treatment, chemotherapy is one of the main treatment strategies. However, the toxicity from non-specific accumulation in normal tissues, narrow therapeutic window and low tolerance all limit chemotherapy drug development in the tumor treatment process (Atkins and Gershell, 2002; Alley et al., 2010; Ashley et al., 2011). In recent decades, scientists have gained an in-depth understanding of cancer biology, taking advantage of some unique features

Abbreviations: ADCs, antibody–drug conjugates; ALCL, anaplastic large cell lymphoma; AML, acute myeloid leukemia; DAR, drug-to-antibody ratio; MDR, multiple drug resistance; MMAE, monomethyl auristatin E; PDBs, pyrrolobenzodiazepine dimers; PEG, polyethylene glycol; PHF, hydroxymethyl-formal; SMCC, succinimidyl-4-(*N*-maleimidomethyl)-cyclohexane-1-carboxylate; SMCC-DM1, succinimidyl 4-(*N*-maleimidomethyl) cyclohexane-1-carboxylate-maytansinoid; sulfo-SPDB-DM4, *N*-succinimidyl-4-(2-pyridyldithio)-2-sulfo butanoate-maytansinoid; val-cit-PABC-MMAF, valine-citrulline-p-aminobenzyl-carbamate-monomethyl auristatin F.

of tumor cells to transform cancer treatment from previous chemotherapy drugs to tumor-targeted therapies. Monoclonal antibodies and polypeptides which bind to specific markers on the tumor cell's surface provide targeted therapeutic approaches and are both less toxic. However, whether they are monoclonal antibodies or peptides, they both lack potency in killing tumor cells.

The treatment strategy of antibodies armed with toxins to selectively kill target cells was first proposed in 1970 (Moolten and Cooperband, 1970). The tumor-targeting drug conjugates integrate targeted biomolecules with therapeutic small molecule toxins to specifically recognize the tumor tissues and kill the tumor cells, thereby improving the therapeutic index of the toxins and the insufficient efficacy of antibodies or peptides. The tumor-targeting drug conjugates mainly compose of ADCs that generally couple antibodies which specifically recognize the surface antigens of tumor cells with chemical toxins which effectively kill tumor tissues through linkers, and ADCs exert killing activity by bringing the chemical toxins into the tumor cells. In general, the antibody specifically binds to the tumor cell surface antigen, and the antigen mediates the endocytosis of the ADC and then releases free toxins (**Figure 1**), but the downsides are that immunogenicity, poor internalization and the instability of the linker give rise to insecurity and ineffectiveness (Chari, 2008). More than 60 ADCs have been in the process of clinical development until 2016 (Carter and Lazar, 2017), there are almost 204 ADCs (**Supplementary Table S1**) that aim for cancer in clinical development by 2018, including at least nine of which have entered phases III and IV clinical trials[1]. It indicates that ADCs are coming to the center-stage of research field in recent years especially in North America (**Figure 2**). However, until today, only ado-trastuzumab emtansine (T-DM1, Kadcyla[@]) and brentuximab vedotin (Adcetris[@]) are approved by FDA and on the market (Mullard, 2013; Thomas et al., 2016). There are many reasons for the dilemma, including the complexity of the composition of the ADC itself, and the fact that the tumor microenvironment or physiological conditions in animals are different from the human so that the evaluation of ADC efficacy by animal models is not applicable to humans. Beck et al. (2017) published a review paper about the strategies and challenges for the next generation of ADCs in 2017. However, ADCs are developing rapidly and some novel technologies may bring new considerations. Thus, this review mainly focuses on imperative factors that are associated with ADC efficacy (**Figure 3**).

THE SELECTION OF ANTIBODY AND ANTIGEN

Normally, the antigen specific to the cancer cell should be a priority after determining the indications for ADC. Ideally, the antigen should express highly and homogeneously on the surface of the cancer cells (Sievers and Senter, 2013; Damelin et al., 2015). When the antibody combines with the antigen specifically, the antibody-antigen complex should be internalized by antigen-mediated endocytosis, and then the free payloads are released through lysosomal trafficking. As a result, the payloads are concentrated in cancer cells and exert the cytotoxic effect (Erickson et al., 2006). Currently, the predominant therapeutic limitations are the ineffectiveness and the off-target toxicities of ADCs, which are caused by the finite internalization and the low expression of antigens to some extent. Therefore, some researchers came up with some approaches to counteract these problems such as utilizing the anti-tumor angiogenesis antibody, non-internalizing ADC, or bispecific antibody.

The Utilization of Anti-tumor Angiogenesis Antibody

Some researchers proposed a strategy that using an anti-tumor angiogenesis ADC to selectively kill cancer cells due to the process without the involvement of internalization, which could improve the deficient efficacy caused by finite internalization. For example, Palumbo et al. (2011) reported that the ADC composes of an anti-angiogenesis LC19 antibody to selectively target to the tumor blood vessels, the strategy showed a long-term anti-tumor effect. However, ADCs of the anti-tumor vessel may elicit off-target toxicities to normal tissues due to non-specificity of antigen expression and resistance of vessel co-option in some particular tumor tissues (Kuczynski et al., 2016). This requires choosing antibodies based on proper antigens. Seaman et al. (2017) applied the anti-CD276 antibody to the ADC to improve the non-specificity. The CD276 expresses in angiogenic tumor vessel, existed vasculature and tumor cells. Moreover, the anti-CD276 antibody is capable of identifying the normal and pathological angiogenesis. The anti-CD276 ADC evaded the vessel co-option and displayed a dual-targeting ability thus displaying effective anti-tumor activity (Seaman et al., 2017).

Preparing Non-internalizing ADCs

An approach to prepare non-internalizing ADCs to target corresponding antigens needed to be developed. For instance, the ADC took advantage of a diabody without an Fc region to target the matching antigen and an additional chemical activator to cut the linker, and then release the free payload to penetrate into tumor cells (Rossin et al., 2018). This strategy is able to increase the anti-tumor activity and avoid some factors can sacrifice the efficacy of ADCs such as interstitial pressure and epithelial barriers from the tumor cells.

The Selection of the Bispecific Antibody

On one hand, in terms of the deficiency of internalization, Li et al. (2016) used a bispecific antibody to target two non-overlapping epitopes of one antigen, which increased the affinity between antibody and antigen. For example, an anti-HER2 biparatopic antibody displayed better internalization, lysosomal trafficking, and degradation of the antibody-antigen complex relative to the traditional T-DM1 (Li et al., 2016). However, the superior affinity also may trigger a controversy about whether the biparatopic ADC would induce on-target toxicities to healthy tissues. Though this study also further indicated that the biparatopic ADC has an acceptable safety profile due to the threshold of antigen.

[1]https://clinicaltrials.gov

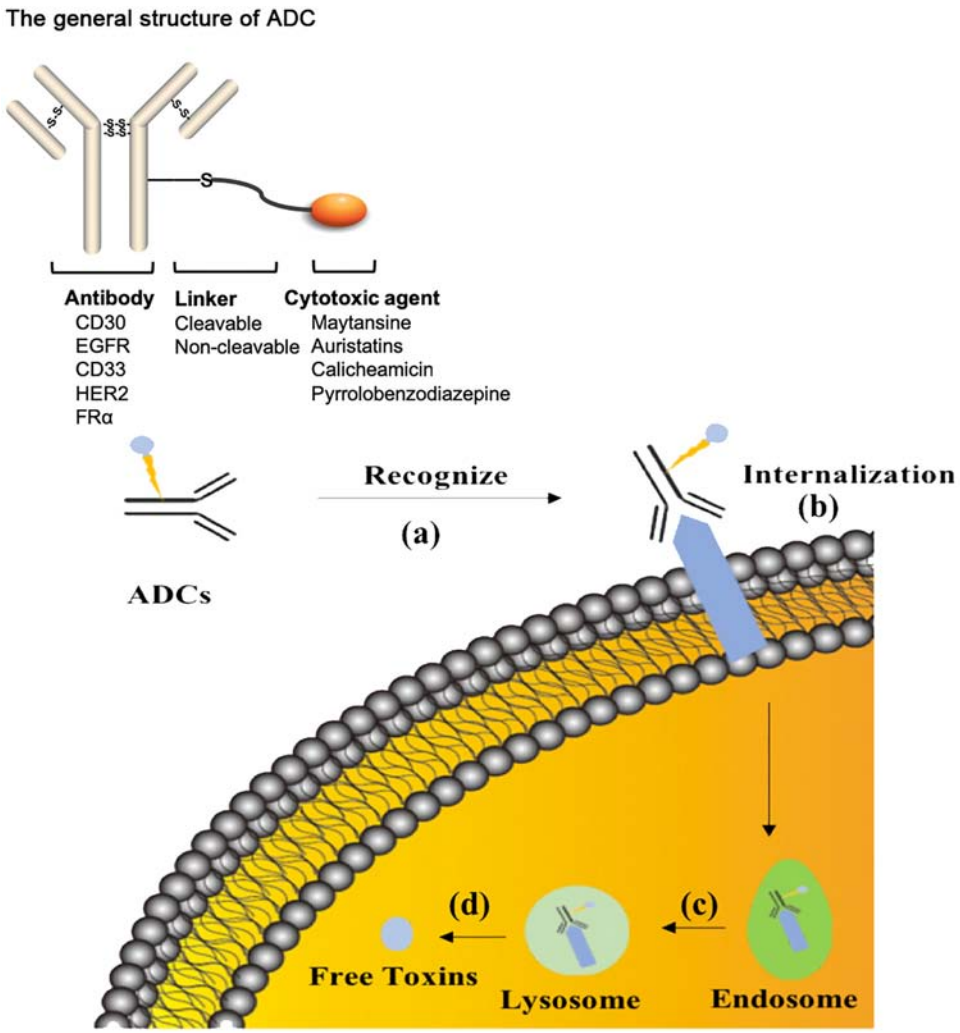

FIGURE 1 | The process of ADCs exerting activity. **(a)** ADCs specifically recognize cancer-associated antigens in the blood system. **(b)** ADCs are internalized into tumor cells during the formation of antibody-antigen complex. **(c)** ADCs are normally transported to lysosome from endosome. **(d)** The linker or antibody are broken in the lysosome conditions to release free toxins. ADCs, antibody drug conjugates.

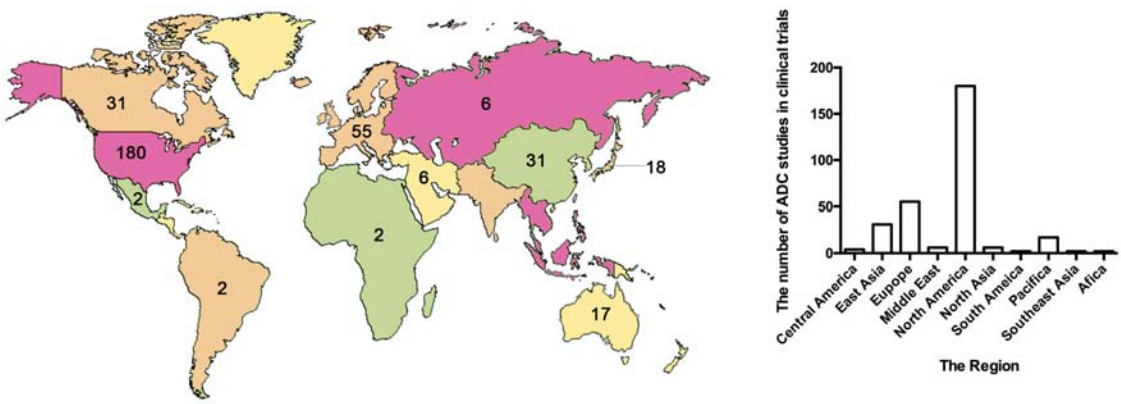

FIGURE 2 | The map and statistical graph depict regions where developed antibody–drug conjugates. The numbers in the figure indicate the amounts of ADCs in the clinical phase of the region. The data comes from ClinicalTrials.gov.

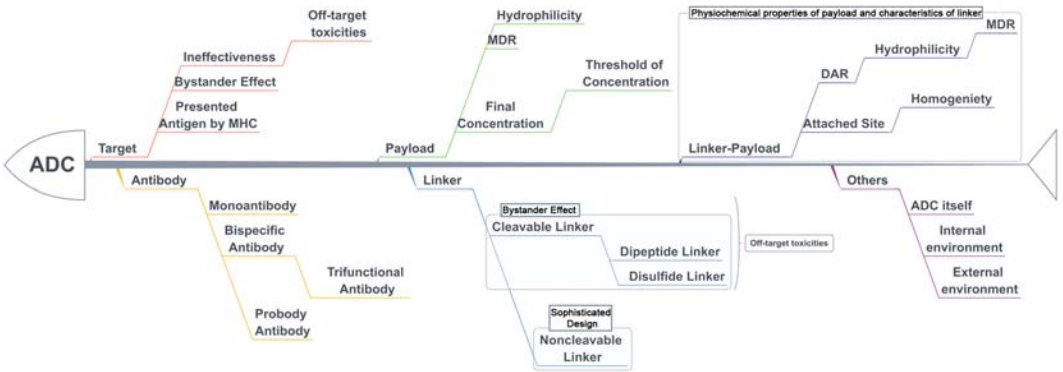

FIGURE 3 | The key parameters associated with efficacy and toxicities with ADCs.

It is unable to form the antibody-antigen complex if the expression level of antigen below the threshold. However, it seems arduous to avoid the problem due to the uncertain threshold. Theoretically, a higher affinity antigen–antibody could make more ADC molecules combine with tumor cells thus having more accumulation, but a lower affinity may allow ADCs to penetrate into tumor cells more effectively. Scientists are still looking for antigen–antibody with proper affinity (Rudnick et al., 2011). It needs further research (Tsumura et al., 2018).

Also, some researchers proposed to use the probody of antibody to solve the on-target toxicities, which may also be applied to ADCs. This strategy used masking peptide to cover up the active sites of the antibody then hydrolysis of the shelter to expose the antibody to target cancer tissues to exert activity (Desnoyers et al., 2013), which allays the indistinct recognition of ADCs in the blood circulation.

On the other hand, the bispecific antibody is able to selectively bind two distinct antigens on a cancer cell to avoid the off-target toxicities. For example, the bispecific antibody simultaneously targets the HER2 and PRLR double positive ($HER2^+/PRLR^+$) breast cancer cells to enhance the internalization and activity of the ADC, and to decrease the off-target toxicities to the healthy cells (Andreev et al., 2017). Nevertheless, targeting double-antigens is ineligible for most heterogeneous tumor cells, since it may trigger their escape mechanism. Furthermore, the bispecific antibody could be used to target the immunosuppressive molecule and tumor-specific antigen on the tumor cells simultaneously to improve the efficacy of ADC. The ADC targeting CD47 that an immunosuppressive receptor and TAA double positive ($CD47^+/TAA^+$) tumor cells could block the immunosuppression to augment the killing activity of the ADC (Dheilly et al., 2017). Currently, there are more than 70 bispecific antibodies applied in clinical trials (see text footnote 1), two of them have used on the market. These specific antibodies seem to change some imperfect phenomena of ADCs (Piccione et al., 2015). Moreover, the trifunctional antibody also could be used to ADC (Krishnamurthy and Jimeno, 2018), which possess an arm to target the tumor cells, the second is used to target T cells, the remaining Fc region to recruit some immune cells. Using the trifunctional antibody to link a small molecule toxin seems to improve the deficient specificity and the killing potency of ADCs. Though the bispecific or trifunctional prospect is promising to improve potency and specificity to increase market competitiveness of ADCs, the challenge of determining the target combination still remains.

The Bystander Effect to Heterogeneous Tumors

Some reports also demonstrated that some ADCs may take advantage of the physical and chemical properties of linkers and the microenvironment of the tumor to release free payloads to kill those adjacent negative-antigen cancer cells. The process is the bystander effect (Kovtun et al., 2006; Okeley et al., 2010). ADC was metabolized to release uncharged and membrane-permeable toxic metabolites after being internalized in positive-antigen cancer, which is able to kill adjacent antigen-negative cancer cells by membrane-penetration (Kellogg et al., 2011). This has a great significance for some heterogeneous tumor cells. Admittedly this was that the bystander effect may also cause non-specific killing of normal cells. Therefore, it requires to have rational selection and design of payloads and linkers based on the target to avoid the adverse effects from bystander effect.

The Selection of Antibody Isotype

Within IgG isotypes, IgG1, IgG2, IgG4 have been used to develop therapeutics, but IgG3 isotypes are not used as therapeutics owing to a significantly faster clearance rate (Jefferis, 2007). Further, most ADCs use IgG1 isotype currently (Beck et al., 2017). IgG1 isotype may exert ADCC (antibody-dependent cell-mediated cytotoxicity) and CDC (complement-dependent cytotoxicity) to improve ADCs activity further, whereas IgG2 and IgG4 are typically deficient in their effector functions (Salfeld, 2007). However, the PD-1 antibodies (Nivolumab and Pembrolizumab) used IgG4 isotype, which may be due to the PD-1 antibody only needing to block the interaction between PD-1 and PD-L1

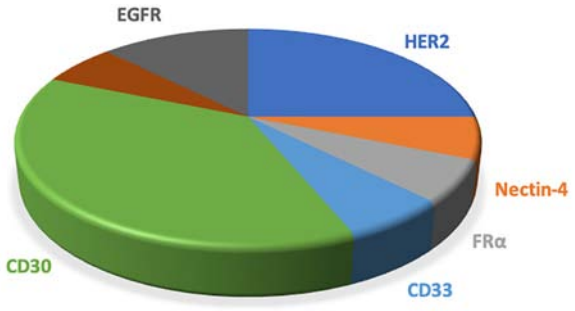

FIGURE 4 | The pie chart shows the antigens applied to the clinical phase III/IV trials of ADCs. ADCs, antibody drug conjugates; MDR, multiple drug resistance; DAR, drug-to-antibody ratio.

to increase immune system function to produce anti-tumor activity, which is needed to avoid the toxicity to T cells from ADCC and CDC. Therefore, the choice of isotype also needs careful consideration.

The Consideration of Antigen

Glycosylation of antigen also could affect the design of ADCs. On the one hand, if glycosylated antigen specifically exists on the tumor cell surface, it will have an important implication to be a target of an ADC. For example, a monoclonal antibody targeting glycosylated PD-L1 (gPD-L1) to disrupt PD-L1/PD-1 interaction. The gPD-L1 is mainly expressed on tumor tissues, which improves non-specific expression of PD-L1 in some immune cells to limit toxicity (Li et al., 2018). On the other hand, the steric structure of a glycosylated antigen plays a certain protective role, which will block the interaction between the antibody and specific sites on the antigen surface. Therefore, we need to have a more comprehensible understanding on designing ADCs.

Most ADCs utilize the antigens on the tumor cells surface, which are limited in their specificity relative to intracellular antigens. Taking advantage of the antigen presentation feature of MHC that caused tumor-specific endogenous antigen expression on the cell surface overcomes the inaccessibility of intracellular antigens. Further, the MHC-I/peptide complex is recognized by the ADCs that mimic the characterization of TCR, which will produce superior specificity and potency (Lai et al., 2018). **Table 1** and **Figure 4** showed the antigens used in phase III/IV trial currently (see text footnote 1).

THE SELECTION OF PAYLOADS

Once the target is determined, the proper choice of payload becomes a critical part of ADC. The final potency of ADCs mainly depends on the concentration of payloads in tumor cells; thus some researchers are dedicated on improving the DAR of ADCs to increase the accumulation of drugs in tumor cells. Zhang et al. (2018b) indicated that activity of the ADC still remains constant though augmenting the payload concentration, and this also could magnify the toxicity to normal tissues at the same time. This suggests that the threshold of payload concentration also needs consideration. In summary, choosing the applicable payloads and designing the appropriate DAR is important for the final concentration of the payloads in tumor cells.

Improving the Efficacy of ADCs

Early ADCs used drugs that have been approved for clinical use such as vinblastine and doxorubicin, but the low clinical activity of these drugs resulted in suboptimal ADCs efficiency. Some cytotoxins were too toxic to be non-target agents in clinical application, but they seemed to be more promising as payloads for ADCs. At present, the dose of the payloads in tumor cells is required to be the picomolar range to kill these cancer cells (Chari et al., 2014). Also, payloads must possess acceptable solubility and decent sites to react with linkers. These all limited the selection of payloads. Currently, most payloads are derivatives of the microtubule inhibitor family, such as the auristatin and maytansine (Beck and Reichert, 2014). Brentuximab vedotin (Adcetris[@]), approved by FDA in 2011, composes of MMAE and cAC10 mAb (chimeric IgG1 antibody) via a protease-cleavable dipeptide linker to target tumor antigen CD30 (also known as TNFRSF8) for the treatment of Hodgkin's lymphoma and ALCL (ki-1 lymphoma) (Senter and Sievers, 2012; Younes et al., 2012). Ado-trastuzumab emtansine (Kadcyla[@]), approved in 2013, consists of a stable thioether linker (SMCC) attached to trastuzumab (anti-human epidermal growth factor receptor-2 antibody, anti-HER2 antibody) and DM1 (maytansine derivative) for the treatment of advanced breast cancer (Lambert and Chari, 2014). Both adopted the microtubule inhibitor family as payloads, yet auristatins and maytansines are only able to exert activity in cell proliferation and they are hydrophobic, which will disturb their activity. Thus, some novel payloads or the original payload structural modifications such as the improvement of hydrophilicity will become the hotspots of the future payload research (Burke et al., 2017). At present, some novel ADCs have better activity and have been through clinical phase III/IV (**Table 1**).

The first commercially available ADC was gemtuzumab ozogamicin (GO) that consists of calicheamicins which damage DNA (Walker et al., 1992) for the treatment of AML. However, GO showed no significant improvement in overall survival (OS) compared with the calicheamicin agent alone, and had a higher mortality rate and was recalled in 2010 (Petersdorf et al., 2013; Kharfan-Dabaja, 2014). This is because calicheamicin is hydrophobic in that almost only 50% could be conjugated, and only approximately 50% of free drugs are eventually released in the conjugated drugs (Beck et al., 2010; Senter and Sievers, 2012), resulting in a significant decrease in potency. To overcome these limitations, some novel targeted DNA agents have been broadly developed. Pyrrolobenzodiazepine dimers (PBDs) have already become a new choice, it may attach to the linker that conjugated to the antibody, and has the ability to overcome MDR relative to the commonly used calicheamicin as a substrate of *P*-glycoprotein (Kung Sutherland et al., 2013; Stein et al., 2018). The IMGN779 (NCT02674763) utilized DGN462 that a novel drug with DNA-alkylating activity also demonstrated better anti-tumor activity and tolerability (Kovtun et al., 2018).

TABLE 1 | Current clinical phase III/IV trials of ADCs.

NCT number	Name	Conditions	Payloads	Target
NCT03523585	DS-8201a	Breast cancer	Topoisomerase I inhibitor	HER2
NCT03734029	DS-8201a	Breast cancer	topoisomerase I inhibitor	HER2
NCT03529110	DS-8201a	Breast cancer	topoisomerase I inhibitor	HER2
NCT03262935	SYD985	Metastatic breast cancer	DUBA	HER2
NCT03474107	Enfortumab vedotin	Ureteral cancer| urothelial cancer| bladder cancer	MMAE	Nectin-4
NCT02631876	Mirvetuximab soravtansine (IMGN853)	Epithelial ovarian cancer| primary peritoneal carcinoma| fallopian tube cancer| ovarian cancer	DM4	FRα
NCT02785900	Vadastuximab talirine (SGN-CD33A; 33A)	Acute myeloid leukemia	PBD	CD33
NCT01990534	Brentuximab Vedotin	Hodgkin lymphoma	MMAE	CD30
NCT03677596	Inotuzumab ozogamicin	Leukemia| precursor b-cell lymphoblastic leukemia-lymphoma| acute lymphoblastic leukemia	Calicheamicins	CD22
NCT02573324	Depatuxizumab mafodotin (ABT-414)	Glioblastoma	MMAF	EGFR
NCT01100502	Brentuximab vedotin (SGN-35)	Disease, Hodgkin	MMAE	CD30
NCT01777152	Brentuximab vedotin	Anaplastic large-cell lymphoma| non-Hodgkin lymphoma| T-cell lymphoma	MMAE	CD30
NCT01909934	Brentuximab vedotin	Anaplastic large-cell lymphoma	MMAE	CD30
NCT03419403	Depatuxizumab mafodotin (ABT-414)	Glioblastoma multiforme	MMAF	EGFR
NCT01712490	Brentuximab vedotin	Hodgkin lymphoma	MMAE	CD30
NCT02166463	Brentuximab vedotin	Hodgkin lymphoma	MMAE	CD30

DUBA, duocarmycin-hydroxybenzamide-azaindole; MMAE, monomethyl auristatin E; MMAF, monomethyl auristatin F; DM4, maytansine 4; PBD, pyrrolobenzodiazepine dimers.

Avoiding MDR

The MDR has always been a barrier and one of the important factors affecting the therapeutic effect in the cancer treatment. The MDR is still an impeditive factor of using ADCs. This is because the essence of ADC's activity is that the payloads in tumor cells exert cytotoxicity, and these payloads may be affected by MDR. Many studies concentrate on the modification of drug-linker that, by increasing hydrophilicity, circumvents MDR caused by the overexpression of efflux pumps because the substrates of MDR1 were hydrophobic in general. Moreover, some novel payloads such as PBD, DGN462, and tubulysins cooperate with ADCs to display better anti-tumor activity in MDR^+ tumor cells (Burke et al., 2018; Kovtun et al., 2018; Stein et al., 2018). ADCs are susceptible to hydrophobicity to be insensible to MDR^+ cells, thereby it is essential to improve the hydrophilicity to escape from MDR to increase the activity of ADCs (Kovtun et al., 2010).

THE MODIFICATION OF LINKER

Although the linker may be not directly correlated with the final potency of ADC (Lee et al., 2018b), the potency of ADC is dictated by the concentration of payload accumulated in tumor cells, and the payload release is determined by the stability of the linker. Thus, the linker is crucial for a perfect ADC, and it determines the stability, efficacy, and even the ability to overcome MDR. The basic requirement of the linker is to make the payload attach to the antibody, stabilize the payload in the circulation system, and is labile to release the free payload into cancer cells when the antigen–antibody complex is formed (Doronina et al., 2006). Currently, linkers are mainly divided into the cleavable linkers and the non-cleavable linkers.

The Comparison of Cleavable Linkers With Non-cleavable Linkers

The cleavable linkers normally take advantage of the difference of tumor microenvironment and normal physiological environment to release the payloads that may be membrane-permeable and can produce the bystander effect. The non-cleavable linkers need to meet the requirement that the antibody and linker must be disconnected after the formation of the antigen–antibody complex enter the lysosomal trafficking. This may cause the bystander effect that is a passive transport process to weaken, caused by the membrane-impermeability

of linker-payloads connected with polar amino acids. Both types of linkers have their advantages and disadvantages, which are applied to the clinical trials (Chari et al., 2014; Bialucha et al., 2017). However, about 2/3 ADCs used cleavable linkers in the current clinical trials (Lambert and Berkenblit, 2018), in which mainly are dipeptide linkers and disulfide linkers. The non-cleavable linkers are not only more stable to escape from the off-target toxicities than cleavable linkers (Lu et al., 2016), but also may overcome the barrier of multiple-drug resistance (MDR) (Shefet-Carasso and Benhar, 2015; Beck et al., 2017; Nasiri et al., 2018) for the reason that the payload connected with polar amino cannot be a substrate of MDR1, which will improve the MDR phenomenon. However, the non-cleavable linkers need a more elaborate process to produce activity such as the internalization and metabolism of the antibody in the lysosome, which is a prerequisite to release active payloads to exert killing activity (Rosenberg, 2006; Lambert and Berkenblit, 2018), and the polar amino-linker-payload also needs a distinct transporter to carry it from the lysosome to cytoplasm to work (Hamblett et al., 2015; Kinneer et al., 2018; Lee et al., 2018b), which makes the design of ADC more complex to limit the utilization of non-cleavable linkers. The cleavable linkers are more vulnerable to lead to off-target toxicities, but the process of exerting effects is more comprehensible thus researchers are dedicated to modifying the cleavable linkers to overcome their weakness and to increase their stability in the circulation (Sanderson et al., 2005; Kellogg et al., 2011).

The Analysis of Cleavable Linkers

The cleavable linker can metabolize some cell-permeable metabolites to exert the bystander killing effect. The cleavable sulfo-SPDB-DM4 linker produced cell-permeable catabolites to display a better activity than non-cleavable SMCC-DM1 linker (Bialucha et al., 2017). Also, the application of the sulfonate group improved hydrophilicity to increase the exposure of ADC to the antigen to promote killing activity. The brentuximab vedotin (SGN-35) took advantage of a cleavable dipeptide linker to release free MMAE, and the MMAE may permeate adjacent cells to exert killing activity which is important to some heterogeneous tumor cells. Moreover, the dipeptide linker offers ADC better stability in the circulation, and is more specific to tumor cells (Katz et al., 2011). The protease cleavage pathway is not restricted to cathepsin B, various cysteine cathepsins can cleavage the dipeptide linker, such as cysteine cathepsins B, K, L, and S. It seems to explain why the dipeptide linkers cannot be insensitive to tumors, caused by the insufficient expression of protease (Caculitan et al., 2017), which is one of the reasons why some protease-sensitive linkers are widely used by ADCs.

In particular, the design of the valine-citrulline (val-cit) linker, the most frequent in dipeptide linkers, needs to consider the connection to the phenol-containing payloads; diverse electron groups affect the degrees of immolation of the linker to influence the different potency of an ADC (Zhang et al., 2018a). However, the val-cit dipeptide linker is not conducive to preclinical research to appraise the efficacy of ADCs due to instability in mice (Dokter et al., 2014). Anami et al. (2018) reported a glutamic acid-val-cit linker replaced val-cit dipeptide linker, which could alleviate the flaw of instability in the mice plasma and retain the cathepsin-mediated cleavage mechanisms, thus boosting preclinical application of some ADCs. The acidic tripeptide linker could increase the polarity of ADCs to improve solubility to increase the therapeutic potency (Anami et al., 2018). However, one of the studies suggests that activity of the ADC with cleavable valine-citrulline-p-aminobenzyl-carbamate-monomethyl auristatin F (val-cit-PABC-MMAF) is much less than the ADC with non-cleavable maleimidocaproyl-MMAF (Doronina et al., 2006), which may be due to the character of payloads rather than the linker. The metabolites of some payloads are more effective than the prototypes. The non-cleavable linkers are not widely applied to ADCs since many payload derivatives attached to an amino cannot satisfy the killing potency of ADCs.

The disulfide linker utilized the difference of glutathione (GSH) levels between the tumor microenvironment and the physiological environment of normal tissues to produce activity (Meister and Anderson, 1983; Dubikovskaya et al., 2008), which is more labile in tumoral hypoxia conditions (de Groot et al., 2001). At present, the main obstacle of the disulfide linker is the instability, which is mainly improved by increasing steric hindrance to relieve the vulnerability. ADCs using the disulfide linkers have inferior potency *in vivo* due to the more rapid clearance of payloads compared with the non-cleavable thioether linkers that displayed more potent activity (Lewis Phillips et al., 2008). The trastuzumab emtansine (T-DM1) consists of non-cleavable thioether linker and a maytansine derivate, which has better anti-breast cancer activity. The linker contained a cyclohexane carboxylate and a maleimidomethyl group. The ionized metabolite cannot kill surrounding normal cells due to its impermeability after ADC metabolized, thus the ADC has a better safety (LoRusso et al., 2011). The non-cleavable linkers are stricter in the choice of antigens compared with cleavable linkers, yet fewer toxicities (Polson et al., 2009). Zhang et al. (2016) reported that using methy- and cyclobutyl-substituted disulfide with efficient immolation demonstrated more potent killing activity than cyclopropyl-substituted disulfide with non-immolation. Also, this reflects that the immolation of the linker is imperative to the potency of ADC (Zhang et al., 2016). However, the anti-tumor activity is more determined by the cleavage of the linkers only when payloads require complete cleaving to exert activity (Caculitan et al., 2017). Thus, new research could focus on developing payloads that do not require the production of pharmacological effects with prototype drugs. Also, future studies could focus on developing some novel technologies of payload-linker to improve the activity of ADCs such as SYD985 based on a cleavable linker-duocarmycin payload (NCT03262935) (Dokter et al., 2014).

THE PAYLOAD-LINKER LINKAGE

With the development of ADCs, the drug-linker linkage that goes hand in hand with the efficacy of ADCs is more critical (Nasiri et al., 2018). In order to give full play to ADCs' activity in tumor cells, it is necessary to effectively design the payload-linker

according to the physicochemical properties of the payloads and the characteristics of the linkers.

The Consideration of the Sites of Payload-Linker

The sites of the payload-linker are essential conditions to consider due to the attaching-sites being correlated with homogeneity that is related to the therapeutic index. In the early stages of ADCs development, the lysine on the antibody was used as the site to attach the linker, which caused great heterogeneity. Later, Adcetris[@] used the cysteine that only eight free cysteines per antibody to link through disulfide bonds, which reduced the ADCs heterogeneity. In recent years, to ensure ADC homogeneity, researchers have developed some site-specific methods, such as THIOMAB (Junutula et al., 2008; Chudasama et al., 2016).

The Modification of Payload-Linker

The drug-linker linkage determines the DAR that are related to the efficacy of ADC. Generally, the therapeutic potency of ADC gradually increases *in vitro* with the increase of DAR whereas the therapeutic index *in vivo* decreases (Hamblett et al., 2004), which may due to with the enhancement of DAR accelerates the clearance of ADC which is closely related to the hydrophobicity of ADC (Lyon et al., 2015). The hydrophobicity is determined by the amounts of payloads per antibody and the design of drug-linker (Doronina et al., 2014). It is the main reason for the failure of ADC in the clinical application that the concentration of payload is deficient to treat tumors on account of the DAR of ADC in clinical stage generally control to 3.5–4 (Beck et al., 2017). Thus, augmenting the hydrophilicity of ADC with high DAR by the design of drug-linker exquisitely will improve the efficacy *in vivo* (Pabst et al., 2017). Some hydrophilic groups such as PEG or PHF may improve this dilemma. Accurately connecting these hydrophilic groups to a linker will effectively improve the efficacy of the ADCs. For example, Trastuzumab–PHF–Vinca ADC with DAR of 20 demonstrated a potent anti-tumor activity and decent pharmacokinetic profile due to the high hydrophilicity of PHF (Yurkovetskiy et al., 2015).

At the same time, MDR^+ tumor cells are insensible to some ADCs due to the fact that many payloads applied to ADCs are hydrophobic, which are the substrates of the MDR1 transporter. By improving the hydrophobicity of the drug-linker, it seems to be able to bypass MDR (Kovtun et al., 2010; Shefet-Carasso and Benhar, 2015).

OTHER PARAMETERS CORRELATED WITH THE EFFICACY OF ADCs

The Relationship Between the Internal Environment and Activity of ADCs

Normally, we consider the internalization that influences the efficacy of ADCs to be regulated by antigen. Recently, Lee et al. (2018a) demonstrated that the internalization may be mainly determined by the cellular environment rather than the antigen, which brought another hint that the development of the ADCs has to consider a variety of parameters besides the choice of target and the design of the linker. The characteristics of tumor cells also affect the activity of ADCs, including the endothelium, interstitial, and epithelial barriers which could limit ADCs uptake in the tumor, resulting in a small fraction of the injected dose reaching the desired tumor target (Perez et al., 2014). Intra-tumor distribution of ADCs also affects the anti-tumor efficacy (Tsumura et al., 2018).

Sometimes the efficacy of the ADCs does not have a positive correlation with the dose of the injection of ADCs. In addition to being interfered by the payload concentration threshold, the activity of ADCs could be affected by the saturation of the antigen–antibody combination, which causes the concentration of the ADCs in the circulation to be higher than the concentration of the corresponding receptors (Mager, 2006). Some antigens may shed from the tumor cells and circulate in the blood system to alleviate invalid combination with antibodies, which is also able to enhance the efficacy of ADCs (Pak et al., 2012). These internal factors seem to be imperative considerations when designing ADCs in the future.

The External Conditions Related to Activity of ADCs

Another point worth attention is the choice of assessment method of safety and efficacy of ADCs. Owing to the ADC subjects to some physical and chemical conditions such as storage conditions, which is able to cause degradation or aggregation of ADCs to influence the assessment of ADCs' activity (Mohamed et al., 2018). Therefore, the assessment method must be considered to some extent.

CONCLUSION AND PERSPECTIVE

With in-depth understandings of antibodies, linkers, and payloads, ADCs have also achieved great development. The linkage strategy and target diversity have already improved the delivery of the payloads to tumor tissues and reduced exposure to normal tissues. With the development of payloads, some novel potent payloads are used by ADCs, which allows researchers to exploit novel linkers to attach the antibody and payloads without disturbing their potency (Dragovich et al., 2018). Furthermore, some irrelevant antigen-target ADCs also may exert toxicity to tumor cells due to the vascular gap of tumors relative to the normal tissues, which is big enough to make ADCs penetrate into tumor cells (Cardillo et al., 2011), indicating the specific recognition of ADCs by tumor tissues on another aspect.

Some prodrug strategies also are used in ADCs design, which modified the toxic payloads to inactive prodrugs, then utilized self-immolation groups and took advantage of the intratumoral environment to reduce the prodrugs to prototype drugs to exert intrinsic activity (Pei et al., 2018). Moreover, nanoparticles combining with the strategy of ACD prodrugs could also increase the activity and circumvent MDR (Qi et al., 2017). The key issues of ADCs are optimization of the appropriate antibody,

the choice of proper antigen, the selection of high-activity cytotoxic payloads, stable linkage technology and optimization of DAR in future development. These strategies will improve the efficacy of ADCs that give them a larger market share to replace chemotherapy drugs in medical therapy in the future. At present, ADCs in clinical trials mainly focus on hematological tumors especially Hodgkin lymphoma, because the CD30 is an ideal target, overexpressed in Hodgin lymphoma consistently. With the deep investigation of the target, more ADCs to cure other types of cancer will expand to clinical applications. However, the development of ADCs is costly to make, marked by Adcetris[@] and Kadcyla[@] imposing more family burdens on patients.

In recent years, peptide-drug conjugates (PDCs) are also on the stage of targeted-drug conjugation therapy and are considered as part of ADCs. PDCs replace antibodies with peptides, which minimize the molecular weight to alleviate the reduction of tumor cell absorption caused by the larger molecular weight of the ADCs. Also, PDCs could possess better homogeneity due to the few of the attached sites of the peptides. The cost-effectiveness of PDCs is critical to alleviate the pressure on patients during treatment. However, PDCs also have some weaknesses that need to be improved. The vulnerability of PDCs in the blood system is a non-negligible obstacle, but it is difficult to improve half-life and reduce off-target toxicity by modifying structure of PDCs without destroying activity. Therefore, we must master more comprehensive knowledge to improve ADCs or PDCs. Whether used alone or in combination with other therapies, the toxicity of ADCs and PDCs must be better understood to adjust the therapeutic index based on the minimum effective dose of the drug in tumor cells and the maximum tolerated dose for normal tissues.

AUTHOR CONTRIBUTIONS

HT wrote the review manuscript. YL, ZY, MS, and WL modified the review. LL and QH edited the review including grammar. The correspondent authors MW and YJ provided the thought.

FUNDING

This work was supported by the National Natural Science Foundation of China and Liaoning Joint Fund Key Program (Grant No. U1608281), the National Natural Science Foundation of China (Grant Nos. 81601370 and 81673475), the Key Laboratory Foundation from Shenyang S&T Projects (Grant No. Z18-4-020), the National Key Research and Development Plan, Digital Diagnosis and Treatment Equipment Research and Development Key Special Project (Grant No. 2017YFC0114203), and the Liaoning Provincial Science and Technology Public Welfare Research Fund Project (Grant No. 20170030).

SUPPLEMENTARY MATERIAL

The Supplementary Material for this article can be found online at: https://www.frontiersin.org/articles/10.3389/fphar.2019.00373/full#supplementary-material

TABLE S1 | The ADCs of cancer therapy in clinical development.

REFERENCES

Alley, S. C., Okeley, N. M., and Senter, P. D. (2010). Antibody-drug conjugates: targeted drug delivery for cancer. *Curr. Opin. Chem. Biol.* 14, 529–537. doi: 10.1016/j.cbpa.2010.06.170

Anami, Y., Yamazaki, C. M., Xiong, W., Gui, X., Zhang, N., An, Z., et al. (2018). Glutamic acid-valine-citrulline linkers ensure stability and efficacy of antibody-drug conjugates in mice. *Nat. Commun.* 9:2512. doi: 10.1038/s41467-018-04982-3

Andreev, J., Thambi, N., Perez Bay, A. E., Delfino, F., Martin, J., Kelly, M. P., et al. (2017). Bispecific antibodies and antibody-drug conjugates (ADCs) bridging HER2 and prolactin receptor improve efficacy of HER2 ADCs. *Mol. Cancer Ther.* 16, 681–693. doi: 10.1158/1535-7163.mct-16-0658

Ashley, C. E., Carnes, E. C., Phillips, G. K., Padilla, D., Durfee, P. N., Brown, P. A., et al. (2011). The targeted delivery of multicomponent cargos to cancer cells by nanoporous particle-supported lipid bilayers. *Nat. Mater* 10, 389–397. doi: 10.1038/nmat2992

Atkins, J. H., and Gershell, L. J. (2002). Selective anticancer drugs. *Nat. Rev. Drug Discov.* 1, 491–492. doi: 10.1038/nrd842

Beck, A., Goetsch, L., Dumontet, C., and Corvaia, N. (2017). Strategies and challenges for the next generation of antibody-drug conjugates. *Nat. Rev. Drug Discov.* 16, 315–337. doi: 10.1038/nrd.2016.268

Beck, A., Haeuw, J. F., Wurch, T., Goetsch, L., Bailly, C., and Corvaia, N. (2010). The next generation of antibody-drug conjugates comes of age. *Discov. Med.* 10, 329–339.

Beck, A., and Reichert, J. M. (2014). Antibody-drug conjugates: present and future. *MABS* 6, 15–17. doi: 10.4161/mabs.27436

Bialucha, C. U., Collins, S. D., Li, X., Saxena, P., Zhang, X., Durr, C., et al. (2017). Discovery and optimization of HKT288, a Cadherin-6-Targeting ADC for the treatment of ovarian and renal cancers. *Cancer Discov.* 7, 1030–1045. doi: 10.1158/2159-8290.cd-16-1414

Burke, P., Hamilton, J., Jeffrey, S., Hunter, J., Doronina, S., Okeley, N., et al. (2017). Optimization of a PEGylated glucuronide-monomethylauristatin e linker for antibody-drug conjugates. *Mol. Cancer Ther.* 16, 116–123. doi: 10.1158/1535-7163.MCT-16-0343

Burke, P. J., Hamilton, J. Z., Pires, T. A., Lai, H. W. H., Leiske, C. I., Emmerton, K. K., et al. (2018). Glucuronide-linked antibody-tubulysin conjugates display activity in MDR+ and heterogeneous tumor models. *Mol. Cancer Ther.* 17, 1752–1760. doi: 10.1158/1535-7163.mct-18-0073

Caculitan, N. G., Dela Cruz Chuh, J., Ma, Y., Zhang, D., Kozak, K. R., Liu, Y., et al. (2017). Cathepsin B Is dispensable for cellular processing of cathepsin b-cleavable antibody-drug conjugates. *Cancer Res.* 77, 7027–7037. doi: 10.1158/0008-5472.can-17-2391

Cardillo, T. M., Govindan, S. V., Sharkey, R. M., Trisal, P., and Goldenberg, D. M. (2011). Humanized anti-Trop-2 IgG-SN-38 conjugate for effective treatment of diverse epithelial cancers: preclinical studies in human cancer xenograft models and monkeys. *Clin. Cancer Res.* 17, 3157–3169. doi: 10.1158/1078-0432.ccr-10-2939

Carter, P. J., and Lazar, G. A. (2017). Next generation antibody drugs: pursuit of the 'high-hanging fruit'. *Nat. Rev. Drug Discov.* 17, 197–223. doi: 10.1038/nrd.2017.227

Chari, R. V. (2008). Targeted cancer therapy: conferring specificity to cytotoxic drugs. *Acc. Chem. Res.* 41, 98–107. doi: 10.1021/ar700108g

Chari, R. V., Miller, M. L., and Widdison, W. C. (2014). Antibody-drug conjugates: an emerging concept in cancer therapy. *Angew Chem. Int. Ed. Engl.* 53, 3796–3827. doi: 10.1002/anie.201307628

Chudasama, V., Maruani, A., and Caddick, S. (2016). Recent advances in the construction of antibody-drug conjugates. *Nat. Chem.* 8, 114–119. doi: 10.1038/nchem.2415

Damelin, M., Zhong, W., Myers, J., and Sapra, P. (2015). Evolving strategies for target selection for antibody-drug conjugates. *Pharm. Res.* 32, 3494–3507. doi: 10.1007/s11095-015-1624-3

de Groot, F. M., Damen, E. W., and Scheeren, H. W. (2001). Anticancer prodrugs for application in monotherapy: targeting hypoxia, tumor-associated enzymes, and receptors. *Curr. Med. Chem.* 8, 1093–1122. doi: 10.2174/0929867013372634

Desnoyers, L. R., Vasiljeva, O., Richardson, J. H., Yang, A., Menendez, E. E., Liang, T. W., et al. (2013). Tumor-specific activation of an EGFR-targeting probody enhances therapeutic index. *Sci. Transl. Med.* 5:207ra144. doi: 10.1126/scitranslmed.3006682

Dheilly, E., Moine, V., Broyer, L., Salgado-Pires, S., Johnson, Z., Papaioannou, A., et al. (2017). Selective blockade of the ubiquitous checkpoint receptor cd47 is enabled by dual-targeting bispecific antibodies. *Mol. Ther.* 25, 523–533. doi: 10.1016/j.ymthe.2016.11.006

Dokter, W., Ubink, R., van der Lee, M., van der Vleuten, M., van Achterberg, T., Jacobs, D., et al. (2014). Preclinical profile of the HER2-targeting ADC SYD983/SYD985: introduction of a new duocarmycin-based linker-drug platform. *Mol. Cancer Therapeu.* 13, 2618–2629. doi: 10.1158/1535-7163.MCT-14-0040-T

Doronina, S. O., Mendelsohn, B. A., Bovee, T. D., Cerveny, C. G., Alley, S. C., Meyer, D. L., et al. (2006). Enhanced activity of monomethylauristatin F through monoclonal antibody delivery: effects of linker technology on efficacy and toxicity. *Bioconjug. Chem.* 17, 114–124. doi: 10.1021/bc0502917

Doronina, S. O., Setter, J. R., Bovee, T. D., Anderson, M. E., Jonas, M., Daniho, S., et al. (2014). Abstract 4470: Elucidating the role of drug-linker hydrophobicity in the disposition of antibody-drug conjugates. *Cancer Res.* 74, 4470–4470. doi: 10.1158/1538-7445.am2014-4470

Dragovich, P. S., Blake, R. A., Chen, C., Chen, J., Chuh, J., den Besten, W., et al. (2018). Conjugation of indoles to antibodies through a novel self-immolating linker. *Chemistry* 24, 4830–4834. doi: 10.1002/chem.201800859

Dubikovskaya, E. A., Thorne, S. H., Pillow, T. H., Contag, C. H., and Wender, P. A. (2008). Overcoming multidrug resistance of small-molecule therapeutics through conjugation with releasable octaarginine transporters. *Proc. Natl. Acad. Sci. U.S.A.* 105, 12128–12133. doi: 10.1073/pnas.0805374105

Erickson, H. K., Park, P. U., Widdison, W. C., Kovtun, Y. V., Garrett, L. M., Hoffman, K., et al. (2006). Antibody-maytansinoid conjugates are activated in targeted cancer cells by lysosomal degradation and linker-dependent intracellular processing. *Cancer Res.* 66, 4426–4433. doi: 10.1158/0008-5472.can-05-4489

Hamblett, K. J., Jacob, A. P., Gurgel, J. L., Tometsko, M. E., Rock, B. M., Patel, S. K., et al. (2015). SLC46A3 is required to transport catabolites of noncleavable antibody maytansine conjugates from the lysosome to the cytoplasm. *Cancer Res.* 75, 5329–5340. doi: 10.1158/0008-5472.can-15-1610

Hamblett, K. J., Senter, P. D., Chace, D. F., Sun, M. M., Lenox, J., Cerveny, C. G., et al. (2004). Effects of drug loading on the antitumor activity of a monoclonal antibody drug conjugate. *Clin. Cancer Res.* 10, 7063–7070. doi: 10.1158/1078-0432.ccr-04-0789

Jefferis, R. (2007). Antibody therapeutics: isotype and glycoform selection. *Expert Opin. Biol. Ther.* 7, 1401–1413. doi: 10.1517/14712598.7.9.1401

Junutula, J. R., Raab, H., Clark, S., Bhakta, S., Leipold, D. D., Weir, S., et al. (2008). Site-specific conjugation of a cytotoxic drug to an antibody improves the therapeutic index. *Nat. Biotechnol.* 26, 925–932. doi: 10.1038/nbt.1480

Katz, J., Janik, J. E., and Younes, A. (2011). Brentuximab vedotin (SGN-35). *Clin. Cancer Res.* 17, 6428–6436. doi: 10.1158/1078-0432.ccr-11-0488

Kellogg, B. A., Garrett, L., Kovtun, Y., Lai, K. C., Leece, B., Miller, M., et al. (2011). Disulfide-linked antibody-maytansinoid conjugates: optimization of in vivo activity by varying the steric hindrance at carbon atoms adjacent to the disulfide linkage. *Bioconjug. Chem.* 22, 717–727. doi: 10.1021/bc100480a

Kharfan-Dabaja, M. A. (2014). A new dawn for gemtuzumab ozogamicin? *Lancet Oncol.* 15, 913–914. doi: 10.1016/S1470-2045(14)70289-X

Kinneer, K., Meekin, J., Tiberghien, A. C., Tai, Y.-T., Phipps, S., Kiefer, C. M., et al. (2018). SLC46A3 as a potential predictive biomarker for antibody-drug conjugates bearing non-cleavable linked maytansinoid and pyrrolobenzodiazepine warheads. *Clin. Cancer Res.* 24, 6570–6582. doi: 10.1158/1078-0432.ccr-18-1300

Kovtun, Y., Noordhuis, P., Whiteman, K. R., Watkins, K., Jones, G. E., Harvey, L., et al. (2018). IMGN779, a novel CD33-targeting antibody-drug conjugate with DNA-alkylating activity, exhibits potent antitumor activity in models of AML. *Mol. Cancer Ther.* 17, 1271–1279. doi: 10.1158/1535-7163.mct-17-1077

Kovtun, Y. V., Audette, C. A., Mayo, M. F., Jones, G. E., Doherty, H., Maloney, E. K., et al. (2010). Antibody-maytansinoid conjugates designed to bypass multidrug resistance. *Cancer Res.* 70, 2528–2537. doi: 10.1158/0008-5472.can-09-3546

Kovtun, Y. V., Audette, C. A., Ye, Y., Xie, H., Ruberti, M. F., Phinney, S. J., et al. (2006). Antibody-drug conjugates designed to eradicate tumors with homogeneous and heterogeneous expression of the target antigen. *Cancer Res.* 66, 3214–3221. doi: 10.1158/0008-5472.can-05-3973

Krishnamurthy, A., and Jimeno, A. (2018). Bispecific antibodies for cancer therapy: a review. *Pharmacol. Ther.* 185, 122–134. doi: 10.1016/j.pharmthera.2017.12.002

Kuczynski, E. A., Yin, M., Bar-Zion, A., Lee, C. R., Butz, H., Man, S., et al. (2016). Co-option of liver vessels and not sprouting angiogenesis drives acquired sorafenib resistance in hepatocellular carcinoma. *J. Natl. Cancer Inst.* 108:djw030. doi: 10.1093/jnci/djw030

Kung Sutherland, M. S., Walter, R. B., Jeffrey, S. C., Burke, P. J., Yu, C., Kostner, H., et al. (2013). SGN-CD33A: a novel CD33-targeting antibody-drug conjugate using a pyrrolobenzodiazepine dimer is active in models of drug-resistant AML. *Blood* 122, 1455–1463. doi: 10.1182/blood-2013-03-491506

Lai, J., Wang, Y., Wu, S. S., Ding, D., Sun, Z. Y., Zhang, Y., et al. (2018). Elimination of melanoma by sortase A-generated TCR-like antibody-drug conjugates (TL-ADCs) targeting intracellular melanoma antigen MART-1. *Biomaterials* 178, 158–169. doi: 10.1016/j.biomaterials.2018.06.017

Lambert, J. M., and Berkenblit, A. (2018). Antibody-drug conjugates for cancer treatment. *Annu. Rev. Med.* 69, 191–207. doi: 10.1146/annurev-med-061516-121357

Lambert, J. M., and Chari, R. V. (2014). Ado-trastuzumab Emtansine (T-DM1): an antibody-drug conjugate (ADC) for HER2-positive breast cancer. *J. Med. Chem.* 57, 6949–6964. doi: 10.1021/jm500766w

Lee, B. C., Chalouni, C., Doll, S., Nalle, S., Darwish, M., Tsai, S. P., et al. (2018a). A novel FRET reagent reveals the intracellular processing of peptide-linked antibody-drug conjugates. . *Bioconjug. Chem.* 29, 2468–2477. doi: 10.1021/acs.bioconjchem.8b00362

Lee, B. C., Chalouni, C., Doll, S., Nalle, S. C., Darwish, M., Tsai, S. P., et al. (2018b). FRET reagent reveals the intracellular processing of peptide-linked antibody-drug conjugates. *Bioconjug. Chem.* 29, 2468–2477. doi: 10.1021/acs.bioconjchem.8b00362

Lewis Phillips, G. D., Li, G., Dugger, D. L., Crocker, L. M., Parsons, K. L., Mai, E., et al. (2008). Targeting HER2-positive breast cancer with trastuzumab-DM1, an antibody-cytotoxic drug conjugate. *Cancer Res.* 68, 9280–9290. doi: 10.1158/0008-5472.can-08-1776

Li, C. W., Lim, S. O., Chung, E. M., Kim, Y. S., Park, A. H., Yao, J., et al. (2018). Eradication of triple-negative breast cancer cells by targeting glycosylated PD-L1. *Cancer Cell* 33, 187.e10–201.e10. doi: 10.1016/j.ccell.2018.01.009

Li, J. Y., Perry, S. R., Muniz-Medina, V., Wang, X., Wetzel, L. K., Rebelatto, M. C., et al. (2016). A biparatopic her2-targeting antibody-drug conjugate induces tumor regression in primary models refractory to or ineligible for HER2-targeted therapy. *Cancer Cell* 29, 117–129. doi: 10.1016/j.ccell.2015.12.008

LoRusso, P. M., Weiss, D., Guardino, E., Girish, S., and Sliwkowski, M. X. (2011). Trastuzumab emtansine: a unique antibody-drug conjugate in development for human epidermal growth factor receptor 2-positive cancer. *Clin. Cancer Res.* 17, 6437–6447. doi: 10.1158/1078-0432.ccr-11-0762

Lu, J., Jiang, F., Lu, A., and Zhang, G. (2016). Linkers having a crucial role in antibody-drug conjugates. *Int. J. Mol. Sci.* 17:561. doi: 10.3390/ijms17040561

Lyon, R. P., Bovee, T. D., Doronina, S. O., Burke, P. J., Hunter, J. H., Neff-LaFord, H. D., et al. (2015). Reducing hydrophobicity of homogeneous antibody-drug conjugates improves pharmacokinetics and therapeutic index. *Nat. Biotechnol.* 33, 733–735. doi: 10.1038/nbt.3212

Mager, D. E. (2006). Target-mediated drug disposition and dynamics. *Biochem. Pharmacol.* 72, 1–10. doi: 10.1016/j.bcp.2005.12.041

Meister, A., and Anderson, M. E. (1983). Glutathione. *Annu. Rev. Biochem.* 52, 711–760. doi: 10.1146/annurev.bi.52.070183.003431

Mohamed, H. E., Mohamed, A. A., Al-Ghobashy, M. A., Fathalla, F. A., and Abbas, S. S. (2018). Stability assessment of antibody-drug conjugate trastuzumab emtansine in comparison to parent monoclonal antibody using orthogonal testing protocol. *J. Pharma. Biomed. Anal.* 150, 268–277. doi: 10.1016/j.jpba.2017.12.022

Moolten, F. L., and Cooperband, S. R. (1970). Selective destruction of target cells by diphtheria toxin conjugated to antibody directed against antigens on the cells. *Science* 169, 68–70. doi: 10.1126/science.169.3940.68

Mullard, A. (2013). Maturing antibody-drug conjugate pipeline hits 30. *Nat. Rev. Drug Discov.* 12, 329–332. doi: 10.1038/nrd4009

Nasiri, H., Valedkarimi, Z., Aghebati-Maleki, L., and Majidi, J. (2018). Antibody-drug conjugates: promising and efficient tools for targeted cancer therapy. *J. Cell Physiol.* 233, 6441–6457. doi: 10.1002/jcp.26435

Okeley, N. M., Miyamoto, J. B., Zhang, X., Sanderson, R. J., Benjamin, D. R., Sievers, E. L., et al. (2010). Intracellular activation of SGN-35, a potent anti-CD30 antibody-drug conjugate. *Clin. Cancer Res.* 16, 888–897. doi: 10.1158/1078-0432.ccr-09-2069

Pabst, M., McDowell, W., Manin, A., Kyle, A., Camper, N., De Juan, E., et al. (2017). Modulation of drug-linker design to enhance in vivo potency of homogeneous antibody-drug conjugates. *J. Control Release* 253, 160–164. doi: 10.1016/j.jconrel.2017.02.027

Pak, Y., Zhang, Y., Pastan, I., and Lee, B. (2012). Antigen Shedding may improve efficiencies for delivery of antibody-based anticancer agents in solid tumors. *Cancer Res.* 72, 3143–3152. doi: 10.1158/0008-5472.CAN-11-3925

Palumbo, A., Hauler, F., Dziunycz, P., Schwager, K., Soltermann, A., Pretto, F., et al. (2011). A chemically modified antibody mediates complete eradication of tumours by selective disruption of tumour blood vessels. *Br. J. Cancer* 104, 1106–1115. doi: 10.1038/bjc.2011.78

Pei, Z., Chen, C., Chen, J., Cruz-Chuh, J. D., Delarosa, R., Deng, Y., et al. (2018). Exploration of pyrrolobenzodiazepine(PBD)-dimers containing disulfide-based prodrugs as payloads for antibody-drug conjugates. *Mol. Pharm.* 15, 3979–3996. doi: 10.1021/acs.molpharmaceut.8b00431

Perez, H. L., Cardarelli, P. M., Deshpande, S., Gangwar, S., Schroeder, G. M., Vite, G. D., et al. (2014). Antibody-drug conjugates: current status and future directions. *Drug Discov. Today* 19, 869–881. doi: 10.1016/j.drudis.2013.11.004

Petersdorf, S. H., Kopecky, K. J., Slovak, M., Willman, C., Nevill, T., Brandwein, J., et al. (2013). A phase 3 study of gemtuzumab ozogamicin during induction and postconsolidation therapy in younger patients with acute myeloid leukemia. *Blood* 121, 4854–4860. doi: 10.1182/blood-2013-01-466706

Piccione, E. C., Juarez, S., Liu, J., Tseng, S., Ryan, C. E., Narayanan, C., et al. (2015). A bispecific antibody targeting CD47 and CD20 selectively binds and eliminates dual antigen expressing lymphoma cells. *MABS* 7, 946–956. doi: 10.1080/19420862.2015.1062192

Polson, A. G., Calemine-Fenaux, J., Chan, P., Chang, W., Christensen, E., Clark, S., et al. (2009). Antibody-drug conjugates for the treatment of non-Hodgkin's lymphoma: target and linker-drug selection. *Cancer Res.* 69, 2358–2364. doi: 10.1158/0008-5472.can-08-2250

Qi, R., Wang, Y., Bruno, P. M., Xiao, H., Yu, Y., Li, T., et al. (2017). Nanoparticle conjugates of a highly potent toxin enhance safety and circumvent platinum resistance in ovarian cancer. *Nat. Commun.* 8:2166. doi: 10.1038/s41467-017-02390-7

Rosenberg, A. S. (2006). Effects of protein aggregates: an immunologic perspective. *AAPS J.* 8, E501–E507. doi: 10.1208/aapsj080359

Rossin, R., Versteegen, R. M., Wu, J., Khasanov, A., Wessels, H. J., Steenbergen, E. J., et al. (2018). Chemically triggered drug release from an antibody-drug conjugate leads to potent antitumour activity in mice. *Nat. Commun.* 9:1484. doi: 10.1038/s41467-018-03880-y

Rudnick, S. I., Lou, J., Shaller, C. C., Tang, Y., Klein-Szanto, A. J., Weiner, L. M., et al. (2011). Influence of affinity and antigen internalization on the uptake and penetration of Anti-HER2 antibodies in solid tumors. *Cancer Res.* 71, 2250–2259. doi: 10.1158/0008-5472.can-10-2277

Salfeld, J. G. (2007). Isotype selection in antibody engineering. *Nat. Biotechnol.* 25, 1369–1372. doi: 10.1038/nbt1207-1369

Sanderson, R. J., Hering, M. A., James, S. F., Sun, M. M., Doronina, S. O., Siadak, A. W., et al. (2005). In vivo drug-linker stability of an anti-CD30 dipeptide-linked auristatin immunoconjugate. *Clin. Cancer Res.* 11(2 Pt 1), 843–852.

Seaman, S., Zhu, Z., Saha, S., Zhang, X. M., Yang, M. Y., Hilton, M. B., et al. (2017). Eradication of tumors through simultaneous ablation of CD276/B7-H3-positive tumor cells and tumor vasculature. *Cancer Cell* 31, 501.e8–515.e8. doi: 10.1016/j.ccell.2017.03.005

Senter, P. D., and Sievers, E. L. (2012). The discovery and development of brentuximab vedotin for use in relapsed Hodgkin lymphoma and systemic anaplastic large cell lymphoma. *Nat. Biotechnol.* 30, 631–637. doi: 10.1038/nbt.2289

Shefet-Carasso, L., and Benhar, I. (2015). Antibody-targeted drugs and drug resistance–challenges and solutions. *Drug Resist. Updat.* 18, 36–46. doi: 10.1016/j.drup.2014.11.001

Sievers, E. L., and Senter, P. D. (2013). Antibody-drug conjugates in cancer therapy. *Annu. Rev. Med.* 64, 15–29. doi: 10.1146/annurev-med-050311-201823

Stein, E., Walter, R., Erba, H., Fathi, A., Advani, A., Lancet, J., et al. (2018). A phase 1 trial of vadastuximab talirine as monotherapy in patients with CD33-positive acute myeloid leukemia. *Blood* 131, 387–396. doi: 10.1182/blood-2017-06-789800

Thomas, A., Teicher, B. A., and Hassan, R. (2016). Antibody-drug conjugates for cancer therapy. *Lancet Oncol.* 17, e254–e262. doi: 10.1016/s1470-2045(16)30030-4

Tsumura, R., Manabe, S., Takashima, H., Koga, Y., Yasunaga, M., and Matsumura, Y. (2018). Influence of the dissociation rate constant on the intra-tumor distribution of antibody-drug conjugate against tissue factor. *J. Control. Release* 284, 49–56. doi: 10.1016/j.jconrel.2018.06.016

Walker, S., Landovitz, R., Ding, W. D., Ellestad, G. A., and Kahne, D. (1992). Cleavage behavior of calicheamicin gamma 1 and calicheamicin T. *Proc. Natl. Acad. Sci. U.S.A.* 89, 4608–4612. doi: 10.1073/pnas.89.10.4608

Younes, A., Yasothan, U., and Kirkpatrick, P. (2012). Brentuximab vedotin. *Nat. Rev. Drug Discov.* 11, 19–20. doi: 10.1038/nrd3629

Yurkovetskiy, A. V., Yin, M., Bodyak, N., Stevenson, C. A., Thomas, J. D., Hammond, C. E., et al. (2015). A Polymer-based antibody-vinca drug conjugate platform: characterization and preclinical efficacy. *Cancer Res.* 75, 3365–3372. doi: 10.1158/0008-5472.can-15-0129

Zhang, D., Le, H., Cruz-Chuh, J. D., Bobba, S., Guo, J., Staben, L., et al. (2018a). Immolation of p-aminobenzyl ether linker and payload potency and stability determine the cell-killing activity of antibody-drug conjugates with phenol-containing payloads. *Bioconjug. Chem.* 29, 267–274. doi: 10.1021/acs.bioconjchem.7b00576

Zhang, D., Yu, S. F., Khojasteh, S. C., Ma, Y., Pillow, T. H., Sadowsky, J. D., et al. (2018b). Intratumoral payload concentration correlates with the activity of antibody-drug conjugates. *Mol. Cancer Ther.* 17, 677–685. doi: 10.1158/1535-7163.mct-17-0697

Zhang, D., Pillow, T. H., Ma, Y., Cruz-Chuh, J. D., Kozak, K. R., Sadowsky, J. D., et al. (2016). Linker immolation determines cell killing activity of disulfide-linked pyrrolobenzodiazepine antibody-drug conjugates. *ACS Med. Chem. Lett.* 7, 988–993. doi: 10.1021/acsmedchemlett.6b00233

Conflict of Interest Statement: The authors declare that the research was conducted in the absence of any commercial or financial relationships that could be construed as a potential conflict of interest.

frontiers in Oncology

ORIGINAL RESEARCH
published: 25 April 2019
doi: 10.3389/fonc.2019.00313

Glesatinib, a c-MET/SMO Dual Inhibitor, Antagonizes P-glycoprotein Mediated Multidrug Resistance in Cancer Cells

*Qingbin Cui[1,2], Chao-Yun Cai[2], Hai-Ling Gao[2,3], Liang Ren[1], Ning Ji[2,4], Pranav Gupta[2], Yuqi Yang[2], Suneet Shukla[5], Suresh V. Ambudkar[5], Dong-Hua Yang[2] and Zhe-Sheng Chen[2]**

[1] School of Public Health, Guangzhou Medical University, Guangdong, China, [2] Department of Pharmaceutical Sciences, College of Pharmacy and Health Sciences, St. John's University, Queens, NY, United States, [3] Department of Histology and Embryology, Clinical Medical College, Weifang Medical University, Weifang, China, [4] Tianjin Key Laboratory on Technologies Enabling Development of Clinical Therapeutics and Diagnostics, School of Pharmacy, Tianjin Medical University, Tianjin, China, [5] Laboratory of Cell Biology, Center for Cancer Research, National Cancer Institute, NIH, Bethesda, MD, United States

OPEN ACCESS

Edited by:
Massimo Broggini, Istituto Di Ricerche Farmacologiche Mario Negri, Italy

Reviewed by:
Fabrizio Martelli, Istituto Superiore di Sanità (ISS), Italy
Kamini Singh, Memorial Sloan Kettering Cancer Center, United States
Sandro Cosconati, Università degli Studi della Campania Luigi Vanvitelli Caserta, Italy

***Correspondence:**
Zhe-Sheng Chen
chenz@stjohns.edu

Specialty section:
This article was submitted to Cancer Molecular Targets and Therapeutics, a section of the journal Frontiers in Oncology

Received: *25 January 2019*
Accepted: *08 April 2019*
Published: *25 April 2019*

Citation:
Cui Q, Cai C-Y, Gao H-L, Ren L, Ji N, Gupta P, Yang Y, Shukla S, Ambudkar SV, Yang D-H and Chen Z-S (2019) Glesatinib, a c-MET/SMO Dual Inhibitor, Antagonizes P-glycoprotein Mediated Multidrug Resistance in Cancer Cells. Front. Oncol. 9:313. doi: 10.3389/fonc.2019.00313

Multidrug resistance (MDR) is one of the leading causes of treatment failure in cancer chemotherapy. One major mechanism of MDR is the overexpressing of ABC transporters, whose inhibitors hold promising potential in antagonizing MDR. Glesatinib is a dual inhibitor of c-Met and SMO that is under phase II clinical trial for non-small cell lung cancer. In this work, we report the reversal effects of glesatinib to P-glycoprotein (P-gp) mediated MDR. Glesatinib can sensitize paclitaxel, doxorubicin, colchicine resistance to P-gp overexpressing KB-C2, SW620/Ad300, and P-gp transfected Hek293/ABCB1 cells, while has no effect to their corresponding parental cells and negative control drug cisplatin. Glesatinib suppressed the efflux function of P-gp to [^{3}H]-paclitaxel and it didn't impact both the expression and cellular localization of P-gp based on Western blot and immunofluorescent analysis. Furthermore, glesatinib can stimulate ATPase in a dose-dependent manner. The docking study indicated that glesatinib interacted with human P-gp through several hydrogen bonds. Taken together, c-Met/SMO inhibitor glesatinib can antagonize P-gp mediated MDR by inhibiting its cell membrane transporting functions, suggesting new application in clinical trials.

Keywords: multidrug resistance, P-gp, glesatinib, reversal effects, mechanism

INTRODUCTION

Multidrug resistance (MDR) is the one of the major challenges in cancer treatment (1). MDR refers to a phenomenon that cancer cell once becomes resistant to one chemotherapeutic, accompanied by cross resistant to other chemotherapeutics that are structurally and mechanistically different (2). MDR is one of the major causes of failure in cancer treatment. The mechanisms of MDR involve dynamic ATP-binding cassette (ABC) transporters (3, 4), oncogenes mutations (5), microenvironment changes (6), reprogramed cancer cell metabolism (7, 8), efficient DNA repairing (9, 10), survived cancer stem cells (11, 12), and activated detoxifying systems (13, 14). Novel effective remedies are urgently needed to circumvent MDR.

ABC transporters are a group of active transporter proteins that have diverse functions and are present in the membrane of both prokaryotes and eukaryotes, acting as protecting enzymes against xenobiotic, including many chemotherapeutics (15, 16). One of the most well studied ABC transporters is P-glycoprotein (P-gp), which is encoded by ABCB1 genes. P-gp contributes in pumping out many different kinds of anticancer drugs, namely, taxanes, anthracyclines, vinca alkaloids, and epipodophyllotoxins (17–24). To counteract the negative regulation of chemotherapy by P-gp, three generations of inhibitors (both specific and non-specific) have been developed and some of them have been introduced into clinical trials (25). However, due to unexpected adverse effects or severely drug-drug interaction, none of them have been approved by FDA (3, 26). There is an unmet need for effective and safe reversal agents for clinical use. Recently, certain tyrosine kinase inhibitors (TKIs) have been found to exert MDR reversal effect via regulating P-gp at non-toxic concentration (27–31), suggesting new regimens in the treatment of resistant cancer. TKI glesatinib (**Figure 1A**), a c-MET/SMO dual inhibitor (32, 33), is now under Phase II clinical trials in combination with Nivolumab in treatment of the non-small cell lung cancer (NSCLC). More importantly, we found that glesatinib can antagonize P-gp mediated MDR. Here, we report the reversal effects of glesatinib and the underlying mechanisms.

MATERIALS AND METHODS

Chemicals

Glesatinib (99% purity as measured by high performance liquid chromatography) was purchased from ChemieTek (Indianapolis, IN). Dulbecco's modified Eagle's Medium (DMEM), bovine serum albumin (BSA), fetal bovine serum (FBS), penicillin/streptomycin and trypsin 0.25% were purchased from Hyclone (GE Healthcare Life Science, Pittsburgh, PA). The monoclonal antibodies for ABCB1 (C219) and GAPDH (MA5-15738), Alexa Fluor 488 conjugated goat anti-mouse IgG secondary antibody were purchased from Thermo Fisher Scientific Inc (Rockford, IL), dimethylsulfoxide (DMSO), 3-(4,5-dimethylthiazol-yl)-2,5-diphenyltetrazolium bromide (MTT), Triton X-100, 4',6-diamidino-2-phenylindole (DAPI), paraformaldehyde, paclitaxel, doxorubicin, colchicine, cisplatin, verapamil and Ko 143 were purchased from Sigma-Aldrich (St. Louis, MO). [^{3}H]-paclitaxel (15 Ci/mmol) was purchased from Moravek Biochemicals, Inc (Brea, CA). All other chemicals were purchased from Sigma Chemical Co (St. Louis, MO).

Cell Lines and Cell Culture

The human epidermoid carcinoma cell line KB-3-1 and its colchicine-selected P-gp-overexpressing KB-C2 cells, the human colon cancer cell line SW620 and its doxorubicin-selected P-gp-overexpressing SW620/Ad300 cells, the NSCLC cell line NCI-H460 and its mitoxantrone-selected ABCG2-overexpressing NCI-H460/MX20 cells, were used for P-gp and ABCG2 reversal study, respectively. The HEK293/pcDNA3.1, HEK293/ABCB1 cells lines were established by transfecting HEK293 cells with either the empty pcDNA3.1 vector or the vector containing full length ABCB1 (HEK293/ABCB1), and were cultured in a medium containing 2 mg/mL of G418. All cell were cultured at 37°C, using 5% CO_2 with DMEM containing 10% FBS and 1% penicillin/streptomycin. All drug resistant cell lines were grown as adherent monolayer in a drug-free culture media for more than 2 weeks prior to their use.

Cytotoxicity and Reversal Experiments

The cytotoxicity and reversal experiments of glesatinib to KB-3-1, KB-C2, SW620, SW620/Ad300, HEK293/pcDNA3.1, HEK293/ABCB1 cells were performed by using the MTT colorimetric assay (34). For reversal experiments, the applied concentrations of glesatinib were 1 and 3 μM according to the results of cytotoxicity experiments. All of the experiments were repeated at least three times, and the mean and standard deviation (SD) values were calculated. Verapamil (3 μM) was used as a positive control inhibitor of P-gp, Ko 143 was used as a positive control inhibitor of ABCG2, cisplatin, a non-P-gp substrate, was used as a negative control.

Western Blot Analysis

Dose-dependent (0, 0.3, 1, 3 μM) and time-dependent (0, 24, 48, 72 h) of glesatinib on the expression of P-gp were determined. Twenty microgram protein cell lysates were loaded in each lane. The presence of P-gp was determined using monoclonal antibody C219 (dilution 1:200). GAPDH was used to confirm equal loading in each lane in the samples prepared from cell lysates. The resulting protein bands were quantified by using Image J software. The detailed protocol of Western blot analysis was carried out as previously described (35).

Immunofluorescence Analysis

SW620, SW620/Ad300 cells were seeded (1×10^4/well) in 24-well plates and cultured at 37°C for 24 h, followed by incubation with 3 μM glesatinib for 0, 24, 48, and 72 h, respectively. Then cells were fixed in 4% paraformaldehyde for 5 min and permeabilized by 0.1% Triton X-100 for 5 min before blocked with 6% BSA for 1 h at 37°C. The presence of P-gp was determined using monoclonal antibody F4 (dilution 1:1000) for incubation at 4°C overnight. Alexa Fluor 488 conjugated secondary antibody (1:1000) was used for incubation at 37°C for 1 h. After washing with iced PBS, DAPI (1 μg/mL) was used to counterstain the nuclei. Immunofluorescence images were collected using an EVOS FL Auto fluorescence microscope (Life Technologies Corporation, Gaithersburg, MD).

ATPase Assay

The vanadate-sensitive ATPase activity of ABCB1 in membrane vesicles of High Five insect cells was measured as previously described (36). Briefly, the membrane vesicles (10 μg of protein) were incubated in ATPase assay buffer [composed by 50 mmol/L MES (pH 6.8), 50 mmol/L KCl, 5 mmol/L sodium azide, 2 mmol/L EGTA, 2 mmol/L DTT, 1 mmol/L ouabain, and 10 mmol/L $MgCl_2$] with or without 0.3 mmol/L vanadate at 37°C for 5 min, then were incubated with different concentrations (ranging from 0 to 40 μM) of glesatinib at 37°C for 3 min. The ATPase reaction was induced by the addition of 5 mM of Mg-ATP, and the total volume was 0.1 mL. After incubation

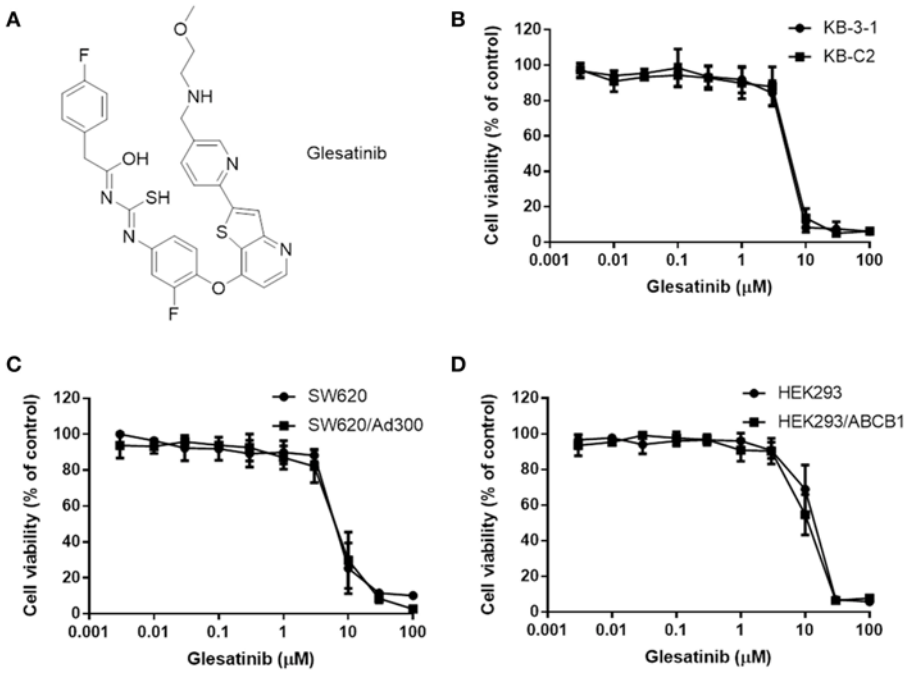

FIGURE 1 | The structure of glesatinib and its cytotoxic effects to three P-gp overexpressing cancer cells. **(A)** Chemical structure of glesatinib. **(B)** Concentration -dependent viability curves for KB-3-1 and KB-C2 cell lines incubated with different concentration of glesatinib for 72 h. **(C)** Concentration-dependent viability curves for SW620 and SW620/Ad300 cell lines incubated with different concentration of glesatinib for 72 h. **(D)** Concentration-dependent viability curves for HEK293/pcDNA3.1 and HEK293/ABCB1 cells incubated with different concentration of glesatinib for 72 h. The cell viability was determined by MTT assay. Data are expressed as mean ± SD, and representative of three independent experiments in triplicate are shown.

at 37°C for 20 min, the reaction was allowed to continue for another 20 min at 37°C and then terminated by adding 100 μL of a 5% SDS solution to the reaction mix. The amount of inorganic phosphate (IP) release was detected at 880 nm using a spectrophotometer.

[^{3}H]-Paclitaxel Accumulation and Efflux Assay

Since glesatinib reversed MDR mediated by P-gp, the reversal mechanism may be related to change of the protein expression or location of P-gp, we used the drug accumulation and efflux assays to determine the reversal mechanism as previously described (27). The accumulation and efflux of [^{3}H]-paclitaxel in KB-3-1 and KB-C2 cells were measured in the absence or presence of glesatinib (1, 3 μM), and verapamil (3 μM) was used as positive control.

Molecular Modeling of Human ABCB1 Homology Model

To reveal more details of the interaction between glesatinib and P-gp, we conducted docking study. All docking experiments were performed following the reported protocols with software Schrodinger 2018–1 (Schrödinger, LLC, New York, NY, 2018) on a Mac Pro 6-core Intel Xenon X5 processor with Macintosh Operating System (OS X El Capitan) (28, 37). Ligand preparation was essentially performed. Human P-gp homology model (4M1M) was established by Dr. S. Aller based on improved mouse P-gp (3G5U). Single-wavelength anomalous diffraction (SAD) phasing was conducted to the full 3.8 Å resolution of the dataset. Non-crystallographic symmetry (NCS) operators were determined from the mouse P-gp structure with the phenix.python script simple_ncs_from_pdb.py. Refinement was conducted with phenix.refine using NCS and secondary structure restraints, restraining NCS-related B-factors, group B-factor and individual B-factor (38). The centroid of some important residues including H61, G64, L65, M68, L339, A342, L975 C343, F942, T945, Q946, Y950, L975, V982, and A985 (39–41). Glide XP docking was performed and the receptor grid for induced-fit docking (IFD) was generated by selecting residues. Then IFD was conducted with the default protocol.

Statistical Analysis

All data are expressed as the mean ± SD. All experiments were repeated at least three times and the data were analyzed using a one-way or two-way ANOVA by GraphPad Prism 7.00 software. Differences were considered significant when $P < 0.05$.

RESULTS

Glesatinib Antagonized MDR in P-gp Overexpressing Cancer Cells

First, the cytotoxicity of glesatinib to P-gp overexpressing cancer cells KB-C2, SW620/Ad300, HEK293/ABCB1, and their parent cells KB-3-1, SW620, HEK293 cells were determined by MTT

assay. As shown in **Figures 1B–D**, the IC_{50}s fell between 5 and 10 μM. Therefore, the non-toxic concentration (IC_{20}) of glesatinib applied in the reversal effects evaluation were 1 and 3 μM.

The reversal effects of glesatinib to P-gp substrates, including doxorubicin, paclitaxel and colchicine were further tested in the aforementioned cancer cells. The non-selective P-gp inhibitor, verapamil was used as a positive control (42), and non-substrate cisplatin was used as a negative control (43). Pretreatment with or without glesatinib with these substrates to P-gp overexpressing cancer cells and their sensitive parent cells were tested to obtain their IC_{50}s.

As shown in **Tables 1**, **2**, the parent cells were sensitive to doxorubicin, paclitaxel and colchicine, and the IC_{50}s were as low as nano-mole. While P-gp overexpressing cancer cell exhibited resistant properties to these chemotherapeutics, resistance fold ranged from 77 to 438. Pretreatment with glesatinib significantly lowered the IC_{50}s of all these three chemotherapeutics to resistant cancer cells. More importantly, glesatinib exhibited similar re-sensitizing effects to P-gp transfected HEK293/ABCB1 cells, suggesting its mechanisms of re-sensitizing to chemotherapeutics were directly or indirectly related to P-gp. In addition, in ABCG2 overexpressing cancer cells NCI-H460/MX20 cells, gleasatinib failed to reverse topotecan (an ABCG substrate) resistance (**Table 2**). These results indicated that glesatinib could antagonize cancer MDR mediated by P-gp, but not MDR mediated by ABCG2.

Glesatinib Did Not Impact the P-gp Expression and Subcellular Localization

The down-regulation or re-localization of P-gp (from cellular membrane to cytosol) may lead to re-sensitization of chemotherapeutics as a result of less extent of efflux or unable to exert its functions (17, 44). We further determined the interaction mechanism of glesatinib with P-gp by examining the P-gp expression and cellular location through Western blotting and immunofluorescence assay. P-gp overexpressing KB-C2 cells were treated with glesatinib at different concentration (0.3, 1, 3 μM for 72 h) or at different time (3 μM for 24, 48, 72 h) and the P-gp expression was examined. SW620/Ad300 cells were treated with 3 μM for 0, 24, 48, 72 h to examine the localization of P-gp. KB-3-1 and SW620 cells were used as negative control in this experiment.

As shown in **Figure 2**, P-gp expression was not impacted by glesatinib either dose- or time-dependently. The immunofluorescence assay results of **Figure 3** showed that after treatment of glesatinib, localization of P-gp had not changed and remained to localize on the cell membrane. These results suggested that glesatinib could not impact the expression and localization of P-gp. We next tested the effects of glesatinib to the efflux functions of P-gp.

Glesatinib Increased the Intracellular [^{3}H]-Paclitaxel Accumulation and Inhibited [^{3}H]-Paclitaxel Efflux in Cancer Cell Lines Overexpressing P-gp

As glesatinib did not alter either P-gp expression or its localization, we set out to test the transporting function of P-gp by examining the cellular accumulation of radioactive [^{3}H]-paclitaxel. As shown in **Figures 4A,B**, in KB-3-1 cells that barely expressed P-gp, [^{3}H]-paclitaxel had not been impacted, and glesatibin had no effects to either the drug accumulation (**Figure 4A**) or efflux (**Figure 4B**).

TABLE 1 | Glesatinib sensitized paclitaxel, colchicine, and doxorubicin to P-gp-overexpressing cell lines (KB-C2 and HEK293/ABCB1 cells).

Treatment	IC_{50} ± SD[a] (RF[b])			
	KB-3-1 (μM)	KB-C2 (μM)	HEK293 (μM)	HEK293/ABCB1 (μM)
Paclitaxel	0.004 ± 0.002 (1.00)	1.755 ± 0.057 (438.75)	0.073 ± 0.027 (1.00)	3.757 ± 0.312 (51.46)
+ Gle (1 μM)	0.004 ± 0.001 (1.00)	0.220 ± 0.026 (55)*	0.122 ± 0.050 (1.67)	0.255 ± 0.084 (3.49)*
+ Gle (3 μM)	0.003 ± 0.001 (0.75)	0.015 ± 0.001 (3.75)*	0.100 ± 0.020 (1.37)	0.047 ± 0.004 (0.64)*
+ Vera (3 μM)	0.003 ± 0.001 (0.75)	0.010 ± 0.002 (2.5)*	0.068 ± 0.003 (0.95)	0.094 ± 0.003 (1.9)*
Doxorubicin	0.032 ± 0.013 (1.00)	2.504 ± 0.487 (78.25)	0.061 ± 0.020 (1.00)	0.631 ± 0.150 (10.34)
+ Gle (1 μM)	0.029 ± 0.003 (0.91)	0.118 ± 0.061 (3.69)*	0.060 ± 0.029 (0.98)	0.072 ± 0.006 (1.18)*
+ Gle (3 μM)	0.028 ± 0.004 (0.88)	0.023 ± 0.010 (0.72)*	0.066 ± 0.009 (1.08)	0.064 ± 0.021 (1.05)*
+ Vera (3 μM)	0.024 ± 0.006 (0.75)	0.024 ± 0.005 (0.75)*	0.061 ± 0.008 (1.00)	0.084 ± 0.009 (1.38)*
Colchicine	0.009 ± 0.002 (1.00)	3.231 ± 0.260 (359.00)	0.066 ± 0.001 (1.00)	1.538 ± 0.090 (23.30)
+ Gle (1 μM)	0.006 ± 0.002 (0.67)	0.993 ± 0.183 (110.33)*	0.058 ± 0.007 (0.88)	0.126 ± 0.106 (1.91)*
+ Gle (3 μM)	0.007 ± 0.001 (0.78)	0.088 ± 0.020 (9.78)*	0.048 ± 0.009 (0.73)	0.047 ± 0.021 (0.71)*
+ Vera (3 μM)	0.009 ± 0.001 (1.00)	0.116 ± 0.035 (12.89)*	0.056 ± 0.006 (0.85)	0.050 ± 0.008 (0.76)*
Cisplatin	2.508 ± 0.432 (1.00)	3.027 ± 0.343 (1.21)	2.660 ± 0.430 (1.00)	3.336 ± 0.451 (1.25)
+ Gle (1 μM)	1.990 ± 0.452 (0.79)	2.676 ± 0.443 (1.07)	1.982 ± 0.253 (0.75)	3.272 ± 0.254 (1.23)
+ Gle (3 μM)	2.031 ± 0.364 (0.81)	2.120 ± 0.152 (0.85)	1.903 ± 0.361 (0.72)	3.394 ± 0.353 (1.28)
+ Vera (3 μM)	2.309 ± 0.641 (0.92)	2.098 ± 0.230 (0.84)	2.388 ± 0.452 (0.90)	3.115 ± 0.433 (1.17)

$P < 0.05$ vs. no inhibitor group.

[a] IC_{50} values represented the mean ± SD of three independent experiments performed in triplicate.

[b] Resistance fold (RF) was calculated by dividing the IC50 values of substrates in the presence or absence of an inhibitor by the IC_{50} values of parental cells without an inhibitor. Gle, Glesatinib; Vera, verapamil.

TABLE 2 | Glesatinib sensitized paclitaxel, colchicine, and doxorubicin to P-gp-overexpressing cell line (SW620/Ad300 cells), but not topotecan to ABCG2-overexpressing cells (NCI-H460/MX20 cells).

Treatment	$IC_{50} \pm SD^a$ (RF^b)		Treatment	$IC_{50} \pm SD^a$ (RF^b)	
	SW620 (μM)	SW620/Ad300 (μM)		NCI-H460 (μM)	NCI-H460/MX20 (μM)
Paclitaxel	0.091 ± 0.015 (1.00)	21.190 ± 6.25 (232.86)	Topotecan	0.063 ± 0.020 (1.00)	6.010 ± 0.530 (95.49)
+ Gle (1 μM)	0.067 ± 0.013 (0.74)	1.969 ± 0.160 (21.63)*	+ Gle (1 μM)	0.060 ± 0.015 (0.95)	6.360 ± 0.127 (100.95)
+ Gle (3 μM)	0.060 ± 0.020 (0.66)	0.257 ± 0.072 (2.82)*	+ Gle (3 μM)	0.040 ± 0.021 (0.63)	7.160 ± 1.193 (113.65)
+ Vera (3 μM)	0.097 ± 0.031 (1.07)	0.646 ± 0.173 (7.10)*	+ Ko 143 (3 μM)	0.051 ± 0.013 (0.81)	0.520 ± 0.130 (8.25)*
Doxorubicin	0.031 ± 0.014 (1.00)	9.950 ± 2.023 (320.97)	Cisplatin	1.640 ± 0.185 (1.00)	2.150 ± 0.498 (1.31)
+ Gle (1 μM)	0.033 ± 0.007 (1.06)	2.397 ± 0.041 (77.32)*	+ Gle (1 μM)	1.699 ± 0.392 (1.04)	1.926 ± 0.297 (1.17)
+ Gle (3 μM)	0.029 ± 0.012 (0.94)	0.271 ± 0.020 (8.74)*	+ Gle (3 μM)	1.513 ± 0.218 (0.92)	2.049 ± 0.187 (1.25)
+ Vera (3 μM)	0.023 ± 0.007 (0.74)	0.288 ± 0.155 (9.29)*	+ Ko 143 (3 μM)	1.686 ± 0.152 (1.03)	2.285 ± 0.138 (1.39)
Cisplatin	1.481 ± 0.676 (1.00)	1.514 ± 0.398 (1.02)			
+ Gle (1 μM)	1.266 ± 0.189 (0.85)	1.676 ± 0.138 (1.13)			
+ Gle (3 μM)	1.166 ± 0.079 (0.79)	1.587 ± 0.329 (1.07)			
+ Vera (3 μM)	1.164 ± 0.107 (0.79)	1.851 ± 0.364 (1.25)			

*$P < 0.05$ vs. no inhibitor group.

[a] IC_{50} values represented the mean ± SD of three independent experiments performed in triplicate.

[b] Resistance fold (RF) was calculated by dividing the IC_{50} values of substrates in the presence or absence of an inhibitor by the IC_{50} values of parental cells without an inhibitor. Gle, Glesatinib; Vera, verapamil.

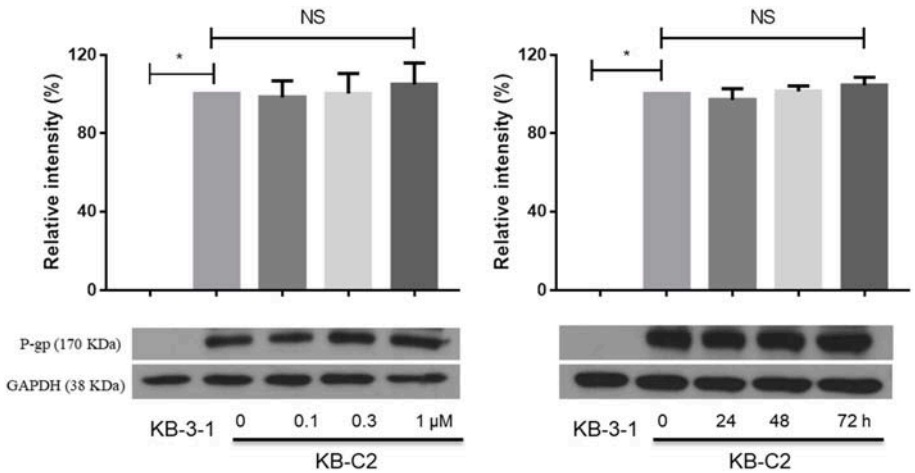

FIGURE 2 | Glesatinib did not affect the protein expression of P-gp transporters in ABCB1 overexpressing cell lines. Detection and relative intensity of ABCB1 expression in KB-C2 cells incubated with 0.3, 1, 3 μM for 72 h and 3 μM for 0, 24, 48, 72 h. Data are mean ± SD, representative of three independent experiments. *$p < 0.05$, compared with control group.

While in P-gp overexpressing KB-C-2 cells, [^{3}H]-paclitaxel accumulation decreased significantly as shown in **Figures 4A,C**. Pretreatment of glesatinib may significantly increase the [^{3}H]-paclitaxel accumulation and inhibited the drug efflux of P-gp. These results indicated that glesatinib may exert its re-sensitizing effects by thwart the transporting function of P-gp.

Glesatinib Stimulated the ATPase Activity of P-gp

ATP hydrolyzed by ATPase was used by P-gp to provide the energy to transport its substrates (45, 46). To further reveal the P-gp inhibitory mechanisms, we determined the effect of glesatinib on the ATPase activity of P-gp transporters by measuring P-gp-mediated ATP hydrolysis in the presence or absence of glesatinib (0–40 μM). As shown in **Figure 5**, Glesatinib stimulated the ATPase activity of P-gp transporters in a dose-dependent manner. The concentration of 50% stimulation was 3.2 μM, and the maximum stimulation was 5.59-fold greater than that of basal level.

Induced-Fit Docking (IFD) Simulation Interactions Between P-gp and Glesatinib

We investigated the potential interaction of glesatinib with P-gp by conducting docking analysis. The best docking score of the binding of glesatinib and human P-gp was −12.639 kcal/mol. The best-scored docked position of glesatinib with P-gp was showed

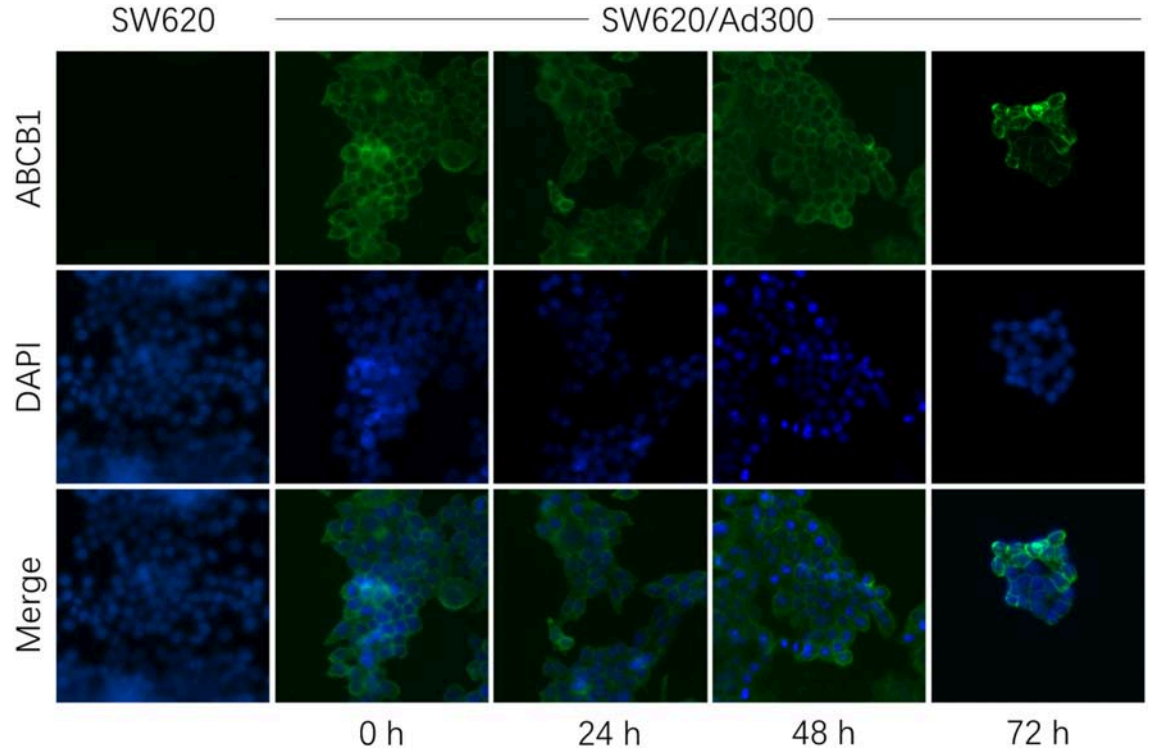

FIGURE 3 | Glesatinib did not affect the localization of ABCB1 transporters in ABCB1 overexpressing cell lines. Sub-cellular localization of ABCB1 expression in SW620/Ad300 cells incubated with 3 μM of glesatinib for 0, 24, 48, and 72 h. ABCB1, green and DAPI (blue) counterstains the nuclei. SW620 cells represented the control group.

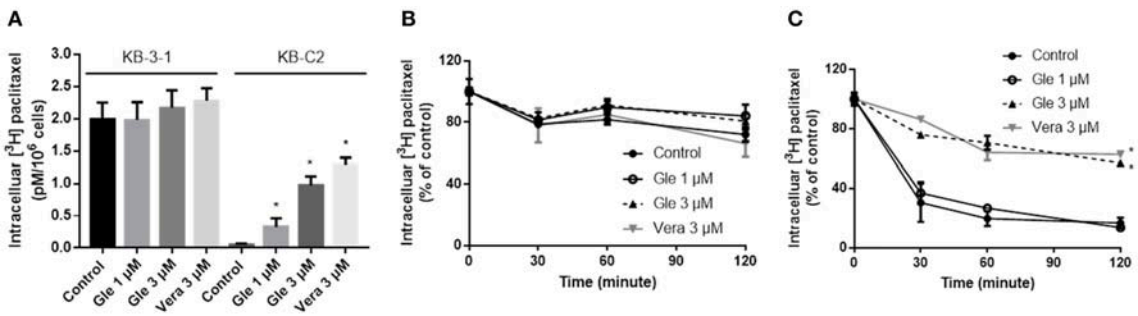

FIGURE 4 | Glesatinib increased the accumulation and inhibited the efflux of [^{3}H]-paclitaxel in P-gp overexpressing KB-C2 cells. **(A)** The effect of glesatinib on the accumulation of [^{3}H]-paclitaxel in KB-3-1 and KB-C2 cell lines. **(B)** The effect of glesatinib on efflux of [^{3}H]-paclitaxel in KB-3-1 and **(C)** KB-C2. Verapamil (3 μM) was used as positive controls. Data are mean ± SD, representative of three independent experiments. *$p < 0.05$, compared with control group. Gle, Glesatinib; Vera, verapamil.

in **Figure 6**. There were two hydrogen bonds between glesatinib and human P-gp, including the hydrogen binding between the amide group of glesatinib and Tyr950 (C=O…HO-Tyr950), in addition with the hydrogen bond between the methoxy group and Asn721 (H_3C-O…H_2N-Asn721). The fluorophenyl group of glesatinib has π-π interaction with both Phe336 and Phe983 of P-gp protein. The thienopyridine group has π-π interaction with the residues Phe728 and Phe983. Interestingly, the acidic microenvironment of tumor (47) could result in the ionization of glesatinib, and the amine cation could form a hydrogen bond with Tyr307 and a π-cation bond with Phe303. These formed various bonds between glesatinib and human P-gp may finally lead to the collapsed P-gp.

DISCUSSION

ABC transporter P-gp functions as the protective enzyme that pumps out xenobiotics including many chemotherapeutics that are its substrates, causing MDR in cancers (3). To counter that, many P-gp inhibitors have been developed and some of them have been tested in clinical trials, while all of them have failed to get approved by US

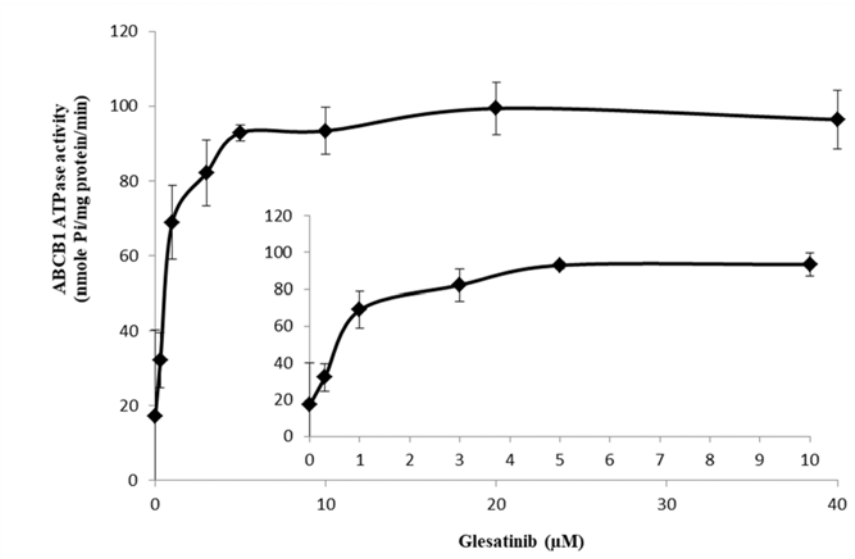

FIGURE 5 | Glesatinib stimulated the ATPase activity of P-gp. Effect of various concentrations of glesatinib on the ATPase activity of P-gp. The inset graphs illustrate the effect of 0–10 μM glesatinib on the ATPase activity of P-gp. Data are mean ± SD, representative of three independent experiments.

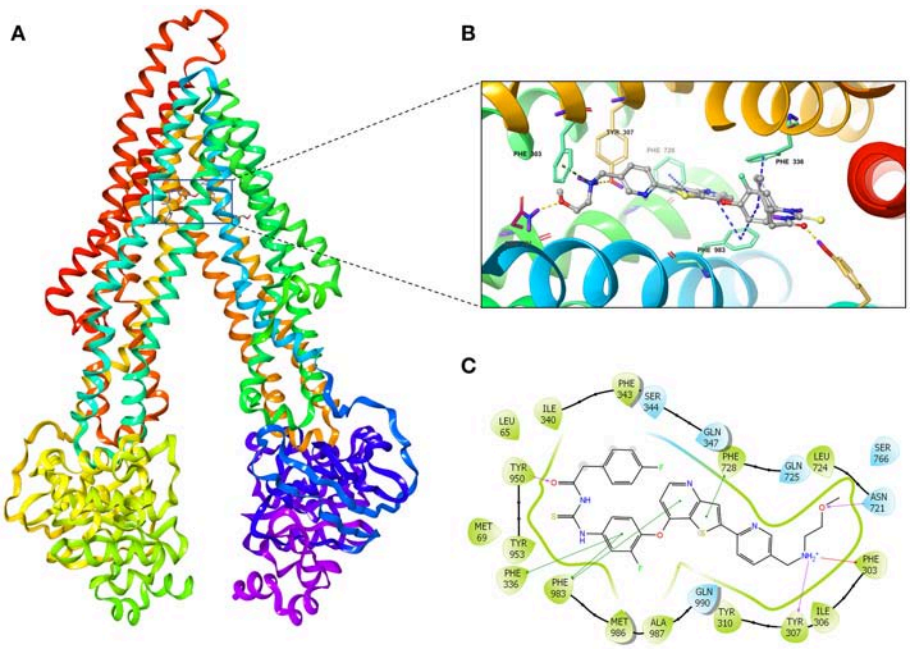

FIGURE 6 | The molecular modeling study of glesatinib with human homology ABCB1. **(A)** Overall view of glesatinib-P-gp complex. **(B)** 3D figure of Docked position of glesatinib within the drug-binding site of human P-gp homology model. Glesatinib was showed as ball and stick mode with the atoms colored: carbon-cyan, nitrogen-blue, oxygen-red, fluorine-green, sulfur-yellow, hydrogen-purple. Important residues were showed as sticks, with the color pattern: carbon-gray, nitrogen-blue, oxygen-red, hydrogen-purple. π-π stacking interactions are indicated with cyan dotted line. π-cation bond is indicated with green dotted line. Hydrogen bonds were showed by the yellow dotted line. **(C)** 2D figure of Docked position of glesatinib within the drug-binding site of human P-gp homology model. The cyan bubbles indicate polar residues and the green bubbles indicate hydrophobic residues. Hydrogen bonds are shown by the purple dotted arrow. π-π stacking interactions are shown by the green lines and π-cation bond is indicated with red line.

FDA due to severely adverse effects (48, 49). Recent studies indicate that certain TKIs may work as regulators of P-gp (2, 50), either inhibiting its expression (51) or impact its functions (35). Combinations of these TKIs and chemotherapeutics hold promising potential in the treatment of MDR cancers.

In this work, we found that MET/SMO dual inhibitor glesatinib, a drug candidate that is now under clinical trials, antagonized P-gp mediated MDR in cancer cells overexpressing P-gp. As shown in SW620/Ad300 and KB-C2 cells, glesatinib could antagonized P-gp mediated resistance by significantly reducing the IC_{50}s of doxorubicin, paclitaxel and colchicine, while had no effects to cisplatin which was not a substrate of P-gp. To confirm these effects were mediated by P-gp, we further tested its reversal effects to P-gp transpected HEK293 cells. Glesatinib exhibited similar effects in HEK293/ABCB1 cells, indicating the effects were mediated by regulating P-gp. We further confirmed that glesatinib did not affect the expression and sub-cellular localization of P-gp, while it could stimulate ATPase, similar as P-gp inhibitor verapamil (45). Importantly, our results showed gleastinib significantly increased the intracellular accumulation of [^{3}H]-paclitaxel and suppressed the efflux effects, which may contribute to the increased cytotoxic effects when used by combination. Finally, the docking study indicated that glesatinib might have strong interaction with P-gp via hydrogen bonds and π-π interaction, leading to the efflux inhibition. This docking result may provide valuable information to develop glesatinib derivatives for better targeting and/or binding.

In conclusion, MET/SMO dual inhibitor Glesatinib antagonized P-gp mediated MDR by inhibiting its efflux functions. This work provided important information for further clinical trials.

AUTHOR CONTRIBUTIONS

QC and Z-SC: conception and design. QC, C-YC, H-LG, NJ, SS, SA, and Z-SC: development of methodology. QC, C-YC, H-LG, PG, and NJ: acquisition of data. QC, C-YC, H-LG, NJ, and Z-SC: analysis and interpretation of data. QC, C-YC, LR, YY, D-HY, and Z-SC: writing, review, and/or revision of the manuscript. All authors read and approved the final manuscript.

ACKNOWLEDGMENTS

We thank Dr. Stephen Aller for providing the human ABCB1 homology model. We thank Dr. Tanaji T. Talele for providing the computing resources for the docking study. We thank Drs. Susan E. Bates and Robert W. Robey (NCI, NIH, Bethesda, MD) for providing the cell lines. We thank the support of Guangzhou Postdoctoral Foundation of International Training for QC and NIH funding (No. 1R15GM116043-01) to Z-SC.

REFERENCES

1. Housman G, Byler S, Heerboth S, Lapinska K, Longacre M, Snyder N, et al. Drug resistance in cancer: an overview. *Cancers*. (2014) 6:1769–92. doi: 10.3390/cancers6031769
2. Shukla S, Chen ZS, Ambudkar SV. Tyrosine kinase inhibitors as modulators of ABC transporter-mediated drug resistance. *Drug Resist Updat.* (2012) 15:70–80. doi: 10.1016/j.drup.2012.01.005
3. Robey RW, Pluchino KM, Hall MD, Fojo AT, Bates SE, Gottesman MM. Revisiting the role of ABC transporters in multidrug-resistant cancer. *Nat Rev Cancer*. (2018) 18:452–64. doi: 10.1038/s41568-018-0005-8
4. Kathawala RJ, Gupta P, Ashby CJ, Chen ZS. The modulation of ABC transporter-mediated multidrug resistance in cancer: a review of the past decade. *Drug Resist Updat.* (2015) 18:1-17. doi: 10.1016/j.drup.2014.11.002
5. Xue M, Cheng J, Zhao J, Zhang S, Jian J, Qiao Y, et al. Outcomes of 219 chronic myeloid leukaemia patients with additional chromosomal abnormalities and/or tyrosine kinase domain mutations. *Int J Lab Hematol.* (2018) 41:94–101. doi: 10.1111/ijlh.12928
6. Taylor S, Spugnini EP, Assaraf YG, Azzarito T, Rauch C, Fais S. Microenvironment acidity as a major determinant of tumor chemoresistance: proton pump inhibitors (PPIs) as a novel therapeutic approach. *Drug Resist Updat.* (2015) 23:69–78. doi: 10.1016/j.drup.2015.08.004
7. Cui Q, Wen S, Huang P. Targeting cancer cell mitochondria as a therapeutic approach: recent updates. *Future Med Chem.* (2017) 9:929–49. doi: 10.4155/fmc-2017-0011
8. Rashmi R, Huang X, Floberg JM, Elhammali AE, McCormick ML, Patti GJ, et al. Radioresistant cervical cancers are sensitive to inhibition of glycolysis and redox metabolism. *Cancer Res.* (2018) 78:1392–403. doi: 10.1158/0008-5472.CAN-17-2367
9. Centurione L, Aiello FB. DNA repair and cytokines: TGF-beta, IL-6, and thrombopoietin as different biomarkers of radioresistance. *Front Oncol.* (2016) 6:175. doi: 10.3389/fonc.2016.00175
10. Yoshimoto K, Mizoguchi M, Hata N, Murata H, Hatae R, Amano T, et al. Complex DNA repair pathways as possible therapeutic targets to overcome temozolomide resistance in glioblastoma. *Front Oncol.* (2012) 2:186. doi: 10.3389/fonc.2012.00186
11. Bekaii-Saab T, El-Rayes B. Identifying and targeting cancer stem cells in the treatment of gastric cancer. *Cancer Am Cancer Soc.* (2017) 123:1303–12. doi: 10.1002/cncr.30538
12. Prieto-Vila M, Takahashi RU, Usuba W, Kohama I, Ochiya T. Drug resistance driven by cancer stem cells and their niche. *Int J Mol Sci.* (2017) 18:E2574. doi: 10.3390/ijms18122574
13. Cui Q, Wang JQ, Assaraf YG, Ren L, Gupta P, Wei L, et al. Modulating ROS to overcome multidrug resistance in cancer. *Drug Resist Updat.* (2018) 41:1–25. doi: 10.1016/j.drup.2018.11.001
14. Zhang G, Wang W, Yao C, Ren J, Zhang S, Han M. Salinomycin overcomes radioresistance in nasopharyngeal carcinoma cells by inhibiting Nrf2 level and promoting ROS generation. *Biomed Pharmacother.* (2017) 91:147–54. doi: 10.1016/j.biopha.2017.04.095
15. Ceballos MP, Rigalli JP, Cere LI, Semeniuk M, Catania VA, Ruiz ML. ABC transporters: regulation and association with multidrug resistance in hepatocellular carcinoma and colorectal carcinoma. *Curr Med Chem.* (2018) doi: 10.2174/0929867325666180105103637. [Epub ahead of print].
16. Chen ZS. ABC transporters in pharmacology/physiology and human diseases. *Curr Pharm Biotechnol.* (2011) 12:569. doi: 10.2174/138920111795163940
17. Fu D. Where is it and how does it get there—intracellular localization and traffic of P-glycoprotein. *Front Oncol.* (2013) 3:321. doi: 10.3389/fonc.2013.00321
18. Zinzi L, Capparelli E, Cantore M, Contino M, Leopoldo M, Colabufo NA. Small and innovative molecules as new strategy to revert MDR. *Front Oncol.* (2014) 4:2. doi: 10.3389/fonc.2014.00002
19. Ezrahi S, Aserin A, Garti N. Basic principles of drug delivery systems—the case of paclitaxel. *Adv Colloid Interface Sci.* (2019) 263:95–130. doi: 10.1016/j.cis.2018.11.004
20. Meyers MB, Scotto KW, Sirotnak FM. P-glycoprotein content and mediation of vincristine efflux: correlation with the level of differentiation in luminal epithelium of mouse small intestine. *Cancer Commun.* (1991) 3:159–65. doi: 10.3727/095535491820873335
21. Bao L, Hazari S, Mehra S, Kaushal D, Moroz K, Dash S. Increased expression of P-glycoprotein and doxorubicin chemoresistance of metastatic breast cancer is regulated by miR-298. *Am J Pathol.* (2012) 180:2490–503. doi: 10.1016/j.ajpath.2012.02.024

22. Frezard F, Pereira-Maia E, Quidu P, Priebe W, Garnier-Suillerot A. P-glycoprotein preferentially effluxes anthracyclines containing free basic versus charged amine. *Eur J Biochem.* (2001) 268:1561–7. doi: 10.1046/j.1432-1327.2001.01989.x
23. Arora A, Shukla Y. Modulation of vinca-alkaloid induced P-glycoprotein expression by indole-3-carbinol. *Cancer Lett.* (2003) 189:167–73. doi: 10.1016/S0304-3835(02)00550-5
24. Leu BL, Huang JD. Inhibition of intestinal P-glycoprotein and effects on etoposide absorption. *Cancer Chemother Pharmacol.* (1995) 35:432–6. doi: 10.1007/s002800050258
25. Palmeira A, Sousa E, Vasconcelos MH, Pinto MM. Three decades of P-gp inhibitors: skimming through several generations and scaffolds. *Curr Med Chem.* (2012) 19:1946–2025. doi: 10.2174/092986712800167392
26. Crowley E, McDevitt CA, Callaghan R. Generating inhibitors of P-glycoprotein: where to, now? *Methods Mol Biol.* (2010) 596:405–32. doi: 10.1007/978-1-60761-416-6_18
27. Ji N, Yang Y, Cai CY, Lei ZN, Wang JQ, Gupta P, et al. Selonsertib (GS-4997), an ASK1 inhibitor, antagonizes multidrug resistance in ABCB1- and ABCG2-overexpressing cancer cells. *Cancer Lett.* (2019) 440–441:82–93. doi: 10.1016/j.canlet.2018.10.007
28. Fan YF, Zhang W, Zeng L, Lei ZN, Cai CY, Gupta P, et al. Dacomitinib antagonizes multidrug resistance (MDR) in cancer cells by inhibiting the efflux activity of ABCB1 and ABCG2 transporters. *Cancer Lett.* (2018) 421:186–98. doi: 10.1016/j.canlet.2018.01.021
29. Gupta P, Zhang YK, Zhang XY, Wang YJ, Lu KW, Hall T, et al. Voruciclib, a potent CDK4/6 inhibitor, antagonizes ABCB1 and ABCG2-mediated multi-drug resistance in cancer cells. *Cell Physiol Biochem.* (2018) 45:1515–28. doi: 10.1159/000487578
30. Zhang YK, Zhang XY, Zhang GN, Wang YJ, Xu H, Zhang D, et al. Selective reversal of BCRP-mediated MDR by VEGFR-2 inhibitor ZM323881. *Biochem Pharmacol.* (2017) 132:29–37. doi: 10.1016/j.bcp.2017.02.019
31. Yang L, Li M, Wang F, Zhen C, Luo M, Fang X, et al. Ceritinib enhances the efficacy of substrate chemotherapeutic agent in human ABCB1-overexpressing leukemia cells *in vitro*, *in vivo* and *ex-vivo*. *Cell Physiol Biochem*. (2018) 46:2487–99. doi: 10.1159/000489655
32. Engstrom LD, Aranda R, Lee M, Tovar EA, Essenburg CJ, Madaj Z, et al. Glesatinib exhibits antitumor activity in lung cancer models and patients harboring MET Exon 14 mutations and overcomes mutation-mediated resistance to type I MET inhibitors in nonclinical models. *Clin Cancer Res.* (2017) 23:6661–72. doi: 10.1158/1078-0432.CCR-17-1192
33. Reungwetwattana T, Liang Y, Zhu V, Ou SI. The race to target MET exon 14 skipping alterations in non-small cell lung cancer: the why, the how, the who, the unknown, and the inevitable. *Lung Cancer.* (2017) 103:27–37. doi: 10.1016/j.lungcan.2016.11.011
34. Shi Z, Tiwari AK, Shukla S, Robey RW, Singh S, Kim IW, et al. Sildenafil reverses ABCB1- and ABCG2-mediated chemotherapeutic drug resistance. *Cancer Res.* (2011) 71:3029–41. doi: 10.1158/0008-5472.CAN-10-3820
35. Ji N, Yang Y, Lei ZN, Cai CY, Wang JQ, Gupta P, et al. Ulixertinib (BVD-523) antagonizes ABCB1- and ABCG2-mediated chemotherapeutic drug resistance. *Biochem Pharmacol.* (2018) 158:274–85. doi: 10.1016/j.bcp.2018.10.028
36. Shukla S, Abel B, Chufan EE, Ambudkar SV. Effects of a detergent micelle environment on P-glycoprotein (ABCB1)-ligand interactions. *J Biol Chem.* (2017) 292:7066–76. doi: 10.1074/jbc.M116.771634
37. Zhang YK, Zhang GN, Wang YJ, Patel BA, Talele TT, Yang DH, et al. Bafetinib (INNO-406) reverses multidrug resistance by inhibiting the efflux function of ABCB1 and ABCG2 transporters. *Sci Rep.* (2016) 6:25694. doi: 10.1038/srep25694
38. Li J, Jaimes KF, Aller SG. Refined structures of mouse P-glycoprotein. *Protein Sci.* (2014) 23:34–46. doi: 10.1002/pro.2387
39. Loo TW, Clarke DM. Mapping the binding site of the inhibitor tariquidar that stabilizes the first transmembrane domain of P-glycoprotein. *J Biol Chem.* (2015) 290:29389–401. doi: 10.1074/jbc.M115.695171
40. Loo TW, Bartlett MC, Clarke DM. Methanethiosulfonate derivatives of rhodamine and verapamil activate human P-glycoprotein at different sites. *J Biol Chem.* (2003) 278:50136–41. doi: 10.1074/jbc.M310448200
41. Loo TW, Clarke DM. Identification of residues in the drug-binding site of human P-glycoprotein using a thiol-reactive substrate. *J Biol Chem.* (1997) 272:31945–8. doi: 10.1074/jbc.272.51.31945
42. Bansal T, Mishra G, Jaggi M, Khar RK, Talegaonkar S. Effect of P-glycoprotein inhibitor, verapamil, on oral bioavailability and pharmacokinetics of irinotecan in rats. *Eur J Pharm Sci.* (2009) 36:580–90. doi: 10.1016/j.ejps.2008.12.005
43. Breier A, Gibalova L, Seres M, Barancik M, Sulova Z. New insight into p-glycoprotein as a drug target. *Anticancer Agents Med Chem.* (2013) 13:159–70. doi: 10.2174/187152013804487380
44. Nobili S, Landini I, Mazzei T, Mini E. Overcoming tumor multidrug resistance using drugs able to evade P-glycoprotein or to exploit its expression. *Med Res Rev.* (2012) 32:1220–62. doi: 10.1002/med.20239
45. Sharom FJ, Yu X, Chu JW, Doige CA. Characterization of the ATPase activity of P-glycoprotein from multidrug-resistant Chinese hamster ovary cells. *Biochem J.* (1995) 308 (Pt 2):381–90. doi: 10.1042/bj3080381
46. Hrycyna CA, Ramachandra M, Ambudkar SV, Ko YH, Pedersen PL, Pastan I, et al. Mechanism of action of human P-glycoprotein ATPase activity. Photochemical cleavage during a catalytic transition state using orthovanadate reveals cross-talk between the two ATP sites. *J Biol Chem.* (1998) 273:16631–4. doi: 10.1074/jbc.273.27.16631
47. Kato Y, Ozawa S, Miyamoto C, Maehata Y, Suzuki A, Maeda T, et al. Acidic extracellular microenvironment and cancer. *Cancer Cell Int.* (2013) 13:89. doi: 10.1186/1475-2867-13-89
48. List AF, Kopecky KJ, Willman CL, Head DR, Slovak ML, Douer D, et al. Cyclosporine inhibition of P-glycoprotein in chronic myeloid leukemia blast phase. *Blood.* (2002) 100:1910–2.
49. Chung FS, Santiago JS, Jesus MF, Trinidad CV, See MF. Disrupting P-glycoprotein function in clinical settings: what can we learn from the fundamental aspects of this transporter? *Am J Cancer Res*. (2016) 6:1583–98.
50. Li W, Zhang H, Assaraf YG, Zhao K, Xu X, Xie J, et al. Overcoming ABC transporter-mediated multidrug resistance: molecular mechanisms and novel therapeutic drug strategies. *Drug Resist Updat.* (2016) 27:14–29. doi: 10.1016/j.drup.2016.05.001
51. Zhang GN, Zhang YK, Wang YJ, Gupta P Jr, Ashby CR, Alqahtani S, et al. Epidermal growth factor receptor (EGFR) inhibitor PD153035 reverses ABCG2-mediated multidrug resistance in non-small cell lung cancer: *in vitro* and *in vivo*. *Cancer Lett.* (2018) 424:19–29. doi: 10.1016/j.canlet.2018.02.040

Conflict of Interest Statement: The authors declare that the research was conducted in the absence of any commercial or financial relationships that could be construed as a potential conflict of interest.

frontiers in Oncology

ORIGINAL RESEARCH
published: 26 April 2019
doi: 10.3389/fonc.2019.00306

Inhibition of SMYD2 Sensitized Cisplatin to Resistant Cells in NSCLC Through Activating p53 Pathway

Lei Shang[1,2] *and Minjie Wei*[1]*

[1] School of Pharmacy, China Medical University, Shenyang, China, [2] Shenyang Medical College, Shenyang, China

The protein lysine methyltransferase SMYD2 has recently emerged as a new enzyme modulate gene transcription or signaling pathways, and involved into tumor progression. However, the role of SMYD2 in drug resistant is still not known. Here, we found that inhibition of SMYD2 by specific inhibitor could enhance the cell sensitivity to cisplatin (CDDP), but not paclitaxel, NVB, and VCR in non-small cell lung cancer (NSCLC). Further study showed that SMYD2 and its substrates were overexpressed in NSCLC resistant cells, and the inhibition of SMYD2 or knockdown by specific siRNA could reverse the cell resistance to cisplatin treatment in NSCLC/CDDP cells. In addition, our data indicated that the inhibition or knockdown SMYD2 inhibit tumor sphere formation and reduce cell migration in NSCLC/CDDP cells, but not in NSCLC parental cells. Mechanistically, inhibition of SMYD2 could enhance p53 pathway activity and induce cell apoptosis through regulating its target genes, including p21, GADD45, and Bax. On the contrary, the sensitivity of cells to cisplatin was decreased after knockdown p53 or in p53 deletion NSCLC cells. The synergistically action was further confirmed by *in vivo* experiments. Taken together, our results demonstrate SMYD2 is involved into cisplatin resistance through regulating p53 pathway, and might become a promising therapeutic target for cisplatin resistance in NSCLC.

Keywords: SMYD2, cisplatin resistance, lung cancer, p53, apoptosis

OPEN ACCESS

Edited by:
Yan-yan YAN,
Shanxi Datong University, China

Reviewed by:
Chiara Ambrogio,
Dana–Farber Cancer Institute, United States
Dawn Sijin Nin,
National University of Singapore, Singapore

***Correspondence:**
Minjie Wei
mjwei@cmu.edu.cn

Specialty section:
This article was submitted to Cancer Molecular Targets and Therapeutics, a section of the journal Frontiers in Oncology

Received: *23 December 2018*
Accepted: *03 April 2019*
Published: *26 April 2019*

Citation:
Shang L and Wei M (2019) Inhibition of SMYD2 Sensitized Cisplatin to Resistant Cells in NSCLC Through Activating p53 Pathway. Front. Oncol. 9:306. doi: 10.3389/fonc.2019.00306

INTRODUCTION

The incidence and mortality of lung cancer ranks at the NO.1 among all kinds of cancer (1). Non-small cell lung cancer (NSCLC) accounts for about 85% of lung cancer (1, 2). The surgery, radiotherapy, chemotherapy, molecular targeting therapy, and immunotherapy are possible choice for NSCLC treatment (2). However, most of NSCLCs are found at advanced stage, so drug-based therapy, mainly including chemotherapy, is considered as the most important approach to treat NSCLCs (3).

The platinum-based chemotherapy, such as cisplatin plus paclitaxel, cisplatin plus NVB, and cisplatin plus VCR, is the first-line treatment approach in NSCLCs (2, 3). However, drug resistance will be inevitable happened after treatment for 1–2 years, which limit the application of chemotherapeutic agents (4, 5). To solve this problem, we should first understand the resistant mechanisms for chemotherapy in NSCLCs. In fact, many previous studies have shown that the upregulation of efflux protein, the mutation of drug target, the activation of by-pass oncogenic pathway, and the accumulation of phenotype change cells contributed to the resistance of chemotherapeutic agents in NSCLCs (6, 7). However, there is still unknown for a large part of NSCLC resistant patients.

SMYD2 was identified as protein methyltransferase which adds methyl-group to its histone and non-histone substrates and epigenetically regulates their function (8, 9). Recently, SMYD2 was observed to involve into the upset and progression of various tumors including leukemia, breast cancer, teratocarcinoma, gastric cancer, and head and neck cancer (10–14). Mechanistically, SMYD2 was found to prompt cell proliferation, block apoptosis, and enhance cell migration and invasion through regulating its substrates methylation status, such as p53 and histone4 (13–15). However, whether this enzyme is involved into drug resistance is still not known.

Here, NSCLC was used to as an example to investigate the role of SMYD2 in chemotherapeutic resistance. Our data showed that SMYD2 was involved into cisplatin resistance, but not paclitaxel, NVB, and VCR. Further study indicated that SMYD2 expression and its activity were increasing in cisplatin resistant NSCLC cells. Mechanistically, SMYD2 prompt cell migration, increase the tumor sphere and block apoptosis, which is dependent on the methylation of $p53^{K370}$. The inhibition or knockdown of SMYD2 model would result in the increasing of sensitivity to cisplatin *in vitro* and *in vivo*. Our results not only elucidate the role of SMYD2 in cisplatin resistance and provide a potential method to reverse cisplatin resistance in NSCLC.

MATERIALS AND METHODS

Cell Lines, Cell Culture, and Treatment

A549 (p53 wide type, KRAS mutation), NCI-H460 (p53 wide type, KRAS mutation), and NCI-H1299 (p53 deletion, KRAS wide type) human lung adenocarcinoma cell lines were purchased from the American Type Culture Collection (ATCC; Manassas, VA, USA). These cancer cells were routinely cultured in RPMI-1640 medium (Gibco, Grand Island, NY, USA) supplemented with 10% fetal bovine serum (FBS; Gibco) and were maintained at 37°C in a humidified incubator with 5% CO_2. The cells were treated with Cisplatin (J&K Scientific Ltd, Beijing, China) at increasing concentrations (ranging from 0.5 to 4 μM) for 3 months.

Compounds and Reagents

BAY-498(SMYD2 inhibitor), AZ505(SMYD2 inhibitor), Cisplatin(CDDP), Vinorelbine(NVB), Paclitaxel (Taxol), and Vincristine sulfate(VCR) was obtained from MedChem Express (Princeton, NJ, USA). The primary antibodies against SMYD2, p53, Cleaved-PARP, and β-actin were obtained from Cell Signaling Technology (Danvers, MA, USA), and the primary antibodies against $p53^{K370Me}$ was purchased from Immunoway Technology (Plano, TX, USA). The pcDNA3-p53 vector was obtained from Addgene.

Cell Viability Assay

In vitro cell viability was determined using the MTT assay. Cells (1×10^5 cells/ml) were seeded in 96-well culture plates. After incubating overnight, the cells were treated with various concentrations of the appropriate agents for 48 h, after which 10 μl of MTT solution (2.5 mg/ml in PBS) was added to each well, and the plates were incubated for an additional 4 h at 37°C. After the samples were centrifuged (2,500 rpm, 10 min), the medium supplemented with MTT was aspirated, and then 100 μl of DMSO was added to each well. The optical density of each well was measured at 570 nm with a Biotek Synergy^{TM} HT Reader (BioTek Instruments, Winooski, VT, USA).

Western Blot Analysis

Western blotting was performed as previously described (14). Briefly, equal amounts of total protein extracts from cultured cells or tissues were fractionated by 10–15% SDS-PAGE before being electrically transferred onto polyvinylidene difluoride (PVDF) membranes, which were sequentially incubated with mouse or rabbit primary antibodies and horseradish peroxidase (HRP)-conjugated secondary antibodies designed to detect the proteins of interest. The indicated secondary antibodies were subsequently reacted with ECL detection reagents (Pierce, Thermo Fisher Scientific, Waltham, MA, USA) and then incubated in a dark room. The relative expression levels of the indicated proteins were normalized to those of β-actin.

Flow Cytometry Analysis

Analyses for apoptosis were conducted with an Annexin V-FITC Apoptosis Detection Kit (BioVision, Mountain View, CA, USA). Cells (1×10^6) were exposed to various inhibitors for 48 h. They were collected by centrifugation and resuspended in 500 μL of 1 × binding buffer. Annexin V-fluorescein isothiocyanate (FITC; 5 μL) and PI (5 μL) were added to the cells. After incubation at room temperature for 5 min in the dark, cells were analyzed by FACS using a flow cytometer (BD Biosciences, San Jose, CA, USA). Cells that stained Annexin V-FITC (apoptosis) were analyzed.

siRNA-Mediated Gene Knockdown

SMYD2 and *p53* knockdown was performed using specific siRNAs purchased from Santa Cruz Biotechnology (Santa Cruz Biotechnology, Santa Cruz, CA, USA). Scramble non-target siRNAs served as negative controls. siRNA was introduced into the indicated cell lines with Lipofectamine RNAiMAX reagent (Thermo Fisher Scientific), according to the manufacturer's instructions, and knockdown efficiency was assessed by western blotting.

Transwell Migration Assay

NCI-H460/CDDP and its parental cell lines migration capacities were tested by Corning transwell assay, according to the manufacturer's instructions. Briefly, the indicated lung cancer cells were treated DMSO, BAY-598 (200 nM), Scramble siRNA, and SMYD2 siRNA (50 nM) for 48 h and then seeded in the upper chamber of the system at a density of 5×10^4 cells/well in serum-free medium (100 μl). The wells in the lower chamber of the system were filled with complete medium. After incubating for 48 h, the cells remaining in the upper chamber were carefully removed with a cotton swab, and the cells that had migrated through the membrane and adhered to its lower surface were fixed with 100% methanol and stained with 0.2% crystal violet. The membrane was then photographed under a microscope,

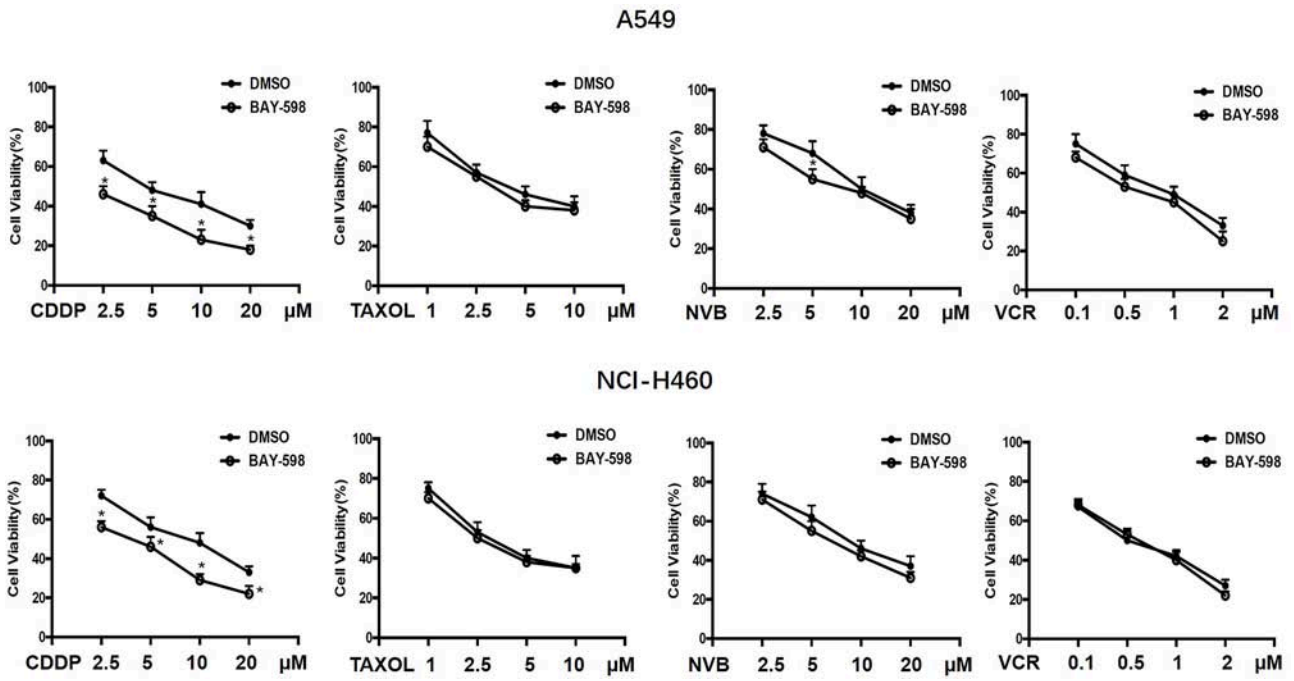

FIGURE 1 | Effects of the combination of chemotherapeutic agents and SMYD2 inhibitor on cell growth in NSCLC cells. The growth of A549 and NCI-H460 cells treated with chemotherapeutic agents, including CDDP, Taxol, NVB, and VCR at different concentrations or combination with SMYD2 inhibitor BAY-598. Cell lines treated with DMSO were used as controls.

and the cells in five predetermined fields were counted at 200× magnification.

Tumor Sphere Formation Assay

NCI-H460/CDDP and its parental cell lines were treated DMSO, BAY-598 (200 nM), Scramble siRNA, and SMYD2 siRNA (50 nM) for 48 h, after which single cells prepared by mechanical and enzymatic dissociation were seeded in 6-well ultra-low attachment plates (Corning, NY, USA) at a density of 1,000 cells/well in serum-free DMEM/F-12 medium supplemented with B27 (1×, Invitrogen, Thermo Fisher Scientific), 20 ng/ml human recombinant bFGF (PeproTech, Rocky Hill, NJ, USA), and 20 ng/ml EGF (PeproTech) for 10–14 days. The cells were then photographed under a microscope.

Luciferase Reporter Gene Assays

NCI-H460/CDDP and its parental cells were plated in 96-well plates. Cells in 96-well plates were transfected with 2 ng pRL-tk (Promega) and 50 ng p53 reporter plasmid (Addgene) for 24 h with the lipofectamine 3000. Cells were treated with DMSO or BAY-598 at indicated concentrations for 24 h. Luciferase activities were evaluated with the Berthold LB960 system (Berthold, DE).

Quantitative PCR Analysis

Total RNA was isolated using an RNeasy Mini Kit (Qiagen, Hilden, Germany), as described in the product insert, and then reverse transcribed with a RevertAid First Strand cDNA Synthesis Kit (Thermo Fisher Scientific). PCR was performed with iQ SYBR Green SuperMix (Bio-Red Laboratories, Hercules, CA, USA) and a CFX96 Real-Time PCR Detection System (Bio-Rad Laboratories). The following primers were used for the experiment: glyceraldehyde-3-phosphate dehydrogenase (*GAPDH*): reverse: 5′-CCCTCAACGACCACTTTGTCA-3′ and forward: 5′-TTCCTCTTGTGCTCTTGCTGG-3′; p21 forward: 5′-TGTACCCTTGTGCCTCGCTC-3′ and reverse: 5′- TGGAGA AGATCAGCCGGCGT-3′; Bax forward: 5′- TTTGCTTCAGGG TTTCATCC-3′ and reverse: 5′- CAGTTGAAGTTGCCGTCA GA-3′; and GADD45 forward: 5′-GGATGCCCTGGAGGAAGT GCT-3′ and reverse: 5′- GGCAGGATCCTTCCATTGAGATGA ATGTG-3′.

Xenografts in Mice

To assess the characteristics of chemotherapy-resistant tumors, we subcutaneously injected viable NCI-H460/CDDP cells (5×10^6/100 μl PBS per mouse), as confirmed by trypan blue staining, into the right flank of 7–8 weeks-old male BALB/C mice. When the average tumor volume reached 100 mm^3, the mice were randomly divided into the following four treatment groups: a control group (saline only, $n = 6$), a AZ505 group (40 mg/kg/qd, i.p.; $n = 6$), an CDDP group (4.0 mg/kg/3 day, i.p.; $n = 6$), and a combination treatment group (AZ505 plus CDDP). After 2 weeks, the mice were sacrificed, and the tumors were excised and stored at −80°C. These experiments were performed in strict accordance with the recommendations in the Guide for the Care and Use of Laboratory Animals of the National Institutes of Health, and the corresponding protocol was approved by the

Animal Experimental Ethics Committee of Shenyang Medical College (Shenyang, Liaoning Province, China).

Statistical Analysis

Differences between the indicated experimental groups were evaluated by one-way ANOVA or Turkey's *post hoc* test with the SPSS 11.5 software package for Windows (SPSS, Chicago, IL, USA). $P < 0.05$ were considered statistically significant ($P < 0.05$, two-tailed test).

RESULTS

The Inhibition of SMYD2 Enhanced the Antigrowth Action of Cisplatin in NSCLC Cells

To explore the possible action of SMYD2 in chemotherapeutic agents in NSCLC, A549 and NCI-H460 cells were treated with various concentrations of the first-line chemotherapeutic agents, including CDDP, Taxol, NVB, and VCR, and combined treatment with SMYD2 inhibitor BAY-598 with non-cytotoxicity concentration (2 μM, cell viability>90%, **Supplementary Figure 1A**). As shown in **Figure 1**, single treatment with CDDP, Taxol, NVB, and VCR could inhibit cell growth at concentration-dependent manner in both cell lines. Addition of SMYD2 inhibitor had no effect on the cell viability when combined with Taxol and VCR, and owned a slightly enhanced inhibition when combined with NVB. Notably, the combination of BAY-598 and CDDP could significantly retard cell growth in both A549 and NCI-H460 cells ($P < 0.05$), suggesting SMYD2 inhibition might be involved into the cell sensitivity to CDDP but not Taxol, VCR, and NVB.

The Expression and Function of SMYD2 in Cisplatin Resistant NSCLC Cells

To clarify the role and function of SMYD2 in CDDP sensitivity of NSCLC cells, we established A549 and NCI-H460 CDDP resistant cell lines. First, we detected the expression level of SMYD2 in parental cell lines and resistant cell lines. Western blot data indicated that SMYD2 was increased in both resistant cell lines as compared to parental cell lines. In consistent with the SMYD2 upregulation in resistant cell lines, the non-histone substrate of SMYD2, $p53^{K370me}$, was also increased in resistant cell lines. The above data demonstrated that the expression and activity of SMYD2 were increased in CDDP resistant cells. Next, to further elucidate the role of SMYD2 in CDDP resistance, we measured the cell viability of NCI-H460/CDDP cells to CDDP after suppression of SMYD2 by specific inhibitor and siRNA. Our data showed, whether inhibition by SMYD2 inhibitor BAY-598 or knockdown by specific siRNA, the cell sensitivity to CDDP would be significantly increased as compared to DMSO or Scramble treated groups ($P < 0.05$). The above data was confirmed by flow cytometry experiments. Treatment with BAY-598 at non-cytotoxic concentration would prompt the apoptosis induced action of CDDP in NCI-H460/CDDP cells. Similarly, knockdown SMYD2 also resulted in the increase of cell apoptosis in CDDP treated NCI-H460/CDDP cells when compared to scramble treated cells. Notably, although the addition of SMYD2 inhibitor or knockdown of SMYD2 could enhance the induction of apoptosis by CDDP in NCI-H460 cells, the level was decreased as compared with resistant cells (**Figure 2C**). The above data indicated that SMYD2 play an important role in CDDP resistance of NSCLC cells.

Inhibition of SMYD2 Reversed Malignant Phenotype of Cisplatin Resistant NSCLC Cells

To further elucidate the role of SMYD2 in CDDP resistance of NSCLC cells, we next assessed the effect of inhibition or knockdown of SMYD2 on cell migration and tumor sphere formation, which are considered as the crucial characteristics of CDDP resistant NSCLC cells (16, 17). Our results showed that cell migration number of NCI-H460/CDDP cells was significant decreased after treated with SMYD2 inhibitor or SMYD2 siRNA as compared to DMSO and Scramble siRNA control, respectively. Furthermore, tumor sphere number of NCI-H460/CDDP cells was also obviously reduced by SMYD2 inhibitor and SMYD2 siRNA. It should be noted that whether addition of BAY-598 or specific siRNA could not significantly affect cell migration number and tumor sphere ability in NCI-H460 cells (**Supplementary Figures 1B–D**). The above results demonstrated that SMYD2 was also involved into the formation of malignant phenotype in CDDP resistant NSCLC cells.

SMYD2 Mediated Cisplatin Resistance Dependent on p53 Regulation in NSCLC Cells

In view of the crucial role of p53 and its epigenetic regulation by SMYD2 (18), we next explore possible role of p53 in SMYD2 mediated CDDP resistance. As shown in **Figure 4A**, knockdown p53 by specific siRNA contributed to the decrease of cell sensitivity to CDDP in NCI-H460/CDDP cells, which owned wide type p53 expression. In addition, the restore of p53 in NCI-H1299 cells (p53 deletion) could lead to the increase of cell sensitivity to CDDP. The above data indicates that the status and expression level of p53 will affect the cell sensitivity of NSCLC cells to CDDP.

In order to explore the effect of SMYD2 on p53 activity, we detected the transcriptional regulation activity of p53 by luciferase assay after treated with BAY-598 in NCI-H460/CDDP and its parental cells. The results showed that BAY-598 could concentration-dependently enhance p53 reporter activity in NCI-H460/CDDP cells (**Figure 4B**). In consistent with reporter assay, BAY-598 treatment also significantly resulted in the upregulation in mRNA level of p53 targeting genes, including p21, GADD45, and Bax (**Figure 4C**), in NCI-H460/CDDP cells. In consistent with resistant cell lines, BAY-598 also could increase p53 reporter activity, p21 and GADD45 expressions in NCI-H460 cells to some extent (**Figure 4B**). On the contrary, BAY-598 treatment could not induce the BAX expression in NCI-H460 cells, suggesting the role of SMYD2 in BAX regulation is different in parental and resistant cells (**Figure 4C**). Furthermore,

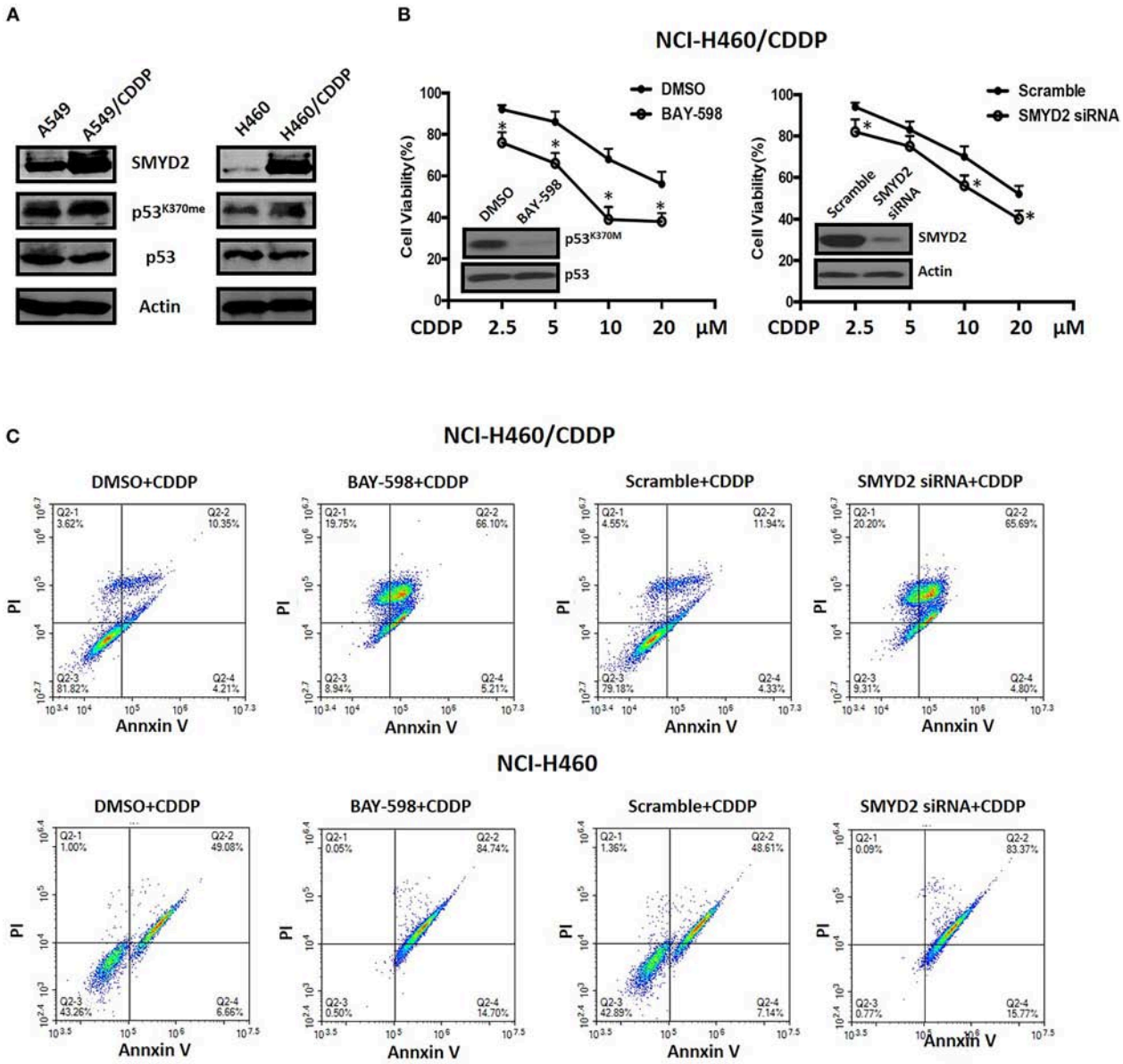

FIGURE 2 | The expression level of SMYD2-related proteins and the effects of genetic or chemical manipulation of SMYD2 on the cell growth of CDDP-resistant and parental NSCLC cells. **(A)** SMYD2, p53, and p53^{K370me} expression levels were measured in CDDP resistant and parental NSCLC cell lines. β-actin was used as a loading control. **(B)** Cell viability was measured in BAY-598-treated or SMYD2-knockdown NCI-H460/CDDP cells treated with CDDP at different concentrations for 36 h. Scramble siRNA or DMSO was used as a control. The efficacy of genetic or chemical manipulation of SMYD2 was confirmed by Western blot in NCI-H460/CDDP cells. **(C)** Cell apoptosis was assessed using Annexin V/PI double staining in BAY-598-treated or SMYD2-knockdown CDDP resistant and parental NCI-H460 cells after treated with CDDP at 10 μM for 48 h. *$P < 0.05$, compared to corresponding control cells.

we also detected the cell apoptosis status of NCI-H460/CDDP and NCI-H460 cells after treated with BAY-598. Our results indicated BAY-598 at 10 μM could induce cell apoptosis in NCI-H460/CDDP cells, but not in NCI-H460 cells (**Figure 4D**), which confirmed the regulation action of Bax, a pro-apoptosis gene, by SMYD2. Taken together, our data suggested that the SMYD2 mediated CDDP resistance through epigenetic regulation of p53.

Inhibition of SMYD2 Sensitized Cisplatin Through Epigenetic Regulation of p53 *in vivo*

To clarify the therapeutic meaning of the above finding, we assessed anti-tumor effect of the combination of SMYD inhibitor and CDDP in NCI-H1299/CDDP xenograft mice. As shown in **Figure 5A**, single treatment with CDDP has no significant effect on tumor growth, indicating the resistant phenotype of

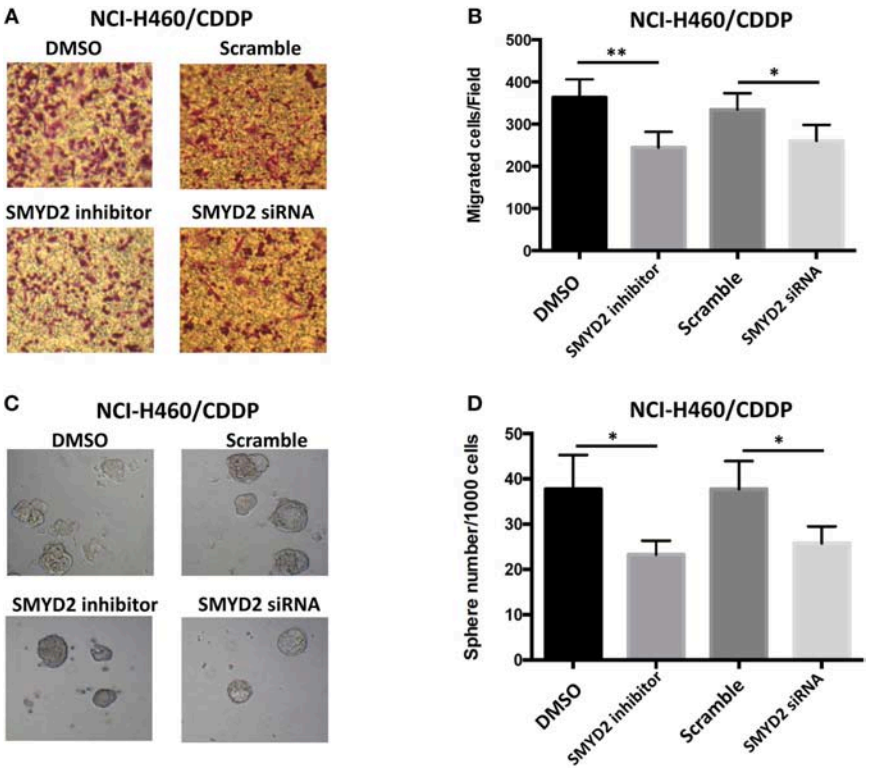

FIGURE 3 | Effects of genetic or chemical manipulation of SMYD2 on the biological characteristics of CDDP-resistant NSCLC cells. **(A,B)** Cell migration was measured in NCI-H460/CDDP cells treated with 2 μM BAY-598 or 50 nM SMYD2 siRNA. Scramble siRNA or DMSO was used as a control. **(C,D)** Tumor sphere was counted in NCI-H460/CDDP cells treated with 2 μM BAY-598 or 50 nM SMYD2 siRNA. Scramble siRNA or DMSO was used as a control. (Scale bars, 100 μm) $^{*}P < 0.05$, $^{**}P < 0.001$, compared to corresponding control cells.

NCI-H1299/CDDP xenograft mice. Similar to CDDP single treatment, single treatment with AZ505, an *in vivo* available SMYD2 inhibitor, only displayed a slightly inhibition on tumor growth. Interestingly, the combination of AZ505 and CDDP could obviously inhibit tumor growth of NCI-H1299/CDDP xenograft mice when compared to vehicle control and single treatment group. In addition, we didn't find the body weight loss in the combination treated group (data not shown), suggesting the combination has no effect on gross toxicity. Next, we further explored the underlying mechanisms using tumor tissue. Western blot data showed that AZ505 single treatment could lead to the decrease of $p53^{K370me}$, whereas CDDP single treatment could slightly increase the level of $p53^{K370me}$ (**Figure 5B**). The combination treatment contributed to a decrease of $p53^{K370me}$. In addition, we found the expression of the clv-PARP, an apoptosis biomarker, was increased in the combination group (**Figure 5B**). In summary, our *in vivo* data showed the inhibition of SMYD2 by AZ505 could sensitize cisplatin antitumor action through epigenetic regulation of p53.

DISCUSSION

Cisplatin(CDDP) is the first line drug for NSCLC patients, therefore, understanding and preventing CDDP resistance are considered as the crucial issue with respect to the treatment of NSCLC (5). Here, we found that SMYD2, a protein methyltransferase, was involved into cisplatin resistance. Furthermore, out data showed that SMYD2 expression and its activity were increasing in cisplatin resistant NSCLC cells. Mechanistically, SMYD2 prompt cell migration, increase the tumor sphere, and block apoptosis, which is dependent on the methylation of $p53^{K370}$. The inhibition or knockdown of SMYD2 model would result in the increasing of sensitivity to cisplatin *in vitro* and *in vivo*. Our findings provide us with a novel perspective epigenetic regulation mechanisms underlying CDDP resistance and define that the combination of SMYD2 inhibitor and CDDP may have promise as treatments for patients with CDDP-resistant NSCLC.

SMYD2 is a protein methyltransferase that catalyzes the methylation of histone substrates, such as H3K4 and H3K36 (18), and non-histone substrates, including p53 (19), Rb (20), HSP90 (21), STAT3, and NF-κB (22). It has been reported that SMYD2 was involved into the upset and progression of various tumors, including leukemia, breast cancer, gastric cancer, and head and neck cancer. Recently, Wang et al. reported SMYD2 inhibition also led to the suppression of cell growth in NSCLC cells (23), suggesting SMYD2 might be involved into lung cancer. Our results demonstrated that SMYD2

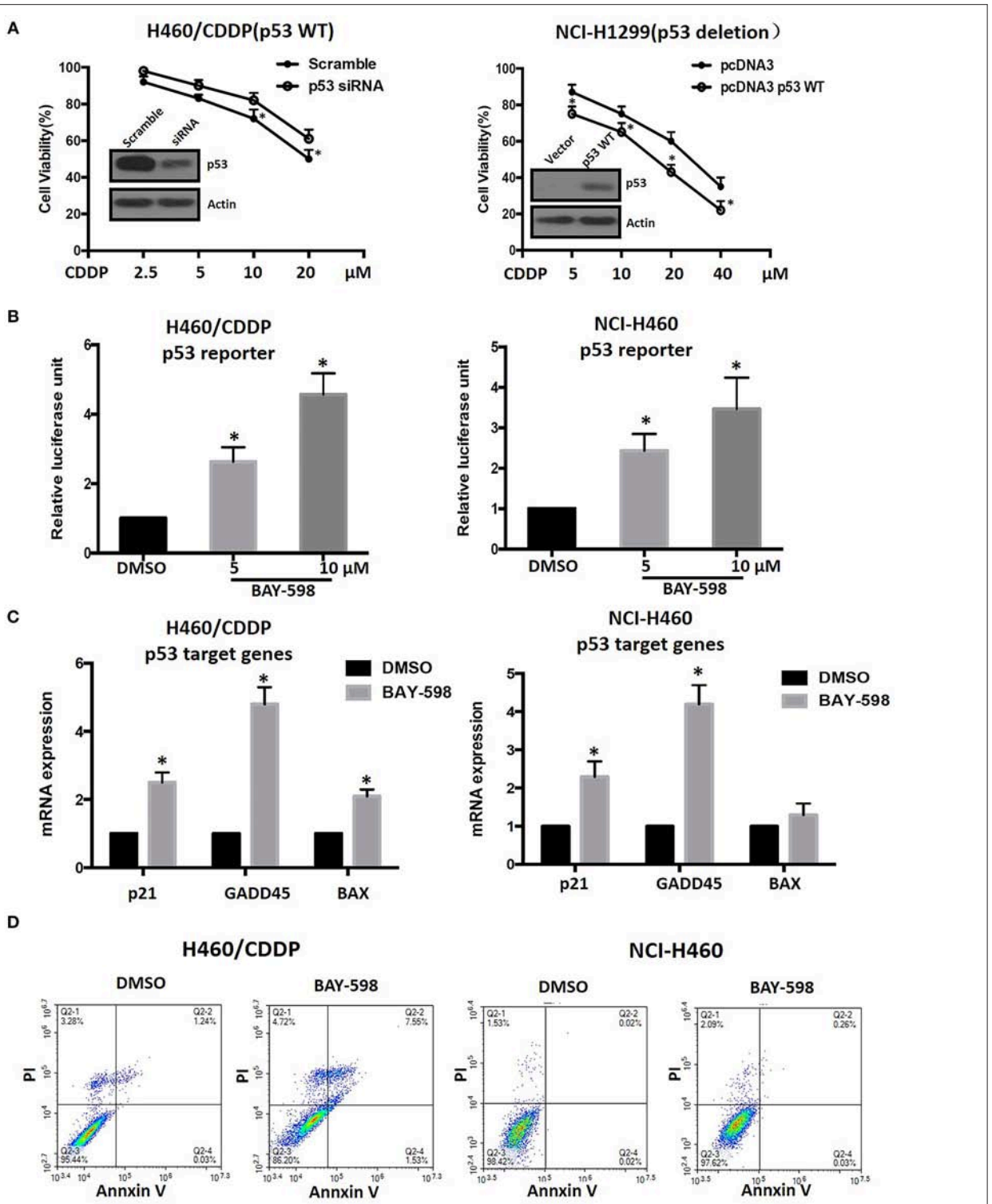

FIGURE 4 | Epigenetic regulation of p53 and its role in CDDP resistance in NSCLC. **(A)** Cell viability in NCI-H460/CDDP (p53 wide type) and NCI-H1299(p53 deletion) cells, with p53 gene manipulation, which were treated with CDDP at different concentrations for 48 h. Scramble siRNA or mock vector was used as a control. The p53 knock-down or restoration efficacy was confirmed by Western Blot. **(B)** The p53 reporter activity was measured in CDDP resistant and parental NCI-H460 cells after treated with BAY-598. The relative luciferase unit was calculated by Luciferase/Renilla and DMSO was considered as 100%. **(C)** The mRNA expression levels of p21, GADD45, and Bax were assessed by real-time RT-PCR in CDDP resistant and parental NCI-H460 cells treated with 10 μM BAY-598. GAPDH was used as a control. **(D)** Cell apoptosis was assessed using Annexin V/PI double staining in CDDP resistant and parental NCI-H460 cells which were treated with BAY-598 at 10 μM concentrations for 48 h. $^*P < 0.05$, compared to corresponding control cells.

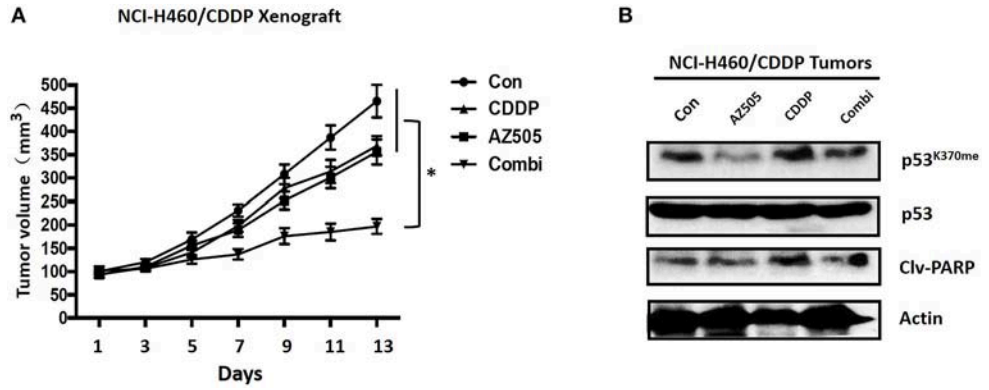

FIGURE 5 | Effects of SMYD2 inhibition and/or CDDP on tumor growth in an CDDP-resistant xenograft model. **(A)** Tumor volume was measured in NCI-H460/CDDP xenografts treated with AZ505, CDDP, or the combination of AZ505 and CDDP. **(B)** The p53 and $p53^{K370me}$, and cleaved PARP(clv-PARP) expression levels were measured in NCI-H460/CDDP xenograft tumor tissues. β-actin was used as a loading control. $^*P < 0.05$, combined treatment group compared to single treatment group and vehicle control.

expression and enzymatic activity levels were upregulated in NSCLC CDDP-resistant cells as compared to parental cells. In addition, either suppressing SMYD2 activity or knocking down SMYD2 would contribute to the increases in sensitivity to CDDP, and the reduction in cell migration and self-renewal ability in CDDP-resistant NSCLC cells, indicating that SMYD2 executes a crucial role in CDDP resistance of NSCLC.

SMYD2 methylates H3K4 and H3K36 would contribute the change of chromatin structure, and subsequently lead to the alteration of its target genes (18). In fact, the important function of SMYD2 was reported to related methylate to its non-histone substrates (9, 24). SMYD2 monomethylates Lys-370 of p53, leading to decreased DNA-binding activity and subsequent transcriptional regulation activity of p53. We found that, as long as the SMYD2 upregulation, the $p53^{K370me}$ level was also increased in CDDP resistant NSCLC cells. Importantly, our data showed that cell sensitivity to CDDP was dependent on wild type p53 level. Inhibition of SMYD2 could induce the increasing of p53 transcription activity and its target gene expression. Taken together, these findings indicate that epigenetic regulation by SMYD2 plays an important role in p53 transcriptional activity and is involved in processes associated with CDDP resistance.

K-RAS is one of the most frequently mutated in human NSCLC (25). Mutation of K-RAS usually results in the activation of oncogenic signaling molecules that regulate cell growth, survival and differentiation by coupling receptor activation to downstream effector pathways (25), and leads to the resistance to tyrosine kinase inhibitors such as gefitinib and erlotinib (26). Therefore, chemotherapy is the standard of treatment for K-RAS mutant NSCLC tumors. Here, our data shown that inhibition of SMYD2 by specific inhibitor can sensitize CDDP efficacy in K-RAS mutated A549 and NCI-H460 cell lines, suggesting epigenetic manipulation might be a promising adjuvant approach to treat K-RAS mutant tumors.

In conclusion, the present study elucidated that the activity of SMYD2 in NSCLC may affect the cell sensitivity to chemotherapeutic agents, especially to CDDP. The elevated SMYD2 mediated CDDP resistance and malignant phenotype in NSCLC, indicating that SMYD2 may be a useful biomarker of CDDP resistance in NSCLC. Inhibition of SMYD2 contributes to the methylation-related activation of p53 and thus results in cell apoptosis. Furthermore, combination treatment with CDDP and an SMYD2 inhibitor had a synergistically antitumor effects in a xenograft model *in vivo*. Given that SMYD2 has reversible effects and is a targetable protein methyltransferase, treatments targeting the protein may be useful for reversing CDDP resistance in NSCLC.

ETHICS STATEMENT

This study was carried out in accordance with the recommendations in the Guide for the Care and Use of Laboratory Animals of the National Institutes of Health, and the corresponding protocol was approved by the Animal Experimental Ethics Committee of Shenyang Medical College (Shenyang, Liaoning Province, China).

AUTHOR CONTRIBUTIONS

All authors listed have made a substantial, direct and intellectual contribution to the work, and approved it for publication.

FUNDING

This work was supported by the National Natural Science Foundation of China (No. 81803476).

SUPPLEMENTARY MATERIAL

The Supplementary Material for this article can be found online at: https://www.frontiersin.org/articles/10.3389/fonc.2019.00306/full#supplementary-material

Supplementary Figure 1 | The effects of genetic or chemical manipulation of SMYD2 on the cell growth, migration, and tumor sphere ability of NCI-H460 cells. **(A)** The growth of A549 and NCI-H460 cells treated with various concentrations SMYD2 inhibitor BAY-598. Cell viability was detected by MTT assay. **(B)** The efficacy of genetic or chemical manipulation of SMYD2 was confirmed by Western blot in NCI-H460 cells. $p53^{K370me}$ and SMYD2 expression levels were measured in NCI-H460 cell lines. The p53 or β-actin was used as a loading control. **(C)** Cell migration was measured in NCI-H460 cells treated with 2 μM BAY-598 or 50 nM SMYD2 siRNA. Scramble siRNA or DMSO was used as a control. **(D)** Tumor sphere was counted in NCI-H460 cells treated with 2 μM BAY-598 or 50 nM SMYD2 siRNA. Scramble siRNA or DMSO was used as a control.

REFERENCES

1. Siegel RL, Miller KD, Jemal A. Cancer statistics, 2016. *CA Cancer J Clin*. (2016) 66:7–30. doi: 10.3322/caac.21332
2. Hirsch FR, Scagliotti GV, Mulshine JL, Kwon R, Curran WJ Jr., Wu YL, et al. Lung cancer: current therapies and new targeted treatments. *Lancet*. (2017) 389:299–311. doi: 10.1016/S0140-6736(16)30958-8
3. Chang A. Chemotherapy, chemoresistance and the changing treatment landscape for NSCLC. *Lung Cancer*. (2011) 71:3–10. doi: 10.1016/j.lungcan.2010.08.022
4. Rivera G, Wakelee HA. Resistance to therapy. *Cancer Treat Res*. (2016) 170:183–202. doi: 10.1007/978-3-319-40389-2_9
5. Kim ES. Chemotherapy resistance in lung cancer. *Adv Exp Med Biol*. (2016) 893:189–209. doi: 10.1007/978-3-319-33826-2
6. Galluzzi L, Vitale I, Michels J, Brenner C, Szabadkai G, Harel-Bellan A, et al. Systems biology of cisplatin resistance: past, present and future. *Cell Death Dis*. (2014) 5:e1257. doi: 10.1038/cddis.2013.428
7. Hardin C, Shum E, Singh AP, Perez-Soler R, Cheng H. Emerging treatment using tubulin inhibitors in advanced non-small cell lung cancer. *Expert Opin Pharmacother*. (2017) 18:701–16. doi: 10.1080/14656566.2017.1316374
8. Brown MA, Sims RJ III, Gottlieb PD, Tucker PW. Identification and characterization of Smyd2: a split SET/MYND domain-containing histone H3 lysine 36-specific methyltransferase that interacts with the Sin3 histone deacetylase complex. *Mol Cancer*. (2006) 5:26. doi: 10.1186/1476-4598-5-26
9. Hamamoto R, Saloura V, Nakamura Y. Critical roles of non-histone protein lysine methylation in human tumorigenesis. *Nat Rev Cancer*. (2015) 15:110–24. doi: 10.1038/nrc3884
10. Sakamoto LH, Andrade RV, Felipe MS, Motoyama AB, Pittella Silva F. SMYD2 is highly expressed in pediatric acute lymphoblastic leukemia and constitutes a bad prognostic factor. *Leuk Res*. (2014) 38:496–502. doi: 10.1016/j.leukres.2014.01.013
11. Li LX, Zhou JX, Calvet JP, Godwin AK, Jensen RA, Li X. Lysine methyltransferase SMYD2 promotes triple negative breast cancer progression. *Cell Death Dis*. (2018) 9:326. doi: 10.1038/s41419-018-0347-x
12. Zhu J, Dou Z, Sammons MA, Levine AJ, Berger SL. Lysine methylation represses p53 activity in teratocarcinoma cancer cells. *Proc Natl Acad Sci USA*. (2016) 113:9822–7. doi: 10.1073/pnas.1610387113
13. Ohtomo-Oda R, Komatsu S, Mori T, Sekine S, Hirajima S, Yoshimoto S, et al. SMYD2 overexpression is associated with tumor cell proliferation and a worse outcome in human papillomavirus-unrelated nonmultiple head and neck carcinomas. *Hum Pathol*. (2016) 49:145–55. doi: 10.1016/j.humpath.2015.08.025
14. Komatsu S, Ichikawa D, Hirajima S, Nagata H, Nishimura Y, Kawaguchi T, et al. Overexpression of SMYD2 contributes to malignant outcome in gastric cancer. *Br J Cancer*. (2015) 112:357–64. doi: 10.1038/bjc.2014.543
15. Sajjad A, Novoyatleva T, Vergarajauregui S, Troidl C, Schermuly RT, Tucker HO, et al. Lysine methyltransferase Smyd2 suppresses p53-dependent cardiomyocyte apoptosis. *Biochim Biophys Acta*. (2014) 1843:2556–62. doi: 10.1016/j.bbamcr.2014.06.019
16. Wang L, Liu X, Ren Y, Zhang J, Chen J, Zhou W, et al. Cisplatin-enriching cancer stem cells confer multidrug resistance in non-small cell lung cancer via enhancing TRIB1/HDAC activity. *Cell Death Dis*. (2017) 8:e2746. doi: 10.1038/cddis.2016.409
17. Xu Y, Jiang Z, Zhang Z, Sun N, Zhang M, Xie J, et al. HtrA1 downregulation induces cisplatin resistance in lung adenocarcinoma by promoting cancer stem cell-like properties. *J Cell Biochem*. (2014) 115:1112–21. doi: 10.1002/jcb.24751
18. Ferguson AD, Larsen NA, Howard T, Pollard H, Green I, Grande C, et al. Structural basis of substrate methylation and inhibition of SMYD2. *Structure*. (2011) 19:1262–73. doi: 10.1016/j.str.2011.06.011
19. Huang J, Perez-Burgos L, Placek BJ, Sengupta R, Richter M, Dorsey JA, et al. Repression of p53 activity by Smyd2-mediated methylation. *Nature*. (2006) 444:629–32. doi: 10.1038/nature05287
20. Saddic LA, West LE, Aslanian A, Yates JR III, Rubin SM, Gozani O, et al. Methylation of the retinoblastoma tumor suppressor by SMYD2. *J Biol Chem*. (2010) 285:37733–40. doi: 10.1074/jbc.M110.137612
21. Hamamoto R, Toyokawa G, Nakakido M, Ueda K, Nakamura Y. SMYD2-dependent HSP90 methylation promotes cancer cell proliferation by regulating the chaperone complex formation. *Cancer Lett*. (2014) 351:126–33. doi: 10.1016/j.canlet.2014.05.014
22. Li LX, Fan LX, Zhou JX, Grantham JJ, Calvet JP, Sage J, et al. Lysine methyltransferase SMYD2 promotes cyst growth in autosomal dominant polycystic kidney disease. *J Clin Invest*. (2017) 127:2751–64. doi: 10.1172/JCI90921
23. Wang R, Deng X, Yoshioka Y, Vougiouklakis T, Park JH, Suzuki T, et al. Effects of SMYD2-mediated EML4-ALK methylation on the signaling pathway and growth in non-small-cell lung cancer cells. *Cancer Sci*. (2017) 108:1203–9. doi: 10.1111/cas.13245
24. Zhang X, Huang Y, Shi X. Emerging roles of lysine methylation on non-histone proteins. *Cell Mol Life Sci*. (2015) 72:4257–72. doi: 10.1007/s00018-015-2001-4
25. Piva S, Ganzinelli M, Garassino MC, Caiola E, Farina G, Broggini M, et al. Across the universe of K-RAS mutations in non-small-cell-lung cancer. *Curr Pharm Des*. (2014) 20:3933–43. doi: 10.2174/13816128113196660761
26. Duffy MJ, O'Donovan N, Crown J. Use of molecular markers for predicting therapy response in cancer patients. *Cancer Treat Rev*. (2011) 37:151–9. doi: 10.1016/j.ctrv.2010.07.004

Conflict of Interest Statement: The authors declare that the research was conducted in the absence of any commercial or financial relationships that could be construed as a potential conflict of interest.

frontiers in Pharmacology

REVIEW
published: 30 April 2019
doi: 10.3389/fphar.2019.00427

USP7: Novel Drug Target in Cancer Therapy

Zhiru Wang[1,2,3], Wenting Kang[1,2], Yinghua You[1,2], Jingru Pang[1,2], Hongmei Ren[1,2], Zhenhe Suo[3]*, Hongmin Liu[1,2]* and Yichao Zheng[1,2]**

[1] School of Pharmaceutical Sciences, Zhenghzou University, Zhengzhou, China, [2] Collaborative Innovation Centre of New Drug Research and Safety Evaluation, Henan Province, and Key Laboratory of Advanced Drug Preparation Technologies, Zhengzhou University, and Key Laboratory of Henan Province for Drug Quality and Evaluation, Ministry of Education of China, Zhengzhou, China, [3] Pathology, Institute of Clinical Medicine, Faculty of Medicine, University of Oslo, Oslo, Norway

Ubiquitin specific protease 7 (USP7) is one of the deubiquitinating enzymes (DUB) that erases ubiquitin and protects substrate protein from degradation. Full activity of USP7 requires the C-terminal Ub-like domains fold back onto the catalytic domain, allowing the remodeling of the active site to a catalytically competent state by the C-terminal peptide. Until now, numerous proteins have been identified as substrates of USP7, which play a key role in cell cycle, DNA repair, chromatin remodeling, and epigenetic regulation. Aberrant activation or overexpression of USP7 may promote oncogenesis and viral disease, making it a target for therapeutic intervention. Currently, several synthetic small molecules have been identified as inhibitors of USP7, and applied in the treatment of diverse diseases. Hence, USP7 may be a promising therapeutic target for the treatment of cancer.

Keywords: deubiquitination, USP7, structure, immune, DNA damage

OPEN ACCESS

Edited by:
Zhe-Sheng Chen,
St. John's University, United States

Reviewed by:
Hong-Yu Hu,
Shanghai Institutes for Biological Sciences (CAS), China
Xiaoming Zha,
China Pharmaceutical University, China

****Correspondence:***
Zhiru Wang
simplearu@163.com
Zhenhe Suo
zhenhe.suo@medisin.uio.no
Hongmin Liu
liuhm@zzu.edu.cn
Yichao Zheng
yichaozheng@zzu.edu.cn

Specialty section:
This article was submitted to Experimental Pharmacology and Drug Discovery, a section of the journal Frontiers in Pharmacology

Received: *28 January 2019*
Accepted: *04 April 2019*
Published: *30 April 2019*

Citation:
Wang Z, Kang W, You Y, Pang J, Ren H, Suo Z, Liu H and Zheng Y (2019) USP7: Novel Drug Target in Cancer Therapy. Front. Pharmacol. 10:427. doi: 10.3389/fphar.2019.00427

INTRODUCTION

Post-translational modification (PTM) is generally enzymatic modification of proteins following protein biosynthesis. Examples of PTM include methylation, acetylation, phosphorylation, glycosylation, ubiquitination, S-nitrosylation, and so on (Chatterjee and Thakur, 2018). As one of the most studied PTMs, ubiquitination involves in the intracellular proteolytic machinery and regulates numerous physical activities in the cell (Dybas et al., 2018). The process of the addition of ubiquitin to a substrate protein is named ubiquitination, which may contribute to the protein degradation. Ubiquitination of target protein can be catalyzed by a cascade reaction comprising the ubiquitin-activating enzymes (E1), the ubiquitin conjugation enzymes (E2) and the ubiquitin ligases (E3). First, ubiquitin is activated by E1 with the participation of ATP and transferred to E2 through a trans-thiolation reaction, and then conjugated to a lysine or α-amino group of the substrate protein in the presence of E3 (Cheon and Baek, 2006). Eventually, proteins labels with more than four ubiquitin molecules can be recognized and subjected to the 26S proteasome at which they are degraded, generating small polypeptides (**Figure 1**).

Deubiquitinating enzymes (DUBs) are responsible for the removal of ubiquitin and keeping the stability of the substrate by rescuing them from degradation (Nijman et al., 2005; Clague et al., 2013). Until now, approximately 100 DUBs have been identified and can be classified into five subclasses based on their Ub-protease domains: ubiquitin-specific proteases (USPs), ubiquitin C-terminal hydrolases (UCHs), ovarian tumor proteases (OTUs), Machado-Joseph disease proteases (MJDs) belonging to cysteine-dependent proteases, and JAB1/MPN/Mov34 (JAMMs) belonging to zinc metalloproteases (Zhou et al., 2018). With approximately 50 members,

the USPs family is the largest one among all the DUB subfamilies. All these members include conserved domains, i.e., three primary functional domains of Cys, His and Asp/Asn boxes which are in charge of the reorganization of ubiquitin conjugated molecules.

Among the members of USP family, ubiquitin specific protease USP7, also known as herpes-associated ubiquitin-specific protease (HAUSP), is a unique deubiquitinating enzyme which was identified in 1997, and it characterized as a novel member of the ubiquitin-specific protease family to interact with herpes simplex virus type 1 immediate-early protein (Vmw110) of the herpes simplex virus type 1 (HSV-1) regulatory protein (Everett et al., 1997). Later, USP7 was found to interact with other viral proteins such as the Epstein-Barr nuclear antigen 1 (EBNA1) of Epstein-Barr virus (EBV) and the vIRF1 (viral interferon regulatory factor 1) protein of Kaposi's sarcoma associated herpesvirus (KSHV) (Holowaty et al., 2003), therefore indicating it as a general target of herpes viruses and giving it the name herpes-associated ubiquitin specific protease. Up to now, USP7 is the most widely studied deubiquitinating enzymes, and is considered as an oncogene by promoting tumor growth and negatively affecting the patient immune response to tumors (Everett, 2014; Lu et al., 2016).

STRUCTURE OF USP7

The full length USP7 includes 1102 amino acids. There are four domains: an N-terminal poly-glutamine stretch (poly Q), the tumor necrosis factor receptor- associated factors (TRAF) domain (amino acids 62–205), the catalytic domain (amino acids 208–560), and the C-terminal tandem ubiquitin-like (Ubl) domain (amino acids 560–1102) (Kim and Sixma, 2017) (**Figure 2A**).

As reported, the amino acids 62–205 of USP7 (**Figure 2B**) bind to EBNA1 (Holowaty et al., 2003), mouse double minute 2 homolog (MDM2) and p53 (Hu et al., 2006; Sheng et al., 2006) through a PA-x-x-S motif (Saridakis et al., 2005), and the TRAF (amino acids 62–205) domain contributes to the nuclear localization of the USP7 (Fernandez-Montalvan et al., 2007). Besides, the USP7 truncation (amino acids 208–1102) performed similar activity as the full length protein (Ma et al., 2010).

Hu et al. (2002) identified a 40 kDa fragment of USP7 as the catalytic domain (amino acids 208–560), which mediates ubiquitin binding and deubiquitination of the substrate. The structure of the catalytic core domain reveals novel three-domain architecture, including Fingers, Palm, and Thumb domains (**Figure 2C**). This catalytic core domain binds to ubiquitin aldehyde, which reveals a conformational change in the active site (Hu et al., 2002). With the aid of molecular dynamics simulations, it is found that the transition of USP7 from the inactive to the active can only be captured when H294 was neutralized with a deprotonated C223 and charged H464. In the inactive apo state, positively charged H294 stabilizes an electrostatic network with W285, E298, and Y224. However, neutral H294 in the active state cannot make charge interactions, so the electrostatic network is disrupted. That would results in the C223 unfavorable backbone angles improved by helical refolding, thus, the active site is formed (Ozen et al., 2018).

Ubl shares the ubiquitin β-grasp fold, however, it lacks the C-terminal Gly–Gly residues that are required for conjugation to a target and is located outside the boundaries of the catalytic core domain (Faesen et al., 2011). There are five Ubl domains that are detected in the C-terminal and are organized in a 2-1-2 manner as Ubl-12, Ubl-3, and Ubl-45 (**Figure 2D**) (Zhu et al., 2007). Among them, Ubl-45 is sufficient to reconstitute the USP7 activation *in vitro* and *in vivo*. In the C-terminal, the 19 residues of USP7 (amino acids 1084–1102) are conserved across species (Faesen et al., 2011). Rouge et al. (2016) revealed how the C terminal 19 amino acids of the USP7 contribute to the enhancement of USP7 activity by stabilizing the ubiquitin binding conformation of the catalytic domain. And the individual point mutations at residues I1100 or I1098 are able to abolish the deubiquitinase activity of USP7 (Rouge et al., 2016).

USP7: ONE PROTEIN, MULTIPLE ROLES

Many proteins have been identified as potential substrates and binding partners of USP7, such as viral proteins, transcription factors, and epigenetic modulators (**Figure 8**), and most of these substrates play important roles in viral replication, immune response, tumor suppression, epigenetic control, and DNA repair. Here, functions of USP7 on these substrate are as detailed below (**Table 1**).

Viral Proteins

EBNA1

EBNA1 of EBV is important for the replication, segregation, and transcriptional activation of latent EBV genomes, it has been implicated in host cell immortalization, and avoids proteasome processing and cell-surface presentation. The amino acids 395–450 of EBNA1 bind to the USP7 N-terminal domain with a dissociation constant of 0.9–2 μM. The △395–450 mutant that selectively disrupted the binding to USP7 was found to increase fourfold EBNA1 replication activity than wild-type, but performed no impact on EBNA1 turnover and cell-surface presentation (Holowaty et al., 2003). As p53 and EBNA1 share similar binding sites with USP7, EBNA1 peptide efficiently competes with p53 peptide for USP7 binding, which results the decreasing stability of p53, and protects cells from apoptosis (Saridakis et al., 2005).

ICP0

Infected cell protein 0 (ICP0) of HSV is a multifunctional protein containing 775 amino acids that acts as a promiscuous trans-activator linked to the degradation of several proteins. The ^{618}PRKCARKT^{625} of ICP0 binds to a negatively charged region on Ubl2, where the residues K620 and K624 of ICP0 form direct contacts with residues D762 and D764 in Ubl2 of USP7 (Pfoh et al., 2015). Overexpression of USP7 had no effect on the mRNA level of ICP0, but could accelerate the mRNA accumulation of thymidine kinase (TK) and gI, which are important for HSV infection of non-replicating cells. The mutations at residues 620

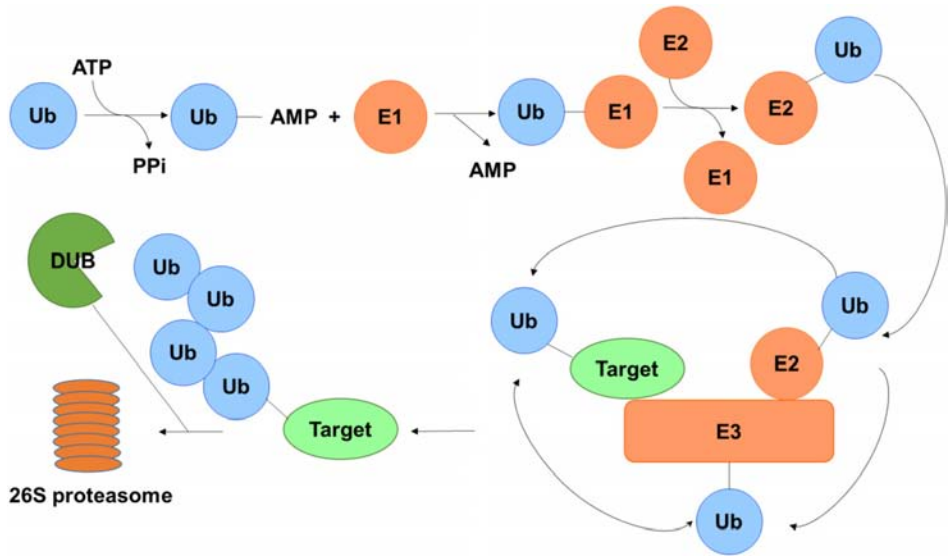

FIGURE 1 | Schematic of the ubiquitin-proteasome system. Ubiquitin is activated by E1 in the presence of ATP and transferred to E2 and then conjugated to a lysine or α-amino group of the substrate protein with the aid of E3. Polyubiquinated targets are recognized and degraded by the 26S proteasome, while the ubiquitin on the substrate can be erased by DUBs to protect it from degradation.

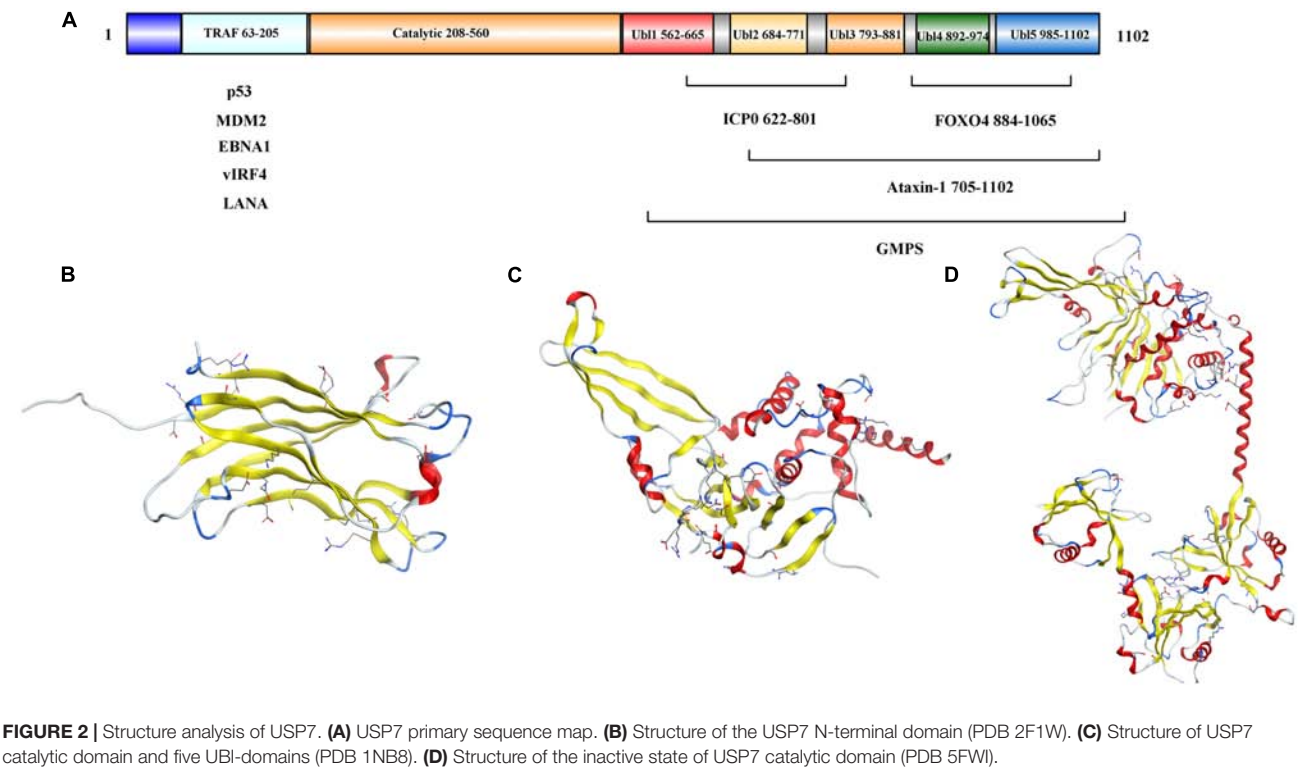

FIGURE 2 | Structure analysis of USP7. **(A)** USP7 primary sequence map. **(B)** Structure of the USP7 N-terminal domain (PDB 2F1W). **(C)** Structure of USP7 catalytic domain and five UBl-domains (PDB 1NB8). **(D)** Structure of the inactive state of USP7 catalytic domain (PDB 5FWI).

to 626 of ICP0 (named as R6702) can abolish the interaction between USP7 and ICP0, and the replication of R6702 in cells cannot be impaired (Kalamvoki et al., 2012). Hence, inhibition of USP7 and/or its interaction with ICP0 using small molecule inhibitors may decrease the virulence of HSV.

vIRFs

Among the vIRFs, vIRF1 could interact with the TRAF domain of USP7 via EGPS motif. The vIRF1 interaction with USP7 can decrease p53 levels by blocking the deubiquitination and stabilization of USP7 on p53. Thus the KSHV could have a

TABLE 1 | Proteins regulated by USP7.

USP7 substrates	Processes	Related cancer	References
EBNA1	Viral proteins		Holowaty et al., 2003
ICP0			Pfoh et al., 2015
vIRFs			Chavoshi et al., 2016; Xiang et al., 2018
LANA			Jager et al., 2012
E1B-55K			Ching et al., 2013
Tat			Ali et al., 2017
Foxp3	Immune response	Non-small cell lung cancer	van Loosdregt et al., 2013; Wang L. et al., 2016
TRIM27		Cervical carcinoma	Cai et al., 2018
NLRP3		Leukemia	Palazon-Riquelme et al., 2018
C-Myc and N-Myc	Oncoproteins	Neuroblastoma	Bhattacharya and Ghosh, 2015
p53	Tumor suppressor proteins	Ovarian cancers	Oliner et al., 1992; Li et al., 2002
DAXX		Breast cancer	Tang et al., 2006
PTEN		Chronic lymphocytic leukemia	Morotti et al., 2014
FOXOs family		Lung carcinoma	Huang et al., 2005
DNMT1	Epigenetics	Colon cancer	Du et al., 2010; Bronner, 2011
SUMO			Lecona et al., 2016
LSD1		Medulloblastoma	Yi et al., 2016
CHK1	DNA damage and repair		Alonso-de Vega et al., 2014
UVSSA			Sarasin, 2012; Zhang et al., 2012
ANXA1		Hela	Park et al., 2015
XPC			He et al., 2014
HLTF, Rad18			Qing et al., 2011
Polη			Qian et al., 2015
RNF168		Breast cancer	Malapelle et al., 2017
PHF8		Breast cancer	Wang Q. et al., 2016
MDC1		Cervical cancer	Su et al., 2018
Wnt/β-catenin signaling pathway	Several canonical signaling pathways	Colorectal cancer	Novellasdemunt et al., 2017
NF-κB signaling pathway		Multiple myeloma	Colleran et al., 2013
NOTCH signaling pathway		Lymphoblastic leukemia	Shan et al., 2018

lifelong infection when p53 is destabilized by USP7 coupled with vIRF1 (Chavoshi et al., 2016). Besides, vIRF3 is expressed in human herpes virus 8 (HHV-8) – infected primary effusion lymphoma (PEL) cells. The vIRF3 has two copies of EGPS, and both support the vIRF3 – USP7 interaction. This interaction plays important roles in PEL cell growth and viability and contributes to the suppression of productive virus replication (Xiang et al., 2018). For another vIRF family member, amino residues 210–216 of KSHV vIRF4 bind to the same surface groove of the USP7 TRAF domain as that can be recognized by MDM2 and p53. Moreover, the amino residues 202–208 of vIRF4 interact with the β-sheet in TRAF domain. The vIRF4-derived vif1 and vif2 peptides can restore p53 dependent apoptosis in wild-type p53 cancer cells by suppressing the USP7 activity. Thus the two peptides may be considered as potential backbones for peptide mimic small molecule inhibitors development for anti-cancer therapies (Lee et al., 2011).

LANA

The viral latency-associated nuclear antigen 1 (LANA) is expressed in all latency KSHV-infected cells and involves in viral latent replication and maintenance of the viral genome. The amino residues 971–986 of LANA interact with TRAF domain of USP7 with similar binding sites as EBNA1, while the △971–986 mutant shows an enhanced ability to replicate latent viral DNA. These results indicate that USP7 may influence accessibility of the viral DNA for latent replication or LANA-mediated viral persistence (Jager et al., 2012). Because of the role of USP7 in EBNA1 – dependent latent replication of EBV, USP7 may play the same role in the replication of latent viral DNA among gamma-1 and gamma-2 herpesviridae.

E1B-55K

Adenovirus E1B protein refers to one or two proteins transcribed from the E1B gene of the adenovirus: a 55 kDa protein and a 19 kDa protein. The N-terminal 79 amino acids of E1B-55K interact with the TRAF domain of USP7. Abrogation of USP7 decreases the protein level of E1B-55K and reduces progeny viral production. Therefore, the small inhibitors of USP7 may be used to treat adenovirus infections (Ching et al., 2013).

Tat

Human immunodeficiency virus (HIV) Tat is synthesized early after infection and mainly responsible for enhancing viral production. USP7 deubiquitinates and stabilizes Tat and enhances HIV-1 production. In turn, HIV-1 infection leads to the overexpression of USP7. These results show that the small inhibitors of USP7 can be used as a novel anti-HIV approach (Ali et al., 2017).

In sum, these results show that USP7 is recruited by these viruses to promote their survival in the host. So we speculate that USP7 may be an attractive target for controlling infection and other malignancies caused by these viruses.

Immune Response

Foxp3

Recent years, more and more reports have identified the importance of USP7 on keeping T regulatory cells (Treg) functions. As the major factor that restrains autoimmune responses, Treg cell expresses the forkhead transcription factor Foxp3, which is necessary for Treg cell development (Bettelli et al., 2005; Laurence et al., 2013). According to a report in 2016, five distinct lysine residues (K249, K251, K263, K267, and K393) in Foxp3 were identified to be ubiquitinated, and Foxp3 can be stabilized by USP7 mediated deubiquitination, resulting in the maintenance of Treg cell

number and function (Wang L. et al., 2016). In fact, a study in 2013 showed that aberrant USP7 overexpression decreases Foxp3 polyubiquitination and protects it from proteasome degradation, resulting in Treg-cell-mediated suppression and tumor growth. On the contrary, USP7 knockdown decreases Foxp3 level and abrogates Treg cell-induced suppression of autoimmune responses *in vitro* and *in vivo* (van Loosdregt et al., 2013).

Later studies gave the mechanism how the level of Foxp3 is regulated. Foxp3 could be ubiquitinated and degraded by the E3 ubiquitin ligase stress inducible protein 1 homology and U-Box containing protein 1 (STUB1). In addition, Foxp3, Heat Shock Protein 70 (Hsp70) and STUB1 associate together as a complex, indicating that these proteins bind and promote Foxp3 ubiquitination (**Figure 3**) (van Loosdregt and Coffer, 2014). Moreover, it is found that mesenchymal stem cells (MSCs) – induced Treg cells express high level of USP7 and low level of STUB1. Besides, Foxp3 mRNA expression was positively associated with USP7 and negatively associated with STUB1 (Khosravi et al., 2018). So, it provides us an opportunity to find a new way to study the unique role of USP7 in Treg cells and makes USP7 as a target in immunology.

TRIM27

Among the binding partners of USP7, tripartite motif 27 (TRIM27) is an ubiquitin E3 ligase that negatively regulates antiviral signaling by promoting the ubiquitination and degradation of TRAF family member-associated NF-κ-B activator – binding kinase 1 (TBK1). USP7 interacts with TRIM27 and forms the USP7-TRIM27-TBK1 complex, and the interaction between USP7 and TRIM27 can be enhanced after Sendai virus (SeV) infection. When USP7 was overexpressed, TRIM27 can be protected from degradation, which contributed to the ubiquitination and degradation of TBK1, resulting in decreased type I interferons (IFNs) signaling (Cai et al., 2018). As IFNs are a series of signaling proteins which are produced and released by host cells to cope with the presence of pathogens, USP7 can enhance the effects of TRIM27 on TBK1-induced IFN – stimulated response element (ISRE) and IFN-β activation (Zaman et al., 2013). Therefore, USP7 may act as a significant host protein to bridge the viral proteins with the antiviral immune response. Therapeutic methods against the USP7-TRIM27 complex may overcome the immune escape mediated by various viruses.

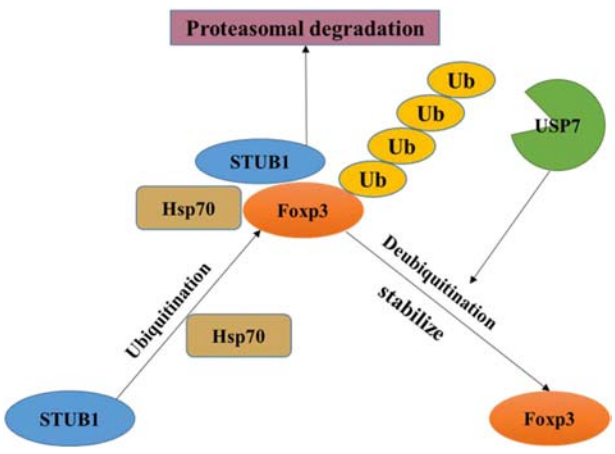

FIGURE 3 | Regulation of Foxp3 by USP7. Foxp3 is ubiquitinated by STUB1 and then produces a complex containing Foxp3, Hsp70 and STUB1, which leading to proteasome degradation of Foxp3. USP7 can remove the ubiquitin on Foxp3 and stabilize it.

NLRP3

USP7 may also impact on regulating NLR family pyrin domain containing 3 (NLRP3) inflammasome activation. NLRP3 is expressed primarily in macrophages as a component of the inflammasome to monitor products of damaged cells such as extracellular ATP and crystalline uric acid. The ubiquitination status of NLRP3 itself can be altered by USP7 and USP47. Furthermore, researchers discovered that the activity of USP7 and USP47 were augmented once the inflammasome was activated. In the meantime, they discovered that abrogation of both USP7 and USP47 resulted in reduction of inflammasome activation (Palazon-Riquelme et al., 2018).

To sum up, there is a remarkable connection between USP7 and immune-associated proteins, and so many studies have shown that the important roles of USP7 on regulating these proteins. It's worth thinking about USP7 inhibitors in combination with immunotherapy will be applied to cancer therapy so that the antitumor effect can be promoted. We hope to see their potential dual antitumor activity will be applied to clinical trials on day.

Oncoproteins

C-Myc and N-Myc

There are three members in Myc family: C-Myc, l-Myc, and N-Myc. Myc family is the most frequent amplified oncogene in human, which contributing to the formation of cancer. Among them, C-Myc and N-Myc are the substrates of USP7. USP7 overexpression can promote C-Myc stability by deubiquitination as well as transformation/transcription domain-associated protein (TRRAP), which is an adaptor protein known as a regulator of C-Myc. On the other hand, C-Myc mRNA can be accumulated by TRRAP indirectly (Bhattacharya and Ghosh, 2015).

N-Myc is another transcription factor that can be stabilized by USP7 via deubiquitination (Tavana et al., 2016). Hence, USP7 inhibitor p5091 was applied to decrease N-Myc expression in a dose dependent manner in neuroblastoma (Tavana et al., 2016). As a consequence, USP7 can be considered as a drug target to modulate C-Myc and N-Myc amount in order to block tumor development.

Tumor Suppressor Proteins

p53

p53 participates in cell cycle arrest, DNA repair, apoptosis, senescence and plays a key role in maintaining normal cell growth (Levine, 1997). USP7 plays a paradoxical role in regulating p53 functions through a variety of mechanisms. On one hand, p53 binds to TRAF domain and C-terminal (amino acids

880–1050) of USP7, and then USP7 ubiquitinates p53 directly and prevents it from degradation. On the other hand, TRAF domain and C-terminal (amino acids 801–1050) of USP7 can interact with MDM2 to increase its stability by erasing the ubiquitin on MDM2, an E3 ligase of p53 (Oliner et al., 1992), and protect it from proteasome degradation. Subsequently, MDM2 ubiquitinates p53 and causes its proteasome degradation, resulting in low expression of p53 in cancer cells (**Figure 4**) (Li et al., 2002, 2004). In addition, MDM2 can also inhibit the transcription of p53 (Wade et al., 2013). Therefore, inhibition of the interaction between MDM2 and p53 can stabilize p53 (Vassilev et al., 2004). It is noteworthy that, crystal structures analysis and binding studies suggest that the MDM2 peptide and p53 peptide bind to the same surface groove in USP7, but MDM2 performs more extensive interaction and stronger affinity (Hu et al., 2006). Taken together, the activation of USP7-MDM2-p53 interaction can promote the occurrence and development of tumors. The design of small molecules that disrupt or prevent the interaction may be an important target for cancer therapy by regulating p53 pathway.

DAXX

Death-domain-associated protein (DAXX) is a highly conserved and developmentally essential nuclear protein, which participates in many cellular processes (Lindsay et al., 2008). The N-terminal 160 amino acids and amino acids 347–570 of DAXX associate with USP7, which are far from the binding sites of MDM2 on DAXX. In unstressed cells, DAXX interacts with USP7 and MDM2, and mediates the stabilization of USP7 on MDM2, thus blocking p53 activation. In response to DNA damage, self-ubiquitination of MDM2 is accelerated when MDM2 is stripped from DAXX and USP7. That is to say, DAXX directs the ligase activity of MDM2 through regulating USP7 (Tang et al., 2006). Recent reports also show that USP7 and DAXX are critical in regulating the correct execution of mitosis by forming a tertiary complex as MDM2/DAXX/USP7 (Zhang et al., 2010). DAXX binding increases USP7 activity toward MDM2. Disassemble the MDM2-DAXX-USP7 complex can increase MDM2 self-ubiquitination and degradation, which leads to the stabilization and accumulation of p53 (Kumar et al., 2018).

PTEN

Phosphatase and tensin homolog (PTEN) is a tumor suppressor gene that displays dual specific phosphatase activity. PTEN inhibits the proliferation and migration of tumor cells (Blanco-Aparicio et al., 2007). It is reported that nuclear PTEN import is promoted by its mono-ubiquitination (Trotman et al., 2007). However, USP7 can remove the mono-ubiquitination of PTEN, triggering its nuclear exclusion and PTEN inactivation (Morotti et al., 2014). Likewise, USP7 inhibitor, P5091, regains PTEN nuclear pool and restores its tumor suppressive functions in chronic lymphocytic leukemia (CLL) (Carra et al., 2017). In addition, PTEN deletion leads to accumulation of activated AKT, and subsequent phosphorylation of MDM2 by AKT (Blanco-Aparicio et al., 2007), which results in the ubiquitination and degradation of p53 (Freeman et al., 2003). Therefore, PTEN deficiency causes p53-dependent cancer-promoting processes. This suggests how important it is to inhibit USP7 to ensure PTEN protein localization and activity.

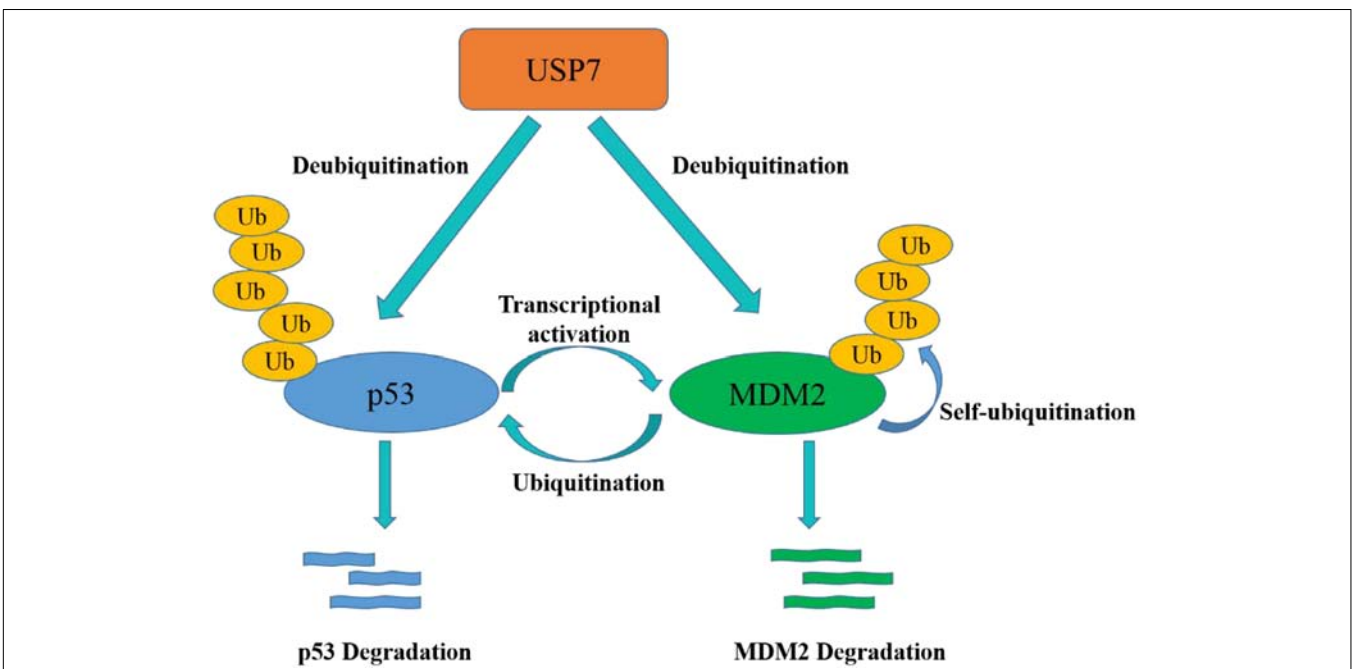

FIGURE 4 | USP7-p53-MDM2 axis interactions control the stability of p53 and MDM2. USP7 can stabilize p53 by deubiquitination, meanwhile, USP7 can also remove the ubiquitin of MDM2, which promotes to p53 degradation.

FOXOs Family

The Forkhead box O (FOXO) family members, including FOXO1, FOXO3, FOXO4 and FOXO6, are transcription factors that take part in regulating several cellular responses, including cell cycle progression and apoptosis and so on (van der Horst and Burgering, 2007). It is reported that USP7 can remove ubiquitin from FOXO1, which is written by Skp2 as an E3 ligase (Huang et al., 2005). Besides, mono-ubiquitination FOXO4 localizes in the nucleus and exhibits stronger transcriptional promotion activity (Brenkman et al., 2008). USP7 can suppress FOXO4 activity due to its deubiquitination and re-localization (van der Horst et al., 2006). In a word, USP7 affects tumor progression by interacting with FOXOs and affecting their activity and localization.

Epigenetics

DNMT1

DNMT1 (DNA methyltransferase 1) contributes to the maintenance of DNA methylation. As reported, USP7 can deubiquitinate and stabilize DNMT1 when its acetylation is erased by histone deacetylase 1 (HDAC1), which protects DNMT1 from proteasome degradation (Bronner, 2011). When the KG linker of DNMT1 is acetylated by Tip60, USP7 breaks away from DNMT1 and results in the degradation of DNMT1 mediated by proteasome system (**Figure 5**) (Du et al., 2010). Thus, HDAC and USP7 inhibitors can be applied in combination for cancer treatment (Cheng et al., 2015).

SUMO

Small ubiquitin related modifier (SUMO) is a ubiquitin-like molecule, which binds to its substrate by E3 SUMO ligase in a similar way as ubiquitination (Geoffroy and Hay, 2009). Like ubiquitin, proteins can be SUMOylated as mono-SUMOylation or poly-SUMOylation, but differently, poly-SUMOylation cannot lead to target degradation directly (Smits and Freire, 2016). Recent research shows that USP7 is associated with DNA synthesis (Smits and Freire, 2016). USP7 associates with an active DNA replication fork and inhibition of USP7 can reduce DNA replication. Moreover, Lecona et al. (2016) identified SUMO2 as a new USP7 substrate and demonstrated that USP7 can deubiquitinate SUMO2 *in vitro* and *in vivo*. However, the fate of SUMO2 after deubiquitination and its biological function are still unclear (Lecona et al., 2016).

LSD1

Histone lysine specific demethylase 1 (LSD1) is the first histone demethylase identified in 2004 and can remove methyl groups of histone H3K4, H3K9 (Shi et al., 2004). As reported, LSD1 can be ubiquitinated by E3 ligase JADE2 (Han et al., 2014). Since ubiquitination of LSD1 is considered as reversible process as ubiquitination and deubiquitination always exit in pair, LSD1 was identified to be deubiquitinated by USP7 and protected it from proteasome degradation (Yi et al., 2016). Besides, patients with high expression of USP7, REST, and LSD1 performed poorer outcomes in medulloblastoma (Callegari et al., 2018). And they found that p53 was a vital downstream transcription factor in the action of USP7 and LSD1.

DNA Damage and Repair

CHK1

USP7 can regulate CHK1 in three manners. The first one is the indirect regulation, USP7 deubiquitinated and prolonged the half-life of Claspin, which leaded to the sustaining phosphorylation of checkpoint kinase 1 (Chk1) in response to genotoxic stress (Faustrup et al., 2009). For the rest two manners, in DNA damage, USP7 deubiquitinates and stabilizes Chk1 via direct deubiquitination in the presence of zinc finger E-box binding homeobox 1 (ZEB1) (Zhang et al., 2014) or not (Alonso-de Vega et al., 2014), while ZEB1 binds to USP7 may result in promoting homologous recombinant-dependent DNA repair and resistant to radiation. In addition, USP7 can also directly regulate the stability of CDC25A, a Cdk-activating phosphatase as the substrate of CHK1, with the aid of brain and reproductive organ expressed protein (BRE). These results show that USP7 is an important modulator of Chk1.

CHFR

Checkpoint with Forkhead and Ring domains (CHFR), a RING family Ub-ligase, is a mitotic checkpoint that delays the transition to metaphase in response to mitotic stress. USP7 binds with CHFR *in vivo* and regulates its stability (**Figure 6**). These results indicate that USP7 may play a role in the cell cycle progression via the deubiquitination of CHFR (Oh et al., 2007).

UVSSA

Transcription-coupled nucleotide excision repair (TC-NER) removes DNA damage of actively transcribed genes. Defect in TC-NER is associated with cockayne syndrome (CS) and ultraviolet – sensitive syndrome (UVSS). Cockayne syndrome B (CSB/ERCC6) and UVSS protein are two important proteins in TC-NER. UVSSA binds with USP7 to stabilize CSB and restores the hypophosphorylated form of RNA polymerase II after UV irradiation (**Figure 6**) (Zhang et al., 2012). UVSSA and USP7 play roles in controlling the fate of stalled RNA polymerase II, the steady-state level of CSB, the efficiency of TC-NER and cell survival following DNA damage (Sarasin, 2012).

ANXA1

ANXA1 is a 37-kDa protein identified as the first member of the annexin superfamily. In response to DNA damage, ANXA1 is cleaved and generates the N-terminal fragment (Ac2-26) and the cleaved form of ANXA1. Both the full length of ANXA1 and Ac2-26 can be translocated to the cell membrane and induce apoptotic cell clearance through recruiting monocytes. The N-terminal of ANXA1 shares the USP7-binding motif sequences (AMVS and ALLS) and interacts with USP7. Hence, USP7 can deubiquitinate and stabilize ANXA1 (**Figure 6**). USP7 may participate in the DDR after UV-induced DNA damage in certain types via ANXA1 (Park et al., 2015).

XPC

Xeroderma pigmentosum complementation group C (XPC) is a critical damage recognition factor which binds to helix-distorting DNA lesions and initiates nucleotide excision repair (NER).

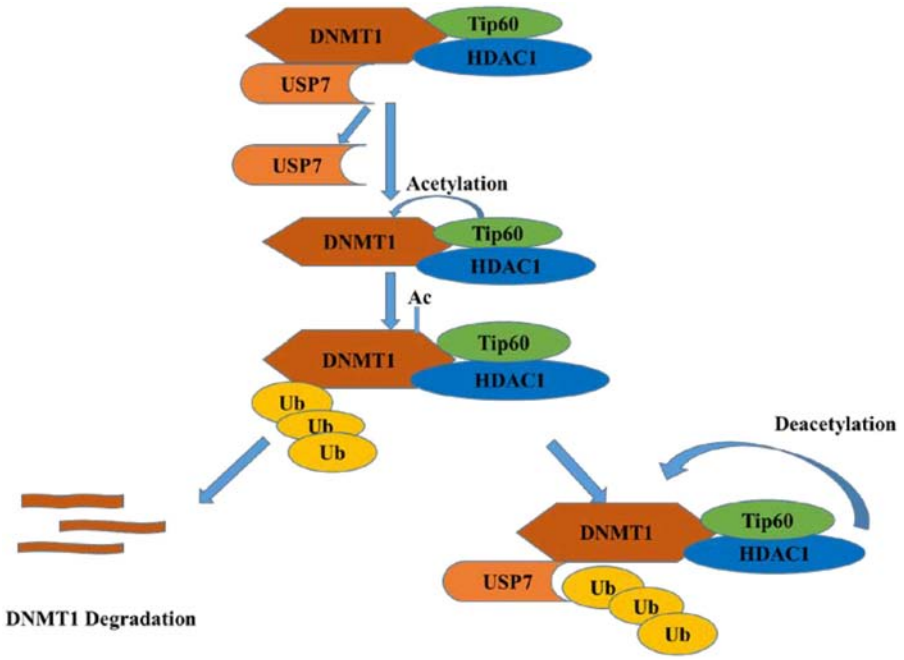

FIGURE 5 | USP7 and HDAC1 protect DNMT1 from degradation while Tip60 acetylates DNMT1 and promotes its degradation.

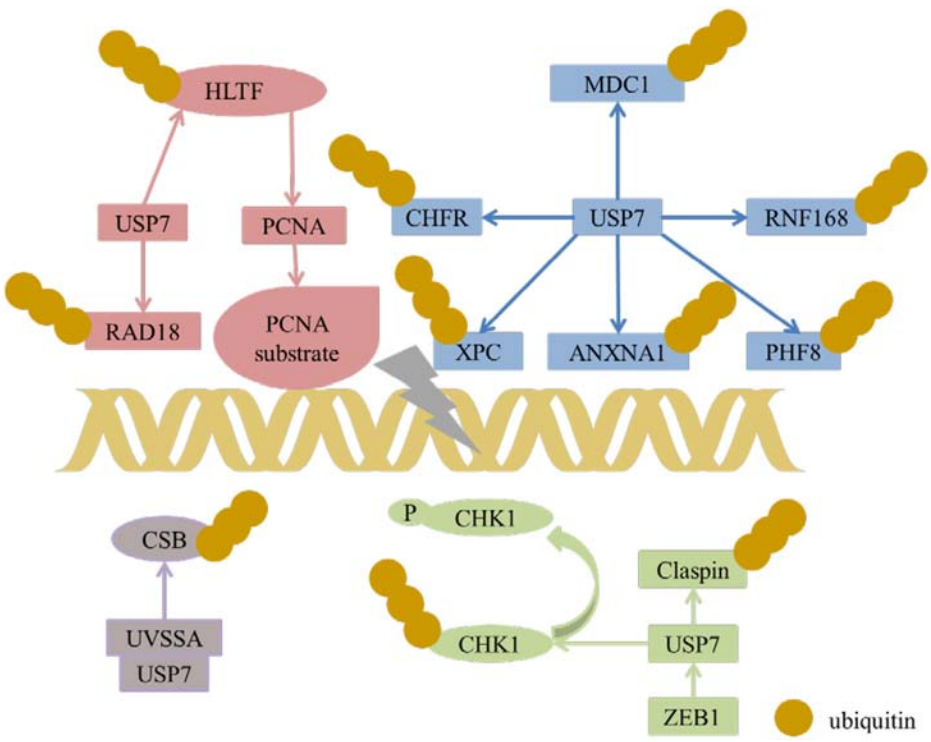

FIGURE 6 | USP7 interacts with a number of substrates in DNA damage response.

During the early stage of NER of UV light-induced DNA lesions, XPC is ubiquitinated. Ubl1 domain (amino acids 560–644) of USP7 can bind and erase the ubiquitination on XPC and prevents XPC from proteolysis (**Figure 6**). Taken together, USP7 plays a vital role in regulating NER through deubiqitinating XPC (He et al., 2014).

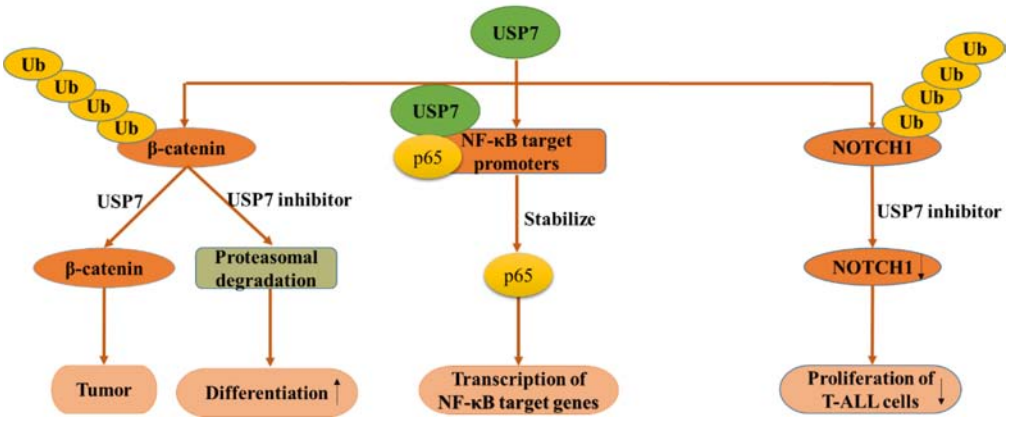

FIGURE 7 | USP7 functions in several canonical signaling pathways. USP7 functions in Wnt/β-catenin signaling pathway **(left)**, NF-κB signaling pathway **(middle)**, NOTCH signaling pathway **(right)**.

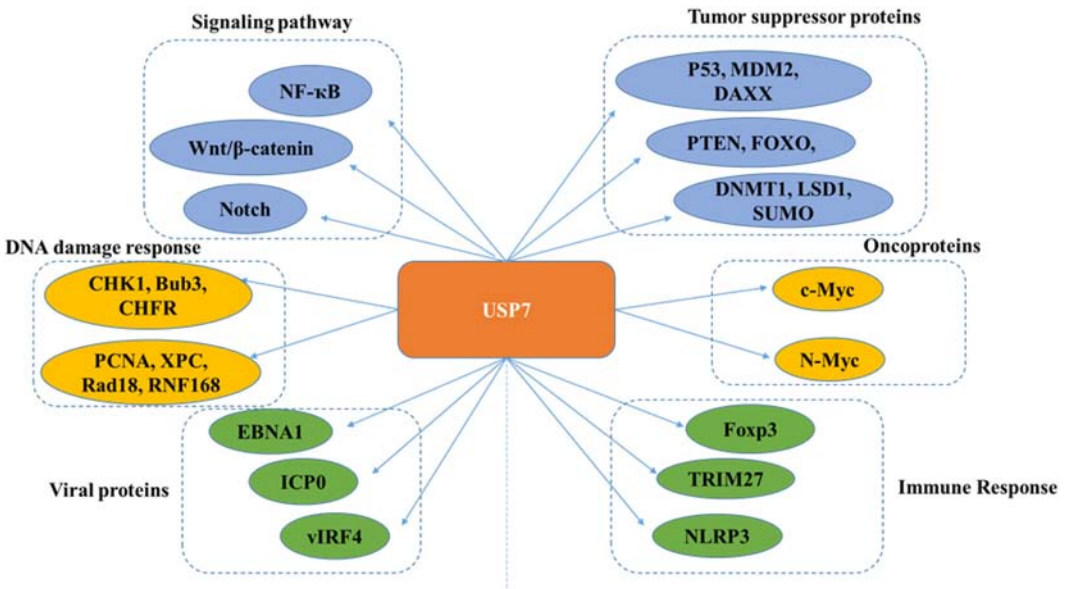

FIGURE 8 | Overview of USP7 functions.

HLTF, Rad18, and Polη

Helicase-like transcription factor (HLTF) is a double-stranded DNA translocase that can promote the polyubiquitination of proliferating cell nuclear antigen (PCNA), while Rad6–Rad18 monoubiquitinates PCNA, both of which make PCNA work as a molecular switch between various DNA damage bypass processes. On one hand, USP7 stabilizes HLTF after genotoxic stress, resulting in prolonging the half-life of HLTF, thus in turn increases polyubiquitination of PCNA (**Figure 6**) (Qing et al., 2011). Besides, USP7 and DNA polymerase eta (Polη), a key player in several DNA damage-tolerance pathways, interact with each other, and USP7 increases UV-induced PCNA ubiquitination through stabilizing Polη and in turn facilitates the recruitment of DNA translesion synthesis (TLS) polymerases to bypass DNA lesions. Therefore USP7 promotes monoUb-PCNA mediated stress-tolerance pathways via the stabilization of Polη. These results provide new mechanistic for USP7-related tumorigenesis and therapeutic strategy (Qian et al., 2015). On the other hand, the amino acids 110–251 of Rad18 interact with USP7 and contain two USP7-binding motifs. Loss of USP7 destabilizes Rad18 and compromises UV-induced PCNA monoubiquitylation and Polη recruitment to stalled replication forks (Zlatanou et al., 2016).

RNF168

During DDR, histone ubiquitination by RNF168 orchestrates the recruitment of downstream DDR factors, e.g., breast cancer type 1 susceptibility protein (BRCA1) and p53 binding protein

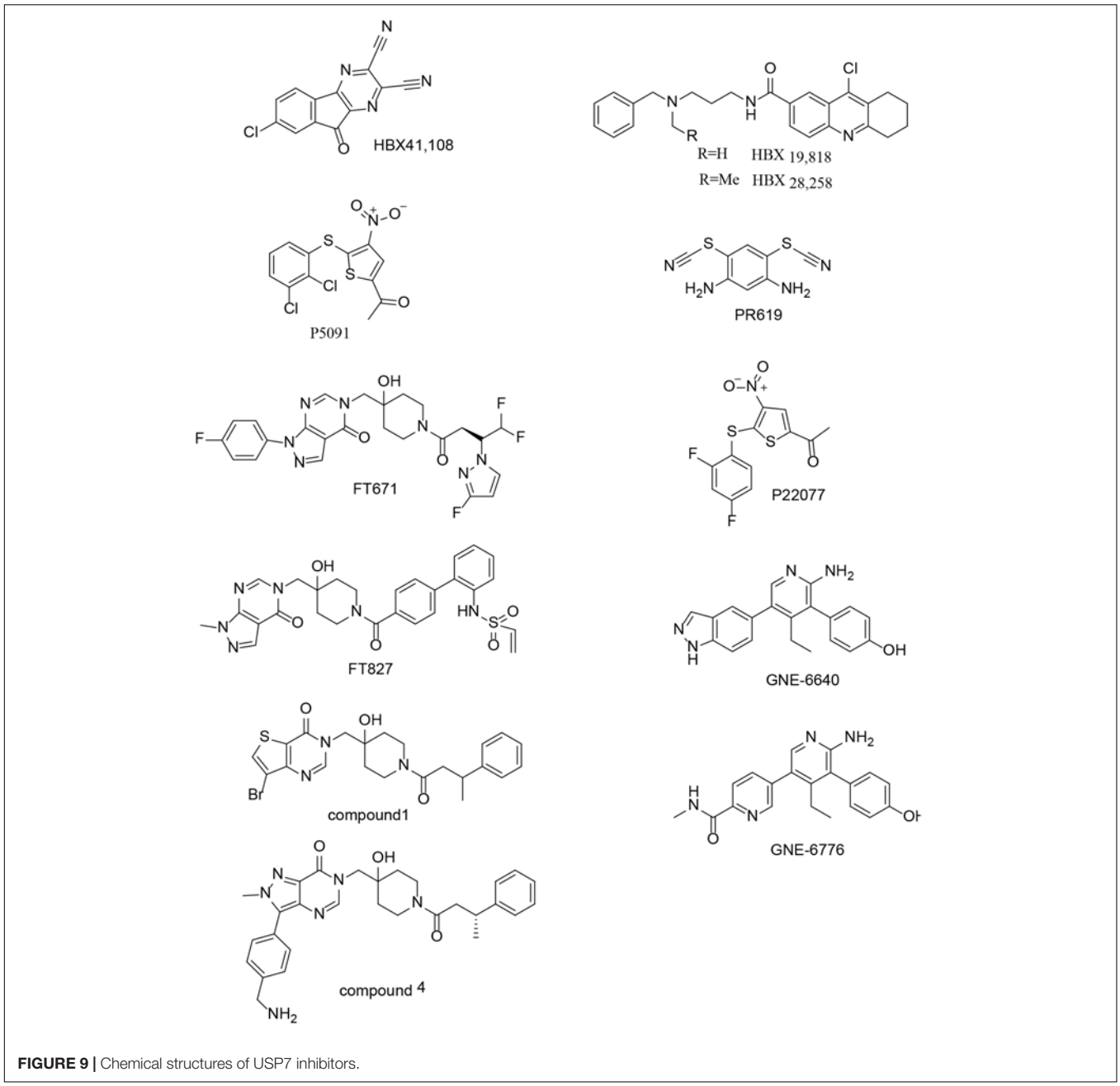

FIGURE 9 | Chemical structures of USP7 inhibitors.

1 (53BP1). The Ubl1 domain of USP7 binds to RNF168 (**Figure 6**). USP7 regulates H2A monoubiquitination and H2A/X polyubiquitination via its regulation on RNF168. In summary, USP7 plays a vital role in regulation of Ub-dependent signaling in DDR via monitoring RNF168 (Malapelle et al., 2017).

PHF8

Plant homeodomain finger-containing protein 8 (PHF8) consists of an N-terminal plant homeodomain and recognizes and binds tri-methyl histone 3 lysine 4 at transcription start sites. The C-terminal region of PHF8 binds with the TRAF domain of USP7, and USP7 promotes the stability of PHF8 via deubiquitinase activity and contributes to the maintenance of genome integrity, which is implemented in DDR (**Figure 6**). The USP7/PHF8 is involved in breast carcinogenesis, indicating these molecules may be as potential targets for breast cancer intervention (Wang Q. et al., 2016).

MDC1

DNA damage checkpoint protein 1 (MDC1) is important for the initiation and amplification of the DDR. USP7 deubiquitinates and stabilizes of MDC1, resulting in sustaining the DDR, while depletion of USP7 influences the engagement of MRE11-RAD50-NBS1(MRN)-MDC1 complex and the

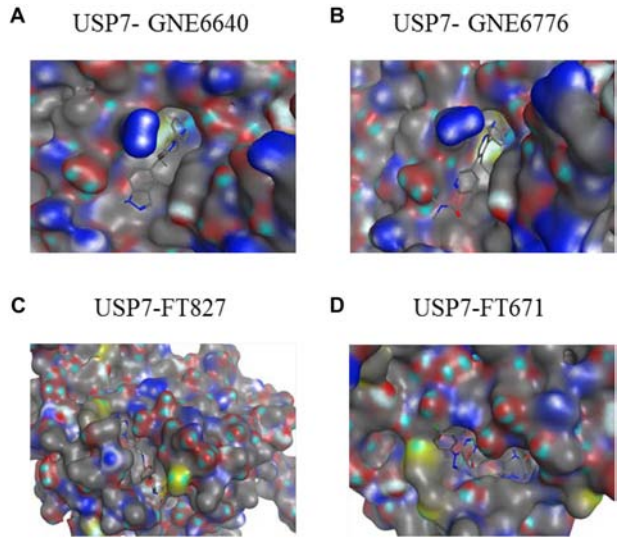

FIGURE 10 | Co-crystal structures of USP7 in complex with inhibitors. The electrostatic surface representation of the CD of USP7 is shown along with compounds **(A)** USP7-GNE6640 (PDB code 5UQV). **(B)** USP7-GNE6776 (PDB code 5UQX). **(C)** USP7-FT827 (PDB code 5NGF). **(D)** USP7-FT671 (PDB code 5NGE). The images were generated with molecular operating environment (MOE).

recruitment of the downstream factors 53BP1 and BRCA1 at DNA lesions. USP7 promotes cervical cancer cell survival and confrere cellular resistance to genotoxic insults via the stabilization of MDC1 (Su et al., 2018).

In a nutshell, USP7 plays a vital role in the DNA damage response (**Figure 6**), and it can be targeted for the treatment of malignancies with DDR defects. Besides, USP7 inhibitors can be combined with genotoxic agents as a novel therapeutic strategy for the treatment of cancer.

USP7 stabilizes HLTF to result in polyubiquitination of PCNA and induces monoubiquitination of PCNA through regulating Rad18. USP7 plays a role in DDR through regulating MDC1, CHFR, XPC, ANXNA1, RNF168, and PHF8. USP7 and UVSSA interact with each other to control steady state of CSB following DNA damage. USP7 can regulate stability of CDC25A via deubiquitination CDC25A directly and through regulating Claspin and CHK1 expression.

Several Canonical Signaling Pathways

Wnt/β-Catenin Signaling Pathway

Wnt signaling was initially found for its function in cancer and embryonic development and then was found responsible for tissue regeneration in adult bone marrow, skin and intestine. β-Catenin, a key element in Wnt signaling pathway, is regulated by diverse PTMs, including ubiquitination (Ma et al., 2014). According to a research in 2017, β-catenin can be deubiquitinated and stabilized by USP7 in adenomatous polyposis coli (APC) truncating mutated colorectal cancer (CRC) but not APC wide type CRC, which resulting in the activation of Wnt pathway (Novellasdemunt et al., 2017). Mechanism study suggested that APC β-catenin inhibitory domain (CID) protects β-catenin from USP7-mediated deubiquitination, while APC lacking CID exposes β-catenin to USP7 for deubiquitination. Hence, abrogation of USP7 in APC-mutated CRC suppresses Wnt activation by regaining β-catenin ubiquitination, which leads to the cell differentiation, and inhibits tumor growth (Novellasdemunt et al., 2017). With the aid of USP7 inhibitor P5091, Wnt pathway can be inactivated by improving ubiquitination and degradation of β-catenin, which provides evidence for the rationality for developing USP7 inhibitors as anti-CRC agent (**Figure 7A**) (An et al., 2017). In a nutshell, USP7 can be considered as a Wnt activator for tumor-specific therapeutic target for most CRCs.

NF-κB Signaling Pathway

Nuclear factor kappa B (NF-κB) signaling pathway is responsible for the transcription of a series of genes that controlling inflammation and immunity. As an essential regulator of Toll-like-receptor (TLR) and tumor necrosis factor receptor (TNFR)-inducible inflammatory gene expression, NF-κB is regulated by USP7 in a research in 2013. Different from other USP7 partners and substrates, NF-κB p65 and USP7 interact together after USP7 is recruited to NF-κB target promoters. Besides, the inhibition of USP7 lead to decreased TLR and TNFR-induced expression of Interleukin (IL-6), TNFα (NF-κB reporter) indicates that the deubiquitination of NF-κB by USP7 may have therapeutic potential (**Figure 7B**) (Colleran et al., 2013).

In 2018, some researchers found that knockout of USP7 dramatically increased the sensitivity of multiple myeloma (MM) cells to bortezomib (BTZ) which led to myeloma cell death and inhibited NF-κB activation by stabilizing IκBα. As expected, usage of USP7 inhibitors also inhibited the activation of NF-κB and the combination of USP7 inhibitor with BTZ triggered the synergistic antitumor activity in bortezomib-resistant MM cells. Taken together, this study provides a new application for USP7 inhibitors alone or in combination with BTZ to overcome BTZ resistance and improve the patient prognosis in MM (Yao et al., 2018).

In all, several reports have illustrated the mechanism that how USP7 and its related proteins regulate NF-κB signaling pathway. However, more deep studies should be conducted to make the mechanism more clearly and logically and there are still great challenges for researchers to face.

NOTCH Signaling Pathway

Notch signaling pathway is highly conserved and presents in most multicellular organisms. This intercellular signaling cascade is involved in cell differentiation, proliferation, and contributes to the fate of cells and occurs in multiple organisms and tissues, containing early T cell development in the thymus and peripheral T cell differentiation (Auderset et al., 2012; Bailis et al., 2013; Amsen et al., 2015). There are four notch receptors in mammals possessing NOTCH1-4 in which NOTCH1 can be stabilized through USP7-mediated deubiquitination. Previous studies have revealed that ubiquitination regulates the stability, activity, and localization of NOTCH1. However, the specific deubiquitinase that affects NOTCH1 protein stability was clarified recently.

Researchers reported that USP7 can deubiquitinate and stabilize NOTCH1 *in vivo* and *in vitro*, on the other hand, knockdown of USP7 increased the ubiquitination of NOTCH1. Used up of USP7 significantly restrained the proliferation of T-cell acute lymphoblastic leukemia (T-ALL) cells *in vitro* and *in vivo*, accompanied by downregulation of the NOTCH1 protein level, suggesting that targeting the USP7/NOTCH1 axis is a novel strategy to combat T-ALL and other NOTCH1-related malignancies (**Figure 7C**) (Shan et al., 2018). Almost at the same time, researchers found USP7 can bind several oncogenes by interacting and stabilizing NOTCH1 and JmjC Domain-Containing Protein 3 (JMJD3) in order to control leukemia growth. What's more, USP7 and NOTCH1 bind T-ALL superenhancers, and inhibition of USP7 leads to a decrease of the transcriptional levels of NOTCH1 targets and T-ALL cell growth *in vitro* and *in vivo*. Therefore, USP7 cooperating with NOTCH1 can improve the oncogenic transcriptional program in T-ALL (Jin et al., 2018).

The functions of USP7 on different signaling pathways indicate the brand new role of USP7 as a great target. To be sure, other classical signaling pathways which may be regulated by USP7 is yet to be found. It provides us a great challenge to find the new mechanisms between USP7 and other classical signaling pathways.

USP7 in Cancer

USP7 is highly expressed in a wide variety of cancers and affects the progression of cancer diseases. Moreover, USP7 assumes different roles in different tumors. In prostate cancer, high expression of USP7 is directly related to tumor invasion (Song et al., 2008). USP7 plays a key role in carcinogenesis via p53-dependent pathways in non-small cell lung carcinoma (NSCLCs) (Masuya et al., 2006). Studies have shown that changes of USP7 regulate colon carcinoma growth and apoptotic sensitivity *in vivo* (Becker et al., 2008). USP7 maintains DNA damage response and promotes cervical cancer, and is positively correlated with poor survival rate in patients with cervical cancer (Su et al., 2018). USP7 regulates human terminal erythroid differentiation by stabilizing GATA1, providing a certain treatment for leukemia (Liang et al., 2019). In short, USP7 plays an important role in a variety of pathologies and is a good target from a therapeutic point of view.

USP7 INHIBITORS

USP7 is a promising target not only for its roles in cellular pathways including regulators of viral proteins, immune response, oncogenes, and DNA damage but also because of its aberrant expression in various cancers. Due to lack of co-crystal structures between USP7 and small molecule inhibitors, there is no potent and selective USP7 inhibitor for a long time (Colland et al., 2009; Altun et al., 2011; Chauhan et al., 2012; Reverdy et al., 2012) (**Figure 9**). However, several groups reported the structures of USP7 in complex with small molecule inhibitors last year (Kategaya et al., 2017; Turnbull et al., 2017) (**Figure 10**) and these structures gives guidance to obtain structure-based small molecule inhibitors.

CONCLUSION AND FUTURE PERSPECTIVES

This review illustrates our current knowledge of USP7, including its source and characterization, structure, binding partners and substrates in various biological processes. Besides, how USP7 regulates various aspects of a cell under both normal and pathological states are elaborated in detail. As the processes of ubiquitination and deubiquitination are extremely dynamic and context-specific, a series of studies have linked USP7 to different cancers. The biology, particularly the immune oncology mechanisms, reveal that USP7 inhibitors would be useful drugs, thus it is vital to develop highly selective and specific inhibitors of USP7. The association of USP7 with several canonical signaling pathways still needs characterized in order to search new targets and regulatory mechanisms. Last but not least, USP7 may be a promising target for cancer therapy and it therefore merits further studies.

AUTHOR CONTRIBUTIONS

ZW discusses the structure of USP7, the viral protein targets of USP7, the DNA damage substrates of USP7 and conclusion. WK talks about the introduction, immune function of USP7, Wnt/β-catenin signaling pathway, and NF-κB signaling pathway. YY illustrates oncoproteins and tumor suppressor proteins. JP states about the epigenetics substrates of USP7. HR talks about the NOTCH signaling pathway. ZS and YZ provide expertise and feedback. HL provides funding.

FUNDING

This work was supported by National Natural Science Foundation of China (Project No. 81602961 for YZ; Project Nos. 81430085 and 81773562 for HL); Outstanding Young Talent Research Fund of Zhengzhou University (Project No. 1521331002 for YZ); National Key Research Program of Proteins (Project No. 2016YFA0501800 for HL; Project No. 2017YFD0501401 for YZ); and Key Research Program of Henan Province (Project No. 161100310100 for HL).

REFERENCES

Ali, A., Raja, R., Farooqui, S. R., Ahmad, S., and Banerjea, A. C. (2017). USP7 deubiquitinase controls HIV-1 production by stabilizing Tat protein. *Biochem. J.* 474, 1653–1668. doi: 10.1042/bcj20160304

Alonso-de Vega, I., Martin, Y., and Smits, V. A. (2014). USP7 controls Chk1 protein stability by direct deubiquitination. *Cell Cycle* 13, 3921–3926. doi: 10.4161/15384101.2014.973324

Altun, M., Kramer, H. B., Willems, L. I., McDermott, J. L., Leach, C. A., Goldenberg, S. J., et al. (2011). Activity-based chemical proteomics accelerates inhibitor

development for deubiquitylating enzymes. *Chem. Biol.* 18, 1401–1412. doi: 10.1016/j.chembiol.2011.08.018

Amsen, D., Helbig, C., and Backer, R. A. (2015). Notch in T Cell differentiation: all things considered. *Trends Immunol.* 36, 802–814. doi: 10.1016/j.it.2015.10.007

An, T., Gong, Y., Li, X., Kong, L., Ma, P., Gong, L., et al. (2017). USP7 inhibitor P5091 inhibits Wnt signaling and colorectal tumor growth. *Biochem. Pharmacol.* 131, 29–39. doi: 10.1016/j.bcp.2017.02.011

Auderset, F., Coutaz, M., and Tacchini-Cottier, F. (2012). The role of notch in the differentiation of CD4(+) T helper cells. *Curr. Top. Microbiol. Immunol.* 360, 115–134. doi: 10.1007/82_2012_227

Bailis, W., Yashiro-Ohtani, Y., Fang, T. C., Hatton, R. D., Weaver, C. T., Artis, D., et al. (2013). Notch simultaneously orchestrates multiple helper T cell programs independently of cytokine signals. *Immunity* 39, 148–159. doi: 10.1016/j.immuni.2013.07.006

Becker, K., Marchenko, N. D., Palacios, G., and Moll, U. M. (2008). A role of HAUSP in tumor suppression in a human colon carcinoma xenograft model. *Cell Cycle* 7, 1205–1213. doi: 10.4161/cc.7.9.5756

Bettelli, E., Dastrange, M., and Oukka, M. (2005). Foxp3 interacts with nuclear factor of activated T cells and NF-kappa B to repress cytokine gene expression and effector functions of T helper cells. *Proc. Natl. Acad. Sci. U.S.A.* 102, 5138–5143. doi: 10.1073/pnas.0501675102

Bhattacharya, S., and Ghosh, M. K. (2015). HAUSP regulates c-MYC expression via de-ubiquitination of TRRAP. *Cell Oncol.* 38, 265–277. doi: 10.1007/s13402-015-0228-6

Blanco-Aparicio, C., Renner, O., Leal, J. F., and Carnero, A. (2007). PTEN, more than the AKT pathway. *Carcinogenesis* 28, 1379–1386. doi: 10.1093/carcin/bgm052

Brenkman, A. B., de Keizer, P. L., van den Broek, N. J., Jochemsen, A. G., and Burgering, B. M. (2008). Mdm2 induces mono-ubiquitination of FOXO4. *PLoS One* 3:e2819. doi: 10.1371/journal.pone.0002819

Bronner, C. (2011). Control of DNMT1 abundance in epigenetic inheritance by acetylation, ubiquitylation, and the histone code. *Sci. Signal.* 4:pe3. doi: 10.1126/scisignal.2001764

Cai, J., Chen, H. Y., Peng, S. J., Meng, J. L., Wang, Y., Zhou, Y., et al. (2018). USP7-TRIM27 axis negatively modulates antiviral type I IFN signaling. *FASEB J.* 32, 5238–5249. doi: 10.1096/fj.201700473RR

Callegari, K., Maegawa, S., Bravo-Alegria, J., and Gopalakrishnan, V. (2018). Pharmacological inhibition of LSD1 activity blocks REST-dependent medulloblastoma cell migration. *Cell Commun. Signal.* 16:60. doi: 10.1186/s12964-018-0275-5

Carra, G., Panuzzo, C., Torti, D., Parvis, G., Crivellaro, S., Familiari, U., et al. (2017). Therapeutic inhibition of USP7-PTEN network in chronic lymphocytic leukemia: a strategy to overcome TP53 mutated/deleted clones. *Oncotarget* 8, 35508–35522. doi: 10.18632/oncotarget.16348

Chatterjee, B., and Thakur, S. S. (2018). Investigation of post-translational modifications in type 2 diabetes. *Clin. Proteomics* 15:32. doi: 10.1186/s12014-018-9208-y

Chauhan, D., Tian, Z., Nicholson, B., Kumar, K. G., Zhou, B., Carrasco, R., et al. (2012). A small molecule inhibitor of ubiquitin-specific protease-7 induces apoptosis in multiple myeloma cells and overcomes bortezomib resistance. *Cancer Cell* 22, 345–358. doi: 10.1016/j.ccr.2012.08.007

Chavoshi, S., Egorova, O., Lacdao, I. K., Farhadi, S., Sheng, Y., and Saridakis, V. (2016). Identification of kaposi sarcoma herpesvirus (KSHV) vIRF1 protein as a novel interaction partner of human deubiquitinase USP7. *J. Biol. Chem.* 291, 6281–6291. doi: 10.1074/jbc.M115.710632

Cheng, J., Yang, H., Fang, J., Ma, L., Gong, R., Wang, P., et al. (2015). Molecular mechanism for USP7-mediated DNMT1 stabilization by acetylation. *Nat. Commun.* 11:7023. doi: 10.1038/ncomms8023

Cheon, K. W., and Baek, K. H. (2006). HAUSP as a therapeutic target for hematopoietic tumors (review). *Int. J. Oncol.* 28, 1209–1215.

Ching, W., Koyuncu, E., Singh, S., Arbelo-Roman, C., Hartl, B., Kremmer, E., et al. (2013). A ubiquitin-specific protease possesses a decisive role for adenovirus replication and oncogene-mediated. *PLoS Pathog.* 9:e1003273. doi: 10.1371/journal.ppat.1003273

Clague, M. J., Barsukov, I., Coulson, J. M., Liu, H., Rigden, D. J., and Urbe, S. (2013). Deubiquitylases from genes to organism. *Physiol. Rev.* 93, 1289–1315. doi: 10.1152/physrev.00002.2013

Colland, F., Formstecher, E., Jacq, X., Reverdy, C., Planquette, C., Conrath, S., et al. (2009). Small-molecule inhibitor of USP7/HAUSP ubiquitin protease stabilizes and activates p53 in cells. *Mol. Cancer Ther.* 8, 2286–2295. doi: 10.1158/1535-7163.mct-09-0097

Colleran, A., Collins, P. E., O'Carroll, C., Ahmed, A., Mao, X., McManus, B., et al. (2013). Deubiquitination of NF-kappaB by ubiquitin-specific protease-7 promotes transcription. *Proc. Natl. Acad. Sci. U.S.A.* 110, 618–623. doi: 10.1073/pnas.1208446110

Du, Z., Song, J., Wang, Y., Zhao, Y., Guda, K., Yang, S., et al. (2010). DNMT1 stability is regulated by proteins coordinating deubiquitination and acetylation-driven ubiquitination. *Sci. Signal.* 3:ra80. doi: 10.1126/scisignal.2001462

Dybas, J. M., Herrmann, C., and Weitzman, M. D. (2018). Ubiquitination at the interface of tumor viruses and DNA damage responses. *Curr. Opin. Virol.* 32, 40–47. doi: 10.1016/j.coviro.2018.08.017

Everett, R. D. (2014). HSV-1 biology and life cycle. *Methods Mol. Biol.* 1444, 1–17. doi: 10.1007/978-1-4939-0428-0_1

Everett, R. D., Meredith, M., Orr, A., Cross, A., Kathoria, M., and Parkinson, J. (1997). A novel ubiquitin-specific protease is dynamically associated with the PML nuclear domain and binds to a herpesvirus regulatory protein. *EMBO J.* 16, 1519–1530. doi: 10.1093/emboj/16.7.1519

Faesen, A. C., Dirac, A. M., Shanmugham, A., Ovaa, H., Perrakis, A., and Sixma, T. K. (2011). Mechanism of USP7/HAUSP activation by its C-terminal ubiquitin-like domain and allosteric regulation by GMP-synthetase. *Mol. Cell* 44, 147–159. doi: 10.1016/j.molcel.2011.06.034

Faustrup, H., Bekker-Jensen, S., Bartek, J., Lukas, J., and Mailand, N. (2009). USP7 counteracts SCFbetaTrCP- but not APCCdh1-mediated proteolysis of Claspin. *J. Cell Biol.* 184, 13–19. doi: 10.1083/jcb.200807137

Fernandez-Montalvan, A., Bouwmeester, T., Joberty, G., Mader, R., Mahnke, M., Pierrat, B., et al. (2007). Biochemical characterization of USP7 reveals post-translational modification sites and structural requirements for substrate processing and subcellular localization. *FEBS J.* 274, 4256–4270. doi: 10.1111/j.1742-4658.2007.05952.x

Freeman, D. J., Li, A. G., Wei, G., Li, H. H., Kertesz, N., Lesche, R., et al. (2003). PTEN tumor suppressor regulates p53 protein levels and activity through phosphatase-dependent and -independent mechanisms. *Cancer Cell* 3, 117–130. doi: 10.1016/s1535-6108(03)00021-7

Geoffroy, M. C., and Hay, R. T. (2009). An additional role for SUMO in ubiquitin-mediated proteolysis. *Nat. Rev. Mol. Cell Biol.* 10, 564–568. doi: 10.1038/nrm2707

Han, X., Gui, B., Xiong, C., Zhao, L., Liang, J., Sun, L., et al. (2014). Destabilizing LSD1 by Jade-2 promotes neurogenesis: an antibraking system in neural development. *Mol. Cell* 55, 482–494. doi: 10.1016/j.molcel.2014.06.006

He, J., Zhu, Q., Wani, G., Sharma, N., Han, C., Qian, J., et al. (2014). Ubiquitin-specific protease 7 regulates nucleotide excision repair through deubiquitinating XPC protein and preventing XPC protein from undergoing ultraviolet light-induced and VCP/p97 protein-regulated proteolysis. *J. Biol. Chem.* 289, 27278–27289. doi: 10.1074/jbc.M114.589812

Holowaty, M. N., Zeghouf, M., Wu, H., Tellam, J., Athanasopoulos, V., Greenblatt, J., et al. (2003). Protein profiling with epstein-barr nuclear antigen-1 reveals an interaction with the herpesvirus-associated ubiquitin-specific protease HAUSP/USP7. *J. Biol. Chem.* 278, 29987–29994. doi: 10.1074/jbc.M303977200

Hu, M., Gu, L., Li, M., Jeffrey, P. D., Gu, W., and Shi, Y. (2006). Structural basis of competitive recognition of p53 and MDM2 by HAUSP/USP7: implications for the regulation of the p53-MDM2 pathway. *PLoS Biol.* 4:e27. doi: 10.1371/journal.pbio.0040027

Hu, M., Li, P., Li, M., Li, W., Yao, T., Wu, J. W., et al. (2002). Crystal structure of a UBP-family deubiquitinating enzyme in isolation and in complex with ubiquitin aldehyde. *Cell* 111, 1041–1054. doi: 10.1016/s0092-8674(02)01199-6

Huang, H., Regan, K. M., Wang, F., Wang, D., Smith, D. I., van Deursen, J. M., et al. (2005). Skp2 inhibits FOXO1 in tumor suppression through ubiquitin-mediated degradation. *Proc. Natl. Acad. Sci. U.S.A.* 102, 1649–1654. doi: 10.1073/pnas.0406789102

Jager, W., Santag, S., Weidner-Glunde, M., Gellermann, E., Kati, S., Pietrek, M., et al. (2012). The ubiquitin-specific protease USP7 modulates the replication of Kaposi's sarcoma-associated herpesvirus latent episomal DNA. *J. Virol.* 86, 6745–6757. doi: 10.1128/jvi.06840-11

Jin, Q., Martinez, C. A., Arcipowski, K. M., Zhu, Y., Gutierrez-Diaz, B. T., Wang, K. K., et al. (2018). USP7 cooperates with NOTCH1 to drive the oncogenic

transcriptional program in T cell leukemia. *Clin. Cancer Res.* 25, 222–239. doi: 10.1158/1078-0432.CCR-18-1740

Kalamvoki, M., Gu, H., and Roizman, B. (2012). Overexpression of the ubiquitin-specific protease 7 resulting from transfection or mutations in the ICP0 binding site accelerates rather than depresses herpes simplex virus 1 gene expression. *J. Virol.* 86, 12871–12878. doi: 10.1128/jvi.01981-12

Kategaya, L., Di Lello, P., Rouge, L., Pastor, R., Clark, K. R., Drummond, J., et al. (2017). USP7 small-molecule inhibitors interfere with ubiquitin binding. *Nature* 550, 534–538. doi: 10.1038/nature24006

Khosravi, M., Bidmeshkipour, A., Cohen, J. L., Moravej, A., Hojjat-Assari, S., Naserian, S., et al. (2018). Induction of CD4(+)CD25(+)FOXP3(+) regulatory T cells by mesenchymal stem cells is associated with modulation of ubiquitination factors and TSDR demethylation. *Stem Cell Res. Ther.* 9:273. doi: 10.1186/s13287-018-0991-1

Kim, R. Q., and Sixma, T. K. (2017). Regulation of USP7: a high incidence of E3 complexes. *J. Mol. Biol.* 429, 3395–3408. doi: 10.1016/j.jmb.2017.05.028

Kumar, S., Brown, A., and Tchounwou, P. B. (2018). Trisenox disrupts MDM2-DAXX-HAUSP complex and activates p53, cell cycle regulation and apoptosis in acute leukemia cells. *Oncotarget* 9, 33138–33148. doi: 10.18632/oncotarget.26025

Laurence, A., Belkaid, Y., and O'Shea, J. J. (2013). A degrading view of regulatory T cells. *Immunity* 39, 201–203. doi: 10.1016/j.immuni.2013.08.017

Lecona, E., Rodriguez-Acebes, S., Specks, J., Lopez-Contreras, A. J., Ruppen, I., Murga, M., et al. (2016). USP7 is a SUMO deubiquitinase essential for DNA replication. *Nat. Struct. Mol. Biol.* 23, 270–277. doi: 10.1038/nsmb.3185

Lee, H. R., Choi, W. C., Lee, S., Hwang, J., Hwang, E., Guchhait, K., et al. (2011). Bilateral inhibition of HAUSP deubiquitinase by a viral interferon regulatory factor protein. *Nat. Struct. Mol. Biol.* 18, 1336–1344. doi: 10.1038/nsmb.2142

Levine, A. J. (1997). p53, the cellular gatekeeper for growth and division. *Cell* 88, 323–331. doi: 10.1016/s0092-8674(00)81871-1

Li, M., Brooks, C. L., Kon, N., and Gu, W. (2004). A dynamic role of HAUSP in the p53-Mdm2 pathway. *Mol. Cell* 13, 879–886. doi: 10.1016/s1097-2765(04)00157-1

Li, M., Chen, D., Shiloh, A., Luo, J., Nikolaev, A. Y., Qin, J., et al. (2002). Deubiquitination of p53 by HAUSP is an important pathway for p53 stabilization. *Nature* 416, 648–653. doi: 10.1038/nature737

Liang, L., Peng, Y., Zhang, J., Zhang, Y., Roy, M., Han, X., et al. (2019). Deubiquitylase USP7 regulates human terminal erythroid differentiation by stabilizing GATA1. *Haematologica*

Lindsay, C. R., Morozov, V. M., and Ishov, A. M. (2008). PML NBs (ND10) and Daxx: from nuclear structure to protein function. *Front. Biosci.* 13, 7132–7142. doi: 10.2741/3216

Lu, Y., Orr, A., and Everett, R. D. (2016). Stimulation of the replication of ICP0-null mutant herpes simplex virus 1 and pp71-deficient human cytomegalovirus by epstein-barr virus tegument protein BNRF1. *J. Virol.* 90, 9664–9673. doi: 10.1128/jvi.01224-16

Ma, J., Martin, J. D., Xue, Y., Lor, L. A., Kennedy-Wilson, K. M., Sinnamon, R. H., et al. (2010). C-terminal region of USP7/HAUSP is critical for deubiquitination activity and contains a second mdm2/p53 binding site. *Arch. Biochem. Biophys.* 503, 207–212. doi: 10.1016/j.abb.2010.08.020

Ma, P., Yang, X., Kong, Q., Li, C., Yang, S., Li, Y., et al. (2014). The ubiquitin ligase RNF220 enhances canonical Wnt signaling through USP7-mediated deubiquitination of beta-catenin. *Mol. Cell Biol.* 34, 4355–4366. doi: 10.1128/mcb.00731-14

Malapelle, U., Morra, F., Ilardi, G., Visconti, R., Merolla, F., Cerrato, A., et al. (2017). USP7 inhibitors, downregulating CCDC6, sensitize lung neuroendocrine cancer cells to PARP-inhibitor drugs. *Lung Cancer* 107, 41–49. doi: 10.1016/j.lungcan.2016.06.015

Masuya, D., Huang, C., Liu, D., Nakashima, T., Yokomise, H., Ueno, M., et al. (2006). The HAUSP gene plays an important role in non-small cell lung carcinogenesis through p53-dependent pathways. *J. Pathol.* 208, 724–732. doi: 10.1002/path.1931

Morotti, A., Panuzzo, C., Crivellaro, S., Pergolizzi, B., Familiari, U., Berger, A. H., et al. (2014). BCR-ABL disrupts PTEN nuclear-cytoplasmic shuttling through phosphorylation-dependent activation of HAUSP. *Leukemia* 28, 1326–1333. doi: 10.1038/leu.2013.370

Nijman, S. M., Luna-Vargas, M. P., Velds, A., Brummelkamp, T. R., Dirac, A. M., Sixma, T. K., et al. (2005). genomic and functional inventory of deubiquitinating enzymes. *Cell* 123, 773–786. doi: 10.1016/j.cell.2005.11.007

Novellasdemunt, L., Foglizzo, V., Cuadrado, L., Antas, P., Kucharska, A., Encheva, V., et al. (2017). USP7 Is a tumor-specific WNT activator for APC-mutated colorectal cancer by mediating beta-catenin deubiquitination. *Cell Rep.* 21, 612–627. doi: 10.1016/j.celrep.2017.09.072

Oh, Y. M., Yoo, S. J., and Seol, J. H. (2007). Deubiquitination of Chfr, a checkpoint protein, by USP7/HAUSP regulates its stability and activity. *Biochem. Biophys. Res. Commun.* 357, 615–619. doi: 10.1016/j.bbrc.2007.03.193

Oliner, J. D., Kinzler, K. W., Meltzer, P. S., George, D. L., and Vogelstein, B. (1992). Amplification of a gene encoding a p53-associated protein in human sarcomas. *Nature* 358, 80–83. doi: 10.1038/358080a0

Ozen, A., Rouge, L., Bashore, C., Hearn, B. R., Skelton, N. J., and Dueber, E. C. (2018). Selectively modulating conformational states of USP7 catalytic domain for activation. *Structure* 26, 72–84.e7. doi: 10.1016/j.str.2017.11.010

Palazon-Riquelme, P., Worboys, J. D., Green, J., Valera, A., Martin-Sanchez, F., Pellegrini, C., et al. (2018). USP7 and USP47 deubiquitinases regulate NLRP3 inflammasome activation. *EMBO Rep.* 19:e44766. doi: 10.15252/embr.201744766

Park, J. J., Lim, K. H., and Baek, K. H. (2015). Annexin-1 regulated by HAUSP is essential for UV-induced damage response. *Cell Death Dis.* 2015:e1654. doi: 10.1038/cddis.2015.32

Pfoh, R., Lacdao, I. K., Georges, A. A., Capar, A., Zheng, H., Frappier, L., et al. (2015). Crystal structure of USP7 ubiquitin-like domains with an ICP0 peptide reveals a novel mechanism used by viral and cellular proteins to target. *PLoS Pathog.* 11:e1004950. doi: 10.1371/journal.ppat.1004950

Qian, J., Pentz, K., Zhu, Q., Wang, Q., He, J., Srivastava, A. K., et al. (2015). USP7 modulates UV-induced PCNA monoubiquitination by regulating DNA polymerase eta stability. *Oncogene* 34, 4791–4796. doi: 10.1038/onc.2014.394

Qing, P., Han, L., Bin, L., Yan, L., and Ping, W. X. (2011). USP7 regulates the stability and function of HLTF through deubiquitination. *J. Cell Biochem.* 112, 3856–3862. doi: 10.1002/jcb.23317

Reverdy, C., Conrath, S., Lopez, R., Planquette, C., Atmanene, C., Collura, V., et al. (2012). Discovery of specific inhibitors of human USP7/HAUSP deubiquitinating enzyme. *Chem. Biol.* 19, 467–477. doi: 10.1016/j.chembiol.2012.02.007

Rouge, L., Bainbridge, T. W., Kwok, M., Tong, R., Di Lello, P., Wertz, I. E., et al. (2016). Molecular understanding of USP7 substrate recognition and C-terminal activation. *Structure* 24, 1335–1345. doi: 10.1016/j.str.2016.05.020

Sarasin, A. (2012). UVSSA and USP7: new players regulating transcription-coupled nucleotide excision repair in human cells. *Genome Med.* 4:44. doi: 10.1186/gm343

Saridakis, V., Sheng, Y., Sarkari, F., Holowaty, M. N., Shire, K., Nguyen, T., et al. (2005). Structure of the p53 binding domain of HAUSP/USP7 bound to Epstein-Barr nuclear antigen 1 implications for EBV-mediated immortalization. *ESE Mol. Cell* 18, 25–36. doi: 10.1016/j.molcel.2005.02.029

Shan, H., Li, X., Xiao, X., Dai, Y., Huang, J., Song, J., et al. (2018). USP7 deubiquitinates and stabilizes NOTCH1 in T-cell acute lymphoblastic leukemia. *Signal. Transduct. Target. Ther.* 3:29. doi: 10.1038/s41392-018-0028-3

Sheng, Y., Saridakis, V., Sarkari, F., Duan, S., Wu, T., Arrowsmith, C. H., et al. (2006). Molecular recognition of p53 and MDM2 by USP7/HAUSP. *Nat. Struct. Mol. Biol.* 13, 285–291. doi: 10.1038/nsmb1067

Shi, Y., Lan, F., Matson, C., Mulligan, P., Whetstine, J. R., Cole, P. A., et al. (2004). Histone demethylation mediated by the nuclear amine oxidase homolog LSD1. *Cell* 119, 941–953. doi: 10.1016/j.cell.2004.12.012

Smits, V. A., and Freire, R. (2016). USP7/HAUSP: a SUMO deubiquitinase at the heart of DNA replication. *Bioessays* 38, 863–868. doi: 10.1002/bies.201600096

Song, M. S., Salmena, L., Carracedo, A., Egia, A., Lo-Coco, F., Teruya-Feldstein, J., et al. (2008). The deubiquitinylation and localization of PTEN are regulated by a HAUSP-PML network. *Nature* 455, 813–817. doi: 10.1038/nature07290

Su, D., Ma, S., Shan, L., Wang, Y., Wang, Y., Cao, C., et al. (2018). Ubiquitin-specific protease 7 sustains DNA damage response and promotes cervical carcinogenesis. *J. Clin. Invest.* 128, 4280–4296. doi: 10.1172/jci120518

Tang, J., Qu, L. K., Zhang, J., Wang, W., Michaelson, J. S., Degenhardt, Y. Y., et al. (2006). Critical role for Daxx in regulating Mdm2. *Nat. Cell Biol.* 8, 855–862. doi: 10.1038/ncb1442

Tavana, O., Li, D., Dai, C., Lopez, G., Banerjee, D., Kon, N., et al. (2016). HAUSP deubiquitinates and stabilizes N-Myc in neuroblastoma. *Nat. Med.* 22, 1180–1186. doi: 10.1038/nm.4180

Trotman, L. C., Wang, X., Alimonti, A., Chen, Z., Teruya-Feldstein, J., Yang, H., et al. (2007). Ubiquitination regulates PTEN nuclear import and tumor suppression. *Cell* 128, 141–156. doi: 10.1016/j.cell.2006.11.040

Turnbull, A. P., Ioannidis, S., Krajewski, W. W., Pinto-Fernandez, A., Heride, C., Martin, A. C. L., et al. (2017). Molecular basis of USP7 inhibition by selective small-molecule inhibitors. *Nature* 550, 481–486. doi: 10.1038/nature24451

van der Horst, A., and Burgering, B. M. (2007). Stressing the role of FoxO proteins in lifespan and disease. *Nat. Rev. Mol. Cell Biol.* 8, 440–450. doi: 10.1038/nrm2190

van der Horst, A., de Vries-Smits, A. M., Brenkman, A. B., van Triest, M. H., van den Broek, N., Colland, F., et al. (2006). FOXO4 transcriptional activity is regulated by monoubiquitination and USP7/HAUSP. *Nat. Cell Biol.* 8, 1064–1073. doi: 10.1038/ncb1469

van Loosdregt, J., and Coffer, P. J. (2014). Post-translational modification networks regulating FOXP3 function. *Trends Immunol.* 35, 368–378. doi: 10.1016/j.it.2014.06.005

van Loosdregt, J., Fleskens, V., Fu, J., Brenkman, A. B., Bekker, C. P., Pals, C. E., et al. (2013). Stabilization of the transcription factor Foxp3 by the deubiquitinase USP7 increases Treg-cell-suppressive capacity. *Immunity* 39, 259–271. doi: 10.1016/j.immuni.2013.05.018

Vassilev, L. T., Vu, B. T., Graves, B., Carvajal, D., Podlaski, F., Filipovic, Z., et al. (2004). In vivo activation of the p53 pathway by small-molecule antagonists of MDM2. *Science* 303, 844–848. doi: 10.1126/science.1092472

Wade, M., Li, Y. C., and Wahl, G. M. (2013). MDM2, MDMX and p53 in oncogenesis and cancer therapy. *Nat. Rev. Cancer* 13, 83–96. doi: 10.1038/nrc3430

Wang, L., Kumar, S., Dahiya, S., Wang, F., Wu, J., Newick, K., et al. (2016). Ubiquitin-specific protease-7 inhibition impairs Tip60-dependent Foxp3+ T-regulatory Cell function and promotes antitumor immunity. *EBioMedicine* 13, 99–112. doi: 10.1016/j.ebiom.2016.10.018

Wang, Q., Ma, S., Song, N., Li, X., Liu, L., Yang, S., et al. (2016). Stabilization of histone demethylase PHF8 by USP7 promotes breast carcinogenesis. *J. Clin. Invest.* 126, 2205–2220. doi: 10.1172/jci85747

Xiang, Q., Ju, H., Li, Q., Mei, S. C., Chen, D., and Choi, Y. B. (2018). Human herpesvirus 8 interferon regulatory factors 1 and 3 mediate replication and latency activities via interactions with USP7 Deubiquitinase. *J. Virol.* 92:e2003–17. doi: 10.1128/jvi.02003-17

Yao, Y., Zhang, Y., Shi, M., Sun, Y., Chen, C., Niu, M., et al. (2018). Blockade of deubiquitinase USP7 overcomes bortezomib resistance by suppressing NF-kappaB signaling pathway in multiple myeloma. *J. Leukoc. Biol.* 104, 1105–1115. doi: 10.1002/JLB.2A1017-420RR

Yi, L., Cui, Y., Xu, Q., and Jiang, Y. (2016). Stabilization of LSD1 by deubiquitinating enzyme USP7 promotes glioblastoma cell tumorigenesis and metastasis through suppression of the p53 signaling pathway. *Oncol. Rep.* 36, 2935–2945. doi: 10.3892/or.2016.5099

Zaman, M. M., Nomura, T., Takagi, T., Okamura, T., Jin, W., Shinagawa, T., et al. (2013). Ubiquitination-deubiquitination by the TRIM27-USP7 complex regulates tumor necrosis factor alpha-induced apoptosis. *Mol. Cell Biol.* 33, 4971–4984. doi: 10.1128/mcb.00465-13

Zhang, P., Wei, Y., Wang, L., Debeb, B. G., Yuan, Y., Zhang, J., et al. (2014). ATM-mediated stabilization of ZEB1 promotes DNA damage response and radioresistance through CHK1. *Nat. Cell Biol.* 16, 864–875. doi: 10.1038/ncb3013

Zhang, X., Gu, L., Li, J., Shah, N., He, J., Yang, L., et al. (2010). Degradation of MDM2 by the interaction between berberine and DAXX leads to potent apoptosis in MDM2-overexpressing cancer cells. *Cancer Res.* 70, 9895–9904. doi: 10.1158/0008-5472.can-10-1546

Zhang, X., Horibata, K., Saijo, M., Ishigami, C., Ukai, A., Kanno, S., et al. (2012). Mutations in UVSSA cause UV-sensitive syndrome and destabilize ERCC6 in transcription-coupled DNA repair. *Nat. Genet.* 44, 593–597. doi: 10.1038/ng.2228

Zhou, J., Wang, J., Chen, C., Yuan, H., Wen, X., and Sun, H. (2018). USP7: target validation and drug discovery for cancer therapy. *Med. Chem.* 14, 3–18. doi: 10.2174/1573406413666171020115539

Zhu, X., Menard, R., and Sulea, T. (2007). High incidence of ubiquitin-like domains in human ubiquitin-specific *proteases*. *Proteins* 69, 1–7. doi: 10.1002/prot.21546

Zlatanou, A., Sabbioneda, S., Miller, E. S., Greenwalt, A., Aggathanggelou, A., Maurice, M. M., et al. (2016). USP7 is essential for maintaining Rad18 stability and DNA damage tolerance. *Oncogene* 35, 965–976. doi: 10.1038/onc.2015.149

Conflict of Interest Statement: The authors declare that the research was conducted in the absence of any commercial or financial relationships that could be construed as a potential conflict of interest.

frontiers in Pharmacology

ORIGINAL RESEARCH
published: 03 May 2019
doi: 10.3389/fphar.2019.00338

Regulation of Wnt Singaling Pathway by Poly (ADP-Ribose) Glycohydrolase (PARG) Silencing Suppresses Lung Cancer in Mice Induced by Benzo(a)pyrene Inhalation Exposure

Wenjuan Dai[1,2†], Yingbin Fu[1†], Yanxia Deng[1†], Zhuoying Zeng[1], Pan Gu[1], Hailong Liu[1], Jianjun Liu[1], Xinyun Xu[1], Desheng Wu[1], Xianru Luo[1], Linqing Yang[1], Jinzhou Zhang[1], Kai Lin[1], Gonghua Hu[2,3] and Haiyan Huang[1]**

[1] Shenzhen Center for Disease Control and Prevention, Shenzhen, China, [2] Jiangxi Provincial Key Laboratory of Preventive Medicine, School of Public Health, Nanchang University, Nanchang, China, [3] Department of Preventive Medicine, Gannan Medical University, Ganzhou, China

OPEN ACCESS

Edited by:
Zhe-Sheng Chen,
St. John's University, United States

Reviewed by:
David W. Koh,
Ohio Northern University,
United States
Shiv K. Gupta,
Mayo Clinic, United States

***Correspondence:**
Gonghua Hu
hgh0129@163.com
Haiyan Huang
hhy424@126.com

[†] These authors have contributed equally to this work

Specialty section:
This article was submitted to Cancer Molecular Targets and Therapeutics, a section of the journal Frontiers in Pharmacology

Received: 13 January 2019
Accepted: 19 March 2019
Published: 03 May 2019

Citation:
Dai W, Fu Y, Deng Y, Zeng Z, Gu P, Liu H, Liu J, Xu X, Wu D, Luo X, Yang L, Zhang J, Lin K, Hu G and Huang H (2019) Regulation of Wnt Singaling Pathway by Poly (ADP-Ribose) Glycohydrolase (PARG) Silencing Suppresses Lung Cancer in Mice Induced by Benzo(a)pyrene Inhalation Exposure. Front. Pharmacol. 10:338. doi: 10.3389/fphar.2019.00338

Benzo(a)pyrene (BaP) is a polycyclic aromatic hydrocarbon that specifically causes cancer and is widely distributed in the environment. Poly (ADP-ribosylation), as a key post-translational modification in BaP-induced carcinogenesis, is mainly catalyzed by poly (ADP-ribose) glycohydrolase (PARG) in eukaryotic organisms. Previously, it is found that PARG silencing can counteract BaP-induced carcinogenesis *in vitro*, but the mechanism remained unclear. In this study, we further examined this process *in vivo* by using heterozygous PARG knockout mice ($PARG^{+/-}$). Wild-type and $PARG^{+/-}$ mice were individually treated with 0 or 10 $\mu g/m^3$ BaP for 90 or 180 days by dynamic inhalation exposure. Pathological analysis of lung tissues showed that, with extended exposure time, carcinogenesis and injury in the lungs of WT mice was progressively worse; however, the injury was minimal and carcinogenesis was not detected in the lungs of $PARG^{+/-}$ mice. These results indicate that PARG gene silencing protects mice against lung cancer induced by BaP inhalation exposure. Furthermore, as the exposure time was extended, the protein phosphorylation level was down-regulated in WT mice, but up-regulated in $PARG^{+/-}$ mice. The relative expression of Wnt2b and Wnt5b mRNA in WT mice were significantly higher than those in the control group, but there was no significant difference in $PARG^{+/-}$ mice. Meanwhile, the relative expression of Wnt2b and Wnt5b proteins, as assessed by immunohistochemistry and Western blot analysis, was significantly up-regulated by BaP in WT mice; while in $PARG^{+/-}$ mice it was not statistically affected. Our work provides initial evidence that PARG silencing suppresses BaP induced lung cancer and stabilizes the expression of Wnt ligands, PARG gene and Wnt ligands may provide new options for the diagnosis and treatment of lung cancer.

Keywords: benzo(a)pyrene, ADP-ribosylation, poly (ADP-ribose) glycohydrolase, Wnt signaling pathway, lung cancer

INTRODUCTION

Benzo(a)pyrene (BaP) is a polycyclic aromatic hydrocarbon that is known to be carcinogenic. It is mainly produced by pyrolysis and incomplete combustion of carbonaceous materials and is widely distributed in both the working and living environment (Liu et al., 2008). A large number of experiments have shown that BaP can induce cancer in various animals (IARC Working Group on the Evaluation of Carcinogenic Risks to Humans, 2010; Kasala et al., 2016). Furthermore, epidemiological studies suggest that BaP is closely associated with human lung cancer (Rojas et al., 2004; Alexandrov et al., 2010; Widziewicz et al., 2018). On the basis of these studies, BaP was classified as a human class I carcinogen by the International Agency for Research on Cancer in 2006 (IARC Working Group on the Evaluation of Carcinogenic Risks to Humans, 2012).

Lung cancer is the most common malignant tumor in the human respiratory system and is extremely harmful to human health. Globally, the morbidity and mortality of lung cancer are among the highest (Ferlay et al., 2015). According to the American Cancer Society, lung cancer leads to the highest number of deaths in both men and women. Recent evidence suggests that the incidence of lung cancer in China is the highest and the mortality is increasing at a rate of 4.5% per year (Chen et al., 2016).

The occurrence of lung cancer is the result of a combination of both environmental and genetic factors, including epigenetic changes which have been proved to contribute to lung cancer development (Hagood, 2014). ADP-ribosylation, as an epigenetic modification, plays a critical role in cell survival and disease development, including cancers (D'Amours et al., 1999; Min et al., 2010; Huang et al., 2012). Poly-ADP-ribosylation can convert nuclear chromatin to a loose state, allowing accessibility of DNA damage repair enzymes to the injury site, thereby promoting DNA damage repair against cytotoxicity and genetic damage. Poly-ADP-ribose glycohydrolase (PARG) can hydrolyze poly (ADP-ribose) on poly (ADP-ribose) polymerase-1 (PARP-1), which promotes the degradation of intracellular poly (ADP-ribose) (PAR) (Rouleau et al., 2004). It is the only known enzyme that can hydrolyze poly (ADP-ribose) in the nucleus (Meyer et al., 2007). Recent studies have shown that PARG gene silencing can increase intracellular poly-ADP-ribosylation to protect cells against cytotoxicity. Li et al. (Li et al., 2016) found that BaP can induce chromosomal aberrations, micronucleus formation, chromatin structure changes and malignant transformation of normal 16HBE cells, but PARG gene silencing can inhibit these abnormalities. Studies have shown that PARG also is associated with tumorigenesis (Miwa and Masutani, 2007), but the exact mechanism of PARG on tumor promotion has not been fully clarified.

In our previous study, 16HBE cells and PARG-deficient cells were treated with 40 μmol/L BaP for a period of time to induce malignant transformation, and by using MeDIP-sequence analysis, it is found that the methylation levels of Wnt2b and Wnt5b genes in the two cells were significantly different. Wnt2b and Wnt5b are key players in the Wnt/β-Catenin signaling pathway (Klaus and Birchmeier, 2008), which has been highly conserved in evolution and is known to control cell growth, differentiation, apoptosis, and self-renewal. This pathway is activated by binding of Wnt ligands to receptors, which increases the stability of β-catenin in the cytoplasm and promotes its translocation to the nucleus, where it modulates the expression of target genes that lead to tumorigenesis (Klaus and Birchmeier, 2008). Studies have shown that this pathway is abnormally activated during the development of lung cancer and may coordinate or antagonize other signaling pathways to regulate proliferation, migration, and invasion in lung cancer (Reya and Clevers, 2005; Berndt and Moon, 2013). Recently, 30–40% of cells in tumor tissues have been shown to express Wnt ligands, which create a microenvironment that is suitable for tumor cells. In a human lung adenocarcinoma model, 70% of cells have abnormal activation of the Wnt pathway, and 80% of cells may be involved in the formation of the tumor microenvironment, which is critical for the progression of lung cancer (Tammela et al., 2017).

Given the decisive role of the Wnt signaling pathway in the development of lung cancer, inhibition of Wnt ligands provides a viable approach for reducing the expansion of lung cancer cell lines. The purpose of this study was to investigate whether PARG gene silencing can inhibit lung cancer development induced by BaP and whether it can regulate the Wnt ligands to inhibit the development of lung cancer. On the basis of our findings, PARG gene and Wnt ligands may constitute a new option for the diagnosis and treatment of lung cancer.

MATERIALS AND METHODS

Materials

BaP (CAS50-32-8, purity ≥96%) was purchased from American Sigma Company, and dissolved in dimethylsulfoxide (DMSO). Other chemicals were purchased from Sigma–Aldrich (St Louis, MO, United States) or Thermo Fisher Scientific (Shanghai, China), unless otherwise stated.

Animals and Treatment

The PARG knockout mice [B6N (Cg)-Parg$^{tm2b(KOMP)Mbp}$/J]were purchased from the Jackson Laboratory, and WT mice (C57BL/6J) were purchased from Guangdong Medical Lab Animal Center. PARG knockout mice were generated by the targeted mutation 2b of the Parg gene resulting in deletion of the full-length isoform of PARG protein ($PARG_{110}$). The strategy of gene targeting is Cre-mediated excision of the parental Parg$^{tm2b(KOMP)Mbp}$ allele resulted in the removal of the promoter-driven neomycin selection cassette and critical exon(s) leaving behind the inserted lacZ reporter sequence. We screened for heterozygous PARG knockout mice ($PARG^{+/-}$) in our study since death of homozygous PARG knockout mice ($PARG^{-/-}$) occurring before the normal life span of an organism, occurring during pregnancy, parturition or lactation. The mice were maintained under semi-specific-pathogen-free conditions with the temperature controlled at 23 ± 2°C and a 12-h light/dark

cycle. We selected 2-month-old $PARG^{+/-}$ and WT mice for this study. The mice were randomly divided into two groups with 6 per group referring to the principles of experimental animal selection and references. And then, they were treated with 0 or 10 $\mu g/m^3$ aerosols through respiratory tract by a dynamic inhalation cabinet (Jiufang Company, Guangzhou) for 90 or 180 days. The dynamic inhalation device makes liquids into aerosols with a diameter of only a few micrometers, which is in line with the actual human exposure to BaP in the air. At the end of the experiment, mice were anesthetized with ether and blood was collected by eyeball sampling. The mice were then euthanized and the lungs were excised rapidly. Half of each lung was stored in 4% paraformaldehyde, and the other half was stored at −80°C. All animal experiments and procedures were approved by the Shenzhen Center for Disease Control and Prevention. Efforts were made to minimize animal suffering and reduce the number of mice used in the experiments.

Genotyping of PARG Knockout Mice

Genomic DNA was purified from mouse tails using TianAMP genomic DNA kits (Tiangen, Beijing, China). The concentration and the quality of DNA were assessed by ultraviolet (UV) absorbance using a NanoDrop ND-2000 spectrophotometer (Thermo Fisher Scientific). The DNA was then amplified by PCR (94°C for 2 min; 10 cycles of 94°C for 20 s, 65°C for 15 s, and 68°C for 10 s; 10 cycles of 94°C for 15 s, 60°C for 15 s, and 72°C for 10 s; 72°C for 2 min, 10°C hold) using primers provided by the Jackson Laboratory (Wild-type Forward: 5′-GAG ATA TCT AAG TCA GAG AAA GGT GGT-3′, Wild-type Reverse: 5′-CCT CCT CTG GTG TGT CTG AAG-3′, Mutant Forward: 5′-CGG TCG CTA CCA TTA CCA GT-3′, Mutant Reverse: 5′-GGT ATC AGC GAT GGT TGT TC-3′). The PCR products were 279 bp for the WT sample, and 279 and 507 bp for the heterozygous PARG knockout ($PARG^{+/-}$) sample.

Hematoxylin and Eosin Staining

Mouse lung tissues were fixed in 4% paraformaldehyde for 48 h, dehydrated in ethanol and embedded in paraffin by using a TissueWave™ 2 Microwave Processor (Thermo Fisher Scientific). Paraffin-fixed tissues were sliced into 5 μm sections, mounted on glass slides, and dried for 1 h. After dewaxing and rehydration, sections were stained with hematoxylin and eosin (Sigma-Aldrich) and examined by light microscopy. The pathology was evaluated by a blinded observer to detect the degree of malignancy.

Real-Time Quantitative PCR

Total RNA was extracted from frozen lung samples with miRNeasy mini kits (Qiagen, China) according to the manufacturer's instructions. Complementary DNA (cDNA) was synthesized from 500 ng of total lung RNA (n = 3 per group) using the PrimeScript™ RT reagent kit (Takara, China). Quantitative PCR (qPCR) was performed on the ABI Prism 7500 system (Applied Biosystems, Foster City, CA, United States) using SYBR select master mix. The mRNA primers were purchased from Sangon Biotech (Shanghai, China) and are listed in **Supplementary Table S1**. Experiments were repeated at least 3 times. The relative level of mRNA for each gene was determined using the $2^{-\Delta\Delta Ct}$ method (Schmittgen and Livak, 2008), and P-values were calculated using the Student's t-test on replicate $2^{-\Delta Ct}$ values for each gene in each treatment group compared to the control group.

Immunohistochemistry

Mouse lung tissues were fixed in 4% paraformaldehyde for 48 h, dehydrated in ethanol and embedded in paraffin by using a TissueWave™ Microwave Processor (Thermo Fisher Scientific). After dewaxing and rehydration, 5 μm-thick coronal sections were incubated in 0.01 M citrate buffer (pH 6.0) with 0.1% Tween-20 at 95–100°C for 10 min for antigen retrieval. For immunochemistry of Wnt2b and Wnt5b (n = 3 per group), the sections were incubated at 4°C overnight with primary antibody (Wnt2b at 1:200 or Wnt5b at 1:50). After being washed with PBST, the sections were stained using the mouse and rabbit-specific HRP/DAB (ABC) detection IHC kit (Abcam, ab64264) and analyzed using an Olympus BX60 compound microscope (Tokyo, Japan).

Western Blot Analysis

Lung proteins (n = 3 per group) were extracted from 30 mg lung tissue with 600 μL lysis buffer (Beyotime, China) and 6 μL protease and phosphatase inhibitor cocktail (Thermo Fisher Scientific, United States) on ice, and then centrifuged and collected. The protein concentration was measured with a BCA protein assay kit (Thermo Fisher Scientific, United States). Each protein sample was combined with loading buffer and heated for 8 min at 100°C. Protein samples were separated on 10% PAGE gels with 5% stacking gels and transferred to PVDF membranes. The membranes were incubated in TBST buffer containing 5% milk at room temperature for 2 h. Subsequently, they were incubated with anti-PARG (mouse monoclonal antibody, 1:100), anti-phosphotyrosine (PY20, mouse monoclonal antibody,1:1000), anti-Wnt2b (rabbit monoclonal antibody, 1:3000), anti-Wnt5b (mouse monoclonal antibody,1:500), or anti-α-tubulin (mouse monoclonal antibody, 1:3000) in TBST buffer for 1.5 h at room temperature. After washing with TBST three times, the membranes were incubated with homologous secondary antibody (anti-rabbit or anti-mouse IgG HRPs) in TBST buffer for 60 min. The membranes were then repeatedly washed with TBST buffer, developed using chemiluminescence reagents from an ECL kit (Pierce ECL, Santa Cruz, CA, United States) and detected on a phosphorimager. The images of the membranes were analyzed by ImageJ software.

Statistical Analysis

The histograms and statistical analyses of the relative expression of each group were completed using Graph-Pad prism 7.0 software (GraphPad Software, Inc.). Data are presented as mean ± SD. Comparisons between two groups were

conducted with the Student's *t*-test. $P < 0.05$ was considered statistically significant.

RESULTS

Genotyping of PARG Knockout Mice

The heterozygous PARG knockout mice were used to characterize the role of PARG in protecting mice from BaP-induced lung cancer. According to the law of Mendelian inheritance, the genotype of the progeny mice may be WT ($PARG^{+/+}$), heterozygous ($PARG^{+/-}$), or homozygous ($PARG^{-/-}$). Based on genomic DNA purified from mouse tails, $PARG^{+/-}$ mice were screened for our study as $PARG^{-/-}$ mice cannot survive to maturity. The PCR product from WT mice was 279 bp, and the PCR products from PARG knockout heteroygotes ($PARG^{+/-}$) were 279 and 507 bp, as shown in **Figure 1A**. After BaP exposure, proteins from the lung tissues were extracted and Western blotting were performed to verify the expression of full-length isoform ($PARG_{110}$). As expected, the expression of $PARG_{110}$ was significantly greater in WT mice than in $PARG^{+/-}$ mice (**Figure 1B**). The results confirm that heterozygous PARG knockout mice were successfully bred in our experiments.

$PARG^{+/-}$ Mice Are Protected From Pathological Changes in Lung Tissues Induced by BaP

To establish a lung cancer model for assessing the effects of heterozygous PARG silencing, we exposed mice to long-term inhalation of BaP and then prepared paraffin sections of lung tissues. Hematoxylin and eosin staining were used to analyze the pathological changes that were observed under light microscopy. As shown in **Figure 2A**, in the lungs of WT mice exposed for 90 days, alveolar diffuse interstitialization occurred, though the alveolar structure was visible; in contrast, the degree of injury in $PARG^{+/-}$ mice was mild with no obvious pathological damage. The results were similar in both male and female mice. After 180-day exposure to BaP, the lungs of the WT mice treated with BaP showed severe alveolar diffuse interstitialization, and the alveolar structure was severely damaged with obvious inflammatory infiltration and abnormal nodules (**Figure 2B**). Comparison between the 90- and 180-d pathology suggests that the degree of lung injury in WT mice treated with BaP was positively correlated with the time of exposure. In $PARG^{+/-}$ mice after 180 days, however, some alveolar interstitial thickening appeared while the alveolar structure was still visible. This suggests that $PARG^{+/-}$ mice were protected from the effects of BaP on lung pathology. A higher magnification was used to examine tumor formation. In WT mice, the number of cells increased abnormally and tumorigenesis could be observed (**Figure 2C**); however, no tumor tissue was found in $PARG^{+/-}$ mice. These results demonstrate that heterozygous PARG gene silencing can inhibit the induction of lung cancer by BaP in mice.

$PARG^{+/-}$ Mice Express Elevated Levels of Phosphorylated Proteins in Lung Tissues After BaP Inhalation Exposure

To determine whether heterozygous PARG silencing affects the overall protein phosphorylation level, we performed Western blot assays using the universal anti-tyrosine phosphorylation monoclonal antibody PY20 with protein extracted from lung tissues. As shown in **Figure 3A**, the levels of total phosphorylated proteins in WT and heterozygous PARG knockout mice were not significantly different from that of the control group after exposure to BaP for 90 days ($P > 0.05$). After 180-d exposure, however, the level of phosphorylated proteins was significantly down-regulated in WT mice ($^*P < 0.05$), but was significantly up-regulated in $PARG^{+/-}$ mice compared with the control group ($^*P < 0.05$). These results indicate that, at an extended BaP exposure time, PARG affects phosphorylation of proteins, which could potentially be associated with the ability of $PARG^{+/-}$ mice to resist tumorigenesis.

PARG Silencing Inhibits the Relative Expression of Wnt2b and Wnt5b mRNA in Lung Tissues After BaP Inhalation Exposure

To further elucidate whether ADP-ribosylation affects the Wnt pathway in $PARG^{+/-}$ mice, we first performed real-time qPCR to detect the relative expression of the Wnt2b and Wnt5b genes. The relative expression of Wnt2b and Wnt5b mRNA was significantly higher in WT mice than in control mice at 90 and 180 days

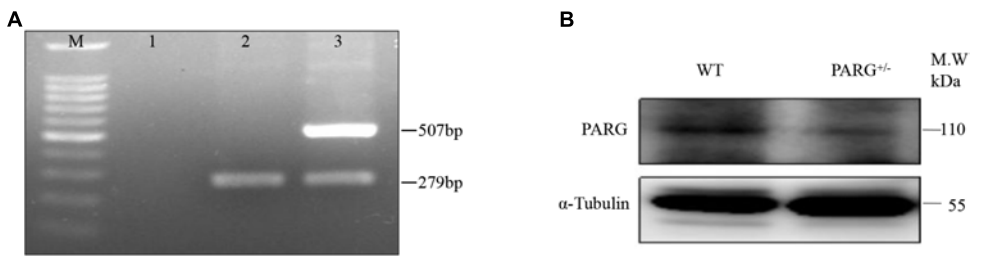

FIGURE 1 | Genotyping of poly (ADP-Ribose) glycohydrolase (PARG) knockout mice. Genotyping of $PARG^{+/-}$ mice. **(A)** Genotyping by PCR. Lane M, 100 bp DNA Marker; Lane 1, blank control; Lane 2, WT mice; and Lane 3, $PARG^{+/-}$ mice. **(B)** Genotyping by Western blotting. The expression of $PARG_{110}$ protein was assessed in lungs from WT and $PARG^{+/-}$ mice.

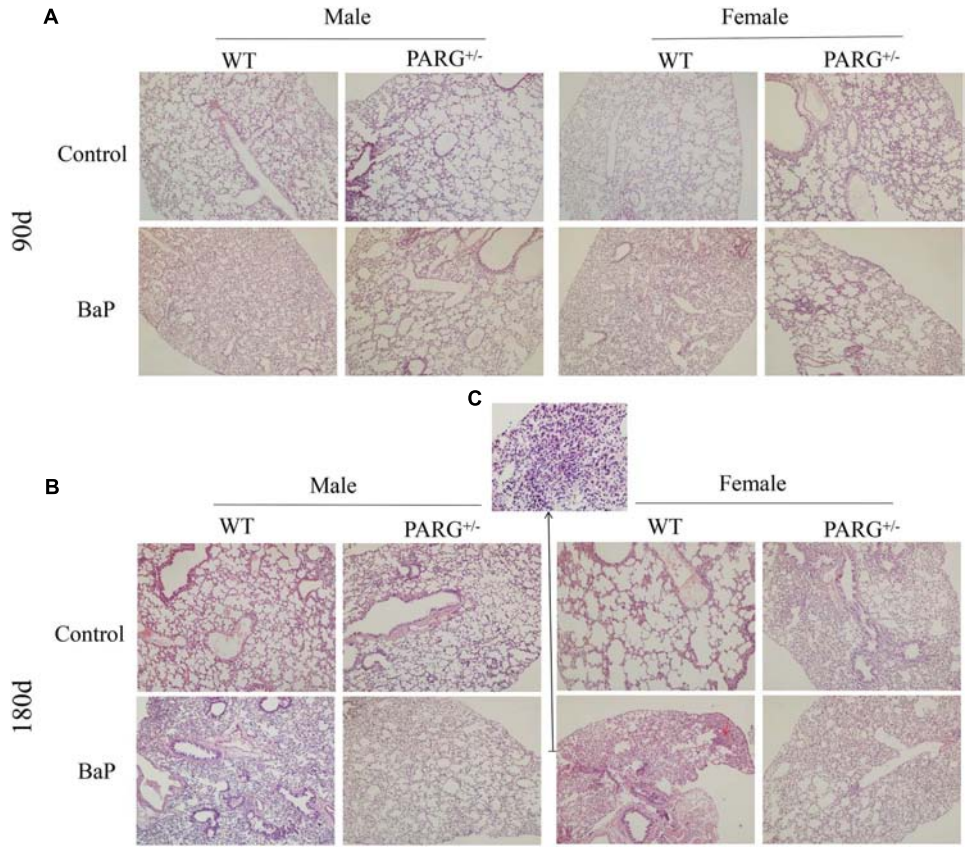

FIGURE 2 | PARG$^{+/-}$ mice are protected from pathological changes in lung tissues induced by BaP inhalation exposure. Pathological changes in lung tissues of WT and PARG$^{+/-}$ mice after benzo(a)pyrene inhalation exposure **(A)** 90-day exposure (×100). **(B)** 180-day exposure to BaP (×100). The red arrows show abnormally increased numbers of cells. **(C)** The magnification of the place pointed by the red arrow in **B**, pathological signs of tumorigenesis (×200). Results are representative of 3 mice from each group.

(***$P < 0.001$), but there were no significant differences in the PARG$^{+/-}$ mice ($P > 0.05$) (**Figure 4**).

PARG Silencing Inhibits the Expression of Wnt2b and Wnt5b Protein in Lung Tissues After BaP Inhalation Exposure

The expression of Wnt2b and Wnt5b at the level of the protein were further confirmed by performing Western blotting and immunohistochemistry. The expression of Wnt2b protein was up-regulated in lungs from WT mice that were treated with BaP for 90 and 180 days (*$P < 0.05$, compared with the control group); however, for PARG$^{+/-}$ mice, no statistically significant differences were observed ($P > 0.05$) (**Figure 5A**). In immunohistochemistry assays, Wnt2b protein (brownish yellow staining) was localized to the cytoplasm, and after 90 and 180 days of BaP inhalation exposure, the expression levels in WT male and female mice were higher for treated vs. control mice; however, for PARG$^{+/-}$ mice, there were no significant differences (**Figure 5B**). Similar results were observed for Wnt5b, though the effect on Wnt5b expression was more obvious at 180 days than at 90 days (**Figures 5C,D**). These findings suggest that PARG gene silencing stabilizes the expression of Wnt2b and Wnt5b after BaP exposure, possibly inhibiting the progression of lung cancer.

DISCUSSION

Metabolically activated BaP is known to cause cytotoxic, teratogenic, genotoxic, mutagenic and carcinogenic effects in many different tissues and cell types from numerous mammalian studies (Miller and Ramos, 2001; van Delft et al., 2010). BaP in cigarette smoking is implicated as one of the main factors in lung cancer (Rubin, 2001). The occurrence of cancer includes three stages: initiation, promoting and progressing. Epigenetic modification, as a bridge between these stages, can involve DNA methylation, microRNA, chromatin remodeling, and histone modification (Bird, 2007). ADP-ribosylation is one of the most important post-translational modifications in tumorigenesis (Klaus and Birchmeier, 2008). Studies showed that the use of PARG inhibitor to suppress PARG activity facilitates oxidative damage-induced PARylation as well as DNA damage repair (Zhang et al., 2015). PARG gene silencing increases the level of poly (ADP-ribosylation) to regulate DNA

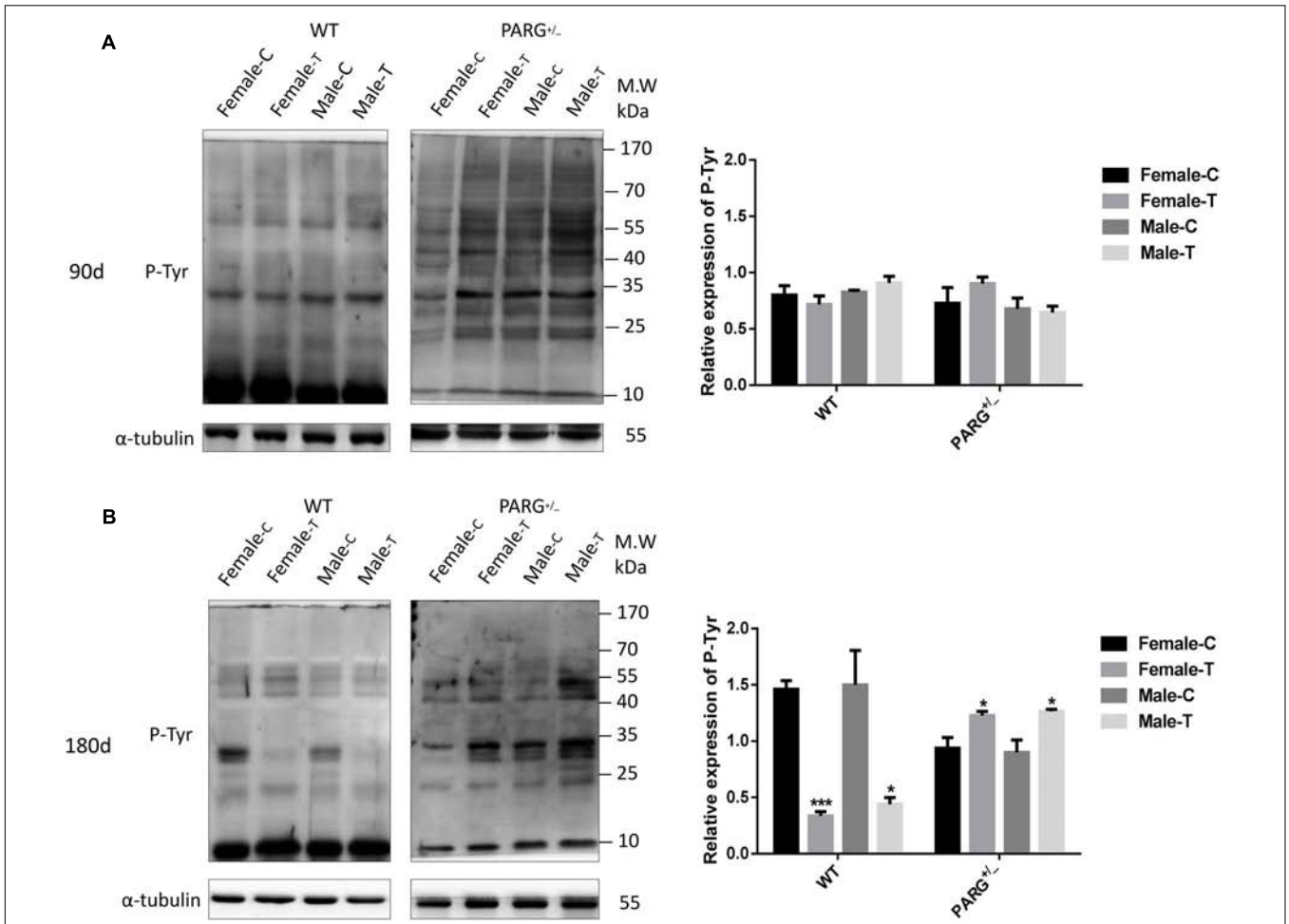

FIGURE 3 | PARG$^{+/-}$ mice express elevated levels of phosphorylated proteins in lung tissues after BaP inhalation exposure. Expression of phosphorylated proteins in lung tissues of mice after BaP inhalation exposure. **(A)** The overall phosphorylation level of proteins in WT and PARG$^{+/-}$ mice that were untreated or were treated with exposure to BaP for 90 days. **(B)** Expression of phosphorylated proteins after 180-day exposure to BaP. Female-C, control untreated female mice; Female-T, treated female mice; Male-C, control untreated male mice; Male-T, treated male mice. $^{*}P < 0.05$, $^{***}P < 0.001$, significant difference in treated compared to untreated mice. Results represent the mean ± SD of 3 mice from each group. Quantification of the phosphorylation levels was performed using ImageJ software.

damage repair and genome stability (Koh et al., 2004). In our previous study, it is determined that *in vitro* PARG silencing inhibits tumorigenesis by dramatically reducing DNA damage, chromosome abnormalities, micronuclei formations, and malignant transformation. To further investigate the possible *in vivo* role of PARG gene silencing, heterozygous PARG knockout mice were utilized. We exposed WT and PARG$^{+/-}$ mice to BaP by dynamic inhalation for 90 and 180 days. Pathological analysis showed that carcinogenesis appeared in the lungs of WT mice and the injury was progressive for 180-day vs. 90-day treatment, while PARG$^{+/-}$ mice showed no carcinogenesis and minimal signs of lung injury. These results suggest that PARG gene silencing can inhibit lung cancer induced by BaP in mice, which is consistent with our *in vitro* results.

In our previous vitro study, we identified two distinct Wnt ligands (Wnt5b and Wnt2b) that are modulated by PARG by using the MeDIP-sequence techniques. This raises the possibility that ADP-ribosylation may affect the carcinogenesis of BaP by regulating the activation of the Wnt signaling pathway after PARG gene silencing. The Wnt pathway consists of three components: the Wnt/β-catenin canonical pathway, the Wnt/Ca^{2+} pathway and the Wnt/polarity pathway (Wodarz and Nusse, 1998). After activation of the canonical pathway, Wnt ligands bind to Frzzled and LRP5/6 on the cell surface to form a trimer, which weakens the stability of a destruction complex composed by β-catenin, Axin, GSK-3β, and APC to prevent the phosphorylated degradation of β-catenin. The concentration of β-catenin increases in the cytoplasm and then is transferred into the nucleus which ultimately activate the expression of downstream target genes (Veeman et al., 2003). During this process, protein phosphorylation, especially tyrosine phosphorylation (P-Tyr), as a major mode of cell signal transduction and regulation of enzyme activity, plays an vital role in the regulation of β-catenin (Ikeda et al., 1998). ADP-ribosylation can promote phosphorylated proteins

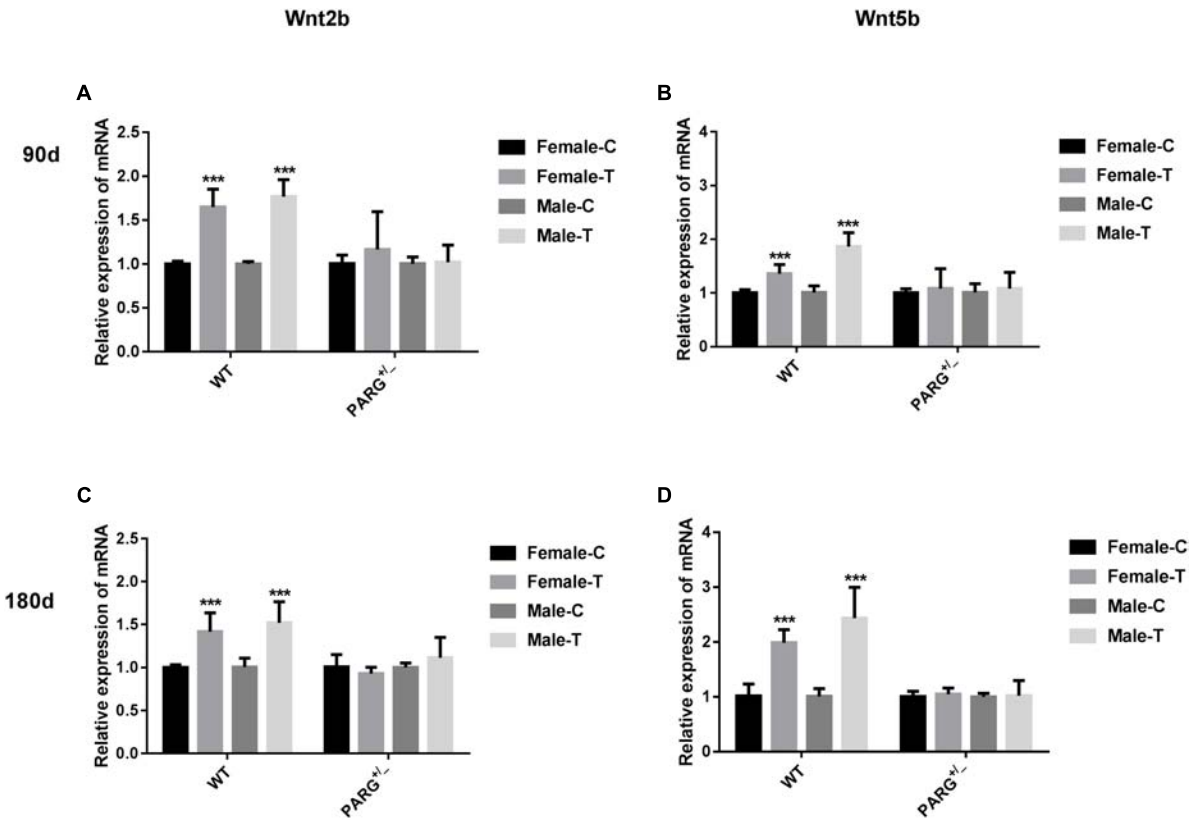

FIGURE 4 | PARG silencing inhibits the relative expression of Wnt2b and Wnt5b mRNA in lung tissues after BaP inhalation exposure. Relative expression of Wnt2b and Wnt5b mRNA in lung tissues of WT and PARG$^{+/-}$ mice after BaP inhalation exposure. The mRNA expression in lungs from WT and PARG$^{+/-}$ mice was measured by real-time quantitative PCR after 90 days (panels **A**,**B**) or 180 days (panels **C**,**D**) of BaP inhalation exposure. Female-C, control untreated female mice; Female-T, treated female mice; Male-C, control untreated male mice; Male-T, treated male mice. ***$P < 0.001$, significant difference was found in treated compared to untreated mice. Results represent the mean ± SD of 3 mice from each group.

to bind to Axin scaffolding proteins, affecting the stability of the key protein β-catenin and regulating the activation of the Wnt pathway (Yang et al., 2016). In the current study, the level of total phosphorylated protein in WT mice and PARG$^{+/-}$ mice was not significantly different after 90-day exposure to BaP. However, after 180 d, phosphorylated protein was significantly reduced in WT mice but was up-regulated in PARG$^{+/-}$ mice compared with the control group. These findings are consistent with the possibility that, as the exposure time of BaP extended, loss of PARG promotes phosphorylation of proteins, which possibly leads to phosphorylated degradation of key proteins in the Wnt pathway; supported by the following studies (Zeng et al., 2005; Kim et al., 2013; Yang et al., 2016). We will try to explore how does PARG regulates protein tyrosine phosphorylation to regulate the Wnt signaling against the progression of lung cancer in our next study.

Wnt ligands play a vital role in the development of lung cancer, and inhibition of Wnt ligands may reduce the expansion of lung cancer cell lines (Tammela et al., 2017). Our results demonstrate that the relative expression of Wnt2b and Wnt5b mRNA was up-regulated in lung tissues of WT mice compared with the control group after 90- and 180-day exposure to BaP. Furthermore, the expression of Wnt2b and Wnt5b protein was up-regulated, though there were no significant differences in Wnt2b and Wnt5b mRNA and protein expression in PARG$^{+/-}$ mice. It suggested that loss of PARG stabilized the expression of Wnt ligands, probably suppressing the activation of the Wnt pathway against the progression of lung cancer.

Wnt2b and Wnt5b are two ligands of the Wnt signaling pathway. Wnt2b mainly acts through the canonical Wnt pathway and binds to receptors on the cell membrane to increase the stability of β-catenin in the cytoplasm and promote its translocation to the nucleus to activate downstream target genes that lead to tumorigenesis (Roelink et al., 1992). Studies have shown that Wnt2b is overexpressed in various cancers (Katoh, 2001; Huang et al., 2015). Wnt5b, on the other hand, is a non-canonical Wnt pathway factor that activates the Wnt/Ca^{2+} pathway or blocks the down-regulation of β-catenin by GSK-3β to prevent the classical Wnt pathway (Kohn and Moon, 2005). Studies have shown that Wnt5b plays different roles in different types of cancers. In some cancers, such as lung cancer, it promotes tumorigenesis, and

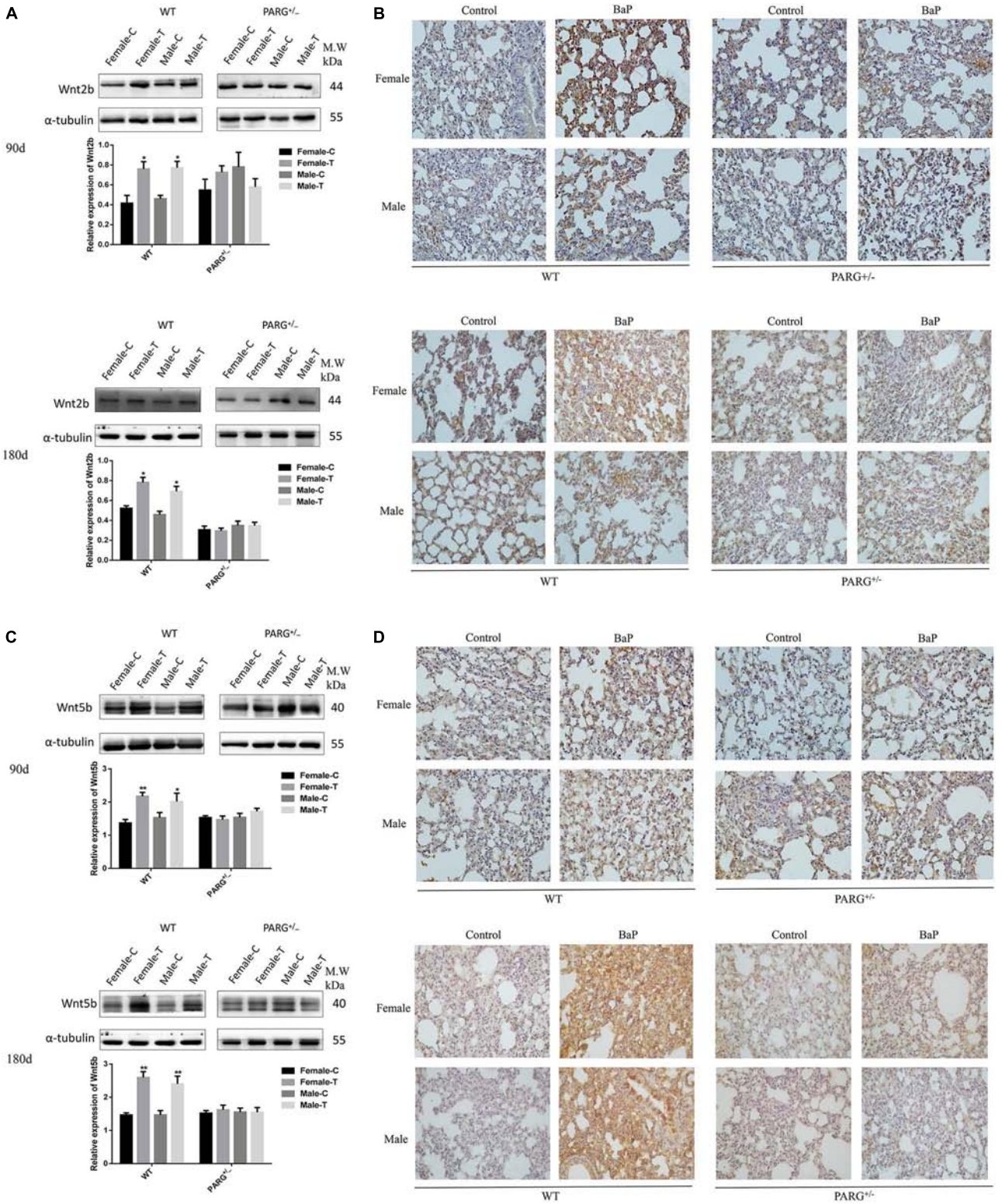

FIGURE 5 | PARG silencing inhibits the expression of Wnt2b and Wnt5b protein in lung tissues after BaP inhalation exposure. Expression of Wnt2b and Wnt5b protein in lung tissues detected by Western blotting and immunohistochemistry. **(A)** Western blotting of Wnt2b expression. **(B)** Immunohistochemical staining of Wnt2b (×200). Protein expression levels are reflected by the area and depth of brownish yellow. **(C)** Western blotting of Wnt5b expression. **(D)** Immunohistochemical staining of Wnt5b (×200). Red arrows indicate Wnt2b and Wnt5b localization in the cytoplasm. Female-C, control untreated female mice; Female-T, treated female mice; Male-C, control untreated male mice; Male-T, treated male mice. $^{*}P < 0.05$, $^{**}P < 0.01$, significant up-regulation in treated vs. control mice.

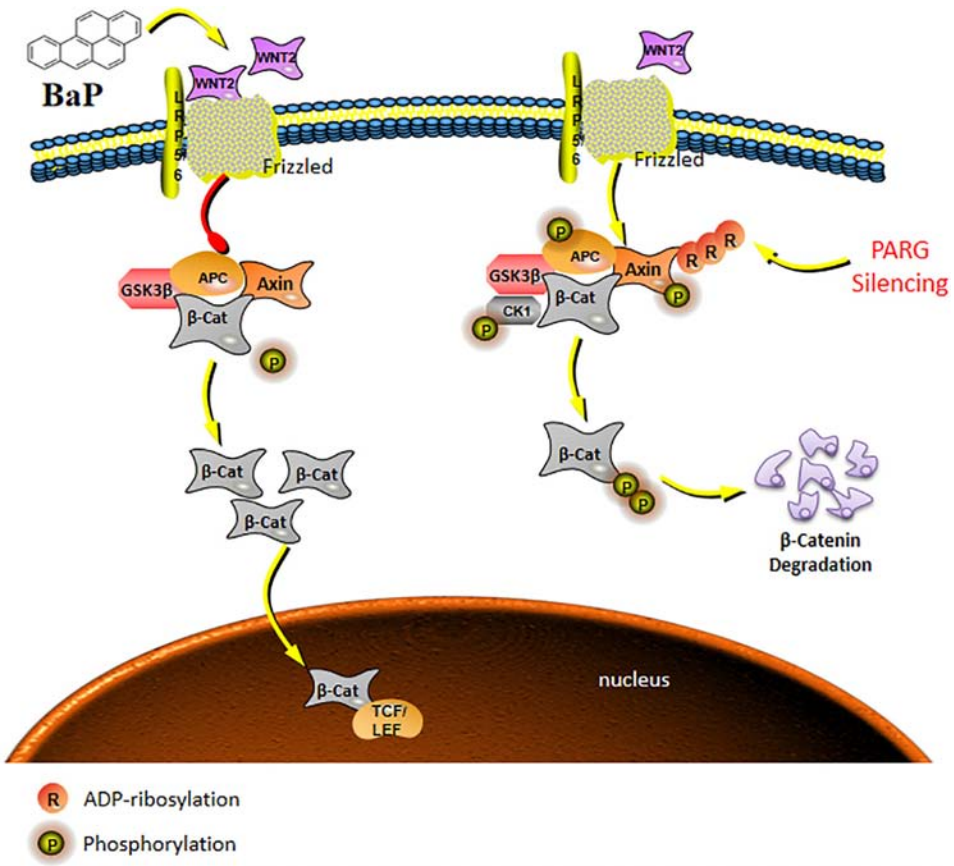

FIGURE 6 | Schematic model of the Wnt/β-catenin signaling pathway regulated by PARG gene silencing during BaP-induced lung cancer. After activation of the canonical pathway, Wnt ligands bind to Frzzled and LRP5/6 on the cell surface to form a trimer, which weakens the stability of a destruction complex composed by β-catenin, Axin, GSK-3β, and APC to prevent the phosphorylated degradation of β-catenin. The concentration of β-catenin increases in the cytoplasm, and then transfers into the nucleus to ultimately activate the expression of downstream target genes. PARG gene silencing may promote binding of phosphorylated proteins to the Axin scaffolding proteins, affecting the stability of the key protein β-catenin, and then suppressing the activation of the Wnt/β-catenin pathway to stabilize the expression of Wnt2b against the progression of lung cancer.

in other cancers, it suppresses tumorigenesis (Kikuchi and Yamamoto, 2008; Harada et al., 2017). On the basis of its different roles in different cancers, Wnt5b may constitute a specific marker for lung cancer screening. In our study, it is found that the up-regulation of Wnt2b was similar at 90 and 180 days, while the up-regulation times of Wnt5b was more obvious at 180 days than at 90 days. These findings may suggest that the Wnt non-canonical pathway increased with extended exposure times, while the classical pathway remains activated at both 90 and 180 days. Specific mechanisms of interaction between the two pathways remains to be further studied.

In conclusion, in the development of lung cancer induced by BaP, the expression of Wnt ligands are up-regulated, which is consistent with current understanding of the role of this pathway. Additionally, PARG gene silencing may regulate the phosphorylation level of proteins to stabilize the expression of Wnt2b, possibly inhibiting the ability of Wnt/β-catenin pathway to drive lung cancer progression as shown in the schematic model in **Figure 6**. The mechanism how PARG gene silencing affects the expression of Wnt5 remains to be futher explored. Understanding of the unresolved issue will contribute to the development of applications of PARG for cancer therapy. Lung cancer is one of the world's most serious threats to human health and has become a global public health problem (Siegel et al., 2018). Therefore, studying the mechanisms of lung cancer provides increased understanding that is relevant to its diagnosis and treatment. Though epigenetic modification is extensive, basic and reversible, its theory and results are gradually being applied to the diagnosis and treatment of cancer (Dawson and Kouzarides, 2012). In this study, it is shown that PARG gene silencing can prevent the occurrence of lung cancer induced by BaP. Our results demonstrate that PARG may be a target for the diagnosis and treatment of lung cancer. Furthermore, the inhibition of Wnt ligands may inhibit lung cancer. These results provide a new potential approach for the treatment of lung cancer. In concludsion, the use of Wnt ligands in the diagnosis of lung cancer and the use of PARG inhibitors as a potential therapeutic against lung cancer is supported.

ETHICS STATEMENT

This study was carried out in accordance with the Principles of Laboratory Animal Care (NIH publication No. 80–23, revised 1985). The protocol was approved by the Regulations for Animal Care and Use Committee of Experimental Animal Center at Shenzhen University.

AUTHOR CONTRIBUTIONS

HH, WD, and JL conceived the project. WD, YF, and YD performed the experiments. WD, YD, DW, XL, LY, and KL analyzed the results. WD, ZZ, PG, HL, JZ, and XX wrote the first draft. All authors revised the manuscript. HH and GH edited and approved the manuscript.

FUNDING

This study was funded by NSFC China (No. 81370080), the Shenzhen Science and Technology Development Fund Project (Nos. JCYJ20170306160932340, JCYJ20170413101713324, JCYJ20160428143634086, and JCYJ20160428142316603) and Sanming Project of Medicine in Shenzhen (SZSM201611090).

SUPPLEMENTARY MATERIAL

The Supplementary Material for this article can be found online at: https://www.frontiersin.org/articles/10.3389/fphar.2019.00338/full#supplementary-material

TABLE S1 | Primers used for real-time quantitative PCR.

REFERENCES

Alexandrov, K., Rojas, M., and Satarug, S. (2010). The critical DNA damage by benzo(a)pyrene in lung tissues of smokers and approaches to preventing its formation. *Toxicol. Lett.* 198, 63–68. doi: 10.1016/j.toxlet.2010.04.009

Berndt, J. D., and Moon, R. T. (2013). Cell biology. Making a point with Wnt signals. *Science* 339, 1388–1389. doi: 10.1126/science.1236641

Bird, A. (2007). Perceptions of epigenetics. *Nature* 447, 396–398. doi: 10.1038/nature05913

Chen, W., Zheng, R., Baade, P. D., Zhang, S., Zeng, H., Bray, F., et al. (2016). Cancer statistics in China, 2015. *CA Cancer J. Clin.* 66, 115–132. doi: 10.3322/caac.21338

D'Amours, D., Desnoyers, S., D'Silva, I., and Poirier, G. G. (1999). Poly(ADP-ribosyl)ation reactions in the regulation of nuclear functions. *Biochem. J.* 342(Pt 2), 249–268.

Dawson, M. A., and Kouzarides, T. (2012). Cancer epigenetics: from mechanism to therapy. *Cell* 150, 12–27. doi: 10.1016/j.cell.2012.06.013

Ferlay, J., Soerjomataram, I., Dikshit, R., Eser, S., Mathers, C., Rebelo, M., et al. (2015). Cancer incidence and mortality worldwide: sources, methods and major patterns in GLOBOCAN 2012. *Int. J. Cancer* 136, E359–E386. doi: 10.1002/ijc.29210

Hagood, J. S. (2014). Beyond the genome: epigenetic mechanisms in lung remodeling. *Physiology* 29, 177–185. doi: 10.1152/physiol.00048.2013

Harada, T., Yamamoto, H., Kishida, S., Kishida, M., Awada, C., Takao, T., et al. (2017). Wnt5b-associated exosomes promote cancer cell migration and proliferation. *Cancer Sci.* 108, 42–52. doi: 10.1111/cas.13109

Huang, C., Ma, R., Xu, Y., Li, N., Li, Z., Yue, J., et al. (2015). Wnt2 promotes non-small cell lung cancer progression by activating WNT/beta-catenin pathway. *Am. J. Cancer Res.* 5, 1032–1046.

Huang, H. Y., Cai, J. F., Liu, Q. C., Hu, G. H., Xia, B., Mao, J. Y., et al. (2012). Role of poly(ADP-ribose) glycohydrolase in the regulation of cell fate in response to benzo(a)pyrene. *Exp. Cell Res.* 318, 682–690. doi: 10.1016/j.yexcr.2012.01.007

IARC Working Group on the Evaluation of Carcinogenic Risks to Humans (2010). IARC monographs on the evaluation of carcinogenic risks to humans. Ingested nitrate and nitrite, and cyanobacterial peptide toxins. *IARC Monogr. Eval. Carcinog. Risks Hum.* 94, 1–412.

IARC Working Group on the Evaluation of Carcinogenic Risks to Humans (2012). Chemical agents and related occupations. *IARC Monogr. Eval. Carcinog. Risks Hum.* 100(Pt F), 9–562.

Ikeda, S., Kishida, S., Yamamoto, H., Murai, H., Koyama, S., and Kikuchi, A. (1998). Axin, a negative regulator of the Wnt signaling pathway, forms a complex with GSK-3beta and beta-catenin and promotes GSK-3beta-dependent phosphorylation of beta-catenin. *EMBO J.* 17, 1371–1384. doi: 10.1093/emboj/17.5.1371

Kasala, E. R., Bodduluru, L. N., Barua, C. C., Madhana, R. M., Dahiya, V., Budhani, M. K., et al. (2016). Chemopreventive effect of chrysin, a dietary flavone against benzo(a)pyrene induced lung carcinogenesis in Swiss albino mice. *Pharmacol. Rep.* 68, 310–318. doi: 10.1016/j.pharep.2015.08.014

Katoh, M. (2001). Differential regulation of WNT2 and WNT2B expression in human cancer. *Int. J. Mol. Med.* 8, 657–660. doi: 10.3892/ijmm.8.6.657

Kikuchi, A., and Yamamoto, H. (2008). Tumor formation due to abnormalities in the beta-catenin-independent pathway of Wnt signaling. *Cancer Sci.* 99, 202–208. doi: 10.1111/j.1349-7006.2007.00675.x

Kim, W., Kim, S. Y., Kim, T., Kim, M., Bae, D. J., Choi, H. I., et al. (2013). ADP-ribosylation factors 1 and 6 regulate Wnt/beta-catenin signaling via control of LRP6 phosphorylation. *Oncogene* 32, 3390–3396. doi: 10.1038/onc.2012.373

Klaus, A., and Birchmeier, W. (2008). Wnt signalling and its impact on development and cancer. *Nat. Rev. Cancer* 8, 387–398. doi: 10.1038/nrc2389

Koh, D. W., Lawler, A. M., Poitras, M. F., Sasaki, M., Wattler, S., Nehls, M. C., et al. (2004). Failure to degrade poly(ADP-ribose) causes increased sensitivity to cytotoxicity and early embryonic lethality. *Proc. Natl. Acad. Sci. U.S.A.* 101, 17699–17704. doi: 10.1073/pnas.0406182101

Kohn, A. D., and Moon, R. T. (2005). Wnt and calcium signaling: beta-catenin-independent pathways. *Cell Calcium* 38, 439–446. doi: 10.1016/j.ceca.2005.06.022

Li, X., Li, X., Zhu, Z., Huang, P., Zhuang, Z., Liu, J., et al. (2016). Poly(ADP-Ribose) glycohydrolase (PARG) silencing suppresses benzo(a)pyrene induced cell transformation. *PLoS One* 11:e0151172. doi: 10.1371/journal.pone.0151172

Liu, G., Niu, Z., Van Niekerk, D., Xue, J., and Zheng, L. (2008). Polycyclic aromatic hydrocarbons (PAHs) from coal combustion: emissions, analysis, and toxicology. *Rev. Environ. Contam. Toxicol.* 192, 1–28. doi: 10.1007/978-0-387-71724-1_1

Meyer, R. G., Meyer-Ficca, M. L., Whatcott, C. J., Jacobson, E. L., and Jacobson, M. K. (2007). Two small enzyme isoforms mediate mammalian mitochondrial poly(ADP-ribose) glycohydrolase (PARG) activity. *Exp. Cell Res.* 313, 2920–2936. doi: 10.1016/j.yexcr.2007.03.043

Miller, K. P., and Ramos, K. S. (2001). Impact of cellular metabolism on the biological effects of benzo[a]pyrene and related hydrocarbons. *Drug Metab. Rev.* 33, 1–35. doi: 10.1081/DMR-100000138

Min, W., Cortes, U., Herceg, Z., Tong, W. M., and Wang, Z. Q. (2010). Deletion of the nuclear isoform of poly(ADP-ribose) glycohydrolase (PARG) reveals its function in DNA repair, genomic stability and tumorigenesis. *Carcinogenesis* 31, 2058–2065. doi: 10.1093/carcin/bgq205

Miwa, M., and Masutani, M. (2007). PolyADP-ribosylation and cancer. *Cancer Sci.* 98, 1528–1535. doi: 10.1111/j.1349-7006.2007.00567.x

Reya, T., and Clevers, H. (2005). Wnt signalling in stem cells and cancer. *Nature* 434, 843–850. doi: 10.1038/nature03319

Roelink, H., Wagenaar, E., and Nusse, R. (1992). Amplification and proviral activation of several Wnt genes during progression and clonal variation of mouse mammary tumors. *Oncogene* 7, 487–492.

Rojas, M., Marie, B., Vignaud, J. M., Martinet, N., Siat, J., Grosdidier, G., et al. (2004). High DNA damage by benzo[a]pyrene 7,8-diol-9,10-epoxide in

bronchial epithelial cells from patients with lung cancer: comparison with lung parenchyma. *Cancer Lett.* 207, 157–163. doi: 10.1016/j.canlet.2003.11.016

Rouleau, M., Aubin, R. A., and Poirier, G. G. (2004). Poly(ADP-ribosyl)ated chromatin domains: access granted. *J. Cell Sci.* 117(Pt 6), 815–825. doi: 10.1242/jcs.01080

Rubin, H. (2001). Synergistic mechanisms in carcinogenesis by polycyclic aromatic hydrocarbons and by tobacco smoke: a bio-historical perspective with updates. *Carcinogenesis* 22, 1903–1930. doi: 10.1093/carcin/22.12.1903

Schmittgen, T. D., and Livak, K. J. (2008). Analyzing real-time PCR data by the comparative C(T) method. *Nat. Protoc.* 3, 1101–1108. doi: 10.1038/nprot.2008.73

Siegel, R. L., Miller, K. D., and Jemal, A. (2018). Cancer statistics, 2018. *CA Cancer J. Clin.* 68, 7–30. doi: 10.3322/caac.21442

Tammela, T., Sanchez-Rivera, F. J., Cetinbas, N. M., Wu, K., Joshi, N. S., Helenius, K., et al. (2017). A Wnt-producing niche drives proliferative potential and progression in lung adenocarcinoma. *Nature* 545, 355–359. doi: 10.1038/nature22334

van Delft, J. H., Mathijs, K., Staal, Y. C., van Herwijnen, M. H., Brauers, K. J., Boorsma, A., et al. (2010). Time series analysis of benzo[A]pyrene-induced transcriptome changes suggests that a network of transcription factors regulates the effects on functional gene sets. *Toxicol. Sci.* 117, 381–392. doi: 10.1093/toxsci/kfq214

Veeman, M. T., Axelrod, J. D., and Moon, R. T. (2003). A second canon. Functions and mechanisms of beta-catenin-independent Wnt signaling. *Dev. Cell* 5, 367–377. doi: 10.1016/S1534-5807(03)00266-1

Widziewicz, K., Rogula-Kozlowska, W., Loska, K., Kociszewska, K., and Majewski, G. (2018). Health risk impacts of exposure to airborne metals and benzo(a)pyrene during episodes of high PM10 concentrations in Poland. *Biomed. Environ. Sci.* 31, 23–36. doi: 10.3967/bes2018.003

Wodarz, A., and Nusse, R. (1998). Mechanisms of Wnt signaling in development. *Annu. Rev. Cell Dev. Biol.* 14, 59–88. doi: 10.1146/annurev.cellbio.14.1.59

Yang, E., Tacchelly-Benites, O., Wang, Z., Randall, M. P., Tian, A., Benchabane, H., et al. (2016). Wnt pathway activation by ADP-ribosylation. *Nat. Commun.* 7:11430. doi: 10.1038/ncomms11430

Zeng, X., Tamai, K., Doble, B., Li, S., Huang, H., Habas, R., et al. (2005). A dual-kinase mechanism for Wnt co-receptor phosphorylation and activation. *Nature* 438, 873–877. doi: 10.1038/nature04185

Zhang, C., Luo, T., Cui, S., Gu, Y., Bian, C., Chen, Y., et al. (2015). Poly(ADP-ribose) protects vascular smooth muscle cells from oxidative DNA damage. *BMB Rep.* 48, 354–359. doi: 10.5483/BMBRep.2015.48.6.012

Conflict of Interest Statement: The authors declare that the research was conducted in the absence of any commercial or financial relationships that could be construed as a potential conflict of interest.

frontiers in Oncology

ORIGINAL RESEARCH
published: 18 June 2019
doi: 10.3389/fonc.2019.00514

Midostaurin Reverses ABCB1-Mediated Multidrug Resistance, an *in vitro* Study

Ning Ji[1,2], *Yuqi Yang*[2], *Chao-Yun Cai*[2], *Jing-Quan Wang*[2], *Zi-Ning Lei*[2], *Zhuo-Xun Wu*[2], *Qingbin Cui*[2], *Dong-Hua Yang*[2], *Zhe-Sheng Chen*[2]* *and Dexin Kong*[1,3]*

[1] *Tianjin Key Laboratory on Technologies Enabling Development of Clinical Therapeutics and Diagnostics, School of Pharmacy, Tianjin Medical University, Tianjin, China,* [2] *Department of Pharmaceutical Sciences, College of Pharmacy and Health Sciences, St. John's University, Queens, NY, United States,* [3] *Research Center, School of Medicine, Tianjin Tianshi College, Tianyuan University, Tianjin, China*

Overexpression of ABC transporters in cancer cells is an underlying mechanism of multidrug resistance (MDR), leading to insensitive response to chemotherapeutic strategies. Thus, MDR is often results in treatment failure in the clinic. In this study, we found midostaurin, a Food and Drug Administration (FDA)-approved anti-leukemia drug, can antagonize ATP-binding cassette subfamily B member 1 (ABCB1)-mediated MDR. Our results indicated that midostaurin has the capacity to antagonize ABCB1-mediated MDR, while no significant reversal effect was found on ATP-binding cassette subfamily G member 2 (ABCG2)-mediated MDR. Our subsequent resistance mechanism studies showed that midostaurin directly inhibited the efflux function of the ABCB1 transporter without alteration of the expression level or the subcellular localization of ABCB1 transporter. In addition, midostaurin inhibited the ATPase activity of ABCB1 transporter in a dose-dependent manner. Moreover, our *in silico* docking study predicted that midostaurin could interact with the substrate-binding sites of ABCB1 transporter. This novel finding could provide a promising treatment strategy that co-administrating midostaurin with anticancer drugs in the clinic could overcome MDR and improve the efficiency of cancer treatment.

Keywords: midostaurin, multidrug resistance, ATP-binding cassette (ABC) transporter, ABC, chemotherapy

OPEN ACCESS

Edited by:
Chun Hei Antonio Cheung, National Cheng Kung University, Taiwan

Reviewed by:
Chung-Pu Wu, Chang Gung University, Taiwan
Csilla Özvegy-Laczka, Institute of Enzymology (MTA), Hungary

***Correspondence:**
Zhe-Sheng Chen
chenz@stjohns.edu
Dexin Kong
kongdexin@tmu.edu.cn

Specialty section:
This article was submitted to Cancer Molecular Targets and Therapeutics, a section of the journal Frontiers in Oncology

Received: *25 January 2019*
Accepted: *29 May 2019*
Published: *18 June 2019*

Citation:
Ji N, Yang Y, Cai C-Y, Wang J-Q, Lei Z-N, Wu Z-X, Cui Q, Yang D-H, Chen Z-S and Kong D (2019) Midostaurin Reverses ABCB1-Mediated Multidrug Resistance, an in vitro Study. Front. Oncol. 9:514. doi: 10.3389/fonc.2019.00514

INTRODUCTION

Multidrug resistance (MDR) in cancer, a phenomenon leading to synchronous resistance of cancer cells to structurally unrelated antineoplastic drugs, is one of the most critical factors responsible for the failure of chemotherapeutics and the poor survival rate of patients (1). Several mechanisms are involved in cancer MDR, including reduced apoptosis, advanced DNA damage repair mechanisms, or altered drug metabolism. However, the most prominent factor is ABC transporter-mediated efflux of antineoplastic drugs (3, 51).

The transport system superfamily of ABC transporters plays critical roles in physiological and pharmacological processes (2). The human ABC protein family has been divided into seven subfamilies (ABCA to ABCG). The ABC transporter family has 49 ABC proteins and 48 of them have identified functions (3, 4). As one of the main contributors, ABCB1 (P-gp/MDR1) is widely expressed not only in the placenta, but in the blood-brain barrier (BBB), intestines, livers and kidneys, in order to protect the body from xenobiotics (5, 6). The ABCB1 transporter also mediates

the transport of a wide range of physiological substrates like lipids, porphyrins, and sterols (7). Furthermore, a broad range of chemotherapeutic drugs are substrates of the ABCB1 transporter, such as taxanes and anthracyclines. ABCB1 transporter significantly increases the efflux of such anticancer drugs, a major reason leading to ABCB1-mediated MDR (8). It has been documented that ABCB1 is strongly related to the chemotherapy prognosis and the progression of malignancy (9). Thus, it is critical to elude MDR by either decreasing the expression level of ABCB1 proteins or inhibiting the efflux function of ABCB1 through specific and potent inhibitors.

Midostaurin, a multi-kinase inhibitor that was originally developed as a protein kinase C (PKC) inhibitor for treatment of patients with solid malignancy (10), has already been approved by the FDA for treatment of acute myelocytic leukemia (AML) with Fms-like tyrosine kinase 3 (FLT3)-mutant subtype (11). It has recently been reported that the combination of midostaurin with standard chemotherapy can significantly prolong overall and event-free survival in patients who suffer from AML with a FLT3 mutation (12). Here, we report the reversal effects of midostaurin on ABCB1-mediated MDR when co-administrated with conventional antineoplastic drugs.

MATERIALS AND METHODS

Chemicals

Midostaurin was obtained from Thermo Fisher Scientific Inc. (Rockford, IL). Bovine serum albumin (BSA), fetal bovine serum (FBS), Dulbecco's modified Eagle's Medium (DMEM), penicillin/streptomycin and 0.25% trypsin were products from Corning Incorporated (Corning, NY). The monoclonal antibody for GAPDH (catalog number MA5-15738, lot number SA247966, clone GA1R), Alexa Fluor 488 conjugated goat anti-mouse IgG secondary antibody, were purchased from Thermo Fisher Scientific Inc. (Rockford, IL). Paclitaxel, doxorubicin, colchicine, cisplatin, mitoxantrone, verapamil, the monoclonal antibodies for ABCB1 (catalog number P7965, lot number 067M4761V, clone F4), dimethylsulfoxide (DMSO), 3-(4,5-dimethylthiazol-yl)-2,5-diphenyltetrazolium bromide (MTT), Triton X-100, 4',6-diamidino-2-phenylindole (DAPI), and paraformaldehyde, were obtained from Sigma-Aldrich (St. Louis, MO). HRP-conjugated rabbit anti-mouse IgG secondary antibody (catalog number 7076S, Lot number 32) were obtained from Cell Signaling Technology Inc. (Danvers, MA). Ko143 was a product from Enzo Life Sciences (Farmingdale, NY). [^{3}H]-paclitaxel (15 Ci/mmol) was purchased from Moravek Biochemicals, Inc. (Brea, CA). All other chemicals were purchased from Sigma Chemical Co (St. Louis, MO).

Cell Lines and Cell Culture

The ABCB1-overexpressing KB-C2 cell line was created by gradually adding colchicine to parental human epidermoid carcinoma KB-3-1 cells, and was kindly provided by Dr. Shin-ichi Akiyama (Kagoshima University, Kagoshima, Japan). The KB-C2 line was cultured in medium containing 2 μg/mL colchicine (13) to maintain its drugresistant characteristics. The SW620/Ad300 cells were cultured in medium with 300 ng/mL doxorubicin (14). KB-3-1, KB-C2, SW620, and SW620/Ad300 cells were used for ABCB1 reversal study. The human non-small cell lung cancer (NSCLC) NCI-H460 cell line and its subline of ABCG2-overexpressing NCI-H460/MX20 cells were used for ABCG2 reversal study. The NCI-H460/MX20 cells were selected by using a high dose of mitoxantrone and maintained in medium with 20 ng/mL mitoxantrone (15). HEK293/pcDNA3.1 and HEK293/ABCB1 were established by transfecting the human embryonic kidney HEK293 cells with empty and ABCB1 expressing vector, respectively (16). SW620 and SW620/Ad300 cells, NCI-H460 and NCI-H460/MX20 cells, were kindly provided by Drs. Susan Bates and Robert Robey (NCI, NIH, Bethesda, MD). HEK293/ABCB1 were kindly provided by Dr. Suresh V. Ambudkar (NCI, NIH, Bethesda, MD). All aforementioned cell lines were maintained in DMEM medium containing 10% fetal bovine serum and 1% penicillin/streptomycin at 37°C in a humidified atmosphere containing 5% CO_2. All cells were grown as an adherent monolayer and drug-resistant cells were grown in drug-free culture media for more than 20 days before assay.

MTT Cytotoxicity Assay

Cell viability was determined by MTT assay as we previously described (17). Each type of cell was harvested and resuspended before being seeded onto a 96-well plate at a final quantity of 5×10^3 cells per well in 160 μL of medium, and was then incubated overnight. Midostaurin and positive control drugs were added 2 h prior to incubation with or without anticancer drugs. After 72 h of further incubation, MTT solution (4 mg/mL) was added to each well and the cells were incubated for an additional 4 h at 37°C. Subsequently, the supernatant was discarded and 100 μL of DMSO was added to each well in order to dissolve the formazan crystals. An accuSkanTM GO UV/Vis Microplate Spectrophotometer from Fisher Sci. (Fair Lawn, NJ) was used to determine the absorbance at 570 nm. The concentration for 50% inhibition of cell viability (IC_{50}) of the anticancer drug was calculated as previously described (18). For positive control drugs, verapamil (3 μM) and Ko143 (3 μM) were used as reference inhibitors to reverse ABCB1- and ABCG2-mediated MDR, respectively. Cisplatin, which is not a substrate of ABCB1 or ABCG2, was used as a negative control chemotherapeutic drug.

Western Blotting and Immunofluorescence Analysis

Western blotting analysis was performed as previously described (19). Briefly, cells were lysed after incubated with or without midostaurin (500 nM) for varying amounts of time (0, 24, 48, and 72 h). The concentration of protein was determined by BCA Protein Assay Kit from Pierce (Rockford, IL). Equal amounts (20 μg) of proteins were subjected to 10% sodium dodecyl sulfate polyacrylamide gel electrophoresis (SDS-PAGE) and transferred to PVDF membranes from Millipore (Billerica, MA). The presence of ABCB1 was determined using monoclonal antibody F4 (dilution 1:500). GAPDH was used as a loading control. The resulting protein bands were analyzed using Image J software. The immunofluorescence assay was performed as previously

described (17). Briefly, after being cultured overnight in 24-well plates, cells (2×10^4/well) were treated with midostaurin for 72 h at 500 nM concentration. Then, cells were fixed in 4% paraformaldehyde for 10 min and permeabilized by 0.1% Triton X-100 for 10 min before being blocked with 6% BSA for 1 h at 37°C. The presence of ABCB1 was determined using monoclonal antibody F4 (dilution 1:100) for incubation at 4°C overnight. Cells were washed with iced PBS after each incubation time. Alexa Fluor 488 (Ex = 499 nm, Em = 519 nm) conjugated secondary antibody (1:1,000) was used after washing with iced PBS. DAPI (Ex = 345 nm, Em = 455 nm) was used to counterstain the nuclei. The cells were washed with ice-cold PBS before being imaged. Immunofluorescence images were collected using an EVOS FL Auto fluorescence microscope from Life Technologies Corporation (Gaithersburg, MD).

Doxorubicin Accumulation and Fluorescence Microscopic Analysis

Cells were grown in 6-well plates and washed twice with phosphate-buffered saline (PBS) before the pre-treatment of 500 nM of midostaurin. After 1 h of midostaurin pretreatment, 10 μM of doxorubicin was then added to each well for further incubation (1 h). Immunofluorescence images were collected using an EVOS FL Auto fluorescence microscope from Life Technologies Corporation (Gaithersburg, MD). Excitation and emission wavelengths of doxorubicin were 475 and 585 nm, respectively.

[^{3}H]-Paclitaxel Accumulation and Efflux Assay

We conducted [^{3}H]-paclitaxel accumulation assay using KB-3-1 and its drug-resistant subline KB-C2 cells. As previously described (20), 5×10^5 cells/well were cultured in 24-well plates overnight before the assay, and midostaurin was added 2 h prior to the addition of [^{3}H]-paclitaxel. After incubating with [^{3}H]-paclitaxel with or without midostaurin for 2 h at 37°C, cells were washed twice with iced PBS, and lysed with 0.25% trypsin before being placed in 5 mL scintillation fluid, and radioactivity was measured in the Packard TRI-CARB 1900CA liquid scintillation analyzer from Packard Instrument (Downers Grove, IL).For the efflux assay, KB-3-1 and KB-C2 cells (20) were incubated with midostaurin for 2 h followed by incubation with [^{3}H]-paclitaxel, with or without midostaurin for 2 h at 37°C. The cells were washed with iced PBS twice and then lysed at various time points (0, 30, 60, and 120 min) with trypsin. Subsequently, cells were placed in 5 mL of scintillation fluid and radioactivity was measured in the Packard TRI-CARB 1900CA liquid scintillation analyzer from Packard Instrument (Downers Grove, IL).

ATPase Assay

The ABCB1-associated ATPase activities were measured using PREDEASY ATPase Kits from TEBU-BIO nv (Boechout, Belgium) with modified protocols. Briefly, cell membranes that overexpressed ABCB1 were thawed and diluted before use. Sodium orthovanadate (Na_3VO_4) was used as an ATPase inhibitor. Various concentrations of midostaurin were incubated with membranes for 5 min. The ATPase reactions were initiated by adding 5 mM Mg^{2+}-ATP. Luminescence signals of P_i were initiated and measured after incubation at 37°C for 40 min with brief mixing. The changes of relative light units were determined by comparing Na_3VO_4-treated samples with midostaurin-treated groups.

Molecular Modeling of Human ABCB1 Homology Model

In silico docking analysis was conducted using software Maestro 11.5 (Schr*ʹ*odinger, LLC, New York, NY, 2018) (21). Human ABCB1 homology model was established by Dr. Aller based on refined mouse ABCB1 (PDB ID: 4M1M) (22). Afterwards, the docking grid at the drug-binding pocket was generated (23). The ligand was essentially prepared to perform glide XP docking with the default protocols.

Statistical Analysis

All data are expressed as the mean ± SD and were analyzed using one-way ANOVA. All experiments were repeated at least three times. Differences were considered significant when $P < 0.05$.

RESULTS

Midostaurin Significantly Antagonized ABCB1-Mediated MDR in ABCB1-Overexpressing Cancer Cells

Firstly, to avoid cytostatic-induced reversal phenomenon, we conducted MTT assays to evaluate the cytostatic effects of midostaurin in the ABCB1-overexpressing cells and corresponding parental cells that we would use. Hence, we could choose concentrations that would not significantly influence cell viability. We conducted further experiments with 200 and 500 nM doses of midostaurin (**Figure 1**).

As shown in **Figure 2**, midostaurin significantly sensitized ABCB1-overexpressing cancer cells KB-C2 (**Figures 2A–C**) and SW620/Ad300 (**Figures 2E–G**) to ABCB1 substrates (doxorubicin, paclitaxel, and colchicine), compared with their control resistance cells, and this sensitization occurred in a dose-dependent manner. At 200 or 500 nM, midostaurin could not alter the IC_{50} values of the above chemotherapeutic drugs to parental KB-3-1 (**Figures 2A–C**) and SW620 (**Figures 2E–G**) cells. In addition, when combined with cisplatin, a platinum drug which is known to not be a substrate of ABCB1, midostaurin showed no significant difference in its cytotoxic effect in neither the resistant cell lines nor the parental cell lines (**Figures 2D,H**). In this study, verapamil, a potent ABCB1 inhibitor, was used as a positive control drug (24).

Midostaurin Significantly Antagonized ABCB1-Mediated MDR in ABCB1-Gene-Transfected Cells

We next evaluated the reversal effect of midostaurin on ABCB1-gene-transfected cells. As shown in **Figure 3**, midostaurin could significantly lower the IC_{50} values of ABCB1 substrate-drugs

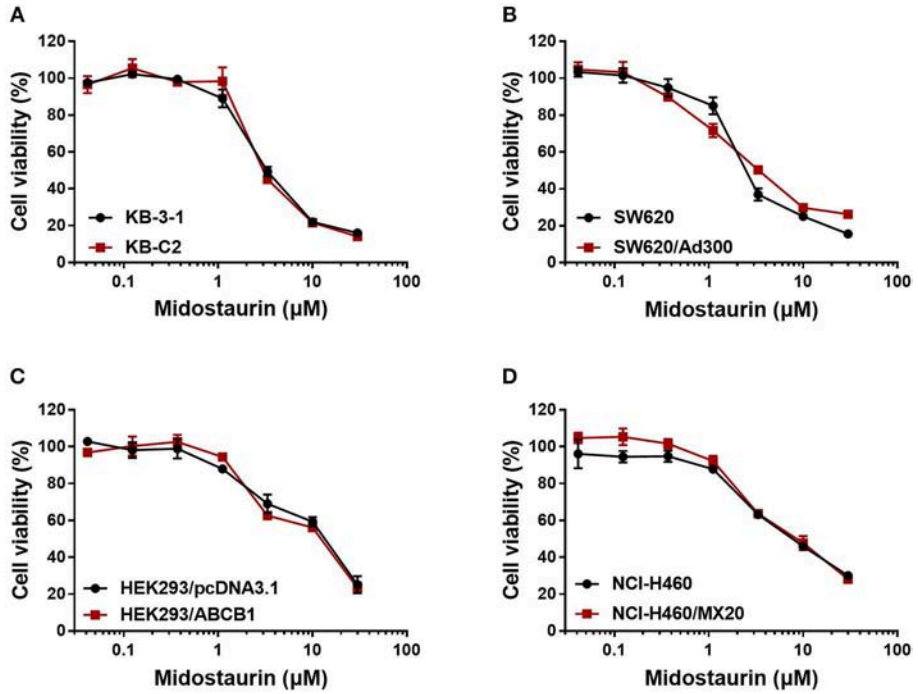

FIGURE 1 | Dose-viability curves of cells used in this study incubated with midostaurin for 72 h. Dose-viability curves for **(A)** KB-3-1 and KB-C2, **(B)** SW620 and SW620/Ad300, **(C)** HEK293/pcDNA3.1 and HEK293/ABCB1, and **(D)** NCI-H460 and NCI-H460/MX20.

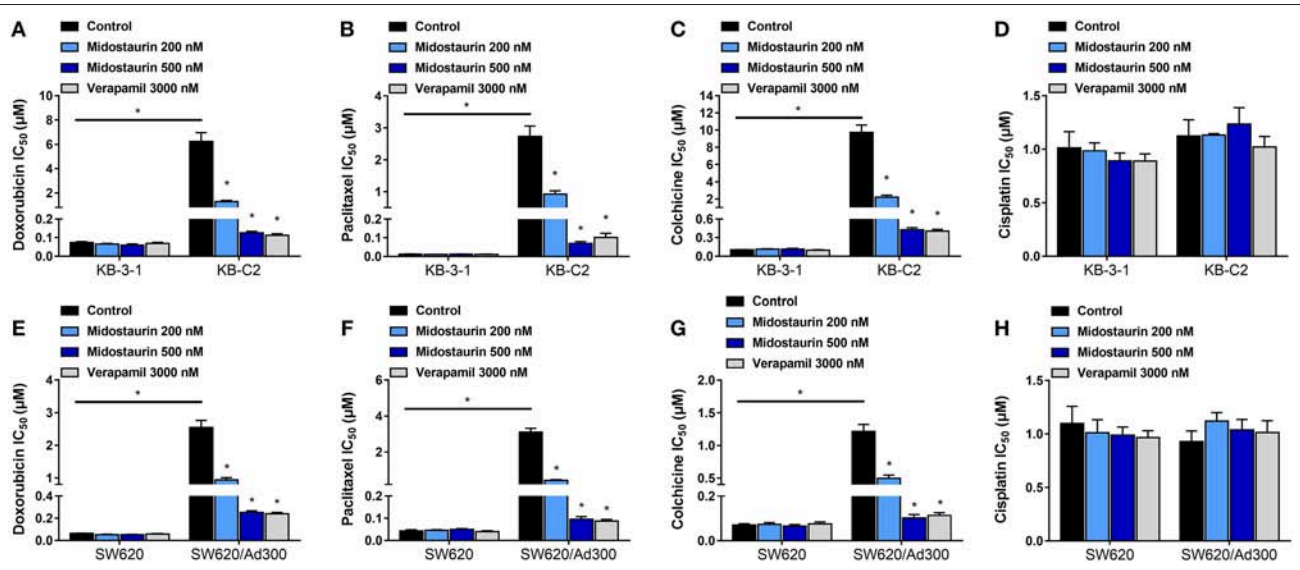

FIGURE 2 | The reversal effect of midostaurin on ABCB1-mediated MDR in ABCB1-overexpression cancer cells. IC_{50} values of **(A)** doxorubicin, **(B)** paclitaxel, **(C)** colchicine, and **(D)** cisplatin in parental KB-3-1 and drug-selected ABCB1-overexpression resistant KB-C2 cells with or without treatment of midostaurin. IC_{50} of **(E)** doxorubicin, **(F)** paclitaxel, **(G)** colchicine, and **(H)** cisplatin in parental SW620 and drug-selected ABCB1-overexpression resistant SW620/Ad300 cells with or without treatment of midostaurin. Data are expressed as mean ± SD, representative of at least three independent experiments. *$p < 0.05$, compared with control group.

(doxorubicin, paclitaxel, and colchicine) to HEK293/ABCB1 cells at 200 and 500 nM in a concentration-dependent manner (**Figures 3A–C**). More importantly, midostaurin did not significantly alter the efficacy of these ABCB1-substrate chemotherapeutic drugs in parental HEK293/pcDNA3.1 cells (**Figures 3A–C**). Furthermore, at 200 or 500 nM,

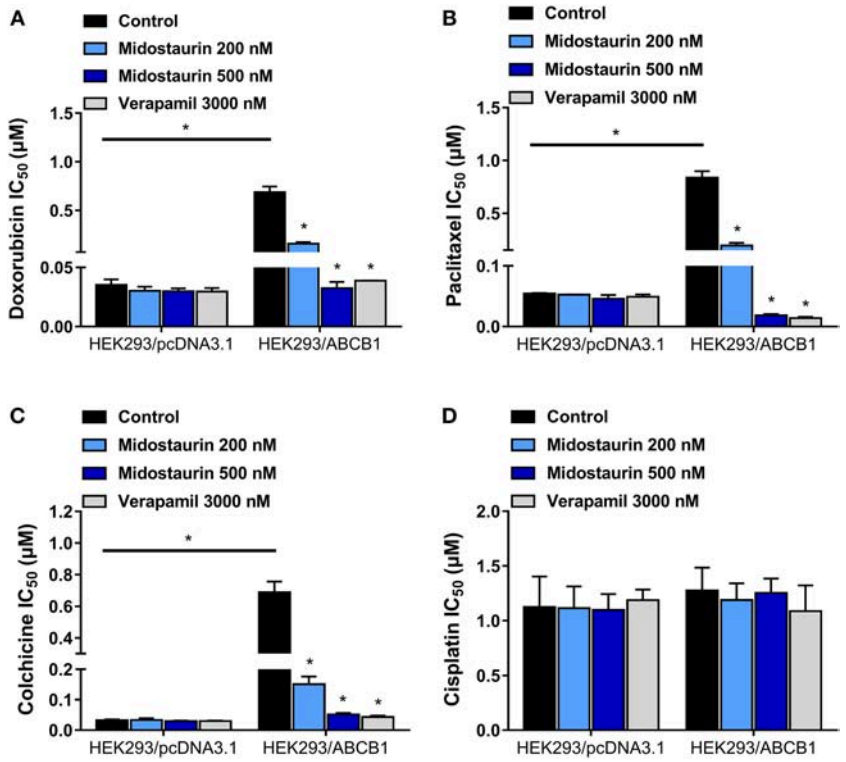

FIGURE 3 | The reversal effect of midostaurin on ABCB1-mediated MDR in ABCB1-gene-transfected cells. IC_{50} values of **(A)** doxorubicin, **(B)** paclitaxel, **(C)** colchicine, and **(D)** cisplatin in parental HEK293/pcDNA3.1 and transfected ABCB1-overexpression HEK293/ABCB1 cells with or without treatment of midostaurin. Data are expressed as mean ± SD, representative of at least three independent experiments. *$p < 0.05$, compared with control group.

midostaurin did not significantly change the IC_{50} values of cisplatin (**Figure 3D**).

Midostaurin Did Not Reverse ABCG2-Mediated MDR

As shown in **Figure 4**, midostautrin (200 and 500 nM) could not significantly lower the IC_{50} value of mitoxantrone, a known substrate of ABCG2-mediated MDR, to drug-selected NCI-H460/MX20 cells. In this study, we chose Ko143 as a positive control drug because it is a potent ABCG2 inhibitor (21). Cisplatin was used as a negative substrate drug as previously described (25).

Midostaurin Did Not Influence the Protein Expression Level or Subcellular Localization of ABCB1 Transporters

The next step was to figure out the mechanism of action of midostaurin. Theoretically, there are varied mechanisms involved in the reversal of ABCB1-mediated MDR. For examples, the reversal effect could be due to down-regulation of ABCB1 protein expression level and/or the change of ABCB1 transporter subcellular localization. To evaluate the effect of midostaurin on the protein level of ABCB1 transporter, we conducted Western blotting and immunofluorescence assays to detect whether midostaurin could impact the ABCB1 protein expression and/or subcellular localization. As shown in **Figure 5A**, after incubation for 24, 48, and 72 h, respectively, midostaurin did not significantly change the expression level of ABCB1 protein (170 kDa) in ABCB1-overexpressing KB-C2 cells. Furthermore, midostaurin did not change the localization of ABCB1 at the subcellular level after incubating for up to 72 h in ABCB1-overexpressing KB-C2 cells (**Figure 5B**). These results suggested that midostaurin influenced neither the expression level nor the subcellular localization of ABCB1 protein even at high concentrations.

Midostaurin Significantly Increased the Intracellular Drug Accumulation in ABCB1-Overexpressing Cancer Cells

The above results indicated that midostaurin could reverse ABCB1-mediated MDR without altering the protein expression level or subcellular localization in ABCB1-overexpressing cancer cells. We then conducted our drug accumulation assay to further understand the mechanism of the reversal effect of midostaurin. Firstly, we conducted our doxorubicin accumulation assay with 500 nM of midostaurin. As shown in **Figure 6A**, midostaurin significantly enhanced the accumulation level of doxorubicin in ABCB1-overexpressing KB-C2 cells. We also conducted our [^{3}H]-paclitaxel accumulation assay to get a digitized result. The intracellular level of [^{3}H]-paclitaxel was measured in

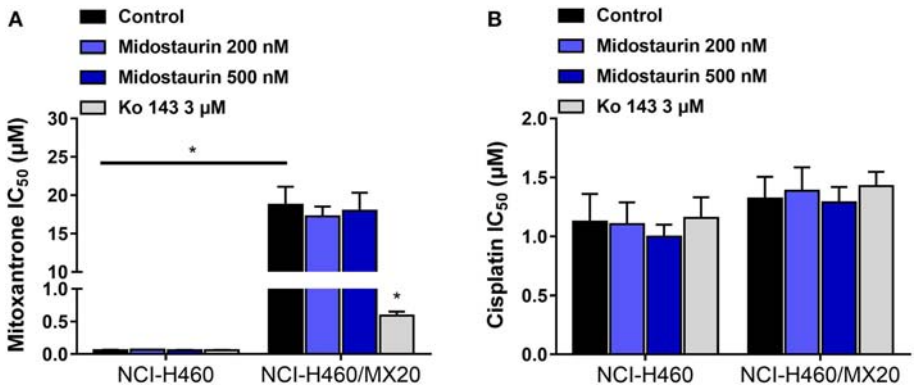

FIGURE 4 | The reversal effect of midostaurin on ABCG2-mediated MDR in ABCG2-overexpression cancer cells. **(A)** IC_{50} values of mitoxantrone in parental NCI-H460 cells and resistant NCI-H460/MX20 cells. **(B)** IC_{50} values of cisplatin in parental NCI-H460 cells and resistant NCI-H460/MX20 cells. *$p < 0.05$, compared with control group.

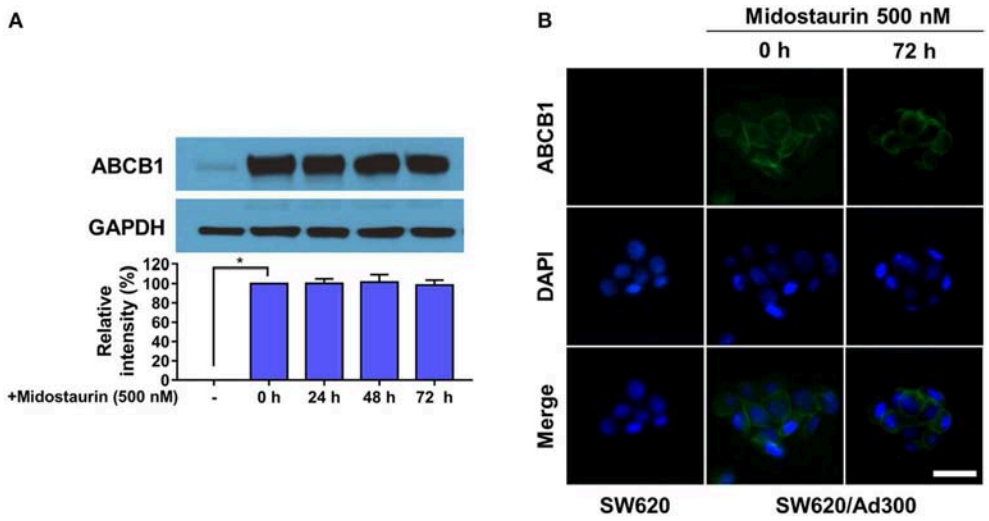

FIGURE 5 | Midostaurin did not alter the protein expression and subcellular localization of ABCB1 transporter. **(A)** Detection and relative intensity of ABCB1 expression in KB-C2 cells incubated with 500 nM of midostaurin for 0, 24, 48, and 72 h. **(B)** Sub-cellular localization of ABCB1 expression in SW620/Ad300 cells incubated with 500 nM of midostaurin for 72 h. Scale bar, 100 μm. *$p < 0.05$, compared with control group.

cells overexpressing ABCB1 transporter in the presence or absence of midostaurin. As shown in **Figure 6B**, midostaurin significantly increased the intracellular levels of [^{3}H]-paclitaxel in ABCB1-overexpressing KB-C2 cells in a dose-dependent manner. However, in parental KB-3-1 cells, no significant change in [^{3}H]-paclitaxel was found. In this study, verapamil was used as a positive control reversal reagent.

Midostaurin Significantly Inhibited the Efflux Function of ABCB1 Transporter in ABCB1-Overexpressing Cancer Cells

The efflux of antineoplastic drugs through ABCB1 transporter is involved in ABCB1-mediated MDR. We conducted an efflux assay at different time points (0, 30, 60, and 120 min) to determine whether midostaurin could inhibit the efflux function of ABCB1 transporter. As shown in **Figures 6C,D**, midostaurin significantly decreased the efflux level of [^{3}H]-paclitaxel in ABCB1-overexpressing KB-C2 cells in a dose-dependent manner, but this change was not shown in parental KB-3-1 cells. These results suggested that midostaurin could significantly increase the accumulation of anticancer drugs by inhibiting the efflux function mediated by ABCB1.

Midostaurin Significantly Inhibited the ATPase Activity of ABCB1 Transporter

The hydrolysis of ATP is the energy source of substrate-efflux mediated by ABCB1. Hence, we conducted the ABCB1-mediated ATP hydrolysis in the presence or absence of midostaurin at 0–40 μM serial concentrations. As shown in **Figure 7A**, midostaurin significantly inhibited the ATPase activity of ABCB1 transporters in a dose-dependent manner. The concentration of midostaurin required to obtain 50% of maximal inhibition

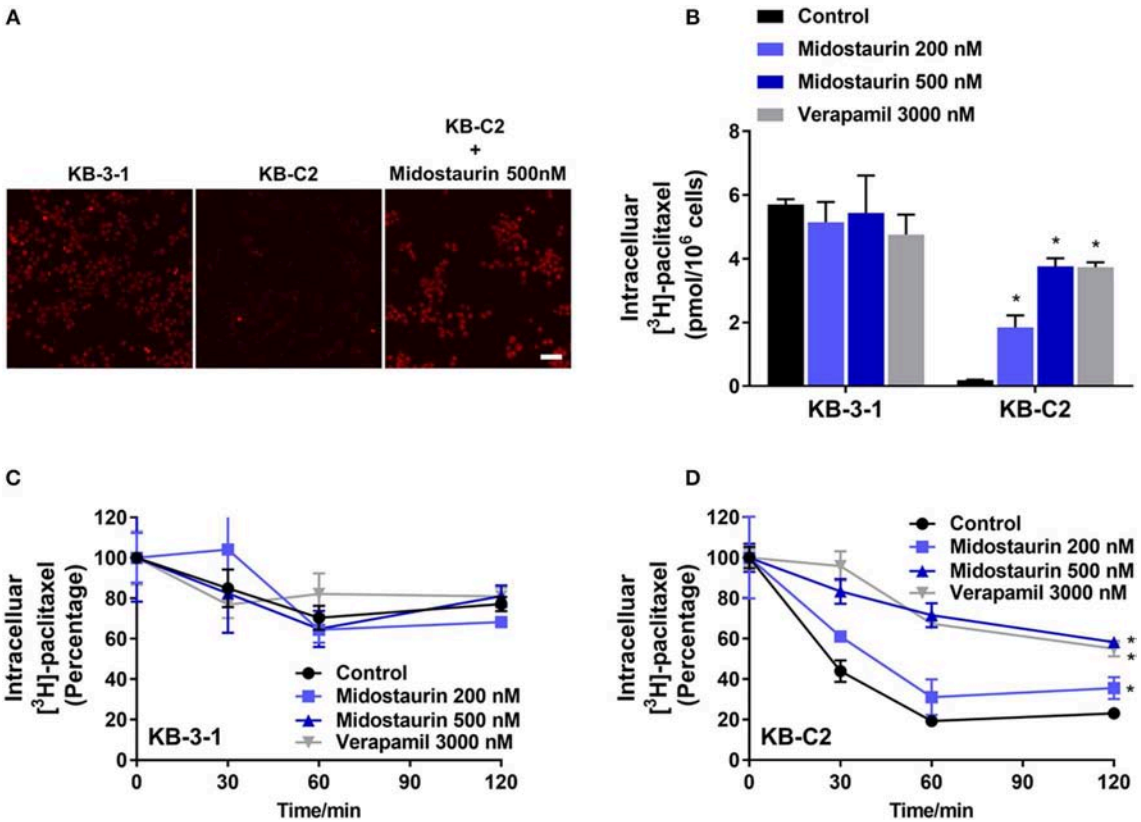

FIGURE 6 | The effect of midostaurin on accumulation and efflux activity in cancer cells overexpression ABCB1 transporter. Scale bar, 50 μm. **(A)** The effect of midostaurin on accumulation of doxorubicin. **(B)** The effect of midostaurin on accumulation of [^{3}H]-paclitaxel in KB-3-1 and KB-C2 cells. **(C,D)** The effects of midostaurin on efflux of [^{3}H]-paclitaxel in KB-3-1 and KB-C2 cells. *$p < 0.05$, compared with control group.

(IC_{50}) was 3.1 μM with the maximum of inhibition being 0.4-fold. These results suggested that midostaurin could inhibit the ATPase activity in ABCB1 transporters by interacting with the drug-binding pocket of these transporters. Therefore, one of the reversal mechanisms of midostraurin includes a reduced energy source for ABCB1 efflux function through inhibition of ATPase activity.

Docking Analysis of the Binding of Midostaurin With ABCB1 Homology Model

The best-scored docked positions of midostaurin with ABCB1 transporter are shown in **Figure 7**. The phenol ring of the methylbenzamide moiety in midostaurin has π-π interactions with the residues Phe336 and Phe983 of human ABCB1 (**Figure 7C**). In addition, midostaurin has hydrophobic interactions with residues of ABCB1 including Met69, Leu339, Ile340, Phe343, Phe728, Met986, and Ala987 (**Figure 7D**), which stabilize midostaurin in the substrate-binding pocket of ABCB1.

DISCUSSION

Growing evidence has shown that the failure of clinical treatment resulting from drug resistance to chemotherapeutic drugs in a series of cancer cell lines is tightly correlated with the overexpression of ABC transporters. It has been widely reported that cancer cells overexpressing ABCB1 transporter is a key factor that could imply poor prognosis as well as low survival rate in cancer patients (26–30). Moreover, genetic polymorphisms in ABC transporters, especially in ABCB1 and ABCG2 transporters, could significantly increase the high risk of death in patients who suffer from colorectal malignancy or non-small cell lung cancer (NSCLC) (31, 32). In recent decades, many small-molecule target drugs have been reported to have the capacity to reverse ABC transporter-mediated MDR, via inhibiting the function, downregulating the protein expressing level, and/or changing the subcellular localization of ABC transporters. Previously, we have reported that selonsertib, ulixertinib, and VS-4718 can significantly antagonize ABC transporter-mediated MDR (21, 23, 33). Unfortunately, there was no successful clinical case study on the therapeutic strategies to develop ABC transporters inhibitors as reversal reagents to reverse drug resistance. Nonetheless, growing evidence has shown that the overexpression of ABC transporters is mainly involved in MDR in cancer, and it is also critical in regulating oral bioavailability of anticancer drugs and reagents. A series of first-line chemotherapeutic drugs, including doxorubicin, paclitaxel and mitoxantrone are substrates of ABC transporters, meaning

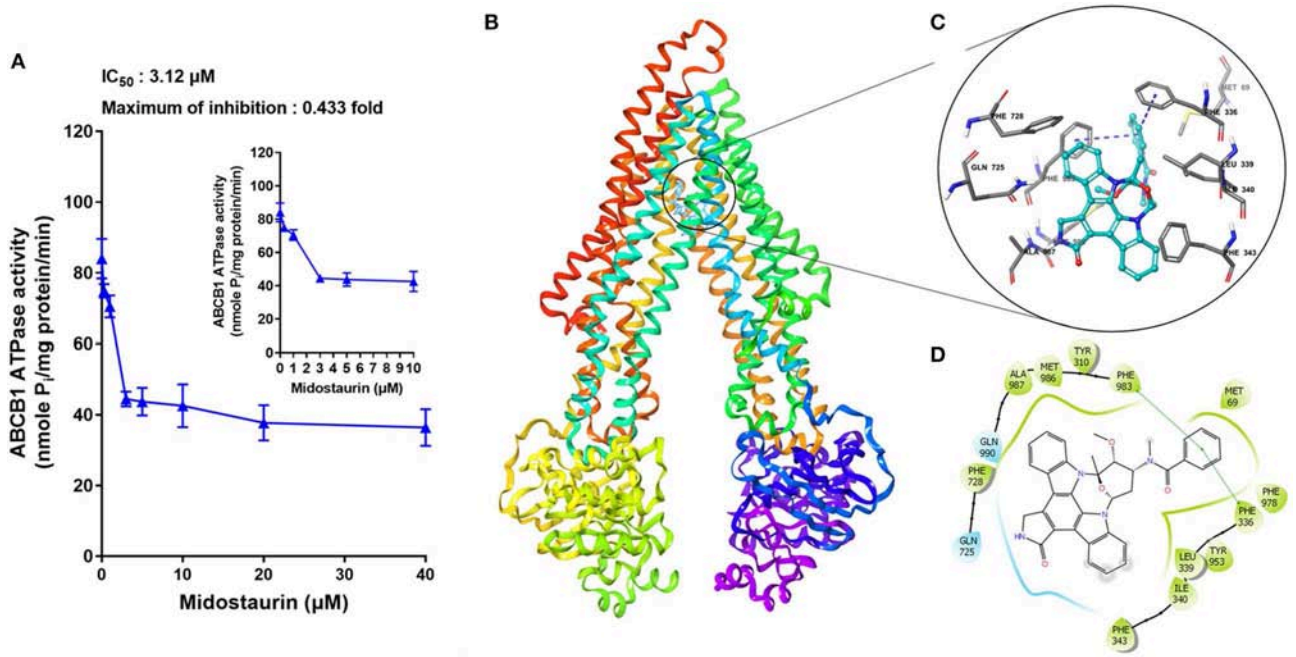

FIGURE 7 | The effects of midostaurin on the ATPase activity of ABCB1 and the molecular modeling study of midostaurin with human homology ABCB1. **(A)** Effect of midostaurin on the ATPase activity of ABCB1. The inset graphs illustrate the effect of 0–10 μM midostaurin on the ATPase activity of ABCB1. Data are mean, representative of three independent experiments. **(B)** Overall view of midostainrin-ABCB1 complex. **(C)** Docked position of midostaurin within the drug-binding site of human ABCB1 homology model by Glide docking. Midostaurin is shown as ball and stick mode with the atoms colored: carbon-cyan, hydrogen-white, nitrogen-blue, oxygen-red. Important residues are shown as sticks with gray color. π-π stacking interactions are indicated with blue dotted short line. **(D)** The two-dimensional ligand-receptor interaction diagram of midostaurin and human ABCB1. The amino acids within 3 Å are shown as colored bubbles, cyan indicates polar residues, and green indicates hydrophobic residues. The green short line shows π-π stacking interaction.

that these anti-cancer drugs will be pumped out from the cancer cells and finally lead to the failure of clinical carcinoma treatment (1–4, 34). Therefore, we confirm that screening small molecules to obtain the inhibitors of ABC transporters is still a potential and effective treatment strategy to circumvent MDR in cancer.

In this *in vitro* study, we evaluated the effect of midostaurin on ABCB1-mediated MDR. We mainly found that midostaurin, at non-toxic concentrations (200 and 500 nM), can significantly overcome ABCB1-mediated MDR in a series of cancer cell lines in a concentration-dependent manner. Firstly, to avoid potential reversal effects caused by the cytostatic effect of midostaurin, we performed our MTT assays to evaluate the anti-proliferative effect of midostaurin in the cells we would use in this study. Based on the results, we conducted further reversal studies using 200 and 500 nM of midostaurin. Our reversal study indicated that midostaurin could significantly reverse ABCB1-mediated MDR in KB-C2 and SW620/Ad300 cells, which were selected by treatment with colchicine or doxorubicin, respectively. Moreover, midostaurin could not alter the efficacy of certain chemotherapy substrate-drugs in their corresponding parental KB-3-1 or SW620 cells. In addition, midostaurin could not antagonize ABCG2-mediated MDR in ABCG2-overexpressing cancer cells NCI-H460/MX20. Based on these results, we hypothesized that the reversal effect of midostaurin was specific to interactions with the ABCB1 transporter. It is notable that we then verified this hypothesis by a reversal study in gene-transfected cells. We found that midostaurin could also lower the IC_{50} values of doxorubicin, paclitaxel, and colchicine in HEK293/ABCB1 cells compared with parental cells in a dose-dependent manner, but not those in parental HEK293/pcDNA3.1 cell line. Furthermore, midostaurin did not sensitize either parental HEK293/pcDNA3.1 cell line or HEK293/ABCB1 cells to cisplatin, a drug that does not use ABCB1 as a substrate. These results suggest that midostaurin exclusively reversed ABCB1-mediated MDR.

The reversal of MDR mediated by ABC transporters may be involved in the down-regulating and/or change of subcellular localization of certain ABC transporters. However, as shown in our Western blotting and immunofluorescence assays, no significant down-regulation of ABCB1 protein was found, and all ABCB1 protein was located on the membrane of KB-C2 cells after incubating with midostaurin for up to 72 h. In other words, these results signified that the mechanisms of midostaurin on the reversal of ABCB1 mediated-MDR were not due to the down-regulating of the protein level or change of subcellular localization of ABCB1 transporters. Nevertheless, as midostaurin is a multi-kinase inhibitor, we could not fully eliminate the possibility

that part of the reversal effect of midostaurin could be associated with its effect to other proteins and/or potential cross-talk with other signals, which may impact the efflux function of ABCB1 transporter, and this needs to be studied further in the future. Further study should also evaluate the potential effect of midostaurin on the protein expression level of ABCB1 with increased concentration or prolonged incubation time. Moreover, a process named post-translational modifications (PTM) plays an important role in proteins, especially transporters' function (35). It has been reported that ABCB1 could be phosphorylated at S661, S667, S671, and S683 to modulate its cell surface trafficking (36), and Pim-1 kinase could prevent ABCB1 from degradation, enabling glycosylation and cell surface expression (36). These clues indicate that it is necessary to further determine the effects of midostaurin on PTM of ABCB1 using higher concentration and/or longer incubation time.

Subsequently, drug accumulation and efflux assays were conducted, so that we could deeply understand the mechanisms of midostaurin on ABC transporter-mediated MDR attenuation. Our results indicated that midostaurin could significantly increase the intracellular concentration of ABCB1 substrate-drugs (doxorubicin and [^{3}H]-paclitaxel) in ABCB1-overexpression KB-C2 cells. Midostaurin could also significantly prevent [^{3}H]-paclitaxel from being pumped out of KB-C2 cells in a concentration-dependent manner. However, there is no significant change in doxorubicin or [^{3}H]-paclitaxel in accumulation or efflux in parental KB-3-1 cells. These novel findings were congruent with our observed reversal effects of midostaurin. Our mechanism study also indicated that midostaurin could increase the accumulation of certain substrate-drugs (doxorubicin and [^{3}H]-paclitaxel) in ABCB1-overexpression cancer cells by targeting the function of ABCB1 transporter.

ABC transporters, including ABCB1, obtain energy via ATP hydrolysis, and this can be modulated by the presence of certain substrates or inhibitors (37, 38). In our ATPase assay, we found that midostaurin could significantly inhibit the ATPase activity of ABCB1 in a dose-dependent manner, and the maximal inhibition level was 0.4-fold. Nevertheless, the accurate binding site of midostaurin with ABCB1 transporter remained unclear. In the *in silico* modeling study, we predicted that midostaurin could interact with the drug-binding pocket in the transmembrane domain (TMD) of ABCB1 transporter.

Midostaurin is an anticancer drug approved by FDA for treatment of AML with FLT3-mutant subtype (11). Over the years, the effect of midostaurin on multidrug resistance mediated by ABCB1 has been investigated independently in great detail. At the very beginning, midostaurin, also known as PKC412 and CGP41215, was developed as a PKC inhibitor, and prior work has documented the effectiveness of midostaurin in reversing MDR. Utz et al. (39) and Fabbro et al. (40) have reported that midostaurin could sensitize CCRF-VCR1000 cells and KB-8551 cells to adriamycin and vinblastine, without altering the ABCB1 mRNA expressing level. As a derivative of staurosporine, midostaurin was also identified to have the capacity to increase doxorubicin accumulation in doxorubicin-resistant cell line A2780/Adr. Meanwhile, midostaurin also acted as a reversal reagent in P-gp mediated leukemia resistance (41, 42). Budworth et al. (43) have explored the reversal effects of midostaurin on P-gp mediated breast cancer MCF7/Adr cell line resistance and Beltran et al. (44) have confirmed that such an effect of midostaurin was related to alterions in the phosphorylation of P-gp. In the study conducted by Courage et al. (45), midostaurin-resistant A549/CGP human lung cancer cell line was identified that overexpressed P-gp, indicated that P-gp may play a key role in midostaurin-mediated MDR. Another research showed that midostaurin could not affect the development of RD cells resistance (RD is a cell line that is resistant to vincristine, and has a mutant P53 but does not have detectable P-gp). This finding, combined with the above evidence, suggests that midostaurin may influence P-gp-mediated MDR (46). Moreover, midostaurin was also documented to alter P-gp efflux function and induce cell death in FLT3 ITD/P-g-positive samples (47). Ganeshaguru et al. (48) studied the effect of midostaurin on malignant cells from B-CLL (B-cell chronic lymphocytic leukemia) patients, and the results showed that nearly 1/3 of B-CLL cells that were originally resistant to chlorambucil and fludarabine were sensitive to midostaurin. P-gp-mediated efflux activity of nearly half of B-CCL cells were observed to be modulated by midostaurin. This novel finding further supported the conclusion that midostaurin could reverse ABCB1-mediated MDR. However, due to technical restrictions in protein structure identification and the incomplete functional research on ABC transporters, few studies systematically explained the exact mechanisms of midostaurin on ABCB1-mediated MDR. In this study, we conducted a series of experiments to verify the reversal effects of midostaurin on ABCB1-mediated MDR in cell lines which were not involved in other studies. Furthermore, we used human ABCB1 homology model to conduct our *in silico* docking study, through which we determined the specific residues that midostaurin would bind to, indicated the potential combining mode of midostaurin with ABCB1 transporter. On the other hand, with the development of pharmacological and molecular biology, various resistant cell lines with definite mechanisms were established and identified. It is necessary to verify the reversal effect and to determine the mechanisms of midostaurin on MDR by utilizing different resistant cell lines. More recently, the results from Hsiao et al. (49) showed that midostaurin could sensitize ABCB1-overexpression KB-V-1, NCI-ADR-RES, and NIH3T3-G185 cells to paclitaxel, colchicine, and vincristine. They also found that midostaurin could enhance colchicine-induced apoptosis effect in KB-V-1 cells, without altering the expression level of ABCB1 transporter. This finding coincides with the results we found when we co-administrated midostaurin with ABCB1-substrate chemotherapeutic drugs. In conclusion, our study demonstrates that midostaurin could overcome ABCB1-mediated MDR by directly inhibiting the efflux function of ABCB1 transporter; as a result, midostaurin can increase the accumulation of antineoplastic drugs. This novel study also suggests that co-administration of midostaurin with certain

substrate-chemotherapeutic drugs of ABCB1 may benefit cancer clinical treatment by circumventing MDR. However, we should not overstate the function of midostautin on MDR before further *in vivo* study and even clinical evaluation is completed as three generations of ABCB1 inhibitors have all failed to be applicable in clinic (50). Admittedly, it remains to be determined whether midostaurin could contribute to improving chemotherapeutic outcome in clinic. More recently, a global study of the efficacy and safety of midostaurin plus chemotherapy in newly diagnosed patients with FLT3 mutation negative (FLT3-MN) acute myeloid leukemia (AML) is recruiting (NCT03512197), and a phase II clinical evaluation is recruiting for midostaurin associated with standard chemotherapy in patients with core-binding factor leukemia (AML FLT3) (NCT03686345). These clinical trials may provide more potent evidence on combined utilization of midostaurin with conventional chemotherapeutic drugs, which would make midostaurin a sensitizing drug, not just a "reversal reagent."

AUTHOR CONTRIBUTIONS

DK and ZC conceived the general idea. NJ, YY, CC, JW, ZL, ZW, and QC performed experiments. NJ, ZC, DY, and DK analyzed the results. NJ, YY, CC, ZL, ZW, and QC wrote the first draft. DK and ZC revised the manuscript.

FUNDING

This work was supported by National Natural Science Foundation of China (81673464), Grant for Major Project of Tianjin for New Drug Development (17ZXXYSY00050), St. John's University Research Seed Grant (No. 579-1110-7002), and the Postgraduate Innovation Fund of 13th Five-Year comprehensive investment, Tianjin Medical University (YJSCX201712).

ACKNOWLEDGMENTS

We would like to thank Dr. Stephen Aller (The University of Alabama at Birmingham, Birmingham) for kindly providing the human ABCB1 homology model. We thank Tanaji T. Talele (St. John's University, New York, NY) for providing the computing resources for the docking analysis. We thank Drs. Susan E. Bates and Robert W. Robey (NCI, NIH, Bethesda, MD) for providing the cell lines. We thank Dr. Yanglu (Princeton University, NJ) for language editing. The first author thanks China Scholarship Council for reimbursing daily expenditures in America.

REFERENCES

1. Szakacs G, Paterson JK, Ludwig JA, Booth-Genthe C, Gottesman MM. Targeting multidrug resistance in cancer. *Nat Rev Drug Discov.* (2006) 5:219–34. doi: 10.1038/nrd1984
2. Dassa E, Bouige P. The ABC of ABCS: a phylogenetic and functional classification of ABC systems in living organisms. *Res Microbiol.* (2001) 152:211–29. doi: 10.1016/S0923-2508(01)01194-9
3. Eckford PD, Sharom FJ. ABC efflux pump-based resistance to chemotherapy drugs. *Chem Rev.* (2009) 109:2989–3011. doi: 10.1021/cr9000226
4. Stavrovskaya AA, Stromskaya TP. Transport proteins of the ABC family and multidrug resistance of tumor cells. *Biochemistry.* (2008) 73:592–604. doi: 10.1134/S0006297908050118
5. Linton KJ. Structure and function of ABC transporters. *Physiology.* (2007) 22:122–30. doi: 10.1152/physiol.00046.2006
6. Linton KJ, Higgins CF. Structure and function of ABC transporters: the ATP switch provides flexible control. *Pflugers Arch.* (2007) 453:555–67. doi: 10.1007/s00424-006-0126-x
7. Wu CP, Ambudkar VS. The pharmacological impact of ATP-binding cassette drug transporters on vemurafenib-based therapy. *Acta Pharm Sin B.* (2014) 4:105–11. doi: 10.1016/j.apsb.2013.12.001
8. Sauna ZE, Smith MM, Muller M, Kerr KM, Ambudkar SV. The mechanism of action of multidrug-resistance-linked P-glycoprotein. *J Bioenerg Biomembr.* (2001) 33:481–91. doi: 10.1023/A:1012875105006
9. Ali MA, Elsalakawy WA. ABCB1 haplotypes but not individual SNPs predict for optimal response/failure in Egyptian patients with chronic-phase chronic myeloid leukemia receiving imatinib mesylate. *Med Oncol.* (2014) 31:279. doi: 10.1007/s12032-014-0279-y
10. Propper DJ, McDonald AC, Man A, Thavasu P, Balkwill F, Braybrooke JP, et al. Phase I and pharmacokinetic study of PKC412, an inhibitor of protein kinase C. *J Clin Oncol.* (2001) 19:1485–92. doi: 10.1200/JCO.2001.19.5.1485
11. Rasko JEJ, Hughes TP. First approved kinase inhibitor for AML. *Cell.* (2017) 171:981. doi: 10.1016/j.cell.2017.11.007
12. Stone RM, Mandrekar SJ, Sanford BL, Laumann K, Geyer S, Bloomfield CD, et al. Midostaurin plus chemotherapy for acute myeloid leukemia with a FLT3 mutation. *N Engl J Med.* (2017) 377:454–64. doi: 10.1056/NEJMoa1614359
13. Akiyama S, Fojo A, Hanover JA, Pastan I, Gottesman MM. Isolation and genetic characterization of human KB cell lines resistant to multiple drugs. *Somat Cell Mol Genet.* (1985) 11:117–26. doi: 10.1007/BF01534700
14. Bates SE, Lee JS, Dickstein B, Spolyar M, Fojo AT. Differential modulation of P-glycoprotein transport by protein kinase inhibition. *Biochemistry.* (1993) 32:9156–64. doi: 10.1021/bi00086a022
15. Robey RW, Honjo Y, van de Laar A, Miyake K, Regis JT, Litman T, et al. A functional assay for detection of the mitoxantrone resistance protein, MXR (ABCG2). *Biochim Biophys Acta.* (2001) 1512:171–82. doi: 10.1016/S0005-2736(01)00308-X
16. Fung KL, Pan J, Ohnuma S, Lund PE, Pixley JN, Kimchi-Sarfaty C, et al. MDR1 synonymous polymorphisms alter transporter specificity and protein stability in a stable epithelial monolayer. *Cancer Res.* (2014) 74:598–608. doi: 10.1158/0008-5472.CAN-13-2064
17. Zhang XY, Zhang YK, Wang YJ, Gupta P, Zeng L, Xu M, et al. Osimertinib (AZD9291), a mutant-selective EGFR inhibitor, reverses ABCB1-mediated drug resistance in cancer cells. *Molecules.* (2016) 21:E1236. doi: 10.3390/molecules21091236
18. Zhang YK, Zhang H, Zhang GN, Wang YJ, Kathawala RJ, Si R, et al. Semi-synthetic ocotillol analogues as selective ABCB1-mediated drug resistance reversal agents. *Oncotarget.* (2015) 6:24277–90. doi: 10.18632/oncotarget.4493
19. Shi Z, Peng XX, Kim IW, Shukla S, Si QS, Robey RW, et al. Erlotinib (Tarceva, OSI-774) antagonizes ATP-binding cassette subfamily B member 1 and ATP-binding cassette subfamily G member 2-mediated drug resistance. *Cancer Res.* (2007) 67:11012–20. doi: 10.1158/0008-5472.CAN-07-2686
20. Sun YL, Kathawala RJ, Singh S, Zheng K, Talele TT, Jiang WQ, et al. Zafirlukast antagonizes ATP-binding cassette subfamily G member 2-mediated multidrug resistance. *Anticancer Drugs.* (2012) 23:865–73. doi: 10.1097/CAD.0b013e328354a196
21. Ji N, Yang Y, Lei ZN, Cai CY, Wang JQ, Gupta P, et al. Ulixertinib (BVD-523) antagonizes ABCB1- and ABCG2-mediated chemotherapeutic drug resistance. *Biochem Pharmacol.* (2018b) 158:274–85. doi: 10.1016/j.bcp.2018.10.028
22. Li J, Jaimes KF, Aller SG. Refined structures of mouse P-glycoprotein. *Protein Sci.* (2014) 23:34–46. doi: 10.1002/pro.2387

23. Ji N, Yang Y, Cai CY, Lei ZN, Wang JQ, Gupta P, et al. VS-4718 antagonizes multidrug resistance in ABCB1- and ABCG2-overexpression cancer cells by inhibiting the efflux function of ABC transporters. *Front Pharmacol.* (2018a) 9:1236. doi: 10.3389/fphar.2018.01236
24. Zhang H, Patel A, Wang YJ, Zhang YK, Kathawala RJ, Qiu LH, et al. The BTK inhibitor ibrutinib (PCI-32765) overcomes paclitaxel resistance in ABCB1- and ABCC10-overexpression cells and tumors. *Mol Cancer Ther.* (2017a) 16:1021–30. doi: 10.1158/1535-7163.MCT-16-0511
25. Zhang YK, Zhang XY, Zhang GN, Wang YJ, Xu H, Zhang D, et al. Selective reversal of BCRP-mediated MDR by VEGFR-2 inhibitor ZM323881. *Biochem Pharmacol.* (2017b) 132:29–37. doi: 10.1016/j.bcp.2017.02.019
26. Marsh S, Somlo G, Li X, Frankel P, King CR, Shannon WD, et al. Pharmacogenetic analysis of paclitaxel transport and metabolism genes in breast cancer. *Pharmacogenomics J.* (2007) 7:362–5. doi: 10.1038/sj.tpj.6500434
27. Campa D, Muller P, Edler L, Knoefel L, Barale R, Heussel CP, et al. A comprehensive study of polymorphisms in ABCB1, ABCC2 and ABCG2 and lung cancer chemotherapy response and prognosis. *Int J Cancer.* (2012) 131:2920–8. doi: 10.1002/ijc.27567
28. Hlavata I, Mohelnikova-Duchonova B, Vaclavikova R, Liska V, Pitule P, Novak P, et al. The role of ABC transporters in progression and clinical outcome of colorectal cancer. *Mutagenesis.* (2012) 27:187–96. doi: 10.1093/mutage/ger075
29. Litviakov NV, Cherdyntseva NV, Tsyganov MM, Denisov EV, Garbukov EY, Merzliakova MK, et al. Changing the expression vector of multidrug resistance genes is related to neoadjuvant chemotherapy response. *Cancer Chemother Pharmacol.* (2013) 71:153–63. doi: 10.1007/s00280-012-1992-x
30. Bartholomae S, Gruhn B, Debatin KM, Zimmermann M, Creutzig U, Reinhardt D, et al. Coexpression of multiple ABC-transporters is strongly associated with treatment response in childhood acute myeloid leukemia. *Pediatr Blood Cancer.* (2016) 63:242–7. doi: 10.1002/pbc.25785
31. Wu H, Kang H, Liu Y, Xiao Q, Zhang Y, Sun M, et al. Association of ABCB1 genetic polymorphisms with susceptibility to colorectal cancer and therapeutic prognosis. *Pharmacogenomics.* (2013) 14:897–911. doi: 10.2217/pgs.13.78
32. Wang F, Huang Z, Zheng K, Zhao H, Hu W. Two SNPs of ATP-binding cassette B1 gene on the risk and prognosis of colorectal cancer. *Int J Clin Exp Pathol.* (2015) 8:3083–9.
33. Ji N, Yang Y, Cai CY, Lei ZN, Wang JQ, Gupta P, et al. Selonsertib (GS-4997), an ASK1 inhibitor, antagonizes multidrug resistance in ABCB1- and ABCG2-overexpression cancer cells. *Cancer Lett.* (2019) 440–441:82–93. doi: 10.1016/j.canlet.2018.10.007
34. Kartal-Yandim M, Adan-Gokbulut A, Baran Y. Molecular mechanisms of drug resistance and its reversal in cancer. *Crit Rev Biotechnol.* (2016) 36:716–26. doi: 10.3109/07388551.2015.1015957
35. Czuba LC, Hillgren KM, Swaan PW. Post-translational modifications of transporters. *Pharmacol Ther.* (2018) 192:88–99. doi: 10.1016/j.pharmthera.2018.06.013
36. Germann UA, Chambers TC, Ambudkar SV, Licht T, Cardarelli CO, Pastan I, et al. Characterization of phosphorylation-defective mutants of human P-glycoprotein expressed in mammalian cells. *J Biol Chem.* (1996) 271:1708–16. doi: 10.1074/jbc.271.3.1708
37. Gottesman MM, Ambudkar SV. Overview: ABC transporters and human disease. *J Bioenerg Biomembr.* (2001) 33:453–8. doi: 10.1023/A:1012866803188
38. Wilkens S. Structure and mechanism of ABC transporters. *F1000Prime Rep.* (2015) 7:14. doi: 10.12703/P7-14
39. Utz I, Hofer S, Regenass U, Hilbe W, Thaler J, Grunicke H, et al. The protein kinase C inhibitor CGP 41251, a staurosporine derivative with antitumor activity, reverses multidrug resistance. *Int J Cancer.* (1994) 57:104–10. doi: 10.1002/ijc.2910570119
40. Fabbro D, Buchdunger E, Wood J, Mestan J, Hofmann F, Ferrari S, et al. Inhibitors of protein kinases: CGP 41251, a protein kinase inhibitor with potential as an anticancer agent. *Pharmacol Ther.* (1999) 82:293–301. doi: 10.1016/S0163-7258(99)00005-4
41. Sedlak J, Hunakova L, Duraj J, Chorvath B, Novotny L. Effects of protein kinase C inhibitor, staurosporine derivative CGP 41 251, on cell cycle, DNA synthesis and drug uptake in neoplastic cell lines. *Anticancer Drugs.* (1995) 6:70–6. doi: 10.1097/00001813-199502000-00008
42. Sedlak J, Hunakova L, Sulikova M, Chorvath B. Protein kinase inhibitor-induced alterations of drug uptake, cell cycle and surface antigen expression in human multidrug-resistant (Pgp and MRP) promyelocytic leukemia HL-60 cells. *Leuk Res.* (1997) 21:449–58. doi: 10.1016/S0145-2126(96)00088-4
43. Budworth J, Davies R, Malkhandi J, Gant TW, Ferry DR, Gescher A. Comparison of staurosporine and four analogues: their effects on growth, rhodamine 123 retention and binding to P-glycoprotein in multidrug-resistant MCF-7/Adr cells. *Br J Cancer.* (1996) 73:1063–8. doi: 10.1038/bjc.1996.205
44. Beltran PJ, Fan D, Fidler IJ, O'Brian CA. Chemosensitization of cancer cells by the staurosporine derivative CGP 41251 in association with decreased P-glycoprotein phosphorylation. *Biochem Pharmacol.* (1997) 53:245–7. doi: 10.1016/S0006-2952(96)00718-6
45. Courage C, Bradder SM, Jones T, Schultze-Mosgau MH, Gescher A. Characterisation of novel human lung carcinoma cell lines selected for resistance to anti-neoplastic analogues of staurosporine. *Int J Cancer.* (1997) 73:763–8.
46. Cocker HA, Tiffin N, Pritchard-Jones K, Pinkerton CR, Kelland LR. *In vitro* prevention of the emergence of multidrug resistance in a pediatric rhabdomyosarcoma cell line. *Clin Cancer Res.* (2001) 7:3193–8.
47. Hunter HM, Pallis M, Seedhouse CH, Grundy M, Gray C, Russell NH. The expression of P-glycoprotein in AML cells with FLT3 internal tandem duplications is associated with reduced apoptosis in response to FLT3 inhibitors. *Br J Haematol.* (2004) 127:26–33. doi: 10.1111/j.1365-2141.2004.05145.x
48. Ganeshaguru K, Wickremasinghe RG, Jones DT, Gordon M, Hart SM, Virchis AE, et al. Actions of the selective protein kinase C inhibitor PKC412 on B-chronic lymphocytic leukemia cells *in vitro*. *Haematologica.* (2002) 87:167–76.
49. Hsiao SH, Lusvarghi S, Huang YH, Ambudkar SV, Hsu SC, Wu CP. The FLT3 inhibitor midostaurin selectively resensitizes ABCB1-overexpression multidrug-resistant cancer cells to conventional chemotherapeutic agents. *Cancer Lett.* (2019) 445:34–44. doi: 10.1016/j.canlet.2019.01.001
50. Palmeira A, Sousa E, Vasconcelos MH, Pinto MM. Three decades of P-gp inhibitors: skimming through several generations and scaffolds. *Curr Med Chem.* (2012) 19:1946–2025. doi: 10.2174/0929867128001 67392
51. Gottesman MM, Fojo T, Bates SE. Multidrug resistance in cancer: role of ATP-dependent transporters. *Nat Rev Cancer.* (2002) 2:48–58. doi: 10.1038 nrc706

Conflict of Interest Statement: The authors declare that the research was conducted in the absence of any commercial or financial relationships that could be construed as a potential conflict of interest.

frontiers in Pharmacology

ORIGINAL RESEARCH
published: 06 August 2019
doi: 10.3389/fphar.2019.00857

An Insight Into the Molecular Mechanism of Berberine Towards Multiple Cancer Types Through Systems Pharmacology

Pengfei Guo[1,2†], Chuipu Cai[1,3†], Xiaoqin Wu[4], Xiude Fan[4], Wei Huang[1], Jingwei Zhou[1], Qihui Wu[1], Yujie Huang[1], Wei Zhao[1], Fengxue Zhang[3], Qi Wang[1,5], Yongbin Zhang[2] and Jiansong Fang[1,4,5]**

[1] Science and Technology Innovation Center, Guangzhou University of Chinese Medicine, Guangzhou, China, [2] Laboratory of Experimental Animal, Guangzhou University of Chinese Medicine, Guangzhou, China, [3] School of Basic Medical Sciences, Guangzhou University of Chinese Medicine, Guangzhou, China, [4] Lerner Research Institute, Cleveland Clinic, Cleveland, OH, United States, [5] Institute of Clinical Pharmacology, Guangzhou University of Chinese Medicine, Guangzhou, China

OPEN ACCESS

Edited by:
Zhe-Sheng Chen,
St. John's University, United States

Reviewed by:
Pranav Gupta,
Massachusetts General Hospital and Harvard Medical School, United States
Shuaishuai Liu,
University of Maryland, United States

***Correspondence:**
Jiansong Fang
fangjs@gzucm.edu.cn;
fangj3@ccf.org
Yongbin Zhang
zyb-73@163.com

†These authors have contributed equally to this work.

Specialty section:
This article was submitted to Cancer Molecular Targets and Therapeutics, a section of the journal Frontiers in Pharmacology

Received: *23 January 2019*
Accepted: *04 July 2019*
Published: *06 August 2019*

Citation:
Guo P, Cai C, Wu X, Fan X, Huang W, Zhou J, Wu Q, Huang Y, Zhao W, Zhang F, Wang Q, Zhang Y and Fang J (2019) An Insight Into the Molecular Mechanism of Berberine Towards Multiple Cancer Types Through Systems Pharmacology. Front. Pharmacol. 10:857. doi: 10.3389/fphar.2019.00857

Over the past several decades, natural products with poly-pharmacological profiles have demonstrated promise as novel therapeutics for various complex diseases, including cancer. Berberine (PubChem CID: 2353), a soliloquies quaternary alkaloid, has been validated to exert powerful effects in many cancers. However, the underlying molecular mechanism is not yet fully elucidated. In this study, we summarized the molecular effects of berberine against multiple cancers based on current available literatures. Furthermore, a systems pharmacology infrastructure was developed to discover new cancer indications of berberine and explore their molecular mechanisms. Specifically, we incorporated 289 high-quality protein targets of berberine by integrating experimental drug–target interactions (DTIs) extracted from literatures and computationally predicted DTIs inferred by network-based inference approach. Statistical network models were developed for identification of new cancer indications of berberine through integration of DTIs and curated cancer significantly mutated genes (SMGs). High accuracy was yielded for our statistical models. We further discussed three typical cancer indications (hepatocarcinoma, lung adenocarcinoma, and bladder carcinoma) of berberine with new mechanisms of actions (MOAs) based on our systems pharmacology framework. In summary, this study systematically provides a powerful strategy to identify potential anti-cancer effects of berberine with novel mechanisms from a systems pharmacology perspective.

Keywords: berberine, cancer, systems pharmacology, drug–target interactions, significantly mutated genes

INTRODUCTION

Natural products with diverse chemical scaffolds have been recognized as an invaluable source of candidates in drug discovery and development for multiple complex diseases, including cancer. Berberine, a plant-derived compound isolated from medicinal plants such as Coptis chinensis and Hydrastis canadensis, had a long history of medicinal application in traditional Chinese medicine

(Ayati et al., 2017). As one of the main alkaloids, berberine has been reported to exert potentially beneficial effects on many cancer types, including breast cancer (Kim et al., 2008), bladder cancer (Yan et al., 2011), and hepatocarcinoma (Liu et al., 2011; Zhu et al., 2016). For example, berberine had shown significant inhibitory effect on hepatocellular carcinoma cells and could reduce the volume and weight of tumors in an H22 transplanted tumor model in mice (Li et al., 2015).

Based on collection of hundreds of berberine-related pharmacological literatures, we systematically summarized eight key mechanisms of anti-cancer effects of berberine, including cell death, cell invasion and metastasis, cell cycle arrest, cell growth, transcription factors, inflammatory factors, angiogenic, chemo-sensitivity, and radio-sensitivity (**Figure 1** and **Supplementary Table S1**). Specifically, apoptosis (programmed cell death) plays a vital role in tumor cell development, differentiation, and proliferation (Ola et al., 2011). Recent study has revealed that berberine could induce apoptosis of human osteosarcoma U2OS cells through inhibiting the PI3K/Akt signaling pathway activation (Chen, 2016). In addition, anti-angiogenesis is a promising strategy for prevention and treatment of multicancer in preclinical or clinical studies in terms of many natural products (Khalid et al., 2016; Kotoku et al., 2016). Previous *in vitro* and *in vivo* experiments have validated that berberine exerted anti-angiogenic effect through inhibiting various proinflammatory and pro-angiogenic factors, including vascular endothelial growth factor (VEGF), interleukin-6 (IL-6), interleukin-2 (IL-2), and metalloproteinase inhibitor (TIMP) (Hamsa and Kuttan, 2012).

Collectively, berberine with polypharmacology has demonstrated its broad anti-cancer properties through targeting various oncogenic pathways and targets. Therefore, systematic exploration of the drug targets of berberine is of great significance for understanding its anti-cancer mechanisms of action (MOAs) and for further excavating its novel cancer indications.

Systems pharmacology-based approaches, as an emerging interdiscipline that combines experimental assays and computational tools, have provided an alternative to understand the therapeutic mechanisms of complex diseases (Fang et al., 2018). Recent studies have demonstrated advanced discovery of new indications for natural products based on systems pharmacology approaches (Fang et al., 2017b; Fang et al., 2019). For example, novel molecular mechanisms of several effective natural products (e.g., resveratrol, quercetin, caffeic acid, and wogonoside) for multiple complex diseases including multi-cancer types and age-related disorders have been identified and validated by various literatures and *in vitro* and *in vivo* experiments (Fang et al., 2017a; Huang et al., 2019). Collectively, systems pharmacology-based approaches have been proved as an effective tool for exploring the poly-pharmacological actions of natural products towards various complex diseases.

In this study, we proposed a systems pharmacology infrastructure to identify new cancer indications of berberine and explore their molecular mechanisms (**Figure 2**). Specifically, we constructed a global DTI network of berberine by integrating both experimentally reported DTIs obtained from literatures and DTIs computationally predicted by our previous predictive network models (Fang et al., 2017c). Besides, a high-quality

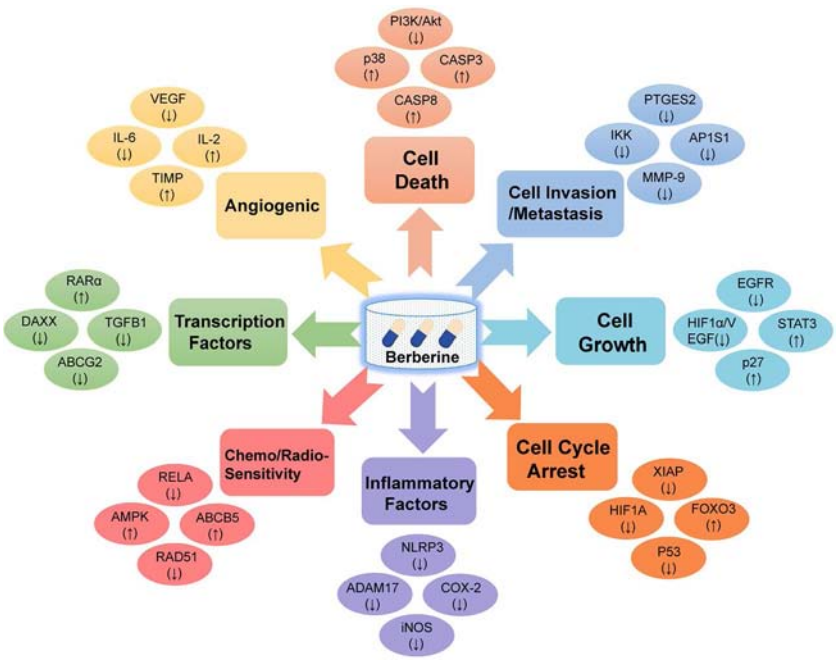

FIGURE 1 | Diagram illustrating the eight potential anti-cancer effects of berberine. Berberine exerts anti-cancer activities *via* targeting various cancer key protein targets, related to cell death, cell invasion and metastasis, cell cycle arrest, cell growth, transcription factors, inflammatory factors, angiogenic, chemo-sensitivity, and radio-sensitivity.

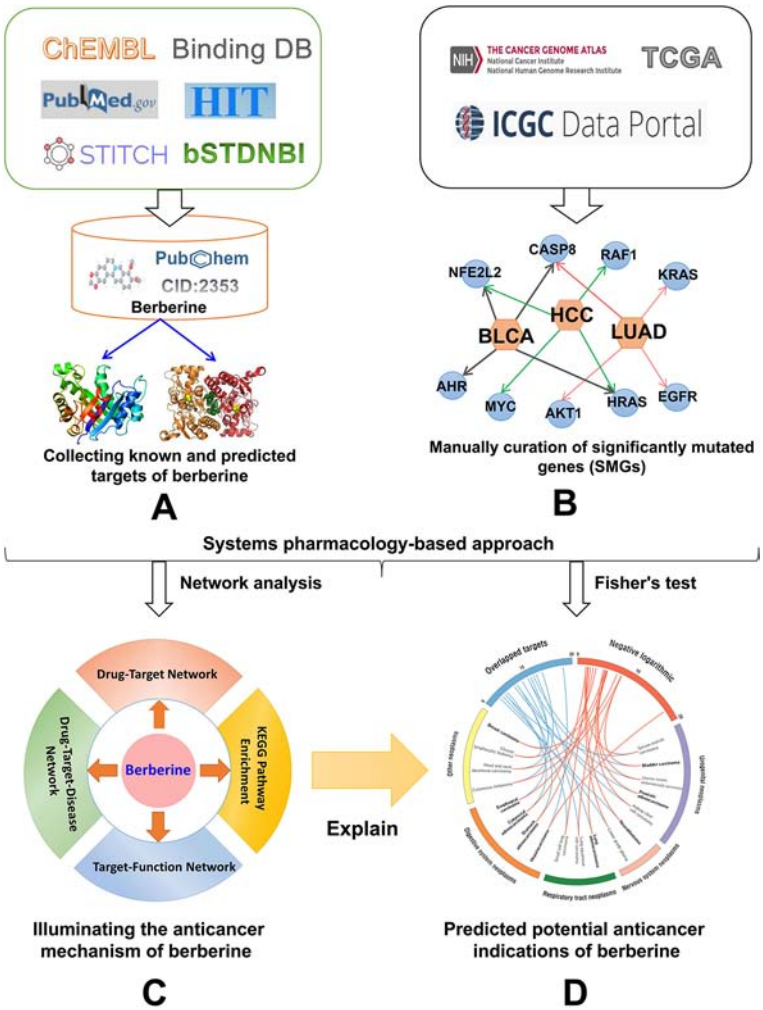

FIGURE 2 | Workflow of a systems pharmacology infrastructure for the identification of cancer indications and exploration of molecular mechanisms of berberine. **(A)** Construction of drug–target network for berberine, **(B)** manual curation of cancer significantly mutated genes (SMGs) for multiple cancer types, **(C)** performing network analyses to explore the anti-cancer mechanism of berberine, and **(D)** statistical network models for prioritizing novel anti-cancer indication of berberine through integrating computationally predicted and known drug targets into the curated cancer SMGs.

collection of significantly mutated genes (SMGs) for multiple cancer types was manually collected. On the basis of curated cancer SMGs and DTIs, we built statistical network models with high accuracy to prioritize new cancer indications of berberine and showcased its potential mechanisms. Overall, this study provides a useful systems pharmacology framework to interpret the multi-scale MOAs of berberine in multiple cancer type management, which may give some enlightenment for further treatment of cancer-associated diseases.

MATERIALS AND METHODS

Collection of Known Targets for Berberine

Known targets of berberine were collected by extracting data from four data sources, including HIT (Ye et al., 2011), STITCH (Kuhn et al., 2014), BindingDB (accessed June 2016) (Gilson et al., 2016), and ChEMBL (Bento et al., 2014). For STITCH, we only kept the targets with experimental evidence score higher than 0.7. We totally obtained 66 known targets *via* integrating the four available databases. Besides, we further gathered 238 extra targets of berberine by manually retrieving large-scale pharmacological literatures from PubMed (https://www.ncbi.nlm.nih.gov) with "berberine [title] and cancer" as search terms (**Supplementary Table S2**). After duplicated targets and DTIs were eliminated from non-*Homo sapiens*, 275 high-quality known DTIs were selected for further study (**Supplementary Table S3**).

Network-Based Target Prediction for Berberine

In a previous study, we have developed statistical network models to predict targets of natural products through a balanced

substructure–drug–target network-based inference (bSDTNBI) approach (Fang et al., 2018). The bSDTNBI method utilizes resource-diffusion processes to prioritize potential targets for natural products through integrating known DTI network, drug–substructure linkages, and new input drug–substructure linkages (Wu et al., 2017). For a new input chemical, each of its substructures equally spreads resources to its neighbor nodes layer by layer, and targets obtaining final resources could be regarded as the potential targets of the new chemical. Four parameters ($\alpha = \beta = 0.1$, $\gamma = -0.5$, and $k = 2$) of bSDTNBI were adopted based on a previous study (Wu et al., 2016). Among them, parameter α was introduced to balance the initial resource allocation of different node types, while β was used to adjust weighted values of different edge types. The third parameter γ was imported to balance the influence of hub nodes in resource-diffusion processes, and the fourth parameter κ denotes the number of resource-diffusion processes. We calculated four substructure items for each compound based on four types of molecular fingerprints from PaDEL-Descriptor (version 2.18) (Yap, 2011), including Substructure (FP4), Klekota-Roth (KR), MACCS, and PubChem. Among the four network models generated with different types of fingerprints, bSDTNBI_KR performed best with the highest values of precision ($P = 0.049$), recall ($R = 0.752$), precision enhancement (Ep = 27.02), recall enhancement (eR = 27.24), and the area under the receiver operating characteristic curve (AUC = 0.959). Finally, the best model built based on KR molecular fingerprint was selected to predict the new targets of berberine. The top 20 predicted candidates were used for further study (**Supplementary Table S3**).

Significantly Mutated Genes (SMG) for Multiple Cancer Types

We collected 804 SMGs for 28 cancer types/subtypes from a previous study (Cheng et al., 2016), including glioblastoma multiforme (GBM), serous ovarian adenocarcinoma (SOC), stomach adenocarcinoma (STAD), colorectal adenocarcinoma (CRAC), breast carcinoma (BRCA), uterine corpus endometrioid (UCEC), medulloblastoma (MBL), acute myeloid leukemia (AML), cutaneous melanoma (CM), lung squamous cell (SQCC), thyroid carcinoma (THCA), lung adenocarcinoma (LUAD), kidney clear cell (CCSK), head and neck squamous (HNSCC), small cell lung (SCLC), lower grade glioma (LGG), bladder carcinoma (BLCA), esophageal carcinoma (EC), prostate adenocarcinoma (PRAD), hepatocarcinoma (HCC), neuroblastoma (NBL), chronic lymphocytic leukemia (CLL), pancreas adenocarcinoma (PAC), multiple myeloma (MM), acute lymphocytic leukemia (ALL), non-small cell lung (NSCLC), diffuse large B-cell lymphoma (DLBCL), and pilocytic astrocytoma (PA). Considering a lack of statistical power if the number of SMG for specific cancer types is lower than 20, we further excluded ALL, NSCLC, DLBCL, and PA. All SMGs are annotated using gene Entrez ID, chromosome location, and the official gene symbols from the National Center for Biotechnology Information (NCBI) database (Zhe and Huang, 2002). Finally, 24 cancer types/subtypes covering 804 SMGs were selected for further study (**Supplementary Table S4**).

Prioritizing Cancer Indications of Berberine

In this study, an integrated statistical network model was generated to prioritize cancer indication of berberine based on drug–target network and cancer SMGs (Cheng et al., 2016; Jiang et al., 2018). We assumed that berberine would exert high potential for the treatment of a specific cancer type if its targets tend to be SMGs of this cancer. For each cancer type/subtype, Fisher's exact test was utilized to calculate the statistical significance of the enrichment of SMGs for each cancer type in target profiles of berberine. The *P*-values were corrected by Benjamini–Hochberg method (Benjamini and Yekutieli, 2001). We set a cutoff adjusted *P*-value threshold (q) < 0.05 to define significantly predicted drug–cancer pairs.

Network Construction

To further explore the multi-scale MOAs of berberine in treating multiple cancer types, three types of networks were constructed by Cytoscape 3.2.1 software (Shannon et al., 2003): 1) drug–target (D-T) network, which presents the relationship between berberine and its targets; 2) target–function (T-F) network, which illustrates the relationship between cancer-related biological processes and SMGs; and 3) drug–target–disease (D-T-D) network, which reflects a global view of the molecular mechanism of berberine against multiple cancer types. After network analysis, the SMGs were further mapped to DAVID database (https://david.ncifcrf.gov/summary.jsp) for extracting the canonical pathways that were highly associated with these targets (Dennis et al., 2003). Finally, circos plot was used to visualize the predicted cancer indications.

RESULTS AND DISCUSSION

Construction of the Drug–Target (D-T) Network for Berberine

The constructed drug–target interaction network (**Figure 3**) of berberine contains 289 interactions, including 275 known targets and 20 predicted targets (**Supplementary Table S3**). *In vitro* and *in vivo* assays in previous studies have validated that five out of the 20 predicted targets could be mediated by berberine, indicating high accuracy of our target prediction approach. These five predicted targets are caspase-3 (CASP3) (Okubo et al., 2017), cellular tumor antigen p53 (TP53) (Qing et al., 2014), caspase-9 (CASP9) (Zhao et al., 2017), nuclear factor NF-kappa-B p105 subunit (NFKB1) (Yu et al., 2014), and mitogen-activated protein kinase 1 (MAPK1) (Song et al., 2015).

We further mapped the 289 protein targets of berberine into the curated cancer SMGs, resulting in 51 cancer-related targets encoded by SMGs (**Supplementary Table S3**). Accumulating evidences indicate that berberine may exert anti-cancer effects through regulating these targets. For instance, signal transducer and activator of transcription 3 (STAT3) are important in

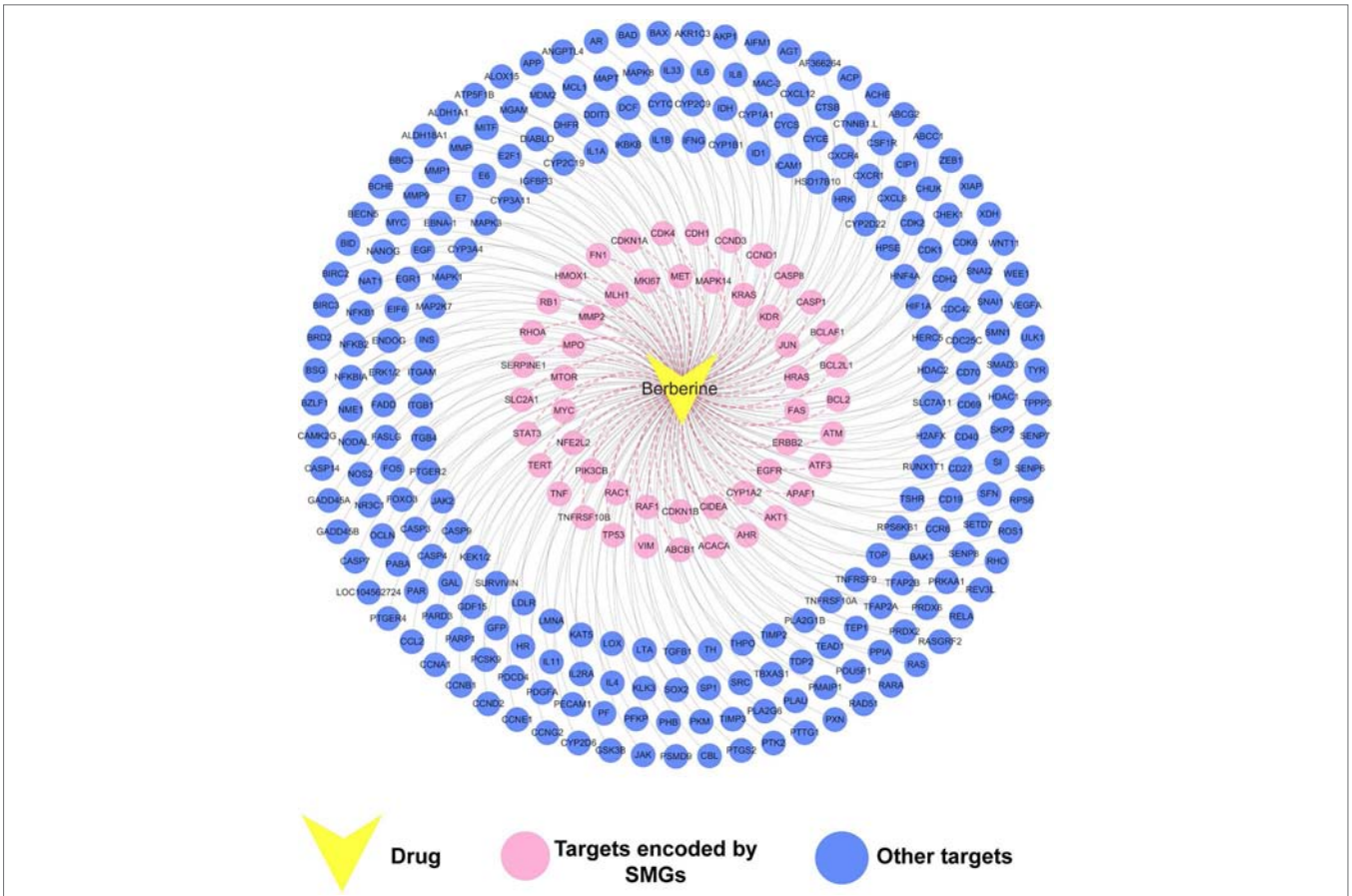

FIGURE 3 | Drug–target (D-T) network of berberine composed of known and predicted targets. The predicted targets were obtained by a balanced substructure–drug–target network-based inference (bSDTNBI) approach. This network includes 289 drug–target interactions connecting berberine and 51 protein targets encoded by significantly mutated genes (SMGs).

various phases of the tumor development, including tumor cell proliferation, survival, invasion, immunosuppression, and inducing and maintaining a pro-carcinogenic inflammatory microenvironment (Fan et al., 2013). A previous study has showed that berberine suppressed tumorigenicity and growth of nasopharyngeal carcinoma (NPC) cells by inhibiting STAT3 activation (Tsang et al., 2013). Recently, a strategy targeting tumor suppressors and apoptosis-related genes provides a rationale for developing more effective approaches and agents for cancer prevention (Sun et al., 2017; López-Cortés et al., 2018; Yamaguchi et al., 2019). Berberine has been observed to activate expression of many tumor apoptosis-related proteins, including caspase-8 (CASP8), tumor necrosis factor-a (TNF-a), and p38 MAPK, and thus induced apoptosis of HeLa cells (Lu et al., 2010). Besides, it has been reported that berberine can decrease expression of mitochondrial-dependent anti-apoptotic factors such as B-cell lymphoma-2 (Bcl-2) and Bcl-2-like protein 1 (BCL2L1) in KB human oral cancer cells (Kim et al., 2015).

Taken together, the observed polypharmacological profiles of berberine motivated us to elucidate its anti-cancer mechanism through systems pharmacology analysis on the interaction between berberine and 51 SMGs.

Elucidating Molecular Mechanisms of Berberine in Cancer Prevention and Treatment

Target–Function Network

As depicted in **Figure 4**, the target–function (T-F) network is composed of 230 T-F pairs connecting 51 SMG targets and 8 cancer-related functional modules based on the DAVID analysis (**Supplementary Table S5**). The eight functional modules include anti-cancer action associated with sustaining proliferative signaling (Huang et al., 2015), resisting cell death (Chidambara Murthy et al., 2012), deregulating cellular energetics (Tan et al., 2015), enabling replicative immortality (Xiong et al., 2015), avoiding immune destruction (Jiang et al., 2017), genome instability and mutation (Li et al., 2014), angiogenesis (Jie et al., 2011), and activating invasion and metastasis (Tang et al., 2009). On average, each SMG target is involved in six cancer-related functional modules. We found that 25 out of 51 SMG targets are associated with more than five functional modules, indicating the higher potential role of these SMG targets related to cancers. Previous studies of berberine in cancer validated the functional analysis of our T-F network. For instance, berberine could induce cell cycle arrest involved in sustaining proliferative signaling in

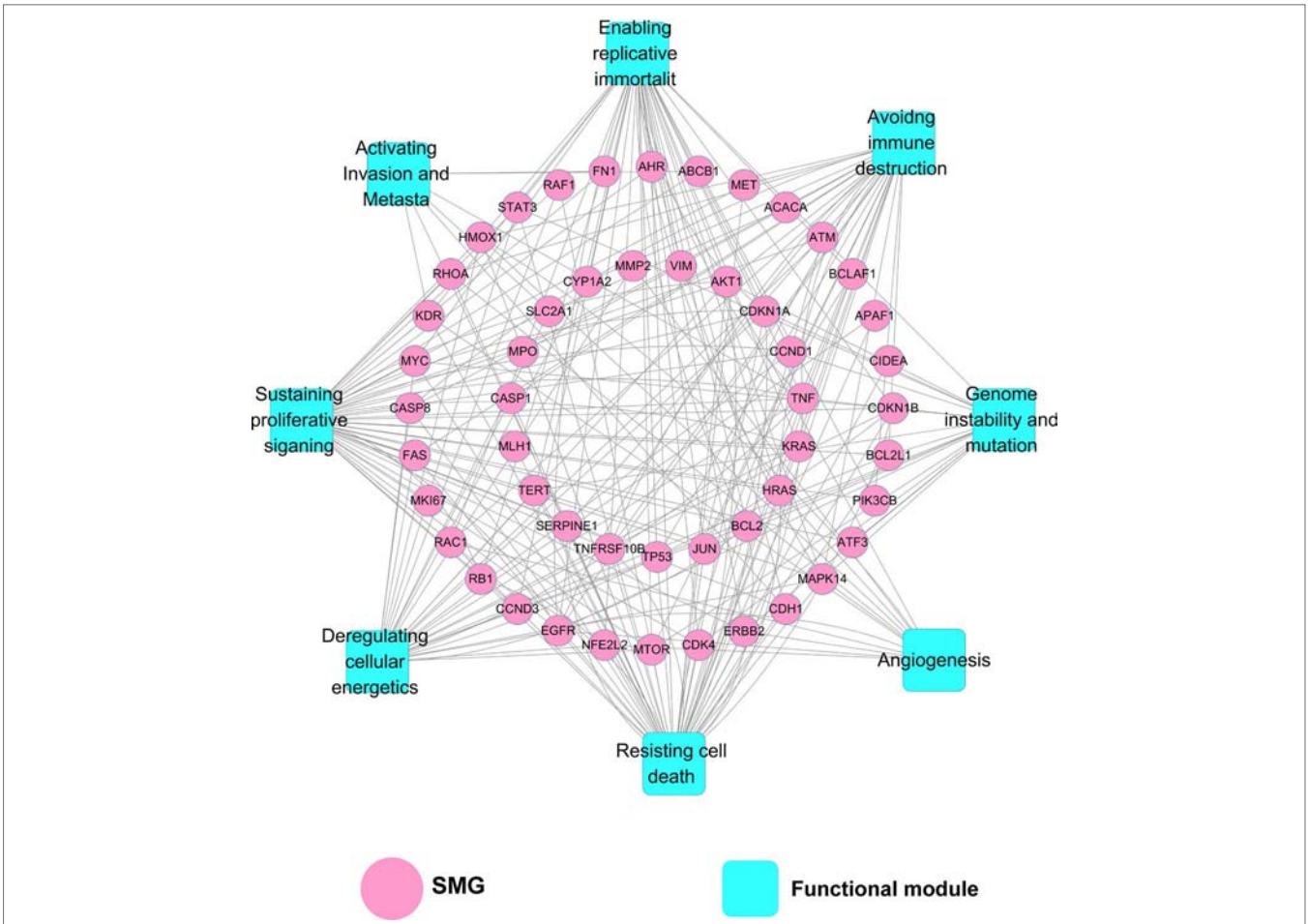

FIGURE 4 | Target–function (T-F) network demonstrating the relationship between cancer-related biological processes and SMGs. A functional module is linked to a target if the target is involved in mechanism of anti-cancer action.

cholangiocarcinoma KKU-213 and KKU-214 cell lines (Puthdee et al., 2017). Berberine was reported to inhibit metastasis and tumor-induced angiogenesis in human cervical cancer cells as well (Chu et al., 2014).

KEGG Enrichment Analysis

In order to further elucidate molecular mechanisms of berberine in cancer prevention and treatment, we performed KEGG pathway enrichment analysis based on the 51 SMGs. After pathways with adjusted P (q) value higher than 0.05 were excluded, 56 enriched pathways related to cancer pathogenesis were obtained (**Supplementary Table S6**).

Among 56 pathways, PI3K-Akt (hsa04151; $q = 2.0 \times 10^{-12}$), p53 (hsa04115; $q = 2.7 \times 10^{-9}$), HIF-1 (hsa04066; $q = 3.9 \times 10^{-9}$), FoxO (hsa04068; $q = 4.9 \times 10^{-9}$), VEGF (hsa04370; $q = 5.7 \times 10^{-7}$), MAPK (hsa04010; $q = 2.5 \times 10^{-6}$), Ras (hsa04014; $q = 6.4 \times 10^{-6}$), Jak-STAT (hsa04630; $q = 9.9 \times 10^{-4}$), mTOR (hsa04150; $q = 1.5 \times 10^{-2}$), AMPK (hsa04152; $q = 1.9 \times 10^{-2}$), and NF-kappa B (hsa04064; $q = 4.0 \times 10^{-2}$) signaling pathways have been confirmed to be associated with berberine in previous literatures (**Table 1**). For example, berberine was reported to inhibit cellular growth and promotes apoptosis by down-regulating PI3K/Akt signaling pathway in breast cancer SKBR-3 cells and hepatoma HepG2 cells (Liu et al., 2011; Kuo et al., 2011). *In vitro* and *in vivo* assays revealed that berberine sensitized drug-resistant breast cancer to doxorubicin (DOX) chemotherapy and directly induced apoptosis through the dose-orchestrated AMPK signaling pathway (Pan et al., 2017). Berberine also induces autophagic cell death through inhibition of mTOR-signaling pathway by suppressing Akt activity and up-regulating P38 MAPK signaling in HepG2 and MHCC97-L cells (Wang et al., 2010). The rest of the 45 enriched pathways prompt the potential anti-cancer acting mechanisms that may be mediated by berberine, which deserve to be validated by experimental assays in the future.

Drug–Target–Diseases Network

We further built a drug–target–diseases (D-T-D) network *via* mapping 51 SMGs targeted by berberine into multiple cancers. As shown in **Figure 5**, the 51 SMGs are related to 24 types of cancer. On average, each cancer links to nine SMGs, while each SMG is connected to 4.6 cancer types. Network analysis showed that the top 6 SMGs connected to the largest number of cancer types are

TABLE 1 | Summary of the 11 enriched pathways validated to be mediated by berberine in previous literatures.

Pathway ID	Pathway name	Genes	*P*-value	PMID
hsa04151	PI3K-Akt signaling pathway	EGFR, HRAS, PIK3CB, MET, TP53, RAF1, BCL2L1, CDK4, KDR, AKT1, CDKN1A, CCND1, KRAS, CDKN1B, CCND3, BCL2, RAC1, MTOR, MYC, FN1	2.03E–12	27081456|25212656
hsa04115	p53 signaling pathway	CDKN1A, CCND1, CCND3, CASP8, SERPINE1, TP53, APAF1, FAS, CDK4, ATM	2.66E–09	20455200
hsa04066	HIF-1 signaling pathway	AKT1, EGFR, HRAS, CCND1, KRAS, PIK3CB, ERBB2, TP53, RAF1, RB1, CDK4	3.89E–09	28775788
hsa04068	FoxO signaling pathway	AKT1, EGFR, HRAS, CCND1, KRAS, PIK3CB, ERBB2, TP53, RAF1, MLH1, CDH1, MYC	4.88E–09	24766860|29360760
hsa04370	VEGF signaling pathway	TNF, MAPK14, BCL2, RAC1, TP53, APAF1, BCL2L1, CASP1	5.72E–07	23869238
hsa04010	MAPK signaling pathway	AKT1, EGFR, HRAS, CCND1, KRAS, PIK3CB, ERBB2, TP53, RAF1, MLH1, CDH1, MYC	2.45E–06	19492307|25212656
hsa04014	Ras signaling pathway	AKT1, EGFR, HRAS, CCND1, KRAS, PIK3CB, ERBB2, TP53, RAF1, RB1, CDK4	6.42E–06	25212656|23159854
hsa04630	Jak-STAT signaling pathway	AKT1, HRAS, KRAS, PIK3CB, JUN, RAC1, RAF1	9.90E–04	26463023
hsa04150	mTOR signaling pathway	TNF, CASP8, APAF1, CASP1	1.50E–02	23159854|20830746
hsa04152	AMPK signaling pathway	EGFR, MAPK14, JUN, RAC1, MET	1.88E–02	28775788
hsa04064	NF-kappa B signaling pathway	TNF, CASP8, APAF1, CASP1	3.97E–02	19107816

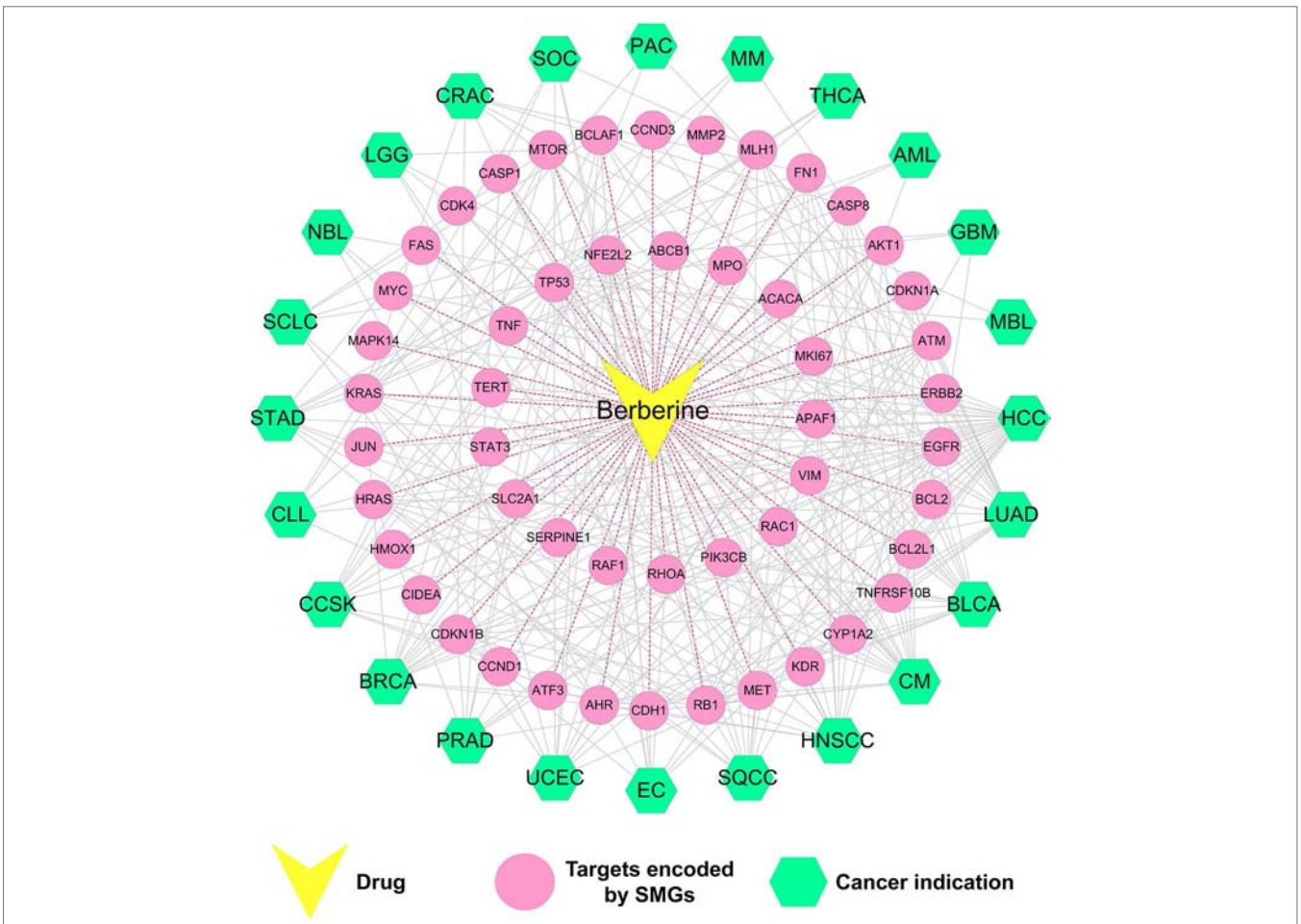

FIGURE 5 | Drug–target–disease (D-T-D) network of berberine. This network shows 51 proteins of berberine encoded by SMGs of 24 types of cancer.

cellular tumor antigen p53 (TP53), gTPase KRas (KRAS), epidermal growth factor receptor (EGFR), retinoblastoma-associated protein (RB1), serine-protein kinase ATM (ATM), and cadherin-1 (CDH1). Among them, EGFR, a key significantly mutated gene of cancer, is involved in the pathological mechanism of 13 cancer types, including LUAD, HNSCC, SQCC, EC, UCEC, PRAD, BRCA, CCSK, CLL,

STAD, LGG, CRAC, and GBM. Previous studies confirmed that berberine can inhibit EGFR signal pathway in several cancer types, including STAD (Wang et al., 2016), PRAD (Huang et al., 2015), and CRAC (Wang et al., 2013). Besides, berberine acts in specific tumor by regulating multiple SMGs. For instance, cellular tumor antigen p53 (TP53) (Wilson et al., 2010), RAC-alpha serine/threonine-protein kinase (AKT1) (López-Cortés et al., 2018), and cyclin-dependent kinase inhibitor 1B (CDKN1B) (Cusan et al., 2018) are highly correlated with breast cancer. Accumulating evidences demonstrated that berberine can inhibit breast cancer by acting on SMGs such as TP53 (Kim et al., 2012; Tan et al., 2015), AKT1 (Kuo et al., 2011), and CDKN1B (Patil et al., 2010).

Briefly, the D-T-D network demonstrated that SMGs targeted by berberine were closely related to multi-cancer types. In the following part, statistical systems pharmacology approach was employed to identify novel cancer indications of berberine and explore the molecular mechanisms.

Systems Pharmacology-Based Prediction of Cancer Indications for Berberine

As shown in **Figure 6**, a statistical systems pharmacology framework is proposed to prioritize novel cancer indications of berberine based on Fisher's exact test analysis. We calculated the therapeutic potential of berberine in 24 cancer indications and obtained 18 cancer indications of which adjusted P (q) values are lower than 0.05 ($q < 0.05$), including HCC ($q < 1.0 \times 10^{-5}$; $-\text{Log10}(q) = 19.25$), LUAD ($q < 1.0 \times 10^{-5}$; $-\text{Log10}(q) = 9.35$), BLCA ($q < 1.0 \times 10^{-5}$; $-\text{Log10}(q) = 9.31$), CM ($q < 1.0 \times 10^{-5}$; $-\text{Log10}(q) = 9.29$), HNSCC ($q < 1.0 \times 10^{-5}$; $-\text{Log10}(q) = 8.52$), SQCC ($q < 1.0 \times 10^{-5}$; $-\text{Log10}(q) = 6.74$), EC ($q < 1.0 \times 10^{-5}$; $-\text{Log10}(q) = 6.66$), UCEC ($q < 1.0 \times 10^{-5}$; $-\text{Log10}(q) = 6.52$), PRAD ($q = 1.15 \times 10^{-5}$; $-\text{Log10}(q) = 6.32$), BRCA ($q = 1.33 \times 10^{-5}$; $-\text{Log10}(q) = 6.26$), CCSK ($q = 2.30 \times 10^{-5}$; $-\text{Log10}(q) = 6.02$), CLL ($q = 0.55 \times 10^{-3}$; $-\text{Log10}(q) = 4.64$), STAD ($q = 1.76 \times 10^{-3}$; $-\text{Log10}(q) = 4.14$), SCLC ($q = 5.33 \times 10^{-3}$; $-\text{Log10}(q) = 3.65$), NBL ($q = 1.29 \times 10^{-2}$; $-\text{Log10}(q) = 3.27$), LGG ($q = 1.67 \times 10^{-2}$; $-\text{Log10}(q) = 3.16$), CRAC ($q = 3.21 \times 10^{-2}$; $-\text{Log10}(q) = 2.87$), and SOC ($q = 3.36 \times 10^{-2}$; $-\text{Log10}(q) = 2.85$) (**Supplementary Table S7**). As listed in **Table 2**, 10 out of the 18 predicted cancer indications of berberine were validated by reported experimental evidences, including HCC, LUAD, BLCA, EC, PRAD, BRCA, STAD, CRAC, and SOC, indicating the high accuracy of our systems pharmacology-based predictive method (success rate = 55.6%).

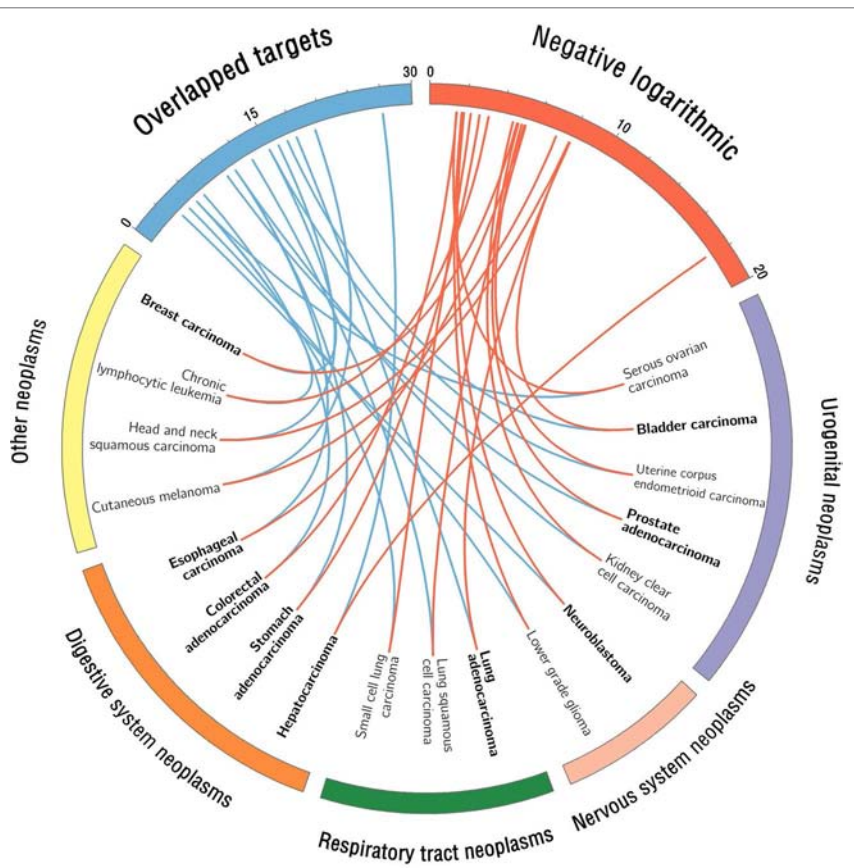

FIGURE 6 | Circos plot visualizes the predicted cancer indications of berberine. The red connected lines represent the calculated $-\text{Log}_{10}(q)$ value of each berberine-cancer type pair based on Fisher's exact test, while the blue ones represent the corresponding number of overlapped targets. The predicted cancer indications with literature validation were highlighted in bold font. We classified the 18 predicted cancer indications into four neoplasm categories according to Medical Subject Headings (MeSH) system (https://www.ncbi.nlm.nih.gov/mesh/68009371).

Among the 18 cancer indications, CM, HNSCC, SQCC, UCEC, CCSK, CLL, SCLC, NBL, and LGG are the unreported cancer indications of berberine, which deserve further preclinical validation. For example, cutaneous melanoma (CM), one of the most aggressive types of cancer, represents a major problem worldwide due to its high incidence and elevated degree of heterogeneity (Jemal et al., 2010; Coricovac et al., 2018). Based on our predictive model, berberine exerted a high potential for anti-CM, with a significant q value [$q < 1.23 \times 10^{-8}$; $-\text{Log10}\ (q) = 9.29$]. Therefore, the potential of berberine in the prevention and treatment of CM deserves to be further validated.

Case Study: Exploring the MOAs of Berberine on Hepatocarcinoma (HCC), Lung Adenocarcinoma (LUAD), and Bladder Carcinoma (BLCA)

To further validate the accuracy of statistical network models and predicted anti-cancer targets of berberine, we selected three typical cancer types [HCC ($q = 5.63 \times 10^{-20}$), LUAD ($q = 4.52 \times 10^{-10}$), and BLCA ($q = 4.92 \times 10^{-10}$)] as case studies to illustrate their anti-cancer MOAs **(Figure 7)**.

Hepatocellular Carcinoma

HCC, the third leading cause of cancer death worldwide, has become one of the most common and prevalent human malignancies in the world (Okubo et al., 2017). *In vitro* assays revealed that berberine can inhibit autophagy in hepatoma cell lines (e.g., HepG2 cells and MHCC97-L cells) by regulating multiple proteins [e.g., mitogen-activated protein kinase 14 (MAPK14), TP53, and phosphatidylinositol 4,5-bisphosphate 3-kinase catalytic subunit beta isoform (PIK3CB)] and pathways (e.g., P38 MAPK signaling), stimulating further development of derivatives for drug-base cancer prevention and treatment (Wang et al., 2010; Liu et al., 2011; Wang et al., 2014). In this study, Fisher's test showed that berberine played a significant role in treatment of liver cancer ($q = 5.63 \times 10^{-20}$). In addition, network analysis revealed that berberine bound with 27 HCC-related SMG targets, suggesting its underlying anti-cancer mechanisms of berberine (**Figure 7**). *In vivo* or *in vitro* data have demonstrated that these SMGs are closely relevant to the treatment of cancer by berberine. For example, berberine can inhibit cell proliferation of HepG2, Hep3B, and SNU-182 through up-regulating protein expression of tumor suppressor genes, such as activating transcription factor 3 (ATF3) (Chuang et al., 2017). Furthermore, study revealed that berberine inhibited expression of BCL2, thus reducing autophagic cell death and mitochondrial apoptosis in liver cancer cells, such as HepG2 and MHCC97-L cells (Hur et al., 2010).

Lung Adenocarcinoma

LUAD is one of the leading causes of cancer-related death both men and women in the United States. Approximately two million people are diagnosed with lung cancer each year (Torre et al., 2016). Berberine was predicted to have anti-LUAD potential ($q = 4.52 \times 10^{-10}$). Some previous *in vivo* and *in vitro* studies confirmed our prediction (Mitani et al., 2001; Zheng et al., 2014). Furthermore, berberine is currently being assessed as an anti-LUAD drug in clinical trials (NCT03486496). As shown in **Figure 7**, berberine interacts with 13 LUAD-related SMGs (e.g., matrix metalloproteinase-2), indicating the underlying MOAs of anti-LUAD of berberine. Matrix metalloproteinases (MMPs), one target displayed in our network, is the major protease of LUAD and is associated with tumor invasion and metastasis (Herbst et al., 2000). Study on human lung cancer cell line A549 confirmed that berberine inhibited invasion and growth of tumor cells through decreasing productions of matrix metalloproteinase-2 (MMP2) (Peng et al., 2006).

Bladder Carcinoma

BLCA is the most common cancer of the urinary system in the United States (Kaufman et al., 2009). In our network model, berberine is predicted to have a significant relationship with

TABLE 2 | Relevant literature evidences of the 18 predicted cancer indications of berberine.

Cancer type	*P*-value (Fisher test)	Adj-*P*	Negative logarithmic	PMID
HCC	5.63E−20	1.35E−18	17.87	26081696|25496992|24942805
LUAD	4.52E−10	1.08E−08	7.96	24766860|26672764|26503561
BLCA	4.92E−10	1.18E−08	7.93	21545798|23065570|10418949
CM	5.12E−10	1.23E−08	7.91	N/A
HNSCC	3.03E−09	7.27E−08	7.14	26503508
SQCC	1.82E−07	4.37E−06	5.36	N/A
EC	2.18E−07	5.23E−06	5.28	28465635|26667771|21858113
UCEC	3.03E−07	7.27E−06	5.14	N/A
PRAD	4.77E−07	1.15E−05	4.94	16505103|26698234|25572870
BRCA	5.53E−07	1.33E−05	4.88	29143794|29414799|28926092
CCSK	9.58E−07	2.30E−05	4.64	N/A
CLL	2.28E−05	5.47E−04	3.26	N/A
STAD	7.32E−05	1.76E−03	2.76	27142767|25837881|18468407
SCLC	2.22E−04	5.33E−03	2.27	N/A
NBL	5.36E−04	1.29E−02	1.89	27235712|19189664|19096576
LGG	6.95E−04	1.67E−02	1.78	N/A
CRAC	1.34E−03	3.21E−02	1.49	23604974|26463023|25954974
SOV	1.40E−03	3.36E−02	1.47	N/A

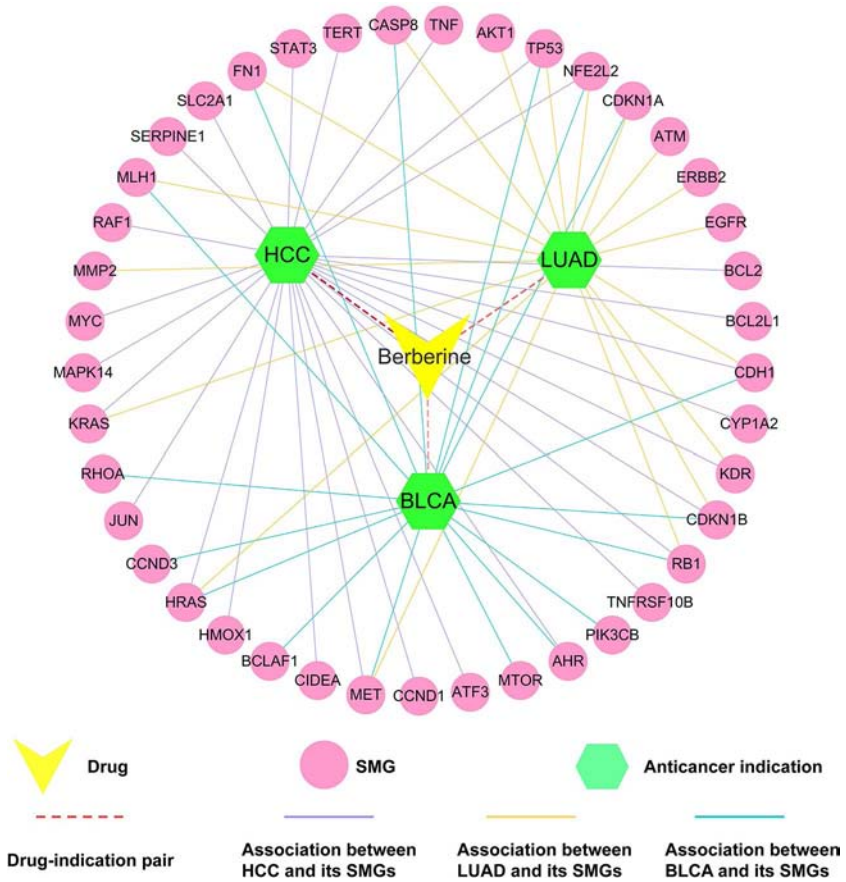

FIGURE 7 | Drug–target–disease (D-T-D) network of berberine on hepatocarcinoma (HCC), lung adenocarcinoma (LUAD), and bladder carcinoma (BLCA). The thickness of the red dotted line represents the predicted association between berberine and three types of tumors.

BLCA ($q = 4.92 \times 10^{-10}$). Meanwhile, our network indicated that berberine interacts with 17 BLCA-related SMGs (e.g., HRAS). According to previous study, the oncogenic ras genes GTPase HRas (HRAS) mutations, endogenously expressed in T24 bladder cancer cell line, were associated with grades and stages of BLCA detected in more than 35% of patients (Buyru et al., 2003). Berberine inhibited cell proliferation and induced cell cycle arrest and apoptosis in BLCA by inhibiting oncogenic H-Ras pathway in BIU-87 and T24 cell lines (Yan et al., 2011).

Taken together, these three case studies against different cancer types (HCC, LUAD, and BLCA) indicate that systems pharmacology approach applied in this study is an effective method for exploring molecular mechanisms of anti-cancer effect of berberine. Meanwhile, the newly predicted tumor types might be promising to further investigate MOAs of berberine.

CONCLUSION

Berberine had been observed to exert multiple biological and pharmacological activities with potential benefits to a variety of complex diseases, including cancer. In this study, we proposed an integrated systems pharmacology infrastructure to identify cancer indications of berberine and explore the underlying molecular mechanisms. This work explores the following new anti-cancer characteristics of berberine: i) Through literature mining, we summarize eight mechanisms of anti-cancer effect of berberine; ii) global drug–target network of berberine is constructed by integrating large-scale experimentally reported targets and computationally predicted targets. Mechanisms of action (MOAs) of various anti-cancer effects of berberine are discussed through current drug–target network; iii) a statistical model is developed to prioritize novel cancer indications of berberine through integrating target profiles of berberine and significantly mutated genes in cancer.

Yet several limitations of our approach should be acknowledged. First, although we have integrated a wide range of DTIs from published literatures and publicly available databases, the incompleteness of current drug–target networks may still exist. Recent studies proved that integration of large-scale gene expression profiles of natural products may help to improve the performance of drug–target network model (Yamanishi et al., 2010; Cheng et al., 2012). Second, as it is extremely difficult to obtain information on the active sites of berberine and mutated domain of proteins from

public sources, the current study could not explain the MOAs from a microcosmic point of view. Third, experimental assays should be performed to further validate the predicted targets and MOAs of anti-cancer effects of berberine in the future.

In summary, the systems pharmacology framework in this study has provided potential strategies to discover the polypharmacology effects of berberine for the prevention and treatment towards multiple cancers.

AUTHOR CONTRIBUTIONS

JF and YZ provided the concept and designed the study. PG and CC conducted the experiments and wrote the manuscript. XW, JZ, XF, QWu, YH, WZ, WH, and FZ participated in the experiments. JF and QWa contributed to revision and proofreading of the manuscript. All authors read and approved the final manuscript.

FUNDING

This work was supported by the National Natural Science Foundation of China (Grants 81603318), the youth scientific research training project of GZUCM (2019QNPY05), Research Fund for Characteristic Innovation Projects of Guangdong Province (2016KTSCX013), and Open Tending Project for the Construction of High-Level University (A1-AFD018171Z11027; A1-AFD018171Z11029).

SUPPLEMENTARY MATERIAL

The Supplementary Material for this article can be found online at: https://www.frontiersin.org/articles/10.3389/fphar.2019.00857/full#supplementary-material

REFERENCES

Ayati, S. H., Fazeli, B., Momtazi-Borojeni, A. A., Afg, C., Pirro, M., and Sahebkar, A. (2017). Regulatory effects of berberine on microRNome in cancer and other conditions. *Crit. Rev. Oncol. Hematol.* 116, 147–158. doi: 10.1016/j.critrevonc.2017.05.008

Bento, A. P., Gaulton, A., Hersey, A., Bellis, L. J., Chambers, J., Davies, M., et al. (2014). The ChEMBL bioactivity database: an update. *Nucleic Acids Res.* 42, 1083–1090. doi: 10.1093/nar/gkt1031

Buyru, N., Tigli, H., Ozcan, F., and Dalay, N. (2003). Ras oncogene mutations in urine sediments of patients with bladder cancer. *J. Biochem. Mol. Biol.* 36, 399–402. doi: 10.5483/BMBRep.2003.36.4.399

Benjamini, Y., and Yekutieli, D. (2001). The control of the false discovery rate in multiple testing under dependency. *Ann. Stat.* 29, 1165–1188. doi: 10.1214/aos/1013699998

Chen, Z. Z. (2016). Berberine induced apoptosis of human osteosarcoma cells by inhibiting phosphoinositide 3 kinase/protein kinase B (PI3K/Akt) signal pathway activation. *Iran. J. Public Health* 45, 578–585.

Cheng, F., Liu, C., Jiang, J., Lu, W., Li, W., Liu, G., et al. (2012). Prediction of drug–target interactions and drug repositioning *via* network-based inference. *PLoS Comput. Biol.* 8, e1002503. doi: 10.1371/journal.pcbi.1002503

Cheng, F., Zhao, J., Fooksa, M., and Zhao, Z. (2016). A network-based drug repositioning infrastructure for precision cancer medicine through targeting significantly mutated genes in the human cancer genomes. *J. Am. Med. Inform. Assoc.* 23, 681–691. doi: 10.1093/jamia/ocw007

Chidambara Murthy, K. N., Jayaprakasha, G. K., and Patil, B. S. (2012). The natural alkaloid berberine targets multiple pathways to induce cell death in cultured human colon cancer cells. *Eur. J. Pharmacol.* 688, 14–21. doi: 10.1016/j.ejphar.2012.05.004

Chu, S. C., Yu, C. C., Hsu, L. S., Chen, K. S., Su, M. Y., and Chen, P. N. (2014). Berberine reverses epithelial-to-mesenchymal transition and inhibits metastasis and tumor-induced angiogenesis in human cervical cancer cells. *Mol. Pharmacol.* 86, 609–623. doi: 10.1124/mol.114.094037

Chuang, T. Y., Wu, H. L., Min, J., Diamond, M., Azziz, R., and Chen, Y. H. (2017). Berberine regulates the protein expression of multiple tumorigenesis-related genes in hepatocellular carcinoma cell lines. *Cancer Cell Int.* 17, 59. doi: 10.1186/s12935-017-0429-3

Coricovac, D., Dehelean, C., Moaca, E. A., Pinzaru, I., Bratu, T., Navolan, D., et al. (2018). Cutaneous melanoma—a long road from experimental models to clinical outcome: a review. *Int. J. Mol. Sci.* 19, E1566. doi: 10.3390/ijms19061566

Cusan, M., Mungo, G., De Marco Zompit, M., Segatto, I., Belletti, B., and Baldassarre, G. (2018). Landscape of CDKN1B mutations in luminal breast cancer and other hormone-driven human tumors. *Front. Endocrinol.* 9, 393. doi: 10.3389/fendo.2018.00393

Dennis, G., Sherman, B. T., Hosack, D. A., Yang, J., Gao, W., Lane, H. C., et al. (2003). DAVID: Database for Annotation, visualization, and Integrated Discovery. *Genome Biol.* 4, R60. doi: 10.1186/gb-2003-4-9-r60

Fan, Q. W., Cheng, C. K., Gustafson, W. C., Charron, E., Zipper, P., Wong, R. A., et al. (2013). EGFR phosphorylates tumor-derived EGFRvIII driving STAT3/5 and progression in glioblastoma. *Cancer Cell* 24, 438–449. doi: 10.1016/j.ccr.2013.09.004

Fang, J., Cai, C., Chai, Y., Zhou, J., Huang, Y., Gao, L., et al. (2019). Quantitative and systems pharmacology 4. Network-based analysis of drug pleiotropy on coronary artery disease. *Eur. J. Med. Chem.* 161, 192–204. doi: 10.1016/j.ejmech.2018.10.020

Fang, J., Cai, C., Wang, Q., Lin, P., Zhao, Z., and Cheng, F. (2017a). Systems pharmacology-based discovery of natural products for precision oncology through targeting cancer mutated genes. *CPT Pharmacometrics Syst. Pharmacol.* 6, 177–187. doi: 10.1002/psp4.12172

Fang, J., Gao, L., Ma, H., Wu, Q., Wu, T., Wu, J., et al. (2017b). Quantitative and systems pharmacology 3. Network-based identification of new targets for natural products enables potential uses in aging-associated disorders. *Front. Pharmacol.* 8, 747. doi: 10.3389/fphar.2017.00747

Fang, J., Liu, C., Wang, Q., Lin, P., and Cheng, F. (2018). In silico polypharmacology of natural products. *Brief. Bioinform.* 19, 1153–1171. doi: 10.1093/bib/bbx045

Fang, J., Wu, Z., Cai, C., Wang, Q., Tang, Y., and Cheng, F. (2017c). Quantitative and systems pharmacology. 1. In silico prediction of drug–target interaction of natural products to enable of new targeted cancer therapy. *J. Chem. Inf. Model.* 57, 2657–2671. doi: 10.1021/acs.jcim.7b00216

Gilson, M. K., Liu, T., Baitaluk, M., Nicola, G., Hwang, L., and Chong, J. (2016). BindingDB in 2015: a public database for medicinal chemistry, computational chemistry and systems pharmacology. *Nucleic Acids Res.* 44, D1045–D1053. doi: 10.1093/nar/gkv1072

Hamsa, T. P., and Kuttan, G. (2012). Antiangiogenic activity of berberine is mediated through the downregulation of hypoxia-inducible factor-1, VEGF, and proinflammatory mediators. *Drug Chem. Toxicol.* 35, 57–70. doi: 10.3109/01480545.2011.589437

Herbst, R. S., Yano, S., Kuniyasu, H., Khuri, F. R., Bucana, C. D., Guo, F., et al. (2000). Differential expression of E-cadherin and type IV collagenase genes predicts outcome in patients with stage I non-small cell lung carcinoma. *Clin. Cancer Res.* 6, 790–797. doi: 10.1159/000007270

Huang, Y., Fang, J., Lu, W., Wang, Z., Wang, Q., Hou, Y., et al. (2019). A systems pharmacology approach uncovers wogonoside as an angiogenesis inhibitor of triple-negative breast cancer by targeting hedgehog signaling. *Cell Chem. Biol.* 26, 1–16. doi: 10.1016/j.chembiol.2019.05.004

Huang, Z. H., Zheng, H. F., Wang, W. L., Wang, Y., Zhong, L. F., Wu, J. L., et al. (2015). Berberine targets epidermal growth factor receptor signaling to suppress prostate cancer proliferation *in vitro*. *Mol. Med. Rep.* 11, 2125–2128. doi: 10.3892/mmr.2014.2929

Hur, J. M., Hyun, M. S., Lim, S. Y., Lee, W. Y., and Kim, D. (2010). The combination of berberine and irradiation enhances anti-cancer effects *via* activation of p38 MAPK pathway and ROS generation in human hepatoma cells. *J. Cell. Biochem.* 107, 955–964. doi: 10.1002/jcb.22198

Jemal, A., Siegel, R., Xu, J., and Ward, E. (2010). Cancer statistics, 2010. *CA Cancer J. Clin.* 60, 277–300. doi: 10.3322/caac.20073

Jiang, X., Lu, W., Shen, X., Wang, Q., Lv, J., Liu, M., et al. (2018). Repurposing sertraline sensitizes non-small cell lung cancer cells to erlotinib by inducing autophagy. *JCI Insight* 3, 98921. doi: 10.1172/jci.insight.98921

Jiang, Y., Huang, K., Lin, X., Chen, Q., Lin, S., Feng, X., et al. (2017). Berberine attenuates NLRP3 inflammasome activation in macrophages to reduce the secretion of interleukin-1β. *Ann. Clin. Lab. Sci.* 47, 720–728.

Jie, S., Li, H., Tian, Y., Guo, D., Zhu, J., Gao, S., et al. (2011). Berberine inhibits angiogenic potential of Hep G2 cell line through VEGF down-regulation *in vitro*. *J. Gastroenterol Hepatol.* 26, 179–185. doi: 10.1111/j.1440-1746.2010.06389.x

Kaufman, D. S., Shipley, W. U., and Feldman, A. S. (2009). Bladder cancer. *Lancet* 374, 239–249. doi: 10.1016/S0140-6736(09)60491-8

Khalid, E. B., Ayman, E. K., Rahman, H., Abdelkarim, G., and Najda, A. (2016). Natural products against cancer angiogenesis. *Tumour Biol.* 37, 1–24. doi: 10.1007/s13277-016-5364-8

Kim, J. B., Lee, K. M., Ko, E., Han, W., Lee, J. E., Shin, I., et al. (2008). Berberine inhibits growth of the breast cancer cell lines MCF-7 and MDA-MB-231. *Planta Med.* 74, 39–42. doi: 10.1055/s-2007-993779

Kim, J. S., Oh, D., Yim, M. J., Park, J. J., Kang, K. R., Cho, I. A., et al. (2015). Berberine induces FasL-related apoptosis through p38 activation in KB human oral cancer cells. *Oncol. Rep.* 33, 1775–1782. doi: 10.3892/or.2015.3768

Kim, S., Han, J., Kim, N. Y., Lee, S. K., Cho, D. H., Choi, M. Y., et al. (2012). Effect of berberine on p53 expression by TPA in breast cancer cells. *Oncol. Rep.* 27, 210–215. doi: 10.3892/or.2011.1480

Kotoku, N., Arai, M., and Kobayashi, M. (2016). Search for anti-angiogenic substances from natural sources. *Chem. Pharm. Bull.* 64, 128–134. doi: 10.1248/cpb.c15-00744

Kuhn, M., Szklarczyk, D., Pletscher-Frankild, S., Blicher, T. H., von Mering, C., Jensen, L. J., et al. (2014). STITCH 4: integration of protein-chemical interactions with user data. *Nucleic Acids Res.* 42, D401–D407. doi: 10.1093/nar/gkt1207

Kuo, H. P., Chuang, T. C., Yeh, M. H., Hsu, S. C., Way, T. D., Chen, P. Y., et al. (2011). Growth suppression of HER2-overexpressing breast cancer cells by berberine *via* modulation of the HER2/PI3K/Akt signaling pathway. *J. Agric. Food Chem.* 59, 8216–8224. doi: 10.1021/jf2012584

Li, J., Li, O., Kan, M., Zhang, M., Shao, D., Pan, Y., et al. (2015). Berberine induces apoptosis by suppressing the arachidonic acid metabolic pathway in hepatocellular carcinoma. *Mol. Med. Rep.* 12, 4572–4577. doi: 10.3892/mmr.2015.3926

Li, Z., Geng, Y. N., Jiang, J. D., and Kong, W. J. (2014). Antioxidant and anti-inflammatory activities of berberine in the treatment of diabetes mellitus. *Evid. Based Complement. Alternat. Med.* 2014, 289264. doi: 10.1155/2014/289264

Liu, B., Wang, G., Yang, J., Pan, X., Yang, Z., and Zang, L. (2011). Berberine inhibits human hepatoma cell invasion without cytotoxicity in healthy hepatocytes. *PLoS One* 6, e21416. doi: 10.1371/journal.pone.0021416

López-Cortés, A., Leone, P. E., Freire-Paspuel, B., Arcos-Villacís, N., Guevara-Ramírez, P., Rosales, F., et al. (2018). Mutational analysis of oncogenic AKT1 gene associated with breast cancer risk in the high altitude ecuadorian mestizo population. *Biomed. Res. Int.* 2018, 1–10. doi: 10.1155/2018/7463832

Lu, B., Hu, M., Liu, K., and Peng, J. (2010). Cytotoxicity of berberine on human cervical carcinoma HeLa cells through mitochondria, death receptor and MAPK pathways, and in-silico drug–target prediction. *Toxicol. In Vitro* 24, 1482–1490. doi: 10.1016/j.tiv.2010.07.017

Mitani, N., Murakami, K., Yamaura, T., Ikeda, T., and Saiki, I. (2001). Inhibitory effect of berberine on the mediastinal lymph node metastasis produced by orthotopic implantation of Lewis lung carcinoma. *Cancer Lett.* 165, 35–42. doi: 10.1016/S0304-3835(00)00710-2

Okubo, S., Uto, T., Goto, A., Tanaka, H., Nishioku, T., Yamada, K., et al. (2017). Berberine induces apoptotic cell death *via* activation of caspase-3 and -8 in HL-60 human leukemia cells: nuclear localization and structure–activity relationships. *Am. J. Chin. Med.* 45, 1497–1511. doi: 10.1142/S0192415X17500811

Ola, M. S., Nawaz, M., and Ahsan, H. (2011). Role of Bcl-2 family proteins and caspases in the regulation of apoptosis. *Mol. Cell Biochem.* 351, 41–58. doi: 10.1007/s11010-010-0709-x

Pan, Y., Zhang, F., Zhao, Y., Shao, D., Zheng, X., Chen, Y., et al. (2017). Berberine enhances chemosensitivity and induces apoptosis through dose-orchestrated AMPK signaling in breast cancer. *J. Cancer* 8, 1679–1689. doi: 10.7150/jca.19106

Patil, J. B., Kim, J., and Jayaprakashaa, G. K. (2010). Berberine induces apoptosis in breast cancer cells (MCF-7) through mitochondrial-dependent pathway. *Eur. J. Pharmacol.* 645, 70–78. doi: 10.1016/j.ejphar.2010.07.037

Peng, P. L., Hsieh, Y. S., Wang, C. J., Hsu, J. L., and Chou, F. P. (2006). Inhibitory effect of berberine on the invasion of human lung cancer cells *via* decreased productions of urokinase-plasminogen activator and matrix metalloproteinase-2. *Toxicol. Appl. Pharmacol.* 214, 8–15. doi: 10.1016/j.taap.2005.11.010

Puthdee, N., Seubwai, W., Vaeteewoottacharn, K., Boonmars, T., Cha'On, U., Phoomak, C., et al. (2017). Berberine induces cell cycle arrest in cholangiocarcinoma cell lines *via* inhibition of NF-κB and STAT3 pathways. *Biol. Pharm. Bull.* 40, 751–757. doi: 10.1248/bpb.b16-00428

Qing, Y., Hu, H., Liu, Y., Feng, T., Meng, W., Jiang, L., et al. (2014). Berberine induces apoptosis in human multiple myeloma cell line U266 through hypomethylation of p53 promoter. *Cell Biol. Int.* 38, 563–570. doi: 10.1002/cbin.10206

Shannon, P., Markiel, A., Ozier, O., Baliga, N. S., Wang, J. T., Ramage, D., et al. (2003). Cytoscape: a software environment for integrated models of biomolecular interaction networks. *Genome Res.* 13, 2498–2504. doi: 10.1101/gr.1239303

Song, Y. C., Lee, Y., Kim, H. M., Hyun, M. Y., Lim, Y. Y., Song, K. Y., et al. (2015). Berberine regulates melanin synthesis by activating PI3K/AKT, ERK and GSK3β in B16F10 melanoma cells. *Int. J. Mol. Med.* 35, 1011–1016. doi: 10.3892/ijmm.2015.2113

Sun, X., Wang, S. C., Wei, Y., Luo, X., Jia, Y., Li, L., et al. (2017). Arid1a has context-dependent oncogenic and tumor suppressor functions in liver cancer. *Cancer Cell* 33, 151–152. doi: 10.1016/j.ccell.2017.12.011

Tan, W., Li, N., Tan, R., Zhong, Z., Suo, Z., Yang, X., et al. (2015). Berberine interfered with breast cancer cells metabolism, balancing energy homeostasis. *Anticancer Agents Med. Chem.* 15, 66–78. doi: 10.2174/1871520614664140910120518

Tang, F., Wang, D., Duan, C., Huang, D., Wu, Y., Chen, Y., et al. (2009). Berberine inhibits metastasis of nasopharyngeal carcinoma 5-8F cells by targeting Rho kinase-mediated Ezrin phosphorylation at threonine 567. *J. Biol. Chem.* 284, 27456–27466. doi: 10.1074/jbc.M109.033795

Tsang, C. M., Cheung, Y. C., Lui, V. W., Yip, Y. L., Zhang, G., Lin, V. W., et al. (2013). Berberine suppresses tumorigenicity and growth of nasopharyngeal carcinoma cells by inhibiting STAT3 activation induced by tumor associated fibroblasts. *BMC Cancer* 13, 619. doi: 10.1186/1471-2407-13-619

Torre, L. A., Siegel, R. L., and Jemal, A. (2016). Lung cancer statistics. *Adv. Exp. Med. Biol.* 893, 1–19. doi: 10.1007/978-3-319-24223-1

Wang, J., Yang, S., Cai, X., Dong, J., Chen, Z., Wang, R., et al. (2016). Berberine inhibits EGFR signaling and enhances the antitumor effects of EGFR inhibitors in gastric cancer. *Oncotarget* 7, 76076–76086. doi: 10.18632/oncotarget.12589

Wang, L., Cao, H., Lu, N., Liu, L., Wang, B., Hu, T., et al. (2013). Berberine inhibits proliferation and down-regulates epidermal growth factor receptor through activation of Cbl in colon tumor cells. *PLoS One* 8, e56666. doi: 10.1371/journal.pone.0056666

Wang, N., Feng, Y., Zhu, M., Tsang, C. M., Man, K., Tong, Y., et al. (2010). Berberine induces autophagic cell death and mitochondrial apoptosis in liver cancer cells: the cellular mechanism. *J. Cell. Biochem.* 111, 1426–1436. doi: 10.1002/jcb.22869

Wang, N., Zhu, M., Wang, X., Tan, H. Y., Tsao, S. W., and Feng, Y. (2014). Berberine-induced tumor suppressor p53 up-regulation gets involved in the regulatory network of MIR-23a in hepatocellular carcinoma. *Biochim. Biophys. Acta.* 1839, 849–857. doi: 10.1016/j.bbagrm.2014.05.027

Wilson, J. R. F., Bateman, A. C., Hanson, H., An, Q., Evans, G., Rahman, N., et al. (2010). A novel HER2-positive breast cancer phenotype arising from germline TP53 mutations. *J. Med. Genet.* 47, 771–774. doi: 10.1136/jmg.2010.078113

Wu, Z., Cheng, F., Li, J., Li, W., Liu, G., and Tang, Y. (2017). SDTNBI: an integrated network and chemoinformatics tool for systematic prediction of drug–target interactions and drug repositioning. *Brief. Bioinform.* 18, 333–347. doi: 10.1093/bib/bbw012

Wu, Z., Lu, W., Wu, D., Luo, A., Bian, H., Li, J., et al. (2016). In silico prediction of chemical mechanism-of-action *via* an improved network-based inference method. *Br. J. Pharmacol.* 173, 3372–3385. doi: 10.1111/bph.13629

Xiong, Y. X., Su, H. F., Lv, P., Ma, Y., Wang, S. K., Miao, H., et al. (2015). A newly identified berberine derivative induces cancer cell senescence by stabilizing endogenous G-quadruplexes and sparking a DNA damage response at the telomere region. *Oncotarget* 6, 35625–35635. doi: 10.18632/oncotarget

Yamaguchi, R., Lartigue, L., and Perkins, G. (2019). Targeting Mcl-1 and other Bcl-2 family member proteins in cancer therapy. *Pharmacol. Ther.* 195, 13–20. doi: 10.1016/j.pharmthera.2018.10.009.

Yamanishi, Y., Kotera, M., Kanehisa, M., and Goto, S. (2010). Drug–target interaction prediction from chemical, genomic and pharmacological data in an integrated framework. *Bioinformatics* 26, i246–i254. doi: 10.1093/bioinformatics/btq176

Yan, K., Zhang, C., Feng, J., Hou, L., Yan, L., Zhou, Z., et al. (2011). Induction of G1 cell cycle arrest and apoptosis by berberine in bladder cancer cells. *Eur. J. Pharmacol.* 661, 1–7. doi: 10.1016/j.ejphar.2011.04.021

Yap, C. W. (2011). PaDEL-descriptor: an open source software to calculate molecular descriptors and fingerprints. *J. Comput. Chem.* 32, 1466–1474. doi: 10.1002/jcc.21707

Ye, H., Ye, L., Kang, H., Zhang, D., Tao, L., Tang, K., et al. (2011). HIT: linking herbal active ingredients to targets. *Nucleic Acids Res.* 39, D1055–D1059. doi: 10.1093/nar/gkq1165

Yu, H., Lee, H., Herrmann, A., Buettner, R., and Jove, R. (2014). Revisiting STAT3 signalling in cancer: new and unexpected biological functions. *Nat. Rev. Cancer.* 14, 736–746. doi: 10.1038/nrc3818

Zhao, Y., Jing, Z., Lv, J., Zhang, Z., Lin, J., Cao, X., et al. (2017). Berberine activates caspase-9/cytochrome *c*-mediated apoptosis to suppress triple-negative breast cancer cells *in vitro* and in *vivo*. *Biomed. Pharmacother.* 95, 18–24. doi: 10.1016/j.biopha.2017.08.045

Zhe, W., and Huang, G. S. (2002). Database resources of the National Center for Biotechnology Information and its application. *Chin. Bull. Life Sci.* 14, 59–62. doi: 10.1007/BF02943277

Zheng, F., Tang, Q., Wu, J. J., Zhao, S. Y., Liang, Z. Y., Li, L., et al. (2014). p38α MAPK-mediated induction and interaction of FOXO3a and p53 contribute to the inhibited-growth and induced-apoptosis of human lung adenocarcinoma cells by berberine. *J. Exp. Clin. Cancer Res.* 33, 36. doi: 10.1186/1756-9966-33-36

Zhu, R. X., Seto, W. K., Lai, C. L., and Yuen, M. F. (2016). Epidemiology of hepatocellular carcinoma in the Asia-Pacific region. *Gut. Liver.* 10, 332–339. doi: 10.5009/gnl15257

Conflict of Interest Statement: The authors declare that the research was conducted in the absence of any commercial or financial relationships that could be construed as a potential conflict of interest.

frontiers in Oncology

ORIGINAL RESEARCH
published: 08 November 2019
doi: 10.3389/fonc.2019.01100

A High-Content Screening Approach to Identify MicroRNAs Against Head and Neck Cancer Cell Survival and EMT in an Inflammatory Microenvironment

Bruno Sangiorgi[1,2], Felipe Canto de Souza[1,2], Ildercílio Mota de Souza Lima[1,2], Josiane Lilian dos Santos Schiavinato[1,2], Amanda Cristina Corveloni[1,2], Carolina Hassibe Thomé[1,3], Wilson Araújo Silva Jr.[1,2], Vitor Marcel Faça[1,3], Dimas Tadeu Covas[1], Marco Antônio Zago[1] and Rodrigo Alexandre Panepucci[1,2]

[1] Center for Cell-Based Therapy (CTC), Regional Blood Center of Ribeirão Preto, Ribeirão Preto, Brazil, [2] Department of Genetics and Internal Medicine, Ribeirão Preto Medical School, University of São Paulo (FMRP-USP), Ribeirão Preto, Brazil, [3] Department of Biochemistry and Immunology, Ribeirão Preto Medical School, University of São Paulo (FMRP-USP), Ribeirão Preto, Brazil

Head and neck squamous cell carcinoma (HNSCC) is among the most common cancer types. Metastasis, the main cause of death by cancer, can be promoted by an inflammatory microenvironment, which induces epithelial-mesenchymal transition (EMT) through a NF-κB-mediated stabilization of Snail. Here, we aimed to explore how microRNAs (miRs) can affect cell survival and EMT in HNSCC cells under an inflammatory microenvironment. By using a high-content screening (HCS) approach, we evaluated alterations in morphometric parameters, as well as expression/localization of Snail/Slug, in HNSCC cells primed with TNF-α. Based on those quantitation, we established the optimal experimental conditions of EMT induction driven by TNF-α. Those conditions were applied to cells transfected with distinct miRs ($N = 31$), followed by clusterization of miRs based on alterations related to cell survival and EMT. The signaling pathways enriched with molecular targets from each group of miRs were identified by *in silico* analyses. Finally, cells were transfected with siRNAs against signaling pathways targeted by miRs with anti-survival/EMT effect and evaluated for alterations in cell survival and EMT. Overall, we observed that TNF-α, at 20 ng/ml, induced EMT-related changes in cell morphology, Snail/Slug expression, and cell migration. Predicted targets of miRs with anti-survival/EMT effect were enriched with targets of NF-κB, PI3K/ATK, and Wnt/beta catenin pathways. Strikingly, individual gene silencing of elements from those pathways, namely *RELA* (NF-kB), *AKT1* (PI3K/AKT), and *CTNNB1* (Wnt/beta catenin) reduced cell survival and/or expression of Snail/Slug in cells stimulated with TNF-α. As a whole, our HCS approach allowed for the identification of miRs capable of inhibiting cell survival

OPEN ACCESS

Edited by:
Zhe-Sheng Chen,
St. John's University, United States

Reviewed by:
Paul B. Fisher,
Virginia Commonwealth University, United States
Weiguo Feng,
Weifang Medical University, China

***Correspondence:**
Rodrigo Alexandre Panepucci
panepucci@hemocentro.fmrp.usp.br

Specialty section:
This article was submitted to Cancer Molecular Targets and Therapeutics, a section of the journal Frontiers in Oncology

Received: *08 December 2018*
Accepted: *07 October 2019*
Published: *08 November 2019*

Citation:
Sangiorgi B, de Souza FC, Mota de Souza Lima I, dos Santos Schiavinato JL, Corveloni AC, Thomé CH, Araújo Silva W Jr, Faça VM, Covas DT, Zago MA and Panepucci RA (2019) A High-Content Screening Approach to Identify MicroRNAs Against Head and Neck Cancer Cell Survival and EMT in an Inflammatory Microenvironment. Front. Oncol. 9:1100. doi: 10.3389/fonc.2019.01100

and EMT considering the presence of an inflammatory microenvironment, also indicating the common signaling pathways and molecular targets most likely to underlie those alterations. These findings may contribute to the development of targeted therapies against HNSCC.

Keywords: head and neck squamous cell carcinoma, high-content screening, microRNAs, epithelial-mesenchymal-transition, inflammation, NF-κB

INTRODUCTION

Head and neck squamous cell carcinoma (HNSCC) comprises a group of upper aerodigestive tract neoplasia and is among the ten types of cancer with the highest incidence and mortality in the world (1). Over the past decades, despite advances in treatment strategies of HNSCC, it was observed a growth in mortality associated with distant metastases (2). Studies to date demonstrated that metastasis initiation is promoted by tumor cells that undergoes epithelial-mesenchymal transition (EMT), a transformation process which cells acquire a mesenchymal-like phenotype and dislodges from the tumor bulk, invading adjacent vessels and entering in the circulation (3).

EMT events are coordinated by transcription factors known as "EMT master regulators," including members of the Snail family: SNAI1 (Snail) and SNAI2 (Slug), which are capable of both silencing and promoting the expression of genes related to epithelial and mesenchymal phenotypes, respectively (4). As a consequence of the "EMT master regulators" activity, cancer cells undergo drastic phenotypic changes in cell morphology: from polygonal to elongated, expression of cell adhesion proteins: downregulation of E-Cadherin and upregulation of N-Cadherin and integrins, expression of structural proteins: upregulation of Vimentin, among others that lead to the formation of mesenchymal cancer cells with migratory/invasive capacities (5).

Increasing literature data have established that, for several types of cancer including HNSCC, the presence of an inflamed tumor microenvironment is associated with tumor progression, the acquisition of EMT-like features by cancer cells and the formation of metastasis (6). In different types of cancer, multiple lines of evidence have supported that inflammatory cytokines secreted by tumor-associated macrophages (which can represent half of the tumor mass), including tumor necrosis factor alpha (TNF-α), are capable of inducing EMT events in cancer cells (7). TNF-α activates the nuclear factor kappa b (NF-κB) signaling pathway, which the main effector p50/p65 (RelA) promotes the nuclear translocation of Snail, thereby inducing EMT (8). Additionally, NF-κB crosstalk with other oncogenic signaling pathways in HNSCC including Ras/MAPK, PI3K/AKT, and Wnt/beta catenin, that collectively promotes cancer cell survival, evasion from apoptosis and therapy resistance (9, 10). Due to the complexity of intracellular signaling pathways and tumor microenvironment in cancer, including HNSCC, a multi-target therapy (targeting multiple signaling pathways) may be an interesting therapeutic approach (11).

MicroRNAs (miRs) are a class of small non-coding RNAs that act predominantly through the destabilization and degradation of multiple targeted messenger RNAs (mRNAs) thereby affecting several biological processes independently (12, 13). In HNSCC, as in other types of cancer, there is mounting evidence that miRs are capable of interfering in multiple cellular processes, such as cancer cell proliferation, invasion, and apoptosis, thereby promoting (oncomiRs) or inhibiting (tumor suppressor miRs) the progression from normal tissue to carcinoma and subsequently metastasis (14, 15). Importantly, the HNSCC oncomiR: miR-21 and tumor suppressor miR: miR-29, are both involved in transcriptional networks that regulates the activity of the NF-κB signaling pathway (14, 16), highlighting the importance of NF-κB as a regulator of both inflammation and tumor progression in HNSCC.

Since its discovery, miRs have been drawing attention due to their capacity to be used either as prognostic biomarkers or in miR-based targeted therapies against cancer (17, 18). Currently, miR-based targeted therapeutic strategies comprehends the delivery of either mimetics of miRs with tumor suppressor activity (microRNA replacement or restoration therapy) or molecules capable of inactivating oncomiRs (microRNA reduction or inhibition therapy) (19). Importantly, a functional study conducted by Lindenbergh-van der Plas and coworkers provided a proof-of-concept that miRs can be used to selectively kill HNSCC cancer cells (20). However, despite the potential use of miRs in drug discovery and therapeutic applications, it is a current challenge to identify, among the several signaling pathways regulated by a given miR, those that has an effective therapeutic value (21).

In the last decade, advances in the High-Content Screening (HCS) approach (cell-based functional screens based on automated microscopy and image analysis) allowed for the quantitative measurement of a broad spectrum of phenotypic alterations at a cellular level (22). Noteworthy, the advantage of the HCS approach to measure the phenotype in a multiparametric fashion makes it especially suited to investigate the pleiotropic effects exerted by miRs (23). In addition, target-prediction tools can also be utilized for the identification of the molecular targets shared by groups of miRs and thereby indicating the ones that are most likely responsible for the observed effects (24). In the present work, through an HCS approach and *in-silico* analysis, we investigated the capacity of miRs to alter the phenotypic features related to tumor progression (e.g., cell survival) and metastasis (e.g., EMT) in HNSCC cells considering the presence of an inflammatory microenvironment. Overall, we have identified miRs capable of inhibiting cell survival and EMT as well as potential targets and signaling pathways involved in the observed effects.

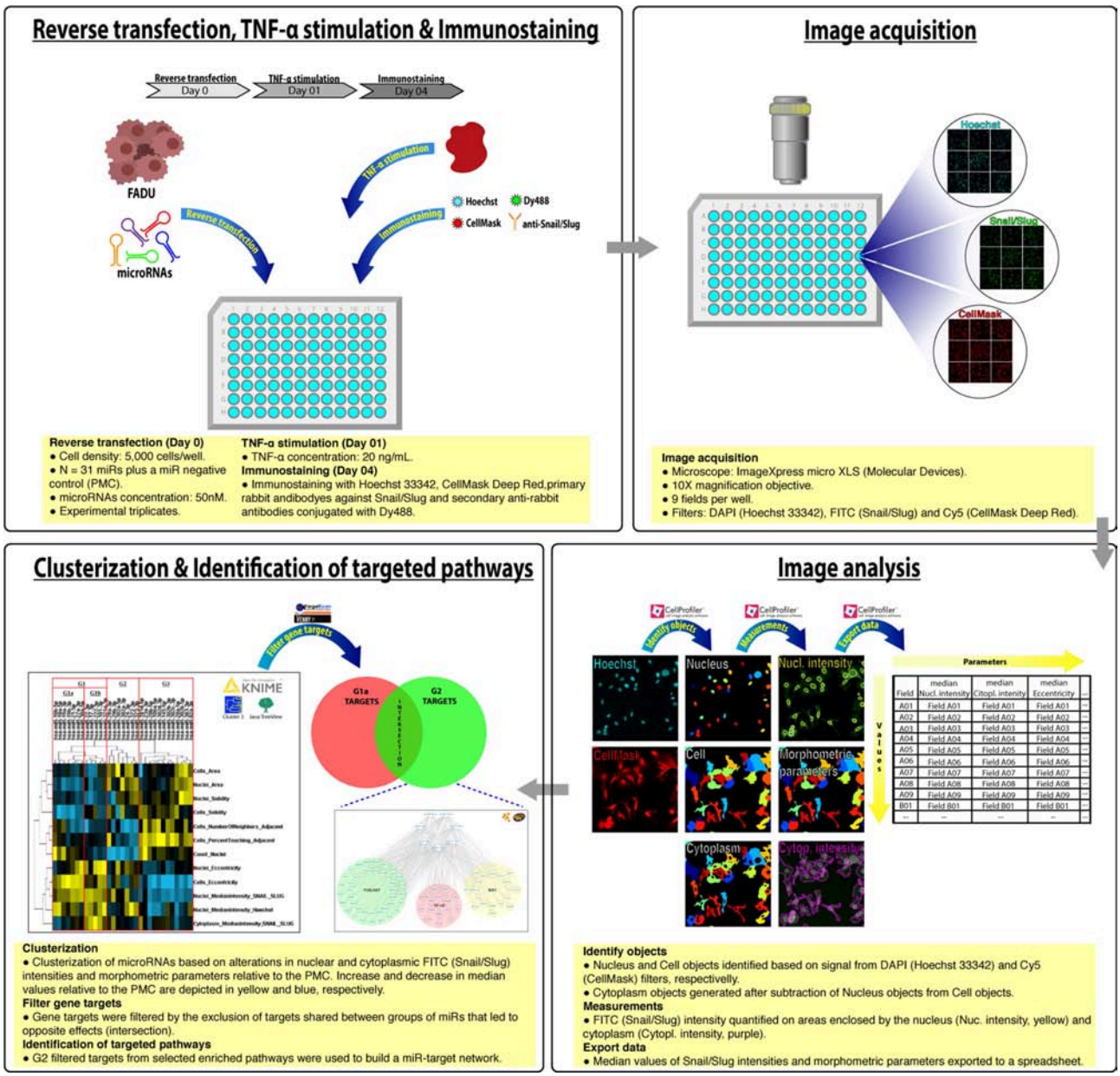

FIGURE 1 | Study design. Reverse transfection, TNF-α stimulation and Immunostaining: Cells from the FADU cell line were transfected (day 0) with microRNAs (N = 31), followed by stimulation with TNF-α (20 ng/mL, Day 01) and immunostaining with primary rabbit antibodies against Snail/Slug, secondary anti-rabbit antibodies conjugated with Dy488, nuclear (Hoechst) and cytoplasmic (CellMask) fluorescent dyes (Day 04). Image acquisition: Images (9 fields per well) were acquired using a 10X objective and excitation/emission filters DAPI (Hoechst), FITC (Snail/Slug), and Cy5 (CellMask), using an ImageXpress Micro XLS HCS system (Molecular Devices). Image analysis: Nuclei and corresponding cytoplasm objects were identified and segmented based on images from DAPI (Hoechst) and Cy5 (CellMask) channels, respectively. FITC (Snail/Slug) intensity on nuclei and cytoplasm, as well as morphometric parameters were then quantified. Median values per field were exported into a spreadsheet. Clusterization and Identification of targeted pathways: Based on alterations in median values per well relative to the PMC, microRNAs were subjected to an unsupervised hierarchical clustering. After the exclusion of genes commonly targeted by miRs from G1a (pro-survival/EMT) and G2 (anti-survival/EMT), genes from signaling pathways targeted by G2 miRs were used to generate a microRNA regulatory network.

MATERIALS AND METHODS

Study Design

The design of this study is illustrated in **Figure 1**. Cells from the FADU cell line were transfected (reverse transfection) into 96 well plates with miR mimetics (N = 31 plus a miR negative control) in experimental triplicates, followed by stimulation with TNF-α (20 ng/mL) for 72 h and immunostaining with primary rabbit antibodies against Snail/Slug, secondary anti-rabbit antibodies conjugated with Dy488, nuclear (Hoechst) and cytoplasmic (CellMask) fluorescent dyes. Images (nine fields per well) were acquired using a 10X objective and excitation/emission filters

DAPI (Hoechst), FITC (Snail/Slug), and Cy5 (CellMask), using an ImageXpress Micro XLS HCS system (Molecular Devices). With aid of CellProfiler, images from filters DAPI (Hoechst) and Cy5 (CellMask) were used to identify nuclear, cell and cytoplasm objects, followed by quantification of nuclear and cytoplasmic median FITC (Snail/Slug) intensity, as well as morphometric parameters. Median values per field were exported into spreadsheets and with help of KNIME software, we obtained the percentage change of the median values per well relative to the miR negative control (PMC). By using Cluster3 and Java TreeView software, we performed a unsupervised hierarchical clustering of miRs by which the four groups of miRs (G1a, G1b, G2, and G4) were identified. With help of KNIME and Targetscan software, we identified the genes targeted by most (N-2, minimum of 4) of the microRNAs in each group. With help of Venny online tool, genes targeted by groups that led to opposite phenotypic effects were identified and excluded from further analyses. With aid of Database for Annotation, Visualization and Integrated Discovery (DAVID, version 6.7) online tool, we identified signaling pathways enriched with filtered targets. With help of the Kyoto Encyclopedia of Genes and Genomes (KEGG) database, the filtered targets from G2 miRs were assigned to the NF-kB, PI3K/AKT, and Wnt/beta-catenin signaling pathways, which were used to generate a microRNA regulatory network with help of Cytoscape software. Based on information from those analyses, secondary functional assays using siRNAs were designed to evaluate the effect, in cell survival and EMT, of interferences in NF-kB, PI3K/AKT, and Wnt/beta-catenin signaling pathways.

Cell Lines

Cells derived from the HNSCC cell lines FADU (oropharynx), HN30 (pharynx), and UMSCC1 (floor of mouth) were cultured in Dulbecco's modified Eagle's medium (DMEM) supplemented with 10% fetal bovine serum (FBS), 50 U/mL penicillin and 50 μg/mL streptomycin. Cells were passaged by using a 10% trypsin solution.

Reagents

Throughout this work, cells were treated with TNF-α (300-01A, PrepoTech, USA) or mitomycin C (MMC, M4287, sigma-aldrich, USA). For immunostaining, we used the nuclear dye Hoechst 33342 (10 μg/mL; H1399, Thermo Scientific, USA) and cytoplasmic dye HCS CellMask Deep Red (5 μg/mL, H10294, Thermo Scientific, USA), primary antibodies: Anti-N-Cadherin mouse IgG2ab mAb (SC-271386, Santa Cruz Biotechnology, USA), Rabbit anti-Snail/Slug (ab180714, abcam, USA), Goat anti-Vimentin (sc-7558, Santa Cruz Biotechnology) and Mouse-anti-Caspase-7 (cleaved caspase-7 p10, clone h207, sc-22179, Santa Cruz Biotechnology, USA), as well as secondary antibodies: Goat anti-Rabbit DyLight 488 (dy488, 35553, Thermo Scientific, USA), Goat anti-Rabbit DyLight 594 (35561, Thermo Scientific, USA) DyLight 488 mouse (35503, Thermo Scientific, USA) and Donkey anti-Goat DyLight 594 (SA5-1088, Thermo Scientific, USA). For western blot, we used the antibodies rabbit anti-snail (#3879, Cell Signaling, USA), rabbit anti-slug (#9585, Cell Signaling, USA), rabbit anti-vimentin (#5741, Cell Signaling, USA), rabbit anti N-cadherin (#13116, Cell Signaling, USA), rabbit anti-β-catenin (#8480, Cell Signaling, USA) and mouse anti-β-actin (sc-81178, Santa Cruz, CA).

Western Blot

For protein extraction and quantification, cells were washed with PBS and disrupted in lyses buffer (20 mM Tris-HCl, 150 mM NaCl, 1 mM Na2EDTA, 1 mM EGTA, 1% Triton X-100, 2.5 mM sodium pyrophosphate, 1 mM β-glycerophosphate, 1 mM Na3VO4 and 1 μg/ml leupeptin). After three sonication cycles at 45 W for 5 min each in a sonicator bath, the samples were centrifuged at 20,000 × g for 30 min at 4°C. The protein concentration was determined by the Bradford method (Bio-Rad, Hercules, CA).

Proteins were submitted to SDS–PAGE and electrotransferred to PVDF membranes (GE Lifesciences, Pittsburgh, PA, USA). Membranes were blocked with 5% non-fat dry milk in 0.1% Tween-TBS and incubated with the primary antibody. After 1 h of incubation with horseradish peroxidase-conjugated goat anti-rabbit IgG (#7074, Cell Signaling) or horse anti-mouse IgG (#7076, Cell Signaling) secondary antibodies The antibody-protein complex was detected using ECL Western Blotting Detection Reagents (GE Lifesciences) using a CCD-Camera (Image QuantLAS 4000 mini, Uppsala, Sweden). Densitometric analysis was performed using the ImageJ software, and bands were normalized to the constitutive protein β-actin.

MicroRNA Mimics and siRNAs

Transfection assays were carried out with human microRNA mimetic molecules (50 nM, Thermo Scientific) or synthetic siRNA molecules (10 nM; **Supplementary File 1**).

Reverse Transfection

Reverse transfection assays were performed using lipofectamine LTX transfection reagent (15338100, Thermo Scientific) and synthetic miRs/siRNAs according to manufacturer's instructions. Transfection efficiency was calculated by evaluating the percentage reduction in cell numbers following transfection with a cytotoxic siRNA against Ubiquitin (siUBC) as compared to cells transfected with a control miR (PMC) or siRNA (siCTR).

Immunostaining

Cells were fixed and permeabilized with a 2% formaldehyde solution in methanol for 20 min at −20°C. Quenching of formaldehyde was achieved by incubation for 15 min with a 0.1 M glycine solution and blocking with a 1% FBS solution for 30 min. Afterwards, cells were incubated for 1 h at room temperature with primary antibodies, followed by incubation for 45 min with a solution containing secondary antibodies and nuclear/cytoplasmic dyes.

Image Analysis

Image analyses were performed with aid of MetaXpress software (Molecular Devices, USA) or CellProfiler (version 2.2.0, Broad Institute, USA). Briefly, images from functional assays that aimed to evaluate only the presence/absence of fluorescent dyes or markers were analyzed using MetaXpress software, whereas CellProfiler was used to analyze images from functional assays

aiming both the evaluation of morphometric parameters and the presence and subcellular localization of fluorescent markers. Data from image analyses were processed with the aid of KNIME software (version 3.2.0).

HCS-Based Functional Assays

Alterations in cell morphology and expression/localization of proteins were assessed through HCS-based functional assays, which comprises of:

i) MiR/siRNA reverse transfection of FADU cells into 96-well culture plates (CLS3603, Corning, USA);
ii) Stimulation or not with TNF-α, 24 h after reverse transfection;
iii) Immunostaining using antibodies, nuclear and cytoplasmic dyes;
iv) Image acquisition (9 fields per well) with aid of an ImageXpress® Micro XLS High-Content Screening (HCS) system (Molecular Devices, USA), using a 10X magnification objective and excitation/emission filters DAPI, FITC, Cy3, Texas Red, and Cy5;
v) Image analysis with aid of MetaXpress (Molecular Devices, USA) or CellProfiler (version 2.2.0, Broad Institute, USA) software.

Migration Assay

Cells were seeded on culture plates specific for migration assays Oris Pro Cell Migration Assay, 96 wells (PROCMA5, Platypus Technologies, USA). After 24 h, cells were treated with 0.2 μg/mL of mitomycin C for 2 h (to suppress proliferation), followed or not by incubation with TNF-a at 20 or 50 ng/mL for 72 h (experimental triplicates). Images were acquired using a 4X phase-contrast objective after cell seeding and at the endpoint using the ImageXpress HCS system. The area occupied by cells was quantified after cell seeding and at the endpoint, which were used to measure cell migration using $M = (Ae/As * 100)-100$, in which M = migration, Ae = Area occupied by cells at the endpoint, As = Area occupied by cells 24 h after seeding.

Clusterization of miRs

A unsupervised hierarchical clustering of miRs was performed with aid of Cluster 3 software (25) and visualized with help of Java TreeView software (26). Groups of miRs were classified as of pro/anti survival/EMT properties based on alterations in the following phenotypic parameters: "count nuclei (cell survival)," "cells eccentricity (EMT)," "Nuclei Median Intensity Snail/Slug (EMT)," and "Cytoplasm Median Intensity Snail/Slug (EMT)."

Identification of Genes and Signaling Pathways Targeted by Groups of miRs

Using the KNIME software (version 3.7) and TargetScan database of predicted miR targets (version 7.1) (27), we created a pipeline to identify the transcripts commonly targeted by most of the miRs contained in each of the identified groups (N-2, minimum of 4). Venn diagrams were generated using Venny 2.1 online tool (bioinfogp.cnb.csic.es/tools/venny) by comparing the identified targets from groups of miRs with opposite phenotypic effects, followed by the exclusion (filtering) of the shared targets. Afterwards, with help of the Database for Annotation, Visualization and Integrated Discovery (DAVID, version 6.7) (28), we identified signaling pathways that were enriched with the filtered targets from each group of miRs.

The filtered targets were assigned to their given signaling pathways according to information available on the Kyoto Encyclopedia of Genes and Genomes (KEGG) database about the following signaling pathways: NF-κB (hsa04064), PI3K/AKT (hsa04151), and Wnt (hsa04310) (29). The miRs and targets from the selected pathways were used to generate a microRNA regulatory network with aid of Cytoscape software (30).

Quantitative PCR (qPCR)

RNA extraction was performed using TRIZOL reagent (Invitrogen Life Technologies, Grand Island, NY, USA) and total RNA was reverse transcribed using the High Capacity cDNA Reverse Transcription Kit (Applied Biosystems, Foster City, CA, USA), according to the manufacturer's instructions. Gene expression qPCR reactions were carried in duplicates with Power SYBR Green Master Mix (Applied Biosystems) and primers for AKT2 (Forward: AAGGATGAAGTCGCTCACAC; Reverse: ACTCCATCACAAAGCACAGG), CCND1 (Forward: CCCGCACGATTTCATTGAAC; Reverse: GGCGGATTGGAAATGAACTTC), GAPDH (Forward: GAAGGTGAAGGTCGGAGTC; Reverse: GAAGATGGTGATGGGATTTC); IL6 (Forward: ATGCAATAACCACCCCTGAC; Reverse: GAGGTGCCCATGCTACATTT); MYC (Forward: CAGATCAGCAACAACCGAAA; Reverse: GGCCTTTTCATTGTTTTCCA) and RELA (Forward: TGACAAGGTGCAGAAAGAGG; Reverse: CACATCAGCTTGCGAAAAGG) using a CFX96 Real-Time PCR system (Bio-Rad). Relative gene expression levels were assessed using the $2^{-\Delta\Delta Ct}$ strategy (31).

Statistics

All statistical analyses were performed with aid of GraphPad Prism software version 5.0. Comparisons between multiple experimental conditions were performed using either unpaired *t*-test or univariate "ONE-WAY Anova" test. Statistical significance was considered at $p < 0.05$.

RESULTS

Stimulation With Tumor Necrosis Factor Alpha Leads to EMT-Related Morphometric Alterations

We performed an HCS-based functional assay in cells primed with TNF-α at different concentrations and time points followed by quantification of morphometric features. Stimulation for 48 h with TNF-α, at all concentrations used (5–50 ng/mL), reduced the percentage of intercellular contact by around 15% while not changing cell eccentricity (elongation). On this same endpoint, we found a trend for increase and decrease in cell area and number of neighboring cells, respectively, in a concentration-dependent manner, attaining significance at 20 and 50 ng/mL. On the other hand, stimulation for 72 h with all TNF-α concentrations used, led to a significant increase in cell

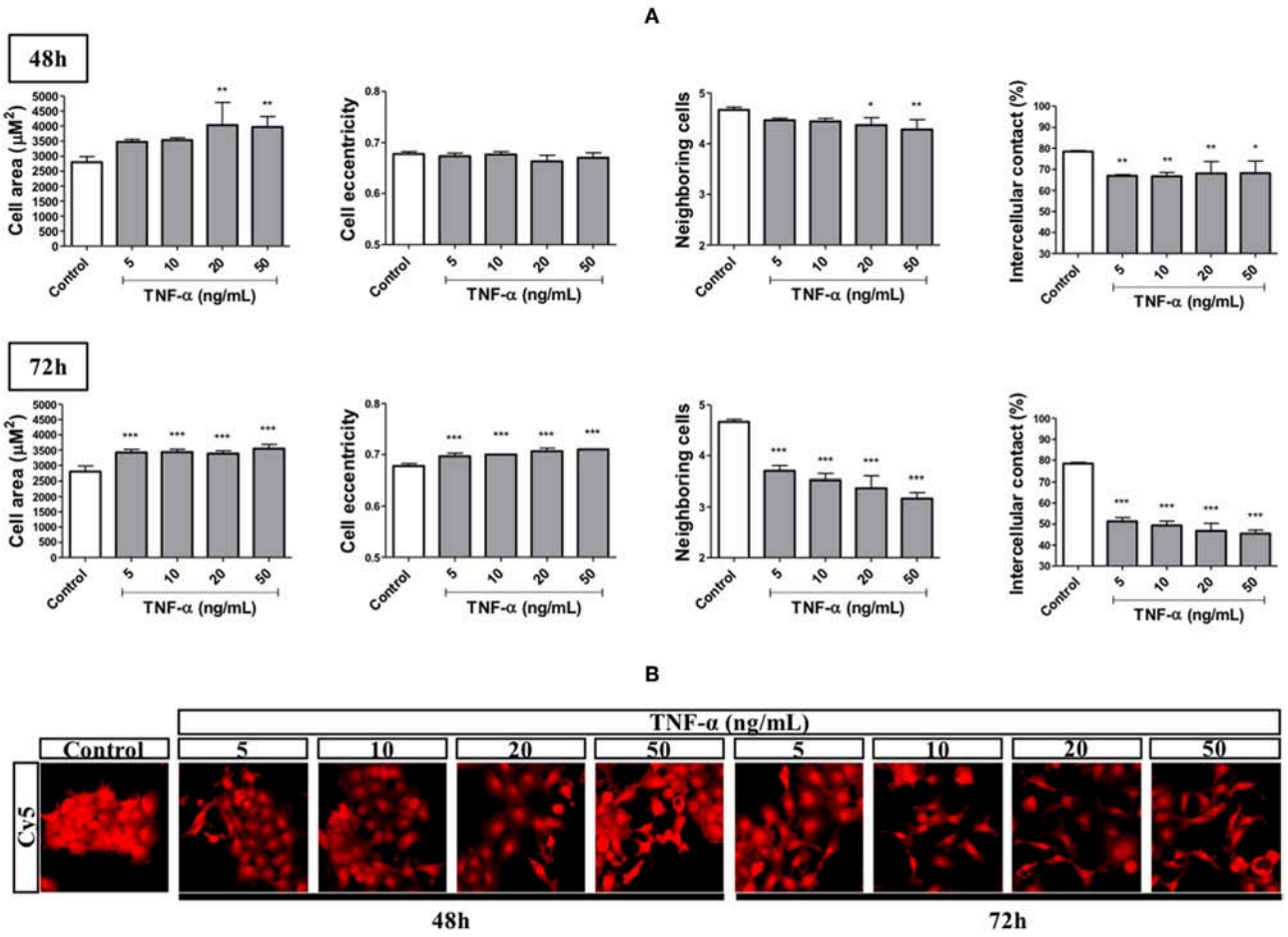

FIGURE 2 | Effects of TNF-α in EMT-related morphometric parameters. The FADU cell line was stimulated or not (Control) with TNF-α (5 to 50 ng/mL), for 48 or 72 h (squares). At the endpoint, the cells were stained with nuclear (Hoechst) and cytoplasmic (CellMask) fluorescent dyes. Images (nine fields per well) were acquired using a 10X objective and excitation/emission filters DAPI (Hoechst) and Cy5 (CellMask), using an ImageXpress Micro XLS HCS system (Molecular Devices). Images were analyzed using CellProfiler, in order to quantify the following parameters: cell area, cell eccentricity, number of neighboring cells and percentage of intercellular contact. **(A)** Quantitative changes (Mean +-SD) in morphometric parameters due to TNF-α stimulation for 48 and 72 h. **(B)** Representative images of cells stimulated with TNF-α for 48 and 72 h. Statistically significant differences (ONE-WAY Anova with Tukey post-test), in comparison to the control condition: $^{*}p < 0.05$; $^{**}p < 0.01$; $^{***}p < 0.001$.

area (around 1,000 μm^2) and cell eccentricity. These changes were accompanied by significant reductions in both the number of neighboring cells (by around 1.5) and the percentage of intercellular contact (by around 30%; **Figure 2**).

Stimulation With Tumor Necrosis Factor Alpha Leads to the Expression of EMT-Related Proteins

An HCS-based functional assay was done in cells primed with TNF-α for 72 h and at different concentrations, with further quantification of changes in the percentage of cells positive for markers of EMT. Generally, we observed that stimulation with TNF-α led to a concentration-dependent increase in the percentage of cells positive for all markers evaluated. More specifically, the higher concentration of 50 ng/mL led to a significant increase in the percentage of cells expressing N-Cadherin in the cytoplasm (from 30 to 50%, approximately). Moreover, the percentage of cells expressing cytoplasmic Vimentin significantly increased by 25% after treatment with TNF-α at 20 and 50 ng/mL. Finally, the percentage of cells expressing Snail/Slug in the nucleus significantly increased at all concentrations of TNF-α, ranging from below 20% (in untreated cells) up to above 60% ate the highest TNF-α concentration.

By western blot, we observed that after 72 h of treatment with TNF-α at 20 ng/mL, the protein levels of Snail and N-Cadherin increased by 2.2- and 5.4- fold in comparison to the untreated control group, respectively. Moreover, the levels of Slug and Vimentin were increased by around 1.1-fold, whereas the protein level of beta-catenin was increased by 1.2-fold (**Figure 3**).

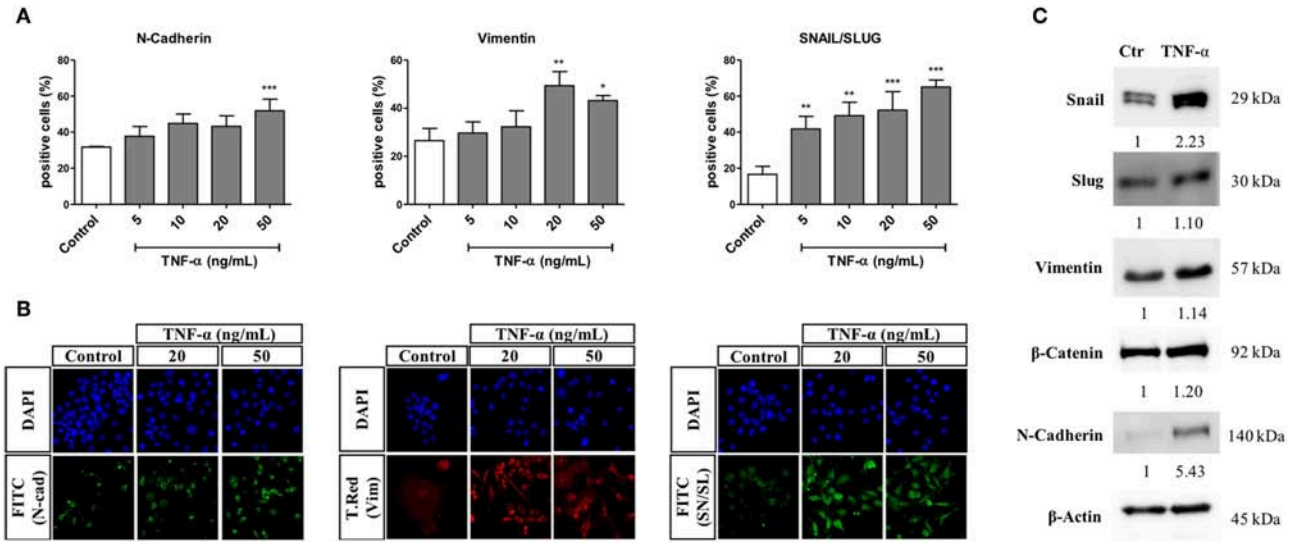

FIGURE 3 | Effects of TNF-α in the expression of EMT-related proteins. The FADU cell line was stimulated or not (Control) with TNF-α (5 to 50 ng/mL), for 72 h, followed by analyses of EMT-related protein levels by immunostaining or western blot. After immunostaining using antibodies against N-cadherin (N-cad), Vimentin (Vim) and Snail/Slug (SN/SL), cells were co-stained with nuclear (Hoechst) and cytoplasmic (CellMask) fluorescent dyes. Images (nine fields per well) were acquired using a 10X objective and excitation/emission filters DAPI (Hoechst), FITC (N-Cadherin and SN/SL), and Texas Red (T.Red; Vimentin), using an ImageXpress Micro XLS HCS system (Molecular Devices). Images were analyzed using MetaXpress, in order to evaluate the percentage of cells positive for each protein in the nucleus or cytoplasm. For western blot, protein detection was achieved using antibodies against Snail, Slug, Vimentin, beta-catenin and N-Cadherin. **(A)** Nuclear or cytoplasmic quantitative changes (Mean +-SD) in protein levels of N-Cadherin, Vimentin and Snail/Slug, as evaluated by immunofluorescence. **(B)** Representative images of stained cells stimulated with TNF-α at 20 and 50 ng/mL. **(C)** Alterations (fold change) in the protein levels of Snail, Slug, Vimentin, beta-catenin and N-Cadherin, as evaluated by western blot after 72 h of TNF-α stimulation (20 ng/mL). Statistically significant differences (ONE-WAY Anova with Tukey post-test), in comparison to the control condition: $^{*}p < 0.05$; $^{**}p < 0.01$; $^{***}p < 0.001$.

Tumor Necrosis Factor Alpha Stimulation Induces Cell Migration

A migration assay was performed in cells treated with mitomycin C and primed with TNF-α at different concentrations, for 72 h. Stimulation with TNF-α at 20 and 50 ng/mL increased the migratory capacity of FADU cells by around 30 and 20%, respectively (**Figure 4**).

HCS-Based miR Screening Identifies miRs With Distinct Effects on Cell Survival and EMT

An HCS-based functional assay was performed in cells transfected with our library of miRs ($N = 31$), followed by priming with TNF-α (20 ng/mL) for 72 h, in order to evaluate changes on morphometric parameters and Snail/Slug levels/localization. We identified miRs that altered cell survival (nuclei count) and EMT-related features including nuclear Snail/Slug levels and morphometric parameters such as cellular/nuclear area, eccentricity and cell distancing relative to the miR negative control. After unsupervised hierarchical clustering, miRs were distributed into three main groups (G1, G2, and G3). Based on distinct alterations in cell survival (nuclei count), G1 was further subdivided into the subgroups G1a and G1b.

MiRs from G3 led to a pro-survival and anti-EMT effect, as seemed by increase in cell survival and epithelial phenotype: tightly packed juxtaposed (higher number of neighboring cells and percentage of touching) round cells (lower eccentricity and higher solidity) with low nuclear Snail/Slug levels. In contrast, the subgroup G1b had the exact opposite phenotypic features (anti-survival and pro-EMT), with low cell counts, high Snail/Slug intensity and interspersed cells with mesenchymal phenotype (high eccentricity and low solidity). Since a higher cell density by itself excerpts a strong inhibitory effect on EMT, while a lower cell density is able to promote it (32), G1b and G3 are hereafter referred as anti-survival and pro-survival miR groups, respectively.

The subgroup G1a promoted cell survival while increasing nuclear Snail/Slug levels and morphological EMT-related features comparable to that of G1b; thus, clearly displaying a pro-survival/EMT effect. Otherwise, miRs from G2 had the strongest negative impact on survival while some of its members were still capable of reducing or preventing the increase of cell eccentricity or nuclear Snail/Slug levels, thereby displaying a anti-survival/EMT effect (**Figure 5**).

Anti-survival/EMT miRs Target Inflammatory-Associated Pathways

After identifying the genes collectively targeted by the miRs from G1a, G1b, G2, and G3, we eliminated targets shared by groups that led to opposite phenotypic effects. Thereby,

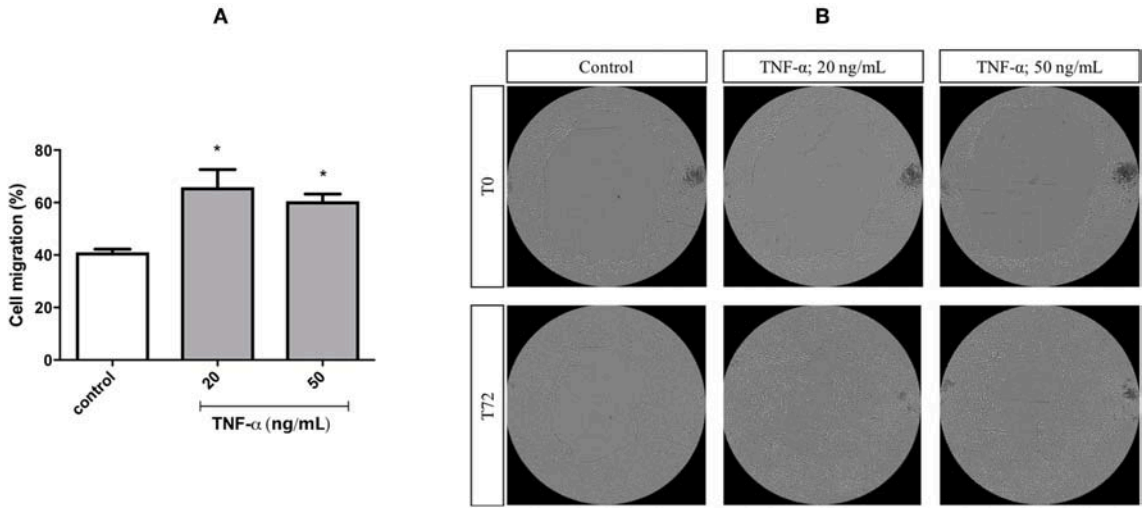

FIGURE 4 | Cell migration of FADU cells following stimulation with TNF-α. The FADU cell line was cultured for 24 h in cell culture plates designed for migration assays, treated with mitomycin for 2 h (to inhibit cell proliferation) and stimulated or not (Control) with TNF-α at 20 or 50 ng/mL for 72 h. Phase-contrast transmitted light images were acquired, with an ImageXpress Micro XLS HCS system (Molecular Devices), using a 4X objective. With aid of CellProfiler, cell migration was quantified based on the percentage of increase in the area occupied by cells. **(A)** Percentage of cell migration after 72 h (Mean +-SD). **(B)** Representative images of different experimental conditions at initial time (T0) and after 72 h (T72). Statistically significant differences (ONE-WAY Anova with Tukey post-test), in comparison to the control condition: $^*p < 0.05$.

targets shared between G1a (pro-survival/EMT) and G2 (anti-survival/EMT), as well as G1b (anti-survival) and G3 (pro-survival) were eliminated from further analyses as they were considered not relevant for the phenotypic effects driven by the groups of miRs (**Supplementary File 2**). Then, the filtered targets were used for enrichment analysis on signaling pathways and biological processes (**Supplementary File 3**). Strikingly, we found that miRs from both G1b (anti-survival) and G2 (anti-survival/EMT) targeted inflammatory pathways including "TNF signaling pathway (G1b)" and "Toll-like receptor signaling pathway (G2)" and shared targets from the following pathways: NF-κB (*IKBKG);* PI3K/AKT (*AKT2*), and MAPK (*MAPK9*). Moreover, we found that miRs from G2 also targeted additional genes (not found in G1b) from the NF-κB and PI3K/AKT pathways including *RELA* and *PIK3R3*, respectively. Finally, the Wnt/beta catenin signaling pathway was also found to be enriched with targets from G2. The miRs from G2 (anti-survival/EMT) and its targets from the NF-κB, PI3K/AKT, and Wnt/beta-catenin signaling pathways were used to generate a microRNA regulatory network (**Figure 6**).

Anti-survival/EMT miRs Reduce the Transcript Levels of Their Direct and Indirect Targets

We evaluated the capacity of three miRs with anti-survival/EMT effects (miR-29b-3p, miR-302a-3p, and miR-372-3p) to reduce the transcript levels of direct predicted targets, as well as indirect downstream transcriptional targets. Overall, with the exception of *CCND1* (an indirect target of the miRs), the targets were downregulated by most of the miRs among the cell lines, however a stronger effect and less variability were observed on the FADU cell line. More specifically, we observed a reduction on the expression levels of the direct target *AKT2*, with the exception of miR-372 (on FADU) and miR-302a (on HN30 and UMSCC1). The same was observed for the direct target *RELA*, with the exception of miR-29b (on HN30 and UMSCC1) and miR-372 (on HN30 and UMSCC1). As for the indirect targets, *MYC* was downregulated with the exception of miR-372 (on FADU) and miR-29b (on HN30 and UMSCC1). Finally, *IL6* was also downregulated by the miRs, with the exception of miR-29b (on FADU), and miR-372 (on HN30 and UMSCC1) (**Figure 7**).

Interferences in Signaling Pathways Targeted by Anti-survival/EMT miRs Partially Recapitulate Their Effects

HCS-based functional assays were done in cells transfected with siRNAs against elements of signaling pathways regulated by the anti-survival/EMT miRs: *RELA* (siRELA, NF-κB pathway), *AKT1* (siAKT1, PI3K/AKT pathway), and *CTNNB1* (siCTNNB1, Wnt/beta-catenin signaling pathway), besides a non-targeting control siRNA (siCTR) and cytotoxic siRNA (siUBC), followed or not by stimulation with TNF-α.

After 72 h of TNF-α stimulation, siRNA-mediated knockdown of *RELA* transcripts led to an expressive reduction in cell number (count nuclei) and number of neighboring cells, while increased cell eccentricity. Silencing the expression of *AKT1* (of high homology with *AKT2*, target of G2) led to a discrete reduction in cell number, while increased cell area and significantly reduced nuclear and cytoplasmic levels of Snail/Slug. Finally, knockdown of *CTNNB1* significantly reduced cell number, cytoplasmic levels

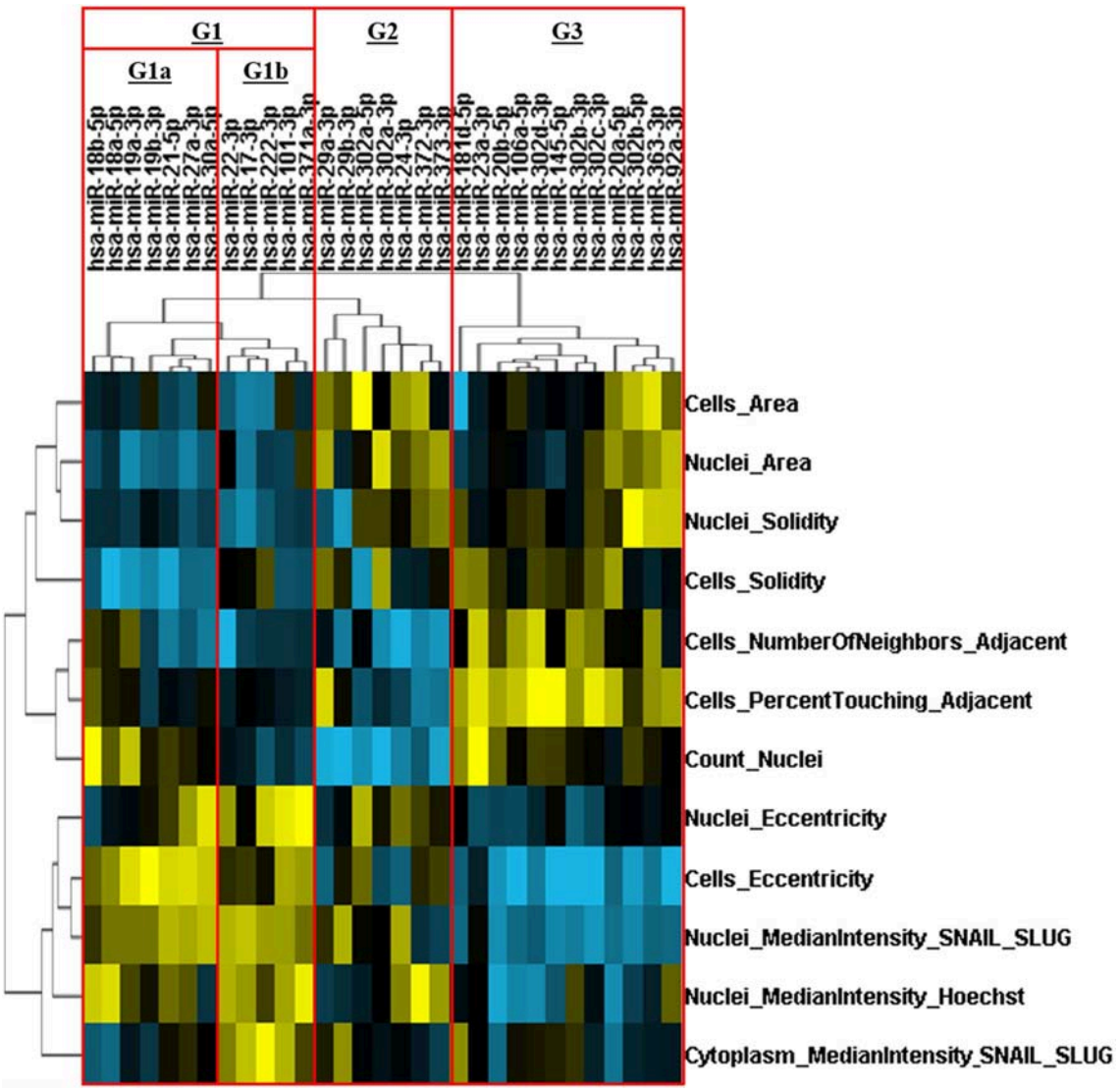

FIGURE 5 | Hierarchical clustering of miRs based on their effects on multiparametric phenotypic alterations. The FADU cell line was transfected with human miRs mimics, for 24 h, followed by stimulation with TNF-α (20 ng/mL) for 72 h. After immunostaining with antibodies against Snail/Slug (SN/SL) and co-staining with nuclear (Hoechst) and cytoplasmic (CellMask) dyes, images were acquired with an ImageXpress Micro XLS HCS system (Molecular Devices), using a 10X objective and excitation/emission filters DAPI (Hoechst), FITC (SN/SL), and Cy5 (CellMask Deep Red). With aid of CellProfiler, we evaluated several morphometric parameters, besides cell quantity (count nuclei) and the presence/location of Snail/Slug. Multiparametric phenotypic profiles, describing the effects of each miR, were obtained and subjected to an unsupervised hierarchical cluster analysis. Heatmap showing the multiparametric phenotypic profiles induced by each miR, and the four groups of miRs identified (G1a, G1b, G2, and G3. Red rectangles). Increase and decrease relative to PMC are depicted in yellow and blue, respectively.

of Snail/Slug and number of neighboring cells, while increased cell area and eccentricity.

Without TNF-α stimulation, the knockdown of the selected targets led to a reduction in cell counts as early as 24 h post-transfection, especially on cells transfected with siRELA, in which the impact was comparable to siUBC (a cytotoxic siRNA). At the same time point, the percentage of apoptotic cells (positive for cleaved caspase-7) transfected with siRELA and siAKT1 was around 25% higher than the control group (10%) but was unaltered on cells transfected with siCTNNB1, which also reduced the cell number. After 48 h of siRNA transfection, in comparison to 24 h after transfection, the number of cells in the control condition had almost doubled (indicating cell proliferation), while only slightly increasing in cells transfected with siAKT1 and siCTNNB1 and further decreasing in cells transfected with siRELA and siUBC. The percentage of apoptotic cells slightly decreased in cells transfected with siAKT1, while increased in cells transfected with siCTNNB1 (although not attaining significance), siRELA and siUBC (**Figure 8**).

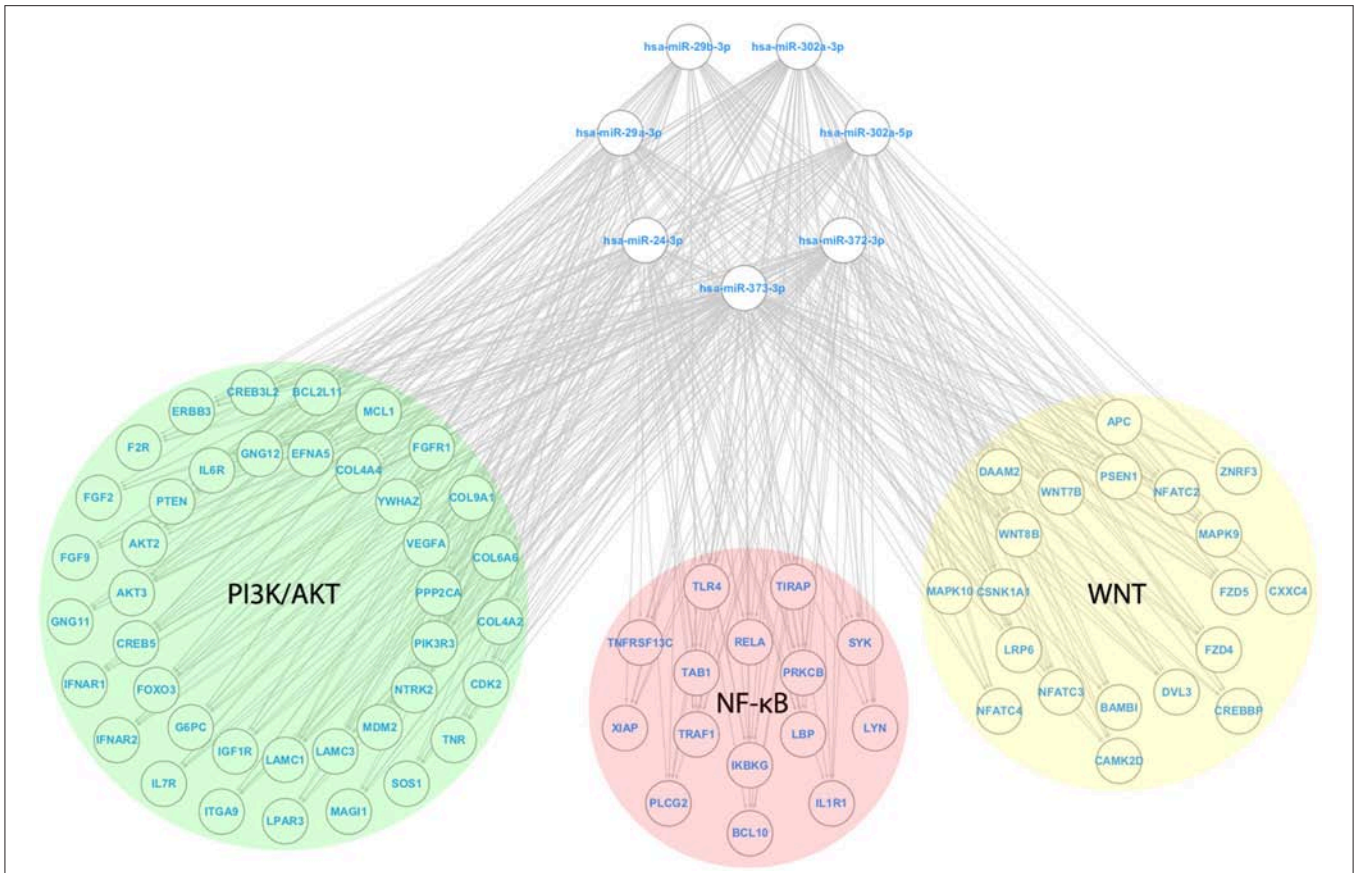

FIGURE 6 | MicroRNA Regulatory network with miRs from the anti-survival/EMT group. A microRNA regulatory network was composed of miRs from the anti-survival/EMT group, along with their targets from the PI3K/AKT (Green circle), NF-κB (Red circle), and Wnt (Yellow circle) signaling pathways. For each pathway, targets from the outer portion of the circle are the ones targeted by no more than 5 miRs, whereas the ones from the inside portion of the circle are the ones targeted by more than 5 miRs (maximum of 7). The following genes are shared between the signaling pathways NF-κB and PI3K/AKT: *IKBKG*, *RELA*, *SYK,* and *TLR4*; NF-κB and WNT: *PRKCB*.

DISCUSSION

Many of the functional studies conducted so far about the impact of small molecules in cancer cell survival disregards the presence of an inflammatory microenvironment, which is known to promote apoptosis resistance, epithelial to mesenchymal transition, among other phenotypic changes that promotes therapy resistance and disease recurrence (7).With that in mind, our study aimed to identify, through functional assays using an HCS approach, miRs and signaling pathways with the potential to suppress both cell survival and EMT features in HNSCC cells considering the presence of an inflammatory microenvironment. This approach should provide evidence if the effect of previously studied miRs translates or not to cancer cells under inflammatory stimuli, as well as to describe the effect of miRs with no known effect in HNSCC cells so far.

Initially, we demonstrated the capacity of TNF-α to promote a broad spectrum of phenotypic changes characterizing EMT, including an increase in nuclear expression of Snail/Slug, mesenchymal markers N-Cadherin and Vimentin, as well as cell eccentricity, inter-cell distancing and cell migration. Interestingly, our results of the western blot assay indicate that Snail, rather than Slug, might be involved in the induction of EMT driven by stimulation with TNF-α. Moreover, the increased levels of beta-catenin after stimulation with TNF-α also indicates a possible role, in our model, for the Wnt/beta-catenin pathway for the induction of EMT. Based on our observations, we concluded that the treatment of cells with TNF-α at 20 ng/mL is the best option to induce FADU cells to EMT, as it promoted strong changes in all parameters evaluated, as well as a superior induction to cell migration in comparison to a higher concentration.

Next, by performing an HCS-based miR screening, we investigated the capacity of 31 human miR mimics to alter phenotypic features related to cell survival and EMT in FADU cells induced to EMT by TNF-α stimulation. Overall, the results from this screening led us to identify four groups of miRs, namely G1a, G1b, G2, and G3, with distinct activity in promoting/inhibiting cell survival and EMT. Among them, two groups had characteristics of oncomiRs: G1a (pro-survival/EMT)

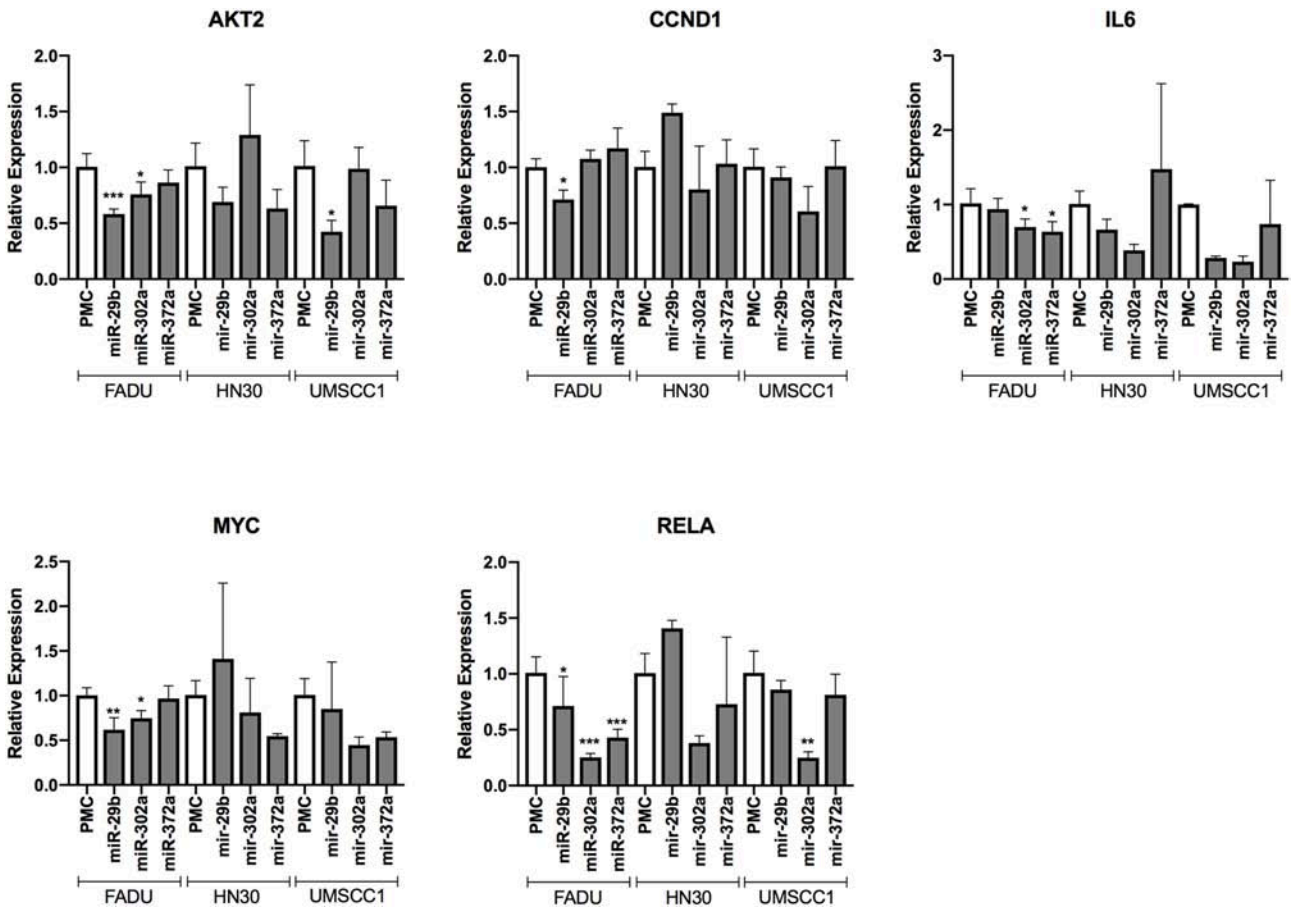

FIGURE 7 | Changes in the transcript levels of direct and indirect targets of anti-survival/EMT miR group following miR transfection. The cell lines FADU, HN30, and UMSCC1 were transfected with PMC (control) or miR mimics from G2 (miR-29b-3p, miR-302a-3p, and miR-372), followed by TNF-α stimulation (20 ng/mL) for 48 h and qPCR with primers for *AKT2*, *CCND1* (cyclin D1), *IL6*, *MYC,* and *RELA*. Alterations in relative gene expression levels, relative to cells transfected with miR-CTR (PMC). Statistically significant differences (*t*-test), in comparison to the reference control group (PMC): $^{*}p < 0.05$; $^{**}p < 0.01$; $^{***}p < 0.001$.

and G3 (pro-survival) whereas the two remaining groups had characteristics of tumor suppressor miRs: G1b (anti-survival) and G2 (anti-survival/EMT). Noteworthy, G1b (anti-survival) also excerpted an pro-EMT effect, while G3 (pro-survival) excerpted a anti-EMT effect, however, as the effects of G1b and G3 in EMT could be a byproduct (i.e., secondary effect) of their alterations in cell survival, those groups were not classified regarding their alterations in EMT (32).

Among the miRs from G1b (anti-survival), it was previously found that miR-101 is downregulated in HNSCC tissues from different anatomical sites, besides having an anti-survival effect on HNSCC cell lines, including FADU (33–35). Additionally, studies conducted with esophageal squamous cell carcinoma (ESCC)-derived cell lines subjected to the ectopic expression of miR-22 (also from G1b) observed a reduction in cell survival and migratory/invasive potential (36, 37). On the other hand, the pro-survival group G3 was mainly composed by miRs from miR-302-367 cluster, which are traditionally associated with pluripotency and malignancy of germ cells tumors (38, 39). In the context of head and neck cancer, overexpression of miR-302a and miR-302b was found in cells derived from HNSCC with characteristics of cancer stem cells including self-renewal and the ability to generate heterogeneous cell populations (40).

The pro-survival/EMT G1a was composed of miRs that are traditionally involved in regulatory mechanisms linking inflammation and tumor progression, including elements of the miR-17-92 cluster, miR-21 (a HNSCC oncomiR) and miR-23a/24/27a cluster (41). Interestingly, Chang and coworkers also observed a pro-survival activity of miR-21, as well as increased expression of miR-21 in primary HNSCC compared to mucosal controls (42). Moreover, in the recent meta-analysis study performed by Lubov et al., it was observed that an increased expression of miR-21 is associated with poor outcome in HNSCC (14). Differently from G1a, G2 (anti-survival/EMT) was composed of miRs from miR-29 family, which displays tumor suppressor activity in several types of cancer, including HNSCC (14, 43). In line with our results, Kinoshita and coworkers observed that the ectopic expression of elements from the mir-29

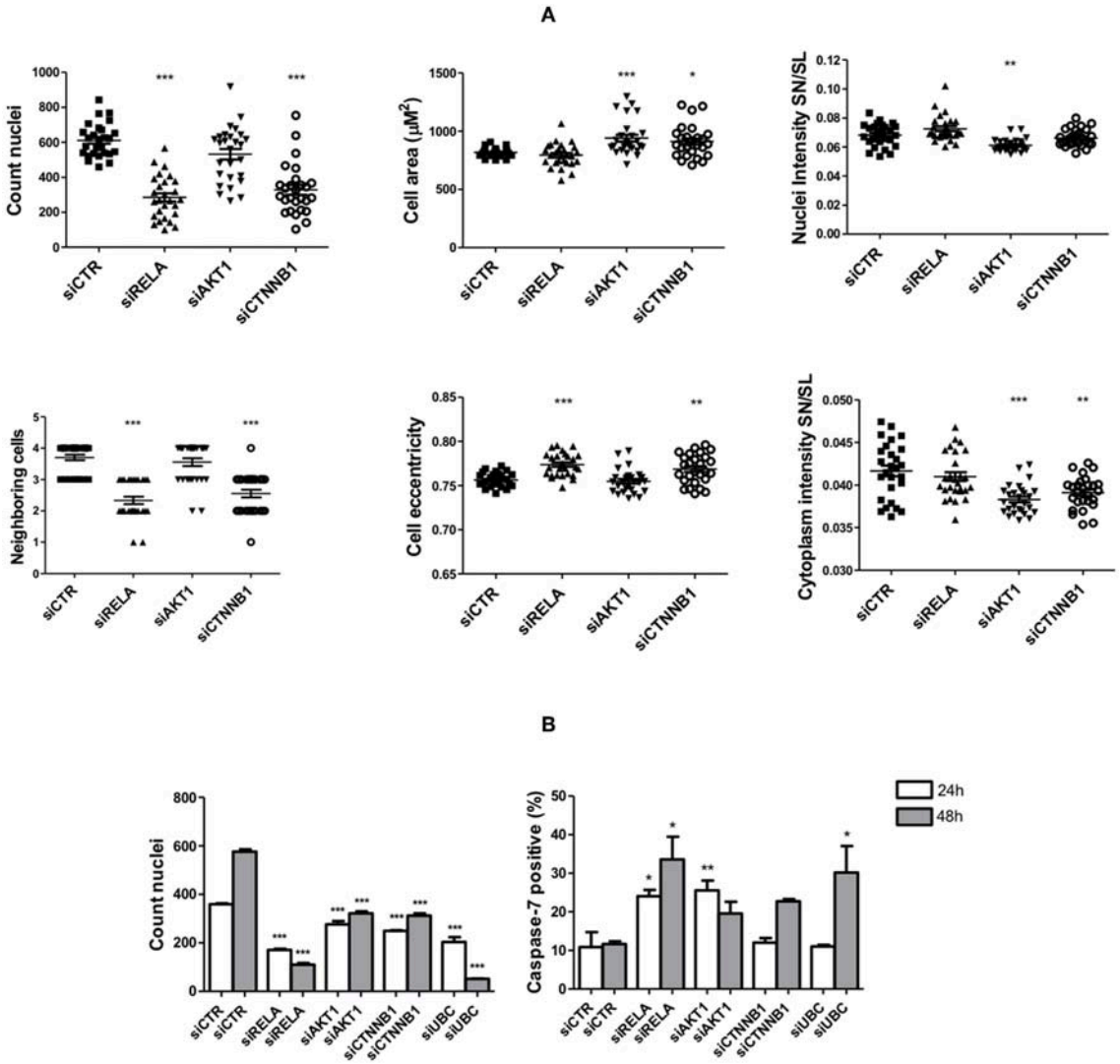

FIGURE 8 | Changes in cell survival and EMT upon interferences in signaling pathways targeted by the anti-survival/EMT group. The FADU cell line was transfected with siRNAs specific for *RELA*, *AKT1*, *CTNNB1*, cytotoxic siUBC, and unspecific siRNA control (siCTR), followed or not by TNF-α stimulation. At the endpoint, images were acquired with an ImageXpress Micro XLS HCS system (Molecular Devices), using a 10X objective and excitation/emission filters DAPI (Hoechst), FITC (SN/SL) and Cy5 (CellMask Deep Red). **(A)** Cells were stimulated for 72 h with TNF-α (20 ng/mL), starting 24 h post-transfection, followed by immunostaining with antibodies against Snail/Slug (SN/SL) and co-staining with nuclear (Hoechst) and cytoplasmic (CellMask) dyes. Alterations in morphometric parameters, cell counts and nuclear/cytoplasmic Snail/Slug due to siRNA transfection as observed after image analysis. **(B)** 24 and 48 h after transfection, cells without TNF-α stimulation were immunostained with antibodies against cleaved Caspase-7 and co-stained with nuclear (Hoechst) and cytoplasmic (CellMask) dyes. Cell counts and percentage of apoptotic cells positive for active caspase-7 as observed after image analysis. Statistically significant differences (ONE-WAY Anova with Tukey post-test), in comparison to the control condition: $*p < 0.05$; $**p < 0.01$; $***p < 0.001$.

family in the FADU cell line resulted in a significant reduction in cell number, as well as in cell migration and invasion (44).

In an effort to identify, among the several targets and signaling pathways regulated by miRs, those that effectively contributed to the observed phenotypic effect, we excluded from further analyses genes that were commonly targeted by groups of miRs that led to opposite phenotypes. Those filtered targets were used in *in silico* enrichment analysis, leading to the identification of specific targets and targeted signaling pathways. Noteworthy, this strategy provided cues on the genes and signaling pathways to be explored to suppress HNSCC tumor growth and metastasis.

By following this strategy, we observed that miRs from G1b (anti-survival) and G2 (anti-survival/EMT) targeted signaling pathways that are associated with the interface between inflammation and tumor initiation/progression, including MAPK, PI3K/AKT and NF-κB pathways (45). However, in comparison to predicted targets from G1b, it was found that miRs from G2 interfered in the PI3K/AKT and NF-κB pathways

in a more extensive manner, also targeting a regulatory subunit of PI3K (PIK3R3), a oncogene that regulates AKT activity, as well as *RELA*, which codes for the canonical subunit (p65) of the NF-κB transcription factor (46, 47). Moreover, miRs from G2 also targeted several elements of the Wnt/beta-catenin signaling pathway. Altogether, our results from *in silico* analyses provided evidence that the anti-survival/EMT effects elicited by miRs from G2 likely derives from an extensive perturbation in PI3K/AKT and NF-κB pathways, besides Wnt signaling pathway. Additionally, by evaluating alterations in gene expression levels of cells transfected with miRs from G2 (anti-survival/EMT) group, we confirmed that elements from the following targeted signaling pathways: NF-κB (*RELA* and *IL6*), PI3K/AKT (*AKT2*), as well as Wnt/beta-catenin (*MYC*) were downregulated after the transfection in most cases.

Additional functional assays were performed with siRNAs against genes from the following signaling pathways regulated by anti-survival/EMT group (G2): *AKT1* (PI3K/AKT pathway); *RELA* (NF-κB pathway); and *CTNNB1* (Wnt pathway) followed or not by stimulation with TNF-α. Noteworthy, though *AKT1* and *CTNNB1* are not directly targeted by the miRs from G2, their use is justified by the central role of those genes in regulating the PI3K/AKT and Wnt/beta-catenin pathways, respectively, which were extensively targeted by those miRs. Therefore, results from our functional assays using siRNAs should not be interpreted as direct link between anti-survival/EMT miRs and a specific target, but rather between miRs and targeted signaling pathways. An exception are observations from siRELA transfections, as *RELA* is not only a central gene in the NF-κB pathway but also a direct target of G2.

By stimulating cells with TNF-α after siRNA transfection, we sought to investigate the individual role of NF-κB, PI3K/AKT, and Wnt/beta-catenin signaling pathways on either cell survival or EMT considering the presence of an inflammatory microenvironment. Interestingly, we found that although gene silencing of *RELA* and *CTNNB1* led to an anti-survival effect whereas silencing *AKT1* led to an anti-EMT effect, none of the siRNAs alone impaired both cell survival and EMT, which indicates that the effects of anti-survival/EMT miRs are most likely due to their potential to interfere in multiple signaling pathways simultaneously. This possibility points out to the potential benefits of a multi-target approach to treat HNSCC, especially considering that so far, clinical trials evaluating the capacity of PI3K inhibitors to treat HNSCC have shown disappointing results (48). In line, a recent study by Li et al. demonstrated that co-targeting EGFR (upstream of PI3K/AKT) and NF-κB pathways led to a superior inhibition of cell survival and xenograph tumor growth, when compared to targeting either pathway alone (49).

By not stimulating cells with TNF-α after siRNA transfection, we aimed to evaluate if the effects coming from the interferences in NF-κB, PI3K/AKT, and Wnt/beta-catenin signaling pathways are influenced by the presence of an inflammatory microenvironment. Additionally, we investigated if effects on cell survival are due to alterations in apoptosis by evaluating the percentage of cells positive for cleaved caspase-7. Strikingly, we found that transfection with siRELA not only dramatically reduced the number of cells but also strongly induced cell-death by apoptosis after 24 h and 48 h. This indicates that interferences in the NF-κB pathway is deleterious to HNSCC cells regardless of stimulation with inflammatory factors. Interestingly, transfection with siAKT1 also followed a similar pattern (although not further increasing apoptosis at 48 h) revealing that an inflammatory stimulation exerts a protective effect on HNSCC cells against the deleterious effect of interferences in the PI3K/AKT pathway. Moreover, although transfection with siCTNNB1 reduced cell count, it did not enhance the number of apoptotic cells 24 h post-transfection, indicating a more prominent role of Wnt signaling toward cell proliferation regardless of TNF-α stimulation.

As a whole, our study identified several molecules that may have the potential to be used for prognosis or miR-based targeted therapies against HNSCC considering the presence of an inflammatory microenvironment. By further investigating the miRs with anti-survival/EMT effects, we found that interferences in the signaling pathways: NF-κB and Wnt/beta-catenin were the ones that most likely contributed for the anti-survival effect, whereas interferences in PI3K/AKT signaling pathway was most likely associated with anti-EMT effect. Future studies using *in vivo* models should shed light into the anti-tumor and anti-metastatic activity of the miRs and targets herein identified.

CONCLUSION

The present work characterized the functional role of a set of human miRs in modulating a broad spectrum of phenotypic alterations related to HNSCC cell survival and EMT in cells under an inflammatory stimulation, as well as the potentially involved signaling pathways. More specifically, the following miR mimetics: miR-24-3p, miR-29a-3p, miR-29b-3p, miR-302a-3p, miR-302a-5p, miR-372-3p, and miR-373-3p were identified as the ones with greatest potential use in microRNA replacement therapies, as they displayed an anti-survival/EMT effect. On the other hand, endogenous miRs herein identified as with pro-survival/EMT effects: miR-18a-5p, miR-18b-5p, miR-19a-3p, miR-19b-3p, miR-21-5p, miR-27a-3p, miR-30a-5p, were identified as the ones with greatest potential use in microRNA inhibition therapies. Additionally, we found that together, interferences on NF-κB, PI3K/AKT, and Wnt/beta-catenin signaling pathways are the ones that most likely driven the anti-survival/EMT effects displayed by miRs. Individual gene silencing of components of those pathways, namely *RELA* (NF-κB), *AKT1* (PI3K/AKT), and *CTNNB1* (Wnt/beta-catenin), partially recapitulated the effects displayed by miRs with anti-survival/EMT effects. Our findings revealed miRs and signaling pathways that might be explored to fight HNSCC tumor growth and metastasis considering the presence an inflammatory microenvironment.

AUTHOR CONTRIBUTIONS

BS, WA, VF, DC, MZ, and RP: study concept. BS, FS, and RP: study design. BS, FS, IM, JS, RP, AC, and CT: data acquisition, analysis, and interpretation. BS: statistical analysis. BS and RP:

manuscript preparation and editing. BS, WA, VF, DC, MZ, and RP: manuscript review.

FUNDING

This work was supported by São Paulo Research Foundation (FAPESP), grants #2013/08135-2 (Center for Cell-Based Therapy - CTC) and #2015/08070-3 (Scholarship for Research Abroad - BPE, RP); and by the National Council for Scientific and Technological Development (CNPq).

SUPPLEMENTARY MATERIAL

The Supplementary Material for this article can be found online at: https://www.frontiersin.org/articles/10.3389/fonc.2019.01100/full#supplementary-material

REFERENCES

1. Torre LA, Bray F, Siegel RL, Ferlay J, Lortet-Tieulent J, Jemal A. Global cancer statistics, 2012. *CA Cancer J Clin.* (2015) 65:87–108. doi: 10.3322/caac.21262
2. Allen CT, Law JH, Dunn GP, Uppaluri R. Emerging insights into head and neck cancer metastasis. *Head Neck.* (2013) 35:1669–78. doi: 10.1002/hed.23202
3. Massague J, Obenauf AC. Metastatic colonization by circulating tumour cells. *Nature.* (2016) 529:298–306. doi: 10.1038/nature17038
4. Lamouille S, Xu J, Derynck R. Molecular mechanisms of epithelial-mesenchymal transition. *Nat Rev Mol Cell Biol.* (2014) 15:178–96. doi: 10.1038/nrm3758
5. Singh M, Yelle N, Venugopal C, Singh SK. EMT: mechanisms and therapeutic implications. *Pharmacol Ther.* (2018) 182:80–94. doi: 10.1016/j.pharmthera.2017.08.009
6. Gao F, Liang B, Reddy ST, Farias-Eisner R, Su X. Role of inflammation-associated microenvironment in tumorigenesis and metastasis. *Curr Cancer Drug Targets.* (2014) 14:30–45. doi: 10.2174/1568009613136660107
7. Suarez-Carmona M, Lesage J, Cataldo D, Gilles C. EMT and inflammation: inseparable actors of cancer progression. *Mol Oncol.* (2017) 11:805–23. doi: 10.1002/1878-0261.12095
8. Wu Y, Zhou BP. TNF-alpha/NF-kappaB/Snail pathway in cancer cell migration and invasion. *Br J Cancer.* (2010) 102:639–44. doi: 10.1038/sj.bjc.6605530
9. Matta A, Ralhan R. Overview of current and future biologically based targeted therapies in head and neck squamous cell carcinoma. *Head Neck Oncol.* (2009) 1:6. doi: 10.1186/1758-3284-1-6
10. Hoesel B, Schmid JA. The complexity of NF-kappaB signaling in inflammation and cancer. *Mol Cancer.* (2013) 12:86. doi: 10.1186/1476-4598-12-86
11. Holohan C, Van Schaeybroeck S, Longley DB, Johnston PG. Cancer drug resistance: an evolving paradigm. *Nat Rev Cancer.* (2013) 13:714–26. doi: 10.1038/nrc3599
12. Bartel DP. MicroRNAs: target recognition and regulatory functions. *Cell.* (2009) 136:215–33. doi: 10.1016/j.cell.2009.01.002
13. Shalgi R, Brosh R, Oren M, Pilpel Y, Rotter V. Coupling transcriptional and post-transcriptional miRNA regulation in the control of cell fate. *Aging.* (2009) 1:762–70. doi: 10.18632/aging.100085
14. Lubov J, Maschietto M, Ibrahim I, Mlynarek A, Hier M, Kowalski LP, et al. Meta-analysis of microRNAs expression in head and neck cancer: uncovering association with outcome and mechanisms. *Oncotarget.* (2017) 8:55511–24. doi: 10.18632/oncotarget.19224
15. Pradhan AK, Emdad L, Das SK, Sarkar D, Fisher PB. The enigma of miRNA regulation in cancer. *Adv Cancer Res.* (2017) 135:25–52. doi: 10.1016/bs.acr.2017.06.001
16. Markopoulos GS, Roupakia E, Tokamani M, Alabasi G, Sandaltzopoulos R, Marcu KB, et al. Roles of NF-kappaB Signaling in the regulation of miRNAs impacting on inflammation in cancer. *Biomedicines.* (2018) 6:E40. doi: 10.3390/biomedicines6020040
17. Castilho RM, Squarize CH, Almeida LO. Epigenetic modifications and head and neck cancer: implications for tumor progression and resistance to therapy. *Int J Mol Sci.* (2017) 18:E1506. doi: 10.3390/ijms18071506
18. Bhome R, Del Vecchio F, Lee GH, Bullock MD, Primrose JN, Sayan AE, et al. Exosomal microRNAs (exomiRs): Small molecules with a big role in cancer. *Cancer Lett.* (2018) 420:228–35. doi: 10.1016/j.canlet.2018.02.002
19. Chakraborty C, Sharma AR, Sharma G, Sarkar BK, Lee SS. The novel strategies for next-generation cancer treatment: miRNA combined with chemotherapeutic agents for the treatment of cancer. *Oncotarget.* (2018) 9:10164–74. doi: 10.18632/oncotarget.24309
20. Lindenbergh-van der Plas M, Martens-de Kemp SR, de Maaker M, van Wieringen WN, Ylstra B, Agami R, et al. Identification of lethal microRNAs specific for head and neck cancer. *Clin Cancer Res.* (2013) 19:5647–57. doi: 10.1158/1078-0432.CCR-12-2295
21. Haefliger B, Prochazka L, Angelici B, Benenson Y. Precision multidimensional assay for high-throughput microRNA drug discovery. *Nat Commun.* (2016) 7:10709. doi: 10.1038/ncomms10709
22. Boutros M, Heigwer F, Laufer C. Microscopy-based high-content screening. *Cell.* (2015) 163:1314–25. doi: 10.1016/j.cell.2015.11.007
23. Serva A, Claas C, Starkuviene V. A potential of microRNAs for high-content screening. *J Nucleic Acids.* (2011) 2011:870903. doi: 10.4061/2011/870903
24. Rupaimoole R, Slack FJ. MicroRNA therapeutics: towards a new era for the management of cancer and other diseases. *Nat Rev Drug Discov.* (2017) 16:203–22. doi: 10.1038/nrd.2016.246
25. de Hoon MJ, Imoto S, Nolan J, Miyano S. Open source clustering software. *Bioinformatics.* (2004) 20:1453–4. doi: 10.1093/bioinformatics/bth078
26. Saldanha AJ. Java Treeview–extensible visualization of microarray data. *Bioinformatics.* (2004) 20:3246–8. doi: 10.1093/bioinformatics/bth349
27. Agarwal V, Bell GW, Nam JW, Bartel DP. Predicting effective microRNA target sites in mammalian mRNAs. *Elife.* (2015) 4:e05005. doi: 10.7554/eLife.05005
28. Huang da W, Sherman BT, Lempicki RA. Systematic and integrative analysis of large gene lists using DAVID bioinformatics resources. *Nat Protoc.* (2009) 4:44–57. doi: 10.1038/nprot.2008.211
29. Kanehisa M, Goto S. KEGG: kyoto encyclopedia of genes and genomes. *Nucleic Acids Res.* (2000) 28:27–30. doi: 10.1093/nar/28.1.27
30. Shannon P, Markiel A, Ozier O, Baliga NS, Wang JT, Ramage D, et al. Cytoscape: a software environment for integrated models of biomolecular interaction networks. *Genome Res.* (2003) 13:2498–504. doi: 10.1101/gr.1239303
31. Livak KJ, Schmittgen TD. Analysis of relative gene expression data using real-time quantitative PCR and the 2(-Delta Delta C(T)) method. *Methods.* (2001) 25:402–8. doi: 10.1006/meth.2001.1262
32. Cichon MA, Nelson CM, Radisky DC. Regulation of epithelial-mesenchymal transition in breast cancer cells by cell contact and adhesion. *Cancer Inform.* (2015) 14:1–13. doi: 10.4137/CIN.S18965
33. Li M, Tian L, Ren H, Chen X, Wang Y, Ge J, et al. MicroRNA-101 is a potential prognostic indicator of laryngeal squamous cell carcinoma and modulates CDK8. *J Transl Med.* (2015) 13:271. doi: 10.1186/s12967-015-0626-6
34. Hui Y, Li Y, Jing Y, Feng JQ, Ding Y. miRNA-101 acts as a tumor suppressor in oral squamous cell carcinoma by targeting CX chemokine receptor 7. *Am J Transl Res.* (2016) 8:4902–11.
35. Wu B, Lei D, Wang L, Yang X, Jia S, Yang Z, et al. MiRNA-101 inhibits oral squamous-cell carcinoma growth and metastasis by targeting zinc finger E-box binding homeobox 1. *Am J Cancer Res.* (2016) 6:1396–407.
36. Yang C, Ning S, Li Z, Qin X, Xu W. miR-22 is down-regulated in esophageal squamous cell carcinoma and inhibits cell migration and invasion. *Cancer Cell Int.* (2014) 14:138. doi: 10.1186/s12935-014-0138-0

37. Qiu K, Huang Z, Huang Z, He Z, You S. miR-22 regulates cell invasion, migration and proliferation *in vitro* through inhibiting CD147 expression in tongue squamous cell carcinoma. *Arch Oral Biol.* (2016) 66:92–7. doi: 10.1016/j.archoralbio.2016.02.013
38. Murray MJ, Nicholson JC, Coleman N. Biology of childhood germ cell tumours, focussing on the significance of microRNAs. *Andrology.* (2015) 3:129–39. doi: 10.1111/andr.277
39. Adlakha YK, Seth P. The expanding horizon of MicroRNAs in cellular reprogramming. *Prog Neurobiol.* (2017) 148:21–39. doi: 10.1016/j.pneurobio.2016.11.003
40. Bourguignon LY, Wong G, Earle C, Chen L. Hyaluronan-CD44v3 interaction with Oct4-Sox2-Nanog promotes miR-302 expression leading to self-renewal, clonal formation, and cisplatin resistance in cancer stem cells from head and neck squamous cell carcinoma. *J Biol Chem.* (2012) 287:32800–24. doi: 10.1074/jbc.M111.308528
41. Tili E, Michaille JJ, Croce CM. MicroRNAs play a central role in molecular dysfunctions linking inflammation with cancer. *Immunol Rev.* (2013) 253:167–84. doi: 10.1111/imr.12050
42. Chang SS, Jiang WW, Smith I, Poeta LM, Begum S, Glazer C, et al. MicroRNA alterations in head and neck squamous cell carcinoma. *Int J Cancer.* (2008) 123:2791–7. doi: 10.1002/ijc.23831
43. Slusarz A, Pulakat L. The two faces of miR-29. *J Cardiovasc Med.* (2015) 16:480–90. doi: 10.2459/JCM.0000000000000246
44. Kinoshita T, Nohata N, Hanazawa T, Kikkawa N, Yamamoto N, Yoshino H, et al. Tumour-suppressive microRNA-29s inhibit cancer cell migration and invasion by targeting laminin-integrin signalling in head and neck squamous cell carcinoma. *Br J Cancer.* (2013) 109:2636–45. doi: 10.1038/bjc.2013.607
45. Raposo TP, Beirao BC, Pang LY, Queiroga FL, Argyle DJ. Inflammation and cancer: till death tears them apart. *Vet J.* (2015) 205:161–74. doi: 10.1016/j.tvjl.2015.04.015
46. Vander Broek R, Mohan S, Eytan DF, Chen Z, Van Waes C. The PI3K/Akt/mTOR axis in head and neck cancer: functions, aberrations, cross-talk, and therapies. *Oral Dis.* (2015) 21:815–25. doi: 10.1111/odi.12206
47. Mitchell S, Vargas J, Hoffmann A. Signaling via the NFkappaB system. *Wiley Interdiscip Rev Syst Biol Med.* (2016) 8:227–41. doi: 10.1002/wsbm.1331
48. Jung K, Kang H, Mehra R. Targeting phosphoinositide 3-kinase (PI3K) in head and neck squamous cell carcinoma (HNSCC). *Cancers Head Neck.* (2018) 3:3. doi: 10.1186/s41199-018-0030-z
49. Li Z, Liao J, Yang Z, Choi EY, Lapidus RG, Liu X, et al. Co-targeting EGFR and IKKbeta/NF-kappaB signalling pathways in head and neck squamous cell carcinoma: a potential novel therapy for head and neck squamous cell cancer. *Br J Cancer.* (2019) 120:306–16. doi: 10.1038/s41416-018-0351-z

Conflict of Interest: The authors declare that the research was conducted in the absence of any commercial or financial relationships that could be construed as a potential conflict of interest.

frontiers in Pharmacology

ORIGINAL RESEARCH
published: 12 September 2018
doi: 10.3389/fphar.2018.01042

CD13 Inhibition Enhances Cytotoxic Effect of Chemotherapy Agents

Jian Zhang[1†], Chunyan Fang[1†], Meihua Qu[1], Huina Wu[1], Xuejuan Wang[1], Hongan Zhang[1], Hui Ma[1], Zhaolin Zhang[2], Yongxue Huang[2], Lihong Shi[1], Shujuan Liang[3], Zhiqin Gao[4], Weiguo Song[1] and Xuejian Wang[1]**

[1] School of Pharmacy, Weifang Medical University, Weifang, China, [2] Weifang Bochuang International Biological Medicinal Institute, Weifang, China, [3] School of Clinical Medicine, Weifang Medical University, Weifang, China, [4] School of Bioscience and Technology, Weifang Medical University, Weifang, China

OPEN ACCESS

Edited by:
Zhe-Sheng Chen,
St. John's University, United States

Reviewed by:
Fabrizio Martelli,
Istituto Superiore di Sanità (ISS), Italy
Qi Xie,
University of California, San Diego, United States
Junjiang Chen,
Hong Kong Polytechnic University, Hong Kong

***Correspondence:**
Weiguo Song
songwg@139.com
Xuejian Wang
wangxuejian@wfmc.edu.cn;
wxj2901@126.com

[†]These authors have contributed equally to this work

Specialty section:
This article was submitted to Cancer Molecular Targets and Therapeutics, a section of the journal Frontiers in Pharmacology

Received: *07 July 2018*
Accepted: *27 August 2018*
Published: *12 September 2018*

Citation:
Zhang J, Fang C, Qu M, Wu H, Wang X, Zhang H, Ma H, Zhang Z, Huang Y, Shi L, Liang S, Gao Z, Song W and Wang X (2018) CD13 Inhibition Enhances Cytotoxic Effect of Chemotherapy Agents. Front. Pharmacol. 9:1042. doi: 10.3389/fphar.2018.01042

Multidrug resistance (MDR) of hepatocellular carcinoma is a serious problem. Although CD13 is a biomarker in human liver cancer stem cells, the relationship between CD13 and MDR remains uncertain. This study uses liver cancer cell model to understand the role of CD13 in enhancing the cytotoxic effect of chemotherapy agents. Cytotoxic agents can induce CD13 expression. CD13 inhibitor, bestatin, enhances the antitumor effect of cytotoxic agents. Meanwhile, CD13-targeting siRNA and neutralizing antibody can enhance the cytotoxic effect of 5-fluorouracil (5FU). CD13 overexpression increases cell survival upon cytotoxic agents treatment, while the knockdown of CD13 causes hypersensitivity of cells to cytotoxic agents treatment. Mechanistically, the inhibition of CD13 leads to the increase of cellular reactive oxygen species (ROS). BC-02 is a novel mutual prodrug (hybrid drug) of bestatin and 5FU. Notably, BC-02 can inhibit cellular activity in both parental and drug-resistant cells, accompanied with significantly increased ROS level. Moreover, the survival time of Kunming mice bearing H22 cells under BC-02 treatment is comparable to the capecitabine treatment at maximum dosage. These data implicate a therapeutic method to reverse MDR by targeting CD13, and indicate that BC-02 is a potent antitumor compound.

Keywords: CD13, MDR, bestatin, BC-02, 5FU

INTRODUCTION

Hepatocellular carcinoma (HCC) is the fifth most common cancer type and the third leading cause of cancer-related deaths worldwide (Mlynarsky et al., 2015). Prognosis remains poor due to the low percentage of patients with HCC eligible for surgery (9–29%) (Tsurusaki and Murakami, 2015), high tumor recurrence rates after resection (60%) (Cheng et al., 2005), and limited benefit of conventional chemotherapy (Cao et al., 2012; Deng et al., 2015). The resistance of cancer cells to structurally and mechanistically unrelated classes of anticancer drugs is known as multidrug resistance (MDR) (Gottesman et al., 2002). And MDR is one of the major causes of chemotherapeutic failure in HCC therapy. Therefore, exploring more effective therapeutic strategies for patients with HCC is urgently needed. Increasing clinical trials have proposed that combination therapy may provide new strategy for chemo-resistance in patients with advanced HCC (Alves et al., 2011; Cervello et al., 2012; Shin and Chung, 2013).

Aminopeptidase N (APN, EC 3.4.11.2), which is also known as CD13, is a type 2 transmembrane Zn-dependent metallopeptidase of the gluzincin superfamily. APN forms a non-covalent bond homodimer on the cellular membrane. It hydrolyzes oligopeptides and releases neutral amino acids from the N-terminal end of small peptides. In human non-small cell lung cancer, pancreatic carcinoma, and prostate cancer, CD13 expression is associated with poor prognosis, and CD13 expression is involved in cancer invasion and metastasis (Tokuhara et al., 2006; Su et al., 2012). CD13 is also a marker for semi-quiescent cancer stem cells (CSCs) in human liver cancer cell lines and clinical liver cancer samples (Haraguchi et al., 2010). CSCs or tumor-initiating cells are responsible for drug resistance and tumor recurrence. CSCs express high level of ATP-binding cassette (ABC) transporters. Suppression of Pim-3 kinase expression by targeting CD13 can reverse MDR in HCC cells. Therefore, ABC transporters and Pim-3 may contribute to CD13 mediated HCC MDR (Guo et al., 2017).

Bestatin, which is a [(2S,3R)-3-amino-2-hydroxy-4-phenylbutanoyl] leucine obtained from the culture filtrates of *Streptomyces olivoreticuli*, is a dipeptide with low molecular mass. It is also a potent competitive inhibitor of CD13 with antitumor activity. Bestatin synergistically enhances the antitumor effects of anticancer drugs in HCC cell lines, and the effects of bestatin are due to the increased intracellular reactive oxygen species (ROS) levels (Yamashita et al., 2016). Our previous data indicated that CD13 inhibitor 4cc synergizes the antitumor effects of 5-fluorouracil (5FU) on human liver cancer cells in a ROS-dependent manner. CD13-neutralizing antibody (clone WM15, CD13 Ab) can also significantly induce ROS production compared with control (Sun et al., 2015).

In the current study, we aim to understand the role of CD13 in MDR and evaluate the antitumor effect of BC-02, a novel mutual prodrug (hybrid drug) of bestatin and 5FU, which can be degraded into bestatin and 5FU (Dou et al., 2017), on drug-resistant tumor cells. CD13 inhibitor bestatin and neutralizing antibody can enhance the sensitivity of tumor cells to cytotoxic agents. CD13 overexpression or knockdown affects the sensitivity of cells to cytotoxic agents. Compound BC-02 can inhibit both parental and drug-resistance tumor cell proliferation more markedly than single treatment of bestatin, 5FU, or a combination of 5FU and bestatin. All together, this study may bring new strategy to reverse MDR in HCC cancer.

MATERIALS AND METHODS

Cell Culture and Reagents

Human hepatocarcinoma cell line PLC/PRF/5, Huh7, H7402, HepG2, and human colon cancer cell HCT116 were maintained in RPMI-1640 supplemented with 10% fetal calf serum (FCS). Human alveolar epithelial cell line A549 was grown in Dulbecco modified Eagle medium supplemented with 10% FCS. The cells were incubated at 37°C in a humidified atmosphere containing 5% CO_2. Lipofection 2000 was purchased from Invitrogen (Cat. 11668-019). siRNA was synthesized by Shanghai GenePharma. Bestatin (Cat. B8385), 5FU (Cat. F6627), and cisplatin (cis-DDP, Cat. P4394) were purchased from Sigma. Gemcitabine (GEM, Cat. G8970), Paclitaxel (PTX, Cat. SP8020), and doxorubicin (DOX, Cat. D8740) were purchased from Solarbio. BC-02 (12a) was synthesized by conjugating bestatin and 5FU as previously described (Jiang et al., 2018).

PLC/PRF/5-5FU Cell Culture

Low dose of 5FU was added into the medium of PLC/PRF/5. When cells need digest and passage, 5FU was also added after cell attachment. For a long time of incubation, higher concentration of 5FU was added. Then cells could survive at 40 μM 5FU.

Flow Cytometry

Determination of CD13 expression by FACS was described previously (Wang et al., 2011). 1×10^5 cells were washed with cold PBS and incubated with PE-conjugated monoclonal antibody targeting CD13 (BD Pharmingen, CD13mAb clone: WM15) for 60 min on ice. Then, the cells were analyzed on FACScan (FACSAria II; Becton-Dickinson). For ROS assay, cells were seeded and exposed to different drug samples. After 5 h incubation, cells were isolated and incubated at 37°C for 30 min with 10 μM 2,7-dichlorofluorescein diacetate (DCFH-DA) in the dark. Then the samples were washed and analyzed on a FACSCan.

Cell Viability Assays

2×10^3 cells/well were seeded in 96-well plate and allowed to grow for 4 h and the drugs were added to the wells at various concentrations. After 48 h, cells were incubated with 1% of 0.5 mg/ml MTT reagent for an additional 4 h. After that, the culture was removed, and the cells were lysed with 100 μl dimethyl sulfoxide (DMSO). The optical density of 570/630 nm was read on a plate reader (M5, MD) to calculate the inhibition rate. The inhibition rate of compounds was calculated by (ODcontrol-ODtested)/ODcontrol × 100%, where OD is the mean value of three replicate wells. The IC_{50} values were determined using ORIGIN 8 software (OriginLab Corporation, Northampton, MA, United States).

Transfection Assay

Cells were seeded on a 96-well plate and transfected with siRNA targeting the sequence of CCGAAATGCCACACTGGTCAA of the human ANPEP (CD13) sequence (NM_001150) (Lai et al., 2012). Non-specific scrambled siRNA duplex was also purchased from GenePharma (Shanghai, China). The transfection protocol was according to the lipofection 2000 instruction.

Lentivirus Infection

Lentivirus particles was supplied by GeneChem. The target of shRNA lentivirus was CCGAAATGCCACACTGGTCAA of the human ANPEP (CD13) sequence (NM_001150). The human ANPEP (CD13) sequence (NM_001150) was inserted into the vector of overexpression lentivirus. CD13 overexpression and knockdown lentivirus all overexpress green fluorescent protein. The procedure was according to the instruction. In brief, lentivirus particles was added into the medium of cells. Twelve hours later, the medium was replaced with completed culture

medium. Then puromycin treatment help to get the stably overexpression or knockdown cells.

Clone Formation Assay

Cells were plated in 6 or 48-well plates for overnight. Then cells were treated with different compounds for about 7–10 days. When the cells grew to visible colonies (>50 cells) the medium was discarded, and the cells were fiand with paraformaldehyde and stained with 0.1% crystal violet. Then clones were counted under an optical microscope.

Western Blot

Either 20 or 30 μg of total protein of each lysate were subjected to 10 or 12% SDS–PAGE and electrotransferred onto PVDF membranes (Cat. IPVH00010, Millipore). Membrane was blocked with BSA and then incubated with primary antibodies. After washing, HRP-conjugated secondary antibodies were incubated. Washed with TBST, the bound antibodies were visualized by enhanced chemiluminescence (ECL, Cat. WBKLS0050, Millipore).

In vivo Anti-tumor Assay

3×10^6 H22 cells were injected to enterocoelia of Kunming mice. And mice were divided into different groups randomly and treated with agents. The survival period was recorded. For drug-resistant cell assay, H22-bearing KM mice were given 86 mg/kg/day capecitabine. After 2 weeks, tumor tissues were dissected from mice and triturated into single cell suspension. Then cells were implanted subcutaneously in KM mouse. Then mice randomized into vehicle and treatment groups, and mice were treated with BC-02 (130 mg/kg/day, ig) and capecitabine (370 mg/kg/day, ig). The mice body weight was monitored. After 2 weeks, all mice were sacrificed and dissected to weigh the tumor tissues. Animal experiment was approved by the Guidelines of the Animal Care and Use Committee of Weifang Medical University. The protocol was approved by the Animal Care and Use Committee of Weifang Medical University.

Statistical Analysis

Data was presented as the mean ± SD, and analyzed by Student's two-tailed *t*-test. The limit of statistical significance was $P < 0.05$. Statistical analysis was done with SPSS/Win11.0 software (SPSS Inc., Chicago, IL, United States).

RESULTS

Cytotoxic Agent Results in Upregulation of CD13 Expression

As shown in **Figure 1A**, after the 5FU treatment, CD13 expression was upregulated in hepatoma tumor cells, such as

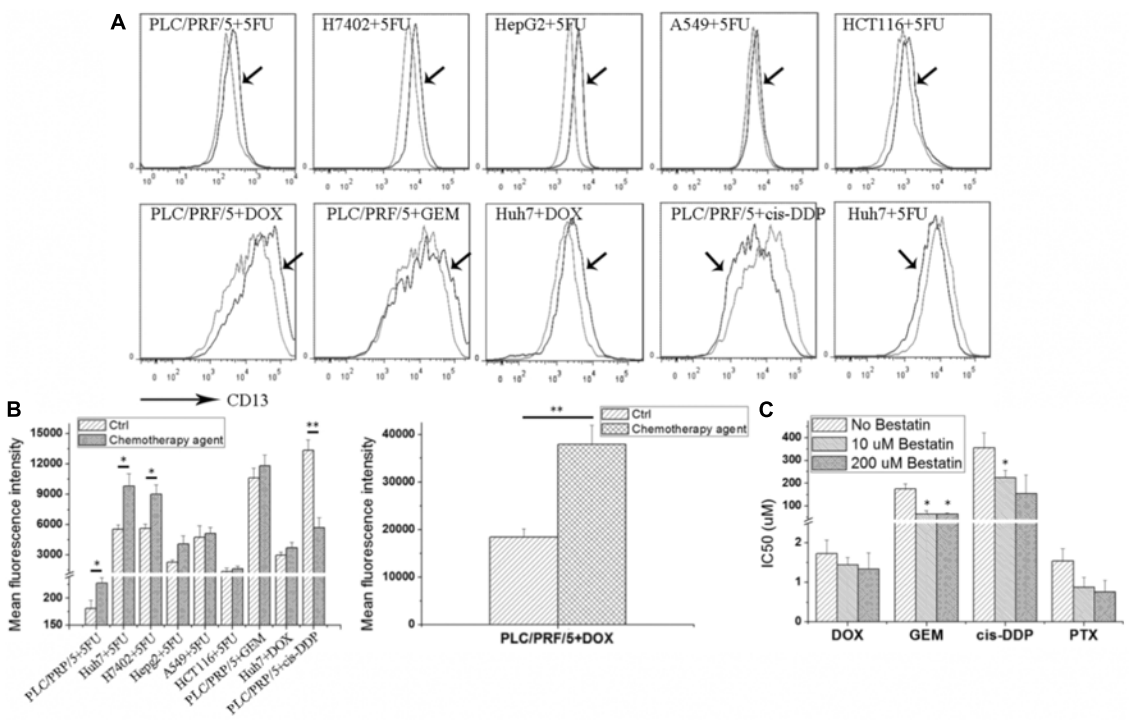

FIGURE 1 | Cytotoxic agents increase CD13 expression, and CD13 inhibitor bestatin enhances the antitumor effect of cytotoxic agents. Different tumor cells were incubated with low cytotoxic agent dosage for 3 days, and CD13 expression was detected **(A)**. Geometric mean fluorescence intensity was shown **(B)**. MTT assay was employed to detect the viability inhibition after cytotoxic agent treatments combined with different bestatin concentrations **(C)**. Data represent mean ± SD ($n = 3$). $^*P < 0.05$ and $^{**}P < 0.01$ vs. Ctrl.

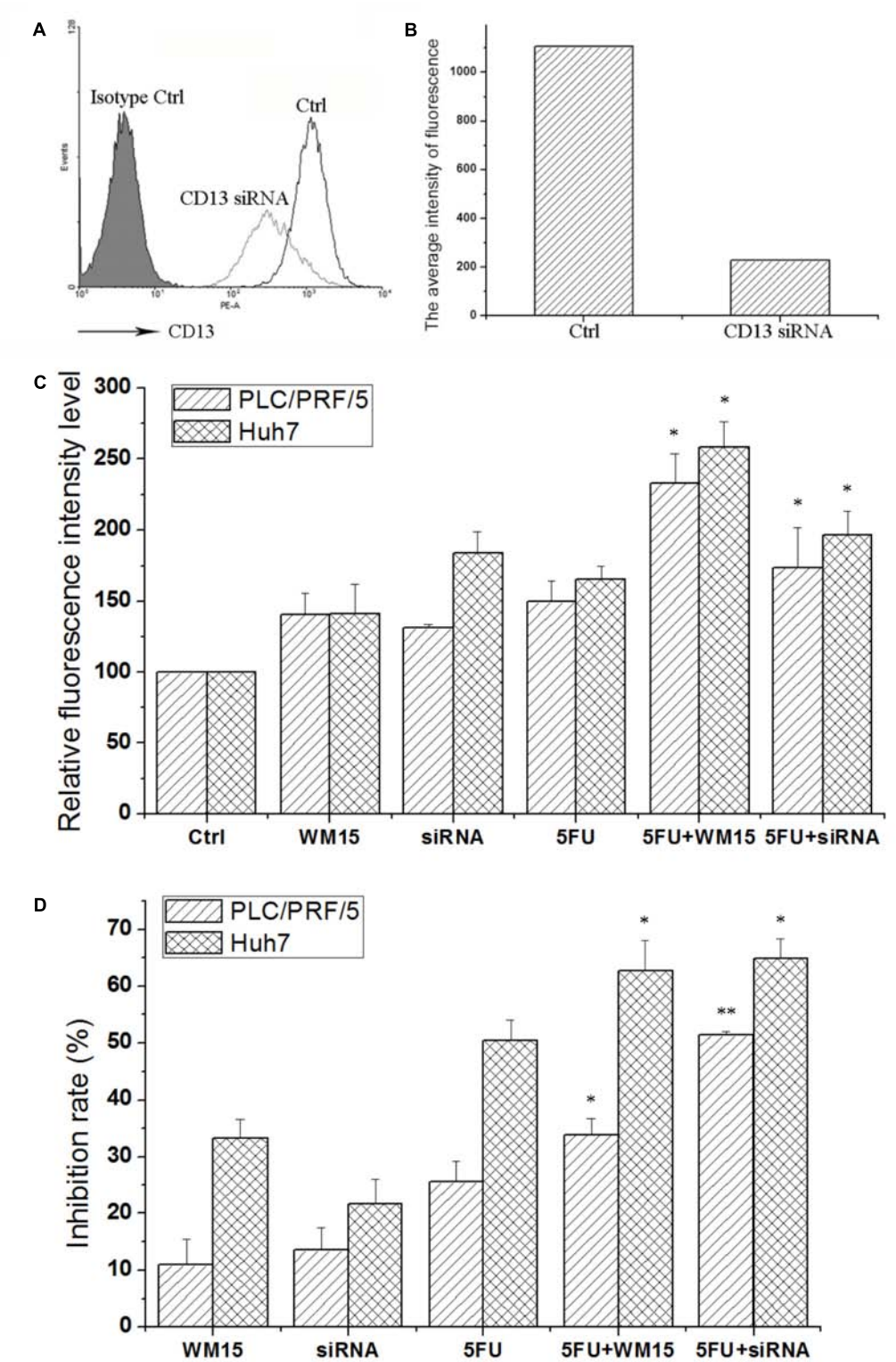

FIGURE 2 | CD13 inhibition enhances the cytotoxic effect of 5FU. PLC/PRF/5 cells were transfected with CD13-targeting siRNA. FCS was used to detect CD13 expression **(A)**. **(B)** The average intensity of fluorescence of one experiment. The results were from a representative of at least three repeated experiments. PLC/PRF/5 and Huh7 cells were treated with CD13-neutralizing antibody, CD13-targeting siRNA, 5FU, a combination of neutralizing antibody and 5FU, and a combination of siRNA and 5FU. Then, ROS level **(C)** and cell viability **(D)** were detected. Data represent mean ± SD ($n = 3$). *$P < 0.05$ vs. 5FU, **$P < 0.01$ vs. 5FU. The transfection protocol was performed according to the instructions of lipofection 2000.

PLC/PRF/5, Huh7, H7402, and HepG2. 5FU could also increase CD13 expression in human alveolar epithelial cell line A549 and human colon cancer cell HCT116. Other cytotoxic agents, such as DOX and GEM, could also increase CD13 expression in PLC/PRF/5 and Huh7 cells. Meanwhile, cis-DDP could decrease CD13 expression of in PLC/PRF/5 cells.

CD13 upregulation induced by cytotoxic agent treatments demonstrated that CD13 may contribute to cell resistance to anticancer drugs. We supposed that CD13 inhibitor should enhance the cytotoxic effect of these agents. Our data indicated that CD13 inhibitor bestatin could enhance the cytotoxic effect of DOX, GEM, cis-DDP, and PTX (**Figure 1B**). Combination of bestatin and cytotoxic agents remarkably inhibited the cell viability of PLC/PRF/5 cells, compared with single treatment of cytotoxic agents (**Figure 1C**). Thus, the increased CD13 expression may protect cells from cytotoxic agents, and CD13 inhibitor bestatin enhances the cytotoxic effect of anticancer drugs.

CD13-Targeting siRNA and Neutralizing Antibody Increase the ROS Level and Inhibit Cell Viability

Although bestatin could enhance the cytotoxic effect of anticancer drugs, off-target effect for small molecular compound was observed. To certify the role of CD13 in protecting cells resistant to cytotoxic agent, CD13-targeting siRNA and neutralizing antibody were employed to suppress CD13. CD13-targeting siRNA could remarkably decrease CD13 expression (**Figures 2A,B**). siRNA and neutralizing antibody could also increase the ROS level in PLC/PRF/5 and Huh7 cells (**Figure 2C**). Compared with single 5FU, a combination of siRNA and neutralizing antibody with 5FU could remarkably increase the ROS level (**Figure 2C**). We also obtained similar result in MTT assay. Compared with single 5FU, siRNA and neutralizing antibody could remarkably enhance the inhibitory effect of 5FU on proliferation (**Figure 2D**). These data prove the importance of

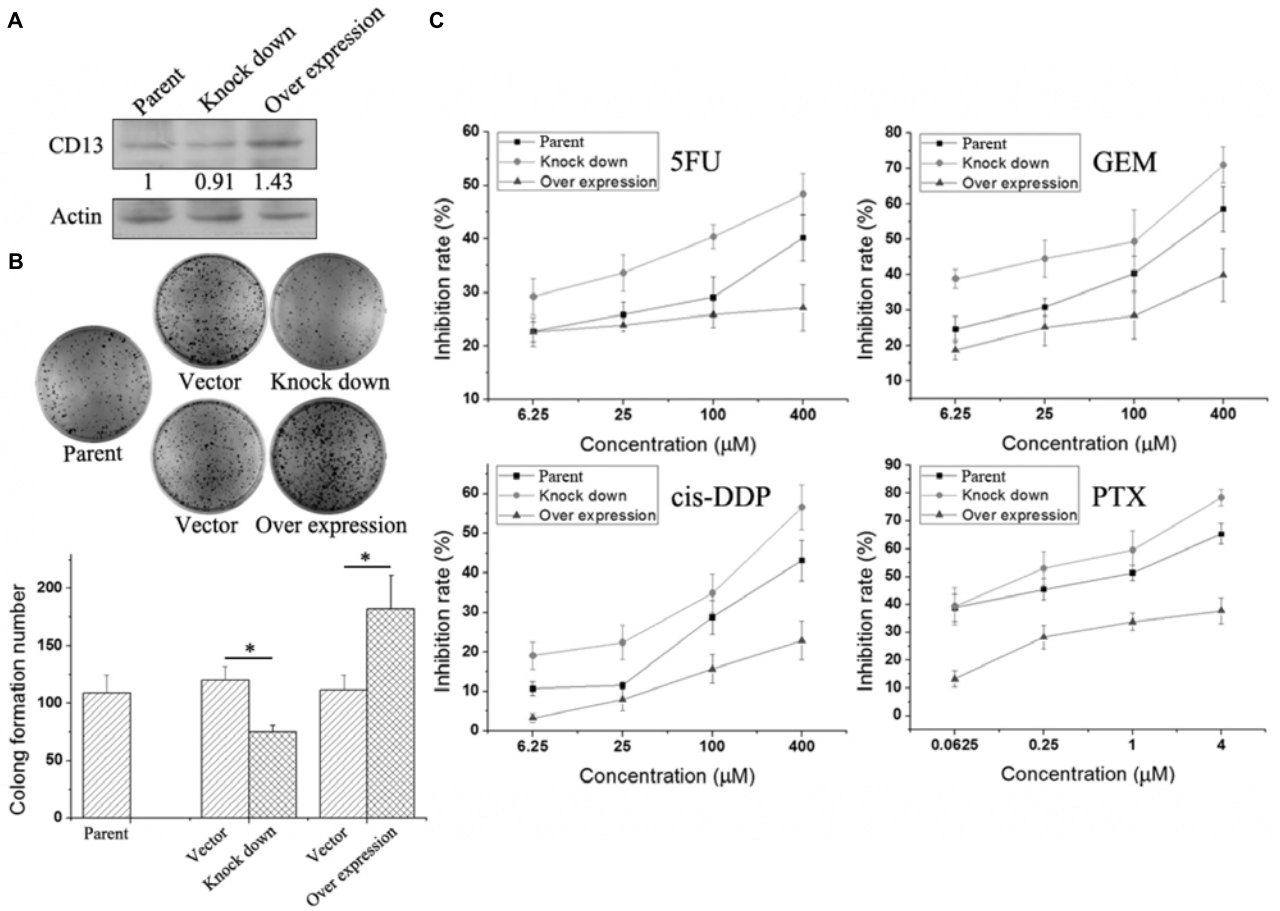

FIGURE 3 | Effect of CD13 expression on drug resistance. PLC/PRF/5 cells were infected with lentivirus. After puromycin screening, PLC/PRF/5 cells with stable CD13 overexpression or knockdown were obtained **(A)**. A representative immunoblot from three independent experiments giving similar results is shown for each western blot experiment. Densitometry for western blot was performed using AlphaEaseFC-v4.0.0 program. 1×10^3 PLC/PRF/5 cells, vector control, stable CD13 overexpression or knockdown PLC/PRF/5 cells were seeded in 6-well plates. Approximately 1 week later, cells were dyed with 0.1% crystal violet, and then photographs were taken **(B)**. The inhibition rate of different cytotoxic agents on overexpressed or knocked down cells were determined **(C)**. Data represent mean ± SD ($n = 3$). *$P < 0.05$.

CD13 in tumor cell proliferation through the modulation of ROS generation.

CD13 Overexpression Induces Cell Resistant to Cytotoxic Agent and CD13 Knockdown Leads to Sensitivity to Cytotoxic Agent

To further verify the relationship between CD13 expression and drug resistance, we used a lentiviral vector to overexpress or knockdown CD13 expression. PLC/PRF/5 cells with stable CD13 overexpression or knockdown were obtained (**Figure 3A**). CD13 overexpression or knockdown could promote or inhibit cell colony formation (**Figure 3B**). Then, we detected the sensitivity of cells to cytotoxic agents. Compared with parental cells, CD13 overexpression induced cell resistance to 5FU, GEM, cis-DDP, and PTX (**Figure 3C**). In addition, CD13 knockdown sensitized cells to cytotoxic agents (**Figure 3C**).

BC-02 Induces Higher ROS Generation Than 5FU and Inhibits Cell Viability

Compound BC-02 can be degraded into bestatin and 5FU (Dou et al., 2017). And BC-02 could inhibit the viability of PLC/PRF/5 and Huh7 cells more effectively, compared with single treatment of bestatin, 5FU, or a combination of 5FU and bestatin (**Figures 4A,B**). Clone formation assay also indicated that BC-02 could potently inhibit the clone formation of PLC/PRF/5 and Huh7 cells compared with 5FU and 1:1 combination group (**Figure 4C**). To verify specificity, we used CD13-neutralizing antibody, which could inhibit clone formation. Meanwhile, a combination of neutralizing antibody and 5FU could markedly inhibit clone formation compared

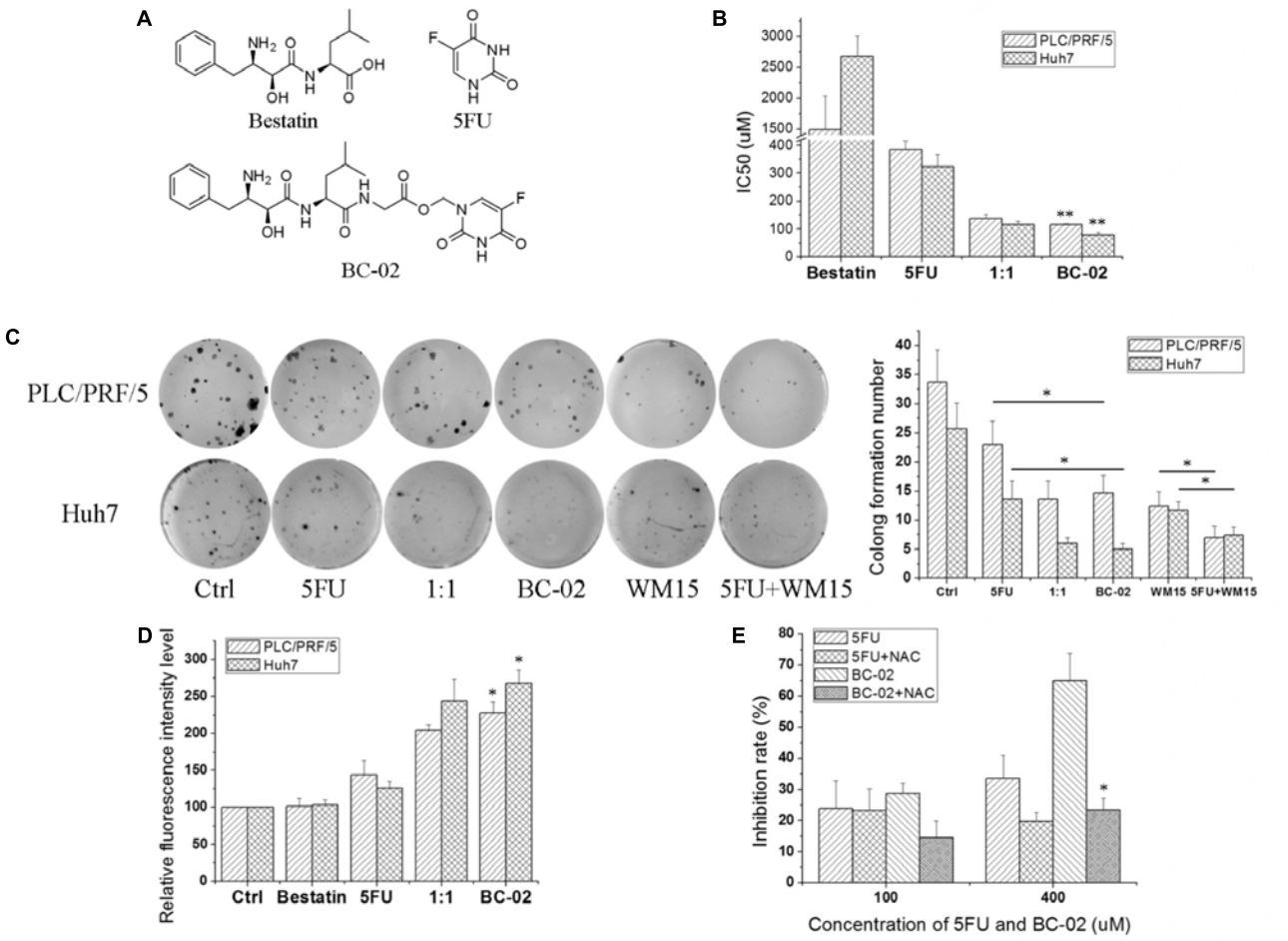

FIGURE 4 | BC-02 increases ROS level and inhibits cell viability. **(A)** The chemical structure of compounds. PLC/PRF/5 and Huh7 cells were treated with bestatin, 5FU, equal bestatin and 5FU molars (1:1), and BC-02 for 48 h. Inhibition rate was determined using MTT assay, and IC50 value was calculated **(B)**. **(C)** 250 PLC/PRF/5 or Huh7 cells were seeded in 48-well plates. After 8 h, 2 μM drugs or 1 μg/ml neutralizing antibody were added. Approximately 1 week later, cells were dyed with 0.1% crystal violet, and then photographs were taken. **(D)** PLC/PRF/5 and Huh7 cells were treated with different drugs for 5 h, and ROS level was detected. **(E)** MTT assay was used to detect the inhibition rate of 5FU, 5FU+500 μM NAC, BC-02, and BC-02+500 μM NAC by using PLC/PRF/5 cells. Data represent mean ± SD ($n = 3$). $^{*}P < 0.05$, $^{**}P < 0.01$.

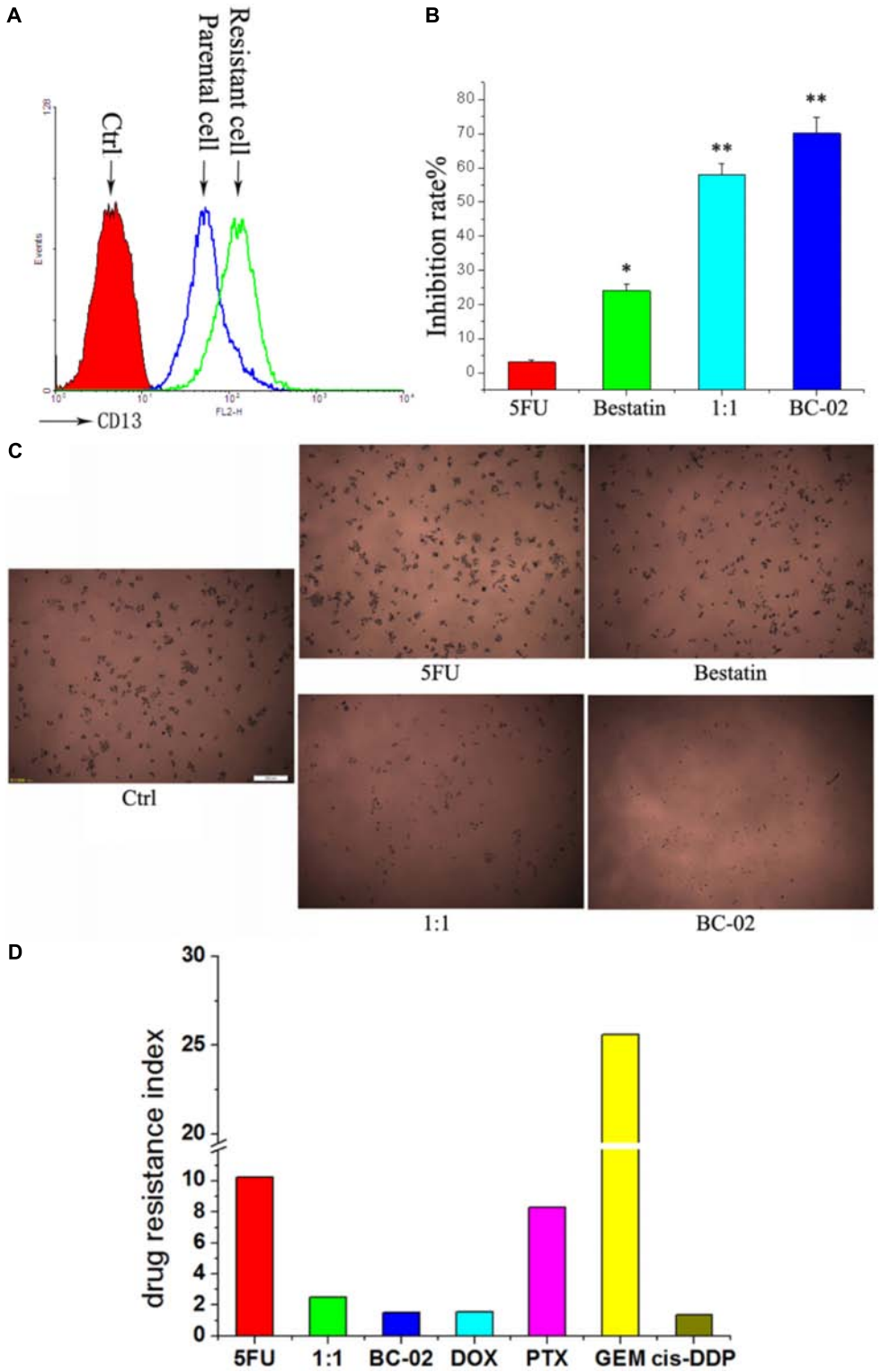

FIGURE 5 | BC-02 inhibits the viability of 5FU-resistant cells. After long period of 5FU incubation, 5FU-resistance PLC/PRF/5 cells (PLC/PRF/5-5FU) can survive at 40 μM 5FU. CD13 expression was detected by FCS **(A)**. The inhibition rate of different drugs at a concentration 100 μM on PLC/PRF/5-5FU cells were determined **(B)**. After MTT was added for 2 h, photographs of cells were taken **(C)**. The IC50 values of different cytotoxic agents on PLC/PRF/5 and PLC/PRF/5-5FU cells were determined using MTT assay. In addition, drug resistance index was calculated using the IC50 value of PLC/PRF/5-5FU cells versus the IC50 value of PLC/PRF/5 cells **(D)**. Data represent mean ± SD ($n = 3$). *$P < 0.05$, **$P < 0.01$ vs. 5FU.

with neutralizing antibody or 5FU alone (**Figure 4C**). Moreover, cellular ROS was detected by FCS. These data indicated that BC-02 could induce significantly higher level of ROS in PLC/PRF/5 and Huh7 cells more effectively, compared with single treatment of bestatin, 5FU, or a combination of 5FU and bestatin (**Figure 4D**). Moreover, ROS scavenger *N*-acetyl-L-cysteine (NAC) could protect cells from the cytotoxic effects of 5FU and BC-02 (**Figure 4E**). All these data together indicated that cell growth was inhibited through CD13 inhibition due to ROS generation.

5FU-Resistant Cancer Cells With Upregulated CD13 Expression Are More Sensitive to BC-02 Than 5FU

It is common to meet chemo-resistance for patients with HCC. Whether the chemo-resistant cells overexpress CD13 and remain sensitive to BC-02? To uncover this problem, we established 5FU-resistant PLC/PRF/5 cells (PLC/PRF/5-5FU) through low dose of 5FU incubation. After a long duration time of incubation with 5FU, PLC/PRF/5-5FU cells could survive at a concentration of 40 μM 5FU. FCS data confirmed that CD13 expression was upregulated in PLC/PRF/5-5FU chemo-resistant cells (**Figure 5A**). Moreover, PLC/PRF/5-5FU cells were resistant to 5FU but sensitive to BC-02 after being treated with 100 μM of either 5FU, bestatin, 5FU+bestatin (1:1), or BC-02 (**Figure 5B**). Photographs were also taken after MTT was added (**Figure 5C**). Almost no cells were observed in the BC-02 group. MTT assay further confirmed that almost no 5FU resistant cancer cells could survive after BC-02 treatment. The IC50 values of different cytotoxic agents to PLC/PRF/5 and PLC/PRF/5-5FU cells were determined, and drug resistance index was calculated using the IC50 value of PLC/PRF/5-5FU cells versus the IC50 value of PLC/PRF/5 cells. PLC/PRF/5-5FU cells were resistant to 5FU, PTX, and GEM, which were sensitive to BC-02, DOX, and cis-DDP, respectively (**Figure 5D**). All these data indicated that both parental and 5FU resistant cancer cells remain sensitive to BC-02.

BC-02 Inhibits H22 Tumor Growth *in vivo*

Capecitabine, a prodrug of 5FU, is used as a first- and second-line drugs for HCC treatment by several clinical trials (Murer et al., 2016; Casadei Gardini et al., 2017). The *in vivo* antitumor activity of capecitabine was stronger than that of 5FU in H22 cell-bearing Kunming (KM) mice transplant model (data not shown). Therefore, capecitabine was chosen as the positive control for our study in antitumor activity evaluation *in vivo*. In lifespan extension assay, H22 cell-bearing KM mice were treated with capecitabine (1 mmol/kg/day, iv), BC-02(①) (0.15 mmol/kg/day, iv), BC-02(②) (0.075 mmol/kg, bid, iv), or BC-02(③) (0.1125 mmol/kg, bid, iv). Both BC-02 and

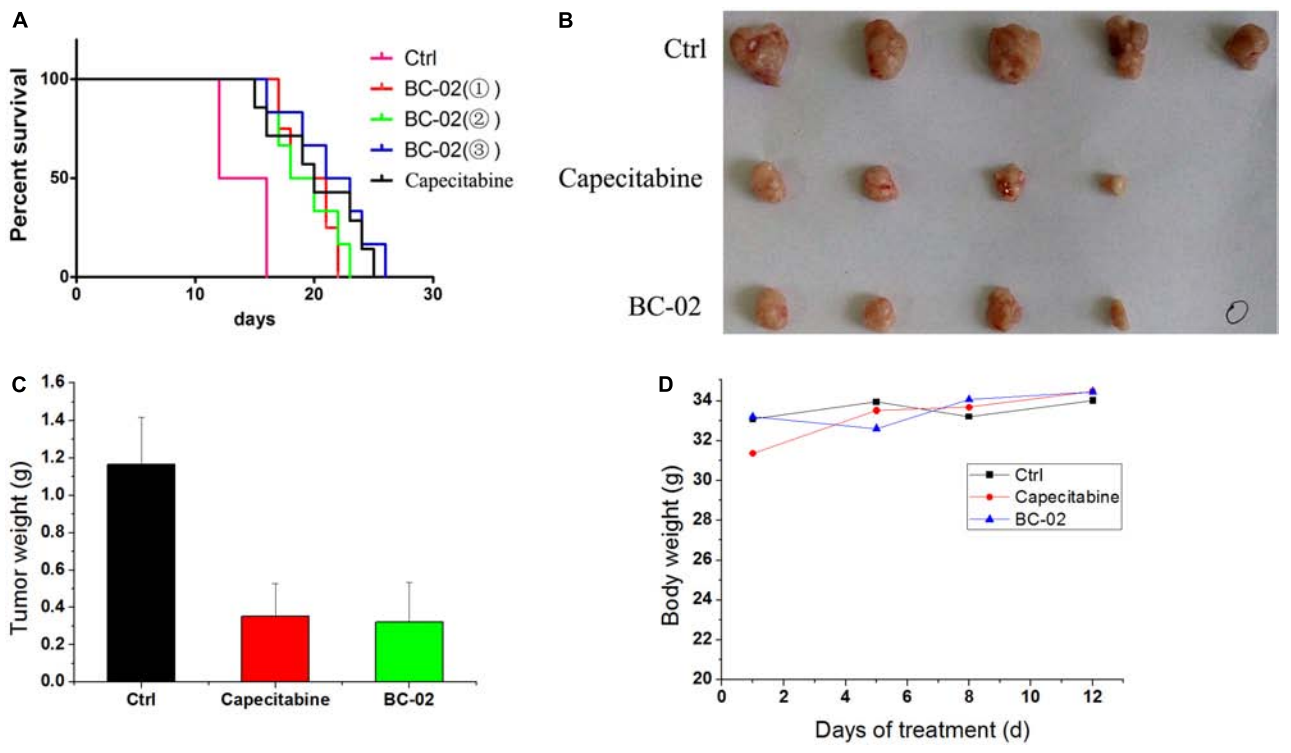

FIGURE 6 | Antitumor activities of BC-02 *in vivo*. 3 × 10^6 H22 cells were injected to the enterocoelia of Kunming mice. Then, mice were divided into different groups and treated with BC-02 and capecitabine, and survival period was recorded **(A)**. Capecitabine-resistant H22 cells was inoculated subcutaneously in KM mice, and they were treated with BC-02 and capecitabine. Then, mice body weight was monitored **(D)**. After 2 weeks, all mice were sacrificed and dissected to weigh tumor tissues **(B,C)**. "○" means no tumor was found.

capecitabine could extend the lifespan of mice, while BC-02(③) (0.1125 mmol/kg, bid, iv) was more potent than capecitabine (**Figure 6A**).

We also detected whether BC-02 inhibit the growth of capecitabine-resistant H22 cell. As described in the method section, capecitabine-resistant H22 cells were implanted subcutaneously in KM mice, and they were treated with BC-02 (130 mg/kg/day, ig) or capecitabine (370 mg/kg/day, ig). Both BC-02 and capecitabine could inhibit tumor growth (**Figures 6B,C**). No decrease in body weight was observed indicating the safety of BC-02 (**Figure 6D**). All together, BC-02 showed potent anti-tumor activity comparable to capecitabine *in vivo*.

DISCUSSION

HCC accounts for 85–90% of all liver cancer (El-Serag, 2011; Chacko and Samanta, 2016). Only a small portion of patients with HCC are available for surgery due to delayed diagnosis (Diaz-Gonzalez et al., 2016; Grandhi et al., 2016; Llovet et al., 2016; Mazzanti et al., 2016; Mazzoccoli et al., 2016). Because of low response rate and high toxicity, many chemotherapy agents have limited usage and can only provide minimal benefit to the survival time of patients with HCC (Simonetti et al., 1997; Connell et al., 2016). In this study, we found that CD13 was a therapeutic target which can reverse tumor cell MDR. Through the inhibition of CD13 activity, bestatin could enhance the cytotoxic effects of 5FU and other chemotherapy agents. Therefore, bestatin can be used as a good strategy for tumor therapy.

CD13 is a biomarker in human liver CSCs (Haraguchi et al., 2010), which are related to cancer MDR, recurrence, and metastasis. Therefore, we detected the relationship between CD13 and MDR. The results showed that CD13 inhibitor bestatin, CD13-neutralizing antibody, and CD13-targeting siRNA all could enhance the cytotoxic effect of 5FU and other chemotherapy agents. CD13 overexpression in PLC/PRF/5 cells could cause resistance to chemotherapy agents, while knocking down of CD13 could make PLC/PRF/5 cells to became sensitive to chemotherapy agents. All of these data together indicated that CD13 is a good therapeutic target to reverse MDR.

CD13-neutralizing antibody and bestatin can increase the ROS level in $CD13^{+}CD90^{-}$ PLC/PRF/5 and $CD13^{+}CD133^{+}$ Huh7 CSCs (Haraguchi et al., 2010). Excess of ROS induces cytotoxicity and apoptosis of cancer cells. Our previous work also indicated that BC-02 impaires the properties of liver CSCs by targeting CD13 and upregulating the intracellular ROS and ROS-induced DNA damage (Dou et al., 2017). APN inhibitor 4cc also synergizes the antitumor effects of 5FU in human liver cancer cells via ROS-mediated drug resistance inhibition and concurrent activation of the mitochondrial pathways of apoptosis (Sun et al., 2015). Therefore, we detected the relationship between CD13 inhibition and ROS. FCS data indicated that CD13 inhibitor bestatin, CD13-neutralizing antibody, and CD13 targeting-siRNA all could enhance the ROS upregulation effect of 5FU in tumor cells. Therefore, through CD13 inhibition, tumor cells cannot resist the ROS upregulation effect of 5FU, thereby leading to proliferation inhibition. Gclm participates in ROS scavenger pathway and encodes the glutamate-cysteine ligase which catalyzes the rate-limiting synthesis step of glutathione (GSH). GSH works as a critical cellular anti-oxidant and reducing agent. Gclm is overexpressed in the $CD13^{+}CD90^{-}$ fraction in PLC/PRF/5 cells (Haraguchi et al., 2010). Therefore, CD13 may protect cells from excessive ROS through up-regulation of Gclm.

Capecitabine has been tested as first- and second-line treatments for HCC by some studies (Murer et al., 2016; Casadei Gardini et al., 2017), and its antitumor activity was higher than that of 5FU in the mice transplant model. In the present assay, the capecitabine dosage was the maximum endurable dosage, while BC-02 was used at a much lower dosage. When treated with equal dosage, BC-02 performed better than capecitabine (data not shown). Moreover, BC-02 (0.1125 mmol/kg, bid, iv) was also more potent than the maximum endurable capecitabine dosage in lifespan assay. Furthermore, BC-02 was also sensitive in capecitabine-resistant H22 model. BC-02 achieved its antitumor activity through ROS upregulation. Silver nanoparticles also increased ROS level and lead to cell apoptosis (Wei et al., 2015). If BC-02 can be made into silver nanoparticles, its antitumor activity will be strengthened.

Li et al. (2015) reports that combining 5FU and bestatin could enhance the anticancer activity of 5FU in human tumor-derived cell lines and an H22 tumor-bearing mouse model. The authors mainly focused on normal tumor cells. In this study, we further indicated that the inhibition of CD13 could reverse the resistance of HCC cells to 5FU. ROS up-regulation is involved in the CD13 suppression induced cell death. However, we didn't detect the ROS generation and elimination molecular. Therefore, the underlying molecular mechanism is still unclear and needs further research.

CONCLUSION

Our study revealed CD13 as a promising target to reverse MDR. Through CD13 inhibition, the cytotoxic effect of chemo-agents will be enhanced via ROS upregulation. By the release of bestatin and 5FU, BC-02 remained sensitive to resistant cells. Taken together, BC-02 can be developed as a potent chemotherapeutic agent for human liver cancer.

AUTHOR CONTRIBUTIONS

JZ and CF participated in most of the experiments, such as cell biology and molecular biology experiments. MQ, HW, and XjuW performed the FCS assay. HZ and HM performed the MTT assay. ZZ and YH performed the mice assay. LS performed the colon assay. SL and ZG directed the data analysis. XjiW and WS designed the project.

FUNDING

This work was supported by National Natural Science Foundation of China (81503108, 31671208, and 81272319), the Project of Shandong Province Higher Educational Science and Technology Program (J15LM58), and Weifang Medical University Doctoral Scientific Research Foundation (2017BSQD12 and 2017BSQD33).

REFERENCES

Alves, R. C., Alves, D., Guz, B., Matos, C., Viana, M., Harriz, M., et al. (2011). Advanced hepatocellular carcinoma. Review of targeted molecular drugs. *Ann. Hepatol.* 10, 21–27.

Cao, H., Phan, H., and Yang, L. X. (2012). Improved chemotherapy for hepatocellular carcinoma. *Anticancer Res.* 32, 1379–1386.

Casadei Gardini, A., Foca, F., Scartozzi, M., Silvestris, N., Tamburini, E., Faloppi, L., et al. (2017). Metronomic capecitabine versus best supportive care as second-line treatment in hepatocellular carcinoma: a retrospective study. *Sci. Rep.* 7:42499. doi: 10.1038/srep42499srep42499

Cervello, M., McCubrey, J. A., Cusimano, A., Lampiasi, N., Azzolina, A., and Montalto, G. (2012). Targeted therapy for hepatocellular carcinoma: novel agents on the horizon. *Oncotarget* 3, 236–260. doi: 10.18632/oncotarget.466

Chacko, S., and Samanta, S. (2016). Hepatocellular carcinoma: a life-threatening disease. *Biomed. Pharmacother.* 84, 1679–1688. doi: 10.1016/j.biopha.2016.10.078

Cheng, H. Y., Wang, X., Chen, D., Xu, A. M., and Jia, Y. C. (2005). The value and limitation of transcatheter arterial chemoembolization in preventing recurrence of resected hepatocellular carcinoma. *World J. Gastroenterol.* 11, 3644–3646. doi: 10.3748/wjg.v11.i23.3644

Connell, L. C., Harding, J. J., and Abou-Alfa, G. K. (2016). Advanced hepatocellular cancer: the current state of future research. *Curr. Treat. Options Oncol.* 17:43. doi: 10.1007/s11864-016-0415-310.1007/s11864-016-0415-3

Deng, G. L., Zeng, S., and Shen, H. (2015). Chemotherapy and target therapy for hepatocellular carcinoma: new advances and challenges. *World J. Hepatol.* 7, 787–798. doi: 10.4254/wjh.v7.i5.787

Diaz-Gonzalez, A., Reig, M., and Bruix, J. (2016). Treatment of hepatocellular carcinoma. *Dig. Dis.* 34, 597–602. doi: 10.1159/000445275000445275

Dou, C., Fang, C., Zhao, Y., Fu, X., Zhang, Y., Zhu, D., et al. (2017). BC-02 eradicates liver cancer stem cells by upregulating the ROS-dependent DNA damage. *Int. J. Oncol.* 51, 1775–1784. doi: 10.3892/ijo.2017.4159

El-Serag, H. B. (2011). Hepatocellular carcinoma. *N. Engl. J. Med.* 365, 1118–1127. doi: 10.1056/NEJMra1001683

Gottesman, M. M., Fojo, T., and Bates, S. E. (2002). Multidrug resistance in cancer: role of ATP-dependent transporters. *Nat. Rev. Cancer* 2, 48–58. doi: 10.1038/nrc706

Grandhi, M. S., Kim, A. K., Ronnekleiv-Kelly, S. M., Kamel, I. R., Ghasebeh, M. A., and Pawlik, T. M. (2016). Hepatocellular carcinoma: from diagnosis to treatment. *Surg. Oncol.* 25, 74–85. doi: 10.1016/j.suronc.2016.03.002S0960-7404(16)30001-9

Guo, Q., Sui, Z. G., Xu, W., Quan, X. H., Sun, J. L., Li, X., et al. (2017). Ubenimex suppresses Pim-3 kinase expression by targeting CD13 to reverse MDR in HCC cells. *Oncotarget* 8, 72652–72665. doi: 10.18632/oncotarget.2019420194

Haraguchi, N., Ishii, H., Mimori, K., Tanaka, F., Ohkuma, M., Kim, H. M., et al. (2010). CD13 is a therapeutic target in human liver cancer stem cells. *J. Clin. Invest.* 120, 3326–3339. doi: 10.1172/JCI4255042550

Jiang, Y., Li, X., Hou, J., Huang, Y., Wang, X., Jia, Y., et al. (2018). Synthesis and biological characterization of ubenimex-fluorouracil conjugates for anti-cancer therapy. *Eur. J. Med. Chem.* 143, 334–347. doi: 10.1016/j.ejmech.2017.11.074

Lai, A., Ghaffari, A., Li, Y., and Ghahary, A. (2012). Microarray-based identification of aminopeptidase N target genes in keratinocyte conditioned medium-stimulated dermal fibroblasts. *J. Cell. Biochem.* 113, 1061–1068. doi: 10.1002/jcb.23438.

Li, J., Wang, X., Hou, J., Huang, Y., Zhang, Y., and Xu, W. (2015). Enhanced anticancer activity of 5-FU in combination with Bestatin: evidence in human tumor-derived cell lines and an H22 tumor-bearing mouse. *Drug Discov. Ther.* 9, 45–52. doi: 10.5582/ddt.2015.01006.

Llovet, J. M., Zucman-Rossi, J., Pikarsky, E., Sangro, B., Schwartz, M., Sherman, M., et al. (2016). Hepatocellular carcinoma. *Nat. Rev. Dis. Primers* 2:16018. doi: 10.1038/nrdp.2016.18

Mazzanti, R., Arena, U., and Tassi, R. (2016). Hepatocellular carcinoma: where are we? *World J. Exp. Med.* 6, 21–36. doi: 10.5493/wjem.v6.i1.21

Mazzoccoli, G., Miele, L., Oben, J., Grieco, A., and Vinciguerra, M. (2016). Biology, epidemiology, clinical aspects of hepatocellular carcinoma and the role of sorafenib. *Curr. Drug Targets* 17, 783–799. doi: 10.2174/1389450117666151209120831

Mlynarsky, L., Menachem, Y., and Shibolet, O. (2015). Treatment of hepatocellular carcinoma: steps forward but still a long way to go. *World J. Hepatol.* 7, 566–574 doi: 10.4254/wjh.v7.i3.566

Murer, F., Pozzan, C., Peserico, G., and Farinati, F. (2016). Capecitabine in advanced hepatocellular carcinoma. *Dig. Liver Dis.* 48, 1260–1261. doi: 10.1016/j.dld.2016.06.037S1590-8658(16)30516-3

Shin, J. W., and Chung, Y. H. (2013). Molecular targeted therapy for hepatocellular carcinoma: current and future. *World J. Gastroenterol.* 19, 6144–6155. doi: 10.3748/wjg.v19.i37.6144

Simonetti, R. G., Liberati, A., Angiolini, C., and Pagliaro, L. (1997). Treatment of hepatocellular carcinoma: a systematic review of randomized controlled trials. *Ann. Oncol.* 8, 117–136. doi: 10.1023/A:1008285123736

Su, L., Cao, J., Jia, Y., Zhang, X., Fang, H., and Xu, W. (2012). Development of synthetic aminopeptidase N/CD13 inhibitors to overcome cancer metastasis and angiogenesis. *ACS Med. Chem. Lett.* 3, 959–964. doi: 10.1021/ml3000758

Sun, Z. P., Zhang, J., Shi, L. H., Zhang, X. R., Duan, Y., Xu, W. F., et al. (2015). Aminopeptidase N inhibitor 4cc synergizes antitumor effects of 5-fluorouracil on human liver cancer cells through ROS-dependent CD13 inhibition. *Biomed. Pharmacother.* 76, 65–72. doi: 10.1016/j.biopha.2015.10.023S0753-3322(15)00241-3

Tokuhara, T., Hattori, N., Ishida, H., Hirai, T., Higashiyama, M., Kodama, K., et al. (2006). Clinical significance of aminopeptidase N in non-small cell lung cancer. *Clin. Cancer Res.* 12, 3971–3978. doi: 10.1158/1078-0432.CCR-06-0338

Tsurusaki, M., and Murakami, T. (2015). Surgical and locoregional therapy of HCC: tace. *Liver Cancer* 4, 165–175. doi: 10.1159/000367739lic-0004-0165

Wang, X., Jing, F., Zhu, H., Fang, H., Zhang, J., and Xu, W. (2011). Activity screening and structure-activity relationship of the hit compounds targeting APN/CD13. *Fundam. Clin. Pharmacol.* 25, 217–228. doi: 10.1111/j.1472-8206.2010.00844.xFCP844

Wei, L., Lu, J., Xu, H., Patel, A., Chen, Z. S., and Chen, G. (2015). Silver nanoparticles: synthesis, properties, and therapeutic applications. *Drug Discov. Today* 20, 595–601. doi: 10.1016/j.drudis.2014.11.014

Yamashita, M., Wada, H., Eguchi, H., Ogawa, H., Yamada, D., Noda, T., et al. (2016). A CD13 inhibitor, ubenimex, synergistically enhances the effects of anticancer drugs in hepatocellular carcinoma. *Int. J. Oncol.* 49, 89–98. doi: 10.3892/ijo.2016.3496

Conflict of Interest Statement: The authors declare that the research was conducted in the absence of any commercial or financial relationships that could be construed as a potential conflict of interest.

frontiers in Pharmacology

RESEARCH SNAPSHOT
published: 11 October 2018
doi: 10.3389/fphar.2018.01160

A Cell Model Suitable for a High-Throughput Screening of Inhibitors of the Wnt/β-Catenin Pathway

*Marina Grimaldi[1,2,3,4], Abdelhay Boulahtouf[1,2,3,4], Corinne Prévostel[1,2,3,4], Alain Thierry[1,2,3,4], Patrick Balaguer[1,2,3,4] and Philippe Blache[1,2,3,4]**

[1] Institut de Recherche en Cancérologie de Montpellier, Montpellier, France, [2] INSERM, U1194, Montpellier, France, [3] Université de Montpellier, Montpellier, France, [4] Institut Régional du Cancer de Montpellier, Montpellier, France

OPEN ACCESS

Edited by:
Yunkai Zhang,
Vanderbilt University Medical Center, United States

Reviewed by:
Zhenfang Du,
Vanderbilt University Medical Center, United States
Mao Wang,
St. John's University, United States

***Correspondence:**
Philippe Blache
philippe.blache@inserm.fr

Specialty section:
This article was submitted to Experimental Pharmacology and Drug Discovery, a section of the journal Frontiers in Pharmacology

Received: *14 August 2018*
Accepted: *24 September 2018*
Published: *11 October 2018*

Citation:
Grimaldi M, Boulahtouf A, Prévostel C, Thierry A, Balaguer P and Blache P (2018) A Cell Model Suitable for a High-Throughput Screening of Inhibitors of the Wnt/β-Catenin Pathway. Front. Pharmacol. 9:1160. doi: 10.3389/fphar.2018.01160

A constitutive activation of the Wnt/β-catenin pathway is an initiating event in colon carcinogenesis. We developed colon cancer cells models that highlight the non-selectivity of previously described inhibitors of the Wnt pathway and we propose our model as a suitable screening system for inhibitors of the pathway.

Keywords: cell models, Wnt/β-catenin pathway, inhibitors, high-throughput screening, colorectal cancer

RESULTS

A constitutive activation of the Wnt/β-catenin signaling pathway is admitted as an initiating event of carcinogenesis in at least 90% of colorectal cancers (Giles et al., 2003). This constitutive activity is mostly due to mutations of the APC tumor suppressor that result in the accumulation of β-catenin in the nucleus where β-catenin interacts with TCFs transcription factors to activate the transcription of target genes like c-myc (Sansom et al., 2007). To date, very few molecules targeting the Wnt pathway have been discovered and none has been yet approved for clinical practice (Kahn, 2014). Therefore, there is a great interest in identifying new inhibitors of Wnt signaling for clinical use.

Luciferase-based reporter assays are widely used for studying gene expression at the transcriptional level. Here, we use such a system to set up a high-throughput screening assay for inhibitors of the Wnt/β-catenin signaling pathway by using DLD-1 cells stably transfected with a luciferase TCF reporter plasmid (Veeman et al., 2003). The choice of a good control was critical given that a previous work dedicated to screen new Wnt inhibitors had recently been retracted due to a non-selective inhibition of the firefly luciferase activity (Li et al., 2017). Besides, a reporter system based on mutated TCF binding sites is available, but has a very low basal luciferase activity and is rather a control for a non-specific activation of the Wnt pathway. Here, we developed a genetically modified DLD-1 cell line model expressing the firefly luciferase under the control of the E2F1 promoter, an independent promoter of the WNT pathway.

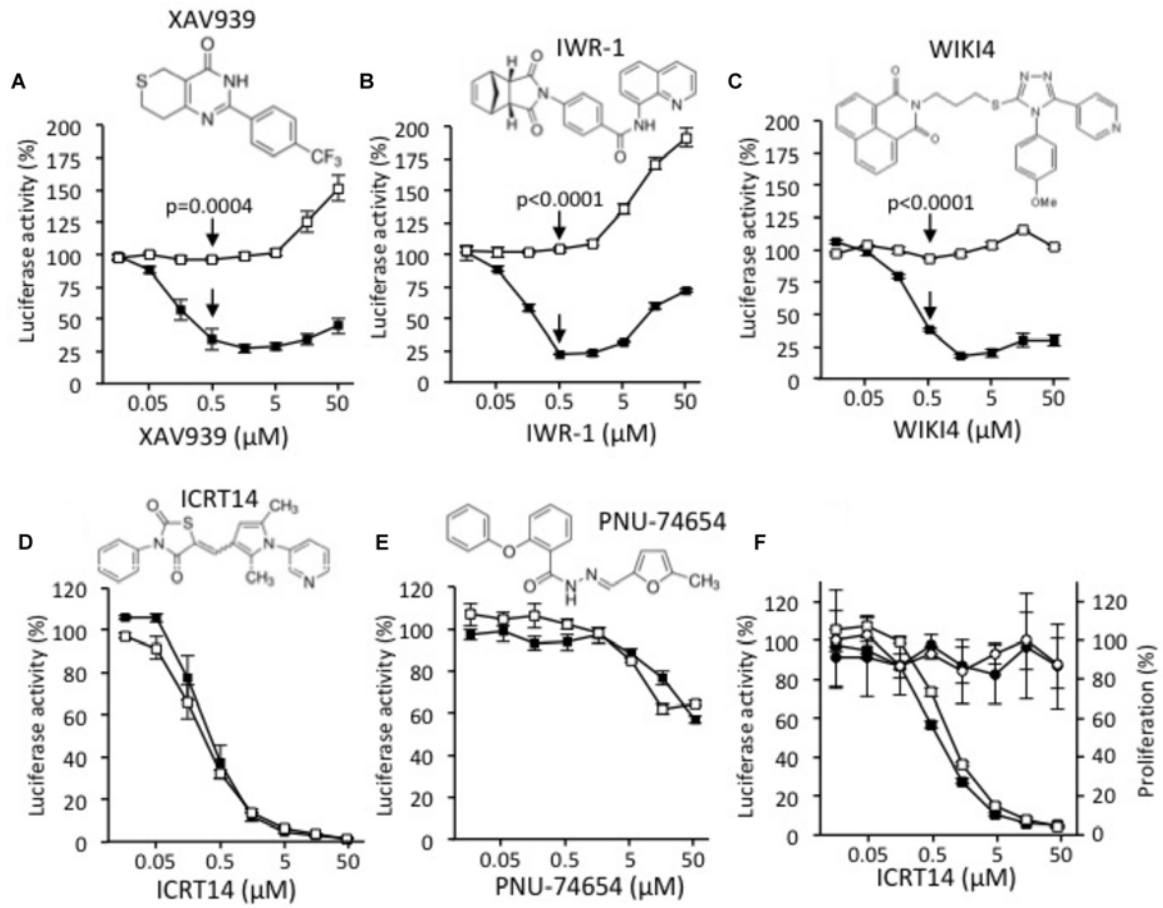

FIGURE 1 | Effects of XAV939 **(A)**, IWR-1 **(B)**, WIKI4 **(C)**, ICRT14 **(D)**, and PNU-74654 **(E)** on luciferase activity of DLD1-Wnt-luc cells (black squares) and of DLD1-luc control cells (white squares). **(F)** MTT assay was performed in presence of ICRT14 on DLD1-Wnt-luc cells (black circles) and on DLD1-luc control cells (white circles). In parallel, luciferase activity of DLD1-Wnt-luc cells (black squares) and of DLD1-luc control cells (white squares) was measured. The Student's *t*-test was performed for doses of 0.5 μM and the probability of error (*p*-value) is indicated by arrows.

Two types of available Wnt inhibitors were used in order to validate the model: the tankyrase (TNKS) inhibitors XAV939 (Huang et al., 2009), IWR-1 (Chen et al., 2009) and WIKI4 (James et al., 2012), and the destabilizers of the TCF/β-catenin complex ICRT14 (Gonsalves et al., 2011) and PNU-74654 (Trosset et al., 2006). TNKS acts as an activator of the Wnt/β-catenin signaling by mediating poly-adenosine diphosphate (ADP) ribosylation of AXIN-1 and -2, two key components of the β-catenin destruction complex whose inhibition enhances β-catenin degradation and consequently inhibits the Wnt/β-catenin signaling (Yamada and Masuda, 2017).

XAV939 (**Figure 1A**), IWR-1 (**Figure 1B**), and WIKI4 (**Figure 1C**) specifically inhibited the activity of the Wnt/β-catenin signaling, with and IC50 of 0.13, 0.21 and 0.28 μM, respectively. However, a side activating effect was observed at doses higher than 1 μM as evidenced by the increase of the luciferase activity observed in the control conditions. Besides, both ICRT14 (**Figure 1D**) and PNU-74654 (**Figure 1E**) behaved as non-selective inhibitors as evidenced by the inhibition of both Wnt dependent and independent luciferase activities. In addition, PNU-74654 was poorly efficient. To further determine whether the apparent inhibitory effect of ICRT14 on the Wnt independent luciferase activity was due to a toxicity, or not, we evaluated the impact of ICRT14 on cells viability by using the MTT system in parallel with measurement of the luciferase activity. As shown in **Figure 1F**, ICRT14 again decreased both Wnt dependent and independent luciferase activities in a dose dependent manner but had no significant effect on cells viability.

MATERIALS AND METHODS

Luciferase and MTT assays were done as we previously described (Molina-Molina et al., 2008). More details about the methods are available in the **Supplementary Material**.

DISCUSSION

With respects to the use of inhibitors previously reported as specific, studies have concluded that biological activities were

regulated by the Wnt/β-catenin pathway. In the present study, we demonstrate that the destabilizers of the TCF/β-catenin complex ICRT14 and PNU-74654 are unspecific inhibitors of the Wnt/β-catenin pathway. Therefore, to test the implication of the Wnt pathway in a biological mechanism, it seems more rationable to use at least one of the specific inhibitors confirmed here. Compared with the original reference system dedicated to test the impact of compounds on the activity of the Wnt/β-catenin signaling pathway, our method was set-up with an adequate control that lowers the number of false positives resulting from a non-specific inhibition of the luciferase enzymatic activity. For example, using our method points out ICRT14 as a non-specific inhibitor of the Wnt/β-catenin signaling pathway. Besides, true positives will have to be dose-dependent tested, and their ability to decrease the proliferation of colon cancer cells will have to be evaluated for further potential therapeutic purposes.

AUTHOR CONTRIBUTIONS

CP, PhB, and PaB designed the study. CP, PhB, and AT drafted the manuscript. MG, AB, and PhB performed the experimental work.

FUNDING

INSERM, the Institut du Cancer de Montpellier, and Lilly France financially supported this work.

SUPPLEMENTARY MATERIAL

The Supplementary Material for this article can be found online at: https://www.frontiersin.org/articles/10.3389/fphar.2018.01160/full#supplementary-material

REFERENCES

Chen, B., Dodge, M. E., Tang, W., Lu, J., Ma, Z., Fan, C.-W., et al. (2009). Small molecule-mediated disruption of Wnt-dependent signaling in tissue regeneration and cancer. *Nat. Chem. Biol.* 5, 100–107. doi: 10.1038/nchembio.137

Giles, R. H., van Es, J. H., and Clevers, H. (2003). Caught up in a Wnt storm: Wnt signaling in cancer. *Biochem. Biophys. Acta* 1653, 1–24.

Gonsalves, F. C., Klein, K., Carson, B. B., Katz, S., Ekas, L. A., Evans, S., et al. (2011). An RNAi-based chemical genetic screen identifies three small-molecule inhibitors of the Wnt/wingless signaling pathway. *Proc. Natl. Acad. Sci. U.S.A.* 108, 5954–5963. doi: 10.1073/pnas.1017496108

Huang, S.-M. A., Mishina, Y. M., Liu, S., Cheung, A., Stegmeier, F., Michaud, G. A., et al. (2009). Tankyrase inhibition stabilizes axin and antagonizes Wnt signalling. *Nature* 461, 614–620. doi: 10.1038/nature08356

James, R. G., Davidson, K. C., Bosch, K. A., Biechele, T. L., Robin, N. C., Taylor, R. J., et al. (2012). WIKI4, a novel inhibitor of tankyrase and Wnt/ß-catenin signaling. *PLoS One* 7:e50457. doi: 10.1371/journal.pone.0050457

Kahn, M. (2014). Can we safely target the WNT pathway? *Nat. Rev. Drug Discov.* 13, 513–532. doi: 10.1038/nrd4233

Li, Y., Oliver, P. G., Lu, W., Pathak, V., Sridharan, S., Augelli-Szafran, C. E., et al. (2017). SRI36160 is a specific inhibitor of Wnt/β-catenin signaling in human pancreatic and colorectal cancer cells. *Cancer Lett.* 389, 41–48. doi: 10.1016/j.canlet.2016.12.030

Molina-Molina, J.-M., Escande, A., Pillon, A., Gomez, E., Pakdel, F., Cavaillès, V., et al. (2008). Profiling of benzophenone derivatives using fish and human estrogen receptor-specific in vitro bioassays. *Toxicol. Appl. Pharmacol.* 232, 384–395. doi: 10.1016/j.taap.2008.07.017

Sansom, O. J., Meniel, V. S., Muncan, V., Phesse, T. J., Wilkins, J. A., Reed, K. R., et al. (2007). Myc deletion rescues Apc deficiency in the small intestine. *Nature* 446, 676–679. doi: 10.1038/nature05674

Trosset, J.-Y., Dalvit, C., Knapp, S., Fasolini, M., Veronesi, M., Mantegani, S., et al. (2006). Inhibition of protein-protein interactions: the discovery of druglike beta-catenin inhibitors by combining virtual and biophysical screening. *Proteins* 64, 60–67. doi: 10.1002/prot.20955

Veeman, M. T., Slusarski, D. C., Kaykas, A., Louie, S. H., and Moon, R. T. (2003). Zebrafish prickle, a modulator of noncanonical Wnt/Fz signaling, regulates gastrulation movements. *Curr. Biol.* 13, 680–685. doi: 10.1016/S0960-9822(03)00240-9

Yamada, T., and Masuda, M. (2017). Emergence of TNIK inhibitors in cancer therapeutics. *Cancer Sci.* 108, 818–823. doi: 10.1111/cas.13203

Conflict of Interest Statement: The authors declare that the research was conducted in the absence of any commercial or financial relationships that could be construed as a potential conflict of interest.

The reviewer ZD and handling Editor declared their shared affiliation.

frontiers in Oncology

REVIEW
published: 02 November 2018
doi: 10.3389/fonc.2018.00507

Targeted p53 on Small-Molecules-Induced Ferroptosis in Cancers

*Weifen Zhang[1], Chengcheng Gai[2], Dejun Ding[1], Fang Wang[3] and Wentong Li[2]**

[1] Department of Pharmacology, Weifang Medical University, Weifang, China, [2] Department of Pathology, Weifang Medical University, Weifang, China, [3] School of Clinical Medicine, Weifang Medical University, Weifang, China

OPEN ACCESS

Edited by:
Zhe-Sheng Chen,
St. John's University, United States

Reviewed by:
Wenjun Wu,
University of Chicago, United States
Pranav Gupta,
Massachusetts General Hospital, Harvard Medical School, United States
De-shen Wang,
Sun Yat-sen University Cancer Center (SYSUCC), China

***Correspondence:**
Wentong Li
liwentong11@163.com

Specialty section:
This article was submitted to Cancer Molecular Targets and Therapeutics, a section of the journal Frontiers in Oncology

Received: *23 September 2018*
Accepted: *16 October 2018*
Published: *02 November 2018*

Citation:
Zhang W, Gai C, Ding D, Wang F and Li W (2018) Targeted p53 on Small-Molecules-Induced Ferroptosis in Cancers. Front. Oncol. 8:507. doi: 10.3389/fonc.2018.00507

Ferroptosis is a type of programmed cell death characterized by the accumulation of lipid reactive oxygen species (L-ROS) driven by the oxidative degeneration of lipids in an iron-dependent manner. The mechanism by which lipid oxidative degradation drives ROS-ferroptosis involves metabolic dysfunctions that result in impaired intracellular metabolic processes and ROS production. Recent studies have found that p53 acts as a positive regulator of ferroptosis by promoting ROS production. p53 directly regulates the metabolic versatility of cells by favoring mitochondrial respiration, leading to ROS-mediated ferroptosis. In mild stress, p53 protects cell survival via eliminating ROS; additionally, in human colorectal cancer, p53 antagonizes ferroptosis by formation of the DPP4–p53 complex. In short, the mechanisms of p53-mediated ROS production underlying cellular response are poorly understood. In the context of recent research results, the indistinct roles of p53 on ROS-mediated ferroptosis are scrutinized to understand the mechanism underlying p53-mediated tumor suppression.

Keywords: p53, ferroptosis, reactive oxygen species, tumor suppression, metabolic gene

INTRODUCTION

Ferroptosis, a new form of cell death, was first described in a high-throughput screening of molecules for selectively inducing cell death in RAS mutant isoform cancer cells (1). As a novel subtype of programmed cell death, ferroptosis is primarily characterized by increased mitochondrial membrane density and volume shrinkage with distinct morphological, biochemical, and genetic differences from other types of cell death, including apoptosis, necrosis, necroptosis, and autophagy; for instance, the typical characteristics of apoptosis, including activated caspases, chromatin condensation, and DNA fragmentation, are absent in ferroptosis (1, 2), the distinctive morphological feature of erastin-treated cells involved smaller mitochondria with increased membrane density (3). In addition, loss of the plasma membrane integrity of necrotic morphological features and formation of double membrane-layered autophagic vacuoles during autophagy are not observed in ferroptosis.

Small molecules belonging to class I and class II ferroptosis-inducing agents trigger ferroptosis via inhibiting cystine-glutamate exchange transporter (*system* X_c^-) and glutathione peroxidase 4 (GPX4), respectively (4). Class I ferroptosis inducers, such as erastin, sorafenib, sulfasalazine and the neurotransmitter glutamate, *system* X_c^-, class II ferroptosis inducers, such as RSL3, FIN56 (5), or altretamine (6) are shown to induce ferroptosis via inhibition of GPX4.

Recent studies have reported that p53 activation is essential for ferroptosis in certain cancers. Since the discovery of p53, its role on tumor suppression in tumorigenesis and cancer therapy has attracted considerable attention. Loss of p53 is a vital event in the tumorigenesis of many human cancers (7, 8). In general, the tumor suppression activity of p53 in response to cellular stress relies on its capability to elicit cell-cycle arrest, apoptosis, and senescence. Nevertheless, recent efforts indicate that other unconventional activities of p53 are also crucial for tumor suppression (9, 10).

Novel roles of p53 on tumor suppression have come to light when a synthetic mutant of p53, incapable of transactivating the majority of known p53 target genes, displays antitumor activities in unstressed organisms and some cancer-prone mouse models (10, 11). A mutant p53 that loses acetylation at some definite residues of the DNA binding domain is disabled to evoke growth arrest, senescence, and apoptosis, thereby inhibiting spontaneous tumor development through sensitizing cells to ferroptosis (12, 13). Given that p53 is a main regulatory factor of critically important cellular biological processes, elucidating the mechanism by which p53 responds to stress may clarify the upstream signaling of ferroptosis. In the context of recent insights, the indistinct roles of p53 signaling in reactive oxygen species (ROS)-mediated ferroptosis via the transcriptional and non-transcriptional regulation of metabolic targets are scrutinized (**Table 1**).

ACTIVATION OF P53 SENSITIZES CELLS TO ROS AND TRIGGERS FERROPTOSIS

Increased accumulation of lipid reactive oxygen species (L-ROS) in an iron-dependent manner is a fundamental characteristic of ferroptosis (14, 27). Metabolic dysfunctions contribute to ferroptosis by elevating the production of ROS independent of mitochondria (5). Thus, several investigations have been devoted to elucidate the regulatory roles of p53 on metabolic targets in ROS production for regulating ferroptosis.

p53 participates in various cellular processes by acting as a DNA binding transcription factor that selectively modulates the expression of target genes. For example, wild-type p53 regulates the transactivation of cytochrome c oxidase 2 (SCO2), favoring mitochondrial respiration over glycolysis (28). In addition, p53 plays a negative regulatory role on glycolysis via transcriptionally modulating glucose transporter (GLUT)1, GLUT4 (24), TP53-induced glycolysis and apoptosis regulator (TIGAR), and glutaminase 2 (GLS2) (15, 29) (**Figure 1**). p53 could also suppress glucose metabolism directly by binding and inhibiting glucose-6-phosphate dehydrogenase (30). Clearly, p53 directly adjusts the metabolic polyfunctionality of cells by supporting mitochodial respiration, leading to ROS-mediated ferroptosis.

MODULATION OF P53 ON THE EXPRESSION OF SLC7A11 TO MEDIATE FERROPTOSIS

p53 Represses SLC7A11 Expression

SLC7A11 (xCT) is a light-chain subunit of the membrane Na^+-dependent *system* X_c^-, which is a disulfide-linked heterodimer composed of SLC7A11 and a heavy-chain subunit (SLC3A2) (31). Previous experiments showed the inconformity in the p53 activation and expression of SLC7A11, which could directly affect ferroptosis in mouse embryonic fibroblast (MEF) cells (32). *System* X_c^- transfers intracellular glutamate to the extracellular space and extracellular cystine into cells (33). Cystine is then converted into cysteine for synthesizing glutathione (GSH), which protects cells from oxidative stress. Inhibition of *system* X_c^- reduces intracellular GSH, resulting in an iron-dependent ferroptosis mediated by the accumulation of L-ROS (23).

Activation of p53 by nutlin-3 markedly decreases SLC7A11 expression in HT-1080 cells with basal *system* X_c^- activity (34). Knockdown of p53 completely abrogates the inhibition of SLC7A11 (35), and *system* X_c^- function and SLC7A11 expression in $p53^{KO}$ cells are insensitive to nutlin-3 (36). Furthermore, microarray analysis confirmed that SLC7A11 is a novel target gene of p53 in a tetracycline-controlled p53-inducible cell line (13). A previous study identified a p53-binding sequence at the 5′ flanking region of the SLC7A11 gene and subsequently confirmed the formation of a p53–DNA complex at the promoter region (13). The transcriptional repression of p53 on SLC7A11 leads to the destruction of cystine import, resulting in declined glutathione production and enhanced ROS-mediated ferroptosis (**Figure 2**).

p53-Dependent Repression of SLC7A11 Is Independent of p53 Mutation

The molecular cascade whereby p53 restrains cystine transfer by suppressing SLC7A11 expression to induce ferroptosis may be conducive to the oncosuppressive roles of p53 (13). Although an acetylation-absent $p53^{3KR}$ (K117/161/162R) variant at certain lysine residues cannot transcriptionally activate gene expression involved in pro-apoptotic and cell cycle arrest, knock-in mice expressing $p53^{3KR}$ are not tumor prone and exhibit similar overall survival with the wild-type mice (12). Similarly, studies on $p53^{25,26}$, a transactivation-compromised mutant variant of p53, displayed intact tumor suppression of $p53^{3KR}$ in the absence of the most downstream genes of p53 (10). Reduced levels of SLC7A11 expression caused by the $p53^{3KR}$ variant in xenograft tumor models lead to an apparent depression of tumor growth (13). This finding indicates that the intact p53-SLC7A11 axis, reserved in the $p53^{3KR}$ variant, promotes the inhibition

TABLE 1 | The mechanisms of transcriptional and post-translational regulation on metabolic genes involving in ferroptosis.

Active style	Targets	Function	References
Transcriptional regulation	GLUT1, GLUT4	Negatively regulates glycolysis by transcriptional repression	(14)
	TIGAR	Negatively regulates glycolysis by transactivation	(15–17)
	GLS2	Favoring aerobic glycolysis over oxidative phosphorylation and contributing to Warburg metabolism	(11, 18–20)
	SCO2	Coupling p53 to mitochondrial respiration provides a possible interpretation for the Warburg phenomenon	(13, 21)
	SLC7A11	Repression of SLC7A11 leads to destruction of cystine import, resulting in declined glutathione production and enhanced ROS-mediated ferroptosis	(9, 15)
	RRAD	Negatively regulates glycolysis	(17)
	SAT1	lipid peroxidation and ROS-induced ferroptosis	(22)
	p21	Slower depletion of intracellular glutathione and a reduced accumulation of toxic L-ROS	(23)
Post-translational regulation	G6PDH	Suppress glucose metabolism directly via binding and inhibiting with G6PDH	(24)
	DPP4	Dismantling of DPP4-p53 complex	(25)
	SOSC1	The regulation of SAT1 by p53 was SOCS1-dependent, stabilizating p53	(26)

of tumorigenesis independent of the conventional tumor suppression mechanisms of p53. Thus, ferroptosis can ensue from the transcriptional repression of SLC7A11 in a p53-dependent mechanism in response to stress, irrespective of p53 mutational status (37).

However, whether cell ferroptosis upon ROS-induced by $p53^{3KR}$ in human cancer cells is similar to that of wild-type p53 remains unclear. In addition, whether cyclophilin D could be a downstream responder of p53 activation has yet to be clarified (38).

Acetylation Is Crucial for p53-Mediated Ferroptosis

p53 activity is controlled by a complex fine-tuning network that includes protein stability, recruitment of co-inhibitor or activator, and various post-translational modifications, such as acetylation, ubiquitination, phosphorylation, and methylation (25, 39). In particular, acetylation of p53 serves a vital role in regulating downstream targets in a promoter-specific activation during stress responses. Acetylation of p53 at K120 by Tip60/MOF is crucial for p53-induced apoptosis (40). Nevertheless, p53-mediated cell cycle arrest is involved in the combinative acetylation of K120 by Tip60/MOF and K164 by CBP/p300 (41). The $p53^{3KR}$ mouse expressing acetylation-deficient p53, similar to the K120/164R mutations in human, displays intact p53-dependent metabolic regulation but lacks p53 functions in pro-apoptosis activity and growth arrest (12).

A recent study has found that p53 is acetylated at lysine residue K98 by acetyltransferase CBP. Acetylation of p53 at K98 lysine residue in mouse does not interfere with the steady-state, DNA-binding abilities and transcriptional activity of p53. However, combinatorial absence of K117/161/162 acetylation and K98 acetylation abrogates p53-mediated transcriptional regulation on SLC7A11, TIGAR, and GLS2 (32).

Binding of p53 With DPP4 Limits Ferroptosis by Regulating SLC7A11

Although p53 induces ferroptosis in a transcription-dependent manner in various cancers, in human colorectal cancer (CRC), it unusually functions in the regulation of erastin-mediated ferroptosis. p53-deficiency contributes to the increased lipid oxidation and GSH downregulation in CRC cells treated with erastin (42). Interestingly, the aforementioned alterations in malondialdehyde and GSH were recovered after transfecting p53 cDNA into $p53^{-/-}$ CRC cells (42).

Depletion of p53 contributing to ferroptosis is involved with interdicting dipeptidyl-peptidase-4 (DPP4) activity in a transcription-independent mechanism. DPP4, a membrane-bound dimeric peptidase, is widely expressed in different cell types and can cleave and degrade various bioactive peptides biologically (43, 44). The function of DPP4 in tumorigenicity has been studied in many tumors (45). Deviant expression of DPP4 is associated with tumor aggressiveness in different cancers (18, 46). Paradoxically, some advanced malignancies, including lung squamous cell carcinoma and endometrial carcinoma, show the absence of DPP4 (22). Thus, DPP4 may play different roles in different backgrounds or cancers, and further studies are needed to elucidate the exact mechanism of DPP4 in cancer.

DPP4 has been related to increased proportion of cancer stem cells and worse prognosis of CRC patients (16). Loss of p53 restrains the nuclear localization of DPP4 and boosts plasma-membrane-associated DPP4-dependent lipid peroxidation in CRC cells; then, the DPP4–NOX complex is formed and facilitates lipid peroxidation-induced ferroptosis. p53 antagonizes ferroptosis in CRC cells by facilitating DPP4 into nuclear to form the DPP4–p53 complex; dismantling of the DPP4–p53 complex can recover the ferroptosis sensitivity of CRC cells to erastin (**Figure 3**). This mechanism differs from the previously recognized role of p53 as a positive regulator of ferroptosis in non-CRC cells (13, 32, 47, 48). Thus, the

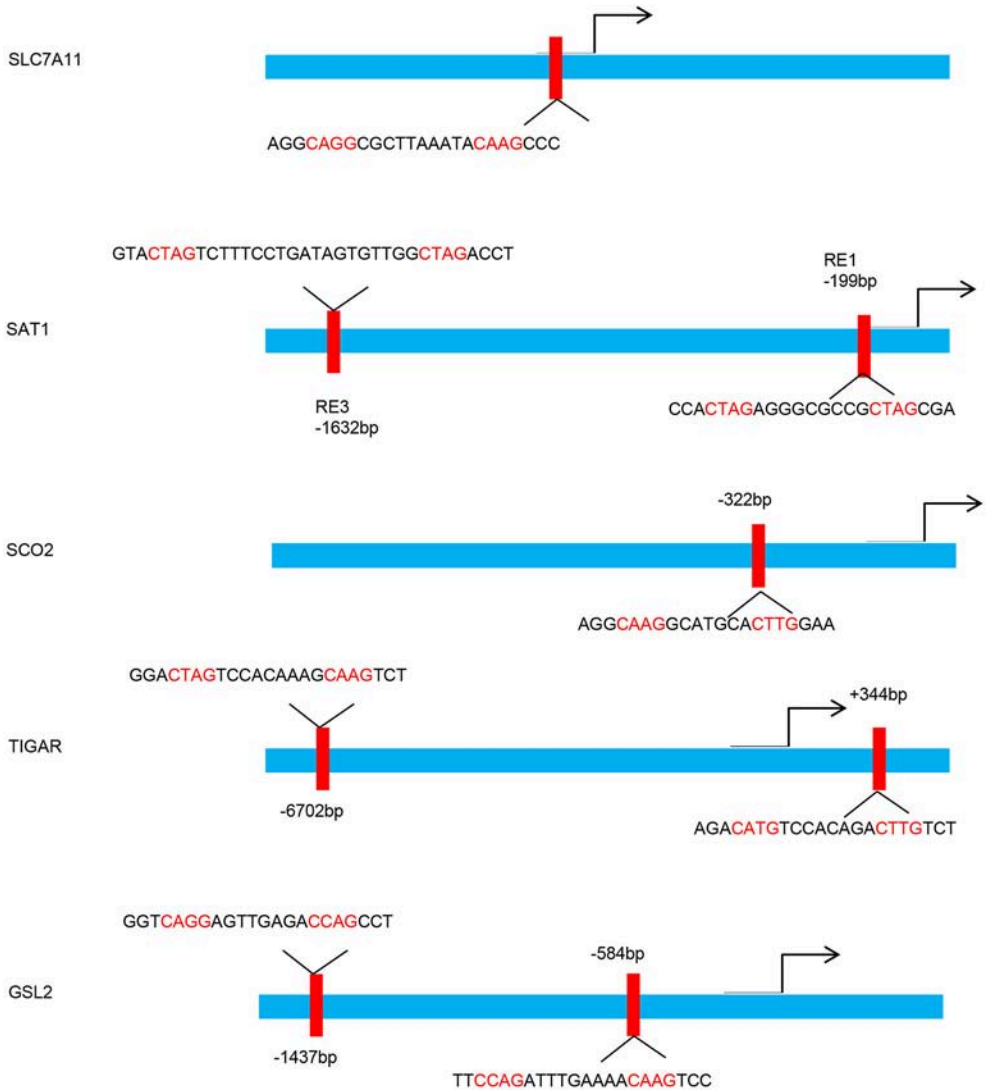

FIGURE 1 | p53 binding sites within the upstream regulatory region of the target gene promoters. Schematic diagram indicates the p53 binding sites within the upstream regulatory region of the SLC7A11, SAT1, SCO2, TIGAR, and GSL2 promoters.

bidirectional regulation of ferroptosis by p53 in a transcription-dependent and transcription-independent manner is dependent on tumor types and background.

However, many vital questions need to be elucidated. First, only two types of CRC cell lines are used in Xie's experiment (42), which is insufficient to prove the role of p53 and DPP4 on ferroptosis in CRC. Second, DPP4 is ubiquitously expressed in various cell types, including different tumors, whereas mutations and deletions of p53 are also common in malignant tumors. Further studies are needed to reveal the mechanism underlying the different roles of the DPP4–p53 complex on the regulation of SLC7A11 in CRC and other types of malignant tumors. Third, whether that p53 favors the localization of DPP4 into nuclear to form the DPP4–p53 complex could be affected by the mutation of p53 or modification of p53, such as acetylation, should be illuminated, and this may provide an answer to the opposite effects of p53 in different cellular context.

P53 REPRESSES THE TIGAR, GLS2, SCO2, AND SAT1 GENES TO MEDIATE FERROPTOSIS

TIGAR Plays an Antioxidant Functions in a p53-Dependent Manner

As a target of p53, TIGAR is prefigured to participate in tumor suppression and plays a role in antioxidant functions, which is in line with its functions in preventing cells from the acquirement of injury (49) (**Figure 2**). Nevertheless, in mouse models, the absence of TIGAR reduces capabilities to regenerate injured intestinal epithelium and represses tumor development with

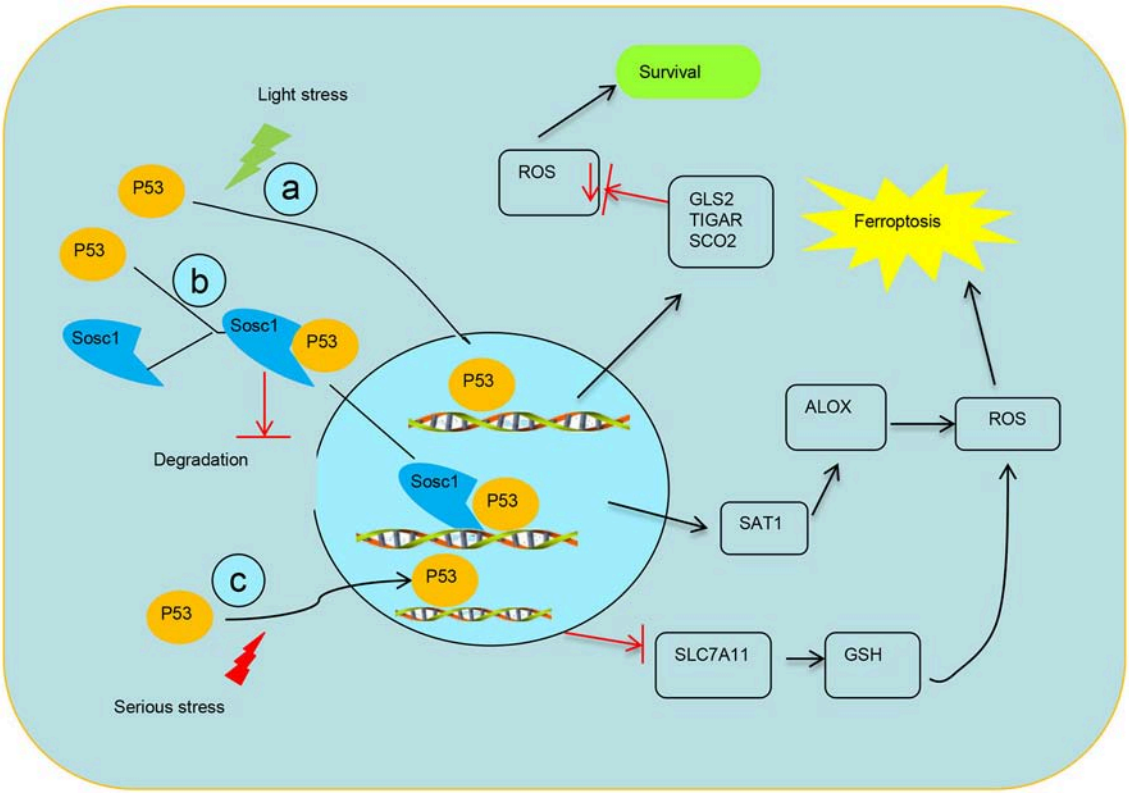

FIGURE 2 | Schematic diagram of transcriptional regulation of p53 on targets. **(a)** p53 transcriptionally represses the expression TIGAR, GLS2, and SCO2 to mediate ferroptosis. **(b)** SOCS1 is required for p53 modulating some target genes and SOCS1–p53 complex preserves a pool of preactive p53 via preventing p53 degradation. **(c)** Modulation of p53 on the expression of SLC7A11 system X_c^- activity to mediate ferroptosis.

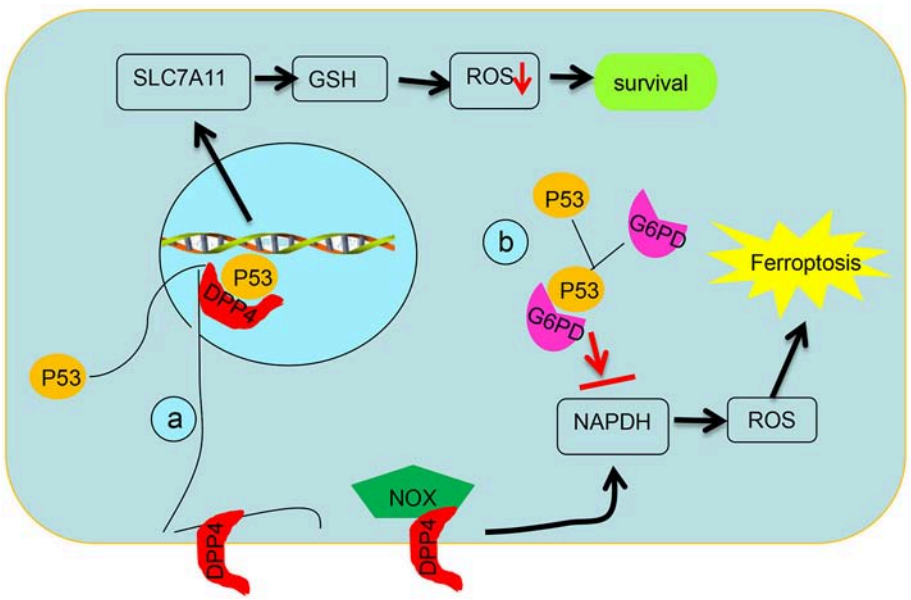

FIGURE 3 | Schematic diagram of post-translational regulation of p53 on targets. **(a)** p53 antagonizes ferroptosis by favoring DPP4 into a nuclear to form of the DPP4–p53 complex and impeding formation of the DPP4–NOX complex, which is required for lipid peroxidation in ferroptosis. **(b)** p53 suppresses glucose metabolism and production of NADPH via inhibiting glucose-6-phosphate dehydrogenase directly.

ROS restriction (50). TIGAR is upregulated in some cancer models and tumor types via a pattern that may be independent on the maintenance of p53 (51, 52). Furthermore, TIGAR expression negatively correlates with p53 expression in human breast cancer (53). p53-independent expression of TIGAR is poorly understood, although some transcription factors, such as SP1, CREB, and other members of the p53 family (p63 and p73), have been implicated in the regulation of p53 (17, 19, 54). In brief, these results highlight that TIGAR functions as a tumor suppressor in response to p53 but might also participate in cancer development when TIGAR expression is deregulated and uncoupled from p53 (20).

GLS2 Plays an Antioxidant Functions in a p53-Dependent Manner

Glutaminolysis plays crucial roles in ferroptosis (27). Glutaminolysis refers to the switch of glutamine into glutamate under the catalysis of GLS1 and GLS2. Although both enzymes are similar in structure and enzyme catalysis, GLS2 is required for ferroptosis (27). Human GLS2 gene is located on chromosome 12q13 and contains two potential p53 binding sites (BS). Adenovirus-mediated expression of p53 binds to both BS1 and BS2, but only BS2 is associated with endogenous p53. These data show that p53, once activated, can directly combine with BS2 in the GLS2 promoter and augment the mRNA expression of GLS2 (21). Upregulation of GLS2 contributes to p53-dependent ferroptosis by favoring aerobic glycolysis over oxidative phosphorylation and contributing to Warburg effect (27, 47, 55, 56) (**Figure 2**).

p53-Mediate Metabolisms via Repressing the SCO2

Synthesis of SCO2 is essential for regulating the cytochrome c oxidase complex, which is the main site of oxygen utilization in eukaryotic cells. The balance between the utilization of respiratory and glycolytic pathways is modulated by SCO2, which is a downstream target of p53 (57) (**Figure 2**). The source of energy from cellular respiration to glycolysis caused by the loss of p53 function resembles metabolic switch toward glycolysis in cancer cells with wild-type p53 when the SCO2 gene is depleted. SCO2 coupling p53 to mitochondrial respiration provides a possible interpretation for the Warburg phenomenon and supplies new ideas as to how p53 influences metabolism and ferroptosis (28).

P53-MEDIATED ACTIVATION OF SAT1 ENGAGES IN FERROPTOSIS

The polyamines, amino acid-derived polycationic alkylamines, are basic for the growth and survival of eukaryotic cells (58). Polyamine metabolism is frequently dysregulated in cancers (59). Spermidine/spermine N1-acetyltransferase 1 (SAT1), a rate-limiting enzyme, catalyzes the acetylation of spermidine and spermine into N1-acetylspermidine and N1-acetylspermine (60).

SAT1 could be highly induced by p53 (48). It is a p53-regulated target in wild-type p53 melanoma cells treated with Nutlin using RNA sequencing and two p53-binding sites have been found on the promoter region of SAT1. SAT1 transcriptionally activated in a p53-dependented manner is critical for lipid peroxidation and ROS-induced ferroptosis, and decreased expression of SAT1 significantly abrogates p53-induced ferroptosis. Elevation of prostaglandin-endoperoxide synthase 2 (PTGS2), a ferroptosis inducer, was identified in high-SAT1-expression xenograft tumors. Ferroptosis induced by SAT1 is arachidonate 15-lipoxygenase (ALOX15) dependent (**Figure 2**). ALOX15 is a lipoxygenase that catalyzes the peroxidation of arachidonic acid, and inhibition of ALOX15 can entirely rescue SAT1-induced ferroptosis. These results are consistent with the previous finding that ALOX15 is a main adjuster with which oxidative stress is transformed into lipid peroxidation and cell death (61). Nevertheless, whether that SAT1 plays a role in tumor suppression remains largely unknown.

SOCS1 REGULATES FERROPTOSIS BY ACTIVATING P53 VIA PHOSPHORYLATION AND STABILIZATION

Suppressor of cytokine signaling (SOCS) family proteins have been implicated as negative feedback regulators of cytokine signaling pathways mediated by JAK-STAT (62). SOCS is involved in tumor development by regulating STATs in the background of aberrant activation of the JAK/STAT5 pathway. In particular, SOCS1 is thought to act as a pivotal tumor suppressor through negative regulation of JAKs and plays vital roles in tumor progression. Downregulated SOCS1 expression in various human cancers has been associated with dysregulation of cytokine receptor signaling pathways (63), whereas upregulated SOCS1 expression is associated with earlier tumor stages and better clinical outcomes in breast cancer (64).

A significant correlation exists between the expression of SOCS1 and the SOCS1-dependent p53 target genes in human fibroblasts, and SOCS1 is required for p53 activation (26, 65). SOCS1-regulated genes overlap with a set of genes induced by oxidized phospholipids, which has been recently linked to ferroptosis (66). The regulation of SAT1 by p53 is SOCS1-dependent, suggesting a role for SOCS1 in ferroptosis. Aside from influencing p53 target gene expression, SOCS1 also plays a general role in senescence by stabilizing the interactions of p53 with protein complexes at DNA damage foci (**Figure 2**). This function of SOCS1 allows the maintenance of a pool of preactive p53 that could be slowly released and contribute to generate a lasting chronic p53 response (67). SOCS1 activates the functions of p53 via facilitating the serine 15 phosphorylation of p53 and stabilizing p53 by interfering with KAP1 (67).

DELAYED FERROPTOSIS ONSET REQUIRES P21

CDKN1A (encoding p21) is a well-characterized target of p53 and key mediator of p53-dependent cell-cycle progression. p21 upregulation could cause a coordinated p53-mediated response that normally decreases cystine import to match the lower

metabolic demands of growth-arrested cells. The impact of p21 on GSH metabolism renders it a reasonable target for inducing ferroptosis in the context of p53 (68). Stabilization of p53 and activation of the p53–p21 axis make many cancer cells insensitive to ferroptosis induced by *system* X_c^- inhibition or direct cystine deprivation. p21-dependent suppression of CDKs may be required to preserve GSH by regulating CDK-regulated metabolic enzymes and inhibit ferroptosis by inducing a complete cell-cycle arrest (69). However, the mechanism through which the p53–p21 axis reduces cellular reliance on *system* X_c^--mediated cystine import and ongoing *de novo* GSH synthesis is unclear (36). Thus, the p53–p21 axis may help cancer cell survive metabolic stress, such as cystine deprivation, by suppressing the onset of ferroptosis, indicating that the p53–p21 transcriptional axis negatively regulates ferroptosis in cancer cells.

S47 POLYMORPHISM OF P53 DECREASES FERROPTOSIS

Aside from mutations that impair p53 activity, single-nucleotide polymorphisms of p53 also alter cancer risk and clinical outcome significantly by impairing p53 signaling. About 20 years earlier, a naturally occurring polymorphism in p53 was discovered in Africans and African Americans; this polymorphism transforms the proline residue adjacent to Ser46 to a serine in human p53 (70). In particular, the Pro47Ser polymorphism (S47) impairs p53 apoptotic and transcriptional functions through reducing phosphorylation on serine 46 (47, 55). The defect in p53 function is traced to a restriction in downstream gene regulation that reduces cell ferroptosis in response to stress (70).

Profound cell death is induced in wild-type MEFs cells treated with erastin. However, cell viability assays certified that S47 MEFs and heterozygote S47/wild-type MEFs are resistant to erastin, especially S47 MEFs (47). Interestingly, treatment with erastin remarkably upregulates GLS2 expression in wild-type cells but not S47 cells, and depletion of GLS2 in wild-type MEFs recapitulates the cell death defect that is exhibited in S47 cells treated with erastin (47). The defective capacity of S47 to transactivate GLS2 might annotate the ferroptosis defect and tumor-prone characteristics of S47 mice (55).

In brief, elucidating the relevancy between p53 and ferroptosis has shown the other features of p53 biology and provided insights into the tumor suppression roles of p53. Clarification of the mechanism provides further insights into exploiting feasible therapeutic means through inducing ferroptosis defined by the occurrence of ROS in p53-retaining tumors. Nevertheless, the roles of p53 in ferroptosis remain formally demonstrated in different contexts due to the appearance of opposite effects in various cancer cells. Moreover, p53 could protect cells from slight stress damage via eliminating ROS, but p53-mediated ferroptosis owing to serious stress in cancer cells relies on the accumulation of ROS. Nevertheless, the mechanism of p53-mediated ROS production underlying cellular response is poorly understood.

AUTHOR CONTRIBUTIONS

WZ and CG took part in the writing of the article. DD and FW participated in the data arrangement and drawing. WL examined and verified the article.

FUNDING

This work was supported by grants from the National Natural Science Foundation of China (81774125, 81572578).

REFERENCES

1. Dixon SJ, Lemberg KM, Lamprecht MR, Skouta R, Zaitsev EM, Gleason CE, et al. Ferroptosis: an iron-dependent form of nonapoptotic cell death. *Cell* (2012) 149:1060–72. doi: 10.1016/j.cell.2012.03.042
2. Xie Y, Hou W, Song X, Yu Y, Huang J, Sun X, et al. Ferroptosis: process and function. *Cell Death Differ.* (2016) 23:369–79. doi: 10.1038/cdd.2015.158
3. Yagoda N, von Rechenberg M, Zaganjor E, Bauer AJ, Yang WS, Fridman DJ, Wolpaw AJ, et al. RAS-RAF-MEK-dependent oxidative cell death involving voltage-dependent anion channels. *Nature* (2007) 447:864–8. doi: 10.1038/nature05859
4. Conrad M, Angeli JP, Vandenabeele P, Stockwell BR. Regulated necrosis: disease relevance and therapeutic opportunities. *Nat Rev Drug Discov.* (2016) 15:348–66. doi: 10.1038/nrd.2015.6
5. Yang WS, SriRamaratnam R, Welsch ME, Shimada K, Skouta R, Viswanathan VS, et al. Regulation of ferroptotic cancer cell death by GPX4. *Cell* (2014) 156:317–31. doi: 10.1016/j.cell.2013.12.010
6. Woo JH, Shimoni Y, Yang WS, Subramaniam P, Iyer A, Nicoletti P, et al. Elucidating compound mechanism of action by network perturbation analysis. *Cell* (2015) 162:441–51. doi: 10.1016/j.cell.2015.05.056
7. Jackson JG, Lozano G. The mutant p53 mouse as a pre-clinical model. *Oncogene* (2013) 32:4325–30. doi: 10.1038/onc.2012.610
8. Wang SJ, Gu W. To be, or not to be: functional dilemma of p53 metabolic regulation. *Curr Opin Oncol.* (2014) 26:78–85. doi: 10.1097/CCO.0000000000000024
9. Junttila MR, Evan GI. p53–a Jack of all trades but master of none. *Nat Rev Cancer* (2009) 9:821–9. doi: 10.1038/nrc2728
10. Brady CA, Jiang D, Mello SS, Johnson TM, Jarvis LA, Kozak MM, et al. Distinct p53 transcriptional programs dictate acute DNA-damage responses and tumor suppression. *Cell* (2011) 145:571–83. doi: 10.1016/j.cell.2011.03.035
11. Jiang D, Brady CA, Johnson TM, Lee EY, Park EJ, Scott MP, et al. Full p53 transcriptional activation potential is dispensable for tumor suppression in diverse lineages. *Proc Natl Acad Sci USA.* (2011) 108:17123–8. doi: 10.1073/pnas.1111245108
12. Li T, Kon N, Jiang L, Tan M, Ludwig T, Zhao Y, et al. Tumor suppression in the absence of p53-mediated cell-cycle arrest, apoptosis, and senescence. *Cell* (2012) 149:1269–83. doi: 10.1016/j.cell.2012.04.026
13. Jiang L, Kon N, Li T, Wang SJ, Su T, Hibshoosh H, et al. Ferroptosis as a p53-mediated activity during tumour suppression. *Nature* (2015) 520:57–62. doi: 10.1038/nature14344
14. Torii S, Shintoku R, Kubota C, Yaegashi M, Torii R, Sasaki M, et al. An essential role for functional lysosomes in ferroptosis of cancer cells. *Biochem J.* (2016) 473:769–77. doi: 10.1042/BJ20150658
15. Hu W, Zhang C, Wu R, Sun Y, Levine A, Feng Z. Glutaminase 2, a novel p53 target gene regulating energy metabolism and antioxidant function. *Proc Natl Acad Sci USA.* (2010) 107:7455–60. doi: 10.1073/pnas.1001006107
16. Pang R, Law WL, Chu AC, Poon JT, Lam CS, Chow AK, et al. A subpopulation of CD26+ cancer stem cells with metastatic capacity in human colorectal cancer. *Cell Stem Cell* (2010) 6:603–15. doi: 10.1016/j.stem.2010.04.001

17. Zou S, Gu Z, Ni P, Liu X, Wang J, Fan Q. SP1 plays a pivotal role for basal activity of TIGAR promoter in liver cancer cell lines. *Mol Cell Biochem.* (2012) 359:17–23. doi: 10.1007/s11010-011-0993-0
18. Yamaguchi U, Nakayama R, Honda K, Ichikawa H, Hasegawa T, Shitashige M, et al. Distinct gene expression-defined classes of gastrointestinal stromal tumor. *J Clin Oncol.* (2008) 26:4100–8. doi: 10.1200/JCO.2007.14.2331
19. Lee P, Hock AK, Vousden KH, Cheung EC. p53- and p73-independent activation of TIGAR expression *in vivo*. *Cell Death Dis.* (2015) 6:e1842. doi: 10.1038/cddis.2015.205
20. Gnanapradeepan K, Basu S, Barnoud T, Budina-Kolomets A, Kung CP, Murphy ME. The p53 tumor suppressor in the control of metabolism and ferroptosis. *Front Endocrinol.* (2018) 9:124. doi: 10.3389/fendo.2018.00124
21. Suzuki S, Tanaka T, Poyurovsky MV, Nagano H, Mayama T, Ohkubo S, et al. Phosphate-activated glutaminase (GLS2), a p53-inducible regulator of glutamine metabolism and reactive oxygen species. *Proc Natl Acad Sci USA.* (2010) 107:7461–6. doi: 10.1073/pnas.1002459107
22. Kajiyama H, Kikkawa F, Ino K, Shibata K, Mizutani S. Expression of CD26/dipeptidyl peptidase IV in endometrial adenocarcinoma and its negative correlation with tumor grade. *Adv Exp Med Biol.* (2003) 524:245–8. doi: 10.1007/0-306-47920-6_29
23. Lo M, Ling V, Wang YZ, Gout PW. The xc- cystine/glutamate antiporter: a mediator of pancreatic cancer growth with a role in drug resistance. *Br J Cancer* (2008) 99:464–72. doi: 10.1038/sj.bjc.6604485
24. Schwartzenberg-Bar-Yoseph F, Armoni M, Karnieli E. The tumor suppressor p53 down-regulates glucose transporters GLUT1 and GLUT4 gene expression. *Cancer Res.* (2004) 64:2627–33. doi: 10.1158/0008-5472.CAN-03-0846
25. Kruse JP, Gu W. Modes of p53 regulation. *Cell* (2009) 137:609–22. doi: 10.1016/j.cell.2009.04.050
26. Mallette FA, Calabrese V, Ilangumaran S, Ferbeyre G. SOCS1, a novel interaction partner of p53 controlling oncogene-induced senescence. *Aging* (2010) 2:445–52. doi: 10.18632/aging.100163
27. Gao M, Monian P, Quadri N, Ramasamy R, Jiang X. Glutaminolysis and transferrin regulate ferroptosis. *Mol Cell* (2015) 59:298–308. doi: 10.1016/j.molcel.2015.06.011
28. Matoba S, Kang JG, Patino WD, Wragg A, Boehm M, Gavrilova O, et al. p53 regulates mitochondrial respiration. *Science* (2006) 312:1650–3. doi: 10.1126/science.1126863
29. Bensaad K, Tsuruta A, Selak MA, Vidal MN, Nakano K, Bartrons R, et al. TIGAR, a p53-inducible regulator of glycolysis and apoptosis. *Cell* (2006) 126:107–20. doi: 10.1016/j.cell.2006.05.036
30. Jiang P, Du W, Wang X, Mancuso A, Gao X, Wu M, et al. p53 regulates biosynthesis through direct inactivation of glucose-6-phosphate dehydrogenase. *Nat Cell Biol.* (2011) 13:310–6. doi: 10.1038/ncb2172
31. Conrad M, Sato H. The oxidative stress-inducible cystine/glutamate antiporter, system x (c) (-) : cystine supplier and beyond. *Amino Acids* (2012) 42:231–46. doi: 10.1007/s00726-011-0867-5
32. Wang SJ, Li D, Ou Y, Jiang L, Chen Y, Zhao Y, et al. Acetylation is crucial for p53-mediated ferroptosis and tumor suppression. *Cell Rep.* (2016) 17:366–73. doi: 10.1016/j.celrep.2016.09.022
33. Bridges RJ, Natale NR, Patel SA. System xc(-) cystine/glutamate antiporter: an update on molecular pharmacology and roles within the CNS. *Br J Pharmacol.* (2012) 165:20–34. doi: 10.1111/j.1476-5381.2011.01480.x
34. Dixon SJ, Patel DN, Welsch M, Skouta R, Lee ED, Hayano M, et al. Pharmacological inhibition of cystine-glutamate exchange induces endoplasmic reticulum stress and ferroptosis. *Elife* (2014) 3:e02523. doi: 10.7554/eLife.02523
35. Gupta AK, Bharadwaj M, Kumar A, Mehrotra R. Spiro-oxindoles as a promising class of small molecule inhibitors of p53-MDM2 interaction useful in targeted cancer therapy. *Top Curr Chem.* (2017) 375:3. doi: 10.1007/s41061-016-0089-0
36. Tarangelo A, Magtanong L, Bieging-Rolett KT, Li Y, Ye J, Attardi LD, et al. p53 suppresses metabolic stress-induced ferroptosis in cancer cells. *Cell Rep.* (2018) 22:569–75. doi: 10.1016/j.celrep.2017.12.077
37. Galluzzi L, Bravo-San Pedro JM, Kroemer G. Ferroptosis in p53-dependent oncosuppression and organismal homeostasis. *Cell Death Differ.* (2015) 22:1237–8. doi: 10.1038/cdd.2015.54
38. Ying Y, Padanilam BJ. Regulation of necrotic cell death: p53, PARP1 and cyclophilin D-overlapping pathways of regulated necrosis? *Cell Mol Life Sci.* (2016) 73:2309–24. doi: 10.1007/s00018-016-2202-5
39. Eischen CM, Lozano G. The Mdm network and its regulation of p53 activities: a rheostat of cancer risk. *Hum Mutat.* (2014) 35:728–37. doi: 10.1002/humu.22524
40. Sykes SM, Mellert HS, Holbert MA, Li K, Marmorstein R, Lane WS, et al. Acetylation of the p53 DNA-binding domain regulates apoptosis induction. *Mol Cell* (2006) 24:841–51. doi: 10.1016/j.molcel.2006.11.026
41. Tang Y, Zhao W, Chen Y, Zhao Y, Gu W. Acetylation is indispensable for p53 activation. *Cell* (2008) 133:612–26. doi: 10.1016/j.cell.2008.03.025
42. Xie Y, Zhu S, Song X, Sun X, Fan Y, Liu J, et al. The tumor suppressor p53 limits ferroptosis by blocking DPP4 activity. *Cell Rep.* (2017) 20:1692–704. doi: 10.1016/j.celrep.2017.07.055
43. Liang PI, Yeh BW, Li WM, Chan TC, Chang IW, Huang CN, et al. DPP4/CD26 overexpression in urothelial carcinoma confers an independent prognostic impact and correlates with intrinsic biological aggressiveness. *Oncotarget* (2017) 8:2995–3008. doi: 10.18632/oncotarget.13820
44. Carl-McGrath S, Lendeckel U, Ebert M, Rocken C. Ectopeptidases in tumour biology: a review. *Histol Histopathol.* (2006) 21:1339–53. doi: 10.14670/HH-21.1339
45. Cordero OJ, Salgado FJ, Nogueira M. On the origin of serum CD26 and its altered concentration in cancer patients. *Cancer Immunol Immunother.* (2009) 58:1723–47. doi: 10.1007/s00262-009-0728-1
46. Stremenova J, Krepela E, Mares V, Trim J, Dbaly V, Marek J, et al. Expression and enzymatic activity of dipeptidyl peptidase-IV in human astrocytic tumours are associated with tumour grade. *Int J Oncol.* (2007) 31:785–92. doi: 10.3892/ijo.31.4.785
47. Jennis M, Kung CP, Basu S, Budina-Kolomets A, Leu JI, Khaku S, et al. An African-specific polymorphism in the TP53 gene impairs p53 tumor suppressor function in a mouse model. *Genes Dev.* (2016) 30:918–30. doi: 10.1101/gad.275891.115
48. Ou Y, Wang SJ, Li D, Chu B, Gu W. Activation of SAT1 engages polyamine metabolism with p53-mediated ferroptotic responses. *Proc Natl Acad Sci USA.* (2016) 113:E6806–12. doi: 10.1073/pnas.1607152113
49. Rajendran R, Garva R, Ashour H, Leung T, Stratford I, Krstic-Demonacos M, et al. Acetylation mediated by the p300/CBP-associated factor determines cellular energy metabolic pathways in cancer. *Int J Oncol.* (2013) 42:1961–72. doi: 10.3892/ijo.2013.1907
50. Cheung EC, Athineos D, Lee P, Ridgway RA, Lambie W, Nixon C, et al. TIGAR is required for efficient intestinal regeneration and tumorigenesis. *Dev Cell* (2013) 25:463–77. doi: 10.1016/j.devcel.2013.05.001
51. Li B, Wang Z, Xie JM, Wang G, Qian LQ, Guan XM, et al. TIGAR knockdown enhanced the anticancer effect of aescin via regulating autophagy and apoptosis in colorectal cancer cells. *Acta Pharmacol Sin.* (2018). doi: 10.1038/s41401-018-0001-2. [Epub ahead of print].
52. Shen M, Zhao X, Zhao L, Shi L, An S, Huang G, et al. Met is involved in TIGAR-regulated metastasis of non-small-cell lung cancer. *Mol Cancer* (2018) 17:88. doi: 10.1186/s12943-018-0839-4
53. Won KY, Lim SJ, Kim GY, Kim YW, Han SA, Song JY, et al. Regulatory role of p53 in cancer metabolism via SCO2 and TIGAR in human breast cancer. *Hum Pathol.* (2012) 43:221–8. doi: 10.1016/j.humpath.2011.04.021
54. Zou S, Wang X, Deng L, Wang Y, Huang B, Zhang N, et al. CREB, another culprit for TIGAR promoter activity and expression. *Biochem Biophys Res Commun.* (2013) 439:481–6. doi: 10.1016/j.bbrc.2013.08.098
55. Basu S, Barnoud T, Kung CP, Reiss M, Murphy ME. The African-specific S47 polymorphism of p53 alters chemosensitivity. *Cell Cycle* (2016) 15:2557–60. doi: 10.1080/15384101.2016.1215390
56. Zhang C, Liu J, Liang Y, Wu R, Zhao Y, Hong X, et al. Tumour-associated mutant p53 drives the Warburg effect. *Nat Commun.* (2013) 4:2935. doi: 10.1038/ncomms3935
57. Qi Z, He J, Su Y, He Q, Liu J, Yu L, et al. Physical exercise regulates p53 activity targeting SCO2 and increases mitochondrial COX biogenesis in cardiac muscle with age. *PLoS ONE* (2011) 6:e21140. doi: 10.1371/journal.pone.0021140
58. Gerner EW, Meyskens FL Jr. Polyamines and cancer: old molecules, new understanding. *Nat Rev Cancer* (2004) 4:781–92. doi: 10.1038/nrc1454

59. Casero RA Jr, Marton LJ. Targeting polyamine metabolism and function in cancer and other hyperproliferative diseases. *Nat Rev Drug Discov.* (2007) 6:373–90. doi: 10.1038/nrd2243
60. Pegg AE. Spermidine/spermine-N(1)-acetyltransferase: a key metabolic regulator. *Am J Physiol Endocrinol Metab.* (2008) 294:E995–1010. doi: 10.1152/ajpendo.90217.2008
61. Shintoku R, Takigawa Y, Yamada K, Kubota C, Yoshimoto Y, Takeuchi T, et al. Lipoxygenase-mediated generation of lipid peroxides enhances ferroptosis induced by erastin and RSL3. *Cancer Sci.* (2017) 108:2187–94. doi: 10.1111/cas.13380
62. Slattery ML, Lundgreen A, Kadlubar SA, Bondurant KL, Wolff RK. JAK/STAT/SOCS-signaling pathway and colon and rectal cancer. *Mol Carcinogen.* (2013) 52:155–66. doi: 10.1002/mc.21841
63. Jiang M, Zhang WW, Liu P, Yu W, Liu T, Yu J. Dysregulation of SOCS-mediated negative feedback of cytokine signaling in carcinogenesis and its significance in cancer treatment. *Front Immunol.* (2017) 8:70. doi: 10.3389/fimmu.2017.00070
64. Sasi W, Jiang WG, Sharma A, Mokbel K. Higher expression levels of SOCS 1,3,4,7 are associated with earlier tumour stage and better clinical outcome in human breast cancer. *BMC Cancer* (2010) 10:178. doi: 10.1186/1471-2407-10-178
65. Calabrese V, Mallette FA, Deschenes-Simard X, Ramanathan S, Gagnon J, Moores A, et al. SOCS1 links cytokine signaling to p53 and senescence. *Mol Cell* (2009) 36:754–67. doi: 10.1016/j.molcel.2009.09.044
66. Kagan VE, Mao G, Qu F, Angeli JP, Doll S, Croix CS, et al. Oxidized arachidonic and adrenic PEs navigate cells to ferroptosis. *Nat Chem Biol.* (2017) 13:81–90. doi: 10.1038/nchembio.2238
67. Saint-Germain E, Mignacca L, Vernier M, Bobbala D, Ilangumaran S, Ferbeyre G. SOCS1 regulates senescence and ferroptosis by modulating the expression of p53 target genes. *Aging* (2017) 9:2137–62. doi: 10.18632/aging.101306
68. Maddocks OD, Berkers CR, Mason SM, Zheng L, Blyth K, Gottlieb E, et al. Serine starvation induces stress and p53-dependent metabolic remodelling in cancer cells. *Nature* (2013) 493:542–6. doi: 10.1038/nature11743
69. Ewald JC, Kuehne A, Zamboni N, Skotheim JM. The yeast cyclin-dependent kinase routes carbon fluxes to fuel cell cycle progression. *Mol Cell* (2016) 62:532–45. doi: 10.1016/j.molcel.2016.02.017
70. Lane D. p53: out of Africa. *Genes Dev.* (2016) 30:876–77. doi: 10.1101/gad.281733.116

Conflict of Interest Statement: The authors declare that the research was conducted in the absence of any commercial or financial relationships that could be construed as a potential conflict of interest.

frontiers in Pharmacology

MINI REVIEW
published: 19 November 2018
doi: 10.3389/fphar.2018.01323

Applications of Ruthenium Complex in Tumor Diagnosis and Therapy

Ke Lin[1], Zi-Zhuo Zhao[2], Hua-Ben Bo[1], Xiao-Juan Hao[3] and Jin-Quan Wang[1]**

[1] School of Bioscience and Biopharmaceutics, Guangdong Province Key Laboratory for Biotechnology Drug Candidates, Guangdong Pharmaceutical University, Guangzhou, China, [2] Department of Ultrasound, Sun Yat-sen Memorial Hospital, Sun Yat-sen University, Guangzhou, China, [3] Manufacturing, Commonwealth Scientific and Industrial Research Organisation, Clayton, VIC, Australia

Ruthenium complexes are a new generation of metal antitumor drugs that are currently of great interest in multidisciplinary research. In this review article, we introduce the applications of ruthenium complexes in the diagnosis and therapy of tumors. We focus on the actions of ruthenium complexes on DNA, mitochondria, and endoplasmic reticulum of cells, as well as signaling pathways that induce tumor cell apoptosis, autophagy, and inhibition of angiogenesis. Furthermore, we highlight the use of ruthenium complexes as specific tumor cell probes to dynamically monitor the active biological component of the microenvironment and as excellent photosensitizer, catalyst, and bioimaging agents for phototherapies that significantly enhance the diagnosis and therapeutic effect on tumors. Finally, the combinational use of ruthenium complexes with existing clinical antitumor drugs to synergistically treat tumors is discussed.

Keywords: ruthenium complexes, antitumor, diagnosis and therapy, drug combinations, synergistic effect

OPEN ACCESS

Edited by:
Zhe-Sheng Chen,
St. John's University, United States

Reviewed by:
Leli Zeng,
Shenzhen University, China
Qingbin Cui,
Guangzhou Medical University, China
Lili Liu,
Guangdong Provincial Occupational Disease Prevention Hospital, China

****Correspondence:***
Xiao-Juan Hao
xiaojuan.hao@csiro.au
Jin-Quan Wang
wangjinquan@gdpu.edu.cn

Specialty section:
This article was submitted to Cancer Molecular Targets and Therapeutics, a section of the journal Frontiers in Pharmacology

Received: *27 September 2018*
Accepted: *29 October 2018*
Published: *19 November 2018*

Citation:
Lin K, Zhao Z-Z, Bo H-B, Hao X-J and Wang J-Q (2018) Applications of Ruthenium Complex in Tumor Diagnosis and Therapy. Front. Pharmacol. 9:1323. doi: 10.3389/fphar.2018.01323

INTRODUCTION

Chemotherapy is an important modality for cancer treatment. Since the introduction of metal chemotherapeutics represented by cisplatinum (**Figure 1A**), numerous metal agents have been developed as antitumor drugs, and platinum-based drugs have become the focus of metal-based antitumor drug research (Harper et al., 2010; Burger et al., 2011; Wang X. et al., 2015). In recent years, the platinum-based drugs have become the first line of anti-cancer drugs because of their significant antitumor efficacy (Jakupec et al., 2008; Gasser et al., 2011; Wang and Guo, 2013). However, there are increasing reports that platinum-based anticancer drugs have severe side effects including myelotoxicity, peripheral neuropathy et al. (Galanski, 2006; Samimi et al., 2007). Therefore, researchers have turned their attention to other potential metal antitumor drugs. Ruthenium complexes have shown remarkable antitumor activity among the numerous metal compounds studied; they possess various advantages over platinum drugs, such as potent efficacy, low toxicity, less drug resistance, and are expected to become a new generation of clinical metal antitumor drugs (Abid et al., 2016; Thota, 2016; Southam et al., 2017).

There are three main oxidation states of ruthenium compounds. The high oxidation state of Ru(IV) compound is unstable, which limited its further development (Duan et al., 2009). Ru(III) complexes have good stability of thermodynamics and kinetics, and can be used as prodrugs under biological circumstances of hypoxia, acidic pH and high level glutathione, showing antitumor effect by reducing to corresponding Ru(II) counterparts *in vivo* (Minchinton and Tannock, 2006; Antonarakis and Emadi, 2010). Ru(II) can directly kill tumor cells *via* multiple

mechanisms (Zeng et al., 2015). Ru(II) complexes have great photophysical and chemical properties as well as multiple exchanging ligands. Combining with their applicability as nanomaterials and they have demonstrated significant antitumor efficacy (Poynton et al., 2017). Generally, the thermodynamic and kinetic stability of Ru(II) compounds are higher than Ru(III) due to their lower oxidation states (Duan et al., 2009). In addition, the nature and net charge of the ligands play important roles in the kinetics of Ru(II) compounds hydration (Abid et al., 2016). Many Ru(II) compounds showed better antitumor activities than their corresponding Ru(III) counterpart *in vivo* (Minchinton and Tannock, 2006; Hartinger et al., 2013). Generally speaking, the following options are viable in improving the water solubility of ruthenium compounds. (i) modifying the ligand structures; (ii) constructing the supramolecular ruthenium compounds; (iii) encapsulating ruthenium compounds into nanomaterial systems. (Suss-Fink, 2010; Jiang et al., 2012; Schmitt et al., 2012).

All the following ruthenium complexes that have progressed to clinical studies, NAMI-A {ImH[*trans*-$RuCl_4$(dmso)(imidazole)]} (**Figure 1B**), KP1019 {indazolium *trans*-[tetrachlorobis(1H-indazole)ruthenate(III)]} (**Figure 1C**), and KP1339, are Ru(III) complexes (Webb et al., 2013). NAMI-A showed potent inhibitory efficacy on tumor metastasis. However, the phase II clinical studies revealed that it caused severe side effects in patients and, therefore, further investigations were not undertaken (Bergamo et al., 2003; Alessio et al., 2004). KP1019 had also failed to be investigated because of its poor water solubility, severe side effects and unsatisfactory efficacy for clinical study, (Hartinger et al., 2006, 2008). To improve the low water solubility of KP1019, researchers designed a more soluble sodium salt complex, KP1339 [Na(*trans*-$RuCl_4$ $(Ind)_2$)] (**Figure 1D**), which is currently used in clinical studies (Heffeter et al., 2010). Using the potent photophysical and chemical properties of Ru(II) complex, researchers have synthesized a photosensitizer TLD1443 (**Figure 1E**), which has immensely enhanced photodynamic therapy (Zeng et al., 2017a). It has a significant therapeutic efficacy on bladder cancer and is currently in phase II clinical trials (Smithen et al., 2017).

Based on the characteristics of ruthenium compound, optimizing its structure with relevant modification is a good strategy to improve its targeting capability and antitumor activity (Blanck et al., 2012). Researchers designed a series of lipophilic ruthenium complexes that effectively increase the uptake efficiency of tumor cells (Svensson et al., 2010; Matson et al., 2011). They found that the difference in the length of alkyl ether chains contributed to the different organelle-targeting properties of ruthenium complexes. Coupling of targeted polypeptides with ruthenium complexes is another effective way to enhance their targeting capability (Chakrabortty et al., 2017). In addition, encapsulating ruthenium complexes into nanomaterials can improve their targeting capability through the enhanced permeation and retention (EPR) effect (Frasconi et al., 2013; Wei et al., 2015). Capitalizing the properties of Ru(II) complexes, researchers have designed a series of nanoruthenium complexes including, Ru(II)-selenium nanoparticles (Sun et al., 2013), Ru(II)-gold nanocomplexes (Rogers et al., 2014), Ru(II)-silicon nanocomplexes (Frasconi et al., 2013), Ru(II)-carbon nanotubes (Wang N. et al., 2015), and some organic and biometallic nanoruthenium complexes (Chakrabortty et al., 2017) with direct antitumor effects. These nanoruthenium complexes can also be used as a good catalyst, photosensitizer and tracer to enhance the therapeutic effect (Chakrabortty et al., 2017).

ANTITUMOR TARGETS AND MECHANISMS OF RUTHENIUM COMPLEXES

Ruthenium complexes show multiple targets and diverse mechanisms for its antitumor properties (**Figure 2**). Some ruthenium complexes act on telomere DNA, some interfere with replication and transcription of DNA, and others inhibit related enzymes (Kurzwernhart et al., 2012; Jain et al., 2018). Furthermore, ruthenium complexes can block the cell cycle (Kou et al., 2012; Wang et al., 2016; De Carvalho et al., 2018) and induce the formation of DNA photocrosslinking products to prevent RNA polymerization enzymes or exonucleases from binding to DNA, thereby causing tumor cell apoptosis (Le Gac et al., 2009; Rickling et al., 2010). Studies have found that some dinuclear and polynuclear Ru(II) polypyridyl complexes bind stably to the G-quadruplex (G4-DNA) structure of telomere DNA (Hiyama et al., 1995; Ambrus et al., 2006), inhibiting telomerase activity and blocking the function of DNA replication, thus, preventing normal cells from developing into immortalized tumor cells (Rajput et al., 2006; Shi et al., 2008). Ruthenium complexes have good topoisomerase (Topo) inhibitory activity (Kurzwernhart et al., 2012); however, some studies have found that inhibition of one type of Topo increases the activity of others (Crump et al., 1999; Vey et al., 1999). To solve this problem, studies have been conducted to synthesize a ruthenium complex with dual inhibitory property on Topo I and Topo II, which significantly inhibits tumor cell proliferation (Du et al., 2011; Zhang et al., 2013). Researchers have also designed a ruthenium complex with dual inhibitory effects on G4-DNA and Topo (Liao et al., 2015), achieving multitarget synergy with strong apoptosis promoting effects on tumor cells. In addition, Hurley and co-workers reported a ruthenium complex with dual stabilizing effects on Topo and G4-DNA, which also inhibited some drug resistant tumor cells (Kim et al., 2003).

In addition, it was found that ruthenium complexes accumulate more in organelles, such as mitochondria, endoplasmic reticulum, and lysosome, than in nucleus (Puckett and Barton, 2007; Groessl et al., 2011). A number of studies have revealed that mitochondria is a key target of ruthenium complexes (Wang et al., 2014; Liu et al., 2015; Wan et al., 2017), because ruthenium complexes can quickly decrease the membrane potential of mitochondria, leading to mitochondrial dysfunction or activating mitochondrial apoptosis pathways. Furthermore, this effect promoted the expression of pro-apoptotic members of the B-cell lymphoma-2 (Bcl-2) family, releasing cytochrome c (Cyto C), and activating cascade reactions of the caspase family members to induce tumor cell apoptosis. The endoplasmic reticulum is a key participant in tumor cell

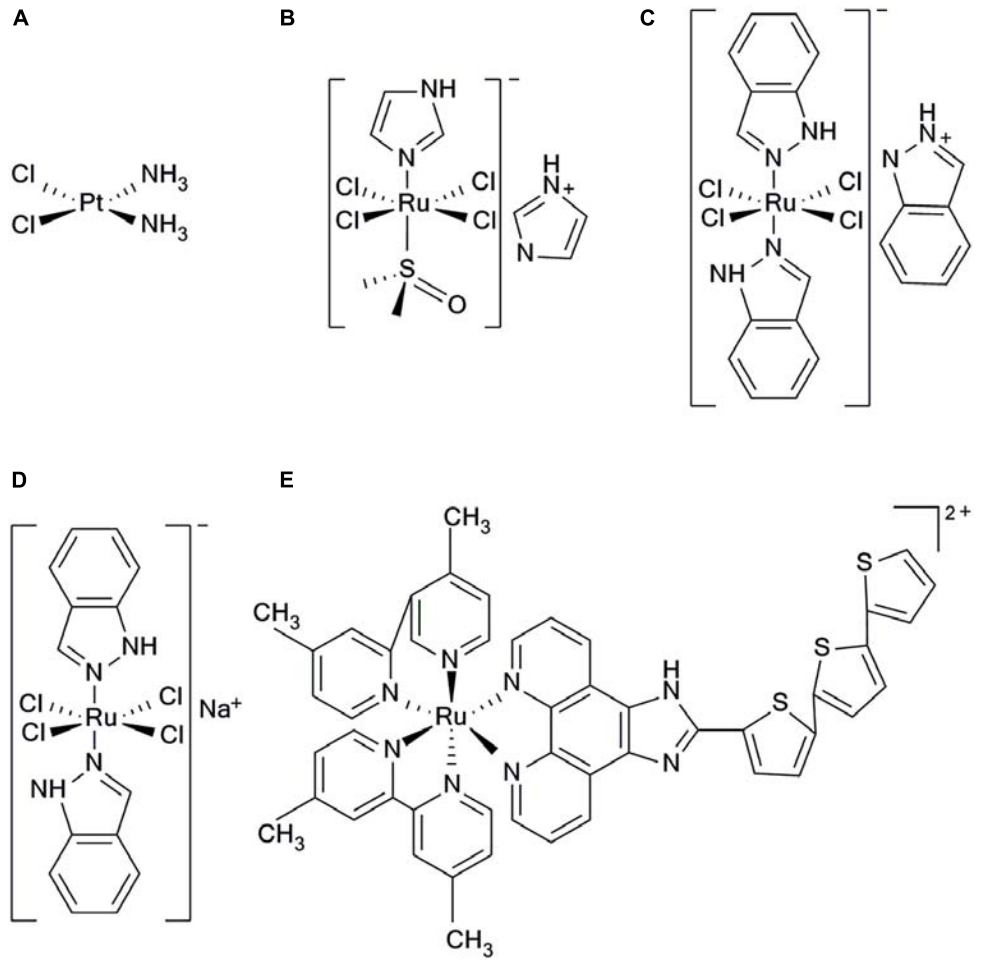

FIGURE 1 | Structure of five clinical complexes; **(A)** Cisplatinum, **(B)** NAMI-A, **(C)** KP1019, **(D)** KP1339, and **(E)** TLD1443.

apoptosis, autophagy, and drug resistance and, thus, is a target in antitumor research (Sano et al., 2012; Fernandez et al., 2015). Ruthenium complexes can target the endoplasmic reticulum, cause oxidative stress or endoplasmic reticulum stress (ERS), and induce tumor cell apoptosis by activating caspase family members (Gill et al., 2013; Sano and Reed, 2013). In addition, ruthenium complexes can target another significant participant in autophagy, the lysosomes, inducing autolysosome production and hydrolase release (Tan et al., 2010; Castonguay et al., 2012; Chen et al., 2016). Thereby, they increase apoptosis of tumor cells (Yuan et al., 2015).

A very important feature of ruthenium complexes is that it is effective against many platinum resistant tumors. Gasser et al. found that $[Ru(dppz)_2(CppH)]^{2+}$ (CppH = 2-(20-pyridyl)-pyrimidine-4-carboxylic acid)] accumulated in the mitochondria. Moreover, this Ru(II) complex showed more cytotoxic effect in cisplatin-resistant A2780/CP70 cells than cisplatin and less cytotoxic than cisplatin in normal MRC-5 cells (Pierroz et al., 2012). Dyson and co-workers also designed some ruthenium complexes which contained ethacrynic acid (EA) ligands that inhibited cisplatin resistant A2780cisR cells (Ang et al., 2007). Moreover, Chao's and Chen's group designed a series of mitochondria-targeted Ru(II) complexes, based on a 2-phenylimidazo[4,5-f] [1,10]phenanthroline (PIP) Ru(II) polypyridyl complexes. These complexes induced apoptosis *via* a mitochondrial pathway and were effective against cisplatin resistant tumor cells (Li et al., 2012c; Wang et al., 2014; Yu et al., 2014).

The membrane structure as a "protective barrier" not only regulates the entry of drug molecules into cells, but also acts as a direct target of drug molecules, effectively killing tumor cells. A number of studies have confirmed that ruthenium complexes directly act on cell membrane, changing its permeability to allow cellular content to flow out of cells and induce cell apoptosis (Deng et al., 2017). Using the photophysical properties of Ru(II) complexes, researchers designed a Ru(II) polypyridine complex that accumulates on mitochondrial membrane and tumor surface membrane. These complexes emit red phosphorescence and produce a large amount of $^1O_2$, thereby causing cytotoxicity and inducing cell apoptosis (Hess et al., 2017; Pal et al., 2018). Chao and colleagues synthesized Ru(II) pyridine complexes with two-photon performance and $^1O_2$ yield, which could serve as a

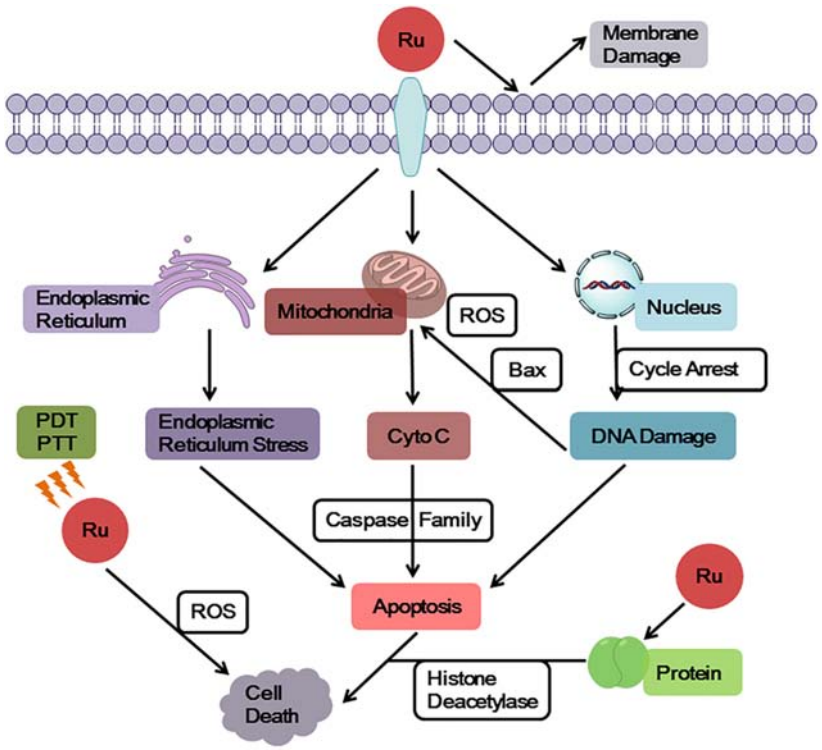

FIGURE 2 | General targets and mechanisms of anticancer action of ruthenium complexes.

photosensitizer to simultaneously target surface membrane and mitochondrial membrane of human cervical carcinoma (HeLa) cells, achieving a dual killing effect (Qiu et al., 2017).

THE USE OF RUTHENIUM COMPLEXES IN DIAGNOSIS AND TREATMENT OF TUMORS

The effective diagnosis and treatment of tumors is a major clinical challenge. Ruthenium complexes have shown promising application prospects to this difficulty. The combination of development and applications of subcellular targeting probes and bio-imaging technologies with the understanding of the occurrence and physiological development of tumors, is expected to facilitate the achievement of tumor-specific diagnosis and therapy. Ru(II) complexes have the advantages of considerable photothermal stability, large stokes shift, long luminescence lifetime, and low toxicity (Gill et al., 2009). They are ideal photosensitizers, catalysts, and imaging agents in phototherapy, and could serve as excellent probes and tracers for subcellular structure localization. Thomas and colleagues reported a lipophilic Ru(II) complex that can be used as a fluorescent probe, targeting the mitochondria and endoplasmic reticulum of human breast cancer cell (MCF-7), and it showed comparable cytotoxicity to that of cisplatin (Gill et al., 2013). In addition to targeting and imaging tumor subcellular structures, ruthenium complexes can also detect and specifically recognize biological components of the microenvironment. As a significant active ingredient in organisms, the level of thiol in tumor tissues can change rapidly. Specific recognition of the thiol level is important for tumor diagnosis and therapy (Dirican et al., 2016; Inal et al., 2017). The Ru(II)-gold nanocomplex synthesized by Chao and co-workers could be used as a specific two-photon probe for thiol level, as it detected biothiol levels in living HeLa cells and mouse hippocampus using two-photon microscopy, which provides a potent tool for molecular biology research in tumors (Zhang et al., 2014). The oxygen allotrope O_2 is an indispensable source of metabolic energy and could be specifically identified and used to monitor the local metabolites of tumor cells, which would facilitate tumor diagnosis and therapy. Keyes and colleagues found that a peptide-bridged dinuclear Ru(II) complex as the mitochondrial fluorescent probe can monitor the dynamic changes of O_2 concentration in mitochondria of HeLa cell, which could be used to monitor the malignant proliferation of tumor cells (Martin et al., 2014). The non-oxygen-dependent Ru(II) complex has been used as a photosensitizer in treating hypoxic tumors. This complex overcomes the limitations of low-depth-effect and low cell killing efficiency of phototherapy, significantly increasing $^1O_2$ production and fluorescence efficiency, thus, enhancing cytotoxicity of ruthenium complex and showing potent therapeutic effects (Volker et al., 2014; Sadhu et al., 2015; Cuello-Garibo et al., 2017).

The development of DNA structure recognition and imaging probes enables us to understand the pathogenesis of cancer at the genetic level, which has enhanced the study of antitumor

drugs. Using the optical switch effect of Ru(II) complex to DNA (Augustyn et al., 2007), a Ru(II) polypyridine complex as a DNA secondary structure recognition probe was designed. The Barton research team reported a selective Ru(II) complex for DNA mismatch detection and fluorescence localization, which effectively reduces the risk of carcinogenesis caused by base mismatches (McConnell et al., 2012). DNA bulge structures are caused by the DNA recombination process, which is likely to cause a frameshift mutation in DNA replication. This structure binds more tightly to DNA repair proteins than it does to normal double-stranded DNA, making the bulge structures a potential binding site for therapeutic drugs (Pieniazek et al., 2011). Keene and colleagues synthesized a series of binuclear Ru(II) complexes that selectively recognize and bind to DNA bulge structures *via* electrostatic interaction and zonal action, and have DNA-targeted repair function (Mulyana et al., 2011; Li et al., 2012a). Z-DNA induces gene deletion, translocation, and other instability (Dumat et al., 2016). Tridentate complexes, $[Ru(tpy)(ptn)]^{2+}$ and $[Ru(dmtpy)(ptn)]^{2+}$, were designed to induce Z-DNA transforms into a stable B-DNA dominant conformation, which effectively decreased the risk of mutations (Li et al., 2012b).

In addition to DNA imaging, some complexes were synthesized by coupling fluorescent Ru(II) complexes with histone deacetylase inhibitors (HDACIs). These complexes specifically recognize and image proteins (Kurzwernhart et al., 2012). Further investigation has found that it not only images and inhibits HDACs, but also produces a large amount of reactive oxygen species (ROS) under light irradiation, showing comparable cytotoxicity to that of cisplatin. Thus, it induces apoptosis of some tumor cells. Photoacoustic imaging (PA) is a novel imaging technique for tissue imaging based on optical absorption coefficients under the action of an imaging agent (Levi et al., 2014). Liu and co-workers used poly(nisopropylacrylamide) as a thermal response switch and $[Ru(bpy)_2(tip)]^{2+}$ as a photosensitizer in combination with gold nanomaterials to synthesize the Ru(II) complex pRu-pNIPAM@RBT (Chen et al., 2017). Under optical stimulation, this complex produces high heat and large amounts of ROS in tumor tissues, and it showed synergistic action in photothermal therapy (PTT) and photodynamic therapy (PDT) against tumors. Ruthenium complexes are good imaging agents for PA. Combination of infrared thermal imaging quantitative analysis and PA data, can be effectively used to distinguish healthy and tumor tissues, which has significantly improved the accuracy and efficiency of tumor therapy (Su et al., 2010).

At the organizational level, tumor cell proliferation and metastasis depend on adequate nutrient supply and angiogenesis. Therefore, blocking tumor angiogenesis is also a key strategy to inhibit tumor growth and migration (Gau et al., 2017). Studies have found that some ruthenium complexes have good antiangiogenic effects and effectively inhibit tumor growth (Silva Sousa et al., 2016). Liu and colleagues designed a fluorescent Ru(II)-selenium nanoparticles (Ru-SeNPs) that significantly inhibited the proliferation of liver carcinoma HepG2 cells. *In vivo* experiments in tumor bearing mice revealed that NAMI-A potently inhibited tumor angiogenesis and migration (Vacca et al., 2002). In another study, the nitric oxide synthase (NOS) pathway was found to play an important role in tumor angiogenesis (Chakraborty and Ain, 2017). Increasing NO levels is positively correlated with tumor growth and migration. Drugs that interfere with the NOS pathway can inhibit tumor angiogenesis. It has been observed that NAMI-A inhibits vascular endothelial growth factor (VEGF)-mediated angiogenesis in tumor tissues by scavenging NO (Morbidelli et al., 2003).

SYNERGISTIC EFFECT OF RUTHENIUM COMPLEXES

Drug combinations are common therapeutic strategies in clinical practices. Combinational drug molecules act on multiple targets and pathways simultaneously, which could enhance their synergistic effects, reduce dosage and side effects, and reduce the risk of drug resistance (Lehar et al., 2009). A ruthenium complex was combined with a second-line antitumor agent ketoconazole (KTZ) in hormone-refractory cancer therapy to form a $RuCl_2(KTZ)_2$ complex, which showed a favorable synergistic effect (Bozic et al., 2013). The combination of these two agents in a C8161 melanoma cell line significantly enhanced the expression of caspase-3 and promoted tumor cell apoptosis. Mechanistic studies have shown that $RuCl_2(KTZ)_2$ has mitochondrial targeting effects, releasing mitochondrial cytochrome c and activating superoxide dismutase (Mn-SOD), thereby facilitating apoptosis. In the melanoma (WM164) cell line, $RuCl_2(KTZ)_2$ displayed a stronger inhibitory effect on tumor cell growth than cisplatin, and induced apoptosis by activating poly-ADP ribose polymerase (PARP) fragmentation and the proapoptotic factor Bcl-2-associated X protein (Bax) expression. $RuCl_2(KTZ)_2$ acts on the P53 signaling pathway to effectively inhibit the proliferation of a variety of adherent tumor cells, and synergizes the anti-epidermal growth factor receptor (EGFR) inhibitor C225MAb to kill resistant spheroids (Gelfo et al., 2016).

Berger and colleagues studied the combinations of ruthenium complexes and first-line anticancer drugs. They found that the clinical drug, ruthenium complex KP1339 combined with multi-kinase inhibitor sorafenib was more effective in the therapy of hepatoma (Hep3B) than KP1339 or sorafenib alone (Heffeter et al., 2013). Specifically, the mean survival of patients was extended by 3.9-fold by the combination, whereas KP1339 and sorafenib alone extended it by 2.4-and 1.9-fold, respectively. The combination of both agents effectively inhibited sorafenib-resistant tumor cells. In-depth investigations have found that the combination substantially increased their intracellular accumulation and, thereby, interfered with the DNA synthesis process, rendering the cells unable to perform effective mitosis, and enhancing apoptosis induction.

In clinical studies, NAMI-A combined with gemcitabine, better inhibited the activity of non-small cell lung cancer cells and reduced tolerance compared with the use of gemcitabine alone, but the combination of both had significant side effects such as neutropenia, anemia, and renal impairment (Leijen et al., 2015). Sava and co-workers identified promising drug combinations with synergistic potential using high-throughput screening (Bergamo et al., 2015). NAMI-A and doxorubicin

were shown to have a potent synergistic antitumor efficacy. NAMI-A effectively increased the accumulation of doxorubicin in breast carcinoma. In *in vivo* studies of mouse MCa mammary carcinoma, this combination increased inhibition of tumor metastasis by 70%, compared to the use of doxorubicin alone. In a lung metastasis preclinical tumor model in mice, both agents demonstrated promising synergistic effects (Marien et al., 2017). However, there were noticeable side effects when the maximum doses were used.

The tumor vasculature is poorly organized, resulting in extravascular permeation of drug molecules (Pries et al., 2010). In addition, the decreased blood flow and oxygen supply affects drug uptake, which is also a major obstacle to effective tumor therapy (Siemann and Horsman, 2015). Studies on the combination of ovarian carcinoma chemotherapeutic doxorubicin and a ruthenium complex RAPTA-C have demonstrated that this combination significantly promoted the apoptosis of A2780 ovarian carcinoma cells compared with either single drug alone (Weiss et al., 2015). Normalization of tumor vasculature induced by apoptosis reduces vascular extravasation, and provides adequate oxygen for oxygen-dependent phototherapy, achieving synergism (Goel et al., 2011). These studies provide valid evidence for the interaction between anti-angiogenesis and antitumor effects.

CONCLUSION AND PERSPECTIVES

Investigation of the antitumor activity of ruthenium complexes has led to gratifying achievements and the identification of some promising antitumor compounds (Chen et al., 2016; Alves de Souza et al., 2017; Zeng et al., 2017b; Zhao et al., 2018). The ruthenium complex showed more potent activities than platinum drugs, and has a significant inhibitory effect on platinum-resistant tumor (Zeng et al., 2016). The peculiarity of ruthenium compounds suggests that the research methods used for investigating platinum-based drugs may not fully be applied in these agents, because the cytotoxic mechanisms of cisplatin and ruthenium are different. The primary target of cisplatin is DNA, but the target of some ruthenium complexes is mitochondria or endoplasmic reticulum. Although they can both regulate cell apoptosis and cell cycle, cisplatin induces a large number of genes related to DNA damage, P53 and apoptosis, while some ruthenium complexes facilitate the expression of oxidative stress and ER stress (Licona et al., 2017).

The existing research achievements should be combined with molecular biology and nanomaterials, applying the advantage of existing tools and methods to develop antitumor drugs with better therapeutic effects, based on these complexes. This prospect is extremely enlightening, and antitumor drugs with better efficacy than that of existing chemotherapeutic drugs, which are ineffective in treating certain tumors, could be developed. Furthermore, the prospective agents could be effective against tumors that have developed drug resistance for their potent efficacy (Wang N. et al., 2015; Purushothaman et al., 2018). The results of clinical studies should be reflectively considered in determining the reasons for the failure of the clinical investigations of NAMI-A and KP1019, which could lead to design drugs with less side effects, greater selectivity, and higher bioavailability. For example, KP1339, the sodium salt of KP1019, which is currently in clinical studies, has better water solubility and transmembrane absorption efficiency than KP1019 (Bytzek et al., 2016). The Ru(II) complex TLD1443, as a promising photosensitizer, significantly enhanced the efficacy of phototherapy and produced less toxicity *in vitro* and *in vivo* (Smithen et al., 2017).

Numerous breakthroughs have been made in the diagnosis and therapy of tumors using ruthenium complexes (Thota et al., 2018). As a probe, the ruthenium complex could be used for target localization and imaging of DNA, the mitochondria, endoplasmic reticulum, and lysosomes, achieving specific identification and dynamic monitoring of thiol and O_2 in tumors (Martin et al., 2014; Zhang et al., 2014). As a tracer, it enhances the understanding of the physiological development of tumors at the genetic level (Wilson et al., 2016; Xu et al., 2016). As photosensitizers and catalysts, these complexes have significant synergistic effects with phototherapies such as PDT, PTT, and photoactivated chemotherapy (PACT) (Chen et al., 2017). The combination of ruthenium complexes and PA imaging technology has significantly improved the accuracy and effectiveness of tumor diagnosis and therapy (Chen et al., 2014). In the therapy of tumors using drug combinations, ruthenium complexes have shown favorable efficacy. The Ru(II) complex combined with KTZ significantly inhibited the proliferation of C8161 melanoma cells and directly killed cisplatin-resistant spheroids (Bozic et al., 2013). KP1339 combined with the first-line anticancer drug sorafenib for hepatic carcinoma, demonstrated a remarkable therapeutic effect (Heffeter et al., 2013). Furthermore, NAMI-A combined with gemcitabine enhanced the inhibitory effect on non-small cell lung cancer while NAMI-A combined with doxorubicin showed potent inhibitory effects on lung metastasis *in vivo* (Bergamo et al., 2015). RAPTA-C and doxorubicin showed synergistically enhanced therapeutic effects on ovarian cancer and some solid tumors (Weiss et al., 2015). However, studies on the synergistic effect of ruthenium complexes are rare, because there are some uncertain factors such as the mechanism of drug synergy and how to choose drugs that cooperate with ruthenium complexes (Zhao et al., 2013; Madani Tonekaboni et al., 2018).

In conclusion, the results of the investigations on drugs combinations with ruthenium complexes are currently unsatisfactory. Perhaps the development and use of high-throughput screening technology and algorithm analysis tools are a viable strategy to promote the study of drug synergistic effects (Aviolat et al., 2018).

Presently, the mechanism of action of ruthenium complexes is unclear, and further research is still needed. Before the ruthenium complex can be used clinically, numerous problems need to be addressed, including strategies to improve the hydrolysis of ruthenium complexes to achieve effective absorption and better metabolism, as well as enhance their cellular penetration to achieve targeted tumor cell death. Furthermore, methods to avoid and alleviate the side effects of ruthenium complexes, enhance their efficacy *via* synergism, and overcome drug resistance are

imperative. The solution to these problems would provide a promising direction for the design and screening of ruthenium complexes, which are of great significance for their use in clinical diagnosis and therapy of tumors.

AUTHOR CONTRIBUTIONS

KL and Z-ZZ drafted and wrote the manuscript. J-QW conceived the idea for the manuscript. H-BB and X-JH provided critical analysis and language editing. All authors contributed to the writing and final approval of the manuscript.

FUNDING

This work was supported by the National Science Foundation of China (No. 21771042) and Natural Science Foundation of Guangdong Province (No. 2016A030310298).

REFERENCES

Abid, M., Shamsi, F., and Azam, A. (2016). Ruthenium complexes: an emerging ground to the development of metallopharmaceuticals for cancer therapy. *Mini Rev. Med. Chem.* 16, 772–786. doi: 10.2174/1389557515666151001142012

Alessio, E., Mestroni, G., Bergamo, A., and Sava, G. (2004). Ruthenium antimetastatic agents. *Curr. Top. Med. Chem.* 4, 1525–1535. doi: 10.2174/1568026043387421

Alves de Souza, C. E., Alves, de Souza, H. M., Stipp, M. C., Corso, C. R., Galindo, C. M., et al. (2017). Ruthenium complex exerts antineoplastic effects that are mediated by oxidative stress without inducing toxicity in Walker-256 tumor-bearing rats. *Free Radic. Biol. Med.* 110, 228–239. doi: 10.1016/j.freeradbiomed.2017.06.011

Ambrus, A., Chen, D., Dai, J., Bialis, T., Jones, R. A., and Yang, D. (2006). Human telomeric sequence forms a hybrid-type intramolecular G-quadruplex structure with mixed parallel/antiparallel strands in potassium solution. *Nucleic Acids Res.* 34, 2723–2735. doi: 10.1093/nar/gkl348

Ang, W. H., De Luca, A., Chapuis-Bernasconi, C., Juillerat-Jeanneret, L., Lo Bello, M., and Dyson, P. J. (2007). Organometallic ruthenium inhibitors of glutathione-S-transferase P1-1 as anticancer drugs. *Chem. Med. Chem.* 2, 1799–1806. doi: 10.1002/cmdc.200700209

Antonarakis, E. S., and Emadi, A. (2010). Ruthenium-based chemotherapeutics: are they ready for prime time? *Cancer Chemother. Pharmacol.* 66, 1–9. doi: 10.1007/s00280-010-1293-1

Augustyn, K. E., Stemp, E. D., and Barton, J. K. (2007). Charge separation in a ruthenium-quencher conjugate bound to DNA. *Inorg. Chem.* 46, 9337–9350. doi: 10.1021/ic701276t

Aviolat, H., Nomine, Y., Gioria, S., Bonhoure, A., Hoffmann, D., Ruhlmann, C., et al. (2018). SynAggreg: a multifunctional high-throughput technology for precision study of amyloid aggregation and systematic discovery of synergistic inhibitor compounds. *J. Mol. Biol.* doi: 10.1016/j.jmb.2018.09.009 [Epub ahead of print].

Bergamo, A., Messori, L., Piccioli, F., Cocchietto, M., and Sava, G. (2003). Biological role of adduct formation of the ruthenium(III) complex NAMI-A with serum albumin and serum transferrin. *Invest. New Drugs* 21, 401–411. doi: 10.1023/A:1026243000320

Bergamo, A., Riedel, T., Dyson, P. J., and Sava, G. (2015). Preclinical combination therapy of the investigational drug NAMI-A^{+} with doxorubicin for mammary cancer. *Invest. New Drugs* 33, 53–63. doi: 10.1007/s10637-014-0175-5

Blanck, S., Maksimoska, J., Baumeister, J., Harms, K., Marmorstein, R., and Meggers, E. (2012). The art of filling protein pockets efficiently with octahedral metal complexes. *Angew. Chem. Int. Ed. Engl.* 51, 5244–5246. doi: 10.1002/anie.201108865

Bozic, I., Reiter, J. G., Allen, B., Antal, T., Chatterjee, K., Shah, P., et al. (2013). Evolutionary dynamics of cancer in response to targeted combination therapy. *eLife* 2:e00747. doi: 10.7554/eLife.00747

Burger, H., Loos, W. J., Eechoute, K., Verweij, J., Mathijssen, R. H., and Wiemer, E. A. (2011). Drug transporters of platinum-based anticancer agents and their clinical significance. *Drug Resist. Updat.* 14, 22–34. doi: 10.1016/j.drup.2010.12.002

Bytzek, A. K., Koellensperger, G., Keppler, B. K., and G Hartinger, C. (2016). Biodistribution of the novel anticancer drug sodium trans-[tetrachloridobis(1H-indazole)ruthenate(III)] KP-1339/IT139 in nude BALB/c mice and implications on its mode of action. *J. Inorg. Biochem.* 160, 250–255. doi: 10.1016/j.jinorgbio.2016.02.037

Castonguay, A., Doucet, C., Juhas, M., and Maysinger, D. (2012). New ruthenium(II)–letrozole complexes as anticancer therapeutics. *J. Med. Chem.* 55, 8799–8806. doi: 10.1021/jm301103y

Chakrabortty, S., Agrawalla, B. K., Stumper, A., Vegi, N. M., Fischer, S., Reichardt, C., et al. (2017). Mitochondria targeted protein-ruthenium photosensitizer for efficient photodynamic applications. *J. Am. Chem. Soc.* 139, 2512–2519. doi: 10.1021/jacs.6b13399

Chakraborty, S., and Ain, R. (2017). Nitric-oxide synthase trafficking inducer is a pleiotropic regulator of endothelial cell function and signaling. *J. Biol. Chem.* 292, 6600–6620. doi: 10.1074/jbc.M116.742627

Chen, G., Xu, M., Zhao, S., Sun, J., Yu, Q., and Liu, J. (2017). Pompon-like RuNPs-Based theranostic nanocarrier system with stable photoacoustic imaging characteristic for accurate tumor detection and efficient phototherapy guidance. *ACS Appl. Mater. Interfaces* 9, 33645–33659. doi: 10.1021/acsami.7b10553

Chen, L., Li, G., Peng, F., Jie, X., Dongye, G., Cai, K., et al. (2016). The induction of autophagy against mitochondria-mediated apoptosis in lung cancer cells by a ruthenium (II) imidazole complex. *Oncotarget* 7, 80716–80734. doi: 10.18632/oncotarget.13032

Chen, Y., Lei, W., Jiang, G., Hou, Y., Li, C., Zhang, B., et al. (2014). Fusion of photodynamic therapy and photoactivated chemotherapy: a novel Ru(II) arene complex with dual activities of photobinding and photocleavage toward DNA. *Dalton Trans.* 43, 15375–15384. doi: 10.1039/c4dt01755b

Crump, M., Lipton, J., Hedley, D., Sutton, D., Shepherd, F., Minden, M., et al. (1999). Phase I trial of sequential topotecan followed by etoposide in adults with myeloid leukemia: a national cancer Institute of Canada clinical trials group study. *Leukemia* 13, 343–347. doi: 10.1038/sj.leu.2401308

Cuello-Garibo, J. A., Meijer, M. S., and Bonnet, S. (2017). To cage or to be caged? The cytotoxic species in ruthenium-based photoactivated chemotherapy is not always the metal. *Chem. Commun.* 53, 6768–6771. doi: 10.1039/c7cc03469e

De Carvalho, N. C., Neves, S. P., Dias, R. B., Valverde, L. F., Sales, C. B. S., Rocha, C. A. G., et al. (2018). A novel ruthenium complex with xanthoxylin induces S-phase arrest and causes ERK1/2-mediated apoptosis in HepG2 cells through a p53-independent pathway. *Cell Death Dis.* 9:79. doi: 10.1038/s41419-017-0104-6

Deng, Z., Gao, P., Yu, L., Ma, B., You, Y., Chan, L., et al. (2017). Ruthenium complexes with phenylterpyridine derivatives target cell membrane and trigger death receptors-mediated apoptosis in cancer cells. *Biomaterials* 129, 111–126. doi: 10.1016/j.biomaterials.2017.03.017

Dirican, N., Dirican, A., Sen, O., Aynali, A., Atalay, S., Bircan, H. A., et al. (2016). Thiol/disulfide homeostasis: a prognostic biomarker for patients with advanced non-small cell lung cancer? *Redox. Rep.* 21, 197–203. doi: 10.1179/1351000215y.0000000027

Du, K. J., Wang, J. Q., Kou, J. F., Li, G. Y., Wang, L. L., Chao, H., et al. (2011). Synthesis, DNA-binding and topoisomerase inhibitory activity of ruthenium(II) polypyridyl complexes. *Eur. J. Med. Chem.* 46, 1056–1065. doi: 10.1016/j.ejmech.2011.01.019

Duan, L., Fischer, A., Xu, Y., and Sun, L. (2009). Isolated seven-coordinate Ru(IV) dimer complex with [HOHOH]- bridging ligand as an intermediate for catalytic water oxidation. *J. Am. Chem. Soc.* 131, 10397–10399. doi: 10.1021/ja9034686

Dumat, B., Larsen, A. F., and Wilhelmsson, L. M. (2016). Studying Z-DNA and B- to Z-DNA transitions using a cytosine analogue FRET-pair. *Nucleic Acids Res.* 44:e101. doi: 10.1093/nar/gkw114

Fernandez, A., Ordonez, R., Reiter, R. J., Gonzalez-Gallego, J., and Mauriz, J. L. (2015). Melatonin and endoplasmic reticulum stress: relation to autophagy and apoptosis. *J. Pineal. Res.* 59, 292–307. doi: 10.1111/jpi.12264

Frasconi, M., Liu, Z., Lei, J., Wu, Y., Strekalova, E., Malin, D., et al. (2013). Photoexpulsion of surface-grafted ruthenium complexes and subsequent release of cytotoxic cargos to cancer cells from mesoporous silica nanoparticles. *J. Am. Chem. Soc.* 135, 11603–11613. doi: 10.1021/ja405058y

Galanski, M. (2006). Recent developments in the field of anticancer platinum complexes. *Recent Pat. Anticancer Drug Discov.* 1, 285–295. doi: 10.2174/157489206777442287

Gasser, G., Sosniak, A. M., and Metzler-Nolte, N. (2011). Metal-containing peptide nucleic acid conjugates. *Dalton Trans.* 40, 7061–7076. doi: 10.1039/c0dt01706j

Gau, D., Veon, W., Capasso, T. L., Bottcher, R., Shroff, S., Roman, B. L., et al. (2017). Pharmacological intervention of MKL/SRF signaling by CCG-1423 impedes endothelial cell migration and angiogenesis. *Angiogenesis* 20, 663–672. doi: 10.1007/s10456-017-9560-y

Gelfo, V., Rodia, M. T., Pucci, M., Dall'Ora, M., Santi, S., Solmi, R., et al. (2016). A module of inflammatory cytokines defines resistance of colorectal cancer to EGFR inhibitors. *Oncotarget* 7, 72167–72183. doi: 10.18632/oncotarget.12354

Gill, M. R., Cecchin, D., Walker, M. G., Mulla, R. S., Battaglia, G., Smythe, C., et al. (2013). Targeting the endoplasmic reticulum with a membrane-interactive luminescent ruthenium(ii) polypyridyl complexdagger Electronic supplementary information (ESI) available: experimental details, characterization of 2 and Fig. S1-S6. See doi: 10.1039/c3sc51725jClick here for additional data file. *Chem. Sci.* 4, 4512–4519. doi: 10.1039/c3sc51725j

Gill, M. R., Garcia-Lara, J., Foster, S. J., Smythe, C., Battaglia, G., and Thomas, J. A. (2009). A ruthenium(II) polypyridyl complex for direct imaging of DNA structure in living cells. *Nat. Chem.* 1, 662–667. doi: 10.1038/nchem.406

Goel, S., Duda, D. G., Xu, L., Munn, L. L., Boucher, Y., Fukumura, D., et al. (2011). Normalization of the vasculature for treatment of cancer and other diseases. *Physiol. Rev.* 91, 1071–1121. doi: 10.1152/physrev.00038.2010

Groessl, M., Zava, O., and Dyson, P. J. (2011). Cellular uptake and subcellular distribution of ruthenium-based metallodrugs under clinical investigation versus cisplatin. *Metallomics* 3, 591–599. doi: 10.1039/c0mt00101e

Harper, B. W., Krause-Heuer, A. M., Grant, M. P., Manohar, M., Garbutcheon-Singh, K. B., and Aldrich-Wright, J. R. (2010). Advances in platinum chemotherapeutics. *Chemistry* 16, 7064–7077. doi: 10.1002/chem.201000148

Hartinger, C. G., Groessl, M., Meier, S. M., Casini, A., and Dyson, P. J. (2013). Application of mass spectrometric techniques to delineate the modes-of-action of anticancer metallodrugs. *Chem. Soc. Rev.* 42, 6186–6199. doi: 10.1039/c3cs35532b

Hartinger, C. G., Jakupec, M. A., Zorbas-Seifried, S., Groessl, M., Egger, A., Berger, W., et al. (2008). KP1019, a new redox-active anticancer agent–preclinical development and results of a clinical phase I study in tumor patients. *Chem. Biodivers.* 5, 2140–2155. doi: 10.1002/cbdv.200890195

Hartinger, C. G., Zorbas-Seifried, S., Jakupec, M. A., Kynast, B., Zorbas, H., and Keppler, B. K. (2006). From bench to bedside–preclinical and early clinical development of the anticancer agent indazolium trans-[tetrachlorobis(1H-indazole)ruthenate(III)] (KP1019 or FFC14A). *J. Inorg. Biochem.* 100, 891–904. doi: 10.1016/j.jinorgbio.2006.02.013

Heffeter, P., Atil, B., Kryeziu, K., Groza, D., Koellensperger, G., Korner, W., et al. (2013). The ruthenium compound KP1339 potentiates the anticancer activity of sorafenib in vitro and in vivo. *Eur. J. Cancer* 49, 3366–3375. doi: 10.1016/j.ejca.2013.05.018

Heffeter, P., Bock, K., Atil, B., Reza Hoda, M. A., Korner, W., Bartel, C., et al. (2010). Intracellular protein binding patterns of the anticancer ruthenium drugs KP1019 and KP1339. *J. Biol. Inorg. Chem.* 15, 737–748. doi: 10.1007/s00775-010-0642-1

Hess, J., Huang, H., Kaiser, A., Pierroz, V., Blacque, O., Chao, H., et al. (2017). Evaluation of the medicinal potential of two ruthenium(II) polypyridine complexes as one- and two-photon photodynamic therapy photosensitizers. *Chemistry* 23, 9888–9896. doi: 10.1002/chem.201701392

Hiyama, E., Hiyama, K., Yokoyama, T., Matsuura, Y., Piatyszek, M. A., and Shay, J. W. (1995). Correlating telomerase activity levels with human neuroblastoma outcomes. *Nat. Med.* 1, 249–255. doi: 10.1038/nm0395-249

Inal, B. B., Emre, H. O., Baran, O., Ahmedov, M., Ozdemir, A. F., Kemerdere, R., et al. (2017). Dynamic thiol-disulphide homeostasis in low-grade gliomas: preliminary results in serum. *Clin. Neurol. Neurosurg.* 161, 17–21. doi: 10.1016/j.clineuro.2017.08.002

Jain, S. S., Anderson, C. M., Sapse, I. A., Lundgren, S. H., Freer, A. K., Hoang, H., et al. (2018). A ruthenium-platinum metal complex that binds to sarcin ricin loop RNA and lowers mRNA expression. *Chem. Commun.* 54, 8987–8990. doi: 10.1039/c8cc02131g

Jakupec, M. A., Galanski, M., Arion, V. B., Hartinger, C. G., and Keppler, B. K. (2008). Antitumour metal compounds: more than theme and variations. *Dalton Trans.* 183–194. doi: 10.1039/b712656p

Jiang, Q., Song, C., Nangreave, J., Liu, X., Lin, L., Qiu, D., et al. (2012). DNA origami as a carrier for circumvention of drug resistance. *J. Am. Chem. Soc.* 134, 13396–13403. doi: 10.1021/ja304263n

Kim, M. Y., Duan, W., Gleason-Guzman, M., and Hurley, L. H. (2003). Design, synthesis, and biological evaluation of a series of fluoroquinoanthroxazines with contrasting dual mechanisms of action against topoisomerase II and G-quadruplexes. *J. Med. Chem.* 46, 571–583. doi: 10.1021/jm0203377

Kou, J. F., Qian, C., Wang, J. Q., Chen, X., Wang, L. L., Chao, H., et al. (2012). Chiral ruthenium(II) anthraquinone complexes as dual inhibitors of topoisomerases I and II. *J. Biol. Inorg. Chem.* 17, 81–96. doi: 10.1007/s00775-011-08316

Kurzwernhart, A., Kandioller, W., Bartel, C., Bachler, S., Trondl, R., Muhlgassner, G., et al. (2012). Targeting the DNA-topoisomerase complex in a double-strike approach with a topoisomerase inhibiting moiety and covalent DNA binder. *Chem. Commun.* 48, 4839–4841. doi: 10.1039/c2cc31040f

Le Gac, S., Rickling, S., Gerbaux, P., Defrancq, E., Moucheron, C., and Kirsch-De Mesmaeker, A. (2009). A photoreactive ruthenium(II) complex tethered to a guanine-containing oligonucleotide: a biomolecular tool that behaves as a "seppuku molecule". *Angew. Chem. Int. Ed. Engl.* 48, 1122–1125. doi: 10.1002/anie.200804503

Lehar, J., Krueger, A. S., Avery, W., Heilbut, A. M., Johansen, L. M., Price, E. R., et al. (2009). Synergistic drug combinations tend to improve therapeutically relevant selectivity. *Nat. Biotechnol.* 27, 659–666. doi: 10.1038/nbt.1549

Leijen, S., Burgers, S. A., Baas, P., Pluim, D., Tibben, M., van Werkhoven, E., et al. (2015). Phase I/II study with ruthenium compound NAMI-A and gemcitabine in patients with non-small cell lung cancer after first line therapy. *Invest. New Drugs* 33, 201–214. doi: 10.1007/s10637-014-0179-1

Levi, J., Sathirachinda, A., and Gambhir, S. S. (2014). A high-affinity, high-stability photoacoustic agent for imaging gastrin-releasing peptide receptor in prostate cancer. *Clin. Cancer Res.* 20, 3721–3729. doi: 10.1158/1078-0432.ccr-13-3405

Li, F., Weber, D. K., Morgan, J. L., Collins, J. G., and Keene, F. R. (2012a). An approach to therapeutic agents through selective targeting of destabilised nucleic acid duplex sequences. *Dalton Trans.* 41, 6528–6535. doi: 10.1039/c2dt12146h

Li, L. Y., Jia, H. N., Yu, H. J., Du, K. J., Lin, Q. T., Qiu, K. Q., et al. (2012b). Synthesis, characterization, and DNA-binding studies of ruthenium complexes $[Ru(tpy)(ptn)]^{2+}$ and $Ru(dmtpy)(ptn)]^{2+}$. *J. Inorg. Biochem.* 113, 31–39. doi: 10.1016/j.jinorgbio.2012.03.008

Li, L., Wong, Y. S., Chen, T., Fan, C., and Zheng, W. (2012c). Ruthenium complexes containing bis-benzimidazole derivatives as a new class of apoptosis inducers. *Dalton Trans.* 41, 1138–1141. doi: 10.1039/c1dt11950h

Liao, G., Chen, X., Wu, J., Qian, C., Wang, Y., Ji, L., et al. (2015). Ruthenium(II) polypyridyl complexes as dual inhibitors of telomerase and topoisomerase. *Dalton Trans.* 44, 15145–15156. doi: 10.1039/c4dt03585b

Licona, C., Spaety, M. E., Capuozzo, A., Ali, M., Santamaria, R., Armant, O., et al. (2017). A ruthenium anticancer compound interacts with histones and impacts differently on epigenetic and death pathways compared to cisplatin. *Oncotarget* 8, 2568–2584. doi: 10.18632/oncotarget.13711

Liu, J., Chen, Y., Li, G., Zhang, P., Jin, C., Zeng, L., et al. (2015). Ruthenium(II) polypyridyl complexes as mitochondria-targeted two-photon photodynamic anticancer agents. *Biomaterials* 56, 140–153. doi: 10.1016/j.biomaterials.2015.04.002

Madani Tonekaboni, S. A., Soltan Ghoraie, L., Manem, V. S. K., and Haibe-Kains, B. (2018). Predictive approaches for drug combination discovery in cancer. *Brief Bioinform.* 19, 263–276. doi: 10.1093/bib/bbw104

Marien, E., Hillen, A., Vanderhoydonc, F., Swinnen, J. V., and Vande Velde, G. (2017). Longitudinal microcomputed tomography-derived biomarkers for lung metastasis detection in a syngeneic mouse model: added value to bioluminescence imaging. *Lab. Invest.* 97, 24–33. doi: 10.1038/labinvest.2016.114

Martin, A., Byrne, A., Burke, C. S., Forster, R. J., and Keyes, T. E. (2014). Peptide-bridged dinuclear Ru(II) complex for mitochondrial targeted monitoring of dynamic changes to oxygen concentration and ROS generation in live mammalian cells. *J. Am. Chem. Soc.* 136, 15300–15309. doi: 10.1021/ja508043q

Matson, M., Svensson, F. R., Norden, B., and Lincoln, P. (2011). Correlation between cellular localization and binding preference to RNA, DNA, and phospholipid membrane for luminescent ruthenium(II) complexes. *J. Phys. Chem. B* 115, 1706–1711. doi: 10.1021/jp109530f

McConnell, A. J., Lim, M. H., Olmon, E. D., Song, H., Dervan, E. E., and Barton, J. K. (2012). Luminescent properties of ruthenium(II) complexes with sterically expansive ligands bound to DNA defects. *Inorg. Chem.* 51, 12511–12520. doi: 10.1021/ic3019524

Minchinton, A. I., and Tannock, I. F. (2006). Drug penetration in solid tumours. *Nat. Rev. Cancer* 6, 583–592. doi: 10.1038/nrc1893

Morbidelli, L., Donnini, S., Filippi, S., Messori, L., Piccioli, F., Orioli, P., et al. (2003). Antiangiogenic properties of selected ruthenium(III) complexes that are nitric oxide scavengers. *Br. J. Cancer* 88, 1484–1491. doi: 10.1038/sj.bjc.6600906

Mulyana, Y., Weber, D. K., Buck, D. P., Motti, C. A., Collins, J. G., and Keene, F. R. (2011). Oligonuclear polypyridylruthenium(II) complexes incorporating flexible polar and non-polar bridges: synthesis, DNA-binding and cytotoxicity. *Dalton Trans.* 40, 1510–1523. doi: 10.1039/c0dt01250e

Pal, M., Nandi, U., and Mukherjee, D. (2018). Detailed account on activation mechanisms of ruthenium coordination complexes and their role as antineoplastic agents. *Eur. J. Med. Chem.* 150, 419–445. doi: 10.1016/j.ejmech.2018.03.015

Pieniazek, S. N., Hingorani, M. M., and Beveridge, D. L. (2011). Dynamical allosterism in the mechanism of action of DNA mismatch repair protein MutS. *Biophys. J.* 101, 1730–1739. doi: 10.1016/j.bpj.2011.08.039

Pierroz, V., Joshi, T., Leonidova, A., Mari, C., Schur, J., Ott, I., et al. (2012). Molecular and cellular characterization of the biological effects of ruthenium(II) complexes incorporating 2-pyridyl-2-pyrimidine-4-carboxylic acid. *J. Am. Chem. Soc.* 134, 20376–20387. doi: 10.1021/ja307288s

Poynton, F. E., Bright, S. A., Blasco, S., Williams, D. C., Kelly, J. M., and Gunnlaugsson, T. (2017). The development of ruthenium(ii) polypyridyl complexes and conjugates for in vitro cellular and in vivo applications. *Chem. Soc. Rev.* 4, 7706–7756. doi: 10.1039/c7cs00680b

Pries, A. R., Hopfner, M., le Noble, F., Dewhirst, M. W., and Secomb, T. W. (2010). The shunt problem: control of functional shunting in normal and tumour vasculature. *Nat. Rev. Cancer* 10, 587–593. doi: 10.1038/nrc2895

Puckett, C. A., and Barton, J. K. (2007). Methods to explore cellular uptake of ruthenium complexes. *J. Am. Chem. Soc.* 129, 46–47. doi: 10.1021/ja0677564

Purushothaman, B., Arumugam, P., Ju, H., Kulsi, G., Samson, A. A. S., and Song, J. M. (2018). Novel ruthenium(II) triazine complex $[Ru(bdpta)(tpy)]^{2+}$ co-targeting drug resistant GRP78 and subcellular organelles in cancer stem cells. *Eur. J. Med. Chem.* 156, 747–759. doi: 10.1016/j.ejmech.2018.07.048

Qiu, K., Wang, J., Song, C., Wang, L., Zhu, H., Huang, H., et al. (2017). Crossfire for two-pphoton photodynamic therapy with fluorinated ruthenium (II) photosensitizers. *ACS Appl. Mater. Interfaces* 9, 18482–18492. doi: 10.1021/acsami.7b02977

Rajput, C., Rutkaite, R., Swanson, L., Haq, I., and Thomas, J. A. (2006). Dinuclear monointercalating RuII complexes that display high affinity binding to duplex and quadruplex DNA. *Chemistry* 12, 4611–4619. doi: 10.1002/chem.200501349

Rickling, S., Ghisdavu, L., Pierard, F., Gerbaux, P., Surin, M., Murat, P., et al. (2010). A rigid dinuclear ruthenium(II) complex as an efficient photoactive agent for bridging two guanine bases of a duplex or quadruplex oligonucleotide. *Chemistry* 16, 3951–3961. doi: 10.1002/chem.200902817

Rogers, N. J., Claire, S., Harris, R. M., Farabi, S., Zikeli, G., Styles, I. B., et al. (2014). High coating of Ru(II) complexes on gold nanoparticles for single particle luminescence imaging in cells. *Chem. Commun.* 50, 617–619. doi: 10.1039/c3cc47606e

Sadhu, K. K., Lindberg, E., and Winssinger, N. (2015). In cellulo protein labelling with Ru-conjugate for luminescence imaging and bioorthogonal photocatalysis. *Chem. Commun.* 51, 16664–16666. doi: 10.1039/c5cc05405b

Samimi, G., Kishimoto, S., Manorek, G., Breaux, J. K., and Howell, S. B. (2007). Novel mechanisms of platinum drug resistance identified in cells selected for resistance to JM118 the active metabolite of satraplatin. *Cancer Chemother. Pharmacol.* 59, 301–312. doi: 10.1007/s00280-006-0271-0

Sano, R., Hou, Y. C., Hedvat, M., Correa, R. G., Shu, C. W., Krajewska, M., et al. (2012). Endoplasmic reticulum protein BI-1 regulates Ca^{2+}-mediated bioenergetics to promote autophagy. *Genes Dev.* 26, 1041–1054. doi: 10.1101/gad.184325.111

Sano, R., and Reed, J. C. (2013). ER stress-induced cell death mechanisms. *Biochim. Biophys. Acta* 1833, 3460–3470. doi: 10.1016/j.bbamcr.2013.06.028

Schmitt, F., Freudenreich, J., Barry, N. P., Juillerat-Jeanneret, L., Suss-Fink, G., and Therrien, B. (2012). Organometallic cages as vehicles for intracellular release of photosensitizers. *J. Am. Chem. Soc.* 134, 754–757. doi: 10.1021/ja207784t

Shi, S., Liu, J., Yao, T., Geng, X., Jiang, L., Yang, Q., et al. (2008). Promoting the formation and stabilization of G-quadruplex by dinuclear RuII complex $Ru_2(obip)L_4$. *Inorg. Chem.* 47, 2910–2912. doi: 10.1021/ic7021209

Siemann, D. W., and Horsman, M. R. (2015). Modulation of the tumor vasculature and oxygenation to improve therapy. *Pharmacol. Ther.* 153, 107–124. doi: 10.1016/j.pharmthera.2015.06.006

Silva Sousa, E. H., Ridnour, L. A., Gouveia, F. S. Jr., Silva da Silva, C. D., Wink, D. A., de Franca Lopes, L. G., et al. (2016). Thiol-activated HNO release from a ruthenium antiangiogenesis complex and HIF-1alpha inhibition for cancer therapy. *ACS Chem. Biol.* 11, 2057–2065. doi: 10.1021/acschembio.6b00222

Smithen, D. A., Yin, H., Beh, M. H., Hetu, M., Cameron, T. S., McFarland, S. A., et al. (2017). Synthesis and photobiological activity of Ru(II) dyads derived from pyrrole-2-carboxylate thionoesters. *Inorg. Chem.* 56, 4121–4132. doi: 10.1021/acs.inorgchem.7b00072

Southam, H. M., Butler, J. A., Chapman, J. A., and Poole, R. K. (2017). The microbiology of ruthenium complexes. *Adv. Microb. Physiol.* 71, 1–96. doi: 10.1016/bs.ampbs.2017.03.001

Su, J. L., Wang, B., Wilson, K. E., Bayer, C. L., Chen, Y. S., Kim, S., et al. (2010). Advances in clinical and biomedical applications of photoacoustic imaging. *Expert Opin. Med. Diagn.* 4, 497–510. doi: 10.1517/17530059.2010.529127

Sun, D., Liu, Y., Yu, Q., Zhou, Y., Zhang, R., Chen, X., et al. (2013). The effects of luminescent ruthenium(II) polypyridyl functionalized selenium nanoparticles on bFGF-induced angiogenesis and AKT/ERK signaling. *Biomaterials* 34, 171–180. doi: 10.1016/j.biomaterials.2012.09.031

Suss-Fink, G. (2010). Arene ruthenium complexes as anticancer agents. *Dalton Trans.* 39, 1673–1688. doi: 10.1039/b916860p

Svensson, F. R., Matson, M., Li, M., and Lincoln, P. (2010). Lipophilic ruthenium complexes with tuned cell membrane affinity and photoactivated uptake. *Biophys. Chem.* 149, 102–106. doi: 10.1016/j.bpc.2010.04.006

Tan, C., Lai, S., Wu, S., Hu, S., Zhou, L., Chen, Y., et al. (2010). Nuclear permeable ruthenium(II) beta-carboline complexes induce autophagy to antagonize mitochondrial-mediated apoptosis. *J. Med. Chem.* 53, 7613–7624. doi: 10.1021/jm1009296

Thota, S. (2016). Editorial: anticancer ruthenium complexes in drug discovery and medicinal chemistry. *Mini Rev. Med. Chem.* 16:771. doi: 10.2174/1389557516101605030034 05

Thota, S., Rodrigues, D. A., Crans, D. C., and Barreiro, E. J. (2018). Ru(II) compounds: next-generation anticancer metallotherapeutics? *J. Med. Chem.* 61, 5805–5821. doi: 10.1021/acs.jmedchem.7b01689

Vacca, A., Bruno, M., Boccarelli, A., Coluccia, M., Ribatti, D., Bergamo, A., et al. (2002). Inhibition of endothelial cell functions and of angiogenesis by the metastasis inhibitor NAMI-A. *Br. J. Cancer* 86, 993–998. doi: 10.1038/sj.bjc.6600176

Vey, N., Kantarjian, H., Beran, M., O'Brien, S., Cortes, J., Koller, C., et al. (1999). Combination of topotecan with cytarabine or etoposide in patients with refractory or relapsed acute myeloid leukemia: results of a randomized phase I/II study. *Invest. New Drugs* 17, 89–95. doi: 10.1023/A:1006271618635

Volker, T., Dempwolff, F., Graumann, P. L., and Meggers, E. (2014). Progress towards bioorthogonal catalysis with organometallic compounds. *Angew. Chem. Int. Ed. Engl.* 53, 10536–10540. doi: 10.1002/anie.201404547

Wan, D., Tang, B., Wang, Y. J., Guo, B. H., Yin, H., Yi, Q. Y., et al. (2017). Synthesis and anticancer properties of ruthenium (II) complexes as potent apoptosis

inducers through mitochondrial disruption. *Eur. J. Med. Chem.* 139, 180–190. doi: 10.1016/j.ejmech.2017.07.066

Wang, J. Q., Zhang, P. Y., Qian, C., Hou, X. J., Ji, L. N., and Chao, H. (2014). Mitochondria are the primary target in the induction of apoptosis by chiral ruthenium(II) polypyridyl complexes in cancer cells. *J. Biol. Inorg. Chem.* 19, 335–348. doi: 10.1007/s00775-013-1069-2

Wang, J.-Q., Zhao, Z.-Z., Bo, H.-B., and Chen, Q.-Z. (2016). Synthesis, characterization, and antitumor properties of ruthenium(II) anthraquinone complexes. *J. Coord. Chem.* 69, 177–189. doi: 10.1080/00958972.2015.1120291

Wang, N., Feng, Y., Zeng, L., Zhao, Z., and Chen, T. (2015). Functionalized multiwalled carbon nanotubes as carriers of ruthenium complexes to antagonize cancer multidrug resistance and radioresistance. *ACS Appl. Mater. Interfaces* 7, 14933–14945. doi: 10.1021/acsami.5b03739

Wang, X., Wang, X., and Guo, Z. (2015). Functionalization of platinum complexes for biomedical applications. *Acc Chem. Res.* 48, 2622–2631. doi: 10.1021/acs.accounts.5b00203

Wang, X., and Guo, Z. (2013). Targeting and delivery of platinum-based anticancer drugs. *Chem. Soc. Rev.* 42, 202–224. doi: 10.1039/c2cs35259a

Webb, M. I., Wu, B., Jang, T., Chard, R. A., Wong, E. W., Wong, M. Q., et al. (2013). Increasing the bioavailability of Ru(III) anticancer complexes through hydrophobic albumin interactions. *Chemistry* 19, 17031–17042. doi: 10.1002/chem.201302671

Wei, L., Lu, J., Xu, H., Patel, A., Chen, Z. S., and Chen, G. (2015). Silver nanoparticles: synthesis, properties, and therapeutic applications. *Drug Discov. Today* 20, 595–601. doi: 10.1016/j.drudis.2014.11.014

Weiss, A., Bonvin, D., Berndsen, R. H., Scherrer, E., Wong, T. J., Dyson, P. J., et al. (2015). Angiostatic treatment prior to chemo- or photodynamic therapy improves anti-tumor efficacy. *Sci. Rep.* 5:8990. doi: 10.1038/srep08990

Wilson, R., Espinosa-Diez, C., Kanner, N., Chatterjee, N., Ruhl, R., Hipfinger, C., et al. (2016). MicroRNA regulation of endothelial TREX1 reprograms the tumour microenvironment. *Nat. Commun.* 7:13597. doi: 10.1038/ncomms13597

Xu, L., Liu, Y. Y., Chen, L. M., Xie, Y. Y., Liang, J. X., and Chao, H. (2016). Mitochondria-targeted ruthenium (II) polypyridyl complexes with benzofuran group for live cell imaging. *J. Inorg. Biochem.* 159, 82–88. doi: 10.1016/j.jinorgbio.2016.02.028

Yu, Q., Liu, Y., Xu, L., Zheng, C., Le, F., Qin, X., et al. (2014). Ruthenium(II) polypyridyl complexes: cellular uptake, cell image and apoptosis of HeLa cancer cells induced by double targets. *Eur. J. Med. Chem.* 82, 82–95. doi: 10.1016/j.ejmech.2014.05.040

Yuan, J., Lei, Z., Wang, X., Zhu, F., and Chen, D. (2015). Ruthenium complex Lambda-WH0402 induces hepatocellular carcinoma LM6 (HCCLM6) cell death by triggering the Beclin-1-dependent autophagy pathway. *Metallomics* 7, 896–907. doi: 10.1039/c5mt00010f

Zeng, L., Chen, Y., Huang, H., Wang, J., Zhao, D., Ji, L., et al. (2015). Cyclometalated ruthenium(II) anthraquinone complexes exhibit strong anticancer activity in hypoxic tumor cells. *Chemistry* 21, 15308–15319. doi: 10.1002/chem.201502154

Zeng, L., Chen, Y., Liu, J., Huang, H., Guan, R., Ji, L., et al. (2016). Ruthenium(II) complexes with 2-phenylimidazo[4,5-f][1,10]phenanthroline derivatives that strongly combat cisplatin-resistant tumor cells. *Sci. Rep.* 6:19449. doi: 10.1038/srep19449

Zeng, L., Gupta, P., Chen, Y., Wang, E., Ji, L., Chao, H., et al. (2017a). The development of anticancer ruthenium(ii) complexes: from single molecule compounds to nanomaterials. *Chem. Soc. Rev.* 46, 5771–5804. doi: 10.1039/c7cs00195a

Zeng, L., Kuang, S., Li, G., Jin, C., Ji, L., and Chao, H. (2017b). A GSH-activatable ruthenium(ii)-azo photosensitizer for two-photon photodynamic therapy. *Chem. Commun.* 53, 1977–1980. doi: 10.1039/c6cc10330h

Zhang, P., Wang, J., Huang, H., Chen, H., Guan, R., Chen, Y., et al. (2014). RuNH2@AuNPs as two-photon luminescent probes for thiols in living cells and tissues. *Biomaterials* 35, 9003–9011. doi: 10.1016/j.biomaterials.2014.07.021

Zhang, P., Wang, J., Huang, H., Qiao, L., Ji, L., and Chao, H. (2013). Chiral ruthenium(II) complexes with phenolic hydroxyl groups as dual poisons of topoisomerases I and IIalpha. *Dalton Trans.* 42, 8907–8917. doi: 10.1039/c3dt50472g

Zhao, S., Nishimura, T., Chen, Y., Azeloglu, E. U., Gottesman, O., Giannarelli, C., et al. (2013). Systems pharmacology of adverse event mitigation by drug combinations. *Sci. Transl. Med.* 5:206ra140. doi: 10.1126/scitranslmed.3006548

Zhao, X., Li, M., Sun, W., Fan, J., Du, J., and Peng, X. (2018). An estrogen receptor targeted ruthenium complex as a two-photon photodynamic therapy agent for breast cancer cells. *Chem. Commun.* 54, 7038–7041. doi: 10.1039/c8cc03786h

Conflict of Interest Statement: The authors declare that the research was conducted in the absence of any commercial or financial relationships that could be construed as a potential conflict of interest.

frontiers in Pharmacology

ORIGINAL RESEARCH
published: 27 November 2018
doi: 10.3389/fphar.2018.01392

Osthole Synergizes With HER2 Inhibitor, Trastuzumab in HER2-Overexpressed N87 Gastric Cancer by Inducing Apoptosis and Inhibition of AKT-MAPK Pathway

Yun Yang[1,2,3], Feng Ren[1], Ziyin Tian[1], Wei Song[4], Binfeng Cheng[5] and Zhiwei Feng[1]**

[1] School of Basic Medical Sciences, Xinxiang Medical University, Xinxiang, China, [2] State Key Laboratory of Antibody Medicine and Targeted Therapy, Shanghai, China, [3] Henan Collaborative Innovation Center of Molecular Diagnosis and Laboratory Medicine, Xinxiang, China, [4] College of Life Science and Engineering, Henan University of Urban Construction, Pingdingshan, China, [5] School of Life Sciences and Technology, Xinxiang Medical University, Xinxiang, China

OPEN ACCESS

Edited by:
Zhe-Sheng Chen,
St. John's University, United States

Reviewed by:
Zhijun Liu,
Weifang Medical University, China
Ru Li,
Stony Brook University, United States
Pranav Gupta,
Harvard Medical School, United States

***Correspondence:**
Yun Yang
jamesyangyun1@126.com
Zhiwei Feng
123066@xxmu.edu.cn

Specialty section:
This article was submitted to Cancer Molecular Targets and Therapeutics, a section of the journal Frontiers in Pharmacology

Received: *17 October 2018*
Accepted: *12 November 2018*
Published: *27 November 2018*

Citation:
Yang Y, Ren F, Tian Z, Song W, Cheng B and Feng Z (2018) Osthole Synergizes With HER2 Inhibitor, Trastuzumab in HER2-Overexpressed N87 Gastric Cancer by Inducing Apoptosis and Inhibition of AKT-MAPK Pathway. Front. Pharmacol. 9:1392. doi: 10.3389/fphar.2018.01392

Background and Purpose: Although trastuzumab has shown considerable activity in the treatment of HER2-positive breast and gastric cancers, a significant proportion of patients do not respond to trastuzumab. Recent studies revealed that osthole, an active coumarin isolated from *Cnidium monnieri* (L.) Cusson possesses potent anti-tumor activity. Here, we for the first time investigated the anti-tumor activity of trastuzumab in combination with osthole in HER2-overexpressing cancers.

Materials and Methods: N87 and SK-BR-3 cell lines, which were HER2-overexpressing cancer cells were used in our study. Cell Counting Kit-8 (CCK-8) assay was utilized to test the inhibitory effects of trastuzumab plus osthole. Combination index (CI) values were calculated using the Chou-Talalay method. Fluorescence-Activated Cell Sorter (FACS) assay was used to examine the cell cycle change and apoptosis upon combinatorial treatment. N87 tumor xenografts were established to evaluate *in vivo* effects of trastuzumab plus osthole. In addition, molecular mechanisms were analyzed by Western blot *in vitro and in vivo*.

Results: As shown in our study, osthole alone exhibited effective anti-tumor activity against HER2-overexpressed N87 gastric cancer cells and SK-BR-3 breast cancer cells, which may be attributed to cell cycle arrest on G2/M phase and apoptosis. More importantly, our data demonstrated that trastuzumab plus osthole was much more potent than either agent alone in inhibiting the growth of N87 cancer cells *in vitro* and *in vivo*, which may be partly explained by the enhanced apoptosis upon the combinatorial treatment. Besides these, we also observed a significant decrease on the phosphorylation of AKT and MAPK in N87 cells when treated with trastuzumab plus osthole compared to either agent alone. Further data from N87 tumor xenografts

revealed that trastuzumab plus osthole exerted their synergistic effects mainly on AKT signaling pathway.

Conclusion: Collectively, these results support the clinical development of combination osthole with trastuzumab for the treatment of HER2-overexpressed gastric cancer.

Keywords: trastuzumab, osthole, gastric cancer, apoptosis, AKT

INTRODUCTION

Amplification of human epidermal growth factor receptor-2 (HER2), an important member of the ErbB family, is found in many solid tumors such as breast cancer and gastric cancer (Han et al., 2014; Yang et al., 2017). HER2 activation is dependent on HER2 homodimers or heterodimers with other ErbB family members, which could stimulate constitutive phosphorylation of HER2 and initiate the key downstream PI3K/AKT pathway or MAPK pathway that results in tumor growth and progression (Agus et al., 2002; Baselga and Swain, 2009; Wang et al., 2017). Trastuzumab is a well-known HER2-targeted humanized antibody that binds to the extracellular domain IV of HER2 and then causes inhibition of activation of downstream pathway (Wang et al., 2012; Li et al., 2013). It was approved by the US Food and Drug Administration (FDA) for clinical use for patients with HER2-overexpressing metastatic breast cancer in 1998, and for HER2-positive metastatic gastric cancer in 2010 (Baselga and Swain, 2009; Zheng et al., 2014). Despite the effectiveness, the majority of trastuzumab-responsive patients developed resistance within 1 year of treatment (Han et al., 2014; Zheng et al., 2014; Yang et al., 2017). Increased levels of membrane-bound EGFR and HER3 or sustained PI3K-AKT pathway activation has been implicated in the resistance to trastuzumab (Baselga and Swain, 2009). Collectively, there is an urgent need to enhance the efficacy of trastuzumab therapy.

Osthole is a natural coumarin, which was first derived from *Cnidium monnieri* (L.) Cusson (Zhang et al., 2015). As we know, osthole has been used in Traditional Chinese Medicine (TCM) for the treatment of cutaneous pruritus, eczema, trichomonas vaginalis infection, and sexual dysfunction for a long time (You et al., 2009; Zhang et al., 2012). Studies also revealed that osthole exhibited many pharmacological and biological activities, including anti-oxidation, anti-osteoporosis, and anti-inflammation (Liao et al., 2010; Chen et al., 2011). Recently, osthole was found to potently inhibit the growth of several types of cancer (Yang et al., 2003; Ye et al., 2013; Wang et al., 2015). However, its molecular mechanism has not been comprehensively elucidated although osthole has shown potent anti-tumor effects. Xu et al. (2011) revealed that osthole treatment caused G2/M arrest and apoptosis via modulating PI3K/Akt signaling pathway in lung cancer A549 cells. Besides, osthole was found to inhibit invasion and metastasis through down-regulation of MMP-5 and MMP-9 level in human lung adenocarcinoma cells (Kao et al., 2012). Moreover, studies revealed that osthole exerted anti-tumor effects on HER2-overexpressed breast cancer through inhibiting the c-Met/Akt/mTOR pathway (Lin et al., 2010; Hung et al., 2011). However, the anti-tumor activity of trastuzumab plus osthole in HER2-overexpressed cancers has not yet been reported.

Herein, we first investigated the anti-tumor effects of osthole alone in HER2-overexpressed N87 gastric cancer cells and SK-BR-3 breast cancer cells. Results revealed that osthole caused G2/M arrest and apoptosis in the two types of cancer cells, especially in SK-BR-3 cells. As we know, trastuzumab was an established anti-tumor therapeutic in treating HER2-positive breast cancer and gastric cancer (Baselga and Swain, 2009; Zheng et al., 2014). Next, we examined the anti-tumor activity of trastuzumab in combination with osthole against N87 and SK-BR-3 cells. Surprisingly, our results for the first time showed that osthole synergistically enhanced the growth-inhibitory effect of trastuzumab against N87 cancer cells *in vitro* and *in vivo*. Moreover, we found that the combination was more potent in inducing apoptosis and reducing the phosphorylation of AKT and MAPK than either agent alone in N87 cells, which may explain the synergistic effect. To conclude, these results shown in our study suggested that the effective regimen by combing trastuzumab with osthole has a great potential to treat HER2-overexpressed gastric cancer in clinics.

MATERIALS AND METHODS

Cell Lines

The human breast cancer cell line SK-BR-3 and gastric cancer cell line N87 were purchased from the American Type Culture Collection (ATCC).

Agents

Osthole was purchased from Shanghai Macklin Biochemical Co., Ltd. (Shanghai, China). It is over 99% pure determined by HPLC. The stock solution of osthole was prepared by dissolving in DMEM with 0.25% ethanol and 0.25% dimethyl sulfoxide (DMSO).

Animals

All experimental protocols were approved by the Animal Experimentation Ethics Committee of Xinxiang Medical University and all efforts were made to minimize animal suffering and reduce the number of animals used. All experiments were performed in accordance with the guideline of the Animal Care and Use Committee of Xinxiang Medical University. Five-week-old female BALB/c nude mice were obtained from the Beijing Vital River Laboratory Animal Technology Co., Ltd. (Beijing, China).

In vitro Cytotoxicity Assays

Cells were plated at a density of 5×10^3 per well and incubated with increasing concentrations of osthole, trastuzumab or the combination. Two days later, cell proliferation was determined using CCK-8 kit (Dojindo, Japan). The percentage of surviving cells was calculated using the following formula: [(A450 of experiment – A450 of background)/(A450 of untreated control – A450 of background)] × 100. Combination index (CI) values were calculated using the Chou-Talalay method by Compusyn software (Han et al., 2014). Drug synergy, addition, and antagonism are defined by C.I. values less than 1.0, equal to 1.0, or greater than 1.0, respectively.

In vivo Therapy Study

N87 cells (1×10^7 per mouse) were inoculated subcutaneously into the right flank of female BALB/c nude mice. When tumor volumes reached an average of about 150 mm^3 on day 8 after inoculation, the mice were randomly divided into four groups of six mice each. Mice were intraperitoneally injected with control IgG (15 mg/kg for two times every week), trastuzumab (15 mg/kg for two times every week), osthole (100 mg/kg once daily) or the combination of trastuzumab (15 mg/kg for two times every week), and osthole (100 mg/kg once daily) for 2 weeks. Tumors were measured with digital calipers, and tumor volumes were calculated by the formula: Volume = Length × $(\text{Width})^2/2$.

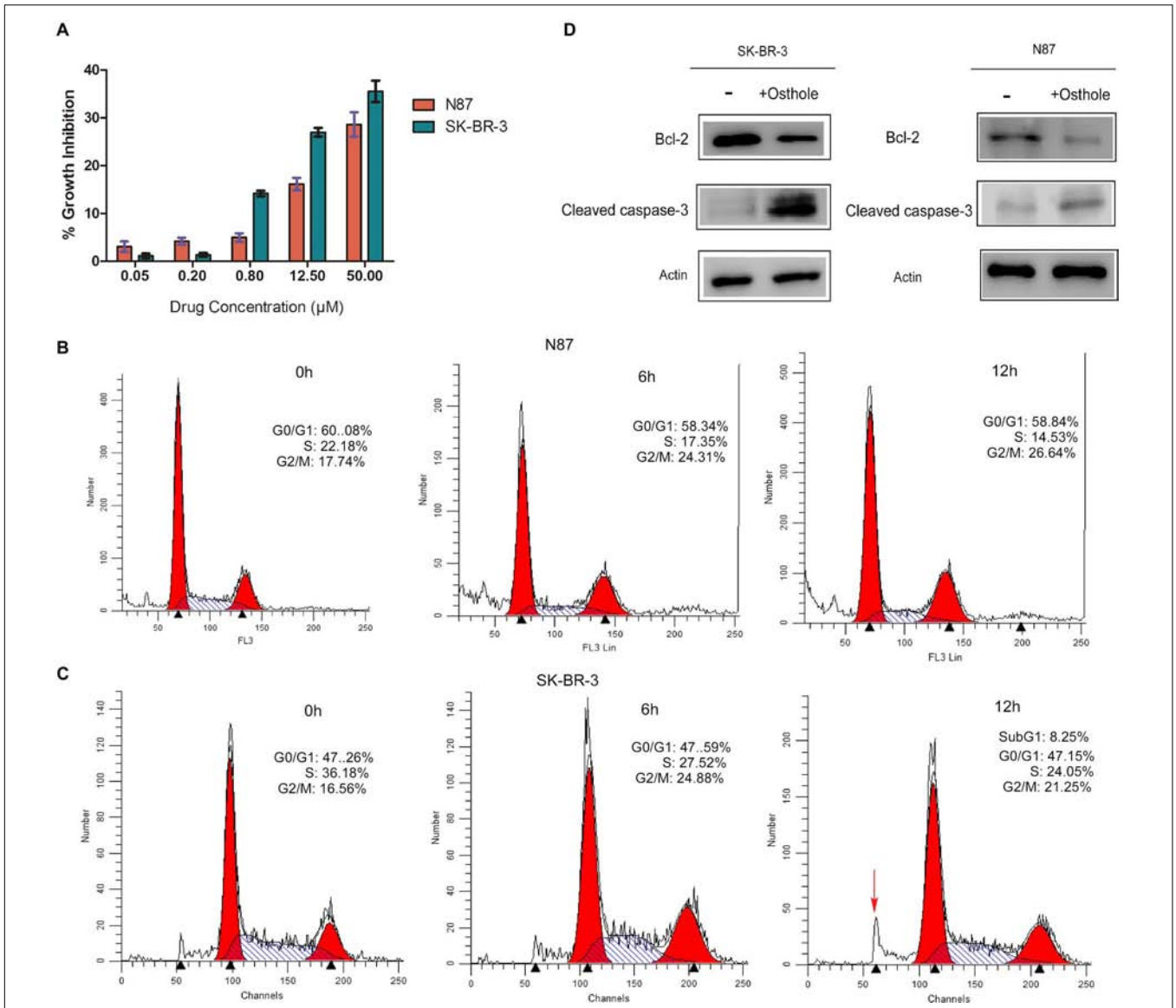

FIGURE 1 | Osthole inhibited the growth of N87 and SK-BR-3 cells and induced cell cycle arrest and apoptosis. **(A)** CCK-8 assay evaluating cell growth of N87 and SK-BR-3 cells upon treatment with increasing concentration of osthole for 48 h. **(B)** Cell cycle analysis of N87 cells following 40 μM osthole treatment for 0, 6, and 12 h by flow cytometry. **(C)** Effects of osthole on cell cycle of SK-BR-3 cells. **(D)** N87 and SK-BR-3 cells were treated with 40 μM osthole for 30 h and cleaved Caspase-3 and Bcl-2 were examined by Western blot.

Immunoblotting

Western blot was performed using established procedures.(Yang et al., 2017) Cells were lysed in lysis buffer (Beijing Dingguo Biotechnology Co., Ltd.), incubated on ice for 30 min and centrifuged for 20 min to remove cell debris. Total cell lysates were subjected to SDS–polyacrylamide and immunoblotted with primary antibodies and HRP-conjugated secondary antibody. After another wash of the membrane, the bands were detected using a super-sensitive ECL solution (Boster Biological Technology Co., Ltd., China), and visualized using an Amersham imager 600 (GE Healthcare Life Sciences, Fairfield, CT, United States).

Cell Cycle Analysis

This assay was performed according to previous report.(Kovtun et al., 2010) Cells (1×10^5/mL) were incubated with osthole for 0, 6, or 12 h at 37° C. Cells were then fixed with 1 mL of 70% ethanol, and DNA content was determined after staining with propidium iodide by flow cytometry. Flow cytometric data were analyzed using FlowJo 7.6 software.

Apoptosis Analysis

Apoptosis analysis was performed by flow cytometry using established procedures (Zhang et al., 2012). For flow cytometry analysis, N87 cells (5×10^6/well) were plated in 6-well plate and treated with osthole (40 μM), trastuzumab (10 μg/mL), or osthole (40 μM) in combination with trastuzumab (10 μg/mL) for 30 h at 37°C. The cells were then labeled with Annexin V and Propidium Iodide (PI; Beijing Dingguo Biotechnology Co., Ltd, Beijing). Apoptotic rates were determined by FACSCalibur flow cytometer (BD Biosciences, Franklin Lakes, NJ, United States) and analyzed by Flowjo software. The percentage of the early apoptosis was calculated by Annexin V (+) and PI (−), while the percentage of the late apoptosis was calculated by Annexin V (+) and PI (+).

Statistical Analysis

Statistical analysis was performed by Student's unpaired t test to identify significant differences unless otherwise indicated. Differences were considered significant at $p < 0.05$.

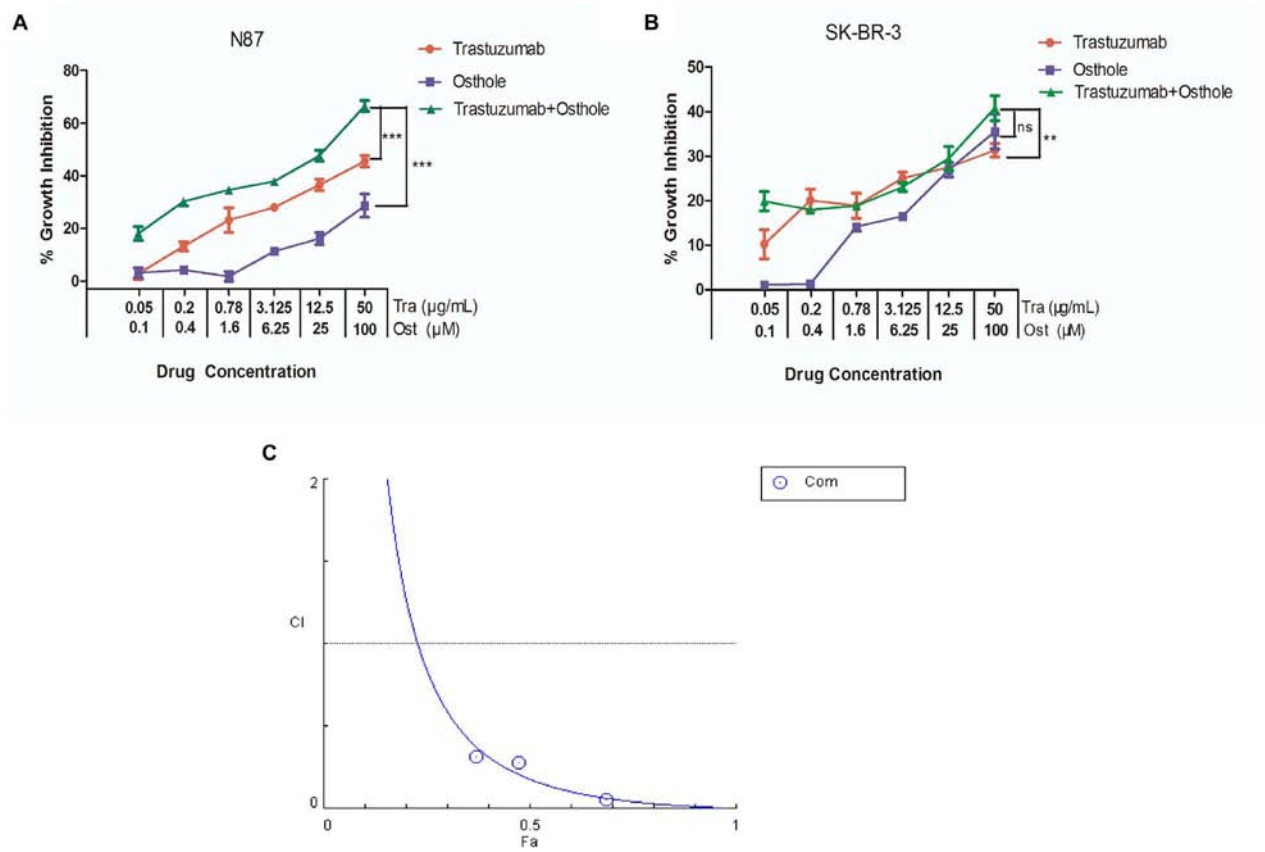

FIGURE 2 | Osthole and trastuzumab synergistically inhibited the *in vitro* growth of N87 cells. **(A)** The inhibitory effects of osthole and trastuzumab combinatorial treatment against N87 cells for 48 h. **(B)** The inhibitory effects of osthole and trastuzumab combinatorial treatment against SK-BR-3 cells for 48 h. **(C)** The synergistic effect of trastuzumab in combination with osthole on the growth of N87 cell line. Combination index (CI) values were calculated at the drug concentration of trastuzumab (3.125 μg/mL) plus osthole (6.25 μM), trastuzumab (12.5 μg/mL) plus osthole (25 μM), trastuzumab (50 μg/mL) plus osthole (100 μM) using the Chou-Talalay method. Drug synergy, addition, and antagonism are defined by C.I. values less than 1.0, equal to 1.0, or greater than 1.0, respectively. Data show the mean ± SD (three independent experiments); *$p < 0.05$; **$p < 0.01$; ***$p < 0.001$. ns, no significant difference.

RESULTS

Osthole Exhibits Growth-Inhibitory Activity Against HER2-Overexpressed N87 and SK-BR-3 Cancer Cells Through Cell Cycle Arrest and Apoptosis

We first examined the inhibitory effects of osthole alone on N87 and SK-BR-3 cell lines. As shown in **Figure 1A**, osthole inhibited the growth of N87 and SK-BR-3 cancer cells in a dose-dependent manner. Additionally, we found that SK-BR-3 cell line responded more sensitively to osthole compared with N87 cell line.

Furthermore, we investigated the effect of osthole on cell cycle arrest and apoptosis in N87 and SK-BR-3 cells. FACS assay showing that osthole significantly elevated the percentage of G2/M phase in both N87 and SK-BR-3 cells when treated for 6 and 12 h compared to control (**Figures 1B,C**). More importantly, elevated sub-G1 population in SK-BR-3 cells was observed after treatment for 12 h. As we know, Bcl-2 was an important anti-apoptotic protein that regulates a late step in the apoptosis pathway (Srinivas et al., 2000; Willis et al., 2007). And Caspase-3 is an important member in Caspase family, which is critical for cytochrome c-dependent apoptosis (Zou et al., 1997). In our study, we found that Bcl-2 was down-regulated and cleaved Caspase-3 was up-regulated after treatment with osthole for 30 h, suggesting apoptosis may be induced following cell cycle arrest in response to osthole treatment in SK-BR-3 and N87 cells (**Figure 1D** and **Supplementary Figure S1**). Taken together, osthole may exert its anti-tumor effects in SK-BR-3 and N87 cells through inducing cell cycle arrest and apoptosis.

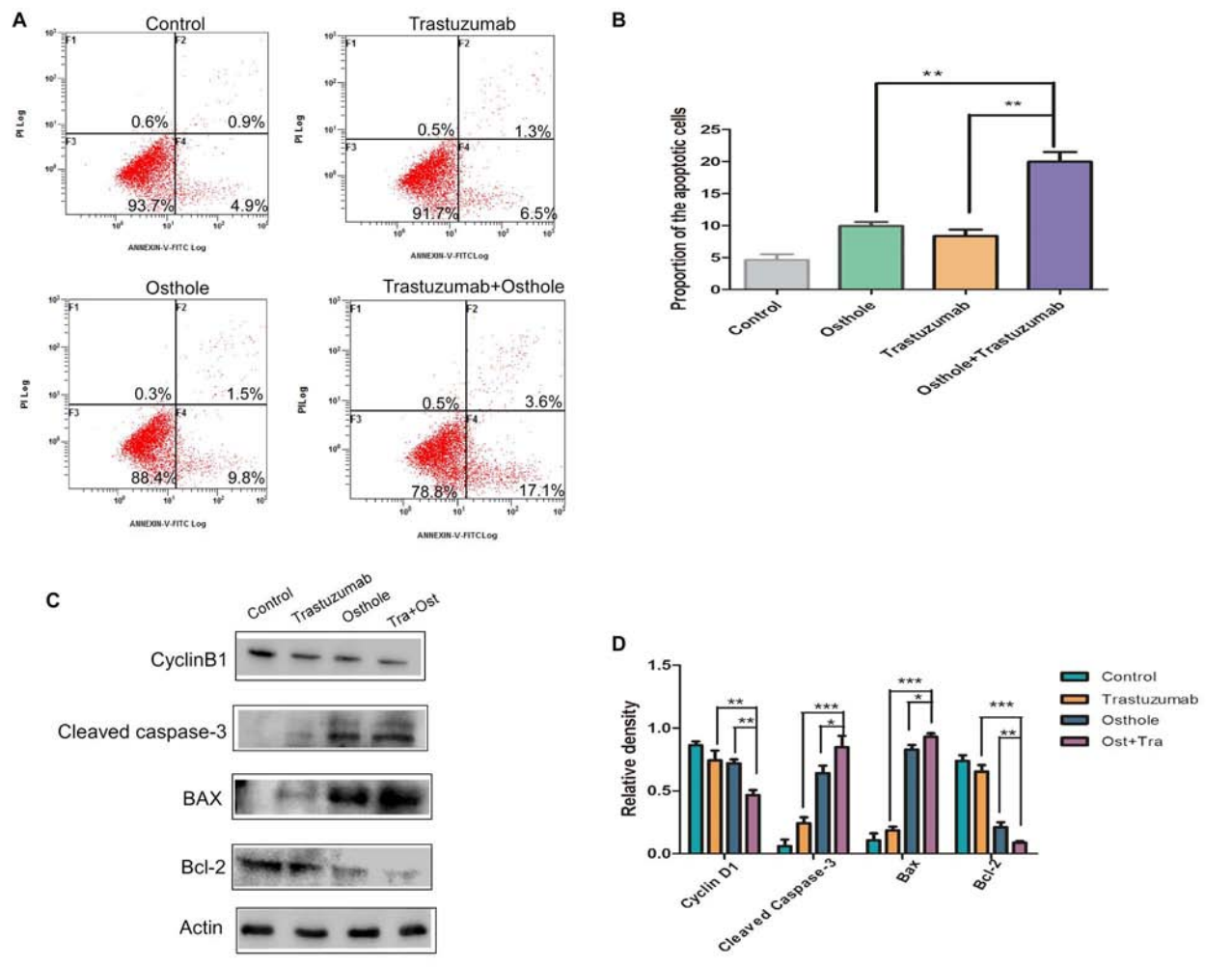

FIGURE 3 | Trastuzumab enhanced osthole-induced apoptosis, which may partly explained the synergistic anti-tumor effect of trastuzumab in combination with osthole. **(A)** Induction of apoptosis of N87 cells after control IgG (10 μg/mL), osthole (40 μM), trastuzumab (10 μg/mL) or the combinatorial treatment for 30 h. Apoptosis was measured by flow cytometry. **(B)** Statistical analysis of the percentages of the apoptotic cells. Data was shown with mean ± SD. **(C)** Cell cycle and apoptosis related protein (CyclinB1, cleaved Caspase-3, Bax or Bcl-2) was examined in N87 cells when treated with control IgG (10 μg/mL), osthole (40 μM), trastuzumab (10 μg/mL), or the combination for 30 h. **(D)** Quantification of Western blot signal intensity analysis is expressed relative to the β-actin loading control by using Image J software. Data show the mean ± SD (three independent experiments); $^{*}p < 0.05$; $^{**}p < 0.01$; $^{***}p < 0.001$.

Trastuzumab and Osthole Act Synergistically on N87 Gastric Cancer Cells *in vitro*

Next, we examined the inhibitory effects of trastuzumab in combination with osthole on N87 and SK-BR-3 cell lines. As shown in **Figures 2A,B**, trastuzumab plus osthole exhibited a significantly greater inhibitory activity than either agent alone in N87 cells, while no marked synergistic effect was found in SK-BR-3 cells.

To further examine whether the combination of trastuzumab with osthole is synergistic, we treated N87 cells with combination of trastuzumab and osthole at various concentrations. Data were analyzed using the method of Chou and Talalay to establish drug C.I. values (Han et al., 2014). Synergy is defined as C.I. values of <1.0, antagonism as C.I. values >1.0, and additivity as CI values equal to 1.0. Our results showed that trastuzumab and osthole synergistically inhibited the growth of N87 cells (**Figure 2C**).

Trastuzumab in Combination With Osthole Synergistically Induced Apoptosis

Furthermore, we investigated whether the co-treatment of trastuzumab with osthole may synergistically induce apoptosis in N87 cells. First, the apoptotic cell percentage was analyzed by flow cytometry following Annexin V and PI staining. Results showed that the percentage of apoptotic cells was significantly increased in the trastuzumab plus osthole treated cells compared to either agent mono-treated cells (**Figures 3A,B**).

And we further assessed the cell extracts for expression of apoptotic markers including cleaved Caspase-3, Bcl-2, and Bax. Compared to treatment with either agent alone, combinatorial treatment significantly up-regulated the level of cleaved Caspase-3 (**Figures 3C,D**). In addition, Bcl-2 was markedly down-regulated, while Bax that was a protein favoring induction of apoptosis was up-regulated in trastuzumab plus osthole treated cells. Besides these, the expression of cell cycle-related molecule, CyclinB1 was significantly decreased in N87 cells upon combinatorial treatment. Taken together, these results suggested the addition of trastuzumab markedly enhanced osthole-induced apoptosis, which may partly explain the superiority of combinatorial treatment.

Effect of Trastuzumab Plus Osthole on AKT and MAPK Signaling Pathway

To further investigate the mechanism that may explain the synergistic effect, we examined the level of AKT, phosphorylated AKT, MAPK, and phosphorylated MAPK in N87 cells treated with trastuzumab in combination with osthole. Compared to trastuzumab or osthole treatment alone, trastuzumab plus osthole more significantly inhibited the phosphorylation of both AKT and MAPK in N87 cell lines (**Figures 4A,B**). Notably, combinatorial treatment resulted in a more effective inhibition on phospho-AKT level than on phospho-MAPK level, whereas there was no substantially decrease in total AKT and MAPK protein levels. Therefore, our results suggested that trastuzumab in combination with osthole may exert their synergistic effect on inhibiting AKT and MAPK pathway, mainly inhibiting the phosphorylation of AKT, which also further explained the superior effects of trastuzumab plus osthole.

Trastuzumab in Combination With Osthole Potently Suppresses the *in vivo* Growth of N87 Cancer Xenografts

To assess the synergistic effect *in vivo*, we examined the therapeutic efficacy of trastuzumab plus osthole for nude mice bearing established N87 tumor xenografts. As shown in **Figures 5A,B** and **Supplementary Figure S2**, our *in vivo*

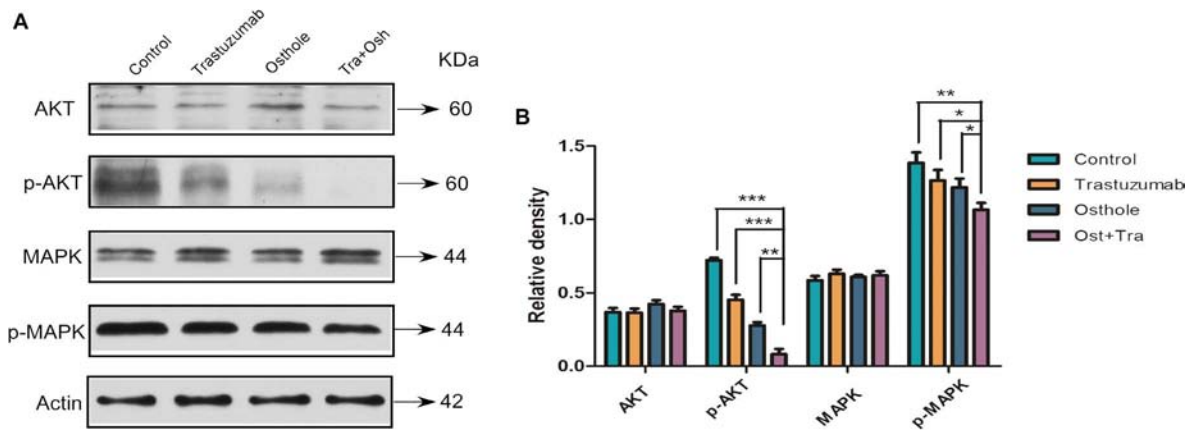

FIGURE 4 | Trastuzumab in combination with osthole blocked AKT pathway in a synergistic manner. **(A)** Immunoblots assessing AKT and MAPK signaling in the N87 cell lines upon treatment with control IgG (10 μg/mL), trastuzumab (10 μg/mL), osthole (40 μM), or trastuzumab (10 μg/mL) plus osthole (40 μM) for 30 h. Data are representative of three independent experiments. **(B)** Quantification of Western blot signal intensity analysis is expressed relative to the β-actin loading control by using Image J software. Data show the mean ± SD (three independent experiments); $^{*}p < 0.05$; $^{**}p < 0.01$; $^{***}p < 0.001$.

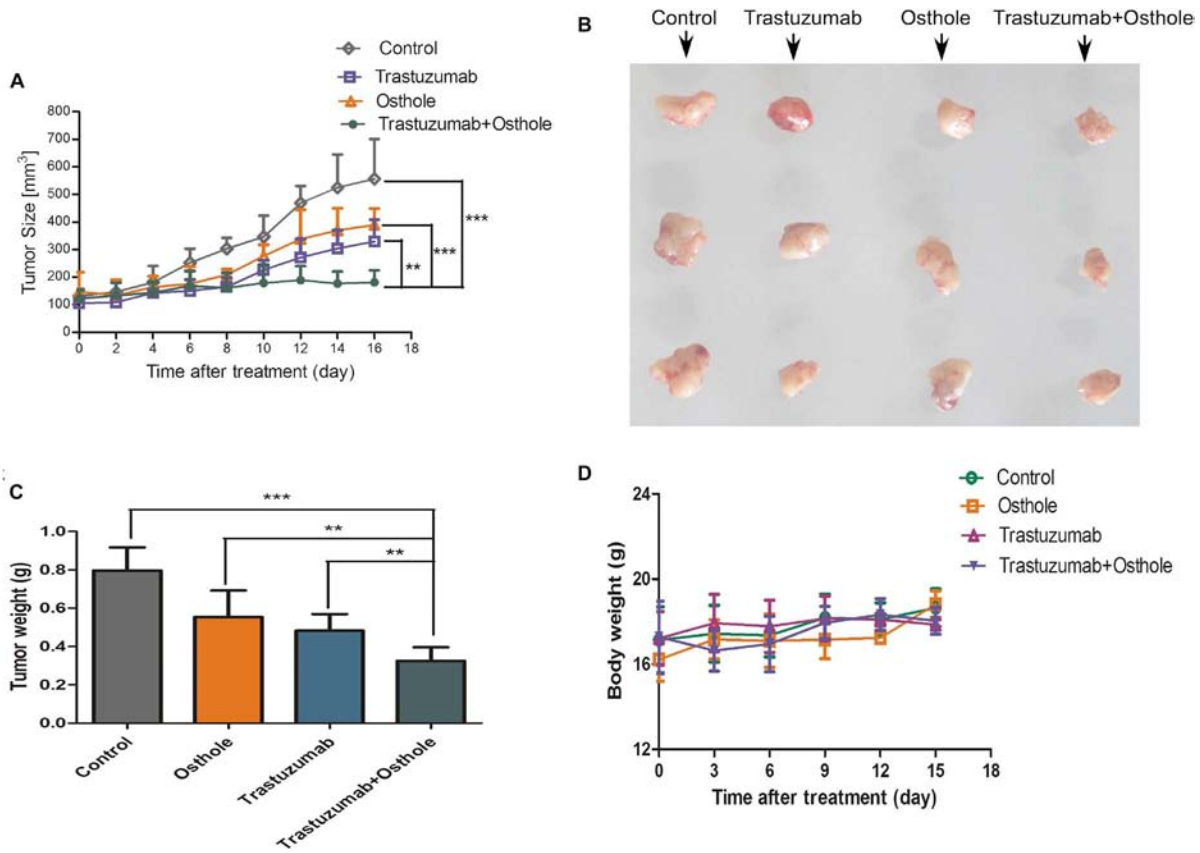

FIGURE 5 | Trastuzumab plus osthole combinatorial treatment inhibits the growth of N87 cancer cells *in vivo*. **(A)** Tumor volume of N87 xenografts after injection with control IgG (15 mg/kg), Trastuzumab (15 mg/kg), Osthole (100 mg/kg), or Trastuzumab (15 mg/kg) plus Osthole (100 mg/kg). **(B)** On day 16 post first injection, xenograft tumors from each group were removed and photographed. Representative tumors in each group were shown. **(C)** After xenograft tumors were removed, these tumors were weighted. **(D)** Effects of agents on tumor-bearing mice body weight were determined using N87 tumor-bearing nude mice. Mice were weighed at regular intervals during the whole period to monitor unspecific toxicity. Data are shown as mean ± SD. (n = 6 mice, each group); $^{**}p < 0.01$; $^{***}p < 0.001$.

experiments showed that the combinatorial therapy of trastuzumab with osthole significantly reduced tumor growth compared to either agent treatment alone. Compared to the control IgG, the treatment with trastuzumab and osthole combination resulted in a 50 % reduction in tumor weight (**Figure 5C**). Consistent with the observations *in vitro*, combinatorial treatment of trastuzumab with osthole resulted in a significant benefit over either agent alone in the N87 xenograft model. Moreover, we also preliminarily evaluated the unspecific-toxicity in these xenografts. As shown in **Figure 5D**, No marked weight loss was observed in trastuzumab plus osthole treated mice compared with that of in the control IgG treated group (p = 0.1934). Thus, our results showed that trastuzumab in combination with osthole exhibited potent inhibitory effects and good tolerance on N87 tumor xenografts.

Trastuzumab in Combination With Osthole Inhibited AKT Signaling Pathway *in vivo*

To further determine if combinatorial treatment caused inhibition of intracellular signaling cascade *in vivo*, we examined tumor samples from treated animals using western blot assay to evaluate the degree to which MAPK or AKT signaling was inhibited. As expected, the level of pAKT in tumors of combinatorial treatment group was more effectively regressed compared to that of in trastuzumab or osthole treatment group while the level of pMAPK was not substantially reduced in tumors from trastuzumab plus osthole treated mice (**Figures 6A,B**). Collectively, these results above may also suggest that trastuzumab plus osthole exerted their synergistic effects mainly on AKT signaling pathway in N87 tumor xenografts.

DISCUSSION

In our study, we for the first time reported the anti-tumor effects of trastuzumab in combination with osthole, a natural coumarin derivative extracted from Traditional Chinese Medicine on N87 gastric cancer cells and investigated the underlying mechanism involved. We first examined the inhibitory effects of osthole on HER2-amplified N87 and SK-BR-3 cells. Results revealed that osthole exhibited potent anti-tumor activity on the two cell lines, especially on SK-BR-3 cells. Previous studies suggested

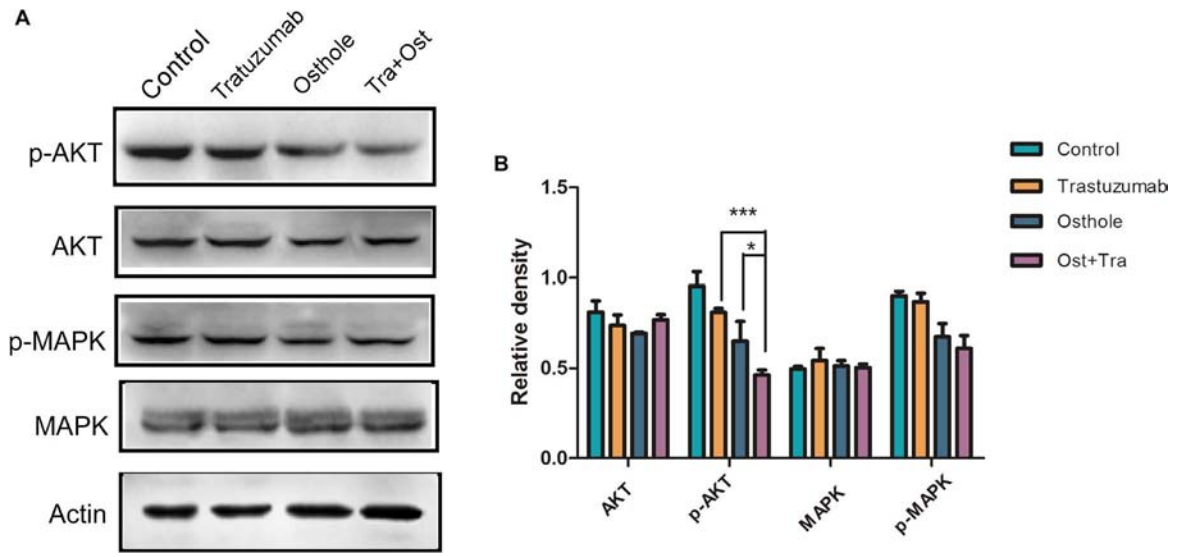

FIGURE 6 | Trastuzumab in combination with osthole inhibited AKT signaling pathway *in vivo*. **(A)** Tumor tissues isolated from N87 xenografts upon treatment with control IgG (15 mg/kg), Trastuzumab (15 mg/kg), Osthole (100 mg/kg), Sor Trastuzumab (15 mg/kg) plus Osthole (100 mg/kg) were then subjected to Western blot to detect the expression of AKT, p-AKT, MAPK and p-AMPK. Data are representative of three independent experiments. **(B)** Quantification of Western blot signal intensity analysis is expressed relative to the -actin loading control by using Image J software. Data show the mean ± SD (three independent experiments); $^{*}p < 0.05$; $^{**}p < 0.01$; $^{***}p < 0.001$.

that osthole could induce G2/M arrest and apoptosis in lung cancer A549 cells and hepatocellular carcinoma HepG2 cells (Xu et al., 2011; Chao et al., 2014). In consistent with these studies, we also found that osthole induced G2/M arrest and apoptosis in HER2-amplified N87 and SK-BR-3 cells. As we know, trastuzumab is a FDA-approved antibody therapeutic that has shown clinical efficacy in treating breast and gastric cancers (Hudis, 2007; Rose and Bekaii-Saab, 2011). Despite the effectiveness, numbers of patients with HER2-positive cancer treated with trastuzumab monotherapy exhibited *de novo* resistance unfortunately (Zhang et al., 2011). Thus, novel therapeutic regimens are urgently needed to enhance the efficacy of trastuzumab-therapy. Surprisingly, we found that osthole could synergistically enhance the inhibitory effect of trastuzumab against HER2-overexpressed N87 cells both *in vitro* and *in vivo*. However, the synergistic effect were not been observed in SK-BR-3 cells, which was the other trastuzumab-sensitive breast cancer cell line. The underlying mechanism explaining the different responses to trastuzumab plus osthole in the two HER2-overexpressed cancer cell lines will be further explored in our following research.

As previously reported, trastuzumab may exert its anti-tumor activity on HER2-overexpressed cancers through inducing apoptosis (Cuello et al., 2001; Milella et al., 2004). And osthole also caused cell cycle arrest and apoptosis in several types of cancer (Xu et al., 2011; Chao et al., 2014; Wang et al., 2016). In our present study, the hypothesis was investigated that if trastuzumab plus osthole may synergistically enhance the effect of apoptosis in N87 cells. As expectedly, our data revealed that trastuzumab in combination with osthole more effectively promoted apoptosis compared to either agent treatment alone.

As we know, studies have demonstrated that PI3K-AKT pathway activity is directly linked to the proliferation and growth of HER2-overexpressing cancer cells and trastuzumab mainly exerted its anti-tumor in inhibiting the HER2-PI3K-AKT pathway (Pal and Mandal, 2012; Li et al., 2013; Han et al., 2014). Recently, Lin et al. (2014) indicated that osthole inhibited IGF-1-induced EMT by blocking PI3K-Akt pathway in brain cancer cells. In our study, we also observed AKT and MAPK phosphorylation were regressed in N87 cells when treated with trastuzumab plus osthole. Especially, AKT phosphorylation was more markedly inhibited in the combinatorial treatment compared to either agent treatment alone, which was also verified in tumor samples from N87 tumor xenografts. Generally speaking, our study partly explained the molecular mechanism involved in the synergistic effects of trastuzumab in combination with osthole on HER2-overexpressed gastric cancer, which may provide a reference for other researchers. In our following study, we will explore if other AKT involved signaling pathway like c-Met/Akt/mTOR pathway may be related to the synergistic anti-tumor effects.

Taken together, our results suggested that osthole, a promising lead compound from traditional Chinese medicine could effectively inhibit N87 and SK-BR-3 cells with HER2-overexpression by causing cell cycle arrest and inducing apoptosis. More importantly, we found that combination of trastuzumab with osthole showed synergistic inhibitory effects on the growth of N87 cells, which may be partly attributed to the enhanced apoptosis. Phosphorylation of AKT were effectively inhibited *in vitro* and *in vivo* when treated with trastuzumab plus

osthole may also contribute to the synergistic effect. Therefore, combination of trastuzumab with osthole provides a new strategy for targeting HER2-overexpressed gastric cancer, which will contribute to enhancing the therapeutic effect of trastuzumab. Based on these results, our study also suggested that osthole can be developed into an adjuvant drug for HER2-targeted therapy in treating HER2-overexpressed gastric cancer. In addition, a novel antibody-drug conjugate may also be designed by conjugating osthole to trastuzumab, which may represent a new therapeutic approach.

CONCLUSION

Our results indicated that osthole alone exhibited effective anti-tumor activity against HER2-overexpressed N87 gastric cancer cells and SK-BR-3 breast cancer cells. Furthermore, osthole could synergistically enhance the inhibitory effect of trastuzumab against HER2-overexpressed N87 cells both *in vitro* and *in vivo*. Moreover, we explored the molecular mechanism involved in the synergistic effects, which may be attributed to the enhanced apoptosis effects and AKT-MAPK signaling pathway blockade. Collectively, these results support the clinical development of osthole plus trastuzumab for the treatment of HER2-overexpressed gastric cancer. Besides, our study may also provide a strategy for testing combinations of HER2-targeting agents with other bioactive constituents isolated from food in clinical studies.

DATA AVAILABILITY STATEMENT

Data arising from this study are contained within the manuscript.

ETHICS STATEMENT

This study was carried out in accordance with the Principle of Laboratory Animal Care (NIH Publication No. 85-23, revised 1985). The protocol was approved by the Animal Ethics Committee of Xinxiang Medical University.

AUTHOR CONTRIBUTIONS

YY and ZF designed the experiments and wrote the manuscript. YY, FR, ZT, WS, and BC carried out the experiments. ZF supervised and corrected the manuscript.

FUNDING

This work was supported by grants from the Natural Science Foundation of China (81703054, 81671226, and 81403161), National Major Scientific and Technological Special Project for "Significant New Drugs Development"(2018ZX09301002001), Key Scientific Research Project of Higher Education of Henan Province, China (17A350012 and 19A310004), Key Science and Technology Program of Henan Province, China (172102310614 and 182102310259), Key Science and Technology Program of Shanghai (16431904700, 16DZ1910400, 16431904100, and 17431901800), and Doctoral Foundation of Xinxiang Medical University (XYBSKYZZ201506).

SUPPLEMENTARY MATERIAL

The Supplementary Material for this article can be found online at: https://www.frontiersin.org/articles/10.3389/fphar.2018.01392/full#supplementary-material

REFERENCES

Agus, D. B., Akita, R. W., Fox, W. D., Lewis, G. D., Higgins, B., Pisacane, P. I., et al. (2002). Targeting ligand-activated ErbB2 signaling inhibits breast and prostate tumor growth. *Cancer Cell* 2, 127–137. doi: 10.1016/S1535-6108(02)00097-1

Baselga, J., and Swain, S. M. (2009). Novel anticancer targets: revisiting ERBB2 and discovering ERBB3. *Nat. Rev. Cancer* 9, 463–475. doi: 10.1038/nrc2656

Chao, X., Zhou, X., Zheng, G., Dong, C., Zhang, W., Song, X., et al. (2014). Osthole induces G2/M cell cycle arrest and apoptosis in human hepatocellular carcinoma HepG2 cells. *Pharm. Biol.* 52, 544–550. doi: 10.3109/13880209.2013.850517

Chen, T., Liu, W., Chao, X., Qu, Y., Zhang, L., Luo, P., et al. (2011). Neuroprotective effect of osthole against oxygen and glucose deprivation in rat cortical neurons: involvement of mitogen-activated protein kinase pathway. *Neuroscience* 183, 203–211. doi: 10.1016/j.neuroscience.2011.03.038

Cuello, M., Ettenberg, S. A., Clark, A. S., Keane, M. M., Posner, R. H., Nau, M. M., et al. (2001). Down-regulation of the erbB-2 receptor by trastuzumab (herceptin) enhances tumor necrosis factor-related apoptosis-inducing ligand-mediated apoptosis in breast and ovarian cancer cell lines that overexpress erbB-2. *Cancer Res.* 61, 4892–4900.

Han, S., Meng, Y., Tong, Q., Li, G., Zhang, X., Chen, Y., et al. (2014). The ErbB2-targeting antibody trastuzumab and the small-molecule SRC inhibitor saracatinib synergistically inhibit ErbB2-overexpressing gastric cancer. *MAbs* 6, 403–408. doi: 10.4161/mabs.27443

Hudis, C. A. (2007). Trastuzumab–mechanism of action and use in clinical practice. *N. Engl. J. Med.* 357, 39–51. doi: 10.1056/NEJMra043186

Hung, C. M., Kuo, D. H., Chou, C. H., Su, Y. C., Ho, C. T., and Way, T. D. (2011). Osthole suppresses hepatocyte growth factor (HGF)-induced epithelial-mesenchymal transition via repression of the c-Met/Akt/mTOR pathway in human breast cancer cells. *J. Agric. Food Chem.* 59, 9683–9690. doi: 10.1021/jf2021489

Kao, S. J., Su, J. L., Chen, C. K., Yu, M. C., Bai, K. J., Chang, J. H., et al. (2012). Osthole inhibits the invasive ability of human lung adenocarcinoma cells via suppression of NF-kappaB-mediated matrix metalloproteinase-9 expression. *Toxicol. Appl. Pharmacol.* 261, 105–115. doi: 10.1016/j.taap.2012.03.020

Kovtun, Y. V., Audette, C. A., Mayo, M. F., Jones, G. E., Doherty, H., Maloney, E. K., et al. (2010). Antibody-maytansinoid conjugates designed to bypass multidrug resistance. *Cancer Res.* 70, 2528–2537. doi: 10.1158/0008-5472.CAN-09-3546

Li, B., Meng, Y., Zheng, L., Zhang, X., Tong, Q., Tan, W., et al. (2013). Bispecific antibody to ErbB2 overcomes trastuzumab resistance through comprehensive blockade of ErbB2 heterodimerization. *Cancer Res.* 73, 6471–6483. doi: 10.1158/0008-5472.CAN-13-0657

Liao, P. C., Chien, S. C., Ho, C. L., Wang, E. I., Lee, S. C., Kuo, Y. H., et al. (2010). Osthole regulates inflammatory mediator expression through modulating NF-kappaB, mitogen-activated protein kinases, protein kinase C, and reactive oxygen species. *J. Agric. Food Chem.* 58, 10445–10451. doi: 10.1021/jf102812t

Lin, V. C., Chou, C. H., Lin, Y. C., Lin, J. N., Yu, C. C., Tang, C. H., et al. (2010). Osthole suppresses fatty acid synthase expression in HER2-overexpressing breast cancer cells through modulating Akt/mTOR pathway. *J. Agric. Food Chem.* 58, 4786–4793. doi: 10.1021/jf100352c

Lin, Y. C., Lin, J. C., Hung, C. M., Chen, Y., Liu, L. C., Chang, T. C., et al. (2014). Osthole inhibits insulin-like growth factor-1-induced epithelial to mesenchymal transition via the inhibition of PI3K/Akt signaling pathway in human brain cancer cells. *J. Agric. Food Chem.* 62, 5061–5071. doi: 10.1021/jf501047g

Milella, M., Trisciuoglio, D., Bruno, T., Ciuffreda, L., Mottolese, M., Cianciulli, A., et al. (2004). Trastuzumab down-regulates Bcl-2 expression and potentiates apoptosis induction by Bcl-2/Bcl-XL bispecific antisense oligonucleotides in HER-2 gene–amplified breast cancer cells. *Clin. Cancer Res.* 10, 7747–7756. doi: 10.1158/1078-0432.CCR-04-0908

Pal, I., and Mandal, M. (2012). PI3K and Akt as molecular targets for cancer therapy: current clinical outcomes. *Acta Pharmacol. Sin.* 33, 1441–1458. doi: 10.1038/aps.2012.72

Rose, J. S., and Bekaii-Saab, T. S. (2011). New developments in the treatment of metastatic gastric cancer: focus on trastuzumab. *Oncol. Targets Ther.* 4, 21–26. doi: 10.2147/OTT.S10188

Srinivas, G., Kusumakumary, P., Nair, M. K., Panicker, K. R., and Pillai, M. R. (2000). Mutant p53 protein, Bcl-2/Bax ratios and apoptosis in paediatric acute lymphoblastic leukaemia. *J. Cancer Res. Clin. Oncol.* 126, 62–67. doi: 10.1007/s004320050010

Wang, L., Peng, Y., Shi, K., Wang, H., Lu, J., Li, Y., et al. (2015). Osthole inhibits proliferation of human breast cancer cells by inducing cell cycle arrest and apoptosis. *J. Biomed. Res.* 29, 132–138. doi: 10.7555/JBR.27.20120115

Wang, L., Yang, L., Lu, Y., Chen, Y., Liu, T., Peng, Y., et al. (2016). Osthole induces cell cycle arrest and inhibits migration and invasion via pten/akt pathways in osteosarcoma. *Cell Physiol. Biochem.* 38, 2173–2182. doi: 10.1159/000445573

Wang, L., Yu, X., Wang, C., Pan, S., Liang, B., Zhang, Y., et al. (2017). The anti-ErbB2 antibody H2-18 and the pan-PI3K inhibitor GDC-0941 effectively inhibit trastuzumab-resistant ErbB2-overexpressing breast cancer. *Oncotarget* 8, 52877–52888. doi: 10.18632/oncotarget.17907

Wang, S., Chen, C., Meng, Y., Hu, S., Zheng, L., Song, J., et al. (2012). Effective suppression of breast tumor growth by an anti-EGFR/ErbB2 bispecific antibody. *Cancer Lett.* 325, 214–219. doi: 10.1016/j.canlet.2012.07.007

Willis, S. N., Fletcher, J. I., Kaufmann, T., van Delft, M. F., Chen, L., Czabotar, P. E., et al. (2007). Apoptosis initiated when BH3 ligands engage multiple Bcl-2 homologs, not Bax or Bak. *Science* 315, 856–859. doi: 10.1126/science.1133289

Xu, X., Zhang, Y., Qu, D., Jiang, T., and Li, S. (2011). Osthole induces G2/M arrest and apoptosis in lung cancer A549 cells by modulating PI3K/Akt pathway. *J. Exp. Clin. Cancer Res.* 30:33. doi: 10.1186/1756-9966-30-33

Yang, L. L., Wang, M. C., Chen, L. G., and Wang, C. C. (2003). Cytotoxic activity of coumarins from the fruits of Cnidium monnieri on leukemia cell lines. *Planta Med.* 69, 1091–1095. doi: 10.1055/s-2003-45188

Yang, Y., Guo, R., Tian, X., Zhang, Z., Zhang, P., Li, C., et al. (2017). Synergistic anti-tumor activity of nimotuzumab in combination with trastuzumab in HER2-positive breast cancer. *Biochem. Biophys. Res. Commun.* 489, 523–527. doi: 10.1016/j.bbrc.2017.06.001

Ye, Y., Han, X., Guo, B., Sun, Z., and Liu, S. (2013). Combination treatment with platycodin D and osthole inhibits cell proliferation and invasion in mammary carcinoma cell lines. *Environ. Toxicol. Pharmacol.* 36, 115–124. doi: 10.1016/j.etap.2013.03.012

You, L., Feng, S., An, R., and Wang, X. (2009). Osthole: a promising lead compound for drug discovery from a traditional Chinese medicine (TCM). *Nat. Prod. Commun.* 4, 297–302.

Zhang, L., Jiang, G., Yao, F., He, Y., Liang, G., Zhang, Y., et al. (2012). Growth inhibition and apoptosis induced by osthole, a natural coumarin, in hepatocellular carcinoma. *PLoS One* 7:e37865. doi: 10.1371/journal.pone.0037865

Zhang, S., Huang, W. C., Li, P., Guo, H., Poh, S. B., Brady, S. W., et al. (2011). Combating trastuzumab resistance by targeting SRC, a common node downstream of multiple resistance pathways. *Nat. Med.* 17, 461–469. doi: 10.1038/nm.2309

Zhang, Z. R., Leung, W. N., Cheung, H. Y., and Chan, C. W. (2015). Osthole: a review on its bioactivities, pharmacological properties, and potential as alternative medicine. *Evid Based Complement. Alternat. Med.* 2015:919616. doi: 10.1155/2015/919616

Zheng, L., Tan, W., Zhang, J., Yuan, D., Yang, J., and Liu, H. (2014). Combining trastuzumab and cetuximab combats trastuzumab-resistant gastric cancer by effective inhibition of EGFR/ErbB2 heterodimerization and signaling. *Cancer Immunol. Immunother.* 63, 581–586. doi: 10.1007/s00262-014-1541-z

Zou, H., Henzel, W. J., Liu, X., Lutschg, A., and Wang, X. (1997). Apaf-1, a human protein homologous to *C. elegans* CED-4, participates in cytochrome c-dependent activation of caspase-3. *Cell* 90, 405–413. doi: 10.1016/S0092-8674(00)80501-2

Conflict of Interest Statement: The authors declare that the research was conducted in the absence of any commercial or financial relationships that could be construed as a potential conflict of interest.

frontiers in Oncology

REVIEW
published: 28 November 2018
doi: 10.3389/fonc.2018.00563

Progresses and Perspectives of Anti-PD-1/PD-L1 Antibody Therapy in Head and Neck Cancers

Bo Yang[1,2], *Tingjun Liu*[1,2], *Yang Qu*[1,2], *Hangbo Liu*[1,2], *Song Guo Zheng*[3], *Bin Cheng*[1,2]* and *Jianbo Sun*[1,2]*

[1] Guanghua School of Stomatology, Hospital of Stomatology, Sun Yat-sen University, Guangzhou, China, [2] Guangdong Provincial Key Laboratory of Stomatology, Sun Yat-sen University, Guangzhou, China, [3] Division of Rheumatology, Penn State Health Milton S. Hershey Medical Center, Hershey, PA, United States

Head and neck cancer is the 6th most common malignancy worldwide and urgently requires novel therapy methods to change the situation of low 5-years survival rate and poor prognosis. Targeted therapy provides more precision, higher efficiency while lower adverse effects than traditional treatments like surgery, radiotherapy, and chemotherapy. Blockade of PD-1 pathway with antibodies against PD-1 or PD-L1 is such a typical targeted therapy which reconstitutes anti-tumor activity of T cell in treatments of cancers, especially those highly expressing PD-L1, including head and neck cancers. There are many clinical trials all over the world and FDA has approved anti-PD-1/PD-L1 drugs for head and neck cancers. However, with the time going, the dark side of this therapy has emerged, including some serious side effects and drug resistance. Novel materials like nanoparticles and combination therapy have been developed to improve the efficacy. At the same time, standards for evaluation of activity and safety are to be established for this new therapy. Here we provide a systematic review with comprehensive depth on the application of anti-PD1/PD-L1 antibodies in head and neck cancer treatment: mechanism, drugs, clinical studies, influencing factors, adverse effects and managements, and the potential future developments.

Keywords: PD-1, PD-L1, immune checkpoint inhibitor, head and neck cancer, immunotherapy, adverse effects

OPEN ACCESS

Edited by:
Jian-ye Zhang,
Guangzhou Medical University, China

Reviewed by:
Alexandre Corthay,
Department of Pathology, Oslo University Hospital, Norway
Karishma Rajani,
Mayo Clinic, United States

***Correspondence:**
Bin Cheng
chengbin@mail.sysu.edu.cn
Jianbo Sun
sunjb3@mail.sysu.edu.cn

Specialty section:
This article was submitted to Cancer Molecular Targets and Therapeutics, a section of the journal Frontiers in Oncology

Received: *23 August 2018*
Accepted: *12 November 2018*
Published: *28 November 2018*

Citation:
Yang B, Liu T, Qu Y, Liu H, Zheng SG, Cheng B and Sun J (2018) Progresses and Perspectives of Anti-PD-1/PD-L1 Antibody Therapy in Head and Neck Cancers. Front. Oncol. 8:563. doi: 10.3389/fonc.2018.00563

INTRODUCTION OF HEAD AND NECK CANCERS

Head and neck cancers are composed of various kinds of epithelial malignant tumors, including oral cancers, maxillofacial cancers, larynx cancers, and many others, almost all of which are head and neck squamous cell carcinoma (HNSCC). Although, there are other pathological types such as verrucous carcinoma, basaloid squamous cell carcinoma, papillary squamous cell carcinoma, they only make up a small percentage (1). HNSCC is the 6th most common malignancy worldwide, with number of 650,000 new cases a year and 350,000 deaths (2). Around 2/3 of patients present with advanced disease, often with regional lymph node involvement, while 10% present with distant metastases (3). According to epidemiological survey, the 5-years survival rate of HNSCC in all stages was about 60%, and the survival rate was even worse for specific primary sites such as hypopharynx. The main causes of head and neck cancers are tobacco and alcohol consumption (1, 4–8). Chewing betel quid is also well-recognized as a risk factor for the cancer of oral cavity (9). And human papillomavirus (HPV) and p53 mutation are related to certain subsets of head

and neck cancers (10–12). About 25% of HNSCC contain HPV genomic DNA (13). However, HPV positivity is a favorable prognostic factor in HNSCC (14). Patients with HPV^+ HNSCC show better responsiveness to radiation, chemotherapy, or both, and might be more susceptive to immunosurveillance of tumor-specific antigens (14).

COMMON TREATMENT STRATEGIES FOR HEAD AND NECK CANCERS

The location of the cancers makes it necessary to take the spiritual and plastic factors into consideration. Primary tumor site, stage, and resectability are also treatment concerns as well as the patient factors such as swallowing, airway, organ preservation, and comorbid illnesses. For plan making, doctors are needed and organized from different departments which include head and neck surgeons, plastic surgeons, medical oncologists, radiation oncologists, radiologists, and dentists (2).

Common treatment strategies for head and neck cancers include surgery, radiotherapy, and chemotherapy. At present, surgery is still the standard therapy for HNSCC. However, surgical operations are limited, owing to the complexity of structures and the need for organ preservation. Most surgeons agree that the carotid artery, the base of the skull, and the invasion of the pre-vertebral muscle tissue are unresectable (2). Moreover, when the tumor is too extensive or there are multiple distant metastases, patients are generally not suitable for surgical treatment. Radiotherapy alone can improve the cure rate of early glottis, tongue, and tonsil cancers (15). However, prolonged interruption of radiotherapy or delayed post-operative radiotherapy may impair the patient's prognosis, which may be due to the proliferation of cancer cells (16). Delivery of radiation remains to be improved with continuous technological progress, and customization of radiation dose and volume (17). Chemotherapy is the core component of local advanced HNSCC treatment (18). Platinum compounds Cisplatin is a standard reagent for combination with radiotherapy or other drugs. Huperzine compounds are active and have been tested in locally advanced HNSCC chemotherapy (19, 20). Concurrent chemotherapy with normo-fractionated radiotherapy (2 Gy/day, 5 days/week, for 5–7 weeks) is used most in current practice (21).

Traditional therapy can result in serious complications, from pain to malnutrition, risk of infection, and psychological distress (21). In order to ameliorate these drawbacks, comprehensive treatments are currently preferred for the advanced tumors. Comprehensive treatments must be well-designed and planned according to the patient's general condition and the stage of tumor development. At present, the treatment of oral and maxillofacial malignant tumors emphasizes the comprehensive treatment based on surgery, especially the triple therapy, which combines surgery with radiotherapy and chemotherapy.

Modern research has been keen on identifying specific molecular targets involved in the occurrence and progression of head and neck cancers. EGFR and VEGF are two main targets which are overexpressed in majority of both precancerous oral lesions and HNSCC (22–24). EGFR can bind to and be activated by different ligands, including the epidermal growth factor (EGF) and transforming growth factor-α (TGF-α) (25). EGFR activation initiates subsequent signaling pathways, eventually resulting in tumor cell resistance to apoptosis and promoting angiogenesis, tumor cell migration, and tumor cell proliferation (**Figure 1**) (25, 26). Current EGFR-targeted therapies include monoclonal antibodies (mAbs) and tyrosine kinase inhibitors (TKIs). Antibodies target the extracellular domain of EGFR while TKIs hinder downstream signaling pathways by binding to the cytoplasmic region of EGFR (27). To date, Cetuximab remains the only FDA-approved EGFR-targeted mAb for the treatment of recurrent/metastatic (R/M) HNSCC. Cetuximab in combination with radiotherapy is a standard treatment option for locally or regionally advanced HNSCC (28). VEGF, is a key regulator of physiological angiogenesis during embryogenesis, skeletal growth, and reproductive functions (29). The biological effects of VEGF, mediated by two receptor tyrosine kinases (RTKs), VEGFR-1 and VEGFR-2, cause receptor TK activation and downstream signaling to stimulate endothelial cell proliferation, vessel permeability, and migration (27). Bevacizumab, a humanized monoclonal antibody targeting VEGF-A, was approved by the FDA for treatment of advanced cancer types. Bevacizumab could increase the sensitivity of HNSCC to radiotherapy in preclinical trials. Bevacizumab was evaluated in phase I and II clinical trials in combination with Erlotinib, an EGFR inhibitor, in patients with R/M HNSCC (30, 31) and the combined treatments increased the complete response rate by ∼15% and median survival by 7.1 months (30). The phase II trial on the combination of Bevacizumab with chemotherapy, radiotherapy or EGFR inhibitors are ongoing.

IMMUNOLOGICAL TARGETED THERAPY

Immunotherapies stimulate host antitumor immune system and can elicit endurable responses in subsets of patients across different types of tumors (**Figure 1**) (32). Immune checkpoints, like cytotoxic T-lymphocyte-associated antigen-4 (CTLA-4) and programmed cell death-1 (PD-1), work as inhibitory pathways, playing an important role in self-tolerance under healthy conditions. Checkpoint inhibitors are part of immunotherapies that enhance antitumor T cell activity by hindering initiation of suppressive signaling pathways of activated T cells. The 2018 Nobel Prize in Physiology or Medicine was recently given to James P. Allison and Tasuku Honjo for their discovery and contribution in cancer immunotherapy correlated with CTLA-4

Abbreviations: APC, antigen presenting cell; ATF, activating transcription factor; CRC, colorectal cancer; GEM, chemotherapy drug gemcitabine; GOx, glucose oxidase; HNSCC, head and neck squamous cell carcinoma; IGF, insulin-like growth factor; NFAT, nuclear factor of activated T cells; NSCLC, non-small cell lung cancer; ORR, objective response rate; OS, overall survival; PIP, phosphatidylinositol; PLGF, placental growth factor; RCC, renal cell carcinoma; ROS, reactive oxygen species; RTK, receptor tyrosine kinases; SAEs, severe adverse events; sPD-1/sPD-L1, soluble PD-1/ soluble PD-L1; TCR, T cell receptors; TGF, transforming growth factor; TILs, tumor-infiltrating lymphocytes; TKIs, tyrosine kinase inhibitors; TNF, tumor necrosis factor; T-NHL, T-cell non-Hodgkin's lymphoma; trAEs, treatment-related adverse events.

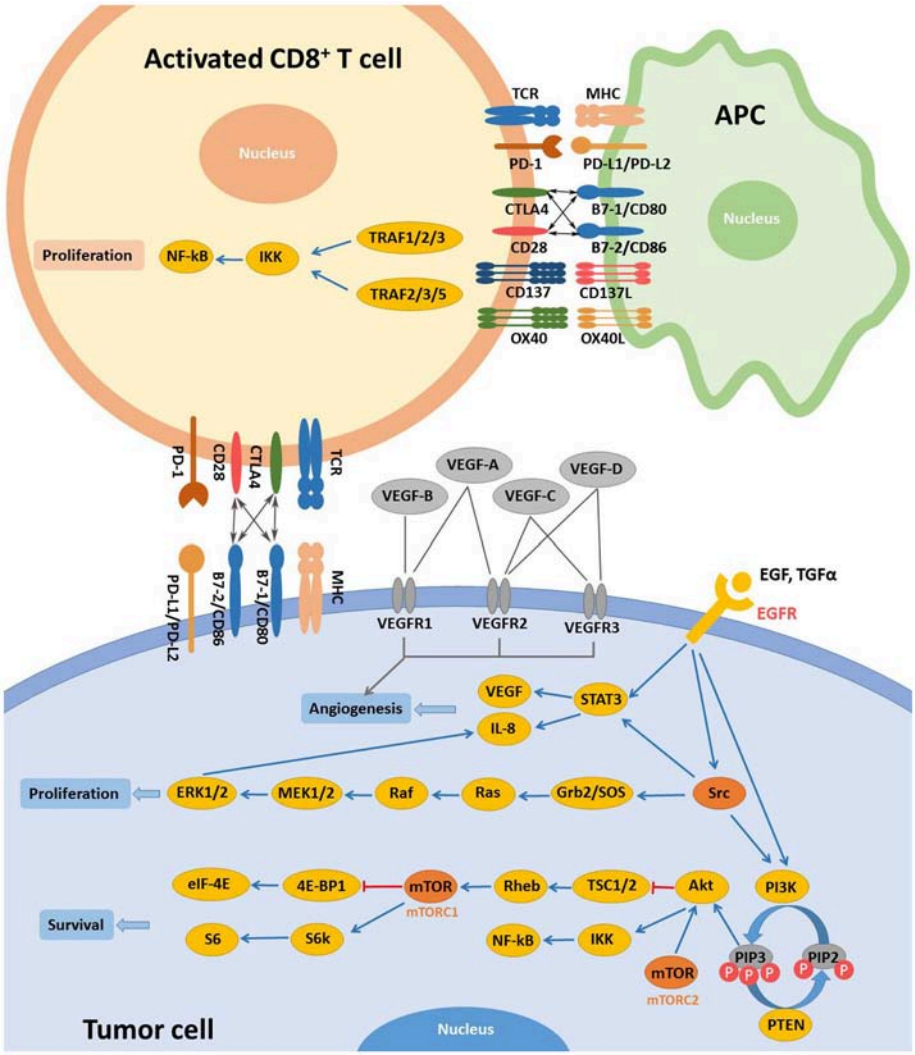

FIGURE 1 | Main targets and related signaling pathways involved in the targeted therapy for R/M HNSCC. Activation of EGFR by extracellular ligands initiates activation of Src, STAT3, and PI3K. Activated Src promotes cell proliferation mainly via RAS/RAF/MAPK pathway. In the PI3K/Akt pathway, phosphorylation of PIP2 is mediated by PI3K while dephosphorylation of PIP3 is controlled by PTEN. Akt could be activated independently by mTORC2 activation. Activation of Akt and mTORC1 inhibit TSC1/2/Rheb and 4E-BP1/eIF-4E downstream signaling, respectively while IKK/NF-kB and S6/S6k pathways are initiated, promoting tumor cell survival. Once activated, other targets, including VEGFR and c-MET, expressed on tumor cells share similar downstream signaling with EGFR. CD137L and OX40L activate CD137 and OX40, respectively. And proliferation of activated T cells is achieved via TRAF/IKK/NF-κB downstream signaling. CTLA-4 and its ligands are also demonstrated. Some pathways were simplified for clearer demonstration.

and PD-1. Other targets such as CD137 and OX40, unlike CTLA-4 and PD-1, work as immune activators and are as well under active investigation for cancer therapy (**Table 1**) (37, 38).

CTLA-4

Cytotoxic T lymphocyte-associated antigen-4 (CTLA-4; also known as CD152) is the first clinically targeted immune checkpoint receptor. CTLA-4, expressed on activated $CD8^+$ effector T cells, mainly regulates the early stage of T cell activation, enhances the activity of effector $CD4^+$ T cell, and inhibits Treg cell-dependent immunosuppression (39, 40). CD28 and CTLA-4 have the same ligands B7-1 (also known as CD80) and B7-2 (also known as CD86); and CTLA-4, compared to CD28, has a much higher affinity for B7-1 (41). CTLA-4 has been proved to be a negative regulator of T cell activation in an effort to prevent autoimmunity, antagonizing the CD28-B7 co-stimulatory signals. Research showed that the blockade of CTLA-4 results in enhanced antitumor immunity (42). Clinical studies using anti-CTLA-4 antibodies demonstrated activity in melanoma. Ipilimumab, an anti-CTLA-4 antibody, was the first targeted immunotherapy to prove a survival advantage for patients with metastatic melanoma. Hence, it was approved by FDA for the treatment of advanced melanoma in 2010 (43). In HNSCC, Yu et al. showed that CTLA4

TABLE 1 | Immunological targeted therapies approved or under investigation for the treatment of head and neck cancers.

Drug	Target	Modality	Status	References
MEDI0562	OX40	Antibody	Phase I Phase Ib Phase IPhase I	NCT03336606 NCT02315066
Urelumab	CD137	Antibody	Phase IPhase I	NCT02110082
PF-05082566	CD137	Antibody	Phase IPhase I	NCT02315066
Ipilimumab	CTLA-4	Antibody	Phase II Phase IPhase I Phase IPhase I	NCT03620123 NCT03098160 NCT02812524
Tremelimumab	CTLA-4	Antibody	Phase III Phase III Phase II Phase II Phase IPhase I-2	NCT02369874 NCT02551159 NCT03624231 NCT03292250 NCT03019003
Pembrolizumab	PD-1	Antibody	Approved	(33, 34)
Nivolumab	PD-1	Antibody	Approved	(35, 36)
Darvalumab	PD-L1	Antibody	Phase III Phase II Phase IPhase I	NCT02551159 NCT02207530 NCT02997332
Avelumab	PD-L1	Antibody	Phase III Phase IPhase I	NCT02952586 NCT02938273
INCB024360	PD-L1	Antibody	Phase IPhase I/2	NCT02318277

PD-1, programmed cell death protein 1; PD-L1, programmed death ligand 1; CTLA-4, cytotoxic T lymphocyte-associated antigen-4.

was upregulated in the tumor-infiltrating lymphocyte (TIL) of HNSCC and the high $CD8^+$/CTLA4 ratio was associated with improved prognosis (44). Further, Jie et al. found that intratumoral Tregs, compared to circulating Tregs, induced higher expression of CTLA-4 in HNSCC (45). Currently, clinical trials of Ipilimumab (NCT02551159, NCT03212469), alone or in combination with other treatments, for HNSCC are in progress (40).

CD137

CD137, a member of TNF receptor superfamily, is widely induced on activated $CD4^+$ T cells, $CD8^+$ T cells, B cells, NK cells, monocytes, and DC. The engagement of CD137 could promote the proliferation of T cells. The introduction of Urelumab, the fully human CD137-agonist mAb, has enabled modulation of CD137 function in immune-oncology, including application in combination with tumor targeting mAb (46). Srivastava et al. (38) confirmed that Cetuximab combined with CD137 agonist was effective in the treatment of HNC. CD137 has provided a new mechanism for the enhancement of Cetuximab (38).

OX40

OX40 is a member of the TNF receptor family and mediates an effective co-stimulation pathway which can enhance T cell memory, proliferation, and antitumor activity in patients with metastatic cancers (47, 48). Overexpression of OX40 in the TIL of patients with HNSCC has been identified (49). Furthermore, Montler et al. have noted co-expression of OX40 with PD-1 and CTLA-4 in a majority of tumor specimens, especially within the Treg population (49). The preclinical model showed the synergistic effects of anti-OX40 and anti-PD1, anti-OX40 and anti-CTLA-4, as well as anti-OX40 and anti-PDL1 (49). Anti-OX40 is currently being tested in early clinical trials of HNSCC, both as monotherapy and in combination with other immunotherapies (37).

ANTI-PD-1/PD-L1 THERAPY

T cells express the inhibitory receptor known as PD-1 on their surfaces to guard our body (50). When bound by its ligands PD-L1 or PD-L2, PD-1 transduces a signal into T cells to attenuate downstream signaling through the PI3K and PKCθ pathways (50, 51), which results in inhibition of T cell activation and proliferation. This protective mechanism is also utilized by tumor cells to escape immune attack through expressing high abundance of PD-L1 ligands on their surfaces.

Anti-PD-1/PD-L1 therapy has been a routine treatment to patients with PD-L1 highly expressing tumor (52). This kind of

immunotherapy could target tumors more precisely. Meanwhile, as anti-PD-1/PD-L1 therapy has been applied to more and more patients, the side effects and the factors hindering the therapeutic effects have been noticed. Thus, combined treatments and better administrating methods have been raised to improve the treatment.

Mechanism of PD-1/PD-L1 Inhibitors

Tumor infiltrating lymphocytes, especially $CD8^+$ T cells, exhibit high levels of PD-1 in HPV^+ HNSCC (12). When PD-1 binds to PD-L1 on tumor cells, T cell proliferation is suppressed and tumor cells are able to evade immune attack more effectively in the tumor microenvironment (12). Since tumors expressing PD-L1, compared to PD-L1–negative tumors, showed improved response to Nivolumab (a PD-1 inhibitor) (53), it is important to investigate the level of PD-L1 expression in tumor microenvironment. One study suggested that patients with HPV^- HNSCC expressed high levels of PD-1 in T cells and PD-L1 in a majority of tumor cells (54). Despite primary tumor sites, PD-L1 has been spotted on metastatic lesions (55). In summary, more than 29% of HPV^- and around 70% of HPV^+ HNSCC express PD-L1, suggesting that the majority of these cancers have potential for responding to PD-1 inhibitors (56). PD-L1 and PD-1 interaction is among the signals beneficial for tumor cells, which also include EGFR signaling, CD 28 stimulation and many others. And there are plenty of downstream pathways as well, which are composed of SHP2, RAS, ZAP70, P13K, and so on (**Figure 2**).

When bond by PD-1 ligands, PD-1 is able to recruit phosphatases including SHP2 toinhibit T cell functions by countering the positive signaling events mediated by the T cell receptors (TCR) and CD28 (50). For instance, they restrain ZAP70 and PI3K–AKT and RAS signaling pathways (50). In conclusion, this lowers down the activation of transcription factors such as AP-1, NFAT, and NF-κB, which are important for T cell activation, proliferation, growth, and survival. Besides, PD-1 is able to inhibit T cell functions by improving the expression of BATF transcription factor to inhibit the effector transcriptional programs. EGFR is an important target for mediating tumor metastasis and adhesion. After combining with epidermal growth factor (EGF), EGFR can deliver positive signaling events downstream. For example, it activates PI3K–AKT and RAS signaling pathways to promote tumor cells proliferation and migration (50). Successful anti-PD-1/PD-L1 therapy requires adequate amount of specific T cells in tumor microenvironment and competent ability of T cells to get enough nutrients (57). Studies have shown aerobic glycolysis is essential for T cells to secrete IFN-γand attack tumor cells. PD-1/PD-L1 inhibitors may help T cells compete for glucose in tumor microenvironment, promoting T cell glycolysis and IFN-γ secretion (57, 58).

Daste et al. reported a case that a 64-years-old patient with HNSCC developed local tumor flare-up under immunotherapy, and a dramatic response was achieved in the following chemotherapy (59). Owing to the "loco-regional phenomena" described in their case study, they suggested that although clinical efficacy was not achieved in this case, immunotherapy might enhance response sensitivity to chemotherapy in patients with HNSCC (59).

Overview of FDA-Approved PD-1 Inhibitors for Head and Neck Cancers

Pembrolizumab

Pembrolizumab was the first anti-PD-1 antibody approved by FDA to treat patients with unresectable or metastatic melanoma who progress after Ipilimumab treatment. It is also approved for the treatment for melanoma patients harboring a *BRAF V600E* mutation, following treatment with a BRAF inhibitor. Pembrolizumab has also been legal for the treatment of non-small-cell lung cancer (NSCLC) without EGFR mutation and ALK rearrangement but with disease progression or following platinum-based chemotherapy (60). In August 2016, FDA approved the use of Pembrolizumab in R/M HNSCC that has progressed on or after platinum-containing chemotherapy (33, 34).

Nivolumab

Nivolumab, a PD-1 inhibitor, has been approved by FDA to treat Hodgkin lymphoma, renal cell carcinoma, NSCLC, and melanoma. Recent breakthrough in the application of Nivolumab in patients with processed HNSCC during chemotherapy or R/M HNSCC after chemotherapy with platinum-based drugs has made Nivolumab second to the Pembrolizumab approved by FDA in HNSCC treatment (35, 36).

CLINICAL STUDIES OF PD-1/PD- L1 INHIBITORS

Inhibiting either PD-1 or PD-L1 function can block the PD-1 pathway. A number of PD-1/PD-L1 inhibitors are being investigated clinically and described in more details below (**Table 2**).

PD-1

Pembrolizumab (MK-3475, Previously Known as Lambrolizumab)

Preclinical anti-tumor effects were demonstrated in animals bearing multiple tumors. The first phase I clinical trial was carried out in patients with advanced solid tumors (61). Results suggested that Pembrolizumab was well-tolerated and associated with durable antitumor activity in multiple solid tumors (61). Two mg/kg per 3 weeks is considered a safe and effective minimum dose of antitumor activity (61). KEYNOTE-012 trial was a multicenter, open-label, phase Ib trial that included patients with R/M HNSCC in one of the cohorts. The objective response rate (ORR) was ∼20% and overall survival (OS) was better in HPV^+ patients (33). Then a larger HNSCC expansion cohort of KEYNOTE-012 reported an ORR of 18.2%, and response rates were similar in HPV^+ and HPV^- patients (62). In a recent single-arm, phase II KEYNOTE-055 study conducted in patients with R/M HNSCC, ORR was 16% and response rates were similar in HPV^+ and HPV^- patients, providing rationale for treatment with Pembrolizumab (NCT02255097) (63).

Monotherapy with Pembrolizumab is being carried out in patients with NSCLC (NCT01840579), advanced solid tumors

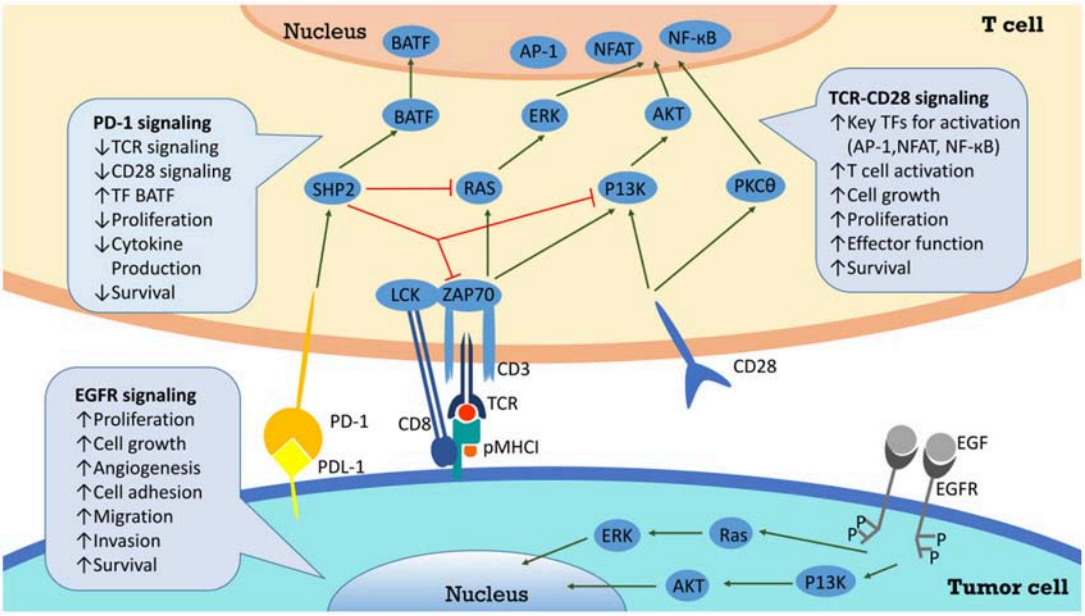

FIGURE 2 | PD-L1/PD-1 signaling pathway and the correlated network. Interaction between PD-L1 and PD-1 on T cells results in inhibition of Zap70 phosphorylation and PI3K activation, and finally attenuates TCR signaling, CD28 mediated co-stimulation, NF-κB, and AP-1 activation, and IL2 production. Through inhibition of T cell via overexpression of PD-L1, cancer cells evade the host immune system.

(NCT01295827) and hematologic malignancies (NCT01953692). Clinical trials of Pembrolizumab focusing on HNSCC are ongoing in comparison to chemotherapy (NCT02358031), in combination with radiotherapy (NCT02707588), and in combination with cisplatin and radiation (NCT02586207).

Nivolumab (MDX-1106, BMS-936558, ONO-4538)

The first phase I clinical trial was conducted in patients with treatment-refractory solid tumors such as advanced metastatic melanoma, colorectal cancer, castrate-resistant prostate cancer, NSCLC, and renal cell carcinoma (64). The study exhibited good tolerance and meaningful antitumor activity of PD-1 inhibitors, and the early results from a follow-up trial (NCT00730639) further confirmed this. It appeared that the PD-1 antibody was well-tolerated and demonstrated anti-tumor activity in many patients whose previous treatment failed (65). In a recent randomized, open-label, phase III clinical trial conducted in patients with R/M HNSCC, the ORR was 26.1% for Nivolumab, demonstrating a survival advantage compared with conventional treatments with ORR of 0% for investigators' choices of therapy (NCT02105636) (66). Ongoing clinical trials focusing on HNSCC include comparison to Cetuximab, Methotrexate or Docetaxel (NCT02105636), combination with Cisplatin, Cetuximab, or IMRT (NCT02764593), and monotherapy (NCT03132038, NCT03012581).

PD-L1

Durvalumab (MEDI4736)

In a phase I/II clinical trial that included a group of HNSCC patients, ORR was 17%, especially higher (25%) in PD-L1^{high} patients. The disease control rate in PD-L1 high subgroup was 44.9%, much greater than that in PD-L1 low or negative subgroup (21.5%) (67). These data support continued clinical development of Durvalumab in HNSCC. Durvalumab is being tested as monotherapy (NCT02207530), in combination with Docetaxel plus Displatin and 5-FU (NCT02997332), and in comparison to Durvalumab plus Tremelimumab (NCT02551159).

Avelumab

Avelumab is an anti-PD-L1 antibody. Studies of Avelumab targeting HNSCC has been scarce. It's currently assessed in combination with Cetuximab and radiotherapy in a phase I trial (NCT02938273), and in combination with standard care in a phase III trial (NCT02952586).

FACTORS INFLUENCING ANTI-PD-1/PD-L1 THERAPY

Gut Microbiota

It has been lately reported that gut microbiome plays important roles in many diseases, including influenza (68), multiple sclerosis (69, 70), diabetes (71), colorectal cancer (68, 72), and many others in various preclinical models, among which gut microbiome may modulate PD-1/PD-L1-based immunotherapy (73–76). Many kinds of bacteria have been proved to facilitate PD-1/PD-L1 blockades, meanwhile, there are bacteria that hamper the treatment (**Table 3**). It is reported that oral gavage of *Bifidobacterium* could achieve the same effects as anti-PD-L1 treatment, and combinational therapy almost eliminated tumor outgrowth, in which enhanced dendritic cell function led to more priming and accumulation of CD8$^+$ T cells in the tumor microenvironment (76). On one hand, *Akkermansia*

TABLE 2 | Clinical Trials on anti-PD-1/PD-L1 in head and neck cancers.

Immune checkpoint	Inhibitor	Other names	NCT-nummer	Phase	Arms	N of pts	Primary endpoint	Recruitment status
PD-1	pembrolizumab	Lambrolizumab/MK-3475 /Keytruda	NCT02586207	Phase I	Pembrolizumab + Cisplatin + Radiation	58	AE	recruiting
			NCT02358031	Phase III	Pembrolizumab vs. Pembrolizumab+Platinum+5-FU vs. Cetuximab+Platinum+5-FU	825	PFS, OS	Active, not recruiting
			NCT02707588	Phase II	Pembrolizumab+radiotherapy vs. Cetuximab+radiotherapy	133	LRC	Active, not recruiting
	nivolumab	Opdivo/BMS-936558/MDX-1106/NIVO/ONO-4538	NCT02764593	Phase I	Nivolumab+Cisplatin vs. Nivolumab+High-dose Cisplatin vs. Nivolumab+Cetuximab vs. Nivolumab+IMRT	40	DLT	Active, not recruiting
			NCT03132038	Phase II	Nivolumab	92	non-progression rate	recruiting
			NCT03012581	Phase II	Nivolumab	300	ORR	recruiting
			NCT02105636	Phase III	Nivolumab vs. Cetuximab/Methotrexate/ Docetaxel	506	OS	Active, not recruiting
PD-L1	Durvalumab	Imfinzi/MEDI4736	NCT02207530	Phase II	Durvalumab	112	ORR	Active, not recruiting
			NCT02997332	Phase I	Durvalumab+Docetaxel+ Cisplatin+5-FU	36	RP2D, DLT	recruiting
			NCT02551159	Phase III	Durvalumab vs. Durvalumab+Tremelimumab vs. SOC	823	OS	Active, not recruiting
	Avelumab	Bavencio	NCT02952586	Phase III	Avelumab+SOC CRT vs. Placebo+SOC CRT	640	PFS	recruiting
			NCT02938273	Phase I	Avelumab+cetuximab+ Radiation therapy	10	toxicity	recruiting
	INCB024360		NCT02318277	Phase I/ II	MEDI4736 + INCB024360	42	DLT, AE, ORR	Active, not recruiting

PD-L1, programmed death-1 ligand; FU, fluorouracil; HNSCC, head and neck squamous cell carcinoma; AE, adverse event; LRC, locoregional control; DLT, dose limiting toxicity; ORR, overall response rate; OS, overall survival; PFS, progression-free survival; SOC, standard of care; CRT, chemoradiation therapy; IMRT, intensity-modulated radiation therapy; RP2D, recommended phase II dose.

muciniphila was screened out to affect the anti-PD-1-based therapy in epithelial tumors in an IL-12 dependent fashion by enhancing the recruitment of $CCR9^+CXCR3^+CD4^+$ T cells (75). Further study in patients also revealed that responding patients had more diverse and abundant bacteria of the *Ruminococcaceae* family, enhanced systemic and antitumor immunity, functioning better in anabolic pathways as well (74). On the other hand, the recent study by Matson V reported *Blautia obeum* and *Roseburia intestinalis* with compromised efficacy of PD-1 blockade (77). These results provide important information for cancer therapy with immune checkpoint inhibitors.

Molecules Regulating PD-1/PD- L1

Some tumors respond more sensitively to anti-PD-1/PD-L1 therapy, while others do not. The mechanisms regulating anti-PD-1/PD-L1 therapy sensitivity have arisen wide attention. Recently, two molecules, CMTM6 and CMTM4, have been reported as PD-L1 protein regulators. CMTM6 could prevent the degradation of PD-L1, maintaining the stability of PD-L1 and facilitating the immune escape of tumors. Interfering either CMTM6 or CMTM4 would hamper the expression of PD-L1. They function through reducing the ubiquitination of PD-L1, prolonging its half-life period. This provides a new target for immunotherapy to enhance the anti-PD-1/PD-L1 treatment (78, 79).

ADVERSE EVENTS OF FDA-APPROVED PD-1 INHIBITORS AND THE RELEVANT MANAGEMENTS FOR HEAD AND NECK CANCERS

The fact that PD-1/PD-L1 axis contributes to the maintenance of self-tolerance implies that immune checkpoint blockade might disturb the balance of immune systems, resulting in treatment-related adverse events (trAEs) (80) (**Table 4**). TrAEs are frequent and occur in up to 80% of patients treated with an PD-1/PD-L1 antibody (81, 82). In the KEYNOTE-012 trial and the KEYNOTE-055 trial, trAEs occured in 63%-65% HNSCC patients treated with Pembrolizumab (33, 63). The most

TABLE 3 | Gut microbiome affecting efficacy of PD-1/PD-L1 treatment.

Effects	Bacteria	Models	Other effects on immune systems	Author/year	References
Enhanced efficacy	*Akkermansiacea muciniphila*	Human/mouse	Upregulating T_{CM}, CD4/Foxp3 ratio in tumor sites and IL-12 production; Increasing IFN- γ production	Bertrand Routy 2018	(75)
	Alistipes indistinctus	Human/mouse	/	Bertrand Routy 2018	(75)
	Bifidobacterium adolescentis	Human	Decreasing peripherally derived Tregs	Matson V 2018	(77)
	Bifidobacterium breve	Mouse	Stimulating DCs directly, inducing DCs maturation and cytokine secretion	Ayelet Sivan 2015	(76)
	Bifidobacterium longum	Mouse	Promoting DCs maturation and inducing cytokine production	Ayelet Sivan 2015	(76)
	Bifidobacterium longum	Human	/	Matson V 2018	(77)
	Collinsella aerofaciens	Human	Decreasing peripherally derived Tregs	Matson V 2018	(77)
	Enterococcus faecium	Human	Decreasing peripherally derived Tregs	Matson V 2018	(77)
	Enterococcus hirae	Human/mouse	Upregulating T_{CM}, CD4/Foxp3 ratio in tumor sites and IL-12 production; Increasing IFN- γ production	Bertrand Routy 2018	(75)
	Klebsiella pneumonia	Human	/	Matson V 2018	(77)
	Parabacteroides merdae	Human	Decreasing peripherally derived Tregs	Matson V 2018	(77)
	Ruminococcaceae	Human/mouse	Increasing effector T cells in peripheral blood and tumors	Gopalakrishnan V 2018	(74)
	Veillonella parvula	Human	/	Matson V 2018	(77)
Compromised efficacy	*Blautia obeum*	Human	/	Matson V 2018	(77)
	Roseburia intestinalis	Human	/	Matson V 2018	(77)

T_{CM} central memory T cell; Treg regulatory T cell; DC dendritic cell.

commonly observed trAEs were fatigue, decreased appetite, rash, hypothyroidism, nausea and diarrhea (63). Grade 3–4 trAEs occurred in around 9–14% of patients who had PD-1 inhibitors treatment. Three deaths were reported due to pulmonary toxicity (53, 82).

By comparing the various organs involved, grade 1–2 trAEs mainly influence the skin and the gut, while grade 3–4 events mainly affect the digestive tract. Data suggest that trAEs usually occur within 3–6 months after the PD-1/PD-L1 blockade treatment (83). Accumulative toxic effects with prolonged treatment of anti-PD-1 were not observed (65).

For T cell tumors, like T-cell non-Hodgkin's lymphoma (T-NHL), anti-PD-1/PD-L1 therapy could render the tumors better proliferative. The reason is in this kind of tumors, T cells don't play the role to attack the tumors, instead, they are the major part of the tumor. It highlights a dangerous possible adverse event of anti-PD-1 treatment (84).

Nivolumab

A randomized, open-label, phase III study was designed to investigate efficacy and safety of Nivolumab for patients with recurrent HNSCC that progressed within 6 months post platinum-based chemotherapy (36). In this trial, the primary end point was OS. Although rates of trAEs of any grade were similar between two groups, fewer events of grade 3 or 4 were observed in the Nivolumab treatment group when treated with Nivolumab than the standard therapy group. Fatigue, nausea, rash, decreased appetite, and pruritus were the most commonly reported trAEs of any grade in patients receiving Nivolumab. Two treatment-related deaths owing to pneumonitis and hypercalcemia were reported in the Nivolumab treatment group (36). Daste et al. (59) reported a case of a patient with HNSCC developed tumor flare-up after therapy with Nivolumab (59).

Pembrolizumab

TrAEs of any grade occurred within an average of 9 weeks after the initiation of Pembrolizumab (85, 86). In the KEYNOTE-012 trial, trAEs of any grade were observed in 63% of patients. The most frequently observed trAEs were fatigue, pruritus, nausea, decreased appetite and rash. Grade 3–4 trAEs were reported in 10 of 60 patients (17%), including increased ALT and AST, hyponatremia, atrial fibrillation and congestive heart failure (33). In the expansion cohort, 62% of patients had trAEs of any grade. The most common trAEs were fatigue, hypothyroidism and decreased appetite. Grade 3–4 trAEs were observed in around 9% of patients, including lowered appetite, facial swelling and

TABLE 4 | Incidents of treatment-related adverse events occurring in patients with head and neck cancers.

	Pembrolizumab 10 mg/kg every 2 weeks Ib/n 60 (33)		Pembrolizumab 200 mg every 2 weeks Ib/n 132 (62)		Pembrolizumab 200 mg every 2 weeks II/n 171 (63)		Nivolumab 3 mg/kg every 2 weeks III/n 236(GLOBAL) (36)		Nivolumab 3 mg/kg every 2 weeks III/n 23(ASIAN) (66)	
Adverse Events	Grade 1–2	Grade 3–4	Grade 1–2	Grade 3–4	Any Grade	Grade 3–5	Any Grade	Grade 3–4	Any Grade	Grade 3–4
Fatigue	20.00%	2.00%	21.00%	0	18.00%	1.00%	14.00%	2.10%	17.40%	0
Decreased appetite	0	0	7.00%	2.00%	5.00%	0	7.20%	0	21.70%	0
Rash	5.00%	2.00%	0	0	2.00%	1.00%	7.60%	0	17.40%	0
Nausea	0	0	5.00%	1.00%	6.00%	0	8.50%	0	8.70%	0
Hypothyroidism	0	0	11.00%	0	9.00%	0	0	0	0	0
Pruritus	12.00%	0	0	0	0	0	7.20%	0	17.40%	0
Diarrhea	2.00%	2.00%	0	0	6.00%	1.00%	6.80%	0	4.30%	0
Abdominal pain	0	0	1.00%	1.00%	0	0	0	0	0	0
Stomatitis	0	0	1.00%	1.00%	0	0	2.10%	0.40%	0	0
Colitis	0	0	0	1.00%	0	0	0	0	0	0
Lymphopenia	0	2.00%	0	0	0	0	0	0	0	0
Atrial fibrillation	0	2.00%	0	0	0	0	0	0	0	0
Congestive cardiac failure	0	2.00%	0	0	0	0	0	0	0	0
Neck abscess	0	2.00%	0	0	0	0	0	0	0	0
Alanine aminotransferase increase	0	3.00%	0	0	4.00%	0	0	0	0	0
Hyponatremia	0	3.00%	0	0	2.00%	1%%	0	0	0	0
Anemia	0	0	0	0	4.00%	2.00%	5.10%	1.30%	0	0
Musculoskeletal pain	2.00%	2.00%	0	0	0	0	1.30%	0	0	0
Immune thrombocytopenic purpura	0	0	0	1.00%	0	0	0	0	0	0
Dysphagia	0	0	1.00%	1.00%	0	0	0	0	0	0
Dehydration	0	0		1.00%	0	0	0	0	0	0
Facial swelling	0	0	2.00%	3.00%	0	0	0	0	0	0
Pneumonitis	0	0	2.00%	2.00%	4.00%	1.00%	0	0	0	0
Hyperglycemia	0	0	1.00%	1.00%	0	0	0	0	0	0
Asthenia	0	0	0	0	0	0	4.20%	0.40%	0	0

pneumonitis (62). In the KEYNOTE-055 trial, around 64% of patients exhibited trAEs. Grade 3–5 trAEs were reported in 15% of patients. One death owing to treatment-related pneumonitis was reported (63).

Severe Immune-Related Adverse Events in Crucial Organs

Myocarditis

Accounting for <0.3% of patients, myocarditis is a rare but severe immune-related adverse event that frequently results in rapid dyspnea and acute heart failure (87). More and more cases of patients with anti-PD-1/PD-L1 treatment-related heart diseases have been reported in recent 3 years (88). Semper et al. (89) reported a case of a patient, diagnosed with squamous cell carcinoma of the lung, developing Nivolumab-induced myocarditis. Three days post the 9th cycle of Nivolumab therapy, the patient with tumor remission developed acute chest pain and severe dyspnea, which was later confirmed to be immunotherapy-related (89). Johnson et al. (87) reported two more cases of patients, diagnosed with metastatic melanoma, developing lethal myocarditis induced by Nivolumab and Ipilimumab combined (87). Läubli et al. (90) reported a case of Pembrolizumab-induced myocarditis. A 73-years-old female patient with metastatic uveal melanoma developed severe Pembrolizumab-induced myocarditis which resulted in potentially life-threatening acute heart failure (90). In 2018, Frigeri et al. (91) reported the patients achieved complete remission of recurrent metastatic pulmonary adenocarcinoma after 7 cycles of Nivolumab administration. Unfortunately, she experienced rapid cardiogenic shock afterwards (91). A fatal case was reported by Matson et al. (92). One patient with NSCLC receiving Nivolumab developed acute heart failure (92). Moslehi et al. (88) have identified altogether 101 cases of severe immune checkpoint inhibitors-induced (ICIs-induced) myocarditis, 46% of which resulted in patients' deaths (88). A more conclusive mechanism of anti-PD-1-induced myocarditis is under investigation (87). Studies revealed that PD-L1 could be found on endothelium. Interaction between PD-1 and its ligands on endothelium is important in limiting T cell responses in the heart and thus controlling immune-mediated cardiac injury (93, 94). One suspected mechanism is that PD-L1 is expressed on the surface of various types of cells and tissues, including tumor cells and cardiac muscle cells. When patients receive anti-PD-1/PD-L1 treatment, owing to the distribution of drugs, T cell responses in cardiac muscles might be disturbed and enhanced, leading to the occurrence of lethal immune-related myocarditis (87, 95).

Pneumonitis

Incidence of pneumonitis of all grades during anti-PD-1 therapy was 2.7% and the incidence of pneumonitis for grade 3 or higher was around 0.8% (96). Patients diagnosed with lung cancers, compared to patients with other types of cancers had higher incidence of treatment-related pneumonitis, with incidence of grade 3 or higher being 1.8% and incidence of deaths being 0.4% (96, 97). In a randomized, open-label, phase II/III study on efficacy and safety of Pembrolizumab for patients with advanced NSCLC, three cases of deaths resulting from treatment-related pneumonitis were reported (85). As in clinical trial of PD-1 blockade treating HNSCC, two treatment-related deaths owing to pneumonitis and hypercalcemia were reported in the Nivolumab group of a randomized, open-label, phase III trial (NCT02105636) (36). In a phase II study, Bauml et al. evaluated efficacy of Pembrolizumab in patients with previously treated refractory head and neck cancers (KEYNOTE-055) and one death owing to immune-related pneumonitis was observed (63).

One patient with NSCLC, after receiving 2 cycles of anti–PD-1 therapy, developed symptoms of pneumonitis and received proper treatment. However, symptoms relapsed; treatments with corticosteroids displayed less efficacy and the patient died. Another case of a female patient with small-cell lung cancer (SCLC), treated with an anti-CTLA-4/PD-1 combination therapy, was reported. The patient showed responsiveness to corticosteroid treatment; with discontinuation of current immunotherapy, the patient recovered from pneumonitis and started next line of anti-tumor therapy (98).

Hepatitis

The incidence of immune-related hepatitis of all grades was around 3.1% and the incidence of grade 3 or higher was 0.5–0.6% (99). For a clinical trial with Pembrolizumab in patients with previously treated NSCLC (KEYNOTE-010), three cases of immune-related hepatitis were reported (97).

Management of Adverse Events

Before confirming the occurrence of immune-related adverse events, specialist should rule out all other possible diagnoses, including but not limited to infection and tumor progression (83). **Figure 3** gives a glimpse of main adverse events in patients receiving anti-PD-1/PD-L1 therapy. The general principle for managing trAEs are suggested as followed: patients with grade 1 adverse events are provided with supportive care; patients with grade 2 events are advised on treatment with topical or systemic steroids (0.5–1 mg/kg/day); patients with grade 3 or 4 events require hospitalization, treatment of steroids, 1–2 mg/kg/day, or discontinuation of the current immunotherapy, depending on specialists' assessments (97, 100). **Table 5** shows the management of some commonly observed trAEs. Most trAEs are manageable with steroids, which should be provided at a sufficient dose and gradually withdrawn. But there are some cases where trAEs may be permanent, and in those scenarios, adverse events can be treated with hormone instead (83, 100).

THE PERSPECTIVES OF ANTI-PD-1/PD-L1 THERAPY IN HEAD AND NECK CANCERS

Figure 4 shows the perspectives of anti-PD-1/PD-L1 therapy.

Criteria to Monitor the Immune-Checkpoint Blockade

Scientists brought up the importance of monitoring immune-checkpoint blockade. As it is a novel therapy for cancers, the response evaluation and biomarkers should be different. Immune-related response criteria is an important concept to evaluate the immunotherapy and is the first step of precision immunotherapy (101). There are many biomarkers of immunotherapy response including PD-L1, other immune-checkpoint molecules, tumor-infiltrating lymphocytes (TILs), IFN-γ (102–104), mutational burden, neoantigens, microsatellite instability, serum markers, radiographic markers, and the "immunoscore" (105) which evaluates the distribution of TILs in the core and in the invasive margin of tumors. A recent study showed that the frequency of $CD14^{+}CD16^{-}HLA^{-}DR^{hi}$ monocytes had strong correlation with progression-free and OS in response to therapy with anti-PD-1. The researchers used single-cell mass cytometry to analyze the immune cell subpopulations in the peripheral blood of patients with stage IV melanoma before and after anti-PD-1 therapy. It is an effective predictive biomarkers of a clinical response (106). Similarly, more predictive biomarkers are expected to be found and used in the near future.

Novel Materials Advancing the Effect

Nanoscale materials have potential as drug delivery systems that assist or advance the treatment in cancers. Some could even respond intelligently to molecular triggers (107, 108). A recent research reported that an autonomous DNA robot was programmed to transport blood coagulation protease thrombin within tubular nanorobot while DNA outside of the nanorobot as both a targeting domain and a molecular trigger. It could target the nucleolin specifically expressed in tumor blood vessels and caused tumor necrosis. Animal experiments with this DNA robot showed promising results (109). As it could carry the blood coagulation protease thrombin that is a type of protein, it would also be able to transport the anti-PD-1/PD-L1 antibody to specific areas with certain DNA targeting domains.

A microneedle, made by hyaluronic acid and pH-sensitive dextran nanoparticles, is developed to encapsulate anti-PD-1 antibody and glucose oxidase. Glucose oxidase can turn blood glucose into gluconic acid and generate an acidic environment in tumors to drive the self-dissociation of nanoparticles and finally substantially release anti-PD-1 antibodies. This newly developed tool with immunotherapy induced more robust immune response in melanoma. And the microneedle could carry more than one antitumor therapeutics like combination of anti-PD-1 and anti-CTLA-4 antibodies to enhance the treatment effect (110).

Years ago, Sun et al. utilized bacterial magnetosomes as drug carriers transporting doxorubicin to treat hepatocellular carcinoma and got a better result compared with the sole

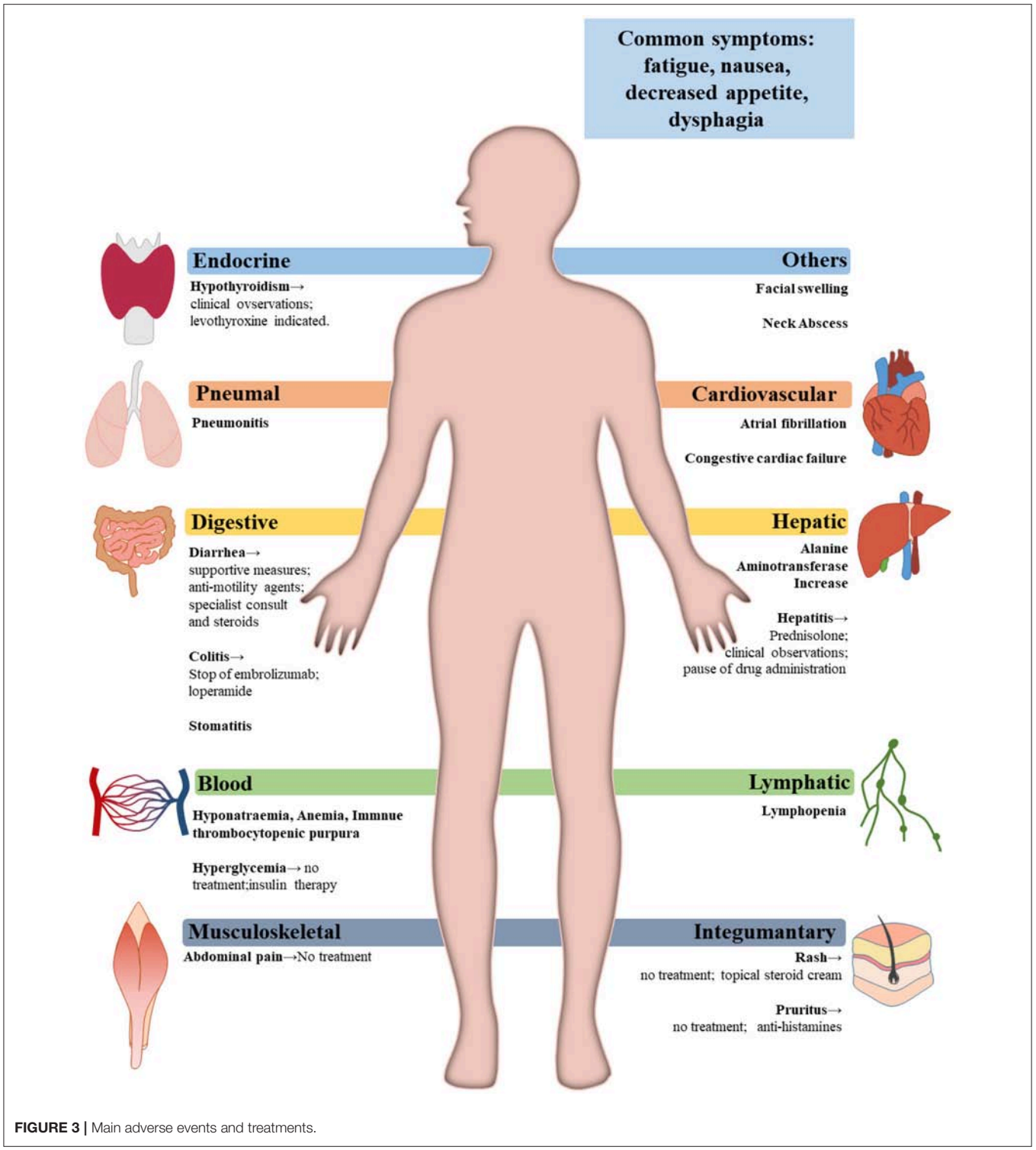

FIGURE 3 | Main adverse events and treatments.

doxorubicin group (111). Immobilization of anti-PD-1/PD-L1 antibodies on magnetic nanoparticles may also provide an efficient local delivery strategy of the drugs for malignant solid tumors. Local magnetic delivery of these immobilized antibodies would increase local concentration while reduce the administration times, total usage and peripheral distribution of the antibodies, reducing the adverse effects. It would be very easy to immobilize antibodies on either biosynthesized or chemical synthesized magnetic nanoparticles since there are a lot of linking methods available (112).

TABLE 5 | Management of treatment-related rash, pneumonitis, thyroid dysfunction and diarrhea (100).

Adverse events	Grade 1–2	Grade 3–4
Rash	≤30% BSA: anti-histamines for pruritus and topical steroid cream for rash.	>30% BSA:skin biopsy is needed and steroids with 1 mg/kg of prednisolone until BSA≤30%.If life-threatening, permanently discontinue drug administration.
Pneumonitis	Clinical or diagnostic observations; delay drug administration; daily monitoring.	Oxygen is needed; stop drug administration; hospitalization; high dose steroids with methylprednisolone; intensive care support.
Thyroid dysfunction	Clinical or diagnostic observations; daily monitoring; for hypothyroidism, levothyroxine indicated; for hyperthyroidism, propranolol is needed.	Hospitalization; specialist consult; clinical observation
Diarrhea	≤6 bowel actions/day: supportive measures; anti-motility agents when needed.	>7 bowel actions/day: hospitalization; specialist consult; clinical observation; steroids with 1–2mg/kg prednisolone.

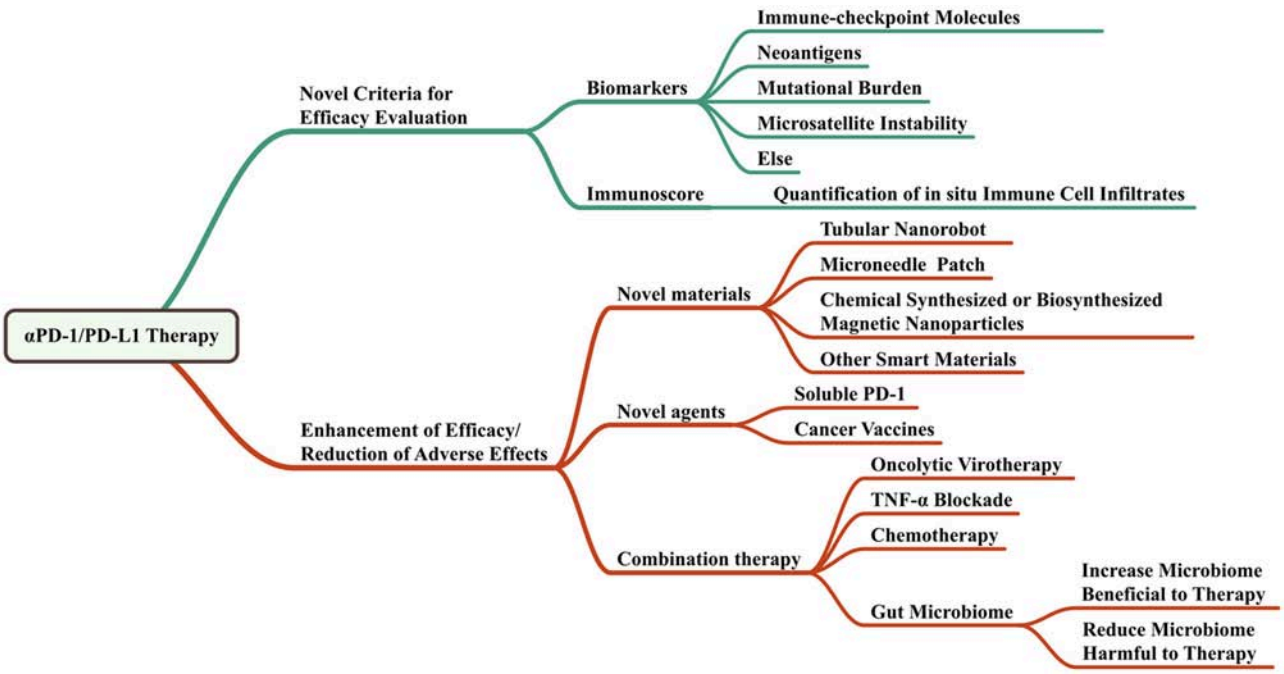

FIGURE 4 | Perspectives of anti-PD-1/PD-L1 therapy.

Novel Agents Providing Similar Blockade Effects of Anti-PD-1/PD-L1 Antibodies

Despite the anti-PD-1/PD-L1 antibodies, soluble PD-1 (sPD-1) peptides may provide similar inhibition effect of PD-1 pathway by competitively binding to PD-L1 expressed on tumor cells. The plasmids expressing sPD-1 peptides could also be developed as gene therapy drugs which turn tumor cells as producers of sPD-1.

Soluble Immune Checkpoint Molecules

In addition to membrane bound form, there are sPD-1 and soluble PD-L1 (sPD-L1). Currently, sPD-1 is thought to be the translational product of the PD-1Δex3 mRNA transcript, and sPD-L1 may be derived from the cleavage of membrane bound PD-L1 by matrix metalloproteinases.

sPD-1 and sPD-L1 can also bind to ligands, thus blocking the PD-1/PD-L1 signaling pathway, resulting in potent peripheral T-cell anti-tumor responses. It's reported that the PD-1 extracellular domain was transfected into tumors by adenoviral vectors and could antagonize the negative regulation of T cells by PD-1/PD-L1 pathway, thus inhibiting tumor growth and prolong survival of mice (113).

Compared with membranous molecules, soluble molecules can not only affect neighboring cells in the tumor microenvironment, but also affect the body farther through the blood circulation, having a wider range of biological effects.

The production and function of the sPD-1 and sPD-L1 require further investigation. sPD-1 and sPD-L1 can be used in immunomodulatory therapy in combination with other antitumor therapy, such as HSP70 vaccine, to enhance the anti-tumor efficacy of tumor vaccine (114). In addition, the soluble forms may be used as an additional biomarker to the membrane bound forms, helping more accurately determine the patient's immune status and predict efficacy (115).

Cancer Vaccines

Up to now, preclinical and recent clinical studies have indicated that combining PD-1 or PD-L1 checkpoint inhibitors with cancer vaccines improves antitumor activity compared with anti-PD-1 or PD-L1 antibody monotherapy alone (116). However, satisfactory results about vaccines targeting PD-1 or PD-L1 checkpoint molecular are few. The DNA vaccines under active study work well but safety is hard to guarantee. In contrast, protein vaccines are low in cost and high in safety. It provides a promising research direction for the future development of cancer treatment. A study using genetic engineering to prepare a Cholera Toxin B based vaccine that targets both mouse MUC1 and mouse PD-1 showed that this fused protein vaccine can produce a stronger immune response (117).

Combination Therapy

Luo et al. (118) developed a nano-vaccine by simply mixing an antigen with a synthesized polymeric nanoparticle, PC7A NP. It delivered tumor antigens to APCs in draining lymph nodes, increasing surface presentation and simultaneously activating type I interferon-triggered genes through STING pathway. Combination of PC7A nano-vaccine with anti-PD-1 antibodies demonstrated increased survival rate in animal tumor models. Tumor growth was completely inhibited when these vaccinated animals were rechallenged with tumor cells, suggesting generation of antitumor memory (118). Researchers found that exploiting the individual tumor mutations as neo-epitopes and utilizing them as vaccines could enhance the immune response to tumors. Some patients even completely responsed to vaccination during combinational therapy with anti-PD-1 (119, 120).

Oncolytic virotherapy has demonstrated promise, however, it only had efficacy in a small fraction of tumor patients. As the virus could upregulate PD-L1 expression on tumor cells, combination of oncolytic virus, and anti-PD-1/PD-L1 therapy could synergistically promote the treatment of cancers. This was tested in colon and ovarian cancer models, but was believed to own wider indications (121).

Recent study revealed that TNF-α blockade prevents death of tumor infiltrating T lymphocyte induced by anti-PD-1 as well as PD-L1 and TIM-3 expression. It is strongly rationalized to develop a combinational therapy with anti-PD-1/PD-L1 and anti-TNF-α in cancer patients (122).

Chemotherapy drug gemcitabine (GEM) and anti-PD-L1 antibodies could be released locally when an engineered reactive oxygen species (ROS)-degradable hydrogel was injected and formed in tumor microenvironment, which contained abundant ROS. Anti-PD-L1-GEM scaffold promoted an tumor regression in the tumor-bearing mice and prevention of tumor recurrence after primary resection (123). In this research, a novel material together with the combination therapy reinforced the effect and reduced side effects of the treatment.

The trends of anti-PD-1/PD-L1 therapy are to enhance the therapy effects while reduce the side effects. It would benefit from the combination of anti-PD-1/PD-L1 antibodies with other checkpoint inhibitors, other suppressor inhibitors, cytokine inhibitors or chemotherapy drugs. Emerging novel materials and delivery strategies like nanorobots, microneedle patches, and magnetic immobilization could help the therapeutics work better in the way of localizing them in the cancer sites or carrying other biomarkers like DNAs or proteins to target better.

AUTHOR CONTRIBUTIONS

BY, TL, YQ, and HL summarized the literature, wrote the manuscript, and prepared figures. SZ and BC provided critical comments and wrote part of the manuscript. JS supervised all the work and wrote the manuscript.

ACKNOWLEDGMENTS

This work was supported by Natural Science Foundation of Guangdong Province (2018A030313563) to JS; Program for Guangdong Introducing Innovative and Entrepreneurial Teams (2016ZT06S252) to JS; Science and Technology Program of Guangzhou (201704020063) to BC; and Special Grant for Precision Medicine from Sun Yat-sen University to BC.

REFERENCES

1. Argiris A, Eng C. Epidemiology, staging, and screening of head and neck cancer. *Cancer Treat Res*. (2003) 114:15–60. doi: 10.1007/0-306-48060-3_2
2. Argiris A, Karamouzis MV, Raben D, Ferris RL. Head and neck cancer. *Lancet* (2008) 371:1695–709. doi: 10.1016/S0140-6736(08)60728-X
3. Albers AE, Strauss L, Liao T, Hoffmann TK, Kaufmann AM. T cell-tumor interaction directs the development of immunotherapies in head and neck cancer. *Clin Dev Immunol*. (2010) 2010:236378. doi: 10.1155/2010/236378
4. Vineis P, Alavanja M, Buffler P, Fontham E, Franceschi S, Gao YT, et al. Tobacco and cancer: recent epidemiological evidence. *J Natl Cancer Inst*. (2004) 96:99–106. doi: 10.1093/jnci/djh014
5. Blot WJ, McLaughlin JK, Winn DM, Austin DF, Greenberg RS, Preston-Martin S, et al. Smoking and drinking in relation to oral and pharyngeal cancer. *Cancer Res*. (1988) 48:3282–87.
6. Tuyns AJ, Esteve J, Raymond L, Berrino F, Benhamou E, Blanchet F, et al., Cancer of the larynx/hypopharynx, tobacco and alcohol: IARC international case-control study in Turin and Varese (Italy), Zaragoza and Navarra (Spain), Geneva (Switzerland) and Calvados (France). *Int J Cancer* (1988) 41:483–91. doi: 10.1002/ijc.2910410403
7. Hashibe M, Boffetta P, Zaridze D, Shangina O, Szeszenia-Dabrowska N, Mates D, et al. Evidence for an important role of alcohol- and aldehyde-metabolizing genes in cancers of the upper aerodigestive tract. *Cancer Epidemiol Biomarkers Prev*. (2006) 15:696–703. doi: 10.1158/1055-9965.EPI-05-0710
8. Sturgis EM, Wei Q. Genetic susceptibility–molecular epidemiology of head and neck cancer. *Curr Opin Oncol*. (2002) 14:310–17. doi: 10.1097/00001622-200205000-00010
9. Warnakulasuriya S. Areca nut use following migration and its consequences. *Addict Biol*. (2002) 7:127–32. doi: 10.1080/13556210120091491
10. D'Souza G, Kreimer AR, Viscidi R, Pawlita M, Fakhry C, Koch WM, et al. Case-control study of human papillomavirus and oropharyngeal cancer. *N Engl J Med*. (2007) 356:1944–56. doi: 10.1056/NEJMoa065497

11. Chan PK, Chor JS, Vlantis AC, Chow TL, Fung SC, Lau CH, et al. Smoking, human papillomavirus infection, and p53 mutation as risk factors in oropharyngeal cancer: a case-control study. *Hong Kong Med J*. (2017) 23 (Suppl. 5):12–16.
12. Lyford-Pike S, Peng S, Young GD, Taube JM, Westra WH, Akpeng B, et al. Evidence for a role of the PD-1:PD-L1 pathway in immune resistance of HPV-associated head and neck squamous cell carcinoma. *Cancer Res.* (2013) 73:1733–41. doi: 10.1158/0008-5472.CAN-12-2384
13. Kreimer AR, Clifford GM, Boyle P, Franceschi S. Human papillomavirus types in head and neck squamous cell carcinomas worldwide: a systematic review. *Cancer Epidemiol Biomarkers Prev*. (2005) 14:467–75. doi: 10.1158/1055-9965.EPI-04-0551
14. Licitra L, Perrone F, Bossi P, Suardi S, Mariani L, Artusi R, et al. High-risk human papillomavirus affects prognosis in patients with surgically treated oropharyngeal squamous cell carcinoma. *J Clin Oncol*. (2006) 24:5630–6. doi: 10.1200/JCO.2005.04.6136
15. Eisbruch A, Marsh LH, Dawson LA, Bradford CR, Teknos TN, Chepeha DB, et al. Recurrences near base of skull after IMRT for head-and-neck cancer: implications for target delineation in high neck and for parotid gland sparing. *Int J Radiat Oncol Biol Phys*. (2004) 59:28–42. doi: 10.1016/j.ijrobp.2003.10.032
16. Bentzen SM. Repopulation in radiation oncology: perspectives of clinical research. *Int J Radiation Biol*. (2003) 79:581–5. doi: 10.1080/09553000310001597002
17. Lin A. Radiation therapy for oral cavity and oropharyngeal cancers. *Dent Clin N Am*. (2018) 62:99–109. doi: 10.1016/j.cden.2017.08.007
18. Cohen EE, Lingen MW, Vokes EE. The expanding role of systemic therapy in head and neck cancer. *J Clin Oncol*. (2004) 22:1743–52. doi: 10.1200/JCO.2004.06.147
19. Argiris A. Induction chemotherapy for head and neck cancer: will history repeat itself? *J Natl Comprehen Cancer Netw*. (2005) 3:393–403. doi: 10.6004/jnccn.2005.0020
20. De Andres L, Brunet J, Lopez-Pousa A, Burgues J, Vega M, Tabernero JM, et al. Randomized trial of neoadjuvant cisplatin and fluorouracil versus carboplatin and fluorouracil in patients with stage IV-M0 head and neck cancer. *J Clin Oncol*. (1995) 13:1493–500. doi: 10.1200/JCO.1995.13.6.1493
21. Epstein JB, Thariat J, Bensadoun RJ, Barasch A, Murphy BA, Kolnick L, et al. Oral complications of cancer and cancer therapy: from cancer treatment to survivorship. *CA Cancer J Clin.* (2012) 62:400–22. doi: 10.3322/caac.21157
22. Young M, Neville B, Chi AC, Lathers D, Boyd-Gillespie M, Day T. Oral premalignant lesions induce immune reactivity to both premalignant oral lesions and head and neck squamous cell carcinoma. *Cancer Immunol Immunother.* (2007) 56:1077–86. doi: 10.1007/s00262-006-0242-7
23. Grandis JR, Tweardy DJ. Elevated levels of transforming growth factor alpha and epidermal growth factor receptor messenger RNA are early markers of carcinogenesis in head and neck cancer. *Cancer Res.* (1993) 53:3579.
24. Minchenko A, Bauer T, Salceda S, Caro J. Hypoxic stimulation of vascular endothelial growth factor expression *in vitro* and *in vivo*. *Lab Investig*. (1994) 71:374–9.
25. Pancari P, Mehra R. Systemic therapy for squamous cell carcinoma of the head and neck. *Surg Oncol Clin N Am*. (2015) 24:437–54. doi: 10.1016/j.soc.2015.03.004
26. Rubin GJ, Melhem MF, Gooding WE, Day R, Holst VA, Wagener MM, et al. Levels of TGF-alpha and EGFR protein in head and neck squamous cell carcinoma and patient survival. *J Natl Cancer Inst*. (1998) 90:824.
27. Ferreira MB, Lima JP, Cohen EE. Novel targeted therapies in head and neck cancer. *Expert Opin Investig Drugs* (2012) 21:281–95. doi: 10.1517/13543784.2012.651455
28. Bonner JA, Harari PM, Giralt J, Azarnia N, Shin DM, Cohen RB, et al. Radiotherapy plus cetuximab for squamous-cell carcinoma of the head and neck. *N Eng J Med.* (2006) 354:567–78. doi: 10.1056/NEJMoa053422
29. Yancopoulos GD, Davis S, Gale NW, Rudge JS, Wiegand SJ, Holash J. Vascular-specific growth factors and blood vessel formation. *Nature* (2000) 407:242–8. doi: 10.1038/35025215
30. Cohen EE, Davis DW, Karrison TG, Seiwert TY, Wong SJ, Nattam S, et al. Erlotinib and bevacizumab in patients with recurrent or metastatic squamous-cell carcinoma of the head and neck: a phase I/II study. *Lancet Oncol*. (2009) 10:247–57. doi: 10.1016/S1470-2045(09)70002-6
31. Burtness B. Commentary: bevacizumab and erlotinib with chemoradiation for head and neck cancer. *Cancer J.* (2011) 17:273–5. doi: 10.1097/PPO.0b013e3182326944
32. Hughes PE, Caenepeel S, Wu LC. Targeted therapy and checkpoint immunotherapy combinations for the treatment of cancer. Trends Immunol. (2016) 37:462–76. doi: 10.1016/j.it.2016.04.010
33. Seiwert TY, Burtness B, Mehra R, Weiss J, Berger R, Eder JP, et al. Safety and clinical activity of pembrolizumab for treatment of recurrent or metastatic squamous cell carcinoma of the head and neck (KEYNOTE-012): an open-label, multicentre, phase Iphase Ib trial, *Lancet Oncol*. (2016) 17:956–65. doi: 10.1016/S1470-2045(16)30066-3
34. Mulvey A. "*FDA Approves Pembrolizumab (Keytruda®), a PD-1 Antibody, for Head And Neck Cancer*". Cancer Research Institute (2016). Available online at: https://www.cancerresearch.org/blog/august-2016/fda-approves-pembrolizumab-keytruda-pd-1-antibody
35. Staff N. "*FDA Approves Nivolumab for Head and Neck Cancer was originally published by the National Cancer Institute*". National Cancer Institute (2016). Available online at: https://www.cancer.gov/news-events/cancer-currents-blog/2016/fda-nivolumab-scchn
36. Ferris RL, Blumenschein G Jr, Fayette J, Guigay J, Colevas AD, Licitra L, et al. Nivolumab for recurrent squamous-cell carcinoma of the head and neck. *N Eng J Med*. (2016) 375:1856–67. doi: 10.1056/NEJMoa1602252
37. Bell RB, Leidner RS, Crittenden MR, Curti BD, Feng Z, Montler R, et al. OX40 signaling in head and neck squamous cell carcinoma: overcoming immunosuppression in the tumor microenvironment. *Oral Oncol.* (2016) 52:1–10. doi: 10.1016/j.oraloncology.2015.11.009
38. Srivastava RM, Trivedi S, Concha-Benavente F, Gibson SP, Reeder C, Ferrone S, et al. CD137 stimulation enhances cetuximab-induced natural killer: dendritic cell priming of antitumor T-cell immunity in patients with head and neck cancer. *Clin Cancer Res*. (2017) 23:707–16. doi: 10.1158/1078-0432.CCR-16-0879
39. Schwartz RH. Costimulation of T lymphocytes: the role of CD28, CTLA-4, and B7/BB1 in interleukin-2 production and immunotherapy. *Cell* (1992) 71:1065–8. doi: 10.1016/S0092-8674(05)80055-8
40. Deng WW, Wu L, Sun ZJ. Co-inhibitory immune checkpoints in head and neck squamous cell carcinoma. *Oral Dis.* (2018) 24:120–3. doi: 10.1111/odi.12746
41. Collins AV, Brodie DW, R.Gilbert JC, Iaboni A, Manso-Sancho R, Walse B, et al. The interaction properties of costimulatory molecules revisited. *Immunity* (2002) 17:201–10. doi: 10.1016/S1074-7613(02)00362-X
42. Leach DR, Krummel MF, Allison JP. Enhancement of antitumor immunity by CTLA-4 blockade. *Science* (1996) 271:1734–36.
43. Pardoll DM. The blockade of immune checkpoints in cancer immunotherapy. *Nat Rev Cancer* (2012) 12:252–64. doi: 10.1038/nrc3239
44. Yu GT, Bu LL, Zhao YY, Mao L, Deng WW, Wu TF, et al. CTLA4 blockade reduces immature myeloid cells in head and neck squamous cell carcinoma. *Oncoimmunology* (2016) 5:e1151594. doi: 10.1080/2162402X.2016.1151594
45. Jie HB, Gildener-Leapman N, Li J, Srivastava RM, Gibson SP, Whiteside TL et al. Intratumoral regulatory T cells upregulate immunosuppressive molecules in head and neck cancer patients. *Br J Cancer* (2013) 109:2629–35. doi: 10.1038/bjc.2013.645
46. Ascierto PA, Kalos M, Schaer DA, Callahan MK, Wolchok JD. Biomarkers for immunostimulatory monoclonal antibodies in combination strategies for melanoma and other tumor types. *Clin Cancer Res*. (2013) 19:1009–20. doi: 10.1158/1078-0432.CCR-12-2982
47. Kjaergaard J, Peng L, Cohen PA, Drazba JA, Weinberg AD, Shu S. Augmentation versus inhibition: effects of conjunctional OX-40 receptor monoclonal antibody and IL-2 treatment on adoptive immunotherapy of advanced tumor. *J Immunol*. (2001) 167:6669–77. doi: 10.4049/jimmunol.167.11.6669
48. Gough MJ, Ruby CE, Redmond WL, Dhungel B, Brown A, Weinberg AD. OX40 agonist therapy enhances CD8 infiltration and decreases immune suppression in the tumor. *Cancer Res.* (2008) 68:5206–15. doi: 10.1158/0008-5472.CAN-07-6484
49. Montler R, Bell RB, Thalhofer C, Leidner R, Feng Z, Fox BA, et al. OX40, PD-1 and CTLA-4 are selectively expressed on tumor-infiltrating T cells in head and neck cancer. *Clin Transl Immunol*. (2016) 5:e70. doi: 10.1038/cti.2016.16

50. Sharpe AH, Pauken KE. The diverse functions of the PD1 inhibitory pathway, Nature reviews. *Immunology* (2018) 18:153–67. doi: 10.1038/nri.2017.108
51. Navarro MN, Cantrell DA. Serine-threonine kinases in TCR signaling. *Nat Immunol*. (2014) 15:808–14. doi: 10.1038/ni.2941
52. Ludin A, Zon LI. Cancer immunotherapy: the dark side of PD-1 receptor inhibition. *Nature* (2017) 552:41–42. doi: 10.1038/nature24759
53. Topalian SL, Hodi FS, Brahmer JR, Gettinger SN, Smith DC, McDermott DF, et al. Safety, activity, and immune correlates of anti-PD-1 antibody in cancer. *N Eng J Med*. (2012) 366:2443–54. doi: 10.1056/NEJMoa1200690
54. Malm IJ, Bruno TC, Fu J, Zeng Q, Taube JM, Westra W, et al. Expression profile and *in vitro* blockade of programmed death-1 in human papillomavirus-negative head and neck squamous cell carcinoma. *Head Neck* (2015) 37:1088–95. doi: 10.1002/hed.23706
55. Brahmer J, Reckamp KL, Baas P, Crinò LW, Eberhardt EE, Poddubskaya E, et al. Nivolumab versus docetaxel in advanced squamous-cell non–small-cell lung cancer. *N Eng J Med*. (2015) 373:123–35. doi: 10.1056/NEJMoa1504627
56. Swanson MS, Sinha UK. Rationale for combined blockade of PD-1 and CTLA-4 in advanced head and neck squamous cell cancer-review of current data. *Oral Oncol.* (2015) 51:12–15. doi: 10.1016/j.oraloncology.2014.10.010
57. Sukumar M, Kishton RJ, Restifo NP. Metabolic reprograming of anti-tumor immunity. *Curr Opin Immunol*. (2017) 46:14–22. doi: 10.1016/j.coi.2017.03.011
58. Gerriets VA, Kishton RJ, Nichols AG, Macintyre AN, Inoue M, Ilkayeva O, et al. Metabolic programming and PDHK1 control $CD4^+$ T cell subsets and inflammation. *J Clin Investig*. (2015) 125:194–207. doi: 10.1172/JCI76012
59. Daste A, de Mones E, Digue L, Francois L, Domblides C, Dupin C, et al. Immunotherapy in head and neck cancer: need for a new strategy? Rapid progression with nivolumab then unexpected response with next treatment. *Oral Oncol*. (2017) 64:e1–3. doi: 10.1016/j.oraloncology.2016.10.020
60. Khoja L, Butler MO, Kang SP, Ebbinghaus S, Joshua AM. Pembrolizumab. *J Immunother Cancer* (2015) 3:36. doi: 10.1186/s40425-015-0078-9
61. Patnaik A, Kang SP, Rasco D, Papadopoulos KP, Elassaiss-Schaap J, Beeram M, et al. Phase I study of pembrolizumab (MK-3475; Anti-PD-1 Monoclonal Antibody) in patients with advanced solid tumors. *Clin Cancer Res*. (2015) 21:4286–93. doi: 10.1158/1078-0432.CCR-14-2607
62. Chow LQM, Haddad R, Gupta S, Mahipal A, Mehra R, Tahara M, et al. Antitumor activity of pembrolizumab in biomarker-unselected patients with recurrent and/or metastatic head and neck squamous cell carcinoma: results from the phase Ib KEYNOTE-012 expansion cohort. *J Clin Oncol.* (2016) 34:3838–45. doi: 10.1200/JCO.2016.68.1478
63. Bauml J, Seiwert TY, Pfister DG, Worden F, Liu SV, Gilbert J, et al. Pembrolizumab for platinum- and cetuximab-refractory head and neck cancer: results from a single-arm, phase ii study. *J Clin Oncol*. (2017) 35:1542–9. doi: 10.1200/JCO.2016.70.1524
64. Brahmer JR, Drake CG, Wollner I, Powderly JD, Picus J, Sharfman WH, et al. Phase I study of single-agent anti-programmed death-1 (MDX-1106) in refractory solid tumors: safety, clinical activity, pharmacodynamics, and immunologic correlates. *J Clin Oncol*. (2010) 28:3167–75. doi: 10.1200/JCO.2009.26.7609
65. Topalian SL, Sznol M, McDermott DF, Kluger HM, Carvajal RD, Sharfman WH, et al. Survival, durable tumor remission, and long-term safety in patients with advanced melanoma receiving nivolumab. *J Clin Oncol.* (2014) 32:1020–30. doi: 10.1200/JCO.2013.53.0105
66. Kiyota N, Hasegawa Y, Takahashi S, Yokota T, Yen CJ, Iwae S, et al. A randomized, open-label, Phase III clinical trial of nivolumab vs. therapy of investigator's choice in recurrent squamous cell carcinoma of the head and neck: a subanalysis of Asian patients versus the global population in checkmate 141. *Oral Oncol.* (2017) 73:138–46. doi: 10.1016/j.oraloncology.2017.07.023
67. Powles T, O'Donnell PH, Massard C, Arkenau HT, Friedlander TW, Hoimes CJ, et al. Efficacy and safety of durvalumab in locally advanced or metastatic urothelial carcinoma: updated results from a Phase I Phase I/2 open-label study. *JAMA Oncol.* (2017) 3:e172411. doi: 10.1001/jamaoncol.2017.2411
68. Rosshart SP, Vassallo BG, Angeletti D, Hutchinson DS, Morgan AP, Takeda K, et al. Wild mouse gut microbiota promotes host fitness and improves disease resistance. *Cell* (2017) 171:1015–28 e1013. doi: 10.1016/j.cell.2017.09.016
69. Cekanaviciute E, Yoo BB, Runia TF, Debelius JW, Singh S, Nelson CA, et al. Gut bacteria from multiple sclerosis patients modulate human T cells and exacerbate symptoms in mouse models. *Proc Natl Acad Sci USA*. (2017) 114:10713–18. doi: 10.1073/pnas.1711235114
70. Berer K, Gerdes LA, Cekanaviciute E, Jia X, Xiao L, Xia Z, et al. Gut microbiota from multiple sclerosis patients enables spontaneous autoimmune encephalomyelitis in mice. *Proc Natl Acad Sci USA*. (2017) 114:10719–24. doi: 10.1073/pnas.1711233114
71. Yu H, Gagliani N, Ishigame H, Huber S, Zhu S, Esplugues E, et al. Intestinal type 1 regulatory T cells migrate to periphery to suppress diabetogenic T cells and prevent diabetes development. *Proc Natl Acad Sci USA*. (2017) 114:10443–8. doi: 10.1073/pnas.1705599114
72. Wong SH, Zhao L, Zhang X, Nakatsu G, Han J, Xu W, et al. Gavage of fecal samples from patients with colorectal cancer promotes intestinal carcinogenesis in germ-free and conventional mice. *Gastroenterology* (2017) 153:1621–33 e1626. doi: 10.1053/j.gastro.2017.08.022
73. Yi M, Yu S, Qin S, Liu Q, Xu H, Zhao W, et al. Gut microbiome modulates efficacy of immune checkpoint inhibitors. *J Hematol Oncol*. (2018) 11:47. doi: 10.1186/s13045-018-0592-6
74. Gopalakrishnan V, Spencer CN, Nezi L, Reuben A, Andrews MC, Karpinets TV, et al. Gut microbiome modulates response to anti-PD-1 immunotherapy in melanoma patients. *Science* (2018) 359:97–103. doi: 10.1126/science.aan4236
75. Routy B, Le Chatelier E, Derosa LC, Duong PM, Alou MT, Daillere R, et al. Gut microbiome influences efficacy of PD-1-based immunotherapy against epithelial tumors. Science (2018) 359:91–97. doi: 10.1126/science.aan3706
76. Sivan A, Corrales L, Hubert N, Williams JB, Aquino-Michaels K, Earley ZM, et al. Commensal *Bifidobacterium* promotes antitumor immunity and facilitates anti-PD-L1 efficacy. *Science* (2015) 350:1084–9. doi: 10.1126/science.aac4255
77. Matson V, Fessler J, Bao R, Chongsuwat T, Zha YY, Alegre ML, et al. The commensal microbiome is associated with anti-PD-1 efficacy in metastatic melanoma patients. *Science* (2018) 359:104–8. doi: 10.1126/science.aao3290
78. Mezzadra R, Sun C, Jae LT, Gomez-Eerland R, de Vries E, Wu W, et al. Identification of CMTM6 and CMTM4 as PD-L1 protein regulators. *Nature* (2017) 549:106–10. doi: 10.1038/nature23669
79. Burr ML, Sparbier CE, Chan YC, Williamson JC, Woods K, Beavis PA, et al. CMTM6 maintains the expression of PD-L1 and regulates anti-tumour immunity. *Nature* (2017) 549:101–5. doi: 10.1038/nature23643
80. Boussiotis VA. Molecular and biochemical aspects of the PD-1 checkpoint pathway. *N Eng J Med*. (2016) 375:1767–78. doi: 10.1056/NEJMra1514296
81. Boutros C, Tarhini A, Routier E, Lambotte O, Ladurie FL, Carbonnel F, et al. Safety profiles of anti-CTLA-4 and anti-PD-1 antibodies alone and in combination. *Nat Rev*. (2016) 13:473–86. doi: 10.1038/nrclinonc.2016.58
82. Brahmer JR, Tykodi SS, Chow QM, Hwu J, Topalian SL, Hwu P, et al. Safety and activity of anti–PD-L1 antibody in patients with advanced cancer. *N Eng J Med*. (2012) 366:2455–65. doi: 10.1056/NEJMoa1200694
83. Michot JM, Bigenwald C, Champiat S, Collins M, Carbonnel F, Postel-Vinay S, et al. Immune-related adverse events with immune checkpoint blockade: a comprehensive review. *Eur J Cancer* (2016) 54:139–48. doi: 10.1016/j.ejca.2015.11.016
84. Wartewig T, Kurgyis Z, Keppler S, Pechloff K, Hameister E, Ollinger R, et al. PD-1 is a haploinsufficient suppressor of T cell lymphomagenesis. *Nature* (2017) 552:121–5. doi: 10.1038/nature24649
85. Herbst RS, Baas P, Kim DW, Felip E, Perez-Gracia JL, Han JY, et al. Pembrolizumab versus docetaxel for previously treated, PD-L1-positive, advanced non-small-cell lung cancer (KEYNOTE-010): a randomised controlled trial. *Lancet* (2016) 387:1540–50. doi: 10.1016/S0140-6736(15)01281-7
86. Robert C, Schachter J, Long GV, Arance A, Grob JJ, Mortier L, et al. Pembrolizumab versus Ipilimumab in advanced melanoma. *N Eng J Med*. (2015) 372:2521–2. doi: 10.1056/NEJMoa1503093
87. Johnson DB, Balko JM, Compton ML, Chalkias S, Gorham J, Xu Y, et al. Fulminant myocarditis with combination immune checkpoint blockade. *N Eng J Med*. (2016) 375:1749–55. doi: 10.1056/NEJMoa1609214
88. Moslehi JJ, Salem JE, Sosman JA, Lebrun-Vignes B, Johnson DB. Increased reporting of fatal immune checkpoint inhibitor-associated myocarditis. *Lancet* (2018) 391:933. doi: 10.1016/S0140-6736(18)30533-6

89. Semper H, Muehlberg F, Schulz-Menger J, Allewelt M, Grohe C. Drug-induced myocarditis after nivolumab treatment in a patient with PDL1-negative squamous cell carcinoma of the lung. *Lung Cancer* (2016) 99:117–19. doi: 10.1016/j.lungcan.2016.06.025
90. Laubli H, Balmelli C, Bossard M, Pfister O, Glatz K, Zippelius A. Acute heart failure due to autoimmune myocarditis under pembrolizumab treatment for metastatic melanoma. *J Immunother Cancer* (2015) 3:11. doi: 10.1186/s40425-015-0057-1
91. Frigeri M, Meyer P, Banfi C, Giraud R, Hachulla AL, Spoerl D, et al. Immune checkpoint inhibitor-associated myocarditis: a new challenge for cardiologists. *Can J Cardiol*. (2018) 34:92.e91–2.e3. doi: 10.1016/j.cjca.2017.09.025
92. Matson DR, Accola MA, Rehrauer WM, Corliss RF. Fatal myocarditis following treatment with the PD-1 inhibitor nivolumab. *J Foren Sci*. (2017) 63:954–7. doi: 10.1111/1556-4029.13633
93. Tarrio ML, Grabie N, Bu DX, Sharpe AH, Lichtman AH. PD-1 protects against inflammation and myocyte damage in T cell-mediated myocarditis. *J Immunol*. (2012) 188:4876–84. doi: 10.4049/jimmunol.1200389
94. Grabie N, Gotsman I, DaCosta R, Pang H, Stavrakis G, Butte MJ, et al. Endothelial programmed death-1 ligand 1 (PD-L1) regulates $CD8^+$ T-cell mediated injury in the heart. *Circulation* (2007) 116:2062–71. doi: 10.1161/CIRCULATIONAHA.107.709360
95. Cheng F, Loscalzo J. Autoimmune cardiotoxicity of cancer immunotherapy. *Trends Immunol*. (2017) 38:77–8. doi: 10.1016/j.it.2016.11.007
96. Nishino M, Giobbie-Hurder A, Hatabu H, Ramaiya NH, Hodi FS. Incidence of programmed cell death 1 inhibitor-related pneumonitis in patients with advanced cancer: a systematic review and meta-analysis. *JAMA Oncol*. (2016) 2:1607–16. doi: 10.1001/jamaoncol.2016.2453
97. O'Kane GM, Labbe C, Doherty MK, Young K, Albaba H, Leighl NB. Monitoring and management of immune-related adverse events associated with programmed cell death protein-1 axis inhibitors in lung cancer. *Oncologist* (2017) 22:70–80. doi: 10.1634/theoncologist.2016-0164
98. Balaji A, Verde F, Suresh K, Naidoo J. Pneumonitis from anti-PD-1/ PD-L1 therapy. *Oncology* (2017) 31 739–46.
99. Zhang X, Ran Y, Wang K, Zhu Y, Li J. Incidence and risk of hepatic toxicities with PD-1 inhibitors in cancer patients: a meta-analysis. *Drug Design Dev Ther*. (2016) 10:3153–61. doi: 10.2147/DDDT.S115493
100. Spain L, Diem S, Larkin J. Management of toxicities of immune checkpoint inhibitors. *Cancer Treat Rev*. (2016) 44:51–60. doi: 10.1016/j.ctrv.2016.02.001
101. Nishino M, Ramaiya NH, Hatabu H, Hodi FS. Monitoring immune-checkpoint blockade: response evaluation and biomarker development. *Nat Rev Clin Oncol*. (2017) 14:655–68. doi: 10.1038/nrclinonc.2017.88
102. Gao J, Shi LZ, Zhao H, Chen J, Xiong L, He Q, et al. Loss of IFN-gamma pathway genes in tumor cells as a mechanism of resistance to anti-CTLA-4 therapy. *Cell* (2016) 167:397–404 e399. doi: 10.1016/j.cell.2016.08.069
103. Overacre-Delgoffe AE, Chikina M, Dadey RE, Yano H, Brunazzi EA, Shayan G, et al. Interferon-gamma drives treg fragility to promote anti-tumor immunity. *Cell* (2017) 169:1130–41 e1111. doi: 10.1016/j.cell.2017.05.005
104. Bifulco CB, Urba WJ. Unmasking PD-1 resistance by next-generation sequencing. *N Eng J Med*. (2016) 375:888–9. doi: 10.1056/NEJMe1606042
105. Galon J, Mlecnik B, Bindea G, Angell HK, Berger A, Lagorce C, et al. Towards the introduction of the 'Immunoscore' in the classification of malignant tumours. *J Pathol*. (2014) 232:199–209. doi: 10.1002/path.4287
106. Krieg C, Nowicka M, Guglietta S, Schindler S, Hartmann FJ, Weber LM, et al. High-dimensional single-cell analysis predicts response to anti-PD-1 immunotherapy. *Nat Med*. (2018) 24:144–53. doi: 10.1038/nm.4466
107. Douglas SM, Bachelet I, Church GM. A logic-gated nanorobot for targeted transport of molecular payloads. *Science* (2012) 335:831–4. doi: 10.1126/science.1214081
108. Modi S, Nizak C, Surana S, Halder S, Krishnan Y. Two DNA nanomachines map pH changes along intersecting endocytic pathways inside the same cell. *Nat Nanotechnol*. (2013) 8:459–67. doi: 10.1038/nnano.2013.92
109. Li S, Jiang Q, Liu S, Zhang Y, Tian Y, Song C, et al. A DNA nanorobot functions as a cancer therapeutic in response to a molecular trigger *in vivo*. *Nat Biotechnol*. (2018) 36:258–64. doi: 10.1038/nbt.4071
110. Wang C, Ye Y, Hochu GM, Sadeghifar H, Gu Z. Enhanced cancer immunotherapy by microneedle patch-assisted delivery of anti-PD1 antibody. *Nano Lett*. (2016) 16:2334–40. doi: 10.1021/acs.nanolett.5b05030
111. Sun JB, Duan JH, Dai SL, Ren J, Zhang YD, Tian JS, et al. *In vitro* and *in vivo* antitumor effects of doxorubicin loaded with bacterial magnetosomes (DBMs) on H22 cells: the magnetic bio-nanoparticles as drug carriers. *Cancer Lett*. (2007) 258:109–17. doi: 10.1016/j.canlet.2007.08.018
112. Sun J, Li Y, Liang XJ, Wang PC. Bacterial magnetosome: a novel biogenetic magnetic targeted drug carrier with potential multifunctions. *J Nanomater*. (2011) 2011:469031–43. doi: 10.1155/2011/469031
113. Elhag OA, Hu XJ, Wen-Ying Z, Li X, Yuan YZ, Deng LF, et al. Reconstructed adeno-associated virus with the extracellular domain of murine PD-1 induces antitumor immunity. *Asian Pacific J Cancer Prev*. (2012) 13:4031–6. doi: 10.7314/APJCP.2012.13.8.4031
114. Wang XH, Zhang GM, He YF, Zhang H, Feng ZH. [Soluble PD-1 can augment anti-tumor immunity induced by HSP70-peptide complex in tumor-bearing mice]. *Chin J Cell Mol Immunol*. (2004) 20:655–8. doi: 10.1007/s11670-004-0048-0
115. Liu C, Jiang J, Gao L, Wang X, Hu X, Wu M, et al. Soluble PD-1 aggravates progression of collagen-induced arthritis through Th1 and Th17 pathways. *Arthritis Res Ther*. (2015) 17:340. doi: 10.1186/s13075-015-0859-z
116. Soares KC, Rucki AA, Wu AA, Olino K, Xiao Q, Chai Y, et al. PD-1/PD-L1 blockade together with vaccine therapy facilitates effector T cell infiltration into pancreatic tumors. *J Immunother*. (2015) 38:1–11. doi: 10.1097/CJI.0000000000000062
117. Qiu L, Lu W, Lin Z, Cai H, Li R. Construction and Humoral Immunological analysis of a fusion protein vaccine that targets MUC1 and PD-1. *Genom Appl Biol*. (2016) 35:513–9. doi: 10.13417/j.gab.035.000513
118. Luo M, Wang H, Wang Z, Cai H, Lu Z, Li Y, et al. A STING-activating nanovaccine for cancer immunotherapy. *Nat Nanotechnol*. (2017) 12:648–54. doi: 10.1038/nnano.2017.52
119. Sahin U, Derhovanessian E, Miller M, Kloke BP, Simon P, Lower M, et al. Personalized RNA mutanome vaccines mobilize poly-specific therapeutic immunity against cancer. *Nature* (2017) 547:222–26. doi: 10.1038/nature23003
120. Ott PA, Hu Z, Keskin DB, Shukla SA, Sun J, Bozym DJ, et al. An immunogenic personal neoantigen vaccine for patients with melanoma. *Nature* (2017) 547:217–21. doi: 10.1038/nature22991
121. Liu Z, Ravindranathan R, Kalinski P, Guo ZS, Bartlett DL. Rational combination of oncolytic vaccinia virus and PD-L1 blockade works synergistically to enhance therapeutic efficacy. *Nat Commun*. (2017) 8:14754. doi: 10.1038/ncomms14754
122. Bertrand F, Montfort A, Marcheteau E, Imbert C, Gilhodes J, Filleron T, et al. TNF alpha blockade overcomes resistance to anti-PD-1 in experimental melanoma. *Nat Commun*. (2017) 8:2256. doi: 10.1038/s41467-017-02358-7
123. Wang C, Wang J, Zhang X, Yu S, Wen D, Hu Q, et al. *In situ* formed reactive oxygen species-responsive scaffold with gemcitabine and checkpoint inhibitor for combination therapy. *Sci Transl Med*. (2018) 10:eaan3682. doi: 10.1126/scitranslmed.aan3682

Conflict of Interest Statement: The authors declare that the research was conducted in the absence of any commercial or financial relationships that could be construed as a potential conflict of interest.

frontiers in Oncology

ORIGINAL RESEARCH
published: 05 December 2018
doi: 10.3389/fonc.2018.00573

Comparative Transcriptomics Unravels Prodigiosin's Potential Cancer-Specific Activity Between Human Small Airway Epithelial Cells and Lung Adenocarcinoma Cells

Bala Davient[1,2], *Jessica Pei Zhen Ng*[1,2], *Qiang Xiao*[3]*, *Liang Li*[4,2]* and *Liang Yang*[1,2,5]*

[1] Singapore Centre for Environmental Life Sciences Engineering, Nanyang Technological University, Singapore, Singapore, [2] School of Biological Sciences, Nanyang Technological University, Singapore, Singapore, [3] Respiratory Medicine, Shunde Hospital, Southern Medical University, The First People's Hospital of Shunde Foshan, Foshan, China, [4] Shenzhen Institute of Advance Technology, Chinese Academy of Sciences, Shenzhen, China, [5] School of Medicine, Southern University of Science and Technology, Shenzhen, China

OPEN ACCESS

Edited by:
Yunkai Zhang,
Vanderbilt University Medical Center, United States

Reviewed by:
Junyi Li,
University of Pittsburgh, United States
Zhenfang Du,
Vanderbilt University Medical Center, United States

***Correspondence:**
Qiang Xiao
xiaoq@mail2.sysu.edu.cn
Liang Li
liang.li@siat.ac.cn
Liang Yang
yangl@sustc.edu.cn

Specialty section:
This article was submitted to Cancer Molecular Targets and Therapeutics, a section of the journal Frontiers in Oncology

Received: *25 September 2018*
Accepted: *15 November 2018*
Published: *05 December 2018*

Citation:
Davient B, Ng JPZ, Xiao Q, Li L and Yang L (2018) Comparative Transcriptomics Unravels Prodigiosin's Potential Cancer-Specific Activity Between Human Small Airway Epithelial Cells and Lung Adenocarcinoma Cells. Front. Oncol. 8:573. doi: 10.3389/fonc.2018.00573

Objective: Non-Small Cell Lung Cancer (NSCLC) is extremely lethal upon metastasis and requires safe and effective systemic therapies to improve a patient's prognosis. Prodigiosin (PG) appears to selectively and effectively target cancer but not healthy cells. However, PG's cancer-specific activity has remained elusive until recently.

Methods: PG's cancer-specific performance was compared to Docetaxel (DTX), Paclitaxel (PTX), and Doxorubicin (DOX) against human lung adenocarcinoma (A549) and human small airway epithelial cells (HSAEC). Combination of PG with DTX, PTX, or DOX in a 1:1 ED50 ratio was also evaluated. MTT assay was used to determine the post-treatment cell viability. RNA-sequencing was used for comparative transcriptomics analysis between A549 and HSAEC treated with 1.0 μM PG for 24 h.

Results: PG reduced A549 cell viability by four-folds greater than HSAEC. In comparison to DTX, PTX and DOX, PG was ~1.7 times more toxic toward A549, and 2.5 times more protective toward HSAEC. Combination of PG in a 1:1 ED50 ratio with DTX, PTX, or DOX failed to exhibit synergistic toxicity toward A549 or protection toward HSAEC. In A549, genes associated in DNA replication were downregulated, while genes directly or indirectly associated in lipid and cholesterol biogenesis were upregulated. In HSAEC, co-upregulation of oncogenic and tumor-suppressive genes was observed.

Conclusion: An overactive lipid and cholesterol biogenesis could have caused A549's autophagy, while a balancing-act between genes of oncogenic and tumor-suppressive nature could have conferred HSAEC heightened survival. Overall, PG appears to be a smart chemotherapeutic agent that may be both safe and effective for NSCLC patients.

Keywords: prodigiosin, small molecule, chemotherapy, lung cancer, selective, RNA-sequencing

INTRODUCTION

Cancer represents a major disease burden to mankind (1–4), and it accounts for almost one out of six deaths worldwide (5). Out of the 8.8 million cancer deaths in 2015, 1.69 million was due to lung cancer (5). The high mortality in patients with lung cancer is often associated with an advanced metastatic disease state (6, 7). In such cases, effective systemic therapies are vital to improve a

patient's prognosis. Targeted therapy, immunotherapy and chemotherapy are all systemic therapies, each with their own strengths and weaknesses.

Targeted therapies can mitigate most side-effects commonly seen in chemotherapy by working on specific mutations unique to cancer cells (8), but their highly specific nature excludes patients whom do not harbor these mutations (9). Almost 80% of all lung cancers are Non-Small Cell Lung Cancer (NSCLC). The most studied target for NSCLC is the Epidermal Growth Factor Receptor (EGFR). There exist three classes of activating EGFR mutations that sensitizes NSCLCs to EGFR Tyrosine Kinase Inhibitors (TKIs). These activating EGFR mutations have been well summarized in the literature (10). Gefitinib, Erlotinib, Afatinib, Osimertinib, and Dacomitinib are a few prominent and promising EGFR TKIs used in NSCLC patients harboring specific activating EGFR mutations. Gefitinib and Erlotinib are inhibitors of a few specific EGFR mutations found in some NSCLC patients and have demonstrated enduring progression free survival for responders (11–13). Although effective, Gefitinib, Erlotinib, and the other EGFR TKIs are beneficial to only a small population of patients as only about 15% of Caucasian and 50% of Asian lung adenocarcinoma patients harbor EGFR mutations (14, 15).

Immunotherapy exploits the patient's own immune system against cancers (16), but its success depends on the cancer's ability to display its unique neoantigens on its outer cell membrane (17–19) to be identified and destroyed by immune cells (20). Cancers can evade immune destruction by expressing Programmed Death (PD) Ligand 1 (PD-L1), which binds to PD-1 receptors on CD8+ T-cells, inhibiting cytotoxic elimination (21). Nivolumab and Pembrolizumab are antibodies against PD-1. Their prevention of interaction with PD-1 allows CD8+ T-cells to eliminate cancer cells such as NSCLCs (22, 23). Anti-PD-1 effectiveness against NSCLC has been reported to positively correlate with the cancer cell's mutation burden, as a high mutation load generates unique neoantigens for T-cell recognition (24). However, response rates of anti-PD-1 in NSCLC patients appears to be low at ∼19% (22, 23, 25).

In contrast to targeted and immunotherapy, chemotherapy offers broader patient coverage and is still the mainstream cancer therapy available for the majority of cancer patients (26). Platinum-based doublet chemotherapies have been indicated as the first-line against NSCLC with response rates ranging from 25 to 35% (27, 28). However, despite better response rates, their inability to distinguish rapidly diving cancer cells from healthy cells could lead to debilitating side-effects such as anemia, nausea, and neurotoxicity (29).

NSCLC urgently require therapies that are effective, have wide coverage, and harbor fewer side effects. Many studies are ongoing to improve systemic therapies for metastatic NSCLC. In terms of chemotherapies, the search for newer and safer treatments, alone or in combination, persists (30–33).

Nature provides a rich source of anti-cancer agents suitable for chemotherapy. Docetaxel (DTX), Paclitaxel (PTX), and Doxorubicin (DOX) are natural compounds that have been used against NSCLC (34, 35). Recently, Prodigiosin (PG), a secondary metabolite from *Serratia marcescens*, was observed to inhibit NSCLC proliferation (36). Interestingly, PG has been reported to exhibit high cancer-specificity (37–39). This means that PG could potentially mitigate common side-effects associated with chemotherapies, making it a smart chemotherapy candidate.

The current understanding of PG's anti-cancer mechanisms of action encompasses cytoplasmic acidification through modulation of H^+/Cl^- symporters, DNA damage through copper-mediated oxidative cleavage, inhibition of topoisomerases, and ATP synthesis reduction through disruption of the mitochondrial proton gradient (40). At the molecular level, PG has been described to initiate autophagy through mTOR deactivation (39) and apoptosis through the disruption of BCL-2 family pro-survival members (39, 41) or downregulation of pro-survival Survivin (40, 42), a member of the inhibitor of apoptosis. In addition, common to many cancers is the dysregulation of p53, a protein that dictates cell survival or cell death upon cell stress. In most cancers, p53 activity is lost and cells attain a permanent survival status. In some reports, PG was able to induce cancer cell apoptosis in a p53-independent manner (43, 44). This reveals that PG could trigger alternative apoptosis pathways.

Altogether, PG appears to be a promising chemotherapeutic agent which warrants further research into its mechanisms of action. At present, there exists limited data on PG's mechanisms of action to draw meaningful links between studies. Here, we add value to the current knowledge by unveiling PG's potential cancer-specific activity through comparative transcriptomics analysis between Human Lung Adenocarcinoma (A549) and Human Small Airway Epithelial Cells (HSAEC), with Human Colorectal Carcinoma Cells (HCT116) as a cancer control. In addition, we also report on PG's *in vitro* effectiveness and safety, based on the degree of cancer cytotoxicity and selectivity, respectively, in comparison to DTX, PTX and DOX.

MATERIALS AND METHODS

Materials

Docetaxel purum (DTX), doxorubicin hydrochloride (DOX), paclitaxel from *Taxus brevifolia* (PTX), prodigiosin hydrochloride from *Serratia marcescens* (PG), and dimethyl sulfoxide (DMSO) were purchased from Sigma (St. Louis, MO, USA). 3-(4,5-Dimethylthiazol-2-yl)-2,5-diphenyltetrazolium bromide (MTT) was purchased from Bio Basic (Amherst, NY, USA). Proteinase K, RNase-Free DNase I and the RNAprotect Cell Reagent were purchased from Qiagen (Hilden, Germany). TURBO™ DNase, Qubit™ dsDNA HS, and RNA HS Assay Kits were purchased from Invitrogen (Waltham, MA, USA). Angencourt RNAClean XP Kit was purchased from Beckman Coulter (Bera, CA, USA). RNA ScreenTape was purchased from Agilent (Santa Clara, CA, USA).

Cell Culture

Primary Small Airway Epithelial Cells; Normal, Human (HSAEC) (ATCC® PCS301-010™), A549 (ATCC® CCL-185™), HCT116 (ATCC® CCL-247™), and the Airway Epithelial Cell Basal Medium (AECBM) with associated growth factors were purchased from the American Type Culture Collection (ATCC) (Manassas, VA, USA). Phosphate Buffered

Saline (PBS) without calcium and magnesium, high glucose Dulbecco's Modified Eagles Media (DMEM) with added L-glutamine, sodium pyruvate, and phenol red, were purchased from GE Healthcare Life Sciences (Logan, UT, USA). Heat-inactivated Fetal Bovine Serum (FBS) of South American origin and Trypsin-EDTA (0.25%) with phenol red were purchased from Gibco (Waltham, MA, USA). HSAEC cells were cultured with 8 mL AECBM while both A549 and HCT116 cells were cultured with 8 mL DMEM supplemented with 10% FBS, which henceforth will be referred to as complete media, in a 75 cm^2 culture flask. All culture flasks were incubated in a humidified atmosphere at 37°C with 5% CO_2. All incubations mentioned henceforth will be referring to these conditions. No *Mycoplasma* testing was performed.

Cell Viability Assay

DTX, PTX, DOX, and PG were reconstituted with DMSO to a stock concentration of 50, 50, 80, and 2 mM, respectively. Drugs were diluted in pre-warmed AECBM or complete media of 37°C. For each drug concentration tested, an equivalent DMSO concentration was created as control (**Supplementary Figure S1**).

At ∼90% cell confluency, cells were split into 96-well flat-bottomed plates at a seed density and final volume of 7,000 cells and 100 μL per well. Cultures were incubated overnight for 24 h. At ∼80% confluency, the spent media was replaced with either the treatment or control media to a final volume of 100 μL per well. The culture plates were incubated for another 48 h.

The MTT shipped in the powdered state was reconstituted with PBS to a final concentration of 5 mg/mL and sterile filtered with a 0.2 μm Acrodisk Syringe Filter (PALL, Port Washington, NY, USA). This was mixed at a 1:1 ratio with serum-free DMEM or AECBM to create the MTT mix. After the 48 h of treatment, the spent drug media was replaced with 100 μL of the MTT mix. The cultures were incubated for an additional 3 h before being homogenized with 150 μL of DMSO. Cell viability was measured with the Infinite® M200 Pro (Tecan, Männedorf, Zürich, Switzerland) microplate reader at 590 nm.

Drug Cytotoxicity Screening

HSAEC and A549 cells, both at passage P6, were split into three 25 cm^2 culture flasks. These cultures were propagated further for two more passages, and at P8, each cell line was considered to have three biological replicates of $n = 3$ (45). The cells were thereafter cultured in 96-well plates as technical duplicates per biological replicate.

DTX, PTX, DOX, and PG's ED50 were pre-determined with A549 cells (**Supplementary Figure S2**). The ED50 for DTX, PTX, DOX, and PG were 0.1, 0.1, 1, and 0.3 μM, respectively. For the combination therapies with PG, drugs were mixed in a 1:1 ED50 ratio. All treatments were first created as eight-fold stock concentrations and were serially diluted by two-folds (i.e., 8:8 to 4:4 till 0.25:0.25). All other steps conducted have been described under the "Cell Viability Assay" section.

RNA Extraction and Quality Controls

HSAEC, A549, and HCT116 at passage number P8 were cultured as technical triplicates in 25 cm^2 culture flasks, and after two more passages, each cell line was considered to have biological triplicates of $n = 3$ (45). At 90% confluency, HSAEC and A549 cells were split at a seed density of 3.0×10^4 cells/cm^2 while HCT116 cells were split at 6.0×10^4 cells/cm^2 into 6-well plates. After 24 h of incubation in 3 mL of AECBM or complete media, the spent media was replaced with 3 mL of either 1.0 μM PG (treatment) or 0.05% DMSO (control). Cells were incubated for another 24 h and thereafter, the media was replaced with 1 mL of RNAprotect Cell Reagent.

Cells were gently agitated on an orbital shaker at 80 revolutions per minute for 10 min. A lysis cocktail comprised of 10 μL 1% β-mercaptoethanol, 20 μL proteinase K, and 800 μL RLT buffer, which was a component from the RNeasy Mini Kit (Qiagen), was homogenized with cells in each well. The RNA extraction was conducted according to instructions found in the RNeasy Mini Kit.

A 30 min on-column DNase I treatment was performed. DNA contamination was further minimized with TURBO™ DNase treatment. Once RNA was purified with the Angencourt RNAClean XP Kit, RNA integrity was verified using the RNA ScreenTape with analysis on the Agilent 2200 TapeStation (Agilent). Using the Qubit™ dsDNA HS and RNA HS Assay Kits, total RNA was quantified fluorometrically via the Qubit™ Fluorometer 2.0 (Invitrogen).

RNA Sequencing and Data Processing

RNA library preparation and sequencing were conducted by an in-house facility at Singapore Centre for Environmental Life Science Engineering (SCELSE). Briefly, library preparation was executed with the Illumina® TruSeq® Stranded messenger RNA Sample Prep Kit (Illumina, San Diego, CA, USA). The output which was cDNA fragments were paired-end sequenced at read lengths of 100 nucleotides via the Illumina® HiSeq 2500 (Illumina) platform.

All samples had a sequencing depth of more than 24 million reads. These reads were processed using the CLC Genomics Workbench Version 11.0.1 (CLC Bio, Aarhus, Denmark). The default settings were used unless otherwise stated. All reads were trimmed with a quality score of 0.05. Using the "RNA-Seq Analysis" function, the trimmed reads were mapped onto the human genome GRCh38 downloaded from the Ensemble database. The maximum number of hits for a read was set to 1. Gene hits were annotated with GRCh38.92 acquired from the Ensemble database. Gene expression was measured as total counts, where each paired-read was considered as 1. A negative binomial test was performed using the workbench's "Differential Expression for RNA-Seq" tool to establish the differentially expressed genes (DEGs). All raw and processed sequence files may be acquired from Gene Expression Omnibus (Accession number: GSE118448).

Functional Analysis

DEG datasets were exported from CLC into the Ingenuity® Pathway Analysis (IPA; Qiagen) Version 44691306 software. A

Log2 Fold-change (Log2FC) of ±1 with a false discovery rate (FDR) adjusted p-value of < 0.05 was applied to the datasets. With these cut-off values, HSAEC had 2,222, A549 had 2,004, and HCT116 had 2,199 DEGs out of 37,258 successfully annotated gene identifiers.

Statistical Analysis

The Welch two-tailed t-test available in GraphPad Prism 8 was applied onto the drug cytotoxicity screening assay datasets. This statistical test considers the data to have been sampled from a Gaussian population but does not presume that the two populations under scrutiny have the same standard deviation. The null hypothesis is defined as the two populations tested having equal means. When $p > 0.05$, the null hypothesis is not rejected, and the interpretation would be that the evidence is not convincing enough to claim that the means of the two populations tested are different.

RESULTS

PG Demonstrated Selective Toxicity Toward A549 but not HSAEC

PG has been known to induce cancer cell death while preserving healthy cell's viability (37–39). Here, we evaluated PG's cancer-specific toxicity with cancer cell line A549 and immortalized human lung small airway epithelial cells (HSAEC; **Figure 1**). At PG's ED50 of 0.3 μM, cell viability of A549 was reduced by 67.7 ± 5.3%, while HSAEC was reduced by 15.6 ± 2.8%. As A549 is a cancer cell line while HSAEC is an immortalized healthy cell line, with both dividing rapidly, the greater reduction in A549 cell viability demonstrates PG's selective toxicity. PG concentrations >0.3 μM exhibited neither enhanced cancer toxicity nor healthy cell protection.

PG Outperformed DTX, PTX, and DOX in Terms of Cancer-Specificity

Here, we define performance as the agent's ability to protect normal cells while being toxic to cancer cells. In other words, the degree of cancer-specificity. Evaluation of DTX, PTX, DOX, and PG's ED50 of 0.1, 0.1, 1.0, and 0.3 μM, respectively, against A549 and HSAEC, revealed PG's superior performance as a cancer-specific agent. At these concentrations, PG preserved HSAEC viability by 2.8, 2.4, and 2.5 times more than DTX, PTX, and DOX, respectively (**Figure 1**). Moreover, PG reduced A549 cell viability at an average of 1.7 times greater than the other agents.

PG Exhibited Poor Performance in Combination With DTX, PTX, or DOX

DTX, PTX, or DOX in a 1:1 ED50 ratio with PG failed to exhibit anti-cancer synergism and were almost equally toxic, if not worst, toward HSAEC as compared to A549. 0.3 μM PG with 0.1 μM DTX reduced HSAEC viability by 63.0 ± 2.6% and A549 by 67.2 ± 3.7% (**Figure 1A**). 0.3 μM PG with 0.1 μM PTX reduced HSAEC viability by 66.4 ± 7.5% and A549 by 63.9 ± 4.3% (**Figure 1B**). 0.3 μM PG with 1.0 μM DOX reduced HSAEC viability by 71.4 ± 2.7% and A549 by 40.4 ± 10.4% (**Figure 1C**). PG in combination with DTX, PTX, or DOX, at 4:4, 2:2, 1:1, 0.5:0.5 or 0.25:0.25 ED50 ratio, failed to exhibit improved toxicity toward A549 with enhanced protection to HSAEC in comparison to 0.3 μM PG alone.

PG Altered Both A549 and HCT116 Cancer Cells' Morphology

To determine if PG's anti-cancer activity can be observed beyond lung adenocarcinoma cells, in addition to A549 cells, we treated HCT116 cells, another cancer type which could serve as a cancer control, with 1.0 μM PG for 24 h prior microscopic visualization. A549 cells were found in low numbers, elongated, shriveled, with a deformed nucleus and non-homogenous cytoplasm (**Figure 1Da**). HCT116 cells appeared rounded-up, detached from culture surfaces, but still adhered to neighboring cells (**Figure 1Db**). Overall, PG demonstrated substantial morphological alterations in both A549 and HCT116 cancer cell lines.

PG's Toxicity Possibly Mitigated Through a "Balancing Act" in HSAEC

To understand how PG protects healthy cells yet kills cancer cells, we conducted an RNA-sequencing experiment with HSAEC, A549 and HCT116 cells treated with 1.0 μM PG for 24 h. Using the top 50 up- and down-regulated genes per cell line, we were able to identify 84 DEGs specifically perturbed in HSAEC. These DEGs had an FDR p-value $< 4.0 \times 10^{-15}$ (**Figure 2**). For comparison validity, these 84 HSAEC-specific DEGs were filtered under two conditions. Firstly, the corresponding DEGs in A549 and HCT116 were required to have an FDR p-value < 0.05, and secondly, the difference in expression in terms of Log2FC with HSAEC had to be $> \pm 1.5$. Under these conditions, 21 DEGs were identified as fit for comparison (**Table 1**).

The 21 DEGs revealed a "balancing act" in HSAEC between genes of oncogenic and tumor-suppressive nature. Oncogenic genes such as *PDK4, RRAGD, HEY1, TSPAN15,* and *SERPINB9* were found overexpressed. At the same time, tumor-suppressive genes such as *MT1G, MT1M, CDKN1C,* and *DCN* were overexpressed. On the other hand, genes of oncogenic nature such as *SHCBP1, CPA4, KRT19, KRT15, and DSG3* were found downregulated. DEGs such as *BMP6, GULP1, AC106865.1, CNTN3, GDAP1, C1orf116, and SDSL* were uncategorizable due to their lack of information.

PG Possibly Induced DNA Replication Inhibition and Metabolic Rewiring in A549 and HCT116

To identify other possible anti-cancer mechanisms associated with PG, we performed a comparative transcriptomics analysis between A549, HCT116 and HSAEC cells treated with 1.0 μM PG for 24 h. A total of 18 DEGs were considered fit for comparison (**Table 2**) based on two conditions. Firstly, the DEGs commonly perturbed between A549 and HCT116 had to be upregulated by at least >2 Log2FC and downregulated by <-1.5 Log2FC. Secondly, the difference between A549 and HSAEC gene expression had to be $> \pm 1.5$ (**Figure 2**).

All commonly downregulated genes between A549 and HCT116 were found associated with DNA replication. These were *MCM10, H2AFX, DSCC1, MCM4,* and *RFC5* (**Table 2**).

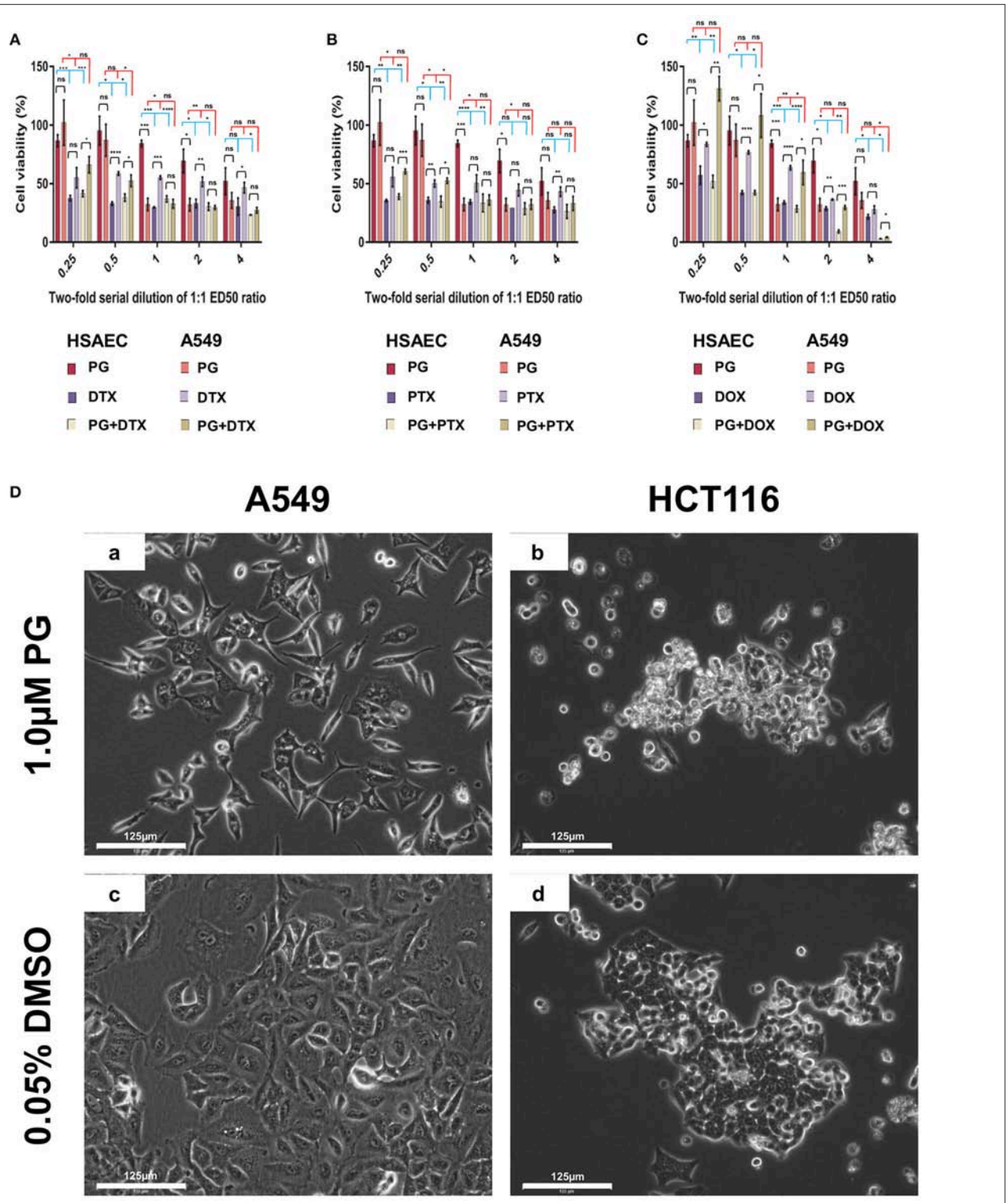

FIGURE 1 | Cell viability of HSAEC and A549 cell measured by the MTT assay after 48-h of PG treatment **(A–C)**. Effects of 1.0 μM PG on A549 and HCT116 cell morphology after 24 h treatment **(Da–Dd)**. **(A)** PG, DTX, and PG+DTX. **(B)** PG, PTX, and PG+PTX. **(C)** PG, DOX, and PG+DOX. Bar graphs represent mean cell viability from biological triplicates ($n = 3$) while the black vertical lines on the bar tops represent standard deviation (SD). A Welch *t*-test was applied to the datasets; black horizontal lines compare drug effects between HSAEC and A549, blue lines compare within HSAEC, and red lines compare within A549 (*$p < 0.05$, **$p < 0.01$, ***$p < 0.001$, ****$p < 0.0001$, and "ns" is not significant). **(Da)** A549 and **(Db)** HCT116 were treated with 1.0 μM PG. **(Dc)** A549 and **(Dd)** HCT116 were treated with 0.05% DMSO as a negative control. Phase-contrast images were acquired at 20X magnification with the EVOS FL Auto 2 microscope. Images have not been enhanced. Scale bars represent 125 μm.

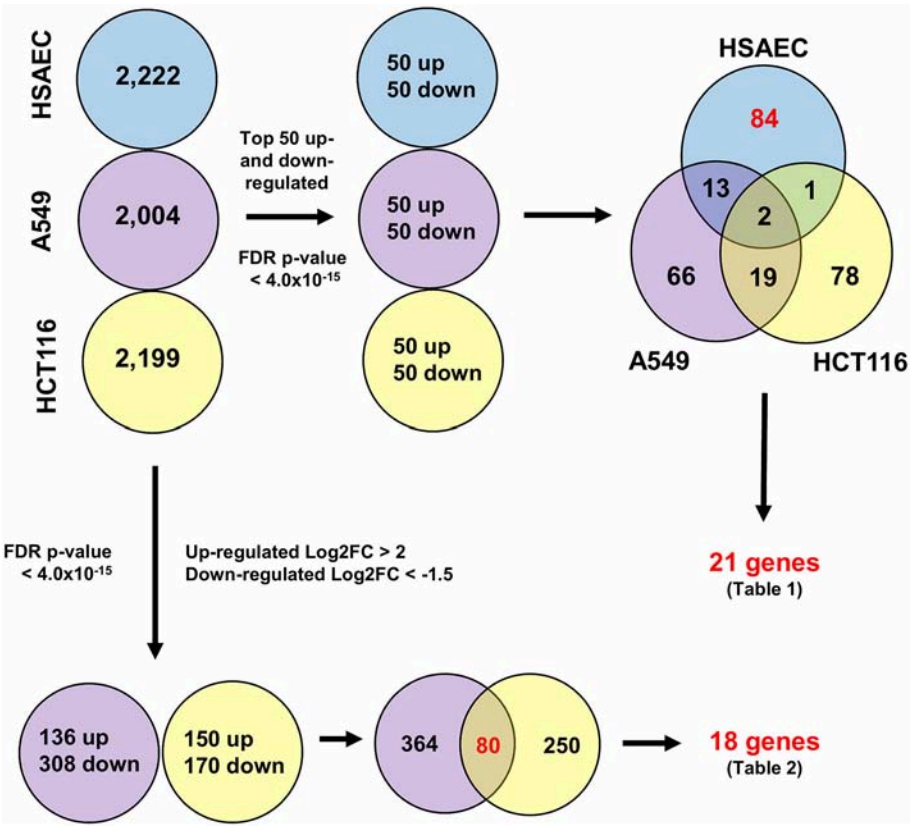

FIGURE 2 | Differentially expressed genes from CLC Workbench for HSAEC, A549 and HCT116 after 24 h treatment with 1.0 μM PG. Blue circles represents HSAEC, purple as A549 and yellow as HCT116. Twenty one genes for **Table 1** were derived from filtering 84 HSAEC-specific genes on the condition that corresponding genes in A549 and HCT116 had an FDR *p*-value < 0.05, and secondly, the difference of A549 and HCT116 gene expression in terms of Log2FC with HSAEC had to be > ± 1.5. Eighteen genes for **Table 2** were derived from filtering 80 genes common to A549 and HCT116 on the condition that corresponding genes in A549 with HSAEC had an FDR *p*-value < 0.05, and secondly, the difference of A549 and HSAEC gene expression in terms of Log2FC with HSAEC had to be > ± 1.5.

Surprisingly, *MCM10* and *DSCC1* expression were severely repressed in HSAEC than in A549 and HCT116. On the other hand, multiple genes associated with lipid and cholesterol metabolism, either directly or indirectly, were found commonly overexpressed between A549 and HCT116. These were *ALDOC, NDRG1, WIPI1, PCSK9, LIPG, MSMO1, MVD, IDI1,* and *ANGPTL4* (**Table 2**). The other genes that were overexpressed yet did not closely associate with the two main categories described here were *MIR210HG, CCNG2, P4HA1,* and *PPM1K* (**Table 2**). Confirmatory repeat experimental data for RNA sequencing result of A549 and HCT116 can be found in **Tables S1,S2**. Further pathway analysis also revealed different upstream regulator activities in PG-treated HSAEC, A549, and HCT116 cells (**Tables S3–S5**).

Based on pathway analysis, and in relation to DNA replication, the "Role of BRCA1 in DNA Damage Response" and the "Mitotic Roles of Polo-Like Kinase" pathways were seen perturbed in all three cell lines but were predicted to be inactivated (**Table 3**). In terms of DNA damage, the "Cell Cycle: G2/M DNA Damage Checkpoint Regulation" pathway was predicted to be activated (**Table 3**). In relation to metabolic rewiring, the "Superpathway of Cholesterol Biosynthesis," the "Cholesterol Biosynthesis III (via Desmosterol)," the "Cholesterol Biosynthesis II (via 24,25-dihydrolanosterol)," and the "Cholesterol Biosynthesis I" pathways were significantly perturbed and predicted to be highly activated (**Table 3**). Furthermore, these cholesterol pathways were not perturbed in HSAEC following PG treatment.

With experimental data, the IPA's Molecule Activity Prediction (MAP) algorithm managed to predict PG-induced mechanistic differences between HSAEC and A549 cells in terms of "Cell Cycle Progression," "Apoptosis," "Cell Survival," "Mitochondrial Respiration," "Glycolysis," "Autophagy," and "Senescence" (**Figure 3**). The overall prediction landscape seems to suggest PG-induced pro-survival in HSAEC but pro-death in A549. Interestingly, "DNA Repair" mechanism was predicted to be inhibited in both cell lines (**Figure 3**).

DISCUSSION

Metastatic lung cancers are extremely lethal and requires effective systemic therapies to improve clinical outcomes for patients (46). PG has demonstrated immense potential as a smart chemotherapeutic candidate. Its most promising feature is its ability to selectively eliminate cancer cells yet protect healthy

TABLE 1 | HSAEC-specific DEGs in comparison with A549 and HCT116 cells after 24 h treatment with 1.0 μM PG.

Gene name	Gene symbol	ENSEMBL ID	Log2FC		
			HSAEC	A549	HCT116
ONCOGENIC NATURED GENES					
Pyruvate Dehydrogenase Kinase 4	PDK4	ENSG00000004799	6.87	1.25	1.62
Ras Related GTP Binding D	RRAGD	ENSG00000025039	4.92	2.03	0.68
Hes Related Family BHLH Transcription Factor with YRPW Motif 1	HEY1	ENSG00000164683	4.54	0.93	1.41
Tetraspanin 15	TSPAN15	ENSG00000099282	4.19	-0.61	1.28
Serpin Family B Member 9	SERPINB9	ENSG00000170542	3.69	-0.78	0.72
SHC Binding and Spindle Associated 1	SHCBP1	ENSG00000171241	-3.73	-2.18	-1.14
Carboxypeptidase A4	CPA4	ENSG00000128510	-3.68	0.49	0.67
Keratin 19	KRT19	ENSG00000171345	-3.48	1.97	0.76
Keratin 15	KRT15	ENSG00000171346	-3.28	1.13	2.00
Desmoglein 3	DSG3	ENSG00000134757	-2.86	–	–
TUMOR-SUPPRESSIVE NATURED GENES					
Metallothionein 1G	MT1G	ENSG00000125144	5.80	–	–
Metallothionein 1M	MT1M	ENSG00000205364	5.64	–	–
Cyclin Dependent Kinase Inhibitor 1C	CDKN1C	ENSG00000129757	4.74	2.84	2.43
Decorin	DCN	ENSG00000011465	3.81	–	–
UNCATEGORIZABLE GENES					
Bone Morphogenetic Protein 6	BMP6	ENSG00000153162	5.49	2.18	-1.41
GULP, Engulfment Adaptor PTB Domain Containing 1	GULP1	ENSG00000144366	4.11	0.78	1.41
–	AC106865.1	ENSG00000250771	4.88	–	–
Contactin 3	CNTN3	ENSG00000113805	4.51	–	–
Ganglioside Induced Differentiation Associated Protein 1	GDAP1	ENSG00000104381	-3.93	-1.12	-0.63
Chromosome 1 Open Reading Frame 116	C1orf116	ENSG00000182795	-3.57	-1.47	1.23
Serine Dehydratase Like	SDSL	ENSG00000139410	-2.88	-0.68	-0.72

Upregulated genes are represented in red, downregulated in blue, and those with no detectable changes with the symbol "-". All genes curated had an FDR p-value $< 4.0 \times 10^{-15}$ *except the following; A549's CDKN1C (0.01) and HEY1 (0.04), HCT116's BMP6 (0.05). Experiments were conducted in biological triplicates of n = 3. Confirmatory repeat experimental data can be found in* ***Supplementary Table S1****.*

cells (37–39). Here, we were able to demonstrate PG's selective elimination of NSCLC by four-folds (**Figures 1A–C**). Beyond lung adenocarcinoma cells, we also showed that PG could cause substantial morphological alterations to colorectal carcinoma cells (**Figure 1D**). When compared to other naturally derived anti-cancer agents such as DTX, PTX, or DOX, PG exhibited heightened protection toward HSAEC while being more toxic to A549. Indeed, PG established itself as a promising cancer-specific agent. However, the random combination with other anti-cancer agents could ameliorate PG's cancer-specific activity and yield an undesirable outcome to healthy cells (**Figures 1A–C**). A rational drug combination approach could increase synergism, hence, greater success in combinatorial chemotherapies. To permit a rational combination of PG with other anti-cancer agents, we require a deeper understanding of the agent's molecular functions.

Previously, a microarray analysis for 1,176 genes was performed on human breast cancer cells treated with PG (44). Out of the 37 significantly perturbed genes (44), there were no similarities found with our study (**Table 2**). The lack of similarities was not unexpected as this could be due to the inherent limitation of the microarray technology (47), or simply because a different cell line was used. Nevertheless, using RNA-sequencing, a genome-wide transcriptomics approach, we were able to identify at least 2,000 significantly perturbed genes per cell line. With broader coverage, we were confident that employing such a technology would permit a more comprehensive analysis.

The comparative transcriptomics analysis between A549 and HCT116 revealed 18 genes that were significantly perturbed by PG (**Table 2**). These genes revealed the possibility of DNA replication inhibition and metabolic rewiring toward enhanced lipid and cholesterol biogenesis. In the study with breast cancer cells, PG was reported to perturb genes related to transcriptional regulation, cell adhesion, cell cycle, and apoptosis (44). Although we have not found perturbations in genes associated with transcriptional regulation or cell adhesion, based on experimental data, we have predicted cell cycle inhibition (**Table 3** and **Figure 3**) and reduced survival fitness in line with apoptosis (**Figure 3**) in A549 cells.

The gene products of *MCM10, MCM4, H2AFX, DSCC1,* and *RFC5* are necessary for DNA replication. However, they were found downregulated in both A549 and HCT116 after PG treatment (**Table 2**). MCM10 plays a crucial role in allowing

TABLE 2 | Common DEGs in both A549 and HCT116 cells after 24 h treatment with 1.0 μM PG.

Gene name	Gene symbol	ENSEMBL ID	Log2FC		
			HSAEC	A549	HCT116
DNA-REPLICATION ASSOCIATED GENES					
Minichromosome Maintenance 10 Replication Initiation Factor	MCM10	ENSG00000065328	-4.67	-3.09	-1.87
H2A Histone Family Member X	H2AFX	ENSG00000188486	-0.96	-2.70	-1.57
DNA Replication and Sister Chromatid Cohesion 1	DSCC1	ENSG00000136982	-3.93	-2.35	-1.55
Minichromosome Maintenance Complex Component 4	MCM4	ENSG00000104738	-0.33	-2.22	-1.87
Replication Factor C Subunit 5	RFC5	ENSG00000111445	-0.51	-2.11	-1.62
LIPID AND CHOLESTEROL METABOLISM ASSOCIATED GENES					
Aldolase, Fructose-Bisphosphate C	ALDOC	ENSG00000109107	1.74	5.36	4.71
N-Myc Downstream Regulated 1	NDRG1	ENSG00000104419	1.08	3.80	2.81
WD Repeat Domain, Phosphoinositide Interacting 1	WIPI1	ENSG00000070540	1.53	3.39	2.50
Proprotein Convertase Subtilisin/Kexin Type 9	PCSK9	ENSG00000169174	1.65	3.27	2.85
Lipase G, Endothelial Type	LIPG	ENSG00000101670	-0.27	2.82	3.35
Methylsterol Monooxygenase 1	MSMO1	ENSG00000052802	0.51	2.76	3.32
Mevalonate Diphosphate Decarboxylase	MVD	ENSG00000167508	0.52	2.48	2.76
Isopentenyl-Diphosphate Delta Isomerase 1	IDI1	ENSG00000067064	0.59	2.34	2.98
Angiopoietin Like 4	ANGPTL4	ENSG00000167772	-1.34	2.19	3.66
OTHER PATHWAYS ASSOCIATED GENES					
MIR210 (MicroRNA 210) Host Gene	MIR210HG	ENSG00000247095	1.00	4.57	3.60
Cyclin G2	CCNG2	ENSG00000138764	0.78	3.15	3.74
Prolyl 4-Hydroxylase Subunit Alpha 1	P4HA1	ENSG00000122884	0.30	2.40	2.68
Protein Phosphatase, Mg2+/Mn2+ Dependent 1K	PPM1K	ENSG00000163644	0.57	2.32	2.15

Upregulated genes are represented in red and downregulated in blue. All genes curated had an FDR p-value $< 4.0 \times 10^{-15}$ *except the following; HSAEC's MIR210HG* (4.09×10^{-15}), *LIPG* (7.17×10^{-3}), *MSMO1* (2.15×10^{-12}), *MVD* (5.92×10^{-10}), *P4HA1* (4.41×10^{-4}), *IDI1* (3.13×10^{-10}), *PPM1K* (8.86×10^{-3}), *MCM10* (3.26×10^{-7}), *H2AFX* (4.09×10^{-15}), *DSCC1* (8.96×10^{-4}), *MCM4* (2.54×10^{-3}), *and RCF5 (0.02). Experiments were conducted as biological triplicates of n = 3. Confirmatory repeat experimental data can be found in* ***Supplementary Table S2***.

CDC45:MCM2-7:GINS helicase to unwind DNA double-strand for replication initiation (48). After DNA has been unwounded, DNA replication requires DSCC1 and RFC5 complexed with other proteins to load Proliferating Cell Nuclear Antigen (PCNA) onto the DNA (49). PCNA is required to clamp DNA polymerase epsilon onto the DNA for replication (50). After DNA synthesis, to maintain genomic integrity, H2AFX serves as a sensor for DNA damage and recruits DNA repair complexes to the area of lesion (51). PG has been reported to cause genotoxicity directly through copper-mediated oxidative cleavage (52), or indirectly through inhibition of topoisomerases (53). One potential mechanism stemming from the downregulation of *H2AFX* is the loss of genomic integrity, induction of cell cycle arrest [*CCNG2* overexpression (**Table 2**) and predicted G2/M DNA damage checkpoint arrest activation (**Table 3**)] and therefore, DNA replication stand-still (54, 55). By throwing the DNA repair mechanisms off-balance [predicted BRCA pathway shutdown (**Table 3**)], genotoxic agents such as PG might increase sensitivity and effectiveness against cancer cells (56, 57).

Metabolic rewiring has been described as an emerging hallmark of cancer (58, 59), and there have been reports of lipid and cholesterol metabolism being drivers of tumorigenesis and progression (60–62). In fact, it has been mentioned that "highly proliferative cancer cells show a strong lipid and cholesterol avidity, which they satisfy by either increasing the uptake of exogenous (or dietary) lipids and lipoproteins or overactivating their endogenous synthesis (that is, lipogenesis and cholesterol synthesis, respectively)" (60). Interestingly, these overactivations were observed only after PG treatment (**Table 2**). ALDOC, MVD, and IDI1 are metabolic enzymes that support lipid and cholesterol biosynthesis. Their gene overexpression could potentially hint at an overactive endogenous lipid and cholesterol biogenesis. *ANGPTL4*, a lipoprotein lipase inhibitor, had a Log2FC difference of 3.53 between healthy HSAEC and cancerous A549 cells. *ANGPTL4* upregulation in A549 cells may have been in response to the overexpression of other lipogenic genes (63). On the flip side, upregulation of *PCKS9* hints at a potential supply cut-off of low-density lipoproteins (LDL) from exogenous sources by reducing LDL receptors (64, 65). As a compensatory mechanism to reduced LDL uptake, *NDRG1* and *LIPG* may have been upregulated to acquire LDL and fatty acids, respectively, from the cell's surroundings (66, 67). *CXCL8*, otherwise known as interleukin-8, has been implicated as a cancer growth factor (68, 69), as well as a molecule that promotes cholesterol accumulation (70). *MSMO1* is also believed to be involved in cholesterol metabolism and cancer (71, 72). Altogether, there may be a possibility that the blockade of exogenous LDL import, compounded with the rampant endogenous demand for lipid and cholesterol biogenesis to support rapidly dividing cancer cells, induced a suicidal metabolic rewiring that eventually led to autophagy (73).

TABLE 3 | Top 10 canonical pathways in A549 and HCT116 cells after 24 h of 1.0 μM PG treatment.

Top 10 Canonical pathways	-log(*p*-value)			Activation z-score		
	HSAEC	A549	HCT116	HSAEC	A549	HCT116
	0.0	15.1		-3.0	4.4	
Superpathway of Cholesterol Biosynthesis						
Cell Cycle Control of Chromosomal Replication				Not predictable		
Cholesterol Biosynthesis III (via Desmosterol)						
Cholesterol Biosynthesis II (via 24,25-dihydrolanosterol)						
Cholesterol Biosynthesis I						
Role of BRCA1 in DNA Damage Response						
Mitotic Roles of Polo-Like Kinase						
Hereditary Breast Cancer Signaling				Not predictable		
Mismatch Repair in Eukaryotes				Not predictable		
Cell Cycle: G2/M DNA Damage Checkpoint Regulation						

Pathways were ranked in descending order of decreasing -log(p-value) of the Fisher's exact test. Dark purple heat-map blocks represent high -log(p-value). Activation z-scores were calculated based on the IPA's pathway activity prediction algorithm. Dark orange heat-map blocks represent the possibility of a highly active pathway, whereas dark blue blocks represent inhibition.

Autophagy is a form of cellular self-cannibalization of cytoplasmic content via lysosomal compartments to recycle cell materials and provide substrates for cellular homeostasis under metabolic stress (74). However, autophagy can be a double-edged sword when it comes to cancers. It could either be pro-tumorigenic or anti-tumorigenic (75, 76). PG is known to bind and inhibit mTORC1 and mTORC2, initiating autophagy in cancer cells (39, 77, 78). We found *WIPI1*, a marker and an important player in autophagy (79, 80), markedly upregulated (**Table 2**). It is unclear if the lipid and cholesterol biosynthesis genes were upregulated to support the *de novo* biogenesis of autophagosomes.

How PG protects healthy cells yet eliminates cancer cells has been a mystery thus far. For the first time, we attempted to unravel PG's cancer-specific mechanisms of action through comparative transcriptomics analysis. Firstly, unlike in A549 and HCT116, there were little to no upregulation in lipid and cholesterol biosynthetic genes and pathways in HSAEC

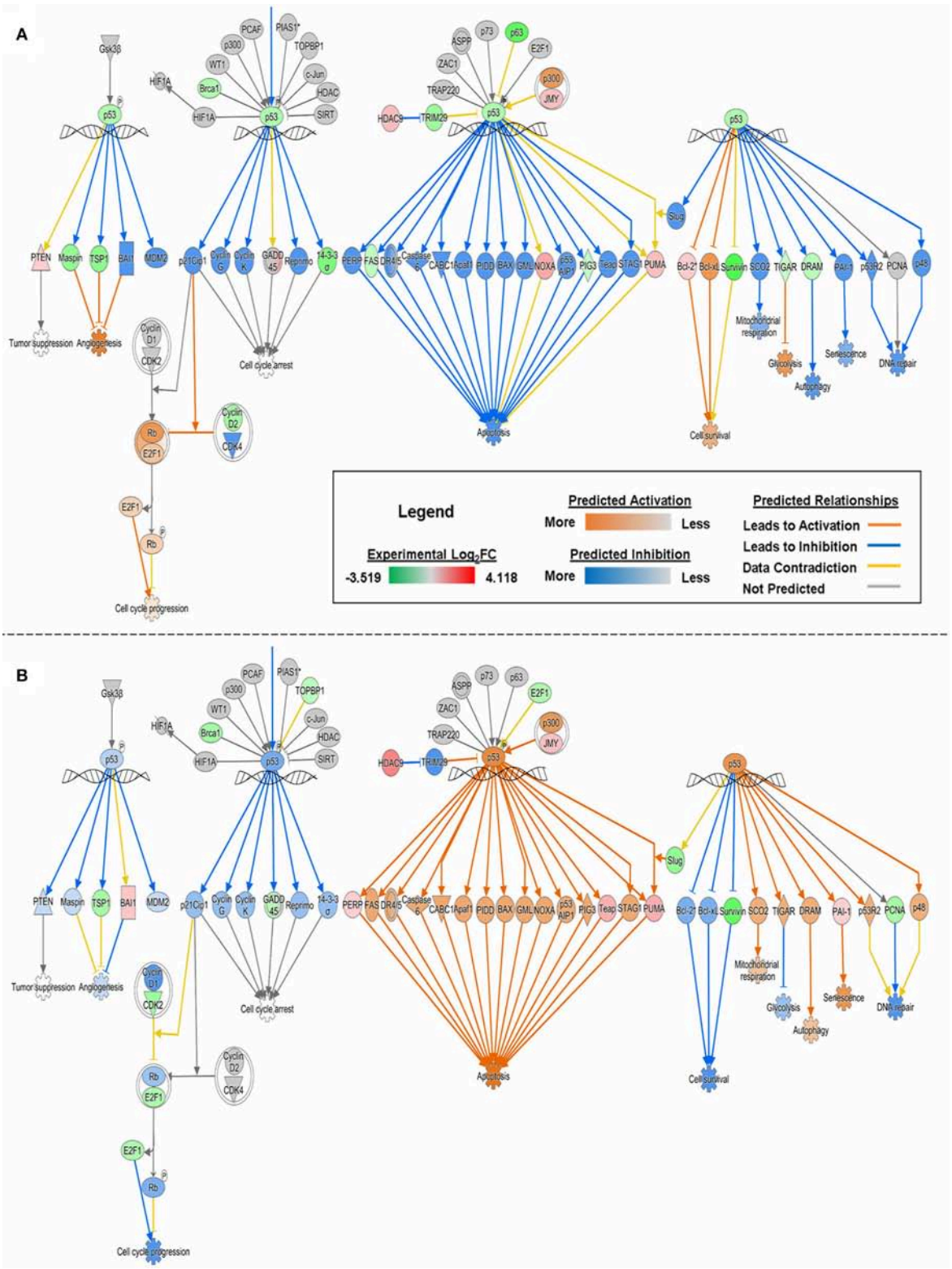

FIGURE 3 | MAP of "p53 Signaling" pathway in **(A)** HSAEC and **(B)** A549 cells treated with 1 μM PG over 24 h. Predictions were calculated based upon DEGs from the experimental dataset overlaid onto the Ingenuity Knowledge Base in IPA. Orange, blue, yellow, and gray lines corresponds to predicted activation, inhibition, contradiction, and the inability to predict an outcome, respectively. Red or green color intensities within shapes reflect the level of upregulation or downregulation, respectively, based upon the experimental Log2FC values. Orange or blue color intensities within shapes reflect the level of predicted activation or inhibition, respectively, based on upon IPA's predictions.

(**Tables 2**, **3**). In fact, the downregulation of *ANGPTL4* suggests an active catabolism of lipoproteins. Secondly, although *WIPI1* was upregulated, it was much lesser than A549, possibly reflecting a weaker autophagic status in HSAEC. Thirdly, the near-normal expression of *H2AFX* suggests that HSAEC may be able to overcome PG's genotoxic stress. However, how this could be possible despite *BRCA1* downregulation (**Figure 3**) and potential BRCA1 pathway inactivation (**Table 3**) is unclear. Fourth, a deep analysis of HSAEC-specific genes perturbed by PG revealed a "balancing act" expression of pro-cancer and anti-cancer genes (**Table 1**). This could potentially assist in HSAEC's viability under PG treatment. Lastly, and surprisingly, *MCM10* and *DSCC1* were found severely downregulated in HSAEC. As PG could inhibit topoisomerases (53), another potential means of PG genotoxicity could be mitigated here as the loss of MCM10 does not permit DNA to unwind for replication (48). Altogether, we suspect that HSAEC may have been conferred protection to PG through DNA replication inhibition, BRCA1-independent DNA repair availability and autophagic resistance.

PG's upregulation of cholesterol pathways in cancer cells and its ability to potentially inhibit DNA replication brings about two immediate concerns that should be addressed in future studies. Firstly, the degree of which PG could inhibit DNA replication in HSAEC should be monitored with cell growth rate compared to A549 and other rapidly dividing cells. This would elucidate the potential clinical benefits PG has over other conventional chemotherapeutics that falls short in protecting rapidly dividing healthy cells. Secondly, the impact of PG treatment with regards to hypercholesterolemia should be assessed *in vivo*. On the other hand, further studies on *MIR210HG,* the second most differentially expressed gene in both A549 and HCT116 (**Table 2**) could potentially highlight novel insights with regards to PG's cancer-specific mechanisms of action. To further improve PG's cancer specificity, chemical modifications may be explored to acquire novel PG analogs or develop targeted drug delivery strategies which studies have already begun (81, 82).

CONCLUSION

Numerous decades of cancer research, drug discovery, and development have led to major improvements in patients' quality of life. Research into systemic therapies for metastatic cancers continues at two major fronts, namely, safety and efficacy. PG appears to be a promising smart chemotherapeutic agent against NSCLC. PG not only demonstrated heightened anti-cancer activity against A549, but this activity was also cancer-specific. Understanding how such an agent differentiates cancerous from healthy cells has been unclear until recently. With RNA-sequencing, a next-generation tool for transcriptomics, we managed to unravel PG's potential cancer-specific mechanisms of action. Through an exogenous cholesterol supply cut-off and an internal overactivation of cholesterol synthesis, PG might have induced cancer cell autophagy to a point whereby self-cannibalization led to cell death. At the same time, through balancing the overexpression of oncogenic and tumor-suppressive genes, healthy cells might have been conferred a heightened survival status by PG. By exposing A549 transcriptome landscape perturbed by PG, we can now conduct further experiments with single or multiplexed knock-outs and knock-downs using CRISPR to yield definitive targets which could aid the development of precision medicine against NSCLC.

AUTHOR CONTRIBUTIONS

BD performed the cell cultures, cytotoxicity assays, RNA extraction, RNA purification, RNA-sequencing data processing in CLC Workbench, and the data analysis in IPA. JN repeated the RNA extraction throughout data analysis in IPA and reproduced the data. LL, QX, and LY conceptualized the study idea and provided material and technical support. BD and LL wrote the manuscript. BD, JN, QX, LL, and LY revised the manuscript.

FUNDING

This work was supported by the National Research Foundation and Ministry of Education Singapore under its Research Centre of Excellence Program (SCELSE), AcRF Tier 2 (MOE2016-T2-1-010) from the Ministry of Education, Singapore and The Marine Science Research and Development Programme (MSRDP-P34) from National Research Foundation, Singapore.

SUPPLEMENTARY MATERIAL

The Supplementary Material for this article can be found online at: https://www.frontiersin.org/articles/10.3389/fonc.2018.00573/full#supplementary-material

REFERENCES

1. Ma X, Yu H. Global burden of cancer. *Yale J Biol Med.* (2006) 79:85–94.
2. Rahib L, Smith BD, Aizenberg R, Rosenzweig AB, Fleshman JM, Matrisian LM. Projecting cancer incidence and deaths to 2030: the unexpected burden of thyroid, liver, and pancreas cancers in the United States. *Cancer Res* (2014) 74:2913–21. doi: 10.1158/0008-5472.Can-14-0155
3. Fidler MM, Bray F, Soerjomataram I. The global cancer burden and human development: a review. *Scand J Public Health* (2018) 46:27–36. doi: 10.1177/1403494817715400
4. Global Burden of Disease Cancer Collaboration. Global, regional, and national cancer incidence, mortality, years of life lost, years lived with disability, and disability-adjusted life-years for 32 cancer groups, 1990 to 2015: a systematic analysis for the global burden of disease study. *JAMA Oncol.* (2017) 3:524–48. doi: 10.1001/jamaoncol.2016.5688
5. World Health Organization. *Cancer key facts [Online]*. (2018). Available online at: http://www.who.int/news-room/fact-sheets/detail/cancer (Accessed 24 May 2018).
6. Herbst RS, Heymach JV, Lippman SM. Lung cancer. *N Engl J Med.* (2008) 359:1367–80. doi: 10.1056/NEJMra0802714
7. Morgensztern D, Ng SH, Gao F, Govindan R. Trends in stage distribution for patients with non-small cell lung cancer: a national cancer database survey. *J Thoracic Oncol.* (2010) 5:29–33. doi: 10.1097/JTO.0b013e3181c5920c
8. Baudino TA. Targeted cancer therapy: the next generation of cancer treatment. *Curr Drug Discov Technol* (2015) 12:3–20. doi: 10.2174/1570163812666150602144310

9. Huang M, Shen A, Ding J, Geng M. Molecularly targeted cancer therapy: some lessons from the past decade. *Trends Pharmacol Sci.* (2014) 35:41–50. doi: 10.1016/j.tips.2013.11.004
10. Kumar A, Petri ET, Halmos B, Boggon TJ. Structure and clinical relevance of the epidermal growth factor receptor in human cancer. *J Clin Oncol.* (2008) 26:1742–51. doi: 10.1200/JCO.2007.12.1178
11. Lynch TJ, Bell DW, Sordella R, Gurubhagavatula S, Okimoto RA, Brannigan BW, et al. Activating mutations in the epidermal growth factor receptor underlying responsiveness of non-small-cell lung cancer to gefitinib. *N Engl J Med.* (2004) 350:2129–39. doi: 10.1056/NEJMoa040938
12. Maemondo M, Inoue A, Kobayashi K, Sugawara S, Oizumi S, Isobe H, et al. Gefitinib or chemotherapy for non–small-cell lung cancer with mutated EGFR. *N Engl J Med.* (2010) 362:2380–8. doi: 10.1056/NEJMoa0909530
13. Morgillo F, Della Corte CM, Fasano M, Ciardiello F. Mechanisms of resistance to EGFR-targeted drugs: lung cancer. *ESMO Open* (2016) 1:e000060. doi: 10.1136/esmoopen-2016-000060
14. Rosell R, Moran T, Queralt C, Porta R, Cardenal F, Camps C, et al. Screening for epidermal growth factor receptor mutations in lung cancer. *N Engl J Med.* (2009) 361:958–67. doi: 10.1056/NEJMoa0904554
15. Shi Y, Au JS-K, Thongprasert S, Srinivasan S, Tsai C-M, Khoa MT, et al. A prospective, molecular epidemiology study of EGFR mutations in asian patients with advanced non-small-cell lung cancer of adenocarcinoma histology (PIONEER). *J Thoracic Oncol.* (2014) 9:154–62. doi: 10.1097/JTO.0000000000000033
16. Farkona S, Diamandis EP, Blasutig IM. Cancer immunotherapy: the beginning of the end of cancer? *BMC Med.* (2016) 14:73. doi: 10.1186/s12916-016-0623-5
17. Restifo NP, Marincola FM, Kawakami Y, Taubenberger J, Yannelli JR, Rosenberg SA. Loss of functional beta 2-microglobulin in metastatic melanomas from five patients receiving immunotherapy. *J Natl Cancer Inst.* (1996) 88:100–8.
18. Shukla SA, Rooney MS, Rajasagi M, Tiao G, Dixon PM, Lawrence MS, et al. Comprehensive analysis of cancer-associated somatic mutations in class I HLA genes. *Nat Biotechnol.* (2015) 33:1152–8. doi: 10.1038/nbt.3344
19. Anagnostou V, Smith KN, Forde PM, Niknafs N, Bhattacharya R, White J, et al. Evolution of neoantigen landscape during immune checkpoint blockade in non-small cell lung cancer. *Cancer Discov.* (2017) 7:264–76. doi: 10.1158/2159-8290.Cd-16-0828
20. Finn, O. J. (2012). Immuno-oncology: understanding the function and dysfunction of the immune system in cancer. *Ann Oncol.* 23(suppl_8):viii6–9. doi: 10.1093/annonc/mds256
21. Juneja VR, McGuire KA, Manguso RT, LaFleur MW, Collins N, Haining WN, et al. PD-L1 on tumor cells is sufficient for immune evasion in immunogenic tumors and inhibits CD8 T cell cytotoxicity. *J Exp Med.* (2017) 214:895–904. doi: 10.1084/jem.20160801
22. Borghaei H, Paz-Ares L, Horn L, Spigel DR, Steins M, Ready NE, et al. Nivolumab versus docetaxel in advanced nonsquamous non–small-cell lung cancer. *N Engl J Med.* (2015) 373:1627–39. doi: 10.1056/NEJMoa1507643
23. Garon EB, Rizvi NA, Hui R, Leighl N, Balmanoukian AS, Eder JP, et al. Pembrolizumab for the treatment of non–small-cell lung cancer. *N Engl J Med.* (2015) 372:2018–28. doi: 10.1056/NEJMoa1501824
24. Rizvi NA, Hellmann MD, Snyder A, Kvistborg P, Makarov V, Havel JJ, et al. Mutational landscape determines sensitivity to PD-1 blockade in non–small cell lung cancer. *Science* (2015) 348:124–8. doi: 10.1126/science.aaa1348
25. Topalian SL, Hodi FS, Brahmer JR, Gettinger SN, Smith DC, McDermott DF, et al. Safety, activity, and immune correlates of anti-PD-1 antibody in cancer. *N Engl J Med.* (2012) 366:2443–54. doi: 10.1056/NEJMoa1200690
26. American Cancer Society. *"Cancer Treatment & Survivorship Facts & Figures 2016-2017".* Atlanta, GA: American Cancer Society (2016). Available online at: https://www.cancer.org/research/cancer-facts-statistics/survivor-facts-figures.html
27. Socinski MA, Bondarenko I, Karaseva NA, Makhson AM, Vynnychenko I, Okamoto I, et al. Weekly nab-paclitaxel in combination with carboplatin versus solvent-based paclitaxel plus carboplatin as first-line therapy in patients with advanced non–small-cell lung cancer: final results of a phase III trial. *J Clin Oncol.* (2012) 30:2055–62. doi: 10.1200/JCO.2011.39.5848
28. Patel JD, Socinski MA, Garon EB, Reynolds CH, Spigel DR, Olsen MR, et al. PointBreak: a randomized phase III study of pemetrexed plus carboplatin and bevacizumab followed by maintenance pemetrexed and bevacizumab versus paclitaxel plus carboplatin and bevacizumab followed by maintenance bevacizumab in patients with stage IIIB or IV nonsquamous non–small-cell lung cancer. *J Clin Oncol.* (2013) 31:4349–57. doi: 10.1200/JCO.2012.47.9626
29. Rajeswaran A, Trojan A, Burnand B, Giannelli M. Efficacy and side effects of cisplatin- and carboplatin-based doublet chemotherapeutic regimens versus non-platinum-based doublet chemotherapeutic regimens as first line treatment of metastatic non-small cell lung carcinoma: a systematic review of randomized controlled trials. *Lung Cancer* (2008) 59:1–11. doi: 10.1016/j.lungcan.2007.07.012
30. Feng L-X, Li M, Liu Y-J, Yang S-M, Zhang N. Synergistic enhancement of cancer therapy using a combination of ceramide and docetaxel. *Int J Mol Sci.* (2014) 15:4201–20. doi: 10.3390/ijms15034201
31. Garon EB, Neidhart JD, Gabrail NY, de Oliveira MR, Balkissoon J, Kabbinavar F. A randomized Phase II trial of the tumor vascular disrupting agent CA4P (fosbretabulin tromethamine) with carboplatin, paclitaxel, and bevacizumab in advanced nonsquamous non-small-cell lung cancer. *OncoTargets Ther.* (2016) 9:7275–83. doi: 10.2147/OTT.S109186
32. Yan X, Ge H, Huang T, Hindra, Yang, D., Teng, Q., et al. (2016). Strain prioritization and genome mining for enediyne natural products. *MBio* 7:6. doi: 10.1128/mBio.02104-16
33. Wang S, Gao A, Liu J, Sun Y. First-line therapy for advanced non-small cell lung cancer with activating EGFR mutation: is combined EGFR-TKIs and chemotherapy a better choice? *Cancer Chemother Pharmacol.* (2018) 81:443–53. doi: 10.1007/s00280-017-3516-1
34. Schiller JH. Current standards of care in small-cell and non-small-cell lung cancer. *Oncology* (2001) 61(Suppl 1):3–13. doi: 10.1159/000055386
35. Huang CY, Ju DT, Chang CF, Muralidhar Reddy P, Velmurugan BK. A review on the effects of current chemotherapy drugs and natural agents in treating non-small cell lung cancer. *Biomedicine* (2017) 7:23. doi: 10.1051/bmdcn/2017070423
36. Hsieh H-Y, Shieh J-J, Chen C-J, Pan M-Y, Yang S-Y, Lin S-C, et al. Prodigiosin down-regulates SKP2 to induce p27(KIP1) stabilization and antiproliferation in human lung adenocarcinoma cells. *Br J Pharmacol.* (2012) 166:2095–108. doi: 10.1111/j.1476-5381.2012.01921.x
37. Montaner B, Pérez-Tomás R. Prodigiosin-induced apoptosis in human colon cancer cells. *Life Sci.* (2001) 68:2025–36. doi: 10.1016/S0024-3205(01)01002-5
38. Hassankhani R, Sam MR, Esmaeilou M, Ahangar P. Prodigiosin isolated from cell wall of Serratia marcescens alters expression of apoptosis-related genes and increases apoptosis in colorectal cancer cells. *Med Oncol.* (2015) 32:366. doi: 10.1007/s12032-014-0366-0
39. Cheng MF, Lin CS, Chen YH, Sung PJ, Lin SR, Tong YW, et al. Inhibitory growth of oral squamous cell carcinoma cancer via bacterial prodigiosin. *Mar Drugs* (2017) 15:7. doi: 10.3390/md15070224
40. Yenkejeh RA, Sam MR, Esmaeillou M. Targeting survivin with prodigiosin isolated from cell wall of Serratia marcescens induces apoptosis in hepatocellular carcinoma cells. *Hum Exp Toxicol.* (2017) 36:402–11. doi: 10.1177/0960327116651122
41. Soto-Cerrato V, Llagostera E, Montaner B, Scheffer GL, Perez-Tomas R. Mitochondria-mediated apoptosis operating irrespective of multidrug resistance in breast cancer cells by the anticancer agent prodigiosin. *Biochem Pharmacol.* (2004) 68:1345–52. doi: 10.1016/j.bcp.2004.05.056
42. Sam MR, Pourpak RS. Regulation of p53 and survivin by prodigiosin compound derived from Serratia marcescens contribute to caspase-3-dependent apoptosis in acute lymphoblastic leukemia cells. *Hum Exp Toxicol.* (2017) 2017:960327117718052. doi: 10.1177/0960327117718052
43. Montaner B, Navarro S, Pique M, Vilaseca M, Martinell M, Giralt E, et al. Prodigiosin from the supernatant of Serratia marcescens induces apoptosis in haematopoietic cancer cell lines. *Br J Pharmacol.* (2000) 131:585–93. doi: 10.1038/sj.bjp.0703614
44. Soto-Cerrato V, Vinals F, Lambert JR, Kelly JA, Perez-Tomas R. Prodigiosin induces the proapoptotic gene NAG-1 via glycogen synthase kinase-3beta activity in human breast cancer cells. *Mol Cancer Ther.* (2007) 6:362–9. doi: 10.1158/1535-7163.Mct-06-0266
45. Cumming G, Fidler F, Vaux DL. Error bars in experimental biology. *J Cell Biol.* (2007) 177:7. doi: 10.1083/jcb.200611141
46. Herbst RS, Morgensztern D, Boshoff C. The biology and management of non-small cell lung cancer. *Nature* (2018) 553:446. doi: 10.1038/nature25183

47. Zhao S, Fung-Leung W-P, Bittner A, Ngo K, Liu X. Comparison of RNA-Seq and microarray in transcriptome profiling of activated T cells. *PLoS ONE* (2014) 9:e78644. doi: 10.1371/journal.pone.0078644
48. Thu YM, Bielinsky A-K. MCM10: one tool for all—integrity, maintenance and damage control. *Semin Cell Dev Biol.* (2014) 30:121–30. doi: 10.1016/j.semcdb.2014.03.017
49. Bermudez VP, Maniwa Y, Tappin I, Ozato K, Yokomori K, Hurwitz J. The alternative Ctf18-Dcc1-Ctf8-replication factor C complex required for sister chromatid cohesion loads proliferating cell nuclear antigen onto DNA. *Proc Natl Acad Sci.* (2003) 100:10237–42. doi: 10.1073/pnas.1434308100
50. Bowman GD, O'Donnell M, Kuriyan J. Structural analysis of a eukaryotic sliding DNA clamp–clamp loader complex. *Nature* (2004) 429:724. doi: 10.1038/nature02585
51. Srivastava N, Gochhait S, de Boer P, Bamezai RNK. Role of H2AX in DNA damage response and human cancers. *Mutat Res Rev.* (2009) 681:180–8. doi: 10.1016/j.mrrev.2008.08.003
52. Melvin MS, Tomlinson JT, Saluta GR, Kucera GL, Lindquist N, Manderville RA. Double-strand DNA cleavage by copper·prodigiosin. *J Am Chem Soc.* (2000) 122:6333–4. doi: 10.1021/ja0000798
53. Montaner B, Castillo-Avila W, Martinell M, Ollinger R, Aymami J, Giralt E, et al. DNA interaction and dual topoisomerase I and II inhibition properties of the anti-tumor drug prodigiosin. *Toxicol Sci.* (2005) 85:870–9. doi: 10.1093/toxsci/kfi149
54. Hakem R. DNA-damage repair; the good, the bad, and the ugly. *Embo J.* (2008) 27:589–605. doi: 10.1038/emboj.2008.15
55. Lal A, Pan Y, Navarro F, Dykxhoorn DM, Moreau L, Meire E, et al. miR-24-mediated down-regulation of H2AX suppresses DNA repair in terminally differentiated blood cells. *Nat Struct Mol Biol.* (2009) 16:492–8. doi: 10.1038/nsmb.1589
56. Atsumi Y, Inase A, Osawa T, Sugihara E, Sakasai R, Fujimori H, et al. The Arf/p53 protein module, which induces apoptosis, down-regulates histone H2AX to allow normal cells to survive in the presence of anti-cancer drugs. *J Biol Chem.* (2013) 288:13269–77. doi: 10.1074/jbc.M112.402560
57. Jongen JMJ, van der Waals LM, Trumpi K, Laoukili J, Peters NA, Schenning-van Schelven SJ, et al. Downregulation of DNA repair proteins and increased DNA damage in hypoxic colon cancer cells is a therapeutically exploitable vulnerability. *Oncotarget* (2017) 8:86296–311. doi: 10.18632/oncotarget.21145
58. Ward PS, Thompson CB. Metabolic reprogramming: a cancer hallmark even warburg did not anticipate. *Cancer Cell* (2012) 21:297–308. doi: 10.1016/j.ccr.2012.02.014
59. Pavlova NN, Thompson CB. The emerging hallmarks of cancer metabolism. *Cell Metab.* (2016) 23:27–47. doi: 10.1016/j.cmet.2015.12.006
60. Beloribi-Djefaflia S, Vasseur S, Guillaumond F. Lipid metabolic reprogramming in cancer cells. *Oncogenesis* (2016) 5:e189. doi: 10.1038/oncsis.2015.49
61. Liu Q, Luo Q, Halim A, Song G. Targeting lipid metabolism of cancer cells: a promising therapeutic strategy for cancer. *Cancer Lett.* (2017) 401:39–45. doi: 10.1016/j.canlet.2017.05.002
62. Luo X, Cheng C, Tan Z, Li N, Tang M, Yang L, et al. Emerging roles of lipid metabolism in cancer metastasis. *Molecular Cancer* (2017) 16:76. doi: 10.1186/s12943-017-0646-3
63. Lim H, Lim Y-M, Kim KH, Jeon YE, Park K, Kim J, et al. A novel autophagy enhancer as a therapeutic agent against metabolic syndrome and diabetes. *Nat Commun.* (2018) 9:1438. doi: 10.1038/s41467-018-03939-w
64. Nassoury N, Blasiole DA, Tebon Oler A, Benjannet S, Hamelin J, Poupon V, et al. The cellular *traffi*cking of the secretory proprotein convertase PCSK9 and its dependence on the LDLR. *Traffic* (2007) 8:718–32. doi: 10.1111/j.1600-0854.2007.00562.x
65. Zhang DW, Lagace TA, Garuti R, Zhao Z, McDonald M, Horton JD, et al. Binding of proprotein convertase subtilisin/kexin type 9 to epidermal growth factor-like repeat A of low density lipoprotein receptor decreases receptor recycling and increases degradation. *J Biol Chem.* (2007) 282:18602–12. doi: 10.1074/jbc.M702027200
66. Pietiainen V, Vassilev B, Blom T, Wang W, Nelson J, Bittman R, et al. NDRG1 functions in LDL receptor trafficking by regulating endosomal recycling and degradation. *J Cell Sci.* (2013) 126(Pt 17):3961–71. doi: 10.1242/jcs.128132
67. Olivecrona G. Role of lipoprotein lipase in lipid metabolism. *Curr Opin Lipidol.* (2016) 27:233–41. doi: 10.1097/mol.0000000000000297
68. Zhu YM, Webster SJ, Flower D, Woll PJ. Interleukin-8/CXCL8 is a growth factor for human lung cancer cells. *Br J Cancer* (2004) 91:1970. doi: 10.1038/sj.bjc.6602227
69. Liu Q, Li A, Tian Y, Wu JD, Liu Y, Li T, et al. The CXCL8-CXCR1/2 pathways in cancer. *Cytokine Growth Factor Rev.* (2016) 31:61–71. doi: 10.1016/j.cytogfr.2016.08.002
70. He M, Zhang W, Dong Y, Wang L, Fang T, Tang W, et al. Pro-inflammation NF-κB signaling triggers a positive feedback via enhancing cholesterol accumulation in liver cancer cells. *J Exp Clin Cancer Res.* (2017) 36:15. doi: 10.1186/s13046-017-0490-8
71. Yang Y-F, Jan Y-H, Liu Y-P, Yang C-J, Su C-Y, Chang Y-C, et al. Squalene synthase induces tumor necrosis factor receptor 1 enrichment in lipid rafts to promote lung cancer metastasis. *Am J Resp Critic Care Med.* (2014) 190:675–87. doi: 10.1164/rccm.201404-0714OC
72. Simigdala N, Gao Q, Pancholi S, Roberg-Larsen H, Zvelebil M, Ribas R, et al. Cholesterol biosynthesis pathway as a novel mechanism of resistance to estrogen deprivation in estrogen receptor-positive breast cancer. *Breast Cancer Res.* (2016) 18:58. doi: 10.1186/s13058-016-0713-5
73. Selwan EM, Finicle BT, Kim SM, Edinger AL. Attacking the supply wagons to starve cancer cells to death. *FEBS Lett.* (2016) 590:885–907. doi: 10.1002/1873-3468.12121
74. Mathew R, Karantza-Wadsworth V, White E. Role of autophagy in cancer. *Nat Rev Cancer* (2007) 7:961. doi: 10.1038/nrc2254
75. Proikas-Cezanne T, Waddell S, Gaugel A, Frickey T, Lupas A, Nordheim A. WIPI-1alpha (WIPI49), a member of the novel 7-bladed WIPI protein family, is aberrantly expressed in human cancer and is linked to starvation-induced autophagy. *Oncogene* (2004) 23:9314–25. doi: 10.1038/sj.onc.1208331
76. Choi KS. Autophagy and cancer. *Exp Mol Med.* (2012) 44:109. doi: 10.3858/emm.2012.44.2.033
77. Espona-Fiedler M, Soto-Cerrato V, Hosseini A, Lizcano JM, Guallar V, Quesada R, et al. Identification of dual mTORC1 and mTORC2 inhibitors in melanoma cells: prodigiosin vs. obatoclax. *Biochem Pharmacol.* (2012) 83:489–96. doi: 10.1016/j.bcp.2011.11.027
78. Cheng S-Y, Chen N-F, Kuo H-M, Yang S-N, Sung C-S, Sung P-J, et al. Prodigiosin stimulates endoplasmic reticulum stress and induces autophagic cell death in glioblastoma cells. *Apoptosis* (2018) 23:314–28. doi: 10.1007/s10495-018-1456-9
79. Tsuyuki S, Takabayashi M, Kawazu M, Kudo K, Watanabe A, Nagata Y, et al. Detection of WIPI1 mRNA as an indicator of autophagosome formation. *Autophagy* (2014) 10:497–513. doi: 10.4161/auto.27419
80. Proikas-Cezanne T, Takacs Z, Donnes P, Kohlbacher O. WIPI proteins: essential PtdIns3P effectors at the nascent autophagosome. *J Cell Sci.* (2015) 128:207–17. doi: 10.1242/jcs.146258
81. Dozie-Nwachukwu SO, Danyuo Y, Obayemi JD, Odusanya OS, Malatesta K, Soboyejo WO. Extraction and encapsulation of prodigiosin in chitosan microspheres for targeted drug delivery. *Mater Sci Eng C Mater Biol Appl.* (2017) 71:268–78. doi: 10.1016/j.msec.2016.09.078
82. Dozie-Nwachukwu SO, Obayemi JD, Danyuo Y, Anuku N, Odusanya OS, Malatesta K, et al. A comparative study of the adhesion of biosynthesized gold and conjugated gold/prodigiosin nanoparticles to triple negative breast cancer cells. *J Mater Sci Mater Med.* (2017) 28:143. doi: 10.1007/s10856-017-5943-2

Conflict of Interest Statement: The authors declare that the research was conducted in the absence of any commercial or financial relationships that could be construed as a potential conflict of interest.

frontiers in Oncology

MINI REVIEW
published: 07 December 2018
doi: 10.3389/fonc.2018.00598

Curaxin CBL0137 Exerts Anticancer Activity via Diverse Mechanisms

Ming-Zhu Jin[1†], *Bai-Rong Xia*[2†], *Yu Xu*[1] *and Wei-Lin Jin*[3,4,5*]

[1] Shanghai Jiao Tong University School of Medicine, Shanghai, China, [2] Department of Gynecology, The Affiliated Tumor Hospital, Harbin Medical University, Harbin, China, [3] Key Laboratory for Thin Film and Microfabrication Technology of Ministry of Education, Department of Instrument Science and Engineering, Shanghai Engineering Center for Intelligent Diagnosis and Treatment Instrument, School of Electronic Information and Electronic Engineering, Institute of Nano Biomedicine and Engineering, Shanghai Jiao Tong University, Shanghai, China, [4] National Center for Translational Medicine, Collaborative Innovational Center for System Biology, Shanghai Jiao Tong University, Shanghai, China, [5] Shaanxi Key Laboratory of Brain Disorders and Institute of Basic and Translational Medicine, Xi'an Medical University, Xi'an, China

Chemotherapy with or without radiation remains the first choice for most cancers. However, intolerant side effects and conventional drug resistance restrict actual clinical efficacy. Curaxin CBL0137 is designed to regulate p53 and nuclear factor-κB simultaneously and to prevent the resistance caused by a single target. Functionally, CBL0137 exhibits an antitumor activity in multiple cancers, including glioblastoma, renal cell carcinoma, melanoma, neuroblastoma, and small cell lung cancer (SCLC). Mechanistically, CBL0137 is originally identified to act by facilitates chromatin transcription (FACT) complex. Further investigations reveal that several pathways, such as NOTCH1 and heat shock factor 1 (HSF1), are involved in the process. CBL0137 has been reported to target cancer stem cells (CSCs) and enhance chemotherapy/monotherapy efficacy. The translational advance of CBL0137 into clinical practice is expected to provide a promising future for cancer treatment.

Keywords: cancer stem cells, CBL0137, chemotherapy, facilitates chromatin transcription, p53

OPEN ACCESS

Edited by:
Zhe-Sheng Chen,
St. John's University, United States

Reviewed by:
Ho Sup Yoon,
Nanyang Technological University, Singapore
Jihong Zhang,
Kunming University of Science and Technology, China
Chao Yan,
Nanjing University, China

***Correspondence:**
Wei-Lin Jin
weilinjin@yahoo.com;
weilinjin@sjtu.edu.cn

[†]*These authors have contributed equally to this work*

Specialty section:
This article was submitted to Cancer Molecular Targets and Therapeutics, a section of the journal Frontiers in Oncology

Received: *24 September 2018*
Accepted: *26 November 2018*
Published: *07 December 2018*

Citation:
Jin M-Z, Xia B-R, Xu Y and Jin W-L (2018) Curaxin CBL0137 Exerts Anticancer Activity via Diverse Mechanisms. Front. Oncol. 8:598. doi: 10.3389/fonc.2018.00598

INTRODUCTION

Cancer harbors several characteristics, including high heterogeneity, diverse gene mutation, or rapid progression; consequently, treating cancer is difficult, and it easily relapses. Remarkable achievements have been observed in treatment approaches, including surgery, radiotherapy, chemotherapy, immunotherapy, and targeted therapy. In particular, targeted therapies, such as HER2 inhibitor lapatinib, EGFR inhibitor erlotinib, BRAF inhibitor dabrafenib, promote treatment (1). However, we have failed to treat cancer. Malignancies, such as glioblastoma, are quite invasive and cannot be entirely removed by surgery. Chemotherapy is hindered by innate and acquired chemoresistance.

Originally, antimalarial agents, including quinacrine, can activate p53 and inhibit nuclear factor-κB (NF-κB) simultaneously (2, 3). These drugs have been used as a reference of curaxins, undergoing some structural changes but maintaining similar functions (2, 4). As a second-generation curaxin, CBL0137 satisfies the requirements for a drug design, that is, full efficacy while inducing the least adverse effects. Further research suggested that CBL0137 exerts an antitumor activity through multiple targets, including facilitates chromatin transcription (FACT), NOTCH1, and heat shock factor 1 (HSF1), in various cancers (**Table 1**). At present, CBL0137 in patients with hematological malignancies (ClinicalTrials.gov Identifier: NCT02931110) and solid tumors are under phase I clinical trials (ClinicalTrials.gov Identifier: NCT01905228). In this review, we

summarized the design of CBL0137, highlighted its antitumor mechanisms through multiple targets, and proposed its potential for clinical applications, especially as a combination drug.

CBL0137: A SECOND-GENERATION CURAXIN

Small molecular inhibitor CBL0137 [1,1′-(9-(2-(isopropylamino)ethyl)-9H-carbazole-3,6-diyl)bis(ethan-1-one) (IUPAC/chemical name)] is a second-generation curaxin. Dermawan et al. (12) found that quinacrine (CBLC-102), a first-generation curaxin, can overcome erlotinib resistance through preconceived mechanisms in non-small cell lung cancer (12). Similar results are also observed in ovarian (13) and breast (14) cancers. Second-generation curaxins, such as CBLC-000, CBLC-100, and CBLC-137 (CBL0137), have more exact targets than first-generation curaxins, such as quinacrine (CBLC-102). In particular, CBL0137 is water soluble because of its chemical structure and better tolerated in mice than other members of curaxins, showing great potential for cancer treatment (2). In addition to the two targets, namely, p53 and NF-κB, CBL0137 can intercalate DNA through FACT without causing any DNA damage or genotoxicity (2, 7, 15), and more targets are under investigation.

FACT: A CORE TARGET FOR CBL0137

FACT, a histone chaperone, contains two subunits of the suppressor of Ty 16 (SPT16) and structure-specific recognition protein 1 (SSRP1), which participates in DNA replication, transcription, repair, mitosis, and cell fate reprogramming (16–18). SPT16 remodels the histone structure after transcription, and SSRP1 recognizes nucleosomes with its high-mobility group (HMG)-1 domain (19, 20). SSRP1 is considered more like a target since it's more amplified in cancers at mRNA and protein levels. FACT is involved in the poor prognosis, malignant transformation, tumorigenesis, and aggressiveness of cancers (9, 16, 21–23). It can recognize the formation of alternative DNA structures and promote the activation of p53 to prevent DNA damage (24); thus FACT is regarded as a sensor for genome instability and mutation, which is one of the ten hallmarks of cancer treatment (24, 25) (**Figure 1**). It is highly expressed in cancer including glioblastoma (GBM) (6), breast cancer (16), and hepatocellular carcinoma (21), but is poor expressed in normal tissues or well-differentiated cells (26).

CBL0137, chemotherapeutic agents, UV radiation, oxygen-free radicals, and hypoxia stress can affect p53 activation (7, 27, 28). With Western Blot analysis, Gasparian et al. (7) have revealed that CBL0137 activates p53 through posttranslational modifications at serine 392 (Ser^{392}) rather than serine 15 (Ser^{15}), which involves casein kinase 2 (CK2) inhibition (7). Previous studies showed that CK2-induced p53 phosphorylation involves FACT. FACT, SPT16, and SSRP1 subunits, can bind to CK2 after CBL0137 is administered, and the SPT16-SSRP1-CK2 complex phosphorylates p53 at Ser^{392} and promotes p53 activation (2, 27) (**Figure 1**). Activated p53 induces apoptosis, promotes DNA repair, and inhibits tumor growth. Extensive evidence has also demonstrated that FACT can promote tumor growth, inhibit apoptosis or cell differentiation and induce cell proliferations through the regulation of multiple genes including TP53, MYC, NF-κB, OCT1, and HSF1 (23) (**Figure 1**).

FACT has recently been reported to correlate with the expression of cancer stem cell (CSC) markers, such as SOX2, OCT4, OLIG2, and NANOG in an adult GBM model. The transcriptional knockdown of FACT or its inhibition with a small molecule (CBL0137) reduces the expression of these genes (5).

CBL0137 EXERTS ANTITUMOR ACTIVITY BY INCREASING P53 AND DECREASING NF-κB SIMULTANEOUSLY

p53 is a classic tumor suppressor protein responsible for the prevention of oncogenic mutation accumulation, tumorigenesis and tumor progression (29). p53 mutation or inactivation is quite common in many cancers (30). p53 activities are regulated by diverse post-translational modifications such as Ser^{15} and Ser^{392} phosphorylation or lysine 382 acetylation and methylation (7, 31). NF-κB is a critical transcription factor in antiapoptosis and cell proliferation, which is activated in inflammation and cancers (32). CBL0137 is originally designed to activate p53 and inhibit NF-κB simultaneously to achieve an enhanced efficacy with modest toxicity (7).

The *in vitro* and *in vivo* experiments of CBL0137 have confirmed the issue. For example, a research on renal cell carcinoma has suggested that CBL0137 intercalates DNA and traps FACT, thereby leading to NF-κB inhibition. FACT binds to CK2 to form a complex, which further induces Ser^{392} phosphorylation of p53; otherwise, p53 is degraded by MDM2 (2, 7, 33) (**Figure 1**). Meanwhile, NF-κB is inhibited by the complex (6). Similar results have been shown in GBM research, temozolomide (TMZ)-resistant A1207, TMZ-responsive U87MG cell lines, and orthotopic model. CBL0137 prolongs the survival of orthotopic A1207 and U87MG models, though it is less effective than TMZ in the latter. Furthermore, 0.6 and 2.0 μM CBL0137 can increase p53 significantly in cell lines. These studies have exhibited the antitumor activity of CBL0137 by targeting p53 and NF-κB, which are the two most common transcription factors in oncogenic and tumor suppressor pathways.

CBL0137 INHIBITS THE SELF-RENEWAL OF CANCER STEM CELLS/TUMOR-INITIATING CELLS THROUGH NOTCH1 ACTIVATION

Therapeutic resistance is a complex phenomenon in cancer treatment, though many mechanisms have been proposed. "The bad seed" CSCs can explain the consequence to some degree (34). Conventional therapies that do not target CSCs may encounter cancer recurrence because CSCs can undergo self-renewal and differentiation (35). Dermawan et al. investigated CBL0137 in GBM and focused on cancer stem-like cells by using CD133 as

TABLE 1 | Targets and induced effects of CBL0137 reported in cancer research.

Indications	Targets	Effects	Experiment models	References
Glioblastoma	SSRP1↓ SOX2↓ OCT4↓ NANOG↓ OLIG2↓ CD133↓	Inhibited proliferation of patient-derived tumor cells	Cell lines Orthotopic mouse models	(5)
Glioblastoma (2)	FACT↓ p53↑ NF-κB↓	Induced Apoptosis and inhibited proliferation Increased survival of TMZ-responsive and -resistant GBM	Cell lines Orthotopic mouse models	(6)
Renal cell carcinoma	p53↑ NF-κB↓	Induced death of tumor cells through FACT with no DNA damage	Cell lines PDX mouse models	(7)
Melanoma	p53↑ NF-κB↓ HSF1↓	Enhanced anti-tumor activity by inhibiting heat shock responses of tumor cells	Cell lines Orthotopic mouse models	(8)
Neuroblastoma	MYCN↓	Reduced tumor initiation and progression	Cell lines TH-MYCN transgenic mouse models	(9)
Neuroblastoma (2)	SSRP1↓ SPT16↓ MYCN↓	Inhibited neuroblastoma cell growth	MYCN transgenic zebrafish	(10)
Small cell lung cancer	NOTCH1↑	Reduced the tumor cell growth Preferentially kills tumor-initiating cells	Cell lines PDX mouse models	(11)

PDX, patient-derived xenograft.

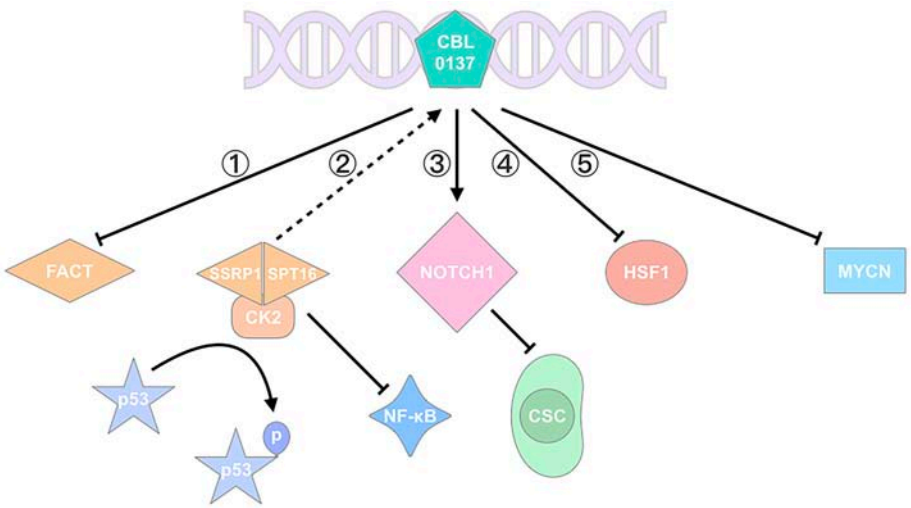

FIGURE 1 | CBL0137 exhibits its antitumor activity via multiple pathways. (1) CBL0137 can target SPT16 and SSRP1, the two subunits of FACT; (2) CBL0137 can induce p53 activation by phosphorylation and NF-κB inhibition, depending on the formation of SPT16-SSRP1-CK2 complex; (3) CBL0137 can reduce the self-renewal of CSCs through NOTCH1 signaling pathway activation; (4) CBL0137 can decrease HSF1 transcription level; (5) CBL0137 can downregulate MYCN expression.

a marker (5). CBL0137 accumulates in brain tissues in orthotopic mouse models, suggesting that it can penetrate the blood brain barrier; oral intake *ad libitum* can also achieve its efficacy. CBL0137 prefers to inhibit CD133+ tumor cell growth with the help of FACT, which is higher in CSCs than non-stem tumor cells. CBL0137 treatment decreases the expression of CD133 and the self-renewal of CSCs, increases asymmetric cell division, prevents tumor initiation and prolongs the survival of tumor-bearing animals (5). A similar consequence has been demonstrated in small cell lung cancer (SCLC) and pancreatic cancer (11, 36). Tumor-initiating cells (TICs) represent those with stemness. CBL0137 preferentially reduces $CD133^{high}$ and $CD44^{high}$ cells (TICs) over $CD133^{low}$ and $CD44^{low}$ (non-TICs) and attenuate the self-renewal of TICs (11).

The stemness of CSCs is well-modulated by stem-cell factors including p53, NF-κB, Sox2, Bmi1, c-Myc, and NOTCH1 (35, 37). Therefore, drugs should target CSCs and CSC-related factors. NOTCH signaling pathway plays a role in oncogenesis, angiogenesis and CSC maintenance (38). It exhibits oncogenic and suppressive roles in different cancers (11). NOTCH1, as a member of the NOTCH family, increases apoptosis and inhibits cell proliferation in SCLC (11). CBL0137 treatment in SCLC prevents SP3 binding to the NOTCH1 promoter, decreases achaete-scute homolog-1 (ASCL1) expression, increases the mRNA expression of NOTCH1, and inhibits CSC renewal. The expression levels of ASCL1 and SP3 are higher in TICs than non-TICs, negatively modulating NOTCH1. Therefore, the tendency of CBL0137 killing TICs may be a result of FACT and NOTCH1, though whether CBL0137 targeting NOTCH1 acts through FACT is unclear in this research (11). CBL0137 can activate NOTCH1 and inhibit the self-renewal of CSCs/TICs (5, 11, 36), thereby facilitating the enhanced prevention of therapeutic resistance and tumor progression.

HSF1 IS INVOLVED IN THE ANTIMELANOMA EFFECT OF CBL0137

Regional chemotherapy via isolated limb perfusion (ILP) is recommended for patients with in-transit extremity melanoma in which mild hyperthermia (42°C compared with 37°C) is adopted, thereby improving drug uptake by tumor cells (8). CBL0137 was then tested for potential use as a regional chemotherapeutic agent on B16 melanoma cell line and tumor-bearing mice. CBL0137 treatment by ILP reduces SSRP1 expression, suppresses HSF1/hsp70 transcription, and causes tumor cell death, and its efficacy can be improved by hyperthermia. Conversely, CBL0137 can downregulate HSF1 to inhibit heat shock responses brought by hyperthermia, thereby increasing tumor cell apoptosis. However, treatment of traditional melphalan had no statistically significant differences between 42 and 37°C. Moreover, the linkage of the ILP drug melphalan can be highly toxic and cause death. By contrast, even 0.1 mg of CBL0137 establishes a strong antitumor activity, suggesting its leakage causes minimal side effects (8). These results explain the antitumor mechanism of CBL0137 from the perspective of hyperthermia and HSF1, suggesting that CBL0137 can be considered as a promising candidate for ILP drug to treat melanoma.

MYCN IN NEUROBLASTOMA: A POTENTIAL INDICATOR OF CBL0137 SENSITIVITY

Approximately 20% of patients with neuroblastoma encounter MYCN amplification, which is a predictor of poor prognosis (9, 39). Considering that the expression of FACT and MYCN is closely related and high in precancerous TH-MYCN$^{+/+}$ neuroblasts, Carter et al. (9) treated TH-MYCN$^{+/+}$ and TH-MYCN$^{+/-}$ mice with CBL0137, which is regarded as the inhibitor of FACT. CBL0137 can downregulate FACT and MYCN expression and inhibit MYCN-driven tumor initiation and progression in MYCN mice and xenografts. In tumor-bearing zebrafish, CBL0137 elicits an inhibitory effect on neuroblastoma (10). Moreover, high-MYCN-expressing cell lines, such as SH-SY5Y and BE(2)C, require a lower IC_{50} of CBL0137 than those expressing normal or relatively low MYCN, suggesting that MYCN expression may be applied to evaluate CBL0137 sensitivity, though further investigation is needed (9).

COMBINATION APPROACH OF CBL0137: THE WAY TO GO

The initial goal of scientists from Clevel and BioLabs Inc. in designing curaxins is to regulate p53 and NF-κB (2). After the "target multiplier" FACT is introduced, the understanding of curaxins has improved. CBL0137 can reduce CSC populations and their stemness (5, 11, 36), which show its promising clinical prospect combined with standard treatment strategies.

The cisplatin resistance of SCLC is likely caused by CSCs. In this research, the combination of CBL0137 and cisplatin at a 1:1 molar ratio remarkably inhibits SCLC tumor growth in H82 xenograft (11). Drug combination delays tumor growth for 30 days and prolongs tumor-bearing mice survival for more than 10 days (11). FACT plays an important role in DNA repair; thus, researchers believed that these results may be due to FACT and its ability to inhibit DNA repair, though this hypothesis has yet to be further investigated (11). However, this hypothesis is partially confirmed in neuroblastoma. Combined with cisplatin, cyclophosphamide, etoposide, or vincristine, CBL0137 can inhibit DNA repair after a double-strand break occurs without genotoxicity. DNA damage markers remarkably increase after etoposide and CBL0137 are administered. The results showed that the effects of CBL0137 are observed in DNA synthesis inhibitors, such as hydroxyurea, rather than microtubule poisons, such as hydroxyurea (9). Another research has shown that the combination of CBL0137 and TMZ does not significantly affect GBM. Combination therapy surpasses CBL0137 monotherapy but not that of TMZ (6). These results are not satisfactory for GBM, but they provide insights into CBL0137 combined with chemotherapy. Further research should be conducted on this area.

Early studies revealed the crosstalk between NF-κB and epidermal growth factor receptor (EGFR), describing them as "partners in cancer" (31, 40–44). In a GBM research, EGFR inhibitor lapatinib and CBL0137 are combined at a 10:1 molar ratio. Lapatinib seldom inhibits CSC growth, which partially explains why it fails to achieve a satisfactory clinical efficacy in GBM treatment (5). The combination of lapatinib and CBL0137 confirms Shostak and Chariot's outlook and presents possibilities for CBL0137 to be applied with targeted therapy.

CONCLUSIONS AND FURTHER DIRECTIONS

Various small molecules, including PRIMA-1, COTI-2, ReACp53, ZMC1, PK7088 (45–51), and CBL0137, target

p53 and have been at preclinical and clinical stages. CBL0137 has a broad antitumor activity in a wide range of cancers, other than targeting p53 (7). CBL0137 can be considered as a candidate for monotherapy and applied to enhance the effectiveness of chemotherapy and targeted therapy, giving it more potential and clinical significance.

However, some concerns still exist. Tumor suppressor protein p53 is important in the oncogenic pathway, and almost 50% of cancers possess mutated or depleted p53; thus, resistance likely exists when one path is blocked. *In vitro* data have also shown that p53-wild type cells are slightly more susceptible to curaxins, including CBL0137-induced cell death, than p53-null cells (7). Discovering how CBL0137 works on those cancers is quite important; in addition, the effect of CBL0137 on the immune system is unknown, and further data support should be obtained to determine whether CBL0137 can synergize with immunotherapy to provide an enhanced efficacy. Further studies on these areas may lead to an in-depth understanding of the mechanism and application of CBL0137.

AUTHOR CONTRIBUTIONS

M-ZJ and B-RX conceived, wrote the manuscript, and completed the figure/table. YX contributed to the writing. W-LJ conceived, organized, and edited the text.

ACKNOWLEDGMENTS

We apologize to those colleagues whose important work could not be cited due to space constraints. This work was in part supported by the 12th undergraduate training programs for innovation of Shanghai Jiao Tong University School of Medicine (No. 1218201), National Natural Science Foundation of China (No. 81872430), the National Key Research and Development Program of China (No. 2017FYA0205302).

REFERENCES

1. Hughes PE, Caenepeel S, Wu LC. Targeted therapy and checkpoint immunotherapy combinations for the treatment of cancer. *Trends Immunol*. (2016) 37:462–76. doi: 10.1016/j.it.2016.04.010
2. Di Bussolo V, Minutolo F. Curaxins: a new family of non-genotoxic multitargeted anticancer agents. *ChemMedChem* (2011) 6:2133–6. doi: 10.1002/cmdc.201100476
3. Maluchenko NV, Chang HW, Kozinova MT, Valieva ME, Gerasimova NS, Kitashov AV, et al. Inhibiting the pro-tumor and transcription factor FACT: Mechanisms. *Mol Biol.* (2016) 50:599–610. doi: 10.1134/S0026893316040087
4. Gurova KV, Hill JE, Guo C, Prokvolit A, Burdelya LG, Samoylova E, et al. Small molecules that reactivate p53 in renal cell carcinoma reveal a NF-kappaB-dependent mechanism of p53 suppression in tumors. *Proc Natl Acad Sci USA*. (2005) 102:17448–53. doi: 10.1073/pnas.0508888102
5. Dermawan JK, Hitomi M, Silver DJ, Wu Q, Sandlesh P, Sloan AE, et al. Pharmacological targeting of the histone chaperone complex FACT preferentially eliminates glioblastoma stem cells and prolongs survival in preclinical models. *Cancer Res*. (2016) 76:2432–42. doi: 10.1158/0008-5472.CAN-15-2162
6. Barone TA, Burkhart CA, Safina A, Haderski G, Gurova KV, Purmal AA, et al. Anticancer drug candidate CBL0137, which inhibits histone chaperone FACT, is efficacious in preclinical orthotopic models of temozolomide-responsive and -resistant glioblastoma. *Neuro Oncol*. (2017) 19:186–96. doi: 10.1093/neuonc/now141
7. Gasparian AV, Burkhart CA, Purmal AA, Brodsky L, Pal M, Saranadasa M, et al. Curaxins: anticancer compounds that simultaneously suppress NF-kappaB and activate p53 by targeting FACT. *Sci Transl Med*. (2011) 3:95ra74. doi: 10.1126/scitranslmed.3002530
8. Kim M, Neznanov N, Wilfong CD, Fleyshman DI, Purmal AA, Haderski G, et al. Preclinical validation of a single-treatment infusion modality that can eradicate extremity melanomas. *Cancer Res*. (2016) 76:6620–30. doi: 10.1158/0008-5472.CAN-15-2764
9. Carter DR, Murray J, Cheung BB, Gamble L, Koach J, Tsang J, et al. Therapeutic targeting of the MYC signal by inhibition of histone chaperone FACT in neuroblastoma. *Sci Transl Med*. (2015) 7:312ra176. doi: 10.1126/scitranslmed.aab1803
10. Zhang X, Dong Z, Zhang C, Ung CY, He S, Tao T, et al. Critical role for GAB2 in neuroblastoma pathogenesis through the promotion of SHP2/MYCN cooperation. *Cell Rep*. (2017) 18:2932–42. doi: 10.1016/j.celrep.2017.02.065
11. De S, Lindner DJ, Coleman CJ, Wildey G, Dowlati A, Stark GR. The FACT inhibitor CBL0137 synergizes with cisplatin in small-cell lung cancer by increasing NOTCH1 expression and targeting tumor-initiating cells. *Cancer Res*. (2018) 78:2396–406. doi: 10.1158/0008-5472.CAN-17-1920
12. Dermawan JK, Gurova K, Pink J, Dowlati A, De S, Narla G, et al. Quinacrine overcomes resistance to erlotinib by inhibiting FACT, NF-kappaB, and cell-cycle progression in non-small cell lung cancer. *Mol Cancer Ther*. (2014) 13:2203–14. doi: 10.1158/1535-7163.MCT-14-0013
13. Khurana A, Roy D, Kalogera E, Mondal S, Wen X, He X, et al. Quinacrine promotes autophagic cell death and chemosensitivity in ovarian cancer and attenuates tumor growth. *Oncotarget* (2015) 6:36354–69. doi: 10.18632/oncotarget.5632
14. Preet R, Mohapatra P, Mohanty S, Sahu SK, Choudhuri T, Wyatt MD, et al. Quinacrine has anticancer activity in breast cancer cells through inhibition of topoisomerase activity. *Int J Cancer* (2012) 130:1660–70. doi: 10.1002/ijc.26158
15. Nesher E, Safina A, Aljahdali I, Portwood S, Wang ES, Koman I, et al. Role of chromatin damage and chromatin trapping of FACT in mediating the anticancer cytotoxicity of DNA-binding small-molecule drugs. *Cancer Res*. (2018) 78:1431–43. doi: 10.1158/0008-5472.CAN-17-2690
16. Fleyshman D, Prendergast L, Safina A, Paszkiewicz G, Commane M, Morgan K, et al. Level of FACT defines the transcriptional landscape and aggressive phenotype of breast cancer cells. *Oncotarget* (2017) 8:20525–42. doi: 10.18632/oncotarget.15656
17. Belotserkovskaya R, Saunders A, Lis JT, Reinberg D. Transcription through chromatin: understanding a complex FACT. *Biochim Biophys Acta* (2004) 1677:87–99. doi: 10.1016/j.bbaexp.2003.09.017
18. Kolundzic E, Ofenbauer A, Bulut SI, Uyar B, Baytek G, Sommermeier A, et al. FACT sets a barrier for cell fate reprogramming in caenorhabditis elegans and human cells. *Dev Cell* (2018) 46:611–26.e12. doi: 10.1016/j.devcel.2018.07.006
19. Draetta GF, Depinho RA. Cancer drug discovery faces the FACT. *Sci Transl Med*. (2011) 3:95ps34. doi: 10.1126/scitranslmed.3002822
20. Bondarenko MT, Maluchenko NV, Valieva ME, Gerasimova NS, Kulaeva OI, Georgiev PG, et al. Structure and function of histone chaperone FACT. *Mol Biol*. (2015) 49:891–904. doi: 10.1134/S0026893315060023
21. Ding Q, He K, Luo T, Deng Y, Wang H, Liu H, et al. SSRP1 contributes to the malignancy of hepatocellular carcinoma and is negatively regulated by miR-497. *Mol Ther*. (2016) 24:903–14. doi: 10.1038/mt.2016.9
22. Koman IE, Commane M, Paszkiewicz G, Hoonjan B, Pal S, Safina A, et al. Targeting FACT complex suppresses mammary tumorigenesis in Her2/neu transgenic mice. *Cancer Prev Res.* (2012) 5:1025–35. doi: 10.1158/1940-6207.CAPR-11-0529
23. Garcia H, Miecznikowski JC, Safina A, Commane M, Ruusulehto A, Kilpinen S, et al. Facilitates chromatin transcription complex is an "accelerator" of tumor transformation and potential marker and target of aggressive cancers. *Cell Rep*. (2013) 4:159–73. doi: 10.1016/j.celrep.2013.06.013

24. Hanahan D, Weinberg RA. Hallmarks of cancer: the next generation. *Cell* (2011) 144:646–74. doi: 10.1016/j.cell.2011.02.013
25. Safina A, Cheney P, Pal M, Brodsky L, Ivanov A, Kirsanov K, et al. FACT is a sensor of DNA torsional stress in eukaryotic cells. *Nucleic Acids Res*. (2017) 45:1925–45. doi: 10.1093/nar/gkw1366
26. Garcia H, Fleyshman D, Kolesnikova K, Safina A, Commane M, Paszkiewicz G, et al. Expression of FACT in mammalian tissues suggests its role in maintaining of undifferentiated state of cells. *Oncotarget* (2011) 2:783–96. doi: 10.18632/oncotarget.340
27. Keller DM, Lu H. p53 serine 392 phosphorylation increases after UV through induction of the assembly of the CK2.hSPT16.SSRP1 complex. *J Biol Chem*. (2002) 277:50206–13. doi: 10.1074/jbc.M209820200
28. Keller DM, Zeng X, Wang Y, Zhang QH, Kapoor M, Shu H, et al. A DNA damage-induced p53 serine 392 kinase complex contains CK2, hSpt16, and SSRP1. *Mol Cell* (2001) 7:283–92. doi: 10.1016/S1097-2765(01)00176-9
29. Kastenhuber ER, Lowe SW. Putting p53 in context. *Cell* (2017) 170:1062–78. doi: 10.1016/j.cell.2017.08.028
30. Cancer Genome Atlas Research N. Comprehensive genomic characterization defines human glioblastoma genes and core pathways. *Nature* (2008) 455:1061–8. doi: 10.1038/nature07385
31. Shi X, Kachirskaia I, Yamaguchi H, West LE, Wen H, Wang EW, et al. Modulation of p53 function by SET8-mediated methylation at lysine 382. *Mol Cell* (2007) 27:636–46. doi: 10.1016/j.molcel.2007.07.012
32. Perkins ND. The diverse and complex roles of NF-kappaB subunits in cancer. *Nat Rev Cancer* (2012) 12:121–32. doi: 10.1038/nrc3204
33. Bykov VJN, Eriksson SE, Bianchi J, Wiman KG. Targeting mutant p53 for efficient cancer therapy. *Nat Rev Cancer* (2018) 18:89–102. doi: 10.1038/nrc.2017.109
34. Colak S, Medema JP. Cancer stem cells–important players in tumor therapy resistance. *FEBS J*. (2014) 281:4779–91. doi: 10.1111/febs.13023
35. Qiu GZ, Sun W, Jin MZ, Lin J, Lu PG, Jin WL. The bad seed gardener: deubiquitinases in the cancer stem-cell signaling network and therapeutic resistance. *Pharmacol Ther*. (2017) 172:127–38. doi: 10.1016/j.pharmthera.2016.12.003
36. Burkhart C, Fleyshman D, Kohrn R, Commane M, Garrigan J, Kurbatov V, et al. Curaxin CBL0137 eradicates drug resistant cancer stem cells and potentiates efficacy of gemcitabine in preclinical models of pancreatic cancer. *Oncotarget* (2014) 5:11038–53. doi: 10.18632/oncotarget.2701
37. Shetzer Y, Solomon H, Koifman G, Molchadsky A, Horesh S, Rotter V. The paradigm of mutant p53-expressing cancer stem cells and drug resistance. *Carcinogenesis* (2014) 35:1196–208. doi: 10.1093/carcin/bgu073
38. Takebe N, Nguyen D, Yang SX. Targeting notch signaling pathway in cancer: clinical development advances and challenges. *Pharmacol Ther*. (2014) 141:140–9. doi: 10.1016/j.pharmthera.2013.09.005
39. Danovi S. Neuroblastoma: as a matter of FACT. *Nat Rev Cancer* (2016) 16:2. doi: 10.1038/nrc.2015.11
40. Shostak K, Chariot A. EGFR and NF-kappaB: partners in cancer. *Trends Mol Med*. (2015) 21:385–93. doi: 10.1016/j.molmed.2015.04.001
41. Yang W, Xia Y, Cao Y, Zheng Y, Bu W, Zhang L, et al. EGFR-induced and PKCepsilon monoubiquitylation-dependent NF-kappaB activation upregulates PKM2 expression and promotes tumorigenesis. *Mol Cell* (2012) 48:771–84. doi: 10.1016/j.molcel.2012.09.028
42. Le Page C, Koumakpayi IH, Lessard L, Mes-Masson AM, Saad F. EGFR and Her-2 regulate the constitutive activation of NF-kappaB in PC-3 prostate cancer cells. *Prostate* (2005) 65:130–40. doi: 10.1002/pros.20234
43. Biswas DK, Cruz AP, Gansberger E, Pardee AB. Epidermal growth factor-induced nuclear factor kappa B activation: a major pathway of cell-cycle progression in estrogen-receptor negative breast cancer cells. *Proc Natl Acad Sci USA*. (2000) 97:8542–7. doi: 10.1073/pnas.97.15.8542
44. Sun L, Carpenter G. Epidermal growth factor activation of NF-kappaB is mediated through IkappaBalpha degradation and intracellular free calcium. *Oncogene* (1998) 16:2095–102. doi: 10.1038/sj.onc.1201731
45. Bykov VJ, Issaeva N, Shilov A, Hultcrantz M, Pugacheva E, Chumakov P, et al. Restoration of the tumor suppressor function to mutant p53 by a low-molecular-weight compound. *Nat Med*. (2002).8:282–8. doi: 10.1038/nm0302-282
46. Salim KY, MalekiVareki S, Danter WR, Koropatnick J. COTI-2, a novel small molecule that is active against multiple human cancer cell lines *in vitro* and *in vivo*. *Oncotarget* (2016) 7:41363–79. doi: 10.18632/oncotarget.9133
47. Soragni A, Janzen DM, Johnson LM, Lindgren AG, Thai-Quynh Nguyen A, Tiourin E, et al. A designed inhibitor of p53 aggregation rescues p53 tumor suppression in ovarian carcinomas. *Cancer Cell* (2016). 29:90–103. doi: 10.1016/j.ccell.2015.12.002
48. Yu X, Vazquez A, Levine AJ, Carpizo DR. Allele-specific p53 mutant reactivation. *Cancer Cell* (2012) 21:614–25. doi: 10.1016/j.ccr.2012.03.042
49. Liu X, Wilcken R, Joerger AC, Chuckowree IS, Amin J, Spencer J, et al. Small molecule induced reactivation of mutant p53 in cancer cells. *Nucleic Acids Res*. (2013). 41:6034–44. doi: 10.1093/nar/gkt305
50. Duffy MJ, Synnott NC, Crown J. Mutant p53 as a target for cancer treatment. *Eur J Cancer* (2017) 83:258–65. doi: 10.1016/j.ejca.2017.06.023
51. Levine AJ. Targeting therapies for the p53 protein in cancer treatments. *Ann Rev Cancer Biol*. (2019) 3:1. doi: 10.1146/annurev-cancerbio-030518-055455

Conflict of Interest Statement: The authors declare that the research was conducted in the absence of any commercial or financial relationships that could be construed as a potential conflict of interest.

frontiers in Oncology

REVIEW
published: 12 December 2018
doi: 10.3389/fonc.2018.00608

CDK 4/6 Inhibitors as Single Agent in Advanced Solid Tumors

Francesco Schettini[1†], Irene De Santo[1†], Carmen G. Rea[1], Pietro De Placido[1], Luigi Formisano[1], Mario Giuliano[1,2], Grazia Arpino[1], Michelino De Laurentiis[3], Fabio Puglisi[4,5], Sabino De Placido[1‡] and Lucia Del Mastro[6,7‡]*

[1] University of Naples Federico II, Naples, Italy, [2] Baylor College of Medicine, Houston, TX, United States, [3] Istituto Nazionale Tumori Fondazione G. Pascale, Naples, Italy, [4] Department of Medicine, University of Udine, Udine, Italy, [5] IRCCS Centro di Riferimento Oncologico Aviano, Aviano, Italy, [6] Policlinico San Martino-IST, Genova, Italy, [7] University of Genova, Genova, Italy

Cyclin-dependent kinases (CDK) 4/6 inhibitors, namely abemaciclib, palbociclib, and ribociclib, interfere with cell cycle progression, induce cell senescence and might promote cancer cell disruption by a cytotoxic T cells-mediated effect. Phase III randomized clinical trials have proven that CDK4/6 inhibitors (CDK4/6i) in combination with several endocrine agents improve treatment efficacy over endocrine agents alone for hormone receptor positive (HR+) HER2 negative (HER2–) metastatic breast cancer (MBC). Based on such results, these combinations have been approved for clinical use. Preclinical studies in cell cultures and mouse models proved that CDK4/6i are active against a broad spectrum of solid tumors other than breast cancer, including liposarcoma, rhabdomyosarcoma, non-small cell lung cancer, glioblastoma multiforme, esophageal cancer, and melanoma. The role of CDK4/6i in monotherapy in several solid tumors is currently under evaluation in phase I, II, and III trials. Nowadays, abemaciclib is the only of the three inhibitors that has received approval as single agent therapy for pretreated HR+ HER2– MBC. Here we review biological, preclinical and clinical data on the role of CDK4/6 inhibitors as single agents in advanced solid tumors.

Keywords: solid tumors, cyclin-dependent kinases, palbociclib, ribociclib, abemaciclib, cell cycle

OPEN ACCESS

Edited by:
Yunkai Zhang,
Vanderbilt University Medical Center, United States

Reviewed by:
Mao Wang,
Memorial Sloan Kettering Cancer Center, United States
Zhenfang Du,
Vanderbilt University Medical Center, United States
Junyi Li,
University of Pittsburgh, United States

***Correspondence:**
Francesco Schettini
francescoschettini1987@gmail.com

†These authors have contributed equally to this work

‡These authors share co-last authorship

Specialty section:
This article was submitted to Cancer Molecular Targets and Therapeutics, a section of the journal Frontiers in Oncology

Received: *26 October 2018*
Accepted: *28 November 2018*
Published: *12 December 2018*

Citation:
Schettini F, De Santo I, Rea CG, De Placido P, Formisano L, Giuliano M, Arpino G, De Laurentiis M, Puglisi F, De Placido S and Del Mastro L (2018) CDK 4/6 Inhibitors as Single Agent in Advanced Solid Tumors. Front. Oncol. 8:608. doi: 10.3389/fonc.2018.00608

INTRODUCTION

The key role of cyclin-dependent kinases (CDK) and D-type Cyclins (CCND) in cell cycle progression from G1 to S phase was discovered more than 20 years ago (1). Since then, it has been demonstrated that several solid tumors present direct modifications of genes codifying for several proteins involved in CCND-CDK activity and regulation (2). As a result, in recent years, small molecule inhibitors which target this mitogenic pathway have been developed. Three of them are currently available for the treatment of metastatic breast cancer (MBC) in combination with aromatase inhibitors or fulvestrant. This review focuses on the role of CCND-CDK in normal cells, on how this pathway is altered in solid tumors and on the activity of CDK4/6 inhibitors (CDK4/6i), as single agents in the treatment of advanced solid tumors in adult patients.

THE ROLE OF CDK IN CELL CYCLE AND SOLID TUMORS

CCND interact with several CDK, including CDK 4/6, forming functional complexes that phosphorylate and inactivate retinoblastoma protein (pRb) (1). This protein operates a negative control on E2F transcription factors, resulting in an inhibition of cell cycle progression. Indeed, E2F modulates the expression of a broad variety of genes implied in cell cycle S1 phase and mitosis. On the opposite, functional CCND-CDK4/6 complexes allow E2F to be released from pRb control and promote the transition from the G1 to the S phase of the cell cycle (**Figure 1**) (1). Cyclin D is important in growth factor signaling and, more in general, is a common downstream pathway for several mitogenic signaling, including phosphatidylinositol 3-kinase (PI3K)/AKT/mammalian target of rapamycin (mTOR), mitogen-activated protein kinase (MAPK), wnt/beta-catenin, janus kinase (JAK)-signal transducer and activator of transcription (STAT), nuclear factor kappa-light-chain-enhancer of activated B cells (NF-kB), and steroid hormone signaling pathways (e.g., estrogen, progesterone, and androgen) (**Figure 1**) (2). CDK 4/6 activity is regulated by the INK4 family of proteins. Among them, $p16^{INK4A}$ appears to be the most relevant, in terms of tumor suppression activity. Several other factors, including $p21^{CIP1}$ and $p27^{KIP1}$ modulate CCND-CDK4/6 complexes' activity in a context-dependent manner (2). Finally, the SMARCB1/INI1/SNF5 tumor suppressor gene directly represses the transcription of the Cyclin-D coding gene CCND1 and increases the expression of CCND-CDK4/6 negative regulators $p16^{INK4A}$ and $p21^{CIP1}$ (2).

In solid tumors, an hyperactivation of the CCND-CDK4/6 activity can occur through: (1) increased activity of upstream mitogenic signaling pathways; (2) aberrant activity of the components of the pathway or their regulators. This latter may depend on various molecular mechanisms, i.e., point mutations, translocations or amplification of CDK4/6, amplification of D-type cyclins, deletions that cause the loss of $p16^{INK4A}$ or pRb expression, epigenetic modifications and downregulation of microRNAs (miRNAs) that target CDK4/6. Alterations of the expression of CCND-CDK4/6-INK4-Rb pathway components or of their direct regulators result in cell cycle progression and cell proliferation and represent a key mechanism of tumorigenesis (2). The solid tumors for which the CCND-CDK4/6-INK4-Rb pathway is more frequently deregulated through direct genetic, epigenetic or transcriptional modifications are breast, head and neck, lung, pancreatic, ovarian and bladder cancer, melanoma, endometrial carcinoma, liposarcoma, neuroblastoma, and malignant rabdoid tumors (3–25). Because of their central role in tumorigenesis and progression, CDK4 and 6 might represent a valid therapeutic target for cancer treatment in a broad spectrum of solid tumors.

Abbreviations: CDK4/6, cyclin-dependent kynases 4 and 6; CDK4/6i, CDK4/6 inhibitors; CCND, cyclin D; PI3K, phosphatidylinositol 3-kinase; mTOR, mammalian target of rapamycin; MAPK, mitogen-activated protein kinase; JAK, janus kinase; STAT, signal transducer and activator of transcription; NF-kB, nuclear factor kappa-light-chain-enhancer of activated B cells; miRNAs, microRNAs; pRb, retinoblastoma protein; ET, endocrine therapy; ER+, estrogen receptor positive; HR+, hormone receptor positive; HER2–, human epidermal growth factor receptor 2 negative; MBC, metastatic breast cancer; BC, breast cancer; GBM, glioblastoma multiforme; WD/DDLS, well-differentiated/dedifferentiated liposarcoma; NSCLC, non-small cell lung cancer; SCLC, small cell lung cancer; GIST, gastrointestinal stromal tumors; PDA, pancreatic ductal adenocarcinoma; EAC, esophageal adenocarcinoma; BBB, blood-brain barrier; ORR, overall response rate; PFS, progression-free survival; mPFS, median progression-free survival; TTP, time to progression; DCR, disease control rate; CBR, clinical benefit rate; DLT, dose-limiting toxicity; MTD, maximum tolerated dose; RP2D, recommended phase II dose; ADRs, adverse reactions; SD, stable disease; PR, partial response; CR, complete response; CI, confidence interval; HR, hazard ratio.

CDK 4/6 INHIBITORS: AN OVERVIEW

Mechanism of Action and Toxicities

After the discovery of CDK 4/6 role in tumorigenesis, several CDK inhibitors have been developed for clinical use. The most recent are selective for CDK4 and CDK6, preventing inhibition of other CDKs activity (1). Three CDK4/6i are currently approved in clinical practice, namely: palbociclib, ribociclib, and abemaciclib. Their mechanism of action is based on the binding to CDK 4 and 6 ATP pocket, which leads to a substantial inactivation of CCND-CDK4/6 complexes, with a subsequent increase in the activity of pRb. The logic consequence is a G1 phase arrest (**Figure 2**). The interference with cell cycle progression results in an increased apoptosis phenomena in tumor cells (1, 2).

Palbociclib and ribociclib are similar in chemical structure, while abemaciclib differs and has a higher CDK4/6 binding power than the other two CDK4/6i. More specifically, abemaciclib shows higher selectivity for the complex CDK4/cyclin D1 compared to the other two compounds, and is 14 times more potent against CDK4 than CDK6 (2, 26). Cell cycle arrest and subsequent apoptosis are sought to be the most relevant mechanism of action of CDK4/6i. However, a very recent study based on mouse models of breast cancer and other solid tumors and on a confirmatory trascriptomic analysis of serial biopsies from a clinical trial involving CDK4/6i in breast cancer, showed that CDK4/6 inhibition might also induce a broad spectrum of immunologic events. More precisely, they seem to increase the antigen presenting capability of tumor cells, while concurrently reducing the immunosuppressive population of T regulator lymphocytes. This could in turn enhance the activation of cytotoxic T cells, which ultimately kill tumor cells (27). However, immunologic effects of CDK4/6i are still object of debate and need further validation/confirmation. Despite a very similar mechanism of action, dose limiting toxicities (DLTs) observed in phase I trials differed, with neutropenia being the DLT for palbociclib, diarrhea and fatigue for abemaciclib, and neutropenia, mucositis, asymptomatic thrombocytopenia, pulmonary embolism, increased creatinine, hyponatriemia, and QTcF prolongation for ribociclib (2, 28). Some of the latter toxicities (such as creatinine increase or thromboembolic events) were also reported for abemaciclib however they did not represent formal DLTs in phase I trials. The most common CDK4/6i toxicities of any grade observed in pivotal phase III trials were neutropenia, leukopenia, fatigue and

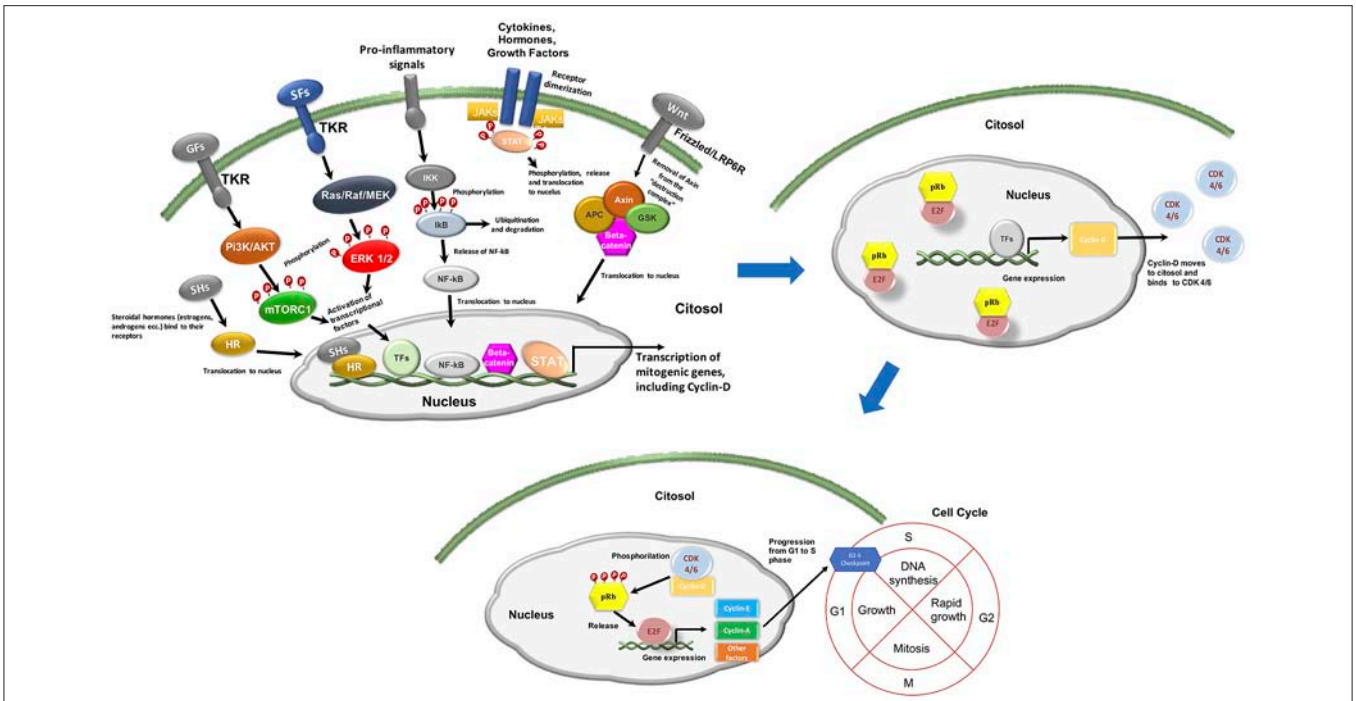

FIGURE 1 | Mitogenic signaling and cell cycle progression. GFs, growth factors; TKR, tyrosine kinase receptor; SFs, survival factors; HR, hormone receptor; SHs, steroidal hormones (i.e., estrogens, androgens); TFs, transcriptional factors.

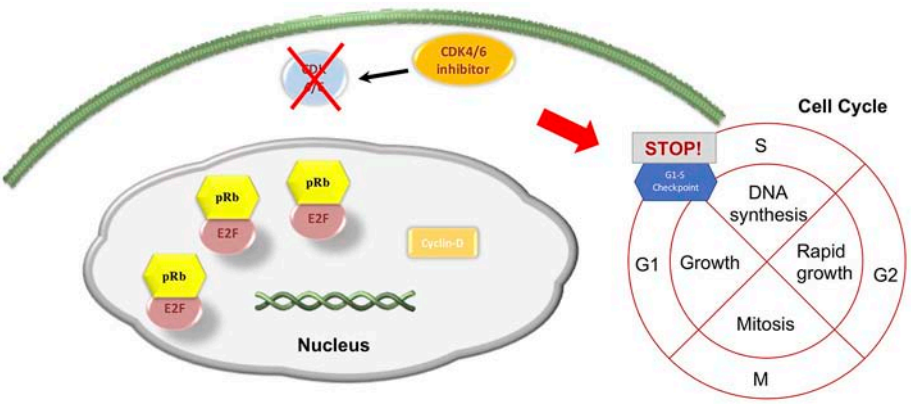

FIGURE 2 | CDK4/6 inhibitors' main effect on cell cycle progression.

nausea for palbociclib (29, 30), neutropenia, nausea, infections, fatigue and diarrhea for ribociclib (31, 32), creatinine increase, diarrhea, fatigue, and neutropenia for abemaciclib (33, 34). The pathophysiology of such toxicities has mostly to be linked to CDK4/6i mechanism of action. Additionally, abemaciclib-induced creatinine increase, might be due to its competitive inhibition of efflux transporters of creatinine (26). A comparison between main pharmacokinetic and pharmacodynamic properties among the three molecules is reported in **Table 1**. All of the three molecules are orally administered and are metabolized by the liver. Palbociclib and ribociclib, due to longer half-life than abemaciclib, can be administered once daily, while abemaciclib needs twice daily administration.

Current Indications

The three inhibitors are currently available for the treatment of hormone receptor positive (HR+) Human Epidermal Growth Factor Receptor 2 negative (HER2–) MBC in combination with an aromatase inhibitor (AI) as first-line endocrine therapy or in combination with fulvestrant in pretreated patients. All of these combinations substantially doubled the comparator in terms of median progression-free survival (PFS) (29–34). Moreover, ribociclib was also studied in combination with tamoxifen or AIs

TABLE 1 | CDK 4/6 inhibitors' pharmacological characteristics.

Drug properties	CDK 4/6 inhibitors		
	Palbociclib	**Ribociclib**	**Abemaciclib**
Bioavailability (35)	46%	Unknown	45%
Protein binding (35)	85%	∼70%	96.3%
Metabolism (35)	Liver	Liver	Liver
Elimination half-life (35)	29 (±5) h	32.0 (29.7–54.7) h	18.3 h
Excretion (35)	74% feces, 18% urine	69% feces, 23% urine	81% feces, 3% urine
IC50 (nM) (2)			
➢ CDK4-cyclin D1	11	10	2
➢ CDK6-cyclin D1-2-3	15	39	10
➢ CDK1-cyclin B	>10,000	113,000	1,627
➢ CDK2-cyclin A-E	>10,000	76,000	504
➢ CDK9-cyclin T	NR	NR	57
MTDs (2)	125 mg	900 mg	200 mg every 12 h
DLTs (2)	Neutropenia	Neutropenia, Mucositis, Asymptomatic thrombocytopenia, Pulmonary embolism, Increased creatinine, Hyponatriemia, QTcF prolongation (>500 ms)	Fatigue
Recommended dose (35)	125 mg/die on a 21-on-28-days schedule	600 mg/die on a 21-on-28-days schedule	200 mg twice daily
Administration (35)	Oral	Oral	Oral

and a GnRH analog (GnRHa) in pre-/perimenopausal setting in the context of the MONALEESA 7 phase III trial (36), which enrolled HR+ HER2– MBC in first line setting and results were in line with those published in the other CDK4/6i pivotal trials. Results and characteristics of the pivotal trials, namely PALOMA 2 and 3, MONALEESA 2, 3, and 7, and MONARCH 2 and 3 are reported in **Table 2**.

SINGLE AGENTS CDK4/6I: CURRENT EVIDENCE

As previously reported, the CCND-CDK4/6-INK4-Rb pathway is frequently deregulated through direct genetic, epigenetic or transcriptional modifications in a broad variety of neoplasms (3–25). Indeed, apart from their use in combination with ET for the treatment of HR+ HER2– MBC, CDK4/6i are also under study as single agent in breast cancer (BC) and other solid tumors. The following paragraphs will resume the current preclinical and clinical evidence supporting this experimental treatment strategy.

Preclinical Evidence

Single agent CDK4/6i have shown consistent activity in preclinical models (38–56). In brief, the most relevant results were observed in *in vivo* and/or *in vitro* models of colon cancer (palbociclib, abemaciclib), glioblastoma (palbociclib, abemaciclib), breast cancer (palbociclib, ribociclib, abemaciclib), prostate carcinoma (palbociclib), sarcomas (palbociclib and ribociclib), pancreatic ductal adenocarcinoma (palbociclib), melanoma (palbociclib, ribociclib, abemaciclib), non-small cell lung cancer (palbociclib, abemaciclib), and esophageal adenocarcinoma (abemaciclib).

Palbociclib

A study demonstrated a potent antitumor activity in different mice models, bearing colon cancer, glioblastoma, breast, and prostate carcinoma xenografts. Palbociclib, given as continuous treatment, was able to arrest growth and induce regression of tumor xenografts. A modest activity was also observed in non-small cell lung cancer (NSCLC) models (38). Palbociclib was also able to arrest the growth of estrogen receptor-positive (ER+) BC cell lines (39). A potent antitumor activity was also demonstrated in an *ex vivo* model of human breast tumors (40). Palbociclib activity was demonstrated on cell lines and intracranial xenografts of glioblastoma multiforme (GBM) (41). In the latter case, the proneural subtype appeared to be the most sensitive to palbociclib activity (42). In ovarian cancer cell lines, Palbociclib induces G0/G1 cell cycle arrest by reducing pRb phosphorylation (43). Palbociclib is also effective in arresting cell cycle progression and blocking proliferation in synovial sarcomas cell lines (44). Another study demonstrated that palbociclib may inhibit cellular growth and induce senescence in liposarcoma cell lines and mice xenografts (45) and in sarcoma cell lines (46). An antiproliferative effect was observed also in rhabdomyosarcoma-derived cell cultures (47). Palbociclib was also studied in immunocompromised mice with subcutaneous and intrasplenic injections of pancreatic ductal adenocarcinoma (PDA) cell lines derived from patients' specimens. The CDK 4/6i significantly disrupted extracellular matrix organization and increased quiescence and apoptosis, decreased invasion, metastatic spread and tumor progression (48).

Ribociclib

Ribociclib as single agent is effective in inhibiting cell growth in liposarcoma cell lines. Moreover, the administration to mice bearing human liposarcoma xenografts resulted in tumor growth inhibition and/or tumor regression. A similar effect was noted in preclinical models of breast cancers with intact estrogen receptor and/or activating aberrations of PIK3CA/HER2 (49). In preclinical models, ribociclib also showed some activity in melanomas with activating mutations of BRAF or NRAS (50).

Abemaciclib

Abemaciclib is effective in inducing cell cycle arrest and tumor growth inhibition in colon cancer and breast cancer cell lines and in mice bearing human melanoma and colon cancer xenografts (51, 52). Abemaciclib, similarly to temozolamide, increased survival in a rat xenograft model of glioblastoma

TABLE 2 | Characteristics of pivotal trials concerning CDK4/6 inhibitors approved for clinical practice.

Characteristics	Pivotal trials						
	Paloma 2 (29)	**Paloma 3 (30)**	**Monaleesa 2 (31)**	**Monaleesa 7 (36)**	**Monaleesa 3 (32)**	**Monarch-3 (33)**	**Monarch-2 (34)**
Combination	Palbociclib + letrozole vs. letrozole	Palbociclib + fulvestrant vs. fulvestrant	Ribociclib + letrozole vs. letrozole	Ribociclib + tamoxifen or AI + GnRHa vs. tamoxifen or AI + GnRHa	Ribociclib + fulvestrant vs. fulvestrant	Abemaciclib + NSAI vs. NSAI	Abemaciclib + fulvestrant vs. fulvestrant
Menopausal status	Post-menopausal (iatrogenic or physiologic)	Post-menopausal (iatrogenic or physiologic)	Post-menopausal	Pre- and perimenopausal	Post-menopausal	Post-menopausal (iatrogenic or physiologic)	Post-menopausal (iatrogenic or physiologic)
Setting	1st line HR+ HER2– MBC	≥1st line HR+ HER2– MBC	1st line HR+ HER2– MBC	1st line HR+ HER2– MBC	≥1st line HR+ HER2– MBC	1st line HR+ HER2– MBC	1st line HR+ HER2– MBC
Median PFS (months)	24.8 vs. 14.5	9.5 vs. 4.6	NR vs. 14.7	23.8 vs. 13.0	20.5 vs. 12.8	NR vs. 14.7	16.4 vs. 9.3
PFS HR (95% Cis); *p*-value*	0.58 (0.46–0.72); $p < 0.001$	0.46 (0.36–0.59); $p < 0.0001$	0.56 (0.43–0.72); $p = 3.29 \times 10^{-6}$	0.553 (0.441–0.694); $p < 0.0001$	0.59 (0.48–0.73); $p = 4.10 \times 10^{-7}$	0.543 (0.409–0.723); $p = 0.000021$	0.553 (0.449–0.681); $p = 0.000021$
ORR	42.1 vs. 34.7%	25 vs. 11%	40.7 vs. 27.5%	51 vs. 36%	41 vs. 9%	59.2 vs. 43.8%	48.1 vs. 21.3%
Trial phase	III	III	III	III	III	III	III
FDA/EMA status	A/A	A/A	A/A	A/NA	A/NA	A/A	A/A

**OS data not mature, yet, except for palbociclib + fulvestrant vs. fulvestrant [HR 0.81 (0.64–1.03); p = 0.043] (37).*
NSAI, non-steroidal aromatase inhibitor; AI, aromatase inhibitor; GnRHa, gonadotropin releasing hormone analog; HR+, ER and/or PgR positive; HER2–, human epidermal growth factor receptor 2 negative; A, approved; NA, not yet approved.

(53), thus suggesting a significant capability to cross the blood-brain barrier (BBB). It was also effective on NSCLC tumor xenografts (54). Abemaciclib was also able to inhibit growth of melanoma tumor xenografts and delay tumor recurrence in combination with vemurafenib. Furthermore, abemaciclib yielded tumor growth regression in a vemurafenib-resistant model, and induced apoptotic cell death in a concentration-dependent manner, suggesting that this drug might be a viable therapeutic option to overcome MAPK-mediated resistance to B-RAF inhibitors in B-RAF V600E melanoma (55). Abemaciclib was also evaluated in preclinical models of esophageal adenocarcinoma (EAC): in tumor cell lines it appeared to increased apoptosis and decrease proliferation while in mice models, it was able to decrease of more than 20% tumor volume (56).

Clinical Evidence

The preclinical data reviewed above offered a solid rationale to test single agent CDK4/6i in clinical trials.

Palbociclib: Completed Trials

Palbociclib was tested in a cohort of 41 patients affected by several solid tumors in the context of a phase I dose escalating study. Tumors had been screened for the presence of pRb. In this trial the maximum tolerated dose (MTD) and recommended phase II dose (RP2D) of single-agent palbociclib was 125 mg/day on a 21-of-28 days schedule. The most frequent G3/4 toxicities were neutropenia, leucopenia and anemia with the first present in 20% of cases, the second in 10% and the latter in 7% of cases. Albeit being a phase I trial, clinical activity was also reported. Among 37 evaluable patients, 27% achieved stable disease (SD) for at least 4 cycles and 16% for at least 10 cycles (57).

Several phase II studies tested palbociclib monotherapy in a broad variety of solid tumors, namely well-differentiated or dedifferentiated liposarcoma (WD/DDLS) (58, 59), NSCLC (60), gastric and esophageal cancer (61), urothelial carcinoma (62), epithelial ovarian cancer (63), HR+ and triple negative (TN) BC (64, 65). The best results were observed in WD/DDLS, ovarian and BC, counterbalanced by overall disappointing results in the other neoplasms. The most frequent grade (G)3/4 adverse reactions (ADRs) were hematologic.

More in details, a phase II study explored the activity and safety of palbociclib on a 200 mg/day on a 14-of-21-days schedule in patients with advanced CDK4-amplified WD/DDLS. The trial enrolled 30 patients. The estimated 12-weeks PFS rate was 66%, far exceeding the expected rate of 40% for an active agent. There was only one partial response (PR) and 19 SD at 12 weeks. Median PFS (mPFS) was 17.9 weeks. The most frequent G3/4 ADRs were neutropenia (50%), leukopenia (47%), thrombocytopenia (30%), lymphopenia (27%), and anemia (17%) (58). In a subsequent study, patients affected by advanced WD/DDLS were treated with standard palbociclib 125 mg for 21 days in 28 days-schedule. The trial results showed a successful PFS at 12 weeks of 57.2% [95% Confidence Interval (CI): 42.4–68.8%]. The median PFS was 17.9 weeks (95% CI: 11.9–24.0 weeks). One complete response (CR) was observed. G3/4 ADRs were primarily hematologic and included neutropenia (33%), without neutropenic fever (59). A clinical trial in previously-treated patients with recurrent or metastatic NSCLC was prematurely halted due to lack of objective tumor responses. Half

of evaluable patients achieved SD. The mPFS was 12.5 weeks. One patient experienced G3 transaminitis and unexpected G4 rhabdomyolysis, supposedly due to concomitant use of high-dose simvastatin. Some patients developed G3 or 4 neutropenia, and G3 thrombocytopenia (60). Single agent palbociclib was also not effective in advanced gastric and esophageal tumors, even if the patients had been selected for Rb expression and despite 19/38 tumors showed amplification of CCND1. The median duration of treatment was of 1.7 months, with a maximum of 5.5 months. No objective responses were observed (61). Similarly, palbociclib was not effective in a phase II trial conducted in patients affected by metastatic urothelial carcinoma with both p16 loss and pRb expression (62). A single arm phase II trial in patients with heavily pretreated epithelial ovarian cancer showed a discreet activity and efficacy for palbociclib as single agent. Thirty percent of patients were progression-free at 6 months, with a median PFS of 3.7 months (95% CI: 1.2–6.2). A 4% of PR and a 65% of SD were observed. The toxicity was minimal. Predictive biomarker analyses are ongoing (63). A phase II study of palbociclib as single agent was conducted in patients with metastatic pRb positive BC. The clinical benefit rate (CBR) at 6 months, composed of all complete responses (CR), PR and SD observed as best responses, was 21%, the median PFS were of 4.1 months (95% CI 2.3–7.7) for patients with ER+ HER2– BC, 18.8 months (95% CI: 5.1—NE) for ER+ HER2+ patients and 1.8 months (95% CI: 0.9—NE) for patients with triple negative (TN) tumors, respectively. Neutropenia (50%) and thrombocytopenia (21%) were the most frequent G3/4 toxicities (64). The TREND study, an Italian multicentre open-label phase II trial, compared single agent palbociclib with palbociclib combined with the same ET received prior to disease progression in post-menopausal women with HR+ HER2– MBC. The trial enrolled 115 patients, the primary endpoint was CBR. In both arms, 67% of pts had the study treatment as second line, 33% as third line, and about 1/3 of pts also had received 1 prior chemotherapy for MBC. The CBR was similar in both arms, 54% (95% CI: 42–67%) observed in the combination one, and 60% (95% CI: 48–73%) with palbociclib alone. The Overall Response Rates (ORR), composed of all CR and PR observed as best responses, were 11% (95% CI: 3–19%) and 7% (95% CI: 0.4–13%) with the combination therapy and palbociclib alone, respectively. The trial was not powered to estimate survival endpoints, however exploratory analyses were performed, with no significant differences observed in PFS ($p = 0.13$) and a longer median duration of clinical benefit for the combination than for the single agent [11.5 months, 95% CI: 8.6–17.8 vs. 6 months, 95% CI: 3.9–9.9; Hazard Ratio (HR): 0.31, 95% CI: 0.1–0.7, p-value 0.001]. Overall, however, the primary endpoint did not differ significantly between the 2 study arms, thereby lending support to the potential use of palbociclib as single agent in pretreated patients with HR+ HER2– MBC (65).

Palbociclib: Ongoing Trials

A number of trials are currently ongoing with single agent palbociclib in several advanced solid tumors.

Results are awaited from the NCT03219554 single arm phase II trial that is evaluating the efficacy of single agent palbociclib in patients with recurrent or metastatic advanced thymic epithelial tumors pretreated with one or more cytotoxic chemotherapy. The primary endpoint is PFS (66). The activity and efficacy of single agent palbociclib will be also evaluated in the Lung-MAP trial, a phase II/III biomarker-driven study for second line therapy of squamous cell lung cancer (SCLC). More specifically, single agent palbociclib will be studied in the context of a sub-study that includes all patients that harbored genetic alterations involving cell-cycle genes. The accrual has been completed and results are awaited (67). A phase II study, the NCT01907607—CYCLIGIST, has also already completed accrual and will evaluate the efficacy of single agent palbociclib in patients with gastrointestinal stromal tumors (GIST) refractory to imatinib and sunitinib. The primary endpoint is the non-progression rate at 4 months (68). Results are also awaited for the NCT01356628. This multicenter single arm phase II trial is exploring the efficacy of single agent palbociclib in advanced hepatocellular carcinoma pretreated with standard therapies. The primary endpoint is the time to disease progression (TTP) (69). Another phase II trial, the NCT02806648—PALBONET, is ongoing to demonstrate the safety and activity of palbociclib in subject affected by pNET with overexpression of CDK4, RB1, and CCND1. Results are awaited (70).

Several trials are currently recruiting participants. The NCT02530320 phase II study is ongoing in patients with oligodendroglioma or recurrent anaplastic oligoastrocytoma with preserved pRb activity. The primary end point is the PFS rate at 6 months (71). Another ongoing single arm phase II study (NCT03242382) will evaluate the efficacy of second-line palbociclib in patients with advanced soft tissue sarcomas with CDK4 overexpression. The primary endpoint is the PFS at 6 months (72). The NCT01037790 phase II clinical trial is studying activity, safety and tolerability of single agent palbociclib in preatreated refractory solid tumors, including metastatic colorectal cancer that harbors the Kras or BRAF mutation, metastatic breast cancer, advanced or metastatic esophageal and/or gastric cancer, cisplatin-refractory, unresectable germ cell tumors and any tumor type if tissue tests positive for CCND1 amplification, CDK4/6 mutation, CCND2 amplification or any other functional alteration at the G1/S checkpoint. Co-primary endpoints are the response rates and the safety and tolerability profile. The trial is currently recruiting participants (73).

Finally, a single arm phase II trial (NCT03454919) in acral melanoma bearing alterations in cell cycle pathways, including CDK4 amplification and/or CCND1 amplification and/or P16 (CDKN2A) loss, is going to start but not yet recruiting patients. The primary end point is PFS (74).

Ribociclib: Completed and Ongoing Trials

The initial phase I dose escalation study of single-agent ribociclib enrolled 128 patients with pRb positive advanced solid tumors and lymphomas. The MTD and RP2D were established as 900 and 600 mg/day, respectively, on a 21-of-28-days schedule. The most relevant G3/4 ADRs were neutropenia (27%), leukopenia (17%), fatigue (2%), and nausea (2%). An asymptomatic QTcF prolongation was observable, but mostly with doses ≥600 mg/day (9% of patients at 600 mg/day; 33% at doses >600 mg/day). Response rates were evaluable for 110 patients, though this was

a phase I trial. There were 3 PR and 43 SD as best response; eight patients were progression-free for more than 6 months (75). Results are awaited for an ongoing phase I study (NCT02345824) that will assess tumor pharmacokinetics and efficacy of ribociclib in patients with recurrent glioblastoma or anaplastic glioma (76).

Several phase II trials of single agent ribociclib are currently ongoing. More specifically, the NCT02571829 trial is assessing the efficacy and safety of ribociclib in patients with advanced WD/DDLS. Patients' recruitment has been completed (77). Another trial is ongoing in patients with advanced neuroendocrine tumors of foregut origin progressed after prior systemic therapy. The primary endpoint is the objective response rate (78). The NCT02300987 randomized study is ongoing in patients with relapsed, refractory, incurable teratoma with recent progression from at least 1 prior line of chemotherapy and for which no additional standard surgical or medical therapy exists. This trial will compare ribociclib to placebo. The primary endpoint is PFS. Recruitment has been completed and results are awaited (79). Another phase II single arm study (NCT03096912) assessing efficacy and safety of ribociclib in patients with advanced WD/DDLS is currently recruiting patients. The primary endpoint is the response to therapy after 36 months, as evaluated by RECIST and Choi criteria (80).

Abemaciclib: Completed Trials

Abemaciclib as single agent was investigated in a multicentre phase I study conducted by Patnaik and colleagues. In this study, the 225 enrolled patients were affected by NSCLC, BC, melanoma, colorectal cancer and GBM. The MTD was 200 mg twice daily and the DLT was G3 fatigue. The most relevant G3 ADRs were diarrhea (5%), nausea (4%), fatigue (7%), vomiting (2%), and neutropenia (7%). Activity data were also reported. Fifteen patients experienced SD for at least 4 cycles, with 3 patients achieving SD for 8, 16, and 26 cycles, respectively. One patient with ovarian cancer had a durable and relevant CA125 response. One patient with KRAS mutant NSCLC had a PR. One patient with NRAS mutant melanoma had a confirmed PR. The ORR was 31% for HR+ BC. Moreover, when also considering patients who achieved SD as a best response, 61% of the overall subjects obtained a clinical response lasting at least 6 months (81, 82). A focus on 49 NSCLC patients was also published. The most relevant G3 ADRs were diarrhea (2%), nausea (4%), fatigue (2%), vomiting (2%), and anemia (2%); there were no G4 events. Activity results were also shown. The disease control rate (DCR = CR + PR + SD) was 51% with 1 confirmed PR. The median duration of SD was 5.6 months and the median PFS was 2.1 months. Twenty patients reached at least 4 cycles and 13 reached at least 6 cycles. Among those 49 patients, 19 were affected by KRAS wildtype tumors, 26 by KRAS mutant tumors and 4 with unknown KRAS status. The DCR was 37% for KRAS wildtype and 54% for KRAS mutant NSCLC, consistently with what observed in xenograft studies. The MTD was 200 mg twice daily (83). A randomized phase III study JUNIPER, has compared abemaciclib plus best supportive care to erlotinib plus best supportive care in patients with metastatic NSCLC with a detectable KRAS mutation who have progressed after platinum-based chemotherapy. The primary endpoint was OS and the study failed to show a significant benefit. Moreover, researchers reported a higher-than-expected OS rate in the control group based on historical data (84, 85).

At present, the most relevant trial involving abemaciclib in monotherapy is the MONARCH-1. Such study was a single arm phase II trial in which the efficacy and safety profile of abemaciclib as a single agent were investigated in HR+ HER2– MBC. The 132 enrolled patients had to be progressed on or after prior ET and must have received at least two prior chemotherapy regimens, at least one but no more than two in the metastatic setting. Abemaciclib was administrated at the dose of 200 mg every 12 h on a continuous schedule. The ORR (primary endpoint) was 19.7% (95% CI, 13.3–27.5), the CBR was 42.4%, mPFS was 6 months (95% CI 4.2–7.5) and median overall survival (OS) was 17.7 months (95% CI, 16 to not reached). In this study the most common ADRs were diarrhea, fatigue, nausea, neutropenia, leukopenia, anemia and increased serum creatinine (86). This trial led to the FDA approval of abemaciclib as single therapy in pretreated patients with HR+ HER2– MBC.

Finally, preliminary results from a Simon 2-stage single arm phase II trial in patients affected by HR+ HER2– MBC, NSCLC or melanoma with brain metastases showed a number of brain partial responses that met the predefined threshold for expanding the trial to stage 2. For each patient cerebrospinal fluid concentration of unbound abemaciclib were comparable and consistent with those in the plasma and tumor tissue (87). This trial provided evidence that abemaciclib is able to cross the BBB in human, coherently with preclinical evidence on mice xenografts (53). The second stage is ongoing.

Abemaciclib: Ongoing Trials

Several ongoing trials with single agent abemaciclib have completed patients' recruitment. An asian phase I study (NCT02014129) is evaluating the safety and toxicities of abemaciclib in advanced solid tumors and lymphomas in Japanese participants (88). Abemaciclib is also currently investigated in GBM at first relapse in the NCT02981940 phase II trial. Tumors must be pRb wild type and carry inactivation of CDKN2A/B or C in the tumor by homozygous deletion. The coprimary endpoint are the intratumoral abemaciclib concentration and the 6-months PFS (89). Another phase II trial (active but no more recruiting), the NCT02450539, is evaluating the efficacy of abemaciclib compared to docetaxel in patients with metastatic squamous NSCLC previously treated with platinum-based chemotherapy. The primary endpoint is PFS (90). A phase II ongoing study (NCT02308020), currently recruiting participants, is evaluating the activity and efficacy of abemaciclib in patients with brain metastases secondary to HR+ breast cancer, NSCLC or melanoma. The primary endpoint is the objective intracranial response rate. Preliminary results have been reported in a previous section of this review (87). Other ongoing trials are currently enrolling participants. More specifically, the NCT02919696 phase I trial is studying abemaciclib in native chinese patients with advanced and/or metastatic cancers (91). A phase II trial (NCT03130439) is also investigating the efficacy and activity of abemaciclib in metastatic triple negative breast cancer expressing pRb. The primary endpoint is the ORR

TABLE 3 | Currently ongoing trials on CDK 4/6 inhibitors as single agent in solid tumors.

	CDK4/6 inhibitor	*N*	Phase and setting	Primary endpoint(s)
NCT03123744	Palbociclib	200	Non-randomized Phase II study of palbociclib in adult subjects with recurrent or refractory advanced cancers with aberration(s) in cyclin (CCN/CDK) signaling.	Response rates in subjects with advanced cancer and aberrations of cyclin pathway gene(s) who are treated with palbociclib
NCT02530320	Palbociclib	40	Phase II pilot, prospective, open label, multicenter clinical trial, to evaluate the safety and efficacy of palbociclib, in patients with oligodendroglioma or recurrent oligoastrocytoma anaplastic with the activity of the protein rb preserved	PFS, PFS6m
NCT03454919	Palbociclib	60	Phase II clinical study on efficacy of palbociclib in advanced acral melanoma with cell cycle gene aberrations	ORR, Complete response and partial response
NCT 03242382	Palbociclib	38	Phase II multicenter trial of palbociclib in second line of advanced sarcomas with CDK4 overexpression.	PFS rate
NCT03219554	Palbociclib	33	Phase II single center, open-label, single arm study of palbociclib treatment in patients with recurrent or metastatic advanced thymic epithelial tumor (TET) after failure of one or more cytotoxic chemotherapy regimens	PFS
NCT01907607	Palbociclib	63	Multicentre single-arm phase II study evaluating the efficacy and safety of orally Palbociclib, 125 mg/day, 21 days on/7 days off, in patients with documented disease progression while on therapy with second line sunitinib for unresectable and/or metastatic GIST.	Efficacy, assessed based on 4-months non-progression
NCT01356628	Palbociclib	23	Phase II study of Palbociclib in the treatment of patients with advanced hepatocellular carcinoma (HCC), a type of adenocarcinoma and the most common type of liver tumor.	Time to disease progression
NCT02806648	Palbociclib	21	Phase II trial to assess the activity and safety of Palbociclib in patients with well and moderately differentiated metastatic pancreatic neuroendocrine tumors (pNET)	Response rates
NCT01037790	Palbociclib	205	Phase II trial is studying the side effects and how well PD 0332991 works in treating patients with refractory solid tumors.	Response rates
NCT02345824	Ribociclib	3	Early-phase study to assess tumor pharmacokinetics and efficacy of the cdk4/6 inhibitor Ribociclib in patients with recurrent glioblastoma or anaplastic glioma	Inhibition of CDK4/CDK6 signaling pathway in cell proliferation
NCT03096912	Ribociclib	30	Phase II single arm study assessing efficacy and safety of Ribociclib in patients with advanced well-differentiated or dedifferentiated liposarcoma	Response to therapy as evaluated by RECIST 1.1 Response to therapy as evaluated by Choi [Time Frame: 36 months]
NCT02571829	Ribociclib	30	Phase II single arm study assessing efficacy and safety of Ribociclib in patients with advanced well-differentiated or dedifferentiated liposarcoma	Response to therapy as evaluated by RECIST 1.1 and Choi [Time Frame: 36 months (24 months accrual period and 12 months follow up period)]
NCT02300987	Ribociclib	10	Randomized, blinded, placebo-controlled, phase II trial of LEE011 in patients with relapsed, refractory, incurable teratoma with recent progression.	Progression free survival (PFS) [Time Frame: at 4 months]
NCT02919696	Abemaciclib	20	Phase I study of Abemaciclib in native Chinese patients with advanced and/or metastatic cancers.	Number of Participants with One or More Drug Related Adverse Events Number of participants with one or more drug related adverse events
NCT02014129	Abemaciclib	12	Phase I study of Abemaciclib in Japanese patients with advanced cancer	Number of Participants with LY2835219 Dose-Limiting Toxicities (DLT)
NCT02981940	Abemaciclib	36	Phase II study of Abemaciclib in recurrent glioblastoma	Intratumoral abemaciclib concentration [Time Frame: 2 years] PFS6m
NCT03130439	Abemaciclib	37	Phase II study of Abemaciclib for patients with retinoblastoma-positive, triple negative metastatic breast cancer.	Objective Response Rate [Time Frame: 2 years] ORR as confirmed Complete Response (CR) or Partial Response (PR) per Response Evaluation Criteria in Solid Tumors (RECIST)
NCT02846987	Abemaciclib	30	Phase II study of Abemaciclib in dedifferentiated liposarcoma	PFS [Time Frame: 12 weeks]
NCT03356587	Abemaciclib	32	Biomarker-driven, open label, single arm, multicentre phase II study of Abemaciclib in patients with recurrent or metastatic head and neck squamous cell carcinoma who failed to platinum-based therapy	Response rate [Time Frame: 24 months]

(Continued)

TABLE 3 | Continued

	CDK4/6 inhibitor	*N*	Phase and setting	Primary endpoint(s)
NCT03356223	Abemaciclib	25	Phase II trial aiming to evaluate the clinical interest of Abemaciclib monotherapy in patients with locally advanced/metastatic head and neck cancer after failure of platinum and Cetuximab or anti-EGFR-based therapy and harboring an homozygous deletion of cdkn2a, and/or an amplification of CCND1 and/or of CDK6	The 8-weeks non-progression rate defined as the rate of patients with complete response (CR), partial response (PR) or stable disease (SD) lasting at least 8 weeks, according to RECIST v1.1 [Time Frame: 8 weeks after start of treatment]
NCT02450539	Abemaciclib	150	Randomized phase II study of Abemaciclib vs. docetaxel in patients with stage iv squamous non-small cell lung cancer previously treated with platinum-based chemotherapy.	PFS
NCT02308020	Abemaciclib	247	Phase 2 study of Abemaciclib in patients with brain metastases secondary to hormone receptor positive breast cancer, non-small cell lung cancer, or melanoma.	Percentage of Participants Achieving Complete Response (CR) or Partial Response (PR): Objective Intracranial Response Rate (OIRR)
NCT03310879	Abemaciclib	38	Phase II study of the cdk4/6 inhibitor Abemaciclib in patients with solid tumors harboring genetic alterations in genes encoding D-type cyclins or amplification of CDK4 or 6.	Progression-free rate

(92). The NCT02846987 phase II trial is currently recruiting patients affected by not surgically resectable locally advanced or recurrent dedifferentiated liposarcoma with any number of prior therapies (including none). The primary endpoint is PFS (93). A biomarker-driven phase II study (NCT03356587) of abemaciclib in patients with recurrent or metastatic head and neck squamous cell carcinoma who failed to platinum-based therapy is also currently recruiting participants. Primary endpoint is response rate (94). Another phase II trial in (NCT03356223) patients with locally advanced/metastatic head and neck cancer is currently evaluating abemaciclib monotherapy after failure of platinum and cetuximab or anti-EGFR-based therapy, but only in tumors harboring a homozygous deletion of CDKN2A, and/or amplification of CCND1 and/or of CDK6. The primary endpoint is the 8-weeks non-progression rate (95). Finally, the NCT03310879 phase II study is testing abemaciclib in patients with solid tumors of non-breast origin harboring genetic alterations in genes encoding D-type Cyclins or amplification of CDK4/6 without therapeutic alternative. The progression-free rate at 4 months is the primary endpoint (96).

Ongoing trials for palbociclib, ribociclib, and abemaciclib are resumed in **Table 3**.

CONCLUSIONS

Albeit it is unquestionable, at present, that CDK 4/6i treatment proved to be more efficacious in combination strategies (e.g., in HR+ HER2– MBC is in combination with endocrine agents), the MONARCH 1 trial results (86) led to the FDA approval of abemaciclib as monotherapy for the treatment of adult patients with HR+ HER2– MBC with disease progression after prior ET and CT received in metastatic setting. This study opened up a new scenario for CDK4/6i, making them suitable as single agent treatment in heavily pretreated MBC. In this perspective, the TREND trial provided some evidence for some activity of palbociclib as single agent in pretreated patients with HR+HER2– MBC (65). A cross-trial comparison of response rate from the MONARCH-1 and TREND trial suggests that abemaciclib might be more effective than palbociclib in the same disease setting. However, this hint should be taken as hypothesis only, given the lack of direct comparisons between the two CDK4/6i. Additionally, there is a strong need for biomarkers predictive of response and resistance to better define which patients could benefit most from these drugs. In fact, mechanisms of resistance to CDK4/6i therapy have yet to be clearly identified. Laboratory evidences suggest that markers of intrinsic resistance might be the pRb loss and subsequent increase in $p16^{INK4A}$, deregulation of cyclin E expression, E2F family members amplification and TP53 mutations (97). Interestingly, a study recently published from Condorelli et al. showed for the first time in human patients that acquired mutations leading to functional loss of pRb encoding gene (RB1) might emerge under treatment with palbociclib and ribociclib, maybe due to selective pressure from the CDK4/6i and might potentially confer therapeutic resistance (98). Results from ongoing trials in solid tumors will surely shed a light on CDK4/6i future development as single agents. It is likely that eventual new treatment indications might be acquired by the three inhibitors in the next future, especially in tumors where few therapeutic options are available, such as sarcomas.

AUTHOR CONTRIBUTIONS

All authors conceived the review. FS, ID, CR, and PD performed the literature search. FS drew the figures. FS, ID, and LD wrote the first draft of the manuscript. All authors revised and approved the final version of the manuscript.

REFERENCES

1. Musgrove EA, Caldon CE, Barraclough J, Stone A, Sutherland RL. Cyclin D as a therapeutic target in cancer. *Nat Rev Cancer* (2011) 45:558–72. doi: 10.1038/nrc3090
2. Hamilton E, Infante JR. Targeting CDK4/6 in patients with cancer. *Cancer Treat Rev.* (2016) 45:129–38. doi: 10.1016/j.ctrv.2016.03.002
3. Cassier P, Trédan O, Seigne C, Lavergne E, Fayette J, Desseigne F, et al. Identifying actionable targets in advanced cancer patients: preliminary results from the Profiler program. *J Clin Oncol.* (2014) 32(5_Suppl.):2621. doi: 10.1200/jco.2014.32.15_suppl.2621
4. Cancer Genome Atlas Network. Comprehensive molecular portraits of human breast tumors. Nature (2012) 490:61–70. doi: 10.1038/nature11412
5. Geradts J, Wilson PA. High frequency of aberrant p16(INK4A) expression in human breast cancer. *Am J Pathol.* (1996) 149:15–20.
6. Lim JT, Mansukhani M, Weinstein IB. Cyclin-dependent kinase 6 associates with the androgen receptor and enhances its transcriptional activity in prostate cancer cells. *Proc Natl Acad Sci USA*. (2005) 102:5156–61. doi: 10.1073/pnas.0501203102
7. Young RJ, Waldeck K, Martin C, Foo JH, Cameron DP, Kirby L, et al. Loss of CDKN2A expression is a frequent event in primary invasive melanoma and correlates with sensitivity to the CDK4/6 inhibitor PD0332991 in melanoma cell lines. *Pigment Cell Melanoma Res.* (2014) 27:590–600. doi: 10.1111/pcmr.12228
8. Reed AL, Califano J, Cairns P, Westra WH, Jones RM, Koch W, et al. High frequency of p16 (CDKN2/MTS-1/INK4A) inactivation in head and neck squamous cell carcinoma. *Cancer Res.* (1996) 56:3630–3.
9. Molenaar JJ, Ebus ME, Koster J, van Sluis P, van Noesel CJ, Versteeg R, et al. Cyclin D1 and CDK4 activity contribute to the undifferentiated phenotype in neuroblastoma. *Cancer Res.* (2008) 68:2599–609. doi: 10.1158/0008-5472.CAN-07-5032
10. Crago AM, Singer S. Clinical and molecular approaches to well differentiated and dedifferentiated liposarcoma. *Curr Opin Oncol.* (2011) 23:373–8. doi: 10.1097/CCO.0b013e32834796e6
11. Singer S, Socci ND, Ambrosini G, Sambol E, Decarolis P, Wu Y, et al. Gene expression profiling of liposarcoma identifies distinct biological types/subtypes and potential therapeutic targets in well-differentiated and dedifferentiated liposarcoma. *Cancer Res.* (2007) 67:6626–36. doi: 10.1158/0008-5472.CAN-07-0584
12. Louis-Brennetot C, Coindre JM, Ferreira C, Pérot G, Terrier P, Aurias A. The CDKN2A/CDKN2B/CDK4/CCND1 pathway is pivotal in well-differentiated and dedifferentiated liposarcoma oncogenesis: an analysis of 104 tumors. *Genes Chromosomes Cancer* (2011) 50:896–907. doi: 10.1002/gcc.20909
13. Zuo L, Weger J, Yang Q, Goldstein AM, Tucker MA, Walker GJ, et al. Germline mutations in the p16INK4a binding domain of CDK4 in familial melanoma. *Nat Genet.* (1996) 12:97–9. doi: 10.1038/ng0196-97
14. Hodis E, Watson IR, Kryukov GV, Arold ST, Imielinski M, Theurillat JP, et al. A landscape of driver mutations in melanoma. *Cell* (2012) 150:251–63. doi: 10.1016/j.cell.2012.06.024
15. Haluska FG, Hodi FS. Molecular genetics of familial cutaneous melanoma. *J Clin Oncol.* (1998) 16:670–82. doi: 10.1200/JCO.1998.16.2.670
16. Potrony M, Puig-Butillé JA, Aguilera P, Badenas C, Carrera C, Malvehy J, et al. Increased prevalence of lung, breast, and pancreatic cancers in addition to melanoma risk in families bearing the cyclin-dependent kinase inhibitor 2A mutation: Implications for genetic counseling. *J Am Acad Dermatol.* (2014) 71:888–95. doi: 10.1016/j.jaad.2014.06.036
17. Dreyling M, Kluin-Nelemans HC, Beà S, Hartmann E, Salaverria I, Hutter G, et al. Update on the molecular pathogenesis and clinical treatment of mantle cell lymphoma: report of the 10th annual conference of the European Mantle Cell Lymphoma Network. *Leuk Lymphoma* (2011) 52:2226–36. doi: 10.3109/10428194.2011.600488
18. Pérez-Galán P, Dreyling M, Wiestner A. Mantle cell lymphoma: biology, pathogenesis, and the molecular basis of treatment in the genomic era. *Blood* (2011) 117:26–38. doi: 10.1182/blood-2010-04-189977
19. Fernandez V, Hartmann E, Ott G, Campo E, Rosenwald A. Pathogenesis of mantle-cell lymphoma: all oncogenic roads lead to dysregulation of cell cycle and DNA damage response pathways. *J Clin Oncol.* (2005) 23:6364–9. doi: 10.1200/JCO.2005.05.019
20. Abou-Zeid AA, Azzam AZ, Kamel NA. Methylation status of the gene promoter of cyclin-dependent kinase inhibitor 2A (CDKN2A) in ovarian cancer. *Scand J Clin Lab Invest.* (2011) 71:542–7. doi: 10.3109/00365513.2011.590224
21. Jackson EM, Sievert AJ, Gai X, Hakonarson H, Judkins AR, Tooke L, et al. Genomic analysis using high-density single nucleotide polymorphism-based oligonucleotide arrays and multiplex ligation-dependent probe amplification provides a comprehensive analysis of INI1/SMARCB1 in malignant rhabdoid tumors. *Clin Cancer Res.* (2009) 15:1923–30. doi: 10.1158/1078-0432.CCR-08-2091
22. Kuwahara Y, Charboneau A, Knudsen ES, Weissman BE. Reexpression of hSNF5 in malignant rhabdoid tumor cell lines causes cell cycle arrest through a p21 (CIP1/WAF1)-dependent mechanism. *Cancer Res.* (2010) 70:1854–65. doi: 10.1158/0008-5472.CAN-09-1922
23. Zhang ZK, Davies KP, Allen J, Zhu L, Pestell RG, Zagzag D, et al. Cell cycle arrest and repression of cyclin D1 transcription by INI1/hSNF5. *Mol Cell Biol.* (2002) 22:5975–88. doi: 10.1128/MCB.22.16.5975-5988.2002
24. Wang X, Wu J, Lin Y, Zhu Y, Xu X, Xu X, et al. MicroRNA-320c inhibits tumorous behaviors of bladder cancer by targeting Cyclin-dependent kinase 6. *J Exp Clin Cancer Res.* (2014) 33:69. doi: 10.1186/s13046-014-0069-6
25. Lin Y, Wu J, Chen H, Mao Y, Liu Y, Mao Q, et al. Cyclin-dependent kinase 4 is a novel target in micoRNA-195-mediated cell cycle arrest in bladder cancer cells. *FEBS Lett.* (2012) 586:442–7. doi: 10.1016/j.febslet.2012.01.027
26. Corona SP, Generali D. Abemaciclib: a CDK4/6 inhibitor for the treatment of HR+/HeR2– advanced breast cancer. *Drug Design Dev Ther.* (2018) 12:321–30. doi: 10.2147/DDDT.S137783
27. Goel S, DeCristo MJ, Watt AC, BrinJones H, Sceneay J, Li BB, et al. CDK4/6 inhibition triggers anti-tumor immunity. *Nature* (2017) 548:471–5. doi: 10.1038/nature23465
28. Knudsen ES, Hutcheson J, Vail P, Witkiewicz AK. Biological specificity of CDK4/6 inhibitors: dose response relationship, *in vivo* signaling, and composite response signature. *Oncotarget* (2017) 8:43678–91. doi: 10.18632/oncotarget.18435
29. Finn RS, Martin M, Rugo HS, Jones S, Im SA, Gelmon K, et al. Palbociclib and letrozole in advanced breast cancer. *N Engl J Med.* (2016) 375:1925–36. doi: 10.1056/NEJMoa1607303
30. Cristofanilli M, Turner NC, Bondarenko I, Ro J, Im SA, Masuda N, et al. Fulvestrant plus palbociclib versus fulvestrant plus placebo for treatment of hormone-receptor-positive, HER2-negative metastatic breast cancer that progressed on previous endocrine therapy (PALOMA-3): final analysis of the multicentre, double-blind, phase 3 randomised controlled trial. *Lancet Oncol.* (2016) 17:425–39. doi: 10.1016/S1470-2045(15)00613-0
31. Hortobagyi GN, Stemmer SM, Burris HA, Yap YS, Sonke GS, Paluch-Shimon S, et al. Ribociclib as first-line therapy for HR-positive, advanced breast cancer. *N Engl J Med.* (2016) 375:1738–48. doi: 10.1056/NEJMoa1609709
32. Slamon DJ, Neven P, Chia S, Fasching PA, De Laurentiis M, Im SA, et al. Phase III randomized study of ribociclib and fulvestrant in hormone receptor–positive, human epidermal growth factor receptor 2–negative advanced breast cancer: MONALEESA-3. *J Clin Oncol.* (2018) 36:2465–72. doi: 10.1200/JCO.2018.78.9909
33. Goetz MP, Toi M, Campone M, Sohn J, Paluch-Shimon S, Huober J, et al. MONARCH 3: abemaciclib as initial therapy for advanced breast cancer. *J Clin Oncol.* (2017) 35:3638–46. doi: 10.1200/JCO.2017.75.6155
34. Sledge GW Jr., Toi M, Neven P, Sohn J, Inoue K, Pivot X, et al. MONARCH 2: abemaciclib in combination with fulvestrant in women with HR+/HER2– advanced breast cancer who had progressed while receiving endocrine therapy. *J Clin Oncol.* (2017) 35:2875–84. doi: 10.1200/JCO.2017.73.7585
35. *Prescription Drug Information, Interactions & Side Effects* (2018). Available online at: https://www.drugs.com
36. Tripathy D, Im SA, Colleoni M, Franke F, Bardia A, Harbeck N, et al. Ribociclib plus endocrine therapy for premenopausal women with hormone-receptor-positive, advanced breast cancer (MONALEESA-7): a randomized phase 3 trial. *Lancet Oncol.* (2018) 19:904–15. doi: 10.1016/S1470-2045(18)30292-4
37. Turner NC, Slamon DJ, Ro J, Bondarenko I, Im SA, Masuda N, et al. Overall survival with palbociclib and fulvestrant in advanced breast cancer. *N Engl J Med.* (2018). doi: 10.1056/NEJMoa1810527

38. Fry DW, Harvey PJ, Keller PR, Elliott WL, Meade M, Trachet E, et al. Specific inhibition of cyclin-dependent kinase 4/6 by PD 0332991 and associated antitumor activity in human tumor xenografts. *Mol Cancer Ther.* (2004) 3:1427–38.
39. Finn RS, Dering J, Conklin D, Kalous O, Cohen DJ, Desai AJ, et al. PD 0332991, a selective cyclin D kinase 4/6 inhibitor, preferentially inhibits proliferation of luminal estrogen receptor-positive human breast cancer cell lines *in vitro*. *Breast Cancer Res.* (2009) 11:R77. doi: 10.1186/bcr2419
40. Dean JL, McClendon AK, Hickey TE, Butler LM, Tilley WD, Witkiewicz AK, et al. Therapeutic response to CDK4/6 inhibition in breast cancer defined by *ex vivo* analyses of human tumors. *Cell Cycle* (2012) 11:2756–61. doi: 10.4161/cc.21195
41. Michaud K, Solomon DA, Oermann E, Kim JS, Zhong WZ, Prados MD, et al. Pharmacologic inhibition of cyclin-dependent kinases 4 and 6 arrests the growth of glioblastoma multiforme intracranial xenografts. *Cancer Res.* (2010) 70:3228–38. doi: 10.1158/0008-5472.CAN-09-4559
42. Wiedemeyer WR, Dunn IF, Quayle SN, Zhang J, Chheda MG, Dunn GP, et al. Pattern of retinoblastoma pathway inactivation dictates response to CDK4/6 inhibition in GBM. *Proc Natl Acad Sci USA.* (2010) 107:11501–6. doi: 10.1073/pnas.1001613107
43. Konecny GE, Winterhoff B, Kolarova T, Qi J, Manivong K, Dering J, et al. Expression of p16 and retinoblastoma deter- mines response to CDK4/6 inhibition in ovarian cancer. *Clin Cancer Res.* (2011) 17:1591–602. doi: 10.1158/1078-0432.CCR-10-2307
44. Vlenterie M, Hillebrandt-Roeffen MH, Schaars EW, Flucke UE, Fleuren ED, Navis AC, et al. Targeting cyclin-dependent kinases in synovial sarcoma: palbociclib as a potential treatment for synovial sarcoma patients. *Ann Surg Oncol.* (2016) 23:2745–52. doi: 10.1245/s10434-016-5341-x
45. Barretina J, Taylor BS, Banerji S, Ramos AH, Lagos-Quintana M, Decarolis PL, et al. Subtype-specific genomic alterations define new targets for soft-tissue sarcoma therapy. *Nat Genet.* (2010) 42:715–21. doi: 10.1038/ng.619
46. Perez M, Muñoz-Galván S, Jiménez-García MP, Marín JJ, Carnero A. Efficacy of CDK4 inhibition against sarcomas depends on their levels of CDK4 and p16ink4 mRNA. *Oncotarget* (2015) 6:40557–74. doi: 10.18632/oncotarget.5829
47. Saab R, Bills JL, Miceli AP, Anderson CM, Khoury JD, Fry DW, et al. Pharmacologic inhibition of cyclin-dependent kinase 4/6 activity arrests proliferation in myoblasts and rhabdomyosarcoma-derived cells. *Mol Cancer Ther.* (2006) 5:1299–308. doi: 10.1158/1535-7163.MCT-05-0383
48. Chou A, Froio D, Nagrial AM, Parkin A, Murphy KJ, Chin VT, et al. Tailored first-line and second-line CDK4-targeting treatment combinations in mouse models of pancreatic cancer. *Gut* (2018) 67:2142–55. doi: 10.1136/gutjnl-2017-315144
49. Zhang YX, Sicinska E, Czaplinski JT, Remillard SP, Moss S, Wang Y, et al. Antiproliferative effects of CDK4/6 inhibition in CDK4-amplified human liposarcoma *in vitro* and *in vivo*. *Mol Cancer Ther.* (2014) 13:2184–93. doi: 10.1158/1535-7163.MCT-14-0387
50. Kim S, et al. LEE011: an orally bioavailable, selective small molecule inhibitor of CDK4/6–reactivating Rb in cancer. *Mol Cancer Ther.* (2014) 12(11_Supplement):PR02. doi: 10.1158/1535-7163.TARG-13-PR02
51. Tate SC, Cai S, Ajamie RT, Burke T, Beckmann RP, Chan EM, et al. Semi mechanistic pharmacokinetic/pharmacodynamic modeling of the antitumor activity of LY2835219, a new cyclin-dependent kinase 4/6 inhibitor, in mice bearing human tumor xenografts. *Clin Cancer Res.* (2014) 20:3763–74. doi: 10.1158/1078-0432.CCR-13-2846
52. Gelbert LM, Cai S, Lin X, Sanchez-Martinez C, Del Prado M, Lallena MJ, et al. Preclinical characterization of the CDK4/6 inhibitor LY2835219: *in-vivo* cell cycle-dependent/independent anti-tumor activities alone/in combination with gemcitabine. *Invest New Drugs* (2014) 32:825–37. doi: 10.1007/s10637-014-0120-7
53. Raub TJ, Wishart GN, Kulanthaivel P, Staton BA, Ajamie RT, Sawada GA, et al. Brain exposure of two selective dual CDK4 and CDK6 inhibitors and the antitumor activity of CDK4 and 6 inhibition in combination with temozolomide in an intracranial glioblastoma xenograft. *Drug Metab Dispos.* (2015) 43:9:1360–71. doi: 10.1124/dmd.114.062745
54. Dempsey JA, Chan EM, Burke TF, Beckmann RP. LY2835219, a selective inhibitor of CDK4 and CDK6, inhibits growth in preclinical models of human cancer. *Cancer Res.* (2013) 73(8_Suppl.):LB-122. doi: 10.1158/1538-7445.AM2013-LB-122
55. Yadav V, Burke TF, Huber L, Van Horn RD, Zhang Y, Buchanan SG, et al. The CDK4/6 inhibitor LY2835219 overcomes vemurafenib resistance resulting from MAPK reactivation and cyclin D1 upregulation. *Mol Cancer Ther.* (2014) 13:2253–63. doi: 10.1158/1535-7163.MCT-14-0257
56. Kosovec JE, Zaidi AH, Omstead AN, Matsui D, Biedka MJ, Cox EJ, et al. CDK4/6 dual inhibitor abemaciclib demonstrates compelling preclinical activity against esophageal adenocarcinoma: a novel therapeutic option for a deadly disease. *Oncotarget* (2017) 8:100421–32. doi: 10.18632/oncotarget.22244
57. Flaherty KT, Lorusso PM, Demichele A, Abramson VG, Courtney R, Randolph SS, et al. Phase I, dose-escalation trial of the oral cyclin-dependent kinase 4/6 inhibitor PD 0332991, administered using a 21-day schedule in patients with advanced cancer. *Clin Cancer Res.* (2012) 18:568–76. doi: 10.1158/1078-0432.CCR-11-0509
58. Dickson MA, Tap WD, Keohan ML, D'Angelo SP, Gounder MM, Antonescu CR, et al. Phase II trial of the CDK4 inhibitor PD0332991 in patients with advanced CDK4-amplified well-differentiated or dedifferentiated liposarcoma. *J Clin Oncol.* (2013) 31:2024–8. doi: 10.1200/JCO.2012.46.5476
59. Dickson MA, Schwartz GK, Keohan ML, D'Angelo SP, Gounder MM, Chi P, et al. Progression-free survival among patients with well-differentiated or dedifferentiated liposarcoma treated with CDK4 inhibitor palbociclib: a phase II clinical trial. *JAMA Oncol.* (2016) 2:937–40. doi: 10.1001/jamaoncol.2016.0264
60. Gopalan PK, Pinder MC, Chiappori A, Ivey AM, Villegas AG, Kaye FJ, et al. A phase II clinical trial of the CDK 4/6 inhibitor palbociclib (PD 0332991) in previously treated, advanced non-small cell lung cancer (NSCLC) patients with inactivated CDKN2A. *J Clin Oncol.* (2014) 32(5_Suppl.):8077. doi: 10.1200/jco.2014.32.15_suppl.8077
61. Karasic TB, O'Hara MH, Teitelbaum UR, Damjanov N, Giantonio BJ, d'Entremont TS, et al. Phase II trial of palbociclib in patients with advanced esophageal or gastric cancer. *J Clin Oncol.* (2018) 36(4_Suppl.):68. doi: 10.1200/JCO.2018.36.4_suppl.68
62. US National Library of Medicine. ClinicalTrials.gov (2018). Available online at: https://clinicaltrials.gov/ct2/show/NCT02334527?term=palbociclib&draw=2&rank=16
63. Konecny GE, Hendrickson AEW, Jatoi A, Burton JK, Paroly J, Glaspy JA, et al. A multicenter open-label phase II study of the efficacy and safety of palbociclib a cyclin-dependent kinases 4 and 6 inhibitor in patients with recurrent ovarian cancer. *J Clin Oncol.* (2016) 34(15_Suppl.):5557. doi: 10.1200/JCO.2016.34.15_suppl.5557
64. DeMichele A, Clark AS, Tan KS, Heitjan DF, Gramlich K, Gallagher M, et al. A phase II trial of an oral CDK 4/6 inhibitor, PD0332991, in advanced breast cancer. *J Clin Oncol.* (2013) 31(15_Suppl.):519. doi: 10.1200/jco.2013.31.15_suppl.519
65. Malorni L, Curigliano G, Minisini AM, Cinieri S, Tondini CA, D'Hollander K, et al. Palbociclib as single agent or in combination with the endocrine therapy received before disease progression for estrogen receptor-positive, HER2-negative metastatic breast cancer: TREnd trial. *Ann Oncol.* (2018) 29:1748–54. doi: 10.1093/annonc/mdy214
66. US National Library of Medicine. ClinicalTrials.gov (2018). Available online at: https://clinicaltrials.gov/ct2/show/NCT03219554?term=palbociclib&draw=7&rank=65
67. Steuer CE, Papadimitrakopoulou V, Herbst RS, Redman MW, Hirsch FR, Mack PC, et al. Innovative clinical trials: the LUNG-MAP study. *Clin Pharmacol Ther.* (2015) 97:488–91. doi: 10.1002/cpt.88
68. US National Library of Medicine. ClinicalTrials.gov (2018). Available online at: https://clinicaltrials.gov/ct2/show/NCT01907607
69. US National Library of Medicine. ClinicalTrials.gov (2018). Available online at: https://clinicaltrials.gov/ct2/show/NCT01356628?term=palbociclib&draw=11&rank=101
70. US National Library of Medicine. ClinicalTrials.gov (2018). Available online at: https://clinicaltrials.gov/ct2/show/NCT02806648
71. US National Library of Medicine. ClinicalTrials.gov (2018). Available online at: https://clinicaltrials.gov/ct2/show/NCT02530320?term=palbociclib&rank=8

72. US National Library of Medicine. ClinicalTrials.gov (2018). Available online at: https://clinicaltrials.gov/ct2/show/NCT03242382?term=palbociclib&draw=4&rank=37
73. US National Library of Medicine. ClinicalTrials.gov (2018). Available online at: https://clinicaltrials.gov/ct2/show/NCT01037790?term=palbociclib&draw=15&rank=145
74. US National Library of Medicine. ClinicalTrials.gov (2018). Available online at: https://clinicaltrials.gov/ct2/show/NCT03454919?term=palbociclib&draw=2&rank=12
75. Infante JR, Cassier PA, Gerecitano JF, Witteveen PO, Chugh R, Ribrag V, et al. A phase I study of the cyclin-dependent kinase 4/6 inhibitor ribociclib (LEE011) in patients with advanced solid tumors and lymphomas. *Clin Cancer Res*. (2016) 22:5696–705. doi: 10.1158/1078-0432.CCR-16-1248
76. US National Library of Medicine. ClinicalTrials.gov (2018). Available online at: https://clinicaltrials.gov/ct2/show/NCT02345824?term=ribociclib&draw=2&rank=4
77. US National Library of Medicine. ClinicalTrials.gov (2018). Available online at: https://clinicaltrials.gov/ct2/show/NCT02571829?term=ribociclib&draw=3&rank=12
78. US National Library of Medicine. ClinicalTrials.gov (2018). Available online at: https://clinicaltrials.gov/ct2/show/NCT02420691?term=ribociclib&draw=5&rank=32
79. US National Library of Medicine. ClinicalTrials.gov (2018). Available online at: https://clinicaltrials.gov/ct2/show/NCT02300987?term=ribociclib&draw=7&rank=60
80. US National Library of Medicine. ClinicalTrials.gov (2018). Available online at: https://clinicaltrials.gov/ct2/show/NCT03096912?term=ribociclib&draw=2&rank=2
81. Patnaik A, Rosen LS, Tolaney SM, Tolcher AW, Goldman JW, Gandhi L, et al. Efficacy and safety of abemaciclib, an inhibitor of CDK4 and CDK6, for patients with breast cancer, non–small cell lung cancer, and other solid tumors. *Cancer Discov*. (2016) 6:740–53. doi: 10.1158/2159-8290.CD-16-0095
82. Shapiro G, Rosen LS, Tolcher AW, Goldman JW, Gandhi L, Papadopoulos KP, et al. A first-in-human phase I study of the CDK4/6 inhibitor, LY2835219, for patients with advanced cancer. *J Clin Oncol*. (2013) 31(15_Suppl.):2500. doi: 10.1200/jco.2013.31.15_suppl.2500
83. Goldman JW, Gandhi L, Patnaik A, Rosen LS, Hilton JF, Papadopoulos KP, et al. Clinical activity of LY2835219, a novel cell cycle inhibitor selective for CDK4 and CDK6, in patients with non-small cell lung cancer. *J Clin Oncol*. (2014) 32(15_Suppl.):8026. doi: 10.1200/jco.2014.32.15_suppl.8026
84. The ASCO Post. *Results From the Phase III JUNIPER Trial Evaluating Abemaciclib in* KRAS-*Mutated, Advanced NSCLC*. The ASCO Post (2017). Available online at: http://www.ascopost.com/News/58135
85. US National Library of Medicine. ClinicalTrials.gov (2018). Available online at: https://clinicaltrials.gov/ct2/show/NCT02152631?term=Abemaciclib&draw=3&rank=19
86. Dickler MN, Tolaney SM, Rugo HS, Cortés J, Diéras V, Patt D, et al. MONARCH 1, a phase II study of abemaciclib, a CDK4 and CDK6 inhibitor, as a single agent, in patients with refractory HR(+)/HER2(−) metastatic breast cancer. *Clin Cancer Res*. (2017) 23:5218–24. doi: 10.1158/1078-0432.CCR-17-0754
87. Tolaney SM, Lin NU, Thornton D, Klise S, Costigan TM, Turner PK, et al. Abemaciclib for the treatment of brain metastases (BM) secondary to hormone receptor positive (HR+), HER2 negative breast cancer. *J Clin Oncol*. (2017) 35:1019. doi: 10.1200/JCO.2017.35.15_suppl.1019
88. US National Library of Medicine. ClinicalTrials.gov (2018). Available online at: https://clinicaltrials.gov/ct2/show/NCT02014129?term=abemaciclib&draw=3&rank=42
89. US National Library of Medicine. ClinicalTrials.gov (2018). Available online at: https://clinicaltrials.gov/ct2/show/NCT02981940?term=Abemaciclib&draw=2&rank=2
90. US National Library of Medicine. ClinicalTrials.gov (2018). Available online at: https://clinicaltrials.gov/ct2/show/NCT02450539?term=Abemaciclib&draw=3&rank=18
91. US National Library of Medicine. ClinicalTrials.gov (2018). Available online at: https://clinicaltrials.gov/ct2/show/NCT02919696?term=Abemaciclib&draw=2&rank=6
92. US National Library of Medicine. ClinicalTrials.gov (2018). Available online at: https://clinicaltrials.gov/ct2/show/NCT03130439?term=Abemaciclib&draw=2&rank=4
93. US National Library of Medicine. ClinicalTrials.gov (2018). Available online at: https://clinicaltrials.gov/ct2/show/NCT02846987?term=Abemaciclib&draw=2&rank=5
94. US National Library of Medicine. ClinicalTrials.gov (2018). Available online at: https://clinicaltrials.gov/ct2/show/NCT03356587?term=Abemaciclib&draw=2&rank=9
95. US National Library of Medicine. ClinicalTrials.gov (2018). Available online at: https://clinicaltrials.gov/ct2/show/NCT03356223?term=Abemaciclib&draw=3&rank=14
96. US National Library of Medicine. ClinicalTrials.gov (2018). Available online at: https://clinicaltrials.gov/ct2/show/NCT03310879?term=Abemaciclib&draw=3&rank=13
97. Condorelli R, Spring L, O'Shaughnessy J, Lacroix L, Bailleux C, Scott V, et al. Polyclonal RB1 mutations and acquired resistance to CDK4/6i in patients with metastatic breast cancer. *Ann Oncol*. (2017) 0:1–6. doi: 10.1093/annonc/mdx784
98. Knudsen ES, Witkiewicz AK. The strange case of CDK4/6 inhibitors: mechanisms, resistance, and combination strategies. *Trends Cancer* (2017) 3:39–55. doi: 10.1016/j.trecan.2016.11.006

Conflict of Interest Statement: The authors declare that the research was conducted in the absence of any commercial or financial relationships that could be construed as a potential conflict of interest.

frontiers in Oncology

ORIGINAL RESEARCH
published: 17 December 2018
doi: 10.3389/fonc.2018.00625

Phage Ligands for Identification of Mesenchymal-Like Breast Cancer Cells and Cancer-Associated Fibroblasts

*Kelvin M. Jones[1], Balasubramanyam Karanam[2], Jacqueline Jones-Triche[3], Maninder Sandey[4], Henry J. Henderson[1], Rajeev S. Samant[5], Samuel Temesgen[6], Clayton Yates[2] and Deepa Bedi[1]**

[1] Department of Biomedical Sciences, College of Veterinary Medicine, Tuskegee University, Tuskegee, AL, United States, [2] Department of Biology, Center for Cancer Research, Tuskegee University, Tuskegee, AL, United States, [3] Department of Biology and Environmental Sciences, Troy University, Troy, AL, United States, [4] Department of Pathobiology, Auburn University, Auburn, AL, United States, [5] Department of Pathobiology, The University of Alabama at Birmingham, Birmingham, AL, United States, [6] Department of Pathobiology, College of Veterinary Medicine, Tuskegee University, Tuskegee, AL, United States

OPEN ACCESS

Edited by:
Zhe-Sheng Chen,
St. John's University, United States

Reviewed by:
Dongmei Zhang,
Jinan University, China
Ning Ji,
Tianjin Medical University, China

***Correspondence:**
Deepa Bedi
dbedi@tuskegee.edu

Specialty section:
This article was submitted to Cancer Molecular Targets and Therapeutics, a section of the journal Frontiers in Oncology

Received: *08 July 2018*
Accepted: *03 December 2018*
Published: *17 December 2018*

Citation:
Jones KM, Karanam B, Jones-Triche J, Sandey M, Henderson HJ, Samant RS, Temesgen S, Yates C and Bedi D (2018) Phage Ligands for Identification of Mesenchymal-Like Breast Cancer Cells and Cancer-Associated Fibroblasts. Front. Oncol. 8:625. doi: 10.3389/fonc.2018.00625

Epithelial to mesenchymal transition (EMT) is believed to be crucial for primary tumors to escape their original residence and invade and metastasize. To properly define EMT, there is a need for ligands that can identify this phenomenon in tumor tissue and *invivo*. A phage-display selection screening was performed to select novel binding phage peptides for identification of EMT in breast cancer. Epithelial breast cancer cell line, MCF-7 was transformed to mesenchymal phenotype by TGF-β treatment and was used for selection. Breast fibroblasts were used for subtractive depletion and breast cancer metastatic cell lines MDA-MB-231, T47D-shNMI were used for specificity assay. The binding peptides were identified, and their binding capacities were confirmed by phage capture assay, phage-based ELISA, immunofluorescence microscopy. The phage peptide bearing the 7-amino acid sequence, LGLRGSL, demonstrated selective binding to EMT phenotypic cells (MCF-7/TGF-β and MDA-MB-231) as compared to epithelial subtype, MCF-7, T47D and breast fibroblasts (Hs578T). The selected phage was also able to identify metastatic breast cancer tumor in breast cancer tissue microarray (TMA). These studies suggest that the selected phage peptide LGLRGSL identified by phage-display library, showed significant ability to bind to mesenchymal-like breast cancer cells/ tissues and can serve as a novel probe/ligand for metastatic breast cancer diagnostic and imaging.

Keywords: Phage display, breast cancer, fibroblasts, EMT, cancer-associated fibroblasts

INTRODUCTION

Breast cancer is the most common cancer in women and the second leading causes of death due to cancer (1). The cause of death in breast cancer is often due metastasis to distant sites, resulting in organ failure accounting for a 5-year survival rate of 23%. Evidences support the observation that metastasis is an early event in breast cancer progression (2), with possibly up to 90% of patients already having metastasis at the time of diagnosis. Studies have shown that dissemination of cancer cells and metastasis into distant organs is often preceded by an epithelial to mesenchymal transition

(EMT) of cancer cells (3), which allows cancer cells to dedifferentiate, acquire mesenchymal including fibroblast-like morphology, enhanced migratory and invasive properties, enabling them to invade through the stroma and migrate and seed to distant organs (4, 5). The concept of EMT in breast cancer has been well demonstrated in numerous *invitro* studies in different normal, malignant mammary epithelial cells and in mouse models of mammary cancers (6, 7). It has been suggested that tumor microenvironment (8) and growth factors such as transforming growth factor-β (TGFβ), epidermal growth factor (EGF), platelet-derived growth factor (PDGF) has a dramatic effect on epithelial phenotype and in promoting motility and invasiveness via the induction of EMT (9, 10). TGFβ treatment changes epithelial cells from cubodial shape to more elongated ones with concomitant loss of epithelial markers and increased expression of mesenchymal markers vimentin, fibronectin and α-smooth muscle actin (11). These EMT markers are also present in activated cancer-associated fibroblasts (CAF's), which contributes to the pathogenesis of tumor progression and invasiveness (12). Several studies support a physiologic role of EMT during tumor progression (13–15) by monitoring EMT progression by the cadherin switch, E-cadherin to N-cadherin, which is normally also present in mesenchymal cells, fibroblasts, neural tissue (16). Similarly, vimentin is also often used to define cancer cells undergoing EMT, is also present in fibroblasts, endothelial cells, cells of the hematopoietic lineages, and glial cells (17, 18). There is a lack of specific ligands that can recognize mesenchymal-like cancer cells and define EMT in tumor and in cancer-associated fibroblasts.

Phage display offers great advantage as a high throughput profiling technology based on peptide libraries present on the surface of bacteriophage. Selective binding of phages from a library with billions of diversified peptides can make a clear distinction between two morphological same but functionally different targets and thus offers a complementary approach for comparative screening. Usually peptides can be displayed on the N-terminus of pIII protein coat protein (pIII phage display), which is displayed at one end of the filamentous phage in 3–5 copies (19) or can be displayed on the N-terminus of all copies of pVIII major coat protein (20). Diversity of pIII or pVIII combinatorial phage library has been exploited extensively to explore the cell surface repertoire of various cancer cells such as colon (21), prostate (22, 23), pancreatic (24), breast (25, 26) and to select many cell surface or cell internalizing peptides. Some of these highly specific and high affinity ligands have been used as diagnostic (24), molecular and targeting agents (27–30). Additionally, lamba (T7) phage display has been used to identify vascular zip codes (31) and markers for angiogenesis (32). These studies and more define the power of using combinatorial phage display to identify molecular differences and interactive regions of the proteins without knowing the nature of interaction.

In this study, we propose a novel and innovative study to use phage display libraries for identification of phages that can specifically and selectively bind to the mesenchymal breast cancer cells *invitro*. Since TGFβ is a known inducer of EMT, we have used a model of TGFβ induced EMT in MCF-7 breast cancer cells, (MCF-7/TGFβ) for selection of EMT-specific phages. CX7C PhD phage library was used for selection of phages binding to MCF-7/TGFβ cells after subtractive depletion from breast fibroblasts. These selected phages were then tested on breast cancer cells that exhibited EMT phenotype (MDA-MB-231 and T47D-shNMI) and breast cancer TMA of primary and metastatic site. The phage peptide LGLRGSL displayed specific binding to the EMT breast cancer cells as well recognized tumor in TMA's at primary as well as metastatic site.

MATERIALS AND METHODS

Materials

PhD CX7C phage library was purchased from New England Biolabs (NEB). Fetal calf serum (FCS) and cell culture media (Dulbecco's modified Eagle's medium, DMEM) was purchased from Sigma (USA). The phage display library contains random peptides constructed at the N terminus of the minor coat protein (cpIII) of M13 phage. The library contains a mixture of 3.1×10^9 individual clones, representing repertoire of phages with 7-mer peptide sequences, which expresses random 7-amino-acid sequences. The *Escherichia coli* host strain ER2738 (F+ strain, New England Biolabs) was used for M13 phage propagation. The human breast cancer cell lines MDA-MB-231, MCF-7 and breast fibroblasts (Hs 578T) were purchased from the American Type Culture Collection. MCF-7 cells were treated 1ng/mL of TGFβ for 16 days. MCF-7, MDA-MB-231, MCF-7/TGFβ, breast cancer cells, and SW620, colon cancer cells, were maintained in DMEM supplemented with 10% fetal bovine serum (Sigma) at 37°C. PC3, prostate cancer cells, were cultured in RPMI1640 media supplemented with 10% FBS at 37°C.Breast fibroblasts (Hs578T) were maintained in special hybricare medium supplemented with 15% FBS (ATCC).

Validation of EMT Marker in MCF7/TGFβ Cells by Western Blot

MCF-7 and MCF-7/TGFβ cells were grown in 25 cm^2 flask to 75–80% confluency. Confluent cells were lysed in ice-cold complete 1x RIPA buffer (PMSF solution, sodium orthovanadate solution, protease inhibitor cocktail solution, and 1x lysis buffer) (Santa Cruz Biotechnology, Santa Cruz, CA, United States). The protein concentration in the samples was quantified using the BCA Protein Assay Kit (Pierce Biotechnology, Rockford, IL, United States). Thirty microgram of protein from each sample was separated by a 4–12% SDS-PAGE gel and then transferred to a 0.2 μm polyvinylidene difluoride (PVDF) membrane. Membranes were blocked with 5% nonfat dry milk in PBS-T for 45 min and then incubated with the E-cad herin (Abcam, UK) or N-cadherin (Abcam, UK) primary antibody (1:1,000) overnight at 4°C. After washing, membranes were incubated with horseradish peroxidase (HRP)-conjugated secondary antibody (1:2,000). Subsequently, membranes were washed and blots were visualized using enhanced chemiluminescence. The membrane was stripped with mild stripping buffer and reprobed with β-actin (Cell Signaling, Danvers, MA, United States) to verify that equal

amount of protein was loaded. The relative quantification was normalized against β-actin using image J image analysis software.

In vitro Phage Selection

Biased protocol for selection of phages was employed as described (26) with some modifications. The PhD phage library (Cx7C) was depleted against a cell culture flask and breast fibroblasts (Hs578T). Unbound phages recovered from the depletion were incubated with confluent MCF-7/TGFβ cells at room temperature for 1 h. Unbound phages were washed away and cell-associated phages were eluted with elution buffer (200 mM glycine-HCl, 1 mg/ml BSA, 0.1 mg/ml phenol red, pH 2.2) for 10 min on ice. The eluate was neutralized with 376 μl of 1 M Tris (pH 9.1). Internalized phages were recovered with lysis buffer [2% CHAPS, 10 mM Tris, 2 mM EDTA (pH 8.0)] after further washing and propagated in bacteria to determine their titer as described previously (29). The results were expressed as a percentage of a ratio of output to input phage. The eluted phage and cell-internalized phage were amplified separately in bacteria and used in the second and third round of selection using the same protocol of depletion of the amplified phages (lysate and eluate) against breast fibroblasts and incubating MCF-7/TGFβ cells with unbound phages recovered from depletion. Sixty phages from the third round of selection were randomly picked and were propagated in the ER2738 bacteria. DNA was isolated form these 60 propagated clones using DNA isolation kit (QIAGEN GmbH, Hilden, Germany) and individual phage DNA sequences were identified. A sequencing primer used was 5′-CCC TCA TAG TTA GCG TAA CG-3′ (−96 gIII sequencing primer, provided in the Ph.D.-CX7C Phage display peptide library kit (NEB, MA).

Cell-Based ELISA and Phage Capture Assay

Selected phage clones were characterized for their selectivity toward EMT cells, MCF-7/TGFβ and MDA-MB-231 breast cancer cells in comparison with epithelial breast cancer cells, MCF-7, T47D, and breast fibroblasts using phage capture assay (29) and cell-based ELISA.

Briefly, in phage capture assay, target cells MCF-7/TGFβ, MDA-MB-231, MCF-7, T47D, T47D-shNMI, breast fibroblasts (Hs578T), PC3 (metastatic prostate cancer cells) and SW620 (metastatic colon cancer cells) were cultured in triplicate to confluence in separate wells of 12-well cell culture plates. Cells were incubated with phage (1×10^{10} pfu) at RT for 1.5 h. Cells were washed with 100 μl washing buffer for 5 min eight times to remove non-specifically interacting unbound phages. Cells were lysed with 50 μl lysis buffer (2.5% CHAPS) for 10 min on a rocker and the lysate containing phages was titered in *E. coli* ER2738 bacterial cells. Phage titer was calculated as a ratio of output to input phage.

ELISA:

Confluent monolayers of MCF-7/TGFβ, MDA-MB-231, MCF-7, T47D, T47D-shNMI and breast fibroblasts (Hs578T) cells were incubated at room temperature with individual phage clones (10^{10} PFU), for 1.5 h at RT. Subsequently, cells were washed with PBS containing 0.1% Tween-20, incubated with primary anti-M13-biotin antibody (1:1,000), for 1 h, at RT. Cells were washed again with PBS containing 0.1% Tween-20, incubated with secondary antibody streptavidin-HRP (1:2,000, 45 min, RT), developed with tetra methyl benzidine and read at absorbance 650 with microplate reader (BioTek).

Phage Capture Assay of Phage Binding to Cancer-Conditioned Media Activated Fibroblasts

Breast fibroblasts (Hs578T) were plated in a 12.5 cm^2 flask cultured until approximately 70% confluent. Once properly confluent, fibroblasts were then cultured in MDA-MB-231 conditioned media or normal fibroblasts media for 72 h. Thereafter, they were exposed to E11 phage (10^8 pfu) for 2 h and analyzed for binding in phage capture assay as described above.

Immunofluorescence Study of Selected Phages

MCF-7, MCF-7/TGFβ, MDA-MB-231 and Hs578T (breast fibroblasts) cells were seeded in 4-well chamber overnight. On next day, cells were fed with fresh medium. Phage LGLRGSL (E11) (10^8 pfu) was added in fresh medium and incubated at RT for 1 h. After removing the unbound phages, cells were washed with wash buffer (0.1% tween-20 in PBS) three times and fixed with 4% formaldehyde for 15 min at 37°C. Thereafter, cells were permeabilized with 0.2% Triton X-100 at RT for 10 min. Then, cells were washed with TBS 3 times. Before incubation with anti-phage antibody, cells were treated with blocking buffer for 30 min at RT. Cells were incubated with M13-pIII monoclonal antibody for 1 h at RT, washed and incubated with the secondary goat anti-mouse IgG antibody labeled with Alexa Flour® 488 (Molecular Probes) (1:500 in PBS containing 1% BSA) for 45 min at RT. Subsequently, cells were washed three times and stained with TOTO-3 for nucleus staining. Prolong Gold Anti-fade Reagents was used on the cells which were then covered with cover slides. Pictures were taken by using the NIKON eclipse TE 2000-E confocal microscope. The fluorescence intensity of the images was quantified using image J software.

Phage Binding to Breast Cancer Tissue Microarrays

The breast tissue microarrays were purchased from Novus Biological (Littleton, CO). TMA included 40 breast cancer infiltrating ductal carcinoma, 10 metastatic lymph node and 9 adjacent normal breast tissues. Clinico-histopathologic characteristics of the subjects in the tissue microarray study included grade, age, hormone status and clinical stage, according to information provided by the suppliers. Tissues were de-paraffinized in xylene, rehydrated in graded alcohols and endogenous peroxidase activity was quenched with 3% hydrogen peroxide for 5 min. Slides were treated with LGLRGSL phage (10^{10} pfu) overnight. Slides were subsequently washed and blocked by 3% goat serum at RT for 1 h in humidity chambers. Slides were then treated with M13-pIII phage monoclonal

antibody (NEB, MA) or Vimentin antibody (Cell Siganling, Danvers, MA, United States) (1:100) and then subsequently with HRP conjugated goat anti-mouse secondary antibody (Jackson Immunoresearch Laboratories Inc., West Grove, PA, United States) for 40 min. The antigen-antibody reaction was visualized after applying diaminobenzidine (Sigma-Aldrich, MO, United States) for 7 min. The slides were counterstained with hematoxylin (Sigma-Aldrich, MO, United States) for 1 min. Slides were dehydrated in alcohols and cleared in xylene baths before being mounted with Permount media.

Statistics

The significance of difference between two variables was assessed by the Student's *t*-test. The difference was considered significant if the *p*-value was <0.05. Data from all experiments are expressed as mean ± standard error (SD). All statistical calculations were performed using GraphPad Prism and Microsoft Excel.

RESULTS

Selection of Phages Binding to Breast Cancer Cells That Have Undergone EMT

MCF-7 (epithelial-luminal subtype) breast cancer cells were transformed into mesenchymal phenotype by long-term treatment with TGFβ (1 ng/mL for 16 days). **Figure 1A** shows the change of MCF-7 breast cancer cells change in morphology upon TGFβ treatment. Since reduction in E-cadherin and upregulation of mesenchyme markers, is a hallmark of metasatatic carcinoma's

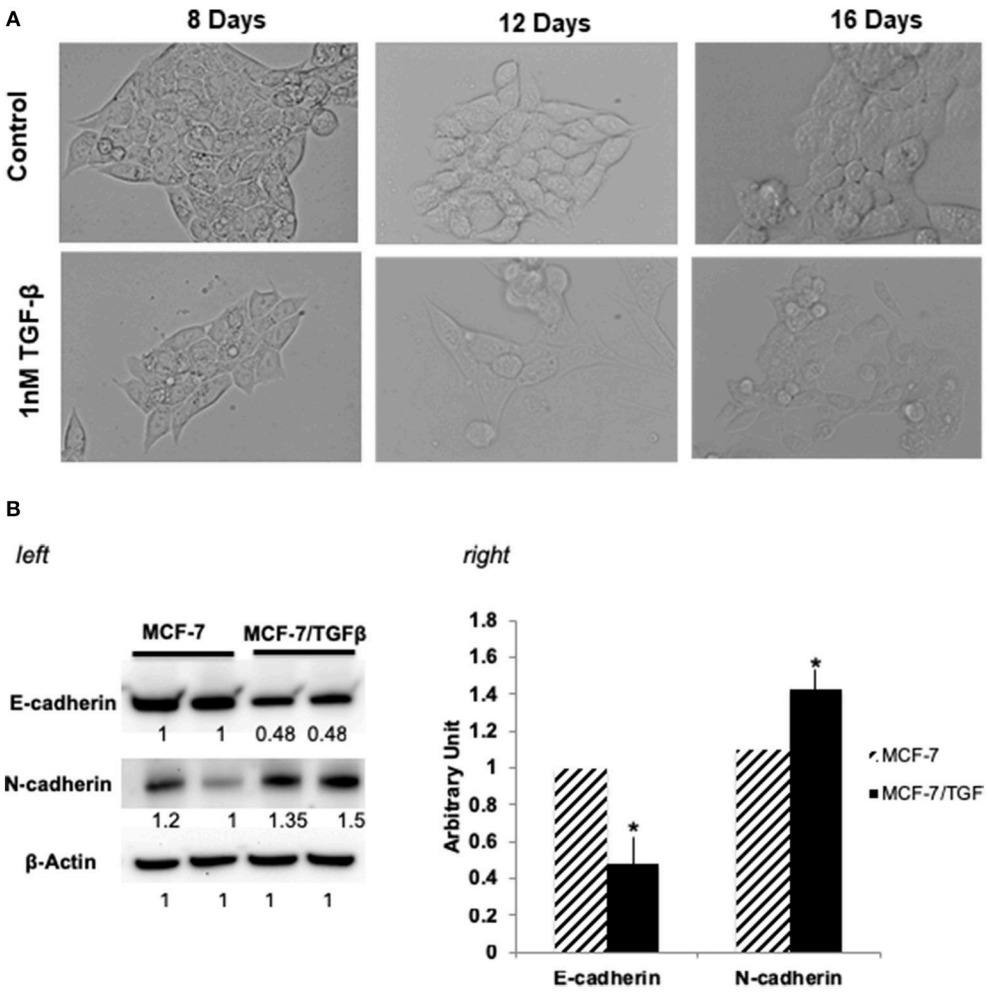

FIGURE 1 | (A) Morphological change in MCF-7 cells during TGFβ –induced EMT. Images of cells treated long term (16 days) with TGFβ showing spindle-shaped morphology as compared with control. Images were acquired by phase contrast microscopy using a 20 × objective. **(B) (left)** Immunoblot analysis of expression of EMT-related proteins. Protein expression levels of E-cadherin in TGFβ-treated MCF-7 cells were markedly decreased, whereas expression levels of N-cadherin and vimentin (mesenchymal markers) were dramatically increased. Numbers below each panel indicate the relative integrated density of the protein band in that lane. **(right)** Quantification analysis of the Western blot data showing the change in EMT markers (E-cadherin and N- cadherin) in MCF-7/TGFβ cells vs. MCF-7 breast cancer cells. The relative quantification was normalized against β-actin using image J image analysis software. All data represent the mean± S.D of three different experiments. *p <0.05, student-*t*-test.

and indication of EMT (33, 34), following treatment MCF-7/TGFβ cells were validated for EMT transition by looking at the protein expression of E-cadherin and N-cadherin (mesenchymal marker) (35). Consistent with literature that (33) demonstrated that TGFβ treatment downregulates E-cadherin expression in MCF-7 cells, our Western blot data confirmed these observations. **Figure 1B** showed downregulation of E-cadherin and upregulation of N-cadherin protein expression in MCF-7/TGFβ cells as compared to MCF-7 cells.

CX7C PhD phage library (NEB) was used to find phage clones that bind with high specificity and selectivity to MCF-7/TGFβ cells. Extensive depletion of the phage library against plastic, breast fibroblasts before enrichment of phage that interact with MCF-7-TGFβ breast cancer cells was employed for a robust selection of phage clones specific for cancer cells. This negative selection step was also performed after each round of panning on the MCF-7-TGFβ cells. Three such rounds of biopanning were performed on and in every round, phage library and sub-library was depleted against breast fibroblasts to preferentially select for phages that did not bind to normal fibroblasts. Phages associated with cells were eluted sequentially with acid and detergents. Titer of the phage increased from one round to another indicating successful enrichment for phage clones that bind to the target MCF-7-TGFβ cells (**Figure 2**). After the third round of selection, 100 phage clones were randomly picked after titering of the eluate and lysate fractions. Their DNA was isolated, sequenced and translated to reveal the sequence of the pIII fusion peptides. In total, 21 phage clones were isolated and classified based on their consensus foreign peptide motifs (**Table 1**).

Selectivity of Phages Toward Mesenchymal-Like Breast Cancer Cells

Phage clones obtained by screening of the CX7C phage library against MCF-7/TGFβ cancer cells were tested for their selective binding toward the target MCF-7/TGFβ, MDA-MB-231, T47D-shNMI cells and not to breast fibroblasts or epithelial subtype breast cancer cells MCF-7 and T47D in phage capture assay (**Figures 3A,B**) and phage based ELISA (**Figure 3C**).

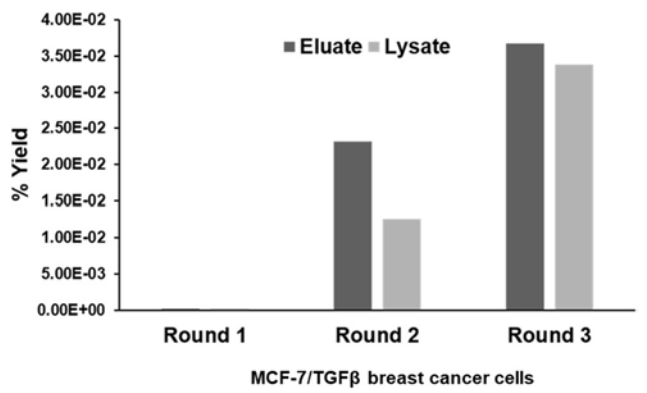

FIGURE 2 | Specific enrichment of eluate and lysate MCF-7/TGFβ cell-binding phage isolated from PhD CX7C library during three rounds of selection. The titer of recovered phages from each round was evaluated by blue plaque-forming assay on agar plates. The phage enrichment rate was calculated as yield (%), which is as output number/input number x100.

These cells lines MCF-7/TGFβ, MDA-MB-231, T47D-NMI exhibit mesenchymal phenotype or markers of EMT and are aggressive, are structurally similar to fibroblasts and expresses markers of EMT and thus are representation of EMT in breast cancer cells. MDA-MB-231 breast cancer cell line exhibit mesenchymal phenotype and are detonated EMT phenotype (36). T47D is an epithelial breast cancer cell line and was transitioned to EMT by silencing a gene, N-myc and STAT interactor (37).

In these assays, some phages demonstrated high selectivity toward EMT cells, while other phage showed selectivity for epithelial breast cancer cells as well as breast fibroblasts. Phages were considered selective if their relative binding to EMT phenotypic cells (MCF-7/TGFβ, MDA-MB-231, and T47D-shNMI) and were at least five times higher than those of epithelial breast cancer cells (MCF-7 and T47D) and breast fibroblasts. KGDYKLF (L42), phage selected from lysate fraction, showed high specificity toward MDA-MB-231 cells but not so selective toward MCF-7/TGFβ, MCF-7 and breast fibroblasts. Phages selected from eluate fraction, LGLRGSL (E11), GTFLFS (E32), and PNLPWVP (E45) were very selective for EMT phenotypic cells (MCF-7/TGFβ, MDA-MB-231, and T47D-shNMI) and

TABLE 1 | Displayed phage peptide sequences from isolated eluate and lysate phages from third round of selection against MCF/TGFβ breast cancer cells.

ELUATE PHAGE PEPTIDE SEQUENCES							
E9	I	L	N	C	M	R	N
E11	L	G	L	R	G	S	L
E12	A	R	K	T	N	P	L
E16	F	N	G	P	H	T	R
E20	T	K	F	H	F	S	G
E25	D	F	L	T	A	R	L
E29	N	T	F	S	W	H	T
E32	G	T	F	L	F	S	
E42	N	T	L	R	T	P	Y
E43	H	H	D	N	V	A	M
E45	P	N	L	P	W	V	P
E46	Y	E	H	H	P	R	I
E48	H	M	R	Q	G	M	A
LYSATE PHAGE PEPTIDE SEQUENCES							
L5	T	H	S	S	W	G	M
L9	N	M	W	E	S	V	P
L10	R	E	G	H	M	G	V
L24	K	D	S	H	E	P	W
L27	T	L	A	T	G	G	M
L30	P	Y	E	P	R	A	T
L42	K	G	D	Y	K	L	F
L45	S	I	L	S	K	N	H
L46	E	R	S	G	M	H	S
L47	H	W	P	A	K	H	I
L49	P	V	L	L	G	E	S

showed more than 10 times binding as compared to its binding to breast fibroblasts (Hs578T) and epithelial breast cancer cells (MCF-7 and T47D) in phage capture assay (**Figure 3A**). Phage E11 was confirmatory toward EMT cells in phage-based ELISA (**Figure 3B**) and thus was chosen for further characterization.

To determine if E11 could recognize EMT phenotype in other cell types of tumor microenvironment, E11 was screened against activated fibroblasts (fibroblasts converted to CAF's by treatment with cancer-conditioned media). E11 demonstrated higher binding (twice as much) to activated-fibroblasts than normal fibroblasts (**Figure 3C**). To see if E11 can recognize EMT on cancer other than breast, E11 was screened against other metastatic cancer cells, PC3 (prostate cancer) and SW620 (colon cancer) in phage capture assay. PC3 is a highly metastatic prostate cancer cell line and exhibits EMT phenotype (38, 39). SW620 are highly tumourigenic, metastatic and exhibit fibroblasts like morphology (40). E11 showed comparable binding to PC3 and SW620 like MDA-MB-231 (**Figure 3D**), which demonstrates that it is binding to a receptor common to metastatic phenotype.

Affirmation of Phages Binding to Target Cells *in vitro* Using Immunofluoresence Analysis

To further affirm the specificity of LGLRGSL (E11) toward breast cancer cells with an EMT phenotype, immunofluorescence microscopy of intact target mesenchymal phenotypic cells (MCF-7/TGF β and MDA-MB-231), control MCF-7 breast cancer cells and breast fibroblasts (Hs578T) was employed. All cells were treated with the phage (10^8 pfu) at RT for 1 h, and subsequently incubated with primary anti-pIII antibody and then stained with secondary anti-mouse Alexa fluor 488 secondary antibody. LGLRGSL (E11) showed almost no binding to breast fibroblasts (**Figure 4A**), some staining to MCF-7 cells (**Figure 4B**), while abundant binding to EMT cells, MCF-7/TGFβ (**Figure 4C**) and MDA-MB-231 (**Figure 4D**) as shown by green fluorescent phage staining and analysis (**Figure 4E**). We did not observe any background antibody as shown in the respective controls of cells treated with just primary and secondary antibodies.

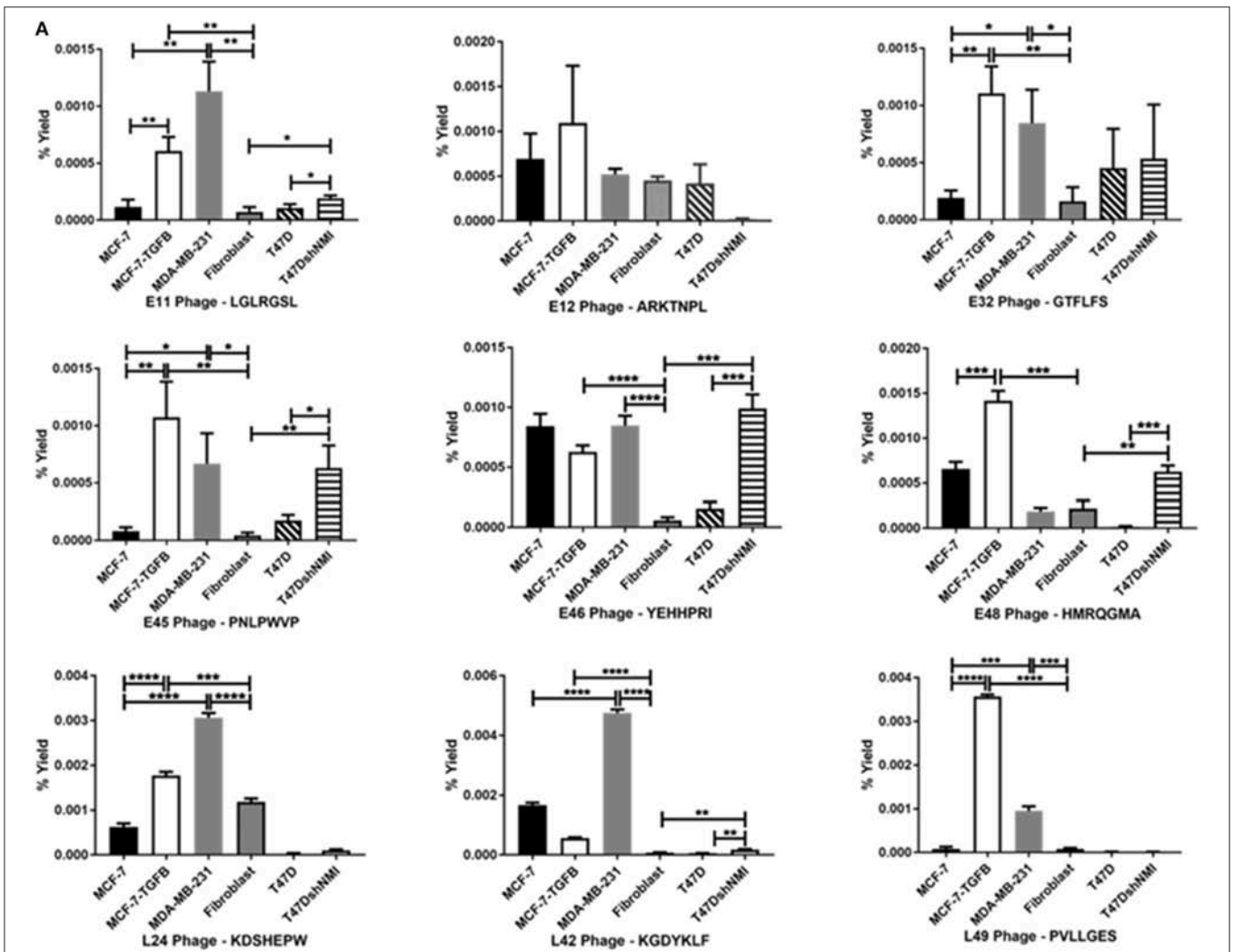

FIGURE 3 | continued

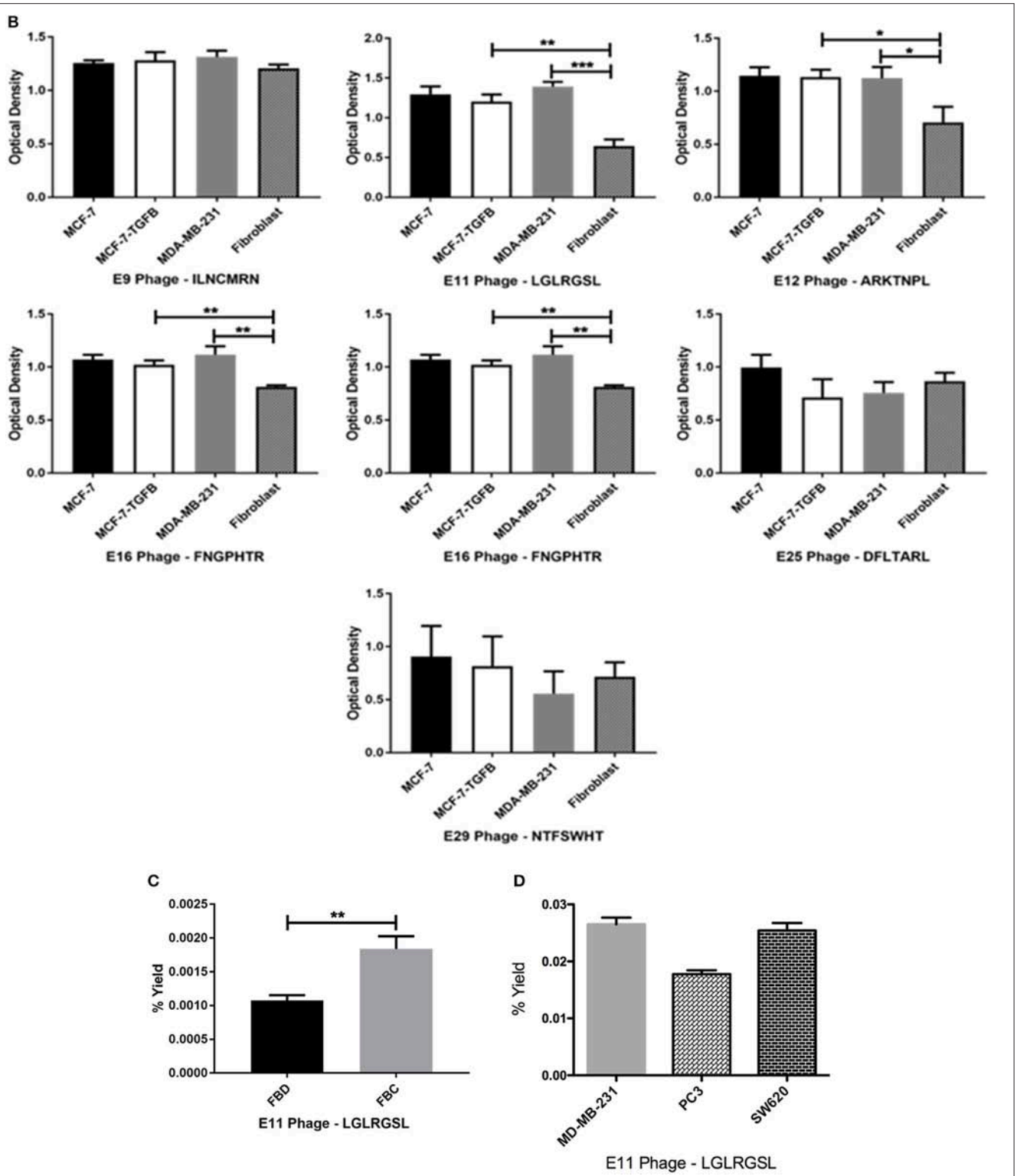

FIGURE 3 | Affinity selected eluate and lysate phage showed higher binding to MCF-7-TGFβ, MDA-MB-231, T47D-shNMI cells as compared to breast fibroblasts, T47D and MCF-7 cells in **(A)** phage capture assay; **(B)** in phage based-ELISA; **(C)** LGLRGSL (E11) was also highly reactive to activated fibroblasts. FBD denotes fibroblasts in normal fibroblast media and FBC denotes fibroblasts in MDA-MB-231 breast cancer cell conditioned media and **(D)** LGLRGSL showed comparable binding to PC3 and SW620 cancer cells as compared to MDA-MB-231 cancer cells. All data represent the mean± S.D. $^{*}p < 0.05$, $^{**}p \leq 0.01$, $^{***}p \leq 0.001$, and $^{****}p \leq 0.0001$.

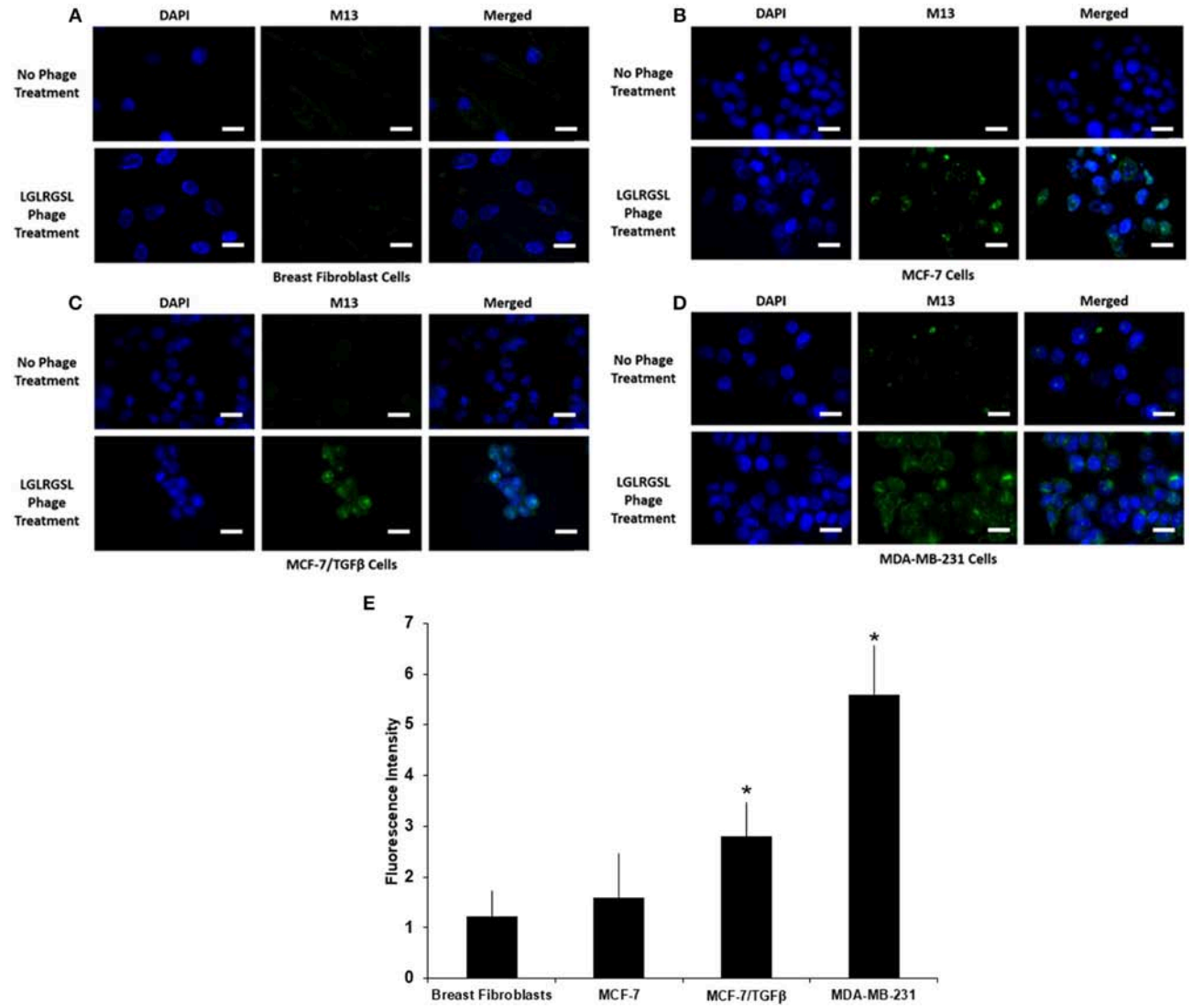

FIGURE 4 | A. Phage peptide LGLRGSL (E11) stained selective to EMT phenotypic cells in immunofluorescence microscopy analysis upper, **(A)** Breast Fibroblast, **(B)** MCF-7, **(C)** MCF-7/TGFβ, and **(D)** MDA-MB-231 cells without phage exposure; stained with DAPI and Alexa 488 secondary antibody, lower, **(A)** Breast Fibroblasts, **(B)**MCF-7, **(C)** MCF-7/TGF β, and **(D)**. MDA-MB-231 exposed to phage; stained with M13 primary antibody, DAPI and Alexa 488 secondary antibody. Scale bar is 20 μm. **(E)** Quantification data of the fluorescence intensity of the Breast fibroblasts, MCF-7, MCF-7/TGFβ, and MDA-MB-231 breast cancer cells. The fluorescence intensity of the images was quantified using Image J software. All data represent the mean± S.D of three different experiments. *p <0.05, student-t-test.

Validation of Phage Peptide Binding to Human Breast Cancer *Exvivo*

Next, we investigated the clinical relevance of these findings by assessing if LGLRGSL (E11) could be used to prospectively identify human invasive ductal carcinoma (IDC) breast tumors with a propensity to metastasize as metastatic cells undergo EMT before metastasizing (41). Immunostaining for phage in human breast cancer tissue indicated phage has substantial staining for invasive ductal breast cancer carcinoma (**Figures 5A–C**, left) and its staining intensity increased in tumors invading into adjacent lymph nodes (**Figure 5D**). Furthermore, we did not observe any binding in normal breast tissues (**Figure 5E**). Interestingly we observed that vimentin, a mesenchymal marker, within the same TMA (**Figures 5A–C**, right) demonstrated a different staining pattern than the LGLRGSL (E11) phage. While vimentin showed stromal staining, phage was immunoreactive to the tumor cells with robust staining around the invasive or leading edge of the tumor-stromal interaction.

DISCUSSION

There is accumulating evidence to show that epithelial cells can undergo transformation into migratory fibroblast-like mesenchymal cells in a process called EMT (Epithelial-to-Mesenchymal Transition). Normally, an embryo and organ development related phenomenon, EMT is believed to be crucial

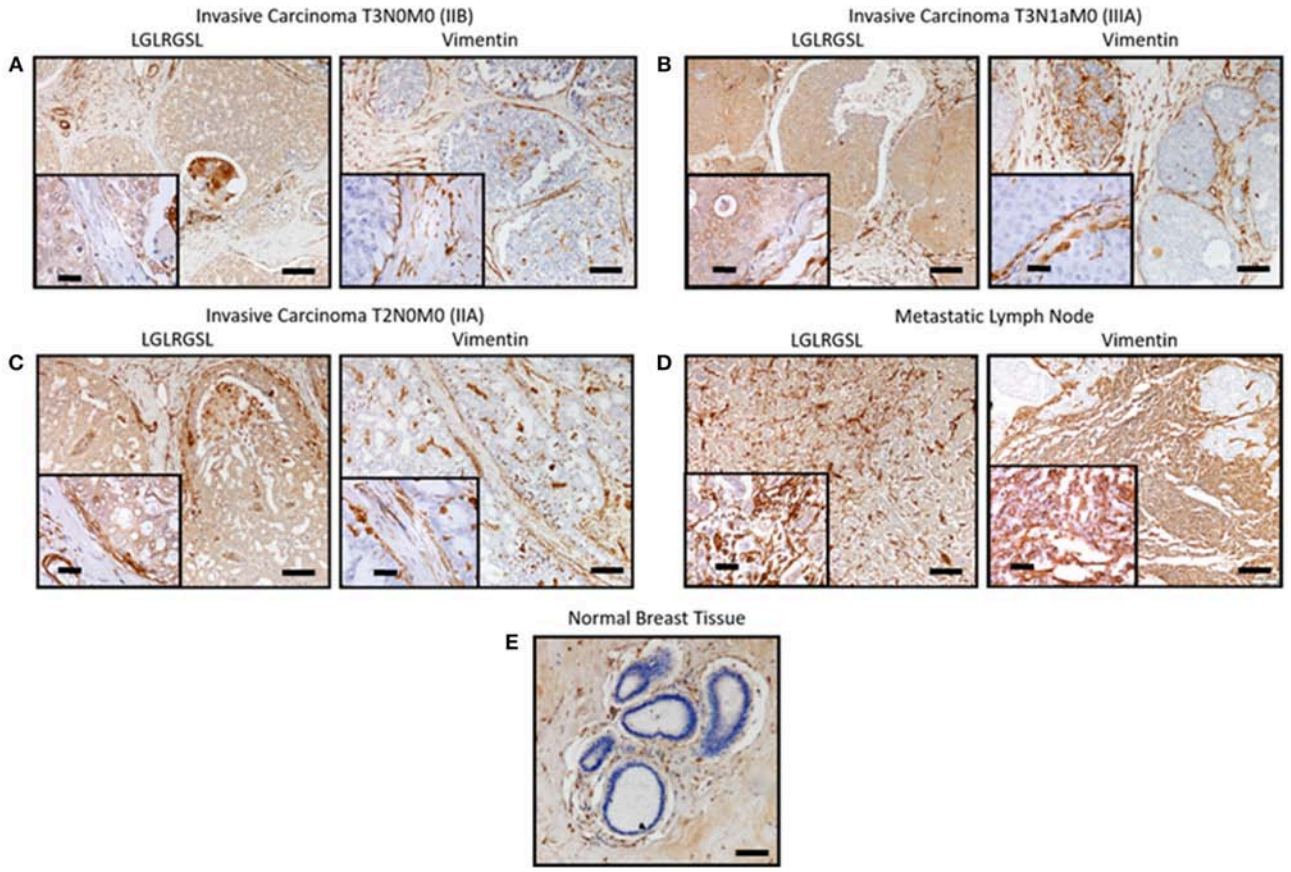

FIGURE 5 | *Ex vivo* phage binding to human breast cancer tissue microarray. Tissue microarray of invasive ductal carcinoma and adjacent normal tissues were incubated with 10^{10} pfu of LGLRGSL phage or Vimentin antibody and then subsequently with M13-pIII antibody for phage and secondary peroxidase antibody for phage and Vimentin, imaged with a digital light microscope. Strong brown staining of the phage and Vimentin was observed in invasive ductal carcinoma sections **(A–C)** and metastasis in lymph nodes, **(D)** while no staining was observed in normal breast tissue, **(E)** Scale Bar is 40 and 10 μm for the inserts.

for primary tumors to escape their original residence and invade and metastasize to other organs such as liver, lungs, bone and brain (42). Moreover, EMT is also a critical determinant of stemness and drug-related relapse (6, 41, 43). EMT of breast cancer cells is, in large part, dependent oncontingent on the tumor microenvironment (44). Because of the close cross-talk between the cancer cells and CAFs, it is evident that the development of cancer cannot be dissociated from its local microenvironment (45). Tumor cells signals stromal fibroblast cells and activate them into cancer-associated fibroblasts (CAFs) to undergo EMT through the stimulation of paracrine growth factors (46, 47) promotes EMT, cell survival (48) and progression (49) of cancer cells. To better understand the events involved from acquiring motility for invasion to seeding in distant organs, there is a need to develop probes that can selectively bind to invasive, metastatic and tumor-progressing CAF's (46). Such ligands can further ascertain the role of EMT in cancer metastasis and could enable the development of new approaches in the management of this disease.

In this study, we have successfully isolated phage ligands using CX7C phage library for EMT transformed breast cancer cells, MCF7/TGFβ and MDA-MB-231 by employing subtractive depletion of phages binding to breast fibroblasts. The optimizing procedures (several rounds of subtractive screening) were performed to improve the probability of successful selection, which is highly dependent on obtaining specific phages with high selectivity. The isolated clones were used in cell-ELISA and *invitro* phage capture assay to confirm their specificity to EMT phenotype cells, MCF-7/TGFβ, MDA-MB-231 and T47D-shNMI cells *in vitro* as compared to epithelial subtype cells, MCF-7, T47D and mesenchymal breast fibroblasts (Hs578T). Phage capture assay and ELISA demonstrated the selective affinity of various phages to EMT phenotype.

The best candidate, LGLRGSL (E11), was then selected for immunocytochemical assays. Immunofluorescence studies confirmed the selectivity of LGLRGSL (E11) to the target mesenchymal-like cells as there was minimal binding to the non-target epithelial breast cancer cells and mesenchymal breast fibroblasts. E11 also bound with great affinity to PC3, prostate cancer cells and SW620, colon cancer cells. It's binding to these other cancer cell type was as comparable as to MDA-MB-231 breast cancer cells. These findings suggest that LGLRGSL (E11) is

recognizing a receptor/antigen on mesenchymal-like cancer cells that are highly invasive and metastatic in nature and would be a useful probe to identify invasive front and metastatic tumor cells. Phage probing to the breast cancer tissue microarray identified tumor representing high grade and lymph node metastasis. When compared to Vimentin, a marker of mesenchymal-like cells metastasis, phage had more positive staining to the invasive front and lymph node metastasis.

More work is needed to characterize LGLRGSL (E11) as ligand binding to EMT marker of cancer origin. One such direction is the identification of the receptors responsible for LGLRGSL (E11) phage binding to the mesenchymal-like cells, that may allow for the discovery of novel cell surface molecules, which may yield future targets for drug design.

In conclusion, the 7-amino acid phage peptide, LGLRGSL, obtained by phage-display technology showed significant ability to bind to EMT breast cancer cells *in vitro* and tissues array *exvivo*. The phage peptide can be used for preparation of targeted devices for drug and gene delivery to metastatic cells; development of probes for molecular imaging of metastasis; and identification and isolation of cancer-specific receptors as potential components for development of therapeutic antibodies, anticancer vaccines and diagnostics.

AUTHOR CONTRIBUTIONS

KJ study design, performed experiments, data analysis and interpretation, and manuscript preparation. KJ, BK, JJ-T, HH and MS: performed experiments and data analysis. RS, ST, CY, and DB project supervision, study design, and manuscript preparation.

ACKNOWLEDGMENTS

This work was supported by SC2CA211028-03 (DB) (NIH/NCI/NIGMS) and U54-MD007585-26 (NIH/RCMI) [CY], U54 CA118623 (NIH/NCI) [CY], (NIH/NCI).

REFERENCES

1. Jemal A, Siegel R, Ward E, Hao Y, Xu J, Thun MJ. Cancer statistics, 2009. *Cancer J Clin.* (2009) 59:225–49. doi: 10.3322/caac.20006
2. Weng D, Penzner JH, Song B, Koido S, Calderwood SK, Gong J. Metastasis is an early event in mouse mammary carcinomas and is associated with cells bearing stem cell markers. *Breast Cancer Res.* (2012) 14:R18. doi: 10.1186/bcr3102
3. Tsai JH, Donaher JL, Murphy DA, Chau S, Yang J. Spatiotemporal regulation of epithelial-mesenchymal transition is essential for squamous cell carcinoma metastasis. *Cancer Cell* (2012) 22:725–36. doi: 10.1016/j.ccr.2012.09.022
4. Menezes ME, Devine DJ, Shevde LA, Samant RS. Dickkopf1: a tumor suppressor or metastasis promoter? *Int J Cancer* (2012) 130:1477–83. doi: 10.1002/ijc.26449
5. Quail DF, Joyce JA. Microenvironmental regulation of tumor progression and metastasis. *Nat Med.* (2013) 19:1423–37. doi: 10.1038/nm.3394
6. Wang Y, Zhou BP. Epithelial-mesenchymal transition in breast cancer progression and metastasis. *Chinese J Cancer* (2011) 30:603–11. doi: 10.5732/cjc.011.10226
7. Trimboli AJ, Fukino K, de Bruin A, Wei G, Shen L, Tanner SM, et al. Direct evidence for epithelial-mesenchymal transitions in breast cancer. *Cancer Res.* (2008) 68:937–45. doi: 10.1158/0008-5472.CAN-07-2148
8. Harris LG, Samant RS, Shevde LA. Hedgehog signaling: networking to nurture a promalignant tumor microenvironment. *Mol Cancer Res.* (2011) 9:1165–74. doi: 10.1158/1541-7786.MCR-11-0175
9. Barcellos-Hoff MH, Akhurst RJ. Transforming growth factor-beta in breast cancer: too much, too late. *Breast Cancer Res.* (2009) 11:202. doi: 10.1186/bcr2224
10. Gotzmann J, Fischer AN, Zojer M, Mikula M, Proell V, Huber H, et al. A crucial function of PDGF in TGF-β-mediated cancer progression of hepatocytes. *Oncogene* (2006) 25:3170–85. doi: 10.1038/sj.onc.1209083
11. Miettinen PJ, Ebner R, Lopez AR, Derynck R. TGF-beta induced transdifferentiation of mammary epithelial cells to mesenchymal cells: involvement of type I receptors. *J Cell Biol.* (1994) 127:2021–36. doi: 10.1083/jcb.127.6.2021
12. Li H, Fan X, Houghton J. Tumor microenvironment: the role of the tumor stroma in cancer. *J Cell Biochem.* (2007) 101:805–15. doi: 10.1002/jcb.21159
13. Mitra A, Menezes ME, Shevde LA. Samant RS, DNAJB6 induces degradation of beta-catenin and causes partial reversal of mesenchymal phenotype. *J Biol Chem.* (2010) 285:24686–94. doi: 10.1074/jbc.M109.094847
14. Moody SE, Perez D, Pan TC, Sarkisian CJ, Portocarrero CP, Sterner CJ, et al. The transcriptional repressor Snail promotes mammary tumor recurrence. *Cancer Cell* (2005) 8:197–209. doi: 10.1016/j.ccr.2005.07.009
15. Morrow KA, Das S, Metge BJ, Ye K, Mulekar MS, Tucker JA, et al. Loss of tumor suppressor Merlin in advanced breast cancer is due to post- translational regulation. *J Biol Chem.* (2011) 286:40376–85. doi: 10.1074/jbc.M111.250035
16. Zeisberg M, Neilson EG. Biomarkers for epithelial-mesenchymal transitions. *J Clin Invest.* (2009) 119:1429–37. doi: 10.1172/JCI36183
17. Franke WW, Schmid E, Osborn M, Weber K. Different intermediate-sized filaments distinguished by immunofluorescence microscopy. *Proc Natl Acad Sci USA.* (1978) 75:5034–8. doi: 10.1073/pnas.75.10.5034
18. Dellagi K, Vainchenker W, Vinci G, Paulin D, Brouet JC. Alteration of vimentin intermediate filament expression during differentiation of human hemopoietic cells. *EMBO J* (1983) 2:1509–14. doi: 10.1002/j.1460-2075.1983.tb01615.x
19. Smith GP, Petrenko VA. Phage Display. *Chem Rev.* (1997) 97:391–410. doi: 10.1021/cr960065d
20. Petrenko VA, Smith GP, Gong X, Quinn T. A library of organic landscapes on filamentous phage. *Protein Eng.* (1996) 9:797–801. doi: 10.1093/protein/9.9.797
21. Kelly KA, Jones DA. Isolation of a colon tumor specific binding peptide using phage display selection. *Neoplasia* (2003) 5:437–44. doi: 10.1016/S1476-5586(03)80046-5
22. Newton JR, Kelly KA, Mahmood U, Weissleder R, Deutscher SL. *In vivo* selection of phage for the optical imaging of PC-3 human prostate carcinoma in mice. *Neoplasia* (2006) 8:772–80. doi: 10.1593/neo.06331
23. Jayanna PK, Bedi D, Deinnocentes P, Bird RC, Petrenko VA. Landscape phage ligands for PC3 prostate carcinoma cells. *Protein Eng Design Select.* (2010) 23:423–30. doi: 10.1093/protein/gzq011
24. Kelly KA, Bardeesy N, Anbazhagan R, Gurumurthy S, Berger J, Alencar H, et al. Targeted nanoparticles for imaging incipient pancreatic ductal adenocarcinoma. *PLoS Med* (2008) 5:e85. doi: 10.1371/journal.pmed.0050085
25. Shukla GS, Krag DN. Cancer cell-specific internalizing ligands from phage displayed β-lactamase-peptide fusion libraries. *Protein Eng Design Select.* (2010) 23:431–40. doi: 10.1093/protein/gzq013
26. Fagbohun OA, Bedi D, Grabchenko NI, Deinnocentes PA, Bird RC, Petrenko VA. Landscape phages and their fusion proteins targeted to breast cancer cells. *Protein Eng Design Select.* (2012) 25:271–83. doi: 10.1093/protein/gzs013
27. Wang T, D'Souza GG, Bedi D, Fagbohun OA, Potturi LP, Papahadjopoulos-Sternberg B, et al. Enhanced binding and killing of target tumor cells by drug-loaded liposomes modified with tumor-specific phage fusion coat protein. *Nanomedicine* (2010) 5:563–74. doi: 10.2217/nnm.10.30
28. Bedi D, Musacchio T, Fagbohun OA, Gillespie JW, Deinnocentes P, Bird RC, et al. Delivery of siRNA into breast cancer cells via phage

fusion protein-targeted liposomes. *Nanomedicine* (2011) 7:315–23. doi: 10.1016/j.nano.2010.10.004
29. Jayanna PK, Bedi D, Gillespie JW, DeInnocentes P, Wang T, Torchilin VP, et al. Landscape Phage Fusion Protein-mediated Targeting of Nanomedicines Enhances their Prostate Tumor Cell Association and Cytotoxic Efficiency. *Nanomedicine* (2010) 6:538–46. doi: 10.1016/j.nano.2010.10.004
30. Rasmussen UB, Schreiber V, Schultz H, Mischler F, Schughart K. Tumor cell-targeting by phage-displayed peptides. *Cancer Gene Ther.* (2002) 9:606–12. doi: 10.1038/sj.cgt.7700476
31. Teesalu T, Sugahara KN, Ruoslahti E. Mapping of vascular ZIP codes by phage display. *Methods Enzymol.* (2012) 503:35–56. doi: 10.1016/B978-0-12-396962-0.00002-1
32. Li XB, Schluesener HJ, Xu SQ. Molecular addresses of tumors: selection by *in vivo* phage display. *Arch Immunol Ther Exp.* (2006) 54:177–81. doi: 10.1007/s00005-006-0026-y
33. Mahdi SH, Cheng H, Li J, Feng R. The effect of TGF-beta-induced epithelial-mesenchymal transition on the expression of intracellular calcium-handling proteins in T47D and MCF-7 human breast cancer cells. *Arch Biochem Biophys.* (2015) 583:18–26. doi: 10.1016/j.abb.2015.07.008
34. Lombaerts M, van Wezel T, Philippo K, Dierssen JWF, Zimmerman RME, Oosting J, et al. E-cadherin transcriptional downregulation by promoter methylation but not mutation is related to epithelial-to-mesenchymal transition in breast cancer cell lines. *Br J Cancer* (2006) 94:661–71. doi: 10.1038/sj.bjc.6602996
35. Nakajima S, Doi R, Toyoda E, Tsuji S, Wada M, Koizumi M, et al. N-cadherin expression and epithelial-mesenchymal transition in pancreatic carcinoma. *Clin Cancer Res.* (2004) 10:4125–33. doi: 10.1158/1078-0432.CCR-0578-03
36. D'Amato NC, Ostrander JH, Bowie ML, Sistrunk C, Borowsky A, Cardiff RD, et al. Evidence for phenotypic plasticity in aggressive triple-negative breast cancer: human biology is recapitulated by a novel model system. *PLoS ONE* (2012) 7:e45684. doi: 10.1371/journal.pone.0045684
37. Devine DJ, Rostas JW, Metge BJ, Das S, Mulekar MS, Tucker JA, et al. Loss of N-Myc interactor promotes epithelial-mesenchymal-transition by activation of TGF-β/SMAD signaling. *Oncogene* (2014) 33:2620–28. doi: 10.1038/onc.2013.215
38. Tai S, Sun Y, Squires JM, Zhang H, Oh WK, Liang CZ, et al. PC3 is a cell line characteristic of prostatic small cell carcinoma. *Prostate* (2011) 71:1668–79. doi: 10.1002/pros.21383
39. Ke XS, Qu Y, Goldfinger N, Rostad K, Hovland R, Akslen LA, et al. Epithelial to mesenchymal transition of a primary prostate cell line with switches of cell adhesion modules but without malignant transformation. *PLoS ONE* (2008) 3:e3368. doi: 10.1371/journal.pone.0003368
40. Hewitt RE, McMarlin A, Kleiner D, Wersto R, Martin P, Tsokos M, et al. Validation of a model of colon cancer progression. *J. Pathol.* (2000) 192:446–54. doi: 10.1002/1096-9896(2000)9999:9999<::AID-PATH775>3.0.CO;2-K
41. Heerboth S, Housman G, Leary M, Longacre M, Byler S, Lapinska K, et al. EMT and tumor metastasis. *Clin Transl Med.* (2015) 4:6. doi: 10.1186/s40169-015-0048-3
42. Seyfried TN, Huysentruyt LC. On the origin of cancer metastasis. *Crit Rev Oncogen.* (2013) 18:43–73. doi: 10.1615/CritRevOncog.v18.i1-2.40
43. Ayob AZ, Ramasamy TS. Cancer stem cells as key drivers of tumour progression. *J Biomed Sci.* (2018) 25:20. doi: 10.1186/s12929-018-0426-4
44. Schedin P, Borges V. Breaking down barriers: the importance of the stromal microenvironment in acquiring invasiveness in young women's breast cancer. *Breast Cancer Res.* (2009) 11:102. doi: 10.1186/bcr2235
45. Ishii G. Crosstalk Between Cancer Associated Fibroblasts and Cancer Cells in the Tumor Microenvironment After Radiotherapy. *EBioMedicine* (2017) 17:7-8. doi: 10.1016/j.ebiom.2017.03.004
46. Kalluri R, Zeisberg M. Fibroblasts in cancer. *Nature reviews. Cancer 6* (2006) 392–401. doi: 10.1038/nrc1877
47. Tejada ML, Yu L, Dong J, Jung K, Meng G, Peale FV, et al. Tumor-driven paracrine platelet-derived growth factor receptor alpha signaling is a key determinant of stromal cell recruitment in a model of human lung carcinoma. *Clin Cancer Res.* (2006) 12:2676–88. doi: 10.1158/1078-0432.CCR-05-1770
48. Martinez-Outschoorn UE, Trimmer C, Lin Z, Whitaker-Menezes D, Chiavarina B, Zhou J, et al. Autophagy in cancer associated fibroblasts promotes tumor cell survival: role of hypoxia, HIF1 induction and NFkappaB activation in the tumor stromal microenvironment. *Cell Cycle* (2010) 9:3515–33. doi: 10.4161/cc.9.17.12928
49. Giannoni E, Bianchini F, Masieri L, Serni S, Torre E, Calorini L, et al. Reciprocal activation of prostate cancer cells and cancer-associated fibroblasts stimulates epithelial-mesenchymal transition and cancer stemness. *Cancer Res.* (2010) 70:6945–56. doi: 10.1158/0008-5472.CAN-10-0785

Conflict of Interest Statement: The authors declare that the research was conducted in the absence of any commercial or financial relationships that could be construed as a potential conflict of interest.

frontiers in Pharmacology

REVIEW
published: 17 December 2018
doi: 10.3389/fphar.2018.01453

Therapeutic Potential of Nitrogen Mustard Based Hybrid Molecules

Yiming Chen[1†], Yuping Jia[2†], Weiguo Song[1] and Lei Zhang[1]*

[1] Department of Medicinal Chemistry, School of Pharmacy, Weifang Medical University, Weifang, China, [2] Shandong Academy of Pharmaceutical Science, Jinan, China

As medicine advances, cancer is still among one of the major health problems, posing significant threats to human health. New anticancer agents features with novel scaffolds and/or unique mechanisms of action are highly desirable for the treatment of cancers, especially those highly aggressive and drug-resistant ones. Nitrogen mustard has been widely used as an anticancer drug since the discovery of its antitumor effect in the 1942. However, the lack of selectivity to cancer cells restricts the wide usage of a mass of nitrogen mustard agents to achieve further clinical significance. Discovery of antitumor hybrids using nitrogen mustards as key functional groups has exhibited enormous potential in the drug development. Introduction of nitrogen mustards resulted in improvement in the activity, selectivity, targetability, safety, pharmacokinetics and pharmacodynamics properties of corresponding lead compounds or agents. Herein, the recently developed nitrogen mustard based hybrids have been introduced in the cancer therapy.

Keywords: antitumor, nitrogen mustard, hybrids, side effects, drug discovery

OPEN ACCESS

Edited by:
Zhe-Sheng Chen,
St. John's University, United States

Reviewed by:
Xiaozhuo Liu,
University at Buffalo, United States
Guannan Zhang,
University of Pennsylvania, United States

***Correspondence:**
Lei Zhang
leiqdu@foxmail.com

† These authors have contributed equally to this work

Specialty section:
This article was submitted to Experimental Pharmacology and Drug Discovery, a section of the journal Frontiers in Pharmacology

Received: *31 October 2018*
Accepted: *27 November 2018*
Published: *17 December 2018*

Citation:
Chen Y, Jia Y, Song W and Zhang L (2018) Therapeutic Potential of Nitrogen Mustard Based Hybrid Molecules. Front. Pharmacol. 9:1453. doi: 10.3389/fphar.2018.01453

INTRODUCTION

In recent years, malignant tumors have become a serious threat to human health due to their worldwide rising incidence and mortality. Second to cardiovascular diseases, cancer contributed the second most mortalities among all diseases (Torre et al., 2015; Ryerson et al., 2016; Lallukka et al., 2017). In recent decades, development of antitumor drugs has achieved significant progress in the treatment of cancer. Since nitrogen mustard, known as an alkylating agent, was proven effective in the treatment of malignant lymphoma in the 1940s, the usage of nitrogen mustard drugs in cancer chemotherapy has a history of over 70 years. At present, nitrogen mustard agents are still used clinically, and targeted modification of nitrogen mustards is an important strategy for the discovery of anticancer drugs. The development of nitrogen mustard derivatives originated from bis(2-chloroethyl) sulfide, which was used as a poison gas during World War II (Gilman, 1963; DeVita and Chu, 2008). After a terrible accident, it was found that bis(2-chloroethyl) sulfide exhibited therapeutic potential on leukemia. Because of its severe toxicity, bis(2-chloroethyl) sulfide was not applied as a antitumor drug for clinical use. However, nitrogen mustard antitumor drugs were developed based on the leukocyte killing effect of bis(2-chloroethyl) sulfide (**Figure 1**).

Nitrogen mustard is a kind of bio-alkylating agent, which can form active electron-deficient intermediates or other compounds with active electrophilic groups *in vivo*. The active intermediates can react electrophilically with some electron-rich groups in bio-macromolecules by forming covalent bonds, and results in activity inhibition of corresponding bio-macromolecules. The mechanism of nitrogen mustards includes DNA binding and cross-linking, thus preventing DNA

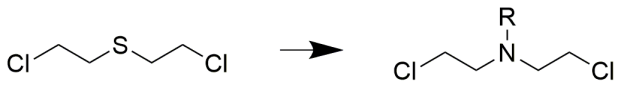

FIGURE 1 | Origin of nitrogen mustards.

replication and cell proliferation. Since its binding to the N7 nitrogen-atoms on DNA guanines with poor selectivity, nitrogen mustard agents are revealed to be toxic to normal cells (Kohn et al., 1987; Bank et al., 1989; Povirk and Shuker, 1994; Di Antonio et al., 2014).

Clinical application of nitrogen mustard compounds has a long history, but the present and future application of nitrogen mustards is limited by disadvantages including poor selectivity and severe adverse reactions (Frei et al., 1988; Sanderson and Shield, 1996; Schobert et al., 2009; Chen et al., 2014). Therefore, enormous effort has been made in the development of nitrogen mustard derivatives, aiming to obtain antitumor nitrogen mustard drugs with high activity and low toxicity (Zarytova et al., 1990). In recent years, the discovery of nitrogen mustard drugs and derivatives has become attractive field in the anticancer therapy. Development of nitrogen mustard based hybrid molecules by introducing druggable fragment, has been considered to be effective strategy in the antitumor drug discovery. Herein, recently development of nitrogen mustard based hybrids was reviewed and provided suggestions for the future study of bifunctional and multitargeted antitumor drugs.

NITROGEN MUSTARD DRUGS

According to different carriers, nitrogen mustard drugs can be classified into several classes, including fatty nitrogen mustard, aromatic nitrogen mustard, amide nitrogen mustard, amino acid and polypeptide nitrogen mustard, and heterocyclic nitrogen mustard.

Chlormethine **1** (**Figure 2**), a fatty nitrogen mustard, is now rarely used for clinic due to its poor selectivity and severe toxicity. The introduction of aromatic rings into nitrogen mustard causes the decrease of electrophilicity of the nitrogen atom. Consequently, aromatic nitrogen mustards are characterized with reduced reactivity and toxicity compared with fatty nitrogen mustard (Goodman and Wintrobe, 1946). Chlorambucil **2** (**Figure 2**) is used clinically for the treatment of ovarian cancer, Hodgkin's disease, chronic lymphocytic leukemia and lymphosarcoma (Galton et al., 1961). Clinical application of chlorambucil is also limited by adverse effects including nausea, vomiting, anemia, bone marrow suppression and neurotoxicity (Springer et al., 1990; Nicolle et al., 2004). Melphalan **3** (**Figure 2**), which takes phenylalanine as the carrier, has exhibited clinical effects on ovarian cancer, breast cancer, lymphoid sarcoma and multiple myeloma (Sarosy et al., 1988). Cyclophosphamide **4** (**Figure 2**), a heterocyclic amide nitrogen mustard, features a board spectrum of anti-malignancy activity, and is commonly utilized in the management of malignant lymphoma, acute lymphoblastic leukemia, multiple myeloma, lung cancer, neuroblastoma, breast cancer, ovarian cancer and nasopharyngeal cancer (Hughes et al., 2018). Moreover, cyclophosphamide has been discovered to be less toxicity than other types of nitrogen mustard drugs, due to the specific metabolic pathway.

NITROGEN MUSTARD BASED HYBRIDS

In recent years, it has been revealed that the conjugation of targeted antitumor drugs or natural molecules with nitrogen mustard drugs provides novel strategies for the discovery of antitumor molecules with improved antitumor effect, selectivity, and reduced toxicity.

Brefeldin A (BFA) **5** (**Figure 3**) is a 16-member macrolide antibiotic with a broad range of pharmacological activities, including antitumor, antiviral and antifungal effects (Rajamahanty et al., 2010; Moon et al., 2012; South et al., 2013; Toda et al., 2015; Grose and Klionsky, 2016; Huang et al., 2017). In the antiproliferative activity assay, BFA exhibited GI_{50} (half maximal growth inhibitory concentration) value of 40 nM against the national cancer institute NCI-60 cancer cell line (Anadu et al., 2006). Although BFA has great potentials to serve as a cancer chemotherapeutic drug, its development is still restricted by major limitations including severe undesirable effects and relatively low selectivity on tumor cells over normal ones (Kikuchi et al., 2003; Seehafer et al., 2013). Several novel BFA-nitrogen mustard conjugates were derived by introducing nitrogen mustards at 4-OH and/or 7-OH of BFA (Han et al., 2018). All the synthesized BFA-nitrogen mustard compounds **5a-i** (**Figure 3**) were assessed for their effectiveness against different tumor cell lines. Several hybrid molecules exhibited potent cytostatic activities and improved selectivity on malignant cells over normal ones. It is revealed that almost all the new BFA-nitrogen mustards showed stronger cytotoxic activities against one or more cell lines than nitrogen mustards and even 5-FU. Among all the tested compounds, molecule **5a** exhibited the most potent antiproliferative effects against various tumor cell lines (with IC_{50} (half maximal inhibitory concentration) values of 4.48, 9.37, 0.2, and 0.84 μM against human leukemia HL-60, human prostate PC-3, human hepatocellular carcinoma Bel-7402 and drug-resistant Bel-7402/5-FU cell lines), respectively. Molecule **5a** also displayed much lower cytotoxicity (IC_{50} < 0.001 μM) than BFA (IC_{50} = 9.74 μM) against normal human hepatic L-O2 cells. Therefore, introduction of nitrogen mustard to toxic natural products could be significant in the improvement the potency and safety of lead compounds.

Evodiamine **6** (**Figure 4**) is a natural quinolone alkaloid widely studied for the treatment of diverse human disorders including Alzheimer's disease, inflammation and especially cancer (Ogasawara et al., 2002; Yu et al., 2013; Lv et al., 2015; Shi L. et al., 2016; Wang et al., 2016; Wu et al., 2016; Fan et al., 2017; Shi et al., 2017). By targeting topoisomerase I and II, evodiamine has induced apoptosis and cell cycle arrest of a broad spectrum of tumor cell lines (Shyu et al., 2006). However, it is revealed that evodiamine is cytotoxic to human normal

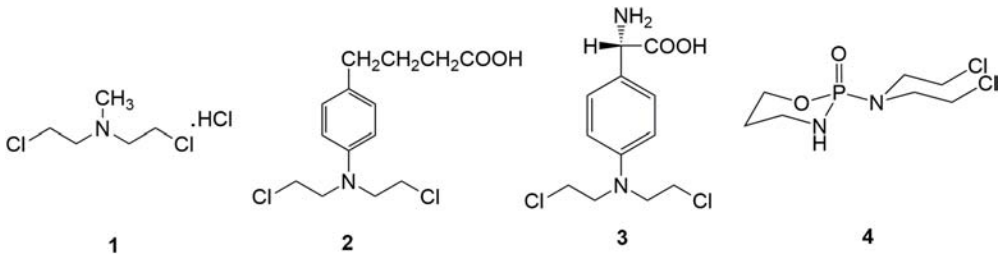

FIGURE 2 | Representative nitrogen mustard agents.

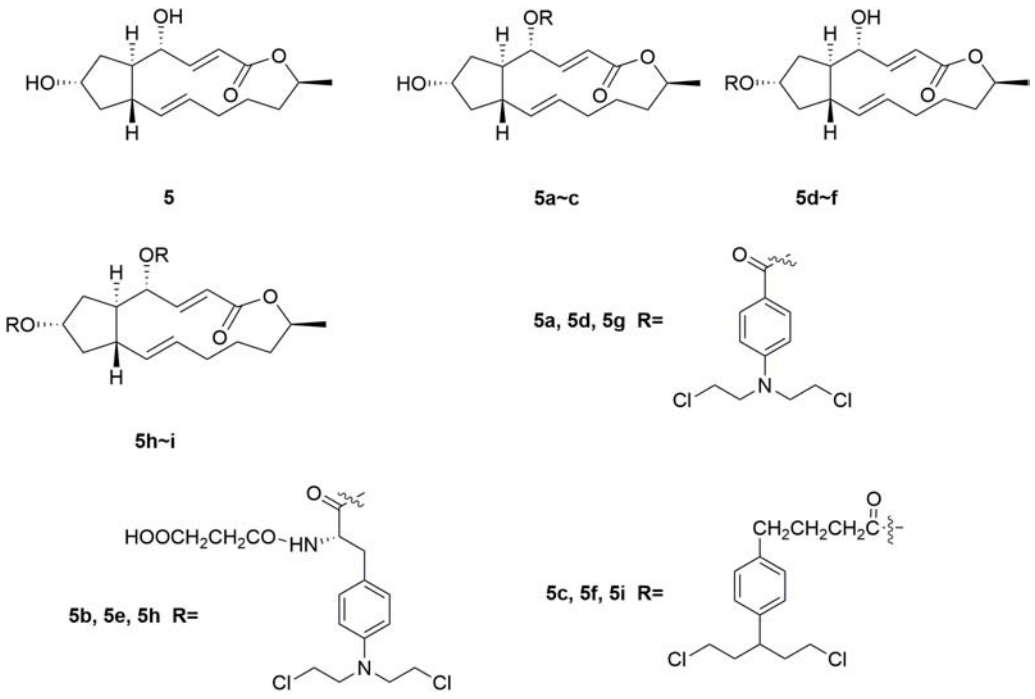

FIGURE 3 | Structures of Brefeldin A-nitrogen mustard hybrids.

cells, such as peripheral blood mononuclear cells (PBMC). In discovery of antitumor agent with improved potency and reduced adverse side effects, conjunct of evodiamine to nitrogen mustards was carried out by Li and coworkers (Hu et al., 2017). The synthesized nitrogen mustard-evodiamine hybrids were evaluated in the antitumor activity assay. Compared with evodiamine (IC_{50} values of 22.87 μM against PBMC cells), all the tested mustard-evodiamine hybrids **7a-d, 8a-d, 9a-d** (**Figure 4**) showed improved safety properties with IC_{50} values of more than 200 μM in inhibition the proliferation of PBMC cells. Remarkably, molecule **9c** revealed potent antiproliferative effects against human liver cancer HepG2, human leukemic THP-1 and HL-60 cell lines with IC_{50} value of 17.04 μM, 4.05 μM and 0.50 μM, respectively. The involved investigations indicated that further drug discovery based on **9c** is promising in the treatment of tumor, such as leukemia. Collectively, introduction of nitrogen mustard moiety has shown significance in the improvement of potency and safety, and the nitrogen mustard hybridation strategy could be productive for the optimization of lead compounds.

Oridonin **10** (**Figure 5**) is a kind of natural diterpenoids, which has a unique, safe, broad antitumor activity (Sun et al., 2006; Cui et al., 2007; Zhou et al., 2007; Bao et al., 2014; Li Y. et al., 2015; Ding et al., 2016; Dong et al., 2016; Shi M. et al., 2016; Liu et al., 2017). However, the utilization of oridonin in cancer chemotherapy was limited by its relatively low potency (Wang et al., 2012; Xu S.T. et al., 2014). Development of oridonin-nitrogen mustard conjugates used for antitumor application has been demonstrated to be promising in the drug discovery (Ding et al., 2013a,b). Several synthetic oridonin-nitrogen mustard conjugates **10a**∼**f** (**Figure 5**), and their anticancer activities evaluated in four human malignant cell lines (human leukemia K562 cells, human breast cancer MCF-7 cells, human hepatocellular carcinoma Bel-7402 cells, and human gastric cancer MCG-803 cells) were reported by Xu and coworkers (Xu S. et al., 2014). All the tested compounds exhibited better

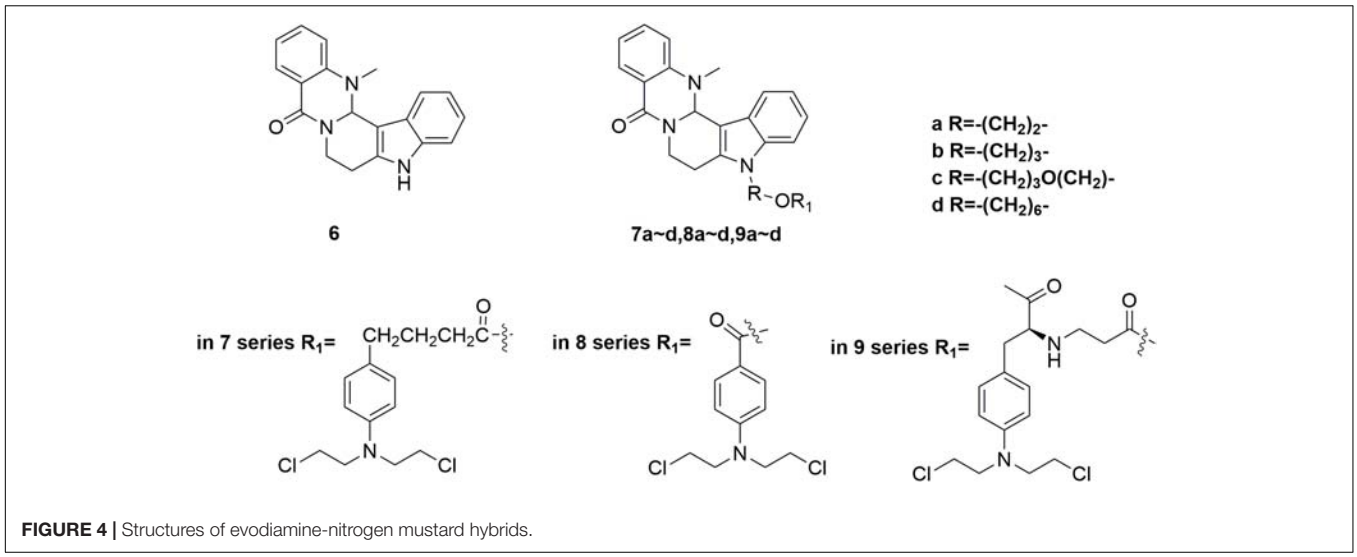

FIGURE 4 | Structures of evodiamine-nitrogen mustard hybrids.

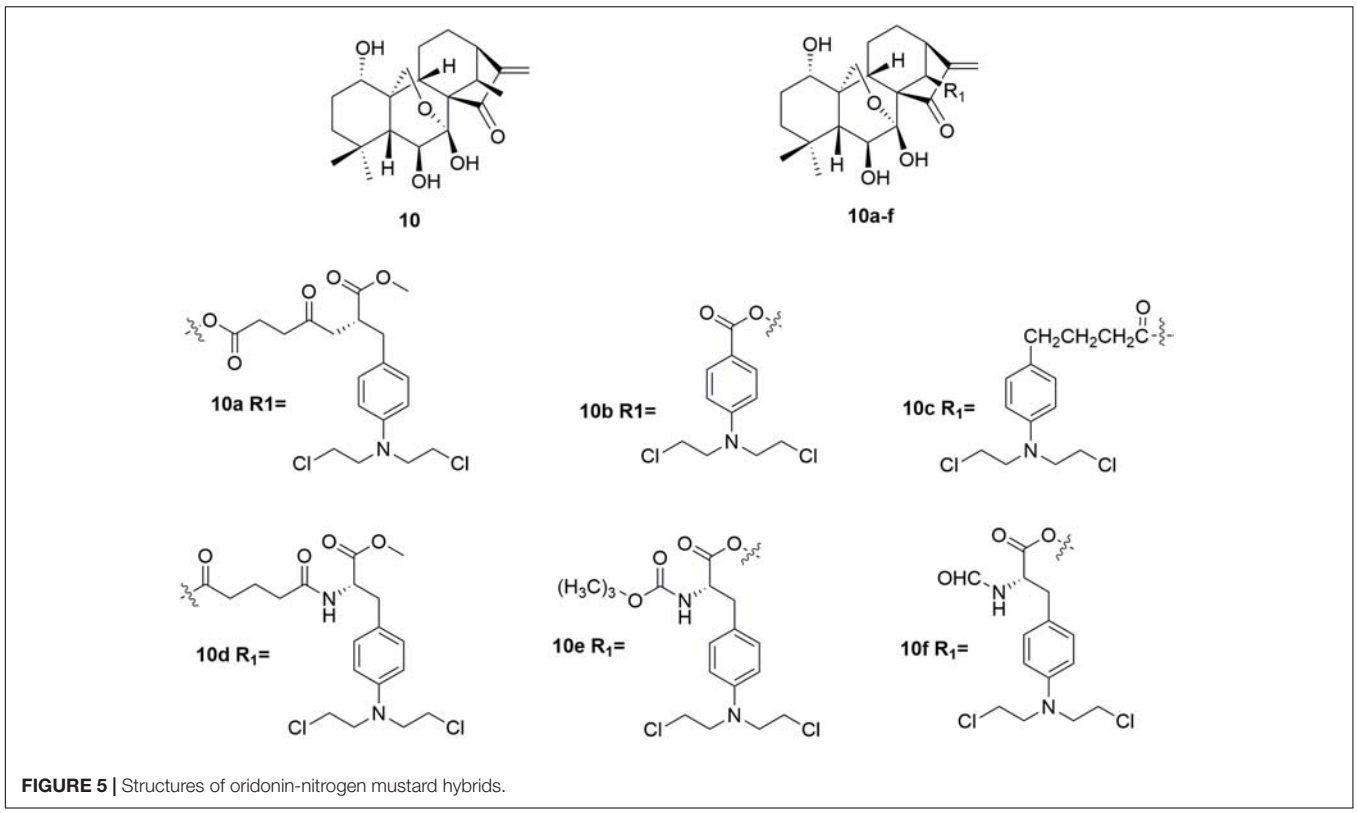

FIGURE 5 | Structures of oridonin-nitrogen mustard hybrids.

antiproliferative effects comparing to the positive control drugs, melphalan, chlorambucil and benzoic acid mustard. Among the synthetic oridonin mustards, compound **10b** was the most potent hybrid against MCF-7 and Bel-7402 cells with IC_{50} values of 0.68 μM and 0.50 μM, respectively. It is also revealed that **10b** and **10c** could inhibit the growth of drug-resistant cancer cells. Notably, molecule **10b** exhibits approximately eight-fold higher selectivity for cancer cells over normal cells, which is significantly higher than its parent oridonin compound and clinically available nitrogen mustard drugs. Collectively, the derived oridonin-nitrogen mustard conjugates exhibited improved activity and safety than the parent fragments, and introduction of nitrogen mustard make contributions to the potency and selectivity of oridonin based hybrids.

In addition to evodiamine, another alkaloid, sophoridine **11** (**Figure 6**) evaluated in detailed for its antitumor potency, was approved by the CFDA in 2005 for treatment several types of cancer, including liver, gastric and lung cancer (Sun et al., 2012; Liu and Liu, 2013; Wang et al., 2014). The sophoridine which could cause apoptotic cell death by inhibiting DNA

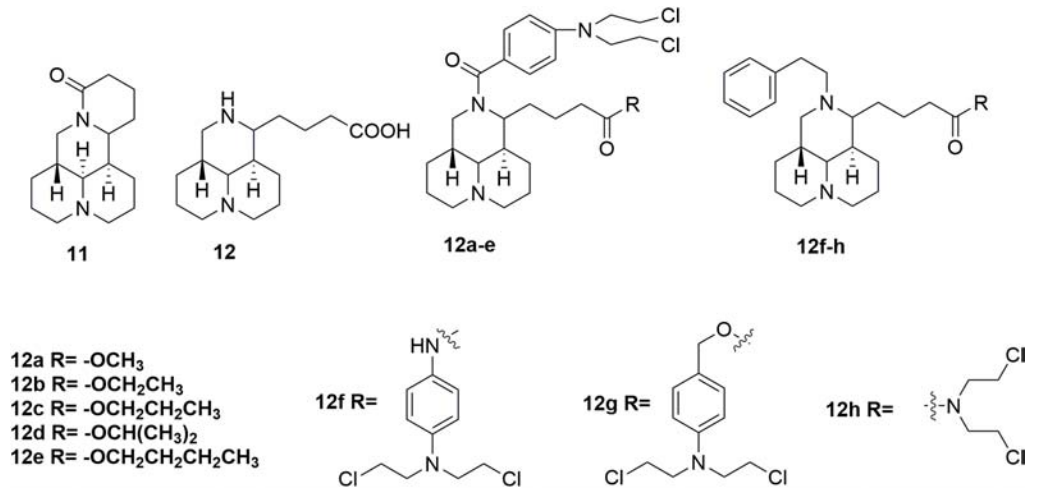

FIGURE 6 | Structures of sophoridine-nitrogen mustard hybrids.

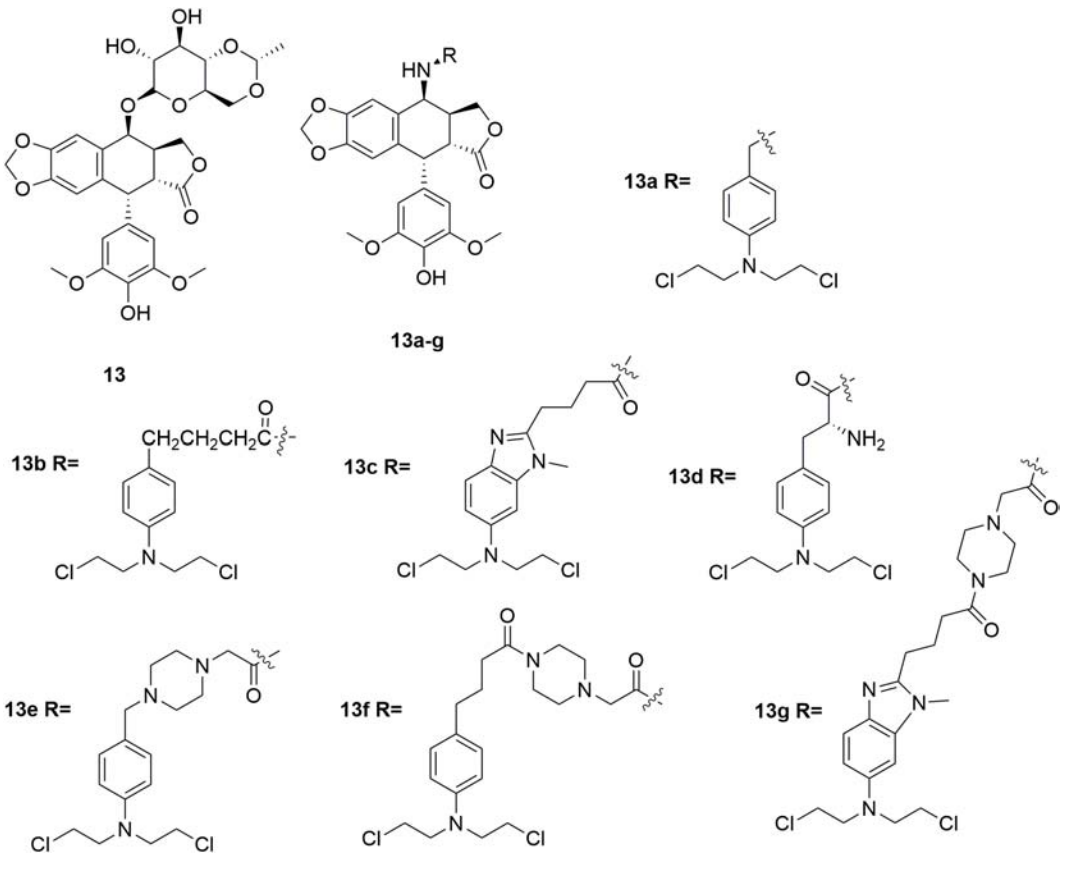

FIGURE 7 | Structures of etoposide-nitrogen mustard hybrids.

topoisomerase I activity and initiate cell cycle arrest at the G0/G1 phase, has high solubility and good safety profiles (Quo et al., 2013). However, the moderate anticancer activity of sophoridine limit its clinical application. Therefore, development of sophoridine derivatives was performed in discovery of more effective drug candidates. The D-ring of sophridine has been opened to generate sophoridinic acid **12** (**Figure 6**) for further structural modification. A series of sophoridinic acid-nitrogen mustard deivatives **12a-h** (**Figure 6**) were derived by modifying 12 nitrogen atom and carboxyl groups of **12** (Li D.D. et al., 2015).

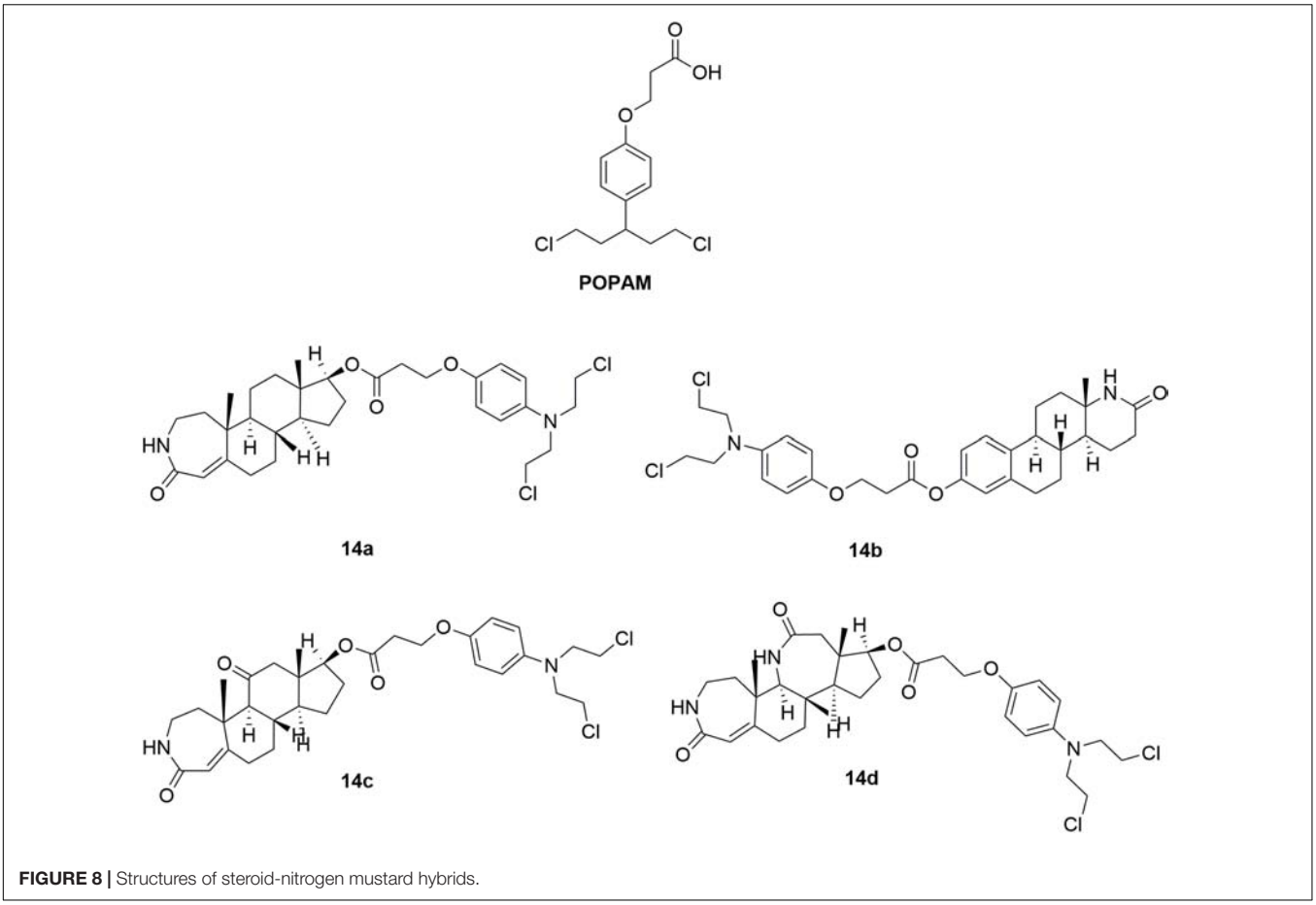

FIGURE 8 | Structures of steroid-nitrogen mustard hybrids.

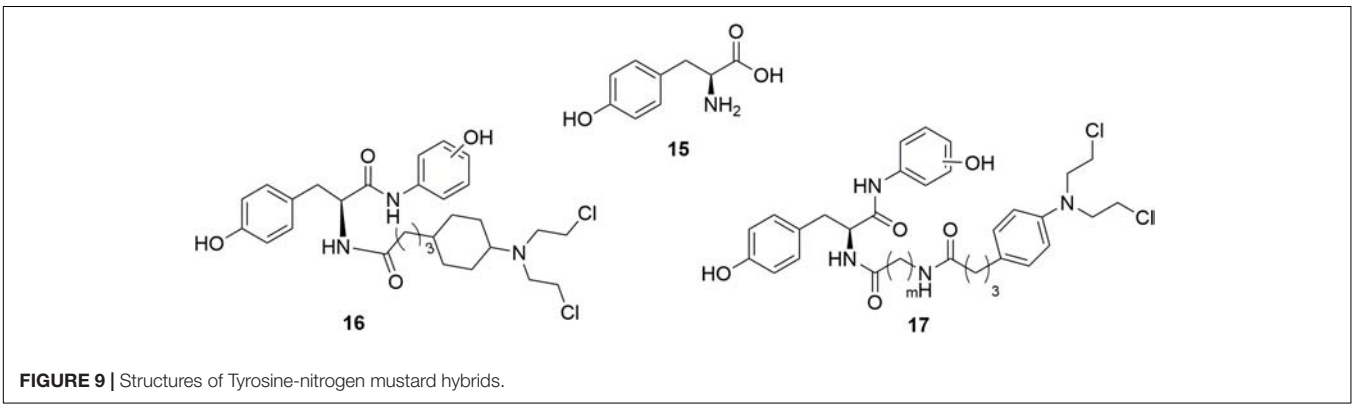

FIGURE 9 | Structures of Tyrosine-nitrogen mustard hybrids.

Compared with sophoridine (IC_{50} > 80 μM against human liver cancer HepG2 cells), several new synthesized hybrids showed improved antitumor activity. Especially compound **12f** showed IC_{50} value of 0.47 μM compared with melphalan (IC_{50} value of 0.41 μM) in the inhibition of HepG2 cells. SAR analysis indicated two promising substituents on the 12-nitrogen atom and carboxyl region, which were helpful for maintaining potent antitumor activity. Moreover, various decorating various substituents may be introduced to these two moieties, regulating the pharmacological effects of the compounds. Introduction of the cyclophosphamide metabolite (phosphamide mustard A) analogs also resulted in hybrids with significantly improved activities compared with sophoridine (Li D. et al., 2018). It is demonstrated that the introduction of nitrogen mustard on sophoridine could significantly improve interactions between sophoridine and DNA-Topo I, and subsequently increase the antitumor activity. Therefore, the study of nitrogen mustard as the parent drug is of great significance in the design and synthesis of antitumor drugs.

Etoposide **13** (**Figure 7**) is a topoisomerase II inhibitor effective in the treatments of various types of cancer including testicular cancer, lung cancer, lymphoma, leukemia,

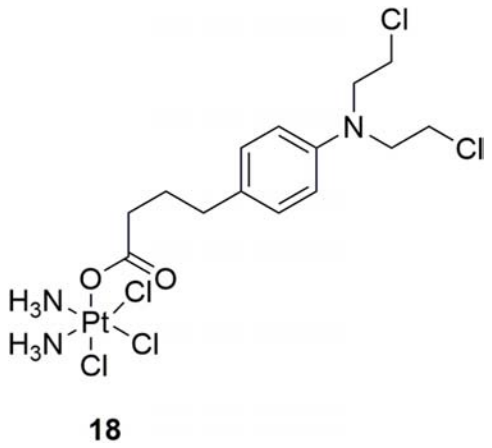

18

FIGURE 10 | Structure of Platinum-nitrogen mustard hybrid.

neuroblastoma, and ovarian cancer (Nitiss, 2009; Pommier and Marchand, 2011; Pommier, 2013). In discovery of etoposide analogs, glycoside moiety of etoposide was replaced by nitrogen mustard moiety designed to alkylate either protein residues on topoisomerase II, or the DNA bases on the DNA-topoisomeraseII complex (Deweese and Osheroff, 2009; Pommier et al., 2010; Wu et al., 2011). Seven N-mustard–epipodophyllotoxin hybrid compounds **13a-g** (**Figure 7**) were synthesized, and demonstrated to target topoisomerase II by kDNA decatenation assay, DNA cleavage assay, cellular ICE assay and the cell cycle analyses (Yadav et al., 2014). The derived molecules also exhibited nitrogen mustard-alike activity as it crosslinked DNA. In the *in vitro* antiproliferative assay, molecule **13e** exhibited the best antiproliferative activity with IC_{50} values of 0.27 μM and 0.85 μM against human leukemia K562 cells and etoposide-resistant K/VP.5 cells, and GI_{50} of 0.71 μM against NCI-60 cells in contrast to the control melphalan (IC_{50} values of 12 μM and 5.3 μM against K562 cells and K/VP.5 cells, and GI_{50} of 29 μM against NCI-60 cells) and etoposide (IC_{50} values of 0.29 μM and 4.9 μM against K562 cells and K/VP.5 cells, and GI_{50} of 12 μM against NCI-60 cells). The results suggested that hybridization of etoposide and nitrogen mustards is promising in the development of highly potent antitumor molecules both by topoisomerase II inhibition as well as DNA alkylation.

In order to decrease toxicity of nitrogen mustards, steroids have been tested as a vehicle to deliver the mustard drugs to a specific target tissue via interaction with steroid receptors (Wall et al., 1969; Catane, 1978). Such conjugates improved the lipophilicity and solubility of the resulting drugs. Development of steroidal alkylating agents has been reviewed by Bérubé and coworkers (Trafalis et al., 2016). Herein, the recently derived novel steroidal lactam derivatives and 3-(4-(bis(2-chloroethyl)amino)phenoxy)propanoic acid (POPAM) (**Figure 8**) conjunctions were described (Trafalis et al., 2016). Four new ester conjugates **14a-d** (**Figure 8**) of steroidal lactams with POPAM were synthesized and tested against human leukemia cell lines *in vitro*. Molecule **14c** was discovered to be the most potent hybrid with IC_{50} values of 90 μM, 65 μM, 80 μM, and 85 μM against human leukemia MOLT-4, CCRF-CEM, JURKAT and SUP-B15 cells compared with melphalan (IC_{50} > 100 μM against all the test cell lines) and POPAM (IC_{50} > 100 μM against all the test cell lines), respectively. In the *in vivo* antiproliferative assay, **14c** also exhibited improved antileukemic activity compared with their alkylating component alone (POPAM). Moreover, in the *in vivo* acute toxicity test, all the derived hybrids had significantly lower acute toxicity (LD_{10} (10% lethal dose) > 80 mg/kg), in contrast to the non-steroidal alkylators POPAM (LD_{10} = 14 mg/kg) and melphalan (LD_{10} = 15 mg/kg). Further investigation revealed that the chemical linkage between the nitrogen mustard and the lactam-steroids seems to both decreased the toxicities of the nitrogen mustards and improved the bioactivity and antitumor effects.

Tyrosine **15** (**Figure 9**), a natural amino acid, has been reported to share some structural similarities to that of the phenol group of estradiol (Anstead et al., 1997). Molecular modeling study indicated that the phenol group of tyrosine also interact with the estrogen receptor binding site in the same manner as the A-ring phenol of estradiol. Therefore, the tyrosine was modified to mimic the structure of estradiol (Muthyala et al., 2003; Descoteaux et al., 2012b). Tyrosinamide, combined tyrosine with hydroxyaniline, was proved to be structurally similar to estradiol. A series of tyrosinamide-nitrogen mustard derivatives were synthesized and tested by Bérubé and coworkers (Descoteaux et al., 2012a). It is revealed that all new compounds showed potent antitumor activities. Among the derived tyrosinamide-chlorambucil hybrids, compound ***m*-16** (**Figure 9**), showed IC_{50} values of 48.61 and 31.25 μM against human breast cancer MDA-MB-231 cells and MCF-7 cells compared with the parent compounds chloramucil (IC_{50} values of 136.85 and 130.36 μM against MDA-MB-231 cell and MCF-7 cells), respectively. Compared with chloramucil (IC_{50} values of 63.17, 66.11, 100.48 and 131.83 μM against human ovarian carcinoma A2780 cells, OVCAR-3 cells, human breast cancer ZR-75-1 cells and MDA-MB-468 cells, respectively), the ***m*-17** (**Figure 9**) showed potent antitumor activity with IC50 values of 31.79, 35.42, and 52.10 μM against OVCAR-3 cells, MDA-MB-468 cells and ZR-75-1 cells, respectively. It is found that all the synthesized tyrosinamide-chlrambucil molecules exhibited improved inhibitory activity in the inhibition of breast, ovarian and uterine cancer cells than the parental chlorambucil. Introduction of tyrosine entity to nitrogen mustards was considered to make contributes to the increased antitumor activity of the derived hybrid molecules.

Platinum-based antineoplastic drugs are usually considered as another class of alkylating agents with high antitumor potency (Jamieson and Lippard, 1999; Wang and Lippard, 2005). Notably, cisplatin is one of the most potent platinum(II) complexes used in cancer chemotherapy by binding to DNA and subsequently interfere with replication and transcription, eventually leading to cellular apoptosis (Abu-Surrah and Kettunen, 2006; Wheate et al., 2010). However, clinical application of cisplatin is limited by its severe adverse effects, including nephrotoxicity, hepatotoxicity, ototoxicity and neurotoxicity, etc. Acquired resistance is also a concern (Brabec et al., 2017). In discovery of more potent

and safe antitumor compounds, conjunction of two different types of DNA-damaging drugs by combining chlorambucil with platinum(IV) complexes was performed by Gou and coworkers (Qin et al., 2017). In the *in vitro* activity assay, molecule **18** (**Figure 10**), a hybrid of cisplatin and chlorambucil, displayed potent antiproliferative activities with IC_{50} values of 3.99 μM, 4.37 μM, 4.97 μM, 2.97 μM, and 4.23 μM against human breast cancer MCF-7, human colon cancer HCT-116, human liver cancer HepG-2, human gastric cancer SGC7901, and cisplatin-resistant SGC7901/CDDP cells, respectively. Compared with chlorambucil, cisplatin, and oxaliplatin, molecule **18** exhibited improved activity in the inhibition of cisplatin resistant SGC7901/CDDP cells. Further studies revealed that molecule **18** induced cell cycle arrest at S/G2 phases (distinct from those of cisplatin and chlorambucil), and revealed ability of overcome drug resistance. Collectively, hybridization of nitrogen mustards and platinum(IV) complexes resulted in conjunctions with improved antitumor potency, and with advantage of overcoming drug resistance of tumor cells.

Several highly potent 1,3,5-triazine scaffold-carrying cytostatic agents have been previously reported as inhibitors of cell proliferation-involved enzymes (Maeda et al., 2000; Riou et al., 2002; Gomez et al., 2003; Kaminski et al., 2004; Mandal et al., 2007; Paquin et al., 2008). Among them, ZSTK474 (**Figure 11**) was discovered to inhibit the growth of tumor cells in human cancer xenografts without toxic effects on critical organs by targeting PI3K (Di Francesco et al., 2000; Vedejs et al., 2003). In the structural modification of current melamine derivatives, a series of melamine-nitrogen mustard derivatives **19a-f** (**Figure 11**) were synthesized by introducing one or more 2-chloroethylamine groups (Kolesinska et al., 2012). It is revealed that all synthesized molecules showed potent antitumor activities. Compared with the positive control chlorambucil (IC_{50} value of 29.14 μM against human breast cancer MCF-7 cells), the obtained molecule **19f** showed potent antitumor activity with IC_{50} value of 18.70 μM against MCF-7 cells. Compound **19a** also exhibited potent antitumor activities with IC_{50} value of 0.62 μM, 0.99 μM, 1.40 μM, 2.06 μM and 3.45 μM against human leukemia Jurkat, human prostate adenocarcinoma LNCaP, human breast adenocarcinoma T47D, human lung adenocarcinoma A549 and human colorectal carcinoma SW707 cells, respectively. Further biological studies suggested that introducing nitrogen mustard into triazine is promising in the increase of antitumor activity by promoting alkylation.

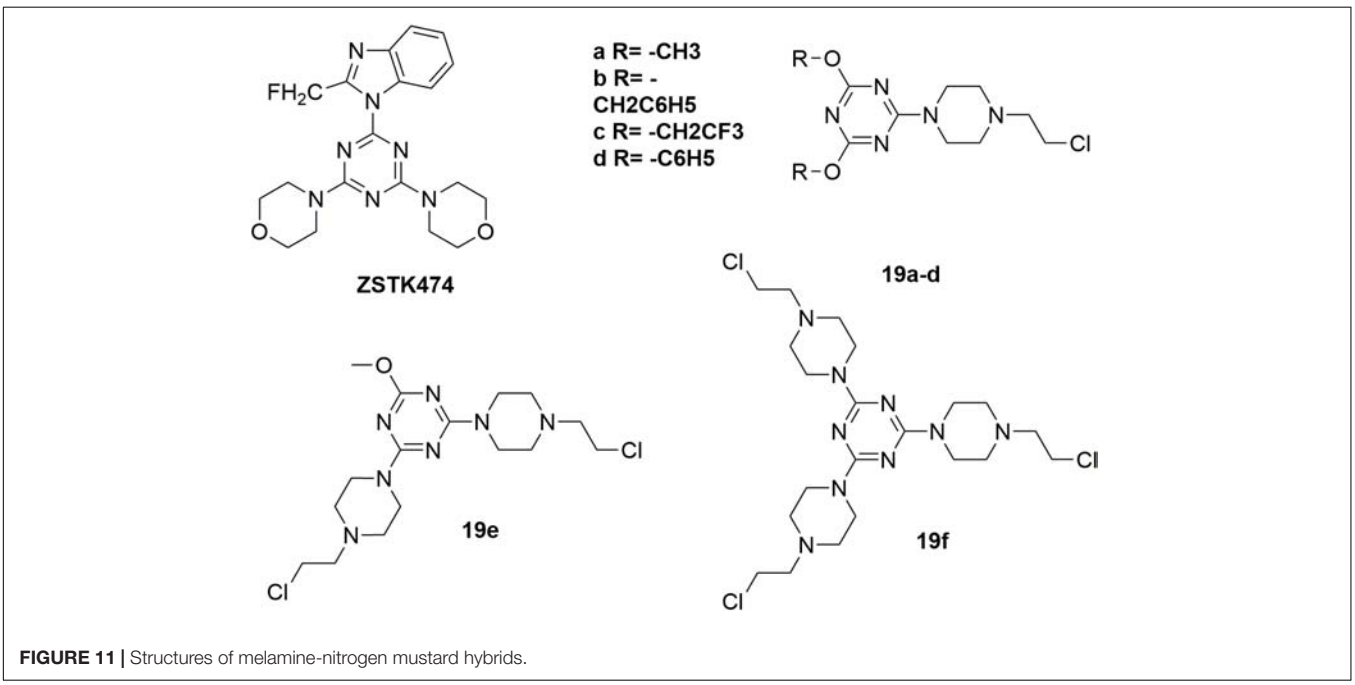

FIGURE 11 | Structures of melamine-nitrogen mustard hybrids.

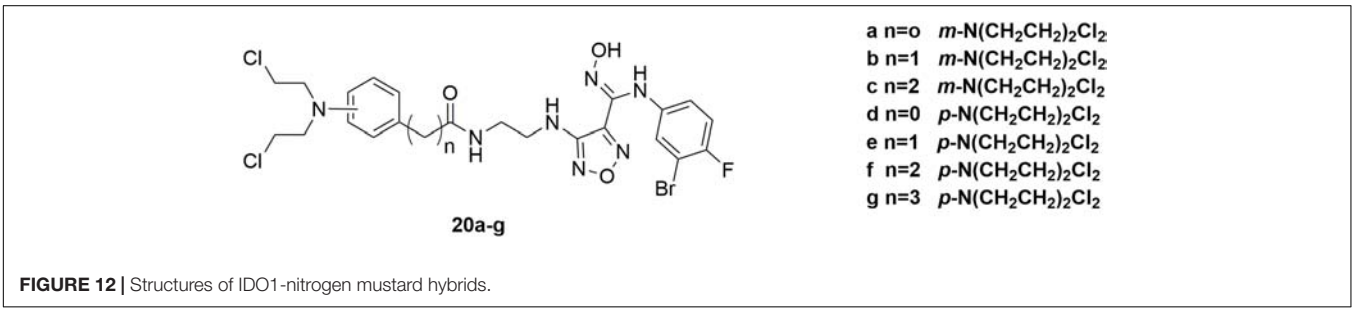

FIGURE 12 | Structures of IDO1-nitrogen mustard hybrids.

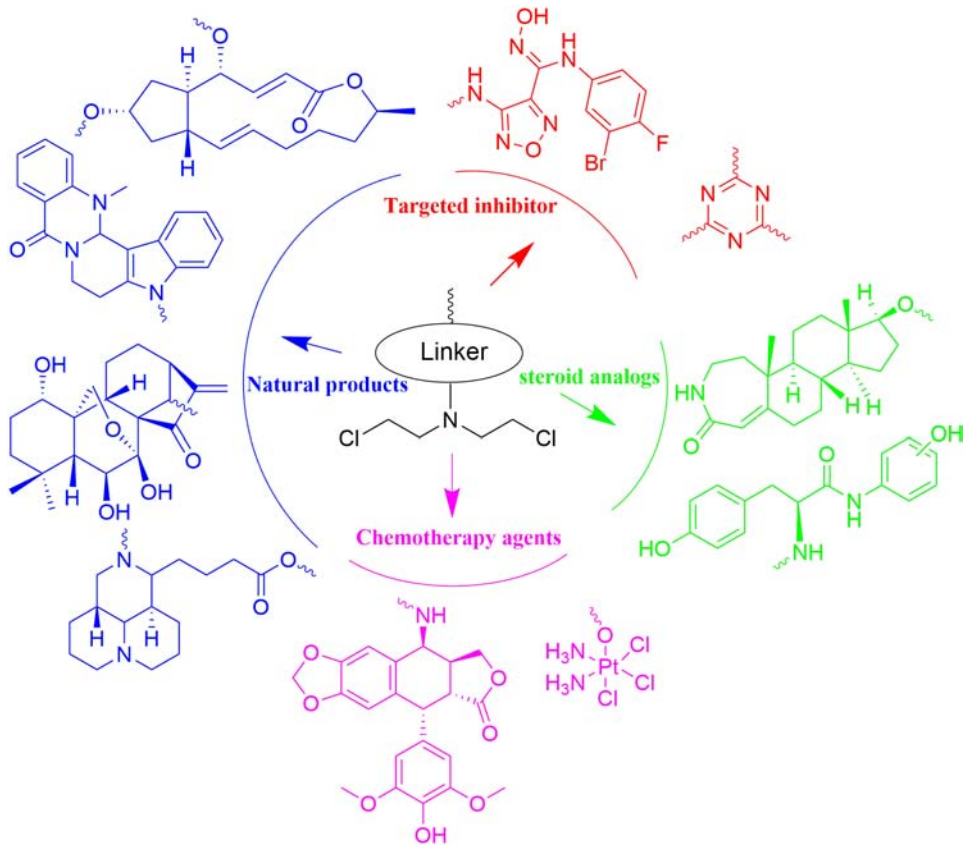

FIGURE 13 | Summary of the nitrogen mustard based hybridization strategy involved in the current article.

Accordingly, introduction of nitrogen mustard is regarded to make contribution to improve the selectivity, activity and lipophilicity of current drug-like cytotoxic derivatives.

IDO1, a heme-containing enzyme, plays an important role in carcinogenesis and its progression by converting Trp to Kyn (Jiang et al., 2015). Both Trp degradation and Kyn accumulation are associated with immune tolerance by affecting T cell activity and altering the tumor microenvironment (Moon et al., 2015). A number of studies showed that the combination of IDO1 inhibitors along with cytotoxic chemotherapeutic agents is an effective strategy in cancer treatment (Muller et al., 2005). However, such a simple combination will inevitably be limited by the severe adverse effects induced by the highly toxic cytotoxic agents and possible drug-drug interactions. Therefore, in discovery of potent antitumor molecules with reduced toxicity, a series of hybrid molecules **20a-g** (**Figure 12**) were synthesized by including the pharmacophores of both IDO1 inhibitors and nitrogen mustards (Fang et al., 2018). All the compounds showed potent antitumor activities compared with the positive drug chlorambucil in the inhibition of murine colorectal carcinoma CT-26, human lung adenocarcinoma A549, human colon cancer HCT116 and human colorectal adenocarcinoma HT-29 cells. Obviously, compound **20a** significantly inhibited IDO1 activity in tumor tissues and reduced Kyn level in plasma with IDO1 inhibitory IC_{50} value of 0.13 μM and antiproliferative EC_{50} (half maximal effect concentration) value of 0.27 μM aganist HeLa cells. Moreover, molecule **20a** exhibited high potent *in vivo* antitumor efficacy (tumor growth inhibition (TGI) = 58.2%) compared with clinical candidate IDO1 inhibitor epacadostat (TGI = 47.5%) in the allograft animal model with CT-26 without remarkable body weight loss or adverse effects. In conclusion, it is revealed that introduction of nitrogen mustard into pharmacophores of IDO1 inhibitors could significantly improve the antitumor activity and reduce toxicity of parent compound in the antitumor evaluation.

CONCLUSION AND PERSPECTIVE

Nitrogen mustards represent the earliest studied DNA cross-linking agents, and application of DNA alkylating agents has been widely utilized for the treatment of cancer for more than 70 years. In spite of their long history, several nitrogen mustard drugs, including cyclophosphamide, chlorambucil, and melphalan, still remained as first line antitumor agents in the management of various types of tumors. However, the clinical application of nitrogen mustards was restricted by their undesired adverse effects, relatively low efficacy compared with targeted antitumor drugs, and drug resistance caused by enhanced drug inactivation, decreased cellular uptake,

enhanced DNA repair and/or DNA damage tolerance. It is generally accepted that cancer has its pathological root in genetical mutations, affecting cell replication. Thus, targeting different proliferative mechanisms by the construction of hybrid anticancer drugs seem to be a promising strategy. Development of nitrogen mustard based hybrids has been revealed to be effective strategy in discovery of antitumor drugs with increased activity, reduced toxicity, and improved physicochemical properties such as the lipophilicity and the solubility.

With N,N-bis(2-chloroethyl)amine as functional group, nitrogen mustards has been hybridized with various drug-like fragments (**Figure 13**). Novel hybrids have been derived with improved potency, selectivity, safety, pharmacokinetics, pharmacodynamics properties and/or broader range of therapeutic activities. Current achievements make development of nitrogen mustard based conjunctions to be attractive area in the cancer treatment. Despite the reported advantages, unexpected side effects caused by introduction of nitrogen mustards also require careful attention in the drug design and biological evaluation. As questioned on the efficacy of twin drugs and prodrugs, it is also necessary to demonstrate advantages of the conjugates linked by ester bond or more stable bonds in comparison with the combined therapy with parental drugs.

AUTHOR CONTRIBUTIONS

YC and YJ participated in most of the literature retrieval and article writing. LZ and WS guided the review and revised the writing.

FUNDING

Some of the materials in this work were supported by National Natural Science Foundation of China (Youth Found, Grant No. 81803343).

REFERENCES

Abu-Surrah, A. S., and Kettunen, M. (2006). Platinum group antitumor chemistry: design and development of new anticancer drugs complementary to cisplatin. *Curr. Med. Chem.* 13, 1337–1357. doi: 10.2174/092986706776872970

Anadu, N. O., Davisson, V. J., and Cushman, M. (2006). Synthesis and anticancer activity of brefeldin A ester derivatives. *J. Med. Chem.* 49, 3897–3905. doi: 10.1021/jm0602817

Anstead, G. M., Carlson, K. E., and Katzenellenbogen, J. A. (1997). The estradiol pharmacophore: ligand structure-estrogen receptor binding affinity relationships and a model for the receptor binding site. *Steroids* 62, 268–303. doi: 10.1016/S0039-128X(96)00242-5

Bank, B. B., Kanganis, D., Liebes, L. F., and Silber, R. (1989). Chlorambucil pharmacokinetics and DNA binding in chronic lymphocytic leukemia lymphocytes. *Cancer Res.* 49, 554–559.

Bao, R. F., Shu, Y. J., Wu, X. S., Weng, H., Ding, Q., Cao, Y., et al. (2014). Oridonin induces apoptosis and cell cycle arrest of gallbladder cancer cells via the mitochondrial pathway. *BMC Cancer* 14:217. doi: 10.1186/1471-2407-14-217

Brabec, V., Hrabina, O., and Kasparkova, J. (2017). Cytotoxic platinum coordination compounds. DNA binding agents. *Coordin. Chem. Rev.* 351, 2–31. doi: 10.1016/j.ccr.2017.04.013

Catane, R. (1978). Clinical experience with estramustine phosphate and predinimustine, two steroidal alkylating agents compounds [proceedings]. *Cancer Treat. Rep.* 62, 1264–1265.

Chen, W. B., Balakrishnan, K., Kuang, Y. Y., Han, Y. Y., Fu, M., Gandhi, V., et al. (2014). Reactive Oxygen Species (ROS) inducible DNA cross-linking agents and their effect on cancer cells and normal lymphocytes. *J. Med. Chem.* 57, 4498–4510. doi: 10.1021/jm401349g

Cui, Q., Tashiro, S., Onodera, S., Minami, M., and Ikejima, T. (2007). Oridonin induced autophagy in human cervical carcinoma HeLa cells through Ras. JNK, and P38 regulation. *J. Pharmacol. Sci.* 105, 317–325. doi: 10.1254/jphs.FP0070336

Descoteaux, C., Brasseur, K., Leblanc, V., Parent, S., Asselin, E., and Berube, G. (2012a). Design of novel tyrosine-nitrogen mustard hybrid molecules active against uterine, ovarian and breast cancer cell lines. *Steroids* 77, 403–412. doi: 10.1016/j.steroids.2011.12.021

Descoteaux, C., Brasseur, K., Leblanc, V., Parent, S., Asselin, E., and Berube, G. (2012b). SAR study of tyrosine-chlorambucil hybrid regioisomers; synthesis and biological evaluation against breast cancer cell lines. *Amino Acids* 43, 923–935. doi: 10.1007/s00726-011-1152-3

DeVita, V. T. Jr., and Chu, E. (2008). A history of cancer chemotherapy. *Cancer Res.* 68, 8643–8653. doi: 10.1158/0008-5472.CAN-07-6611

Deweese, J. E., and Osheroff, N. (2009). The DNA cleavage reaction of topoisomerase II: wolf in sheep's clothing. *Nucleic Acids Res.* 37, 738–748. doi: 10.1093/nar/gkn937

Di Antonio, M., McLuckie, K. I. E., and Balasubramanian, S. (2014). Reprogramming the mechanism of action of chlorambucil by coupling to a G-Quadruplex ligand. *J. Am. Chem. Soc.* 136, 5860–5863. doi: 10.1021/ja5014344

Di Francesco, A. M., Hargreaves, R. H., Wallace, T. W., Mayalarp, S. P., Hazrati, A., Hartley, J. A., et al. (2000). The abnormal cytotoxicities of 2,5-diaziridinyl-1,4-benzoquinone-3-phenyl esters. *Anti Cancer Drug Des.* 15, 347–359.

Ding, C. Y., Zhang, Y. S., Chen, H. J., Yang, Z. D., Wild, C., Chu, L. L., et al. (2013a). Novel nitrogen-enriched oridonin analogues with thiazole-fused a-ring: protecting group-free synthesis, enhanced anticancer profile, and improved aqueous solubility. *J. Med. Chem.* 56, 5048–5058. doi: 10.1021/jm400367n

Ding, C. Y., Zhang, Y. S., Chen, H. J., Yang, Z. D., Wild, C., Ye, N., et al. (2013b). Oridonin ring a-based diverse constructions of enone functionality: identification of novel dienone analogues effective for highly aggressive breast cancer by inducing apoptosis. *J. Med. Chem.* 56, 8814–8825. doi: 10.1021/jm401248x

Ding, Y., Ding, C. Y., Ye, N., Liu, Z. Q., Wold, E. A., Chen, H. Y., et al. (2016). Discovery and development of natural product oridonin-inspired anticancer agents. *Eur. J. Med. Chem.* 122, 102–117. doi: 10.1016/j.ejmech.2016.06.015

Dong, X. J., Liu, F. Y., and Li, M. L. (2016). Inhibition of nuclear factor kappa B transcription activity drives a synergistic effect of cisplatin and oridonin on HepG2 human hepatocellular carcinoma cells. *Anticancer Drugs* 27, 286–299. doi: 10.1097/CAD.0000000000000329

Fan, X., Zhu, J. Y., Sun, Y., Luo, L., Yan, J., Yang, X., et al. (2017). Evodiamine inhibits Zymosan-induced inflammation in vitro and in vivo: inactivation of NF-kappa B by inhibiting I kappa B alpha phosphorylation. *Inflammation* 40, 1012–1027. doi: 10.1007/s10753-017-0546-0

Fang, K., Dong, G. Q., Wang, H. Y., He, S. P., Wu, S. C., Wang, W., et al. (2018). Improving the potency of cancer immunotherapy by dual targeting of IDO1 and DNA. *ChemMedChem* 13, 30–36. doi: 10.1002/cmdc.201700666

Frei, E. III, Teicher, B. A., Holden, S. A., Cathcart, K. N., and Wang, Y. Y. (1988). Preclinical studies and clinical correlation of the effect of alkylating dose. *Cancer Res.* 48, 6417–6423.

Galton, D. A., Wiltshaw, E., Szur, L., and Dacie, J. V. (1961). The use of chlorambucil and steroids in the treatment of chronic lymphocytic leukaemia. *Br. J. Haematol.* 7, 73–98. doi: 10.1111/j.1365-2141.1961.tb00321.x

Gilman, A. (1963). The initial clinical trial of nitrogen mustard. *Am. J. Surg.* 105, 574–578. doi: 10.1016/0002-9610(63)90232-0

Gomez, D., Aouali, N., Londono-Vallejo, A., Lacroix, L., Megnin-Chanet, F., Lemarteleur, T., et al. (2003). Resistance to the short term antiproliferative activity of the G-quadruplex ligand 12459 is associated with telomerase overexpression and telomere capping alteration. *J. Biol. Chem.* 278, 50554–50562. doi: 10.1074/jbc.M308440200

Goodman, L. S., and Wintrobe, M. M. (1946). Nitrogen mustard therapy; use of methyl-bis (beta-chloroethyl) amine hydrochloride and tris (beta-chloroethyl) amine hydrochloride for Hodgkin's disease, lymphosarcoma, leukemia and certain allied and miscellaneous disorders. *J. Am. Med. Assoc.* 132, 126–132. doi: 10.1001/jama.1946.02870380008004

Grose, C., and Klionsky, D. J. (2016). Alternative autophagy, brefeldin A and viral trafficking pathways. *Autophagy* 12, 1429–1430. doi: 10.1080/15548627.2016.1203489

Han, T., Tian, K. T., Pan, H. Q., Liu, Y. X., Xu, F. X., Li, Z. L., et al. (2018). Novel hybrids of brefeldin A and nitrogen mustards with improved antiproliferative selectivity: design, synthesis and antitumor biological evaluation. *Eur. J. Med. Chem.* 150, 53–63. doi: 10.1016/j.ejmech.2018.02.088

Hu, X., Wang, Y., Xue, J. J., Han, T., Jiao, R. W., Li, Z. L., et al. (2017). Design and synthesis of novel nitrogen mustard-evodiamine hybrids with selective antiproliferative activity. *Bioorg. Med. Chem. Lett.* 27, 4989–4993. doi: 10.1016/j.bmcl.2017.10.014

Huang, H. R., Liu, T., Guo, J. X., Yu, L., Wu, X. F., He, Y., et al. (2017). Brefeldin A enhances docetaxel-induced growth inhibition and apoptosis in prostate cancer cells in monolayer and 3D cultures. *Bioorg. Med. Chem. Lett.* 27, 2286–2291. doi: 10.1016/j.bmcl.2017.04.047

Hughes, E., Scurr, M., Campbell, E., Jones, E., Godkin, A., and Gallimore, A. (2018). T-cell modulation by cyclophosphamide for tumour therapy. *Immunology* 154, 62–68. doi: 10.1111/imm.12913

Jamieson, E. R., and Lippard, S. J. (1999). Structure, recognition, and processing of cisplatin-DNA adducts. *Chem. Rev.* 99, 2467–2498. doi: 10.1021/cr980421n

Jiang, T. Z., Sun, Y. Y., Yin, Z. C., Feng, S., Sun, L. P., and Li, Z. Y. (2015). Research progress of indoleamine 2,3-dioxygenase inhibitors. *Future Med. Chem.* 7, 185–201. doi: 10.4155/fmc.14.151

Kaminski, Z. J., Kolesinska, B., and Markowicz, S. W. (2004). Synthesis and cytostatic properties of monoterpene derivatives of cyanuric and isocyanuric acids. *Acta. Pol. Pharm.* 61(Suppl.), 29–32.

Kikuchi, S., Shinpo, K., Tsuji, S., Yabe, I., Niino, M., and Tashiro, K. (2003). Brefeldin A-induced neurotoxicity in cultured spinal cord neurons. *J. Neurosci. Res.* 71, 591–599. doi: 10.1002/jnr.10479

Kohn, K. W., Hartley, J. A., and Mattes, W. B. (1987). Mechanisms of DNA sequence selective alkylation of guanine-N7 positions by nitrogen mustards. *Nucleic Acids Res.* 15, 10531–10549. doi: 10.1093/nar/15.24.10531

Kolesinska, B., Barszcz, K., Kaminski, Z. J., Drozdowska, D., Wietrzyk, J., and Switalska, M. (2012). Synthesis and cytotoxicity studies of bifunctional hybrids of nitrogen mustards with potential enzymes inhibitors based on melamine framework. *J. Enzyme Inhib. Med. Chem.* 27, 619–627. doi: 10.3109/14756366.2011.604482

Lallukka, T., Millear, A., Pain, A., Cortinovis, M., and Giussani, G. (2017). GBD 2015 Mortality and Causes of Death Collaborators. Global, regional, and national life expectancy, all-cause mortality, and cause-specifi c mortality for 249 causes of death, 1980-2015: a systematic analysis for the Global Burden of Disease Study 2015 (vol 388, pg 1459, 2016). *Lancet* 389:E1.

Li, D., Dai, L., Zhao, X., Zhi, S., Shen, H., and Yang, Z. (2018). Novel sophoridine derivatives bearing phosphoramide mustard moiety exhibit potent antitumor activities in vitro and in vivo. *Molecules* 23:E1960. doi: 10.3390/molecules23081960

Li, D. D., Dai, L. L., Zhang, N., and Tao, Z. W. (2015). Synthesis, structure-activity relationship and biological evaluation of novel nitrogen mustard sophoridinic acid derivatives as potential anticancer agents. *Bioorg. Med. Chem. Lett.* 25, 4092–4096. doi: 10.1016/j.bmcl.2015.08.035

Li, Y., Wang, Y., Wang, S. H., Gao, Y. J., Zhang, X. F., and Lu, C. H. (2015). Oridonin phosphate-induced autophagy effectively enhances cell apoptosis of human breast cancer cells. *Med. Oncol.* 32:365. doi: 10.1007/s12032-014-0365-1

Liu, J. B., and Liu, Y. Q. (2013). Influence of Erbanxiao solution on inhibiting angiogenesis in stasis toxin stagnation of non-small cell lung cancer. *J. Tradit. Chin. Med.* 33, 303–306. doi: 10.1016/S0254-6272(13)60169-7

Liu, M., Wang, W. G., Sun, H. D., and Pu, J. X. (2017). Diterpenoids from Isodon species: an update. *Nat. Prod. Rep.* 34, 1090–1140. doi: 10.1039/c7np00027h

Lv, Q. L., Xue, Y., Li, G. D., Zou, L. F., Zhang, X., Ying, M. F., et al. (2015). Beneficial effects of evodiamine on P2X(4)-mediated inflammatory injury of human umbilical vein endothelial cells due to high glucose. *Int. Immunopharmacol.* 28, 1044–1049. doi: 10.1016/j.intimp.2015.08.020

Maeda, M., Ligo, M., Tsuda, H., Fujita, H., Yonemura, Y., Nakagawa, K., et al. (2000). Antimetastatic and antitumor effects of 2,4-diamino-6-(pyridine-4-yl)-1,3,5-triazine (4PyDAT) on the high lung metastatic colon 26 tumor in mice. *Anti Cancer Drug Des.* 15, 217–223.

Mandal, S., Berube, G., Asselin, E., Mohammad, I., Richardson, V. J., Gupta, A., et al. (2007). A novel series of potent cytotoxic agents targeting G2/M phase of the cell cycle and demonstrating cell killing by apoptosis in human breast cancer cells. *Bioorg. Med. Chem. Lett.* 17, 4955–4960. doi: 10.1016/j.bmcl.2007.06.033

Moon, J. L., Kim, S. Y., Shin, S. W., and Park, J. W. (2012). Regulation of brefeldin A-induced ER stress and apoptosis by mitochondrial NADP(+)-dependent isocitrate dehydrogenase. *Biochem. Bioph. Res. Commun.* 417, 760–764. doi: 10.1016/j.bbrc.2011.12.030

Moon, Y. W., Hajjar, J., Hwu, P., and Naing, A. (2015). Targeting the indoleamine 2,3-dioxygenase pathway in cancer. *J. Immunother. Cancer* 3:51. doi: 10.1186/s40425-015-0094-9

Muller, A. J., DuHadaway, J. B., Donover, P. S., Sutanto-Ward, E., and Prendergast, G. C. (2005). Inhibition of indoleamine 2,3-dioxygenase, an immunoregulatory target of the cancer suppression gene Bin1, potentiates cancer chemotherapy. *Nat. Med.* 11, 312–319. doi: 10.1038/nm1196

Muthyala, R. S., Carlson, K. E., and Katzenellenbogen, J. A. (2003). Exploration of the bicyclo[3.3.1]nonane system as a template for the development of new ligands for the estrogen receptor. *Bioorg. Med. Chem. Lett.* 13, 4485–4488. doi: 10.1016/j.bmcl.2003.08.061

Nicolle, A., Proctor, S. J., and Summerfield, G. P. (2004). High dose chlorambucil in the treatment of lymphoid malignancies. *Leuk. Lymphoma* 45, 271–275. doi: 10.1080/10428190310001595704

Nitiss, J. L. (2009). Targeting DNA topoisomerase II in cancer chemotherapy. *Nat. Rev. Cancer* 9, 338–350. doi: 10.1038/nrc2607

Ogasawara, M., Matsunaga, T., Takahashi, S., Saiki, I., and Suzuki, H. (2002). Anti-invasive and metastatic activities of evodiamine. *Biol. Pharm. Bull.* 25, 1491–1493. doi: 10.1248/bpb.25.1491

Paquin, I., Raeppel, S., Leit, S., Gaudette, F., Zhou, N., Moradei, O., et al. (2008). Design and synthesis of 4-[(s-triazin-2-ylamino)methyl]-N-(2-aminophenyl)-benzamides and their analogues as a novel class of histone deacetylase inhibitors. *Bioorg. Med. Chem. Lett.* 18, 1067–1071. doi: 10.1016/j.bmcl.2007.12.009

Pommier, Y. (2013). Drugging topoisomerases: lessons and challenges. *ACS Chem. Biol.* 8, 82–95. doi: 10.1021/cb300648v

Pommier, Y., Leo, E., Zhang, H., and Marchand, C. (2010). DNA topoisomerases and their poisoning by anticancer and antibacterial drugs. *Chem. Biol.* 17, 421–433. doi: 10.1016/j.chembiol.2010.04.012

Pommier, Y., and Marchand, C. (2011). Interfacial inhibitors: targeting macromolecular complexes. *Nat. Rev. Drug Discov.* 11, 25–36. doi: 10.1038/nrd3404

Povirk, L. F., and Shuker, D. E. (1994). DNA damage and mutagenesis induced by nitrogen mustards. *Mutat. Res.* 318, 205–226. doi: 10.1016/0165-1110(94)90015-9

Qin, X. D., Fang, L., Chen, F. H., and Gou, S. H. (2017). Conjugation of platinum(IV) complexes with chlorambucil to overcome cisplatin resistance via a "joint action" mode toward DNA. *Eur. J. Med. Chem.* 137, 167–175. doi: 10.1016/j.ejmech.2017.05.056

Quo, L., Xue, T. Y., Xu, W., and Gao, J. Z. (2013). Matrine promotes G(0)/G(1) arrest and down-regulates cyclin D1 expression in human rhabdomyosarcoma cells. *Panminerva Med.* 55, 291–296.

Rajamahanty, S., Alonzo, C., Aynehchi, S., Choudhury, M., and Konno, S. (2010). Growth inhibition of androgen-responsive prostate cancer cells with brefeldin A targeting cell cycle and androgen receptor. *J. Biomed. Sci.* 17:5. doi: 10.1186/1423-0127-17-5

Riou, J. F., Guittat, L., Mailliet, P., Laoui, A., Renou, E., Petitgenet, O., et al. (2002). Cell senescence and telomere shortening induced by a new series of specific G-quadruplex DNA ligands. *Proc. Natl. Acad. Sci. U.S.A.* 99, 2672–2677. doi: 10.1073/pnas.052698099

Ryerson, A. B., Eheman, C. R., Altekruse, S. F., Ward, J. W., Jemal, A., Sherman, R. L., et al. (2016). Annual report to the nation on the status of cancer, 1975-2012, featuring the increasing incidence of liver cancer. *Cancer* 122, 1312–1337. doi: 10.1002/cncr.29936

Sanderson, B. J., and Shield, A. J. (1996). Mutagenic damage to mammalian cells by therapeutic alkylating agents. *Mutat. Res.* 355, 41–57. doi: 10.1016/0027-5107(96)00021-8

Sarosy, G., Leyland-Jones, B., Soochan, P., and Cheson, B. D. (1988). The systemic administration of intravenous melphalan. *J. Clin. Oncol.* 6, 1768–1782. doi: 10.1200/JCO.1988.6.11.1768

Schobert, R., Biersack, B., Dietrich, A., Knauer, S., Zoldakova, M., Fruehauf, A., et al. (2009). Pt(II) complexes of a combretastatin A-4 analogous chalcone: effects of conjugation on cytotoxicity, tumor specificity, and long-term tumor growth suppression. *J. Med. Chem.* 52, 241–246. doi: 10.1021/jm801001d

Seehafer, K., Rominger, F., Helmchen, G., Langhans, M., Robinson, D. G., Ozata, B., et al. (2013). Synthesis and biological properties of novel brefeldin a analogues. *J. Med. Chem.* 56, 5872–5884. doi: 10.1021/jm400615g

Shi, C. S., Li, J. M., Chin, C. C., Kuo, Y. H., Lee, Y. R., and Huang, Y. C. (2017). Evodiamine induces cell growth arrest, apoptosis and suppresses tumorigenesis in human urothelial cell carcinoma cells. *Anticancer. Res.* 37, 1149–1159. doi: 10.21873/anticanres.11428

Shi, L., Yang, F., Luo, F., Liu, Y., Zhang, F., Zou, M. J., et al. (2016). Evodiamine exerts anti-tumor effects against hepatocellular carcinoma through inhibiting beta-catenin-mediated angiogenesis. *Tumor Biol.* 37, 12791–12803. doi: 10.1007/s13277-016-5251-3

Shi, M., Lu, X. J., Zhang, J., Diao, H., Li, G. M., Xu, L., et al. (2016). Oridonin, a novel lysine acetyltransferases inhibitor, inhibits proliferation and induces apoptosis in gastric cancer cells through p53-and caspase-3-mediated mechanisms. *Oncotarget* 7, 22623–22631. doi: 10.18632/oncotarget.8033

Shyu, K. G., Lin, S., Lee, C. C., Chen, E., Lin, L. C., Wang, B. W., et al. (2006). Evodiamine inhibits in vitro angiogenesis: implication for antitumorgenicity. *Life Sci.* 78, 2234–2243. doi: 10.1016/j.lfs.2005.09.027

South, P. F., Harmeyer, K. M., Serratore, N. D., and Briggs, S. D. (2013). H3K4 methyltransferase Set1 is involved in maintenance of ergosterol homeostasis and resistance to Brefeldin A. *Proc. Natl. Acad. Sci. U.S.A.* 110, E1016–E1025. doi: 10.1073/pnas.1215768110

Springer, C. J., Antoniw, P., Bagshawe, K. D., Searle, F., Bisset, G. M., and Jarman, M. (1990). Novel prodrugs which are activated to cytotoxic alkylating agents by carboxypeptidase G2. *J. Med. Chem.* 33, 677–681. doi: 10.1021/jm00164a034

Sun, H. D., Huang, S. X., and Han, Q. B. (2006). Diterpenoids from Isodon species and their biological activities. *Nat. Prod. Rep.* 23, 673–698. doi: 10.1039/b604174d

Sun, Q., Sattayakhom, A., Backs, J., Stremmel, W., and Chamulitrat, W. (2012). Role of myocyte enhancing factor 2B in epithelial myofibroblast transition of human gingival keratinocytes. *Exp. Biol. Med.* 237, 178–185. doi: 10.1258/ebm.2011.011261

Toda, T., Watanabe, M., Kawato, J., Kadin, M. E., Higashihara, M., Kunisada, T., et al. (2015). Brefeldin a exerts differential effects on anaplastic lymphoma kinase positive anaplastic large cell lymphoma and classical Hodgkin lymphoma cell lines. *Br. J. Haematol.* 170, 837–846. doi: 10.1111/bjh.13508

Torre, L. A., Bray, F., Siegel, R. L., Ferlay, J., Lortet-Tieulent, J., and Jemal, A. (2015). Global cancer statistics, 2012. *Cancer J. Clin.* 65, 87–108. doi: 10.3322/caac.21262

Trafalis, D., Geromichalou, E., Dalezis, P., Nikoleousakos, N., and Sarli, V. (2016). Synthesis and evaluation of new steroidal lactam conjugates with aniline mustards as potential antileukemic therapeutics. *Steroids* 115, 1–8. doi: 10.1016/j.steroids.2016.07.009

Vedejs, E., Naidu, B. N., Klapars, A., Warner, D. L., Li, V. S., Na, Y., et al. (2003). Synthetic enantiopure aziridinomitosenes: preparation, reactivity, and DNA alkylation studies. *J. Am. Chem. Soc.* 125, 15796–15806. doi: 10.1021/ja030452m

Wall, M. E., Abernethy, G. S. Jr., Carroll, F. I., and Taylor, D. J. (1969). The effects of some steroidal alkylating agents on experimental animal mammary tumor and leukemia systems. *J. Med. Chem.* 12, 810–818. doi: 10.1021/jm00305a021

Wang, C. Y., Bai, X. Y., and Wang, C. H. (2014). Traditional chinese medicine: a treasured natural resource of anticancer drug research and development. *Am. J. Chin. Med.* 42, 543–559. doi: 10.1142/S0192415X14500359

Wang, D., and Lippard, S. J. (2005). Cellular processing of platinum anticancer drugs. *Nat. Rev. Drug Discov.* 4, 307–320. doi: 10.1038/nrd1691

Wang, L., Li, D. H., Xu, S. T., Cai, H., Yao, H. Q., Zhang, Y. H., et al. (2012). The conversion of oridonin to spirolactone-type or enmein-type diterpenoid: synthesis and biological evaluation of ent-6,7-seco-oridonin derivatives as novel potential anticancer agents. *Eur. J. Med. Chem.* 52, 242–250. doi: 10.1016/j.ejmech.2012.03.024

Wang, Z. Y., Liu, J. G., Li, H., and Yang, H. M. (2016). Pharmacological effects of active components of chinese herbal medicine in the treatment of Alzheimer's disease: a review. *Am. J. Chin. Med.* 44, 1525–1541. doi: 10.1142/S0192415X16500853

Wheate, N. J., Walker, S., Craig, G. E., and Oun, R. (2010). The status of platinum anticancer drugs in the clinic and in clinical trials. *Dalton Trans.* 39, 8113–8127. doi: 10.1039/c0dt00292e

Wu, C. C., Li, T. K., Farh, L., Lin, L. Y., Lin, T. S., Yu, Y. J., et al. (2011). Structural basis of type II topoisomerase inhibition by the anticancer drug etoposide. *Science* 333, 459–462. doi: 10.1126/science.1204117

Wu, W. S., Chien, C. C., Chen, Y. C., and Chiu, W. T. (2016). Protein Kinase RNA-like endoplasmic reticulum kinase-mediated Bcl-2 protein phosphorylation contributes to evodiamine-induced apoptosis of human renal cell carcinoma cells. *PLoS One* 11:e0160484. doi: 10.1371/journal.pone.0160484

Xu, S., Pei, L. L., Wang, C. Q., Zhang, Y. K., Li, D. H., Yao, H. Q., et al. (2014). Novel hybrids of natural oridonin-bearing nitrogen mustards as potential anticancer drug candidates. *ACS Med. Chem. Lett.* 5, 797–808. doi: 10.1021/ml500141f

Xu, S. T., Pei, L. L., Li, D. H., Yao, H., Cai, H., Yao, H. Q., et al. (2014). Synthesis and antimycobacterial evaluation of natural oridonin and its enmein-type derivatives. *Fitoterapia* 99, 300–306. doi: 10.1016/j.fitote.2014.10.005

Yadav, A. A., Wu, X., Patel, D., Yalowich, J. C., and Hasinoff, B. B. (2014). Structure-based design, synthesis and biological testing of etoposide analog epipodophyllotoxin-N-mustard hybrid compounds designed to covalently bind to topoisomerase II and DNA. *Bioorg. Med. Chem.* 22, 5935–5949. doi: 10.1016/j.bmc.2014.09.014

Yu, H., Jin, H., Gong, W., Wang, Z., and Liang, H. (2013). Pharmacological actions of multi-target-directed evodiamine. *Molecules* 18, 1826–1843. doi: 10.3390/molecules18021826

Zarytova, V. F., Ivanova, E. M., and Chasovskikh, M. N. (1990). [Synthesis of steroid-containing oligonucleotides and their alkylating derivatives]. *Bioorg. Khim.* 16, 610–616.

Zhou, G. B., Kang, H., Wang, L., Gao, L., Liu, P., Xie, J., et al. (2007). Oridonin, a diterpenoid extracted from medicinal herbs, targets AML1-ETO fusion protein and shows potent antitumor activity with low adverse effects on t(8;21) leukemia in vitro and in vivo. *Blood* 109, 3441–3450. doi: 10.1182/blood-2006-06-032250

Conflict of Interest Statement: The authors declare that the research was conducted in the absence of any commercial or financial relationships that could be construed as a potential conflict of interest.

frontiers in Oncology

ORIGINAL RESEARCH
published: 18 December 2018
doi: 10.3389/fonc.2018.00631

Oxymatrine and Cisplatin Synergistically Enhance Anti-tumor Immunity of CD8$^+$ T Cells in Non-small Cell Lung Cancer

Jin Ye[1†], Man-Man Zou[2†], Pei Li[1], Xi-Jun Lin[1], Qi-Wei Jiang[3], Yang Yang[3], Jia-Rong Huang[3], Meng-Ling Yuan[3], Zi-Hao Xing[3], Meng-Ning Wei[3], Yao Li[3], Zhi Shi[3] and Hui Liu[2]**

[1] Department of Otolaryngology-Head and Neck Surgery, The Third Affiliated Hospital, Sun Yat-sen University, Guangzhou, China, [2] Division of Pulmonary and Critical Care, Department of Internal Medicine, The Third Affiliated Hospital, Sun Yat-sen University, Guangzhou, China, [3] Guangdong Provincial Key Laboratory of Bioengineering Medicine, Department of Cell Biology & Institute of Biomedicine, National Engineering Research Center of Genetic Medicine, College of Life Science and Technology, Jinan University, Guangzhou, China

Oxymatrine (OMT) has shown broad antitumor activities for the treatment of several types of cancers. However, little is known about its effect on anti-tumor immunity. Combination therapy is a potentially promising strategy of cancer to enhance anticancer activity, overcome drug resistance, and lower treatment failure rate. In the present study, we demonstrated that the combination of OMT with cisplatin (DDP) synergistically inhibited non-small cell lung cancer (NSCLC) cells growth when co-cultured with peripheral blood mononuclear cells *in vitro*. Furthermore, the combination of OMT with DDP significantly inhibited the growth of Lewis lung cancer (LLC) mouse xenograft tumors. Flow cytometry analysis revealed that OMT and DDP synergistically increase the CD8$^+$/ regulatory T cells ratio and enhanced more CD8$^+$ T cells secreted cytokines of IFN-γ, TNF-α, and IL-2 *in vivo*. Mechanistically, upregulation of *miR-155* and downregulation of suppressor of cytokine signaling-1 (*SOCS1*) were confirmed as a target signaling pathway to positively regulate the anti-tumor response of CD8$^+$ T cells. Overall, OMT in combination with DDP showed outstanding synergistic anti-tumor immunity, suggesting that this beneficial combination may offer a potential immunotherapy for NSCLC patients.

Keywords: oxymatrine, cisplatin, CD8$^+$ T cells, anti-tumor immunity, NSCLC

OPEN ACCESS

Edited by:
Yan-yan Yan,
Shanxi Datong University, China

Reviewed by:
Hua Zhu,
The Ohio State University, United States
Xiao Qian Chen,
Huazhong University of Science and Technology, China

****Correspondence:***
Zhi Shi
tshizhi@jnu.edu.cn
Hui Liu
liuhui27@mail.sysu.edu.cn

[†]These authors have contributed equally to this work

Specialty section:
This article was submitted to Cancer Molecular Targets and Therapeutics, a section of the journal Frontiers in Oncology

Received: *12 November 2018*
Accepted: *04 December 2018*
Published: *18 December 2018*

Citation:
Ye J, Zou M-M, Li P, Lin X-J, Jiang Q-W, Yang Y, Huang J-R, Yuan M-L, Xing Z-H, Wei M-N, Li Y, Shi Z and Liu H (2018) Oxymatrine and Cisplatin Synergistically Enhance Anti-tumor Immunity of CD8$^+$ T Cells in Non-small Cell Lung Cancer. Front. Oncol. 8:631. doi: 10.3389/fonc.2018.00631

INTRODUCTION

Lung cancer is the leading cause of cancer-related death worldwide (1), and non-small cell lung cancer (NSCLC) accounts for approximately 85% of the whole lung cancer cases (2). Despite years of researches for early diagnosis and standard treatment, the prognosis for patients with lung cancer remains dismal, and 5-year survival rate remains <15% (3–6). T cell–mediated anti-tumor immunotherapy emerges as a promising treatment for human malignancies, in which CD8$^+$ T cells [cytotoxic T lymphocytes (CTLs)] represent a major of the cell-mediated anti-tumor response via providing host immune protection against intracellular pathogens and cancers (7, 8). However,

progressive tumors can escape immune recognition and attack by smartly establishing an immune tolerance involving immunosuppressive T lymphocytes (9, 10). In particular, regulatory T cells (T_{reg}) are proposed as key components of the immune suppressive tumor microenvironment with strong suppressive capacities toward $CD4^+$ and $CD8^+$ T lymphocytes, B cells, and dendritic cells etc. (11). Further, Baras et al. demonstrated that the $CD8^+/T_{reg}$ ratio in tumor infiltrating lymphocytes (TIL) densities rather than the two independent parameters was significantly associated with cisplatin-based neoadjuvant chemotherapy (12). MicroRNAs (miRNAs) have been confirmed as global regulators of gene expression programs that regulate specific target genes at the post-transcriptional level (13). Some of them have been identified as targets for anti-cancer therapeutics (14), and effects on tumor-infiltrating immune cells has become a hot spot besides their functions in cancer cells recent years (15). *miR-155* is an ancient regulator of the immune system (16). Elegant et al. demonstrated that *miR-155* was required for $CD8^+$ T cell responses in defending against infection and cancer by silencing suppressor of cytokine signaling-1 (*SOCS1*) (17, 18). Initial evidence has also unraveled the crucial role of *miR-155* in dendritic cells functions in multiple types of cancers (19, 20). Altogether, these studies suggested the pivotal functions of *miR-155* in various T cell subsets as they respond to solid tumors.

Cisplatin (DDP)-based doublet remains the foundation of treatment for the patients with NSCLC in the modern era (21). The resistance of NSCLC cells to DDP is also an emergent problem, therefore developing more effective strategies for the treatment of NSCLC is urgently required. Combination chemotherapy is identified as a potentially promising approach to enhance anticancer activity, overcome drug resistance, and lower treatment failure rate (22, 23). Oxymatrine (OMT) is a main alkaloid extracted from roots of Sophora species with a broad range of bioactivities. Especially, extensive researches have reported that OMT have anticancer effects by inducing cell cycle arrest, apoptosis and inhibition of angiogenesis in various cancer cells *in vitro* and *in vivo* (24). In the previous studies, immunoregulatory effects of OMT on hepatitis B of mice, rheumatoid arthritis in rats and mastitis in mice have been confirmed (25–27). Considering the extensive effects of OMT, we investigate the effect of OMT in combination with DDP on anti-tumor immunity in NSCLC and elucidate the potential mechanism.

MATERIALS AND METHODS

Cell Culture and Reagents

Human A549 NSCLC cell line and mouse Lewis lung cancer (LLC) cell line were cultured in Dulbecco' s modified Eagle's medium (DMEM) with 10% fetal bovine serum (FBS), penicillin (100 U/ml), and streptomycin (100 ng/ml) at 37°C with 5% CO_2 in a humidified incubator. OMT and DDP were ordered from Dalian Meilun Biotechnology and Qilu Pharmaceutical, respectively. OMT and DDP were dissolved in phosphate-buffered saline (PBS) on stock concentration (1 M and 10 mM, respectively) and stored at −20°C. Other reagents were purchased from Shanghai Sangon Biotech unless otherwise noted.

Cell Viability Assay

Freshly-isolated peripheral blood mononuclear cells (PBMCs) were suspended in DMED culture medium and seeded into a 96-well plate at a density of 1×10^4 cells/well and treated with various concentrations of drugs in three parallel wells for 72 h. CCK-8 (Dojindo Molecular Technologies, Shanghai, China) was then added to each well according to the protocol of the manufacture. The absorbance was measured at wavelengths of 450 nm after incubation with CCK-8 solution at 37°C for 4 h. Cells viability assay of A549 and LLC cells were measured using methylthiazolyldiphenyl-tetrazolium bromide (MTT) (28). Briefly, tumor cells were distributed (5,000 cells/well) into 96-well plates containing agents at different concentrations. After 3 days, MTT was added to each well at a final concentration of 0.5 mg/ml. After incubation for 4 h, the medium and MTT solution were removed from each well, and formazan crystals were dissolved in 100 μl of DMSO. Absorbance was measured at wavelengths of 570 nm. All absorbance was detected by Multiscan Spectrum (Thermo Fisher). The concentrations required to inhibit growth by 50% (IC_{50}) were calculated from survival curves using the Bliss method (29). Studies relative to human in this article were approved by the ethics committee of the Third Affiliated Hospital, Sun Yat-sen University (Approval No: [2014]2-17).

Tumor Cells/PBMCs Co-culture

After adherence of tumor cells into 6-well plates (target cells, 4×10^5 cells/well), a certain amount of PBMCs (effector cells) suspended in the appropriate DMEM pulsed with 10% FBS were added. Four ratios of effector cells to target cells, 0:1, 2:1, 4:1, and 6:1 were designed. After treated with OMT and DDP alone or combination, target cells (tumor cells) and effector cells (PBMCs) were co-cultured for 24 h at 37°C in 5% CO_2. The cellular remaining viable tumor cells were photographed under microscope (OLYMPUS IX71) and quantified, respectively.

Mice Xenograft Tumor Assay

Age-suitable C57BL/6 female mice were obtained from Vital River Laboratory Animal Technology (Beijing), and all mice have been maintained with sterilized food and water. All animal experimental procedures were approved by the Institutional Animal Care and Use Committee of Sun Yat-sen University (Approval No: IACUC-DB-17-0502). Briefly, female C57BL/6 mice within 6 weeks old and 20 g weight were used for each group. Each mouse was injected subcutaneously with LLC cells (2×10^6 in 100 μl of PBS) in right scapular region. When the subcutaneous tumors were approximately 0.3×0.3 cm^2 (two perpendicular diameters) in size, mice were randomized into four groups. Mice were injected intraperitoneally with vehicle alone (0.9% saline), OMT alone (100 mg/kg body weight per day), DDP alone (2 mg/kg body weight every 2 day), or a combination of OMT and DDP (administration method is as same as the relevant single drug group). The body weights of mice and the two perpendicular diameters (A and B) of tumors were recorded

TABLE 1 | The primer sequences for real time PCR (mouse).

miR-155 (RT)	5′-GTCGTATCCAGTGCAGGGTCCGAGGTATTCGCACTGGATACGACACCCCT-3′
miR-155 (F)	5′-GTCGTATCCAGTGCAGGGTCCGAGGTATTCGCACTGGATACGACACCCCT-3′
miR-155 (R)	5′-GTCGTATCCAGTGCAGGGTCCGAGGTATTCGCACTGGATACGACAAAATA-3′
U6 (RT)	5′-GTCGTATCCAGTGCAGGGTCCGAGGTATTCGCACTGGATACGACAAAATA-3
U6 (F)	5′-GCGCGTCGTGAAGCGTTC-3
U6 (R)	5′-GTGCAGGGTCCGAGGT-3
SOCS1 (F)	5′-CTGCGGCTTCTATTGGGGAC-3
SOCS1 (R)	5′-AAAAGGCAGTCGAAGGTCTCG-3
β-actin (F)	5′-CCTTCTTGGGTATGGAATCCTG-3
β-actin (R)	5′-CAATGCCTGGGTACATGGTG-3

every day. The tumor volumes (V) were calculated according to the formula:

$$V = \pi/6(1/2(A + B))^3$$

The mice were anesthetized after the experiment, and tumors were excised from the mice and weighted. Heparin anticoagulated peripheral blood, spleens and tumors were collected for further use. The rate of inhibition (IR) was calculated according to the formula below:

IR = 1-Mean tumor weight of experimental group/Mean tumor weight of control group × 100%.

Flow Cytometric Analysis

PBMCs and spleen lymphocytes were collected with Ficoll-diatrizoate (LTS1077, tbdscience, Tianjin) according to the protocol of the manufacture. For the separation of tumor infiltrating lymphocytes from LLC-bearing mice, xenograft tumors were mechanically disrupted into 1 mm^3 pieces and digested chemically in 7 ml of dissociation medium (DMEM medium plus with 10% FBS, collagenase type IV (5 mg/ml), DNase I (1 mg/ml), and hyaluronidase (1 mg/ml) for 30 min at 37°C followed by filtration through a 70 μm cell strainer (NEST Biotechnology, Wuxi). Dissociated tumor cells were washed twice by PBS. Erythrocytes were lysed by red blood cell lysing buffer (BD Pharmigen) if necessary. The following antibodies were used for staining: Fc block (anti-CD16/32, Cat: 553142), CD3 APC-A750 (Cat: 557596), CD8a BV510 (Cat: 563068), CD4a FITC (Cat: 553046), Foxp3 PE (Cat: 563101), CD45 Percp-cy5.5 (Cat: 550994), IFN-γ FITC (Cat: 554411), TNF-α (Cat: 554420), anti-IL-2 (eBioscience, Cat: 12-7021-81), PE Rat IgG2a, κ Isotype Control (Cat: 553930), FITC Rat IgG1, κ Isotype Control (Cat: 554684), APC Rat IgG1, κ Isotype Control (Cat: 554686), and Rat IgG2b kappa Isotype Control (eBioscience, Cat: 12-4031-82). As regards the concentrations of antibodies, 2 μl/test was used in PBMCs and spleen lymphocytes samples and 3 μl/test in TIL flow cytometry. All antibodies were purchased from BD Pharmigen unless otherwise noted. Briefly, all samples were block with anti-CD16/32 for 20 min on room temperature and then stained with appropriate antibodies for 30 min on ice. Anti-mouse FoxP3 staining (eBioscience, Cat: 00-5523) was used for intracellular staining according to the manufacturer's instructions. For intracellular staining of IFN-γ, TNF-α, and IL-2, single-cell suspensions were incubated at 37°C for 5 h in the presence of Cell Stimulation Cocktail (eBioscience, Cat: 85-00-4975-93) according to the manufacturer's protocol. Zombie Violet™ Fixable Viability Kit (Biolegend, Cat: 423113) was required to distinguish live/dead cells in tumor flow cytometry. Appropriate isotype control antibodies were used to determine the gating strategies.

$CD8^+$ T Cell Isolation

Freshly-separated single-cells of splenocytes were obtained according to the procedure above. For splenocytes $CD8^+$ T cells isolation, $CD8^+$ T cells were sorted by MACS (Miltenyi, Bergisch Gladbach, Germany) as described in the manufacturer's protocols. The purity of $CD8^+$ T cells was >95%, confirmed by flow cytometry.

Reverse Transcription Quantitative PCR

Total RNAs were extracted using RNeasy Mini Kit (Qiagen, Duesseldorf, Germany) in accordance with the manufacturer's instructions. We used 0.1 μg total RNAs as the template to synthesize cDNA via reverse transcription reaction through GoScript™ Reverse Transcription System kit (Promega) according to the manufacturer's instructions. For miRNA detection, equal RNA from each sample was reverse-transcribed to cDNA by means of specific miRNA stem-loop primers. Subsequently, quantitative real-time polymerase chain reactions were ran on Roche-LightCycler-480 by LightCycler 480 SYBR Green I Master. *β-actin* and *U6* were used as internal normalization controls. All assays were performed following the manufacturer's instructions. All sequences of primers listed in **Table 1** were synthesized by Sangon Biotech (Shanghai, China). The thermal cycling conditions include 5 min at 95°C, and 40 cycles of 10 s at 95°C and 20 s at 55°C. Samples were run in triplicate and differences in gene expression were calculated using the $2^{-\text{cycle threshold}}$ method (30, 31).

Statistical Analysis

All results were presented as mean ± standard deviation (SD). Comparisons between the treated and untreated groups were performed with Student's *t*-test. All data were analyzed using GraphPad Prism 5 and a values of $P < 0.05$ was set statistically significant.

RESULTS

OMT and DDP Synergistically Inhibit the Growth of NSCLC Cells Co-cultured With PBMCs *in vitro*

In the present study, we firstly investigate the effects of OMT and DDP on NSCLC cells and PBMCs. Cell survival was assessed by MTT assay. As shown in **Figures 1A,B**, the survival of all used cells was decreased in a dose-dependent manner *in vitro* after OMT or DDP treatment. OMT and DDP exhibited significant cytotoxicity against A549 and LLC cells, but weaker cytotoxicity against human and mice PBMCs. To assess the anti-tumor effects of OMT and DDP on growth of NSCLC cells in the presence of PBMCs, co-cultured NSCLC cells (target cells) with PBMCs (effect cells) at ratios of 1:0, 1:2, 1:4, and 1:6 were treated with OMT and DDP alone or combination. As showed in **Figure 1C**, after co-treatment with OMT and DDP, the survival of cancer cells were significantly reduced in comparison with OMT or DDP alone without PBMCs. Strikingly, the growth of tumor cells were more potently inhibited by OMT or (and) DDP administration when co-cultivated in combination with PBMCs at all target/effector cells ratio, and especially the ratio of target/effect cells at 1:6 exhibited most effective inhibition. These results suggest that OMT and DDP synergistically inhibit the growth of lung cancer cells when co-cultured with PBMCs *in vitro*.

OMT and DDP Synergistically Inhibit the NSCLC Xenografts Growth *in vivo*

To examine the synergistic anti-tumor effects of OMT and DDP *in vivo*, we generated the xenograft tumor models by transplanting LLC cells into C57BL/6 mice. As shown in **Figures 2A–C**, compared with OMT or DDP alone treatment, co-treatment OMT with DDP significantly inhibited the growth of subcutaneous tumors by diminishing the volume and weight of tumors. The inhibition rate of tumor growth in the co-treatment group reached 94.19%, which was obviously higher than that in either single treatment group (**Figure 2E**). In addition, mice body weights in DDP alone or co-treatment groups were lower than those of control group (**Figure 2D**). These data suggest that OMT and DDP can synergistically inhibit the NSCLC xenograft growth *in vivo*.

OMT and DDP Synergistically Increase the $CD8^+/T_{reg}$ Ratio *in vivo*

The interaction of immune system in malignant diseases is heralded as one of the most important advances in oncology. We speculated that heightened tumor regression after OMT and DDP treatments may be caused by strong anti-tumor immunity. The cytotoxic T lymphocytes (CTLs, also $CD8^+$ T cells, marked as $CD3^+CD8^+$ T cells) are pivotal immune cells directed against tumor cells susceptible to cell lysis, but $CD4^+Foxp3^+$ regulatory T cells (T_{reg}) disturb antitumor immunity by suppressing the activities of effector T cells. Our flow cytometry data revealed that compared with OMT or DDP alone treatment, co-treatment OMT with DDP significantly increased $CD8^+$ T cells percentage in PBMCs and spleen lymphocytes, and decreased T_{regs} cells percentage in PBMCs and tumor infiltrating lymphocytes (**Figures 3A–C**). Furthermore, compared with OMT or DDP alone treatment, co-treatment OMT with DDP significantly increased the $CD8^+/T_{reg}$ ratio in PBMCs, spleen lymphocytes and tumor infiltrating lymphocytes (**Figure 3D**). These results indicate that OMT and DDP can synergistically increase the $CD8^+/T_{reg}$ ratio *in vivo*.

OMT and DDP Synergistically Enhance $CD8^+$ T Cells Anti-tumor Immune Response

We further evaluated the immune status of $CD8^+$ T cells in mice bearing LLC, since $CD8^+$ T cells play a pivotal role in anti-tumor immunity. As shown in **Figures 4A,B**, compared with OMT or DDP alone treatment, co-treatment OMT with DDP significantly induced the increased intracellular IFN-γ and TNF-α and the decreased intracellular IL-2 in spleen lymphocytes, and the increased intracellular IFN-γ, TNF-α, and IL-2 in tumor infiltrating lymphocytes, suggesting that OMT and DDP synergistically enhance $CD8^+$ T cells anti-tumor immune response.

OMT and DDP Synergistically Upregulate *miR-155* and Downregulate *SOCS1* Expressions in Splenic $CD8^+$ T Cells

MiR-155 plays a key role in tumor immune response by targeting *SOCS1* (16). We detected *miR-155* and *SOCS1* expressions in splenic $CD8^+$ T cells. As shown in **Figure 5**, compared with OMT or DDP alone treatment, co-treatment with OMT and DDP significantly upregulated *miR-155* and downregulate *SOCS1* expressions in splenic $CD8^+$ T cells.

DISCUSSION

Natural products play an important role in the prevention and treatment of cancer and other disease in the world (32, 33). Our study clearly indicates that the combination of OMT and DDP synergistically enhanced NSCLC cells growth inhibition, $CD8^+/_{Treg}$ ratio and $CD8^+$ T cells anti-tumor immune response with the upregulation of *miR-155* and the silence of *SOCS1*. It has been reported that cancer immunotherapy has been a hot spot in the treatment of NSCLC (34). T_{reg} cells are highly immune suppressive cells and play central roles in the maintenance of self-tolerance and immune homeostasis (35). It can inhibit anti-tumor immunity in NSCLC by suppressing effector T cells directly by cell interaction or indirectly via the secretion of soluble factor-mediated suppression (36). We previously have reported that higher $T_{reg}/CD8^+$ ratio in tumor was an independent factor for poor response to platinum-based chemotherapy, but $CD8^+$ and T_{reg} tumor infiltrating lymphocytes was not correlated with any clinicopathological features in advanced NSCLC patients (37). Current findings on the model of mice bearing LLC have suggested that co-treatment OMT with DDP significantly enhanced the $CD8^+/T_{reg}$ ratio in comparison with single agent groups, which is also in agreement

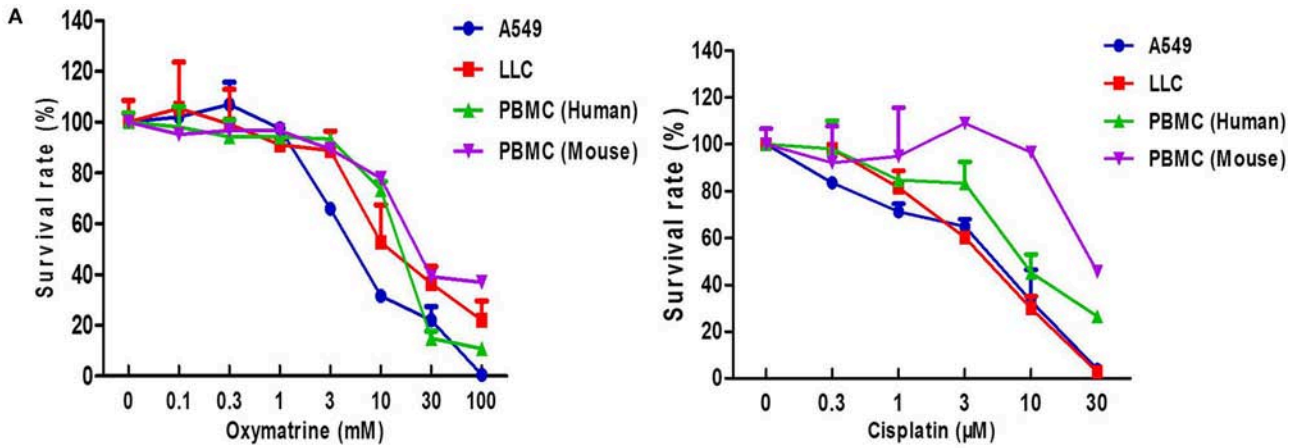

B

Summary of IC50 values of oxymatrine and cisplatin in the indicated cells.

Cell line	A549	LLC	PBMC (Human)	PBMC (Mouse)
Oxymatrine (mM)	5.35±1.24	12.54±0.99	18.09±0.16	23.27±1.58
Cisplatin (μM)	8.14±2.64	5.83±0.66	9.52±0.42	28.96±0.96

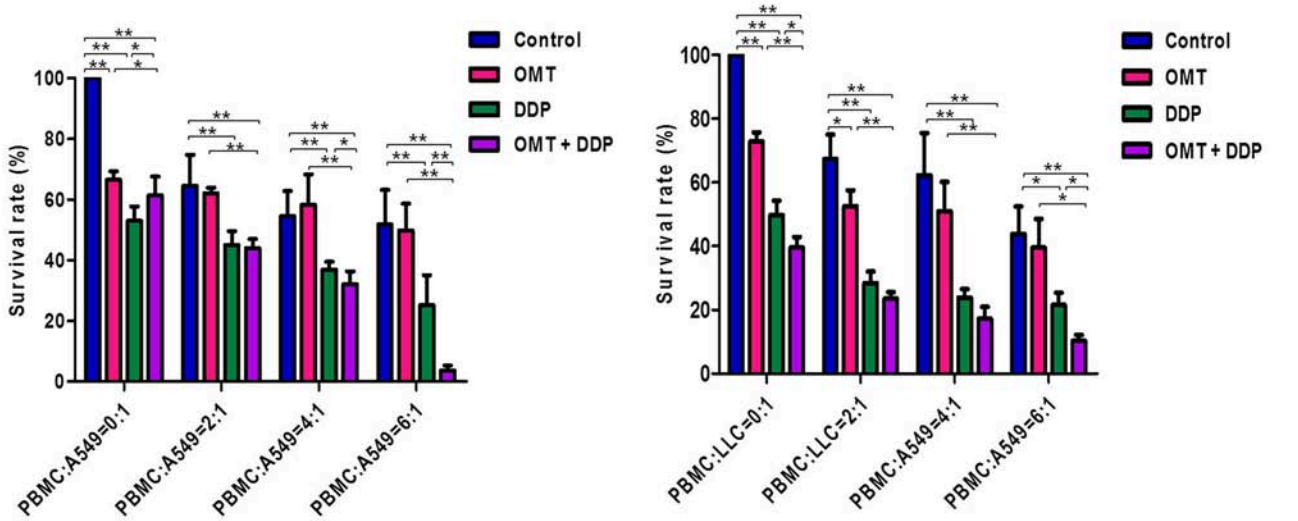

FIGURE 1 | OMT and DDP synergistically inhibit the growth of NSCLC cells co-cultured with PBMCs *in vitro*. Cells were treated with the indicated concentrations of OMT or DDP for 72 h, and cell survival was determined by MTT or CCK-8 assay and summary survival curves **(A)** and IC_{50} values in the indicated cells **(B)** were shown. Co-cultured NSCLC cells (target cells) with PBMCs (effect cells) at ratios of 1:0, 1:2, 1:4, and 1:6 were treated with OMT (3 mM) and DDP (2 μM) alone or combination for 24 h. Quantified results were shown in **(C).** The values presented are the means ± SD for each group. $^{*}P < 0.05$ and $^{**}P < 0.01$ *vs.* corresponding control.

with other clinical evidence that decreased $CD8^{+}/T_{reg}$ ratio among tumor infiltrating lymphocytes are correlated with poor prognosis in various types of human cancers (38–40). However, there are differences between the results of the present study and a report by Zhang et al. which demonstrated that higher ratio of $CD8^{+}/ T_{reg}$ was significantly associated with poor overall

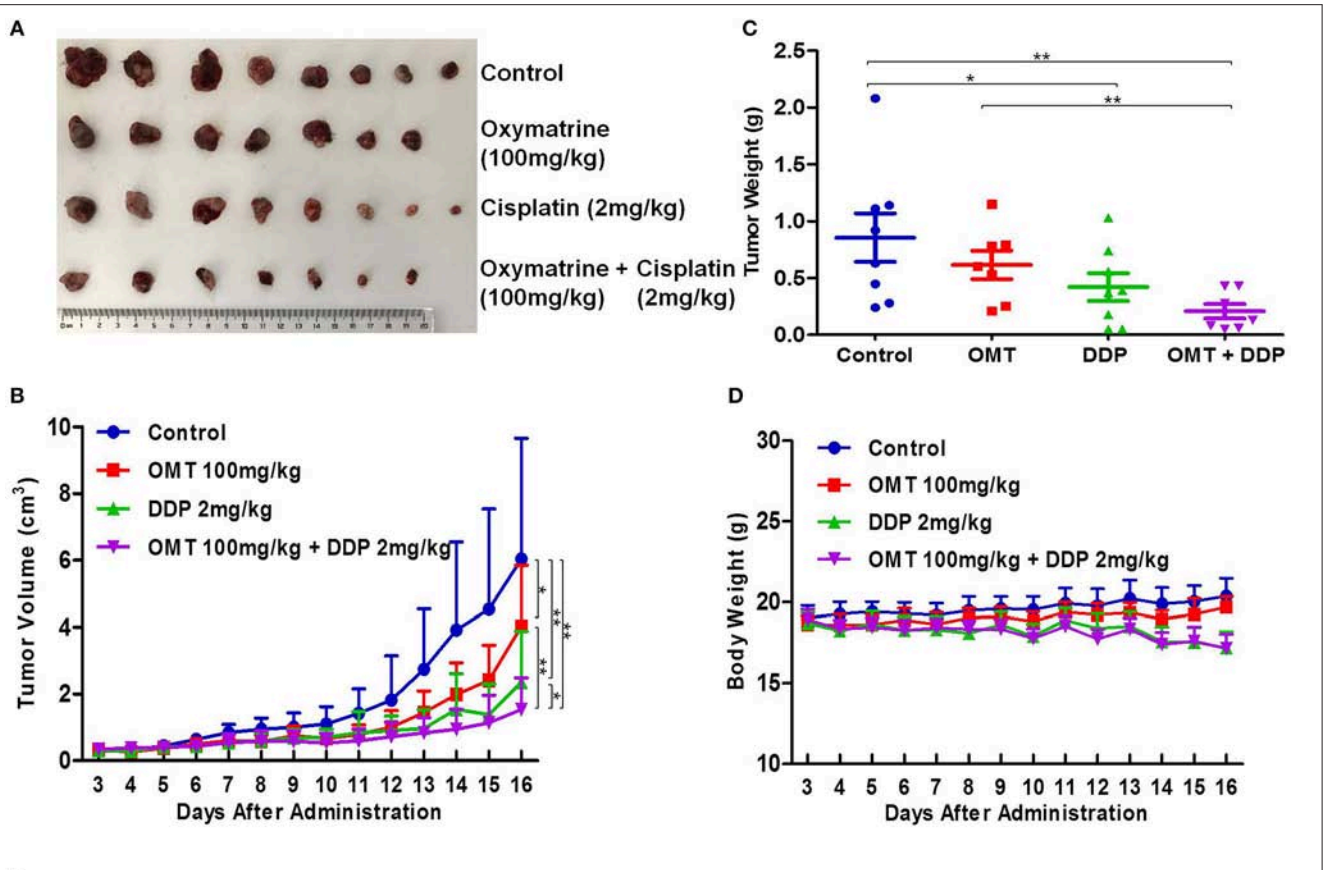

E

Summary of oxymatrine and cisplatin on the growth of LLC xenografts in C57BL/6 mice

Groups	Before Expriment		After Expriment		Weight of Tumor (g)	Inhibition(%)
	Mice (n)	Weight (g)	Mice (n)	Weight (g)		
Control	8	19.04±0.77	8	20.37±1.10	0.86±0.61	
Oxymatrine	7	18.64±0.52	7	19.69±0.66	0.55±0.36	52.32
Cisplatin	8	18.71±0.68	8	17.18±1.00	0.42±0.34*	67.44*
OMT + DDP	7	18.93±0.64	7	17.17±0.86	0.19±0.17**	94.19**

FIGURE 2 | OMT and DDP synergistically inhibit NSCLC xenografts growth *in vivo*. Each mouse was injected subcutaneously with LLC cells (2×10^6 in 100 μl of PBS) in right scapular region. When the subcutaneous tumors were approximately 0.3×0.3 cm^2 (two perpendicular diameters) in size, mice were randomized into four groups, and were injected intraperitoneally with vehicle alone (0.9% saline), OMT alone (100 mg/kg body weight per day), DDP alone (2 mg/kg body weight every 2 day), or a combination of OMT and DDP (administration method is as same as the relevant single drug group). The body weights and tumor volumes of mice were recorded. The mice were anesthetized after experiment, and tumors were excised from the mice and weighted. The original tumors **(A)**, tumor volumes **(B)**, tumor weights **(C)**, body weights **(D)**, and summary data **(E)** were shown. The values presented are the means ± SD for each group. $^*P < 0.05$ and $^{**}P < 0.01$ vs. corresponding control.

survival and progression-free survival in early nasopharyngeal carcinoma stage patients (41). Different chemotherapeutic regimens and tumor context may contribute to these differences.

It is well-known that $CD8^+$ effector T cells have a critical role in elimination of tumors. Previous studies showed that IFN-γ, TNF-α, and IL-2-expressing $CD8^+$ T cells are instrumental in anti-tumor immune response (42). IFN-γ-expressing T cells are essential in repressing tumor growth which promotes host responses to tumors. Moreover, IFN-γ can execute direct anti-proliferative, pro-apoptotic and anti-angiogenesis actions on various tumor cells (43). TNF-α is another multifunctional cytokine, which mediates anticancer adaptive immune response. In the report of Ando et al. TNF-α might be an effective therapy in some cases of NSCLC that have acquired resistance to gefitinib (44). IL-2 acts crossroads functions in activation and cell growth of T and NK cells and it can promote $CD8^+$ T cells and natural killer cells cytolytic activities in response to antigen (45). In lung

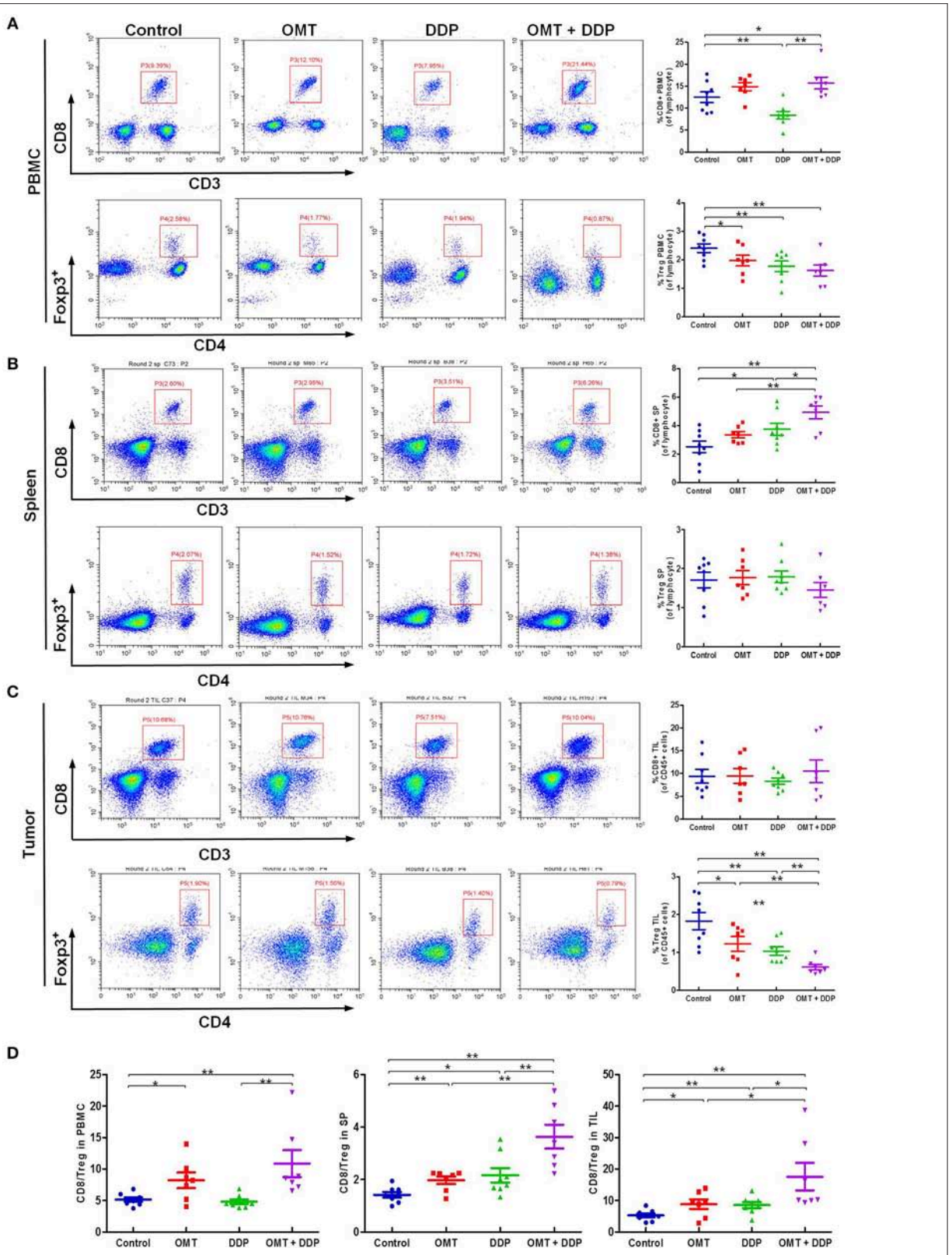

FIGURE 3 | OMT and DDP synergistically increase the $CD8^+/T_{reg}$ ratio *in vivo*. Isolated PBMCs, spleen lymphocytes and tumor infiltrating lymphocytes were stained with indicated antibodies and analyzed by flow cytometry. Representative flow plots and quantified results of $CD8^+$ T cells and T_{reg} cells in PBMCs **(A)**, spleen lymphocytes **(B),** and tumor infiltrating lymphocytes **(C)** were shown. The $CD8^+/T_{reg}$ ratios were quantified **(D)**. $^*P < 0.05$ and $^{**}P < 0.01$ vs. corresponding control.

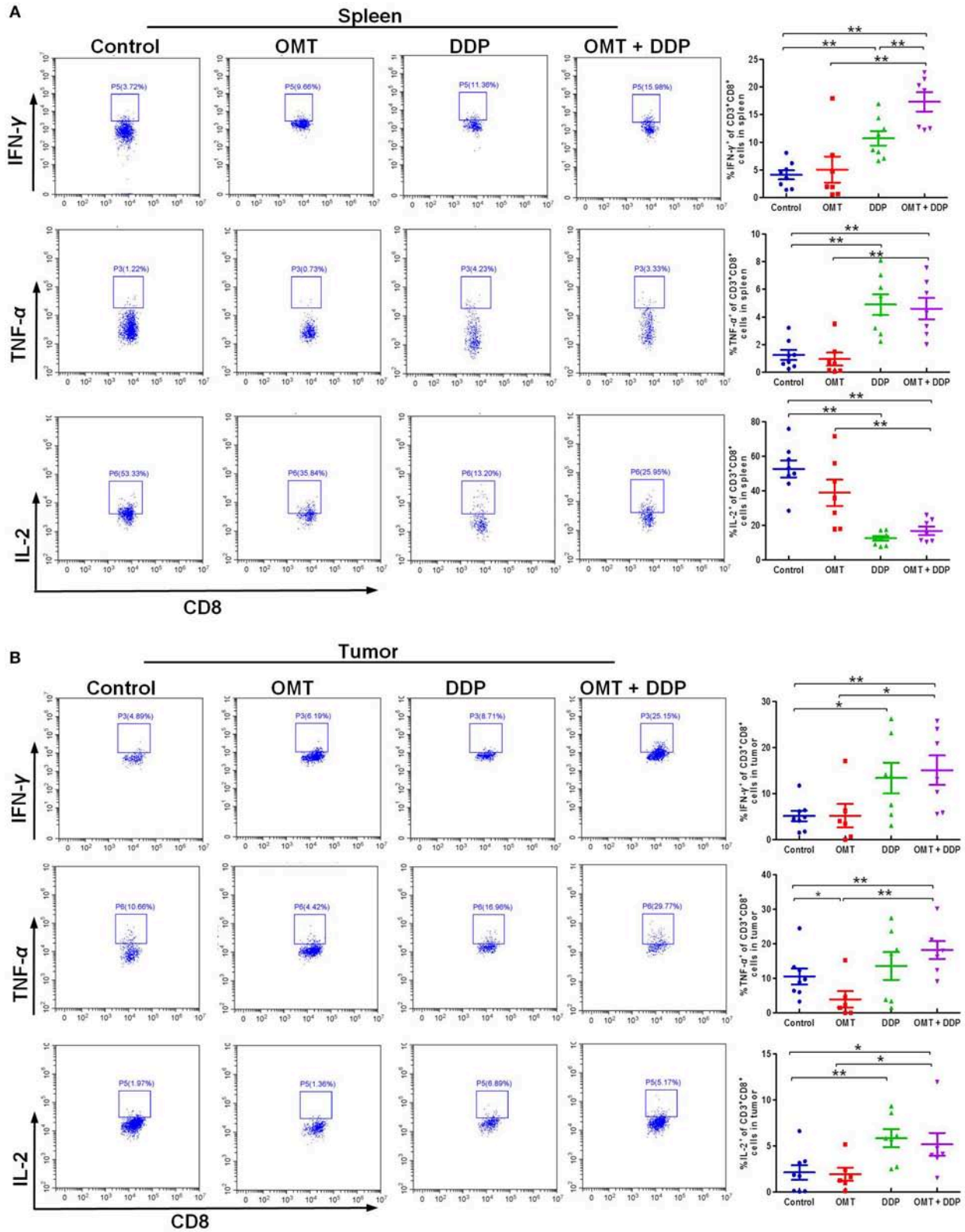

FIGURE 4 | OMT and DDP synergistically enhance $CD8^+$ T cells anti-tumor immune response. Spleen lymphocytes and tumor infiltrating lymphocytes were isolated, and intracellular IFN-γ, TNF-α, and IL-2 were determined by flow cytometry. Representative flow plots and quantified results of intracellular IFN-γ, TNF-α, and IL-2 expression in $CD8^+$ T cells of spleen lymphocytes **(A)** and tumor infiltrating lymphocytes **(B)** were shown. $^*P < 0.05$ and $^{**}P < 0.01$ vs. corresponding control.

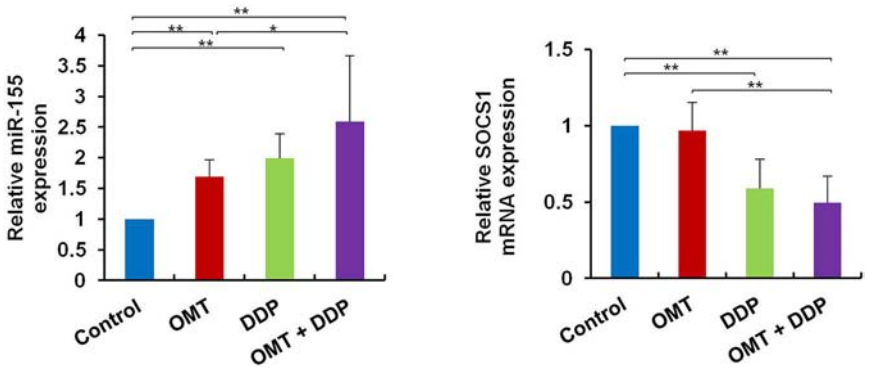

FIGURE 5 | OMT and DDP synergistically upregulate *miR-155* and downregulate *SOCS1* expressions in splenic CD8$^+$ T cells. Splenocytes CD8$^+$ T cells were separated by magnetic bead from MACS and the total RNAs were extracted immediately. Expression of *miR-155* and *SOCS1* in splenic CD8$^+$ T cells were determined by RT-qPCR. *U6* and β-actin were used as the normal controls. Data shown are representative of three independent experiments. *P <0.05 and **P < 0.01 vs. corresponding control.

cancer patients, IL-2 treatment reverses CD8$^+$ T cells exhaustion and markedly increases Granzyme B and IFN-γ in malignant pleural effusion. Our study indicated that OMT in combination with DDP significantly upregulated the production of IFN-γ and TNF-α in CD8$^+$ T cells compared with the single agent both in the splenocytes and tumor infiltrating lymphocytes. Nevertheless, expression of IL-2 is declined in splenocytes and increased in tumor infiltrating lymphocytes, inversely. These differences indicated the complexities of the effects of chemotherapeutic drugs in different immune organs. Since IL-2 is essential for the development and maintenance of T_{reg} (45), declined IL-2 secretion may be able to decrease the immune suppressive T_{reg}. This may be another manner to enhance CD8$^+$ T cells anti-tumor response to a certain extent.

One particular miRNA, *miR-155*, has emerged as a central regulator in immune homeostasis and antitumor immunity recent years (16, 46). *MiR-155* silencing promotes solid tumor growth through increasing the recruitment and functions of myeloid-derived suppressor cells in tumor microenvironment (47). Strikingly, *miR-155* can augments effector CD8$^+$ T-cell anti-tumor immunity against viruses and cancer (17, 18, 48, 49). In detail, *miR-155* overexpression and silence of its target *SOCS1* in CD8$^+$ T cells enhanced the antitumor response and augmented tumor destruction (17). According to Ji et al.'s report, *miR-155* restrained the expression of *SOCS1*, one of the negative regulators of signal transducer and activator of transcription 5 (*STAT5a*), and constitutively active *STAT5a* recapitulated the survival advantages conferred by miR-155 (18). In addition, it is reported that *miR-155* shapes cytokine signaling via downregulation of *SOCS1* in T_{reg} subsets. Consistently, these findings consider *miRNA-155* and its target *SOCS1* as key regulators of effector CD8$^+$ T cells that can be modulated to potentiate immunotherapies for cancers. In our study, increased *miR-155* and decreased *SOCS1* expressions in splenic CD8$^+$ T cells are much agreement with the aforementioned investigations, which demonstrated that co-treatment OMT with DDP can enhanced antitumor immunity via *miR-155-SOCS1* signaling pathway in mice bearing LLC tumor. Further researches need to elucidate the effects of "loss or gain" functions of *miR-155* gene in our mice NSCLC model when OMT co-treatment with DDP. Moreover, antitumor immunity is most complicated involved in effector and immunosuppressive networks in the tumor microenvironment. In addition to CD8$^+$ T cells and T_{regs}, dendritic cells, natural killer cells, suppressive dysfunctional dendritic cells and macrophagocytes, these are essential immunogenic elements to skew the balance of pro- and anti-tumor forces toward tumor-specific immunity (50). Their immunomodulated functions in our present study need to be further investigated.

Collectively, the present study offers the first evidence that OMT and DDP synergistically inhibit the growth of NSCLC cells when co-culture with PBMCs *in vitro*. Further *in vivo* studies provide strong evidence that combinational treatment OMT with DDP shows outstanding synergistic anticancer effect by tipping a favor anti-tumor immunity, suggesting this beneficial combination may offer a promising treatment option for NSCLC patients.

ETHICS STATEMENT

Studies relative to human in this article were approved by the ethics committee of the Third Affiliated Hospital, Sun Yat-sen University (Approval No: [2014]2-17). All animal experiments were performed strictly in accordance with the Guidelines for the Care and Use of Laboratory Animals (No. 55 issued by Ministry of Health, China on January 25, 1998), and experimental procedure were approved by the Institutional Animal Care and Use Committee of Sun Yat-sen University (Approval No: IACUC-DB-17-0502).

AUTHOR CONTRIBUTIONS

JY, M-MZ, ZS, and HL designed the experiments, performed the experiments, analyzed the data, and wrote the paper. PL, X-JL, Q-WJ, YY, J-RH, M-LY, Z-HX, M-NW, and YL performed the experiments. All authors read and approved the final manuscript.

FUNDING

This work was supported by funds from the National Key Research and Development Program of China No. 2017YFA0505104 (ZS), the National Natural Science Foundation of China Nos. 81772540 (ZS) and 81472760 (HL), the Guangdong Natural Science Funds for Distinguished Young Scholar No. 2014A030306001 (ZS), the Guangdong Special Support Program for Young Talent No. 2015TQ01R350 (ZS), the Science and Technology Program of Guangdong Nos. 2016A050502027 (ZS) and 2014A020212078 (HL), the Science and Technology Program of Guangzhou No. 201704030058 (ZS).

REFERENCES

1. Siegel R, Naishadham D, Jemal A. Cancer statistics, 2013. *CA Cancer J Clin*. (2013) 63:11–30. doi: 10.3322/caac.21166
2. Molina JR, Yang P, Cassivi SD, Schild SE, Adjei AA. Non-small cell lung cancer: epidemiology, risk factors, treatment, and survivorship. *Mayo Clin Proc*. (2008) 83:584–94. doi: 10.1016/S0025-6196(11)60735-0
3. Rosell R, Karachaliou N. Lung cancer in 2014: optimizing lung cancer treatment approaches. *Nat Rev Clin Oncol*. (2015) 12:75–6. doi: 10.1038/nrclinonc.2014.225
4. Thomas A, Liu SV, Subramaniam DS, Giaccone G. Refining the treatment of NSCLC according to histological and molecular subtypes. *Nat Rev Clin Oncol*. (2015) 12:511–26. doi: 10.1038/nrclinonc.2015.90
5. Bansal P, Osman D, Gan GN, Simon GR, Boumber Y. Recent advances in immunotherapy in metastatic NSCLC. *Front Oncol*. (2016) 6:239. doi: 10.3389/fonc.2016.00239
6. Blais N, Hirsh V. Chemotherapy in metastatic NSCLC - new regimens (pemetrexed, nab-paclitaxel). *Front Oncol*. (2014) 4:177. doi: 10.3389/fonc.2014.00177
7. Pluhar GE, Pennell CA, Olin MR. CD8(+) T Cell-independent immune-mediated mechanisms of anti-tumor activity. *Crit Rev Immunol*. (2015) 35:153–72. doi: 10.1615/CritRevImmunol.2015013607
8. Zhang N, Bevan MJ. CD8(+) T cells: foot soldiers of the immune system. *Immunity* (2011) 35:161–8. doi: 10.1016/j.immuni.2011.07.010
9. Berendt MJ. T-cell-mediated suppression of anti-tumor immunity. An explanation for progressive growth of an immunogenic tumor. *J Exp Med*. (1980) 151:69–80. doi: 10.1084/jem.151.1.69
10. Smyth MJ, Godfrey DI, Trapani JA. A fresh look at tumor immunosurveillance and immunotherapy. *Nat Immunol*. (2001) 2:293–9. doi: 10.1038/86297
11. Shevach EM. Mechanisms of foxp3+ T regulatory cell-mediated suppression. *Immunity* (2009) 30:636–45. doi: 10.1016/j.immuni.2009.04.010
12. Baras AS, Drake C, Liu JJ, Gandhi N, Kates M, Hoque MO, et al. The ratio of CD8 to Treg tumor-infiltrating lymphocytes is associated with response to cisplatin-based neoadjuvant chemotherapy in patients with muscle invasive urothelial carcinoma of the bladder. *Oncoimmunology* (2016) 5:e1134412. doi: 10.1080/2162402X.2015.1134412
13. Bartel DP. MicroRNAs: target recognition and regulatory functions. *Cell* (2009) 136:215–33. doi: 10.1016/j.cell.2009.01.002
14. Li Z, Rana TM. Therapeutic targeting of microRNAs: current status and future challenges. *Nat Rev Drug Discov*. (2014) 13:622–38. doi: 10.1038/nrd4359
15. Paladini L, Fabris L, Bottai G, Raschioni C, Calin GA, Santarpia L. Targeting microRNAs as key modulators of tumor immune response. *J Exp Clin Cancer Res*. (2016) 35:103. doi: 10.1186/s13046-016-0375-2
16. Vigorito E, Kohlhaas S, Lu D, Leyland R. miR-155: an ancient regulator of the immune system. *Immunol Rev*. (2013) 253:146–57. doi: 10.1111/imr.12057
17. Dudda JC, Salaun B, Ji Y, Palmer DC, Monnot GC, Merck E, et al. MicroRNA-155 is required for effector CD8+ T cell responses to virus infection and cancer. *Immunity* (2013) 38:742–53. doi: 10.1016/j.immuni.2012.12.006
18. Ji Y, Wrzesinski C, Yu ZY, Hu JH, Gautam S, Hawk NV, et al. miR-155 augments CD8(+) T-cell antitumor activity in lymphoreplete hosts by enhancing responsiveness to homeostatic gamma(c) cytokines. *Proc Natl Acad Sci USA*. (2015) 112:476–81. doi: 10.1073/pnas.1422916112
19. Dunand-Sauthier I, Santiago-Raber ML, Capponi L, Vejnar CE, Schaad O, Irla M, et al. Silencing of c-Fos expression by microRNA-155 is critical for dendritic cell maturation and function. *Blood* (2011) 117:4490–500. doi: 10.1182/blood-2010-09-308064
20. Wang J, Iwanowycz S, Yu F, Jia X, Leng S, Wang Y, et al. microRNA-155 deficiency impairs dendritic cell function in breast cancer. *Oncoimmunology* (2016) 5:e1232223. doi: 10.1080/2162402X.2016.1232223
21. Fennell DA, Summers Y, Cadranel J, Benepal T, Christoph DC, Lal R, et al. Cisplatin in the modern era: the backbone of first-line chemotherapy for non-small cell lung cancer. *Cancer Treat Rev*. (2016) 44:42–50. doi: 10.1016/j.ctrv.2016.01.003
22. Bozic I, Reiter JG, Allen B, Antal T, Chatterjee K, Shah P, et al. Evolutionary dynamics of cancer in response to targeted combination therapy. *Elife* (2013) 2:e00747. doi: 10.7554/eLife.00747
23. Diyabalanage HV, Granda ML, Hooker JM. Combination therapy: histone deacetylase inhibitors and platinum-based chemotherapeutics for cancer. *Cancer Lett*. (2013) 329:1–8. doi: 10.1016/j.canlet.2012.09.018
24. Liu Y, Xu Y, Ji W, Li X, Sun B, Gao Q, et al. Anti-tumor activities of matrine and oxymatrine: literature review. *Tumour Biol*. (2014) 35:5111–9. doi: 10.1007/s13277-014-1680-z
25. Sang X, Wang R, Han Y, Zhang C, Shen H, Yang Z, et al. T cell–associated immunoregulation and antiviral effect of oxymatrine in hydrodynamic injection HBV mouse model. *Acta Pharm Sin B* (2017) 7:311–8. doi: 10.1016/j.apsb.2017.02.005
26. Ma A, Yang Y, Wang Q, Wang Y, Wen J, Zhang Y. Antiinflammatory effects of oxymatrine on rheumatoid arthritis in rats via regulating the imbalance between Treg and Th17 cells. *Mol Med Rep*. (2017) 15:3615–22. doi: 10.3892/mmr.2017.6484
27. Yang Z, Yin R, Cong Y, Yang Z, Zhou E, Wei Z, et al. Oxymatrine lightened the inflammatory response of LPS-induced mastitis in mice through affecting NF-kappaB and MAPKs signaling pathways. *Inflammation* (2014) 37:2047–55. doi: 10.1007/s10753-014-9937-7
28. Lv G, Sun D, Zhang J, Xie X, Wu X, Fang W, et al. Lx2-32c, a novel semi-synthetic taxane, exerts antitumor activity against prostate cancer cells *in vitro* and *in vivo*. *Acta Pharm Sin B* (2017) 7:52–8. doi: 10.1016/j.apsb.2016.06.005
29. Li W-S, Yang Y, Liu J-J, Shen L, Shi Z, Wu J. Scaffold diversity-oriented synthesis of limonoid dimers: discovery of an axially chiral agent with *in vivo* anti-breast cancer activity. *Org Chem Front*. (2018) 5:1079–91. doi: 10.1039/C8QO00154E
30. Li P, Yang Y, Liu H, Yang AK, Di JM, Tan GM, et al. MiR-194 functions as a tumor suppressor in laryngeal squamous cell carcinoma by targeting Wee1. *J Hematol Oncol*. (2017) 10:32. doi: 10.1186/s13045-017-0402-6
31. Yang Y, Guan D, Lei L, Lu J, Liu JQ, Yang G, et al. H6, a novel hederagenin derivative, reverses multidrug resistance *in vitro* and *in vivo*. *Toxicol Appl Pharmacol*. (2018) 341:98–105. doi: 10.1016/j.taap.2018.01.015
32. Jiang QW, Cheng KJ, Mei XL, Qiu JG, Zhang WJ, Xue YQ, et al. Synergistic anticancer effects of triptolide and celastrol, two main compounds from thunder god vine. *Oncotarget* (2015) 6:32790–804. doi: 10.18632/oncotarget.5411
33. Jiang Q-W, Chen M-W, Cheng K-J, Yu P-Z, Wei X, Shi Z. Therapeutic potential of steroidal alkaloids in cancer and other diseases. *Med Res Rev*. (2016) 36:119–43. doi: 10.1002/med.21346
34. Anagnostou VK, Brahmer JR. Cancer immunotherapy: a future paradigm shift in the treatment of non-small cell lung cancer. *Clin Cancer Res*. (2015) 21:976–84. doi: 10.1158/1078-0432.CCR-14-1187
35. Takeuchi Y, Nishikawa H. Roles of regulatory T cells in cancer immunity. *Int Immunol*. (2016) 28:401–9. doi: 10.1093/intimm/dxw025
36. Zhang D, Chen Z, Wang DC, Wang X. Regulatory T cells and potential inmmunotherapeutic targets in lung cancer. *Cancer Metastasis Rev*. (2015) 34:277–90. doi: 10.1007/s10555-015-9566-0

37. Liu H, Zhang T, Ye J, Li H, Huang J, Li X, et al. Tumor-infiltrating lymphocytes predict response to chemotherapy in patients with advance non-small cell lung cancer. *Cancer Immunol Immunother* (2012) 61:1849–56. doi: 10.1007/s00262-012-1231-7
38. Shen Z, Zhou S, Wang Y, Li RL, Zhong C, Liang C, et al. Higher intratumoral infiltrated Foxp3+ Treg numbers and Foxp3+/CD8+ ratio are associated with adverse prognosis in resectable gastric cancer. *J Cancer Res Clin Oncol*. (2010) 136:1585–95. doi: 10.1007/s00432-010-0816-9
39. Sato E, Olson SH, Ahn J, Bundy B, Nishikawa H, Qian F, et al. Intraepithelial CD8+ tumor-infiltrating lymphocytes and a high CD8+/regulatory T cell ratio are associated with favorable prognosis in ovarian cancer. *Proc Natl Acad Sci USA*. (2005) 102:18538–43. doi: 10.1073/pnas.0509182102
40. Liu F, Lang R, Zhao J, Zhang X, Pringle GA, Fan Y, et al. CD8(+) cytotoxic T cell and FOXP3(+) regulatory T cell infiltration in relation to breast cancer survival and molecular subtypes. *Breast Cancer Res Treat*. (2011) 130:645–55. doi: 10.1007/s10549-011-1647-3
41. Zhang YL, Li J, Mo HY, Qiu F, Zheng LM, Qian CN, et al. Different subsets of tumor infiltrating lymphocytes correlate with NPC progression in different ways. *Mol Cancer* (2010) 9:4. doi: 10.1186/1476-4598-9-9
42. Yang J, Liu R, Deng Y, Qian J, Lu Z, Wang Y, et al. MiR-15a/16 deficiency enhances anti-tumor immunity of glioma-infiltrating CD8+ T cells through targeting mTOR. *Int J Cancer* (2017) 141:2082–92. doi: 10.1002/ijc.30912
43. Ikeda H, Old LJ, Schreiber RD. The roles of IFN gamma in protection against tumor development and cancer immunoediting. *Cytokine Growth Factor Rev*. (2002) 13:95–109. doi: 10.1016/S1359-6101(01)00038-7
44. Ando K, Ohmori T, Inoue F, Kadofuku T, Hosaka T, Ishida H, et al. Enhancement of sensitivity to tumor necrosis factor alpha in non-small cell lung cancer cells with acquired resistance to gefitinib. *Clin Cancer Res*. (2005) 11(24 Pt 1):8872–9. doi: 10.1158/1078-0432.CCR-05-0811
45. Liao W, Lin JX, Leonard WJ. Interleukin-2 at the crossroads of effector responses, tolerance, and immunotherapy. *Immunity* (2013) 38:13–25. doi: 10.1016/j.immuni.2013.01.004
46. Lind EF, Ohashi PS. Mir-155, a central modulator of T-cell responses. *Eur J Immunol.* (2014) 44:11–5. doi: 10.1002/eji.201343962
47. Wang J, Yu F, Jia X, Iwanowycz S, Wang Y, Huang S, et al. MicroRNA-155 deficiency enhances the recruitment and functions of myeloid-derived suppressor cells in tumor microenvironment and promotes solid tumor growth. *Int J Cancer* (2015) 136:E602–13. doi: 10.1002/ijc.29151
48. Huffaker TB, Lee SH, Tang WW, Wallace JA, Alexander M, Runtsch MC, et al. Antitumor immunity is defective in T cell-specific microRNA-155-deficient mice and is rescued by immune checkpoint blockade. *J Biol Chem*. (2017) 292:18530–41. doi: 10.1074/jbc.M117.808121
49. Huffaker TB, Hu R, Runtsch MC, Bake E, Chen X, Zhao J, et al. Epistasis between microRNAs 155 and 146a during T cell-mediated antitumor immunity. *Cell Rep*. (2012) 2:1697–709. doi: 10.1016/j.celrep.2012.10.025
50. Zou W. Immunosuppressive networks in the tumour environment and their therapeutic relevance. *Nature Rev Cancer* (2005) 5:263–74. doi: 10.1038/nrc1586

Conflict of Interest Statement: The authors declare that the research was conducted in the absence of any commercial or financial relationships that could be construed as a potential conflict of interest.

frontiers in Oncology

MINI REVIEW
published: 22 January 2019
doi: 10.3389/fonc.2019.00018

Salt-Inducible Kinase 2: An Oncogenic Signal Transmitter and Potential Target for Cancer Therapy

Fangyu Chen[1,2†], *Liuwei Chen*[2†], *Qin Qin*[1†] *and Xinchen Sun*[1*]

[1] *Department of Radiation Oncology, The First Affiliated Hospital of Nanjing Medical University, Nanjing, China,* [2] *The First School of Clinical Medicine, Nanjing Medical University, Nanjing, China*

Salt-inducible kinase (SIK), which belongs to the sucrose non-fermenting 1/AMP-activated protein kinase family, was first discovered in the adrenal cortex of a rat on a high-salt diet. As an isoform of the SIK family, SIK2 modulates various biological functions and acts as a signal transmitter in various pathways. Compared with that in adjacent normal tissues, the expression of SIK2 is significantly higher in multiple types of tumors, which indicates its pivotal effect in oncogenesis. Studies on SIK2 have recently underlined its role in several signaling pathways, including the PI3K-Akt-mTOR pathway, the Hippo-YAP pathway, the LKB1-HDAC axis, and the cAMP-PKA axis. Moreover, a few small-molecule SIK2 inhibitors have been found to be able to rescue the oncogenicity of SIK2 during tumor development and reverse its abnormal activation of downstream pathways. In this mini-review, we discuss the results of *in vivo* and *in vitro* studies regarding the SIK2 mechanism in different signaling pathways, particularly their regulation of cancer cells. This work may provide new ideas for targeting SIK2 as a novel therapeutic strategy in tumor therapy.

Keywords: salt-inducible kinase, SIK2, cancer, signaling pathway, target therapy

OPEN ACCESS

Edited by:
Zhe-Sheng Chen,
St. John's University, United States

Reviewed by:
Yun Dai,
Virginia Commonwealth University, United States
Luca Tamagnone,
Institute for Cancer Research and Treatment (IRCC), Italy
Xingxiang Pu,
Hunan Cancer Hospital, China

***Correspondence:**
Xinchen Sun
Sunxinchen2012@163.com

These authors have contributed equally to this work

Specialty section:
This article was submitted to Cancer Molecular Targets and Therapeutics, a section of the journal Frontiers in Oncology

Received: *09 October 2018*
Accepted: *07 January 2019*
Published: *22 January 2019*

Citation:
Chen F, Chen L, Qin Q and Sun X (2019) Salt-Inducible Kinase 2: An Oncogenic Signal Transmitter and Potential Target for Cancer Therapy. Front. Oncol. 9:18. doi: 10.3389/fonc.2019.00018

INTRODUCTION

Plasma ion balances regulate a wide range of cellular processes from cell proliferation to mitochondrial functions. The plasma concentrations of Na+ and K+ have been proven to play a vital role in the biosynthesis of aldosterone in the adrenal cortex. Studies have shown that changes in plasma ion concentration can target biomembrane ion channels, such as Na+-K+-ATPase to regulate extra- and intracellular ion balances (1, 2). As a major part of this ion modulation network, salt-inducible kinase (SIK) was first discovered in 1999 by Okamoto et al. in the adrenal cortex of a rat on a high-salt diet. SIK is a serine/threonine protein kinase that belongs to the sucrose non-fermenting 1/AMP-activated protein kinase (SNF1/AMPK) family. The SIK family comprises three isoforms, namely, SIK1, SIK2, and SIK3, all of which may act as metabolic transmitters. The SIK2 gene is located on chromosome 11 and encodes for the SIK2 protein, which has 926 amino acids and three domains (3, 4). The C-terminal domain of the SIK protein contains numerous unique sites that can be phosphorylated by different protein kinases and transmit various stimulation signals involved in different biological processes, including cell growth and apoptosis (4–8). In many malignant tumors, such as breast cancer, lung cancer, melanoma, primary liver

cancer, and ovarian cancer, SIK expression is significantly different from that in adjacent tissues (9–14).

Growing evidence has proven that the expression and action of SIK2 are tissue-specific. The cellular and subcellular distributions of SIK should be considered to determine its mechanism. Earlier investigations demonstrate that SIK2 maintains cell homeostasis via modulation of cAMP response element binding protein (CREB)-mediated gene transcription during starvation, which may be a possible mechanism for cancer cell survival under stress, such as chemoradiotherapy (15). SIK2 reduces glucose uptake in muscle cells and white adipocytes and downregulates lipogenesis and ketogenesis by phosphorylating the glucose-activated histone acetyltransferase coactivator p300 (16). SIK2 modulates several subtle cellular signaling pathways, and its abundant expression in melanoma and ovarian tumors is suggestive of its pivotal function in tumor development (13, 17). Thus, in this mini-review, we discuss the specific role and related signaling pathways of SIK2 in tumorigenesis. Our findings indicate the potential application of SIK2 as a therapeutic target for cancers.

SIK FAMILY AND THEIR FUNCTIONS

The structures of the SIK isoforms are shown in **Figure 1**. The three isoforms are similar to one another, particularly in three domains: a kinase domain near the N-terminal, a central SNF1 protein kinase homology (SNH) domain, and a phosphorylation domain near the C-terminal (3). SIK1 is a 776-amino acid protein with a kinase domain in the region of residues 27–278, an SNH domain in the region of residues 301–354, and a domain enriched with PKA-dependent phosphorylation sites in the region of residues 567–613. Similarly, SIK2 is a 931-amino acid protein with a kinase domain in the region of residues 20–271, an SNH domain in the region of residues 293–346, and a phosphorylation domain in the region of residues 577–623. Finally, SIK3 is a 1,263-amino acid protein with a kinase domain in the region of residues 8–259, an SNH domain in the region of residues 283–336, and a phosphorylation domain in the region of residues 486–518. Initial studies have found that SIK1 is most abundant in the adrenal cortex and an important regulator in the early phase of hormonal stimulation of the adrenal cortex (4, 18), adipose tissue (6), and neural tissue (19). It may overexpress in several non-adipose tissues, such as in the ovaries and lungs, and act as an oncogenic signal transmitter during the occurrence and progression of tumors in the aforementioned organs (18–20). Unlike SIK1, SIK2 modulates several subtle cellular signaling pathways, and the increased expression of SIK2 in adipose and neuronal tissues indicates its pivotal role in lipid metabolism and neural physiology. SIK2 promotes insulin resistance and diabetes by reducing glucose uptake in muscles and white adipose tissues and inhibiting gluconeogenesis (7). SIK2 is overexpressed in several cancer cell lines and boosts cancer cell tolerance to different stresses, such as deprivation of nutrients and taxol chemotherapy (21). It plays a proinflammatory role by repressing IL-10 secretion of regulatory macrophages (22). However, little is known about why the structural similarity of the SIK family leads to different biological functions.

SIK2 AND THE PI3K-Akt-mTOR PATHWAY

The expression level of SIK2 in cancers is significantly higher than that in adjacent and surrounding normal tissues, which suggests that SIK2 is critical in tumorigenesis and tumor development. Miranda et al. found that the loss of SIK2 reduces G1/S transition, delays mitotic progression, and decreases Akt phosphorylation levels (17). They also confirmed that SIK2 is overexpressed in adipocyte-rich metastatic deposits compared with ovarian primary lesions and that adipocytes activate SIK2 in ovarian cancer cells in a calcium-dependent manner. Following adipocyte-induced stimulation, the activated SIK2 alters metabolic effects in ovarian cancer cells by inhibiting acetyl-CoA carboxylase and promoting fatty acid oxidation. p85α, the regulatory subunit of the PI3K complex, was previously identified as a putative SIK2 substrate during chemical genetic screening. The identified p85α phosphorylation site (S154) resides in the known SIK2 phosphorylation consensus sequence L-x-[HKR]-[ST]-x-S-X(3)-L at L149–L158 (LYRTQSSSNL). Incubation of recombinant full-length SIK2 or its kinase domain with a peptide corresponding to L149–L158 of p85α confirmed that SIK2 catalyzes the phosphorylation of this sequence. More importantly, full-length SIK2, but not the kinase-inactive mutant, phosphorylated p85α was confirmed in isotopic labeling assay. Phosphopeptide mapping of p85α following incubation with SIK2 (kinase domain or full-length) revealed that the former was phosphorylated at S154 in the BH domain. The BH domain is thought to bind to proteins that modulate PI3K activity. Downstream S154 phosphorylation also appears to increase in an SIK2-dose-dependent manner. siRNA-mediated depletion or chemical inhibition confirms that SIK2 is required for p85α S154 phosphorylation. Moreover, p85α phosphorylation and concomitant Akt phosphorylation can be triggered by calcium-mediated SIK2 activation. Consistent with these observations, incubation of the PI3K complex with recombinant SIK2 leads to a profound increase in PI3K activity *in vitro* (up to 13.8-fold), while chemical inhibition of SIK2 induces a dose-dependent reduction in PI3K activity to its basal level. These data confirm that p85α is a direct catalytic substrate of SIK2 and that SIK2 S154 phosphorylation significantly increases the activity of the PI3K-Akt pathway in ovarian cancer cells.

While most reports suggest that SIK2 is an oncogenic marker, one study in Turkey claimed that SIK2 is a potential tumor suppressor in breast cancer (23); SIK2 expression was reportedly reduced in tumor tissues and breast cancer cell lines compared with that in normal counterparts. The researchers also found SIK2-mediated attenuation of proliferation and survival of breast cancer cells with parallel inhibition of the Ras-Erk and PI3K-Akt pathways. However, the mechanisms underlying the reduction of SIK2 levels in cancer tissues were not discussed. Thus, research into the mechanism of SIK2 loss will help future scholars better understand tumor transformation in breast tissue and design new treatment strategies.

SIK2 AND THE HIPPO-YAP PATHWAY

The Hippo pathway is a highly conserved growth regulatory signaling pathway that was first discovered in *Drosophila*. It can

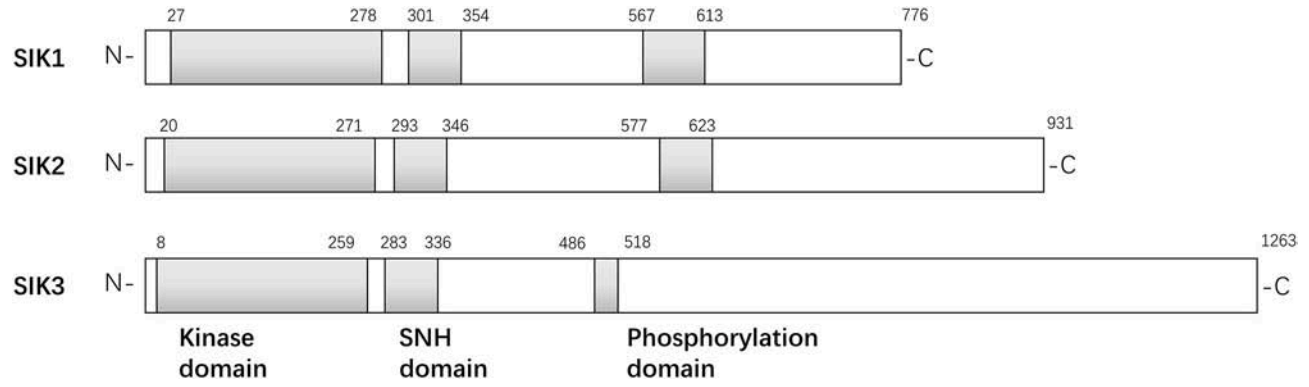

FIGURE 1 | Structures of isoforms in SIK family.

block the downstream pro-growth transcriptional co-activator Yorkie (Yki), which is homologous to mammalian Yes-associated protein (YAP), and exert its regulatory effects on organ size, cell proliferation, and apoptosis during organ development (24, 25). YAP has been shown to be highly expressed in various human tumors, such as endometrial carcinoma, primary liver cancer, and oral squamous cell carcinoma. Activation of YAP can remove tumor cell contact inhibition, leading to tumor metastasis (25–27). Tsujiura et al. immunohistochemically analyzed YAP in endometrial carcinoma tissue samples and found that the high expression of YAP in the nucleus is closely associated with higher tumor grading and staging, lymphatic/blood vessel invasion, increased recurrence, and metastasis. They then confirmed these results at the cellular level in knockdown and overexpression assays. Recent studies have demonstrated that YAP restricts the activity of the cell cycle checkpoints ATM and ChK2 to enable cancer cells to enter the cell cycle and mitosis after chemoradiotherapy despite unrepaired DNA damage, resulting in tumor growth, chemoradiotherapy resistance, and ongoing proliferation (28).

Wehr et al. characterized Drosophila salt-inducible kinase (sik2) as an upstream inhibitor of the Hippo pathway (29). sik2 has been identified as the ortholog of human SIK2. Activated sik2 phosphorylates Ser413 of the scaffold protein Salvador (Sav), a major part of the core kinase complex of the Hippo pathway, and subsequently abolishes the inhibition of the proto-oncogene Yki. In addition, sik2 directly induces the expression of Yki and facilitates Yki-dependent tissue overgrowth. Coincidentally, both SIK2 and YAP have been proven to be oncogenes in ovarian cancer. Research has confirmed a close interaction between the PI3K-Akt-mTOR and Hippo-YAP pathways via SIK2 (**Figure 2**). On the one hand, YAP directly activates PI3K-Akt-mTOR and alters cellular biological functions (30, 31). YAP also increases pAkt-S473 levels and suppresses apoptosis by induction of insulin-like growth factor 2 expression (28). On the other hand, mTOR complex 2 enhances the oncogenicity of YAP through phosphorylation of the Hippo pathway component AMOTL2 (32). These observations reveal that mutual activation between the PI3K-Akt-mTOR and Hippo-YAP pathways caused by SIK2 may be crucial in tumorigenesis. However, the precise role of SIK2 in these intersecting pathways is not well-understood, and future studies are still desperately needed to elucidate the related detailed mechanisms.

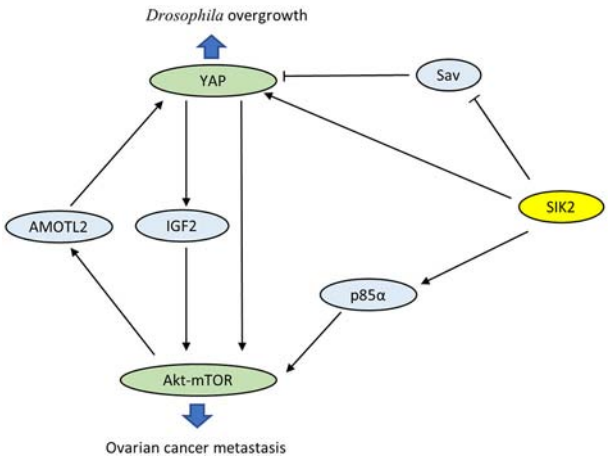

FIGURE 2 | Crosstalk between the PI3K-Akt-mTOR pathway and the Hippo-Yap pathway via SIK2.

SIK2 AND THE LKB1-HDAC SIGNALING AXIS

Epigenetic studies have confirmed that DNA acetylation modification is closely related to tumorigenesis, tumor invasion, and chemoradiotherapy resistance (33–35). The abnormal activation and overexpression of histone deacetylase (HDAC) down-regulates tumor suppressor genes and exhibits tumor-promoting effects. Using kinase domain-focused CRISPR techniques, researchers screened all dependent kinase in acute myeloid leukemia (AML), focusing subsequent experiments on SIK3, which scored strongly in MOLM-13 and MV4-11 AML cells and in a more intermediate fashion in other AML cell lines (36). Liver kinase B1 (LKB1) was also identified to show an AML-biased pattern of dependence. Since SIK3 is homologous to SIK1

and SIK2, further studies were conducted to determine whether a broader requirement exists for SIKs in cancer. By performing dual targeting of each SIK gene combination in 17 AML cell lines, researchers observed a broad AML-specific requirement for SIK2 + SIK3 resembling the pattern of LKB1 dependence with a bias for lines with mixed lineage leukemia fusions. In cDNA rescue assays, LKB1 was found to phosphorylate and activate SIK3 in AML. The SIK3 mutant was unable to maintain the proliferation of MOLM-13 cells, while a phosphomimetic allele of SIK3 rescued the proliferation arrest caused by inactivating LKB1. The reverse of SIK3 dependence for AML proliferation was observed during dual CRISPR targeting of HDAC4. Western blotting revealed reductions in HDAC4 phosphorylation upon genetic targeting of SIK3 or chemical inhibition of SIK. Taken together, these results indicate that the function of SIK3 is critical in AML and that inhibition of HDAC4 is one of the key functions of SIK3 in supporting AML proliferation.

Histone H3 lysine 27 acetylation (H3K27ac) is linked to the relevant downstream activity in the LKB1-SIK pathway, and ChIP-seq has confirmed that LKB1/SIK3-dependent H3K27ac coincides with sites of transcription factor MEF2C occupancy. While LKB1/SIK3 knockout or following SIK inhibitor HG-9-91-01 treatment did not change MEF2C protein expression, HG-9-91-01 exposure led to increased HDAC4 binding to MEF2C-bound sites. Epigenomic analysis suggests that LKB1-SIK signaling is critical in AML to prevent HDAC4 from inactivating the function of MEF2C on chromatin. These genetic experiments suggest that co-inhibition of SIK2 + SIK3 could be the ideal strategy to achieve potent MEF2C inhibition in AML. Since MEF2C is maladjusted in lymphoid malignancies, LKB1-SIK signaling is likely to be important in other hematopoietic cancers (37).

SIK2 AND THE cAMP-PKA SIGNALING AXIS

The G protein αs (GNAS) gene encodes the Gαs stimulatory subunit of G proteins, which mediate G-protein-coupled receptor signaling, a major mechanism that links multiple environmental stimuli with intracellular responses (38). The primary target is adenylyl cyclase, which generates the second messenger cAMP, which, in turn, activates downstream protein kinase A (PKA). In many tissues, GNAS–cAMP-PKA signaling is required during cell dormancy and cell growth (39–43). However, multiple types of human cancers show gain-of-function variations in this pathway (38). For example, loss of p53 promotes the advent of GNAS R201C mutations and induces malignant transformation in pancreatic benign tumors in the KGC mice model, which can rapidly develop cystic pancreatic tumors (44–47). Mutated GNAS R201C supports pancreatic tumor growth via cAMP-PKA signaling, which subsequently phosphorylates SIKs (SIK1, SIK2, and SIK3) and prevents them from phosphorylating downstream targets (48). Also, small molecule pan-SIK inhibitors (HG-9-91-01 and KIN-112) prevent the growth of KGC organoids after silencing GNAS, and their effects are directly proportional to the degree of SIK inhibition. Compared with wild-type SIK2, the SIK2-S4A mutant, which is resistant to cAMP-PKA activation, strongly inhibits the proliferation of KGC-like organs. In particular, SIK^{KO} rescues both organoid growth *in vitro* and subcutaneous tumor growth following GNAS R201C silencing, and these findings have been confirmed in human pancreatic ductal adenocarcinomas (PDA). Thus, the cAMP-PKA-SIK2 signaling pathway is a conserved tumorigenic mechanism in pancreatic tumor cells. The mutant GNAS drives downstream PKA-SIK2 axis and promotes lipid hydrolysis in addition to lipid synthesis and remodeling. While SIK2 is known to maintain cell homeostasis and energetic metabolism, particularly glucose and fatty acid oxidation (15), the suppression of SIK2 mediated by GNAS-PKA will inhibit the phosphorylation of its downstream CREB-regulated transcription co-activator (CRTC) and others (**Figure 3**). Then it will promote lipids absorption and synthesis, and the abundant lipids in tumor cells provide substrates for structural, signaling, and metabolic purposes, which explains why SIK2 act as a tumor suppressor in PDA.

While SIK2 is deemed to be a tumor promoter in most cases, in the context of GNAS mutated PDA, it is supposed to be a tumor suppressor, mainly because SIK2 plays different roles in different tissue and cells, similar to cAMP/PKA signaling. Given the context-dependent tumor-promoting and -suppressing roles of SIK2, administration of SIK2 inhibitors in GPCR-mutated or other overactive cAMP-PKA cancer types should be attempted with extremely caution to avoid potential pro-tumor effects. More investigations are necessary to clarify these issues and promote the use of SIK2 inhibitors in tumor therapy.

SIK2 IN CANCER THERAPY

Previous studies on SIK2 have reported its regulation of energetic metabolism, mostly based on its signaling pathways and the downstream role of LKB1 in adipocytes. Studies on SIK2 have recently underlined its role in several signaling pathways related to tumorigenesis. Clinical and pathological data indicate that

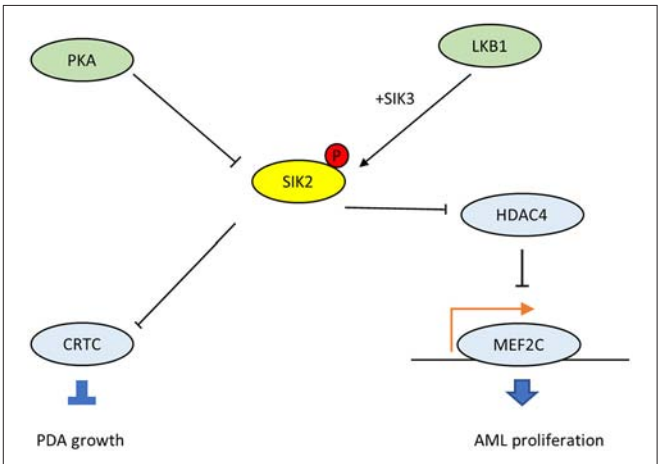

FIGURE 3 | The dichotomous oncogenic roles of SIK2 in the LKB1-HDAC axis and the cAMP-PKA axis.

SIK2 is a potential oncogenic marker in ovarian (17, 49), prostate (50), osteosarcoma (51), and colorectal (52) cancers by controlling different cellular mechanisms. Intriguingly, two studies report that SIK2 may act as a tumor suppressor in breast cancer and PDA. Since SIK2 plays a distinct role in different tissues and divergent pathways, its dysregulation may lead to conflicting phenotypes. Initial studies on SIK2 maily focused on its role in energetic metabolism, particularly in glucose, and lipids oxidation during starvation. The functions of SIK2 may be unique in cells that are involved in glycolipid metabolism, such as hepatocyte and pancreatic cells. As a consequence, SIK2 may act as both tumor promoter and suppressor due to the diversity of cancer cell types or different genetic background. The SIK2 inhibitors HG-9-91-01, ARN-3236, and KIN-112 have succeeded in cancer therapy approaches, validated in cultured cells and *in vivo* animal models (17, 36, 48), although additional optimization of these small molecules is required for therapeutic investigation. Further evaluation of these small molecules is necessary to achieve potent SIK2 inhibition in the uncontrolled signaling pathways of tumor cells while preserving the homeostatic and tumor-protective functions of SIK2 in other cell types.

CONCLUSION

In this mini-review, we discussed the role of the newly identified protein kinase, SIK2, in tumorigenesis, specifically focusing on different signaling pathways involving SIK2. SIKs present significant physiological functions, including novel roles in tumorigenesis and tumor progression. While most studies reveal SIK2 to be a tumor promoter, some claims indicate that SIK2 provides protection from cancer. Thus, the dichotomous function and mechanism between SIK2 and cancer must be further elucidated. As described earlier, SIK2 targeting may be applied as a novel strategy for treating multiple cancer types. Future studies to investigate the molecular mechanisms underlying the precise role of SIK2 in intersecting signaling pathways, as well as the therapeutic effects of SIK2 in preclinical and clinical trials, are recommended.

AUTHOR CONTRIBUTIONS

FC, LC, and QQ contributed to conception and manuscript writing. XS participated in its coordination and modification. All authors read and approved the final manuscript.

FUNDING

This work was supported by the National Natural Science Foundation of China (No. 81472809, No. 81502653, No. 81672983, No.81874217), A Project Funded by the Priority Academic Program Development of Jiangsu Higher Education Institutions (PAPD) (JX10231801), Young Medical Key Talents of Jiangsu Province (grant number QNRC2016572) and the Six Major Talent Peak Project of Jiangsu Province (No.2013-WSN-040).

REFERENCES

1. Muller J. Regulation of aldosterone biosynthesis. Physiological and clinical aspects. *Monogr Endocrinol.* (1987) 29:1–364.
2. Nussdorfer GG. Cytophysiology of the adrenal cortex. *Int Rev Cytol.* (1986) 98:1–405.
3. Katoh Y, Takemori H, Horike N, Doi J, Muraoka M, Min L, et al. Salt-inducible kinase (SIK) isoforms: their involvement in steroidogenesis and adipogenesis. *Mol Cell Endocrinol.* (2004) 217:109–12. doi: 10.1016/j.mce.2003.10.016
4. Wang Z, Takemori H, Halder SK, Nonaka Y, Okamoto M. Cloning of a novel kinase (SIK) of the SNF1/AMPK family from high salt diet-treated rat adrenal. *FEBS Lett.* (1999) 453:135–9. doi: 10.1016/S0014-5793(99)00708-5
5. Dentin R, Liu Y, Koo SH, Hedrick S, Vargas T, Heredia J, et al. Insulin modulates gluconeogenesis by inhibition of the coactivator TORC2. *Nature* (2007) 449:366–9. doi: 10.1038/nature06128
6. Horike N, Takemori H, Katoh Y, Doi J, Min L, Asano T, et al. Adipose-specific expression, phosphorylation of Ser794 in insulin receptor substrate-1, and activation in diabetic animals of salt-inducible kinase-2. *J Biol Chem.* (2003) 278:18440–7. doi: 10.1074/jbc.M211770200
7. Muraoka M, Fukushima A, Viengchareun S, Lombes M, Kishi F, Miyauchi A, et al. Involvement of SIK2/TORC2 signaling cascade in the regulation of insulin-induced PGC-1alpha and UCP-1 gene expression in brown adipocytes. *Am J Physiol Endocrinol Metab.* (2009) 296:E1430–9. doi: 10.1152/ajpendo.00024.2009
8. Wang Y, Li G, Goode J, Paz JC, Ouyang K, Screaton R, et al. Inositol-1,4,5-trisphosphate receptor regulates hepatic gluconeogenesis in fasting and diabetes. *Nature* (2012) 485:128–32. doi: 10.1038/nature10988
9. Ahmed AA, Lu Z, Jennings NB, Etemadmoghadam D, Capalbo L, Jacamo RO, et al. SIK2 is a centrosome kinase required for bipolar mitotic spindle formation that provides a potential target for therapy in ovarian cancer. *Cancer Cell* (2010) 18:109–21. doi: 10.1016/j.ccr.2010.06.018
10. Bricambert J, Miranda J, Benhamed F, Girard J, Postic C, Dentin R. Salt-inducible kinase 2 links transcriptional coactivator p300 phosphorylation to the prevention of ChREBP-dependent hepatic steatosis in mice. *J Clin Invest.* (2010) 120:4316–31. doi: 10.1172/JCI41624
11. Charoenfuprasert S, Yang YY, Lee YC, Chao KC, Chu PY, Lai CR, et al. Identification of salt-inducible kinase 3 as a novel tumor antigen associated with tumorigenesis of ovarian cancer. *Oncogene* (2011) 30:3570–84. doi: 10.1038/onc.2011.77
12. Cheng H, Liu P, Wang ZC, Zou L, Santiago S, Garbitt V, et al. SIK1 couples LKB1 to p53-dependent anoikis and suppresses metastasis. *Sci Signal.* (2009) 2:ra35. doi: 10.1126/scisignal.2000369
13. Horike N, Kumagai A, Shimono Y, Onishi T, Itoh Y, Sasaki T, et al. Downregulation of SIK2 expression promotes the melanogenic program in mice. *Pigment Cell Melanoma Res.* (2010) 23:809–19. doi: 10.1111/j.1755-148X.2010.00760.x
14. Imielinski M, Berger AH, Hammerman PS, Hernandez B, Pugh TJ, Hodis E, et al. Mapping the hallmarks of lung adenocarcinoma with massively parallel sequencing. *Cell* (2012) 150:1107–20. doi: 10.1016/j.cell.2012.08.029
15. Du J, Chen Q, Takemori H, Xu H. SIK2 can be activated by deprivation of nutrition and it inhibits expression of lipogenic genes in adipocytes. *Obesity* (2008) 16:531–8. doi: 10.1038/oby.2007.98
16. Zhang ZN, Gong L, Lv S, Li J, Tai X, Cao W, et al. SIK2 regulates fasting-induced PPAR alpha activity and ketogenesis through p300. *Sci Rep.* (2016) 6:23317. doi: 10.1038/srep23317
17. Miranda F, Mannion D, Liu S, Zheng Y, Mangala LS, Redondo C, et al. Salt-inducible kinase 2 couples ovarian cancer cell metabolism with survival at the adipocyte-rich metastatic niche. *Cancer Cell* (2016) 30:273–89. doi: 10.1016/j.ccell.2016.06.020
18. Lin X, Takemori H, Katoh Y, Doi J, Horike N, Makino A, et al. Salt-inducible kinase is involved in the ACTH/cAMP-dependent protein kinase signaling

in Y1 mouse adrenocortical tumor cells. *Mol Endocrinol.* (2001) 15:1264–76. doi: 10.1210/mend.15.8.0675
19. Feldman JD, Vician L, Crispino M, Hoe W, Baudry M, Herschman HR. The salt-inducible kinase, SIK, is induced by depolarization in brain. *J Neurochem.* (2000) 74:2227–38. doi: 10.1046/j.1471-4159.2000.0742227.x
20. Ruiz JC, Conlon FL, Robertson EJ. Identification of novel protein kinases expressed in the myocardium of the developing mouse heart. *Mech Dev.* (1994) 48:153–64. doi: 10.1016/0925-4773(94)90056-6
21. Du WQ, Zheng JN, Pei DS. The diverse oncogenic and tumor suppressor roles of salt-inducible kinase (SIK) in cancer. *Expert Opin Ther Targets* (2016) 20:477–85. doi: 10.1517/14728222.2016.1101452
22. MacKenzie KF, Clark K, Naqvi S, McGuire VA, Noehren G, Kristariyanto Y, et al. PGE(2) induces macrophage IL-10 production and a regulatory-like phenotype via a protein kinase A-SIK-CRTC3 pathway. *J Immunol.* (2013) 190:565–77. doi: 10.4049/jimmunol.1202462
23. Zohrap N, Saatci O, Ozes B, Coban I, Atay HM, Battaloglu E, et al. SIK2 attenuates proliferation and survival of breast cancer cells with simultaneous perturbation of MAPK and PI3K/Akt pathways. *Oncotarget* (2018) 9:21876–92. doi: 10.18632/oncotarget.25082
24. Gumbiner BM, Kim NG. The Hippo-YAP signaling pathway and contact inhibition of growth. *J Cell Sci.* (2014) 127 (Pt. 4):709–17. doi: 10.1242/jcs.140103
25. Zeng Q, Hong W. The emerging role of the hippo pathway in cell contact inhibition, organ size control, and cancer development in mammals. *Cancer Cell* (2008) 13:188–92. doi: 10.1016/j.ccr.2008.02.011
26. Fernandez LA, Kenney AM. The Hippo in the room: a new look at a key pathway in cell growth and transformation. *Cell Cycle* (2010) 9:2292–9. doi: 10.4161/cc.9.12.11919
27. Zhao B, Ye X, Yu J, Li L, Li W, Li S, et al. TEAD mediates YAP-dependent gene induction and growth control. *Genes Dev.* (2008) 22:1962–71. doi: 10.1101/gad.1664408
28. Fernandez LA, Squatrito M, Northcott P, Awan A, Holland EC, Taylor MD, et al. Oncogenic YAP promotes radioresistance and genomic instability in medulloblastoma through IGF2-mediated AKT activation. *Oncogene* (2012) 31:1923–37. doi: 10.1038/onc.2011.379
29. Wehr MC, Holder MV, Gailite I, Saunders RE, Maile TM, Ciirdaeva E, et al. Salt-inducible kinases regulate growth through the Hippo signalling pathway in Drosophila. *Nat Cell Biol.* (2013) 15:61–71. doi: 10.1038/ncb2658
30. Jiang J, Chang W, Fu Y, Gao Y, Zhao C, Zhang X, et al. SAV1 represses the development of human colorectal cancer by regulating the Akt-mTOR pathway in a YAP-dependent manner. *Cell Prolif.* (2017) 50:e12351. doi: 10.1111/cpr.12351
31. Zhang Y, Yuan J, Zhang X, Yan F, Huang M, Wang T, et al. Angiomotin promotes the malignant potential of colon cancer cells by activating the YAP-ERK/PI3K-AKT signaling pathway. *Oncol Rep.* (2016) 36:3619–26. doi: 10.3892/or.2016.5194
32. Artinian N, Cloninger C, Holmes B, Benavides-Serrato A, Bashir T, Gera J. Phosphorylation of the hippo pathway component AMOTL2 by the mTORC2 kinase promotes YAP signaling, resulting in enhanced glioblastoma growth and invasiveness. *J Biol Chem.* (2015) 290:19387–401. doi: 10.1074/jbc.M115.656587
33. Frame FM, Pellacani D, Collins AT, Simms MS, Mann VM, Jones GD, et al. HDAC inhibitor confers radiosensitivity to prostate stem-like cells. *Br J Cancer* (2013) 109:3023–33. doi: 10.1038/bjc.2013.691
34. Marampon F, Megiorni F, Camero S, Crescioli C, McDowell HP, Sferra R, et al. HDAC4 and HDAC6 sustain DNA double strand break repair and stem-like phenotype by promoting radioresistance in glioblastoma cells. *Cancer Lett.* (2017) 397:1–11. doi: 10.1016/j.canlet.2017.03.028
35. Roos WP, Krumm A. The multifaceted influence of histone deacetylases on DNA damage signalling and DNA repair. *Nucleic Acids Res.* (2016) 44:10017–30. doi: 10.1093/nar/gkw922
36. Tarumoto Y, Lu B, Somerville TDD, Huang YH, Milazzo JP, Wu XS, et al. LKB1, Salt-inducible kinases, and MEF2C are linked dependencies in acute myeloid leukemia. *Mol Cell* (2018) 69:1017–27 e6. doi: 10.1016/j.molcel.2018.02.011
37. Homminga I, Pieters R, Langerak AW, de Rooi JJ, Stubbs A, Verstegen M, et al. Integrated transcript and genome analyses reveal NKX2–1 and MEF2C as potential oncogenes in T cell acute lymphoblastic leukemia. *Cancer Cell* (2011) 19:484–97. doi: 10.1016/j.ccr.2011.02.008
38. O'Hayre M, Vazquez-Prado J, Kufareva I, Stawiski EW, Handel TM, Seshagiri S, et al. The emerging mutational landscape of G proteins and G-protein-coupled receptors in cancer. *Nat Rev Cancer* (2013) 13:412–24. doi: 10.1038/nrc3521
39. Drelon C, Berthon A, Sahut-Barnola I, Mathieu M, Dumontet T, Rodriguez S, et al. PKA inhibits WNT signalling in adrenal cortex zonation and prevents malignant tumour development. *Nat Commun.* (2016) 7:12751. doi: 10.1038/ncomms12751
40. He X, Zhang L, Chen Y, Remke M, Shih D, Lu F, et al. The G protein alpha subunit Galphas is a tumor suppressor in Sonic hedgehog-driven medulloblastoma. *Nat Med.* (2014) 20:1035–42. doi: 10.1038/nm.3666
41. Iglesias-Bartolome R, Torres D, Marone R, Feng X, Martin D, Simaan M, et al. Inactivation of a Galpha(s)-PKA tumour suppressor pathway in skin stem cells initiates basal-cell carcinogenesis. *Nat Cell Biol.* (2015) 17:793–803. doi: 10.1038/ncb3164
42. Pattabiraman DR, Bierie B, Kober KI, Thiru P, Krall JA, Zill C, et al. Activation of PKA leads to mesenchymal-to-epithelial transition and loss of tumor-initiating ability. *Science* (2016) 351:aad3680. doi: 10.1126/science.aad3680
43. Xing F, Luan Y, Cai J, Wu S, Mai J, Gu J, et al. The anti-warburg effect elicited by the cAMP-PGC1alpha pathway drives differentiation of glioblastoma cells into astrocytes. *Cell Rep.* (2017) 18:468–81. doi: 10.1016/j.celrep.2016.12.037
44. Amato E, Molin MD, Mafficini A, Yu J, Malleo G, Rusev B, et al. Targeted next-generation sequencing of cancer genes dissects the molecular profiles of intraductal papillary neoplasms of the pancreas. *J Pathol.* (2014) 233:217–27. doi: 10.1002/path.4344
45. Bailey P, Chang DK, Nones K, Johns AL, Patch AM, Gingras MC, et al. Genomic analyses identify molecular subtypes of pancreatic cancer. *Nature* (2016) 531:47–52. doi: 10.1038/nature16965
46. Zehir A, Benayed R, Shah RH, Syed A, Middha S, Kim HR, et al. Mutational landscape of metastatic cancer revealed from prospective clinical sequencing of 10,000 patients. *Nat Med.* (2017) 23:703–13. doi: 10.1038/nm.4333
47. Cancer Genome Atlas Research Network. Electronic address aadhe, Cancer Genome Atlas Research Network. Integrated Genomic Characterization of Pancreatic Ductal Adenocarcinoma. *Cancer Cell* (2017) 32:185–203 e13. doi: 10.1016/j.ccell.2017.07.007
48. Patra KC, Kato Y, Mizukami Y, Widholz S, Boukhali M, Revenco I, et al. Mutant GNAS drives pancreatic tumourigenesis by inducing PKA-mediated SIK suppression and reprogramming lipid metabolism. *Nat Cell Biol.* (2018) 20:811–22. doi: 10.1038/s41556-018-0122-3
49. Yang FC, Tan BC, Chen WH, Lin YH, Huang JY, Chang HY, et al. Reversible acetylation regulates salt-inducible kinase (SIK2) and its function in autophagy. *J Biol Chem.* (2013) 288:6227–37. doi: 10.1074/jbc.M112.431239
50. Bon H, Wadhwa K, Schreiner A, Osborne M, Carroll T, Ramos-Montoya A, et al. Salt-inducible kinase 2 regulates mitotic progression and transcription in prostate cancer. *Mol Cancer Res.* (2015) 13:620–35. doi: 10.1158/1541-7786.MCR-13-0182-T
51. Liu J, Zhu H, Zhong N, Jiang Z, Xu L, Deng Y, et al. Gene silencing of USP1 by lentivirus effectively inhibits proliferation and invasion of human osteosarcoma cells. *Int J Oncol.* (2016) 49:2549–57. doi: 10.3892/ijo.2016.3752
52. Liu Y, Gao S, Chen X, Liu M, Mao C, Fang X. Overexpression of miR-203 sensitizes paclitaxel (Taxol)-resistant colorectal cancer cells through targeting the salt-inducible kinase 2 (SIK2). *Tumour Biol.* (2016) 37:12231–9. doi: 10.1007/s13277-016-5066-2

Conflict of Interest Statement: The authors declare that the research was conducted in the absence of any commercial or financial relationships that could be construed as a potential conflict of interest.

frontiers in Pharmacology

ORIGINAL RESEARCH
published: 22 January 2019
doi: 10.3389/fphar.2019.00004

Liver-Targeted Combination Therapy Basing on Glycyrrhizic Acid-Modified DSPE-PEG-PEI Nanoparticles for Co-delivery of Doxorubicin and Bcl-2 siRNA

Guixiang Tian[1†], Ruiyan Pan[2†], Bo Zhang[2†], Meihua Qu[2], Bo Lian[1], Hong Jiang[1], Zhiqin Gao[1] and Jingliang Wu[1*]*

[1] School of Bioscience and Technology, Weifang Medical University, Weifang, China, [2] School of Pharmacy, Weifang Medical University, Weifang, China

OPEN ACCESS

Edited by:
Zhe-Sheng Chen,
St. John's University, United States

Reviewed by:
Yingfang Fan,
Zhujiang Hospital, Southern Medical University, China
Hua Zhu,
The Ohio State University, United States

***Correspondence:**
Zhiqin Gao
zhiqingao2013@163.com
Jingliang Wu
jlwu2008@163.com

† These authors have contributed equally to this work

Specialty section:
This article was submitted to Cancer Molecular Targets and Therapeutics, a section of the journal Frontiers in Pharmacology

Received: 20 November 2018
Accepted: 04 January 2019
Published: 22 January 2019

Citation:
Tian G, Pan R, Zhang B, Qu M, Lian B, Jiang H, Gao Z and Wu J (2019) Liver-Targeted Combination Therapy Basing on Glycyrrhizic Acid-Modified DSPE-PEG-PEI Nanoparticles for Co-delivery of Doxorubicin and Bcl-2 siRNA. Front. Pharmacol. 10:4. doi: 10.3389/fphar.2019.00004

Combination therapy based on nano-sized drug delivery system has been developed as a promising strategy by combining two or more anti-tumor mechanisms. Here, we prepared liver-targeted nanoparticles (GH-DPP) composed of 1,2-distearoyl-sn-glycero-3-phosphoethanolamine-polyethylene glycol-polyetherimide (DSPE-PEG-PEI) with Glycyrrhetinic acid-modified hyaluronic acid (GA-HA) for co-delivery of doxorubicin (DOX) and Bcl-2 siRNA. Particles size, zeta potential and morphology were determined for the drug-loaded GH-DPP nanoparticles (siRNA/DOX/GH-DPP). Cellular uptake and *in vitro* cytotoxicity were analyzed against HepG2 cells. *In vivo* bio-distribution and anti-tumor therapeutic effects of siRNA/DOX/GH-DPP were evaluated in H22-bearing mice. The results showed that siRNA/DOX/GH-DPP nanoparticles were nearly spherical and showed dose-dependent cytotoxicity against HepG2 cells. Compared to Glycyrrhetinic acid-free co-delivery system (siRNA/DOX/DPP) and GH-DPP nanoparticles for delivery of DOX or Bcl-2 siRNA alone, siRNA/DOX/GH-DPP nanoparticles could induce more cellular apoptosis, and showed higher anti-tumor effect. Herein GH-DPP nanoparticles could simultaneously deliver both chemotherapy drugs and siRNA into the tumor region, exhibiting great potential in anti-tumor therapy.

Keywords: combination therapy, nanoparticles, delivery, liver cancer, glycyrrhizic acid

INTRODUCTION

Liver cancer is one of prevalent cancers with high mortality rate around the world, and traditional chemotherapy is one effective approach used in anti-cancer therapy (Gravitz, 2014; Sia et al., 2017). However, many chemotherapeutic agents, such as DOX and paclitaxel, have many clinical limitations owing to severe system toxicity, non-specific targeting, and the development of multidrug resistance (MDR) (Zahreddine and Borden, 2013).

To improve selectivity toward liver cancer cells, an effective strategy is to design nano-sized carrier to realize liver-targeted delivery (Shamay et al., 2018). Recently, nanoparticles have been

proved to have the advantages in drug delivery with low system toxicity (Wei et al., 2015; Zeng et al., 2017; Arms et al., 2018). Many nano-sized drug delivery systems, such as natural and synthetic polymer nanoparticles, metal nanoparticles, and polymer-drug conjugates, have been investigated for delivery of anti-tumor drugs (Ekladious et al., 2018; Liu et al., 2018; Maeki et al., 2018). The nano-vehicles basing on phosphoethanolamine-polyethylene glycol polymers (PEG-PE) represent a promising nanoparticles delivery system owing to biocompatibility, prolonged circulation, and accumulation in tumors by the enhanced permeability and retention (EPR) effect (Perche et al., 2012; Kohay et al., 2017). In the past decade, many efforts have been made to prepare liver-targeting nano-carriers, which were modified by sugars, antibodies, and other ligands (Singh et al., 2016; Zhu et al., 2016; Yan et al., 2017; Wu J. et al., 2018). Glycyrrhetinic acid (GA), a metabolite of glycyrrhizin, has attracted growing interest in anti-hepatoma therapy (Wu J. et al., 2018). It has been reported that GA-modified nano-carriers could significantly improve liver-targeting efficiency and inhibit liver cancer development.

Moreover, development of MDR in cancer cells was a major cause of the failure in clinical chemotherapy. Bcl-2, an anti-apoptosis protein, is distributed on the endoplasmic reticulum, the outer membrane of nuclear and mitochondrion. Up-regulation of Bcl-2 expression was one of the mechanisms responsible for MDR, leading to the activation of anti-apoptotic pathways (Yin et al., 2014). The Bcl-2 siRNA, an antisense oligonucleotide sequence of Bcl-2, could silence the expression of Bcl-2 gene, resulting in cell apoptosis of liver cancer (Sun et al., 2018).

To overcome the limitations of traditional chemotherapy in clinical antitumor therapy, combination drug strategy has been applied as a novel anti-tumor therapy. It is based on co-delivery nanoparticles system for combination of chemotherapeutics with other treatment approaches like RNAi (Zuckerman and Davis, 2015). The nanoparticles can simultaneously co-deliver two or more drugs to tumor region and thus improve the cancer therapeutic effect by synergistic/combined therapy effect, and reverse the multi-drug resistance (MDR) (Zhang et al., 2016; Sun et al., 2018).

In previous study, we have prepared GA-modified hyaluronic acid micelles for DOX delivery (Wu et al., 2016). Hyaluronic acid (HA), a negatively charged polysaccharide, is present in the extracellular matrix and synovial fluids (Knopf-Marques et al., 2016). It can cover on the shell of positive nano-carriers, such as PEI-PE, chitosan, dendrimer, to decrease the uptake rate by reticuloendothelial systems (Nguyen and Alsberg, 2014; Zhao et al., 2016; Wickens et al., 2017; Parmar et al., 2018).

In this study, DSPE-PEG-PEI and GA-HA conjugates were synthesized, and GH-DPP nanoparticles were prepared for co-delivery of DOX and Bcl-2 siRNA (**Figure 1**). The characteristics of the drug-loaded nanoparticles were investigated using dynamic light scattering, transmission electron microscopy (TEM) and UV-Vis spectrophotometer. The *in vitro* cytotoxicity and cellular uptake of siRNA/DOX/GH-DPP were investigated against HepG2 cells. And the *in vivo* bio-distribution and anti-tumor effect were explored.

MATERIALS AND METHODS

Materials and Cell Lines

Branched poly(ethyleneimine) (PEI, Mw 1.8 kDa) was purchased from Sigma Aldrich (United States). DOX was purchased from Dalian Meilun Biology Technology Co., Ltd., (Dalian, China). 4-(4,6-dimethoxy-1,3,5-triazin-2-yl)-4-methylmorpholinium ch loride (DMT–MM) were purchased from Shanghai Medpep Co., Ltd., (Shanghai, China) 1,2-distearoyl-sn-glycero-3-phosphoethanolamine-N-[succinimidyl (polyethylene glycol) -2000] (DSPE-PEG-NHS) was purchased from Xi'an Rixi Technology Co., Ltd., (Xi'an, China). Bcl-2 siRNA and FITC-labeled siRNA were purchased from Guangzhou RiboBio Co., Ltd., (Guangzhou, China). 3-(4, 5-dimethylthiazol-2-yl)-2, 5-diphenyltetrazolium bromide (MTT) was purchased from Sigma Aldrich (United States). Fetal bovine serum and RPMI-1640 medium (RPMI) were purchased from Beijing Solarbio Co., Ltd., (Beijing, China). All other reagents were of commercial special grade and used without further purification.

Human hepatic cell line (HepG2), human lung adenocarcinoma cell line (A549) and murine HCC cells (H22) were obtained from the China Center for Type Culture Collection (Wuhan, China). Female BALB/c mice (weight: 18 ± 2 g) were supplied by the Experimental Animal Center of Weifang Medical University (Weifang, China), and approved by the WFMU Animal Research Ethics Committee.

Synthesis of HA-GA and DSPE-PEG-PEI Conjugates

GA-HA conjugate (GH) was synthesized using HA as a hydrophilic segment and GA as a hydrophobic segment (Wu et al., 2016). In brief, GA–NH_2 was obtained by adding ethylene diamine to the GA solution in the presence of DMT-MM. And the GA–HA conjugate was synthesized by the chemical modification of GA–NH_2 to HA chain.

Syntheses of DSPE-PEG-PEI (DPP) were conducted in one steps as shown in **Figure 2**. Briefly, PEI was dissolved in DMSO (10 mL) in a 25 mL glass flask, and then functional DSPE-PEG-NHS was added into the reaction solution under stirring. The reaction solution was stirred for 24 h at room temperature. The product was purified by dialysis against distilled water (MWCO 8000-14000 Da), lyophilized, and the chemical structure was confirmed by ^{1}H NMR (in D_2O, 300 MHz).

Preparation and Characteristics of Drug-Loaded GH-DPP Nanoparticles

siRNA/DOX/GH-DPP nanoparticles were prepared by three steps. Firstly, DOX was loaded into the core of DPP nanoparticles via a dialysis method. In brief, DOX • HCl was stirred with triethylamine (1.3-fold molar quantity of DOX) in DMF, and the DPP conjugates were dispersed in formamide. Then the DOX solution was added slowly to the DPP solution, followed by stirring overnight. The mixed system was dialyzed against deionized water. The solution in the dialysis bag was freeze-dried to obtain DOX-loaded DPP nanoparticles (DOX/DPP). Secondly, the DPP nanoparticles for co-delivery

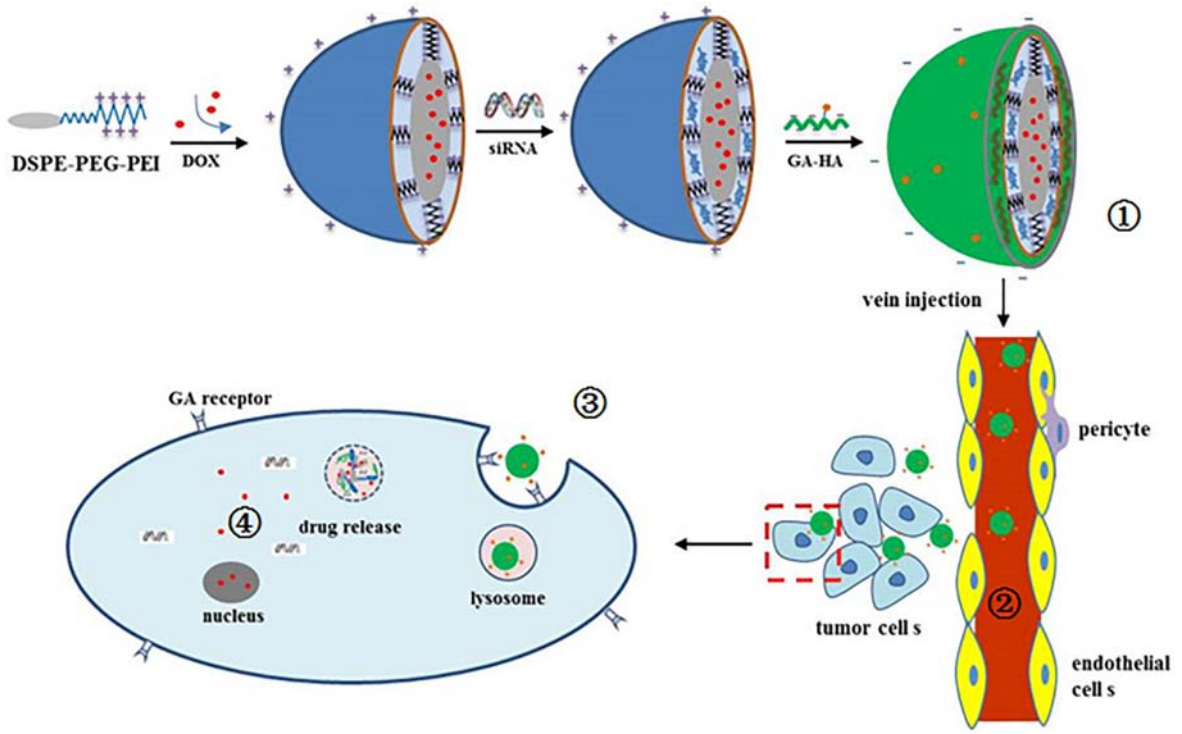

FIGURE 1 | Schematic illustration of ①preparation of siRNA/DOX/GH-DPP nanoparticles, ②liver-targeted drug delivery via blood cycle, ③cellular uptake, and ④pH-triggered release of Bcl-2 siRNA and DOX.

of DNA and siRNA were prepared by electrovalent interaction. The sequences of Bcl-2 siRNA were as follows: (sense) 5′ – GUACAUCCAUUAUAAGCUGUCdTdT-3′, (anti-sense) 5′ – GACAGCUUAUAAUGGAUGUACdTdT-3′. DOX/DPP nanoparticles were incubated with Bcl-2 siRNA in deionized water. In order to obtain the proper mass ratio of DPP to siRNA, the same amount of siRNA was incubated with different concentrations of DOX/DPP nanopaticles solutions for 1 h. The mass ratios of DOX/DPP to siRNA was set as 100:512, 100:256, 100:128, 100:64, 100:32, 100:16, and 100:8, respectively. The binding ability of DOX/DPP and siRNA was investigated by agarose gel retardation assay, followed by electrophoretic mobility shift assay via a UV gel imaging system. The proper mass ratio of DOX/DPP to siRNA was selected for preparation of siRNA/DOX/DPP nanoparticles. Thirdly, GA-HA conjugate was mixed with siRNA/DOX/DPP nanoparticles to prepare siRNA/DOX/GH-DPP by stirring slowly for 1 h. Then drug-loaded nanoparticles were freeze-dried, and the lyophilized power was stored at 4°C. The GH-DPP nanoparticles for delivery of DOX or siRNA alone were prepared as control.

The particle size and ζ potential of siRNA/DOX/GH-DPP nanoparticles were measured using a dynamic laser scattering method with a wavelength of 633 nm at 25°C. The detection angle was set to 90°. The polydispersingindex (PdI) was used to evaluate the size distribution. The concentration of siRNA/DOX/GH-DPP nanoparticles was kept 1 mg/mL, and all measurements were performed in triplicate. The morphology of siRNA/DOX/GH-DPP nanoparticles was observed by electron microscopy. One drop of drug-loaded nanoparticles solution were placed on a copper grid, and dried at room temperature. The sample was examined using a transmission electron microscope.

To evaluate the loading efficiency (LE) and encapsulation efficiency (EE) of GH/DPP nanoparticles, siRNA/DOX/GH-DPP nanoparticles were dissolved in formamide by gently heating, and measured using UV–Vis spectrophotometer at 480 nm. The concentration of DOX in the GH/DPP micelles was obtained using the standard curve. Then LE and EE were calculated using the following equation (1) and (2):

$$\mathrm{LE}(\%) = \mathrm{Ws}/\mathrm{Wt} \times 100\% \quad (1)$$

$$\mathrm{EE}(\%) = \mathrm{Ws}/\mathrm{Wa} \times 100\% \quad (2)$$

Ws = the amount of DOX measured in the GH/DPP nanoparticles; Wt = the total weight of siRNA/DOX/GH-DPP nanoparticles; and Wa = the initial amount of the DOX•HCl added.

In vitro Drug Release From GH-DPP Nanoparticles

The release of DOX and siRNA from GH-DPP nanoparticles was investigated in PBS buffer (pH 7.4 and 5.0) (Wang et al., 2016). 1 mg/mL siRNA/DOX/GH-DPP nanoparticles was dispersed in

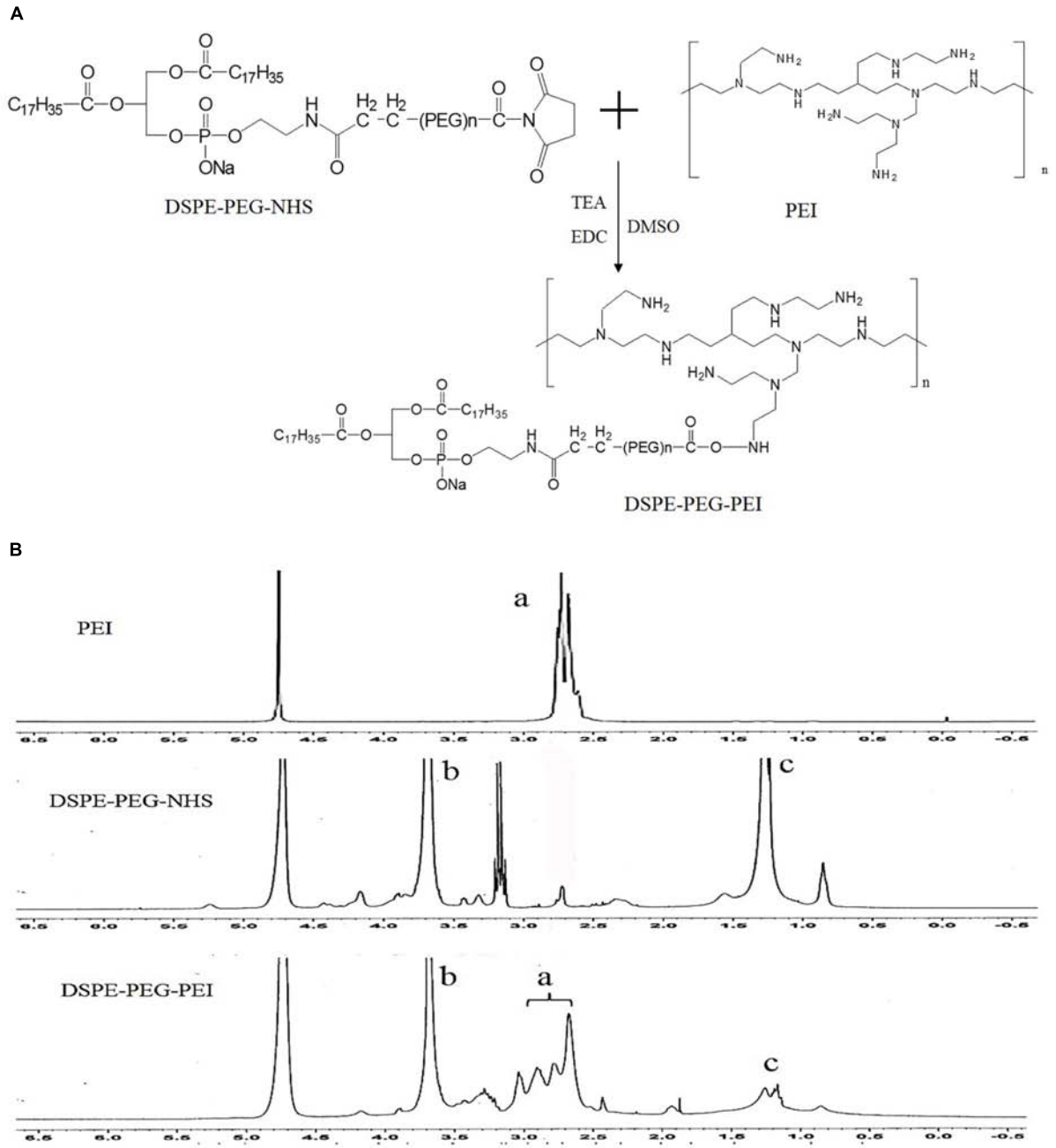

FIGURE 2 | Synthesis of DSPE-PEG-PEI conjugate. **(A)** Synthetic route of DSPE-PEG-PEI conjugate. **(B)** ^{1}H-NMR spectra of PEI, DSPE-PEG-NHS and DSPE-PEG-PEI (a: peaks of PEI; b and c: peaks of DSPE-PEG-NHS).

5 mL PBS, and the solution was placed in a dialysis bag (MWCO of 1000 and 20000 for DOX and siRNA, respectively). Then, the dialysis bag was placed in 20 mL of PBS buffer at 37°C under a shaking speed of 100 rpm. At predetermined time intervals, 1 mL of release media was taken out and 1 mL of fresh PBS buffer was added. The DOX and siRNA content was tested by UV-Vis spectroscopyat 480 and 260 nm, respectively. The release of DOX and siRNA was calculated by standard curve. The test was performed in triplicate.

Cytotoxicity Assay of siRNA/DOX/GH-DPP Nanoparticles

The cytotoxicity of blank DPP and GH-DPP nanoparticles against HepG2 and A549 cells was evaluated by MTT assay. Briefly, the tumor cells were seeded in 96-well plates (1×10^4 cells/well) and incubated for 48 h. Then, the cells were co-cultured with different concentrations (1, 10, 20, 50, and 100 μg/ml) of DPP or GH-DPP nanoparticles, respectively. After 48 h, 20 μL of MTT reagents (5 mg/mL) was added for another

4 h incubation at 37°C. The media were replaced with 200 μL of DMSO. The absorbance at 490 nm was measured using a Bio-Rad Microplate Reader (Model 680, Richmond, VA, United States).

The cytotoxicity of siRNA/DOX/GH-DPP nanoparticles was evaluated by MTT assay against HepG2 and A549 cells. The cells were incubated with the culture media containing free DOX, DOX/GH-DPP, siRNA/GH-DPP, siRNA/DOX/DPP and siRNA/DOX/GH-DPP nanoparticles at different DOX concentrations (0.01, 0.1, 0.5, 1, 2, and 5 μg/mL), respectively. The cytotoxicity of drug formulations was shown as a cell viability percentage with respect to the untreated tumor cells. All the experiments were repeated thrice.

Cellular Uptake Analysis

Cellular uptake of DOX and FITC-labeled siRNA was monitored by fluorescent microscopy (BX40, Olympus, Japan). HepG2 cells were seeded in a 12-well plate at a density of 1×10^5 cells/well at 37°C. After the cells reached 75% confluence, the media were replaced with fresh media containing free DOX and siRNA, siRNA/DOX/DPP, siRNA/DOX/GH-DPP nanoparticles, respectively. After 4 h, the cells were washed three times by cold PBS, and fixed with 4% paraformaldehyde solution. The intracellular localization of DOX was visualized by fluorescence microscope.

Western Blotting Analysis

Suppression of the BCL-2 protein was determined by Western blot using bicin-choninic acid protein assay kit (BCA, Invitrogen, United States). Sample proteins (30 μg) was subjected to electrophoresis in 10% sodium dodecyl sulfate polacrylamine gel. And the protein was transferred to polyvinylidene difluoride membranes, followed by incubation with non-fat milk for 1 h, and with antibody against BCL-2 and β-action (1:1000 dilution) for 12 h at 4°C. The membranes were washed thrice in TBST, and incubated with HRP conjugated goat anti-rabbit IgG (1:5000, Santa Cruz Biotech., United States) for 1 h. the complexes were visualized using chemiluminescence kit (KeyGEN, China).

In vivo Near-Infrared Fluorescence Imaging (NIFI)

In vivo biodistribution of the drug-loaded GH-DPP nanoparticles was monitored via near-infrared fluorescence imaging system. Preparation of DiR loaded GH-DPP nanoparticles was as followed: GH-DPP and DiR were dis-solved in methanol, and the solution was dripped to deionized water by a micro-syringe pump under magnetic stirring. The mixture system was dialyzed against deionized water for 48 h. The final concentration of DiR for tail vein injection was 40 μg/mL. The tumor-bearing mice model was established by subcutaneous inoculation of H22 cells in the flank of BALB/c female mice. When the volume of the tumor grew to approximately 100 mm^3, the mice were randomly divided into three groups. DiR was used as a fluorescence agent. DiR-loaded DPP and DiR-loaded GH-DPP nanoparticles were prepared, respectively. Free DiR, DiR-loaded DPP and DiR-loaded GH-DPP nanoparticles were administrated by intravenous injection. The *in vivo* near-infrared fluorescence imaging was performed at pre-determined times (2, 6, 12, and 24 h), using the Xenogen IVIS Spectrum from Caliper Life Sciences (Ex was 745 nm, Em was 835 nm).

Anti-tumor Effect Analysis

The therapeutic effects of drug-loaded GH-DPP nanoparticles were investigated through evaluation of their anti-tumor effects using H22 tumor-bearing mice as model. When the tumor size reached about 100 mm^3, H22-bearing mice was randomly divided into sever groups (five mice per group). The mice were administrated by physiological saline (control), blank GH-DPP nanoparticles, free DOX●HCl, siRNA/GH-DPP, DOX/GH-DPP, siRNA/DOX/DPP, and siRNA/DOX/GH-DPP nanoparticles, respectively. Drug treatment was set at a dose of 5 mg DOX/kg body weight every other day. The body weight and tumor volume was measured every day. Finally, all of the mice were sacrificed, and the tumors were harvested. The tumor volume was calculated by follow equation:

$$Vt = d^2 \times L/2$$

L is the longest diameter of tumor; d is the shortest diameter of tumor; and Vt is the tumor volume.

Statistical Analysis

All results are presented as mean ± S.D., $n = 3$ parallel samples. The data were analyzed by Student's *t*-test for comparison of two groups. A *p*-value less than 0.05 was considered to be significant.

Synthesis of DSPE-PEG-PEI Conjugates

Bi-functional DSPE-PEG-NHS was used to conjugate with PEI via the primary amine reactive NHS ester moiety at weakly basic pH, thus avoiding the conjugation and crosslinking of the maleimide groups to the amine functions of PEI, which occurs at higher pH (pH > 8). The structure of DSPE-PEG-NHS, PEI and resulting DSPE-PEG-PEI copolymer were verified by ^{1}H NMR. The peaks of PEG (3.6 ppm, -CH_2O-), DSPE (1.0–1.5 ppm, -CH_2-) and PEI (2.5–3.0 ppm, CH_2-N) were confirmed. The^{1}H-NMR spectrum of DSPE-PEG-PEI in D_2O exhibited characteristic peaks at 2.5–3.0 ppm (peaks of PEI), 3.6 ppm (peaks of PEG) and 1.0–1.5 ppm (peaks of DSPE), indicating that PEI was successfully introduced to the DSPE-PEG-NHS molecular.

Preparation and Physicochemical Characteristics of Drug-Loaded Nanoparticles

Doxorubicin and Bcl-2 siRNA were loaded in DPP or GH/DPP copolymers, named as siRNA/DOX/DPP and siRNA/DOX/GH-DPP, respectively. The characterization of DOX-loaded nanoparticles was shown in **Table 1**. The average particles size of siRNA/DOX/GH-DPP was bigger than that of siRNA/DOX/DPP, while the ζ potential was lower in siRNA/DOX/GH-DPP. The result was due to the coverage of GA-HA conjugate, resulting in bigger particles size and less ζ potential. LE and EE of DOX in siRNA/DOX/GH-DPP nanoparticles were measured by UV spectrophotometer. When the feed ratio of DOX to DPP was 10%, the EE and LE of DOX was 86.1 and 8.02%, respectively.

TABLE 1 | The particle size, polydispersity index (PDI) and zeta potential of siRNA/DOX/DPP and siRNA/DOX/GH-DPP ($n = 3$).

	Size (nm)	PDI	Zeta (mV)	EE[b](%)	DL[b](%)
siRNA/DOX/DPP	157.2 ± 5.7	0.272 ± 0.05	12.75 ± 2.19	87.4 ± 2.7	8.32 ± 1.4
siRNA/DOX/GH-DPP	185.4 ± 6.4[a]	0.294 ± 0.04	−2.64 ± 1.73[a]	86.1 ± 3.1	8.02 ± 1.6

[a] $P < 0.05$ siRNA/DOX/DPP vs siRNA/DOX/GH-DPP. [b] DOX loadeding.

To obtain the co-delivery system of DOX and siRNA, DOX/DPP and siRNA with different mass ratio were mixed and tested by gel retardation assay. **Figure 3A** showed that the fraction of free DNA disappeared at 100:16, suggesting that DOX/DPP could condense DNA efficaciously when the mass ratio of DPP to siRNA was over 100:16. The siRNA/DOX/DPP and siRNA/DOX/GH-DPP nanoparticles were well-separated with a rather narrow size distribution (**Figures 3B,C**). As shown in **Figures 3D,E**, the co-delivery system exhibited sphere in shape. Stability studies showed that drug-loaded GH-DPP nanoparticles were more stable than drug-loaded DPP nanoparticles under physiological conditions (**Supplementary Figure S1**).

DOX and siRNA Release From siRNA/DOX/GH-DPP Nanoparticles

The release of DOX and siRNA from siRNA/DOX/GH-DPP or siRNA/DOX/DPP nanoparticles was conducted in pH 7.4 and pH 5.0. The siRNA and DOX released from GA-DPP or DPP were time-dependent (**Figure 4**). Both GH-DPP and DPP nanoparticles showed a rapid release at pH 5.0. By contrast, the drug release was slower at pH 7.4. The possible explanation is that the electrostatic interaction between positive segments (PEI) and negative segments (siRNA, GA-HA) is weak at lower pH value, leading to rapid release of the drug from the nano-carriers (Sun et al., 2018). Compared to siRNA/DOX/GH-DPP nanoparticles, the siRNA/DOX/DPP released more drugs at the same time. This may due to the fact the coverage layer (GA-HA) could delay the release of DOX from GH-DPP nanoparticles (Manna et al., 2010).

In vitro Cytotoxicity of siRNA/DOX/GH-DPP Nanoparticls

The cytotoxicity of blank nano-carriers was determined using the MTT assay. The cytotoxicity of two blank nano-carriers was below 15% at the concentration of 10 to 100 μg/mL (**Figure 5A**). The results suggested that DPP and GH-DPP nanoparticles could be used in drug delivery materials due to their negligible toxicity.

The viability of A549 and HepG2 cells was evaluated after incubations with free DOX, DOX/GH-DPP, siRNA/GH-DPP, siRNA/DOX/DPP, and siRNA/DOX/GH-DPP nanoparticles for 48 h. **Figure 5B** showed that all of five drug formulations exhibited similar dose-dependent cytotoxic effects, and that the co-delivery nanoparticles groups (siRNA/DOX/DPP and siRNA/DOX/GH-DPP) showed higher cytotoxicity compared to free drug treatment groups. The half maximal inhibitory concentration (IC50 value) of siRNA/DOX/DPP and siRNA/DOX/GH-DPP nanoparticles against HepG2 cells was measured to be 1.02 and 0.76 DOX μg/mL, respectively, which were lower than that of free DOX (1.86 DOX μg/mL). The results suggested that co-delivery nanoparticles for DOX and Bcl-2 siRNA could enhanced inhibitory effect of DOX. This was due to the fact that sensitivity of HepG2 cells to DOX was enhanced owing to down-regulation of BCL-2 by RNA interference (Cao et al., 2011). As shown in **Figures 5C,D**, siRNA/DOX/GH-DPP nanoparticles exhibited higher toxicity against HepG2 cells than other DOX formulations, while, it was different at same treatment with A549 cells. The possible explanation was that GA-receptors were over-expressed on HepG2 cells, which enhanced cellular uptake of DOX and siRNA via GA receptor-mediated endocytosis. Whereas, the siRNA/DOX/GH-DPP nanoparticles against A549 cells showed lower cytotoxicity than siRNA/DOX/ DPP nanoparticles. The different cytotoxicity against HepG2 cells and A549 cells might due to different expressed level of GA-receptor on two tumor cells (Tian et al., 2010).

Cellular Uptake of siRNA/DOX/GH-DPP Nanoparticles and Suppression of BCL-2 Expression

The cellular uptake of siRNA/DOX/GH-DPP nanoparticles was investigated through fluorescence microscope. Green and red fluorescence signals indicate the uptake of siRNA and DOX, respectively, while blue fluorescence signals show the nuclei stained with DAPI. Overlays of three fluorescence picture revealed the distribution of DOX and siRNA in the cytoplasm. As shown in **Figure 6A**, there were obvious red fluorescence signals in cytoplasm of HepG2 cells incubating with three drug formulations, indicating that DOX was taken up by tumor cells. There was little green fluorescence signals in the group treated by mixture of free DOX and siRNA, indicating that little siRNA were taken up by tumor cells. Compared to drug-loaded DPP nanoparticles, stronger green fluorescence signals were found in HepG2 cells incubating with DOX/GH-DPP nanoparticles. This result was due to the coverage of GA-HA conjugate, which increase the amounts of drugs via GA-receptor-mediated endocytosis. The down-regulation of BCL-2 gene in HepG2 cells was assessed by western blot assays. After treated with siRNA/DOX/DPP and siRNA/DOX/GH-DPP nanoparticles, the expression of BCL-2 protein was inhibited obviously in comparison with the control group (**Figures 6B,C**), suggesting that the up-regulation of BCL-2 in HepG2 cells could be reversed by RNA interference basing on GH-DPP nanoparticles.

In vivo Biodistribution of GH-DPP Nanoparticles

DiR-loaded nanoparticles were prepared to investigate the biodistribution of GH-DPP *in vivo* (Frangioni, 2003). After injection of DiR formulations, fluorescence signals could be monitored in liver and tumor. As shown in **Figure 7**, there were strong fluorescence signals in the tumor for DiR-loaded nanoparticles compared to free DiR, indicating the nano-carrier

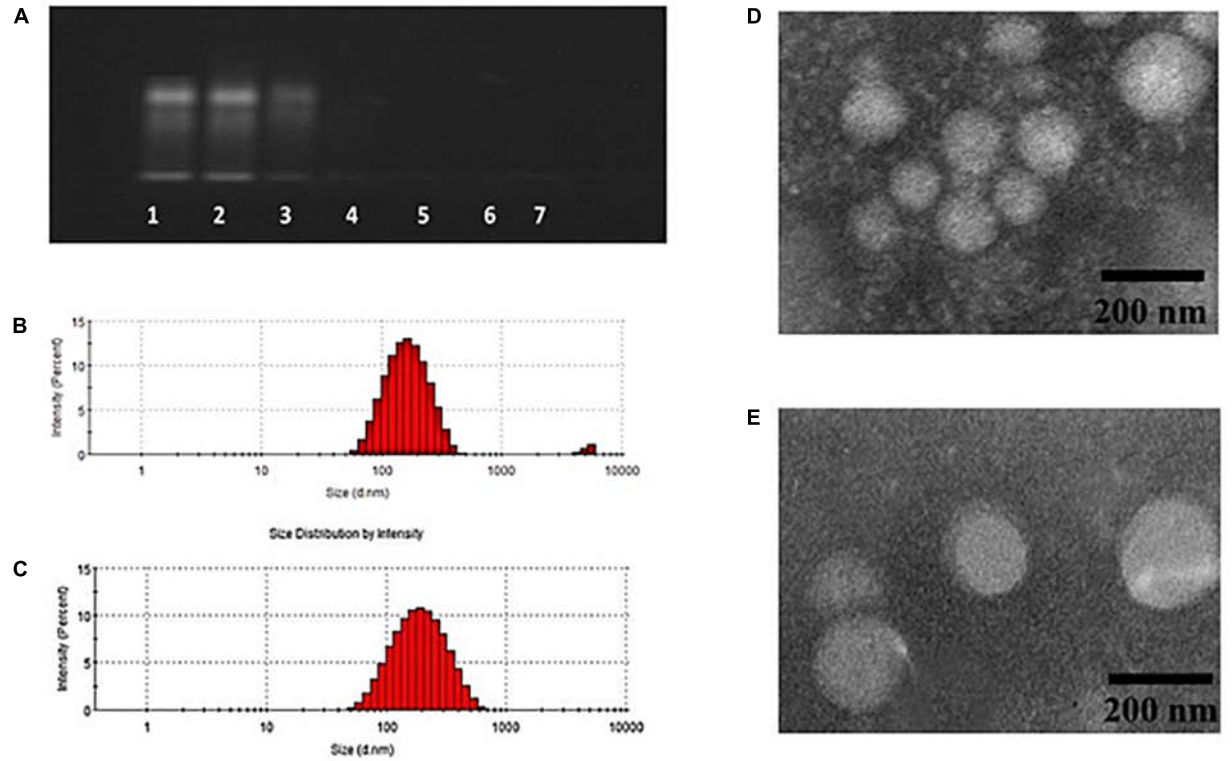

FIGURE 3 | Characteristics of siRNA/DOX-loaded GH-DPP nanoparticles. **(A)** The siRNA retardation assay of GH-DPP at the mass ratio of DPP to siRNA from 100:256 to 100:4 (1, 100:128; 2, 100:64; 3, 100:32; 4, 100:16; 5, 100:8; 6, 100:4). **(B–C)** Particle size distribution of siRNA/DOX/ DPP and siRNA/DOX/GH-DPP nanoparticles. **(D–E)** TEM image of siRNA/DOX/ DPP and siRNA/DOX/GH-DPP nanoparticles.

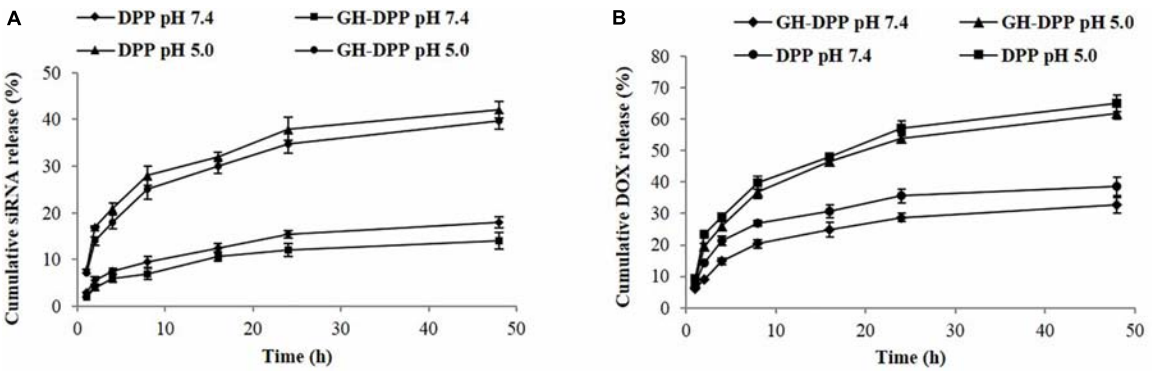

FIGURE 4 | Release profile of siRNA and DOX-loaded nanoparticles. **(A)** siRNA release from GH-DPP or DPP nanoparticles in pH 7.4 or 5.0, respectively. **(B)** DOX release from GH-DPP or DPP nanoparticles in pH 7.4 or 5.0, respectively.

could enhance drug accumulation in tumor region (Nichols and Bae, 2014). Moreover, the fluorescence intensity of DiR-loaded GH-DPP nanoparticles in the tumor was greater than that of DiR-loaded DPP nanoparticles. This may be due to the fact that GH-DPP nanoparticles increased accumulation in the liver cancer cells via liver-targeting delivery, and decreased the uptake by normal cells. After injection for 24 h, major organs and tumors were extracted for fluorescent intensity evaluation. Similar to DiR biodistribution in **Figure 7A**, the DiR-loaded GH-DPP treatment group show strongest fluorescent signals in tumor region (**Figure 7B**).

In vivo Anti-tumor Effect of siRNA/DOX/GH-DPP Nanoparticles

The combination of DOX and Bcl-2-siRNA was used in anti-hepatoma therapy. The anti-tumor effect of siRNA/DOX/GH-DPP nanoparticles was evaluated in the H22

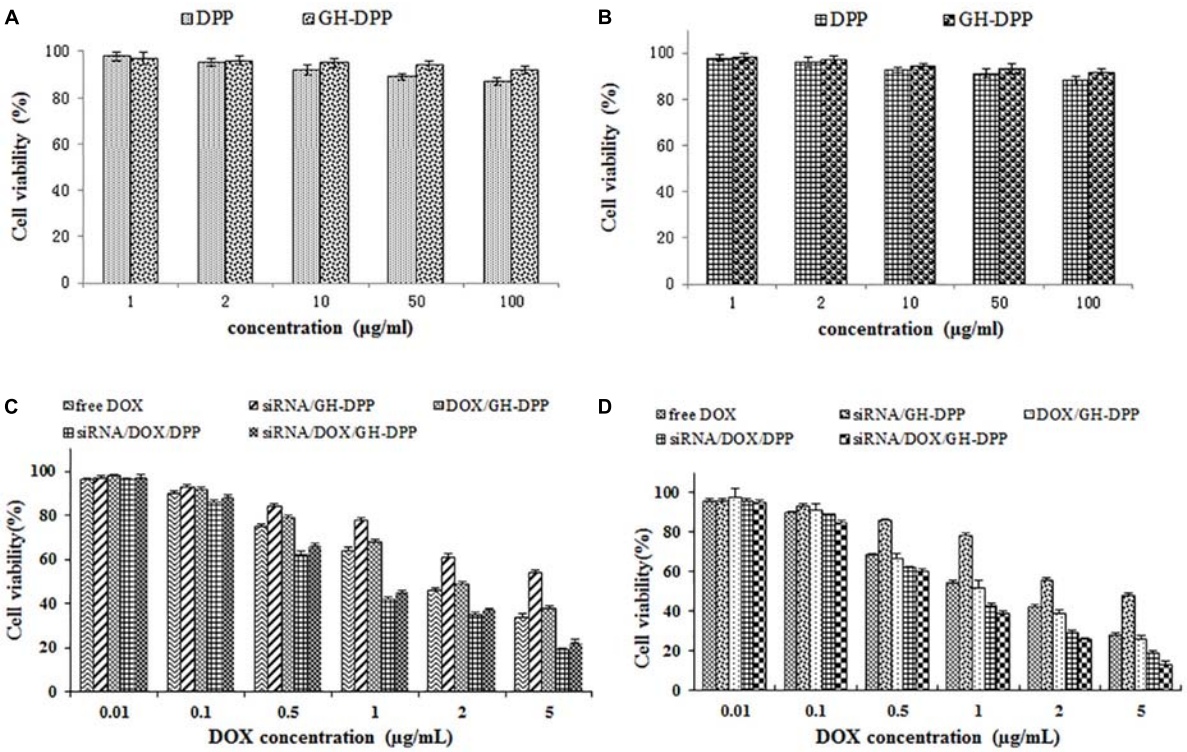

FIGURE 5 | The cell viability of blank nanoparticles against **(A)** A549 cells and **(B)** HepG2 cells for 48 h. The cell viability of drug formulations against **(C)** A549 cells and **(D)** HepG2 cells for 48 h.

tumor-bearing mice. As shown in **Figure 8**, the groups treated with saline and blank GH-DPP nanoparticles showed a rapid growth in tumor size, and no significant difference was observed between the blank GH-DPP group and the control group, indicating that the GH-DPP nanoparticles was biocompatible. In contrast, the groups treated with drug formulations showed obvious growth inhibition. *In vivo* tumor inhibition ratio (IR) of co-delivery nanoparticles for DOX and Bcl-2 siRNA was higher than GH-PDD nanoparticles for delivery of DOX or siRNA alone, indicating that combined therapy of DOX and Bcl-2 siRNA improved antitumor efficacy. Interestingly, siRNA/DOX/GH-DPP nanoparticles showed stronger anti-tumor effect than siRNA/DOX/DPP nanoparticles. This may be due to GA-HA conjugate promoting the accumulation of drug-loaded nanoparticles in tumor region, resulting in higher anti-hepatoma efficacy than siRNA/DOX/DPP nanoparticles.

Figure 8B showed that the body weight of mice treated with free DOX was lower than those treated with drug-loaded nanoparticles, indicating that GH-DPP nanoparticles decreased the systemic toxicity of DOX. As shown in **Figure 8E**, obvious intercellular vacuolation and dissolution of myocardial fibers were observed in the group of free DOX, indicating that the injection of free DOX induced significant cardiotoxicity. By contrast, there was no obvious degeneration of myocardial fibers in the groups which were injected by drug-loaded nanoparticles. These results showed that combined therapy basing on nano-carriers improved the anti-tumor effect and alleviated the systemic toxicity of DOX.

The tumors were extracted for H and E staining to evaluate the antitumor effect. As shown in **Figure 8F**, tumor cells treated with co-delivery system exhibited obvious karyolysis and pyknosis with more cytoplasmic vacuolation in comparison to single drug formulation, indicating that combination therapy exhibited higher antitumor effect. In comparison with siRNA/DOX/DPP nanoparticles, the siRNA/DOX/GH-DPP nanoparticles induced more shrunk nuclei and lower cellular density, suggesting that introduction of GA-HA promote the liver-targeting delivery of drugs, resulting in more effective treatment. The expression of BCL-2 protein was evaluated in the tumor by immunohistochemical assay. The high expression of BCL-2 protein was observed in the groups of free DOX and DOX/GH-DPP nanoparticles. By comparison, the group treated with co-delivery systems showed obvious suppression of BCL-2 expression (Cao et al., 2011).

DISCUSSION

Liver cancer has become one of the highest incidences of malignant tumor in the world. Conventional chemotherapy has severe system toxicity, and always fails in MDR (Perez-Herrero and Fernandez-Medarde, 2015). Some efforts have been focused on the combination of two or more therapeutic approaches

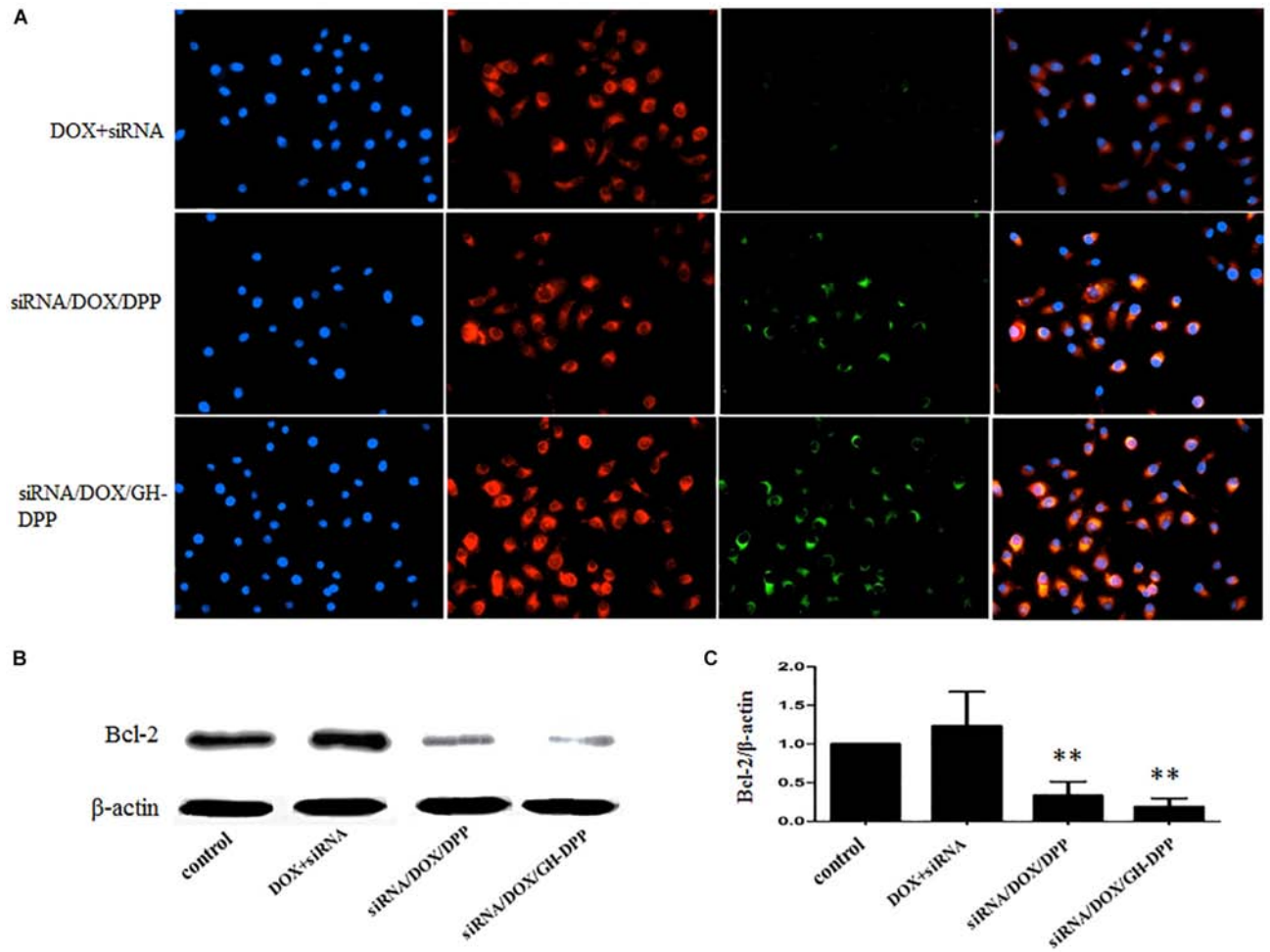

FIGURE 6 | Cellular uptake and western blot analyses. **(A)** The images of HepG2 cells treated with mixture of free DOX and FITC-labeled siRNA, siRNA/DOX/DPP or siRNA/DOX/GH-DPP nanoparticles for 4 h, respectively. FITC channel (green) for FITC-labeled siRNA, TRITC channel (red) for DOX, and DAPI channel (blue) for nucleus were presented simultaneously. **(B,C)** Protein expression of BCL-2 evaluated by western blot analysis with different treatments. $^{**}P < 0.01$ vs. control.

with different mechanisms. The combination of chemotherapy drugs and RNA interference has attracted more attention for the enhanced sensitivity of drugs against tumor cells due to the silence of oncogene (Li et al., 2018). Moreover, nanoparticles for drug delivery have been proven as the useful vehicles of anti-tumor drugs or gene for liver-targeting delivery. The nano-carriers could accumulate in tumor region via active-targeted manner when they are modified by liver-targeting moiety, resulting in loss of side effect from drugs (Chen et al., 2014).

In this study, we prepared the GH-DPP nanoparticles for co-delivery of DOX and Bcl-2 siRNA for liver cancer therapy. The siRNA/DOX/GH-DPP nanoparticles were spherical in shape, negative in zeta potential with an average particle size of 185.4 nm. There was an obvious difference in zeta potential between siRNA/DOX/GH-DPP (negative) and siRNA/DOX/DPP nanoparticles (positive). This was due to the introduction of the negatively charged GA-HA conjugate which induced the shift of surface charge of nano-carriers. The co-delivery system of DOX and Bcl-2 siRNA showed time-dependent sustained release *in vitro*. Compared to DPP nanoparticles, GH-DPP nanoparticles showed slower DOX release. This might due to the fact the coverage layer (GA-HA) delay the release of DOX from GH-DPP.

In vitro cytotoxicity test showed that siRNA/DOX/GH-DPP nanoparticles exhibited a better therapeutic effect than delivering DOX or Bcl-2 siRNA alone. This is due to that fact that co-delivery of DOX and Bcl-2 siRNA produce a synergistic anti-tumor effect in which sensitivity of HepG2 cells to DOX was enhanced owing to down-regulation of BCL-2 by RNA interference. Moreover, siRNA/DOX/GH-DPP nanoparticles exhibited higher cytotoxicity than siRNA/DOX/DPP nanoparticles against HepG2 cells (GA-receptor over-expressed). Interestingly, the cytotoxicity of siRNA/DOX/GH-DPP against A549 cells (no GA-receptor) was lower than that of siRNA/DOX/DPP. The possible explanation was that the introduction of GA-HA conjugate promotes the cellular uptake of drug-loaded GH-DPP nanoparticles by HepG2

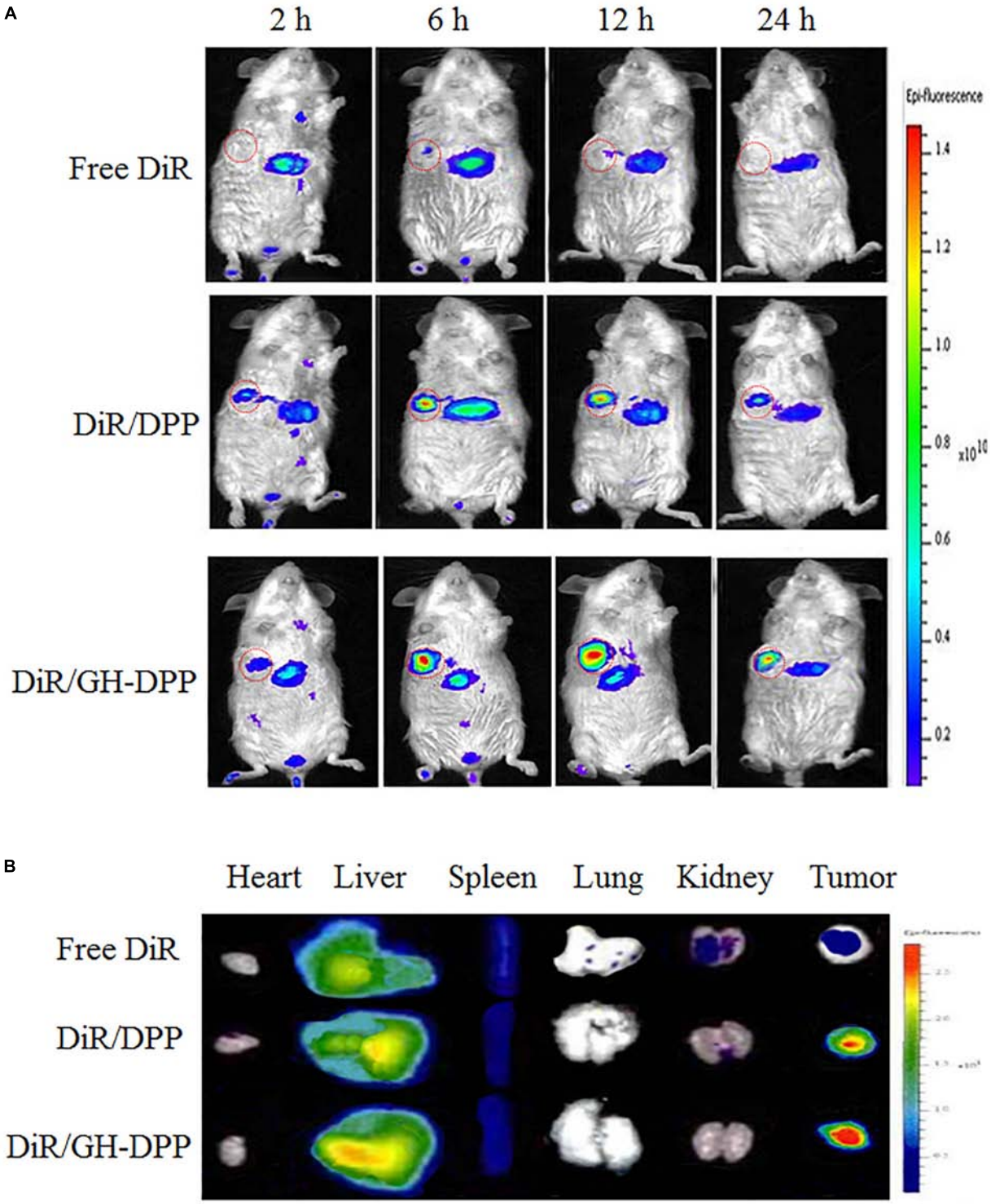

FIGURE 7 | (A) Real-time NIRF images of H22 tumors-bearing mice after tail vein injection of free DiR, DiR/DPP and DiR/GH-DPP nanoparticles for 24 h. The tumors are circled in red. **(B)** *Ex vivo* NIRF images of organs and tumors excised at 24 h.

cells via GA-receptor-mediated endocytosis, leading to higher cytotoxicity (Wu J. et al., 2018). However, there was no GA receptor on A549 cells, and drug-loaded DPP nanoparticles (positive charged) were easily taken up by tumor cells, resulting in higher cytotoxicity than drug-loaded GH-DPP nanoparticles (negative charged).

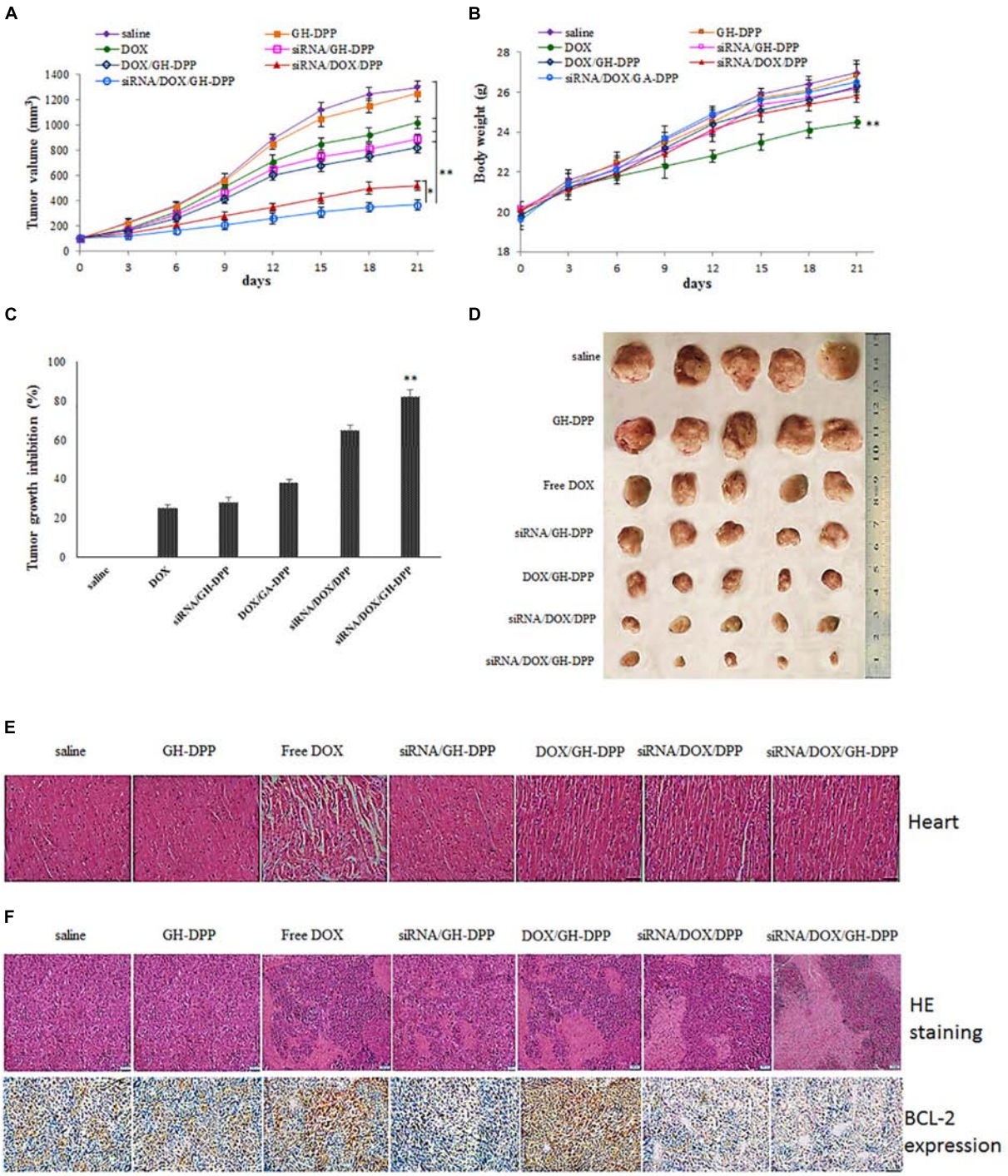

FIGURE 8 | Inhibition of tumor growth by injection of physiological saline (control), blank GH-DPP nanoparticles, free DOX, siRNA/DPP, DOX/DPP, siRNA/DOX/DPP or siRNA/DOX/GH-DPP nanoparticles, respectively. **(A)** Tumor growth curves; **(B)** Body weight changes; **(C)** The tumor growth inhibition rate; **(D)** excised tumors of each group; **(E)** Histological observation of heart for H22 tumor-bearing mice treated with different drug formulations; **(F)** The histological features of H22 subcutaneous tumor sections are characterized by H and E and BCL-2 immunohistochemical analysis. The data represent the mean of the tumor volume or body weight from five mice ± SD; $^{*}P < 0.05$ and $^{**}P < 0.01$.

Figure 6A showed that DOX or siRNA can be effectively taken up by HepG2 cells compared with mixture of free DOX and siRNA. There were stronger fluorescence signals in HepG2 cells incubated with drug-loaded GH-DPP than drug-loaded DPP nanoparticles. This result may be due to the coverage of GA-HA conjugate, which increase the amounts of cellular uptake

via GA-receptor-mediated endocytosis (Yan et al., 2018). *In vivo* near-infrared fluorescence imaging shows that the fluorescence intensity of DiR-loaded GH-DPP nanoparticles in the tumor was greater than that of DiR-loaded DPP nanoparticles. This may be due to the fact that DiR-loaded GH-DPP nanoparticles could be accumulated in the tumor tissue by liver-targeting delivery manner (Fan et al., 2015).

As shown in **Figure 8**, there was no significant difference in body weight and cardiotoxicity between the blank GH-DPP group and the control group. By contrast, the treatment of free DOX induced obvious intercellular vacuolation and dissolution of myocardial fibers, showing significant cardiotoxicity. This result suggested that the GH-DPP nanoparticles were biocompatible and useful for the delivery of chemotherapy drugs (Sun et al., 2018). Compared with nano-formulations for delivery DOX or siRNA alone, siRNA/DOX/GH-DPP nanoparticles showed stronger anti-tumor effect, indicating combination therapy could improve the anti-tumor efficiency by enhancing the sensitivity of cancer cells for chemotherapy drugs through inhibiting the expression of Bcl-2 protein (Chen et al., 2014). Compared to siRNA/DOX/DPP nanoparticles, siRNA/DOX/GH-DPP nanoparticles exhibit stronger antitumor effect. These results showed that the introduction of GA-HA conjugate was helpful to promote the accumulation of drug-loaded nanoparticles in tumor region, resulting in higher anti-hepatoma efficacy (Cai et al., 2016).

CONCLUSION

Doxorubicin-loaded DPP nanoparticles were self-assembled and then complexed successively with Bcl-2 siRNA and GA-HA conjugate to prepare a co-delivery system. The GH-DPP nanoparticles could simultaneously deliver siRNA and DOX into HepG2 cells, and GA-receptor-mediated internalization significantly increased the cellular uptake efficiency. *In vitro* and *in vivo* anti-tumor effects revealed that siRNA/DOX/GH-DPP nanoparticles could suppress the expression of Bcl-2 gene, enhanced cell apoptosis, and exhibited higher anti-tumor effect. The results showed that GH-DPP nanoparticles are efficient nano-carrier for co-delivery of siRNA and hydrophobic drug in combined therapy.

ETHICS STATEMENT

Animal studies were conducted according to the Regulation on Experimental Animals of Animal Research Ethics Committee of WeiFang Medical University.

AUTHOR CONTRIBUTIONS

JW, GT, and BZ designed the experiments. GT, BZ, and JW prepared the drug-loaded GH-DPP nanoparticles. GT, HJ, ZG, and RP performed *in vitro* anti-tumor analysis. BL, ZG, and RP made the anti-tumor effect *in vivo*. MQ, BZ, RP, and JW wrote the manuscript and contributed to data analyses.

FUNDING

This study was financially supported by National Science Foundation of China (8180346, 81871892, and 31671208), Natural Science Foundation of Shandong Province (ZR2018BH041 and ZR2017LC002), the Higher Education Science and Technology Project of Shandong Province (J17KA141), Medical and Health Technology Development Program in Shandong Province (2016WS0673) and Project of traditional Chinese Medicine Technology Development Program in Shandong Province (2017-212).

SUPPLEMENTARY MATERIAL

The Supplementary Material for this article can be found online at: https://www.frontiersin.org/articles/10.3389/fphar.2019.00004/full#supplementary-material

REFERENCES

Arms, L., Smith, D. W., Flynn, J., Palmer, W., Martin, A., Woldu, A., et al. (2018). Advantages and limitations of current techniques for analyzing the biodistribution of nanoparticles. *Front. Pharmacol.* 9:802. doi: 10.3389/fphar.2018.00802

Cai, Y., Xu, Y., Chan, H. F., Fang, X., He, C., and Chen, M. (2016). Glycyrrhetinic acid mediated drug delivery carriers for hepatocellular carcinoma therapy. *Mol. Pharm.* 13, 699–709. doi: 10.1021/acs.molpharmaceut.5b00677

Cao, N., Cheng, D., Zou, S., Ai, H., Gao, J., and Shuai, X. (2011). The synergistic effect of hierarchical assemblies of siRNA and chemotherapeutic drugs co-delivered into hepatic cancer cells. *Biomaterials* 32, 2222–2232. doi: 10.1016/j.biomaterials.2010.11.061

Chen, W., Yuan, Y., Cheng, D., Chen, J., Wang, L., and Shuai, X. (2014). Co-delivery of doxorubicin and siRNA with reduction and pH dually sensitive nanocarrier for synergistic cancer therapy. *Small* 10, 2678–2687. doi: 10.1002/smll.201303951

Ekladious, I., Colson, Y. L., and Grinstaff, M. W. (2018). Polymer-drug conjugate therapeutics: advances, insights and prospects. *Nat. Rev. Drug Discov.* doi: 10.1038/s41573-018-0005-0 [Epub ahead of print].

Fan, Y., Sahdev, P., Ochyl, L. J., Akerberg, J., and Moon, J. J. (2015). Cationic liposome-hyaluronic acid hybrid nanoparticles for intranasal vaccination with subunit antigens. *J. Control. Release* 208, 121–129. doi: 10.1016/j.jconrel.2015.04.010

Frangioni, J. V. (2003). In vivo near-infrared fluorescence imaging. *Curr. Opin. Chem. Biol.* 7, 626–634.

Gravitz, L. (2014). Liver cancer. *Nature* 516:S1. doi: 10.1038/516S1a

Knopf-Marques, H., Pravda, M., Wolfova, L., Velebny, V., Schaaf, P., Vrana, N. E., et al. (2016). Hyaluronic acid and its derivatives in coating and delivery systems: applications in tissue engineering, regenerative medicine and immunomodulation. *Adv. Healthc. Mater.* 5, 2841–2855. doi: 10.1002/adhm.201600316

Kohay, H., Sarisozen, C., Sawant, R., Jhaveri, A., Torchilin, V. P., and Mishael, Y. G. (2017). PEG-PE/clay composite carriers for doxorubicin: effect of composite

structure on release, cell interaction and cytotoxicity. *Acta Biomater.* 55, 443–454. doi: 10.1016/j.actbio.2017.04.008

Li, Y., Thambi, T., and Lee, D. S. (2018). Co-delivery of drugs and genes using polymeric nanoparticles for synergistic cancer therapeutic effects. *Adv. Healthc. Mater.* 7:1700886. doi: 10.1002/adhm.201700886

Liu, X. L., Chen, S., Zhang, H., Zhou, J., Fan, H. M., and Liang, X. J. (2018). Magnetic nanomaterials for advanced regenerative medicine: the promise and challenges. *Adv. Mater.* 30:e1804922. doi: 10.1002/adma.201804922

Maeki, M., Kimura, N., Sato, Y., Harashima, H., and Tokeshi, M. (2018). Advances in microfluidics for lipid nanoparticles and extracellular vesicles and applications in drug delivery systems. *Adv. Drug Deliv. Rev.* 128, 84–100. doi: 10.1016/j.addr.2018.03.008

Manna, U., Dhar, J., Nayak, R., and Patil, S. (2010). Multilayer single-component thin films and microcapsules via covalent bonded layer-by-layer self-assembly. *Chem. Commun.* 46, 2250–2252. doi: 10.1039/b924240f

Nguyen, M. K., and Alsberg, E. (2014). Bioactive factor delivery strategies from engineered polymer hydrogels for therapeutic medicine. *Prog. Polym. Sci.* 39, 1236–1265. doi: 10.1016/j.progpolymsci.2013.12.001

Nichols, J. W., and Bae, Y. H. (2014). EPR: evidence and fallacy. *J. Control Release* 190, 451–464. doi: 10.1016/j.jconrel.2014.03.057

Parmar, M. B., Meenakshi Sundaram, D. N., K C, R. B., Maranchuk, R., Montazeri Aliabadi, H., Hugh, J. C., et al. (2018). Combinational siRNA delivery using hyaluronic acid modified amphiphilic polyplexes against cell cycle and phosphatase proteins to inhibit growth and migration of triple-negative breast cancer cells. *Acta Biomater.* 66, 294–309. doi: 10.1016/j.actbio.2017.11.036

Perche, F., Patel, N. R., and Torchilin, V. P. (2012). Accumulation and toxicity of antibody-targeted doxorubicin-loaded PEG-PE micelles in ovarian cancer cell spheroid model. *J. Control Release* 164, 95–102. doi: 10.1016/j.jconrel.2012.09.003

Perez-Herrero, E., and Fernandez-Medarde, A. (2015). Advanced targeted therapies in cancer: drug nanocarriers, the future of chemotherapy. *Eur. J. Pharm. Biopharm.* 93, 52–79. doi: 10.1016/j.ejpb.2015.03.018

Shamay, Y., Shah, J., Isik, M., Mizrachi, A., Leibold, J., Tschaharganeh, D. F., et al. (2018). Quantitative self-assembly prediction yields targeted nanomedicines. *Nat. Mater.* 17, 361–368. doi: 10.1038/s41563-017-0007-z

Sia, D., Villanueva, A., Friedman, S. L., and Llovet, J. M. (2017). Liver cancer cell of origin, molecular class, and effects on patient prognosis. *Gastroenterology* 152, 745–761. doi: 10.1053/j.gastro.2016.11.048

Singh, B., Jang, Y., Maharjan, S., Kim, H. J., Lee, A. Y., Kim, S., et al. (2016). Combination therapy with doxorubicin-loaded galactosylated poly(ethyleneglycol)-lithocholic acid to suppress the tumor growth in an orthotopic mouse model of liver cancer. *Biomaterials* 116, 130–144. doi: 10.1016/j.biomaterials.11.040

Sun, W., Chen, X., Xie, C., Wang, Y., Lin, L., Zhu, K., et al. (2018). Co-delivery of doxorubicin and Anti-BCL-2 siRNA by pH-responsive polymeric vector to overcome drug resistance in *in vitro* and *in vivo* hepg2 hepatoma model. *Biomacromolecules* 19, 2248–2256. doi: 10.1021/acs.biomac.8b00272

Tian, Q., Zhang, C. N., Wang, X. H., Wang, W., Huang, W., Cha, R. T., et al. (2010). Glycyrrhetinic acid-modified chitosan/poly(ethylene glycol) nanoparticles for liver-targeted delivery. *Biomaterials* 31, 4748–4756. doi: 10.1016/j.biomaterials.2010.02.042

Wang, F. Z., Xing, L., Tang, Z. H., Lu, J. J., Cui, P. F., Qiao, J. B., et al. (2016). Codelivery of doxorubicin and shAkt1 by poly(ethylenimine)-glycyrrhetinic acid nanoparticles to induce autophagy-mediated liver cancer combination therapy. *Mol. Pharm.* 13, 1298–1307. doi: 10.1021/acs.molpharmaceut.5b00879

Wei, L., Lu, J., Xu, H., Patel, A., Chen, Z. S., and Chen, G. (2015). Silver nanoparticles: synthesis, properties, and therapeutic applications. *Drug Discov. Today* 20, 595–601. doi: 10.1016/j.drudis.2014.11.014

Wickens, J. M., Alsaab, H. O., Kesharwani, P., Bhise, K., Amin, M., Tekade, R. K., et al. (2017). Recent advances in hyaluronic acid-decorated nanocarriers for targeted cancer therapy. *Drug Discov. Today* 22, 665–680. doi: 10.1016/j.drudis.2016.12.009

Wu, F., Li, X., Jiang, B., Yan, J., Zhang, Z., Qin, J., et al. (2018). Glycyrrhetinic acid functionalized nanoparticles for drug delivery to liver cancer. *J. Biomed. Nanotechnol.* 14, 1837–1852. doi: 10.1166/jbn.2018.2638

Wu, J., Yuan, J., Ye, B., Wu, Y., Xu, Z., Chen, J., et al. (2018). Dual-responsive core crosslinking glycopolymer-drug conjugates nanoparticles for precise hepatocarcinoma therapy. *Front. Pharmacol.* 9:663. doi: 10.3389/fphar.2018.00663

Wu, J. L., Tian, G. X., Yu, W. J., Jia, G. T., Sun, T. Y., and Gao, Z. Q. (2016). pH-responsive hyaluronic acid-based mixed micelles for the hepatoma-targeting delivery of doxorubicin. *Int. J. Mol. Sci.* 17, 364. doi: 10.3390/ijms17040364

Yan, G., Wang, J., Hu, L., Wang, X., Yang, G., Fu, S., et al. (2017). Stepwise targeted drug delivery to liver cancer cells for enhanced therapeutic efficacy by galactose-grafted, ultra-pH-sensitive micelles. *Acta Biomater.* 51, 363–373. doi: 10.1016/j.actbio.2017.01.031

Yan, T., Cheng, J., Liu, Z., Cheng, F., Wei, X., Huang, Y., et al. (2018). Acid-sensitive polymeric vector targeting to hepatocarcinoma cells via glycyrrhetinic acid receptor-mediated endocytosis. *Mater. Sci. Eng. C Mater. Biol. Appl.* 87, 32–40. doi: 10.1016/j.msec.02.013

Yin, T., Wang, P., Li, J., Wang, Y., Zheng, B., Zheng, R., et al. (2014). Tumor-penetrating codelivery of siRNA and paclitaxel with ultrasound-responsive nanobubbles hetero-assembled from polymeric micelles and liposomes. *Biomaterials* 35, 5932–5943. doi: 10.1016/j.biomaterials.2014.03.072

Zahreddine, H., and Borden, K. L. (2013). Mechanisms and insights into drug resistance in cancer. *Front. Pharmacol.* 4:28. doi: 10.3389/fphar.2013.00028

Zeng, L., Gupta, P., Chen, Y., Wang, E., Ji, L., Chao, H., et al. (2017). The development of anticancer ruthenium(ii) complexes: from single molecule compounds to nanomaterials. *Chem. Soc. Rev.* 46, 5771–5804. doi: 10.1039/c7cs00195a

Zhang, X., Wang, Q., Qin, L., Fu, H., Fang, Y., Han, B., et al. (2016). EGF-modified mPEG-PLGA-PLL nanoparticle for delivering doxorubicin combined with Bcl-2 siRNA as a potential treatment strategy for lung cancer. *Drug Deliv.* 23, 2936–2945. doi: 10.3109/10717544.2015.1126769

Zhao, Y., Wang, W., Guo, S., Wang, Y., Miao, L., Xiong, Y., et al. (2016). PolyMetformin combines carrier and anticancer activities for in vivo siRNA delivery. *Nat. Commun.* 7:11822. doi: 10.1038/ncomms11822

Zhu, D., Tao, W., Zhang, H., Liu, G., Wang, T., Zhang, L., et al. (2016). Docetaxel (DTX)-loaded polydopamine-modified TPGS-PLA nanoparticles as a targeted drug delivery system for the treatment of liver cancer. *Acta Biomater.* 30, 144–154. doi: 10.1016/j.actbio.2015.11.031

Zuckerman, J. E., and Davis, M. E. (2015). Clinical experiences with systemically administered siRNA-based therapeutics in cancer. *Nat. Rev. Drug Discov.* 14, 843–856. doi: 10.1038/nrd4685

Conflict of Interest Statement: The authors declare that the research was conducted in the absence of any commercial or financial relationships that could be construed as a potential conflict of interest.

frontiers in Pharmacology

ORIGINAL RESEARCH
published: 23 January 2019
doi: 10.3389/fphar.2019.00001

Pathway Based Analysis of Mutation Data Is Efficient for Scoring Target Cancer Drugs

Marianna A. Zolotovskaia[1,2], Maxim I. Sorokin[3,4,5], Anna A. Emelianova[5], Nikolay M. Borisov[3,4], Denis V. Kuzmin[5], Pieter Borger[6], Andrew V. Garazha[4] and Anton A. Buzdin[1,3,5]*

[1] Oncobox Ltd., Moscow, Russia, [2] Department of Oncology, Hematology and Radiotherapy of Pediatric Faculty, Pirogov Russian National Research Medical University, Moscow, Russia, [3] The Laboratory of Clinical Bioinformatics, IM Sechenov First Moscow State Medical University, Moscow, Russia, [4] Omicsway Corp., Walnut, CA, United States, [5] Science-Educational Center Department, M. M. Shemyakin and Yu. A. Ovchinnikov Institute of Bioorganic Chemistry, Russian Academy of Sciences, Moscow, Russia, [6] Laboratory of the Swiss Hepato-Pancreato-Biliary, Department of Surgery, Transplantation Center, University Hospital Zurich, Zurich, Switzerland

Despite the significant achievements in chemotherapy, cancer remains one of the leading causes of death. Target therapy revolutionized this field, but efficiencies of target drugs show dramatic variation among individual patients. Personalization of target therapies remains, therefore, a challenge in oncology. Here, we proposed molecular pathway-based algorithm for scoring of target drugs using high throughput mutation data to personalize their clinical efficacies. This algorithm was validated on 3,800 exome mutation profiles from The Cancer Genome Atlas (TCGA) project for 128 target drugs. The output values termed Mutational Drug Scores (MDS) showed positive correlation with the published drug efficiencies in clinical trials. We also used MDS approach to simulate all known protein coding genes as the putative drug targets. The model used was built on the basis of 18,273 mutation profiles from COSMIC database for eight cancer types. We found that the MDS algorithm-predicted hits frequently coincide with those already used as targets of the existing cancer drugs, but several novel candidates can be considered promising for further developments. Our results evidence that the MDS is applicable to ranking of anticancer drugs and can be applied for the identification of novel molecular targets.

Keywords: cancer, DNA mutation, molecular pathways, biomarker, target drugs, tyrosine kinase inhibitors, nibs, mabs

OPEN ACCESS

Edited by:
Zhe-Sheng Chen,
St. John's University, United States

Reviewed by:
Honglin Jiang,
University of California, San Francisco, United States
Nelson Shu-Sang Yee,
Penn State Milton S. Hershey Medical Center, United States

****Correspondence:***
Marianna A. Zolotovskaia
zolotovskaya@oncobox.com

Specialty section:
This article was submitted to Cancer Molecular Targets and Therapeutics, a section of the journal Frontiers in Pharmacology

Received: *07 November 2018*
Accepted: *03 January 2019*
Published: *23 January 2019*

Citation:
Zolotovskaia MA, Sorokin MI, Emelianova AA, Borisov NM, Kuzmin DV, Borger P, Garazha AV and Buzdin AA (2019) Pathway Based Analysis of Mutation Data Is Efficient for Scoring Target Cancer Drugs. Front. Pharmacol. 10:1. doi: 10.3389/fphar.2019.00001

INTRODUCTION

Globally, cancer is one of the major causes of death (Centers for Disease Control and Prevention, 2017). For several decades, chemotherapy remains a key treatment for many cancers, often with impressive success rates. For example, its use in testicular cancer turned near complete mortality to >90% disease-specific survival (Hanna and Einhorn, 2014; Oldenburg et al., 2015). However, most of the advanced cancers remain incurable and/or unresponsive using standard chemotherapy approaches, frequently develop resistance to treatments and relapse (Vasey, 2003; Housman et al., 2014). More recently, a new generation of drugs has been developed that specifically target functional tumor marker molecules. These medicines termed *Target drugs* have one or a few

specific molecular targets in a cell (Druker et al., 2001a,b; Sawyers, 2004; Spirin et al., 2017). They have greater selectivity and generally lower toxicity than the conventional chemotherapy (Joo et al., 2013). Structurally, they can be either low molecular mass inhibitor molecules or monoclonal antibodies (Padma, 2015). The repertoire of their molecular targets is permanently growing and now includes receptor and intracellular tyrosine kinases (Baselga, 2006), vascular endothelial growth factor (Rini, 2009), immune checkpoint molecules such as PD1, PDL1, and CTLA4 (Azoury et al., 2015), poly(ADP-ribose) polymerase (Anders et al., 2010), mTOR inhibitors (Xie et al., 2016), hormone receptors (Ko and Balk, 2004), proteasomal components (Kisselev et al., 2012), ganglioside GD2 (Suzuki and Cheung, 2015), and cancer-specific fusion proteins (Giles et al., 2005). For many cancers, the emergence of target drugs was highly beneficial. For example, trastuzumab (anti-HER2 monoclonal antibody) and other related medications at least doubled median survival time in patients with metastatic HER2-positive breast cancer (Hudis, 2007; Nahta and Esteva, 2007). In melanoma, immune checkpoint inhibitors, and anti-BRAF target drugs like Vemurafenib and Dabrafenib dramatically increased the patient's chances to respond to treatment and to increase survival (Chapman et al., 2011; Prieto et al., 2012). Target drugs were also of a great advantage for inoperable kidney cancer, before almost uncurable (Ghidini et al., 2017).

The efficiencies of target drugs vary from patient to patient (Ma and Lu, 2011) and the results of clinical trials clearly evidence that the drugs considered inefficient for an overall cohort of a given cancer type, may be beneficial for a small fraction of the patients (Zappa and Mousa, 2016). For example, the anti-EGFR drugs gefitinib and erlotinib showed little advantage in the randomized trials on patients with non-small cell lung cancer. However, ∼10-15% of the patients responded to the treatment and had longer survival characteristics. It was further understood that these patients had activating mutations of *EGFR* gene and that these mutations, therefore, can predict response to the EGFR-targeting therapies (Gridelli et al., 2011). Interestingly, the same approach was ineffective in colorectal cancer, where EGFR-mutated status had no predictive power for the anti-EGFR drugs cetuximab and panitumumab. In the latter case, it is the wild-type status of *KRAS* gene (∼60% of all the cases) that is indicative of tumor response to these drugs (Grothey and Lenz, 2012).

The price for inefficient treatment is high as it is converted from decreased patient's survival characteristics and overall clinical expenses. There are currently more than 200 different anticancer target drugs approved in different countries, and this number grows every year (Law et al., 2014). However, the predictive molecular diagnostic tests are available for only a minor fraction of drugs, in a minor fraction of cancer types (Hornberger et al., 2005; Le Tourneau et al., 2014; Buzdin et al., 2018). This makes the clinician's decision on drug prescription a difficult task somewhat similar to finding needle in a haystack. The problem of choosing the right medication for the right patient is currently well understood, so US FDA(Food and Drug Administration) strongly recommends any new target drug emerging on the market to be supplied with the companion diagnostics test[1]. It is, therefore, of a great importance to identify robust predictive biomarkers of target drug efficacy, for as many cancer-drug combinations as possible. Recently, a new generation of molecular markers has been proposed involving gene combinations and even entire molecular pathways (Gu et al., 2011; Li et al., 2014; Toren and Zoubeidi, 2014). Here, the biomarkers used are not just a single gene or single locus-based mutation, expression or epigenetic features, but rather the aggregated combinations of those, crosslinking the physiologically relevant gene products (Diamandis, 2014; Sanchez-Vega et al., 2018; Zaim et al., 2018). The pathway-based approach has been better developed for the high throughput gene expression data (Khatri et al., 2012; Buzdin A. A. et al., 2017; Buzdin et al., 2018) where the *Pathway Activation Strength (PAS)* may be used as an aggregated biomarker (Buzdin et al., 2014). The formulas for *PAS* calculation may be different; they normally consider relative concentrations of gene products, internal molecular architecture of pathways and gene coexpression patterns (Ozerov et al., 2016; Aliper et al., 2017; Buzdin et al., 2018). *PAS* was shown to be more efficient as a biomarker than the individual gene expression data (Borisov et al., 2014, 2017), and *PAS* biomarkers were further generated for a plethora of normal and pathological conditions, including cancer response to treatments (Kurz et al., 2017; Petrov et al., 2017; Spirin et al., 2017; Wirsching et al., 2017; Sorokin et al., 2018).

Furthermore, a method for ranking of more than a 100 of target anticancer drugs has been recently published based on the *PAS* scoring and the pathway enrichments by the molecular targets of drugs (Artemov et al., 2015). This approach termed *Drug Scoring* was experimentally shown promising for drugs prescription to advanced solid tumor patients (Buzdin A. et al., 2017; Buzdin et al., 2018; Poddubskaya et al., 2018). However, good quality expression profiles required for *PAS*-based *Drug Scoring* frequently cannot be obtained due to apparent lack of biopsy biomaterials and RNA degradation. To our knowledge, so far there were no published reports on the application of gene mutation data for *Drug Scoring*.

In this study, for the first time we proposed and tested 10 alternative pathway-based *Drug Scoring* algorithms utilizing mutations data. These algorithms were used for the data from 3,800 published cancer mutation profiles representing eight tumor localizations and validated using the published clinical trials data. We showed that several mutation-based *Drug Scoring* methods can be used efficiently for predicting the effectiveness of target drugs. This has been evidenced by statistically significant positive correlations between *Drug Score* ratings of individual

Abbreviations: CDS length, Coding DNA Sequence Length; COSMIC, Catalog Of Somatic Mutations In Cancer; FDA, Food and Drug Administration; ICGC, International Cancer Genome Consortium; MDS, Mutational Drug Scores; MR, Mutation rate; nMR, Normalized mutation rate; NIH, The National Institutes of Health; PAS, Pathway Activation Strength; PI, Pathway instability; TCGA, The Cancer Genome Atlas; TC, Target Conversion.

[1]For Consumers - Personalized Medicine and Companion Diagnostics Go Hand-in-Hand Available at: https://www.fda.gov/ForConsumers/ucm407328.htm [Accessed October 15, 2018].

drugs and their therapeutic success reflected by the completed phases of clinical trials for the respective cancer types. We also used the best *Drug Scoring* algorithm to simulate all known protein coding genes as the potential drug targets. We found that the algorithm-predicted most efficient targets are highly congruent with the molecular targets already used by the real anticancer drugs.

MATERIALS AND METHODS

Mutation Data

The human mutation dataset was obtained from the Catalog Of Somatic Mutations In Cancer (COSMIC) (Forbes et al., 2017). COSMIC aggregates and annotates mutation data from various sources by providing lists of verified somatic mutations. We downloaded the data from COSMIC website, version 76. The complete dataset includes 6,651,236 somatic mutation records for 20,528 genes in 19,434 tumor samples of 37 primary localizations.

The Algorithm Validation Dataset

For the validation of drug scoring algorithms, we extracted mutation data only for the primary localizations containing at least 100 samples indexed in COSMIC and originally taken from The Cancer Genome Atlas (TCGA) project (Tomczak et al., 2015; Forbes et al., 2017) because of the uniform sequencing and data processing pipeline used there. For the algorithm validation dataset, we totally took 3,800 tumor mutation profiles from eight primary localizations: central nervous system, kidney, large intestine (including cecum, colon, and rectum), liver, lung, ovary, stomach, thyroid gland (**Table 1**).

The COSMIC data were processed with script written in R (version 3.4.3) to obtain mutation profile for each tumor[1]. The processed data is available as **Supplementary Data Sheet 1**.

The Dataset for Prediction of Potential Molecular Targets

We used the full COSMIC dataset to increase the statistical significance and to investigate the effectiveness of potential target drugs for a maximum range of cancer localizations. However, we excluded the samples related to cell cultures or tumor xenograft to standardize the analysis. We excluded records having the following marks in the "Sample source" field: organoid culture, short-term culture, cell-line, xenograft. Thus, the final dataset included 6,027,881 mutations records in 18,273 in tumor samples of 35 primary localizations. The COSMIC data were processed with script written in R (version 3.4.3) to return mutation rates for all genes[2]. The processed data is available as **Supplementary Data Sheet 2**.

TABLE 1 | The structure of algorithm validation dataset.

Localization (COSMIC nomenclature)	Number of samples	Disease, its abbreviation
Central nervous system	657	Gliomas, GL
Kidney	601	Kidney cancer, KC
Large intestine	620	Colorectal cancer, CRC
Liver	188	Hepatic cancer, HC
Lung	569	Non-small cell lung cancer, NSCLC
Ovary	474	Ovarian cancer, OVC
Stomach	288	Stomach cancer, STC
Thyroid	403	Thyroid cancer, THC

Clinical Trials Data

We extracted clinical trials data from the web sites of NIH (the National Institutes of Health)[3] and US FDA[4]. They were processed by manually curation of web data as of July 2017. The processed clinical trials data used for the correlation studies are shown on **Supplementary Table 1**.

Molecular Pathways Data

The gene contents data about 3,125 human molecular pathways used to calculate mutation drug scores were extracted from Reactome (Croft et al., 2014), NCI Pathway Interaction Database (Schaefer et al., 2009), Kyoto Encyclopedia of Genes and Genomes (Kanehisa and Goto, 2000), HumanCyc (Romero et al., 2004), Biocarta (Nishimura, 2001), Qiagen[5]. For drug scores calculation, we used only the 1,752 pathways including at least 10 gene products because of previously reported poor theoretical data aggregation effect for smaller pathways (Borisov et al., 2017). The information about molecular specificities of 128 anticancer target drugs were obtained from databases DrugBank (Law et al., 2014) and ConnectivityMap (Lamb et al., 2006).

Data Presentation

The results were visualized using package ggplot2 (Wickham, 2009).

RESULTS

In this study, we developed a molecular pathway-based method of target drug scoring using high throughput mutation data.

Algorithms of Mutation Drug Scoring

The principle of *Mutation Drug Scoring (MDS)* methods proposed here deals with quantization of mutation enrichment for the molecular pathways having molecular targets of a drug under investigation. Overall, they are based on the rationale that the greater is the mutation level of the respective pathways, the higher will be the expected drug efficiency. The mutation enrichment of a molecular pathway called pathway instability (*PI*) is calculated based on the relative *mutation rates* (*MR*) of its member genes. Under *mutations*, we meant here the changes in protein coding sequence understood as such in the Catalog of Somatic Mutations in Cancer (COSMIC) v.76 database (Forbes et al., 2016). COSMIC is the world's largest database of somatic

[2]Cosmic v76 processing Available at: https://gitlab.com/White_Knight/cosmic76_processing/tree/master [Accessed October 22, 2018].
[3]ClinicalTrials.gov Available at: https://clinicaltrials.gov/ [Accessed July 25, 2017]
[4]U S Food and Drug Administration Home Page Available at: https://www.fda.gov/ [Accessed July 25, 2017].
[5]QIAGEN - Sample to Insight Available at: https://www.qiagen.com/us/shop/genes-and-pathways/pathway-central/ [Accessed September 19, 2018].

mutations relating to human cancers. We used only Genome-wide Screen Data to estimate *MR* correctly. This part of COSMIC consists of peer reviewed large-scale genome screening data and data from the validated sources such as The Cancer Genome Atlas (TCGA) and International Cancer Genome Consortium (ICGC).

Mutation rate (*MR*) is calculated according to the formula:

$$MR_{n,g} = \frac{N\ mut(\ n,g)}{N\ samples\ (g)},$$

where $MR_{n,g}$ is *MR* of a gene *n* in a group of samples *g*; *N mut(n,g)* is the total number of mutations for gene *n* in a group of samples *g*; *N samples (g)* is the number of samples in a group *g*. The *MR* values strongly positively correlated with the lengths of gene coding DNA sequence (CDS; data not shown). In order to remove bias linked with the CDS length, we took for further consideration a normalized value termed *Normalized Mutation Rate* (*nMR*) expressed by the formula:

$$nMR_n = \frac{1000 * MR_n}{Length\ CDS\ (n)},$$

where nMR_n is the *nMR* of a gene *n*; MR_n is the *MR* of a gene *n*; *Length CDS(n)* is the length of CDS of gene *n* in nucleotides. Indeed, normalization of this metric enabled to terminate any CDS-linked bias (data not shown).

To determine if gene *n* is included in pathway *p*, we introduced a Boolean flag *pathway-gene indicator* $PG_{n,p}$ expressed by the formula:

$$PG_{n,p} = \begin{cases} 1, \text{ pathway } p \text{ includes gene } n, \\ 0, \text{ pathway } p \text{ doesn't include gene } n; \end{cases}$$

The *Pathway Instability* (*PI*) score is then calculated as follows:

$$PI_p = \sum\nolimits_n nMR_n PG_{n,p},$$

where PI_p is pathway instability score for a pathway *p*; nMR_n is the *normalized* mutation rate of a gene *n*, $PG_{n,p}$ is pathway-gene indicator for gene *n* and pathway *p*. *Pathway instability score* characterizes the mutation enrichment of a pathway (Pathway instability is an effective new mutation-based type of cancer biomarkers, 2018, in preparation). To formalize if gene *n* is molecular target of drug *d*, we introduced another Boolean flag *drug target index*, $DTI_{d,n}$:

$$\mathrm{DTI_{d,n}} = \begin{cases} 1, \text{ drug } d \text{ has target gene } n, \\ 0, \text{ drug } d \text{ doesn}'\text{t have target gene } n \end{cases}$$

To complete *DTI* database for this study, we used the data about molecular specificities of 128 target drugs extracted from the databases DrugBank (Law et al., 2014) and Connectivity Map (Lamb et al., 2006).

To link *PI* scores and estimated drug efficiencies, the following basic formula was proposed for the calculation of *Mutation Drug Score* (*MDS*):

$$\mathbf{MDS_d} = \sum\nolimits_{\mathbf{n}} \mathbf{DTI_{d,n}} \sum\nolimits_p PG_{n,p}\ PI_p, \quad (1)$$

where *d* is drug name; *n* is gene name; *p* is pathway name; MDS_d is *MDS* for drug *d*; $DTI_{d,n}$ is drug target index for drug *d* and gene *n*; PI_p is *Pathway Instability* of pathway *p*; $PG_{n,p}$ is pathway-gene indicator for gene *n* and pathway *p*.

The above basic formula (*1*) was modified to generate several alternative methods of drug scoring.

- *Pathway size-normalized*. Since molecular pathways include considerably different number of genes varying from dozens to hundreds, we proposed a modification of the calculation method (*1*) where normalization is performed for *MDS* on the respective number of genes for each *PI* member:

$$MDS\_N_d = \sum\nolimits_n \mathbf{DTI_{d,n}} \sum\nolimits_p PG_{n,p}\ PI_p/k_p, \quad (2)$$

where k_p is number of genes in pathway *p*.

- *Single count-normalized*. Impact of each gene participating in pathways targeted by drug *d* is counted only once:

$$\mathbf{MDS\_gene_d} = \sum\nolimits_n \mathbf{nMR}_n\ \mathbf{GII}_{d,n}, \quad (3)$$

where $GII_{d,n}$ – Boolean flag *gene involvement index*,

$$\mathrm{GII}_{d,n} = \begin{cases} 1, \text{ gene } n \text{ participates in at least one pathway targeted by drug } d \\ 0, \text{ gene } n \text{ doesn}'\text{t participate in pathways targeted by drug } d \end{cases}$$

- *Number of pathways-normalized*. *MDS* for drug *d* is normalized on the number of its targeted molecular pathways.

$$\mathbf{MDS\_m_d} = MDS_d/m_\mathbf{d}, \quad (4)$$

where m_d – number of pathways targeted by drug *d*.

- *Number of pathways-normalized*. *MDS_N* is additionally normalized on the number of pathways targeted by drug *d* (m_d).

$$\mathbf{MDS\_N\_m_d} = MDS\_N/m_d \quad (5)$$

- *Number of target genes-normalized*. MDS_b_d is additionally normalized on the number of target genes for drug *d*, (b_d).

$$\mathbf{MDS\_b_d} = MDS_d/b_d \quad (6)$$

- *Number of target genes-normalized MDS_N*. *MDS_N*, normalized on the number of target genes for drug *d*, (b_d).

$$\mathbf{MDS\_N\_b_d} = \mathbf{MDS\_N}/b_d \quad (7)$$

- *Number of target genes-normalized MDS_gene*. *MDS_gene*, normalized on the number of target genes for drug *d*, (b_d).

$$\mathbf{MDS\_gene\_b_d} = MDS\_gene/b_d \quad (8)$$

- *Target genes dependent only*. *MDS2* is calculated considering only mutation frequencies of target genes.

$$\mathbf{MDS2_d} = \sum\nolimits_p PG_{n,p} \sum\nolimits_n \mathbf{DTI_{d,n}} nMR_n \quad (9)$$

- *Single count-normalized, target genes dependent only. MDS2_gene* is calculated, considering each target gene for drug *d* only one time.

$$\mathbf{MDS2\_gene_d} = \sum\nolimits_n \mathbf{DTI_{d,n}}\ NMR_n\ \mathbf{GII}_{d,n} \qquad (10)$$

For these algorithms of mutation-based drug scoring, we next compared their congruences with the published clinical trials data.

Validation of Mutation Drug Scoring (MDS) Algorithms on Clinical Trials Data

We calculated different versions of *MDS* according to formulae (1–10) for 128 anticancer target drugs, for eight cancer types (**Supplementary Data Sheet 3**). We examined somatic mutation profiles for 3,800 samples of the following primary tumor localizations: large intestine (including cecum, colon and rectum), lung, kidney, stomach, ovarian, central nervous system, liver, thyroid (**Table 1**).

Mutation profiles were extracted from COSMIC v76 database (Forbes et al., 2016). To validate the *MDS* algorithms, we selected only tumor samples related to TCGA project because it was the largest source of biosamples profiled using a single deep sequencing and bionformatic pipeline (Tomczak et al., 2015). Molecular specificities of drugs were obtained from DrugBank (Law et al., 2014) and Connectivity Map (Lamb et al., 2006) databases. The information about clinical approval and the completion of phases of clinical trials for 128 target drugs for the above eight tumor localizations was taken from the web sites of NIH and US FDA. To measure completion of clinical investigations for a drug, we introduced the metric termed *Clinical Status*. These values are congruent with the apparent efficiencies of drugs for the given cancer types. The same drugs most frequently had different clinical statuses for the different cancer types.

The *Clinical Status* varied in a range from 0 to 1 proportional to the top phase of clinical trials passed by a drug for a given cancer type. The *Clinical Status* grows incrementally depending on the completion of the clinical trials phases 1–4, while the later phases have a greater specific weight, because they allow to more accurately determine clinical efficacy of a drug (**Table 2**).

TABLE 2 | Clinical Status of drug, according of the top passed phases of clinical trials.

Phase of clinical trials	Clinical status
Phase I ongoing	0.1
Phase I/II ongoing (Phase I completed)	0.2
Phase II ongoing	0.3
Phase II completed	0.4
Phase III ongoing	0.7
Phase III completed	0.85
Phase IV (drug approved and marketed)	1

The complete *Clinical Status* information for 128 drugs under investigation is shown on **Supplementary Table 1**. The major limitation of this approach is that only the drugs that had been already clinically investigated for the respective tumor type can be ranked in such a way.

To investigate the capacities of different versions of *Mutation Drug Scores* to successfully predicts clinical efficiencies of drugs, we analyzed how ranks of *MDS* values correlated with Clinical Status of drugs. We calculated correlations and compared distributions of the Spearman correlation coefficients. To calculate correlations, we took all cancer mutation profiles together without separation on cancer types (**Figure 1**).

Overall, the markedly better correlations were seen for the *MDS* and *MDS_N* types of drug scoring (**Figure 1**). We next analyzed the cancer type-specific distributions (**Figure 2**). It was seen that both *MDS* and *MDS_N* scores positively correlated with the drugs clinical efficiencies in all the localizations investigated, thus confirming their top status among the drug scoring algorithms. Among those, *MDS* showed best overall

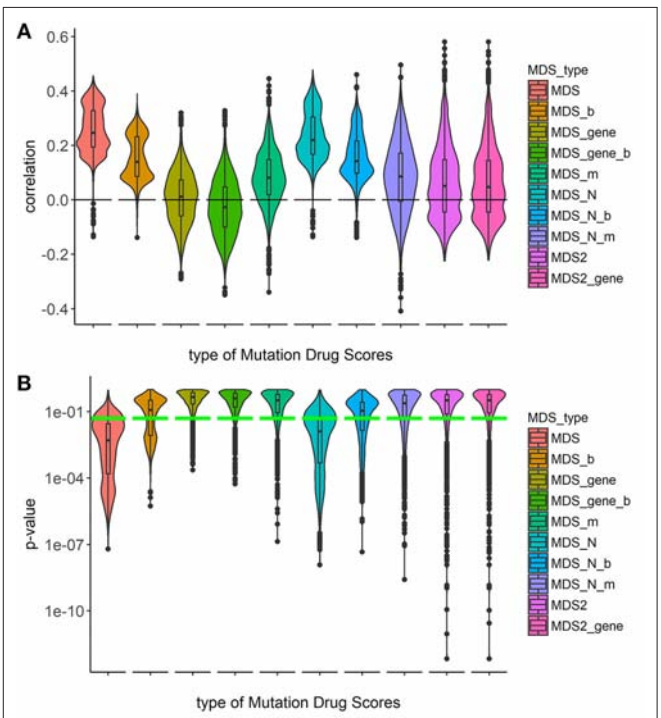

FIGURE 1 | Correlation between Clinical Status and MDS rank for 10 types of drug scoring in eight cancer types at once. **(A)** Distributions of Spearman correlation coefficients between Clinical Status and MDS rank for 128 target drugs in 3,800 tumor samples. MDS rank of a drug was calculated as the individual drug's position in the rating (from top to low) of all drugs under investigation. Ten violin plots distributed along X-axis, each represent a particular type of drug scoring. The Y-axis reflects density distributions of correlations between Clinical Status and MDS ranks. Boxes indicate the second and third quartiles of distribution, black dots indicate outliers. **(B)** The plot demonstrates the distributions of *p*-value for the correlation coefficients between Clinical Status and MDS rank for 128 target drugs in the same tumor samples. The horizontal green line corresponds to $p = 0.05$.

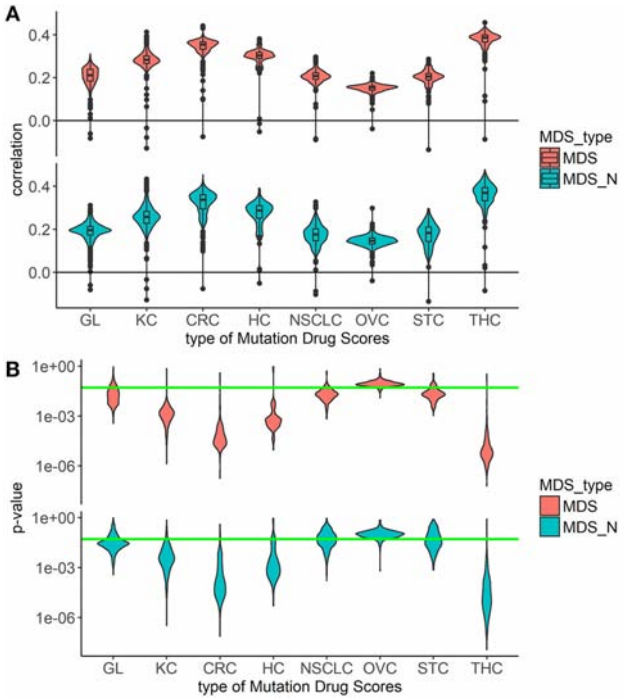

FIGURE 2 | Correlation between Clinical Status and MDS rank for two best types of drug scoring in eight cancer types separately. **(A)** Distributions of Spearman correlation coefficients between Clinical Status and MDS rank for 128 target drugs in eight tumor types. MDS rank of a drug was calculated as the drug's position in the rating (from top to low) of all drugs under study. The drug scoring methods are shown in horizontal lines, and the cancer types are placed vertically. The violin plots distributed along X-axis, each represent a particular cancer type. The Y-axis reflects density distributions of correlations between Clinical Status and MDS ranks. Boxes indicate the second and third quartiles of distribution, black dots indicate outliers. **(B)** The plot shows the distributions of *p*-value for the correlation coefficients between Clinical Status and MDS rank for 128 target drugs in the same tumor types. The horizontal green line corresponds to $p = 0.05$.

functional characteristics and was, therefore, used in further analyses.

Application of MDS for Identification of Possible Target Genes

We next tested the *MDS* algorithm for its capacity to identify potentially valuable drug targets. To this end, we modeled a situation when each gene specifically corresponds to one target drug. Those simulated, or virtual drugs, also were specific each to only one gene product. Using the database of 1,752 molecular pathways, we were able to calculate *MDS* for 8,736 *virtual drugs* specific to the same number of genes included in these pathways. For this analysis, we used 18,273 full-exome tumor mutation profiles from the COSMIC v76 database. Top 30 molecular targets with highest *MDS* values and already clinically approved cancer drugs specific for these molecular targets are listed on **Table 3**. The complete *MDS* calculation data are given in **Supplementary Table 2**.

We next ranked all the *virtual* drugs according to their *MDS* values and compared if the same molecular targets are already exploited by the *existing* 128 target cancer drugs (**Figure 3**).

TABLE 3 | Top 30 molecular targets sorted by MDS and clinically approved drugs using these molecular targets.

Potential molecular targets	MDS	Existing relevant drugs
PIK3CA	387.11	Idelalisib
PIK3R1	371.31	
MAPK1	354.75	
MAPK3	343.81	
HRAS	343.66	
PIK3CB	313.02	Idelalisib
AKT1	305.54	Perifosine
PIK3R2	302.74	
PIK3CD	293.15	Idelalisib
KRAS	291.42	
PIK3R3	290.07	
MAP2K1	288.80	Binimetinib, cobimetinib, selumetinib, trametinib
NRAS	287.90	
PIK3R5	279.34	
RAF1	271.72	Dabrafenib, regorafenib, sorafenib
MAPK8	267.73	
MAP2K2	257.33	Binimetinib, cobimetinib, selumetinib, trametinib
TP53	255.89	
GRB2	254.36	
SOS1	243.39	
RAC1	239.32	
MAPK9	233.01	
EGFR	232.80	Afatinib, brigatinib, cetuximab, erlotinib, flavopiridol, foretinib, gefitinib, lapatinib, masitinib, nimotuzumab, osimertinib, panitumumab, vandetanib, necitumumab
MAPK14	224.08	
MAPK10	222.51	
EGF	214.20	
RELA	212.43	
PRKCA	211.99	
NFKB1	211.63	Thalidomide
AKT2	205.38	Perifosine

To do this, we introduced an auxiliary value termed *Target Conversion* (*TC*). It reflects the percentage share of *known* molecular targets among *predicted* molecular targets.

$$\mathbf{TC} = \frac{\textbf{\textit{number of known}} \textbf{ molecular targets}}{\textbf{\textit{number of predicted}} \textbf{ molecular targets}} * \mathbf{100\%}$$

For the overall (complete) list of potential molecular targets, *TC* was 2.17%. However, there was an clear-cut incremental *TC* growth trend when the potential molecular targets were sorted in the ascending order of *MDS* value (**Figure 3A**, shown for deciles of the potential targets). The greater *TC* value exceeding 10% was

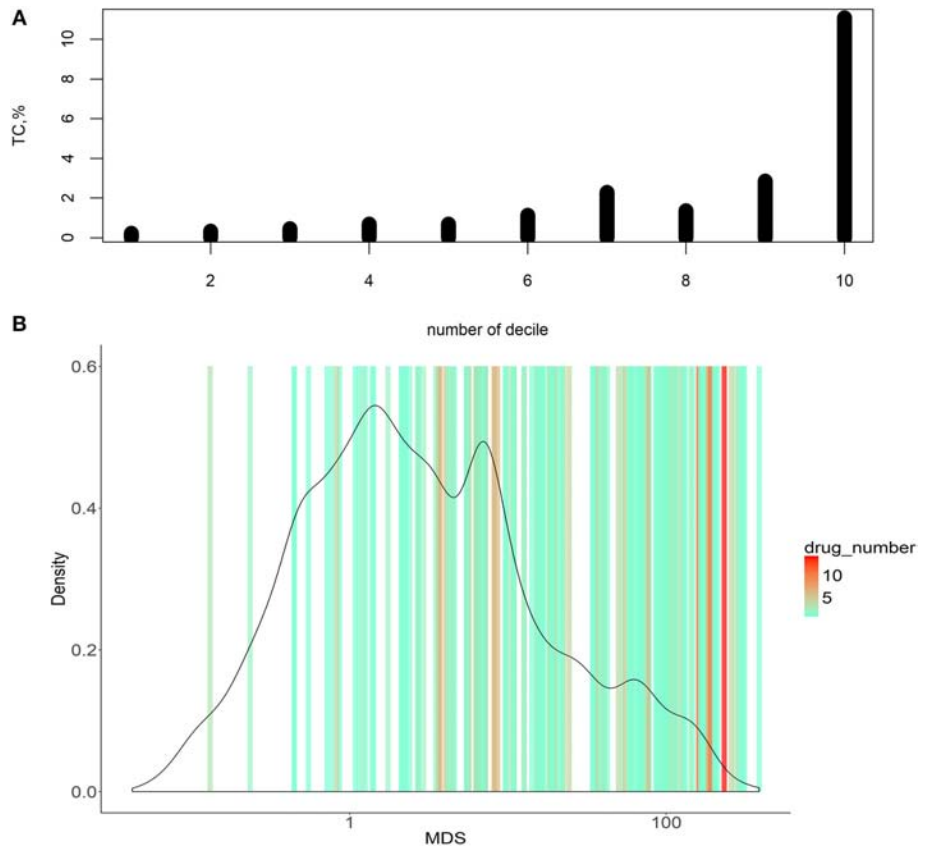

FIGURE 3 | Dependence of MDS and occurrence of molecular targets in approved cancer drugs. **(A)** Deciles of potential molecular targets sorted in ascending order according to MDS value. TC was calculated for each decile, shown on vertical axes. **(B)** Distribution of MDS values among the potential molecular drug targets. The color scale on the graph indicates densities of clinically approved cancer drugs exploiting the respective molecular targets.

observed for the decile of molecular targets having the highest *MDS* values.

Molecular targets with the highest *MDS* are clearly enriched by the existing clinically approved drugs compared to those with low *MDS* scores (**Figure 3A**). On the other hand, target genes with higher *MDS* are covered by a bigger number of approved drugs per target, as many drugs have common molecular specificities (**Figure 3B**).

The present algorithm for scoring potential drug targets considers a cumulative mutation enrichment of molecular pathways. For the example shown on **Figure 4** (Nectin adhesion pathway), most genes involved in a pathway are mutated in cancers, see the color scale. The mutation enrichment of a pathway may characterize its overall involvement in malignization. According to the present conception of drug scoring, the maximum efficiency of drug can be obtained by acting on the most strongly affected molecular pathways.

DISCUSSION

In this study, we report a new bioinformatic instrument of ranking target anticancer drugs using high throughput gene mutation data. We proposed here 10 different versions of molecular pathway-based *mutation drug scoring*. At least two types of this scoring could provide output data positively correlated with the clinical trials data for 128 drugs in all eight tumor localizations tested. We hope that the pathway-based mutation drug scoring approach has a potential of helping clinical oncologists to implement personalized selection of target drugs based on the individual, the patient's tumor-specific high throughput mutation profile.

We showed that the same approach can be applied to identify potentially efficient molecular targets in experimental oncology. The educated choice of new drug targets is one of the main tasks in pharmacology (Schenone et al., 2013). Experimental search for new efficient drug targets is still time consuming, laborious, and expensive (Haggarty et al., 2003), so since recently a credit is frequently given to computational predictive algorithms (Rifaioglu et al., 2018).

The history of computational prediction of drug targets began with prediction of druggability based on the structure of targets and biomedical text mining (Cheng et al., 2007; Zhu et al., 2007). Several methods have been also proposed based on known links between drugs and genes (Luo et al., 2017). Further development of bioinformatic methods allowed to apply for this task a set of systems approaches based on networks of molecular interactions (Mani et al., 2008).

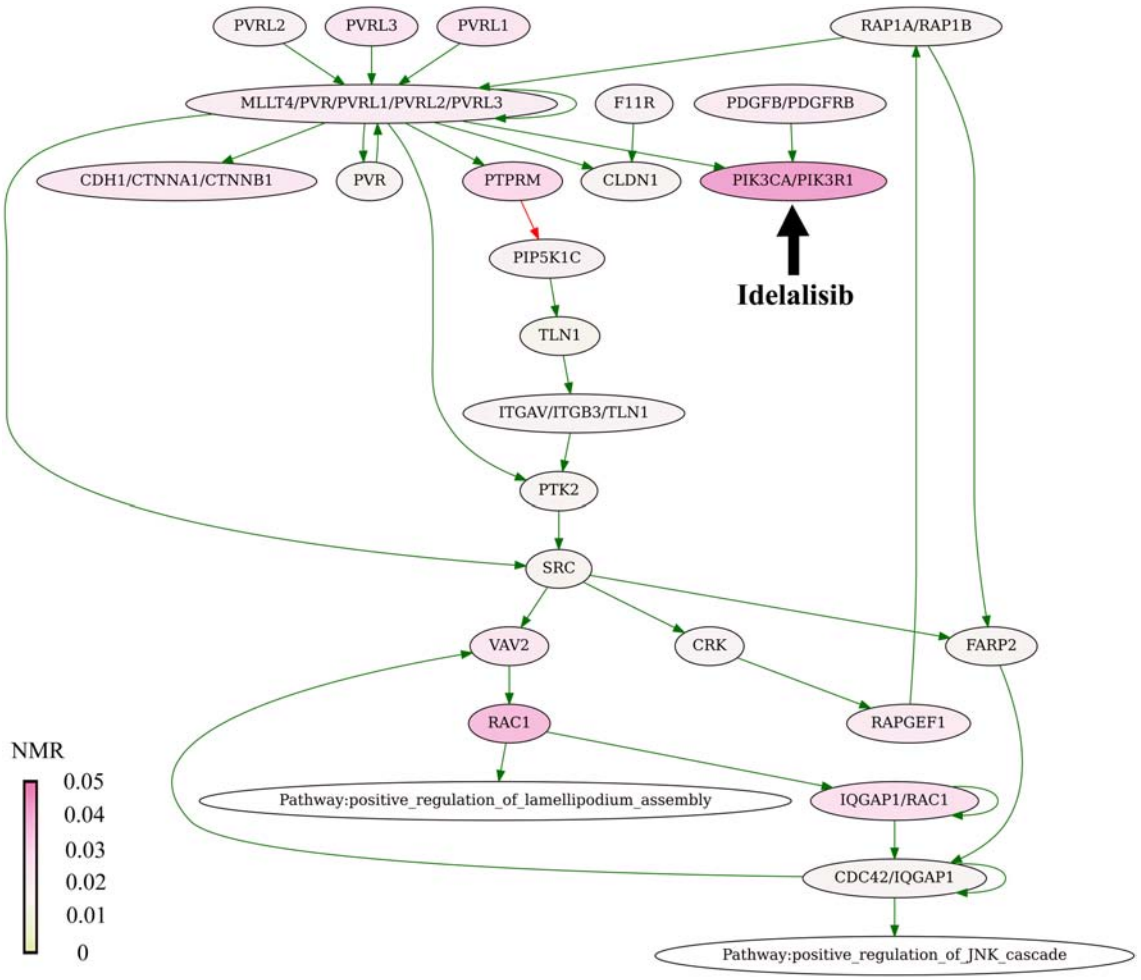

FIGURE 4 | Mutation enrichment of Nectin adhesion pathway. The pathway is targeted by Idelalisib. The pathway structure is taken from the NCI database (Schaefer et al., 2009). The mutation burden was visualized using Oncobox pathway plot tool. The color scale reflects mutation levels of the corresponding nodes on the pathway graph. The green arrows indicate activation, red arrow—inhibition, bold black arrow indicates molecular target of Idelalisib.

Our results provide principal evidence that the mutation drug scoring is applicable to ranking of anticancer drugs. On the other hand, our data suggest that these drug scoring algorithms can be applied for the identification of novel molecular targets for the prospective anticancer drugs. Although many genes with high *MDS* already serve as molecular targets of the approved cancer drugs, there is a number of top *MDS* genes that are not yet covered by the existing medications. This latter fraction of genes, therefore, can be considered a source of potential targets for new drug developments. For example, the following top 100 *MDS* genes can be mentioned that are not yet covered by approved or experimental cancer or antineoplastic drugs [according to DrugBank (Law et al., 2014), DGIdb (Cotto et al., 2018), FDA[6], HMDB (Wishart et al., 2018), Tocris[7], GeneCards (Safran et al., 2010) databases]: *GRB2, SOS1,SOS2, SHC1, GNB1, CREB1, GNG2, GNAQ, GNB5, GNAI2. Three* of them (*GRB2, GNG2, CREB1*) are the targets of approved non-oncological drugs (Pegademase bovine, Naloxone, Adenosine monophosphate, Citalopram, Halothane), thus illustrating *MDS* method potential in drug repurposing.

This study can be regarded as proof-of concept trial of *MDS* approach exemplified by bigger proportion of real cancer targets among the genes with higher *MDS* values. In this application, we assessed integral *MDS* for all cancer types. However, in further applications the same approach can be used for any specific tumor type or subtype to identify targets that may seem most promising for this particular disease. This could be valuable, for example, for drugs repurposing among the different tumor types and for more effectively identifying the patient cohorts in clinical trials

The present mutation drug scoring approach scores the molecular pathway instability caused by accumulation of mutations and ranks drugs according to a simple rationale—the higher is mutation burden of a pathway, the greater may be the efficiency of a drug targeting this pathway. We hope

[6]U S Food and Drug Administration Home Page Available at: https://www.fda.gov/ [Accessed July 25, 2017].

[7]Tocris Bioscience Available at: https://www.tocris.com/ [Accessed December 21, 2018].

these findings will be interesting to those working in the fields of oncology, drug discovery, systems biomedicine, high throughput mutation data analysis, personalized medicine and molecular diagnostics.

DATA AVAILABILITY STATEMENT

The datasets analyzed for this study can be found in the COSMIC repository (COSMICv76; CosmicGenomeScreensMutantExport.tsv.gz, https://cancer.sanger.ac.uk/cosmic/download).

AUTHOR CONTRIBUTIONS

MZ developed algorithms, did mutation drug scoring analyses, planned the research and wrote the manuscript. PB planned the research, extracted and filtered cancer mutation data. AG planned the research and developed algorithms. MS completed the molecular pathway database. DK completed and processed Clinical Status database. AE organized the information about molecular specificities of anticancer target drugs. NB developed algorithms, did statistical analyses, and planned the research. AB completed Clinical Status database, developed algorithms, planned the research, and wrote the manuscript.

FUNDING

This study was supported by the Oncobox research program in digital oncology, by the Russian Science Foundation grant no. 18-15-00061, by Amazon and Microsoft Azure grants for cloud-based computational facilities for this project.

SUPPLEMENTARY MATERIAL

The Supplementary Material for this article can be found online at: https://www.frontiersin.org/articles/10.3389/fphar.2019.00001/full#supplementary-material

Supplementary Data Sheet 1 | Mutation profiles for 3800 TCGA tumor samples obtained from COSMIC v76.

Supplementary Data Sheet 2 | Normalized mutation rate for genes that mutated in 18273 tumor samples from COSMIC v76.

Supplementary Data Sheet 3 | Mutation drug scores for 3800 TCGA tumor samples for 10 versions of drug scoring algorithm. The dataset contains 10 tables that match the 10 methods of drug scoring.

Supplementary Table 1 | The complete clinical status information for 128 target drugs in eight cancer localizations.

Supplementary Table 2 | Mutation Drug Scores for 8736 virtual drugs specific to the same number of genes.

REFERENCES

Aliper, A. M., Korzinkin, M. B., Kuzmina, N. B., Zenin, A. A., Venkova, L. S., Smirnov, P. Y., et al. (2017). Mathematical justification of expression-based pathway activation scoring (PAS). *Methods Mol. Biol.* 1613, 31–51. doi: 10.1007/978-1-4939-7027-8_3

Anders, C. K., Winer, E. P., Ford, J. M., Dent, R., Silver, D. P., Sledge, G. W., et al. (2010). Poly(ADP-Ribose) polymerase inhibition: andquot;targetedandquot; therapy for triple-negative breast cancer. *Clin. Cancer Res.* 16, 4702–4710. doi: 10.1158/1078-0432.CCR-10-0939

Artemov, A., Aliper, A., Korzinkin, M., Lezhnina, K., Jellen, L., Zhukov, N., et al. (2015). A method for predicting target drug efficiency in cancer based on the analysis of signaling pathway activation. *Oncotarget* 6, 29347–29356. doi: 10.18632/oncotarget.5119

Azoury, S. C., Straughan, D. M., and Shukla, V. (2015). Immune checkpoint inhibitors for cancer therapy: clinical efficacy and safety. *Curr. Cancer Drug Targets* 15, 452–462. doi: 10.2174/1568009615061508051 45120

Baselga, J. (2006). Targeting tyrosine kinases in cancer: the second wave. *Science* 312, 1175–1178. doi: 10.1126/science.1125951

Borisov, N., Suntsova, M., Sorokin, M., Garazha, A., Kovalchuk, O., Aliper, A., et al. (2017). Data aggregation at the level of molecular pathways improves stability of experimental transcriptomic and proteomic data. *Cell Cycle* 16, 1810–1823. doi: 10.1080/15384101.2017.1361068

Borisov, N. M., Terekhanova, N. V., Aliper, A. M., Venkova, L. S., Smirnov, P. Y., Roumiantsev, S., et al. (2014). Signaling pathways activation profiles make better markers of cancer than expression of individual genes. *Oncotarget* 5, 10198–10205. doi: 10.18632/oncotarget.2548

Buzdin, A., Sorokin, M., Garazha, A., Sekacheva, M., Kim, E., Zhukov, N., et al. (2018). Molecular pathway activation - new type of biomarkers for tumor morphology and personalized selection of target drugs. *Semin. Cancer Biol.* 53, 110–124. doi: 10.1016/j.semcancer.2018.06.003

Buzdin, A., Sorokin, M., Glusker, A., Garazha, A., Poddubskaya, E., Shirokorad, V., et al. (2017). Activation of intracellular signaling pathways as a new type of biomarkers for selection of target anticancer drugs. *J. Clin. Oncol.* 35:e23142. doi: 10.1200/JCO.2017.35.15_suppl.e23142

Buzdin, A. A., Prassolov, V., Zhavoronkov, A. A., and Borisov, N. M. (2017). Bioinformatics meets biomedicine: oncofinder, a quantitative approach for interrogating molecular pathways using gene expression data. *Methods Mol. Biol.* 1613, 53–83. doi: 10.1007/978-1-4939-7027-8_4

Buzdin, A. A., Zhavoronkov, A. A., Korzinkin, M. B., Venkova, L. S., Zenin, A. A., Smirnov, P. Y., et al. (2014). Oncofinder, a new method for the analysis of intracellular signaling pathway activation using transcriptomic data. *Front. Genet.* 5:55. doi: 10.3389/fgene.2014.00055

Centers for Disease Control and Prevention (2017). *Leading Causes of Death and Numbers of Deaths, by Sex, Race, and Hispanic Origin: United States, 1980 and 2016.*

Chapman, P. B., Hauschild, A., Robert, C., Haanen, J. B., Ascierto, P., Larkin, J., et al. (2011). Improved survival with vemurafenib in melanoma with BRAF V600E mutation. *N. Engl. J. Med.* 364, 2507–2516. doi: 10.1056/NEJMoa1103782

Cheng, A. C., Coleman, R. G., Smyth, K. T., Cao, Q., Soulard, P., Caffrey, D. R., et al. (2007). Structure-based maximal affinity model predicts small-molecule druggability. *Nat. Biotechnol.* 25, 71–75. doi: 10.1038/nbt1273

Cotto, K. C., Wagner, A. H., Feng, Y. Y., Kiwala, S., Coffman, A. C., Spies, G., et al. (2018). DGIdb 3.0: a redesign and expansion of the drug–gene interaction database. *Nucleic Acids Res.* 46, D1068–D1073. doi: 10.1093/nar/gkx1143

Croft, D., Mundo, A. F., Haw, R., Milacic, M., Weiser, J., Wu, G., et al. (2014). The reactome pathway knowledgebase. *Nucleic Acids Res.* 42, D472–D477. doi: 10.1093/nar/gkt1102

Diamandis, E. P. (2014). Towards identification of true cancer biomarkers. *BMC Med.* 12:156. doi: 10.1186/s12916-014-0156-8

Druker, B. J., Sawyers, C. L., Kantarjian, H., Resta, D. J., Reese, S. F., Ford, J. M., et al. (2001a). Activity of a specific inhibitor of the BCR-ABL tyrosine kinase in the blast crisis of chronic myeloid leukemia and acute lymphoblastic leukemia with the Philadelphia chromosome. *N. Engl. J. Med.* 344, 1038–1042. doi: 10.1056/NEJM200104053441402

Druker, B. J., Talpaz, M., Resta, D. J., Peng, B., Buchdunger, E., Ford, J. M., et al. (2001b). Efficacy and safety of a specific inhibitor of the BCR-ABL tyrosine kinase in chronic myeloid leukemia. *N. Engl. J. Med.* 344, 1031–1037. doi: 10.1056/NEJM200104053441401

Forbes, S. A., Beare, D., Bindal, N., Bamford, S., Ward, S., Cole, C. G., et al. (2016). COSMIC: high-resolution cancer genetics using the catalogue of somatic mutations in cancer. *Curr. Protoc. Hum. Genet.* 91, 10.11.1–10.11.37. doi: 10.1002/cphg.21

Forbes, S. A., Beare, D., Boutselakis, H., Bamford, S., Bindal, N., Tate, J., et al. (2017). COSMIC: somatic cancer genetics at high-resolution. *Nucleic Acids Res.* 45, D777–D783. doi: 10.1093/nar/gkw1121

Ghidini, M., Petrelli, F., Ghidini, A., Tomasello, G., Hahne, J. C., Passalacqua, R., et al. (2017). Clinical development of mTor inhibitors for renal cancer. *Expert Opin. Investig. Drugs* 26, 1229–1237. doi: 10.1080/13543784.2017.1384813

Giles, F. J., Cortes, J. E., and Kantarjian, H. M. (2005). Targeting the kinase activity of the BCR-ABL fusion protein in patients with chronic myeloid leukemia. *Curr. Mol. Med.* 5, 615–623. doi: 10.2174/156652405774641115

Gridelli, C., De Marinis, F., Di Maio, M., Cortinovis, D., Cappuzzo, F., and Mok, T. (2011). Gefitinib as first-line treatment for patients with advanced non-small-cell lung cancer with activating epidermal growth factor receptor mutation: review of the evidence. *Lung Cancer* 71, 249–257. doi: 10.1016/j.lungcan.2010.12.008

Grothey, A., and Lenz, H. J. (2012). Explaining the unexplainable: EGFR antibodies in colorectal cancer. *J. Clin. Oncol.* 30, 1735–1737. doi: 10.1200/JCO.2011.40.4194

Gu, Y., Zhao, W., Xia, J., Zhang, Y., Wu, R., Wang, C., et al. (2011). Analysis of pathway mutation profiles highlights collaboration between cancer-associated superpathways. *Hum. Mutat.* 32, 1028–1035. doi: 10.1002/humu.21541

Haggarty, S. J., Koeller, K. M., Wong, J. C., Butcher, R. A., and Schreiber, S. L. (2003). Multidimensional chemical genetic analysis of diversity-oriented synthesis-derived deacetylase inhibitors using cell-based assays. *Chem. Biol.* 10, 383–396. doi: 10.1016/S1074-5521(03)00095-4

Hanna, N., and Einhorn, L. H. (2014). Testicular cancer: a reflection on 50 years of discovery. *J. Clin. Oncol.* 32, 3085–3092. doi: 10.1200/JCO.2014.56.0896

Hornberger, J., Cosler, L. E., and Lyman, G. H. (2005). Economic analysis of targeting chemotherapy using a 21-gene RT-PCR assay in lymph-node-negative, estrogen-receptor-positive, early-stage breast cancer. *Am. J. Manag. Care* 11, 313–324.

Housman, G., Byler, S., Heerboth, S., Lapinska, K., Longacre, M., Snyder, N., et al. (2014). Drug resistance in cancer: an overview. *Cancers* 6, 1769–1792. doi: 10.3390/cancers6031769

Hudis, C. A. (2007). Trastuzumab — mechanism of action and use in clinical practice. *N. Engl. J. Med.* 357, 39–51. doi: 10.1056/NEJMra043186

Joo, W. D., Visintin, I., and Mor, G. (2013). Targeted cancer therapy–are the days of systemic chemotherapy numbered? *Maturitas* 76, 308–314. doi: 10.1016/j.maturitas.2013.09.008

Kanehisa, M., and Goto, S. (2000). KEGG: kyoto encyclopedia of genes and genomes. *Nucleic Acids Res.* 28, 27–30. doi: 10.1093/nar/28.1.27

Khatri, P., Sirota, M., and Butte, A. J. (2012). Ten years of pathway analysis: current approaches and outstanding challenges. *PLoS Comput. Biol.* 8:e1002375. doi: 10.1371/journal.pcbi.1002375

Kisselev, A. F., van der Linden, W. A., and Overkleeft, H. S. (2012). Proteasome inhibitors: an expanding army attacking a unique target. *Chem. Biol.* 19, 99–115. doi: 10.1016/j.chembiol.2012.01.003

Ko, Y. J., and Balk, S. P. (2004). Targeting steroid hormone receptor pathways in the treatment of hormone dependent cancers. *Curr. Pharm. Biotechnol.* 5, 459–470. doi: 10.2174/1389201043376616

Kurz, S., Thieme, R., Amberg, R., Groth, M., Jahnke, H. G., Pieroh, P., et al. (2017). The anti-tumorigenic activity of A2M-A lesson from the naked mole-rat. *PLoS ONE* 12:e0189514. doi: 10.1371/journal.pone.0189514

Lamb, J., Crawford, E. D., Peck, D., Modell, J. W., Blat, I. C., Wrobel, M. J., et al. (2006). The connectivity map: using gene-expression signatures to connect small molecules, genes, and disease. *Science* 313, 1929–1935. doi: 10.1126/science.1132939

Law, V., Knox, C., Djoumbou, Y., Jewison, T., Guo, A. C., Liu, Y., et al. (2014). DrugBank 4.0: shedding new light on drug metabolism. *Nucleic Acids Res.* 42, D1091–D1097. doi: 10.1093/nar/gkt1068

Le Tourneau, C., Paoletti, X., Servant, N., Bièche, I., Gentien, D., Rio Frio, T., et al. (2014). Randomised proof-of-concept phase II trial comparing targeted therapy based on tumour molecular profiling vs conventional therapy in patients with refractory cancer: results of the feasibility part of the SHIVA trial. *Br. J. Cancer* 111, 17–24. doi: 10.1038/bjc.2014.211

Li, H., Zeng, J., and Shen, K. (2014). PI3K/AKT/mTOR signaling pathway as a therapeutic target for ovarian cancer. *Arch. Gynecol. Obstet.* 290, 1067–1078. doi: 10.1007/s00404-014-3377-3

Luo, Y., Zhao, X., Zhou, J., Yang, J., Zhang, Y., Kuang, W., et al. (2017). A network integration approach for drug-target interaction prediction and computational drug repositioning from heterogeneous information. *Nat. Commun.* 8:573. doi: 10.1038/s41467-017-00680-8

Ma, Q., and Lu, A. Y. (2011). Pharmacogenetics, pharmacogenomics, and individualized medicine. *Pharmacol. Rev.* 63, 437–459. doi: 10.1124/pr.110.003533

Mani, K. M., Lefebvre, C., Wang, K., Lim, W. K., Basso, K., Dalla-Favera, R., et al. (2008). A systems biology approach to prediction of oncogenes and molecular perturbation targets in B-cell lymphomas. *Mol. Syst. Biol.* 4:169. doi: 10.1038/msb.2008.2

Nahta, R., and Esteva, F. J. (2007). Trastuzumab: triumphs and tribulations. *Oncogene* 26, 3637–3643. doi: 10.1038/sj.onc.1210379

Nishimura, D. (2001). BioCarta. *Biotech. Softw. Internet Rep.* 2, 117–120. doi: 10.1089/152791601750294344

Oldenburg, J., Aparicio, J., Beyer, J., Cohn-Cedermark, G., Cullen, M., Gilligan, T., et al. (2015). Personalizing, not patronizing: the case for patient autonomy by unbiased presentation of management options in stage I testicular cancer. *Ann. Oncol.* 26, 833–838. doi: 10.1093/annonc/mdu514

Ozerov, I. V., Lezhnina, K. V., Izumchenko, E., Artemov, A. V., Medintsev, S., Vanhaelen, Q., et al. (2016). *In silico* pathway activation network decomposition analysis (iPANDA) as a method for biomarker development. *Nat. Commun.* 7:13427. doi: 10.1038/ncomms13427

Padma, V. V. (2015). An overview of targeted cancer therapy. *BioMedicine* 5:19. doi: 10.7603/s40681-015-0019-4

Petrov, I., Suntsova, M., Ilnitskaya, E., Roumiantsev, S., Sorokin, M., Garazha, A., et al. (2017). Gene expression and molecular pathway activation signatures of MYCN-amplified neuroblastomas. *Oncotarget* 8, 83768–83780. doi: 10.18632/oncotarget.19662

Poddubskaya, E. V., Baranova, M. P., Allina, D. O., Smirnov, P. Y., Albert, E. A., Kirilchev, A. P., et al. (2018). Personalized prescription of tyrosine kinase inhibitors in unresectable metastatic cholangiocarcinoma. *Exp. Hematol. Oncol.* 7:21. doi: 10.1186/s40164-018-0113-x

Prieto, P. A., Yang, J. C., Sherry, R. M., Hughes, M. S., Kammula, U. S., White, D. E., et al. (2012). CTLA-4 blockade with ipilimumab: long-term follow-up of 177 patients with metastatic melanoma. *Clin. Cancer Res.* 18, 2039–2047. doi: 10.1158/1078-0432.CCR-11-1823

Rifaioglu, A. S., Atas, H., Martin, M. J., Cetin-Atalay, R., Atalay, V., and Dogan, T. (2018). Recent applications of deep learning and machine intelligence on in silico drug discovery: methods, tools and databases. *Brief. Bioinform.* doi: 10.1093/bib/bby061. [Epub ahead of print].

Rini, B. I. (2009). Vascular endothelial growth factor-targeted therapy in metastatic renal cell carcinoma. *Cancer* 115, 2306–2312. doi: 10.1002/cncr.24227

Romero, P., Wagg, J., Green, M. L., Kaiser, D., Krummenacker, M., and Karp, P. D. (2004). Computational prediction of human metabolic pathways from the complete human genome. *Genome Biol.* 6:R2. doi: 10.1186/gb-2004-6-1-r2

Safran, M., Dalah, I., Alexander, J., Rosen, N., Iny Stein, T., Shmoish, M., et al. (2010). GeneCards Version 3: the human gene integrator. *Database* 2010:baq020. doi: 10.1093/database/baq020

Sanchez-Vega, F., Mina, M., Armenia, J., Chatila, W. K., Luna, A., La, K. C., et al. (2018). Oncogenic signaling pathways in the cancer genome atlas. *Cell* 173, 321–337.e10. doi: 10.1016/j.cell.2018.03.035

Sawyers, C. (2004). Targeted cancer therapy. *Nature* 432, 294–297. doi: 10.1038/nature03095

Schaefer, C. F., Anthony, K., Krupa, S., Buchoff, J., Day, M., Hannay, T., et al. (2009). PID: the pathway interaction database. *Nucleic Acids Res.* 37, D674–D679. doi: 10.1093/nar/gkn653

Schenone, M., Dancík, V., Wagner, B. K., and Clemons, P. A. (2013). Target identification and mechanism of action in chemical biology and drug discovery. *Nat. Chem. Biol.* 9, 232–240. doi: 10.1038/nchembio.1199

Sorokin, M., Kholodenko, R., Grekhova, A., Suntsova, M., Pustovalova, M., Vorobyeva, N., et al. (2018). Acquired resistance to tyrosine kinase inhibitors

may be linked with the decreased sensitivity to X-ray irradiation. *Oncotarget* 9, 5111–5124. doi: 10.18632/oncotarget.23700

Spirin, P., Lebedev, T., Orlova, N., Morozov, A., Poymenova, N., Dmitriev, S. E., et al. (2017). Synergistic suppression of t(8;21)-positive leukemia cell growth by combining oridonin and MAPK1/ERK2 inhibitors. *Oncotarget* 8, 56991–57002. doi: 10.18632/oncotarget.18503

Suzuki, M., and Cheung, N. K. (2015). Disialoganglioside GD2 as a therapeutic target for human diseases. *Expert Opin. Ther. Targets* 19, 349–362. doi: 10.1517/14728222.2014.986459

Tomczak, K., Czerwinska, P., and Wiznerowicz, M. (2015). The cancer genome atlas (TCGA): an immeasurable source of knowledge. *Contemp. Oncol.* 19, A68–77. doi: 10.5114/wo.2014.47136

Toren, P., and Zoubeidi, A. (2014). Targeting the PI3K/Akt pathway in prostate cancer: challenges and opportunities (Review). *Int. J. Oncol.* 45, 1793–1801. doi: 10.3892/ijo.2014.2601

Vasey, P. A. (2003). Resistance to chemotherapy in advanced ovarian cancer: mechanisms and current strategies. *Br. J. Cancer* 89, S23–S28. doi: 10.1038/sj.bjc.6601497

Wickham, H. (2009). *Ggplot2 : Elegant Graphics for Data Analysis*. New York, NY: Springer-Verlag.

Wirsching, A., Melloul, E., Lezhnina, K., Buzdin, A. A., Ogunshola, O. O., Borger, P., et al. (2017). Temporary portal vein embolization is as efficient as permanent portal vein embolization in mice. *Surgery* 162, 68–81. doi: 10.1016/j.surg.2017.01.032

Wishart, D. S., Feunang, Y. D., Marcu, A., Guo, A. C., Liang, K., Vázquez-Fresno, R., et al. (2018). HMDB 4.0: the human metabolome database for 2018. *Nucleic Acids Res.* 46, D608–D617. doi: 10.1093/nar/gkx1089

Xie, J., Wang, X., and Proud, C. G. (2016). mTOR inhibitors in cancer therapy. *F1000Research* 5:F1000 Faculty Rev-2078. doi: 10.12688/f1000research.9207.1

Zaim, S. R., Li, Q., Schissler, A. G., and Lussier, Y. A. (2018). Emergence of pathway-level composite biomarkers from converging gene set signals of heterogeneous transcriptomic responses. *Pac. Symp. Biocomput.* 23, 484–495. doi: 10.1142/9789813235533_0044

Zappa, C., and Mousa, S. A. (2016). Non-small cell lung cancer: current treatment and future advances. *Transl. Lung Cancer Res.* 5, 288–300. doi: 10.21037/tlcr.2016.06.07

Zhu, S., Okuno, Y., Tsujimoto, G., and Mamitsuka, H. (2007). Application of a new probabilistic model for mining implicit associated cancer genes from OMIM and medline. *Cancer Inform.* 2, 361–371. doi: 10.1177/117693510600200025

Conflict of Interest Statement: MS, NB, AG were employed by company Omicsway Corp. MZ, AB were employed by company Oncobox Ltd.

The remaining authors declare that the research was conducted in the absence of any commercial or financial relationships that could be construed as a potential conflict of interest.

frontiers in Oncology

MINI REVIEW
published: 23 January 2019
doi: 10.3389/fonc.2019.00015

Progression on Citrullination of Proteins in Gastrointestinal Cancers

*Shuzheng Song and Yingyan Yu**

Department of Surgery, Ruijin Hospital, Shanghai Jiao Tong University School of Medicine, Shanghai Key Laboratory for Gastric Neoplasms, Shanghai, China

The citrullination modification (Cit) of proteins has received increasing attention in recent years. This kind of protein modification was first discovered in autoimmune diseases such as rheumatoid arthritis. The citrullination modification process is catalyzed by the peptidyl arginine deiminases (PADIs) family. A well-known citrullination of histone involves the key mechanism of neutrophil extracellular traps (NETs) of inflammation in the peripheral blood. Further studies revealed that citrullination modification of proteins also involves in carcinogenesis in human being. Citrullinated proteins disturbed the stability of proteins and caused DNA damages. There is increasing evidence that citrullinated proteins can be used as potential targets for cancer diagnosis or treatment. This review introduces the concept of citrullination modification of proteins, substrate proteins, examining methods and biological significances.

Keywords: citrullination, proteins, histone, PADIs, molecular targets

OPEN ACCESS

Edited by:
Zhe-Sheng Chen,
St. John's University, United States

Reviewed by:
Kathy Keqin LI,
Georgia State University, United States
Qingyuan Zhang,
Ningxia Medical University, China
Qi Liu,
Tongji University, China

****Correspondence:***
Yingyan Yu
yingyan3y@sjtu.edu.cn

Specialty section:
This article was submitted to Cancer Molecular Targets and Therapeutics, a section of the journal Frontiers in Oncology

Received: *18 November 2018*
Accepted: *04 January 2019*
Published: *23 January 2019*

Citation:
Song S and Yu Y (2019) Progression on Citrullination of Proteins in Gastrointestinal Cancers. Front. Oncol. 9:15. doi: 10.3389/fonc.2019.00015

INTRODUCTION

Proteins are the main executor of life activities. The epigenetics and post-translational modification of proteins, such as phosphorylation, acetylation, glycosylation, methylation, ubiquitination and citrullination have been found to play important roles on pathogenesis and carcinogenesis (1–3). Citrullination of proteins is a new kind of post-translational modification, which has been reported to be involved in large numbers of autoimmune diseases and cancers. This review focuses on the mechanisms, regulation, and the clinical significance of citrullinated proteins in the field of gastrointestinal diseases.

DEFINITION OF CITRULLINATED PROTEINS

Citrullination of protein refers to the process by which the peptidyl arginine residue is converted to citrulline by a catalytic enzyme (**Figure 1**). Since this process is accompanied by the removal of an amino group, it is also called a peptidyl arginine deamination reaction. This chemical reaction is accompanied by a change in electrostatic charge, which may affect the folding state and function of protein, especially on histones. To date, it has been confirmed that arginine residues of dozens of proteins can undergo citrullination modifications. The substrates could be enolase, vimentin, keratin, filaggrin, serine protease inhibitors, proteases and metabolic enzymes (4). Moreover, arginine residues of histones such as H3R2/R8/R17/R26, H4R3, H2A, and H1 could be citrullinated by peptidyl arginine deiminases (PADIs) (5–8).

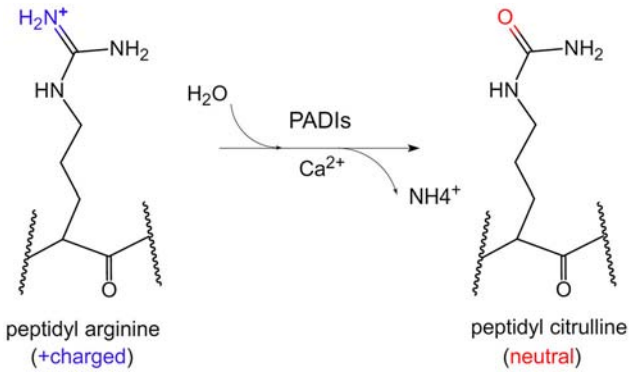

FIGURE 1 | The chemical conversion process of protein citrullination. In the presence of calcium ions, PADIs could catalyze the formation of peptidyl citrulline from peptidyl arginine, which removes an amino group, accompanied by the positive charge becoming electrically neutral.

Citrullination of proteins is catalyzed by PADIs, which include five isoenzymes (PADI1-4 and PADI6) in humans. The genes of these five isozymes are located on chromosome 1p36.13. The coding regions of PADIs are about 2k in size, and consist of three parts: the nitrogen end, middle part and catalytic groups of carbon end. Regarding the subcellular localization, the PADI4 is located in the nucleus with a nuclear localization signal, while others are mainly localized in the cytosol (9) (**Figure 2**). PADI2 had been shown to be undergoing nuclear translocation in some cells for modifying histones (10). Therefore, citrullinated modification of histones may catalyzed by PADI4 and PADI2. The citrullination of proteins occurs in various life processes, including regulation of gene expression, immune response and protein degradation (10, 11). The citrullination of proteins is also associated with carcinogenesis in the stomach (12, 13), the large intestine (13–15), the pancreas (16), the liver (13), and so on.

CITRULLINATION OF NON-HISTONE PROTEINS

Citrullination of proteins could be induced by chemical compounds. Qu et al. reported that the antiparasitic drug nitazoxanide could induce citrullination of protein β-catenin in colorectal cancer cells via up-regulation of PADI2 enzyme. Citrullination of β-catenin resulted in the instability of the protein, and then inhibited the Wnt signaling pathway. ING4, a tumor suppressor protein, was identified as a substrate of PADI4 enzyme. Citrullination of ING4 interfered with its interaction with p53, and then decreased the tumor suppressor function in colon cancer cells (17). On the other hand, some research indicated that DNA damage induced PADI4, and then increased the citrullination of NPM1 and lamine C, which inhibited cell growth through the p53 pathway in colon cancer cells (18). Cantarino and colleagues found that down-regulation of PADI2 is an early event in the pathogenesis of colorectal cancer and is associated with poor prognosis (14). Overexpression of PADI2 inhibited cell growth and was accompanied with an increase in citrullinated protein in colon cancer cells. Overexpression of PADI2 did not increase cell apoptosis, but arrested the cell cycle in G1 phase (15). The exact effect of citrullination of proteins on cancer should be studied further.

Citrullination of proteins is not only detected in *in vitro* experiments, but also in human blood. Ordóñez et al. (19) reported that up-regulation of citrullinated antithrombin in peripheral blood of patients with rheumatoid arthritis and colorectal cancer predicted higher risk of thrombosis. Yuzhalin et al. (20) found that PADI4 could be secreted into the extracellular matrix by colorectal cancer cells, catalyzing the citrullination of proteins, thereby promoting distant metastasis of cancer cells to liver. Increased PADI4 could be found in the peripheral blood of patients with various malignancies such as gastric cancer, lung cancer, hepatocellular carcinoma, esophageal squamous cell carcinoma and breast cancer (13, 21). Until now, multiple proteins have been found as substrates of citrullination, including NF-κB p65 (22), CXCL8 (23), CXCL12 (24), E2F-1 (25), GSK3β (26), MEK1 (27), VEGFR2 (28), and so on. Obviously, citrullination of proteins involve double-sided roles in promoting both inflammation and anti-inflammation, as well as cancer promotion and inhibition.

CITRULLINATION OF HISTONE PROTEINS

Citrullinated modification of histones is an epigenetic event. As introduced above, both PADI2 and PADI4 involve the citrullination process of histones in the nucleus. Recently, increased citrullinated histone H3 (H3Cit) has been considered a novel prognostic blood marker in patients with advanced cancer, due to its higher levels compared to healthy controls (29). PADI2 has been found playing an important role in mediating histone H3Cit modification, and promoting disease progression in some non-digestive cancers (30, 31). McNee et al. (32) found that PADI2 could up-regulate IL-6 expression by catalyzing H3R26Cit of bone marrow mesenchymal stem cells of multiple myeloma, which ultimately lead to chemo-resistance to bortezomib. PADI4 is another important enzyme in catalyzing the citrullination of histones. DNA damage could activate the PADI4-p53 network and catalyze histone chaperone protein, nucleophosmin (NPM1) (18). In addition, DNA damage could catalyze citrullination of the arginine 3 residue of histone H4 (H4R3cit) through the p53-PADI4 pathway in non-small cell lung cancer (33).

CITRULLINATION OF PROTEINS AND IMMUNE RESPONSE

The immune system is a major weapon against cancer. Citrullination of proteins exist widely in immune-related diseases and cancers. Makrygiannakis and colleagues examined biopsy tissues from rheumatoid arthritis, myositis, tonsillitis and inflammatory bowel disease via immunohistochemistry. They found that there is a significant increase in citrullinated proteins in inflammatory tissues, compared to corresponding normal controls (34). The immune system is composed of innate immunity and acquired immunity. Neutrophils are a member of

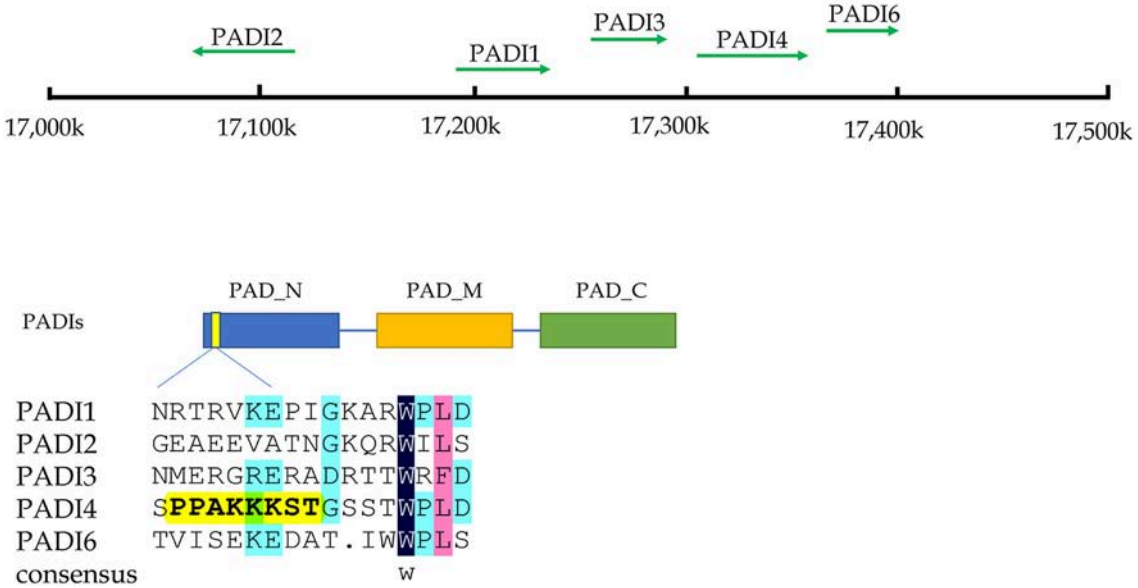

FIGURE 2 | The chromosome location and structural characteristics of PADIs family. Five PADIs genes (PADI 1, 2, 3, 4, and 6) are located in the p36.13 of chromosome 1 across a region of approximately 500 k bases. PADIs members have similar structural regions, which can be divided into three sections: nitrogen zone, middle zone, and carbon end catalytic zone. Only PADI4 contains a nuclear localization signal at the nitrogen end of sequence, implying that PADI4 may play a role in the cell nucleus.

the cells of innate immunity. In process of clearing bacteria, the neutrophils secrete cell DNA, histones, and intracellular proteins to the extracellular space or circulatory system, forming so-called neutrophil extracellular traps (NETs). The citrullination of histones is involved in the process of NETs. In this process, PADI4 mediates the citrullination of histones, and results in the unwinding of DNA and subsequently excreting into the extracellular space (35–37). NETs are a self-protective mechanism against harmful bacteria. Recently, Thalin et al. found that H3Cit was significantly increased in the peripheral blood of advanced cancer patients (29). The proportion of H3Cit-positive neutrophils was increased in more serious patients. The expression level of H3Cit of serum was strongly correlated with the neutrophil activation markers, such as neutrophil elastase, myeloperoxidase and NETs-induced factors IL-6, as well as IL-8. Therefore, H3Cit is considered a useful blood biomarker for evaluating inflammatory response and prognosis in advanced cancers. Up-regulation of NETs was also identified in pancreatic ductal adenocarcinoma. The histone modification of H3Cit was proposed as a marker of NETs (16). In the pancreas, stimulating factors such as pancreatic juice could induce NETs in pancreatic ducts. Excess in NETs blocks the pancreatic duct and eventually causes pancreatitis (38).

In the cancer immunity area, the new epitopes caused by post-translational modification of proteins may provide a novel target for cancer-specific immune therapy. The condition of the cancer microenvironment including nutrient deficiency, hypoxia, redox stress and DNA damage could irritate active expression of PADIs, and catalyze production of citrullinated peptides. Increased content of citrullinated peptides may be a good target for the immune system. The cancer-specific microenvironment could induce the immune response by citrullinated peptides, and this is non-toxic and safe to the host. Carbohydrate metabolizing enzyme α-enolase is a substrate of citrullinated modification. Cook et al. (39) found that citrullination significantly induced elevation of α-enolase in Th1 immune cells, while unmodified wild-type peptides of α-enolase did not show this efficacy. Citrullinated peptides of α-enolase also induced CD4+ T activation (40, 41). The results suggested that developing tumor vaccines against citrullinated peptides of α-enolase may be a useful strategy (39). The function of citrullinated protein epitope has revealed promising utility in anti-cancer immunity.

DETECTION AND BIOLOGICAL SIGNIFICANCE OF CITRULLINATION MODIFICATION

Citrullination modification of proteins has been reported in several fields of cancer research. Along with the progression of biomedical techniques, detection and identification of citrullinated proteins in complex biological systems becomes more feasible. Clinically, the detection of anti-cyclic citrulline antibody has been used as an assistive method for diagnosis and monitoring clinical rheumatoid arthritis (42, 43). Since the citrullination modification itself leads to 1Da mass change only,

detection of the change of low abundance is still a challenging work. Phenylglyoxal (PG) could be covalently bonded with citrullinated residues specifically, and used for specific probes of labeling citrullinated proteins. The reaction could be colored by coupling dyes such as rhodamine (Rh) or biotin, and then identified by ELISA or mass spectrometry (13, 21, 29, 42, 43). By means of this technology, more and more antigens with citrullinated modification could be found, which will provide new targets for diagnosis and treatment of cancers.

In an animal experiment, Mohamed and colleagues found that nanomaterials could induce production of citrullinated protein and auto-antibodies in mice. In their study, after injection of nickel nanowires into mice, the levels of citrullinated protein and PADIs enzymes were elevated in the spleen, kidney and lymph nodes of mice, implying a systemic response to environmental materials (44). Their results suggested that safety of the nanoparticles needs to be evaluated further. Citrullination modification of proteins may be an important event for the host to recognize foreign antigens. Citrullinated proteins may be recognized as new antigens, and are promising for targeted therapy or CAR-T/NK cell-specific recognition targets.

Inhibitors of PADIs demonstrated strong potential of anti-autoimmune and anti-cancer functions *in vitro* and *in vivo*. PADI4 is the only member of the PADI family containing a nuclear localization signal, and can citrullinate many substrates including histones. PADI4 functions as a corepressor of p53 and cooperates with a histone deacetylase HDAC2 to repress the expression of tumor suppressor genes. Chlor-amidine (Cl-amidine) is a pan-PADI inhibitor that shows inhibitory effects on several members of PADIs family. However, its higher IC50 (150–200 μM) limit its preclinical exploration in cancer study and treatment (44–47). Recently, Wang and colleagues found a lead compound, YW3-56, which could activate a cohort of p53 target genes, and realize inhibitory efficacy on the mTORC1 signaling pathway, thereby disturbing autophagy and inhibiting cancerous cell growth (45). However, since the feature of a pan-PADIs inhibitor, Cl-amidine, is still be used in experimental study (48), and many new small molecule inhibitors of PADI4 are being developed by pharmacologists (49).

In summary, compared to other modification of proteins, citrullination modification is relatively novel. The exact regulatory mechanisms and biological significance in carcinogenesis are largely unclear. As shown in **Figure 3**, many substrates of citrullination modification are very important in life processes and development of cancers. The accurate identification of citrullination sites may help researchers to elucidate the underlying molecular mechanisms of citrullination and designing drugs for related human diseases. Several groups made efforts to predict citrullination sites by bioinformatics. Ju and Wang (50) provided a user-friendly web-server for CKSAAP_CitrSite. Zhang et al. (51) published their pioneering work of maximum-relevance-minimum-redundancy to analyze citrullination sites, and constructed classifier by random forest algorithm. We believe that in citrullination research area, bioinformatics will provide some useful insights and assistance.

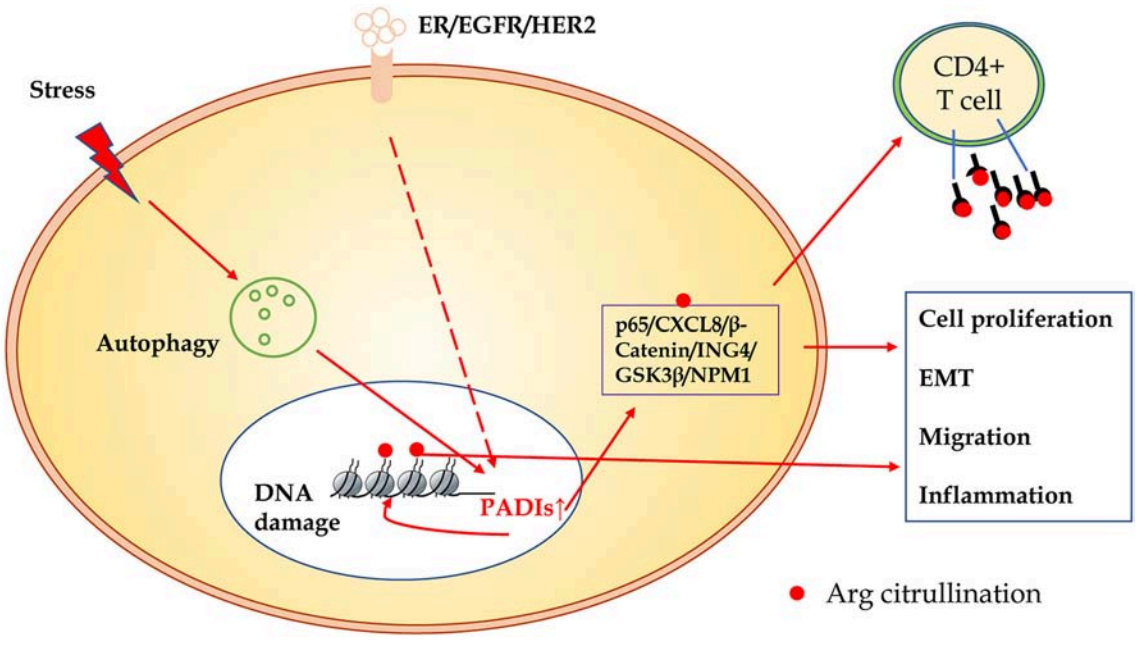

FIGURE 3 | The schematic presentation of citrullinated modification of proteins and its biological significance. PADIs enzymes are activated through receptors of ER/EGFR/HER2, oxidative stress, hypoxia, and other microenvironment factors, which initiate autophagy and DNA damage. Increased PADIs catalyze citrullination modification of histones and non-histone proteins, and result in cell proliferation, epithelial-mesenchymal transition, migration, and inflammation. Citrullinated proteins as a new antigen may activate immune response of T cells or induce specific antibodies.

AUTHOR CONTRIBUTIONS

SS and YY were involved in concept and design. All authors wrote, reviewed and revised the manuscript.

FUNDING

This project was supported by National Key R&D Program of China (2017YFC0908300, 2016YFC1303200), the National Natural Science Foundation of China (81772505), Shanghai Science and Technology Committee (18411953100), the Cross-Institute Research Fund of Shanghai Jiao Tong University (YG2017ZD01, YG2015MS62), Innovation Foundation of Translational Medicine of Shanghai Jiao Tong University School of Medicine (15ZH4001, TM201617, and TM201702), and Technology Transfer Project of Science & Technology Department Shanghai Jiao Tong University School of Medicine.

REFERENCES

1. Bettermann K, Benesch M, Weis S, Haybaeck J. SUMOylation in carcinogenesis. *Cancer Lett.* (2012) 316:113–25. doi: 10.1016/j.canlet.2011.10.036
2. Okudela K, Mitsui H, Suzuki T, Woo T, Tateishi Y, Umeda S, et al. Expression of HDAC9 in lung cancer–potential role in lung carcinogenesis. *Int J Clin Exp Pathol.* (2014) 7:213–20.
3. Chrun ES, Modolo F, Daniel FI. Histone modifications: a review about the presence of this epigenetic phenomenon in carcinogenesis. *Pathol Res Pract.* (2017) 213:1329–39. doi: 10.1016/j.prp.2017.06.013
4. Tilvawala R, Nguyen SH, Maurais AJ, Nemmara VV, Nagar M, Salinger AJ, et al. The rheumatoid arthritis-associated citrullinome. *Cell Chem Biol.* (2018) 25:691–704.e6. doi: 10.1016/j.chembiol.2018.03.002
5. Hagiwara T, Nakashima K, Hirano H, Senshu T, Yamada M. Deimination of arginine residues in nucleophosmin/B23 and histones in HL-60 granulocytes. *Biochem Biophys Res Commun.* (2002) 290:979–83. doi: 10.1006/bbrc.2001.6303
6. Arita K, Shimizu T, Hashimoto H, Hidaka Y, Yamada M, Sato M. Structural basis for histone N-terminal recognition by human peptidylarginine deiminase 4. *Proc Natl Acad Sci USA.* (2006) 103:5291–6. doi: 10.1073/pnas.0509639103
7. Saiki M, Watase M, Matsubayashi H, Hidaka Y. Recognition of the N-terminal histone H2A and H3 peptides by peptidylarginine deiminase IV. *Protein Pept Lett.* (2009) 16:1012–6. doi: 10.2174/092986609789055449
8. Christophorou MA, Castelo-Branco G, Halley-Stott RP, Oliveira CS, Loos R, Radzisheuskaya A, et al. Citrullination regulates pluripotency and histone H1 binding to chromatin. *Nature* (2014) 507:104–8. doi: 10.1038/nature12942
9. Nakashima K, Hagiwara T, Yamada M. Nuclear localization of peptidylarginine deiminase V and histone deimination in granulocytes. *J Biol Chem.* (2002) 277:49562–8. doi: 10.1074/jbc.M208795200
10. Amin B, Voelter W. Human deiminases: isoforms, substrate specificities, kinetics, and detection. *Prog Chem Org Nat Prod.* (2017) 106:203–40. doi: 10.1007/978-3-319-59542-9_2
11. Fert-Bober J, Giles JT, Holewinski RJ, Kirk JA, Uhrigshardt H, Crowgey EL, et al. Citrullination of myofilament proteins in heart failure. *Cardiovasc Res.* (2015) 108:232–42. doi: 10.1093/cvr/cvv185
12. Zheng Y, Zhao G, Xu B, Liu C, Li C, Zhang X, et al. PADI4 has genetic susceptibility to gastric carcinoma and upregulates CXCR2, KRT14 and TNF-alpha expression levels. *Oncotarget* (2016) 7:62159–76. doi: 10.18632/oncotarget.11398
13. Guo W, Zheng Y, Xu B, Ma F, Li C, Zhang X, et al. Investigating the expression, effect and tumorigenic pathway of PADI2 in tumors. *Onco Targets Ther.* (2017) 10:1475–85. doi: 10.2147/OTT.S92389
14. Cantariño N, Musulén E, Valero V, Peinado MA, Perucho M, Moreno V, et al. Downregulation of the deiminase PADI2 is an early event in colorectal carcinogenesis and indicates poor prognosis. *Mol Cancer Res.* (2016) 14:841–8. doi: 10.1158/1541-7786.MCR-16-0034
15. Funayama R, Taniguchi H, Mizuma M, Fujishima F, Kobayashi M, Ohnuma S, et al. Protein-arginine deiminase 2 suppresses proliferation of colon cancer cells through protein citrullination. *Cancer Sci.* (2017) 108:713–8. doi: 10.1111/cas.13179
16. Boone BA, Orlichenko L, Schapiro NE, Loughran P, Gianfrate GC, Ellis JT, et al. The receptor for advanced glycation end products (RAGE) enhances autophagy and neutrophil extracellular traps in pancreatic cancer. *Cancer Gene Ther.* (2015) 22:326–34. doi: 10.1038/cgt.2015.21
17. Guo Q, Fast W. Citrullination of inhibitor of growth 4 (ING4) by peptidylarginine deminase 4 (PAD4) disrupts the interaction between ING4 and p53. *J Biol Chem.* (2011) 286:17069–78. doi: 10.1074/jbc.M111.230961
18. Tanikawa C, Ueda K, Nakagawa H, Yoshida N, Nakamura Y, Matsuda K. Regulation of protein Citrullination through p53/PADI4 network in DNA damage response. *Cancer Res.* (2009) 69:8761–9. doi: 10.1158/0008-5472.CAN-09-2280
19. Ordóñez A, Yélamos J, Pedersen S, Miñano A, Conesa-Zamora P, Kristensen SR, et al. Increased levels of citrullinated antithrombin in plasma of patients with rheumatoid arthritis and colorectal adenocarcinoma determined by a newly developed ELISA using a specific monoclonal antibody. *Thromb Haemost.* (2010) 104:1143–9. doi: 10.1160/TH10-05-0297
20. Yuzhalin AE, Gordon-Weeks AN, Tognoli ML, Jones K, Markelc B, Konietzny R, et al. Colorectal cancer liver metastatic growth depends on PAD4-driven citrullination of the extracellular matrix. *Nat Commun.* (2018) 9:4783. doi: 10.1038/s41467-018-07306-7
21. Chang X, Han J, Pang L, Zhao Y, Yang Y, Shen Z. Increased PADI4 expression in blood and tissues of patients with malignant tumors. *BMC Cancer* (2009) 9:40. doi: 10.1186/1471-2407-9-40
22. Sun B, Dwivedi N, Bechtel TJ, Paulsen JL, Muth A, Bawadekar M, et al. Citrullination of NF-kappaB p65 promotes its nuclear localization and TLR-induced expression of IL-1beta and TNFalpha. *Sci Immunol.* (2017) 2:eaal3062. doi: 10.1126/sciimmunol.aal3062
23. Proost P, Loos T, Mortier A, Schutyser E, Gouwy M, Noppen S, et al. Citrullination of CXCL8 by peptidylarginine deiminase alters receptor usage, prevents proteolysis, and dampens tissue inflammation. *J Exp Med.* (2008) 205:2085–97. doi: 10.1084/jem.20080305
24. Struyf S, Noppen S, Loos T, Mortier A, Gouwy M, Verbeke H, et al. Citrullination of CXCL12 differentially reduces CXCR4 and CXCR7 binding with loss of inflammatory and anti-HIV-1 activity via CXCR4. *J Immunol.* (2009) 182:666–74. doi: 10.4049/jimmunol.182.1.666
25. Ghari F, Quirke AM, Munro S, Kawalkowska J, Picaud S, McGouran J, et al. Citrullination-acetylation interplay guides E2F-1 activity during the inflammatory response. *Sci Adv.* (2016) 2:e1501257. doi: 10.1126/sciadv.1501257
26. Stadler SC, Vincent CT, Fedorov VD, Patsialou A, Cherrington BD, Wakshlag JJ, et al. Dysregulation of PAD4-mediated citrullination of nuclear GSK3beta activates TGF-beta signaling and induces epithelial-to-mesenchymal transition in breast cancer cells. *Proc Natl Acad Sci USA.* (2013) 110:11851–6. doi: 10.1073/pnas.1308362110
27. Qin H, Liu X, Li F, Miao L, Li T, Xu B, et al. PAD1 promotes epithelial-mesenchymal transition and metastasis in triple-negative breast cancer cells by regulating MEK1-ERK1/2-MMP2 signaling. *Cancer Lett.* (2017) 409:30–41. doi: 10.1016/j.canlet.2017.08.019
28. Sase T, Arito M, Onodera H, Omoteyama K, Kurokawa MS, Kagami Y, et al. Hypoxia-induced production of peptidylarginine deiminases and citrullinated proteins in malignant glioma cells. *Biochem Biophys Res Commun.* (2017) 482:50–6. doi: 10.1016/j.bbrc.2016.10.154
29. Thålin C, Lundström S, Seignez C, Daleskog M, Lundström A, Henriksson P, et al. Citrullinated histone H3 as a novel prognostic blood marker in patients with advanced cancer. *PLoS ONE* (2018) 13:e0191231. doi: 10.1371/journal.pone.0191231

30. Wang L, Song G, Zhang X, Feng T, Pan J, Chen W, et al. PADI2-mediated citrullination promotes prostate cancer progression. *Cancer Res.* (2017) 77:5755–68. doi: 10.1158/0008-5472.CAN-17-0150
31. DeVore SB, Young CH, Li G, Sundararajan A, Ramaraj T, Mudge J, et al. Histone citrullination represses miRNA expression resulting in increased oncogene mRNAs in somatolactotrope cells. *Mol Cell Biol.* (2018) 38:e00084-18. doi: 10.1128/MCB.00084-18
32. McNee G, Eales KL, Wei W, Williams DS, Barkhuizen A, Bartlett DB, et al. Citrullination of histone H3 drives IL-6 production by bone marrow mesenchymal stem cells in MGUS and multiple myeloma. *Leukemia* (2017) 31:373–81. doi: 10.1038/leu.2016.187
33. Tanikawa C, Espinosa M, Suzuki A, Masuda K, Yamamoto K, Tsuchiya E, et al. Regulation of histone modification and chromatin structure by the p53-PADI4 pathway. *Nat Commun.* (2012) 3:676. doi: 10.1038/ncomms1676
34. Makrygiannakis D, af Klint E, Lundberg IE, Löfberg R, Ulfgren AK, Klareskog L, et al. Citrullination is an inflammation-dependent process. *Ann Rheum Dis.* (2006) 65:1219–22. doi: 10.1136/ard.2005.049403
35. Neeli I, Khan SN, Radic M. Histone deimination as a response to inflammatory stimuli in neutrophils. *J Immunol.* (2008) 180:1895–902. doi: 10.4049/jimmunol.180.3.1895
36. Wang Y, Li M, Stadler S, Correll S, Li P, Wang D, et al. Histone hypercitrullination mediates chromatin decondensation and neutrophil extracellular trap formation. *J Cell Biol.* (2009) 184:205–13. doi: 10.1083/jcb.200806072
37. Honda M, Kubes P. Neutrophils and neutrophil extracellular traps in the liver and gastrointestinal system. *Nat Rev Gastroenterol Hepatol.* (2018) 15:206–21. doi: 10.1038/nrgastro.2017.183
38. Leppkes M, Maueröder C, Hirth S, Nowecki S, Günther C, Billmeier U, et al. Externalized decondensed neutrophil chromatin occludes pancreatic ducts and drives pancreatitis. *Nat Commun.* (2016) 7:10973. doi: 10.1038/ncomms10973
39. Cook K, Daniels I, Symonds P, Pitt T, Gijon M, Xue W, et al. Citrullinated alpha-enolase is an effective target for anti-cancer immunity. *Oncoimmunology* (2018) 7:e1390642. doi: 10.1080/2162402X.2017.1390642
40. Brentville VA, Metheringham RL, Gunn B, Symonds P, Daniels I, Gijon M, et al. Citrullinated vimentin presented on MHC-II in tumor cells is a target for CD4+ T-cell-mediated antitumor immunity. *Cancer Res.* (2016) 76:548–60. doi: 10.1158/0008-5472.CAN-15-1085
41. Durrant LG, Metheringham RL, Brentville VA. Autophagy, citrullination and cancer. *Autophagy* (2016) 12:1055–6. doi: 10.1080/15548627.2016.1166326
42. Bicker KL, Subramanian V, Chumanevich AA, Hofseth LJ, Thompson PR. Seeing citrulline: development of a phenylglyoxal-based probe to visualize protein citrullination. *J Am Chem Soc.* (2012) 134:17015–8. doi: 10.1021/ja308871v
43. Lewallen DM, Bicker KL, Subramanian V, Clancy KW, Slade DJ, Martell J, et al. Chemical proteomic platform to identify citrullinated proteins. *ACS Chem Biol.* (2015) 10:2520–8. doi: 10.1021/acschembio.5b00438
44. Mohamed BM, Boyle NT, Schinwald A, Murer B, Ward R, Mahfoud OK, et al. Induction of protein citrullination and auto-antibodies production in murine exposed to nickel nanomaterials. *Sci Rep.* (2018) 8:679. doi: 10.1038/s41598-017-19068-1
45. Wang Y, Li P, Wang S, Hu J, Chen XA, Wu J, et al. Anticancer peptidylarginine deiminase (PAD) inhibitors regulate the autophagy flux and the mammalian target of rapamycin complex 1 activity. *J Biol Chem.* (2012) 287:25941–53. doi: 10.1074/jbc.M112.375725
46. Mondal S, Parelkar SS, Nagar M, Thompson PR. Photochemical control of protein arginine deiminase (PAD) activity. *ACS Chem Biol.* (2018) 13:1057–65. doi: 10.1021/acschembio.8b00053
47. Bozdag M, Dreker T, Henry C, Tosco P, Vallaro M, Fruttero R, et al. Novel small molecule protein arginine deiminase 4 (PAD4) inhibitors. *Bioorg Med Chem Lett.* (2013) 23:715–9. doi: 10.1016/j.bmcl.2012.11.102
48. Witalison EE, Cui X, Hofseth AB, Subramanian V, Causey CP, Thompson PR, et al. Inhibiting protein arginine deiminases has antioxidant consequences. *J Pharmacol Exp Ther.* (2015) 353:64–70. doi: 10.1124/jpet.115.222745
49. Witalison EE, Cui X, Causey CP, Thompson PR, Hofseth LJ. Molecular targeting of protein arginine deiminases to suppress colitis and prevent colon cancer. *Oncotarget* (2015) 6:36053–62. doi: 10.18632/oncotarget.5937
50. Ju Z, Wang SY. Prediction of citrullination sites by incorporating k-spaced amino acid pairs into Chou's general pseudo amino acid composition. *Gene* (2018) 664:78–83. doi: 10.1016/j.gene.2018.04.055
51. Zhang Q, Sun X, Feng K, Wang S, Zhang YH, Wang S, et al. Predicting citrullination sites in protein sequences using mRMR method and random forest algorithm. *Comb Chem High Throughput Screen.* (2017) 20:164–73. doi: 10.2174/1386207319666161227124350

Conflict of Interest Statement: The authors declare that the research was conducted in the absence of any commercial or financial relationships that could be construed as a potential conflict of interest.

frontiers in Pharmacology

ORIGINAL RESEARCH
published: 24 January 2019
doi: 10.3389/fphar.2019.00010

A Smart pH-Sensitive Delivery System for Enhanced Anticancer Efficacy via Paclitaxel Endosomal Escape

Yihua Yang[1,2], Zhe Wang[3], Ying Peng[1], Jinsong Ding[1] and Wenhu Zhou[1]**

[1] Xiangya School of Pharmaceutical Sciences, Central South University, Changsha, China, [2] Jiangsu Key Laboratory of New Drug Research and Clinical Pharmacy, School of Pharmaceutical Sciences, Xuzhou Medical University, Xuzhou, China, [3] Xiangya International Academy of Translational Medicine, Central South University, Changsha, China

Micelles are highly attractive nano-drug delivery systems for targeted cancer therapy. While they have been demonstrated to significantly alleviate the side-effects of their cargo drugs, the therapy outcomes are usually suboptimal partially due to ineffective drug release and endosome entrapment. Stimulus-responsive nanoparticles have allowed controlled drug release in a smart fashion, and we want to use this concept to design novel micelles. Herein, we reported pH-sensitive paclitaxel (PTX)-loaded poly (ethylene glycol)-phenylhydrazone-dilaurate (PEG-BHyd-dC_{12}) micelles (PEG-BHyd-dC_{12}/PTX). The micelles were spherical, with an average particle size of ∼135 nm and a uniform size distribution. The pH-responsive properties of the micelles were certified by both colloidal stability and drug release profile, where the particle size was strikingly increased accompanied by faster drug release as pH decreased from 7.4 to 5.5. As a result, the micelles exhibited much stronger cytotoxicity than the pH-insensitive counterpart micelles against various types of cancer cells due to the hydrolysis of the building block polymers and subsequent rapid PTX release. Overall, these results demonstrate that the PEG-BHyd-dC_{12} micelle is a promising drug delivery system for cancer therapy.

Keywords: pH-sensitive, micelles, cancer, paclitaxel, endosomal escape

OPEN ACCESS

Edited by:
Zhe-Sheng Chen,
St. John's University, United States

Reviewed by:
Lei Zhang,
Fujian Institute of Research on the Structure of Matter (CAS), China
Qi Liu,
Johns Hopkins Medicine, United States

****Correspondence:***
Jinsong Ding
dingjs0221@163.com
Wenhu Zhou
zhouwenhuyaoji@163.com

Specialty section:
This article was submitted to Cancer Molecular Targets and Therapeutics, a section of the journal Frontiers in Pharmacology

Received: *10 July 2018*
Accepted: *07 January 2019*
Published: *24 January 2019*

Citation:
Yang Y, Wang Z, Peng Y, Ding J and Zhou W (2019) A Smart pH-Sensitive Delivery System for Enhanced Anticancer Efficacy via Paclitaxel Endosomal Escape. Front. Pharmacol. 10:10. doi: 10.3389/fphar.2019.00010

INTRODUCTION

With the development of nanotechnology, various materials such as polymers, lipid, and metals (oxides), have been widely applied to design drug delivery system, especially for cancer therapy (Farokhzad and Langer, 2009). Nanoparticles based on the above materials have been demonstrated to realize controlled drug release and effectively targeting drug delivery (Wilczewska et al., 2012). To this end, micelles composed of amphipathic copolymers have received wide attention owing to their attractive features, such as small and uniform size, tumor targeting ability *via* the enhanced permeability and retention (EPR) effect, high stability in aqueous solution and excellent biocompatibility (Felber et al., 2012; Liu J. et al., 2014; Wang et al., 2018).

However, albeit with the extensive research efforts, the clinical translations of micelles from bench to bedsides are rather limited, partially due to their suboptimal therapy outcomes caused by

the inefficient drug release at the tumor site and the endosomal entrapment of micelles (Kanamala et al., 2016). Plain micelles exhibit relatively slow drug release rate, which may result in ineffective drug concentration inside targeted cells (Wu et al., 2013). To mitigate these issues, smarter micelles are desired to be equipped with endosomal escape and rapid drug release abilities, which could be able to provide sufficient drug concentration for effective killing of the tumor cells.

To achieve such goals, environmentally sensitive polymers that can respond to different stimuli to trigger drug release have been extensively investigated, such as light (Liu et al., 2012; Cao et al., 2013), temperature (Kim et al., 2010; Wang et al., 2014), ultrasound (Yin et al., 2013; Ahmed et al., 2015), magnetic field (Ao et al., 2014; Deng et al., 2015), pH (Liu Y. et al., 2014; Yuba et al., 2017), redox properties (Yin et al., 2015; Zhang et al., 2016), and enzyme activity (Rao and Khan, 2013; Harnoy et al., 2014). Among of them, the pH-sensitive polymeric micelle appears to be a highly appealing candidate due to the intrinsic differences between solid tumors and the surrounding normal tissues in terms of their relative acidity. The pH-sensitive polymer micelles were devised based on copolymers composed of hydrophobic and hydrophilic polymers linked *via* acid-liable bonds, including hydrazone (Mo et al., 2012), benzoic imine (Yuan et al., 2012), oxime (Liu B. et al., 2014), acetal (Li et al., 2016), ester (Gao et al., 2018) and orthoester (Tang et al., 2011). Hydrolysis of the acid-labile bonds leads to rapid drug release at an acidic pH.

Herein, we synthesized the amphiphilic polymer PEG-BHyd-dC_{12} via an acid-labile hydrazone bond and constructed pH-responsive micelles. The hydrophilic PEG segment on micelles surface affords high colloidal stability *in vitro* and long circulation time *in vivo*, while it is readily departed from micelles at the tumor site under acid conditions, which is beneficial for cellular uptake (Du et al., 2011). Paclitaxel (PTX), one of the most effective antitumor drugs, was encapsulated into micelles due to its hydrophobic nature, and released in a pH-responsive manner. For comparison, the pH-insensitive counterpart polymer of PEG-BAmi-dC_{12} was also synthesized for micelles preparation. The physicochemical characterization, colloidal stability, drug release, cellular uptake, and *in vitro* cytotoxicity of the micelles were evaluated.

MATERIALS AND METHODS

Chemicals and Reagents

Paclitaxel (PTX), 1-ethyl-3-[3-dimethylaminopropyl] carbodiimide hydrochloride (EDC), *N*-hydroxysulfosuccinimide (NHS), 4-dimethylaminopyridine (DMAP), lauroyl chloride, α-methoxy-x-amino-poly(ethylene glycol) (Mn = 2000) (MeO-PEG2000-NH_2) were purchased from Shanghai Aladdin Reagent Co. Ltd. (Shanghai, China). mPEG-hydrazide (Mn = 2000) was from Seebio Biotech, Inc. (Shanghai, China), and 3,5-dihydroxybenzaldehyde was from Bide Pharmatech Ltd. (Shanghai, China). 3,5-Dihydroxybenzoic acid was obtained from Saen Chemical Technology Co. Ltd. (Shanghai, China). Potassium hydroxide (KOH), tetrahydrofuran (THF), dimethyl sulfoxide (DMSO), petroleum ether, ethyl acetate were purchased from Sinopharm Chemical Reagent Co., Ltd. (Shanghai, China). 3-(4,5-dimethylthiazol-2-yl)-2,5-diphenyl tetrazolium bromide (MTT), coumarine (Cou-6) and 4′,6-diamidino-2-phenylindole (DAPI) were obtained from Sigma-Aldrich Co. (St. Louis, MO, United States). Lysotracker red was supplied from Beyotime Institute of Biotechnology (Jiangsu, China). Dulbecco's modified Eagle's medium (DMEM), RPMI 1640, penicillin, streptomycin, phosphate buffered saline (PBS), fetal bovine serum (FBS) were purchased from Gibco Life Technologies, Inc. (Carlsbad, CA, United States). Human lung cancer cells (A549), human breast cancer cells (MDA-MB-231), human ovarian cancer cells (A2780) were obtained from Xiangya cell center (Changsha, China). PTX-resistant human lung cancer cells (A549/T) was bought from Gefan Biotechnology Co., Ltd. (Shanghai, China).

Synthesis of the pH-Sensitive Copolymer PEG-BHyd-dC_{12}

3,5-Dihydroxybenzaldehyde was dissolved in THF, followed by the addition of KOH. Lauroyl chloride was added dropwise into the above mixture and vigorously stirred for 6 h to yield 3,5-dilaurate benzaldehyde. The purified 3,5-dilaurate benzaldehyde and mPEG-hydrazide were dissolved in ethyl alcohol and stirred for 24 h. After purification, the final amphiphilic polymer PEG-BHyd-dC_{12} was obtained.

Synthesis of the pH-Insensitive Copolymer PEG-BAmi-dC_{12}

First, lauroyl chloride was added dropwise to a mixture of 3,5-dihydroxybenzoic acid with KOH in anhydrous acetone at 0°C under stirring to obtain 3,5-dilaurate benzoic acid. Then, 3,5-dilaurate benzoic acid, EDC, DMAP and NHS were dissolved into DMSO and stirred at room temperature for 2 h, followed by the addition of MeO-PEG2000-NH_2. The resulting solution was dialyzed and subsequently lyophilized to obtain PEG-BAmi-dC_{12}.

Characterization of Copolymers

The ^{1}H-NMR spectra of PEG-BHyd-dC_{12} and PEG-BAmi-dC_{12} were recorded using a Bruker Avance 400 MHz NMR spectrometer (Varian, United States) with deuterated chloroform ($CDCl_3$) as the solvent. The self-assembly behavior of polymers was investigated by the fluorescence probe technique (Xiong et al., 2017). First, 100 μL of pyrene in acetone (2.9×10^{-2} mM) was evaporated to form a thin film on the flask bottom. Then, various concentrations of polymer solutions (from 0.1 μg/mL to 200 μg/mL) were added to the pyrene-coated vials and stored in the dark overnight. The fluorescence intensity ratio of I_{337}/I_{334} in the emission spectra of pyrene was calculated and plotted against the logarithm of the polymer concentrations. The CMC value was obtained based on the fluorescence excitation spectra of the mixed solution.

Preparation of Micelles

PTX-loaded micelles were prepared by a thin-film hydration method. In brief, PEG-BHyd-dC_{12} or PEG-BAmi-dC_{12} (20.0 mg) and PTX (1 mg) were dissolved in dichloromethane (4 mL).

The solution was evaporated under reduced pressure to form a uniform film. Deionized water (10 mL) was added and rotated for another 1 h. The obtained colloidal solution was then centrifuged at 3,000 rpm for 10 min and filtered through 0.45 μm pore size filter, followed by lyophilization. Blank micelles were prepared in a similar way in the absence of PTX.

Characterization of Micelles

The particle size, PDI, and zeta potential measurement were determined by dynamic light scattering (DLS) method using a Malvern Zeta Sizer Nano series (Nano ZS, Malvern Instruments, United Kingdom) at 25°C. The morphologies of the micelles were observed using transmission electron microscopy (TEM) (Titan G2-F20, FEI, United States).

The determination of PTX was carried out using a high-performance liquid chromatography (HPLC) system (LC-2010, Shimadzu, Tokyo, Japan). The chromatographic column was an ODS C_{18} (250 × 4.6 mm, 5 μm, Diamonsil, Beijing, China). The mobile phase consisted of mixtures of acetonitrile and water (55:45, v/v). The flow rate was 1 $mL{\cdot}min^{-1}$, and the detection wavelength was 227 nm. Micelles were centrifuged in an ultrafiltration tube (MWCO 10 kDa) at 5,000 rpm for 10 min and filtered through 0.22 μm filter to remove the unloaded PTX. PTX-loaded micelles were disrupted by methanol. The PTX loading content (LC) and encapsulated efficiency (EE) were calculated using the following formulae:

$$\text{EE (\%)} = \text{Amount of PTX in micelles/Amount of PTX fed initially} \times 100\%$$

$$\text{LC (\%)} = \text{Amount of PTX in micelles/Amount of PTX-loaded micelles} \times 100\%$$

Colloidal Stability

Micelles were incubated with 10% FBS or 10 mM phosphate buffer solutions (pH 7.4, 6.5, and 5.5) at 37°C for 72 h, and the size was measured by DLS at different intervals.

In vitro Drug Release

The release study was assessed by the dialysis method. The release media was PBS solutions containing 0.5% Tween-80 with different pH values (5.5, 6.5, and 7.4). Typically, 2 mL of PTX-loaded micelles was placed in a dialysis bag (MWCO 3500) and dialyzed against 25 mL of buffer medium under mechanical shaking (100 rpm) at 37°C. At predetermined time intervals, 2 mL of release medium was withdrawn and replenished with an equal volume of fresh medium. The released PTX was detected by HPLC.

Cell Culture

A549 and A549/T cells were maintained in RPMI 1640 medium supplemented with 10% FBS, penicillin (50 U/mL) and streptomycin (50 U/mL) in a 5% CO_2 atmosphere at 37°C. MDA-MB-231 and A2780 were maintained in DMEM medium supplemented with 10% FBS, penicillin (50 U/mL) and streptomycin (50 U/mL) in a 5% CO_2 atmosphere at 37°C.

Intracellular Distribution

Cou-6 loaded micelles were constructed according to the above method, except the drug was replaced with Cou-6. A549 cells were seeded on glass coverslips in the 24-well plates at a density of 4×10^4 per well. After culturing for 24 h, Cou-6 loaded micelles ([Cou-6] = 200 ng/mL) were added and incubated for 1 h. Alternatively, the cells were incubated with Cou-6 loaded micelles for 1 h, then washed and cultured in fresh media for another 3 h. Then, the medium was replaced with 70 nM lysotracker red and incubated for another 1 h. Afterward, the cells were fixed with 4% formaldehyde for 20 min at room temperature and visualized using a CLSM (LSM 780, Carl Zeiss, Jena, German).

Cellular Uptake

A549 cells were seeded in 6-well plates with a density of 3×10^5 cells per well and incubated overnight, and then, the medium was replaced with Cou-6 loaded micelles at final Cou-6 concentration of 200 ng/mL. After 1 h or 4 h of incubation, the cells were harvested and quantified by flow cytometry (FACSVerse, BD, United States).

Cytotoxicity Assay

The cytotoxicity of micelles with or without an anticancer drug was determined by MTT assay. The cells were seeded in a 96-well plate at a density of 6,000 cells per well and maintained for 24 h. The medium was then replaced with the micelles and further incubated for 72 h. Then, 20 μL of MTT solution (5 mg/mL) was added to each well of the plate for another 4 h. Subsequently, 100 μL of DMSO was added to dissolve the formazan crystals, and the absorbance was measured at 570 nm by a microplate reader (ELX800, Bio-Tek, United States). The untreated cells were used as controls.

Hemolysis Tests

The hemocompatibility of micelles was evaluated by hemolysis assay (Yang et al., 2016). First, fresh rabbit blood was extracted from the heart of a rabbit. Subsequently, erythrocytes were obtained by centrifugation at 3,000 rpm for 15 min and washed with normal saline (NS). Serial dilutions of micelles were then added to the 2% erythrocytes (v/v) and incubated for 2 h at 37°C in a thermostatic water bath. Finally, the mixtures were centrifuged at 3,500 rpm for 15 min, and the supernatant of all samples was measured for UV absorbance (A) at 540 nm. NS and 0.5% Triton X-100 were regarded as the negative and positive controls, respectively. The hemolysis ratio was calculated as follows:

$$\text{Hemolysis (\%)} = (A_{\text{sample}} - A_{\text{control}(-)})/(A_{\text{control}(+)} - A_{\text{control}(-)})$$

Statistical Analysis

The data were expressed as the mean ± standard deviation (SD). Statistical analysis was performed using a two-tailed Student's *t*-test and analysis of variance (ANOVA) with the aid of SPSS 23.0 software. Differences were considered statistically significant when *p*-values were less than 0.05.

RESULTS AND DISCUSSION

Synthesis and Characterizations of Copolymers

The synthesis schemes of PEG-BHyd-dC_{12} and PEG-BAmi-dC_{12} were illustrated in **Figures 1A,B**. To synthesize the PEG-BHyd-dC_{12} di-block amphiphilic polymer, the hydrophobic fragment of 3,5-dilaurate benzaldehyde was conjugated with the hydrophilic fragment of PEG through the linkage of hydrazone. The 3,5-dihydroxybenzaldehyde was first reacted with lauroyl chloride to form a 3,5-dilaurate benzaldehyde intermediate with a yield of 90%, and then the aldehyde group on 3,5-dilaurate benzaldehyde reacted with the hydrazine groups on mPEG-hydrazide to give PEG-BHyd-dC_{12} with a final yield was 69%. All of the synthetic compounds were characterized by ^{1}H-NMR spectra (**Figures 1C,D**), which were in good agreement with their depicted structures as described in the following:

^{1}H NMR of intermediate compound 3,5-dilaurate benzaldehyde: ^{1}H NMR (400 MHz, $CDCl_3$) δ (ppm) 0.91 (6H, t, -CH_3), 1.21–1.45 (32H, m, -$(CH_2)_n$), 1.75 (4H, m, CO-βH), 2,59 (4H, t, CO-αH), 7.20 (1H, t, 4-ArH), 7.52 (2H, d, 2,6-ArH), 9.98 (1H, s, -CHO).

^{1}H NMR of PEG-BHyd-dC_{12}: ^{1}H NMR (400 MHz, $CDCl_3$) δ (ppm) 0.89 (6H, t, -CH_3), 1.22–1.45 (32H, m, -$(CH_2)_n$), 1.74 (4H, m, CO-βH), 2,54 (4H, t, CO-αH), 3.39 (3H, s, -OCH_3 from PEG), 3.50–3.84 ((-OCH_2CH_2-)$_n$), 4.19 (2H, s, CO-αH, from PEG), 6.94 (1H, t, 4-ArH), 7.41 (2H, d, 2,6-ArH), 8.24 (1H, s, -NH), 10.5 (1H, s, -CH = N).

As for PEG-BHyd-dC_{12}, the characteristic peaks at 3.5–3.84 ppm were from PEG, and the proton peak at 10.5 ppm indicated the formation of the hydrazone bond. In addition, the absence of proton peak of aldehyde (9.98 ppm) suggested that free 3,5-dilaurate benzaldehyde was removed in the purified PEG-BHyd-dC_{12}.

^{1}H NMR of intermediate compound 3,5-dilaurate benzoic acid: ^{1}H NMR (400 MHz, $CDCl_3$) δ (ppm) 0.90 (6H, t, -CH_3), 1.21–1.44 (32H, m, -$(CH_2)_n$), 1.71 (4H, m, CO-βH), 2,61 (4H, t, CO-αH), 7.20 (1H, t, 4-ArH), 7.72 (2H, d, 2,6-ArH).

^{1}H NMR of PEG-BAmi-dC_{12}: ^{1}H NMR (400 MHz, $CDCl_3$) δ (ppm) 0.90 (6H, t, -CH_3), 1.22–1.45 (32H, m, -$(CH_2)_n$), 1.75 (4H, m, CO-βH), 2,58 (4H, t, CO-αH), 3.40 (3H, s, -OCH_3 from PEG), 3.50–3.84 ((-OCH_2CH_2-)$_n$), 7.06 (1H, t, 4-ArH), 7.45 (2H, d, 2, 6-ArH), 7.79 (1H, d, -CONH).

The characteristic peaks of PEG (3.50–3.84 ppm) were obvious, and the peak of new amide bond can be seen at 7.79 ppm for PEG-BAmi-dC_{12}.

CMC Measurement

As amphiphilic materials, a key parameter for their applications as a nanocarrier is their CMC. Micelles can be formed at concentrations above the CMC. The CMC values of PEG-BHyd-dC_{12} and PEG-BAmi-dC_{12} were determined by a well-established method using pyrene as a fluorescence probe, resulting in

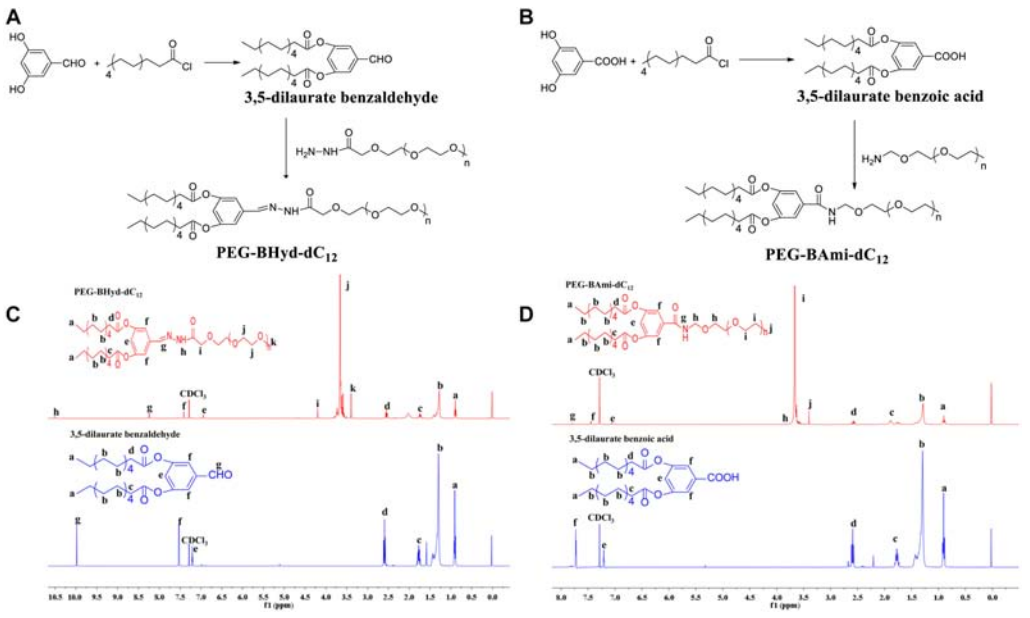

FIGURE 1 | Synthesis and characterization of PEG-BHyd-dC_{12} **(A,C)** and PEG-BAmi-dC_{12} **(B,D)**. The synthesis of PEG-BHyd-dC_{12} **(A)** and PEG-BAmi-dC_{12} **(B)**, H1-NMR spectrum of PEG-BHyd-dC_{12} **(C)**, and PEG-BAmi-dC_{12} **(D)**.

7.5 μg/mL for PEG-BHyd-dC$_{12}$ and 5.6 μg/mL for PEG-BAmi-dC$_{12}$ (**Figure 2**). These CMC values were within the typical concentration range for most polymeric micelle CMCs, which can be directly applied *in vivo* (Maysinger et al., 2007; Diezi et al., 2010; Owen et al., 2012). It is reasonable that these two polymers have comparable CMC values, as their structures are nearly identical; they only differed at the junction between the hydrophobic and hydrophilic blocks (one with a hydrazone bond and the other with an amide bond). Therefore, PEG-BAmi-dC$_{12}$ is an excellent control to study the pH-responsive property of PEG-BHyd-dC$_{12}$ for drug delivery.

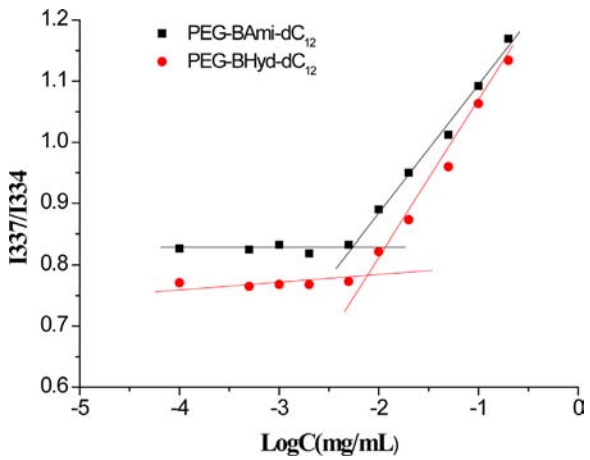

FIGURE 2 | The CMC curve of PEG-BHyd-dC$_{12}$ and PEG-BAmi-dC$_{12}$.

Preparation and Characterization of Micelles

From the above experiments, we have demonstrated that both PEG-BHyd-dC$_{12}$ and PEG-BAmi-dC$_{12}$ were able to self-assemble into micelles at very low concentrations, implying their applicability for the development of a nano-drug delivery system. We next used these polymers to prepare micelles, and the hydrophobic PTX was used a model to encapsulate into the hydrophobic core of the micelles (**Figure 3A**). The pH-sensitive micelles (PEG-BHyd-dC$_{12}$/PTX) were prepared using a standard thin-film hydration method. After removing the organic solvents, the solution appeared to be semi-transparent with light-blue opalescence (Inset in **Figure 3B**, left), suggesting the successful preparation of nano-sized micelles. The particle size was approximately 135 nm as determined by DLS (**Figure 3B**, left); this size is suitable for passive accumulation in the tumor tissue through the EPR effect (Danhier et al., 2010). From TEM, the micelles were well dispersed with spherical morphology (Inset in **Figure 3B**, left). The LC efficiency of PEG-BHyd-dC$_{12}$/PTX was 3% (**Figure 3C**), which was comparable to many other PTX-loading micelles reported previously, and was sufficient for subsequent *in vitro*/*in vivo* therapeutic applications (Lee et al., 2003; Zhu et al., 2010; Mei et al., 2015).

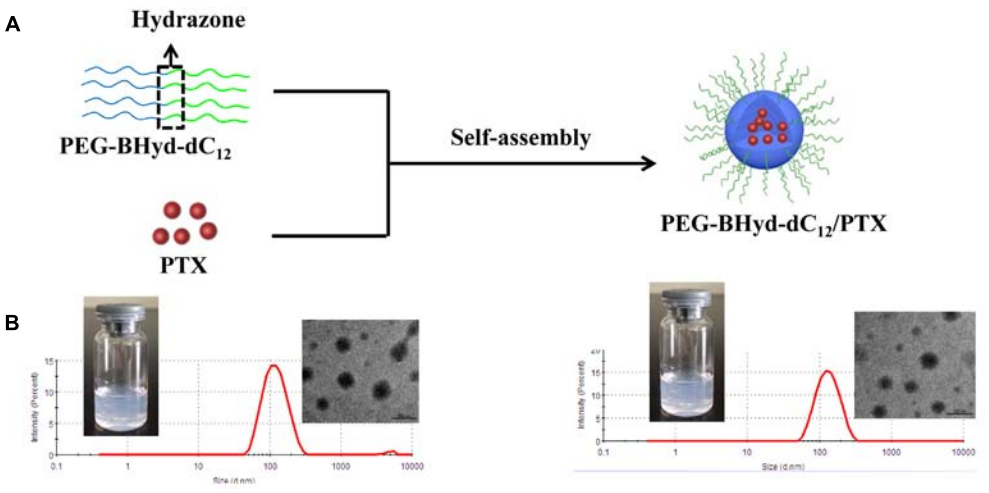

C

	Size (nm)	PDI	EE (%)	LC (%)
PEG-BHyd-dC$_{12}$/PTX	135.50±0.24	0.25±0.019	65.53±3.11	3.2±1.12
PEG-BAmi-dC$_{12}$/PTX	127.30±0.28	0.23±0.017	67.65±2.98	3.1±1.09

FIGURE 3 | Preparation and characterization of micelles. Schematic preparation **(A)**, appearance, size distribution, and TEM images (**B**, left presents PEG-BHyd-dC$_{12}$/PTX, right presents PEG-BAmi-dC$_{12}$/PTX), characterization **(C)**. Data were presented as mean ± standard deviation (SD; n = 3).

By using the same method, the pH-insensitive PEG-BAmi-dC$_{12}$/PTX micelles were also prepared and characterized (**Figure 3B**, right; **Figure 3C**). Interestingly, these two types of micelles displayed quite similar properties in terms of appearance, particle size, morphology and drug loading efficiency. Therefore, a parallel comparison between these micelles can be made for their *in vitro/in vivo* biological performance, which can be rationalized by the pH-responsive bond linkage.

Colloidal Stability

The colloidal stability of the micelles was first studied under different buffer solutions. Interestingly, with pH decrease from 7.4 to 6.5 and 5.5, the particle size of PEG-BHyd-dC$_{12}$/PTX markedly increased, while it remained unchanged for PEG-BAmi-dC$_{12}$/PTX (**Figure 4A**). This can be rationalized by the pH-responsive property of the PEG-BHyd-dC$_{12}$/PTX, which could swell and then collapse at lower pH (Li et al., 2016; Qiu et al., 2017). We also challenged the micelles with 10% FBS, and both types of micelles were quite stable even after 72 h incubation (**Figure 4B**). Therefore, the pH-sensitive micelles were stable in blood circulation and can rapidly collapse to release the payload under acidic conditions.

In vitro Drug Release

The release behavior of PTX from polymeric micelles was evaluated under various conditions at 37°C. Different buffer solutions were employed to simulate the micro-environment of the blood circulation (pH 7.4), tumor tissue (pH 6.5), and endosome (pH 5.5). We first studied the performance of pH-sensitive PEG-BHyd-dC$_{12}$/PTX micelles. At pH 7.4, almost no PTX was released in the initial 4 h, which was followed by a sustained release phase with only 38% PTX release after 48 h (**Figure 5A**, black trace). Therefore, the micelles can stably encapsulate PTX for a long time, which is important for decreasing the side effects and increasing the drug accumulation in tumor sites. By lowering the pH to 6.5, a notable increase in drug release was observed at each time point (**Figure 5A**, blue trace). With further decrease of the pH to 5.5, the micelles showed an even higher rate of drug release (**Figure 5A**, red trace). After 48 h, the cumulative drug release was 50% and 65%, respectively, significantly higher than that at pH 7.4 (∼40%), indicating a good pH-responsive capability. This pH-responsive drug release profile can be ascribed to the hydrazone bond between the hydrophilic and hydrophobic chains of the polymer. As the pH decreases, the hydrazone bond tends to hydrolyse

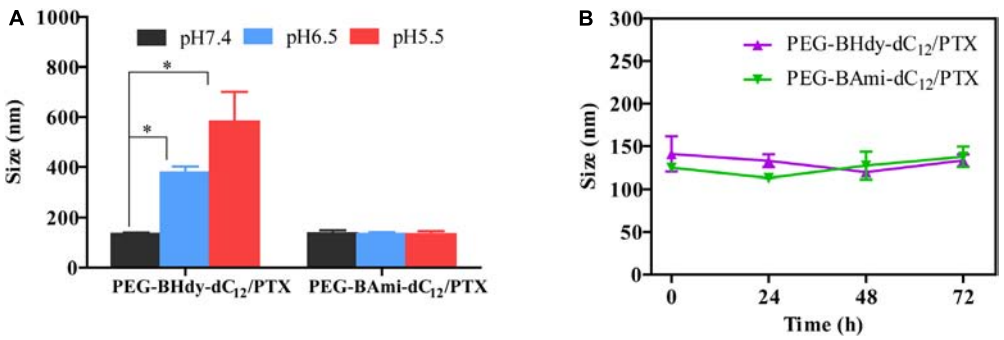

FIGURE 4 | Colloidal stability of micelles. Size change of PEG-BHyd-dC$_{12}$/PTX micelles and PEG-BAmi-dC12/PTX micelles in phosphate buffers with different pH values **(A)** and 10% FBS **(B)** at 37°C for 72 h. The pHs were buffered by disodium hydrogen phosphate and sodium dihydrogen phosphate with total phosphate concentration of 10 mM. Data were shown as mean ± SD (n = 3). *p < 0.05.

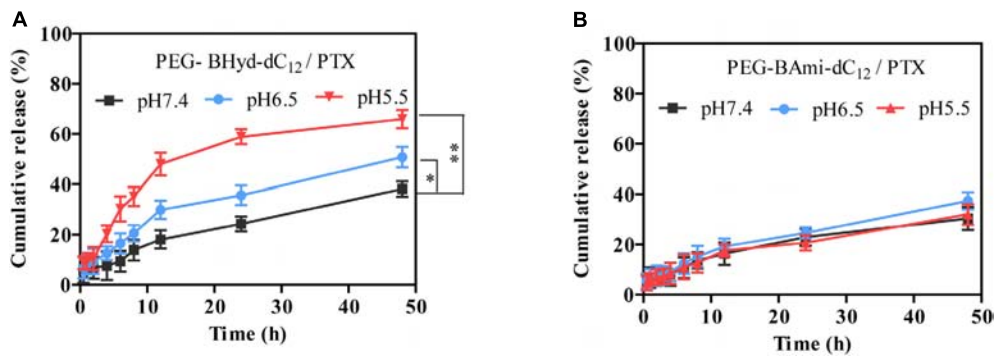

FIGURE 5 | Release profiles of PEG-BHyd-dC$_{12}$/PTX micelles **(A)** and PEG-BAmi-dC12/PTX micelles **(B)** at different pHs at 37°C. The pHs were buffered by disodium hydrogen phosphate and sodium dihydrogen phosphate with total phosphate concentration of 10 mM. Data were shown as mean ± SD (n = 3). *p < 0.05, **p < 0.01.

and thus the micelles collapse, resulting in burst drug release.

As a control, we also performed the drug release experiment with pH-insensitive PEG-BAmi-dC_{12}/PTX micelles. In this case, slow and sustained drug release was seen under different conditions, and pH had little effect on the rate of drug release, giving a cumulative drug release of less than 40% after 48 h (**Figure 5B**). Considering the structural difference

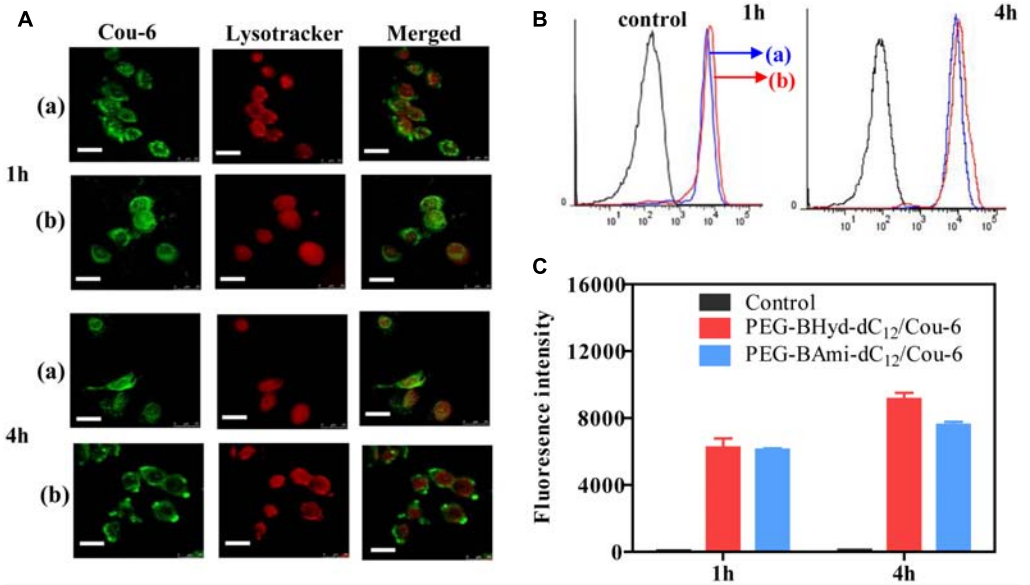

FIGURE 6 | Cellular uptake studies of PEG-BHyd-dC_{12}/Cou-6 and PEG-BAmi-dC_{12}/Cou-6 in A549 cells by using CLSM **(A)**, flow cytometry **(B)**, fluorescence intensities quantified from **B (C)**. The (a) indicated PEG-BAmi-dC12/Cou-6 while the (b) represented PEG-BHyd-dC_{12}/Cou-6. The scale bar is 25 μm.

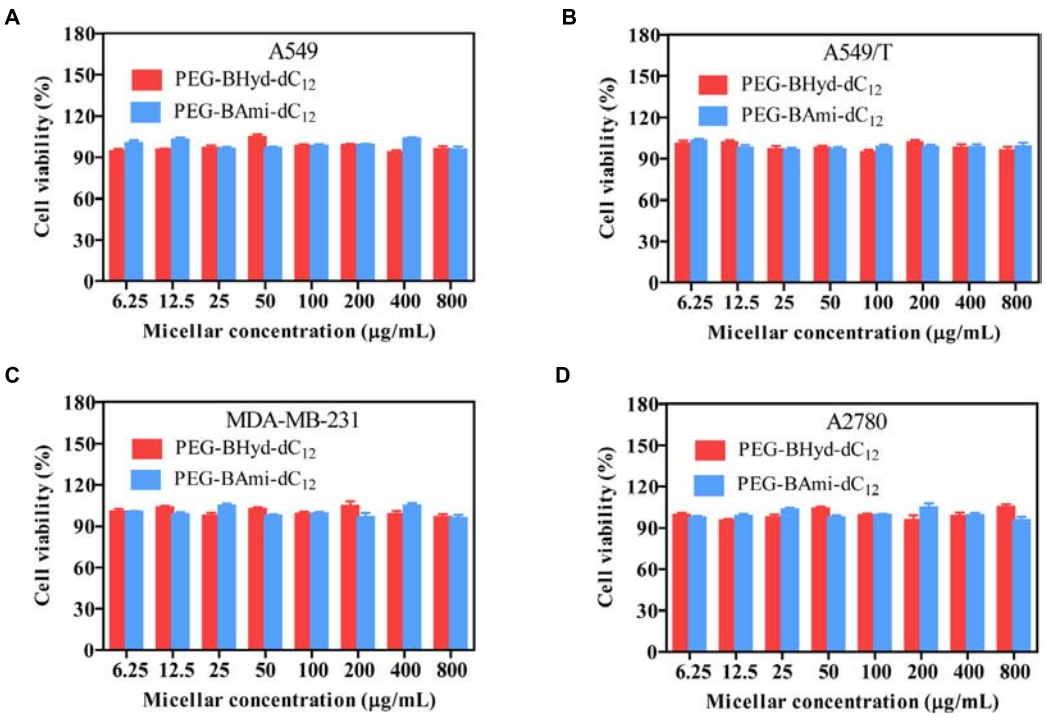

FIGURE 7 | Cell viability of blank micelles after incubating with A549 **(A)**, A549/T **(B)**, MDA-MB-231 **(C)**, and A2780 **(D)** cells for 72 h. Data were shown as mean ± SD (n = 4).

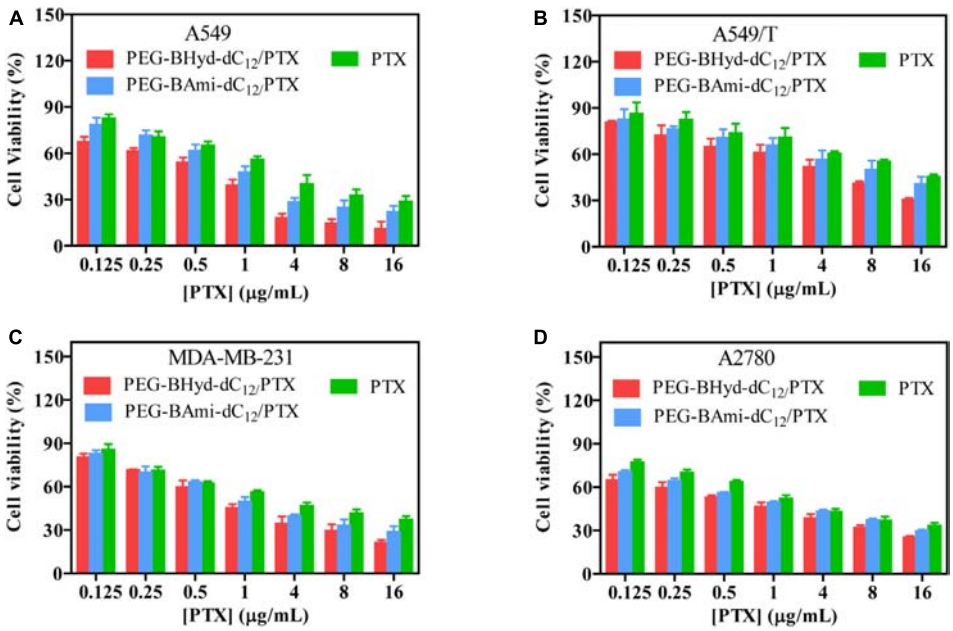

FIGURE 8 | Cell viability of PTX-loaded micelles and free PTX after incubating with A549 **(A)**, A549/T **(B)**, MDA-MB-231 **(C)**, and A2780 **(D)** cells for 72 h. Data were shown as mean ± SD (n = 4).

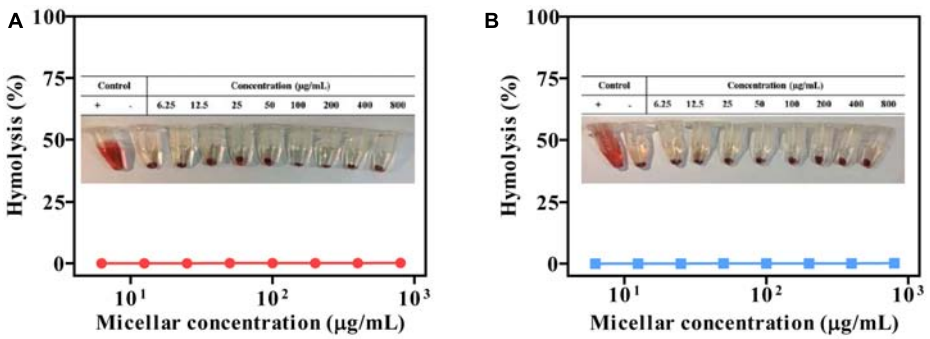

FIGURE 9 | Compatibility studies of micelles (pH 7.4). PEG-BHyd-dC12 **(A)** and PEG-BAmi-dC12 **(B)**. "+" represents positive control by using 0.5% Triton X-100, and "–" represents negative control of non-treatment.

TABLE 1 | IC_{50} value of the micelles and free PTX to A549, A549/T, MDA-MB-231, and A2780 cells for 72 h incubation (mean ± SD, n = 4).

	IC_{50} (μg/mL)			
	A549	**A549/T**	**MDB-MA-231**	**A2780**
PTX	1.87 ± 0.08	11.17 ± 1.15	2.99 ± 0.37	2.01 ± 0.04
PEG-BHyd-dC_{12}/PTX	0.57 ± 0.16*▲	3.04 ± 1.13*▲	1.16 ± 0.06*▲	0.75 ± 0.08**▲
PEG-BAmi-dC_{12}/PTX	1.10 ± 0.06#	6.77 ± 0.30#	1.64 ± 0.13#	1.33 ± 0.13#

*PTX vs. PEG-BHyd-dC_{12}/PTX, *$p < 0.05$, **$p < 0.01$; PTX vs. PEG-BAmi-dC_{12}/PTX, #$p < 0.05$; PEG-BHyd-dC_{12}/PTX vs. PEG-BAmi-dC_{12}/PTX, ▲$p < 0.05$.*

between PEG-BHyd-dC_{12}/PTX and PEG-BAmi-dC_{12}/PTX, these results further demonstrated critical role of the hydrazone bond for the pH-sensitive property of the PEG-BHyd-dC_{12}/PTX micelles.

Intracellular Uptake Study

Having demonstrated the pH-responsive property of the PEG-BAmi-dC_{12}/PTX micelles, we next studied the performance of the micelles inside cells. To conveniently track the micelles inside cells, Cou-6 (a hydrophobic green fluorophore) instead of PTX was encapsulated into micelles, and the acidic organelles (i.e., lysosomes and endosomes) were stained by Lysotracker red. A549 cancer cell line was used as a model since PTX has been widely used in clinic for lung cancer therapy (Singla et al., 2002). From confocal laser scanning microscopy (CLSM), substantial green fluorescence was observed for both types of micelles after 1 h incubation (**Figure 6A**), indicating a high level of cellular

internalization. To visualize the co-localization of micelles and endo/lysosomes, we merged the green and red channels, and the emergence of orange spots indicated the localization of micelles in the endo/lysosomes. Both PEG-BHyd-dC_{12}/Cou-6 and PEG-BAmi-dC_{12}/Cou-6 micelles showed obvious spots after 1 h of incubation, consistent with the endocytosis pathway of the micelles (Zhang et al., 2017).

We next studied the intracellular performance of the micelles. To do this, the cells were washed and cultured in fresh media so that further internalization of micelles was avoided. After 4 h incubation, the pH-insensitive micelles were still largely entrapped into the endo/lysosomes. In contrast, the orange spots of pH-sensitive micelles were weakened, and green color was evenly distributed throughout the cytoplasm, which showed minimal co-localization with the red fluorescence of the endo/lysosomes. The micelles detached from endosome due to hydrolysis of copolymer under acidic organelles, which facilitated efficient release of drug. Therefore, successful endo/lysosomal escape of pH-sensitive micelles was indicated. It is known that the successful escape of a nano-delivery system from the intracellular endosome/lysosome for drug release is a key issue in determining their therapeutic efficiency (Qiu et al., 2017). After cellular uptake, micelles were first entrapped into endosome/lysosome (Chou et al., 2011; Varkouhi et al., 2011). Once entering the endo/lysosomes, the pH-sensitive micelles were disassembled because of pH-triggered hydrolysis of the acid-labile chemical linkage, and the drug rapidly escaped from the endosome/lysosome, resulting in pH-triggered intracellular burst release (Fang et al., 2016).

To have a quantitative understanding, we next performed flow cytometry experiments to study the uptake of micelles by A549 cells (**Figures 6B,C**). After 1 h incubation, there was no difference in intensity between pH-sensitive and pH-insensitive micelles. Interestingly, after 4 h, the fluorescence from pH-responsive micelles was considerably higher than that of pH-insensitive micelles (**Figure 6C**), in agreement with a previous report (Qiu et al., 2017). While the pH-responsiveness of micelles has little effect on cell uptake process, the relative lower fluorescence for PEG-BAmi-dC_{12}/PTX was likely due to the efflux of the micelles from cells to medium. As has been demonstrated, the endo/lysosome entrapped micelles can be pumped out by ATP-binding cassette protein B1 (ABCB1) transporter (Sakai-Kato et al., 2012). Since the pH-responsive micelles collapse faster in endo/lysosome, relatively less micelles were cleared from cells by this pump-out process, resulting in stronger fluorescence inside cells.

Cytotoxicity Assay

Cytotoxicity studies were performed by incubating micelles with different types of cells for 72 h, and cell viability was measured by MTT assay. The cytotoxicity of the polymers was tested by incubating the cells with blank micelles (without PTX loading), and all types of cells remained >90% viability with concentration up to 800 μg/mL, indicating high biocompatibility (**Figure 7**). As for A549, at the highest PTX concentration (16 μg/mL), the viabilities of cells incubated with PEG-BHyd-dC_{12}/PTX, PEG-BAmi-dC_{12}/PTX and free PTX dropped to 11%, 22%, and 28%, respectively, showing high toxicity to cancer cells (**Figure 8A**). The anti-cancer capability was quantified by measuring the half-maximal inhibitory concentration (IC_{50}), which was in order of PEG-BHyd-dC_{12}/PTX (0.57 μg/mL) < PEG-BAmi-dC_{12}/PTX (1.1 μg/mL) < free PTX (1.87 μg/mL) (**Table 1**). Therefore, PEG-BHyd-dC_{12}/PTX exhibited the highest activity, which was attributable to the pH-responsive property for rapid endo/lysosome drug escape to enhance the antitumor effect.

To test the generality, we further performed the anti-tumor assay by using MDA-MB-231 and A2780 cells, and analogous results were observed (**Figures 8C,D**). The PEG-BHyd-dC_{12}/PTX displayed the best anti-cancer activity, followed by PEG-BAmi-dC_{12}/PTX and then free PTX. Therefore, such micelles can be implemented for different types of cancer therapy. As one limitation of PTX for long-term cancer treatment is the acquired drug resistance by cancer cells (Yusuf et al., 2003), we also tested whether the nano-systems could reverse drug resistance by using PTX-resistant A549/T cells as a proof-of-concept. The cytotoxicity of PTX and micelles was also dose dependent (**Figure 8B**), while the overall IC_{50} value was much higher due to the drug resistance (**Table 1**). Notably, cytotoxicity of PEG-BHyd-dC_{12}/PTX was 3.7-fold higher than that of free PTX, which may be useful to reverse drug resistance.

Hemolysis Assay

The biocompatibility of polymeric micelles is the prerequisite for biomedical application. We studied this property by using hemolysis assay. Typically, the micelles were incubated with erythrocytes, and the release of hemoglobin was measured to quantify the erythrocyte-damaging properties (Nogueira et al., 2013). The positive control of 0.5% Triton X-100 showed obvious hemolysis, as high as 100%, while the micelles produced less than 2% at different concentration (**Figure 9**). Therefore, the micelles were highly biocompatible and can be directly administrated by intravenous injection.

CONCLUSION

In this work, pH-sensitive PTX-loaded PEG-BHyd-dC_{12} micelles were constructed and characterized. These nanoparticles exhibited pH-dependent drug release profile and endosomal escape ability after intracellular delivery, and displayed enhanced anti-tumor activity compared with the pH-insensitive counterpart micelles and the free PTX. All of these results suggested that the PEG-BHyd-dC_{12} micelles-based drug delivery system is a promising drug carrier for targeted cancer treatment.

AUTHOR CONTRIBUTIONS

YY performed the cell experiments and wrote the manuscript. ZW performed the synthesis and characterization. YP performed drug release. JD and WZ designed the experiments.

FUNDING

Thanks to the supported of the Innovation-Driven Project of Central South University (Grant No. 20170030010004), National Natural Science Foundation of China (Grant Nos. 81573374 and 81502997), Key Laboratory Breeding Base of Hunan Oriented Fundamental and Applied Research in Innovative Pharmaceutics (Grant No. 2016TP1029), Hunan Engineering Research Center for Optimization of Drug Formulation and Early Clinical Evaluation (Grant No. 2015TP2005), and Director Fund of Jiangsu Key Laboratory of New Drug Research and Clinical Pharmacy (Grant No. ZR-XY201406).

REFERENCES

Ahmed, S. E., Martins, A. M., and Husseini, G. A. (2015). The use of ultrasound to release chemotherapeutic drugs from micelles and liposomes. *J. Drug Target.* 23, 16–42. doi: 10.3109/1061186X.2014.954119

Ao, L., Wang, B., Liu, P., Huang, L., Yue, C., Gao, D., et al. (2014). A folate-integrated magnetic polymer micelle for MRI and dual targeted drug delivery. *Nanoscale* 6, 10710–10716. doi: 10.1039/c4nr02484b

Cao, J., Huang, S., Chen, Y., Li, S., Li, X., Deng, D., et al. (2013). Near-infrared light-triggered micelles for fast controlled drug release in deep tissue. *Biomaterials* 34, 6272–6283. doi: 10.1016/j.biomaterials.2013.05.008

Chou, L. Y., Ming, K., and Chan, W. C. (2011). Strategies for the intracellular delivery of nanoparticles. *Chem. Soc. Rev.* 40, 233–245. doi: 10.1039/c0cs00003e

Danhier, F., Feron O., and Préat, V. (2010). To exploit the tumor microenvironment: passive and active tumor targeting of nanocarriers for anti-cancer drug delivery. *J. Control. Release* 148, 135–146. doi: 10.1016/j.jconrel.2010.08.027

Deng, L., Ren, J., Li, J., Leng, J., Qu, Y., Lin, C., et al. (2015). Magnetothermally responsive star-block copolymeric micelles for controlled drug delivery and enhanced thermo-chemotherapy. *Nanoscale* 7, 9655–9663. doi: 10.1039/c5nr00642b

Diezi, T. A., Bae, Y., and Kwon, G. S. (2010). Enhanced stability of PEG-block-poly(N-hexyl stearate l-aspartamide) micelles in the presence of serum proteins. *Mol. Pharm.* 7, 1355–1360. doi: 10.1021/mp100069p

Du, J. Z., Du, X. J., Mao, C. Q., and Wang, J. (2011). Tailor-made dual pH-sensitive polymer-doxorubicin nanoparticles for efficient anticancer drug delivery. *J. Am. Chem. Soc.* 133, 17560–17563. doi: 10.1021/ja207150n

Fang, X. B., Zhang, J. M., Xie, X., Liu, D., He, C. W., Wan, J. B., et al. (2016). pH-sensitive micelles based on acid-labile pluronic F68-curcumin conjugates for improved tumor intracellular drug delivery. *Int. J. Pharm.* 502, 28–37. doi: 10.1016/j.ijpharm.2016.01.029

Farokhzad, O. C., and Langer, R. (2009). Impact of nanotechnology on drug delivery. *ACS Nano* 3, 16–20. doi: 10.1021/nn900002m

Felber, A. E., Dufresne, M. H., and Leroux, J. C. (2012). pH-sensitive vesicles, polymeric micelles, and nanospheres prepared with polycarboxylates. *Adv. Drug Deliv. Rev.* 64, 979–992. doi: 10.1016/j.addr.2011.09.006

Gao, Y., Xiao, Y., Liu, S., and Yu, J. (2018). Camptothecin prodrug nanomicelle based on a boronate ester-linked diblock copolymer as the carrier of doxorubicin with enhanced cellular uptake. *J. Biomater. Sci. Polym. Ed.* 29, 160–180. doi: 10.1080/09205063.2017.1406632

Harnoy, A. J., Rosenbaum, I., Tirosh, E., Ebenstein, Y., Shaharabani, R., Beck, R., et al. (2014). Enzyme-responsive amphiphilic PEG-dendron hybrids and their assembly into smart micellar nanocarriers. *J. Am. Chem. Soc.* 136, 7531–7534. doi: 10.1021/ja413036q

Kanamala, M., Wilson, W. R., Yang, M., Palmer, B. D., and Wu, Z. (2016). Mechanisms and biomaterials in pH-responsive tumour targeted drug delivery: a review. *Biomaterials* 85, 152–167. doi: 10.1016/j.biomaterials.2016.01.061

Kim, T. H., Chen, Y., Mount, C. W., Gombotz, W. R., Li, X., and Pun, S. H. (2010). Evaluation of temperature-sensitive, indocyanine green-encapsulating micelles for noninvasive near-infrared tumor imaging. *Pharm. Res.* 27, 1900–1913. doi: 10.1007/s11095-010-0190-y

Lee, S. C., Kim, C., Kwon, I. C., Chung, H., and Jeong, S. Y. (2003). Polymeric micelles of poly(2-ethyl-2-oxazoline)-block-poly(epsilon-caprolactone) copolymer as a carrier for paclitaxel. *J. Control. Release* 89, 437–446. doi: 10.1016/S0168-3659(03)00162-7

Li, M., Gao, M., Fu, Y., Chen, C., Meng, X., Fan, A., et al. (2016). Acetal-linked polymeric prodrug micelles for enhanced curcumin delivery. *Colloids Surf. B Biointerfaces* 140, 11–18. doi: 10.1016/j.colsurfb.2015.12.025

Liu, B., Chen, H., Li, X., Zhao, C., Liu, Y., Zhu, L., et al. (2014). pH-responsive flower-like micelles constructed via oxime linkage for anticancer drug delivery. *RSC Adv.* 4, 48943–48951. doi: 10.1039/c4ra08719d

Liu, G., Chen, C., Li, D., Wang, S., and Ji, J. (2012). Near-infrared light-sensitive micelles for enhanced intracellular drug delivery. *J. Mater. Chem.* 22, 16865–16871. doi: 10.1039/c2jm00045h

Liu, J., Huang, Y., Kumar, A., Tan, A., Jin, S., Mozhi, A., et al. (2014). pH-sensitive nano-systems for drug delivery in cancer therapy. *Biotechnol. Adv.* 32, 693–710. doi: 10.1016/j.biotechadv.2013.11.009

Liu, Y., Feng, L., Liu, T., Zhang, L., Yao, Y., Yu, D., et al. (2014). Multifunctional pH-sensitive polymeric nanoparticles for theranostics evaluated experimentally in cancer. *Nanoscale* 6, 3231–3242. doi: 10.1039/c3nr05647c

Maysinger, D., Lovrić, J., Eisenberg, A., and Savić, R. (2007). Fate of micelles and quantum dots in cells. *Eur. J. Pharm. Biopharm.* 65, 270–281. doi: 10.1016/j.ejpb.2006.08.011

Mei, D., Lin, Z., Fu, J., He, B., Gao, W., Ma, L., et al. (2015). The use of α-conotoxin ImI to actualize the targeted delivery of paclitaxel micelles to α7 nAChR-overexpressing breast cancer. *Biomaterials* 42, 52–65. doi: 10.1016/j.biomaterials.2014.11.044

Mo, G., Hu, X., Liu, S., Yue, J., Wang, R., Huang, Y., et al. (2012). Influence of coupling bonds on the anti-tumor activity of polymer-pirarubicin conjugates. *Eur. J. Pharm. Sci.* 46, 329–335. doi: 10.1016/j.ejps.2012.02.013

Nogueira, D. R., Tavano, L., Mitjans, M., Perez, L., Infante, M. R., and Vinardell, M. P. (2013). *In vitro* antitumor activity of methotrexate via pH-sensitive chitosan nanoparticles. *Biomaterials* 34, 2758–2772. doi: 10.1016/j.biomaterials.2013.01.005

Owen, S. C., Chan, D. P., and Shoichet, M. S. (2012). Polymeric micelle stability. *Nano Today* 7, 53–65. doi: 10.1016/j.nantod.2012.01.002

Qiu, L., Zhu, M., Gong, K., Peng, H., Ge, L., Zhao, L., et al. (2017). pH-triggered degradable polymeric micelles for targeted anti-tumor drug delivery. *Mater. Sci. Eng. C Mater. Biol. Appl.* 78, 912–922. doi: 10.1016/j.msec.2017.04.137

Rao, J., and Khan, A. (2013). Enzyme sensitive synthetic polymer micelles based on the azobenzene motif. *J. Am. Chem. Soc.* 135, 14056–14059. doi: 10.1021/ja407514z

Sakai-Kato, K., Ishikura, K., Oshima, Y., Tada, M., Suzuki, T., Ishii-Watabe, A., et al. (2012). Evaluation of intracellular trafficking and clearance from HeLa cells of doxorubicin-bound block copolymers. *Int. J. Pharm.* 423, 401–409. doi: 10.1016/j.ijpharm.2011.12.022

Singla, A. K., Garg, A., and Aggarwal, D. (2002). Paclitaxel and its formulations. *Int. J. Pharm.* 235, 179–192. doi: 10.1016/S0378-5173(01)00986-3

Tang, R., Ji, W., Panus, D., Palumbo, R. N., and Wang, C. (2011). Block copolymer micelles with acid-labile ortho ester side-chains: synthesis, characterization, and enhanced drug delivery to human glioma cells. *J. Control. Release* 151, 18–27. doi: 10.1016/j.jconrel.2010.12.005

Varkouhi, A. K., Scholte, M., Storm, G., and Haisma, H. J. (2011). Endosomal escape pathways for delivery of biologicals. *J. Control. Release* 151, 220–228. doi: 10.1016/j.jconrel.2010.11.004

Wang, X., Li, S., Wan, Z., Quan, Z., and Tan, Q. (2014). Investigation of thermo-sensitive amphiphilic micelles as drug carriers for chemotherapy in cholangiocarcinoma in vitro and in vivo. *Int. J. Pharm.* 463, 81–88. doi: 10.1016/j.ijpharm.2013.12.046

Wang, Z., Deng, X., Ding, J., Zhou, W., Zheng, X., and Tang, G. (2018). Mechanisms of drug release in pH-sensitive micelles for tumour targeted drug delivery system: a review. *Int. J. Pharm.* 535, 253–260. doi: 10.1016/j.ijpharm.2017.11.003

Wilczewska, A. Z., Niemirowicz, K., Markiewicz, K. H., and Car, H. (2012). Nanoparticles as drug delivery systems. *Pharmacol. Rep.* 64, 1020–1037. doi: 10.1016/s1734-1140(12)70901-5

Wu, H., Zhu, L., and Torchilin, V. P. (2013). pH-sensitive poly(histidine)-PEG/DSPE-PEG co-polymer micelles for cytosolic drug delivery. *Biomaterials* 34, 1213–1222. doi: 10.1016/j.biomaterials.2012.08.072

Xiong, D., Zhang, X., Peng, S., Gu, H., and Zhang, L. (2017). Smart pH-sensitive micelles based on redox degradable polymers as DOX/GNPs carriers for controlled drug release and CT imaging. *Colloids Surf. B Biointerfaces* 163, 29–40. doi: 10.1016/j.colsurfb.2017.12.008

Yang, M., Ding, J., Zhang, Y., Chang, F., Wang, J., Gao, Z., et al. (2016). Activated macrophage-targeted dextran–methotrexate/folate conjugate prevents deterioration of collagen-induced arthritis in mice. *J. Mater. Chem. B* 4, 2102–2113. doi: 10.1039/c5tb02479j

Yin, T., Wang, L., Yin, L., Zhou, J., and Huo, M. (2015). Co-delivery of hydrophobic paclitaxel and hydrophilic AURKA specific siRNA by redox-sensitive micelles for effective treatment of breast cancer. *Biomaterials* 61, 10–25. doi: 10.1016/j.biomaterials.2015.05.022

Yin, T., Wang, P., Li, J., Zheng, R., Zheng, B., Cheng, D., et al. (2013). Ultrasound-sensitive siRNA-loaded nanobubbles formed by hetero-assembly of polymeric micelles and liposomes and their therapeutic effect in gliomas. *Biomaterials* 34, 4532–4543. doi: 10.1016/j.biomaterials.2013.02.067

Yuan, Z., Que, Z., Cheng, S., Zhuo, R., and Li, F. (2012). pH-triggered blooming of 'nano-flowers' for tumor intracellular drug delivery. *Chem. Commun.* 48, 8129–8131. doi: 10.1039/c2cc34225a

Yuba, E., Yamaguchi, A., Yoshizaki, Y., Harada, A., and Kono, K. (2017). Bioactive polysaccharide-based pH-sensitive polymers for cytoplasmic delivery of antigen and activation of antigen-specific immunity. *Biomaterials* 120, 32–45. doi: 10.1016/j.biomaterials.2016.12.021

Yusuf, R. Z., Duan, Z., Lamendola, D. E., Penson, R. T., and Seiden, M. V. (2003). Paclitaxel resistance: molecular mechanisms and pharmacologic manipulation. *Curr. Cancer Drug Targets* 3, 1–19. doi: 10.2174/1568009033333754

Zhang, J., Zhao, X., Chen, Q., Yin, X., Xin, X., Li, K., et al. (2017). Systematic evaluation of multifunctional paclitaxel-loaded polymeric mixed micelles as a potential anticancer remedy to overcome multidrug resistance. *Acta Biomater.* 50, 381–395. doi: 10.1016/j.actbio.2016.12.021

Zhang, P., Zhang, H., He, W., Zhao, D., Song, A., and Luan, Y. (2016). Disulfide-linked amphiphilic polymer-docetaxel conjugates assembled redox-sensitive micelles for efficient antitumor drug delivery. *Biomacromolecules* 17, 1621–1632. doi: 10.1021/acs.biomac.5b01758

Zhu, C., Jung, S., Luo, S., Meng, F., Zhu, X., Park, T. G., et al. (2010). Co-delivery of siRNA and paclitaxel into cancer cells by biodegradable cationic micelles based on PDMAEMA-PCL-PDMAEMA triblock copolymers. *Biomaterials* 31, 2408–2416. doi: 10.1016/j.biomaterials.2009.11.077

Conflict of Interest Statement: The authors declare that the research was conducted in the absence of any commercial or financial relationships that could be construed as a potential conflict of interest.

frontiers in Oncology

ORIGINAL RESEARCH
published: 25 January 2019
doi: 10.3389/fonc.2019.00025

Molecular, Biological and Structural Features of V_L CDR-1 Rb44 Peptide, Which Targets the Microtubule Network in Melanoma Cells

*Natalia Girola[1], Pedro T. Resende-Lara[2], Carlos R. Figueiredo[1,3], Mariana H. Massaoka[4], Ricardo A. Azevedo[1], Rodrigo L. O. R. Cunha[5], Luciano Polonelli[6] and Luiz R. Travassos[1,7]**

[1] Department of Microbiology, Immunology and Parasitology, Experimental Oncology Unit, Federal University of São Paulo, São Paulo, Brazil, [2] Computational Biology and Bioinformatics Laboratory, Federal University of ABC, Santo André, Brazil, [3] Department of Molecular and Clinical Cancer Medicine, University of Liverpool, Liverpool, United Kingdom, [4] Cancer Focus, São Paulo, Brazil, [5] Chemical Biology Laboratory, Natural and Human Sciences Center, Federal University of ABC, Santo André, Brazil, [6] Unit of Biomedical, Biotechnological and Translational Sciences, Department of Medicine and Surgery, Universitá degli Studi di Parma, Parma, Italy, [7] Recepta Biopharma, São Paulo, Brazil

OPEN ACCESS

Edited by:
Jian-ye Zhang, Guangzhou Medical University, China

Reviewed by:
Chakrabhavi Dhananjaya Mohan, University of Mysore, India
César de la Fuente, Massachusetts Institute of Technology, United States

***Correspondence:**
Luiz R. Travassos
luiztravassos@gmail.com

Specialty section:
This article was submitted to Cancer Molecular Targets and Therapeutics, a section of the journal Frontiers in Oncology

Received: *21 August 2018*
Accepted: *08 January 2019*
Published: *25 January 2019*

Citation:
Girola N, Resende-Lara PT, Figueiredo CR, Massaoka MH, Azevedo RA, Cunha RLOR, Polonelli L and Travassos LR (2019) Molecular, Biological and Structural Features of V_L CDR-1 Rb44 Peptide, Which Targets the Microtubule Network in Melanoma Cells. Front. Oncol. 9:25. doi: 10.3389/fonc.2019.00025

Microtubules are important drug targets in tumor cells, owing to their role in supporting and determining the cell shape, organelle movement and cell division. The complementarity-determining regions (CDRs) of immunoglobulins have been reported to be a source of anti-tumor peptide sequences, independently of the original antibody specificity for a given antigen. We found that, the anti-Lewis B mAb light-chain CDR1 synthetic peptide Rb44, interacted with microtubules and induced depolymerization, with subsequent degradation of actin filaments, leading to depolarization of mitochondrial membrane-potential, increase of ROS, cell cycle arrest at G2/M, cleavage of caspase-9, caspase-3 and PARP, upregulation of Bax and downregulation of Bcl-2, altogether resulting in intrinsic apoptosis of melanoma cells. The *in vitro* inhibition of angiogenesis was also an Rb44 effect. Peritumoral injection of Rb44L1 delayed growth of subcutaneously grafted melanoma cells in a syngeneic mouse model. L1-CDRs from immunoglobulins and their interactions with tubulin-dimers were explored to interpret effects on microtubule stability. The opening motion of tubulin monomers allowed for efficient L1-CDR docking, impairment of dimer formation and microtubule dissociation. We conclude that Rb44 V_L-CDR1 is a novel peptide that acts on melanoma microtubule network causing cell apoptosis *in vitro* and melanoma growth inhibition *in vivo*.

Keywords: metastatic melanoma, microtubule, tubulin, peptide, complementarity-determining region, apoptosis

INTRODUCTION

The polymerization dynamics of cytoskeleton molecules is crucial to the survival and to the energetic and mechanistic properties of cells and organisms. As important polymers in the mitotic process, microtubules are targets of anticancer drugs, with several compounds already being studied (1, 2).

Microtubule targeting agents (MTAs) exert inhibitory effects on cell proliferation, with cell cycle arrest at G2-M and induction of apoptosis (3). They may act as vascular-targeting drugs, disrupting microtubules in endothelial cells, which affects the blood supply in the tumor tissue (4). Microtubules also induce maturation and migration of dendritic cells, which are essential to the immune response (5).

MTAs can be divided into mechanistic acting categories as they either stabilize or destabilize microtubules (6). Microtubule-stabilizing agents such as paclitaxel and docetaxel bind to the taxane-binding site on β-tubulin, inhibiting microtubule depolymerization and intensifying its polymerization. Recently, Taxol/Paclitaxel has been described as first billion-dollar anticancer drug (7). Microtubule-destabilizing agents including colchicine and vinca alkaloid, typically bind to sites located at the intra-dimer interface and near the GTP binding site on β-tubulin, respectively. Such interactions induce inhibition of microtubule polymerization and promote depolymerization (8, 9). Although these agents are widely used in medicine, particularly paclitaxel and vinca alkaloids, drug resistance and side effects such as neurotoxicity, are significant limitations to MTAs clinical success (10, 11).

In the last decade, peptides displaying anticancer properties have been studied as promising alternative agents for cancer therapy (12, 13). Peptides are mostly non-genotoxic, have high affinity and selectivity for molecular targets on cancer cells, low cost production with feasible synthesis of derivatives, exhibiting low antigenicity and good tissue penetration (14, 15). Peptides can also be conjugated to large molecules to improve pharmacokinetics (16). Peptides can be displayed on the phage surface giving rise to specific sequences targeting different tissues or be developed from internal regions of transcription factors (17). Peptides and derivatives from natural sources such as marine animals and insects have been described with preferential antitumor activity without affecting normal cells (18, 19). Complementarity-determining regions (CDRs) of immunoglobulins (Igs) have been found to exhibit with high frequency, antiinfective, immunomodulatory, and antitumor activities (20–22).

Synthetic peptides corresponding to the Ig hypervariable CDRs, may display antitumor activities *in vivo*, as well as cytotoxic effects *in vitro* including cell cycle arrest, inhibition of tumor cell migration and invasion, induction of apoptosis, disruption of cytoskeleton dynamics (22–28), and many others.

We have previously described a novel bioactive mAb V_L CDR 1 peptide (C36L1), displaying *in vitro* and *in vivo* anti-tumor activities. Depolymerization of microtubules, leading to cytotoxic and cytostatic effects mediated by Rho-GTPase, PTEN, and PI3K/Akt signaling, have been characterized (26).

Presently, we investigated a V_L CDR1-derived synthetic peptide, Rb44, expressed in a anti-Lewis B monoclonal antibody, focusing on structural, biological and molecular docking properties, in comparison with two other V_L CDR1 peptides (Rb29L1 and C36L1), to understand the mechanism of action of Ig-CDR derived, apoptotic peptides targeting microtubules. Rb44L1 exerted both *in vitro* and *in vivo* anti-melanoma activities and inhibited endothelial cell sprouting *in vitro*.

MATERIALS AND METHODS

Peptides

The L1 CDR amino acid sequences were obtained from the anti-Lewis B mAb antibody, V_L Rb44L1 (RSSQTITHGNGNTYLY-$_{NH2}$), and from the anti-A34 mAb, V_L Rb29L1 (RSSTSLLHGNGNTYLT-$_{NH2}$) according to Kabat et al. (29) CDR definition. The peptide sequences were purchased from Peptide 2.0 (Chantilly, VA) at 95–98% purity. All peptides were amidated at the C-terminus. Peptides were diluted in 1% DMSO-RPMI medium. In some experiments a scrambled Rb44L1 (Scr44) peptide was used (SIGTYSTRNYQHNLTG-$_{NH2}$). The previously described C36L1 (KSSQSVFYSSNNKNYLA-$_{NH2}$) was comparatively studied for molecular modeling.

Tumor Cell Lines and Cell Culture

B16F10-Nex2 subline of murine melanoma cells was isolated at the Experimental Oncology Unit (UNONEX) of Federal University of São Paulo (UNIFESP) and registered in the Banco de Células do Rio de Janeiro (BCRJ), no. 0342. The original B16F10 cell line was obtained from the Ludwig Institute for Cancer Research (LICR), São Paulo Branch. Human melanoma cell line A2058; human carcinoma cell lines of colon, HCT-8; uterine cervix, SiHa; and breast, MCF-7; murine fibroblasts, 3T3-NIH; and human fibroblasts, GM637, were provided by the Ludwig Institute for Cancer Research and were a gift from Dr. Luiz F. Lima Reis (Hospital Sírio-Libanez, São Paulo). Human umbilical vein endothelial cells (HUVEC) were kindly provided by the Department of Immunology, Institute of Biomedical Sciences (University of São Paulo). Both cell lines were cultured at 37°C, under humid atmosphere and 5% CO_2, in RPMI-1640 medium for tumorigenic cell lines and DMEM for non-tumorigenic ones, in both cases supplemented with 10 mM N-2-hydroxyethylpiperazine-N2 ethane sulfonic acid (HEPES), 24 mM sodium bicarbonate, 40 mg/L gentamicin, pH 7.2 and 10% fetal bovine serum (FBS).

Cell Viability Assay

For IC_{50} determination, 1×10^4 tumorigenic and non-tumorigenic cell lines were seeded in 96-well plates and treated at different concentrations ranging from 0 to 1 mM of Rb44L1 and Rb29L1 peptides for 24 h. Viable cells were quantified using the MTT (3-[4,5-dimethylthiazol-2-yl]-2,5-diphenyltetrazolium bromide) (Sigma-Aldrich, St. Louis, MO) assay. After incubation, 5 μL of MTT solution (5 mg/ml) was added to the cells, followed by incubation for 3 h at 37°C. Absorbance was measured in a microplate reader at 570 nm (SpectraMax-M2, Molecular Devices Software Pro 5.4, Sunnyvale, CA). IC_{50} was calculated using GraFit 5 data analysis software (Version 5.0.13).

Chromatin Condensation and DNA Fragmentation Assays

Apoptotic melanoma cells treated with Rb44L1 peptide were examined by TUNEL staining, using the *in situ* Cell Death Detection Kit according with the manufacture's instruction (Roche Applied Science, Madison, WI). B16F10-Nex2 melanoma cells (1×10^4) were seeded on 96-well clear-bottom black

polystyrene microplate and incubated with 0, 130 and 260 μM of Rb44L1 peptide for 18 h. After incubation, cells were fixed in formaldehyde 2% for 20 min at room temperature, washed in PBS, and incubated with Hoechst 33342 (Invitrogen, Eugene, OR), at 10 μg/mL final concentration in the reaction buffer and TUNEL enzymatic substrate. Cells were washed and images were acquired and analyzed in a Cytell Cell image cytometer (GE Healthcare, Little Chalfont, UK).

Annexin V and Propidium Iodide Labeling

B16F10-Nex2 cells (5×10^5) were cultured in 6-well plates and further incubated with Rb44L1 at 0, 80 and 100 μM for 18 h at 37°C. After incubation, the Annexin V-FITC Apoptosis Detection Kit (Sigma-Aldrich, St. Louis, MO) was used and cells labeled with propidium iodide (PI) and FITC annexin V (AV) were analyzed by flow cytometry (BD Bioscience FACSCanto II equipment, Franklin Lakes, NJ), using FlowJo software (TreeStar Inc., Ashland, OR).

Cell Cycle Analysis

B16F10-Nex2 (5×10^5) cells were seeded in conical centrifugation tubes and incubated with 65 μM Rb44L1 peptide for 16 h in suspension. After incubation, the cells were washed with PBS and fixed in ethanol 70% for 1 h at 4°C. Cells were then washed again with PBS and stained with propidium iodide (PI) solution (50 μg/ml PI, 0.1 mg/ml RNAse A) for 20 min at 4°C in the dark. DNA fluorescence staining was acquired by FACSCalibur flow cytometer (Becton Dickinson, San Jose, CA). FlowJo software (Tree Star Inc., Ashland, OR) was used for post-acquisition analysis (20.000 events per sample). The microtubule depolymerizing CA4 (combretastatin A4, Sigma-Adrich, St. Louis, MO) was used at 75 μM as positive control of G2/M cell cycle arrest.

Transmission Electron Microscopy

B16F10-Nex2 cells (1×10^6) were seeded in 6-well plates. Cells were then incubated with peptide Rb44L1 at 260 μM for 18 h at 37°C. Fixation, dehydration and staining of the samples were performed as previously described (23). Jeol 1200 EXII electron microscope (Tokyo, Japan) was used for image acquisition.

Mitochondrial Membrane Potential ($\Delta\psi m$)

B16F10-Nex2 cells (1×10^4) were pre-incubated with the cationic lipophilic dye tetramethylrhodamine ethyl ester (TMRE) at 20 nM for 30 min, and then with peptide Rb44L1 at 0, 130, and 260 μM for 6 h. After the incubation period, images of living cells were acquired and analyzed by Cytell Cell Imaging System (GE Healthcare, Little Chalfont, UK).

Superoxide Anion Measurement

Superoxide anion production was measured by dihydroethidium (DHE) assay. Briefly, 1×10^4 cells cultivated on 96-well clear-bottom black plate were pre-incubated with DHE for 30 min at 37°C. Rb44L1 was added at 130 and 260 μM concentrations and fluorescence units were quantified after 16 h in a microplate reader (Molecular Devices M2, Sunnyvale, CA) adjusted for excitation at 370 nm and emission at 420 nm. As positive control, cells were treated with 5 mM of H_2O_2 at 37°C for 20 min, and the negative control run with no peptide.

Cell Lysate Extracts and Western Blotting

B16F10-Nex2 cells (10^6) were incubated with 0 and 130 μM of Rb44L1 peptide for different times (1, 3, 6, 8, and 24 h). After incubation, cells were washed in PBS and lysed with 300 μL of SDS sample buffer (62.5 mM Tris-HCl, pH 6.8 at 25°C, 2% w/v SDS, 10% glycerol, 50 mM DTT, 0.01% w/v bromophenol blue). Proteins from whole cell extracts were analyzed by Western blotting as previously described (20). The following primary, highly specific monoclonal antibodies, were used: rabbit anti-Bcl-2, -Bcl-xl, -Bax, -caspase-9 and cleaved caspase-9, -caspase-3 and cleaved caspase-3, -Parp and cleaved Parp, and -GAPDH (for total protein loading control), with secondary anti-rabbit IgG conjugated with horseradish peroxidase (HRP). All antibodies were purchased from Cell Signaling Technology (Beverly, MA) except for anti-GAPDH, acquired from Sigma-Aldrich (St. Louis, MO). Immunoreaction was revealed using the Luminata™ Forte solution (Millipore, Billerica, MA) and images were acquired using Uvitec Cambridge (Cambridge, UK). The molecular mass of each protein was estimated based on a pre-stained protein standard (Spectra Multicolor, ThermoScientific, Waltham, MA). Full-length Western blotting membranes are displayed in **Figure S1**.

In vitro Angiogenesis Assay

The basement matrix Geltrex™ (Invitrogen, Eugene, OR) was added (30 μl/well) to coat a 96-well plate and allowed to polymerize for 40 min at 37°C. HUVEC cells (5×10^3) suspended in RPMI medium supplemented with 0.2% of fetal calf serum were plated alone (control) or mixed with 5 μM of Rb44L1 peptide. The cells were incubated at 37°C for 6 h and images were captured with a microscope digital camera (Olympus, Tokyo, Japan). The numbers of pro-angiogenic structures (typically closed compartments or rings formed after endothelial cell sprouting) were counted from 3 different wells.

Ethics Statement

The present study is part of Project 2010/51423-0 granted by the São Paulo State Research Support Foundation (FAPESP), Brazil. The protocols used for animal experiments were carried out in accordance with the Ethics Committee of Federal University of São Paulo, Brazil and have been approved via document CEP 1234/2011.

Mice and Subcutaneous Melanoma Model

Eight-week-old male C57Bl/6 mice were acquired from the Center for Development of Experimental Models (CEDEME) at Federal University of São Paulo (UNIFESP), Brazil. The Ethics Committee for Animal Experimentation (UNIFESP) approved protocols of animal experiments. In the subcutaneous (s.c.) melanoma model, male C57Bl/6 mice (five per group) were subcutaneously grafted in the right flank with 1×10^5 syngeneic B16F10-Nex2 melanoma cells. Animals were subjected to 5 peritumoral daily doses of 300 μg (total 10 mg/kg) of Rb44L1. DMSO (1%) in PBS, was the vehicle control. Treatment started

after the tumor size reached 80 mm^3 as measured with a caliper. The tumor volume (V) was calculated by the formula $V = 0.52 \times d^2 \times D$, where d and D are short and long diameters of the tumor, respectively, measured every other day. Mice were euthanized at the end of experiments or when the tumor size reached the maximum allowed volume of 3,000 mm^3.

Live-Cell Imaging of Microtubule Dynamics

Real-time fluorescence microscopy of living B16F10-Nex2 melanoma cells previously modified by viral transduction for the expression of green fluorescent tubulin (CellLight® Reagents −2.0 BacMam, Life Technologies), was used to investigate the peptide interaction with microtubules. Viable green fluorescence protein (GFP) tubulin-expressing cells (1×10^4) were incubated with Rb44L1 and Rb29L1 at 260 μM and fluorescent images were taken at 10-min intervals during 2 h using the time-lapse BioStation fluorescence microscope (Nikon Instruments, Inc, Melville, NY). For instance, humidity, temperature (37°C) and CO_2 (5%) were carefully controlled. Fluorescence analysis and quantification were performed with the ImageJ software and the video was processed with the NIS-Elements analysis software (Nikon, Tokyo) and Adobe After Effects software.

Fluorescence Staining of F-Actin

B16F10-Nex2 cells (5×10^4) were seeded in 24-well microplates and incubated with different concentrations of Rb44L1 (0, 130 and 260 μM) for 30 min and 3 h. After incubation, cells were fixed in 3.7% of formaldehyde for 20 min at 4°C, blocked (1% BSA, 5% SFB, 0.1% Triton in 1X PBS) for 30 min at room temperature and stained with Hoechst 33342 (Invitrogen, Eugene, OR) and anti-phalloidin conjugated with FITC for 1 h at 37°C. Images were acquired and analyzed by Cytell Cell Imaging System (GE healthcare, Little Chalfont, UK).

System Preparation and Molecular Dynamics

De novo peptide structure prediction was made by Pep-Fold3 webserver (30). We obtained the tubulin structure from PDB 4TV9 (31) (chains A and B). Protonation analysis was made by PROPKA3 (32). Energy minimization was carried out on GROMACS 5.1 (33) using CHARMM36 force field (34). Systems were built by CHARMM-GUI webserver (35, 36) with TIP3P water molecules (37) and counter ions, when charge balancing was required. Simulations consisted of 5,000 steps of steepest descent energy minimization, followed by 25 ps of NVT equilibration dynamics for L1-CDR peptides and 10 ns for tubulin. A NPT production molecular dynamics of 100 ns was carried out on GROMACS 5.1 using CHARMM36 force field for each system. Secondary structure assignment and hydrogen bonds (H-bonds) were analyzed by using VMD (38) plugins. H-bonds distance cut-off was set up at 3.0 Å with angle cut-off of 20°. All further MD analyses were made by GROMACS 5.1.

Normal Mode Calculations and Generation of Low-Energy Conformations

Normal mode analysis (NMA) was performed using CHARMM c41b1 (39) and CHARMM36 force filed using DIMB (40) module and excluding CMAP (41). A distance dependent dielectric constant was employed to treat the electrostatic shielding by the solvent as described by Philot et al. (42). We used the mode 08 (open/close of tubulin monomers) as directional constraint to generate low-energy conformers along the mode trajectory using the VMOD algorithm in CHARMM as depicted by Louet et al. (43). The restraints were applied only on Cα atoms and the energy was computed for all atoms. The structures were displaced from 0.0 Å to +6.0 Å (open direction) using steps of 1.0 Å, resulting in 7 intermediate low-energy structures along the mode.

Molecular Docking

In order to obtain different structures to perform molecular docking, we clustered the MD trajectory of each peptide. All MD frames were fitted to the reference structure and clustered with GROMOS method by using GROMACS 5.1, with a backbone RMSD cutoff of 2.0 Å for Rb29 and Rb44 and 5.0 Å for C36 (since the last is very flexible) resulting in 3, 11, and 8 different clusters, respectively. The center structure of each peptide cluster was then used in docking simulations, performed with Hex 8.0 (44). Hex depicts proteins as rigid bodies and makes a blind search through protein surface while it evaluates the interaction correlation by using the fast Fourier transformation algorithm. As described in Meissner et al. (45), solvation and desolvation effects were treated as surface phenomena, since the Hex algorithm models the interaction, excluding volume and complementarity of form. Approximately 350 solutions were found for each combination. We used BINANA 1.2 (46) as a rescore method to investigate the specific molecular basis guiding the interaction between tubulin and peptides.

Chemiluminescent Dot-Blotting

Peptide Rb44L1 binding to microtubule structures was determined by chemiluminescent (CL) dot-blotting as described elsewhere (26) with some modifications. Peptides C36L1 (positive control), Rb44L1, scrambled-Rb44L1 (Scr44) at 10 μg/10 μL each, or vehicle (1% DMSO in milli-Q water), were applied on nitrocellulose membranes. They were blocked with 5% BSA in 0.05% PBS-Tween 20. B16F10-Nex2 cell protein lysate (50 μg/ml), prepared with non-denaturing protein extraction buffer according to the manufacturer's instructions (Cell Signaling, Beverly, MA), was applied onto the nitrocellulose membranes and incubated overnight at 4°C. After washing, membranes were incubated with anti-alpha tubulin antibody (Sigma-Aldrich, St. Louis, MO) for 1 h at 37°C followed by anti-rabbit IgG-HRP antibody for 1 h at 37°C. Immunoreactivity was determined using the Luminata™ Forte solution (Millipore, Billerica, MA). Images were acquired by Uvitec Cambridge (Cambridge, UK) with 1-min membrane exposure time. No reactivity with the control peptide was observed. To investigate the influence of GTP and Mn^{2+} on the peptide binding with α-tubulin, the membranes coated with 10 μg Rb44L1 or scrambled (Scr44) peptide were blotted with or without 1 mM GTP (Cytoskeleton, Denver, CO) and/or 1 mM $Mn_2SO_4H_2O$ (Sigma-Aldrich, St. Louis, MO) added to the cell lysate (50 μg/ml), for 2 h at 37°C. Chemiluminescence was detected as described above but with short membrane exposure time (20 s).

Tubulin Polymerization Assay

Microtubule polymerization was evaluated using the Tubulin Polymerization Assay kit (Cytoskeleton, Inc., Denver, CO). Rb44L1 (130 μM) or Scr44 (130 μM); colchicine (50 μM); Rb44L1 (130 μM) + colchicine (50 μM), diluted with 1% DMSO in distilled water were added to 50 μl of the tubulin reaction mix with optimized volumes for inhibitor detection containing 2 mg/ml or 1 mg/ml of tubulin in 80 mM PIPES (piperazine-N-N'-bis [2- ethane sulfonic acid] sodium salt), pH 6.9, 2 mM $MgCl_2$, 0.5 mM EGTA (ethylene glycol-bis N,N,N',N'- tetra acetic acid), 60% v/v glycerol, 1 mM GTP, and 10 μM of the fluorescent reporter. The black, flat bottom, half area 96-well plate, with the samples, was examined in a fluorescence microplate reader (SpectraMax-M2e, Molecular Devices, Sunnyvale, CA) every 1 min at 340 nm of excitation and 410 nm of emission for 40 or 180 min. To monitor the tubulin polymerization in the same condition as of the dot blotting assay, the reaction was prepared as described above with 2 mg/ml of purified tubulin in 0.1% of BSA in PBS and 3.4% of cell lysis buffer, without cell lysate.

Statistical Analysis

The software GraphPad Prism 5.0 (San Diego, CA) was utilized for all tests. Statistical differences between groups were compared by Student's *t*-test. Differences in survival time and rate were evaluated by the Kaplan-Meier survival curves. *P*-values are indicated as $^{*}p < 0.05$, $^{**}p < 0.01$ and, $^{***}p < 0.001$.

RESULTS

L1-CDR Peptides Differ in Dynamic Features

Peptides Rb44L1 and Rb29L1 were studied in comparison with peptide (C36L1), which exerts cytotoxicity by depolymerization of microtubules and displays antitumor activities, as previously investigated (26).

In spite of the sequence similarity, the dynamics of L1-CDRs were very different from each other. Rb29L1 assumed a stable β-hairpin conformation, with residues ^{5}SLL and ^{13}TYL forming the β-sheet (**Figures 1A,B**). In turn, Rb44L1 showed only an intermittent β-bridge between residues ^{5}TI and ^{14}YL (**Figures 1C,D**). C36L1, however, did not assume any ordered structure (**Figures 1E,F**). Root-mean-squared deviation (RMSD) of backbone heavy atoms and Cα root-mean-squared fluctuation (RMSF) calculations were performed to evaluate structure stability along the molecular dynamics (MD). Results confirmed the stability of Rb29L1, while C36L1 showed several conformational shifts (**Figure 1G**). Flexibility analysis confirmed this profile (**Figure 1H**). H-bonds formation during the dynamics could address these structural differences among the peptides. Rb29L1 showed more internal H-bonds than the other peptides, therefore it is more rigid. **Table 1** summarizes these interactions. The trajectories of each peptide MD were clustered, according to RMSD, onto representative conformations to perform docking simulations (**Figure S2**).

In vitro Cytotoxicity of CDR Peptides

We investigated the anti-tumor potential of two L1-CDR-derived peptides: Rb44L1 from anti-Lewis B mAb and Rb29L1 from anti-A34 mAb. The IC_{50} values were determined for the Rb44L1 and Rb29L1 against different tumorigenic and non-tumorigenic cell lines (**Table 2**). Peptide Rb44L1 showed the lowest IC_{50} values as compared to Rb29L1. The concentrations of 130 μM (IC_{50}) and 260 μM (IC_{100}), respectively, were therefore used in the subsequent experiments with B16F10-Nex2 melanoma cells. Rb44L1, was less active against non-tumorigenic cells, including murine and human fibroblasts, 3T3-NIH and GM637 cell lines. In the concentration range of 0 to 0.140 mM, no cytotoxicity was observed in these cells. Rb29L1 IC_{50} values were 3- to 10-fold higher than those of Rb44L1 in tumorigenic cell lines.

Rb44L1 Induces Apoptosis

Changes in the dynamics of the cytoskeleton have been implicated in the induction of apoptosis. Here, we show that Rb44L1 induced morphological alterations typical of apoptotic cell death such as cellular shrinkage, membrane blebs and cell rounding-up with pseudopodia retraction in B16F10-Nex2 melanoma cells when incubated with peptide at IC_{50} (130 μM) and IC_{100} (260 μM) for 18 h (**Figure 2A**). Chromatin condensation was observed in 95% and 98% of tumor cells treated with Rb44L1 at 130 and 260 μM, respectively, for 18 h. DNA fragmentation was determined by green positive TUNEL staining in B16F10-Nex2 cells treated with 130 and 260 μM of Rb44L1 (**Figures 2B,C**). Both DNA condensation and fragmentation were significantly higher in Rb44L1-treated cells as compared with the negative control (for chromatin condensation, $^{**}p < 0.01$ at 130 μM, $^{***}p < 0.001$ at 260 μM; and for DNA fragmentation, $^{***}p < 0.001$ at both concentrations). Additionally, we observed that Rb44L1 could significantly enhance the translocation of phosphatidylserine (PS) to the outer leaflet of the plasma membrane, indicating early apoptosis. We observed a significant increase in the number of early apoptotic events in cells treated with Rb44L1 at 80 and 100 μM, in comparison with untreated control cells (**Figure 2D**). Finally, Rb44L1 inhibited cell proliferation with cell cycle arrest, at 65 μM (**Figure 2E**). The S-phase area decreased from 22.3 to 13.4%, with increase of the G2/M phase (from 21.8 to 33.5%). Microtubule depolymerizing combretastatin-A4 was used as positive control.

Morphological and Functional Alterations in Mitochondria and ROS Production

Transmission electron microscopy (TEM) of Rb44L1-treated B16F10-Nex2 cells, at 260 μM for 18 h, showed condensed chromatin, nuclear membrane detachment, enlarged, and vacuolated mitochondria with damaged cristae surrounded by heavily injured cytoplasmic organelles compared to untreated cells (**Figure 3A**). The collapse of the mitochondria transmembrane potential ($\Delta\psi m$) was observed on early incubation with Rb44L1 (0, 130, and 260 μM). After 6 h, reduction of TMRE fluorescence (53 and 94% reduction in cells treated with 130 and 260 μM, respectively; $^{**}p < 0.01$ and $^{***}p < 0.001$ in relation to untreated cells) was observed indicating mitochondrial damage in these cells (**Figure 3B**).

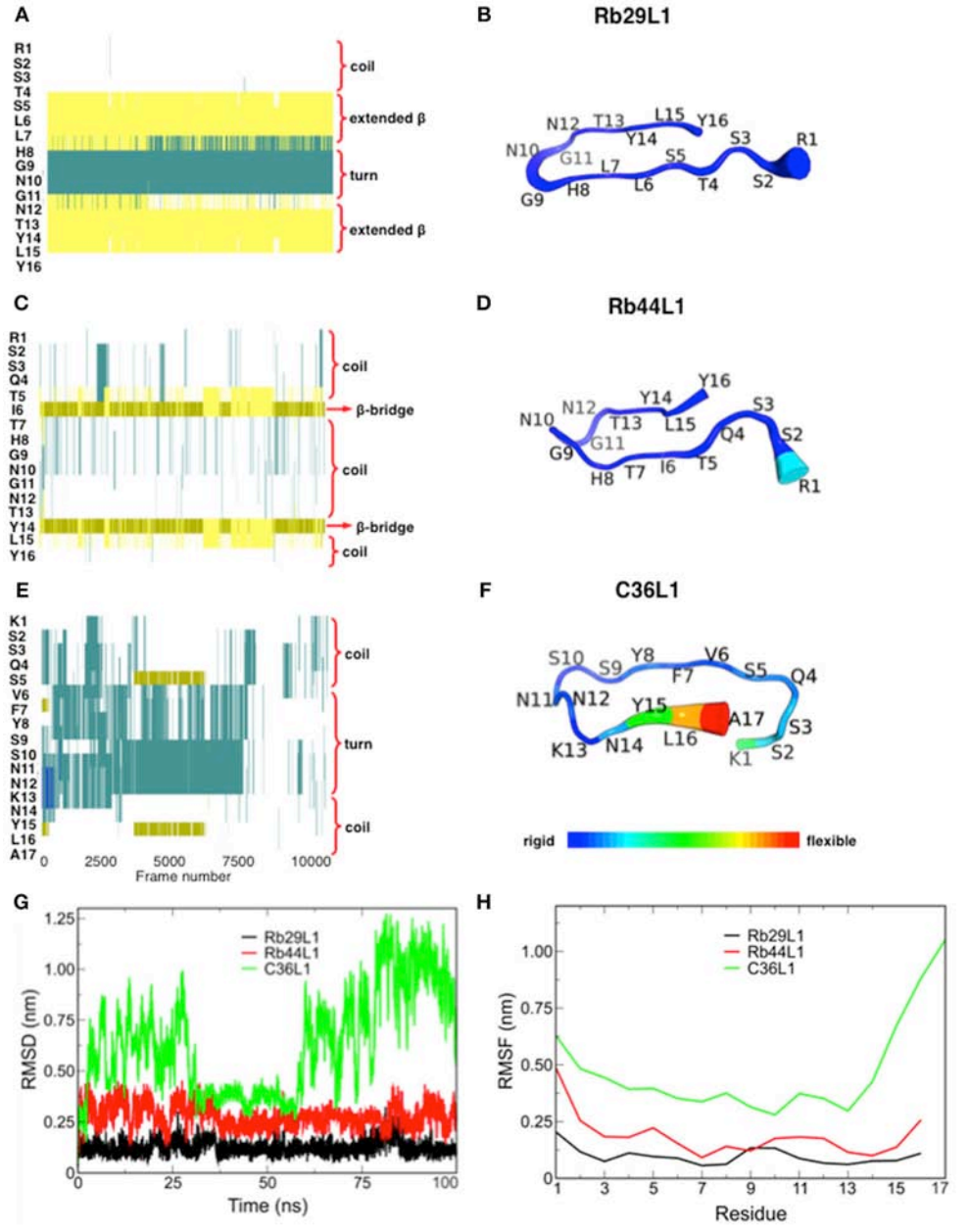

FIGURE 1 | Secondary structure assignment during molecular dynamics and structural analysis of L1-CDRs. **(A,B)** Rb29L1 assumes a stable β-hairpin conformation during MD, showing a well established β-sheet between residues ^{5}SLL and ^{13}TYL; **(C,D)** Rb44L1 shows a recurrent β-bridge between residues ^{5}TI and ^{14}YL; **(E,F)** C36L1 presents the most flexible conformation, in its majority composed by turn and coil. Secondary structure color code: turn, in green; extended conformation (β-sheet), in yellow; isolated bridge, in gold; 3-10 helix, in blue; coil, in white; **(G)** root-mean-squared deviation of backbone atoms of Rb29L1, Rb44L1, and C36L1. Rb29L1 remains nearly at the same conformation during all MD, an effect also seen for Rb44L1, although with less intensity. C36L1, nonetheless, presented a great conformational variation; **(H)** root-mean-squared fluctuations of Cα atoms of Rb29L1, Rb44L1 and C36L1. Cα fluctuation, or flexibility, follows RMSD pattern. Rb29L1 presents a rigid structure while Rb44L1 and C36L1 are more flexible, the latter more pronounced.

Tumor cells were incubated with Rb44L1 at 130 and 260 μM for 16 h and ROS levels were detected using DHE dye measured by fluorimetry. Hydrogen peroxide (H_2O_2) was used as positive control (Control +) at 5 mM. Accumulation of ROS (59% in relation to untreated cells; $^{***}p < 0.001$) was observed in cells treated with Rb44L1 at both concentrations (**Figure 3C**).

Rb44L1 Elicited Caspase Activation

Different pro- and anti-apoptotic proteins in total cell lysates were evaluated by Western blotting in Rb44L1-treated B16F10-Nex2 cells at 130 μM and different incubation periods. We observed that Rb44L1 induced early increase of pro-apoptotic Bax protein, followed by the cleavage of caspase-9, caspase-3 and

TABLE 1 | Hydrogen bonds formation during molecular dynamics of L1-CDR peptides*.

Hydrogen bonds	Occupancy (%)
Rb29L1	
ARG1-Side-NH1 – TYR16-Side-OT1	34.94
ARG1-Side-NH1 – TYR16-Side-OT2	17.56
ARG1-Side-NH2 – TYR16-Side-OT1	17.78
ARG1-Side-NH2 – TYR16-Side-OT2	37.64
SER3-Side-OG – TYR16-Side-OT1	27.63
SER3-Side-OG – TYR16-Side-OT2	18.97
THR4-Main-N – TYR16-Side-OT1	11.7
THR4-Main-N – TYR16-Side-OT2	27.13
LEU6-Main-N – TYR14-Main-O	42.05
HIS8-Main-N – ASN12-Main-O	43.21
TYR14-Main-N – LEU6-Main-O	36.03
TYR16-Main-N – THR4-Main-O	43.64
TYR16-Side-OH – HIS8-Side-NE2	17.83
Rb44L1	
THR7-Main-N – THR13-Main-O	36.35
LEU15-Main-N – THR5-Main-O	54.47
C36L1	
ALA17-Main-N – GLN4-Main-O	11.51

Only interactions with ≥ 10% occupancy are shown.

TABLE 2 | IC_{50} values of the bioactive peptide Rb44L1 and control Rb29L1 against tumorigenic and non-tumorigenic lineages after 16 h of incubation.

Cell lineages	IC_{50} (μM) ± SD	
	Rb44L1	Rb29L1
B16F10-Nex2	130 ± 5.8	465 ± 67
A2058	66 ± 2.0	265 ± 16
MCF-7	134 ± 2.4	858 ± 53
SIHA	51 ± 6.6	773 ± 61
HCT-8	81 ± 1.5	821 ± 57
3T3-NIH*	>140	>140
GM637*	>140	>140

*Non-tumorigenic cell lines.

PARP, together with downregulation of anti-apoptotic protein Bcl-2 (**Figure 3D**). GAPDH was used as loading control.

Rb44L1 Inhibited Angiogenesis *in vitro*

The cytotoxicity of Rb44L1 at different concentrations was assayed in the HUVEC lineage (**Figure 4A**). A non-cytotoxic concentration was used for the inhibition of endothelial cell (HUVEC) sprouting in Geltrex™ Matrix. Rb44L1 at 5 μM for 6 h, significantly inhibited 90% of endothelial cell sprouting, with the number of compartments built by intercellular connections being compared to that of the control ($^{**}p < 0.01$; **Figures 4B,C**).

Antitumor Activity *in vivo* Against Subcutaneous Melanoma

The *in vivo* antitumor activity was also investigated in a subcutaneously grafted, syngeneic murine melanoma model. Peritumoral injections of Rb44L1 at 15 mg/Kg significantly delayed tumor volume progression ($^{**}p < 0.01$), and also prolonged mice survival ($^{**}p < 0.01$) (**Figures 4D,E**). Mice were euthanized at the scheduled end of experiments, or before, should the tumors ulcerate or reach the maximum allowed volume of 3,000 mm^3.

Rb44L1 Interacts With Microtubules and Induces Cytoskeleton Disruption in Melanoma Cells

Disruption of the microtubule integrity in B16F10-Nex2 cells was monitored during the incubation with Rb44L1 and Rb29L1. Microtubules were assessed by live-cell imaging using B16F10-Nex2 cells previously transduced with a genetic modified insect virus (baculovirus) containing a tubulin-green fluorescent fusion-protein construct (CellLight®, Life Technologies). The fluorescence of live murine melanoma cells was monitored and quantified for 2 h during incubation with 260 μM of Rb44L1 and Rb29L1. The Rb44L1 peptide drastically reduced microtubule fluorescence compared to the negative control (**Figures 5A,B**), indicating that the microtubule network was depolymerized during the incubation with Rb44L1, whereas no depolymerization was seen in Rb29L1 treated cells. A representative video showing the kinetics of microtubule depolymerization in B16F10-Nex2 cells during the incubation with Rb44L1 and Rb29L1 is available in **Video S1**.

In addition to investigating whether Rb44L1 would also affect the integrity of F-actin, the reaction was assessed simultaneously using a phalloidin-FITC probe, as described in methods. We observed that F-actin integrity was completely lost after 3 h of incubation with Rb44L1 at 260 and 130 μM (**Figure 5C**). Actin degradation occurred after the microtubule disruption process, as evidenced in the cytoskeleton integrity quantification analysis (**Figure 5D**), suggesting that actin filaments were disrupted as a consequence of microtubule depolymerization ($^{*}p < 0.05$ comparing microtubule and actin disruption). Less than 55 or 65% of cytotoxicity was seen when testing both concentrations of Rb44L1 at 260 and 130 μM, respectively, in the first hours of incubation (**Figure S3**).

Normal Modes Expose Nonexchangeable Nucleotide and Colchicine Binding Sites

Normal mode analysis (NMA) was employed to investigate the opening motion of tubulin monomers. We hypothesized that this opening motion would be required to expose the nucleotide binding site located at α-tubulin (N-site) and dimer interface. Such exposition could favor the efficient docking of L1-CDR peptides and impair the tubulin dimer assembly, finally leading to microtubule dissociation. This motion was verified as the normal mode 8 (**Figures 6A,B**). Using the VMOD routine implemented on CHARMM, we performed a mass-weighted displacement of tubulin structure along mode 8, to produce energy-relaxed structures with gradually exposed nucleotide site. Tubulin residues originally in contact with GTP (contacts within 4.5 Å) showed a solvent-accessible surface area (SASA) of 511

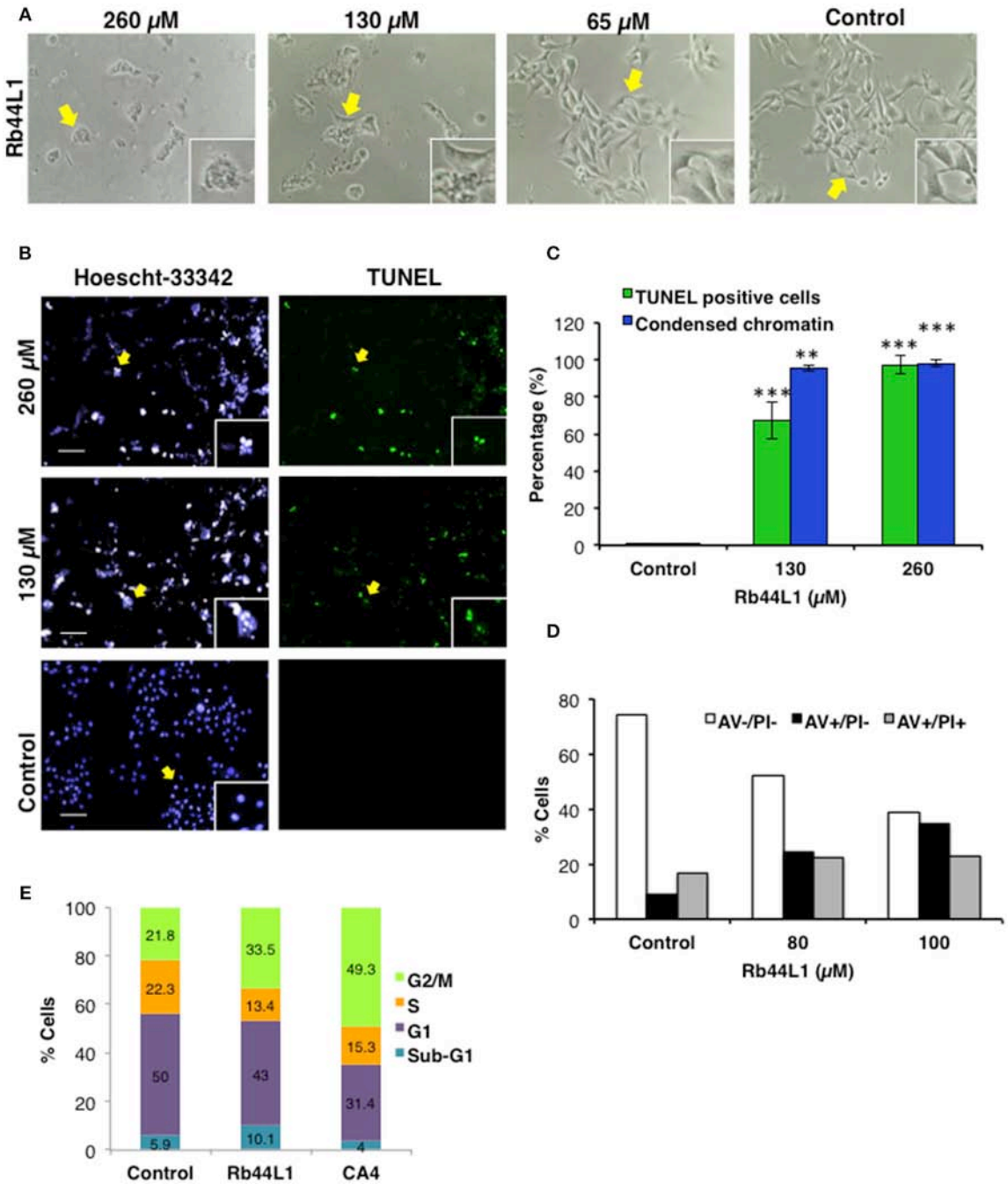

FIGURE 2 | Rb44L1 induces apoptosis in melanoma cells. **(A)** morphological changes were analyzed by light microscopy. Representative images of cells treated with different doses of Rb44L1 or untreated cells (control). Arrows indicate inserts (x200, magnification); **(B)** representative images of chromatin condensation (Hoescht 33342, blue) and DNA fragmentation (TUNEL, green) of tumor cells treated with different concentrations of Rb44L1 for 18 h. Scale bar represents 50 μm; **(C)** percentage of TUNEL positive cells and condensed nuclei. $^{**}p < 0.01$ and $^{***}p < 0.001$ in comparison to untreated cells; **(D)** percentage of apoptotic cells determined by the externalization of phosphatidylserine; **(E)** cell cycle of B16F10-Nex2 cells after incubation with Rb44L1 at 65 μM for 16 h. Percent tumor cells at Sub-G1, G1, S, and G2/M phases are indicated. CA4 was used as positive control.

Å² at the crystallographic structure (PDB 4TV9), while the same residues were more exposed after a displacement of 6 Å, presenting a SASA of 588 Å² (**Figures 6C,D**). The same occurred for the colchicine site, which presented a SASA of 225 Å² before the displacement and 236 Å² after mass-weighted displacement of 6 Å.

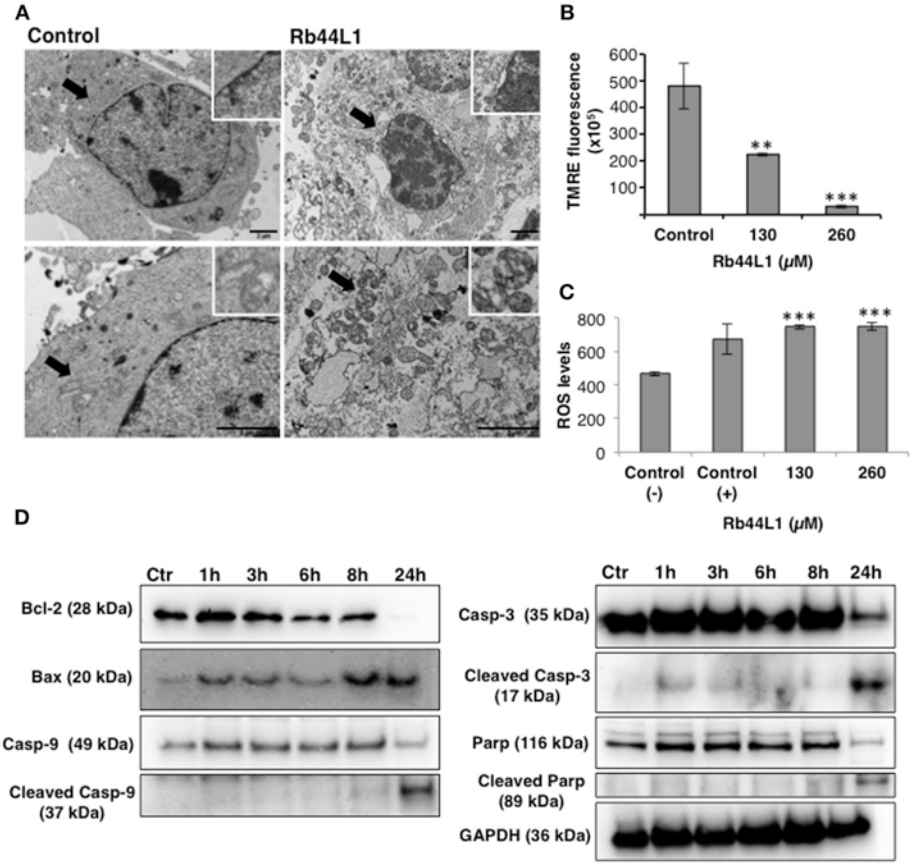

FIGURE 3 | Rb44L1 induces morphological alterations in mitochondria. **(A)** B16F10-Nex2 cells were treated with 260 μM of Rb44L1 for 18 h and examined by transmission electron microscopy. Representative micrographs of untreated cells (control) and Rb44L1 treated cells. Arrows indicate mitochondrial ultrastructure in the inserts; scale bar represents 2 μm; **(B)** loss of mitochondrial transmembrane potential in B16F10-Nex2 cells treated with 130 and 260 μM of Rb44L1 for 6 h, probed with red TMRE. $^{**}p < 0.01$ and $^{***}p < 0.001$ in comparison to the control; **(C)** enhanced superoxide anion production observed by DHE staining in B16F10-Nex2 cells treated with different concentrations of Rb44L1 for 16 h, vehicle control (Control −) and 5 mM H_2O_2 as positive control (Control +). The conversion of DHE to ethidium by oxidation was acquired at 370 nm (excitation) and 420 nm (emission). $^{***}p < 0.001$ in relation to control (−); **(D)** levels of apoptosis related proteins in Rb44L1-treated melanoma cells. Time-dependent effect on cell signaling of B16F10-Nex2 incubated with Rb44L1 at 130 μM. Levels of total and cleaved caspase-3,−9, cleaved PARP, Bax, Bcl-2, and Bcl-xl during Rb44-induced apoptosis are shown by Western blotting. GAPDH was used as loading control. A single cell-lysate sample was used in the same experiment and the Western blotting membranes were processed in parallel for antibody reactivity. Uncropped, full-length blottings are shown in **Figure S1**.

Docking Studies Reveal the Importance of Electrostatic Interactions

Docking calculations were performed using 7 tubulin structures generated from NMA displacement against the central structure of each L1-CDR peptide cluster (3 for Rb29L1, 11 for Rb44L1, and 8 for C36L1). In every docking round, an average of 350 different solutions was calculated. We then evaluated the best solution from Hex with BINANA to better understand the key binding characteristics governing the interaction.

Results indicated less favorable interactions for Rb29L1 than C36L1 and Rb44L1 in almost all displacements (as summarized in **Table 3**, detailed in **Table S1**, respectively), according to experimental results. At the best pose for Rb44L1 (docked with tubulin displaced by 2 Å) the ^{1}R side-chain is buried in the cavity formed between tubulin monomers, participating in 3 of 6 H-bonds and 2 salt-bridges (**Figures 7A,C,E,G**). In fact, interactions involving ^{1}R were observed in all displacements except at 3 Å and 4 Å. This indicates the putative importance of this residue to maintain the interaction with tubulin. When the ^{1}R is replaced by alanine, the results showed a systematic worsening of energy values (as summarized in **Table 3**, detailed in **Table S1**). Biological assays confirmed this prediction since the R1A substitution in Rb44L1 was not cytotoxic to B16F10-Nex2 cells, in the 0 to 500 μM range (data not shown). C36L1 pose analysis also indicated the involvement of a basic residue governing the interaction with tubulin. The ^{13}K was present participating of H-bond, salt-bridge or cation-pi interactions in all tubulin displacements but at 5 Å. At the best pose–docked with tubulin displaced by 4 Å, ^{13}K appeared in two H-bonds and in a salt-bridge (**Figures 7B,D,F,H**). Moreover, its side-chain was also buried in a cavity between tubulin monomers. On the other hand, although Rb29L1 had a greater number of H-bonds, the lack of

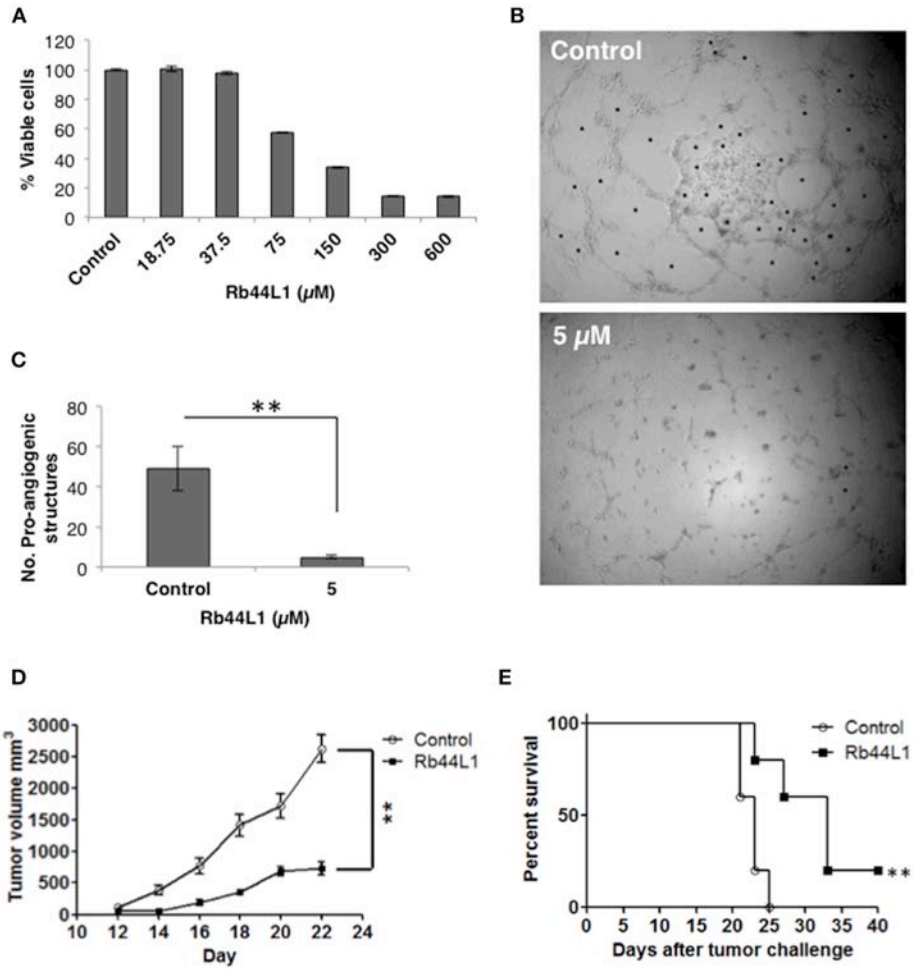

FIGURE 4 | Rb44L1 inhibits HUVEC sprouting on Geltrex^{TM} Matrix. **(A)** dose-response curve of Rb44L1 on HUVEC cells; **(B,C)** Inhibition by Rb44L1 (5 μM) on HUVEC sprouting on Geltrex^{TM} Matrix to form closed proangiogenic structures; $^{**}p < 0.01$ compared to untreated control. Rb44L1 prevents tumor progression. **(D)** 1×10^5 syngeneic B16F10-Nex2 cells were subcutaneously injected in C57Bl/6 mice. Peritumoral daily doses of 300 μg of Rb44L1 peptide were administered during five consecutive days. Tumor volume was measured and documented during the treatment period. $^{**}p < 0.01$ in comparison with control group treated with PBS; **(E)** survival of C57Bl/6 challenged mice after treatment with Rb44L1 or PBS (control). $^{**}p < 0.01$ in relation to control group.

charged residues would contribute to predicted energies higher than the other peptides.

Docking Studies Showed the L1-CDR Interactions Preferentially at the Nonexchangeable Nucleotide-Binding Site

We evaluated the best docking pose for both Rb44L1 and C36L1 in relation to the exposed nucleotide and colchicine binding sites. Rb44L1 interacted with three residues of the N-site (^{11}Q, ^{69}D, and ^{71}E) and with one residue of the colchicine site (^{252}K). The ^{1}R participated in all interactions. C36L1, however, interacted with different residues of the N- site (^{71}E, ^{11}Q, ^{224}Y, ^{206}N, ^{177}V) and one residue of colchicine site (^{179}T). These interactions depended on ^{13}K and ^{11}N residues of the C36L1 peptide (**Figures 8A,B**). Rb29L1 showed interactions with tubulin similarly with those of C36L1 (^{177}V, ^{179}T, ^{206}N, and ^{224}Y). In contrast, there were interactions shared with Rb44L1 and C36L1 (^{11}Q and ^{71}E), which were absent in Rb29L1 (**Figure 8C**). Taken together, these results showed that tubulin-opening motion corresponded to a decrease of summed electrostatic energy values of the displaced structures (**Figure 8D**).

Both Rb44L1 and C36L1 interacted with the region of helices α2, α3 and α8 of α-tubulin subunit, and showed differences in relation to β-tubulin monomer. While Rb44L1 interacts with loops α1β1 and α7α8, C36L1 interacts with loop β9α11 and helix α11. The overlapping of C36L1 and Rb44L1 best poses showed residues ^{13}K and ^{1}R occupying the same region at the tubulin dimer interface, that is blocked by residues ^{70}LEPT of α-tubulin and ^{243}PGQL of β-tubulin in a minimized structure (**Figure 8E**). Rb44L1 interaction with α-tubulin subunit was further confirmed using a chemiluminescence dot-blotting assay. We observed that Rb44L1 significantly bound to α-tubulin present in B16F10-Nex2 cell extract, as compared to the negative

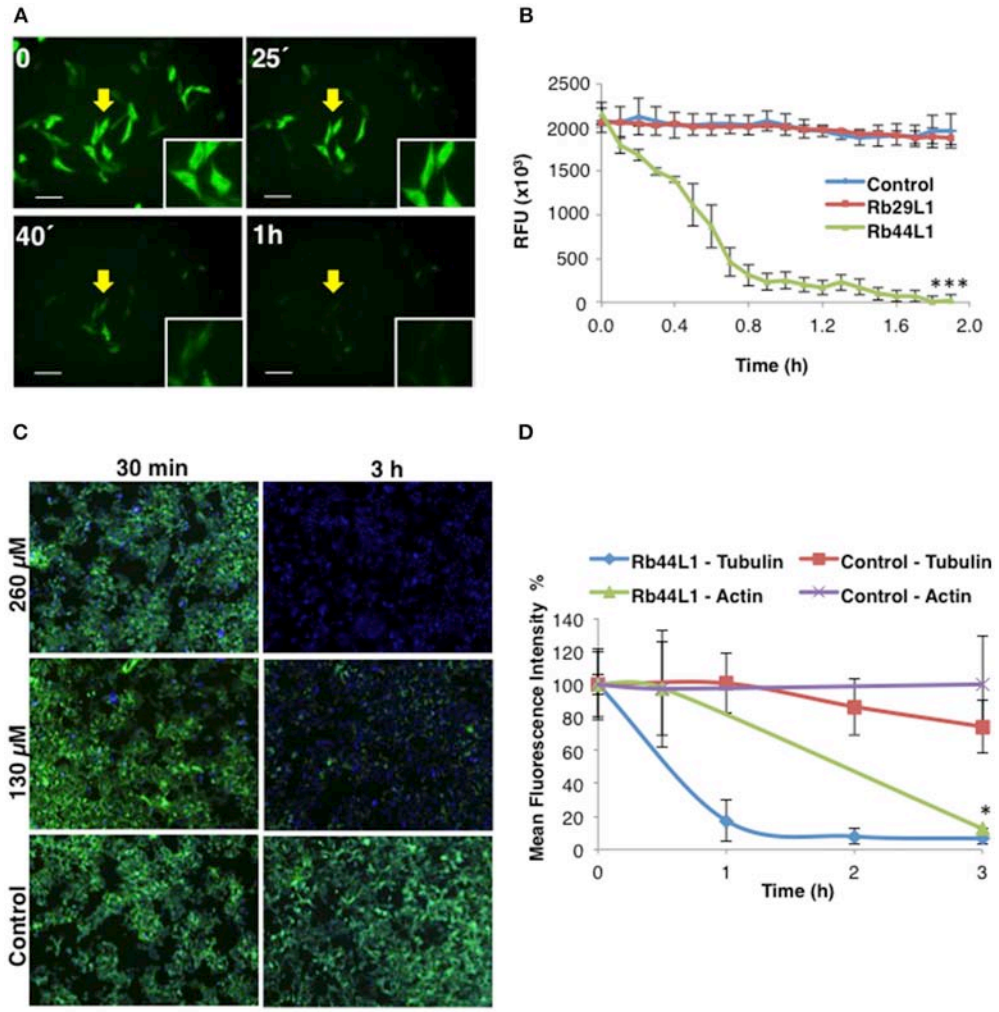

FIGURE 5 | Rb44L1 targets microtubules and disrupts tubulin assembly. **(A)** B16F10-Nex2 cells expressing baculovirus-transduced fluorescent tubulin were incubated with Rb44L1 at 260 μM; representative image of microtubule integrity is shown. Scale bar represents 50 μm; **(B)** microtubule dissociation was quantified in Rb44L1 and Rb29L1 treated cells and expressed as fluorescence decreased intensity and complete dispersion. ***$p < 0.001$ in comparison to untreated cells; **(C)** representative images of B16F10-Nex2 cells treated for different times with 130 and 260 μM of Rb44L1. Merged images of phalloidin-FITC and Hoescht 33342 staining are shown; **(D)** loss of actin and tubulin assembly integrity in Rb44L1 treated cells was quantified and compared. Results are expressed by fluorescence intensity. *$p < 0.05$ comparing microtubules and actin disruption.

control and the scrambled peptide (Scr44), which was inactive. The C36L1 peptide was used as a positive control (**Figure 8F**). Different concentrations of the coated peptide Rb44L1 were tested and we found 10 μg/10 μl to give the best resolution in the dot-blotting (**Figure S4**). Interaction with β-actin was also evaluated and no reaction was seen (data not shown). As the docking studies revealed that the Rb44L1 interacted preferentially close to the N-site, we investigated the influence of additional GTP and Mn^{2+} on the peptide binding to α-tubulin in a dot-blotting assay with fixed peptide and melanoma cell lysate as a source of α-tubulin (monomeric, modified, dimeric). The peptide binding was enhanced in the presence of both GTP and Mn^{2+}, but not with these agents added separately (**Figure S5**). Since the GTP N-site is nonexchangeable and non-catalytic, most likely the addition of GTP and Mn^{2+} triggered tubulin assembly by interacting on the E-site. Oligomeric tubulin bound to the peptide explains the increased reactivity with anti-α-tubulin antibody used to reveal the dot-blotting assay.

Rb44L1 Inhibits Purified Tubulin Assembly

The microtubule destabilization effect of Rb44L1 was also evaluated using a fluorescence recombinant tubulin polymerization assay kit (Cystoskeleton, Inc., Denver, CO). In this setting and starting with 2 mg/ml tubulin, 0.2 mg/ml of Rb44L1 delayed tubulin assembly and reduced approximately 1/4 of the total assembly capacity compared to the control (***$p < 0.001$) and the scrambled peptide, Scr44 (**Figures 9A,B**). This effect was significantly more evident at half the tubulin concentration (1 mg/ml) and 0.2 mg/ml of Rb44L1 (***$p < 0.001$

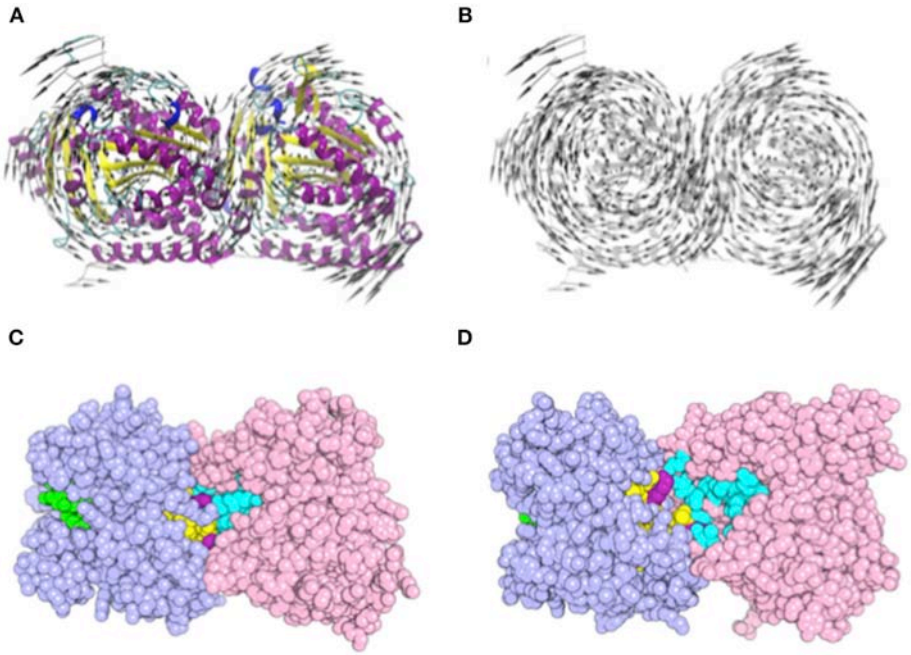

FIGURE 6 | Motion representation of normal mode 8 and nucleotide/colchicine site exposition as a result of α/β-tubulin displacement. **(A)** cartoon representation of α/β-tubulin normal mode 8. The circular motion in opposite directions of each tubulin monomer promotes the exposition of a nucleotide and colchicine binding sites; **(B)** highlight of vector directions. Vectors are placed into Cα atoms of each residue. Secondary structure color code: turn in green; β-sheet in yellow; β-bridge in gold; α-helix in purple; G, 3-10 helix in blue; and C, Coil in white. **(C,D)** α/β-tubulin crystallographic structure (PDB 4TV9) where atoms are represented as spheres. **(C)** comparison of GTP N-site (cyan), colchicine (yellow), and GTP E-site (green) site exposition between **(C)** α/β-tubulin crystallographic structure (PDB 4TV9); and **(D)** α/β-tubulin displaced by 6 Å along normal mode 8. Atoms are represented as spheres and residues present in both colchicine, and GTP N-site are colored in purple. α-Tubulin is represented in light-pink and β-tubulin in light-blue.

compared to the control). Polymerization was inhibited in 3/4 followed by depolymerization, after approximately 150 min incubation (**Figures 9C,D**). Since colchicine is a well-known microtubule inhibitor and has a binding-site mostly on β-tubulin, we assayed the effect of simultaneous addition of colchicine and Rb44L1. Increased inhibition of tubulin assembly was observed with this combination, suggesting independent interaction sites of Rb44L1 and colchicine, $^{***}p < 0.001$ compared to the colchicine alone (**Figure 9E**). It should be pointed out that single drugs such as the MT- depolymerizing colchicine and the MT-polymerizing paclitaxel when used in combination, the depolymerization effect has predominated (47).

DISCUSSION

The microtubules together with various stabilizing and destabilizing molecules display many important physiological functions. Due to their indispensability in the mitotic cell division, microtubules have been selected as preferred anticancer targets. Indeed, microtubule directed drugs are among the most commonly prescribed agents in cancer chemotherapy (2). Recently, anti-tumor peptides targeting microtubules (26) have been studied as tubulin interacting ligands that may evolve to be used in cancer therapy.

Novel anti-tumor peptides may have advantages over mAbs and tyrosine-kinase inhibitors, such as low cost, high specificity and potency due to their compatibility with targeted proteins, ability to penetrate the cell membrane, reduced immunogenicity, and improved safety (48). For example, the ADH-1 (Exherin), is an anticancer peptide distributed by Adhex Technologies®, which targets N-cadherin and induced partial and complete protective responses in patients with metastatic melanoma (49).

The microtubule destabilizing Ig V_L CDR1 peptide (C36L1) triggered cytotoxic and cytostatic effects on melanoma cells *in vitro* (23). Besides C36L1, we found that another CDR-L1 derived peptide, from anti-Lewis B mAb, exhibited similar cytotoxic mechanisms, targeting microtubules (MT). In the present work, we studied the molecular structure and biological effects of different L1-CDR-derived peptides: C36L1, Rb44L1 and Rb29L1 on microtubules. We analyzed the structure of L1-CDR-destabilizing MT peptides C36L1 and Rb44L1, as compared to the inactive one, Rb29L1. The latter demonstrated the most stable and rigid structure, assuming a β-hairpin conformation with several high occupancy H-bonds. Rb44L1 showed less rigidity as compared to Rb29L1, with a stable β-bridge conformation, while C36L1 was the most flexible peptide among them.

The biological effects of the peptides were examined and Rb44L1 showed the highest cytotoxic activity, selectively in different cancer cell lines with no significant effects on non-tumorigenic cell lines (**Table 2**).

Morphological and biochemical changes during tumor cells incubation with cytotoxic concentrations of Rb44L1 were

TABLE 3 | Key binding characteristics governing tubulin and L1-CDR interaction.

	Displacement (Å)						
	0	**1**	**2**	**3**	**4**	**5**	**6**
Rb29L1							
Energy*	434.76	751.84	383.90	−60.19	800.12	**−101.62**	−37.13
H-bonds	2	3	5	4	8	**1**	8
Salt-bridges	–	1	–	–	–	–	–
Cation-pi	–	–	1	–	–	–	–
T-stacking	–	–	–	–	–	–	1
Hydrophobic contacts	27	69	33	45	57	**60**	58
C36L1							
Energy*	−41.64	−186.92	15.15	−59.66	**−287.46**	195.54	−271.06
H-bonds	7	2	2	2	**6**	–	4
Salt-bridges	1	1	1	1	**1**	–	–
Cation-pi	–	–	1	–	–	–	1
T-stacking	–	–	–	–	–	–	–
Hydrophobic contacts	60	67	56	45	**42**	59	87
Rb44L1							
Energy*	216.31	−169.17	**−300.48**	45.49	−70.64	−30.10	−165.28
H-bonds	4	2	**6**	3	1	3	3
Salt-bridges	1	–	**2**	–	–	–	–
Cation-pi	–	–	–	–	–	–	–
T-stacking	–	–	–	–	–	–	–
Hydrophobic contacts	51	57	**61**	47	47	56	64
Rb44L1-R1A							
Energy*	253.99	45.25	−52.26	35.38	−37.68	−78.29	**−125.58**
H-bonds	2	3	3	–	2	3	**4**
Salt-bridges	–	–	–	–	–	–	–
Cation-pi	–	–	–	–	–	–	–
T-stacking	–	–	–	–	–	–	–
Hydrophobic contacts	41	53	51	46	47	56	**64**

*Best poses are highlighted in bold (energy values in kJ/mol).*Predicted summed electrostatic energy by atom-type pair according to Gasteiger partial charges.*

observed. Apoptosis was recognized by the remarkable shrinkage of the cytoplasm, roundup cells with pseudopodia retraction and shriveling without cell lysis, genomic DNA condensation and fragmentation, and exposure of phosphatidylserine at the surface of peptide-treated cells (50). The intrinsic pathway involves the functional deregulation of mitochondria, which may culminate in activation of caspases and the cascade of events that drives to cell death (51, 52). Early disruption of mitochondrial membrane potential, as evidenced by time-lapse fluorescence microscopy and TEM, together with later production of ROS, cleavage of caspase-9, caspase-3, the PARP, upregulation of Bax and downregulation of Bcl-2 were effects induced by Rb44L1, and they are all consistent with the intrinsic pathway of apoptosis (53, 54), strongly suggesting that this is the main *in vitro* cytotoxic mechanism of the peptide in melanoma cells.

P53 is activated in response to different stresses leading tumor cells to apoptosis and growth arrest (55). In this regard, accumulation of active p53 may also be attributed to disintegration of the cytoskeleton. Microtubule targeted-drugs are one of the main stimuli able to increase levels and activate p53 (56).

The main mechanism that seems to be involved in the intrinsic apoptosis by Rb44L1 peptide is the early disruption of the microtubules in melanoma cells. Rb44L1 destabilized labeled microtubules during early stages of incubation, as observed by fluorescence microscopy. In contrast, Rb29L1 did not affect the microtubule dynamics, under the same conditions.

The actin cytoskeleton integrity was also evaluated, as observed by fluorescence microscopy. Rb44L1 induced the degradation of actin filaments in melanoma cells to a maximum effect after 3 h of tumor cell treatment with this peptide. Alterations of actin dynamics are sufficient to induce apoptosis. They involve changes in F-actin levels, in the flux of actin through the filament pool, or both (57). In addition, F-actin depolymerization has been implicated in reduced MMP and elevated ROS production, together with shortening of cell lifespan (58), as observed in melanoma cells treated with Rb44L1. The peptide, however, did not directly interact with F-actin to induce depolymerization as suggested by a late kinetics, which follows microtubule depolymerization. In fact, the actin cytoskeleton integrity has been shown to be highly dependent on the microtubule dynamics (59, 60), which is crucial in tumor cells constantly entering the mitotic program as compared to non-tumorigenic cells (2). Cellular functions depend on the crosstalk between microtubules and actin filaments, in which specific proteins bind to microtubules and actin filaments simultaneously, promoting co-organization and coupled growth of both networks (61). Both cytoskeleton constituents are intrinsically related and rearranged during the progress of apoptosis. Important events are regulated by ROCK kinases that actively regulate the actomyosin contractile ring, a process facilitated by the early disruption of microtubules. Protrusions of the plasma membrane also called apoptotic bodies or blebs, are formed, with subsequent depolymerization of actin filaments (62).

Rb44L1 interaction with microtubules and induction of their depolymerization with subsequent degradation of actin filaments increased the number of tumor cells in the G2/M phase leading to a mitotic catastrophe. Such effects, coupled to inhibited angiogenesis as observed *in vitro,* are consistent with the described effects of other microtubule targeting drugs (2, 63). A schematic illustration of the effects induced by Rb44L1 on melanoma cells is detailed in the **Figure 10**.

Most importantly, this peptide showed a promising antitumor protective effect against subcutaneously grafted melanoma, with no systemic toxicity being observed.

Once proteins exist in equilibrium of multiple conformations in solution, we used a theoretical approach that mixed analyses of molecular dynamics and normal modes, to sample distinct structural states of α/β-tubulin dimer. This hybrid methodology allowed for the assignment of both local and collective motions of the system, that are essential dynamic features related to conformational selection and induced fit, respectively (64–66).

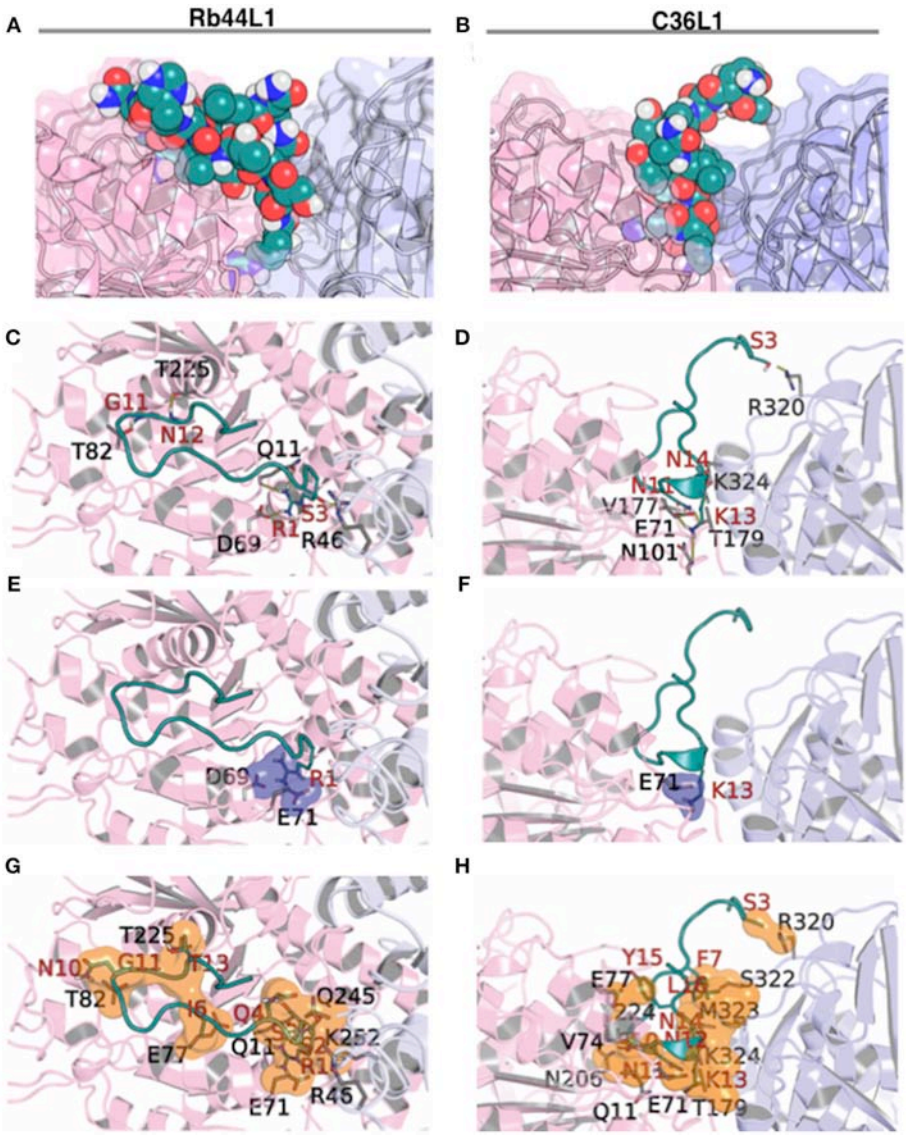

FIGURE 7 | Rb44L1 and C36L1 interactions with α/β-tubulin displaced by 2 Å and 4 Å, respectively. **(A,B)** surface complementarity; **(C,D)** hydrogen bonds formed; **(E,F)** salt bridges form a tiny pocket demonstrated in navy blue surface; **(G,H)** hydrophobic contacts form pockets represented by orange surface. α-Tubulin is represented in light-pink and β-tubulin in light-blue.

Microtubules are dynamic cellular structures that switch between growing and pruning cycles both *in vivo* and *in vitro*. Stabilization or destabilization of microtubule dynamics is promoted by a number of endogenous and exogenous compounds that regulate the process in different ways, either by competition with GTP (67), structural modification of the protein-protein interface between α and β monomers (8, 31, 68) or by allosteric mechanisms (69). One of the most frequently described mechanisms is the ligand binding at the colchicine site on β-tubulin, which is spatially next to an α-tubulin nucleotide binding site, with nonexchangeable, noncatalytic characteristics, known as N-site. Therefore, we explored the exposition of both binding sites as a molecular docking strategy, since their coupling might trigger the structural destabilization of tubulin dimer exerted by some L1-CDR peptides.

The tubulin heterodimer has two guanine binding sites: at the exchangeable, catalytic site (E-site) on the β chain, GTP is hydrolyzed to GDP during microtubule assembly; the nonexchangeable, noncatalytic site (N-site), on the α chain, is always occupied by GTP, suggesting that it may function as a structural cofactor of tubulin (70). Divalent cations have high affinity for both sites and their binding is associated to the structural stability of tubulin dimer (71). Mg^{2+} is a well-established ion required for microtubule assembly and stability, and contributes to strong GTP binding to the E-site (72). Q-band EPR and electron spin echo envelope modulation spectroscopy

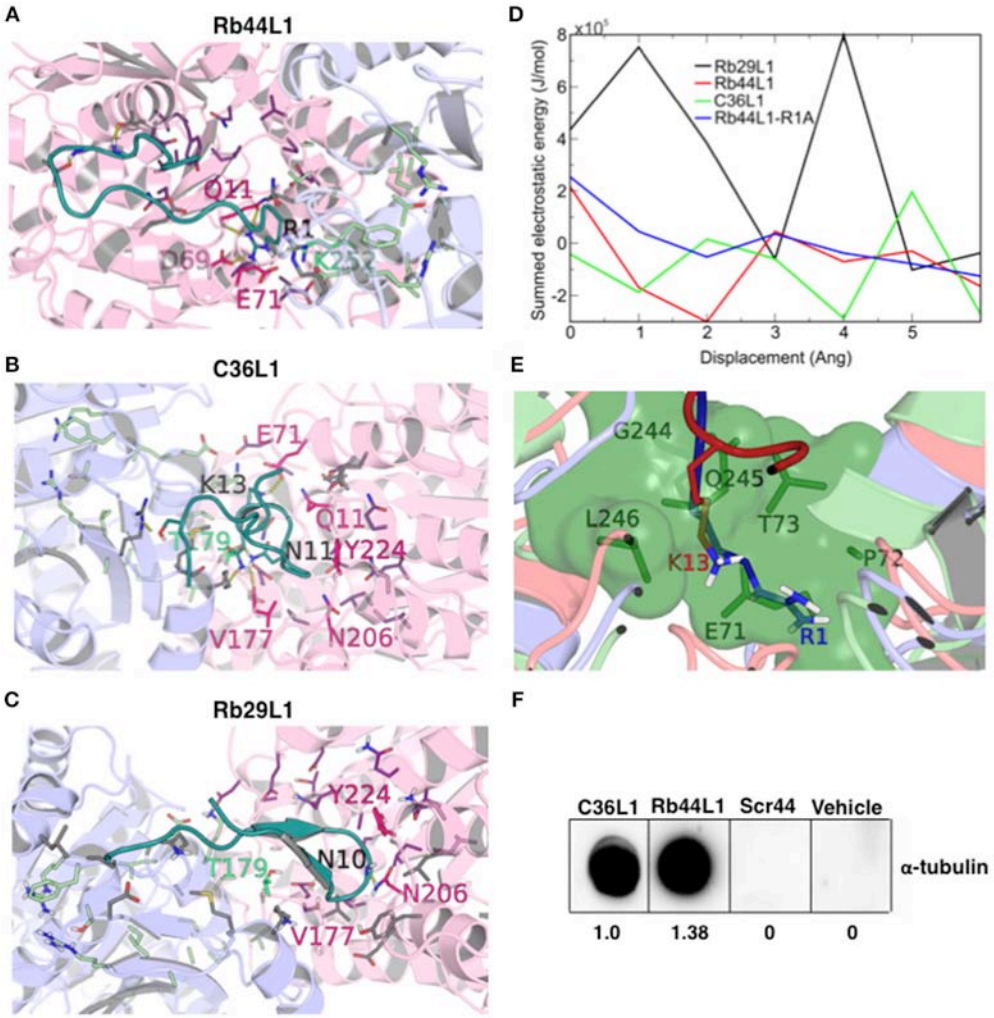

FIGURE 8 | CDR-L1 docking poses in relation to α/β-tubulin N-site and colchicine binding sites and energy re-score of docked complexes. **(A)** Rb44L1; **(B)** C36L1; **(C)** Rb29L1 best docking pose highlighting their position in relation to residues at N-site and colchicine binding sites. α-Tubulin is represented in light-pink and β-tubulin in light-blue. N-site and colchicine binding site residues are represented as purple and pale green, respectively, whereas those that interact with the CDRs are hot pink and lime green for nucleotide and colchicine binding site, respectively. The camera was inverted 170° on the y-axis and 80° on the x-axis for better visualization of the C36L1 and Rb29L1 interactions; **(D)** summed electrostatic energy of Rb29L1, Rb44L1, C36L1 and Rb44L1-R1A complexed with α/β-tubulin at different displacements; **(E)** overlapping of Rb44L1 and C36L1 docked complexes. Residues ^{1}R and ^{13}K of Rb44L1 (blue) and C36L1 (red), respectively, occupy the same region at the tubulin dimer interface, that is blocked by residues ^{70}LEPT of α-tubulin and ^{243}PGQL of β-tubulin at minimized structure (green surface); **(F)** Rb44L1 binds to tubulin present in the lysate of B16F10-Nex2 cells. Dot-blottings were performed by coating the nitrocellulose membranes with 10 μg of C36L1, Rb44L1, scrambled-Rb44L1 (Scr44), and vehicle (1% DMSO in milli-Q water). Experimental and control dot-blottings were performed as described in methods. Quantitation of dots was performed using ImageJ, and are represented as arbitrary units.

showed that Mn^{2+} at both N and E-sites directly coordinated to the triphosphate of GTP, proving that the divalent cation at both sites directly interacts with GTP (73). Mn^{2+} slowly exchanged for Mg^{2+} at the N-site and other divalent and trivalent cations may also exchange at this site and play a role in the assembly of microtubules (74, 75). Chelation of divalent cations in general, inhibits the assembly of tubulin dimers.

L1-CDR peptides bound at the nucleotide/colchicine binding site at the dimer interface, but most of the interactions were made at the N-site. The best solution of Rb44L1 peptide was in an α/β-tubulin semi-open state. We observed that the ^{1}R is a key residue for interaction with tubulin dimer. The mutation of this residue for alanine, weakened the interaction, increasing the free energy. This result was further corroborated by experimental assays. Interestingly, the ^{13}K of C36L1 used the same tubulin cavity as that of ^{1}R of Rb44L1, although C36L1 best docking pose was observed in an open conformation. This polar pocket may play an important role in tubulin depolymerization induced by L1-CDR peptides since the inactive Rb29L1 did not present a favorable interaction on this region.

The inactivity of Rb29L1 peptide is noteworthy, since its sequence is quite similar to Rb44L1 except between residues 4

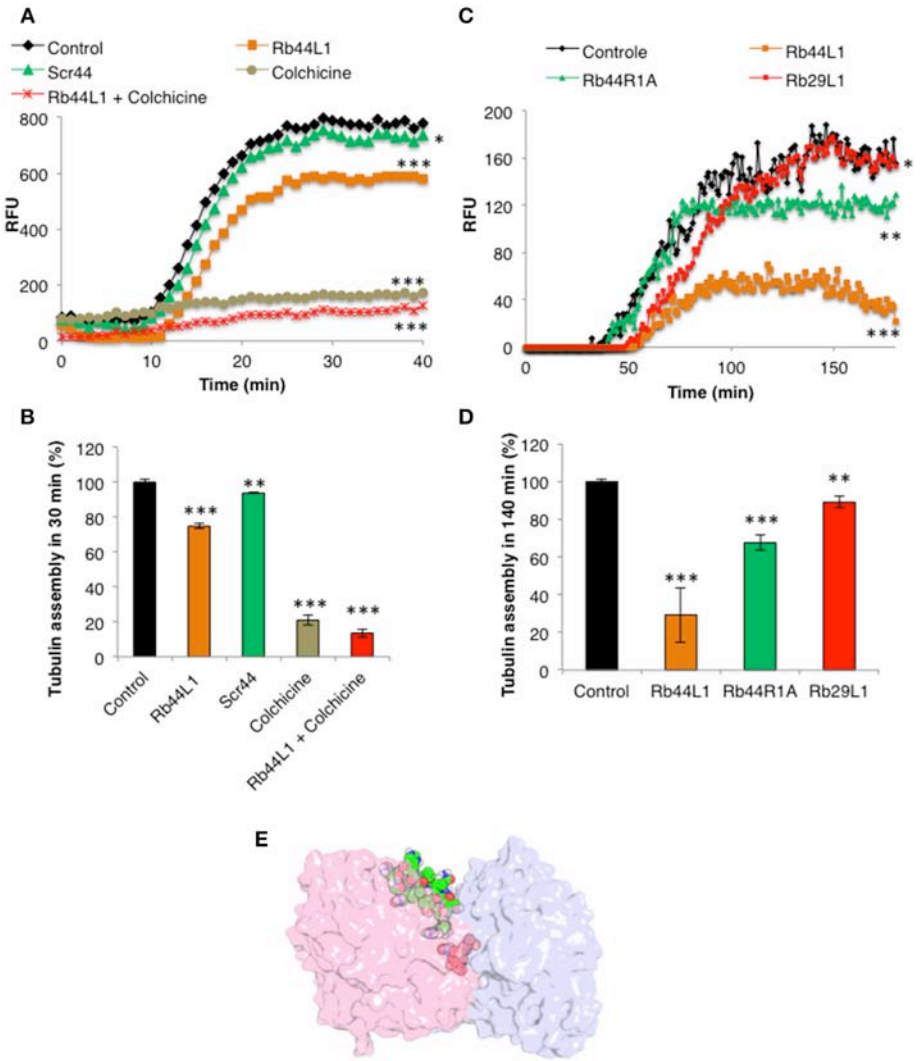

FIGURE 9 | Effects of Rb44L1 on microtubule assembly. **(A)** Polymerization kinetics in presence of Rb44L1 and Scr44 (130 μM) with purified fluorescent tubulin at 2 mg/ml. Inhibition by colchicine (50 μM) was assayed alone or in combination with Rb44L1. **(B)** bar graph represents the percentage of tubulin assembly measured at 30 min from kinetic curve demonstrated in **(A)**. **(C)** Rb44L1, Rb29L1, and Rb44R1A were incubated with tubulin at 1 mg/ml and polymerization/destabilization was measured. **(D)** bar graph represents the percentage of tubulin assembly measured at 140 min from kinetic curve demonstrated in **(C)**. $^{*}p < 0.05$, $^{**}p < 0.01$, and $^{***}p < 0.001$ in comparison to the control **(E)** structural alignment between the best pose from molecular docking and PDB 4O2B (chains A and B) illustrating the possibility of Rb44L1 (green) and colchicine (red) interact concomitantly with α/β-tubulin at its interface. PDB4O2B was firstly aligned with PDB4TV9, and then the comparison was made. α-Tubulin is represented in light-pink and β-tubulin in light-blue.

and 7, which is TSLL in the former peptide and QTIT in the latter. Interestingly, the most favorable docking poses showed a different interaction pattern with tubulin, since Rb44L1 QTIT residues were less solvent exposed than Rb29L1 TSLL residues, which are 70 $Å^2$ more exposed to solvent. This is a direct consequence of the observed R interaction pattern with buried tubulin residues (^{69}D and ^{11}Q) in the N-site, and could be related to the observed activity differences.

A dot-blotting assay showed that in the presence of both GTP and Mn^{2+}, but not with these agents added separately, the Rb44L1 peptide bound with increased affinity to the tubulin α-chains of monomeric, modified or dimeric substrates from a tumor cell lysate. This may have occurred by the GTP-E site induced oligomerization of tubulin dimers present in the cell lysate during incubation, indicating that under the conditions used, the dot-blotting assay with fixed peptide did not impair tubulin assembly on the latter (**Figure S6**).

In contrast, what is the possible mechanism triggering Rb44L1 depolymerization of tubulin? We found that the surface overlapping of the docked conformation of the peptide and the closed α/β-tubulin revealed that the peptide represents a steric constraint to the protein in this conformation. The effect noticed in the overlapping regions of ^{1}R, ^{3}S, and ^{12}N residues, and the peptide size

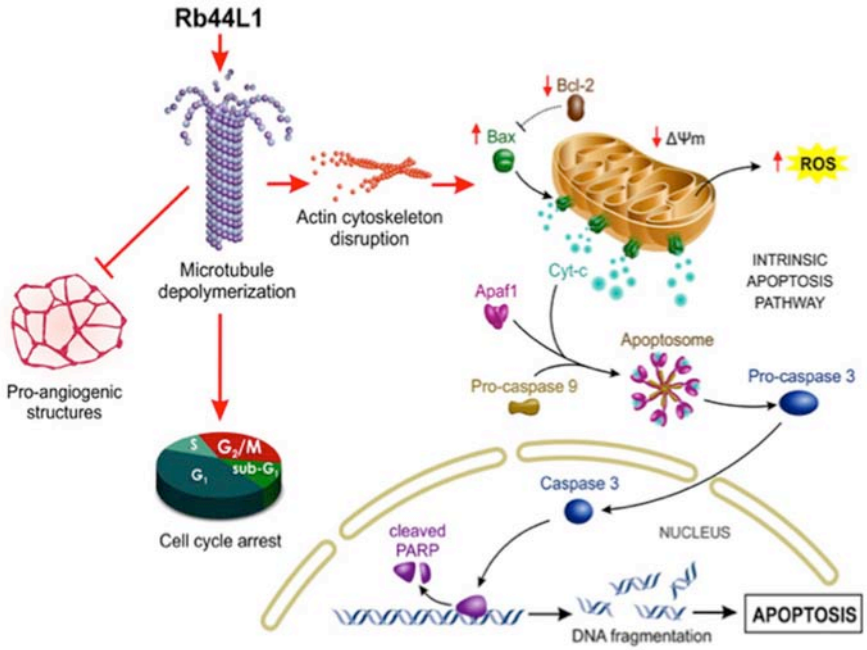

FIGURE 10 | Schematic illustration of proposed Rb44L1 effects on melanoma cells. Rb44L1 peptide interacts at the tubulin monomers' interface in microtubules promoting depolymerization. Alteration of microtubule dynamics led to actin filaments degradation, disrupting the cytoskeleton integrity. In response to changes in the environment, mitochondria produce high amounts of ROS and release co-factors that trigger intrinsic apoptosis. Upon activation by binding to and neutralization of Bcl-2, insertion of Bax into mitochondrial outer membrane form pores to allow the passage of proteins from the intermembrane space to the cytosol. It involves the disruption of mitochondrial membrane potential ($\Delta\psi m$) followed by release of cytochrome c in the cytosol that binds to Apaf-1, ATP, and pro-caspase 9 to form an oligomeric apoptosome, which results in the caspase cascade initiation. Activation of caspase 3 by caspase 9 is responsible for the proteolytic cleavage of the nuclear enzyme Parp-1, which abolishes its DNA repair ability and induces DNA fragmentation in cells undergoing apoptosis. In addition, Rb44L1 inhibited pro-angiogenic structure formation *in vitro* and induced cell cycle arrest at G2/M. Abbreviations: Apaf-1, Apoptotic protease activating factor 1; Cyt-c, Cytochrome-c; ROS, Reactive oxygen species; $\Delta\psi m$, Mitochondrial membrane potential; Bcl-2, B-cell lymphoma 2; Bax, Bcl-2 associated X protein; Parp-1, Poly [ADP-ribose] polymerase 1. The illustration was designed by Carolina de Amat.

of 1675.0 $Å^3$, which preclude the α/β-tubulin return to a closed conformation, is a source of structure destabilization (**Video S2**).

Taken together, we propose that Rb44L1 peptide is a novel candidate to be developed as a drug, acting on the microtubule network of tumor cells. Molecular docking on tubulin monomers in opening motion, and the possible mechanisms of action leading to microtubule depolymerization were explored in comparison with other Ig CDR-L1 derived peptides, all tested against *in vitro* models of melanoma cells.

DATA AVAILABILITY STATEMENT

Datasets are available on request. The raw data supporting the conclusions of this manuscript will be made available by the authors, without undue reservation, to any qualified researcher.

ETHICS STATEMENT

This study was carried out in accordance with the recommendations of the Ethics Committee of Federal University of São Paulo, Brazil for animal manipulation and experimental procedures. Animals were provided by Centro de desenvolvimento de modelos experimentais para medicina e biologia (CEDEME), of Federal University of São Paulo. The protocol was approved by the Ethics Committee of Federal University of São Paulo, Brazil via document CEP 1234/2011.

AUTHOR CONTRIBUTIONS

NG and CF performed the biological experiments, analyzed data, and designed the figures. MM carried out annexin V and propidium iodide labeling analysis and designed **Figure 2D**. RA carried out the cell cycle analysis and designed **Figure 2E**. PR-L and RC carried out all the chemical analysis. NG wrote the manuscript and LP and LT designed the research project. All authors reviewed and approved the manuscript.

FUNDING

This work was supported by Fundação de Amparo a Pesquisa do Estado de São Paulo (Fapesp), grant 10/51423-0 and by the National Council for Scientific and Technological Development (CNPq).

ACKNOWLEDGMENTS

The authors acknowledge Carolina de Amat for the illustration of Rb44L1 effects.

SUPPLEMENTARY MATERIAL

The Supplementary Material for this article can be found online at: https://www.frontiersin.org/articles/10.3389/fonc.2019.00025/full#supplementary-material

REFERENCES

1. Stanton RA, Gernert KM, Nettles JH, Aneja R. Drugs that target dynamic microtubules: a new molecular perspective. *Med Res Rev.* (2011) 31:443–81. doi: 10.1002/med.20242
2. Jordan MA, Wilson L. Microtubules as a target for anticancer drugs. *Nat Rev Cancer* (2004) 4:253–65. doi: 10.1038/nrc1317
3. Jordan A, Hadfield JA, Lawrence NJ, McGown AT. Tubulin as a target for anticancer drugs: agents which interact with the mitotic spindle. *Med Res Rev.* (1998) 18:259–96. doi: 10.1002/(SICI)1098-1128(199807)18:43.3.CO;2-T
4. Tozer GM, Kanthou C, Parkins CS, Hill SA. The biology of the combretastatins as tumour vascular targeting agents. *Int J Exp Pathol.* (2002) 83:21–38. doi: 10.1046/j.1365-2613.2002.00211.x
5. Mizumoto N, Gao J, Matsushima H, Ogawa Y, Tanaka H, Takashima A. Discovery of novel immunostimulants by dendritic-cell-based functional screening. *Blood* (2005) 106:3082–9. doi: 10.1182/blood-2005-03-1161
6. Dumontet C, Jordan MA. Microtubule-binding agents: a dynamic field of cancer therapeutics. *Nat Rev Drug Discov.* (2010) 9:790–803. doi: 10.1038/nrd3253
7. Uzma F, Mohan CD, Hashem A, Konappa NM, Rangappa S, Kamath PV, et al. Endophytic fungi-alternative sources of cytotoxic compounds: a review. *Front Pharmacol.* (2018) 9:309. doi: 10.3389/fphar.2018.00309
8. Prota AE, Danel F, Bachmann F, Bargsten K, Buey RM, Pohlmann J, et al. The novel microtubule-destabilizing drug BAL27862 binds to the colchicine site of tubulin with distinct effects on microtubule organization. *J Mol Biol.* (2014) 426:1848–60. doi: 10.1016/j.jmb.2014.02.005
9. Prota AE, Bargsten K, Zurwerra D, Field JJ, Diaz JF, Altmann KH, et al. Molecular mechanism of action of microtubule-stabilizing anticancer agents. *Science* (2013) 339:587–90. doi: 10.1126/science.1230582
10. Fojo T, Menefee M. Mechanisms of multidrug resistance: the potential role of microtubule-stabilizing agents. *Ann Oncol.* (2007) 18 (Suppl. 5):v3–8. doi: 10.1093/annonc/mdm172
11. Quasthoff S, Hartung HP. Chemotherapy-induced peripheral neuropathy. *J Neurol.* (2002) 249:9–17. doi: 10.1007/PL00007853
12. Xiao YF, Jie MM, Li BS, Hu CJ, Xie R, Tang B, et al. Peptide-based treatment: a promising cancer therapy. *J Immunol Res.* (2015) 2015:1–13. doi: 10.1155/2015/761820
13. Thundimadathil J. Cancer treatment using peptides: current therapies future prospects. *J Amino Acids* (2012) 2012:967347. doi: 10.1155/2012/967347
14. Fosgerau K, Hoffmann T. Peptide therapeutics: current status future directions. *Drug Discov Today* (2015) 20:122–8. doi: 10.1016/j.drudis.2014.10.003
15. Bhutia SK, Maiti TK. Targeting tumors with peptides from natural sources. *Trends Biotechnol.* (2008) 26:210–7. doi: 10.1016/j.tibtech.2008.01.002
16. Srivatsan A, Ethirajan M, Pey SK, Dubey S, Zheng X, Liu TH, et al. Conjugation of cRGD peptide to chlorophyll a based photosensitizer (HPPH) alters its pharmacokinetics with enhanced tumor-imaging photosensitizing (PDT) efficacy. *Mol Pharm.* (2011) 8:1186–97. doi: 10.1021/mp200018y
17. Massaoka MH, Matsuo AL, Figueiredo CR, Girola N, Farias CF, Pasqualoto K, et al. A subtraction tolerization method of immunization allowed for Wilms' tumor protein-1 (WT1) identification in melanoma discovery of an antitumor peptide sequence. *J Immunol Methods* (2014) 414:11–9. doi: 10.1016/j.jim.2014.08.003
18. Suarez-Jimenez GM, Burgos-Hernez A, Ezquerra-Brauer JM. Bioactive peptides depsipeptides with anticancer potential: sources from marine animals. *Mar Drugs* (2012) 10:963–86. doi: 10.3390/md10050963
19. Torres MDT, Andrade GP, Sato RH, Pedron CN, Manieri TM, Cerchiaro G, et al. Natural redesigned wasp venom peptides with selective antitumoral activity. *Beilstein J Org Chem.* (2018) 14:1693–703. doi: 10.3762/bjoc.14.144
20. Gabrielli E, Pericolini E, Cenci E, Ortelli F, Magliani W, Ciociola T, et al. Antibody complementarity-determining regions (CDRs): a bridge between adaptive innate immunity. *PLoS ONE* (2009) 4:e8187. doi: 10.1371/journal.pone.0008187
21. Polonelli L, Ciociola T, Magliani W, Zanello PP, D'Adda T, Galati S, et al. Peptides of the constant region of antibodies display fungicidal activity. *PLoS ONE* (2012) 7:e34105. doi: 10.1371/journal.pone.0034105
22. Polonelli L, Ponton J, Elguezabal N, Moragues MD, Casoli C, Pilotti E, et al. Antibody complementarity-determining regions (CDRs) can display differential antimicrobial, antiviral antitumor activities. *PLoS ONE* (2008) 3:e2371. doi: 10.1371/journal.pone.0002371
23. Dobroff AS, Rodrigues EG, Juliano MA, Friaca DM, Nakayasu ES, Almeida IC, et al. Differential antitumor effects of IgG IgM monoclonal antibodies their synthetic complementarity-determining regions directed to new targets of B16F10-Nex2 melanoma cells. *Transl Oncol.* (2010) 3:204–17. doi: 10.1593/tlo.09316
24. Arruda DC, Santos LC, Melo FM, Pereira FV, Figueiredo CR, Matsuo AL, et al. Travassos: beta-Actin-binding complementarity-determining region 2 of variable heavy chain from monoclonal antibody C7 induces apoptosis in several human tumor cells is protective against metastatic melanoma. *J Biol Chem.* (2012) 287:14912–22. doi: 10.1074/jbc.M111.322362
25. Figueiredo CR, Matsuo AL, Massaoka MH, Polonelli L, Travassos LR. Anti-tumor activities of peptides corresponding to conserved complementary determining regions from different immunoglobulins. *Peptides* (2014) 59:14–9. doi: 10.1016/j.peptides.2014.06.007
26. Figueiredo CR, Matsuo AL, Azevedo RA, Massaoka MH, Girola N, Polonelli L, et al. A novel microtubule de-stabilizing complementarity-determining region C36L1 peptide displays antitumor activity against melanoma *in vitro in vivo*. *Sci Rep.* (2015) 5:14310. doi: 10.1038/srep14310
27. Girola N, Matsuo AL, Figueiredo CR, Massaoka MH, Farias CF, Arruda DC, et al. The Ig VH complementarity-determining region 3-containing Rb9 peptide, inhibits melanoma cells migration invasion by interactions with Hsp90 an adhesion G-protein coupled receptor. *Peptides* (2016) 85:1–15. doi: 10.1016/j.peptides.2016.08.006
28. Rabaça AN, Arruda DC, Figueiredo CR, Massaoka MH, Farias CF, Tada DB, et al. AC-1001 H3 CDR peptide induces apoptosis signs of autophagy *in vitro* exhibits antimetastatic activity in a syngeneic melanoma model. *FEBS Open Bio.* (2016) 6:885–901. doi: 10.1002/2211-5463.12080
29. Kabat EA, Wu TT, Bilofsky H. Unusual distributions of amino acids in complementarity-determining (hypervariable) segments of heavy light chains of immunoglobulins their possible roles in specificity of antibody-combining sites. *J Biol Chem.* (1977) 252:6609–16.
30. Lamiable A, Thevenet P, Rey J, Vavrusa M, Derreumaux P, Tuffery P. PEP-FOLD3: faster *de novo* structure prediction for linear peptides in solution in complex. *Nucleic Acids Res.* (2016) 44:W449–54. doi: 10.1093/nar/gkw329
31. Prota AE, Bargsten K, Diaz JF, Marsh M, Cuevas C, Liniger M, et al. A new tubulin-binding site pharmacophore for microtubule-destabilizing anticancer drugs. *Proc Natl Acad Sci USA.* (2014) 111:13817–21. doi: 10.1073/pnas.1408124111
32. Olsson MH, Sondergaard CR, Rostkowski M, Jensen JH. PROPKA3: consistent treatment of internal surface residues in empirical pKa predictions. *J Chem Theory Comput.* (2011) 7:525–37. doi: 10.1021/ct100578z
33. Van Der Spoel D, Lindahl E, Hess B, Groenhof G, Mark AE, Berendsen HJ. GROMACS: fast, flexible, free. *J Comput Chem.* (2005) 26:1701–18. doi: 10.1002/jcc.20291
34. Huang J, MacKerell ADJr. CHARMM36 all-atom additive protein force field: validation based on comparison to NMR data. *J Comput Chem.* (2013) 34:2135–45. doi: 10.1002/jcc.23354
35. Jo S, Kim T, Iyer VG, Im W. CHARMM-GUI: a web-based graphical user interface for CHARMM. *J Comput Chem.* (2008) 29:1859–65. doi: 10.1002/jcc.20945

36. Lee J, Cheng X, Swails JM, Yeom MS, Eastman PK, Lemkul JA, et al. CHARMM-GUI input generator for NAMD, GROMACS, AMBER, OpenMM, CHARMM/OpenMM simulations using the CHARMM36 additive force field. *J Chem Theory Comput.* (2016) 12:405–13. doi: 10.1021/acs.jctc.5b00935
37. Boonstra S, Onck PR, Giessen E. CHARMM TIP3P water model suppresses peptide folding by solvating the unfolded state. *J Phys Chem B* (2016) 120:3692–8. doi: 10.1021/acs.jpcb.6b01316
38. Humphrey W, Dalke A, Schulten K. VMD: visual molecular dynamics. *J Mol Graph.* (1996) 14:33–8, 27–8. doi: 10.1016/0263-7855(96)00018-5
39. Brooks BR, Brooks CL III, Mackerell ADJr, Nilsson L, Petrella RJ, Roux B, et al. CHARMM: the biomolecular simulation program. *J Comput Chem.* (2009) 30:1545–614. doi: 10.1002/jcc.21287
40. Perahia D, Mouawad L. Computation of low-frequency normal modes in macromolecules: improvements to the method of diagonalization in a mixed basis application to hemoglobin. *Comput Chem.* (1995) 19:241–6. doi: 10.1016/0097-8485(95)00011-G
41. Buck M, Bouguet-Bonnet S, Pastor RW, MacKerell ADJr. Importance of the CMAP correction to the CHARMM22 protein force field: dynamics of hen lysozyme. *Biophys J.* (2006) 90:L36–8. doi: 10.1529/biophysj.105.078154
42. Philot EA, Perahia D, Braz AS, Costa MG, Scott LP. Binding sites hydrophobic pockets in human thioredoxin 1 determined by normal mode analysis. *J Struct Biol.* (2013) 184:293–300. doi: 10.1016/j.jsb.2013.09.002
43. Louet M, Perahia D, Martinez J, Floquet N. A concerted mechanism for opening the GDP binding pocket release of the nucleotide in hetero-trimeric G-proteins. *J Mol Biol.* (2011) 411:298–312. doi: 10.1016/j.jmb.2011.05.034
44. Ritchie DW, Venkatraman V. Ultra-fast FFT protein docking on graphics processors. *Bioinformatics* (2010) 26:2398–405. doi: 10.1093/bioinformatics/btq444
45. Meissner GO, de Resende Lara PT, Scott LP, Braz AS, Chaves-Moreira D, Matsubara FH, et al. Molecular cloning *in silico* characterization of knottin peptide, U2-SCRTX-Lit2:from brown spider (Loxosceles intermedia) venom glands. *J Mol Model.* (2016) 22:196. doi: 10.1007/s00894-016-3067-0
46. Durrant JD, McCammon JA. BINANA: a novel algorithm for lig-binding characterization. *J Mol Graph Model.* (2011) 29:888–93. doi: 10.1016/j.jmgm.2011.01.004
47. Bombuwala K, Kinstle T, Popik V, Uppal SO, Olesen JB, Vina J, et al. Colchitaxel, a coupled compound made from microtubule inhibitors colchicine paclitaxel. *Beilstein J Org Chem.* (2006) 2:13. doi: 10.1186/1860-5397-2-13
48. Miller MJ, Foy KC, Kaumaya PT. Cancer immunotherapy: present status, future perspective, a new paradigm of peptide immunotherapeutics. *Discov Med.* (2013) 15:166–76.
49. Augustine CK, Yoshimoto Y, Gupta M, Zipfel PA, Selim MA, Febbo P, et al. Targeting N-cadherin enhances antitumor activity of cytotoxic therapies in melanoma treatment. *Cancer Res.* (2008) 68:3777–84. doi: 10.1158/0008-5472.CAN-07-5949
50. Galluzzi L, Vitale I, Abrams JM, Alnemri ES, Baehrecke EH, Blagosklonny MV, et al. Molecular definitions of cell death subroutines: recommendations of the nomenclature committee on cell death 2012. *Cell Death Differ.* (2012) 19:107–20. doi: 10.1038/cdd.2011.96
51. Elmore S. Apoptosis: a review of programmed cell death. *Toxicol Pathol.* (2007) 35:495–516. doi: 10.1080/01926230701320337
52. Thornberry NA, Lazebnik Y. Caspases: enemies within. *Science* (1998) 281:1312–6. doi: 10.1126/science.281.5381.1312
53. Kroemer G, Galluzzi L, Brenner C. Mitochondrial membrane permeabilization in cell death. *Physiol Rev.* (2007) 87:99–163. doi: 10.1152/physrev.00013.2006
54. Desouza M, Gunning PW, Stehn JR. The actin cytoskeleton as a sensor mediator of apoptosis. *Bioarchitecture* (2012) 2:75–87. doi: 10.4161/bioa.20975
55. Jimenez GS, Khan SH, Stommel JM, Wahl GM. p53 regulation by post-translational modification nuclear retention in response to diverse stresses. *Oncogene* (1999) 18:7656–65. doi: 10.1038/sj.onc.1203013
56. Giannakakou P, Nakano M, Nicolaou KC, O'Brate A, Yu J, Blagosklonny MV, et al. Enhanced microtubule-dependent trafficking p53 nuclear accumulation by suppression of microtubule dynamics. *Proc Natl Acad Sci USA*. (2002) 99:10855–60. doi: 10.1073/pnas.132275599
57. Franklin-Tong VE, Gourlay CW. A role for actin in regulating apoptosis/programmed cell death: evidence spanning yeast, plants animals. *Biochem J.* (2008) 413:389–404. doi: 10.1042/BJ20080320
58. Boldogh IR, Pon LA. Interactions of mitochondria with the actin cytoskeleton. *Biochim Biophys Acta* (2006) 1763:450–62. doi: 10.1016/j.bbamcr.2006.02.014
59. Akhshi TK, Wernike D, Piekny A. Microtubules actin crosstalk in cell migration division. *Cytoskeleton* (2014) 71:1–23. doi: 10.1002/cm.21150
60. Rodriguez OC, Schaefer AW, Mato CA, Forscher P, Bement WM, Waterman-Storer CM. Conserved microtubule-actin interactions in cell movement morphogenesis. *Nat Cell Biol.* (2003) 5:599–609. doi: 10.1038/ncb0703-599
61. Elie A, Prezel E, Guerin C, Denarier E, Ramirez-Rios S, Serre L, et al. Tau co-organizes dynamic microtubule actin networks. *Sci Rep*. (2015) 5:9964. doi: 10.1038/srep09964
62. Ávila MO, Vega AF, Maraver JG, Paz MV, Lavera I, Mata M, et al. The apoptotic microtubule network during the execution phase of apoptosis. In: Ntuli T, editor. *Cell Death - Autophagy, Apoptosis and Necrosis*. London: INTECH (2015). 299–329.
63. Rapino F, Naumann I, Fulda S. Bortezomib antagonizes microtubule-interfering drug-induced apoptosis by inhibiting G2/M transition MCL-1 degradation. *Cell Death Dis*. (2013) 4:e925. doi: 10.1038/cddis.2013.440
64. Csermely P, Palotai R, Nussinov R. Induced fit, conformational selection independent dynamic segments: an extended view of binding events. *Trends Biochem Sci*. (2010) 35:539–46. doi: 10.1016/j.tibs.2010.04.009
65. Nussinov R, Ma B, Tsai CJ. Multiple conformational selection induced fit events take place in allosteric propagation. *Biophys Chem*. (2014) 186:22–30. doi: 10.1016/j.bpc.2013.10.002
66. Tobi D, Bahar I. Structural changes involved in protein binding correlate with intrinsic motions of proteins in the unbound state. *Proc Natl Acad Sci USA*. (2005) 102:18908–13. doi: 10.1073/pnas.0507603102
67. Winder BS, Strgaard CS, Miller MG. The role of GTP Binding microtubule-associated proteins in the inhibition of microtubule assembly by carbendazim. *Toxicol Sci*. (2001) 59:138–46. doi: 10.1093/toxsci/59.1.138
68. Ravelli RB, Gigant B, Curmi PA, Jourdain I, Lachkar S, Sobel A, et al. Insight into tubulin regulation from a complex with colchicine a stathmin-like domain. *Nature* (2004) 428:198–202. doi: 10.1038/nature02393
69. Brindisi M, Maramai S, Brogi S, Fanigliulo E, Butini S, Guarino E, et al. Development of novel cyclic peptides as pro-apoptotic agents. *Eur J Med Chem*. (2016) 117:301–20. doi: 10.1016/j.ejmech.2016.04.001
70. Spiegelman BM, Penningroth SM, Kirschner MW. Turnover of tubulin the N site GTP in Chinese hamster ovary cells. *Cell* (1977) 12:587–600. doi: 10.1016/0092-8674(77)90259-8
71. Menendez M, Rivas G, Diaz JF, Andreu JM. Control of the structural stability of the tubulin dimer by one high affinity bound magnesium ion at nucleotide N-site. *J Biol Chem*. (1998) 273:167–76. doi: 10.1074/jbc.273.1.167
72. Croom HB, Correia JJ, Baty LT, Williams RCJr. Release of exchangeably bound guanine nucleotides from tubulin in a magnesium-free buffer. *Biochemistry* (1985) 24:768–75.
73. Correia JJ. Effects of antimitotic agents on tubulin-nucleotide interactions. *Pharmacol Ther*. (1991) 52:127–47.
74. Correia JJ, Beth AH, Williams RCJr. Tubulin exchanges divalent cations at both guanine nucleotide-binding sites. *J Biol Chem*. (1988) 263:10681–6.
75. Buttlaire DH, Czuba BA, Stevens TH, Lee YC, Himes RH. Manganous ion binding to tubulin. *J Biol Chem*. (1980) 255:2164–8.

Conflict of Interest Statement: The authors declare that the research was conducted in the absence of any commercial or financial relationships that could be construed as a potential conflict of interest.

frontiers in Oncology

ORIGINAL RESEARCH
published: 28 January 2019
doi: 10.3389/fonc.2019.00002

Celastrol Inhibits the Growth of Ovarian Cancer Cells *in vitro* and *in vivo*

Li-Na Xu[1†], Na Zhao[1†], Jin-Yan Chen[2†], Piao-Piao Ye[1], Xing-Wei Nan[1], Hai-Hong Zhou[1], Qi-Wei Jiang[3], Yang Yang[3], Jia-Rong Huang[3], Meng-Ling Yuan[3], Zi-Hao Xing[3], Meng-Ning Wei[3], Yao Li[3], Zhi Shi[3] and Xiao-Jian Yan[1,4*]*

[1] Department of Gynecology, The First Affiliated Hospital of Wenzhou Medical University, Wenzhou, China, [2] Department of Gynecology, The Second Affiliated Hospital of Zhejiang University School of Medicine, Hangzhou, China, [3] Department of Cell Biology and Institute of Biomedicine, National Engineering Research Center of Genetic Medicine, Guangdong Provincial Key Laboratory of Bioengineering Medicine, College of Life Science and Technology, Jinan University, Guangzhou, China, [4] Center for Uterine Cancer Diagnosis & Therapy Research of Zhejiang Province, Women's Hospital and Institute of Translational Medicine, Zhejiang University School of Medicine, Zhejiang, China

OPEN ACCESS

Edited by:
Yan-Yan Yan,
Shanxi Datong University, China

Reviewed by:
Changliang Shan,
Nankai University, China
Nana Zhang,
Chinese Academy of Medical Sciences, China

***Correspondence:**
Zhi Shi
tshizhi@jnu.edu.cn
Xiao-Jian Yan
yxjbetter@126.com

[†]These authors have contributed equally to this work

Specialty section:
This article was submitted to Cancer Molecular Targets and Therapeutics, a section of the journal Frontiers in Oncology

Received: 06 December 2018
Accepted: 02 January 2019
Published: 28 January 2019

Citation:
Xu L-N, Zhao N, Chen J-Y, Ye P-P, Nan X-W, Zhou H-H, Jiang Q-W, Yang Y, Huang J-R, Yuan M-L, Xing Z-H, Wei M-N, Li Y, Shi Z and Yan X-J (2019) Celastrol Inhibits the Growth of Ovarian Cancer Cells in vitro and in vivo. Front. Oncol. 9:2. doi: 10.3389/fonc.2019.00002

Celastrol is a natural triterpene isolated from the Chinese plant Thunder God Vine with potent antitumor activity. However, the effect of celastrol on the growth of ovarian cancer cells *in vitro* and *in vivo* is still unclear. In this study, we found that celastrol induced cell growth inhibition, cell cycle arrest in G2/M phase and apoptosis with the increased intracellular reactive oxygen species (ROS) accumulation in ovarian cancer cells. Pretreatment with ROS scavenger N-acetyl-cysteine totally blocked the apoptosis induced by celastrol. Additionally, celastrol inhibited the growth of ovarian cancer xenografts in nude mice. Altogether, these findings suggest celastrol is a potential therapeutic agent for treating ovarian cancer.

Keywords: celastrol, reactive oxygen species, N-acetyl-cysteine, apoptosis, ovarian cancer

INTRODUCTION

Ovarian cancer is the most lethal gynecologic cancer and the fifth leading cause of female cancer-related deaths in the United States in 2018 (1). Because of the late stage diagnoses, the prognosis of ovarian cancer remains poor, despite advances in aggressive surgery and combination chemotherapy (2–4). Current treatments for ovarian cancer are far from satisfactory, therefore it is of considerable interest to develop novel therapeutic agents to improve the outcomes of ovarian cancer.

Celastrol is a natural triterpene isolated from the Chinese plant Thunder God Vine (*Tripterygium wilfordii*),which has been reported with a wide range of bioactivities, such as antitumor (5), anti-inflammatory (6), antidiabetic activities (7) and antihypertensive (8). Celastrol has shown the potent antitumor activity in various cancers including prostate, breast, liver, colon, and lung (9–13). Although celastrol is able to induce apoptosis and inhibit proliferation, migration and invasion in ovarian cancer cells *in vitro* (14–16), the effect of celastrol on the growth of ovarian cancer cells *in vivo* is still unknown. Here, we have comprehensively investigated the antitumor activity of celastrol in ovarian cancer cells *in vitro* and *in vivo*.

MATERIALS AND METHODS

Cells Lines and Reagents

The human ovarian cancer lines A2780 and SKOV3 were cultured in Dulbecco's modified Eagle's medium (DMEM) supplemented with 10% fetal bovine serum (FBS), penicillin (100 U/ml) and

streptomycin (100 ng/ml) at 37°C with 5% CO2 in a humidified incubator. Celastrol was purchased from Shanghai Tauto Biotechnology. N-acetyl-L-cysteine (NAC) and dihydroethidium (DHE) were purchased from Sigma-Aldrich. Methythiazolyldiphenyl-tetrazolium bromide (MTT), propidium iodide (PI) and other chemicals were purchased from Shanghai Sangon Biotech. Anti-p27 (610241), Anti-Cyclin B1 (554177), and Anti-Cyclin E (51-1459GR) antibodies were from BD Biosciences. Anti-RAF1 (SC-133) antibodies were from Santa Cruz Biotechnology. Anti-PARP (9542), Anti-AKT (4691), Anti-pAKT S473 (4060), Anti-ERK (4695), Anti-pERK T202/T204 (4370), Anti-JNK (9252), Anti-pJNK T183/Y185 (4668), Anti-p38 (9212), Anti-pp38 T180/Y182 (4511) antibodies were from Cell Signaling Technologies. Anti-GAPDH (LK9002T) antibodies were from Tianjin Sungene Biotech.

MTT Assay

Cells were seeded into a 96-well plate at a density of 0.5 $\times 10^4$ cells/well. Then, different concentrations of celastrol (10 μL/well) were added to designated wells. After 72 h, 10 μL of MTT was added to each well at a final concentration of 0.5 mg/ml, and the plate was further incubated for 4 h, allowing viable cells to change the yellow MTT into dark-blue formazan crystals. Subsequently, the medium was discarded and 50 μL of dimethylsulfoxide (DMSO) was added to each well to dissolve the formazan crystals. The absorbance in individual well was determined at 570 nm by multidetection microplate reader 680 (BioRad, PA, USA). The concentrations required to inhibit growth by 50% (IC_{50}) were calculated from survival curves using the Bliss method (17).

Cell Cycle Analysis

Cells were harvested and washed twice with cold PBS and then fixed with 70% ice-cold ethanol at 4°C for 30 min. After centrifugation at 200 × g for 10 min, cells were washed twice with PBS, resuspended with 0.5 mL PBS containing PI (50 μg/mL), Triton X-100(0.1%, v/v), 0.1% sodium citrate, and DNase-free RNase (100 μg/mL), and detected by flow cytometry (FCM) after 15 min incubation in the dark at room temperature. Fluorescence was measured at an excitation wave length of 480 nm through a FL-2 filter. Data were analyzed using ModFit LT 3.0 software (Becton Dickinson) (18, 19).

Apoptosis Analysis

Cell apoptosis was evaluated with FCM assay. Briefly, cells were harvested and washed twice with cold PBS, then stained with Annexin V-FITC and PI in the binding buffer, and detected by FACSCalibur FCM (BD, CA, USA) after 15 min incubation in

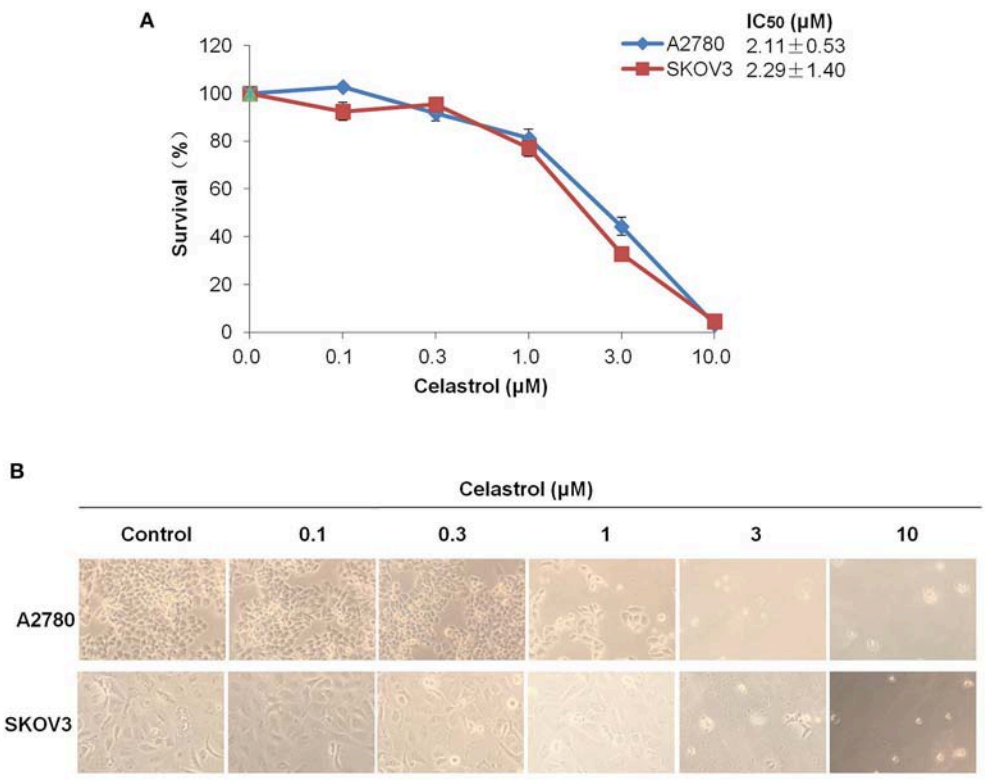

FIGURE 1 | Celastrol inhibited the growth of ovarian cancer cells *in vitro*. **(A)** The growth curves, IC_{50} values and **(B)** phase-contrast images of A2780 and SKOV3 cells treated with the indicated concentrations of celastrol (0, 0.1, 0.3, 1, 3, and 10 μM) for 72 h. Cell survival was measured by MTT assay, and the IC_{50} values of celastrol in each cell lines were calculated.

the dark at room temperature. Fluorescence was measured at an excitation wave length of 480 nm through FL-1 (530 nm) and FL-2 (585 nm) filters. The early apoptotic cells (Annexin V positive only) and late apoptotic cells (Annexin V and PI positive) were quantified (20).

Western Blot Analysis

Cells were harvested and washed twice with cold PBS and then resuspended and lysed in RIPA buffer (1% NP-40, 0.5% sodium deoxycholate, 0.1% SDS, 10 ng/mL PMSF, 0.03% aprotinin, and 1 μM sodium orthovanadate) at 4°C for 30 min.

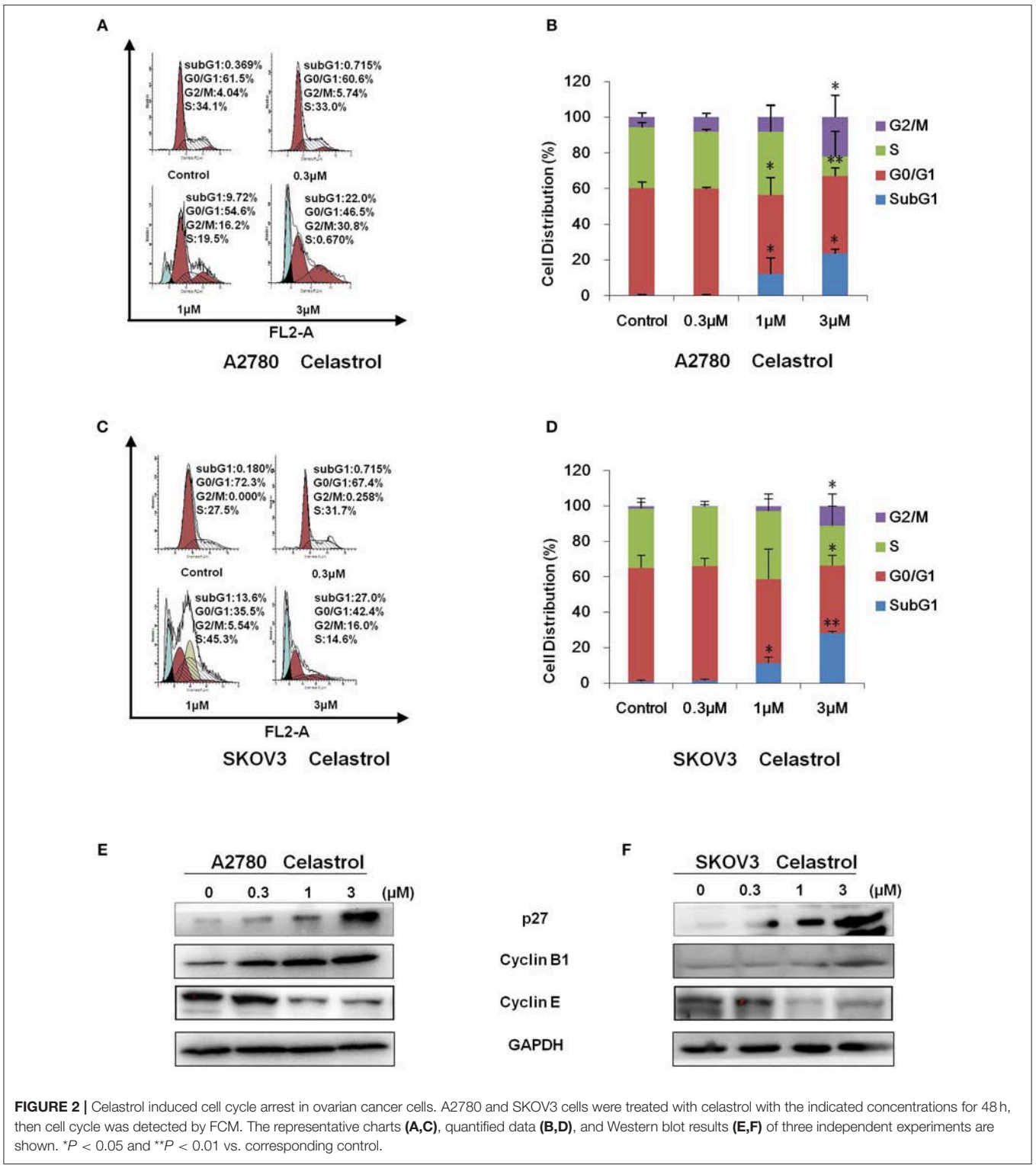

FIGURE 2 | Celastrol induced cell cycle arrest in ovarian cancer cells. A2780 and SKOV3 cells were treated with celastrol with the indicated concentrations for 48 h, then cell cycle was detected by FCM. The representative charts **(A,C)**, quantified data **(B,D)**, and Western blot results **(E,F)** of three independent experiments are shown. *$P < 0.05$ and **$P < 0.01$ vs. corresponding control.

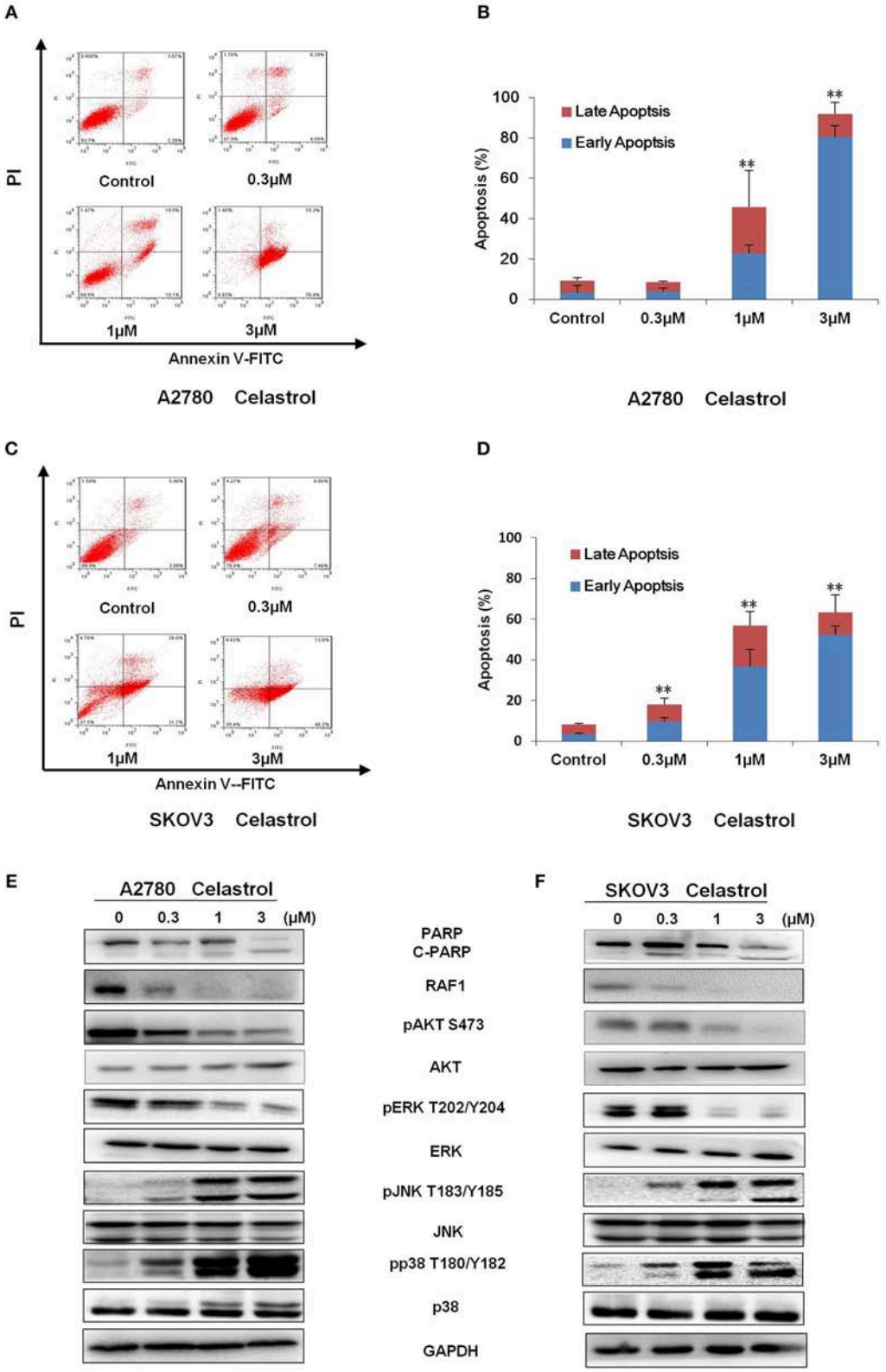

FIGURE 3 | Celastrol induced apoptosis in ovarian cancer cells. A2780 and SKOV3 cells were treated with celastrol with the indicated concentrations for 48 h, then cell apoptosis was detected by FCM. The representative charts **(A,C)**, quantified data **(B,D)**, and Western blot results **(E,F)** of three independent experiments are shown. The same GAPDH image of **Figure 2** has been used as loading control. $^{**}P < 0.01$ vs. corresponding control.

Lysates were centrifuged at 14,000 × g for 10 min and supernatants were collected. Proteins were separated on 12% SDS-PAGE gels and transferred to polyvinylidene difluoride membranes. Membranes were blocked with 5% BSA and incubated with the indicated primary antibodies. Corresponding horseradish peroxidase-conjugated secondary antibodies were used against each primary antibody. Proteins were detected using the chemiluminescent detection reagents and films (21, 22).

Reactive Oxygen Species Assay

Cells were incubated with 10 μM of DHE at 37°C for 30 min, washed twice with PBS, and microphotographed under a conventional fluorescent microscope (Olympus, Japan) immediately. For each well, 5 fields were taken randomly. Then, cells were rapidly digested, harvested and washed twice with cold PBS, and detected by FCM. The DHE Fluorescence intensity was measured and quantified at an excitation wave length of 518 nm through PE filters (23, 24).

Nude Mice Xenograft Assay

Balb/c nude mice were obtained from the Guangdong Medical Laboratory Animal Center and maintained with sterilized food and water. This study was carried out in accordance with the recommendations of the Guidelines for the Care and Use of Laboratory Animals, and the protocol were approved by the Institutional Animal Care and Use Committee of Jinan University. Four female nude mice with 4–5 weeks old and 20–22 g weight were used for each group. Each mouse was injected subcutaneously with A2780 cells (4×10^6 in 100 μl of medium) under the left and right shoulders. Mice were randomized into two groups, when the subcutaneous tumors were approximately 0.3×0.3 cm^2 (two perpendicular diameters) in size, and were injected intraperitoneally with vehicle alone (0.5% methylcellulose) and celastrol (2 mg/kg) every day. The body weights of mice and the two perpendicular diameters (A and B) of tumors were recorded every day. The tumor volume (V) was calculated as:

$$V = \pi/6\ (1/2(A + B))^3$$

The mice were anaesthetized after experiment, and tumor tissue was excised from the mice and weighted. The rate of inhibition (IR) was calculated according to the formula:

IR=1-Mean tumor weight of experimental group/Mean tumor weight of control group × 100% (25)

Statistical Analysis

A student's *t*-test was used to compare individual data points between two groups. A *P*-value of < 0.05 was set as the criterion for statistical significance.

RESULTS

Celastrol Inhibited the Growth of Ovarian Cancer Cells *in vitro*

To access the effect of celastrol on ovarian cancer cells, we treated two ovarian cancer cell lines A2780 and SKOV3 with the increasing concentrations of celastrol range from 0.1 to 10 μM for 72 h. As shown in **Figures 1A,B**, the results of MTT assay revealed that the growth of two ovarian cancer cell lines was similarly inhibited by celastrol in a dose-dependent manner with the IC_{50} values were 2.11 and 2.29 μM in A2780 and SKOV3 respectively. These data suggested that celastrol inhibits the growth of ovarian cancer cells.

Celastrol Induced Cell Cycle Arrest in Ovarian Cancer Cells

To determine whether celastrol is able to induce cell cycle arrest, cell cycle distribution was examined after celastrol treatment. A2780 and SKOV3 cells were treated with 0.3, 1 and 3 μM of celastrol for 48 h, then stained with PI and examined by FCM. As shown in **Figures 2A–D**, celastrol induced the accumulation in Sub G1 and G2/M phase and reduction in G0/G1 and S phase in two ovarian cancer cell lines. Next, the cell cycle related proteins were detected by Western Blot. As shown in **Figures 2E,F**, increased p27 and Cyclin B1 and decreased Cyclin E proteins were detected in celastrol-treated A2780 and SKOV3 cells. Together, these results indicated that celastrol induces cell cycle arrest in ovarian cancer cells.

Celastrol Induced Apoptosis in Ovarian Cancer Cells

To determine whether celastrol could induce cell apoptosis, A2780 and SKOV3 cells were treated with indicated concentrations of celastrol for 48 h, apoptosis was assessed by FCM with Annexin V/PI staining. As shown in **Figures 3A–D**, celastrol dose-dependently induced early stage of apoptosis (Annexin V+/PI–) and late stage of apoptosis (Annexin V+/PI+) in both cells. Treatment of celastrol upregulated the protein expressions of cleaved-PARP, pp38 T180/Y182 and pJNK T183/Y185 but downregulated the protein expressions of pERK T202/Y204, pAKT S473 and RAF1 (**Figures 3E,F**). Consequently, these results suggest that celastrol induces cell apoptosis in ovarian cancer cells.

ROS Generation Was Critical for Celastrol-Induced Apoptosis in Ovarian Cancer Cells

Numerous antitumor agents demonstrate antitumor activity via ROS-dependent activation of apoptotic cell death (26, 27). It has previously been reported that the elevated intracellular ROS mediated celastrol-induced apoptosis in several human cancer cells (28). Thus, we surmised that celastrol caused apoptosis in ovarian cancer cells was due to excessive ROS generation. Firstly, the cellular ROS was tagged by DHE fluorescence staining in celastrol-treated cells. As shown in **Figure 4**, celastrol enhanced the detectable red fluorescent signals of DHE in both A2780 and SKOV3 cells, suggesting the intracellular ROS levels were increased after celastrol treatment. Then we pre-treated A2780 and SKOV3 cells with NAC (a specific ROS scavenger), Celastrol-induced cell apoptosis were totally attenuated by NAC in both ovarian cancer cells

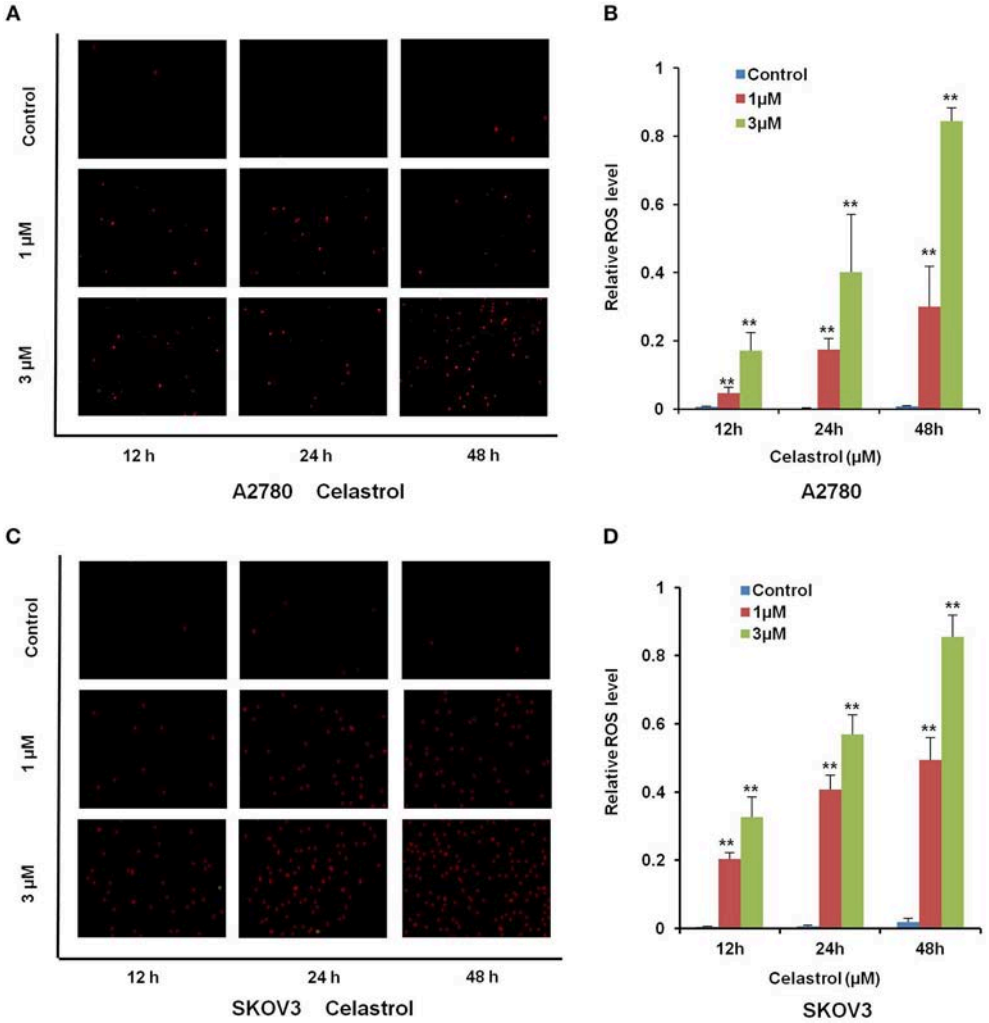

FIGURE 4 | Celastrol enhanced the intracellular ROS levels in ovarian cancer cells. A2780 and SKOV3 cells were treated with celastrol with indicated times and concentrations, stained with DHE, photographed and quantified respectively under fluorescent microscope and FCM. The representative micrographs **(A,C)** and quantified results **(B,D)** were shown. $^{**}P < 0.01$ vs. corresponding control.

(**Figure 5**). Collectively, these results suggest that ROS generation was critical for celastrol-induced apoptosis in ovarian cancer cells.

Celastrol Inhibited the Tumor Growth of Ovarian Cancer in Nude Mice

To confirm the antitumor effects of celastrol *in vivo*, A2780 subcutaneous xenograft tumors were generated in the nude mice. As shown in **Figures 6A–E**, treatment of celastrol did inhibit the growth of A2780 xenograft tumors with the inhibition ratio of 28.60% by diminishing the tumor volumes and weights. Furthermore, mice body weight in celastrol group was close to that of control group, suggesting that celastrol at the indicated dose did not cause toxicity in mice (**Figure 6C**).

DISCUSSION

Natural products attract more and more attention in the prevention and treatment of cancer in recent years. Products from the plant *Tripterygium wilfordii*, including celastrol and triptolide, are of special attention because of its superior anti-tumor activities against a variety of cancer types, and therefore are the traditional herb medicines considered to have the most potential in modern cancer therapy. For the treatment of ovarian cancer, triptolide has been shown to inhibit the proliferation, migration and invasion of ovarian cancer in multiple pathways (29–31) and demonstrated to exert efficacy in preclinical models (32). Celastrol has also been reported to induce apoptosis and inhibit proliferation, migration and invasion in ovarian cancer cells *in vitro* (14, 16), but the mechanism for its anti-tumor effect and the effect of celastrol on the growth of ovarian cancer cells *in vivo* are not fully understood. In our present study,

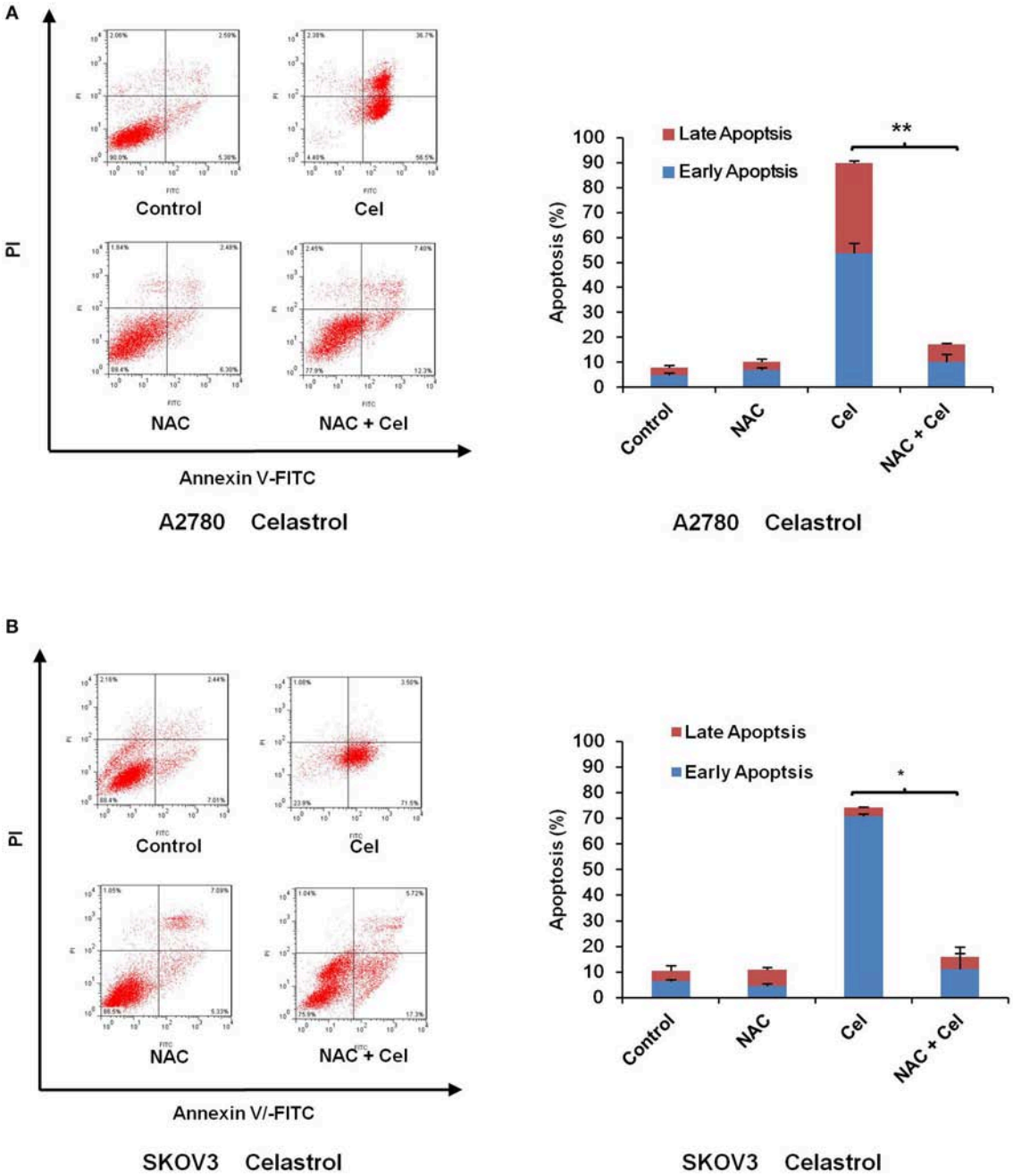

FIGURE 5 | NAC impeded celastrol-induced cell apoptosis. A2780 and SKOV3 cells were treated with 3 μM celastrol for 48 h in the presence or absence of 5 mM NAC pretreated for 1 h. The apoptosis was detected by FCM. The apoptosis charts and quantified data **(A,B)** were shown. *$P < 0.05$ and **$P < 0.01$ vs. corresponding control.

we have demonstrated that celastrol mediated dose-dependent anti-growth effects on human ovarian cancer cell lines SKOV3 and A2780. The IC_{50} value after 72 h treatment with celastrol ranged from 2 to 3 μM in these two human ovarian cancer cell lines, similarly to the IC_{50} value of celastrol of ovarian cancer in other articles (15, 16). We have also shown that celastrol induced both the early and late stage of apoptosis and cell cycle arrest in G2/M phase with obvious up-regulation of cleaved-PARP, pp38 T180/Y182, pJNK T183/Y185, p27 and Cyclin B1 and down-regulation of pERK T202/Y204, pAKT S473, RAF1 and Cyclin E in a dose-dependent manner. Similar with our results, celastrol can induce the activation of JNK and inactivation of AKT in multiple myeloma cells RPMI-8226 (33), activation of p38 in ovarian cancer cells OVCAR-8 and colorectal cancer

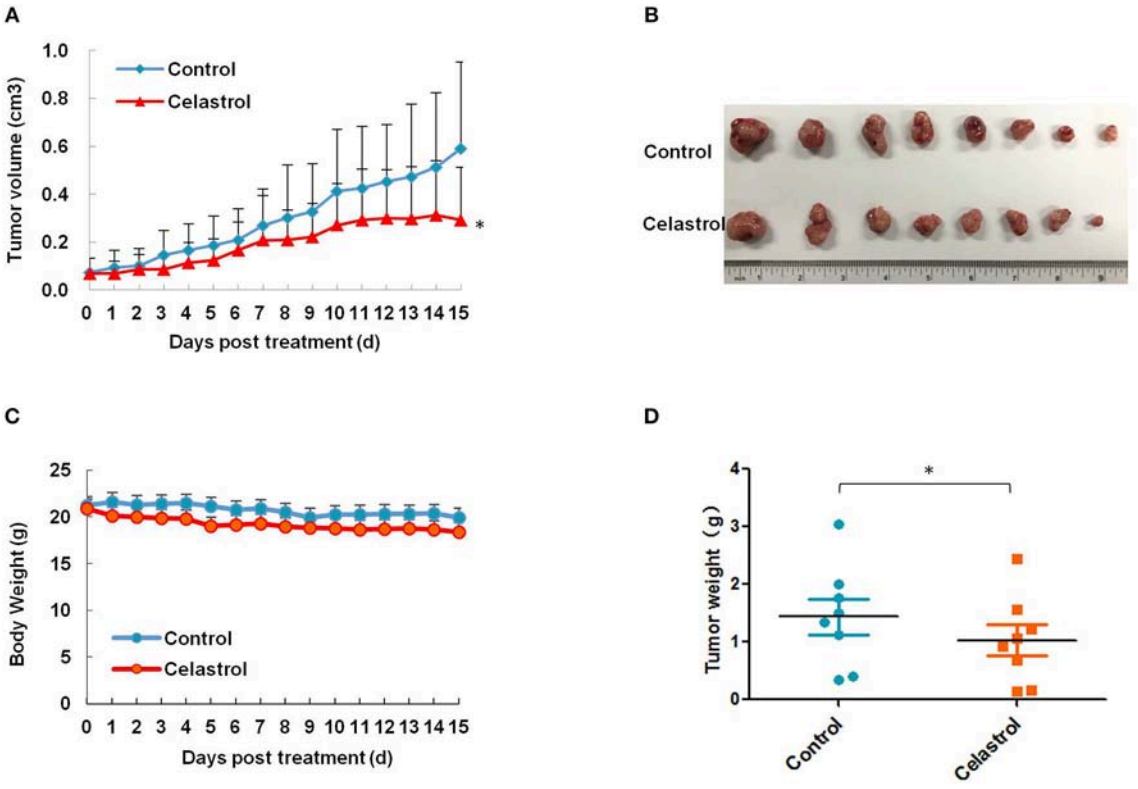

E

Cell	Groups	Before Experiment		After Experiment		Weight of	Inhibition(%)
		Mice	Weight(g)	Mice	Weight(g)	Tumors(g)	
A2780	Control	4	21.19±1.03	4	19.95±0.60	1.44±0.88	
	Celastrol	4	20.91±0.80	4	18.40±1.48	1.03±0.75	28.60*

FIGURE 6 | Celastrol inhibited the tumor growth of ovarian cancer in nude mice. Each mouse was injected subcutaneously with A2780 cells (4×10^6 in 100 μl of medium) under the left and right shoulders. When the subcutaneous tumors were approximately 0.3 × 0.3 cm in size, mice were randomized into two groups, and received intraperitoneal injection of vehicle alone (0.5% methylcellulose) or celastrol (2 mg/kg) every day. The body weight and tumor volume were recorded every day. After experiment, the mice were anesthetized, and tumor tissue was excised from the mice and weighted. The tumor volume **(A)**, original tumors **(B)**, body weight **(C)**, tumor weight **(D)**, and summary data **(E)** were shown. *$P < 0.05$ vs. corresponding control.

cells SW620 cells (34) and inactivation of ERK in hepatoma cells Hep3B (35). Furthermore, celastrol inhibited the growth of A2780 ovarian cancer subcutaneous xenograft tumors in nude mice by diminishing the tumor volumes and weights, and mice body weight in celastrol group was close to that of control group. These *in vitro* and *in vivo* data strongly indicate that celastrol may be a appropriate candidate for treating ovarian cancer.

Biological roles of ROS were intricate and important in cancer cells (36). The intracellular ROS plays a significant role in regulating multifarious cell physiological process such as growth, differentiation, death and so on (37). ROS changes the cellular redox condition, induces DNA damage and influences the activities of tumor suppressor or oncogene, thereby involving in the initiation and progression of cancer (38, 39). Lots of studies have shown that cancer cells normally produce more ROS than normal cells (40). Interestingly, accumulating evidence suggests that cancer cells are more vulnerable to ROS-induced death because they are under the increased oxidative stress (41). A variety of agents like YM155, dinaciclib and triptolide may be selectively toxic to tumor cells because they enhanced intracellular oxidant stress and push these already stressed cells beyond their limitation (24, 38, 42, 43). In addition, previous studies have demonstrated that ROS plays a pivotal role in celastrol-induced apoptosis in multiple cancers, such as colon cancer, liver cancer, osteosarcoma, etc. (9, 28, 44). In this study, we have found that the intracellular ROS levels were increased after celastrol treatment, and pre-treated with ROS scavenger NAC totally attenuated celastrol-induced cell apoptosis in ovarian cancer cells. It has been reported that celastrol enhanced the intracellular ROS to induce apoptosis by inhibiting mitochondrial respiratory chain

complex I activity in lung cancer H1299 cells (45). Whether celastrol induces ROS accumulation to trigger apoptosis in the same way in ovarian cancer cells need to be further investigated.

In summary, our data have shown that celastrol induced cell growth inhibition, cell cycle arrest in G2/M phase and apoptosis with the increased intracellular ROS accumulation in ovarian cancer cells *in vitro* and *in vivo*. Pretreatment with NAC totally blocked the apoptosis induced by celastrol. Altogether, these findings suggest celastrol is a potential therapeutic agent for treating ovarian cancer.

AUTHOR CONTRIBUTIONS

L-NX, NZ, J-YC, ZS, and X-JY designed the experiments, performed the experiments, analyzed the data, and wrote the paper. X-WN, H-HZ, P-PY, Q-WJ, YY, J-RH, M-LY, Z-HX, M-NW, and YL performed the experiments. All authors read and approved the final manuscript.

FUNDING

This work was supported by funds from the National Key Research and Development Program of China (No. 2017YFA0505104 to ZS), the National Natural Science Foundation of China (No. 81772540 to ZS and No. 81503293 to X-JY), the Guangdong Natural Science Funds for Distinguished Young Scholar (No. 2014A030306001 to ZS), the Guangdong Special Support Program for Young Talent (No. 2015TQ01R350 to ZS), the Science and Technology Program of Guangdong (No. 2016A050502027 to ZS) and the Science and Technology Program of Guangzhou (No. 201704030058 to ZS), the Zhejiang major disease diagnosis and treatment technology research center (No. JBZX-201803 to X-JY).

REFERENCES

1. Siegel RL, Miller KD, Jemal A. Cancer statistics, 2018. *CA Cancer J Clin* (2018) 68:7–30. doi: 10.3322/caac.21442
2. Torre LA, Trabert B, DeSantis CE, Miller KD, Samimi G, Runowicz CD, et al. Ovarian cancer statistics, 2018. *CA Cancer J Clin.* (2018) 68:284–96. doi: 10.3322/caac.21456
3. Fields EC, McGuire WP, Lin L, Temkin SM. Radiation treatment in women with Ovarian cancer: past, present, and future. *Front Oncol.* (2017) 7:177. doi: 10.3389/fonc.2017.00177
4. Ohman AW, Hasan N, Dinulescu DM. Advances in tumor screening, imaging, and avatar technologies for high-grade serous ovarian cancer. *Front Oncol.* (2014) 4:322. doi: 10.3389/fonc.2014.00322
5. Uttarkar S, Dasse E, Coulibaly A, Steinmann S, Jakobs A, Schomburg C, et al. Targeting acute myeloid leukemia with a small molecule inhibitor of the Myb/p300 interaction. *Blood* (2016) 127:1173–82. doi: 10.1182/blood-2015-09-668632
6. Lin L, Sun Y, Wang D, Zheng S, Zhang J, Zheng C. Celastrol ameliorates ulcerative colitis-related colorectal cancer in mice via suppressing inflammatory responses and epithelial-mesenchymal transition. *Front Pharmacol.* (2015) 6:320. doi: 10.3389/fphar.2015.00320
7. Liu J, Lee J, Salazar Hernandez MA, Mazitschek R, Ozcan U. Treatment of obesity with celastrol. *Cell* (2015) 161:999–1011. doi: 10.1016/j.cell.2015.05.011
8. Wong KF, Yuan Y, Luk JM. *Tripterygium wilfordii* bioactive compounds as anticancer and anti-inflammatory agents. *Clin Exp Pharmacol Physiol.* (2012) 39:311–20. doi: 10.1111/j.1440-1681.2011.05586.x
9. Jiang QW, Cheng KJ, Mei XL, Qiu JG, Zhang WJ, Xue YQ, et al. Synergistic anticancer effects of triptolide and celastrol, two main compounds from thunder god vine. *Oncotarget* (2015) 6:32790–804. doi: 10.18632/oncotarget.5411
10. Jang SY, Jang SW, Ko J. Celastrol inhibits the growth of estrogen positive human breast cancer cells through modulation of estrogen receptor alpha. *Cancer Lett.* (2011) 300:57–65. doi: 10.1016/j.canlet.2010.09.006S0304-3835(10)00429-5
11. Yang H, Chen D, Cui QC, Yuan X, Dou QP. Celastrol, a triterpene extracted from the Chinese "Thunder of God Vine," is a potent proteasome inhibitor and suppresses human prostate cancer growth in nude mice. *Cancer Res.* (2006) 66:4758–65. doi: 10.1158/0008-5472.CAN-05-4529
12. Li YJ, Sun YX, Hao RM, Wu P, Zhang LJ, Ma X, et al. miR-33a-5p enhances the sensitivity of lung adenocarcinoma cells to celastrol by regulating mTOR signaling. *Int J Oncol.* (2018) 52:1328–38. doi: 10.3892/ijo.2018.4276
13. Jannuzzi AT, Kara M, Alpertunga B. Celastrol ameliorates acetaminophen-induced oxidative stress and cytotoxicity in HepG2 cells. *Hum Exp Toxicol.* (2018) 37:742–51. doi: 10.1177/0960327117734622
14. Li X, Wang H, Ding J, Nie S, Wang L, Zhang L, et al. Celastrol strongly inhibits proliferation, migration and cancer stem cell properties through suppression of Pin1 in ovarian cancer cells. *Eur J Pharmacol.* (2018) 842:146–56. doi: 10.1016/j.ejphar.2018.10.043
15. Wang Z, Zhai Z, Du X. Celastrol inhibits migration and invasion through blocking the NF-kappaB pathway in ovarian cancer cells. *Exp Ther Med.* (2017) 14:819–24. doi: 10.3892/etm.2017.4568ETM-0-0-4568
16. Zhang H, Li J, Li G, Wang S. Effects of celastrol on enhancing apoptosis of ovarian cancer cells via the downregulation of microRNA21 and the suppression of the PI3K/AktNFkappaB signaling pathway in an *in vitro* model of ovarian carcinoma. *Mol Med Rep.* (2016) 14:5363-8. doi: 10.3892/mmr.2016.5894
17. Shi Z, Liang YJ, Chen ZS, Wang XW, Wang XH, Ding Y, et al. Reversal of MDR1/P-glycoprotein-mediated multidrug resistance by vector-based RNA interference *in vitro* and *in vivo*. *Cancer Biol Ther.* (2006) 5:39–47.
18. Chen X, Gong L, Ou R, Zheng Z, Chen J, Xie F, et al. Sequential combination therapy of ovarian cancer with cisplatin and gamma-secretase inhibitor MK-0752. *Gynecol Oncol.* (2016) 140:537–44. doi: 10.1016/j.ygyno.2015.12.011
19. Lv M, Qiu JG, Zhang WJ, Jiang QW, Qin WM, Yang Y, et al. Wallichinine reverses ABCB1-mediated cancer multidrug resistance. *Am J Transl Res* (2016) 8:2969–80.
20. Shi Z, Park HR, Du Y, Li Z, Cheng K, Sun SY, et al. Cables1 complex couples survival signaling to the cell death machinery. *Cancer Res.* (2015) 75:147–58. doi: 10.1158/0008-5472.CAN-14-0036
21. Zheng DW, Xue YQ, Li Y, Di JM, Qiu JG, Zhang WJ, et al. Volasertib suppresses the growth of human hepatocellular carcinoma *in vitro* and *in vivo*. *Am J Cancer Res* (2016) 6:2476–88.
22. Yang Y, Qiu JG, Li Y, Di JM, Zhang WJ, Jiang QW, et al. Targeting ABCB1-mediated tumor multidrug resistance by CRISPR/Cas9-based genome editing. *Am J Transl Res* (2016) 8:3986-94.
23. Xie FF, Pan SS, Ou RY, Zheng ZZ, Huang XX, Jian MT, et al. Volasertib suppresses tumor growth and potentiates the activity of cisplatin in cervical cancer. *Am J Cancer Res.* (2015) 5:3548–59.
24. Hou LJ, Huang XX, Xu LN, Zhang YY, Zhao N, Ou RY, et al. YM155 enhances docetaxel efficacy in ovarian cancer. *Am J Transl Res.* (2018) 10:696–708.
25. Yuan ML, Li P, Xing ZH, Di JM, Liu H, Yang AK, et al. Inhibition of WEE1 suppresses the tumor growth in laryngeal squamous cell carcinoma. *Front Pharmacol.* (2018) 9:1041. doi: 10.3389/fphar.2018.01041
26. Gong LH, Chen XX, Wang H, Jiang QW, Pan SS, Qiu JG, et al. Piperlongumine induces apoptosis and synergizes with cisplatin or paclitaxel

in human ovarian cancer cells. *Oxid Med Cell Longev*. (2014) 2014:906804. doi: 10.1155/2014/906804
27. Geng YD, Zhang C, Lei JL, Yu P, Xia YZ, Zhang H, et al. Walsuronoid B induces mitochondrial and lysosomal dysfunction leading to apoptotic rather than autophagic cell death via ROS/p53 signaling pathways in liver cancer. *Biochem Pharmacol*. (2017) 142:71–86. doi: 10.1016/j.bcp.2017.06.134
28. Li HY, Zhang J, Sun LL, Li BH, Gao HL, Xie T, et al. Celastrol induces apoptosis and autophagy via the ROS/JNK signaling pathway in human osteosarcoma cells: an *in vitro* and *in vivo* study. *Cell Death Dis* (2015) 6:e1604. doi: 10.1038/cddis.2014.543
29. Zhao H, Yang Z, Wang X, Zhang X, Wang M, Wang Y, et al. Triptolide inhibits ovarian cancer cell invasion by repression of matrix metalloproteinase 7 and 19 and upregulation of E-cadherin. *Exp Mol Med* (2012) 44:633–41. doi: 10.3858/emm.2012.44.11.072
30. Wang Y, Liu T, Li H. Enhancement of triptolide-loaded micelles on tumorigenicity inhibition of human ovarian cancer. *J Biomater Sci Polym Ed*. (2016) 27:545–56. doi: 10.1080/09205063.2015.1131667
31. Hu H, Huang G, Wang H, Li X, Wang X, Feng Y, et al. Inhibition effect of triptolide on human epithelial ovarian cancer via adjusting cellular immunity and angiogenesis. *Oncol Rep* (2018) 39:1191–6. doi: 10.3892/or.2017.6158
32. Patil S, Lis LG, Schumacher RJ, Norris BJ, Morgan ML, Cuellar RA, et al. Phosphonooxymethyl Prodrug of Triptolide: Synthesis, Physicochemical Characterization, and Efficacy in Human Colon Adenocarcinoma and Ovarian Cancer Xenografts. *J Med Chem*. (2015) 58:9334–44. doi: 10.1021/acs.jmedchem.5b01329
33. Kannaiyan R, Manu KA, Chen L, Li F, Rajendran P, Subramaniam A, et al. Celastrol inhibits tumor cell proliferation and promotes apoptosis through the activation of c-Jun N-terminal kinase and suppression of PI3 K/Akt signaling pathways. *Apoptosis* (2011) 16:1028–41. doi: 10.1007/s10495-011-0629-6
34. Zhu H, Liu XW, Ding WJ, Xu DQ, Zhao YC, Lu W, et al. Up-regulation of death receptor 4 and 5 by celastrol enhances the anti-cancer activity of TRAIL/Apo-2L. *Cancer Lett*. (2010) 297:155–64. doi: 10.1016/j.canlet.2010.04.030S0304-3835(10)00260-0
35. Ma J, Han LZ, Liang H, Mi C, Shi H, Lee JJ, et al. Celastrol inhibits the HIF-1alpha pathway by inhibition of mTOR/p70S6K/eIF4E and ERK1/2 phosphorylation in human hepatoma cells. *Oncol Rep*. (2014) 32:235–42. doi: 10.3892/or.2014.3211
36. Halliwell B. The antioxidant paradox: less paradoxical now? *Br J Clin Pharmacol*. (2013) 75:637–44. doi: 10.1111/j.1365-2125.2012.04272.x
37. Murphy MP, Holmgren A, Larsson NG, Halliwell B, Chang CJ, Kalyanaraman B, et al. Unraveling the biological roles of reactive oxygen species. *Cell Metab*. (2011) 13:361–6. doi: 10.1016/j.cmet.2011.03.010
38. Chen XX, Xie FF, Zhu XJ, Lin F, Pan SS, Gong LH, et al. Cyclin-dependent kinase inhibitor dinaciclib potently synergizes with cisplatin in preclinical models of ovarian cancer. *Oncotarget* (2015) 6:14926–39. doi: 10.18632/oncotarget.3717
39. Sabharwal SS, Schumacker PT. Mitochondrial ROS in cancer: initiators, amplifiers or an Achilles' heel? *Nat Rev Cancer* (2014) 14:709–21. doi: 10.1038/nrc3803
40. Szatrowski TP, Nathan CF. Production of large amounts of hydrogen peroxide by human tumor cells. *Cancer Res* (1991) 51:794–8.
41. Schumacker PT. Reactive oxygen species in cancer cells: live by the sword, die by the sword. *Cancer Cell* (2006) 10:175–6. doi: 10.1016/j.ccr.2006.08.015
42. Li R, Jia Z, Trush MA. Defining ROS in biology and medicine. *React Oxyg Species (Apex)* (2016) 1:9–21. doi: 10.20455/ros.2016.803
43. Tan BJ, Chiu GN. Role of oxidative stress, endoplasmic reticulum stress and ERK activation in triptolide-induced apoptosis. *Int J Oncol*. (2013) 42:1605–12. doi: 10.3892/ijo.2013.1843.
44. Liu X, Gao RW, Li M, Si CF, He YP, Wang M, et al. The ROS derived mitochondrial respirstion not from NADPH oxidase plays key role in Celastrol against angiotensin II-mediated HepG2 cell proliferation. *Apoptosis* (2016) 21:1315–26. doi: 10.1007/s10495-016-1294-6
45. Chen G, Zhang X, Zhao M, Wang Y, Cheng X, Wang D, et al. Celastrol targets mitochondrial respiratory chain complex I to induce reactive oxygen species-dependent cytotoxicity in tumor cells. *BMC Cancer* (2011) 11:170. doi: 10.1186/1471-2407-11-170

Conflict of Interest Statement: The authors declare that the research was conducted in the absence of any commercial or financial relationships that could be construed as a potential conflict of interest.

frontiers in Oncology

ORIGINAL RESEARCH
published: 30 January 2019
doi: 10.3389/fonc.2019.00022

Inhibition of FAK Signaling Elicits Lamin A/C-Associated Nuclear Deformity and Cellular Senescence

*Hsiang-Hao Chuang[1], Pei-Hui Wang[1], Sheng-Wen Niu[2], Yen-Yi Zhen[2], Ming-Shyan Huang[3], Michael Hsiao[4,5] and Chih-Jen Yang[1,6,7]**

[1] Division of Pulmonary and Critical Care Medicine, Department of Internal Medicine, Kaohsiung Medical University Hospital, Kaohsiung Medical University, Kaohsiung, Taiwan, [2] Division of Nephrology, Department of Internal Medicine, Kaohsiung Medical University Hospital, Kaohsiung Medical University, Kaohsiung, Taiwan, [3] Department of Internal Medicine, E-Da Cancer Hospital, School of Medicine, I-Shou University, Kaohsiung, Taiwan, [4] Genomics Research Center, Academia Sinica, Taipei, Taiwan, [5] Department of Biochemistry, College of Medicine, Kaohsiung Medical University, Kaohsiung, Taiwan, [6] Department of Internal Medicine, Kaohsiung Municipal Ta-Tung Hospital, Kaohsiung Medical University, Kaohsiung, Taiwan, [7] Department of Respiratory Therapy, College of Medicine, Kaohsiung Medical University, Kaohsiung, Taiwan*

Focal adhesion kinase (FAK) is a non-receptor kinase that facilitates tumor aggressiveness. The effects of FAK inhibition include arresting proliferation, limiting metastasis, and inhibiting angiogenesis. PF-573228 is an ATP-competitive inhibitor of FAK. Treating lung cancer cells with PF-573228 resulted in FAK inactivation and changes in the expressions of lamin A/C and nuclear deformity. Since lamin A/C downregulation or deficiency was associated with cellular senescence, the senescence-associated β-galactosidase (SA-β-gal) assay was used to investigate whether PF-573228 treatment drove cellular senescence, which showed more SA-β-gal-positive cells in culture. p53 is known to play a pivotal role in mediating the progression of cellular senescence, and the PF-573228-treated lung cancer cells resulted in a higher p53 expression level. Subsequently, the FAK depletion in lung cancer cells was employed to confirm the role of FAK inhibition on cellular senescence. FAK depletion and pharmacological inhibition of lung cancer cells elicited similar patterns of cellular senescence, lamin A/C downregulation, and p53 upregulation, implying that FAK signaling is associated with the expression of p53 and the maintenance of lamin A/C levels to shape regular nuclear morphology and manage anti-senescence. Conversely, FAK inactivation led to p53 upregulation, disorganization of the nuclear matrix, and consequently cellular senescence. Our data suggest a new FAK signaling pathway, in that abolishing FAK signaling can activate the senescence program in cells. Triggering cellular senescence could be a new therapeutic approach to limit tumor growth.

Keywords: non-small cell lung cancer, senescence, focal adhesion kinase, nuclear deformity, lamin A/C

OPEN ACCESS

Edited by:
Zhe-Sheng Chen,
St. John's University, United States

Reviewed by:
Shiv K. Gupta,
Mayo Clinic, United States
Ji-Ye Yin,
Central South University, China

****Correspondence:***
Chih-Jen Yang
chjeya@cc.kmu.edu.tw

Specialty section:
This article was submitted to Cancer Molecular Targets and Therapeutics, a section of the journal Frontiers in Oncology

Received: *24 October 2018*
Accepted: *08 January 2019*
Published: *30 January 2019*

Citation:
Chuang H-H, Wang P-H, Niu S-W, Zhen Y-Y, Huang M-S, Hsiao M and Yang C-J (2019) Inhibition of FAK Signaling Elicits Lamin A/C-Associated Nuclear Deformity and Cellular Senescence. Front. Oncol. 9:22. doi: 10.3389/fonc.2019.00022

INTRODUCTION

Focal adhesion kinase (FAK) is a multifunctional non-receptor tyrosine kinase that participates in a variety of signaling axes (1–5). In response to extracellular stimuli, FAK translocates to the focal adhesion complex, and mediates molecular signaling for cellular events (6–9). In focal adhesion, FAK cascades signal the focal adhesion complex to promote cell proliferation and migration

(4, 9, 10). In addition to the focal adhesion complex and cytoplasm, FAK is also present in the cell nucleus (3, 11). Nuclear FAK acts as a cotranscriptional factor in gene transcription and is involved in p53 degradation, in contrast to its enzymatic function in protein phosphorylation (3, 11, 12). Whereas, FAK in the focal adhesion complex affects the expressions of cyclin B1 and cyclin D1 to program tumor cell proliferation (6, 13, 14), nuclear FAK elicits p53 degradation to drive cell cycle progression (11, 12).

The biological roles of FAK in cell migration and proliferation have also been implicated in pathological progression and in the development of cancer. There are several lines of evidence suggesting that FAK activity can manipulate tumor phenotypes, leading to uncontrolled proliferation, neovascularization, and metastasis (5, 15, 16), and the FAK signaling to tumor cell propagation represents tumorigenic capacity (5, 11). Given the crucial roles of FAK in these malignant processes, FAK is regarded to be a potential target for anti-cancer therapy (17, 18). Experiments have shown that FAK depletion results in silencing of cancer-promoting gene expressions in human hepatocellular carcinoma (HCC) xenotransplants in nude and severe combined immunodeficiency (SCID) mice (19). Moreover, the enzymatic function of FAK involves in proliferation and metastasis (9, 15, 20). Suppressing the catalytic activity of FAK or sequestering FAK in the cytoplasm has been reported to potentially perturb FAK signaling, which implies that chemical inhibitors of the enzymatic activity of FAK may be a pharmacological strategy to limit cancer growth and metastasis (6, 7, 21, 22).

Triggering cell apoptosis and arresting cell cycle progression with pharmacological regimens are common strategies to limit tumor cell growth. FAK inhibition represents an anti-cancer therapeutic strategy, as FAK inhibitors have effects on anti-angiogenesis, anti-proliferation, and anti-invasion effects (5, 15, 23). Besides, inducing cellular senescence in tumor cells could be a new therapeutic approach to limit tumor cell growth (24). Although therapy-induced senescence (TIS) in cancer cells may result from deficient apoptosis (25), driving cancer cells to cellular senescence could be a way to limit tumor propagation (26). In general, chemotherapy-induced DNA damage, telomere shortening, and oncogenic stress are the three main pathological causes of senescence (24, 27–32), and the induction of cellular senescence with these drug regimens is a side effect. Cases of β-gal-positive lung cancer biopsies in response to chemotherapy have been reported (24, 29, 33). Inducing cellular senescence could be a new approach to limit cancer growth based on phenotypic aging without DNA damage or genomic instability (31, 34). Chromatin or nuclear skeleton disorganization could be a cause of cellular senescence instead of oncogenic stress and replicative failure (8, 26).

Recent pharmacological advances in cancer therapy have led to an increased focus on developing chemical compounds that are able to target specific molecules in tumor cells to both improve efficacy and lower toxicity (4, 35). PF-573228, which competes with ATP binding to abolish the catalytic function of FAK, can inhibit the phosphorylation of FAK at tyrosine 576/577 and FAK kinase function (36, 37). Consequently, PF-573228 efficiently suppresses both the growth and metastasis of epithelial carcinoma (4, 36). The pharmacological effects of PF-573228 have been characterized based on the inhibition of FAK catalytic activity (36). In this study, we hypothesized that inhibiting the enzymatic function of FAK would stop lung cancer cell growth and invasion. Interestingly, the enzymatic inactivation of FAK resulted in nuclear deformity. When we investigated the cause and effect of nuclear deformity by PF-573228, we observed that p53 upregulation, lamin A/C downregulation, and cellular senescence in the lung cancer cells exposed to PF-573228. Strikingly, perturbation of FAK signaling led to downregulation of lamin A/C and cellular senescence rather than proliferative arrest, and halted migration of the lung cancer cells. These results showed that treatment with a FAK inhibitor could be a therapeutic approach to abrogate tumor growth. In addition, these findings revealed the crucial role of FAK signaling in anti-senescence, and that inhibition of FAK resulted in the progression of senescence.

MATERIALS AND METHODS

Materials

Detailed information on the materials is listed in **Supplementary Table S1**.

Cell Culture and Drug Treatment

A549 cells, H1299 cells, and H460 cells were purchased from ATCC. The cells were cultured in RPMI 1640 medium supplemented with 10% fetal bovine serum (FBS) at 37°C in a humidified atmosphere at 5% CO_2, and treated with PF-573228 (TOCRIS, Bristol, UK) at concentrations of 0, 0.1, 1, or 10 μM.

Western Blot Analysis

The cells were harvested and lysed in 1x RIPA buffer (Merck, Darmstadt, Germany) containing protease and phosphatase inhibitors. The protein concentration was determined using a Bio-Rad DC protein assay kit (Bio-Rad, California, USA). For Western blot analysis, 30 μg of total protein was applied to SDS-PAGE and transferred to a PVDF membrane. The membranes were blocked in 5% skim milk for 2 h in TBST buffer (20 mM Tris-Cl, 150 mM NaCl, 0.1% Tween 20, pH 7.4). After blocking, the membranes were probed with the primary antibody overnight. Antibodies against FAK, p-FAK, cyclin B1, p53, and lamin A/C were used in immunoblotting. The given protein bands were identified by horseradish peroxidase-conjugated secondary antibodies and developed with an enhanced chemiluminescence solution.

Flow Cytometry Cell Cycle Analysis

The cells were harvested and washed with PBS buffer, and then fixed in 70% (v/v) ethanol. The fixed cells were stained with propidium iodide solution and injected into an Attune NxT Flow Cytometer (Life Tech, California, USA) to analyze the cell cycle profile.

Immunofluorescent Staining and Immunofluorescent Microscopic Imaging

A Leica DMi8S epifluorescence microscope (Wetzlars, Germany) equipped with an X-Cite XCT10A (Lumen Dynamics,

Wiesbaden, Germany) light source, filters and objectives (10x, 20x, 40x, and 63x) was used to observe fluorescent signals in the cells. In addition to epifluorescence, confocal images were captured using an OLYMPUS FV1000 confocal laser scanning microscope equipped with a light source, filters and objectives (10x, 20x, 40x, 63x, and 100x). Cells were seeded on 12-mm coverslips in a 24-well culture plate. The cells were harvested and fixed in 4% paraformaldehyde in PBS for 10 min, and permeabilized in 0.5% Triton in PBS for 5 min. After fixation, the cells were subjected to immunofluorescent staining with antibodies recognizing FAK and emerin. Phalloidin-TRITC was used as an additional reagent. Cell nuclei were stained with 0.2 μg/mL 4′, 6-diamidino-2-phenylindole (DAPI).

Senescence-Associated β-Galactosidase Staining

The cells were fixed with 4% paraformaldehyde for 15 min. After fixation, acidic β-galactosidase (SA-β-gal) was assayed in senescence assay buffer (1 mg/mL 5-bromo-4-chloro-3-indolyl β D-galactopyranoside (X-gal), 5 mM $K_3Fe(CN)_6$, 5 mM $K_4Fe(CN)_6$, 2 mM $MgCl_2$, 150 mM NaCl, 40 mM citric acid, and 40 mM Na_2HPO_4 at pH 6.0) in the dark at 37°C for 16 h. SA-β-gal activity was detected based on SA-β-gal-hydrolyzed X-gal, which produces a blue color. All chemical reagents were purchased from Sigma-Aldrich.

Cell Growth Assay

The cells were trypsinized, resuspended in 1xPBS, and stained with trypan blue (Sigma-Aldrich). The number of cells was counted with a hemocytometer.

Lentiviral Production and Infection

Lentivirus-associated plasmids encoding luciferase, and FAK short hairpin RNA (shRNA) were obtained from the National RNAi Core Facility of Academia Sinica, Taiwan. The production and infection of lentiviruses were performed according to the guidelines of the National RNAi Core Facility.

Statistical Analysis

The experimental data were digitized and analyzed. Data are presented as the mean ± the standard error of the mean (SEM). One-way ANOVA was used to compare digitized data and measurements from independent experiments in two or more groups, and the Student's *T*-test was used to compare two independent samples. A $p < 0.05$ was considered to indicate a statistically significant difference.

RESULTS

PF-573228 Causes Cessation of the Propagation of Lung Cancer Cells

Focal adhesion signaling is involved in cell proliferation, and FAK plays a key role in the focal adhesion complex that relays focal adhesion signals to the cell proliferation program (9, 15). Given the role of FAK signaling in tumor growth and metastasis, we hypothesized that inhibiting the catalytic activity of FAK may disrupt FAK signaling and blunt tumor cell proliferation. Therefore, we treated three distinct non-small cell lung cancer cell lines (A549 lung adenocarcinoma cells and H460 and H1299 large cell carcinoma cells) with PF-573228, an enzymatic inhibitor of FAK. PF-573228 was administered to the lung cancer cells for 4 days at three doses: 0.1, 1, or 10 μM. The growth curves showed that 10 μM PF-573228 effectively induced cessation of cell growth (**Figures 1A–C**).

We then examined the expression level of the cell cycle regulator cyclin B1, which has been reported to be a downstream effector of FAK signaling. Western blot analysis showed that cyclin B1 expression levels were much lower after the cells were exposed to 10 μM PF-573228 (**Figures 1D–F**). To further characterize the effect of PF-573228 treatment on cell cycle progression, we analyzed the cell cycle distribution using flow cytometry analysis. The results showed that a low PF-573228 concentration had little influence on cell cycle progression (**Figures 1G–I**), whereas a high PF-573228 concentration (10 μM) halted cell cycle progression at the G2/M transition (**Figures 1J,K**). This showed that PF-573228 treatment effectively suppressed multiplication of lung cancer cells.

PF-573228 Administration Inactivates FAK

Since phosphorylation of FAK at Tyr-576 and Tyr-577 (p-FAK) represents enzymatic activation of FAK (37), an antibody against p-FAK was used to confirm the kinase activity of FAK and verify the effect of PF-573228 on FAK inactivation. FAK activity was practically blocked by 10 μM PF-573228 in A549 cells (**Figures 2A,C**). To further confirm the inactivation of FAK by PF-573228 treatment, we also examined the phosphorylation of tyrosine 397 in FAK (pTyr-397). The results showed that the intensity of pTyr-397 was decreased after PF-573228 treatment (**Figure S1**). FAK is a key regulator of integrin signaling for focal adhesion assembly (38, 39). In addition to FAK inhibition, PF-573228 has been shown to perturb integrin-based signaling for focal adhesion maturation (36).

Treatment of the lung cancer cells with PF-573228 resulted in failure of FAK activation, and translocation to focal adhesion was observed in immunofluorescent imaging (**Figure 2B**). When the cells were cultured in PF-573228-free medium, more FAK translocated to focal adhesions, which appeared as plaque-like patterns in the cell periphery that formed at the tips of stress fibers, as visualized in cells stained with phalloidin-labeled F-actin and an antibody against FAK (**Figure 2B**). By contrast, in the A549 cells treated with PF-573228, only a few FAK molecules translocated to focal adhesions, and tiny FAK-based focal adhesions formed at the tips of F-actin bundles, indicating failure of focal adhesion maturation (**Figure 2B**). The sizes of focal adhesions were measured and the areas of FAK at the tips of the actin stress fibers were digitized using Image Pro software. The sizes of focal adhesions ranged from 12 to 28 μm^2 in the cells without PF-573228 treatment, whereas the extent of FAK-based focal adhesion was approximately 3–12 μm^2 after PF-573228 treatment (**Figure 2D**).

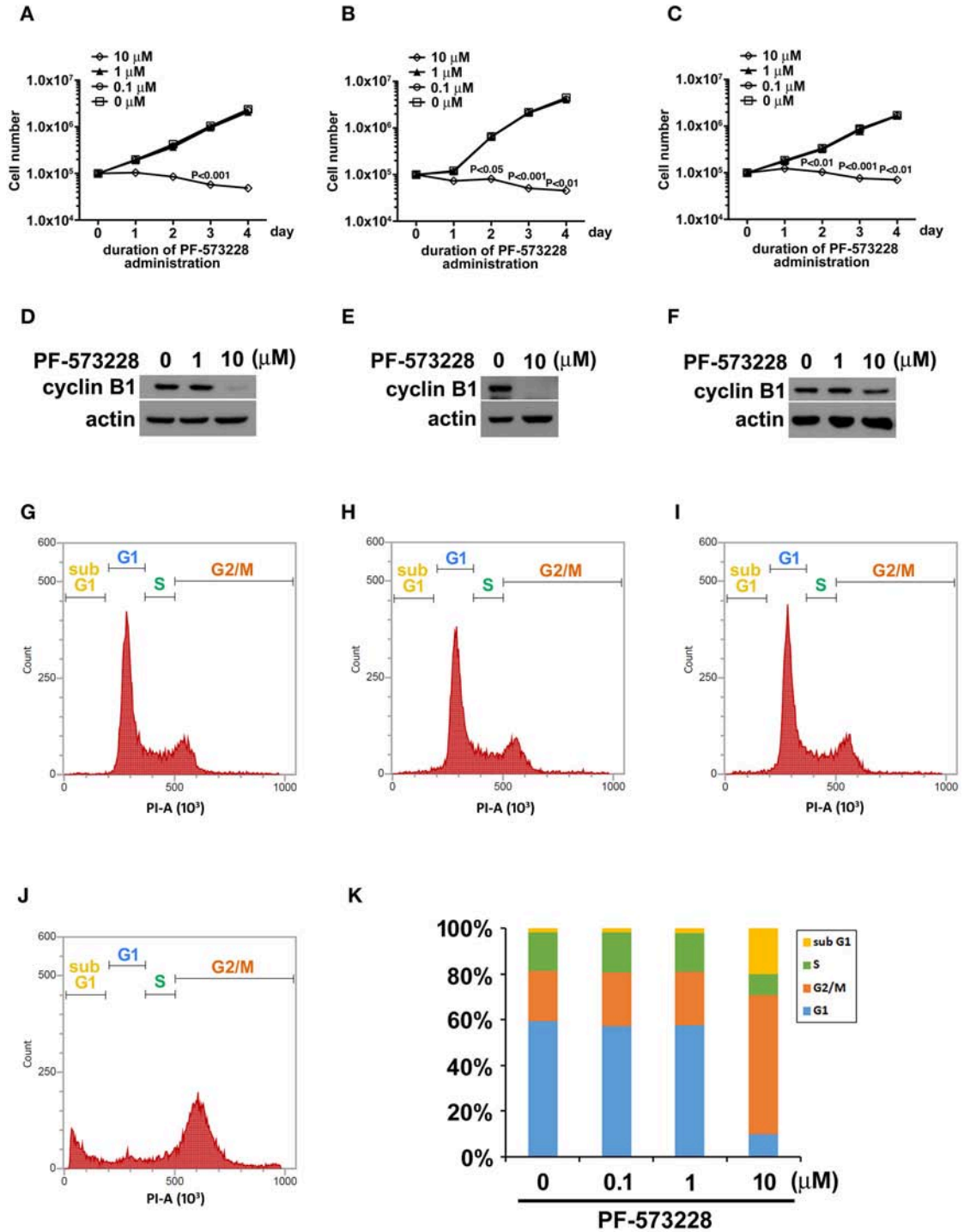

FIGURE 1 | PF-573228 inhibited lung cancer cell growth. Three different types of lung cancer cells, **(A)** A549 lung adenocarcinoma and **(B)** H460, and **(C)** H1299 large cell carcinoma, were selected for the PF-573228 administration regimen. Cell growth curves of the three lung cancer cell lines treated with various doses of PF-573228 for 4 days were established. The administration of PF-573228 at 10 μM to the lung cancer cells effectively suppressed cell growth *in vitro*, as proliferative activity totally ceased in the cells exposed to 10 μM PF-573228. **(D)** On the third day, PF-573228-treated cells were harvested and subjected to Western blot analysis for cyclin B1. Cyclin B1 levels were much higher in A549 cells with 1 μM PF-573228 or without PF-573228 treatment than in the cells treated with higher concentrations of PF-573228. **(E)** After 10 μM PF-573228 treatment, cyclin B1 levels declined markedly in H460 cells. **(F)** PF-573228 administration slightly reduced cyclin B1 levels in H1299 cells. A549 cells were harvested and subjected to flow cytometry analysis for cell cycle profiling after PF-573228 treatment for 3 days. The concentrations of PF-573228 were 0 μM **(G)**, 0.1 μM **(H)**, 1 μM **(I)** and 10 μM **(J)**, respectively, **(K)** After 10 μM PF-573228 treatment, the G2/M ratio was significantly extended. The apoptotic ratio was also increased in A549 cells with 10 μM PF-573228 treatment.

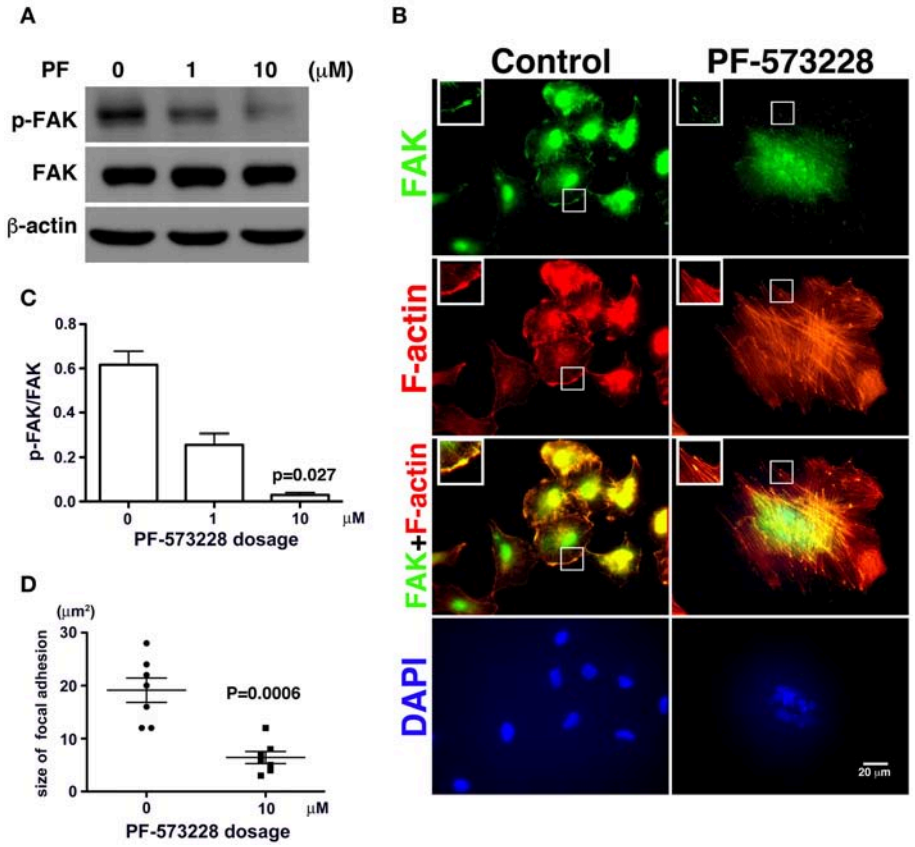

FIGURE 2 | PF-573228 as a catalytic inhibitor inactivated the kinase function of FAK. **(A)** FAK expression levels and FAK activity, as measured by the phosphorylation of FAK at tyrosine 576 and 577, were quantified by Western blot analysis after treatment of lung cancer cells with PF-573228 for 3 days. **(B)** The cells were stained with phalloidin to visualize F-actin (red) and a FAK antibody to visualize the FAK distribution (green). In cells without PF-573228 administration, FAK translocated to focal adhesions at the tips of actin stress fibers, and the focal adhesions were relatively large. When cells were exposed to 10 μM PF-573228, FAK translocation to focal adhesions was reduced, and the sizes of the focal adhesions were smaller. Nuclei in cells treated with PF-573228 were deformed, as visualized with DAPI staining, whereas most nuclei in cells without PF-573228 treatment were oval shaped. **(C)** The p-FAK/FAK ratios in the cells with exposure to 1 μM and 10 μM PF-573228 were reduced to less than half and one tenth compared with the cells without PF-573228 treatment, respectively. **(D)** The sizes of FAK-based focal adhesions were 19 μm^2 on average in the cells without PF-573228 treatment and 6.4 μm^2 on average in the cells without PF-573228 treatment.

Aberrant Nuclear Appearance and Lamin A/C Downregulation Occur Concurrently in the Lung Cancer Cells Exposed to PF-573228

In the absence of PF-573228, most cells contained oval or round nuclei, as visualized by DAPI staining (**Figure 2B**). Interestingly, a distorted nuclear morphology was observed in the A549 cells treated with PF-573228 (**Figure 2B**). As DAPI staining was insufficient to clearly visualize the nuclear appearance in detail, an antibody against emerin (40), a nuclear inner membrane protein, was used to visualize the nuclear shape in the PF-573228-treated A549 cells. Emerin staining revealed that the cells without PF-573228 treatment harbored oval-like nuclei. By contrast, most nuclei were larger and had irregular shapes with invagination in the cells upon exposure to 10 μM PF-573228 (**Figure 3A**).

Lamin A/C is the nuclear skeleton responsible for maintaining and stabilizing the nuclear architecture (41–44). Because interrupting FAK signaling resulted in nuclear deformity (**Figure 2B**), changes in lamin A/C expression levels were assessed. The effects of FAK signaling on the expressions of lamin A/C and other nuclear skeletal proteins inferred that the nuclear deformity caused by PF-573228 was attributable to changes in lamin A/C expression.

To investigate changes in lamin A/C expressions in cells exposed to PF-573228, PF-573228-treated cells were harvested and subjected to Western blot analysis. Inhibition of FAK activity led to lower p-FAK levels (**Figures 3B,C**) and deformed nuclei in the lung cancer cells (**Figure 3A**). To quantify the expressions of lamin A and C, the intensities of their protein bands were normalized to β-actin (**Figure 3B**). The expressions of lamin A and C were much lower in the A549, H460, and H1299 cells treated with PF-573228 compared to those without PF-573228 treatment (**Figure 3B** and **Figures S2A,B**). The lamin A and C band intensities were quantified and plotted in bar charts. The ratios of lamin A/β-actin and lamin C/β-actin in A549 cells exposed to PF-573228 were reduced by one third and one half, respectively, compared to A549 cells without PF-573228

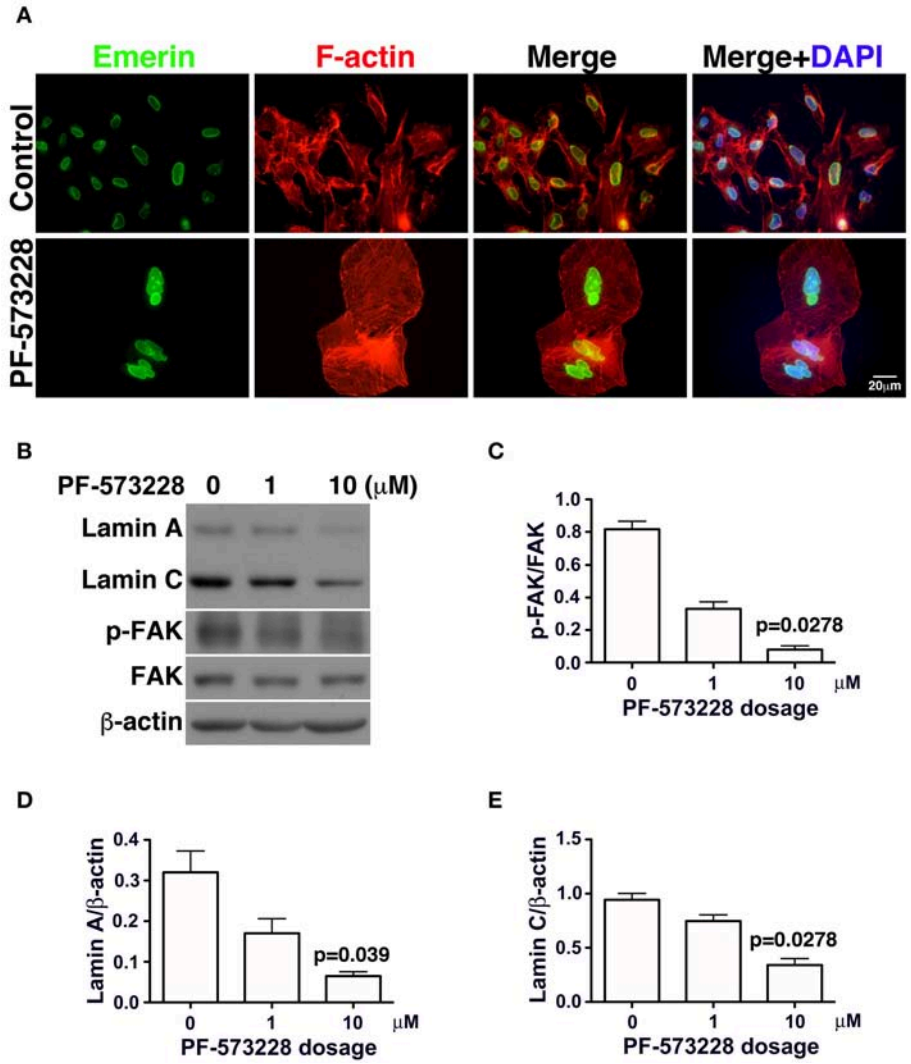

FIGURE 3 | Downregulation of lamin A and lamin C and nuclear deformity in A549 cells exposed to PF-573228. **(A)** After PF-573228 treatment of A549 cells, the cells were fixed and stained with phalloidin to label F-actin (red) and an antibody against emerin (green) to outline the nuclear shape. Cells treated with PF-573228 were extremely large and had deformed nuclei, whereas mostly oval-like nuclei were present in the cells without PF-573228 treatment. **(B)** The cells treated with 10 μM PF-573228 exhibited a decrease in p-FAK levels. Lamin A and lamin C expression levels were much lower in A549 cells exposed to 10 μM PF-573228. **(C)** The p-FAK/FAK ratios in A549 cells exposed to 1 μM and 10 μM PF-573228 were less than half and one tenth of those in A549 cells without PF-573228 treatment, respectively. **(D,E)** Decreased lamin A and lamin C levels appeared in A549 cells treated with PF-573228.

treatment (**Figures 3D,E**). Similar trends of downregulation of lamin A and lamin C by PF-573228 treatment were also detected in the two other lung cancer cell lines (**Figures S2A,B**).

Lung Cancer Cells Are Destined to Senescence After Inhibition of FAK Enzymatic Function

Mutant LMNA, mutations that affect lamin A/C expression, and lamin A/C depletion in cells have been associated with premature aging and cellular senescence (8, 30, 32, 42, 45). Based on the concurrent lamin A/C downregulation and nuclear deformity observed in lung cancer cells exposed to PF-573228 (**Figures 3A,B**), we examined the development of cellular senescence in lung cancer cells treated with PF-573228. The SA-β-gal activity in cells was assayed by *in situ* staining using the chromogenic substrate X-gal, which colored SA-β-gal-positive cells blue. As noted in **Figure 4A**, blue cells were clearly visible in the cells treated with PF-573228 (**Figure 4A**), whereas a sporadic distribution of blue-colored cells was observed in the cells without PF-573228 treatment (**Figure 4A**). The bar chart in **Figure 4B** shows that nearly 90% of the cells exposed to a higher dose of PF-573228 were positive for SA-β-gal, compared to ∼20% of the cells exposed to a lower dose of PF-573228, and ∼1% of the cells without PF-573228 treatment.

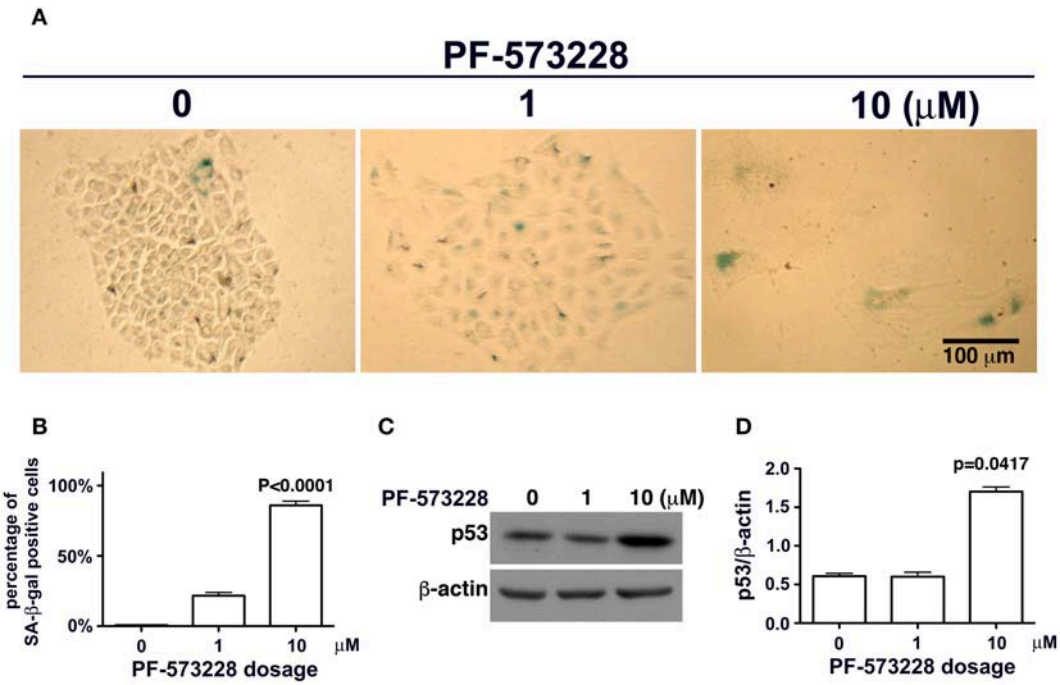

FIGURE 4 | Cellular senescence occurred in lung cancer cells after FAK inhibition. **(A)** A549 cells were exposed to 0, 1 μM, or 10 μM PF-573228 for 7 days. SA-β-gal-positive cells appeared sporadically in cells without PF-573228 treatment. The cells treated with 1 μM PF-573228 were slightly enlarged, with few β-gal-positive cells. The cells treated with 10 μM PF-573228 were quite large, and most were β-gal positive. **(B)** The ratio of SA-β-gal-positive cells to the total population was calculated and plotted in a bar chart. SA-β-gal-positive cells represented <1% of the total A549 cell population without PF-573228 treatment, ∼21% in the 1 μM PF-573228-treated A549 cell population, and more than 80% in the 10 μM PF-573228-treated A549 cell population. **(C)** A549 cells were treated with 0, 1, or 10 μM PF-573228 for 4 days. p53 was not obviously increased in 1 μM PF-573228 treated-A549 cells and was significantly elevated in 10 μM PF-573228-treated A549 cells. **(D)** p53 levels approximately tripled in A549 cells exposed to 10 μM PF-573228 compared to cells with or without 1 μM PF-573228 treatment.

Upregulation of p53 in Cells Exposed to PF-573228

Disruption of FAK signaling by PF-573228 caused cellular senescence. However, the mechanisms by which inhibition of FAK signaling affects senescence programming remain unclear. Cellular senescence in chemotherapy-affected cancer cells has been observed in several studies (24, 29, 46). In addition, clinical studies have reported that p53 plays a role in the development of cellular senescence in chemotherapy-affected cancer cells (46, 47). p53 is known to be a transcription factor in programed senescence and cell cycle arrest (48), and it may play a similar role in the cellular senescence program in lung cancer cells exposed to PF-573228 as in cells in which FAK signaling is interrupted.

To investigate whether or not p53 plays a role in PF-573228-induced cellular senescence, p53 expression levels were examined in PF-573228-treated cells. Western blot analysis showed that p53 expression levels increased significantly by more than 3-fold compared to cells without PF-573228 treatment and cells treated with a low concentration of PF-573228 (**Figures 4C,D**, and **Figure S3**).

Engagement of FAK Signaling With Nuclear Integrity and p53 Expression

FAK is not the only molecule targeted by PF-573228 (36). Although FAK enzymatic activity was blocked by PF-573228 administration, off-target effects could also have turned off other kinases, for example, cyclin-dependent kinases. Therefore, signaling perturbations of other kinases may have caused the pathogenic senescence in the lung cancer cells.

If FAK has an anti-senescence effect, FAK depletion would cause anti-senescence to fail and escalate senescence programing. To clarify the role of loss of FAK signaling in the development of cellular senescence and nuclear deformity with changes in lamin A and lamin C expressions, we used an shRNA targeting FAK to deplete the expression of FAK in lung cancer cells. After introducing shFAK into lung cancer cells, cells harboring shFAK were selected. To assess FAK knockdown, two shFAK clones were selected for Western blot analysis and senescence assays, which showed that shFAK successfully caused FAK depletion in A549, H460, and H1299 cells (**Figure 5A** and **Figure S4A**). In addition, the impact of FAK depletion on the downregulation of lamin C and cyclin B1 and upregulation of p53 was validated (**Figure 5A** and **Figure S4A**). We also assessed nuclear appearance using emerin staining, which revealed that A549 cells without FAK depletion harbored oval-like nuclei. By contrast, the ratio of nuclei harboring slightly larger and irregular shapes was increased in the cells with FAK depletion (**Figure 5B**). Similar results were obtained in the H460 and H1299 cells (**Figures S4B,C**). In addition, lung cancer cells harboring shLuc or shFAK were subjected to senescence assays, which revealed

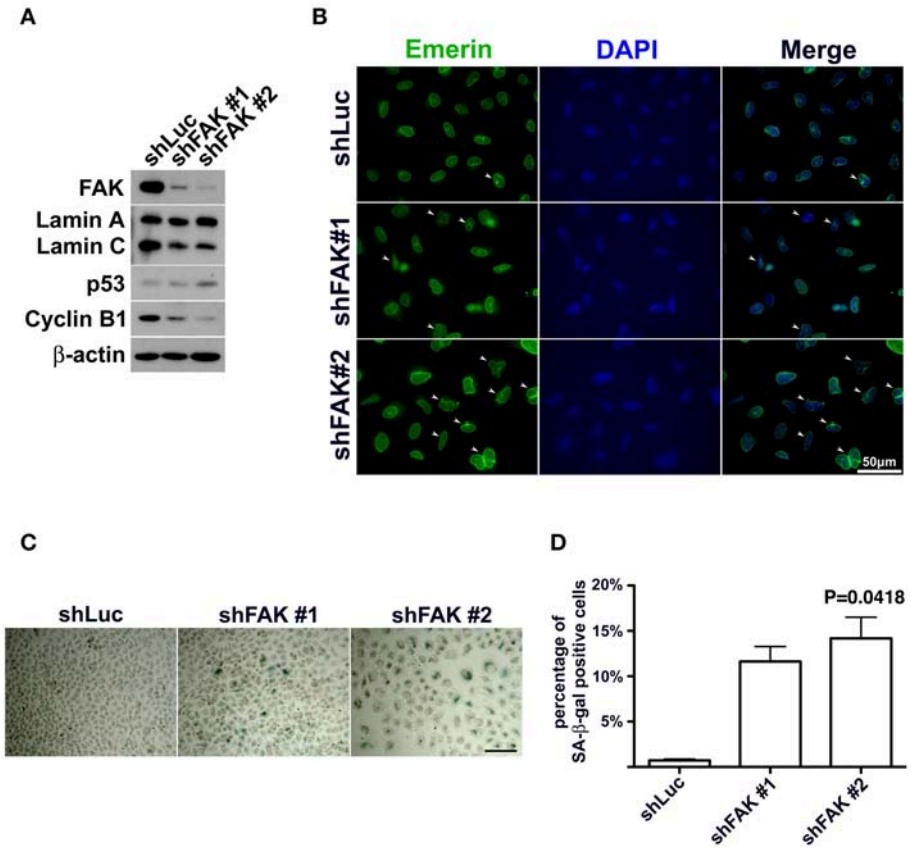

FIGURE 5 | FAK depletion resulted in nuclear deformity and cellular senescence. **(A)** A549 cells with FAK depletion by shRNA were seeded and incubated for 7 days. Western blot analysis revealed low FAK levels in the cells with shFAK and higher levels in the cells with shLuc. Upon FAK depletion, lamin C and cyclin B1 levels decreased, and p53 expression levels increased. **(B)** The cells were fixed and stained with an antibody against emerin (green) to outline the nuclear shape. Cells with FAK depletion were slightly larger, with a higher proportion of deformed nuclei (arrowhead), whereas mostly oval-like nuclei were present in cells without FAK depletion. (Scale bar, 50 μm) **(C)** SA-β-gal-positive cells were sporadically visible in A549 cells with shLuc. By contrast, more SA-β-gal-positive cells were observed among cells with shFAK. (Scale bar, 100 μm) **(D)** The bar chart shows that <1% of the cells in the shLuc population were SA-β-gal-positive, whereas more than 10% of the shFAK cell population was SA-β-gal positive.

more SA-β-gal-positive A549 cells harboring shFAK (**Figure 5C**). By contrast, few SA-β-gal-positive cells were visible in those harboring shLuc. The SA-β-gal-positive cells represented ∼0.7% of the shLuc A549 population. In the two shFAK cell clones, SA-β-gal-positive cells represented ∼11 and 15%, respectively (**Figure 5D**). Similar results were observed in H460 and H1299 cells (**Figures S4D–F**). However, H460 cells grew in single and multiple layers (**Figure S4D**), and it was difficult to measure the ratio of SA-β-gal-positive cells.

Senescent Cells Reactivate Their Proliferative Activity After PF-573228 Withdrawal From Cell Culture

Aging and cellular senescence are often present in replicative failure, oncogenic induction, and telomere shortening (8, 34, 49). In clinical cases, chemotherapy or radiation has been shown to induce cellular senescence, and DNA damage or genomic instability is thought to be the pathological cause. Therapy-induced senescence can be classified as replicative senescence (24, 27, 33, 48), and replicative senescence is able to cease tumor growth (47, 50). However, this cellular senescence is reversible (31, 51, 52). Senescent cells expressing low levels of p16 have been shown to reversibly exit senescence when p53 expression levels fall (52).

In this study, FAK signaling downregulated the expression of p53, and inhibition of FAK signaling upregulated the expression of p53 in A549 cells (**Figures 4C,D**, **5A**). The A549 cells that entered senescence due to PF-573228 administration exhibited regrowth and return to a non-senescent state after withdrawal of PF-573228 from the culture (**Figures 6A–C**). The proliferative activity of A549 cells was based on cyclin B1 expression after the cells were incubated in PF-573228-free medium (**Figure 6D**).

Restoration of Lamin a and Lamin C Expressions in Senescent Lung Cancer Cells After PF-573228 Withdrawal

We then tested whether senescence in lung cancer cells with FAK inhibition was reversible or irreversible. The three lung

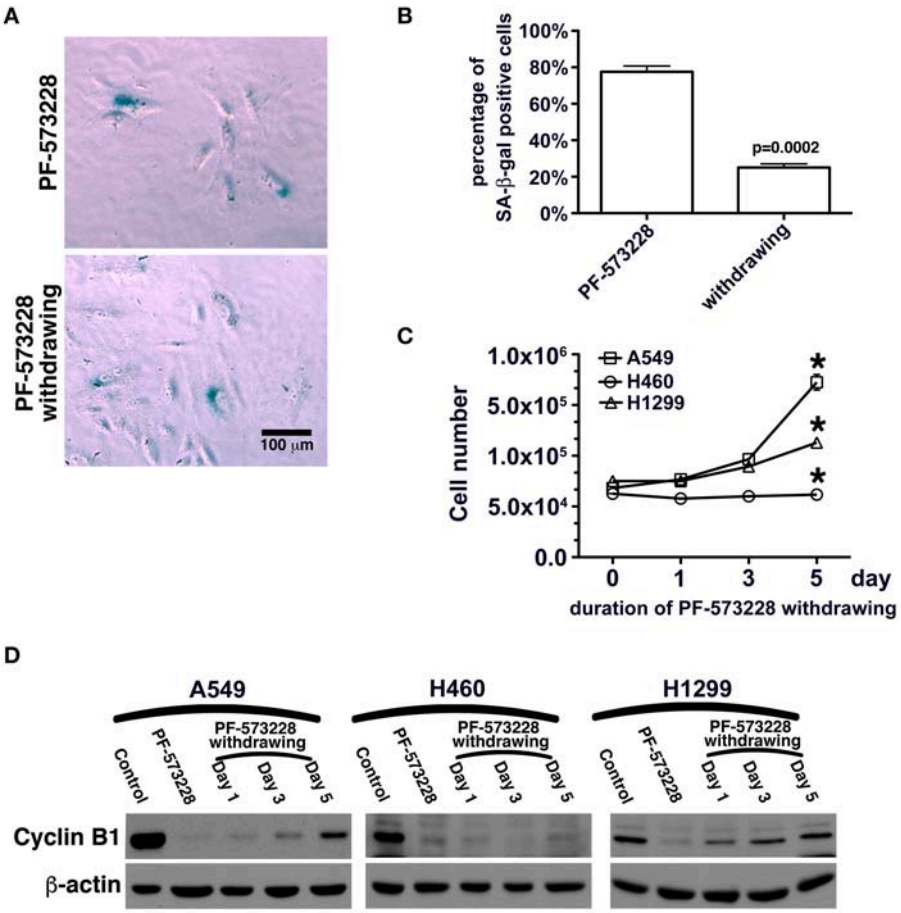

FIGURE 6 | Recovery of the proliferative activity of lung cancer cells after PF-573228 withdrawal. **(A)** The population of SA-β-gal-positive A549 cells declined after the cells were released from PF-573228 inhibition. **(B)** The proportion of SA-β-gal-positive A549 cells was ~80% when cells were exposed to PF-573228, and only 25% after PF-573228 withdrawal. **(C)** Initially, the cells were senescent, and proliferation ceased in the three lung cancer cell lines with PF-573228 treatment. After PF-573228 withdrawal, the A549 cells grew exponentially, H1299 cells grew linearly, and H460 cells continued to exhibit cessation of division. **(D)** When cells were exposed to PF-573228, cyclin B1 expression level was extremely low. After the cells were released from PF-573228 inhibition, cyclin B1 levels gradually increased in A549 cells and H1299 cells. However, cyclin B1 remained at low levels in H460 cells after PF-573228 withdrawal. *$P < 0.05$.

cancer cells lines were cultured in medium containing 10 μM PF-573228 to induce cell senescence in a 5-day induction course, after which the expressions of lamin A and lamin C decreased (**Figure 7A**). After the induction of senescence, PF-573228 withdrawal was scheduled over 6 days. Lamin A and lamin C expressions in A549 cells and H1299 cells gradually recovered after PF-573228 withdrawal (**Figures 7A,B**). By contrast, lamin A and lamin C levels in H460 cells remained lower when senescent H460 cells were incubated in PF-573228-free medium (**Figures 7A,B**). After PF-573228 withdrawal, senescent A549 cells escaped from senescence, as the SA-β-gal-positive A549 cell population declined to nearly half by the fifth day of PF-73228 withdrawal (**Figure 8A**).

DISCUSSION

FAK is a signaling mediator of integrin-based signaling and is associated with epidermal growth factor receptor (EGFR) signaling (23, 53). FAK-associated cross-talk between EGFR and integrin pathways have been shown to lead to tumor growth and metastasis in lung cancer (39, 53–55). Phosphorylation at tyrosine 576/577 (p-FAK) has been reported to result in catalytic activity and to be involved in tumor cell proliferation and metastasis (2, 12, 15, 16). Therefore, inhibition of the enzymatic function of FAK has been proposed to be a therapeutic strategy to limit tumor growth, angiogenesis, and metastasis (5, 7, 16, 23). In the present study, we tested the pharmacological effect of PF-573228 on inhibiting FAK activity and limiting lung cancer cell growth. When lung cancer cells were treated with PF-573228, an abnormal nuclear shape was observed. A similar cytological phenomenon has been reported in previous studies (56), however the molecular mechanism has not been clearly elucidated. In addition, nuclear lobulation and distorted nuclear morphology have been reported in cells with the LNMA mutation or lamin A/C downregulation (41–43). The LNMA mutation or lamin A/C downregulation has been shown to result in nuclear distortion

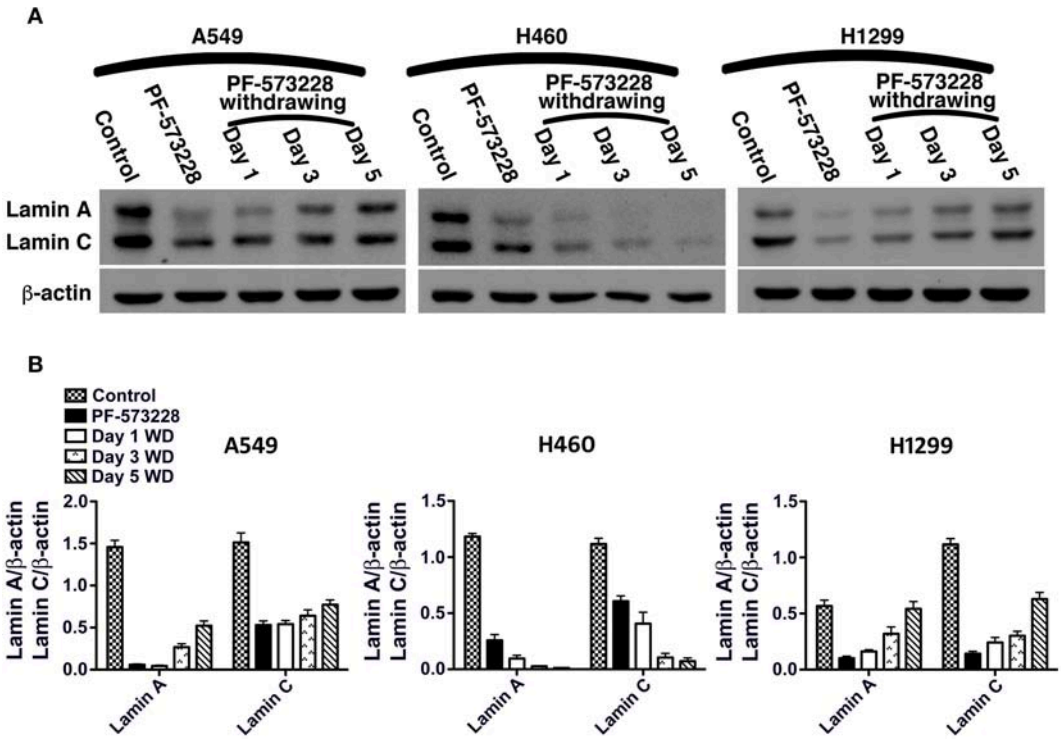

FIGURE 7 | Restoration of lamin A and lamin C expressions in lung cancer cells after PF-573228 withdrawal (WD). **(A)** The senescent cells were released from PF-573228 inhibition for the indicated period. Western blot analysis revealed that the expression levels of lamin A and lamin C were gradually restored in A549 cells and H1299 cells. However, the lamin A and lamin C levels remained lower in H460 cells when senescent H460 cells were incubated in PF-573228-free medium. **(B)** The expression levels of lamin A and lamin C in A549 cells increased after the cells were released from PF-573228 inhibition. However, H460 cells expressed lower levels of lamin A and lamin C when exposed to PF-573228, and lamin A and lamin C expression in H460 cells remained lower when PF-573228-treated cells were cultured in PF-573228-free medium. Lamin A and lamin C levels in H1299 cells decreased when cells were exposed to PF-573228. After PF-573228 withdrawal, the expression levels of lamin A and lamin C gradually increased in H1299 cells previously treated with PF-573228.

with a pathogenic tendency to develop aging and senescence (8, 30, 42, 57). The nuclear deformity in PF-573228-treated lung cancer cells (**Figures 2B**, **3A–C**) supports a pathophysiological impact from the inactivation of FAK signaling to downregulate lamin A/C.

In this study, we examined the expressions of lamin A/C and assayed SA-β-gal activity in lung cancer cells exposed to PF-573228. Our experimental results demonstrated that FAK inhibition and FAK depletion elicited similar downregulation of lamin A/C, upregulation of p53, and cellular senescence (**Figures 4A,C,D**, **5A,C**). These results imply that FAK signaling regulates the expression of lamin A/C to maintain a regular nuclear shape and activate anti-senescence programs (**Figure 8B**). The finding that FAK signaling affects lamin A/C expressions and influences the cellular context in which lamin A/C organizes the nuclear architecture is an important biological theme. The degradation of lamin A/C has recently been reported to be regulated by Akt1 or cdk5 signaling (30, 58). Akt signaling was shown to slightly alter the amount of lamin A/C in cells, but this small change in lamin A/C expressions did not seem to have a notable effect on nuclear shape. On the other hand, nuclear FAK has also been shown to act as a transactivator to regulate gene expressions and stem cell differentiation rather than stem cell renewal (59). In addition, nuclear FAK and Oct-4 have been shown to coordinate gene expression programming with the expression of Oct-4 in stem cell renewal. However, the role of nuclear FAK in gene expression programming does not seem to be associated with changes in lamin A/C expressions. Furthermore, we found that PF-573228 treatment does not dramatically affect nuclear translocation of FAK in A549 cells (**Figure S5**). This implied that FAK-mediated signaling to maintain lamin A/C expression may not be through transcriptional regulation. By contrast, inactivation of FAK signaling or nestin silencing (30) has been shown to significantly downregulate lamin A/C and cause round or oval nuclei to become lobulated or irregular in shape. Our results indicated that FAK-mediated signaling is crucial to maintain nuclear shape and, potentially, for chromatin reorganization.

In addition to the downregulation of lamin A/C, this study showed that FAK inhibition-mediated p53 upregulation also played a crucial role in cellular senescence, and that p53 was increased during FAK inhibition either by a small compound or shRNA-mediated downregulation. Lim et al. demonstrated that nuclear FAK could promote p53 downregulation via enhanced Mdm2-dependent p53 ubiquitination in a kinase-independent manner (11). However, in our study, both the amount of

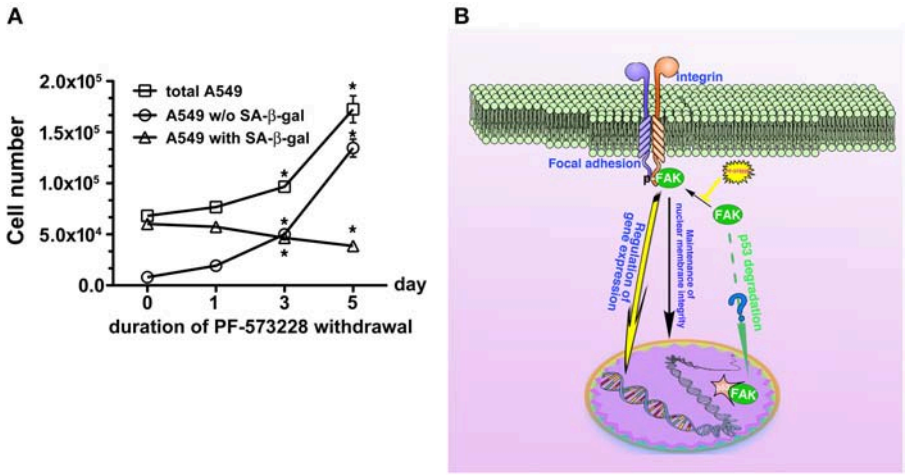

FIGURE 8 | Disruption of FAK signaling with cellular senescence. Reactivation of FAK signaling was observed in A549 cells in which senescence was induced by 5 days of PF-573228 treatment after PF-573228 withdrawal. **(A)** The proportion of SA-β-gal-positive A549 cells declined to half when the senescent cells were cultured in PF-573228-free medium. In addition, A549 cells grew exponentially after A549 cells were released from inhibition by 10 μM PF-573228. *$P < 0.05$. **(B)** The proposed scheme shows that integrin-based signaling activates FAK to trigger cell proliferation, to manage lamin A/C expression to maintain nuclear shape and program anti-senescence. Blockade of FAK signaling by PF-573228 induced cell cycle arrest and senescence.

FAK protein and its enzymatic function affected the expression level of p53. PF-573228 treatment suppressed the enzymatic activity of FAK but did not significantly affect its abundance. However, an obvious effect on cell senescence was observed in the inhibitor treatment group. This result implies an important role of FAK enzymatic function in suppressing senescence. Downstream signaling such as the PI3K/Akt axis may play a critical role in modulating Mdm2 function and p53 regulation, and p53 activation may suppress cell proliferation and further trigger senescence. However, FAK inhibition also repressed the proliferation of p53 null cancer cells such as H1299 cells and induced senescence. FAK inhibition also reduced lamin A/C expressions in H1299 cells, with changes in chromatin integrity followed by the induction of senescence. These observations indicate that the induction of cellular senescence by perturbations in lamin A/C-mediated chromatin alterations is independent of p53 (30, 34, 60).

Downregulation or degradation of lamin A/C and upregulation of p53 by PF-573228 treatment or FAK depletion are the main causes of cellular senescence. Baell et al. reported that inhibition of histone acetyltransferase could induce cellular senescence (26), and that the pharmacological effects of VM-8014 and VM-1119 on chromatin remodeling caused cellular senescence (26). The induction of senescence by PF-573228, VM-8014, and VM-1119 may also be due to defective chromatin remolding. Because FAK and lamin A/C are also involved in chromatin remodeling (43, 55, 61), this cellular senescence is likely to be reversible (**Figures 6A–C**, **8A**). Therefore, when the enzymatic activity of FAK is restored, lamin A/C and cyclin B1 expression levels recover (**Figures 7A,B**, **6D**).

Inhibition of FAK signaling may have a therapeutic role in limiting cancer cell growth. In the present study, we demonstrated that disruption of the FAK signaling pathway led to cellular senescence in lung cancer cells. We also tested the sensitivity of human normal lung epithelial cells, BEAS-2B, to PF-573228 treatment. It appeared that a high concentration of PF-573228 could attenuate the propagation of BEAS-2B cells. However, the BEAS-2B cells cultured in medium containing serum still underwent cell cycle progression with a low proliferative rate (**Figure S6A**). This implies that oncogene addiction occurs in lung cancer cells for FAK signaling (54). We also evaluated whether FAK inhibition causes cellular senescence in BEAS-2B cells. The results showed that a high dose of PF-573228 treatment promoted cellular senescence in BEAS-2B cells (**Figures S6B,C**). However, the ratio of SA-β-gal positive cells was <3% (**Figure S6C**). This implies that normal cells are more insensitive to high concentrations of PF-573228 than lung cancer cells and FAK inhibitors have a therapeutic potential for cancer treatment. However, there was no evidence showing that FAK signaling can result in anti-senescence and convert senescent cells to non-senescent cells upon FAK inhibitor withdrawal in A549 cells (**Figures 8A,B**). We calculated the ratios of SA-β-gal-positive and SA-β-gal-negative A549 cells after PF-573228 withdrawal and plotted curves with the timing of PF-573228 withdrawal. The slope of the curve for SA-β-gal-negative cells over 5 days indicated a reduction of 5,402 cells per day in the linear variation of SA-β-gal-negative cell numbers (**Figure 8A**). SA-β-gal-negative cells increased exponentially after PF-573228 withdrawal in A549 cells, and the curves of the SA-β-gal-negative cell growth were convergent with the growth curve of total A549 cells (**Figure 8A**). These results may be due to reversion of some of the senescent cells to non-senescent cells, as described in the schematic representation of FAK signaling in anti-senescence and PF-573228 treatment signaling cellular senescence (**Figure 8B**).

Previously, therapeutic outcomes were measured in terms of anti-angiogenesis, anti-proliferation, and anti-invasion

(16, 39, 62). In this study, FAK inhibition limited lung cancer cell propagation by inducing cellular senescence (**Figure 8B**). Driving cell senescence programing is a new trend for the treatment of tumor diseases (26), as this therapeutic approach does not chemically elicit genomic evolution in cancer cells and does not severely damage non-cancer cells (63). Although cellular senescence does not kill tumor cells, limiting cancer growth could eliminate cancer cell malignancy. However, cellular senescence is an inducer of autophagy (64) and increases susceptibility to cell-mediated cytotoxicity by activated killer cells (65). Furthermore, FAK inhibition also increases immune surveillance (66). Consequently, FAK appears to be an attractive target for pharmacological strategies for cancer therapy. Our data reveal a signaling pathway for senescence and support a therapeutic strategy for cancer.

AUTHOR CONTRIBUTIONS

H-HC, Y-YZ, and C-JY conceptualized and designed this study. P-HW devised the methodology. H-HC, P-HW, and Y-YZ performed the experiments. S-WN and Y-YZ performed formal analysis. M-SH and MH provided the resources. H-HC and Y-YZ wrote the draft. M-SH, MH, and C-JY reviewed and edited the manuscript. All authors reviewed the manuscript.

FUNDING

This work was supported by the Ministry of Science and Technology [MOST 102-2314-B-037-028-MY3] to C-JY; Kaohsiung Municipal Ta-Tung Hospital [grant number KMTTH-106-006]. This research was also supported by Academia Sinica and Ministry of Science and Technology [MOST 106-0210-01-15-02, MOST 107-0210-01-19-01] to MH.

ACKNOWLEDGMENTS

We thank Dr. Lee, Che-Hsin for technical assistance for the flow cytometry analysis.

SUPPLEMENTARY MATERIAL

The Supplementary Material for this article can be found online at: https://www.frontiersin.org/articles/10.3389/fonc.2019.00022/full#supplementary-material

REFERENCES

1. Oktay M, Wary KK, Dans M, Birge RB, Giancotti FG. Integrin-mediated activation of focal adhesion kinase is required for signaling to Jun NH2-terminal kinase and progression through the G1 phase of the cell cycle. *J Cell Biol*. (1999) 145:1461–9. doi: 10.1083/jcb.145.7.1461
2. Schaller MD, Parsons JT. Focal adhesion kinase: an integrin-linked protein tyrosine kinase. *Trends Cell Biol*. (1993) 3:258–62. doi: 10.1016/0962-8924(93)90053-4
3. Lim ST. Nuclear FAK: a new mode of gene regulation from cellular adhesions. *Mol Cells* (2013) 36:1–6. doi: 10.1007/s10059-013-0139-1
4. Kleinschmidt EG, Schlaepfer DD. Focal adhesion kinase signaling in unexpected places. *Curr Opin Cell Biol*. (2017) 45:24–30. doi: 10.1016/j.ceb.2017.01.003
5. Sulzmaier FJ, Jean C, Schlaepfer DD. FAK in cancer: mechanistic findings and clinical applications. *Nat Rev Cancer* (2014) 14:598–610. doi: 10.1038/nrc3792
6. Zhao J, Bian ZC, Yee K, Chen BP, Chien S, Guan JL. Identification of transcription factor KLF8 as a downstream target of focal adhesion kinase in its regulation of cyclin D1 and cell cycle progression. *Mol Cell* (2003) 11:1503–15. doi: 10.1016/S1097-2765(03)00179-5
7. Zhao JH, Reiske H, Guan JL. Regulation of the cell cycle by focal adhesion kinase. *J Cell Biol*. (1998) 143:1997–2008.
8. Cao K, Blair CD, Faddah DA, Kieckhaefer JE, Olive M, Erdos MR, et al. Progerin and telomere dysfunction collaborate to trigger cellular senescence in normal human fibroblasts. *J Clin Invest*. (2011) 121:2833–44. doi: 10.1172/JCI43578
9. Lee FY, Zhen YY, Yuen CM, Fan R, Chen YT, Sheu JJ, et al. The mTOR-FAK mechanotransduction signaling axis for focal adhesion maturation and cell proliferation. *Am J Transl Res*. (2017) 9:1603–17.
10. Ruest PJ, Roy S, Shi E, Mernaugh RL, Hanks SK. Phosphospecific antibodies reveal focal adhesion kinase activation loop phosphorylation in nascent and mature focal adhesions and requirement for the autophosphorylation site. *Cell Growth Differ*. (2000) 11:41–8.
11. Lim ST, Chen XL, Lim Y, Hanson DA, Vo TT, Howerton K, et al. Nuclear FAK promotes cell proliferation and survival through FERM-enhanced p53 degradation. *Mol Cell* (2008) 29:9–22. doi: 10.1016/j.molcel.2007.11.031
12. Canel M, Byron A, Sims AH, Cartier J, Patel H, Frame MC, et al. Nuclear FAK and runx1 cooperate to regulate IGFBP3, cell-cycle progression, and tumor growth. *Cancer Res*. (2017) 77:5301–12. doi: 10.1158/0008-5472.CAN-17-0418
13. Ding Q, Grammer JR, Nelson MA, Guan JL, Stewart JE, Jr. Gladson CL. p27Kip1 and cyclin D1 are necessary for focal adhesion kinase regulation of cell cycle progression in glioblastoma cells propagated *in vitro* and *in vivo* in the scid mouse brain. *J Biol Chem*. (2005) 280:6802–15. doi: 10.1074/jbc.M409180200
14. Liu TJ, LaFortune T, Honda T, Ohmori O, Hatakeyama S, Meyer T, et al. Inhibition of both focal adhesion kinase and insulin-like growth factor-I receptor kinase suppresses glioma proliferation *in vitro* and *in vivo*. *Mol Cancer Ther*. (2007) 6:1357–67. doi: 10.1158/1535-7163.MCT-06-0476
15. Pirone DM, Liu WF, Ruiz SA, Gao L, Raghavan S, Lemmon CA, et al. An inhibitory role for FAK in regulating proliferation: a link between limited adhesion and RhoA-ROCK signaling. *J Cell Biol*. (2006) 174:277–88. doi: 10.1083/jcb.200510062
16. Parsons JT, Slack-Davis J, Tilghman R, Roberts WG. Focal adhesion kinase: targeting adhesion signaling pathways for therapeutic intervention. *Clin Cancer Res*. (2008) 14:627–32. doi: 10.1158/1078-0432.CCR-07-2220
17. Cance WG, Kurenova E, Marlowe T, Golubovskaya V. Disrupting the scaffold to improve focal adhesion kinase-targeted cancer therapeutics. *Sci Signal*. (2013) 6:pe10. doi: 10.1126/scisignal.2004021
18. Carter BZ, Mak PY, Wang X, Yang H, Garcia-Manero G, Mak DH, et al. Focal adhesion kinase as a potential target in AML and MDS. *Mol Cancer Ther*. (2017) 16:1133–44. doi: 10.1158/1535-7163.MCT-16-0719
19. Gnani D, Romito I, Artuso S, Chierici M, De Stefanis C, Panera N, et al. Focal adhesion kinase depletion reduces human hepatocellular carcinoma growth by repressing enhancer of zeste homolog 2. *Cell Death Differ*. (2017) 24:889–902. doi: 10.1038/cdd.2017.34
20. Schwartz MA, Assoian RK. Integrins and cell proliferation: regulation of cyclin-dependent kinases via cytoplasmic signaling pathways. *J Cell Sci*. (2001) 114:2553–60.
21. Zhang HM, Keledjian KM, Rao JN, Zou T, Liu L, Marasa BS, et al. Induced focal adhesion kinase expression suppresses apoptosis by activating NF-kappaB signaling in intestinal epithelial cells. *Am J Physiol Cell Physiol*. (2006) 290:C1310–20. doi: 10.1152/ajpcell.00450.2005

22. Livshits G, Kobielak A, Fuchs E. Governing epidermal homeostasis by coupling cell-cell adhesion to integrin and growth factor signaling, proliferation, and apoptosis. *Proc Natl Acad Sci USA* (2012) 109:4886–91. doi: 10.1073/pnas.1202120109
23. Fan H, Guan JL. Compensatory function of Pyk2 protein in the promotion of focal adhesion kinase (FAK)-null mammary cancer stem cell tumorigenicity and metastatic activity. *J Biol Chem*. (2011) 286:18573–82. doi: 10.1074/jbc.M110.200717
24. Ewald JA, Desotelle JA, Wilding G, Jarrard DF. Therapy-induced senescence in cancer. *J Natl Cancer Inst*. (2010) 102:1536–46. doi: 10.1093/jnci/djq364
25. Schosserer M, Grillari J, Breitenbach M. The dual role of cellular senescence in developing tumors and their response to cancer therapy. *Front Oncol*. (2017) 7:278. doi: 10.3389/fonc.2017.00278
26. Baell JB, Leaver DJ, Hermans SJ, Kelly GL, Brennan MS, Downer NL, et al. Inhibitors of histone acetyltransferases KAT6A/B induce senescence and arrest tumour growth. *Nature* (2018) 560:253–7. doi: 10.1038/s41586-018-0387-5
27. Ewald JA, Jarrard DF. Decreased skp2 expression is necessary but not sufficient for therapy-induced senescence in prostate cancer. *Transl Oncol*. (2012) 5:278–87. doi: 10.1593/tlo.12181
28. Gibadulinova A, Pastorek M, Filipcik P, Radvak P, Csaderova L, Vojtesek B, et al. Cancer-associated S100P protein binds and inactivates p53, permits therapy-induced senescence and supports chemoresistance. *Oncotarget* (2016) 7:22508–22. doi: 10.18632/oncotarget.7999
29. Roberson RS, Kussick SJ, Vallieres E, Chen SY, Wu DY. Escape from therapy-induced accelerated cellular senescence in p53-null lung cancer cells and in human lung cancers. *Cancer Res*. (2005) 65:2795–803. doi: 10.1158/0008-5472.CAN-04-1270
30. Zhang Y, Wang J, Huang W, Cai J, Ba J, Wang Y, et al. Nuclear Nestin deficiency drives tumor senescence via lamin A/C-dependent nuclear deformation. *Nat Commun*. (2018) 9:3613. doi: 10.1038/s41467-018-05808-y
31. Wright WE, Pereira-Smith OM, Shay JW. Reversible cellular senescence: implications for immortalization of normal human diploid fibroblasts. *Mol Cell Biol*. (1989) 9:3088–92. doi: 10.1128/MCB.9.7.3088
32. Lenain C, Gusyatiner O, Douma S, van den Broek B, Peeper DS. Autophagy-mediated degradation of nuclear envelope proteins during oncogene-induced senescence. *Carcinogenesis* (2015) 36:1263–74. doi: 10.1093/carcin/bgv124
33. Demaria M, O'Leary MN, Chang J, Shao L, Liu S, Alimirah F, et al. Cellular senescence promotes adverse effects of chemotherapy and cancer relapse. *Cancer Discov*. (2017) 7:165–76. doi: 10.1158/2159-8290.CD-16-0241
34. Prieur A, Besnard E, Babled A, Lemaitre JM. p53 and p16(INK4A) independent induction of senescence by chromatin-dependent alteration of S-phase progression. *Nat Commun*. (2011) 2:473. doi: 10.1038/ncomms1473
35. Singh Y, Palombo M, Sinko PJ. Recent trends in targeted anticancer prodrug and conjugate design. *Curr Med Chem*. (2008) 15:1802–26. doi: 10.2174/092986708785132997
36. Slack-Davis JK, Martin KH, Tilghman RW, Iwanicki M, Ung EJ, Autry C, et al. Cellular characterization of a novel focal adhesion kinase inhibitor. *J Biol Chem*. (2007) 282:14845–52. doi: 10.1074/jbc.M606695200
37. Lietha D, Cai X, Ceccarelli DF, Li Y, Schaller MD, Eck MJ. Structural basis for the autoinhibition of focal adhesion kinase. *Cell* (2007) 129:1177–87. doi: 10.1016/j.cell.2007.05.041
38. Eke I, Deuse Y, Hehlgans S, Gurtner K, Krause M, Baumann M, et al. beta(1)Integrin/FAK/cortactin signaling is essential for human head and neck cancer resistance to radiotherapy. *J Clin Invest*. (2012) 122:1529–40. doi: 10.1172/JCI61350
39. Shibue T, Weinberg RA. Integrin beta1-focal adhesion kinase signaling directs the proliferation of metastatic cancer cells disseminated in the lungs. *Proc Natl Acad Sci USA* (2009) 106:10290–5. doi: 10.1073/pnas.0904227106
40. Shimojima M, Yuasa S, Motoda C, Yozu G, Nagai T, Ito S, et al. Emerin plays a crucial role in nuclear invagination and in the nuclear calcium transient. *Sci Rep*. (2017) 7:44312. doi: 10.1038/srep44312
41. Piekarowicz K, Machowska M, Dratkiewicz E, Lorek D, Madej-Pilarczyk A, Rzepecki R. The effect of the lamin A and its mutants on nuclear structure, cell proliferation, protein stability, and mobility in embryonic cells. *Chromosoma* (2017) 126:501–17. doi: 10.1007/s00412-016-0610-9
42. Goldman RD, Shumaker DK, Erdos MR, Eriksson M, Goldman AE, Gordon LB, et al. Accumulation of mutant lamin A causes progressive changes in nuclear architecture in Hutchinson-Gilford progeria syndrome. *Proc Natl Acad Sci USA* (2004)101:8963–8. doi: 10.1073/pnas.0402943101
43. Dechat T, Pfleghaar K, Sengupta K, Shimi T, Shumaker DK, Solimando L, et al. Nuclear lamins: major factors in the structural organization and function of the nucleus and chromatin. *Genes Dev*. (2008) 22:832–53. doi: 10.1101/gad.1652708
44. Goldman RD, Gruenbaum Y, Moir RD, Shumaker DK, Spann TP. Nuclear lamins: building blocks of nuclear architecture. *Genes Dev*. (2002) 16:533–47. doi: 10.1101/gad.960502
45. Liao CY, Anderson SS, Chicoine NH, Mayfield JR, Academia EC, Wilson JA, et al. Rapamycin reverses metabolic deficits in lamin A/C-deficient mice. *Cell Rep*. (2016) 17:2542–52. doi: 10.1016/j.celrep.2016.10.040
46. Schmitt CA, Fridman JS, Yang M, Lee S, Baranov E, Hoffman RM, et al. A senescence program controlled by p53 and p16INK4a contributes to the outcome of cancer therapy. *Cell* (2002) 109:335–46. doi: 10.1016/S0092-8674(02)00734-1
47. Rufini A, Tucci P, Celardo I, Melino G. Senescence and aging: the critical roles of p53. *Oncogene* (2013) 32:5129–43. doi: 10.1038/onc.2012.640
48. Jackson JG, Pant V, Li Q, Chang LL, Quintas-Cardama A, Garza D, et al. p53-mediated senescence impairs the apoptotic response to chemotherapy and clinical outcome in breast cancer. *Cancer Cell* (2012) 21:793–806. doi: 10.1016/j.ccr.2012.04.027
49. Shay JW, Wright WE. Senescence and immortalization: role of telomeres and telomerase. *Carcinogenesis* (2005) 26:867–74. doi: 10.1093/carcin/bgh296
50. Lidzbarsky G, Gutman D, Shekhidem HA, Sharvit L, Atzmon G. Genomic instabilities, cellular senescence, and aging: *in vitro*, *in vivo* and aging-like human syndromes. *Front Med*. (2018) 5:104. doi: 10.3389/fmed.2018.00104
51. Martinez-Zamudio RI, Robinson L, Roux PF, Bischof O. SnapShot: cellular senescence pathways. *Cell* (2017) 170:816. e1. doi: 10.1016/j.cell.2017.07.049
52. Beausejour CM, Krtolica A, Galimi F, Narita M, Lowe SW, Yaswen P, et al. Reversal of human cellular senescence: roles of the p53 and p16 pathways. *EMBO J*. (2003) 22:4212–22. doi: 10.1093/emboj/cdg417
53. Weinstein B. Relevance of the concept of oncogene addiction to hormonal carcinogenesis and molecular targeting in cancer prevention and therapy. *Adv Exp Med Biol*. (2008) 617:3–13. doi: 10.1007/978-0-387-69080-3_1
54. Weinstein IB, Joe A. Oncogene addiction. *Cancer Res*. (2008) 68:3077–80. discussion. 3080. doi: 10.1158/0008-5472.CAN-07-3293
55. Luo SW, Zhang C, Zhang B, Kim CH, Qiu YZ, Du QS, et al. Regulation of heterochromatin remodelling and myogenin expression during muscle differentiation by FAK interaction with MBD2. *EMBO J*. (2009) 28:2568–82. doi: 10.1038/emboj.2009.178
56. Rao L, Perez D, White E. Lamin proteolysis facilitates nuclear events during apoptosis. *J Cell Biol*. (1996) 135:1441–55. doi: 10.1083/jcb.135.6.1441
57. DiLoreto R, Murphy CT. The cell biology of aging. *Mol Biol Cell* (2015) 26:4524–31. doi: 10.1091/mbc.E14-06-1084
58. Naeem AS, Zhu Y, Di WL, Marmiroli S, O'Shaughnessy RF. AKT1-mediated Lamin A/C degradation is required for nuclear degradation and normal epidermal terminal differentiation. *Cell Death Differ*. (2015) 22:2123–32. doi: 10.1038/cdd.2015.62
59. Villa-Diaz LG, Kim JK, Laperle A, Palecek SP, Krebsbach PH. Inhibition of focal adhesion kinase signaling by integrin alpha6beta1 supports human pluripotent stem cell self-renewal. *Stem Cells* (2016) 34:1753–64. doi: 10.1002/stem.2349
60. Moiseeva O, Lessard F, Acevedo-Aquino M, Vernier M, Tsantrizos YS, Ferbeyre G. Mutant lamin A links prophase to a p53 independent senescence program. *Cell Cycle* (2015) 14:2408–21. doi: 10.1080/15384101.2015.1053671
61. Mei L, Xiong WC. FAK interaction with MBD2: a link from cell adhesion to nuclear chromatin remodeling? *Cell Adh Migr*. (2010) 4:77–80. doi: 10.4161/cam.4.1.10343
62. Xu B, Lefringhouse J, Liu Z, West D, Baldwin LA, Ou C, et al. Inhibition of the integrin/FAK signaling axis and c-Myc synergistically disrupts ovarian cancer malignancy. *Oncogenesis* (2017) 6:e295. doi: 10.1038/oncsis.2016.86
63. Yates LR, Desmedt C. Translational genomics: practical applications of the genomic revolution in breast cancer. *Clin Cancer Res*. (2017) 23:2630–9. doi: 10.1158/1078-0432.CCR-16-2548
64. Gerland LM, Peyrol S, Lallemand C, Branche R, Magaud JP, Ffrench M. Association of increased autophagic inclusions labeled for

beta-galactosidase with fibroblastic aging. *Exp Gerontol*. (2003) 38:887–95. doi: 10.1016/S0531-5565(03)00132-3

65. Petti C, Molla A, Vegetti C, Ferrone S, Anichini A, Sensi M. Coexpression of NRASQ61R and BRAFV600E in human melanoma cells activates senescence and increases susceptibility to cell-mediated cytotoxicity. *Cancer Res*. (2006) 66:6503–11. doi: 10.1158/0008-5472.CAN-05-4671
66. Jiang H, Hegde S, Knolhoff BL, Zhu Y, Herndon JM, Meyer MA, et al. Targeting focal adhesion kinase renders pancreatic cancers responsive to checkpoint immunotherapy. *Nat Med*. (2016) 22:851–60. doi: 10.1038/nm.4123

Conflict of Interest Statement: The authors declare that the research was conducted in the absence of any commercial or financial relationships that could be construed as a potential conflict of interest.

frontiers in Oncology

SYSTEMATIC REVIEW
published: 01 February 2019
doi: 10.3389/fonc.2019.00030

Molecular Targeted Therapy in the Treatment of Chordoma: A Systematic Review

Tong Meng[1,2,3†], *Jiali Jin*[4†], *Cong Jiang*[5], *Runzhi Huang*[1], *Huabin Yin*[2,3*], *Dianwen Song*[2,3*] *and Liming Cheng*[1,6*]

[1] Division of Spine, Department of Orthopedics, Tongji Hospital Affiliated to Tongji University School of Medicine, Shanghai, China, [2] Shanghai Bone Tumor Institution, Shanghai, China, [3] Department of Orthopedics, Shanghai General Hospital, School of Medicine, Shanghai Jiaotong University, Shanghai, China, [4] Department of Central Laboratory, Shanghai Tenth People's Hospital of Tongji University, School of Medicine, School of Life Sciences and Technology, Tongji University, Shanghai, China, [5] Beth Israel Deaconess Medical Center, BIDMC Cancer Center, Harvard Medical School, Cancer Research Institute, Boston, MA, United States, [6] Key Laboratory of Spine and Spinal Cord Injury Repair and Regeneration, Ministry of Education, Tongji University, Shanghai, China

Objectives: Chordoma is a rare bone malignancy that affects the spine and skull base. Treatment dilemma leads to a high rate of local relapse and distant metastases. Molecular targeted therapy (MTT) is an option for advanced chordoma, but its therapeutic efficacy and safety have not been investigated systematically. Therefore, a systematic review was conducted on studies reporting MTT regimens for chordoma.

Methods: Clinical trials, case series and case reports on chordoma MTT were identified using MEDLINE, Cochrane library and EMBASE, and systematically reviewed. Data on clinical outcomes, such as median overall survival, progression-free survival, response rate and adverse events (AEs) were extracted and analyzed.

Results: Thirty-three eligible studies were selected for the systematic review, which indicated that imatinib and erlotinib were the most frequently used molecular targeted inhibitors (MTIs) for chordoma. For PDGFR-positive and/or EGFR-positive chordoma, clinical benefits were achieved with acceptable AEs. Monotherapy is preferred as the first-line of treatment, and combined drug therapy as the second-line treatment. In addition, the brachyury vaccine has shown promising results.

Conclusions: The selection of MTIs for patients with advanced or relapsed chordoma should be based on gene mutation screening and immunohistochemistry (IHC). Monotherapy of TKIs is recommended as the first-line management, and combination therapy (two TKIs or TKI plus mTOR inhibitor) may be the choice for drug-resistant chordoma. Brachyury vaccine is a promising therapeutic strategy and requires more clinical trials to evaluate its safety and efficacy.

Keywords: molecular targeted therapy, bone tumor, chordoma, systematic review, imatinib, erlotinib

OPEN ACCESS

Edited by:
Jian-ye Zhang,
Guangzhou Medical University, China

Reviewed by:
Claudia Palena,
National Cancer Institute (NCI), United States
Victor C. Kok,
Asia University, Taiwan

***Correspondence:**
Huabin Yin
yinhuabin@aliyun.com
Dianwen Song
osongdianwen@126.com
Liming Cheng
limingcheng@tongji.edu.cn

[†]These authors have contributed equally to this work and share first authorship

Specialty section:
This article was submitted to Cancer Molecular Targets and Therapeutics, a section of the journal Frontiers in Oncology

Received: *05 November 2018*
Accepted: *10 January 2019*
Published: *01 February 2019*

Citation:
Meng T, Jin J, Jiang C, Huang R, Yin H, Song D and Cheng L (2019) Molecular Targeted Therapy in the Treatment of Chordoma: A Systematic Review. Front. Oncol. 9:30. doi: 10.3389/fonc.2019.00030

INTRODUCTION

Chordoma is a relatively rare malignant bone tumor with an incidence of 0.08 per 100,000 (1). It accounts for 1–4% of all bone malignancies, and ∼20% of primary spine tumors (2). Although it can occur at any segment of the spine, the predominant site of chordoma are fused segments like clivus and sacrococcyx (3). It is an indolent malignancy that progresses slowly, but exhibits strong local aggressiveness and often grows into huge masses that compress vital nerves and blood vessels (4). In addition, since chordoma is usually unresponsive to the conventional radiotherapy and cytotoxic chemotherapy, surgery is the primary therapeutic option (1, 5). Large case series including our previous one have shown that a total resection of the tumor, with the goal of negative microscopic margins, is crucial for long-term positive outcomes (6). However, the complex anatomy of the spine and the relatively large tumor volume make a clean resection technically challenging, leading to a high rate of local relapse and distant metastases (7). Regarding to this advanced setting, conventional therapeutic methods were shown to be not highly effective (1). Therefore, novel therapeutic strategies are needed to prolong patients' survival and improve the quality of life.

Pathologically, chordoma arises from residual notochord cells within the vertebral body (8), as verified on the basis of genetic and immuno-phenotypic biomarkers (9). New insights into the molecular mechanism underlying chordoma have also identified novel therapeutic targets (5). Molecular targeted therapy (MTT) in chordoma includes (1) imatinib and dasatinib against platelet-derived growth factor receptors (PDGFR) and stem cell factor receptor (KIT) (10, 11); (2) erlotinib, lapatinib, gefitinib, and cetuximab against epidermal growth factor receptor (EGFR) and erbB-2/human epidermal growth factor receptor 2 (HER2/neu) (12, 13); (3) sorafenib, pazopanib, and sunitinib that target angiogenic factors like vascular endothelial growth factor receptor (VEGFR) (14–16); and (4) temsirolimus and sirolimus that target the phosphoinositide 3-kinase (PI3K)/AKT/mammalian target of rapamycin (mTOR) pathway (17).

The indications for MTTs in chordoma patients are largely based on a few prospective clinical trials, small retrospective studies, and even case reports (10–17). However, the efficacy and safety of MTT regimens in chordoma patients, as well as the underlying molecular mechanisms, lack systematic investigation. Therefore, we conducted a systematic review on MTT regimens in chordoma patients to determine the clinical outcomes and underlying molecular mechanisms.

MATERIALS AND METHODS

Search Strategy

For this systematic review, we used standard procedures from PRISMA guidelines (18). A comprehensive, systematic search was performed using MEDLINE (via PubMed), Cochrane Library and EMBASE. To find appropriate studies in MEDLINE, we used a combination of terms related to the MeSH terms "Chordoma/drug therapy" OR the free-text searching "Chordoma" AND ("targeted therapy OR inhibitor OR inhibit OR inhibition"). This search was further modified as appropriate for Cochrane Library and EMBASE. Initial search was performed on January 17, 2018 and repeated on July 1, 2018.

Eligibility Criteria

Studies were deemed eligible for the assessment of MTTs in patients with chordoma, irrespective of previous and subsequent other treatment. Only English language publications were included. For clinical trials, case series and case reports published exclusively in abstract or news form, only those containing new data were analyzed. For literature reviews, new personal unpublished data is also included. Reference lists of selected studies and previous reviews associated with similar topics were screened manually. New clinical trials for chordoma were found from Chordoma Foundation, ClinicalTrials.gov, EU Clinical Trials Register and WHO International Clinical Trials Registry Platform. Although gray literature (such as unpublished reports, conference abstracts and dissertations) might provide some negative results and decrease the publication bias, we did not access them, because they were usually not peer reviewed and might be later published in peer-reviewed journals.

Data Extraction and Synthesis

After removal of duplicates, titles and abstracts of all identified publications were systematically screened by two independent reviewers (MT and YHB). Discrepancies between reviewers were resolved by discussion. When eligibility criteria seemed to be met, the two reviewers (MT and YHB) independently assessed retrieved full texts and extracted information. If disagreements were still remained, the third reviewer (SDW) helped to reach an agreement. We contacted with the Chordoma Foundation in order to get helpful information. Additionally, we corresponded with researchers clarify study eligibility if the published study was unclear, although responses were poor. Extracted data were study characteristics (study design, first author, year of publication), patient characteristics (total number, history of treatment) and tumor characteristics (gene mutation and immunohistochemistry), MTT information (type of agents, dosage, course of treatment and adverse events), evaluation criteria (Choi's criteria, the response evaluation criteria in solid tumor (RECIST), clinical and radiological or metabolic response), and survival (duration of follow-up, progression-free survival and overall survival).

RESULTS

Search Results

The flow-chart for the selection and exclusion of relevant publications is shown in **Figure 1**. We identified 293 studies in the initial screening, and after removing duplicates and papers based on their titles and abstracts, selected 64 publications for full-text assessment. Twenty-seven studies met our inclusion criteria, and six more were included—three from manually searching the reference list of the selected articles, two from repeated search and one with the help of the Chordoma

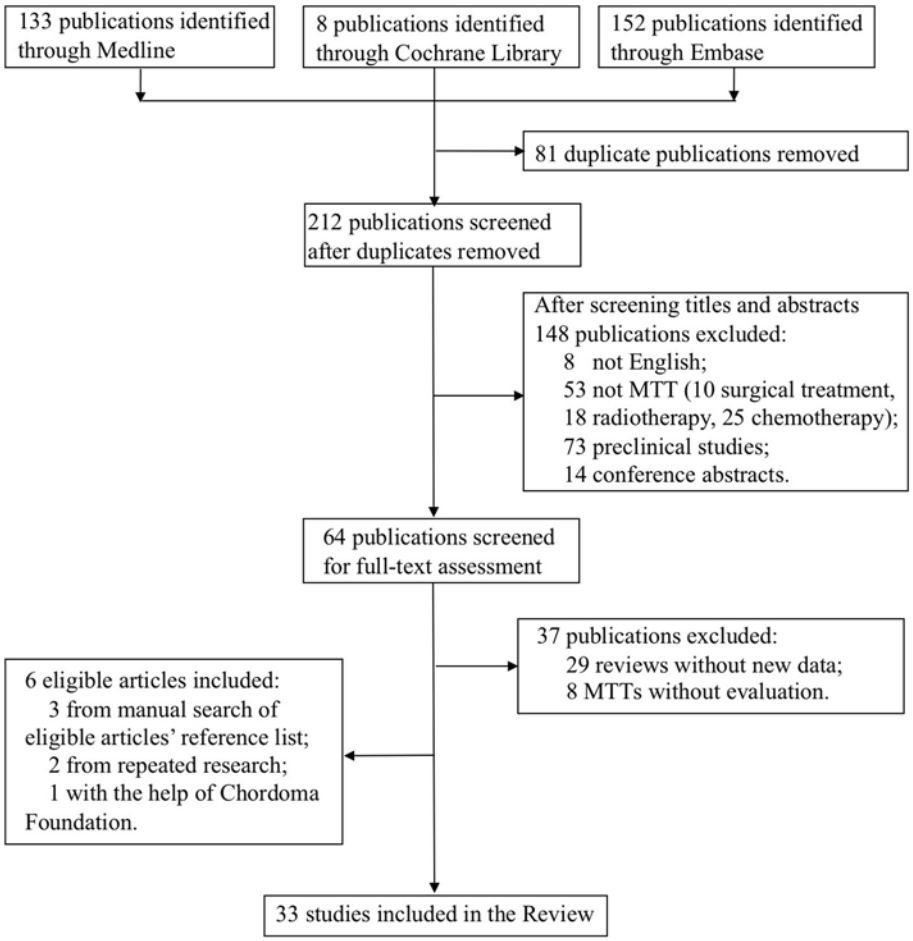

FIGURE 1 | PRISMA flow diagram of the study selection process.

Foundation. Finally, 33 studies were included in this systematic review.

Study Characteristics

Among 33 studies, nine studies were clinical trials (10–12, 14, 15, 19–22), with eight retrospective case series (16, 17, 23–28), and 16 case reports (13, 29–43). Imatinib was assessed in 18 studies with a total of 221 patients (10, 16, 17, 19, 23–28, 32, 34–36, 38, 39, 41, 42), erlotinib in 10 studies with 16 patients (13, 17, 22, 33, 35, 38, 40–42), cetuximab in five studies (seven patients) (13, 30, 31, 33, 41), sorafenib in four studies (65 patients) (15, 17, 21, 37), pazopanib in four studies with seven patients (16, 28, 41, 43) and sunitinib in three studies with 11 patients (14, 17, 28). Sirolimus, thalidomide, bevacizumab, gefitinib, linsitinib, and everolimus were accessed in two studies each (13, 22, 25, 28–31, 33, 34, 40–42), whereas dasatinib (32 patients) (11), lapatinib (18 patients) (12), rapamycin (one patients) (34), temosirolimus (one patients) (17) and yeast-brachyury (GI-6301) vaccine (11 patients) (20) were only analyzed in one study each (**Figures 2** and **3**). Monotherapy of MTTs was reported in 24 studies (10–12, 14–17, 20, 21, 23, 24, 26–28, 32, 34–39, 41, 43, 44) with combination therapy in 13 studies (13, 19, 22, 25, 28–31, 33, 39–42).

RECIST evaluation criteria was used in 19 studies (10–15, 17, 19, 20, 22, 25–28, 32, 40, 42, 43, 45) and Choi's criteria is applied in three studies (11, 12, 25). Twenty-one studies were evaluated by clinical/radiological or metabolic responses (16, 23–27, 29–43). Adverse events (AEs) were reported in 25 studies, including hematological anomalies like anemia, thrombocytopenia, as well as non-hematological AEs like fatigue, fever, anorexia, QTc prolongation, abnormal liver function, nausea, and vomiting (10–15, 19, 22, 23, 26–38, 40, 43, 45).

Efficacy and Safety of MTT Regimens in Chordoma Patients

PDGFR Inhibitors (Table 1)

Imatinib mesylate (IM), a specific tyrosine kinase inhibitor (TKI) targeting PDGFR and KIT (10, 46), was the most frequently-used MTT in chordoma patients. Eighteen studies investigated the therapeutic efficacy of IM on 221 patients (10, 16, 17, 19, 23–28, 32, 34–36, 38, 39, 41, 42), including three clinical trials (10, 19,

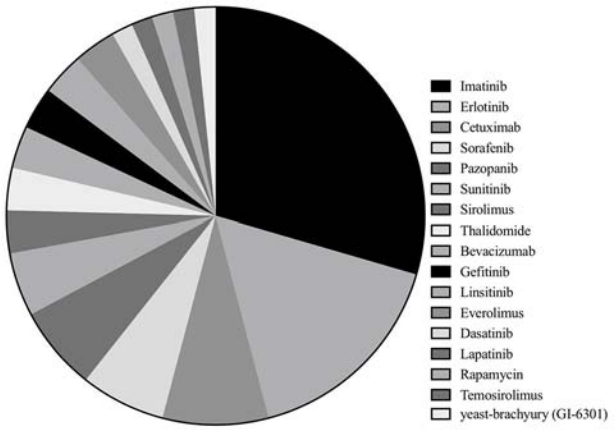

FIGURE 2 | Of the included studies, the proportion of studies reporting each molecular targeted inhibitor.

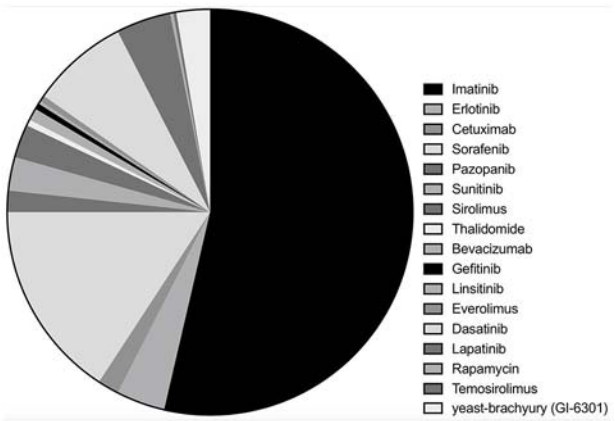

FIGURE 3 | Of the included chordoma patients, the proportion of patients received each molecular targeted inhibitor.

28), seven retrospective case series (16, 17, 23–27), and eight case reports (32, 34–36, 38, 39, 41, 42). Fourteen studies (204 patients) analyzed the efficacy of imatinib as monotherapy (10, 16, 17, 23, 24, 26–28, 32, 34–36, 39, 41), of which four studies (181 patients) used RECIST and 3 were focused on PDGFRβ-expressing chordoma. In these four studies, four patients achieved partial response (PR) (2.2%), 133 cases sustained stable disease (SD) (73.5%) and 44 cases experienced progressive disease (PD) (24.3%) (10, 17, 26, 27, 32). Clinical/radiological or metabolic responses were evaluated in 13 studies (85 patients), with 33 patients achieving PR (38.8%), 23 patients sustaining SD (27.1%) and 29 patients experiencing PD (34.1%) (16, 23, 24, 26–28, 32, 34–36, 38, 39, 41). Five of the above studies (73 patients) focused on PDGFRβ-expressing chordoma, with 45.2% PR, 31.5% SD, and 23.3% PD cases (23, 24, 26, 27, 36), and eight studies included 12 patients that experienced PD within a short period of time.

Progression-free survival (PFS) and overall survival (OS) are important indices of clinical outcome, and they were reported in two large case-studies (10, 27). Stacchiotti et al. conducted a phase II trial in 56 patients with chordoma, and the median PFS and OS were 9 and 35 months, respectively (10). A retrospective study on 46 chordoma patients reported a median PFS of 9.9 months (27).

AEs were reported in eight studies (10, 23, 27, 32, 34, 36), with skin rash being the most common, followed by oedema, chronic anemia, fatigue and fluid retention (10, 26). Subacute intraventricular hemorrhage was seen in one case of clivus chordoma treated with imatinib (36).

Dasatinib, an inhibitor of PDGFR and Src, was evaluated in a phase II study (NCT00464620) (11) on 32 patients. The median PFS and 6 months PFS rate were 6.3 months and 54%, respectively. The 2- and 5-years OS rate were 43 and 18%, respectively. Six patients had an objective response (OR) according to Choi criteria and one for RECIST. Fatigue, fever, anorexia, nausea, and vomiting occurred in more than 5% of the patients.

EGFR Inhibitors (Table 2)

Erlotinib was the most commonly used anti-EGFR agent and was analyzed in 10 studies (16 patients) for the treatment of chordoma (13, 17, 22, 32, 33, 35, 38, 40–42), including one clinical trials (22), one retrospective case study (17) and eight case reports (13, 17, 22, 32, 33, 35, 38, 40–42). Monotherapy with erlotinib was used in five studies (nine patients) (17, 32, 35, 38, 42), three (seven patients) of which were evaluated by RECIST (17, 32, 42), reporting PR in two patients and SD in five patients. Three case reports were evaluated by clinical/radiological or metabolic responses (32, 35, 38). All achieved PR and significant tumor bulk reduction was seen in two patients (70 and 46%, respectively). Skin rashes were commonly seen in the erlotinib-treated patients.

Lapatinib monotherapy was evaluated in a phase II clinical trial on 18 patients with EGFR-positive chordoma (12). Six patients achieved PR and seven sustained SD, with the median PFS of 6 months according to the Choi criteria. In contrast, all patients had SD by RECIST criteria with the median PFS of 8 months. Most patients experienced G $\geq$ 2 AEs.

Combined therapy with EGFR inhibitors was used in seven studies (eight patients) (13, 22, 30, 31, 33, 40, 41). Erlotinib was also the most common agents used in the combined MTT regimens (five studies, seven patients) (13, 22, 33, 40, 41).

Linsitinib, an inhibitor of IGF-1R/insulin receptor (INSR), was evaluated in a phase I study in combination with erlotinib (NCT00739453) (22). One patient with chordoma achieved PR for 18 months according to RECIST, with a PFS of 5 years. AEs included QTc prolongation, abnormal liver function, hyperglycemia and anorexia (22, 40).

The anti-EGFR monoclonal antibody (mAb) cetuximab was applied in combination with erlotinib in one patient with EGFR-positive chordoma, and he had a SD for 6 months (41). However, four patients with EGFR-negative chordoma experienced PD after receiving the same regimen. The treatment failure prompted a switch to bevacizumab, an anti-VEGF mAb (13, 33). Following this change, two patients achieved PR and another two presented SD. Treatment-related fatigue was observed in one patient (13, 33). Combined regimen of cetuximab and gefitinib was also effective in two cases of EGFR-positive chordoma (30, 31), where

TABLE 1 | Molecular targeted therapy of chordomas with PDGFR inhibitors (imatinib, dasatinib).

References	Study design	Levels of evidence	Sample size	Conditions	IHC positive	Drug (dosage)	Median treatment time (months)	AEs	Outcomes			Median follow-up (months)	Median PFS (months)	Median OS (months)
									Choi's criteria	RECIS	TRMR			
Stacchiotti et al. (10)	Phase II	IV	56	Advanced chordoma	PDGFRB/ PDGFB	Imatinib (800 mg/day)	9.1	Grade 3 toxicity: 72%	—	PR: 2%; SD: 70%; PD: 28%	—	26.4	9.2	35
Casali et al. (23)	Case series	IV	6	Advanced chordoma	PDGFRB	Imatinib (800 mg/day)	—	Toxicity: 33.3%	—	—	PR: 66.6%; SD: 16.7%; PD: 16.7%	—	—	—
Hindiet al. (27)	Case series	IV	46	Advanced chordoma	PDGFB/ PDGFRB	Imatinib (800 mg/day)	—	Toxicity: 87.5%	—	PR: 0; SD: 74%; PD: 26%	PR: 40%; SD: 28%; PD: 32%	24.5	9.9	30
Geoerger et al. (24)	Case series	IV	3	Chordoma	PDGFB/ PDGFRB/KIT	Imatinib (800 mg/day)	—	—	—	—	PR: 67%; SD: 33%	—	—	—
Ferraresi et al. (26)	Case series	IV	17	Advanced chordoma	PDGFRB	Imatinib (800 mg/day)	—	—	—	SD	PR: 54%; SD + PD: 46%	—	—	—
Launay et al. (35)	Case report	V	1	Advanced chordoma	EGFR	Imatinib (600 mg/day)	—	None	—	—	PD	—	—	—
Singhal et al. (32)	Case report	V	1	Recurrent chordoma	EMA/ cytokeratins	Imatinib (600 mg/day)	—	Grade 2 skin rash	—	—	PD	—	—	—
Trapani et al. (42)	Case report	V	1	Recurrent chordoma	PDGFRB, EGFR, pS6	Imatinib (400 mg/day) + everolimus	—	—	—	PD	—	—	—	—
Stacchiotti et al. (25)	Case series	IV	10	Advanced chordoma	mTOR effectors (AKT, S6) PDGFR	Imatinib (400 mg/day) + sirolimus (2 mg/day)	9	Grade 3 toxicity 30%	PR: 78%; SD: 11%; PD: 11%	PR: 11%; SD: 78%; PD: 11%	PR: 78%	—	—	—
Lebellec et al. (17)	Case series	IV	62	Advanced chordoma	—	Imatinib	—	—	—	PR: 5%; SD: 69%; PD: 26%	—	—	—	—
Adenis et al. (19)	Phase I	IV	7	Chordoma	—	MC (50 mg two times daily) + imatinib (400 mg/day)	—	Anemia, Nausea, vomiting, Fatigue	—	Long-lasting SD, PD at last	—	—	10.2	—
Lipplaa et al. (28)	Case series	IV	2	Metastatic chordoma	VEGFR	Imatinib	9		—	—	PD	—	—	—
Lipplaa et al. (28)	Case series	IV	1	Metastatic chordoma	VEGFR	Imatinib + sirolimus	—	Grade 2 fatigue, intermittent diarrhea	—	—	PD	—	—	—
Mercier et al. (36)	Case report	V	1	Recurrent chordoma	PDGFRB	Imatinib (400–800 mg/day)	2.25	Intracranial hemorrhage	—	—	PD	—	—	—

(Continued)

TABLE 1 | Continued

References	Study design	Levels of evidence	Sample size	Conditions	IHC positive	Drug (dosage)	Median treatment time (months)	AEs	Outcomes			Median follow-up (months)	Median PFS (months)	Median OS (months)
									Choi's criteria	RECIS	TRMR			
Chay et al. (34)	Case report	V	1	Recurrent chordoma	–	Imatinib	1.25	Persistent vomiting	–	–	PD	–	–	–
Houessinon et al. (38)	Case report	V	1	Recurrent chordoma	–	Imatinib (400–800 mg/day)	5	–	–	–	PD	–	–	–
Rohatgi et al. (39)	Case report	V	2	Metastatic chordoma	–	Imatinib (800 mg/day)	–	–	–	–	PR	–	60	–
Migliorini et al. (41)	Case report	V	2	Recurrent chordoma	Brachyury, EGFR, p53	Imatinib	–	–	–	–	PD	–	–	–
Jagersberg et al. (16)	Case series	V	2	Recurrent chordoma	–	Imatinib	–	–	–	–	PD	–	9	–
Schuetze et al. (11)	Phase II	IV	32	Incurable chordoma by conventional treatments	Src family of kinases, PDGFR, KIT, ephrin	Dasatinib (50–100 mg twice daily)	4	Grade 3 toxicity: 39.7%; Grade 4 toxicity: 6.9%	OR: 18.75%	OR: 3.125%	–	–	6.3	–

IHC, immunohistochemistry; AEs, adverse events; RMR, radiological or metabolic response; PR, partial response; SD, stable disease; PD, progressive disease; TVR, tumor volume regression; MC, metronomic cyclophosphamide.

one achieved a PR for 9 months and the other had a 44% reduction in tumor bulk. Pronounced AEs, such as rash, acne, diarrhea, and skin defects, were reported in both cases (30, 31).

VEGFR Inhibitors (Table 3)

Sorafenib, a TKI against VEGFR and PDGFR, was assessed in four studies (15, 17, 21, 37). A phase II trial was conducted on 27 patients with chordomas (NCT00874874) (15), and OR was observed in one patient as per RECIST. The 12 months PFS and OS rates were 73.0 and 86.5%, respectively. In a study on 11 patients treated with sorafenib, PR was obtained in one patient, with SD in nine patients and PD in one patient according to RECIST (17). Another study assessing sorafenib reported a PFS of 12 months (37). However, sorafenib was limited by severe AEs like thrombocytopenia and diarrhea, and the rates of grade 3 and 4 toxicity were 77.8 and 14.8%, respectively.

Sunitinib, a multi-targeting TKI against VEGFR and PDGFR, was assessed in three studies (14, 17, 28). A phase II trial on sunitinib was conducted on nine patients (14), four of which achieved SD according to RECIST, concurrent to a qualitative decrease in tumor density, along with a median PFS of 12 months (14). Two patients treated with sunitinib had at least SD according to RECIST (17, 28), and one achieved a PR after a 27 months SD (28). The major toxicities were of grade 1 or 2 (14).

Pazopanib, another VEGFR inhibitor, was analyzed in seven patients (16, 28, 41, 43), of which four sustained SD with the median PFS of 15 months and the remaining three experienced PD. Thalidomide, an inhibitor of VEGF, was used as a second-line treatment for chordoma after failure of imatinib, rapamycin and other chemotherapy (29, 34). While one patient achieved a 50% tumor reduction, another experienced a PD (29, 34). In addition, severe toxicities of grade 3 and 4 were reported in both cases.

Other Molecular Targeted Inhibitors (MTIs) (Table 4)

Monotherapy with the mTOR inhibitors rapamycin and everolimus were ineffective in chordoma patients (34, 41). The combined MTT regimen of everolimus and imatinib resulted in sustained SD in one patient, with a PFS of 16 months (42). In addition, IM plus sirolimus was used in 10 patients with IM-refractory chordoma and activated mTOR (25). Nine patients were assessed, of which one achieved PR, seven sustained SD and one experienced PD according to RECIST. According to Choi criteria, seven patients achieved PR, and one sustained SD and one experienced PD. The same MTT regimen was also used against IM- and sunitinib-refractory chordoma but was not effective due to short of the mTOR expression (28). A phase I trial evaluated the effect of IM plus metronomic cyclophosphamide (MC)-based chemotherapy on 7 IM- and sunitinib-refractory chordoma patients (19). The median PFS was 10.2 months, and the 12 months PFS and OS rates were 42.9 and 85.7%, respectively according to RECIST. No dose-limiting toxicity and drug pharmacokinetic interactions were observed.

Brachyury Vaccine (Table 4)

A phase I dose-escalation trial using a recombinant *Saccharomyces cerevisiae* (yeast) vaccine encoding brachyury (GI-6301) was conducted on 11 patients (20), and 10 evaluable

TABLE 2 | Molecular targeted therapy of chordomas with EGFR inhibitors (erlotinib, linsitinib, cetuximab, lapatinib, gefitinib).

References	Study design	Levels of evidence	Sample size	Conditions	IHC positive	Drug (dosage)	Median treatment time (months)	AEs	Outcomes			Median follow-up (months)	Median PFS (months)	Median OS (months)
									Choi's criteria	RECIST	RMR			
Launay et al. (35)	Case report	V	1	Advanced chordoma	EGFR	Erlotinib (150 mg/day)	40	None	—	—	TVR (70%)	40	12	40
Singhal et al. (32)	Case report	V	1	Recurrent chordoma	EMA, cytokeratins	Erlotinib (150 mg/day)	18	Grade 2 skin rash	—	PR	TVR (46%)	18	11	18
Trapani et al. (42)	Case report	V	1	Recurrent chordoma	PDGFR-β, EGFR, pS6	Erlotinib (150 mg/day)	—	—	—	PD (4 months), SD (16 months)	—	—	—	—
Asklund et al. (13)	Case report	V	3	Recurrent chordoma	—	Erlotinib (100–150 mg/day) + cetuximab;	—	Infection	—	—	—	—	—	—
Asklund et al. (13)	Case report	V	3	Recurrent chordoma	—	Erlotinib 100–150 mg/day + bevacizumab 10 mg/kg*week	—	Infection	—	PR: 33%, SD: 67%	—	—	—	—
Aleksic et al. (40)	Case report	V	1	Recurrent chordoma	brachyury, EGFR, IGF-1R	Erlotinib (100 mg/day) + linsitinib (50 mg/day)	61	Toxicity ≤ grade 2	—	PR	TVR	69	60	69
Lebellec et al. (17)	Case series	IV	5	Advanced chordoma	—	Erlotinib	—	—	—	PR: 20%, SD: 80%	—	—	4	—
Macaulay et al. (22)	Phase I	V	1	Advanced chordoma	—	Erlotinib + linsitinib	—	—	—	—	—	—	—	—
Migliorini et al. (41)	Case report	V	1	Recurrent and metastatic chordoma	Brachyury, EGFR, p53	Erlotinib + cetuximab	—	—	—	—	SD	—	—	—
Asklund et al. (33)	Case report	V	1	Advanced chordoma	—	Erlotinib + cetuximab	—	—	—	—	PD	—	—	—
Asklund et al. (33)	Case report	V	1	Advanced chordoma	—	Erlotinib + bevacizumab	—	—	—	—	TVR	—	—	—
Houessinon et al. (38)	Case report	V	1	Recurrent chordoma	—	Erlotinib (150 mg/day)	28	A moderate rash and diarrhea	—	—	PR	—	28	—
Stacchiotti et al. (12)	Phase II	V	18	Advanced chordoma	EGFR and HER2/neu	Lapatinib (1,500 mg/day)	—	G ≥ 2 toxicity	PR: 33%, SD: 39%, PD: 28%	PR: 40%, SD: 50%, PD: 10%	—	10.5	6 (Choi); 8 (RECIST)	25

(Continued)

TABLE 2 | Continued

References	Study design	Levels of evidence	Sample size	Conditions	IHC positive	Drug (dosage)	Median treatment time (months)	AEs	Outcomes			Median follow-up (months)	Median PFS (months)	Median OS (months)
									Choi's criteria	RECIST	RMR			
Lindén et al. (31)	Case report	V	1	Recurrent and metastatic chordoma	—	Cetuximab 500 mg/week + gefitinib 250 mg/day	4	Facial acne	—	—	TVR (44%)	4	4	4
Hof et al. (30)	Case report	V	1	Recurrent and metastatic chordoma	EGFR	Cetuximab 500 mg/week + gefitinib 250 mg/day	12	Facial acne, diarrhea and skin defects	—	—	TVR	12	12	12

IHC, immunohistochemistry; AEs, adverse events; RMR, radiological or metabolic response; PR, partial response; SD, stable disease; PD, progressive disease; TVR, tumor volume regression.

patients showed a median PFS of 8.3 months. One patient achieved PR, with eight sustaining SD and one experiencing PD at 3 months according to RECIST. Seven patients had no evidence of PD, giving a clinical benefit rate of 70% at 5 months. The most common AEs were injection site reactions.

Ongoing and planned clinical trials on chordoma MTT are listed in **Table 5**.

DISCUSSION

Novel therapeutic strategies against chordoma are urgently needed to prolong the overall survival and relieve symptoms. Elucidation of the underlying molecular mechanisms of chordoma have helped identify numerous potential therapeutic targets (47, 48), and several anti-chordoma agents are currently being tested in animal models and clinical trials. This systematic review is focused on the pharmacological management of chordoma patients and the clinical outcomes. Furthermore, the molecular mechanisms of MTT action have also been assessed.

Molecular Targets

Chordoma is a genetically heterogeneous tumor with frequent imbalances of large chromosomal regions. Somatic duplications of the notochordal transcription factor brachyury (47, 48), chromosomal copy loss of phosphatase and tensin homolog (PTEN) (49), tuberous sclerosis complex (TSC) (50), cyclin-dependent kinase inhibitor 2A and 2B (CDKN2A and CDKN2B) (51), SMARCB1 (49), and PIK3CA (9) mutations are key aspects of chordoma pathogenesis, and therefore potential targets.

RTKs are the key players in the development and progression of chordoma, and their mutated forms can activate signaling cascades resulting in dysregulation of many essential proteins. Therefore, mutational analyses and IHC can greatly assist oncologists to determine the optimal inhibitors (52–56). It needs to be emphasized that mutations in the molecular targets are clinically more relevant than their immunoreactivity, since target overexpression is not always driven by the activation of the corresponding signaling pathway. For example, high levels of EGFR in the chordoma cell line JHC7 was not accompanied by activated EGFR signaling (57).

Indications and Evaluation Criteria for MTTs

MTTs are not the first treatment options for chordoma, and only recommended for advanced or recurrent chordoma that are unresponsive to either surgical resection or radiotherapy.

The outcomes of MTTs is often difficult to evaluate in chordoma. Choi's criteria is based on changes in tumor size and density following contrast administration in CT or MRI (58). A radiological PR is defined as $\geq$10% decrease in tumor size or $\geq$15% decrease in tumor density/contrast enhancement in CT/MRI. RECIST defines PR as $\geq$20% decrease in tumor growth, which occurs later than that required for Choi criteria. Therefore, RECIST is not fully adequate to evaluate the clinical response in chordoma (59). Clinical/radiological and metabolic responses include symptom relief, anti-tumor effects (such as liquefaction) and changes in tumor density in the CT scan,

TABLE 3 | Molecular targeted therapy with VEGF and VEGFR inhibitors (sorafenib, sunitinib, thalidomide, pazopanib).

References	Study design	Levels of evidence	Sample size	Conditions	IHC positive	Drug (dosage)	Median treatment time (months)	AEs	Outcomes			Median follow-up (months)	Median PFS (months)	Median OS (months)
									Choi's criteria	RECIS	TRMR			
Bompas et al. (15)	Phase II	IV	27	Locally advanced and metastatic chordoma	—	Sorafenib (800 mg/day)	8.7	Grade 3 (77.8%); grade 4 (14.8%)	—	OR: 4%; PR: 4%; SD + PD: 92%	—	—	PFS rates: 6 m (85.3%), 9 m (73.0%), 12 m (73.0%)	OS rates: 6 m (100%), 9 m (86.5%), 12 m (86.5%)
Lebellec et al. (21)	Phase II	IV	26	Advanced chordoma	—	Sorafenib	—	—	—	—	—	—	—	—
Lebellec et al. (17)	Case series	IV	11	Advanced chordoma	—	Sorafenib	—	—	—	PR: 9%; SD: 82%; PD: 9%	—	—	—	—
Svoboda et al. (37)	Case report	IV	1	Recurrent and metastatic chordoma	—	Sorafenib (200 mg/day)	—	Thrombocytopenia; diarrhea		—	SD	—	12	—
George et al. (14)	Phase II	IV	9	Advanced chordoma	VEGFR, PDGFRB	Sunitinib (37.5 mg/day)	—	Grade 1 or 2 (fatigue, diarrhea, hypertension)	—	SD: 44%; PD: 56%	—	—	—	—
Lipplaa et al. (28)	Case series	IV	1	Metastatic chordoma	VEGFR	Sunitinib (37.5–50 mg/day)	—	Grade 2 nausea, fatigue	—	PR	TVR	—	27	—
Lebellec et al. (17)	Case series	IV	1	Advanced chordoma	—	Sunitinib	—	—	—	—	—	—	—	—
Schonegger et al. (29)	Case report	V	1	Recurrent and metastatic chordoma	—	Thalidomide	12	—	—	—	PD	—	—	—
Chay et al. (34)	Case report	V	1	Recurrent chordoma	—	Thalidomide (100–300 mg/day)	23+	—	—	—	TVR (more than 50%)	—	21	—
Lipplaa et al. (28)	Case series	IV	4	Unresectable or metastatic chordoma	VEGFR	Pazopanib (600–800 mg/day)	—	Grade 2 diarrhea, fatigue	—	SD: 50%; PD: 50%	—	—	8.5	—
Ribeiro et al. (43)	Case report	V	1	Recurrent chordoma	Cytokeratins, EMA and vimentin	Pazopanib (800 mg/day)	—	Grade 3 neutropenia	—	SD	TVR (23.1%)	—	15	—
Migliorini et al. (41)	Case report	V	1	Recurrent chordoma	Brachyury, EGFR, p53	Pazopanib	6	—	—	—	PD	—	—	—
Jagersberg et al. (16)	Case series	IV	1	Recurrent chordoma	—	Pazopanib	—	—	—	—	PR	—	24	—

IHC, immunohistochemistry; AEs, adverse events; RMR, radiological or metabolic response; OR, objective response; PR, partial response; SD, stable disease; PD, progressive disease; TVR, tumor volume regression.

TABLE 4 | Molecular targeted therapy of chordomas with other inhibitors (rapamycin, temsirolimus, yeast brachyury vaccine).

References	Study design	Levels of evidence	Sample size	Conditions	IHC positive	Drug (dosage)	Median treatment time (months)	AEs	Outcomes			Median follow-up (months)	Median PFS (months)	Median OS (months)
									Choi's criteria	RECIS	TRMR			
Chay et al. (34)	Case report	V	1	Recurrent chordoma	–	Rapamycin	2	–	–	–	PD	–	–	–
Migliorini et al. (41)	Case report	V	1	Recurrent and metastatic chordoma	Brachyury, EGFR, p53	Everolimus	–	–	–	–	PD	–	–	–
Lebellec et al. (17)	Case series	IV	1	Advanced chordoma	–	Temsirolimus	–	–	–	–	SD	–	–	–
Migliorini et al. (41)	Case report	V	1	Recurrent chordoma	Brachyury	Pembrolizumab	6	–	–	–	TVR	–	6	–
Heery et al. (20)	Phase I	IV	11	Advanced chordoma	–	Yeast-brachyury (GI-6301) vaccine (40-80 YU)	–	–	–	PR: 10%; SD: 80%; PD: 10%	–	–	8.3	–

IHC, immunohistochemistry; AEs, adverse events; RMR, radiological or metabolic response; PR, partial response; SD, stable disease; PD, progressive disease; TVR, tumor volume regression.

reduction in contrast enhancement in MR, and maximum standardized uptake (SUVmax) in PET (23). However, typical tumor tissue characteristics like component and scirrhosity may also affect tumor-related symptoms, even in the absence of any changes in tumor size, resulting in incorrect readings.

MTTs for Chordoma

Imatinib was the first effective agent tested against chordoma, and is currently the most commonly used MTIs (23). Most patients with PDGFRβ-positive chordoma benefited from imatinib treatment and avoided rapid PD, likely due to tumor necrosis and intra-tumoral subacute bleeding that manifest as liquefaction (36). A dosage of 800 mg/day is recommended, except in cases of high toxicity. The major AEs associated with imatinib include oedema, chronic anemia, fatigue and even subacute intraventricular hemorrhage (36).

Several trials have also reported the ineffectiveness of imatinib in chordoma (19, 28, 32, 35, 38, 42). In such cases, EGFR inhibitor is the second line of treatment, since PDGFRβ activation can also stimulate EGFR, given an EGFR gene copy number gain (CNG) or strong intra-tumoral EGFR staining is detected. Around 40% of chordoma patients show CNG of the chromosome band 7p12, where EGFR is located. Erlotinib has shown a good clinical effect EGFR-positive chordoma, and could serve as the second choice for imatinib-refractory chordoma (32, 35). The combination of gefitinib and cetuximab, two other inhibitors of EGFR, showed improved clinical benefits and decreased AEs (30, 31).

HER2/neu is involved in EGFR dimer formation, and the possibility of heterodimerization increases the sensitivity of EGFR-positive chordoma to 54% (60). Lapatinib, a bi-specific inhibitor blocking both EGFR and HER2/neu, achieved 33.3% PR and 38.9% SD as per Choi criteria and 100% SD according to RECIST in EGFR-positive chordoma (12). Afatinib, another bi-specific inhibitor of EGFR and HER2/neu, was the only agent which showed cytotoxic effects across multiple chordoma cell lines in a drug sensitivity assessment (57). On this basis, a new clinical trial on the effects of afatinib is currently enrolling patients (NCT03083678).

IGF signaling is also important in chordoma tumorigenesis, since IGF-1 and IGF-1R have been detected in 92 and 76% of chordoma tissues (61), and are absent in benign notochordal cell tumor and fetal notochord (52). Linsitinib, an IGF-1R inhibitor, was assessed in two studies (22, 40), and effectively controlled chordoma progression in combination with erlotinib (22, 40).

VEGF levels are significantly higher in chordoma tissues and associated with angiogenesis (62). Five VEGFR or VEGF inhibitors (sorafenib, sunitinib, pazopanib, thalidomide, bevacizumab) were evaluated in this systematic review. Although occasional severe AEs were observed occasionally, sorafenib, sunitinib, and pazopanib monotherapy resulted in substantial clinical effects. Although thalidomide was effective against drug-resistant chordomas, severe toxicities limit its clinical application. Bevacizumab can be used as a supplement for erlotinib in drug-resistant chordomas, and their combination showed good clinical effect and high tolerance. A new phase II trial evaluating the efficacy and safety of regorafenib, a

TABLE 5 | Clinical trials programs of chordomas in progress.

Official title	Trial registration number	Type	Medical condition:	Interventions	Mechanism	Sites	Status
Nilotinib with radiation for high risk chordoma	NCT01407198	Phase I	Histologically confirmed chordoma	Nilotinib (daily 200–400 mg BID) Radiation therapy	A Bcr-Abl kinase inhibitor	USA	Active, not recruiting
Study of Imatinib, a platelet-derived growth factor receptor inhibitor, and LBH589, a histone deacetylase inhibitor, in the treatment of newly diagnosed and recurrent chordoma	NCT01175109	Phase I	Histologically confirmed chordoma	Imatinib + LBH589	Imatinib: a PDGFR inhibitor LBH589: a HDAC inhibitor	USA	Unknown
CDK4/6 inhibition in locally advanced/metastatic chordoma	NCT03110744 EUDRACT 2016-004660-19	Phase II	Locally advanced or metastatic chordoma refractory to tyrosine kinase inhibitors	Palbociclib	A CDK4/6 inhibitor	Germany	Recruiting
Afatinib in locally advanced and metastatic chordoma	NCT03083678	Phase II	Locally advanced or metastatic, pathologically proven, EGFR expressing chordoma	Afatinib (40 mg/day)	A Her2 and EGFR kinases inhibitor	Italy, Netherlands, UK	Not yet recruiting
Phase I safety study of stereotactic radiosurgery with concurrent and adjuvant PD-1 antibody nivolumab in subjects with recurrent or advanced chordoma	NCT02989636	Phase I	Histologically confirmed chordoma	Nivolumab Stereotactic Radiosurgery	Nivolumab: a PD-1 Antibody	USA	Recruiting
A randomized, double-blind, phase 2 trial of GI-6301 (Yeast-Brachyury Vaccine) vs. placebo in combination with standard of care definitive radiotherapy in locally advanced, unresectable, chordoma	NCT02383498	Phase II	Histologically confirmed chordoma	GI-6301 Vaccine (Yeast-Brachyury) GI-6301 Placebo Radiotherapy	A heat-killed, recombinant yeast-based vaccine engineered to express the transcription factor, Brachyury	USA	Recruiting
Phase II trial of the immune checkpoint inhibitor nivolumab in patients with select rare CNS cancers	NCT03173950	Phase II	Primary brain sarcoma including chordoma	Nivolumab	A PD-1 Antibody	USA	Recruiting
A phase II trial of dasatinib in advanced sarcomas	NCT00464620	Phase II	Unresectable, recurrent, or metastatic soft tissue or bone sarcoma including chordoma	Dasatinib (70 mg, twice daily)	An inhibitor of Src family of kinases, PDGFR, KIT, ephrin	USA	Active, not recruiting
DART: dual anti-CTLA-4 and anti-PD-1 blockade in rare tumors	NCT02834013	Phase II	Rare tumors including chordoma	Ipilimumab Nivolumab	Ipilimumab: a CTLA-4 inhibitor Nivolumab: a PD-1 inhibitor	USA	Recruiting
A phase II, multicenter study of the EZH2 inhibitor tazemetostat in adult subjects with INI1-negative tumors or relapsed/refractory synovial sarcoma	NCT02601950 EUDRACT 2015-002469-41	Phase II	Poorly differentiated chordoma (or other chordoma with sponsor approval)	Tazemetostat (800 mg BID)	An EZH2 Inhibitor	USA, Australia, Belgium, Canada, France, Germany, Italy, Taiwan, UK	Recruiting
A phase 1 study of the EZH2 inhibitor tazemetostat in pediatric subjects with relapsed or refractory INI1-negative tumors or synovial sarcoma	NCT02601937 EUDRACT 2015-002468-18	Phase I	INI1-negative tumors including chordoma	Tazemetostat	An EZH2 Inhibitor	USA, Australia, Canada, Denmark, France, Germany, Italy, Netherlands, UK	Active, not recruiting

(Continued)

TABLE 5 | Continued

Official title	Trial registration number	Type	Medical condition:	Interventions	Mechanism	Sites	Status
A phase II multi-arm study to test the efficacy of immunotherapeutic agents in multiple sarcoma subtypes	NCT02815995	Phase II	Advanced and/or metastatic sarcoma including chordoma	Durvalumab Tremelimumab	Durvalumab: a PD-L1 inhibitor; Tremelimumab: a CTLA-4 inhibitor	USA	Recruiting
A randomized phase II study of Durvalumab (MEDI4736) and Tremelimumab compared to doxorubicin in patients with advanced or metastatic soft tissue sarcoma.	EUDRACT 2016-004750-15	Phase II	Advanced or metastatic soft tissue sarcoma including chordoma	Durvalumab Tremelimumab	Durvalumab: a PD-L1 inhibitor; Tremelimumab: a CTLA-4 inhibitor	Germany	Ongoing
A phase I, open-label, multiple-ascending dose trial to investigate the safety, tolerability, pharmacokinetics, biological and clinical activity of MSB0011359C in subjects with metastatic or locally advanced solid tumors and expansion to selected indications	NCT02517398	Phase I	Solid tumors including chordoma	MSB0011359C (M7824)	A PD-L1 inhibitor	USA	Recruiting
An open-label phase 1 trial to evaluate the safety and tolerability of a Modified Vaccinia Ankara (MVA) priming followed by fowlpox booster vaccines modified to express brachyury and T-cell costimulatory molecules (MVA-BN-Brachyury/FPV-Brachyury)	NCT03349983	Phase I	Metastatic or unresectable locally advanced malignant solid tumors including chordoma	MVA-BN-Brachyury FPV-Brachyury	A brachyury vaccine	USA	Recruiting
An open phase I clinical study assessing safety and tolerability of MVX-ONCO-1 in patients with solid tumor who are not/not any longer amenable to standard therapy	NCT02193503	Phase I	—	MVX-ONCO-1	An autologous tumor vaccine	Switzerland	Recruiting
Secured access to pembrolizumab for adult patients with selected rare cancer types	NCT03012620 EUDRACT 2016-002260-14	Phase II	Unresectable, recurrent, or metastatic soft tissue or bone sarcoma including chordoma	Pembrolizumab	A PD-L1 inhibitor	France	Recruiting
A randomized phase II, placebo-controlled, multicenter study evaluating efficacy and safety of regorafenib in patients with metastatic bone sarcomas	NCT02389244	Phase II	Advanced metastatic cancer in progression including chordoma	Regorafenib Placebo	A multi-kinase inhibitor; angiogenesis inhibitor	France	Recruiting
Phase 2 study on imatinib in combination with RAD001 in advanced chordoma	EUDRACT 2010-021755-34	Phase II	PDGFRB and mTOR (or S6 or 4BP1) positive advanced chordoma	Imatinib Everolimus	Imatinib: a PDGFRB inhibitor Everolimus: a mTOR inhibitor	Italy	Ongoing
A phase 2, single arm, European multi-center trial evaluating the efficacy of afatinib as first-line or later-line treatment in advanced chordoma.	EUDRACT 2016-002766-31	Phase II	Metastatic or unresectable chordoma	Afatinib	A Her2 and EGFR kinases inhibitor	Netherlands	Ongoing
Phase II study of lapatinib in EGFR/HER2NEU positive advanced chordoma	EUDRACT 2009-014456-29	Phase II	Advanced EGFR/Her2Neu positive chordoma	Lapatinib	EGFR/Her2Neu inhibitor	Germany	Ongoing

PDGFR, platelet-derived growth factor receptor; HDAC, histone deacetylase; Her2, human epidermal growth factor receptor 2; EGFR, epidermal growth factor receptor; PD-1, programmed cell death protein 1; CTLA4, cytotoxic T lymphocyte antigen 4.

multi-kinase inhibitor of VEGFR, is ongoing in France for metastatic bone sarcoma (NCT02389244).

Chordomas with indication of anti-RTK agents may also relapse or progress early. In TKI-resistant chordomas, p-AKT is a relative reliable indicator and its persistent expression following tyrphostin treatment resulted in relapse and progression (54). AKT is activated by mTOR, its downstream molecules (RPS6 and eIF4E), and Stat3. The combination of the antagonists of upstream RTKs and downstream mTOR/PI3K/MAPK/Stat not only synergistically reduced chordoma growth by avoiding the negative feedback loop (63) and PI3K-dependent feedback loop (64), but also significantly decreased the cytotoxicity of either agent (65). For example, monotherapy of rapamycin or everolimus was ineffective against tumor progression (34, 41), while combining imatinib with everolimus or sirolimus induced good clinical effects in 3 studies (12 patients) (25, 28, 42). Therefore, the combined therapy can be considered for drug-resistant chordoma.

Mutations in the downstream effectors of RTKs, like PTEN and PIK3CA, also impair TKI response (66, 67). PTEN deficient chordoma cell lines exhibit increased proliferation, reduced apoptosis and enhanced migration in chordoma cell lines (68). Reintroduction of PTEN in tumor cells increased their therapeutic sensitivity to PDGFR inhibitors, and the combination of histone deacetylase (HDAC) and PDGFR inhibitors effectively reduced the growth and invasion of chordoma cells, irrespective of PTEN status (69). On this basis, a new phase I trial of Imatinib and LBH589 (a HDAC inhibitor) is ongoing in chordoma patients (NCT01175109).

Chordomas frequently show deletions in the SMARCB1 locus (49). SMARCB1 directly antagonizes the histone methyltransferase EZH2 and regulates the cell-cycle by activating CDKN2A (45). A phase I trial on the EZH2 inhibitor tazemetostat, confirmed complete or partial responses were observed in two children with chordoma according to RECIST (NCT02601937) (45). Therefore, another phase II clinical trial on tazemetostat is ongoing in patients with SMARCB1/INI1 deleted chordoma (NCT02601950).

The loss of chromosome 9 or 9p region, which contains CDKN2A, has been reported in some chordoma patients (51). The inactivation of CDKN2A universally activates the CDK4/6 and Rb pathways (70), which are highly expressed in the chordoma tissues (71). The CDK4/6 inhibitors palbociclib and LY2835219 inhibited chordoma cell growth and proliferation *in vitro* efficiently (72, 73). A phase II clinical trial on palbociclib is currently enrolling patients with chordoma (NCT031 10744).

Somatic duplications of the notochordal transcription factor brachyury was demonstrated in chordoma, and enhanced tumor growth by activating YAP (9, 47, 48). Preclinical studies have shown that a recombinant *Saccharomyces cerevisiae* (yeast) vaccine encoding brachyury (GI-6301) activates human T cells *in vitro*. A phase II GI-6301 dose-escalation trial showed a 70% clinical benefit rate in chordoma patients (20). A phase II clinical trial on the combination of GI-6301 and radiotherapy is currently enrolling chordoma patients in the United States (NCT02383498). Additionally, a phase I trial of a Modified Vaccinia Ankara (MVA)-brachyury and a fowlpox (FPV)-brachyury vaccines is currently ongoing in patients with solid tumors, including chordoma (NCT03349983).

Limitations

In order to decrease the selection bias, this systematic review screened all published studies enrolling chordoma patients treated with MTT, including clinical trials, case series and even case reports, and provides the most detailed information. However, there were some limitations that need to be addressed. We included case reports on account of the rarity of chordoma and the paucity of available studies. However, a case report might overemphasize the final results due to lack of strong results. In addition, we only included English language publications which can also increase the selection bias. Furthermore, the baseline conditions of the patients and the evaluation criteria were not consistent across studies which is another factor contributing to selection bias. Therefore, large prospective randomized clinical trials are warranted to help clinicians determine the optimum treatment modality for chordoma patients.

CONCLUSIONS

The selection of MTIs for patients with advanced or relapsed chordoma should be based on gene mutation screening and immunohistochemistry (IHC). Monotherapy of TKIs is recommended as the first-line treatment. Combined therapy (two TKIs or TKI plus mTOR inhibitor) may be the choice for drug-resistant chordoma. Brachyury vaccine is a promising therapeutic strategy and requires more clinical trials to evaluate its safety and efficacy.

AUTHOR CONTRIBUTIONS

TM did the literature search, data and data analysis, and led the writing of the review. HY, JJ, and RH contributed to the design, data collection, and analysis. HY, DS, and LC contributed their experience of clinical practice in chordoma to ensure the relevance of findings. JJ and CJ contributed their experience in the discussion of the molecular mechanism underlying chordoma and drug interaction.

FUNDING

This work was supported in part by the National Natural Science Foundation of China [grant numbers 81702659, 81772856] and National Key R&D Program of China [grant numbers 2016YFA0100800].

ACKNOWLEDGMENTS

We acknowledge the contributions of Josh Sommer of the Chordoma Foundation, who assisted with the revision of concept and the final manuscript.

REFERENCES

1. Walcott BP, Nahed BV, Mohyeldin A, Coumans JV, Kahle KT, Ferreira MJ. Chordoma: current concepts, management, and future directions. *Lancet Oncol.* (2012) 13:e69–76. doi: 10.1016/S1470-2045(11)70337-0
2. Mcmaster ML, Goldstein AM, Bromley CM, Ishibe N, Parry DM. Chordoma: incidence and survival patterns in the United States, 1973–1995. *Cancer Causes Control.* (2001) 12:1–11. doi: 10.1023/A:1008947301735
3. Chugh R, Tawbi H, Lucas DR, Biermann JS, Schuetze SM, Baker LH. Chordoma: the nonsarcoma primary bone tumor. *Oncologist* (2007) 12:1344–50. doi: 10.1634/theoncologist.12-11-1344
4. Casali PG, Stacchiotti S, Sangalli C, Olmi P, Gronchi A. Chordoma. *Curr Opin Oncol.* (2007) 19:367–70. doi: 10.1097/CCO.0b013e3281214448
5. Stacchiotti S, Sommer J. Building a global consensus approach to chordoma: a position paper from the medical and patient community. *Lancet Oncol.* (2015) 16:e71–83. doi: 10.1016/S1470-2045(14)71190-8
6. Meng T, Yin H, Li B, Li Z, Xu W, Zhou W, et al. Clinical features and prognostic factors of patients with chordoma in the spine: a retrospective analysis of 153 patients in a single center. *Neuro Oncol.* (2015) 17:725–32. doi: 10.1093/neuonc/nou331
7. Stacchiotti S, Casali PG, Lo Vullo S, Mariani L, Palassini E, Mercuri M, et al. Chordoma of the mobile spine and sacrum: a retrospective analysis of a series of patients surgically treated at two referral centers. *Ann Surg Oncol.* (2010) 17:211–9. doi: 10.1245/s10434-009-0740-x
8. Arain A, Hornicek FJ, Schwab JH, Chebib I, Damron TA. Chordoma arising from benign multifocal notochordal tumors. *Skeletal Radiol.* (2017) 46:1745–52. doi: 10.1007/s00256-017-2727-1
9. Tarpey PS, Behjati S, Young MD, Martincorena I, Alexandrov LB, Farndon SJ, et al. The driver landscape of sporadic chordoma. *Nat Commun.* (2017) 8:890. doi: 10.1038/s41467-017-01026-0
10. Stacchiotti S, Longhi A, Ferraresi V, Grignani G, Comandone A, Stupp R, et al. Phase II study of imatinib in advanced chordoma. *J Clin Oncol.* (2012) 30:914–20. doi: 10.1200/JCO.2011.35.3656
11. Schuetze SM, Bolejack V, Choy E, Ganjoo KN, Staddon AP, Chow WA, et al. Phase 2 study of dasatinib in patients with alveolar soft part sarcoma, chondrosarcoma, chordoma, epithelioid sarcoma, or solitary fibrous tumor. *Cancer* (2017) 123:90–7. doi: 10.1002/cncr.30379
12. Stacchiotti S, Tamborini E, Lo Vullo S, Bozzi F, Messina A, Morosi C, et al. Phase II study on lapatinib in advanced EGFR-positive chordoma. *Ann Oncol.* (2013) 24:1931–6. doi: 10.1093/annonc/mdt117
13. Asklund T, Sandstrom M, Shahidi S, Riklund K, Henriksson R. Durable stabilization of three chordoma cases by bevacizumab and erlotinib. *Acta Oncol.* (2014) 53:980–4. doi: 10.3109/0284186X.2013.878472
14. George S, Merriam P, Maki RG, Van Den Abbeele AD, Yap JT, Akhurst T, et al. Multicenter phase II trial of sunitinib in the treatment of nongastrointestinal stromal tumor sarcomas. *J Clin Oncol.* (2009) 27:3154–60. doi: 10.1200/JCO.2008.20.9890
15. Bompas E, Le Cesne A, Tresch-Bruneel E, Lebellec L, Laurence V, Collard O, et al. Sorafenib in patients with locally advanced and metastatic chordomas: a phase II trial of the French Sarcoma Group (GSF/GETO). *Ann Oncol.* (2015) 26:2168–73. doi: 10.1093/annonc/mdv300
16. Jagersberg M, El Rahal A, Dammann P, Merkler D, Weber DC, Schaller K. Clival chordoma: a single-centre outcome analysis. *Acta Neurochir (Wien).* (2017) 159:1815–23. doi: 10.1007/s00701-017-3163-7
17. Lebellec L, Chauffert B, Blay JY, Le Cesne A, Chevreau C, Bompas E, et al. Advanced chordoma treated by first-line molecular targeted therapies: outcomes and prognostic factors. A retrospective study of the French Sarcoma Group (GSF/GETO) and the Association des Neuro-Oncologues d'Expression Francaise (ANOCEF). *Eur J Cancer* (2017) 79:119–28. doi: 10.1016/j.ejca.2017.03.037
18. Liberati A, Altman DG, Tetzlaff J, Mulrow C, Gotzsche PC, Ioannidis JP, et al. The PRISMA statement for reporting systematic reviews and meta-analyses of studies that evaluate healthcare interventions: explanation and elaboration. *BMJ* (2009) 339:b2700. doi: 10.1136/bmj.b2700
19. Adenis A, Ray-Coquard I, Italiano A, Chauzit E, Bui-Nguyen B, Blay JY, et al. A dose-escalating phase I of imatinib mesylate with fixed dose of metronomic cyclophosphamide in targeted solid tumours. *Br J Cancer* (2013) 109:2574–8. doi: 10.1038/bjc.2013.648
20. Heery CR, Singh BH, Rauckhorst M, Marte JL, Donahue RN, Grenga I, et al. Phase I trial of a yeast-based therapeutic cancer vaccine (GI-6301) targeting the transcription factor brachyury. *Cancer Immunol Res.* (2015) 3:1248–56. doi: 10.1158/2326-6066.CIR-15-0119
21. Lebellec L, Bertucci F, Tresch-Bruneel E, Bompas E, Toiron Y, Camoin L, et al. Circulating vascular endothelial growth factor (VEGF) as predictive factor of progression-free survival in patients with advanced chordoma receiving sorafenib: an analysis from a phase II trial of the french sarcoma group (GSF/GETO). *Oncotarget* (2016) 7:73984–94. doi: 10.18632/oncotarget.12172
22. Macaulay VM, Middleton MR, Eckhardt SG, Rudin CM, Juergens RA, Gedrich R, et al. Phase I dose-escalation study of linsitinib (OSI-906) and erlotinib in patients with advanced solid tumors. *Clin Cancer Res.* (2016) 22:2897–907. doi: 10.1158/1078-0432.CCR-15-2218
23. Casali PG, Messina A, Stacchiotti S, Tamborini E, Crippa F, Gronchi A, et al. Imatinib mesylate in chordoma. *Cancer* (2004) 101:2086–97. doi: 10.1002/cncr.20618
24. Geoerger B, Morland B, Ndiaye A, Doz F, Kalifa G, Geoffray A, et al. Target-driven exploratory study of imatinib mesylate in children with solid malignancies by the Innovative Therapies for Children with Cancer (ITCC) European Consortium. *Eur J Cancer* (2009) 45:2342–51. doi: 10.1016/j.ejca.2009.03.007
25. Stacchiotti S, Marrari A, Tamborini E, Palassini E, Virdis E, Messina A, et al. Response to imatinib plus sirolimus in advanced chordoma. *Ann Oncol.* (2009) 20:1886–94. doi: 10.1093/annonc/mdp210
26. Ferraresi V, Nuzzo C, Zoccali C, Marandino F, Vidiri A, Salducca N, et al. Chordoma: clinical characteristics, management and prognosis of a case series of 25 patients. *BMC Cancer* (2010) 10:22. doi: 10.1186/1471-2407-10-22
27. Hindi N, Casali PG, Morosi C, Messina A, Palassini E, Pilotti S, et al. Imatinib in advanced chordoma: a retrospective case series analysis. *Eur J Cancer* (2015) 51:2609–14. doi: 10.1016/j.ejca.2015.07.038
28. Lipplaa A, Dijkstra S, Gelderblom H. Efficacy of pazopanib and sunitinib in advanced axial chordoma: a single reference centre case series. *Clin Sarcoma Res.* (2016) 6:19. doi: 10.1186/s13569-016-0059-x
29. Schonegger K, Gelpi E, Prayer D, Dieckmann K, Matula C, Hassler M, et al. Recurrent and metastatic clivus chordoma: systemic palliative therapy retards disease progression. *Anticancer Drugs* (2005) 16:1139–43. doi: 10.1097/00001813-200511000-00015
30. Hof H, Welzel T, Debus J. Effectiveness of cetuximab/gefitinib in the therapy of a sacral chordoma. *Onkologie* (2006) 29:572–4. doi: 10.1159/000096283
31. Linden O, Stenberg L, Kjellen E. Regression of cervical spinal cord compression in a patient with chordoma following treatment with cetuximab and gefitinib. *Acta Oncol.* (2009) 48:158–9. doi: 10.1080/02841860802266672
32. Singhal N, Kotasek D, Parnis FX. Response to erlotinib in a patient with treatment refractory chordoma. *Anticancer Drugs* (2009) 20:953–5. doi: 10.1097/CAD.0b013e328330c7f0
33. Asklund T, Danfors T, Henriksson R. PET response and tumor stabilization under erlotinib and bevacizumab treatment of an intracranial lesion non-invasively diagnosed as likely chordoma. *Clin Neuropathol.* (2011) 30:242–6. doi: 10.5414/NP300371
34. Chay WY, Teo M, Sittampalam K, Toh HC. Effective use of thalidomide in the treatment of recurrent metastatic chordoma. *J Clin Oncol.* (2011) 29:e477–80. doi: 10.1200/JCO.2010.34.2139
35. Launay SG, Chetaille B, Medina F, Perrot D, Nazarian S, Guiramand J, et al. Efficacy of epidermal growth factor receptor targeting in advanced chordoma: case report and literature review. *BMC Cancer* (2011) 11:423. doi: 10.1186/1471-2407-11-423

36. Mercier F, Guiot MC, Bojanowski MW. Treatment of chordoma with imatinib complicated by intracranial hemorrhage: a case showing dissociation between biological effect and therapeutic outcome. *J Neurooncol.* (2012) 107:435–7. doi: 10.1007/s11060-011-0767-2
37. Svoboda RM, Mackay D, Welsch MJ, Anderson BE. Multiple cutaneous metastatic chordomas from the sacrum. *J Am Acad Dermatol.* (2012) 66:e246–7. doi: 10.1016/j.jaad.2011.07.037
38. Houessinon A, Boone M, Constans JM, Toussaint P, Chauffert B. Sustained response of a clivus chordoma to erlotinib after imatinib failure. *Case Rep Oncol.* (2015) 8:25–9. doi: 10.1159/000371843
39. Rohatgi S, Ramaiya NH, Jagannathan JP, Howard SA, Shinagare AB, Krajewski KM. Metastatic chordoma: report of the two cases and review of the literature. *Eurasian J Med.* (2015) 47:151–4. doi: 10.5152/eurasianjmed.2015.52
40. Aleksic T, Browning L, Woodward M, Phillips R, Page S, Henderson S, et al. Durable response of spinal chordoma to combined inhibition of IGF-1R and EGFR. *Front Oncol.* (2016) 6:98. doi: 10.3389/fonc.2016.00098
41. Migliorini D, Mach N, Aguiar D, Vernet R, Landis BN, Becker M, et al. First report of clinical responses to immunotherapy in 3 relapsing cases of chordoma after failure of standard therapies. *Oncoimmunology* (2017) 6:e1338235. doi: 10.1080/2162402X.2017.1338235
42. Trapani D, Conforti F, De Pas T. EGFR Inhibition in a pretreated sacral chordoma: a role for erlotinib? Case Report and a Brief Review of Literature. *Transl Med UniSa* (2017) 16:30–3.
43. Ribeiro M, De Sousa MC, Hanna SA, Maldaun MVC, Kurimori CO, De Lima L, et al. Tumor reduction with pazopanib in a patient with recurrent lumbar chordoma. *Case Rep Oncol Med.* (2018) 2018:4290131. doi: 10.1155/2018/4290131
44. Mcpherson CM, Suki D, Mccutcheon IE, Gokaslan ZL, Rhines LD, Mendel E. Metastatic disease from spinal chordoma: a 10-year experience. *J Neurosurg Spine* (2006) 5:277–80. doi: 10.3171/spi.2006.5.4.277
45. Chi S, Fouladi M, Shukla N, Bourdeaut F, Margol A, Makin G, et al. Phase 1 study of the EZH2 inhibitor, tazemetostat, in children with relapsed or refractory INI1-negative tumors including rhabdoid tumors, epithelioid sarcoma, chordoma, and synovial sarcoma. *Mol Cancer Ther.* (2018) 17:1. doi: 10.1158/1535-7163
46. Tamborini E, Miselli F, Negri T, Lagonigro MS, Staurengo S, Dagrada GP, et al. Molecular and biochemical analyses of platelet-derived growth factor receptor (PDGFR) B, PDGFRA, and KIT receptors in chordomas. *Clin Cancer Res.* (2006) 12:6920–8. doi: 10.1158/1078-0432.CCR-06-1584
47. Presneau N, Shalaby A, Ye H, Pillay N, Halai D, Idowu B, et al. Role of the transcription factor T (brachyury) in the pathogenesis of sporadic chordoma: a genetic and functional-based study. *J Pathol.* (2011) 223:327–35. doi: 10.1002/path.2816
48. Shah SR, David JM, Tippens ND, Mohyeldin A, Martinez-Gutierrez JC, Ganaha S, et al. Brachyury-YAP regulatory axis drives stemness and growth in cancer. *Cell Rep.* (2017) 21:495–507. doi: 10.1016/j.celrep.2017.09.057
49. Choy E, Macconaill LE, Cote GM, Le LP, Shen JK, Nielsen GP, et al. Genotyping cancer-associated genes in chordoma identifies mutations in oncogenes and areas of chromosomal loss involving CDKN2A, PTEN, and SMARCB1. *PLoS ONE* (2014) 9:e101283. doi: 10.1371/journal.pone.0101283
50. Lee-Jones L, Aligianis I, Davies PA, Puga A, Farndon PA, Stemmer-Rachamimov A, et al. Sacrococcygeal chordomas in patients with tuberous sclerosis complex show somatic loss of TSC1 or TSC2. *Genes Chromosomes Cancer* (2004) 41:80–5. doi: 10.1002/gcc.20052
51. Hallor KH, Staaf J, Jonsson G, Heidenblad M, Vult Von Steyern F, Bauer HC, et al. Frequent deletion of the CDKN2A locus in chordoma: analysis of chromosomal imbalances using array comparative genomic hybridisation. *Br J Cancer* (2008) 98:434–42. doi: 10.1038/sj.bjc.6604130
52. Sommer J, Itani DM, Homlar KC, Keedy VL, Halpern JL, Holt GE, et al. Methylthioadenosine phosphorylase and activated insulin-like growth factor-1 receptor/insulin receptor: potential therapeutic targets in chordoma. *J Pathol.* (2010) 220:608–17. doi: 10.1002/path.2679
53. Tamborini E, Virdis E, Negri T, Orsenigo M, Brich S, Conca E, et al. Analysis of receptor tyrosine kinases (RTKs) and downstream pathways in chordomas. *Neuro Oncol.* (2010) 12:776–89. doi: 10.1093/neuonc/noq003
54. De Castro CV, Guimaraes G, Aguiar S Jr, Lopes A, Baiocchi G, Da Cunha IW, et al. Tyrosine kinase receptor expression in chordomas: phosphorylated AKT correlates inversely with outcome. *Hum Pathol.* (2013) 44:1747–55. doi: 10.1016/j.humpath.2012.11.024
55. Akhavan-Sigari R, Gaab MR, Rohde V, Abili M, Ostertag H. Prognostic significance of immunohistochemical expression of VEGFR2 and iNOS in spinal chordoma. *Eur Spine J.* (2014) 23:2416–22. doi: 10.1007/s00586-014-3417-5
56. Hu Y, Mintz A, Shah SR, Quinones-Hinojosa A, Hsu W. The FGFR/MEK/ERK/brachyury pathway is critical for chordoma cell growth and survival. *Carcinogenesis* (2014) 35:1491–9. doi: 10.1093/carcin/bgu014
57. Magnaghi P, Salom B, Cozzi L, Amboldi N, Ballinari D, Tamborini E, et al. Afatinib is a new therapeutic approach in chordoma with a unique ability to target EGFR and brachyury. *Mol Cancer Ther.* (2018) 17:603–13. doi: 10.1158/1535-7163.MCT-17-0324
58. Choi H, Charnsangavej C, Faria SC, Macapinlac HA, Burgess MA, Patel SR, et al. Correlation of computed tomography and positron emission tomography in patients with metastatic gastrointestinal stromal tumor treated at a single institution with imatinib mesylate: proposal of new computed tomography response criteria. *J Clin Oncol.* (2007) 25:1753–9. doi: 10.1200/JCO.2006.07.3049
59. Eisenhauer EA, Therasse P, Bogaerts J, Schwartz LH, Sargent D, Ford R, et al. New response evaluation criteria in solid tumours: revised RECIST guideline (version 1.1). *Eur J Cancer* (2009) 45:228–47. doi: 10.1016/j.ejca.2008.10.026
60. Stommel JM, Kimmelman AC, Ying H, Nabioullin R, Ponugoti AH, Wiedemeyer R, et al. Coactivation of receptor tyrosine kinases affects the response of tumor cells to targeted therapies. *Science* (2007) 318:287–90. doi: 10.1126/science.1142946
61. Scheipl S, Froehlich EV, Leithner A, Beham A, Quehenberger F, Mokry M, et al. Does insulin-like growth factor 1 receptor (IGF-1R) targeting provide new treatment options for chordomas? A retrospective clinical and immunohistochemical study. *Histopathology* (2012) 60:999–1003. doi: 10.1111/j.1365-2559.2012.04186.x
62. Akhavan-Sigari R, Gaab MR, Rohde V, Brandis A, Tezval H, Abili M, et al. Expression of vascular endothelial growth factor receptor 2 (VEGFR-2), inducible nitric oxide synthase (iNOS), and Ki-M1P in skull base chordoma: a series of 145 tumors. *Neurosurg Rev.* (2014) 37:79–88. doi: 10.1007/s10143-013-0495-5
63. Roux PP, Shahbazian D, Vu H, Holz MK, Cohen MS, Taunton J, et al. RAS/ERK signaling promotes site-specific ribosomal protein S6 phosphorylation via RSK and stimulates cap-dependent translation. *J Biol Chem.* (2007) 282:14056–64. doi: 10.1074/jbc.M700906200
64. Carracedo A, Ma L, Teruya-Feldstein J, Rojo F, Salmena L, Alimonti A, et al. Inhibition of mTORC1 leads to MAPK pathway activation through a PI3K-dependent feedback loop in human cancer. *J Clin Invest.* (2008) 118:3065–74. doi: 10.1172/JCI34739
65. Yang C, Schwab JH, Schoenfeld AJ, Hornicek FJ, Wood KB, Nielsen GP, et al. A novel target for treatment of chordoma: signal transducers and activators of transcription 3. *Mol Cancer Ther.* (2009) 8:2597–605. doi: 10.1158/1535-7163.MCT-09-0504
66. Ohashi K, Maruvka YE, Michor F, Pao W. Epidermal growth factor receptor tyrosine kinase inhibitor-resistant disease. *J Clin Oncol.* (2013) 31:1070–80. doi: 10.1200/JCO.2012.43.3912
67. Chen K, Mo J, Zhou M, Wang G, Wu G, Chen H, et al. Expression of PTEN and mTOR in sacral chordoma and association with poor prognosis. *Med Oncol.* (2014) 31:886. doi: 10.1007/s12032-014-0886-7
68. Han S, Polizzano C, Nielsen GP, Hornicek FJ, Rosenberg AE, Ramesh V. Aberrant hyperactivation of akt and Mammalian target of rapamycin complex 1 signaling in sporadic chordomas. *Clin Cancer Res.* (2009) 15:1940–6. doi: 10.1158/1078-0432.CCR-08-2364
69. Lee DH, Zhang Y, Kassam AB, Park MJ, Gardner P, Prevedello D, et al. Combined PDGFR and HDAC inhibition overcomes PTEN disruption in chordoma. *PLoS ONE* (2015) 10:e0134426. doi: 10.1371/journal.pone.0134426
70. Wang L, Zehir A, Nafa K, Zhou N, Berger MF, Casanova J, et al. Genomic aberrations frequently alter chromatin regulatory genes in chordoma. *Genes Chromosomes Cancer* (2016) 55:591–600. doi: 10.1002/gcc.22362

71. Bosotti R, Magnaghi P, Di Bella S, Cozzi L, Cusi C, Bozzi F, et al. Establishment and genomic characterization of the new chordoma cell line Chor-IN-1. *Sci Rep*. (2017) 7:9226. doi: 10.1038/s41598-017-10044-3
72. Liu T, Shen JK, Choy E, Zhang Y, Mankin HJ, Hornicek FJ, et al. CDK4 Expression in chordoma: a potential therapeutic target running title: CDK4 expression in chordoma. *J Orthop Res*. (2018) 36:1581–9. doi: 10.1002/jor.23819
73. Levy J. *Chordoma Foundation In Vivo Drug Screening Program*. Chordoma Foundation (2018). Available online at: https://figshare.com/projects/Chordoma_Foundation_In_Vivo_Drug_Screening_Program/25948 (accessed January 25, 2018).

Conflict of Interest Statement: The authors declare that the research was conducted in the absence of any commercial or financial relationships that could be construed as a potential conflict of interest.

frontiers in Pharmacology

REVIEW
published: 01 February 2019
doi: 10.3389/fphar.2019.00065

PD-1/PD-L1 Inhibitors in Cervical Cancer

Yuncong Liu[1,2†], Li Wu[2†], Ruizhan Tong[1], Feiyue Yang[2], Limei Yin[1,3], Mengqian Li[1,3], Liting You[1,3], Jianxin Xue[1,3] and You Lu[1,3*]*

[1] West China School of Medicine, Sichuan University, Chengdu, China, [2] Department of Gynaecological Oncology, Guizhou Provincial People's Hospital, Guiyang, China, [3] Department of Thoracic Oncology, Cancer Center, West China Hospital, Sichuan University, Chengdu, China

Cervical cancer is one of the most common gynecological tumors, and the majority of early-stage cervical cancer patients achieve good recovery through surgical treatment and concurrent chemoradiotherapy (CCRT). However, for patients with recurrent, persistent, metastatic cervical cancer, effective treatment is rare, except for bevacizumab combined with chemotherapy. Programmed cell death-1/programmed cell death-ligand 1 (PD-1/PD-L1) inhibitors might be a novel choice to improve the clinical outcomes of these patients. Thus far, some pivotal trials, including Keynote 028, Keynote 158 and Checkmate 358, have indicated established clinical benefit of PD-1/PD-L1 inhibitors in cervical cancer. In light of these data, the FDA has approved pembrolizumab for patients with recurrent or metastatic cervical cancer with disease progression during or after chemotherapy. There are also some ongoing studies that may provide more evidence for the PD-1/PD-L1 pathway as a therapeutic target in cervical cancer. In this review, we have summarized the status and application of PD-1/PD-L1 inhibitors in clinical trials for the treatment of cervical cancer and suggested some future directions in this field.

Keywords: cervical cancer, programmed cell death-1/programmed cell death-ligand 1 (PD-1/PD-L1), immune checkpoint inhibitors, immunotherapy, human papillomavirus (HPV)

OPEN ACCESS

Edited by:
Yan-Yan Yan,
Shanxi Datong University, China

Reviewed by:
Daniel Olive,
Aix-Marseille Université, France
Jingying Zhou,
The Chinese University of Hong Kong, China

****Correspondence:***
Jianxin Xue
radjianxin@163.com
You Lu
radyoulu@hotmail.com

† These authors have contributed equally to this work

Specialty section:
This article was submitted to Cancer Molecular Targets and Therapeutics, a section of the journal Frontiers in Pharmacology

Received: *27 November 2018*
Accepted: *18 January 2019*
Published: *01 February 2019*

Citation:
Liu Y, Wu L, Tong R, Yang F, Yin L, Li M, You L, Xue J and Lu Y (2019) PD-1/PD-L1 Inhibitors in Cervical Cancer. Front. Pharmacol. 10:65. doi: 10.3389/fphar.2019.00065

INTRODUCTION

Cervical cancer is one of the most common gynecological tumors. More than 569,847 women are diagnosed with cervical cancer annually worldwide, resulting in over 311,365 deaths (Bray et al., 2018). Although the incidence of cervical cancer has been greatly reduced by the use of HPV vaccines and cervical cancer screening (Goodman, 2015), cervical cancer is second in terms of morbidity among gynecological tumors in developing countries (Sahasrabuddhe et al., 2012). Over 70% of cervical cancer cases diagnosed in developing countries are locally invasive or metastatic, contributing to the high mortality rate of cervical cancer. The 5-year OS rate of local cervical cancer can achieve approximately 75–85% through effective treatments such as surgery CCRT, etc. (Chen et al., 2015). Nevertheless, the 5-year OS of recurrent, persistent, metastatic cervical cancer is only approximately 15%. The poor prognosis is mainly due to limited therapeutic options (Guitarte et al., 2014). The majority of these patients can only be treated with palliative

Abbreviations: AE, adverse event; APCs, antigen-presenting cells; CCRT, concurrent chemoradiotherapy; CRs, complete responses; CRT, chemoradiotherapy; CTLA-4, cytotoxic T-lymphocyte-associated protein-4; hfRT, hyperfraction radiotherapy; HNSCC, head and neck squamous cell carcinoma; HPV, human papillomavirus; mAb, monoclonal antibody; NSCLC, non-small cell lung cancer; ORR, objective response rate; OS, overall survival rate; PD-1/PD-L1, programmed cell death-1/programmed cell death-ligand 1; PFS, progression-free survival; PRs, partial responses; SCCs, squamous cell cancers; TILs, tumor infiltrating lymphocytes; uPRs, unconfirmed partial responses.

chemotherapy (Boussios et al., 2016), in which platinum-based chemotherapies were the prior choice (Monk et al., 2009). In 2014, the GOG 240 trial indicated that when bevacizumab was added to the chemotherapy, the ORR was improved from 36 to 48% (Tewari et al., 2014), and the OS could be prolonged from 13 to 17 months for recurrent, persistent, metastatic cervical cancer, thus laying the foundation for the first-line choice of combining bevacizumab with chemotherapy for this population (Tewari et al., 2017). However, for those who progress during the first-line treatment, the lack of effective second-line treatment remains to be the main reason for the high mortality rate (Minion and Tewari, 2018). Currently, immune checkpoint inhibitors (Schumacher and Schreiber, 2015), especially PD-1/PD-L1 inhibitors (Constantinidou et al., 2018), have achieved favorable efficacy in treating multiple solid tumors (Gettinger et al., 2018), including cervical cancer (Borcoman and Le Tourneau, 2017). Accumulating evidence has demonstrated that PD-1/PD-L1 inhibitors may be a promising approach for cervical cancer treatment.

IMMUNE CHECKPOINT INHIBITORS

Numerous immunomodulatory therapies are being investigated in clinical trials with diverse potential targets, including PD-1/PD-L1, CTLA-4, Tim-3, ICOS, 4-1BB, and OX-40. Among these novel targets, ICOS (Amatore et al., 2018), 4-1BB (Compte et al., 2018), and OX-40 (Polesso et al., 2018) are costimulatory receptors, while PD-1/PD-L1 (Raedler, 2015), CTLA-4 (Lheureux et al., 2018), and Tim-3 (Gorris et al., 2018) are negative immune regulators of T cells. Currently, only CTLA-4 inhibitors (Hodi et al., 2010) and PD-1/PD-L1 inhibitors (Bagcchi, 2014) have been approved by the FDA. CTLA-4 integrates with the costimulatory molecules CD80 (B7-1) and CD86 (B7-2) that express on the surfaces of APCs (Fife and Bluestone, 2008), while PD-L1 is expressed on a wide variety of cell types, including tumor-associated fibroblasts, tumor cells, APCs, etc. (Boussiotis, 2016). As a result, CTLA-4 inhibits T cell activation within secondary lymphoid organs (Kurup et al., 2017), but PD-1/PD-L1 chiefly regulates T cell function within peripheral tissues and the tumor microenvironment (Pardoll, 2012). Therefore, PD-1/PD-L1 signaling is more specific to tumor than CTLA-4 signaling, and inhibitors of PD-1/PD-L1 may cause less damage to healthy tissue (Boussiotis, 2016; Minion and Tewari, 2018) (**Figure 1**).

Based on the above mechanism, ipilimumab (monoclonal anti-CTLA-4), the first immune checkpoint inhibitor, approved for melanoma, had little clinical benefit until the emergence of pembrolizumab, and the combination of the two drugs further improved treatment efficacy in malignant melanoma (Wang et al., 2017). To date, another mAb for CTLA-4, tremelimumab, has not been approved for the treatment in any type of cancer. However, mAbs targeting PD-1 [pembrolizumab (Paz-Ares et al., 2018), nivolumab (Long et al., 2018), and cemiplimab (Sidaway, 2018)] and PD-L1 [atezolizumab (Hsu et al., 2018), durvalumab (Siu et al., 2018), and avelumab (Le Tourneau et al., 2018)] have presented clinical advantages in malignant melanoma, advanced NSCLC, urothelial cancer (Zhang and Li, 2018) and other tumors (Lim et al., 2018) (**Table 1**). In addition, extensive research has been carried out on gynecological tumors, such as ovarian cancer (Liu and Zamarin, 2018) and breast cancer (Julia et al., 2018), and clinical researches on cervical cancer are ongoing. At present, some initial results have been achieved.

THEORETICAL BASIS FOR PD-1/PD-L1 INHIBITORS IN CERVICAL CANCER

The PD-1/PD-L1 axis is one of the most well-known immune-checkpoint pathways with a mechanism of immune evasion for cancer cells and thus inhibiting the immune response in various kinds of solid tumors, including cervical cancer Cancer Genome Atlas Research Network et al. (2017). In brief, PD-L1 expresses on the surface of cervical tumor cells, APCs and TILs, while the PD-1-positive cells were mostly identified as T cells in the stroma of cervical tumors. For the expression of PD-1 in the tumor stroma of cervical cancer, Meng et al. (2018) reported that 60.82% (59/97) of the patients exhibited PD-1 expression, while another study showed PD-1 expression in 46.97% (31/66) of the patients (Feng et al., 2018).

To date, numerous studies have investigated the expression of PD-L1 in cervical cancer (Yang et al., 2013; Chen et al., 2016). The expression of PD-L1 has been reported in 34.4–96% of cervical carcinoma tissues, while expression of PD-L1 in histologically normal cervical tissues was rarely found (Enwere et al., 2017). Opal Reddy et al. (2017) showed that PD-L1 expression was positive in 32 of 93 (34.4%) cervical carcinoma samples, subcategorically in 28 of 74 (37.8%) SCCs, 2 of 7 (28.6%) adenosquamous carcinomas, and 2 of 12 (16.7%) endocervical adenocarcinomas. In another study, PD-L1 expression was found in 96% of the samples (Enwere et al., 2017). Specifically, for cervical SCC, PD-L1 expression was found in 80% (56/70) cases (Mezache et al., 2015). In the TCGA database for cervical SCCs, the amplification or gain of PD-L1 was found in 28 of 129 (22%) cases (Dijkstra et al., 2016). In addition, PD-L1 can also be expressed on TILs, which plays a role in antitumor response inhibition. A study found that for cervical SCCs samples, the expression rates of PD-L1 on cancer cells and TILs were 59.1 and 47.0%, respectively (Feng et al., 2018). Collectively, these data suggest that both PD-L1 and PD-1 are widely expressed in cervical cancer tumor cells and stroma, providing potential therapeutic targets for PD-1/PD-L1 inhibitors.

Notoriously, persistent HPV infection is involved in the pathogenesis of cervical cancer and is related to its prognosis. Several teams have interrogated whether HPV infection could affect PD-L1 expression in cervical cancer and found that HPV positivity was positively correlated with increased PD-L1 expression (Mezache et al., 2015; Liu et al., 2017).

Considerable effort has been made to dissect the underlying mechanism of the association between HPV status and PD-L1 expression in HPV-related solid tumors, mainly HNSCC and cervical cancer. In HPV-HNSCCs, membranous expression of PD-L1 and significant increased levels of mRNA of IFN-γ were found in the tonsillar crypts, As tonsillar crypts witnesses the initial HPV infection, and IFN-γ induces PD-L1 expression, this

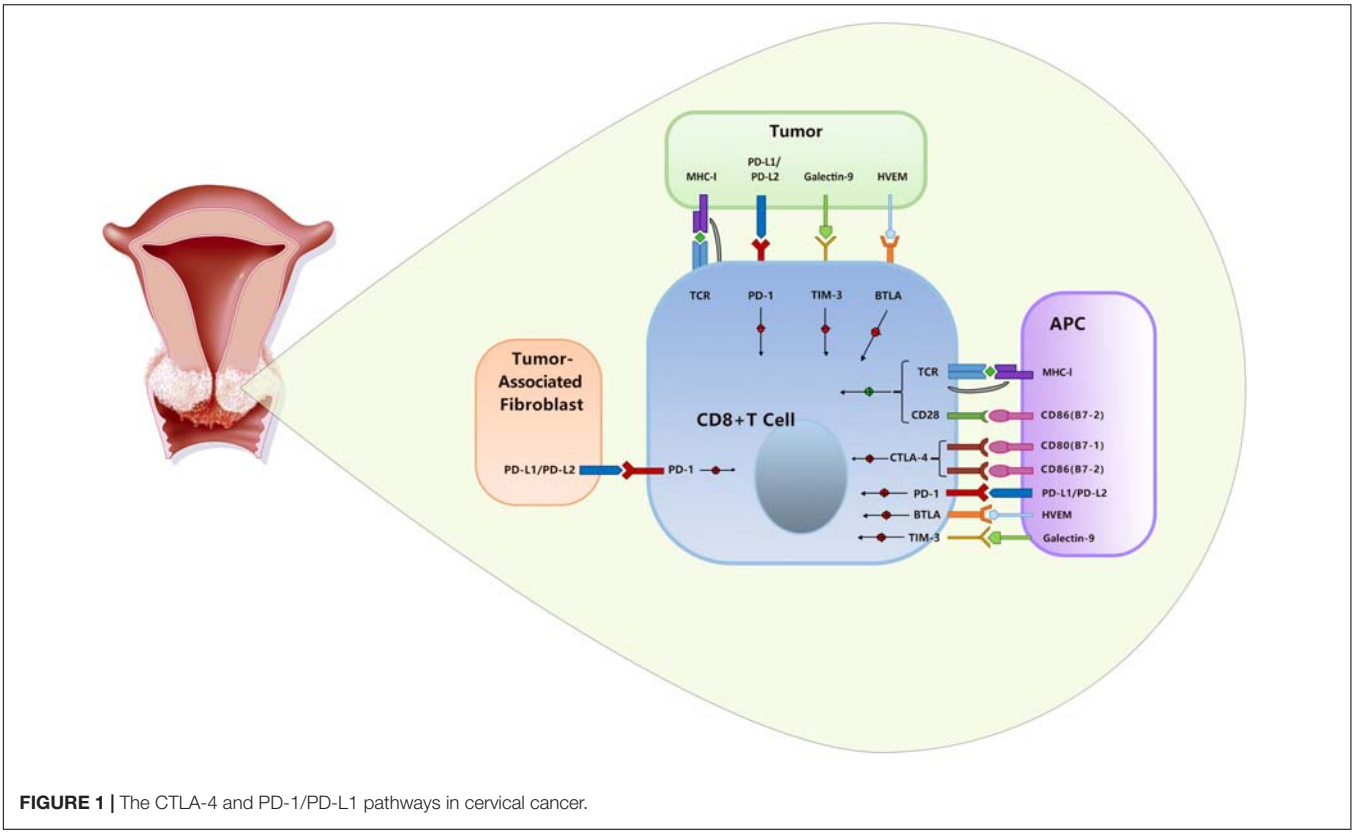

FIGURE 1 | The CTLA-4 and PD-1/PD-L1 pathways in cervical cancer.

evidence might support the role of the PD-1/PD-L1 interaction in creating an "immune-privileged" site for initial viral infection and subsequent adaptive immune resistance (Franzen et al., 2018). In another study, DNA methylation of PD-L1 was inversely correlated with PD-L1 mRNA expression ($p \leq 0.002$) and was further significantly associated with HPV infection in the TCGA cohort, indicating that DNA methylation of PD-L1 is associated with transcriptional silencing and HPV infection in HNSCCs (Balermpas et al., 2017). In cervical cancer, Qin et al. (2017) indicated that HPV-induced somatic mutations and a multitude of neoantigens, which played a crucial role in the inhibitory tumor microenvironment and could lead to notable alterations among checkpoint-related genes such as CTLA-4, PD-1, and PD-L1. Specifically, PD-L1 showed a positive correlation with ENO1, PRDM1, OVOL1, and MNT, all of which are related master regulators of HPV16 E6 and E7 (Qin et al., 2017). Of

TABLE 1 | The characteristics of the clinical application of monoclonal antibodies (mAbs) of immune checkpoint inhibitors in cervical cancer.

Target	Drug (trade name)	Antibody type	Formerly name	Manufacturer	Time to market (FDA)	Indications
CTLA-4	Ipilumumab (Yervoy)	IgG1	–	BMS	March, 2011	Melanoma, colorectal cancer, renal cell carcinoma
	Tremelimumab	IgG2	Ticilimumb, CP-675,206	Pfizer	–	Undergoing human trials has not attained approval for any
PD-1	Pembrolizumab (Keytruda)	IgG4	MK-3475 Lambrolizumab	MSD	September, 2014	Advanced melanoma, non-small cell lung cancer, Hodgkin's lymphoma, and head and neck SCC[1]
	Nivolumab (Opdivo)	IgG4	BMS-9365580 NO-4538	BMS	December, 2014	Metastatic melanoma, squamous non-small cell lung cancer, renal cell carcinoma
	Cemiplimab (REGN2810)	IgG4	–	Sanofi	September, 2018 (EMA[2])	squamous cell skin cancer (EMPOWER-CSCC 1)
PD-L1	Durvalumab (Imfiniz)	IgGlK	–	AstraZeneca	May, 2017	Bladder cancer, NSCLC[3]
	Atezolizumab (Tecentriq)	IgGl	–	Roche	April, 2016	Lung cancer, bladder cancer, advanced triple negative breast cancer

[1]SCC, squamous cell cancers; [2]EMA, European Medicines Agency; [3]NSCLC, non-small cell lung cancer.

TABLE 2 | Clinical research outcomes on PD-1/PD-L1 inhibitors in cervical cancer.

Study	Author	Study population (n)	Phase	Treatment arm(s)	Principal results	Toxicity	Significance
REGN2810	Papadopoulos et al., 2016	Advanced solid tumors	I	Cemiplimab	62.8% patients had disease control	No dose-limiting toxicities	Higher response rate when combined with radiation suggesting abscopal responses
Keynote 028	Frenel et al., 2017	Recurrent cervical cancer with PD-L1 positive tumors (24)	Ib	Pembrolizumab 10 mg/kg q2w	ORR[1] 17% (95% CI: 5–37%)	Grade=3 AE[2] including rash and proteinuria	Well-tolerated and active in cervical cancer
Keynote 158	Schellens et al., 2017	Recurrent cervical cancer with progression or intolerance to standard therapy (82)	II	Pembrolizumab 200 mg/kg q2w	Preliminary results: ORR[1] 17% (95% CI: 8–31%); patients with >27 weeks of follow up, ORR 27% (95% CI: 8–55%)	Grades 3–4 AE[2] included AST/ALT[3] elevation and pyrexia	Demonstrates activity in cervical cancer and increasing response with a longer duration of follow-up
Checkmate 358	Hollebecque et al., 2017	Recurrent or metastatic HPV[4]-related cancers (19)	I–II	Nivolumab 240 mg q2w	Preliminary results: ORR[1] 26% (95% CI: 9.1–51.2%) in cervical cancer patients	Grade 3–4 AE[2] included hyponatremia, syncope, diarrhea and hepatocellular injury	Durable responses demonstrated in cervical cancer patients, with at least 6 months duration

[1]ORR, objective response rate; [2]AE, adverse event; [3]AST/ALT, aspartate transaminase/alanine transaminase; [4]HPV, human papillomavirus.

note, a single-arm, phase II study investigated durvalumab in patients with recurrent/metastatic HNSCCs (n = 112) and found that HPV-positive patients had a higher response rate and better survival than that of the HPV-negative patients (Zandberg et al., 2018). Nevertheless, for cervical cancer, the association of HPV status and the efficacy of PD-1/PD-L1 inhibitors is not yet certain due to the paucity of available data.

Several studies have probed the role of PD-L1 expression in the prognosis and therapeutic efficacy of cervical cancer. These results separately proved that an increase in PD-L1 expression was positively associated with tumor metastasis (Yang et al., 2017), tumor progression (Hsu et al., 2018) and poor prognosis in cervical cancer (Heeren et al., 2016). In this regard, the negative relationship between HPV infection and the clinical outcomes of cervical cancer may be partially attributed to the PD-L1 expression induced by HPV infection (Yang et al., 2017). For patients with locally advanced cervical adenocarcinoma and adenosquamous carcinoma treated with CRT, the underexpression of PD-L1 was a prognostic factor for tumor relapse (p = 0.041), indicating that PD-L1 expression might be a novel biomarker for CRT outcome (Lai et al., 2017).

CLINICAL RESEARCH OUTCOMES OF PD-1/PD-L1 INHIBITORS IN CERVICAL CANCER

Since 2015, multiple clinical trials have been conducted to explore the application of PD-1/PD-L1 antibodies in cervical cancer. To date, four studies have yielded preliminary results (**Table 2**). Keynote 028 (a phase Ib study) and Keynote 158 (a phase II study) evaluated pembrolizumab at the dose of 10 mg/kg and 200 mg/kg, respectively, in recurrent, metastatic cervical cancer. In Keynote 028 (Frenel et al., 2017), 24 patients were enrolled, and the overall response rate (RECIST v1.1) was 17% (95% CI: 5 to 37%). In terms of toxicity, 5 patients experienced grade 3 AEs (NCI-CTCAE 3.0), while no grade 4 AEs was observed. In Keynote 158 (Schellens et al., 2017), 98 patients with recurrent or metastatic cervical cancer were enrolled. With a median follow-up time of 11.7 months, the ORR in 77 patients was 14.3% (95% CI: 7.4 to 24.1%), including 2.6% of the patients with CRs and 11.7% of patients with PRs, whereas no response was observed in patients without PD-L1 expression in tumor cells. The most frequent serious adverse reactions included anemia (7%), fistula (4.1%), hemorrhage (4.1%), and infection (4.1%). Based on Keynote 158, the FDA approved pembrolizumab on June 12, 2018, for advanced cervical cancer with disease progression during or after chemotherapy[1]. Checkmate 358 (Hollebecque et al., 2017) (phases I–II studies) adopted nivolumab (200 mg/kg q2w) for the treatment of recurrent, metastatic cervical cancer and resulted in an ORR of 26.3%. The disease control rate was 70.8%. The related grades 3–4 toxic effects included hyponatremia, syncope, diarrhea, and hepatocellular injury. From these three studies, pembrolizumab and nivolumab showed promising antitumor effects and were well-tolerated in patients with recurrent or metastatic cervical cancer. However, due to a limited follow-up time, PFS and OS were not reported. Additionally, the REGN2810 study (Papadopoulos et al., 2016), a phase I multicenter study, assessed REGN2810 (a PD-1 mAb) as a monotherapy and in combination with hfRT, in combination with cyclophosphamide (CTX) or with CTX + hfRT in patients with advanced solid tumors, including cervical cancer. This study adopted a dose escalation design, and as of February 2016, no dose-limiting

[1]https://www.fda.gov/Drugs/InformationOnDrugs/ApprovedDrugs/ucm610572.htm

TABLE 3 | Ongoing clinical research on PD-1/PD-L1 in cervical cancer.

Clinical trial code	Study	Study population (n)	Phase	Treatment arm(s)	Primary outcome measures	Secondary outcome measures
NCT02257528	Nivolumab in Treating Patients with Persistent, Recurrent, or Metastatic Cervical Cancer (NRG-GYO-02)	Recurrent or metastatic cervical cancer (25)	II	Nivolumab	ORR[1] [5 y]; AE[2] [100 d]	PFS[3] [5 y], OS[4] [5 y]
NCT03298893	Nivolumab in Association with Radiotherapy and Cisplatin in Locally Advanced Cervical Cancers Followed by Adjuvant Nivolumab for up to 6 Months (NiCOL)	Locally advanced cervical cancer (21)	III	Nivolumab	DLT[5] [11 w]	ORR[1] [2 m], PFS[3] [2 y], DFS[6] [2 y], SAE[7] [100 d], AE[2] [100 d], etc.
NCT03257267	Study of REGN2810 in Adults with Cervical Cancer (GOG 3016/ENGOT-cx9) (EMPOWER-Cervical)	Recurrent or metastatic platinum-refractory cervical cancer (436)	III	Cemiplimab (REGN2810)	OS[4] [32 m]	PFS[3] [32 m], ORR[1] [32 m], DOR[8] [32 m], Quality of life (QOL) [100 w]
NCT03104699	Phase 1/2 Study of AGEN2034 in Advanced Tumors and Cervical Cancer	Advanced cervical cancer (75)	I–II	AGEN2034	DLTs[5] [3 w], MTD[9] [1 y], BOR[10] [1 y]	Cmax[11] [1 y], AUC[12] [1 y], PFS[3] [1 y], DOR[8] [1 y], OS[4] [1 y]
NCT03518606	Metronomic Oral Vinorelbine Plus Anti-PD-L1/Anti-CTLA4 ImmunothErapy in Patients with Advanced Solid Tumors (MOVIE)	Advanced solid tumors (150) including cervical cancer	I–II	Durvalumab +Tremelimumab +metronomic Vinorelbine	Phase I: MTD[9] and RP2D[13] [9 m] Phase II: CBR[14] [24 m]	None
NCT03556839	Platinum Chemotherapy Plus Paclitaxel with Bevacizumab and Atezolizumab in Metastatic Carcinoma of the Cervix	Carcinoma of the cervix, stage IVB (404)	III	Atezolizumab	OS[4] [48 m]	PFS[3] [48 m], ORR[1] [48 m], DOR[8] [48 m], AE[2] [48 m], etc.
NCT01975831	A Phase 1 Study to Evaluate MEDI4736 in Combination with Tremelimumab	Solid tumors (106) including cervical cancer	I	MEDI4736 (Durvalumab)+Trem elimumab	AE[2] [1 y]	AUC[12], Cmax[11] [15 m], PFS[3] [15 m], OS[4] [15 m], etc.
NCT02914470	Pilot Study of Durvalumab and Vigil in Advanced Women's Cancers (PROLOG)	Solid tumors (12) including cervical cancer	I	Durvalumab and Vigil	Toxicity [30 d]	ORR[1] [120 m]
NCT02725489	Pilot Study of Durvalumab and Vigil in Advanced Women's Cancers	Solid tumors (15) including cervical cancer	II	Vigil+durvalumab	AEs[2] [90 d]	ORR[1] [12 m], Disease status [12 m], IFNγ-ELISPOT conversion rate [12 w]
NCT02921269	Atezolizumab and Bevacizumab in Treating Patients with Recurrent, Persistent, or Metastatic Cervical Cancer	Recurrent, persistent, or metastatic cervical cancer (22)	II	Atezolizumab +Bevac izumab	ORR[1] [2 y]	PFS[3] [2 y], OS[4] [2 y] AE[2] [30 d], PD-L1, etc.
NCT03635567	Efficacy and Safety Study of First-line Treatment with Pembrolizumab (MK-3475) Plus Chemotherapy Versus Placebo Plus Chemotherapy in Women with Persistent, Recurrent, or Metastati Cervical Cancer (MK-3475-826/KEYNOTE-826)	Cervical cancer (600) c	I–II	Pembrolizumab	PFS[3] [2y] OS[4] [2 y]	ORR[1] [2 y], DOR[8] [2 y], etc.
NCT03144466	A Study of Pembrolizumab And Platinum with Radiotherapy in Cervix Cancer (PAPAYA)	Cervical cancer (26)	I	Pembrolizum	MTD[9] [2 y] ab Efficacy [2 y]	OS[4] [2 y], PFS[3] [2 y], etc.
NCT03255252	Assessment Study to Evaluate Specific Immune Response in Locally Advanced Cervix Cancer After Radio-chemotherapy (IMMUVIX)	Cervical cancer (100)	II	Cisplatin	Expression of CD8+CD39+PD1+	Effect on 1-year DFS[6] of other putative biomarkers (CD73, CD39, PD1 and Tim3)
NCT03559803	A Prospective Study of Monitoring Immune Response in Locally Advanced Cervix Cancer(GHR002)	Cervical cancer(50)	Not appli cable	Cisplatin	PD-L1 [3w, 2 m]	PD1+CD4+T [3w, 2 m], PD1+CD8+T [3w, 2 m], TCR[3w, 2 m]

[1]ORR, objective response rate; [2]AE, adverse event; [3]PFS, progression-free survival; [4]OS, overall survival rate; [5]DLT, dose limiting toxicity; [6]DFS, disease-free survival; [7]SAE, serious adverse event; [8]DOR, duration of response; [9]MTD, maximum tolerated dose; [10]BOR, best overall response; [11]Cmax, maximum plasma concentration; [12]AUC, area under curve; [13]RP2D, phase II recommended dose; [14]CBR, clinical benefit response.

toxicity (DLT) was observed. The most common treatment-related AEs were fatigue (n = 14, 24.1%), arthralgia (n = 7, 12.1%), and nausea (n = 6, 10.3%). Additionally, 4 patients experienced grade $\geq$ 3 AEs. For 9/22 (40.9%) patients who received REGN2810 + hfRT and 2/21 (9.5%) patients who received REGN2810 monotherapy, they were determined to have partial/uPRs, suggesting that the treatment response was augmented by the addition of hfRT.

ONGOING CLINICAL RESEARCH ON PD-1/PD-L1 IN CERVICAL CANCER

As of September 2018, 11 clinical trials have been conducted, mainly in patients with persistent, recurrent, or metastatic cervical cancer, with only three studies on patients with locally advanced cervical cancer. Twenty to thirty cases were intended to be included in the majority of these studies, while there were only three studies (Keynote 826, GOG 3016/ENGOT-cx9, and NCT03556839) in which more than 200 cases were intended to be included. Except for the two studies (IMMUVIX, GHR002) aimed at exploring the immune status of PD-1/PD-L1 in patients with locally advanced cervical cancer, the remaining 12 studies all looked into the applicability of PD-1/PD-L1 inhibitors in cervical cancer. Of these 12 studies, there are 2 studies on nivolumab, 2 on pembrolizumab, 4 on durvalumab, 2 on atezolizumab, 1 on cemiplimab (REGN2810) and 1 on AGEN2034. For PD-1 inhibitors, the difference between the 2 studies on nivolumab is the study population. NRG-GYO-02 was conducted in patients with persistent, recurrent, or metastatic cervical cancer, while the NiCOL study enrolled more patients with locally advanced cervical cancer. The main difference between the two studies on pembrolizumab is that KEYNOTE-826 adopted pembrolizumab in combination with chemotherapy versus placebo, while PAPAYA mainly adopted pembrolizumab in combination with platinum and radiotherapy. The GOG 3016/ENGOT-cx9 (EMPOWER-Cervical) study is an important phase III clinical study to advance the clinical application of cemiplimab (REGN2810) in advanced cervical cancer. NCT03104699 is a phase I/II clinical study on AGEN2034, another PD-1 inhibitor, in advanced solid tumors that includes 75 cases of cervical cancer. In terms of treatment combinations, tremelimumab (a fully human mAb against CTLA-4), Vigil vaccine for cervical cancer, bevacizumab, and chemotherapy were paired with PD-1/PD-L1 inhibitors throughout these studies (**Table 3**).

CONCLUSION

Although there are a few studies suggesting the potential feasibility of PD-1/PD-L1 inhibitors for the treatment of cervical cancer, a consideration should be made for the clinical application of PD-1/PD-L1 inhibitors. The inadequate number of cases included and the insufficient follow-up time are the main defects of all the studies, leading to the unavailability of data regarding OS, PFS, AEs, drug resistance and the treatment mechanism as well. These data are very pivotal not only for obtaining a more convincing result, but also for guiding physicians to select the appropriate patients for PD-1/PD-L1 inhibitors.

Currently, most of these studies, including ongoing studies, are mostly limited to recurrent, persistent, metastatic cervical cancer, which accounts for only a minor portion of patients with cervical cancer. There are several future directions that can be given more attention. First, the latest evidence suggests a clinical benefit of PD-1/PD-L1 inhibitors as neoadjuvant therapy in lung cancer (Lommatzsch et al., 2018). For patients with early-stage cervical cancer, studies in a small sample size can be conducted to investigate PD-1/PD-L1 inhibitors with attempted surgical treatment or to prevent post-operative recurrence. Second, for patients with locally advanced cervical cancer who are not sensitive to CCRT or who relapse in the short term after initial treatment, PD-1/PD-L1 inhibitors may be a useful treatment, and we are looking forward to the research targeting this population. Third, for locally advanced cervical cancer patients, whether PD-1/PD-L1 inhibitors can achieve better therapeutic efficacy in tumors with higher PD-L1 expression before CCRT begins will provide a better understanding of the effects of these inhibitors. Finally, since PD-L1 expression is correlated with HPV status, more studies are warranted to provide further insights into the association of HPV status and the efficacy of PD-1/PD-L1 inhibitors in patients with cervical cancer. Combining the level of HPV DNA with the expression of PD-L1 may also provide a novel predictive biomarker of the efficacy of PD-1/PD-L1 inhibitors and the prognosis of patients with cervical cancer.

AUTHOR CONTRIBUTIONS

JX and YoL conceived the review. YuL and LYi searched the literature. YuL, LYi, LW, FY, ML, LY, and RT critically appraised the literature and wrote and all authors approved the final version of the manuscript.

FUNDING

This work was supported by National Natural Science Foundation of China (grants 81672982 and 81602670) and Sichuan Provincial Research Foundation for Basic Research (No. 18YYJC1284).

REFERENCES

Amatore, F., Gorvel, L., and Olive, D. (2018). Inducible co-stimulator (ICOS) as a potential therapeutic target for anti-cancer therapy. *Expert. Opin. Ther. Targets* 22, 343–351. doi: 10.1080/14728222.2018.1444753

Bagcchi, S. (2014). Pembrolizumab for treatment of refractory melanoma. *Lancet Oncol.* 15:e419. doi: 10.1016/S1470-2045(14)70348-1

Balermpas, P., Martin, D., Wieland, U., Rave-Frank, M., Strebhardt, K., Rodel, C., et al. (2017). Human papilloma virus load and PD-1/PD-L1, CD8(+) and FOXP3 in anal cancer patients treated with chemoradiotherapy: rationale for

immunotherapy. *Oncoimmunology* 6:e1288331. doi: 10.1080/2162402X.2017.1288331

Borcoman, E., and Le Tourneau, C. (2017). Pembrolizumab in cervical cancer: latest evidence and clinical usefulness. *Ther. Adv. Med. Oncol.* 9, 431–439. doi: 10.1177/1758834017708742

Boussios, S., Seraj, E., Zarkavelis, G., Petrakis, D., Kollas, A., Kafantari, A., et al. (2016). Management of patients with recurrent/advanced cervical cancer beyond first line platinum regimens: where do we stand? A literature review. *Crit. Rev. Oncol. Hematol.* 108, 164–174. doi: 10.1016/j.critrevonc.2016.11.006

Boussiotis, V. A. (2016). Molecular and biochemical aspects of the PD-1 checkpoint pathway. *N. Engl. J. Med.* 375, 1767–1778. doi: 10.1056/NEJMra1514296

Bray, F., Ferlay, J., Soerjomataram, I., Siegel, R. L., Torre, L. A., and Jemal, A. (2018). Global cancer statistics 2018: globocan estimates of incidence and mortality worldwide for 36 cancers in 185 countries. *CA Cancer J. Clin.* 68, 394–424. doi: 10.3322/caac.21492

Cancer Genome Atlas Research Network, Albert Einstein College of Medicine, Analytical Biological Services, Barretos Cancer Hospital, Baylor College of Medicine, Beckman Research Institute of City of Hope, et al. (2017). Integrated genomic and molecular characterization of cervical cancer. *Nature* 543, 378–384. doi: 10.1038/nature21386

Chen, J., Gu, W., Yang, L., Chen, C., Shao, R., Xu, K., et al. (2015). Nanotechnology in the management of cervical cancer. *Rev. Med. Virol.* 25(Suppl. 1), 72–83. doi: 10.1002/rmv.1825

Chen, Z., Pang, N., Du, R., Zhu, Y., Fan, L., Cai, D., et al. (2016). Elevated expression of programmed death-1 and programmed death ligand-1 negatively regulates immune response against cervical cancer cells. *Med. Inflamm.* 2016:6891482. doi: 10.1155/2016/6891482

Compte, M., Harwood, S. L., Munoz, I. G., Navarro, R., Zonca, M., Perez-Chacon, G., et al. (2018). A tumor-targeted trimeric 4-1BB-agonistic antibody induces potent anti-tumor immunity without systemic toxicity. *Nat. Commun.* 9:4809. doi: 10.1038/s41467-018-07195-w

Constantinidou, A., Alifieris, C., and Trafalis, D. T. (2018). Targeting programmed cell death -1 (PD-1) and ligand (PD-L1): a new era in cancer active immunotherapy. *Pharmacol. Ther.* 18, 30173–30176. doi: 10.1016/j.pharmthera.2018.09.008

Dijkstra, K. K., Voabil, P., Schumacher, T. N., and Voest, E. E. (2016). Genomics- and transcriptomics-based patient selection for cancer treatment with immune checkpoint inhibitors: a review. *JAMA Oncol.* 2, 1490–1495. doi: 10.1001/jamaoncol.2016.2214

Enwere, E. K., Kornaga, E. N., Dean, M., Koulis, T. A., Phan, T., Kalantarian, M., et al. (2017). Expression of PD-L1 and presence of CD8-positive T cells in pre-treatment specimens of locally advanced cervical cancer. *Mod. Pathol.* 30, 577–586. doi: 10.1038/modpathol.2016.221

Feng, Y. C., Ji, W. L., Yue, N., Huang, Y. C., and Ma, X. M. (2018). The relationship between the PD-1/PD-L1 pathway and DNA mismatch repair in cervical cancer and its clinical significance. *Cancer Manag. Res.* 10, 105–113. doi: 10.2147/CMAR.S152232

Fife, B. T., and Bluestone, J. A. (2008). Control of peripheral T-cell tolerance and autoimmunity via the CTLA-4 and PD-1 pathways. *Immunol. Rev.* 224, 166–182. doi: 10.1111/j.1600-065X.2008.00662.x

Franzen, A., Vogt, T. J., Muller, T., Dietrich, J., Schrock, A., Golletz, C., et al. (2018). PD-L1 (CD274) and PD-L2 (PDCD1LG2) promoter methylation is associated with HPV infection and transcriptional repression in head and neck squamous cell carcinomas. *Oncotarget* 9, 641–650. doi: 10.18632/oncotarget.23080

Frenel, J. S., Le Tourneau, C., O'neil, B., Ott, P. A., Piha-Paul, S. A., Gomez-Roca, C., et al. (2017). Safety and efficacy of pembrolizumab in advanced, programmed death ligand 1-positive cervical cancer: results from the phase Ib KEYNOTE-028 trial. *J. Clin. Oncol.* 35, 4035–4041. doi: 10.1200/JCO.2017.74.5471

Gettinger, S., Horn, L., Jackman, D., Spigel, D., Antonia, S., Hellmann, M., et al. (2018). Five-year follow-up of nivolumab in previously treated advanced non-small-cell lung cancer: results from the CA209-003 study. *J. Clin. Oncol.* 36, 1675–1684. doi: 10.1200/JCO.2017.77.0412

Goodman, A. (2015). HPV testing as a screen for cervical cancer. *BMJ* 350:h2372. doi: 10.1136/bmj.h2372

Gorris, M. A. J., Halilovic, A., and Rabold, K. (2018). Eight-color multiplex immunohistochemistry for simultaneous detection of multiple immune checkpoint molecules within the tumor microenvironment. *J. Immunol.* 200, 347–354. doi: 10.4049/jimmunol.1701262

Guitarte, C., Alagkiozidis, I., Mize, B., Stevens, E., Salame, G., and Lee, Y. C. (2014). Glassy cell carcinoma of the cervix: a systematic review and meta-analysis. *Gynecol. Oncol.* 133, 186–191. doi: 10.1016/j.ygyno.2014.01.048

Heeren, A. M., Punt, S., Bleeker, M. C., Gaarenstroom, K. N., Van Der Velden, J., Kenter, G. G., et al. (2016). Prognostic effect of different PD-L1 expression patterns in squamous cell carcinoma and adenocarcinoma of the cervix. *Mod. Pathol.* 29, 753–763. doi: 10.1038/modpathol.2016.64

Hodi, F. S., O'day, S. J., Mcdermott, D. F., Weber, R. W., Sosman, J. A., Haanen, J. B., et al. (2010). Improved survival with ipilimumab in patients with metastatic melanoma. *N. Engl. J. Med.* 363, 711–723. doi: 10.1056/NEJMoa1003466

Hollebecque, A., Meyer, T., Moore, K. N., Machiels, J.-P. H., De Greve, J., López-Picazo, J. M., et al. (2017). An open-label, multicohort, phase I/II study of nivolumab in patients with virus-associated tumors (CheckMate 358): efficacy and safety in recurrent or metastatic (R/M) cervical, vaginal, and vulvar cancers. *J. Clin. Oncol.* 35:5504. doi: 10.1200/JCO.2017.35.15_suppl.5504

Hsu, P. C., Li, S. H., and Yang, C. T. (2018). Recurrent pneumonitis induced by atezolizumab (anti-programmed death ligand 1) in NSCLC patients who previously experienced anti-programmed death 1 immunotherapy-related pneumonitis. *J. Thorac. Oncol.* 13, e227–e230. doi: 10.1016/j.jtho.2018.06.022

Julia, E. P., Amante, A., Pampena, M. B., Mordoh, J., and Levy, E. M. (2018). Avelumab, an IgG1 anti-PD-L1 immune checkpoint inhibitor, triggers NK cell-mediated cytotoxicity and cytokine production against triple negative breast cancer cells. *Front. Immunol.* 9:2140. doi: 10.3389/fimmu.2018.02140

Kurup, S. P., Obeng-Adjei, N., Anthony, S. M., Traore, B., Doumbo, O. K., Butler, N. S., et al. (2017). Regulatory T cells impede acute and long-term immunity to blood-stage malaria through CTLA-4. *Nat. Med.* 23, 1220–1225. doi: 10.1038/nm.4395

Lai, Y. L., Chen, L. C., Huang, C. Y., Chiang, S. F., Liang, J. A., Chao, K. S. C., et al. (2017). PD-L1 as the prognostic immune biomarker for predicting the relapse of locally advanced cervical adenocarcinoma and adenosquamous carcinoma treated with definitive chemoradiation therapy. *Int. J. Radiat. Oncol. Biol. Phys.* 99, E299–E300. doi: 10.1016/j.ijrobp.2017.06.1318

Le Tourneau, C., Hoimes, C., Zarwan, C., Wong, D. J., Bauer, S., Claus, R., et al. (2018). Avelumab in patients with previously treated metastatic adrenocortical carcinoma: phase 1b results from the JAVELIN solid tumor trial. *J. Immunother. Cancer* 6:111. doi: 10.1186/s40425-018-0424-9

Lheureux, S., Butler, M. O., Clarke, B., Cristea, M. C., Martin, L. P., Tonkin, K., et al. (2018). Association of ipilimumab with safety and antitumor activity in women with metastatic or recurrent human papillomavirus-related cervical carcinoma. *JAMA Oncol.* 4:e173776. doi: 10.1001/jamaoncol.2017.3776

Lim, M., Xia, Y., Bettegowda, C., and Weller, M. (2018). Current state of immunotherapy for glioblastoma. *Nat. Rev. Clin. Oncol.* 15, 422–442. doi: 10.1038/s41571-018-0003-5

Liu, C., Lu, J., Tian, H., Du, W., Zhao, L., Feng, J., et al. (2017). Increased expression of PDL1 by the human papillomavirus 16 E7 oncoprotein inhibits anticancer immunity. *Mol. Med. Rep.* 15, 1063–1070. doi: 10.3892/mmr.2017.6102

Liu, Y. L., and Zamarin, D. (2018). Combination immune checkpoint blockade strategies to maximize immune response in gynecological cancers. *Curr. Oncol. Rep.* 20:94. doi: 10.1007/s11912-018-0740-8

Lommatzsch, M., Bratke, K., and Stoll, P. (2018). Neoadjuvant PD-1 blockade in resectable lung cancer. *N. Engl. J. Med.* 379:e14. doi: 10.1056/NEJMc1808251

Long, G. V., Tykodi, S. S., Schneider, J. G., Garbe, C., Gravis, G., Rashford, M., et al. (2018). Assessment of nivolumab exposure and clinical safety of 480 mg every 4 weeks flat-dosing schedule in patients with cancer. *Ann. Oncol.* 29, 2208–2213. doi: 10.1093/annonc/mdy408

Meng, Y., Liang, H., Hu, J., Liu, S., Hao, X., Wong, M. S. K., et al. (2018). PD-L1 Expression correlates with tumor infiltrating lymphocytes and response to neoadjuvant chemotherapy in cervical cancer. *J. Cancer* 9, 2938–2945. doi: 10.7150/jca.22532

Mezache, L., Paniccia, B., Nyinawabera, A., and Nuovo, G. J. (2015). Enhanced expression of PD L1 in cervical intraepithelial neoplasia and cervical cancers. *Mod. Pathol.* 28, 1594–1602. doi: 10.1038/modpathol.2015.108

Minion, L. E., and Tewari, K. S. (2018). Cervical cancer - state of the science: from angiogenesis blockade to checkpoint inhibition. *Gynecol. Oncol.* 148, 609–621. doi: 10.1016/j.ygyno.2018.01.009

Monk, B. J., Sill, M. W., Mcmeekin, D. S., Cohn, D. E., Ramondetta, L. M., Boardman, C. H., et al. (2009). Phase III trial of four cisplatin-containing doublet combinations in stage IVB, recurrent, or persistent cervical carcinoma: a gynecologic oncology group study. *J. Clin. Oncol.* 27, 4649–4655. doi: 10.1200/JCO.2009.21.8909

Papadopoulos, K. P., Crittenden, M. R., Johnson, M. L., Lockhart, A. C., Moore, K. N., and Falchook, G. S. (2016). A first-in-human study of REGN2810, a monoclonal, fully human antibody to programmed death-1 (PD-1), in combination with immunomodulators including hypofractionaed radiotherapy (hfRT). *J. Clin. Oncol.* 34:3024. doi: 10.1200/JCO.2016.34.15_suppl.3024

Pardoll, D. M. (2012). The blockade of immune checkpoints in cancer immunotherapy. *Nat. Rev. Cancer* 12, 252–264. doi: 10.1038/nrc3239

Paz-Ares, L., Luft, A., Vicente, D., Tafreshi, A., Gumus, M., Mazieres, J., et al. (2018). Pembrolizumab plus chemotherapy for squamous non-small-cell lung cancer. *N. Engl. J. Med.* 379, 2040–2051. doi: 10.1056/NEJMoa1810865

Polesso, F., Weinberg, A., and Moran, A. E. (2018). Late stage tumor regression after PD-L1 blockade with a concurrent OX40 agonist. *Cancer Immunol. Res.* doi: 10.1158/2326-6066.CIR-18-0222 [Epub ahead of print].

Qin, Y., Ekmekcioglu, S., Forget, M. A., Szekvolgyi, L., Hwu, P., Grimm, E. A., et al. (2017). Cervical cancer neoantigen landscape and immune activity is associated with human papillomavirus master regulators. *Front. Immunol.* 8:689. doi: 10.3389/fimmu.2017.00689

Raedler, L. A. (2015). Opdivo (Nivolumab): second PD-1 inhibitor receives FDA approval for unresectable or metastatic melanoma. *Am. Health Drug Benefits* 8, 180–183.

Reddy, O. L., Shintaku, P. I., and Moatamed, N. A. (2017). Programmed death-ligand 1 (PD-L1) is expressed in a significant number of the uterine cervical carcinomas. *Diagn. Pathol.* 12:45. doi: 10.1186/s13000-017-0631-6

Sahasrabuddhe, V. V., Parham, G. P., Mwanahamuntu, M. H., and Vermund, S. H. (2012). Cervical cancer prevention in low- and middle-income countries: feasible, affordable, essential. *Cancer Prevent. Res.* 5, 11–17. doi: 10.1158/1940-6207.CAPR-11-0540

Schellens, J. H. M., Marabelle, A., Zeigenfuss, S., Ding, J., Pruitt, S. K., and Chung, H. C. (2017). Pembrolizumab for previously treated advanced cervical squamous cell cancer:preliminary results from the phase 2 KEYNOTE-158 study. *J. Clin. Oncol.* 35:5514. doi: 10.1200/JCO.2017.35.15_suppl.5514

Schumacher, T. N., and Schreiber, R. D. (2015). Neoantigens in cancer immunotherapy. *Science* 348, 69–74. doi: 10.1126/science.aaa4971

Sidaway, P. (2018). Cemiplimab effective in cutaneous SCC. *Nat. Rev. Clin. Oncol.* 15:472. doi: 10.1038/s41571-018-0056-5

Siu, L. L., Even, C., Mesia, R., Remenar, E., Daste, A., Delord, J. P., et al. (2018). Safety and efficacy of durvalumab with or without tremelimumab in patients with PD-L1-low/negative recurrent or metastatic HNSCC: the phase 2 CONDOR randomized clinical trial. *JAMA Oncol.* doi: 10.1001/jamaoncol.2018.4628[Epub ahead of print].

Tewari, K. S., Sill, M. W., Long, H. J. III, Penson, R. T., Huang, H., Ramondetta, L. M., et al. (2014). Improved survival with bevacizumab in advanced cervical cancer. *N. Engl. J. Med.* 370, 734–743. doi: 10.1056/NEJMoa1309748

Tewari, K. S., Sill, M. W., Penson, R. T., Huang, H., Ramondetta, L. M., Landrum, L. M., et al. (2017). Bevacizumab for advanced cervical cancer: final overall survival and adverse event analysis of a randomised, controlled, open-label, phase 3 trial (gynecologic oncology group 240). *Lancet* 390, 1654–1663. doi: 10.1016/S0140-6736(17)31607-0

Wang, J., Chmielowski, B., Pellissier, J., Xu, R., Stevinson, K., and Liu, F. X. (2017). Cost-Effectiveness of pembrolizumab versus ipilimumab in ipilimumab-naive patients with advanced melanoma in the United States. *J. Manag. Care Spec. Pharm.* 23, 184–194. doi: 10.18553/jmcp.2017.23.2.184

Yang, W., Lu, Y. P., Yang, Y. Z., Kang, J. R., Jin, Y. D., and Wang, H. W. (2017). Expressions of programmed death (PD)-1 and PD-1 ligand (PD-L1) in cervical intraepithelial neoplasia and cervical squamous cell carcinomas are of prognostic value and associated with human papillomavirus status. *J. Obstet. Gynaecol. Res.* 43, 1602–1612. doi: 10.1111/jog.13411

Yang, W., Song, Y., Lu, Y. L., Sun, J. Z., and Wang, H. W. (2013). Increased expression of programmed death (PD)-1 and its ligand PD-L1 correlates with impaired cell-mediated immunity in high-risk human papillomavirus-related cervical intraepithelial neoplasia. *Immunology* 139, 513–522. doi: 10.1111/imm.12101

Zandberg, D. P., Algazi, A. P., Jimeno, A., Good, J. S., Fayette, J., Bouganim, N., et al. (2018). Durvalumab for recurrent or metastatic head and neck squamous cell carcinoma: results from a single-arm, phase II study in patients with > / = 25% tumour cell PD-L1 expression who have progressed on platinum-based chemotherapy. *Eur. J. Cancer* 107, 142–152. doi: 10.1016/j.ejca.2018.11.015

Zhang, S., and Li, W. (2018). The effort in exploration of a definitive predictive factor from PD-1/PD-L1 blockade in advanced or metastatic urothelial cancer. *J. Clin. Oncol.* 36, 3056–3057. doi: 10.1200/JCO.2018.79.1400

Conflict of Interest Statement: The authors declare that the research was conducted in the absence of any commercial or financial relationships that could be construed as a potential conflict of interest.

frontiers in Oncology

MINI REVIEW
published: 06 February 2019
doi: 10.3389/fonc.2019.00040

The CXCL8-CXCR1/2 Axis as a Therapeutic Target in Breast Cancer Stem-Like Cells

*Pier Adelchi Ruffini**

Research and Development Department, Dompé farmaceutici S.p.A., Milan, Italy

Cancer stem-like cells (CSC) have been targeted by different strategies over the last decade. This mini review focuses on preclinical and clinical results obtained by interfering with chemokine receptors CXCR1 and CXCR2 in breast cancer. This strategy is currently being tested in a randomized, double blind phase 2 clinical trial.

Keywords: CXCR1, CXCL8, cancer stem-like cells, reparixin, breast cancer

OPEN ACCESS

Edited by:
Zhe-Sheng Chen,
St. John's University, United States

Reviewed by:
Vijay Pandey,
National University of Singapore, Singapore
Fabrizio Martelli,
Istituto Superiore di Sanità (ISS), Italy

***Correspondence:**
Pier Adelchi Ruffini
pieradelchi.ruffini@dompe.com

Specialty section:
This article was submitted to Cancer Molecular Targets and Therapeutics, a section of the journal Frontiers in Oncology

Received: *30 October 2018*
Accepted: *15 January 2019*
Published: *06 February 2019*

Citation:
Ruffini PA (2019) The CXCL8-CXCR1/2 Axis as a Therapeutic Target in Breast Cancer Stem-Like Cells. Front. Oncol. 9:40. doi: 10.3389/fonc.2019.00040

Cancer stem-like cells (CSC) have been the focus of several clinical investigations testing different strategies for a more effective anticancer treatment through inhibition of this unique cell population (1). Targeting the CXCL8-CXCR1/2 axis is one such strategy that has moved from preclinical models to an ongoing randomized phase 2 clinical trial in breast cancer.

CXCL8 (formerly IL-8) is a chemokine whose biological effects are mediated by two G-protein-coupled receptors: **CXCR1** and **CXCR2** (2). CXCL8 has been reported to play multiple roles in cancer, such as increasing proliferation, angiogenesis, invasion, and metastases (3). In **breast cancer**, recent evidence points to this chemokine as a key regulator of CSC activity (4).

PRECLINICAL EVIDENCE IN BREAST CANCER

In breast cancer, tumor cells capable of forming tumors in immunocompromised mice (i.e., CSC by a functional definition) are identified by the expression of either the enzyme aldehyde dehydrogenase (ALDH) (5) and/or the $CD24^{-}/CD44^{+}$ phenotype (6), representing two largely non-overlapping cell populations. CXCR1 was identified as a druggable target on breast cancer CSC identified by the expression of ALDH, while its expression was almost undetectable on bulk (i.e., non-CSC) tumor cells (7). In keeping, breast cancer CSC were shown to proliferate *in vitro* in response to the addition of exogenous CXCL8 while a small molecular weight antagonist of CXCR1/2 (**reparixin**) (8) or a blocking anti-CXCR1 (but not anti-CXCR2) monoclonal antibody were both able to deplete CSC *in vitro* (9). A FAS-FASL mediated bystander effect killed the vast majority of bulk tumor cells *in vitro*, suggesting the possibility of synergistic effects with chemotherapy (9). In human breast cancer cell lines or breast cancer patient-derived xenografts orthotopically implanted in mice, the combination of weekly docetaxel and reparixin for 4 weeks was more effective than either treatment alone in reducing tumor size (9). However, in tumors recovered from mice that had been treated with reparixin, either alone or in combination with chemotherapy, CSC proportion was far lower than in tumors recovered from mice receiving chemotherapy alone (9). These results were framed in a model where, following administration of chemotherapy, CXCL8 and FASL are released by dying bulk tumor cells. Engagement of CXCR1 on the surface of CSC by CXCL8 shelters CSC from apoptotic signals delivered by FASL. To the contrary, when CXCR1 signaling on CSC is blocked by reparixin these cells undergo FASL-mediated apoptosis. Evidence provided later by independent laboratories supports this model. First, as originally reported by Ginestier and coworkers, tumor cells exposed to taxane

in vitro release CXCL8 (10). Also, Triple-Negative Breast Cancer (TNBC) tumor cells recovered from immunocompromised mice following two doses of paclitaxel displayed a marked and dose-dependent increase in mammosphere forming efficiency as compared with untreated mice (10). Furthermore, and again in line with the original report by Ginestier, administration of a CXCR1 inhibitor reduced CSC percentage *in vitro*. Consistent findings were later reported by an independent group (11). Second, in breast cancer patients with pleural effusions and/or ascites CXCL8 levels were measured and tumor cells recovered and cultured *in vitro* (4). A direct correlation was observed between CXCL8 levels and CSC activity by means of mammosphere formation (4). Surface CXCR1 was detected on the majority of mammosphere cells, and the effects of exogenous CXCL8 on mammosphere formation were blocked by a CXCR1/2 inhibitor, SCH563705 (4).

The relative contribution of CXCR1 inhibition and paclitaxel in this model were further investigated in CSC-enriched mammospheres from the human TNBC cell line MDA-MB231. The combination treatment displayed a synergistic effect on mammosphere number and an additive effect on mammosphere volume as compared with either treatment alone (12). Different than paclitaxel, which increased the number of dead cells, reparixin increased the number of non-proliferating cells, and the combination treatment exerted both effects (12). In keeping with previous reports (9), also in MDA-MB231-derived tumorspheres reparixin activity was mediated by inhibition of the FAK/AKT pathway which is unaffected by paclitaxel. When the effects on cell cycle were investigated, a shift of tumor cells in S phase or a block in G2 phase were observed upon paclitaxel and combination treatment, respectively. In keeping, cyclin B1, which is responsible for the cell cycle progression from G2 to S phase, was also inhibited by the combination treatment (12). Furthermore, paclitaxel + reparixin treatment induced "cell senescence by decreasing PI3K-Akt activation paralleled by a decrease of the cytosolic p-FOXO3A (inactive) and by an increase of p27" (12). The effects on cell cycle, cyclin B1 and p-FAK levels recorded upon exposure to reparixin were reproduced using neutralizing anti-CXCR1 and anti-CXCL8 monoclonal antibodies, thus providing indirect evidence of the ability of reparixin to downregulate CXCL8-CXCR1signaling pathway (12).

Another set of experiments aimed at testing the hypothesis that inhibition of CSC would reduce metastatic spread. First, it was shown that reparixin administration reduced metastasis formation in mice following injection of luciferase-transfected human breast cancer cells into the bloodstream (9). Second, the suppressive activity of CXCR1 inhibition on the metastatic process was tested in a mouse model of brain metastases by the TNBC cell line MDA-MB231. In the absence of brain metastases, reparixin does not cross the blood brain barrier (BBB). However, in the presence of brain metastases and an allegedly damaged BBB, reparixin can be found in the central nervous system (12). When treatment was started on the same day when tumor cells were injected, a significant decrease of both the number and the volume of brain metastases was observed following single agent (i.e., reparixin or paclitaxel) as well as the combination treatment. When treatment was started at day 7 following tumor cell injection and continued until day 21, a significant reduction of the number of brain metastases was observed only following combination treatment, which also showed a trend toward an inhibitory effect on metastases volume (12).

PRECLINICAL EVIDENCE IN TUMORS OTHER THAN BREAST CANCER

Anti-tumor and anti CSC activity of reparixin has been demonstrated in human epithelial thyroid cancer *in vitro* and *in vivo* (13). Reparixin ability to inhibit stemness (evaluated by stemness marker expression and tumorsphere formation) and epithelial-mesenchymal transition (EMT) (evaluated at both the biochemical and functional level) of thyroid cancer was shown to be dependent, different than in breast cancer (9), on its activity on both CXCR1 and CXCR2 (13).

In malignant melanoma, CXCR1/2 inhibition reduced the percentage of ALDH+ cells in human tumors growing in nude athymic mice (14).

In pancreatic cancer (15) a positive correlation was found between CXCR1 and both CD44 and CD133 stemness marker expression. Exogenous CXCL8 added to pancreatic cancer cells *in vitro* increased their invasion ability, tumorsphere formation, and CSC population and addition of a CXCR1-blocking monoclonal antibody was able to revert all these effects (15).

CLINICAL TRIALS IN BREAST CANCER

In a phase Ib study (NCT02001974) (16), patients with HER-2 negative metastatic breast cancer not known to be refractory to paclitaxel who had received no more than three lines of cytotoxic chemotherapy in the metastatic setting were enrolled in cohorts of 3–6 patients to receive escalating doses of the CXCR1/2 inhibitor reparixin oral tablets three times per day (t.i.d.) from day 1 to 21 in combination with a fixed dose of weekly paclitaxel (80 mg/m^2) on days 1, 8, and 15 of a 28-days cycle, for as long as clinical benefit was observed. Primary objectives were the assessment of the safety of the combination and the pharmacokinetic (PK) profile of oral reparixin. Expansion of the highest dose cohort was foreseen to gain additional PK and safety data. Cohorts 1–3 received reparixin 400, 800, and 1,200 mg t.i.d. respectively. In cycle 1 only, patients received a 3 days course of reparixin alone (day −3 to −1) at the assigned dose for the cohort, for purpose of obtaining single agent PK data.

Thirty-three patients were enrolled in the study. Eighty-three percent of patients had visceral disease, and the majority had two or more sites of metastasis. 20/33 patients had received prior (neo)adjuvant chemotherapy, and 16 of these patients had received a taxane in the (neo)adjuvant setting. 19/33 had received chemotherapy in the metastatic setting, with 11 having one prior metastatic regimen and eight having two or more chemotherapy regimens. Thirty patients were evaluated for safety. There were no dose limiting toxicities in any cohort. Most adverse reactions (ADR) were of grade 1 (79.8%), with only 2.7% grade 3 ADR. There was no apparent dose effect of increasing reparixin dose

on the incidence, severity or profile of treatment emergent adverse events (TEAE) experienced by the treatment groups, and there were no clinically significant differences between the treatment groups with regards to laboratory measurements, vital signs, ECG, and physical examination assessments. Twenty-seven patients were evaluated for antitumor activity. In total, 8/27 patients had a confirmed RECIST response. Of responding patients, all but one were from cohort 3. Median time to progression (TTP) (95% C.I.) for the 3 cohorts were 58 days (44-infinity) for cohort 1, 67 days (58–82) for cohort 2 and 162 days (60–229) for cohort 3. Remarkably, there were long term remissions among patients treated (16). In this trial, it was not possible to obtain optional serial biopsies of tumor tissue at study entry and during treatment from any patient. However, blood-based biomarkers of CSC were explored. The circulating biomarkers included Circulating Tumor Cell (CTC) enumeration, evaluation of ALDEFLUOR, and EMT transcription factors in peripheral blood, and serum cytokine measurements. Unfortunately, no clear pattern of change in any of these markers was observed. This is likely related to multiple issues, including but not limited to small sample size, low CTC number in the enrolled patient population leading to limited tumor material for testing, and high baseline heterogeneity in the measurements.

Operable breast cancer is a more suitable clinical setting to evaluate the ability of a novel agent to reduce the number of CSC following treatment, as they can be measured on readily available tumor tissue. Thus, after reviewing safety data from the second cohort of the above trial, a window-of-opportunity, pilot trial (NCT01861054) of single agent reparixin was started (17).

Patients with previously untreated HER-2 negative operable breast cancer not eligible for neo(adjuvant) treatment were divided into two cohorts, i.e., group A: histologically proven ER^+ and/or PgR^+ and group B: ER^-/PgR^- breast cancer (i.e., TNBC). This design allowed potential to identify the cohort of patients who might benefit the most from this treatment in later stage clinical trials. Oral reparixin was administered at 1,000 mg t.i.d. for 21 consecutive days before curative surgery. Core biopsies were taken at baseline (day −14 to 0) and at the completion of therapy (day 21). The primary objectives of this study were to evaluate the effects of orally administered reparixin on CSC in the primary tumor and the tumor microenvironment and to evaluate the safety of oral reparixin. Signal of activity was defined as a ≥20% reduction of CSC (defined by either the $ALDH^+$ or $CD24^-/CD44^+$ phenotype) in tumor tissue from baseline values as measured by flow cytometry accompanied by a consistent reduction of the same cell population by immunohistochemistry (IHC).

A total of 20 patients were enrolled, 18 of whom in group A. Signal of activity was detected by flow cytometry in the majority of patients (18), but the very low numbers of CSC hindered the possibility to confirm flow cytometry results by IHC. However, the later published evidence that the two breast cancer CSC populations (i.e., $ALDH^+$ and $CD24^-/CD44^+$) investigated reside in different areas of primary breast tumors and can transition from one phenotype to the other (19) might affect the reliability of CSC counts in this patient population. More in general, the clinical relevance of a ≥20% reduction of CSC following a single 21-day course of reparixin in this patient population is unknown and was beyond the scope of this trial.

From a safety standpoint, also in this trial reparixin appeared to be well-tolerated with 10/20 patients experiencing one or more ADR, all of which of grade ≤2. Neither TEAE leading to treatment discontinuation nor delays in surgery due to TEAE were recorded.

CONCLUSIONS

Evidence for a CXCL8-CXCR1/2 axis in CSC has been reported by independent laboratories and offers a potential therapeutic target. Clinical trials aimed at testing the effective targeting of CSC through this axis have been conducted in breast cancer, where the most information is available from preclinical research. Reparixin appeared to be well-tolerated, however, such trials were faced with several issues for efficacy evaluation, e.g., the very low numbers of CSC in primary operable breast cancer. To circumvent this limitation, circulating markers for monitoring the effect of anti-CSC agents were explored but these assays turned out to be inadequate.

Future prospects for CSC targeting agents include the development of reliable assays to measure stem cell number and/or activity (20) in serial biopsies from accessible tumors (e.g., window-of-opportunity trials), and alternative endpoints in clinical trials in the metastatic setting. One possible endpoint is the development of metastases at new sites (21), which can have also clinical significance (22). In keeping with preclinical findings (9, 12), it is hypothesized that an effective anti-CSC treatment will impact on development of new metastases while progression of pre-existing metastases is more consistent with proliferation of non-CSC, bulk tumor cells that should be addressed by chemotherapy.

As concerns CXCR1/2 inhibition, a randomized, placebo-controlled clinical trial (NCT02370238) of weekly paclitaxel with and without reparixin in front line treatment of metastatic TNBC has completed enrolment. Identification of clinical (e.g., disease sensitivity to chemotherapy) and/or cellular/molecular biomarkers of patients most likely to benefit from treatment represents a future direction of research, while analysis of time to new metastasis may fuel development of this strategy in the (neo)adjuvant setting, also leveraging on safety data generated in metastatic patients.

AUTHOR CONTRIBUTIONS

The author confirms being the sole contributor of this work and has approved it for publication.

ACKNOWLEDGMENTS

The author is grateful to Sonia Amicarella (Dompé farmaceutici S.p.A.) for assistance with formatting the manuscript.

REFERENCES

1. Ramos EK, Hoffmann AD, Gerson SL, Liu H. New opportunities and challenges to defeat cancer stem cells. *Trends Cancer* (2017) 3:780–96. doi: 10.1016/j.trecan.2017.08.007
2. Zlotnik A, Yoshie O. The chemokine superfamily revisited. *Immunity* (2012) 36:705–16. doi: 10.1016/j.immuni.2012.05.008
3. Waugh DJ, Wilson C. The interleukin-8 pathway in cancer. *Clin Cancer Res.* (2008) 14:6735–41. doi: 10.1158/1078-0432.ccr-07-4843
4. Singh JK, Farnie G, Bundred NJ, Simoes BM, Shergill A, Landberg G, et al. Targeting CXCR1/2 significantly reduces breast cancer stem cell activity and increases the efficacy of inhibiting HER2 via HER2-dependent and -independent mechanisms. *Clin Cancer Res.* (2013) 19:643–56. doi: 10.1158/1078-0432.ccr-12-1063
5. Ginestier C, Hur MH, Charafe-Jauffret E, Monville F, Dutcher J, Brown M, et al. ALDH1 is a marker of normal and malignant human mammary stem cells and a predictor of poor clinical outcome. *Cell Stem Cell* (2007) 1:555–67. doi: 10.1016/j.stem.2007.08.014
6. Al-Hajj M, Wicha MS, Benito-Hernandez A, Morrison SJ, Clarke MF. Prospective identification of tumorigenic breast cancer cells. *Proc Natl Acad Sci USA.* (2003) 100:3983–8. doi: 10.1073/pnas.0530291100
7. Charafe-Jauffret E, Ginestier C, Iovino F, Wicinski J, Cervera N, Finetti P, et al. Breast cancer cell lines contain functional cancer stem cells with metastatic capacity and a distinct molecular signature. *Cancer Res.* (2009) 69:1302–13. doi: 10.1158/0008-5472.can-08-2741
8. Bertini R, Allegretti M, Bizzarri C, Moriconi A, Locati M, Zampella G, et al. Noncompetitive allosteric inhibitors of the inflammatory chemokine receptors CXCR1 and CXCR2: prevention of reperfusion injury. *Proc Natl Acad Sci USA.* (2004) 101:11791–6. doi: 10.1073/pnas.0402090101
9. Ginestier C, Liu S, Diebel ME, Korkaya H, Luo M, Brown M, et al. CXCR1 blockade selectively targets human breast cancer stem cells *in vitro* and in xenografts. *J Clin Invest.* (2010) 120:485–97. doi: 10.1172/jci39397
10. Bhola NE, Balko JM, Dugger TC, Kuba MG, Sanchez V, Sanders M, et al. TGF-beta inhibition enhances chemotherapy action against triple-negative breast cancer. *J Clin Invest.* (2013) 123:1348–58. doi: 10.1172/jci65416
11. Samanta D, Gilkes DM, Chaturvedi P, Xiang L, Semenza GL. Hypoxia-inducible factors are required for chemotherapy resistance of breast cancer stem cells. *Proc Natl Acad Sci USA.* (2014) 111:E5429–38. doi: 10.1073/pnas.1421438111
12. Brandolini L, Cristiano L, Fidoamore A, De Pizzol M, Di Giacomo E, Florio TM, et al. Targeting CXCR1 on breast cancer stem cells: signaling pathways and clinical application modelling. *Oncotarget* (2015) 6:43375–94. doi: 10.18632/oncotarget.6234
13. Liotti F, De Pizzol M, Allegretti M, Prevete N, Melillo RM. Multiple anti-tumor effects of Reparixin on thyroid cancer. *Oncotarget* (2017) 8:35946–61. doi: 10.18632/oncotarget.16412
14. Kemp DM, Pidich A, Larijani M, Jonas R, Lash E, Sato T, et al. Ladarixin, a dual CXCR1/2 inhibitor, attenuates experimental melanomas harboring different molecular defects by affecting malignant cells and tumor microenvironment. *Oncotarget* (2017) 8:14428–42. doi: 10.18632/oncotarget.14803
15. Chen L, Fan J, Chen H, Meng Z, Chen Z, Wang P, et al. The IL-8/CXCR1 axis is associated with cancer stem cell-like properties and correlates with clinical prognosis in human pancreatic cancer cases. *Sci Rep.* (2014) 4:5911. doi: 10.1038/srep05911
16. Schott AF, Goldstein LJ, Cristofanilli M, Ruffini PA, McCanna S, Reuben JM, et al. Phase Ib pilot study to evaluate reparixin in combination with weekly paclitaxel in patients with HER-2-negative metastatic breast cancer. *Clin Cancer Res.* (2017) 23:5358–65. doi: 10.1158/1078-0432.ccr-16-2748
17. Goldstein L, Sparano J, Perez R, Vito C, Reuben J, Landis M, et al. Abstract OT2-6-03: a single arm, preoperative, pilot study to evaluate the safety and biological effects of orally administered reparixin in early breast cancer patients who are candidates for surgery. *Cancer Res.* (2013) 73(24 Suppl.):OT2-6-03-OT02-06-03. doi: 10.1158/0008-5472.sabcs13-ot2-6-03
18. Goldstein LJ, Perez RP, Yardley DA, Han LK, Reuben JM, McCanna S, et al. Abstract CT057: a single-arm, preoperative, pilot study to evaluate the safety and biological effects of orally administered reparixin in early breast cancer patients who are candidates for surgery. *Cancer Res.* (2016) 76(14 Suppl.):CT057-CT057. doi: 10.1158/1538-7445.am2016-ct057
19. Liu S, Cong Y, Wang D, Sun Y, Deng L, Liu Y, et al. Breast cancer stem cells transition between epithelial and mesenchymal states reflective of their normal counterparts. *Stem Cell Rep.* (2014) 2:78–91. doi: 10.1016/j.stemcr.2013.11.009
20. Saygin C, Matei D, Majeti R, Reizes O, Lathia JD. Targeting cancer stemness in the clinic: from hype to hope. *Cell Stem Cell* (2019) 24:25–40. doi: 10.1016/j.stem.2018.11.017
21. Giuliano M, Giordano A, Jackson S, De Giorgi U, Mego M, Cohen EN, et al. Circulating tumor cells as early predictors of metastatic spread in breast cancer patients with limited metastatic dissemination. *Breast Cancer Res.* (2014) 16:440. doi: 10.1186/s13058-014-0440-8
22. Twelves C, Cortes J, Kaufman PA, Yelle L, Awada A, Binder TA, et al. "New" metastases are associated with a poorer prognosis than growth of pre-existing metastases in patients with metastatic breast cancer treated with chemotherapy. *Breast Cancer Res.* (2015) 17:150. doi: 10.1186/s13058-015-0657-1

Conflict of Interest Statement: PAR is a full time employee of Dompé farmaceutici S.p.A.

frontiers in Pharmacology

ORIGINAL RESEARCH
published: 06 February 2019
doi: 10.3389/fphar.2019.00075

Iron-Chelated Polydopamine Decorated Doxorubicin-Loaded Nanodevices for Reactive Oxygen Species Enhanced Cancer Combination Therapy

*Xu-Jing Li[1†], Wen-Tong Li[1,2†], Zi-Hao-Ran Li[1], Li-Ping Zhang[3], Cheng-Cheng Gai[1], Wei-Fen Zhang[2,3] and De-Jun Ding[2,3]**

[1] Department of Pathology, Weifang Medical University, Weifang, China, [2] Collaborative Innovation Center for Target Drug Delivery System, Weifang Medical University, Weifang, China, [3] College of Pharmacy, Weifang Medical University, Weifang, China

OPEN ACCESS

Edited by:
Zhe-Sheng Chen,
St. John's University, United States

Reviewed by:
Xuan Zhou,
George Washington University, United States
Jiwei Cui,
Shandong University, China

***Correspondence:**
De-Jun Ding
dejunding@wfmc.edu.cn

† These authors have contributed equally to this work

Specialty section:
This article was submitted to Cancer Molecular Targets and Therapeutics, a section of the journal Frontiers in Pharmacology

Received: *11 December 2018*
Accepted: *21 January 2019*
Published: *06 February 2019*

Citation:
Li X-J, Li W-T, Li Z-H-R, Zhang L-P, Gai C-C, Zhang W-F and Ding D-J (2019) Iron-Chelated Polydopamine Decorated Doxorubicin-Loaded Nanodevices for Reactive Oxygen Species Enhanced Cancer Combination Therapy. Front. Pharmacol. 10:75. doi: 10.3389/fphar.2019.00075

Combination therapy which enhances efficacy and reduces toxicity, has been increasingly applied as a promising strategy for cancer therapy. Here, a reactive oxygen species (ROS) that enhanced combination chemotherapy nanodevices was fabricated based on the Fe-chelated polydopamine (PDA) nanoparticles (NPs). The structure was characterized by dynamic light scattering-autosizer, transmission electron microscopy, energy dispersive spectroscopy, and Fourier-transform infrared (FT-IR) spectrophotometer. The *in vitro* drug release profile triggered by low intracellular pH indicated that the system demonstrated controlled therapeutic activity. *In vitro* cell uptake studies showed that doxorubicin (DOX)-loaded Fe-PDA/ folic acid (FA)-polyethylene glycol (DOX@Fe-PDA/FA-PEG) had a strong uptake capacity and can be rapidly internalized by MCF-7 cells. The *in vitro* experiments demonstrated that DOX@Fe-PDA/FA-PEG triggered the intracellular ROS overproduction, thereby enhancing its therapeutic effect on breast cancer. In summary, this experiment demonstrated the novel DOX-loaded composite NPs used as a potential targeted nanocarrier for breast cancer treatment, which could be a promising therapeutic strategy against breast cancer.

Keywords: polydopamine, combination therapy, reactive oxygen species, doxorubicin, breast cancer

INTRODUCTION

As one of the most common malignant tumors among women, breast cancer is the second and common cause of cancer-related death in women (Wood et al., 2017; Bray et al., 2018). Chemotherapy has become one of the most mature and common treatment option for breast cancer (Fisher et al., 1998; Miller et al., 2016; Spiegel and Koontz, 2018). Doxorubicin (DOX) is an anthracycline non-specific broad-spectrum anticancer drug that is widely used to treat breast cancer. Doxorubicin can exert its effects by elevating reactive oxygen species (ROS) thereby activating of caspase and ultimately leading to apoptosis (Russell and Cotter, 2015; Chakravarti et al., 2016). However, serious side effects, such as myelosuppression, cardiotoxicity, and drug resistance, are the major clinical chemotherapeutic drawbacks of DOX.

It has been proposed that combination therapeutics plays a synergistic effect and can enhance efficacy and reduce the toxicity of chemotherapy (Xu et al., 2015; Camacho et al., 2016; Kemp et al., 2016; Seo et al., 2017). Dayton et al. (2011) reported that the use of HO-3867, which is a synthetic curcumin analog, combined with DOX, in low doses to achieve enhanced cell death and reduced myocardial toxicity. And the increased generation of ROS, thereby resulting in oxidative damage to the cellular constituents, is widely exploited for therapeutic benefits on cancer (Matés and Sánchez-Jiménez, 2000; Schumacker Paul, 2015; Zhou et al., 2016). Fe, which plays a role in several types of cell death, has long been associated with toxicity because it induces hydroxyl radical (OH·), which is a ROS formed via Fenton reaction (Dixon and Stockwell, 2013; Shen et al., 2018; Zhang et al., 2018). Using ROS-producing agents could enhance the anticancer activity of DOX in cancer therapy through ROS-mediated apoptosis (Xia et al., 2017; Wu et al., 2017), autophagy (Fong et al., 2012), and ferroptosis (Zheng et al., 2017). Fan et al. (2014) identified the synergistic effect of DOX/ selenocystine sensitized to DOX by through ROS overproduction. Dai et al. (2018) fabricated assembled metal-phenolic network Nps as a novel ROS promoted synergistic nanomedicine platform for cancer therapy. This observation inspires us to import an iron-supply system in combination with DOX to elicit a synergistic effect on the cancer therapy.

Recently, researchers attempted to build some drug carrier systems to load and transport DOX overcoming the low bioavailability, poor absorption, and high toxicity of DOX (Xu et al., 2015; Kemp et al., 2016; Indermun et al., 2018). Particularly, polydopamine (PDA), which is a natural-inspired polymer, is an appealing material as drug carrier due to its good biocompatibility (Lynge et al., 2015; Indermun et al., 2018; Ryu et al., 2018). Considering its abundant aromatic rings, PDA NPs could be an efficient platform for loading DOX through π–π stacking and hydrogen-bonding interactiron. Meanwhile, the existence of phenolic hydroxyl groups on the surface makes it suitable for further modification with PEG, which could endow nanoparticles excellent physiological stability of NPs (Liu et al., 2014). More attractively, the phenolic surface have excellent chelating ability with metal ions such as Mn (Miao et al., 2015; Xi et al., 2017), Cu (Ge et al., 2017), and Fe (Li et al., 2016).

Keep all the issues in mind, we hypothesized that the Fe-chelated PDA nanoparticles with DOX loading could act as an Fe-supply system used for Fe and DOX combined cancer theranostics, as shown in **Figure 1**. The designed DOX@Fe-PDA/folic acid (FA)-PEG could be provided with several advantages, as follows: (Wood et al., 2017) Combination therapy. The chemotherapy drug DOX undergoes redox cycles to generate and increase H_2O_2 in living cells. The released Fe from PDA further reacts with H_2O_2 to generate hydroxyl radical via Fenton reaction and induces cell death. In combination with Fe, DOX was prone to kill cancer cells efficiently (Bray et al., 2018). Biocompatibility and safety. PDA, which is a natural biopolymer, possesses biocompatibility. The coated PEG and chelated Fe of PDA Nps were metabolic. Meanwhile, the pH-triggered release performance of PDA in tumor microenvironment, avoids damage to surrounding tissues. The PEG-coating can help Nps to ameliorate long-term circulation (Fisher et al., 1998). Tumor targeted. Considering folate receptor overexpression on the surface of breast cancer cells, the FA conjugated NPs may improve cell uptake via receptor mediated endocytosis. In summary, the DOX@Fe-PDA/FA-PEG system could be used as potential combination chemotherapy nanodevice for breast cancer treatment.

MATERIALS AND METHODS

NPs Synthesis

The synthesis of NPs was modified based on the previously introduced procedure (Li et al., 2016). In brief, 4.08 mg $FeCl_3$ and 15 mg dopamine plus 10 mL of water were mixed and stirred at room temperature for 1 h. Then 500 mg Tris was added, and the mixture was stirred at room temperature for 1.5 h. The mixture was centrifuged at 12000 rpm for 15 min to obtain Fe-PDA NPs. A total of 3.85 mL Fe-PDA NPs (5.2 mg/mL) were mixed with 20 mg FA-PEG-SH, 4.7 mg Tris, and 100 μL *tris*(2-carboxyethyl)phosphine (8 mg/mL). The mixture was vigorously stirred for 1 h at room temperature. Then, the FA-PEG modified NPs (Fe-PDA/PEG-FA) were purified via centrifugation and washed with deionized water.

Drug Loading

A total of 2 mg adriamycin hydrochloride were added into 300 μL of dimethyl sulfoxide and 8.2 μL of triethylamine was added. The mixture was stirred in dark at room temperature for 12 h to desalinate hydrochloride. Then, the neutral DOX (2 mg) above-mentioned was added dropwise to 1 mL of Fe-PDA/FA-PEG NPs (10 mg/mL). Afterward, Tris (2.42 mg) was added and volume of 3 mL was obtained by adding distilled water. After vigorous stirring for 24 h in the dark, free DOX was removed via centrifugation at 12000 rpm for 10 min, then washed with phosphate buffer solution (PBS) and stored at 4°C in the dark. The DOX loading capacity of NPs was determined by UV-Vis spectrophotometer at the wavelength of 480 nm. The encapsulation efficiency (EE) of DOX was calculated by the following equation: EE = (initial amount of feeding drugs – free drugs)/initial amount of feeding drugs.

NPs Characterization

The size and Zeta potential of the prepared NPs were measured by dynamic light scattering-autosizer (DLS) on Zetasizer Nano ZS90 (Malvern Instruments, Malvern, United Kingdom). The liquid sample was sonicated before measurement. Three independent test results were recorded. The shape and surface morphology of the NPs were imaged by a transmission electron microscope (TEM, JEM-1230; JEOL, Tokyo, Japan). TEM, energy dispersive X-ray spectroscopy (EDS) and corresponding EDS-mapping were adopted for morphology and elemental distribution analyses on the JEM-1230 electron microscope operated at 200 kV. The chemical composition and structural changes of NPs were analyzed by Fourier transform infrared (FT-IR) spectroscopy (VERTEX 70; Bruker, Bremen, Germany). The IR spectra

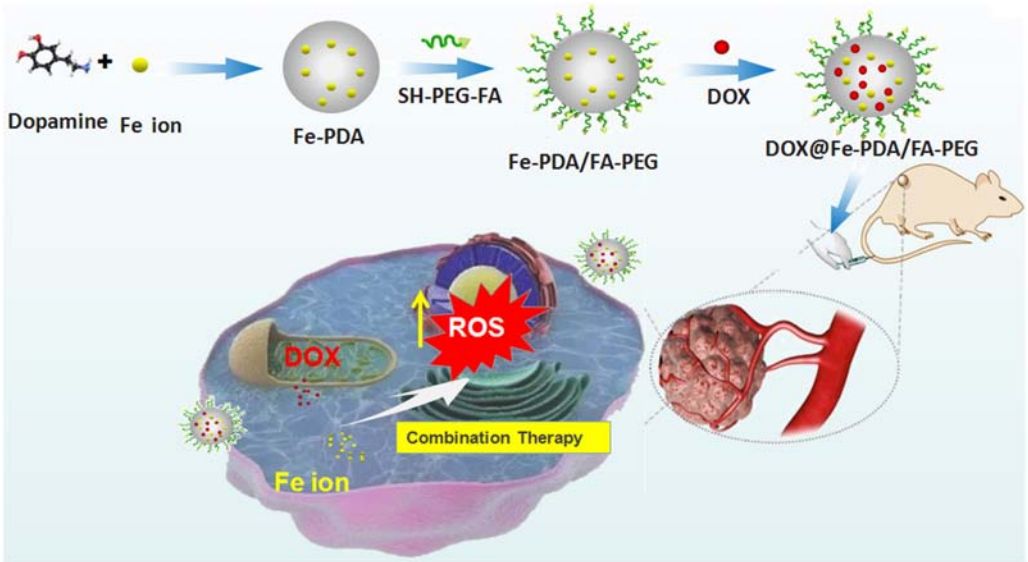

FIGURE 1 | Schematic representation of DOX@Fe-PDA/PEG-FA synthesis, targeted cell uptake and intracellular drug release and combination therapy.

of the samples were obtained in the range of 4000 and 500 cm^{-1}.

In vitro Drug Release Profiles

The *in vitro* DOX release behavior of DOX@Fe-PDA/FA-PEG was tested as reported previously (Liu et al., 2014). Briefly, DOX@Fe-PDA/FA-PEG was dispersed in 2 mL PBS with the pH of either 7.2 or 5.5. The tube was shaken at 37°C with 100 rpm in dark. At appropriate time points, the full release buffer was collected via centrifugation at 12000 rpm for 10 min, and replaced with 2 mL of fresh PBS. The amount of released drug DOX was quantified by a UV spectrophotometer at the wavelength of 480 nm. The correlation between the accumulative DOX released from NPs and time was plotted.

Cell Culture

The *in vitro* cell cytotoxicity cellular uptake and ROS measurement were assessed on human breast cancer cell line MCF-7, which was purchased from American Type Culture Collection. Cells were incubated at 37°C with modified Eagle's medium (MEM) containing 10% fetal bovine serum (FBS), 100 U/mL penicillin, and 100 mg/mL streptomycin in a 5% CO_2 atmosphere.

Cellular Uptake Study

A total of 2×10^5 cells/well MCF-7 cells were seeded in 6-well plates for 24 h. Then, the samples (free DOX, DOX@Fe-PDA/FA-PEG) were added to each well (equivalent DOX concentration of 10 μg/mL) and the cells were incubated at 37°C for an appropriate time at an additional of 24 h. Afterward, the cells were washed with PBS and stained by Hoechst 33342 (Sangon Biotech, Shanghai, China). Confocal laser scanning microscopy (CLSM) imaging was performed on LSM 410 fluorescence microscope (Zeiss, Jena, Germany). The fluorescence signal of DOX was excited at 488 nm and measured at 610 nm. The fluorescence signal stained by Hoechst 33342 was excited at 405 nm and detected at 490 nm.

In vitro Cytotoxicity by Using MTT Assay

MCF-7 cells were seeded in 96-well plates at a density of 5000 cells per well and incubated in 100 mL of medium for 24 h to allow attachment. Then, the cells were incubated with free DOX and DOX@Fe-PDA/FA-PEG (DOX concentration of 0.1093, 0.2187, 04375, 0.875, 1.75, and 3.5 μg/mL) for 24 and 48 h, respectively. A total of 20 μL MTT solution (5 mg/mL) were added to each well and incubated for 4 h. The crystals were dissolved by adding DMSO. The optical density value of each well was measured at 490 nm by an iMark plate reader (Bio-Rad, Berkeley, CA, United States). All data were obtained in quadruplicate.

Intracellular ROS Content Measurement

MCF-7 cells were seeded on 6-well plates at a density of 2×10^5 cells per well. Then the cells were incubated with free DOX and DOX@Fe-PDA/FA-PEG (equivalent DOX concentration of 10 μg/mL) for 8 h at 37°C. Afterward, diluted 2′,7′-dichlorofluorescein diacetate (DCFH-DA; Solarbio, Beijing, China), which is a cell-permeable fluorescent probe, were added. Then, the cells were placed in a 6-well plate at 37°C and incubated for another 30 min. The cells were washed for three times with serum-free medium to remove DCFH-DA completely and finally observed using fluorescence microscope.

Data Analysis Methodology

All experiments were performed at least three times unless otherwise stated. All experimental data were expressed as

mean ± SD and both were treated with SPSS 18.0 (SPSS, Chicago, IL, United States).

RESULTS AND DISCUSSION

DOX@ Fe-PDA/FA-PEG Synthesis and Characterization

The design and synthetic strategy of DOX@Fe-PDA/FA-PEG is shown in **Figure 1**. First, the Fe-PDA was synthesized using an oxidative self-polymerization method according to previously literature (Li et al., 2016). In addition, folic acid conjugated PEG was introduced to modify the PDA in enhancing the targeting effect and improving the stability of the NPs. Finally, DOX was loaded via diffusion in an aqueous media. The mean hydrodynamic sizes of DOX@PDA/FA-PEG, DOX@Fe-PDA/FA-PEG and the unloaded Fe-PDA/FA-PEG were 239.5 ± 28.82, 267.7 ± 34.16, and 283.22 ± 21.6 nm, respectively, with a narrow size distribution as demonstrated in **Figure 2A**. This particle size is theoretically suitable for cellular uptake and tumor cell permeation duo to EPR effect (Maeda, 2015). Zeta potential plays a key role in the stability and penetration through cell membranes for Nps (Bhattacharjee, 2016). Considering the presence of the carboxyl group of FA, the zeta potentials of all NPs are negative (**Supplementary Figure 1**), thereby indicating that these Nps were stable *in vivo* by electrostatic repulsion, which is the basis of drug delivery (Wu et al., 2011). The zeta potential of Fe-PDA/FA-PEG (−30 mV) is slightly lower than that of Fe-PDA/FA-PEG loaded with DOX (−27.2 mV) (**Supplementary Figure 1**), thereby suggesting that the positively charged amino groups on DOX partially neutralized the negative charge.

The morphologies of Fe-PDA/FA-PEG (wihout DOX loaded), DOX@PDA/FA-PEG (without Fe chelated), DOX@Fe-PDA/FA-PEG were observed by TEM. The results revealed that the DOX-loaded PDA/FA-PEG exhibited a spherical and uniform morphology (**Figure 2B**). The particle size observed by TEM was substantially the same as the particle size measured by DLS. Scanning electron microscopy used to perform accurate elemental analysis of Nps. Using dark field image (DFI) characterization, electron energy loss spectroscopy (EELS), energy dispersive spectroscopy (EDS), and corresponding element mapping (EDS mapping) (**Figure 3**) clearly show the morphological structure of the nanoparticles and distribution of four elements (C, N, O, Fe). The results showed that the coexistence of C, N, O, and Fe signals coexisted in the EDS spectra of Fe-PDA and Fe-PDA/FA-PEG. The uniform distribution of C, N, O, and Fe was confirmed by EDS element mapping. This result indicated the success and dispersion loads of Fe, PDA, and PEG in the DOX-loaded Fe-PDA/FA-PEG and unloaded Fe-PDA/FA-PEG. However, in the EDS element mapping of PDA, only C, N, and O signals coexisted and were distributed, thereby indicating the success and dispersion load of PDA and PEG in the DOX-loaded PDA/FA-PEG. Further, the FR-IR was performed to evaluat the surface characterization. As shown in **Supplementary Figure 2**, the, the characteristic peaks of N-H bending vibration appearing at 1512, 1589, and 3250 cm^{-1}. The peaks at 1493 and 1445 cm^{-1} can be ascribed to the existence of FA. Compared with PDA, the peaks of PEG at 1128 cm^{-1} (C-O-C stretching) were observed.

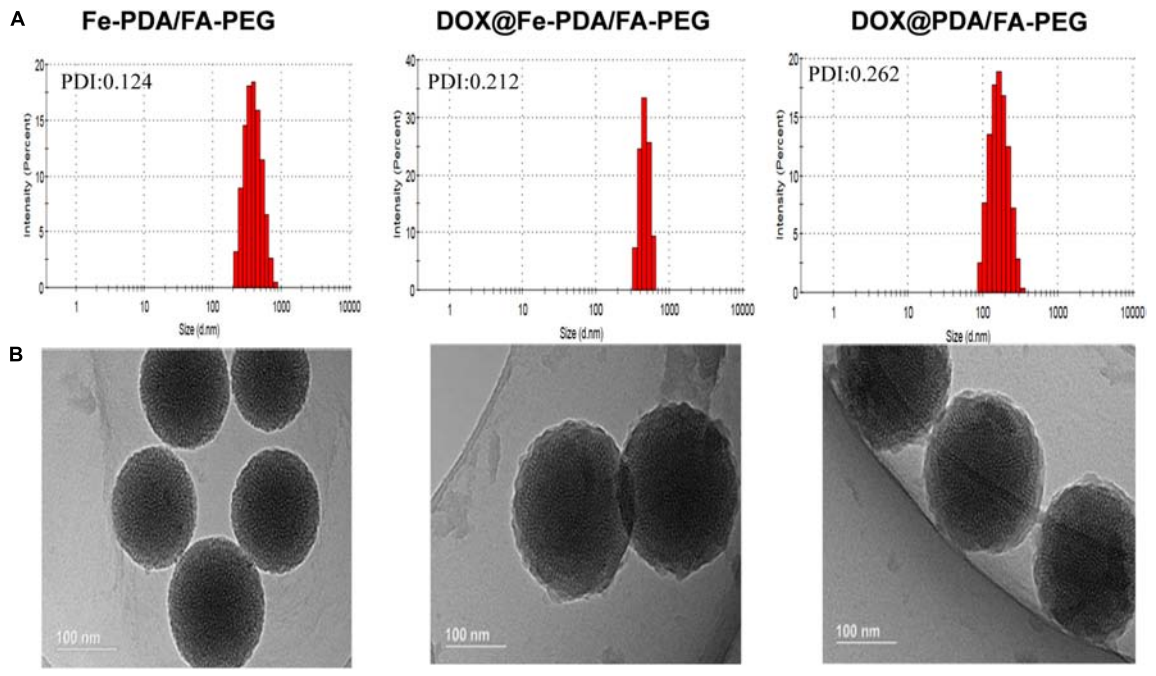

FIGURE 2 | The characterization of different nanoparticl nanoparticles. **(A)** Size distributions of Fe-PDA/FA-PEG, DOX@Fe-PDA/FA-PEG, DOX@PDA/FA-PEG. **(B)** TEM image of PDA/FA-PEG, DOX@Fe-PDA/FA-PEG, DOX@PDA/FA-PEG. Scale bar: 100 nm.

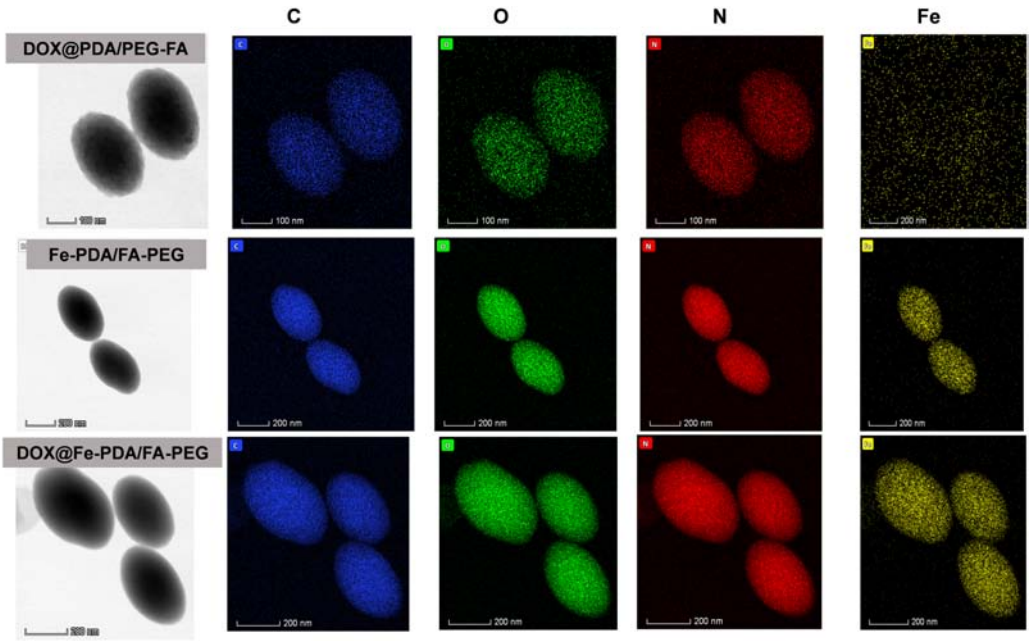

FIGURE 3 | Dark-field image, and corresponding area-elemental mappings of PDA/FA-PEG, DOX@Fe-PDA/FA-PEG, DOX@PDA/FA-PEG. Scale bar: 50 nm.

In vitro pH-Stimuli Release Study

At a drug to Fe-PDA/FA-PEG feeding ratio of 1:5 in weight, the encapsulation efficiency of DOX in the Fe-PDA/FA-PEG was 76.6 ± 5.2% determined by UV-Vis absorption spectrophotometer. As PDA NPs exist abundant aromatic rings and phenolic hydroxyl groups, the DOX was loaded through π−π stacking and hydrogen-bonding interaction. Subsequently, the pH dependent release capability of DOX@Fe-PDA/FA-PEG was investigated at 37°C under the pH levels of 7.2 and 5.5. The accumulative drug release kinetics curves are shown in **Figure 4**. The drug release of both the DOX-loaded Fe-PDA/FA-PEG was significantly pH-dependent. As shown in **Figure 4**, the release of the drug was as low as 25.5% at the of pH 7.2 within 36 h, and even 30.1% within 48 h. However, under acidic conditions, the release amount reached 34.6% within 8 h at the pH of 5.5, and the release rate at 48 h was 47.2%. This indicated that the drug-loaded Nps can cause the drug release under acidic condition, mainly due to the extremely high pH responsiveness of the PDA-modified NPs. This phenomenon allowed the rapid drug release at low pH. Considering the acidic microenvironment of the tumor and intracellular acidic endosomes and lysosomes, drugs are released only after being phagocytized by lysosomes in tumor cells, thereby effectively reducing drug waste and enhancing the antitumor effects by rapidly increasing the lysosome concentration (Duo et al., 2017).

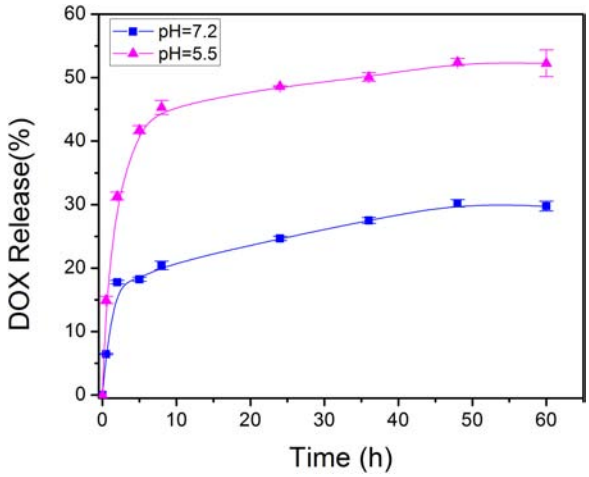

FIGURE 4 | *In vitro* drug release profile of DOX@Fe-PDA/FA-PEG in media with different pH value (pH 7.2 and 5.5).

Cellular Uptake

To study the cellular uptake and the intracellular distribution, we investigated the intracellular delivery of free DOX by using a confocal microscopy. **Figure 5A** shows the fluorescence of DOX distrubuted in the cytoplasm and cell nuclei after incubation with free DOX for 1 h. However the red flourescence with NPS observed in nucleus was not obvious. Based on the different intracellular fates of DOX, it was indicated that the NPs were internalized into cell mainly via endocytic pathway. And then we continued to incubate for another 9 h and observed under a fluorescence microscope as shown in **Figure 5B**. Apparently, the uptake intensities of DOX-loaded NPs was higher than that of free DOX, and it was contributed by the targeting effect of folate receptor. Moreover, the cell uptake intensities of DOX-loaded NPs were positive correlation with incubation time. While the fluorescence intensity of free DOX

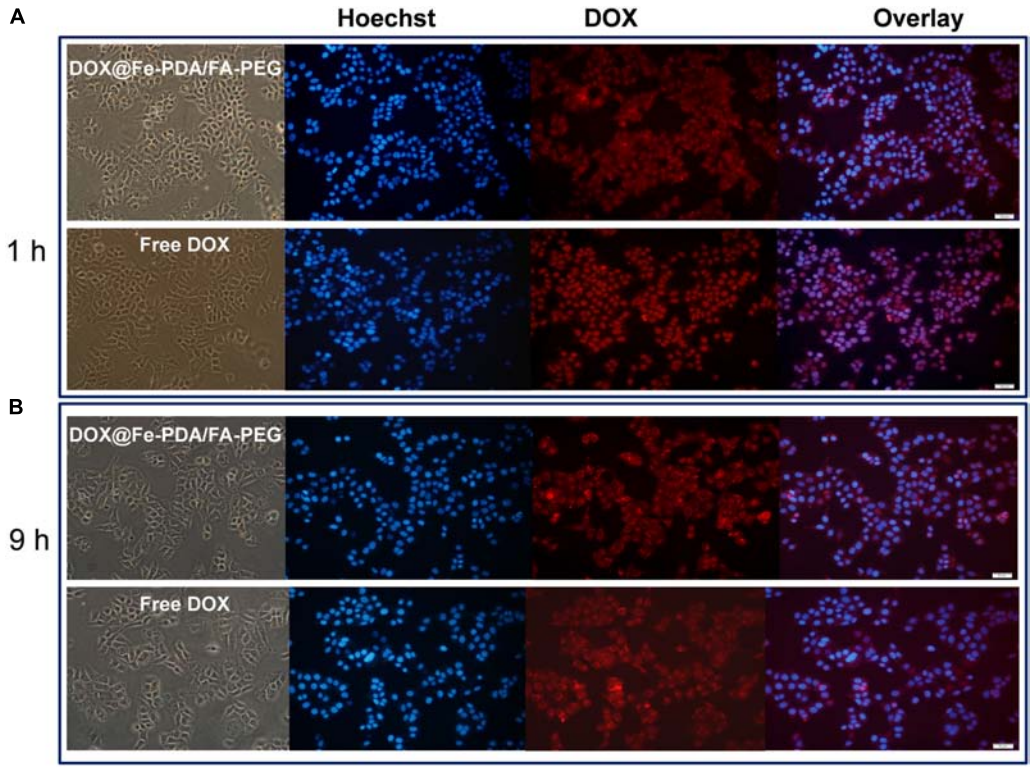

FIGURE 5 | Confocal laser scanning microscopy (CLSM) images of MCF-7 cells after incubation with free DOX, DOX-@ Fe-PDA/FA-PEG for 1 h **(A)**, and 9 h **(B)**. The cells were stained by Hoechst (blue) and drug DOX was red.

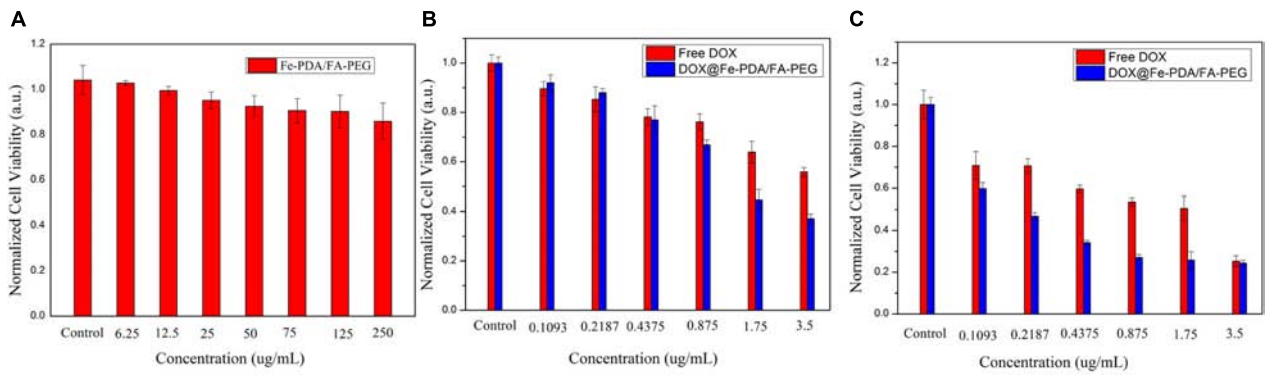

FIGURE 6 | Relative viabilities of MCF-7 cells after incubated with PDA/FA-PEG for 48 h **(A)** and free DOX and DOX@Fe-PDA/FA-PEG at different concentrations 24 h **(B)** and 48 h **(C)**.

in the cells is weaker than that of the doxorubicin-loaded NPs, indicating that the intracellular free DOX decays with time. According to the *in vitro* drug release profiles, this phenomenon proves that the DOX-loaded Nps have a sustained release effect, which may help to enhance the cytotoxicity of DOX.

Cytotoxicity of DOX-Loaded NPs

To assess the cytotoxicity of DOX@Fe-PDA/FA-PEG, we performed the MTT assays. In order to confirm the high biocompatibility and safety of the NPs, we incubated the Fe-PDA/FA-PEG NPs with MCF-7 cells. As shown in **Figure 6A**, the Fe-PDA/FA-PEG NPs without drug-loading exhibited a negligible cytotoxicity the concentration ranging from 0 to 250 μg/mL for 48 h. This result suggested that the prepared material possessed high biocompatibility and low cell cytotoxicity. Then, we compared the results of cytotoxicity of free DOX and DOX-loaded Nps at 24 and 48 h. **Figures 6B,C** shows the cytotoxicity of DOX on MCF-7 was time and dose-dependent. As the DOX concentration and incubation time prolonged, the

greater the toxicity of the drug to MCF-7 cell. Apparently, the cytotoxicity of DOX-loaded Fe-PDA/FA-PEG NPs was greater than that free DOX, thereby demonstrating that Fe enhanced the killing effect of DOX on the MCF-7 cells. And it was found that the 48 h of incubation exhibited a considerable killing effect on MCF-7 cells than 24 h. This result further confirmed the sustained release of NPs.

ROS Detection

Reactive oxygen species -induced cell death has been a widely uesed strategy for tumor therapy (Matés and Sánchez-Jiménez, 2000; Dixon and Stockwell, 2013; Schumacker Paul, 2015; Zhou et al., 2016). As we know, DOX could activate nicotinamide adenine dinucleotide phosphate oxidases, and further produce ROS, which contribute to anticancer drug-induced toxicity (Chakravarti et al., 2016; Seo et al., 2017). Recently, synergistic approaches by using ROS-producing agents with DOX have attracted considerable attention (Xia et al., 2017). Intriguingly, the presence of Fe (II and III) contributes to the enhanced chemotherapy efficacy by converting the accumulated H_2O_2 to the hydroxyl radical via Fenton reactions (Dixon and Stockwell, 2013). To explore the underlying mechanism of enhanced antiproliferating effects of DOX@Fe-PDA/FA-PEG further, we quantified the intracellular ROS by using 2′-7′-dichlorofuorescin diacetate. Compared with the control group, green fluorescence was observed after incubation with DOX and DOX@Fe-PDA/FA-PEG (**Figure 7**). In addition, cells treated with DOX-loaded Fe-PDA/FA-PEG had the highest fluorescence intensity, thereby indicating the highest ROS production. The results showed that the cells treated with DOX loaded Fe-PDA/FA-PEG can synergistically produce ROS to kill tumor cells. DOX used to undergo redox cycles to generate high H_2O_2 levels inside the cancer cells. After endocytosis by tumor cells, the DOX@Fe-PDA/FA-PEG was decomposed by the acidic microenvironment. The elevated H_2O_2 of DOX can be further catalyzed by Fe ions via Fenton reaction to generate abundant highly toxic resulting in enhancing anticancer effects of DOX through oxidative damage to DNA, protein, and lipid (Matés and Sánchez-Jiménez, 2000; Schumacker Paul, 2015; Zhou et al., 2016). Previous investigations have developed iron-based nanomaterials, including iron nanometallic glasses and iron oxide, have been employed to upregulation of ROS by using the situ Fenton reaction (Zhang et al., 2016; Liu et al., 2018; Tang et al., 2018). However, current iron-based nanomaterials is far from satisfactory. Some of the nanomaterials such as Fe^0 nanoparticles (Zhang et al., 2016) and iron oxide nanoplatform (Liu et al., 2018), are difficult to fabricate and the synthetic conditions generally are harsh and complicated. In this work, we synthesized the iron-chelated PDA NPs via a one-pot reaction and the FA-PEG as the surface ligand for tumor homing with a low cost and biocompable biocompatibility. And the pH-stimuli release profiles included being highly selective and logical, and amenable to activation by endogenous stimuli. This strategy present an approach for synergistic combination of ROS and chemotherapy to enhance the anticancer efficacy.

CONCLUSION

In this study, we successfully fabricated a novel nanocarrier on the basis of Fe-chelated PDA nanoparticles used for Fe and DOX combined cancer theranostics through ROS over-generation. The obtained DOX@Fe-PDA/FA-PEG Nps had a hydrodynamic size of about 250 nm, and the structure was characterized by DLS, TEM, EDS, and FT-IR. The *in vitro* drug release profile triggered by low intracellular pH indicated that the system demonstrated controlled therapeutic activity. Further, *in vitro* cell uptake studies indicate that DOX-loaded Fe-PDA /FA-PEG can be internalized by MCF-7 cells and exhibited high targeting efficiency due to specific recognition. The *in vitro* experiments demonstrated that DOX@Fe-PDA/FA-PEG trigged the intracellular ROS overproduction, thereby enhancing the therapeutic effect on breast cancer. Taken together, this study provides a strategy to harness Fe-PAD nanocarrier for Fe and DOX combined cancer theranostics.

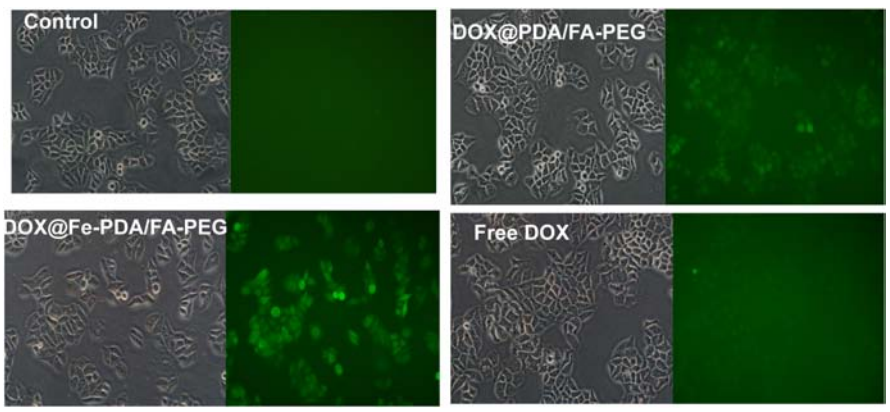

FIGURE 7 | The intracellular ROS stained with DCFH-DA in MCF-7 cells after incubation with free DOX, DOX@Fe-PDA/FA-PEG, DOX@PDA/FA-PEG for 8 h were measured by fluorescence microscopic.

AUTHOR CONTRIBUTIONS

X-JL and W-TL performed the experiments and drafted the manuscript. Z-H-RL and L-PZ prepared and characterized the NPs. C-CG and performed the statistical design of the experiments. W-FZ and D-JD conceived the initial idea. All authors helped to correct and polish the manuscript and read and approved the final manuscript.

FUNDING

The authors are grateful for the generous financial support of the Project of Shandong Province Higher Educational Science and Technology Program (Grant No. J18KA279), National Natural Science Foundation of China (Grant No. 81774125), Project of Collaborative Innovation Center for Target Drug Delivery System of Weifang Medical University (2017), and College Students' Technology Innovation Project of Weifang Medical University (Grant No. KX2017045).

ACKNOWLEDGMENTS

We appreciate the experimental assistance of bachelor students Ling-Yan Liao, Ruo-Bing Liu, Yajing Ji, and Yanan Li.

SUPPLEMENTARY MATERIAL

The Supplementary Material for this article can be found online at: https://www.frontiersin.org/articles/10.3389/fphar.2019.00075/full#supplementary-material

REFERENCES

Bhattacharjee, S. (2016). DLS and zeta potential – what they are and what they are not? *J. Controll. Release* 235, 337–351. doi: 10.1016/j.jconrel.2016.06.017

Bray, F., Ferlay, J., Soerjomataram, I., Siegel, R. L., Torre, L. A., and Jemal, A. (2018). Global cancer statistics 2018: GLOBOCAN estimates of incidence and mortality worldwide for 36 cancers in 185 countries. *CA Cancer J. Clin.* 68, 394–424. doi: 10.3322/caac.21492

Camacho, K. M., Menegatti, S., Vogus, D. R., Pusuluri, A., Fuchs, Z., Jarvis, M., et al. (2016). DAFODIL: a novel liposome-encapsulated synergistic combination of doxorubicin and 5FU for low dose chemotherapy. *J. Controll. Release* 229, 154–162. doi: 10.1016/j.jconrel.2016.03.027

Chakravarti, B., Yang, J., Luo, Z., and Ahlers, K. E. (2016). Contribution of NADPH oxidase (Nox)-derived reactive oxygen species (ROS) to doxorubicin-induced cardiomyopathy mediated by regulator of g protein signaling 6 (RGS6). *FASEB J.* 30:939.3. doi: 10.1096/fasebj.30.1_supplement.939.3

Dai, Y., Yang, Z., Cheng, S., Wang, Z., Zhang, R., Zhu, G., et al. (2018). Toxic reactive oxygen species enhanced synergistic combination therapy by self-assembled metal-phenolic network nanoparticles. *Adv. Mat.* 30:1704877. doi: 10.1002/adma.201704877

Dayton, A., Selvendiran, K., Meduru, S., Khan, M., Kuppusamy, M. L., Naidu, S., et al. (2011). Amelioration of doxorubicin-induced cardiotoxicity by an anticancer-antioxidant dual-function compound, HO-3867. *J. Pharmacol. Exp. Ther.* 339:350. doi: 10.1124/jpet.111.183681

Dixon, S. J., and Stockwell, B. R. (2013). The role of iron and reactive oxygen species in cell death. *Nat. Chem. Biol.* 10:9. doi: 10.1038/nchembio.1416

Duo, Y., Li, Y., Chen, C., Liu, B., Wang, X., Zeng, X., et al. (2017). DOX-loaded pH-sensitive mesoporous silica nanoparticles coated with PDA and PEG induce pro-death autophagy in breast cancer. *RSC Adv.* 7, 39641–39650. doi: 10.1039/C7RA05135B

Fan, C., Zheng, W., Fu, X., Li, X., Wong, Y.-S., and Chen, T. (2014). Strategy to enhance the therapeutic effect of doxorubicin in human hepatocellular carcinoma by selenocystine, a synergistic agent that regulates the ROS-mediated signaling. *Oncotarget* 5, 2853–2863. doi: 10.18632/oncotarget.1854

Fisher, B., Bryant, J., Wolmark, N., Mamounas, E., Brown, A., Fisher, E. R., et al. (1998). Effect of preoperative chemotherapy on the outcome of women with operable breast cancer. *J. Clin. Oncol.* 16, 2672–2685. doi: 10.1200/jco.1998.16.8.2672

Fong, M. Y., Jin, S., Rane, M., Singh, R. K., Gupta, R., and Kakar, S. S. (2012). Withaferin a synergizes the therapeutic effect of doxorubicin through ROS-mediated autophagy in ovarian cancer. *PLoS One* 7:e42265. doi: 10.1371/journal.pone.0042265

Ge, R., Lin, M., Li, X., Liu, S., Wang, W., Li, S., et al. (2017). Cu2+-loaded polydopamine nanoparticles for magnetic resonance imaging-guided pH- and near-infrared-light-stimulated thermochemotherapy. *ACS Appl. Mat. Interfaces* 9, 19706–19716. doi: 10.1021/acsami.7b05583

Indermun, S., Govender, M., Kumar, P., Choonara, Y. E., and Pillay, V. (2018). "2 - Stimuli-responsive polymers as smart drug delivery systems: classifications based on carrier type and triggered-release mechanism," in *Stimuli Responsive Polymeric Nanocarriers for Drug Delivery Applications*, Vol. 1, eds A. S. H. Makhlouf and N. Y. Abu-Thabit (Sawston: Woodhead Publishing), 43–58. doi: 10.1016/B978-0-08-101997-9.00002-3

Kemp, J. A., Shim, M. S., Heo, C. Y., and Kwon, Y. J. (2016). "Combo" nanomedicine: co-delivery of multi-modal therapeutics for efficient, targeted, and safe cancer therapy. *Adv. Drug Deliv. Rev.* 98, 3–18. doi: 10.1016/j.addr.2015.10.019

Li, Y., Xie, Y., Wang, Z., Zang, N., Carniato, F., Huang, Y., et al. (2016). Structure and function of iron-loaded synthetic melanin. *ACS Nano* 10, 10186–10194. doi: 10.1021/acsnano.6b05502

Liu, Y., Ai, K., and Lu, L. (2014). Polydopamine and its derivative materials: synthesis and promising applications in energy, environmental, and biomedical fields. *Chem. Rev.* 114, 5057–5115. doi: 10.1021/cr400407a

Liu, Y., Ji, X., Tong, W. W. L., Askhatova, D., Yang, T., Cheng, H., et al. (2018). Engineering multifunctional RNAi nanomedicine to concurrently target cancer hallmarks for combinatorial therapy. *Angew. Chem. Int. Ed.* 57, 1510–1513. doi: 10.1002/anie.201710144

Lynge, M. E., Schattling, P., and Städler, B. (2015). Recent developments in poly(dopamine)-based coatings for biomedical applications. *Nanomedicine* 10, 2725–2742. doi: 10.2217/nnm.15.89

Maeda, H. (2015). Toward a full understanding of the EPR effect in primary and metastatic tumors as well as issues related to its heterogeneity. *Adv. Drug Deliv. Rev.* 91, 3–6. doi: 10.1016/j.addr.2015.01.002

Matés, J. M., and Sánchez-Jiménez, F. M. (2000). Role of reactive oxygen species in apoptosis: implications for cancer therapy. *Int. J. Biochem. Cell Biol.* 32, 157–170. doi: 10.1016/S1357-2725(99)00088-6

Miao, Z.-H., Wang, H., Yang, H., Li, Z.-L., Zhen, L., and Xu, C.-Y. (2015). Intrinsically Mn2+-chelated polydopamine nanoparticles for simultaneous magnetic resonance imaging and photothermal ablation of cancer cells. *ACS Appl. Mat. Interfaces* 7, 16946–16952. doi: 10.1021/acsami.5b06265

Miller, K. D., Siegel, R. L., Lin, C. C., Mariotto, A. B., Kramer, J. L., Rowland, J. H., et al. (2016). Cancer treatment and survivorship statistics, 2016. *CA Cancer J. Clin.* 66, 271–289. doi: 10.3322/caac.21349

Russell, E. G., and Cotter, T. G. (2015). "Chapter six - new insight into the role of reactive oxygen species (ROS) in cellular signal-transduction processes," in *International Review of Cell and Molecular Biology*, Vol. 319, ed. K. W. Jeon (Cambridge, MA: Academic Press), 221–254.

Ryu, J. H., Messersmith, P. B., and Lee, H. (2018). Polydopamine surface chemistry: a decade of discovery. *ACS Appl. Mat. Interfaces* 10, 7523–7540. doi: 10.1021/acsami.7b19865

Schumacker Paul, T. (2015). Reactive oxygen species in cancer: a dance with the devil. *Cancer Cell* 27, 156–157. doi: 10.1016/j.ccell.2015.01.007

Seo, S. U., Kim, T. H., Kim, D. E., Min, K.-J., and Kwon, T. K. (2017). NOX4-mediated ROS production induces apoptotic cell death via down-regulation of c-FLIP and Mcl-1 expression in combined treatment with thioridazine and curcumin. *Redox Biol.* 13, 608–622. doi: 10.1016/j.redox.2017.07.017

Shen, Z., Song, J., Yung, B. C., Zhou, Z., Wu, A., and Chen, X. (2018). Cancer therapy: emerging strategies of cancer therapy based on ferroptosis. *Adv. Mat.* 30:1870084. doi: 10.1002/adma.201870084

Spiegel, D. Y., and Koontz, B. F. (2018). Meeting the needs of long-term survivors: a testament to success in the care of patients with cancer. *Cancer* 124, 2488–2490. doi: 10.1002/cncr.31381

Tang, Z., Liu, Y., He, M., and Bu, W. (2018). Chemodynamic therapy: tumour microenvironment-mediated fenton and fenton-like reactions. *Angew. Chem. Int. Ed.* 58, 946–956. doi: 10.1002/anie.201805664

Wood, R., Mitra, D., de Courcy, J., and Iyer, S. (2017). Patient-reported quality of life and treatment satisfaction in patients With HR+/HER2-advanced/metastatic breast cancer. *Clin. Ther.* 39, 1719–1728. doi: 10.1016/j.clinthera.2017.07.009

Wu, H., Liu, S., Gong, J., Liu, J., Zhang, Q., Leng, X., et al. (2017). VCPA, a novel synthetic derivative of α-tocopheryl succinate, sensitizes human gastric cancer to doxorubicin-induced apoptosis via ROS-dependent mitochondrial dysfunction. *Cancer Lett.* 393, 22–32. doi: 10.1016/j.canlet.2017.02.007

Wu, L., Zhang, J., and Watanabe, W. (2011). Physical and chemical stability of drug nanoparticles. *Adv. Drug Deliv. Rev.* 63, 456–469. doi: 10.1016/j.addr.2011.02.001

Xi, J., Da, L., Yang, C., Chen, R., Gao, L., Fan, L., et al. (2017). Mn2+-coordinated PDA@DOX/PLGA nanoparticles as a smart theranostic agent for synergistic chemo-photothermal tumor therapy. *Int. J. Nanomed.* 2017, 3331–3345. doi: 10.2147/IJN.S132270

Xia, J., Inagaki, Y., Gao, J., Qi, F., Song, P., Han, G., et al. (2017). Combination of cinobufacini and doxorubicin increases apoptosis of hepatocellular carcinoma cells through the Fas- and mitochondria-mediated pathways. *Am. J. Chin. Med.* 45, 1537–1556. doi: 10.1142/s0192415x17500835

Xu, X., Ho, W., Zhang, X., Bertrand, N., and Farokhzad, O. (2015). Cancer nanomedicine: from targeted delivery to combination therapy. *Trends Mol. Med.* 21, 223–232. doi: 10.1016/j.molmed.2015.01.001

Zhang, C., Bu, W., Ni, D., Zhang, S., Li, Q., Yao, Z., et al. (2016). Synthesis of iron nanometallic glasses and their application in cancer therapy by a localized fenton reaction. *Angew. Chem. Int. Ed.* 55, 2101–2106. doi: 10.1002/anie.201510031

Zhang, W., Gai, C., Ding, D., Wang, F., and Li, W. (2018). Targeted p53 on small-molecules-induced ferroptosis in cancers. *Front. Oncol.* 8:507. doi: 10.3389/fonc.2018.00507

Zheng, D.-W., Lei, Q., Zhu, J.-Y., Fan, J.-X., Li, C.-X., Li, C., et al. (2017). Switching apoptosis to ferroptosis: metal–organic network for high-efficiency anticancer therapy. *Nano Lett.* 17, 284–291. doi: 10.1021/acs.nanolett.6b04060

Zhou, Z., Song, J., Nie, L., and Chen, X. (2016). Reactive oxygen species generating systems meeting challenges of photodynamic cancer therapy. *Chem. Soc. Rev.* 45, 6597–6626. doi: 10.1039/C6CS00271D

Conflict of Interest Statement: The authors declare that the research was conducted in the absence of any commercial or financial relationships that could be construed as a potential conflict of interest.

frontiers in Oncology

CASE REPORT
published: 07 February 2019
doi: 10.3389/fonc.2019.00055

Bevacizumab Combined With Oxaliplatin/Capecitabine in Patient With Refractory and Recurrent Mucinous Adenocarcinoma of the Appendix: A Case Report

Wenzhi Liu[1†], Lili Liu[2†], Ruoyu Wang[1†], Guanyu Gong[1,3], Xinjia Ding[4], Bin Yang[3,5], Yun Bao[1], Zhiqiang Wang[1], Bo Zhang[4], Dewei Zhao[1], Fei Wu[1] and Yan Ding[1,5*]*

[1] The Institute for Translational Medicine, The Affiliated Zhongshan Hospital of Dalian University, Dalian, China, [2] Department of Oncology, The Second Affiliated Hospital of Dalian Medical University, Dalian, China, [3] Genomic Future Inc., Lexington, MA, United States, [4] Department of Neurosurgery, The Second Affiliated Hospital of Dalian Medical University, Dalian, China, [5] Department of Pediatrics, Children's Hospital of Boston, Harvard Medical School, Boston, MA, United States

OPEN ACCESS

Edited by:
Yunkai Zhang,
Vanderbilt University Medical Center,
United States

Reviewed by:
Antonio Rozzi,
INI, Istituto Neurotraumatologico Italiano, Italy
Daekyu Sun,
University of Arizona, United States

***Correspondence:**
Fei Wu
wufei0348@126.com
Yan Ding
yan.ding@childrens.harvard.edu

[†] These authors have contributed equally to this work

Specialty section:
This article was submitted to Cancer Molecular Targets and Therapeutics, a section of the journal Frontiers in Oncology

Received: 30 November 2018
Accepted: 21 January 2019
Published: 07 February 2019

Citation:
Liu W, Liu L, Wang R, Gong G, Ding X, Yang B, Bao Y, Wang Z, Zhang B, Zhao D, Wu F and Ding Y (2019) Bevacizumab Combined With Oxaliplatin/Capecitabine in Patient With Refractory and Recurrent Mucinous Adenocarcinoma of the Appendix: A Case Report. Front. Oncol. 9:55. doi: 10.3389/fonc.2019.00055

Primary appendiceal adenocarcinoma with peritoneal pseudomyxoma (PPM) has a high recurrence rate and refractory to medical interventions such as repetitive debulking surgery and systemic chemotherapy. Genome-based targeted therapy for such cases has not been well-documented. Here we present a 63-years-old women, who was diagnosed with recurrent mucinous adenocarcinoma of the appendix with local invasions and peritoneal carcinomatosis, was refractory to systemic chemotherapy after surgery. We used a regime developed using whole exome sequencing. Somatic mutations in the genes encoding VEGFR2, FGFR1, FGFR2, FGFR3, and KRAS were identified in the patient's tumor tissue. The patient was then treated with bevacizumab plus oxaliplatin. After 4 months of treatment, pelvic CT showed dramatic reduction of pseudomyoma and a decline of CA199 level from 5436.7 to 1121.4 U/ml. Continual treatment with bevacizumab-capecitabine remained effective and the patient's CA199 level further decreased to 401.26 U/ml according to the follow-up examination on Aug 15th, 2018. Results from this study show the evidence of gene mutations involving VEGF signal activation in the recurrence of appendiceal adenocarcinoma. Our results also suggest the association of these mutations with the effectiveness of anti-VEGF treatment using bevacizumab. Therefore, the screening of gene mutations involved in VEGF signaling and targeted therapy with anti-VEGF drugs may provide a new option to manage refractory/recurrent advanced-stage appendiceal adenocarcinoma.

Keywords: appendiceal adenocarcinoma, peritoneal carcinomatosis, next generation sequencing, bevacizumab, targeted therapy

BACKGROUND

Primary adenocarcinoma of the appendix is a rare malignancy and accounts for 0.4% of gastrointestinal tumors, according to a report of national cancer institute (NCI) (1). Mucinous adenocarcinoma is the most common histological subtype (37%), followed by colonic and carcinoid subtypes (2). The clinical presentations of appendiceal cancer are vague until advanced stage. As a

result, early diagnosis of appendiceal cancer is often difficult. Common complications of late stage disease include rupture and acute appendicitis (accounting for ∼1% appendectomy cases) (3), local invasion and peritoneal carcinomatosis (PC)/peritoneal pseudomyxoma (PPM) (4, 5). The advanced stage has a poor overall survival rate with median survival time of 5.2–12.6 months (5). Currently there is no standard medical care for the disseminated late-stage appendiceal cancer with PC/PPM. It has been generally recommended to perform cytoreductive surgery (CRS) combined with perioperative hyperthermic intraperitoneal chemotherapy (HIPEC) or postoperative intraperitoneal chemotherapy (EPIC) with mitomycin C, cisplatin, 5-FU, or a combination (5, 6). Unfortunately, most appendiceal cancer patients with PC/PPM experience recurrent and refractory to treatment, and fail to repetitive surgery and systemic chemotherapy (6).

Targeted therapy has been successfully used to treat many types of cancers including colorectal cancer. However, to the best of our knowledge, genome-based targeted therapy for the appendiceal cancer has never been reported. In the present case, a patient was diagnosed with mucinous adenocarcinoma of the appendix with peritoneal carcinomatosis and multiple local invasions. The patient received routine treatments by CRS-HEPIC-EPIC but relapsed after 1 year. Then the patient's condition deteriorated continuously and experienced recurrent and refractory to the treatment. Using whole exome sequencing and targeted medicine, optimal therapeutical efficacy was achieved with a gradual remission and remains progression-free until now.

CASE PRESENTATION

A 63-years-old Chinese female presented with asymptomatic palpable abdominal mass, increased carbohydrate antigen 19-9 (CA-199) level and pelvic mass on CT scan. An opening surgery observed an appendiceal mass involving the entire layer of the appendix, rupture, invasion of bilateral ovaries, wide-spreading nodular implantations with pseudomyxoma in peritoneal cavity, greater omentum, small intestine mesentery and hepatic and splenic regions. Debulking surgery with peritoneal nodule ablation and mucus reduction was performed in Beijing 301 Hospital. Postoperative pathology confirmed mucinous adenocarcinoma of the appendix T4NxM1, stage IV with peritoneal carcinomatosis (**Figure 1**). After surgery, the patient received one time standard perioperative hyperthermic intraperitoneal chemotherapy (HIPEC) with mitomycin C. Because of the excessive peritoneal carcinomatosis, the patient was given three cycles of postoperative intraperitoneal chemotherapy (EPIC) with 5-FU plus mitomycin C. The patient remained symptom free for 1 year until she developed progressive abdominal distension, loss of appetite and worsening nourishment. The patient failed to response to further systemic chemotherapy, and a large number of PPM (**Figures 2A,B**). Then a second surgery was performed, intestinal obstruction by mucous cavities was observed, and a colostomy was given. Shortly after operation, cetuximab, a monoclonal antibody binding to and inhibiting EGFR, was given to the patient for 20 days (yet without gene testing) at a local hospital, but failed to show any improvement. By then the patient had tried all available approved options and became refractory to the treatments.

TABLE 1 | Mutated genes identified in the present case of mucinous adenocarcinoma.

AKT1	ATM	CSFIR	ERBB2	FGFR1	FGFR2	FGFR3	FLT3
GNA11	JAK3	KDR	KIT	KRAS	NOTCH1	PIK3CA	PET
SMARCB1	SMO	STK11	TP53				

At the time when the patient visited us, she was severely wasted, with progressive abdominal distension and elevated CA-199 level at 5436.7 U/ml. Considering her weak constitution and failure of previous interventions, alternative treatment strategies, especially a rationally designed targeted therapy, emerged to be the last-ditch option to the patient. Targeted therapy is usually based on a patient's genomic profile by genetic testing. In order to find the accurate target, we decided to use the paraffin-embedded surgical tumor tissue from the patient, and detect gene mutations using the TruSeq Rapid Capture Exome Kit for whole exome sequencing (WES) on the Illumina NextSeq500 sequencing platform. The WES data was then analyzed using OncoDecoder™ (Genomic Future, Inc. USA). Several key gene mutations were identified including a missense mutation p.Gln472His (exon 11) in KDR/VEGFR-2, a missense mutation p.Arg281Gln (exon 8) in FGFR1, a missense mutation p.Lys296Arg (exon 7) in FGFR2, a missense mutation p.Thr654Ser (exon 14) in FGFR3 and a missense mutation p.Gly12Asp (exon 2) in KRAS. Additional 38 gene mutations including TP53, ERBB2, KIT, GNA11, and JAK3 were also detected (**Table 1**).

Although no NCCN-guided targeted therapy regime for appendiceal mucinous adenocarcinoma is documented as of to-date, there are two approved drugs for colorectal cancer may be considered as potential candidates: bevacizumab and cetuximab. Bevacizumab is a monoclonal antibody blocking the VEGF ligand, and bevacizumab in combination with standard chemotherapy has been approved by FDA as first line treatment for metastatic colorectal cancer (7, 8). We predicted that bevacizumab may be a suitable targeted drug candidate for our case based on the following three reasons: Firstly, the gene testing results showed several mutations involving KDR/VEGFR-2, FGFR1, FGFR2, and FGFR3. Although these mutations are currently classified as variation of uncertain significance (VUS), hyperactive VEGF pathway is a common event in colorectal cancer and contributes to tumor metastatic activity (9). A recent study from the MD Anderson cancer center showed improved average overall survival and progression-free survival by providing anti-VEGF treatment to patients diagnosed with unresectable appendiceal epithelial neoplasm (yet no gene

Abbreviations: CT, computed tomography; PC, peritoneal carcinomatosis; PPM, peritoneal pseudomyxoma; CRS, cytoreductive surgery; HIPEC, hyperthermic intraperitoneal chemotherapy; EPIC, intraperitoneal chemotherapy; VEGFR, Vascular endothelial growth factor receptor; FGFR, Fibroblast growth factor receptor.

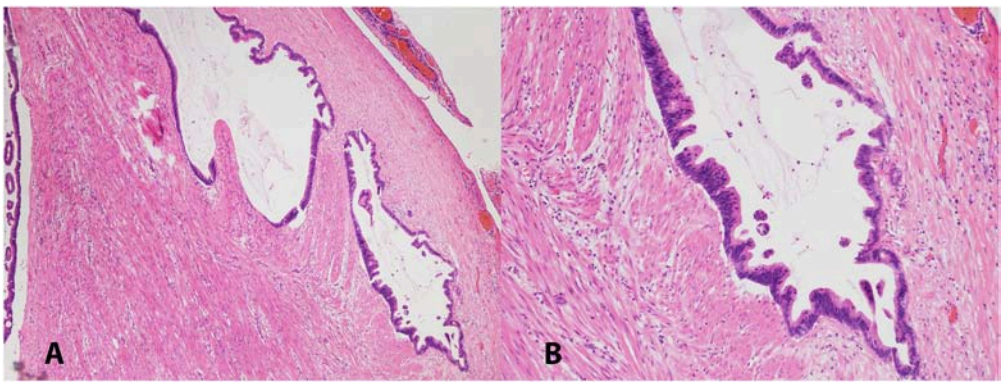

FIGURE 1 | Low (**A**, 40X) and high (**B**, 100X) magnification pictures of appendiceal mucinous adenocarcinoma. H&E stained.

testing was performed) (10). This finding suggests that VEGF hyperactivity could be a common event in appendiceal cancer, and bevacizumab could be a promising targeted drug. Next, it has been known that the efficacy of certain EGFR monoclonal antibody drugs, including cetuximab and panitumumab, could be affected by KRAS mutation (6). Indeed, in the present case, we identified KRAS p.Gly12Asp missense mutation, which could cause inefficient response to cetuximab (11). However, the efficacy of bevacizumab for colorectal cancer treatment has been testified to be independent from KRAS mutation (8). Thirdly, there was no contraindication of bevacizumab usage to the patient. The common risk factors include low WBC count, high blood pressure, impaired heart function and poor renal function.

Under our advice, the patient received treatment of bevacizumab (7.5 mg/Kg, in total 450 mg, IV-GTT) plus oxaliplatin (130 mg/m^2, in total 200 mg IV-GTT) on day 1 every 3 weeks for 6 cycles since August, 2016. Follow-up examination after treatment showed significant improvement of the patient's condition, and CT scan imaging results showed dramatic reduction of her peritoneal mucus (as shown in **Figures 2C,D**). In addition, the patient's CA-199 level decreased from 5,436.7 U/ml (before treatment) to 1121.4 U/ml (after treatment). Afterwards, the patient received continuous maintenance treatment using bevacizumab (7.5 mg/Kg, in total 450 mg, IV-GTT on day 1 each 3 weeks) plus capecitabine (1,500 mg, oral, twice a day) for days 1 to 14 until now. The patient has been followed up routinely to evaluate the treatment efficacy and to monitor the adverse effects. The main adverse effects were numbness in the hands and feet, dry nose and epistaxis, dry throat, fatigue, loss of appetite. The patient has been progression-free as of recent follow-up on September 26th, 2018 with the most recent CA-199 being 401.26 U/ml on August 15th, 2018.

DISCUSSION

Primary adenocarcinoma of the appendix is a rare neoplasm with an incidence of 1.2 cases per 100,000 people each year (12). The prognosis of appendiceal adenocarcinoma varies depending on the histology types, including colonic-type adenocarcinoma, typical carcinoid, mucinous adenocarcinoma, and singlet ring cell adenocarcinoma (3). The mucinous adenocarcinoma is similar to the ovarian adenocarcinoma, and peritoneal dissemination is a frequent metastatic route (12). Like most colorectal cancers, the appendiceal adenocarcinoma presents with non-specific symptoms and is difficult to be diagnosed preoperatively (4, 5). As a result, it is often found at an advanced stage in which the disease has already spread within abdomen (5). Appendiceal adenocarcinoma-derived peritoneal carcinomatosis (PC) or peritoneal pseudomyxoma (PPM) is a very poor prognostic factor with average life expectancy between half and 1 year (5). In the present case, the patient presented with asymptomatic abdominal mass, local invasions to greater omentum and fallopian tubes and peritoneal carcinomatosis with multiple pseudomyxoma cavities at the initial visit.

The management of mucinous appendiceal adenocarcinoma varies depending on the stages and does not have standard guideline. Right hemicolectomy remains the treatment of choice for the early stage local or regional appendiceal adenocarcinoma (5, 6). CRS-HIPEC or EPIC is usually recommended for the appendiceal or colonic-type carcinoma with confined peritoneal metastasis (5). However, there is no standardized protocol for HIPEC or EPIC (5), and it only achieved complete response in some patients (5, 6). In our case, the patient received CRS-HIPEC-EPIC regime but relapse of peritoneal carcinomatosis occurred 1 year later. Systemic 5-fluorouracil-based chemotherapy was barely beneficial.

Recently, genome-based precision medicine has made great progress to treat a variety of cancers, including colorectal cancer (13). Targeted drugs feature high efficiency and low toxicity. To the best of our knowledge, genome-based targeted therapy for metastatic appendiceal adenocarcinoma has not yet been reported. In order to seek for appropriate targeted therapy for the patient with recurrent and refractory appendiceal cancer, we performed whole exome sequencing with the patient surgical pathology tissue at our genetic testing lab. Several

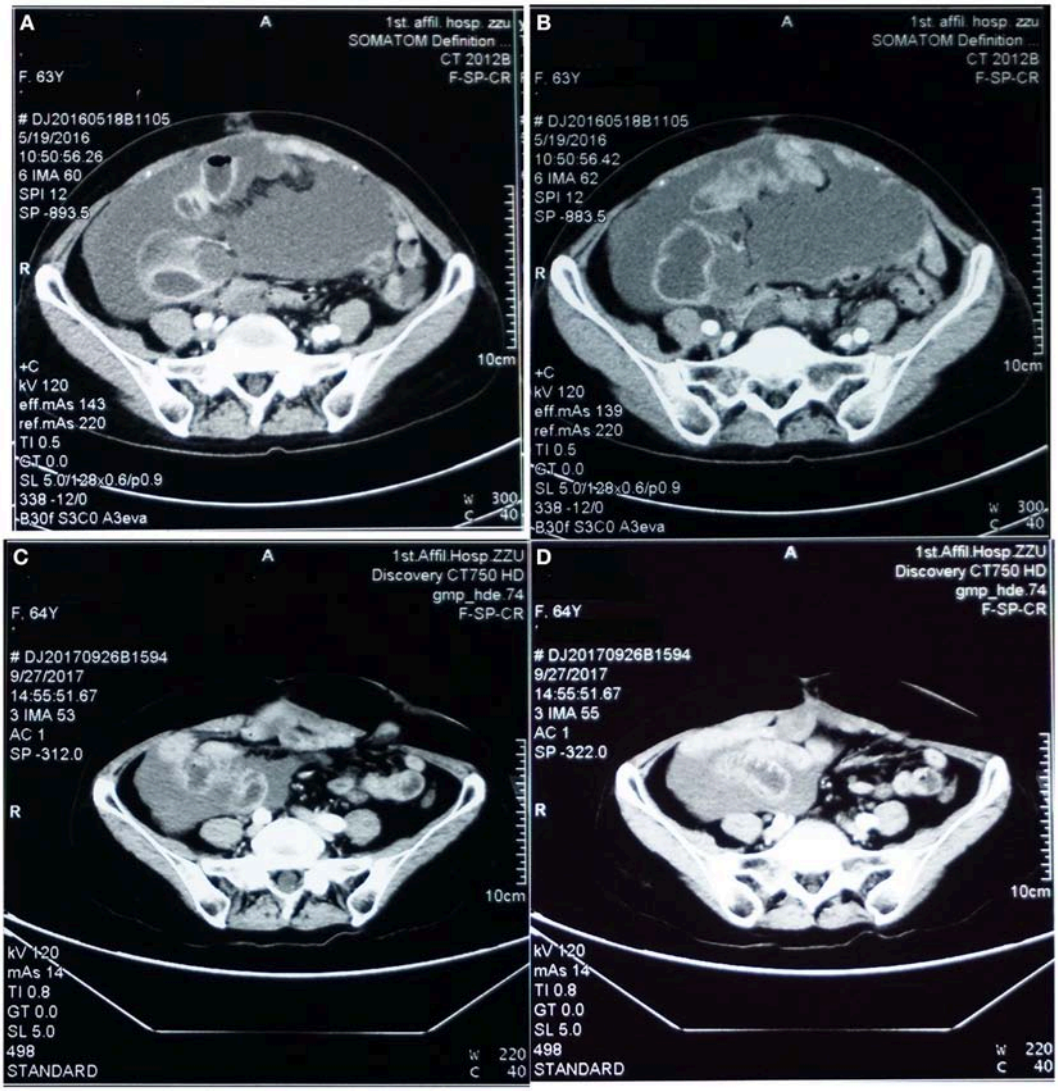

FIGURE 2 | Pelvic CT images before **(A,B)** vs. after **(C,D)** targeted therapy. **(A,B)** Prior to targeted therapy, images showed intraperitoneal multiple nodules, and a large number of peritoneal cavities filled up with mucus. **(C,D)** After targeted therapy using bevacizumab and oxaliplatin, image on the same sections showed significantly reduced peritoneal nodules and mucous cavities, suggesting stabilization of disease progression and partial response.

candidate target gene mutations involved in the angiogenesis pathway including KDR/VEGFR-2 and FGFR1, FGFR2, FGFR3 were identified. Both VEGF and FGF pathways function as angiogenetic mediators to promote metastasis of many neoplasms (9). Based on the gene mutation profile, the patient received the bevacizumab-oxaliplatin regime and then the bevacizumab-capecitabine as maintenance treatment. The results showed great effectiveness of the treatment and the patient remains progression-free and continuous decrease of CA-199 level as of to-date. The use of bevacizumab for metastatic appendiceal cancer treatment has been reported in a recent study (10). However, the treatment achieved therapeutical benefits in some patients but not the others, owing to the fact that no gene testing was performed before treatment (10). Therefore, our case report is the first study demonstrating evidence-based therapy for metastatic mucinous appendiceal adenocarcinoma. Indeed, we argue that certain level of cost-effective gene testing may be necessary prior to administration of targeted drugs in order to avoid the abuse of targeted medicines. A good example could be found in our case that the blind usage of anti-EGFR drug cetuximab without prior detection of KRAS mutation from the patient pathology tissue failed to achieve any treatment benefit.

In conclusion, accurate detection of gene mutation can help clinicians to make the optimal choice of individualized targeted drugs, and improve the prognosis and life quality of patients. The present report is one case and limited and waits for more cases to be filled in to expand our knowledge

about the genome mutations and personalized medicine of appendiceal cancer.

ETHICS STATEMENT

The patient of this case report agreed and provided written informed consent in accordance with the Declaration of Helsinki. Written informed consent was obtained from the patient for the purpose of publication of the present case report and any relevant images.

AUTHOR CONTRIBUTIONS

All authors listed have made a substantial, direct and intellectual contribution to the work, and approved it for publication.

REFERENCES

1. Hesketh KT. The management of primary adenocarcinoma of the vermiform appendix. *Gut* (1963) 4:158. doi: 10.1136/gut.4.2.158
2. Turaga KK, Pappas SG, Gamblin T. Importance of histologic subtype in the staging of appendiceal tumors. *Ann Surg Oncol.* (2012) 19:1379–85. doi: 10.1245/s10434-012-2238-1
3. Connor SJ, Hanna GB, Frizelle FA. Appendiceal tumors: retrospective clinicopathologic analysis of appendiceal tumors from 7,970 appendectomies. *Dis Colon Rectum* (1998) 41:75–80. doi: 10.1007/BF02236899
4. Ruoff C, Hanna L, Zhi W, Shahzad G, Gotlieb V, Salf MW. Cancers of the appendix: review of the literatures. *ISRN Oncol.* (2011) 2011:728579. doi: 10.5402/2011/728579
5. Winder T, Lenz HJ. Mucinous adenocarcinomas with intra-abdominal dissemination: a review of current therapy. *Oncologist* (2010) 15:836–44. doi: 10.1634/theoncologist.2010-0052
6. Pietrantonio F, Maggi C, Fanetti G, Iacovelli R, Di Bartolomeo M, Ricchini F, et al. FOLFOX-4 chemotherapy for patients with unresectable or relapsed peritoneal pseudomyxoma. *Oncologist* (2014) 19:845–50. doi: 10.1634/theoncologist.2014-0106
7. Saltz LB, Clarke S, Díaz-Rubio E, Scheithauer W, Figer A, Wong R, et al. Bevacizumab in combination with oxaliplatin-based chemotherapy as first-line therapy in metastatic colorectal cancer: a randomized phase III study. *J Clin Oncol.* (2008) 26:2013–9. doi: 10.1200/JCO.2007.14.9930.
8. Bencsikova B, Bortlicek Z, Halamkova J, Ostrizkova L, Kiss I, Melichar B, et al. Efficacy of bevacizumab and chemotherapy in the first-line treatment of metastatic colorectal cancer: broadening KRAS-focused clinical view. *BMC Gastroenterol.* (2015) 15:37. doi: 10.1186/s12876-015-0266-6
9. Ellis LM, Takahashi Y, Liu W, Shaheen RM. Vascular endothelial growth factor in human colon cancer: biology and therapeutic implications. *Oncologist.* (2000) 5 (Suppl. 1):11–5. doi: 10.1634/theoncologist.5-suppl_1-11
10. Choe JH, Overman MJ, Fournier KF, Royal RE, Ohinata A, Rafeeq S, et al. Improved survival with anti-VEGF therapy in the treatment of unresectable appendiceal epithelial neoplasms. *Ann Surg Oncol.* (2015) 22:2578–84. doi: 10.1245/s10434-014-4335-9
11. Karapetis CS, Khambata-Ford S, Jonker DJ, O'Callaghan CJ, Tu D, Tebbutt NC, et al. K-ras mutations and benefit from cetuximab in advanced colorectal cancer. *N Engl J Med.* (2008) 359:1757–65. doi: 10.1056/NEJMoa0804385
12. Arellano ML, Gonzalez-Dominguez Y, Molina-Ortiz F, Garceau MAH, Cantero R, Rodriguez-Montes JA. Primary adenocarcinoma of the appendix: experience at La Paz University Hospital of Madrid (1967-2014). *Int J Surg Open* (2016) 4:23–6. doi: 10.1016/j.ijso.2016.06.003
13. Linnekamp JF, Wang X, Medema JP, Vermeulen L. Colorectal cancer heterogeneity and targeted therapy: a case for molecular disease subtypes. *Cancer Res.* (2015) 75:245–9. doi: 10.1158/0008-5472.CAN-14-2240

Conflict of Interest Statement: The authors declare that the research was conducted in the absence of any commercial or financial relationships that could be construed as a potential conflict of interest.

frontiers in Pharmacology

REVIEW
published: 14 February 2019
doi: 10.3389/fphar.2019.00009

A Natural Isoquinoline Alkaloid With Antitumor Activity: Studies of the Biological Activities of Berberine

Da Liu[1,2], Xue Meng[1,2], Donglu Wu[1,2], Zhidong Qiu[1,2] and Haoming Luo[1,2]**

[1] Department of Pharmacy, Changchun University of Chinese Medicine, Changchun, China, [2] Key Laboratory of Effective Components of Traditional Chinese Medicine, Changchun University of Chinese Medicine, Changchun, China

Coptis, a traditional medicinal plant, has been used widely in the field of traditional Chinese medicine for many years. More recently, the chemical composition and bioactivity of Coptis have been studied worldwide. Berberine is a main component of Rhizoma Coptidis. Modern medicine has confirmed that berberine has pharmacological activities, such as anti-inflammatory, analgesic, antimicrobial, hypolipidemic, and blood pressure-lowering effects. Importantly, the active ingredient of berberine has clear inhibitory effects on various cancers, including colorectal cancer, lung cancer, ovarian cancer, prostate cancer, liver cancer, and cervical cancer. Cancer, ranked as one of the world's five major incurable diseases by WHO, is a serious threat to the quality of human life. Here, we try to outline how berberine exerts antitumor effects through the regulation of different molecular pathways. In addition, the berberine-mediated regulation of epigenetic mechanisms that may be associated with the prevention of malignant tumors is described. Thus, this review provides a theoretical basis for the biological functions of berberine and its further use in the clinical treatment of cancer.

Keywords: berberine, biological activities, antitumor, autophagy, epigenetic effects

OPEN ACCESS

Edited by:
Zhe-Sheng Chen,
St. John's University, United States

Reviewed by:
Di Wang,
Jilin University, China
Min Ye,
Peking University, China

****Correspondence:***
Zhidong Qiu
Qiuzd@ccucm.edu.cn
Haoming Luo
luo.haoming@163.com

Specialty section:
This article was submitted to Cancer Molecular Targets and Therapeutics, a section of the journal Frontiers in Pharmacology

Received: *21 November 2018*
Accepted: *07 January 2019*
Published: *14 February 2019*

Citation:
Liu D, Meng X, Wu D, Qiu Z and Luo H (2019) A Natural Isoquinoline Alkaloid With Antitumor Activity: Studies of the Biological Activities of Berberine. Front. Pharmacol. 10:9. doi: 10.3389/fphar.2019.00009

INTRODUCTION

Natural medicine plays a very important role in novel drug discovery (Zhang et al., 2013; Zhang L. et al., 2017). In recent years, many natural products have been confirmed to play an important role in cancer prevention and therapy (Tao et al., 2015; Zhang et al., 2015, 2016; Meng et al., 2018). Coptis chinensis is a valuable Chinese medicine used commonly in China. The medicinal parts are the dried rhizome of *Coptis chinensis* Franch., *Coptis deltoidea* C.Y.Cheng, and P.K.Hsiao, or *Coptis teeta* Wall (Wang et al., 2015b). It has been reported that Coptis exerts antibacterial, immune-enhancing, anti-ulcer, hypoglycemic, detoxifying, antitumor, and other pharmacological

Abbreviations: AP-1, activating protein 1; AMPK, AMP-activated protein kinase; BTG2, B-cell translocation gene 2; Bax, BCL2 associated X; BBC3, BCL2-binding component 3; CCNB, cyclin B; CCND, cyclin D; CCNE, cyclin E; CDK, cyclin-dependent kinases; CDKN1A/p21, cyclin-dependent kinase inhibitor; COX2, cyclooxygenase-2; DNMT, DNA methyltransferase; EGFR, epidermal growth factor receptor; GMCSF, granulocyte-macrophage colony-stimulating factor; GADD45, growth arrest and DNA damage-inducible 45; HCC, hepatocellular carcinoma cells; HAT, histone acetyltransferase; HDAC, histone deacetylase; HIF1α, hypoxia-induced factor α; INOS, inducible NO synthase; IL-8, interleukin-8; MMPs, matrix metalloproteinases; NSCLC, non-small cell lung cancer cells; NF-κB, nuclear factor kappa B; PARP, poly-ADP ribose polymerase; PGE2, prostaglandin E2; STAT3, signal transducer and activator of transcription 3; SIRT, sirtuins; Bcl-2, the B cell lymphoma-2; TNF, tumor necrosis factor; uPA, urokinase-type plasminogen activator; VEGF, vascular endothelial growth factor.

effects (Imenshahidi and Hosseinzadeh, 2016). Coptis is mainly used for the adjuvant treatment of depression, coronary heart disease, diabetes, liver cancer, and other malignant tumors. There are several active ingredients of Coptis chinensis, such as berberine (BBR), palmatine, coptisine, jatrorrhizine, worenine, columbamine, cedarone, obakunone, obakulactone, magnoflorine, and ferulic acid; berberine is the main bioactive component of Coptis chinensis and is present at a content of 5.20–7.69%. Consequently, it has become one of the natural small-molecule drugs used commonly in the clinical setting treatment for chronic disease such like diabetes (Cicero and Baggioni, 2016; Tabeshpour et al., 2017).

Berberine hydrochloride, the more commonly available salt form of berberine, is a quaternary ammonium isoquinoline alkaloid with the chemical formula $C_{20}H_{18}ClNO_4$ (**Figure 1**) that forms yellow needle-like crystals (Neag et al., 2018). Berberine was originally used as a broad-spectrum antibacterial drug. Extensive research revealed a wide range of pharmacological activities, including antibacterial, anti-inflammatory, antihypertensive, hypolipidemic, and antidiarrheal effects. In addition, berberine exhibits inhibitory effects on a variety of tumors (Xu et al., 2017), such as esophageal cancer. Many studies (Kumar et al., 2015; Foroutan F. et al., 2018; Foroutan T. et al., 2018; Mirhadi et al., 2018) have confirmed that berberine affects the development of tumor cells through the inhibition of tumor cell growth and the induction of apoptosis and cell cycle arrest (Iizuka et al., 2000; Kong et al., 2004; Tang and Feng, 2009; Xue et al., 2013; Signorelli et al., 2017).

It is reported that 8.2 million people die of cancer every year globally and that this number is continuously rising; according to the American Cancer Society, cancer is the cause of more than 600,000 deaths every year in the United States, a mortality rate second only to heart disease (Khalil et al., 2016; Walker et al., 2017). Owing to the seriousness of this situation, scientific approaches to the prevention and control of cancer have become a major public health issue (Gu et al., 2015; Viegas et al., 2017).

It has long been believed that the occurrence and development of tumors are attributable to only genetic abnormalities, which include gene mutations, translocations, and chromatin insertions (Dupont et al., 2009; Li et al., 2018). However, in recent years, the emergence and progress of genome sequencing technology have led to the rapid development of epigenetics and many researchers have determined that epigenetics plays an important role in the regulation of tumors. Epigenetic changes are reversible, heritable changes in gene expression and protein function in which the genomic DNA sequence remains unchanged (Biswas and Rao, 2018). Epigenetic changes can regulate gene expression at multiple levels, for example, at the DNA level through DNA methylation, at the RNA level through non-coding RNA regulation, at the protein level through histone modification, and at the chromatin level through chromatin remodeling. The continuous presence of these mechanisms in cell division allows cells to retain their respective characteristics, respond to intrinsic cellular signals, and participate in cell evolution and adaptation to environmental changes. Many research studies have confirmed that epigenetic mechanisms are implicated in tumorigenesis through the regulation of oncogene activation and tumor suppressor gene inactivation. For example, DNA methylation can inactivate tumor suppressor genes, abnormal histone acetylation can change tumor-associated gene expression, and non-coding microRNAs can result in dysregulation of tumor suppressor genes (Blandino et al., 2014; Wong and Chim, 2015). It is of note that different epigenetic modifications in cells often interact with each other in a synergistic manner to maintain body's homeostasis through the regulation of the expression of key genes, and that when abnormal changes occur, they may cause a variety of diseases, including tumors (Vijayaraghavalu et al., 2013). Recent evidence has suggested that epigenetic modifications may be involved in the processes tumor cells use to shape a microenvironment suitable for their own growth (Honda et al., 2006). There are a large number of active substances, such as growth factors, inflammatory factors, and proteases, in the tumor microenvironment and these participate in the various processes of tumorigenesis through their own functional properties or mediated signaling pathways (Booth and Gutierrez-Hartmann, 2015). Epigenetic modifications are involved in the regulation of the secretory processes of these biomolecules or their mediated signaling pathways (Li et al., 2018). From the perspective of the tumor development process, the regulation of epigenetic modification in the tumor microenvironment occurs at various stages of tumorigenesis, progression, and metastasis, and is one of the important tools for diversifying between tumor cells and the tumor microenvironment. That is to say, tumors may have specific epigenetic modification characteristics that may lead to changes in cell biological characteristics and malignant transformation. Therefore, an exploration the mechanism of tumor biology from the perspective of epigenetics is of great significance.

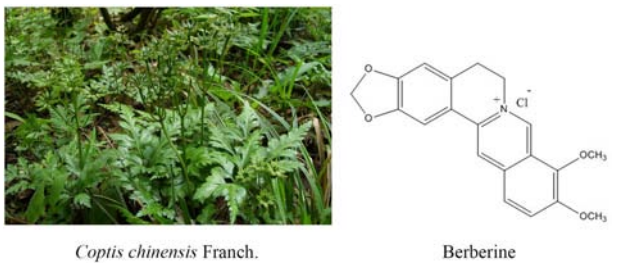

FIGURE 1 | *Coptis chinensis* Franch. and chemical structure of berberine.

THE BIOLOGICAL EFFICACY OF BERBERINE

Berberine Inhibits the Migration and Invasion of Tumor Cells

Migration and invasion are the basic characteristics of tumor cells. Therefore, it is valuable to study whether berberine can affect the migration and invasion ability of tumor cells. It is well known that E-cadherin and *N*-Cadherin proteins are closely

related to cell migration and invasion. Moreover, E-cadherin is not only an important mediator that regulates cell-cell adhesion, but also an important molecule in the maintenance of the morphology and structural integrity of epithelial cells (Qi et al., 2014; Shi et al., 2017). There is a large amount of experimental evidence suggesting that berberine can inhibit the migration and invasion of tumor cells. In human lung cancer A549 cells, berberine increased the expression of E-cadherin protein in a concentration- and time-dependent manner (Li et al., 2018), and significantly downregulated the expression of *N*-cadherin; these changes inhibited invasion and metastasis. MMPs are a class of important proteins that are involved in that the degradation of the extracellular matrix barrier, which is the first step in tumor cell metastasis (Hao et al., 2017). Studies have shown that berberine inhibits the expression of MMP2 and MMP9 in a time- and concentration-dependent manner. Simultaneously, berberine also regulates the expression of MMPs through the inhibition of the transfer of p-STAT3 to the nucleus, which affects its activity. Wang X et al. found that berberine was an effective inhibitor of the invasion and migration of HCC cells. Berberine treatment of HCC cells downregulated the expression of cox-2, NF-κB, uPA, and MMP9 in a dose-dependent manner (Sengupta et al., 2017). In summary, the data strongly suggest that berberine has an important role in the regulation of cadherin- and MMP-mediated pathways, which leads to inhibitory effects on cancer migration and invasion (**Table 1**).

Furthermore, Jin Y. et al. (2017) showed that the effect of berberine on the metastatic potential of cancer cells may be mediated by the activation of the AMPK signaling pathway, which reduces the activity of ERK and the expression of COX-2, thereby inhibiting the adhesion, migration, and invasion of tumor cells. Moreover, berberine inhibited tumor cells through signaling pathways, including the NF-κB and AMPK pathways. Studies have demonstrated that berberine prevents tumor cells from producing IL-8 and blocks NF-κb signaling pathway, ultimately inhibiting endometrial cancer metastasis, and that colon cancer cell migration was inhibited by targeting AMPK signaling (Li et al., 2014).

Vascular endothelial growth factor, the most important angiogenic factor secreted from tumor cells, stimulates tumor neovascularization through an increase in the mitogenic and survival properties of vascular endothelial cells. Berberine not only reduces the expression of SC-M1 cells with normal oxygen content and low oxygen content. VEGF also directly inhibits the proliferation and migration of umbilical vein epithelial cells. Berberine treatment in B16F-10 melanoma cells reduced the expression of VEGF mRNA and inhibited angiogenesis. Inflammation plays an important role in tumor angiogenesis, which is mainly manifested through the activation of NF-κB to regulate VEGF, and results have shown that berberine treatment of tumor cells significantly inhibited NF-κB and ultimately decreased the expression of VEGF and IL-8 in tumor cells (Hamsa and Kuttan, 2011; Siveen and Kuttan, 2011). In addition, berberine significantly inhibited the VEGF-induced migration and invasion of human umbilical vein endothelial cells HUVEC in a dose-dependent manner, and significantly reduced the expression of COX-2, Inos, and VEGF mRNA and downregulated pro-angiogenic factors to inhibit angiogenesis (Naveen et al., 2016; Wang et al., 2018). These results indicated the critical effects of berberine on the HIF1α/VEGF pathway.

Angiogenesis plays an important role in tumor growth, as progression and metastasis are prerequisites for solid tumor growth. The angiogenic process is therefore a target for the inhibition of tumor growth and metastasis (Ma et al., 2008) Studies have shown that berberine can reduce the levels of IL-1β, IL-6, TNF, and GMCSF in the serum of tumor-inoculated animals and inhibit the elevation of NO and TNF-α, inflammatory mediators involved in angiogenesis. Wang Y et al. inferred that berberine suppressed the growth and metastasis of endometrial cancer cells via miR-101/COX2, and berberine is also known to inhibit tumors via the COX-2/PGE2 signaling pathway. The transcription of miR-101 is up-regulated by berberine through AP-1 to regulate the transcription of COX-2 in EC cells (Wu et al., 2012). The high expression of p-STAT3 in malignant tumor cells and the expression level of p-STAT3 in tumor tissues, the more obvious the proliferation and metastasis of tumor cells (Munir et al., 2000).

Berberine Inhibits Tumor Cell Proliferation (Autophagy, Apoptosis)

Apoptosis is an ideal form of cell death in cancer therapy because it generally does not cause an inflammatory response. Thus, the induction of apoptosis is one of the various mechanisms that inhibit the growth of tumor cells (Yakata et al., 2007). It has also been reported that berberine significantly inhibited the proliferation of human prostate cancer PC3 cells (Huang et al., 2015). In recent years, studies have shown that the proliferation of renal cell cancer cells can be effectively inhibited by berberine; when a certain concentration of berberine is treated to renal cell cancer cells, the effects continue for some time. The inhibitory effect of berberine on the tumor cells gradually increased, and it was found that the effect of inhibitory effect was greatest for treatment times of up to 48 h. In addition, the total apoptotic rate of renal tumor cells detected by a double staining method showed that after treatment of renal cell cancer cell lines A498 and 786-0 with different concentrations of berberine, the rate of total apoptosis in cells gradually increased as the concentration of the drug increased (Wang et al., 2015a; Liu et al., 2017a,b, 2018).

Berberine induces apoptosis in tumor cells, mainly through upregulation of pro-apoptotic genes and downregulation of apoptosis-inhibiting genes. For example, berberine can upregulate the expression of the pro-apoptotic protein BAD in HL-60 cells and downregulate the expression of anti-apoptotic protein Bcl-2 to achieve regulation of tumor cell apoptosis. In addition, apoptosis can be induced by the mitochondrial/caspase pathway, DNA cleavage induces tumor cell apoptosis, tumor cell apoptosis is induced by inflammatory factors, and tumor cell apoptosis is induced by cyclooxygenase. For example, berberine treatment of liver cancer cells revealed that DNA fragments, caspase-3, and caspase-8 were activated, which was followed by the activation of PARP, and the release of cytochrome c to inhibit tumor metastasis (Mistry et al., 2017).

Studies have showed that berberine can regulate apoptosis-associated proteins. Caspase cleavage is a typical phenomenon in apoptosis cells. Thus, numerous reports have used the detection of this cleavage to clarify the role of berberine in the induction of apoptosis. For example, berberine decreased the expression of Bcl-2 and survivin and, conversely, increased the expression of the pro-apoptotic genes Bax and cleaved caspase-3 in a dose-dependent manner in human ovarian cancer SKOV3 cells (Su et al., 2015). Moreover, the treatment of berberine to treat human colorectal adenocarcinoma (HCT-15) cells significantly increased the expression of spliced caspase-3 and the mitochondrial apoptosis-related protein Bax, and significantly decreased the expression of Bcl-2 and survivin, finally inducing apoptosis (Agnarelli et al., 2018). Berberine inhibited the proliferation of human cervical cancer Ca Ski cells through alteration of the ratio of p53 and Bax/Bcl-2 proteins, upregulation of ROS, and enhancement of caspase-3 activity to induce apoptosis (Kalaiarasi et al., 2016). In addition, berberine induced the proliferation of BIU-87 and T24 cells through the inhibition of protein expression, the induction of G1 cell cycle arrest, and the induction of apoptosis via the caspase-3 and caspase-9 pathways (Lu et al., 2015). Agnarelli A et al. treated U343 cells and MIA PaCa-2 cells with 50 μM berberine for 48 h, and found that the activity of caspase-3 was decreased in U343 cells and increased in MIA PaCa-2 cells. Therefore, they concluded that berberine promoted the apoptosis of tumor cells (Katona et al., 2014). It has been reported that berberine induces Bax activation in human lung cancer A549 cells, enables p53 pathway-mediated cytochrome c release, and leads to the activation of caspase signaling ultimately causing apoptosis (Shi et al., 2013). The reported data also showed that berberine induced cancer cell apoptosis mainly through the regulation of the expression of caspases and Bcl-2; this results in the release of cytochrome c and the activation of the mitochondria-dependent apoptotic pathway to promote apoptosis in PC3 cells (Wang et al., 2017).

Autophagy is one type of cellular self-protection mechanism, consisting mainly of the degradation of macromolecular material and damaged organelles in cytoplasm after autophagosome formation with lysosomes. The products of degradation are used to restore cell homeostasis. There are three forms of cell autophagy: macro-autophagy, micro-autophagy, and autophagy, which are mediated by different molecular chaperones. Autophagy is involved in many of the physiological and pathological processes of cells, and there is a close relationship between autophagy and tumorigenesis. The effects of autophagy vary in different cell lines and maybe inhibitory or stimulatory. In addition, the occurrence of autophagy is regulated by various signal pathways. Recent experimental studies have shown that berberine inhibits the proliferation of colon cancer cells through the downregulation of the expression of EGFR and that it activates autophagy and apoptosis through the p38 signaling pathway to inhibit the proliferation of HCT-15 cells. Similarly, in berberine-treated HCT-15 cells, the autophagy marker proteins ATG5 and LC3 were upregulated in a time-dependent manner (Zhang L. et al., 2017), indicating that berberine induced autophagy in HCT-15 cells. These data demostrate a role of Berberin in regulating cancer cell proliferation (**Tables 1**, **2**).

Berberine Arrests Tumor Cell Cycle

Many studies have shown that low concentrations of berberine arrest human osteosarcoma U20S cells in the G1 phase through the induction of DNA double-strand breaks that activate the p53-p21 pathway. In contrast to low concentrations of berberine, high concentrations induce arrest in the G2/M phase, but do not depend on the p53-p21 pathway (Yang et al., 2015; Li et al., 2017). Other studies demonstrated that berberine significantly inhibited human ovarian cancer cells (HEY and SKOV3 cells) in a time- and dose-dependent manner. It is demonstrated that that berberine exerts a significant inhibitory effect on human gastric cancer MGC 80 3 cells in a dose-dependent manner. Using laser confocal microscopy, the nucleus condenses, and apoptotic bodies are seen, which indicate that berberine can inhibit the proliferation of MGC 80 3 cells and arrest cells in the G0/G1 phase to inhibit the proliferation of tumor cells *in vitro*.

B-cell translocation gene 2 is a transient early-response gene induced by p53. It is a member of the gene family that regulates cell proliferation and is an important bridge molecule that links

TABLE 1 | Inhibitory effects of berberine on tumor migration and invasion.

Cell lines	Mechanism	Reference
Human non-small cell lung cancer (A549)	N-Cadherin↓ E-cadherin↑	Li et al., 2018
Hepatocellular carcinoma (HCC) cells	COX-2↓,NF-κB↓ UPA,MMP-9↓	Sengupta et al., 2017
Endothelial canjcer colon cells	IL-8↓, NF-κB↓ AMPK↑	Li et al., 2014
Mouse melanoma cell (B16F-10)	VEGF mRNA↓	Siveen and Kuttan, 2011; Hamsa and Kuttan, 2011
Human umbilical vein endothelial cells (HUVEC)	COX-2↓, iNOS↓, VEGF mRNA↓	Ma et al., 2008
Human endometrial cancer cell lines(AN3 CA and HEC-1-A)	COX-2↓ PEG-2↓	Wu et al., 2012

TABLE 2 | Inhibitory effects of berberine on tumor cell proliferation.

Cell Lines	Mechanism	Reference
Liver cancer cells	Caspase-3↑, Caspase-8↑,PARP↑	Mistry et al., 2017
Human ovarian cancer cell (SKOV3)	Bcl-2↓ Bax↑, Cleaved-Caspase-3↑,	Su et al., 2015
Colorectal adenocarcinoma cell line (HCT-15)	EGFR↓, Bcl-2↓, Survivin↓ ATG5↑, Bax↑, LC3↑	Agnarelli et al., 2018
Human cervical cancer cell (CaSki)	p53↑, Bax/Bcl-2↑ ROS↑, Caspase-3↑	Kalaiarasi et al., 2016
Human bladder cancer cell (BIU-87, T24)	Caspase-3↑, Caspase-9↑	Lu et al., 2015
Human pancreatic carcinoma cell (MIA PaCa-2)	Caspase-3↑ P53↓	Katona et al., 2014

p53, pRB, the cell cycle, cell proliferation, and differentiation. The current body of evidence indicates that berberine can promote the cell cycle arrest of human hepatoma HEPG2 cells in the G1 phase through the upregulation of BTG2 and the downregulation of cyclin D1, consequently inhibiting the proliferation of hepatoma cells and inducing apoptosis.

Cyclin is one of the target proteins that regulate the G1 phase. As a proto-oncogene, it is involved in the regulation of the cell cycle, and its overexpression is closely related to the occurrence and development of tumors. Berberine has a variety of effects on the cell cycle; for example, it can arrest the G2/M phase in the cell growth cycle through a reduction in the expression of cyclin B1 and increase in the expression of Wee1, which stops the tumor cells in the early stage of DNA synthesis (G1) and late DNA synthesis (G2). The induction of tumor cell apoptosis through the downregulation of cyclin E expression and upregulation of p21 expression, which causes G1 arrest in HEY and SKOV3 cells and downregulates Bcl-2 protein expression and upregulates Bax protein expression. Berberine treatment of MDA-MB-231 and MCF-7 human breast cancer cells dose-dependently caused G0/G1 arrest, which was possibly associated with a decrease in the cell cycle regulation protein cyclin B1. Furthermore, it increased the expression of CDC4 and cyclin B1 through an increase in the expression of CDC2 and caspase-3 in human hepatoma HepG2 cells, causing arrest in the S and G2/M phases, and activating the AMPK signaling pathway to induce the apoptosis of HepG2 cells (Chidambaram et al., 2012; Murthy et al., 2012; Balestrieri et al., 2018). Li et al. demonstrated that berberine regulates the PI3K-AKT and MAPK signaling pathways in PTC (the most common subtype) and ATC (the most malignant and aggressive subtype), leading to mitochondrial apoptosis, G0/G1 cell cycle arrest, increased Bax/Bcl-2, cleaved caspase-3, p21, and decreased cyclin E1, CDK2, and vimentin were verified by western blotting (Waterbeemd et al., 2013). The combination of drugs upregulated the expression of the cell cycle-dependent kinase inhibitory proteins p27 and p21, and downregulated the expression of cyclin D1, CDK2, and CDK4-cyclin.

In addition, studies have reported that berberine can bind to topoisomerase (TOP1), which hinders the synthesis of S phase cells and prevents cell proliferation.

Effects of Berberine in Compatibility

With the identification of numerous anti-tumor drugs, research of cancer therapy has gradually shifted from a focus on monotherapy to combined therapy. More and more reports have demonstrated that berberine combined with radio-therapy or chemotherapy drugs can achieve better anti-tumor effect. For instance, berberine combined with gamma-radiation enhance the anti-cancer effects, including inducing apoptosis and ROS generation (Jung-Mu et al., 2009). Also, berberine sensitizes lung cancer cells to radiation via autophagy both *in vitro* and *in vivo* (Peng et al., 2008). Indicated an adjuvant role in radio-therapy of cancer. Another major anti-cancer therapy is chemotherapy, several novel chemotherapy drugs such like doxorubicin, rapamycin were texted combined with berberine, and showed a more effective result. It is reported that berberine sensitizes mutliple human cancer cells to the anticancer effects of doxorubicin (Tong et al., 2012). More details and drugs were summarized in **Table 3**, which clarified that berberine synergistic work with chemotherapy drugs in anti-tumor proliferation through inducing cell cycle arrest, apoptosis, as well as autophagy. These data have laid theoretical foundation for the combined therapy in clinic trial.

EPIGENETIC EFFECTS OF BERBERINE ON TUMORS

For many years, researchers have been studying and developing drugs for cancer prevention and treatment. Chinese medicines, such as berberine, are commonly used as drugs. As an active ingredient of Coptis, berberine is inevitably closely related to the occurrence and development of tumors (Wang-Johanning et al., 2008; Coward et al., 2014; Delga-docruzata et al., 2015; Dkhil et al., 2015). Extensive research has led scholars to conclude that, ultimately, the antitumor effect of berberine may be related to epigenetic effects. The following is a brief description of the methods through which berberine regulates tumor cells, including migration, proliferation, and apoptosis, through epigenetic mechanisms.

DNA Methylation

DNA methylation refers to the covalent attachment of the fifth carbon atom of cytosine on the CpG dinucleotide to the methyl group through the action of DNMT, which is modified to 5-methylcytosine. DNA methylation is a potential epigenetic mechanism involving a variety of biological processes. The DNMT family consists of three main members: DNMT1, DNMT3A, and DNMT3B. DNMT1 mainly maintains DNA methylation status and DNMT3A and DNMT3B catalyze new DNA methylations (Kalinkova et al., 2018; Li et al., 2018; Puneet et al., 2018). Human CpG exists mainly in two forms: one is dispersed in genomic DNA; the other is highly aggregated to form CpG islands, which are present in the promoter region or the first exon region of various genes. In the human genome, the CpG site is usually in an unmethylated state in the CpG islands, but in a methylated outside the CpG islands. When tumors occur, the degree of unmethylation of CpG sites outside CpG islands increases, whereas the CpG sites in CpG islands are highly methylated, causing a decrease in the overall methylation level of the genome, as well as certain gene CpG islands. Local methylation levels are abnormally elevated, leading to genomic instabilities, such as chromosomal instability, the activation of proto-oncogenes, and the silencing of tumor suppressor genes (Qing et al., 2014; Crawford et al., 2018; Lee and Gang, 2018; Sanna et al., 2018). DNA methylation abnormalities are mainly divided into the hypomethylation state of proto-oncogenes and the hypermethylation state of tumor suppressor genes. The most studied of these is the hypermethylation of tumor suppressor genes. It is of interest that berberine has been found to inhibit the expression of human DNA methyltransferases DNMT1 and DNMT3B in multiple myeloma U266 cells. For example, berberine can alter the CpG methylation of p53

TABLE 3 | Berberine combined with chemotherapy drugs.

Combined With	Cells	Mechnisms/Effect	Reference
2-deoxy-D-glucose	Human lymphoblastoid TK6 cells	BBR combined with the glucose analog 2-deoxy-D-glucose (2-dG) synergistic inducing the apoptosis of human lymphoblastoid TK6 cells	Halicka et al., 2017
5-Fluorouracil	Gastric cancer cells AGS	BBR sensitized gastric cancer cells to 5-FU, the combination shows a synergistic inhibition of surviving and STAT3 level	Pandey et al., 2015
Cinnamaldehyde	Lung carcinogenesis A549 cell	BBR combined with cinnamaldehyde prevented A549 cell substance permeability via AMPK-reduced AQP-1 expression	Meng et al., 2017
Cisplatin	Breast cancer MCF-7	BBR sensitized MCF-7 cells to cisplatin through inducing DNA breaks and caspase-3-dependent apoptosis	Zhao et al., 2016
D-limonene	Human gastric carcinoma cell line MGC803	BBR in combination with d-limonene showed synergistic anticancer effects on MGC803 cells through inducing cell-cycle arrest, ROS production, and apoptosis via the mitochondria-mediated intrinsic pathway	Zhang et al., 2014
Doxorubicin	Murine melanoma B16F10 cells	BBR combined with Doxorubicin inhibit melanoma tumor growth through casepase-3 dependtent apoptosis	Mittal et al., 2014
	Lung cancer cell lines	BBR sensitizes lung cancer cells to Doxorubicin by promoting STAT3 degradation, inhibiting doxorubicin mediated STAT3 activation.	Zhu et al., 2015
Evodiamine	Breast cancer MCF-7	BBR in combination with evodiamine inducing cell cycle arrest and apoptosis, further inhibit MCF-7 prolieration	Du et al., 2017
Hsp90 inhibitor NVP-AUY922	Colorectal cancer	BBR combined with NVP-AUY922 inhibit proliferation of colorectal cancer via mutiple pathways	Su et al., 2015
Metformin	NSCLC	BBR combined with metformin synergistic induced cell cycle arrest, as well as reduced migration and invasion of NSCLC cells	Zheng et al., 2018
Rapamycin	Human hepatoma cell SMMC7721 cells	BBR combined with rapamycin can improve HCC therapy through inhibiting the mTOR signaling pathway	Guo et al., 2014
S-allyl-cysteine (SAC)	Human liver cancer HepG2 cells	BBR combined with SAC effectively reduced Rb-phosphorylation resulting insignificant nuclear E2F presence, further inhibiting cancer cell proliferation	Sengupta et al., 2017
	DEN+CCl4 induced hepatocarcinoma	BBR in combination with SAC inhibited Akt mediated cell proliferation, and inducing PP2A/JNK mediated apoptosis.	Sengupta et al., 2014
Sorafenib	Human liver cancer SMMC-7721 and HepG2 cells	berberine combined with sorafenib inhibited the proliferation of liver cancer cells by inducing cancer cell apoptosis.	Huang Y. et al., 2018
Tamoxifen	Breast cancer MCF-7	BBR sensitized MCF-7 cells to tamoxifen via inducing the G1 phase arrest and activating apoptosis.	Wen et al., 2016
Tetrahydropalmatine	MDA-MB-231 breast cancer cells	BBR combined with tetrahydropalmatine synergistic inhibited the proliferation of MDA-MB-231	Zhao et al., 2014
TPD7	T-cell acute lymphoblastic leukemia cell	BBR combined with TPD7 induced G1 -phase cell-cycle arrest of T-cell acute lymphoblastic leukemia cell.	Ma et al., 2017

DNA, affect the mRNA expression of key apoptosis-related proteins, and increases apoptosis in U266 cells, and thereby leads to cell cycle arrest. Although the hypomethylation of the p53 promoter can regulate apoptosis-related genes, such as GADD45, Bax, PMAIP1, BBC3, CCNB1, CCND3, and CCNE1. Specifically, in the p53 pathway, CDKN1A, GADD45B, Bax, PMAIP1, and BBC3 were upregulated, and CCNB1, CCND3, and CCNE1 were downregulated, which suggested that berberine activated the p53 signaling pathway through the impairment of U266 cells. In addition, results have shown that treatment of colorectal cancer cells with berberine results in a significant increase in the expression of DNMT1 and DNMT3A in the presence of TGF-β1; this hypermethylation in the promoter CpG island leads to further silencing of TSG, which results in tumor cell proliferation (Riaz et al., 2015; Asadi et al., 2018; Nardi et al., 2018).

Histone Modification

Histones play an important role in gene expression and tumorigenesis and development. The nucleosome is the basic constituent unit of chromatin. A nucleosome is an octamer composed of histones H2A, H2B, H3, and H4 and DNA entangled on the outside of the 147 base pairs. Histones not only protect the DNA structure and genetic information, but also participate in the regulation of gene expression. The extracellular amino terminus of histones can be modified by a variety of

TABLE 4 | Epigenetic regulation of berberine on tumor.

Type of Regulation	Cell Lines	Mechanism	Reference
DNA methylation	Multiple myeloma	DNMT1↓, DNMT3B↓ CDKN1A↑, GADD45B↑ Bax↑, PMAIP1↑	Asadi et al., 2018; Riaz et al., 2015; Nardi et al., 2018
	U266 cells	CCNB1↓, CCND3↓, CCNE1↓	
Histone Modification	Human non small cell lung cancer A549	HDAC↓MMP2↓ MMP9↓	Huang et al., 2017
	U266 cells	CBP/P300↑ SIRT3↑	Sun et al., 2017
MicroRNA	Human U266 multiple myeloma cells	miRNA21, Bcl-2↓	Hashiguchi et al., 2017
	Colon cancer	miR-152↓; miR-429↓ miR-29a↓	Hu et al., 2013

enzymes to form specific "histone codes" that alter the "open" or "closed" state of the local chromatin structure, or determine which proteins bind to specific DNA regions. Consequently, they regulate the various functions of DNA, including transcription and damage repair. Histone acetylation is highly dynamic and is coordinated by HATs and HDACs, and occurs at the amino-specific lysine residues of histones (Stevens et al., 1984; Yan et al., 2001; Bhat et al., 2018; Georgoff et al., 2018; Liu et al., 2018; Rahnamoun et al., 2018). Histone modification is a major determinant of the epigenetic silencing of genes and the regulation of cellular processes. Histone modifications often occur at the amino terminus of histones, and modifications of various chemical groups are acceptable due to exposure to chromatin (Oliver et al., 2013; Bennetzen and Wang, 2014; Hoen and Bureau, 2015; Yamada et al., 2015; Zhang et al., 2015; Li and Zhao, 2016; Rayan et al., 2016; Jiang et al., 2018; Salimian et al., 2018; Shang et al., 2018; Yan et al., 2018; Sahebi et al., 2018; Zhang L. et al., 2018; Zhang S. et al., 2018). The most widely studied are the acetylation and methylation of lysine K on histone H3 and H4. Histone acetylation plays an important role in the epigenetic theory proposed in recent years. Histone acetylation can affect the chromatin structure in cells, and thus participate in the transcriptional regulation of genes at specific sites, playing an important role in cell growth and differentiation. With a deeper understanding of the mechanism of histone acetylation in gene transcriptional regulation, the role of HDAC inhibitors in tumor therapy has received increasing attention (Sun et al., 2017).

CBP and p300 proteins with acetylase activity are transcriptional coactivators and hematopoietic tumor suppressors. Studies have shown that berberine can upregulate the expression of CBP/P300 and SIRT3 in U266 cells, and downregulate the expression of HDAC8; however, in HL-60/ADR and KG1-α cells, CBP/P300 and SIRT3 were also upregulated, but HDAC8 did not change significantly. Histone acetylation maintains its balance through HAT and HDAC. Berberine downregulated HDAC in human lung cancer A549 cells, which resulted in decreased expression of the metalloproteinases MMP-2 and MMP-9 mRNA and protein, inhibiting cell migration and invasion (Huang et al., 2017). Simultaneously, another study has shown that berberine treatment of A549 cells significantly reduced the expression of class I, II-a, II-b, and IV mRNA, histone H3, and H4 hyperacetylation.

MicroRNA

MicroRNAs (miRNAs) are short-chain non-coding RNAs of 19–22 nucleotides in length that bind to the 3′UTR in target mRNAs, thereby degrading or blocking the translation of target mRNAs. It plays an important role in the growth, differentiation, apoptosis, and tumor cell development. miRNAs can regulate the expression of multiple tumor-associated genes. In accordance with the function of miRNAs, they can be divided into two types: oncogenes or tumor suppressor genes (Hu et al., 2013). Not only can it act directly as a proto-oncogene or a tumor suppressor gene, but also regulate the expression of other proto-oncogenes or tumor suppressor genes. miRNAs play a central role in many cellular biology processes, and their dysregulation is a ubiquitous feature in tumors. Epigenetic effects have been shown to be a major cause of miRNA dysregulation in tumors (Hashiguchi et al., 2017). In the TGF-β1-induced colorectal cancer model, berberine significantly decreased the expression of miR-152

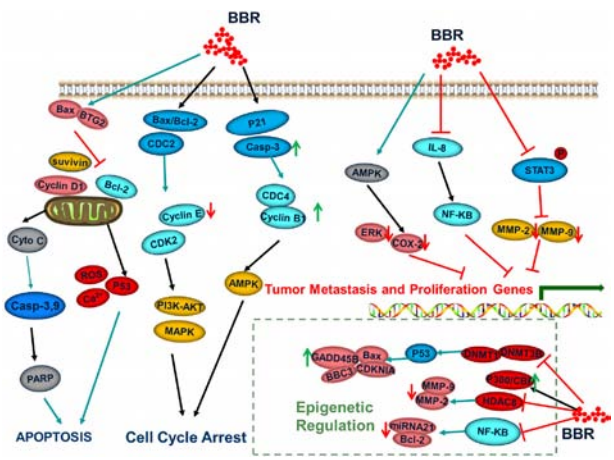

FIGURE 2 | Signaling pathways regulated by berberine.

(targeting DNMT1), miR-429 (targeting DNMT3A), and miR-29a (targeting DNMT3A/3B), which suggested that berberine inactivates some tumor suppressor factors, including DNMT1 and DNMT3A/3B, through the regulation of the expression of the above miRNAs during colon cancer development. Furthermore, other evidence has suggested that berberine treatment of human U266 multiple myeloma cells led to the inhibition of NF-κB nuclear translocation via Set9-mediated lysine methylation, which resulted in decreased miRNA21 and Bcl-2 expression, inducing the cells to produce ROS and promoting cell apoptosis. Berberine treatment of colorectal cancer cells increased the expression of miR-200a-5p and decreased the expression of miR-429. These epigenetic regulation affected by Berberine was briefly summarized in **Table 4**.

SUMMARY AND FUTURE PERSPECTIVES

The importance of epigenetic regulation in the occurrence and development of tumors is now an established fact. An increasing body of research has been devoted to the exploration of epigenetic molecular markers for the early diagnosis, treatment, and prognosis of tumors. Simultaneously, epigenetic drugs provide a new direction for the treatment of tumors owing to the reversibility and ease of regulation of epigenetics. At present, the anticancer drugs that inhibit the proliferation of malignant tumor cells via induction of apoptosis or that regulate signal transduction are mostly multi-targeted (He et al., 2010). Berberine is a natural isoquinoline alkaloid that significantly contributed to the development of anticancer drugs (**Figure 2**). Given the continuous development in the field of medicine and the extension of research and development in the field of medicine, berberine has gained attention of researchers owing to the combination of multiple effects. Berberine is not irreplaceable with respect to its traditional pharmacological activities, such as antibacterial, anti-inflammatory, and antiviral effects (Huang S.X. et al., 2018). Moreover, the efficacy of the antihypertensive, antitumor, and hypolipidemic effects has also become a "hot topic" in contemporary research. Berberine regulates the molecular mechanisms that cause tumor cells through a variety of signaling pathways, confirming the potential therapeutic effects in a variety of tumor cells. However, there are few reports on the effects of berberine on the epigenetic functions of tumors. Epigenetics is also the main controlling factor of oncogenes in the development of cancer. Therefore, the application of epigenetic properties of berberine in the treatment of malignant tumors offers broad prospects for drug development. At the same time, extended research into epigenetics has provided a new strategy to understand the various characteristics of tumors, optimize the early diagnosis of tumors, and improve the prognosis of patients. In future, basic research and clinical transformations in the epigenetics of cancer will provide new strategies for the precise diagnosis and treatment of cancer.

AUTHOR CONTRIBUTIONS

DL contributed significantly to analysis and manuscript preparation. XM contributed significantly to manuscript preparation. DW helped to writing the manuscript. ZQ and HL contributed to the conception of the study.

FUNDING

This work was supported by the National Natural Science Foundation of China (Grant No. 81803680). Jilin Province Science and Technology Development Project in China (Grant Nos. 20170307031 and YY20180520050JH).

REFERENCES

Agnarelli, A., Natali, M., Garciagil, M., Pesi, R., Tozzi, M. G., Ippolito, C., et al. (2018). Cell-specific pattern of berberine pleiotropic effects on different human cell lines. *Sci. Rep.* 8:10599. doi: 10.1038/s41598-018-28952-3

Asadi, R., Omrani, M. D., Ghaedi, H., Mirfakhraie, R., Azargashb, E., Habibi, M., et al. (2018). Premutations of fmr1 cgg repeats are not related to idiopathic premature ovarian failure in iranian patients: a case control study. *Gene* 676, 189–194. doi: 10.1016/j.gene.2018.07.034

Balestrieri, E., Argaw-Denboba, A., Gambacurta, A., Cipriani, C., Bei, R., Serafino, A., et al. (2018). Human endogenous retrovirus k in the crosstalk between cancer cells microenvironment and plasticity: a new perspective for combination therapy. *Front. Microbiol.* 9:1448. doi: 10.3389/fmicb.2018.01448

Bennetzen, J. L., and Wang, H. (2014). The contributions of transposable elements to the structure, function, and evolution of plant genomes. *Annu. Rev. Plant Biol.* 65:505. doi: 10.1146/annurev-arplant-050213-035811

Bhat, A. V., Hora, S., Pal, A., Jha, S., and Taneja, R. (2018). Stressing the (epi) genome: dealing with reactive oxygen species in cancer. *Antioxid. Redox Signal.* 29, 1273–1292. doi: 10.1089/ars.2017.7158

Biswas, S., and Rao, C. M. (2018). Epigenetic tools (The Writers, the readers and the erasers) and their implications in cancer therapy. *Eur. J. Pharmacol.* 837, 8–24. doi: 10.1016/j.ejphar.2018.08.021

Blandino, G., Fazi, F., Donzelli, S., Kedmi, M., Saschen, A., Muti, P., et al. (2014). Tumor suppressor microrna: a novel non-coding alliance against cancer. *FEBS Lett.* 588, 2639–2652. doi: 10.1016/j.febslet.2014.03.033

Booth, A. K., and Gutierrez-Hartmann, A. (2015). Signaling pathways regulating pituitary lactotrope homeostasis and tumorigenesis. *Adv. Exp. Med. Biol.* 846, 37–59. doi: 10.1007/978-3-319-12114-7_2

Chidambaram, A., Fillmore, H. L., Van Meter, T. E., Dumur, C. I., Band roaddus, W. C., (2012). Novel report of expression and function of CD97 in malignant gliomas: correlation with Wilms tumor 1 expression and glioma cell invasiveness. *J. Neurosurg.* 116, 843–853. doi: 10.3171/2011.11.JNS111455

Cicero, A. F., and Baggioni, A. (2016). Berberine and its role in chronic disease. *Adv. Exp. Med. Biol.* 928:27. doi: 10.1007/978-3-319-41334-1_2

Coward, W. R., Feghalibostwick, C. A., Jenkins, G., Knox, A. J., and Pang, L. (2014). A central role for g9a and ezh2 in the epigenetic silencing of cyclooxygenase-2 in idiopathic pulmonary fibrosis. *FASEB J.* 28, 3183–3196. doi: 10.1096/fj.13-241760

Crawford, B., Craig, Z., Mansell, G., White, I., Spaull, S., Imm, J., et al. (2018). DNA methylation and inflammation marker profiles associated with a history of depression. *Hum. Mol. Genet.* 27, 2840–2850. doi: 10.1093/hmg/ddy199

Delga-docruzata, L., Zhang, W., Mcdonald, J. A., Tsai, W. Y., Valdovinos, C., Falci, L., et al. (2015). Dietary modifications, weight loss, and changes in

metabolic markers affect global dna methylation in hispanic, african american, and afro-caribbean breast cancer survivors. *J. Nutr.* 145:783. doi: 10.3945/jn.114.202853

Dkhil, M. A., Metwaly, M. S., Saleh, A. Q., Sherif, N. E., Denis, D., Omar, S. Y. A., et al. (2015). Anti-eimeria activity of berberine and identification of associated gene expression changes in the mouse jejunum infected with eimeria papillata. *Parasitol. Res.* 114, 1–13. doi: 10.1007/s00436-015-4344-z

Du, J., Sun, Y., Lu, Y. Y., Lau, E., Zhao, M., Zhou, Q. M., et al. (2017). Berberine and evodiamine act synergistically against human breast cancer mcf-7 cells by inducing cell cycle arrest and apoptosis. *Anticancer Res.* 37, 6141–6151.

Dupont, C., Armant, D. R., and Brenner, C. A. (2009). Epigenetics: definition, mechanisms and clinical perspective. *Semin. Reprod. Med.* 27, 351–357. doi: 10.1055/s-0029-1237423

Foroutan, F., Alba, A. C., Stein, M., Krakovsky, J., Chien, K. G. W., Chih, S., et al., (2018). Validation of the International Society for Heart and Lung Transplantation primary graft dysfunction instrument in heart transplantation. *J. Heart Lung Transplant.* doi: 10.1016/j.healun.2018.12.007 [Epub ahead of print].

Foroutan, T., Farhadi, A., Abroun, S., and Mohammad Soltani, B. (2018). Adipose derived stem cells affect miR-145 and p53 expressions of co-cultured hematopoietic stem cells. *Cell J.* 19, 654–659. doi: 10.22074/cellj.2018.4393

Georgoff, P. E., Nikolian, V. C., Higgins, G., Chtraklin, K., Eidy, H., Ghandour, M. H., et al. (2018). Valproic acid induces pro-survival transcriptomic changes in swine subjected to traumatic injury and hemorrhagic shock. *J. Trauma Acute Care Surg.* 84:1. doi: 10.1097/TA.0000000000001763

Gu, L., Frommel, S. C., Oakes, C. C., Simon, R., Grupp, K., Gerig, C. Y., et al. (2015). Baz2a (tip5) is involved in epigenetic alterations in prostate cancer and its overexpression predicts disease recurrence. *Nat. Genet.* 47:22. doi: 10.1038/ng.3165

Guo, N., Yan, A., Gao, X., Chen, Y., He, X., Hu, Z., et al. (2014). Berberine sensitizes rapamycin-mediated human hepatoma cell death in vitro. *Mol. Med. Rep.* 10, 3132–3138. doi: 10.3892/mmr.2014.2608

Halicka, H. D., Garcia, J., Li, J., Zhao, H., and Darzynkiewicz, Z. (2017). Synergy of 2-deoxy-d-glucose combined with berberine in inducing the lysosome/autophagy and transglutaminase activation-facilitated apoptosis. *Apoptosis* 22, 229–238. doi: 10.1007/s10495-016-1315-5

Hamsa, T. P., and Kuttan, G. (2011). Studies on anti-metastatic and anti-invasive effects of harmine using highly metastatic murine b16f-10 melanoma cells. *J. Environ. Pathol. Toxicol. Oncol.* 30:123. doi: 10.1615/JEnvironPatholToxicolOncol.v30.i2.40

Hao, D. C., He, C. N., and Shen, J. (2017). Anticancer chemodiversity of ranunculaceae medicinal plants molecular mechanisms and functions. *Curr. Genomics* 18, 39–59. doi: 10.2174/1389202917666160803151752

Hashiguchi, Y., Kawano, S., Goto, Y., Yasuda, K., Kaneko, N., Sakamoto, T., et al. (2017). Tumor-suppressive roles of Δnp63β-mir-205 axis in epithelial-mesenchymal transition of oral squamous cell carcinoma via targeting zeb1 and zeb2. *J. Cell. Physiol.* 233, 6565–6577. doi: 10.1002/jcp.26267

He, X. Y., Chen, J. X., Zhang, Z., Li, C. L., Peng, Q. L., and Peng, H. M. (2010). The let-7a microrna protects from growth of lung carcinoma by suppression of k-ras and c-myc in nude mice. *J. Cancer Res. Clin. Oncol.* 136, 1023–1028. doi: 10.1007/s00432-009-0747-5

Hoen, D. R., and Bureau, T. E. (2015). Discovery of novel genes derived from transposable elements using integrative genomic analysis. *Mol. Biol. Evol.* 32, 1487–1506. doi: 10.1093/molbev/msv042

Honda, H., Pazin, M. J., Ji, H., Wernyj, R. P., and Morin, P. J. (2006). Crucial roles of sp1 and epigenetic modifications in the regulation of the cldn4 promoter in ovarian cancer cells. *J. Biol. Chem.* 281:21433. doi: 10.1074/jbc.M603767200

Liu, H. C., Lämke, J., Lin, S. Y., Hung, M. J., Liu, K. M., Charng, Y. Y., et al. (2018). Distinct heat shock factors and chromatin modifications mediate the organ-autonomous transcriptional memory of heat stress. *Plant J.* 95, 401–413. doi: 10.1111/tpj.13958

Hu, H., Li, K., Wang, X., Liu, Y., Lu, Z. G., Dong, R. H., et al. (2013). Set9, NF-κB, and microRNA-21 mediate berberine-induced apoptosis of human multiple myeloma cells. *Acta Pharmacol. Sin.* 34:157. doi: 10.1038/aps.2012.161

Huang, C., Liu, H., Gong, X. L., Wu, L. Y., and Wen, B. (2017). Effect of evodiamine and berberine on the interaction between dnmts and target micrornas during malignant transformation of the colon by tgf-β1. *Oncol. Rep.* 37, 1637–1645. doi: 10.3892/or.2017.5379

Huang, S. X., Qiu, G., Cheng, F. R., Pei, Z., Yang, Z., Deng, X. H., et al. (2018). Berberine protects secondary injury in mice with traumatic brain injury through anti-oxidative and anti-inflammatory modulation. *Neurochem. Res.* 43, 1–12. doi: 10.1007/s11064-018-2597-5

Huang, Y., Wang, K., Gu, C., Yu, G., Zhao, D., Mai, W., et al. (2018). Berberine, a natural plant alkaloid, synergistically sensitizes human liver cancer cells to sorafenib. *Oncol. Rep.* 40, 1525–1532. doi: 10.3892/or.2018.6552

Huang, Z. H., Zheng, H. F., Wang, W. L., Wang, Y., Zhong, L. F., Wu, J. L., et al. (2015). Berberine targets epidermal growth factor receptor signaling to suppress prostate cancer proliferation in vitro. *Mol. Med. Rep.* 11:2125. doi: 10.3892/mmr.2014.2929

Iizuka, N., Miyamoto, K., Okita, K., Tangoku, A., Hayashi, H., Yosino, S., et al. (2000). Inhibitory effect of coptidis rhizoma and berberine on the proliferation of human esophageal cancer cell lines. *Cancer Lett.* 148, 19–25. doi: 10.1016/S0304-3835(99)00264-5

Imenshahidi, M., and Hosseinzadeh, H. (2016). Berberis vulgaris and berberine. *Phytother. Res.* 30, 1745–1764. doi: 10.1002/ptr.5693

Jiang, L., Xue, W., and Wang, Y. (2018). Inhibition of miR-31a-5p decreases inflammation by down-regulating IL-25 expression in human dermal fibroblast cells (CC-2511 cells) under hyperthermic stress via Wnt/β-catenin pathway. *Biomed. Pharmacother.* 107, 24–33. doi: 10.1016/j.biopha.2018.07.142

Jin, Y., Liu, S., Ma, Q., Xiao, D., and Chen, L. (2017). Berberine enhances the ampk activation and autophagy and mitigates high glucose-induced apoptosis of mouse podocytes. *Eur. J. Pharmacol* 794, 106–114. doi: 10.1016/j.ejphar.2016.11.037

Jung-Mu, H., Mee-Sun, H., Sang-Yong, L., Woo-Yiel, L., and Dongho, K. (2009). The combination of berberine and irradiation enhances anti-cancer effects via activation of p38 mapk pathway and ros generation in human hepatoma cells. *J. Cell. Biochem.* 107, 955–964. doi: 10.1002/jcb.22198

Kalaiarasi, A., Anusha, C., Sankar, R., Rajasekaran, S., John, M. J., Muthusamy, K., et al. (2016). Plant isoquinoline alkaloid berberine exhibits chromatin remodeling by modulation of histone deacetylase to induce growth arrest and apoptosis in the a549 cell line. *J. Agric. Food Chem.* 64:9542. doi: 10.1021/acs.jafc.6b04453

Kalinkova, L., Zmetakova, I., Smolkova, B., Minarik, G., Sedlackova, T., Kajabova, V. H., et al. (2018). Decreased methylation in the SNAI2 and ADAM23 genes associated with de-differentiation and haematogenous dissemination in breast cancers. *BMC Cancer* 18:875. doi: 10.1186/s12885-018-4783-x

Katona, B. W., Liu, Y., Ma, A., Jin, J., and Hua, X. (2014). Ezh2 inhibition enhances the efficacy of an egfr inhibitor in suppressing colon cancer cells. *Cancer Biol. Ther.* 15:11. doi: 10.4161/15384047.2014.972776

Khalil, I., Colombara, D. V., Forouzanfar, M. H., Troeger, C., Daoud, F., Moradi-Lakeh, M., et al. (2016). Burden of diarrhea in the eastern mediterranean region, 1990–2013: findings from the global burden of disease study 2013. *Am. J. Trop. Med. Hyg.* 95, 1319–1329. doi: 10.4269/ajtmh.16-0339

Kong, W., Wei, J., Abidi, P., Lin, M., Inaba, S., Li, C., et al. (2004). Berberine is a novel cholesterol-lowering drug working through a unique mechanism distinct from statins. *Nat. Med.* 7, 464–464. doi: 10.1016/S1567-5688(06)81865-9

Kumar, A., Ekavali, Chopra, K., Mukherjee, M., Pottabathini, R., and Dhull, D. K. (2015). Current knowledge and pharmacological profile of berberine: an update. *Eur. J. Pharmacol.* 761, 288–297. doi: 10.1016/j.ejphar.2015.05.068

Lee, C., and Gang, J. (2018). A label-free detection of ndei endonuclease activity by using dna-templated silver nanoclusters. *J. Nanosci. Nanotechnol.* 18:6339. doi: 10.1166/jnn.2018.15657

Li, B., Wang, Z., Wu, H., Xue, M., Lin, P., Wang, S., et al. (2018). Epigenetic regulation of cxcl12 plays a critical role in mediating tumor progression and the immune response in osteosarcoma. *Cancer Res.* 78:3938. doi: 10.1158/0008-5472.can-17-3801

Li, C. H., Wu, D. F., Ding, H., Zhao, Y., Zhou, K. Y., and Xu, D. F. (2014). Berberine hydrochloride impact on physiological processes and modulation of twist levels in nasopharyngeal carcinoma cne-1 cells. *Asian Pac. J. Cancer Prev.* 15, 1851–1857. doi: 10.7314/APJCP.2014.15.4.1851

Li, J., Liu, F., Jiang, S., Liu, J., Chen, X., Zhang, S., et al. (2018). Berberine hydrochloride inhibits cell proliferation and promotes apoptosis of non-small

cell lung cancer via the suppression of the mmp2 and bcl-2/bax signaling pathways. *Oncol. Lett.* 15:7409. doi: 10.3892/ol.2018.8249

Li, L., Wang, X., Sharvan, R., Gao, J., Qu, S., Li, L., et al. (2017). Berberine could inhibit thyroid carcinoma cells by inducing mitochondrial apoptosis, g0/g1 cell cycle arrest and suppressing migration via pi3k-akt and mapk signaling pathways. *Biomed. Pharmacother.* 95, 1225–1231. doi: 10.1016/j.biopha.2017.09.010

Li, L., and Zhao, G. (2016). Downregulation of microrna-218 relieves neuropathic pain by regulating suppressor of cytokine signaling 3. *Int. J. Mol. Med.* 37:851. doi: 10.3892/ijmm.2016.2455

Li, N., Xu, F., Cheng, J., Zhang, Y., Huang, G., Zhu, J., et al. (2018). Perfluorocarbon nanocapsules improve hypoxic microenvironment for the tumor ultrasound diagnosis and photodynamic therapy. *J. Biomed. Nanotechnol.* 14, 2162–2171. doi: 10.1166/jbn.2018.2656

Li, W., Li, Q., Kang, S., Same, M., Zhou, Y., Sun, C., et al. (2018). Cancerdetector: ultrasensitive and non-invasive cancer detection at the resolution of individual reads using cell-free dna methylation sequencing data. *Nucleic Acids Res.* 46:e89.

Liu, L., Chen, L., Jiang, C., Guo, J., Xie, Y., Kang, L., et al. (2017a). Berberine inhibits the lps-induced proliferation and inflammatory response of stromal cells of adenomyosis tissues mediated by the lps/tlr4 signaling pathway. *Exp. Therap. Med.* 14:6125. doi: 10.3892/etm.2017.5316

Liu, L., Luo, N., Guo, J., Xie, Y., Chen, L., and Cheng, Z. (2017b). Berberine inhibits growth and inflammatory invasive phenotypes of ectopic stromal cells: imply the possible treatment of adenomyosis. *J. Pharmacol. Sci.* 137, 5–11. doi: 10.1016/j.jphs.2017.12.001

Lu, W., Du, S., and Wang, J. (2015). Berberine inhibits the proliferation of prostate cancer cells and induces g0/g1 or g2/m phase arrest at different concentrations. *Mol. Med. Rep.* 11, 3920–3924. doi: 10.3892/mmr.2014.3139

Ma, C. Y., Shen, S. C., Huang, D. W., Chang, H. M., and Wu, J. S. B. (2008). Growth inhibition and induction of apoptosis in u937 cells by coptis chinensis extract. *J. Food Sci.* 73, H127–H133. doi: 10.1111/j.1750-3841.2008.00837.x

Ma, W., Zhu, M., Yang, L., Yang, T., and Zhang, Y., (2017). Synergistic effect of TPD7 and berberine against leukemia jurkat cell growth through regulating ephrin-B2 signaling. *Phytother. Res.* 31, 1392–1399.

Meng, F. C., Wu, Z. F., Yin, Z. Q., Lin, L. G., Wang, R., and Zhang, Q. W. (2018). Coptidis rhizoma and its main bioactive components: recent advances in chemical investigation, quality evaluation and pharmacological activity. *Chinese Med.* 13:13. doi: 10.1186/s13020-018-0171-3

Meng, M., Geng, S., Du, Z., Yao, J., Zheng, Y., Li, Z., et al. (2017). Berberine and cinnamaldehyde together prevent lung carcinogenesis. *Oncotarget* 8:76385. doi: 10.18632/oncotarget.20059

Mirhadi, E., Rezaee, M., and Malaekehnikouei, B. (2018). Nano strategies for berberine delivery, a natural alkaloid of berberis. *Biomed. Chromatogr. BMC* 1060:e4279. doi: 10.1002/bmc.4279

Mistry, B. M., Keum, Y. S., Pandurangan, M., Kim, D. H., Moon, S. H., Kadam, A. A., et al. (2017). Synthesis and evaluation of antioxidant and cytotoxicity of the n-mannich base of berberine bearing benzothiazole moieties. *Anti-cancer Agents Med. Chem.* 17, 1652–1660. doi: 10.2174/1871520617666170710180549

Mittal, A., Tabasum, S., and Singh, R. P. (2014). Berberine in combination with doxorubicin suppresses growth of murine melanoma b16f10 cells in culture and xenograft. *Phytomedicine* 21, 340–347. doi: 10.1016/j.phymed.2013.09.002

Munir, I., Fukunaga, K., Kanasaki, H., Miyazaki, K., Ohba, T., Okamura, H., et al. (2000). Expression of cyclooxygenase 2 by prostaglandin e2 in human endometrial adenocarcinoma cell line hec-1b1. *Biol. Reprod.* 63, 933–941. doi: 10.1095/biolreprod63.3.933

Murthy, K. N. C., Kim, J., Vikram, A., and Patil, B. S. (2012). Differential inhibition of human colon cancer cells by structurally similar flavonoids of citrus. *Food Chem.* 132, 27–34. doi: 10.1016/j.foodchem.2011.10.014

Nardi, I., Reno, T., Yun, X., Sztain, T., Wang, J., Dai, H., et al. (2018). Triptolide inhibits Wnt signaling in NSCLC through upregulation of multiple Wnt inhibitory factors via epigenetic modifications to Histone H3. *Int. J. Cancer* 143, 2470–2478. doi: 10.1002/ijc.31756

Naveen, C. R., Gaikwad, S., and Agrawalrajput, R. (2016). Berberine induces neuronal differentiation through inhibition of cancer stemness and epithelial-mesenchymal transition in neuroblastoma cells. *Phytomed. Int. J. Phytother. Phytopharmacol.* 23, 736–744. doi: 10.1016/j.phymed.2016.03.013

Neag, M. A., Mocan, A., Echeverría, J., Pop, R. M., Bocsan, C. I., Crişan, G., et al. (2018). Berberine: botanical occurrence, traditional uses, extraction methods, and relevance in cardiovascular, metabolic, hepatic, and renal disorders. *Front. Pharmacol.* 9:557. doi: 10.3389/fphar.2018.00557

Oliver, K. R., Mccomb, J. A., and Greene, W. K. (2013). Transposable elements: powerful contributors to angiosperm evolution and diversity. *Genome Biol. Evol.* 5, 1886–1901. doi: 10.1093/gbe/evt141

Pandey, A., Vishnoi, K., Mahata, S., Tripathi, S. C., Misra, S. P., Misra, V., et al. (2015). Berberine and curcumin target survivin and stat3 in gastric cancer cells and synergize actions of standard chemotherapeutic 5-fluorouracil. *Nutr. Cancer Int. J.* 67, 1293–1304. doi: 10.1080/01635581.2015.1085581

Peng, P. L., Kuo, W. H., Tseng, H. C., and Chou, F. P., (2008). Synergistic tumor-killing effect of radiation and berberine combined treatment in lung cancer: the contribution of autophagic cell death. *Int. J. Radiat. Oncol. Biol. Phys.* 70, 529–542. doi: 10.1016/j.ijrobp.2007.08.034

Puneet, Kazmi, H. R., Kumari, S., Tiwari, S., Khanna, A., and Narayan, G. (2018). Epigenetic mechanisms and events in gastric cancer-emerging novel biomarkers. *Pathol. Oncol. Res.* 2, 1–14. doi: 10.1007/s12253-018-0410-z

Qi, H. W., Xin, L. Y., Xu, X., Ji, X. X., and Fan, L. H. (2014). Epithelial-to-mesenchymal transition markers to predict response of berberine in suppressing lung cancer invasion and metastasis. *J. Trans. Med.* 12:22. doi: 10.1186/1479-5876-12-22

Qing, Y., Hu, H., Liu, Y., Feng, T., Meng, W., Jiang, L., et al. (2014). Berberine induces apoptosis in human multiple myeloma cell line u266 through hypomethylation of p53 promoter. *Cell Biol. Int.* 38, 563–570. doi: 10.1002/cbin.10206

Rahnamoun, H., Lee, J., Sun, Z., Lu, H., Ramsey, K. M., Komives, E. A., et al. (2018). RNAs interact with BRD4 to promote enhanced chromatin engagement and transcription activation. *Nat. Struct. Mol. Biol.* 25:687. doi: 10.1038/s41594-018-0102-0

Rayan, N. A., Rosario, R. C. H. D., and Prabhakar, S. (2016). Massive contribution of transposable elements to mammalian regulatory sequences. *Semin. Cell Dev. Biol.* 57, 51–56. doi: 10.1016/j.semcdb.2016.05.004

Riaz, S. K., Saeed, M., and Malik, M. F. (2015). Clinical and therapeutic implications of histone acetylation in breast cancer. *West Indian Med. J.* 65, 337–344. doi: 10.7727/wimj.2014.297

Sahebi, M., Hanafi, M. M., van Wijnen, A. J., Rice, D., Rafii, M. Y., Azizi, P., et al. (2018). Contribution of transposable elements in the plant's genome. *Gene* 665, 155–166. doi: 10.1016/j.gene.2018.04.050

Salimian, N., Peymani, M., Ghaedi, K., and Esfahani, M. (2018). Modulation in mir-200a/sirt1axis is associated with apoptosis in mpp+-induced sh-sy5y cells. *Gene* 674, 24–30. doi: 10.1016/j.gene.2018.06.061

Sanna, L., Marchesi, I., Melone, M. A. B., and Bagella, L. (2018). The role of enhancer of zeste homolog 2: from viral epigenetics to the carcinogenesis of hepatocellular carcinoma. *J. Cell. Physiol.* 233, 6508–6517. doi: 10.1002/jcp.26545

Sengupta, D., Chowdhury, K. D., Chatterjee, S., Sarkar, A., Paul, S., Sur, P. K., et al. (2017). Modulation of adenylate cyclase signaling in association with mkk3/6 stabilization under combination of sac and berberine to reduce hepg2 cell survivability. *Apoptosis* 22, 1–18. doi: 10.1007/s10495-017-1407-x

Sengupta, D., Chowdhury, K. D., Sarkar, A., Paul, S., and Sadhukhan, G. C., (2014). Berberine and S allyl cysteine mediated amelioration of DEN+ CCl4 induced hepatocarcinoma. *Biochim. Biophys. Acta (BBA)-Gen. Subjects* 1840, 219–244. doi: 10.1016/j.bbagen.2013.08.020

Shang, A., Bylipudi, S., and Bieszczad, K. M. (2018). Inhibition of histone deacetylase 3 via rgfp966 facilitates cortical plasticity underlying unusually accurate auditory associative cue memory for excitatory and inhibitory cue-reward associations. *Behav. Brain Res.* 356, 453–469. doi: 10.1016/j.bbr.2018.05.036

Shi, H. L., Wu, X. J., Liu, Y., and Xie, J. Q. (2013). Berberine counteracts enhanced il-8 expression of ags cells induced by evodiamine. *Life Sci.* 93, 830–839. doi: 10.1016/j.lfs.2013.09.010

Shi, Y., Zhao, Y., Shao, N., Ye, R., Lin, Y., Zhang, N., et al. (2017). Overexpression of microrna-96-5p inhibits autophagy and apoptosis and enhances the

proliferation, migration and invasiveness of human breast cancer cells. *Oncol. Lett.* 13, 4402–4412. doi: 10.3892/ol.2017.6025

Signorelli, C., Odone, A., Ciorba, V., Cella, P., Audisio, R. A., Lombardi, A., et al. (2017). Human papillomavirus 9-valent vaccine for cancer prevention: a systematic review of the available evidence. *Epidemiol. Infect.* 145:21. doi: 10.1017/s0950268817000747

Siveen, K. S., and Kuttan, G. (2011). Thujone inhibits lung metastasis induced by b16f-10 melanoma cells in c57bl/6 mice. *Can. J. Physiol. Pharmacol.* 89:691. doi: 10.1139/y11-067

Stevens, M. S., Aliabadi, Z., and Moore, M. R. (1984). Associated effects of sodium butyrate on histone acetylation and estrogen receptor in the human breast cancer cell line mcf-7. *Biochem. Biophys. Res. Commun.* 119, 132–138. doi: 10.1016/0006-291X(84)91628-0

Su, Y. H., Tang, W. C., Cheng, Y. W., Sia, P., Huang, C. C., Lee, Y. C., et al. (2015). Targeting of multiple oncogenic signaling pathways by hsp90 inhibitor alone or in combination with berberine for treatment of colorectal cancer. *BBA – Mol. Cell Res.* 1853, 2261–2272. doi: 10.1016/j.bbamcr.2015.05.012

Sun, W., Zhang, L., and Li, R. (2017). Overexpression of miR-206 ameliorates chronic constriction injury-induced neuropathic pain in rats via the MEK/ERK pathway by targeting brain-derived neurotrophic factor. *Neurosci. Lett.* 646, 68–74. doi: 10.1016/j.neulet.2016.12.047

Tabeshpour, J., Imenshahidi, M., and Hosseinzadeh, H. (2017). A review of the effects ofberberis vulgarisand its major component, berberine, in metabolic syndrome. *Iran. J. Basic Med. Sci.* 20, 557–568. doi: 10.22038/IJBMS.2017.8682

Tang, J., and Feng, Y. S. (2009). Berberine and coptidis rhizoma as novel antineoplastic agents: a review of traditional use and biomedical investigations. *J. Ethnopharmacol.* 126, 5–17. doi: 10.1016/j.jep.2009.08.009

Tao, Y., Lin, Y., She, Z., Lin, M., Chen, P., and Zhang, J. (2015). Anticancer activity and mechanism investigation of beauvericin isolated from secondary metabolites of the mangrove endophytic fungi. *Anti-Cancer Agents Med. Chem.* 15, 258–266. doi: 10.2174/1871520614666140825112255

Tong, N., Zhang, J., Chen, Y., Zhubo, L. I., Luo, Y., Zuo, H., et al. (2012). Berberine sensitizes mutliple human cancer cells to the anticancer effects of doxorubicin in vitro. *Oncol. Lett.* 3, 1263–1267. doi: 10.3892/ol.2012.644

Viegas, S., Ladeira, C., Costaveiga, A., Perelman, J., and Gajski, G. (2017). Forgotten public health impacts of cancer – An overview. *Arh. Hig. Rada. Toksikol.* 68:287. doi: 10.1515/aiht-2017-68-3005

Vijayaraghavalu, S., Dermawan, J. K., and Cheriyath, V. (2013). Highly synergistic effect of sequential treatment with epigenetic and;anticancer drugs to overcome drug resistance in breast cancer cells is;mediated via activation of p21 gene expression leading to g2/m cycle;arrest. *Mol. Pharm.* 10, 337–352. doi: 10.1021/mp3004622

Walker, D. K., Edwards, R. L., Bagcivan, G., and Bakitas, M. A. (2017). Cancer and palliative care in the united states, turkey, and malawi: developing global collaborations. *Asia-Pacific J. Oncol. Nurs.* 4, 209–219. doi: 10.4103/apjon.apjon_31_17

Wang, J., Kang, M., Wen, Q., Qin, Y. T., Wei, Z. X., Xiao, J. J., et al. (2017). Berberine sensitizes nasopharyngeal carcinoma cells to radiation through inhibition of sp1 and emt. *Oncol. Rep.* 37, 2425–2432. doi: 10.3892/or.2017.5499

Wang, N., Feng, Y., Cheung, F., Wang, X., Zhang, Z., and Feng, Y. (2015a). A chinese medicine formula gegen qinlian decoction suppresses expansion of human renal carcinoma with inhibition of matrix metalloproteinase-2. *Integr. Cancer Ther.* 14:75. doi: 10.1177/1534735414550036

Wang, N., Tan, H. Y., Li, L., Yuen, M. F., and Feng, Y. (2015b). Berberine and coptidis rhizoma as potential anticancer agents: recent updates and future perspectives. *J. Ethnopharmacol.* 176, 35–48. doi: 10.1016/j.jep.2015.10.028

Wang, S., Xiao, Z., Hong, Z., Jiao, H., Zhu, S., Zhao, Y., et al. (2018). FOXF1 promotes angiogenesis and accelerates bevacizumab resistance in colorectal cancer by transcriptionally activating VEGFA. *Cancer Lett.* 439, 78–90. doi: 10.1016/j.canlet.2018.09.026

Wang-Johanning, F., Radvanyi, L., Rycaj, K., Plummer, J. B., Yan, P., Sastry, K. J., et al. (2008). Human endogenous retrovirus k triggers an antigen-specific immune response in breast cancer patients. *Cancer Res.* 68, 5869–5877. doi: 10.1158/0008-5472.CAN-07-6838

Waterbeemd, B. V. D., Mommen, G. P. M., Pennings, J. L. A., Eppink, M. H., Wijffels, R. H., Pol, L. A. V. D., et al. (2013). Quantitative proteomics reveals distinct differences in the protein content of outer membrane vesicle vaccines. *J. Proteome Res.* 12, 1898–1908. doi: 10.1021/pr301208g

Wen, C., Wu, L., Fu, L., Zhang, X., and Zhou, H. (2016). Berberine enhances the anti-tumor activity of tamoxifen in drug-sensitive MCF-7 and drug-resistant MCF-7/TAM cells. *Mol. Med. Rep.* 14, 2250–2256. doi: 10.3892/mmr.2016.5490

Wong, K. Y., and Chim, C. S. (2015). DNA methylation of tumor suppressor protein-coding and non-coding genes in multiple myeloma. *Epigenomics* 7, 985–1001. doi: 10.2217/epi.15.57

Wu, Y. Q., Chen, X. S., and Chai, J. B. (2012). The involvement of the cd40-cd40l pathway in activated platelet-induced changes in huvec cox-2 and pparα expression. *Inflammation* 35, 1184–1190. doi: 10.1007/s10753-011-9427-0

Xu, Z., Feng, W., Shen, Q., Yu, N., Yu, K., Wang, S., et al. (2017). Rhizoma coptidis and berberine as a natural drug to combat aging and aging-related diseases via anti-oxidation and ampk activation. *Aging Dis.* 8, 760–777. doi: 10.14336/AD.2016.0620

Xue, M., Yang, M. X., Zhang, W., Li, X. M., Gao, D. H., Ou, Z. M., et al. (2013). Characterization, pharmacokinetics, and hypoglycemic effect of berberine loaded solid lipid nanoparticles. *Int. J. Nanomed.* 8(Issue 1), 4677–4687. doi: 10.2147/IJN.S51262

Yakata, Y., Nakayama, T., Yoshizaki, A., Kusaba, T., and Sekine, I. (2007). Expression of p-stat3 in human gastric carcinoma: significant correlation in tumour invasion and prognosis. *Int. J. Oncol.* 30, 437–442. doi: 10.3892/ijo.30.2.437

Yamada, K., Mizukoshi, E., Sunagozaka, H., Arai, K., Yamashita, T., Takeshita, Y., et al. (2015). Response to importance of confounding factors in assessing fatty acid compositions in patients with non-alcoholic steatohepatitis. *Liver Int.* 35, 1773–1773. doi: 10.1111/liv.12755

Yan, L., Yang, X., and Davidson, N. E. (2001). Role of dna methylation and histone acetylation in steroid receptor expression in breast cancer. *J. Mamm. Gland Biol. Neoplasia* 6, 183–192. doi: 10.1023/a:1011308707512

Yan, X. T., Zhao, Y., and Cheng, X. L. (2018). Inhibition of mir-200b/mir-429 contributes to neuropathic pain development through targeting zinc finger e box binding protein-1. *J. Cell Physiol.* 233, 4815–4824. doi: 10.1002/jcp.26284

Yang, M., Yang, Y., Cui, H., Guan, Z., Yang, Y., Zhang, H., et al. (2015). The natural compound gambogic acid radiosensitizes nasopharyngeal carcinoma cells under hypoxic conditions. *Tumori* 102:135. doi: 10.5301/tj.5000411

Zhang, J., Lai, Z., Huang, W., Ling, H., Lin, M., Tang, S., et al. (2017). Apicidin inhibited proliferation and invasion and induced apoptosis via mitochondrial pathway in non-small cell lung cancer glc-82 cells. *Anti-cancer Agents Med. Chem.* 17, 1374–1382. doi: 10.2174/1871520617666170419120044

Zhang, J., Yi, T., Liu, J., Zhao, Z., and Chen, H. (2013). Quercetin induces apoptosis via the mitochondrial pathway in kb and kbv200 cells. *J. Agric. Food Chem.* 61, 2188–2195. doi: 10.1021/jf305263r

Zhang, J., Zhang, H., and Zi, T. (2015). Overexpression of microrna-141 relieves chronic constriction injury-induced neuropathic pain via targeting high-mobility group box 1. *Int. J. Mol. Med.* 36:1433. doi: 10.3892/ijmm.2015.2342

Zhang, J. Y., Huang, W. J., Sun, H. M., Liu, Y., Zhao, X. Q., Tang, S. L., et al. (2017). Structure identification and in vitro anticancer activity of lathyrol-3-phenylacetate-5,15-diacetate. *Molecules* 22:1412. doi: 10.3390/molecules22091412

Zhang, J. Y., Lin, M. T., Tung, H. Y., Tang, S. L., Yi, T., Zhang, Y. Z., et al. (2016). Bruceine d induces apoptosis in human chronic myeloid leukemia k562 cells via mitochondrial pathway. *Am. J. Cancer Res.* 6:819.

Zhang, J. Y., Lin, M. T., Zhou, M. J., Yi, T., Tang, Y. N., Tang, S. L., et al. (2015). Combinational treatment of curcumin and quercetin against gastric cancer mgc-803 cells in vitro. *Molecules* 20, 11524–11534. doi: 10.3390/molecules200611524

Zhang, L., Fang, Y., Xu, X. F., and Jin, D. Y. (2017). Moscatilin induces apoptosis of pancreatic cancer cells via reactive oxygen species and the jnk/sapk pathway. *Mol. Med. Rep.* 15, 1195–1203. doi: 10.3892/mmr.2017.6144

Zhang, L., Wang, Y., Wang, L., Yin, G., Li, W., Xian, Y., et al. (2018). miR-23c suppresses tumor growth of human hepatocellular carcinoma by attenuating ERBB2IP. *Biomed. Pharmacother.* 107, 424–432. doi: 10.1016/j.biopha.2018.07.155

Zhang, S., Chang, M., Zhou, Z., Dai, X., and Xu, Z. (2018). Pdhs-elm: computational predictor for plant dnase i hypersensitive sites based on extreme learning machines. *Mol. Genet. Genomics* 293, 1035–1049. doi: 10.1007/s00438-018-1436-3

Zhang, X. Z., Wang, L., Liu, D. W., Tang, G. Y., Zhang, H. Y., et al. (2014). Synergistic inhibitory effect of berberine and d-limonene on human gastric carcinoma cell line MGC803. *J. Med. Food* 17, 955–962. doi: 10.1089/jmf.2013.2967

Zhao, Y., Gao, J. L., Ji, J. W., Gao, M., Yin, Q. S., Qiu, Q. L., et al. (2014). Cytotoxicity enhancement in MDA-MB-231 cells by the combination treatment of tetrahydropalmatine and berberine derived from *Corydalis yanhusuo* WT Wang. *J. Int. Ethnopharmacol.* 3:68. doi: 10.5455/jice.20140123040224

Zhao, Y., Jing, Z., Li, Y., and Mao, W., (2016). Berberine in combination with cisplatin suppresses breast cancer cell growth through induction of dna breaks and caspase-3-dependent apoptosis. *Oncol. Rep.* 36, 567–572. doi: 10.3892/or.2016.4785

Zheng, F., Wu, J., Tang, Q., Xiao, Q., Wu, W., Hann, S. S., et al. (2018). The enhancement of combination of berberine and metformin in inhibition of DNMT1 gene expression through interplay of SP1 and PDPK1. *J. Cell Mol. Med.* 22, 600–612. doi: 10.1111/jcmm.13347

Zhu, T., Li, L. L., Xiao, G. F., Luo, Q. Z., Liu, Q. Z., Yao, K. T., et al. (2015). Berberine increases doxorubicin sensitivity by suppressing stat3 in lung cancer. *Am. J. Chin. Med.* 43, 1487–1502. doi: 10.1142/S0192415X15500846

Conflict of Interest Statement: The authors declare that the research was conducted in the absence of any commercial or financial relationships that could be construed as a potential conflict of interest.

frontiers in Oncology

ORIGINAL RESEARCH
published: 21 February 2019
doi: 10.3389/fonc.2019.00100

Wheat Germ Agglutinin as a Potential Therapeutic Agent for Leukemia

Bradley Ryva[1], *Keman Zhang*[2], *Abhishek Asthana*[2], *Derek Wong*[1], *Yorleny Vicioso*[1] *and Reshmi Parameswaran*[1,2,3]*

[1] Department of Pathology, School of Medicine, Case Western Reserve University, Cleveland, OH, United States, [2] Division of Hematology/Oncology, Department of Medicine, School of Medicine, Case Western Reserve University, Cleveland, OH, United States, [3] The Case Comprehensive Cancer Center, Case Western Reserve University School of Medicine, Cleveland, OH, United States

Dietary lectins are carbohydrate-binding proteins found in food sources. We used a panel of seven dietary lectins to analyze cytotoxicity against hematological cancers. Wheat germ agglutinin (WGA), even at low doses, demonstrated maximum toxicity toward acute myeloid leukemia (AML) cells. Using AML cell lines, we show time- and dose-dependent killing by WGA. We also show that low doses of WGA kills primary patient AML cells, irrespective of subtype, with no significant toxicity to normal cells. WGA caused AML cell agglutination, but failed to agglutinate RBC's at this dose. WGA, primarily, binds to *N*-acetyl-D-glucosamine (GlcNAc) and is also reported to interact with sialic-acid-containing glycoconjugates and oligosaccharides. After neuraminidase pre-treatment, which catalyzes the hydrolysis of terminal sialic acid residues, AML cells were less sensitive to WGA-induced cell death. AML cells were also not sensitive to succinyl-WGA, which does not react with sialic acid. Incubation with LEL lectin, which recognizes GlcNAc or SNA, which binds preferentially to sialic acid attached to terminal galactose in α-2,6 and to a lesser degree α-2,3 linkage, did not alter AML cell viability. These data indicate that WGA-induced AML cell death is dependent on both GlcNAc binding and interaction with sialic acids. We did not observe any *in vitro or in vivo* toxicity of WGA toward normal cells at the concentrations tested. Finally, low doses of WGA injection demonstrated significant *in vivo* toxicity toward AML cells, using xenograft mouse model. Thus, WGA is a potential candidate for leukemia therapy.

Keywords: WGA, leukemia, therapy, lectin, GlcNAc

OPEN ACCESS

Edited by:
Zhe-Sheng Chen,
St. John's University, United States

Reviewed by:
Daekyu Sun,
University of Arizona, United States
Kajian Hou,
Guangzhou University of Chinese Medicine, China
Minfeng Chen,
Jinan University, China

***Correspondence:**
Reshmi Parameswaran
rxp278@case.edu

Specialty section:
This article was submitted to Cancer Molecular Targets and Therapeutics, a section of the journal Frontiers in Oncology

Received: *13 September 2018*
Accepted: *04 February 2019*
Published: *21 February 2019*

Citation:
Ryva B, Zhang K, Asthana A, Wong D, Vicioso Y and Parameswaran R (2019) Wheat Germ Agglutinin as a Potential Therapeutic Agent for Leukemia. Front. Oncol. 9:100. doi: 10.3389/fonc.2019.00100

INTRODUCTION

Lectins, carbohydrate-binding proteins, have been well characterized for more than 40 years (1). Because they are present in many of our major staple foods, such as wheat, potato, soy, and tomato, they play an important role for humans (2). Their true biological function is as a pesticide and anti-fungal, preventing disease from spreading and killing the plant or organism (3). Lectins, also present in animals and fungi, are classified by evolutionary origin, three-dimensional structure, and binding specificity (4, 5). In the last 10 years, with technological improvements in protein structural analysis, lectins have been organized into seven families. Most lectins are within the legume, chitin-binding (hevein domain), type 2 ribosome-inactivating, and monocot mannose-binding lectin families; but there are also jacalin-related, amaranthin, and Cucurbitacea phloem families (6).

Lectins have wide-ranging biological activity at cellular, tissue, and organism levels. *In vitro*, it has been demonstrated that incubation with lectin from red kidney bean lead to T cell proliferation and increased cytokine production (7). Haas et al. demonstrated that certain dietary lectins can cause IL-4 and IL-13 release from basophils (8), while Gong et al. demonstrated that plant lectins can activate NLRP3 inflammasome in macrophages, although at concentrations outside of normal physiological conditions (9). Recently it has been shown that certain lectins can activate toll-like receptors (TLRs) in a distinct, yet comparable, fashion to activation by pathogens. Specifically, the lectin ArtinM leads to TLR activation, resulting in increased pro-inflammatory cytokine release (10). Since their first isolations, lectins have been known to agglutinate cells, including red blood cells (11). When lectins are ingested, they have effects on tissues and organs, partially because they are not digested by gut enzymes (12) but pass through the gut wall and enter the circulation (13, 14). Lectins have also been shown to cause gut inflammation and have been potentially linked to autoimmune disease, such as rheumatoid arthritis (15). Besides this biological activity toward normal tissues, lectins have been shown to exhibit specific effects on cancer cells.

Many lectins have demonstrated cytotoxic and anti-proliferative effect on cancer cells. In the early 1980s, it was shown that lectin from *Griffonia simplicifolia* administered to mice *in vivo* was cytotoxic toward ascites tumor cells (16). Miyoshi et al. showed that rice bran agglutinin (RBA) caused apoptosis and cell cycle disruption on human U937 monoblastic leukemia cells (17). Lectins like *Concanavalin* A, *Griffonia simplicifolia* (GSA-1A4), and *Phaseolus vulgaris* were shown to be toxic toward melanoma cell lines (18). Finally, Wang et al. looked at various lectins and their effects on cancers of the liver, chorion, skin, and bone. They determined that lectins from mushroom, soybean, and potato had varying impacts on these cell lines (19). Of the lectins tested, wheat germ agglutinin (WGA) had the most profound cytotoxic effects against these cell lines.

WGA, the lectin derived from wheat germ, binds specifically to *N*-Acetyl-D-glucosamine (GlcNAc). It has been reported that WGA also binds *N*-acetyl-neuraminic (sialic) acid; however more recently it has been characterized as interacting with sialic acid residues on glyconjugates and oligosaccharides (20). WGA is one of the most characterized and studied lectins. While studying the effect of WGA on normal gut epithelium, it was determined that WGA can bind the apical side of gut-like cells and alter the cell membrane permeability (21). Pellegrina et al. also quantified whether the amount of wheat consumed in the normal diet is toxic. They concluded that in order to reach toxic levels more than 1 kilogram of uncooked pasta would need to be consumed in one meal (21). Despite the limited toxicity to normal tissues, it has been shown that WGA is toxic to pancreatic, liver, bone (osteosarcoma), and skin (melanoma) cancer in low doses (18, 19, 22). WGA causes killing via apoptosis and cell cycle arrest in melanoma and human monoblastic leukemia (14, 17). It may also work in a novel apoptotic fashion that is Fas-, caspase-3, Bax, and Bak independent (23). Recently, there is evidence that WGA can kill via a completely different pathway. It has been demonstrated that WGA induces paraptosis-like cell death in cervical carcinoma cells (24). These different modes of killing, dependent on target cells, makes WGA an intriguing protein to study.

Because lectins, specifically wheat germ agglutinin, have been shown to be cytotoxic toward pancreatic cancer, osteosarcoma, hepatoma, etc. (19, 22), we screened three hematological malignancies [acute myeloid leukemia (AML), acute lymphoblastic leukemia (ALL), and non-Hodgkin lymphoma (NHL)] against a panel of lectins. AML is a common childhood leukemia. In patients who acquire the malignancy in adulthood it has a low survival rate (25). ALL is the most common pediatric cancer. If relapse occurs, patients have an even lower survival rate (26). NHL is an umbrella term for many different malignancies that originate in the lymphoid system (27). Because of this broad category, NHL is one of the most common cancers in the United States and the American Cancer Society estimates that more than 70,000 cases will be diagnosed in 2018 (28). Because these three cancer types are very common impacting large numbers of people, we looked at the cytotoxic effects of various lectins on these cancer cells.

Abbreviations: WGA, Wheat germ agglutinin; AML, acute myeloid leukemia, ALL, acute lymphoid leukemia; NHL, non-Hodgkin Lymphoma; sWGA, Succinyl-WGA; LEL, *L. esculentum* lectin; SNA, *S. nigra*; *N*-acetyl-D-neuraminic (sialic) acid; GlcNAc, *N*-acetyl-D-glucosamine.

METHODS

Cell Culture

Human acute myeloid leukemia cell lines, OCI-AML3 and HL-60, obtained from DMSZ and American Type Culture collection, respectively, were cultured in sterile RPMI-1640 medium (R8758) with 10% Serum Plus II and 5% penicillin streptomycin. Human acute lymphoblastic leukemia cell lines, ALL-1 and ALL-2, were cultured in MEM medium (M4526) with 20% FBS. ALL-1 NSG cell line had been passaged through mice before freezing and usage. Human non-Hodgkin lymphoma cell lines, JVM2 and OCI-Ly10, were cultured in RPMI complete medium and in Iscove's DMEM (10-016CV) (20% SPII and 1% Glutamax), respectively. Non-cancerous control cells, HEK293 and OP9, were cultured in DMEM (sc-224478) and MEM, respectively. All cell lines were cultured at 37°C and 5% carbon dioxide. When cells reached confluency, they were passaged.

Patient Samples

Primary patient AML cells were ordered from the Hematopoietic Stem Cell Core Facility at Case Western Reserve University and cultured in RPMI-1640 complete medium (10% FBS). Peripheral blood mononuclear cells (PBMCs), isolated from blood, were obtained from the Hematopoietic Stem Cell Core Facility at Case Western and cultured in RPMI-1640 complete medium (10% Serum Plus II). Human blood was also obtained from Hematopoietic Stem Cell Core Facility at Case Western Reserve University.

Lectins

Lectins from: *Pisum sativum* (L5380), *Arachis hypogaea* (L0881), *Triticum vulgaris* (L9640), *Glycine max* (L1395), *Phaseolus vulgaris* (61764), *Agaricus bisprous* (L5640), *Lycopersicon esculentum* (L2886) were purchased from Sigma-Aldrich, dissolved in sterile phosphate-buffered saline (PBS), and stored at 4°C in a concentration of 1 mg/mL. Succinyl-WGA (W0110) and wheat germ agglutinin FITC-conjugate (L4895), were purchased at Vector Laboratories and Sigma-Aldrich, respectively. These variants were also dissolved in sterile phosphate-buffered saline (PBS) and stored at 4°C in a concentration of 1 mg/mL. Lectin from *Sambucus nigra* (ZB0106) was purchased from Vector Laboratories. Detailed information on each lectin is included in **Table 1** and obtained from Sigma-Aldrich product sheets.

Reagents

Neuraminidase (N7885) was purchased from Sigma-Aldrich and stored at 4°C. Propidium Iodide/RNAase staining kit (P40875) was obtained from Cell Signaling Technology. Annexin V Apoptosis Detection Kit with PI (640914) was purchased from BioLegend. Trypan blue (T8154) was purchase from Sigma-Aldrich. Alsever's Solution was prepared using Sally E. Grimes's protocol (29). Citric acid (1940) and Sodium chloride (BP-358-10) was purchased from Sigma-Aldrich, while Sodium citrate (S-4641) and D-glucose (G-5767) were purchased from Fisher Scientific.

Cell Death Assay

HL60 and OCI cells were seeded in 12-well plates at a concentration of 250,000 cells/mL (1 mL per well). Cells were treated with WGA at various concentrations on day 0, then again at 24 h intervals up until the final day of measurement. Two microliter PBS were added as a negative control. Cell count and cell viability were assessed using 1:1 trypan blue staining (Sigma-Aldrich) and an automated cell counter (Bio-Rad TC-20). Measurements were conducted in triplicate. Data was graphed and analyzed using GraphPad Prism 7.

Apoptosis Assay

Cells were treated with 2 μg/mL WGA for 24 h. Cells were centrifuged at 300 × *g* for 5 min and the supernatant was removed. The pellet was washed with PBS and resuspended in 100 μL Annexin V/ Propidium iodide (AV/PI) buffer. Samples and positive controls were incubated with 3 μL of Annexin V antibody and 10 μL of Propidium Iodide for 15 min at room temperature. The samples were run using fluorescence-activated cell sorting (FACS BD Accuri™C6). 20,000 events were recorded per sample. AV/PI kit from Biolegend, USA was used to perform apoptosis assay.

Cell Cycle Analysis

Cells were seeded at 250,000 cells per mL in 4 mL and treated with WGA. Cells were spun at 600 rpm for 5 min and washed with PBS twice. Pellet was resuspended in PBS and vortexed to make single cell suspension. While vortexing the sample, 1 mL of ice-cold 70% ethanol was added. Samples were incubated overnight in −20°C. Then, samples were pelleted, washed, resuspended in PBS, and incubated with 100 μL of Propidium Iodide at room temperature for 15 min. Samples were analyzed with FACS, counting 10,000 events. Events collected were gated on live cell populations, avoiding debris and aggregate populations.

For cell aggregation/agglutination assay, HL-60, OCI, and healthy human white blood cells (WBCs) were seeded in 12-well plates at a concentration of 250,000 cells/mL (1 mL per well). Cells were treated with either 2 μg/mL WGA or with 2 μL PBS as a negative control. After 20 h treatment, cells were assessed at 10x magnification using bright field microscopy (Leica DM IL LED) and captured using Leica LAS X imaging software.

WGA Binding

WGA-FITC working stock was made by diluting the 1 μg/mL stock solution. HL-60 AML cells were seeded at 250,000 cells per mL and treated with 0.5 μg/mL WGA-FITC at 37°C. At each time point, samples were washed with PBS and analyzed using FACS.

Sialic Acid-Based Treatments

Cells were treated with succinylated-WGA (sWGA) at 2 μg/mL at 37°C for 24 h. Samples were counted using trypan blue. For neuraminidase pre-treatment, the protocol described in Schwarz et al. where 4 million cells in 2 mL serum free media are incubated with 50 mU/mL neuraminidase for 1 h at 37°C was used (22). Samples were washed twice in complete media and seeded in wells at 250,000 cells/mL. Samples were treated with WGA in the same manner as described above. Cells were stained with Propidium iodide and cell viability was determined using flow cytometry.

E-670 Cell Proliferation Assays

OCI AML-3 and HL-60 cell lines were labeled with 1 mM cell proliferation Dye eFluor 670™ (Thermo Fisher Scientific) as per manufacturer's instructions. After staining cells were washed two times and cultured at 37°C in media alone or in the presence of 2.5 μg/mL WGA for the indicated times. Proliferation of live cells was assessed via flow cytometry (Accuri 6C).

In vitro Toxicity

Two AML patient samples were treated in the absence or presence of with 2 μg/mL WGA for 24 h at 37°C. The samples were analyzed for viability by flow cytometry. OP9 and HEK293 cells were plated and incubated for 24 h with doses of WGA. Confocal images were acquired using EVOS® XL Core Imaging System.

Hemagglutination (HA) Assay

The protocol designed by Virapur® was modified as follows (30). Acquired mouse blood was stored in prepared Alsever's solution. After three washes in PBS, 10% blood stock solution was made in PBS. A working stock (5%) solution was made using the 10% stock and PBS. A serial dilution of WGA (50 μg to 0.09 μg/mL) was prepared using a round-bottomed 96-well plate. 0.0 μg/mL WGA was used as a negative control. The plate was incubated for 30–60 min at room temperature and images were taken. The plates were analyzed by looking for "buttons" in each well. Diffuse blood in the well is analyzed as hemagglutination. Experiments were performed on human blood, as well, but the blood was

TABLE 1 | All lectins used and their name, source, molecular weight, and sugar specificities.

Lectin	Source[a]	Molecular weight[b] (kDa)	Sugar specificity[c]
Wheat germ agglutinin (WGA)	*T. vulgaris* (wheat)	36	$(GlcNAc)_2$ & NeuNAc
Succinyl-Wheat germ agglutinin (sWGA)	*T. vulgaris* (wheat)	36	$(GlcNAc)_2$
Pisum sativum agglutinin (PSA)	*P. sativum(pea)*	49	α-man
Peanut agglutinin (PNA)	*A. hypogaea* (peanut)	120	Gal-β(1→ 3)-GalNAc
Soybean agglutinin (SBA)	*Glycine max* (soy)	110	GalNAc
Phytohemagglutinin (PHA)	*P. vulgaris* (red kidney bean)	126/128	Oligosaccharide
Agaricus bisporus lectin (ABL)	*A. bisporus* (mushroom)	58.5	β-gal(1→ 3)GalNAc
Lycopersicon esculentum lectin (LEL)	*L. esculentum* (tomato)	71	$(GlcNAc)_3$
Sambucus nigra lectin (SNA)	*S. nigra* (elderberry)	140	αNeuNAc(2→ 6)gal & GalNAc

Information obtained from Sigma-Aldrich data sheets.
[a,b,c]All values and specificities from Sigma Aldrich product information sheet.

not stored in Alsever's solution because it already contains the anti-coagulant heparin.

In vivo Toxicity

Twelve-week-old C57BL mice were given WGA (2 mg/kg) by intraperitoneal injection on days 1, 4, and 8. Mouse weights were also taken throughout the time of administration. After WGA administration was completed, the mice were sacrificed and spleen, kidney, and liver were harvested and fixed in formalin. H&E staining was completed at the Immunohistochemistry Core Facility at CWRU. Blood was collected in EDTA-coated tubes and analyzed using HemaVet.

Xenograft *in vivo* Model

NSG mice were subcutaneously injected with 5×10^6 HL-60 cells to generate solid AML xenograft mice model, followed by three intra-tumor injection of WGA or PBS.

Statistical Analysis

Data were analyzed using unpaired Student's *t*-test. All experiments were done in triplicate ($n = 3$). *P*-values in figures correspond to: ns = non-significant (>0.05), $^*P < 0.05$, $^{**}P < 0.01$, $^{***}P < 0.001$. All graphs were made and statistical analyses were performed using GraphPad Prism program.

RESULTS

Lectins Demonstrate Variable Cytotoxic Activity Toward Different Cancers

In order to determine how WGA killing compares to other lectin treatment, we looked at a panel of varied lectins. Cytotoxic effects of seven different dietary lectins at 2.0 μg/mL were tested toward AML, ALL, and NHL. Two cell lines from each disease type were used. Wheat germ agglutinin (WGA) consistently showed significant cytotoxicity toward all five cancer cell lines, except OCI-Ly10. As shown in **Figure 1**, WGA-mediated cell killing of OCI-AML3 ($p = 0.0028$), HL60 ($p = 0.0005$), ALL-1 ($p = 0.0058$), ALL-2 ($p = 0.03$), and JVM2 ($p = 0.009$) were statistically significant (**Figures 1A–C**). All other lectins tested did not show significant cytotoxic activity toward these cancer cells. Binding specificities of all these lectins are detailed in **Table 1**.

WGA Binds and Kills Cancer Cells in a Dose- and Time-Dependent Manner

We were interested at which dose and time WGA would be most effective, so we looked at binding and killing at different doses and time points. We utilized a FITC-labeled WGA at 0.5 μg/mL, in order to analyze cellular binding using flow cytometry at a sub-lethal WGA dose. From the flow cytometry data, it is evident that within 45 min of incubation with WGA, the lectin is bound to the surface of the OCI-AML3 cells. This binding is present up to 24-h after incubation (**Figure 2A**). We also wanted to elucidate the relationship between binding and killing, so we looked at binding of WGA to OCI-Ly10 compared to HL-60 AML. We show that there is a significant reduction in WGA-binding to OCI-Ly10 (**Figure 2B**). This reduction in binding coincides with the absence of WGA-induced cell killing of OCI-Ly10 (**Figure 1C**).

Sensitivity of AML cells to WGA up to 4 days was calculated using OCI-AML3 and HL-60 cell lines, using four different doses. Significant killing for HL-60, occurred at 1.0, 2.0, and 4.0 μg/mL, starting from day 1 of WGA treatment (**Figure 2C**). We analyzed cell killing at day 1, 2, 3, and 4. At day 4, almost all cells were killed except for 0.5 μg/mL WGA treated wells. Viable cell count data shows that most of the cells were killed at day 1 itself. Dose kinetics of OCI-AML3 cells show significant killing at 2.0 and 4.0 μg/ml WGA (**Figure 2D**). HL-60 was more sensitive to WGA induced cell death, even at 1.0 μg/ml, while OCI-AML3 was sensitive to 2.0 μg/ml WGA.

WGA Kills Different Subtypes of Primary Patient AML Cells

In order to further evaluate our findings using AML cell lines, we tested if WGA has same effect on primary cells derived from AML patients. AML can be divided into eight different subclasses (M0-M7) based on the differentiation status, according to the French-American-British (FAB) classification (31). AML also can be divided into subtypes based on WHO classification of genetic abnormalities (32). Primary acute myeloid leukemia blood samples from two AML patients (subtype M1 and M5) were treated with 2 μg/mL WGA for 24 h and analyzed by flow cytometry. The flow cytometry count of viable cells (as determined by analyzing forward and side scatter) demonstrates very significant cell killing at this dose of WGA for both

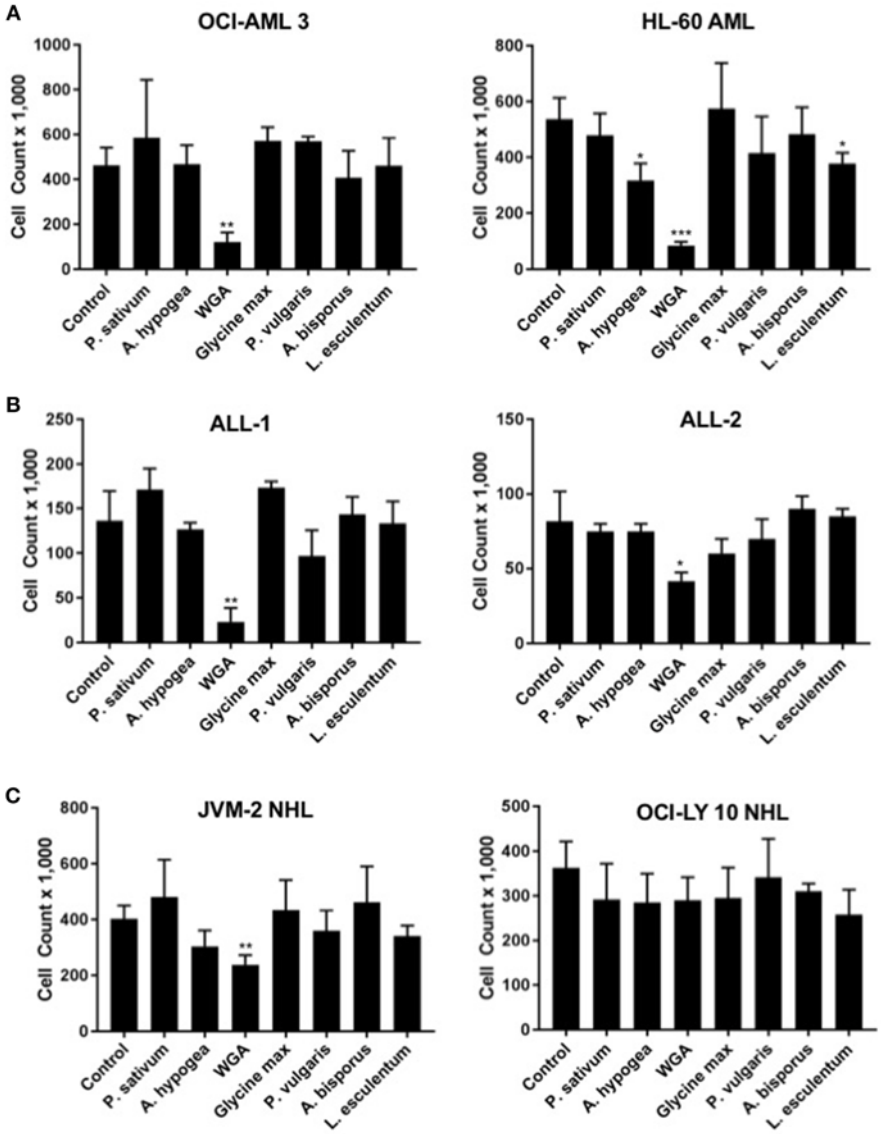

FIGURE 1 | Lectins demonstrate variable toxicities to cancer types. **(A)** Viable cell count of AML (OCI-AML3 and HL-60) cells treated with different dietary lectins as indicated. **(B)** Viable cell count of ALL (ALL-1 and ALL-2) cells treated with different dietary lectins as indicated. **(C)** Viable cell count of NHL (JVM2 and OCI-Ly10) cells treated with different dietary lectins as indicated. All seven lectins administered at 2 μg/mL for 24 h for all cell types. Un-labeled bars were non-significant compared to control. $^{*}p < 0.05$, $^{**}p < 0.01$, $^{***}p < 0.001$, and ns > 0.05.

patient samples ($p = 0.0001$) (**Figure 3A**). Further, we analyzed sensitivity of seven more different AML subtypes to WGA induced killing and found that all six subtypes except M2 subtype showed significant cell killing after exposure to 1.0 and 2.0 μg/ml WGA (**Figure 3B**). M2 subtype with MDS related changes showed maximum killing, even after exposure to 1.0 μg/ml WGA (**Figure 3B**).

After confirming WGA induced cell death in different AML cell lines and patient cells, we wanted to elucidate the specific method of cell killing that WGA utilizes toward AML cells by focusing on cell death and cell cycle. Annexin V (AV)/Propidium Iodide (PI) stain can be used to distinguish between necrotic and apoptotic cell death. AV staining works by binding to phosphatidylserine, which normally resides on the inner cell membrane. However, in early apoptosis, the cellular membrane undergoes changes where phosphatidylserine is present on the outer membrane. PI staining works due to cell membrane rupture, which allows the stain to enter the cell which are in late apoptotic phase or undergoing necrotic death. Flow cytometry scatter demonstrates that at 2 μg/mL there are AV+ and PI+ cells. There is a significant difference between AV–/PI–, AV+, and AV+/PI+ of control and treated HL-60 AML cells ($p = 0.0002$, $p = 0.0068$, $p = 0.0006$). However, there was no statistical difference between PI+ (alone) of control and treated

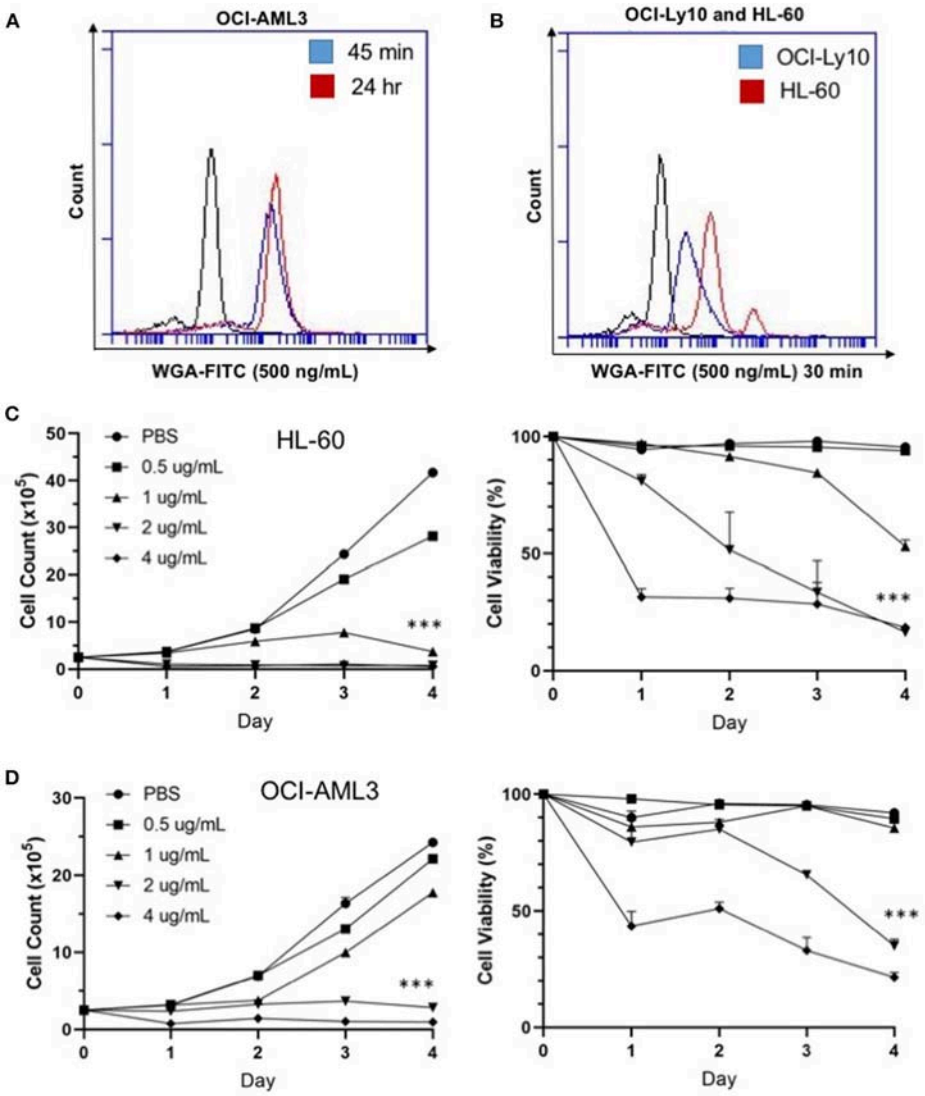

FIGURE 2 | WGA binds and kills in a dose- and time-dependent manner. **(A)** OCI-AML3 cells treated with WGA-FITC (500 ng/mL) and analyzed for binding using flow cytometry. Binding to cells at 45 min (blue peak) and 24 h (red peak) compared to control (black peak). **(B)** OCI-Ly10 and HL-60 cells treated with WGA-FITC (500 ng/mL) for 30 min and analyzed for binding using flow cytometry. **(C,D)** Viable cell count and percent viability of HL-60 **(C)** and **(D)** OCI-AML3 with WGA treatment (0.5, 1.0, 2.0, and 4.0 μg/mL) for 1–4 days, counted using trypan blue. ***$p < 0.001$.

(**Figure 3C**). There is also a significant difference between control and treated cells if all positively staining populations (AV+, AV+/PI+, PI+) are grouped together ($p = 0.0002$). Because it has been shown in the literature that WGA can disrupt cell cycle (14, 17), we tested AML cell cycle changes after being incubated with WGA. Fixing cells and staining with PI allows for the different phases of the cell cycle to be distinguished. Flow cytometry analysis shows that OCI-AML3 cells incubated with 2 μg/mL WGA for 24 h have non-significant changes to G_0/G_1, S, and G_2/M phases compared to untreated control cells (**Figure 3D**). In order to analyze the effect of WGA on cell proliferation, we performed E-670 cell proliferation analysis of OCI-AML3 and HL-60 cells before and after 16 and 24 h of WGA treatment (**Figure 3E**). We did not see any significant changes in staining of these cells. Since WGA induced AML cell killing is a rapid process happening within 24 h, we could not analyze further time points.

WGA Induced AML Cell Death Depends on Both Interaction With Sialic Acid and GlcNAc Binding

WGA binds primarily to GlcNAc and also interacts with sialic-acid containing glyconjugates and oligosaccharides. We tested which binding activity of WGA contributes to its cancer killing activity. Neuraminidase, also called sialidase, is an enzyme that

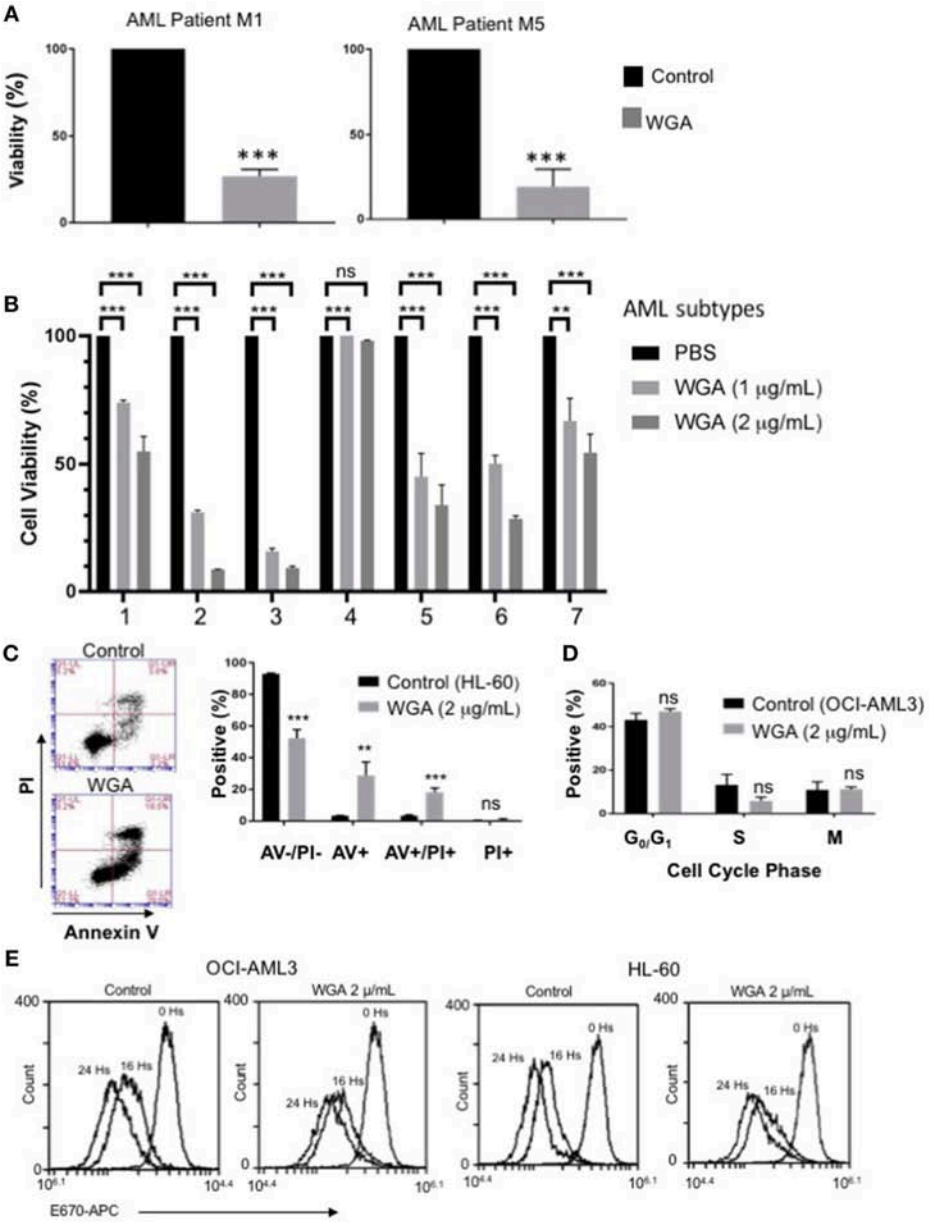

FIGURE 3 | WGA is toxic to primary patient cells and kills AML cells without altering cell cycle. **(A,B)** Percent viability calculated using FSC/SSC live gating of primary AML patient cells belonging to different subtypes **(A)** M1&M5 **(B)** M4Eo; inv16 (1), AML with MDS related changes (2), M2 with MDS-related changes (3), M2(4), CEBPA;c-Kit;TET2(5), NPM1;IDH1(6), IDH1;DNMT3a;FLT3-TKD;trisomy8(7) all treated with or without 2 μg/mL WGA for 24 h. Control was standardized to one hundred percent. **(C)** Annexin V/Propidium Iodide staining of HL-60 cells treated with WGA (2.0 μg/mL) for 24 h. **(D)** Cell cycle analysis of gated live OCI-AML3 cells treated with WGA (2 μg/mL) for 24 h. **(E)** E-670 cell proliferation assays using OCI-AML-3 and HL-60 cell lines in media alone or in the presence of 2.5 μg/mL WGA for the indicated times. Proliferation of live cells was assessed via flow cytometry (Accuri 6C). $^{**}p < 0.01$, $^{***}p < 0.001$, and ns > 0.05.

can catalyze the hydrolysis of sialic acid glycosidic linkages. After neuraminidase pre-treatment, the sialic acid should be cleaved off the cell membrane. Hence, to determine the role of sialic acid interaction with WGA in WGA-mediated cancer cytotoxicity, we pre-treated HL-60 cells with neuraminidase (50 mU/mL) for 2 h and then incubated with 4 μg/mL WGA for 4 h. After treatment, we stained the cells with Propidium iodide and analyzed using flow cytometry. There was a significant increase in PI staining in the WGA-treated groups with and without neuraminidase ($p = 0.0001$, $p = 0.0002$, respectively) (**Figure 4B**). However, when the cells were pre-treated with neuraminidase followed by WGA treatment, the amount of PI staining is significantly reduced compared to cells treated with WGA alone ($p = 0.0033$) (**Figure 4B**). We used FITC-labeled WGA at sub-toxic levels (500 ng/mL) analyzed with flow cytometry to confirm that neuraminidase reduced WGA binding.

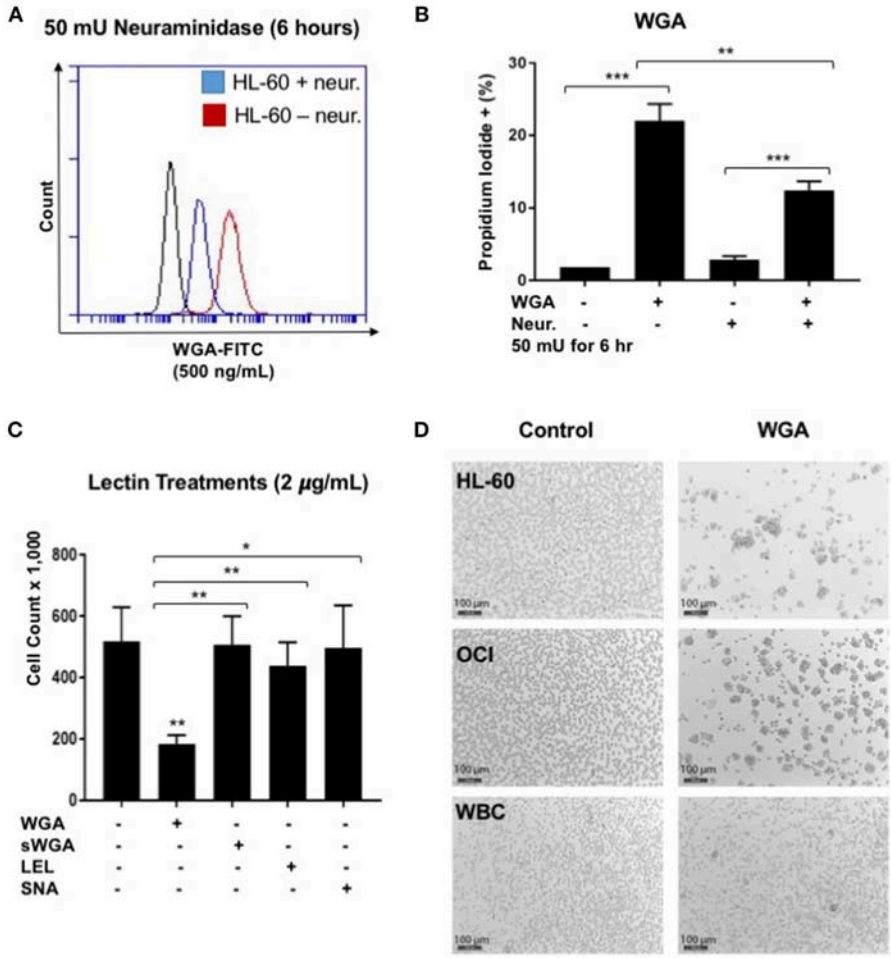

FIGURE 4 | WGA effect on AML is sialic acid dependent. **(A)** HL-60 cells treated with WGA-FITC (500 ng/mL) to analyze WGA binding using flow cytometry. Cells untreated with neuraminidase (red peak) were overlaid with cells treated with neuraminidase (50 mU/mL) for 6 h. **(B)** Percentage Propidium iodide positive HL-60 cells treated with WGA (4 μg/mL) for 4 h were analyzed with flow cytometry. HL-60 cells were either untreated or pre-treated with neuraminidase (50 mU/mL) for 2 h. **(C)** Viable cell count of OCI-AML3 cells treated with 2 μg/mL WGA, sWGA, LEL, and SNA for 24 h counted using trypan blue. **(D)** HL-60, OCI, and healthy human white blood cells (WBCs) treated with either 2 μg/mL WGA or with 2 μL PBS as a negative control and after 20 h treatment, cells were assessed at 10× magnification using bright field microscopy. Scale bar 100 μm shown. $^{*}p < 0.05$, $^{**}p < 0.01$, $^{***}p < 0.001$, and ns > 0.05.

At 6 h, there was a noticeable reduction in binding to HL-60 cells (**Figure 4A**).

We also wanted to look at other lectins, specific for the carbohydrate moieties WGA interacts with. Succinyl-WGA is a modified form of WGA that only binds GlcNAc. We used succinyl-WGA to determine the role of GlcNAc binding in WGA cytotoxicity. We found a significant difference between OCI-AML3 cells treated with succinylated-WGA and unmodified WGA ($p = 0.0237$) (**Figure 4C**), showing that the sialic acid interaction is important for WGA-induced killing. Cells treated with 2 μg/mL SNA lectin, which are specific for sialic acid attached to terminal galactose in α-2,6 and to a lesser degree α-2,3 linkage, are not affected compared to control (**Figure 4C**). OCI-AML3 cells treated with 2 μg/mL LEL, which binds GlcNAc, are also not affected compared to control (**Figure 4C**); however, HL-60 cells treated with LEL showed a significant decrease ($p = 0.0302$) (**Figure 1A**). We also observed cell aggregation/agglutination in HL-60 and OCI-AML3 cells preceding cell death (**Figure 4D**). WGA did not agglutinate normal white blood cells (WBC's) at this concentration and time point (**Figure 4D**).

WGA Exhibits Limited Toxicity to Normal Cells *in vitro* and *in vivo*

At this point, we had demonstrated WGA kills leukemia cells at 1.0–2.0 μg/mL, but we could not discount indiscriminate killing. Because of this concern, we tested various non-cancerous cells with WGA. Propidium iodide staining and flow cytometry analysis shows no significant changes between peripheral blood mononuclear cells treated without WGA and with 0.5, 1.0, and 2.0 μg/mL WGA (**Figure 5A**). OP9, a stromal cell line, was treated with 2.0 μg/mL WGA and no significant morphological changes were apparent microscopically. The cells were not detached from the plates and maintained normal shape

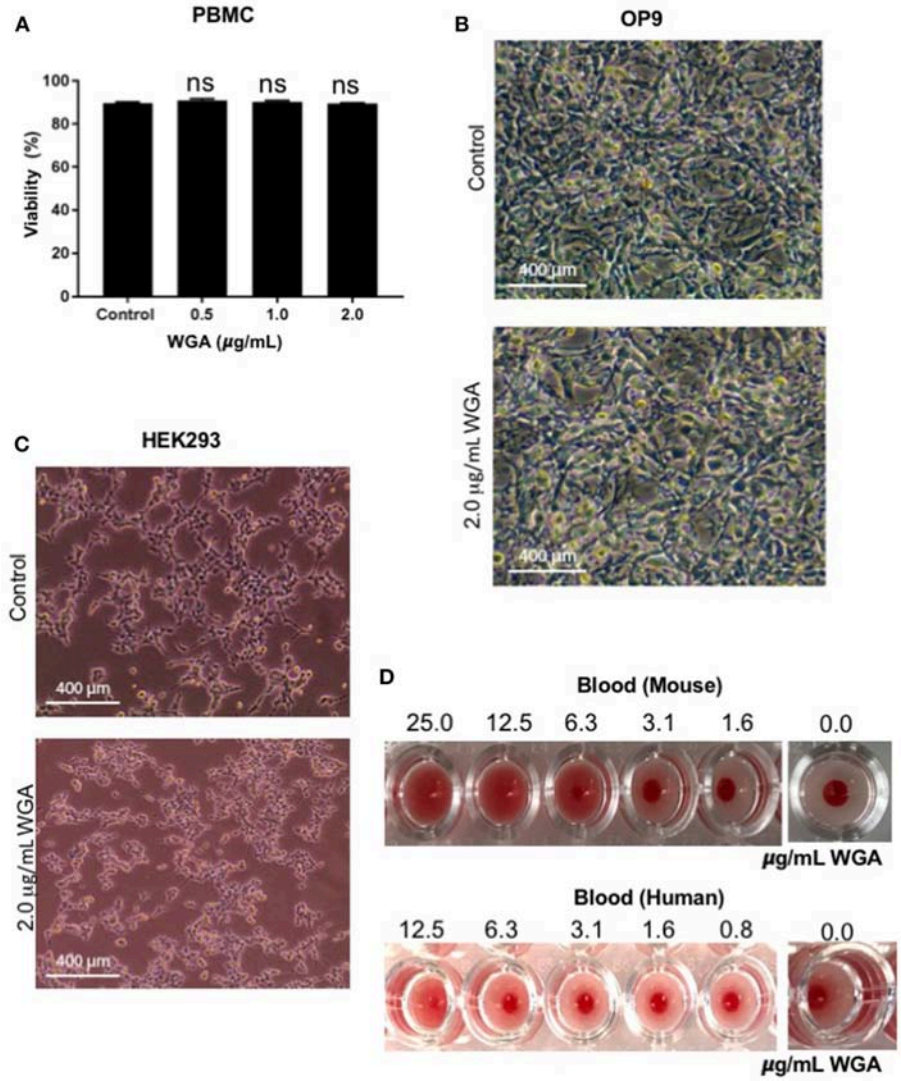

FIGURE 5 | WGA treatment exhibits little or no toxicity toward normal cells *in vitro*. **(A)** Viable peripheral blood mononuclear cells (PBMCs) treated with 0.5, 1.0, and 2.0 μg/mL WGA for 24 h were calculated by PI uptake using flow cytometry. **(B)** Light microscopy of OP9 stromal cells showing phenotype. Cells were treated with 2.0 μg/mL WGA for 24 h and imaged. Scale bar 400 mm shown. **(C)** Light microscopy of HEK293 cells showing phenotype. Cells were treated with 2.0 μg/mL WGA for 24 h and imaged. Scale bar 400 mm shown. **(D)** Hemagglutination assay on 96-well micro-plate of mouse and human blood using serial dilution of WGA (25 to 1.6 μg and 12.5 to 0.8 μg, respectively). Absence of lectin control (0.0 μg) for mouse and human blood are included. ns > 0.05.

(**Figure 5B**). HEK293 cells were also treated with 2.0 μg/mL WGA and imaged. There were no morphological changes after incubation (**Figure 5C**). All these data points to the different toxicity of WGA toward cancer cells and normal cells. Because WGA is known to cause red blood cell (RBC) agglutination (20), we wanted to test whether the WGA dose we are using for the cytotoxic assay causes agglutination in mouse and human RBCs. Hemagglutination assays of human and murine blood after exposure to WGA demonstrated lack of hemagglutination at the indicated doses used. This is evident by the button of blood settled to the bottom of the well. A positive hemagglutination result is diffuse blood in the well as shown in the higher doses imaged (**Figure 5D**).

Finally, because we had determined effect of WGA on normal cells *in vitro*, we tested whether WGA is toxic *in vivo*. We conducted a study to obtain information of WGA dose toxicity where WGA was injected (2 mg/kg) by IP to 2 C57BL/6 mice on days 1, 4, and 8. Mice were sacrificed on day 9 for further analysis (**Figure 6A**). Age and sex-matched, non-treated mice served as controls. The mortality and changes to body weight, clinical signs, gross observation, organ weight, and histopathology of principal organs (spleen, liver and kidney) were monitored. We found no mortalities, WGA treatment-related clinical signs, changes to the body and organ weights, or gross and histopathological findings (**Figures 6B,C**). Since some reports say WGA can cross blood brain barrier (BBB) (33), we analyzed

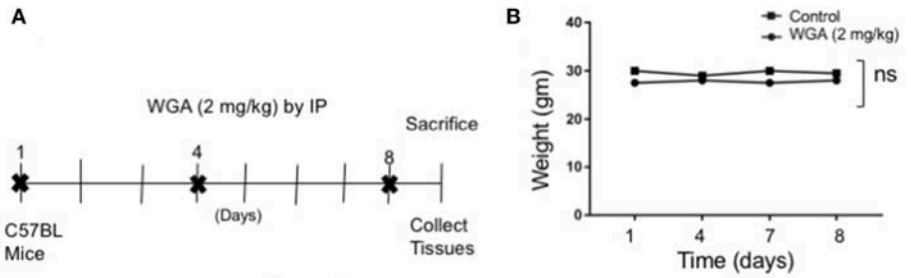

E

	Control	WGA (2 mg/kg)	NORMAL VALUES
WBC (K/µL)	9.91	7.21	1.8 – 10.7
NE	4.855	1.92	0.1 – 2.4
LY	3.965	4.93	0.9 – 9.3
MO	0.365	0.16	0.0 – 0.4
EO	.59	0.17	0.0 – 0.2
BA	.13	0.06	0.0 – 0.2
NE %	46.22	26.61	6.6 – 38.9
LY %	42.815	68.33	55.8 – 91.6
MO%	4.17	2.12	0.0 – 7.5
EO%	5.545	2.33	0.0 – 3.9
BA%	1.2145	0.63	0.0 – 2.0
RBC (M/µL)	6.585	4.725	6.36 – 9.42
Hb (g/dL)	9.55	6.95	11.0 – 15.1
HCT %	30.55	22.4	35.1 – 45.4

FIGURE 6 | WGA treatment demonstrated little toxicity to normal cells *in vivo*. **(A)** Treatment scheme where 2 mg/kg WGA was IP administered to two mice on days 1, 4, and 8. Mice were sacrificed on day 9. **(B)** Weights of mice treated with WGA during duration of treatment. **(C)** Histological analysis of WGA-treated tissues. Spleen, liver, and kidney stained with H&E and imaged by light microscopy at 10X magnification. Scale bar 400 µm shown **(D)** Histological analysis of Hematoxylin&Eosin stained brain tissues from PBS and WGA (5 mg/kg) injected mice. Scale bar 100 µm shown **(E)** HEMAVET blood toxicity analysis of treated mice after sacrifice compared to control mice and normal values. Normal values were given with HemaVet instructions. ns > 0.05.

brain tissue from WGA (5 mg/kg) and PBS injected C57BL/6 mice. Histochemical stainings of brain sections showed normal structures comparable to PBS injected mice, with no signs of toxicity (**Figure 6D**).

We also analyzed different blood cells using HEMAVET. WGA-treated mice displayed cell counts within normal ranges as shown in **Figure 6E**, except for slightly reduced red blood cell count values, such as RBC, hemoglobin, and hematocrit levels (**Figure 6E**). These suggest that WGA at this dose is safe to use *in vivo*.

WGA Induced AML Cell Killing in Xenograft Mouse Model

We further evaluated WGA killing of AML cells *in vivo* using a xenograft mouse model. Severely immunodeficient NSG mice were used for this study. HL-60 AML cells were injected subcutaneously (s.c.) into NSG mice and injected WGA intra-tumorally at days 6, 8, and 10 (**Figure 7A**). Mice tumor volume was measured every alternate day and WGA injected mice showed a very significant inhibition in tumor progression, compared to PBS injected mice (**Figures 7B,C**). We sacrificed

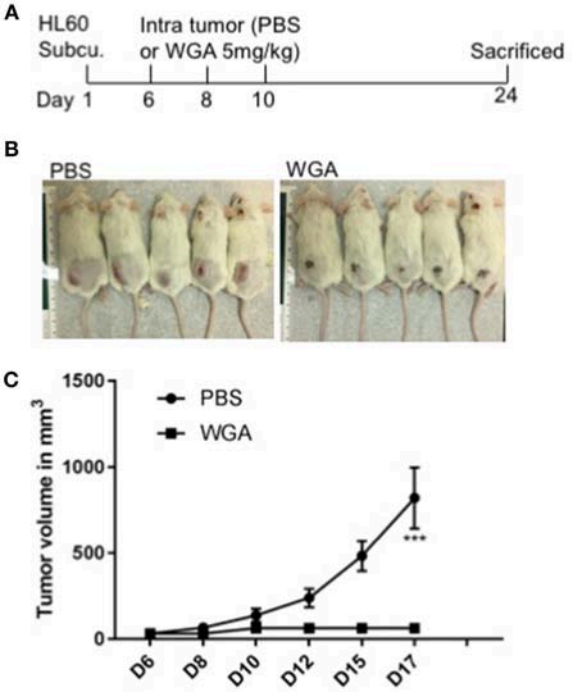

FIGURE 7 | WGA induced AML cell killing in xenograft mouse model. **(A)** Treatment scheme- HL-60 cells injected at day 1 and at day 6, 8 and 10 WGA 5mg/kg injected intratumorally and mice were sacrificed at day 24. **(B)** Pictures of mice treated with PBS or WGA **(C)** Graph showing tumor volume (mm^3) of PBS and WGA injected mice. ***$p < 0.001$.

these mice at day 24. Tumors in PBS injected mice reached volume upto 1,000 mm^3, while there were no measurable tumors in WGA injected mice. NSG mice lack mature lymphocytes including B cells, T cells and NK cells, so it is highly likely that AML cell killing by WGA lectin seen in this model is a direct anti-leukemic effect by WGA. Mice injected with WGA did not show any obvious signs of toxicity suggesting that this therapeutic strategy may be safe, and it is worthy of further development for AML, provided route of administration is optimized.

DISCUSSION

Dietary lectins, particularly wheat germ agglutinin, have been shown to have important anti-cancer properties (18, 19, 22). However, knowledge of lectins' impact on hematological malignancies, such as AML, ALL, and NHL, is lacking. Because these malignancies are in need of potential new treatments, exploring dietary lectins can be a valuable starting point. The panel of lectins chosen encompasses various carbohydrate binding specifities and sizes, as well as sources of origin. We demonstrated that lectins' effects on cancer is variable, with the vast majority of dietary lectins having no impact at all on cancer cell viability. WGA showed significant cell killing against five cell lines tested (out of six). WGA was ineffective against OCI-Ly10. Normal cells were also insensitive to doses of WGA, where it showed significant killing activity against cancer cells. High concentrations of WGA will kill normal cells as well, so choosing the right dose of WGA is key to the success of treatment. We demonstrate the dose specificity of WGA with AML cells showing a significant cytotoxic effect on AML cells but not with the normal cells. WGA killed all AML subtypes tested except M2, this has to be tested further using many M2 patient samples and if WGA fails to kill this particular subtype, it has to be studied further. The exact reasons for this specificity is not known. WGA binds to GlcNAc and it also interacts with sialic-acid containing glyconjugates and oligosaccharides. Since most of the cancer cells are hyper O-GlcNAcylated and hyper silalylated (34–39), we could speculate that it might be the differences in levels of GlcNAc expression and presence of sialylation on cell membrane in different cells which accounts for WGA's cell binding and toxicity specificity. At higher doses, the mechanism of cell killing may be agglutination of cell membrane.

Our data and the literature show the importance of both sialic acid and GlcNAc in the cytotoxicity of WGA. However, the role of each carbohydrate moiety in the lectin-induced death of cells might vary from cell to cell. Sialic acid-specific lectins and GlcNAc-specific lectins were not able to kill AML cells on their own, signifying both properties are necessary for cell killing. If sialic acid is removed using neuraminidase, there is a reduction in binding and killing. The dual interaction to both carbohydrate moieties might be required because of the different locations of the carbohydrates within the cells. The sialic acid interaction may occur outside the cell on the cell membrane, while the GlcNAc binding may occur within the cell after internalization as proposed by Schwarz et al. (22). However, this mechanism of action may be specific to the pancreatic cancer cells used in the study. Further studies are required to understand any AML cell specific mechanism. Sialic acid and GlcNAc interaction within the cell upon internalization may also be key to the cell killing effects. These cell specific differences could also be why the method of killing varies by cancer type. Mechanisms of cytotoxicity by WGA includes apoptosis, necrosis, paraptosis, and cell cycle arrest. Our data demonstrates WGA induces apoptosis and necrosis, but cell cycle analysis revealed no significant differences.

WGA injected into the tumor arrested tumor growth in an NSG xenograft AML model. PBS injected mice had large tumors as expected, which excludes the possibility that intratumoral injection procedure has any effect on tumor growth. Since we used severely immune-compromised mice which lacks a proper innate immune response, the AML killing effect observed might be solely from WGA's direct effect on AML. Studies in the past suggested the possibility that WGA has harmful effects, however, several recent studies have re-evaluated many of those assumptions and suggested that WGA dangers are either non-existent or have limited effects (40, 41). Importantly, the *in vitro* and *in vivo* concentrations of WGA used in this study is very low and no toxicity is reported using this low concentration. Interestingly, more recently dietary lectins including WGA have been associated with the beneficial effect on health, including reduced risks of type 2 diabetes, cardiovascular disease, some types of cancer and weight management (41). Chronic exposure

of high doses of WGA can lead to toxic effects like development of anti WGA antibodies, platelet aggregation or red blood cell (RBC) agglutination. We used low doses of WGA and short exposure timings, where these kind of toxicity is not a concern. WGA has been shown to elicit pro-inflammatory conditions, and its toxic effects could only be seen at a very high dose (of 7 g/kg body weight over a period of 10 days) in the normal gastrointestinal tract of rats, suggesting that WGA being non-toxic in a huge range (21, 40). A final word on toxicity or atoxicity of WGA is pending due to lack of *in vivo* studies, whereas microgram range of WGA used for targeting or carrier system is unlikely to provoke toxic effects (40).

The current therapies for treatment of AML include chemotherapy, radiation therapy, and stem cell transplant. These therapies rely on cell killing and differentiation which lead to cell death. AML treatment regimen can also change depending on the age and health of the patient. In a young patient, induction therapy of high doses of cytarabine and daunorubicin will be used to clear as much of the tumor burden as possible. Once the tumor is cleared, lower doses of these drugs will be used for maintenance. In older and unhealthy patients, these high doses are contraindicated because of their toxicity and potential life-threatening effects. In the AML M3 subtype acute promyelocytic leukemia (APL), ATRA and arsenic trioxide can be used (42). Common side effects of cytarabine include headache, nausea, vomiting, and low blood counts, while less common side effects include flu-like symptoms, loss of appetite, and pain in the hands, feet, and eyes (43). The side effects of daunorubicin's include nausea, vomiting, diarrhea, and hair loss (44). Because of the complexity of AML and its multiple subtypes, the treatment of AML has changed very little over the last few decades. Because of these factors, exploring WGA as a potential therapeutic is worthwhile. The side effects of WGA, such as adverse toxicity and hemagglutination, could be curtailed if administered at low doses.

We show that dietary lectins may be a unique therapeutic tool against hematological malignancies because of their cytotoxic potential and limited toxicity to normal cells and tissues. We characterized the effects on one subtype, OCI-AML3, leaving open the exploration of many other cancer types and conditions, such as drug-resistance and relapse. Characterization of WGA-killing may also lead to more information on novel cell killing pathways. Insights into WGA as a drug-delivery system (45, 46), might also be utilized in combination with our findings to develop potential targeted treatments for hematological malignancies.

ETHICS STATEMENT

Case Western Reserve University's Institution's Animal Care and Use Committee (IACUC) reviewed and approved the Animal Experimentation performed in this study and followed IACUC guide lines and protocol. Mice were maintained in ARC facility at Case Western Reserve University under a 12-h day-night cycle and had *ad libitum* access to food and water. Human samples from normal donors and leukemia patients were obtained from Hematopoietic Stem Cell Core Facility located in Case Western Reserve University. Discarded human blood samples were used in this study and informed consent documents were approved by the University Hospitals Case Medical Center Institutional Review Board.

AUTHOR CONTRIBUTIONS

BR: performed experiments, data analysis, and writing. KZ: performed *in vivo* xenograft experiment. AA: performed *in vivo* toxicity experiments. DW: performed some of the *in vitro* experiments. YV: performed some of the *in vitro* experiments. RP: conceived the idea, analyzed data, wrote and edited manuscript.

FUNDING

St. Baldrick's Foundation (RP), Mizutani foundation for Glycoscience (RP), The Andrew McDonough B+ Foundation (RP), Velosano Foundation (RP) grants and NIH 1R21CA201775-01A1 (RP).

ACKNOWLEDGMENTS

This research was supported by the Athymic Animal and Hemapoietic Biorepository and Cellular therapy core facilities, Shared Resources of the Case Comprehensive Cancer Center (P30CA043703) for their support and funding. We thank Dr. Distelhorst who gifted JVM2 and OCI-Ly10 and Sarah Groft who gifted SNA lectin.

REFERENCES

1. Sharon N, Lis H. Lectins: cell-agglutinating and sugar-specific proteins. *Science* (1972) 177:949–59. doi: 10.1126/science.177.4053.949
2. Etzler ME. Distribution and function of plant lectins. In: Liener IE, Sharon N, Goldstein IJ, editors. *The Lectins: Properties, Functions, and Applications in Biology and Medicine*. Orlando, FL: Academic Press. (1986). p. 371–91. doi: 10.1016/B978-0-12-449945-4.50011-7
3. Vandenborre G, Van Damme E, Smagghe G. Natural products: plant lectins as important tools in controlling pest insects. In: Rami Horowitz, A. editor. *Biorational Control of Arthropod Pests- Application and Resistance Management*. Springer Verlag (2009). p. 163–87.
4. Peumans WJ, Van Damme EJ. Lectins as plant defense proteins. *Plant Physiol*. (1995) 109:347–52. doi: 10.1104/pp.109.2.347
5. Fujimoto Z, Tateno H, Hirabayashi J. Lectin structures: classification based on the 3-D structures. *Methods Mol Biol*. (2014) 1200:579–606. doi: 10.1007/978-1-4939-1292-6_46
6. Damme EJMV, Peumans WJ, Barre A, Rougé P. Plant lectins: a composite of several distinct families of structurally and evolutionary related proteins with diverse biological roles. *Critic Rev Plant Sci*. (2010) 575–692. doi: 10.1080/07352689891304276
7. Hubbard SC, Kranz DM, Longmore GD, Sitkovsky MV, Eisen HN. Glycosylation of the T-cell antigen-specific receptor and its potential role in lectin-mediated cytotoxicity. *Proc Natl Acad Sci USA*. (1986) 83:1852–6. doi: 10.1073/pnas.83.6.1852

8. Haas H, Falcone FH, Schramm G, Haisch K, Gibbs BF, Klaucke J, et al. Dietary lectins can induce *in vitro* release of IL-4 and IL-13 from human basophils. *Eur J Immunol.* (1999) 29:918–27. doi: 10.1002/(SICI)1521-4141(199903)29:03<918::AID-IMMU918>3.0.CO;2-T
9. Gong T, Wang X, Yang Y, Yan Y, Yu C, Zhou R, et al. Plant lectins activate the NLRP3 inflammasome to promote inflammatory disorders. *J Immunol.* (2017) 198:2082–92. doi: 10.4049/jimmunol.1600145
10. Ricci-Azevedo R, Roque-Barreira MC, Gay NJ. Targeting and recognition of toll-like receptors by plant and pathogen lectins. *Front Immunol.* (2017) 8:1820. doi: 10.3389/fimmu.2017.01820
11. Goldstein IJ, Hayes CE. The lectins: carbohydrate-binding proteins of plants and animals. *Adv Carbohydr Chem Biochem.* (1978) 35:127–340. doi: 10.1016/S0065-2318(08)60220-6
12. Pusztai A, Grant G. Assessment of lectin inactivation by heat and digestion. *Methods Mol Med.* (1998) 9:505–14.
13. Kilpatrick DC, Pusztai A, Grant G, Graham C, Ewen SW. Tomato lectin resists digestion in the mammalian alimentary canal and binds to intestinal villi without deleterious effects. *FEBS Lett.* (1985) 185:299–305. doi: 10.1016/0014-5793(85)80927-3
14. Kim M, Rao MV, Tweardy DJ, Prakash M, Galili U, Gorelik E. Lectin-induced apoptosis of tumour cells. *Glycobiology* (1993) 3:447–53. doi: 10.1093/glycob/3.5.447
15. Vasconcelos IM, Oliveira JT. Antinutritional properties of plant lectins. *Toxicon* (2004) 44:385–403. doi: 10.1016/j.toxicon.2004.05.005
16. Eckhardt AE, Malone BN, Goldstein IJ. Inhibition of Ehrlich ascites tumor cell growth by Griffonia simplicifolia I lectin *in vivo*. *Cancer Res.* (1982) 42:2977–9.
17. Miyoshi N, Koyama Y, Katsuno Y, Hayakawa S, Mita T, Ohta T, et al. Apoptosis induction associated with cell cycle dysregulation by rice bran agglutinin. *J Biochem.* (2001) 130:799–805. doi: 10.1093/oxfordjournals.jbchem.a003051
18. Lorea P, Goldschmidt D, Darro F, Salmon I, Bovin N, Gabius HJ, et al. *In vitro* characterization of lectin-induced alterations on the proliferative activity of three human melanoma cell lines. *Melanoma Res.* (1997) 7:353–63. doi: 10.1097/00008390-199710000-00001
19. Wang H, Ng TB, Ooi VE, Liu WK. Effects of lectins with different carbohydrate-binding specificities on hepatoma, choriocarcinoma, melanoma and osteosarcoma cell lines. *Int J Biochem Cell Biol.* (2000) 32:365–72. doi: 10.1016/S1357-2725(99)00130-2
20. Van Damme JM. *Handbook of Plant Lectins: Properties and Biomedical Applications*. Chichester: John Wiley & Sons (1998).
21. Dalla Pellegrina C, Rizzi C, Mosconi S, Zoccatelli G, Peruffo A, Chignola R. Plant lectins as carriers for oral drugs: is wheat germ agglutinin a suitable candidate? *Toxicol Appl Pharmacol.* (2005) 207:170–8. doi: 10.1016/j.taap.2005.01.001
22. Schwarz RE, Wojciechowicz DC, Picon AI, Schwarz MA, Paty PB. Wheatgerm agglutinin-mediated toxicity in pancreatic cancer cells. *Br J Cancer* (1998) 80:1754–62. doi: 10.1038/sj.bjc.6690593
23. Gastman B, Wang K, Han J, Zhu ZY, Huang X, Wang GQ, et al. A novel apoptotic pathway as defined by lectin cellular initiation. *Biochem Biophys Res Commun.* (2004) 316:263–71. doi: 10.1016/j.bbrc.2004.02.043
24. Tsai TL, Wang HC, Hung CH, Lin PC, Lee YS, Chen HHW, et al. Wheat germ agglutinin-induced paraptosis-like cell death and protective autophagy is mediated by autophagy-linked FYVE inhibition. *Oncotarget* (2017) 8:91209–22. doi: 10.18632/oncotarget.20436
25. Brown CM, Larsen SR, Iland HJ, Joshua DE, Gibson J. Leukaemias into the 21st century: part 1: the acute leukaemias. *Intern Med J.* (2012) 42:1179–86. doi: 10.1111/j.1445-5994.2012.02938.x
26. Puckett Y, Chan O. *Cancer, Leukemia, Lymphocytic, Acute (ALL)*. Treasure Island, FL: StatPearls Publishing (2017).
27. Nogai H, Dorken B, Lenz G. Pathogenesis of non-Hodgkin's lymphoma. *J Clin Oncol.* (2011) 29:1803–11. doi: 10.1200/JCO.2010.33.3252
28. *Key Statistics for Non-Hodgkin Lymphoma.* (2018). Available online at: https://www.cancer.org/cancer/non-hodgkin-lymphoma/about/key-statistics.html
29. Grimes SE. *A Basic Laboratory Manual for Small Scale Production and Testing of I-2 Newcastle Disease Vaccine.* (2002). Available online at: http://www.fao.org/docrep/005/ac802e/ac802e00.htm
30. Assay Services. *VIRAPUR, LLC, Hemagglutination (HA) Assay Protocol.* (2018). Available online at: http://www.virapur.com/assay_services/assay_services.php
31. Bennett JM, Catovsky D, Daniel MT, Flandrin G, Galton DA, Gralnick HR, et al. Proposed revised criteria for the classification of acute myeloid leukemia. A report of the French-American-British Cooperative Group. *Ann Intern Med.* (1985) 103:620–5. doi: 10.7326/0003-4819-103-4-620
32. Döhner H, Estey E, Grimwade D, Amadori S, Appelbaum FR, Büchner T, et al. Diagnosis and management of AML in adults: 2017 ELN recommendations from an international expert panel. *Blood* (2017) 129:424–47. doi: 10.1182/blood-2016-08-733196
33. Villegas JC, Broadwell RD. Transcytosis of protein through the mammalian cerebral epithelium and endothelium. II Adsorptive-transcytosis of WGA-HRP and the blood-brain and brain-blood barriers. *J Neurocytol.* (1993) 22:67–80. doi: 10.1007/BF01181571
34. Zhang X, Qiao Y, Wu Q, Chen Y, Zou S, Liu X, et al. The essential role of YAP O-GlcNAcylation in high-glucose-stimulated liver tumorigenesis. *Nat Commun.* (2017) 8:15280. doi: 10.1038/ncomms15280
35. Fardini Y, Dehennaut V, Lefebvre T, Issad T. O-GlcNAcylation: A New Cancer Hallmark? *Front Endocrinol.* (2013) 4:99. doi: 10.3389/fendo.2013.00099
36. Shi Y, Tomic J, Wen F, Shaha S, Bahlo A, Harrison R, et al. Aberrant O-GlcNAcylation characterizes chronic lymphocytic leukemia. *Leukemia* (2010) 24:1588–98. doi: 10.1038/leu.2010.152
37. Asthana A, Ramakrishnan P, Vicioso Y, Zhang K, Parameswaran R. Hexosamine Biosynthetic Pathway (HBP) inhibition leads to AML cell differentiation and cell death. *Mol Cancer Ther.* (2018) 17:2226–37. doi: 10.1158/1535-7163.MCT-18-0426.
38. Bull C, Stoel MA, den Brok MH, Adema GJ. Sialic acids sweeten a tumor's life. *Cancer Res.* (2014) 74:3199–204. doi: 10.1158/0008-5472.CAN-14-0728
39. Pearce OM, Laubli H. Sialic acids in cancer biology and immunity. *Glycobiology* (2016) 26:111–28. doi: 10.1093/glycob/cwv097
40. Gabor F, Bogner E, Weissenboeck A, Wirth M. The lectin–cell interaction and its implications to intestinal lectin-mediated drug delivery. *Adv Drug Delivery Rev.* (2004) 56:459–80. doi: 10.1016/j.addr.2003.10.015
41. Van Buul VJ, Brouns FJPH. Health effects of wheat lectins: a review. *J Cereal Sci.* (2014) 59:112–7. doi: 10.1016/j.jcs.2014.01.010
42. *Treating Acute Myeloid Leukemia.* (2018). Available online at: https://www.cancer.org/cancer/acute-myeloid-leukemia/treating.html
43. Cancer CC. *Cytarabine - Drug Information – Chemocare.* (2018). Available online at: http://chemocare.com/chemotherapy/drug-info/cytarabine.aspx
44. Cancer CC. *Daunorubicin - Drug Information – Chemocare.* (2018). Available online at: http://chemocare.com/chemotherapy/drug-info/daunorubicin.aspx
45. Plattner VE, Wagner M, Ratzinger G, Gabor F, Wirth M. Targeted drug delivery: binding and uptake of plant lectins using human 5637 bladder cancer cells. *Eur J Pharm Biopharm.* (2008) 70:572–6. doi: 10.1016/j.ejpb.2008.06.004
46. Wang C, Ho PC, Lim LY. Wheat germ agglutinin-conjugated PLGA nanoparticles for enhanced intracellular delivery of paclitaxel to colon cancer cells. *Int J Pharm.* (2010) 400:201–10. doi: 10.1016/j.ijpharm.2010.08.023

Conflict of Interest Statement: The authors declare that the research was conducted in the absence of any commercial or financial relationships that could be construed as a potential conflict of interest.

frontiers in Oncology

ORIGINAL RESEARCH
published: 12 March 2019
doi: 10.3389/fonc.2019.00137

Glucose-Regulated Protein 78 Signaling Regulates Hypoxia-Induced Epithelial–Mesenchymal Transition in A549 Cells

*Ling-Ling Sun, Chang-Ming Chen, Jue Zhang, Jing Wang, Cai-Zhi Yang and Li-Zhu Lin**

Integrative Cancer Centre, the First Affiliated Hospital of Guangzhou University of Chinese Medicine, Guangzhou, China

Objective: Metastasis and therapeutic resistance are the major determinants of lung cancer progression and high mortality. Epithelial–mesenchymal transition (EMT) plays a key role in the metastasis and therapeutic resistance. Highly expressed glucose-regulated protein 78 (GRP78) is a poor prognostic factor in lung cancer and possibly correlated with EMT. This study aims to examine whether the up-regulation of GRP78 is involved in EMT in lung adenocarcinoma and explore the underlying downstream molecular pathways.

Study Design: EMT was assessed by analysis of cell morphology and expression of EMT protein markers in A549 cells under normoxia, hypoxia and silencing GRP78 conditions. The expression levels of Smad2/3, Src, and MAPK (p38, ERK, and JNK) proteins were examined by Western blot analysis under hypoxia and treatments with phosphorylation inhibitors.

Results: Under hypoxic conditions, the EMT morphology significantly changed and the GRP78 expression was significantly up-regulated in A549 cells compared with those in normoxia control. The expression and phosphorylation levels of smad2/3, Src, p38, ERK, and JNK were also upregulated. When GRP78 was silenced, EMT was inhibited, and the levels of phospho-smad2/3, phospho-Src, phospho-p38, phospho-ERK, and phospho-JNK were suppressed. When the activation of Smad2/3, Src, p38, ERK, and JNK was inhibited, EMT was also inhibited. The inhibition effect on EMT by these phosphorylation inhibitors was found to be weaker than that of GRP78 knockdown.

Conclusions: Hypoxia-induced EMT in A549 cells is regulated by GRP78 signaling pathways. GRP78 promotes EMT by activating Smad2/3 and Src/MAPK pathways. Hence, GRP78 might be a potential target for treatment of lung adenocarcinoma.

Keywords: lung cancer, lung adenocarcinoma, epithelial mesenchymal transition, hypoxia, glucose-regulated protein 78, GRP78

OPEN ACCESS

Edited by:
Zhe-Sheng Chen,
St. John's University, United States

Reviewed by:
Qi Xie,
University of California, San Diego, United States
JiaXing Zhang,
Sun Yat-sen University, China

****Correspondence:***
Li-Zhu Lin
lizhulin26@yahoo.com

Specialty section:
This article was submitted to Cancer Molecular Targets and Therapeutics, a section of the journal Frontiers in Oncology

Received: *09 December 2018*
Accepted: *15 February 2019*
Published: *12 March 2019*

Citation:
Sun L-L, Chen C-M, Zhang J, Wang J, Yang C-Z and Lin L-Z (2019) Glucose-Regulated Protein 78 Signaling Regulates Hypoxia-Induced Epithelial–Mesenchymal Transition in A549 Cells. Front. Oncol. 9:137. doi: 10.3389/fonc.2019.00137

INTRODUCTION

Lung cancer is the leading cause of cancer death worldwide; according to the estimated data from GLOBOCAN in 2012, one of five cancer deaths is due to lung cancer (1.59 million deaths, 19.4% of the total cancer deaths) (1). Despite significant progress in the development of new therapies for lung cancer, metastasis and therapeutic resistance remain the major determinants of lung cancer progression and high mortality (2).

Mounting evidence demonstrated that epithelial–mesenchymal transition (EMT) is involved in the metastasis and therapeutic resistance of lung cancer. EMT refers to the biological process by which epithelial cells are transformed into mesenchymal phenotypes through specific procedures. EMT inhibits the expression of E-cadherin and cytokeratin in epithelial cells, upregulates the expression of N-cadherin and vimentin in mesenchymal cells and promotes the ability of cells to secrete matrix metalloproteinase and fibronectin. EMT can be induced by various factors, such as TGF-beta, which increases the expression of key nuclear transcription factors including Twist, Snail and ZEB (3) and causes phenotypic changes by activating intrinsic cellular signal molecules including Src, MAPK, Smad2/3, and other signals (4–6).

Hypoxia is a common hallmark of several human malignancies and an independent and unfavorable prognostic factor associated with the occurrence of EMT (7–9). Previous studies found that cAMP-dependent protein kinase, hypoxia factor Hif-1alpha(HIF1a) and unfolded protein response can potentiate EMT; moreover, treatment with insulin-like growth factor 1 receptor inhibitor reverses hypoxia-induced EMT (8–11), However, the mechanisms of hypoxia-induced EMT remain unknown. Understanding the biology of hypoxia-induced EMT and their implications in therapeutic relapse may provide new crucial approaches for development of improved therapeutic strategies.

The 78-kDa glucose-regulated protein (GRP78), also known as BiP and HSPA5, is highly expressed in many types of cancers, including lung, hepatocellular cancer, and breast cancer (12–15). It could inhibit apoptosis of cancer cells, and induce chemoresistance of cancer (16–18). What's more, it is closely related to EMT. Zhang et al. (19) reported that high expressed GRP78 induced EMT in hepatocellular carcinoma cell lines. Lizardo et al. (20) that up-regulation of GRP78 in metastatic cancer cells is necessary for lung metastasis in some highly metastatic cell line models, such as osteosarcomas and murine mammary adenocarcinoma. Zhang et al. (21) demonstrated that overexpressing GRP78 facilitated the expression and secretion of TGF-beta1, which further activated EMT. However, Chang et al. (22) stated that overexpressing GRP78 inhibited the metastasis of colon cancer through EMT biomarkers. Thus far, the relationship between GRP78 expression and EMT remains controversial. Whether GRP78 expression has causality link with EMT in lung cancer also remains unknown. Hence, the present study aims to examine the role of up-regulation of GRP78 in EMT in lung adenocarcinoma and explore the downstream molecular pathways involved.

METHODS

Cell Culture and Conditioning

Human lung adenocarcinoma A549 cells were purchased from the Cell Bank of the Chinese Academy of Sciences (Shanghai, China) and cultured in RPMI-1640 medium (Gibco, USA) supplied with 10% FBS (Gibco, USA) and 100 U/ml penicillin/streptomycin in 5% CO_2 incubator at 37°C. The medium was changed every 3 days. The cells were treated with normal O_2 as control.

A549 cells were cultured with 2% O_2 for hypoxia condition. The concentration of protein inhibitors for treatment of A549 cells were as follows: 550 nM SB505124 (phospho-Smad2/3 inhibitor), 25 nM KX2-391 (phospho-Src inhibitor), 100 nM JNK-IN-8 (phospho-JNK inhibitor), 2.5 μM SB203580 (phospho-p38 inhibitor), and 1.5 μM FR180204 (phospho-ERK). All of the inhibitors were purchased from Celleck Chemicals (USA).

Assessment of Cell Morphology

Morphological changes were examined using phase-contrast microscopy (Olympus, Japan).

Real-Time Quantitative Fluorescent PCR

Experiments were performed following the methods in our previous study. The cells were collected to extract total RNA using Trizol method. The cDNA was synthesized with Prime Script TMRT Master Mix (RR036A; Takara, Japan) through reverse transcription and used as template to amplify target genes with real-time quantitative fluorescent PCR with SYBR® Premix Ex TaqII (RR820A; Takara, Japan). The specific primers (Invitrogen, USA) of each transcription factor (Snail1, Snail2, Twist, ZEB1 and ZEB2) were also based on such study (23). The reaction condition was 95°C for 30 s, followed by 95°C for 5 s and 60°C for 30 s with 40 cycles. The amplified productions were quantitatively analyzed with 2-ΔΔCt method. All tests were repeated three times.

Western Blot Analysis

Experiments were performed following the methods in our previous study. The specific program and concentration of each antibody were also based on such study (23). Briefly, the protein was extracted with PIRA buffer and centrifuged at 12,000 g for 15 min at 4°C. Fifty microgram total proteins were separated with 10%SDS-PAGE. After electrophoresis, proteins were blotted to polyvinylidene fluoride (PVDF) membranes and then blocked with 5% skim milk powder with 0.1% Tween-20. The blots were then probed at 4°C overnight with the relevant primary antibodies respectively, and incubated in 4°C for overnight. The membranes were rinsed with TBST for 3 times, 10 min each time. Then secondary goat anti-rabbit or anti-mouse IgG-HRP antibodies were added for incubation in room temperature for 2 h. The membranes were rinsed with TBST for 3 times, and 10 min per time. Then the membranes were developed with ECL (Beijing Kangwei Biotech, China) and taken photos to analyze the relative expression of proteins with GAPDH as internal referral. All tests were repeated three times.

Immunofluorescence Staining

Cells were cultured on six-well chamber slides for immunofluorescent staining. The cells were fixed in 4% paraformaldehyde for 30 min at room temperature. After washing with PBS three times for 10 min each time, the cells were permeabilised with 0.1% Triton X-100 in PBS for 15 min. After three washes with PBS, the cells were blocked with 5%

BSA for 30 min at room temperature. The cells were incubated with the indicated GRP78 antibody (1:250) overnight at 4°C, washed three times with PBS and incubated with fluorescent secondary antibodies. Nuclear staining was performed in the dark with DAPI at room temperature. Phase contrast and fluorescent microscopy was performed using an NikonTi-U Inverted Fluorescence Microscope (Nikon, Japan).

Plasmid Transfection and Identification

GRP78 short hairpin RNA(GRP78shRNA) eukaryotic expression plasmid was designed and synthesized by Invitrogen, USA. Transfection and identification were conducted according to the protocol of Lipofectamine 3000. using previously published methods (24). Briefly, 7.5 μl Lipofectamine 3000 Reagent was diluted with 125 μl Opti-MEM media, then blended with a diluted plasmid DNA which diluted by 10 μl P3000 Reagent and 125 μl Opti-MEM media. After incubating for 5 min, the overall mixture was added into the culture cells and cultured for 72 h. The cells carrying green fluorescence are plasmids transfected successfully in inverted microscope. 20 μg/ml blasticidin was used to screen the cells and the maintenance concentration of blasticidin is 10 μg/ml. Blank shRNA was used as a control. The mRNA and protein expression levels of GRP78 decreased by 70 and 85.33%, respectively, suggesting successful transfection.

Statistical Analysis

Data were expressed as mean ± SD. Comparison between two groups was performed with *t*-test for independent samples. Comparison among multiple groups was performed with one-way ANOVA following LSD (equal variances) or Dunnett's *t*-test (unequal variances). $P<0.05$ was set as the significance level. All analyses were performed using SPSS 22.0 software.

RESULTS

Activation of EMT by Hypoxia in A549 Cells

A549 cells cultured under hypoxia condition for 72 h showed morphological changes, from oblate fusiform-shaped epithelial cells to elongated spindle-shaped mesenchymal cells (**Figure 1A**). The expression levels of EMT-related genes including Snail1, Snail2, Twist, ZEB1, and ZEB2 were increased by approximately three times under hypoxic condition compared with that in the control group. The Western blot analysis showed that the protein expression of E-cadherin (biomarker of epithelial phenotype) under hypoxia found to be approximately three times less than that in the control group. The expression levels of vimentin and fibronectin (biomarker of mesenchymal phenotype) were increased by 1.48 and 1.22 times, respectively, under hypoxia condition compared with that in the control group ($P < 0.05$ compared with Normoxia, **Figures 1B,C**).

Expression of GRP78 Under Normoxia and Hypoxia Conditions

The expression and location of the GRP78 protein in A549 cells under hypoxia and normoxia conditions were determined by immunofluorescence staining. Under normoxia condition, GRP78 (green fluorescence) showed weak staining intensity and was mainly distributed in the cytoplasm (**Figure 1A**). By contrast, under hypoxia, A549 cells showed an elongated spindle-shaped mesenchymal phenotype, and GRP78 showed strong staining intensity and was mainly distributed in the cytoplasm and cell membrane (**Figure 1A**). The Western blot analysis showed that the expression of GRP78 in A549 cells under hypoxia was found to be 1.36 times more than that under normoxia (**Figure 1B**).

Effect of GRP78 Knockdown on the Expression of EMT Markers

The expression of GRP78 in GRP78 knockdown A549 cells under hypoxia was reduced by 70% compared with that under hypoxia. In A549 cells transfected with GRP78 shRNA under hypoxia, the expression levels of vimentin and fibronectin significantly decreased by 52 and 60%, respectively. Meanwhile, the mRNA expression levels of transcription factors (Snail1, Snail2, Twist, ZEB1, and ZEB2) were significantly inhibited under hypoxia condition and decreased by approximately 70% compared with that in the normoxia group (**Figures 1B,C**). The significant change in the expression of EMT biomarkers and its transcription factor mRNAs after GRP78 knockdown indicated that GRP78 might play an important role in hypoxia-induced EMT.

Expression of Smad2/3, Src, p38, ERK and JNK in A549 Cells Under Hypoxia Condition

The expression levels of phosphorylated Smad2/3, p38, and JNK in A549 cells significantly increased by approximately 2.4 times under hypoxia condition compared with those under normoxia condition, whereas the levels of the phosphorylated Src and ERK increased by approximately 1.8 times (all $p < 0.05$, **Figure 2A**). Hence, these signaling pathways were activated under hypoxia condition.

The inhibitors of Smad2/3, Src, p38, ERK, and JNK were used to treat A549 cells under hypoxia condition to further verify the relationship between these signaling molecules with hypoxia-induced EMT. The expression levels of EMT protein markers and transcription factor mRNAs were also examined. The changes in EMT protein markers and transcription factor mRNAs in A549 cells were approximately similar to that in the group treated with Smad2/3 and Src inhibitors. The levels of vimentin, fibronectin and mRNAs decreased by approximately 50%, whereas that of E-cadherin increased by 2-fold compared with those in the cells under hypoxia. The change in the three other groups was found to be smaller than that in the group treated with Smad2/3 and Src inhibitors. The levels of vimentin, fibronectin and mRNAs were reduced by approximately 30%. Hence, EMT is inhibited in A549 cells when the activation of Smad2/3, Src, p38, ERK, and JNK proteins is inhibited under hypoxia (**Figure 2B**).

The changes in the expression of EMT protein markers were compared in A549 cells transfected by GRP78shRNA or treated by different protein inhibitors under hypoxia condition. The changes in the mRNA expression of EMT markers and signaling molecules were the most evident in GRP78 knockdown cells ($P < 0.05$ compared with the other groups, **Figures 3A,B**). Similar results were obtained on the protein expression of signaling molecules (Smad2/3, Src, p38, ERK, and JNK). After GRP78

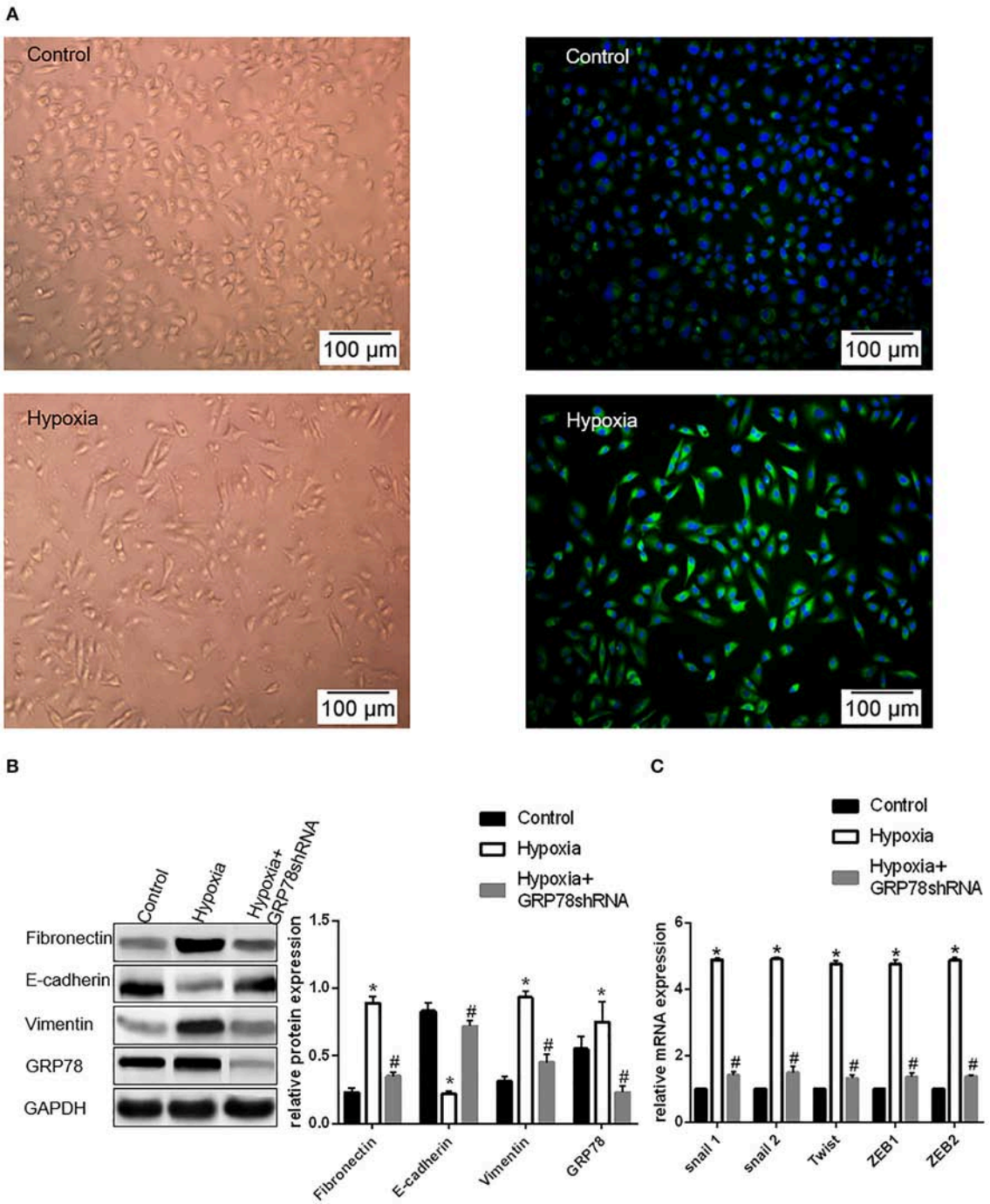

FIGURE 1 | Up-regulation of GRP78 plays an important role in hypoxia-induced EMT in A549 cells. **(A)** A549 cells acquire spindle-shaped mesenchymal morphology after 72 h of 2% O_2 hypoxia (left, 100×). GRP78 (green fluorescence) is highly expressed in A549 cells with spindle-shaped mesenchymal morphology (right, 100×). **(B)** EMT-related markers (E-cadherin, Vimentin and Fibronectin) and GRP78 were examined by Western blot analysis (left). GAPDH was used as internal control. The protein relative value (GAPDH) is plotted in the right panel (mean ± SD in three separate experiments). *$P < 0.05$, compared with A549 cells under the condition of normal oxygen, the expression of E-cadherin decreases, while those of Vimentin and Fibronectin increase in A549 cells under hypoxia (2% O_2 72 h). The expression of GRP78 also increases in A549 cells under hypoxia. #$P < 0.05$, compared with the A549 cells under the condition of hypoxia; the expression of E-cadherin increases, and those of Vimentin and Fibronectin decrease in GRP78 knockdown A549 cells under hypoxia. **(C)** EMT-related genes including Snail1, Snail2, Twist, ZEB1, and ZEB2 were examined by real-time quantitative PCR; mRNA expression relative value (control group) is plotted (mean ± SD in three separate experiments). *$P < 0.05$, compared with A549 cells in the control group, the mRNA expression levels of EMT-related genes including Snail1, Snail2, Twist, ZEB1, and ZEB2 increase under hypoxic condition (2% O_2 72 h); #$P < 0.05$, compared with A549 cells under the condition of hypoxia, the mRNA expression levels of EMT-related genes decrease in GRP78 knockdown A549 cells under hypoxia.

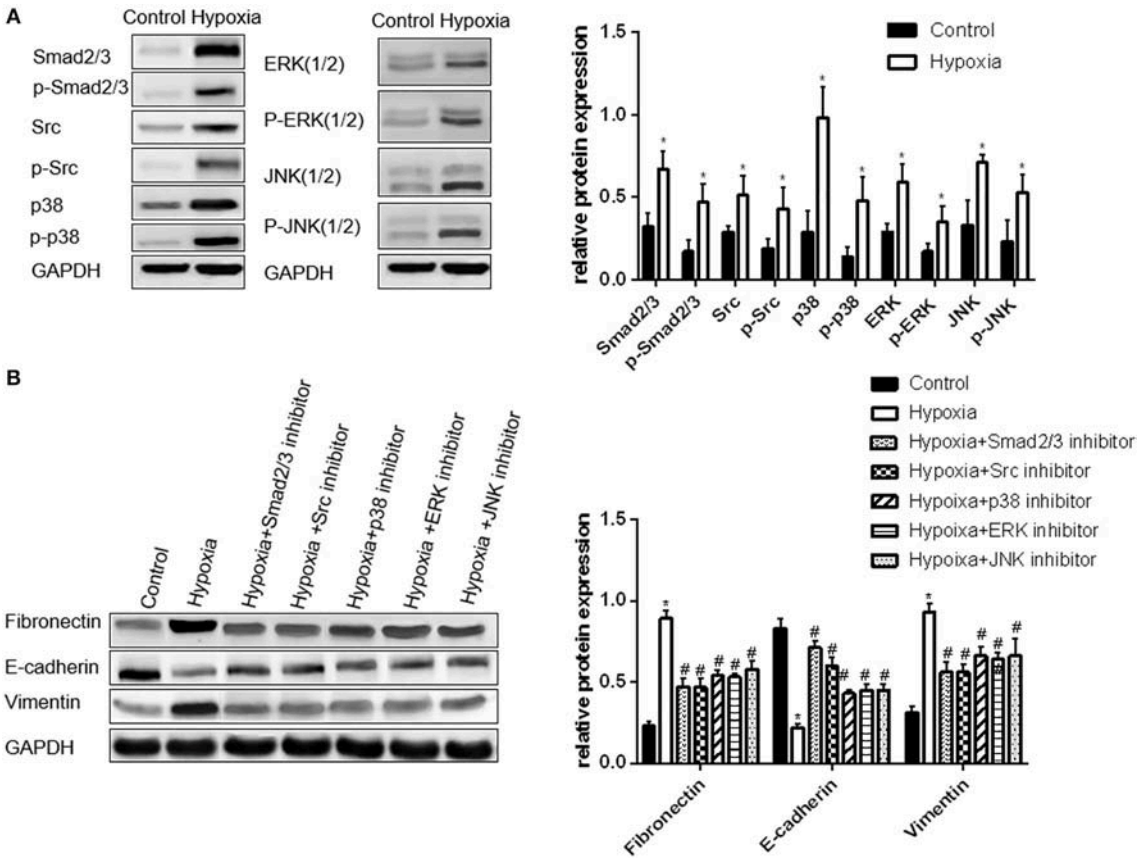

FIGURE 2 | Activation of Smad2/3, Src, p38, ERK, and JNK is important in hypoxia-induced EMT in A549 cells. **(A)** Smad2/3, Src, p38, ERK, JNK, and their phosphorylated forms were examined by Western blot analysis (left). GAPDH was used as internal control. The protein relative value (GAPDH) is plotted in the right panel (mean ± SD in three separate experiments). *$P < 0.05$, compared with A549 cells in the normal oxygen environments, the Smad2/3, Src, and MAPK proteins of A549 cells are highly regulated and activated in hypoxia environments. **(B)** EMT markers were examined by Western blot analysis (left). GAPDH was used as internal control. The protein relative value (GAPDH) is plotted in the right panel (mean ± SD in three separate experiments). *$P < 0.05$, compared with A549 cells in the normal oxygen environments, the EMT process of A549 cells under hypoxia is activated; #$P < 0.05$, compared with A549 cells in the hypoxia environments, the EMT process of A549 cells under hypoxia is inhibited separately by Smad2/3, Src, p38, ERK, and JNK inhibitors. The expression levels of Fibronectin and Vimentin decrease, and that of E-cadherin increases.

silencing, the expression of Smad2/3, Src, p38, ERK, and JNK and their phosphorylated proteins in hypoxia cells was significantly inhibited compared with that in the vehicle control under hypoxia ($P < 0.05$, **Figures 3C, 4A**).

Different effects were observed on the expression of the signaling molecules after inhibition of a particular pathway. After Smad2/3 inhibition, the expression of the four other signaling molecules did not significantly change ($P > 0.05$, **Figures 4A,B**). After inhibition of Src, JNK, ERK, and p38 pathways, the expression of Smad2/3 was not significantly changed (P>0.05, **Figures 4A,C**). After inhibiting Src, the activation of p38, ERK, and JNK (MAPK pathway) was also inhibited ($P < 0.05$, **Figures 4A,D**).

DISCUSSION

This study shows that GRP78 highly expressed under hypoxia condition is likely to play an essential role in hypoxia-induced EMT in A549 cells. This main finding is supported by the following observations: (1) the expression of GRP78 was significantly elevated under hypoxia condition and closely associated with the changes in the EMT markers; (2) GRP78 silencing significantly inhibited hypoxia-induced EMT markers; and (3) GRP78 silencing inhibited the expression of several signaling molecules, especially Smad2/3. This work is the first to demonstrate that GRP78 has a causal relationship with hypoxia-induced EMT in lung adenocarcinoma. Hence, targeted inhibition on GRP78 might could hamper EMT, which could further inhibit metastasis and overcome therapeutic resistance.

GRP78 was highly expressed in lung cancer cells under hypoxia condition; this finding is consistent with those reported by Song and Pi (25, 26). Chronic hypoxia induced GRP78 in human cancer cells possibly through the protein kinase C-epsilon/ERK/AP-1 signaling cascade (25).

A causal relationship between high GRP78 expression and EMT was confirmed by the GRP78 knock-down experiment. A very strong correlation was found between changes in the expression of GRP78 and EMT markers. Previous studies

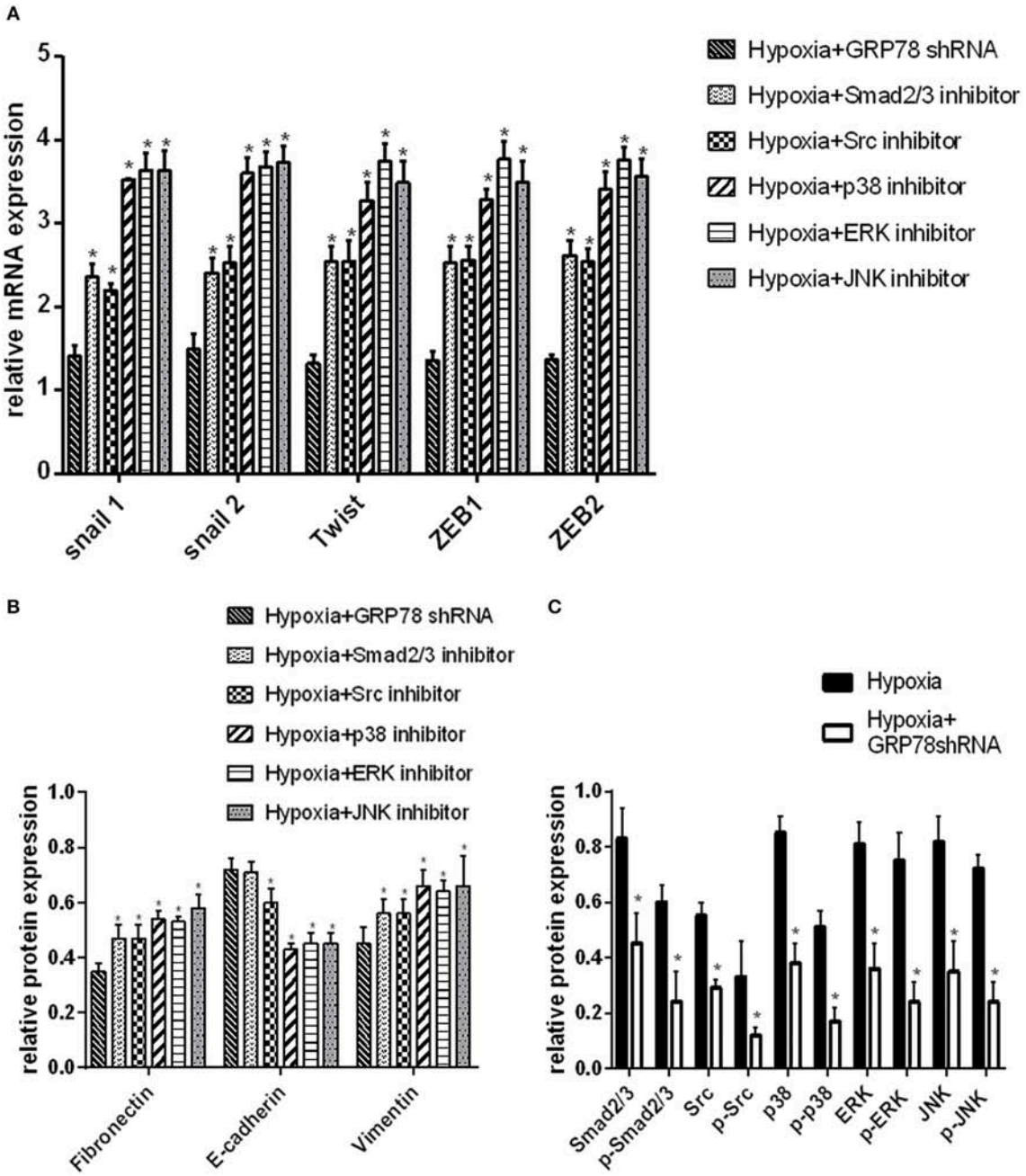

FIGURE 3 | GRP78 is the upper reaches of the Smad2/3, Src and MAPK pathways in hypoxia-induced EMT in A549 cells. **(A)** The mRNA relative value (control group) of EMT transcription factors is plotted (mean ± SD in three separate experiments). *$P < 0.05$, compared with EMT transcription factors in A549 cells under hypoxia condition separately inhibited by Smad2/3, Src, p38, ERK, and JNK inhibitors, the expression is higher than that in GRP78 knockdown A549 cells under hypoxia. **(B)** The protein relative value (GAPDH) of EMT markers was examined by Western blot analysis and plotted (mean ± SD in three separate experiments). *$P <$ 0.05, compared with EMT markers of A549 cells under hypoxia condition separately inhibited by Smad2/3, Src, p38, ERK, and JNK inhibitors, the expression is higher than that in GRP78 knockdown A549 cells in the hypoxia. **(A,B)** indicate that the inhibition effect of GRP78 silencing is more powerful than those of the five other inhibitors. **(C)** The protein relative values (GAPDH) of Smad2/3, Src, p38, ERK, JNK, and their phosphorylated forms were examined by Western blot analysis and plotted (mean ± SD in three separate experiments). *$P < 0.05$, compared with A549 cells under hypoxia, the expression levels of Smad2/3, Src, p38, ERK, JNK, and their activation forms decrease compared with those in GRP78 knockdown A549 cells under hypoxia. After GRP78 silencing, the expression and activation of these proteins are inhibited significantly.

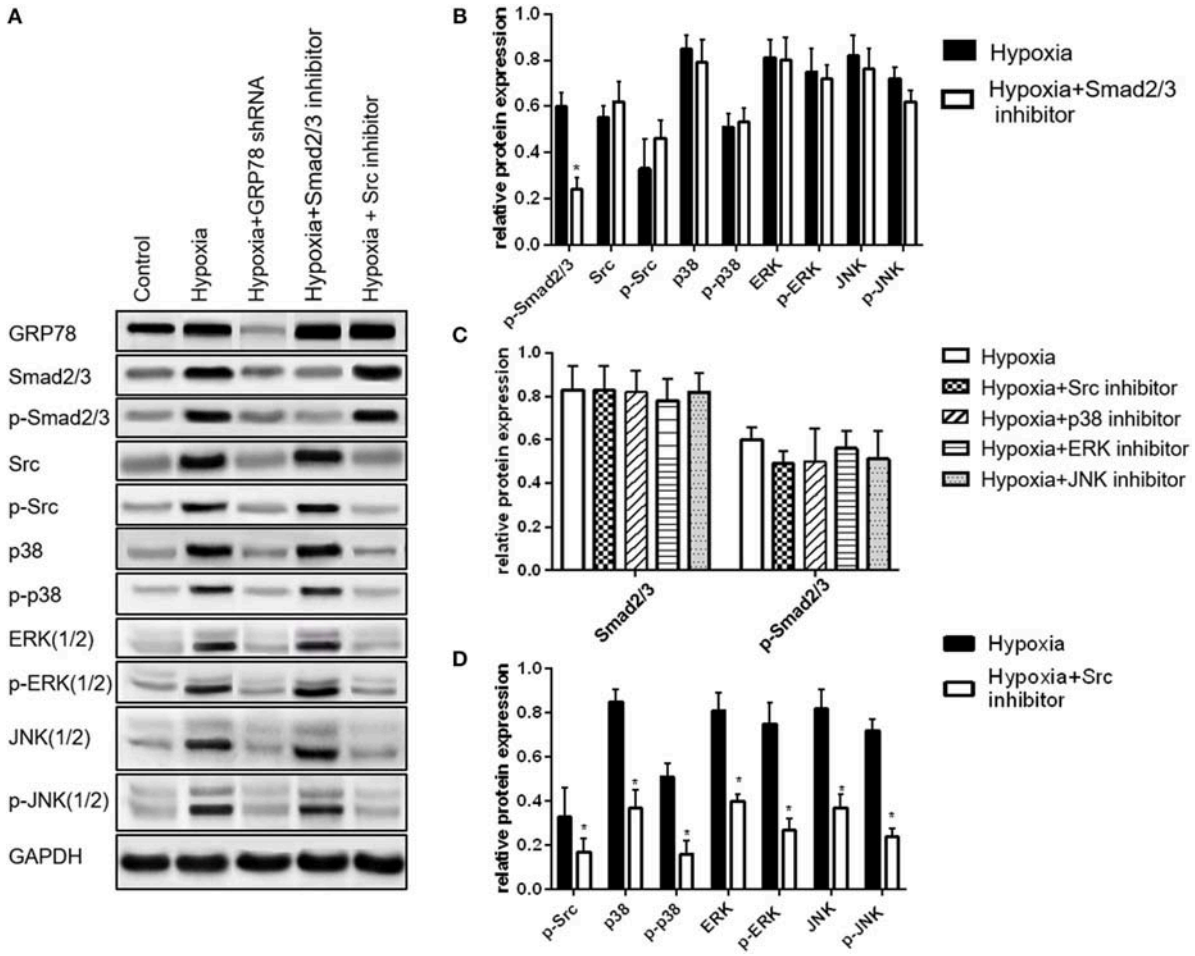

FIGURE 4 | Smad2/3 and Src/MAPK are two dependent signaling pathways in hypoxia-induced EMT in A549 cells. **(A)** Smad2/3, Src, p38, ERK, JNK, and their phosphorylated forms were examined by Western blot analysis. **(B)** Compared with the expression levels of Src, JNK, p38, ERK, and their activation forms in A549 cells under hypoxia, their expression levels do not change after inhibiting the activation of Smad2/3. **(C)** Compared with the expression levels of Smad2/3 and p-Smad2/3 in A549 cells under hypoxia, their expression does not change after inhibiting the activation of Src, JNK, ERK and p38. **(D)** $^*P < 0.05$, compared with the expression levels of p38, ERK, JNK (three forms of MAPK) and their activated forms in A549 cells under hypoxia, their expression levels decrease after inhibiting the activation of Src. MAPK is the downstream pathway of Src.

suggested that other methods for silencing GRP78 could inhibit EMT. For example, neutralization of endogenous GRP78 on the cell surface with the anti-GRP78 antibody inhibited the ability of adhesion and invasion of hepatocellular carcinoma cell lines Mahlavu and SMMC7721 (19). The mitigation of GRP78 up-regulation by using short hairpin RNA or treatment with the small molecule IT-139 inhibited metastatic growth in the lung microenvironment in four highly metastatic cell line models (three human osteosarcomas and one murine mammary adenocarcinoma) (20). However, no rational interpretation is available regarding the inconsistency on the relationship between GRP78 expression and EMT in colorectal cancer.

The mechanism of GRP78 downstream signaling for EMT promotion has been demonstrated. Cell surface GRP78 can accelerate breast cancer cell proliferation and migration by activating STAT3 (27). We found two key molecular pathways (Smad2/3 and Src/MAPK) of GRP78 that may play an important role in hypoxia-induced EMT by using multiple protein inhibitors. These findings were consistent with those of previous works. Li et al. reported that overexpressing or knocking down GRP78 induced the corresponding activation or inhibition of the Smad2/3 pathway in colon cancer cells (28). Zhao et al. reported that GRP78 interacted directly with Src, thereby promoting the phosphorylation of Src in hepatocellular cancer cells (29). Tanjore et al. also suggested that the combination of the Smad2/3 inhibitor (SB431542) and the Src kinase inhibitor (PP2) blocked the EMT of alveolar epithelial cells induced by ER stress inducer tunicamycin, which also induced high GRP78 expression (30). In the present study, the activation of the Smad2/3 and Src/MAPK pathways follows the same trend with the up-regulation of GRP78; moreover, knockdown of GRP78 inhibited the activation of Smad2/3 and Src, suggesting a causal link between GRP78

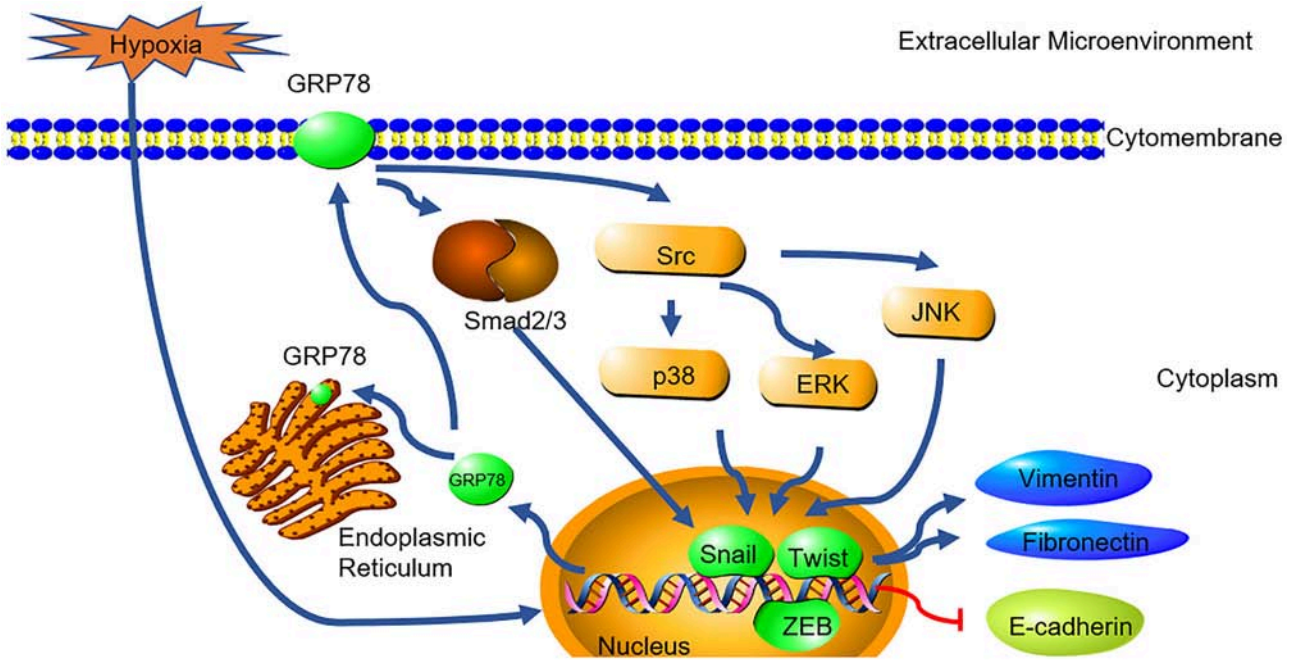

FIGURE 5 | GRP78 mediates hypoxia-induced EMT through smad2/3 and SRC/MAPK signaling. Hypoxia induced the high expression of GRP78. High expressed GRP78 activated the smad2/3 and Src/MAPK pathway. The pathway activated the expression of EMT transcription factor (snail, Twist and ZEB) and collaborated with them to induce the expression of Fibronectin, Vimentin and inhibit the expression of E-cadherin.

and activation of the two pathways in lung cancer. Smad2/3 inhibition did not interact with the inhibition of Src, p38, ERK, and JNK. By contrast, inhibiting the activation of Src was accompanied by the inhibition of p38, ERK, and JNK. Hence, the Smad2/3 and Src/MAPK pathways are two independent downstream signaling pathways of GRP78 during hypoxia-induced EMT in A549 cells. However, we did not perform the knockdown experiment of Smad2/3 and Src, and the co-immunoprecipitation experiment; as such, we cannot provide additional evidence for such link. And the control shRNA was not applied in the present study, which might limiting its evidence.

Other pitfall of the present study is that we have not explored the relationship between GRP78 and HIF1a, which is a key regulator on hypoxia induced EMT. But there are some evidences in other cell lines, that the expression of GRP78 is regulated by HIF1a (31). What's more, all the results in the study are limited to one cell line, limiting its evidence.

In summary, this study demonstrated the possible causal link between GRP78 and hypoxia-induced EMT in A549 cells (**Figure 5**). Together with its roles in anti-apoptosis and chemoresistance, it indicates that GRP78 might be a potential target for treatment of lung adenocarcinoma. Further, studies are needed to elucidate the exact mechanisms involved in the GRP78-EMT pathway in hypoxia and their relevant clinical significance.

DATA AVAILABILITY

All datasets generated for this study are included in the manuscript and/ or the supplementary files.

AUTHOR CONTRIBUTIONS

L-ZL and L-LS: designed the experiments. L-LS, C-MC, and JW: performed the experiments. JZ and C-ZY: analyzed the data. L-LS and C-ZY: prepared the figures. L-LS and JZ: wrote the main manuscript. All authors reviewed the manuscript.

FUNDING

This study was supported by grant from the National Natural Science Foundation of China (NSFC) (Nos. 81403227 to L-LS and 81573870 to L-ZL).

ACKNOWLEDGMENTS

We would like to thank the colleagues from First Affiliated Hospital of Guangzhou University of Chinese Medicine, China. We would also like to thank the support from Prof. Chunguang Li, Prof. Xiaoshu Zhu, Prof. Alan Bensussan from the Western Sydney University, Australia and Prof. Kevin Chang from New South Wales Association of Chinese Medicine, Australia.

REFERENCES

1. Ferlay J, Soerjomataram I, Dikshit R, Eser S, Mathers C, Rebelo M, et al. Cancer incidence and mortality worldwide: sources, methods and major patterns in GLOBOCAN 2012. *Int J Cancer*. (2015) 136:E359–86. doi: 10.1002/ijc.29210
2. Zhao Y, Adjei AA. New strategies to develop new medications for lung cancer and metastasis. *Cancer Metastasis Rev*. (2015) 34:265–75. doi: 10.1007/s10555-015-9553-5
3. Skovierova H, Okajcekova T, Strnadel J, Vidomanova E, Halasova E. Molecular regulation of epithelial-to-mesenchymal transition in tumorigenesis (Review). *Int J Mol Med*. (2018) 41:1187–200. doi: 10.3892/ijmm.2017.3320
4. Xu J, Lamouille S, Derynck R. TGF-beta-induced epithelial to mesenchymal transition. *Cell Res*. (2009) 19:156–72. doi: 10.1038/cr.2009.5
5. Patel A, Sabbineni H, Clarke A, Somanath PR. Novel roles of Src in cancer cell epithelial-to-mesenchymal transition, vascular permeability, microinvasion and metastasis. *Life Sci*. (2016) 157:52–61. doi: 10.1016/j.lfs.2016.05.036
6. Zhao L, Li X, Song N, Li A, Hou K, Qu X, et al. Src promotes EGF-induced epithelial-to-mesenchymal transition and migration in gastric cancer cells by upregulating ZEB1 and ZEB2 through AKT. *Cell Biol Int*. (2018) 42:294–302. doi: 10.1002/cbin.10894
7. Ruan J, Zhang L, Yan L, Liu Y, Yue Z, Chen L, et al. Inhibition of hypoxia-induced epithelial mesenchymal transition by luteolin in non-small cell lung cancer cells. *Mol Med Rep*. (2012) 6:232–8. doi: 10.3892/mmr.2012.884
8. Shaikh D, Zhou Q, Chen T, Ibe JC, Raj JU, Zhou G. cAMP-dependent protein kinase is essential for hypoxia-mediated epithelial-mesenchymal transition, migration, and invasion in lung cancer cells. *Cell Signal*. (2012) 24:2396–406. doi: 10.1016/j.cellsig.2012.08.007
9. Nurwidya F, Takahashi F, Kobayashi I, Murakami A, Kato M, Minakata K, et al. Treatment with insulin-like growth factor 1 receptor inhibitor reverses hypoxia-induced epithelial-mesenchymal transition in non-small cell lung cancer. *Biochem Biophys Res Commun*. (2014) 455:332–8. doi: 10.1016/j.bbrc.2014.11.014
10. Barriga EH, Maxwell PH, Reyes AE, Mayor R. The hypoxia factor Hif-1alpha controls neural crest chemotaxis and epithelial to mesenchymal transition. *J Cell Biol*. (2013) 201:759–76. doi: 10.1083/jcb.201212100
11. Shen X, Xue Y, Si Y, Wang Q, Wang Z, Yuan J, et al. The unfolded protein response potentiates epithelial-to-mesenchymal transition (EMT) of gastric cancer cells under severe hypoxic conditions. *Med Oncol*. (2015) 32:447. doi: 10.1007/s12032-014-0447-0
12. Su R, Li Z, Li H, Song H, Bao C, Wei J, et al. Grp78 promotes the invasion of hepatocellular carcinoma. *BMC Cancer*. (2010) 10:20. doi: 10.1186/1471-2407-10-20
13. Sun Q, Hua J, Wang Q, Xu W, Zhang J, Zhang J, et al. Expressions of GRP78 and Bax associate with differentiation, metastasis, and apoptosis in non-small cell lung cancer. *Mol Biol Rep*. (2012) 39:6753–61. doi: 10.1007/s11033-012-1500-8
14. Chang YW, Chen HA, Tseng CF, Hong CC, Ma JT, Hung MC, et al. De-acetylation and degradation of HSPA5 is critical for E1A metastasis suppression in breast cancer cells. *Oncotarget*. (2014) 5:10558–70. doi: 10.18632/oncotarget.2510
15. Chen HA, Chang YW, Tseng CF, Chiu CF, Hong CC, Wang W, et al. E1A-mediated inhibition of HSPA5 suppresses cell migration and invasion in triple-negative breast cancer. *Ann Surg Oncol*. (2015) 22:889–98. doi: 10.1245/s10434-014-4061-3
16. Roller C, Maddalo D. The molecular chaperone GRP78/BiP in the development of chemoresistance: mechanism and possible treatment. *Front Pharmacol*. (2013) 4:10. doi: 10.3389/fphar.2013.00010
17. Xie J, Tao ZH, Zhao J, Li T, Wu ZH, Zhang JF, et al. Glucose regulated protein 78 (GRP78) inhibits apoptosis and attentinutes chemosensitivity of gemcitabine in breast cancer cell via AKT/mitochondrial apoptotic pathway. *Biochem Biophys Res Commun*. (2016) 474:612–9. doi: 10.1016/j.bbrc.2016.03.002
18. Gifford JB, Hill R. GRP78 Influences Chemoresistance and Prognosis in Cancer. *Curr Drug Targets*. (2018) 19:701–8. doi: 10.2174/1389450118666170615100918
19. Zhang XX, Li HD, Zhao S, Zhao L, Song HJ, Wang G, et al. The cell surface GRP78 facilitates the invasion of hepatocellular carcinoma cells. *Biomed Res Int*. (2013) 2013:917296. doi: 10.1155/2013/917296
20. Lizardo MM, Morrow JJ, Miller TE, Hong ES, Ren L, Mendoza A, et al. Upregulation of glucose-regulated protein 78 in metastatic cancer cells is necessary for lung metastasis progression. *Neoplasia*. (2016) 18:699–710. doi: 10.1016/j.neo.2016.09.001
21. Zhang L, Li Z, Fan Y, Li H, Li Z, Li Y. Overexpressed GRP78 affects EMT and cell-matrix adhesion via autocrine TGF-beta/Smad2/3 signaling. *Int J Biochem Cell Biol*. (2015) 64:202–11. doi: 10.1016/j.biocel.2015.04.012
22. Chang YJ, Chen WY, Huang CY, Liu HH, Wei PL. Glucose-regulated protein 78 (GRP78) regulates colon cancer metastasis through EMT biomarkers and the NRF-2/HO-1 pathway. *Tumour Biol*. (2015) 36:1859–69. doi: 10.1007/s13277-014-2788-x
23. Chen CM, Sun LL, Fang RM, Lin LZ. YiQi ChuTan recipe inhibits epithelial mesenchymal transition of A549 cells under hypoxia. *Cell Mol Biol (Noisy-le-grand)*. (2016) 62:10–5. doi: 10.14715/cmb/2016.62.1.3
24. Chen C, Sun L, Lin L. Construction of eukaryotic expression vector for glucose regulated protein 78-shRNA and establishment of stably transfected A549 cell line. *Chi J Biologic*. (2016) 29:348–53. doi: 10.13200/j.cnki.cjb.001289
25. Song MS, Park YK, Lee JH, Park K. Induction of glucose-regulated protein 78 by chronic hypoxia in human gastric tumor cells through a protein kinase C-epsilon/ERK/AP-1 signaling cascade. *Cancer Res*.(2001) 61:8322–30. Available online at: http://cancerres.aacrjournals.org/content/61/22/8322
26. Pi L, Li X, Song Q, Shen Y, Lu X, Di B. Knockdown of glucose-regulated protein 78 abrogates chemoresistance of hypopharyngeal carcinoma cells to cisplatin induced by unfolded protein in response to severe hypoxia. *Oncol Lett*. (2014) 7:685–92. doi: 10.3892/ol.2013.1753
27. Yao X, Liu H, Zhang X, Zhang L, Li X, Wang C, et al. Cell surface GRP78 accelerated breast cancer cell proliferation and migration by activating STAT3. *PLoS ONE*. (2015) 10:e0125634. doi: 10.1371/journal.pone.0125634
28. Li Z, Zhang L, Zhao Y, Li H, Xiao H, Fu R, et al. Cell-surface GRP78 facilitates colorectal cancer cell migration and invasion. *Int J Biochem Cell Biol*. (2013) 45:987–94. doi: 10.1016/j.biocel.2013.02.002
29. Zhao S, Li H, Wang Q, Su C, Wang G, Song H, et al. The role of c-Src in the invasion and metastasis of hepatocellular carcinoma cells induced by association of cell surface GRP78 with activated alpha2M. *BMC Cancer*. (2015) 15:389. doi: 10.1186/s12885-015-1401-z
30. Tanjore H, Cheng DS, Degryse AL, Zoz DF, Abdolrasulnia R, Lawson WE, et al. Alveolar epithelial cells undergo epithelial-to-mesenchymal transition in response to endoplasmic reticulum stress. *J Biol Chem*. (2015) 290:3277. doi: 10.1074/jbc.A110.181164
31. Lee JH, Yoon YM, Lee SH. Hypoxic preconditioning promotes the bioactivities of mesenchymal stem cells via the HIF-1alpha-GRP78-Akt Axis. *Int J Mol Sci*. (2017) 18:E1320. doi: 10.3390/ijms18061320

Conflict of Interest Statement: The authors declare that the research was conducted in the absence of any commercial or financial relationships that could be construed as a potential conflict of interest.

frontiers in Oncology

ORIGINAL RESEARCH
published: 27 February 2019
doi: 10.3389/fonc.2019.00080

Targeting uPAR by CRISPR/Cas9 System Attenuates Cancer Malignancy and Multidrug Resistance

*Kun Wang†, Zi-Hao Xing†, Qi-Wei Jiang, Yang Yang, Jia-Rong Huang, Meng-Ling Yuan, Meng-Ning Wei, Yao Li, Sheng-Te Wang, Kun Liu and Zhi Shi**

Guangdong Provincial Key Laboratory of Bioengineering Medicine, Department of Cell Biology and Institute of Biomedicine, College of Life Science and Technology, Jinan University, National Engineering Research Center of Genetic Medicine, Guangzhou, China

Urokinase plasminogen activator receptor (uPAR), a member of the lymphocyte antigen 6 protein superfamily, is overexpressed in different types of cancers and plays an important role in tumorigenesis and development. In this study, we successfully targeted uPAR by CRISPR/Cas9 system in two human cancer cell lines with two individual sgRNAs. Knockout of uPAR inhibited cell proliferation, migration and invasion. Furthermore, knockout of uPAR decreases resistance to 5-FU, cisplatin, docetaxel, and doxorubicin in these cells. Although there are several limitations in the application of CRISPR/Cas9 system for cancer patients, our study offers valuable evidences for the role of uPAR in cancer malignancy and drug resistance.

Keywords: cancer, uPAR, CRISPR/Cas9, malignancy, drug resistance

OPEN ACCESS

Edited by:
Yan-yan Yan,
Shanxi Datong University, China

Reviewed by:
Zui Pan,
University of Texas at Arlington, United States
Hui Yang,
Second Affiliated Hospital of Guangzhou Medical University, China

***Correspondence:**
Zhi Shi
tshizhi@jnu.edu.cn

†These authors have contributed equally to this work

Specialty section:
This article was submitted to Cancer Molecular Targets and Therapeutics, a section of the journal Frontiers in Oncology

Received: *25 December 2018*
Accepted: *29 January 2019*
Published: *27 February 2019*

Citation:
Wang K, Xing Z-H, Jiang Q-W, Yang Y, Huang J-R, Yuan M-L, Wei M-N, Li Y, Wang S-T, Liu K and Shi Z (2019) Targeting uPAR by CRISPR/Cas9 System Attenuates Cancer Malignancy and Multidrug Resistance. Front. Oncol. 9:80. doi: 10.3389/fonc.2019.00080

INTRODUCTION

Urokinase plasminogen activator (uPA) receptor (uPAR), also known as CD87 and encoded by PLAUR gene, is a member of the lymphocyte antigen 6 protein superfamily (1). uPAR is a glycoprotein consisting of 313 amino acid residues with only the extracellular domain, no transmembrane and intracellular structures, and is attached to the cell membrane via glycosylphosphatidylinositol anchors (1). uPAR binds to and activates uPA to cleaving plasminogen to plasmin, thus triggering the remodeling of extracellular matrix and playing a key role in cell adhesion, migration, proliferation, and survival (2). Besides uPA, uPAR can interact with other proteins, including vitronectin, integrins, and EGFR, etc to regulate multiple signal pathways (2). Compared to normal tissues, uPAR is highly expressed in many human cancers including lung, breast, gastric, colorectal, pancreatic, bladder, and prostate cancers, etc (3). The expression of uPAR in these cancers promotes the proliferation, metastasis, and invasion of cancer cells (3). Therefore, uPAR may be an important biomarker and target for cancers. Indeed, many inhibitors of uPAR have been developed. The inhibitors blocks the interaction of uPAR with uPA, including: small molecules UK1 (4), WX-UK1 (5), WX-671 (6), etc; peptides Mupain-1 (7), AE105 (8), ATF (9), etc; and monoclonal antibody ATN-291 (10). In addition, there are inhibitors that inhibit the interaction of uPAR with integrins, including: peptides P25 (11), a325 (12), H245A (13), etc; and monoclonal antibody ATN-658 (14). However, the poor affinity and bioavailability limit the application of these inhibitors in clinic. Consequently, it is necessary to develop new approaches to target uPAR for treatment cancer and other diseases.

The RNA-guided clustered regularly interspaced short palindromic (CRISPR) in combination with a CRISPR-associated nuclease 9 (Cas9) nuclease system is a novel gene editing technology by delivering the Cas9 complexed with a synthetic guide RNA (gRNA) into a cell to cut the desired genome location, allowing existing genes to be removed and/or new ones added (15). Due to the advantages of faster, cheaper, more accurate, and efficient, CRISPR/Cas9 system has been widely used as a basic biology research tool, development of biotechnology products and potentially to treat diseases (16). In this study, we used CRISPR/Cas9 system targeting uPAR to verify the role of uPAR in cancers.

MATERIALS AND METHODS

Cells and Reagents

The two multidrug resistant cancer cell lines HCT8/T and KB_{V200} were cultured in Dulbecco's modified Eagle's medium (DMEM) with 10% FBS, penicillin (100 U/ml) and streptomycin (100 ng/ml) at 37°C in a humidified atmosphere of 5% CO_2. Restriction endonuclease BsmBI was from New England Biolabs. Polyetherimide (PEI) was from Ploysciences. Cisplatin was from Shandong Qilu Pharmaceutical. 5-FU, docetaxel, and doxorubicin were from LC Laboratories. Puromycin was from Selleck Chemicals. Methylthiazolyldiphenyl-tetrazolium bromide (MTT) was from ApexBio Technology. Anti-uPAR (D121140) antibody was from Shanghai sangon biotech. Anti-Vinculin antibody (BM1611) was from Wuhan Boster Biotech.

Vector Generation, Lentivirus Production, and Transduction

LentiCRISPRv2 vector (from Addgene #52961) was digested with BsmBI and ligated with annealed oligonucleotides (uPAR-sg1-F: 5′-CACCGGACCAACGGGGATTGCCGTG-3′, uPAR-sg1-R: 5′-AA-ACCACGGCAATCCCCGTTGGTCC-3′; uPAR-sg2-F: 5′-CACCGGGACCACGATCGTGCGCTTG-3′, uPAR-sg2-R: 5′-AAACCAAGCGCACGATCGTGGTCCC-3′). HEK293T were transfected using PEI at 70% confluency with recombinant vectors and packaging vectors pMD2G and psPAX2. Viral supernatant was harvested 96 h after transfection and stored at −80°C. HCT-8/T and KB_{V200} cells were transducted with viral supernatant containing 10 μg/ml polybrene, and were selected with 100 and 10 μg/ml puromycin respectively to establish the stable cell lines.

Genomic PCR and Sequencing Analysis

The genomic DNA of cells was extracted with the QuickExtract DNA extraction kit following the manufacturer's protocol and amplified with a pair of primers (Detection 1-F: 5′-GACAACGGACAGACTGGAA-3′, Detection 1-R: 5′-CCGAATCGCTCTAAGTGG-3′) designed for the target region of interest using a Pfu DNA polymerase. Followed by agarose gel electrophoresis and ethidium bromide staining, the purified PCR products were sequencing with an ABI 3131xl Genetic analyzer.

Western Blot Analysis

Cells were harvested and lysed in RIPA buffer (1% NP-40, 0.5% sodium deoxycholate, 0.1%SDS, 10 ng/ml PMSF, 0.03% aprotinin, 1 μM sodium orthovanadate) at 4°C for 30 min. Lysates were centrifuged for 10 min at 14,000×g and supernants were stored at −80°C as whole cell extracts. Protein concentration was quantified using with Bradford assay. Proteins were separated on 10% SDS-PAGE gels and transferred to polyvinylidene difluoride membranes. Membranes were blocked with 5% BSA and incubated with the indicated primary antibodies. Corresponding horseradish peroxidase-conjugated secondary antibodies were used against each primary antibody. Proteins were detected using the chemiluminescent detection reagents and films.

Cell Morphology Assay

Cells were seeded on glass cover slips for 24 h and then fixed in 4% paraformaldehyde for 20 min and permeabilized with 0.1% Triton X-100 for 15 min at room temperature. The coverslips were incubated in the dark with 100 nM rhodamine-phalloidin at room temperature for 30 min. Nuclei were counterstained with 100 nM DAPI. The coverslips were rinsed in PBS and inverted on a drop of anti-fade mounting media on a glass slide. Then, these slides were sealed with neutral balsam and viewed under the confocal microscope.

Cell Viability Assay

Cells were seeded into a 96-well plate at a density of 5,000 cells/well and treated with various concentrations of agents for 72 h. Then 10 μl MTT was added to each well at a final concentration of 0.5 mg/ml. After incubation for 4 h, formazan crystals were dissolved in 50 μl of DMSO, and absorbance at 570 nm was measured by plate reader. The concentrations required to inhibit growth by 50% (IC_{50}) were calculated from survival curves as previously described (17).

Sphere Formation Assay

Cells were trypsinized, suspended in medium containing 0.3% agar and 10% FBS and seeded at a density of 5×10^2 cells/well in a 12-well plate. The agar–cell mixture was plated onto a bottom layer with 0.5% agar. Then treated cells were incubated in a humidified incubator and fresh medium was added every 3 days. Two weeks later, colonies were analyzed microscopically.

Cell Migration Assay

Cells were seeded into a 6-well plate, and reached 80–90% confluence, the cell monolayer was wounded using a sterilized 10 μl pipette tip and washed with PBS two times. Cells were allowed to migrate for 12, 24, and 36 h in serum-free medium, and the wounds were observed and captured. The gap lengths were measured from the photomicrographs.

Cell Invasion Assay

Cell invasion assays were performed with a modified Boyden chamber (Corning) containing matrigel-coated polycarbonate membrane filter (6.5 mm diameter, 8 μm pore size). Cells were plated in the upper chamber and the lower chamber contained medium with 10% FBS, and incubated for 24 h

at 37°C in 5% CO_2. Non-migrated cells were scraped from the upper surface of the membrane, and migrated cells remaining on the bottom surface were photographed and counted.

Statistical Analysis

The experimental data of this paper are the results of three independent repetitions. The data obtained is presented in the form of an average and a standard deviation. Statistical analysis

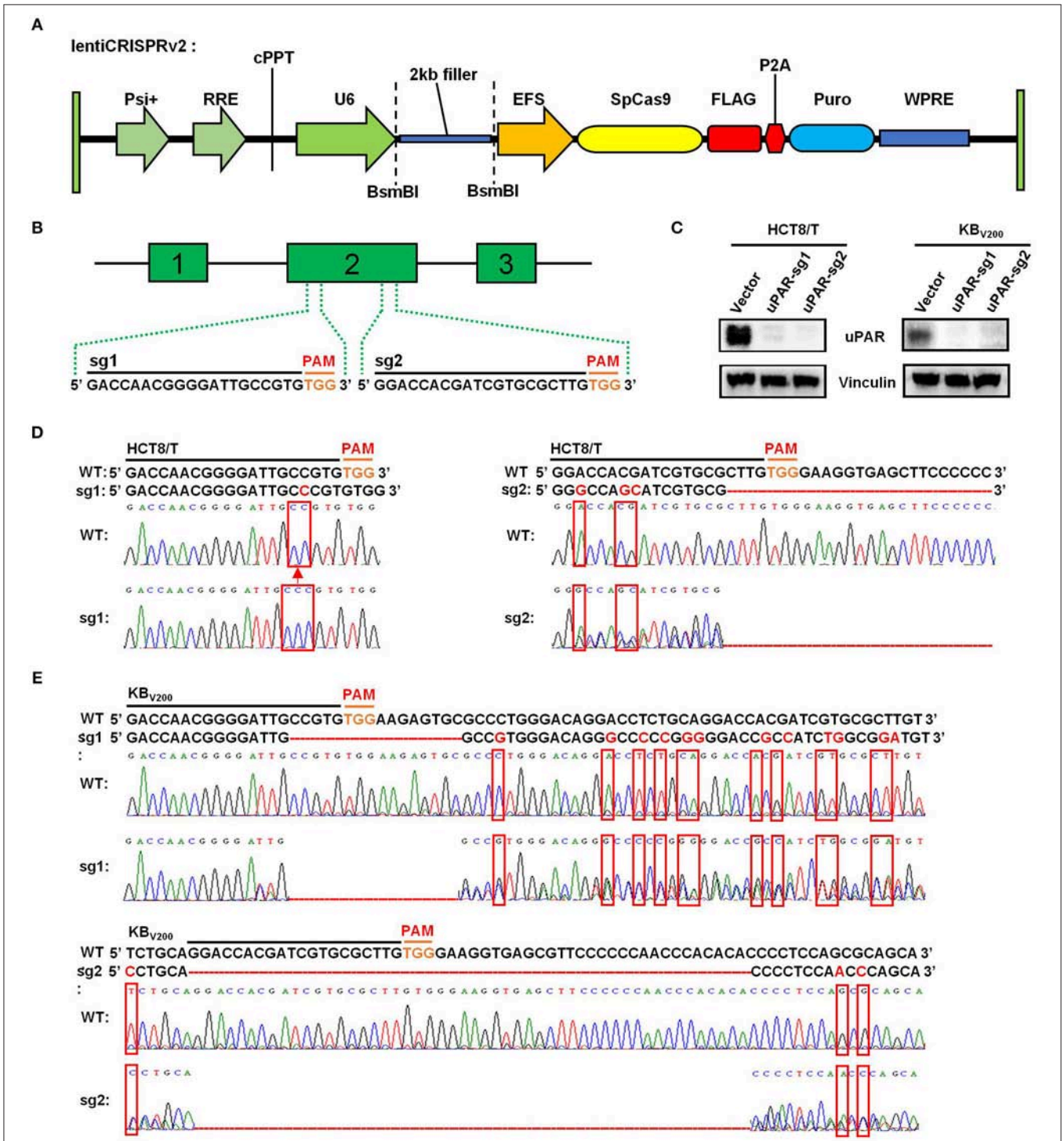

FIGURE 1 | Knockout of uPAR by CRISPR/Cas9 system. **(A)** The map of lentiCRISPRv2 vector. **(B)** The locations and sequences of two sgRNAs of uPAR. **(C)** The protein expression levels of uPAR were examined by Western blot, and vinculin was used as loading control. The genomic DNA of cells was amplified and sequenced by the designed primers. The sequencing comparison and original data of HCT8/T **(D)** and KB_{V200} **(E)** cells are shown.

of data differences using *t*-test method. A *P*-value of <0.05 was set as the criterion for statistical significance.

RESULTS

Knockout of uPAR by CRISPR/Cas9 System

To target uPAR with CRISPR/Cas9 system, we firstly used lentiCRISPRv2 vector which expresses both hSpCas9 and the chimeric guide RNA (**Figure 1A**) linked respectively, with two targeting sequences from exon 2 of human uPAR gene (PLAUR) end with a 5′NGG3′ PAM (protospacer adjacent motif) sequence (**Figure 1B**). Then, the two successfully generated vectors expressed sgRNA1 (sg1) or sgRNA2 (sg2) to target uPAR were identified by sequencing. To establish cell lines stably expressed sgRNA to target uPAR, HCT8/T, and KB_{V200} cells were selected with puromycin after transduction with LentiCRISPRv2 viral supernatant. As shown in **Figure 1C**, the protein levels of uPAR were undetectable by western blot in both HCT8/T and KB_{V200} cells stably expressed either sg1 or sg2. To further identify the genomic change of targeting uPAR by CRISPR/Cas9 system, the genomic DNA of cells was extracted and amplified using the designed primers by PCR reaction. The sequencing results of PCR productions showed that 1 base was inserted into the target position of HCT8/T uPAR-sg1 cells and 3 base mismatches and a large deletion in the target position of HCT8/T uPAR-sg2 cells (**Figure 1D**). There were 16 base deletions and 12 base mismatches in the target position of KB_{V200} uPAR-sg1 cells and 51 base deletions and 3 base mismatches in the target position of KB_{V200} uPAR-sg2 cells (**Figure 1E**). These data suggest that cells with stable knockout of uPAR by CRISPR/Cas9 system were successfully established.

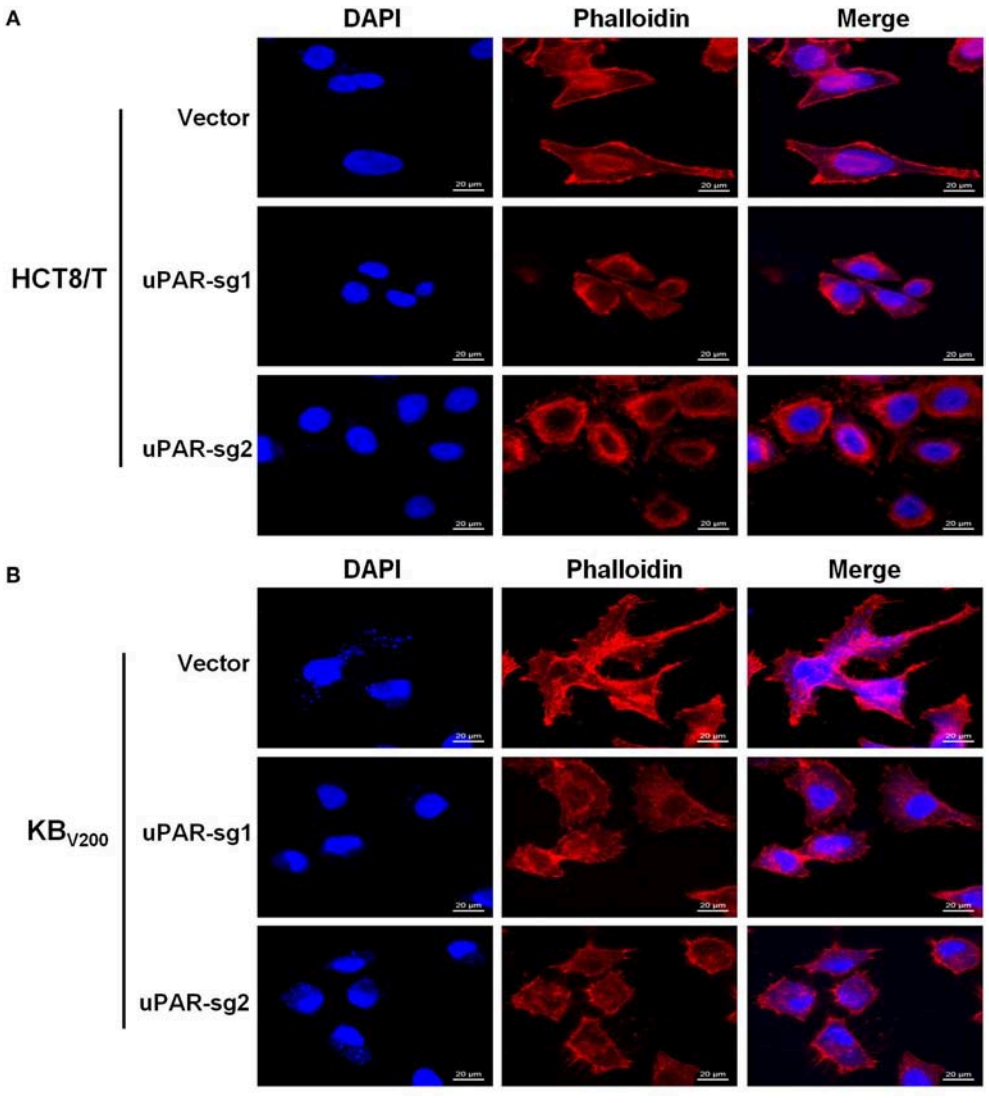

FIGURE 2 | Knockout of uPAR alters cell morphology. The morphology of HCT8/T **(A)** and KB_{V200} **(B)** cells was obtained with confocal microscope.

Knockout of uPAR Alters Cell Morphology

To explore the effect of knockout of uPAR on cell morphology, we stained cells with Rhodamine-labeled phalloidin and DAPI. The results showed that HCT8/T and KB_{V200} cells with uPAR knockout underwent morphologic changes from spindle-shaped phenotype to round phenotype (**Figures 2A,B**), indicating that knockout of uPAR alters cell morphology.

Knockout of uPAR Attenuates Cell Proliferation

To investigate the effect of knockout of uPAR on cell proliferation, we detected cell proliferation by MTT and sphere formation assays. As shown in **Figure 3A**, knockout of uPAR inhibited the growth of HCT8/T and KB_{V200} cells. Further sphere formation assay showed that knockout of uPAR reduced the sphere number and size of HCT8/T and KB_{V200} cells (**Figures 3B–E**). These results suggest that knockout of uPAR attenuates cell proliferation.

Knockout of uPAR Inhibits Cell Migration

To examine the effect of knockout of uPAR by CRISPR/Cas9 on cell migration, wound healing assay was used to detect cell migration. The results showed that cell migration was reduced in HCT8/T and KB_{V200} cells with uPAR knockout (**Figure 4**), indicating that knockout of uPAR inhibits cell migration.

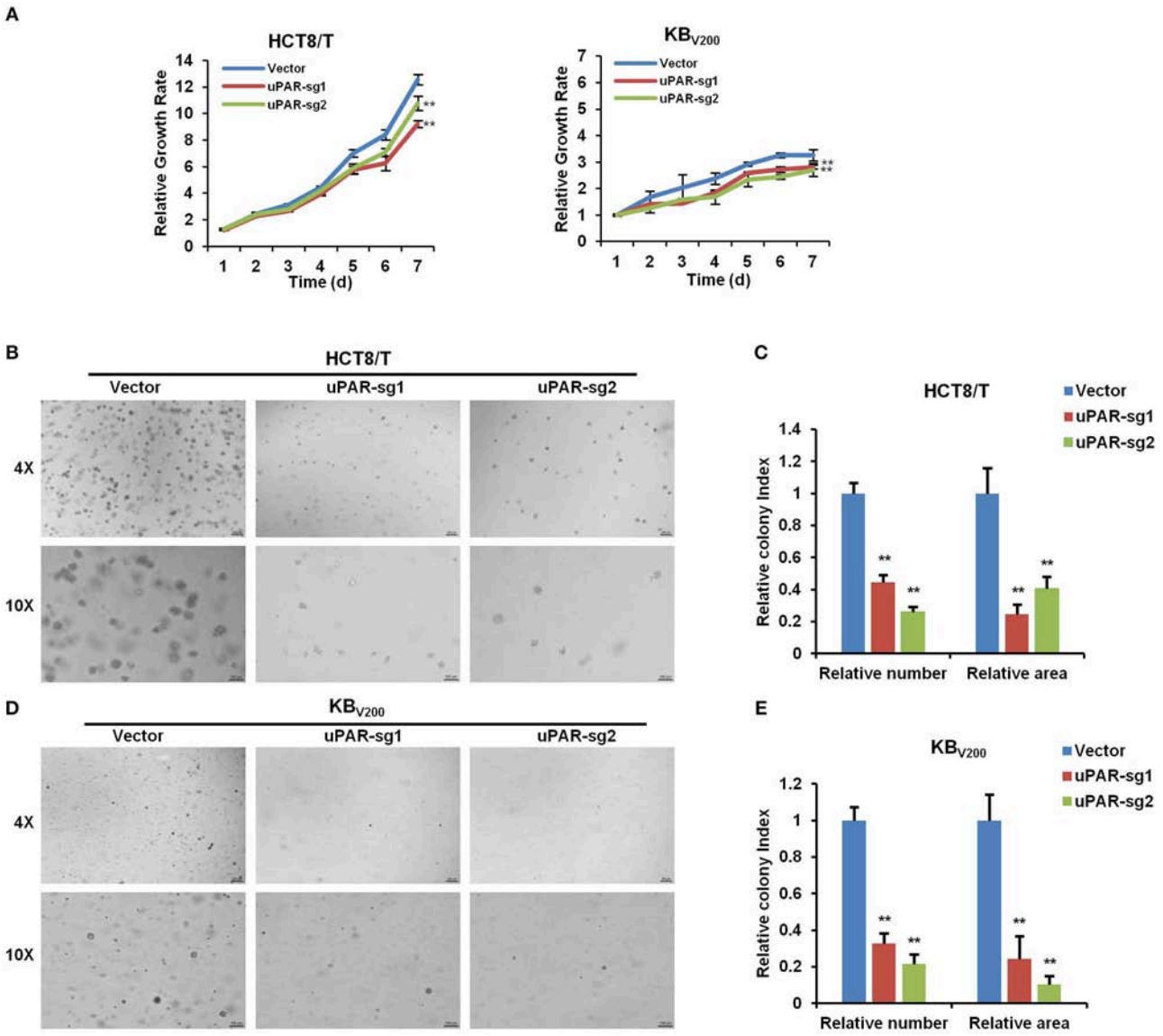

FIGURE 3 | Knockout of uPAR attenuates cell proliferation. **(A)** Cell proliferation was evaluated by MTT assay. Representative spheres images and quantification of HCT8/T **(B,C)** and KB_{V200} **(D,E)** cells were determined by sphere formation assay. $^{**}P < 0.01$ vs. corresponding control.

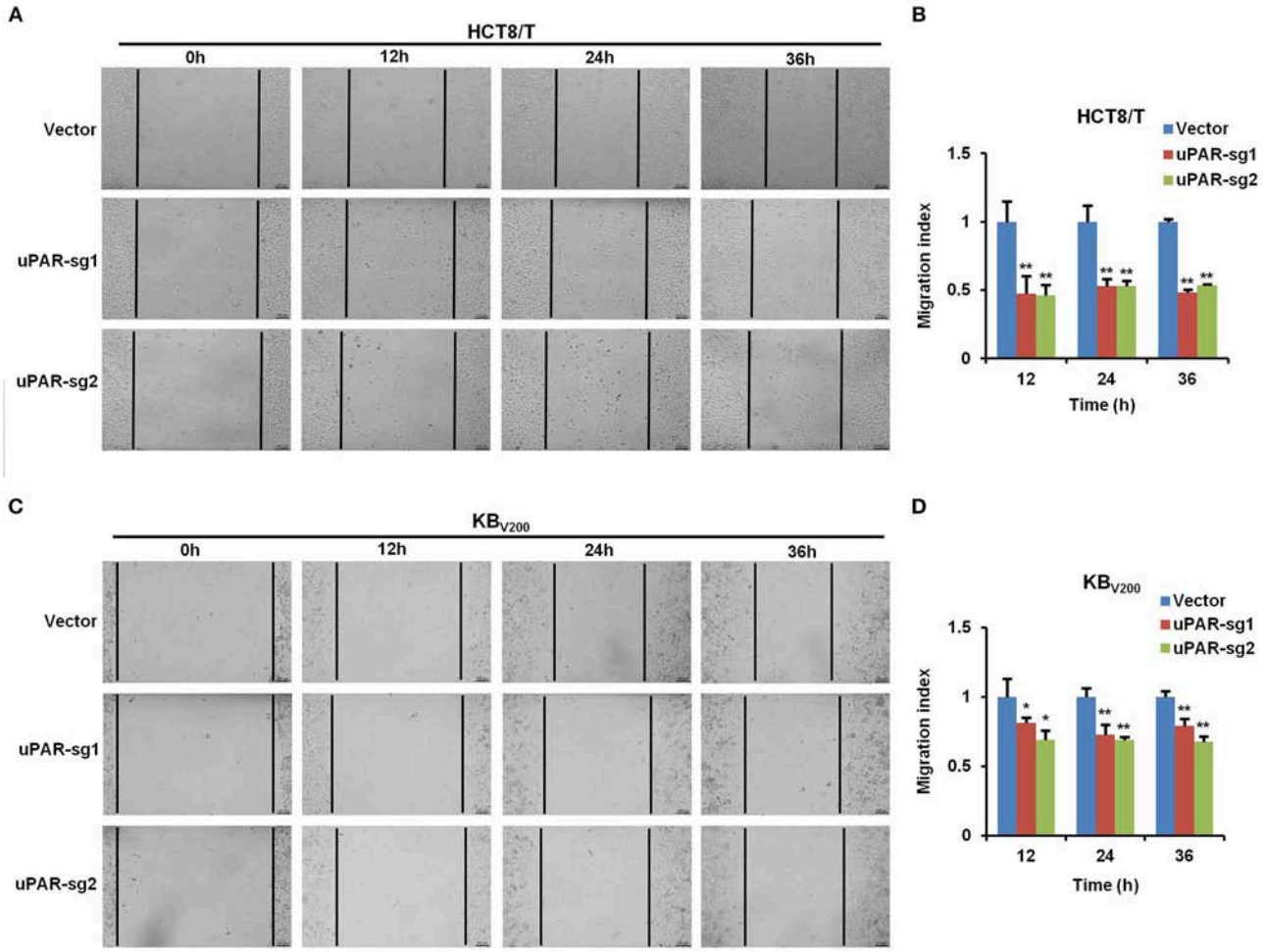

FIGURE 4 | Knockout of uPAR inhibits cell migration. Cell migration was determined with wound healing assay. Representative migration images and quantification of HCT8/T **(A,B)** and KB_{V200} **(C,D)** cells were shown. $^{*}P < 0.05$ and $^{**}P < 0.01$ vs. corresponding control.

Knockout of uPAR Inhibits Cell Invasion

To further evaluate the effect of knockout of uPAR by CRISPR/Cas9 on cell invasion, transwell assay was used to detect cell invasion. As shown in **Figure 5**, cell invasion was reduced in HCT8/T and KB_{V200} cells with uPAR knockout, suggesting that knockout of uPAR inhibits cell invasion.

Knockout of uPAR Decreases Multidrug Resistance

To study the effect of knockout of uPAR by CRISPR/Cas9 on multidrug resistance, four chemotherapeutical drugs 5-FU, cisplatin, docetaxel, and doxorubicin were used to treat cells, and cell survival was detected by MTT assays. As shown in **Figure 6**, the cell survival curves shifted to downward, and IC_{50} values of these four drugs were reduced in HCT8/T and KB_{V200} cells with uPAR knockout. These data indicate that knockout of uPAR suppresses multidrug resistance.

DISCUSSION

Recently, it has been demonstrated that knockout of uPAR using CRISPR/Cas9 system in mouse neuroblastoma Neuro 2A cells inhibit cell proliferation, reduce the number of Ki-67 positive cells, and down-regulate the mRNA expression level of TrkC receptor (18). In the current study, we successfully targeted uPAR in two cancer cell lines by CRISPR/Cas9 system with two individual sgRNAs. Knockout of uPAR suppresses cell proliferation, migration and invasion. Moreover, knockout of uPAR decreases resistance to 5-FU, cisplatin, docetaxel, and doxorubicin in these cells. Previous studies have shown that high expression of uPAR leads to small cell lung cancer, head and neck squamous cell carcinoma, and malignant pleural mesothelioma resistant to chemotherapy (19–21). uPAR promotes the resistance to tamoxifen in breast cancer by activated ERK1/2 activity (22), and confers the resistance to gefitinib in non-small-cell lung cancer through activated EGFR/pAKT/survivin signal pathway (23). Therefore, uPAR plays important roles not only in cancer malignancy but also in drug resistance.

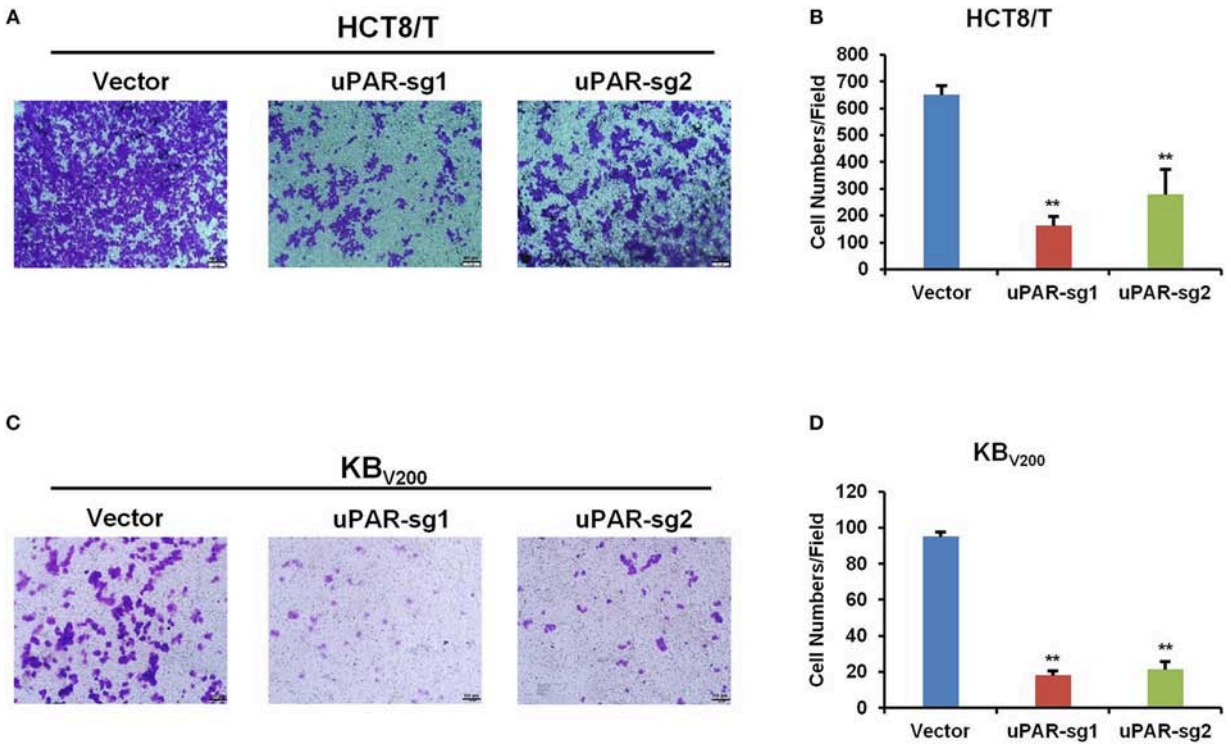

FIGURE 5 | Knockout of uPAR inhibits cell invasion. Cell invasion was determined with transwell assay. Representative invasion images and quantification of HCT8/T **(A,B)** and KB_{V200} **(C,D)** cells were shown. $^{**}P < 0.01$ vs. corresponding control.

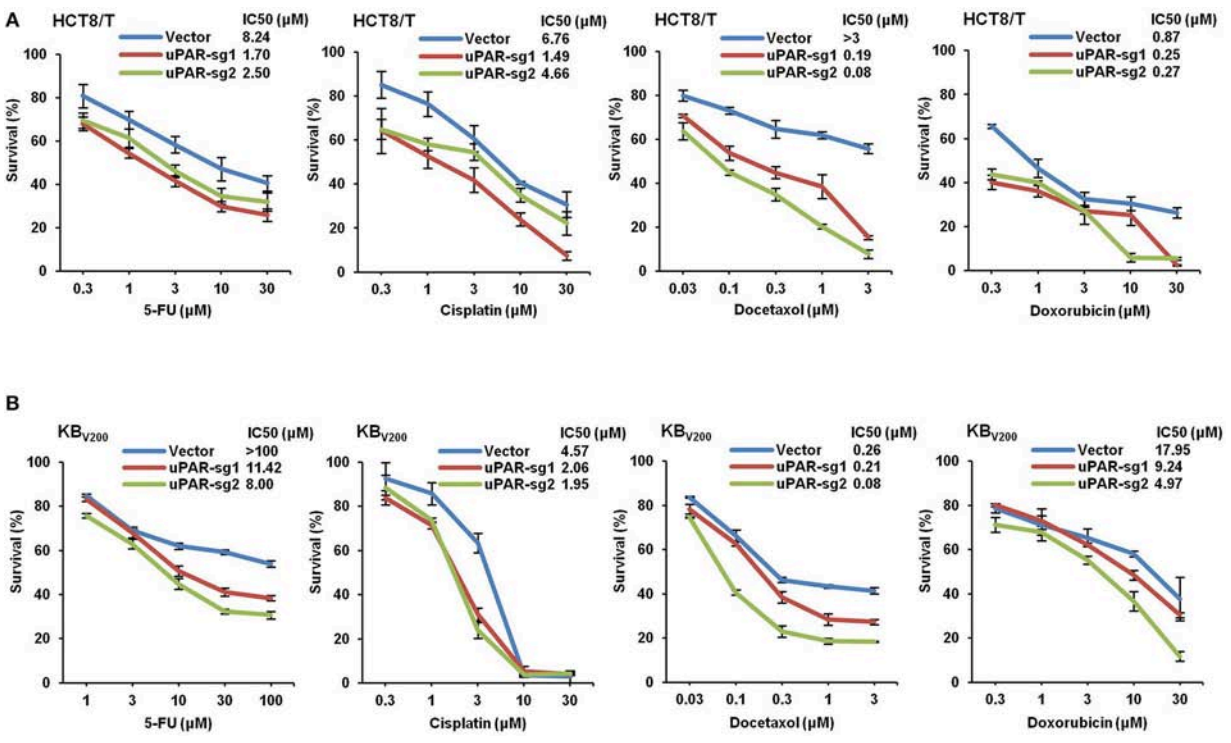

FIGURE 6 | Knockout of uPAR decreases multidrug resistance. Cells survival was measured by MTT assay. The representative growth curve of HCT8/T **(A)** and KB_{V200} **(B)** cells treated with the indicated concentrations of 5-FU, cisplatin, docetaxel, and doxorubicin for 72 h were shown.

CRISPR/Cas9 system has been widely applied in exploring the molecular mechanism of tumorigenesis, generating the models for cancer research and identifying the targets for cancer treatment, etc. A genome-wide CRISPR screen shows that loss-of-function mutations of some genes including NF2, PTEN, CDKN2A, TRIM72, FGA, miR-152, miR-345, and so on are able to drive tumor growth and metastasis in a mouse model (24). Using CRISPR/Cas9 technology to target MAN2A1-FER fusion gene inhibits tumor proliferation and metastasis in the mouse models of prostate and liver cancer (25). Colorectal cancer from normal human intestinal epithelium organoids are generated by introducing mutations in the tumor suppressor genes APC, SMAD4 and TP53, and oncogenes KRAS and/or PIK3CA with CRISPR/Cas9 system (26, 27). Liver tumors in mice are occurred by using hydrodynamic injection of CRISPR/Cas9 plasmids and sgRNAs that directly target the tumor suppressor genes PTEN and p53 (28). Mouse pancreatic ductal adenocarcinoma models are established by introducing 13 sgRNAs of different tumor suppressor genes into expression vectors and then transferred them to mouse pancreatic tissue (29). CDC25A is identifies as a determinant of sensitivity to ATR inhibitors by a genome-wide CRISPR screen (30). Deletion of genes such as NF1 and MED12 with CRISPR/Cas9 system is associated with resistance to vemurafenib (31). Moreover, the combination of CRISPR/Cas9 gene editing technology and immunotherapy, especially with CAR-T cell therapy, will have enormous therapeutic potential in leukemia, lymphoma, and some solid tumors (32, 33). Using CRISPR/Cas9 system can produce universal CAR-T cells by simultaneously targeting TCR and HLA-I (34) and enhanced CAR-T cells by deleting T cell inhibitory receptor or signaling molecule genes such as PD1 and CTLA4 (33, 35). We previously have demonstrated that targeting ABCB1 by CRISPR/Cas9-based genome editing reverses ABCB1-mediated multidrug resistance in cancer cells, resulting in the increase of the sensitivity and intracellular accumulation of the anti-cancer drugs (36). Although there are several limitations such as off-targets and delivery in the clinical application of CRISPR/Cas9 technology, it is believed that CRISPR/Cas9 system will benefit cancer patients in the near future.

In summary, our results have demonstrated that targeting uPAR by CRISPR/Cas9-based genome editing causes knockout of uPAR in human cancer cell lines, resulting in attenuation of cell proliferation, migration, invasion and multidrug resistance. Our study offers valuable evidences for the role of uPAR in cancer malignancy and drug resistance.

AUTHOR CONTRIBUTIONS

KW, Z-HX, and ZS designed the experiments, performed the experiments, analyzed the data, and wrote the paper. Q-WJ, YY, J-RH, M-LY, M-NW, YL, S-TW, and KL performed the experiments. All authors read and approved the final manuscript.

FUNDING

This work was supported by funds from the National Key Research and Development Program of China No. 2017YFA0505104 ZS, the National Natural Science Foundation of China No. 81772540 ZS, the Guangdong Natural Science Funds for Distinguished Young Scholar No. 2014A030306001 ZS, the Guangdong Special Support Program for Young Talent No. 2015TQ01R350 ZS, the Science and Technology Program of Guangdong No. 2016A050502027 ZS, the Science and Technology Program of Guangzhou No. 201704030058 ZS.

REFERENCES

1. Mahmood N, Mihalcioiu C, Rabbani SA. Multifaceted role of the urokinase-type plasminogen activator (uPA) and its receptor (uPAR): diagnostic, prognostic, and therapeutic applications. *Front Oncol.* (2018) 8:24. doi: 10.3389/fonc.2018.00024
2. Smith HW, Marshall CJ. Regulation of cell signalling by uPAR. *Nat Rev Mol Cell Biol.* (2010) 11:23–36. doi: 10.1038/nrm2821
3. Noh H, Hong S, Huang S. Role of urokinase receptor in tumor progression and development. *Theranostics.* (2013) 3:487–95. doi: 10.7150/thno.4218
4. Setyono-Han B, Sturzebecher J, Schmalix WA, Muehlenweg B, Sieuwerts AM, Timmermans M, et al. Suppression of rat breast cancer metastasis and reduction of primary tumour growth by the small synthetic urokinase inhibitor WX-UK1. *Thromb Haemost.* (2005) 93:779–86. doi: 10.1160/TH04-11-0712
5. Zhu M, Gokhale VM, Szabo L, Munoz RM, Baek H, Bashyam S, et al. Identification of a novel inhibitor of urokinase-type plasminogen activator. *Mol Cancer Ther.* (2007) 6:1348–56. doi: 10.1158/1535-7163.MCT-06-0520
6. Heinemann V, Ebert MP, Pinter T, Bevan P, Neville NG, Mala C. Randomized phase II trial with an uPA inhibitor (WX-671) in patients with locally advanced nonmetastatic pancreatic cancer. *J Clin Oncol.* (2010) 28:4060. doi: 10.1200/jco.2010.28.15_suppl.4060
7. Andersen LM, Wind T, Hansen HD, Andreasen PA. A cyclic peptidylic inhibitor of murine urokinase-type plasminogen activator: changing species specificity by substitution of a single residue. *Biochem J.* (2008) 412:447–57. doi: 10.1042/BJ20071646
8. Ploug M, Ostergaard S, Gardsvoll H, Kovalski K, Holst-Hansen C, Holm A, et al. Peptide-derived antagonists of the urokinase receptor. Affinity maturation by combinatorial chemistry, identification of functional epitopes, and inhibitory effect on cancer cell intravasation. *Biochemistry.* (2001) 40:12157–68. doi: 10.1021/bi010662g
9. Luparello C, Del Rosso M. *In vitro* anti-proliferative and anti-invasive role of aminoterminal fragment of urokinase-type plasminogen activator on 8701-BC breast cancer cells. *Eur J Cancer.* (1996) 32A:702–7. doi: 10.1016/0959-8049(95)00657-5
10. Mazar AP, Ahn RW, O'Halloran TV. Development of novel therapeutics targeting the urokinase plasminogen activator receptor (uPAR) and their translation toward the clinic. *Curr Pharm Des.* (2011) 17:1970–8. doi: 10.2174/138161211796718152
11. Ahmed N, Oliva K, Wang Y, Quinn M, Rice G. Downregulation of urokinase plasminogen activator receptor expression inhibits Erk signalling with concomitant suppression of invasiveness due to loss of uPAR-beta 1 integrin complex in colon cancer cells. *Brit J Cancer.* (2003) 89:374–84. doi: 10.1038/sj.bjc.6601098
12. Zhang F, Tom CC, Kugler MC, Ching TT, Kreidberg JA, Wei Y, et al. Distinct ligand binding sites in integrin alpha 3 beta 1 regulate matrix adhesion and cell-cell contact. *J Cell Biol.* (2003) 163:177–88. doi: 10.1083/jcb.200304065
13. Ghosh S, Johnson JJ, Sen R, Mukhopadhyay S, Liu Y, Zhang F, et al. Functional relevance of urinary-type plasminogen activator receptor-alpha3beta1 integrin association in proteinase regulatory pathways. *J Biol Chem.* (2006) 281:13021–9. doi: 10.1074/jbc.M508526200

14. Kenny HA, Leonhardt P, Ladanyi A, Yamada SD, Montag A, Im HK, et al. Targeting the urokinase plasminogen activator receptor inhibits ovarian cancer metastasis. *Clin Cancer Res.* (2011) 17:459–71. doi: 10.1158/1078-0432.CCR-10-2258
15. Barrangou R, Doudna JA. Applications of CRISPR technologies in research and beyond. *Nat Biotechnol.* (2016) 34:933–41. doi: 10.1038/nbt.3659
16. Fellmann C, Gowen BG, Lin PC, Doudna JA, Corn JE. Cornerstones of CRISPR-Cas in drug discovery and therapy. *Nat Rev Drug Discov.* (2017) 16:89–100. doi: 10.1038/nrd.2016.238
17. Yuan ML, Li P, Xing ZH, Di JM, Liu H, Yang AK, et al. Inhibition of WEE1 suppresses the tumor growth in laryngeal squamous cell carcinoma. *Front Pharmacol.* (2018) 9:1041. doi: 10.3389/fphar.2018.01041
18. Rysenkova KD, Semina EV, Karagyaur MN, Shmakova AA, Dyikanov DT, Vasiluev PA, et al. CRISPR/Cas9 nickase mediated targeting of urokinase receptor gene inhibits neuroblastoma cell proliferation. *Oncotarget.* (2018) 9:29414–30. doi: 10.18632/oncotarget.25647
19. Gutova M, Najbauer J, Gevorgyan A, Metz MZ, Weng Y, Shih CC, et al. Identification of uPAR-positive chemoresistant cells in small cell lung cancer. *PLoS ONE.* (2007) 2:e243. doi: 10.1371/journal.pone.0000243
20. Cortes-Dericks L, Carboni GL, Schmid RA, Karoubi G. Putative cancer stem cells in malignant pleural mesothelioma show resistance to cisplatin and pemetrexed. *Int J Oncol.* (2010) 37:437–44. doi: 10.3892/ijo-0000692
21. Huang Z, Wang L, Wang Y, Zhuo Y, Li H, Chen J, et al. Overexpression of CD147 contributes to the chemoresistance of head and neck squamous cell carcinoma cells. *J Oral Pathol Med.* (2013) 42:541–6. doi: 10.1111/jop.12046
22. Eastman BM, Jo M, Webb DL, Takimoto S, Gonias SL. A transformation in the mechanism by which the urokinase receptor signals provides a selection advantage for estrogen receptor-expressing breast cancer cells in the absence of estrogen. *Cell Signal.* (2012) 24:1847–55. doi: 10.1016/j.cellsig.2012.05.011
23. Zhou J, Kwak KJ, Wu Z, Yang D, Li J, Chang M, et al. PLAUR confers resistance to gefitinib through EGFR/P-AKT/Survivin signaling pathway. *Cell Physiol Biochem.* (2018) 47:1909–24. doi: 10.1159/000491071
24. Chen S, Sanjana NE, Zheng K, Shalem O, Lee K, Shi X, et al. Genome-wide CRISPR screen in a mouse model of tumor growth and metastasis. *Cell.* (2015) 160:1246–60. doi: 10.1016/j.cell.2015.02.038
25. Chen ZH, Yu YP, Zuo ZH, Nelson JB, Michalopoulos GK, Monga S, et al. Targeting genomic rearrangements in tumor cells through Cas9-mediated insertion of a suicide gene. *Nat Biotechnol.* (2017) 35:543–50. doi: 10.1038/nbt.3843
26. Matano M, Date S, Shimokawa M, Takano A, Fujii M, Ohta Y, et al. Modeling colorectal cancer using CRISPR-Cas9-mediated engineering of human intestinal organoids. *Nat Med.* (2015) 21:256–62. doi: 10.1038/nm.3802
27. Drost J, van Jaarsveld RH, Ponsioen B, Zimberlin C, van Boxtel R, Buijs A, et al. Sequential cancer mutations in cultured human intestinal stem cells. *Nature.* (2015) 521:43–7. doi: 10.1038/nature14415
28. Xue W, Chen S, Yin H, Tammela T, Papagiannakopoulos T, Joshi NS, et al. CRISPR-mediated direct mutation of cancer genes in the mouse liver. *Nature.* (2014) 514:380–4. doi: 10.1038/nature13589
29. Maresch R, Mueller S, Veltkamp C, Oellinger R, Friedrich M, Heid I, et al. Multiplexed pancreatic genome engineering and cancer induction by transfection-based CRISPR/Cas9 delivery in mice. *Nat Commun.* (2016) 7:10770. doi: 10.1038/ncomms10770
30. Ruiz S, Mayor-Ruiz C, Lafarga V, Murga M, Vega-Sendino M, Ortega S, et al. A genome-wide CRISPR screen identifies CDC25A as a determinant of sensitivity to ATR inhibitors. *Mol Cell.* (2016) 62:307–13. doi: 10.1016/j.molcel.2016.03.006
31. Shalem O, Sanjana NE, Hartenian E, Shi X, Scott DA, Mikkelsen TS, et al. Genome-Scale CRISPR-Cas9 knockout screening in human cells. *Science.* (2014) 343:84–7. doi: 10.1126/science.1247005
32. Maus MV, Grupp SA, Porter DL, June CH. Antibody-modified T cells: CARs take the front seat for hematologic malignancies. *Blood.* (2014) 123:2625–35. doi: 10.1182/blood-2013-11-492231
33. Ren JT, Zhao YB. Advancing chimeric antigen receptor T cell therapy with CRISPR/Cas9. *Protein Cell.* (2017) 8:634–43. doi: 10.1007/s13238-017-0410-x
34. Ren JT, Liu XJ, Fang CY, Jiang SG, June CH, Zhao YB. Multiplex genome editing to generate universal CAR T cells resistant to PD1 inhibition. *Clin Cancer Res.* (2017) 23:2255–66. doi: 10.1158/1078-0432.CCR-16-1300
35. Hoos A. Development of immuno-oncology drugs - from CTLA4 to PD1 to the next generations. *Nat Rev Drug Discov.* (2016) 15:235–47. doi: 10.1038/nrd.2015.35
36. Yang Y, Qiu JG, Li Y, Di JM, Zhang WJ, Jiang QW, et al. Targeting ABCB1-mediated tumor multidrug resistance by CRISPR/Cas9-based genome editing. *Am J Transl Res.* (2016) 8:3986–94.

Conflict of Interest Statement: The authors declare that the research was conducted in the absence of any commercial or financial relationships that could be construed as a potential conflict of interest.

frontiers in Pharmacology

ORIGINAL RESEARCH
published: 01 March 2019
doi: 10.3389/fphar.2019.00140

Integrated Bioinformatics Analysis the Function of RNA Binding Proteins (RBPs) and Their Prognostic Value in Breast Cancer

Ke Wang[1]†, Ling Li[2]†, Liang Fu[2], Yongqiang Yuan[2], Hongying Dai[2], Tianjin Zhu[2], Yuxi Zhou[3] and Fang Yuan[3]*

[1] Clinical Laboratory, Yongchuan People's Hospital of Chongqing, Chongqing, China, [2] Clinical Laboratory, Yongchuan Hospital of Chongqing Medical University, Chongqing, China, [3] Yidu Cloud (Beijing) Technology Co., Ltd., Beijing, China

Background and Purpose: Breast cancer is one of the leading causes of death among women. RNA binding proteins (RBPs) play a vital role in the progression of many cancers. Functional investigation of RBPs may contribute to elucidating the mechanisms underlying tumor initiation, progression, and invasion, therefore providing novel insights into future diagnosis, treatment, and prognosis.

Methods: We downloaded RNA sequencing data from the cancer genome atlas (TCGA) by UCSC Xena and identified relevant RBPs through an integrated bioinformatics analysis. We then analyzed biological processes of differentially expressed genes (DEGs) by DAVID, and established their interaction networks and performed pathway analysis through the STRING database to uncover potential biological effects of these RBPs. We also explored the relationship between these RBPs and the prognosis of breast cancer patients.

Results: In the present study, we obtained 1092 breast tumor samples and 113 normal controls. After data analysis, we identified 90 upregulated and 115 downregulated RBPs in breast cancer. GO and KEGG pathway analysis indicated that these significantly changed genes were mainly involved in RNA processing, splicing, localization and RNA silencing, DNA transposition regulation and methylation, alkylation, mitochondrial gene expression, and transcription regulation. In addition, some RBPs were related to histone H3K27 methylation, estrogen response, inflammatory mediators, and translation regulation. Our study also identified five RBPs associated with breast cancer prognosis. Survival analysis found that overexpression of DCAF13, EZR, and MRPL13 showed worse survival, but overexpression of APOBEC3C and EIF4E3 showed better survival.

Conclusion: In conclusion, we identified key RBPs of breast cancer through comprehensive bioinformatics analysis. These RBPs were involved in a variety of biological and molecular pathways in breast cancer. Furthermore, we identified five RBPs as a potential prognostic biomarker of breast cancer. Our study provided novel insights to understand breast cancer at a molecular level.

Keywords: breast cancer, RNA binding protein, integrated bioinformatics analysis, survival, prognosis

OPEN ACCESS

Edited by:
Jian-ye Zhang,
Guangzhou Medical University, China

Reviewed by:
Zhi Shi,
Jinan University, China
Changliang Shan,
Nankai University, China

****Correspondence:***
Ke Wang
wk125@126.com

† These authors have contributed equally to this work

Specialty section:
This article was submitted to Cancer Molecular Targets and Therapeutics, a section of the journal Frontiers in Pharmacology

Received: *12 November 2018*
Accepted: *06 February 2019*
Published: *01 March 2019*

Citation:
Wang K, Li L, Fu L, Yuan Y, Dai H, Zhu T, Zhou Y and Yuan F (2019) Integrated Bioinformatics Analysis the Function of RNA Binding Proteins (RBPs) and Their Prognostic Value in Breast Cancer. Front. Pharmacol. 10:140. doi: 10.3389/fphar.2019.00140

INTRODUCTION

Breast cancer is the most commonly diagnosed cancer and a main cause of cancer death among women. In 2018, there was an estimated 2.1 million newly diagnosed female breast cancer cases worldwide, accounting for about 25% of cancer cases among women (Bray et al., 2018). In recent years, with great progress in medical technology, the diagnosis incidence of breast cancer has increased year by year, and the age of onset or diagnosis has consequently become younger. Breast cancer is aggressive and has a high recurrence rate. Currently, the diagnosis of breast cancer mainly relies on pathological assessments, imaging tests, and tumor markers (McDonald et al., 2016), which creates difficulty for meeting clinical requirements. In order to reduce the recurrence rate and mortality of breast cancer patients, and to improve their quality of life, it is vital to increase ability in surveillance, early detection and diagnosis. Over the years there has been an increase of molecular research on early diagnosis, drug resistance and prognosis, and it is therefore valuable to find new molecular markers on the occurrence, progression, and prognosis, to further expand this research.

RNA-binding proteins (RBPs) are abundant and ubiquitously expressed in cells. They play a central and conserved role in gene regulation (Gerstberger et al., 2014b), and act as important participants and coordinators to maintain genome integrity (Nishida et al., 2017). RBPs have extensive capabilities including regulating stability, maturation, posttranscriptional regulation of mRNA stability, splicing, editing and translation, mRNA localization and polyadenylation, which ultimately impacts the expression of every gene in the cell (Campos-Melo et al., 2014; Gerstberger et al., 2014a). Although it is known that post-transcription contributes to tumor initiation and progression, the role of RBPs in cancer remain relatively unexplored (Wurth and Gebauer, 2015).

There is a large number of Human RBPs, but very few have been studied in depth, such as AGO2, Nova, PTB, HuR, AUF1, TTP, CUGBP2 which are known for their role in many regulation processes, including interacting with non-coding RNAs (Iadevaia and Gerber, 2015), controlling intracellular localization of non-coding RNAs (Glisovic et al., 2008), methylation (Harvey et al., 2017), forming the RNA induce silencing complex (Connerty et al., 2015), and alternative splicing (Paronetto et al., 2010). RBPs participate in comprehensive biological processes, such as reproductive development, tumorigenesis and apoptosis, and is therefore closely related to many human diseases. A systematic functional study of RBPs will be helpful to understand the function and mechanism of non-coding RNA, but will also have a significant applied value in studying the pathogenesis of diseases and in the screening of innovative drug targets.

Currently, genes and signaling pathways that participate in breast cancer tumorigenesis and progression remain to be further investigated. Exploring new genes and pathways associated with breast cancer may help to identify potential molecular mechanisms, diagnostic markers and therapeutic targets (Wang et al., 2018). High-throughput genomic analysis techniques can be applied to screening for differentially expressed genes (DEGs) and to understand the relevant pathways and protein interaction networks (Vogelstein et al., 2013). In this study, we downloaded breast cancer data from the cancer genome atlas (TCGA), and selected differential expressed RBPs to perform gene ontology (GO), KEGG pathways and an interaction network and survival analysis. The study identified a number of RBPs involved in breast cancer. Some of which might be used as potential prognostic biomarkers in the future.

RESULTS

Identification of Differently Expressed RBPs (DEGs)

The database analysis contained 1092 breast tumor samples and 113 no-tumor control samples. We conducted a deep analysis of 1912 RBPs and a total of 205 RBPs were identified, including 90 upregulated and 115 downregulated RBPs (**Supplementary Table S1**). We also constructed an expression heat map for all DEGs (**Figure 1**).

Functional and Pathway Enrichment Analysis of DEGs

To determine the function and mechanisms of these RBPs, all DEGs were divided into two groups (upregulated group and down-regulated group), and submitted to the David database for

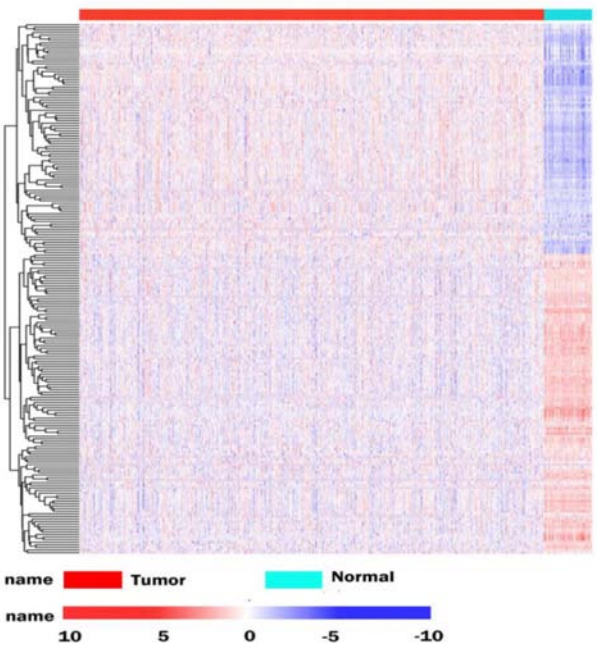

FIGURE 1 | Differentially expressed RBPs in BRCA cancer. Unsupervised clustering analysis was performed using the pheatmap function, using complete and Euclidean as metrics in R, based on log2-transformed FPKM values. The columns are samples and the rows are RBPs. The blue represents down-regulation, while red represents up-regulation.

GO analysis. We then conducted a KEGG pathway analysis for all DEGs. We found that upregulated DEGs were significantly enriched in RNA processing, RNA binding, mRNA binding, and located in the non-membrane-bounded organelle, intracellular non-membrane-bounded organelle, ribonucleoprotein complex, intracellular organelle lumen, organelle lumen, membrane-enclosed lumen, nuclear lumen, and the nucleolus (**Table 1**). The GO result of down-regulated DEGs were significantly enriched in the RNA processing, posttranscriptional regulation of gene expression, mRNA metabolic process, mRNA processing, regulation of translation and the RNA binding, and these genes mainly consisted of the chromatoid body, P granule, germ plasm, pole plasm, intracellular non-membrane-bounded organelle and the non-membrane-bounded organelle (**Table 1**).

TABLE 1 | GO enrichment analysis results of differentially up-regulated genes and down-regulated genes (DEGs).

	Term	*P* value	FDR
Up-regulated genes (DEGs)	RNA processing	3.23E-06	0.00478286
	Non-membrane-bounded organelle	4.53E-13	5.56E-10
	Intracellular non-membrane-bounded organelle	4.53E-13	5.56E-10
	Ribonucleoprotein complex	5.00E-11	6.15E-08
	Intracellular organelle lumen	1.81E-09	2.22E-06
	Organelle lumen	3.09E-09	3.80E-06
	Membrane-enclosed lumen	4.90E-09	6.02E-06
	Nuclear lumen	1.32E-06	0.00162684
	Nucleolus	1.59E-06	0.00194848
	RNA binding	5.78E-16	6.77E-13
	mRNA binding	2.37E-05	0.02904478
Down-regulated genes (DEGs)	RNA processing	1.41E-10	2.21E-07
	Posttranscriptional regulation of gene expression	2.29E-09	3.58E-06
	mRNA metabolic process	1.81E-08	2.82E-05
	mRNA processing	2.40E-07	3.74E-04
	Regulation of translation	1.05E-06	0.00164623
	Chromatoid body	2.05E-06	0.00250038
	P granule	3.57E-06	0.00436073
	Germ plasm	3.57E-06	0.00436073
	Pole plasm	3.57E-06	0.00436073
	Intracellular non-membrane-bounded organelle	1.94E-05	0.02370618
	Non-membrane-bounded organelle	1.94E-05	0.02370618
	RNA binding	1.46E-23	1.83E-20

TABLE 2 | The KEGG pathway analysis of all DEGs.

Term	*P* value
Dorso-ventral axis formation	4.18E-03
Fatty acid elongation in mitochondria	3.11E-02
Pathogenic *Escherichia coli* infection	2.06E-02

According to the KEGG pathway enrichment analysis, all DEGs mainly participated in Dorso-ventral axis formation, fatty acid elongation in mitochondria and pathogenic *Escherichia coli* infection (**Table 2**).

Protein-Protein Interaction Network Building and Interrelation Analysis Between Pathways

To better understand the role of these differentially expressed RBPS in breast cancer development, we constructed co-expression networks. All DEGs were submitted to STRING 10.5, we obtained 294 PPI nodes, 174 edges, and a *p*-value of PPI concentration <1.00–16, while also including the result of the GO and KEGG pathway. In the biological process, there was mainly enrichment in the regulation of transcription, translation level and epigenetics, and it also played an important role in histone modification, mitochondrial gene expression, cell metabolism, production of inflammatory mediators and estrogen response. The cellular components are significantly located in the ribosome, mitochondria, chromosomes, and the telomeres, etc. Molecular functions showed that they can bind to a variety of RNA and specific regions, and were closely related to regulated enzymes activity, including various metabolic and gene expressions, modification and regulation of enzymes, and also bound to steroid hormones and estrogen receptors. For KEGG pathway analysis, it was mainly enriched in Glycolysis/Gluconeogenesis, mRNA surveillance pathway, RNA degradation and pathogenic *E. coli* infection. Then, we constructed the PPI network of these DEGs using Cytoscape (**Figure 2A**). Two topological features, degree and betweenness, were calculated to identify candidate hub nodes. The higher the two quantitative values of a gene, the greater the importance within the network (Liu et al., 2018b). The co-expression network revealed that ELAVL2, VIM, MRPS12, HSPE1, EZH2, HIST1H4B, and MRPL13 played a vital role in the progression of breast cancer, and we further selected important modules of target genes through MCODE (**Figures 2B,C**). Finally, we used the ClueGO to externalize all biological processes (**Figures 3A,B**) and the interaction modes of molecular functions (**Figures 4A,B**).

Survival Analysis

The correlation between RBP expression and overall survival was assessed using both the Cox regression analysis and the Kaplan-Meier estimation method. Then, survival correlation $P < 0.05$ and key RBPs were selected to analyze their correlation with survival prognosis. After that we used both the Kaplan-Meier estimates and the log-rank test to assess the significant differences of the two-group survival curves. As shown in the **Figure 5**, the expression of selected target genes in tumor and normal tissues was significantly different. In addition, patients with highly expressed RBPs of EZR, DCAF13, and MRPL13 showed lower survival, but patients with highly expressed RBPs of APOBEC3C, EIF4E3 showed better survival (**Figure 5**). Therefore these genes could be potential biomarkers for breast cancer prognosis.

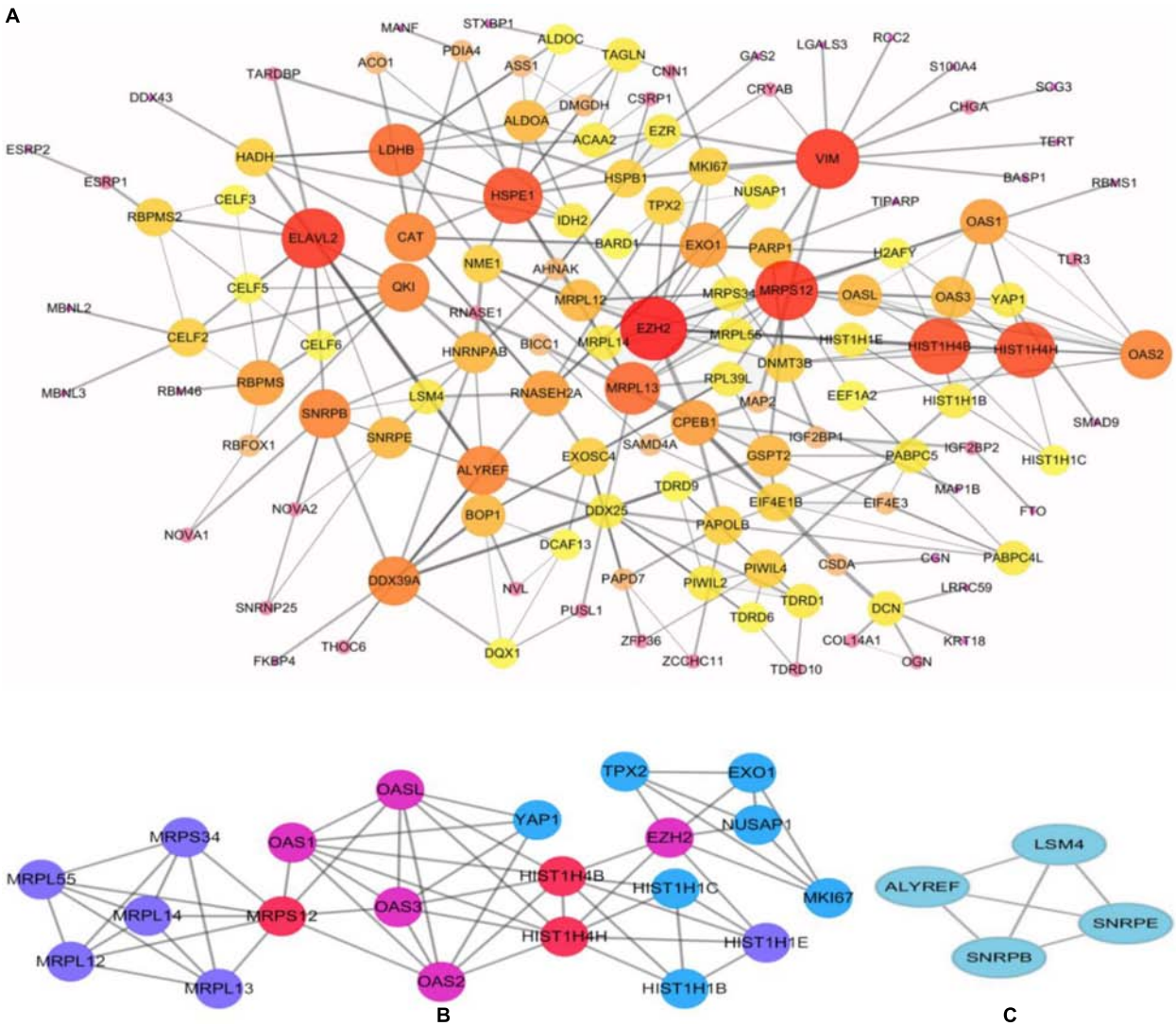

FIGURE 2 | Construction of protein-protein interaction (PPI) network. **(A)** Modules inferred from protein-protein interaction network. Elected important modules of target gene (**B**,**C**) MCODE score >4, nodes >4.

MATERIALS AND METHODS

Data Sources Analysis

The corresponding clinical data was downloaded from the following website http://gdac.broadinstitute.org/. Combined with the RNA-seq expression data set, 1075 patients had clinical information available including age, gender and disease stage. The details have been listed in **Supplementary Table S1**. We downloaded the RBPs expression data (TOIL RSEM expected count and FPKM) processed by the Toil pipeline (Vivian et al., 2017) based on RNA sequencing (RNA-Seq) for TCGA Pan-Cancer cohort from the website https://xena.ucsc.edu/. The data included the 60498 genes annotated by GENCODE version 23. We then used custom Perl script to extract the data from BRCA cancer, for subsequent analysis. We applied the Voom function (Law et al., 2014) in the Limma package, to estimate DEGs between tumor and normal tissues for BRCA cancer. Those with a fold change ≥ 1 and FDR < 0.05 were considered to have statistical significance. We further identified significantly dysregulated RBPs based on our RBP catalog. Unsupervised clustering of differentially expressed RBPs was performed based on log2-transformed FPKM values using the "pheatmap" package in R.

GO Functional and Pathway Enrichment Analysis

In order to comprehensively analyze the biological functions of these RBPS, we used the GO and kyoto encyclopedia of genes and genomes (KEGG) analysis by The database for annotation, visualization and integrated discovery (DAVID) version 6.7. The GO Term analysis included the

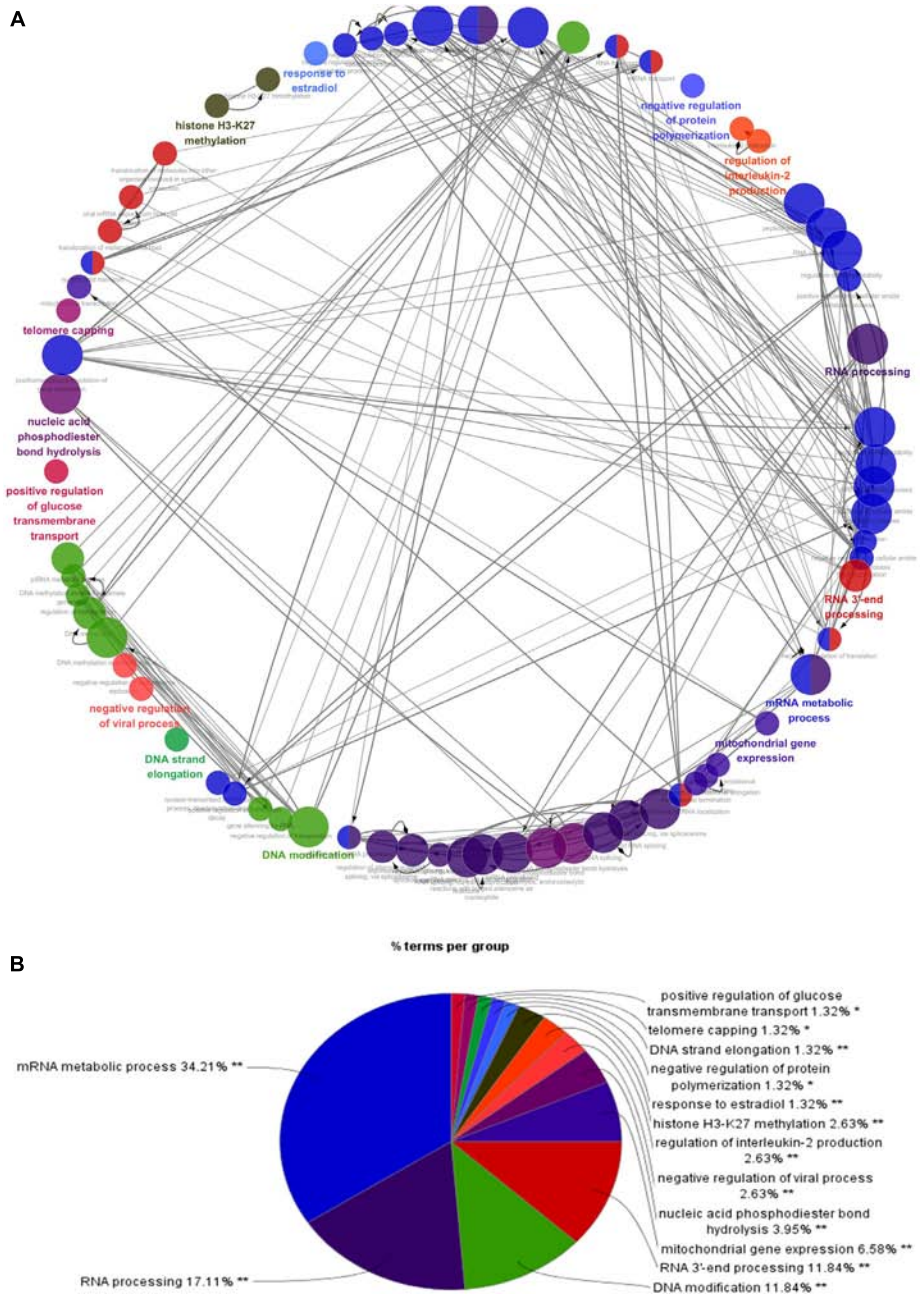

FIGURE 3 | Interrelation analysis between pathways (biological process). **(A)** Interrelation between biological process pathways. **(B)** The proportion of each pathway.

biological process, cellular component and the molecular function. Both $P < 0.05$ and FDR < 0.05 were considered statistically significant.

Protein Interaction Network (PPI) and Pathways Interaction Analysis Building

SRTING version 10.5 was used to evaluate the protein interaction information of all DEGs, and their biological functions were also obtained. Then, the interaction network of these proteins was visualized by Cytoscape3.6.0, and important modules both MCODE score and node number > 4 were selected by the MCODE plug in to Cytoscape version 3.6.0. Furthermore, the pathway enrichment of $P < 0.05$ was analyzed by the ClueGO plug to Cytoscape version 3.6.0.

Statistical Analysis

The correlation of RBP expression and overall survival was assessed using both the Cox regression analysis and the Kaplan-Meier estimation method, based on the "survival"

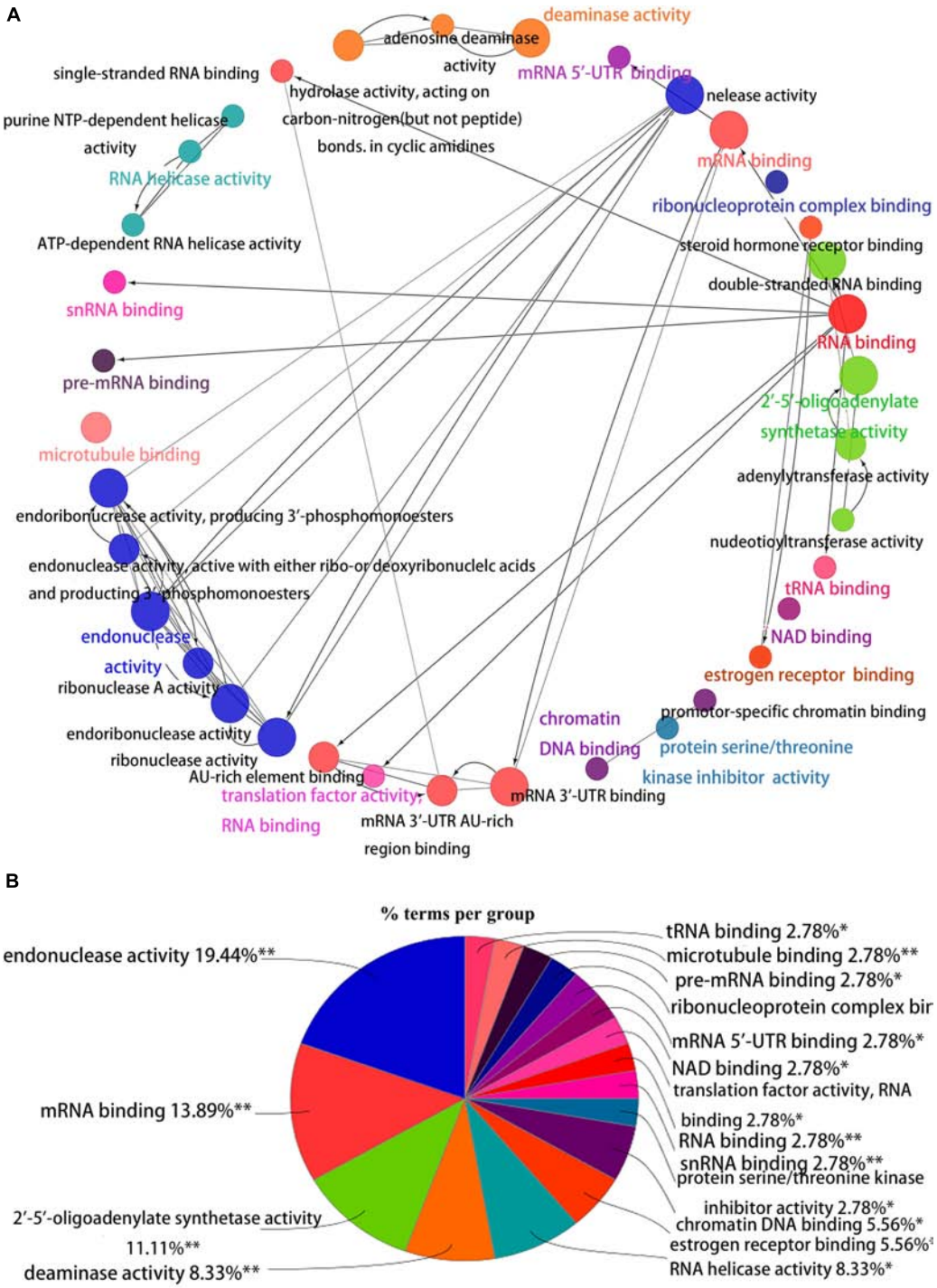

FIGURE 4 | Interrelation analysis between pathways molecular functions. **(A)** Interrelation between molecular functions pathways. **(B)** The proportion of each pathway.

package in R. For the Cox regression analysis, the RBP was evaluated as a continuous variable with age and gender as additional covariables. For the Kaplan-Meier estimates, we defined the high-expression group and low-expression group using the median RBP expression value as a cut-off point. A significant difference of two-group survival curves was assessed by a log-rank test. $P < 0.05$ was considered as statistically significant.

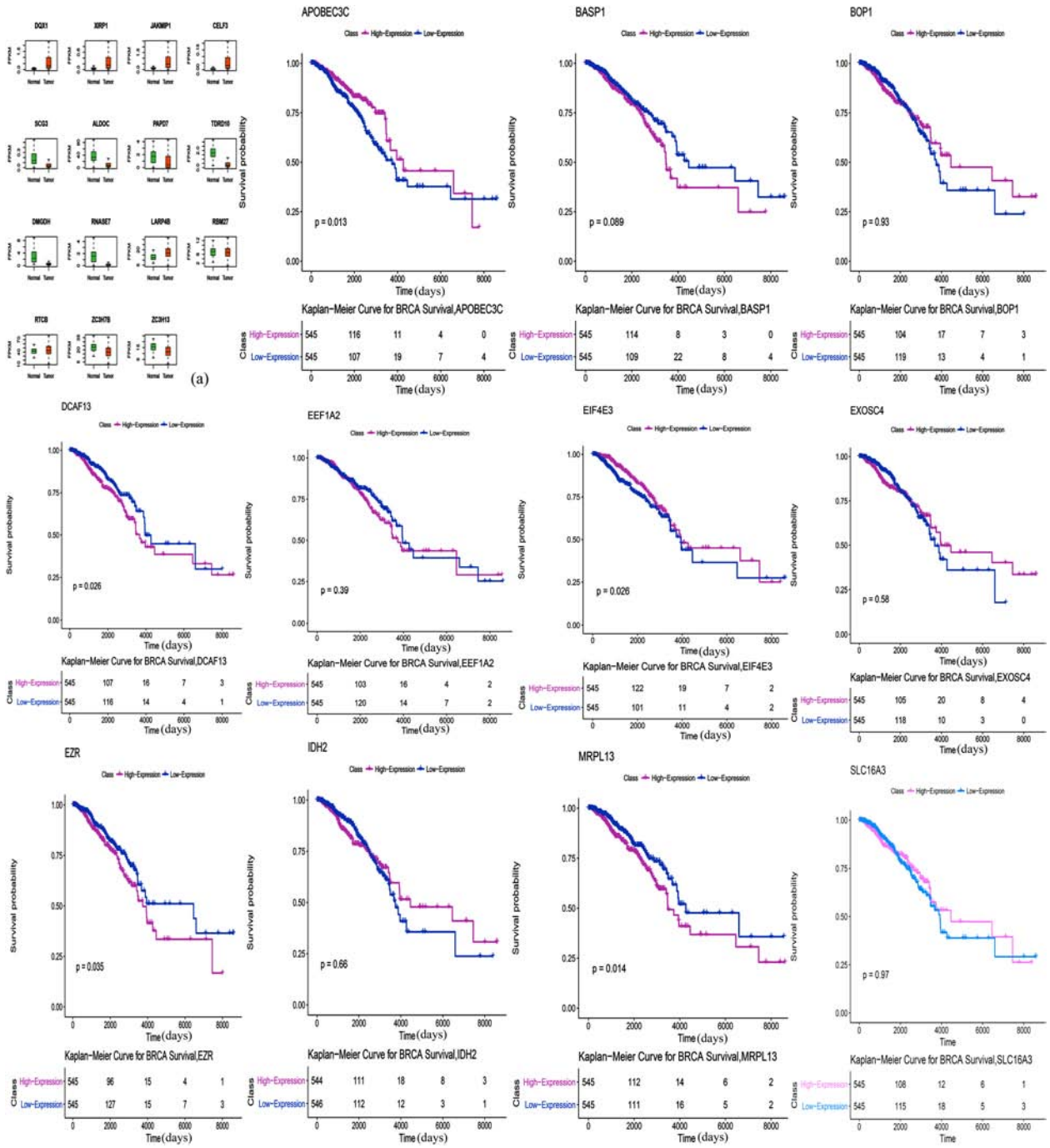

FIGURE 5 | Survival Kaplan-Meier Estimate (EZR $p = 0.035$, DCAF13 $p = 0.026$, MRPL13 $p = 0.014$, APOBEC3C $p = 0.013$, and EIF4E3 $p = 0.026$). Expression of selected target genes in tumor and normal tissues was significantly different.

DISCUSSION

Currently, cancer causes more death than coronary heart diseases or stroke does (Lin et al., 2017a). In recent years, although molecular targeted therapy has improved treatment effect, breast cancer is still the primary cause of death among women. During clinical practice, biomarkers that indicate the grade malignancy, metastasis and the prognosis of breast cancer are needed. Microarray and high-throughput sequencing technologies provide effective tools for deciphering key genetic or epigenetic changes in the occurrence of cancer, as well as promising biomarkers

for cancer diagnosis, treatment, and prognosis (Kulasingam and Diamandis, 2008; Cancer Genome Atlas Research and Network, 2014). Our study integrated TCGA RNA sequencing data, and identified DEGs between tumor and normal tissue. We analyzed relevant biological pathways, constructed protein interaction networks and performed survival analyses to explore biological functions and clinical application of these RBPs.

The biological functions of these DEGs were obtained using the GO and KEGG pathway analysis. Firstly, the enrichment of cell components is mainly located in the ribosome, exonuclease, endonuclease, spliceosome and the ribonuclease, which are important sites protecting the transmission of biological information. The ribosome is a key organelle that performs protein synthesis. The mutation of the ribosomal protein regulates the translation and activity of p53, finally resulting in diseases, and cancers (Goudarzi and Lindstrom, 2016). A number of RBPs exist in exonuclease, endonuclease and sites with DNA damage, which may participate in DNA damage repair (Goudarzi and Lindstrom, 2016). In addition, RBPs are widely present in spliceosome. Expression of eukaryotic genes is often accompanied by the RNA splicing process, especially in the alternative splicing of RNA, which could produce tissue and development specific mRNA. For example, Sam68 can result in drug resistance and poor prognosis by regulating the expression ratio of cyclinD1, an alternative splicing in breast cancer (Paronetto et al., 2010). Some RBPs also expressed in the telomere and telomerase and regulate their activity. Telomere play an important role in regulating cell growth and division. Some studies have found that telomerase activity was suppressed in normal tissues but was reactivated in tumors. Telomerase is overexpressed in 80–95% of cancers and is likely to participate in cell malignant transformation (Ruden and Puri, 2013). During the analysis of cellular components, we also found the occurrence of RBPs in the exosome, which could cause tumor invasion and metastasis, immune escape and therapeutic resistance. For example, SYNCRIP, as a component of the miRNA sorting mechanism, in hepatocyte exosomes, can directly bind to specific miRNA rich in exosomes, and regulates miRNA localization (Santangelo et al., 2016).

Secondly, in terms of molecular function, RPBs can bind to various RNAs such as pre-mRNA, Sn RNA, tRNA, mRNA and regulates the activity of various enzymes, such as hydrolytic enzyme, purine metabolic enzyme, and enzymes involved in DNA synthesis, repair, and RNA metabolism. Furthermore, some RBPs also bind to estrogen and steroid hormone receptors. For example, MSI2 is highly expressed in ER(+) breast cancer, and its expression is significantly correlated with ESR1 expression, which affects the growth of breast cancer cells, by changing the function of ESR1 (Kang et al., 2017).

Next, for the biological process, the function enrichment of differential RBPs mainly occurred in RNA processing, splicing, localization, transport, hydrolysis, and RNA silencing. It participates in transposition regulation, methylation, and alkylation of DNA. Some RBPs were also related to histone H3K27 methylation, inflammatory mediators, and translation regulation. Our findings are consistent with the consensus that multiple genes, multiple molecules, and multiple pathways are involved in breast cancer. Although the relationship with breast cancer remains unclear, some RBPs have been reported in other cancers. HuR can promote the growth of colorectal cancer cell by regulating mRNA expression (Lopez de Silanes et al., 2003). CRD-BP can regulate many mRNAs with coding for cancer-related genes, including Gli1, PTEN, PTEN, ptlcp1, MAPK4, MDR1, IGF2, H19, c-myc, etc. (Fakhraldeen et al., 2015). HNRNPA2B1 controls the replacement splicing for the pre-mRNA of cancer-related genes, and which is up-regulated in diverse cancers (Stockley et al., 2014). HuR can bind with DNMT3b and maintain its stability, thus affecting abnormal DNA methylation (Lopez de Silanes et al., 2009). Numerous studies reported that a change of mitochondrial function plays a key role in all kinds of cancers (Tao et al., 2015; Lin et al., 2017b; Zhang J.Y. et al., 2017; Zhang J. et al., 2017), and RBPs involved in the expression and transcription regulation of mitochondrial genes, such as LRPPRC, GRSF1, SLIRP, and other RBPs can interact with mt-RNA to affect the expression and metabolism of mitochondrial transcripts (Dong et al., 2017). The incidence of breast cancer and female estrogen levels are closely related. Some RBPs can respond with estrogen, for example, through Nova1, 17-b estradiol can regulate the replacement splicing of estrogen receptor b in the brain of aging female mice (Shults et al., 2018). Then, the results of the KEGG pathway analysis indicated that these RBPs may affect the occurrence and development of breast cancer through glycolysis, glycosylation, mRNA monitoring pathways, and RNA degradation regulation. RPBs have various basic biological functions, especially the function of RNA which has been studied widely. Other RBPs functions should therefore be studies further.

By constructing a protein network for DEGs, we found that breast cancer is associated with immune response, splicing, transcript regulation, and intercellular signaling transduction. HSPE1 is a member of the heat shock protein family (Hsp10) E, which usually acts as a chaperone to assist protein folding in the mitochondria, which is highly expressed in various cancers, such as lung cancer, pancreatic cancer and bladder cancer. Some studies reported that it may protect cancer cells from apoptosis, and facilitate the immune escape of cancer, by down-regulating the immune response (Rappa et al., 2016; Liu et al., 2018a). ELAVL2 is a neurospecific RNA binding protein, which is involved in splicing and transcript trafficking to regulate protein localization (Berto et al., 2016). Elevated methylation of ELAVL2 was shown in high Gleason scores of prostate tumors (Wu et al., 2016). VIM is expressed in a variety of cell types and is responsible for maintaining cell shape, cytoplasmic integrity, and stabilizing cytoskeletal. It is also involved in immune responses, attachment, migration, and cell signaling in tissues. Previous studies have shown that vimentin regulated Ras, Slug and TGF glows in cancer cells, which is necessary for EMT induction. It is also highly expressed in various tumors such as lung cancer, breast cancer and gastric cancer, and is

closely related to invasion, metastasis and the poor prognosis of tumors (Satelli and Li, 2011; Virtakoivu et al., 2015). High expressions of EZH2 is associated with malignancy and hyper-invasiveness in a variety of cancers. EZH2 can activate NF-κB targets and NOTCH1 in breast cancer cells, which has also been implicated in the transcriptional activation of gene expression in breast cancer. Research has shown that it induces the expression of genes that are regulated by the estrogen receptor (ER) and Wnt signaling transcription factors, by physically bridging between the ER and components of Wnt signaling (Kim and Roberts, 2016).

These RBPS may lead to breast cancer by regulating mitochondrial translation, splicing of pre-mRNA, activation of RNase L, and histone modifications through two modules selected from the PPI network. It has been reported that the upregulation of mitochondrial translation may meet the energy needs of cancer cells in human tumors, but the mechanism of its tumorigenesis remains unclear. There are many studies targeting the inhibition of mitochondrial translation in various cell types, to obliterate cancer stem cells. Currently, suppressing mitochondrial translation is considered a valuable therapeutic target (Kim et al., 2017). RNase L was activated through the synthesis of 2′, 5′ -oligoadenylic acid by OAS (OAS1, OAS2, and OAS3). It was found that the activated OAS-RNase L system can degrade virus and cell RNA, promote cell apoptosis, and inhibit protein synthesis (Bhosle et al., 2016). In addition, single nucleotide polymorphisms of OAS are associated with cancer, such as OAS1 SNP rs2660 AA (Mandal et al., 2011). However, no studies reported the exact role of OAS in breast cancer. As we know, epigenetic change is involved in the initiation and progression of cancer, which includes histone modifications and DNA methylation. Studies have shown that the regulation of histone is gene specific, but their function is diversified. Histone cluster 1 can interact with some regulatory factors, such as inhibiting p53-dependent chromatin transcription, and maintaining or establishing specific DNA methylation patterns (Perez-Magan et al., 2010). It has been demonstrated that the function of protecting DNA with histone may be an independent prognostic factor for better survival of cervical cancer patients (Li et al., 2017). Furthermore, splicing affects the expression of most genes, and eventually influences the levels of proteins. In the module, SNRPE, SNRPB, and ALYREF participate in the splicing of pre-mRNA. Knockdown SNRPE significantly reduces the expressed level of mTOR mRNA and protein, and is accompanied by the imbalance of the mTOR pathway, which activates abnormal mTOR signaling and which can result in the growth and metastasis of tumor cells (Quidville et al., 2013).

Finally, we performed a survival analysis and found five genes that are associated with survival in breast cancer patients. The overexpression of DCAF13, EZR, and MRPL13 in patients were associated with lower survival, which reveals that these genes might be associated with tumor invasion, progression and poor prognosis. Whereas, overexpression of APOBEC3C and EIF4E3 in patients were associated with better survival, suggesting their potential role as tumor suppressor genes. DCAF13 is amplified in all kinds of cancers. Studies have shown that overexpression of DCAF13 in hepatocellular carcinoma is significantly correlated with low survival and it may be involved in the regulation of cell cycle (Cao et al., 2017). It also reported that the E3 ligase formed by DCAF13, CUL4B and DDB1, could induce ubiquitination of tumor suppressor PTEN *in vivo* and *in vitro* (Chen et al., 2018). Mutated or inactivated PTEN was helpful to infiltrate and spread cancer cells. As a member of the ERM protein family, Ezrin has been linked to molecules that control the phosphatidylinositol-3-kinase, AKT, Erk1/2 MAPK and Rho pathways, which are functionally involved in regulating cell survival, proliferation and migration, and it is an indicator of poor prognosis of multiple cancers (Hunter, 2004). It has been shown that overexpressed EZR in a nude mice phantom of pancreatic cancer, can increase the number of metastasis and is closely related to the progression of malignant cancer (Meng et al., 2010). MRPL13 is a mitochondrial ribosomal protein. Loss of MRPL13 can lead to the loss of mitochondrial DNA, and eventually lead to the loss of the ability of mitochondrial coding proteins (Gruschke et al., 2010). In a study, reduced MRPL13 expression in hepatocellular carcinoma was a key factor in the regulation of mitochondrial ribosome and subsequent OXPHOS deficiency, which regulates the aggressive activity of liver cancer cells (Lee et al., 2017). APOBEC can mediate c-to-t mutagenesis in various cancers, while the APOBEC3 gene family is overexpressed in breast cancer and other cancer cells and tissues. Some studies suggest that it is regulated by estrogen in breast cancer (Long et al., 2013). At present, there are few studies about APOBEC3C in breast cancer, and some studies have found that it should play a positive role in the invasiveness and prognosis of hepatocellular carcinoma (Zhang et al., 2015). EIF4E3 belongs to the EIF4E family of translational initiation factors that interact with the 5-prime cap structure of mRNA. A study demonstrated that EIF4E3 relies on cap-binding activity to act as a tumor suppressor and compete with the growth-promoting functions of EIF4E. In fact, reduced EIF4E3 levels in high-expressed EIF4E cancers suggests that EIF4E3 underlies a clinically relevant inhibitory mechanism that is lost in some malignancies (Osborne et al., 2013). Other studies also found that EIF4E3 can impede oncogenic transformation (Volpon et al., 2013).

Over all, we identified key genes and related pathways through bioinformatics analysis of differential expressions of RBPs in breast cancer. These RBPs may be involved in the occurrence, development, invasion and metastasis of breast cancer. The survival analysis suggested that DCAF13, EZR, MRPL13, APOBEC3C, and EIF4E3 might have a prognostic value for breast cancer. Future *in vitro* and *in vivo* studies are needed to verify the functions of these genes.

DATA AVAILABILITY

Publicly available datasets were analyzed in this study. This data can be found here: https://xena.ucsc.edu/.

AUTHOR CONTRIBUTIONS

LL and KW conceived and designed the experiments. LF, YY, TZ, and HD analyzed the data. LL, YZ, and FY wrote the manuscript. All authors reviewed and approved the final manuscript.

FUNDING

This study was supported by the Natural Science Foundation Project of Yongchuan People's Hospital of Chongqing (Grant No. YCPH2019001). Chongqing Health and the Health Committee and Chongqing Science and Technology Commission (Grant No. 2018MSXM020) and the Natural Science Foundation Project of Yongchuan (Grant No. Ycstc.2017nc5020).

SUPPLEMENTARY MATERIAL

The Supplementary Material for this article can be found online at: https://www.frontiersin.org/articles/10.3389/fphar.2019.00140/full#supplementary-material

REFERENCES

Berto, S., Usui, N., Konopka, G., and Fogel, B. L. (2016). ELAVL2-regulated transcriptional and splicing networks in human neurons link neurodevelopment and autism. *Hum. Mol. Genet.* 25, 2451–2464. doi: 10.1093/hmg/ddw110

Bhosle, S. M., Hunt, A., and Chaudhary, J. (2016). A modified coupled spectrophotometric method to detect 2-5 oligoadenylate synthetase activity in prostate cell lines. *Biol. Proced. Online* 18:9. doi: 10.1186/s12575-016-0038-x

Bray, F., Ferlay, J., Soerjomataram, I., Siegel, R. L., Torre, L. A., and Jemal, A. (2018). Global cancer statistics 2018: GLOBOCAN estimates of incidence and mortality worldwide for 36 cancers in 185 countries. *CA Cancer. J. Clin.* 68, 394–424. doi: 10.3322/caac.21492

Campos-Melo, D., Droppelmann, C. A., Volkening, K., and Strong, M. J. (2014). RNA-binding proteins as molecular links between cancer and neurodegeneration. *Biogerontology* 15, 587–610. doi: 10.1007/s10522-014-9531-2

Cancer Genome Atlas Research and Network (2014). Comprehensive molecular characterization of gastric adenocarcinoma. *Nature* 513, 202–209. doi: 10.1038/nature13480

Cao, J., Hou, P., Chen, J., Wang, P., Wang, W., Liu, W., et al. (2017). The overexpression and prognostic role of DCAF13 in hepatocellular carcinoma. *Tumour Biol.* 39:1010428317705753. doi: 10.1177/1010428317705753

Chen, Z., Zhang, W., Jiang, K., Chen, B., Wang, K., Lao, L., et al. (2018). MicroRNA-300 regulates the ubiquitination of PTEN through the CRL4B(DCAF13) E3 ligase in osteosarcoma cells. *Mol. Ther. Nucleic Acids* 10, 254–268. doi: 10.1016/j.omtn.2017.12.010

Connerty, P., Ahadi, A., and Hutvagner, G. (2015). RNA Binding Proteins in the miRNA Pathway. *Int. J. Mol. Sci.* 17:31. doi: 10.3390/ijms17010031

Dong, Y., Yoshitomi, T., Hu, J. F., and Cui, J. (2017). Long noncoding RNAs coordinate functions between mitochondria and the nucleus. *Epigen. Chromatin* 10:41. doi: 10.1186/s13072-017-0149-x

Fakhraldeen, S. A., Clark, R. J., Roopra, A., Chin, E. N., Huang, W., Castorino, J., et al. (2015). Two isoforms of the RNA binding protein, coding region determinant-binding protein (CRD-BP/IGF2BP1), are expressed in breast epithelium and support clonogenic growth of breast tumor cells. *J. Biol. Chem.* 290, 13386–13400. doi: 10.1074/jbc.M115.655175

Gerstberger, S., Hafner, M., Ascano, M., and Tuschl, T. (2014a). Evolutionary conservation and expression of human RNA-binding proteins and their role in human genetic disease. *Adv. Exp. Med. Biol.* 825, 1–55. doi: 10.1007/978-1-4939-1221-6-1

Gerstberger, S., Hafner, M., and Tuschl, T. (2014b). A census of human RNA-binding proteins. *Nat. Rev. Genet.* 15, 829–845. doi: 10.1038/nrg3813

Glisovic, T., Bachorik, J. L., Yong, J., and Dreyfuss, G. (2008). RNA-binding proteins and post-transcriptional gene regulation. *FEBS Lett.* 582, 1977–1986. doi: 10.1016/j.febslet.2008.03.004

Goudarzi, K. M., and Lindstrom, M. S. (2016). Role of ribosomal protein mutations in tumor development. *Int. J. Oncol.* 48, 1313–1324. doi: 10.3892/ijo.2016.3387

Gruschke, S., Grone, K., Heublein, M., Holz, S., Israel, L., Imhof, A., et al. (2010). Proteins at the polypeptide tunnel exit of the yeast mitochondrial ribosome. *J. Biol. Chem.* 285, 19022–19028. doi: 10.1074/jbc.M110.113837

Harvey, R., Dezi, V., Pizzinga, M., and Willis, A. E. (2017). Post-transcriptional control of gene expression following stress: the role of RNA-binding proteins. *Biochem. Soc. Trans.* 45, 1007–1014. doi: 10.1042/BST20160364

Hunter, K. W. (2004). Ezrin, a key component in tumor metastasis. *Trends Mol. Med.* 10, 201–204. doi: 10.1016/j.molmed.2004.03.001

Iadevaia, V., and Gerber, A. P. (2015). Combinatorial control of mRNA fates by RNA-binding proteins and non-coding RNAs. *Biomolecules* 5, 2207–2222. doi: 10.3390/biom5042207

Kang, M. H., Jeong, K. J., Kim, W. Y., Lee, H. J., Gong, G., Suh, N., et al. (2017). Musashi RNA-binding protein 2 regulates estrogen receptor 1 function in breast cancer. *Oncogene* 36, 1745–1752. doi: 10.1038/onc.2016.327

Kim, H.-J., Maiti, P., and Barrientos, A. (2017). Mitochondrial ribosomes in cancer. *Semin. Cancer Biol.* 47, 67–81. doi: 10.1016/j.semcancer.2017.04.004

Kim, K. H., and Roberts, C. W. (2016). Targeting EZH2 in cancer. *Nat. Med.* 22, 128–134. doi: 10.1038/nm.4036

Kulasingam, V., and Diamandis, E. P. (2008). Strategies for discovering novel cancer biomarkers through utilization of emerging technologies. *Nat. Clin. Pract. Oncol.* 5, 588–599. doi: 10.1038/ncponc1187

Law, C. W., Chen, Y., Shi, W., and Smyth, G. K. (2014). Voom: precision weights unlock linear model analysis tools for RNA-seq read counts. *Genome Biol.* 15:R29. doi: 10.1186/gb-2014-15-2-r29

Lee, Y. K., Lim, J. J., Jeoun, U. W., Min, S., Lee, E. B., Kwon, S. M., et al. (2017). Lactate-mediated mitoribosomal defects impair mitochondrial oxidative phosphorylation and promote hepatoma cell invasiveness. *J. Biol. Chem.* 292, 20208–20217. doi: 10.1074/jbc.M117.809012

Li, X., Tian, R., Gao, H., Yang, Y., Williams, B. R. G., Gantier, M. P., et al. (2017). Identification of a histone family gene signature for predicting the prognosis of cervical cancer patients. *Sci. Rep.* 7:16495. doi: 10.1038/s41598-017-16472-5

Lin, M., Bi, H., Yan, Y., Huang, W., Zhang, G., Zhang, G., et al. (2017a). Parthenolide suppresses non-small cell lung cancer GLC-82 cells growth via B-Raf/MAPK/Erk pathway. *Oncotarget* 8, 23436–23447. doi: 10.18632/oncotarget.15584

Lin, M., Tang, S., Zhang, C., Chen, H., Huang, W., Liu, Y., et al. (2017b). Euphorbia factor L2 induces apoptosis in A549 cells through the mitochondrial pathway. *Acta Pharm. Sin. B* 7, 59–64. doi: 10.1016/j.apsb.2016.06.008

Liu, X., Weng, Y., Liu, P., Sui, Z., Zhou, L., Huang, Y., et al. (2018a). Identification of PGAM1 as a putative therapeutic target for pancreatic ductal adenocarcinoma metastasis using quantitative proteomics. *Onco Targets Ther.* 11, 3345–3357. doi: 10.2147/OTT.S162470

Liu, X., Wu, J., Zhang, D., Bing, Z., Tian, J., Ni, M., et al. (2018b). Identification of potential key genes associated with the pathogenesis and prognosis of gastric cancer based on integrated bioinformatics analysis. *Front. Genet.* 9:265. doi: 10.3389/fgene.2018.00265

Long, J., Delahanty, R. J., Li, G., Gao, Y. T., Lu, W., Cai, Q., et al. (2013). A common deletion in the APOBEC3 genes and breast cancer risk. *J. Natl. Cancer Inst.* 105, 573–579. doi: 10.1093/jnci/djt018

Lopez de Silanes, I., Fan, J., Yang, X., Zonderman, A. B., Potapova, O., Pizer, E. S., et al. (2003). Role of the RNA-binding protein HuR in colon carcinogenesis. *Oncogene* 22, 7146–7154. doi: 10.1038/sj.onc.1206862

Lopez de Silanes, I., Gorospe, M., Taniguchi, H., Abdelmohsen, K., Srikantan, S., Alaminos, M., et al. (2009). The RNA-binding protein HuR regulates DNA methylation through stabilization of DNMT3b mRNA. *Nucleic Acids Res.* 37, 2658–2671. doi: 10.1093/nar/gkp123

Mandal, S., Abebe, F., and Chaudhary, J. (2011). 2′-5′ oligoadenylate synthetase 1 polymorphism is associated with prostate cancer. *Cancer* 117, 5509–5518. doi: 10.1002/cncr.26219

McDonald, E. S., Clark, A. S., Tchou, J., Zhang, P., and Freedman, G. M. (2016). Clinical diagnosis and management of breast cancer. *J. Nucl. Med.* 57(Suppl. 1), 9S–16S. doi: 10.2967/jnumed.115.157834

Meng, Y., Lu, Z., Yu, S., Zhang, Q., Ma, Y., and Chen, J. (2010). Ezrin promotes invasion and metastasis of pancreatic cancer cells. *J. Transl. Med.* 8:61. doi: 10.1186/1479-5876-8-61

Nishida, K., Kuwano, Y., Nishikawa, T., Masuda, K., and Rokutan, K. (2017). RNA binding proteins and genome integrity. *Int. J. Mol. Sci.* 18:1341. doi: 10.3390/ijms18071341

Osborne, M. J., Volpon, L., Kornblatt, J. A., Culjkovic-Kraljacic, B., Baguet, A., and Borden, K. L. (2013). eIF4E3 acts as a tumor suppressor by utilizing an atypical mode of methyl-7-guanosine cap recognition. *Proc. Natl. Acad. Sci. U.S.A.* 110, 3877–3882. doi: 10.1073/pnas.1216862110

Paronetto, M. P., Cappellari, M., Busa, R., Pedrotti, S., Vitali, R., Comstock, C., et al. (2010). Alternative splicing of the cyclin D1 proto-oncogene is regulated by the RNA-binding protein Sam68. *Cancer Res.* 70, 229–239. doi: 10.1158/0008-5472.CAN-09-2788

Perez-Magan, E., Rodriguez de Lope, A., Ribalta, T., Ruano, Y., Campos-Martin, Y., Perez-Bautista, G., et al. (2010). Differential expression profiling analyses identifies downregulation of 1p, 6q, and 14q genes and overexpression of 6p histone cluster 1 genes as markers of recurrence in meningiomas. *Neuro Oncol.* 12, 1278–1290. doi: 10.1093/neuonc/noq081

Quidville, V., Alsafadi, S., Goubar, A., Commo, F., Scott, V., Pioche-Durieu, C., et al. (2013). Targeting the deregulated spliceosome core machinery in cancer cells triggers mTOR blockade and autophagy. *Cancer Res.* 73, 2247–2258. doi: 10.1158/0008-5472.Can-12-2501

Rappa, F., Pitruzzella, A., Marino Gammazza, A., Barone, R., Mocciaro, E., Tomasello, G., et al. (2016). Quantitative patterns of Hsps in tubular adenoma compared with normal and tumor tissues reveal the value of Hsp10 and Hsp60 in early diagnosis of large bowel cancer. *Cell Stress Chaperones* 21, 927–933. doi: 10.1007/s12192-016-0721-5

Ruden, M., and Puri, N. (2013). Novel anticancer therapeutics targeting telomerase. *Cancer Treat. Rev.* 39, 444–456. doi: 10.1016/j.ctrv.2012.06.007

Santangelo, L., Giurato, G., Cicchini, C., Montaldo, C., Mancone, C., Tarallo, R., et al. (2016). The RNA-binding protein SYNCRIP is a component of the hepatocyte exosomal machinery controlling microRNA sorting. *Cell Rep.* 17, 799–808. doi: 10.1016/j.celrep.2016.09.031

Satelli, A., and Li, S. (2011). Vimentin in cancer and its potential as a molecular target for cancer therapy. *Cell. Mol. Life Sci.* 68, 3033–3046. doi: 10.1007/s00018-011-0735-1

Shults, C. L., Dingwall, C. B., Kim, C. K., Pinceti, E., Rao, Y. S., and Pak, T. R. (2018). 17beta-estradiol regulates the RNA-binding protein Nova1, which then regulates the alternative splicing of estrogen receptor beta in the aging female rat brain. *Neurobiol. Aging* 61, 13–22. doi: 10.1016/j.neurobiolaging.2017.09.005

Stockley, J., Villasevil, M. E., Nixon, C., Ahmad, I., Leung, H. Y., and Rajan, P. (2014). The RNA-binding protein hnRNPA2 regulates beta-catenin protein expression and is overexpressed in prostate cancer. *RNA Biol.* 11, 755–765. doi: 10.4161/rna.28800

Tao, Y. W., Lin, Y. C., She, Z. G., Lin, M. T., Chen, P. X., and Zhang, J. Y. (2015). Anticancer activity and mechanism investigation of beauvericin isolated from secondary metabolites of the mangrove endophytic fungi. *Anticancer Agents Med. Chem.* 15, 258–266. doi: 10.2174/1871520614666140825112255

Virtakoivu, R., Mai, A., Mattila, E., De Franceschi, N., Imanishi, S. Y., Corthals, G., et al. (2015). Vimentin-ERK signaling uncouples slug gene regulatory function. *Cancer Res.* 75, 2349–2362. doi: 10.1158/0008-5472.CAN-14-2842

Vivian, J., Rao, A. A., Nothaft, F. A., Ketchum, C., Armstrong, J., Novak, A., et al. (2017). Toil enables reproducible, open source, big biomedical data analyses. *Nat. Biotechnol.* 35, 314–316. doi: 10.1038/nbt.3772

Vogelstein, B., Papadopoulos, N., Velculescu, V. E., Zhou, S., Diaz, L. A. Jr., and Kinzler, K. W. (2013). Cancer genome landscapes. *Science* 339, 1546–1558. doi: 10.1126/science.1235122

Volpon, L., Osborne, M. J., Culjkovic-Kraljacic, B., and Borden, K. L. (2013). eIF4E3, a new actor in mRNA metabolism and tumor suppression. *Cell Cycle* 12, 1159–1160. doi: 10.4161/cc.24566

Wang, Y., Zhang, Y., Huang, Q., and Li, C. (2018). Integrated bioinformatics analysis reveals key candidate genes and pathways in breast cancer. *Mol. Med. Rep.* 17, 8091–8100. doi: 10.3892/mmr.2018.8895

Wu, Y., Davison, J., Qu, X., Morrissey, C., Storer, B., Brown, L., et al. (2016). Methylation profiling identified novel differentially methylated markers including OPCML and FLRT2 in prostate cancer. *Epigenetics* 11, 247–258. doi: 10.1080/15592294.2016.1148867

Wurth, L., and Gebauer, F. (2015). RNA-binding proteins, multifaceted translational regulators in cancer. *Biochim. Biophys. Acta* 1849, 881–886. doi: 10.1016/j.bbagrm.2014.10.001

Zhang, J. Y., Huang, W. J., Sun, H. M., Liu, Y., Zhao, X. Q., Tang, S. L., et al. (2017). Structure identification and in vitro anticancer activity of lathyrol-3-phenylacetate-5,15-diacetate. *Molecules* 22:1412. doi: 10.3390/molecules22091412

Zhang, J., Lai, Z., Huang, W., Ling, H., Lin, M., Tang, S., et al. (2017). Apicidin inhibited proliferation and invasion and induced apoptosis via mitochondrial pathway in non-small cell lung cancer GLC-82 cells. *Anticancer Agents Med. Chem.* 17, 1374–1382. doi: 10.2174/1871520617666170419120044

Zhang, Y., Delahanty, R., Guo, X., Zheng, W., and Long, J. (2015). Integrative genomic analysis reveals functional diversification of APOBEC gene family in breast cancer. *Hum. Genomics* 9:34. doi: 10.1186/s40246-015-0056-9

Conflict of Interest Statement: YZ and FY were employed by company Yidu Cloud Technology Co.

The remaining authors declare that the research was conducted in the absence of any commercial or financial relationships that could be construed as a potential conflict of interest.

frontiers in Oncology

ORIGINAL RESEARCH
published: 01 March 2019
doi: 10.3389/fonc.2019.00120

MiR-1-3p Inhibits Lung Adenocarcinoma Cell Tumorigenesis via Targeting Protein Regulator of Cytokinesis 1

*Tao Li, Xiuxiu Wang, Lijun Jing and Yu Li**

Department of Respiratory Diseases, Qilu Hospital of Shandong University, Jinan, China

Lung adenocarcinoma (LUAD) is one of the most lethal malignancies, posing a threat to human health. However, the molecular mechanisms underlying LUAD development remain largely unknown. In this study, we found that miR-1-3p was significantly downregulated in human LUAD tissues and cell lines and played an inhibitory role in LUAD cell tumorigenesis, as evidenced by the significantly reduced viability, migration, and invasion of LUAD cells in response to miR-1-3p overexpression. Mechanistically, microRNA (miR)-1-3p physically interacted with the 3′-untranslated region (UTR) of protein regulator of cytokinesis 1 (PRC1) mRNA, leading to downregulation of PRC1. Overexpression of PRC1 reversed the inhibitory effects of miR-1-3p on LUAD cell tumorigenesis, suggesting that the miR-1-3p/PRC1 axis is majorly involved in suppressing LUAD development and progression. Consistently, PRC1 was dramatically induced in LUAD tissues and cell lines as well as associated with a poor prognosis in LUAD patients. Taken together, our study identified the miR-1-3p/PRC1 axis as an important regulatory mechanism contributing to LUAD inhibition and provided valuable clues for the future development of therapeutic strategies against LUAD.

Keywords: lung adenocarcinoma, miR-1-3p, protein regulator of cytokinesis 1, malignant behavior, mechanism

OPEN ACCESS

Edited by:
Jian-ye Zhang,
Guangzhou Medical University, China

Reviewed by:
Frank Arfuso,
Curtin University, Australia
Kuzhuvelil B. Harikumar,
Rajiv Gandhi Centre for Biotechnology, India

****Correspondence:***
Yu Li
qlliyures@163.com

Specialty section:
This article was submitted to Cancer Molecular Targets and Therapeutics, a section of the journal Frontiers in Oncology

Received: *13 November 2018*
Accepted: *11 February 2019*
Published: *01 March 2019*

Citation:
Li T, Wang X, Jing L and Li Y (2019) MiR-1-3p Inhibits Lung Adenocarcinoma Cell Tumorigenesis via Targeting Protein Regulator of Cytokinesis 1. Front. Oncol. 9:120. doi: 10.3389/fonc.2019.00120

INTRODUCTION

Lung adenocarcinoma (LUAD) is the most common subtype of non-small cell lung cancer (NSCLC), accounting for 80–85% of all lung cancers; worldwide, approximately 40% of all lung cancer patients are diagnosed with LUAD (1). Compared to other subtypes of NSCLC, LUAD has a higher incidence and a shorter survival time among patients, with a 5-year survival rate as low as 10–15% (2, 3); thus, LUAD poses a serious threat to human health. Currently, chemotherapy is a relatively effective therapeutic option for NSCLC (4). However, the existence and development of intrinsic or acquired chemoresistance greatly limit the application of chemotherapy in cancer treatment. Therefore, there is still an urgent need to develop novel therapeutic strategies against LUAD that are based on the mechanisms underlying the development and progression of LUAD.

MicroRNAs (miRNAs) are a class of small endogenous non-coding RNA molecules (∼22 nucleotides) found in animals and plants that are responsible for the degradation or translation repression of mRNAs by binding to the 3′-untranslated region (UTR) of target mRNAs (5). A variety of miRNAs have been identified as novel biomarkers or promising therapeutic targets of human malignant tumors. Among them, miR-1-3p plays an antitumor role in multiple cancer

types, including rhabdomyosarcoma as well as lung, thyroid, prostatic, bladder, colorectal, and hepatocellular carcinomas (6–11). However, the role of miR-1-3p in LUAD has not yet been investigated. In addition, the association between miR-1-3p and its target genes may deepen our understanding of the molecular mechanisms contributing to LUAD development, thus facilitating the discovery of improved therapies for LUAD.

The microtubule-associated protein regulator of cytokinesis 1 (PRC1) has been found to be majorly involved in the organization of antiparallel microtubules in the central spindle during cytokinesis. The human PRC1 gene, located on chromosome 15q26.1, encodes a 620-amino-acid protein with a molecular weight of 71 kDa (3). An abnormally high expression of PRC1 has been observed in breast cancer (12), bladder cancer (13), hepatocellular carcinoma (14), and pancreatic cancer (15), which suggests a promotive role of PRC1 in tumorigenesis. However, it remains largely unknown whether there is a functional association between miR-1-3p and the regulation of PRC1 in LUAD. In this study, we examined the role of miR-1-3p in LUAD growth and metastasis as well as the underlying mechanism.

MATERIALS AND METHODS

Tissue Samples From LUAD Patients

Human LUAD tissues were collected from LUAD patients undergoing pulmonary resection or bronchoscopy biopsy, and normal tissues adjacent to cancer were collected from LUAD patients undergoing pulmonary resection at Qilu Hospital between May and September 2018. None of the patients had received chemotherapy or radiotherapy prior to surgery. All the fresh samples were stored in RNAlater Stabilization Solution (Ambion) at −80°C until use. This study was approved by the Ethics Committee of Shandong University, and written informed consent was obtained from all patients prior to enrollment in the present study. The clinicopathological characteristics of the patients are shown in **Supplementary Table 1**.

Cell Culture

Three LUAD cell lines (A549, H1299, and H1975 cells) and a human alveolar epithelial cell line (HPAEpiC) were purchased from the Cell Bank of the Type Culture Collection of the Chinese Academy of Sciences (Shanghai, China). The cells were maintained in RPMI 1640 medium (Gibco, USA) containing 10% fetal bovine serum (Gibco, USA), 100 U/mL penicillin, and 100 μg/mL streptomycin in a humidified atmosphere of 5% CO_2 at 37°C. Cells in the exponential phase of growth were used for the following experiments.

Construction of the miR-1-3p Overexpression Cell Lines

The pre-miR-1-3p sequences were synthesized by Biosune Biotechnology Company (Shanghai, China) and cloned into the lentiviral vector pGIPZ. Lentivirus was produced in HEK293T cells using the packaging vectors psPAX2 and pMD2.G. The cells were infected with lentivirus for 24 h and then cultured for 1 week in medium containing 2 μg/mL puromycin (Merck Millipore, USA) for screening to acquire cells with stable expression of miR-1-3p.

Transient Transfection

The miR-1-3p mimic and its negative control (NC) were chemically synthesized by GenePharma Co., Ltd. (Shanghai, China). The cells were transiently transfected with 50 nM miR-1-3p mimic or 50 nM NC (Boshang, Inc., China) using Lipofectamine 2000 (Invitrogen; Thermo Fisher Scientific, Inc.), according to the manufacturer's protocol. The cells were harvested at 24 or 48 h after the transfection. The NC was a scrambled oligonucleotide that does not encode any known miRNA. The transfection efficiency was confirmed by detecting the miR-1-3p expression level using the SYBR green (Takara)-based real-time quantitative polymerase chain reaction (qPCR) system.

RNA Isolation and qPCR

Total RNA was extracted from the cells using Trizol reagents (Invitrogen; Thermo Fisher Scientific, Inc.), according to the manufacturer's instructions. The cDNA of miRNA was synthesized with the One Step PrimeScript miRNA cDNA Synthesis Kit (Takara Biotechnology, Co., Ltd., Dalian, China). qPCR was performed using the SYBR green Premix Ex Taq II (Takara Biotechnology, Co., Ltd.) with the Step One Plus Real-Time PCR System (Applied Biosystems; Thermo Fisher Scientific, Inc.). The expression of U6 was used as an internal control. The primers for miR-1-3p are indicated in **Supplementary Table 2**.

Western Blot Analysis

The cells were lysed in ice-cold RIPA lysis buffer, and the cell lysates were obtained by centrifugation at 12,000 rpm and 4°C for 10 min. The protein concentration was determined using the bicinchoninic acid method. The protein samples (5–10 μg) were separated by sodium dodecyl sulfate–polyacrylamide gel electrophoresis, followed by transfer to polyvinylidene difluoride membranes, and then immunoblotted with the indicated antibodies. After blocking with 5% nonfat milk, the membranes were incubated with the respective primary antibody overnight at 4°C, followed by incubation with the horseradish peroxidase-coupled secondary antibody for 1 h at room temperature. The protein bands were visualized using enhanced chemiluminescence reagents (PerkinElmer) with an ImageQuant LAS 4000 system (GE Healthcare Life Sciences). The following antibodies were used: anti-PRC1, anti-fibronectin, anti-N-cadherin, anti-vimentin, and anti-β-actin (Cell Signaling Technology).

3-(4,5-Dimethylthiazol-2-yl)-2,5-Diphenyltetrazolium Bromide (MTT) Assay

The cells were seeded into 96-well plates at a density of 2,000 cells/well and grown for 5 days. After the addition of 100 μL of 5 mg/mL MTT solution, the cells were incubated for an additional 4 h at 37°C, and then the supernatant was removed and dissolved in 100 μL of dimethyl sulfoxide (Sigma-Aldrich).

Cell viability was assessed on the 1st, 2nd, 3rd, 4th, and 5th day. The absorbance of each well was measured in triplicate using an iMark Microplate Absorbance Reader (Bio-Rad).

Luciferase Reporter Assay

Luciferase reporter constructs containing wild-type (WT) or mutant PRC1 3′-UTR (pmirGLO-PRC1-WT or pmirGLO-PRC1-mut, respectively) were generated by GenePharma Inc. (Shanghai, China). The cells were cotransfected with 25 ng of PRC1 3′-UTR reporter constructs and 20 nM miR-1-3p mimic using Lipofectamine 2,000 (Invitrogen) in 24-well plates. At 24 h after transfection, luciferase assays were performed using the Dual-Luciferase reporter assay system (Promega). *Renilla* luciferase activity was used to normalize the luciferase activity of the PRC1 3′-UTR reporter constructs.

In vivo Tumorigenicity Assays

Four-week-old male BALB/c nude mice were purchased from the Shanghai Laboratory Animal Center of the Chinese Academy of Sciences (Shanghai, China). The mice were randomly divided into two groups and injected subcutaneously with A549 cells (2×10^6 cells/mouse, $n = 5$ mice/group) that were infected with either control lentivirus or miR-1-3p-overexpressing lentivirus. Tumor growth was monitored by measuring the tumor diameter. Tumor

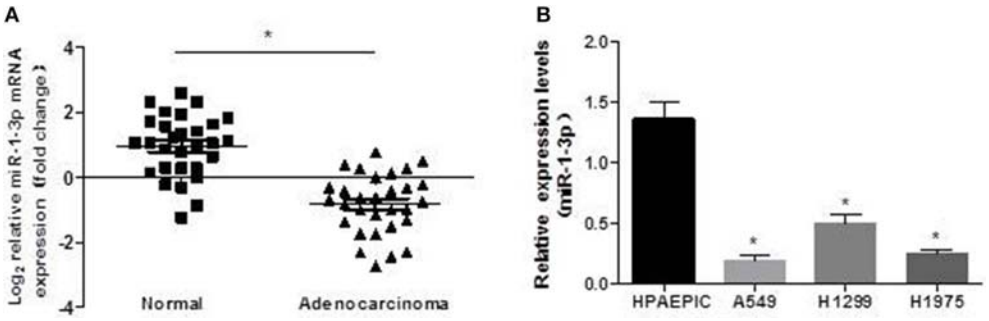

FIGURE 1 | Expression pattern of miR-1-3p in human LUAD tissues and cell lines. qPCR was performed to determine the expression levels of miR-1-3p in human LUAD tissues **(A)** and cell lines **(B)**, as indicated. *$P < 0.05$ in **(A)** ($n = 30$); *$P < 0.05$ vs. HPAEpiCs in **(B)** ($n = 3$).

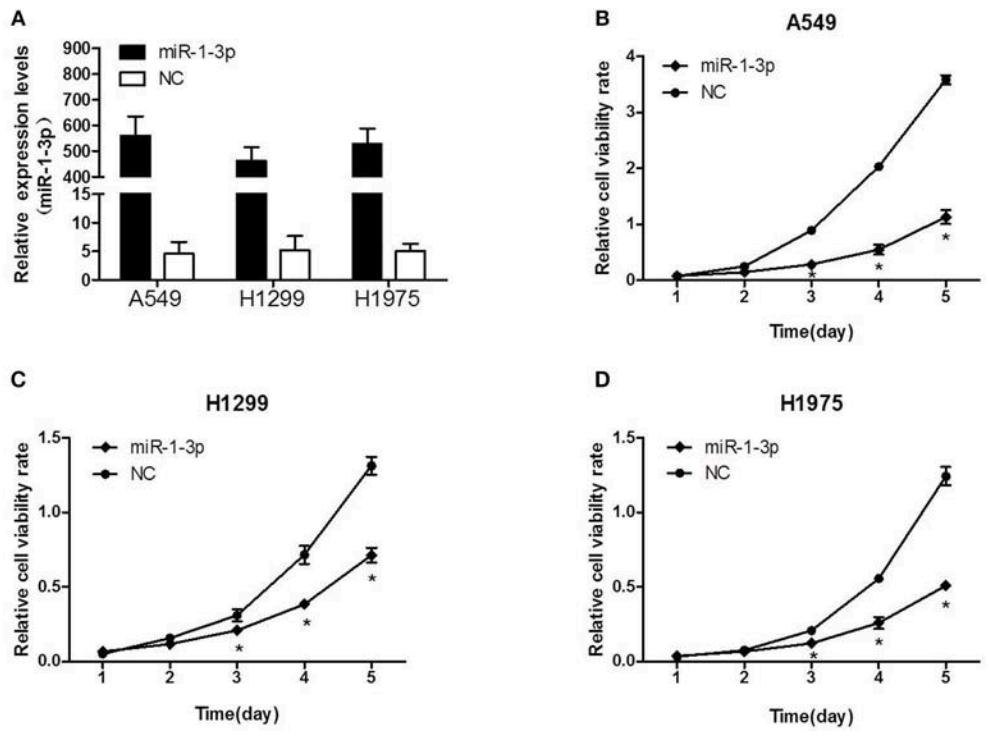

FIGURE 2 | The effect of miR-1-3p overexpression on LUAD cell viability. **(A)** qPCR was performed to validate the overexpression efficiency of miR-1-3p in A549, H1299, and H1975 cells. **(B–D)** The MTT assay was performed to measure the viability of miR-1-3p-overexpressing A549, H1299, and H1975 cells. *$P < 0.05$ vs. the corresponding negative control (NC) groups ($n = 3$).

volume was calculated according to the formula TV (cm^3) = a × b^2 × π/6, where a is the longest diameter and b is the shortest diameter. The mice were sacrificed after 3 weeks, and then the tumors were excised and weighed. All animal experiments were approved by the Shandong University Animal Care and Use Committee.

Bioinformatics Analyses

PRC1 genetic alterations and copy number variation in LUAD were retrieved from the cBioPortal for Cancer Genomics (http://www.cbioportal.org/) (16, 17). The Cancer Genome Atlas RNA expression data of LUAD tissues were processed and analyzed by the Cancer Genomics Browser (https://xena.ucsc.edu/welcome-to-ucsc-xena/) (18). The PRC1 expression levels and copy number variation were analyzed by Proteinatlas (https://www.proteinatlas.org/), Oncomine (www.oncomine.org) (19), and Gene Expression Profiling Interactive Analysis (http://gepia.cancer-pku.cn/) in LUAD and normal lung tissues via immunohistochemistry. Kaplan–Meier plots (http://kmplot.com/analysis/) (20) were used to analyze the overall survival of the LUAD patients.

Statistical Analysis

Statistical analysis was performed using GraphPad Prism 6.0 (GraphPad Software, La Jolla, CA, USA). Data are expressed as the mean ± standard deviation. Comparison between two groups was performed using the Student's *t*-test or the Mann-Whitney *U*-test. The correlation between the expression levels of miR-1 and PRC1 was analyzed using Pearson's correlation analysis. LUAD tissues with lower miR-1 and PRC1 expression than the median expression were assigned to the low-expression group, whereas those with higher miR-1 and PRC1 expression than the median expression were assigned to the high-expression group. Associations between the clinicopathological features and the expression levels of miR-1 and PRC1 were analyzed using the χ^2 test. Overall survival curves were determined according to the Kaplan–Meier method. A $p < 0.05$ was considered statistically significant.

RESULTS

MiR-1-3p Is Downregulated in Human LUAD Tissues and Cell Lines

To investigate the possible role of miR-1-3p in LUAD development, we first examined the expression levels of miR-1-3p in human LUAD tissues and cell lines. As shown in **Figure 1A**, miR-1-3p expression was significantly decreased in LUAD tissues, compared with the matched adjacent normal lung tissues. Similarly, marked downregulation of miR-1-3p was also observed in the human LUAD cell lines A549, H1299, and H1975,

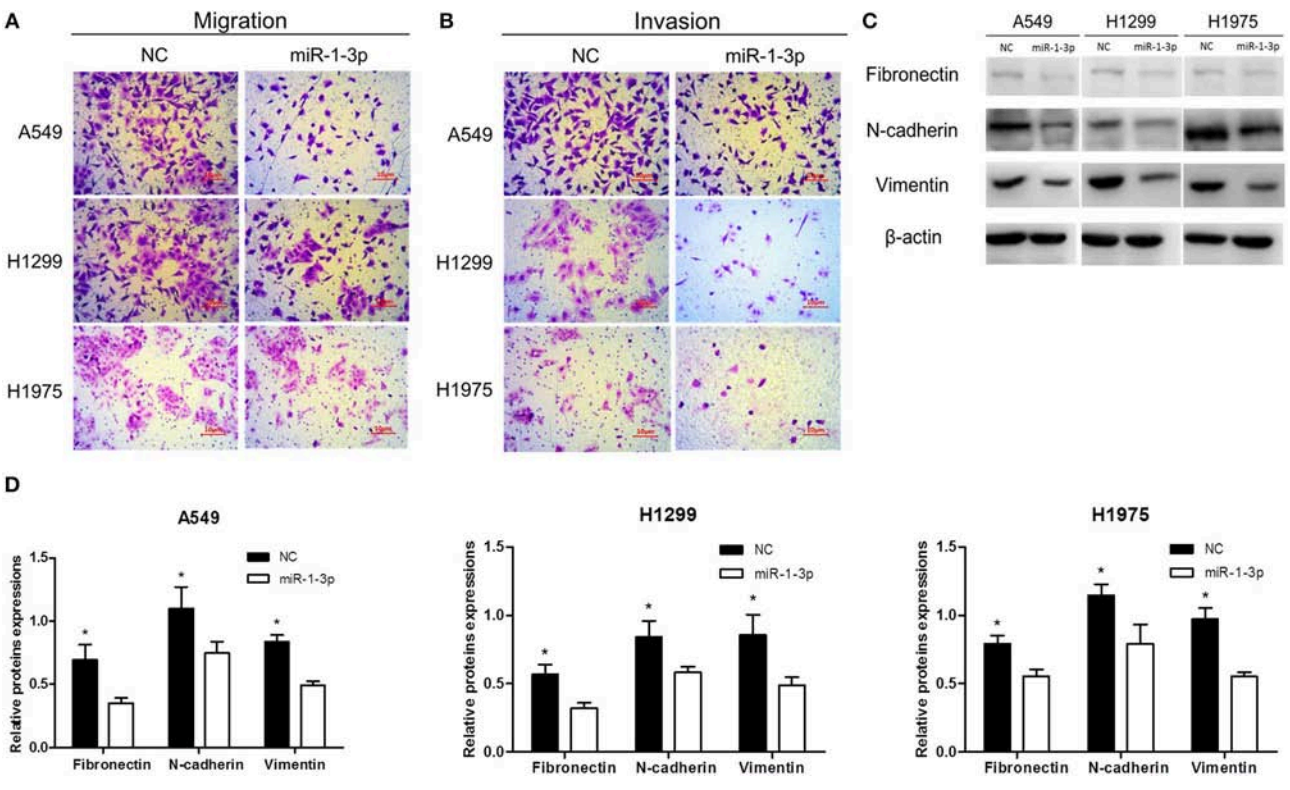

FIGURE 3 | The effect of miR-1-3p overexpression on LUAD cell migration and invasion as well as epithelial-mesenchymal transition. Transwell assays for migration **(A)** and invasion **(B)** of miR-1-3p-overexpressing LUAD cells. **(C)** Western blot assay for the expression of the indicated mesenchymal markers. β-Actin was used as an internal control. **(D)** Quantification of the western blot assay results shown in **(C)**. *$P < 0.05$ vs. miR-1-3p groups in **(C)** ($n = 3$).

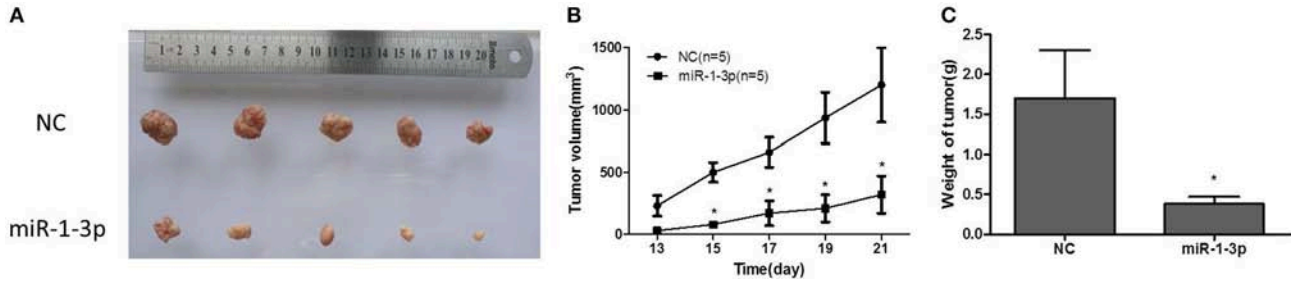

FIGURE 4 | The effect of miR-1-3p overexpression on tumorigenesis *in vivo*. **(A)** Overexpression of miR-1-3p reduced LUAD cell-derived tumor growth in a xenograft model. **(B)** Summary of the tumor growth data; the error bars indicate the standard deviation. **(C)** miR-1-3p overexpression results in a decline of tumor weight. $^*P < 0.05$.

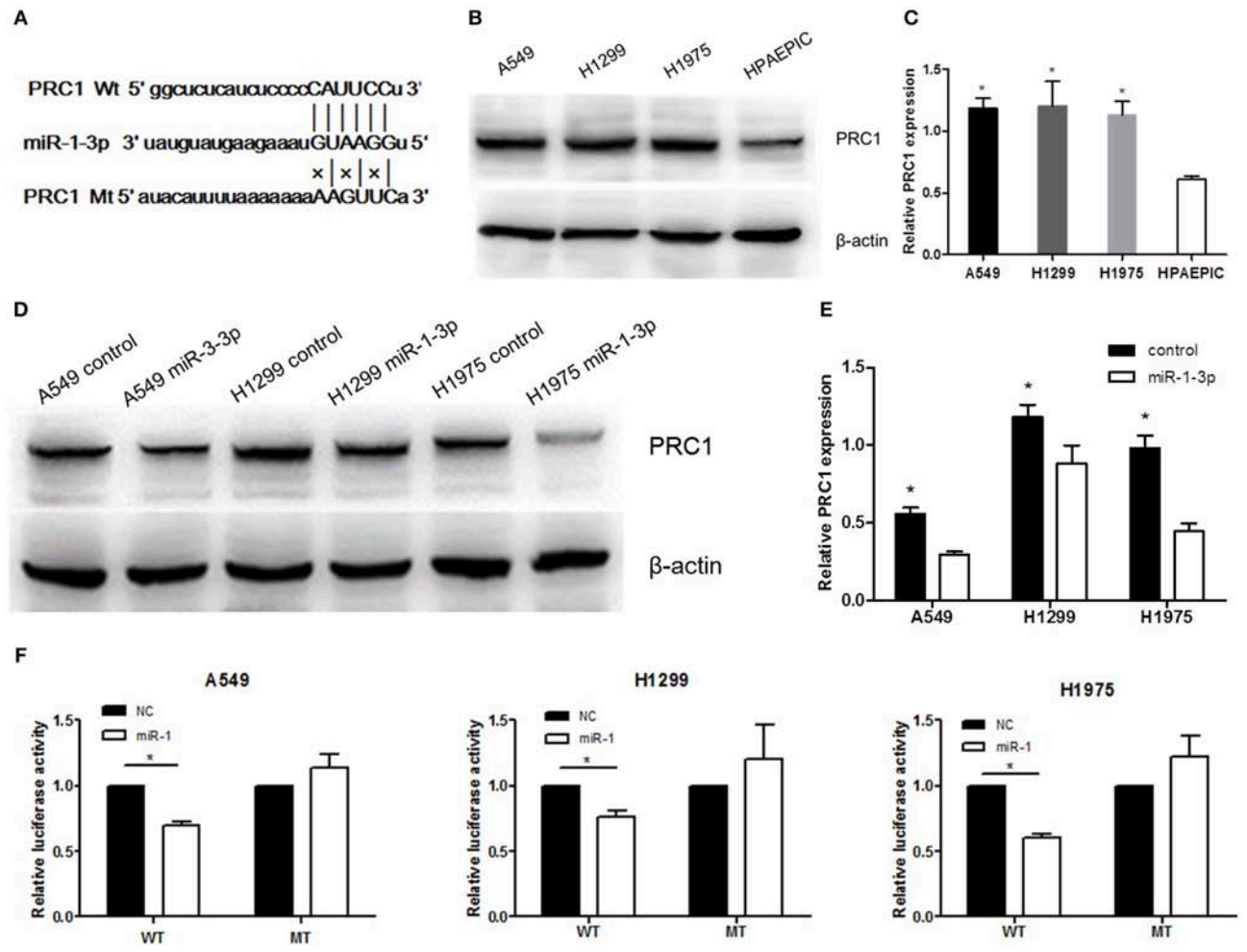

FIGURE 5 | PRC1 is a direct target of miR-1-3p in LUAD cells. **(A)** The putative miR-1-3p-binding sites in PRC1 3′-UTR and the mutated binding sites are shown. **(B,D)** Western blot analysis of PRC1 expression in the nontransfected negative control (NC)- or miR-1-3p-transfected LUAD cells. β-Actin was used as an internal control. **(C)** Quantification of the western blot assay results shown in **(B)**. $^*P < 0.05$ vs. HPAEpiCs ($n = 3$). **(E)** Quantification of the western blot assay results shown in **(D)**. $^*P < 0.05$ vs. the miR-1-3p groups ($n = 3$). **(F)** Luciferase reporter assay for LUAD cells transfected with wild-type (WT) or mutated (MT) pGL3-3′-UTR. The luciferase activity was normalized to *Renilla* luciferase activity. $^*P < 0.05$ ($n = 3$).

compared with the normal HPAEpiCs (**Figure 1B**). These *in vivo* and *in vitro* results suggest that miR-1-3p may play an inhibitory role in LUAD development.

Overexpression of miR-1-3p Suppresses LUAD Cell Viability *in vitro*

Next, we sought to investigate whether miR-1-3p indeed plays a role in suppressing LUAD development using a gain-of-function assay. As shown in **Figure 2A**, transfection of the miR-1-3p mimic led to a dramatic increase in miR-1-3p expression in the LUAD cell lines A549, H1299, and H1975. Importantly, overexpression of miR-1-3p significantly inhibited the viability of these three cell lines in a time-dependent manner, compared with the NC groups (**Figures 2B–D**). These results demonstrate that miR-1-3p is sufficient to suppress LUAD cell growth *in vitro*.

Overexpression of miR-1-3p Inhibits LUAD Cell Migration and Invasion *in vitro*

To further investigate whether miR-1-3p inhibits LUAD progression, Transwell assays were performed to examine the effects of miR-1-3p overexpression on LUAD cell migration and invasion. As shown in **Figures 3A,B**, overexpression of miR-1-3p resulted in a significant decrease in LUAD cell migration and invasion abilities, compared with the NC groups. Consistently, overexpression of miR-1-3p markedly suppressed epithelial-mesenchymal transition (EMT), a process contributing to tumor metastasis, as evidenced by downregulation of the mesenchymal markers fibronectin, N-cadherin, and vimentin (**Figures 3C,D**). These data suggest that miR-1-3p overexpression may suppress LUAD progression through reducing LUAD cell migration and invasion as well as inhibiting EMT in these cells.

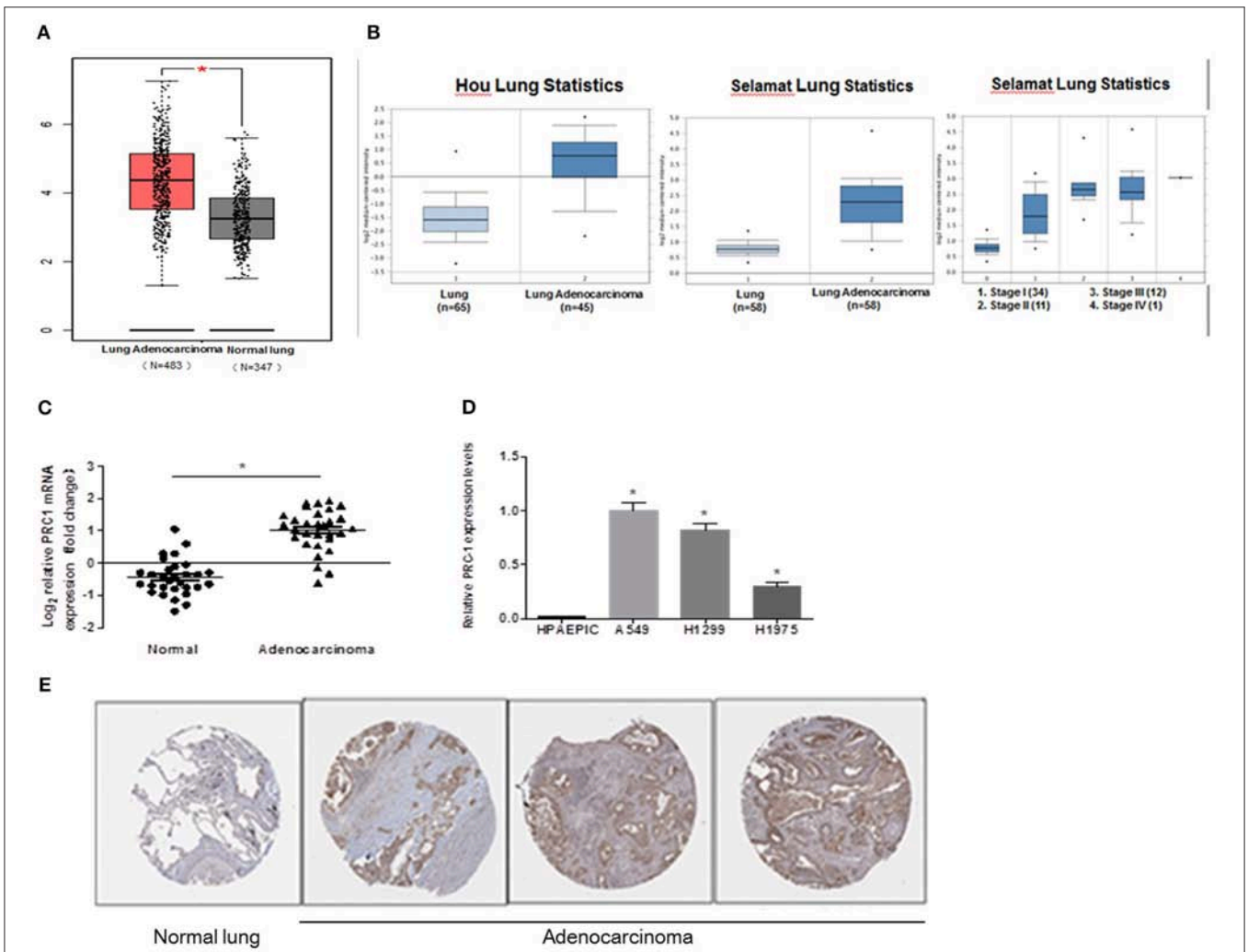

FIGURE 6 | Expression pattern of PRC1 in LUAD tissues and cell lines. **(A)** The data of copy number variation in LUAD from The Cancer Genome Atlas cohort. **(B)** The mRNA expression of PRC1 in different TNM staging groups in Oncomine. **(C)** qPCR analysis of PRC1 expression in LUAD tissues ($n = 30$). **(D)** qPCR analysis of PRC1 expression in LUAD cells and HPAEpiCs. **(E)** Representative images of the immunohistochemical staining of PRC1 from The Human Protein Atlas in LUAD and normal lung tissues. *$P < 0.05$ in **(C)** ($n = 30$); *$P < 0.05$ vs. HPAEpiCs in **(D)** ($n = 3$).

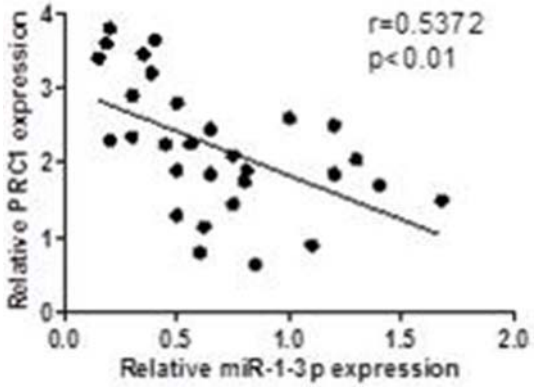

FIGURE 7 | Association between the miR-1-3p and PRC-1 levels in LUAD patients. The PRC1 and miR-1 levels were determined by qPCR in LUAD tissues and matched adjacent normal tissues ($n = 30$).

miR-1-3p Inhibits Xenograft Tumor Growth of LUAD Cells

To further explore whether miR-1-3p overexpression could suppress LUAD growth *in vivo*, human LUAD A549 cells with and without miR-1-3p overexpression were subcutaneously inoculated into nude mice. At 1 week after inoculation, all mice had developed detectable tumors. However, at 3 weeks after inoculation, the mice bearing tumors with miR-1-3p overexpression demonstrated a dramatic decrease in the tumor size and weight (**Figures 4A–C**), compared to the control groups. These results show that overexpression of miR-1-3p inhibits tumorigenesis *in vivo*.

PRC1 Is a Direct Target Gene of miR-1-3p

To further examine the mechanism underlying miR-1-3p-mediated suppression of LUAD development and progression, we employed the TargetScan computational algorithm to predict the target genes of miR-1-3p (21). The results indicated complementary base-pairing between miR-1-3p and the 3′-UTR of PRC1 (**Figure 5A**), suggesting that PRC1 may be a target gene of miR-1-3p. To verify this finding, we detected the expression of PRC1 in LUAD cells. As shown in **Figures 5B,C**, the protein expression of PRC1 was markedly induced in LUAD cells, compared with normal HPAEpiCs, consistent with the expression pattern of miR-1-3p in LUAD tissues and cells. Importantly, miR-1-3p overexpression led to downregulation of PRC1 in LUAD cells (**Figures 5D,E**), confirming that PRC1 is a downstream target of miR-1-3. To determine whether PRC1 is directly targeted by miR-1-3p, we performed a mutation assay through introducing a PRC1 3′-UTR mutation in the pmirGLO vector. The results demonstrated that the PRC1 3′-UTR mutation had no significant effect on the luciferase activity in miR-1-3p-transfected LUAD cells, compared with that in the NC-transfected cells (**Figure 5F**), suggesting that WT PRC1 3′-UTR is essential for the function of miR-1-3p. Taken together, our data show that PRC1 is a direct downstream target gene of miR-1-3p.

PRC1 Is Induced in LUAD Tissues and Cell Lines

To determine whether PRC1 contributes to LUAD development and progression, we examined the expression profile of PRC1 in LUAD tissues using the publicly accessible database Oncomine. As shown in **Figure 6A**, the mRNA expression levels of PRC1 were significantly enhanced in the LUAD tissues, compared with the normal lung tissues. In addition, we also analyzed the mRNA expression of PRC1 in LUAD tissues using two microarray datasets from the Hou and Selamat lung cancer groups, which were downloaded from Oncomine. The results demonstrated that the mRNA expression of PRC1 was significantly induced in the LUAD tissues of these groups and positively correlated with the tumor, lymph node, metastasis (TNM) staging of LUAD (**Figure 6B**). These findings were further confirmed by our mRNA expression data of PRC1 and the immunohistochemical staining of PRC1 in human LUAD tissues and matched adjacent normal lung tissues (**Figures 6C,E**). For the *in vitro* study, the mRNA levels of PRC1 were dramatically increased in the LUAD cell lines A549, H1299, and H1975, compared to those in normal HPAEpiCs (**Figure 6D**). Collectively, these results suggest that PRC1 may be involved in LUAD development and progression.

Correlation of miR-1-3p/PRC1 and Clinicopathological Characteristics of LUAD Patients

To investigate whether the miR-1-3p/PRC1 axis plays a role in LUAD development, we first analyzed the association between the miR-1-3p and PRC1 levels in LUAD tissues. The results revealed that the miR-1-3p levels were negatively correlated with the PRC1 mRNA expression ($r = -0.5858$; $P < 0.01$; **Figure 7**) in the LUAD tissues. Importantly, low levels of miR-1-3p and high levels of PRC1 were strongly associated with the TNM stage, lymph node metastasis, and distant metastasis (**Table 1**). These data suggest that LUAD development may be at least partially attributable to the miR-1-3p/PRC1 axis.

miR-1-3p Inhibits LUAD Cell Metastasis via PRC1

To determine whether miR-1-3p-mediated suppression of PRC1 expression is a major mechanism inhibiting LUAD development and progression, we cotransfected LUAD cells with miR-1-3p and a PRC1-overexpression plasmid for Transwell assays. The plasmid transfection efficacy of miR-1-3p and PRC1 was validated in **Figures 8A,B**. We found that miR-1-3p significantly inhibited the migration and invasion of three LUAD cell lines and that the inhibitory effects of miR-1-3p were markedly reversed by PRC1 overexpression (**Figures 8C–E**), suggesting that miR-1-3p inhibits LUAD cell metastasis in a PRC1-depedent manner and the miR-1-3p/PRC1 axis is majorly involved in LUAD development and progression.

Overexpression of PRC1 Is Associated With a Poor Prognosis in LUAD Patients

MiR-1-3p functions through suppressing PRC1 expression, suggesting a promotive role of PRC1 in LUAD development. To

TABLE 1 | The clinicopathological characteristics of 30 lung adenocarcinoma patients.

Clinicopathological features	*n*	Percent (%)	PRC1 expression		*p*	miR-1-3p expression		*p*
			Low ($n = 9$)	High ($n = 21$)		Low ($n = 18$)	High ($n = 12$)	
GENDER								
Male	19	63.33	7	12	0.419	11	9	0.694
Female	11	36.67	2	9	–	7	3	–
AGE (YEARS)								
≤60	13	43.33	6	7	0.123	8	5	1.000
>60	17	56.67	3	14	–	10	7	–
TUMOR SIZE								
T1 and T2	6	20.00	1	5	0.637	4	2	1.000
T3 and T4	24	80.00	8	16	–	14	10	–
TNM STAGE								
I and II	7	23.33	5	2	0.014	1	6	0.009
III and IV	23	76.67	4	19	–	17	6	–
LYMPHATIC METASTASIS								
Negative	12	40.00	8	4	0.001	2	10	0.000
Positive	18	60.00	1	17	–	16	2	–
DISTANT METASTASIS								
M0	12	40.00	7	5	0.013	3	9	0.002
M1	18	60.00	2	16	–	15	3	–

TNM, tumor, lymph node, metastasis stage.

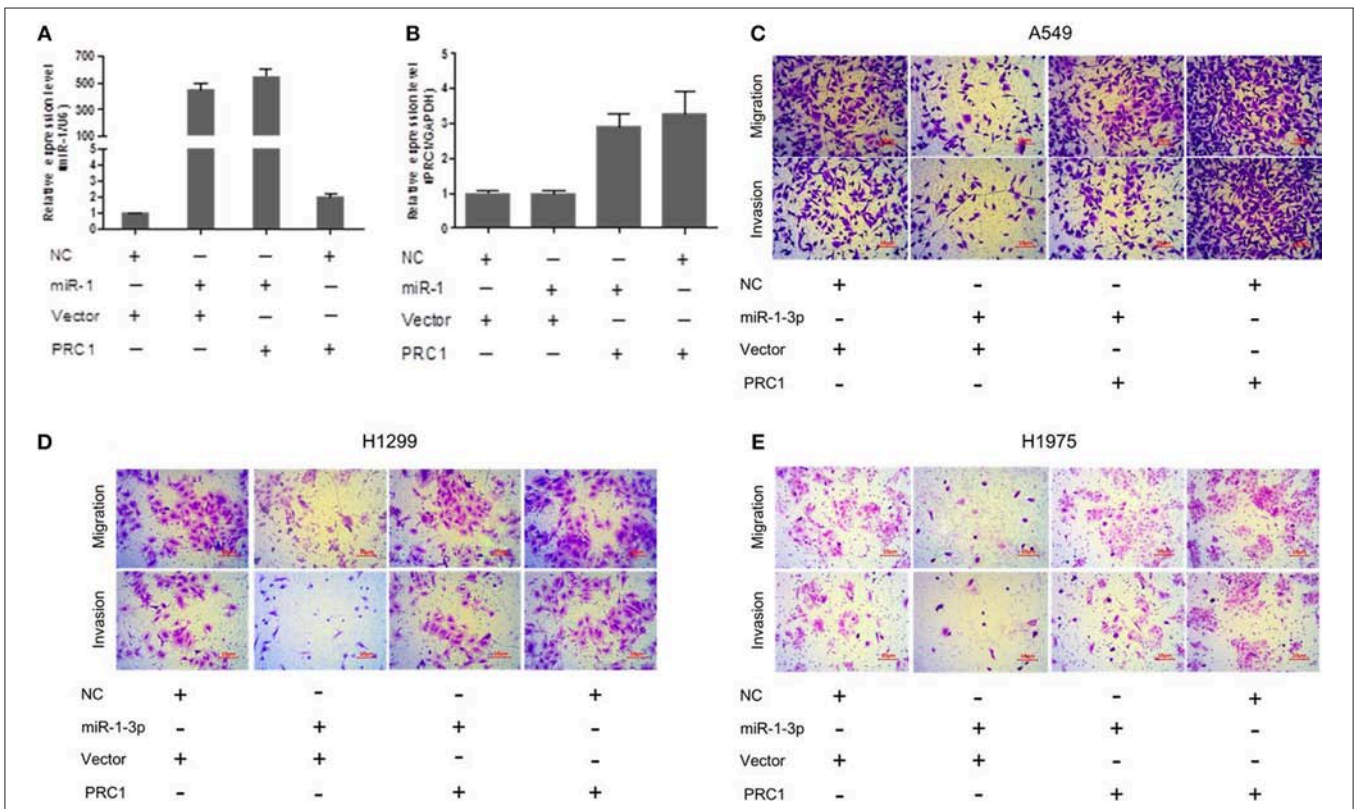

FIGURE 8 | miR-1-3p inhibits LUAD cell migration and invasion via PRC1. **(A,B)** qPCR analysis of the transfection efficiency of the miR-1-3p mimic and the PRC1-overexpression plasmid in LUAD cells. **(C–E)** Transwell assays for migration and invasion of LUAD cells transfected with the miR-1-3p mimic and/or the PRC1-overexpression plasmid.

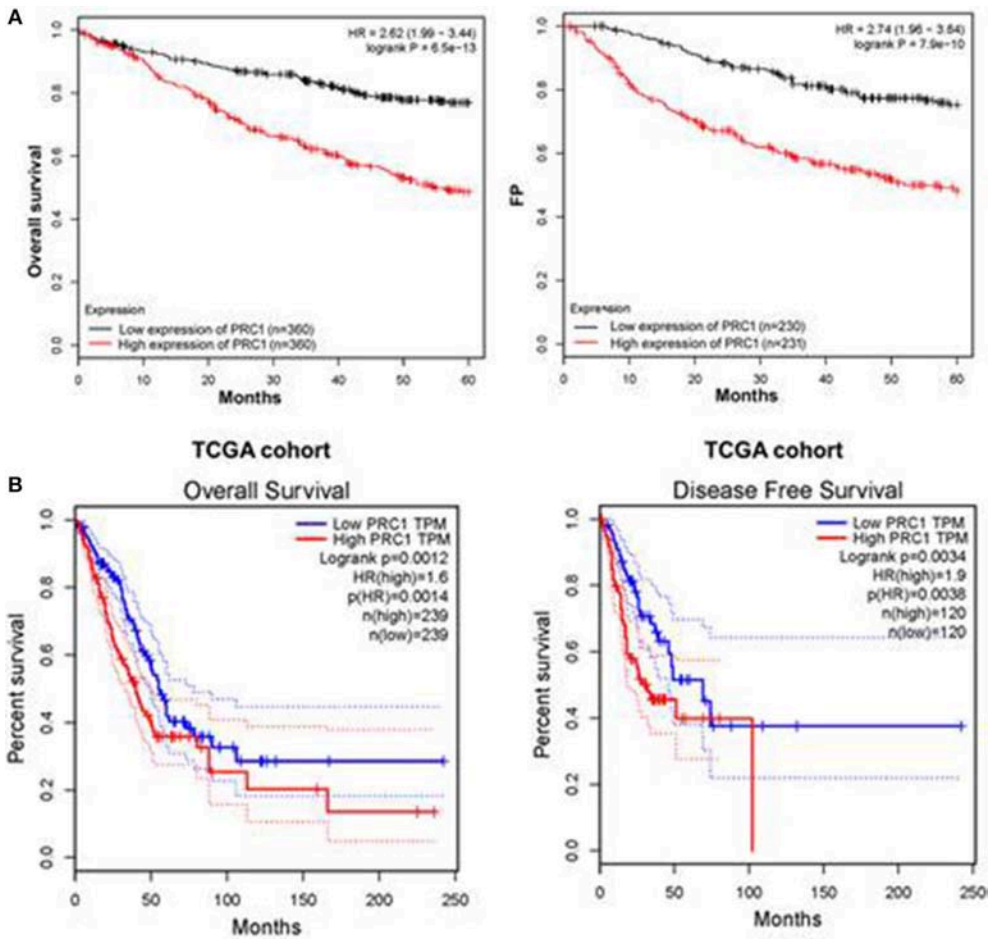

FIGURE 9 | Overexpression of PRC1 is associated with a poor prognosis in LUAD patients. **(A)** The prognostic effect of PRC1 in LUAD patients was evaluated using Kaplan–Meier plots. **(B)** The overall and disease-free survival rates in LUAD patients with different PRC1 expression patterns were evaluated for The Cancer Genome Atlas (TCGA) cohort.

confirm this, we examined the prognostic effect of PRC1 in LUAD patients from a public database by performing Kaplan–Meier analysis (http://www.kmplot.com). The results showed that the LUAD patients with a higher mRNA expression of PRC1 had shorter overall and disease-free survival times than those with a lower mRNA expression of PRC1 (**Figures 9A,B**). These data suggest that PRC1 overexpression may serve as a biomarker of a poor prognosis for LUAD patients, further supporting our findings that miR-1-3p plays a key role in inhibiting LUAD development through targeting PRC1.

DISCUSSION

Carcinogenesis of LUAD is a complex and multistage process involving the regulation of a wide range of genes by miRNAs (22–24). Among them, miR-1-3p, a muscle-specific miRNA, has been shown to play a key role in skeletal muscle differentiation and have inhibitory effects on the growth, migration, and invasion of LUAD (25). The present study revealed that miR-1-3p was significantly downregulated in LUAD tissues and cells. Lower levels of miR-1-3p were strongly associated with a higher TNM stage, earlier lymph node metastasis, and more distant metastasis. Therefore, miR-1-3p is suggested as a tumor suppressor in LUAD. The detection of miR-1-3p expression may be a valuable tool to evaluate the invasion and metastasis of LUAD.

There are hundreds of possible target genes of miR-1-3p, among which PRC1 is a critical protein in cytokinesis and characterized as a mitotic spindle-associated cyclin-dependent kinase substrate (26). Previous studies have provided evidence that PRC1 is involved in different types of cancer (27, 28). Loss of PRC1 leads to the accumulation of bi- and multi-nucleated cells in lung cancer, which further supports its role as the major central spindle organizer in cytokinesis (29). In view of our findings that miR-1-3p overexpression inhibits LUAD cell viability, there is a possibility that the function of PRC1 in apoptosis and senescence is due to induction of miR-1-3p. In this study, we demonstrated that the function of miR-1-3p could be suppressed by dysregulated expression of PRC1. In accordance with the above-mentioned studies, we confirmed that the overexpression of PRC1 significantly promoted the viability, invasion, and migration of LUAD cells. A higher PRC1

expression was also related to a worse outcome in patients with LUAD. Because Wnt/β-catenin signaling is dysregulated in lung cancer (30) and the overexpression of Wnt proteins (Wnt1 and Wnt5a) is significantly associated with adverse outcomes in lung cancer patients (31), we speculate that the miR-1-3p/PRC1 axis participates in dysregulation of Wnt/β-catenin signaling in LUAD development (32); however, this hypothesis requires further investigation. Although our study demonstrated that the miR-1-3p/PRC1 axis is a major mechanism underlying LUAD development, we do not exclude the possibility that other miRNAs or protein regulators besides miR-1-3p/PRC1 are also involved in LUAD pathogenesis. Therefore, more research is needed.

In summary, we identified miR-1-3p as a novel regulator of PRC1 in LUAD. A high PRC1 expression correlates with a poor prognosis in LUAD patients. Thus, targeting miR-1-3p/PRC1 may be a potential therapeutic intervention for the treatment of LUAD.

ETHICS STATEMENT

The Ethics Committee of Qilu Hospital at Shandong University approved this study [KYLL-2018 (KS)-156]. All participants in this study provided informed consent.

AUTHOR CONTRIBUTIONS

TL designed the questionnaire and drafted the manuscript. XW did the statistical analysis. TL and LJ did the relationship analysis and collected the data. YL conceived the study, supervised and reviewed the entire study, and edited the manuscript.

SUPPLEMENTARY MATERIAL

The Supplementary Material for this article can be found online at: https://www.frontiersin.org/articles/10.3389/fonc.2019.00120/full#supplementary-material

REFERENCES

1. Siegel RL, Miller KD, Jemal A. Cancer statistics. *CA Cancer J Clin.* (2017) 67:7–30. doi: 10.3322/caac.21387
2. Zhang W, Fan J, Chen Q, Lei C, Qiao B, Liu Q. SPP1 and AGER as potential prognostic biomarkers for lung adenocarcinoma. *Oncol Lett.* (2018) 15:7028–36. doi: 10.3892/ol.2018.8235
3. Jiang W, Jimenez G, Wells NJ, Hope TJ, Wahl GM, Hunter T, et al. PRC1: a human mitotic spindle-associated CDK substrate protein required for cytokinesis. *Mol Cell.* (1998) 2:877–85. doi: 10.1016/S1097-2765(00)80302-0
4. Peters S, Popat S, Reinmuth N, De Ruysscher D, Kerr KM, Peters S, et al. Metastatic non-small-cell lung cancer (NSCLC): ESMO clinical practice guidelines for diagnosis, treatment and follow-up. *Ann Oncol.* (2012) 23(Suppl. 7):vii56–64. doi: 10.1093/annonc/mds226
5. Leva GD, Croce CM. The role of microRNAs in the tumorigenesis of ovarian cancer. *Front Oncol.* (2013) 3:153. doi: 10.3389/fonc.2013.00153
6. Han C, Yu Z, Duan Z, Kan Q. Role of microRNA-1 in human cancer and its therapeutic potentials. *Biomed Res Int.* (2014) 2014:428371. doi: 10.1155/2014/428371
7. Li J, Guan J, Long X, Wang Y, Xiang X. mir-1-mediated paracrine effect of cancer-associated fibroblasts on lung cancer cell proliferation and chemoresistance. *Oncol Rep.* (2016) 35:3523–31. doi: 10.3892/or.2016.4714
8. Li SM, Wu HL, Yu X, Tang K, Wang SG, Ye ZQ, et al. The putative tumour suppressor miR-1–3p modulates prostate cancer cell aggressiveness by repressing E2F5 and PFTK1. *J Exp Clin Cancer Res.* (2018) 37:219. doi: 10.1186/s13046-018-0895-z
9. Diniz GP, Lino CA, Moreno CR, Senger N, Barreto-Chaves MLM. MicroRNA-1 overexpression blunts cardiomyocyte hypertrophy elicited by thyroid hormone. *J Cell Physiol.* (2017) 232:3360–8. doi: 10.1002/jcp.25781
10. Gao L, Yan P, Guo FF, Liu HJ, Zhao ZF. MiR-1–3p inhibits cell proliferation and invasion by regulating BDNF-TrkB signaling pathway in bladder cancer. *Neoplasma.* (2018) 65:89–96. doi: 10.4149/neo_2018_161128N594
11. Zhu D, Sun Y, Zhang D, Dong M, Jiang G, Zhang X, et al. miR1 inhibits the progression of colon cancer by regulating the expression of vascular endothelial growth factor. *Oncol Rep.* (2018) 40:589–98. doi: 10.3892/or.2018.6463
12. Shimo A, Nishidate T, Ohta T, Fukuda M, Nakamura Y, Katagiri T. Elevated expression of protein regulator of cytokinesis 1, involved in the growth of breast cancer cells. *Cancer Sci.* (2007) 98:174–81.doi: 10.1111/j.1349-7006.2006.00381.x
13. Kanehira M, Katagiri T, Shimo A, Takata R, Shuin T, Miki T, et al. Oncogenic role of MPHOSPH1, a cancer-testis antigen specific to human bladder cancer. *Cancer Res.* (2007) 67:3276–85. doi: 10.1158/0008-5472.CAN-06-3748
14. Chen J, Rajasekaran M, Xia H, Zhang X, Kong SN, Sekar K, et al. The microtubule-associated protein PRC1 promotes early recurrence of hepatocellular carcinoma in association with the Wnt/beta-catenin signalling pathway. *Gut.* (2016) 65:1522–34. doi: 10.1136/gutjnl-2015-310625
15. Nakamura T, Furukawa Y, Nakagawa H, Tsunoda T, Ohigashi H, Murata K, et al. Genome-wide cDNA microarray analysis of gene expression profiles in pancreatic cancers using populations of tumor cells and normal ductal epithelial cells selected for purity by laser microdissection. *Oncogene.* (2004) 23:2385–400. doi: 10.1038/sj.onc.1207392
16. Gao J, Aksoy BA, Dogrusoz U, Dresdner G, Gross B, Sumer SO, et al. Integrative analysis of complex cancer genomics and clinical profiles using the cBioPortal. *Sci Signal.* (2013) 6:pl1. doi: 10.1126/scisignal.2004088
17. Cerami E, Gao J, Dogrusoz U, Gross BE, Sumer SO, Aksoy BA, et al. The cBio cancer genomics portal: an open platform for exploring multidimensional cancer genomics data. *Cancer Discov.* (2012) 2:401–4. doi: 10.1158/2159-8290.CD-12-0095
18. Zhu J, Sanborn JZ, Benz S, Szeto C, Hsu F, Kuhn RM, et al. The UCSC cancer genomics browser. *Nat Methods.* (2009) 6:239–40. doi: 10.1038/nmeth0409-239
19. Rhodes DR, Yu J, Shanker K, Deshpande N, Varambally R, Ghosh D, et al. ONCOMINE: a cancer microarray database and integrated data-mining platform. *Neoplasia.* (2004) 6:1–6. doi: 10.1016/S1476-5586(04)80047-2
20. Gyorffy B, Surowiak P, Budczies J, Lánczky A. Online survival analysis software to assess the prognostic value of biomarkers using transcriptomic data in non-small-cell lung cancer. *PLoS ONE.* (2013) 8:e82241. doi: 10.1371/journal.pone.0082241
21. Jiao D, Chen J, Li Y, Tang X, Wang J, Xu W, et al. miR-1–3p and miR-206 sensitizes HGF-induced gefitinib-resistant human lung cancer cells through inhibition of c-Met signalling and EMT. *J Cell Mol Med.* (2018) 22:3526–36. doi: 10.1111/jcmm.13629
22. Nadal E, Chen G, Gallegos M, Lin L, Ferrer-Torres D, Truini A, et al. Epigenetic inactivation of microRNA-34b/c predicts poor disease-free survival in early-stage lung adenocarcinoma. *Clin Cancer Res.* (2013) 19:6842–52. doi: 10.1158/1078-0432.CCR-13-0736
23. Yu QQ, Wu H, Huang X, Shen H, Shu YQ, Zhang B, et al. MiR-1 targets PIK3CA and inhibits tumorigenic properties of A549 cells. *Biomed Pharmacother.* (2014) 68:155–61. doi: 10.1016/j.biopha.2014.01.005
24. Singh A, Happel C, Manna SK, Acquaah-Mensah G, Carrerero J, Kumar S, et al. Transcription factor NRF2 regulates miR-1 and miR-206 to drive tumorigenesis. *J Clin Invest.* (2013) 123:2921–34. doi: 10.1172/JCI 66353
25. Chiu KL, Lin YS, Kuo TT, Lo CC, Huang YK, Chang HF, et al. ADAM9 enhances CDCP1 by inhibiting miR-1 through EGFR signaling

activation in lung cancer metastasis. *Oncotarget*. (2017) 8:47365–78. doi: 10.18632/oncotarget.17648
26. Zhan P, Zhang B, Xi GM, Wu Y, Liu HB, Liu YF, et al. PRC1 contributes to tumorigenesis of lung adenocarcinoma in association with the Wnt/beta-catenin signaling pathway. *Mol Cancer*. (2017) 16:108. doi: 10.1186/s12943-017-0682-z
27. Brynychova V, Ehrlichova M, Hlavac V, Nemcova-Furstova V, Pecha V, Leva J, et al. Genetic and functional analyses do not explain the association of high PRC1 expression with poor survival of breast carcinoma patients. *Biomed Pharmacother.* (2016) 83:857–64. doi: 10.1016/j.biopha.2016.07.047
28. Hanselmann S, Wolter P, Malkmus J, Gaubatz S. The microtubule-associated protein PRC1 is a potential therapeutic target for lung cancer. *Oncotarget*. (2018) 9:4985–97. doi: 10.18632/oncotarget.23577
29. Glotzer M. The 3Ms of central spindle assembly: microtubules, motors and MAPs. *Nat Rev Mol Cell Biol*. (2009) 10:9–20. doi: 10.1038/nrm2609
30. Stewart DJ. Wnt signaling pathway in non-small cell lung cancer. *J Natl Cancer Inst*. (2014) 106:djt356. doi: 10.1093/jnci/djt356
31. Jin J, Zhan P, Qian H, Wang X, Katoh M, Phan K, et al. Prognostic value of wingless-type proteins in non-small cell lung cancer patients: a meta-analysis. *Transl Lung Cancer Res*. (2016) 5:436–42. doi: 10.21037/tlcr.2016.08.08
32. Anton R, Chatterjee SS, Simundza J, Cowin P, Dasgupta R. A systematic screen for micro-RNAs regulating the canonical Wnt pathway. *PLoS ONE*. (2011) 6:e26257. doi: 10.1371/journal.pone.0026257

Conflict of Interest Statement: The authors declare that the research was conducted in the absence of any commercial or financial relationships that could be construed as a potential conflict of interest.

frontiers in Pharmacology

MINI REVIEW
published: 05 March 2019
doi: 10.3389/fphar.2019.00208

Inhibitors of Human ABCG2: From Technical Background to Recent Updates With Clinical Implications

Yu Toyoda, Tappei Takada and Hiroshi Suzuki*

Department of Pharmacy, The University of Tokyo Hospital, Faculty of Medicine, The University of Tokyo, Tokyo, Japan

The ATP-binding cassette transporter G2 (ABCG2; also known as breast cancer resistance protein, BCRP) has been suggested to be involved in clinical multidrug resistance (MDR) in cancer like other ABC transporters such as ABCB1 (*P*-glycoprotein). As an efflux pump exhibiting a broad substrate specificity localized on cellular plasma membrane, ABCG2 excretes a variety of endogenous and exogenous substrates including chemotherapeutic agents, such as mitoxantrone and several tyrosine kinase inhibitors. Moreover, in the normal tissues, ABCG2 is expressed on the apical membranes and plays a pivotal role in tissue protection against various xenobiotics. For this reason, ABCG2 is recognized to be an important determinant of the pharmacokinetic characteristics of its substrate drugs. Although the clinical relevance of reversing the ABCG2-mediated MDR has been inconclusive, an appropriate modulation of ABCG2 function during chemotherapy should logically enhance the efficacy of anti-cancer agents by overcoming the MDR phenotype and/or improving their pharmacokinetics. To confirm this possibility, considerable efforts have been devoted to developing ABCG2 inhibitors, although there is no clinically available substance for this purpose. As a clue for addressing this issue, this mini-review provides integrated information covering the technical backgrounds necessary to evaluate the ABCG2 inhibitory effects on the target compounds and a current update on the ABCG2 inhibitors. This essentially includes our recent findings, as we serendipitously identified febuxostat, a well-used agent for hyperuricemia as a strong ABCG2 inhibitor, that possesses some promising potentials. We hope that an overview described here will add value to further studies involving in the multidrug transporters.

Keywords: BCRP, cancer chemotherapy, drug repurposing, febuxostat, Ko143, multidrug resistance, tumor lysis syndrome, vesicle transport

OPEN ACCESS

Edited by:
Yunkai Zhang,
Vanderbilt University Medical Center, United States

Reviewed by:
Tomohiro Terada,
Shiga University of Medical Science, Japan
Ning Ji,
Tianjin Medical University, China
Shinobu Ohnuma,
Tohoku University, Japan

****Correspondence:***
Tappei Takada
tappei-tky@umin.ac.jp

Specialty section:
This article was submitted to Experimental Pharmacology and Drug Discovery, a section of the journal Frontiers in Pharmacology

Received: *25 December 2018*
Accepted: *19 February 2019*
Published: *05 March 2019*

Citation:
Toyoda Y, Takada T and Suzuki H (2019) Inhibitors of Human ABCG2: From Technical Background to Recent Updates With Clinical Implications. Front. Pharmacol. 10:208. doi: 10.3389/fphar.2019.00208

INTRODUCTION

Two decades ago, the ABC transporter G2 (ABCG2) was discovered in drug-resistant cancer cells and human placenta (Allikmets et al., 1998; Doyle et al., 1998; Miyake et al., 1999). Thereafter, many studies were conducted to determine the role of ABCG2 in developing MDR in cancer. Moreover, in the first decade, *in vivo* studies using *Abcg2* knockout mice (Jonker et al., 2002)

Abbreviations: ABC, ATP-binding cassette; BBB, blood–brain barrier; CML, chronic myeloid leukemia; EC_{50}, half-maximal effective concentration; FTC, fumitremorgin C; IC_{50}, half-maximal inhibitory concentration; MDR, multidrug resistance; TKI, tyrosine kinase inhibitor, TLS, tumor lysis syndrome.

coupled with biochemical characterizations revealed the importance of ABCG2 in the biological defense mechanisms against xenobiotics (Vlaming et al., 2009). Indeed, ABCG2—a 655-amino acid protein working as a homodimer on cellular plasma membranes (Robey et al., 2009)—is expressed not only in cancer cells but also in several normal tissues, such as brush border membranes of epithelium in the intestine and of proximal tubules in the kidney, bile canalicular membranes of the hepatocytes in the liver, luminal membranes of the mammary gland epithelium, and blood-facing membranes of the endothelial cells forming the BBB. In these tissues ABCG2 plays a pivotal role in the extrusion of various endogenous and exogenous substrates including drugs (Mizuno et al., 2004, 2007; Adachi et al., 2005; Hirano et al., 2005; Jonker et al., 2005; Ando et al., 2007). Hence, this transporter is recognized as an important determinant of the pharmacokinetic characteristics profiles of various drugs (Giacomini et al., 2010).

In the next decade, after identifying ABCG2 as a physiologically important urate transporter, a positive relationship between ABCG2 dysfunction and increased risk of human diseases, such as gout and hyperuricemia was revealed (Matsuo et al., 2009; Woodward et al., 2009; Ichida et al., 2012; Higashino et al., 2017). In addition to the sulfate conjugates of endogenous steroids (Suzuki et al., 2003) and porphyrins (Zhou et al., 2005; Robey et al., 2009), phytoestrogen sulfate conjugates (van de Wetering and Sapthu, 2012) and a uremic toxin indoxyl sulfate (Takada et al., 2018) were added in the growing list of ABCG2 substrates. Contrary to these advances in understanding the pathophysiological importance of ABCG2, the clinical relevance of reversing ABCG2-mediated MDR has been inconclusive (Robey et al., 2018).

ABCG2 overexpression can render the cancer cells resistant to the ABCG2 substrate chemotherapy agents, such as mitoxantrone, doxorubicin, SN-38, and several TKIs. To the best of our knowledge, no published clinical trial has ever succeeded in reversing the ABCG2-mediated MDR. This is because, despite a lot of efforts in ABCG2 inhibitor development, chemical knock-out/down of ABCG2 in clinical situations has not been achieved yet due to the lack of an appropriate candidate molecule. We herein describe some well-used experimental systems to evaluate the ABCG2 inhibitory activity, followed by a recent update on the ABCG2 inhibitors that includes a potent substance, febuxostat.

TECHNICAL BACKGROUND FOR FUNCTIONAL VALIDATION

Various experimental models are available to examine the functions of the ABC transporters. Mainly focusing on ABCG2, with a current update this section introduces some *in vitro* and *in vivo* models that have been used in ABC transporter field. Broadly, the *in vitro* models are classified into two types, namely membrane-based systems and cell-based systems (**Figure 1**).

Plasma Membrane Vesicle-Based Methods

Preparation of Plasma Membrane Vesicles

In mammals, most of the ABC transporters are membrane proteins and work as an efflux pump involved in the transport of its substrates from the cytosol, either to the extracellular space or into organelles by an ATP-dependent manner. Therefore, isolation of the target ABC protein-enriched cell membrane is the first step for biochemical analyses. For ABCG2, sucrose density gradient ultracentrifugation for the isolation of plasma membrane fraction is generally employed to prepare plasma membrane vesicles from ABCG2-expressing cells (related notes are inscribed in the legend of **Figure 1**). For this purpose, not only mammalian cells but also insect cells [e.g., baculovirus-infected Sf9 cells (Saito et al., 2006)] could be used as host cells. Nonetheless, for easy and convenient preparation of ABCG2-expressing cells, we here recommend plasmid-based overexpression in non-polarized cells exhibiting high transfection efficiency, such as HEK293 cells (Miyata et al., 2016).

Vesicle Transport Assay

Vesicle transport assay is a well-established *in vitro* method employed to quantitatively evaluate ABC transporter function. The presence of ATP-dependent active transport across the cell membrane was directly proved using this method (Ishikawa, 1989). In this assay, ATP-regeneration components—enough amount of creatine phosphate and creatine kinase—are employed to maintain ATP levels in the reaction mixtures during prolonged incubation, and AMP is used as an alternative of ATP for the ATP-deficient controls. After incubation for the transport reaction, the plasma membrane vesicles are washed by filtration and then the intravesicularly accumulated substances are detected. To make this process more convenient and sensitive, radiolabeled or fluorescent substrates are usually used; alternatively, mass spectrometry is used (Toyoda et al., 2016; Takada et al., 2018). With ABCG2, [^{14}C]-urate (Miyata et al., 2016; Stiburkova et al., 2016; Higashino et al., 2017) and [^{3}H]-estrone sulfate (Suzuki et al., 2003) are well-used radiolabeled substrates that exhibit comparatively lower background signal for the quantitative detection due to their relatively hydrophilic properties. Additionally, non-radiolabeled experiments are conducted by the combined use of hematoporphyrin (a fluorescent ABCG2 substrate) and gel filtration techniques (Tamura et al., 2006).

ATPase Assay

Since ABC protein is driven by the free energy of ATP hydrolysis, ATPase activity is recognized as an indicator of the substrate transport. In this assay, the release of inorganic phosphate from ATP coupled with the transport of substrates is estimated using a colorimetric method, such as malachite green procedure (Baykov et al., 1988). This catalytic assay is relatively convenient for estimating the activity of some ABC proteins that prefer lipophilic compounds as their substrates because the non-specifically adsorbed substrates on the vesicles interfere with the measurement of direct transport. Considering that ABCB1 activity has been well

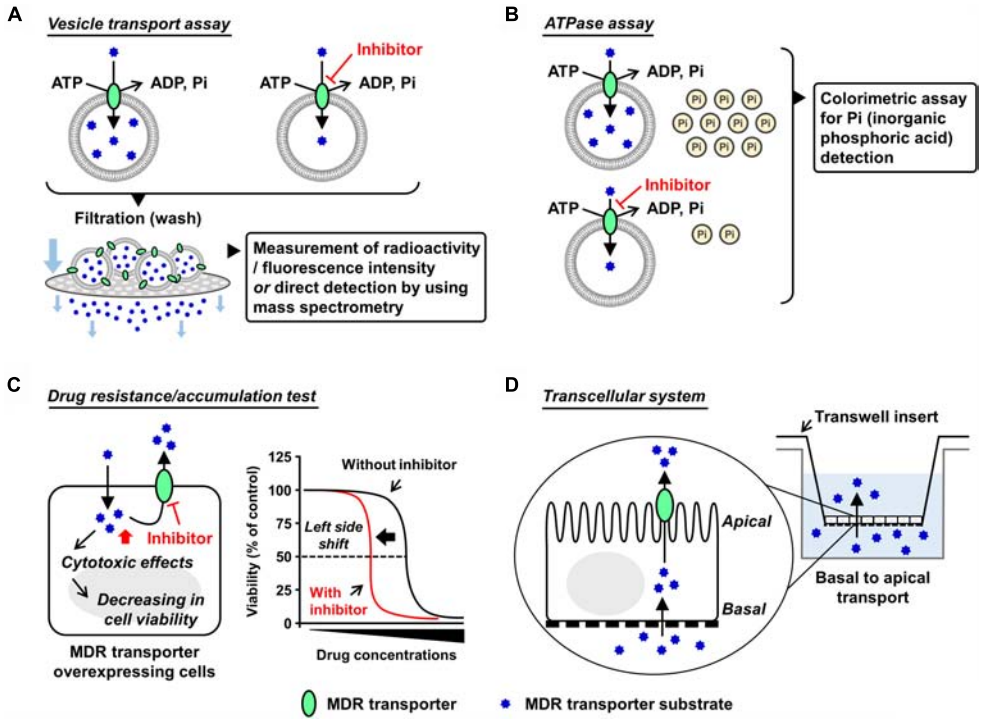

FIGURE 1 | Schematic illustrations of each *in vitro* assay. Generally used *in vitro* models which are classified into membrane-based systems and cell-based systems (Hegedus et al., 2009) are shown. In the former systems, investigators can use culture cell-derived plasma membrane vesicles or reconstituted proteoliposomes as described in the main text. In the latter systems, aside from a couple of exceptions using *Xenopus laevis* oocytes (Nakanishi et al., 2003; Woodward et al., 2009), mammalian cells expressing target ABC protein are generally used. **(A,B)** Plasma membrane vesicle- or proteoliposome-based methods: vesicle transport assay **(A)** and ATPase assay **(B)**. Both plasma membrane vesicles and reconstituted proteoliposomes are applicable to the vesicle transport assay and the ATPase assay. Of note, the final step of the vesicle preparation—gentle homogenization of isolated membrane fraction—is empirically important for the formation of inside-out plasma membrane vesicles, whose outer faces are the cytoplasmic aspects of the parent membranes. Although the resulting plasma membrane vesicles are the mixture of inside-out and right-side-out components, without any separation of the right-side-out vesicles they are generally stored at –80°C and subjected to further assays. This is because that in these *in vitro* assays, only ABC proteins embedded in the inside-out vesicles have their ABCs outside of the vesicles and can use ATP in the reaction mixture for their transport function. In other words, the ABC proteins in the right-side-out vesicles cannot work due to an inaccessibility of the ABCs with ATP. Additionally, ABCG2-enriched plasma membrane vesicles are used for a biochemical analysis to study interactions of candidate chemicals with ABCG2 at the substrate-binding sites, known as the photoaffinity labeling of ABCG2 with [^{125}I]-iodoarylazido-prazosin (Shukla et al., 2006). **(C,D)** Cell-based methods: drug resistance/accumulation test **(C)** and transcellular system **(D)**. MDR, multidrug resistance.

studied based on the ATPase assay, this method will be appropriate when investigators would need to compare the inhibitory effects of target compounds on ABCB1 and ABCG2 (Zhang et al., 2016; Guo et al., 2018). Nonetheless, since the ATPase assay does not evaluate the direct transport, regarding ABCG2, we recommend the vesicle transport assay for more precise evaluation.

Proteoliposome-Based Methods

An artificial lipid membrane system characterized by the reconstitution of purified ABC protein into proteoliposomes (Ambudkar et al., 1998; Jackson et al., 2018) is also a powerful technique. The ABC protein-contained proteoliposomes can be used as an alternative to the plasma membrane vesicles, and their detailed preparation methods are described previously (Geertsma et al., 2008). Additionally, this approach serves as the first choice in the functional studies involving the ABC proteins localized on the organelle membrane (Okamoto et al., 2018).

Cell-Based Methods

Drug Resistance/Accumulation Test

The cells overexpressing MDR machinery show lower sensitivity against its substrate drugs exhibiting cytotoxic or anti-proliferative effects compared to their parent cells, indicating that the ABC protein-expressing cells have higher half maximal effective concentration (EC_{50}) values for cytotoxic transporter substrates. In such situations, co-treatment of the transporter inhibitors with the substrate decreases the EC_{50} values, which is depicted as a left-side shift of cell viability curve in the cytotoxic assay. Additionally, if fluorescence transporter substrates are available, flow cytometry analyses addressing their intracellular accumulation will be useful for inhibitor screening (Murakami et al., 2017; Wu et al., 2017).

Transcellular System

To investigate the transcellular transport of substances, monolayer culture of polarized cells expressing target transporter(s) in Transwell® inserts system has been used (Hegedus et al.,

2009). For instance, using double-transfected Madin-Darby canine kidney II cells overexpressing both organic anion-transporting polypeptide 1B1 (OATP1B1, a basal uptake transporter) and ABCG2 (an apical efflux transporter), an earlier study has observed an enhanced vectorial transport of [^{3}H]estrone sulfate—an ABCG2 substrate that cannot passively penetrate the plasma membrane—from the basal to the apical side (Matsushima et al., 2005). A similar strategy employing ABCG2-expressing polarized cells was used for *in vitro* studies investigating the active secretion of drugs and toxins into milk via ABCG2 (Wassermann et al., 2013; Ito et al., 2015). Of note, in this transcellular system, endogenous transporters and metabolic reactions in the cells may affect apparent transport activities of target transporters.

In vivo Evaluation Methods

Xenograft Models

Athymic nude mice models with MDR-xenografts have been used to test whether co-administration of a potential MDR inhibitor with an anti-cancer agent can reverse the MDR phenotype (Tiwari et al., 2013; Zhang et al., 2017, 2018). In such models, the obtained results could be affected by the difference in the origin of the transplanted cancer cells. This concern might be important while xenograft models are studied.

Focusing on Pharmacokinetic Characteristics

To examine the *in vivo* effects of different chemicals on the target ABC transporter, its pharmacokinetic role has been focused (Robey et al., 2018). With ABCG2, the pharmacokinetic parameters related to the intestinal absorption or the brain distribution of ABCG2 substrate drugs will be good indicators for ABCG2 activity *in vivo*. For example, pre-dosing of enough quantity of ABCG2 inhibitors increased the bioavailability of sulphasalazine—an ABCG2 substrate—in wild-type mice. This was, however, not observed in *Abcg2*-knockout mice, suggesting the *in vivo* inhibition of Abcg2 (Kusuhara et al., 2012; Miyata et al., 2016). Interestingly, the utility of a combination of brain-specific firefly luciferase transgenic mice and D-luciferin, a chemiluminescent luciferase substrate transported by ABCG2 (Zhang et al., 2007) to investigate the *in vivo* inhibitory effects of test compounds on ABCG2 in the BBB was reported (Bakhsheshian et al., 2016). Further methodological progress will aid evaluation of *in vivo* ABCG2 function.

Structure-Based *in silico* Approaches

A main approach to abolish MDR is to discover specific inhibitors of the drug-efflux pump. For this purpose, quantitative structure-activity relationship (QSAR) analysis among the series of compounds can serve for the design of lead inhibitors (Nicolle et al., 2009; Ishikawa et al., 2012; Marighetti et al., 2013; Shukla et al., 2014). With ABCG2, since three-dimensional structures of this protein determined by cryo-electron microscopy (EM) were very recently presented (Taylor et al., 2017; Jackson et al., 2018), a deeper understanding of the chemicals–ABCG2 interactions will be achieved as described below.

HISTORY AND RECENT UPDATE OF THE ABCG2 INHIBITORS

As a MDR machinery in cancer cells and an important drug gatekeeper in tissues like the intestine and the brain, ABCG2 is involved in the efficacy of cancer chemotherapy in patients treated with ABCG2 substrate anti-cancer drugs. To achieve appropriate modulation of ABCG2 by small molecules, the inhibitory potency of various compounds against ABCG2 activity has been extensively evaluated. In this section, we highlight the history and recent update of ABCG2 inhibitors.

Overview of the History of ABCG2 Inhibitors

The first ABCG2 inhibitor reported was FTC, a mycotoxin produced by *Aspergillus fumigatus* (Rabindran et al., 1998, 2000). The *in vivo* use of FTC was unfortunately precluded due to its neurotoxicity. Among the FTC derivatives, Ko143 was identified as a highly potent ABCG2 inhibitor *in vivo* as it was less neurotoxic than the native FTC and was not overtly toxic to mice (Allen et al., 2002). Cell-based assays showed that the EC_{90} concentrations of Ko143 were 23 nM (Abcg2-mediated mitoxantrone resistance), 5.5 μM (ABCB1-mediated paclitaxel resistance) and >8 μM (ABCC1-mediated etoposide resistance), respectively; these results indicated that Ko143 inhibits ABCG2 stronger than ABCB1 and ABCC1, but is not selective to ABCG2 (Allen et al., 2002). Furthermore, from a series of ABCB1 inhibitors, some ABCG2 inhibitors, such as elacridar (GF120918) (Allen et al., 1999; Kruijtzer et al., 2002) and tariquidar (XR9576) (Robey et al., 2004) are frequently used in basic research as well as Ko143.

To date, the molecular bases relating to the chemical inhibition of ABCG2 are not fully understood. The cryo-EM structures of ABCG2 (Taylor et al., 2017) and ABCG2 bound to Ko143 derivatives or tariquidar (Jackson et al., 2018) will be an important to address this issue. Besides, another group of researchers has revealed the structural characteristics of ABCG2 protein critical for its function based on a molecular modeling approach combined with biochemical characterizations of ABCG2 mutants (Khunweeraphong et al., 2017). Previous studies employing the QSAR approaches predicted some structural requirements of compounds for interacting with ABCG2 as an inhibitor (Ishikawa et al., 2012; Mao and Unadkat, 2015); not being true for all ABCG2 inhibitors, the representative features are lipophilicity, planner structure, and amine bonded to one carbon of a heterocyclic ring. Furthermore, a virtual screening strategy employing a ligand-based *in silico* classification model to predict the inhibitory potential of drugs toward ABCG2 presented some favorable outcomes (Montanari et al., 2017). Integration of these findings will contribute to providing a basis for the design of new ABCG2 inhibitors.

Hitherto, many studies focusing on the chemicals–ABCG2 interactions identified a large number of ABCG2 inhibitors with diverse chemical structures (Mao and Unadkat, 2015; Wiese, 2015; Pena-Solorzano et al., 2017; Silbermann et al., 2019). An expanding list of the ABCG2 inhibitors, which include ABCG2

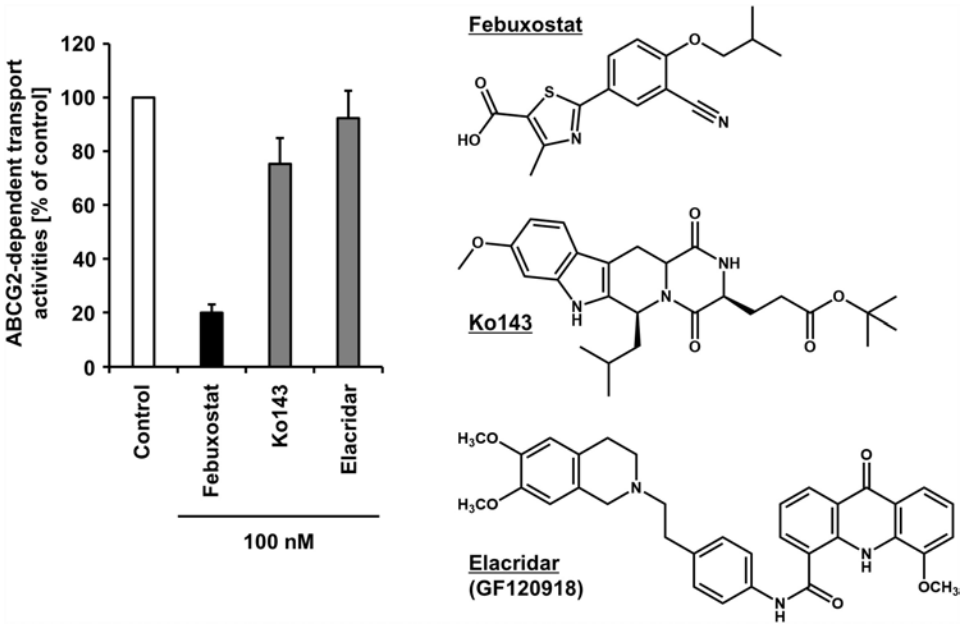

FIGURE 2 | Inhibitory effect of febuxostat against ABCG2 is stronger than that of Ko143 and elacridar, two well-used ABCG2 inhibitors. Febuxostat is known as an oral hypouricemic agent inhibiting xanthine oxidoreductase, a key enzyme for uric acid production. **(Left)** Effect of each compound on the transport activity of ABCG2 are shown. Data from our previous study under CC BY license (Miyata et al., 2016) are shown graphically, in which in the absence (vehicle control) or presence of 100 nM of each compound, the ATP-dependent urate transport activities of ABCG2 were measured using the vesicle transport assay. Data are expressed as the mean ± SD, $n = 3$. Of note, the half-maximal inhibitory concentration (IC_{50}) of febuxostat against the urate transport activity of ABCG2 was 27 nM in the previous study. **(Right)** Chemical structures of each compound are depicted.

substrates (competitive inhibitors), contains such drugs on the market as TKIs and anti-HIV drugs [some of them are often ABCG2 substrates (Polgar et al., 2008; Mao and Unadkat, 2015)] and such dietary phytochemicals as flavonoids and rotenoids. Nevertheless, to the best of our knowledge, the clinical use of such chemicals for ABCG2 inhibition has not yet been achieved probably due to concerns on safety and/or *in vivo* efficacy of them, which may have been common reasons responsible for the failure of the clinical development of ABCG2 inhibitors. Recent studies importantly showed that two potential anti-cancer compounds under clinical development could competitively inhibit both ABCG2 and ABCB1 (Ji et al., 2018a,b).

Febuxostat, a Highly Potent ABCG2 Inhibitor Applicable in Clinical Situations

Regarding the difficulty in the clinical applications of existing ABCG2 inhibitors, our recent study may open up further avenues, in which febuxostat—an approved agent for hyperuricemia globally used in clinical situations—was serendipitously identified as a strong ABCG2 inhibitor both *in vitro* and *in vivo* (Miyata et al., 2016). Using the vesicle transport assay, we revealed that febuxostat inhibits ABCG2 more strongly than Ko143 and elacridar (**Figure 2**). This indicates that febuxostat has a superior safety profile and better inhibitory ability against ABCG2 compared to these two compounds. Moreover, the study demonstrated that the IC_{50} of febuxostat against urate transport activity of ABCG2 (0.027 μM) was lower than its maximum plasma unbound concentrations reported in humans (0.09 μM), suggesting that febuxostat might inhibit human ABCG2 at a clinically used dose. Thus, febuxostat can be a promising candidate as a potential ABCG2 inhibitor in humans. The structural characteristics and molecular mechanisms of febuxostat as an ABCG2 inhibitor remain to be elucidated, as well as the effects of febuxostat on the function of other ABC transporters, including ABCB1.

Febuxostat will be used in cancer chemotherapy more frequently because recently this drug has been approved in Europe and Japan for the prophylaxis of TLS. TLS is a potentially life-threatening condition caused by an abrupt release of intracellular metabolites after tumor cell lysis in cancer patients on chemotherapy (Alakel et al., 2017). It is the most common treatment-related emergency in patients with hematologic malignancies and characterized by metabolic abnormalities including hyperuricemia that triggers several mechanisms resulting in acute kidney injury. Appropriate control of serum uric acid is therefore important in the prevention of TLS. Recent studies demonstrated that febuxostat—an oral hypouricemic agent—can successfully prevent TLS in cancer patients (Spina et al., 2015; Tamura et al., 2016). In such situations, since the patients will be treated with febuxostat before and during chemotherapy, there would be drug-drug interactions between febuxostat and ABCG2 substrate anti-cancer agents.

Importantly, ABCG2 is reportedly expressed on the malignant hematopoietic and the lymphoid cells frequently; its expression in several types of human leukemia has been investigated

(Jordanides et al., 2006; Eechoute et al., 2011; Stacy et al., 2013). Considering that initiating cells in CML arises from a multipotent hematopoietic stem cell (HSC), together with high expression of ABCG2 in human HSCs (Zhou et al., 2001; Scharenberg et al., 2002), overexpression of ABCG2 has been considered to confer drug resistance ability to the CML stem cell population (Brendel et al., 2007). However, the clinical relevance of ABCG2 inhibition in CML patients from the view point of reversing MDR remains to be clarified. Since several TKIs used for CML are ABCG2 substrates (Hira and Terada, 2018), the combination use of febuxostat may be a future research topic.

Additionally, ABCG2 expressed in tumor cells is reportedly involved in the efflux of photosensitizers in 5-aminolevulinic acid-based photodynamic therapy (Ishikawa et al., 2015). Hence, febuxostat might enhance the efficacy of this minimally invasive modality for treating solid cancers by accumulating photosensitizers in the target cells. The details are discussed in our previous report (Miyata et al., 2016).

CONCLUSION AND PERSPECTIVE

Here, we summarized some key experimental systems that will continuously contribute to generating novel ABCG2 inhibitors and described an overview of the current update of ABCG2 inhibitors. Among them, febuxostat will be one of the most promising candidates for clinical use. Considering that dysfunctional *ABCG2* genotypes, which are summarized in a recent review (Heyes et al., 2018), alter the pharmacokinetic characteristics of ABCG2 substrate drugs such as several TKIs (Hira and Terada, 2018) and rosuvastatin (Keskitalo et al., 2009), ABCG2 inhibitors will also exert similar effects in humans. As a beneficial application of this clinical possibility, we have proposed a novel concept named febuxostat-boosted therapy (Miyata et al., 2016), in which febuxostat is expected to enhance the bioavailability of ABCG2 substrate drugs. For a similar purpose, ritonavir and cobicistat are used as pharmacokinetic boosters inhibiting cytochrome P450 3A4, a major pathway of drug metabolism, to increase the plasma concentrations of certain drugs (Shah et al., 2013). No pharmacokinetic enhancer targeting transporter proteins has been, however, successfully evaluated in clinical trials. In this context, the potential benefits of the febuxostat-boosted therapy should be validated in the near future. Furthermore, this concept could also be applied to enhance the BBB penetration of ABCG2 substrate drugs for brain cancer chemotherapy. Despite the potential risks of adverse events in the combination therapy, further clinical studies to elucidate whether febuxostat is beneficial in enhancing the efficacy of pharmacotherapy via ABCG2 inhibition are warranted.

AUTHOR CONTRIBUTIONS

YT researched the data for the manuscript, provided substantial contributions to discussion of its content, and wrote the manuscript. TT contributed to the discussion and the writing of the manuscript. HS critiqued the manuscript and provided intellectual inputs. All the authors reviewed and edited the manuscript before submission and have made final approval of the manuscript.

FUNDING

This work and relating our findings were supported by the JSPS KAKENHI Grant Numbers 15H05610 to YT, 16H1808 and 18KK0247 to TT, 22136015 to HS; TT has received research grants from Gout Research Foundation, The Uehara Memorial Foundation, Mochida Memorial Foundation for Medical and Pharmaceutical Research, The Takeda Medical Foundation, and MSD Life Science Foundation, Public Interest Incorporated Foundation.

ACKNOWLEDGMENTS

The authors would like to acknowledge Drs. Hiroshi Miyata, Hirotaka Matsuo, and Kimiyoshi Ichida for their contribution to our studies highlighted in this mini-review article as well as Drs. Toshihisa Ishikawa and Yuichi Sugiyama for their previous mentorships and encouragements.

REFERENCES

Adachi, Y., Suzuki, H., Schinkel, A. H., and Sugiyama, Y. (2005). Role of breast cancer resistance protein (Bcrp1/Abcg2) in the extrusion of glucuronide and sulfate conjugates from enterocytes to intestinal lumen. *Mol. Pharmacol.* 67, 923–928. doi: 10.1124/mol.104.007393

Alakel, N., Middeke, J. M., Schetelig, J., and Bornhauser, M. (2017). Prevention and treatment of tumor lysis syndrome, and the efficacy and role of rasburicase. *Onco Targets Ther.* 10, 597–605. doi: 10.2147/OTT.S103864

Allen, J. D., Brinkhuis, R. F., Wijnholds, J., and Schinkel, A. H. (1999). The mouse Bcrp1/Mxr/Abcp gene: amplification and overexpression in cell lines selected for resistance to topotecan, mitoxantrone, or doxorubicin. *Cancer Res.* 59, 4237–4241.

Allen, J. D., Van Loevezijn, A., Lakhai, J. M., Van Der Valk, M., Van Tellingen, O., Reid, G., et al. (2002). Potent and specific inhibition of the breast cancer resistance protein multidrug transporter in vitro and in mouse intestine by a novel analogue of fumitremorgin C. *Mol. Cancer Ther.* 1, 417–425.

Allikmets, R., Schriml, L. M., Hutchinson, A., Romano-Spica, V., and Dean, M. (1998). A human placenta-specific ATP-binding cassette gene (ABCP) on chromosome 4q22 that is involved in multidrug resistance. *Cancer Res.* 58, 5337–5339.

Ambudkar, S. V., Lelong, I. H., Zhang, J., and Cardarelli, C. (1998). Purification and reconstitution of human P-glycoprotein. *Methods Enzymol.* 292, 492–504. doi: 10.1016/S0076-6879(98)92038-9

Ando, T., Kusuhara, H., Merino, G., Alvarez, A. I., Schinkel, A. H., and Sugiyama, Y. (2007). Involvement of breast cancer resistance protein (ABCG2) in the biliary excretion mechanism of fluoroquinolones. *Drug Metab. Dispos.* 35, 1873–1879. doi: 10.1124/dmd.107.014969

Bakhsheshian, J., Wei, B. R., Hall, M. D., Simpson, R. M., and Gottesman, M. M. (2016). In vivo bioluminescent imaging of ATP-binding cassette transporter-mediated efflux at the blood-brain barrier. *Methods Mol. Biol.* 1461, 227–239. doi: 10.1007/978-1-4939-3813-1_19

Baykov, A. A., Evtushenko, O. A., and Avaeva, S. M. (1988). A malachite green procedure for orthophosphate determination and its use in alkaline

phosphatase-based enzyme immunoassay. *Anal. Biochem.* 171, 266–270. doi: 10.1016/0003-2697(88)90484-8

Brendel, C., Scharenberg, C., Dohse, M., Robey, R. W., Bates, S. E., Shukla, S., et al. (2007). Imatinib mesylate and nilotinib (AMN107) exhibit high-affinity interaction with ABCG2 on primitive hematopoietic stem cells. *Leukemia* 21, 1267–1275. doi: 10.1038/sj.leu.2404638

Doyle, L. A., Yang, W., Abruzzo, L. V., Krogmann, T., Gao, Y., Rishi, A. K., et al. (1998). A multidrug resistance transporter from human MCF-7 breast cancer cells. *Proc. Natl. Acad. Sci. U.S.A.* 95, 15665–15670. doi: 10.1073/pnas.95.26.15665

Eechoute, K., Sparreboom, A., Burger, H., Franke, R. M., Schiavon, G., Verweij, J., et al. (2011). Drug transporters and imatinib treatment: implications for clinical practice. *Clin. Cancer Res.* 17, 406–415. doi: 10.1158/1078-0432.CCR-10-2250

Geertsma, E. R., Nik Mahmood, N. A., Schuurman-Wolters, G. K., and Poolman, B. (2008). Membrane reconstitution of ABC transporters and assays of translocator function. *Nat. Protoc.* 3, 256–266. doi: 10.1038/nprot.2007.519

Giacomini, K. M., Huang, S. M., Tweedie, D. J., Benet, L. Z., Brouwer, K. L., Chu, X., et al. (2010). Membrane transporters in drug development. *Nat. Rev. Drug Discov.* 9, 215–236. doi: 10.1038/nrd3028

Guo, C., Liu, F., Qi, J., Ma, J., Lin, S., Zhang, C., et al. (2018). A novel synthetic dihydroindeno[1,2-b] indole derivative (LS-2-3j) reverses ABCB1- and ABCG2-mediated multidrug resistance in cancer cells. *Molecules* 23:E3264. doi: 10.3390/molecules23123264

Hegedus, C., Szakacs, G., Homolya, L., Orban, T. I., Telbisz, A., Jani, M., et al. (2009). Ins and outs of the ABCG2 multidrug transporter: an update on in vitro functional assays. *Adv. Drug Deliv. Rev.* 61, 47–56. doi: 10.1016/j.addr.2008.09.007

Heyes, N., Kapoor, P., and Kerr, I. D. (2018). Polymorphisms of the multidrug Pump ABCG2: a systematic review of their effect on protein expression, function, and drug pharmacokinetics. *Drug Metab. Dispos.* 46, 1886–1899. doi: 10.1124/dmd.118.083030

Higashino, T., Takada, T., Nakaoka, H., Toyoda, Y., Stiburkova, B., Miyata, H., et al. (2017). Multiple common and rare variants of ABCG2 cause gout. *RMD Open* 3:e000464. doi: 10.1136/rmdopen-2017-000464

Hira, D., and Terada, T. (2018). BCRP/ABCG2 and high-alert medications: biochemical, pharmacokinetic, pharmacogenetic, and clinical implications. *Biochem. Pharmacol.* 147, 201–210. doi: 10.1016/j.bcp.2017.10.004

Hirano, M., Maeda, K., Matsushima, S., Nozaki, Y., Kusuhara, H., and Sugiyama, Y. (2005). Involvement of BCRP (ABCG2) in the biliary excretion of pitavastatin. *Mol. Pharmacol.* 68, 800–807. doi: 10.1124/mol.105.014019

Ichida, K., Matsuo, H., Takada, T., Nakayama, A., Murakami, K., Shimizu, T., et al. (2012). Decreased extra-renal urate excretion is a common cause of hyperuricemia. *Nat. Commun.* 3:764. doi: 10.1038/ncomms1756

Ishikawa, T. (1989). ATP/Mg2+-dependent cardiac transport system for glutathione S-conjugates. A study using rat heart sarcolemma vesicles. *J. Biol. Chem.* 264, 17343–17348.

Ishikawa, T., Kajimoto, Y., Inoue, Y., Ikegami, Y., and Kuroiwa, T. (2015). Critical role of ABCG2 in ALA-photodynamic diagnosis and therapy of human brain tumor. *Adv. Cancer Res.* 125, 197–216. doi: 10.1016/bs.acr.2014.11.008

Ishikawa, T., Saito, H., Hirano, H., Inoue, Y., and Ikegami, Y. (2012). Human ABC transporter ABCG2 in cancer chemotherapy: drug molecular design to circumvent multidrug resistance. *Methods Mol. Biol.* 910, 267–278. doi: 10.1007/978-1-61779-965-5_11

Ito, N., Ito, K., Ikebuchi, Y., Toyoda, Y., Takada, T., Hisaka, A., et al. (2015). Prediction of drug transfer into milk considering breast cancer resistance protein (BCRP)-mediated transport. *Pharm. Res.* 32, 2527–2537. doi: 10.1007/s11095-015-1641-2

Jackson, S. M., Manolaridis, I., Kowal, J., Zechner, M., Taylor, N. M. I., Bause, M., et al. (2018). Structural basis of small-molecule inhibition of human multidrug transporter ABCG2. *Nat. Struct. Mol. Biol.* 25, 333–340. doi: 10.1038/s41594-018-0049-1

Ji, N., Yang, Y., Cai, C. Y., Lei, Z. N., Wang, J. Q., Gupta, P., et al. (2018a). VS-4718 antagonizes multidrug resistance in ABCB1- and ABCG2-overexpressing cancer cells by inhibiting the efflux function of ABC transporters. *Front. Pharmacol.* 9:1236. doi: 10.3389/fphar.2018.01236

Ji, N., Yang, Y., Lei, Z. N., Cai, C. Y., Wang, J. Q., Gupta, P., et al. (2018b). Ulixertinib (BVD-523) antagonizes ABCB1- and ABCG2-mediated chemotherapeutic drug resistance. *Biochem. Pharmacol.* 158, 274–285. doi: 10.1016/j.bcp.2018.10.028

Jonker, J. W., Buitelaar, M., Wagenaar, E., Van Der Valk, M. A., Scheffer, G. L., Scheper, R. J., et al. (2002). The breast cancer resistance protein protects against a major chlorophyll-derived dietary phototoxin and protoporphyria. *Proc. Natl. Acad. Sci. U.S.A.* 99, 15649–15654. doi: 10.1073/pnas.202607599

Jonker, J. W., Merino, G., Musters, S., Van Herwaarden, A. E., Bolscher, E., Wagenaar, E., et al. (2005). The breast cancer resistance protein BCRP (ABCG2) concentrates drugs and carcinogenic xenotoxins into milk. *Nat. Med.* 11, 127–129. doi: 10.1038/nm1186

Jordanides, N. E., Jorgensen, H. G., Holyoake, T. L., and Mountford, J. C. (2006). Functional ABCG2 is overexpressed on primary CML CD34+ cells and is inhibited by imatinib mesylate. *Blood* 108, 1370–1373. doi: 10.1182/blood-2006-02-003145

Keskitalo, J. E., Zolk, O., Fromm, M. F., Kurkinen, K. J., Neuvonen, P. J., and Niemi, M. (2009). ABCG2 polymorphism markedly affects the pharmacokinetics of atorvastatin and rosuvastatin. *Clin. Pharmacol. Ther.* 86, 197–203. doi: 10.1038/clpt.2009.79

Khunweeraphong, N., Stockner, T., and Kuchler, K. (2017). The structure of the human ABC transporter ABCG2 reveals a novel mechanism for drug extrusion. *Sci. Rep.* 7:13767. doi: 10.1038/s41598-017-11794-w

Kruijtzer, C. M., Beijnen, J. H., Rosing, H., ten Bokkel Huinink, W. W., Schot, M., Jewell, R. C., et al. (2002). Increased oral bioavailability of topotecan in combination with the breast cancer resistance protein and P-glycoprotein inhibitor GF120918. *J. Clin. Oncol.* 20, 2943–2950. doi: 10.1200/JCO.2002.12.116

Kusuhara, H., Furuie, H., Inano, A., Sunagawa, A., Yamada, S., Wu, C., et al. (2012). Pharmacokinetic interaction study of sulphasalazine in healthy subjects and the impact of curcumin as an in vivo inhibitor of BCRP. *Br. J. Pharmacol.* 166, 1793–1803. doi: 10.1111/j.1476-5381.2012.01887.x

Mao, Q., and Unadkat, J. D. (2015). Role of the breast cancer resistance protein (BCRP/ABCG2) in drug transport–an update. *AAPS J.* 17, 65–82. doi: 10.1208/s12248-014-9668-6

Marighetti, F., Steggemann, K., Hanl, M., and Wiese, M. (2013). Synthesis and quantitative structure-activity relationships of selective BCRP inhibitors. *ChemMedChem* 8, 125–135. doi: 10.1002/cmdc.201200377

Matsuo, H., Takada, T., Ichida, K., Nakamura, T., Nakayama, A., Ikebuchi, Y., et al. (2009). Common defects of ABCG2, a high-capacity urate exporter, cause gout: a function-based genetic analysis in a Japanese population. *Sci. Transl. Med.* 1:5ra11. doi: 10.1126/scitranslmed.3000237

Matsushima, S., Maeda, K., Kondo, C., Hirano, M., Sasaki, M., Suzuki, H., et al. (2005). Identification of the hepatic efflux transporters of organic anions using double-transfected Madin-Darby canine kidney II cells expressing human organic anion-transporting polypeptide 1B1 (OATP1B1)/multidrug resistance-associated protein 2, OATP1B1/multidrug resistance 1, and OATP1B1/breast cancer resistance protein. *J. Pharmacol. Exp. Ther.* 314, 1059–1067. doi: 10.1124/jpet.105.085589

Miyake, K., Mickley, L., Litman, T., Zhan, Z., Robey, R., Cristensen, B., et al. (1999). Molecular cloning of cDNAs which are highly overexpressed in mitoxantrone-resistant cells: demonstration of homology to ABC transport genes. *Cancer Res.* 59, 8–13.

Miyata, H., Takada, T., Toyoda, Y., Matsuo, H., Ichida, K., and Suzuki, H. (2016). Identification of febuxostat as a new strong ABCG2 inhibitor: potential applications and risks in clinical situations. *Front. Pharmacol.* 7:518. doi: 10.3389/fphar.2016.00518

Mizuno, N., Suzuki, M., Kusuhara, H., Suzuki, H., Takeuchi, K., Niwa, T., et al. (2004). Impaired renal excretion of 6-hydroxy-5,7-dimethyl-2-methylamino-4-(3-pyridylmethyl) benzothiazole (E3040) sulfate in breast cancer resistance protein (BCRP1/ABCG2) knockout mice. *Drug Metab. Dispos.* 32, 898–901.

Mizuno, N., Takahashi, T., Kusuhara, H., Schuetz, J. D., Niwa, T., and Sugiyama, Y. (2007). Evaluation of the role of breast cancer resistance protein (BCRP/ABCG2) and multidrug resistance-associated protein 4 (MRP4/ABCC4) in the urinary excretion of sulfate and glucuronide metabolites of edaravone (MCI-186; 3-methyl-1-phenyl-2-pyrazolin-5-one). *Drug Metab. Dispos.* 35, 2045–2052. doi: 10.1124/dmd.107.016352

Montanari, F., Cseke, A., Wlcek, K., and Ecker, G. F. (2017). Virtual screening of DrugBank reveals two drugs as new BCRP inhibitors. *SLAS Discov.* 22, 86–93. doi: 10.1177/1087057116657513

Murakami, M., Ohnuma, S., Fukuda, M., Chufan, E. E., Kudoh, K., Kanehara, K., et al. (2017). Synthetic analogs of curcumin modulate the function of multidrug resistance-linked ATP-binding cassette transporter ABCG2. *Drug Metab. Dispos.* 45, 1166–1177. doi: 10.1124/dmd.117.076000

Nakanishi, T., Doyle, L. A., Hassel, B., Wei, Y., Bauer, K. S., Wu, S., et al. (2003). Functional characterization of human breast cancer resistance protein (BCRP, ABCG2) expressed in the oocytes of *Xenopus laevis*. *Mol. Pharmacol.* 64, 1452–1462. doi: 10.1124/mol.64.6.1452

Nicolle, E., Boumendjel, A., Macalou, S., Genoux, E., Ahmed-Belkacem, A., Carrupt, P. A., et al. (2009). QSAR analysis and molecular modeling of ABCG2-specific inhibitors. *Adv. Drug Deliv. Rev.* 61, 34–46. doi: 10.1016/j.addr.2008.10.004

Okamoto, T., Kawaguchi, K., Watanabe, S., Agustina, R., Ikejima, T., Ikeda, K., et al. (2018). Characterization of human ATP-binding cassette protein subfamily D reconstituted into proteoliposomes. *Biochem. Biophys. Res. Commun.* 496, 1122–1127. doi: 10.1016/j.bbrc.2018.01.153

Pena-Solorzano, D., Stark, S. A., Konig, B., Sierra, C. A., and Ochoa-Puentes, C. (2017). ABCG2/BCRP: specific and nonspecific modulators. *Med. Res. Rev.* 37, 987–1050. doi: 10.1002/med.21428

Polgar, O., Robey, R. W., and Bates, S. E. (2008). ABCG2: structure, function and role in drug response. *Expert Opin. Drug Metab. Toxicol.* 4, 1–15. doi: 10.1517/17425255.4.1.1

Rabindran, S. K., He, H., Singh, M., Brown, E., Collins, K. I., Annable, T., et al. (1998). Reversal of a novel multidrug resistance mechanism in human colon carcinoma cells by fumitremorgin C. *Cancer Res.* 58, 5850–5858.

Rabindran, S. K., Ross, D. D., Doyle, L. A., Yang, W., and Greenberger, L. M. (2000). Fumitremorgin C reverses multidrug resistance in cells transfected with the breast cancer resistance protein. *Cancer Res.* 60, 47–50.

Robey, R. W., Pluchino, K. M., Hall, M. D., Fojo, A. T., Bates, S. E., and Gottesman, M. M. (2018). Revisiting the role of ABC transporters in multidrug-resistant cancer. *Nat. Rev. Cancer* 18, 452–464. doi: 10.1038/s41568-018-0005-8

Robey, R. W., Steadman, K., Polgar, O., Morisaki, K., Blayney, M., Mistry, P., et al. (2004). Pheophorbide a is a specific probe for ABCG2 function and inhibition. *Cancer Res.* 64, 1242–1246. doi: 10.1158/0008-5472.CAN-03-3298

Robey, R. W., To, K. K., Polgar, O., Dohse, M., Fetsch, P., Dean, M., et al. (2009). ABCG2: a perspective. *Adv. Drug Deliv. Rev.* 61, 3–13. doi: 10.1016/j.addr.2008.11.003

Saito, H., Hirano, H., Nakagawa, H., Fukami, T., Oosumi, K., Murakami, K., et al. (2006). A new strategy of high-speed screening and quantitative structure-activity relationship analysis to evaluate human ATP-binding cassette transporter ABCG2-drug interactions. *J. Pharmacol. Exp. Ther.* 317, 1114–1124. doi: 10.1124/jpet.105.099036

Scharenberg, C. W., Harkey, M. A., and Torok-Storb, B. (2002). The ABCG2 transporter is an efficient Hoechst 33342 efflux pump and is preferentially expressed by immature human hematopoietic progenitors. *Blood* 99, 507–512. doi: 10.1182/blood.V99.2.507

Shah, B. M., Schafer, J. J., Priano, J., and Squires, K. E. (2013). Cobicistat: a new boost for the treatment of human immunodeficiency virus infection. *Pharmacotherapy* 33, 1107–1116. doi: 10.1002/phar.1237

Shukla, S., Kouanda, A., Silverton, L., Talele, T. T., and Ambudkar, S. V. (2014). Pharmacophore modeling of nilotinib as an inhibitor of ATP-binding cassette drug transporters and BCR-ABL kinase using a three-dimensional quantitative structure-activity relationship approach. *Mol. Pharm.* 11, 2313–2322. doi: 10.1021/mp400762h

Shukla, S., Robey, R. W., Bates, S. E., and Ambudkar, S. V. (2006). The calcium channel blockers, 1,4-dihydropyridines, are substrates of the multidrug resistance-linked ABC drug transporter, ABCG2. *Biochemistry* 45, 8940–8951. doi: 10.1021/bi060552f

Silbermann, K., Shah, C. P., Sahu, N. U., Juvale, K., Stefan, S. M., Kharkar, P. S., et al. (2019). Novel chalcone and flavone derivatives as selective and dual inhibitors of the transport proteins ABCB1 and ABCG2. *Eur. J. Med. Chem.* 164, 193–213. doi: 10.1016/j.ejmech.2018.12.019

Spina, M., Nagy, Z., Ribera, J. M., Federico, M., Aurer, I., Jordan, K., et al. (2015). FLORENCE: a randomized, double-blind, phase III pivotal study of febuxostat versus allopurinol for the prevention of tumor lysis syndrome (TLS) in patients with hematologic malignancies at intermediate to high TLS risk. *Ann. Oncol.* 26, 2155–2161. doi: 10.1093/annonc/mdv317

Stacy, A. E., Jansson, P. J., and Richardson, D. R. (2013). Molecular pharmacology of ABCG2 and its role in chemoresistance. *Mol. Pharmacol.* 84, 655–669. doi: 10.1124/mol.113.088609

Stiburkova, B., Miyata, H., Zavada, J., Tomcik, M., Pavelka, K., Storkanova, G., et al. (2016). Novel dysfunctional variant in ABCG2 as a cause of severe tophaceous gout: biochemical, molecular genetics and functional analysis. *Rheumatology* 55, 191–194. doi: 10.1093/rheumatology/kev350

Suzuki, M., Suzuki, H., Sugimoto, Y., and Sugiyama, Y. (2003). ABCG2 transports sulfated conjugates of steroids and xenobiotics. *J. Biol. Chem.* 278, 22644–22649. doi: 10.1074/jbc.M212399200

Takada, T., Yamamoto, T., Matsuo, H., Tan, J. K., Ooyama, K., Sakiyama, M., et al. (2018). Identification of ABCG2 as an exporter of uremic toxin indoxyl sulfate in mice and as a crucial factor influencing CKD progression. *Sci. Rep.* 8:11147. doi: 10.1038/s41598-018-29208-w

Tamura, A., Watanabe, M., Saito, H., Nakagawa, H., Kamachi, T., Okura, I., et al. (2006). Functional validation of the genetic polymorphisms of human ATP-binding cassette (ABC) transporter ABCG2: identification of alleles that are defective in porphyrin transport. *Mol. Pharmacol.* 70, 287–296.

Tamura, K., Kawai, Y., Kiguchi, T., Okamoto, M., Kaneko, M., Maemondo, M., et al. (2016). Efficacy and safety of febuxostat for prevention of tumor lysis syndrome in patients with malignant tumors receiving chemotherapy: a phase III, randomized, multi-center trial comparing febuxostat and allopurinol. *Int. J. Clin. Oncol.* 21, 996–1003. doi: 10.1007/s10147-016-0971-3

Taylor, N. M. I., Manolaridis, I., Jackson, S. M., Kowal, J., Stahlberg, H., and Locher, K. P. (2017). Structure of the human multidrug transporter ABCG2. *Nature* 546, 504–509. doi: 10.1038/nature22345

Tiwari, A. K., Sodani, K., Dai, C. L., Abuznait, A. H., Singh, S., Xiao, Z. J., et al. (2013). Nilotinib potentiates anticancer drug sensitivity in murine ABCB1-, ABCG2-, and ABCC10-multidrug resistance xenograft models. *Cancer Lett.* 328, 307–317. doi: 10.1016/j.canlet.2012.10.001

Toyoda, Y., Takada, T., and Suzuki, H. (2016). Halogenated hydrocarbon solvent-related cholangiocarcinoma risk: biliary excretion of glutathione conjugates of 1,2-dichloropropane evidenced by untargeted metabolomics analysis. *Sci. Rep.* 6:24586. doi: 10.1038/srep24586

van de Wetering, K., and Sapthu, S. (2012). ABCG2 functions as a general phytoestrogen sulfate transporter in vivo. *FASEB J.* 26, 4014–4024. doi: 10.1096/fj.12-210039

Vlaming, M. L., Lagas, J. S., and Schinkel, A. H. (2009). Physiological and pharmacological roles of ABCG2 (BCRP): recent findings in Abcg2 knockout mice. *Adv. Drug Deliv. Rev.* 61, 14–25. doi: 10.1016/j.addr.2008.08.007

Wassermann, L., Halwachs, S., Baumann, D., Schaefer, I., Seibel, P., and Honscha, W. (2013). Assessment of ABCG2-mediated transport of xenobiotics across the blood-milk barrier of dairy animals using a new MDCKII in vitro model. *Arch. Toxicol.* 87, 1671–1682. doi: 10.1007/s00204-013-1066-9

Wiese, M. (2015). BCRP/ABCG2 inhibitors: a patent review (2009-present). *Expert Opin. Ther. Pat.* 25, 1229–1237. doi: 10.1517/13543776.2015.1076796

Woodward, O. M., Kottgen, A., Coresh, J., Boerwinkle, E., Guggino, W. B., and Kottgen, M. (2009). Identification of a urate transporter, ABCG2, with a common functional polymorphism causing gout. *Proc. Natl. Acad. Sci. U.S.A.* 106, 10338–10342. doi: 10.1073/pnas.0901249106

Wu, C. P., Hsiao, S. H., Murakami, M., Lu, Y. J., Li, Y. Q., Huang, Y. H., et al. (2017). Alpha-mangostin reverses multidrug resistance by attenuating the function of the multidrug resistance-linked ABCG2 transporter. *Mol. Pharm.* 14, 2805–2814. doi: 10.1021/acs.molpharmaceut.7b00334

Zhang, G. N., Zhang, Y. K., Wang, Y. J., Gupta, P., Ashby, C. R. Jr., Alqahtani, S., et al. (2018). Epidermal growth factor receptor (EGFR) inhibitor PD153035 reverses ABCG2-mediated multidrug resistance in non-small cell lung cancer: in vitro and in vivo. *Cancer Lett.* 424, 19–29. doi: 10.1016/j.canlet.2018.02.040

Zhang, W., Chen, Z., Chen, L., Wang, F., Li, F., Wang, X., et al. (2017). ABCG2-overexpressing H460/MX20 cell xenografts in athymic nude mice maintained original biochemical and cytological characteristics. *Sci. Rep.* 7:40064. doi: 10.1038/srep40064

Zhang, Y., Bressler, J. P., Neal, J., Lal, B., Bhang, H. E., Laterra, J., et al. (2007). ABCG2/BCRP expression modulates D-Luciferin based bioluminescence imaging. *Cancer Res.* 67, 9389–9397. doi: 10.1158/0008-5472.CAN-07-0944

Zhang, Y. K., Zhang, G. N., Wang, Y. J., Patel, B. A., Talele, T. T., Yang, D. H., et al. (2016). Bafetinib (INNO-406) reverses multidrug resistance by inhibiting the efflux function of ABCB1 and ABCG2 transporters. *Sci. Rep.* 6:25694. doi: 10.1038/srep25694

Zhou, S., Schuetz, J. D., Bunting, K. D., Colapietro, A. M., Sampath, J., Morris, J. J., et al. (2001). The ABC transporter Bcrp1/ABCG2 is expressed in a wide variety of stem cells and is a molecular determinant of the side-population phenotype. *Nat. Med.* 7, 1028–1034. doi: 10.1038/nm0901-1028

Zhou, S., Zong, Y., Ney, P. A., Nair, G., Stewart, C. F., and Sorrentino, B. P. (2005). Increased expression of the Abcg2 transporter during erythroid maturation plays a role in decreasing cellular protoporphyrin IX levels. *Blood* 105, 2571–2576. doi: 10.1182/blood-2004-04-1566

Conflict of Interest Statement: TT and HS have a patent pending.

The remaining author declares that the research was conducted in the absence of any commercial or financial relationships that could be construed as a potential conflict of interest.

frontiers in Pharmacology

ORIGINAL RESEARCH
published: 21 February 2019
doi: 10.3389/fphar.2019.00137

MiR-409-3p Inhibits Cell Proliferation and Invasion of Osteosarcoma by Targeting Zinc-Finger E-Box-Binding Homeobox-1

*Liang Wu†, Yiming Zhang†, Zhongyue Huang, Huijie Gu, Kaifeng Zhou, Xiaofan Yin and Jun Xu**

Minhang Hosptial, Fudan University, Shanghai, China

Osteosarcoma (OS) is the most common bone cancer worldwide. There is evidence that microRNA-409 (miR-409-3p) is involved in tumorigenesis and cancer progression, however, its possible role in OS requires clarification. In the present study, we evaluated the expression level, clinical significance, and mode of action of miR-409-3p in OS. The miR-409-3p levels were diminished in the OS cells and tissues compared with associated adjacent non-tumor tissues and a non-cancer osteoplastic cell line. Low miR-409-3p expression levels were associated with clinical stage and distant metastasis in patients with OS. Resumption of miR-409-3p expression attenuated OS cell proliferation and invasion. Additionally, based on informatics analyses, we predicted that zinc-finger E-box-binding homeobox-1 (ZEB1) is a possible target of miR-409-3p. This hypothesis was confirmed using luciferase reporter assays, reverse transcription-quantitative real-time polymerase chain reaction, and Western blot analyses. The findings of the current study indicated that ZEB1 was up-regulated in the OS tissues and cell lines, and that this up-regulation was inversely proportional to miR-409-3p expression levels. Furthermore, down-regulation of ZEB1 decreased OS cell invasion and proliferation, illustrating that the tumor suppressive role of miR-409-3p in OS cells may be exerted *via* negative regulation of ZEB1. Taken together, our observations highlight the potential role of miR-409-3p as a tumor suppressor in OS partially through down-regulation of ZEB1 and suggest that miR-409-3p has potential applications in OS treatment.

Keywords: osteosarcoma, microRNA-409, molecular mechanism, zinc-finger E-box-binding homeobox-1, invasion

OPEN ACCESS

Edited by:
Jian-ye Zhang,
Guangzhou Medical University, China

Reviewed by:
Jianmeng Wang,
First Affiliated Hospital of Jilin University, China
Jixue Wang,
Jilin University, China

***Correspondence:**
Jun Xu
Aline_Adam@126.com

†These authors have contributed equally to this work

Specialty section:
This article was submitted to Cancer Molecular Targets and Therapeutics, a section of the journal Frontiers in Pharmacology

Received: *22 October 2018*
Accepted: *06 February 2019*
Published: *21 February 2019*

Citation:
Wu L, Zhang Y, Huang Z, Gu H, Zhou K, Yin X and Xu J (2019) MiR-409-3p Inhibits Cell Proliferation and Invasion of Osteosarcoma by Targeting Zinc-Finger E-Box-Binding Homeobox-1. Front. Pharmacol. 10:137. doi: 10.3389/fphar.2019.00137

INTRODUCTION

Osteogenic sarcoma (osteosarcoma; OS) is among the most common forms of bone cancer globally. The incidence ranges from 4 to 5 cases per million among children and teenagers (Gill et al., 2013; Tang et al., 2014). The OS tumors are always located in the distal femur or proximal tibia, and tumors in these regions present a high tendency to destroy adjacent normal tissues (Cates, 2016; Righi et al., 2016). Despite considerable advances in treatment strategies such as surgery, radiotherapy, chemotherapy and new antineoplastic agent (Li et al., 2015), cases with metastatic or recurrent OS have an inferior prognosis, and the likelihood of long-term survival for patients

with advanced OS remains very low (Anderson, 2015; Isakoff et al., 2015). Genetic and epigenetic variations and potential environmental factors that block mesenchymal stem cell differentiation into osteoblasts contribute to OS tumorigenesis and tumor development (Sun et al., 2015; Li et al., 2018; Zhang et al., 2018), however, the detailed and complex molecular mechanisms underlying OS development remain largely unknown. Therefore, the molecular mechanisms underlying OS formation and progression require investigation to facilitate the development of novel therapeutic approaches for application in patients with OS.

MicroRNAs (miRNAs) are a subtype of endogenous, non-coding, single-stranded, short RNAs, with an approximate range in length of 19–25 nucleotides (Esteller, 2011). miRNAs can regulate the expression of protein-coding genes by binding to complementary sequences in the 3′-untranslated regions (3′ UTRs) of target genes, causing translational repression or mRNA cleavage (Bartel, 2004). miRNAs play key roles in various cellular processes, including apoptosis, cell proliferation, differentiation, angiogenesis, invasion, and metastasis (Gambari et al., 2016). Recently, the abnormal expression of miRNAs has been implicated in the etiology and development of various human cancers (Chen et al., 2016; Li and Wang, 2016; Wang et al., 2016). The potential biological roles of several miRNAs abnormally expressed in OS during its tumorigenesis have also been highlighted. For example, miR-422a expression is down-regulated in OS cell lines and tissues. Conversely, high levels of miR-422a expression can suppress OS cell invasion and proliferation, and improve paclitaxel and cisplatin-mediated apoptosis (Liu et al., 2016). Therefore, there is a need to explore the potential role of miRNA expression in OS and to unravel the underlying primary molecular mechanisms, which may provide information useful for designing new and efficient therapeutic strategies aimed at curing OS.

The effect of miR-409-3p has been investigated in various human malignancies, including breast (Ma et al., 2016), gastric (Zheng et al., 2012), colon (Tan et al., 2016), and prostate (Josson et al., 2015) cancers, however, its role of miR-409-3p in OS remains unclear. Latest study confirmed the interaction of miR-409-3p and ZEB1 played a role in the progression process of non-small cell lung cancer, indicating ZEB1 acted as a direct target of miR409-3p and could be modulated by miR-409-3p (Qu et al., 2018). Herein, we hypothesis there exists the miR-409-3p/ZEB1 axis in OS and report the first investigation of the expression levels, clinical significance, and biological functions of miR-409-3p in OS, as well as its underlying molecular mechanism.

MATERIALS AND METHODS

Ethics Statement

All study participants voluntarily provided written consent before entering the study. We obtained the approval of The Ethics Committee of the Minhang Hospital, Zhongshan Hospital, Fudan University for Disease Control and Prevention. The methodology used in this study completely conformed to the recommendations of CONSORT 2010.

Tissue Specimens

Forty-nine pairs of osteosarcoma tumor and adjacent non-tumor tissues were collected from patients with osteosarcoma at Minhang Hospital, Zhongshan Hospital, Fudan University. No participants underwent chemotherapy or radiotherapy before surgery. All tissues samples were directly transferred into liquid nitrogen and were stored at −80°C until RNA extraction.

Cell Lines

OS cell lines, including HOS (GDC76) and MG63 (GDC074) were obtained directly from the Chinese Academy of Medical Sciences (Beijing, China) Cell Resource Center. A non-cancer osteoblastic cell line (hFOB 1.19 CRL-11372) was obtained from the American Type Culture Collection (ATCC; Manassas, VA, United States). All cells were incubated in Dulbecco's modified Eagle medium (DMEM; Gibco, Invitrogen Life Technologies, Carlsbad, CA, United States) supplemented with 10% fetal bovine serum (FBS; Gibco, Invitrogen Life Technologies, Carlsbad, CA, United States). All experimental cells were maintained at 37°C in 5% (*V*/*V*) carbon dioxide (CO_2) and passaged every 2–3 days.

Cells were then seeded in 6-well plates at a density of 50–60% confluence for transfection. After overnight incubation, cells were transfected with miR-409-3p mimics, negative control miRNA mimics (miR-NC), ZEB1 siRNA, or scrambled siRNA (GenePharma, Shanghai, China), using Lipofectamine 2000 transfection reagent (Invitrogen, Carlsbad, CA, United States), according to the manufacturer's guidelines. Post-transfection (6 h), the culture medium was changed to DMEM containing 10% FBS.

Reverse Transcription-Quantitative Real-Time Polymerase Chain Reaction (RT–qPCR)

RNA was extracted using Trizol reagent (Invitrogen, Carlsbad, CA, United States), following the manufacturer's directions. A TaqMan Micro-RNA Reverse Transcription Kit (Applied Biosystems, Foster City, CA, United States) was used to reverse-transcribe miRNA, and qPCR performed using a TaqMan Micro-RNA PCR Kit (Applied Biosystems, Foster City, CA, United States). Reverse transcription of mRNA was performed using the M-MLV Reverse Transcription system (Promega Corporation, Madison, WI, United States). To determine *ZEB1* mRNA expression levels we used the primers: forward 5′-AGGCAATAGGTTTTGAGGGCCAT-3′ and reverse 5′-TGCACCTTCTGTCTCGGTTTCTT-3′ and SYBR Premix Ex Taq (TaKaRa, Dalian, China). Endogenous U6 small nuclear RNA (primers: forward, 5′-CTCGCTTCGGCAGCACA-3′; reverse, 5′-AACGCTTCACGAATTTGCGT-3′) was amplified as an internal control for miR-409-3p, and β-actin (primers: forward, 5′-AGCGAGCATCCCCCAAAGTT-3′; reverse, 5′-GGGCACGAAGGCTCATCATT-3′) was amplified as an internal control for *ZEB1* mRNA. All RT-qPCR experiments were conducted using an ABI7500 Real-time PCR system (Applied Biosystems, Carlsbad, CA, United States). Relative mRNA or miRNA expression levels were quantified using the $2^{-\Delta\Delta Ct}$ method (Livak and Schmittgen, 2001).

3-(4,5-Dimethylthiazol-2-yl)-2,5-Diphenyltetrazolium Bromide (MTT) Assay

Post-transfection (24 h), cells were re-seeded into 96-well plates at 3,000 per well. Cells were maintained at 37°C in 5% (*V*/*V*) CO_2 for 4 days. Then, cell proliferation was tested at the indicated times using the MTT assay (Sigma, St. Louis, MO, United States). In brief, 0.5 mg/mL MTT solution was added to cells, which were then incubated at 37°C for a further 4 h. Subsequently, we added 150.0 μL DMSO (Sigma, St. Louis, MO, United States) into each to dissolve the formazan crystals. Spectrometric absorbance was determined using a microplate reader (Bio-Rad Laboratories Inc., Hercules, CA, United States) at a wavelength of 490 nm.

Cell Invasion Assay

After 48 h transfection, cells were collected and suspended in FBS-free culture medium. Then, 5×10^4 cells were added into upper chambers of a 24-well Transwell Permeable Support device (8-μm pores, Costar; Corning Incorporated, Corning, NY, United States) coated with Matrigel (BD Biosciences, San Jose, CA, United States), while 500.0 μL culture medium containing 20% FBS was added to the lower chambers and cells incubated at 37°C in 5% CO_2 for 48 h. We removed cells in the upper chambers using cotton swabs, then invaded cells were fixed with methanol, stained with 0.5% crystal violet, washed, and dried in air. An inverted microscope (Olympus Corporation, Tokyo, Japan) (200 × magnification) was used to calculate the number of invading cells in five randomly selected fields.

Prediction of miR-409-3p Targets and Luciferase Reporter Assays

Two miRNA targeted-gene databases, TargetScan[1] and miRanda[2], were used to predict target genes of miR-409-3p. HEK293T cells (ATCC) were seeded into 24-well plates at 40–50% confluence. After 24 h, cells were transfected with miR-409-3p mimics or miR-NC and pmirGLO-ZEB1-3′UTR-mutant (Mut) (GenePharma) or pmirGLO-ZEB1-3′UTR-wild-type (Wt) using Lipofectamine 2000. Cells were maintained at 37°C in 5% (*V*/*V*) CO_2 for 48 h and luciferase reporter assays conducted using the Dual-Luciferase Reporter Assay System (Promega Corporation, Madison, WI, United States). Renilla luciferase was used as an internal control.

Western Blot Analyses

Cells were harvested after transfection for 72 h and lysed with RIPA Lysis Buffer (Beyotime Institute of Biotechnology, Haimen, China). Protein concentrations were determined using a BCA assay kit (Pierce™; Thermo Fisher Scientific, Inc.). Equal amounts of protein were separated by SDS-PAGE, transferred to polyvinylidene difluoride membranes (Millipore, MA, United States), blocked with 5% skimmed milk for 2 h at room temperature, then incubated overnight at 4°C with mouse anti-human GAPDH monoclonal antibody (sc-137179; 1:1000 dilution; Santa Cruz Biotechnology) or mouse anti-human ZEB1 monoclonal antibody (sc-81428; 1:1000 dilution; Santa Cruz Biotechnology, CA, United States). Membranes were then washed three times using Tris-buffered saline containing 0.1% Tween-20 and probed with horseradish peroxidase-conjugated secondary immunoglobulin G goat anti-mouse (catalog no, sc-2005; 1:10,000) for 2 h at room temperature. Protein bands were visualized using enhanced chemiluminescence reagents (Bio-Rad Laboratories Inc., Hercules, CA, United States) and band densities analyzed using AlphaEase FC software (version 4.0.1; ProteinSimple, San Jose, CA, United States).

Statistical Analyses

Data were presented as means ± S.D. or box plots. We used SPSS 17.0 software (SPSS Inc., Chicago, IL, United States) for data analyses. Differences among groups were evaluated using one-way ANOVA corrected for multiple comparisons or Student's *t*-tests. The χ^2-test was used to evaluate associations between miR-409-3p expression levels and clinicopathological factors. Spearman's correlation analysis was used to determine the correlation between miR-409-3p and *ZEB1* mRNA expression levels. All statistical tests were two-sided; $P < 0.05$ were considered statistically significant.

RESULTS

MiR-409-3p Was Downregulated in OS Tissues and Cell Lines

RT-qPCR was used to evaluate miR-409-3p expression levels in OS tumor and adjacent non-tumor tissues. Expression of miR-409-3p was lower in OS tissues than that in adjacent non-tumor and normal tissue controls (**Figure 1A**, $P < 0.05$). Moreover, remarkable low levels of MiR-409-3p expression were detected in two OS cell lines relative to those in a non-cancer osteoblastic cell line (hFOB 1.19) (**Figure 1B**, $P < 0.05$).

Relationship Between miR-409-3p Expression and OS Clinicopathological Factors

We also determined the relationship between miR-409-3p expression levels and OS clinicopathological factors. Our data showed that low miR-409-3p expression levels were significantly associated with advanced clinical stage ($P = 0.035$) and distant metastasis ($P = 0.030$), however, there were no significance associations with other clinicopathological factors, including sex ($P = 0.961$), age ($P = 0.804$), and tumor size ($P = 0.851$) (**Table 1**).

MiR-409-3p Reduces OS Cell Proliferation and Invasion

To investigate the role of miR-409-3p in OS, we transfected MG63 and HOS cells with miR-409-3p mimics, and used RT-qPCR to determine miR-409-3p expression levels (**Figure 2A**, $P < 0.05$). We investigated the role of miR-409-3p in OS cell proliferation using MTT assays conducted in MG63 and HOS cells transfected with miR-409-3p mimics or miR-NC. Expression

[1] http://www.targetscan.org/index.html

[2] http://www.microrna.org

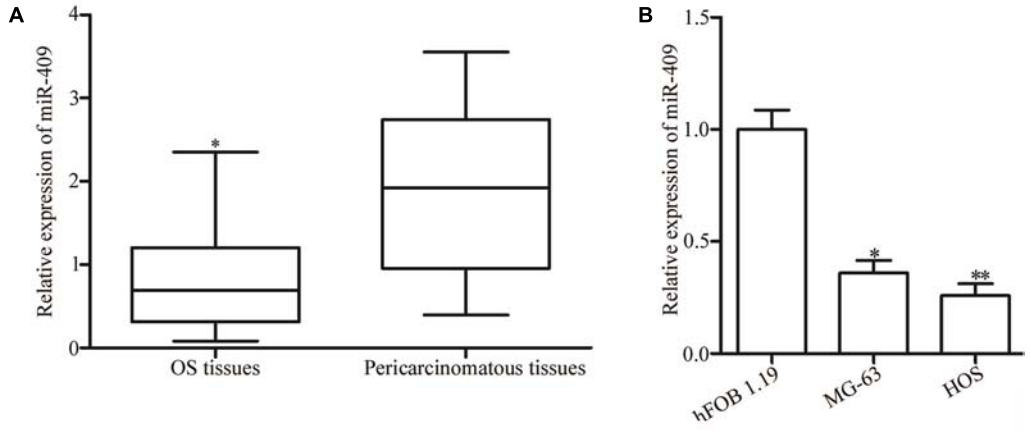

FIGURE 1 | Expression of miR-409-3p in OS tissues and cell lines. **(A)** Relative expression levels of miR-409-3p in 49 paired OS tumor and adjacent non-tumor tissues were evaluated by RT-qPCR. **(B)** Expression of miR-409-3p in OS cell lines compared with that in a non-cancer osteoblastic cell line (hFOB1.19). miR-409-3p, microRNA-409. OS, osteosarcoma. *$P < 0.05$, **$P < 0.01$ compared with the control group.

TABLE 1 | Correlation of microRNA-409 expression with clinicopathological feature of osteosarcoma.

Variables	Case number	microRNA-409 expression		*P*
		Low	High	
Sex				0.961
Male	31	17	14	
Female	18	10	8	
Age (years)				0.804
< 20*	21	12	9	
≥ 20	28	15	13	
Tumor size (cm)				0.851
< 8	26	14	12	
≥ 8	23	13	10	
Clinical stage				0.035*
I-II	23	9	14	
III-IV	26	18	8	
Distant metastasis				0.030*
Present	24	17	7	
Absent	25	10	15	

**These participants were above 16 years age. *P < 0.05.*

of miR-409-3p led to a significant decline in MG63 and HOS cell proliferation (**Figure 2B**, $P < 0.05$). Similarly, the invasion capacity of HOS and MG63 cells transfected with miR-NC or miR-409-3p mimics was estimated using a cell invasion assay. As illustrated in **Figure 2C**, the introduction of miR-409-3p mimics into HOS and MG63 cells resulted in a considerable decline of invasion ability relative to the miR-NC group ($P < 0.05$). These observations suggested that miR-409-3p has a crucial role in the suppression of OS growth and metastasis.

A Potential miR-409-3p Target in OS

We then investigated the molecular mechanisms underlying the tumor suppression caused by miR-409-3p in OS by predicting its potential targets using bioinformatics analysis. The 3′ UTR of *ZEB1* was predicted to contain an miR-409-3p seed match at position 1280-1286 and has previously been reported as extensively upregulated in OS and participates in the regulation of OS tumorigenesis and progression (Shen et al., 2012; Li et al., 2016; Liu and Lin, 2016); therefore, we primarily focused on ZEB1 (**Figure 3A**) in this study. To validate the prediction, we performed luciferase reporter assays in HEK293T cells transfected with plasmids containing Mut and Wt ZEB 3′ UTR, along with miR-409-3p mimics or miR-NC. Luciferase activity was markedly downregulated in cells transfected with Wt ZEB1-3′ UTR and miR-409-3p mimics (**Figure 3B**, $P < 0.01$), however, no significant difference was observed in cells transfected with mutated ZEB1-3′ UTR and miR-409-3p mimics, suggesting that miR-409-3p could directly target the 3′ UTR of *ZEB1*. Additionally, RT-qPCR data showed that restoration of miR-409-3p expression led to down-regulation of *ZEB1* mRNA expression in MG63 and HOS cells (**Figure 3C**, $P < 0.01$). Moreover, Western blot analysis demonstrated that miR-409-3p reduced ZEB1 protein expression in MG63 and HOS cells (**Figure 3D**, $P < 0.05$). *In vivo* assay showed the protein levels in tumor tissues were significantly lower than those in adjacent normal tissues (**Figure 3E**, $P < 0.01$). To summarize, Our data demonstratedthat ZEB1 is potentially a direct target gene of miR-409-3p in OS.

Upregulation of ZEB1 in OS Tissues and Negative Correlation of Its Expression With That of miR-409-3p

ZEB1 is recognized as a direct target gene of miR-409-3p in OS; therefore, we next investigated whether miR-409-3p expression levels were negatively correlated with those of *ZEB1* in OS. Therefore, we performed RT-qPCR to evaluate *ZEB1* mRNA expression levels and found that they were higher in OS specimens than adjacent non-tumor tissues (**Figure 4A**, $P < 0.05$). Moreover, Spearman's correlation analysis indicated an inverse relationship between miR-409-3p and *ZEB1* mRNA

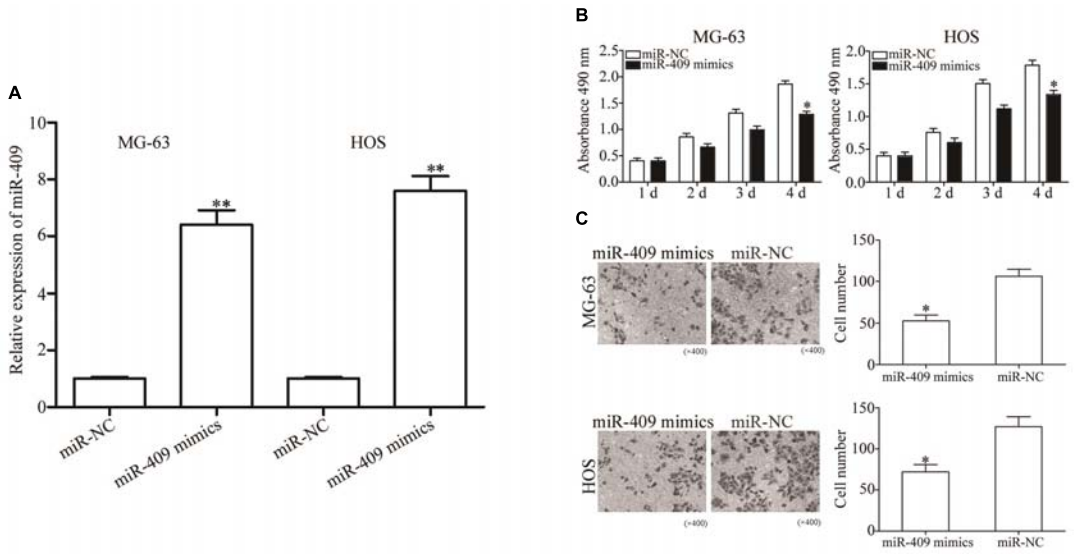

FIGURE 2 | The effects of miR-409-3p overexpression on cell proliferation and invasion in OS. **(A)** Relative expression of miR-409-3p in MG63 and HOS cells following transfection with miR-409-3p mimics or miR-NC. **(B)** MTT assays were performed to assess the effect of miR-409-3p overexpression on MG63 and HOS cells proliferation. **(C)** Cell invasion assays were conducted in MG63 and HOS cells following transfection with miR-409-3p mimics or miR-NC. miR-409, microRNA-409-3p (magnification, ×200). OS, osteosarcoma. miR-NC, negative control microRNA mimics. $^{*}P < 0.05$, $^{**}P < 0.01$ compared with the control group.

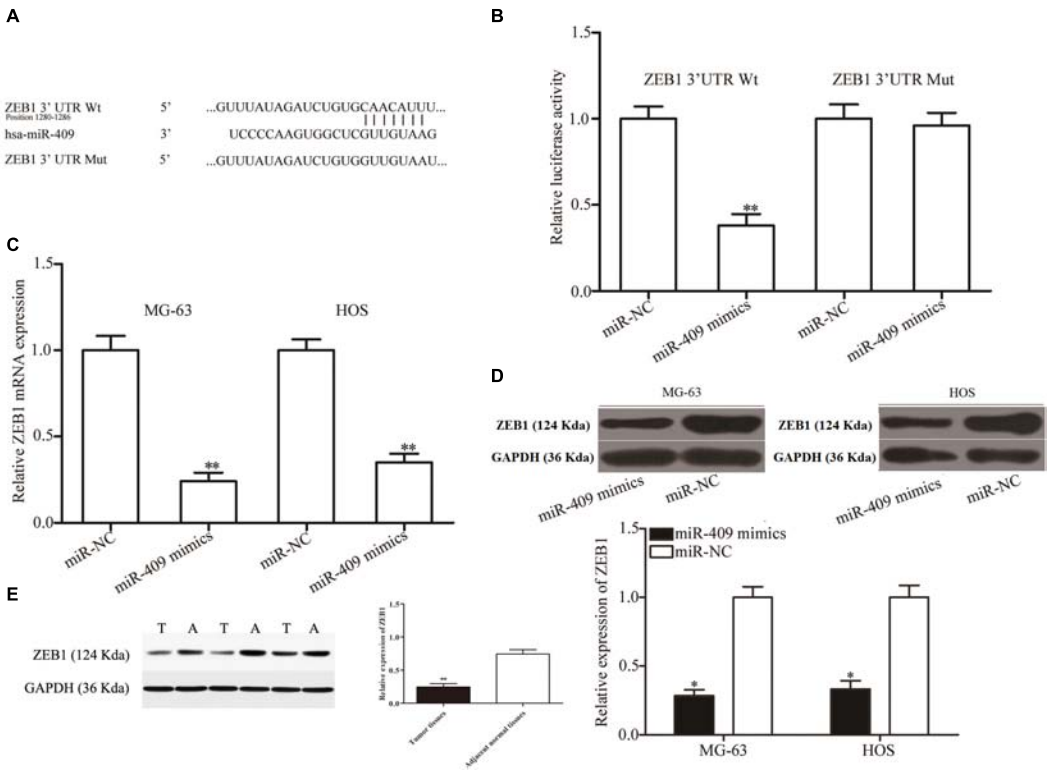

FIGURE 3 | ZEB1 is a direct target of miR-409-3p in OS. **(A)** *ZEB1* 3′ UTR sequences containing wild type and mutant miR-409-3p binding sites. **(B)** Luciferase reporter assays performed in HEK293T cells co-transfected with miR-409-3p mimics or miR-NC, and pmirGLO-ZEB1-3′UTR Wt or pmirGLO-ZEB1-3′UTR Mut. After transfection (48 h), cells were collected and luciferase activities measured. ZEB1 mRNA **(C)** and protein **(D)** were detected in MG63 and HOS cells transfected with miR-409-3p mimics or miR-NC. miR-409, microRNA-409-3p. **(E)** Protein levels of ZEB1 in tumor tissues and adjacent normal tissues. OS, osteosarcoma. miR-NC, negative control microRNA mimics. Wt, wild type. Mut, mutant. ZEB1, Zinc-finger E-box-binding Homeobox-1. $^{*}P < 0.05$, $^{**}P < 0.01$ compared with the control group.

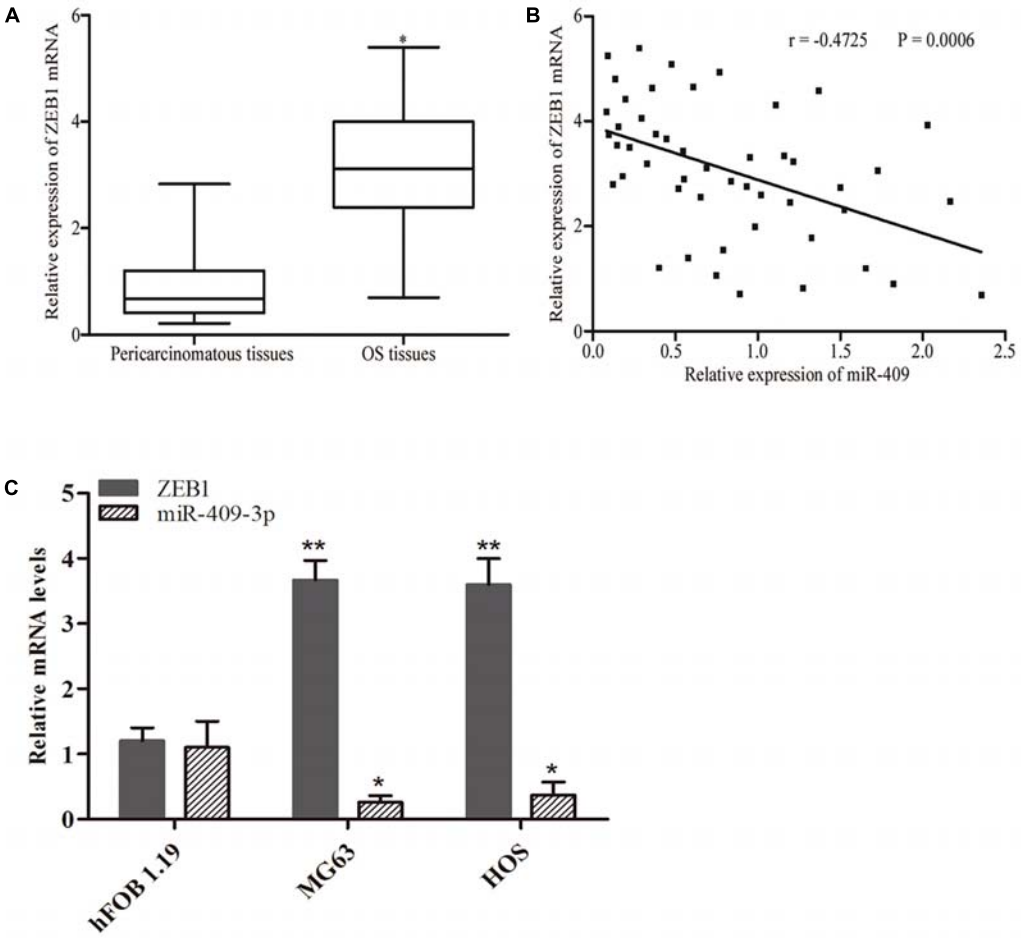

FIGURE 4 | Inverse correlation between miR-409-3p and *ZEB1* mRNA expression levels in OS tissues. **(A)** RT-qPCR analysis showing that *ZEB1* mRNA levels were increased in OS tissues. **(B)** Spearman's correlation analysis of the association between miR-409-3p and *ZEB1* mRNA in OS tissues. **(C)** Expressions of miR-409-3p and *ZEB1* mRNA in cell lines. miR-409, microRNA-409-3p. OS, osteosarcoma. ZEB1, Zinc-finger E-box-binding Homeobox-1. mRNA, message RNA. $^{*}P < 0.05$, $^{**}P < 0.01$ compared with the control group.

expression (**Figure 4B**, r = -0.4725, P = 0.0006) in OS tissue samples. As shown in **Figure 4C**, we observed higher expression of *ZEB1* mRNA and lower expression of miR-409-3p in tumor cell lines, when compared to normal cell line. Our results further confirm ZEB1 as a potential target of miR-409-3p in OS.

Inhibition of ZEB1 Has Similar Effects to Those of miR-409-3p Overexpression in OS Cells

To explore the biological roles of ZEB1 in response to miR-409-3p inhibition in OS, we investigated whether ZEB1 knockdown mimicked the effects of miR-409-3p overexpression in OS cells. ZEB1-targeting siRNA was used to knockdown ZEB1 expression in HOS and MG63 cells. As shown in **Figure 5A**, ZEB1 protein was successfully knocked down in HOS and MG63 cells transfected with ZEB1 siRNA ($P < 0.01$). MTT and cell invasion assays showed that knockdown of ZEB1 by the introduction of ZEB1 siRNA suppressed MG63 and HOS cell proliferation (**Figure 5B**, $P < 0.05$) and invasion (**Figure 5C**, $P < 0.05$), suggesting that negative regulation of ZEB1 may mediate the tumor suppressive effects of miR-409-3p in OS cells.

DISCUSSION

Dysregulation of miRNAs is a frequent event in various types of human cancer and has a pivotal role in the instigation of tumorigenesis and tumor progression where miRNAs can function as oncogenes or tumor suppressor genes (Fenger et al., 2014; Vanas et al., 2016). Furthermore, targeting miRNA with various types of chemically modified oligonucleotides has the potential to alter miRNA functions, providing a theoretical foundation for miRNA-based targeted therapy for specific human cancers (Trang et al., 2010; Imani et al., 2017; Tsai et al., 2017). Thus, research into the expression levels, biological roles, and fundamental molecular mechanisms of miRNAs has the potential to stimulate the development of novel approaches to

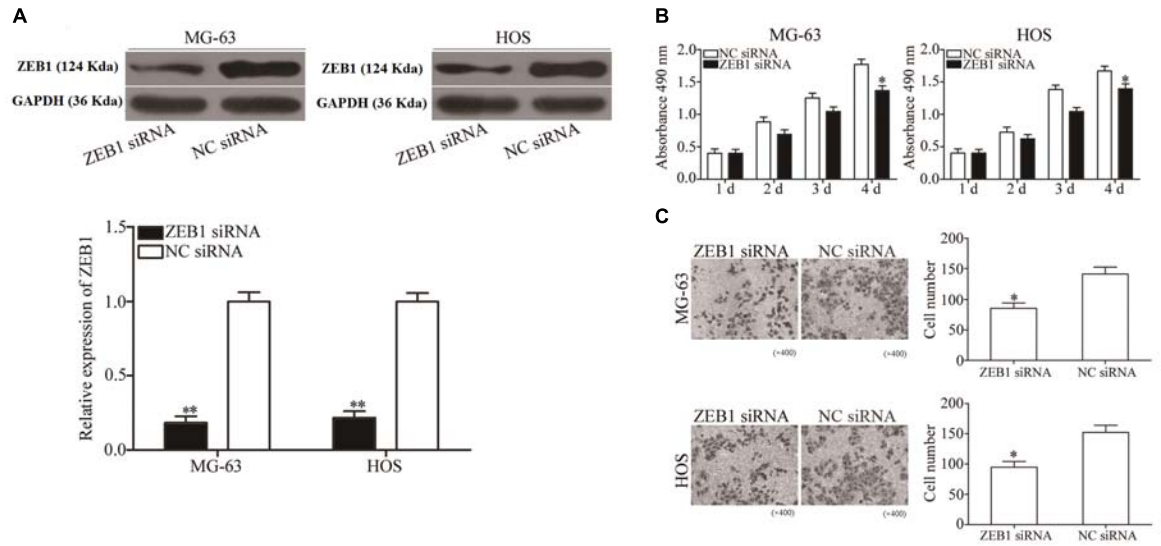

FIGURE 5 | ZEB1 under-expression has similar effects to miR-409-3p over-expression on OS cell proliferation and invasion. **(A)** ZEB1 protein expression was detected in MG63 and HOS cells transfected with ZEB1 siRNA or NC siRNA. MTT **(B)** and cell invasion **(C)** assays were conducted in MG63 and HOS cells transfected with ZEB1 siRNA or NC siRNA. miR-409, microRNA-409-3p (magnification, × 200). OS, osteosarcoma. ZEB1, Zinc-finger E-box-binding Homeobox-1. mRNA, message RNA. siRNA, small interfering RNA. NC, negative control. $^{*}P < 0.05$, $^{**}P < 0.01$ compared with the control group.

the treatment of different types of cancer. Our data demonstrated that miR-409-3p expression levels were significantly down-regulated in OS tissues and cells relative to adjacent non-tumor tissues and a non-cancer osteoblastic cell line, respectively. Our observations are consistent with the findings of Ma et al. in breast cancer tissues and cell lines (Zheng et al., 2012). Additionally, reduced miR-409-3p expression levels were associated with clinical stage and distant metastasis in patients with OS, and our results also demonstrate that expression of miR-409-3p suppressed proliferation and invasion of OS cells. Furthermore, our data suggest that ZEB1 is a functional target of miR-409-3p in OS.

Recently, several studies have reported roles for abnormal miR-409-3p expression in the initiation and progression of various human cancers. For example, Josson et al. found that miR-409-3p expression was elevated in prostate cancer and that its re-expression in normal prostate fibroblasts resulted in a cancer-associated stroma-like phenotype, and miR-409-3p was released in extracellular vesicles to induce cancer initiation and epithelial-to-mesenchymal transition both *in vitro* and *in vivo* (Josson et al., 2015). Zheng et al. (2012) showed that miR-409-3p expression levels were decreased in gastric cancer and that they were negatively associated with tumor-node-metastasis stage and lymph node metastasis in patients with gastric cancer. Upregulation of miR-409-3p attenuated gastric cancer cell motility *in vitro* and decreased their ability to induce distal pulmonary metastases and peritoneal diffusion *in vivo* (Zheng et al., 2012). Tan et al. (2016) found that miR-409-3p was expressed at low levels in colon tumors and that its expression was negatively correlated with resistance to oxaliplatin. Ectopic expression of miR-409-3p improved the chemosensitivity of oxaliplatin-sensitive and oxaliplatin-resistant colon cancer cells (Tan et al., 2016). Therefore, miR-409-3p is a strong candidate for a new therapeutic target for the treatment of cancer because of its essential roles in cancer initiation and progression.

MiR-409-3p target identification is essential for understanding its potential functions in OS and developing novel targeted therapies for improving OS treatment. Potential miR-409-3p target genes have been previously reported; for example, Beclin-1 in colon cancer (Tan et al., 2016), radixin in gastric cancer (Zheng et al., 2012), and Ras suppressor 1 and stromal antigen 2 in prostate cancer (Josson et al., 2015). In the current study, we identified ZEB1 as a novel direct target of miR-409-3p in OS. Based on bioinformatics analysis, we predicted that *ZEB1* contains a miR-409-3p seed match at position 1280–1286 of the *ZEB1* 3′ UTR. Luciferase reporter assays demonstrated that miR-409-3p directly targeted the 3′ UTR of *ZEB1*. Furthermore, Western blot and RT-qPCR analysis indicated that endogenous miR-409-3p has a negative regulatory effect on *ZEB1* mRNA and protein expression in OS cells. Moreover, ZEB1 expression was high in OS tissues and inversely associated with that of miR-409-3p expression and knockdown of ZEB1 led to decreased OS cell proliferation and invasion, similar to miR-409-3p overexpression.

ZEB1, a member of the deltaEF1 family of two-handed zinc-finger transcription factors, maps to the short arm of human chromosome 10 (Zhang et al., 2019). ZEB1 expression is abnormally upregulated in various types of human cancer, including thyroid (Zhang et al., 2016), cervical (Ma et al., 2015), gastric (Jia et al., 2012), endometrial (Feng et al., 2014), and prostate (Drake et al., 2009) cancers. Accumulating evidence shows that ZEB1 has crucial roles during cancer initiation and progression (Kenney et al., 2011; Jia et al., 2012; Liu et al., 2012). In OS, Shen et al. reported that ZEB1 is highly

expressed in tumor tissues and that its levels are significantly associated with lung metastasis. The signal network of ZEB1 involved in malignant transformation in various types of tumor is complicated. All of the upstream and downstream molecules participate in activating the signaling pathways in cell survival, senescence, chemosensitivity and immune escape, which may trigger the regulation of miR-409-3p. These findings suggest that inhibition of OS has the potential to be a novel and effective therapeutic target with the aim of curing this type of cancer. The limitations of this study include that we did not investigate the effects of ectopic ZEB1 over-expression on cell proliferation and invasion activity of miR-409-3p-expressing osteosarcoma cells and that the number of samples in this study is small thus multi-center trial is still needed.

CONCLUSION

In conclusion, here we establish for the first time that miR-409-3p expression is down-regulated in OS tissues and cell lines. Decreased miR-409-3p expression levels were associated with clinical stage and distant metastasis. MiR-409-3p targets ZEB1, which may be associated with OS carcinogenesis and progression, leading to inhibition of OS cell proliferation and invasion. Thus, the miR-409-3p/ZEB1 axis can be considered a novel therapeutic target for OS treatment. Further research is needed to explore whether the potential of miR-409-3p/ZEB1 can be realized to treat OS.

AUTHOR CONTRIBUTIONS

These studies were conceived of and designed by all authors. Experiments were performed by LW and YZ. Data analysis, data interpretation, manuscript preparations were done by ZH, HG, KZ, XY, and JX.

FUNDING

The work was supported by General Projects of Shanghai Health State Planning Commission (No. 201640219).

ACKNOWLEDGMENTS

We thank Australian Saqlain Abbas for helping us in editing our manuscript.

REFERENCES

Anderson, M. E. (2015). Update on survival in osteosarcoma. *Orthop. Clin. North Am.* 2016, 283–292. doi: 10.1016/j.ocl.2015.08.022

Bartel, D. P. (2004). MicroRNAs: genomics, biogenesis, mechanism, and function. *Cell* 116, 281–297. doi: 10.1016/S0092-8674(04)00045-5

Cates, J. M. (2016). Utility of examination of biopsy tracts in osteosarcoma resection specimens. *Am. J. Clin. Pathol.* 146, 324–327. doi: 10.1093/ajcp/aqw119

Chen, X., Chen, X. G., Hu, X., Song, T., Ou, X., Zhang, C., et al. (2016). MiR-34a and miR-203 inhibit survivin expression to control cell proliferation and survival in human osteosarcoma cells. *J. Cancer* 7, 1057–1065. doi: 10.7150/jca.15061

Drake, J. M., Strohbehn, G., Bair, T. B., Moreland, J. G., and Henry, M. D. (2009). ZEB1 enhances transendothelial migration and represses the epithelial phenotype of prostate cancer cells. *Mol. Biol. Cell* 20, 2207–2217. doi: 10.1091/mbc.E08-10-1076

Esteller, M. (2011). Non-coding RNAs in human disease. *Nat. Rev. Genet.* 12, 861–874. doi: 10.1038/nrg3074

Feng, G., Wang, X., Cao, X., Shen, L., and Zhu, J. (2014). ZEB1 expression in endometrial biopsy predicts lymph node metastases in patient with endometrial cancer. *Dis. Markers* 2014:680361. doi: 10.1155/2014/680361

Fenger, J. M., Bear, M. D., Volinia, S., Lin, T. Y., Harrington, B. K., London, C. A., et al. (2014). Overexpression of miR-9 in mast cells is associated with invasive behavior and spontaneous metastasis. *BMC Cancer* 14:84. doi: 10.1186/1471-2407-14-84

Gambari, R., Brognara, E., and Spandidos, D. A. (2016). Targeting oncomiRNAs and mimicking tumor suppressor miRNAs: new trends in the development of miRNA therapeutic strategies in oncology (Review). *Int. J. Oncol.* 49, 5–32. doi: 10.3892/ijo.2016.3503

Gill, J., Ahluwalia, M. K., Geller, D., and Gorlick, R. (2013). New targets and approaches in osteosarcoma. *Pharmacol. Ther.* 137, 89–99. doi: 10.1016/j.pharmthera.2012.09.003

Imani, S., Wei, C., Cheng, J., Khan, M. A., Fu, S., Yang, L., et al. (2017). MicroRNA-34a targets epithelial to mesenchymal transition-inducing transcription factors (EMT-TFs) and inhibits breast cancer cell migration and invasion. *Oncotarget* 8, 21362–21379. doi: 10.18632/oncotarget.15214

Isakoff, M. S., Bielack, S. S., and Meltzer, P. (2015). Osteosarcoma: current treatment and a collaborative pathway to success. *J. Clin. Oncol.* 33, 3029–3035. doi: 10.1200/JCO.2014.59.4895

Jia, B., Liu, H., Kong, Q., and Li, B. (2012). Overexpression of ZEB1 associated with metastasis and invasion in patients with gastric carcinoma. *Mol. Cell Biochem.* 366, 223–229. doi: 10.1007/s11010-012-1299-6

Josson, S., Gururajan, M., Sung, S. Y., Hu, P., Shao, C., Zhau, H. E., et al. (2015). Stromal fibroblast-derived miR-409 promotes epithelial-to-mesenchymal transition and prostate tumorigenesis. *Oncogene* 34, 2690–2699. doi: 10.1038/onc.2014.212

Kenney, P. A., Wszolek, M. F., Rieger-Christ, K. M., Neto, B. S., Gould, J. J., Harty, N. J., et al. (2011). Novel ZEB1 expression in bladder tumorigenesis. *BJU Int.* 107, 656–663. doi: 10.1111/j.1464-410X.2010.09489.x

Li, C., Xu, W., Ding, J., Zhang, Y., Wang, J., Zhuang, X., et al. (2015). Micellization of antineoplastic agent to significantly upregulate efficacy and security. *Macromol. Biosci.* 15, 328–341. doi: 10.1002/mabi.201400356

Li, R. Z., and Wang, L. M. (2016). Decreased microRNA-452 expression and its prognostic significance in human osteosarcoma. *World J. Surg. Oncol.* 14:150. doi: 10.1186/s12957-016-0900-y

Li, S., Zhang, T., Xu, W., Ding, J., Yin, F., Xu, J., et al. (2018). Sarcoma-targeting peptide-decorated polypeptide nanogel intracellularly delivers shikonin for upregulated osteosarcoma necroptosis and diminished pulmonary metastasis. *Theranostics* 8, 1361–1375. doi: 10.7150/thno.18299

Li, Y., Zeng, C., Tu, M., Jiang, W., Dai, Z., Hu, Y., et al. (2016). MicroRNA-200b acts as a tumor suppressor in osteosarcoma via targeting ZEB1. *Onco. Targets Ther.* 9, 3101–3111. doi: 10.2147/OTT.S96561

Liu, C., and Lin, J. (2016). Long noncoding RNA ZEB1-AS1 acts as an oncogene in osteosarcoma by epigenetically activating ZEB1. *Am. J. Transl. Res.* 8, 4095–4105.

Liu, M., Xiusheng, H., Xiao, X., and Wang, Y. (2016). Overexpression of miR-422a inhibits cell proliferation and invasion, and enhances chemosensitivity in osteosarcoma cells. *Oncol. Rep.* 36, 3371–3378. doi: 10.3892/or.2016.5182

Liu, Z., Sun, B., Qi, L., Li, H., Gao, J., and Leng, X. (2012). Zinc finger E-box binding homeobox 1 promotes vasculogenic mimicry in colorectal cancer through induction of epithelial-to-mesenchymal transition. *Cancer Sci.* 103, 813–820. doi: 10.1111/j.1349-7006.2011.02199.x

Livak, K. J., and Schmittgen, T. D. (2001). Analysis of relative gene expression data using real-time quantitative PCR and the 2(-Delta Delta C(T) Method. *Methods* 25, 402–408. doi: 10.1006/meth.2001.1262

Ma, Y., Zheng, X., Zhou, J., Zhang, Y., and Chen, K. (2015). ZEB1 promotes the progression and metastasis of cervical squamous cell carcinoma via the promotion of epithelial-mesenchymal transition. *Int. J. Clin. Exp. Pathol.* 8, 11258–11267.

Ma, Z., Li, Y., Xu, J., Ren, Q., Yao, J., and Tian, X. (2016). MicroRNA-409-3p regulates cell invasion and metastasis by targeting ZEB1 in breast cancer. *IUBMB Life* 68, 394–402. doi: 10.1002/iub.1494

Qu, R., Chen, X., and Zhang, C. (2018). LncRNA ZEB1-AS1/miR-409-3p/ZEB1 feedback loop is involved in the progression of non-small cell lung cancer. *Biochem. Biophys. Res. Commun.* 507, 450–456. doi: 10.1016/j.bbrc.2018.11.059

Righi, A., Gambarotti, M., Sbaraglia, M., Sisto, A., Ferrari, S., Tos, A. P., et al. (2016). p16 expression as a prognostic and predictive marker in high grade localized osteosarcoma of the extremities: an analysis of 357 cases. *Hum. Pathol.* 58, 15–23. doi: 10.1016/j.humpath.2016.07.023

Shen, A., Zhang, Y., and Yang, H. (2012). Overexpression of ZEB1 relates to metastasis and invasion in osteosarcoma. *J. Surg. Oncol.* 105, 830–834. doi: 10.1002/jso.23012

Sun, L., Li, Y., Zhang, J., Li, H., Li, B., and Ye, Z. (2015). Prognostic value of pathologic fracture in patients with high grade localized osteosarcoma: a systemic review and meta-analysis of cohort studies. *J. Orthop. Res.* 33, 131–139. doi: 10.1002/jor.22734

Tan, S., Shi, H., Ba, M., Lin, S., Tang, H., Zeng, X., et al. (2016). miR-409-3p sensitizes colon cancer cells to oxaliplatin by inhibiting Beclin-1-mediated autophagy. *Int. J. Mol. Med.* 37, 1030–1038. doi: 10.3892/ijmm.2016.2492

Tang, J., Shen, L., Yang, Q., and Zhang, C. (2014). Overexpression of metadherin mediates metastasis of osteosarcoma by regulating epithelial-mesenchymal transition. *Cell Prolif.* 47, 427–434. doi: 10.1111/cpr.12129

Trang, P., Medina, P. P., Wiggins, J. F., Ruffino, L., Kelnar, K., Omotola, M., et al. (2010). Regression of murine lung tumors by the let-7 microRNA. *Oncogene* 29, 1580–1587. doi: 10.1038/onc.2009.445

Tsai, S. C., Lin, C. C., Shih, T. C., Tseng, R. J., Yu, M. C., Lin, Y. J., et al. (2017). The miR-200b-ZEB1 circuit regulates diverse stemness of human hepatocellular carcinoma. *Mol. Carcinog.* 56, 2035–2047. doi: 10.1002/mc.22657

Vanas, V., Haigl, B., Stockhammer, V., and Sutterluty-Fall, H. (2016). MicroRNA-21 increases proliferation and cisplatin sensitivity of osteosarcoma-derived cells. *PLoS One* 11:e0161023. doi: 10.1371/journal.pone.0161023

Wang, G. C., He, Q. Y., Tong, D. K., Wang, C. F., Liu, K., Ding, C., et al. (2016). MiR-367 negatively regulates apoptosis induced by adriamycin in osteosarcoma cells by targeting KLF4. *J. Bone Oncol.* 5, 51–56. doi: 10.1016/j.jbo.2016.02.002

Zhang, Y., Liu, G., Wu, S., Jiang, F., Xie, J., and Wang, Y. (2016). Zinc finger E-box-binding homeobox 1: its clinical significance and functional role in human thyroid cancer. *Onco. Targets Ther.* 9, 1303–1310. doi: 10.2147/OTT.S96723

Zhang, Y., Wang, F., Li, M., Yu, Z., Qi, R., Ding, J., et al. (2018). Self-Stabilized hyaluronate nanogel for intracellular codelivery of doxorubicin and cisplatin to osteosarcoma. *Adv. Sci.* 5:1700821. doi: 10.1002/advs.201700821

Zhang, Y., Xu, L., and Li, A. (2019). The roles of ZEB1 in tumorigenic progression and epigenetic modifications. *Biomed. Pharmacother.* 110, 400–408. doi: 10.1016/j.biopha.2018.11.112

Zheng, B., Liang, L., Huang, S., Zha, R., Liu, L., Jia, D., et al. (2012). MicroRNA-409 suppresses tumour cell invasion and metastasis by directly targeting radixin in gastric cancers. *Oncogene* 31, 4509–4516. doi: 10.1038/onc.2011.581

Conflict of Interest Statement: The authors declare that the research was conducted in the absence of any commercial or financial relationships that could be construed as a potential conflict of interest.

frontiers in Oncology

ORIGINAL RESEARCH
published: 15 March 2019
doi: 10.3389/fonc.2019.00150

Targeting TF-AKT/ERK-EGFR Pathway Suppresses the Growth of Hepatocellular Carcinoma

Shan-Zhou Huang[1,2†], Meng-Ning Wei[3†], Jia-Rong Huang[3†], Zi-Jian Zhang[4], Wen-Ji Zhang[3], Qi-Wei Jiang[3], Yang Yang[3], Huan-Yu Wang[5], Hui-Lin Jin[1], Kun Wang[3], Zi-Hao Xing[3], Meng-Ling Yuan[3], Yao Li[3], Xiao-Shun He[2], Zhi Shi[2*] and Qi Zhou[1,6*]*

[1] Department of Hepatic Surgery, The First Affiliated Hospital, Sun Yat-sen University, Guangzhou, China, [2] Organ Transplant Center, The First Affiliated Hospital, Sun Yat-sen University, Guangzhou, China, [3] Guangdong Provincial Key Laboratory of Bioengineering Medicine, Department of Cell Biology and Institute of Biomedicine, National Engineering Research Center of Genetic Medicine, College of Life Science and Technology, Jinan University, Guangzhou, China, [4] Department of Hepatobiliary Surgery, The Seventh Affiliated Hospital of Sun Yat-sen University, Shenzhen, China, [5] Department of Thyroid and Breast Surgery, Nanshan District People's Hospital, Shenzhen, China, [6] Department of General Surgery, Hui Ya Hospital of The First Affiliated Hospital, Sun Yat-sen University, Huizhou, China

Tissue factor (TF) is a transmembrane glycoprotein to initiate blood coagulation and frequently overexpressed in a variety of tumors. Our previous study has showed that the expression of TF is upregulated and correlated with prognosis in hepatocellular carcinoma (HCC). However, the role and molecular mechanism of TF in the growth of HCC are still unclear. *In vitro* and *in vivo* functional experiments were performed to determine the effect of TF on the growth of HCC cells. A panel of biochemical assays was used to elucidate the underlying mechanisms. TF could promote the growth of HCC *in vitro* and *in vivo* by activating both ERK and AKT signaling pathways. TF induced EGFR upregualtion, and inhibition of EGFR suppressed TF-mediated HCC growth. In addition, TF protein expression was correlated with EGFR in HCC tissues. TF promotes HCC growth by upregulation of EGFR, and TF as well as EGFR may be potential therapeutic targets of HCC.

Keywords: hepatocellular carcinoma, tissue factor, epidermal growth factor receptor, AKT/ERK, tumor growth

OPEN ACCESS

Edited by:
Yunkai Zhang,
Vanderbilt University Medical Center, United States

Reviewed by:
Chuan Wang,
Auburn University, United States
Shujue Lan,
Institute of Biochemistry and Cell Biology, Shanghai Institutes for Biological Sciences (CAS), China
Jing Zhao,
Fourth Military Medical University, China

****Correspondence:***
Zhi Shi
tshizhi@jnu.edu.cn
Xiao-Shun He
gdtrc@163.com
Qi Zhou
zhouqi@mail.sysu.edu.cn

† These authors have contributed equally to this work

Specialty section:
This article was submitted to Cancer Molecular Targets and Therapeutics, a section of the journal Frontiers in Oncology

Received: *25 January 2019*
Accepted: *22 February 2019*
Published: *15 March 2019*

Citation:
Huang S-Z, Wei M-N, Huang J-R, Zhang Z-J, Zhang W-J, Jiang Q-W, Yang Y, Wang H-Y, Jin H-L, Wang K, Xing Z-H, Yuan M-L, Li Y, He X-S, Shi Z and Zhou Q (2019) Targeting TF-AKT/ERK-EGFR Pathway Suppresses the Growth of Hepatocellular Carcinoma. Front. Oncol. 9:150. doi: 10.3389/fonc.2019.00150

INTRODUCTION

Hepatocellular carcinoma (HCC) is the fifth most lethal cancers worldwide, while China accounted for more than half of all cases and deaths in 2012 (1). More than 400,000 people die from liver cancer and over 450,000 new cases are diagnosed in China each year (2). Though the treatments for HCC have been greatly advanced in recent years, the outcome of HCC is still unoptimistic. Postoperative recurrence, the main reason for poor survival of HCC patients, mainly owes to the tendency of the invasion and metastasis of HCC cells (3, 4). Therefore, understanding the mechanism of HCC tumorigenesis and progression is critical to improve the clinical outcome of HCC patients.

Tissue factor (TF, also known as platelet tissue factor, factor III, thromboplastin, or CD142, encoded by the F3 gene) is a 47 kD transmembrane glycoprotein that contains 263 amino acid residues totally including a 219 amino acid extracellular region, a 23 amino acid hydrophobic transmembrane region, and a 21 amino acids C-terminal intracellular tail (5). Originally, TF is found on the surface of intravascular cells, such as platelets, leukocytes, and endothelial cells and

functions as the principal initiator of the extrinsic coagulation cascade by binding with circulating factor VII or VIIα (FVII/VIIα) (6). Recently, TF is frequently overexpressed in a variety of tumors, including breast cancer, colorectal carcinoma, gastric cancer, non-small cell lung, and pancreatic ductal carcinoma, etc. (7). We and other groups have reported that the expression of TF is upregulated and correlated with prognosis in HCC (8–10). In the current study, we investigate the role and molecular mechanism of TF in the growth of HCC cells.

MATERIALS AND METHODS

Patients and Tissue Specimens

A total 144 HCC tissues were obtained from patients who underwent curative resection between Jan 2008 and Dec 2010 at the First Affiliated Hospital, Sun Yat-sen University. None of the patients received neoadjuvant radiotherapy or chemotherapy before surgery. Signed informed consents were obtained from all patients. The study was approved by the ethics committee of the First Affiliated Hospital, Sun Yat-sen University.

Cell Culture and Reagents

The human HCC cell lines HepG2, BEL-7402, SK-HEP1, SMMC-7721, and normal hepatic cell line LO2 were from China Center for Type Culture Collection and cultured in Dulbecco's modified Eagle's medium (DMEM) supplemented with 10% fetal bovine serum (FBS), penicillin (100 U/ml) and streptomycin (100 ng/ml) in a humidified incubator at 37°C with 5% CO_2 atmosphere. U0126, LY294002, and Gefitinib were from ApexBio. Anti-TF (ab17375) and Anti-Ki-67 (2724-1) were from Abcam. Anti-pAKT (4060), Anti-AKT (4691), Anti-pERK (4370), and Anti-ERK (4695) antibodies were from Cell Signaling Technologies. Anti-EGFR (SC-03) and Anti-c-Myc (SC-40) antibodies were from Santa Cruz Biotechnology. Anti-β-actin

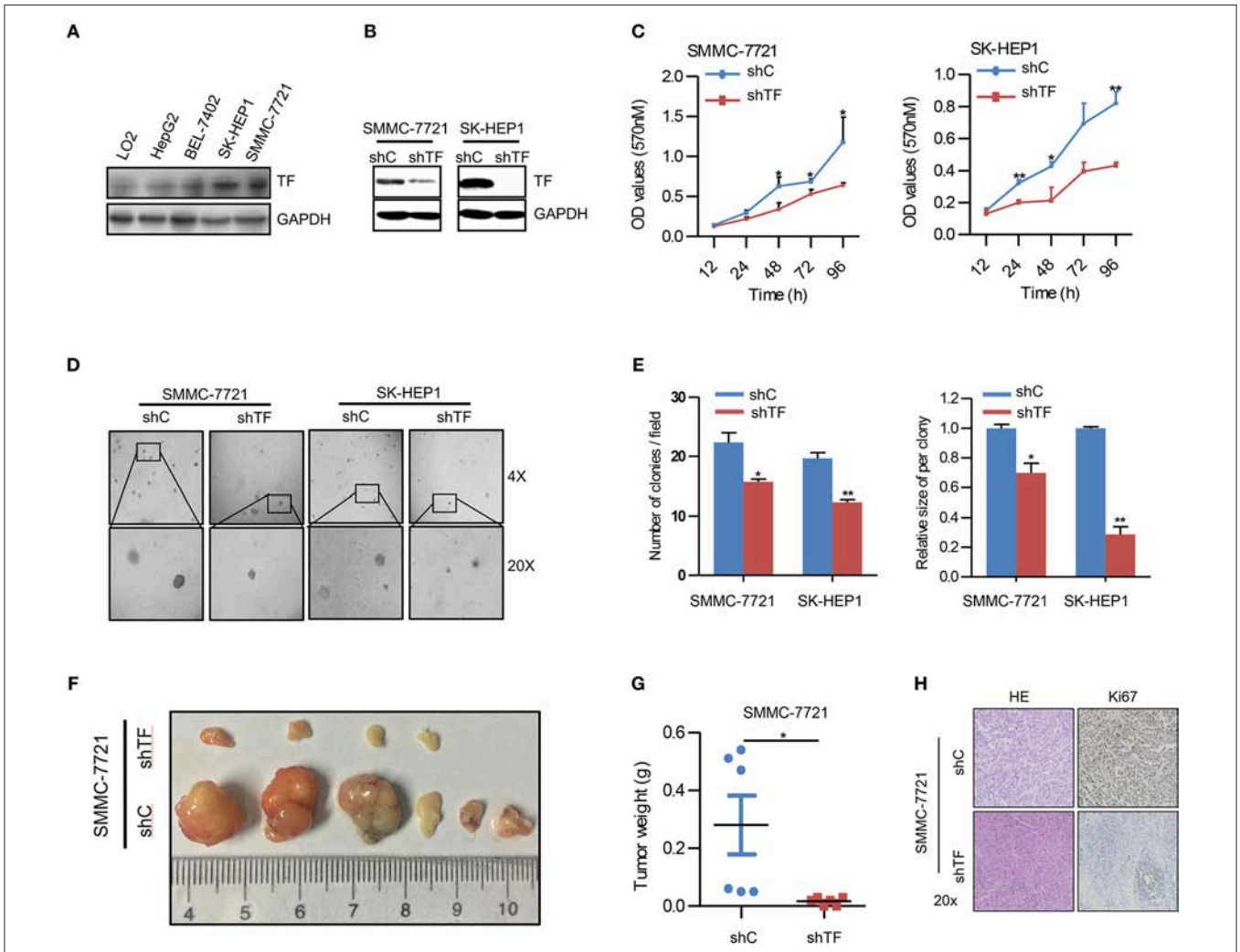

FIGURE 1 | Knockdown of TF inhibits the growth of HCC. **(A,B)** Western blot analysis of the protein expressions in the indicated cells. **(C)** Cell growth of the indicated cells as determined with MTT assay. **(D)** Representative images and **(E)** quantification of the indicated cells sphere as determined with sphere formation assay. **(F)** The indicated subcutaneous tumors and **(G)** tumor weight of nude mice were shown. **(H)** Representative images of H&E and Ki-67 staining in the indicated tumor sections as determined with IHC assay. Error bars, mean ± SD. *$p < 0.05$ and **$p < 0.01$ [two-tailed Student's *t*-test **(C,E,G)**].

(LK9001T) and Anti-GAPDH (LK9002T) antibodies were from Tianjin Sungene Biotech.

Plasmid Construction and Lentivirus Production

The human TF cDNA was cloned into pLVX-AcGFP1-N1 lentiviral vector, and shRNA targeting human TF mRNA (5′-GCGCUUCAGGCACUACAAA-3′) was cloned into pLKO.1 lentiviral vector. Lentivirus was packaged in HEK293T cells and collected from the medium supernatant. Stable cell lines were established by infecting lentivirus into cells, followed by puromycin selection (11, 12).

siRNA Transfection

The EGFR siRNA (sense sequences: 5′- CUGACUCCGUCCAGUAUUGAU−3′) and negative control siRNA were synthesized by Guangzhou Ribobio. Each siRNA solution was mixed gently with the respective volume of the X-tremeGENE siRNA Transfection Reagent and allowed to form transfection mixture for 20 min. Cells were cultured in 6-well plate with DMEM until 50% of confluence and added with the transfection mixture for 24 h before the next experiment (13, 14).

Western Blot

Cells were harvested and washed twice with cold PBS, then resuspended and lysed in RIPA buffer (1% NP-40, 0.5% sodium deoxycholate, 0.1% SDS, 10 ng/ml PMSF, 0.03% aprotinin, 1 μM sodium orthovanadate) at 4°C for 30 min. Lysates were centrifuged for 10 min at 14,000 × g and supernatants were stored at −80°C as whole cell extracts. Proteins were separated on 12% SDS-PAGE gels and transferred to polyvinylidene difluoride membranes. Membranes were blocked with 5% BSA and incubated with the indicated primary antibodies. Corresponding horseradish peroxidase-conjugated secondary antibodies were used against each primary antibody. Signals were detected using

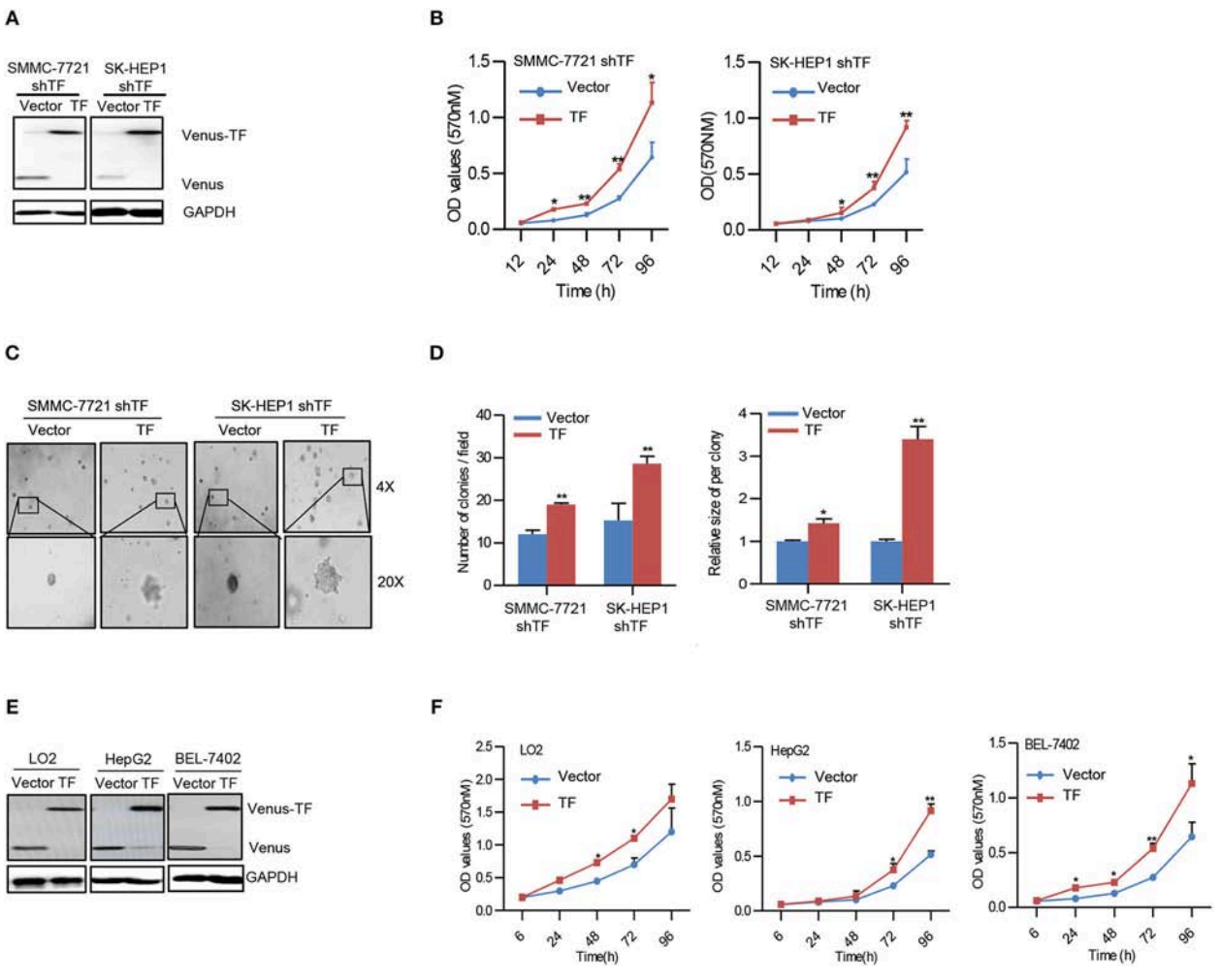

FIGURE 2 | Overexpression of TF promotes the growth of HCC. **(A,E)** Western blot analysis of the protein expressions in the indicated cells. **(B,F)** Cell growth of the indicated cells as determined with MTT assay. **(C)** Representative images and **(D)** quantification of the indicated cells sphere as determined with sphere formation assay. Error bars, mean ± SD. *$p < 0.05$ and **$p < 0.01$ [two-tailed Student's *t*-test **(B,D,F)**].

the ChemiDoc XRS chemiluminescent gel imaging system (Bio-RAD) (15, 16).

MTT Assay

Cells were seeded into a 96-well plate at a density of 0.5–1 × 10^4 cells/well and treated with various concentrations of agents. After 3 days, 3-(4, 5-dimethylthiazolyl-2)-2, 5-diphenyltetrazolium bromide (MTT) was added to each well at a final concentration of 0.5 mg/ml. After incubation for 4 h, the medium and MTT solution were removed from each well, and formazan crystals were dissolved in 100 μl of DMSO. Absorbance was measured at 570 nm by Multiscan Spectrum (Thermofisher) (17, 18).

Sphere Formation Assay

Cells were trypsinized, suspended in medium containing 0.3% agar and 10% FBS and seeded at a density of 5 × 10^2 cells/well in a 12-well plate. The agar–cell mixture was plated onto a bottom layer with 0.5% agar. Then treated cells were incubated in a humidified incubator and fresh medium was added every 3 days. Two weeks later, colonies were analyzed microscopically (19, 20).

Nude Mice Xenograft Tumor Assay

The female Balb/c nude mice with 5 weeks old and 16–18 g weight were obtained from the Shanghai SLAC Laboratory Animal Co and maintained with sterilized food and water. For xenograft tumor assay, 4 × 10^6 cells in 100 μl of DMEM were injected subcutaneously under the shoulder of six mice per group. The mice were anesthetized after experiment, and tumors or lungs were removed, weighed, and sectioned. All experimental procedures were approved by the Institutional Animal Care and Use Committee of Jinan University (21, 22).

Immunohistochemistry Assay

Immunohistochemistry (IHC) assay was performed with a microwave-enhanced avidin-biotin staining method. Formalin-fixed, paraffin embedded human HCC tissue array and subcutaneous tumors in mice were stained with antibodies, respectively, using a microwave-enhanced avidin-biotin staining method. To quantify the protein expression, the following formula was used: IHC score = percentage of positive cells × intensity score. The intensity was scored as follows: 0, negative (no staining); 1, weak (light yellow); 2, moderate (yellow brown); and 3, intense (brown) (23, 24).

Statistical Analysis

Statistical analyses were performed using SPSS 19.0 for Windows (SPSS) and Graph-Pad Prism 6. Data were expressed as the mean ± standard deviation (SD) from at least three independent experiments. Quantitative data between two groups were compared using the Student's *t*-test. Categorical data

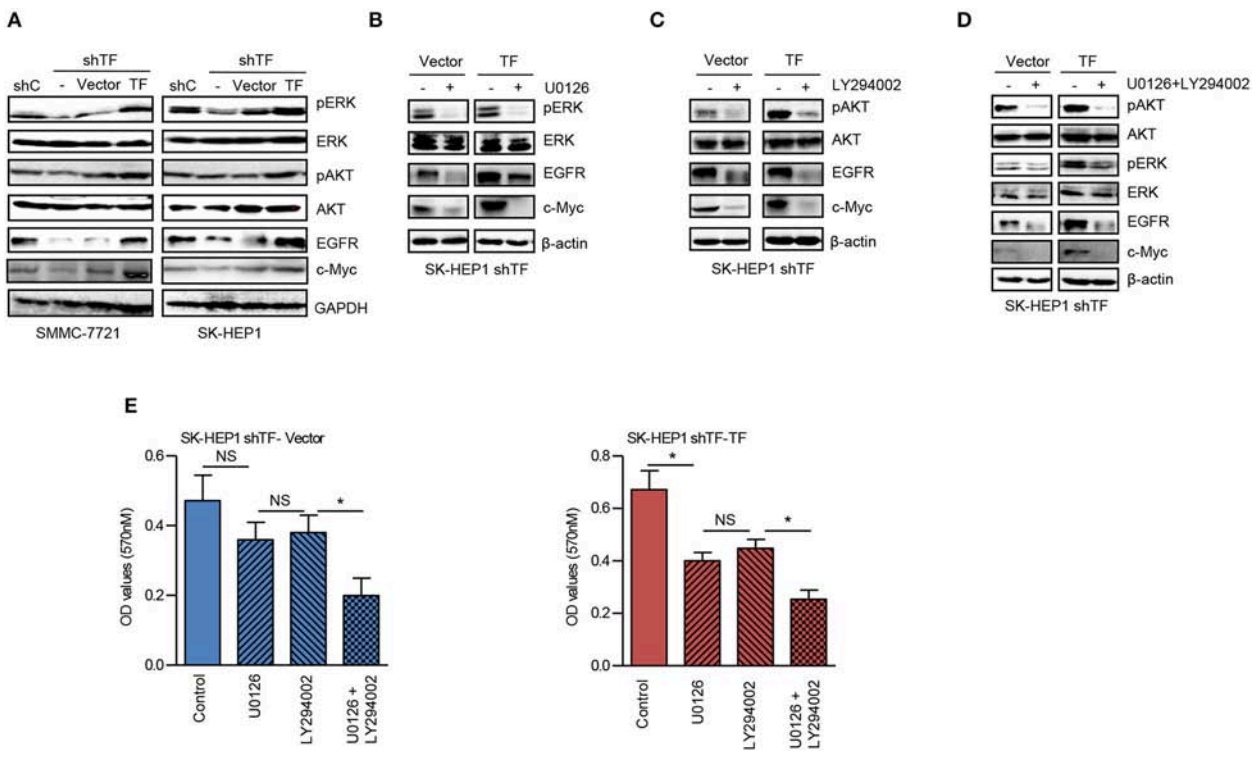

FIGURE 3 | TF promotes the growth of HCC by activating both ERK and AKT signaling pathways. **(A)** Western blot analysis of the protein expressions in the indicated cells. SK-HEP1 shTF-Vector and SK-HEP1 shTF-TF cells were treated with/without U0126 and LY294002 at the concentration of 10 μM for 24 h. **(B–D)** Western blot and **(E)** MTT assay analysis of the protein expressions and cell growth. Error bars, mean ± SD. *$p < 0.05$ (two-tailed Student's *t*-test **E**).

were analyzed by the χ^2 test or Fisher exact test. Correlations between different protein expressions level were determined using Spearman's rank analysis. The $p < 0.05$ was considered as statistical significance. $^{*}p < 0.05$; $^{**}p < 0.01$; NS: no statistical significance.

RESULTS

Knockdown of TF Inhibits the Growth of HCC

To explore the potential biological function of TF in HCC, we first examined the protein expression of TF in human HCC cell lines including HepG2, BEL-7402, SK-HEP1, SMMC-7721, and normal hepatic cell line LO2. Notably, all HCC cell lines displayed higher protein levels of TF than normal hepatic cell line, and SK-HEP1 and SMMC-7721 cells showed the highest protein levels of TF in all cells (**Figure 1A**). To further investigate the role of TF in HCC malignancy, we generated the cells with shRNA-mediated stable knockdown of endogenous TF in both SK-HEP1 and SMMC-7721 cells (**Figure 1B**). Knockdown of TF decreased the cell amounts, sphere numbers and sizes in both SK-HEP1 and SMMC-7721 cells as detected by MTT and sphere formation assays (**Figures 1C–E**). Additionally, the data of subcutaneous tumor models in nude mice showed that TF knockdown inhibited the growth of SMMC-7721 xenografts by decreasing the volumes and weights of tumors as well as the numbers of $Ki67^{+}$ proliferating cells (**Figures 1F–H**).

Overexpression of TF Promotes the Growth of HCC

To confirm the effect of TF on HCC growth, we performed rescue experiments by ectopic expression of TF in both TF-silenced SMMC-7721 and SK-HEP1 cells (**Figure 2A**). Ectopic expression of TF increased the cell amounts, sphere numbers, and sizes in both TF-silenced SMMC-7721 and SK-HEP1 cells (**Figures 2B–D**). Furthermore, overexpression of TF increased the cell amounts in LO2, HepG2, and BEL-7402 cells (**Figures 2E, F**). Taken together, these results suggest that TF can promote the growth of HCC.

TF Promotes the Growth of HCC by Activating Both ERK and AKT Signaling Pathways

To further explore the molecular mechanism of TF-promoted HCC growth, we detected the downstream signaling pathway of TF. As shown in **Figure 3A**, knockdown of TF decreased the protein levels of phosphorylated ERK (pERK), phosphorylated AKT (pAKT), and their downstream transcriptional factor c-Myc in both SMMC-7721 and SK-HEP1 cells. While ectopic expression of TF increased the protein levels of pERK, pAKT and c-Myc in both TF-silenced SMMC-7721 and SK-HEP1 cells. Interesting, the protein level of EGFR was downregulated in TF-silenced HCC cells and upregulated in TF-overexpressed HCC cells (**Figure 3A**). To define the roles of ERK and AKT in TF-mediated HCC growth, we examined the effects of MEK inhibitor U0126 and PI3K inhibitor LY294002 on the growth of both SK-HEP1 shTF-Vector and -TF cells. Treatment with U0126 or/and LY294002 decreased the protein levels of EGFR, c-Myc, pERK or/and pAKT in both SK-HEP1 shTF-Vector and -TF cells (**Figures 3B–D**). However, with U0126 or LY294002 alone inhibited the growth only in SK-HEP1 shTF-TF cells but not in SK-HEP1 shTF-Vector cells. After treating with the combination of U0126 and LY294002 significantly

TABLE 1 | The correlation between TF and EGFR protein expressions in HCC tissues.

		TF expression			*P*
		High	**Low**	**Total**	**r**
EGFR expression	High	82	9	91	< 0.001
	Low	23	30	53	0.668
		105	39	144	

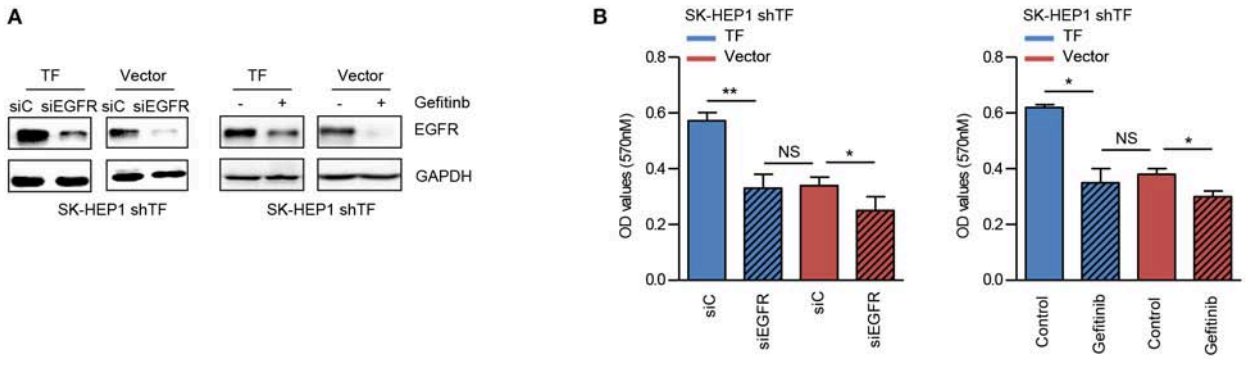

FIGURE 4 | Inhibition of EGFR suppresses TF-mediated HCC growth. SK-HEP1 shTF-Vector and SK-HEP1 shTF-TF cells were transfected with siControl or siEGFR or treated with/without gefinib at the concentration of 10 μM for 24 h. **(A)** Western blot and **(B)** MTT assay analysis of the protein expressions and cell growth. Error bars, mean ± SD. $^{*}p < 0.05$ and $^{**}p < 0.01$ (two-tailed Student's *t*-test **B**).

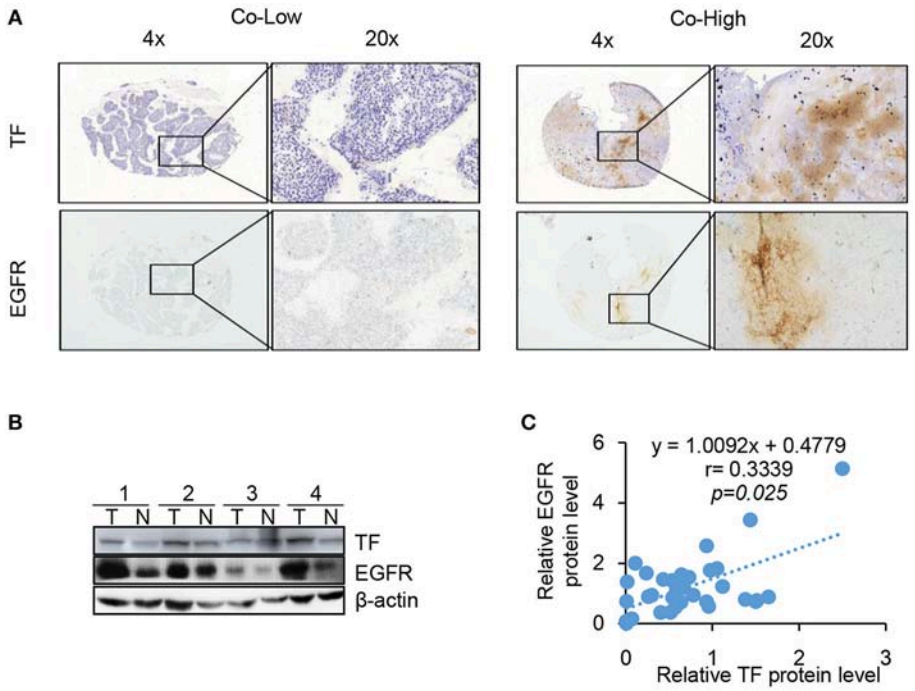

FIGURE 5 | TF protein expression is correlated with EGFR and poor HCC patient prognosis. TF and EGFR protein expressions in 144 HCC tissues were examined with IHC assay. **(A)** Representative images of positive and negative expression of both TF and EGFR were shown at 4 X and 20 X magnification. **(B)** Representative images of western blot analysis of TF and EGFR protein expression in the paired HCC tissues and adjacent normal tissues. **(C)** Spearman's rank correlation test showed the correlation between TF and EGFR protein expressions by Western blot.

inhibited the growth in both SK-HEP1 shTF-Vector and -TF cells (**Figure 3E**). In short, these data suggest that TF promotes the growth of HCC by activating both ERK and AKT signaling pathways.

Inhibition of EGFR Suppresses TF-Mediated HCC Growth

EGFR has been identified as a key player in the development of HCC (25). To verify the role of EGFR in TF-mediated HCC growth, we examined the effects of EGFR siRNA and EGFR inhibitor gefitinib on the growth of both SK-HEP1 shTF-Vector and -TF cells. EGFR siRNA or gefitinib decreased the protein levels of EGFR in both SK-HEP1 shTF-Vector and -TF cells (**Figure 4A**). Furthermore, EGFR siRNA or gefitinib inhibited the growth more significantly in SK-HEP1 shTF-TF cells than in SK-HEP1 shTF-Vector cells, indicating that inhibition of EGFR suppresses TF-mediated HCC growth (**Figure 4B**).

TF Protein Expression Is Correlated With EGFR in HCC Tissues

Our results clearly demonstrate that EGFR is regulated by TF in cell culture. To determine whether this is also the case in tumor tissues, we compared the protein levels of TF and EGFR in human 144 HCC tissues by IHC assay. High TF and EGFR staining were present in 105 (72.9%) and 91 (63.2%) out of 144 HCC tissues, respectively. Results of representative tissues with co-low or co-high staining of TF and EGFR were shown in **Figure 5A**. The expression of TF was highly correlated with the expression of EGFR in HCC tissues (**Table 1** and **Figures 5B, C**).

DISCUSSION

It has been demonstrated that TF-induced tumor progression need the activation of intracellular signaling pathways, where TF cytoplasmic domain couples to proteolytic activation of the protease activated receptor (PAR) 2 and subsequently activates ERK, AKT and other signaling pathways (26). For example, TF was involved in retinoblastoma cell proliferation via activating both ERK and AKT signaling pathways (27). Knockdown of TF suppressed human lung adenocarcinoma growth *in vitro* and *in vivo* through inhibiting both ERK and AKT signaling pathways (28). Similarly, our results showed that TF promoted the growth of HCC *in vitro* and *in vivo* by activating both ERK and AKT signaling pathways. Inhibition of ERK and AKT blocked TF-mediated growth of HCC. Therefore, activation of both ERK and AKT signaling pathways is indispensable for TF-promoted the growth of HCC.

EGFR is a member of ErbB/HER family of transmebrane receptor tyrosine kinases. It is activated by specific ligands resulting in the activation of multiple intracellular signaling pathways including ERK, AKT. Those signaling pathways is related to cell proliferation, migration and invasion (29–31). The gene expression of EGFR is regulated by the transcription factor c-Myc (32). In this study, we found that TF could enhance

the expression of c-Myc and EGFR, and inhibition of ERK and AKT could block TF-induced c-Myc and EGFR upregulation. Phosphorylation of serine 62 amino acid residues by ERK prevents c-Myc protein from degradation (33). AKT stabilizes c-Myc protein by phosphorylation and inactivation of GSK-3β which phosphorylated threonine 58 amino acid residues of c-Myc to promote c-Myc degradation (33).

Inhibition of EGFR with either small molecule inhibitors or specific antibodies has achieved promising results in the preclinical HCC models. In human HCC cells, gefitinib, erlotinib or cetuximab could induce growth inhibition, cell cycle arrest and apoptosis (34–36). In the orthotopic HCC models, gefitinib significantly inhibited the growth and metastasis of HCC tumors, and enhanced by the combination with cisplatin (37, 38). However, the outcome of targeting EGFR in HCC was modest in the clinical trials. When used as a single agent in HCC patients, erlotinib only acquired moderate effects (39, 40), and cetuximab showed no antitumor activity (41). Treatment failure with EGFR inhibitors in HCC patients may cause by many reasons, such as the levels and mutations of EGFR, EMT status of tumor cells, etc. (42–44). In the current study, we found that treatment with EGFR siRNA or gefitinib suppressed the growth more significantly in the TF highly expressed HCC cells, suggesting that the levels of TF in tumor cells may influence the effects of EGFR inhibitors. Furthermore, our IHC data showed that both positive ratios of TF and EGFR protein in the HCC tissue were 72.9% (105/144) and 63.2% (91/144), respectively. The expression of TF was highly correlated with the expression of EGFR in HCC tissues. Therefore, it may be valuable to investigate the relation of TF expressions and EGFR inhibitors effects in the future studies.

CONCLUSIONS

Our results provide proof-of-principle insights into a novel mechanism driven by TF on HCC growth and suggest that TF and EGFR may be potential therapeutic targets of HCC.

DATA AVAILABILITY

The datasets generated for this study are available on request to the corresponding author.

AUTHOR CONTRIBUTIONS

S-ZH, M-NW, J-RH, Z-JZ, W-JZ, Q-WJ, and YY performed experiments. H-YW, H-LJ, KW, Z-HX, M-LY, and YL collected and analyzed data. X-SH, ZS, and QZ prepared the manuscript.

FUNDING

This work was supported by funds from the National Natural Science Foundation of China Nos. 81661148049 and 81772540 (ZS), the Guangdong Natural Science Funds for Distinguished Young Scholar No. 2014A030306001 (ZS), the Guangdong Special Support Program for Young Talent No. 2015TQ01R350 (ZS), the Science and Technology Program of Guangdong Nos. 201300000187 (QZ) and 2016A050502027 (ZS), the Science and Technology Program of Guangzhou No. 201704030058 (ZS), the Science and Technology Program of Huizhou (170520181743174/2017Y229 and 180529101741637/2018Y305), and the Program Sci-tech Research Development of Guangdong Province 2014A020212717 (QZ).

REFERENCES

1. Torre LA, Bray F, Siegel RL, Ferlay J, Lortet-Tieulent J, Jemal A. Global cancer statistics, 2012. *CA Cancer J Clin.* (2015) 65:87–108. doi: 10.3322/caac.21262
2. Chen W, Zheng R, Baade PD, Zhang S, Zeng H, Bray F, et al. Cancer statistics in China, 2015. *CA Cancer J Clin.* (2016) 66:115–32. doi: 10.3322/caac.21338
3. Sun T, Liu H, Ming L. Multiple roles of autophagy in the sorafenib resistance of hepatocellular carcinoma. *Cell Physiol Biochem.* (2017) 44:716–27. doi: 10.1159/000485285
4. Li C, Chen J, Zhang K, Feng B, Wang R, Chen L. Progress and prospects of long noncoding RNAs (lncRNAs) in hepatocellular carcinoma. *Cell Physiol Biochem.* (2015) 36:423–34. doi: 10.1159/000430109
5. Versteeg HH, Spek CA, Peppelenbosch MP, Richel DJ. Tissue factor and cancer metastasis: the role of intracellular and extracellular signaling pathways. *Mol Med.* (2004) 10:6–11. doi: 10.2119/2003-00047.Versteeg
6. Mackman N. Role of tissue factor in hemostasis, thrombosis, and vascular development. *Arterioscler Thromb Vasc Biol.* (2004) 24:1015–22. doi: 10.1161/01.ATV.0000130465.23430.74
7. Ruf W. Tissue factor and cancer. *Thromb Res.* (2012) 130(Suppl. 1):S84–87. doi: 10.1016/j.thromres.2012.08.285
8. Zhou Q, Huang T, Wang YF, Zhou XB, Liang LJ, Peng BG. Role of tissue factor in hepatocellular carcinoma genesis, invasion and metastasis. *Chin Med J.* (2011) 124:3746–51.
9. Kaido T, Oe H, Yoshikawa A, Mori A, Arii S, Imamura M. Tissue factor is a useful prognostic factor of recurrence in hepatocellular carcinoma in 5-year survivors. *Hepatogastroenterology.* (2005) 52:1383–7.
10. Poon RT, Lau CP, Ho JW, Yu WC, Fan ST, Wong J. Tissue factor expression correlates with tumor angiogenesis and invasiveness in human hepatocellular carcinoma. *Clin Cancer Res.* (2003) 9:5339–45.
11. Yang Y, Qiu JG, Li Y, Di JM, Zhang WJ, Jiang QW, et al. Targeting ABCB1-mediated tumor multidrug resistance by CRISPR/Cas9-based genome editing. *Am J Transl Res.* (2016) 8:3986–94.
12. Shi Z, Li Z, Li ZJ, Cheng K, Du Y, Fu H, et al. Cables1 controls p21/Cip1 protein stability by antagonizing proteasome subunit alpha type 3. *Oncogene.* (2015) 34:2538–45. doi: 10.1038/onc.2014.171
13. Luo Y, Jiang QW, Wu JY, Qiu JG, Zhang WJ, Mei XL, et al. Regulation of migration and invasion by toll-like receptor-9 signaling network in prostate cancer. *Oncotarget.* (2015) 6:22564–74. doi: 10.18632/oncotarget.4197
14. Zhang WJ, Li Y, Wei MN, Chen Y, Qiu JG, Jiang QW, et al. Synergistic antitumor activity of regorafenib and lapatinib in preclinical models of human colorectal cancer. *Cancer Lett.* (2017) 386:100–9. doi: 10.1016/j.canlet.2016.11.011
15. Lv M, Qiu JG, Zhang WJ, Jiang QW, Qin WM, Yang Y, et al. Wallichinine reverses ABCB1-mediated cancer multidrug resistance. *Am J Transl Res.* (2016) 8:2969–80.
16. Chen X, Gong L, Ou R, Zheng Z, Chen J, Xie F, et al. Sequential combination therapy of ovarian cancer with cisplatin and gamma-secretase inhibitor MK-0752. *Gynecol Oncol.* (2016) 140:537–44. doi: 10.1016/j.ygyno.2015.12.011
17. Lin M, Bi H, Yan Y, Huang W, Zhang G, Tang S, et al. Parthenolide suppresses non-small cell lung cancer GLC-82 cells growth via B-Raf/MAPK/Erk pathway. *Oncotarget.* (2017) 8:23436–47. doi: 10.18632/oncotarget.15584
18. Gong LH, Chen XX, Wang H, Jiang QW, Pan SS, Qiu JG, et al. Piperlongumine induces apoptosis and synergizes with cisplatin or paclitaxel

in human ovarian cancer cells. *Oxid Med Cell Longev.* (2014) 2014:906804. doi: 10.1155/2014/906804
19. Li P, Yang Y, Liu H, Yang AK, Di JM, Tan GM, et al. MiR-194 functions as a tumor suppressor in laryngeal squamous cell carcinoma by targeting wee1. *J Hematol Oncol.* (2017) 10:32. doi: 10.1186/s13045-017-0402-6
20. Jiang QW, Cheng KJ, Mei XL, Qiu JG, Zhang WJ, Xue YQ, et al. Synergistic anticancer effects of triptolide and celastrol, two main compounds from thunder god vine. *Oncotarget.* (2015) 6:32790–804. doi: 10.18632/oncotarget.5411
21. Zheng DW, Xue YQ, Li Y, Di JM, Qiu JG, Zhang WJ, et al. Volasertib suppresses the growth of human hepatocellular carcinoma *in vitro* and *in vivo*. *Am J Cancer Res.* (2016) 6:2476–88.
22. Mei XL, Yang Y, Zhang YJ, Li Y, Zhao JM, Qiu JG, et al. Sildenafil inhibits the growth of human colorectal cancer *in vitro* and *in vivo*. *Am J Cancer Res.* (2015) 5:3311–24.
23. Shi Z, Park HR, Du Y, Li Z, Cheng K, Sun SY, et al. Cables1 complex couples survival signaling to the cell death machinery. *Cancer Res.* (2015) 75:147–58. doi: 10.1158/0008-5472.CAN-14-0036
24. Qiu JG, Zhang YJ, Li Y, Zhao JM, Zhang WJ, Jiang QW, et al. Trametinib modulates cancer multidrug resistance by targeting ABCB1 transporter. *Oncotarget.* (2015) 6:15494–509. doi: 10.18632/oncotarget.3820
25. Berasain C, Avila MA. The EGFR signalling system in the liver: from hepatoprotection to hepatocarcinogenesis. *J Gastroenterol.* (2014) 49:9–23. doi: 10.1007/s00535-013-0907-x
26. Han X, Guo B, Li Y, Zhu B. Tissue factor in tumor microenvironment: a systematic review. *J Hematol Oncol.* (2014) 7:54. doi: 10.1186/s13045-014-0054-8
27. Lee BJ, Kim JH, Woo SH, Kim DH, Yu YS. Tissue factor is involved in retinoblastoma cell proliferation via both the akt and extracellular signal-regulated kinase pathways. *Oncol Rep.* (2011) 26:665–70. doi: 10.3892/or.2011.1314
28. Xu C, Gui Q, Chen W, Wu L, Sun W, Zhang N, et al. Small interference RNA targeting tissue factor inhibits human lung adenocarcinoma growth *in vitro* and *in vivo*. *J Exp Clin Cancer Res.* (2011) 30:63. doi: 10.1186/1756-9966-30-63
29. Grant S, Qiao L, Dent P. Roles of ERBB family receptor tyrosine kinases, and downstream signaling pathways, in the control of cell growth and survival. *Front Biosci.* (2002) 7:d376–89. doi: 10.2741/grant
30. Normanno N, De Luca A, Bianco C, Strizzi L, Mancino M, Maiello MR, et al. Epidermal growth factor receptor (EGFR) signaling in cancer. *Gene.* (2006) 366:2–16. doi: 10.1016/j.gene.2005.10.018
31. Ma P, Fu Y, Chen M, Jing Y, Wu J, Li K, et al. Adaptive and acquired resistance to EGFR inhibitors converge on the MAPK pathway. *Theranostics.* (2016) 6:1232–43. doi: 10.7150/thno.14409
32. Perini G, Diolaiti D, Porro A, Della Valle G. *In vivo* transcriptional regulation of n-myc target genes is controlled by E-box methylation. *Proc Natl Acad Sci USA.* (2005) 102:12117–22. doi: 10.1073/pnas.0409097102
33. Sears R, Nuckolls F, Haura E, Taya Y, Tamai K, Nevins JR. Multiple ras-dependent phosphorylation pathways regulate Myc protein stability. *Genes Dev.* (2000) 14:2501–14. doi: 10.1101/gad.836800
34. Okano J, Matsumoto K, Nagahara T, Murawaki Y. Gefitinib and the modulation of the signaling pathways downstream of epidermal growth factor receptor in human liver cancer cells. *J Gastroenterol.* (2006) 41:166–76. doi: 10.1007/s00535-005-1736-3
35. Hopfner M, Sutter AP, Huether A, Schuppan D, Zeitz M, Scherubl H. Targeting the epidermal growth factor receptor by gefitinib for treatment of hepatocellular carcinoma. *J Hepatol.* (2004) 41:1008–16. doi: 10.1016/j.jhep.2004.08.024
36. Huether A, Hopfner M, Sutter AP, Schuppan D, Scherubl H. Erlotinib induces cell cycle arrest and apoptosis in hepatocellular cancer cells and enhances chemosensitivity towards cytostatics. *J Hepatol.* (2005) 43:661–9. doi: 10.1016/j.jhep.2005.02.040
37. Matsuo M, Sakurai H, Saiki I. ZD1839, a selective epidermal growth factor receptor tyrosine kinase inhibitor, shows antimetastatic activity using a hepatocellular carcinoma model. *Mol Cancer Ther.* (2003) 2:557–61.
38. Zhu BD, Yuan SJ, Zhao QC, Li X, Li Y, Lu QY. Antitumor effect of gefitinib, an epidermal growth factor receptor tyrosine kinase inhibitor, combined with cytotoxic agent on murine hepatocellular carcinoma. *World J Gastroenterol.* (2005) 11:1382–6. doi: 10.3748/wjg.v11.i9.1382
39. Philip PA, Mahoney MR, Allmer C, Thomas J, Pitot HC, Kim G, et al. Phase II study of erlotinib (OSI-774) in patients with advanced hepatocellular cancer. *J Clin Oncol.* (2005) 23:6657–63. doi: 10.1200/JCO.2005.14.696
40. Thomas MB, Chadha R, Glover K, Wang X, Morris J, Brown T, et al. Phase 2 study of erlotinib in patients with unresectable hepatocellular carcinoma. *Cancer.* (2007) 110:1059–67. doi: 10.1002/cncr.22886
41. Zhu AX, Stuart K, Blaszkowsky LS, Muzikansky A, Reitberg DP, Clark JW, et al. Phase 2 study of cetuximab in patients with advanced hepatocellular carcinoma. *Cancer.* (2007) 110:581–9. doi: 10.1002/cncr.22829
42. Lanaya H, Natarajan A, Komposch K, Li L, Amberg N, Chen L, et al. EGFR has a tumour-promoting role in liver macrophages during hepatocellular carcinoma formation. *Nat Cell Biol.* (2014) 16:972–7. doi: 10.1038/ncb3031
43. Su MC, Lien HC, Jeng YM. Absence of epidermal growth factor receptor exon 18-21 mutation in hepatocellular carcinoma. *Cancer Lett.* (2005) 224:117–21. doi: 10.1016/j.canlet.2004.10.010
44. Fuchs BC, Fujii T, Dorfman JD, Goodwin JM, Zhu AX, Lanuti M, et al. Epithelial-to-mesenchymal transition and integrin-linked kinase mediate sensitivity to epidermal growth factor receptor inhibition in human hepatoma cells. *Cancer Res.* (2008) 68:2391–9. doi: 10.1158/0008-5472.CAN-07-2460

Conflict of Interest Statement: The authors declare that the research was conducted in the absence of any commercial or financial relationships that could be construed as a potential conflict of interest.

frontiers in Oncology

ORIGINAL RESEARCH
published: 22 March 2019
doi: 10.3389/fonc.2019.00175

Schistosoma japonicum MiRNA-7-5p Inhibits the Growth and Migration of Hepatoma Cells via Cross-Species Regulation of S-Phase Kinase-Associated Protein 2

Chao Hu[1], *Shanli Zhu*[1], *Jing Wang*[1], *Yu Lin*[1], *Li Ma*[1], *Liufang Zhu*[1], *Pengyue Jiang*[1], *Zhengli Li*[1] *and Weiqing Pan*[1,2]*

[1] *Institute for Infectious Diseases and Vaccine Development, Tongji University School of Medicine, Shanghai, China,*
[2] *Department of Tropical Diseases, Second Military Medical University, Shanghai, China*

OPEN ACCESS

Edited by:
Yunkai Zhang,
Vanderbilt University Medical Center, United States

Reviewed by:
Yang Li,
University of Arizona, United States
Hui Wang,
Vanderbilt University, United States

***Correspondence:**
Weiqing Pan
wqpan0912@aliyun.com

Specialty section:
This article was submitted to Cancer Molecular Targets and Therapeutics, a section of the journal Frontiers in Oncology

Received: *24 October 2018*
Accepted: *28 February 2019*
Published: *22 March 2019*

Citation:
Hu C, Zhu S, Wang J, Lin Y, Ma L, Zhu L, Jiang P, Li Z and Pan W (2019) Schistosoma japonicum MiRNA-7-5p Inhibits the Growth and Migration of Hepatoma Cells via Cross-Species Regulation of S-Phase Kinase-Associated Protein 2. Front. Oncol. 9:175. doi: 10.3389/fonc.2019.00175

MicroRNAs (miRNAs) play important roles in human diseases, such as cancer. Human miRNA-7-5p is a tumor suppressor miRNA that inhibits tumor growth by regulating multiple oncogenic signal pathways. Recently, studies revealed that plant miRNAs could regulate mammalian gene expression in a cross-kingdom manner. *Schistosoma japonicum* miRNA-7-5p (designated as sja-miR-7-5p) is conserved between the parasites and mammals. Thus, we investigated whether sja-miR-7-5p has similar antitumor activity to its mammalian counterpart. We first showed that sja-miR-7-5p was detected in host hepatocytes during *S. japonicum* infection. The sja-miR-7-5p mimics significantly inhibited the growth, migration, and colony formation of mouse and human hepatoma cell lines *in vitro*, and induced G1/G0 cell cycle arrest. In a xenograft animal model, the tumor volume and weight were significantly reduced in mice inoculated with hepatoma cells transfected with sja-miR-7-5p mimics compared with those transfected with NC miRNAs. Furthermore, the antitumor activity of sja-miR-7-5p was suggested by cross-species downregulation of the S-phase kinase-associated protein 2 gene in the host. Thus, sja-miR-7-5p is translocated into hepatocytes and exerts its anti-cancer activities in mammals, implying that sja-miR-7-5p might strengthen host resistance to hepatocellular carcinoma during schistosome infection.

Keywords: ***Schistosoma japonicum*, microRNA, hepatoma cell, SKP2, cross-species regulation**

INTRODUCTION

The primary pathology of schistosomiasis caused by *S. japonicum* is egg-induced granuloma and fibrosis. The female adult worms living in the host mesenteric veins lay numerous eggs, and most of them are trapped in the liver tissues via the portal venous system, causing a granulomatous reaction and fibrosis. The parasite eggs in the granuloma are surrounded by host cells, including immunocytes, hepatic mesenchymal cells, and hepatocytes (1). Our previous studies indicated that *S. japonicum* secretes many microRNAs (miRNAs), including *Schistosoma*-specific and conserved miRNAs (2), and parasite miRNA-containing exosomes (2).

MiRNAs are a class of highly conserved, small non-coding RNAs, with a length of about 20–24 nucleotides (nt) that post-transcriptionally regulate gene expression through complete or incomplete binding to their target mRNAs (3). MiRNAs have extensive effects on not only physiological processes, but also on the progression of many human diseases, such as cancers (4, 5). Aberrant miRNA expression promotes the occurrence and development of various cancers (6–8); however, some miRNAs can exert therapeutic effects on multiple cancers through regulation of tumor-related genes, including those that control tumor cell growth or apoptosis (9, 10). Interestingly, miRNAs derived from plants can regulate the expression of their target genes in mammals in a cross-kingdom manner (11–13). For example, miR-159 derived from plants was detectable in human sera and inhibited breast cancer growth by targeting the human transcription factor 7 (*TCF7*) gene (13). Accumulating evidence indicates that heterogeneous miRNAs can modulate cell functions in mammals. However, it remains unclear how the plant miRNAs can survive the passage through the gastrointestinal tract following ingestion.

Unlike plant miRNAs, which need to pass through the gastrointestinal tract before release into the host serum or entering host cells, schistosomal miRNAs from eggs trapped in liver tissue may be directly transferred to the neighboring host cells. Thus, we hypothesized that parasite miRNAs from the eggs might be translocated into neighboring hepatocytes to exert various biological effects, including some that are beneficial to the host, for example, strengthening the resistance of the host to diseases such as cancer, as do plant-derived miRNAs (13). Human miRNA-7-5p (designated as hsa-miR-7-5p) is a tumor suppressor miRNA that regulates multiple oncogenic signal pathways and reverses drug resistance in certain cancers (14–17). Our previous study identified a *S. japonicum* miRNA-7-5p (designated as sja-miR-7-5p) that is conserved between the parasite and mammals, i.e., there is an identical seed sequence (2–8 nt at the 5′ region) in both parasites and mammalian miRNA-7-5p, despite there being 6 nt differences in the rest of the sequence. Thus, it would be interesting to investigate if sja-miR-7-5 secreted by *S. japonicum* has a similar antitumor activity to hsa-miR-7-5p. In the present study, we demonstrated that sja-miR-7-5p is present in hepatocytes during the *S. japonicum* infection and the sja-miR-7-5p exerts anticancer effects on multiple hepatoma cells (assessed using *in vitro* and *in vivo* models) by targeting the S-phase kinase-associated protein 2(*SKP2*) gene, which is a component of the SCF (Skp1-Cullin 1-F-box) E3 ubiquitin-ligase complex. Previous studies have shown that overexpression of the *SKP2* gene was observed in many cancers, such as in liver cancer (18), prostate cancer (19), lymphoma (20), melanoma (21), and breast cancer (22), which plays an important role in regulating cellular proliferation and cancer progression, mainly by targeting cell cycle regulators in an ubiquitin-dependent manner, followed by 26S proteasome degradation (23). In addition, the *SKP2* overexpression also enhanced tumor cell invasion (24), metastasis (25), and resistance to apoptosis (26), and was associated with tumor aggressiveness (27) and poor prognosis (28).

Abbreviations: *S. japonicum*, *Schistosoma japonicum*; HCC, hepatocellular cancer; SKP2, S-phase kinase associated protein 2; P27(also known as CDKN1B), cyclin dependent kinase inhibitor 1B; MMP9, matrix metallopeptidase 9; miRNA, microRNA; siRNA, small interfering RNA; NC, negative control; Mock, mock control.

MATERIALS AND METHODS

Infection of Mice With *S. japonicum* Cercariae

Animal experiments were performed in accordance with the Guide for the Care and Use of Laboratory Animals of the National Institutes of Health, and approved by the Internal Review Board of Tongji University School of Medicine. The animal surgeries were undertaken under sodium pentobarbital anesthesia. Cercariae of *S. japonicum* were provided by National Institute of Parasitic Disease, Chinese Center for Disease Control and Prevention (CDC). 36 six-week-old male C57BL/6J mice (18–20 g, 3 mice per group), purchased from experimental animal center of the Second Military Medical University and housed under specific pathogen-free conditions, were percutaneously infected with 50 or 100 cercariae of *S. japonicum* per mouse (50 for collection of infected hepatocytes and 100 for collection of early stage parasites). For collection of parasites, the hepatic schistosomula were isolated from the portal system and mesenteric veins of infected mice at 7, 14, and 42 days post-infection (dpi). In addition, 42 days male and female adult worms were manually separated under a light microscope. The eggs were isolated with a traditional method, as described by Cai et al. (29). All the freshly isolated parasites were washed three times with PBS (pH 7.4) and were immediately used for extraction of total RNA or frozen at −80°C until being subjected to further analysis.

Isolation of Primary Mouse Hepatocytes

The primary mouse hepatocytes were isolated by a two-step collagenase perfusion procedure, as described by He et al. (30) with minor modifications. Briefly, after infection, livers of the infected mice collected at various time points of 7, 9, 11, 14, 28, and 42 dpi ($n = 5$) along with the livers of uninfected mice were initially *in situ* digested with 0.03% collagenase type IV and then further digested with 0.08% collagenase type IV at 37°C in a shaking bath for 30 min. The single cell suspensions were harvested by filtration through 400-mesh sieves for removal of the remaining tissue debris and parasite eggs. Next, hepatocytes were isolated by centrifugation of the resulting cell suspensions at 50×g for 4 min and further purified by centrifugation at 50 × g for 4 min. Purified hepatocytes were resuspend in DMEM containing 20 μg/ml Ribonuclease A (Sigma-Aldrich, USA) at 37°C for 30 min to eliminate any miRNA that might be released by schistosome eggs. After washing with PBS for three times, the cell pellet was immediately used for extraction of total RNA or frozen at −80°C until used.

Cell Proliferation Assay

Cells (2×10^5) were seeded in a 6-well plate overnight, respectively. Then cells were transfected with sja-miR-7-5p

mimics or NC mimics, respectively, four replicates per group. And 24 h later, cells were digested and seeded in a 96-well plate (2×10^3) for 1, 2, 3, and 4 d. At each indicated time, 10 μL Cell Counting Kit-8(CCK-8, Dojindo, Japan) was added to each well and cells were incubated for 1 h at 37 °C, then, using the Microplate reader (Bio-Tek, USA) to measure the abosorbance at 450 nm.

Cell Cycle Analysis

Cells (1×10^5) were seeded in a 12-well plate overnight, respectively. Then, cells were transfected with sja-miR-7-5p mimics or NC mimics, respectively, three replicates per group. And 48 h later, cells were collected and fixed with ice-cold 75%(v/v) ethanol and stored at 4°C overnight, then, cells were washed and resuspended in 200 μL phosphate-buffered saline (PBS) contained with 0.05 mg/mL RNase A (Beyotime, China) and 25 mg/mL propidium iodide (PI) (Beyotime, China), cell cycle was determined by the FACSverse flow cytometer (BD Biosciences, USA).

Colony Formation Assay

Cells (2×10^5) were seeded in a 6-well plate overnight, then cells were transfected with sja-miR-7-5p mimics or NC mimics, respectively. And 24 h later, cells were digested and 200 cells in 500 μL complete medium were seeded in 24-well plate, three replicates per group. After incubation for 8 days, then cells were

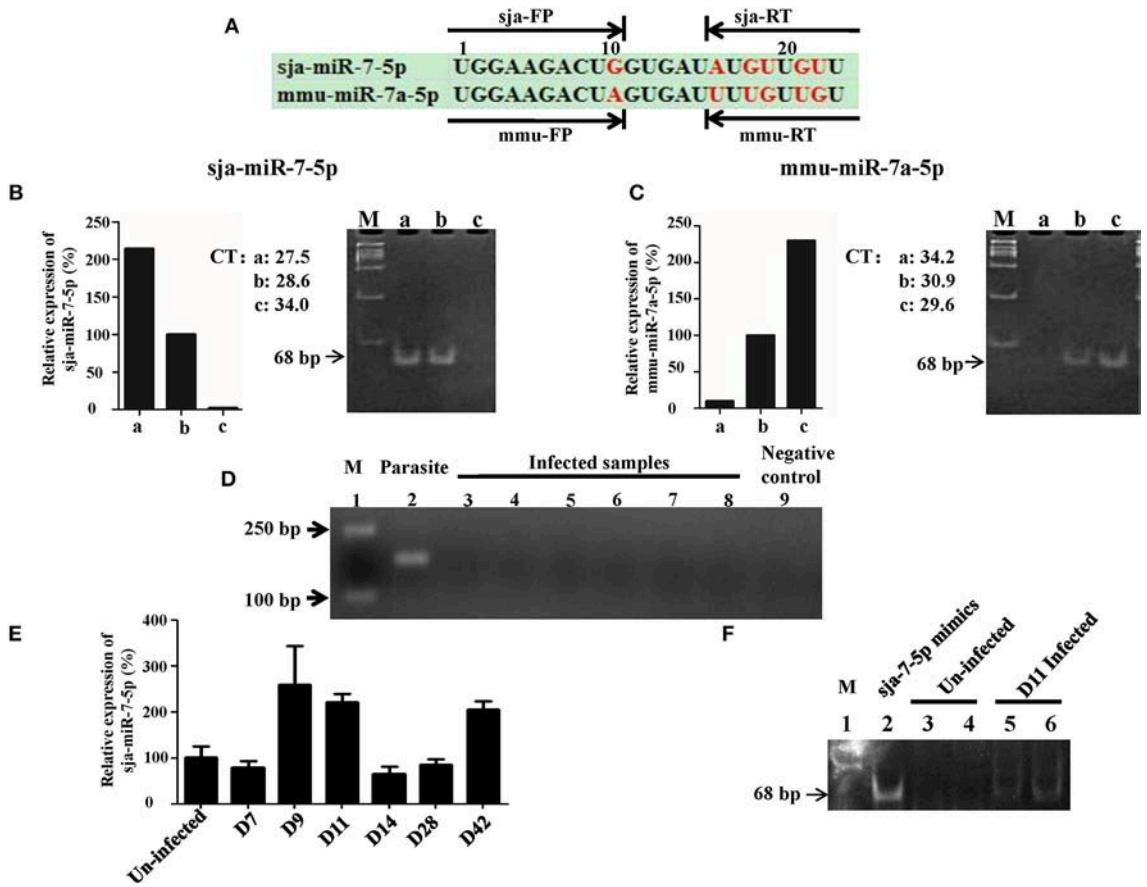

FIGURE 1 | Detection of sja-miR-7-5p in infected hepatocytes**. (A)** A schematic diagram represents two sets of primers of reverse transcription stem-loop primer (RT) and forward primer (FP) for sja-miR-7-5p or mmu-miR-7a-5p, respectively. **(B,C)** Preparation of RNA samples: a. 200 ng *Schistosoma japonicum* egg RNA; b. mixture of equal amount of *Schistosoma japonicum* egg RNA (100 ng) and Hepa1-6 cell RNA (100 ng); c. 200 ng Hepa1-6 cell RNA. The three RNA templates were transcribed into cDNA using the corresponding reverse transcription stem-loop primer, respectively, which were used for qRT-PCR by the corresponding forward primer and common reverse primer, respectively. The PCR products were separated by polyacrylamide gel electrophoresis (PAGE). As shown in B and C, the two sets of primers can effectively distinguished the sja-miR-7-5p and mmu-miR-7a-5p, e.g., the set of sja-miR-7-5p RT and forward primer FP amplified the sja-miR-7-5p [**(B)**, lane a and b] but not mmu-miR-7a-5p (lane c), while the set of mmu-miR-7a-5p RT and forward primer FP generated the mmu-miR-7a-5p but not the sja-miR-7-5p **(C)**. **(D)** Analysis of the RNA samples to ensure no contamination with parasite RNA: the RNA samples used for the above analysis were detected as described in Method by PCR for presence of the NADH gene of *S. japonicum*. Lane 1: marker. Lane 2: parasite positive control: RNA samples of *S. japonicum* eggs as described above. Lane 3–8: six samples of infected hepatocytes with RNase pre-incubation. Lane 9: negative control without the template. **(E)** qRT-PCR analysis of sja-miR-7-5p in the infected hepatocytes at various days after infection; **(F)** 12% PAGE analysis showing sja-miR-7-5p PCR product (68 bp) from the infected hepatocytes: Lane 1: marker; Lane 2: sja-miR-7-5p mimics positive control; Lanes 3 and 4: two uninfected hepatocyte samples with pre-incubation with RNase; Lanes 5 and 6: two infected hepatocyte samples at day 11 post-infection with the pre-incubation. Data are presented as the mean ± SD, $n = 3$.

fixed in methanol for 30 min, followed by staining in crystal violet for 15 min. The number of colonies containing > 50 cells was counted under a light microscope.

Tumor Xenograft Animal Model

Male athymic nude mice were housed and manipulated according to the protocols approved by the Shanghai Medical Experimental Animal Care Commission. Hepa1-6 cells or HepG2 cells were transfected with sja-miR-7-5p mimics or NC mimics, respectively. And 24 h later, for each mouse, 1×10^6 cells in 100 μL PBS after treated with sja-miR-7-5p mimics were injected subcutaneously to the left scapula, while cells after treated with NC mimics were injected subcutaneously to the right scapula, respectively. Tumor volume was measured at 2, 4, 6, and 7 d after injection, At day 7, the mice were sacrificed and tumors were separated to measure their weight and volume. Tumor volume was measured using the formula: $0.5 \times L \times S^2$, where L is the longest diameter of tumor and S is the shortest diameter of tumor. The content of sja-miR-7-5p mimics transfected into the tumor cells measured by quantitative real-time reverse transcription PCR (qRT-PCR), the protein level of SKP2 was determined by Western blotting. And also the expression of Ki67 in the tumor was measured by immunohistochemistry (IHC) as described under this section.

Immunohistochemistry

To determine Ki67 expression in xenograft tumor tissues from the athymic nude mice, immunohistochemistry (IHC) was performed as described previously (31), Antibody against Ki67 was used (1:50 dilution).

Statistical Analysis

All experiments were performed in triplicate and the results were presented as mean ± standard deviation (mean ± SD). All data were analyzed by one-way ANOVA using the software GraphPad Prism 5.0(GraphPad Software, Inc. La Jolla, CA, USA). A value of $P < 0.05$ was considered statistically significant.

RESULTS

Presence of sja-miR-7-5p in Infected Hepatocytes

We first investigated whether sja-miR-7-5p was present in the host liver cells during schistosome infection. For this purpose, we designed a set of two sets primers that could distinguish the sja-miR-7-5p from corresponding miRNA derived from mouse (mmu-miR-7-5p) and human (hsa-miR-7-5p). The sja-miR-7-5p has an identical seed sequence (2–8 nt at the 5' region), but

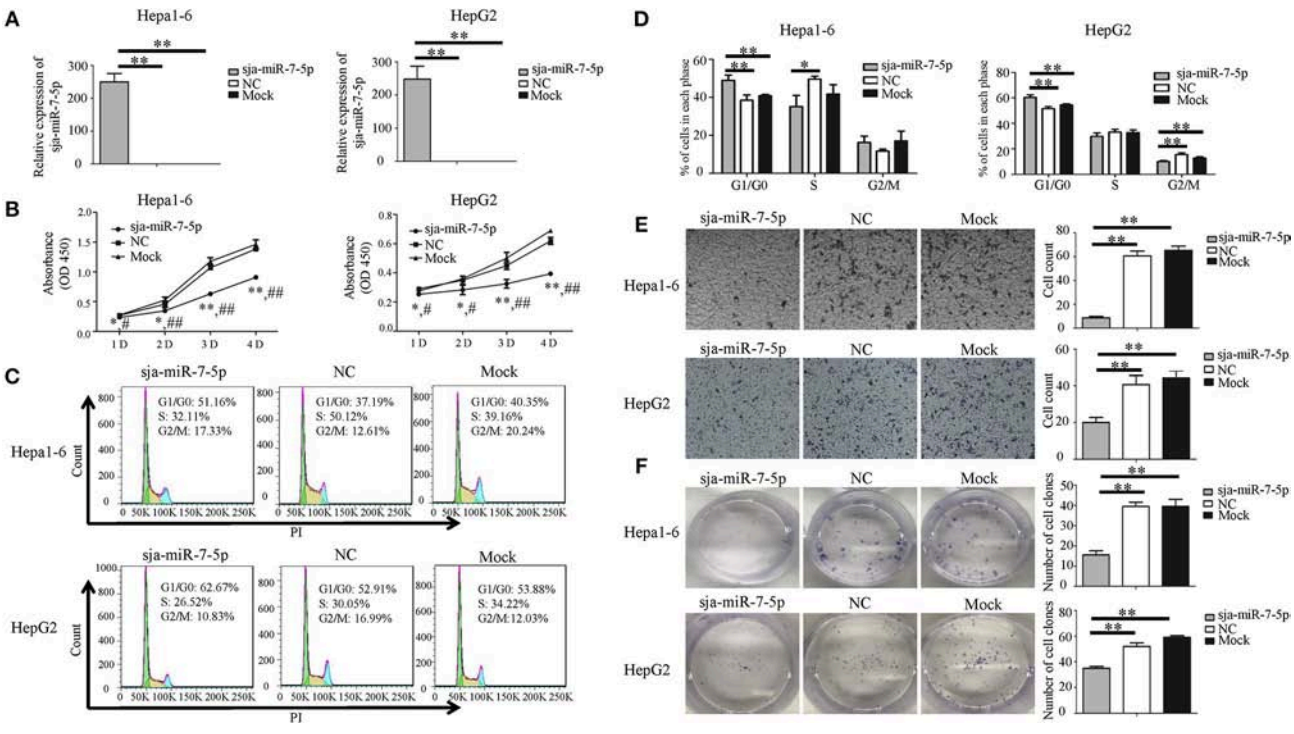

FIGURE 2 | Sja-miR-7-5p inhibits cell proliferation and migration of Hepa1-6 and HepG2 cells *in vitro*. **(A–F)** Hepa1-6 and HepG2 cells were transfected with sja-miR-7-5p mimics and NC (negative control) mimics, respectively, and 48 h later [except for the cell counting kit-8(CCK-8) assay, which was 24 h later], the expression of sja-miR-7-5p was determined using qRT-PCR (A). Cell proliferation was evaluated by CCK-8 assay at 1, 2, 3, and 4 days **(B)**, data are presented as the mean ± SD, $n = 3$, $^*p < 0.05$ or $^{**}p < 0.01$ indicates the comparison between the two groups of sja-miR-7-5p and NC; $\#p < 0.05$ or $\#\#p < 0.01$ indicates the comparison between the groups of sja-miR-7-5p and Mock. Cell cycle was determined by flow cytometry analysis **(C,D)**. Cell migration was evaluated using Transwell inserts without matrigel coating **(E)**. The ability to form cell clones was determined using a colony formation assay **(F)**. Data are presented as the mean ± SD, $n = 3$, $^*p < 0.05$, $^{**}p < 0.01$.

there are 6 nt differences in the rest of the sequence among the species (**Figure 1A**, and **Figure S1**), which allowed us to design sets of specific primers for the mmu-miR-7a-5p (mmu-FP/RT) and the sja-miR-7-5(sja- FP/RT). We first tested specificity of the primers using the RNA samples derived from *S. japonicum* eggs (a), mouse Hepa1-6 cell line (c), and mixture of equal amount of a and c (b). As shown in **Figures 1B,C**, the sja-FP/RT pair primers successfully generated the sja-miR-7a-5p from the samples of a and b, but not c (**Figure 1B**), while the mmu-FP/RT pair primers generated the mmu-miR-7a-5p from the sample b and c, but not a (**Figure 1C**). These data indicated that the two sets of primers can effectively distinguish the sja-miR-7-5p and mmu-miR-7a-5p, and no cross reaction between the mmu-FP/RT and sja-FP/RT primers. All the primers are listed in **Table S1**.

We next used the sja-FP/RT primers for detection of presence of sja-miR-7-5p in the liver cells of infected mice with *S. japonicum*. We prepared RNA samples from the infected liver cells, and carefully analyzed the samples to ensure no contamination with parasite RNA (**Figure 1D**). We showed that sja-miR-7-5p was detected by using qRT-PCR in the hepatocytes from infected mice at the early stage (i.e., days 9 and 11 post infection) and the late stage of infection (day 42) (**Figure 1E**). The presence of this parasite miRNA was further verified by PCR (**Figure 1F**) and cloning and sequencing of the PCR product showed identical sequence of sja-miR-7-5p (**Figure S2A**). In addition, we showed that sja-miR-7-5p was expressed at all these stages, and higher expression of sja-miR-7-5p was detected in adult males compared with that in adult females (**Figure S2B**). These findings indicated that this sja-miR-7-5p is present in the host liver cells during schistosome infection.

Inhibition of Proliferation and Migration of Hepatoma Cells by Sja-miR-7-5p

To investigated the effects of sja-miR-7-5p on the growth of hepatoma cells *in vitro,* both mouse and human hepatoma cells (e.g., Hepa1-6 cells and HepG2 cells) were transfected with the sja-miR-7-5p mimics, NC (a negative control mimics that has no target gene in mice and human) and Mock (transfection reagents only). As shown in **Figure 2A**, the sja-miR-7-5p mimics were effectively transfected into both cell lines. The schistosomal miRNA significantly suppressed the proliferation of both cell lines, as measured by the CCK-8 assay (**Figure 2B**), and substantially arrested the cell cycle at G1/G0 phase, as detected by flow cytometry (**Figures 2C,D**). We also showed that transfection of the sja-miR-7-5p mimics significantly suppressed cell migration, as assessed using the Transwell inserts without matrigel coating (**Figure 2E**) and by the wound-healing assay (**Figures S3B,C**) compared with the NC or Mock control cells. Colony formation assays showed that sja-miR-7-5p inhibited colony formation of hepatoma cells to a greater extent that those in the NC group or Mock group (**Figure 2F**). In addition, the Hepa1-6 cells transfected with sja-miR-7-5p mimics grew bigger and rounder compared with those in the NC or Mock control cells (**Figure S3A**). These data indicated that sja-miR-7-5p inhibited growth, migration, and colony formation of both mouse and human hepatoma cells and arrested their cell cycle

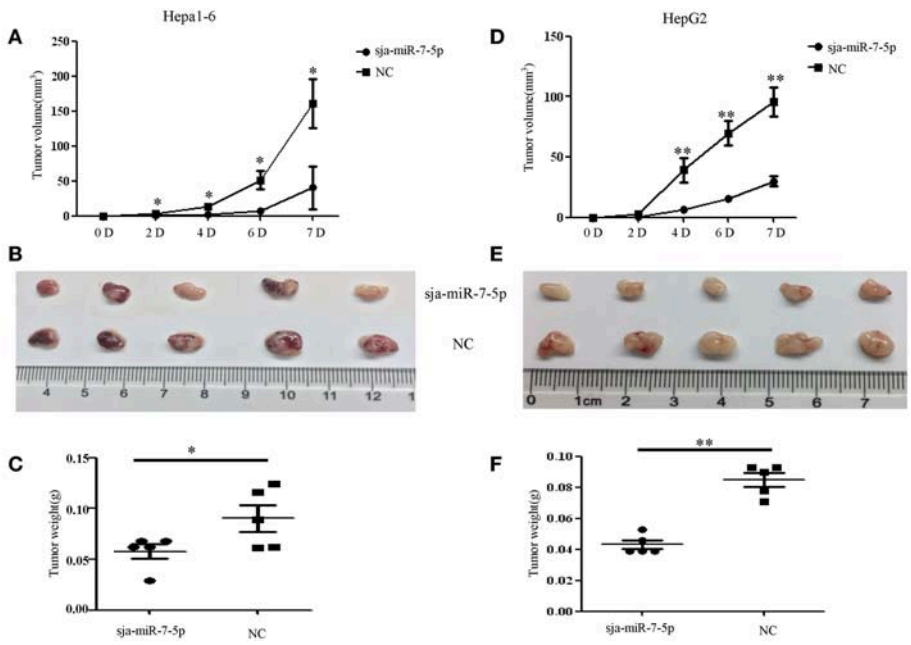

FIGURE 3 | Sja-miR-7-5p inhibits hepatoma cell growth *in vivo*. **(A–F)** Hepa1-6 and HepG2 cells were transfected with sja-miR-7-5p mimics or NC mimics, respectively, and then the sja-miR-7-5p-treated cells (1×10^6) were injected subcutaneously to the left scapula of athymic nude mice, and the NC-treated cells were injected subcutaneously into the right scapula ($n = 5$), respectively. Tumor volumes were measured at days 2, 4, 6, and 7 after injection. At day 7, the mice were sacrificed and tumors were separated to measure their weight and volume, **(A–C)** for Hepa1-6 cells, **(D–F)** for HepG2 cells. Data are presented as the mean ± SD, $n = 5$, $^*p < 0.05$, $^{**}p < 0.01$.

at G1/G0 phase *in vitro*, indicating that the schistosomal miRNA is also a tumor suppressor.

Sja-miR-7-5p-Mediated Inhibition of Hepatoma Cell Growth *in vivo*

To further investigate whether sja-miR-7-5p inhibits growth of liver cancer cells *in vivo*, both Hepa1-6 and HepG2 cells were transfected with sja-miR-7-5p mimics or NC mimics, and then injected subcutaneously to the left and right scapula of athymic nude mice to generate subcutaneous tumors. The tumor volume was measured at days 2, 4, 6, and 7 after injection. At day 7, mice were sacrificed and tumors were excised to measure their weight and volume. The results showed that both the tumor volume and weight were significantly reduced in the mice inoculated with Hepa1-6 cells transfected with sja-miR-7-5p mimics compared with those in mice receiving cells transfected with NC miRNAs (**Figures 3A–C**). Similar results were obtained with the human cell line of HepG2 (**Figures 3D–F**). These data indicated that sja-miR-7-5p suppressed tumor growth *in vivo*.

SKP2 Is a Direct Target of Sja-miR-7-5p

To determine the molecular mechanisms by which sja-miR-7-5p inhibits hepatoma cell growth, we used the online software miRDB (32) (http://www.mirdb.org/miRDB/index.html), MR-microT (33) (http://diana.imis.athena-innovation.gr/DianaTools/index.php?r=mrmicrot/index) and RNAhybrid (34) (http://bibiserv.techfak.uni-bielefeld.de/rnahybrid?id=rnahybrid_view_submission).

To search for potential targets of sja-miR-7-5p. We identified the gene encoding S-phase kinase-associated protein 2(*SKP2*) as a potential target for sja-miR-7-5p, because a binding site was located at the 3' UTR of the both murine and human *SKP2* gene that perfectly matched the seed sequence of sja-miR-7-5p. In addition, the *SKP2* gene in human has been characterized as an oncogene during tumorigenesis (21, 35–38).

To investigate the relationship between sja-miR-7-5p and *SKP2* gene in both human and mouse, first, we constructed two plasmids that contain the luciferase reporter gene: One was the pmirGLO-*SKP2*-WT construct in which the firefly luciferase gene is fused to the 3' UTR of *SKP2* gene; the other was the pmirGLO-*SKP2*-MT in which the seven nucleotides in the miRNA binding site were mutated (**Figure 4A**). The constructs were simultaneously transfected with sja-miR-7-5p mimics or NC mimics into both Hepa1-6 cells and HepG2 cells. As shown in **Figure 4B**, the luciferase activity was significantly decreased in the cells transfected with the pmirGLO-*SKP2*-WT but not with the pmirGLO-*SKP2*-MT, indicating that sja-miR-7-5p mimics could directly bind to the site in the 3′ UTR of the *SKP2* gene, while the mutations in the seed sequence abrogated the inhibitory effect.

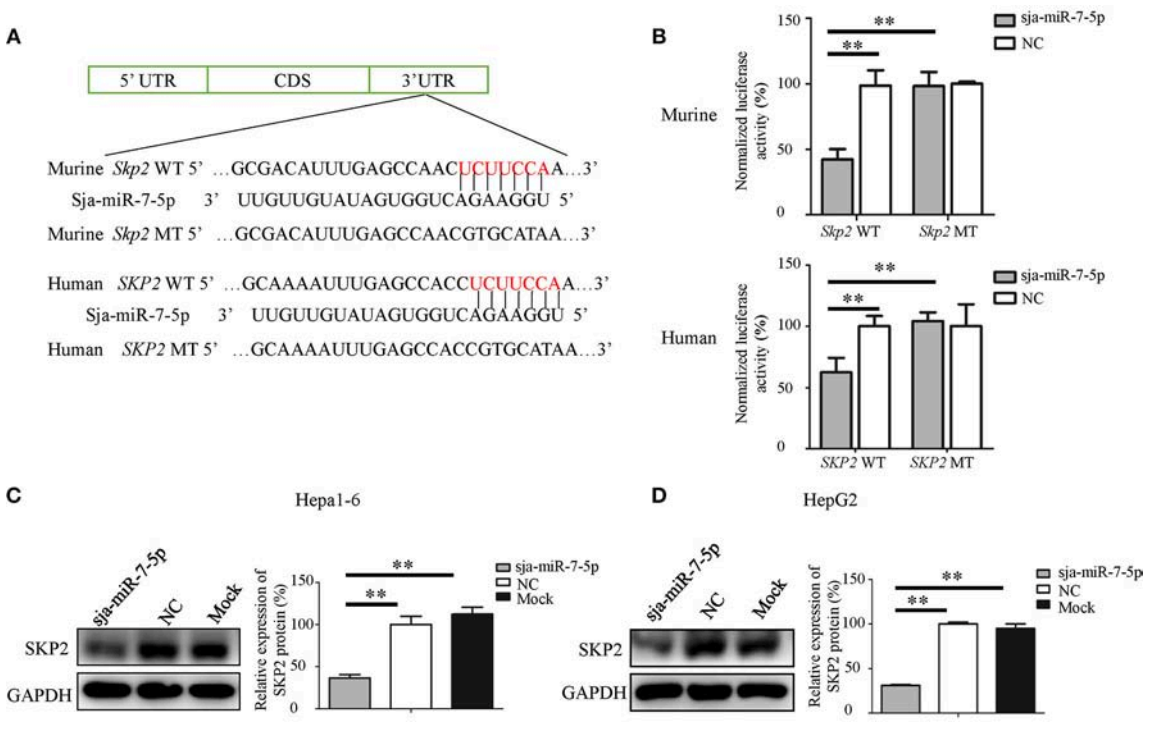

FIGURE 4 | *SKP2* (encoding S-phase kinase-associated protein 2) is a direct target of sja-miR-7-5p. **(A)** A schematic diagram representing the wild-type or mutant 3' untranslated region (UTR) sites of murine *Skp2* and human *SKP2* genes targeted by sja-miR-7-5p. **(B)** A dual-luciferase reporter assay was used to measure the activity of the reporter gene, and the firefly luciferase activity was normalized to renilla luciferase activity. **(C,D)** The protein levels of murine SKP2 **(C)** and human SKP2 **(D)** were measured using western blotting after transfection with sja-miR-7-5p mimics or NC mimics, respectively. Data are presented as the mean ± SD, $n = 3$, $^{**}p < 0.01$.

We then detected the level of the SKP2 protein in both Hepa1-6 or HepG2 cells transfected with sja-miR-7-5p mimics using Western blotting. We found that sja-miR-7-5p downregulated the levels of SKP2 in both Hepa1-6 cells and HepG2 cells compared with that in cells transfected with NC or Mock controls (**Figures 4C,D**).

Sja-miR-7-5p-Mediated Suppression of the Hepatoma Cell Growth Through Downregulation of SKP2 Expression

To investigate whether sja-miR-7-5p inhibits the growth of hepatoma cells through inhibition of SKP2 expression, both Hepa1-6 cells and HepG2 cells were transfected with the *SKP2* small interfering RNAs (siRNAs). We showed that both murine *Skp2* siRNA (SKP2-786) and human *SKP2* siRNA (SKP2-1291) significantly reduced the SKP2 expression in Hepa1-6 cells and HepG2 cells, respectively, at both transcriptional and translational levels detected by qRT-PCR and Western blotting (**Figure 5A**). Importantly, similar to the observations in the sja-miR-7-5p mimics-treated cells, the transfected Hepa1-6 cells and HepG2 cells with the siRNA showed cell cycle arrest at the G0/G1 phase (**Figures 5C,D**), and inhibition of cell proliferation (**Figure 5B**), cell migration (**Figure 5E**), and colony formation (**Figure 5F**), whereas these inhibitory effects were not observed in the cells treated with the NC siRNA. The phenotypes of the cells treated with *SKP2* siRNA were similar to those of sja-miR-7-5p mimics-treated cells, which suggested that the inhibitory effects of the schistosome miRNA on hepatoma cells function by downregulating SKP2 expression.

We also detected the expression of *SKP2* gene in the subcutaneous tumors generated by Hepa1-6 or HepG2 cells transfected with sja-miR-7-5p or NC mimics, respectively. As shown in **Figures 6A,B**, the transfected sja-miR-7-5p was detectable in the tumors on day 7 after injection. We then detected the SKP2 protein level using Western blotting, which showed that the level of SKP2 was significantly decreased in the tumors of both Hepa1-6 and HepG2 cells receiving sja-miR-7-5p compared with that in tumors from cells transfected with the NC control (**Figures 6C,D**). Meanwhile, we evaluated the proliferation of the tumor cells using immunohistochemistry (IHC) for Ki67, which showed that the protein level of Ki67 was also significantly decreased in tumor cells transfected with sja-miR-7-5p compared with that in cells transfected with the NC control (**Figure 6E**). These data further suggested that sja-miR-7-5p inhibited proliferation

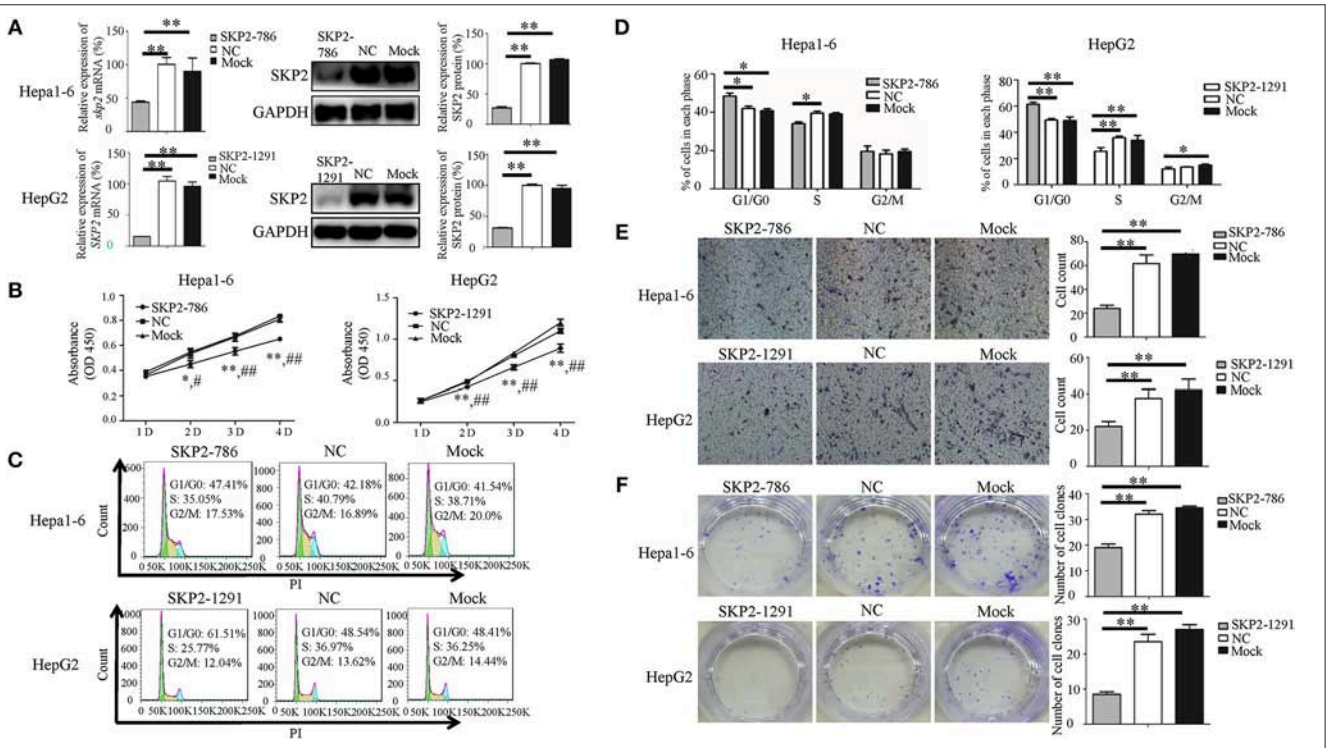

FIGURE 5 | Knockdown of *SKP2* inhibits cell proliferation and migration of Hepa1-6 and HepG2 cells *in vitro*. **(A–F)** Hepa1-6 and HepG2 cells were transfected with *SKP2* siRNA and negative control (NC) siRNA, respectively, and 48 h later (except for the cell counting kit-8(CCK-8) assay, which was 24 h later), the expression of *SKP2* was determined using qRT-PCR and western blotting **(A)**. Cell proliferation was evaluated using the CCK-8 assay at 1, 2, 3, and 4 d **(B)**, data are presented as the mean ± SD, $n = 3$, $^{*}p < 0.05$ or $^{**}p < 0.01$ indicates the comparison between the two groups of sja-miR-7-5p and NC; $\#p < 0.05$ or $\#\#p < 0.01$ indicates the comparison between the two groups of sja-miR-7-5p and Mock. Cell cycle was determined using flow cytometry analysis **(C,D)**. Cell migration was evaluated by using Transwell inserts without matrigel coating **(E)**. The ability to form cell clones was determined using a colony formation assay **(F)**. Data are presented as the mean ± SD, $n = 3$, $^{*}p < 0.05$, $^{**}p < 0.01$.

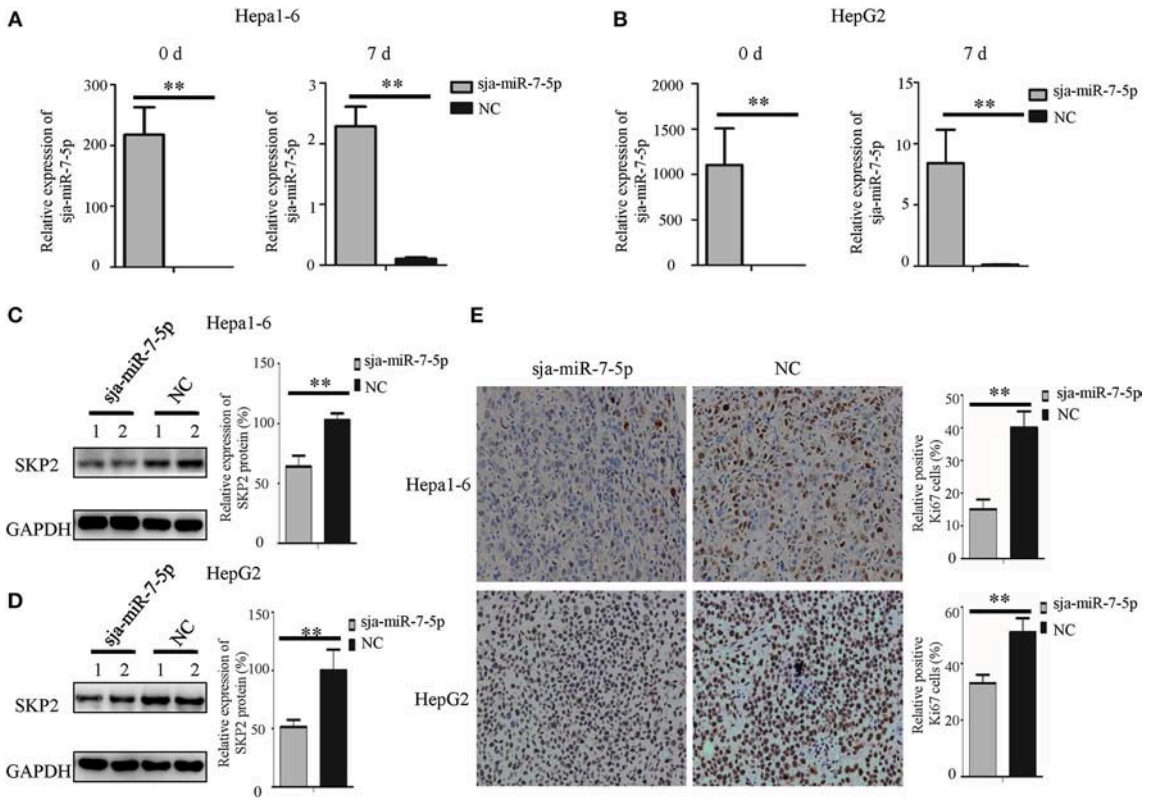

FIGURE 6 | Sja-miR-7-5p inhibits the expression of SKP2 and Ki67 within hepatoma cell tumors. **(A,B)**The content of sja-miR-7-5p mimics after transfection into tumor cells was measured using qRT-PCR before inoculation (0 d) and after sacrifice (7 d), with U6 as the internal control, **(A)** for Hepa1-6 cells, **(B)** for HepG2 cells. Data are presented as the mean ± SD, $n = 5$, $^{**}p < 0.01$. **(C,D)** The protein level of SKP2 was determined by Western blotting, with glyceraldehyde-3-phosphate (GAPDH) as the internal control, **(C)** for Hepa1-6 cells, **(D)** for HepG2 cells. **(E)** The level of Ki67 in tumors was determined using immunohistochemistry.

of both Hepa1-6 cells and HepG2 cells via downregulation of SKP2 expression.

To further explore the molecular mechanism by which sja-miR-7-5p exerts its antitumor activities, we detected the expression of two downstream nodes of SKP2, e.g., P27 [also known as cyclin dependent kinase inhibitor 1B (CDKN1B)] and matrix metalloproteinase 9(MMP9), using Western blotting. We found that sja-miR-7-5p downregulated the level of SKP2, which led to significantly increased levels of P27 and reduced levels of MMP9 in the cells receiving sja-miR-7-5p mimics compared with those in the cells receiving the NC mimics (**Figure 7A**). In addition, transfection of the hepatoma cells with the murine *Skp2* siRNA generated a similar outcome to that in cells transfected with sja-miR-7-5p mimics (**Figure 7B**). These data suggested that sja-miR-7-5p exerts its antitumor activity by targeting *SKP2* to elevate P27 levels, which led to suppression of tumor cell growth, and reducing MMP9 levels, resulting in inhibition of cell migration.

DISCUSSION

Hsa-miR-7-5p is well-characterized as a tumor suppressor miRNA that suppresses survival, proliferation, invasion, and migration of multiple cancer cells, as well as increasing the sensitivity of resistant tumor cells to therapeutics. The molecular mechanism underpinning its anticancer activities involves regulation of multiple signaling related genes such as *PI3K/Akt*, *FAK*, *KLF4*, and *REGγ* (10, 39–41). This miRNA has therapeutic potential for human cancers (42). Our previous studies identified a conserved miR-7-5p from *S. japonicum*, sja-miR-7-5p, that has an identical seed sequence to those of hsa-miR-7-5p and mouse mmu-miR-7-5p, although there are 6 nt differences in the rest of the sequence of the miRNA among species. In this study, we have demonstrated that the schistosome miRNA, sja-miR-7-5p, is present in host hepatocytes during schistosome infection, and the *in vitro* transfection of sja-miR-7-5p mimics into hepatoma cells led to cell cycle arrest and inhibition of cell proliferation, colony formation, and cell migration. Furthermore, we showed that sja-miR-7-5p suppressed the growth of both human and mouse hepatoma cells in a xenograft animal model. Analysis of the molecular mechanisms revealed that sja-miR-7-5p exerts its activities by targeting the *SKP2* gene, which is involved in regulation of cell viability and migration. Thus, the present data indicated that the schistosome sja-miR-7-5p is also a tumor suppressor miRNA that may have therapeutic potential for human cancers. In addition, both the presence of

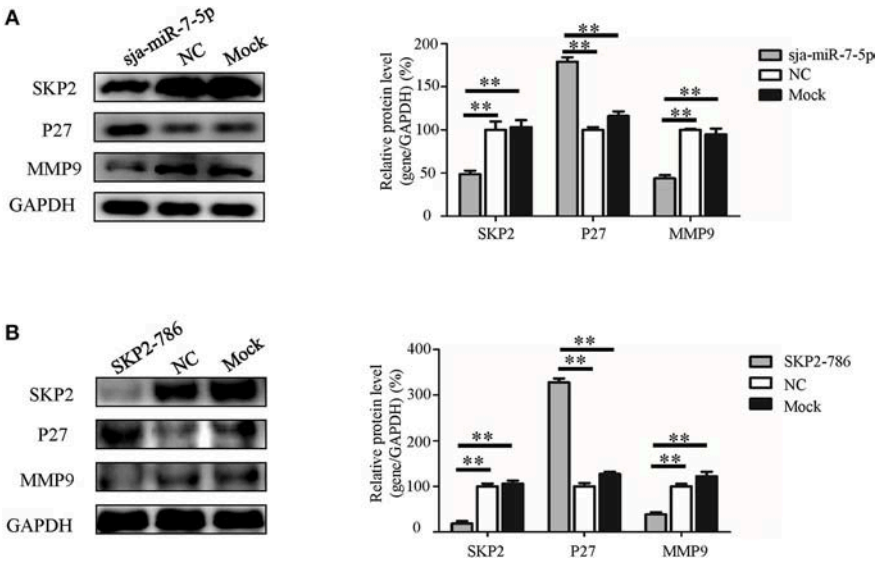

FIGURE 7 | The molecular mechanism whereby sja-miR-7-5p exerts its antitumor activity in hepatoma cells. **(A,B)** In Hepa1-6 cells, the protein levels of SKP2, P27, and MMP9 were measured by Western blotting after transfection with sja-miR-7-5p mimics **(A)** or *Skp2* siRNA **(B)** and their corresponding negative controls, with glyceraldehyde-3-phosphate (GAPDH) as the internal control. Data are presented as the mean ± SD, $n = 3$, $^{**}p < 0.01$.

this miRNA in host hepatocytes and its antitumor effects on human hepatoma cells suggest that schistosome non-small RNA-mediated anticarcinogenic effects might exist in the host liver during schistosome infection.

Infection with several parasites, such as *Opisthorchis viverrini* and *Clonorchis sinensis,* has been reported to be associated with cancer (43, 44). Schistosomiasis is a neglected tropical parasitic disease, affecting approximately 210 million people worldwide. Infection with *Schistosoma haematobium* is associated with bladder cancer (43, 44). However, for infection with *S. japonicum*, the association with hepatocellular carcinoma (HCC) is less evident, although a potential association with colorectal cancer was reported (45). The large retrospective epidemiological surveys conducted in highly endemic areas for schistosomiasis in China showed no correlation between HCC and *S. japonicum* infection (46). Although several other epidemiological and case–control studies proposed a potential association between HCC and *S. japonicum* infection, the evidences for the association remain a matter of debate because the schistosomiasis patients are highly associated with HBV and HCV infections, which are hepatic carcinogens (47). However, accumulating evidence indicates that chronic inflammation plays an important role in carcinogenesis (48). For *S. japonicum* infection, the liver-trapped eggs induce severe hepatic chronic inflammation and fibrosis that could be risk factors for HCC (49). These factors derived from *S. japonicum* infection should contribute to HCC, but this does not seem to happen in *S. japonicum* schistosomiasis. Therefore, we speculated that the *S. japonicum* eggs trapped in the liver might play a dual role in the HCC occurrence and development, i.e., carcinogenic and anticancer activities, similar to those reported for the protozoan *Trypanosoma cruzi*, which has carcinogenic and anticancer activities during infection (50). This study demonstrated that a non-coding small RNA secreted by *S. japonicum,* sja-miR-7-5p, perhaps together with other miRNAs derived from the parasite, could be translocated into liver cells during parasitic infection, and exerts anticancer activity, implying that the *S. japonicum*-producing non-coding small RNAs may, in part, contribute to the anticancer activities in the infected host.

As described above, mammalian miR-7-5p exerts its anticancer activities through regulation of multiple target genes such as *PI3K/Akt*, *FAK* and *KLF4*. To identify the target gene of the parasite sja-miR-7-5p, we first used three online software to search for its potential target genes. We found 5 target gene candidates (*Skp2, Psme3, Pik3cd, Klf4, and Hoxb5*) that were consistently predicted by the three software and involved in tumor-related signaling pathway. Three of them (i.e., *Pik3cd, Klf4, Hoxb5*) were excluded through analysis of their expression in hepatoma cells transfected with the sja-miR-7-5p mimics. Although both *Skp2* and *Psme3* genes were validated as target gene by luciferase reporter assay, our experimental data with *Skp2* and *Psme3* siRNA showed that only the hepatoma cell transfected with the *Skp2* siRNA produced similar phenotype to that of sja-miR-7-5p mimics-treated cells. Thus, *Skp2* gene has been identified as the target gene of sja-miR-7-5p.

SKP2, also known as P45, FBL1, FLB1, and FBXL1, is a component of the SCF (Skp1-Cullin 1-F-box) E3 ubiquitin-ligase complex. Many studies have reported that SKP2 is overexpressed in various cancers of different organs, including the liver (18), colon (51), breast (52), prostate (53), and stomach (54). *SKP2* is characterized as an oncogene, and is involved in modulation of the cell cycle, cell growth, and survival by regulation of

its downstream node molecules, such as P27, P16, P21, P57, E2F-1, and c-MYC in an ubiquitin-dependent manner, followed by 26S proteasome degradation (23). Previous studies showed that loss of *SKP2* reduced the migration and invasion abilities of oral squamous cell carcinoma cells by downregulating the expression of MMP2 and MMP9 (55). The best-known substrate of SKP2 is the cyclin dependent kinase (CDK) inhibitor, P27. Overexpression of SKP2 leads to reduction of P27, which is strongly associated with aggressive tumor behavior and poor clinical outcome (19, 36, 56), while knockdown of *SKP2* resulted in the accumulation of P27, causing cell cycle arrest at G1/G0 phase (57). However, the relationship between miR-7-5p and *SKP2* has not yet been reported in HCC. In the present study, we found that in liver cancer cells, including Hepa1-6 cells and HepG2 cells, sja-miR-7-5p inhibited the growth and migration of both mouse and human hepatoma cells by targeting *SKP2* to elevate the expression of P27 and decrease the expression of MMP9. These data were consistent with the results of experiments using the *SKP2* siRNA, and with the outcome of a study in which miRNA-7-5p could suppress cell proliferation of CHO cells partly by targeting *skp2* (58). Therefore, our data demonstrated that sja-miR-7-5p suppresses hepatoma cell growth and migration by downregulating *SKP2*.

The present study demonstrated that sja-miR-7-5p is present in infected hepatocytes, selectively affects the growth and migration of human and mouse tumor cells by targeting the *SKP2* gene, implying that sja-miR-7-5p might strengthen resistance of host to cancer during schistosome infection.

DATA AVAILABILITY

All datasets generated for this study are included in the manuscript and/or the **Supplementary Files**.

AUTHOR CONTRIBUTIONS

CH and WP conceived and designed the study. CH, SZ, JW, YL, LM, LZ, PJ, and ZL performed the experiments. CH, SZ, and WP analyzed the data. CH and WP wrote the manuscript. All authors read and approved the final manuscript.

FUNDING

This study was supported by the National Natural Science Foundation of China (81430051).

ACKNOWLEDGMENTS

We thank the staff of the National Institute of Parasitic Disease, Chinese Center for Disease Control and Prevention for their help with parasite infections.

SUPPLEMENTARY MATERIAL

The Supplementary Material for this article can be found online at: https://www.frontiersin.org/articles/10.3389/fonc.2019.00175/full#supplementary-material

REFERENCES

1. Colley DG, Bustinduy AL, Secor WE, King CH. Human schistosomiasis. *Lancet.* (2014) 383:2253–64. doi: 10.1016/S0140-6736(13)61949-2
2. Zhu SL, Wang S, Lin Y, Jiang PY, Cui XB, Wang XY, et al. Release of extracellular vesicles containing small RNAs from the eggs of *Schistosoma japonicum*. *Parasit Vectors.* (2016) 9:574. doi: 10.1186/s13071-016-1845-2
3. Bartel DP. MicroRNAs: Genomics, biogenesis, mechanism, and function. *Cell.* (2004) 116:281–97. doi: 10.1016/S0092-8674(04)00045-5
4. Calin GA, Croce CM. MicroRNA signatures in human cancers. *Nat Rev Cancer.* (2006) 6:857–66. doi: 10.1038/nrc1997
5. Berindan-Neagoe I, Monroig PD, Pasculli B, Calin GA. MicroRNAome genome: a treasure for cancer diagnosis and therapy. *Ca-a Cancer J Clini.* (2014) 64:311–36. doi: 10.3322/caac.21244
6. Mi Y, Zhang D, Jiang W, Weng J, Zhou C, Huang K, et al. miR-181a-5p promotes the progression of gastric cancer via RASSF6-mediated MAPK signalling activation. *Cancer Lett.* (2017) 389:11–22. doi: 10.1016/j.canlet.2016.12.033
7. Xue X, Fei X, Hou W, Zhang Y, Liu L, Hu R. miR-342-3p suppresses cell proliferation and migration by targeting AGR2 in non-small cell lung cancer. *Cancer Lett.* (2018) 412:170–8. doi: 10.1016/j.canlet.2017.10.024
8. Zhu Y, Gu J, Li Y, Peng C, Shi M, Wang X, et al. MiR-17-5p enhances pancreatic cancer proliferation by altering cell cycle profiles via disruption of RBL2/E2F4-repressing complexes. *Cancer Lett.* (2018) 412:59–68. doi: 10.1016/j.canlet.2017.09.044
9. Hatziapostolou M, Polytarchou C, Aggelidou E, Drakaki A, Poultsides GA, Jaeger SA, et al. An HNF4 alpha-miRNA inflammatory feedback circuit regulates hepatocellular oncogenesis. *Cell.* (2011) 147:1233–47. doi: 10.1016/j.cell.2011.10.043
10. Fang YX, Xue JL, Shen Q, Chen JZ, Tian L. MicroRNA-7 inhibits tumor growth and metastasis by targeting the phosphoinositide 3-kinase/Akt pathway in hepatocellular carcinoma. *Hepatology.* (2012) 55:1852–62. doi: 10.1002/hep.25576
11. Zhang L, Hou DX, Chen X, Li DH, Zhu LY, Zhang YJ, et al. Exogenous plant MIR168a specifically targets mammalian LDLRAP1: evidence of cross-kingdom regulation by microRNA. *Cell Res.* (2012) 22:107–26. doi: 10.1038/cr.2011.158
12. Zhou Z, Li XH, Liu JX, Dong L, Chen Q, Liu JL, et al. Honeysuckle-encoded atypical microRNA2911 directly targets influenza A viruses. *Cell Res.* (2015) 25:39–49. doi: 10.1038/cr.2014.130
13. Chin AR, Fong MY, Somlo G, Wu J, Swiderski P, Wu XW, et al. Cross-kingdom inhibition of breast cancer growth by plant miR159. *Cell Res.* (2016) 26:217–28. doi: 10.1038/cr.2016.13
14. Liu HX, Huang J, Peng J, Wu XX, Zhang Y, Zhu WL, et al. Upregulation of the inwardly rectifying potassium channel Kir2.1 (KCNJ2) modulates multidrug resistance of small-cell lung cancer under the regulation of miR-7 and the Ras/MAPK pathway. *Mol Cancer.* (2015) 14:59. doi: 10.1186/s12943-015-0298-0
15. Liu HX, Wu XX, Huang J, Peng J, Guo LL. miR-7 modulates chemoresistance of small cell lung cancer by repressing MRP1/ABCC1. *Int J Exp Pathol.* (2015) 96:240–7. doi: 10.1111/iep.12131
16. Suto T, Yokobori T, Yajima R, Morita H, Fujii T, Yamaguchi S, et al. MicroRNA-7 expression in colorectal cancer is associated with poor prognosis and regulates cetuximab sensitivity via EGFR regulation. *Carcinogenesis.* (2015) 36:338–45. doi: 10.1093/carcin/bgu242
17. Cheng MW, Shen ZT, Hu GY, Luo LG. Prognostic significance of microRNA-7 and its roles in the regulation of cisplatin resistance in lung

adenocarcinoma. *Cell Physiol Biochem.* (2017) 42:660–72. doi: 10.1159/000477884
18. Lee SW, Li CF, Jin G, Cai Z, Han F, Chan CH, et al. Skp2-dependent ubiquitination and activation of LKB1 is essential for cancer cell survival under energy stress. *Mol Cell.* (2015) 57:1022–33. doi: 10.1016/j.molcel.2015.01.015
19. Wang Z, Gao D, Fukushima H, Inuzuka H, Liu P, Wan L, et al. Skp2: a novel potential therapeutic target for prostate cancer. *Biochim Biophys Acta.* (2012) 1825:11–7. doi: 10.1016/j.bbcan.2011.09.002
20. Seki R, Okamura T, Koga H, Yakushiji K, Hashiguchi M, Yoshimoto K, et al. Prognostic significance of the F-box protein Skp2 expression in diffuse large B-cell lymphoma. *Am J Hematol.* (2003) 73:230–5. doi: 10.1002/ajh.10379
21. Rose AE, Wang G, Hanniford D, Monni S, Tu T, Shapiro RL, et al. Clinical relevance of SKP2 alterations in metastatic melanoma. *Pigment Cell Melanoma Res.* (2011) 24:197–206. doi: 10.1111/j.1755-148X.2010.00784.x
22. Radke S, Pirkmaier A, Germain D. Differential expression of the F-box proteins Skp2 and Skp2B in breast cancer. *Oncogene.* (2005) 24:3448–58. doi: 10.1038/sj.onc.1208328
23. Bochis OV, Irimie A, Pichler M, Berindan-Neagoe I. The Role of Skp2 and its Substrate CDKN1B (p27) in colorectal cancer. *J Gastrointes Liver Dis.* (2015) 24:225–34. doi: 10.15403/jgld.2014.1121.242.skp2
24. Hung WC, Tseng WL, Shiea J, Chang HC. Skp2 overexpression increases the expression of MMP-2 and MMP-9 and invasion of lung cancer cells. *Cancer Lett.* (2010) 288:156–61. doi: 10.1016/j.canlet.2009.06.032
25. Yokoi S, Yasui K, Mori M, Iizasa T, Fujisawa T, Inazawa J. Amplification and overexpression of SKP2 are associated with metastasis of non-small-cell lung cancers to lymph nodes. *Am J Pathol.* (2004) 165:175–80. doi: 10.1016/S0002-9440(10)63286-5
26. Shi C, Pan BQ, Shi F, Xie ZH, Jiang YY, Shang L, et al. Sequestosome 1 protects esophageal squamous carcinoma cells from apoptosis via stabilizing SKP2 under serum starvation condition. *Oncogene.* (2018) 37:3260–74. doi: 10.1038/s41388-018-0217-0
27. Osoegawa A, Yoshino I, Tanaka S, Sugio K, Kameyama T, Yamaguchi M, et al. Regulation of p27 by S-phase kinase-associated protein 2 is associated with aggressiveness in non-small-cell lung cancer. *J Clin Oncol.* (2004) 22:4165–73. doi: 10.1200/JCO.2004.01.035
28. Zhu CQ, Blackhall FH, Pintilie M, Iyengar P, Liu N, Ho J, et al. Skp2 gene copy number aberrations are common in non-small cell lung carcinoma, and its overexpression in tumors with ras mutation is a poor prognostic marker. *Clin Cancer Res.* (2004) 10:1984–91. doi: 10.1158/1078-0432.CCR-03-0470
29. Cai PF, Piao XY, Hao LL, Liu S, Hou N, Wang H, et al. A deep analysis of the small non-coding RNA population in *Schistosoma japonicum* eggs. *PLoS ONE.* (2013) 8:64003. doi: 10.1371/journal.pone.0064003
30. He X, Xie J, Zhang DM, Su Q, Sai X, Bai RP, et al. Recombinant adeno-associated virus-mediated inhibition of microRNA-21 protects mice against the lethal schistosome infection by repressing both IL-13 and transforming growth factor beta 1 pathways. *Hepatology.* (2015) 61:2008–17. doi: 10.1002/hep.27671
31. Yin XD, Xiang TX, Li LL, Su XW, Shu XS, Luo XR, et al. DACT1, an antagonist to Wnt/beta-catenin signaling, suppresses tumor cell growth and is frequently silenced in breast cancer. *Breast Cancer Res.* (2013) 15:R23. doi: 10.1186/bcr3399
32. Wong N, Wang XW. miRDB: an online resource for microRNA target prediction and functional annotations. *Nucl Acids Res.* (2015) 43:D146–52. doi: 10.1093/nar/gku1104
33. Reczko M, Maragkakis M, Alexiou P, Grosse I, Hatzigeorgiou AG. Functional microRNA targets in protein coding sequences. *Bioinformatics.* (2012) 28:771–6. doi: 10.1093/bioinformatics/bts043
34. Kruger J, Rehmsmeier M. RNAhybrid: microRNA target prediction easy, fast and flexible. *Nucl Acids Res.* (2006) 34:W451–4. doi: 10.1093/nar/gkl243
35. Lim MS, Adamson A, Lin ZS, Perez-Ordonez B, Jordan RCK, Tripp S, et al. Expression of Skp2, a p27(Kip1) ubliquitin ligase, in malignant lymphoma: correlation with p27(Kip1) and proliferation index. *Blood.* (2002) 100:2950–6. doi: 10.1182/blood.V100.8.2950
36. Shapira M, Ben-Izhak O, Linn S, Futerman B, Minkov I, Hershko DD. The prognostic impact of the ubiquitin ligase subunits Skp2 and Cks1 in colorectal carcinoma. *Cancer.* (2005) 103:1336–46. doi: 10.1002/cncr.20917
37. Hershko DD. Oncogenic properties and prognostic implications of the ubiquitin ligase Skp2 in cancer. *Cancer.* (2008) 112:1415–24. doi: 10.1002/cncr.23317
38. Schuler S, Diersch S, Hamacher R, Schmid RM, Saur D, Schneider G. SKP2 confers resistance of pancreatic cancer cells towards TRAIL-induced apoptosis. *Int J Oncol.* (2011) 38:219–25. doi: 10.3892/ijo_00000841
39. Kong XJ, Li GP, Yuan Y, He Y, Wu XL, Zhang WJ, et al. MicroRNA-7 Inhibits Epithelial-to-mesenchymal transition and metastasis of breast cancer cells via targeting FAK expression. *PLoS ONE.* (2012) 7:e41523. doi: 10.1371/journal.pone.0041523
40. Okuda H, Xing F, Pandey PR, Sharma S, Watabe M, Pai SK, et al. miR-7 suppresses brain metastasis of breast cancer stem-like cells by modulating KLF4. *Cancer Res.* (2013) 73:1434–44. doi: 10.1158/0008-5472.CAN-12-2037
41. Shi Y, Luo XR, Li P, Tan JX, Wang XY, Xiang TXS, et al. miR-7-5p suppresses cell proliferation and induces apoptosis of breast cancer cells mainly by targeting REG gamma. *Cancer Lett.* (2015) 358:27–36. doi: 10.1016/j.canlet.2014.12.014
42. Kalinowski FC, Brown RAM, Ganda C, Giles KM, Epis MR, Horsham J, et al. microRNA-7: a tumor suppressor miRNA with therapeutic potential. *Int J Biochem Cell Biol.* (2014) 54:312–7. doi: 10.1016/j.biocel.2014.05.040
43. Bouvard V, Baan R, Straif K, Grosse Y, Secretan B, El Ghissassi F, et al. A review of human carcinogens–Part B: biological agents. *Lancet Oncol.* (2009) 10:321–2. doi: 10.1016/S1470-2045(09)70096-8
44. IARC Working Group on the Evaluation of Carcinogenic Risks to Humans. Biological agents. Volume 100 B. A review of human carcinogens. *IARC Monogr Eval Carcinog Risks Hum.* (2012) 100:1–441.
45. Chen MG. Assessment of morbidity due to Schistosoma japonicum infection in China. *Infect Dis Poverty.* (2014) 3:6. doi: 10.1186/2049-9957-3-6
46. Liu BQ, Rong ZP, Sun XT, Wu YP, Gao RQ. Geographical correlation between colorectal cancer and schistosomiasis in China. *Zhongguo Yi Xue Ke Xue Yuan Xue Bao*. (1983) 5:173–7.
47. Arzumanyan A, Reis HM, Feitelson MA. Pathogenic mechanisms in HBV- and HCV-associated hepatocellular carcinoma. *Nat Rev Cancer.* (2013) 13:123–35. doi: 10.1038/nrc3449
48. Zhang R, Takahashi S, Orita S, Yoshida A, Maruyama H, Shirai T, et al. p53 gene mutations in rectal cancer associated with schistosomiasis japonica in Chinese patients. *Cancer Lett.* (1998) 131:215–21. doi: 10.1016/S0304-3835(98)00154-2
49. Takemura Y, Kikuchi S, Inaba Y. Epidemiologic study of the relationship between schistosomiasis due to *Schistosoma japonicum* and liver cancer/cirrhosis. *Am Journal Tropi Med Hygiene.* (1998) 59:551–6. doi: 10.4269/ajtmh.1998.59.551
50. van Tong H, Brindley PJ, Meyer CG, Velavan TP. Parasite infection, carcinogenesis and human malignancy. *EBioMedicine.* (2017) 15:12–23. doi: 10.1016/j.ebiom.2016.11.034
51. Fujita T, Liu WJ, Doihara H, Wan Y. Regulation of Skp2-p27 axis by the Cdh1/anaphase-promoting complex pathway in colorectal tumorigenesis. *Am J Pathol.* (2008) 173:217–28. doi: 10.2353/ajpath.2008.070957
52. Liu J, Wei XL, Huang WH, Chen CF, Bai JW, Zhang GJ. Cytoplasmic Skp2 expression is associated with p-Akt1 and predicts poor prognosis in human breast carcinomas. *PLoS ONE.* (2012) 7:e52675. doi: 10.1371/journal.pone.0052675
53. Moro L, Arbini AA, Marra E, Greco M. Up-regulation of Skp2 after prostate cancer cell adhesion to basement membranes results in BRCA2 degradation and cell proliferation. *J Biol Chem.* (2006) 281:22100–7. doi: 10.1074/jbc.M604636200
54. Ma XM, Liu Y, Guo JW, Liu JH, Zuo LF. Relation of overexpression of S phase kinase-associated protein 2 with reduced expression of p27 and PTEN in human gastric carcinoma. *World J Gastroenterol.* (2005) 11:6716–21. doi: 10.3748/wjg.v11.i42.6716
55. Yamada SI, Yanamoto S, Naruse T, Matsushita Y, Takahashi H, Umeda M, et al. Skp2 Regulates the Expression of MMP-2 and MMP-9, and enhances the invasion potential of oral squamous cell carcinoma. *Pathol Oncol Res.* (2016) 22:625–32. doi: 10.1007/s12253-016-0049-6

56. Wang Z, Fukushima H, Inuzuka H, Wan L, Liu P, Gao D, et al. Skp2 is a promising therapeutic target in breast cancer. *Front Oncol.* (2012) 1:18702. doi: 10.3389/fonc.2011.00057
57. Ding L, Li R, Han X, Zhou Y, Zhang H, Cui Y, et al. Inhibition of Skp2 suppresses the proliferation and invasion of osteosarcoma cells. *Oncol Rep.* (2017) 38:933–40. doi: 10.3892/or.2017.5713
58. Sanchez N, Gallagher M, Lao N, Gallagher C, Clarke C, Doolan P, et al. MiR-7 Triggers Cell Cycle Arrest at the G1/S Transition by Targeting Multiple Genes Including Skp2 and Psme3. *PLoS ONE.* (2013) 8:e65671. doi: 10.1371/journal.pone.0065671

Conflict of Interest Statement: The authors declare that the research was conducted in the absence of any commercial or financial relationships that could be construed as a potential conflict of interest.

frontiers in Oncology

MINI REVIEW
published: 29 March 2019
doi: 10.3389/fonc.2019.00194

Epigenetic Enzyme Mutations: Role in Tumorigenesis and Molecular Inhibitors

Mei Han†, Lina Jia†, Wencai Lv, Lihui Wang and Wei Cui**

Department of Pharmacology, Shenyang Pharmaceutical University, Shenyang, China

Epigenetic modifications, such as DNA methylation and histone modification, result in heritable changes in gene expression without changing the DNA sequence. Epigenetic regulatory enzymes such as DNA methyltransferases, histone methyltransferases, and histone deacetylases are involved in epigenetic modification. Studies have shown that the dysregulation caused by changes in the amino acid sequence of these enzymes is closely correlated with tumor onset and progression. In addition, certain amino acid changes in the metabolic enzyme isocitrate dehydrogenase (IDH) are linked to altered epigenetic modifications in tumors. Some small molecule inhibitors targeting these aberrant enzymes have shown promising anti-cancer efficacy in preclinical and clinical trials. For example, the small molecule inhibitor ivosidenib, which targets IDH1 with a mutation at R132, has been approved by the FDA for the clinical treatment of acute myeloid leukemia. In this review, we summarize the recurrent "hotspot" mutations in these enzymes in various tumors and their role in tumorigenesis. We also describe candidate inhibitors of the mutant enzymes which show potential therapeutic value. In addition, we introduce some previously unreported mutation sites in these enzymes, which may be related to tumor development and provide opportunities for future study.

Keywords: DNMT, mutation, small molecule inhibitors, tumor, histone modification enzyme

OPEN ACCESS

Edited by:
Zhe-Sheng Chen,
St. John's University, United States

Reviewed by:
Jing Tan,
Sun Yat-sen University, China
Maria Rosa Ciriolo,
University of Rome Tor Vergata, Italy

****Correspondence:***
Lihui Wang
lhwang@syphu.edu.cn
Wei Cui
cuiwei@syphu.edu.cn

† These authors have contributed equally to this work

Specialty section:
This article was submitted to Cancer Molecular Targets and Therapeutics, a section of the journal Frontiers in Oncology

Received: *25 December 2018*
Accepted: *06 March 2019*
Published: *29 March 2019*

Citation:
Han M, Jia L, Lv W, Wang L and Cui W (2019) Epigenetic Enzyme Mutations: Role in Tumorigenesis and Molecular Inhibitors. Front. Oncol. 9:194. doi: 10.3389/fonc.2019.00194

INTRODUCTION

The term "epigenetics" describes inheritable changes of gene expression with no alteration of the DNA sequence (1). As the field of epigenetics has expanded, the connection between epigenetic changes and the occurrence and development of tumors has received more attention (2). The structure of chromatin is the basis for modulating gene expression: euchromatin has an open structure that is typically associated with active transcription, while heterochromatin is tightly compacted and usually associated with transcriptional repression. Epigenetic modification such as DNA methylation and histone modification are important for regulating chromatin structure and therefore gene expression. These modifications are catalyzed by epigenetic regulatory enzymes, including DNA methyltransferases, histone methyltransferases and histone deacetylases.

Recent studies have shown that the dysregulation (e.g., overexpression) of these enzymes plays a crucial role in tumorigenesis. Some small molecule inhibitors targeting these aberrantly expressed epigenetic regulatory enzymes have been approved by the FDA for the treatment of certain cancers. For example, the small molecule inhibitor 5-azacytidine, which targets the DNA methyltransferase DNMT3A, has been approved for clinical treatment of patients with acute lymphoblastic leukemia (AML) (3), and belinostat, which targets histone deacetylases (HDACs)

in peripheral T-cell lymphoma (PTCL), was approved for use in 2014 (4). In addition, the inhibitor EPZ6438, which targets EZH2, a histone methyltransferase, has been approved for testing in the clinic (5).

In recent years, increasing evidence has shown that epigenetic regulatory enzymes are mutated in various types of cancer, and mutations of these enzymes are closely related to the malignant phenotype (6, 7). Hence, inhibitors that target these mutant enzymes have gradually entered preclinical and clinical research. In this review, we first summarize the epigenetic regulatory enzymes and their mutations in different types of tumors, and then we explain how the mutations are correlated with tumorigenesis. Finally, we present some small molecule inhibitors which target epigenetic regulatory enzymes, especially their mutated forms, and may have potential therapeutic value in the future.

DNMTS AND THEIR MUTATIONS IN CANCER

DNMTs in Cancer

DNA methylation, which is one of the major epigenetic regulatory mechanisms, plays a crucial role in many life processes (8). In eukaryotic cells, DNA methylation is a stable gene silencing modification that is copied during DNA replication (9). DNA methylation predominately occurs at cytosine residues in 5′-CpG-3′ dinucleotides, with S-adenosyl methionine (SAM) as the methyl donor (10). In mammals, DNA methylation is catalyzed by enzymes in the DNA methyltransferase (DNMT) family, mainly DNMT1, DNMT3A, and DNMT3B. DNMT1 maintains the methylation status of newly replicated (hemi-methylated) DNA, whereas DNMT3A and DNMT3B are responsible for *de novo* DNA methylation (11). The mechanism by which DNA methylation regulates gene expression involves blocking the binding of transcription factors to DNA and the recruitment of proteins containing a methylated CpG-binding domain to inhibit gene expression in tumor cells (12). The methylation profiles in different cells are not the same, and this has functional consequences. In normal cells, gene promoters containing CpG islands are usually unmethylated, which maintains the chromatin in an open structure, and hence enhances the transcription of the gene. However, in tumor cells, the CpG island-containing promoters of tumor suppressor genes are usually methylated, and thus the euchromatin is converted to compacted heterochromatin (13). These findings indicate that DNA methylation regulates tumorigenesis and progression by inhibiting the expression of tumor suppressor genes.

DNMT Mutations in Cancer

Recently, studies have shown that mutations of DNMT family, especially DNMT3A, are prominent features of many tumors and can lead to malignant transformation (14). DNMT3A is one of the most frequently mutated DNA methyltransferase in AML (6) and myelodysplastic syndromes (MDS) (15). Some reports have shown that mutations in DNMT3A are present in up to 20% of AML cases and are associated with poor prognosis (8, 16). Although a large number of mutations in the DNMT3A have been reported, ∼50% of the changes are in the catalytic domain at position R882 (most commonly R882H) (8, 17, 18). **Table 1** shows DNMT3A mutations, including hotspots and non-reported mutation sites, in various tumors. In addition, mutations in DNMT1 have been described in colorectal (29), prostate and hematological malignancies (30). The gene encoding DNMT3B was reported to be mutated in immunodeficiency syndrome, but mutations have rarely been reported in tumors (31). In addition, except DNMTs' mutations in various cancers, DNA hydroxymethylase TET2, which catalyzes the conversion of 5-methyl-cytosine to 5-hydroxymethyl-cytosine, has been reported in recent years for its mutations in various diseases, especially AML and MDS (32). The above results indicated that the mutations in DNMT and its related enzyme are frequent, which suggesting the potential role of them in tumorigenesis.

Function of DNMT Mutations

Mutations in DNMTs are closely correlated with the biological characteristics of malignant tumors and they increase the ability of cancer cells to undergo proliferation, migration, colony formation, and self-renewal. Recently, the relationship between the DNMT3A R882C mutation and the migration of tumor cells has been investigated *in vitro* (33). The results showed that the OCI-AML3 cell line, which carries the R882C mutation, had a greater migration ability than cell lines carrying wild-type (WT) DNMT3A, and infiltrated into the meninges of mice after intravenous infusion. This indicates that the DNMT3A R882 mutation contributes to the enhanced migration of malignant cells. It was also shown that the DNMT3A R882H mutation increases the proliferative capacity of hematopoietic cells and actively promotes the growth of monocytes and macrophages (33). Mechanistically, DNMT3A R882 mutant proteins interact with polycomb repressive complex 1 (PRC1) to block the differentiation of hematopoietic stem cells and lymphocytes by down-regulating differentiation-associated genes (34). Furthermore, cells with DNMT3A R882 mutations have a higher colony forming capacity than WT cells (34). In addition, it was reported that DNMT3A R882 mutations may induce chemotherapy resistance in AML patients. Guryanova et al. reported that the DNMT3A R882H mutation increases the risk of AML patients being resistant to anthracycline therapy by dysregulating nucleosome remodeling (35). Some reports have shown that the DNMT3A R882 mutation was negatively correlated with the prognosis of AML patients. The 5-year overall survival of AML patients with DNMT3A mutations was significantly shorter than AML patients without such mutations (36, 37). Accordingly, Delhommeau et al. reported that TET2 mutations are early events in patients with some MDS and secondary AML and confirmed the important role of TET2 in maintaining the balance between hematopoietic cell survival, growth and differentiation (38). Studies have shown that leukemia-associated missense mutations impair the enzymatic activity of TET2 and lead to a decrease in the genomic level of 5-hydroxymethyl-cytosine, which disrupts normal hematopoiesis and may accelerate leukemia formation (32). All of the above

TABLE 1 | Epigenetic regulatory enzymes mutation sites and their function in different types of cancer.

Enzyme	Gain-of-function mutation	Function of mutation	Non-reported mutation	Cancer type (references)	Inhibitor
DNMT3A	R882(H/C/P);	Migration;	Y735F, V716F, R729(Q/H/W), R803S, R736H, K829R, P718L, C497Y, D781G, G646V, A741V, F909C, M801V;	**Leukemia (6, 8, 16)**	5-azacytidine;
	R882C	Proliferation;	R792H, G26V, S708C, G412W, A254P, E629D, G293W, V763F, R771Q, Y533C, Q485H, K680R, S878P, E725V, R209P, P59L,	Lung cancer	Dichlone;
		Colony formation;	R379L, M864I, R326P, P804S, V258M, W327G, C494S, S312F, D781H, G413S, S669C, A116S, F909S, R458Q, R55H, Y724C,		SYC-52221;
		Blocking differentiation	V563M, D857V, W795C, P89R, D618N, Y735C, V560L, G570W, M78I, D279V, E392D, M224V, Q248R, V895M, V401L,		EPZ004777;
			G685V, C559Y, E854Q, G49R, G890C, E323K, P709L, Y359C, E213D, G746V, P58L, R885S, V687F, P425T		EPZ5676;
					(pan-inhibitors)
EZH2	Y641(S/H/F/N), A687V, A677G, Y646H;	Migration;	E740K, R679H, G159R, N670K, S271F, W113C, K660R, K660E, D185H, T53M, D183E, M701V, Y447H, V702G, C642S, T144I,	**Lymphoma (19–21)**	EPZ005687;
		Proliferation;	E636D, R685H, D659A, F672L;		GSK126;
	Y641(S/H/N/F), Y646(S/H);	Tumor growth;	S533L, R342Q, R216(Q/W), P132S, P219S, G2(D/S), D316G, R34P, P746S, S229L, S405L, T4(I/P), D142V, A226V, S228F,	**Melanoma (22)**	EPZ-6438;
		Poor prognosis;	P426S, R355G, C530W, G704S, G459E, R81S, P417Q, R456S, P535H, R382M, P262H, P631H, L338F, S474F, E391K, P527L,		CPI-1205;
			N366S, K510R, V675M, D511N, A590V, H521Y, I651T;		(pan-inhibitors)
	Y646H, A687V		K426Q, S652(C/F), P493A, I633M, T467P, S624C, K550T, I150V, E173Q, H129D, Q653E, K545T, L315V, Q648E, S647C;	Breast cancer	
			K510R, E374Q, Q548E, N310S, A340T, P262(L/T/I), R685G, E650Q, R308L, A715V, A622, R497Q, D233Y, R34L, E341K,	Lung cancer	
			R64M, D186N, K39E, H613Q, S647C, Q66R, R357L, E312K, Q94R, P481S, F667L, H502Q, R52I, G5R, S647F, R527W,S40C		
IDH1	R132(C/S/G/H/L);	Proliferation;	G339E, G161R;	**Glioma (7, 23)**	Ivosidenib (specific
	R132(C/H);	Migration;	V178I, G370D, S210N, R20Q;	**Lymphoma (24)**	targeting mutant
	R132(C/G/H);	Colony formation;	R119Q, E306D, T106M;	**Prostate cancer (25)**	IDH1 in R132);
	R132(C/S/G/L);	Blocking differentiation;	N349S;	**Cholangiocarcinoma (26)**	FT-2120 (specific
	R132(C/G/L);	Angiogenesis;	C297S, Q198P, N171T, M182V;	**Hepatic carcinoma (27)**	targeting mutant
	R132(C/H);	Inhibition of apoptosis	D160E, D79N, T327A, G263V, L88F, K217N, Y235C, R338T, K81N, K151N, A179D, I189V, E84Q;	Breast cancer	IDH1 in R132); IDH-305 (specific
	R132(C/L)		R49C, M290I, Q228R, E361K, E360K, S94P, A341V, G339W, G284V, A282V;	Melanoma	targeting mutant
			I102T, E28Q, R109K, D375Y, A179D, Y34C, I333V, V294L, I189F, A193S,	Lung cancer	IDH1);
			D299E, G175V, G221(L/V/W), L359F, E262Q, K406E		AGI-881 (pan-
			T302R, R119W, G310V, I380F, N961		inhibitor)
DH2	R172(S/K/G/W/M);	Proliferation;	G383V, K251N;	**Glioma (7, 28)**	Enasidenib
	R172(K/G/M/S);	Migration;	H430Y, R140(Q/L/G), D225N, N156I;	**Lymphoma (24)**	(specific targeting
	R172K;	Colony formation;	I62V, I61V;	**Prostate cancer (25)**	mutant IDH2);
	R172(K/S);	Blocking differentiation;	S301L, N156S, R60G, F270S, I419T;	**Hepatic carcinoma (27)**	AGI-881(pan-
	R172K	Angiogenesis;	R122(C/S), I139F, G137E, G387W, E68K, M248I, P198T, G176N, A321V,	Melanoma	inhibitor)
			M221I, R362W;	Lung cancer	
			R188W, H273D, Q267E, S249G, Q322K, I62M;	Breast cancer	
			I240V, F192L, T146S, E345K;		
HDAC2	–	–	Q354L, D175N, D231H, S118P, K466Q, N470I;	Leukemia	–
			M65V, G28R, A257T, P102A, R78(L/W), L42F, D456N, A120V, C101F, E109Q, A122S, D426Y	Lung cancer	

Publications reporting cancers with the indicated gain-of-function mutations are in bold. Non-reported mutations in the same proteins were identified from the cBioPortal website.

observations show that mutations in DNMT3A and TET2, to some extent, promote oncogenesis, and tumor progression.

HMTS AND THEIR MUTATIONS IN CANCER

HMTs in Cancer

Histone methylation is involved in the regulation of various biological processes such as gene expression, DNA repair, differentiation, replication and growth (39). Histone methyltransferases catalyze the transfer of the methyl group of SAM to histone arginine or lysine residues. A number of HMTs have been identified, including histone lysine methyltransferases (HKMTs) and histone arginine methyltransferases (HRMTs), which have specific substrates and residues. EZH2 belongs to the HKMT family and is frequently overexpressed in various cancerous tissue types such as breast, prostate and lung (19, 20, 40).

HMT Mutations in Cancer

EZH2 is a histone methyltransferase that catalyzes the trimethylation of arginine 27 in histone H3 (H3K27). Reports of EZH2 mutations in cancer have increased in recent years. Mutations in epigenetic regulatory enzymes are either gain-of-function or loss-of-function (3). EZH2 gain-of-function mutations were previously reported in lymphoma, and the probability of EZH2 mutation in melanoma was recently reported to be about 2%. Popov et al. found that 27% of follicular lymphoma cases had EZH2 mutations at 3 recurrent hotspots (Y646, A682, and A692) (24). Other gain-of-function hotspot mutations including Y641, A677, and A687 in the catalytic SET domain of EZH2 are prevalent, accounting for ∼10–24% of non-Hodgkin's lymphoma (26). In addition to these hotspot mutations, we have summarized some non-reported mutation sites that have yet to be studied, as shown in **Table 1**.

Function of HMT Mutations

The dysregulation of H3K27 trimethylation (H3K27me3) is important in human tumorigenesis (25), and some reports have shown that mutant EZH2 increases the level of H3K27me3 in follicular lymphoma, germinal center B-cell type diffuse large B-cell lymphomas (21, 24, 41) and metastatic skin melanoma (42). The level of H3K27 monomethylation and dimethylation in cancer cells and tumor tissues with heterozygous EZH2 mutations at Y641 and A677 is decreased, while the level of H3K27 trimethylation is increased, resulting from the changed substrate preference of the mutant enzymes (22, 41). Barsotti et al. revealed that cells with a gain-of-function EZH2 mutation at Y641 displayed enhanced motility compared to control cells, forming highly dynamic collective migrating chains under 3D culture conditions (42). The Y641 EZH2 gain-of-function mutant cells also had a significant growth advantage in melanoma xenografts. Others have reported that mutations in EZH2 can promote lymphocyte proliferation and maintain the enhanced histone methyltransferase activity *in vivo*, subsequently increasing tumorigenicity (26). Somatic mutations in EZH2 have been shown in many reports to correlate with poor prognosis in patients with AML and myeloproliferative neoplasms (6, 43). Thus, mutations in EZH2 may contribute to the enhancement of the malignant phenotype.

HMT-RELATED ENZYMES AND THEIR MUTATIONS IN CANCER

HMT-Related Enzymes in Cancer

Isocitrate dehydrogenase (IDH) plays a key role in the Kreb's cycle, catalyzing the conversion of isocitrate into α-ketoglutarate (α-KG). The two major human IDH proteins, IDH1 and IDH2, are not HMTs, but their mutant forms indirectly contribute to effects on histone methylation by catalyzing the conversion of α-KG to 2-hydroxyglutarate (2-HG). Accumulation of 2-HG can inhibit the activity of a broad range of histone demethylases, inducing hypermethylation which is observed in certain cancers such as gliomas (44). In addition, high levels of 2-HG can inhibit α-KG-dependent prolyl hydroxylase, which is important for the degradation of hypoxia-inducible factor (HIF)-1α, a regulator of histone demethylases (7, 23, 28). Mutated forms of IDH therefore mimic the effects of HMTs.

HMT-Related Enzyme Mutations in Cancer

As mentioned above, specific mutants of IDH can catalyze the conversion of α-KG to 2-HG, and 2-HG inhibits not only histone demethylases but also TET DNA demethylases. This can cause increased methylation of both DNA and histones (3). Therefore, mutant IDH may be an oncoprotein and 2-HG may be an "oncometabolite" (7). In recent years, hotspot mutations in IDH1/2 have been reported in various tumors (**Table 1**). It has been reported that mutations of IDH1 and IDH2 occur in the vast majority of low-grade gliomas and secondary high-grade gliomas, and also in some cases of AML (27). In addition, IDH mutations have been found in solid tumors such as cholangiocarcinoma and prostate cancer (45, 46). The hotspot mutation of IDH1 is located at R132, while the hotspot mutation of IDH2 is located at R172, which is homologous to R132 in IDH1. We also found that other mutations of IDH1, including G339(E/W), R49C, R119(Q/W), and V294L, may be hotspot mutations in various tumors (**Table 1**). In addition to mutations in the enzyme of IDH family in the Kreb's cycle, two other metabolic enzymes involved in epigenetic regulation, SDH and FH, have also been reported in recent years to mutate in germline frequently. Ciccarone et al. concluded that SDH mutations in germline are responsible for the formation of hereditary paragangliomas and adrenal gland pheochromocytoma, whereas FH mutations are typical of hereditary leiomyomatosis and renal cell cancer (HLRCC) (47).

Function of HMT-Related Enzyme Mutations

Several groups have investigated the effect of IDH hotspot mutations, which mimic the activity of HMTs, in cancer. Cohen et al. elucidated that mutant IDH can trigger tumorigenesis. In detail, they found that somatic mutations in IDH1 at R132 or IDH2 at R172 led to increased risk of glioma, hemangiomas and chondrosarcoma, and they demonstrated that the mutated IDH contributed to the increased cell proliferation, colony

formation, and inability to differentiate (7). In addition, Fu et al. showed that the IDH2 R172 mutation accelerated the migration and growth of C6 glioma cells by increasing the stability of HIF-1α (48). They also reported that IDH mutations promoted glioma cell metastasis and resistance to chemotherapy through up-regulation of the HIF-1α signaling pathway (49). IDH mutations also play an important role in blocking cell differentiation. Mutant IDH blocks hepatocyte differentiation by inhibiting the HNF-4α pathway (50). Other studies have shown that high levels of 2-HG caused by mutations in IDH can inhibit histone and DNA demethylases, resulting in hypermethylation of histones and DNA which eventually blocks cell differentiation (51, 52). Interestingly, there is no significant difference in the median overall survival rate of intrahepatic cholangiocarcinoma patients with mutant or WT IDH (53). In general, mutated IDH catalyzes the production of high levels of 2-HG, which has multiple effects including the inhibition of α-KG-dependent prolyl hydroxylase, which leads to the accumulation of HIF-1α in cells. This results in the induction of HIF-1α target genes that influence growth, migration, differentiation and angiogenesis as well as cell apoptosis (7), ultimately promoting tumor onset and progression (see **Figure 1**).

HDACS, HATS, AND THEIR MUTATIONS IN CANCER

Histone acetylation is an important epigenetic modification that mainly occurs in the N-terminal region of the histone tail. This modification weakens the binding between histones and DNA, which relaxes the chromatin and enhances gene expression (54). Histone acetyltransferases (HATs) mediate the acetylation in histones, whereas histone deacetylases (HDACs) catalyze the removal of acetyl groups from histones. The HATs are mainly divided into five major families, including GCN5/PCAF, MYST, TAFII250, CBP/p300, and SRC (55). The HDACs are divided into four classes. Class I HDACs include HDAC1, HDAC2, HDAC3, HDAC8; class II HDACs are further divided into two groups, class IIa (HDAC4, HDAC5, HDAC7, HDAC9) and class IIb (HDAC6, HDAC10); class III contains SIRT1-7; and class IV contains one enzyme, HDAC11 (56, 57). Class I, II, and IV HDACs are all Zn^{2+}-dependent enzymes, while class III HDACs do not show any sequence similarity to the other three classes and depend on NAD+ as a co-factor (56, 57). By reversing the histone acetylation status, HDACs mostly regulate the expression of tumor suppressor genes (4). The dysregulation of HATs and HDACs is correlated with the occurrence and development of various diseases, including cancer.

Mutations in genes encoding HDACs are associated with the progression of tumors, owing to the abnormal transcription of key genes that regulate important cellular functions such as cell proliferation, cell cycle regulation and apoptosis. Some studies have shown that HDACs are mutated in certain cancers. For example, somatic mutations of HDAC1 were detected in ∼8% of dedifferentiated human liposarcomas, and the dysfunction of HDAC2 expression caused by a frame-shift mutation was investigated in human epithelial cancers and in colorectal cancer (58). **Table 1** summarizes some of the mutated sites in HDAC2, which may correlate with the development and progression of tumors. However, most of the mutations in HDACs have not been studied and require further investigation. In addition to the discovery that HDACs are mutated in a variety of cancers, there have been many reports in recent years that the HAT CREBBP somatic mutations are more frequent in lymphomas, lung cancer, urothelial carcinoma, and other human tumor types. Jiang et al. reported that somatic mutations in CREBBP occur in 6.4–22.3% of patients with DLBCL and 30.8–68% of follicular lymphoma. Their findings suggest that CREBBP mutation can promote lymphomagenesis *in vivo* (59). Similarly, the results of Jia et al. showed that *CREBBP* acts as a tumor suppressor gene, and its inactivating mutations can promote tumorigenesis of pre-neoplastic neuroendocrine cells and accelerate small cell lung cancer in the autochthonous mouse model (60). The above results suggested that the mutations in HATs and HDACs, although relative low in frequency, might also be involved into the carcinogenesis in various tumors.

INHIBITORS TARGETING MUTATIONS OF EPIGENETIC REGULATORY ENZYMES

Inhibitors Targeting DNMT Mutants

The DNMT inhibitors 5-azacytidine and decitabine (5-aza-2′-deoxycytidine) have already been approved by the FDA (3). These inhibitors are nucleoside analogs which are incorporated into DNA and then covalently trap DNMTs. The results of research by Xu et al. showed that 5-azacytidine might be a suitable drug for the treatment of AML with DNMT3A mutations (8). In a study comparing small molecule inhibitors of DNMT3A R882H, compound 9 (dichlone) displayed superior efficacy, indicating its potential for targeting mutant DNMT3A (61). Interestingly, a recent study showed that targeting DOT1L, a histone lysine methyltransferase without a SET domain, also has an obvious antitumor effect in DNMT3A mutant leukemia. Rau et al. found that the DOT1L inhibitors SYC-52221 and EPZ004777 decreased tumor cell proliferation and induced cell apoptosis, cycle arrest and terminal differentiation in DNMT3A mutant cell lines in a dose- and time-dependent manner (62). Furthermore, they reported that the DOT1L inhibitor EPZ5676 showed promising efficacy in a nude mouse xenograft model of AML with mutant DNMT3A (62). Since pharmacological inhibitors of DOT1L have been tested in clinical trials, DOT1L may be an indirect therapeutic target for the treatment of AML with DNMT3A mutations. These results suggesting a novel approach for treating patients with DNMT3A mutations.

For the TET2, although inhibitors targeting TET2 mutations have not yet been developed, the results of Bejar et al. indicated that cells in MDS patients with TET2-deficient are more sensitive to azacitidine treatment, and this suggests that patients with MDS carrying the TET2 mutation can improve their response to hypomethylating agents (63). However, the detailed mechanisms mediating this process need further study.

Inhibitors Targeting EZH2 Mutants

Recently, studies have shown that small molecule inhibitors can effectively target tumors driven by EZH2 mutations.

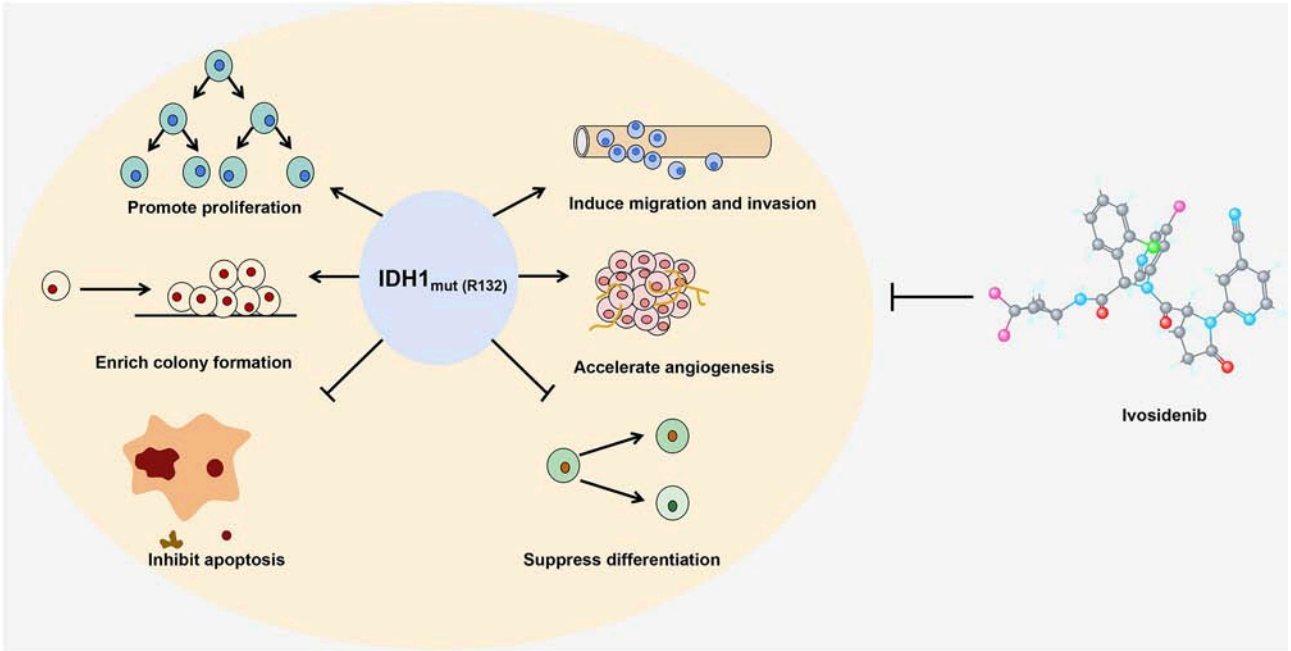

FIGURE 1 | The IDH1 R132 mutant is shown as an example to illustrate how a gain-of-function mutation in an epigenetic enzyme affects the growth and differentiation of cells. Ivosidenib, a specific inhibitor of the IDH1 R132 mutant, is shown at the right.

Knutson et al. have reported that the SAM-competitive EZH2 inhibitor EPZ005687, which is highly selective for EZH2 over other methyltransferases, significantly reduced the viability of lymphoma cell lines carrying the EZH2 Y641 and A677 mutations (64). McCabe et al. discovered that GSK126 is a SAM-competitive small molecule inhibitor of EZH2 methyltransferase activity that efficiently and selectively reduced H3K27me3 levels and reactivated the silenced target genes of polycomb repressive complex 2 (PRC2) (41). Their results also revealed that GSK126 effectively inhibited the proliferation of EZH2-mutant diffuse large B-cell lymphoma (DLBCL) cell lines and retarded the growth of EZH2-mutant DLBCL xenografts in mice (41). In addition, EPZ-6438, another selective inhibitor of EZH2, exerted potent antitumor activity against EZH2-mutant non-Hodgkin's lymphoma (65). Also, CPI-1205, an orally available selective inhibitor of EZH2, killed cells in both EZH2-WT and EZH2-mutant B-cell non-Hodgkin's lymphoma by altering PRC2 target gene expression in a dose- and time-dependent manner (5). All of the above inhibitors markedly reduced the high level of H3K27 trimethylation caused by EZH2 mutations, indicating that inhibition of EZH2 methyltransferase activity may be an effective way of treating EZH2 mutant lymphomas. EPZ005687 is currently in preclinical research, whereas GSK126, EPZ-6438 and CPI-1205 are under phase I/II investigation to assess their efficacy in patients with non-Hodgkin's lymphoma and certain solid tumors (5). In view of the high rate of EZH2 mutation in certain cancers, the application of these inhibitors in the clinic is expected to be successful in the future.

However, in addition to focusing on the effects of the EZH2 inhibitor itself on EZH2 mutant enzymes, we also need to consider the use of EZH2 inhibitors in synthetic lethality. Recently, targeting chromatin deficiency in cancer based on synthetic lethality has been used in cancer treatment. Synthetic lethality defines a relationship between two genes, where the loss of either gene is compatible with cell viability, but the loss of both genes causes cell death. Morel *et al.* summarized that the deficiency of SMARCB1, ARID1A, SMARCA4, and PBRM1, which constitute the chromatin remodeling complex SWI/SNF subunit, led to an EZH2 oncogenic dependence in tumor cells, and pharmacological EZH2 inhibitors such as tazemetostat induced dramatic tumor shrinkage in these subunits-deficient tumors (66). Therefore, synthetic lethality strategy may pave the way to potential epigenetic drugs targets.

Inhibitors Targeting IDH Mutants

Inhibitors targeting mutant IDH enzymes have also been widely investigated. In preclinical studies, it is reported that inhibitors targeting mutated forms of IDH1 and IDH2 can inhibit the growth of glioma cells and induce the differentiation of primary human IDH mutant AML cells *in vitro* (67). Encouragingly, clinical studies of inhibitors targeting mutated IDH have entered the phase I stage, and two inhibitors have been approved by the FDA for clinical use (68). For example, enasidenib (AG-221), a novel-specific small molecule inhibitor targeting mutant IDH2, was approved by the FDA in August 2017 for the treatment of relapsed AML (69). Another novel specific small molecule inhibitor, ivosidenib (AG-120), was approved by the FDA in July 2018 for clinical treatment of relapsed and refractory AML. Ivosidenib targets IDH1 with a mutation at the R132 site (see **Figure 1**) (70). Three other small molecule inhibitors, AGI-881,

IDH305, and FT-2102, are currently in phase I clinical trials. AGI-881 is a non-specific small molecule inhibitor which can target the mutant forms of both IDH1 and IDH2, whereas IDH-305 and FT-2102 target mutant IDH1 (68). These inhibitors prevent the reduction of α-KG to 2-HG by binding to the active site of the mutated IDH enzyme. High levels of 2-HG can inhibit DNA and histone demethylation, leading to hypermethylation. Borodovsky et al. have demonstrated that hypomethylating agents strongly induce differentiation, reduce colony formation ability, and suppress the growth of IDH mutant cells *in vivo* (71). Therefore, inhibitors targeting DNA and histone modifications may have potential therapeutic value. The DNA methyltransferase inhibitors decitabine (DAC) and 5-azacytidine have been approved by the FDA for clinical application and may have a therapeutic effect on tumors caused by IDH mutations (72). These findings also suggest that there is crosstalk among different epigenetic regulatory enzymes. In contrast to IDH mutation inhibitors, studies on inhibitors targeting SDH and FH mutations are currently lagging behind, which may lay the foundation for the development of new anti-tumor drugs.

CONCLUSION AND PERSPECTIVES

DNA methylation and histone modification are common epigenetic changes in eukaryotes, and the dysregulation of epigenetic regulatory enzymes is closely related to the onset and progression of various types of cancer. Mutations, especially gain-of-function mutations, may be responsible for some changes in epigenetic enzyme activity. Mutant epigenetic regulatory enzymes, and mutant forms of IDH that affect epigenetic changes, can enhance the ability of cancer cells to proliferate, migrate and form colonies. Therefore, these mutations are closely related to tumor onset and progression. Some inhibitors that specifically target the mutant forms of epigenetic regulatory enzymes and IDH have now entered clinical trials. The potential therapeutic effects of these inhibitors on tumors caused by mutations are summarized in **Figure 1**.

Many of the mechanisms by which mutations cause changes in the activity or function of epigenetic regulatory enzymes are not fully understood. Elucidation of these mechanisms may drive our understanding of the characteristics of different tumors. Further research into drugs that target these mutant enzymes will also accelerate the process of individualized treatment of tumors.

DATA AVAILABILITY

Publicly available datasets were analyzed in this study. This data can be found here: http://www.cbioportal.org.

AUTHOR CONTRIBUTIONS

MH contributes to draft manuscript and analysis the data. LJ contributes to draft manuscript. WL contributes to analysis the data. LW and WC contribute to design and draft the manuscript.

FUNDING

This work was financially supported by the National Natural Science Foundation of China (No. 81673652, 81572947, 81773780, 81773216), the Natural Science Foundation of Liaoning Province (No. 20170540841, 20180550076), the Scientific Research Fund of Liaoning Provincial Education Department (No. 2017LFW01) and the Science Foundation of Shenyang Pharmaceutical University (No. DFJJ2018210).

REFERENCES

1. Egger G, Liang G, Aparicio A, Jones PA. Epigenetics in human disease and prospects for epigenetic therapy. *Nature*. (2004) 429:457–63. doi: 10.1038/nature02625
2. Lund AH, Lohuizen MV. Epigenetics and cancer. *Genes Dev*. (2004) 18:2315–35. doi: 10.1101/gad.1232504
3. Carlberg C, Molnár F. Cancer epigenomics. *Hum Epigenomics*. (2018) 159–74. doi: 10.1007/978-981-10-7614-5_10
4. Mottamal M, Zheng S, Huang T, Wang G. Histone deacetylase inhibitors in clinical studies as templates for new anticancer agents. *Molecules*. (2015) 20:3898–941. doi: 10.3390/molecules20033898
5. Gulati N, Béguelin W, Giulino-Roth L. Enhancer of zeste homolog 2 (EZH2) inhibitors. *Leuk Lymphoma*. (2018) 59:1574–85. doi: 10.1080/10428194.2018.1430795
6. Tatton-Brown K, Seal S, Ruark E, Harmer J, Ramsay E, Rahman N, et al. Mutations in the DNA methyltransferase gene DNMT3A cause an overgrowth syndrome with intellectual disability. *Nat Genet*. (2014) 46:385–8. doi: 10.1038/ng.2917
7. Cohen AL, Holmen SL, Colman H. IDH1 and IDH2 mutations in gliomas. *Curr Neurol Neurosci Rep*. (2013) 13:345. doi: 10.1007/s11910-013-0345-4
8. Xu J, Wang YY, Dai YJ, Zhang W, Zhang WN, Xiong SM, et al. DNMT3A Arg882 mutation drives chronic myelomonocytic leukemia through disturbing gene expression/DNA methylation in hematopoietic cells. *Proc Natl Acad Sci USA*. (2014) 111:2620–5. doi: 10.1073/pnas.1400150111
9. Ballestar E. The impact of chromatin in human cancer: linking DNA methylation to gene silencing. *Carcinogenesis*. (2002) 23:1103–9. doi: 10.1093/carcin/23.7.1103
10. Singal R, Ginder GD. DNA methylation. *Blood*. (1999) 93:4059–70. doi: 10.1016/S0887-7963(99)80035-2
11. Chen QW, Zhu XY, Li YY, Meng ZQ. Epigenetic regulation and cancer. *Oncol Rep*. (2014) 31:523–32. doi: 10.3892/or.2013.2913
12. Boyes J, Bird A. DNA methylation inhibits transcription indirectly via a methyl-CpG binding protein. *Cell*. (1991) 64:1123–34. doi: 10.1016/0092-8674(91)90267-3
13. Costello JF, Frühwald MC, Smiraglia DJ, Rush LJ, Robertson GP, Gao X, et al. Aberrant CpG-island methylation has non-random and tumour-type–specific patterns. *Nat Genet*. (2000) 24:132–8. doi: 10.1038/72785
14. Baylin SB, Jones PA. A decade of exploring the cancer epigenome — biological and translational implications. *Nat Rev Cancer*. (2011) 11:726–34. doi: 10.1038/nrc3130
15. Yamashita Y, Yuan J, Suetake I, Suzuki H, Ishikawa Y, Choi YL, et al. Array-based genomic resequencing of human leukemia. *Oncogene*. (2010) 29:3723–31. doi: 10.1038/onc.2010.117
16. Elsayed GM, Fahmi AEA, Shafik NF, Elshimy RAA, Abd Elhakeem HK, Attea SA. Study of DNA methyl transferase 3A mutation in acute myeloid leukemic patients. *Egypt J Med Hum Genet*. (2018) 19:315–9. doi: 10.1016/j.ejmhg.2018.05.005
17. Russler-Germain DA, Spencer DH, Young MA, Lamprecht TL, Miller CA, Fulton R, et al. The R882H DNMT3A mutation associated with AML

dominantly inhibits wild-type DNMT3A by blocking its ability to form active tetramers. *Cancer Cell*. (2014) 25:442–54. doi: 10.1016/j.ccr.2014.02.010
18. Pløen GG, Nederby L, Guldberg P, Hansen M, Ebbesen LH, Jensen UB, et al. Persistence of DNMT3A mutations at long-term remission in adult patients with AML. *Br J Haematol*. (2014) 167:478–86. doi: 10.1111/bjh.13062
19. Varambally S, Dhanasekaran SM, Zhou M, Barrette TR, Kumar-Sinha C, Sanda MG, et al. The polycomb group protein EZH2 is involved in progression of prostate cancer. *Nature*. (2002) 419:624–9. doi: 10.1038/nature01075
20. Behrens C, Solis LM, Lin H, Yuan P, Tang X, Kadara H, et al. EZH2 Protein Expression Associates with the early pathogenesis, tumor progression, and prognosis of non-small cell lung carcinoma. *Clin Cancer Res*. (2013) 19:6556–65. doi: 10.1158/1078-0432.ccr-12-3946
21. Zhou Z, Gao J, Popovic R, Wolniak K, Parimi V, Winter JN, et al. Strong expression of EZH2 and accumulation of trimethylated H3K27 in diffuse large B-cell lymphoma independent of cell of origin and EZH2 codon 641 mutation. *Leuk Lymphoma*. (2015) 56:2895–901. doi: 10.3109/10428194.2015.1006220
22. Sneeringer CJ, Scott MP, Kuntz KW, Knutson SK, Pollock RM, Richon VM, et al. Coordinated activities of wild-type plus mutant EZH2 drive tumor-associated hypertrimethylation of lysine 27 on histone H3 (H3K27) in human B-cell lymphomas. *Proc Natl Acad Sci USA*. (2010) 107:20980–5. doi: 10.1073/pnas.1012525107
23. Kickingereder P, Sahm F, Radbruch A, Wick W, Heiland S, Deimling A, et al. Wiestler, B. (2015). IDH mutation status is associated with a distinct hypoxia/angiogenesis transcriptome signature which is non-invasively predictable with rCBV imaging in human glioma. *Sci Rep*. 5:16238. doi: 10.1038/srep16238
24. Bodor C, Grossmann V, Popov N, Okosun J, O'Riain C, Tan K, et al. EZH2 mutations are frequent and represent an early event in follicular lymphoma. *Blood*. (2013) 122:3165–8. doi: 10.1182/blood-2013-04-496893
25. Souroullas GP, Jeck WR, Parker JS, Simon JM, Liu J-Y, Paulk J, et al. An oncogenic Ezh2 mutation induces tumors through global redistribution of histone 3 lysine 27 trimethylation. *Nat Med*. (2016) 22:632–40. doi: 10.1038/nm.4092
26. Majer CR, Jin L, Scott MP, Knutson SK, Kuntz KW, Keilhack H, et al. A687V EZH2 is a gain-of-function mutation found in lymphoma patients. *FEBS Lett*. (2012) 586:3448–51. doi: 10.1016/j.febslet.2012.07.066
27. Dang L, Jin S, Su SM. IDH mutations in glioma and acute myeloid leukemia. *Trends Mol Med*. (2010) 16:387–97. doi: 10.1016/j.molmed.2010.07.002
28. Pollard PJ, Loenarz C, Mole DR, McDonough MA, Gleadle JM, Schofield CJ, et al. Regulation of Jumonji-domain-containing histone demethylases by hypoxia-inducible factor (HIF)-1α. *Bioch J*. (2008) 416:387–94. doi: 10.1042/bj20081238
29. Kanai Y, Ushijima S, Nakanishi Y, Sakamoto M, Hirohashi S. Mutation of the DNA methyltransferase (DNMT) 1 gene in human colorectal cancers. *Cancer Lett*. (2003) 192:75–82. doi: 10.1016/s0304-3835(02)00689-4
30. Yang L, Rau R, Goodell MA. DNMT3A in haematological malignancies. *Nat Rev Cancer*. (2015) 15:152–65. doi: 10.1038/nrc3895
31. Hansen RS, Wijmenga C, Luo P, Stanek AM, Canfield TK, Weemaes CMR, et al. The DNMT3B DNA methyltransferase gene is mutated in the ICF immunodeficiency syndrome. *Proc Natl Acad Sci USA*. (1999) 96:14412–7. doi: 10.1073/pnas.96.25.14412
32. Ko M, Bandukwala HS, An J, Lamperti ED, Thompson EC, Hastie R, et al. Ten-Eleven-Translocation 2 (TET2) negatively regulates homeostasis and differentiation of hematopoietic stem cells in mice. *Proc Natl Acad Sci USA*. (2011) 108:14566–71. doi: 10.1073/pnas.1112317108
33. Xu J, Zhang W, Yan XJ, Lin XQ, Li W, Mi JQ, et al. DNMT3A mutation leads to leukemic extramedullary infiltration mediated by TWIST1. *J Hematol Oncol*. (2016) 9:106. doi: 10.1186/s13045-016-0337-3
34. Koya J, Kataoka K, Sato T, Bando M, Kato Y, Tsuruta-Kishino T, et al. DNMT3A R882 mutants interact with polycomb proteins to block haematopoietic stem and leukaemic cell differentiation. *Nat Commun*. (2016) 7:10924. doi: 10.1038/ncomms10924
35. Guryanova OA, Shank K, Spitzer B, Luciani L, Koche RP, Garrett-Bakelman FE, et al. DNMT3A mutations promote anthracycline resistance in acute myeloid leukemia via impaired nucleosome remodeling. *Nat Med*. (2016) 22:1488–95. doi: 10.1038/nm.4210
36. Ley TJ, Ding L, Walter MJ, McLellan MD, Lamprecht T, Larson DE, et al. DNMT3A mutations in acute myeloid leukemia. *New Engl J Med*. (2010) 363:2424–33. doi: 10.1056/nejmoa1005143
37. Ferreira HJ, Heyn H, Vizoso M, Moutinho C, Vidal E, Gomez A, et al. DNMT3A mutations mediate the epigenetic reactivation of the leukemogenic factor MEIS1 in acute myeloid leukemia. *Oncogene*. (2015) 35:3079–82. doi: 10.1038/onc.2015.359
38. Delhommeau F, Dupont S, Valle VD, James C, Trannoy S, Massé A, et al. Mutation inTET2in Myeloid Cancers. *New Engl J Med*. (2009) 360:2289–301. doi: 10.1056/nejmoa0810069
39. Wei S, Li C, Yin Z, Wen J, Meng H, Xue L, et al. Histone methylation in DNA repair and clinical practice: new findings during the past 5-years. *J Cancer*. (2018) 9:2072–81. doi: 10.7150/jca.23427
40. Simon JA, Lange CA. Roles of the EZH2 histone methyltransferase in cancer epigenetics. *Mutat Res Fund Mol Mech Mutag*. (2008) 647:21–9. doi: 10.1016/j.mrfmmm.2008.07.010
41. McCabe MT, Ott HM, Ganji G, Korenchuk S, Thompson C, Van Aller GS, et al. EZH2 inhibition as a therapeutic strategy for lymphoma with EZH2-activating mutations. *Nature*. (2012) 492:108–12. doi: 10.1038/nature11606
42. Barsotti AM, Ryskin M, Zhong W, Zhang W-G, Giannakou A, Loreth C, et al. Epigenetic reprogramming by tumor-derived EZH2 gain-of-function mutations promotes aggressive 3D cell morphologies and enhances melanoma tumor growth. *Oncotarget*. (2015) 6:2928–38. doi: 10.18632/oncotarget.2758
43. Vannucchi AM, Lasho TL, Guglielmelli P, Biamonte F, Pardanani A, Pereira A, et al. Mutations and prognosis in primary myelofibrosis. *Leukemia*. (2013) 27:1861–9. doi: 10.1038/leu.2013.119
44. Saldanha SN, Tollefsbol TO. Epigenetic approaches to cancer therapy. *Epigenet Hum Dis*. (2018) 219–47. doi: 10.1016/b978-0-12-812215-0.00007-8
45. Kipp BR, Voss JS, Kerr SE, Barr Fritcher EG, Graham RP, Zhang L, et al. Isocitrate dehydrogenase 1 and 2 mutations in cholangiocarcinoma. *Hum Pathol*. (2012) 43:1552–8. doi: 10.1016/j.humpath.2011.12.007
46. Ghiam AF, Cairns RA, Thoms J, Dal Pra A, Ahmed O, Meng A, et al. IDH mutation status in prostate cancer. *Oncogene*. (2011) 31:3826. doi: 10.1038/onc.2011.546
47. Ciccarone F, Vegliante R, Di Leo L, Ciriolo MR. The TCA cycle as a bridge between oncometabolism and DNA transactions in cancer. *Sem Cancer Biol*. (2017) 47:50–6. doi: 10.1016/j.semcancer.2017.06.008
48. Fu Y, Zheng Y, Li K, Huang R, Zheng S, An N, et al. Mutations in isocitrate dehydrogenase 2 accelerate glioma cell migration via matrix metalloproteinase-2 and 9. *Biotechnol Lett*. (2011) 34:441–6. doi: 10.1007/s10529-011-0800-8
49. Fu Y, Zheng S, Zheng Y, Huang R, An N, Liang A, et al. Glioma derived isocitrate dehydrogenase-2 mutations induced up-regulation of HIF-1α and β-catenin signaling: Possible impact on glioma cell metastasis and chemo-resistance. *Int J Biochem Cell Biol*. (2012) 44:770–5. doi: 10.1016/j.biocel.2012.01.017
50. Saha SK, Parachoniak CA, Ghanta KS, Fitamant J, Ross KN, Najem MS, et al. Mutant IDH inhibits HNF-4α to block hepatocyte differentiation and promote biliary cancer. *Nature*. (2014) 513:110–4. doi: 10.1038/nature13441
51. Figueroa ME, Abdel-Wahab O, Lu C, Ward PS, Patel J, Shih A, et al. Leukemic IDH1 and IDH2 Mutations result in a hypermethylation phenotype, disrupt TET2 function, and impair hematopoietic differentiation. *Cancer Cell*. (2010) 18:553–67. doi: 10.1016/j.ccr.2010.11.015
52. Lu C, Ward PS, Kapoor GS, Rohle D, Turcan S, Abdel-Wahab O, et al. IDH mutation impairs histone demethylation and results in a block to cell differentiation. *Nature*. (2012) 483:474–8. doi: 10.1038/nature10860
53. Goyal L, Govindan A, Sheth RA, Nardi V, Blaszkowsky LS, Faris JE, et al. Prognosis and clinicopathologic features of patients with advanced stage Isocitrate Dehydrogenase (IDH) Mutant and IDH wild-type intrahepatic cholangiocarcinoma. *Oncologist*. (2015) 20:1019–27. doi: 10.1634/theoncologist.2015-0210
54. Kelly AD, Issa JPJ. The promise of epigenetic therapy: reprogramming the cancer epigenome. *Curr Opin Genet Dev*. (2017) 42:68–77. doi: 10.1016/j.gde.2017.03.015

55. Marmorstein R, Roth SY. Histone acetyltransferases: function, structure, and catalysis. *Curr Opin Genet Dev*. (2001) 11:155–61. doi: 10.1016/s0959-437x(00)00173-8
56. Yanginlar C, Logie C. HDAC11 is a regulator of diverse immune functions. *Biochim Biophys Acta Gene Regul Mech*. (2018) 1861:54–9. doi: 10.1016/j.bbagrm.2017.12.002
57. Wang L, Beier UH, Akimova T, Dahiya S, Han R, Samanta A, et al. Histone/protein deacetylase inhibitor therapy for enhancement of Foxp3+ T-regulatory cell function posttransplantation. *Am J Transpl*. (2018) 18:1596–603. doi: 10.1111/ajt.14749
58. Ropero S, Esteller M. The role of histone deacetylases (HDACs) in human cancer. *Mol Oncol*. (2007) 1:19–25. doi: 10.1016/j.molonc.2007.01.001
59. Jiang Y, Ortega-Molina A, Geng H, Ying H-Y, Hatzi K, Parsa S, et al. CREBBP inactivation promotes the development of HDAC3-dependent lymphomas. *Cancer Disc*. (2016) 7:38–53. doi: 10.1158/2159-8290.cd-16-0975
60. Jia D, Augert A, Kim DW, Eastwood E, Wu N, Ibrahim AH, et al. Crebbp loss drives small cell lung cancer and increases sensitivity to HDAC inhibition. *Cancer Disc*. (2018) 8:1422–37. doi: 10.1158/2159-8290.cd-18-0385
61. Emperle M, Rajavelu A, Kunert S, Arimondo PB, Reinhardt R, Jurkowska RZ, et al. The DNMT3A R882H mutant displays altered flanking sequence preferences. *Nucleic Acids Res*. (2018) 46:3130–9. doi: 10.1093/nar/gky168
62. Rau RE, Rodriguez BA, Luo M, Jeong M, Rosen A, Rogers JH, et al. DOT1L as a therapeutic target for the treatment of DNMT3A-mutant acute myeloid leukemia. *Blood*. (2016) 128:971–81. doi: 10.1182/blood-2015-11-684225
63. Bejar R, Lord A, Stevenson K, Bar-Natan M, Perez-Ladaga A, Zaneveld J, et al. TET2 mutations predict response to hypomethylating agents in myelodysplastic syndrome patients. *Blood*. (2014) 124:2705–12. doi: 10.1182/blood-2014-06-582809
64. Knutson SK, Wigle TJ, Warholic NM, Sneeringer CJ, Allain CJ, Klaus CR, et al. A selective inhibitor of EZH2 blocks H3K27 methylation and kills mutant lymphoma cells. *Nat Chem Biol*. (2012) 8:890–6. doi: 10.1038/nchembio.1084
65. Knutson SK, Kawano S, Minoshima Y, Warholic NM, Huang K-C, Xiao Y, et al. Selective inhibition of EZH2 by EPZ-6438 leads to potent antitumor activity in EZH2-mutant non-hodgkin lymphoma. *Mol Cancer Ther*. (2014) 13:842–54. doi: 10.1158/1535-7163.mct-13-0773
66. Morel D, Almouzni G, Soria JC, Postel-Vinay S. Targeting chromatin defects in selected solid tumors based on oncogene addiction, synthetic lethality and epigenetic antagonism. *Ann Oncol*. (2016) 28:254–69. doi: 10.1093/annonc/mdw552
67. Dang L, Yen K, Attar EC. IDH mutations in cancer and progress toward development of targeted therapeutics. *Ann Oncol*. (2016) 27:599–608. doi: 10.1093/annonc/mdw013
68. Montalban-Bravo G, DiNardo CD. The role of IDH mutations in acute myeloid leukemia. *Future Oncol*. (2018) 14:979–93. doi: 10.2217/fon-2017-0523
69. Kim ES. Enasidenib: first global approval. *Drugs*. (2017) 77:1705–11. doi: 10.1007/s40265-017-0813-2
70. Popovici-Muller J, Lemieux RM, Artin E, Saunders JO, Salituro FG, Travins J, et al. Discovery of AG-120 (Ivosidenib): a first-in-class mutant IDH1 inhibitor for the treatment of IDH1 mutant cancers. *ACS Med Chem Lett*. (2018) 9:300–5. doi: 10.1021/acsmedchemlett.7b00421
71. Borodovsky A, Salmasi V, Turcan S. 5-azacytidine reduces methylation, promotes differentiation and induces tumor regression in a patient-derived IDH1 mutant glioma xenograft. *Oncotarget*. (2013) 4:1737–47. doi: 10.18632/oncotarget.1408
72. Roy DM, Walsh LA, Chan TA. Driver mutations of cancer epigenomes. *Protein Cell*. (2014) 5:265–96. doi: 10.1007/s13238-014-0031-6

Conflict of Interest Statement: The authors declare that the research was conducted in the absence of any commercial or financial relationships that could be construed as a potential conflict of interest.

frontiers in Oncology

ORIGINAL RESEARCH
published: 02 April 2019
doi: 10.3389/fonc.2019.00185

CACNA2D3 Enhances the Chemosensitivity of Esophageal Squamous Cell Carcinoma to Cisplatin via Inducing Ca^{2+}-Mediated Apoptosis and Suppressing PI3K/Akt Pathways

Changjun Nie[1,2,3,4†], *Xiaohui Qin*[4†], *Xiaoyan Li*[1,2,3†], *Baoqing Tian*[1,2,3], *Ying Zhao*[1,2,3], *Yuan Jin*[1,2,3], *Yadan Li*[1,2,3], *Qiang Wang*[1,2,3], *Dingyuan Zeng*[4], *An Hong*[1,2,3*] *and Xiaojia Chen*[1,2,3*]

[1] Department of Cell Biology, Institute of Biomedicine, Jinan University, Guangzhou, China, [2] National Engineering Research Center of Genetic Medicine, Guangzhou, China, [3] Guangdong Provincial Key Laboratory of Bioengineering Medicine, Guangzhou, China, [4] Department of Medical Genetics, Liuzhou Maternal and Children Healthcare Hospital, Liuzhou, China

Resistance to platinum-based combination chemotherapy is the main cause of poor prognosis in patients with advanced esophageal squamous cell carcinoma (ESCC). Previously, we showed that CACNA2D3 (voltage-dependent subunit alpha 2 delta 3 of a calcium channel complex) was significantly downregulated and functioned as a tumor suppressor in ESCC, but its role in the chemosensitivity of ESCC to cisplatin remained unknown. Here, we found that the expression of CACNA2D3 was significantly associated with poor platinum response in ESCC patients from the Gene Expression Omnibus database. Overexpression of CACNA2D3 increased sensitivity to cisplatin in ESCC *in vitro*, whereas knockdown of CACNA2D3 increased cisplatin resistance. CACNA2D3 promoted cisplatin-induced apoptosis by modulating intracellular Ca^{2+} stores. *In vivo* experiments further showed that overexpression of CACNA2D3 enhanced cisplatin anti-tumor effects in a xenograft mouse model. CACNA2D3 overexpression also resulted in the attenuation of PI3K and Akt phosphorylation. Treatment with the PI3K/Akt inhibitor LY294002 restored the chemosensitivity of CACAN2D3-knockdown cells to cisplatin. In conclusion, the results of the current study indicate that CACAN2D3 enhances the chemosensitivity of ESCC to cisplatin via inducing Ca^{2+}-mediated apoptosis and suppressing PI3K/Akt pathways. Therefore, regulating the expression of CACNA2D3 is a potential new strategy to increase the efficacy of cisplatin in ESCC patients.

Keywords: CACNA2D3, chemosensitivity, ESCC, voltage-gated calcium channel, LY294002

OPEN ACCESS

Edited by:
Yunkai Zhang,
Vanderbilt University Medical Center, United States

Reviewed by:
Leyuan Liu,
Texas A&M University, United States
Zhenfang Du,
Vanderbilt University Medical Center, United States

***Correspondence:**
An Hong
tha@jnu.edu.cn
Xiaojia Chen
tchenxj@jnu.edu.cn;
carolcxj@qq.com

†These authors have contributed equally to this work

Specialty section:
This article was submitted to Cancer Molecular Targets and Therapeutics, a section of the journal Frontiers in Oncology

Received: *24 January 2019*
Accepted: *04 March 2019*
Published: *02 April 2019*

Citation:
Nie C, Qin X, Li X, Tian B, Zhao Y, Jin Y, Li Y, Wang Q, Zeng D, Hong A and Chen X (2019) CACNA2D3 Enhances the Chemosensitivity of Esophageal Squamous Cell Carcinoma to Cisplatin via Inducing Ca^{2+}-Mediated Apoptosis and Suppressing PI3K/Akt Pathways. Front. Oncol. 9:185. doi: 10.3389/fonc.2019.00185

INTRODUCTION

Esophageal cancer (EC) is a fatal digestive tract malignancy (1). EC is composed of two major histologic subtypes: adenocarcinoma and squamous cell carcinoma. Esophageal squamous cell carcinoma (ESCC) is more common in Southeast and Central Asia (2, 3). China is a high incidence area for ESCC, especially in Linzhou and Cixian of North China (4). Esophagectomy is the usual method for the treatment of early esophageal cancer. However, most ESCC patients are diagnosed at an advanced stage when surgery is no longer effective. Recently, the use of comprehensive perioperative therapies has dramatically improved the therapeutic efficacy of ESCC, particularly with respect to long-term survival (5–7). A cisplatin-based regimen is widely used as the first-line treatment in advanced ESCC (8–10). However, cisplatin chemotherapy is often limited by natural and acquired resistance. Consequently, it is critical to identify potential resistance mechanisms in order to restore tumor cell sensitivity to cisplatin.

The human *CACNA2D3* gene is located on the short arm of chromosome 3 at position 3p21.1, a common region of allelic deletion, and has been found to possess a potential tumor suppressor function in multiple tumor types, including gastric cancer (11–13), nasopharyngeal cancer (14), breast cancer (15), renal cell cancer neuroblastoma (16), lung cancer (17), and glioma (18). The promoter of CACNA2D3 was shown to be highly methylated in gastric cancer, and this was associated with a low survival rate (12). Similarly, suppression of CACNA2D3 by methylation was found to promote the metastatic phenotype of breast cancer (15). Another study showed that CACNA2D3 could increase intracellular Ca^{2+} levels and promote apoptosis in nasopharyngeal cancer and glioma, causing changes in the network of tumor-suppressive properties and inducing upregulation of Nemo-like kinase (NLK) through the non-canonical Wnt/Ca^{2+} signaling pathway (14, 18). In neuroblastomas with poor prognosis, the expression of CACNA2D3 is often downregulated (19, 20). Our previous study also identified CACNA2D3 as a tumor suppressor gene, and methylation of its promoter and allele deletion could inhibit its expression in ESCC (21). Recently, CACNA2D3 was implicated in the development of chemoresistance. The downregulation of CACNA2D3 was detected in five cytarabine-resistant leukemic cell lines compared with parental cells (22). However, the underlying mechanism by which CACNA2D3 might function in chemosensitivity has not been identified.

In this study, we aimed to investigate the function of CACNA2D3 in cisplatin-based chemotherapy of ESCC and discover its underlying mechanisms. We found that the expression of CACNA2D3 was significantly associated with poor platinum response in ESCC patients. Overexpression of CACNA2D3 significantly sensitized ESCC cell lines to cisplatin, while CACNA2D3 knockdown induced cellular resistance to cisplatin. Further research showed that CACNA2D3 overexpression enhanced cisplatin-induced apoptosis by modulating intracellular Ca^{2+}. Moreover, CACNA2D3 overexpression resulted in the attenuation of PI3K and Akt phosphorylation. LY294002 is a commonly used PI3K/AKT pathway inhibitor, and treatment with LY294002 could restore the chemosensitivity of CACAN2D3-knockdown cells to cisplatin.

MATERIALS AND METHODS

Cell Lines and Reagents

Six ESCC cell lines (KYSE30, KYSE140, KYSE180, KYSE410, KYSE510, and KYSE520) were purchased from DSMZ, the German Resource Centre for Biological Material (23). The short tandem repeat (STR) analysis technique was used to periodically identify all cell lines. Cell lines were cultured in RPMI1640 medium (Hyclone, Logan, UT, USA) supplemented with 10% fetal bovine serum and 1 × penicillin/streptomycin (100 units/mL, 100 μg/mL) (Gibco, NY, USA) at 37°C in a humidified incubator (5% CO_2/95% air). Cisplatin was acquired from Sigma. LY294002 was purchased from Selleck.

Plasmid Constructs and Stable Transfection

CACNA2D3 cDNA was amplified from normal human esophageal epithelial cells. The eukaryotic expression vector pcDNA3.1 (+) (Invitrogen, Carlsbad, CA, USA) was used for cloning the human CACNA2D3 gene. Then pcDNA3.1-CACNA2D3 was transfected into the ESCC cell line KYSE30 using Lipofectamine™ 3000 (Invitrogen, Carlsbad, CA, USA). The empty vector was used as a negative control. KYSE30 cells stably expressing CACNA2D3 were screened with 500 μg/ml G418.

RNA Interference

Small interfering RNA (siRNA) (SR310953) targeting CACNA2D3 and scrambled negative control siRNA (SR30004) were purchased from OriGene. After transfection for 48 h, the relative expression of CACNA2D3 was detected by quantitative real-time PCR (qRT-PCR) and western blotting.

Cell Viability Assay

A Cell Counting Kit-8 (CCK-8) assay (Dojindo, Kumamoto, Japan) was performed to measure cell viability. Cells were seeded at a density of 1×10^4 cells/well in 96-well plates and incubated with serial dilutions of cisplatin for 72 h. The CCK-8 reagent and RPMI-1640 were diluted in a 1:9 ratio and used to replace the original medium. After incubation at 37°C for 2.5 h, absorbance at a wavelength of 450 nm was measured using a microplate reader. Three independent experiments were conducted. Half maximal inhibitory concentration (IC50) was calculated to evaluate cell resistance to cisplatin using GraphPad Prism 5.0.

Colony Formation Assay

Cells were seeded at a density of 1.5×10^3 cells/well in six-well plates and treated with respective concentrations of cisplatin. After incubation for 10–14 days, the cell colonies were fixed with ethanol for 30 min and then stained with 0.1% crystal violet for 15 min. Colonies (≥50 cells) were counted. All assays were independently performed in triplicate.

Intracellular Calcium Assay

The fluorescent probe Fluo-3 AM assay (Beyotime, Haimen, China) was used to measure intracellular Ca^{2+} concentrations. Cells were washed twice with phosphate-buffered saline (PBS) and then loaded with Fluo-3 AM (1 μM) for 30 min in the dark at 37°C. When Fluo-3 AM penetrates the cellular membrane, it is hydrolyzed by cellular esterases to Fluo-3. Fluo-3 emits green fluorescence when combined with Ca^{2+}. The intracellular Ca^{2+} concentration was measured by flow cytometric analysis.

Apoptosis Assays

Apoptosis in ESCC cells treated with or without cisplatin were evaluated using an Annexin V-FITC/propidium iodide (PI) kit (Beyotime, Haimen, China). In brief, cells were digested, washed, and centrifuged twice with cold PBS. After fixing in 75% ethanol for 3 h, cells were stained with Annexin V-FITC and PI at room temperature for 30 min. Then, cells were measured by flow cytometry with FL-1 (530 nm) and FL-2 (585 nm) at an excitation wave length of 480 nm. The data were quantified using the FlowJo software.

Mitochondrial Membrane Potential Array

The mitochondrial membrane potential ($\Delta\Psi m$) was analyzed using a JC-1 assay kit (Beyotime, Haimen, China). JC-1 is a fluorescent probe for detecting mitochondrial membrane potential; it accumulates in the mitochondrial matrix and forms a red fluorescent polymer under high membrane potential. When the mitochondrial membrane potential is low, JC-1 exists as a monomer and produces green fluorescence. The cells were trypsinized and stained with JC-1 (10 mg/mL) at 37°C for 20 min. After being washed twice in PBS, cells were analyzed by flow cytometry using emission wavelengths of 590 and 525 nm.

Quantitative Real-Time PCR

Total RNA was extracted from ESCC cells using TRIzol reagent (Invitrogen, Carlsbad, CA, USA). First-strand cDNA was synthesized using the Reverse Transcription System (Promega, Wisconsin, USA), and mRNA expression levels were measured by qRT-PCR using a CFX96 Touch™ Real-Time PCR Detection System with SYBR Green Dye mixes (Applied Biosystems, Foster City, CA, USA). The PCR primers used for q-PCR were as follows. CACNA2D3: forward (5′-AGGGATTCACGG TTATGCCTT-3′), reverse (5′-GCCACACCTAAACCCTTT GTC-3′); β-Actin, forward (5′-GCTTGTCCAAGAGTGCAT GGT-3′), reverse (5′-CAGGGCTGGTTCTCGATGG-3′). The amplification parameters were: 5 min denaturation at 94°C, 40 cycles of denaturation 15 s at 94°C, 15 s annealing at 60°C, and 15 s elongation at 72°C, with final extension for 10 min at 72°C. The results were normalized to an internal standard with β-actin, and gene expression was analyzed using the $2^{-\Delta\Delta CT}$ method.

Tumor Xenograft Models

BALB/c nude mice (specific pathogen-free grade, 4–5 weeks old, and 15–20 g in weight) were purchased from Guangdong Medical Laboratory Animal Center (Guangzhou, China). The animals were raised at Jinan University Experimental Animal Management Center. KYSE30-CACNA2D3 cells and KYSE30-vector cells (6×10^6) were subcutaneously inoculated into the right armpit of each nude mouse. Tumor-bearing nude mice were randomly assigned to one of two groups of five mice: the treatment group mice received intraperitoneal injection cisplatin (2 mg/kg, twice per week for 4 weeks), and the control group mice were injected with PBS. Tumor volumes (mm^3) were calculated by the formula $V = 0.5 \times L \times W^2$. The mice were sacrificed and the tumors were isolated, weighed, and imaged. This study was carried out in accordance with the principles of the Basel Declaration and recommendations of the Guide for the Care and Use of Laboratory Animals, US National Institutes of Health (NIH Publication No. 85–23, revised 1996). The protocol was approved by the Laboratory Animal Ethics Committee of Jinan University.

Immunohistochemistry

Immunohistochemical staining was performed with primary antibodies against CACNA2D3 (Novus Biological, Littleton, CO, USA). Sections of xenografts from mice were deparaffinized with xylene and rehydrated in alcohol baths, then incubated in 3% hydrogen peroxide for 20 min to block endogenous peroxidase activity. Antigen retrieval was performed by microwave antigen retrieval in a citric acid buffer (pH 6.0). The slides were subsequently incubated with primary antibodies at 4°C overnight and then incubated with biotinylated secondary antibodies at room temperature for 30 min, followed by incubation with horseradish peroxidase (HRP)-streptavidin for 30 min. Finally, diaminobenzidine (DAB) staining and hematoxylin counterstaining were performed. All samples were observed through a high-power light microscope.

TUNEL Analysis

A colorimetric TUNEL apoptosis assay kit (Beyotime, Haimen, China) was used to identify apoptotic cells in the xenograft. Sections of xenograft from mice were deparaffinized, rehydrated, and incubated with proteinase K for 5 min at 37°C. Endogenous peroxidase was inactivated by treatment with 0.3% hydrogen peroxide for 20 min at room temperature. The sections were washed in PBS and incubated with a labeling buffer containing TdT at 37°C for 1 h, before being incubated with HRP-streptavidin for 30 min. Finally, the sections were incubated with DAB solution for coloration. All samples were observed through a high-power light microscope.

RNA Sequencing (RNA-seq) and Sequencing Analysis

Equal amounts of RNA samples were used to construct strand-specific RNA libraries, following the manufacturer's standard procedures. The libraries were sequenced on a HiSeq X Ten (Illumina, San Diego, CA, USA) platform in PE150 mode. The index of the reference genome was built using Bowtie v2.2.3 (24). Differentially expressed genes (DEGs) were identified using DESeq2 (25). The thresholds for DEGs were set as false discovery rate (FDR) ≤ 0.05 and $|\log_2$ fold change$| \geq 1$. Gene ontology (GO; http://www.geneontology.org) classification analysis was performed for DEGs, including molecular function,

cellular component, and biological process information (26). The Kyoto Encyclopedia of Genes and Genomes (KEGG; http://www.kegg.jp) was used for systematic analysis of the signaling pathways involving the DEGs (27), and related pathways were evaluated by gene set enrichment analysis (GSEA; http://software.broadinstitute.org/gsea/) (28).

Western Blot Assay

Western blot analysis was performed according to conventional methods. Antibodies against Akt, phosphor-Akt, PI3K, phosphor-PI3K, and GAPDH were from Cell Signaling Technology.

Statistical Analysis

Statistical analysis was performed using GraphPad Prism 5.0 and SPSS 19.0. Data were expressed as mean ± standard deviation (S.D.). Significant differences between two independent groups were identified by student's *t*-test and expressed as $^{*}p < 0.05$, $^{**}p < 0.01$, or $^{***}p < 0.001$.

RESULTS

Downregulation of CACNA2D3 Is Correlated With Chemoresistance in ESCC

To analyze the relationship between the expression of CACNA2D3 and chemoresistance in ESCC, we screened microarray data predicting the response of esophageal cancer patients to neoadjuvant chemotherapy from the Gene Expression Omnibus (GSE45670) (29). As shown in **Figure 1A**, the expression of CACNA2D3 in the neoadjuvant chemotherapy responder group was significantly higher than that in the non-responder group ($p < 0.05$). We further investigated the association of CACNA2D3 expression with chemotherapeutic response in ESCC cell lines by calculating the IC50 values of cisplatin during treatment. Six ESCC cell lines were treated with different concentrations of cisplatin. The IC50 dose was calculated in each cell, and qRT-PCR was used to determine the expression level of CACNA2D3. The results showed that the IC50 value of cisplatin was negatively correlated with CACNA2D3 expression in ESCC cell lines (**Figures 1B,C**). These observations indicated that CACNA2D3 might regulate chemosensitivity in ESCC.

CACNA2D3 Enhances Cisplatin Sensitivity in ESCC

To investigate the role of CACNA2D3 in regulating cisplatin sensitivity in ESCC cells, a KYSE30 cell line stably expressing CACNA2D3 (30-CAC) was constructed. Control cells were transfected with empty vector (30-Vec). The expression of CACNA2D3 was determined by western blotting and qRT-PCR (**Figure 2A**). CCK8 assays showed that overexpression of CACNA2D3 (30-CAC) could significantly increase the cells' chemosensitivity to cisplatin compared with controls (30-Vec) (**Figure 2B**). The sensitivity of 30-CAC cells to cisplatin was more than twice that of 30-Vec control cells, based on the IC50 value (**Figure 2C**). In colony formation experiments, we also found that overexpression of CACNA2D3 combined with cisplatin could inhibit the formation of clones more significantly (**Figure 2D**). We next examined whether knocking down CACNA2D3 would contribute to cisplatin resistance in ESCC. The results showed that specific siRNA against CACNA2D3 could significantly suppress the expression of CACNA2D3 up to 48 h after transfection in KYSE180 (**Figure 2E**). Knockdown of CACNA2D3 (180-siCAC) significantly induced cisplatin resistance compared with the scrambled siRNA (180-scr) (**Figure 2F**). The IC50 value of 180-siCAC was higher than that of 180-scr cells ($p < 0.001$) (**Figure 2G**). CACNA2D3 knockdown resulted in significantly higher colony formation efficiency in 180-siCAC cells than in control cells in the presence of cisplatin (**Figure 2H**). Taken together, the data showed that CACNA2D3 sensitized ESCC cells to cisplatin.

CACNA2D3 Enhances Cisplatin-Induced Apoptosis Through the Mitochondria-Dependent Pathway

CACNA2D3, as a regulatory subunit, has been reported to elevate the influx of extracellular Ca^{2+} into cells. In our study, Ca^{2+} levels were detected by Fluo-3 AM staining to evaluate their relationship with CACNA2D3 expression levels. CACNA2D3-overexpressing KYSE30 cells (30-CAC) showed significantly increased intracellular Ca^{2+} compared with the control cells (30-Vec), whereas knockdown of CACNA2D3 in KYSE180 cells (180-siCAC) caused a decrease in intracellular Ca^{2+} levels compared with control cells (180-scr) (**Figure 3A**). As Ca^{2+} can induce mitochondrial permeability changes and regulate the initiation phase of apoptosis, we performed an apoptosis assay to evaluate the effect of CACNA2D3 on the apoptosis of ESCC cells. Surprisingly, CACNA2D3 overexpression did not affect ESCC cell apoptosis, but promoted cisplatin-induced apoptosis. The percentage of apoptotic cells in 30-CAC cells increased by 24.8 ± 3.9% with cisplatin treatment, compared with 13.3 ± 1.7% in 30-Vec cells. In KYSE180 cells, cisplatin increased apoptosis by 14.2 ± 2.3% in 180-siCAC cells and by 32.3 ± 3.2% in 180-scr cells (**Figures 3B,C**). In addition, the JC-1 probe was used to assess changes in mitochondrial membrane potential in ESCC cells treated with cisplatin. As shown in **Figures 3D,E**, with cisplatin treatment, the membrane potential of 30-Vec cells decreased by 14.3 ± 2.5%, while that of 30-CAC cells decreased by 25.5 ± 1.6%. In KYSE180 cells, the membrane potential decreased by 24.2 ± 1.8% in 180-scr cells and by 9.6 ± 3.4% in 180-siCAC cells. Western blot analysis demonstrated that the ratios of cleaved Caspase9/Caspase9 and cleaved Caspase3/Caspase3 in CACNA2D3-overexpressing KYSE30 cells were higher than those in the control cells. Conversely, these ratios decreased in 180-siCAC cells treated with cisplatin compared with 180-scr cells (**Figure 3F**). Taken together, these results suggested that CACNA2D3 sensitized ESCC cells to cisplatin through enhancing mitochondria-mediated apoptosis.

CACNA2D3 Increases Cisplatin Sensitivity *in vivo*

In order to better understand the role of CACNA2D3 in cisplatin sensitivity *in vivo*, we established a subcutaneous

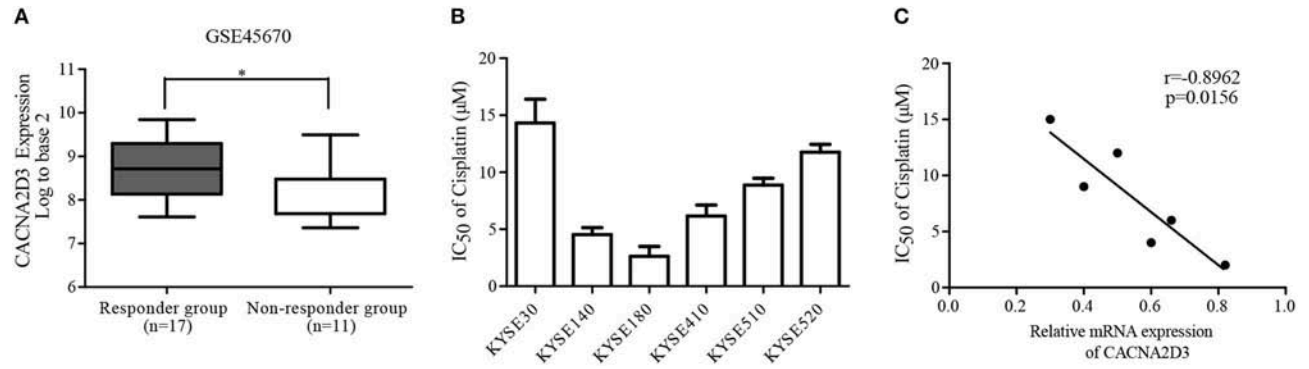

FIGURE 1 | Downregulation of CACNA2D3 is associated with poor chemotherapy response in ESCC. **(A)** Box and whisker plot of CACNA2D3 mRNA levels in neoadjuvant chemotherapy responder and non-responder groups (GSE45670). *$p < 0.05$. **(B)** IC50 values for cisplatin in six ESCC cell lines. Cells were treated with a range of concentrations of cisplatin for 72 h, and IC50 was calculated. Data are represented as the mean ± SD of three independent experiments. **(C)** Correlation of CACNA2D3 mRNA levels and IC50 values for cisplatin in six ESCC cell lines. r, Pearson correlation coefficient.

xenograft model by injecting CACNA2D3-overexpressing cells and control cells into BALB/c-nude mice. When the tumor volumes reached about 100 mm^3, 2 mg/kg cisplatin was injected intraperitoneally twice per week for 4 weeks, while the control group received PBS. As shown in **Figure 4A**, we found that overexpression of CACNA2D3 and cisplatin both inhibited the growth of xenografts. However, CACNA2D3 overexpression in combination with cisplatin could more significantly inhibit the tumorigenic ability of ESCC cells. The mean tumor size (**Figure 4B**) and weight (**Figure 4C**) in the CACNA2D3 overexpression group were significantly lower than those in the vector control group after cisplatin treatment. Moreover, immunohistochemical staining showed that the expression of CACNA2D3 was increased in the CACNA2D3-overexpressing tumors compared with the control tumors (**Figure 4D**). TUNEL analysis also revealed that the apoptosis rate of CACNA2D3 overexpression cells was significantly higher than that of the control cells after cisplatin treatment (**Figure 4E**). These results together indicated that CACNA2D3 increased cisplatin sensitivity *in vivo*.

CACANA2D3 Regulates the Sensitivity of ESCC to Cisplatin Through Inhibiting the PI3K/Akt Pathways

To better understand the molecular mechanism underlying CACNA2D3-enhanced ESCC cisplatin sensitivity, we compared the gene expression profiles of CACNA2D3 stably overexpressed KYSE30 cells with those of control cells using RNA-seq after cisplatin treatment, and identified 2439 DEGs (FDR < 0.05, $|\log_2$ fold change$| \geq 1$) between the two groups. A total of 1,137 genes were upregulated, and 1,302 genes were downregulated (**Figure 5A**). We further explored the biological functions of DEGs by GO, KEGG, and GSEA pathway enrichment analyses. Using the DAVID online GO database for comprehensive analysis, we found that CACNA2D3 was associated with multiple processes, including metabolic processes, biological regulation, regulation of biological processes, and response to stimulus (**Figure 5B**). KEGG database analysis revealed that multiple signaling pathway pathways were highly enriched, including "PI3K-Akt signaling pathway," "Pathways in cancer," "MAPK signaling pathway," and "ABC transporters" (**Figure 5C**). GSEA also showed that the CACNA2D3-regulated genes were enriched in the cell growth pathway and PI3K-Akt-mTOR signaling pathway (**Figure 5D**). Western blotting showed that CACNA2D3 dramatically suppressed the phosphorylation of PI3K and Akt, and the suppression persisted in the presence of cisplatin (**Figure 5E**). These results indicated that CACNA2D3 enhanced cisplatin sensitivity by inhibiting the PI3K/Akt pathway.

LY294002 Restores the Sensitivity of ESCC to Cisplatin in CACNA2D3-Knockdown Cells

For the rescue experiments, we treated CACNA2D3-knockdown cells with Akt inhibitor LY294002. Western blotting showed that LY294002 inhibited Akt activation in 180-siCAC cells and 180-scr cells (**Figure 6A**). The CACNA2D3-knockdown cells showed significantly higher sensitivity to cisplatin after treatment with LY294002 (**Figure 6B**). The effect of LY294002 on the IC50 reduction caused by cisplatin was significantly stronger in 180-siCAC cells than in 180-scr cells (**Figure 6C**). The colony formation assays also demonstrated that the combination of cisplatin and LY294002 suppressed colony formation more significantly in 180-siCAC cells than in control cells (**Figure 6D**). These results suggest that inhibition of the Akt signaling pathway can restore the chemosensitivity of CACNA2D3-knockdown cells to cisplatin.

DISCUSSION

ESCC is a cancer of the digestive system with high incidence in China. Although therapeutic strategies for ESCC have advanced considerably, its mortality rate remains high, and further efforts are needed to improve patient prognosis. Cisplatin is widely used

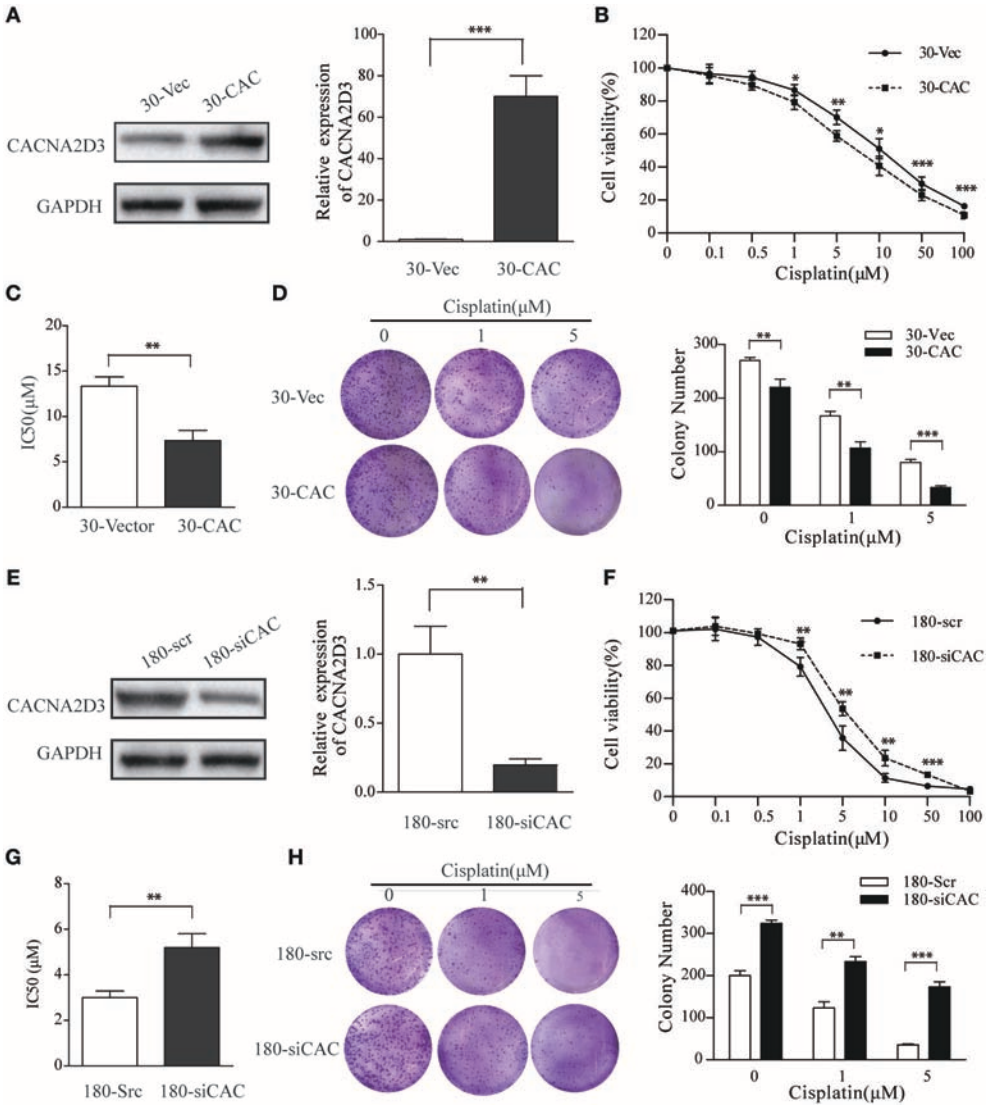

FIGURE 2 | CACNA2D3 promotes chemosensitivity to cisplatin *in vitro*. **(A,E)** Stable expression of CACNA2D3 in KYSE30 cells generated by pCDNA3.1-CACNA2D3 transfection and silencing of CACNA2D3 in KYSE180 cells by siRNA were examined by western blotting and qRT-PCR. GAPDH and β-Actin were employed as a loading control. **(B,F)** CACNA2D3-overexpressing KYSE30 cells and CACNA2D3-knockdown cells were treated with cisplatin at the indicated concentrations for 72 h. The number of viable cells was measured by CCK-8 assay. **(C,G)** IC50 values were calculated using linear or logarithmic regression ($R^2 > 0.9$). Values are presented as the mean ± SD of three wells. **(D,H)** Colony forming assays were used to determine colony forming ability after cisplatin treatment. Data are presented as the mean ± SD of three wells. $^{**}p < 0.01$, $^{***}p < 0.001$.

in the clinical chemotherapy of various types of human tumors, including esophageal, gastric, testicular, bladder, ovarian, and lung cancers (30–32). However, cisplatin resistance is often the biggest obstacle to the success of chemotherapy. Therefore, it is extremely important to be able to predict cisplatin response before chemotherapy, in order to select the most appropriate treatment strategy for patients.

Calcium ions (Ca^{2+}) are vital intracellular second messengers involved in multiple functions of cells, including proliferation, differentiation, fertilization, development, muscle contraction, cell death, learning, and memory (33–35). The voltage-gated calcium channel is a multi-subunit protein complex consisting of a channel-forming α1 subunit and three regulatory subunits, α2δ, β, and γ (36–38). CACNA2D3 encodes one of the α2δ subunits. Our previous study identified CACNA2D3 as a novel tumor suppressor gene for ESCC. Downregulation of CACNA2D3 predicted poor prognosis. Exogenous expression of CACNA2D3 can strongly inhibit cell growth, migration, and invasion, and induce apoptosis (21). In the current study, we first found that the expression of CACNA2D3 was higher in a platinum-based neoadjuvant chemotherapy responder group than in the non-responder group. Based on a serious of assays *in vitro* and *in vivo*, we confirmed the effect of CACNA2D3 on the chemosensitivity of cisplatin in ESCC cells.

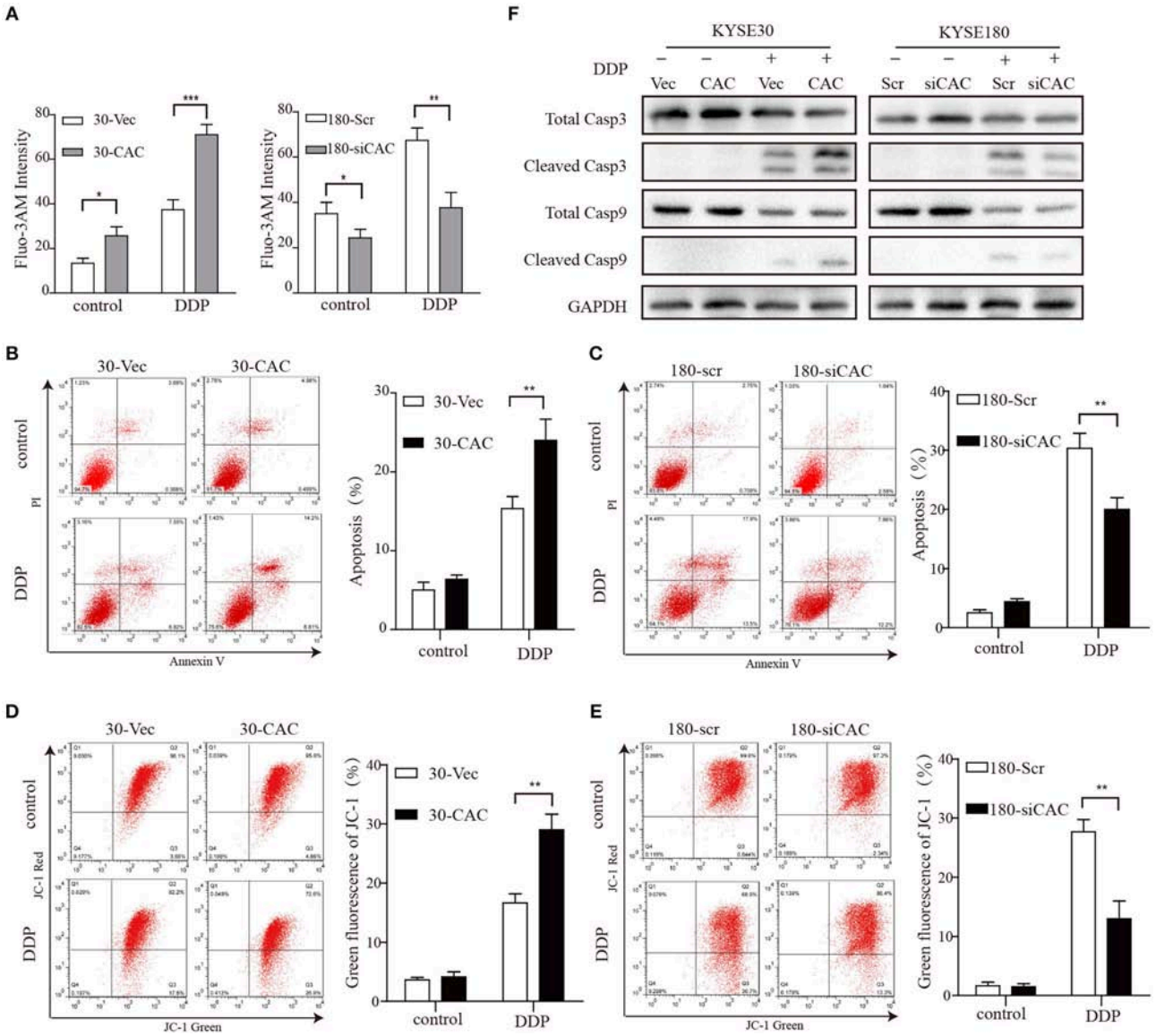

FIGURE 3 | CACNA2D3 enhances cisplatin-induced apoptosis through mitochondria-dependent pathway. **(A)** Intracellular Ca^{2+} levels were detected by fluorescence-activated cell sorting (FACS) with Fluo-3 AM. **(B,C)** Annexin V/PI staining in CACNA2D3 overexpression and knockdown cell lines treated with cisplatin for 48 h; apoptosis was analyzed by FACS. The percentages of apoptotic cells are presented as the mean ± SD of three independent experiments. **(D,E)** The mitochondrial membrane potential was measured using fluorescent dye JC-1 after treatment with cisplatin for 48 h. Percentages of green fluorescence from JC-1 in cells are presented as the mean ± SD of three independent experiments. **(F)** Levels of cleaved caspase-3, total caspase-3, cleaved caspase-9, and total caspase-9 proteins were analyzed by western blotting in CACNA2D3-overexpressing and knockdown cell lines treated with or without cisplatin. $^{*}p < 0.05$; $^{**}p < 0.01$; $^{***}p < 0.001$.

Cisplatin is a conventional chemotherapy drug. It is activated upon entering the cell, when its chloride atoms are replaced by water molecules. The resulting hydrolytic product is an effective electrophilic reagent, which can react with any nucleophile, including DNA, RNA, and proteins. DNA is the primary target of cisplatin. Cisplatin tends to bind to the N7 site of purine bases to form a DNA adduct, causing DNA damage in cancer cells, blocking cell division, and leading to apoptosis (39–41). Several mechanisms of cisplatin resistance have been discovered, including reduced intracellular drug accumulation, increased activity of efflux pumps, changed drug targets, lost mismatch-repair ability, and escape apoptosis (42–44). The voltage-dependent calcium channel α2δ subunits have been found to regulate extracellular Ca^{2+} influx (45). Our study consistently demonstrated that the overexpression of CACNA2D3 increased the uptake of intracellular free Ca^{2+} in ESCC. Apoptosis is closely related to increased intracellular Ca^{2+} concentration. Here, we found that CACNA2D3 overexpression

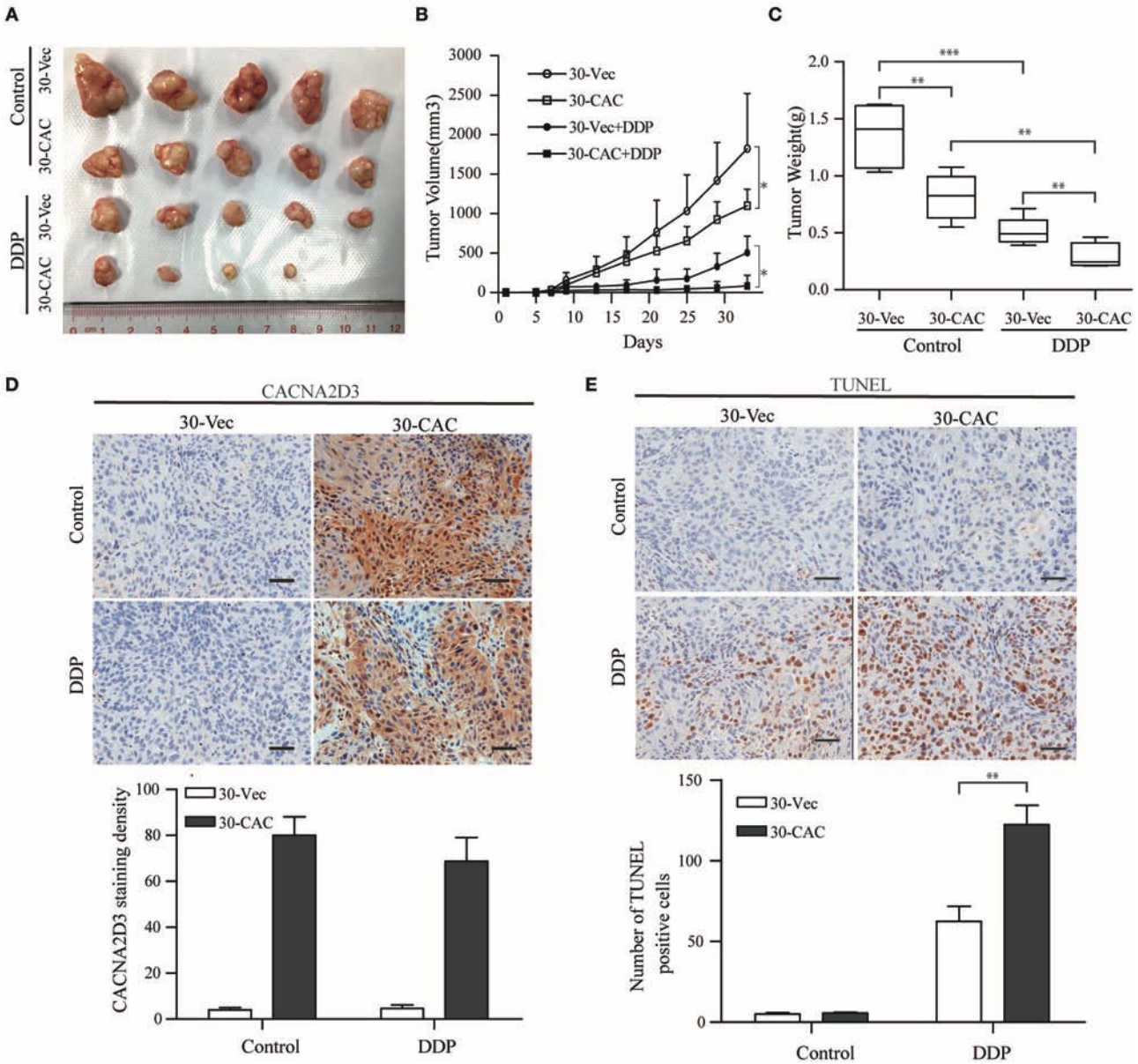

FIGURE 4 | CACNA2D3 increases chemosensitivity of ESCC cells to cisplatin *in vivo*. **(A)** Representative images of xenografted tumors derived from Balb/c-nu mice at day 33. **(B)** The mice in the treatment groups were intraperitoneally injected with 2 mg/kg every 3 days. Tumor volumes were measured at 4 days intervals. Data are presented as mean ± SD. **(C)** Tumor weights were measured after mice were sacrificed. **(D)** Detection of CACNA2D3 from tumor sections by immunohistochemical staining. Quantification was performed by calculating the percentage of the staining intensities using ImageJ. **(E)** TUNEL staining of tumor sections from each group; the number of TUNEL-positive cells was quantified by counting. $^{*}p < 0.05$; $^{**}p < 0.01$; $^{***}p < 0.001$.

did not in itself affect the apoptosis rate of ESCC cells; however, it significantly increased cisplatin-induced apoptosis. Mitochondria often have a decisive role in stimulus-induced apoptosis. Mitochondrial membrane destruction and infiltration are common phenomena related to apoptosis. Excessive Ca^{2+} accumulation inside mitochondria is thought to be a powerful apoptosis stimulator that induces mitochondrial membrane depolarization and activates downstream caspases and finally induces apoptosis (46, 47). We confirmed that ectopic expression of CACNA2D3 led to depolarization of the mitochondrial membrane potential after cisplatin treatment. Moreover, the immunoblotting results showed that CACNA2D3 overexpression activated caspase-3 and caspase-9 in ESCC cells. CACNA2D3 and cisplatin synergistically induce apoptosis by increasing Ca^{2+}-dependent collapse of mitochondrial membrane potential, indicating that CACNA2D3 enhances cisplatin-induced apoptosis by activating the mitochondrial pathway.

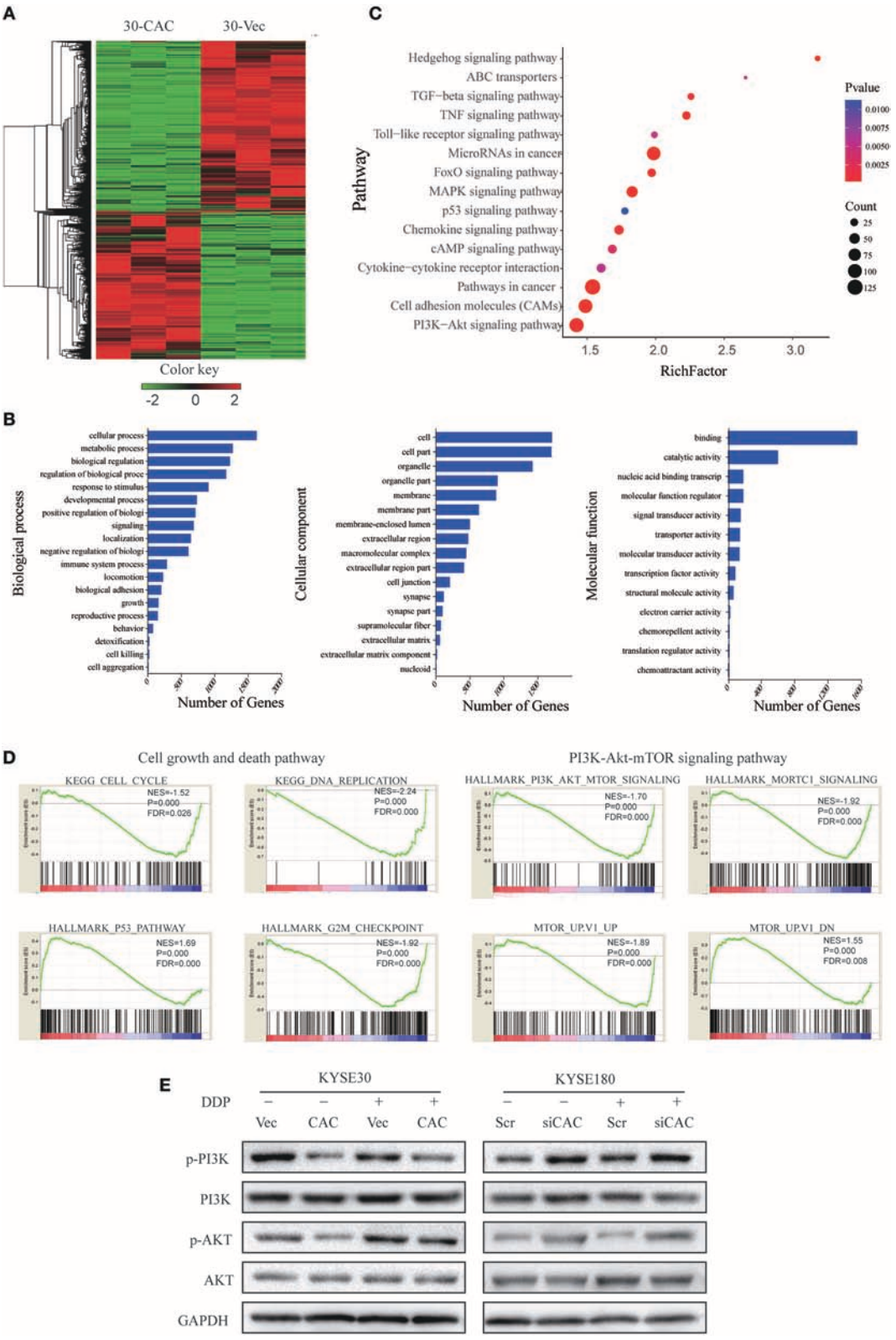

FIGURE 5 | CACANA2D3 regulated the sensitivity of ESCC to cisplatin through inhibiting the PI3K/Akt pathways. **(A)** DEG heatmap and hierarchical clustering results for CACNA2D3-overexpressing KYSE30 ESCC cells. Red and green indicate high and low gene expression, respectively. **(B)** GO enrichment analysis of the DEGs. The genes were divided into three categories: cellular component, biological process, and molecular function genes. **(C)** KEGG pathway enrichment analysis

(Continued)

FIGURE 5 | of differentially expressed pathways upon CACNA2D3 overexpression. The ordinates represent the enriched KEGG pathway. $p < 0.05$ was considered statistically significant. **(D)** GSEA analysis of differentially expressed pathways upon CACNA2D3 overexpression. NES, normalized enrichment score. **(E)** Levels of P-PI3K, PI3K, P-Akt, and Akt proteins were analyzed by western blotting in CACNA2D3-overexpressing and knockdown cell lines treated with or without cisplatin.

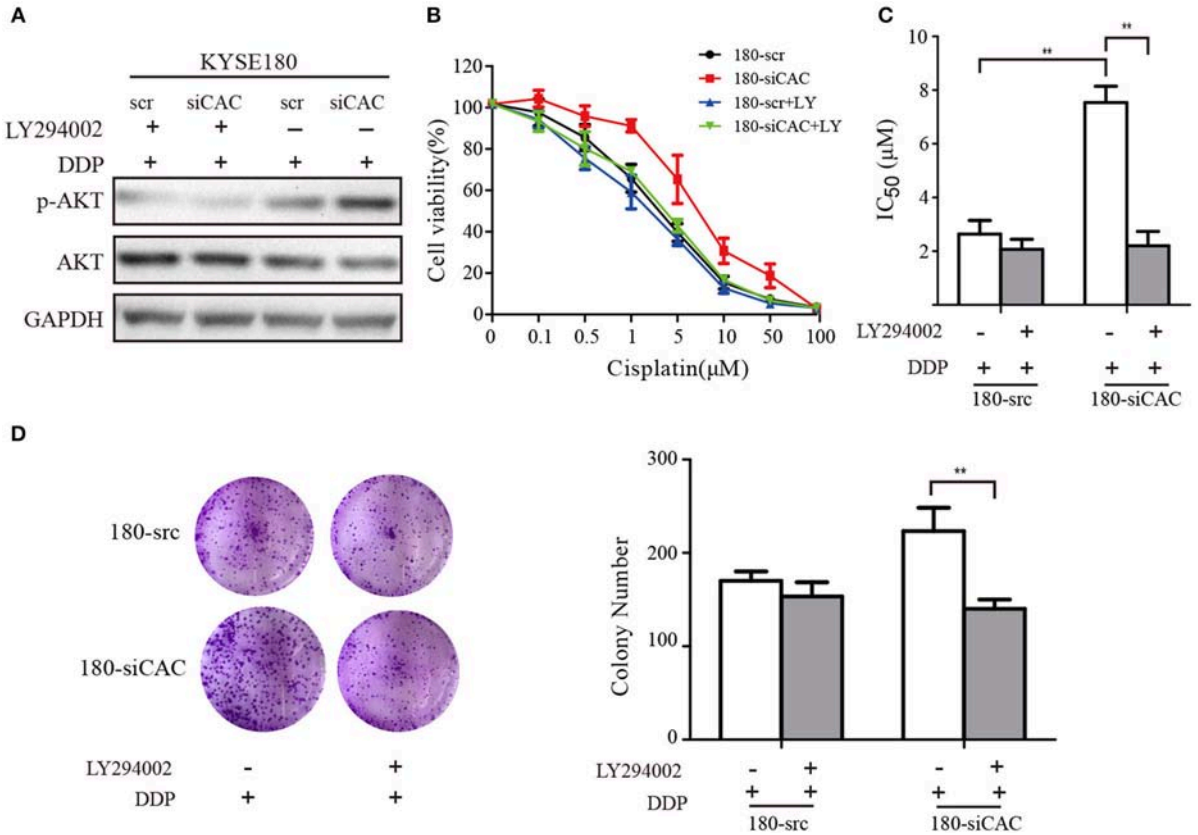

FIGURE 6 | LY294002 restores the sensitivity of ESCC to cisplatin in CACNA2D3-knockdown cells. **(A)** CACNA2D3-knockdown KYSE180 cells and control cells were treated with cisplatin at the indicated concentrations with or without LY294002 for 72 h. Levels of P-Akt and Akt proteins were analyzed by western blotting. **(B)** The number of viable cells was measured by CCK-8 assay. **(C)** IC50 values were calculated using linear or logarithmic regression (R2 > 0.9). Data are presented as the mean ± SD from triplicate wells. **(D)** Colony forming assays were used to determine the colony forming ability after cisplatin with or without LY294002 treatment. Data are presented as the mean ± SD from three wells. $^{**}p < 0.01$.

To systematically investigate the underlying molecular mechanism mediating CACNA2D3-induced ESCC cisplatin sensitivity, we compared the expression profiles of KYSE30 cells with and without CACNA2D3 overexpression after cisplatin treatment using RNA-seq. By pathway enrichment analyses, we found that CACNA2D3 could inhibit DNA replication and block ESCC cells in the G2/M phase by inhibiting the expression of p53, as shown in our previous study (21). We also found the PI3K/Akt pathway to be inactivated in CACNA2D3-overexpressing ESCC cells. The PI3K/Akt signaling pathway has important roles in promoting cell growth, proliferation, invasion, angiogenesis, and drug resistance. In-depth studies of the relationship between the PI3K/Akt signaling pathway and drug resistance have led to this pathway being considered as a new target for chemotherapy drug resistance therapy (48, 49). Here, we found that the phosphorylation of PI3K and Akt was blocked in CACNA2D3-overexpressing KYSE30 cells. Consistently, when CACNA2D3 was knocked down in KYSE180 cells, the phosphorylation level of Akt showed a significant increase. Interestingly, our data also showed that blockade of the PI3K/Akt pathway by LY294002 in CACNA2D3-knockdown cells could restore chemosensitivity to cisplatin.

In summary, in this work we first proved that the expression of CACNA2D3 was associated with chemosensitivity in ESCC patients treated with cisplatin-based therapy. Moreover, CACNA2D3 increased chemosensitivity to cisplatin in cell experiments and xenograft tumors, indicating that it could be used as a tumor marker to predict and improve patients' response to cisplatin. We further found that CACNA2D3 regulated cisplatin-induced apoptosis and decreased Akt phosphorylation. Detection of CACNA2D3 expression might be helpful for individualized treatment of ESCC patients.

AUTHOR CONTRIBUTIONS

CN, XC, and AH designed the study. CN, XQ, XL, YZ, YJ, YL, and QW performed the experiments. CN, XQ, XL, DZ, and BT analyzed the data. CN, XL, and XC wrote the paper.

FUNDING

This work was supported by grants from the National Natural Science Foundation of China (grants 81360365, 81472337, 81473131), the National Key Basic Research Program of China (973 Program) (grant 2015CB553706), the Science & Technology Program of Guangdong province (grant 2016A020217012), the Science &Technology Program of Guangzhou (grant 2016201604030039), and the Guangxi Natural Science Foundation of China (grant 2014GXNSFBA118205, 2017GXNSFAA198157). We thank Yuying Zhou and Shujun Guo from the Institute of Biomedicine of Jinan University for technical assistance.

REFERENCES

1. Ferlay J, Soerjomataram I, Dikshit R, Eser S, Mathers C, Rebelo M, et al. Cancer incidence and mortality worldwide: sources, methods and major patterns in GLOBOCAN 2012. *Int J Cancer*. (2015) 136:E359–86. doi: 10.1002/ijc.29210
2. Arnold M, Soerjomataram I, Ferlay J, Forman, D. Global incidence of oesophageal cancer by histological subtype in 2012. *Gut*. (2015) 64:381–7. doi: 10.1136/gutjnl-2014-308124
3. Zhang Y. Epidemiology of esophageal cancer. *World J Gastroenterol.* (2013) 19:5598–606. doi: 10.3748/wjg.v19.i34.5598
4. Lin Y, Totsuka Y, He Y, Kikuchi S, Qiao Y, Ueda J, et al. Epidemiology of esophageal cancer in Japan and China. *J epidemiol.* (2013) 233–42. doi: 10.2188/jea.JE20120162
5. Ando N, Iizuka T, Ide H, Ishida K, Shinoda M, Nishimaki T, et al. Surgery plus chemotherapy compared with surgery alone for localized squamous cell carcinoma of the thoracic esophagus: a Japan clinical oncology group study–JCOG9204. *J Clin Oncol.* (2003) 21:4592–6. doi: 10.1200/JCO.2003.12.095
6. Iinuma H, Fukushima R, Inaba T, Tamura J, Inoue T, Ogawa E, et al. Phase I clinical study of multiple epitope peptide vaccine combined with chemoradiation therapy in esophageal cancer patients. *J Transl Med.* (2014) 12:84. doi: 10.1186/1479-5876-12-84
7. Lyu X, Huang J, Mao Y, Liu Y, Feng Q, Shao K, et al. Adjuvant chemotherapy after esophagectomy: is there a role in the treatment of the lymph node positive thoracic esophageal squamous cell carcinoma? *J Surg Oncol.* (2014) 110:864–8. doi: 10.1002/jso.23716
8. Kato K, Muro K, Minashi K, Ohtsu A, Ishikura S, Boku N, et al. Phase II study of chemoradiotherapy with 5-fluorouracil and cisplatin for Stage II-III esophageal squamous cell carcinoma: JCOG trial (JCOG 9906). *Int J Rad Oncol Biol Phys.* (2011) 81: 684–90. doi: 10.1016/j.ijrobp.2010.06.033
9. Miyazaki T, Sohda M, Tanaka N, Suzuki S, Ieta K, Sakai M, et al. Phase I/II study of docetaxel, cisplatin, and 5-fluorouracil combination chemoradiotherapy in patients with advanced esophageal cancer. *Cancer Chemother Pharmacol.* (2015) 75:449–55. doi: 10.1007/s00280-014-2659-6
10. Hashimoto J, Kato K, Ito Y, Kojima T, Akimoto T, Daiko H, et al. Phase II feasibility study of preoperative concurrent chemoradiotherapy with cisplatin plus 5-fluorouracil and elective lymph node irradiation for clinical stage II/III esophageal squamous cell carcinoma. *Int J Clin Oncol.* (2018) 24:60–7. doi: 10.1007/s10147-018-1336-x
11. Yuasa Y, Nagasaki H, Akiyama Y, Hashimoto Y, Takizawa T, Kojima K, et al. DNA methylation status is inversely correlated with green tea intake and physical activity in gastric cancer patients. *Int J Cancer*. (2009) 124:2677–82. doi: 10.1002/ijc.24231
12. Wanajo A, Sasaki A, Nagasaki H, Shimada S, Otsubo T, Owaki S, et al. Methylation of the calcium channel-related gene, CACNA2D3, is frequent and a poor prognostic factor in gastric cancer. *Gastroenterology*. (2008) 135:580–90. doi: 10.1053/j.gastro.2008.05.041
13. Qu Y, Dang S, Hou P. Gene methylation in gastric cancer. *Clin Chim Acta*. (2013) 424:53–65. doi: 10.1016/j.cca.2013.05.002
14. Wong AM, Kong KL, Chen L, Liu M, Wong AM, Zhu C, et al. Characterization of CACNA2D3 as a putative tumor suppressor gene in the development and progression of nasopharyngeal carcinoma. *Int J Cancer*. (2013) 133:2284–95. doi: 10.1002/ijc.28252
15. Palmieri C, Rudraraju B, Monteverde M, Lattanzio L, Gojis O, Brizio R, et al. Methylation of the calcium channel regulatory subunit alpha2delta-3 (CACNA2D3) predicts site-specific relapse in oestrogen receptor-positive primary breast carcinomas. *Br J Cancer*. (2012) 107:375–81. doi: 10.1038/bjc.2012.231
16. Hanke S, Bugert P, Chudek J, Kovacs G. Cloning a calcium channel alpha2delta-3 subunit gene from a putative tumor suppressor gene region at chromosome 3p21.1 in conventional renal cell carcinoma. *Gene.* (2001) 264: 69–75. doi: 10.1016/S0378-1119(00)00600-4
17. Tai AL, Mak W, Ng PK, Chua DT, Ng MY, Fu L, et al. High-throughput loss-of-heterozygosity study of chromosome 3p in lung cancer using single-nucleotide polymorphism markers. *Cancer Res.* (2006) 66:4133–8. doi: 10.1158/0008-5472.CAN-05-2775
18. Jin Y, Cui D, Ren J, Wang K, Zeng T, Gao L. CACNA2D3 is downregulated in gliomas and functions as a tumor suppressor. *Mol Carcinogene.* (2017) 56: 945–59. doi: 10.1002/mc.22548
19. De Preter K, Vandesompele J, Heimann P, Yigit N, Beckman S, Schramm A, et al. Human fetal neuroblast and neuroblastoma transcriptome analysis confirms neuroblast origin and highlights neuroblastoma candidate genes. *Genome Biol.* (2006) 7:R84. doi: 10.1186/gb-2006-7-9-r84
20. Thorell K, Bergman A, Caren H, Nilsson S, Kogner P, Martinsson T, et al. Verification of genes differentially expressed in neuroblastoma tumours: a study of potential tumour suppressor genes. *BMC Med Genom.* (2009) 2:53. doi: 10.1186/1755-8794-2-53
21. Li Y, Zhu CL, Nie CJ, Li JC, Zeng TT, Zhou J, et al. Investigation of tumor suppressing function of CACNA2D3 in esophageal squamous cell carcinoma. *PLoS ONE.* (2013) 8:e60027. doi: 10.1371/journal.pone.0060027
22. Negoro E, Yamauchi T, Urasaki Y, Nishi R, Hori H, Ueda T. Characterization of cytarabine-resistant leukemic cell lines established from five different blood cell lineages using gene expression and proteomic analyses. *Int J Oncol.* (2011) 38:911–9. doi: 10.3892/ijo.2011.933
23. Shimada Y, Imamura M, Wagata T, Yamaguchi N, Tobe T. Characterization of 21 newly established esophageal cancer cell lines. *Cancer*. (1992) 69:277–84. doi: 10.1002/1097-0142(19920115)69:2<277::AID-CNCR2820690202>3.0.CO;2-C
24. Langmead B, Trapnell C, Pop M, Salzberg SL. Ultrafast and memory-efficient alignment of short DNA sequences to the human genome. *Genome Biol.* (2009) 10:R25. doi: 10.1186/gb-2009-10-3-r25
25. Love MI, Huber W, Anders S. Moderated estimation of fold change and dispersion for RNA-seq data with DESeq2. *Genome Biol.* (2014) 15:550. doi: 10.1186/s13059-014-0550-8
26. Ashburner M, Ball CA, Blake JA, Botstein D, Butler H, Cherry JM, et al. Gene ontology: tool for the unification of biology. The gene ontology consortium. *Nat Genet.* (2000) 25:25–9. doi: 10.1038/75556
27. Huang da W, Sherman BT, Lempicki RA. Systematic and integrative analysis of large gene lists using DAVID bioinformatics resources. *Nat Protocol*. (2009) 4: 44–57. doi: 10.1038/nprot.2008.211
28. Subramanian A, Tamayo P, Mootha VK, Mukherjee S, Ebert BL, Gillette MA, et al. Gene set enrichment analysis: a knowledge-based approach for interpreting genome-wide expression profiles. *Proc Natl Acad Sci USA*. (2005) 102:15545–50. doi: 10.1073/pnas.0506580102
29. Wen J, Yang H, Liu MZ, Luo KJ, Liu H, Hu Y, et al. Gene expression analysis of pretreatment biopsies predicts the pathological response of esophageal

squamous cell carcinomas to neo-chemoradiotherapy. *Ann Oncol.* (2014) 25:1769–74. doi: 10.1093/annonc/mdu201
30. Sersa G, Stabuc B, Cemazar M, Miklavcic D, Rudolf Z. Electrochemotherapy with cisplatin: clinical experience in malignant melanoma patients. *Clin Cancer Res.* (2000) 6:863–7.
31. Kelland L. The resurgence of platinum-based cancer chemotherapy. *Nat Rev Cancer.* (2007) 7:573–84. doi: 10.1038/nrc2167
32. Galluzzi L, Vitale I, Michels J, Brenner C, Szabadkai G, Harel-Bellan A, et al. Systems biology of cisplatin resistance: past, present and future. *Cell Death Dis.* (2014) 5: e1257. doi: 10.1038/cddis.2013.428
33. Berridge MJ, Bootman MD, and Lipp P. Calcium–a life and death signal. *Nature*. (1998) 395: 645–8. doi: 10.1038/27094
34. Webb SE, Miller AL. Calcium signalling during embryonic development. *Nat Rev Mol Cell Biol*. (2003) 4:539–51. doi: 10.1038/nrm1149
35. Monteith GR, McAndrew D, Faddy HM, Roberts-Thomson SJ. Calcium and cancer: targeting Ca^{2+} transport. *Nat Rev Cancer.* (2007) 7:519–30. doi: 10.1038/nrc2171
36. Gong HC, Hang J, Kohler W, Li L, Su TZ. Tissue-specific expression and gabapentin-binding properties of calcium channel alpha2delta subunit subtypes. *J Membr Biol.* (2001) 184:35–43. doi: 10.1007/s00232-001-0072-7
37. Davies A, Hendrich J, Van Minh AT, Wratten J, Douglas L, Dolphin AC. Functional biology of the alpha(2)delta subunits of voltage-gated calcium channels. *Trends Pharmacol Sci.* (2007) 28:220–8. doi: 10.1016/j.tips.2007.03.005
38. Qin N, Yagel S, Momplaisir ML, Codd EE, D'Andrea MR. Molecular cloning and characterization of the human voltage-gated calcium channel alpha(2)delta-4 subunit. *Mol Pharmacol.* (2002) 62: 485–96. doi: 10.1124/mol.62.3.485
39. Siddik ZH. Cisplatin: mode of cytotoxic action and molecular basis of resistance. Oncogene (2003) 22: 7265-79. doi: 10.1038/sj.onc.1206933
40. Wang D, Lippard SJ. Cellular processing of platinum anticancer drugs. *Nat Rev Drug Disc.* (2005) 4:307–20. doi: 10.1038/nrd1691
41. Johnstone TC, Suntharalingam K, Lippard SJ. The next generation of platinum drugs: targeted Pt(II) agents, nanoparticle delivery, and Pt(IV) prodrugs. *Chem Rev.* (2016) 116:3436–86. doi: 10.1021/acs.chemrev.5b00597
42. Hall MD, Okabe M, Shen DW, Liang XJ, Gottesman MM. The role of cellular accumulation in determining sensitivity to platinum-based chemotherapy. *Ann Rev Pharmacol Toxicol.* (2008) 48: 495–535. doi: 10.1146/annurev.pharmtox.48.080907.180426
43. Holohan C, Van Schaeybroeck S, Longley DB, Johnston PG. Cancer drug resistance: an evolving paradigm. *Nat Rev Cancer.* (2013) 13:714–26. doi: 10.1038/nrc3599
44. Ferreira JA, Peixoto A, Neves M, Gaiteiro C, Reis CA, Assaraf YG, et al. Mechanisms of cisplatin resistance and targeting of cancer stem cells: Adding glycosylation to the equation. *Drug Resist Updates*. (2016) 24:34–54. doi: 10.1016/j.drup.2015.11.003
45. Dolphin AC. The alpha2delta subunits of voltage-gated calcium channels. *Biochim Biophys Acta.* (2013) 1828:1541–9. doi: 10.1016/j.bbamem.2012.11.019
46. Wang X. The expanding role of mitochondria in apoptosis. *Genes Dev.* (2001) 15:2922–33.
47. Gogvadze V, Orrenius S, Zhivotovsky B. Multiple pathways of cytochrome c release from mitochondria in apoptosis. *Biochim Biophys Acta*. (2006) 1757: 639–47. doi: 10.1016/j.bbabio.2006.03.016
48. West KA, Castillo SS, Dennis PA Activation of the PI3K/Akt pathway and chemotherapeutic resistance. *Drug Resist Updates*. (2002) 5:234–48. doi: 10.1016/S1368-7646(02) 00120-6
49. Burris HA III. Overcoming acquired resistance to anticancer therapy: focus on the PI3K/AKT/mTOR pathway. *Cancer Chemother Pharmacol.* (2013) 71:829–42. doi: 10.1007/s00280-012-2043-3

Conflict of Interest Statement: The authors declare that the research was conducted in the absence of any commercial or financial relationships that could be construed as a potential conflict of interest.

frontiers in Pharmacology

ORIGINAL RESEARCH
published: 05 April 2019
doi: 10.3389/fphar.2019.00356

Copper Chaperone for Superoxide Dismutase Promotes Breast Cancer Cell Proliferation and Migration *via* ROS-Mediated MAPK/ERK Signaling

Yanping Li[1†], Ronghui Liang[1†], Xiaoya Zhang[1], Jiyan Wang[2], Changliang Shan[1,2], Shuangping Liu[3]*, Leilei Li[1]* and Shuai Zhang[4]**

[1]Biomedical Translational Research Institute, Jinan University, Guangzhou, China, [2]State Key Laboratory of Medicinal Chemical Biology, College of Pharmacy and Tianjin Key Laboratory of Molecular Drug Research, Nankai University, Tianjin, China, [3]Department of Pathology, Medical School, Dalian University, Dalian, China, [4]School of Integrative Medicine, Tianjin University of Traditional Chinese Medicine, Tianjin, China

Copper chaperone for superoxide dismutase (CCS) is a critical component of oxidation–reduction system and functions as a potential tumor promoter in several cancers. However, the function and clinical significance of CCS in breast cancer remain unclear. Here, we found CCS was highly expressed in breast cancer, where it promoted breast cancer cell proliferation and migration. Suppression of CCS expression was sufficient to attenuate the phosphorylation level of ERK1/2 and increase the accumulation of reactive oxygen species (ROS). Mechanistically, we found that knockdown of CCS decreases the activity of ERK1/2 mediated by the accumulation of ROS, which leads to the inhibition of cell proliferation and migration. In summary, these results indicated that CCS promotes the growth and migration of breast cancer cells *via* regulating the ERK1/2 activity mediated by ROS.

Keywords: breast cancer, CCS, ROS, MAPK/ERK, proliferation, migration

OPEN ACCESS

Edited by:
Jian-ye Zhang,
Guangzhou Medical University, China

Reviewed by:
Bolin Liu,
Louisiana State University, United States
Xinliang Mao,
Soochow University, China

***Correspondence:**
Changliang Shan
changliangshan@nankai.edu.cn
Shuangping Liu
liushuangping@dlu.edu.cn
Leilei Li
89509306@qq.com
Shuai Zhang
shuaizhang@tjutcm.edu.cn

†These authors have contributed equally to this work

Specialty section:
This article was submitted to Cancer Molecular Targets and Therapeutics, a section of the journal Frontiers in Pharmacology

Received: *12 January 2019*
Accepted: *21 March 2019*
Published: *05 April 2019*

Citation:
Li Y, Liang R, Zhang X, Wang J, Shan C, Liu S, Li L and Zhang S (2019) Copper Chaperone for Superoxide Dismutase Promotes Breast Cancer Cell Proliferation and Migration via ROS-Mediated MAPK/ERK Signaling. Front. Pharmacol. 10:356. doi: 10.3389/fphar.2019.00356

INTRODUCTION

Breast cancer is the leading cause of cancer-related deaths in women worldwide (Christofori, 2006; Bray et al., 2018). Breast cancer patients with metastases have an extremely poor prognosis (Gupta et al., 2005; Bacac and Stamenkovic, 2008; Thiery, 2009; Chaffer and Weinberg, 2011; Valastyan and Weinberg, 2011). Thus, exploring new targets for breast cancer treatment is important.

Copper, a redox-active transition metal essential for most living organisms, serves as a catalytic cofactor for enzymes that function in antioxidant defense, iron homeostasis, cellular respiration, and a variety of biochemical processes (Mandinov et al., 2003; Lowndes and Harris, 2005; Ashino et al., 2010; Xu et al., 2016; Sciegienka et al., 2017). The uncontrolled accumulation of copper could lead to increased oxidative stress and inappropriate binding to macromolecules. Copper chaperone for superoxide dismutase (CCS) delivers copper to specific cellular destinations and to superoxide dismutase (SOD1) (Kawamata and Manfredi, 2008; Ulloa, 2009). Mounting evidences

suggest that CCS plays a crucial role in oxidative metabolism (Kawamata and Manfredi, 2008; Leitch et al., 2009; Suzuki et al., 2013a; Wang et al., 2015). Blockade of the copper-trafficking chaperone CCS contributes to the increased cellular reactive oxygen species (ROS) level due to the overall accumulation of copper inside the cells and the decreased SOD1 activity (Ulloa, 2009). Wang et al reported that inhibiting CCS blocks lung cancer and leukemia cell growth (Wang et al., 2015). In addition, they show that blocking copper trafficking induces cellular oxidative stress and reduces cellular ATP levels. The reduced level of ATP results in activation of the AMP-activated protein kinase that leads to reduced lipogenesis. However, the mechanisms underlying the relationship between CCS and tumorigenesis are still largely unknown, although the positive correlation between CCS and redox homeostasis has been revealed (Wang et al., 2015). Therefore, this study aimed to explore the critical role and molecular mechanism of CCS in migration and proliferation of breast cancer.

In aforementioned study by Wang et al, a CCS inhibitor was developed and shown to have the same effect as knocking down CCS in cancer cells (Wang et al., 2015). However, the precise role of CCS in migration and proliferation of breast cancer cells is unknown. In the present study, we report that CCS is highly expressed in breast cancer tissues and invasive breast cancer cells and promotes cell proliferation and migration. Furthermore, we found that inhibition of CCS by shRNA or an inhibitor blocks breast cancer proliferation and migration by triggering ROS mediated ERK activity. These results suggest that metastasis-prone breast cancer cells reprogram oxidative metabolism to promote cell proliferation and migration. Targeting CCS may represent a promising approach for selectively causing cell proliferation and migration in breast cancer cells.

MATERIALS AND METHODS

Reagents and Antibodies

DC_AC50, a CCS inhibitor, was provided by the Shanghai Institute of Materia Medica of the Chinese Academy of Sciences. U0126-EtOH (catalog number: S1102) was purchased from Selleck. Antibody against phospho-p44/42 MAPK (Erk1/2) (Thr202/Tyr204) (1:1000 times dilution) (catalog number: 4370S), p44/42 MAPK (Erk1/2) (1:1000 times dilution) (catalog number: 4695S), phpspho-MEK1/2 (Ser217/221) (1:1000 times dilution) (catalog number: 9154S), MEK1/2 (1:1000 times dilution) (catalog number: 8727S), β-actin (1:1000 times dilution) (catalog number: 8457S), mouse IgG (1:3000 times dilution) (catalog number: 7076S), and rabbit IgG (1:3000 times dilution) (catalog number: 7074S) were from cell signaling technology. Anti-Superoxide Dismutase 4 (1:500 times dilution) (catalog number: ab167170) was from Abcam. Anti-Flag tag (1:1000 times dilution) (catalog number: 66008) was from proteintech. CCS shRNA was purchased from Open Biosystems, Huntsville, AL. The sequence of targeted CCS shRNA was as follows: 5′-CCGGCTGATTATTGATGAGGGAGAACTCGAGTTCTCCC TCATCAATA ATCAGTTTTTG-3′. Lipofectamine RNA iMAX was purchased from Invitrogen. The sequences of targeted CCS siRNA were as follows: sense: 5′-GUCUUGGUACACACCAC UCUA-3′; Antisense: 5′-UAGAGUGGUGUGUACCAAGAC-3′.

Abbreviations: AMP, Adenosine Monophosphate; ATP, Adenosine Triphosphate; CCS, Copper Chaperone for Superoxide Dismutase; ERK, Extracellular Regulated Protein Kinases; MAPK, Mitogen-Activated Protein Kinase; NAC, N-Acetyl-L-cysteine; ROS, Reactive Oxygen Species; PCR, Polymerase Chain Reaction; PEI, Polymine; PVDF, Polyvinylidene Fluoride; qRT-PCR, Real-time Quantitative Reverse Transcription-PCR; SDS-PAGE, Sodium Dodecyl Sulfate Polyacrylamide Gel Electropheresis; ShRNA, Short Hairpin RNA; SiRNA, Small Interfering RNA; SOD1, Superoxide Dismutase; TCGA, The Cancer Genome Atlas.

Cell Culture and Cell Lines

The human breast cancer cell lines MDA-MB-231, MCF-7, SUM159, and T47D were obtained from American Type Culture Collection (Manassas, USA). The human normal epithelial lung cell line BEAS-2B was gifted from Dr. Chenglai Xia (Guangzhou Medical University, Guangdong, China). MDA-MB-231, MCF-7, SUM159, and T47D cells were cultured in Dulbecco Modified Eagle Medium (DMEM) with 10% fetal bovine serum (FBS, ExCell Bio). BEAS-2B cells were cultured in RPMI 1640 medium with 10% FBS. For routine passages, cultures were split 1:3 when they reached 80–90% confluences. All experiments were performed on exponentially growing cells.

Plasmid Construction and Lentivirus Packaging

Exogenous human CCS CDS sequence was inserted into pLVX-3FLAG plasmid. Primer sequences were as follows: pLVX-3FLAG-CCS: 5′-CGGGATCCATGGCTTCGGATTCGG-3′ (forward) and 5′-CCCTCGAGTCAAAGGTGGGCAGG-3′ (reverse). Exogenous pCDH-HA-MEK plasmid was gifted from Dr. ShiZhi (JinanUniversity, Guangdong, China). For transient transfections, cells were grown to 80% confluency and transfected with plasmids using PEI Transfection Reagent (Invitrogen, USA) according to the manufacturer's protocol. Stable knockdown of endogenous CCS was achieved by using lentiviral vector harboring shRNA construct. 5′-CCGGCTGATTATTGATGAGG GAGAACTCGAGTTCTCCCTCATCAATAATCAGTTTTTG-3′. We generated CCS stable knockdown cell lines by infected lentiviral shRNA and selected by antibiotic puromycin. The knockdown effective was confirmed by western blot. PLKO.1 is the name of the lentiviral vector as a control.

Small Interference RNA Transfection

MDA-MB-231, MCF-7, and BEAS-2B cells (2×10^5) were seeded into 6-well plates and cultured in a humidified incubator at 37°C and 5% CO_2 for 24 h. Cells were transfected with a negative control siRNA (NC-siRNA) and siRNA targeting CCS by Lipofectamine RNA iMAX (Invitrogen corporation). Transfected cells were cultured for 48°C before being used for further experiments. The sequences of targeted CCS siRNA were 5′-GUCUUGGUACACACCACUCUA-3′. The sequences of negative control siRNA were 5′-UUCUCCGAACGUGUCACGUTT-3′(forward). All siRNA sequences were purchased from the Invitrogen Ribobio corporation of Guangzhou.

Real-Time Quantitative Reverse Transcription-PCR

Total cellular RNA was extracted using the Eastep & Super RNA Extract reagent Kit (Promega). cDNA was generated from purified RNA using PrimeSciptTM RT reagent Kit (Takara) according to the manufacturer's instructions. Gene expression levels and PCR efficiency, along with its standard error, were calculated using the Bio-Rad CFX Manager, version 3.1 (Bio-Rad), The efficiencies were nearly 100%, allowing the use of the $2^{-\triangle\triangle Ct}$ method for calculating the relative gene expression levels and reference gene normalization using β-actin. All PCR runs were performed in triplicate, and the data analyzed by CFX Manager software (Bio-Rad). Primer sequences were as following: CCS: 5′-CATCGAGG GAACTATTGACG-3′ (forward) and 5′-ATGCTCCATCAGGGT TAAAG-3′(reverse); β-actin:5′-ACGTGGACATCCGCAAAG-3′ (forward) and 5′-GACTCGTCATACTCCTGCTTG-3′ (reverse).

Cell Proliferation Assay

Cell proliferation assays were performed by seeding 5×10^4 cells in 6-well plates and culturing the cells at 37°C. Relative cell proliferation was determined by cell numbers recorded at 4 days after being seeded and normalized to that of each of the cell lines at the starting time (t = 0 h).

Western Blot Analysis

Cells were lysed with lysis buffer (1.5 M NaCl, 1 M HEPES [pH = 7.0], 1% NP40, 0.1 M $Na_4P_2O_7$, 0.1 M NaF, 0.1 M Na_3VO_4, protease inhibitor) on ice 30 min and then centrifuged at 12,000 rpm for 15 min at 4°C. Protein samples were separated by 12%.

SDS-PAGE and transferred onto PVDF membranes (Millipore). The membranes were blocked with 5% non-fat milk for 2 h and then incubated overnight at 4°C with the primary antibody and 1 h at room temperature with secondary antibody. Signals were detected using luminol substrate solution.

Transwell Migration Assay

For the Transwell (24-well insert, 8 mm pore size with polycarbonate membrane; Corning Costar, Lowell, MA, USA) migration assays, 600-mL media supplemented with 10% FBS was added to the lower chamber, and the cells resuspended in serum-free media were added to the upper insert after transfection. Transwell membranes were fixed and stained using crystal violet after specified time. The cells adhering to the lower surface of the membrane were counted under a light microscope (Olympus, Tokyo, Japan) at a magnification of 200.

Wound Healing Assay

To determine cell motility, cells were seeded into 6-well plates and grown to 90% confluence. A monolayer of the cells was then scratched with a sterile micropipette tip, followed by washing with PBS to remove cellular debris. The cell migration was observed and counted under a light microscope (Olympus, Tokyo, Japan) at a magnification of 200. The cells that migrated across the black lines were counted in three randomly chosen fields from each triplicate treatment.

Intracellular Reactive Oxygen Species (ROS) Production

The amount of intracellular ROS was measured by detecting dichlorodihydrofluorescein, which is the cleavage product of carboxy-H_2DCFDA (Invitrogen) by ROS. A total of 200,000 cells were seeded in 6-well plate. Twenty-four hours after seeding, cells were washed with PBS and loaded with 12.5 μM carboxy-H_2DCFDA for 60 min. The cells were harvested, resuspended in PBS, and analyzed using a FACS (BD Biosciences; excitation and emission at 490 and 530 nm, respectively).

Bioinformatics Analysis

The public Gene Expression Omnibus datasets (GSE9574 and GSE21422) and the TCGA (The Cancer Genome Atlas) dataset were used for bioinformatics analysis.

Statistical Analysis

The concentration of DC_AC50 required to reduce cell proliferation by 50% (IC50) was determined graphically using the Dose-response-Stimulation function in GraphPad Prism7 (San Diego, CA, United States). Statistical analyses of the significance of differences between groups were performed using Student's t-test with GraphPad Prism7. All data were obtained from three independent experiments performed in triplicate and were presented as the mean ± standard error. $p < 0.05$ was considered to indicate a statistically significant difference.

RESULTS

Higher CCS Gene Expression in Breast Cancer Patients

Bioinformatics analysis has been used to discover previously unknown function of genes associated with cancer. To determine the role of CCS in human breast cancer, we first examined the expression of CCS utilizing Gene Expression Omnibus (GEO) profiles; we found that the expression of CCS was higher in breast cancer tissue than in noncancerous tissue (**Figure 1A,** GSE9574). We also confirmed these finding using The Cancer Genome Atlas (TCGA) dataset. CCS expression was also significantly higher in breast cancer tissue than in noncancerous tissue in the Cancer Genome Atlas (TCGA) (**Figure 1B**). In addition, we also found that the expression of CCS was higher in invasive ductal carcinoma (IDC) than in ductal carcinoma (DCIS) (**Figure 1A,** GSE21422). To validate these findings, we checked CCS expression in various breast cancer cells lines. CCS was differentially expressed in several breast cancer cell lines, including MCF-7, T47D, MDA-MB-231, and SUM159. Of note, the expression of CCS was higher in T47D and MDA-MB-231 cell lines compared to MCF-7 and SUM159 cells (**Figure 1D**). All these findings indicate the potential role of CCS in tumor formation and progression.

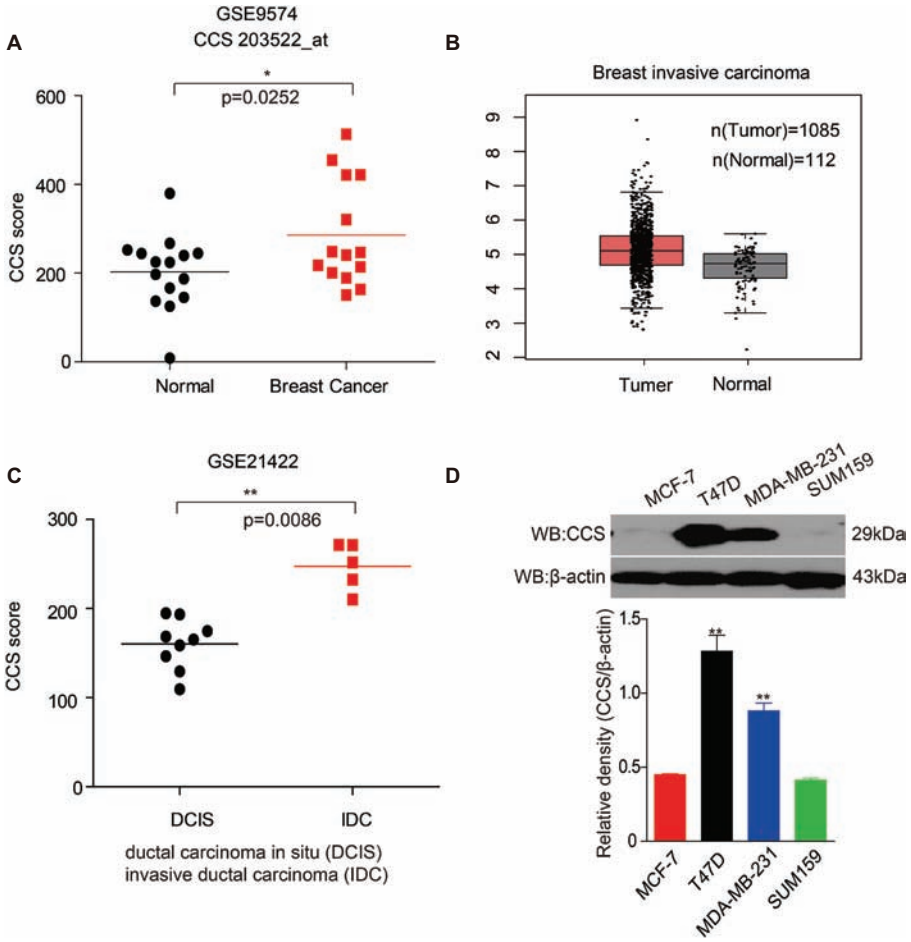

FIGURE 1 | Up-regulation of CCS is associated with cell proliferation and metastasis in human breast cancer. **(A)** CCS expression was analyzed in normal and breast cancer cells using Gene Expression Omnibus (GEO) profiles (GSE9574). **(B)** CCS expression was determined in normal and breast cancer cells in TCGA. **(C)** CCS expression was analyzed in ductal carcinoma in situ (DCIS) and invasion ductal carcinoma (IDC) using Gene Expression Omnibus (GEO) profiles (GSE21422). **(D)** CCS protein levels were analyzed in the majority of a spectrum of diverse human breast cancer cells, including MCF-7, MDA-MB-231, SUM159, and T47D by western blotting. *$p < 0.05$; **$p < 0.01$.

CCS Promotes Breast Cancer Cell Proliferation *in vitro*

We found that the expression of CCS was higher in breast cancer tissue than in noncancerous tissue, suggesting the potential role of CCS in breast cancer cell proliferation. To test our hypothesis, we generated stable cell lines in which CCS was knocked down in MDA-MB-231 cells (**Figure 2A** lower) and exogenously expressed in MCF-7 and SUM159 cells (**Figures 2B,C** lower). Cell number counting assays showed that knockdown of CCS reduced the proliferation of MDA-MB-231 cells (**Figure 2A** upper), while exogenous expression of CCS demonstrated the opposite effect (**Figures 2B,C** upper). To validate these findings, we knocked down the expression of CCS in MDA-MB-231, MCF-7, and BEAS-2B cells using siRNA. Cell number counting assays showed that knockdown of CCS significantly inhibited the proliferation of metastasis-prone breast cancer cell lines MDA-MB-231 but did not have any effect on the proliferation of breast cancer MCF-7 cells or normal BEAS-2B cells (**Figures 2D–F**). Real-time PCR was used to determine the knockdown efficiency of CCS by siRNA (**Figure 2G**). Next, we sought to explore the role DC_AC50, a potent and selective CCS inhibitor, in breast cancer. DC_AC50 has been shown to inhibit the proliferation of acute leukemia cells (Wang et al., 2015). We treated cells with DC_AC50 and found that MCF-7 cells exhibited significantly higher resistance to DC_AC50 than MDA-MB-231 cells (**Figure 2H**). Meanwhile, DC_AC50 treatment resulted in decreased cell proliferation of MDA-MB-231 cells in a time and dose-dependent manner (**Figure 2I**). These results imply that CCS plays an important role in breast cancer cell proliferation and suggests that CCS is a promising anti-cancer target.

CCS Promotes Breast Cancer Cells Migration

We found that the expression of CCS was higher in invasive ductal carcinoma than in ductal carcinoma (**Figure 1C**), suggesting the potential role of CCS in promoting breast cancer migration.

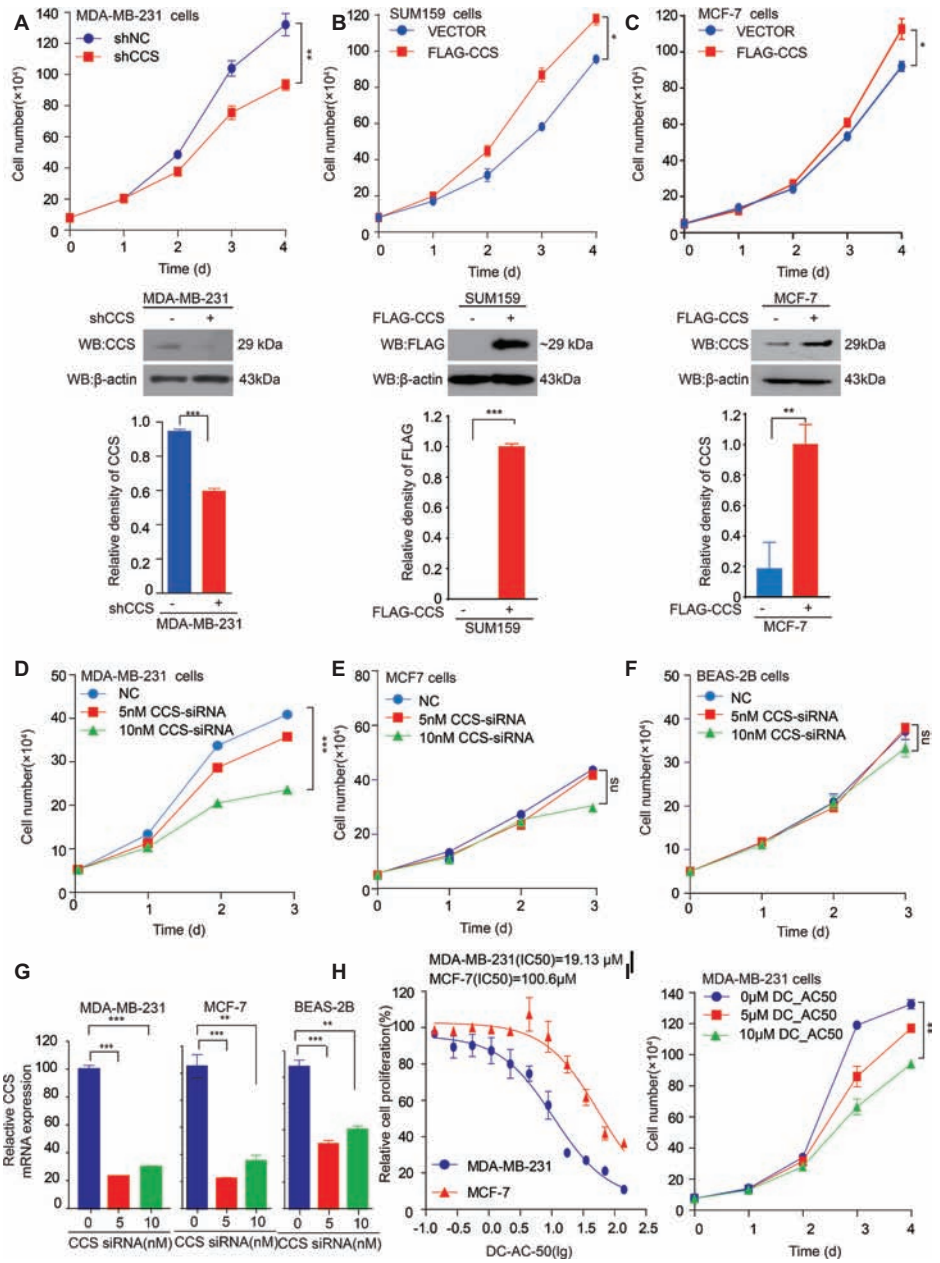

FIGURE 2 | CCS promotes breast cancer cell proliferation. **(A)** Cell proliferation was determined by cell number counting assays in CCS stable knockdown MDA-MB-231 cells, and the knockdown efficiency was determined by western blotting. **(B)** Cell proliferation was determined by cell number counting assays in CCS overexpressing SUM159 cells, and CCS expression was determined by western blotting. **(C)** Cell proliferation was determined by cell number counting assays in CCS overexpressing MCF-7 cells, and CCS expression was determined by western blotting. **(D–F)** Cell proliferation was determined by cell number counting assays in MDA-MB-231 cells **(D)**, MCF-7 cells **(E)**, and normal human BEAS-2B cells **(F)**, which were transiently transfected with increasing concentrations of CCS siRNA and control siRNA. **(G)** The relative CCS mRNA level was determined by q-PCR in MDA-MB-231, MCF-7and BEAS-2B cells, which were transiently transfected with increasing concentrations of CCS siRNA and control siRNA. **(H)** The sensitivities of MDA-MB-231 and MCF-7 cells to DC_AC50 were determined by cell number counting assays when the cells were treated with increasing concentrations of DC_AC50 for 48 h. **(I)** Cell proliferation was determined by cell count assays in MDA-MB-231 cells treated with increasing concentrations of DC_AC50. All results performed above are presented as mean ± SD from three independent experiments. *$p < 0.05$; **$p < 0.01$; ***$p < 0.001$, ns: not significant.

Next, we explore the role of CCS in the motility of the breast cancer cells. We performed a transwell migration assay that showed knockdown of CCS significantly inhibited breast cell migratory abilities in MDA-MB-231 (**Figure 3A**), while exogenous express CCS exhibited the opposite effects in MCF-7 and SUM159 cells (**Figures 3B,C**). To validate these finding, we treated MDA-MB-231 with CCS inhibitor, DC_AC50, and performed a transwell migration assay. We found that DC_AC50 blocked MDA-MB-231 cell migration in a dose-dependent manner (**Figure 3D**). In addition, we also assessed migration of MDA-MB-231 in a wound

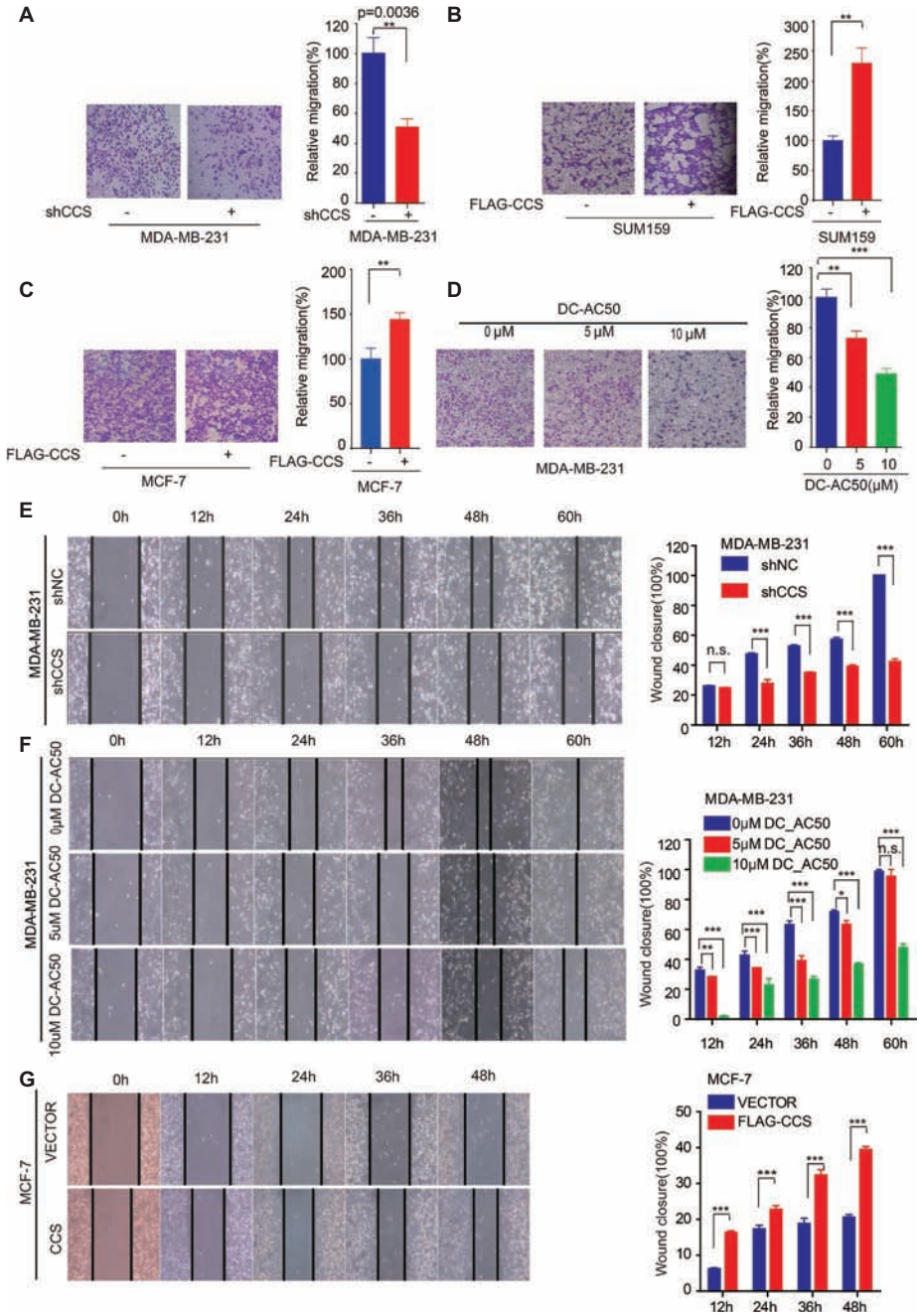

FIGURE 3 | CCS promotes breast cancer cell migration. **(A)** Cell migration in CCS knockdown and control MDA-MB-231 cells was determined by transwell migration assay (Boyden chamber assay). **(B)** Cell migration in CCS overexpressing and control SUM159 cells was determined by transwell migration assay. **(C)** Cell migration in CCS overexpressing and control MCF-7 cells was determined by transwell migration assay. **(D)** Cell migration in CCS overexpressing and control MDA-MB-231 cells with increasing concentrations of DC_AC50 was determined by transwell migration assay. **(E)** Cell migration in CCS knockdown and control MDA-MB-231 cells was also determined by wound healing assay. **(F)** Cell migration in MDA-MB-231 cells treated with increasing concentrations of DC_AC50 was determined by wound healing assay. **(G)** Cell migration in CCS overexpressing and control MCF-7 cells was determined by the wound healing assay. The modified migration assay was evaluated by calculating the ratio of the cell numbers through the chamber or wound closure after the wound healing assay. All results performed above are presented as mean ± SD from three independent experiments. $^{*}p < 0.05$; $^{**}p < 0.01$; $^{***}p < 0.001$, ns: not significant.

healing assay. We found that knockdown or inhibition of CCS dramatically suppressed MDA-MB-231 cell migratory abilities (**Figures 3E,F**). To consolidate our findings, we overexpressed FLAG tagged CCS in MCF-7 cells. As expected, overexpression of CCS accelerated breast cancer cell migration in a wound healing assay (**Figure 3G**). Taken together, our results suggest that CCS plays an important role in promoting breast cancer cells migration.

CCS Promotes Breast Cancer Migration *via* MAPK/ERK Signaling

Activation of survival signaling has been shown to play an essential role in tumor development (Baud and Karin, 2001). Several studies have demonstrated that the MAPK/ERK signaling pathway is activated in cancer cells to promote cancer cell proliferation, migration, and invasion (Rajalingam et al., 2005; El Touny et al., 2014). Therefore, we examined whether

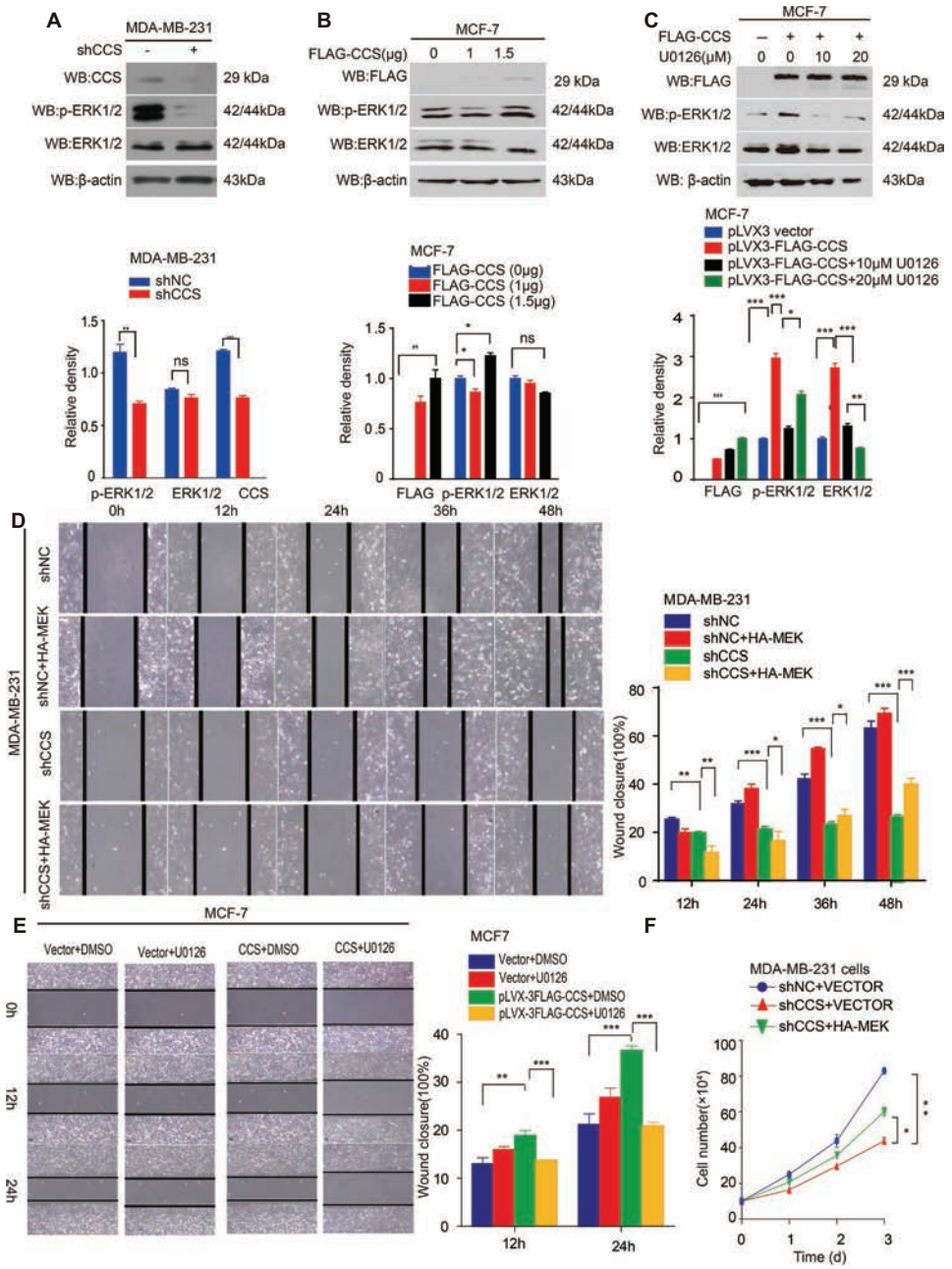

FIGURE 4 | CCS promotes breast cancer cell migration and cell proliferation *via* ERK1/2 activity. **(A)** Phosphorylated ERK1/2 and total ERK1/2 levels were determined in CCS knockdown MDA-MB-231 cells by western blotting. **(B)** Phosphorylated ERK1/2 and total ERK1/2 levels were determined in CCS overexpressing MCF-7 cells by western blotting. **(C)** Phosphorylated ERK1/2 and total ERK1/2 levels were determined in CCS overexpressing MCF-7 cells treated with increasing concentrations of U0126 for 12 h by western blotting. **(D)** Cell migration in CCS knockdown and control MDA-MB-231 cells as determined by wound healing assay when overexpressing exogenous HA-tagged MEK. **(E)** Cell migration in CCS overexpressing and control MCF-7 cells treated with U0126 was determined by wound healing assay. The modified migration assay was evaluated by calculating the ratio of the cell numbers through the chamber or wound closure after the wound healing assay. **(F)** Cell proliferation was determined by cell number counting assays in CCS stable knockdown MDA-MB-231 cells with overexpression of exogenous HA-tagged MEK. All results performed above are presented as mean ± SD from three independent experiments. $^{*}p < 0.05$; $^{**}p < 0.01$; $^{***}p < 0.001$, ns not significant.

MAPK/ERK signaling is involved in CCS mediated cell proliferation and migration. To test this hypothesis, we examined the ERK1/2 and MEK1/2 activity in CCS knockdown MDA-MB-231 cells. Western blotting shows that the activity of ERK1/2 was drastically decreased in CCS knockdown MDA-MB-231 cells (**Figure 4A**). Additionally, overexpression of FLAG tagged CCS increased the activity of ERK1/2 in MCF-7 cells (**Figure 4B**), but the increased activity of ERK1/2 was blocked in MCF-7 with ERK inhibitor U0126 (**Figure 4C**). To validate the role of MAPK signaling in the process of CCS-induced migration and proliferation in breast cancer cells, we first reactivated ERK by transfecting exogenous HA tagged MEK into MDA-MB-CCS-KD cells. As expect, the replenishment of MEK in MDA-MB-231-CCS-KD cells could partially rescue the capability of migration in MDA-MB-231-CCS-KD cells due to the reactivation of ERK1/2 (**Figure 4D**). Secondly, we demonstrated that inhibition of MEK with U0126 treatment inhibited CCS-induced cell migration (**Figure 4E**). Thirdly, overexpression of MEK in MDA-MB-231-CCS-KD cells partially rescues the decreased cell proliferation in CCS knockdown MDA-MB-231 cells (**Figure 4F**). These results suggest that activation of the MAPK/ERK pathway is essential for the CCS-promoted migration abilities and cell proliferation of breast cancer cells.

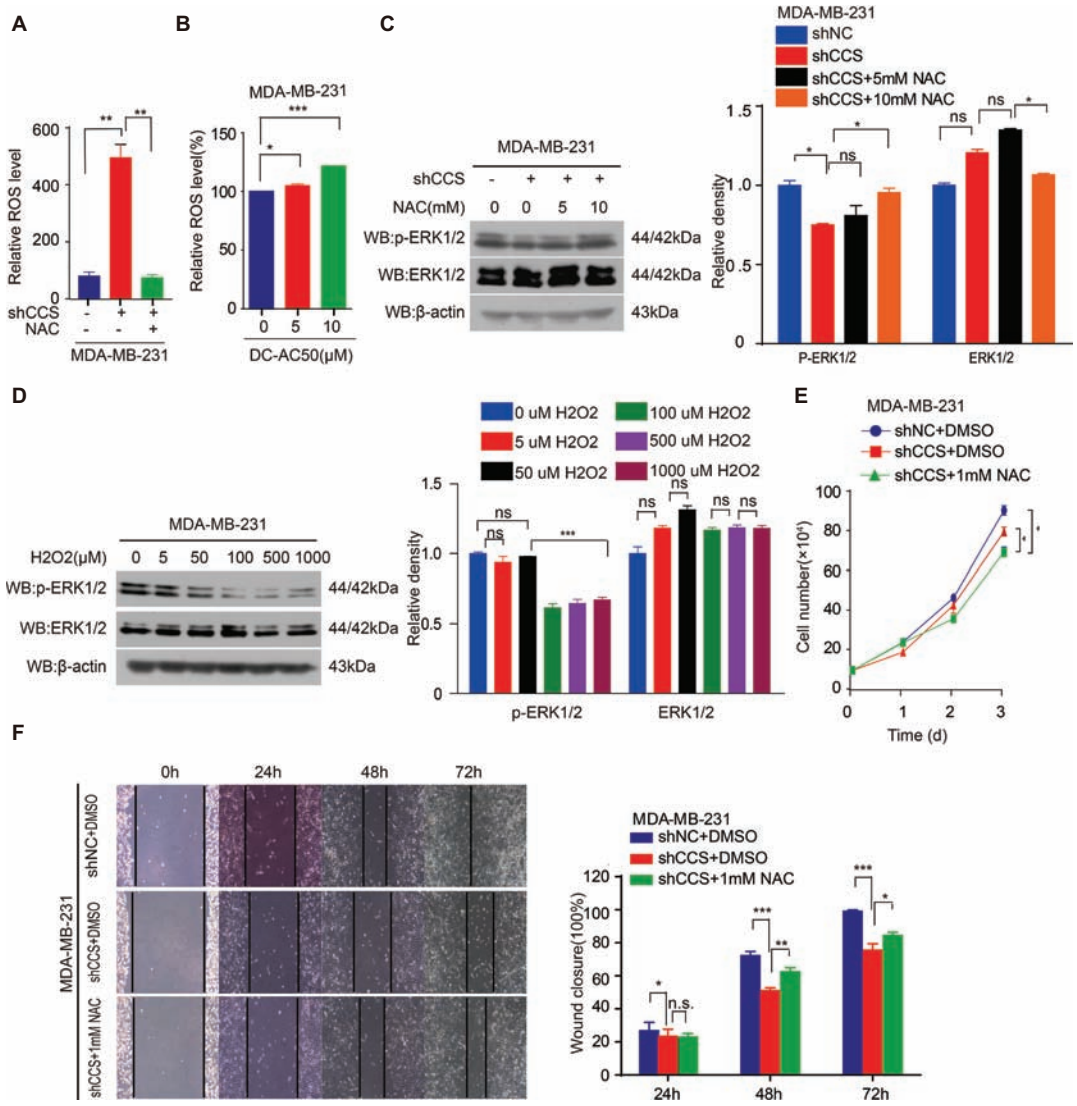

FIGURE 5 | CCS promotes breast cancer cell migration and cell proliferation via ERK1/2 activity mediated by ROS. **(A)** Knockdown of CCS increased ROS level in MDA-MB-231 cells, which was rescued by treatment with 1 mM NAC. **(B)** Treatment with DC_AC50 (5, 10 μM) induced ROS elevation in MDA-MB-231 cells. **(C)** Western blot analysis of total and phosphorylated ERK1/2 levels. β-actin was used as a loading control. Reduced ERK1/2 activity by CCS knockdown was rescued by treatment with NAC (5, 10 mM) for 12 h. **(D)** H_2O_2 significantly abolished ERK1/2 activity in MDA-MB-231cells after 12 h. **(E)** Cell proliferation assays showed that NAC (1 mM) treatment partially rescued the decreased cell proliferation in CCS knockdown MDA-MB-231 cells. **(F)** Wound healing assays showed that NAC (1 mM) treatment partially rescued the decreased cell migration in CCS knockdown MDA-MB-231 cells. All results performed above are presented as mean ± SD from three independent experiments. $^{*}p < 0.05$; $^{**}p < 0.01$; $^{***}p < 0.001$, ns: not significant.

CCS Activates MAPK/ERK Signaling *via* ROS

The inhibition of CCS leads to increased ROS levels. Thus, we hypothesized that CCS regulates the activity of ERK1/2 through ROS. To test this hypothesis, we examined ROS levels in MDA-MB-231 cells treated with CCS shRNA or DC_AC50. Indeed, we found that knockdown or inhibition of CCS significantly increases the cellular ROS levels (**Figures 5A,B**), while the increased ROS was blocked by treating cells with antioxidant N-Acetyl-L-cysteine (NAC; **Figure 5A**). In addition, we also observed that NAC abrogates the decreased activity of ERK1/2 in CCS knockdown MDA-MB-231 cells (**Figure 5C**). Consistently, we also found that H_2O_2 impaired phosphorylation of ERK1/2 in a dose-dependent manner but did not affect the total expression level of ERK1/2 (**Figure 5D**). Finally, we found that NAC could rescue the decreased cell proliferation and migration of MDA-MB-231 CCS knockdown cells (**Figures 5E,F**). These results further support the idea that inhibition of CCS induces a ROS overload, which impairs MAPK/ERK signaling to attenuate cancer cell proliferation. The combined results presented here also establish CCS as a viable anticancer target and copper trafficking as a new pathway for future therapeutic development.

DISCUSSION

Rapid cellular growth and migratory abilities play a crucial role in tumorigenesis and metastasis, which have been recognized to be associated with ROS levels (Aykin-Burns et al., 2009; Doskey et al., 2016). Those cells that survive oxidative stress stand a good chance to have acquired adaptive mechanisms to counteract the potential toxic effects of elevated ROS and to promote cell-survival pathways (Irmak et al., 2003). CCS, a co-enzyme of SOD1, is a critical component of the oxidation–reduction system in cancer, and its differential expression in different types of breast cancer suggests a relationship between CCS and cancer cell growth and migration (**Figure 6**). However, the link between CCS-activated ROS and the occurrence and development of tumors is still in its infancy.

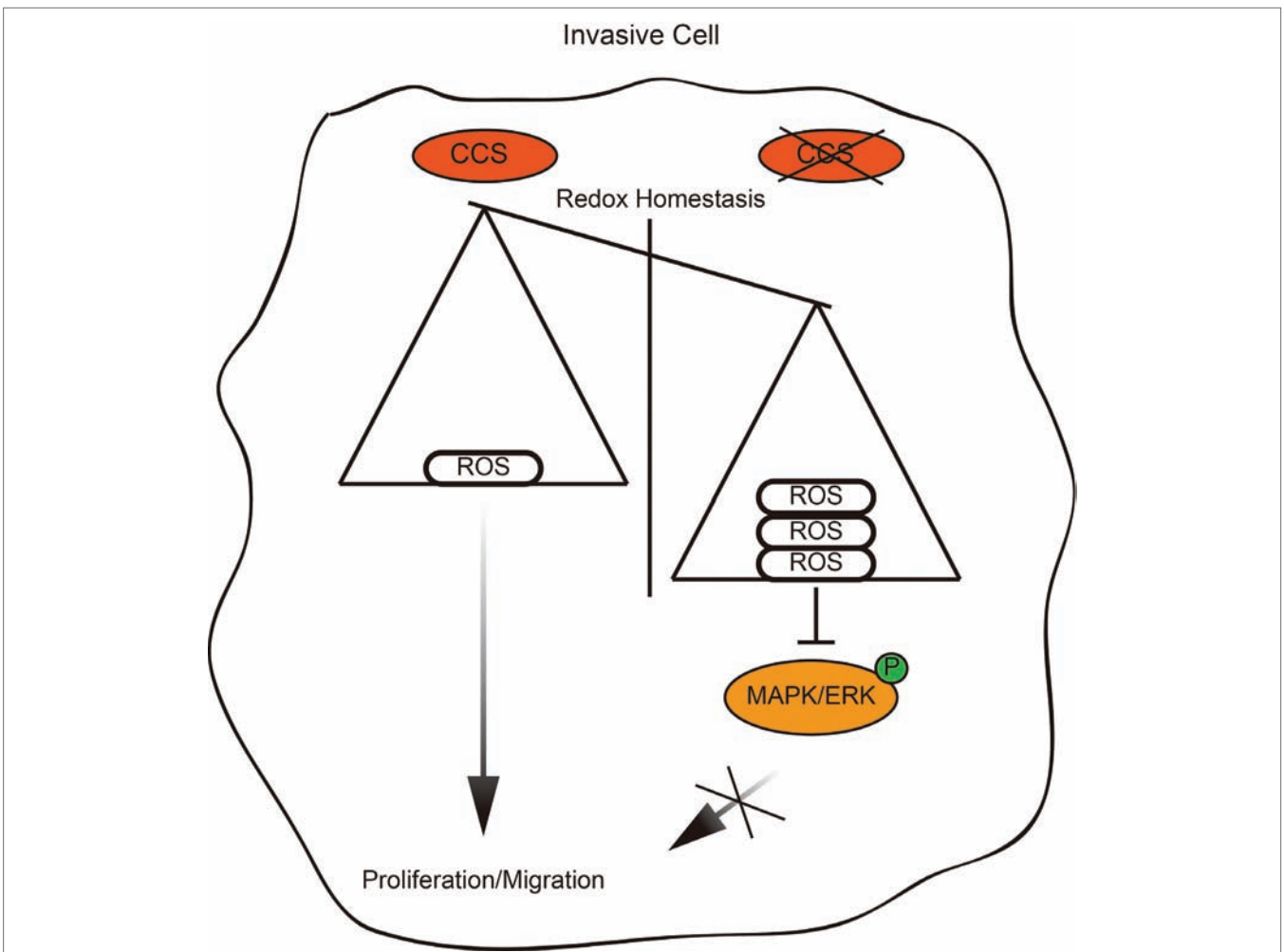

FIGURE 6 | Proposed working model. Schematic model shows that the role and mechanism of CCS in promoting breast cancer cell proliferation and migration.

In this study, we utilized MDA-MB-231 cells (triple-negative breast cancer) and MCF-7 cells (estrogen receptor positive breast cancer) as human cell line models and identified a novel function and mechanism of CCS in facilitating breast cancer cell proliferation and migration. This novel mechanism provides a link between oxidative metabolism and survival signaling. Wang et al. reported that inhibition of CCS leads to a selective suppression of cancer cell proliferation (Wang et al., 2015). Consistent with this, we found that knockdown of CCS significantly reduced cell proliferation in MDA-MB-231 cells but not MCF-7. Interestingly, we revealed a novel function of CCS in regulating migration of breast cancer cells by transwell and wound healing assays. In all, we show that CCS not only plays a vital role in cell proliferation, but it also drives breast cancer migration.

Previous evidence has shown that CCS serves as a co-enzyme of SOD1 to activate its catalytic activity, which is a critical component of oxidation–reduction system (Suzuki et al., 2013b). Since ROS associated oxidative stress has been proven to play important roles in several cancer types and served as promising target for therapy (Perše, 2013; Sosa et al., 2013), we hypothesized that dysregulated ROS levels provide a second signal for CCS-induced proliferation and migration in breast cancer cells. In our study, we showed that knockdown or inhibition of CCS led to increased total ROS levels in MDA-MB-231. ROS overload blocks the activation of the MAPK/ERK pathway, which plays a critical role in tumor formation and progression (Berger et al., 2017; Mayo et al., 2017). By mimicking oxidative stress with H_2O_2 treatment, we were able to suppress the phosphorylation level of ERK1/2, which could be reversed upon treatment with antioxidant NAC. Furthermore, we found that the activation of MAPK/ERK pathways was essential for CCS-induced cell proliferation and migration. Treatment of MCF-7 with U0126-EtOH, a highly selective ERK kinase inhibitor, diminished CCS-induced migration. Conversely, overexpression of MEK enhanced the phosphorylation level of ERK1/2 and partially rescued migration in CCS knockdown MDA-MB-231 cells.

In summary, CCS-mediated ROS decreases the activation of ERK1/2, resulting in attenuation of cell proliferation and migration. Thus, CCS may be a therapeutic strategy to suppress tumor growth and metastasis.

AUTHOR CONTRIBUTIONS

RL and YL performed and analyze all the experiments. XZ and JW drafted the work an provided intellectual content. LL and CS edited the language and figures. CS, SL and SZ designed the study and wrote the manuscript.

FUNDING

This work was supported by the Science and Technology Program of Guangzhou (Grant 201807010003), the Program from the Science and Technology Department of Guangdong Province of China (Grant 2017A030313890), and the National Nature Science Foundation of China (31560312, 81672781 and 81702746). This work was also supported by the China Postdoctoral Science Foundation (2017M612839), the Fundamental Research Funds for the Central Universities (21616323, 21617433), and the Program of Introducing Talents of Discipline to Universities (111 Project, No. B16021).

ACKNOWLEDGMENTS

We thank Dr. Shannon Elf (The University of Chicago) for critical review and edit of the manuscript.

REFERENCES

Ashino, T., Sudhahar, V., Urao, N., Oshikawa, J., Chen, G. F., Wang, H., et al. (2010). Unexpected role of the copper transporter ATP7A in PDGF-induced vascular smooth muscle cell migration. *Circ. Res.* 107, 787–799. doi: 10.1161/CIRCRESAHA.110.225334

Aykin-Burns, N., Ahmad, I. M., Zhu, Y., Oberley, L. W., and Spitz, D. R. (2009). Increased levels of superoxide and H_2O_2 mediate the differential susceptibility of cancer cells versus normal cells to glucose deprivation. *Biochem. J.* 418, 29–37. doi: 10.1042/BJ20081258

Bacac, M., and Stamenkovic, I. (2008). Metastatic cancer cell. *Annu. Rev. pathmechdis. Mech. Dis.* 3, 221–247. doi: 10.1146/annurev.pathmechdis.3.121806.151523

Baud, V., and Karin, M. (2001). Signal transduction by tumor necrosis factor and its relatives. *Trends Cell Biol.* 11, 372–377. doi: 10.1016/S0962-8924(01)02064-5

Berger, M. D., Stintzing, S., Heinemann, V., Yang, D., Cao, S., Sunakawa, Y., et al. (2017). Impact of genetic variations in the MAPK signaling pathway on outcome in metastatic colorectal cancer patients treated with first-line FOLFIRI and bevacizumab: data from FIRE-3 and TRIBE trials. *Ann. Oncol.* 28, 2780–2785. doi: 10.1093/annonc/mdx412

Bray, F., Ferlay, J., Soerjomataram, I., Siegel, R. L., Torre, L. A., and Jemal, A. (2018). Global cancer statistics 2018: GLOBOCAN estimates of incidence and mortality worldwide for 36 cancers in 185 countries. *CA Cancer J. Clin.* 68, 394–424. doi: 10.3322/caac.21492

Chaffer, C. L., and Weinberg, R. A. (2011). A perspective on cancer cell metastasis. *Science* 331, 1559–1564. doi: 10.1126/science.1203543

Christofori, G. (2006). New signals from the invasive front. *Nature* 441:444. doi: 10.1038/nature04872

Doskey, C. M., Buranasudja, V., Wagner, B. A., Wilkes, J. G., Du, J., Cullen, J. J., et al. (2016). Tumor cells have decreased ability to metabolize H_2O_2: implications for pharmacological ascorbate in cancer therapy. *Redox Biol.* 10, 274–284. doi: 10.1016/j.redox.2016.10.010

El Touny, L. H., Vieira, A., Mendoza, A., Khanna, C., Hoenerhoff, M. J., and Green, J. E. (2014). Combined SFK/MEK inhibition prevents metastatic outgrowth of dormant tumor cells. *J. Clin. Invest.* 124, 156–168. doi: 10.1172/JCI70259

Gupta, P. B., Mani, S., Yang, J., Hartwell, K., and Weinberg, R. A. (2005). The evolving portrait of cancer metastasis. *Cold Spring Harbor Symposia on Quantitative Biology* 70, 291–297. doi: 10.1101/sqb.2005.70.033

Irmak, M. B., Ince, G., Ozturk, M., and Cetin-Atalay, R. (2003). Acquired tolerance of hepatocellular carcinoma cells to selenium deficiency: a selective survival mechanism? *Cancer Res.* 63, 6707–6715. doi: 10.1016/S0165-4608(02)00795-1

Kawamata, H., and Manfredi, G. (2008). Different regulation of wild-type and mutant Cu, Zn superoxide dismutase localization in mammalian mitochondria. *Hum. Mol. Genet.* 17, 3303–3317. doi: 10.1093/hmg/ddn226

Leitch, J. M., Jensen, L. T., Bouldin, S. D., Outten, C. E., Hart, P. J., and Culotta, V. C. (2009). Activation of Cu, Zn-superoxide dismutase in the absence of oxygen and the copper chaperone CCS. *J. Biol. Chem.* 284, 21863–21871. doi: 10.1074/jbc.M109.000489

Lowndes, S. A., and Harris, A. L. (2005). The role of copper in tumour angiogenesis. *J. Mammary Gland Biol. Neoplasia* 10, 299–310. doi: 10.1007/s10911-006-9003-7

Mandinov, L., Mandinova, A., Kyurkchiev, S., Kyurkchiev, D., Kehayov, I., Kolev, V., et al. (2003). Copper chelation represses the vascular response to injury. *Proc. Natl. Acad. Sci.* 100, 6700–6705. doi: 10.1073/pnas.1231994100

Mayo, J. C., Hevia, D., Quiros-Gonzalez, I., Rodriguez-Garcia, A., Gonzalez-Menendez, P., Cepas, V., et al. (2017). IGFBP 3 and MAPK/ERK signaling mediates melatonin-induced antitumor activity in prostate cancer. *J. Pineal Res.* 62:e12373. doi: 10.1111/jpi.12373

Perše, M. (2013). Oxidative stress in the pathogenesis of colorectal cancer: cause or consequence? *Biomed. Res. Int.* 2013. doi: 10.1155/2013/725710

Rajalingam, K., Wunder, C., Brinkmann, V., Churin, Y., Hekman, M., Sievers, C., et al. (2005). Prohibitin is required for Ras-induced Raf–MEK–ERK activation and epithelial cell migration. *Nat. Cell Biol.* 7:837. doi: 10.1038/ncb1283

Sciegienka, S. J., Solst, S. R., Falls, K. C., Schoenfeld, J. D., Klinger, A. R., Ross, N. L., et al. (2017). D-penicillamine combined with inhibitors of hydroperoxide metabolism enhances lung and breast cancer cell responses to radiation and carboplatin via H_2O_2-mediated oxidative stress. *Free Radic. Biol. Med.* 108, 354–361. doi: 10.1016/j.freeradbiomed.2017.04.001

Sosa, V., Moliné, T., Somoza, R., Paciucci, R., Kondoh, H., and LLeonart, M. E. (2013). Oxidative stress and cancer: an overview. *Ageing Res. Rev.* 12, 376–390. doi: 10.1016/j.arr.2012.10.004

Suzuki, Y., Ali, M., Fischer, M., and Riemer, J. (2013a). Human copper chaperone for superoxide dismutase 1 mediates its own oxidation-dependent import into mitochondria. *Nat. Commun.* 4, 1–9. doi: 10.1038/ncomms3430

Suzuki, Y., Ali, M., Fischer, M., and Riemer, J. (2013b). Human copper chaperone for superoxide dismutase 1 mediates its own oxidation-dependent import into mitochondria. *Nat. Commun.* 4:2430. doi: 10.1038/ncomms3430

Thiery, J. P. (2009). Metastasis: alone or together? *Curr. Biol.* 19, R1121–R1123. doi: 10.1016/j.cub.2009.11.001

Ulloa, J. L. (2009). *The copper chaperone as a dual regulator of effects related to oxidative stress and chromatin remodeling*. (ProQuest Dissertations Publishing: The Johns Hopkins University), 3339899.

Valastyan, S., and Weinberg, R. A. (2011). Tumor metastasis: molecular insights and evolving paradigms. *Cell* 147, 275–292. doi: 10.1016/j.cell.2011.09.024

Wang, J., Luo, C., Shan, C., You, Q., Lu, J., Elf, S., et al. (2015). Inhibition of human copper trafficking by a small molecule significantly attenuates cancer cell proliferation. *Nat. Chem.* 7, 968–979. doi: 10.1038/nchem.2381

Xu, S., Hoshan, L., and Chen, H. (2016). Improving lactate metabolism in an intensified CHO culture process: productivity and product quality considerations. *Bioprocess Biosyst. Eng.* 39, 1689–1702. doi: 10.1007/s00449-016-1644-3

Conflict of Interest Statement: The authors declare that the research was conducted in the absence of any commercial or financial relationships that could be construed as a potential conflict of interest.

frontiers in Oncology

ORIGINAL RESEARCH
published: 10 April 2019
doi: 10.3389/fonc.2019.00258

A Novel Antibody-Toxin Conjugate to Treat Mantle Cell Lymphoma

*Gulam M. Rather[1], Siang-Yo Lin[1], Hongxia Lin[1], Zoltan Szekely[2] and Joseph R. Bertino[1]**

[1] Departments of Pharmacology and Medicine, Rutgers Cancer Institute of New Jersey, Rutgers, The State University of New Jersey, New Brunswick, NJ, United States, [2] Department of Pharmaceutics, Ernest Mario School of Pharmacy, Rutgers, The State University of New Jersey, Piscataway, NJ, United States

Matriptase is a transmembrane serine protease, synthesized as an inactive single-chain zymogen on the endoplasmic reticulum and transported to the plasma membrane. Matriptase is activated in different epithelial and some B-cell malignancies and changes its conformation and activity is inhibited mainly by its endogenous inhibitor HAI-1. Activated matriptase plays a key role in tumor initiation as well as tumor progression, including invasiveness, and metastasis. To target the anti-mitotic toxin (monomethyl auristatin-E) to activated matriptase, a novel antibody to activated matriptase was conjugated with this toxin via a valine-citrulline-PABA linker. In a previous study, this antibody-toxin conjugate was found to be effective against triple negative breast cancer cell lines and xenografts, alone, or in combination with cisplatin (1). In this study, we examined the anti-tumor effect of the antibody toxin conjugate (ADC) against activated matriptase positive mantle cell lymphoma cell lines (JeKo-1, Maver, Mino, and Z138). This ADC was cytotoxic to these cell lines with IC_{50}s between 5 and 14 μg/mL. The ADC also showed a dose dependent anti-tumor effect on the JeKo-1 xenograft in mice without toxicity.

Keywords: activated matriptase, antibody drug conjugate, monomethyl auristatin-E, mantle cell lymphoma, xenograft

OPEN ACCESS

Edited by:
Zhe-Sheng Chen,
St. John's University, United States

Reviewed by:
Lokesh Jain,
Merck, United States
Jianhua Yang,
Baylor College of Medicine, United States

***Correspondence:**
Joseph R. Bertino
bertinoj@cinj.rutgers.edu

Specialty section:
This article was submitted to Cancer Molecular Targets and Therapeutics, a section of the journal Frontiers in Oncology

Received: *15 August 2018*
Accepted: *21 March 2019*
Published: *10 April 2019*

Citation:
Rather GM, Lin S-Y, Lin H, Szekely Z and Bertino JR (2019) A Novel Antibody-Toxin Conjugate to Treat Mantle Cell Lymphoma. Front. Oncol. 9:258. doi: 10.3389/fonc.2019.00258

INTRODUCTION

Mantle Cell Lymphoma (MCL), represents 6- percent of all lymphoma cases, and currently the survival time is 4–5 years, shorter compared to other hematologic malignancies (2–4). MCL cells express CD20, aberrant expression of CD5, and due to a translocation t(11;14)(q13;q32), overexpression of cyclin-D1, encoded by the CCND1 gene located on chromosome 11, which mediates cell cycle progression through the G1 phase (5, 6). The currently used drugs to treat MCL patients include bortezomib, ibrutinib, rituximab, bendamustine, and combinations of these drugs.

Matriptase, a glycoprotein (80–90 kDa), is a member of type II transmembrane serine proteases. It is synthesized as a latent single-chain structure and with many regulatory mechanisms and functions (7, 8), and is activated through an auto-activation step resulting in a disulfide-linked-two-chain structure. Following activation, matriptase is rapidly inactivated by its endogenous inhibitor HAI-1. This activated matriptase-HAI-1 complex remains present in most epithelial carcinomas and some B-cell malignancies (9–11). Importantly, while matriptase is present in a latent form on epithelial cells and B-cells, activated matriptase expression is mainly restricted to the membranes of epithelial tumors, and some B-cell malignancies, in particular MCL (10–12).

Of importance, given the increase in reactive oxygen species (ROS) and the acidic environment of solid tumors (ROS), these environments activate the matriptase zymogen (13–21).

In this study we show that a novel anti-matriptase antibody toxin (Monomethyl auristatin-E, MMAE) conjugate potently inhibited growth of mantle cell lymphoma cell lines (JeKo-1, Maver, Mino and Z138) and caused significant growth inhibition of the JeKo-1 xenograft *in vivo*.

MATERIALS AND METHODS

Animals

NOD/SCID/IL2 receptor gamma chain null (NOD/SCID/IL2rg^{null}, NSG) mice were obtained from the Jackson Laboratory (Bar Harbor, ME).

Materials

For cell culture, RPMI 1640, and fetal bovine serum were from Invitrogen (Fisher Scientific).

Cell Culture

The MCL cells (JeKo-1, Mino, Maver, and Z138) were cultured in 1X RPMI Media 1,640 (Life Technologies) containing 10% fetal bovine serum (FBS) at 37°C and 5% carbon dioxide. All the cell lines were obtained from American Type Culture Collection (ATCC) and were checked for mycoplasma by MycoAlert™ mycoplasma detection kit (Lonza USA).

Western Blotting

The MCL cells were scraped into a micro centrifuge tube from petri-dishes after 75% confluency. After centrifugation, cell pellets were lysed in lysis buffer (20 mM Tris, pH 7.4) containing 1% triton-X100, a commercial protease inhibitor cocktail (Roche) and 1 mM 5,5′-dithio-bis(2-nitrobenzoic acid) (DTNB). Since, DTNB interferes with the Bradford reagent (Bio-Rad Laboratories), equal volume of protein samples was resolved by 10% SDS-PAGE, without any boiling and under non-reducing sample buffer conditions and transferred onto a nitrocellulose membrane (Bio-Rad Laboratories). After blocking the membrane with 5% non-fat dry milk prepared in Tris buffered saline with 0.1% Tween-20 (TBST), the membrane was incubated with the desired primary antibody M69 at 4°C overnight. The membrane was washed thrice in TBST and then incubated for 2 h at room temperature with the appropriate peroxidase-conjugated secondary antibody. Bands were visualized using an enhanced chemiluminescence kit (Pierce). Anti-glyceraldehyde 3-phosphate dehydrogenase (GAPDH) (from Millipore) and was used as a control. Anti-HAI-1, anti-Vinculin and anti-mouse secondary antibody were from Santa Cruz Biotechnologies. Anti-mouse secondary antibody was used to probe the ADC (mouse antibody recognizing human activated matriptase) and also to probe GAPDH, HAI-1, and Vinculin which are mouse generated.

Cytotoxicity Assay

Five thousand cells per well were plated in RPMI 1,640 media supplemented with 10% FBS. After overnight culture, media was removed and fresh media containing the ADC was added and incubated for different time periods. To assess cell viability, the MCL cell lines with or without drug treatment were collected and cell viability was determined using the Vi-CELL™ Series Cell Viability Analyzer (Beckman Coulter, Carlsbad, CA). The 50% inhibitory concentration (IC_{50}; the drug concentration required to obtain 50% cell kill compared to control) was determined using the non-linear regression curve fit of the graphs drawn by GraphPad Prism 4 software (GraphPad Software Inc., CA). All experiments were performed in triplicate, and all experiments were repeated at least three times.

Migration Assay

MCL (suspension cells) cells were treated with ADC (IC_{50}) for 48 h and washed twice with IX PBS. The cells were then serum starved for 1.5 h in FBS-free RPMI at 37°C and 5% carbon dioxide in presence of ADC. Three hundred microliters of FBS-free RPMI (8×10^5 cells) were added to the top chamber of a cell culture insert (24-well format) of eight-micron pore size (Corning). Cells were treated with ADC (IC_{50}) throughout the experiment (means ADC is present in FBS-free media in inserts as well as in the lower well of that insert). Inserts had been previously transferred to wells containing 700 mL of RPMI (containing 10% FBS) with or without ADC. After 24 h of incubation at 37°C and 5% carbon dioxide, cells were collected from both insert chamber and lower well (of 24-well plate) and checked for viability using the Vi-CELL™ Series Cell Viability Analyzer (Beckman Coulter, Carlsbad, CA). The percent viable cells migrated toward FBS (in lower well) of total viable cells added in insert, were plotted against ADC treatment. Each experiment was done at-least three times and in four replicates.

Animal Studies

The JeKo-1 cell line was used for anti-tumor studies. Cells ($10 \times 10^{6)}$ in 100 μL of PBS were injected subcutaneously into the right flank of 6-week-old NSG female mice. Once tumors were palpable, the mice were randomized to different groups. Mice were treated i.p. with the ADC, and treatment periods were indicated by arrows. Saline was used as a control treatment. Tumor size and body weights were measured twice a week and the tumor volume was calculated using the formula width^2 × (length/2). Results are presented as mean ± SEM.

Histologic Preparation and Immunohistochemistry Staining

Samples were fixed in 4% formalin and paraffin-embedded. Immunohistochemistry was performed on 4 μm sections with antibodies to Ki67 (Santa Cruz Biotechnologies, USA) and Cleaved caspase-3 (Cell Signaling Technology USA #9661). Sections were developed and stained with hematoxylin and eosin using standard methods. All histological preparations and immunostaining were conducted by the Rutgers Cancer Institute of New Jersey Biospecimen Repository and Histopathology Core.

Statistical Analysis

Statistical analysis was performed using Prism software (GraphPad). In all cases, ANOVA followed by two-tailed,

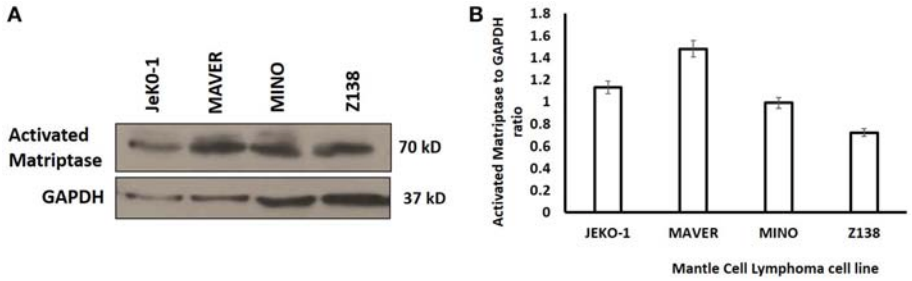

FIGURE 1 | (A) Western Blot analysis of activated matriptase expression in Mantle Cell Lymphoma cells (JeKo-1, MAVER, MINO, and ZI38). Equal volume of lysate was loaded in 10% SDS-PAGE (see methods). **(B)** Activated matriptase to GAPDH ratio for all the four mantle cell lymphoma cell lines.

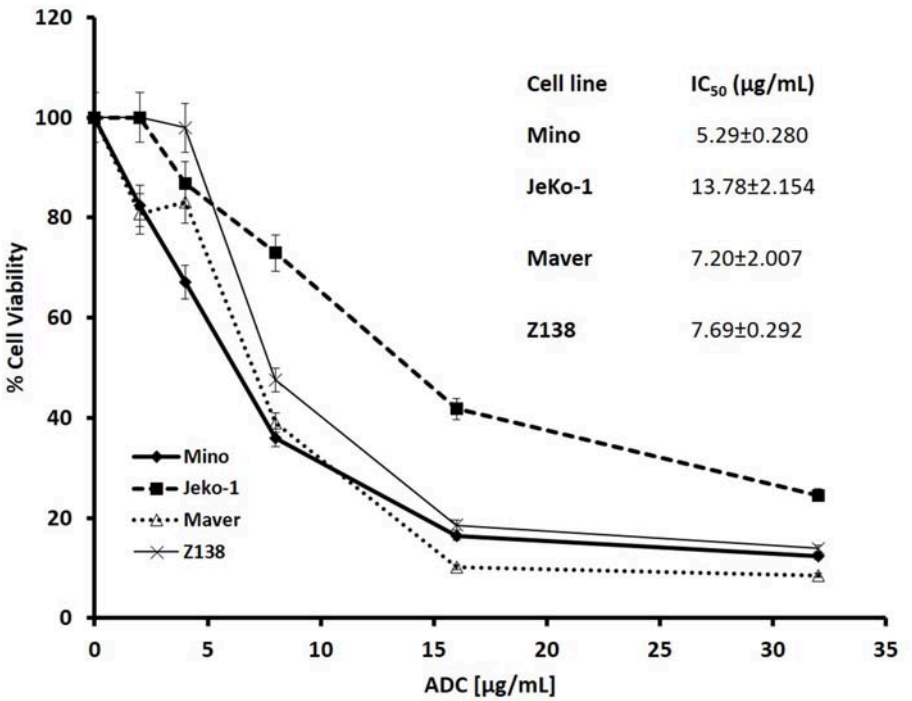

FIGURE 2 | Cytotoxicity of M69-MMAE conjugate (ADC) against different MCL cell lines. Five thousand cells/well were plated in a 96-well plate and the cells were treated the next day with the ADC for 72 h. Cytotoxicity of the ADC was measured by trypan blue dye exclusion method using a Vi-Cell XR© cell viability analyzer (Beckman Coulter). All the reading points were carried out in triplicates. The IC_{50} values (insert) are calculated using GraphPad Prism 4 software. Results are presented as mean ± SEM.

unpaired Student *t*-tests was performed to analyze statistical differences between groups. *P*-values of <0.05 were considered statistically significant.

Antibody-Toxin Conjugate Preparation and Characterization

The anti-matriptase antibody (M69) was generated against purified activated matriptase-HAI complex from human milk as described by Lin et al. (22). Seattle Genetics' valine-citrulline-PABA linker technology was used for conjugation of a potent tubulin-inhibitor, monomethyl auristatin-E (MMAE) to the M69 antibody. The valine-citrulline dipeptide based linker has been shown to be stable in circulation but cleavable by cathepsin B in the lysosome to generate free drug (23). Copper free click chemistry is used to load the toxin in a stoichiometrically controlled manner to M69 antibody under very mild conditions. The technology involves conjugating the linker-toxin with the lysine side chains on the antibody surface. The conjugation procedure does not affect the disulfide bridges between cysteines of the antibody, thus maintaining the structure of the antibody without any loss of antibody activity by misfolding or dissociation of antibody chains. Analysis by mass spectrometry (HR-MALDI-TOF) showed an increase of 7,000 Da average M.W. corresponding to an average of 3.5 toxin (MMAE) molecules linked to each mAb molecule (1).

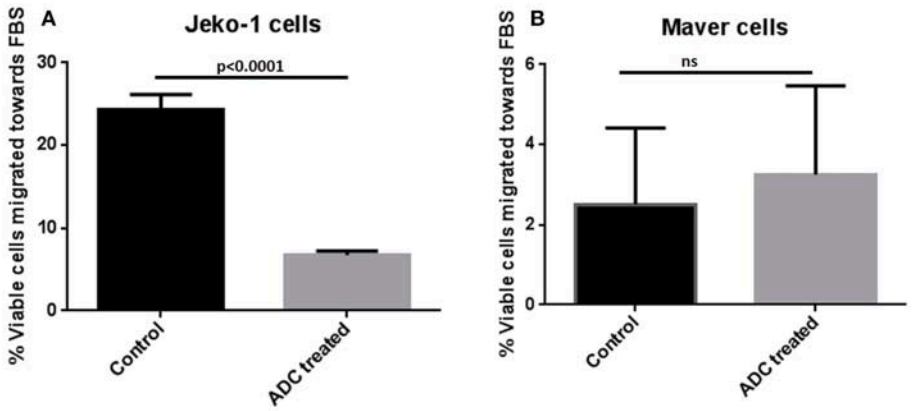

FIGURE 3 | Effect of ADC on migration of MCL cell lines *in vitro*. **(A)** JeKo-1 **(B)** Maver cells. Cells were treated with ADC for 48 h and washed twice with 1X PBS and starved for 1.5 h in FBS-free RPMI and then added in a cell culture insert having 8-micron pore size in 300 μl of FBS-free RPMI (with and without ADC). The insert was transferred to a well containing 700 μl of FBS-containing RPMI (with and without ADC) for 24 h at 37°C and 5% carbon dioxide. Cells were checked for viability from both insert and lower well using the Vi-CELL^{TM} Series Cell Viability Analyzer (Beckman Coulter, Carlsbad, CA). The percent viable cells migrated toward the lower well (having FBS-RPMI) of total viable cells added in insert were plotted against ADC treatment. Each experiment was done at-least three times and in four replicates. Results are presented as mean ± SEM.

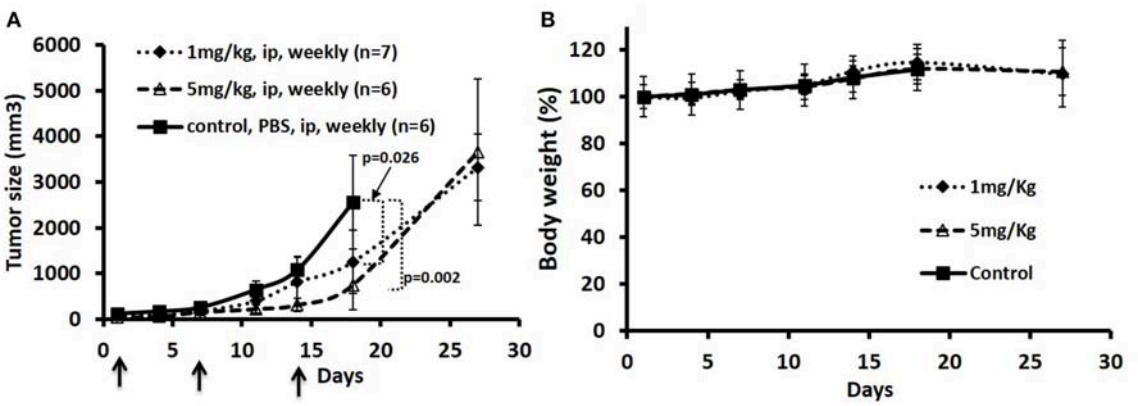

FIGURE 4 | Treatment of JeKo-1 xenografts in mice using different doses of matriptase-MMAE conjugate (ADC). **(A)** Xenograft studies with M69-MMAE. NOD/SCID mice were inoculated with 10 × 10^6 JeKo-1 cells in PBS in the right flanks. When the tumor was palpable (100–200 mm^3), mice ($n = 19$) were randomized into: control (antibody alone), 1 and 5 mg/kg M69-MMAE treatment groups. M69-MMAE was administrated by i.p. weekly x 2. Tumor volume was measured twice a week. Tumor volumes were calculated using the formula $width^2$ x (length/2). Results are presented as mean ± SEM **(B)** Mice body weight change in the control and treatment groups. Treatments are shown by arrows.

RESULTS

In vitro Cytotoxicity of M69-MMAE (ADC) Against Mantle Cell Lymphoma (MCL) Cell Lines

Activated matriptase expression was evaluated in different MCL cell lines (JeKo-1, Mino, Maver, and Z138) by Western blotting using the M-69 antibody that recognizes activated matriptase alone or in complex with HAI-1. The four cell lines showed increased levels of activated matriptase, although the level of expression varied (**Figure 1**). The expression level of hepatocyte growth factor activator inhibitor (HAI)-1 protein in mantle cells is shown in **Figure S1**.

Cytotoxicity studies showed that the ADC decreased the viability of all the cell lines (**Figure 2**) with IC_{50}s at single digit μg/ml of the conjugate. As 3.5 molecules of toxin are bound on the average to each antibody molecule, the IC_{50} values for the toxin ranged from 125 to 611 pM. Based on the IC_{50} values, Mino, Maver and Z138 cells were 1.8–2.6-fold more sensitive to ADC compared to JeKo-1. In order to check whether the ADC is stable in media, the ADC was incubated (37°C and 5% carbon dioxide) in complete media (RPMI with 10% FBS) for 48 h before used for cytotoxicity test and it was found that 48 h incubated ADC and fresh ADC are equally effective against Maver cell line as shown in **Figure S2**. In order to study the role of matriptase in metastasis and invasiveness, the ADC was found to inhibit the migration of JeKo-1 cells *in vitro*. Of interest, only a small percent of cell from the Maver cell line migrated as compared to the JeKo-1 cell line, and the ADC did not enhance migration (**Figure 3**).

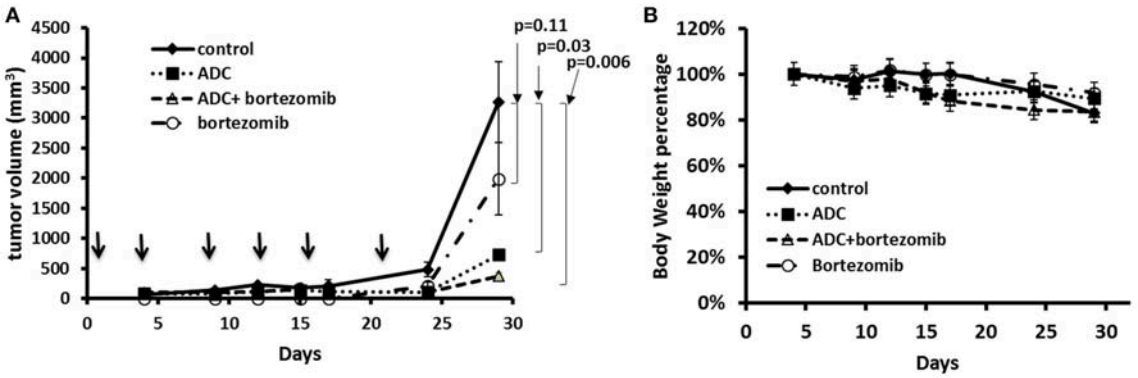

FIGURE 5 | Treatment of JeKo-1 xenografts in mice using the matriptase-MMAE conjugate (ADC) and bortezomib. **(A)** Xenograft studies with M69-MMAE and bortezomib. NOD/SCID mice were inoculated with 10 × 106 JeKo-1 cells in PBS in the right flank. When tumors were palpable, mice were randomized into control, bortezomib, M69-MMAE, and bortezomib plus M69-MMAE treatment groups. M69-MMAE (5 mg/kg) was administrated by i.p. twice weekly for 3 weeks. Bortezomib (0.75 mg/kg) was given i.p. weekly. Bortezomib and M69-MMAE were given together with the same dose schedule. Tumor volume was measured twice a week, and the tumor volume calculated using the formula width^2 x (length/2). Results are presented as mean ± SEM. **(B)** Mice body weight percentage during the treatment. Treatments are shown by arrows.

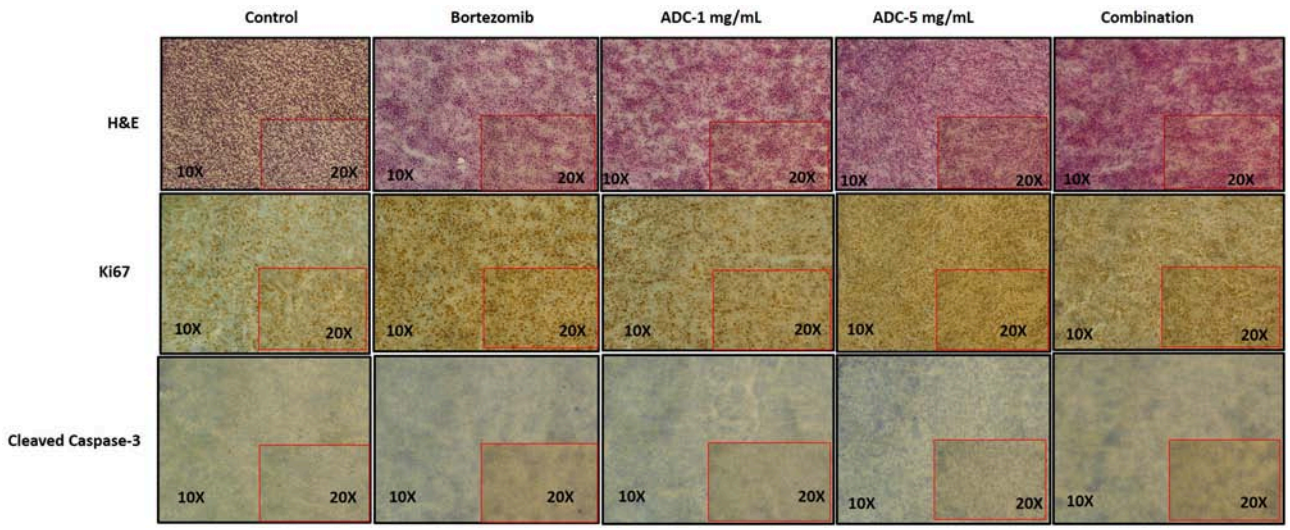

FIGURE 6 | Immunohistochemistry staining of JeKo-1 tumors extracted from mice in **Figures 4**, **5** against various biomarkers. The tumors were harvested from control, 1 and 5 mg/kg (i.p. weekly) M69-MMAE treatment groups from experiment four and Bortezomib and M69-MMAE combination (Bortezomib (0.75 mg/kg, i.p. weekly and M69-MMAE, 5mg/kg i.p. twice weekly) from experiment five. Ki67 staining showing proliferation of JeKo-1; and Cleaved caspase-3 showing the apoptotic cell death. The tonsil tissue was used as a positive control for various IHC staining.

JeKo-1 Xenograft Studies

To test the anti-tumor effects of the ADC in one of the MCL tumors in a mouse model, we elected to test the JeKo-1 cell line. We tested two dose schedules of the ADC: 1 vs. 5 mg/Kg administered i.p. weekly. The 5 mg/Kg weekly dose was more effective than the 1 mg/Kg dose. Even at the higher dose, there were no signs of toxicity as measured by observation and weight loss (**Figure 4**). Previous studies with the naked antibody showed that it had no anti-tumor activity *per se* (1).

As bortezomib is used to treat MCL, alone and in combination, we also tested the ADC in combination with bortezomib in a JeKo-1 xenograft study. Using a similar inoculum, this tumor grows rapidly in NOD-SCID-gamma mice, and the biweekly 5 mg/kg dose schedule, both bortezomib and the ADC caused marked tumor growth inhibition ($p = 0.006$). The combination of bortezomib and the ADC was more effective than either drug alone (**Figure 5**).

We harvested the tumors at the end of the experiment and then used immunohistochemistry to test for various biomarkers. **Figure 6** showed that there was no significant change in Ki-67 staining; however, cleaved caspase-3 staining (apoptosis) showed a significant increase in the combination group (ADC with bortezomib) compared to either drug alone.

DISCUSSION

Brentuximab vedotin (Adcetris), consisting of an antibody that targets CD30, conjugated with MMAE is approved for the treatment of Hodgkin disease, as well anaplastic large cell lymphoma (ALCL) (24). CAT-3888 (BL22), another immunotoxin, which targets the CD22 antigen on certain lymphoma cells, attached to a bacterial Pseudomonas exotoxin, PE38, has shown activity against hairy cell leukemia (HCL) in early clinical trials (25). CAT-8015 (moxetumomab pasudotox), an updated version of this drug, is now being studied for use against lymphomas (26).

Our novel antibody against activated matriptase, overexpressed in B-cell lymphoma and epithelial tumors and involved in tumorogenesis, invasiveness and metastasis (27–29), conjugated with the tubulin binding, mitotic inhibitor toxin, monomethyl auristatin E (MMAE), demonstrates that activated matriptase is a bonafide target for use with antibodies that recognize activated matriptase, armed with a toxin. The pre-incubated ADC was as potent as the non-incubated fresh ADC, indicating that the ADC was stable in FBS and media. The *in vitro* experiments also confirmed that this ADC showed significant inhibition of migration of JeKo-1 cells. No observable toxicity was found with this ADC, however, as this is a mouse antibody that recognizes human, but not mouse matriptase, other toxic effects of the ADC would not be noted. We currently have constructed a chimeric matriptase antibody, suitable for toxicity studies in a primate model and for Phase I trials in humans.

Future plans are to use this ADC alone and in combination with other chemotherapeutic drugs (bortezomib and ibrutinib) in primary MCL xenografts with the goal of generating additional sufficient preclinical data to allow for future clinical development.

ETHICS STATEMENT

All the cell line studies were performed through Rutgers Cancer Institute of New Jersey using protocols approved by the Rutgers Environmental Health and Safety (REHS). Animal experiments were conducted in accordance with Rutgers Cancer Institute of New Jersey Animal Care and Use Committee guidelines using an approved protocol number 15-040.

AUTHOR CONTRIBUTIONS

GR, S-YL, HL, ZS, and JRB conception and design, development of methodology, analysis and interpretation of data (e.g., statistical analysis, biostatistics, computational analysis), writing, review, and/or revision of the manuscript, and administrative, technical, or material support (i.e., reporting or organizing data, constructing databases). GR, S-YL, and HL acquisition of data (provided animals, acquired and managed patients, provided facilities, etc.). S-YL, ZS (for ADC conjugation study), and JRB (overall) study supervision.

ACKNOWLEDGMENTS

This work was supported in part by a Breast Cancer Research Foundation grant to JRB. The author acknowledges Dr. Lin CY and Dr. Johnson M (Georgetown Medical School, USA) for their generous M69-antibody gift. An abstract of this work was published [The American Society of Hematology annual meeting 2017 (Blood 2017 130:5159)].

SUPPLEMENTARY MATERIAL

The Supplementary Material for this article can be found online at: https://www.frontiersin.org/articles/10.3389/fonc.2019.00258/full#supplementary-material

Figure S1 | Western Blot analysis showing the hepatocyte growth factor activator inhibitor (HAI)-1 expression in Mantle Cell Lymphoma cells (Lane1: JEKO-1, Lane 2: MAVER). 10% SDS-PAGE was used.

Figure S2 | Cytotoxicity of M69-MMAE conjugate (ADC) after 48 h incubation in complete media against Maver cell line. Five thousand cells/well were plated in a 96-well plate and the cells were treated the next day with the ADC (fresh and 48 h incubated one) for 72 h. Cytotoxicity was measured using an MTS assay. All the reading points were carried out in triplicates. Results are presented as mean ± SEM.

REFERENCES

1. Rather GM, Lin SY, Lin H, Banach-Petrosky W, Hirshfield KM, Lin CY, et al. Activated matriptase as a target to treat breast cancer with a drug conjugate. *Oncotarget.* (2018) 9:25983–92. doi: 10.18632/oncotarget.25414
2. Shah BD, Martin P, Sotomayor EM. Mantle cell lymphoma: a clinically heterogeneous disease in need of tailored approaches. *Cancer Control.* (2012) 19:227–35. doi: 10.1177/107327481201900307
3. Vose JM. Mantle cell lymphoma: 2012 update on diagnosis, risk-stratification, and clinical management. *Am J Hematol.* (2012) 87:604–9. doi: 10.1002/ajh.23176
4. Dreyling M, Geisler C, Hermine O, Kluin-Nelemans HC, Le Gouill S, Rule S, et al. Newly diagnosed and relapsed mantle cell lymphoma: ESMO clinical practice guidelines for diagnosis, treatment and follow-up. *Ann Oncol.* (2014) 25 (Suppl. 3):iii83–92. doi: 10.1093/annonc/mdu264
5. Williams ME, Swerdlow SH. Cyclin D1 overexpression in non-Hodgkin's lymphoma with chromosome 11 bcl-1 rearrangement. *Ann Oncol.* (1994) 5 (Suppl. 1):71–3. doi: 10.1093/annonc/5.suppl_1.S71
6. Yin CC, Luthra R. Molecular detection of t(11;14)(q13;q32) in mantle cell lymphoma. *Methods Mol Biol.* (2013) 999:211–6. doi: 10.1007/978-1-62703-357-2_14
7. Uhland K. Matriptase and its putative role in cancer. *Cell Mol Life Sci.* (2006) 63:2968–78. doi: 10.1007/s00018-006-6298-x
8. List K, Bugge TH, Szabo R. Matriptase: potent proteolysis on the cell surface. *Mol Med.* (2006) 12:1–7. doi: 10.2119/2006-00022.List
9. Murai N, Miyake Y, Tsuzuki S, Inouye K, Fushiki T. Involvement of the cytoplasmic juxtamembrane region of matriptase in its exclusive localization to the basolateral membrane domain of Madin-Darby canine kidney epithelial cells. *Cytotechnology.* (2009) 59:169–76. doi: 10.1007/s10616-009-9205-0
10. Oberst M, Anders J, Xie B, Singh B, Ossandon M, Johnson M, et al. Matriptase and HAI-1 are expressed by normal and malignant epithelial cells *in vitro* and *in vivo*. *Am J Pathol.* (2001) 15:1301–11. doi: 10.1016/S0002-9440(10)64081-3
11. Benaud CM, Oberst M, Dickson RB, Lin C-Y. Deregulated activation of matriptase in breast cancer cells. *Clin Exp Metastasis.* (2002) 19:639–49. doi: 10.1023/A:1020985632550

12. Chou FP, Chen YW, Zhao XF, Xu-Monette ZY, Young KH, Gartenhaus RB, et al. Imbalanced matriptase pericellular proteolysis contributes to the pathogenesis of malignant B-Cell lymphomas. *Am J Pathol.* (2013) 183:1306–17. doi: 10.1016/j.ajpath.2013.06.024
13. Chen CJ, Wu BY, Tsao PI, Chen CY, Wu MH, Chan YLE, et al. Increased matriptase zymogen activation in inflammatory skin disorders. *Am J Physiol Cell Physiol.* (2011) 300:C406–15. doi: 10.1152/ajpcell.00403.2010
14. Tseng IC, Xu H, Chou FP, Li G, Vazzano AP, Kao JPY, et al. Matriptase activation, an early cellular response to acidosis. *J Biol Chem.* (2010) 285:3261–70. doi: 10.1074/jbc.M109.055640
15. Kato Y, Ozawa S, Miyamoto C, Maehata Y, Suzuki A, Maeda T, et al. Acidic extracellular microenvironment and cancer. *Cancer Cell Int.* (2013) 13:89. doi: 10.1186/1475-2867-13-89
16. Gupta SC, Singh R, Pochampally R, Watabe K, Mo Y-Y. Acidosis promotes invasiveness of breast cancer cells through ROS-AKT-NF-κB pathway. *Oncotarget.* (2014) 5:12070–82. doi: 10.18632/oncotarget.2514
17. Gatenby RA, Gillies RJ. Why do cancers have high aerobic glycolysis? *Nat Rev Cancer.* (2004) 4:891–9. doi: 10.1038/nrc1478
18. Bailey KM, Wojtkowiak JW, Hashim AI, Gillies RJ. Targeting the metabolic microenvironment of tumors. *Adv Pharmacol.* (2012) 65:63–107. doi: 10.1016/B978-0-12-397927-8.00004-X
19. Choi SYC, Collins CC, Gout PW, Wang Y. Cancer-generated lactic acid: a regulatory, immunosuppressive metabolite. *J Pathol.* (2013) 203:350–5. doi: 10.1002/path.4218
20. Gillies RJ, Verduzco D, Gatenby RA. Evolutionary dynamics of carcinogenesis and why targeted therapy does not work. *Nat Rev Cancer.* (2012) 12:487–93. doi: 10.1038/nrc3298
21. Wojtkowiak JW, Verduzco D, Schramm KJ, Gillies RJ. Drug resistance and cellular adaptation to tumor acidic pH microenvironment. *Mol Pharm.* (2011) 8:2032–8. doi: 10.1021/mp200292c
22. Lin CY, Anders J, Johnson M, Dickson RB. Purification and characterization of a complex containing matriptase and a Kunitz-type serine protease inhibitor from human milk. *J Biol Chem.* (1999) 274:18237–42. doi: 10.1074/jbc.274.26.18237
23. Sanderson RJ, Hering MA, James SF, Sun MM, Doronina SO, Siadak AW, et al. *In vivo* drug-linker stability of an anti-CD30 dipeptide-linked auristatin immunoconjugate. *Clin Cancer Res.* (2005) 11:843–52. Available online at: http://clincancerres.aacrjournals.org/content/11/2/843
24. Zhao B, Chen R, O'Connor OA, Gopal AK, Ramchandren R, Goy A, et al. Brentuximab vedotin, an antibody–drug conjugate, in patients with CD30-positive haematologic malignancies and hepatic or renal impairment. *Br J Clin Pharmacol.* (2016) 82:696–705. doi: 10.1111/bcp.12988
25. Kreitman RJ, Wilson WH, Stetler-Stevenson M, Noel P, FitzGerald DJ, Pastan I. Long term results of BL22 (CAT-3888) in multiply relapsed hairy cell leukemia. *Blood.* (2009) 114:3442. Available online at: http://www.bloodjournal.org/content/114/22/3442
26. Alderson RF, Kreitman RJ, Chen T, Yeung P, Herbst R, Fox JA, et al. CAT-8015: a second-generation pseudomonas exotoxin A-based immunotherapy targeting CD22 -expressing hematological malignancies. *Clin Cancer Res.* (2009) 15:832–9. doi: 10.1158/1078-0432.CCR-08-1456
27. Ko CJ, Huang CC, Lin HY, Juan CP, Lan SW, Shyu HY, et al. Androgen-induced TMPRSS2 activates matriptase and promotes extracellular matrix degradation, prostate cancer cell invasion, tumor growth, and metastasis. *Cancer Res.* (2015) 75:2949–60. doi: 10.1158/0008-5472.CAN-14-3297
28. Mukai S, Yorita K, Kawagoe Y, Katayama Y, Nakahara K, Kamibeppu T, et al. Matriptase and MET are prominently expressed at the site of bone metastasis in renal cell carcinoma: immunohistochemical analysis. *Hum Cell.* (2015) 28:44–50. doi: 10.1007/s13577-014-0101-3
29. Tsai CH, Teng CH, Tu YT, Cheng TS, Wu SR, Ko CJ, et al. HAI-2 suppresses the invasive growth and metastasis of prostate cancer through regulation of matriptase. *Oncogene.* (2014) 33:4643–52. doi: 10.1038/onc.2013.41

Conflict of Interest Statement: S-YL and JRB are founders of Xiconic, LLC. ZS is an officer of Xiconic, LLC.

The remaining authors declare that the research was conducted in the absence of any commercial or financial relationships that could be construed as a potential conflict of interest.

frontiers in Oncology

ORIGINAL RESEARCH
published: 10 April 2019
doi: 10.3389/fonc.2019.00250

Nanocarriers of Fe_3O_4 as a Novel Method for Delivery of the Antineoplastic Agent Doxorubicin Into HeLa Cells *in vitro*

Kun-kun Xia[1,2†], Yong Lyu[2†], Wei-tang Yuan[2], Gui-xian Wang[2], Harrison Stratton[3], Shui-jun Zhang[1] and Jie Wu[1,3]*

[1] Department of Hepatobiliary and Pancreatic Surgery, First Affiliated Hospital of Zhengzhou University, Zhengzhou, China, [2] Department of Colon and Rectal Surgery, First Affiliated Hospital of Zhengzhou University, Zhengzhou, China, [3] Department of Neurobiology, Barrow Neurological Institute, St. Joseph's Hospital and Medical Center, Phoenix, AZ, United States

OPEN ACCESS

Edited by:
Yan-yan Yan,
Shanxi Datong University, China

Reviewed by:
Cheng Xiao,
Xuzhou Medical University, China
Yixian Wang,
California State University,
Los Angeles, United States

***Correspondence:**
Jie Wu
jie.wu@dignityhealth.org;
jiewubni@gmail.com

[†]These authors have contributed equally to this work

Specialty section:
This article was submitted to Cancer Molecular Targets and Therapeutics, a section of the journal Frontiers in Oncology

Received: 28 December 2018
Accepted: 19 March 2019
Published: 10 April 2019

Citation:
Xia K, Lyu Y, Yuan W, Wang G, Stratton H, Zhang S and Wu J (2019) Nanocarriers of Fe_3O_4 as a Novel Method for Delivery of the Antineoplastic Agent Doxorubicin Into HeLa Cells in vitro. Front. Oncol. 9:250. doi: 10.3389/fonc.2019.00250

Here we report the synthesis and *in vitro* characterization of a redox-sensitive, magnetically inducible nanoparticle carrier system based on the doxorubicin (DOX) drug delivery model. Each quantal nanocarrier unit consists of a magnetite Fe_3O_4 nanoparticle core that is further encapsulated in self-assembled micelles of the redox-responsive polyethylene glycol derivative, DSPE-SS-mPEG. The nanocarrier system was prepared using a combination of ultrasonication and dialysis to produce the microenvironment sensitive delivery system. The final synthesized and DOX-loaded magnetic nanocarriers had an average size of ∼150 nm when assembled with a 6.9% DOX payload. The release rate of DOX from these redox-responsive magnetic nanocarriers was shown to be accelerated *in vitro* when in the presence of glutathione (GSH). Furthermore, we demonstrated that more redox-responsive magnetic nanocarriers could be taken up by HeLa cells when a local magnetic field was applied. Once internalized within a cell, the micelles of the outer nanocarrier complex were broken down in the presence of higher concentrations of GSH, which accelerated the release of DOX. This produces a particle with dual operating characteristics that can be controlled via a specific cellular environment coupled with an exogenously applied signal in the form of a magnetic field triggering release.

Keywords: redox-responsive, Fe_3O_4, nanocarriers, drug delivery, HeLa cells

INTRODUCTION

Chemotherapy is the most commonly used approach to treating cancer. Traditionally, the chemotherapeutic agents (doxorubicin, paclitaxel, etc.) are systemically delivered through intravenous injection. While this is often an effective approach and can successfully eliminate malignant cell populations, treatment-associated morbidity is often significant (1). Quite frequently this is a result of unintended action of the therapeutic agent at non-specific cellular targets causing injury to healthy somatic cells in addition to the desired effect on malignant cells (2–6). Despite this large unintended effect on healthy cells of the patient, chemotherapy remains a pillar of cancer treatment due to its efficacy, particularly when used as part of a multimodal treatment plan. At the intersection of the potency of chemotherapy as a curative agent and the extensive side effect

profile causing wide-ranging cytotoxicity lays a rationale that suggests transport of the chemotherapeutic agent directly to the tumor site, which avoids systematic exposure, may alleviate unintentional cytotoxic effects on healthy tissue. This concept has existed in the medical literature for quite some time, but only recently has progress in functionalization of mesoscopic carrier particles led to significant progress in realizing this goal. There are now several readily available preparations for a medical oncology approach to cancer treatment that utilizes nanotechnology, in the form of nanoparticle assemblies, to facilitate the transport of highly potent cytotoxic compounds more selectively into tumor sites with restricted systemic circulating concentrations (7–9). These nanoparticles can be constructed such that they resist degradation or internalization except at the target tissue of interest where they are then able to deposit and release their payload at the site of the malignancy and not in healthy tissue (10–12). These particles can also be used to focus energy from external radiative sources into tumor masses acting to physically damage the cancerous cells in addition to the chemical damage affected by the pharmacological agent (13). This is an elegant solution to the problem of how to transport chemotherapeutic drugs to the tumor site without leakage and subsequently release a drug into the tumor-specific microenvironment is an important issue that needs to be solved in the treatment of cancer. The rise of nanotechnology has provided a new set of tools for use in solving this problem of targeted drug delivery (14–17).

The use of nanoparticles as a carrier vehicle for the targeted delivery of chemotherapeutic drugs has the potential to greatly reduce collateral damage to non-cancerous human tissues and organs (18, 19). For example, by modifying the surface of a nanoparticle with intelligent molecules, the nano drug carriers can stimulate drug release in response to the particular micro-environment of pathological tissues to reduce the incidence of healthy cell damage and selectively kill cancer cells (20–22). The study of nano drug carriers provides a new direction for the delivery of care in addition to the traditional cancer treatment approaches already in use and possesses significant potential for future clinical applications (20, 23, 24). In this study, we constructed spherical nanoparticle carriers containing doxorubicin (an antineoplastic drug) with a diameter of about 150 nm. We provide functional data to demonstrate that the entry of the drug carriers into HeLa cells can be enhanced in a magnetic field and the release of the drug can be facilitated by elevating the concentration of glutathione (GSH), resulting in the demise of HeLa cells. As several cancer cells have high intracellular GSH concentrations, using the constructed nanoparticle carriers may achieve satisfying efficacy in killing cancer cells, while causing only minor damage in normal tissue (25–27).

MATERIALS AND METHODS

Materials

The Fe_3O_4 nanoparticles were prepared using a thermal decomposition method described previously (28). DSPE-SS-mPEG 2000 was purchased from Xi'an Ruixi Biotechnology Co. (Xi'an, China), Doxorubicin hydrochloride (DOX·HCl) and GSH were purchased from Sigma-Aldrich (St. Louis, MO, USA), dimethyl sulfoxide (DMSO) and triethylamine (TEA) were obtained from Shanghai Chemical Co. (Shanghai, China) (29).

Human cervical adenocarcinoma (HeLa) cells were purchased from the China Center for Type Culture Collection (Wuhan University) and cultured in Dulbecco's modified Eagle's medium (DMEM, Gibco Life, Grand Island, NY, USA) supplemented with 10% fetal bovine serum (FBS, HyClone, Logan, UT), 2×10^{-3} M L-glutamine and 1% antibiotics mixture (10,000 U of penicillin and 10 mg of streptomycin) (Gibco). The cells were incubated in a humidified atmosphere containing 5% CO_2 at 37°C.

Preparation of Nanocarriers

DOX-loaded redox-responsive magnetic nanocarriers were prepared using an ultrasonication-dialysis method. Briefly, DOX·HCl (10 mg) was stirred in DMSO (5 mL) with twice the number of mole of TEA for 2 h to obtain the DOX base. 80 mg of DSPE-SS-mPEG was added to the solution, which was stirred at room temperature for another 2 h. Meanwhile, the Fe_3O_4 nanoparticles (20 mg) were dissolved in 10 mL of (tetrahydrofuran) THF. The above two solutions were mixed and added to ultrapure water (25 mL) with ultrasonication. The mixed solution was then transferred into a dialysis tube and dialyzed against ultrapure water for 48 h at room temperature. Similarly, DOX-free nanocarriers were prepared using the above mentioned protocol without the addition of DOX.

Characterization of Nanocarriers

The size of the nanocarriers in aqueous solution was measured using a Zetasizer analyzer (Malvern Zetasizer Nano, Zen 3690+MPT2, Malvern, UK). Ultrastructural features and surface geometry of the synthesized nanocarriers was observed by transmission electron microscopy (TEM) (Tecnai G2 F20 S-TWIN electron microscope, FEI company. the USA) at an accelerating voltage of 200 kV.

DOX-loaded nanocarriers were dissolved in DMSO to determine the total content of loaded drug. The DOX content in DMSO was determined by high-performance liquid chromatography (HPLC, Agilent) using a calibration curve obtained from DOX/DMSO solutions containing a known concentration of DOX.

For Fe_3O_4 content measurement, the weighed, freeze-dried nanocarriers were digested in a 1 M HCl solution. The resulting digestion product was then analyzed for atomic species using inductively coupled plasma-atomic emission spectroscopy (TCP-AES, Thermo Electron, USA).

Redox-Triggered Disassembly of Nanocarriers

The change in the size of redox-responsive magnetic nanocarriers in response to 20 mM GSH in PBS (0.01 M, pH 7.4) was measured using dynamic light scattering (DLS). Briefly, 20 mM GSH was added to 1.5 mL of PBS containing nanocarriers within a glass cell. The solution was then placed in a shaking water bath at 37°C, oscillating at 150 rpm. At varying intervals following agitation, the size of nanocarrier particles contained in solution was assessed using DLS.

In vitro Redox-Triggered Release of DOX From DOX-Loaded Nanocarriers

The *in vitro* release profile of nanocarriers was investigated using dialysis of DOX-loaded nanocarriers in two different media: PBS or PBS supplemented with 20 mM GSH. Each solution was diluted to 1.5 mg/mL and 5 mL of the solution was transferred into a membrane tubing. The tubing with the solution was immersed in a tube containing 50 mL of the buffer solution in a shaking water bath at 37°C to acquire the "sink" condition. At predetermined intervals, 20 mL of the external buffer was withdrawn and replaced with a fresh solution of the corresponding buffer. The amount of DOX released was determined using HPLC.

Cell TEM Imaging

For TEM imaging, HeLa cells were incubated with DOX-loaded nanocarriers at a final DOX concentration of 5 μg/mL in DMEM for 2 h at 37°C in the presence or absence of an externally applied magnetic field. The culture medium was removed and the cells were pre-fixed with 2.5% glutaraldehyde in PBS at 4°C for 2 h and post-fixed with 1% osmium tetroxide in PBS at 4°C for 2 h. The cells were then dehydrated using serially increasing concentrations of ethanol and flat embedded in Epon 812. After polymerization at 60°C for 48 h, ultrathin sections (60–80 nm) were trimmed and further stained with uranyl acetate and lead citrate. Micrographs of the stained samples were collected with an FEI Tecnaio G220 TWIN Transmission Electron Microscope.

Cell Viability Assay

To evaluate the anti-tumor activity of DOX-loaded nanocarriers, the cytotoxicity of DOX-loaded nanocarriers or free DOX against HeLa cells was evaluated *in vitro* using the MTT assay. HeLa cells were seeded into a 96-well plate at a density of 4.0×10^3 cells/well in 100 μL of complete DMEM. The cells were cultured for 24 h at 37°C in a 5% CO_2 atmosphere. Subsequently, the cells were incubated with DOX-loaded nanocarriers or free DOX for 24 h at 37°C with or without the presence of an external magnetic field. DOX-loaded nanocarriers or free DOX were diluted in complete DMEM to a final DOX concentration ranging from 0.4 to 40 μg/mL. After the incubation, 10 μL of MTT solution (5 mg/mL in PBS 7.4) was added to each well and incubated for 4 h. The media with MTT solution was removed and 200 μL of DMSO was added to dissolve the formazan crystals and further incubated for 15 min at 37°C. The absorbance readings were recorded using a microplate spectrophotometer (PowerWave XS2, BioTek Instruments, USA) at a wavelength of 540 nm. The cell viability was normalized to that of cells cultured in complete DMEM. The dose-effect curves were plotted and data are presented as the average ± SD ($n = 4$).

Confocal Laser Scanning Microscopy (CLSM) Observation

CLSM was used to examine the intracellular distribution of DOX. HeLa cells were seeded on coverslips in the wells of a 24-well plate at a density of 4.0×10^4 cells/well in 1 mL of complete DMEM. The cells were incubated for 24 h at 37°C in a 5% CO_2 atmosphere. The cells were incubated with DOX-loaded nanocarriers at a final DOX concentration of 5 μg/mL in DMEM for 2 h at 37°C with or without an external magnetic field. After removal of the medium, the cells were washed three times with cold PBS, fixed with 1 mL of 4% paraformaldehyde for 30 min at 4°C, and stained with 2-(4-amidinophenyl)-6-indolecarbamidine dihydrochloride (DAPI, Roche) for 10 min. Finally, the slides were mounted with 10% glycerol solution and viewed using a LeicaTCS SP8 (Leica Microscopy Systems Ltd., Germany).

TABLE 1 | Properties of DOX-free and DOX-loaded nanocarriers.

DOX-free nanocarriers			DOX-loaded nanocarriers			
Size (nm)	PDI	Fe content (wt%)	Size (nm)	PDI	Fe content (wt%)	PLC (wt%)
131	0.26	14.7	150	0.19	13.3	4.6

RESULTS AND DISCUSSION

Characterization of Nanocarriers

The particle size and polydispersity (PDI) of DOX-free or DOX-loaded nanocarriers were determined by DLS, as shown in **Table 1**. The prepared DOX-free nanocarriers and DOX-loaded nanocarriers (**Figure 1A**) were determined to be 131 or 150 nm respectively, with a narrow size distribution, thereby making them suitable as anticancer drug carriers. The morphology of the redox-responsive magnetic nanocarriers was observed using TEM. **Figure 1B** shows the morphology of the nanocarriers. Because DSPE-SS-mPEG does not significantly attenuate electron scattering under TEM, nanocarriers are largely present as isolated clusters of Fe_3O_4 nanoparticles with a spherical shape. The drug loading content values of DOX-loaded nanocarriers was 4.6% (**Table 1**). Whereas, the Fe content of DOX-free or DOX-loaded nanocarriers was 14.7 and 13.3%, respectively (**Table 1**).

The Redox-Responsive Stability of Nanocarriers

Disulfide linkages are known to be readily reduced into free thiols in the presence of reducing agents. To demonstrate the responsiveness, the size change of redox-responsive magnetic nanocarriers in response to 20 mM GSH in PBS was measured by DLS. **Figure 2** shows that the average size of the nanocarriers gradually increased within the first 15 min after the addition of GSH. The size increased from 131 to 340 nm in 15 min, indicating the detachment of hydrophilic PEG shells from the nanocarriers and the enhanced hydrophobic interaction of the inner core. After 1 h, two populations at 547 nm and 1,038 nm were observed, however, after 3 h, the complete destruction of the nanocarriers was observed, and no nanoparticles were detected in the solution.

In vitro Redox-Responsive DOX Release

The drug release behavior of the DOX-loaded nanocarriers was investigated in PBS at 37°C in the presence or absence of

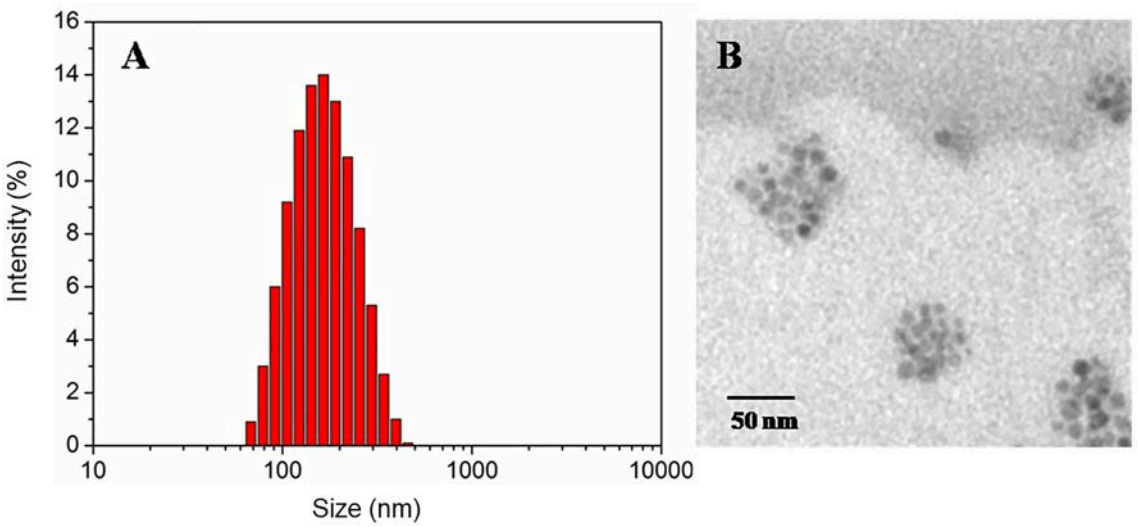

FIGURE 1 | The size distribution by DLS **(A)**, and TEM micrographs **(B)** of redox-responsive magnetic nanocarriers.

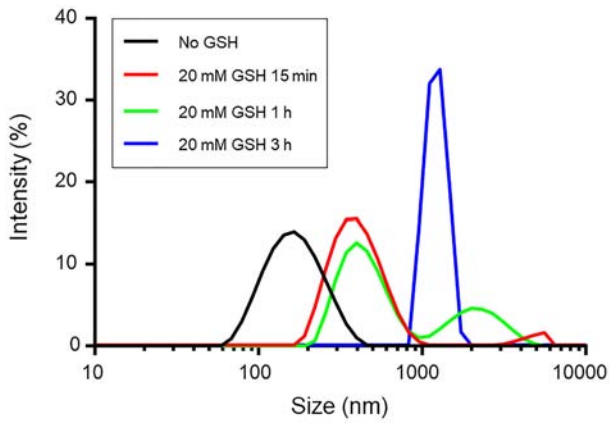

FIGURE 2 | The size change of redox-responsive magnetic nanocarriers in response to 20 mM GSH in PBS determined by DLS measurement.

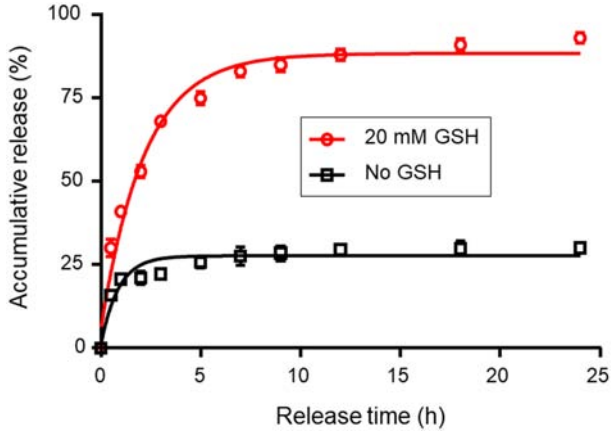

FIGURE 3 | Redox-triggered release of DOX from redox-responsive magnetic nanocarriers in PBS with or without 20 mM GSH. The standard deviation for each data point was averaged over three samples ($n = 3$).

GSH (20 mM). **Figure 3** shows the accumulative drug release profiles as a function of time. **Figure 3** demonstrates that the release of DOX from nanocarriers was markedly correlated with the presence or absence of GSH. The release of DOX from nanocarriers was accelerated by the addition of GSH to the media. In the presence of 20 mM GSH, nanocarriers rapidly released DOX, such that 93.8% of the DOX dose was released within 24 h. However, only 28.7% of DOX was released in the absence of GSH. This difference might be due to cleavage of disulfide bonds, thereby causing the destruction of the nanocarriers and the accelerated release of encapsulated DOX.

Cell TEM Imaging

The rapid accumulation of DOX-loaded nanocarriers was found to be magnetically inducible *in vitro* and was characterized using TEM. When HeLa cells were incubated for 2 h with DOX-loaded nanocarriers in either the presence or absence of a magnetic field, the accumulation of nanocarriers was found to be altered. TEM images demonstrating this observation are shown in **Figure 4**. The heavily electro-dense iron-containing nanoparticles are reproduced in the TEM images as a significantly darker region in contrast to the cellular environment, which facilitated identification of relative particle density between groups. The number of magnetic nanoparticles in cells significantly increased when a magnetic field was applied (**Figure 4B**), suggesting that the presence of a magnetic field enhanced the accumulation of nanocarriers in cells.

Cell Viability Assay

The *in vitro* cytotoxicity of DOX-loaded nanocarriers and free DOX was evaluated using the MTT assay. **Figure 5** shows the

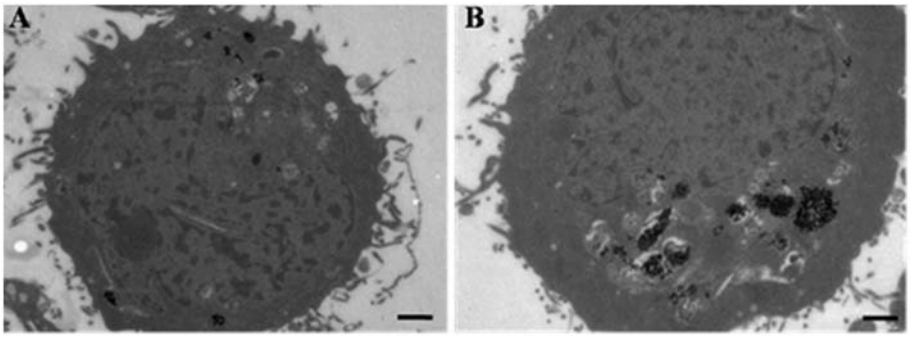

FIGURE 4 | TEM images of HeLa cells incubated with DOX-loaded nanocarriers in the absence **(A)** or presence **(B)** of a magnetic field. Scale bar is 1 μm.

resulting levels of observed cytotoxicity measured as a function of DOX concentration from 0.4 to 40 μg/mL. All test conditions exhibited a dose-dependent cytotoxic effect of the treatment on the population of viable and metabolically active HeLa cells. DOX-loaded nanocarriers exhibited lower cytotoxicity to HeLa cells with or without the magnetic field, as compared to free DOX at the same DOX dose (**Figure 5A**). As a control experiment, we performed a group of experiments using nanocarriers without DOX and examined cytotoxicity under magnetic and non-magnetic conditions, suggesting that the nanocarriers alone did not exhibit cytotoxicity (**Figure 5B**). Given that DOX is a small molecule, it can be quickly transported into cells and enter nuclei by passive diffusion. Furthermore, we found that the presence of a local magnetic field could significantly increase the cytotoxicity of DOX-loaded nanocarriers. This process may be due to the magnetic field increasing cellular uptake of nanocarriers, and once internalized, the redox-responsive nanocarriers are destroyed by high levels of GSH. The DOX is then rapidly released from the destroyed redox-responsive nanocarriers. Taken together these results indicate that the DOX-loaded nanocarriers can achieve both magnetic targeting and reduction-sensitive release simultaneously.

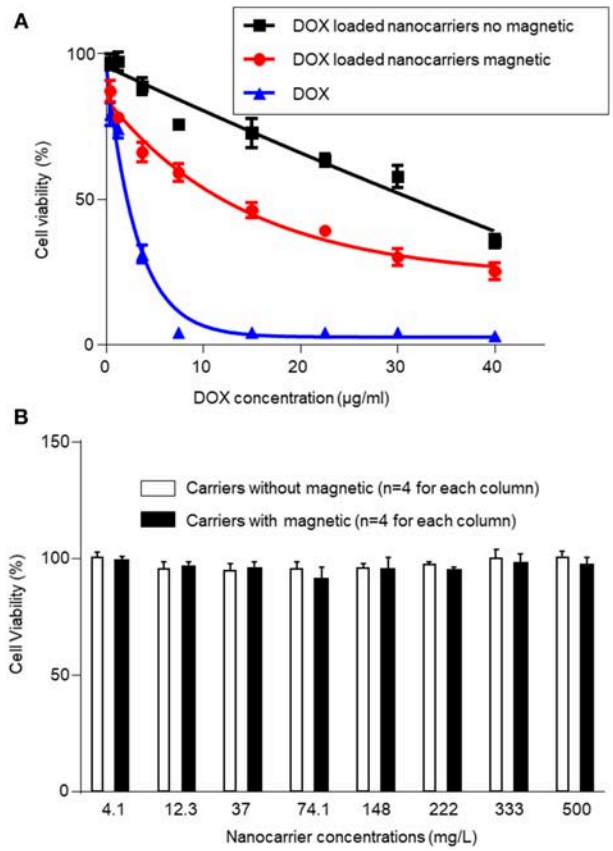

FIGURE 5 | Cytotoxicity of DOX-loaded magnetic nanocarriers and free DOX in HeLa cells with or without magnetic field after incubation for 24 h **(A)**. **(B)** In control experiments, we examined cytotoxicity using magnetic nanocarriers alone with or without magnetic field after incubation for 24 h, and found no cytotoxicity. The standard deviation for each data point was averaged over four samples ($n = 4$) for **(A,B)**.

In vitro Cellular Uptake of DOX-Loaded Nanocarriers

The cellular uptake of the nanocarriers and the intracellular location of the encapsulated DOX was monitored by CLSM in HeLa cells. The nuclei of HeLa cells were stained with DAPI, which presented blue fluorescence to distinguish from the red fluorescence of the labeled DOX. **Figure 6** shows CLSM images of HeLa cells incubated with DOX-loaded nanocarriers for 2 h with or without magnet field treatment. As shown in **Figure 6**, we found that cells incubated with DOX-loaded nanocarriers with applied magnetic field demonstrated stronger DOX fluorescence compared to no applied magnetic field. This phenomenon is primarily a result of the magnetic field increase in the cellular uptake of the DOX-loaded nanocarriers. Our results indicate that these nanocarriers are responsive to either magnetic or redox stimulated activation and are therefore suitable for application as anticancer drug carriers.

CONCLUSION

In this article, we use the amphiphilic copolymer DSPE-SS-mPEG, which is connected by disulfide bonds. Afterward, the

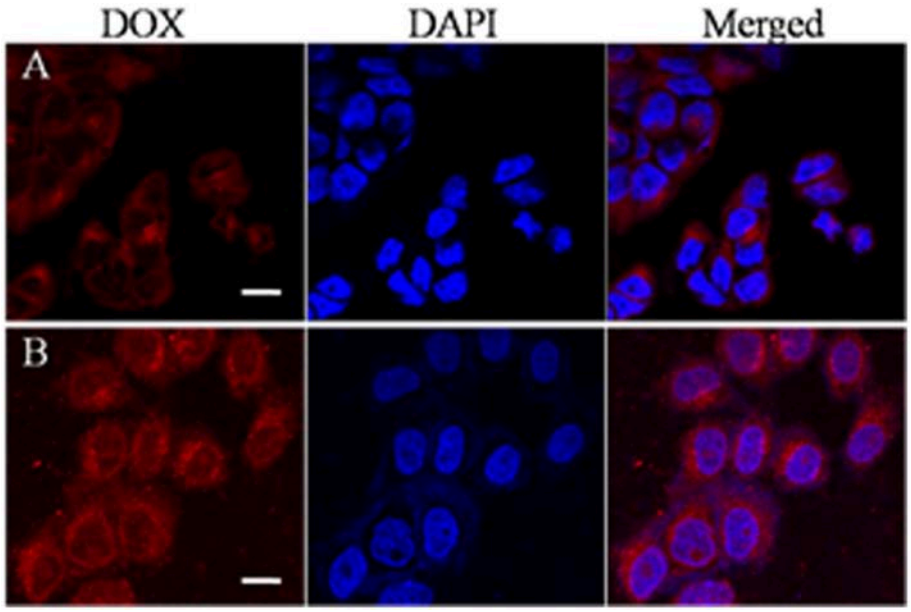

FIGURE 6 | CLSM images of HeLa cells after treatment with DOX-loaded magnetic nanocarriers for 2 h in the absence **(A)** or presence **(B)** of a magnetic field. Scale bar is 15 μm.

magnetic Fe_3O_4 nanoparticles and the hydrophobic drug are made by the self-assembly of the amphiphilic copolymer. DOX is encapsulated in the amphiphilic copolymer to form a magnetic nano drug controlled release system which is sensitive and responds to a reducing environment. This controlled release system can dissociate the disulfide bonds in the presence of dithiothreitol, thereby triggering the release system to disintegrate and expel the drug.

When the DOX-loaded nanocarrier is transported into the cell, intracellular GSH breaks the disulfide bonds, resulting in the disintegration of the transport system and the release of DOX. It is a well-designed enzyme-responsive magnetic-field controlled release system and provides a new foundation for building an efficient and safe nanoscale drug delivery system.

AUTHOR CONTRIBUTIONS

KX and YL equally contributed to this work, conducted the experiments, analyzed data, prepared original figures, and revised the manuscript. WY and GW participated in experimental design, analyzed the data, and revised the manuscript. HS analyzed the data and revised the manuscript. SZ designed the experiments and revised the manuscript. JW designed the experiments and analyzed the data, finalized the figures, and wrote the manuscript.

ACKNOWLEDGMENTS

This work was supported by the Science and Technology Department of Henan Province (Grant # 192102310411) and the Education Department of Henan Province (Grant # 19A320043).

REFERENCES

1. Yasui H. Safe handling of cancer chemotherapy drugs. *Gan to kagaku ryoho Cancer Chemother.* (2016) 43:503–8.
2. Paez JG, Jänne PA, Lee JC, Tracy S, Greulich H, Gabriel S, et al. EGFR mutations in lung cancer: correlation with clinical response to gefitinib therapy. *J Sci.* (2004) 304:1497–500. doi: 10.1126/science.1099314
3. Kerr JF, Winterford CM, Harmon BV. Apoptosis. Its significance in cancer and cancer therapy. *J Cancer.* (1994) 73:2013–26. doi: 10.1002/1097-0142(19940415)73:8<2013::AID-CNCR2820730802>3.0.CO;2-J
4. Wang CY, Mayo MW, Baldwin AS. TNF-and cancer therapy-induced apoptosis: potentiation by inhibition of NF-κB. *J Sci.* (1996) 274:784–7. doi: 10.1126/science.274.5288.784
5. Lowe SW, Bodis S, McClatchey A, Remington L, Ruley HE, Fisher DE, et al. p53 status and the efficacy of cancer therapy *in vivo*. *J Sci.* (1994) 266:807–10. doi: 10.1126/science.7973635
6. Brown JM, Giaccia AJ. The unique physiology of solid tumors: opportunities (and problems) for cancer therapy. *J Cancer Res.* (1998) 58:1408–16.
7. Anselmo AC, Mitragotri S. Nanoparticles in the clinic. *Bioeng Transl Med.* (2016) 1:10–29. doi: 10.1002/btm2.10003
8. Wicki A, Witzigmann D, Balasubramanian V, Huwyler J. Nanomedicine in cancer therapy: challenges, opportunities, and clinical applications. *J Control Release.* (2015) 200:138–57. doi: 10.1016/j.jconrel.2014.12.030
9. Mi Y, Wolfram J, Mu C, Liu X, Blanco E, Shen H, et al. Enzyme-responsive multistage vector for drug delivery to tumor tissue. *Pharmacol Res.* (2016) 113(Pt A):92–9. doi: 10.1016/j.phrs.2016.08.024
10. Bigall NC, Curcio A, Leal MP, Falqui A, Palumberi D, Di Corato R, et al. Magnetic nanocarriers with tunable pH dependence for controlled loading and release of cationic and anionic payloads. *Adv Mater.* (2011) 23:5645–50. doi: 10.1002/adma.201103505
11. Nagaoka H, Sato Y, Xie X, Hata H, Eguchi M, Sakurai N, et al. Coupling stimuli-responsive magnetic nanoparticles with antibody-antigen

detection in immunoassays. *Anal Chem.* (2011) 83:9197–200. doi: 10.1021/ac201814n
12. Ruan G, Vieira G, Henighan T, Chen A, Thakur D, Sooryakumar R, et al. Simultaneous magnetic manipulation and fluorescent tracking of multiple individual hybrid nanostructures. *Nano Lett.* (2010) 10:2220–4. doi: 10.1021/nl1011855
13. Jain S, Hirst DG, O'Sullivan JM. Gold nanoparticles as novel agents for cancer therapy. *Br J Radiol.* (2012) 85:101–13. doi: 10.1259/bjr/59448833
14. Ferrari M. Cancer nanotechnology: opportunities and challenges. *J. Nat Rev Cancer.* (2005) 5:161–71. doi: 10.1038/nrc1566
15. Farokhzad OC, Langer R. Nanomedicine: developing smarter therapeutic and diagnostic modalities. *J Adv Drug Del Rev.* (2006) 58:1456–9. doi: 10.1016/j.addr.2006.09.011
16. Riehemann K, Schneider SW, Luger TA, Godin B, Ferrari M, Fuchs H. Nanomedicine? challenge and perspectives. *J Angewandte Chemie Int Edn.* (2009) 48:872–97. doi: 10.1002/anie.200802585
17. Peer D, Karp JM, Hong S, Farokhzad OC, Margalit R, Langer R. Nanocarriers as an emerging platform for cancer therapy. *J Nat Nanotechnol.* (2007) 2:751–60. doi: 10.1038/nnano.2007.387
18. Xu R, Zhang G, Mai J, Deng X, Segura-Ibarra V, Wu S, et al. An injectable nanoparticle generator enhances delivery of cancer therapeutics. *Nat Biotechnol.* (2016) 34:414–8. doi: 10.1038/nbt.3506
19. Lucky SS, Idris NM, Huang K, Kim J, Li Z, Thong PS, et al. *In vivo* Biocompatibility, biodistribution and therapeutic efficiency of titania coated upconversion nanoparticles for photodynamic therapy of solid oral cancers. *Theranostics.* (2016) 6:1844–65. doi: 10.7150/thno.15088
20. von Maltzahn G, Park JH, Lin KY, Singh N, Schwoppe C, Mesters R, et al. Nanoparticles that communicate *in vivo* to amplify tumour targeting. *Nat Mater.* (2011) 10:545–52. doi: 10.1038/nmat3049
21. Sun S, Murray CB, Weller D, Folks L, Moser A. Monodisperse FePt nanoparticles and ferromagnetic FePt nanocrystal superlattices. *Science.* (2000) 287:1989–92. doi: 10.1126/science.287.5460.1989
22. Gao W, Kagan D, Pak OS, Clawson C, Campuzano S, Chuluun-Erdene E, et al. Cargo-towing fuel-free magnetic nanoswimmers for targeted drug delivery. *Small.* (2012) 8:460–7. doi: 10.1002/smll.201101909
23. Jain RK, Stylianopoulos T. Delivering nanomedicine to solid tumors. *J Nat Rev Clin Oncol.* (2010) 7:653–64. doi: 10.1038/nrclinonc.2010.139
24. Farokhzad OC, Langer R. Impact of nanotechnology on drug delivery. *J ACS Nano.* (2009) 3:16–20. doi: 10.1021/nn900002m
25. Hong R, Han G, Fernandez JM, Kim BJ, Forbes NS, Rotello VM. Glutathione-mediated delivery and release using monolayer protected nanoparticle carriers. *J Am Chem Soc.* (2006) 128:1078–9. doi: 10.1021/ja056726i
26. Chong SF, Chandrawati R, Stadler B, Park J, Cho J, Wang Y, et al. Stabilization of polymer-hydrogel capsules via thiol-disulfide exchange. *Small.* (2009) 5:2601–10. doi: 10.1002/smll.200900906
27. Jones DP, Carlson JL, Samiec PS, Sternberg P, Jr, Mody VC Jr, Reed RL, et al. Glutathione measurement in human plasma. Evaluation of sample collection, storage and derivatization conditions for analysis of dansyl derivatives by HPLC. *Clin Chim Acta.* (1998) 275:175–84.
28. Park J, An K, Hwang Y, Park JG, Noh HJ, Kim JY, et al. Ultra-large-scale syntheses of monodisperse nanocrystals. *J Nat Mater.* (2004) 3:891–5. doi: 10.1038/nmat1251
29. Xu ZC, Shen CM, Hou YL, Gao HJ, Sun SH. Oleylamine as both reducing agent and stabilizer in a facile synthesis of magnetite nanoparticles. *Chem Mater.* (2009) 21:1778–80. doi: 10.1021/cm802978z

Conflict of Interest Statement: The authors declare that the research was conducted in the absence of any commercial or financial relationships that could be construed as a potential conflict of interest.

frontiers in Oncology

PERSPECTIVE
published: 16 April 2019
doi: 10.3389/fonc.2019.00263

Identification of Genetic Mutations in Cancer: Challenge and Opportunity in the New Era of Targeted Therapy

Jing Jin[1†], Xu Wu[2,3†], Jianhua Yin[2,3], Mingxing Li[2,3], Jing Shen[2,3], Jing Li[4], Yueshui Zhao[2,3], Qijie Zhao[2,3], Jingbo Wu[1], Qinglian Wen[1], Chi Hin Cho[2,3], Tao Yi[5], Zhangang Xiao[2]* and Liping Qu[6]*

[1] Department of Oncology, The Affiliated Hospital of Southwest Medical University, Southwest Medical University, Luzhou, China, [2] Laboratory of Molecular Pharmacology, Department of Pharmacology, School of Pharmacy, Southwest Medical University, Luzhou, China, [3] South Sichuan Institute of Translational Medicine, Luzhou, China, [4] Department of Oncology and Hematology, Hospital (T.C.M) Affiliated to Southwest Medical University, Luzhou, China, [5] School of Chinese Medicine, Hong Kong Baptist University, Hong Kong, China, [6] College of Pharmacy, Chengdu University of Traditional Chinese Medicine, Chengdu, China

OPEN ACCESS

Edited by:
Yan-yan Yan,
Shanxi Datong University, China

Reviewed by:
Shengpeng Wang,
University of Macau, China
Maria Munoz Caffarel,
Biodonostia Health Research Institute, Spain
Tinghong Ye,
Sichuan University, China

***Correspondence:**
Tao Yi
yitao@hkbu.edu.hk
Zhangang Xiao
xzg555898@hotmail.com

[†]These authors have contributed equally to the work

Specialty section:
This article was submitted to Cancer Molecular Targets and Therapeutics, a section of the journal Frontiers in Oncology

Received: 25 January 2019
Accepted: 22 March 2019
Published: 16 April 2019

Citation:
Jin J, Wu X, Yin J, Li M, Shen J, Li J, Zhao Y, Zhao Q, Wu J, Wen Q, Cho CH, Yi T, Xiao Z and Qu L (2019) Identification of Genetic Mutations in Cancer: Challenge and Opportunity in the New Era of Targeted Therapy. Front. Oncol. 9:263. doi: 10.3389/fonc.2019.00263

The introduction of targeted therapy is the biggest success in the treatment of cancer in the past few decades. However, heterogeneous cancer is characterized by diverse molecular alterations as well as multiple clinical profiles. Specific genetic mutations in cancer therapy targets may increase drug sensitivity, or more frequently result in therapeutic resistance. In the past 3 years, several novel targeted therapies have been approved for cancer treatment, including drugs with new targets (i.e., anti-PD1/PDL1 therapies and CDK4/6 inhibitors), mutation targeting drugs (i.e., the EGFR T790M targeting osimertinib), drugs with multiple targets (i.e., the EGFR/HER2 dual inhibitor neratinib) and drug combinations (i.e., encorafenib/binimetinib and dabrafenib/trametinib). In this perspective, we focus on the most up-to-date knowledge of targeted therapy and describe how genetic mutations influence the sensitivity of targeted therapy, highlighting the challenges faced within this era of precision medicine. Moreover, the strategies that deal with mutation-driven resistance are further discussed. Advances in these areas would allow for more targeted and effective therapeutic options for cancer patients.

Keywords: targeted therapy, cyclin-dependent kinases 4/6, somatic mutation, resistance, EGFR, PD-1/PD-L1

INTRODUCTION

Targeted therapies usually present with high selectivity, target precisely to specific gene or protein, and exert a biological function with minimal side effects (1), which has distinguished them from most conventional non-specific chemotherapeutic drugs. Targeted therapy has thus been regarded as the biggest success in the treatment of cancer in the past few decades. Many novel promising agents have been experimentally designed and developed and are increasingly entering clinical evaluation. However, the frequently observed alterations in the drug targets have posed a big challenge to successful cancer treatment. Genetic mutations in cancer are resulted from both inherited and environmental factors. In a recent report, it is demonstrated that a large proportion of cancer-related mutations

are due to randomized DNA replication errors (2). Notably, the mutations in cancer therapy targets can greatly affect drug sensitivity. Mutation-driven drug resistance is very common in cancer. The efficacy of targeted therapy is thus largely dependent on the mutation profile of tumors in patients. Accurate molecular and genetic profiling of tumor cells is becoming a routine practice before the introduction of targeted therapy in patients.

In recent years, great progress has been made in targeted therapy discovery. Notably, many new drugs are designed primarily based on specific genetic background. For instance, nearly 40–50% of metastatic cutaneous melanoma possess v-raf murine sarcoma viral oncogene homolog B1 (BRAF) mutations (3), and ∼90% of these BRAF mutations are caused by substitution of glutamic acid for valine at codon 600 (V600E) (4). Two selective BRAF inhibitors vemurafenib and dabrafenib were approved for the treatment of patients with BRAF-V600E mutation, showing improved progression-free survival (5). In November 2018, the U.S. Food and Drug Administration (FDA) approved an inhibitor of tropomyosin receptor kinases (TRKs), larotrectinib, for treatment of any type of solid tumors with TRK gene fusion (6). This is the second targeted therapy approved not for specific cancer types but for any cancers with specific mutations. Targeted therapies are becoming more precise.

In this perspective, we focus on the updated knowledge of targeted therapy in the last 3 years and describe how genetic mutations influence sensitivity of targeted therapy, highlighting the challenges faced within this era of precision medicine. Moreover, the strategies dealing with mutation-driven resistance are further discussed.

INFLUENCE OF GENETIC MUTATION ON SENSITIVITY OF TARGETED THERAPY

It is well-acknowledged that mutations in therapeutic targets can increase or decrease drug sensitivity (**Table 1**). The main challenge of targeted therapy today is the identification of particular cancer mutations which affect efficacy of targeted therapies as well as the identification of a specific group of patients most likely or unlikely to respond to certain targeted therapies. Despite the great challenges, in the last 3 years, we have seen significant progress in targeted therapy (**Table 2**), largely owing to the rise of large-scale sequencing technology and big data analysis. Several novel targets, including the programmed death-1/programmed death-ligand 1 (PD1/PDL1) and cyclin-dependent kinases 4 and 6 (CDK4/6), have been validated, with several new targeted drugs being approved. Some newly approved drugs are directly designed to deal with some known activating mutations, such as the T790M mutation in epidermal growth factor receptor (EGFR). Moreover, many new findings have been added to our knowledge of how mutations influence targeted therapies [e.g., the inhibitors of human epidermal growth factor receptor 2 (HER2) and anaplastic lymphoma kinase (ALK)]. Here, based on the most updated research in the last 3 years, we summarize the recent advances of several targeted therapies.

Anti-PD1/PDL1 Therapies

So far, there are a total of 6 anti-PD1/PDL1 therapies that have been approved by the FDA. Notably, in 2017, a PD1 antibody pembrolizumab was approved for the treatment of any solid tumor with a mismatch repair deficiency or a microsatellite instability. Monotherapy of PD1/PDL1 blockade has received great success in many types of cancers (21, 22). However, there are certain patients that are gradually developing resistance after an initial response (23). Mutation-driven resistance of anti-PD1/PDL1 therapies has recently been studied in a small number of cancer patients. Zaretsky et al. reported that mutations of JAK1/JAK2 led to the desensitization of cancer cells to IFN-γ and contributed to an acquired resistance of pembrolizumab in patients with melanoma (23). Moreover, in one resistant patient, a frame-shift deletion in exon 1 of the β-2-microglobulin was detected, which may result in the loss of expression of surface the MHC class I (23). More studies are advocated to explore the acquired resistance of immune checkpoint inhibitors.

Resistance of CDK4/6 Inhibitors

Currently, three CDK 4/6 selective targeting inhibitors, palbociclib, ribociclib, and abemaciclib have been approved to treat breast cancer. CDK4/6 inhibitors are increasingly used in clinical settings, but patients eventually show disease progression and the major reasons remain unclear (24). Dysregulation of cyclin D1-CDK4/6-retinoblastoma (Rb) pathway has been implicated in hormone receptor positive (HR^+) breast cancer and in chemotherapeutic drug-resistance. Rb is usually intact in HR^+ breast cancer and is important for the efficacy of CDK4/6-inhibitors in the treatment of breast cancer (25). It is indicated that T47D cells that become resistant to CDK4/6 inhibitors, develop CCNE1 amplification or Rb1 loss (26). Moreover, the acquisition of multiple *de novo* somatic Rb1 mutations in metastatic breast cancer patients may result in the emergence of a resistance to CDK 4/6 inhibitors (24). Until now, there has been no report on CDK4/6 mutations in cancer patients and their effect on efficacy of CDK4/6 inhibitors.

EGFR and Different Generation of Tyrosine Kinase Inhibitors (TKIs)

EGFR is a prevalent target in several human cancers, such as lung, breast, colorectal, thyroid, and melanoma cancer. In lung cancer, several generations of small-molecular inhibitors have been developed to target the EGFR tyrosine kinases (27), such as inhibitors gefitinib, erlotinib, osimertinib, and necitumumab. The EGFR mutation in non-small cell lung cancer (NSCLC) was first identified in 2004, and the major missense and deletion mutation of EGFR in NSCLC occurs in the tyrosine kinase-coding domain in exons 18–21 (28). The L858R mutation in the exon 21 and exon-19 frame deletion are the most commonly detected mutation types of EGFR, representing 50 and 40% of tumor patients, respectively (7). These two types of mutations are sensitive to EGFR tyrosine kinase inhibitors (TKIs) in NSCLC. The first-generation TKIs, gefitinib and erlotinib,

TABLE 1 | Therapeutic response of targeted therapy in mutant cancers.

Drugs	Sensitivity	Target mutations	Cancer types	Reference
Gefitinib	+	EGFR-L858R	Lung cancer	(7)
Erlotinib	+	EGFR-L858R	Lung cancer	(7)
Gefitinib	–	EGFR-T789M	Lung cancer	(8)
Osimertinib	+	EGFR-T790M	Lung cancer	(9)
Osimertinib	–	EGFR-L718Q	Lung cancer	(10)
Trastuzumab	–	HER2-A859T, -G776L	Lung cancer	(11)
Afatinib	+	HER2-p.Tyr772_Ala775dup	Lung cancer	(12)
Neratinib	–	HER2-T798I, -L869R	Breast cancer	(13)
Lapatinib	–	HER2-T798M	Breast cancer	(14)
Trastuzumab	–	HER2-T798M	Breast cancer	(14)
Neratinib	+	HER2-S310, -L755, -V777, -G778_P780dup, and -Y772_A775dup	Breast, cervical and biliary cancers	(15)
Crizotinib	–	ALK-C1156Y, -L1196M	Lung cancer	(16, 17)
Lorlatinib	–	ALK-L1198F	Lung cancer	(18)
2,4-Pyrimidinediamine derivative	–	EML4-ALK-C1156Y, -L1196M	Lung cancer	(19)
TAE684	–	EML4-ALK-L1152R	Lung cancer	(20)
Dabrafenib	+	BRAF-V600E	Melanoma	(5)

TABLE 2 | Cancer targeted therapy approved by FDA in 2017 and 2018.

Drugs	Targets	Cancer types
Pembrolizumab (2017)	PD-1	Solid tumor with mismatch repair deficiency or microsatellite instability
Cemiplimab (2018)	PD-1	Squamous cell carcinoma
Durvalumab (2017)	PD-L1	Urothelial carcinoma
Avelumab (2017)	PD-L1	Merkel cell carcinoma, urothelial carcinoma
Brigatinib (2018)	ALK	ALK-positive NSCLC
Lorlatinib (2018)	ALK	ALK-positive NSCLC
Ribociclib (2017)	CDK4/6	Breast cancer
Abemaciclib (2017)	CDK4/6	Breast cancer
Niraparib (2017)	PARP	Ovarian cancer, peritoneal cancer
Dacomitinib (2018)	EGFR	NSCLC with EGFR exon 19 deletion or exon 21 L858R substitution mutations
Talazoparib (2018)	PARP	Breast cancer with germline BRCA mutations
Duvelisib (2018)	PI3Kδ, PI3Kγ	Chronic lymphocytic leukemia, small lymphocytic lymphoma
Larotrectinib (2018)	TRKs	Solid tumor with TRK gene fusion
Neratinib (2017)	EGFR/HER2	HER2-amplified breast cancer

have a high selective inhibitory activity against both wild-types and these sensitive mutant EGFR (29). Previous studies show that gefitinib and erlotinib are important for the first-line treatment of NSCLC patients with the sensitive EGFR mutations (30, 31). On the other hand, another mutation T790M, a secondary EGFR mutation emerging in NSCLC, can lead to the resistance of more than half of patients' TKIs treatment (32). Very recently, the third-generation TKI inhibitor osimertinib has been approved to effectively target to EGFR T790M mutation with a response rate of 61% in NSCLC, significantly extending the overall survival in patients with the T790M mutation (9). However, the further mutation of a residue in the P-loop (L718Q) has been found to cause resistance to osimertinib (10). Nevertheless, though diverse EGFR mutations are present, the overall survival of lung cancer patients is markedly improved with TKI therapy.

HER2 and Its Inhibitors

In breast cancer, the overall HER2 mutation rate is ∼1.6% (25 out of 1,499 patients). In a study by Bose et al., seven HER2 somatic mutations including G309A, D769H, D769Y, V777L, P780ins, V842I, and R896C, have been identified as activating mutations (33). Several patients with HER2 activating mutations are resistant to the reversible HER2 inhibitor lapatinib, but sensitive to the irreversible HER2 inhibitor neratinib. Neratinib as a dual inhibitor of HER2 and EGFR was approved by FDA in 2017. It has been shown that the HER2 L755S mutation results in an acquired resistance to lapatinib in breast cancer, which could be overcome by the neratinib (34). In another study, the HER2-T798I gatekeeper mutation in breast cancer patients with a AHER2-L869R mutation was identified as a mechanism of acquired resistance to neratinib (13). The trial of neratinib has also been conducted in colorectal cancer

(CRC) patients. The HER2 gene amplification and mutation in CRC can lead to the resistance of EGFR-targeted therapies cetuximab and panitumumab (35, 36). A negative effect of neratinib monotherapy has recently been confirmed in 12 CRC patients with different tumors harboring HER2 mutations (15). There were no positive therapeutic response and the median PFS was only 1.8 months, indicating that monotherapy with neratinib is ineffective. The underlying mechanisms still require further investigations.

ALK and Different Generation of ALK Inhibitors

ALK has long been identified as a therapeutic target in cancer. The first ALK inhibitor crizotinib was approved by the FDA in 2011 (37). Although most NSCLC patients respond to this drug, tumors become resistant after 1–2 years of treatment. Around 1/3 of crizotinib-resistant tumors harbor mutations within the ALK kinase domain. The most commonly observed mutations of L1196M and G1269A lead to a decreased affinity for crizotinib (38). Other ALK point mutations, such as L1152R, C1156Y, I1171T, F1174L, G1202R, and S1206Y, are also associated with crizotinib resistance (39). Another oncoprotein of fusion-type tyrosine kinase, the EML4-ALK, results from the inversion within the short arm of the human chromosome 2 in 4–5% of cases of NSCLC (40). Two mutations of EML4-ALK, C1156Y, and L1196M, confer a significant resistance to ALK inhibitors, such as crizotinib and PDD (2,4-pyrimidinediamine derivative) (19). The EML4-ALK C1156Y mutation can contribute to a higher resistance to PDD than those in the L1196M mutant form. It is reported that a candidate ALK inhibitor TAE684 can bind to these mutant kinases, which may have potency in overcoming the mutation-driven resistance (41). The new generation ALK inhibitors lorlatinib and brigatinib were approved in 2018 for the treatment of patients with ALK-rearranged NSCLC. Lorlatinib has been demonstrated to inhibit resistant ALK mutations, including ALK G1202R (16). However, Shaw et al. showed that an ALK L1198F mutation together with the C1156Y mutation results in the resistance of lorlatinib in a patient with metastatic ALK-rearranged NSCLC (18). However, the L1198F mutation re-sensitized crizotinib treatment of a resistant tumor. It was demonstrated that both lorlatinib and brigatinib can overcome crizotinib resistance in NSCLC patients (42, 43). Moreover, when brigatinib was combined with anti-EGFR antibody, it was effective against EGFR triple-mutant cells *in vitro* and *in vivo* (44).

STRATEGIES FOR OVERCOMING MUTATION-DRIVEN RESISTANCE

Mutations in cancer therapy targets usually result in the loss of functions and the accumulation of dysfunctional proteins in tumors (45). Moreover, many mutants have oncogenic gain-of-function (GOF) activities including increased tumor proliferation, metastasis and drug resistance (46). Notably, tumor cells that receive targeted therapy may lead to an overactivation of the by-pass signaling pathways to develop resistance. In most cases, multiple alterations are observed in a resistant tumor.

Recently, many strategies dealing with mutation-driven drug resistance have been proposed and evaluated both experimentally and clinically. The traditional chemotherapy concept of "one ligand to one receptor" for a biological response is inadequate. The treatment of a particular type of cancer with the prescriptive drugs involves many special genes, interacting with their respective targets and triggering a series of biological responses. The concept of using multi-drug therapy and seeking multifunctional compounds that can efficiently interact with various targets might be feasible (47). Currently, to overcome mutation-driven drug resistance, the main strategies include: (1) the design of new mutation-targeted compounds to restore wide-type protein activities, to delete mutants or to influence downstream targets; (2) the application of combinational therapy or new compounds for multiple targeting. Here, we give some examples of how to overcome mutation-driven resistance of targeted therapy.

Dacomitinib, an Irreversible Pan-ERBB Inhibitor, Targeting EGFR Activating Mutants

Recently, dacomitinib was approved to use for metastatic NSCLC with EGFR exon 19 deletion or exon 21 L858R substitution mutations. In a randomized, multicenter, open-label, phase III trial (ARCHER 1050), the patients with newly diagnosed advanced NSCLC and one EGFR mutation (exon 19 deletion or L858R) received a 45 mg/day dose of oral dacomitinib or a 250 mg/day gefitinib for 28 days. In the dacomitinib group, the progression-free survival (14.7 months, 95% CI 11.1–16.6) was significantly longer than that in the gefitinib group (9.2 months, 95% CI 9.1–11.0) (48). This investigation supports the dacomitinib as the first line therapy for EGFR-mutation NSCLC patients.

Dacomitinib is initially designed for irreversible pan-ERBB inhibition. As a small-molecule covalent binding inhibitor of enzymatically active HER family tyrosine kinases EGFR and HER2, it may act as a potent inhibitor of EGFR T790M mutation (49). Additionally, dacomitinib significantly inhibits both wild-type and the gefitinib-resistant ERBB2 mutation in lung cancer. Based on an in-depth investigation, dacomitinib is an effective drug that may treat NSCLC patients with a T790M-related acquired resistance to gefitinib or erlotinib (8). It has been indicated that dacomitinib significantly improves progression-free survival in EGFR-mutation NSCLC patients and is considered as a new treatment option for this population.

Encorafenib/Binimetinib and Dabrafenib/Trametinib for Dual Inhibition of BRAF and MEK

The FDA approved dabrafenib plus trametinib for the anaplastic thyroid cancer (ATC) with BRAF-V600E mutation in May 2018, as well as for the adjuvant treatment of BRAF V600E/K-mutated melanoma in April 2018. Previous studies revealed that dabrafenib plus trametinib have shown substantial antitumor activity in patients with previously treated BRAF-V600E mutated metastatic NSCLC and untreated BRAFV-600E mutated NSCLC (50, 51). Trametinib is an orally administered MEK1/MEK2

inhibitor that suppresses RAF-dependent MEK phosphorylation and persistently inhibits phosphorylated ERK (a substrate of MEK) (52). Dabrafenib is a reversible and high-efficiency ATP-competitive inhibitor of RAF kinases, especially the mutant BRAF (53). Subbiah et al. reported that the overall response rate of dabrafenib plus trametinib applied in BRAF V600E-mutated ATC (complete reaction plus partial reaction to the best overall response) is 69% (54). In contrast to BRAF inhibitor monotherapy, it has longer progression-free survival and overall survival. Overall, the most common adverse events include fatigue, pyrexia and nausea (54), consistent with previous reports in advanced or metastatic melanoma and NSCLC (50). Dabrafenib plus trametinib is the first regimen approved to have significant clinical efficacy in BRAF V600E-mutated ATC.

In June 2018, the FDA approved the combination of BRAF inhibitor encorafenib and the MEK inhibitor binimetinib for treatment of patients with unresectable or metastatic melanoma with a BRAF-V600E or -V600K mutation. It is the third BRAF/MEK inhibitor combination approved following the dabrafenib/trametinib and vemurafenib/cobimetinib combinations (55). The main adverse events for encorafenib plus binimetinib when applied to BRAF-V600 mutant melanoma are gastrointestinal reactions, including nausea, diarrhea and vomiting. Additionally, this combination has a lower calorific value and photosensitivity than other available BRAF-MEK inhibitor combinations do (56). Considerable evidence supports that the median progression-free survival was 14.9 months with encorafenib plus binimetinib, compared with 7.3 months with vemurafenib (57). Therefore, it is an effective therapeutic option in patients with unresectable or metastatic melanoma, with a BRAF V600E or V600K mutation.

CONCLUSIONS

In the new era of targeted therapy, treatment options are increasingly based on the precise molecular and genetic profiling of tumor cells (58). Currently, the main challenge for further novel drug development in targeted therapy is the clarification of specific molecular mechanisms underlying the varied forms of tumors in clinic. It has been acknowledged that cancer is caused by a set of driver mutations. In this regard, it is of great significance to: (1) identify and validate key mutant genes and proteins in cancers as new targets; (2) identify patients most likely and unlikely to benefit from certain targeted therapies; (3) evaluate the mechanism of mutation-driven drug resistance. In past decades, several key mutations which influence drug sensitivity have been identified in various cancers. In order to deal with mutation-driven drug resistance, new methods and drugs have been discovered and approved for clinical use (47). Even so, detailed individualized treatment strategies targeting specific tumorigenesis and drug resistant mechanisms are still required. Advances in these areas would allow for more targeted and effective therapeutic options for more cancer patients.

AUTHOR CONTRIBUTIONS

ML, JS, JL, YZ, JW, LQ, and QW were responsible for the review of the literature. JJ, JY, XW, QZ, CC, and ML wrote the manuscript. XW and LQ drew the Tables. XW, TY, and ZX designed the study and contributed with the valuable discussion and revision of the manuscript.

FUNDING

This work was supported by the National Natural Science Foundation of China (Grant nos. 81503093, 81602166, and 81672444) and the Joint Funds of the Southwest Medical University and Luzhou (2016LZXNYD-T01, 2017LZXNYD-Z05, and 2017LZXNYD-J09). The funding from National Natural Science Foundation of China (Grant nos. 81503093) will cover open access fee.

REFERENCES

1. Scotti L, Mendonca Junior FJ, Ishiki HM, Ribeiro FF, Singla RK, Barbosa Filho JM, et al. Docking studies for multi-target drugs. *Curr Drug Targ.* (2017) 18:592–604. doi: 10.2174/1389450116666150825111818
2. Tomasetti C, Li L, Vogelstein B. Stem cell divisions, somatic mutations, cancer etiology, and cancer prevention. *Science.* (2017) 355:1330–4. doi: 10.1126/science.aaf9011
3. Curtin JA, Fridlyand J, Kageshita T, Patel HN, Busam KJ, Kutzner H, et al. Distinct sets of genetic alterations in melanoma. *N Engl J Med.* (2005) 353:2135–47. doi: 10.1056/NEJMoa050092
4. Davies H, Bignell GR, Cox C, Stephens P, Edkins S, Clegg S, et al. Mutations of the BRAF gene in human cancer. *Nature.* (2002) 417:949–54. doi: 10.1038/nature00766
5. Hauschild A, Grob JJ, Demidov LV, Jouary T, Gutzmer R, Millward M, et al. Dabrafenib in BRAF-mutated metastatic melanoma: a multicentre, open-label, phase 3 randomised controlled trial. *Lancet.* (2012) 380:358–65. doi: 10.1016/s0140-6736(12)60868-x
6. Drilon A, Laetsch TW, Kummar S, DuBois SG, Lassen UN, Demetri GD, et al. Efficacy of larotrectinib in TRK fusion–positive cancers in adults and children. *N Engl J Med.* (2018) 378:731–9. doi: 10.1056/NEJMoa1714448
7. Shigematsu H, Lin L, Takahashi T, Nomura M, Suzuki M, Wistuba II, et al. Clinical and biological features associated with epidermal growth factor receptor gene mutations in lung cancers. *J Natl Cancer Inst.* (2005) 97:339–46. doi: 10.1093/jnci/dji055
8. Kobayashi S, Boggon TJ, Dayaram T, Janne PA, Kocher O, Meyerson M, et al. EGFR mutation and resistance of non-small-cell lung cancer to gefitinib. *N Engl J Med.* (2005) 352:786–92. doi: 10.1056/NEJMoa044238
9. Mok TS, Wu YL, Ahn MJ, Garassino MC, Kim HR, Ramalingam SS, et al. Osimertinib or platinum-pemetrexed in EGFR T790M-positive lung cancer. *N Engl J Med.* (2017) 376:629–40. doi: 10.1056/NEJMoa1612674
10. Callegari D, Ranaghan KE, Woods CJ, Minari R, Tiseo M, Mor M, et al. L718Q mutant EGFR escapes covalent inhibition by stabilizing a non-reactive conformation of the lung cancer drug osimertinib. *Chem Sci.* (2018) 9:2740–9. doi: 10.1039/c7sc04761d
11. Cappuzzo F, Bemis L, Varella-Garcia M. HER2 mutation and response to trastuzumab therapy in non-small-cell lung cancer. *N Engl J Med.* (2006) 354:2619–21. doi: 10.1056/NEJMc060020
12. De Greve J, Teugels E, Geers C, Decoster L, Galdermans D, De Mey J, et al. Clinical activity of afatinib (BIBW 2992) in patients with lung

adenocarcinoma with mutations in the kinase domain of HER2/neu. *Lung Cancer.* (2012) 76:123–7. doi: 10.1016/j.lungcan.2012.01.008
13. Hanker AB, Brewer MR, Sheehan JH, Koch JP, Sliwoski GR, Nagy R, et al. An acquired HER2(T798I) gatekeeper mutation induces resistance to neratinib in a patient with HER2 mutant-driven breast cancer. *Cancer Discov.* (2017) 7:575–85. doi: 10.1158/2159-8290.cd-16-1431
14. Rexer BN, Ghosh R, Narasanna A, Estrada MV, Chakrabarty A, Song Y, et al. Human breast cancer cells harboring a gatekeeper T798M mutation in HER2 overexpress EGFR ligands and are sensitive to dual inhibition of EGFR and HER2. *Clin Cancer Res.* (2013) 19:5390–401. doi: 10.1158/1078-0432.ccr-13-1038
15. Hyman DM, Piha-Paul SA, Won H, Rodon J, Saura C, Shapiro GI, et al. HER kinase inhibition in patients with HER2- and HER3-mutant cancers. *Nature.* (2018) 554:189–94. doi: 10.1038/nature25475
16. Katayama R, Lovly CM, Shaw AT. Therapeutic targeting of anaplastic lymphoma kinase in lung cancer: a paradigm for precision cancer medicine. *Clin Cancer Res.* (2015) 21:2227–35. doi: 10.1158/1078-0432.ccr-14-2791
17. Shaw AT, Kim DW, Mehra R, Tan DS, Felip E, Chow LQ, et al. Ceritinib in ALK-rearranged non-small-cell lung cancer. *N Engl J Med.* (2014) 370:1189–97. doi: 10.1056/NEJMoa1311107
18. Shaw AT, Friboulet L, Leshchiner I, Gainor JF, Bergqvist S, Brooun A, et al. Resensitization to crizotinib by the lorlatinib ALK resistance mutation L1198F. *N Engl J Med.* (2016) 374:54–61. doi: 10.1056/NEJMoa1508887
19. Choi YL, Soda M, Yamashita Y, Ueno T, Takashima J, Nakajima T, et al. EML4-ALK mutations in lung cancer that confer resistance to ALK inhibitors. *N Engl J Med.* (2010) 363:1734–9. doi: 10.1056/NEJMoa1007478
20. Sasaki T, Koivunen J, Ogino A, Yanagita M, Nikiforow S, Zheng W, et al. A novel ALK secondary mutation and EGFR signaling cause resistance to ALK kinase inhibitors. *Cancer Res.* (2011) 71:6051–60. doi: 10.1158/0008-5472.can-11-1340
21. Hamid O, Robert C, Daud A, Hodi FS, Hwu WJ, Kefford R, et al. Safety and tumor responses with lambrolizumab (anti-PD-1) in melanoma. *N Engl J Med.* (2013) 369:134–44. doi: 10.1056/NEJMoa1305133
22. Peters S, Kerr KM, Stahel R. PD-1 blockade in advanced NSCLC: a focus on pembrolizumab. *Cancer Treat Rev.* (2018) 62:39–49. doi: 10.1016/j.ctrv.2017.10.002
23. Zaretsky JM, Garcia-Diaz A, Shin DS, Escuin-Ordinas H, Hugo W, Hu-Lieskovan S, et al. Mutations associated with acquired resistance to PD-1 blockade in melanoma. *N Engl J Med.* (2016) 375:819–29. doi: 10.1056/NEJMoa1604958
24. Condorelli R, Spring L, O'Shaughnessy J, Lacroix L, Bailleux C, Scott V, et al. Polyclonal RB1 mutations and acquired resistance to CDK 4/6 inhibitors in patients with metastatic breast cancer. *Ann Oncol.* (2018) 29:640–5. doi: 10.1093/annonc/mdx784
25. Cancer Genome Atlas Network. (2012). Comprehensive molecular portraits of human breast tumours. *Nature.* 490, 61–70. doi: 10.1038/nature11412
26. Herrera-Abreu MT, Palafox M, Asghar U, Rivas MA, Cutts RJ, Garcia-Murillas I, et al. Early adaptation and acquired resistance to CDK4/6 inhibition in estrogen receptor-positive breast cancer. *Cancer Res.* (2016) 76:2301–13. doi: 10.1158/0008-5472.can-15-0728
27. Renhowe PA. Inhibitors of growth factor receptor kinase-dependent signaling pathways in anticancer chemotherapy–clinical progress. *Curr Opin Drug Discov Devel.* (2002) 5:214. doi: 10.2174/09298670246 06957
28. Pao W, Miller V, Zakowski M, Doherty J, Politi K, Sarkaria I, et al. EGF receptor gene mutations are common in lung cancers from "never smokers" and are associated with sensitivity of tumors to gefitinib and erlotinib. *Proc Natl Acad Sci USA.* (2004) 101:13306–11. doi: 10.1073/pnas.04052 20101
29. Morin MJ. From oncogene to drug: development of small molecule tyrosine kinase inhibitors as anti-tumor and anti-angiogenic agents. *Oncogene.* (2000) 19:6574–83. doi: 10.1038/sj.onc.1204102
30. Inoue A, Kobayashi K, Usui K, Maemondo M, Okinaga S, Mikami I, et al. First-line gefitinib for patients with advanced non-small-cell lung cancer harboring epidermal growth factor receptor mutations without indication for chemotherapy. *J Clin Oncol.* (2009) 27:1394–400. doi: 10.1200/JCO.2008.18.7658
31. Maemondo M, Inoue A, Kobayashi K, Sugawara S, Oizumi S, Isobe H, et al. Gefitinib or chemotherapy for non-small-cell lung cancer with mutated EGFR. *N Engl J Med.* (2010) 362:2380–8. doi: 10.1056/NEJMoa0909530
32. Bell DW, Gore I, Okimoto RA, Godin-Heymann N, Sordella R, Mulloy R, et al. Inherited susceptibility to lung cancer may be associated with the T790M drug resistance mutation in EGFR. *Nat Genet.* (2005) 37:1315–6. doi: 10.1038/ng1671
33. Bose R, Kavuri SM, Searleman AC, Shen W, Shen D, Koboldt DC, et al. Activating HER2 mutations in HER2 gene amplification negative breast cancer. *Cancer Discov.* (2013) 3:224–37. doi: 10.1158/2159-8290.cd-12-0349
34. Xu X, De Angelis C, Burke KA, Nardone A, Hu H, Qin L, et al. HER2 Reactivation through acquisition of the HER2 L755S mutation as a mechanism of acquired resistance to HER2-targeted therapy in HER2(+) breast cancer. *Clin Cancer Res.* (2017) 23:5123–34. doi: 10.1158/1078-0432.ccr-16-2191
35. Dienstmann R, Tabernero J. Spectrum of gene mutations in colorectal cancer: implications for treatment. *Cancer J.* (2016) 22:149–55. doi: 10.1097/ppo.0000000000000191
36. Ross JS, Fakih M, Ali SM, Elvin JA, Schrock AB, Suh J, et al. Targeting HER2 in colorectal cancer: the landscape of amplification and short variant mutations in ERBB2 and ERBB3. *Cancer.* (2018) 124:1358–73. doi: 10.1002/cncr.31125
37. Ou SH. Crizotinib: a novel and first-in-class multitargeted tyrosine kinase inhibitor for the treatment of anaplastic lymphoma kinase rearranged non-small cell lung cancer and beyond. *Drug Des Devel Ther.* (2011) 5:471–85. doi: 10.2147/dddt.s19045
38. Kimura AGM. Molecularly targeted therapy: past, present and future. *Chemotherapy* 1:105. doi: 10.4172/2167-7700.1000105
39. Zhang S, Wang F, Keats J, Zhu X, Ning Y, Wardwell SD, et al. Crizotinib-resistant mutants of EML4-ALK identified through an accelerated mutagenesis screen. *Chem Biol Drug Des.* (2011) 78:999–1005. doi: 10.1111/j.1747-0285.2011.01239.x
40. Soda M, Choi YL, Enomoto M, Takada S, Yamashita Y, Ishikawa S, et al. Identification of the transforming EML4-ALK fusion gene in non-small-cell lung cancer. *Nature.* (2007) 448:561–6. doi: 10.1038/nature05945
41. Heuckmann JM, Holzel M, Sos ML, Heynck S, Balke-Want H, Koker M, et al. ALK mutations conferring differential resistance to structurally diverse ALK inhibitors. *Clin Cancer Res.* (2011) 17:7394–74. doi: 10.1158/1078-0432.ccr-11-1648
42. Zhang S, Anjum R, Squillace R, Nadworny S, Zhou T, Keats J, et al. The potent ALK inhibitor brigatinib (AP26113) overcomes mechanisms of resistance to first- and second-generation ALK inhibitors in preclinical models. *Clin Cancer Res.* (2016) 22:5527–38. doi: 10.1158/1078-0432.ccr-16-0569
43. Shaw AT, Felip E, Bauer TM, Besse B, Navarro A, Postel-Vinay S, et al. Lorlatinib in non-small-cell lung cancer with ALK or ROS1 rearrangement: an international, multicentre, open-label, single-arm first-in-man phase 1 trial. *Lancet Oncol.* (2017) 18:1590–9. doi: 10.1016/s1470-2045(17)30680-0
44. Uchibori K, Inase N, Araki M, Kamada M, Sato S, Okuno Y, et al. Brigatinib combined with anti-EGFR antibody overcomes osimertinib resistance in EGFR-mutated non-small-cell lung cancer. *Nat Commun.* (2017) 8:14768. doi: 10.1038/ncomms14768
45. Iranzo J, Martincorena I, Koonin EV. Cancer-mutation network and the number and specificity of driver mutations. *Proc Natl Acad Sci USA.* (2018) 115:E6010–9. doi: 10.1073/pnas.1803155115
46. Yue X, Zhao Y, Xu Y, Zheng M, Feng Z, Hu W. Mutant p53 in cancer: accumulation, gain-of-function, and therapy. *J Mol Biol.* (2017) 429:1595–606. doi: 10.1016/j.jmb.2017.03.030
47. Wang L, Wang H, Song D, Xu M, Liebmen M. New strategies for targeting drug combinations to overcome mutation-driven drug resistance. *Semin Cancer Biol.* (2017) 42:44–51. doi: 10.1016/j.semcancer.2016.11.002
48. Wu YL, Cheng Y, Zhou X, Lee KH, Nakagawa K, Niho S, et al. Dacomitinib versus gefitinib as first-line treatment for patients with EGFR-mutation-positive non-small-cell lung cancer (ARCHER 1050): a randomised, open-label, phase 3 trial. *Lancet Oncol.* (2017) 18:1454–66. doi: 10.1016/s1470-2045(17)30608-3
49. Engelman JA, Zejnullahu K, Gale CM, Lifshits E, Gonzales AJ, Shimamura T, et al. PF00299804, an irreversible pan-ERBB inhibitor, is effective in lung cancer models with EGFR and ERBB2 mutations that are resistant to gefitinib. *Cancer Res.* (2007) 67:11924–32. doi: 10.1158/0008-5472.can-07-1885

50. Chen G, McQuade JL, Panka DJ, Hudgens CW, Amin-Mansour A, Mu XJ, et al. Clinical, molecular, and immune analysis of dabrafenib-trametinib combination treatment for BRAF inhibitor-refractory metastatic melanoma: a phase 2 clinical trial. *JAMA Oncol.* (2016) 2:1056–64. doi: 10.1001/jamaoncol.2016.0509
51. Planchard D, Smit EF, Groen HJM, Mazieres J, Besse B, Helland A, et al. Dabrafenib plus trametinib in patients with previously untreated BRAF(V600E)-mutant metastatic non-small-cell lung cancer: an open-label, phase 2 trial. *Lancet Oncol.* (2017) 18:1307–16. doi: 10.1016/s1470-2045(17)30679-4
52. Gilmartin AG, Bleam MR, Groy A, Moss KG, Minthorn EA, Kulkarni SG, et al. GSK1120212 (JTP-74057) is an inhibitor of MEK activity and activation with favorable pharmacokinetic properties for sustained *in vivo* pathway inhibition. *Clin Cancer Res.* (2011) 17:989–1000. doi: 10.1158/1078-0432.ccr-10-2200
53. Puszkiel A, Noe G, Bellesoeur A, Kramkimel N, Paludetto MN, Thomas-Schoemann A, et al. Clinical pharmacokinetics and pharmacodynamics of dabrafenib. *Clin Pharmacokinet.* (2019) 58:451–67. doi: 10.1007/s40262-018-0703-0
54. Subbiah V, Kreitman RJ, Wainberg ZA, Cho JY, Schellens JHM, Soria JC, et al. Dabrafenib and trametinib treatment in patients with locally advanced or metastatic BRAF V600-mutant anaplastic thyroid cancer. *J Clin Oncol.* (2018) 36:7–13. doi: 10.1200/jco.2017.73.6785
55. Dummer R, Ascierto PA, Gogas HJ, Arance A, Mandala M, Liszkay G, et al. Overall survival in patients with BRAF-mutant melanoma receiving encorafenib plus binimetinib versus vemurafenib orencorafenib (COLUMBUS): a multicentre, open-label, randomised, phase 3 trial. *Lancet Oncol.* (2018b) 19:1315–27. doi: 10.1016/s1470-2045(18)30497-2
56. Sullivan RJ, Weber JS, Patel SP, Dummer R, Miller WH, Cosgrove D, et al. A phase Ib/II study of BRAF inhibitor (BRAFi) encorafenib (ENCO) plus MEK inhibitor (MEKi) binimetinib (BINI) in cutaneous melanoma patients naive to BRAFi treatment. *J Clin Oncol.* (2015) 33:9007–9007. doi: 10.1200/jco.2015.33.15_suppl.9007
57. Dummer R, Ascierto PA, Gogas HJ, Arance A, Mandala M, Liszkay G, et al. Encorafenib plus binimetinib versus vemurafenib or encorafenib in patients with BRAF-mutant melanoma (COLUMBUS): a multicentre, open-label, randomised phase 3 trial. *Lancet Oncol.* (2018) 19:603–15. doi: 10.1016/s1470-2045(18)30142-6
58. Huang M, Shen A, Ding J, Geng M. Molecularly targeted cancer therapy: some lessons from the past decade. *Trends Pharmacol Sci.* (2014) 35:41–50. doi: 10.1016/j.tips.2013.11.004

Conflict of Interest Statement: The authors declare that the research was conducted in the absence of any commercial or financial relationships that could be construed as a potential conflict of interest.

frontiers in Oncology

ORIGINAL RESEARCH
published: 16 April 2019
doi: 10.3389/fonc.2019.00274

Synthesis and Anticancer Activity Evaluation of Novel Phenanthridine Derivatives

Minghui Wan†, Lei Zhang†, Yiming Chen, Qiang Li, Wenli Fan, Qingxia Xue, Fang Yan and Weiguo Song**

School of Pharmacy, Weifang Medical University, Weifang, China

Based on the structure of sanguinarine, fourteen phenanthridine derivatives were designed and synthesized in the current study. The cytotoxic activities of synthesized compounds were evaluated against five human cancer cell lines (MCF-7, PC3, Hela, A549, and HepG2 cell lines) via MTT assay. Among all the compounds tested, molecule **8a** exhibited significant cytotoxic activity against MCF-7 cells with a IC_{50} value of 0.28 μM. A following up enzymatic assay indicated that compound **8a** could inhibit the activity of DNA topoisomerase I/II. Further mechanistic studies performed in the MCF-7 cell line revealed that compound **8a** could arrest cell cycle in S phase and induce cell apoptosis via downregulation of Bcl-2 and upregulation of Bax. Collectively, a potent DNA topoisomerase inhibitor (**8a**) was discovered, which exhibited potential as a candidate chemotherapeutic agent for the management of tumors in the present study.

Keywords: phenanthridine, anticancer, topoisomerase, apoptosis, cell cycle arrest

OPEN ACCESS

Edited by:
Zhe-Sheng Chen,
St. John's University, United States

Reviewed by:
Xiangbao Meng,
Peking University, China
Pranav Gupta,
Harvard Medical School,
United States

****Correspondence:***
Fang Yan
yanfang303@163.com
Weiguo Song
songwg@139.com

†These authors have contributed equally to this work

Specialty section:
This article was submitted to Cancer Molecular Targets and Therapeutics, a section of the journal Frontiers in Oncology

Received: *24 February 2019*
Accepted: *25 March 2019*
Published: *16 April 2019*

Citation:
Wan M, Zhang L, Chen Y, Li Q, Fan W, Xue Q, Yan F and Song W (2019) Synthesis and Anticancer Activity Evaluation of Novel Phenanthridine Derivatives. Front. Oncol. 9:274. doi: 10.3389/fonc.2019.00274

INTRODUCTION

Sanguinarine (SA) belongs to the chrysene-skeleton-based heterocyclic benzo [c] phenanthridine alkaloids family (**Figure 1**), which are widely distributed in plants, such as *Sanguinaria canadensis* and *Papaveraceae* (1–3). Although SA was isolated in the late 1940s (4), extensive research focusing on the molecular mechanism of its anti-tumor effects has commenced only recently (5). SA has attracted extensive attention because of its significant biological activities, including anti-tumor (6, 7), anti-inflammatory, anti-angiogenesis, antiplatelet, antiviral, and anti-fungal effects (8–11). The flat polyaromatic structure of SA enabled it to directly interact with DNA (12). SA-induced cell cycle arrest and apoptosis was found to not only be caused by DNA damage, but also to be a combined result of targeting other cell structures, such as topoisomerases (Top) (13, 14), antiapoptotic protein (6, 15, 16), and mitochondrial membranes (17, 18).

Previous studies reported that SA might interfere with mitochondrial membranes and induce apoptosis in the CEM leukemia cell line HL-60 (18, 19) and KB carcinoma cell line (17). The potential mechanism was associated with nuclear factor (NF-κB) activation (1), mitochondria damage induced caspase activation (20), and increased expression of Bax/Bcl-2 (21, 22). The proapoptotic effects of SA have significant potential in the development of novel antitumor agents with SA as a lead compound. In addition, SA elicited G0/G1 cell cycle arrest (23), which can be associated with the translocation of cyclin D1 and Top II from nucleus to cytoplasm (24, 25). Additionally, NF-κB, AP-1, MMP-9, and STAT3 inhibition were also observed following SA treatment (26–28) and subsequently resulted in suppressed cancer cell metastasis. Moreover,

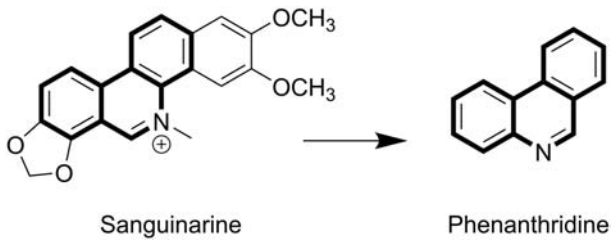

FIGURE 1 | The structures of SA and phenanthridine.

abolishment of VEGF-induced AKT activation was also proposed as another potential mechanism for the antiangiogenic activity of SA (29, 30), which was believed to contribute to its anti-tumor effects in the animal models of melanoma (31) and colorectal cancer (26).

SA exhibited significant potential in the development of new antitumor drugs, as indicated from the results of a wide range of *in vitro* and *in vivo* investigations. Due to the structure of multiple aromatic rings, further development of SA as antitumor agent is restricted by its low solubilities and severe side effects. To discover SA analogs with improved solubilities and activities, a series of phenanthridine derivatives with reduced aromaticities were designed and synthesized using phenanthridine as a core scaffold. All the derived compounds were identified with ^{13}C NMR, ^{1}H NMR, HRMS, and biologically evaluated against MCF-7 (human breast cancer), PC3 (human prostatic cancer), Hela (human cervical cancer), A549 (human lung cancer), and HepG2 (human hepatocellular carcinoma) cell lines. During further investigation of the underlying mechanism, molecular techniques such as flow cytometry, hoechst 33258 staining and western blotting were utilized with the representative compounds synthesized in the current study.

Chemistry

The synthetic pathway of phenanthridine derivatives is shown in **Scheme 1**. As illustrated, amino protection of starting material **1** was performed to afforded compound **2**. The following bromine substitution and deprotection of amino group were carried out to generate intermediate **4**. Preparation of intermediate **5** was performed by Suzuki coupling of 2-bromoaniline derivatives with corresponding phenylboronic acids. Treatment of intermediate **5** under acidic condition yielded compound **6**, and subsequent dehydration of compound **6** afforded 2-isocyanobiphenyls derivatives **7a**-**t**. In the presence of benzoyl peroxide, phenanthridine derivatives **8a**-**n** were derived by reacting of 2-isocyanobiphenyls derivatives with carbon tetrachloride (32).

Cytotoxicity Assay

The cytotoxicity of synthesized compounds was evaluated against five tumor cell lines (A549, PC3, MCF-7, HepG2, and Hela) via MTT assay. Initially, two doses of each compound (5 and 1 μmol/L) were evaluated. As shown in **Table 1**, compounds **8a**, **8b**, **8d**, **8e**, **8l**, **8m**, and **8n** exhibited significant inhibitory activities against MCF-7, PC3, and Hela cells at the dose of 5 μmol/L. However, when compared with the lead compound SA, molecule **8d**, **8l**, and **8n** exhibited lower inhibitory activity at the dose of 1 μmol/L.

Based on the data mentioned above, compounds **8a**, **8b**, **8e**, and **8m** were selected for further test with more doses against the tumor cell lines. The IC_{50} values of these compounds were summarized in **Table 2**, all the four compounds exhibited potent cytotoxicity against the five tumor cell lines tested compared with the positive control SA and clinically used antitumor drug Etoposide (VP 16). The results indicated that compounds **8a** and **8m** exhibited potent activities against all the tested cancer cell lines. Molecule **8a** ($IC_{50} = 0.28 \pm 0.08$) showed potency of over 6 times higher than SA ($IC_{50} = 1.77 \pm 0.06$) in the inhibition of MCF-7 cells, and molecule **8m** ($IC_{50} = 0.39 \pm 0.08$) exhibited 8.9 times of potency comparing to SA ($IC_{50} = 3.49 \pm 0.41$) in the inhibition of HepG2 cells. Therefore, **8a**, **8b**, **8e**, and **8m** were selected for further mechanistical studies.

Topoisomerase Inhibition Assay

To elucidate the target profiles of the cytotoxic compounds (**8a**, **8b**, **8e**, and **8m**), the inhibitory effects of these compounds were tested against human DNA Top I and IIα by relaxing assay using pBR322 DNA. 10-hydroxy camptothecin (OPT) and VP 16 were used as a positive control for Top I and IIα inhibition, respectively. The Top I/II were able to completely convert the supercoiled DNA to open circular form in the absence of inhibitors (**Figure 2,** lane B). In contrast, positive control (OPT/VP 16) and active compounds inhibited the activity of Top, which affected the unwinding of the supercoiled DNA, leading to a band pattern similar to the negative control (**Figure 2**). As shown in **Figure 2A**, positive control OPT and SA inhibited the activity of both Top I and Top IIα. Compound **8a** exhibited weak Top I inhibition, which was similar to OPT. In the Top IIα test, all the tested compounds exhibited potent DNA Top IIα inhibitory activities at the concentration of 100 μM (**Figure 2B**). Based on the above findings, molecule **8a** with most potent cytotoxicity and enzymatic inhibitory activities is chosen as a potential candidate for further investigation.

Cell Cycle Analysis

To elucidate the effects of molecule **8a** on cell cycle distributions, MCF-7 cells were treated with various doses of molecule **8a** (0, 0.15, 0.3, and 0.6 μM) for 24 h. As shown in **Figure 3**, compound **8a** treatment led to significant accumulation of MCF-7 cells at S phase (from 18.86 to 42.99%) dose-dependently. While reduced cells at the G2/M phase was detected from 23.46 to 10.45% (0.15 μM), 8.69% (0.3 μM), and 5.62% (0.6 μM) following treatment with compound **8a** dose-dependently. These results suggest that compound **8a** exhibited a significant antitumor effect and led to MCF-7 cell cycle arrest at the S phase in a dose-dependent manner.

Cell Apoptosis Assay

To further investigate the role of apoptosis in the antitumor effect of compound **8a**, Hoechst 33258 staining was performed to investigate the nuclear morphological changes following molecule **8a** treatment on MCF-7 cells. Hoechst 33258 is a

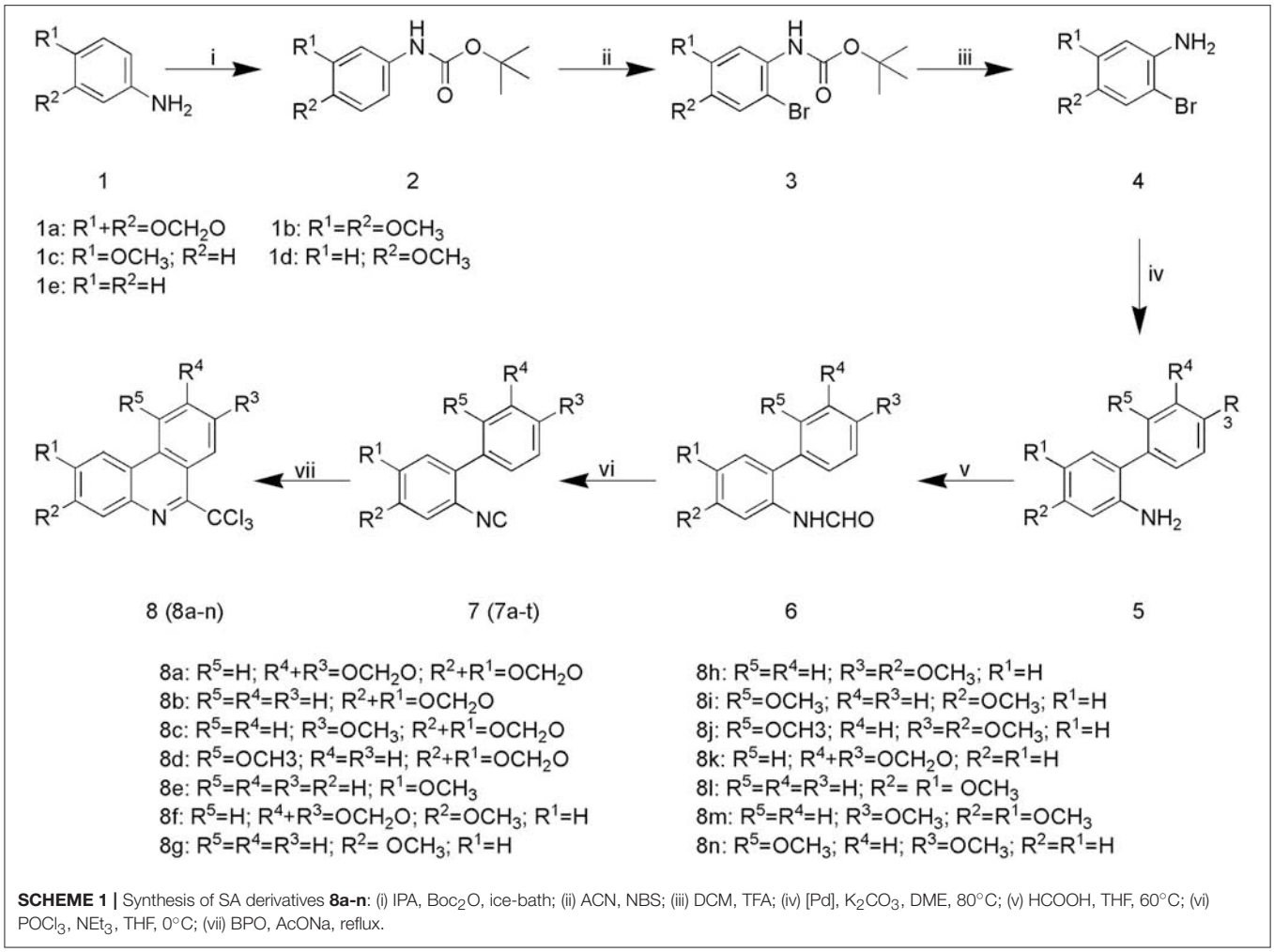

SCHEME 1 | Synthesis of SA derivatives **8a-n**: (i) IPA, Boc_2O, ice-bath; (ii) ACN, NBS; (iii) DCM, TFA; (iv) [Pd], K_2CO_3, DME, 80°C; (v) HCOOH, THF, 60°C; (vi) $POCl_3$, NEt_3, THF, 0°C; (vii) BPO, AcONa, reflux.

fluorescent stain used to label DNA; live cells nuclei will be stained with uniformly light blue and apoptotic cells nuclei will be stained with bright blue because of chromatin condensation. As shown in **Figure 4A**, higher levers of apoptotic cells with nuclear condensation, nuclear fragmentation and enhanced brightness were detected in the cells following treatment with various doses of molecule **8a** (0.15, 0.3, and 0.6 μM). To quantify the number of apoptotic cells and to distinguish early apoptosis and secondary necrosis, MCF-7 cells were stained with annexin V-FITC/PI. As shown in **Figure 4B**, after treatment with difference doses of compound **8a** (0, 0.15, 0.3, and 0.6 μM), the percentage of apoptotic cells were significantly increased from 11.16% of the control to 14.35, 22.79, and 28.98%, respectively, indicating that induction of cell apoptosis contributes to the antitumor effect of compound **8a**.

Protein Expressions of Bcl-2 and Bax

Apoptosis is a heavily regulated cell death process influenced by a series of regulatory molecules (33). The mitochondria-dependent pathway has been described as an important signaling pathway of cell apoptosis regulated by the Bcl-2 family including the pro- and anti-apoptotic proteins such as Bax (pro-apoptotic protein) and Bcl-2 (anti-apoptotic protein) (34–36). Moreover, the ratio of Bax/Bcl-2 is important for apoptosis induced by the mitochondrial pathway. Therefore, the effect of compound **8a** on the levels of Bax and Bcl-2 was evaluated in MCF-7 cells. The results indicated that compound **8a** could significantly downregulate Bcl-2 levels and upregulate Bax levels in MCF-7 cells, increasing the ratio of Bax/Bcl-2 in a dose-dependent manner (**Figure 5**). Collectively, these results suggest that compound **8a** induced apoptosis by regulating the expression of apoptosis-related proteins.

CONCLUSIONS

Based on the structure of sanguinarine, fourteen phenanthridine derivatives **8a**-**m** were synthesized and evaluated for their cytotoxic activity against five different human cancer cell lines. Among the evaluated compounds, **8a** exhibited a broad spectrum of anti-proliferative activities against all the tested cancer cell lines. Further mechanistic assay revealed that compound **8a** could inhibit the activity of both DNA Top I and Top II, as well as preventing cell transition

TABLE 1 | The inhibitory activity on tumor cell of phenanthridine derivatives[a].

Compound[b]	MCF-7 (%)		PC3 (%)		Hela (%)	
	5 μM	1 μM	5 μM	1 μM	5 μM	1 μM
8a	95.66	71.50	91.21	78.47	88.50	58.76
8b	93.66	58.29	89.77	64.16	84.90	54.01
8c	25.06	19.56	25.32	<5	19.66	16.00
8d	83.17	27.48	81.72	43.50	58.92	28.78
8e	95.36	60.07	88.65	73.04	83.80	23.52
8f	36.73	15.99	15.65	<5	16.26	<5
8g	18.23	23.76	<5	<5	<5	<5
8h	31.23	16.30	26.40	<5	15.74	8.61
8i	16.15	13.60	<5	<5	<5	<5
8j	62.18	14.00	64.62	<5	37.46	7.47
8k	19.74	32.60	12.81	<5	8.14	<5
8l	94.05	34.75	89.37	42.52	81.62	32.25
8m	97.83	89.34	95.26	88.75	87.57	80.26
8n	72.26	49.63	64.61	<5	30.69	9.72
SA	98.29	53.86	96.42	95.60	96.13	64.41
VP16	41.84	13.67	38.39	22.39	29.18	17.42

[a]*Values are average of three determinations and deviation of data results is <20%.*
[b]*All compounds were dissolved in DMSO for testing.*

TABLE 2 | The IC_{50}^{a} of phenanthridine derivatives.

Compound	IC_{50} (μM) [a]				
	MCF-7	PC3	Hela	A549	HepG2
8a	0.28 ± 0.08	0.30 ± 0.06	0.48 ± 0.07	0.89 ± 0.07	0.70 ± 0.09
8b	0.77 ± 0.04	0.76 ± 0.01	0.66 ± 0.12	0.85 ± 0.03	1.23 ± 0.08
8e	0.61 ± 0.03	0.45 ± 0.04	1.93 ± 0.02	0.89 ± 0.09	2.21 ± 0.14
8m	0.24 ± 0.08	0.22 ± 0.04	0.49 ± 0.02	0.85 ± 0.04	0.39 ± 0.08
SA	1.77 ± 0.06	1.67 ± 0.33	1.07 ± 0.06	2.68 ± 0.18	3.49 ± 0.41
VP16	>10	>10	>10	>10	>10

[a]*IC_{50} values are represented as mean ±SD (n = 3).*

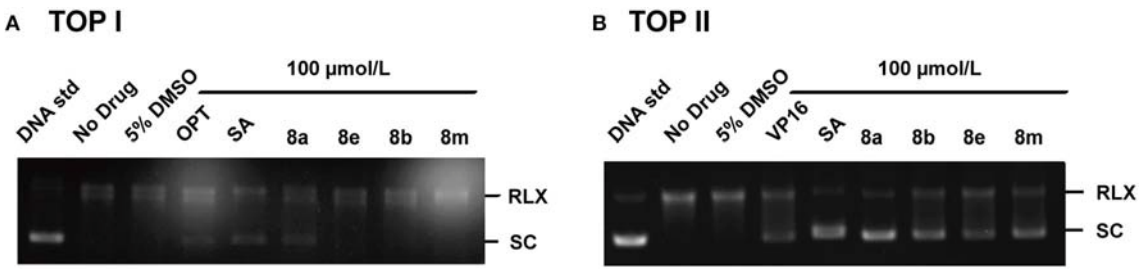

FIGURE 2 | Effects of phenanthridine derivatives and positive control on human Top I **(A)**/IIa **(B)**. Native superhelix pBR322 was incubated at 37°C for 30 min with 2 units of human Top I/IIα in the absence (lane 2) or presence of compound at concentration 100 μM. One hundred micromolar OPT, VP 16, and SA were used as positive controls, respectively. Negatively supercoiled pBR322 (SC) and relaxed DNA (RLX) were shown. DNA samples were run on agarose gel followed by Genecolour I TM staining.

from S to G2 phase dose-dependently. Apoptosis studies against MCF-7 cells indicated that downregulation of Bcl-2 and upregulation of Bax expression may contribute to the anti-proliferative activities. In summary, these findings suggest that molecule **8a** is a potent lead compound in the derived phenanthridine derivatives. Further molecule **8a** based structural

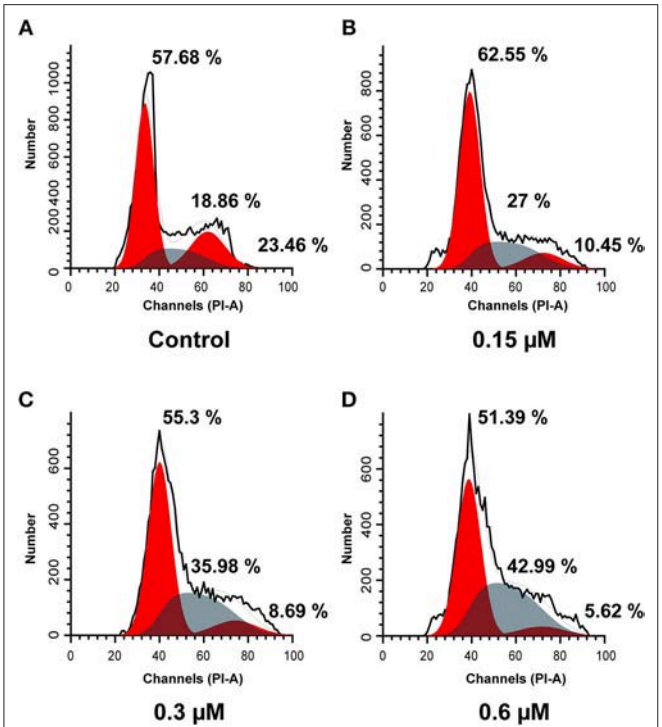

FIGURE 3 | Cell cycle analysis using PI staining of compound **8a** on MCF-7 cells. Cells were treated with compound **8a** at 0.15 **(B)**, 0.3 **(C)**, and 0.6 **(D)** μM for 24 h, compared with the control **(A)**. Cell cycle were detected by flow cytometry.

modification may be beneficial in the discovery of novel anticancer agents with improved antitumor activity and reduced side effects.

MATERIALS AND METHODS

Chemistry

All chemicals were obtained from commercial suppliers and used without further purification. Reactions progress was detected by thin layer chromatography (TLC) and visualized under UV light. Two hundred to three hundred mesh silica gel was used for column chromatography. All compounds were characterized by ^{13}C NMR, ^{1}H NMR, and HRMS. ^{1}H and ^{13}C NMR spectra were recorded on Mercury Plus-400 with internal standard used TMS and recorded in parts per million (ppm). Date were reported as s (singlet), br (broad), s (singlet), d (doublet), t (triplet), q (quartet), m (multiplet), and coupling constant (J) in hertz (Hz). Melting point was determined by MP 100 Automatic Melting Point Apparatus.

Representative Procedure for the Synthesis of Compounds 7a-t

To dissolve compound **6**, THF and NEt_3 was added, the solution was added to $POCl_3$ (11 mmol) until the solution was cooled to 0°C. The reaction was quenched by saturated Na_2CO_3 until complete consumption of starting material, monitored by TLC. The solution of the crude product was extracted with ethyl acetate, and organic layer was dried over Na_2SO_4 and evaporated to dryness. The residue was purified by column chromatography with silica gel (200–300 mesh).

2-isocyano-3′,4′-Methylenedioxy-4,5-methylenedioxy-1,1′-biphenyl (7a)

Yellowish -white solid, Yield 78%; Mp (154.4–156.1°C); ^{1}H NMR (400 MHz, $CDCl_3$) δ 6.90 (d, J = 8.9 Hz, 4H), 6.78 (s, 1H), 6.05 (s, 2H), 6.01 (s, 2H).

2-isocyano-4,5-methylenedioxy-1,1′-biphenyl (7b)

Brown solid, Yield 80%; Mp (90.1–90.3°C); ^{1}H NMR (400 MHz, $CDCl_3$) δ 7.54–7.30 (m, 5H), 6.91 (s, 1H), 6.82 (s, 1H), 6.05 (s, 2H).

2-isocyano-4,5-methylenedioxy-4′-methoxy-1,1′-biphenyl (7c)

White solid, Yield 81%; Mp (132–133.1°C);^{1}H NMR (400 MHz, $CDCl_3$) δ 7.39 (d, J = 8.7 Hz, 2H), 6.98 (d, J = 8.7 Hz, 2H), 6.90 (s, 1H), 6.80 (s, 1H), 6.05 (s, 2H), 3.85 (s, 3H).

2-isocyano-4,5-methylenedioxy-2′-methoxy-1,1′-biphenyl (7d)

Yellowish-white solid, Yield 82%; Mp (139.4–140.7°C); ^{1}H NMR (400 MHz, $CDCl_3$) δ 7.43–7.34 (m, 1H), 7.20 (dd, J = 7.5, 1.8 Hz, 1H), 7.07–6.96 (m, 2H), 6.90 (s, 1H), 6.79 (s, 1H), 6.05 (s, 2H), 3.83 (s, 3H).

2-isocyano-4,5-methylenedioxy-2′,4′-dimethoxy-1,1′-biphenyl (7e)

Brown solid, Yield 79%; Mp (161.4–161.9°C); ^{1}H NMR (400 MHz, $CDCl_3$) δ 7.10 (s, 1H), 6.88 (s, 1H), 6.77 (s, 1H), 6.56 (dt, J = 5.2, 2.5 Hz, 2H), 6.04 (s, 2H), 3.85 (s, 3H), 3.81 (s, 3H).

2-isocyano-3′,4′-methylenedioxy-5-methoxy-1,1′-biphenyl (7f)

Yellowish-white solid, Yield 81%; Mp (119.6–120.1°C); ^{1}H NMR (400 MHz, $CDCl_3$) δ 7.58 (d, J = 8.6 Hz, 1H), 7.12 (d, J = 1.7 Hz, 1H), 7.09–6.95 (m, 4H), 6.10 (s, 2H), 3.84 (s, 3H).

2-isocyano-5-methoxy-1,1′-biphenyl (7g)

Black oil, Yield 83%; ^{1}H NMR (400 MHz, $CDCl_3$) δ 7.62 (d, J = 8.7 Hz, 1H), 7.58–7.42 (m, 5H), 7.08–6.99 (m, 2H), 3.85 (s, 3H).

2'-isocyano-3,4-methylenedioxy-1,1′-biphenyl (7h)

Green solid, Yield 85%; Mp (71.6–73.9°C); ^{1}H NMR (400 MHz, $CDCl_3$) δ 6.02 (s, 2H), 7.02–6.94 (m, 2H), 6.94–6.87 (m, 1H), 7.46 (d, J = 9.3 Hz, 1H), 7.43–7.30 (m, 3H).

2'-isocyano-2,4-dimethoxy-1,1′-biphenyl (7i)

Yellowish-white solid, Yield 79%; Mp (90.1–90.5°C); ^{1}H NMR (400 MHz, $CDCl_3$) δ 7.41 (ddd, J = 8.9, 7.4, 1.8 Hz, 2H), 7.38–7.29 (m, 2H), 7.18–7.10 (m, 1H), 6.58 (dd, J = 5.7, 2.2 Hz, 2H), 3.86 (s, 3H), 3.81 (s, 3H).

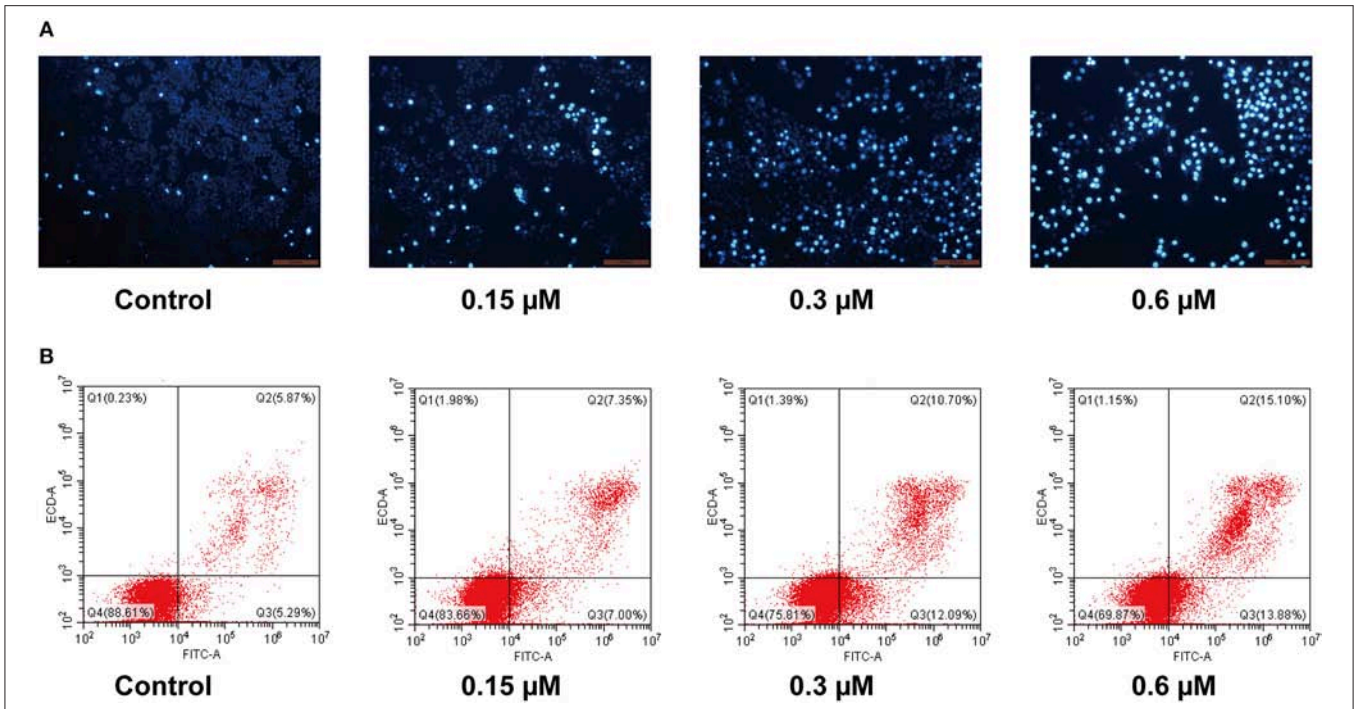

FIGURE 4 | Pro-apoptotic effect of compound **8a** on MCF-7 cells. **(A)** Apoptotic assay by Hoechst 33258. MCF-7 cells were treated with compound **8a** at 0.15, 0.3, and 0.6 μM for 24 h, and then cells were stained with Hoechst 33258 and visualized under a fluorescent microscope. **(B)** Apoptotic assay by flow cytometry. MCF-7 cells were treated with compound **8a** at 0.15, 0.3, and 0.6 μM for 24 h. Then cells were stained with Annexin V-FITC/PI and were detected by flow cytometry analysis.

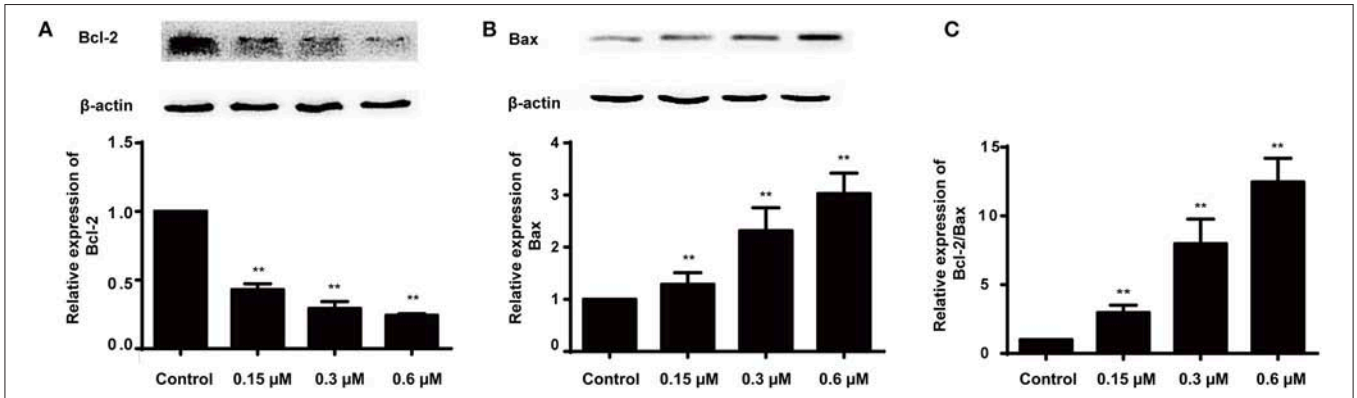

FIGURE 5 | Effects of **8a** on the expressions of Bcl-2 **(A)**, Bax **(B)** and the expression ratio **(C)** in MCF-7 cells. The cells were treated with different concentrations (0.15, 0.3, and 0.6 μM) for 24 h; β-actin served as an internal control. All date were represented as mean ± SD ($n = 3$). $^{**}p < 0.01$, compared with control group.

2′-isocyano-2,4,5′-trimethoxy-1,1′-biphenyl (7j)

Yellow solid, Yield 80%; Mp (104.6–104.9°C); ^{1}H NMR (400 MHz, $CDCl_3$) δ 7.35 (d, $J = 8.4$ Hz, 1H), 7.14 (d, $J = 8.9$ Hz, 1H), 6.88–6.79 (m, 2H), 6.58 (dd, $J = 5.4$, 2.3 Hz, 2H), 3.86 (s, 3H), 3.82 (s, 6H).

2-isocyano-3′,4′-methylenedioxy-4-methoxy-1,1′-biphenyl (7k)

Yellowish-white solid, Yield 75%; Mp (120.6–120.9°C); ^{1}H NMR (400 MHz, $CDCl_3$) δ 7.28 (d, $J = 8.4$ Hz, 1H), 7.02–6.86 (m, 5H), 6.02 (s, 2H), 3.85 (s, 3H).

2-isocyano-4-methoxy-1,1′-biphenyl (7l)

Yellow solid, Yield 78%; Mp (117.3–117.6°C); ^{1}H NMR (400 MHz, $CDCl_3$) δ 7.53–7.43 (m, 4H), 7.43–7.36 (m, 1H), 7.33 (d, $J = 9.0$ Hz, 1H), 7.05–6.97 (m, 2H), 3.86 (s, 3H).

2-isocyano-4,4′-dimethoxy-1,1′-biphenyl (7m)

Yellowish brown solid, Yield 83%; Mp (102.4–102.8°C); ^{1}H NMR (400 MHz, $CDCl_3$) δ 7.44–7.37 (m, 2H), 7.30 (d, $J = 9.0$ Hz, 1H), 6.99 (d, $J = 9.0$ Hz, 4H), 3.85 (d, $J = 4.0$ Hz, 6H).

2-isocyano-2′,4-dimethoxy-1,1′-biphenyl (7n)
White solid, Yield 82%; Mp (125.5–126°C); ^{1}H NMR (400 MHz, $CDCl_3$) δ 7.48–7.34 (m, 1H), 7.33–7.17 (m, 2H), 7.08–6.94 (m, 4H), 3.84 (d, J = 5.4 Hz, 6H).

2-isocyano-2′,4,4′-trimethoxy-1,1′-biphenyl (7o)
Yellowish-white solid, Yield 80%; Mp (105.9–107.3°C); ^{1}H NMR (400 MHz, $CDCl_3$) δ 7.26 (d, J = 1.7 Hz, 1H), 7.12 (d, J = 8.9 Hz, 1H), 7.01–6.93 (m, 2H), 6.61–6.53 (m, 2H), 3.90–3.79 (m, 9H).

2-isocyano-3′,4′-methylenedioxy-4,5-dimethoxy-1,1′-biphenyl (7p)
Brown solid, Yield 84%; Mp (171.7–172.3°C); ^{1}H NMR (400 MHz, $CDCl_3$) δ 6.99–6.86 (m, 4H), 6.80 (s, 1H), 6.02 (s, 2H), 3.91 (d, J = 2.5 Hz, 6H).

2-isocyano-4,5-dimethoxy-1,1′-biphenyl (7q)
Yellowish-white solid, Yield 82%; Mp (139.4–139.9°C); ^{1}H NMR (400 MHz, $CDCl_3$) δ 7.27 (s, 1H), 7.01 (s, 1H), 3.85 (d, J = 3.7 Hz, 5H), 7.58–7.47 (m, 3H), 7.47–7.39 (m, 1H).

2-isocyano-4,4′,5-trimethoxy-1,1′-biphenyl (7r)
Yellowish brown solid, Yield 84%; Mp (102.7–103.7°C); ^{1}H NMR (400 MHz, $CDCl_3$) δ 7.43 (d, J = 8.7 Hz, 2H), 7.00 (d, J = 8.7 Hz, 2H), 6.93 (s, 1H), 6.82 (s, 1H), 3.92 (d, J = 1.5 Hz, 6H), 3.86 (s, 3H).

2-isocyano-2′,4,5-trimethoxy-1,1′-biphenyl (7s)
Yellow solid, Yield 83%; Mp (103–103.6°C); ^{1}H NMR (400 MHz, $CDCl_3$) δ 7.44–7.35 (m, 1H), 7.28–7.20 (m, 1H), 7.09–6.98 (m, 2H), 6.94 (s, 1H), 6.82 (s, 1H), 3.94–3.82 (m, 9H).

2-isocyano-2′,4,4′,5-tetramethoxy-1,1′-biphenyl (7t)
Yellowish-white solid, Yield 82%; Mp (123.4–123.9°C); ^{1}H NMR (400 MHz, $CDCl_3$) δ 7.15 (d, J = 8.9 Hz, 1H), 6.92 (s, 1H), 6.79 (s, 1H), 6.57 (dq, J = 4.2, 2.4 Hz, 2H), 3.91 (s, 3H), 3.88 (s, 3H), 3.86 (s, 3H), 3.82 (s, 3H).

Representative Procedure for the Synthesis of Compounds 8a-8n

A mixture was produced of 2-isocyanobiphenyls derivatives (0.5 mmol), benzoyl peroxide (0.6 mmol), AcONa (1.0 mmol) in CCl_4 (2 mL) under an atmosphere of N_2. The reaction was stirred under reflux until complete consumption of starting material, monitored by TLC (about 16h). The solution of the crude product was extracted with ethyl acetate. The organic layers were washed with a saturated solution of $NaHCO_3$ and dried over Na_2SO_4 and evaporated to dryness. The residue was purified by column chromatography with silica gel (200–300 mesh) to afford the product 6-trichloromethylphenanthridine.

2,3-methylenedioxy-8,9-methylenedioxy-6-(trichloromethyl)phenanthridine (8a)
Yellow solid, Yield 40%; Mp (198.7–199.6°C); ^{1}H NMR (400 MHz, $CDCl_3$): δ 8.23 (s, 1H), 7.77 (s, 1H), 7.67 (s, 1H), 7.53 (s, 1H), 6.18 (d, J = 8.5 Hz, 4H); ^{13}C NMR(101 MHz, DMSO): δ 151.43, 150.27, 149.97, 149.09, 148.77, 147.57, 133.32, 129.68, 128.98, 115.89, 107.21, 104.01, 103.18, 102.90, 101.57, 100.33; HRMS (ESI) *m/z* 383.9592 (M+H).

2,3-methylenedioxy-6-(trichloromethyl)phenanthridine (8b)
Yellowish solid, Yield 39%; Mp (175.4–176.5°C); ^{1}H NMR(400 MHz, $CDCl_3$): δ 8.92 (d, J = 8.4 Hz, 1H), 8.49 (d, J = 8.2 Hz, 1H), 7.91–7.78 (m, 2H), 7.68 (t, J = 7.6 Hz, 1H), 7.60 (s, 1H), 6.19 (s, 2H); ^{13}C NMR(101 MHz, DMSO): δ 150.59, 150.37, 150.29, 137.46, 134.81, 131.31, 127.60, 127.04, 124.18, 121.88, 119.36, 107.77, 103.08, 100.50; HRMS (ESI) *m/z* 339.9696 (M+H).

2,3-methylenedioxy-8-methoxy-6-(trichloromethyl)phenanthridine (8c)
Brown solid, Yield 41%; Mp (93.8–95.0°C); ^{1}H NMR(400 MHz, $CDCl_3$) δ 8.12–8.05 (m, 8H), 7.80 (s, 1H), 7.67 (t, J = 7.5 Hz, 4H), 6.17 (s, 2H), 4.01 (s, 3H); ^{13}C NMR(101 MHz, DMSO) δ 167.67, 163.08, 162.77, 135.60, 134.08, 133.34, 131.07, 130.82, 129.93, 129.87, 129.78, 129.70, 129.31, 129.01, 128.45, 124.97; HRMS (ESI) *m/z* 369.9804 (M+H).

2,3-methylenedioxy-10-methoxy-6-(trichloromethyl)phenanthridine(8d)
Yellow solid; Yield 38%; Mp (219.7–222.3°C); ^{1}H NMR (400 MHz, DMSO) δ 7.95 (d, J = 6.3 Hz, 1H), 7.81 (t, J = 8.3 Hz, 1H), 7.59 (d, J = 3.6 Hz, 2H), 7.31 (t, J = 7.8 Hz, 1H), 6.32 (s, 2H), 3.69 (s, 3H); HRMS (ESI) *m/z* 369.9804 (M+H).

2-methoxy-6-(trichloromethyl)phenanthridine (8e)
Yellowish-white solid; Yield 37%; Mp (119–120.9°C); ^{1}H NMR (400 MHz, $CDCl_3$): δ 8.96 (d, J = 8.2 Hz, 1H), 8.65 (d, J = 8.4 Hz, 1H), 8.19 (d, J = 9.0 Hz, 1H), 7.94–7.83 (m, 2H), 7.80–7.71 (m, 1H), 7.42 (dd, J = 9.0, 2.7 Hz, 1H), 4.05 (s, 3H); ^{13}C NMR (101 MHz, DMSO): δ 160.62, 149.93, 135.31, 134.27, 132.51, 131.38, 128.05, 127.82, 126.70, 124.59, 120.53, 120.27, 104.00, 98.71, 56.46; HRMS (ESI) *m/z* 325.9901 (M+H).

8,9-methylenedioxy-3-methoxy-6-(trichloromethyl)phenanthridine (8f)
Brown solid; Yield 32%; Mp (197.5–197.8°C); ^{1}H NMR (400 MHz, $CDCl_3$) δ 8.36–8.19 (m, 2H), 7.91 (s, 1H), 7.59 (d, J = 2.7 Hz, 1H), 7.35 (dd, J = 9.1, 2.7 Hz, 1H), 6.20 (s, 2H), 4.00 (s, 3H); ^{13}C NMR (101 MHz, DMSO): δ 160.32, 151.87, 141.76, 133.80, 124.77, 120.86, 119.65, 115.39, 109.96, 108.77, 104.45, 103.88, 103.25, 101.29, 100.64, 56.08; HRMS (ESI) *m/z* 369.9798 (M+H).

3-methoxy-6-(trichloromethyl)phenanthridine (8g)
Yellow solid; Yield 26%; Mp (175.1–175.3°C); ^{1}H NMR (400 MHz, $CDCl_3$): δ 8.93 (d, J = 8.7 Hz, 1H), 8.62 (d, J = 8.4 Hz, 1H), 8.48 (d, J = 9.1 Hz, 1H), 7.90–7.81 (m, 1H), 7.72–7.63 (m, 2H), 7.44–7.36 (m, 1H), 4.02 (s, 3H). ^{13}C NMR (101 MHz, DMSO): δ 160.81, 152.92, 142.01, 135.11, 131.94, 127.91, 126.82, 124.58, 123.65, 120.95, 119.09,119.06, 110.67, 98.60, 56.13. HRMS (ESI) *m/z* 325.9899 (M+H).

3,8-dimethoxy-6-(trichloromethyl)phenanthridine (8h)
Yellow solid; Yield 40%; Mp (146.7–147.2°C); ^{1}H NMR (400 MHz, $CDCl_3$): δ 8.52 (d, J = 9.2 Hz, 1H), 8.39 (d, J = 9.1 Hz, 1H), 8.28 (d, J = 2.6 Hz, 1H), 7.63 (d, J = 2.7 Hz, 1H), 7.50 (dd, J = 9.2, 2.6 Hz, 1H), 7.38 (dd, J = 9.1, 2.7 Hz, 1H), 4.01 (d, J = 2.4 Hz, 6H); ^{13}C NMR (101 MHz, DMSO): δ 160.06, 157.07, 151.84, 141.12, 129.60, 125.46, 124.08, 122.20, 121.18, 120.32, 119.35, 110.40, 108.81, 56.07, 55.91; HRMS (ESI) *m/z* 356.0009 (M+H).

3,10-dimethoxy-6-(trichloromethyl)phenanthridine (8i)
Yellow solid; Yield 37%; Mp (149.9–150.9°C). ^{1}H NMR (400 MHz, $CDCl_3$): δ 9.46 (d, J = 9.5 Hz, 1H), 8.60 (d, J = 8.5 Hz, 1H), 7.72–7.56 (m, 2H), 7.41–7.29 (m, 2H), 4.16 (s, 3H), 4.02 (s, 3H); ^{13}C NMR (101 MHz, DMSO) δ 159.78, 157.90, 152.59, 142.64, 129.33, 127.12, 125.28, 120.88, 120.27, 120.03, 118.54, 113.19, 110.92, 56.63, 55.97; HRMS (ESI) *m/z* 356.0009 (M+H).

3,8,10-trimethoxy-6-(trichloromethyl)phenanthridine (8j)
Yellow solid; Yield 35%; Mp (97–97.3°C); ^{1}H NMR (400 MHz, $CDCl_3$): δ 7.98 (d, J = 2.3 Hz, 1H), 7.70–7.60 (m, 3H), 7.35 (dd, J = 9.5, 2.9 Hz, 1H), 4.12 (s, 3H), 4.01 (d, J = 2.9 Hz, 6H); ^{13}C NMR (101 MHz, DMSO): δ 162.77, 159.25, 159.09, 157.44, 135.58, 130.82, 129.78, 129.00, 128.38, 120.61, 120.42, 110.71, 103.67, 101.47, 56.84, 55.95, 55.92; HRMS (ESI) *m/z* 386.0112 (M+H).

8,9-methylenedioxy-6-(trichloromethyl)phenanthridine (8k)
Yellowish solid; Yield 32%; Mp (164.4–165°C); ^{1}H NMR (400 MHz, $CDCl_3$) δ 8.43–8.36 (m, 1H), 8.30 (s, 1H), 8.27–8.20 (m, 1H), 8.02 (s, 1H), 7.73 (tt, J = 7.1, 5.3 Hz, 2H), 6.24 (d, J = 16.4 Hz, 2H); ^{13}C NMR (101 MHz, DMSO) δ 151.82, 151.22, 148.15, 140.03, 133.36, 130.68, 129.57, 125.30, 123.39, 118.56, 116.49, 114.73, 104.69, 103.41, 101.84; HRMS (ESI) *m/z* 339.9697 (M+H).

2,3-dimethoxy-6-(trichloromethyl)phenanthridine (8l)
Yellow solid; Yield 43%; Mp (174.5–176.1°C); ^{1}H NMR (400 MHz, $CDCl_3$): δ 8.95 (d, J = 8.6 Hz, 1H), 8.58 (d, J = 8.4 Hz, 1H), 8.16–8.08 (m, 4H), 7.86 (s, 2H), 7.74–7.58 (m, 4H), 7.49 (t, J = 7.8 Hz, 4H), 4.16 (s, 3H), 4.11 (s, 3H); ^{13}C NMR (101 MHz, DMSO): δ 167.75, 151.93, 151.86, 133.29, 131.16, 129.69, 128.99, 127.70, 126.77, 124.17, 119.98, 119.33, 110.56, 102.99, 56.68, 56.30; HRMS (ESI) *m/z* 356.0010 (M+H).

2,3,8-trimethoxy-6-(trichloromethyl)phenanthridine (8m)
Yellow solid; Yield 39%; Mp (125.5–126.9°C); ^{1}H NMR (400 MHz, $CDCl_3$): δ 8.48 (d, J = 9.1 Hz, 1H), 8.29 (d, J = 2.5 Hz, 1H), 7.77 (s, 1H), 7.62 (s, 1H), 7.50 (dd, J = 9.2, 2.6 Hz, 1H), 4.14 (s, 3H), 4.09 (s, 3H), 4.02 (s, 3H); ^{13}C NMR (101 MHz, DMSO): δ 157.06, 152.00, 151.26, 149.05, 135.36, 129.09, 128.95, 126.01, 121.63, 120.63, 120.29, 110.36, 108.35, 102.47, 56.64, 56.23, 55.89; HRMS (ESI) *m/z* 386.0115 (M+H).

8,10-dimethoxy-6-(trichloromethyl) phenanthridine (8n)
Yellow solid; Yield 39%; Mp (161.3–162°C); ^{1}H NMR (400 MHz, $CDCl_3$): δ 9.45–9.38 (m, 1H), 8.28–8.21 (m, 1H), 8.01 (d, J = 2.3 Hz, 1H), 7.71 (dd, J = 6.5, 3.5 Hz, 2H), 7.00 (d, J = 2.4 Hz, 1H), 4.13 (s, 3H), 4.02 (s, 3H); ^{13}C NMR (101 MHz, DMSO): δ 160.02, 158.37, 151.25, 139.93, 130.95, 130.05, 128.51, 127.15, 124.74, 122.76, 119.71, 103.62, 101.98, 99.01, 56.93, 56.04; HRMS (ESI) *m/z* 356.0007 (M+H).

Pharmacology

Cell Culture

A549, PC3, MCF-7, HepG2 and Hela cell lines were obtained from the Chinese Academy of Sciences Cell Bank. A549, Hela and PC3 were cultured in RPMI-1640 medium supplemented with 10% FBS, MCF-7 cells were maintained in MEM medium supplemented with 10% FBS, HepG2 cells were cultured in DMEM medium supplemented with 10% FBS. All the cell lines were cultured at humidified atmosphere containing 5% CO_2 at 37°C. The stock solutions (20 mM) of phenanthridine derivatives were prepared in DMSO and added at desired concentrations to the cell culture. DMSO concentration did not exceed 1:1,000 in the final culture.

MTT Assay

Cytotoxic activities of the phenanthridine derivatives was evaluated by MTT assay. The stock solutions of phenanthridine derivatives were diluted with culture medium. The cells were seeded in 96-well plates at a density 5 × 10^3 cells per well and incubated until confluency 90–95%, then each well was treated with 100 μL medium containing the desired concentrations of phenanthridine derivatives and incubated for 48 h. 20 μL MTT working solution (5 mg/mL) was then added to each well and incubated for another 4 h. At the end of incubation, the medium was carefully removed, and 200 μL DMSO was added. The optical density at 490 nm and 630 nm were then measured with a microplate reader (MODEL). The percentage of cell growth inhibition was calculated with the following equation: % inhibition = [1–(Sample group OD_{490} - Sample group OD_{630})/(Control group OD_{490}-Control group OD_{630})] × 100%. The IC_{50} values were calculated with Origin 7.5 software, and standard deviations of the IC_{50} values were obtained from at least 3 independent experiments.

DNA Top I and IIα Relaxation Assay *In vitro*

The human Top I and IIα inhibitory activity was determined by agarose gel electrophoresis. Reaction mixture was prepared with 0.5 μg pBR322 supercoiled DNA (TaKaRa) and human Top I (TaKaRa) or IIα (TopoGEN) enzyme in the absence or presence of compound in the Top reaction buffer (Top I: DNA Top I buffer 2 μL, DNA Top I 1U, 0.1% BSA 2 μL and sterile water up to 20 μL; Top IIα: DNA Top IIα buffer A 2 μL, DNA Top IIα buffer B 2 μL, DNA Top IIα 1U and sterile water up to 20 μL). After 30 min of incubation at 37°C, the reaction mixture was electrophoresed on 0.8% agarose gel at 80 V for 50 min with TAE running buffer. The gel was then immersed in the Genecolour I TM staining solution for 45 min and photographed under UV light.

Cell Cycle Assay

MCF-7 cells in logarithmic growth phase were seeded in 6-well plates (6 × 10^5 cells/well) and incubated with different doses of compound **8a** (0, 0.15, 0.3, and 0.6 μM) for 24 h. Cells were then washed twice with cold PBS and fixed in 70% precooled ethanol at 4°C for 12 h. After the fixation, cells were washed again with PBS

and stained with PI/RNase A for 30 min at room temperature, and eventually subjected to flow cytometry (CytoFLEX, Beckman Coulter). for cell cycle distribution determination.

Hoechst 33258 Staining

MCF-7 cells in logarithmic growth phase were seeded in 6-well plates (4×10^5 cells/well) and incubated with different doses of compound **8a** (0, 0.15, 0.3, and 0.6 μM) for 24 h. Cells were then washed twice with PBS and stained with Hoechst 33258 working solution for 30 min at 37°C under 5% CO_2. The morphological changes of apoptotic cells were observed with a fluorescence microscope (Leica DMI 4000B) with blue filter.

Annexin V/PI Detection

MCF-7 cells in logarithmic growth phase were seeded in 6-well plates (4×10^5 cells/well) and incubated with different doses of compound **8a** (0, 0.15, 0.3, and 0.6 μM) for 24 h. After the incubation, cells were washed with PBS, collected, resuspended with binding buffer from the Annexin V-FITC kit (Thermo fisher Co., USA), and then added with 5 μl annexin V-FITC and mixed gently. After 10 min of incubation, 1 μl PI was added to each sample and mixed gently. After incubation at room temperature for another 20 min in the dark, cells were subjected to flow cytometer (CytoFLEX, Beckman Coulter).

Western Blotting

MCF-7 cells were incubated with different doses of compound **8a** (0, 0.15, 0.3, and 0.6 μM) for 24 h, and then total cell proteins were extracted with RIPA buffer supplemented with 1:100 protease inhibitor (info) and phosphatase inhibitor (info). Sample protein concentrations were determined with BCA assay (ComWin Biotech Co., Beijing, China), then equal amounts of protein (30 μg) were mixed with sampling buffer and denatured for 5 min at 100°C. Resulting samples were then subjected to Sodium dodecyl sulfate-polyacrylamide electrophoresis (SDS-PAGE). After electrophoresis, proteins were transferred to polyvinylidene difluoride (PVDF) membrane (Millipore) and blocked with 5% fat-free dry milk in 1×Tris-buffered saline (TBST) for 2 h at room temperature. Membranes were then probed with Bcl-2 (rabbit, 1:1,000, Santa Cruz, CA), Bax (rabbit, 1:1,000, Santa Cruz, CA) and β-actin antibodies at 4°C overnight. The membranes were then washed with TBST three times and incubated with anti-rabbit secondary antibody (Santa Cruz, CA) and visualized with ECL-detecting reagents (ComWin Biotech Co., Beijing, China). The images were obtained from 6000 pro (Clinx Science Instruments Co., Ltd., Shanghai, China) and analyzed with Image Studio Lite software.

Statistical Analysis

Results were expressed as mean ± standard deviation (SD) of three independent experiments performed in triplicates ($n = 3$). SPSS 19.0 software were used for statistical analysis and the means between two groups were compared by one way analysis of variance (ANOVA) with Dunnett's test, $P < 0.05$ was considered significant.

DATA AVAILABILITY

The raw data supporting the conclusions of this manuscript will be made available by the authors, without undue reservation, to any qualified researcher.

AUTHOR CONTRIBUTIONS

WS and FY designed the project. MW, YC, QL, and QX performed the experiments. MW and LZ analyzed the data and wrote the manuscript. All authors discussed the results and contributed to the manuscript.

FUNDING

This work was supported by National Natural Science Foundation of China (Youth Found, Grant No. 81803343).

REFERENCES

1. Chaturvedi MM, Kumar A, Darnay BG, Chainy GB, Agarwal S, Aggarwal BB. Sanguinarine (pseudochelerythrine) is a potent inhibitor of NF-kappaB activation, IkappaBalpha phosphorylation, and degradation. *J Biol Chem.* (1997) 272:30129–34. doi: 10.1074/jbc.272.48.30129
2. Croaker A, King GJ, Pyne JH, Anoopkumar-Dukie S, Liu L. *Sanguinaria canadensis*: traditional medicine, phytochemical composition, biological activities and current uses. *Int J Mol Sci.* (2016) 17:17091414. doi: 10.3390/ijms17091414
3. Achkar IW, Mraiche F, Mohammad RM, Uddin S. Anticancer potential of sanguinarine for various human malignancies. *Future Med Chem.* (2017) 9:933–50. doi: 10.4155/fmc-2017-0041
4. Sarkar SM. Isolation from argemone oil of dihydrosanguinarine and sanguinarine; toxicity of sanguinarine. *Nature.* (1948) 162:265. doi: 10.1038/162265a0
5. Kalogris C, Garulli C, Pietrella L, Gambini V, Pucciarelli S, Lucci C, et al. Sanguinarine suppresses basal-like breast cancer growth through dihydrofolate reductase inhibition. *Biochem Pharmacol.* (2014) 90:226–34. doi: 10.1016/j.bcp.2014.05.014
6. Slaninová I, Pěnčíková K, Urbanová J, Slanina J, Táborská E. Antitumour activities of sanguinarine and related alkaloids. *Phytochemistry Rev.* (2014) 13:51–68. doi: 10.1007/s11101-013-9290-8
7. Zhang R, Wang G, Zhang PF, Zhang J, Huang YX, Lu YM, et al. Sanguinarine inhibits growth and invasion of gastric cancer cells via regulation of the DUSP4/ERK pathway. *J Cell Mol Med.* (2017) 21:1117–27. doi: 10.1111/jcmm.13043
8. Eun JP, Koh GY. Suppression of angiogenesis by the plant alkaloid, sanguinarine. *Biochem Biophys Res Commun.* (2004) 317:618–24. doi: 10.1016/j.bbrc.2004.03.077
9. Miao F, Yang XJ, Zhou L, Hu HJ, Zheng F, Ding XD, et al. Structural modification of sanguinarine and chelerythrine and their antibacterial activity. *Nat Prod Res.* (2011) 25:863–75. doi: 10.1080/14786419.2010.482055
10. Yang XJ, Miao F, Yao Y, Cao FJ, Yang R, Ma YN, et al. *In vitro* antifungal activity of sanguinarine and chelerythrine derivatives against phytopathogenic fungi. *Molecules.* (2012) 17:13026–35. doi: 10.3390/molecules171113026
11. Cee VJ, Chavez FJr, Herberich B, Lanman BA, Pettus LH, Reed AB, et al. Discovery and optimization of macrocyclic quinoxaline-pyrrolo-dihydropiperidinones as potent pim-1/2 kinase inhibitors. *ACS Med Chem Lett.* (2016) 7:408–12. doi: 10.1021/acsmedchemlett.5b00403

12. Maiti M, Nandi R, Chaudhuri K. Sanguinarine: a monofunctional intercalating alkaloid *FEBS Lett.* (1982) 142:280–4.
13. Champoux JJ. DNA topoisomerases: structure, function, and mechanism. *Annu Rev Biochem.* (2001) 70:369–413. doi: 10.1146/annurev.biochem.70.1.369
14. Wang JC. Cellular roles of DNA topoisomerases: a molecular perspective. *Nat Rev Mol Cell Biol.* (2002) 3:430–40. doi: 10.1038/nrm831
15. Chen XM, Zhang M, Fan PL, Qin YH, Zhao HW. Chelerythrine chloride induces apoptosis in renal cancer HEK-293 and SW-839 cell lines. *Oncol Lett.* (2016) 11:3917–24. doi: 10.3892/ol.2016.4520
16. Wang X, Tanaka M, Krstin S, Peixoto HS, Wink M. The interference of selected cytotoxic alkaloids with the cytoskeleton: an insight into their modes of action. *Molecules.* (2016) 21:906. doi: 10.3390/molecules21070906
17. Chang MC, Chan CP, Wang YJ, Lee PH, Chen LI, Tsai YL, et al. Induction of necrosis and apoptosis to KB cancer cells by sanguinarine is associated with reactive oxygen species production and mitochondrial membrane depolarization. *Toxicol Appl Pharmacol.* (2007) 218:143–51. doi: 10.1016/j.taap.2006.10.025
18. Kaminskyy V, Kulachkovskyy O, Stoika R. A decisive role of mitochondria in defining rate and intensity of apoptosis induction by different alkaloids. *Toxicol Lett.* (2008) 177:168–81. doi: 10.1016/j.toxlet.2008.01.009
19. Vrba J, Dolezel P, Vicar J, Ulrichova J. Cytotoxic activity of sanguinarine and dihydrosanguinarine in human promyelocytic leukemia HL-60 cells. *Toxicol In Vitro.* (2009) 23:580–8. doi: 10.1016/j.tiv.2009.01.016
20. Adhami VM, Aziz MH, Mukhtar H, Ahmad N. Activation of prodeath Bcl-2 family proteins and mitochondrial apoptosis pathway by sanguinarine in immortalized human HaCaT keratinocytes. *Clin Cancer Res.* (2003) 9:3176–82.
21. Ahsan H, Reagan-Shaw S, Breur J, Ahmad N. Sanguinarine induces apoptosis of human pancreatic carcinoma AsPC-1 and BxPC-3 cells via modulations in Bcl-2 family proteins. *Cancer Lett.* (2007) 249:198–208. doi: 10.1016/j.canlet.2006.08.018
22. Liu Y, Jiao R, Ma ZG, Liu W, Wu QQ, Yang Z, et al. Sanguinarine inhibits angiotensin II-induced apoptosis in H9c2 cardiac cells via restoring reactive oxygen species-mediated decreases in the mitochondrial membrane potential. *Mol Med Rep.* (2015) 12:3400–8. doi: 10.3892/mmr.2015.3841
23. Lee B, Lee SJ, Park SS, Kim SK, Kim SR, Jung JH, et al. Sanguinarine-induced G1-phase arrest of the cell cycle results from increased p27KIP1 expression mediated via activation of the Ras/ERK signaling pathway in vascular smooth muscle cells. *Arch Biochem Biophys.* (2008) 471:224–31. doi: 10.1016/j.abb.2008.01.008
24. Holy J, Lamont G, Perkins E. Disruption of nucleocytoplasmic trafficking of cyclin D1 and topoisomerase II by sanguinarine. *BMC Cell Biol.* (2006) 7:13. doi: 10.1186/1471-2121-7-13
25. Xu JY, Meng QH, Chong Y, Jiao Y, Zhao L, Rosen EM, et al. Sanguinarine inhibits growth of human cervical cancer cells through the induction of apoptosis. *Oncol Rep.* (2012) 28:2264–70. doi: 10.3892/or.2012.2024
26. Pica F, Balestrieri E, Serafino A, Sorrentino R, Gaziano R, Moroni G, et al. Antitumor effects of the benzophenanthridine alkaloid sanguinarine in a rat syngeneic model of colorectal cancer. *Anticancer Drugs.* (2012) 23:32–42. doi: 10.1097/CAD.0b013e32834a0c8e
27. Sun M, Liu C, Nadiminty N, Lou W, Zhu Y, Yang J, et al. Inhibition of Stat3 activation by sanguinarine suppresses prostate cancer cell growth and invasion. *Prostate.* (2012) 72:82–9. doi: 10.1002/pros.21409
28. Park SY, Jin ML, Kim YH, Lee SJ, Park G. Sanguinarine inhibits invasiveness and the MMP-9 and COX-2 expression in TPA-induced breast cancer cells by inducing HO-1 expression. *Oncol Rep.* (2014) 31:497–504. doi: 10.3892/or.2013.2843
29. Basini G, Bussolati S, Santini SE, Grasselli F. Sanguinarine inhibits VEGF-induced angiogenesis in a fibrin gel matrix. *Biofactors.* (2007) 29:11–8. doi: 10.1002/biof.5520290102
30. Dong XZ, Zhang M, Wang K, Liu P, Guo DH, Zheng XL, et al. Sanguinarine inhibits vascular endothelial growth factor release by generation of reactive oxygen species in MCF-7 human mammary adenocarcinoma cells. *Biomed Res Int.* (2013) 2013:517698. doi: 10.1155/2013/517698
31. De Stefano I, Raspaglio G, Zannoni GF, Travaglia D, Prisco MG, Mosca M, et al. Antiproliferative and antiangiogenic effects of the benzophenanthridine alkaloid sanguinarine in melanoma. *Biochem Pharmacol.* (2009) 78:1374–81. doi: 10.1016/j.bcp.2009.07.011
32. Zhou Y, Wu C, Dong X, Qu J. Synthesis of 6-trichloromethylphenanthridines by transition metal-free radical cyclization of 2-isocyanobiphenyls. *J Org Chem.* (2016) 81:5202–8. doi: 10.1021/acs.joc.6b00885
33. Fuchs Y, Steller H. Programmed cell death in animal development and disease. *Cell.* (2011) 147:742–58. doi: 10.1016/j.cell.2011.10.033
34. Nunez G, Clarke MF. The Bcl-2 family of proteins: regulators of cell death and survival. *Trends Cell Biol.* (1994) 4:399–403. doi: 10.1016/0962-8924(94)90053-1
35. Boise LH, Gottschalk AR, Quintans J, Thompson CB. Bcl-2 and Bcl-2-related proteins in apoptosis regulation. *Curr Top Microbiol Immunol.* (1995) 200:107–21. doi: 10.1007/978-3-642-79437-7_8
36. Zhang H, Xu Q, Krajewski S, Krajewska M, Xie Z, Fuess S, et al. BAR: An apoptosis regulator at the intersection of caspases and Bcl-2 family proteins. *Proc Natl Acad Sci USA.* (2000) 97:2597–602. doi: 10.1073/pnas.97.6.2597

Conflict of Interest Statement: The authors declare that the research was conducted in the absence of any commercial or financial relationships that could be construed as a potential conflict of interest.

frontiers in Oncology

MINI REVIEW
published: 17 April 2019
doi: 10.3389/fonc.2019.00268

Diverse Mechanisms of BRAF Inhibitor Resistance in Melanoma Identified in Clinical and Preclinical Studies

Stephen A. Luebker and Scott A. Koepsell*

Department of Pathology and Microbiology, University of Nebraska Medical Center, Omaha, NE, United States

BRAF inhibitor therapy may provide profound initial tumor regression in metastatic melanoma with BRAF V600 mutations, but treatment resistance often leads to disease progression. A multi-center analysis of BRAF inhibitor resistant patient tissue samples detected genomic changes after disease progression including multiple secondary mutations in the MAPK/Erk signaling pathway, mutant BRAF copy number gains, and BRAF alternative splicing as the predominant putative mechanisms of resistance, but 41.7% of samples had no known resistance drivers. *In vitro* models of BRAF inhibitor resistance have been developed under a wide variety of experimental conditions to investigate unknown drivers of resistance. Several *in vitro* models developed genetic alterations observed in patient tissue, but others modulate the response to BRAF inhibitors through increased expression of receptor tyrosine kinases. Both secondary genetic alterations and expression changes in receptor tyrosine kinases may increase activation of MAPK/Erk signaling in the presence of BRAF inhibitors as well as activate PI3K/Akt signaling to support continued growth. Melanoma cells that develop resistance *in vitro* may have increased dependence on serine or glutamine metabolism and have increased cell motility and metastatic capacity. Future studies of BRAF inhibitor resistance *in vitro* would benefit from adhering to experimental parameters that reflect development of BRAF inhibitor resistance in patients through using multiple cell lines, fully characterizing the dosing strategy, and reporting the fold change in drug sensitivity.

Keywords: melanoma, BRAF inhibitor, vemurafenib, dabrafenib, cell line, drug resistance, metabolism, invasion

OPEN ACCESS

Edited by:
Zhe-Sheng Chen,
St. John's University, United States

Reviewed by:
Karishma Rajani,
Mayo Clinic, United States
Yun Dai,
Virginia Commonwealth University, United States

****Correspondence:***
Stephen A. Luebker
stephen.luebker@unmc.edu

Specialty section:
This article was submitted to Cancer Molecular Targets and Therapeutics, a section of the journal Frontiers in Oncology

Received: *19 December 2018*
Accepted: *25 March 2019*
Published: *17 April 2019*

Citation:
Luebker SA and Koepsell SA (2019) Diverse Mechanisms of BRAF Inhibitor Resistance in Melanoma Identified in Clinical and Preclinical Studies. Front. Oncol. 9:268. doi: 10.3389/fonc.2019.00268

INTRODUCTION

Melanoma makes up 6% of estimated new cancer cases in men and 4% in women, and incidence has been increasing since 1975 (1). BRAF mutations occur in more than 50% of cutaneous melanomas, and BRAF V600E occurs most frequently, which confers constitutive monomeric activation of BRAF kinase activity (2, 3). The identification of oncogenic BRAF signaling increased interest in targeted inhibitors toward mutant BRAF variants, and the FDA has approved two targeted BRAF inhibitors, vemurafenib in 2011 and dabrafenib in 2013, for treatment of non-resectable BRAF V600E/K mutant melanoma. Despite the rapid response and short-term increases in patient survival, resistance to BRAF inhibition persists. In 2017, combination therapy of dabrafenib plus the MEK inhibitor, trametinib was FDA approved for treatment of melanoma to forestall the development of BRAF inhibitor resistance. This review summarizes the potential events driving

BRAF inhibitor resistance detected in patient tissue and contrasts them with *in vitro* studies of BRAF inhibitor resistance through comparison of methods and results.

BRAF Inhibitor Resistance in Patients With Melanoma

Phase-3 clinical trials of vemurafenib treatment for BRAF V600E/K melanoma demonstrated improvements in median progression-free survival relative to dacarbazine (6.9 months vs. 1.6 months) and increased median overall survival (13.6 vs. 9.7 months) (4). Phase-3 clinical trials of dabrafenib treatment for BRAFV600E melanoma observed improvements in median progression free survival relative to dacarbazine (5.1 vs. 2.7 months) (5). Phase-3 clinical trials of dabrafenib and trametinib combination therapy vs. dabrafenib alone found increased median progression-free survival (11.1 vs. 8.8 months) and increased median overall survival (25.1 vs. 18.7 months) (6). Treatment with BRAF/MEK inhibitors often provides remarkable disease regression initially, but resistance to therapy frequently develops within 12 months as indicated by median progression-free survival.

BRAF inhibitor resistance in melanoma is supported through recovery of MAPK/Erk signaling or activation of PI3K/Akt signaling. These pathways may be activated through mutations, copy-number alterations, or changes in expression. A summary diagram including these signaling pathways and a breakdown of common alterations supporting BRAF inhibitor resistance are illustrated in **Figure 1**. A multi-center analysis of BRAF inhibitor resistance combining three comprehensive genome sequencing studies of pre-treatment and post-progression cases of melanoma identified resistance driving events in 58.3% (77/132) of samples obtained from 100 individuals, but failed to identify any known mechanism of resistance in the remaining 41.7% of samples (7). Johnson et al. provide a complete breakdown of the frequency of the resistance mechanisms within this combined data set. Multiple resistance mechanisms were observed within individual samples and unique resistance mechanisms were observed between samples from the same patient. BRAF amplification and alternative splicing were observed most frequently followed by NRAS mutations and MEK1/2 mutations. Mutations in the PI3K/Akt pathway are less frequently observed in patient samples. Despite increased median progression-free survival when treating patients with dabrafenib plus trametinib relative to dabrafenib alone, treatment resistance still develops. Patients treated with dabrafenib/trametinib combination therapy developed alterations in the same genes that support single-agent resistance including MEK1/2 mutations, BRAF amplification, BRAF alternative splicing, and NRAS mutations between pre-treatment and post-progression samples (8, 9). Clinical studies of BRAF inhibitor resistance leave an incomplete picture of the diverse set of mechanisms supporting BRAF inhibitor resistance. This review summarizes recent studies in which BRAF inhibitor resistance was induced stochastically in cell lines via prolonged exposure to a BRAF inhibitor. Major mechanisms identified in these studies are included in **Figure 1** and discussed in more detail in this review.

BRAF Inhibitor Resistance in Melanoma Cell Lines

Receptor Tyrosine Kinase Expression

Receptor tyrosine kinases may act as upstream activators of MAPK/Erk signaling, and increased expression in BRAF inhibitor resistant cells has been described in multiple studies. Shaffer et al. demonstrated that resistance to BRAF inhibitors in WM989 and WM983B cells occurs through non-heritable, transient expression of multiple resistance-associated genes including receptors like AXL receptor tyrosine kinase (AXL), epidermal growth factor receptor (EGFR), fibroblast growth factor receptor 1 (FGFR1), and platelet-derived growth factor receptor beta (PDGFRB) among others (10). Other studies have detected expression changes in these genes but do not point to a single pattern of expression change. Nazarian et al. demonstrated that increased expression of PDGFRB conferred resistance to M229 and M238 cells, but Jazirehi et al. found that resistant M238 cells had increased expression of EGFR and decreased expression of PDGFRB (11, 12). Shao et al. found resistant WM793 and M238 cells both had increased PDGFRB but decreased Insulin-like growth factor 1 receptor (IGF1R) expression (13). Increased PDGFRB expression has also been described in resistant A375 cells (14). In two other studies using A375 cells, increased expression of fibroblast growth factor receptor 3 (FGFR3) expression was associated with BRAF inhibitor resistance (15, 16). Resistant A375 cells have also been shown to increase expression of IGF1R while resistant SKMEL28 cells increased expression of PDGFRB (17). In a separate study, resistant SKMEL28 cells had increased expression of both EGFR and PDGFRB (18). Jazirehi et al. found that resistant M249 cells had increased expression of EGFR, KIT proto-oncogene receptor tyrosine kinase (KIT), MET proto-oncogene receptor tyrosine kinase (MET), and PDGFRB with decreased IGF1R (11). Resistance-associated gene expression may occur through loss of SOX10 expression and gain of JUN, AP-1, and TEAD transcription factor activity (10). EGFR expression may be regulated through MITF expression, but both increased and decreased MITF expression have been observed in BRAF inhibitor resistant cell lines (19, 20). Sun et al. demonstrated that miR-7 was significantly downregulated in resistant A375 and MEL-CV cells, and exogenous expression could reduce resistance with EGFR, IGF1R, CRAF, and AXL as potential targets (21). Overall, changes in growth factor expression are inconsistent between studies using the same cell lines. Increased expression of any growth factor receptor that activates MAPK/Erk may potentially drive resistance in melanoma.

Secondary MAPK/Erk Mutations

In addition to upstream activation of MAPK/Erk through receptor tyrosine kinases, increased MAPK/Erk signaling may be achieved through direct alteration to members of the RAS/RAF/MEK/Erk signaling cascade. Secondary BRAF mutations and alternative BRAF splicing have been shown to induce vemurafenib resistance in multiple cell lines (19, 22). In a patient derived xenograft model, increased BRAF V600E expression sustained resistance, and cells demonstrated

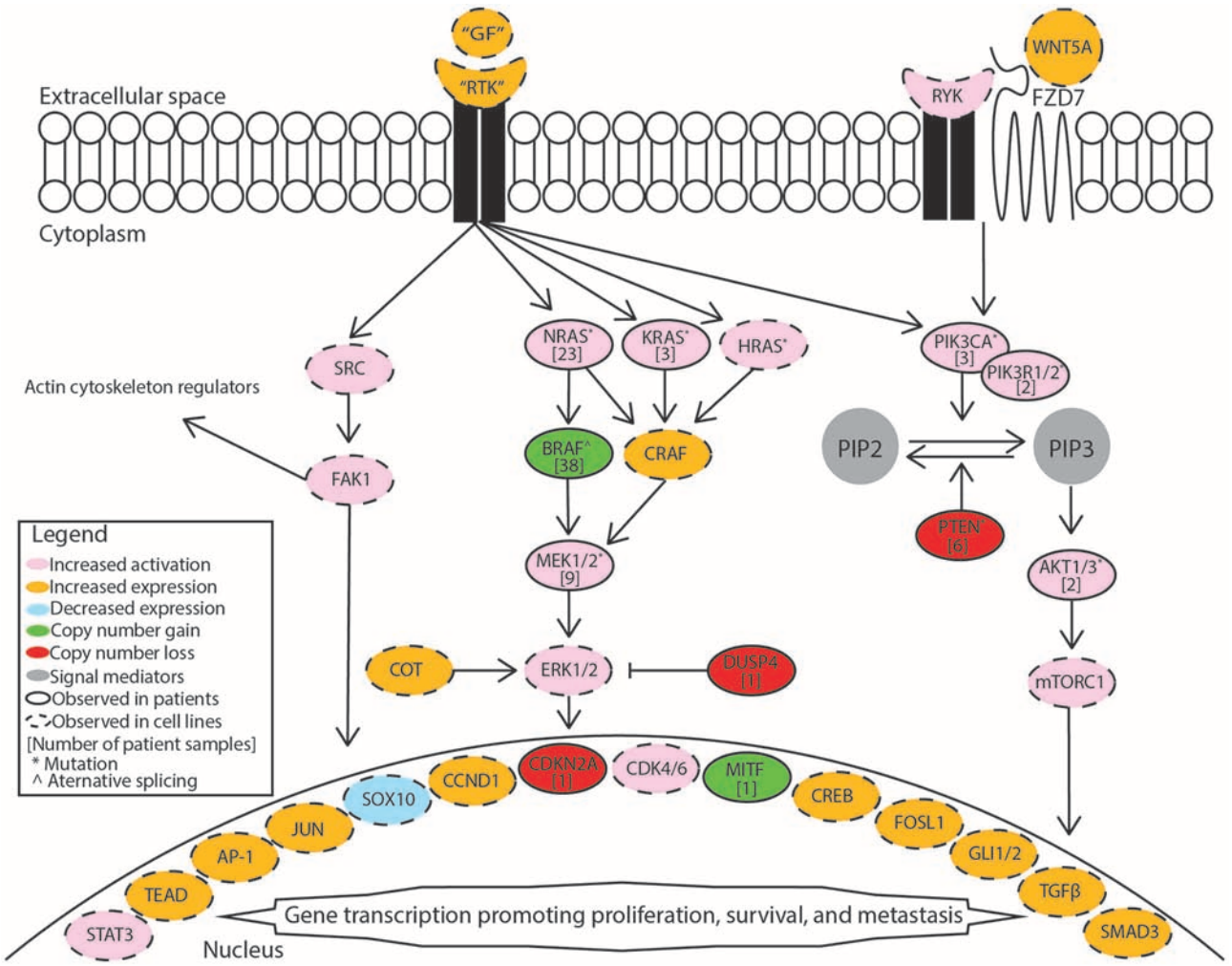

FIGURE 1 | Mechanisms supporting BRAF inhibitor resistance in melanoma. Receptor tyrosine kinases (RTK) include AXL receptor tyrosine kinase (AXL), epidermal growth factor receptor (EGFR), fibroblast growth factor receptor 1 (FGFR1), fibroblast growth factor receptor 3 (FGFR3), platelet-derived growth factor receptor beta (PDGFRB), MET proto-oncogene receptor tyrosine kinase (MET), and KIT proto-oncogene receptor tyrosine kinase (KIT). Growth factors (GF) correspond to the specific receptor tyrosine kinase. The MAPK/Erk pathway includes the Ras GTPases (N/K/HRAS), Serine/threonine-protein kinase B-raf (BRAF), RAF proto-oncogene serine/threonine-protein kinase (CRAF), mitogen-activated and extracellular signal-regulated kinase kinase 1 or 2 (MEK1/2), extracellular signal-regulated kinase 1 or 2 (ERK1/2), cancer Osaka thyroid (COT), and dual specificity protein phosphatase 4 (DUSP4). The PI3K/Akt pathway includes phosphatidylinositol-4,5-bisphosphate 3-kinase catalytic subunit alpha (PIK3CA), phosphatidylinositol 3-kinase regulatory subunit 1 or 2 (PIK3R1/2), phosphatidylinositol 4,5-bisphosphate (PIP2), phosphatidylinositol 3,4,5-trisphosphate (PIP3), phosphatase and tensin homolog (PTEN), AKT serine/threonine kinase 1 or 2 (AKT1/2), mammalian target of rapamycin complex 1 (mTORC1). Src signaling factors include SRC proto-oncogene non-receptor tyrosine kinase (SRC) and focal adhesion kinase 1 (FAK1). Transcription factors include signal transducer and activator of transcription 3 (STAT3), TEA domain transcription factor protein family (TEAD), activator protein 1 complex (AP-1), Jun proto-oncogene AP-1 transcription factor subunit (JUN), SRY-box 10 (SOX10), melanocyte inducing transcription factor (MITF), cyclic AMP responsive element binding protein family (CREB), FOS like 1 AP-1 transcription factor subunit (FOSL1), GLI family zinc finger 1 or 2 (GLI1/2), transforming growth factor beta (TGFβ), SMAD family member 3 (SMAD3). Cell cycle regulators included cyclin D1 (CCND1), cyclin dependent kinase 4 or 6 (CDK4/6). Non-canonical Wnt signaling mediators include receptor like tyrosine kinase (RYK), frizzled class receptor 7 (FZD7), and Wnt family member 5A (WNT5A).

drug-dependence for continued proliferation (23). Resistant tumors derived from 1205LU cells in a mouse xenograft model contained distinct alternative BRAF splicing events in two tumors and HRAS Q61K mutation in one tumor (24). Other alterations within RAS/RAF/MEK/Erk cascade have been observed in SKMEL28, A375, COLO829, and M249 cells, including COT overexpression and NRAS Q61K mutation (12, 17). Dabrafenib resistant A375 and MEL-RMU cells were found to have mutations in MEK1 and NRAS as previously described in vemurafenib resistant cells (25, 26). NRAS mutations may also make cell lines cross-resistant to MEK inhibitors due to elevated PI3K/Akt signaling (27). Resistant A375 cells were found to have an NRAS G13R mutation, high expression of CRAF, and increased Akt phosphorylation (28). Resistant A375 cells with a KRAS K117N also had elevated expression of CRAF and activation of Akt (29). Resistant M249 cells and M376 cells with secondary NRAS mutations had increased Akt activation (30). Resistant WM793 cells with

secondary NRAS Q61K mutation require CRAF expression and SHOC2 scaffold protein to re-activate MAPK/Erk (31). *In vitro* models of BRAF inhibitor resistance indicate that secondary mutations may support increased activation of MAPK/Erk in the presence of inhibitor or support sustained growth through activation of PI3K/Akt signaling.

Alternative Resistance Pathways

Downstream effectors of PI3K/Akt activation promote survival of resistant cells. PI3K/Akt activation upregulates AEBP1 through increased CREB binding, and increased AEBP1 leads to IκBα degradation and NF-κB activation (32). A375, SKMEL28, and WM239 cells resistant to either dabrafenib or vemurafenib all had increased expression of Mcl-1 relative to their pre-treatment counterparts, which promotes cell survival through inhibition of apoptosis, and Mcl-1 expression may be regulated by STAT, cAMP, and NF-κB binding sites (33). Growth factor receptors may also cross activate PI3K/Akt separately or in addition to MAPK/Erk activation. Resistance induced in SKMEL28 cells increased expression of EGFR and activated Akt (34). Resistant LM17 cells had increased IGF1R expression as well as increased Akt phosphorylation (35). Increased expression of WNT5A in A375 and MEL-264 was correlated with increased phosphorylation of Akt and activation of RYK and FZD7 receptors supporting non-canonical Wnt signaling (36). PI3K/Akt activation in multiple BRAF inhibitor resistant melanoma cell lines also up-regulates of FOSL1, which drives secretion of multiple factors from tumor cells that support surrounding tumor growth (37). Melanoma cells may support the resistance of surrounding cells in addition to other stromal cells. Hepatocyte growth factor (HGF) secretion by surrounding stromal cells in co-culture supports tumor growth in the presence of BRAF inhibitors through activation of the MET receptor tyrosine kinase and downstream MAPK/Erk activation (38). The adaptive resistance of melanoma cells may be supported through both neighboring cancer and non-cancer cells. MAPK/Erk signaling and/or PI3K/Akt signaling may be activated in BRAF inhibitor resistant cells frequently through common mechanisms.

Phenotypic Changes in BRAF Inhibitor Resistant Cell Lines

Increased Motility and Invasion

Resistant cell lines acquire a more invasive phenotype characterized by increased cell motility and metastatic capacity. Multiple studies have noted increased invasive capacity of BRAF inhibitor resistant melanoma cell lines, and recent proteomic studies of melanoma cell lines before and after developing BRAF inhibitor resistance have specifically characterized differences in kinase expression and changes in phosphorylation. Quantitative phosphoproteomics of vemurafenib resistant LM-MEL-28 cells demonstrated increased activation of MAPK/Erk signaling and de-phosphorylation of key cytoskeletal regulators (39). Activity-based protein profiling of kinases in WM164, WM793, A375, and 1205LU cells detected increased ATP uptake by FAK1, SLK, LYN, PRKDC, and KCC2D, but overall changes between cell lines showed differences in differential phosphorylation (40). Phospho-array analysis and quantitative phosphoproteomics identified increased EGFR phosphorylation in vemurafenib resistant A375 and COLO829 cell lines leading to Src family kinase phosphorylation and STAT3 activation, which was associated with increased invasion and phosphorylation of cytoskeletal proteins (41). The increase in cytoskeletal remodeling also has downstream effects in cell signaling. For example, actin remodeling has been shown to increase YAP/TAZ nuclear localization in BRAF inhibitor resistant melanoma cells, and YAP/TAZ nuclear localization increases expression of EGFR, AKT, and MYC (42). The expression of receptor tyrosine kinases is associated with the invasive behavior of melanoma cell lines through increased metalloprotease expression. EGFR signaling was found to drive resistance in SKMEL28 cells, and resistance was also associated with upregulation of MMP2 and downregulation of the MMP regulator, TIMP2 (43). Increased expression of EGFR in SKMEL28 cells was also correlated with increased activation of Non-canonical Hedgehog Signaling (GLI1, GLI2, TGFβ, and SMAD3), and inhibition of GLI1 and GLI2 increased vemurafenib sensitivity while decreasing invasiveness (44). Dabrafenib resistant A375 cells had increased expression of epithelial to mesenchymal transition markers including CD90 and decreased expression of E-cadherin with increased cell motility (45). A separate study of dabrafenib resistant A375 cells also detected increased secretion of VEGFA and MMP9, which was associated with increased invasiveness (46).

Metabolism

Alterations in the metabolism of BRAF inhibitor resistant cells have also been described, including increased dependence on serine or glutamine. Vemurafenib resistant SKMEL28 were dependent on serine metabolism, and knockout of PHGDH or depletion of serine in the media reduced viability of resistant cells (47). Additionally, vemurafenib resistant M229 and M249 cells or vemurafenib/selumetinib dual treatment resistant M249 cells had increased glutamine uptake and were dependent on glutamine for survival independently of the underlying mechanism of resistance (48). More complex metabolic reprogramming may occur during the development of BRAF inhibitor resistance. Gene set enrichment of KEGG pathways using quantitative phosphoproteomic analysis of vemurafenib resistant LM-MEL-28 cells detected enrichment in DNA replication and cell cycle but decreases in glycolysis/gluconeogenesis, fatty acid metabolism, valine/leucine/isoleucine degradation, pyruvate metabolism, and tryptophan metabolism (39).

Future Directions of *in vitro* Research

McDermott et al. have recently published a general review of important considerations for developing *in vitro* resistance to targeted inhibitors and chemotherapeutic agents in cancer cell lines (49). Important considerations for *in vitro* models of BRAF inhibitor resistance in melanoma cell lines include choice of cell line, dosing strategy, and resistant cell selection criteria. Examples of current methods that have been applied to A375 cells are summarized in **Table 1**. This review focuses on studies that

develop resistant cell lines through drug treatment and excludes studies of primary resistance or genetically induced resistance.

Selecting Cell Lines

The first major consideration in this type of model is the degree of heterogeneity between cells. There is a great deal of cell-to-cell heterogeneity in melanoma *in vivo* (51). Sub-clones may harbor mutations conferring primary resistance to BRAF inhibitors. Selection of single-cell derived clones may reduce the heterogeneity observed within a single cell line. Studies show that there are genetic differences between cell lines and tumors *in vivo*, and only a few cell lines are most frequently used (52–56). *In vitro* resistance studies would benefit from using multiple cell lines to compare resistance mechanisms and potential novel combination therapy outcomes. The use of multiple cell lines also helps verify findings by highlighting mechanisms observed across cells types as opposed to findings that are specific only to that clone or test system.

Treatment Strategy

The treatment strategy employed to induce resistance in cell lines *in vitro* may or may not represent how the drug is administered clinically. Vemurafenib is administered as 960 mg tablets twice daily and reaches an average maximum plasma concentration of 4.8 ± 3.34 μg/ml after 8 h and 61.4 ± 22.76 μg/ml after 168 h with a half-life of 34.1 ± 19.66 h (57). Dabrafenib is administered as 150 mg oral tablets twice daily and reaches an average maximum plasma concentration of 986 ng/ml in a median 2 h with a half-life of 5 h (58). Both dabrafenib and vemurafenib quickly reach a high plasma concentration and have long half-lives, which would be best represented by continuously treating cells to develop resistance. Fofaria et al. employed a pulsed treatment strategy, which includes a treatment window followed by a recovery period, to generate vemurafenib resistant cell lines (33). A pulsed treatment strategy does not reflect how the drug is administered clinically. However, it has been shown that lower vemurafenib plasma concentration was significantly associated with higher likelihood of tumor progression, and patients had high inter-individual variability in vemurafenib plasma concentration (13.0–109.8 μg/ml) (59). Others have noted that the melanoma cell lines may become dependent on the presence of the BRAF inhibitor for continued growth and continuous treatment is often required, which may potentially be mitigated through a pulsed treatment method (13, 28, 34, 60). Mechanisms regulating development of resistance in each type of model may be different, and clear distinctions should be made between which type of model was employed. Data obtained from studies that use drug exposure methods never observed in patients should be interpreted with caution.

Defining Resistance

There is no standard for defining when a cell line is drug resistant. The selection criteria used to define treatment resistance critically influences results. Ideally the fold change in drug sensitivity should be reported along with the duration of drug exposure. Treatment durations for studies of A375 cells range from 6 days to 1 year of treatment, and fold change in drug sensitivity

TABLE 1 | *In vitro* BRAF inhibitor resistance in A375 melanoma cells.

References	Drug details	Treatment strategy	Dose (μM)	Clonal selection	Time to resistance	IC50 (μM)	Resistance driver	Pathway reactivation
Cordaro et al. (45)	Dabrafenib	Increasing continuous	NA	None	4 weeks	0.0095–110.5	Undetermined	Undetermined
Greger et al. (25)	Dabrafenib	Increasing continuous	up to 1.6	Single cell derived clones	NA	0.028 to >10	MEK1 K59del	pErk
Caporali et al. (46)	Dabrafenib	Increasing continuous	0.001–1.5	None	4 months	0.001041 to >10	Undetermined	pErk and pAkt
Zeiderman et al. (50)	Vemurafenib	Continuous	1	None	1 year	NA	Undetermined	Undetermined
Smyth et al. (14)	Vemurafenib	Continuous	2	None	3 weeks	0.087 to > 10	Undetermined	Undetermined
Jameson et al. (17)	Vemurafenib	Continuous	1	Colonies by limiting dilution	4-6 weeks	0.287–13.47	PDGFRB overexpression	Undetermined
Graziani et al. (28)	Vemurafenib	Increasing continuous	up to 2.5	None	3 months	1.47–20.37	NRAS G13R and CRAF overexpression	pErk and pAkt
Anastas et al. (36)	Vemurafenib	Increasing continuous	2	None	10 weeks	NA	WNT5A overexpression	pAkt
Yadav et al. (15)	Vemurafenib	Increasing continuous	0.2–2	None	4 months	0.085–4.8	FGFR3 phosphorylation	pErk
Girotti et al. (41)	Vemurafenib	Increasing continuous	0.1–2	None	2 months	0.155–5.76	EGFR phosphorylation	pErk and pAkt
Ji et al. (19)	Vemurafenib	Increasing continuous	0.5–10	None	NA	> 10-fold	BRAF splicing	pErk and pAkt
Muller et al. (20)	Vemurafenib	Increasing continuous	up to 3	None	NA	NA	MITF loss	pErk
Sharma et al. (40)	Vemurafenib	Continuous	2.5	None	3 months	NA	Undetermined	Undetermined
Wang et al. (18)	Vemurafenib	Increasing continuous	up to 2.5	None	3 months	0.57–28.9	PDGFRB overexpression	pERK and pAKT
Sun et al. (21)	Vemurafenib	Increasing continuous	up to 2	None	6 months	NA	EGFR, IGF1R, and CRAF overexpression	pERK
Obenauf et al. (37)	Vemurafenib	Increasing continuous	1–3	Low density seeding colonies	8 weeks	NA	EGFR and MET overexpression	pERK
Su et al. (29)	Vemurafenib	Increasing continuous	NA	None	3 months	86–119-fold	KRAS K117N	pERK and pAKT
Fofaria et al. (33)	Vemurafenib	Pulsed	0.2–10	None	1 year	0.1–3	Undetermined	pERK

ranges from 3x to more than 100x (**Table 1**). Correlation to drug levels observed in patients should also be considered. Care must also be taken when reporting drug sensitivity since common colorimetric assays may not be accurate or reproducible due to variations in growth rate; a cell counting based method should be employed when possible (61, 62). Multiple studies have observed changes in cell line growth rate after developing treatment resistance, which may be dependent on the presence of drug (13, 34, 47, 60). Growth rate changes may confound the measurement of drug sensitivity between treatment resistant and pre-treatment cells.

CONCLUSION

Although treatment with BRAF inhibitors provides rapid response in most patients, treatment resistance persists. The few clinical studies of BRAF inhibitor resistance in patients indicate that genetic alterations that activate MAPK/Erk make up half of resistance mechanisms. Preclinical studies of BRAF inhibitor resistance in melanoma support the mechanisms observed in patients and indicate that the development of resistance is more complex than single mutations. *In vitro* models may be very helpful in studying mechanisms in the other half of patients with no known genetic driver of BRAF inhibitor resistance. Overall, BRAF inhibitor resistance depends on oncogenic signaling through reactivation of MAPK/Erk or activation of PI3K/Akt, which may be acquired by directly affecting genes in each pathway, by upregulation of receptor tyrosine kinases, or by affecting downstream signaling. BRAF inhibitor resistance increases invasiveness through changes in phosphorylation actin cytoskeleton regulators and increased extracellular matrix metalloprotease expression. Resistant cells have also been shown to undergo metabolic reprogramming characterized by increased glutamine or serine dependence. A375 cells have been used to model BRAF inhibitor resistance across multiple studies, but the methods and conclusions vary. To improve preclinical *in vitro* research, future studies of BRAF inhibitor resistance in melanoma should include multiple cell lines, consider a continuous-dose treatment strategy, and report drug sensitivity in order to facilitate better comparison across studies.

AUTHOR CONTRIBUTIONS

All authors listed have made a substantial, direct and intellectual contribution to the work, and approved it for publication.

FUNDING

This work was funded by the University of Nebraska Medical Center Chancellor's Program of Excellence Physician-Scientist Training Program.

REFERENCES

1. Siegel RL, Miller KD, Jemal A. Cancer statistics, 2018. *CA Cancer J Clin.* (2018) 68:7–30. doi: 10.3322/caac.21442
2. Zhang T, Dutton-Regester K, Brown KM, Hayward NK. The genomic landscape of cutaneous melanoma. *Pigment Cell Melanoma Res.* (2016) 29:266–83. doi: 10.1111/pcmr.12459
3. Menzies AM, Haydu LE, Visintin L, Carlino MS, Howle JR, Thompson JF, et al. Distinguishing clinicopathologic features of patients with V600E and V600K BRAF-mutant metastatic melanoma. *Clin Cancer Res.* (2012) 18:3242–9. doi: 10.1158/1078-0432.CCR-12-0052
4. McArthur GA, Chapman PB, Robert C, Larkin J, Haanen JB, Dummer R, et al. Safety and efficacy of vemurafenib in BRAF(V600E) and BRAF(V600K) mutation-positive melanoma (BRIM-3): extended follow-up of a phase 3, randomised, open-label study. *Lancet Oncol.* (2014) 15:323–32. doi: 10.1016/S1470-2045(14)70012-9
5. Hauschild A, Grob JJ, Demidov LV, Jouary T, Gutzmer R, Millward M, et al. Dabrafenib in BRAF-mutated metastatic melanoma: a multicentre, open-label, phase 3 randomised controlled trial. *Lancet.* (2012) 380:358–65. doi: 10.1016/S0140-6736(12)60868-X
6. Long GV, Stroyakovskiy D, Gogas H, Levchenko E, de Braud F, Larkin J, et al. Dabrafenib and trametinib versus dabrafenib and placebo for Val600 BRAF-mutant melanoma: a multicentre, double-blind, phase 3 randomised controlled trial. *Lancet.* (2015) 386:444–51. doi: 10.1016/S0140-6736(15)60898-4
7. Johnson DB, Menzies AM, Zimmer L, Eroglu Z, Ye F, Zhao S, et al. Acquired BRAF inhibitor resistance: a multicenter meta-analysis of the spectrum and frequencies, clinical behaviour, and phenotypic associations of resistance mechanisms. *Eur J Cancer.* (2015) 51:2792–9. doi: 10.1016/j.ejca.2015.08.022
8. Wagle N, Van Allen EM, Treacy DJ, Frederick DT, Cooper ZA, Taylor-Weiner A, et al. MAP kinase pathway alterations in BRAF-mutant melanoma patients with acquired resistance to combined RAF/MEK inhibition. *Cancer Discov.* (2014) 4:61–8. doi: 10.1158/2159-8290.CD-13-0631
9. Long GV, Fung C, Menzies AM, Pupo GM, Carlino MS, Hyman J, et al. Increased MAPK reactivation in early resistance to dabrafenib/trametinib combination therapy of BRAF-mutant metastatic melanoma. *Nat Commun.* (2014) 5:5694. doi: 10.1038/ncomms6694
10. Shaffer SM, Dunagin MC, Torborg SR, Torre EA, Emert B, Krepler C, et al. Rare cell variability and drug-induced reprogramming as a mode of cancer drug resistance. *Nature.* (2017) 546:431–5. doi: 10.1038/nature22794
11. Jazirehi AR, Nazarian R, Torres-Collado AX, Economou JS. Aberrant apoptotic machinery confers melanoma dual resistance to BRAF(V600E) inhibitor and immune effector cells: immunosensitization by a histone deacetylase inhibitor. *Am J Clin Exp Immunol.* (2014) 3:43–56.
12. Nazarian R, Shi H, Wang Q, Kong X, Koya RC, Lee H, et al. Melanomas acquire resistance to B-RAF(V600E) inhibition by RTK or N-RAS upregulation. *Nature.* (2010) 468:973–7. doi: 10.1038/nature09626
13. Shao Y, Aplin AE. BH3-only protein silencing contributes to acquired resistance to PLX4720 in human melanoma. *Cell Death Differ.* (2012) 19:2029–39. doi: 10.1038/cdd.2012.94
14. Smyth T, Paraiso KHT, Hearn K, Rodriguez-Lopez AM, Munck JM, Haarberg HE, et al. Inhibition of HSP90 by AT13387 delays the emergence of resistance to BRAF inhibitors and overcomes resistance to dual BRAF and MEK inhibition in melanoma models. *Mol Cancer Ther.* (2014) 13:2793–804. doi: 10.1158/1535-7163.MCT-14-0452
15. Yadav V, Zhang X, Liu J, Estrem S, Li S, Gong XQ, et al. Reactivation of mitogen-activated protein kinase (MAPK) pathway by FGF receptor 3 (FGFR3)/Ras mediates resistance to vemurafenib in human B-RAF V600E mutant melanoma. *J Biol Chem.* (2012) 287:28087–98. doi: 10.1074/jbc.M112.377218
16. Yadav V, Burke TF, Huber L, Van Horn RD, Zhang Y, Buchanan SG, et al. The CDK4/6 inhibitor LY2835219 overcomes vemurafenib resistance resulting from MAPK reactivation and cyclin D1 upregulation. *Mol Cancer Ther.* (2014) 13:2253–63. doi: 10.1158/1535-7163.MCT-14-0257

17. Jameson KL, Mazur PK, Zehnder AM, Zhang J, Zarnegar B, Sage J, et al. IQGAP1 scaffold-kinase interaction blockade selectively targets RAS-MAP kinase-driven tumors. *Nat Med.* (2013) 19:626–30. doi: 10.1038/nm.3165
18. Wang J, Chen J, Miller DD, Li W. Synergistic combination of novel tubulin inhibitor ABI-274 and vemurafenib overcome vemurafenib acquired resistance in BRAFV600E melanoma. *Mol Cancer Ther.* (2014) 13:16–26. doi: 10.1158/1535-7163.MCT-13-0212
19. Ji Z, Erin Chen Y, Kumar R, Taylor M, Jenny Njauw CN, Miao B, et al. MITF Modulates Therapeutic Resistance through EGFR Signaling. *J Invest Dermatol.* (2015) 135:1863–72. doi: 10.1038/jid.2015.105
20. Muller J, Krijgsman O, Tsoi J, Robert L, Hugo W, Song C, et al. Low MITF/AXL ratio predicts early resistance to multiple targeted drugs in melanoma. *Nat Commun.* (2014) 5:5712. doi: 10.1038/ncomms6712
21. Sun X, Li J, Sun Y, Zhang Y, Dong L, Shen C, et al. miR-7 reverses the resistance to BRAFi in melanoma by targeting EGFR/IGF-1R/CRAF and inhibiting the MAPK and PI3K/AKT signaling pathways. *Oncotarget.* (2016) 7:53558–70. doi: 10.18632/oncotarget.10669
22. Choi J, Landrette SF, Wang T, Evans P, Bacchiocchi A, Bjornson R, et al. Identification of PLX4032-resistance mechanisms and implications for novel RAF inhibitors. *Pigment Cell Melanoma Res.* (2014) 27:253–62. doi: 10.1111/pcmr.12197
23. Das Thakur M, Salangsang F, Landman AS, Sellers WR, Pryer NK, Levesque MP, et al. Modelling vemurafenib resistance in melanoma reveals a strategy to forestall drug resistance. *Nature.* (2013) 494:251–5. doi: 10.1038/nature11814
24. Basile KJ, Abel EV, Dadpey N, Hartsough EJ, Fortina P, Aplin AE. *In vivo* MAPK reporting reveals the heterogeneity in tumoral selection of resistance to RAF inhibitors. *Cancer Res.* (2013) 73:7101–10. doi: 10.1158/0008-5472.CAN-13-1628
25. Greger JG, Eastman SD, Zhang V, Bleam MR, Hughes AM, Smitheman KN, et al. Combinations of BRAF, MEK, and PI3K/mTOR inhibitors overcome acquired resistance to the BRAF inhibitor GSK2118436 dabrafenib, mediated by NRAS or MEK mutations. *Mol Cancer Ther.* (2012) 11:909–20. doi: 10.1158/1535-7163.MCT-11-0989
26. Gowrishankar K, Snoyman S, Pupo GM, Becker TM, Kefford RF, Rizos H. Acquired resistance to BRAF inhibition can confer cross-resistance to combined BRAF/MEK inhibition. *J Invest Dermatol.* (2012) 132:1850–9. doi: 10.1038/jid.2012.63
27. Atefi M, von Euw E, Attar N, Ng C, Chu C, Guo D, et al. Reversing melanoma cross-resistance to BRAF and MEK inhibitors by co-targeting the AKT/mTOR pathway. *PLoS ONE.* (2011) 6:e28973. doi: 10.1371/journal.pone.0028973
28. Graziani G, Artuso S, De Luca A, Muzi A, Rotili D, Scimeca M, et al. A new water soluble MAPK activator exerts antitumor activity in melanoma cells resistant to the BRAF inhibitor vemurafenib. *Biochem Pharmacol.* (2015) 95:16–27. doi: 10.1016/j.bcp.2015.03.004
29. Su F, Bradley WD, Wang Q, Yang H, Xu L, Higgins B, et al. Resistance to selective BRAF inhibition can be mediated by modest upstream pathway activation. *Cancer Res.* (2012) 72:969–78. doi: 10.1158/0008-5472.CAN-11-1875
30. Atefi M, Titz B, Tsoi J, Avramis E, Le A, Ng C, et al. CRAF R391W is a melanoma driver oncogene. *Sci Rep.* (2016) 6:27454. doi: 10.1038/srep27454
31. Kaplan FM, Kugel CH III, Dadpey N, Shao Y, Abel EV, Aplin AE. SHOC2 and CRAF mediate ERK1/2 reactivation in mutant NRAS-mediated resistance to RAF inhibitor. *J Biol Chem.* (2012) 287:41797–807. doi: 10.1074/jbc.M112.390906
32. Hu W, Jin L, Jiang CC, Long GV, Scolyer RA, Wu Q, et al. AEBP1 upregulation confers acquired resistance to BRAF (V600E) inhibition in melanoma. *Cell Death Dis.* (2013) 4:e914. doi: 10.1038/cddis.2013.441
33. Fofaria NM, Frederick DT, Sullivan RJ, Flaherty KT, Srivastava SK. Overexpression of Mcl-1 confers resistance to BRAFV600E inhibitors alone and in combination with MEK1/2 inhibitors in melanoma. *Oncotarget.* (2015) 6:40535–56. doi: 10.18632/oncotarget.5755
34. Thang ND, Nghia PT, Kumasaka MY, Yajima I, Kato M. Treatment of vemurafenib-resistant SKMEL-28 melanoma cells with paclitaxel. *Asian Pac J Cancer Prev.* (2015) 16:699–705. doi: 10.7314/APJCP.2015.16.2.699
35. Vergani E, Vallacchi V, Frigerio S, Deho P, Mondellini P, Perego P, et al. Identification of MET and SRC activation in melanoma cell lines showing primary resistance to PLX4032. *Neoplasia.* (2011) 13:1132–42. doi: 10.1593/neo.111102
36. Anastas JN, Kulikauskas RM, Tamir T, Rizos H, Long GV, von Euw EM, et al. WNT5A enhances resistance of melanoma cells to targeted BRAF inhibitors. *J Clin Invest.* (2014) 124:2877–90. doi: 10.1172/JCI70156
37. Obenauf AC, Zou Y, Ji AL, Vanharanta S, Shu W, Shi H, et al. Therapy-induced tumour secretomes promote resistance and tumour progression. *Nature.* (2015) 520:368–72. doi: 10.1038/nature14336
38. Straussman R, Morikawa T, Shee K, Barzily-Rokni M, Qian ZR, Du J, et al. Tumour micro-environment elicits innate resistance to RAF inhibitors through HGF secretion. *Nature.* (2012) 487:500–4. doi: 10.1038/nature11183
39. Parker R, Vella LJ, Xavier D, Amirkhani A, Parker J, Cebon J, et al. Phosphoproteomic analysis of cell-based resistance to BRAF inhibitor therapy in melanoma. *Front Oncol.* (2015) 5:95. doi: 10.3389/fonc.2015.00095
40. Sharma R, Fedorenko I, Spence PT, Sondak VK, Smalley KS, Koomen JM. Activity-based protein profiling shows heterogeneous signaling adaptations to BRAF inhibition. *J Proteome Res.* (2016) 15:4476–89. doi: 10.1021/acs.jproteome.6b00613
41. Girotti MR, Pedersen M, Sanchez-Laorden B, Viros A, Turajlic S, Niculescu-Duvaz D, et al. Inhibiting EGF receptor or SRC family kinase signaling overcomes BRAF inhibitor resistance in melanoma. *Cancer Discov.* (2013) 3:158–67. doi: 10.1158/2159-8290.CD-12-0386
42. Kim MH, Kim J, Hong H, Lee SH, Lee JK, Jung E, et al. Actin remodeling confers BRAF inhibitor resistance to melanoma cells through YAP/TAZ activation. *EMBO J.* (2016) 35:462–78. doi: 10.15252/embj.201592081
43. Sandri S, Faiao-Flores F, Tiago M, Pennacchi PC, Massaro RR, Alves-Fernandes DK, et al. Vemurafenib resistance increases melanoma invasiveness and modulates the tumor microenvironment by MMP-2 upregulation. *Pharmacol Res.* (2016) 111:523–33. doi: 10.1016/j.phrs.2016.07.017
44. Faiao-Flores F, Alves-Fernandes DK, Pennacchi PC, Sandri S, Vicente AL, Scapulatempo-Neto C, et al. Targeting the hedgehog transcription factors GLI1 and GLI2 restores sensitivity to vemurafenib-resistant human melanoma cells. *Oncogene.* (2017) 36:1849–61. doi: 10.1038/onc.2016.348
45. Cordaro FG, De Presbiteris AL, Camerlingo R, Mozzillo N, Pirozzi G, Cavalcanti E, et al. Phenotype characterization of human melanoma cells resistant to dabrafenib. *Oncol Rep.* (2017) 38:2741–51. doi: 10.3892/or.2017.5963
46. Caporali S, Alvino E, Lacal PM, Levati L, Giurato G, Memoli D, et al. Targeting the PI3K/AKT/mTOR pathway overcomes the stimulating effect of dabrafenib on the invasive behavior of melanoma cells with acquired resistance to the BRAF inhibitor. *Int J Oncol.* (2016) 49:1164–74. doi: 10.3892/ijo.2016.3594
47. Ross KC, Andrews AJ, Marion CD, Yen TJ, Bhattacharjee V. Identification of the serine biosynthesis pathway as a critical component of BRAF inhibitor resistance of melanoma, pancreatic, and non-small cell lung cancer cells. *Mol Cancer Ther.* (2017) 16:1596–609. doi: 10.1158/1535-7163.MCT-16-0798
48. Hernandez-Davies JE, Tran TQ, Reid MA, Rosales KR, Lowman XH, Pan M, et al. Vemurafenib resistance reprograms melanoma cells towards glutamine dependence. *J Transl Med.* (2015) 13:210,015-0581-2. doi: 10.1186/s12967-015-0581-2
49. McDermott M, Eustace AJ, Busschots S, Breen L, Crown J, Clynes M, et al. *in vitro* development of chemotherapy and targeted therapy drug-resistant cancer cell lines: a practical guide with case studies. *Front Oncol.* (2014) 4:40. doi: 10.3389/fonc.2014.00040
50. Zeiderman MR, Egger ME, Kimbrough CW, England CG, Dupre TV, McMasters KM, et al. Targeting of BRAF resistant melanoma via extracellular matrix metalloproteinase inducer receptor. *J Surg Res.* (2014) 190:111–8. doi: 10.1016/j.jss.2014.02.021
51. Tirosh I, Izar B, Prakadan SM, Wadsworth MH II, Treacy D, Trombetta JJ, et al. Dissecting the multicellular ecosystem of metastatic melanoma by single-cell RNA-seq. *Science.* (2016) 352:189–96. doi: 10.1126/science.aad0501
52. Domcke S, Sinha R, Levine DA, Sander C, Schultz N. Evaluating cell lines as tumour models by comparison of genomic profiles. *Nat Commun.* (2013) 4:2126. doi: 10.1038/ncomms3126
53. Jiang G, Zhang S, Yazdanparast A, Li M, Pawar AV, Liu Y, et al. Comprehensive comparison of molecular portraits between cell lines and tumors in breast cancer. *BMC Genomics.* (2016) 17(Suppl. 7):525,016-2911-z. doi: 10.1186/s12864-016-2911-z

54. Sinha R, Winer AG, Chevinsky M, Jakubowski C, Chen YB, Dong Y, et al. Analysis of renal cancer cell lines from two major resources enables genomics-guided cell line selection. *Nat Commun.* (2017) 8:15165. doi: 10.1038/ncomms15165
55. Vincent KM, Findlay SD, Postovit LM. Assessing breast cancer cell lines as tumour models by comparison of mRNA expression profiles. *Breast Cancer Res.* (2015) 17:114,015-0613-0. doi: 10.1186/s13058-015-0613-0
56. Vincent KM, Postovit LM. Investigating the utility of human melanoma cell lines as tumour models. *Oncotarget.* (2017) 8:10498–509. doi: 10.18632/oncotarget.14443
57. Grippo JF, Zhang W, Heinzmann D, Yang KH, Wong J, Joe AK, et al. A phase I, randomized, open-label study of the multiple-dose pharmacokinetics of vemurafenib in patients with BRAF V600E mutation-positive metastatic melanoma. *Cancer Chemother Pharmacol.* (2014) 73:103–11. doi: 10.1007/s00280-013-2324-5
58. Falchook GS, Long GV, Kurzrock R, Kim KB, Arkenau HT, Brown MP, et al. Dose selection, pharmacokinetics, and pharmacodynamics of BRAF inhibitor dabrafenib (GSK2118436). *Clin Cancer Res.* (2014) 20:4449–58. doi: 10.1158/1078-0432.CCR-14-0887
59. Funck-Brentano E, Alvarez JC, Longvert C, Abe E, Beauchet A, Funck-Brentano C, et al. Plasma vemurafenib concentrations in advanced BRAFV600mut melanoma patients: impact on tumour response and tolerance. *Ann Oncol.* (2015) 26:1470–5. doi: 10.1093/annonc/mdv189
60. Tap WD, Gong KW, Dering J, Tseng Y, Ginther C, Pauletti G, et al. Pharmacodynamic characterization of the efficacy signals due to selective BRAF inhibition with PLX4032 in malignant melanoma. *Neoplasia.* (2010) 12:637–49. doi: 10.1593/neo.10414
61. He Y, Zhu Q, Chen M, Huang Q, Wang W, Li Q, et al. The changing 50% inhibitory concentration (IC50) of cisplatin: a pilot study on the artifacts of the MTT assay and the precise measurement of density-dependent chemoresistance in ovarian cancer. *Oncotarget.* (2016) 7:70803–21. doi: 10.18632/oncotarget.12223
62. Clark NA, Hafner M, Kouril M, Williams EH, Muhlich JL, Pilarczyk M, et al. GRcalculator: an online tool for calculating and mining dose-response data. *BMC Cancer.* (2017) 17:3689–3. doi: 10.1186/s12885-017-3689-3

Conflict of Interest Statement: The authors declare that the research was conducted in the absence of any commercial or financial relationships that could be construed as a potential conflict of interest.

frontiers in Oncology

ORIGINAL RESEARCH
published: 18 April 2019
doi: 10.3389/fonc.2019.00304

A Novel Citrullinated Modification of Histone 3 and Its Regulatory Mechanisms Related to IPO-38 Antibody-Labeled Protein

*Shuzheng Song, Zhen Xiang, Jun Li, Jun Ji, Ranlin Yan, Zhenggang Zhu and Yingyan Yu**

Department of Surgery, Ruijin Hospital affiliated to Shanghai Jiao Tong University School of Medicine, Shanghai Key Laboratory for Gastric Neoplasms, Shanghai, China

IPO-38 is a potential biomarker for early diagnosis of gastric cancer that we recently identified. Although we characterized its chemical nature as a nucleosome histone, we suspected the existence of histone modification for the IPO-38 antibody-labeled protein. Here, we used a commercially available modified histone peptide array to identify the type and site of histone modification labeled by the IPO-38 monoclonal antibody. In protein array analysis, the citrulline modification of histone 3 on arginine 26 (H3R26Cit) yielded the strongest signal. Although peptidyl arginine deiminase-2 and -4 (PADI2 and PADI4, respectively) can catalyze the conversion of arginine to citrulline, we observed that only PADI4 expression correlated with the citrulline histone modification of H3R26Cit. Overexpression of PADI4, via transfection of a eukaryotic expression vector, and knockdown of PADI4 gene expression, by a PADI4 CRISPR/Cas9 vector, confirmed the crucial function of PADI4 on the increased level of H3R26Cit in gastric cancer cell lines. By immunoprecipitation and immunoblotting, we found an interaction between H3R26Cit and H3K27me3. Our study established the first link between the IPO-38 antigen and citrullinated histone 3, and clarified the upstream regulatory enzyme PADI4. The new findings suggest an important role for the citrullination modification of histone in gastric cancer biology, and should help us optimize the development of a sensitive and specific diagnostic reagent.

Keywords: IPO-38, histone modification, citrullination, PADI4, biomarker

OPEN ACCESS

Edited by:
Zhe-Sheng Chen,
St. John's University, United States

Reviewed by:
Ger J. M. Pruijn,
Radboud University Nijmegen, Netherlands
Qi Liu,
Tongji University, China
Qingyuan Zhang,
Ningxia Medical University, China

****Correspondence:***
Yingyan Yu
yingyan3y@sjtu.edu.cn

Specialty section:
This article was submitted to Cancer Molecular Targets and Therapeutics, a section of the journal Frontiers in Oncology

Received: *21 January 2019*
Accepted: *02 April 2019*
Published: *18 April 2019*

Citation:
Song S, Xiang Z, Li J, Ji J, Yan R, Zhu Z and Yu Y (2019) A Novel Citrullinated Modification of Histone 3 and Its Regulatory Mechanisms Related to IPO-38 Antibody-Labeled Protein. Front. Oncol. 9:304. doi: 10.3389/fonc.2019.00304

INTRODUCTION

Gastric cancer is a disease with high morbidity and mortality rates worldwide, especially in East Asia. Data from GLOBOCAN 2018 show there are 1,033,701 new cases and 782,685 death cases of gastric cancer all over the world (1). Currently, methods are limited for early diagnosis of gastric cancer. Patients are often diagnosed with gastric cancer at an advanced stage with poor prognosis. Therefore, early diagnosis is a key to improving the outcome of patients. Our group proposed a candidate biomarker IPO-38 for diagnosis of gastric cancer (2). Assaying IPO-38 provides significantly higher specificity and sensitivity (56.7 and 93.3%, respectively), over routinely used biomarkers CEA, CA199, and CA72-4. IPO-38 has long been used as a cell proliferation nuclear antigen (3, 4). Although we identified it as a member of the histone protein family based on mass spectrometry, we considered that the histone was modified chemically (2).

Protein function is specified by appropriately folded secondary structure and post-translational modifications, including acetylation, methylation, phosphorylation, and citrullination (5). Histone modification plays an important role in maintaining homeostasis. Disorders of histone modification associate with cancer, neurological diseases, as well as autoimmune diseases (6, 7). Histone modifications potentially alter the electrical charge between histones and DNA duplexes, impacting chromatin organization and transcription. Histone modifications also affect gene regulation by modulating binding with transcription factors (6–8). In addition, histone modifications are involved in the formation of neutrophil extracellular traps (NETs), a crucial process for microbe clearance (9), which also plays a role on cancer metastasis through protein citrullination in peripheral blood (10–12).

Specific antibody analysis and mass spectrometry are commonly used for detection of histone modifications. However, the number of histone-specific antibodies is limited, which has restricted progress in studying histone modifications and functions. Mass spectrometry potentially overcomes the defect of insufficient antibodies to some extent, but trypsin digestion in the sample pretreatment step often destroys many modification sites, and ultimately reduces sensitivity (13). In 2010, a new histone modified peptide array was developed, promoting research to understand the function, metabolism, and significance of histone modifications (14–16).

To clarify the histone modification characteristics and biological significance of the IPO-38 antigen, we used the modified peptide array to identify the IPO-38 monoclonal antibody-binding protein. We characterized the novel modified histone H3, and identified that PADI4 is a key enzyme catalyzing citrullination modification of histone 3.

MATERIALS AND METHODS

Modified Histone Peptide Array Analysis

MODified™ Histone Peptide Array from Active motif (Active Motif, California, USA) is a histone modified polypeptide chip of 59 single-site histone modifications and different permutations in 384 dot matrixes. Each chip is divided into left and right wings and repeating lattice arrangement. The chip was first blocked with 5% BSA (Sangon Biotech, Shanghai, China) for 1 h at room temperature, and then incubated with IPO-38 monoclonal antibody (1:1000, Thermo Fisher, Massachusetts, USA) overnight at 4°C. The next day, the chip was washed three times with 1×PBST [1×PBS with 0.1% (v/v) Tween-20], and then incubated with HRP-labeled goat anti-mouse IgM second antibody for 1 h at room temperature (1:5000, Sangon Biotech, Shanghai, China). After incubation, the chip was again washed with 1×PBST three times and the signal was detected using ECL luminescent reagent (Meilun, Shanghai China), in a chemiluminometer (Tanon, Shanghai, China). The histone modification sites and signal intensity analysis were conducted with the special software provided by Active Motif (https://www.activemotif.com/catalog/668).

Cell Culture

Gastric cancer cell lines, SGC7901, MKN45, HGC27, and BGC823, were purchased from the Cell Bank of the Chinese Academy of Sciences (Shanghai, China). Gastric cancer cell lines, Hs746T, AGS, and NCI-N87, were purchased from the American Type Culture Collection (ATCC, Maryland, USA), and the human gastric mucosal cells, GES1, and 293T cells were preserved in our laboratory. Cell lines were cultured in 37°C culture incubator with 5% carbon dioxide using RPMI 1640 or DMEM medium (Hyclone, Utah, USA) containing 10% FBS (Gibco, New York, USA) according to the manufacturer's instructions.

Construction of PADI2 and PADI4 Eukaryotic Expression Vectors and PADI4 CRISPR/Cas9 Vector

Primers were designed for the coding region sequences of the PADI2 (NM_007365.2), PADI4 (NM_012387.2), and the restriction sites for the eukaryotic expression vector pCDH-CMV-MCS-EF1-Puro (SBI, California, USA). The high-fidelity PCR enzyme KOD plus neo (Toyobo, Osaka, Japan) was used to amplify the coding region sequences of PADI2 and PADI4 from a 293T cell cDNA library. Agarose gel (1%) electrophoresis was used to confirm the PCR product size, and T4 ligase (NEB, Massachusetts, USA) was used to link the target fragment to the empty linear vector after digestion. Competent TNF5α cells (Tiangen, Shanghai, China) were transformed with the expression vectors, and three positive colonies were selected for sequencing to verify the plasmid.

CRISPR/Cas9 vector targeting PADI4 (NM_012387.2) was constructed using the lentiCRISPRv2 vector, which was a gift from the Feng Zhang lab at MIT. The online guide RNA design website (http://crispr.mit.edu) was used to design the target sequence near the transcription start site of PADI4. The top two scored sequences were selected as the gene editing sites for primers (gRNA1: 5′-GGGACGAGCTAGCCCGACGA-3′; gRNA2: 5′-TCACACGGATCAATGTCCCC-3′). In this study we adopted an all-in-one method. Primers designed according to the two gRNA sequences and the tracRNA-U6 vector sequences were used to produce a gRNA1-tracRNA-U6-gRNA2 fragment. Then the proper fragment was ligated into the lentiCRISPRv2 vector and verified by sequencing.

Lentiviral Packaging and Stable Cell Line Screening

The constructed eukaryotic expression vector and gene knockdown vector were transfected into the 293T cells with the packaging plasmids psPAX2 and pMD2.G using Lipofectamine 2000 (Thermo Fisher, Massachusetts, USA). The lentivirus was harvested 48 h after transfection, and the lentivirus supernatant was filtered using a 0.45 μm filter. One day prior to infection, the three cell lines (AGS, SGC7901, and MKN45) were plated at 2×10^5 cells per well in 6-well tissue culture plates. The lentivirus was added into the separate cell lines, and polybrene was added at a density of 6 ng/ul (Sigma, California, USA). After 24 h, the infection medium was removed and replaced

with normal culture medium. After 48 h, the cell lines were screened using 2 ng/μl puromycin (Sangon Biotech, Shanghai, China), and a stable cell line was formed after 1 week of continuous selection.

Western Blot

Whole cellular protein was extracted using RIPA lysis buffer (Beyotime, Shanghai, China) containing a protease inhibitor cocktail (Roche, Basel, Switzerland). The cytoplasmic and nuclear protein fractions were isolated using a Nuclear and Cytoplasmic Protein Extraction Kit (Beyotime, Shanghai, China) according to the manufacturer's instructions. Protein samples were separated by SDS-PAGE gel containing 10% acrylamide, electrophoresis and transferred to a 0.45 μm PVDF membrane (Millipore, Massachusetts, USA). The transferred membranes were blocked with 5% BSA for 1 h at room temperature. Then the membranes were incubated with the corresponding primary antibodies: mouse anti-human IPO-38 monoclonal antibody (1:1000, Thermo Fisher, Massachusetts, USA); rabbit anti-human H3K27ac polyclonal antibody, rabbit anti-human H3R26Cit/H3K27me3 monoclonal antibody, and mouse anti-human PADI4 monoclonal antibody (1:1000, Abcam, Cambridge, UK); rabbit anti-human EZH2 monoclonal antibody (1:1000, CST, Boston, Massachusetts USA), rabbit anti-human PADI2 polyclonal antibody, (1:1000, Proteintech, Chicago, Illinois, USA), and HRP-labeled mouse anti-human GAPDH monoclonal antibody (1:2000, Proteintech, Chicago, Illinois, USA), and mouse anti-human histone H3 monoclonal antibody (1:1000, Abcam, Cambridge, UK) as an internal reference antibody overnight at 4°C. The next day, 1×TBST buffer [10 mM Tris-HCl, pH 8.0, 150 mM NaCl, 0.1% (v/v) Tween-20] was used to wash the membranes 3 times for 10 min each time at RT. HRP-labeled goat anti-rabbit or mouse IgG secondary antibody (1:5000, Proteintech, Chicago, Illinois, USA) of the corresponding species was incubated for 1 h at RT. HRP-labeled goat anti-mouse IgM secondary antibody (Sangon Biotech, Shanghai, China) was used as the second antibody for the IPO-38 IgM monoclonal antibody. After the incubation of the secondary antibody, the membranes were washed 3 times for 10 min each time at RT with 1×TBST buffer, and then the signal was detected in the chemiluminometer using ECL luminescent solution (Meilun, Shanghai China).

Histone Immunoprecipitation

To reduce the interference of non-histone proteins and nucleotides, we used enzymatic digestion to obtain histones for further immunoprecipitation. After collecting the cell pellet, we used the hypotonic buffer [0.3 M sucrose, 60 mM KCl, 15 mM NaCl, 5 mM $MgCl_2$, 0.1 mM EGTA, 15 mM Tris-HCl pH 7.5, 5 mM sodium butyrate, 0.4% NP40, and Complete™ EDTA-free protease inhibitor mixture (Roche, Basel, Switzerland)] to rupture the cell membrane, and then collected the nuclear pellet. Nuclear deposition concentration was measured by nanodrop (Thermo Fisher, Massachusetts, USA), and 200 U/5 μg of micrococcal nuclease (NEB, Massachusetts, USA) was used to digest the nucleosome at 37°C for 6 min. EDTA (Sigma, California, USA) was added to stop the reaction. After centrifugation, the supernatant, which contains histone DNA complexes, namely nucleosomes, was collected, and concentration was measured. The appropriate amount of lysate was taken as input, and the remainder was divided into 3 groups, and 20 μl of protein A/G magnetic beads (Thermo Fisher, Massachusetts, United States), and 5 μg of anti-H3K27me3 antibody, anti-H3K27ac antibody, or normal rabbit IgG (CST, Boston, Massachusetts, USA) was added to each sample of lysate. After incubating overnight at 4°C on a shaker, the complexes were washed with RIPA buffer three times in the magnetic frame (Invitrogen, California, USA). Finally, the bound proteins were eluted into 1×SDS loading buffer (Beyotime, Shanghai, China). The subsequent steps followed the immunoblotting protocol described above, and the rabbit anti-human H3R26Cit polyclonal antibody was used to detect the corresponding histone modification.

Immunofluorescence

The MKN45 and SGC7901 cancer cell lines (5×10^3 cells per plate) were seeded on a fluorescence chamber culture plate. After the cells fully stretched and adhered to the plate 12 h later, they were fixed in 4% paraformaldehyde for 15 min at RT, and the cell and nuclear membranes were permeabilized in 0.5% Triton X-100 (Sangon Biotech, Shanghai, China) for 20 min at RT. The plate was washed 3 times for 5 min with 1×PBS. Goat serum (Sangon Biotech, Shanghai, China) was used for antigen blocking for 1 h at RT. After blocking, the samples were incubated with mouse anti-human PADI4 monoclonal antibody (1:100) and rabbit anti-human PADI2 polyclonal antibody (1:100) at 4°C overnight in a wet box. The plate was then washed with 1×PBST three times for 5 min each, and incubated with Alexa Fluor 488 goat anti-mouse red fluorescent secondary antibody and Alexa Fluor 555 goat anti-rabbit green fluorescent secondary antibody (1:250, Invitrogen, California, USA) at RT in the dark for 1 h. Nuclei were stained for 5 min at room temperature in the dark with DAPI (Sigma, California, USA). Finally, plates were washed 3 times for 5 min with 1×PBST. Fluorescence signal could be observed and the fluorescent images were taken with a fluorescence microscope (Nikon, Tokyo, Japan).

Real-Time PCR

Total mRNA was extracted from the cell lines using Trizol (Invitrogen, California, USA), according to the manufacturer's protocol. The obtained mRNA was reverse transcribed using the ReverTra Ace® qPCR RT Kit (Toyobo, Osaka, Japan). The mRNA levels of PADI2, PADI4, EZH2, KDM6A, KDM6B, and GAPDH were detected using the following specific primers: Primers for PADI2, forward: 5′- GCACCTACCTCTGGACC GAT-3′, reverse: 5′-ACACGTGTTCCGAGTGCTTC-3′, product length 81 bp; primers for PADI4, forward: 5′- GACCCCC AAGGACTTCTTCA-3′, reverse: 5′-GCTGCACTTGG AGGACAGTT-3′, product length 115 bp; primers for EZH2, forward: 5′-CATACGCTTTTCTGTAGGCGA-3′, reverse: 5′-TCCGCTTATAAGTGTTGGGTG-3′, product length 82

bp; primers for KDM6A, forward: 5′-TCTCCAAAAGTCCT TGGAAGC-3′, reverse: 5′-AAGGCATCCTGAACTTTCCC-3′, product length 96 bp; primers for KDM6B, forward: 5′-TACAGA CCCTCGAAATCCCA-3′, reverse: 5′-CAGGGTCTTGGTGG AGAAGA-3′, product length 88 bp; and primers for GAPDH, forward: 5′-ACGGATTTGGTCGTATTGGGCG-3′, reverse: 5′-CTCCTGGAAGATGGTGATGG-3′, product length 212 bp. The qPCR reaction was carried out in a Roche Light cycler 480 PCR machine (Roche, Basel, Switzerland) using SYBR Green PCR master mix (Life Technologies, California, USA).

Statistical Analysis

The mRNA expression data analysis was performed by Student's *t*-test using GraphPad Prism 8.0.1 software (GraphPad Software, San Diego, California, USA). Differences were considered statistically significant when $P < 0.05$.

RESULTS

Identification of Histone Modifications Marked by the IPO-38 Monoclonal Antibody

The IPO-38 monoclonal antibody detects proteins with a molecular weight around 15 kDa in total cellular protein lysates of human gastric epithelial cells (GES1) and gastric cancer cell lines (SGC7901 and NCI-N87) (**Figure 1A**). After incubating the modified histone peptide chip with the IPO-38 monoclonal antibody, 10 high intensity signals were obtained that corresponded to: H3R26Cit-K27me2, H3R26Cit-K27me1, H3R26Cit-K27me3, H3R26Cit, H3K27ac, H3R26me2a-K27ac, H3K12ac-K16ac-K20ac, H3R26me2s-K27ac, H3K16ac-K20ac, and H3K12ac-K16ac-K20me2 (**Figures 1B–D**). Results were duplicated on the left and right wings of the chip (**Figure 1B**), and signal intensities aligned well and showed good consistency (**Figure 1C**). Specific analysis of modified histone peptides revealed that the highest specificity of IPO-38 antibody-binding was for H3R26Cit, followed by the H3K27me2 modification (**Figure 1E**). We noticed that the signal intensity of H3R26Cit site was significantly enhanced when the adjacent site H3K27 was methylated. In particular, the presence of K27me2 modification resulted in 3-fold up-regulation of signaling intensity than that of R26Cit alone based on signaling intensity analysis. Immunoblotting using an antibody specific for H3R26Cit correlated well with protein levels detected using the IPO-38 antibody in the gastric cancer cell lysates (**Figure 1F**).

Expression Levels of H3R26Cit and Related Catalytic Enzyme PADIs

Since PADI2 or PADI4 catalyzes the conversion of arginine to citrulline in humans, we examined the protein levels of PADI2, PADI4, and H3R26Cit in several human gastric cancer cell lines. We observed that the basal expression level of H3R26Cit was higher in SGC7901 and MKN45 cells, and basal expression of PADI4 was also higher in those cancer cell lines. No significant difference of PADI2 was found in those cancer cell lines (**Figure 2A**). The mRNA expression level of PADI2 and PADI4 was lower in cancer cell lines, compared to GES1 control cells, by q-RT-PCR (**Figure 2B**), though PADI4 protein levels were higher in SGC7901 and MKN45 cells. There was discrepancy between the mRNA and protein levels of PADI2 and PADI4. By immunofluorescence microscopy, PADI2 was shown to localize in both the cytoplasm and nucleus, whereas PADI4 was found only in the nucleus (**Figure 2C**).

The Impact of PADI2 and PADI4 Overexpression and Knockdown on H3R26Cit Level

PADI2 and PADI4 eukaryotic expression vectors were packaged with lentivirus. Although PADI4 protein level was higher in SGC7901 and MKN45 cell lines (**Figure 2A**), but they took longer exposure time with ECL luminescence reagent (2 min). Then we chose a PADI4 low expression AGS cell line and a PADI4 moderate expression SGC7901 cell line for the overexpression study, and SGC7901 and MKN-45 cells were used for the knockdown study. After PADI2 and PADI4 were successfully expressed, we examined the expression level of H3R26Cit (**Figures 3A,B**). Overexpression of PADI4 significantly increased intracellular expression of H3R26Cit, compared to PADI2 overexpression, shown by both Western blot with shorter exposure time (2 s) (**Figure 3C**).

The "all-in-one" single plasmid dual target PADI4 gene knockdown system was constructed using CRISPR/Cas9 technology, which targeted a dual target near the PADI4 transcription start site (**Figure 3D**). The plasmid was packaged with lentivirus and SGC7901 and MKN45 cell lines were infected. The puromycin was used to select a stable cell line. The significant decrease in the expression level of PADI4 in experimental cells was accompanied by a decrease in the expression level of H3R26Cit (**Figure 3E**).

Analysis of Interaction Between H3R26Cit and Other Post-translational Modification

Since H3K27ac and H3K27me3 were also highlighted in the modified histone peptide array, we analyzed the interaction between H3R26Cit and other histone modifications. As shown in **Figure 4A**, overexpression of PADI4 resulted in a significant decrease of H3K27me3 levels in AGS and SGC7901 cells, but led to increased expression of H3K27ac. To clarify the potential crosstalk between H3R26Cit and H3K27me, we extracted nucleosomes from cell nucleus by means of the micrococcal nuclease method, and performed immunoprecipitations using H3K27me3 and H3K27ac antibodies. H3R26Cit was not detected in the H3K27me3 pull-down product, but co-precipitated with H3K27ac (**Figure 4B**), which supports an interaction between H3R26Cit and H3K27ac. We further examined expression levels of EZH2, an H3K27me3 methyltransferase, and KDM6A/KDM6B demethylases after PADI4 overexpression. The expression level of EZH2 was significantly decreased in SGC7901 and AGS cells ($P < 0.001$), while the expression level of KDM6A was significantly increased ($P = 0.037$; $P = 0.0046$, for SGC7901 and AGS cells, respectively). The expression

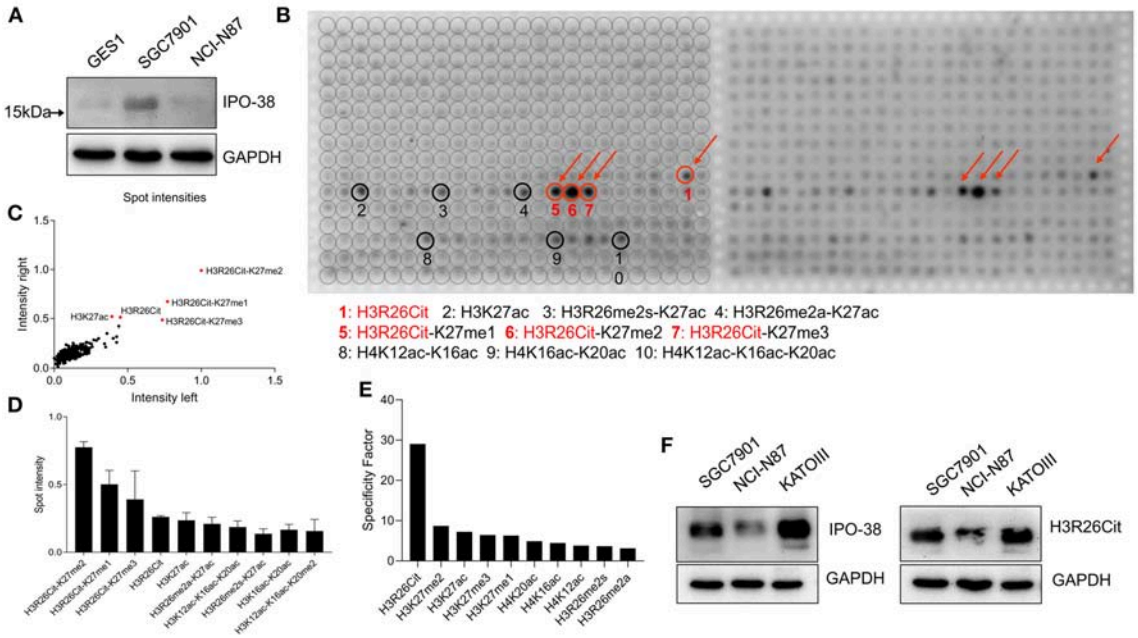

FIGURE 1 | Analysis of histone modification peptide array using IPO-38 monoclonal antibody. **(A)** The protein expression of IPO-38 in gastric mucosal cell GES-1 and gastric cancer cell lines. **(B)** Presentation of signal intensity on modified histone peptide array based on incubation with the IPO-38 monoclonal antibody. **(C)** The consistency assay of two repeated detections on the modified histone peptide array. **(D)** The top 10 histone modifications with the strongest binding to the IPO-38 monoclonal antibody. **(E)** The top 10 histone modification sites with the best specificity for IPO-38 monoclonal antibody binding. **(F)** Comparison of H3R26Cit and IPO-38 protein levels in three gastric cancer cell lines.

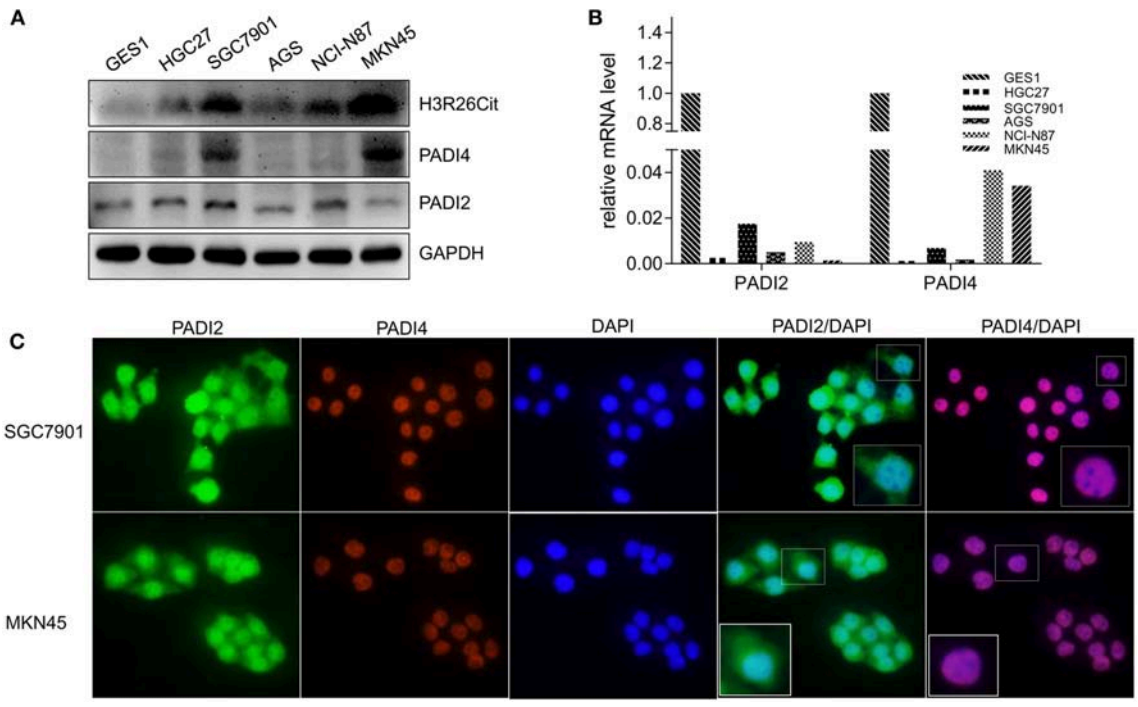

FIGURE 2 | Analysis of basal expression of H3R26Cit and its catalytic enzymes PADIs. **(A)** The protein expression of H3R26Cit, PADI2, and PADI4 in GES-1 gastric mucosa cells and several gastric cancer cell lines. **(B)** The expression of PADI2 and PADI4 mRNA in GES-1 gastric mucosa cells and several gastric cancer cell lines. **(C)** Subcellular localization of PADI2 and PADI4 proteins in SGC7901 and MKN45 gastric cancer cell lines.

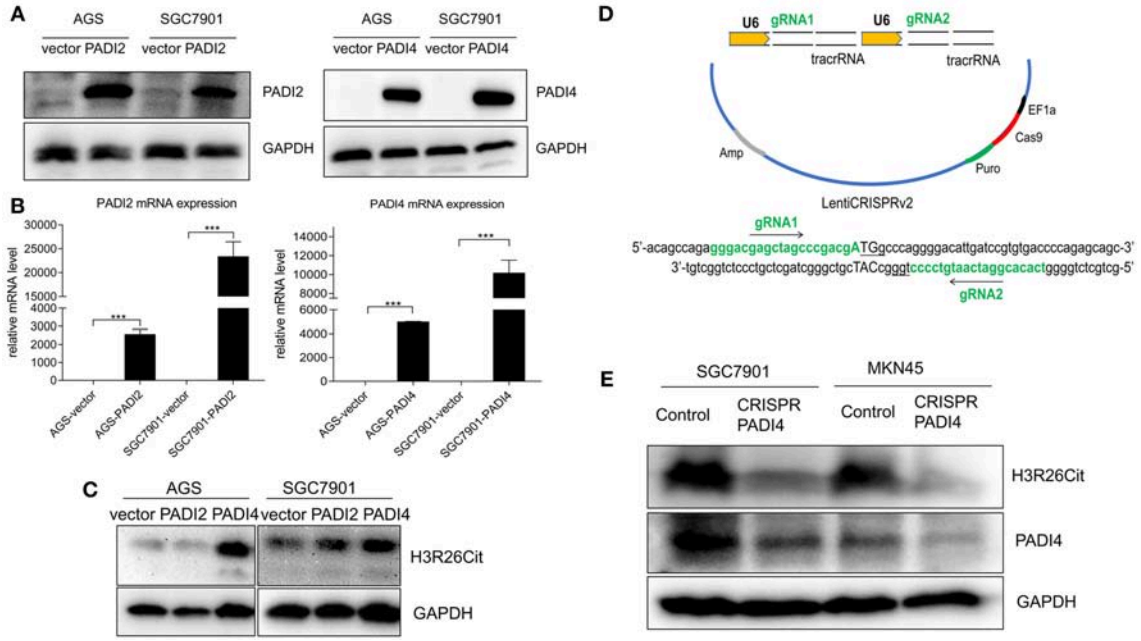

FIGURE 3 | The influence of PADI2 and PADI4 overexpression or knockdown on H3R26Cit. **(A)** Detection of protein level changes after overexpression of PADI2 and PADI4. **(B)** Detection of mRNA level changes after overexpression of PADI2 and PADI4 (*** indicates $P < 0.001$). **(C)** The protein level of H3R26Cit is significantly increased after enforcing PADI4 expression, compared to enforcing PADI2 expression. **(D)** Schematic diagram of the construction of CRISPR/Cas9 all-in-one plasmid system with a double target on the PADI4 gene. **(E)** The protein level of H3R26Cit is significantly decreased after knockdown of PADI4 in both SGC7901 and MKN45 gastric cancer cell lines.

level of KDM6B was increased to some extent ($P = 0.46$; $P = 0.012$) (**Figure 4C**). A significant down-regulation of EZH2 in the nucleus was found; as internal controls, GAPDH was only expressed in the cytoplasm and histone 3 was only expressed in nucleus (**Figure 4D**). The results suggest that PADI4 not only catalyzes H3R26Cit modification, but also influences the activities of EZH2, KDM6A, and KDM6B, as reflected in the decreased level of H3K27me3 in the nucleus (**Figure 4E**).

DISCUSSION

IPO-38 is a diagnostic biomarker for gastric cancer identified in our previous clinical proteome study. We proposed that the protein labeled by IPO-38 monoclonal antibody was a nucleosome histone and suspected it was a modified histone H2B (2). We could not, however, clarify the exact histone modification due to insufficient methods.

In recent years, the relationship between histone modification and tumorigenesis has attracted greater attention. Technologies for detecting and studying histone modifications have been developed and greatly improved. Using the self-developed chromatin immunoprecipitation-based microarray method (ChIP-chip) technology, Heintzman and coworkers demonstrated that cell-specific histone modifications bound to cell-specific enhancers affect cell-specific gene expression spectrum (17). Cejas et al. developed fixed-tissue chromatin immunoprecipitation sequencing, which enables reliable extraction of soluble chromatin from formalin-fixed paraffin-embedded tissues for accurate detection of histone marks. By using multiple histone marks, they generated chromatin state maps and identified cis-regulatory elements in clinical samples for various tumor types (18).

In the current study, a modified histone peptides array was used. This protein array covers 59 different combinations of post-translational modifications such as methylation, acetylation, phosphorylation, and citrullination in up to four different modifications per peptide (15, 16). This array is suitable for assessing the specificity of histone-modified antibodies and for analyzing interactions between different histone modification sites. The processing is straightforward, similar to Western blotting, and used in different molecular oncology laboratories (15, 16, 19). By means of this protein array, we characterized the antigen labeled by the IPO-38 antibody as H3R26Cit, which could interact with H3K27me and form a H3R26Cit-H3K27me complex. This new finding suggests that detection of H3K27me may be helpful to recognize H3R26Cit indirectly.

Previously, most studies on histone modifications focused on acetylation, methylation, and phosphorylation. The studies of histone citrullination are limited, especially for gastric cancer. Protein citrullination, also known as deamination, refers to a post-translational modification of arginine to citrulline (20, 21). Studies on the relationship between histone citrullination and tumors have mainly focused on histone H3. Thalin and coworkers reported that elevated H3Cit in peripheral blood predicted poor prognosis for advanced cancer

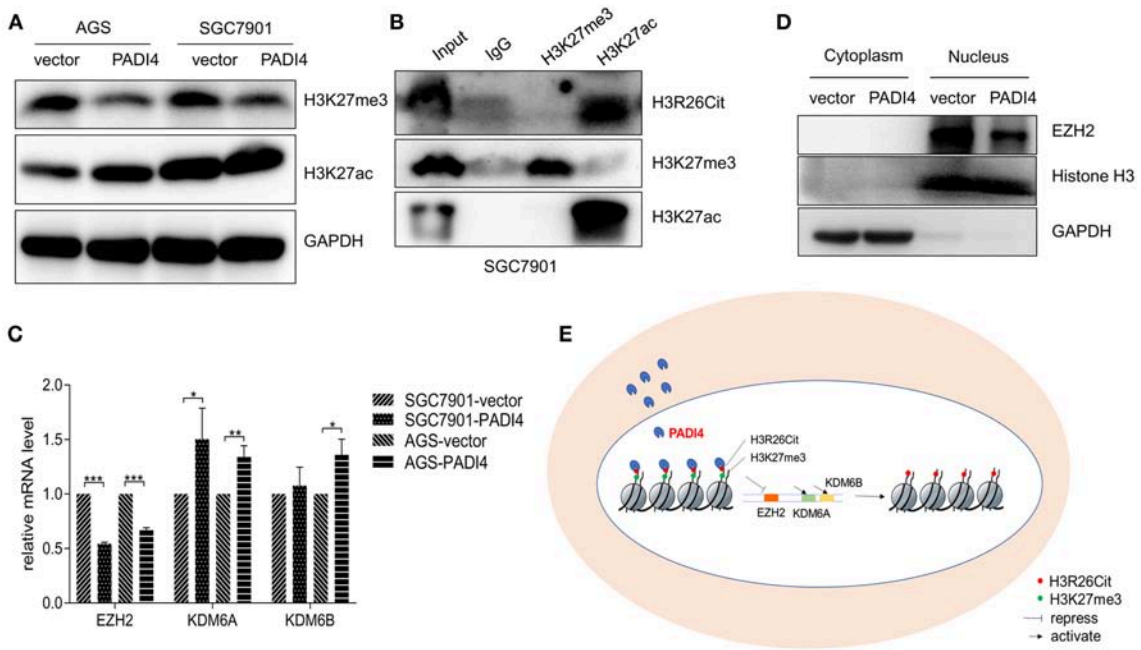

FIGURE 4 | Interaction assay of H3R26Cit and other post-translational modifications. **(A)** An increase in the level of H3K27ac protein and decreased H3K27me3 protein level were observed in both AGS and SGC7901 gastric cancer cell lines in which PADI4 was overexpressed. **(B)** Immunoprecipitation was performed by H3K27me3 and H3K27ac antibodies. H3R26Cit was not detected in the H3K27me3 pull-down product, but was found in the H3K27ac pull-down product. **(C)** Effect of PADI4 overexpression on mRNA expression of the H3K27 methyltransferase EZH2 and demethylases, KDM6A and KDM6B (*, **, and *** represent $P < 0.05$, $P < 0.01$, and $P < 0.001$, respectively) **(D)** EZH2 expression assay revealed that the protein was located in nucleus, and its expression level was decreased after PADI4 overexpression, with histone 3 and GAPDH serving as internal controls. **(E)** Schematic diagram of influences on histone modifications of H3R26Cit and H3K27me3 after PADI4 overexpression.

patients including colorectal cancer, gastric cancer, and breast cancer (10). Neutrophil extracellular traps (NETs) could be a source of citrullinated histones in the blood. PADI4 mediates histone citrullination in NETs formation (11, 22, 23). Protein citrullination also participates in the regulation of stem cell pluripotency, cancer-related genes, and immune responses (24–27). Although we characterized the antigen labeled by IPO-38 antibody, the exact clinical significance of citrullinated histone 3 needs further investigation.

The protein citrullination refers to a chemical conversion of arginine to citrulline, which is catalyzed by peptidylarginine deiminases (PADIs) in human beings (28). Among PADIs family, PADI4 carries a nuclear localization signal, and is mainly located in the nucleus (29). PADI2 might also undergo nuclear translocation in some cells to modify histones (26). Since both PADI4 and PADI2 might be involved in the citrullination of histones, we examined the expression levels of H3R26Cit, PADI4, and PADI2 synchronously and confirmed that PADI4, but not PADI2, regulates H3R26Cit formation. In addition, we found that the expression levels of mRNA and protein of PADI2 and PADI4 was inconsistent, which might be attributed to post-transcriptional modification of mRNA or post-translational modification of protein (30, 31).

In addition to intracellular histone citrullination, PADI4 in neutrophils can facilitate histone citrullination of NETs. This kind of extracellular histone modification facilitated ovarian cancer premetastatic niche formation in the omentum. Interfering NETs formation could inhibit cancer metastasis (32). Yuzhalin and colleagues indicated that extracellular histone modifications can promote liver metastasis of colorectal cancer (12). Therefore, protein citrullination of the extracellular matrix and microenvironment may play an important role on tumor progression. Higher levels of PADI4 have been reported in peripheral blood in several types of cancers (33).

Histone modification is a complex area. The precise correlation of H3R26Cit and H3K27me3 or H3K27ac is largely unknown. In this paper, we identified the crosstalk between H3R26Cit and H3K27me3, which was mentioned by other study before (34). According to our results, the binding ability of IPO-38 antibody to antigen might be affected by their crosstalk, but more experiments need to be done. EZH2 is an enzyme that mediates methylation of H3K27me3 (34). EZH2 was found up-regulated in melanoma, lymphoma, breast cancer, and prostate cancer, and related to promoting tumorigenesis, cell proliferation, and epithelial mesenchymal transition (35). KDM6A and KDM6B are enzymes involved in demethylation of H3K27me3 (36). Although we found that overexpression of PADI4 influences the expression levels of H3K27me3 and H3R26Cit, we did not find a confirm correlation between expression of PADI4 and methylation-related enzymes such as

EZH2, KDM6A, and KDM6B. Our study clarified that PADI4 is a main regulatory enzyme of histone citrullination, at least in gastric cancer. This discovery will be used to optimize the sensitivity and specificity of IPO-38 as a diagnostic reagent for gastric cancer.

Since the technical limitations, we did not analyze the clinical correlations. Next, we prepare to immunize mice with synthetic histone-modified polypeptide antigen to obtain specific monoclonal antibody, and then perform immunohistochemistry by new developed specific monoclonal antibody. We will establish a sandwich ELISA reagent to examine blood samples from patients.

AUTHOR CONTRIBUTIONS

SS and YY formulated the experimental concept and design. ZX, JL, JJ, and RY performed experiments. ZZ and YY supported the research. All authors wrote, reviewed, and revised the manuscript.

FUNDING

This project was supported by National Key R&D Program of China (2016YFC1303200, 2017YFC0908300), the National Natural Science Foundation of China (81772505), Shanghai Science and Technology Committee (18411953100), the Cross-Institute Research Fund of Shanghai Jiao Tong University (YG2017ZD01, YG2015MS62), Innovation Foundation of Translational Medicine of Shanghai Jiao Tong University School of Medicine (15ZH4001, TM201617, and TM 201702), Zhangjiang special development fund for key project (2017-05-HP-C1086-012), and Technology Transfer Project of Science & Technology Department of Shanghai Jiao Tong University School of Medicine.

REFERENCES

1. Bray F, Ferlay J, Soerjomataram I, Siegel RL, Torre LA, Jemal AJ. *Global Cancer Statistics 2018: GLOBOCAN Estimates of Incidence and Mortality Worldwide for 36 Cancers in 185 Countries*. (2018). 68:394–424. doi: 10.3322/caac.21492
2. Hao Y, Yu Y, Wang L, Yan M, Ji J, Qu Y, et al. IPO-38 is identified as a novel serum biomarker of gastric cancer based on clinical proteomics technology. *J Proteome Res*. (2008) 7:3668–77. doi: 10.1021/pr700638k
3. Sidorenko SP, Vetrova EP, Iurchenko OV, Shlapatskaia LN, Berdova AG, Elenskaia AM, et al. Monoclonal antibodies of the IPO series in studying and diagnosing malignant lymphoproliferative diseases. *Gematologiia i Transfuziologiia*. (1990) 35:19–22.
4. Thosaporn W, Iamaroon A, Pongsiriwet S, Ng KH. A comparative study of epithelial cell proliferation between the odontogenic keratocyst, orthokeratinized odontogenic cyst, dentigerous cyst, and ameloblastoma. *Oral Dis*. (2004) 10:22–6. doi: 10.1046/j.1354-523X.2003.00974.x
5. Tan MJ, Luo H, Lee S, Jin FL, Yang JS, Montellier E, et al. Identification of 67 histone marks and histone lysine crotonylation as a new type of histone modification. *Cell*. (2011) 146:1015–27. doi: 10.1016/j.cell.2011.08.008
6. Portela A, Esteller M. Epigenetic modifications and human disease. *Nat Biotechnol*. (2010) 28:1057–68. doi: 10.1038/nbt.1685
7. Audia JE, Campbell RM. Histone modifications and cancer. *Cold Spring Harb Perspect Biol*. (2016) 8:a019521. doi: 10.1101/cshperspect.a019521
8. Berger SL. Histone modifications in transcriptional regulation. *Curr Opin Genet Dev*. (2002) 12:142–8. doi: 10.1016/S0959-437X(02)00279-4
9. Dwivedi N, Radic M. Citrullination of autoantigens implicates NETosis in the induction of autoimmunity. *Ann Rheum Dis*. (2014) 73:483–91. doi: 10.1136/annrheumdis-2013-203844
10. Thalin C, Lundstrom S, Seignez C, Daleskog M, Lundstrom A, Henriksson P, et al. Citrullinated histone H3 as a novel prognostic blood marker in patients with advanced cancer. *PLoS ONE*. (2018) 13:e0191231. doi: 10.1371/journal.pone.0191231
11. Honda M, Kubes P. Neutrophils and neutrophil extracellular traps in the liver and gastrointestinal system. *Nat Rev Gastroenterol Hepatol*. (2018) 15:206–21. doi: 10.1038/nrgastro.2017.183
12. Yuzhalin AE, Gordon-Weeks AN, Tognoli ML, Jones K, Markelc B, Konietzny R, et al. Colorectal cancer liver metastatic growth depends on PAD4-driven citrullination of the extracellular matrix. *Nat Commun*. (2018) 9:4783. doi: 10.1038/s41467-018-07306-7
13. Yuan ZF, Arnaudo AM, Garcia BA. Mass spectrometric analysis of histone proteoforms. *Annu Rev Anal Chem*. (2014) 7:113–28. doi: 10.1146/annurev-anchem-071213-015959
14. Kungulovski G, Kycia I, Tamas R, Jurkowska RZ, Kudithipudi S, Henry C, et al. Application of histone modification-specific interaction domains as an alternative to antibodies. *Genome Res*. (2014) 24:1842–53. doi: 10.1101/gr.170985.113
15. Bock I, Dhayalan A, Kudithipudi S, Brandt O, Rathert P, Jeltsch A. Detailed specificity analysis of antibodies binding to modified histone tails with peptide arrays. *Epigenetics*. (2011) 6:256–63. doi: 10.4161/epi.6.2.13837
16. Bock I, Kudithipudi S, Tamas R, Kungulovski G, Dhayalan A, Jeltsch A. Application of Celluspots peptide arrays for the analysis of the binding specificity of epigenetic reading domains to modified histone tails. *BMC Biochem*. (2011) 12:48. doi: 10.1186/1471-2091-12-48
17. Heintzman ND, Hon GC, Hawkins RD, Kheradpour P, Stark A, Harp LF, et al. Histone modifications at human enhancers reflect global cell-type-specific gene expression. *Nature*. (2009) 459:108–12. doi: 10.1038/nature07829
18. Cejas P, Li L, O'Neill NK, Duarte M, Rao P, Bowden M, et al. Chromatin immunoprecipitation from fixed clinical tissues reveals tumor-specific enhancer profiles. *Nat Med*. (2016) 22:685–91. doi: 10.1038/nm.4085
19. Mann M, Cortez V, Vadlamudi R. PELP1 oncogenic functions involve CARM1 regulation. *Carcinogenesis*. (2013) 34:1468–75. doi: 10.1093/carcin/bgt091
20. Makrygiannakis D, Af Klint E, Lundberg IE, Lofberg R, Ulfgren AK, Klareskog L, et al. Citrullination is an inflammation-dependent process. *Ann Rheum Dis*. (2006) 65:1219–22. doi: 10.1136/ard.2005.049403
21. Ordonez A, Yelamos J, Pedersen S, Minano A, Conesa-Zamora P, Kristensen SR, et al. Increased levels of citrullinated antithrombin in plasma of patients with rheumatoid arthritis and colorectal adenocarcinoma determined by a newly developed ELISA using a specific monoclonal antibody. *Thromb Haemost*. (2010) 104:1143–9. doi: 10.1160/TH10-05-0297
22. Neeli I, Khan SN, Radic M. Histone deimination as a response to inflammatory stimuli in neutrophils. *J Immunol*. (2008) 180:1895–902. doi: 10.4049/jimmunol.180.3.1895
23. Wang Y, Li M, Stadler S, Correll S, Li P, Wang D, et al. Histone hypercitrullination mediates chromatin decondensation and neutrophil extracellular trap formation. *J Cell Biol*. (2009) 184:205–13. doi: 10.1083/jcb.200806072
24. McNee G, Eales KL, Wei W, Williams DS, Barkhuizen A, Bartlett DB, et al. Citrullination of histone H3 drives IL-6 production by bone marrow mesenchymal stem cells in MGUS and multiple myeloma. *Leukemia*. (2017) 31:373–81. doi: 10.1038/leu.2016.187
25. DeVore SB, Young CH, Li G, Sundararajan A, Ramaraj T, Mudge J, et al. Histone citrullination represses miRNA expression resulting in increased oncogene mRNAs in somatolactotrope cells. *Mol Cell Biol*. (2018) 38:e00084–18. doi: 10.1128/MCB.00084-18
26. Amin B, Voelter W. Human deiminases: isoforms, substrate specificities, kinetics, and detection. *Prog Chem Org Nat Prod*. (2017) 106:203–40. doi: 10.1007/978-3-319-59542-9_2

27. Fert-Bober J, Giles JT, Holewinski RJ, Kirk JA, Uhrigshardt H, Crowgey EL, et al. Citrullination of myofilament proteins in heart failure. *Cardiovasc Res*. (2015) 108:232–42. doi: 10.1093/cvr/cvv185
28. Bicker KL, Thompson PR. The protein arginine deiminases: structure, function, inhibition, and disease. *Biopolymers*. (2013) 99:155–63. doi: 10.1002/bip.22127
29. Nakashima K, Hagiwara T, Yamada M. Nuclear localization of peptidylarginine deiminase V and histone deimination in granulocytes. *J Biol Chem*. (2002) 277:49562–8. doi: 10.1074/jbc.M208795200
30. Pradet-Balade B, Boulme F, Beug H, Mullner EW, Garcia-Sanz JA. Translation control: bridging the gap between genomics and proteomics? *Trends Biochem Sci*. (2001) 26:225–9. doi: 10.1016/S0968-0004(00)01776-X
31. El Hajj P, Gilot D, Migault M, Theunis A, van Kempen LC, Sales F, et al. SNPs at miR-155 binding sites of TYRP1 explain discrepancy between mRNA and protein and refine TYRP1 prognostic value in melanoma. *Br J Cancer*. (2015) 113:91–8. doi: 10.1038/bjc.2015.194
32. Lee W, Ko SY, Mohamed MS, Kenny HA, Lengyel E, Naora H. Neutrophils facilitate ovarian cancer premetastatic niche formation in the omentum. *J Exp Med*. (2018) 216:176–94. doi: 10.1084/jem.20181170
33. Chang X, Han J, Pang L, Zhao Y, Yang Y, Shen Z. Increased PADI4 expression in blood and tissues of patients with malignant tumors. *BMC Cancer*. (2009) 9:40. doi: 10.1186/1471-2407-9-40
34. Clancy KW, Russell AM, Subramanian V, Nguyen H, Qian Y, Campbell RM, et al. Citrullination/methylation crosstalk on histone H3 regulates ER-target gene transcription. *ACS Chem Biol*. (2017) 12:1691–702. doi: 10.1021/acschembio.7b00241
35. Margueron R, Reinberg D. The Polycomb complex PRC2 and its mark in life. *Nature*. (2011) 469:343–9. doi: 10.1038/nature 09784
36. Greer EL, Shi Y. Histone methylation: a dynamic mark in health, disease and inheritance. *Nat Rev Genet*. (2012) 13:343–57. doi: 10.1038/nrg3173

Conflict of Interest Statement: The authors declare that the research was conducted in the absence of any commercial or financial relationships that could be construed as a potential conflict of interest.

frontiers in Oncology

REVIEW
published: 24 April 2019
doi: 10.3389/fonc.2019.00297

Gene Therapy Leaves a Vicious Cycle

*Reena Goswami[1], Gayatri Subramanian[2], Liliya Silayeva[1], Isabelle Newkirk[1], Deborah Doctor[1], Karan Chawla[2], Saurabh Chattopadhyay[2], Dhyan Chandra[3], Nageswararao Chilukuri[1] and Venkaiah Betapudi[1,4]**

[1] Neuroscience Branch, Research Division, United States Army Medical Research Institute of Chemical Defense, Aberdeen, MD, United States, [2] Department of Medical Microbiology and Immunology, University of Toledo College of Medicine and Life Sciences, Toledo, OH, United States, [3] Roswell Park Comprehensive Cancer Center, Buffalo, NY, United States, [4] Department of Physiology and Biophysics, Case Western Reserve University, Cleveland, OH, United States

The human genetic code encrypted in thousands of genes holds the secret for synthesis of proteins that drive all biological processes necessary for normal life and death. Though the genetic ciphering remains unchanged through generations, some genes get disrupted, deleted and or mutated, manifesting diseases, and or disorders. Current treatment options—chemotherapy, protein therapy, radiotherapy, and surgery available for no more than 500 diseases—neither cure nor prevent genetic errors but often cause many side effects. However, gene therapy, colloquially called "living drug," provides a one-time treatment option by rewriting or fixing errors in the natural genetic ciphering. Since gene therapy is predominantly a viral vector-based medicine, it has met with a fair bit of skepticism from both the science fraternity and patients. Now, thanks to advancements in gene editing and recombinant viral vector development, the interest of clinicians and pharmaceutical industries has been rekindled. With the advent of more than 12 different gene therapy drugs for curing cancer, blindness, immune, and neuronal disorders, this emerging experimental medicine has yet again come in the limelight. The present review article delves into the popular viral vectors used in gene therapy, advances, challenges, and perspectives.

Keywords: gene therapy, viral vectors, modern medicines, diseases and disorders, clinical trials

OPEN ACCESS

Edited by:
Zhe-Sheng Chen,
St. John's University, United States

Reviewed by:
Paul B. Fisher,
Virginia Commonwealth University, United States
Rocco Savino,
Università degli studi Magna Græcia di Catanzaro, Italy

***Correspondence:**
Venkaiah Betapudi
Venkbetapudi@gmail.com

Specialty section:
This article was submitted to Cancer Molecular Targets and Therapeutics, a section of the journal Frontiers in Oncology

Received: *11 January 2019*
Accepted: *01 April 2019*
Published: *24 April 2019*

Citation:
Goswami R, Subramanian G, Silayeva L, Newkirk I, Doctor D, Chawla K, Chattopadhyay S, Chandra D, Chilukuri N and Betapudi V (2019) Gene Therapy Leaves a Vicious Cycle. Front. Oncol. 9:297. doi: 10.3389/fonc.2019.00297

INTRODUCTION

The human genome contains ~25,000 genes that encode a wide variety of proteins colloquially called the building blocks and workhorses of the cell to drive every biological process necessary for life and death (1–4). Though the genetic ciphering remains largely unchanged through generations, some genes go awry due to mutations, and disruptions or deletions (5). These underlying and inevitable genetic changes translate into altered protein functions affecting normal cell structures, functions, and their physiological roles manifesting into a serious disease or deficiency or disorder (6, 7). According to the Genetic and Rare Diseases Information Center (GARD) and Global Genes®, the leading rare disease patient advocacy organization in the world, dysfunctional genes account for 80% of the total 7,136 diseases reported to date. Nearly 30 million people in the United States alone and more than 300 million people in the rest of the world are affected by genetic diseases; unfortunately, half of them are estimated to be children. According to the National Center for Advancing Translational Sciences (NCATS), only 500 human diseases are treatable with an estimated 10,000 drugs available to date, underscoring the necessity to develop new drugs and treatment options.

Although a significant advancement has been made in developing modern medicine, including chemotherapy, radiation, and surgery, many drugs are synthetic chemicals designed to alter the body's chemistry and create dependency overtime, and offer only temporary relief by reducing disease symptoms and increasing lifespan. These issues are partly addressed by developing protein therapy based on transcription factors, signaling proteins, gene editing enzymes, growth factors, engineered protein scaffolds, hormones, blood factors, thrombolytes, antibodies, and antigens. Some of them, especially the monoclonal antibody-based drugs including Humira, Rituxan, Avastin, Herceptin, Remicade, Lucentis, Enbrel, Synazis, and several others, are being used to treat cancer, diabetes, autoimmune disorders, infectious diseases, and others (8). In fact, both protein and peptide-based drugs have emerged as a major class of therapeutics with nearly 380 marketed pharmaceuticals available in the world (9). However, these protein-based therapies are facing many challenges including low solubility and bioavailability, *in vivo* physicochemical instability, short circulating half-life, penetrability *in vivo*, biodistribution, and causing toxicity in large amounts (10–15). Another adverse effect of introducing therapeutic proteins into a patient's body is that it may result in severe immune responses, inflammation, and fever (16). To add to the woes, the production and manufacturing of high quality therapeutic proteins have become highly complex activity (17). In fact, more than 5,000 critical steps are involved in developing a single therapeutic protein (8). Therefore, the quotient of unpredictability is very high in developing both chemical and protein-based therapies. Gene therapy, on the other hand, leads to long-lasting production of the desired therapeutic protein and can localize protein expression to an area of the body, fixing the problem at its source (18). Also, prognosis for a large number of incurable diseases appears grim, which is why gene therapy presents itself as a breakthrough alternative with immense potential to provide a one-time treatment option for a complete cure as well as disease and disorder prevention. Gene therapy is an emerging experimental treatment that delivers functional genes into a patient's body to counter or replace malfunctioning ones, thus curing disease without pharmacological intervention, radiotherapy, or surgery. This modern approach has the potential to offer complete protection against lethal nerve gases (13, 19–22) and treat monogenic and cardiovascular diseases, immunodeficiency, cancer, and more (23–27). Apart from genetic defects, several other diseases that cannot be treated with drugs or antibodies can be cured with gene therapy. In addition, every prescribed and non-prescribed drug comes with unwanted side effects, ranging from minor discomfort to death. According to Drugwatch®, a non-profit drug information network and organization, an estimated four million patients in the USA alone visit doctors annually due to adverse effects of prescription drugs. Hence, gene therapy that aligns with the natural human genetic transcriptome has the potential to become an unquestionable choice for complete treatment of diseases, disorders, and infectious diseases.

Gene therapy appears simple in principle but involves identification of affected gene(s), cloning and loading of a wild type or recombinant healthy version in a suitable vector for optimal delivery and expression in the target cells or tissue and thus has seen its fair share of hurdles. Because it often uses repurposed viruses to deliver therapeutic genes, gene therapy has been caught in a vicious cycle for nearly two decades owing to immune response, insertional mutagenesis, viral tropism, off-target activity, unwanted clinical outcomes (ranging from illness to death of participants in clinical trials), and patchy regulations (23, 28–31). This led to a sharp decline in research funding for basic, preclinical development and vector production via individual investigators grants such as R01 and program grants. Thus, with limited information of preclinical data and vector production, the number of clinical trials conducted worldwide did not rise steadily from 1999 to 2015 (32). Furthermore, funding of the actual clinical trial was not guaranteed even vectors have been produced and certified for human use at significant cost. The American Society of Gene Therapy has taken lead in fixing this fragmented funding method by making many recommendations including the elimination of redundant regulatory processes and establishment of the National Gene Vector Laboratories (NGVL) to review vector production and toxicology. Now, with new technological advances in gene delivery and editing methods, increased enthusiasm of clinicians and drug companies, the advent of several viral-based drugs in the market, and the potential to provide a one-time treatment option without corrupting the genetic code, gene therapy is breaking free of this cycle. Undoubtedly, the resurgent interest in offering gene therapy-based treatments is one of the most defining developments in the pharmaceutical industry and is expected to have far-reaching implications on curing dangerous diseases in the future. With an estimated US $11 billion market in the next 10 years, both clinical trials and pharmaceutical industry are anticipated to benefit immensely from gene therapy. Here, we describe popular viral vectors used in gene therapy and gene therapy drugs available in the market.

GENE THERAPY AND ITS KINDS

While the idea of gene therapy has been around for the past 80 years, Professor William Szybalski's demonstration in 1962 on correcting a genetic defect by delivering foreign DNA into mammalian cells is regarded as its birth (33). The Food and Drug Administration (FDA) defines gene therapy as products that "mediate their effects by transcription and/or translation of transferred genetic material and/or by integrating into the host genome and that are administered as nucleic acids, viruses, or genetically engineered microorganisms," and the European Medicines Agency (EMA) describes gene therapy medicinal product (GTMP) as a "biological medicinal product that contains an active substance which contains or consists of a recombinant nucleic acid used in or administered to humans to regulate, repair, replace, add or delete genetic sequences and its therapeutic, prophylactic or diagnostic effect relates directly to the recombinant nucleic acid sequence it contains, or to the product of genetic expression of this sequence" (32, 34). Typically, DNA, mRNA, siRNA, miRNA, and anti-sense

oligonucleotides are the genetic materials used for therapeutic delivery into a defective target cell or tissue to restore a specific gene function or turn off a gene responsible for disease or disorder development (35). Other methods include swapping the mutated gene for a functional gene using homologous recombination, repairing the mutated gene using selective reverse mutation, and regulating the mutated gene (36). Gene therapy allows the delivery of therapeutic genetic material to any specific cell or tissue and or organs of the body for treatment.

Based on the type of cells or tissues targeted for gene delivery and treatment, gene therapy is divided into germ-line and somatic cell gene therapies. Germ-line gene therapy involves genetic manipulation of the reproductive cells sperm and egg to make heritable changes. The potential of germ line therapy was successfully demonstrated in mouse, rat, rabbit, sheep, cattle, goat, and pig (37–40) but not in humans because of a moratorium due to ethical reasons, lack of advanced tools, and societal consensus (41–46). However, with recent technological advances in genome editing and gene delivery methods, renewal of debates on revisiting germ line therapy appears not far from reality (47–50). Therefore, the present review is focused on somatic cell gene therapy.

SOMATIC CELL GENE THERAPY

In somatic cell gene therapy, every cell except sperm and egg is targeted for therapeutic treatment. It is considered safe because genetic changes remain in the patient and are not passed onto the offspring. However, the requirement of skill set and sophistication in delivering a therapeutic gene into the target cells or tissue of the patient elevates the quotient for an unpredictable clinical outcome. Therefore, many advanced methods are being developed to deliver therapeutic genetic materials, and they are broadly divided into *ex vivo*, *in situ,* and *in vivo* methods. *Ex vivo,* also called "outside the living body" method, involves isolating the cells to be treated from the patient, modifying them with a therapeutic gene, and re-introducing into the patient's body. Hepatocytes in the liver, retina photoreceptors in the eye, stem cells in the bone marrow, and T lymphocytes have been the focus of this method (43). Recently, the FDA has approved Kymriah™, a groundbreaking prescription cancer treatment that uses the patient's own white blood cells or T cells for inserting the CD19 gene *ex vivo* (51). After being re-introduced into the patient's blood, these genetically engineered T cells will have greater ability to target cancer cells. Less side effects than other methods, no risk of reaching germ-line cells, minimized immune response, and less renal clearance are other advantages of *ex vivo* method (52–54). Zalmoxis™ is another advanced somatic cell therapy product recently approved by the EMA for treating serious blood cancers such as certain types of leukemia and lymphomas. Zalmoxis™ consists of donor lymphocytes transfected with Herpes simplex virus-1 thymidine kinase (HSV-TK) and truncated low affinity nerve growth factor receptor (ΔLNGF). *In situ* delivery, or "in position" delivery, involves administration of the desired genetic material directly into the target cells or tissue. For example, Neovasculgen®, a plasmid vector carrying vascular endothelial growth factor (VEGF) gene, is directly injected into the target ischemic tissue to stimulate blood vessel growth (55–57). This method is being explored to cure cystic fibrosis, muscular dystrophy, and cancer but still requires more technological advancement in delivery methods for a successful clinical outcome (58–60). Though delivering genetic material by this method works well for localized conditions, it cannot be used for treating systemic disorders. The last and most important method of gene delivery is *in vivo*, or "in the living body." In this method, viral, or non-viral vectors are used to deliver the therapeutic material to the defective target cells or tissue in the body (**Figure 1**). A wide variety of physical and chemical methods including needles, gene guns, electroporation, sonoporation, photoporation, magnetofection, hydroporation, mechanical massage, lipid, calcium phosphate, silica, and gold nanoparticles are being used to deliver genetic material to target cells. However, none of them is more efficient than viruses in delivering therapeutic genetic materials to the target cells due to their inherent shortcomings and operational complexity. The present review article is focused on viral vectors only.

VIRUSES IN DELIVERING THERAPEUTIC GENES

There has been a quite bit of resentment in availing the benefits of viruses due to ignorance, bad rap, and skewed view. In fact, the human body offers shelter to viruses, fungi, protozoa, and worms by adopting appropriate mechanisms for mutual benefits in order to survive and thrive (61). For example, viruses offer immunity against bacterial pathogens and tumor cells, and modulate gut bacterial genes to improve host digestion (62). Though the word *virus* implies mortality and morbidity, viruses are considered nature's genetic engineers because of their ability to infect most kinds of organisms including bacteria, humans, animals, and plants. Also, viruses help certain plants to survive in extreme weather conditions (62). We have identified powerful viral promoters and enhancer elements that can be used to construct plasmid vectors for high level expression of foreign proteins (63, 64). They have an advantage over others by carrying several genes encoding structural and non-structural proteins to infect and propagate in host cells. Some viruses have the ability to transduce the cells they infect, i.e., stably express a gene along with the host's genome. They allow manipulation of their genome and removal of virulent genes without losing the ability to infect host cells. This makes them nearly dead or not alive, and the versatile biological entities, a pragmatic reason to accept them as sophisticated biological tools for delivering foreign genetic materials into eukaryotic cells. For example, we have manipulated and reconstituted Sendai viral envelopes containing only the fusion glycoprotein to deliver a reporter gene to liver *in vivo* (65). In fact, viral vectors were the first carriers of nucleic acids used in gene therapy (18).

Because of their abundance on the earth and difference in genetic makeup, many viruses are being used in preclinical and clinical investigations but each comes with its own unique

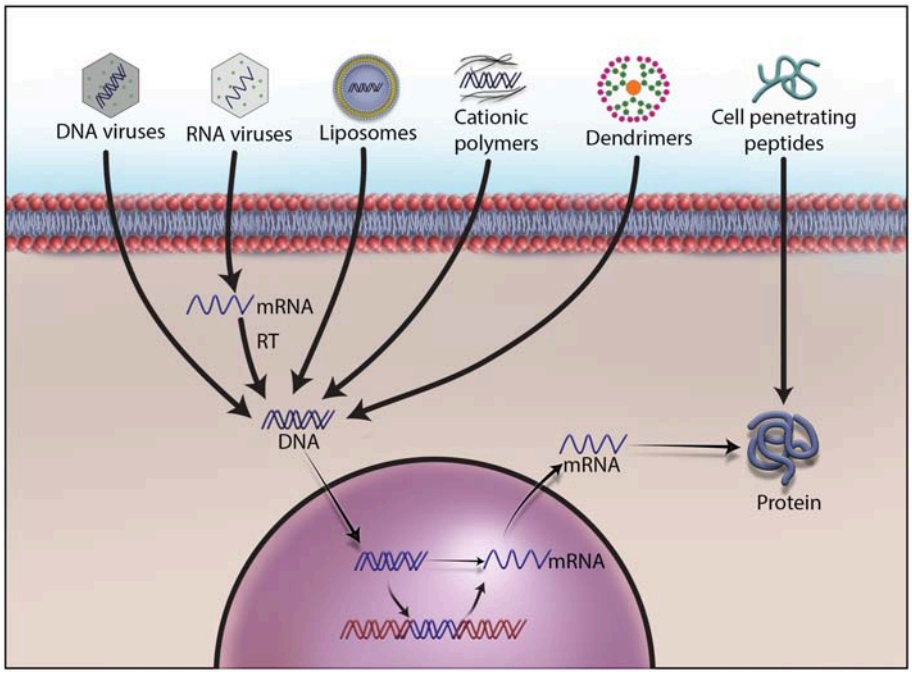

FIGURE 1 | Different methods to deliver therapeutic DNA and proteins to target cells. Non-viral gene delivery methods have many advantages over viral vectors in gene therapy. They do not cause immunogenicity and carcinogenicity, and can deliver a large size of therapeutic DNA efficiently with a low price tag. As no one-size-fits-all solution to therapeutic DNA delivery exits, development, and formulations remain the main focus of research on non-viral methods.

advantages and disadvantages. Therefore, finding a suitable vector to deliver therapeutic genetic material has become a challenge to make gene therapy a viable and better treatment option than conventional methods. Part of the challenge is therapeutic DNA's inability to pass through the cell membrane because of its large size and negative charge. Also, the therapeutic DNA needs to escape the cellular endonucleases and renal clearance. An ideal vector should have enough space to transport large therapeutic genes, high transduction efficiency, and the ability to provide long-term and stable expression, as well as target specific cells, avoid random insertion of the therapeutic gene into the host genome, and infect mitotic as well as post-mitotic cells. It should not be immunogenic or pathogenic, should not cause inflammation and should possess the ability to be manufactured on a large scale. Research on developing novel viral vectors is advancing steadily with a special focus on substituting pathogenic genes with therapeutic DNA (66). In fact, non-pathogenic, replication-defective, and human-friendly viral vectors are being used in more than 70% of the ongoing gene therapy clinical trials worldwide (67). One particularly popular use of viral vectors, such as adenovirus, Seneca Valley virus, poliovirus, vaccinia virus, herpes simplex virus, reovirus, Coxsackievirus, parvovirus, Newcastle disease virus, vesicular stomatitis virus, and measles virus, is in the form of oncolytic viruses (OV). In 2016 alone, more than 40 clinical trials using OV were conducted (68). OV destroy malignant cancer cells by specifically replicating in those cells to effectively lyse them as well as induce a robust antitumor immune response. OV selectively replicate in tumor cells through a variety of methods such as virus-specific receptors on the cells. They can be used to deliver anti-angiogenesis genes, suicide genes, immunostimulatory genes, and DNA encoding small nucleic acids. Apart from carrying immunostimulatory genes, OV can induce an immune response by releasing cell debris and viral antigens (68). Many other innovative approaches are being developed to use viral vectors for treating diseases and disorders. Since Edward Tatum's initial proposal to repurpose viruses for therapeutic gene delivery in 1966, gene therapy has come a long way from the construction of many types of viral vectors to their use in more than 3,000 clinical trials to date (32, 69, 70). However, during this incredible journey with obscure regulations, gene therapy has experienced a few undesired clinical outcomes due to off-target effects, cytotoxicity, viral transmissibility, impurity, and an immune response to the viral vector itself (68). Nonetheless, diseases for which a cure has been attempted include β-thalassemia, X-linked severe combined immunodeficiency (X-SCID), adenosine deaminase deficiency (ADA-SCID), cystic fibrosis, hemophilia, liver enzyme ornithine transcarbamylase (OTC) deficiency, head and neck cancer, metastatic melanoma, HIV, Leber's congenital amaurosis, Wiskott-Aldrich syndrome (WAS), metachromatic leukodystrophy (MLD), and severe lipoprotein lipase deficiency disorder (LPLD) (52, 71). In fact, the possibilities for gene therapy-mediated treatments are endless because virtually every cell in the human body is a potential target for genetic manipulation. Viruses display specificity in infecting cell types;

therefore, viral vectors can be selected based on the type of cell that needs gene delivery. Here, we describe some widely used viral vectors in gene therapy.

ADENOVIRUS (AV)

AV was the first viral vector developed for gene therapy and was approved for clinical trials in 1990. It was isolated from human adenoid tissue-derived cell cultures for the first time in 1953, hence the term adenovirus, and included in a diverse family of non-enveloped double-stranded DNA (dsDNA) viruses called *Adenoviridae* (72). According to the Centers for Disease Control and Prevention (CDC), AV rarely causes serious illness and death in healthy individuals but immuno-compromised individuals may develop a wide range of illnesses including the common cold, sore throat, bronchitis, pneumonia, diarrhea, conjunctivitis, fever, and neurologic disease. As of today, there are 57 human AV serotypes isolated and classified into seven categories based on their properties of agglutination (73, 74). AV carries a linear dsDNA ranging from 26 to 45 kb in a medium sized (∼100 nm) non-enveloped icosahedral viral particle composed of penton and hexon subunits. While the hexon subunits form a major part of the viral capsid coat and carry antigenic motifs, the penton subunits constitute fiber and knob domains required for infection (75). The fiber knob domain initiates AV infection by binding to a variety of proteins such as MHC-1 α2 subunit, CD46, sialic acid saccharides on glycoproteins, coxsackievirus, and AV receptor (CAR) expressed on cell surface (76). The interaction between arginine-glycine-aspartic acid (RGD) sequence of the fiber penton subunit and αν integrins on the cell surface drives endocytosis of viral particle and completion of viral infection (77–79). This creates broad tissue tropism and a nodal for AV transduction efficiency, giving an opportunity to manipulate binding sites for CAR and other ligands to de-target AV infection, an essential feature of popular viral vectors used in gene therapy. Therefore, since its discovery, AV has been repurposed through the deletion of its pathogenic genes.

Based on the expression of AV genes during infection and multiplication, its genome is organized into early (E1, E2a, E2b, E3, and E4), intermediate (IVA2 and IX), and late genes (L1, L2, L3, L4, and L5). Also, its genome carries non-coding inverted terminal repeat (ITR) sequences, ψ packaging sequences, and many viral RNAs (75, 80, 81). The genome of AV has been manipulated many times to develop safe and efficient vectors for gene therapy applications. The first-generation vectors with a partial deletion of E1 or E3 genes do not replicate or display oncogenicity but can deliver less than an 8 kb gene and display leaky expression of viral proteins, strong immune response, and contamination with replication-competent virus (82). To circumvent this, second-generation vectors were created by deleting E2A, E2B, and E4 from the genome of the first-generation AV vectors. However, their production has become complicated, and they do not prevent leaky expression of viral proteins and rapid loss of therapeutic gene expression, and thus have lost enthusiasm for their widespread use in gene therapy (83, 84). The third-generation vectors, otherwise known as gutless or helper-dependent AV vectors, lack all viral genes except the ψ and ITR sequences. They have received special attention because of their capacity to carry larger therapeutic genes (up to 37 kb in size), their ability to display long-term transgene expression, and lesser contamination with replicating virus particles. They are also less immunogenic than first- and second-generation vectors (85). The third-generation vectors were successfully used to express transgenes for about 2 years in animals with no adverse effects (86, 87). Co-transduction of these vectors with Sleeping Beauty transposon along with FLP recombinase was used to insert a FIX gene in the chromosome of dogs suffering from hemophilia B and expressed for up to 960 days (88, 89). Recently, they were successfully used for the long-term expression of a gene encoding an alanine-glyoxylate aminotransferase (AGT) in patients with primary hyperoxaluria type 1 (PH1), a rare kidney disorder that causes recurrent kidney stones (90).

Since AV vectors allow episomal or stable insertion of therapeutic genes, they carry advantages over vectors that integrate into cellular DNA. This provides clinicians an opportunity to offer appropriate treatment for patients with different diseases or disorders. For instance, AV is suitable for treating cancers and offering bioscavenger-mediated short-term protection against nerve gases and other chemical weapons. As depicted in **Figure 2**, we have demonstrated an AV-mediated episomal insertion of *PON1*, *BChE*, and *PD* bioscavenger genes in the liver to express and secrete proteins to detoxify the circulating lethal nerve gases for 10–15 days in mice (13, 20–22, 36). Since the immune system has the natural ability to detect and destroy abnormal cells in our body, new AV vectors that can induce immune response and destroy target cells have been developed. For example cancer cells can go undetected by reducing the expression of tumor antigens on their surfaces, inducing immune cell inactivation, and releasing substances in the microenvironment to promote their growth and survival. Therefore, new oncolytic adenoviruses that effectively induce immune response, and specifically target and lyse tumor cells are being created by replacing their native E1A promoter with tumor-specific promoters and genetically modified CAR, a highly expressed AV receptor in tumor cells (68, 91). For example, the CV706 and OBP-30 AV vectors carry the viral E1A gene under prostate cancer-specific antigen promoter and telomerase reverse transcriptase promoter, respectively (92). Other engineered oncolytic adenoviruses target the components of tumor cells and their microenvironment and inhibit their proliferation by expressing antibodies, relaxin, hyaluronidase, and inhibitors of metalloproteinases to hinder angiogenesis and proper function of the extracellular matrix (91, 93). Oncolytic adenoviral vectors that induce autophagy-related immunogenic cell death were also developed to treat cancer (94). A novel oncolytic AV vector expressing an interfering long non-coding RNA (lncRNA) to inhibit 12 oncogenic miRNAs has been constructed in order to perform selective killing of tumor cells (95). AV vectors carrying complementary sequences of liver-specific miRNA-122a incorporated into 3'-UTR of *E2A, E4,* or *pIX* to reduce the leaky expression of viral genes and hepatotoxicity were developed (96). In addition, AV vectors with *E1A* carrying mutations complementary to retinoblastoma (RB) or p53 gene mutations

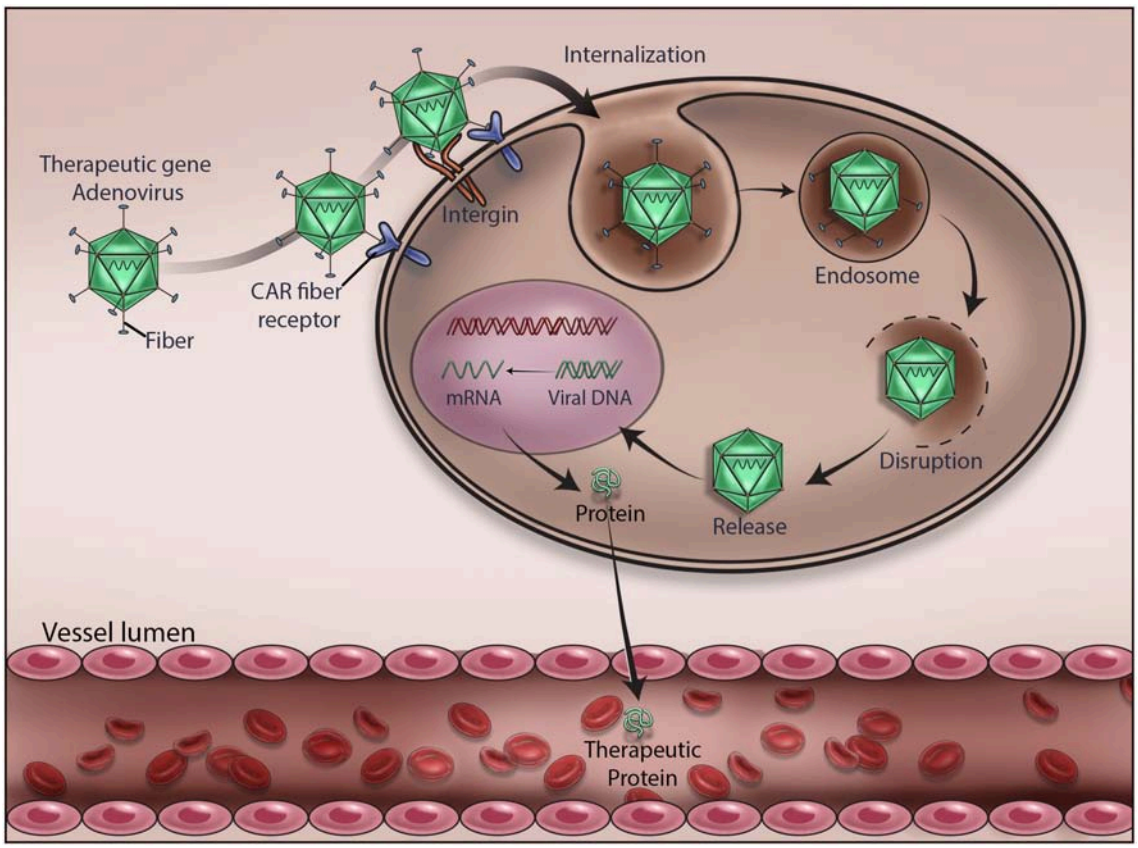

FIGURE 2 | Mechanism of adenovirus-mediated delivery of a therapeutic DNA. Upon infection, adenovirus delivers the encapsulated therapeutic DNA into the cytoplasm of the target cells. Various stages of viral gene delivery, *viz* cell attachment, internalization, endocytosis, uncoating, transcription and translation of the therapeutic protein, are shown.

in tumor cells that can specifically replicate and lyse tumor cells were created (92).

Despite many technological improvements made in vector design and production, there are still certain issues that have to be addressed for better clinical outcome. For example, infecting target cells with the optimal amount of highly purified AV particles is critical for the successful insertion of a therapeutic gene. Recently, it was shown that 10^{10}-10^{12} AV particles per patient are required for a successful Ebola vaccination (97). Production of such high titer virus with no or minimal empty vector contamination is still a formidable challenge. Also, high prevalence of anti-AV vector immunity in the human population and differential expression of CAR and other receptor proteins on target cells have been serious issues in clinical trials (98, 99). For example, the transduction efficiency of the widely used AV serotype 5 in gene therapy is dampened by the prevalence of neutralizing antibodies in the human population (100, 101). An estimated 80% of the human population is believed to carry antibodies against AV serotype 5, resulting in a significant transduction deficiency and stimulation of inflammatory shock (102). There has been a positive correlation between body fat and the presence of circulating antibodies against AV serotype 36 in humans (103). In addition, during systemic administration, the tendency of AV vectors to undergo sequestration in the liver has prevented efficient transgene transduction and displayed severe hepatotoxicity, even causing the death of a clinical trial participant (104, 105). This was due to the binding of blood coagulation factor FV and FX to the hyper variable region (HPV) of AV hexon subunit (106, 107). Therefore, mutating the HPV site in such a way that it neither activates complementary pathway nor interacts with FX could be an ideal way to resolve the liver sequestration issue. Attempts are being made to improve the safety of AV vectors by treating with chemicals and developing chimeric and hybrid vectors to minimize inflammation and immunogenicity (108, 109). For example, the chimeric AV serotype 5 vector carrying receptor-binding epitopes derived from other human AV serotype 3, serotype 35, and serotype 43 displayed low seroprevalence and low affinity for CAR (110, 111). Similarly, the chimeric human AV serotype 5/3, consisting of receptor epitopes derived from serotype 3 and 5, showed high binding affinity for CD46, an AV receptor commonly expressed on many solid tumors. It was thus found to be particularly useful in targeting solid tumors (112, 113). Another CD46-targeted chimeric AV vector derived from human serotype 5 and 35 has been shown to be suitable for transducing vascular smooth muscle cells, treating colorectal cancers, and ischemic wounds

as well as manipulating T-cells (114–117). Novel chimeric AV vectors developed from AV serotypes 5 and 11 and 3 and 11 were found very effective in exclusively targeting glioma and colon cancer cells, respectively (118, 119). Other types of chimeric vectors were also derived entirely from low prevalent human and non-human AV serotypes such as human AV serotype 26, canine AV serotype 2, and chimpanzee serotype 3. For example, the chimeric AV vector developed from human AV serotype 26 and chimpanzee AV serotype 5 has been used successfully for Ebola vaccination in animal models (120, 121). A novel hybrid vector developed from AV serotype 5 and alpha virus was found very useful for the expression of transgenes in malignant hematopoietic cells (122). Many laboratories have developed a library of AV vectors that carry random-peptides on their fiber knobs in order to overcome the paucity of cancer-specific ligands (123–125). This resulted in the generation of many AV vectors that are specific to prostate and pancreatic cancer as well as glioma (123, 125–128). One such vector carrying pancreatic cancer-targeting ligand has shown strong oncolytic effect in primary pancreatic neuroendocrine tumors and appears promising as a next-generation therapy (129). Given the advancements made in developing safe and efficient AV vectors, their choice for delivering therapeutic genes has become apparent in clinical trials.

ADENO-ASSOCIATED VIRUS (AAV)

AAV is yet another popular viral vector used in gene therapy. This small microbe was first isolated as a contaminant in the simian adenovirus preparation and then named adeno-associated virus (AAV) by the Bob Atchison group at Pittsburgh University and the Wallace Rowe group at the NIH (130, 131) and later found in a wide range of animal samples including human, non-human primates, avian, bovine, reptiles, pigs, sea lions, bats, and caprine samples. The 4.7-kb-long single-stranded DNA (ssDNA) packed inside a non-enveloped viral particle carries p5, p19, and p40 promoters as well as rep and cap genes flanked by two 145 nucleotide-long inverted terminal repeats (ITR) and no polymerase gene (132, 133). While ITRs having palindromic sequences base pair to allow synthesis of cDNA, both rep and cap genes undergo alternate splicing to express replication proteins (Rep78, Rep68, Rep52, and Rep40), capsid or virion proteins (VP1, VP2, and VP3), and an assembly activating protein (AAP), respectively (134). Being a non-structural protein, AAP assists virion proteins in capsid formation (135). VP1, VP2, and VP3 expressed from p40 promoter at a ratio of 1:1:10 form the outer capsid of the virion. These capsid proteins carry phospholipase domain to protect virions from the onslaught of intracellular protease system (136). Unlike other viruses, AAV requires a few other helper proteins, agents or viruses such as AV, herpes simplex virus type I/II, pseudorabies virus, cytomegalovirus, genotoxic agents, UV radiation, or hydroxyurea to infect cells and complete replication (137). AAV can also be generated by providing the missing genes E1a, E1b, E2a, E4orf6, and VA that are needed for viral infection. These genes are often cloned in pXX6 helper plasmid and used to co-transfect HEK293 cells along with AAV expression plasmid (rep-cap plasmid) to produce AAV (134, 138). Therapeutic genes are cloned in the AAV expression plasmid carrying ITR sequences, and their size can be increased by cotransfecting another plasmid carrying rep-cap genes or by generating virus in rep-cap stable cells. Since the formation of dsDNA from its ssDNA is the rate-limiting step of viral infection, gene delivery, and expression in the target cells, a self-complementary viral dsDNA (scAAV) is developed; however, it reduces the capacity of AAV vectors to deliver a therapeutic gene (139, 140). AAV inserts a therapeutic gene in the genome of target cells to provide long-term transgene expression. For instance, the gene expressing FIX blood coagulation factor in one individual of a cohort persisted for more than 10 years during a clinical trial (141). AAV inserts a therapeutic gene in the host genome at a specific location on the q arm of chromosome 19 (142, 143). Despite having no large homology regions, more than 70% of the transgene integration events occur within this site; however, the underlying mechanism remains unknown. But AAV lacking its rep-cap genes can deliver a therapeutic gene in the episomal form without inserting into the genome of the target cells. The therapeutic gene in the episomal form can develop into a chromatin-like structure and remain quiescent in cells for months to years without damaging the patient's body. Recently, we have used AAV vectors to make episomal insertion and expression of a bioscavenger gene in the liver cells for about 6 months (unpublished results). This allows clinicians to apply AAV-mediated gene therapy to treat a wide variety of diseases or disorders.

AAV displays broad tropism but requires the expression of heparin sulfate proteoglycan, $\alpha_v\beta_5$ integrin, $\alpha_5\beta_1$ integrin, fibroblast growth factor receptor 1, platelet-derived growth factor receptor, hepatocyte growth factor receptor, epidermal growth factor receptor, laminin receptor, and sialic acid moieties on the surface of target cells for efficient transduction and delivery of a therapeutic gene. Recently, AAVR has been identified as a universal host cell receptor for AAV infections (144). Although every serotype has the ability to infect cells, transport to nucleus, uncoat, and insert its genome into the host's chromosome or leave in the episomal form, not all 13 AAV serotypes isolated to date use the same receptor repertoire on host cell surface for infection (145, 146). This makes AAV a very useful system for a specific cell or tissue type transduction. For example, AAV1 displays high transduction efficiency of muscles, neurons, heart, and retinal pigment epithelium. AAV2 has been shown to infect many types of cancer cells, neurons, kidney, retinal pigment epithelium, and photoreceptor cells. AAV2 is the only serotype that can infect and delivery a therapeutic gene to kidney. AAV4 and AAV5 serotypes infect retina and retinal pigment epithelium, respectively. While AAV6 displays strong tropism for heart, AAV7 has some bias for liver (147). AAV6 is also effective in infecting airway epithelial cells (148). AAV8 and AAV9 have displayed successful infection of lymphoma and HPV tumors, respectively (149). AAV8 is the only serotype that infects pancreas, and it was extensively used to express a therapeutic *FIX* in the liver to treat hemophilia in clinical trials (150). AAV tropism was further refined by mixing the capsid proteins of one serotype with the genome of another serotype. For example, AAV2/5 serotype, which

transduces neurons more efficiently than the parental AAV2, was generated by packaging AAV2 genome in AAV5 capsid proteins. Another example, the pseudotyped AAV8 and AAV9, can cross the endothelial barrier of blood vessels to target muscles (66). For increasing transduction efficiency, hybrid AAV serotypes were also generated by mixing the capsid proteins of multiple serotypes with the genome of another serotype. For example, AAV-DJ serotype that consists of a hybrid capsid is generated by mixing the capsid proteins of eight different AAV serotypes. This made AAV-DJ to display higher transduction efficiency than any other wild type serotype *in vitro* and high infectivity of a broad range of tissue *in vivo*. Its mutant, AAV-DJ8 serotype, displays high infectivity of brain. AAVHSC, a new class of genetic vector isolated from hematopoietic stem cells, has been shown to be ideal for manipulating stem cells (151). Since more than 50% of the adult human population carries AAV neutralizing antibodies, a wide range of mosaic or hybrid vectors were generated by engineering and *de novo* shuffling of capsid proteins (152, 153). For example, the AAV2.5 hybrid vector generated by combining the muscle tropism determinants of AAV1 with parental AAV2 displays immune evasion of their neutralizing antibodies (154). The other hybrid vectors AAV6.2, AAV2i8, AAVrh10, and AAVrh32.33 were found beneficial for intravenous delivery, reduction of liver sequestration, and T-cell response in the clinic, respectively (138, 155–157). Since CpG motifs are responsible for immune response and failure of many clinical trials, AAV vectors were further refined by deleting CpG motifs, known ligands of Toll-like receptor 9 (TLR9), to reduce immune response for maximal expression of a transgene in clinical trials (158). Cre-recombination-based AAV variants are also developed to allow efficient transgene expression in the central nervous system, muscle, and liver (159, 160). Also, the AAV-CRISPR/Cas9 system has been developed to perform *in vivo* genome editing and broaden therapeutic horizons (161).

HERPES SIMPLEX VIRUS (HSV)

Herpes simplex viruses are believed to have tremendous potential as a preventative and therapeutic vaccine against cancer and other diseases because of their ability to evade the immune system and circulating anti-viral drugs, deliver multiple genes, infect a wide variety of cells, pose low risk of adverse health effects, and multiply specifically in tumor cells. They are large enveloped viruses that carry a linear dsDNA of 120–240 kb and infect reptiles, birds, fish, amphibians, and mammals. There are eight known human herpesviruses: herpes simplex virus-1 (HSV-1), herpes simplex virus-2 (HSV-2), human cytomegalovirus (HCMV), varicella-zoster virus (VZV), Epstein-Barr virus (EBV), Kaposi's sarcoma-associated herpesvirus (KSHV), and human herpesviruses 6 and 7 grouped under alpha, beta, and gamma genera. Though they share common virion structure and replication cycle, and many other biological properties, there is a significant difference in their tropism, infection, and clinical manifestations. Some of their genes show homology with regions of human chromosomes. Here, we delve into HSV that infects ∼60% of the human population worldwide and mainly transmits through contact, especially oral-oral contact (162). After infecting oral or genital epithelial cells, HSV enters neurons to establish lifelong latent infection and reactivates periodically causing fever, blisters, cold sores, genital herpes stromal keratitis, blindness, cancer, and encephalitis. Both HSV-1 and HSV-2 carry envelope and sub-envelope structures called tegument and a regular icosahedral capsid consisting of a relatively large dsDNA of 153 kb encoding ∼200 proteins (163). Nearly half of the total 84 genes present in the HSV genome encode proteins required for virus replication, and many were found unnecessary for delivering therapeutic genes. Several genes involved in virulence and immune evasion, and those considered non-essential for viral life cycle *in vivo* were also identified. HSV-1 is relatively less pathogenic than HSV-2 and is, therefore, ideal for vector development and gene therapy (164). HSV infects cells by using its envelope glycoprotein B, glycoprotein C, and glycoprotein D to bind cell surface particles and transmembrane receptors such as heparin sulfate, herpesvirus entry mediator (HVEM), nectin-1, and 3-O sulfated heparin sulfate. While the nectin receptors provide a strong point of viral interaction with the host cell, the other viral envelope proteins, especially glycoprotein B, glycoprotein D, glycoprotein H, glycoprotein L, and HVEM, create an entry pore for the viral capsid. The viral capsid enters through capsid pore and travels through the cytoplasm to the nucleus in order to inject its DNA content. HSV evades the immune system by secreting its immediate-early protein, ICP47, and inducing a transporter associated antigen processing (TAP) protein to block MHC class I antigen presentation on the cell surface. HSV-1 infects many types of mitotic and post-mitotic cells including neurons (36). After infection, HSV induces the expression of the virion host shutoff protein (VHS or UL41) to inhibit protein synthesis by degrading the host mRNA. This makes way for viral replication and lysis of the host cells.

The HSV genome carries immediate-early, early, and late genes for replication and allows creation of replication-competent, replication-incompetent, and helper-dependent vectors, or amplicon vectors, for preclinical and clinical studies. The replication-competent vectors have the capacity to deliver transgenes up to 50 kb in size or the entire locus since treatment of certain diseases requires huge therapeutic gene cassettes carrying complex regulatory elements. These vectors can replicate selectively in cancer cells and have less virulence because of deleted genes. They do not insert transgenes in the host chromosomes and are therefore used primarily as oncolytic viruses to treat glioma, melanoma and ovarian cancers and to stimulate an immune response (66). They are further refined by using tumor specific promoters to express viral genes and target tumor-specific receptors. These vectors with robust replication capacity are believed to enhance intramural vector distribution and lyse tumor cells very effectively. These vectors are generally constructed by homologous recombination in eukaryotic cells by co-transfecting the viral genome and a plasmid carrying the therapeutic gene flanked by the sequences homologous to the target locus on viral genome to undergo recombination. The replication-incompetent vectors are created by either mutating or deleting several immediate early genes including ICP4 and ICP27 that are essential for replication and, therefore, can grow

only in specifically designed cell lines complemented transiently. For example, Vero-7b cell line is capable of providing in trans the proteins encoded by deleted viral genes (165). They are safe and non-inflammatory advanced vector platforms known to persist and express in the nerve cells for life and therefore used to treat neuropathic, inflammatory, and cancer-associated pain (166–168). The helper-dependent HSV vectors, or amplicon vectors, carry deletions in one or more non-essential genes and retain the ability to replicate *in vitro* but are compromised *in vivo* in a context-dependent manner (169, 170). These viruses are the same as wild type HSV, with plasmids containing a packaging signal and the gene of interest. Amplicons have the ability to accommodate a very large therapeutic sequence up to 100 kb in size but have production and stability issues. The replication-incompetent vectors and amplicons have been used to express genes in the nervous system, muscle, heart, and liver.

RETROVIRUS (RV)

Retroviruses are spherical (∼100 nm in diameter) and enveloped microbes belonging to a *Retroviridae* family that comprises foamy virus, human immunodeficiency virus (HIV-1), simian immunodeficiency virus (SIV), bovine immunodeficiency virus, feline immunodeficiency virus, equine infectious anemia virus (EIAV), murine leukemia virus (MLV), bovine leukemia virus, Rous sarcoma virus (RSV), spleen necrosis virus (SNV), and mouse mammary tumor virus. Unlike all other RNA viruses, these viruses are capable of reverse transcribing their genetic blueprint of positive, single-stranded RNA into dsDNA, and inserting it into the host cell genome. RVs carry a non-covalently linked dimers (two copies) of RNA genetic material probably as a fail-safe mechanism for producing genomic DNA and increasing viral RNA diversity due to interstrand recombination (171). Thus, RNA dimerization has been viewed as a prerequisite for RV genome encapsidation and life cycle. With restricted vertebrate hosts, these viruses are divided into exogenous retroviruses (XRV) and endogenous retroviruses (ERV). While the XRVs transmit horizontally among hosts, the ERVs inherit vertically in the genome of their hosts (172). By scattering all over chromosomes and comprising nearly eight percent of the human genome, the ERVs are thought to be relics of ancient retroviral germline infections and believed to play a role of friend or foe in human life (173–175). The two most common types of retroviruses are gammaretrovirus and lentivirus, which are derived from MLV and HIV-1, respectively. The genome of gammaretrovirus has three essential genes, *gag, pol* and *env*, and is flanked on both sides by long terminal repeats (LTRs). *Gag* inserts viral genome mRNA into virions when assembling, *pol* is the reverse transcriptase, integrase, and protease encoding gene, and *env encodes the surface and the transmembrane glycoprotein*. Also, RV genome carries a cis-acting ψ packaging element that involves in regulating the essential process of packaging the RV mRNA into viral capsid during replication. In addition, RV genome carries RNA dimerization signal element. With U3, R, U5 elements, the LTRs display promoter/enhancer activity for gene transcriptional regulation. RVs use their envelope proteins to bind a variety of receptor molecules such as murine cationic amino acid transporter (mCAT), a sodium-dependent Pi transporter (PiT2), xenotropic and polytropic retrovirus receptor 1 (XPR1), CD4, CD46, CD150, and the RD114-and-D-type-retrovirus/alanine-serine-cysteine transporter 2 (RDR/ASCT2) expressed on different cell surfaces to initiate infection, a critical step in determining the target cell tropism of the virus. This leads to a conformational change in the envelope proteins, leading to the entry of virus into the cytoplasm via fusion or endocytosis. With the help of the host cell proteins, the endosome travels through cytoplasm to eject its RNA. After the RNA reverse transcription takes place, viral DNA is integrated into the host cell chromatin, transcribed into RNA with 5' Cap and 3' poly(A) tail, and translated into viral proteins that assemble and bud from the plasma membrane to complete the life cycle with extracellular maturation (171). The matured RVs can infect a wide variety of somatic cells including embryonic stem cells, hematopoietic and neural stem cells. With active nuclear elements, these vectors can transduce therapeutic genes into proliferating cells only and are, therefore, ideal for targeting specifically cancer cells. A downside to gammaretrovirus is that it has broad species specificity, leaving the possibility of transducing undesired cells, faulty reverse transcription, intracellular restriction factors, and risk of insertional mutagenesis. The major difference between gammaretrovirus and lentivirus is that lentivirus can infect post-mitotic cells. It requires four plasmids for production: the *gag* and *pol* plasmid, the *rev* plasmid to transport mRNA into the cytoplasm, VSV-G for membrane fusion and the gene of interest. Other retroviruses require three plasmids: the *gag* and *pol* plasmid, the VSV-G plasmid and the gene of interest. Transient or stable co-expression of all these plasmids in HEK293T packaging cell lines produces RV vector particles carrying no replication-competent virions that are essential for research and therapeutic purposes. Using these cell lines, methods to produce clinical grade RV particles at a concentration of 10^6 to10^7/ml are optimized (176). As *gag*/*pol* and *env* expression constructs carry no ψ packaging and RNA dimerization element, viral structural proteins only recognize the ψ-containing RV vector construct resulting in a preferential packaging of RV vector genomes into infectious particles. After entry of the particle into the host cell, only the RNA of the RV vector construct is reverse transcribed and stably integrated into the host genome. This method prevents generation of replication competent retroviral vector progeny during therapeutic viral particles production. Lentivirus has been used to treat X-SCID, cancers and monogenic diseases. For example, self-inactivating lentiviral vectors can engineer T cells with receptors to better target tumors when treating cancer. Recently, we have successfully used lentiviral vectors to deliver an anti-angiogenic Kininogen gene to budding blood vessels (177, 178). There have been no reports of significant adverse effects from the lentivirus (37).

Some advantages of using retroviruses are that they can accommodate a 9–12-kb-large insert size for the gene of interest and produce high titers. The most significant disadvantages are lack of cell specificity and the possibility of insertional mutagenesis (18). The enzyme "integrase" inserts copies of the retroviral genome into the host cell chromosomes but there

is a risk of inserting the genome copy into an unfavorable location such as a tumor suppressor gene or an oncogene, which would lead to uncontrolled cell division (36). It is critical to evaluate the risk of insertional mutagenesis for each retroviral vector. Gammaretroviral vectors have a tendency to integrate near gene regulatory regions, which can pose a significant risk. For example, patients in a cohort of 20 died due to leucosis development in a clinical trial (179). On the other hand, lentiviral vectors tend to integrate into the body of genes, leading to lower risk of genotoxicity (52). A possible step to address this issue would be to use self-inactivating retroviral vectors that are transcriptionally inactive. Since mature T cells are relatively resistant to oncogenic transformation by RV, developing T cell-based therapeutic approaches to treat cancer and other diseases would be another approach to avoid insertional mutagenesis. Recently, a non-integrating RV-based CRISPR/Cas9 vectors have been created for targeted gene knockout (180). Creating such vectors to target specific genes would help developing therapeutic approaches without insertional mutagenesis issue. Renal fibrosis was treated by using high-fidelity RV-based CRISPR/Cas9 vectors (181). Development of similar vectors would not only address insertional mutagenesis issue but also radically transform basic and applied biomedical research. Also, using AAV vector which inserts a therapeutic gene selectively into known chromosome 19 sequences would be another possibility. Using zinc finger nucleases or including certain sequences such as the β-globin locus control region to direct the site of integration to specific chromosomal sites is yet another way to minimize the risks. However, further studies are needed to address this issue by designing specific vectors and understanding the frequency of insertional mutagenesis, and role of other factors involved. Insertional mutagenesis is an issue that will likely be solved in the coming years. Until then, the use of retroviruses remains a concern. Nonetheless, over 500 gene therapy clinical trials have been conducted using retrovirus to date.

GENE THERAPY DRUGS IN THE MARKET

Despite many technological challenges and barriers, more than a dozen gene therapy-based drugs have entered the world pharmaceutical market to date (**Figure 3**). The first gene therapy drug, Gendicine™, was developed by Shenzhen SiBiono GeneTech for the treatment of patients with tumors carrying a mutated p53 gene, a common cause for more than 50% of all types of human cancers. The State Food Drug Administration of China approved Gendicine™ for the treatment of head and neck squamous cell carcinoma on October 16, 2003 (182, 183). However, the USFDA has turned down Introgen's Advexin, another AV-based viral drug that uses p53 due to concerns about the safety of the AV vectors after Jesse Gelsinger died in 1999 while participating in a clinical trial but no information is available about the submission of Gendicine™ clinical data for approval from the USFDA to date. Gendicine™, a replication defective AV loaded with wild-type p53 gene, is given to patients by less invasive intramural injections and or intracavity infusions. According to the manufacturer, a single dose of this viral drug, costing less than US $400, is given to patients once a week for 8 weeks as a cure. After injection, the therapeutic activity of p53 activated by target tissue cellular stress induces cell-cycle arrest, DNA repair, apoptosis, senescence, and autophagy to cause tumor growth regression. Gendicine™ has been given to more than 30,000 cancer patients, and it has displayed an exemplary safety record with no significant side effects to date (14). According to the manufacturer, Gendicine™ has shown a higher response rate when combined with chemotherapy and radiotherapy in comparison with standard therapies alone. Because Gendicine™ is injected directly into tumors and becomes useless for treating tumors neither detectable nor accessible, other advanced replication-defective AV-based drugs, such as Advexin and SCH-58500, that carry wild type p53 gene were developed to target all tumors in the patient's body in an intravenous injection; however, neither Advexin and SCH-58500 has entered the pharmaceutical market to date. However, Oncorine™, another replication defective AV-based drug that carries p53 gene to cure head and neck cancer, made it to the Chinese pharmaceutical market in 2005. According to the manufacturer, Shanghai Sunway Biotech Co., the curative effective of Oncorine™ combined with chemotherapy is superior to chemotherapy alone with a good safety profile. Since low transduction is a major issue with these approved replication defective AV drugs, more advanced tumor-specific p53-expressing conditionally replicating AV vectors such as ONYX 015, AdDelta24-p53, SG600-p53, H101, and OBP-702 have been developed but none of them is approved for cancer treatment to date. As many clinicians prefer cancer management rather than a cure due to the complex nature of the disease, the future of oncolytic viral therapy demands further advancement in vector design and discovery of appropriate therapeutic genes for better treatment.

The next advanced gene therapy drug, Rexin-G™, a chimeric retrovector loaded with a cytocidal dominant negative cyclin G1 gene to target and kill solid tumors, was approved by the Philippines FDA in 2005. Rexin-G™ developed by Epeius Biotechnologies Corporation was designated by the US FDA as an orphan drug for pancreatic cancer. After intravenous injection, this viral drug carrying a motif derived from von Willebrand coagulation factor (vWF) on its surface selectively binds receptors and collagenous proteins exposed heavily in tumor microenvironment in order to fuse, enter, uncoat, and insert its genetic material randomly in the chromosomes of the actively dividing tumor cells only (184). Recent clinical studies confirmed its safety, anti-tumor activity, and potential to increase survival time and survival rate of patients. Recently, another retrovirus-based drug, Strimvelis™, was approved in Europe to treat an ultra-rare immunodeficiency syndrome, ADA-SCID, or Bubble Boy Syndrome, a fatal and life-threatening disease due to lymphopenia, and recurrent and opportunistic infections. A bone marrow transplant from a young child donor with matched leukocyte antigen is the recommended treatment for ADA-SCID patients, but the availability of a suitable donor is challenging. Therefore, Strimvelis™ is designed and developed to offer *ex vivo* gene therapy and involves use of RV to insert copies of the ADA gene into the chromosomes of stem cells extracted from the

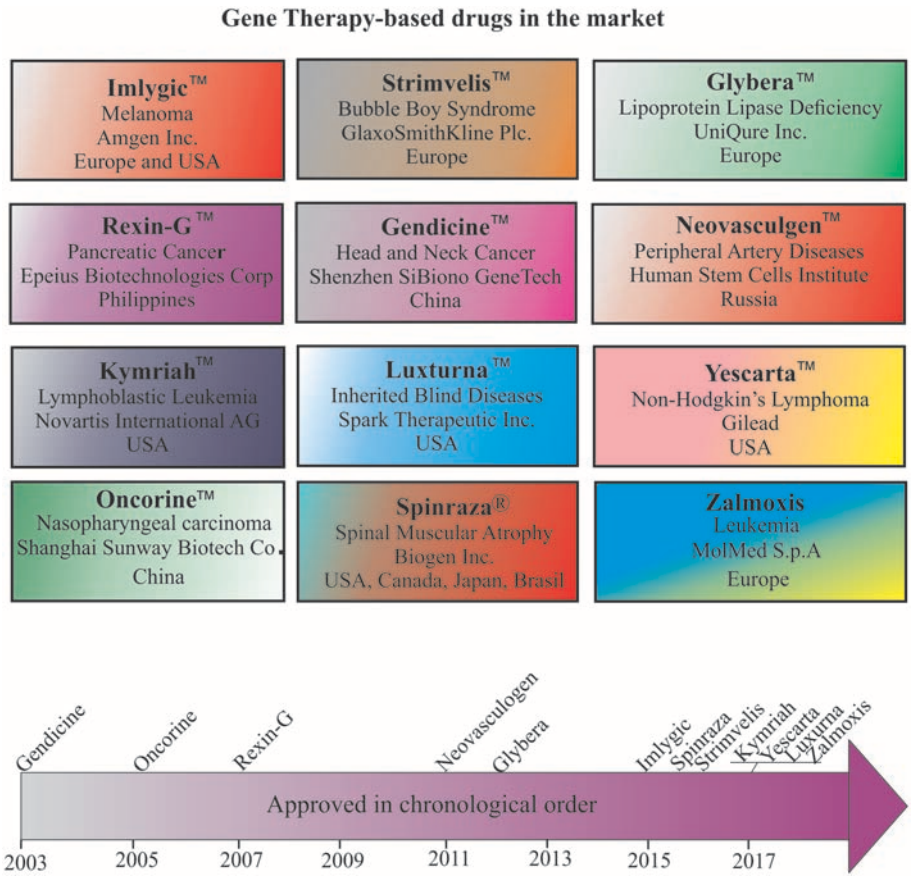

FIGURE 3 | Gene therapy drugs in the pharmaceutical market and a timeline of their approval.

bone marrow of patients. The stem cells carrying the ADA gene are then reintroduced into the patients whose bodies can express protein to repair their immune system on their own. This drug, with a list price of $714,000, is available for ADA-SCID patients without a donor that has matched human leukocyte antigen (HLA). Clinical studies revealed a 100% remission rate for Strimvelis™ (**Table 2**). Nonetheless, there is now a push toward using self-inactivating retroviral vectors that have less risk of insertional mutagenesis, especially self-inactivating HIV-1-based lentiviral vectors (185). A few months ago, the FDA approved Kymriah™, a lentivirus-based chimeric antigen receptor T cell (CAR-T) therapy for acute lymphoblastic leukemia (186). The underlying mechanism of this cancer type disease development still remains unknown, but patients carry abnormal lymphocytes in many of their body parts. Kymriah™ was developed by Novartis in collaboration with the University of Pennsylvania to treat patients with non-Hodgkin lymphoma (NHL) and B-cell acute lymphoblastic leukemia (ALL). Kymriah™ is a novel immunocellular therapy that uses a patient's own reprogrammed T cells with a transgene encoding CAR to identify and eliminate CD19-expressing malignant and non-malignant cells; overall remission rate with the therapy is 83% (**Table 2**). The autologous peripheral blood T cells are reprogrammed to carry intracellular 4-1BB and CD3-zeta costimulatory domains fused with a murine single-chain antibody fragment in its CAR to recognize CD19 increase, cellular expansion, and persistence. Yescarta™ is another retrovirus-based CAR-T cell immunotherapy developed by Kite, a Gilead company, and approved by the FDA in 2017. This breakthrough hematologic cancer drug is a customized treatment generated using an NHL patient's own T-cells to help fight lymphoma. The patient's T-cells are collected and genetically modified using a RV to generate a CAR consisting of anti-CD19 CAR-T cells linked to CD28 and CD3-zeta co-stimulatory domains. This drug is specifically designed to treat diffuse large B-cell lymphoma (DLBCL), a common aggressive NHL that accounts for three out of every five cases. According to the manufacturer, ∼7,500 patients with refractory DLBCL are qualified to receive Yescarta treatment in the USA alone. With a list price of $373,000 in the USA, Yescarta is believed to get approval for the European market in the near future. Zalmoxis is another T-cell based medicine designated an orphan drug and approved by the EMA for treating certain leukaemias and lymphomas. This is used as an add-on treatment in patients who received hematopoietic a stem cell transplant (HSCT) from a partially matched donor to restore the immune system. This is a somatic cell therapy product consisting of T-cells that

are genetically modified using a RV to express ΔNGFR and HSV-TK Mut2 suicide genes. This drug sometimes attacks the patient's body by causing graft-vs.-host disease, but the suicide gene makes these T cells become susceptible to ganciclovir or valganciclovir medicine commonly given to treat and prevent further disease development.

Neovasculgen™, a non-viral first-in-class gene therapy drug developed by the Russian Human Stem Cells Institute, has been available since 2012 for the treatment of atherosclerotic peripheral arterial disease (PAD) including critical limb ischemia. Intramuscular injection of a single dose of this drug, costing less than $50, delivers a plasmid DNA-carrying VEGF gene cloned under a CMV promoter and stimulates angiogenesis and blood supply to decrease the risk of amputation and death in patients suffering from PAD. A recent post-marketing surveillance study revealed a significant increase in pain-free walking distance by PAD patients and confirmed the therapeutic efficacy of this drug (56, 57). Recently, Spinraza® has become the first approved treatment for the rare and often fatal disease spinal muscular atrophy (SMA). SMA patients suffer muscle strength affecting their ability to sit, stand, and breathe. SMA is caused by widespread splicing defects due to mutations in survival motor neuron 1 (*SMN*1), a ubiquitously expressed cytoplasmic and nuclear protein involved in transcriptional regulation, biogenesis of small ribonucleoproteins, telomerase regeneration, and intracellular trafficking. Although the SMA patients carry its paralog *SMN*2, low-level expression due to alternative pre-mRNA splicing appears responsible for this disease development. Therefore, Spinraza carrying *SMN*2-directed antisense oligonucleotides is designed and developed to resurrect normal SMN2 protein expression in SMA patients. This non-viral drug developed by Biogen Inc. has received orphan drug status and was approved for treating all types of SMA in the USA, Canada, Japan, the European Union, Switzerland, Australia, South Korea, Chile, and Brazil. Spinraza solution upon intravenous and or intrathecal administration enters many cells in the body and induces SMN2 protein expression. According to the manufacturer, this medicine, with a list price of $125,000 per injection, costs $750,000 per year for the first year and hundreds of thousands of dollars every year for the rest of patient's life. An AAV-mediated drug designed to express SMN1 protein in patients was developed by a Novartis company, AveXis Inc., and may become available for the treatment of SMA in the near future.

The first AAV1-based drug, Alipogene tiparvovec, or Glybera™, was approved by the EMA to treat LPLD, a rare monogenic genetic disorder characterized by accumulation of triglycerides in plasma due to mutations in *LPL*. Glybera™ carrying correct copies of *LPL* was developed by UniQure Inc., and widely heralded as the "the first gene therapy" in the Western world (**Figure 3**). However, only one or two people in every one million are estimated to carry LPLD, and despite Glybera' s demonstrated potential in curing LPLD, it was withdrawn from the market due to low patient demand. Recently, another AAV-based drug has entered the pharmaceutical market to treat Leber congenital amaurosis, an inherited visual dysfunction characterized by pigmented retina, wandering nystagmus, and amaurotic pupils and caused by a mutation in the *RPE65* (187). Upon completion of the late-stage clinical trials, this AAV2-based voretigene neparvovec, Luxturna™, has been designated by the FDA as a breakthrough therapy and an orphan drug for the treatment of choroideremia. Clinical trials revealed a remarkable improvement in the patients' ability to see in dim light (188). According to the manufacturer, Spark Therapeutics, Inc., Philadelphia, USA, Luxturna™ has successfully cured one blind America's Got Talent semifinalist, Christian Guardino. Recently, Luxturna™ has become the first viral-based drug approved by the FDA to treat blindness. Luxturna™, loaded with wildtype *RPE65*, will be given to patients with confirmed biallelic *RPE65* mutation-associated retinal dystrophy to restore their vision within a few months. Since Luxturna™ comes with a record sticker price, the manufacturing company offers an outcome-based rebate arrangement with a long-term durability measure and payment option over multiple years. Another AAV-based drug is poised to enter the pharmaceutical market in the near future to treat choroideremia, an X-linked inherited retinal dystrophy that causes night blindness and a constricted visual field.

Recently, the USFDA approved an HSV-based drug called T-VEC (Imlygic™) Talimogene Laherparepvec, developed by BioVex Inc., and now acquired by Amgen for melanoma treatment. T-VEC directly kills metastatic melanoma cells and enhances the immune response against them. According to the manufacturer, this advanced oncolytic virus replicates in the tumor cells and synthesizes granulocyte-macrophage colony stimulating factor (GM-CSF), resulting in tumor-lysis and release of tumor antigen, which can then trigger an immune response. The target areas include cutaneous, subcutaneous and nodal lesions. Imlygic™ also serves as an *in-situ* vaccine (189). The T-VEC treatment course involves a series of HSV injections into the melanoma lesions for 6 months for a complete cure. T-VEC was approved also in Europe and Australia for melanoma treatment. G47Δ or DS-1647 is a third generation oncolytic HSV developed by Daiichi-Sankyo Ltd., Japan, and Professor Tomoki Todo at the University of Tokyo for the treatment of malignant glioma. This has shown excellent safety and efficacy in treating glioma in preclinical and clinical studies and has been designated as an orphan drug and "Sakigake," or ahead of the world, by the Ministry of Health, Labor and Welfare of Japan (190). However, this drug is not available for the treatment of cancer patients to date. In addition, a few more drugs are available in the market for treating different diseases (**Table 2**).

GENE THERAPY DRUGS IN CLINICAL TRIALS

The world's first gene therapy clinical study was conducted to test a viral-mediated drug at the NIH in 1989, and now 3704 gene therapy studies from 204 countries are listed in the US Government's clinical trials database to date (**Figure 4A**). More than 50% of them are being conducted in the USA alone. Recently, the US government has removed NIH special oversight rules on gene therapy studies, and the USFDA has

decided to consider gene therapy drugs like other medications for approval in order to make gene therapy a therapeutic reality for patients. These clinical studies are testing both viral and non-viral gene therapy drugs to find cures for a wide variety of human diseases, disorders, and infectious diseases. While the majority of these clinical studies are focused on treating cancer, and immune and digestive diseases, skin diseases are yet to receive momentum (**Figure 4B**). These ongoing gene therapy clinical studies are delivering a wide variety of therapeutic cytotoxic/suicide, tumor suppressor, vaccine antigen, cytokine, receptor, replication inhibitor, and anti-angiogenic genes. Some of the therapeutic genes, vectors, targeted diseases, and their manufacturers are mentioned in **Table 1**. A large number of non-viral vectors are being used to deliver these therapeutic genes, but viruses dominate as successful vectors in the ongoing clinical studies. The most popular viral vectors being used in clinical studies are AV, AAV, HSV, and RV.

AV-MEDIATED GENE THERAPIES IN CLINICAL TRIALS

Both AV and RV vectors are being used in more than 50% of the ongoing viral-mediated clinical studies (**Figure 4C**). The main focus of these are on vaccination and oncolytic therapies. For example, an AV-mediated Theragene (Ad5-yCD/mutTKSR39rep-ADP) delivers a double suicide gene to target stage III pancreatic cancer. AV is being used to deliver the p53 gene in phase II trials to treat recurrent ovarian epithelial, fallopian tube, and primary peritoneal cancer as well as hepatocellular carcinoma (NCT02435186). Also, AV vectors are being used to deliver anti-angiogenic and immunostimulatory genes to treat prostate cancer and malignant pleural mesothelioma (NCT02555397 and NCT01119664). A significant antitumor activity has been demonstrated in phase I-III clinical trials when an AV-based Onyx-015 that undergoes replication selectively in tumors was applied in combination with chemotherapy (14, 191). Vaccination using AV, along with other viruses such as the modified vaccinia Ankara virus (MVA), retrovirus, Sendai virus, and vaccinia virus, is being tested in many clinical trials. AV vectors are also being tested in delivering therapeutic genes for treating malaria, anthrax, HIV, influenza, hepatitis B and C, and severe hemophilia, as well as cardiovascular and many more diseases. AV vectors carrying site-specific endonucleases are being used to edit the CCR5 gene in hematopoietic stem or progenitor cells in AIDS clinical trials (192). The lack of functional dendritic cells in the brain has been attributed to the growth of one of the most aggressive and malignant tumors called gliomas. AV vectors are being used to empower the immune system by expressing the HSV-1 derived thymidine kinase (HSV-1 TK) and cytokine fms-like tyrosine kinase 3 ligand (Flt3L) in the brain. While HSV-1 TK converts ganciclovir into phospho-ganciclovir, a toxic compound to dividing glioma cells, Flt3L differentiates precursors into dendritic cells and acts as a chemokine for dendritic cells resulting into killing of glioma cells and release of tumor antigens in the tumor microenvironment. This follows release of HMGB1, a TLR2 agonist that activates dendritic cells and stimulates dendritic cells loaded with glioma antigens to migrate to the cervical lymph nodes to prime a systemic CD8+ T cytotoxic killing of glioma cells without causing brain toxicity and autoimmunity (193). The median survival of glioma patient is under 2 years and the ongoing clinical trials with DNX-2401, a replication-competent oncolytic AV capable of infecting and killing glioma cells by stimulating an anti-tumor immune response revealed favorable safety profile and prolonged survival of glioma patients (194, 195). Enadenotucirev, a non-natural chimeric oncolytic AV that can retain anti-tumor activity despite intravenous delivery, showed a predictable and manageable safety profile in several advanced cancer patients in phase I clinical studies (196). With encouraging clinical outcome being observed in a large number of ongoing clinical trials, especially in treating cancer, AV-mediated gene therapy is anticipated to make a significant impact on eradicating cancer in the near future.

Although the AV-mediated gene therapy carries a unique advantage over other systems, several concerns must be addressed to offer treatment without side effects. For instance, further improvement in vector development technologies is essential to avoid activation of the endogenous signal transduction pathways and production of cytokines due to anti-vector immune responses that can potentially complicate the clinical outcomes. The necessity of integrin and CAR protein expression on the surface of target cells or tissue to allow efficient infection of AV limits the prospects of treating many diseases. Therefore, generation of novel AV vectors that can infect and transduce target cell or tissue with high specificity, express transgenes up to the therapeutic requirement, induce low organ toxicity and inflammation, and can be detected easily *in vivo* is the need of the hour. Understanding the disease-specific biomarkers, designing and engineering novel AV capsids carrying cell or tissue-specific receptor binding epitopes can reduce the occurrence of unwanted clinical outcome. Since the presence of AV-neutralizing antibodies varies from patient to patient, designing and developing personalized patient-specific capsids can be a promising approach to cure diseases in the future. Development of AV particles that resist inactivation by serum proteins is necessary to promote intravenous administration of therapeutic particles during treatment. Development of strategies to avoid dose-associated toxicity is needed. In addition, contamination with replication-competent virus still remains a serious issue in large scale production of AV preparation for therapeutic purposes (197). Therefore, further advancement in the production of purified AV and AV-based gene delivery technologies is required for using gene therapy to its full potential.

AAV-MEDIATED GENE THERAPIES IN CLINICAL TRIALS

AAV vectors are being used in more than 200 ongoing clinical studies to treat a wide variety of diseases and disorders worldwide. After the approval of the AAV-based drugs Gendicine and Luxturna, another AAV-based drug is poised to enter the

TABLE 1 | Naked DNA and viral-mediated drugs in clinical trials.

Viral Drug/ Intervention	Company/Sponsor	Gene/Ab/Ligand	Disease/Disorder	Vector	Currentstatus	Clinical trial number
Theragene®	SNUBH	CD/TKrep	Cancer	AV	Phase I	NCT02894944
Ad5-Gag	BDHCMU	Gag	AIDS vaccine	AV	Phase I	NCT02762045
AdMA3	BCCA	MG1MA3	Solid tumor	AV	Phase I	NCT02285816
Ad/L523S	CCF	L523S	Lung Cancer	AV	Phase I	NCT00062907
AdAg85A	MUMC	Ag85A	Tuberculosis	AV	Phase I	NCT02337270
Ad35.CS.01	SUSM	CS.01	Malaria	AV	Phase I	NCT00371189
dAd5GNE	WCMC	GNE	Cocaine	AV	Phase I	NCT02455479
ChAd63-METRAP	CCVTM	METRAP	Malaria	AV	Phase I	NCT03084289
Ad5FGF-4	Angionetics	FGF	Angina	AV	Phase III	NCT02928094
AAV5-hFIX	UniQure	hFIX	Hemophilia B	AAV	Phase I/II	NCT02396342
AAV2-GDNF	NIH	GDNF	Parkinson's	AAV	Phase I	NCT01621581
AAV OPTIRPE65	MEH	OPTIRPE65	Eye Diseases	AAV	Phase I/II	NCT02946879
AAV2hAQP1	NIH	hAQP1	AADC	AAV	Phase I	NCT02852213
rAAV1-PG9DP	SCRC	PG9DP	HIV	AAV	Phase I	NCT01937455
scAVV9.CB.CLN6	NCH	CB.CLN6	Batten Disease	AAV	Phase I/II	NCT02725580
SPK-8011	Spark Thera.	FVII	Hemophilia A	AAV	Phase I/II	NCT03003533
scAAV9.U1ahSGSH	Abeona Thera.	SGSH	MPS III	AAV	Phase I/II	NCT02716246
LentiGlobin BB305	Bluebird Bio	HBB	β Thalassemia	LV	Phase III	NCT03207009
Sin-γ- RV-ADA	BCH	ADA	SCID-X1	γ-RV	Phase I/II	NCT01129544
Anti-MAGE-A3-DP4	NIH	TCR	Cancer	RV	Phase II	NCT02111850
Anti-EGFRvIII CAR PBL	NIH	CAR	Glioma	RV	Phase I/II	NCT01454596
Filgrastim	FHCRC	Filgrastim	FA	RV	Phase I	NCT01331018
MO32(NSC 733972)	UA	IL-12	Gliosarcoma	HSV-1	Phase I	NCT02062827
OrienX010	Oriengene Bio	GM-CSF	Melanoma	HSV-1	Phase I	NCT03048253
HSV1716	NCH	ICP34.5	Neuroblastoma	HSV	Phase I	NCT00931931
NP2	Diamyd Inc.	PENK	Cancer Pain	HSV-1	Phase I	NCT00804076
G207	UA	+ radiation	Brain tumor	HSV-1	Phase I	NCT02457845
SGT-94	SynerGene	RB94	Solid tumors	DNA	Phase I	NCT01517464
CYL2-02	InvivoGen	SST2+DCK	Cancer	DNA	Phase II	NCT02806687

SNUBH, Seoul National University Bundang Hospital; BDHCMU, Beijing Ditan Hospital of Capital Medical University; BCCA, Vancouver Cancer Centre Vancouver, British Columbia Canada; CCF, Cancer Center of Florida; MUMC, McMaster University Medical Center; SUSM, Stanford University School of Medicine; WCMC, Weill Medical College of Cornell University; CCVTM, Centre for Clinical Vaccinology and Tropical Medicine; MEH, Moorfield's Eye Hospital; AADC, Aromatic L-amino Acid Decarboxylase Deficiency; SCRC, Surrey Clinical Research Centre; NCH, Nationwide Children's Hospital; BCH, Boston Children's Hospital; TCR, T cell receptor; FHCRC, Fred Hutchinson Cancer Research Center; FA, Fanconi Anemia; UA, University of Alabama; Oriengene Bio, Oriengene Biotechnology Ltd; PENK, Preproenkephalin.

pharmaceutical market in the near future to treat Choroideremia, an X-linked inherited retinal dystrophy that causes night blindness and a constricted visual field. Mutations in *REP1* encoding Rab escort protein 1, a protein involved in lipid modification of Rab proteins, have been implicated in the development of Choroideremia. Patients that received AAV-REP1 therapy showed a significant increase in their visual acuity (198). The product of *CNGB3* provides instructions for making the β-subunit of the cone photoreceptor cyclic nucleotide-gated (CNG) channel, but mutations lead to a defective photoreceptor, decreased visual acuity, and total color blindness, or achromatopsia. In a phase I/II clinical trial sponsored by Applied Genetic Technologies Corporation, AAV was used to deliver *CNGB3* for the successful treatment of achromatopsia (187). AAV is being tested to cure another eye disease, Leber's hereditary optic neuropathy (LHON), a maternally transmitted common mitochondrial disorder caused by point mutations in mitochondrial DNA and impairment of ATP generation. The LHON disease is characterized by apoplectic, bilateral, and severe visual loss. In an ongoing phase I interventional clinical trial, scAAV2 is being used to deliver the P1ND4 gene to rescue visual loss in five legally blind patients (NCT02161380). P1ND4 is a synthetic nuclear encoding gene involved in mitochondrial oxidative phosphorylation. The initial results obtained from this study have showed an improved acuity in two of five patients with no serious adverse events (199). Since treating diseases of the central nervous system is challenging due to the blood brain barrier (BBB), many AAV vectors, especially AAV1, AAV2, AAV5, AAV8, and AAV9, are found to be very useful in transducing neurons (200), and therefore, many AAV-mediated treatments are being tested to cure lysosomal storage disorders, Alzheimer's disease, Parkinson's disease, amyotrophic lateral sclerosis (ALS), epilepsy, spinal muscular atrophy type 1, metachromatic leukodystrophy, aromatic L-amino acid

TABLE 2 | The cellular and gene therapy products available in the market.

Drug	Company	Therapeutic	Disease/Disorder	Remission
Luxturna™	Spark Therapeutics	*RPE65*	Inherited blindness	93%
Kymriah™	Novartis	CAR-T	Leukemia (ALL)	80%
Glybera®	uniQure	*LPL*	LPLD	NA
Gendicine®	Benda Pharmaceutical	*p53*	Head and neck cancer	67%
Strimvelis™	GlaxoSmithKline	HSC	ADA-SCID	100%
Oncorine™	Shanghai Sunway Biotech	*p53*	Head and neck cancer	NA
Neovasculogen™	Human Stem Cell Institute	*VEGF*	PAD and CLI	90%
SPRS-therapy®	Human Stem Cell Institute	Fibroblasts	Skin damage	75%
laViv™	Fibrocell Science	Fibroblasts	Nasolabial fold Wrinkles	57%
Provenge™	Valeant Pharmaceuticals	Dendritic cells	Prostate cancer	38%
Imlygic™	Biogen	ICP34.5 & GM-CSM	Melanoma	50%
Carticel™	Genzyme	Chondrocyte	Knee cartilage injury	92%
Rexin-G™	Epeius Biotechnologies	Cyclin G1	Breast cancer, Sarcoma	40%

CAR-T, Chimeric antigen receptor T- cell; ALL, Acute lymphoblastic leukemia; LPL, Lipoprotein lipase; LPLD, Lipoprotein lipase deficiency; ADA, SCID—Adenosine deaminase severe combined immunodeficiency; HSC, Hematopoietic stem cell; VEGF, Vascular endothelial growth factor; PAD, Peripheral arterial disease; CLI, Critical limb ischemia; ICP34.5, Infected cell protein 34.5; GM, CSF-Granulocyte-macrophage colony stimulating factor.

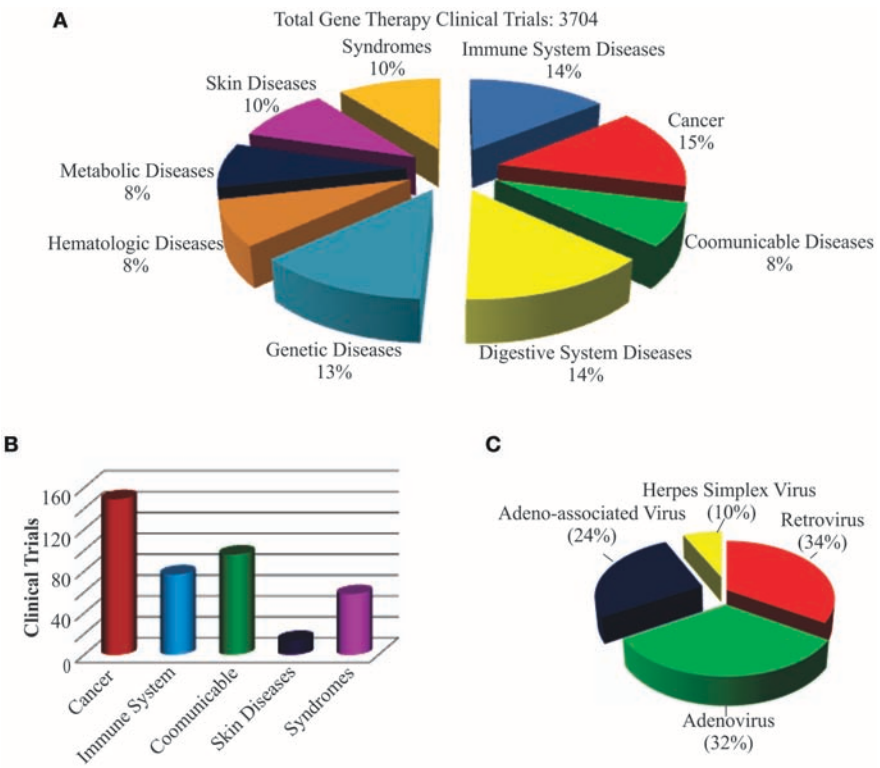

FIGURE 4 | Recent trends in gene therapy research and clinical trials. **(A)** Different diseases being treated by gene therapy in clinical trials. The clinical studies database was searched for the total number of gene therapies conducted in the world to treat different diseases to date. The main focus of the clinical trials was found to be treating cancer, immune, digestive, and genetic diseases. **(B)** Clinical trials actively recruiting patients for testing gene therapy-mediated medicines in curing diseases. This includes both viral and non-viral vector-mediated gene therapies. A relatively large number of clinical trials are recruiting cancer patients for testing different gene therapy-based medicines. **(C)** Different recombinant viral vectors being tested in gene therapy-based treatments.

decarboxylase (AADC) deficiency, and Batten disease. Like AV, AAV is yet another useful viral vector for cancer gene therapy. Several AAV vectors are being used to test the expression of anti-angiogenic, cytotoxic, cytokine, and tumor suppressor genes, small RNAs, antigens, and antibodies for cancer cures. A large number of preclinical studies revealed successful treatment with AAV-mediated gene therapy for improved tumor regression (201–206). AAV is considered a powerful vector in targeting

the liver for treating hematological diseases. Complete treatment of severe hemophilia B by delivering *FIX* in patients was described as the "holy grail" of gene therapy clinical application (207). In ongoing phase I/II clinical trials, *FVIII* and *FIX* are being delivered to hemophilia A and B patients, respectively (NCT03003533, NCT02484092).

Although AAV vectors are non-pathogenic and safe, and found among the commonly used platforms for gene delivery in preclinical and clinical studies, their potential application in gene therapy is limited by the inability to deliver a therapeutic gene more than 5.0 kb in size, immunogenicity of capsid proteins, difficulty in producing a large supply, requirement of large doses of highly purified vectors, broad tropism, and presence of an extensive anti-AAV immunity in human populations (208–211). Adding empty vectors of AAV to the final vector preparations to serve as a decoy and developing new vectors with high transduction and gene expression potential as well as better understanding of T-cell response to all AAV serotypes in clinical settings would reduce inflammation, immune response, and other viral particle-associated side effects because capsid is the primary interface with the target cell that defines pharmacological, immunological, and molecular properties (150, 207, 212, 213). Therefore, designing and developing more chimeric capsid proteins are critical to generate disease- and cell- or tissue-specific viral particles. For example, substitution of tyrosine to phenylalanine in the AAV capsid protein has enhanced the transduction efficiency with reduced toxicity (214). Better understanding of the underlying mechanisms of intracellular transportation of AAV particles in a disease-specific setting will help developing strategies to improve gene delivery efficacy. AAV vectors are commonly delivered to patients by systemic, intramural, central nervous system, cardiac, and pulmonary delivery but certain sites of the human body elicit no immune response to injection of antigens or viral particles because the BBB prevents the entry of antibodies or resting lymphocytes and the absence of traditional antigen-presenting cells. Therefore, applying AAV particles to patients through immune-privileged sites, such as the central nervous system, mucosal surfaces, eye, placenta, fetus, testicles, and articular cartilage, could be a better option to avoid T-cell response. For example, AAV vectors injected intraparenchymally into the central nervous system to treat Batten's, Canavan, and Parkinson's diseases showed little or no adaptive immune response in many clinical trials (155, 215–218). Monitoring T-cell response in patients by using advanced tools especially multicolor flow cytometry, mass cytometry, and enzyme-linked immunospot (ELISpot) assay will minimize the risk of the unexpected clinical outcome (209). Also, for reduced T-cell response and optimal expression of a therapeutic gene, intramuscular instead of systematic injection of AAV particles is recommended because healthy muscles express only low levels of MHC class I antigens (209, 219). Use of immunosuppressive drugs was found safe to maintain therapeutic gene expression in many clinical trials (150, 220, 221), and their use could be an option for better clinical outcome, but maintenance of transgene expression remains unpredictable. Although AAV offers the expression of a therapeutic gene for nearly 1 year without integrating into the host's chromosomes, applying CRISPR/Cas9 technology would resolve long-term expression and mutagenesis issues. Production of high titers of purified AAV particles by employing ionic iodixanol gradients and ion exchange chromatography instead of using the toxic CsCl is also important for the success of gene therapy (222, 223). Recent developments in the production of high quality AAV particles from transfection efficient HEK293 cell suspensions in shaker flasks and WAVE bioreactors free of all animal and human products will certainly improve the success of gene therapy application (224). This system was further improved by changing the NaCl concentration in the medium and optimizing conditions for Expi293F cell infection by helper herpes simplex virus (HSV) (225). However, contamination of the final AAV particle preparation with HSV cannot be ruled out. The AAV particles generated from the baculovirus expression system carry low levels of VP1 capsid protein, so high doses are used in clinical trials to increase transduction efficiency at the expense of immune response (226). No disease caused by AAV infection has been reported to date but repression of PPP1R12C gene promoter in host cells by the rep proteins of AAV2 is clearly a concern (227). Therefore, more efforts are necessary to smooth out the landscape surrounding AAV for its more pronounced clinical benefits in gene therapy.

HSV-MEDIATED GENE THERAPIES IN CLINICAL TRIALS

More than 90 gene therapy clinical trials have been conducted using HSV as a vector to deliver therapeutic genes for curing various diseases to date. They have been extensively used for tumor therapy and vaccine development. After the advent of HSV-based T-VEC drug for melanoma treatment, many HSV vectors are being used to deliver suicide genes to treat anaplastic thyroid cancer (228). Since immunotherapy is currently a hot topic in cancer research and gaining more attention; oncolytic viruses are often combined with immune checkpoint blockades such as T-VEC combined with anti-PD1 Pembrolizumab, anti-CTLA-4 Ipilimumab, and neoadjuvant to increase their therapeutic potential (68). Also, the oncolytic HSV-1 carrying four copies of miR-145 target sites combined with radiation has been shown to be more effective than radiation alone (122, 229). A current phase I clinical trial uses an engineered HSV rRp450 designed to kill cancer cells in order to treat liver metastases and primary liver tumors (NCT01071941). HSV is also used as a transneuronal tracer defining connections among neurons by virtue of traversing synapses (230). HSV has much potential in treating problems of the urinary system. A recent study reports HSV-1 as a vector for delivering poreless TRPV1 channels or protein phosphatase 1α to reduce bladder over-activity in rats (231). HSV-mediated treatment also alleviated bladder pain. These have the potential to offer treatment to cases of overactive bladder (OAB) and interstitial cystitis/bladder pain syndrome (IC/BPS). However, infectivity of solid tumors, leakage, off target viral replication, sequestration, and delivery methods are still hampering the progress of HSV-mediated oncolytic viral therapy.

Although the nervous system is the natural site for HSV latency, the full potential of HSV-mediated gene therapy in treating nerve diseases is yet to be discovered. Several studies treating chronic pain were successful in animal models but very few have reached clinical trials to date. HSV vectors have certainly promising perspectives in clinic trials but detailed understanding of virus-host interaction will minimize cytotoxicity and biohazards generation. Recently, strategies to develop transduction efficient, alternate vector entry and transcriptionally retargeted oncolytic HSV viruses were reviewed (232–234). The therapeutic potential of amplicons is still undermined by production and stability issues; therefore, focus needs to be on improving vector design, construction, and production technology. Developing new HSV vectors carrying genes that enhance tumor cell lysis will increase oncolytic therapeutic efficacy. While gliomas do not express miR-124, it is highly expressed in normal brain, and designing HSV vectors carrying the same could be a promising approach to treat glioma. The full potential of expression libraries created by using HSV vectors in regenerative medicine is yet to be seen in curing human diseases (235). Since oncolytic virus therapy is considered a major breakthrough in treating cancer after the success of radiation and immunotherapies, development of safe and tumor-selective new HSV vectors is necessary for its promising future. Optimizing vector delivery methods especially to solid tumors and in immune-compromised patients will certainly improve oncolytic viral therapy. Exploring their roles in gene editing and repair will expand the horizons of gene therapy.

RV-MEDIATED GENE THERAPIES IN CLINICAL TRIALS

RV vectors can be applied to cure a wide variety of diseases and disorders such as cancer, HIV, ADA-SCID, melanoma, WAS, and many others. Though the majority of retinal gene therapy trials use AAV, some use lentivirus because of its larger gene capacity. For example, Usher syndrome causes hearing loss, less vestibular function, and a pigmented retina (187). Currently, a phase II trial is underway to use lentivirus to deliver a 5.0-kb *MYO7A*. Additionally, a phase II trial that is projected to deliver *ABCA4* by lentivirus to treat Stargadt disease, an inherited macular degeneration that causes cell degeneration, is underway (187). Furthermore, lentivirus is a favorable vector to treat sickle cell anemia because of the advantages it offers, including a large transgene capacity, stable long-term expression, and safer integration (236). A single base substitution in the β-globin gene causes the erythrocyte sickling characteristic of sickle cell anemia. Treatments for sickle cell anemia are transitioning into self-inactivating lentivirus with a deletion in the U3 region of the 3' LTR, which has a safer integration profile (236). A clinical trial sponsored by Bluebird Bio used LentiGlobin BB305, which delivered β-globin T87Q. Clinical results showed 24% anti-sickling (NCT03207009). For treating immunodeficiency, there have been adverse effects reported in the past by gammaretroviral vectors. In the treatment of X-linked SCID, CD34+ hematopoietic stem cells were transduced with murine gammaretroviral vector, which led to an increase in immune function, but 5 patients developed T cell leukemia because of insertional mutagenesis into oncogenes (185). In the treatment of WAS, a gammaretroviral vector expressing *WAS* transgene delivered to patients caused 7 out of 10 to develop leukemia (185). Recently, self-inactivating lentivirus was used to treat five patients with X-linked SCID. Two patients had restoration of immune function even 2–3 years after treatment (237). A current phase I/II clinical trial is using a self-inactivating gammaretrovirus to treat SCID-X1 (NCT01129544). Other current clinical trials include a phase II trial using a retroviral vector to transfer ADA into hematopoietic stem cells to treat ADA-SCID (NCT00598481). A replicating Toca 511 RV vector is being used in a phase I trial to treat recurrent high-grade glioma (NCT02598011). RV is being used in a phase I/II trial to transduce white blood cells with the CAR-T cell receptor to target mesothelin for patients with metastatic cancer (NCT01583686). Donor T cells are being transduced with RV to express the caspase-9 suicide gene in a phase I trial to treat cancer (NCT01494103). Duchenne muscular dystrophy occurs when a lack of dystrophin expression causes muscle degeneration. In a proof-of-concept study, the full-length sequence of dystrophin was spread over two co-packaged RNA copies and delivered via a lentiviral vector. The vector integrated and gave long-term expression of dystrophin (238). Additionally, a RV vector expressing MazF endoribonuclease is being used to transduce CD4+ T cells to treat HIV in a phase I trial (NCT01787994). AIDS-related non-Hodgkin lymphoma is being treated in a phase I clinical trial that transduces stem cells with genes for HIV RNA using lentivirus in order to evoke an immune response (NCT01961063).

Since immunity is the primary barrier for the success of viral gene therapy, it is critical to design viral vectors that can subvert the complement system. The LTRs of RV serve as promoters, enhancers, binding sites for various nuclear proteins, chromatin modulators, and polyadenylation signals. Therefore, applying genetic engineering and CRISPR technology will avoid exacerbating the insertional mutagenesis issue. This issue can also be avoided by using non-integrating RV vectors or integrase inhibitors during treatment. The RV-mediated gene therapy will immensely benefit from developing technologies to guide and monitor transgene insertion in the host cell chromatin. Although RV vectors can deliver a transgene up to 10 kb in size, production of high titer virus, chromatin structure, and epigenetic modification near the insertion site still remain issues in clinical applications. Thus, better RV vectors are needed for future gene therapy applications. Since viral infection depends on the expression of target cell surface receptors and viral envelope protein, designing and constructing to produce efficient and cell-, tissue- and disease-specific recombinant RV vectors are necessary to obtain the expected clinical outcome. New RV vectors with optimized LTRs, created by replacing promoter/enhancer elements with cell- and tissue-specific promoters and enhancer sequences, will boost their use in curing many diseases with fewer or no side effects. Novel RV vectors are needed to transduce heart and other body organs for their wide spread use in gene therapy. Introduction of miRNA binding sites in the viral RNA has been suggested to control posttranscriptional regulation of

disease-causing genes (239). The use of advanced RV vectors carrying the woodchuck posttranscriptional regulatory element (wPRE) to increase transgene mRNA stability, export, and translatability will help to accomplish better clinical outcome (240). As delivering genetic information in the form of RNA is an increasingly popular method, RVs carrying no RT or integrase are poised to play a significant role in a gene editing, vaccination, tumor therapy, gene therapy, transdifferentiation, reprogramming, and other biotechnological applications in the near future (241).

RISKS ASSOCIATED WITH VIRAL VECTORS

Since an estimated 10^{31} virus-like particles exist on the Earth and they are present in the blood, nose, mouth, lung, vagina, gastrointestinal tract, conjunctiva, skin, and the mammalian genome, viruses appear to play a major role in human life (242, 243). The general concerns with viral vectors are the risks of an immune response, off-target effects, inflammation, and insertional mutagenesis. An immune response could make a viral treatment less efficient, or the resulting creation of antibodies could preclude a second dosage of the same virus (244–248). Inflammation was seen as a worst-case scenario in the 1999 death of Jesse Gelsinger caused by a very high dosage of adenovirus (249). Tailoring the viral dose to the patient, however, can better control this risk. Also, insertional mutagenesis is a major obstacle that the gene therapy field must overcome. The risk of inserting a gene into a tumor suppressor gene or activating an oncogene is present for the vectors that integrate into the unwanted locations of the genome, such as retrovirus. To counter this, vectors can be used that do not integrate readily into the genome. Additionally, self-inactivating vectors can be manufactured that do not contain their own promoter; rather, another internal promoter in the cell is used. This leads to less genotoxicity and is a safer alternative to traditional integrating vectors (52). Other concerns are that viral vectors are only relevant for monogenic disorders because of their limited DNA-carrying capability. However, HSV-1 is an example of a virus that has enough carrying capacity for multiple genes. Additionally, dual vector systems, such as dual vector adeno-associated virus, have larger transgene capacities. Also, finding the appropriate virus to infect the desired cells is often difficult, and there is the risk that the virus could cross the Weismann barrier and infect germ line cells. Furthermore, viruses are generally susceptible to genetic variations. Integration into undesirable sites such as regulatory, oncogenes or tumor-suppressor genes would be undesirable. Deletion of virulence genes may affect their ability to infect or integrate with the host chromosome, thus compromising their effectiveness as vectors. Additionally, a social stigma is associated with viral therapy. Most patients would be concerned about being infected by a live virus—a concern also held about viral vaccines. Since their ubiquitous presence is a reality, why shouldn't humankind start accepting them as wonderful molecular biological tools with which to build novel and powerful medicine?

CHALLENGES AND THE WAY FORWARD

Since its birth in the 1960s, gene therapy has come quite a long way by providing an alternate one-time treatment option for cancer, metabolic disorders, and neuronal, immune, and infectious diseases. Notably, it has been able to treat beta thalassemia, Leber's congenital amaurosis, severe immunodeficiency diseases such as ADA-SCID, and more. However, the full potential of gene therapy is yet to be witnessed in regenerative medicine, a branch of translational medicine where engineering or regenerating human cells, tissue or organs enables restoration or establishment of normal function. With recent impressive results observed in vaginal gene therapy in preclinical trials, gene therapy is poised to enter the clinical phase for treating infectious diseases in the near future (250). Both viral and non-viral vectors can be used to deliver DNA, each of which has its own advantages and disadvantages. Additionally, genome-editing technology is an up-and-coming method of delivering DNA to specific parts of the genome. With all of these breakthroughs have come hurdles, such as the death of Jesse Gelsinger in 1999 and the development of leukemia in patients who have been treated for WAS and ADA-SCID. The ethical concerns of patients must be heeded as well. However, these challenges do not reflect a flaw in the concept. Simply, more research is needed to avoid technical issues such as the production of viral particles in large scale, formulations for long-term storage stability, immune responses, and insertional mutagenesis. Loading of viral particles with a therapeutic gene during production is mostly done by transient transfections, a rate-limiting step in large scale production of viral particles. Alternate approaches such as stable cell lines expressing capsid proteins and insect cells based baculovirus expression systems would be useful for mass production of viral particles. This underdeveloped modern medicine needs discovery and engineering of better viral vectors to deliver therapeutic genes precisely to the target diseased cells or tissue.

Gene therapy is a rapidly expanding field, and it seems that scientists have only scratched the surface of its potential. The more that is discovered about how to optimize gene delivery vectors, the closer this field gets to delivering wide-scale solutions to modern medicine. The future of gene therapy moves toward engineering safer and more efficient vectors, combining multiple existing strategies such as viral vectors with genetic engineering technologies, and personalizing all characteristics of gene therapy treatments to the patient, as it has been shown that host genetic variants affect the efficacy of vector-mediated gene delivery (251). This includes understanding of the repertoire of receptors on a target cell in diseased conditions to help in designing appropriate capsid proteins for viral particles. Although the full panoply of gene therapy's might is yet be witnessed, it has enormous potential to shed light on human afflictions, add value to patients' lives, and contribute to future economic growth. Although gene therapy currently shares less than one percent of the total $1.2 trillion world annual pharmaceutical market, it is expected to create approximately a $12 billion market in the next 10 years. According to a market research and advisory

company, Allied Market Research, cancer gene therapy alone has created a $289 million market in 2016 but it is expected to reach $2,082 million by 2023. Gaining popularity among the global medicinal community, gene therapy has become an attractive market for companies and investors. However, the ethical acceptance and advancement in the technology to avoid unwanted clinical outcomes are critical for driving its market growth. Also, the translation of laboratory studies to animal studies and then to clinical trials is a long, tedious, and expensive process to ensure the safety of patients. As a result, if the USFDA, with its patchy regulations, continues its approval rate, providing gene therapies for all the genetic diseases will take many years to come. Therefore, a new perspective on creating a conducive atmosphere for improving this modern cutting-edge gene therapy technology is necessary to transform the lives of patients with severe genetic illnesses, infectious diseases, and disorders. As mentioned elsewhere, knowledge has no boundaries, and there exist unlimited methods to develop a novel invention; every bump in the investigating path can be considered an inspiration and source of energy to advance research, a never-ending learning process.

AUTHOR CONTRIBUTIONS

VB and RG conceived the concept and wrote the manuscript, and the other authors listed made substantial, direct intellectual contributions to the work, and approved it for publication.

FUNDING

Funding for this work was provided by Joint Science and Technology Office (JSTO), Defense Threat Reduction Agency (DTRA), Department of the Army, Department of Defense, United States of America.

ACKNOWLEDGMENTS

Authors thank Mr. Abraham A. James for his artwork and Ms. Neehar Mishra for her comments, and Dr. Manubhai Patel and the late Dr. Douglas M. Cerasoli for their unconditional support. Authors apologize to the scientists whose contributions to gene therapy could not be acknowledged because of space limitations.

REFERENCES

1. Avery OT, Macleod CM, McCarty M. Studies on the chemical nature of the substance inducing transformation of pneumococcal types : induction of transformation by a desoxyribonucleic acid fraction isolated from Pneumococcus Type Iii. *J Exp Med*. (1944) 79:137–58.
2. Crawford GE, Holt IE, Mullikin JC, Tai D, Blakesley R, Bouffard G, et al. Identifying gene regulatory elements by genome-wide recovery of DNase hypersensitive sites. *Proc Natl Acad Sci USA*. (2004) 101:992–7. doi: 10.1073/pnas.0307540100
3. Omenn GS, Lane L, Lundberg EK, Beavis RC, Overall CM, Deutsch EW. Metrics for the Human Proteome Project 2016: progress on identifying and characterizing the human proteome, including post-translational modifications. *J Proteome Res*. (2016) 15:3951–60. doi: 10.1021/acs.jproteome.6b00511
4. Thul PJ, Lindskog C. The human protein atlas: a spatial map of the human proteome. *Protein Sci*. (2018) 27:233–44. doi: 10.1002/pro.3307
5. Loewe L, Hill WG. The population genetics of mutations: good, bad and indifferent. *Philos Trans R Soc Lond B Biol Sci*. (2010) 365:1153–67. doi: 10.1098/rstb.2009.0317
6. Barney M. Mutations: The raw material for evolution? *Acts & Facts*. (2007) 36:10.
7. Joel CL. Mutations are the raw materials of evolution. *Nat Educ Knowledge*. (2011) 3:10.
8. Lagasse HA, Alexaki A, Simhadri VL, Katagiri NH, Jankowski W, Sauna ZE, et al. Recent advances in (therapeutic protein) drug development. *F1000Res*. (2017) 6:113. doi: 10.12688/f1000research.9970.1
9. Usmani SS, Bedi G, Samuel JS, Singh S, Kalra S, Kumar P, et al. THPdb: Database of FDA-approved peptide and protein therapeutics. *PLoS ONE*. (2017) 12:e0181748. doi: 10.1371/journal.pone.0181748
10. Mata DG, Rezk PE, Sabnekar P, Cerasoli DM, Chilukuri N. Investigation of evolved paraoxonase-1 variants for prevention of organophosphorous pesticide compound intoxication. *J Pharmacol Exp Ther*. (2014) 349:549–58. doi: 10.1124/jpet.114.213645
11. Chilukuri N, Parikh K, Sun W, Naik R, Tipparaju P, Doctor BP, et al. Polyethylene glycosylation prolongs the circulatory stability of recombinant human butyrylcholinesterase. *Chem Biol Interact*. (2005) 157–158:115–21. doi: 10.1016/j.cbi.2005.10.013
12. Chilukuri N, Sun W, Naik RS, Parikh K, Tang L, Doctor BP, et al. Effect of polyethylene glycol modification on the circulatory stability and immunogenicity of recombinant human butyrylcholinesterase. *Chem Biol Interact*. (2008) 175:255–60. doi: 10.1016/j.cbi.2008.05.020
13. Duysen EG, Parikh K, Aleti V, Manne V, Lockridge O, Chilukuri N. Adenovirus-mediated human paraoxonase1 gene transfer to provide protection against the toxicity of the organophosphorus pesticide toxicant diazoxon. *Gene Ther*. (2011) 18:250–7. doi: 10.1038/gt.2010.136
14. Zhang WW, Li L, Li D, Liu J, Li X, Li W, et al. The first approved gene therapy product for cancer Ad-p53 (Gendicine): 12 years in the clinic. *Hum Gene Ther*. (2018) 29:160–79. doi: 10.1089/hum.2017.218
15. Thakur A, Huang M, Lum LG. Bispecific antibody based therapeutics: strengths and challenges. *Blood Rev*. (2018) 32:339–47. doi: 10.1016/j.blre.2018.02.004
16. Spicer CD, Jumeaux C, Gupta B, Stevens MM. Peptide and protein nanoparticle conjugates: versatile platforms for biomedical applications. *Chem Soc Rev*. (2018) 47:3574–620. doi: 10.1039/c7cs00877e
17. Walsh G. Biopharmaceutical benchmarks 2014. *Nat Biotechnol*. (2014) 32:992–1000. doi: 10.1038/nbt.3040
18. Ibraheem D, Elaissari A, Fessi H. Gene therapy and DNA delivery systems. *Int J Pharm*. (2014) 459:70–83. doi: 10.1016/j.ijpharm.2013.11.041
19. Chilukuri N, Duysen EG, Parikh K, Sun W, Doctor BP, Lockridge O, et al. Adenovirus-mediated gene transfer of human butyrylcholinesterase results in persistent high-level transgene expression *in vivo*. *Chem Biol Interact*. (2008) 175:327–31. doi: 10.1016/j.cbi.2008.04.009
20. Chilukuri N, Duysen EG, Parikh K, diTargiani R, Doctor BP, Lockridge O, et al. Adenovirus-transduced human butyrylcholinesterase in mouse blood functions as a bioscavenger of chemical warfare nerve agents. *Mol Pharmacol*. (2009) 76:612–7. doi: 10.1124/mol.109.055665
21. Aleti V, Reddy GB, Parikh K, Arun P, Chilukuri N. Persistent and high-level expression of human liver prolidase *in vivo* in mice using adenovirus. *Chem Biol Interact*. (2013) 203:191–5. doi: 10.1016/j.cbi.2012.08.021
22. Mata DG, Sabnekar P, Watson CA, Rezk PE, Chilukuri N. Assessing the stoichiometric efficacy of mammalian expressed paraoxonase-1 variant I-F11 to afford protection against G-type nerve agents. *Chem Biol Interact*. (2016) 259:233–41. doi: 10.1016/j.cbi.2016.04.013
23. Dunbar CE, High KA, Joung JK, Kohn DB, Ozawa K, Sadelain M. Gene therapy comes of age. *Science*. (2018) 359:eaan4672.. doi: 10.1126/science.aan4672
24. Prondzynski M, Mearini G, Carrier L. Gene therapy strategies in the treatment of hypertrophic cardiomyopathy. *Pflugers Arch-Eur J Physiol*. (2018) P. 1–9. doi: 10.1007/s00424-018-2173-5.

25. Hidai C, Kitano H. Nonviral gene therapy for cancer: a review. *Diseases*. (2018) 6:E57. doi: 10.3390/diseases6030057
26. Esrick EB, Bauer DE. Genetic therapies for sickle cell disease. *Semin Hematol*. (2018) 55:76–86. doi: 10.1053/j.seminhematol.2018.04.014
27. Prakash V, Moore M, Yanez-Munoz RJ. Current progress in therapeutic gene editing for monogenic diseases. *Mol Ther*. (2016) 24:465–74. doi: 10.1038/mt.2016.5
28. Verma IM, Somia N. Gene therapy - promises, problems and prospects. *Nature*. (1997) 389:239. doi: 10.1038/38410
29. Cotrim AP, Baum BJ. Gene therapy: some history, applications, problems, and prospects. *Toxicol Pathol*. (2008) 36:97–103. doi: 10.1177/0192623307309925
30. Jafarlou M, Baradaran B, Saedi TA, Jafarlou V, Shanehbandi D, Maralani M, et al. An overview of the history, applications, advantages, disadvantages and prospects of gene therapy. *J Biol Regul Homeost Agents*. (2016) 30:315–21.
31. Giacca M. *Ethical and Social Problems OG Gene Therapy*. Milan:Springer (2010).
32. Hanna E, Remuzat C, Auquier P, Toumi M. Gene therapies development: slow progress and promising prospect. *J Mark Access Health Policy*. (2017) 5:1265293. doi: 10.1080/20016689.2017.1265293
33. Szybalska EH, Szybalski W. Genetics of human cess line. IV. DNA-mediated heritable transformation of a biochemical trait. *Proc Natl Acad Sci USA*. (1962) 48:2026–34.
34. Wirth T, Parker N, Yla-Herttuala S. History of gene therapy. *Gene*. (2013) 525:162–9. doi: 10.1016/j.gene.2013.03.137
35. Chen C, Yang Z, Tang X. Chemical modifications of nucleic acid drugs and their delivery systems for gene-based therapy. *Med Res Rev*. (2018) 38:829–69. doi: 10.1002/med.21479
36. Misra S. Human gene therapy: a brief overview of the genetic revolution. *J Assoc Physicians India*. (2013) 61:127–33.
37. Cartier-Lacave N, Ali R, Yla-Herttuala S, Kato K, Baetschi B, Lovell-Badge R, et al. Debate on Germline Gene Editing. *Hum Gene Ther Methods*. (2016) 27:135–42. doi: 10.1089/hgtb.2016.28999.deb
38. Wolf E, Schernthaner W, Zakhartchenko V, Prelle K, Stojkovic M, Brem G. Transgenic technology in farm animals–progress and perspectives. *Exp Physiol*. (2000) 85:615–25.
39. Jaenisch R. Transgenic animals. *Science*. (1988) 240:1468–74.
40. Gordon JW, Scangos GA, Plotkin DJ, Barbosa JA, Ruddle FH. Genetic transformation of mouse embryos by microinjection of purified DNA. *Proc Natl Acad Sci USA*. (1980) 77:7380–4.
41. McCarthy M. Scientists call for moratorium on clinical use of human germline editing. *BMJ*. (2015) 351:h6603. doi: 10.1136/bmj.h6603
42. Travis J. Genetic engineering. Germline editing dominates DNA summit. *Science*. (2015) 350:1299–300. doi: 10.1126/science.350.6266.1299
43. Naldini L. Gene therapy returns to centre stage. *Nature*. (2015) 526:351–60. doi: 10.1038/nature15818
44. Cohen IG, Adashi EY. Science and regulation. The FDA is prohibited from going germline. *Science*. (2016) 353:545–6. doi: 10.1126/science.aag2960
45. LaBarbera AR. Proceedings of the International Summit on Human Gene Editing: a global discussion-Washington, D.C., December 1-3, 2015. *J Assist Reprod Genet*. (2016) 33:1123–7. doi: 10.1007/s10815-016-0753-x
46. Hildt E. Human germline interventions-think first. *Front Genet*. (2016) 7:81. doi: 10.3389/fgene.2016.00081
47. Pergament E. The promise of gene therapy. *Curr Opin Obstet Gynecol*. (2016) 28:132–5. doi: 10.1097/GCO.0000000000000255
48. Vassena R, Heindryckx B, Peco R, Pennings G, Raya A, Sermon K, Veiga A. Genome engineering through CRISPR/Cas9 technology in the human germline and pluripotent stem cells. *Hum Reprod Update*. (2016) 22:411–9. doi: 10.1093/humupd/dmw005
49. Portin P. [New possibilities will open up in human gene therapy]. *Duodecim*. (2016) 132:26–32.
50. Calos MP. Genome editing techniques and their therapeutic applications. *Clin Pharmacol Ther*. (2017) 101:42–51. doi: 10.1002/cpt.542
51. Morrow T. Novartis's kymriah: harnessing immune system comes with worry about reining in costs. *Manag Care*. (2017) 26:28–30.
52. Kaufmann KB, Buning H, Galy A, Schambach A, Grez M. Gene therapy on the move. *EMBO Mol Med*. (2013) 5:1642–61. doi: 10.1002/emmm.201202287
53. Herrero MJ, Sabater L, Guenechea G, Sendra L, Montilla AI, Abargues R, et al. DNA delivery to *'ex vivo'* human liver segments. *Gene Ther*. (2012) 19:504–12. doi: 10.1038/gt.2011.144
54. Suhonen J, Ray J, Blomer U, Gage FH, Kaspar B. *Ex vivo* and *in vivo* gene delivery to the brain. *Curr Protoc Hum Genet*. (2006) Chapter 13:Unit 13 3. doi: 10.1002/0471142905.hg1303s51
55. Deev RV, Bozo IY, Mzhavanadze ND, Voronov DA, Gavrilenko AV, Chervyakov YV, et al. pCMV-vegf165 Intramuscular Gene Transfer is an Effective Method of Treatment for Patients With Chronic Lower Limb Ischemia. *J Cardiovasc Pharmacol Ther*. (2015) 20:473–82. doi: 10.1177/1074248415574336
56. Deev R, Plaksa I, Bozo I, Isaev A. Results of an International postmarketing surveillance study of pl-VEGF165 Safety and Efficacy in 210 Patients with Peripheral Arterial Disease. *Am J Cardiovasc Drugs*. (2017) 17:235–42. doi: 10.1007/s40256–016-0210–3
57. Deev R, Plaksa I, Bozo I, Mzhavanadze N, Suchkov I, Chervyakov Y, et al. Results of 5-year follow-up study in patients with peripheral artery disease treated with PL-VEGF165 for intermittent claudication. *Ther Adv Cardiovasc Dis*. (2018) 12:237–46. doi: 10.1177/1753944718786926
58. Manunta MD, Tagalakis AD, Attwood M, Aldossary AM, Barnes JL, Munye MM, et al. Delivery of ENaC siRNA to epithelial cells mediated by a targeted nanocomplex: a therapeutic strategy for cystic fibrosis. *Sci Rep*. (2017) 7:700. doi: 10.1038/s41598–017-00662–2
59. Nance ME, Hakim CH, Yang NN, Duan D. Nanotherapy for duchenne muscular dystrophy. *Wiley Interdiscip Rev Nanomed Nanobiotechnol*. (2017). 10:e1472. doi: 10.1002/wnan.1472
60. Guan X, Guo Z, Wang T, Lin L, Chen J, Tian H, et al. A pH-Responsive Detachable PEG shielding strategy for gene delivery system in cancer therapy. *Biomacromolecules*. (2017) 18:1342–9. doi: 10.1021/acs.biomac.7b00080
61. Roossinck MJ. Move over, bacteria! Viruses make their mark as mutualistic microbial symbionts. *J Virol*. (2015) 89:6532–5. doi: 10.1128/jvi.02974–14
62. Roossinck MJ, Bazan ER. Symbiosis: viruses as intimate partners. *Annu Rev Virol*. (2017) 4:123–39. doi: 10.1146/annurev-virology-110615–042323
63. Viswanathan P, Betapudi V, Kumar MS, Rasheedi S, Vrati S, Bashyam MD, Hasnain SE. The homologous region sequence (hr1) of Autographa californica multinucleocapsid polyhedrosis virus can enhance transcription from non-baculoviral promoters in mammalian cells. *J Biol Chem*. (2003) 278:52564–71. doi: 10.1074/jbc.M309351200
64. Betapudi V, Viswanathan P, Habib S, Hasnain SE. An additional copy of the homologous region (hr1) sequence in the Autographa californica multinucleocapsid polyhedrosis virus genome promotes hyperexpression of foreign genes. *Biochemistry*. (2004) 43:8143–51. doi: 10.1021/bi049953q
65. Ramani K, Hassan Q, Betapudi V, Hasnain SE, Sarkar DP. Site-specific gene delivery *in vivo* through engineered Sendai viral envelopes. *Proc Natl Acad Sci USA*. (1998) 95:11886–90.
66. Giacca M Zacchigna S. Virus-mediated gene delivery for human gene therapy. *J Control Release*. (2012) 161:377–88. doi: 10.1016/j.jconrel.2012.04.008
67. Yin H, Kanasty RL, Eltoukhy AA, Vegas AJ, Dorkin JR Anderson DG. Non-viral vectors for gene-based therapy. *Nat Rev Genet*. (2014) 15:541–55. doi: 10.1038/nrg3763
68. Lawler SE, Speranza MC, Cho CF, Chiocca EA. Oncolytic viruses in cancer treatment: a review. *JAMA Oncol*. (2017) 3:841–9. doi: 10.1001/jamaoncol.2016.2064
69. Tatum EL. Molecular biology, nucleic acids, and the future of medicine. *Perspect Biol Med*. (1966) 10:19–32.
70. Ginn SL, Alexander IE. Gene therapy: progress in childhood disease. *J Paediatr Child Health*. (2012) 48:466–71. doi: 10.1111/j.1440–1754.2011.02204.x
71. Ginn SL, Alexander IE, Edelstein ML, Abedi MR, Wixon J. Gene therapy clinical trials worldwide to 2012 - an update. *J Gene Med*. (2013) 15:65–77. doi: 10.1002/jgm.2698
72. Rowe WP, Huebner RJ, Gilmore LK, Parrott RH, Ward TG. Isolation of a cytopathogenic agent from human adenoids undergoing spontaneous degeneration in tissue culture. *Proc Soc Exp Biol Med*. (1953) 84:570–3.
73. Crystal RG. Adenovirus: the first effective *in vivo* gene delivery vector. *Hum Gene Ther*. (2014) 25:3–11. doi: 10.1089/hum.2013.2527

74. Rauschhuber C, Noske N, Ehrhardt A. New insights into stability of recombinant adenovirus vector genomes in mammalian cells. *Eur J Cell Biol*. (2012) 91:2–9. doi: 10.1016/j.ejcb.2011.01.006
75. Nemerow GR, Stewart PL, Reddy VS. Structure of human adenovirus. *Curr Opin Virol*. (2012) 2:115–21. doi: 10.1016/j.coviro.2011.12.008
76. Shayakhmetov DM, Lieber A. Dependence of adenovirus infectivity on length of the fiber shaft domain. *J Virol*. (2000) 74:10274–86.
77. Bai M, Harfe B, Freimuth P. Mutations that alter an Arg-Gly-Asp (RGD) sequence in the adenovirus type 2 penton base protein abolish its cell-rounding activity and delay virus reproduction in flat cells. *J Virol*. (1993) 67:5198–205.
78. Wickham TJ, Segal DM, Roelvink PW, Carrion ME, Lizonova A, Lee GM Kovesdi I. Targeted adenovirus gene transfer to endothelial and smooth muscle cells by using bispecific antibodies. *J Virol*. (1996) 70:6831–8.
79. Sharma P, Martis PC, Excoffon KJ. Adenovirus transduction: More complicated than receptor expression. *Virology*. (2017) 502:144–51. doi: 10.1016/j.virol.2016.12.020
80. Davison AJ, Benko M, Harrach B. Genetic content and evolution of adenoviruses. *J Gen Virol*. (2003) 84:2895–908. doi: 10.1099/vir.0.19497–0
81. Majhen D, Ambriovic-Ristov A. Adenoviral vectors–how to use them in cancer gene therapy? *Virus Res*. (2006) 119:121–33. doi: 10.1016/j.virusres.2006.02.001
82. Liu Q, Muruve DA. Molecular basis of the inflammatory response to adenovirus vectors. *Gene Ther*. (2003) 10:935–40. doi: 10.1038/sj.gt.3302036
83. Amalfitano A, Hauser MA, Hu H, Serra D, Begy CR, Chamberlain JS. Production and characterization of improved adenovirus vectors with the E1, E2b, and E3 genes deleted. *J Virol*. (1998) 72:926–33.
84. Wen S, Schneider DB, Driscoll RM, Vassalli G, Sassani AB, Dichek DA. Second-generation adenoviral vectors do not prevent rapid loss of transgene expression and vector DNA from the arterial wall. *Arterioscler Thromb Vasc Biol*. (2000) 20:1452–8.
85. Sakhuja K, Reddy PS, Ganesh S, Cantaniag F, Pattison S, Limbach P, et al. Optimization of the generation and propagation of gutless adenoviral vectors. *Hum Gene Ther*. (2003) 14:243–54. doi: 10.1089/10430340360535797
86. Alba R, Bosch A, Chillon M. Gutless adenovirus: last-generation adenovirus for gene therapy. *Gene Ther*. (2005) 12 (Suppl. 1):S18–27. doi: 10.1038/sj.gt.3302612
87. Vetrini F, Ng P. Gene therapy with helper-dependent adenoviral vectors: current advances and future perspectives. *Viruses*. (2010) 2:1886–917. doi: 10.3390/v2091886
88. Hausl MA, Zhang W, Muther N, Rauschhuber C, Franck HG, Merricks EP, et al. Hyperactive sleeping beauty transposase enables persistent phenotypic correction in mice and a canine model for hemophilia B. *Mol Ther*. (2010) 18:1896–906. doi: 10.1038/mt.2010.169
89. Hausl M, Zhang W, Voigtlander R, Muther N, Rauschhuber C, Ehrhardt A. Development of adenovirus hybrid vectors for Sleeping Beauty transposition in large mammals. *Curr Gene Ther*. (2011) 11:363–74.
90. Castello R, Borzone R, D'Aria S, Annunziata P, Piccolo P, Brunetti-Pierri N. Helper-dependent adenoviral vectors for liver-directed gene therapy of primary hyperoxaluria type 1. *Gene Ther*. (2016) 23:129–34. doi: 10.1038/gt.2015.107
91. Rosewell Shaw A, Suzuki M. Recent advances in oncolytic adenovirus therapies for cancer. *Curr Opin Virol*. (2016) 21:9–15. doi: 10.1016/j.coviro.2016.06.009
92. Russell SJ, Peng KW, Bell JC. Oncolytic virotherapy. *Nat Biotechnol*. (2012) 30:658–70. doi: 10.1038/nbt.2287
93. Dai B, Roife D, Kang Y, Gumin J, Rios Perez MV, Li X, et al. Preclinical Evaluation of Sequential Combination of Oncolytic Adenovirus Delta-24-RGD and phosphatidylserine-targeting antibody in pancreatic ductal adenocarcinoma. *Mol Cancer Ther*. (2017) 16:662–70. doi: 10.1158/1535–7163.MCT-16–0526
94. Tazawa H, Kuroda S, Hasei J, Kagawa S, Fujiwara T. Impact of autophagy in oncolytic adenoviral therapy for cancer. *Int J Mol Sci*. (2017) 18:E1479. doi: 10.3390/ijms18071479
95. Ji W, Sun B, Su C. Targeting MicroRNAs in cancer gene therapy. *Genes (Basel)*. (2017) 8:E21. doi: 10.3390/genes8010021
96. Shimizu K, Sakurai F, Tomita K, Nagamoto Y, Nakamura S, Katayama K, et al. Suppression of leaky expression of adenovirus genes by insertion of microRNA-targeted sequences in the replication-incompetent adenovirus vector genome. *Mol Ther Methods Clin Dev*. (2014) 1:14035. doi: 10.1038/mtm.2014.35
97. Ledgerwood JE, DeZure AD, Stanley DA, Coates EE, Novik L, Enama ME, et al. Chimpanzee Adenovirus Vector Ebola Vaccine. *N Engl J Med*. (2017) 376:928–38. doi: 10.1056/NEJMoa1410863
98. Capone S, D'Alise AM, Ammendola V, Colloca S, Cortese R, Nicosia A, et al. Development of chimpanzee adenoviruses as vaccine vectors: challenges and successes emerging from clinical trials. *Expert Rev Vaccines*. (2013) 12:379–93. doi: 10.1586/erv.13.15
99. Appaiahgari MB, Vrati S. Adenoviruses as gene/vaccine delivery vectors: promises and pitfalls. *Expert Opin Biol Ther*. (2015) 15:337–51. doi: 10.1517/14712598.2015.993374
100. Barouch DH, Kik SV, Weverling GJ, Dilan R, King SL, Maxfield LF, et al. International seroepidemiology of adenovirus serotypes 5, 26, 35, and 48 in pediatric and adult populations. *Vaccine*. (2011) 29:5203–9. doi: 10.1016/j.vaccine.2011.05.025
101. Wang X, Xing M, Zhang C, Yang Y, Chi Y, Tang X, et al. Neutralizing antibody responses to enterovirus and adenovirus in healthy adults in China. *Emerg Microbes Infect*. (2014) 3:e30. doi: 10.1038/emi.2014.30
102. Fausther-Bovendo H, Kobinger GP. Pre-existing immunity against Ad vectors: humoral, cellular, and innate response, what's important? *Hum Vaccin Immunother*. (2014) 10:2875–84. doi: 10.4161/hv.29594
103. Atkinson RL, Dhurandhar NV, Allison DB, Bowen RL, Israel BA, Albu JB, et al. Human adenovirus-36 is associated with increased body weight and paradoxical reduction of serum lipids. *Int J Obes (Lond)*. (2005) 29:281–6. doi: 10.1038/sj.ijo.0802830
104. Imperiale MJ. Keeping adenovirus away from the liver. *Cell Host Microbe*. (2008) 3:119–20. doi: 10.1016/j.chom.2008.02.007
105. Wilson JM. Lessons learned from the gene therapy trial for ornithine transcarbamylase deficiency. *Mol Genet Metab*. (2009) 96:151–7. doi: 10.1016/j.ymgme.2008.12.016
106. Kalyuzhniy O, Di Paolo NC, Silvestry M, Hofherr SE, Barry MA, Stewart PL, et al. Adenovirus serotype 5 hexon is critical for virus infection of hepatocytes *in vivo*. *Proc Natl Acad Sci USA*. (2008) 105:5483–8. doi: 10.1073/pnas.0711757105
107. Irons EE, Flatt JW, Doronin K, Fox TL, Acchione M, Stewart PL, et al. Coagulation factor binding orientation and dimerization may influence infectivity of adenovirus-coagulation factor complexes. *J Virol*. (2013) 87:9610–9. doi: 10.1128/jvi.01070–13
108. Yoon AR, Hong J, Kim SW, Yun CO. Redirecting adenovirus tropism by genetic, chemical, and mechanical modification of the adenovirus surface for cancer gene therapy. *Expert Opin Drug Deliv*. (2016) 13:843–58. doi: 10.1517/17425247.2016.1158707
109. Brunetti-Pierri N, Ng P. Gene therapy with helper-dependent adenoviral vectors: lessons from studies in large animal models. *Virus Genes*. (2017) 53:684–91. doi: 10.1007/s11262–017-1471-x
110. Abbink P, Lemckert AA, Ewald BA, Lynch DM, Denholtz M, Smits S, et al. Comparative seroprevalence and immunogenicity of six rare serotype recombinant adenovirus vaccine vectors from subgroups B and D. *J Virol*. (2007) 81:4654–63. doi: 10.1128/jvi.02696–06
111. Belousova N, Mikheeva G, Xiong C, Stagg LJ, Gagea M, Fox PS, et al. Native and engineered tropism of vectors derived from a rare species D adenovirus serotype 43. *Oncotarget*. (2016) 7:53414–29. doi: 10.18632/oncotarget.10800
112. Trinh HV, Lesage G, Chennamparampil V, Vollenweider B, Burckhardt CJ, Schauer S, et al. Avidity binding of human adenovirus serotypes 3 and 7 to the membrane cofactor CD46 triggers infection. *J Virol*. (2012) 86:1623–37. doi: 10.1128/jvi.06181–11
113. Tuve S, Wang H, Ware C, Liu Y, Gaggar A, Bernt K, et al. A new group B adenovirus receptor is expressed at high levels on human stem and tumor cells. *J Virol*. (2006) 80:12109–20. doi: 10.1128/jvi.01370–06
114. Parker AL, White KM, Lavery CA, Custers J, Waddington SN, Baker AH. Pseudotyping the adenovirus serotype 5 capsid with both the fibre and penton of serotype 35 enhances vascular smooth muscle cell transduction. *Gene Ther*. (2013) 20:1158–64. doi: 10.1038/gt.2013.44

115. Guo L, Li X, Yang S, Xu Y, Tao R, Wulan H, et al. A highly infectious chimeric adenovirus expressing basic fibroblast growth factor exerts potent targeted therapy for rabbit ear chronic ischemic wounds. *Plast Reconstr Surg*. (2014) 134:248e-56e. doi: 10.1097/prs.0000000000000364
116. Cho YS, Do MH, Kwon SY, Moon C, Kim K, Lee K, et al. Efficacy of CD46-targeting chimeric Ad5/35 adenoviral gene therapy for colorectal cancers. *Oncotarget*. (2016) 7:38210–23. doi: 10.18632/oncotarget.9427
117. Zhang WF, Shao HW, Wu FL, Xie X, Li ZM, Bo HB, et al. Influence of cell physiological state on gene delivery to T lymphocytes by chimeric adenovirus Ad5F35. *Sci Rep*. (2016) 6:22688. doi: 10.1038/srep22688
118. Pesonen S, Kangasniemi L, Hemminki A. Oncolytic adenoviruses for the treatment of human cancer: focus on translational and clinical data. *Mol Pharm*. (2011) 8:12–28. doi: 10.1021/mp100219n
119. Li X, Mao Q, Wang D, Xia H. A novel Ad5/11 chimeric oncolytic adenovirus for improved glioma therapy. *Int J Oncol*. (2012) 41:2159–65. doi: 10.3892/ijo.2012.1674
120. Sykes C, Reisman M. Ebola: working toward treatments and vaccines. *P T*. (2015) 40:521–5.
121. Tapia MD, Sow SO, Lyke KE, Haidara FC, Diallo F, Doumbia M, et al. Use of ChAd3-EBO-Z Ebola virus vaccine in Malian and US adults, and boosting of Malian adults with MVA-BN-Filo: a phase 1, single-blind, randomised trial, a phase 1b, open-label and double-blind, dose-escalation trial, and a nested, randomised, double-blind, placebo-controlled trial. *Lancet Infect Dis*. (2016) 16:31–42. doi: 10.1016/s1473–3099(15)00362-x
122. Yang Y, Xiao F, Lu Z, Li Z, Zuo H, Zhang Q, et al. Development of a novel adenovirus-alphavirus hybrid vector with RNA replicon features for malignant hematopoietic cell transduction. *Cancer Gene Ther*. (2013) 20:429–36. doi: 10.1038/cgt.2013.37
123. Miura Y, Yoshida K, Nishimoto T, Hatanaka K, Ohnami S, Asaka M, et al. Direct selection of targeted adenovirus vectors by random peptide display on the fiber knob. *Gene Ther*. (2007) 14:1448–60. doi: 10.1038/sj.gt.3303007
124. Lupold SE, Kudrolli TA, Chowdhury WH, Wu P, Rodriguez R. A novel method for generating and screening peptides and libraries displayed on adenovirus fiber. *Nucleic Acids Res*. (2007) 35:e138. doi: 10.1093/nar/gkm914
125. Miura Y, Yamasaki S, Davydova J, Brown E, Aoki K, Vickers S, et al. Infectivity-selective oncolytic adenovirus developed by high-throughput screening of adenovirus-formatted library. *Mol Ther*. (2013) 21:139–48. doi: 10.1038/mt.2012.205
126. Nishimoto T, Yamamoto Y, Yoshida K, Goto N, Ohnami S, Aoki K. Development of peritoneal tumor-targeting vector by *in vivo* screening with a random peptide-displaying adenovirus library. *PLoS ONE*. (2012) 7:e45550. doi: 10.1371/journal.pone.0045550
127. Nishimoto T, Yoshida K, Miura Y, Kobayashi A, Hara H, Ohnami S, et al. Oncolytic virus therapy for pancreatic cancer using the adenovirus library displaying random peptides on the fiber knob. *Gene Ther*. (2009) 16:669–80. doi: 10.1038/gt.2009.1
128. Wu P, Kudrolli TA, Chowdhury WH, Liu MM, Rodriguez R, Lupold SE. Adenovirus targeting to prostate-specific membrane antigen through virus-displayed, semirandom peptide library screening. *Cancer Res*. (2010) 70:9549–53. doi: 10.1158/0008–5472.can-10–1760
129. Yamamoto Y, Nagasato M, Rin Y, Henmi M, Ino Y, Yachida S, et al. Strong antitumor efficacy of a pancreatic tumor-targeting oncolytic adenovirus for neuroendocrine tumors. *Cancer Med*. (2017) 6:2385–97. doi: 10.1002/cam4.1185
130. Atchison RW, Casto BC, Hammon WM. Adenovirus-associated defective virus particles. *Science*. (1965) 149:754–6.
131. Hoggan MD, Blacklow NR, Rowe WP. Studies of small DNA viruses found in various adenovirus preparations: physical, biological, and immunological characteristics. *Proc Natl Acad Sci USA*. (1966) 55:1467–74.
132. Laughlin CA, Westphal H, Carter BJ. Spliced adenovirus-associated virus RNA. *Proc Natl Acad Sci USA*. (1979) 76:5567–71.
133. Marcus CJ, Laughlin CA, Carter BJ. Adeno-associated virus RNA transcription *in vivo*. *Eur J Biochem*. (1981) 121:147–54.
134. Grieger JC, Samulski RJ. Adeno-associated virus vectorology, manufacturing, and clinical applications. *Methods Enzymol*. (2012) 507:229–54. doi: 10.1016/B978–0-12–386509-0.00012–0
135. Sonntag F, Schmidt K, Kleinschmidt JA. A viral assembly factor promotes AAV2 capsid formation in the nucleolus. *Proc Natl Acad Sci USA*. (2010) 107:10220–5. doi: 10.1073/pnas.1001673107
136. Jay FT, Laughlin CA, Carter BJ. Eukaryotic translational control: adeno-associated virus protein synthesis is affected by a mutation in the adenovirus DNA-binding protein. *Proc Natl Acad Sci USA*. (1981) 78:2927–31.
137. Carter BJ. Adeno-associated virus and the development of adeno-associated virus vectors: a historical perspective. *Mol Ther*. (2004) 10:981–9. doi: 10.1016/j.ymthe.2004.09.011
138. Vandenberghe LH, Breous E, Nam HJ, Gao G, Xiao R, Sandhu A, et al. Naturally occurring singleton residues in AAV capsid impact vector performance and illustrate structural constraints. *Gene Ther*. (2009) 16:1416–28. doi: 10.1038/gt.2009.101
139. McCarty DM, Monahan PE, Samulski RJ. Self-complementary recombinant adeno-associated virus (scAAV) vectors promote efficient transduction independently of DNA synthesis. *Gene Ther*. (2001) 8:1248–54. doi: 10.1038/sj.gt.3301514
140. McCarty DM, Fu H, Monahan PE, Toulson CE, Naik P, Samulski RJ. Adeno-associated virus terminal repeat (TR) mutant generates self-complementary vectors to overcome the rate-limiting step to transduction *in vivo*. *Gene Ther*. (2003) 10:2112–8. doi: 10.1038/sj.gt.3302134
141. Buchlis G, Podsakoff GM, Radu A, Hawk SM, Flake AW, Mingozzi F, et al. Factor IX expression in skeletal muscle of a severe hemophilia B patient 10 years after AAV-mediated gene transfer. *Blood*. (2012) 119:3038–41. doi: 10.1182/blood-2011–09-382317
142. Kotin RM, Siniscalco M, Samulski RJ, Zhu XD, Hunter L, Laughlin CA, et al. Site-specific integration by adeno-associated virus. *Proc Natl Acad Sci USA*. (1990) 87:2211–5.
143. Samulski RJ, Zhu X, Xiao X, Brook JD, Housman DE, Epstein N, et al. Targeted integration of adeno-associated virus (AAV) into human chromosome 19. *Embo J*. (1991) 10:3941–50.
144. Pillay S, Meyer NL, Puschnik AS, Davulcu O, Diep J, Ishikawa Y, et al. An essential receptor for adeno-associated virus infection. *Nature*. (2016) 530:108–12. doi: 10.1038/nature16465
145. Gao G, Vandenberghe LH, Alvira MR, Lu Y, Calcedo R, Zhou X, et al. Clades of Adeno-associated viruses are widely disseminated in human tissues. *J Virol*. (2004) 78:6381–8. doi: 10.1128/jvi.78.12.6381–6388.2004
146. Weitzman MD, Linden RM. Adeno-associated virus biology. *Methods Mol Biol*. (2011) 807:1–23. doi: 10.1007/978–1-61779–370-7_1
147. Zincarelli C, Soltys S, Rengo G, Rabinowitz JE. Analysis of AAV serotypes 1–9 mediated gene expression and tropism in mice after systemic injection. *Mol Ther*. (2008) 16:1073–80. doi: 10.1038/mt.2008.76
148. Strobel B, Duechs MJ, Schmid R, Stierstorfer BE, Bucher H, Quast K, et al. Modeling pulmonary disease pathways using recombinant adeno-associated virus 6.2. *Am J Respir Cell Mol Biol*. (2015) 53:291–302. doi: 10.1165/rcmb.2014–0338MA
149. Luo H, Chen Y, Ye Z, Sun X, Shi Y, Luo Q, et al. Evaluation of the Association Between Common Genetic Variants Near the ABCA1 Gene and Primary Angle Closure Glaucoma in a Han Chinese Population. *Invest Ophthalmol Vis Sci*. (2015) 56:6248–54. doi: 10.1167/iovs.15–16741
150. Nathwani AC, Nienhuis AW, Davidoff AM. Our journey to successful gene therapy for hemophilia B. *Hum Gene Ther*. (2014) 25:923–6. doi: 10.1089/hum.2014.2540
151. Smith LJ, Ul-Hasan T, Carvaines SK, Van Vliet K, Yang E, Wong KK Jr, et al. Gene transfer properties and structural modeling of human stem cell-derived AAV. *Mol Ther*. (2014) 22:1625–34. doi: 10.1038/mt.2014.107
152. Murphy SL, Li H, Zhou S, Schlachterman A, High KA. Prolonged susceptibility to antibody-mediated neutralization for adeno-associated vectors targeted to the liver. *Mol Ther*. (2008) 16:138–45. doi: 10.1038/sj.mt.6300334
153. Zinn E, Pacouret S, Khaychuk V, Turunen HT, Carvalho LS, Andres-Mateos E, et al. *In silico* reconstruction of the viral evolutionary lineage yields a potent gene therapy vector. *Cell Rep*. (2015) 12:1056–68. doi: 10.1016/j.celrep.2015.07.019
154. Bowles DE, McPhee SW, Li C, Gray SJ, Samulski JJ, Camp AS, et al. Phase 1 gene therapy for Duchenne muscular dystrophy using

a translational optimized AAV vector. *Mol Ther*. (2012) 20:443–55. doi: 10.1038/mt.2011.237
155. Worgall S, Sondhi D, Hackett NR, Kosofsky B, Kekatpure MV, Neyzi N, et al. Treatment of late infantile neuronal ceroid lipofuscinosis by CNS administration of a serotype 2 adeno-associated virus expressing CLN2 cDNA. *Hum Gene Ther*. (2008) 19:463–74. doi: 10.1089/hum.2008.022
156. Mays LE, Vandenberghe LH, Xiao R, Bell P, Nam HJ, Agbandje-McKenna M, et al. Adeno-associated virus capsid structure drives CD4-dependent CD8+ T cell response to vector encoded proteins. *J Immunol*. (2009) 182:6051–60. doi: 10.4049/jimmunol.0803965
157. Lin SW, Hensley SE, Tatsis N, Lasaro MO, Ertl HC. Recombinant adeno-associated virus vectors induce functionally impaired transgene product-specific CD8+ T cells in mice. *J Clin Invest*. (2007) 117:3958–70. doi: 10.1172/jci33138
158. Faust SM, Bell P, Cutler BJ, Ashley SN, Zhu Y, Rabinowitz JE, et al. CpG-depleted adeno-associated virus vectors evade immune detection. *J Clin Invest*. (2013) 123:2994–3001. doi: 10.1172/jci68205
159. Deverman BE, Pravdo PL, Simpson BP, Kumar SR, Chan KY, Banerjee A, et al. Cre-dependent selection yields AAV variants for widespread gene transfer to the adult brain. *Nat Biotechnol*. (2016) 34:204–9. doi: 10.1038/nbt.3440
160. Choudhury SR, Fitzpatrick Z, Harris AF, Maitland SA, Ferreira JS, Zhang Y, et al. *In vivo* selection yields AAV-B1 capsid for central nervous system and muscle gene therapy. *Mol Ther*. (2016) 24:1247–57. doi: 10.1038/mt.2016.84
161. Ran FA, Cong L, Yan WX, Scott DA, Gootenberg JS, Kriz AJ, et al. *in vivo* genome editing using Staphylococcus aureus Cas9. *Nature*. (2015) 520:186–91. doi: 10.1038/nature14299
162. Lin C, Li H, Hao M, Xiong D, Luo Y, Huang C, et al. Increasing the efficiency of CRISPR/Cas9-mediated precise genome editing of HSV-1 virus in human cells. *Sci Rep*. (2016) 6:34531. doi: 10.1038/srep34531
163. Marconi P, Fraefel C, Epstein AL. Herpes simplex virus type 1 (HSV-1)-derived recombinant vectors for gene transfer and gene therapy. *Methods Mol Biol*. (2015) 1254:269–93. doi: 10.1007/978–1-4939–2152-2_20
164. Goins WF, Huang S, Cohen JB, Glorioso JC. Engineering HSV-1 vectors for gene therapy. *Methods Mol Biol*. (2014) 1144:63–79. doi: 10.1007/978–1-4939–0428-0_5
165. Krisky DM, Wolfe D, Goins WF, Marconi PC, Ramakrishnan R, Mata M, et al. Deletion of multiple immediate-early genes from herpes simplex virus reduces cytotoxicity and permits long-term gene expression in neurons. *Gene Ther*. (1998) 5:1593–603. doi: 10.1038/sj.gt.3300766
166. Wolfe D, Mata M, Fink DJ. A human trial of HSV-mediated gene transfer for the treatment of chronic pain. *Gene Ther*. (2009) 16:455–60. doi: 10.1038/gt.2009.17
167. Goss JR, Cascio M, Goins WF, Huang S, Krisky DM, Clarke RJ, et al. HSV delivery of a ligand-regulated endogenous ion channel gene to sensory neurons results in pain control following channel activation. *Mol Ther*. (2011) 19:500–6. doi: 10.1038/mt.2010.246
168. Artusi S, Miyagawa Y, Goins WF, Cohen JB, Glorioso JC. Herpes simplex virus vectors for gene transfer to the central nervous system. *Diseases*. (2018) 6:E74. doi: 10.3390/diseases6030074
169. Advani SJ, Weichselbaum RR, Whitley RJ, Roizman B. Friendly fire: redirecting herpes simplex virus-1 for therapeutic applications. *Clin Microbiol Infect*. (2002) 8:551–63. doi: 10.1046/j.1469-0691.2002.00432.x
170. Argnani R, Lufino M, Manservigi M, Manservigi R. Replication-competent herpes simplex vectors: design and applications. *Gene Ther*. (2005) 12 (Suppl.1):S170–7. doi: 10.1038/sj.gt.3302622
171. Maetzig T, Galla M, Baum C, Schambach A. Gammaretroviral vectors: biology, technology and application. *Viruses*. (2011) 3:677–713. doi: 10.3390/v3060677
172. Hayward A. Origin of the retroviruses: when, where, and how? *Curr Opin Virol*. (2017) 25:23–7. doi: 10.1016/j.coviro.2017.06.006
173. Kassiotis G, Stoye JP. Making a virtue of necessity: the pleiotropic role of human endogenous retroviruses in cancer. *Philos Trans R Soc Lond B Biol Sci*. (2017) 372:20160277. doi: 10.1098/rstb.2016.0277
174. Meyer TJ, Rosenkrantz JL, Carbone L, Chavez SL. Endogenous retroviruses: with us and against Us. *Front Chem*. (2017) 5:23. doi: 10.3389/fchem.2017.00023
175. Buzdin AA, Prassolov V, Garazha AV. Friends-enemies: endogenous retroviruses are major transcriptional regulators of human DNA. *Front Chem*. (2017) 5:35. doi: 10.3389/fchem.2017.00035
176. Schambach A, Swaney WP, van der Loo JC. Design and production of retro- and lentiviral vectors for gene expression in hematopoietic cells. *Methods Mol Biol*. (2009) 506:191–205. doi: 10.1007/978–1-59745–409-4_14
177. Betapudi V, Shukla M, Alluri R, Merkulov S, McCrae KR. Novel role for p56/Lck in regulation of endothelial cell survival and angiogenesis. *Faseb J*. (2016) 30:3515–26. doi: 10.1096/fj.201500040
178. Shukla M, Betapudi V, Alluri RK, Merkulov S, Hale J, Lathia J, et al. Regulation of the tumor microenvironment by high molecular weight kininogen. *Blood*. (2016) 128:1394
179. Hacein-Bey-Abina S, Garrigue A, Wang GP, Soulier J, Lim A, Morillon E, et al. Insertional oncogenesis in 4 patients after retrovirus-mediated gene therapy of SCID-X1. *J Clin Invest*. (2008) 118:3132–42. doi: 10.1172/jci35700
180. Knopp Y, Geis FK, Heckl D, Horn S, Neumann T, Kuehle J, et al. Transient retrovirus-based CRISPR/Cas9 all-in-one particles for efficient, targeted gene knockout. *Mol Ther Nucleic Acids*. (2018) 13:256–74. doi: 10.1016/j.omtn.2018.09.006
181. Xu X, Tan X, Tampe B, Wilhelmi T, Hulshoff MS, Saito S, et al. High-fidelity CRISPR/Cas9- based gene-specific hydroxymethylation rescues gene expression and attenuates renal fibrosis. *Nat Commun*. (2018) 9:3509. doi: 10.1038/s41467–018-05766–5
182. Pearson S, Jia H, Kandachi K. China approves first gene therapy. *Nat Biotechnol*. (2004) 22:3–4. doi: 10.1038/nbt0104–3
183. Garber K. China approves world's first oncolytic virus therapy for cancer treatment. *J Natl Cancer Inst*. (2006) 98:298–300. doi: 10.1093/jnci/djj111
184. Kim S, Federman N, Gordon EM, Hall FL, Chawla SP. Rexin-G((R)), a tumor-targeted retrovector for malignant peripheral nerve sheath tumor: a case report. *Mol Clin Oncol*. (2017) 6:861–5. doi: 10.3892/mco.2017.1231
185. Kuo CY, Kohn DB. Gene therapy for the treatment of primary immune deficiencies. *Curr Allergy Asthma Rep*. (2016) 16:39. doi: 10.1007/s11882–016-0615–8
186. Ruella M, Kenderian SS. Next-generation chimeric antigen receptor t-cell therapy: going off the shelf. *BioDrugs*. (2017) 31:473–81. doi: 10.1007/s40259–017-0247–0
187. Sengillo JD, Justus S, Cabral T, Tsang SH. Correction of monogenic and common retinal disorders with gene therapy. *Genes (Basel)*. (2017) 8:E53. doi: 10.3390/genes8020053
188. MacLaren RE, Groppe M, Barnard AR, Cottriall CL, Tolmachova T, Seymour L, et al. Retinal gene therapy in patients with choroideremia: initial findings from a phase 1/2 clinical trial. *Lancet*. (2014) 383:1129–37. doi: 10.1016/S0140–6736(13)62117–0
189. Breitbach CJ, Lichty BD, Bell JC. Oncolytic viruses: therapeutics with an identity crisis. *EBioMedicine*. (2016) 9:31–6. doi: 10.1016/j.ebiom.2016.06.046
190. Fukuhara H, Ino Y, Todo T. Oncolytic virus therapy: A new era of cancer treatment at dawn. *Cancer Sci*. (2016) 107:1373–9. doi: 10.1111/cas.13027
191. Kirn D. Clinical research results with dl1520 (Onyx-015), a replication-selective adenovirus for the treatment of cancer: what have we learned? *Gene Ther*. (2001) 8:89–98. doi: 10.1038/sj.gt.3301377
192. Saydaminova K, Ye X, Wang H, Richter M, Ho M, Chen H, et al. Efficient genome editing in hematopoietic stem cells with helper-dependent Ad5/35 vectors expressing site-specific endonucleases under microRNA regulation. *Mol Ther Methods Clin Dev*. (2015) 1:14057. doi: 10.1038/mtm.2014.57
193. Lowenstein PR, Castro MG. Evolutionary basis of a new gene- and immune-therapeutic approach for the treatment of malignant brain tumors: from mice to clinical trials for glioma patients. *Clin Immunol*. (2018) 189:43–51. doi: 10.1016/j.clim.2017.07.006
194. Tejada S, Diez-Valle R, Dominguez PD, Patino-Garcia A, Gonzalez-Huarriz M, Fueyo J, et al. DNX-2401, an oncolytic virus, for the treatment of newly diagnosed diffuse intrinsic pontine gliomas: a case report. *Front Oncol*. (2018) 8:61. doi: 10.3389/fonc.2018.00061
195. Stepanenko AA, Chekhonin VP. Recent advances in oncolytic virotherapy and immunotherapy for glioblastoma: a glimmer of hope in the search for an effective therapy? *Cancers (Basel)*. (2018) 10 E492. doi: 10.3390/cancers10120492

196. Machiels JP, Salazar R, Rottey S, Duran I, Dirix L, Geboes K, et al. A phase 1 dose escalation study of the oncolytic adenovirus enadenotucirev, administered intravenously to patients with epithelial solid tumors (EVOLVE). *J Immunother Cancer*. (2019) 7:20. doi: 10.1186/s40425–019-0510–7
197. Kallel H, Kamen AA. Large-scale adenovirus and poxvirus-vectored vaccine manufacturing to enable clinical trials. *Biotechnol J*. (2015) 10:741–7. doi: 10.1002/biot.201400390
198. Edwards TL, Jolly JK, Groppe M, Barnard AR, Cottriall CL, Tolmachova T, et al. Visual Acuity after Retinal Gene Therapy for Choroideremia. *N Engl J Med*. (2016) 374:1996–8. doi: 10.1056/NEJMc1509501
199. Feuer WJ, Schiffman JC, Davis JL, Porciatti V, Gonzalez P, Koilkonda RD, et al. Gene therapy for leber hereditary optic neuropathy: initial results. *Ophthalmology*. (2016) 123:558–70. doi: 10.1016/j.ophtha.2015.10.025
200. Hocquemiller M, Giersch L, Audrain M, Parker S, Cartier N. Adeno-associated virus-based gene therapy for CNS diseases. *Hum Gene Ther*. (2016) 27:478–96. doi: 10.1089/hum.2016.087
201. Mahendra G, Kumar S, Isayeva T, Mahasreshti PJ, Curiel DT, Stockardt CR, et al. Antiangiogenic cancer gene therapy by adeno-associated virus 2-mediated stable expression of the soluble FMS-like tyrosine kinase-1 receptor. *Cancer Gene Ther*. (2005) 12:26–34. doi: 10.1038/sj.cgt.7700754
202. Li ZB, Chen YX, Zhao JY, Lu J. Effects of pharmacological concentrations of estrogens on growth of 3AO human ovarian cancer cells. *Yi Chuan Xue Bao*. (2006) 33:782–92. doi: 10.1016/s0379–4172(06)60111-x
203. Ma H, Liu Y, Liu S, Kung HF, Sun X, Zheng D, et al. Recombinant adeno-associated virus-mediated TRAIL gene therapy suppresses liver metastatic tumors. *Int J Cancer*. (2005) 116:314–21. doi: 10.1002/ijc.20982
204. Tu SP, Cui JT, Liston P, Huajiang X, Xu R, Lin MC, et al. Gene therapy for colon cancer by adeno-associated viral vector-mediated transfer of survivin Cys84Ala mutant. *Gastroenterology*. (2005) 128:361–75.
205. Wu S, Meng L, Wang S, Wang W, Xi L, Tian X, et al. Reversal of the malignant phenotype of cervical cancer CaSki cells through adeno-associated virus-mediated delivery of HPV16 E7 antisense RNA. *Clin Cancer Res*. (2006) 12:2032–7. doi: 10.1158/1078–0432.ccr-05–2567
206. Ho DT, Wykoff-Clary S, Gross CS, Schneider D, Jin F, Kretschmer PJ, et al. Growth inhibition of an established A431 xenograft tumor by a full-length anti-EGFR antibody following gene delivery by AAV. *Cancer Gene Ther*. (2009) 16:184–94. doi: 10.1038/cgt.2008.68
207. Nathwani AC, Reiss UM, Tuddenham EG, Rosales C, Chowdary P, McIntosh J, et al. Long-term safety and efficacy of factor IX gene therapy in hemophilia B. *N Engl J Med*. (2014) 371:1994–2004. doi: 10.1056/NEJMoa1407309
208. Mingozzi F, Maus MV, Hui DJ, Sabatino DE, Murphy SL, Rasko JE, et al. CD8(+) T-cell responses to adeno-associated virus capsid in humans. *Nat Med*. (2007) 13:419–22. doi: 10.1038/nm1549
209. Ertl HCJ, High KA. Impact of AAV capsid-specific T-cell responses on design and outcome of clinical gene transfer trials with recombinant adeno-associated viral vectors: an evolving controversy. *Hum Gene Ther*. (2017) 28:328–37. doi: 10.1089/hum.2016.172
210. Calcedo R, Vandenberghe LH, Gao G, Lin J, Wilson JM. Worldwide epidemiology of neutralizing antibodies to adeno-associated viruses. *J Infect Dis*. (2009) 199:381–90. doi: 10.1086/595830
211. Boutin S, Monteilhet V, Veron P, Leborgne C, Benveniste O, Montus MF, et al. Prevalence of serum IgG and neutralizing factors against adeno-associated virus (AAV) types 1, 2, 5, 6, 8, and 9 in the healthy population: implications for gene therapy using AAV vectors. *Hum Gene Ther*. (2010) 21:704–12. doi: 10.1089/hum.2009.182
212. Vandenberghe LH, Wang L, Somanathan S, Zhi Y, Figueredo J, Calcedo R, et al. Heparin binding directs activation of T cells against adeno-associated virus serotype 2 capsid. *Nat Med*. (2006) 12:967–71. doi: 10.1038/nm1445
213. Mingozzi F, Anguela XM, Pavani G, Chen Y, Davidson RJ, Hui DJ, et al. Overcoming preexisting humoral immunity to AAV using capsid decoys. *Sci Transl Med*. (2013) 5:194ra92. doi: 10.1126/scitranslmed.3005795
214. Zhong L, Li B, Jayandharan G, Mah CS, Govindasamy L, Agbandje-McKenna M, et al. Tyrosine-phosphorylation of AAV2 vectors and its consequences on viral intracellular trafficking and transgene expression. *Virology*. (2008) 381:194–202. doi: 10.1016/j.virol.2008.08.027
215. McPhee SW, Janson CG, Li C, Samulski RJ, Camp AS, Francis J, et al. Immune responses to AAV in a phase I study for Canavan disease. *J Gene Med*. (2006) 8:577–88. doi: 10.1002/jgm.885
216. Davidson BL, Stein CS, Heth JA, Martins I, Kotin RM, Derksen TA, et al. Recombinant adeno-associated virus type 2, 4, and 5 vectors: transduction of variant cell types and regions in the mammalian central nervous system. *Proc Natl Acad Sci USA*. (2000) 97:3428–32. doi: 10.1073/pnas.050581197
217. Eberling JL, Jagust WJ, Christine CW, Starr P, Larson P, Bankiewicz KS, et al. Results from a phase I safety trial of hAADC gene therapy for Parkinson disease. *Neurology*. (2008) 70:1980–3. doi: 10.1212/01.wnl.0000312381.29287.ff
218. LeWitt PA, Rezai AR, Leehey MA, Ojemann SG, Flaherty AW, Eskandar EN, et al. AAV2-GAD gene therapy for advanced Parkinson's disease: a double-blind, sham-surgery controlled, randomised trial. *Lancet Neurol*. (2011) 10:309–19. doi: 10.1016/s1474–4422(11)70039–4
219. Daar AS, Fuggle SV, Fabre JW, Ting A, Morris PJ. The detailed distribution of HLA-A, B, C antigens in normal human organs. *Transplantation*. (1984) 38:287–92.
220. Nathwani AC, Tuddenham EG, Rangarajan S, Rosales C, McIntosh J, Linch DC, et al. Adenovirus-associated virus vector-mediated gene transfer in hemophilia B. *N Engl J Med*. (2011) 365:2357–65. doi: 10.1056/NEJMoa1108046
221. Ferreira V, Twisk J, Kwikkers K, Aronica E, Brisson D, Methot J, et al. Immune responses to intramuscular administration of alipogene tiparvovec (AAV1-LPL(S447X)) in a phase II clinical trial of lipoprotein lipase deficiency gene therapy. *Hum Gene Ther*. (2014) 25:180–8. doi: 10.1089/hum.2013.169
222. Zolotukhin S, Byrne BJ, Mason E, Zolotukhin I, Potter M, Chesnut K, et al. Recombinant adeno-associated virus purification using novel methods improves infectious titer and yield. *Gene Ther*. (1999) 6:973–85. doi: 10.1038/sj.gt.3300938
223. Grieger JC, Choi VW, Samulski RJ. Production and characterization of adeno-associated viral vectors. *Nat Protoc*. (2006) 1:1412–28. doi: 10.1038/nprot.2006.207
224. Grieger JC, Soltys SM, Samulski RJ. Production of recombinant adeno-associated virus vectors using suspension HEK293 cells and continuous harvest of vector from the culture media for GMP FIX and FLT1 clinical vector. *Mol Ther*. (2016) 24:287–97. doi: 10.1038/mt.2015.187
225. Adamson-Small L, Potter M, Byrne BJ, Clement N. Sodium chloride enhances recombinant adeno-associated virus production in a serum-free suspension manufacturing platform using the herpes simplex virus system. *Hum Gene Ther Methods*. (2017) 28:1–14. doi: 10.1089/hgtb.2016.151
226. Smith RH, Levy JR, Kotin RM. A simplified baculovirus-AAV expression vector system coupled with one-step affinity purification yields high-titer rAAV stocks from insect cells. *Mol Ther*. (2009) 17:1888–96. doi: 10.1038/mt.2009.128
227. Dutheil N, Smith SC, Agundez L, Vincent-Mistiaen ZI, Escalante CR, Linden RM, et al. Adeno-associated virus Rep represses the human integration site promoter by two pathways that are similar to those required for the regulation of the viral p5 promoter. *J Virol*. (2014) 88:8227–41. doi: 10.1128/jvi.00412–14
228. Kalimuthu S, Oh JM, Gangadaran P, Zhu L, Lee HW, Jeon YH, et al. Genetically engineered suicide gene in mesenchymal stem cells using a Tet-On system for anaplastic thyroid cancer. *PLoS ONE*. (2017) 12:e0181318. doi: 10.1371/journal.pone.0181318
229. Li JM, Kao KC, Li LF, Yang TM, Wu CP, Horng YM, et al. MicroRNA-145 regulates oncolytic herpes simplex virus-1 for selective killing of human non-small cell lung cancer cells. *Virol J*. (2013) 10:241. doi: 10.1186/1743–422x-10–241
230. Norgren RB Jr. Lehman MN. Herpes simplex virus as a transneuronal tracer. *Neurosci Biobehav Rev*. (1998) 22:695–708.
231. Majima T, Funahashi Y, Takai S, Goins WF, Gotoh M, Tyagi P, et al. Herpes simplex virus vector-mediated gene delivery of poreless TRPV1 channels reduces bladder overactivity and nociception in rats. *Hum Gene Ther*. (2015) 26:734–42. doi: 10.1089/hum.2015.026

232. Campadelli-Fiume G, Petrovic B, Leoni V, Gianni T, Avitabile E, Casiraghi C, et al. Retargeting strategies for oncolytic herpes simplex viruses. *Viruses*. (2016) 8:63. doi: 10.3390/v8030063
233. Lou W, Ji F, Fu J, Han Z, Di W, Zhang N. Transcriptional retargeting of herpes simplex virus for cell-specific replication to control cancer. *J Cancer Res Clin Oncol*. (2018) 144:2107. doi: 10.1007/s00432–017-2566–4
234. Uchida H, Hamada H, Nakano K, Kwon H, Tahara H, Cohen JB, et al. Oncolytic herpes simplex virus vectors fully retargeted to tumor-associated antigens. *Curr Cancer Drug Targets*. (2018) 18:162–70. doi: 10.2174/1568009617666170206105855
235. Wolfe D, Craft AM, Cohen JB, Glorioso JC. A herpes simplex virus vector system for expression of complex cellular cDNA libraries. *J Virol*. (2010) 84:7360–8. doi: 10.1128/jvi.02388–09
236. Hoban MD, Orkin SH, Bauer DE. Genetic treatment of a molecular disorder: gene therapy approaches to sickle cell disease. *Blood*. (2016) 127:839–48. doi: 10.1182/blood-2015–09-618587
237. De Ravin SS, Wu X, Moir S, Anaya-O'Brien S, Kwatemaa N, Littel P, et al. Lentiviral hematopoietic stem cell gene therapy for X-linked severe combined immunodeficiency. *Sci Transl Med*. (2016) 8:335ra57. doi: 10.1126/scitranslmed.aad8856
238. Counsell JR, Asgarian Z, Meng J, Ferrer V, Vink CA, Howe SJ, et al. Lentiviral vectors can be used for full-length dystrophin gene therapy. *Sci Rep*. (2017) 7:44775. doi: 10.1038/srep44775
239. Brown BD, Venneri MA, Zingale A, Sergi Sergi L, Naldini L. Endogenous microRNA regulation suppresses transgene expression in hematopoietic lineages and enables stable gene transfer. *Nat Med*. (2006) 12:585–91. doi: 10.1038/nm1398
240. Schambach A, Bohne J, Baum C, Hermann FG, Egerer L, von Laer D, et al. Woodchuck hepatitis virus post-transcriptional regulatory element deleted from X protein and promoter sequences enhances retroviral vector titer and expression. *Gene Ther*. (2006) 13:641–5. doi: 10.1038/sj.gt.3302698
241. Schott JW, Morgan M, Galla M, Schambach A. Viral and Synthetic RNA vector technologies and applications. *Mol Ther*. (2016) 24:1513–27. doi: 10.1038/mt.2016.143
242. Breitbart M, Rohwer F. Here a virus, there a virus, everywhere the same virus? *Trends Microbiol*. (2005) 13:278–84. doi: 10.1016/j.tim.2005.04.003
243. Carding SR, Davis N, Hoyles L. Review article: the human intestinal virome in health and disease. *Aliment Pharmacol Ther*. (2017) 46:800–15. doi: 10.1111/apt.14280
244. Chattopadhyay S, Sen GC. Tyrosine phosphorylation in Toll-like receptor signaling. *Cytokine Growth Factor Rev*. (2014) 25:533–41. doi: 10.1016/j.cytogfr.2014.06.002
245. Chattopadhyay S, Sen GC. RIG-I-like receptor-induced IRF3 mediated pathway of apoptosis (RIPA): a new antiviral pathway. *Protein Cell*. (2017) 8:165–8. doi: 10.1007/s13238–016-0334-x
246. Chattopadhyay S, Sen GC. dsRNA-activation of TLR3 and RLR signaling: gene induction-dependent and independent effects. *J Interferon Cytokine Res*. (2014) 34:427–36. doi: 10.1089/jir.2014.0034
247. Fensterl V, Chattopadhyay S, Sen GC. No love lost between viruses and interferons. *Annu Rev Virol*. (2015) 2:549–72. doi: 10.1146/annurev-virology-100114–055249
248. Subramanian G, Kuzmanovic T, Zhang Y, Peter CB, Veleeparambil M, Chakravarti R, et al. A new mechanism of interferon's antiviral action: Induction of autophagy, essential for paramyxovirus replication, is inhibited by the interferon stimulated gene, TDRD7. *PLoS Pathog*. (2018) 14:e1006877. doi: 10.1371/journal.ppat.1006877
249. Stolberg SG. The biotech death of Jesse Gelsinger. *N Y Times Mag*. (1999):136–40, 49–50.
250. Rodriguez-Gascon A, Del Pozo-Rodriguez A, Isla A, Solinis MA. Vaginal gene therapy. *Adv Drug Deliv Rev*. (2015) 92:71–83. doi: 10.1016/j.addr.2015.07.002
251. Suwanmanee T, Ferris MT, Hu P, Gui T, Montgomery SA, Pardo-Manuel de Villena F, et al. Toward Personalized Gene Therapy: Characterizing the Host Genetic Control of Lentiviral-vector-mediated hepatic gene delivery. *Mol Ther Methods Clin Dev*. (2017) 5:83–92. doi: 10.1016/j.omtm.2017.03.009

Disclaimer: The views expressed in this review article are those of the author(s) and do not reflect the official policy of the Department of Army, Department of Defense, or the U.S. Government.

Conflict of Interest Statement: The authors declare that that they have no affiliations with or involvement in any organization or entity with any financial interest (such as honoraria; educational grants; participation in speakers' bureaus; membership, employment, consultancies, stock ownership, or other equity interest; and expert testimony or patent-licensing arrangements), or non-financial interest (such as personal or professional relationships, affiliations, knowledge or beliefs) in the subject matter or materials discussed in this manuscript.

frontiers in Pharmacology

REVIEW
published: 24 April 2019
doi: 10.3389/fphar.2019.00373

The Analysis of Key Factors Related to ADCs Structural Design

Haichao Tang[1,2], Yan Liu[3], Zhaojin Yu[1,2], Mingli Sun[1,2], Lu Lin[1,2], Wensi Liu[1,2], Qiang Han[1,2], Minjie Wei[1,2] and Ying Jin[3]**

[1] Department of Pharmacology, School of Pharmacy, China Medical University, Shenyang, China, [2] Liaoning Engineering Technology Research Center for the Research, Development and Industrialization of Innovative Peptide Drugs, China Medical University, Shenyang, China, [3] Liaoning Research Institute of Family Planning, Shenyang, China

Antibody–drug conjugates (ADCs) have developed rapidly in recent decades. However, it is complicated to map out a perfect ADC that requires optimization of multiple parameters including antigens, antibodies, linkers, payloads, and the payload-linker linkage. The therapeutic targets of the ADCs are expected to express only on the surface of the corresponding target tumor cells. On the contrary, many antigens usually express on normal tissues to some extent, which could disturb the specificity of ADCs and limit their clinical application, not to mention the antibody is also difficult to choose. It requires to not only target and have affinity with the corresponding antigen, but it also needs to have a linkage site with the linker to load the payloads. In addition, the linker and payload are indispensable in the efficacy of ADCs. The linker is required to stabilize the ADC in the circulatory system and is brittle to release free payload while the antibody combines with antigen. Also, it is a premise that the dose of ADCs will not kill normal tissues and the released payloads are able to fulfill the killing potency in tumor cells at the same time. In this review, we mainly focus on the latest development of key factors affecting ADCs progress, including the selection of antibodies and antigens, the optimization of payload, the modification of linker, payload-linker linkage, and some other relevant parameters of ADCs.

Keywords: antibody–drug conjugates, precision choice antibody and antigen, elaborate modification linkers, proper payloads, optimized linker-payload linkage

OPEN ACCESS

Edited by:
Zhe-Sheng Chen,
St. John's University, United States

Reviewed by:
Xiaolan Deng,
Beckman Research Institute of City of Hope, United States
Liwu Fu,
Sun Yat-sen University, China
Zhaoqian Liu,
Xiangya Hospital, Central South University, China

****Correspondence:***
Minjie Wei
weiminjiecmu@163.com
Ying Jin
13998830123@139.com

Specialty section:
This article was submitted to Cancer Molecular Targets and Therapeutics, a section of the journal Frontiers in Pharmacology

Received: *17 January 2019*
Accepted: *26 March 2019*
Published: *24 April 2019*

Citation:
Tang H, Liu Y, Yu Z, Sun M, Lin L, Liu W, Han Q, Wei M and Jin Y (2019) The Analysis of Key Factors Related to ADCs Structural Design. Front. Pharmacol. 10:373. doi: 10.3389/fphar.2019.00373

INTRODUCTION

In traditional tumor treatment, chemotherapy is one of the main treatment strategies. However, the toxicity from non-specific accumulation in normal tissues, narrow therapeutic window and low tolerance all limit chemotherapy drug development in the tumor treatment process (Atkins and Gershell, 2002; Alley et al., 2010; Ashley et al., 2011). In recent decades, scientists have gained an in-depth understanding of cancer biology, taking advantage of some unique features

Abbreviations: ADCs, antibody–drug conjugates; ALCL, anaplastic large cell lymphoma; AML, acute myeloid leukemia; DAR, drug-to-antibody ratio; MDR, multiple drug resistance; MMAE, monomethyl auristatin E; PDBs, pyrrolobenzodiazepine dimers; PEG, polyethylene glycol; PHF, hydroxymethyl-formal; SMCC, succinimidyl-4-(*N*-maleimidomethyl)-cyclohexane-1-carboxylate; SMCC-DM1, succinimidyl 4-(*N*-maleimidomethyl) cyclohexane-1-carboxylate-maytansinoid; sulfo-SPDB-DM4, *N*-succinimidyl-4-(2-pyridyldithio)-2-sulfo butanoate-maytansinoid; val-cit-PABC-MMAF, valine-citrulline-p-aminobenzyl-carbamate-monomethyl auristatin F.

of tumor cells to transform cancer treatment from previous chemotherapy drugs to tumor-targeted therapies. Monoclonal antibodies and polypeptides which bind to specific markers on the tumor cell's surface provide targeted therapeutic approaches and are both less toxic. However, whether they are monoclonal antibodies or peptides, they both lack potency in killing tumor cells.

The treatment strategy of antibodies armed with toxins to selectively kill target cells was first proposed in 1970 (Moolten and Cooperband, 1970). The tumor-targeting drug conjugates integrate targeted biomolecules with therapeutic small molecule toxins to specifically recognize the tumor tissues and kill the tumor cells, thereby improving the therapeutic index of the toxins and the insufficient efficacy of antibodies or peptides. The tumor-targeting drug conjugates mainly compose of ADCs that generally couple antibodies which specifically recognize the surface antigens of tumor cells with chemical toxins which effectively kill tumor tissues through linkers, and ADCs exert killing activity by bringing the chemical toxins into the tumor cells. In general, the antibody specifically binds to the tumor cell surface antigen, and the antigen mediates the endocytosis of the ADC and then releases free toxins (**Figure 1**), but the downsides are that immunogenicity, poor internalization and the instability of the linker give rise to insecurity and ineffectiveness (Chari, 2008). More than 60 ADCs have been in the process of clinical development until 2016 (Carter and Lazar, 2017), there are almost 204 ADCs (**Supplementary Table S1**) that aim for cancer in clinical development by 2018, including at least nine of which have entered phases III and IV clinical trials[1]. It indicates that ADCs are coming to the center-stage of research field in recent years especially in North America (**Figure 2**). However, until today, only ado-trastuzumab emtansine (T-DM1, Kadcyla[@]) and brentuximab vedotin (Adcetris[@]) are approved by FDA and on the market (Mullard, 2013; Thomas et al., 2016). There are many reasons for the dilemma, including the complexity of the composition of the ADC itself, and the fact that the tumor microenvironment or physiological conditions in animals are different from the human so that the evaluation of ADC efficacy by animal models is not applicable to humans. Beck et al. (2017) published a review paper about the strategies and challenges for the next generation of ADCs in 2017. However, ADCs are developing rapidly and some novel technologies may bring new considerations. Thus, this review mainly focuses on imperative factors that are associated with ADC efficacy (**Figure 3**).

THE SELECTION OF ANTIBODY AND ANTIGEN

Normally, the antigen specific to the cancer cell should be a priority after determining the indications for ADC. Ideally, the antigen should express highly and homogeneously on the surface of the cancer cells (Sievers and Senter, 2013; Damelin et al., 2015). When the antibody combines with the antigen specifically, the antibody-antigen complex should be internalized by antigen-mediated endocytosis, and then the free payloads are released through lysosomal trafficking. As a result, the payloads are concentrated in cancer cells and exert the cytotoxic effect (Erickson et al., 2006). Currently, the predominant therapeutic limitations are the ineffectiveness and the off-target toxicities of ADCs, which are caused by the finite internalization and the low expression of antigens to some extent. Therefore, some researchers came up with some approaches to counteract these problems such as utilizing the anti-tumor angiogenesis antibody, non-internalizing ADC, or bispecific antibody.

The Utilization of Anti-tumor Angiogenesis Antibody

Some researchers proposed a strategy that using an anti-tumor angiogenesis ADC to selectively kill cancer cells due to the process without the involvement of internalization, which could improve the deficient efficacy caused by finite internalization. For example, Palumbo et al. (2011) reported that the ADC composes of an anti-angiogenesis LC19 antibody to selectively target to the tumor blood vessels, the strategy showed a long-term anti-tumor effect. However, ADCs of the anti-tumor vessel may elicit off-target toxicities to normal tissues due to non-specificity of antigen expression and resistance of vessel co-option in some particular tumor tissues (Kuczynski et al., 2016). This requires choosing antibodies based on proper antigens. Seaman et al. (2017) applied the anti-CD276 antibody to the ADC to improve the non-specificity. The CD276 expresses in angiogenic tumor vessel, existed vasculature and tumor cells. Moreover, the anti-CD276 antibody is capable of identifying the normal and pathological angiogenesis. The anti-CD276 ADC evaded the vessel co-option and displayed a dual-targeting ability thus displaying effective anti-tumor activity (Seaman et al., 2017).

Preparing Non-internalizing ADCs

An approach to prepare non-internalizing ADCs to target corresponding antigens needed to be developed. For instance, the ADC took advantage of a diabody without an Fc region to target the matching antigen and an additional chemical activator to cut the linker, and then release the free payload to penetrate into tumor cells (Rossin et al., 2018). This strategy is able to increase the anti-tumor activity and avoid some factors can sacrifice the efficacy of ADCs such as interstitial pressure and epithelial barriers from the tumor cells.

The Selection of the Bispecific Antibody

On one hand, in terms of the deficiency of internalization, Li et al. (2016) used a bispecific antibody to target two non-overlapping epitopes of one antigen, which increased the affinity between antibody and antigen. For example, an anti-HER2 biparatopic antibody displayed better internalization, lysosomal trafficking, and degradation of the antibody-antigen complex relative to the traditional T-DM1 (Li et al., 2016). However, the superior affinity also may trigger a controversy about whether the biparatopic ADC would induce on-target toxicities to healthy tissues. Though this study also further indicated that the biparatopic ADC has an acceptable safety profile due to the threshold of antigen.

[1]https://clinicaltrials.gov

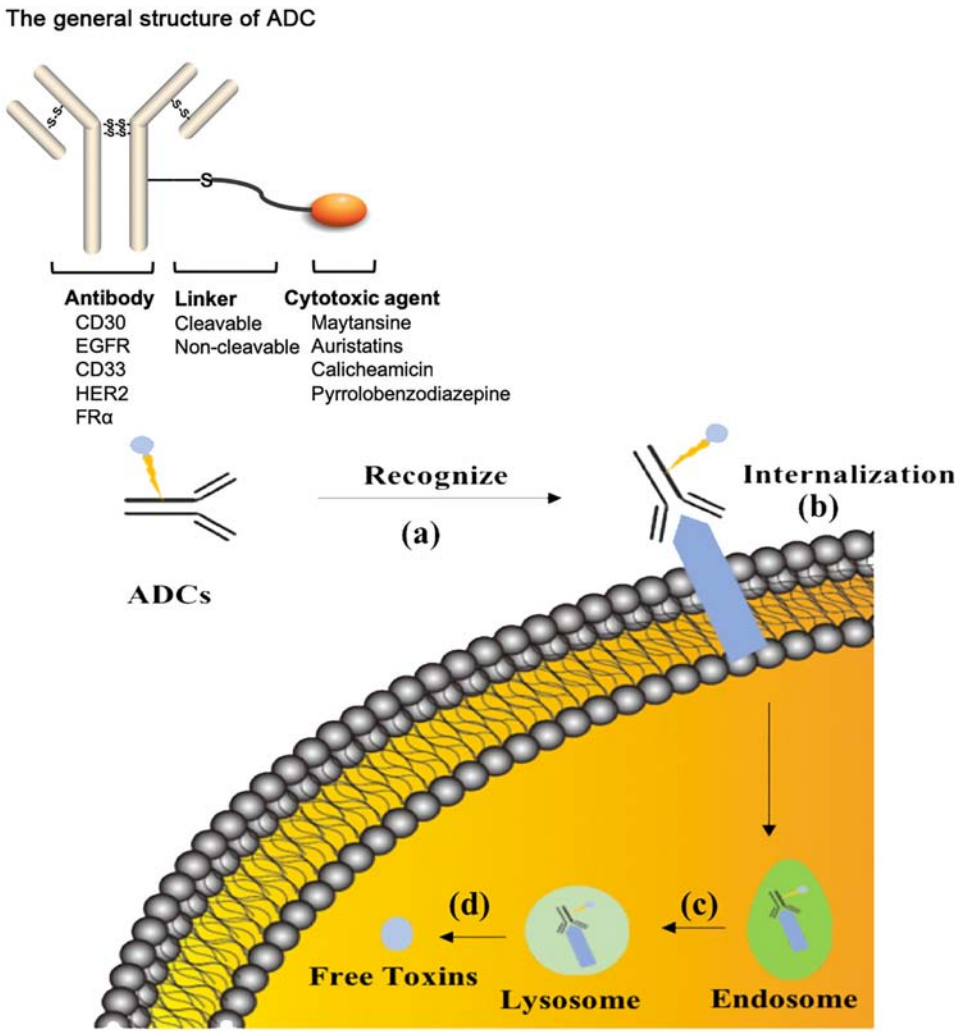

FIGURE 1 | The process of ADCs exerting activity. **(a)** ADCs specifically recognize cancer-associated antigens in the blood system. **(b)** ADCs are internalized into tumor cells during the formation of antibody-antigen complex. **(c)** ADCs are normally transported to lysosome from endosome. **(d)** The linker or antibody are broken in the lysosome conditions to release free toxins. ADCs, antibody drug conjugates.

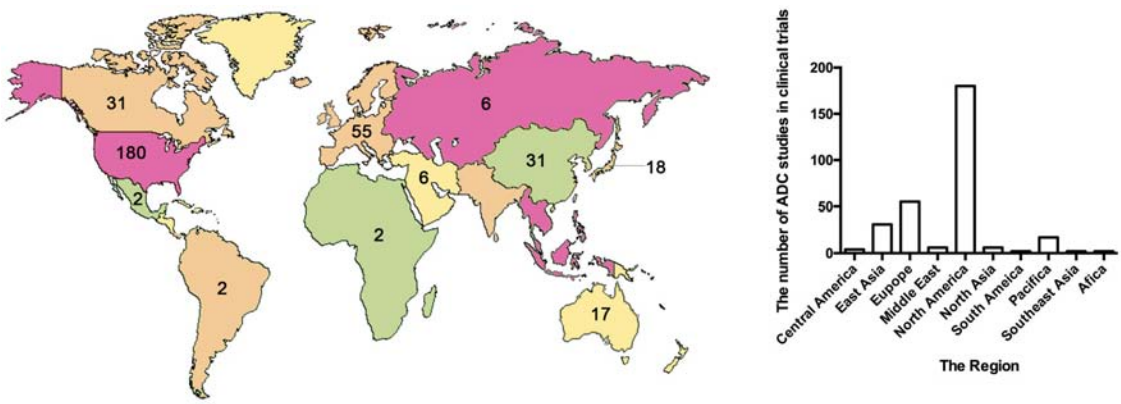

FIGURE 2 | The map and statistical graph depict regions where developed antibody–drug conjugates. The numbers in the figure indicate the amounts of ADCs in the clinical phase of the region. The data comes from ClinicalTrials.gov.

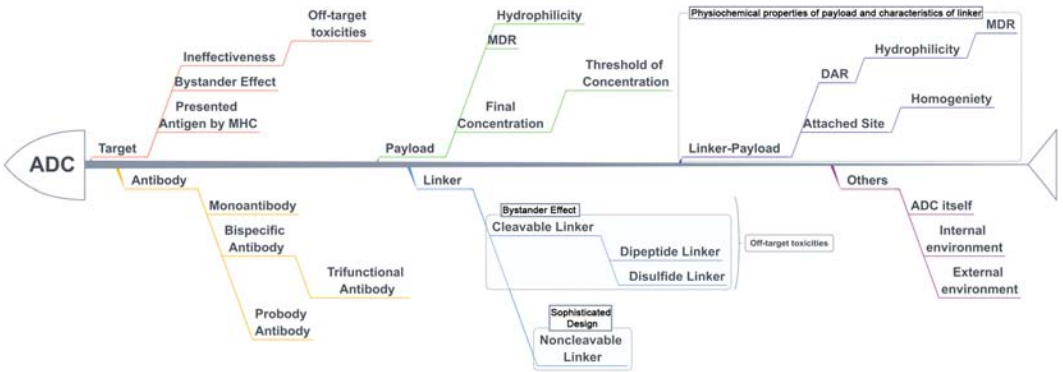

FIGURE 3 | The key parameters associated with efficacy and toxicities with ADCs.

It is unable to form the antibody-antigen complex if the expression level of antigen below the threshold. However, it seems arduous to avoid the problem due to the uncertain threshold. Theoretically, a higher affinity antigen–antibody could make more ADC molecules combine with tumor cells thus having more accumulation, but a lower affinity may allow ADCs to penetrate into tumor cells more effectively. Scientists are still looking for antigen–antibody with proper affinity (Rudnick et al., 2011). It needs further research (Tsumura et al., 2018).

Also, some researchers proposed to use the probody of antibody to solve the on-target toxicities, which may also be applied to ADCs. This strategy used masking peptide to cover up the active sites of the antibody then hydrolysis of the shelter to expose the antibody to target cancer tissues to exert activity (Desnoyers et al., 2013), which allays the indistinct recognition of ADCs in the blood circulation.

On the other hand, the bispecific antibody is able to selectively bind two distinct antigens on a cancer cell to avoid the off-target toxicities. For example, the bispecific antibody simultaneously targets the HER2 and PRLR double positive ($HER2^+/PRLR^+$) breast cancer cells to enhance the internalization and activity of the ADC, and to decrease the off-target toxicities to the healthy cells (Andreev et al., 2017). Nevertheless, targeting double-antigens is ineligible for most heterogeneous tumor cells, since it may trigger their escape mechanism. Furthermore, the bispecific antibody could be used to target the immunosuppressive molecule and tumor-specific antigen on the tumor cells simultaneously to improve the efficacy of ADC. The ADC targeting CD47 that an immunosuppressive receptor and TAA double positive ($CD47^+/TAA^+$) tumor cells could block the immunosuppression to augment the killing activity of the ADC (Dheilly et al., 2017). Currently, there are more than 70 bispecific antibodies applied in clinical trials (see text footnote 1), two of them have used on the market. These specific antibodies seem to change some imperfect phenomena of ADCs (Piccione et al., 2015). Moreover, the trifunctional antibody also could be used to ADC (Krishnamurthy and Jimeno, 2018), which possess an arm to target the tumor cells, the second is used to target T cells, the remaining Fc region to recruit some immune cells. Using the trifunctional antibody to link a small molecule toxin seems to improve the deficient specificity and the killing potency of ADCs. Though the bispecific or trifunctional prospect is promising to improve potency and specificity to increase market competitiveness of ADCs, the challenge of determining the target combination still remains.

The Bystander Effect to Heterogeneous Tumors

Some reports also demonstrated that some ADCs may take advantage of the physical and chemical properties of linkers and the microenvironment of the tumor to release free payloads to kill those adjacent negative-antigen cancer cells. The process is the bystander effect (Kovtun et al., 2006; Okeley et al., 2010). ADC was metabolized to release uncharged and membrane-permeable toxic metabolites after being internalized in positive-antigen cancer, which is able to kill adjacent antigen-negative cancer cells by membrane-penetration (Kellogg et al., 2011). This has a great significance for some heterogeneous tumor cells. Admittedly this was that the bystander effect may also cause non-specific killing of normal cells. Therefore, it requires to have rational selection and design of payloads and linkers based on the target to avoid the adverse effects from bystander effect.

The Selection of Antibody Isotype

Within IgG isotypes, IgG1, IgG2, IgG4 have been used to develop therapeutics, but IgG3 isotypes are not used as therapeutics owing to a significantly faster clearance rate (Jefferis, 2007). Further, most ADCs use IgG1 isotype currently (Beck et al., 2017). IgG1 isotype may exert ADCC (antibody-dependent cell-mediated cytotoxicity) and CDC (complement-dependent cytotoxicity) to improve ADCs activity further, whereas IgG2 and IgG4 are typically deficient in their effector functions (Salfeld, 2007). However, the PD-1 antibodies (Nivolumab and Pembrolizumab) used IgG4 isotype, which may be due to the PD-1 antibody only needing to block the interaction between PD-1 and PD-L1

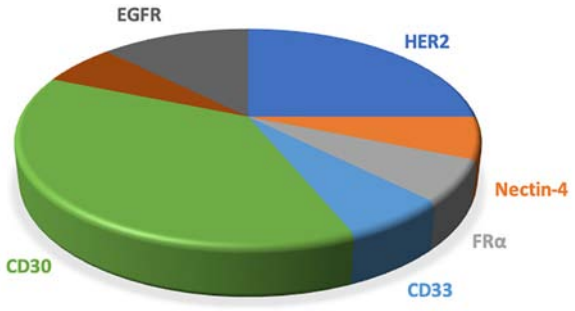

FIGURE 4 | The pie chart shows the antigens applied to the clinical phase III/IV trials of ADCs. ADCs, antibody drug conjugates; MDR, multiple drug resistance; DAR, drug-to-antibody ratio.

to increase immune system function to produce anti-tumor activity, which is needed to avoid the toxicity to T cells from ADCC and CDC. Therefore, the choice of isotype also needs careful consideration.

The Consideration of Antigen

Glycosylation of antigen also could affect the design of ADCs. On the one hand, if glycosylated antigen specifically exists on the tumor cell surface, it will have an important implication to be a target of an ADC. For example, a monoclonal antibody targeting glycosylated PD-L1 (gPD-L1) to disrupt PD-L1/PD-1 interaction. The gPD-L1 is mainly expressed on tumor tissues, which improves non-specific expression of PD-L1 in some immune cells to limit toxicity (Li et al., 2018). On the other hand, the steric structure of a glycosylated antigen plays a certain protective role, which will block the interaction between the antibody and specific sites on the antigen surface. Therefore, we need to have a more comprehensible understanding on designing ADCs.

Most ADCs utilize the antigens on the tumor cells surface, which are limited in their specificity relative to intracellular antigens. Taking advantage of the antigen presentation feature of MHC that caused tumor-specific endogenous antigen expression on the cell surface overcomes the inaccessibility of intracellular antigens. Further, the MHC-I/peptide complex is recognized by the ADCs that mimic the characterization of TCR, which will produce superior specificity and potency (Lai et al., 2018). **Table 1** and **Figure 4** showed the antigens used in phase III/IV trial currently (see text footnote 1).

THE SELECTION OF PAYLOADS

Once the target is determined, the proper choice of payload becomes a critical part of ADC. The final potency of ADCs mainly depends on the concentration of payloads in tumor cells; thus some researchers are dedicated on improving the DAR of ADCs to increase the accumulation of drugs in tumor cells. Zhang et al. (2018b) indicated that activity of the ADC still remains constant though augmenting the payload concentration, and this also could magnify the toxicity to normal tissues at the same time. This suggests that the threshold of payload concentration also needs consideration. In summary, choosing the applicable payloads and designing the appropriate DAR is important for the final concentration of the payloads in tumor cells.

Improving the Efficacy of ADCs

Early ADCs used drugs that have been approved for clinical use such as vinblastine and doxorubicin, but the low clinical activity of these drugs resulted in suboptimal ADCs efficiency. Some cytotoxins were too toxic to be non-target agents in clinical application, but they seemed to be more promising as payloads for ADCs. At present, the dose of the payloads in tumor cells is required to be the picomolar range to kill these cancer cells (Chari et al., 2014). Also, payloads must possess acceptable solubility and decent sites to react with linkers. These all limited the selection of payloads. Currently, most payloads are derivatives of the microtubule inhibitor family, such as the auristatin and maytansine (Beck and Reichert, 2014). Brentuximab vedotin (Adcetris[@]), approved by FDA in 2011, composes of MMAE and cAC10 mAb (chimeric IgG1 antibody) via a protease-cleavable dipeptide linker to target tumor antigen CD30 (also known as TNFRSF8) for the treatment of Hodgkin's lymphoma and ALCL (ki-1 lymphoma) (Senter and Sievers, 2012; Younes et al., 2012). Ado-trastuzumab emtansine (Kadcyla[@]), approved in 2013, consists of a stable thioether linker (SMCC) attached to trastuzumab (anti-human epidermal growth factor receptor-2 antibody, anti-HER2 antibody) and DM1 (maytansine derivative) for the treatment of advanced breast cancer (Lambert and Chari, 2014). Both adopted the microtubule inhibitor family as payloads, yet auristatins and maytansines are only able to exert activity in cell proliferation and they are hydrophobic, which will disturb their activity. Thus, some novel payloads or the original payload structural modifications such as the improvement of hydrophilicity will become the hotspots of the future payload research (Burke et al., 2017). At present, some novel ADCs have better activity and have been through clinical phase III/IV (**Table 1**).

The first commercially available ADC was gemtuzumab ozogamicin (GO) that consists of calicheamicins which damage DNA (Walker et al., 1992) for the treatment of AML. However, GO showed no significant improvement in overall survival (OS) compared with the calicheamicin agent alone, and had a higher mortality rate and was recalled in 2010 (Petersdorf et al., 2013; Kharfan-Dabaja, 2014). This is because calicheamicin is hydrophobic in that almost only 50% could be conjugated, and only approximately 50% of free drugs are eventually released in the conjugated drugs (Beck et al., 2010; Senter and Sievers, 2012), resulting in a significant decrease in potency. To overcome these limitations, some novel targeted DNA agents have been broadly developed. Pyrrolobenzodiazepine dimers (PBDs) have already become a new choice, it may attach to the linker that conjugated to the antibody, and has the ability to overcome MDR relative to the commonly used calicheamicin as a substrate of *P*-glycoprotein (Kung Sutherland et al., 2013; Stein et al., 2018). The IMGN779 (NCT02674763) utilized DGN462 that a novel drug with DNA-alkylating activity also demonstrated better anti-tumor activity and tolerability (Kovtun et al., 2018).

TABLE 1 | Current clinical phase III/IV trials of ADCs.

NCT number	Name	Conditions	Payloads	Target
NCT03523585	DS-8201a	Breast cancer	Topoisomerase I inhibitor	HER2
NCT03734029	DS-8201a	Breast cancer	topoisomerase I inhibitor	HER2
NCT03529110	DS-8201a	Breast cancer	topoisomerase I inhibitor	HER2
NCT03262935	SYD985	Metastatic breast cancer	DUBA	HER2
NCT03474107	Enfortumab vedotin	Ureteral cancer| urothelial cancer| bladder cancer	MMAE	Nectin-4
NCT02631876	Mirvetuximab soravtansine (IMGN853)	Epithelial ovarian cancer| primary peritoneal carcinoma| fallopian tube cancer| ovarian cancer	DM4	FRα
NCT02785900	Vadastuximab talirine (SGN-CD33A; 33A)	Acute myeloid leukemia	PBD	CD33
NCT01990534	Brentuximab Vedotin	Hodgkin lymphoma	MMAE	CD30
NCT03677596	Inotuzumab ozogamicin	Leukemia| precursor b-cell lymphoblastic leukemia-lymphoma| acute lymphoblastic leukemia	Calicheamicins	CD22
NCT02573324	Depatuxizumab mafodotin (ABT-414)	Glioblastoma	MMAF	EGFR
NCT01100502	Brentuximab vedotin (SGN-35)	Disease, Hodgkin	MMAE	CD30
NCT01777152	Brentuximab vedotin	Anaplastic large-cell lymphoma| non-Hodgkin lymphoma| T-cell lymphoma	MMAE	CD30
NCT01909934	Brentuximab vedotin	Anaplastic large-cell lymphoma	MMAE	CD30
NCT03419403	Depatuxizumab mafodotin (ABT-414)	Glioblastoma multiforme	MMAF	EGFR
NCT01712490	Brentuximab vedotin	Hodgkin lymphoma	MMAE	CD30
NCT02166463	Brentuximab vedotin	Hodgkin lymphoma	MMAE	CD30

DUBA, duocarmycin-hydroxybenzamide-azaindole; MMAE, monomethyl auristatin E; MMAF, monomethyl auristatin F; DM4, maytansine 4; PBD, pyrrolobenzodiazepine dimers.

Avoiding MDR

The MDR has always been a barrier and one of the important factors affecting the therapeutic effect in the cancer treatment. The MDR is still an impeditive factor of using ADCs. This is because the essence of ADC's activity is that the payloads in tumor cells exert cytotoxicity, and these payloads may be affected by MDR. Many studies concentrate on the modification of drug-linker that, by increasing hydrophilicity, circumvents MDR caused by the overexpression of efflux pumps because the substrates of MDR1 were hydrophobic in general. Moreover, some novel payloads such as PBD, DGN462, and tubulysins cooperate with ADCs to display better anti-tumor activity in MDR^+ tumor cells (Burke et al., 2018; Kovtun et al., 2018; Stein et al., 2018). ADCs are susceptible to hydrophobicity to be insensible to MDR^+ cells, thereby it is essential to improve the hydrophilicity to escape from MDR to increase the activity of ADCs (Kovtun et al., 2010).

THE MODIFICATION OF LINKER

Although the linker may be not directly correlated with the final potency of ADC (Lee et al., 2018b), the potency of ADC is dictated by the concentration of payload accumulated in tumor cells, and the payload release is determined by the stability of the linker. Thus, the linker is crucial for a perfect ADC, and it determines the stability, efficacy, and even the ability to overcome MDR. The basic requirement of the linker is to make the payload attach to the antibody, stabilize the payload in the circulation system, and is labile to release the free payload into cancer cells when the antigen–antibody complex is formed (Doronina et al., 2006). Currently, linkers are mainly divided into the cleavable linkers and the non-cleavable linkers.

The Comparison of Cleavable Linkers With Non-cleavable Linkers

The cleavable linkers normally take advantage of the difference of tumor microenvironment and normal physiological environment to release the payloads that may be membrane-permeable and can produce the bystander effect. The non-cleavable linkers need to meet the requirement that the antibody and linker must be disconnected after the formation of the antigen–antibody complex enter the lysosomal trafficking. This may cause the bystander effect that is a passive transport process to weaken, caused by the membrane-impermeability

of linker-payloads connected with polar amino acids. Both types of linkers have their advantages and disadvantages, which are applied to the clinical trials (Chari et al., 2014; Bialucha et al., 2017). However, about 2/3 ADCs used cleavable linkers in the current clinical trials (Lambert and Berkenblit, 2018), in which mainly are dipeptide linkers and disulfide linkers. The non-cleavable linkers are not only more stable to escape from the off-target toxicities than cleavable linkers (Lu et al., 2016), but also may overcome the barrier of multiple-drug resistance (MDR) (Shefet-Carasso and Benhar, 2015; Beck et al., 2017; Nasiri et al., 2018) for the reason that the payload connected with polar amino cannot be a substrate of MDR1, which will improve the MDR phenomenon. However, the non-cleavable linkers need a more elaborate process to produce activity such as the internalization and metabolism of the antibody in the lysosome, which is a prerequisite to release active payloads to exert killing activity (Rosenberg, 2006; Lambert and Berkenblit, 2018), and the polar amino-linker-payload also needs a distinct transporter to carry it from the lysosome to cytoplasm to work (Hamblett et al., 2015; Kinneer et al., 2018; Lee et al., 2018b), which makes the design of ADC more complex to limit the utilization of non-cleavable linkers. The cleavable linkers are more vulnerable to lead to off-target toxicities, but the process of exerting effects is more comprehensible thus researchers are dedicated to modifying the cleavable linkers to overcome their weakness and to increase their stability in the circulation (Sanderson et al., 2005; Kellogg et al., 2011).

The Analysis of Cleavable Linkers

The cleavable linker can metabolize some cell-permeable metabolites to exert the bystander killing effect. The cleavable sulfo-SPDB-DM4 linker produced cell-permeable catabolites to display a better activity than non-cleavable SMCC-DM1 linker (Bialucha et al., 2017). Also, the application of the sulfonate group improved hydrophilicity to increase the exposure of ADC to the antigen to promote killing activity. The brentuximab vedotin (SGN-35) took advantage of a cleavable dipeptide linker to release free MMAE, and the MMAE may permeate adjacent cells to exert killing activity which is important to some heterogeneous tumor cells. Moreover, the dipeptide linker offers ADC better stability in the circulation, and is more specific to tumor cells (Katz et al., 2011). The protease cleavage pathway is not restricted to cathepsin B, various cysteine cathepsins can cleavage the dipeptide linker, such as cysteine cathepsins B, K, L, and S. It seems to explain why the dipeptide linkers cannot be insensitive to tumors, caused by the insufficient expression of protease (Caculitan et al., 2017), which is one of the reasons why some protease-sensitive linkers are widely used by ADCs.

In particular, the design of the valine-citrulline (val-cit) linker, the most frequent in dipeptide linkers, needs to consider the connection to the phenol-containing payloads; diverse electron groups affect the degrees of immolation of the linker to influence the different potency of an ADC (Zhang et al., 2018a). However, the val-cit dipeptide linker is not conducive to preclinical research to appraise the efficacy of ADCs due to instability in mice (Dokter et al., 2014). Anami et al. (2018) reported a glutamic acid-val-cit linker replaced val-cit dipeptide linker, which could alleviate the flaw of instability in the mice plasma and retain the cathepsin-mediated cleavage mechanisms, thus boosting preclinical application of some ADCs. The acidic tripeptide linker could increase the polarity of ADCs to improve solubility to increase the therapeutic potency (Anami et al., 2018). However, one of the studies suggests that activity of the ADC with cleavable valine-citrulline-p-aminobenzyl-carbamate-monomethyl auristatin F (val-cit-PABC-MMAF) is much less than the ADC with non-cleavable maleimidocaproyl-MMAF (Doronina et al., 2006), which may be due to the character of payloads rather than the linker. The metabolites of some payloads are more effective than the prototypes. The non-cleavable linkers are not widely applied to ADCs since many payload derivatives attached to an amino cannot satisfy the killing potency of ADCs.

The disulfide linker utilized the difference of glutathione (GSH) levels between the tumor microenvironment and the physiological environment of normal tissues to produce activity (Meister and Anderson, 1983; Dubikovskaya et al., 2008), which is more labile in tumoral hypoxia conditions (de Groot et al., 2001). At present, the main obstacle of the disulfide linker is the instability, which is mainly improved by increasing steric hindrance to relieve the vulnerability. ADCs using the disulfide linkers have inferior potency *in vivo* due to the more rapid clearance of payloads compared with the non-cleavable thioether linkers that displayed more potent activity (Lewis Phillips et al., 2008). The trastuzumab emtansine (T-DM1) consists of non-cleavable thioether linker and a maytansine derivate, which has better anti-breast cancer activity. The linker contained a cyclohexane carboxylate and a maleimidomethyl group. The ionized metabolite cannot kill surrounding normal cells due to its impermeability after ADC metabolized, thus the ADC has a better safety (LoRusso et al., 2011). The non-cleavable linkers are stricter in the choice of antigens compared with cleavable linkers, yet fewer toxicities (Polson et al., 2009). Zhang et al. (2016) reported that using methy- and cyclobutyl-substituted disulfide with efficient immolation demonstrated more potent killing activity than cyclopropyl-substituted disulfide with non-immolation. Also, this reflects that the immolation of the linker is imperative to the potency of ADC (Zhang et al., 2016). However, the anti-tumor activity is more determined by the cleavage of the linkers only when payloads require complete cleaving to exert activity (Caculitan et al., 2017). Thus, new research could focus on developing payloads that do not require the production of pharmacological effects with prototype drugs. Also, future studies could focus on developing some novel technologies of payload-linker to improve the activity of ADCs such as SYD985 based on a cleavable linker-duocarmycin payload (NCT03262935) (Dokter et al., 2014).

THE PAYLOAD-LINKER LINKAGE

With the development of ADCs, the drug-linker linkage that goes hand in hand with the efficacy of ADCs is more critical (Nasiri et al., 2018). In order to give full play to ADCs' activity in tumor cells, it is necessary to effectively design the payload-linker

according to the physicochemical properties of the payloads and the characteristics of the linkers.

The Consideration of the Sites of Payload-Linker

The sites of the payload-linker are essential conditions to consider due to the attaching-sites being correlated with homogeneity that is related to the therapeutic index. In the early stages of ADCs development, the lysine on the antibody was used as the site to attach the linker, which caused great heterogeneity. Later, Adcetris[@] used the cysteine that only eight free cysteines per antibody to link through disulfide bonds, which reduced the ADCs heterogeneity. In recent years, to ensure ADC homogeneity, researchers have developed some site-specific methods, such as THIOMAB (Junutula et al., 2008; Chudasama et al., 2016).

The Modification of Payload-Linker

The drug-linker linkage determines the DAR that are related to the efficacy of ADC. Generally, the therapeutic potency of ADC gradually increases *in vitro* with the increase of DAR whereas the therapeutic index *in vivo* decreases (Hamblett et al., 2004), which may due to with the enhancement of DAR accelerates the clearance of ADC which is closely related to the hydrophobicity of ADC (Lyon et al., 2015). The hydrophobicity is determined by the amounts of payloads per antibody and the design of drug-linker (Doronina et al., 2014). It is the main reason for the failure of ADC in the clinical application that the concentration of payload is deficient to treat tumors on account of the DAR of ADC in clinical stage generally control to 3.5–4 (Beck et al., 2017). Thus, augmenting the hydrophilicity of ADC with high DAR by the design of drug-linker exquisitely will improve the efficacy *in vivo* (Pabst et al., 2017). Some hydrophilic groups such as PEG or PHF may improve this dilemma. Accurately connecting these hydrophilic groups to a linker will effectively improve the efficacy of the ADCs. For example, Trastuzumab–PHF–Vinca ADC with DAR of 20 demonstrated a potent anti-tumor activity and decent pharmacokinetic profile due to the high hydrophilicity of PHF (Yurkovetskiy et al., 2015).

At the same time, MDR^+ tumor cells are insensible to some ADCs due to the fact that many payloads applied to ADCs are hydrophobic, which are the substrates of the MDR1 transporter. By improving the hydrophobicity of the drug-linker, it seems to be able to bypass MDR (Kovtun et al., 2010; Shefet-Carasso and Benhar, 2015).

OTHER PARAMETERS CORRELATED WITH THE EFFICACY OF ADCs

The Relationship Between the Internal Environment and Activity of ADCs

Normally, we consider the internalization that influences the efficacy of ADCs to be regulated by antigen. Recently, Lee et al. (2018a) demonstrated that the internalization may be mainly determined by the cellular environment rather than the antigen, which brought another hint that the development of the ADCs has to consider a variety of parameters besides the choice of target and the design of the linker. The characteristics of tumor cells also affect the activity of ADCs, including the endothelium, interstitial, and epithelial barriers which could limit ADCs uptake in the tumor, resulting in a small fraction of the injected dose reaching the desired tumor target (Perez et al., 2014). Intra-tumor distribution of ADCs also affects the anti-tumor efficacy (Tsumura et al., 2018).

Sometimes the efficacy of the ADCs does not have a positive correlation with the dose of the injection of ADCs. In addition to being interfered by the payload concentration threshold, the activity of ADCs could be affected by the saturation of the antigen–antibody combination, which causes the concentration of the ADCs in the circulation to be higher than the concentration of the corresponding receptors (Mager, 2006). Some antigens may shed from the tumor cells and circulate in the blood system to alleviate invalid combination with antibodies, which is also able to enhance the efficacy of ADCs (Pak et al., 2012). These internal factors seem to be imperative considerations when designing ADCs in the future.

The External Conditions Related to Activity of ADCs

Another point worth attention is the choice of assessment method of safety and efficacy of ADCs. Owing to the ADC subjects to some physical and chemical conditions such as storage conditions, which is able to cause degradation or aggregation of ADCs to influence the assessment of ADCs' activity (Mohamed et al., 2018). Therefore, the assessment method must be considered to some extent.

CONCLUSION AND PERSPECTIVE

With in-depth understandings of antibodies, linkers, and payloads, ADCs have also achieved great development. The linkage strategy and target diversity have already improved the delivery of the payloads to tumor tissues and reduced exposure to normal tissues. With the development of payloads, some novel potent payloads are used by ADCs, which allows researchers to exploit novel linkers to attach the antibody and payloads without disturbing their potency (Dragovich et al., 2018). Furthermore, some irrelevant antigen-target ADCs also may exert toxicity to tumor cells due to the vascular gap of tumors relative to the normal tissues, which is big enough to make ADCs penetrate into tumor cells (Cardillo et al., 2011), indicating the specific recognition of ADCs by tumor tissues on another aspect.

Some prodrug strategies also are used in ADCs design, which modified the toxic payloads to inactive prodrugs, then utilized self-immolation groups and took advantage of the intratumoral environment to reduce the prodrugs to prototype drugs to exert intrinsic activity (Pei et al., 2018). Moreover, nanoparticles combining with the strategy of ACD prodrugs could also increase the activity and circumvent MDR (Qi et al., 2017). The key issues of ADCs are optimization of the appropriate antibody,

the choice of proper antigen, the selection of high-activity cytotoxic payloads, stable linkage technology and optimization of DAR in future development. These strategies will improve the efficacy of ADCs that give them a larger market share to replace chemotherapy drugs in medical therapy in the future. At present, ADCs in clinical trials mainly focus on hematological tumors especially Hodgkin lymphoma, because the CD30 is an ideal target, overexpressed in Hodgin lymphoma consistently. With the deep investigation of the target, more ADCs to cure other types of cancer will expand to clinical applications. However, the development of ADCs is costly to make, marked by Adcetris[@] and Kadcyla[@] imposing more family burdens on patients.

In recent years, peptide-drug conjugates (PDCs) are also on the stage of targeted-drug conjugation therapy and are considered as part of ADCs. PDCs replace antibodies with peptides, which minimize the molecular weight to alleviate the reduction of tumor cell absorption caused by the larger molecular weight of the ADCs. Also, PDCs could possess better homogeneity due to the few of the attached sites of the peptides. The cost-effectiveness of PDCs is critical to alleviate the pressure on patients during treatment. However, PDCs also have some weaknesses that need to be improved. The vulnerability of PDCs in the blood system is a non-negligible obstacle, but it is difficult to improve half-life and reduce off-target toxicity by modifying structure of PDCs without destroying activity. Therefore, we must master more comprehensive knowledge to improve ADCs or PDCs. Whether used alone or in combination with other therapies, the toxicity of ADCs and PDCs must be better understood to adjust the therapeutic index based on the minimum effective dose of the drug in tumor cells and the maximum tolerated dose for normal tissues.

AUTHOR CONTRIBUTIONS

HT wrote the review manuscript. YL, ZY, MS, and WL modified the review. LL and QH edited the review including grammar. The correspondent authors MW and YJ provided the thought.

FUNDING

This work was supported by the National Natural Science Foundation of China and Liaoning Joint Fund Key Program (Grant No. U1608281), the National Natural Science Foundation of China (Grant Nos. 81601370 and 81673475), the Key Laboratory Foundation from Shenyang S&T Projects (Grant No. Z18-4-020), the National Key Research and Development Plan, Digital Diagnosis and Treatment Equipment Research and Development Key Special Project (Grant No. 2017YFC0114203), and the Liaoning Provincial Science and Technology Public Welfare Research Fund Project (Grant No. 20170030).

SUPPLEMENTARY MATERIAL

The Supplementary Material for this article can be found online at: https://www.frontiersin.org/articles/10.3389/fphar.2019.00373/full#supplementary-material

TABLE S1 | The ADCs of cancer therapy in clinical development.

REFERENCES

Alley, S. C., Okeley, N. M., and Senter, P. D. (2010). Antibody-drug conjugates: targeted drug delivery for cancer. *Curr. Opin. Chem. Biol.* 14, 529–537. doi: 10.1016/j.cbpa.2010.06.170

Anami, Y., Yamazaki, C. M., Xiong, W., Gui, X., Zhang, N., An, Z., et al. (2018). Glutamic acid-valine-citrulline linkers ensure stability and efficacy of antibody-drug conjugates in mice. *Nat. Commun.* 9:2512. doi: 10.1038/s41467-018-04982-3

Andreev, J., Thambi, N., Perez Bay, A. E., Delfino, F., Martin, J., Kelly, M. P., et al. (2017). Bispecific antibodies and antibody-drug conjugates (ADCs) bridging HER2 and prolactin receptor improve efficacy of HER2 ADCs. *Mol. Cancer Ther.* 16, 681–693. doi: 10.1158/1535-7163.mct-16-0658

Ashley, C. E., Carnes, E. C., Phillips, G. K., Padilla, D., Durfee, P. N., Brown, P. A., et al. (2011). The targeted delivery of multicomponent cargos to cancer cells by nanoporous particle-supported lipid bilayers. *Nat. Mater* 10, 389–397. doi: 10.1038/nmat2992

Atkins, J. H., and Gershell, L. J. (2002). Selective anticancer drugs. *Nat. Rev. Drug Discov.* 1, 491–492. doi: 10.1038/nrd842

Beck, A., Goetsch, L., Dumontet, C., and Corvaia, N. (2017). Strategies and challenges for the next generation of antibody-drug conjugates. *Nat. Rev. Drug Discov.* 16, 315–337. doi: 10.1038/nrd.2016.268

Beck, A., Haeuw, J. F., Wurch, T., Goetsch, L., Bailly, C., and Corvaia, N. (2010). The next generation of antibody-drug conjugates comes of age. *Discov. Med.* 10, 329–339.

Beck, A., and Reichert, J. M. (2014). Antibody-drug conjugates: present and future. *MABS* 6, 15–17. doi: 10.4161/mabs.27436

Bialucha, C. U., Collins, S. D., Li, X., Saxena, P., Zhang, X., Durr, C., et al. (2017). Discovery and optimization of HKT288, a Cadherin-6-Targeting ADC for the treatment of ovarian and renal cancers. *Cancer Discov.* 7, 1030–1045. doi: 10.1158/2159-8290.cd-16-1414

Burke, P., Hamilton, J., Jeffrey, S., Hunter, J., Doronina, S., Okeley, N., et al. (2017). Optimization of a PEGylated glucuronide-monomethylauristatin e linker for antibody-drug conjugates. *Mol. Cancer Ther.* 16, 116–123. doi: 10.1158/1535-7163.MCT-16-0343

Burke, P. J., Hamilton, J. Z., Pires, T. A., Lai, H. W. H., Leiske, C. I., Emmerton, K. K., et al. (2018). Glucuronide-linked antibody-tubulysin conjugates display activity in MDR+ and heterogeneous tumor models. *Mol. Cancer Ther.* 17, 1752–1760. doi: 10.1158/1535-7163.mct-18-0073

Caculitan, N. G., Dela Cruz Chuh, J., Ma, Y., Zhang, D., Kozak, K. R., Liu, Y., et al. (2017). Cathepsin B Is dispensable for cellular processing of cathepsin b-cleavable antibody-drug conjugates. *Cancer Res.* 77, 7027–7037. doi: 10.1158/0008-5472.can-17-2391

Cardillo, T. M., Govindan, S. V., Sharkey, R. M., Trisal, P., and Goldenberg, D. M. (2011). Humanized anti-Trop-2 IgG-SN-38 conjugate for effective treatment of diverse epithelial cancers: preclinical studies in human cancer xenograft models and monkeys. *Clin. Cancer Res.* 17, 3157–3169. doi: 10.1158/1078-0432.ccr-10-2939

Carter, P. J., and Lazar, G. A. (2017). Next generation antibody drugs: pursuit of the 'high-hanging fruit'. *Nat. Rev. Drug Discov.* 17, 197–223. doi: 10.1038/nrd.2017.227

Chari, R. V. (2008). Targeted cancer therapy: conferring specificity to cytotoxic drugs. *Acc. Chem. Res.* 41, 98–107. doi: 10.1021/ar700108g

Chari, R. V., Miller, M. L., and Widdison, W. C. (2014). Antibody-drug conjugates: an emerging concept in cancer therapy. *Angew Chem. Int. Ed. Engl.* 53, 3796–3827. doi: 10.1002/anie.201307628

Chudasama, V., Maruani, A., and Caddick, S. (2016). Recent advances in the construction of antibody-drug conjugates. *Nat. Chem.* 8, 114–119. doi: 10.1038/nchem.2415

Damelin, M., Zhong, W., Myers, J., and Sapra, P. (2015). Evolving strategies for target selection for antibody-drug conjugates. *Pharm. Res.* 32, 3494–3507. doi: 10.1007/s11095-015-1624-3

de Groot, F. M., Damen, E. W., and Scheeren, H. W. (2001). Anticancer prodrugs for application in monotherapy: targeting hypoxia, tumor-associated enzymes, and receptors. *Curr. Med. Chem.* 8, 1093–1122. doi: 10.2174/0929867013372634

Desnoyers, L. R., Vasiljeva, O., Richardson, J. H., Yang, A., Menendez, E. E., Liang, T. W., et al. (2013). Tumor-specific activation of an EGFR-targeting probody enhances therapeutic index. *Sci. Transl. Med.* 5:207ra144. doi: 10.1126/scitranslmed.3006682

Dheilly, E., Moine, V., Broyer, L., Salgado-Pires, S., Johnson, Z., Papaioannou, A., et al. (2017). Selective blockade of the ubiquitous checkpoint receptor cd47 is enabled by dual-targeting bispecific antibodies. *Mol. Ther.* 25, 523–533. doi: 10.1016/j.ymthe.2016.11.006

Dokter, W., Ubink, R., van der Lee, M., van der Vleuten, M., van Achterberg, T., Jacobs, D., et al. (2014). Preclinical profile of the HER2-targeting ADC SYD983/SYD985: introduction of a new duocarmycin-based linker-drug platform. *Mol. Cancer Therapeu.* 13, 2618–2629. doi: 10.1158/1535-7163.MCT-14-0040-T

Doronina, S. O., Mendelsohn, B. A., Bovee, T. D., Cerveny, C. G., Alley, S. C., Meyer, D. L., et al. (2006). Enhanced activity of monomethylauristatin F through monoclonal antibody delivery: effects of linker technology on efficacy and toxicity. *Bioconjug. Chem.* 17, 114–124. doi: 10.1021/bc0502917

Doronina, S. O., Setter, J. R., Bovee, T. D., Anderson, M. E., Jonas, M., Daniho, S., et al. (2014). Abstract 4470: Elucidating the role of drug-linker hydrophobicity in the disposition of antibody-drug conjugates. *Cancer Res.* 74, 4470–4470. doi: 10.1158/1538-7445.am2014-4470

Dragovich, P. S., Blake, R. A., Chen, C., Chen, J., Chuh, J., den Besten, W., et al. (2018). Conjugation of indoles to antibodies through a novel self-immolating linker. *Chemistry* 24, 4830–4834. doi: 10.1002/chem.201800859

Dubikovskaya, E. A., Thorne, S. H., Pillow, T. H., Contag, C. H., and Wender, P. A. (2008). Overcoming multidrug resistance of small-molecule therapeutics through conjugation with releasable octaarginine transporters. *Proc. Natl. Acad. Sci. U.S.A.* 105, 12128–12133. doi: 10.1073/pnas.0805374105

Erickson, H. K., Park, P. U., Widdison, W. C., Kovtun, Y. V., Garrett, L. M., Hoffman, K., et al. (2006). Antibody-maytansinoid conjugates are activated in targeted cancer cells by lysosomal degradation and linker-dependent intracellular processing. *Cancer Res.* 66, 4426–4433. doi: 10.1158/0008-5472.can-05-4489

Hamblett, K. J., Jacob, A. P., Gurgel, J. L., Tometsko, M. E., Rock, B. M., Patel, S. K., et al. (2015). SLC46A3 is required to transport catabolites of noncleavable antibody maytansine conjugates from the lysosome to the cytoplasm. *Cancer Res.* 75, 5329–5340. doi: 10.1158/0008-5472.can-15-1610

Hamblett, K. J., Senter, P. D., Chace, D. F., Sun, M. M., Lenox, J., Cerveny, C. G., et al. (2004). Effects of drug loading on the antitumor activity of a monoclonal antibody drug conjugate. *Clin. Cancer Res.* 10, 7063–7070. doi: 10.1158/1078-0432.ccr-04-0789

Jefferis, R. (2007). Antibody therapeutics: isotype and glycoform selection. *Expert Opin. Biol. Ther.* 7, 1401–1413. doi: 10.1517/14712598.7.9.1401

Junutula, J. R., Raab, H., Clark, S., Bhakta, S., Leipold, D. D., Weir, S., et al. (2008). Site-specific conjugation of a cytotoxic drug to an antibody improves the therapeutic index. *Nat. Biotechnol.* 26, 925–932. doi: 10.1038/nbt.1480

Katz, J., Janik, J. E., and Younes, A. (2011). Brentuximab vedotin (SGN-35). *Clin. Cancer Res.* 17, 6428–6436. doi: 10.1158/1078-0432.ccr-11-0488

Kellogg, B. A., Garrett, L., Kovtun, Y., Lai, K. C., Leece, B., Miller, M., et al. (2011). Disulfide-linked antibody-maytansinoid conjugates: optimization of in vivo activity by varying the steric hindrance at carbon atoms adjacent to the disulfide linkage. *Bioconjug. Chem.* 22, 717–727. doi: 10.1021/bc100480a

Kharfan-Dabaja, M. A. (2014). A new dawn for gemtuzumab ozogamicin? *Lancet Oncol.* 15, 913–914. doi: 10.1016/S1470-2045(14)70289-X

Kinneer, K., Meekin, J., Tiberghien, A. C., Tai, Y.-T., Phipps, S., Kiefer, C. M., et al. (2018). SLC46A3 as a potential predictive biomarker for antibody-drug conjugates bearing non-cleavable linked maytansinoid and pyrrolobenzodiazepine warheads. *Clin. Cancer Res.* 24, 6570–6582. doi: 10.1158/1078-0432.ccr-18-1300

Kovtun, Y., Noordhuis, P., Whiteman, K. R., Watkins, K., Jones, G. E., Harvey, L., et al. (2018). IMGN779, a novel CD33-targeting antibody-drug conjugate with DNA-alkylating activity, exhibits potent antitumor activity in models of AML. *Mol. Cancer Ther.* 17, 1271–1279. doi: 10.1158/1535-7163.mct-17-1077

Kovtun, Y. V., Audette, C. A., Mayo, M. F., Jones, G. E., Doherty, H., Maloney, E. K., et al. (2010). Antibody-maytansinoid conjugates designed to bypass multidrug resistance. *Cancer Res.* 70, 2528–2537. doi: 10.1158/0008-5472.can-09-3546

Kovtun, Y. V., Audette, C. A., Ye, Y., Xie, H., Ruberti, M. F., Phinney, S. J., et al. (2006). Antibody-drug conjugates designed to eradicate tumors with homogeneous and heterogeneous expression of the target antigen. *Cancer Res.* 66, 3214–3221. doi: 10.1158/0008-5472.can-05-3973

Krishnamurthy, A., and Jimeno, A. (2018). Bispecific antibodies for cancer therapy: a review. *Pharmacol. Ther.* 185, 122–134. doi: 10.1016/j.pharmthera.2017.12.002

Kuczynski, E. A., Yin, M., Bar-Zion, A., Lee, C. R., Butz, H., Man, S., et al. (2016). Co-option of liver vessels and not sprouting angiogenesis drives acquired sorafenib resistance in hepatocellular carcinoma. *J. Natl. Cancer Inst.* 108:djw030. doi: 10.1093/jnci/djw030

Kung Sutherland, M. S., Walter, R. B., Jeffrey, S. C., Burke, P. J., Yu, C., Kostner, H., et al. (2013). SGN-CD33A: a novel CD33-targeting antibody-drug conjugate using a pyrrolobenzodiazepine dimer is active in models of drug-resistant AML. *Blood* 122, 1455–1463. doi: 10.1182/blood-2013-03-491506

Lai, J., Wang, Y., Wu, S. S., Ding, D., Sun, Z. Y., Zhang, Y., et al. (2018). Elimination of melanoma by sortase A-generated TCR-like antibody-drug conjugates (TL-ADCs) targeting intracellular melanoma antigen MART-1. *Biomaterials* 178, 158–169. doi: 10.1016/j.biomaterials.2018.06.017

Lambert, J. M., and Berkenblit, A. (2018). Antibody-drug conjugates for cancer treatment. *Annu. Rev. Med.* 69, 191–207. doi: 10.1146/annurev-med-061516-121357

Lambert, J. M., and Chari, R. V. (2014). Ado-trastuzumab Emtansine (T-DM1): an antibody-drug conjugate (ADC) for HER2-positive breast cancer. *J. Med. Chem.* 57, 6949–6964. doi: 10.1021/jm500766w

Lee, B. C., Chalouni, C., Doll, S., Nalle, S., Darwish, M., Tsai, S. P., et al. (2018a). A novel FRET reagent reveals the intracellular processing of peptide-linked antibody-drug conjugates. . *Bioconjug. Chem.* 29, 2468–2477. doi: 10.1021/acs.bioconjchem.8b00362

Lee, B. C., Chalouni, C., Doll, S., Nalle, S. C., Darwish, M., Tsai, S. P., et al. (2018b). FRET reagent reveals the intracellular processing of peptide-linked antibody-drug conjugates. *Bioconjug. Chem.* 29, 2468–2477. doi: 10.1021/acs.bioconjchem.8b00362

Lewis Phillips, G. D., Li, G., Dugger, D. L., Crocker, L. M., Parsons, K. L., Mai, E., et al. (2008). Targeting HER2-positive breast cancer with trastuzumab-DM1, an antibody-cytotoxic drug conjugate. *Cancer Res.* 68, 9280–9290. doi: 10.1158/0008-5472.can-08-1776

Li, C. W., Lim, S. O., Chung, E. M., Kim, Y. S., Park, A. H., Yao, J., et al. (2018). Eradication of triple-negative breast cancer cells by targeting glycosylated PD-L1. *Cancer Cell* 33, 187.e10–201.e10. doi: 10.1016/j.ccell.2018.01.009

Li, J. Y., Perry, S. R., Muniz-Medina, V., Wang, X., Wetzel, L. K., Rebelatto, M. C., et al. (2016). A biparatopic her2-targeting antibody-drug conjugate induces tumor regression in primary models refractory to or ineligible for HER2-targeted therapy. *Cancer Cell* 29, 117–129. doi: 10.1016/j.ccell.2015.12.008

LoRusso, P. M., Weiss, D., Guardino, E., Girish, S., and Sliwkowski, M. X. (2011). Trastuzumab emtansine: a unique antibody-drug conjugate in development for human epidermal growth factor receptor 2-positive cancer. *Clin. Cancer Res.* 17, 6437–6447. doi: 10.1158/1078-0432.ccr-11-0762

Lu, J., Jiang, F., Lu, A., and Zhang, G. (2016). Linkers having a crucial role in antibody-drug conjugates. *Int. J. Mol. Sci.* 17:561. doi: 10.3390/ijms17040561

Lyon, R. P., Bovee, T. D., Doronina, S. O., Burke, P. J., Hunter, J. H., Neff-LaFord, H. D., et al. (2015). Reducing hydrophobicity of homogeneous antibody-drug conjugates improves pharmacokinetics and therapeutic index. *Nat. Biotechnol.* 33, 733–735. doi: 10.1038/nbt.3212

Mager, D. E. (2006). Target-mediated drug disposition and dynamics. *Biochem. Pharmacol.* 72, 1–10. doi: 10.1016/j.bcp.2005.12.041

Meister, A., and Anderson, M. E. (1983). Glutathione. *Annu. Rev. Biochem.* 52, 711–760. doi: 10.1146/annurev.bi.52.070183.003431

Mohamed, H. E., Mohamed, A. A., Al-Ghobashy, M. A., Fathalla, F. A., and Abbas, S. S. (2018). Stability assessment of antibody-drug conjugate trastuzumab emtansine in comparison to parent monoclonal antibody using orthogonal testing protocol. *J. Pharma. Biomed. Anal.* 150, 268–277. doi: 10.1016/j.jpba.2017.12.022

Moolten, F. L., and Cooperband, S. R. (1970). Selective destruction of target cells by diphtheria toxin conjugated to antibody directed against antigens on the cells. *Science* 169, 68–70. doi: 10.1126/science.169.3940.68

Mullard, A. (2013). Maturing antibody-drug conjugate pipeline hits 30. *Nat. Rev. Drug Discov.* 12, 329–332. doi: 10.1038/nrd4009

Nasiri, H., Valedkarimi, Z., Aghebati-Maleki, L., and Majidi, J. (2018). Antibody-drug conjugates: promising and efficient tools for targeted cancer therapy. *J. Cell Physiol.* 233, 6441–6457. doi: 10.1002/jcp.26435

Okeley, N. M., Miyamoto, J. B., Zhang, X., Sanderson, R. J., Benjamin, D. R., Sievers, E. L., et al. (2010). Intracellular activation of SGN-35, a potent anti-CD30 antibody-drug conjugate. *Clin. Cancer Res.* 16, 888–897. doi: 10.1158/1078-0432.ccr-09-2069

Pabst, M., McDowell, W., Manin, A., Kyle, A., Camper, N., De Juan, E., et al. (2017). Modulation of drug-linker design to enhance in vivo potency of homogeneous antibody-drug conjugates. *J. Control Release* 253, 160–164. doi: 10.1016/j.jconrel.2017.02.027

Pak, Y., Zhang, Y., Pastan, I., and Lee, B. (2012). Antigen Shedding may improve efficiencies for delivery of antibody-based anticancer agents in solid tumors. *Cancer Res.* 72, 3143–3152. doi: 10.1158/0008-5472.CAN-11-3925

Palumbo, A., Hauler, F., Dziunycz, P., Schwager, K., Soltermann, A., Pretto, F., et al. (2011). A chemically modified antibody mediates complete eradication of tumours by selective disruption of tumour blood vessels. *Br. J. Cancer* 104, 1106–1115. doi: 10.1038/bjc.2011.78

Pei, Z., Chen, C., Chen, J., Cruz-Chuh, J. D., Delarosa, R., Deng, Y., et al. (2018). Exploration of pyrrolobenzodiazepine(PBD)-dimers containing disulfide-based prodrugs as payloads for antibody-drug conjugates. *Mol. Pharm.* 15, 3979–3996. doi: 10.1021/acs.molpharmaceut.8b00431

Perez, H. L., Cardarelli, P. M., Deshpande, S., Gangwar, S., Schroeder, G. M., Vite, G. D., et al. (2014). Antibody-drug conjugates: current status and future directions. *Drug Discov. Today* 19, 869–881. doi: 10.1016/j.drudis.2013.11.004

Petersdorf, S. H., Kopecky, K. J., Slovak, M., Willman, C., Nevill, T., Brandwein, J., et al. (2013). A phase 3 study of gemtuzumab ozogamicin during induction and postconsolidation therapy in younger patients with acute myeloid leukemia. *Blood* 121, 4854–4860. doi: 10.1182/blood-2013-01-466706

Piccione, E. C., Juarez, S., Liu, J., Tseng, S., Ryan, C. E., Narayanan, C., et al. (2015). A bispecific antibody targeting CD47 and CD20 selectively binds and eliminates dual antigen expressing lymphoma cells. *MABS* 7, 946–956. doi: 10.1080/19420862.2015.1062192

Polson, A. G., Calemine-Fenaux, J., Chan, P., Chang, W., Christensen, E., Clark, S., et al. (2009). Antibody-drug conjugates for the treatment of non-Hodgkin's lymphoma: target and linker-drug selection. *Cancer Res.* 69, 2358–2364. doi: 10.1158/0008-5472.can-08-2250

Qi, R., Wang, Y., Bruno, P. M., Xiao, H., Yu, Y., Li, T., et al. (2017). Nanoparticle conjugates of a highly potent toxin enhance safety and circumvent platinum resistance in ovarian cancer. *Nat. Commun.* 8:2166. doi: 10.1038/s41467-017-02390-7

Rosenberg, A. S. (2006). Effects of protein aggregates: an immunologic perspective. *AAPS J.* 8, E501–E507. doi: 10.1208/aapsj080359

Rossin, R., Versteegen, R. M., Wu, J., Khasanov, A., Wessels, H. J., Steenbergen, E. J., et al. (2018). Chemically triggered drug release from an antibody-drug conjugate leads to potent antitumour activity in mice. *Nat. Commun.* 9:1484. doi: 10.1038/s41467-018-03880-y

Rudnick, S. I., Lou, J., Shaller, C. C., Tang, Y., Klein-Szanto, A. J., Weiner, L. M., et al. (2011). Influence of affinity and antigen internalization on the uptake and penetration of Anti-HER2 antibodies in solid tumors. *Cancer Res.* 71, 2250–2259. doi: 10.1158/0008-5472.can-10-2277

Salfeld, J. G. (2007). Isotype selection in antibody engineering. *Nat. Biotechnol.* 25, 1369–1372. doi: 10.1038/nbt1207-1369

Sanderson, R. J., Hering, M. A., James, S. F., Sun, M. M., Doronina, S. O., Siadak, A. W., et al. (2005). In vivo drug-linker stability of an anti-CD30 dipeptide-linked auristatin immunoconjugate. *Clin. Cancer Res.* 11(2 Pt 1), 843–852.

Seaman, S., Zhu, Z., Saha, S., Zhang, X. M., Yang, M. Y., Hilton, M. B., et al. (2017). Eradication of tumors through simultaneous ablation of CD276/B7-H3-positive tumor cells and tumor vasculature. *Cancer Cell* 31, 501.e8–515.e8. doi: 10.1016/j.ccell.2017.03.005

Senter, P. D., and Sievers, E. L. (2012). The discovery and development of brentuximab vedotin for use in relapsed Hodgkin lymphoma and systemic anaplastic large cell lymphoma. *Nat. Biotechnol.* 30, 631–637. doi: 10.1038/nbt.2289

Shefet-Carasso, L., and Benhar, I. (2015). Antibody-targeted drugs and drug resistance–challenges and solutions. *Drug Resist. Updat.* 18, 36–46. doi: 10.1016/j.drup.2014.11.001

Sievers, E. L., and Senter, P. D. (2013). Antibody-drug conjugates in cancer therapy. *Annu. Rev. Med.* 64, 15–29. doi: 10.1146/annurev-med-050311-201823

Stein, E., Walter, R., Erba, H., Fathi, A., Advani, A., Lancet, J., et al. (2018). A phase 1 trial of vadastuximab talirine as monotherapy in patients with CD33-positive acute myeloid leukemia. *Blood* 131, 387–396. doi: 10.1182/blood-2017-06-789800

Thomas, A., Teicher, B. A., and Hassan, R. (2016). Antibody-drug conjugates for cancer therapy. *Lancet Oncol.* 17, e254–e262. doi: 10.1016/s1470-2045(16)30030-4

Tsumura, R., Manabe, S., Takashima, H., Koga, Y., Yasunaga, M., and Matsumura, Y. (2018). Influence of the dissociation rate constant on the intra-tumor distribution of antibody-drug conjugate against tissue factor. *J. Control. Release* 284, 49–56. doi: 10.1016/j.jconrel.2018.06.016

Walker, S., Landovitz, R., Ding, W. D., Ellestad, G. A., and Kahne, D. (1992). Cleavage behavior of calicheamicin gamma 1 and calicheamicin T. *Proc. Natl. Acad. Sci. U.S.A.* 89, 4608–4612. doi: 10.1073/pnas.89.10.4608

Younes, A., Yasothan, U., and Kirkpatrick, P. (2012). Brentuximab vedotin. *Nat. Rev. Drug Discov.* 11, 19–20. doi: 10.1038/nrd3629

Yurkovetskiy, A. V., Yin, M., Bodyak, N., Stevenson, C. A., Thomas, J. D., Hammond, C. E., et al. (2015). A Polymer-based antibody-vinca drug conjugate platform: characterization and preclinical efficacy. *Cancer Res.* 75, 3365–3372. doi: 10.1158/0008-5472.can-15-0129

Zhang, D., Le, H., Cruz-Chuh, J. D., Bobba, S., Guo, J., Staben, L., et al. (2018a). Immolation of p-aminobenzyl ether linker and payload potency and stability determine the cell-killing activity of antibody-drug conjugates with phenol-containing payloads. *Bioconjug. Chem.* 29, 267–274. doi: 10.1021/acs.bioconjchem.7b00576

Zhang, D., Yu, S. F., Khojasteh, S. C., Ma, Y., Pillow, T. H., Sadowsky, J. D., et al. (2018b). Intratumoral payload concentration correlates with the activity of antibody-drug conjugates. *Mol. Cancer Ther.* 17, 677–685. doi: 10.1158/1535-7163.mct-17-0697

Zhang, D., Pillow, T. H., Ma, Y., Cruz-Chuh, J. D., Kozak, K. R., Sadowsky, J. D., et al. (2016). Linker immolation determines cell killing activity of disulfide-linked pyrrolobenzodiazepine antibody-drug conjugates. *ACS Med. Chem. Lett.* 7, 988–993. doi: 10.1021/acsmedchemlett.6b00233

Conflict of Interest Statement: The authors declare that the research was conducted in the absence of any commercial or financial relationships that could be construed as a potential conflict of interest.

frontiers in Oncology

ORIGINAL RESEARCH
published: 25 April 2019
doi: 10.3389/fonc.2019.00313

Glesatinib, a c-MET/SMO Dual Inhibitor, Antagonizes P-glycoprotein Mediated Multidrug Resistance in Cancer Cells

*Qingbin Cui[1,2], Chao-Yun Cai[2], Hai-Ling Gao[2,3], Liang Ren[1], Ning Ji[2,4], Pranav Gupta[2], Yuqi Yang[2], Suneet Shukla[5], Suresh V. Ambudkar[5], Dong-Hua Yang[2] and Zhe-Sheng Chen[2]**

[1] School of Public Health, Guangzhou Medical University, Guangdong, China, [2] Department of Pharmaceutical Sciences, College of Pharmacy and Health Sciences, St. John's University, Queens, NY, United States, [3] Department of Histology and Embryology, Clinical Medical College, Weifang Medical University, Weifang, China, [4] Tianjin Key Laboratory on Technologies Enabling Development of Clinical Therapeutics and Diagnostics, School of Pharmacy, Tianjin Medical University, Tianjin, China, [5] Laboratory of Cell Biology, Center for Cancer Research, National Cancer Institute, NIH, Bethesda, MD, United States

OPEN ACCESS

Edited by:
Massimo Broggini, Istituto Di Ricerche Farmacologiche Mario Negri, Italy

Reviewed by:
Fabrizio Martelli, Istituto Superiore di Sanità (ISS), Italy
Kamini Singh, Memorial Sloan Kettering Cancer Center, United States
Sandro Cosconati, Università degli Studi della Campania Luigi Vanvitelli Caserta, Italy

***Correspondence:**
Zhe-Sheng Chen
chenz@stjohns.edu

Specialty section:
This article was submitted to Cancer Molecular Targets and Therapeutics, a section of the journal Frontiers in Oncology

Received: *25 January 2019*
Accepted: *08 April 2019*
Published: *25 April 2019*

Citation:
Cui Q, Cai C-Y, Gao H-L, Ren L, Ji N, Gupta P, Yang Y, Shukla S, Ambudkar SV, Yang D-H and Chen Z-S (2019) Glesatinib, a c-MET/SMO Dual Inhibitor, Antagonizes P-glycoprotein Mediated Multidrug Resistance in Cancer Cells. Front. Oncol. 9:313. doi: 10.3389/fonc.2019.00313

Multidrug resistance (MDR) is one of the leading causes of treatment failure in cancer chemotherapy. One major mechanism of MDR is the overexpressing of ABC transporters, whose inhibitors hold promising potential in antagonizing MDR. Glesatinib is a dual inhibitor of c-Met and SMO that is under phase II clinical trial for non-small cell lung cancer. In this work, we report the reversal effects of glesatinib to P-glycoprotein (P-gp) mediated MDR. Glesatinib can sensitize paclitaxel, doxorubicin, colchicine resistance to P-gp overexpressing KB-C2, SW620/Ad300, and P-gp transfected Hek293/ABCB1 cells, while has no effect to their corresponding parental cells and negative control drug cisplatin. Glesatinib suppressed the efflux function of P-gp to [^{3}H]-paclitaxel and it didn't impact both the expression and cellular localization of P-gp based on Western blot and immunofluorescent analysis. Furthermore, glesatinib can stimulate ATPase in a dose-dependent manner. The docking study indicated that glesatinib interacted with human P-gp through several hydrogen bonds. Taken together, c-Met/SMO inhibitor glesatinib can antagonize P-gp mediated MDR by inhibiting its cell membrane transporting functions, suggesting new application in clinical trials.

Keywords: multidrug resistance, P-gp, glesatinib, reversal effects, mechanism

INTRODUCTION

Multidrug resistance (MDR) is the one of the major challenges in cancer treatment (1). MDR refers to a phenomenon that cancer cell once becomes resistant to one chemotherapeutic, accompanied by cross resistant to other chemotherapeutics that are structurally and mechanistically different (2). MDR is one of the major causes of failure in cancer treatment. The mechanisms of MDR involve dynamic ATP-binding cassette (ABC) transporters (3, 4), oncogenes mutations (5), microenvironment changes (6), reprogramed cancer cell metabolism (7, 8), efficient DNA repairing (9, 10), survived cancer stem cells (11, 12), and activated detoxifying systems (13, 14). Novel effective remedies are urgently needed to circumvent MDR.

ABC transporters are a group of active transporter proteins that have diverse functions and are present in the membrane of both prokaryotes and eukaryotes, acting as protecting enzymes against xenobiotic, including many chemotherapeutics (15, 16). One of the most well studied ABC transporters is P-glycoprotein (P-gp), which is encoded by ABCB1 genes. P-gp contributes in pumping out many different kinds of anticancer drugs, namely, taxanes, anthracyclines, vinca alkaloids, and epipodophyllotoxins (17–24). To counteract the negative regulation of chemotherapy by P-gp, three generations of inhibitors (both specific and non-specific) have been developed and some of them have been introduced into clinical trials (25). However, due to unexpected adverse effects or severely drug-drug interaction, none of them have been approved by FDA (3, 26). There is an unmet need for effective and safe reversal agents for clinical use. Recently, certain tyrosine kinase inhibitors (TKIs) have been found to exert MDR reversal effect via regulating P-gp at non-toxic concentration (27–31), suggesting new regimens in the treatment of resistant cancer. TKI glesatinib (**Figure 1A**), a c-MET/SMO dual inhibitor (32, 33), is now under Phase II clinical trials in combination with Nivolumab in treatment of the non-small cell lung cancer (NSCLC). More importantly, we found that glesatinib can antagonize P-gp mediated MDR. Here, we report the reversal effects of glesatinib and the underlying mechanisms.

MATERIALS AND METHODS

Chemicals

Glesatinib (99% purity as measured by high performance liquid chromatography) was purchased from ChemieTek (Indianapolis, IN). Dulbecco's modified Eagle's Medium (DMEM), bovine serum albumin (BSA), fetal bovine serum (FBS), penicillin/streptomycin and trypsin 0.25% were purchased from Hyclone (GE Healthcare Life Science, Pittsburgh, PA). The monoclonal antibodies for ABCB1 (C219) and GAPDH (MA5-15738), Alexa Fluor 488 conjugated goat anti-mouse IgG secondary antibody were purchased from Thermo Fisher Scientific Inc (Rockford, IL), dimethylsulfoxide (DMSO), 3-(4,5-dimethylthiazol-yl)-2,5-diphenyltetrazolium bromide (MTT), Triton X-100, 4',6-diamidino-2-phenylindole (DAPI), paraformaldehyde, paclitaxel, doxorubicin, colchicine, cisplatin, verapamil and Ko 143 were purchased from Sigma-Aldrich (St. Louis, MO). [^{3}H]-paclitaxel (15 Ci/mmol) was purchased from Moravek Biochemicals, Inc (Brea, CA). All other chemicals were purchased from Sigma Chemical Co (St. Louis, MO).

Cell Lines and Cell Culture

The human epidermoid carcinoma cell line KB-3-1 and its colchicine-selected P-gp-overexpressing KB-C2 cells, the human colon cancer cell line SW620 and its doxorubicin-selected P-gp-overexpressing SW620/Ad300 cells, the NSCLC cell line NCI-H460 and its mitoxantrone-selected ABCG2-overexpressing NCI-H460/MX20 cells, were used for P-gp and ABCG2 reversal study, respectively. The HEK293/pcDNA3.1, HEK293/ABCB1 cells lines were established by transfecting HEK293 cells with either the empty pcDNA3.1 vector or the vector containing full length ABCB1 (HEK293/ABCB1), and were cultured in a medium containing 2 mg/mL of G418. All cell were cultured at 37°C, using 5% CO_2 with DMEM containing 10% FBS and 1% penicillin/streptomycin. All drug resistant cell lines were grown as adherent monolayer in a drug-free culture media for more than 2 weeks prior to their use.

Cytotoxicity and Reversal Experiments

The cytotoxicity and reversal experiments of glesatinib to KB-3-1, KB-C2, SW620, SW620/Ad300, HEK293/pcDNA3.1, HEK293/ABCB1 cells were performed by using the MTT colorimetric assay (34). For reversal experiments, the applied concentrations of glesatinib were 1 and 3 μM according to the results of cytotoxicity experiments. All of the experiments were repeated at least three times, and the mean and standard deviation (SD) values were calculated. Verapamil (3 μM) was used as a positive control inhibitor of P-gp, Ko 143 was used as a positive control inhibitor of ABCG2, cisplatin, a non-P-gp substrate, was used as a negative control.

Western Blot Analysis

Dose-dependent (0, 0.3, 1, 3 μM) and time-dependent (0, 24, 48, 72 h) of glesatinib on the expression of P-gp were determined. Twenty microgram protein cell lysates were loaded in each lane. The presence of P-gp was determined using monoclonal antibody C219 (dilution 1:200). GAPDH was used to confirm equal loading in each lane in the samples prepared from cell lysates. The resulting protein bands were quantified by using Image J software. The detailed protocol of Western blot analysis was carried out as previously described (35).

Immunofluorescence Analysis

SW620, SW620/Ad300 cells were seeded (1×10^4/well) in 24-well plates and cultured at 37°C for 24 h, followed by incubation with 3 μM glesatinib for 0, 24, 48, and 72 h, respectively. Then cells were fixed in 4% paraformaldehyde for 5 min and permeabilized by 0.1% Triton X-100 for 5 min before blocked with 6% BSA for 1 h at 37°C. The presence of P-gp was determined using monoclonal antibody F4 (dilution 1:1000) for incubation at 4°C overnight. Alexa Fluor 488 conjugated secondary antibody (1:1000) was used for incubation at 37°C for 1 h. After washing with iced PBS, DAPI (1 μg/mL) was used to counterstain the nuclei. Immunofluorescence images were collected using an EVOS FL Auto fluorescence microscope (Life Technologies Corporation, Gaithersburg, MD).

ATPase Assay

The vanadate-sensitive ATPase activity of ABCB1 in membrane vesicles of High Five insect cells was measured as previously described (36). Briefly, the membrane vesicles (10 μg of protein) were incubated in ATPase assay buffer [composed by 50 mmol/L MES (pH 6.8), 50 mmol/L KCl, 5 mmol/L sodium azide, 2 mmol/L EGTA, 2 mmol/L DTT, 1 mmol/L ouabain, and 10 mmol/L $MgCl_2$] with or without 0.3 mmol/L vanadate at 37°C for 5 min, then were incubated with different concentrations (ranging from 0 to 40 μM) of glesatinib at 37°C for 3 min. The ATPase reaction was induced by the addition of 5 mM of Mg-ATP, and the total volume was 0.1 mL. After incubation

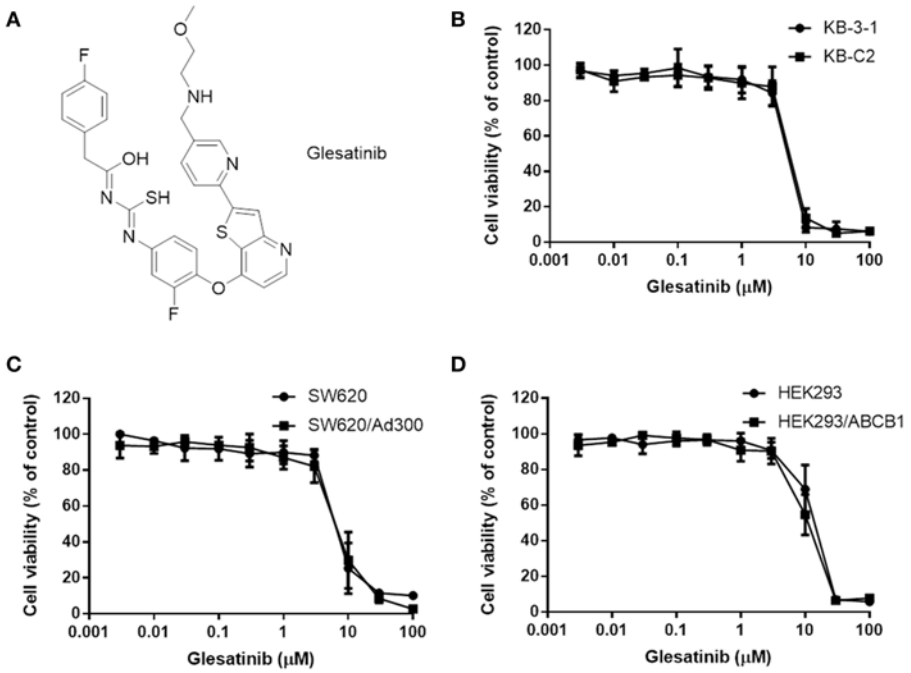

FIGURE 1 | The structure of glesatinib and its cytotoxic effects to three P-gp overexpressing cancer cells. **(A)** Chemical structure of glesatinib. **(B)** Concentration -dependent viability curves for KB-3-1 and KB-C2 cell lines incubated with different concentration of glesatinib for 72 h. **(C)** Concentration-dependent viability curves for SW620 and SW620/Ad300 cell lines incubated with different concentration of glesatinib for 72 h. **(D)** Concentration-dependent viability curves for HEK293/pcDNA3.1 and HEK293/ABCB1 cells incubated with different concentration of glesatinib for 72 h. The cell viability was determined by MTT assay. Data are expressed as mean ± SD, and representative of three independent experiments in triplicate are shown.

at 37°C for 20 min, the reaction was allowed to continue for another 20 min at 37°C and then terminated by adding 100 μL of a 5% SDS solution to the reaction mix. The amount of inorganic phosphate (IP) release was detected at 880 nm using a spectrophotometer.

[^{3}H]-Paclitaxel Accumulation and Efflux Assay

Since glesatinib reversed MDR mediated by P-gp, the reversal mechanism may be related to change of the protein expression or location of P-gp, we used the drug accumulation and efflux assays to determine the reversal mechanism as previously described (27). The accumulation and efflux of [^{3}H]-paclitaxel in KB-3-1 and KB-C2 cells were measured in the absence or presence of glesatinib (1, 3 μM), and verapamil (3 μM) was used as positive control.

Molecular Modeling of Human ABCB1 Homology Model

To reveal more details of the interaction between glesatinib and P-gp, we conducted docking study. All docking experiments were performed following the reported protocols with software Schrodinger 2018–1 (Schrödinger, LLC, New York, NY, 2018) on a Mac Pro 6-core Intel Xenon X5 processor with Macintosh Operating System (OS X El Capitan) (28, 37). Ligand preparation was essentially performed. Human P-gp homology model (4M1M) was established by Dr. S. Aller based on improved mouse P-gp (3G5U). Single-wavelength anomalous diffraction (SAD) phasing was conducted to the full 3.8 Å resolution of the dataset. Non-crystallographic symmetry (NCS) operators were determined from the mouse P-gp structure with the phenix.python script simple_ncs_from_pdb.py. Refinement was conducted with phenix.refine using NCS and secondary structure restraints, restraining NCS-related B-factors, group B-factor and individual B-factor (38). The centroid of some important residues including H61, G64, L65, M68, L339, A342, L975 C343, F942, T945, Q946, Y950, L975, V982, and A985 (39–41). Glide XP docking was performed and the receptor grid for induced-fit docking (IFD) was generated by selecting residues. Then IFD was conducted with the default protocol.

Statistical Analysis

All data are expressed as the mean ± SD. All experiments were repeated at least three times and the data were analyzed using a one-way or two-way ANOVA by GraphPad Prism 7.00 software. Differences were considered significant when $P < 0.05$.

RESULTS

Glesatinib Antagonized MDR in P-gp Overexpressing Cancer Cells

First, the cytotoxicity of glesatinib to P-gp overexpressing cancer cells KB-C2, SW620/Ad300, HEK293/ABCB1, and their parent cells KB-3-1, SW620, HEK293 cells were determined by MTT

assay. As shown in **Figures 1B–D**, the IC_{50}s fell between 5 and 10 μM. Therefore, the non-toxic concentration (IC_{20}) of glesatinib applied in the reversal effects evaluation were 1 and 3 μM.

The reversal effects of glesatinib to P-gp substrates, including doxorubicin, paclitaxel and colchicine were further tested in the aforementioned cancer cells. The non-selective P-gp inhibitor, verapamil was used as a positive control (42), and non-substrate cisplatin was used as a negative control (43). Pretreatment with or without glesatinib with these substrates to P-gp overexpressing cancer cells and their sensitive parent cells were tested to obtain their IC_{50}s.

As shown in **Tables 1**, **2**, the parent cells were sensitive to doxorubicin, paclitaxel and colchicine, and the IC_{50}s were as low as nano-mole. While P-gp overexpressing cancer cell exhibited resistant properties to these chemotherapeutics, resistance fold ranged from 77 to 438. Pretreatment with glesatinib significantly lowered the IC_{50}s of all these three chemotherapeutics to resistant cancer cells. More importantly, glesatinib exhibited similar re-sensitizing effects to P-gp transfected HEK293/ABCB1 cells, suggesting its mechanisms of re-sensitizing to chemotherapeutics were directly or indirectly related to P-gp. In addition, in ABCG2 overexpressing cancer cells NCI-H460/MX20 cells, gleasatinib failed to reverse topotecan (an ABCG substrate) resistance (**Table 2**). These results indicated that glesatinib could antagonize cancer MDR mediated by P-gp, but not MDR mediated by ABCG2.

Glesatinib Did Not Impact the P-gp Expression and Subcellular Localization

The down-regulation or re-localization of P-gp (from cellular membrane to cytosol) may lead to re-sensitization of chemotherapeutics as a result of less extent of efflux or unable to exert its functions (17, 44). We further determined the interaction mechanism of glesatinib with P-gp by examining the P-gp expression and cellular location through Western blotting and immunofluorescence assay. P-gp overexpressing KB-C2 cells were treated with glesatinib at different concentration (0.3, 1, 3 μM for 72 h) or at different time (3 μM for 24, 48, 72 h) and the P-gp expression was examined. SW620/Ad300 cells were treated with 3 μM for 0, 24, 48, 72 h to examine the localization of P-gp. KB-3-1 and SW620 cells were used as negative control in this experiment.

As shown in **Figure 2**, P-gp expression was not impacted by glesatinib either dose- or time-dependently. The immunofluorescence assay results of **Figure 3** showed that after treatment of glesatinib, localization of P-gp had not changed and remained to localize on the cell membrane. These results suggested that glesatinib could not impact the expression and localization of P-gp. We next tested the effects of glesatinib to the efflux functions of P-gp.

Glesatinib Increased the Intracellular [^{3}H]-Paclitaxel Accumulation and Inhibited [^{3}H]-Paclitaxel Efflux in Cancer Cell Lines Overexpressing P-gp

As glesatinib did not alter either P-gp expression or its localization, we set out to test the transporting function of P-gp by examining the cellular accumulation of radioactive [^{3}H]-paclitaxel. As shown in **Figures 4A,B**, in KB-3-1 cells that barely expressed P-gp, [^{3}H]-paclitaxel had not been impacted, and glesatibin had no effects to either the drug accumulation (**Figure 4A**) or efflux (**Figure 4B**).

TABLE 1 | Glesatinib sensitized paclitaxel, colchicine, and doxorubicin to P-gp-overexpressing cell lines (KB-C2 and HEK293/ABCB1 cells).

Treatment	IC_{50} ± SD[a] (RF[b])			
	KB-3-1 (μM)	KB-C2 (μM)	HEK293 (μM)	HEK293/ABCB1 (μM)
Paclitaxel	0.004 ± 0.002 (1.00)	1.755 ± 0.057 (438.75)	0.073 ± 0.027 (1.00)	3.757 ± 0.312 (51.46)
+ Gle (1 μM)	0.004 ± 0.001 (1.00)	0.220 ± 0.026 (55)*	0.122 ± 0.050 (1.67)	0.255 ± 0.084 (3.49)*
+ Gle (3 μM)	0.003 ± 0.001 (0.75)	0.015 ± 0.001 (3.75)*	0.100 ± 0.020 (1.37)	0.047 ± 0.004 (0.64)*
+ Vera (3 μM)	0.003 ± 0.001 (0.75)	0.010 ± 0.002 (2.5)*	0.068 ± 0.003 (0.95)	0.094 ± 0.003 (1.9)*
Doxorubicin	0.032 ± 0.013 (1.00)	2.504 ± 0.487 (78.25)	0.061 ± 0.020 (1.00)	0.631 ± 0.150 (10.34)
+ Gle (1 μM)	0.029 ± 0.003 (0.91)	0.118 ± 0.061 (3.69)*	0.060 ± 0.029 (0.98)	0.072 ± 0.006 (1.18)*
+ Gle (3 μM)	0.028 ± 0.004 (0.88)	0.023 ± 0.010 (0.72)*	0.066 ± 0.009 (1.08)	0.064 ± 0.021 (1.05)*
+ Vera (3 μM)	0.024 ± 0.006 (0.75)	0.024 ± 0.005 (0.75)*	0.061 ± 0.008 (1.00)	0.084 ± 0.009 (1.38)*
Colchicine	0.009 ± 0.002 (1.00)	3.231 ± 0.260 (359.00)	0.066 ± 0.001 (1.00)	1.538 ± 0.090 (23.30)
+ Gle (1 μM)	0.006 ± 0.002 (0.67)	0.993 ± 0.183 (110.33)*	0.058 ± 0.007 (0.88)	0.126 ± 0.106 (1.91)*
+ Gle (3 μM)	0.007 ± 0.001 (0.78)	0.088 ± 0.020 (9.78)*	0.048 ± 0.009 (0.73)	0.047 ± 0.021 (0.71)*
+ Vera (3 μM)	0.009 ± 0.001 (1.00)	0.116 ± 0.035 (12.89)*	0.056 ± 0.006 (0.85)	0.050 ± 0.008 (0.76)*
Cisplatin	2.508 ± 0.432 (1.00)	3.027 ± 0.343 (1.21)	2.660 ± 0.430 (1.00)	3.336 ± 0.451 (1.25)
+ Gle (1 μM)	1.990 ± 0.452 (0.79)	2.676 ± 0.443 (1.07)	1.982 ± 0.253 (0.75)	3.272 ± 0.254 (1.23)
+ Gle (3 μM)	2.031 ± 0.364 (0.81)	2.120 ± 0.152 (0.85)	1.903 ± 0.361 (0.72)	3.394 ± 0.353 (1.28)
+ Vera (3 μM)	2.309 ± 0.641 (0.92)	2.098 ± 0.230 (0.84)	2.388 ± 0.452 (0.90)	3.115 ± 0.433 (1.17)

*$P < 0.05$ vs. no inhibitor group.

[a] IC_{50} values represented the mean ± SD of three independent experiments performed in triplicate.

[b] Resistance fold (RF) was calculated by dividing the IC50 values of substrates in the presence or absence of an inhibitor by the IC_{50} values of parental cells without an inhibitor. Gle, Glesatinib; Vera, verapamil.

TABLE 2 | Glesatinib sensitized paclitaxel, colchicine, and doxorubicin to P-gp-overexpressing cell line (SW620/Ad300 cells), but not topotecan to ABCG2-overexpressing cells (NCI-H460/MX20 cells).

Treatment	$IC_{50} \pm SD^a$ (RF^b)		Treatment	$IC_{50} \pm SD^a$ (RF^b)	
	SW620 (μM)	SW620/Ad300 (μM)		NCI-H460 (μM)	NCI-H460/MX20 (μM)
Paclitaxel	0.091 ± 0.015 (1.00)	21.190 ± 6.25 (232.86)	Topotecan	0.063 ± 0.020 (1.00)	6.010 ± 0.530 (95.49)
+ Gle (1 μM)	0.067 ± 0.013 (0.74)	1.969 ± 0.160 (21.63)*	+ Gle (1 μM)	0.060 ± 0.015 (0.95)	6.360 ± 0.127 (100.95)
+ Gle (3 μM)	0.060 ± 0.020 (0.66)	0.257 ± 0.072 (2.82)*	+ Gle (3 μM)	0.040 ± 0.021 (0.63)	7.160 ± 1.193 (113.65)
+ Vera (3 μM)	0.097 ± 0.031 (1.07)	0.646 ± 0.173 (7.10)*	+ Ko 143 (3 μM)	0.051 ± 0.013 (0.81)	0.520 ± 0.130 (8.25)*
Doxorubicin	0.031 ± 0.014 (1.00)	9.950 ± 2.023 (320.97)	Cisplatin	1.640 ± 0.185 (1.00)	2.150 ± 0.498 (1.31)
+ Gle (1 μM)	0.033 ± 0.007 (1.06)	2.397 ± 0.041 (77.32)*	+ Gle (1 μM)	1.699 ± 0.392 (1.04)	1.926 ± 0.297 (1.17)
+ Gle (3 μM)	0.029 ± 0.012 (0.94)	0.271 ± 0.020 (8.74)*	+ Gle (3 μM)	1.513 ± 0.218 (0.92)	2.049 ± 0.187 (1.25)
+ Vera (3 μM)	0.023 ± 0.007 (0.74)	0.288 ± 0.155 (9.29)*	+ Ko 143 (3 μM)	1.686 ± 0.152 (1.03)	2.285 ± 0.138 (1.39)
Cisplatin	1.481 ± 0.676 (1.00)	1.514 ± 0.398 (1.02)			
+ Gle (1 μM)	1.266 ± 0.189 (0.85)	1.676 ± 0.138 (1.13)			
+ Gle (3 μM)	1.166 ± 0.079 (0.79)	1.587 ± 0.329 (1.07)			
+ Vera (3 μM)	1.164 ± 0.107 (0.79)	1.851 ± 0.364 (1.25)			

*$P < 0.05$ vs. no inhibitor group.

[a] IC_{50} values represented the mean ± SD of three independent experiments performed in triplicate.

[b] Resistance fold (RF) was calculated by dividing the IC_{50} values of substrates in the presence or absence of an inhibitor by the IC_{50} values of parental cells without an inhibitor. Gle, Glesatinib; Vera, verapamil.

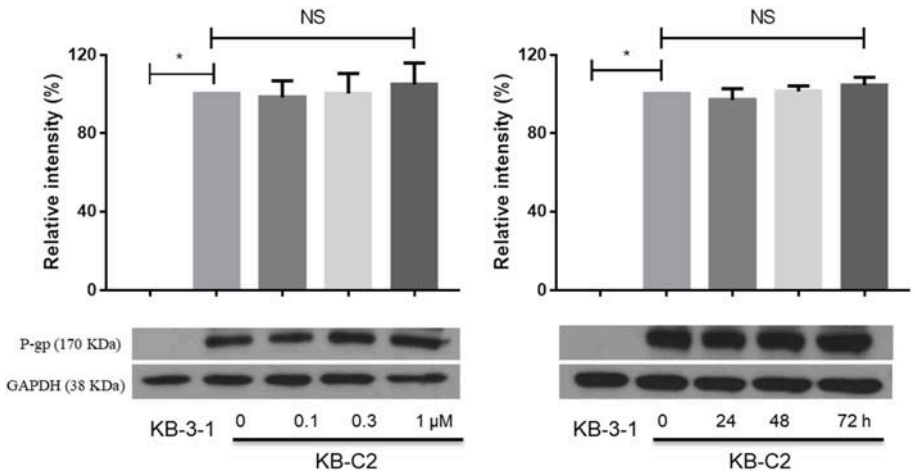

FIGURE 2 | Glesatinib did not affect the protein expression of P-gp transporters in ABCB1 overexpressing cell lines. Detection and relative intensity of ABCB1 expression in KB-C2 cells incubated with 0.3, 1, 3 μM for 72 h and 3 μM for 0, 24, 48, 72 h. Data are mean ± SD, representative of three independent experiments. *$p < 0.05$, compared with control group.

While in P-gp overexpressing KB-C-2 cells, [^{3}H]-paclitaxel accumulation decreased significantly as shown in **Figures 4A,C**. Pretreatment of glesatinib may significantly increase the [^{3}H]-paclitaxel accumulation and inhibited the drug efflux of P-gp. These results indicated that glesatinib may exert its re-sensitizing effects by thwart the transporting function of P-gp.

Glesatinib Stimulated the ATPase Activity of P-gp

ATP hydrolyzed by ATPase was used by P-gp to provide the energy to transport its substrates (45, 46). To further reveal the P-gp inhibitory mechanisms, we determined the effect of glesatinib on the ATPase activity of P-gp transporters by measuring P-gp-mediated ATP hydrolysis in the presence or absence of glesatinib (0–40 μM). As shown in **Figure 5**, Glesatinib stimulated the ATPase activity of P-gp transporters in a dose-dependent manner. The concentration of 50% stimulation was 3.2 μM, and the maximum stimulation was 5.59-fold greater than that of basal level.

Induced-Fit Docking (IFD) Simulation Interactions Between P-gp and Glesatinib

We investigated the potential interaction of glesatinib with P-gp by conducting docking analysis. The best docking score of the binding of glesatinib and human P-gp was −12.639 kcal/mol. The best-scored docked position of glesatinib with P-gp was showed

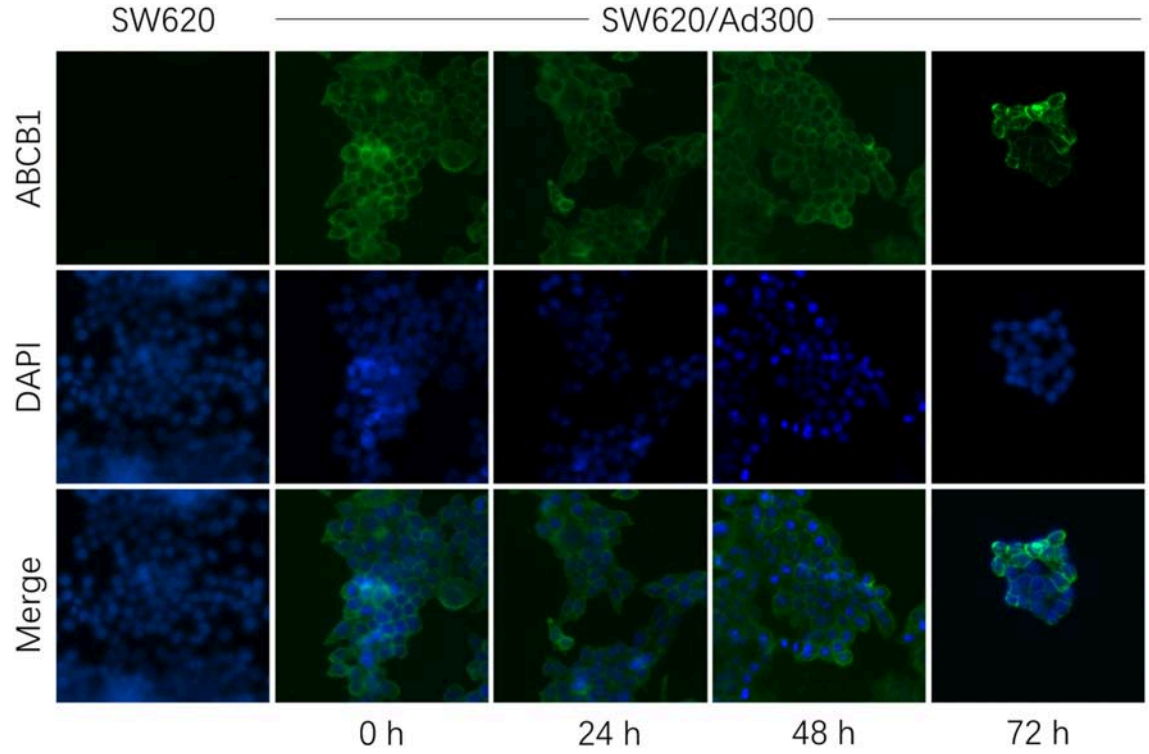

FIGURE 3 | Glesatinib did not affect the localization of ABCB1 transporters in ABCB1 overexpressing cell lines. Sub-cellular localization of ABCB1 expression in SW620/Ad300 cells incubated with 3 μM of glesatinib for 0, 24, 48, and 72 h. ABCB1, green and DAPI (blue) counterstains the nuclei. SW620 cells represented the control group.

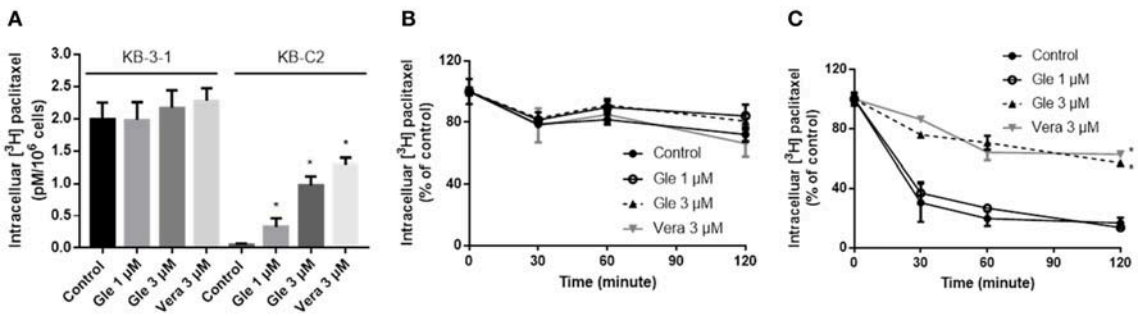

FIGURE 4 | Glesatinib increased the accumulation and inhibited the efflux of [^{3}H]-paclitaxel in P-gp overexpressing KB-C2 cells. **(A)** The effect of glesatinib on the accumulation of [^{3}H]-paclitaxel in KB-3-1 and KB-C2 cell lines. **(B)** The effect of glesatinib on efflux of [^{3}H]-paclitaxel in KB-3-1 and **(C)** KB-C2. Verapamil (3 μM) was used as positive controls. Data are mean ± SD, representative of three independent experiments. *$p < 0.05$, compared with control group. Gle, Glesatinib; Vera, verapamil.

in **Figure 6**. There were two hydrogen bonds between glesatinib and human P-gp, including the hydrogen binding between the amide group of glesatinib and Tyr950 (C=O…HO-Tyr950), in addition with the hydrogen bond between the methoxy group and Asn721 (H_3C-O…H_2N-Asn721). The fluorophenyl group of glesatinib has π-π interaction with both Phe336 and Phe983 of P-gp protein. The thienopyridine group has π-π interaction with the residues Phe728 and Phe983. Interestingly, the acidic microenvironment of tumor (47) could result in the ionization of glesatinib, and the amine cation could form a hydrogen bond with Tyr307 and a π-cation bond with Phe303. These formed various bonds between glesatinib and human P-gp may finally lead to the collapsed P-gp.

DISCUSSION

ABC transporter P-gp functions as the protective enzyme that pumps out xenobiotics including many chemotherapeutics that are its substrates, causing MDR in cancers (3). To counter that, many P-gp inhibitors have been developed and some of them have been tested in clinical trials, while all of them have failed to get approved by US

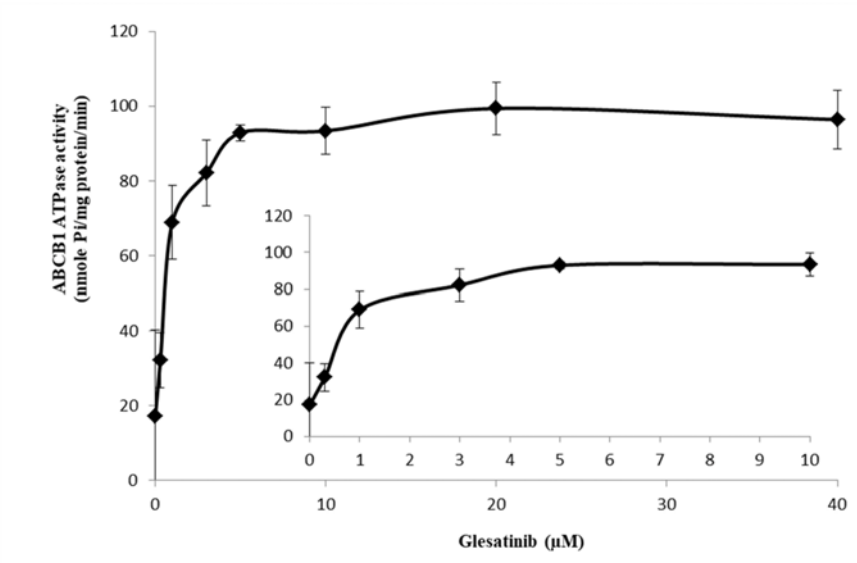

FIGURE 5 | Glesatinib stimulated the ATPase activity of P-gp. Effect of various concentrations of glesatinib on the ATPase activity of P-gp. The inset graphs illustrate the effect of 0–10 μM glesatinib on the ATPase activity of P-gp. Data are mean ± SD, representative of three independent experiments.

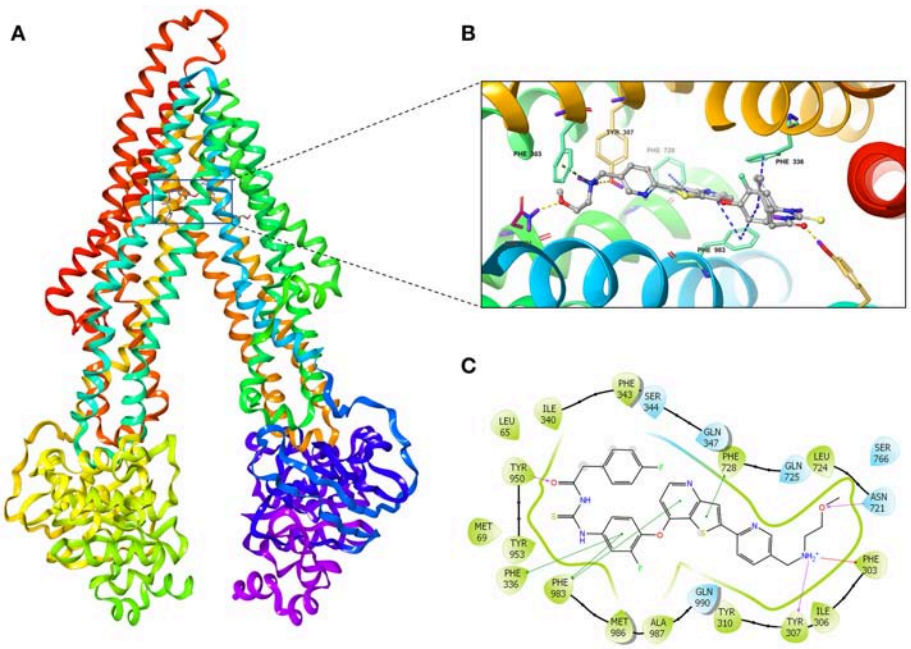

FIGURE 6 | The molecular modeling study of glesatinib with human homology ABCB1. **(A)** Overall view of glesatinib-P-gp complex. **(B)** 3D figure of Docked position of glesatinib within the drug-binding site of human P-gp homology model. Glesatinib was showed as ball and stick mode with the atoms colored: carbon-cyan, nitrogen-blue, oxygen-red, fluorine-green, sulfur-yellow, hydrogen-purple. Important residues were showed as sticks, with the color pattern: carbon-gray, nitrogen-blue, oxygen-red, hydrogen-purple. π-π stacking interactions are indicated with cyan dotted line. π-cation bond is indicated with green dotted line. Hydrogen bonds were showed by the yellow dotted line. **(C)** 2D figure of Docked position of glesatinib within the drug-binding site of human P-gp homology model. The cyan bubbles indicate polar residues and the green bubbles indicate hydrophobic residues. Hydrogen bonds are shown by the purple dotted arrow. π-π stacking interactions are shown by the green lines and π-cation bond is indicated with red line.

FDA due to severely adverse effects (48, 49). Recent studies indicate that certain TKIs may work as regulators of P-gp (2, 50), either inhibiting its expression (51) or impact its functions (35). Combinations of these TKIs and chemotherapeutics hold promising potential in the treatment of MDR cancers.

In this work, we found that MET/SMO dual inhibitor glesatinib, a drug candidate that is now under clinical trials, antagonized P-gp mediated MDR in cancer cells overexpressing P-gp. As shown in SW620/Ad300 and KB-C2 cells, glesatinib could antagonized P-gp mediated resistance by significantly reducing the IC_{50}s of doxorubicin, paclitaxel and colchicine, while had no effects to cisplatin which was not a substrate of P-gp. To confirm these effects were mediated by P-gp, we further tested its reversal effects to P-gp transpected HEK293 cells. Glesatinib exhibited similar effects in HEK293/ABCB1 cells, indicating the effects were mediated by regulating P-gp. We further confirmed that glesatinib did not affect the expression and sub-cellular localization of P-gp, while it could stimulate ATPase, similar as P-gp inhibitor verapamil (45). Importantly, our results showed gleastinib significantly increased the intracellular accumulation of [^{3}H]-paclitaxel and suppressed the efflux effects, which may contribute to the increased cytotoxic effects when used by combination. Finally, the docking study indicated that glesatinib might have strong interaction with P-gp via hydrogen bonds and π-π interaction, leading to the efflux inhibition. This docking result may provide valuable information to develop glesatinib derivatives for better targeting and/or binding.

In conclusion, MET/SMO dual inhibitor Glesatinib antagonized P-gp mediated MDR by inhibiting its efflux functions. This work provided important information for further clinical trials.

AUTHOR CONTRIBUTIONS

QC and Z-SC: conception and design. QC, C-YC, H-LG, NJ, SS, SA, and Z-SC: development of methodology. QC, C-YC, H-LG, PG, and NJ: acquisition of data. QC, C-YC, H-LG, NJ, and Z-SC: analysis and interpretation of data. QC, C-YC, LR, YY, D-HY, and Z-SC: writing, review, and/or revision of the manuscript. All authors read and approved the final manuscript.

ACKNOWLEDGMENTS

We thank Dr. Stephen Aller for providing the human ABCB1 homology model. We thank Dr. Tanaji T. Talele for providing the computing resources for the docking study. We thank Drs. Susan E. Bates and Robert W. Robey (NCI, NIH, Bethesda, MD) for providing the cell lines. We thank the support of Guangzhou Postdoctoral Foundation of International Training for QC and NIH funding (No. 1R15GM116043-01) to Z-SC.

REFERENCES

1. Housman G, Byler S, Heerboth S, Lapinska K, Longacre M, Snyder N, et al. Drug resistance in cancer: an overview. *Cancers*. (2014) 6:1769–92. doi: 10.3390/cancers6031769
2. Shukla S, Chen ZS, Ambudkar SV. Tyrosine kinase inhibitors as modulators of ABC transporter-mediated drug resistance. *Drug Resist Updat.* (2012) 15:70–80. doi: 10.1016/j.drup.2012.01.005
3. Robey RW, Pluchino KM, Hall MD, Fojo AT, Bates SE, Gottesman MM. Revisiting the role of ABC transporters in multidrug-resistant cancer. *Nat Rev Cancer*. (2018) 18:452–64. doi: 10.1038/s41568-018-0005-8
4. Kathawala RJ, Gupta P, Ashby CJ, Chen ZS. The modulation of ABC transporter-mediated multidrug resistance in cancer: a review of the past decade. *Drug Resist Updat.* (2015) 18:1-17. doi: 10.1016/j.drup.2014.11.002
5. Xue M, Cheng J, Zhao J, Zhang S, Jian J, Qiao Y, et al. Outcomes of 219 chronic myeloid leukaemia patients with additional chromosomal abnormalities and/or tyrosine kinase domain mutations. *Int J Lab Hematol.* (2018) 41:94–101. doi: 10.1111/ijlh.12928
6. Taylor S, Spugnini EP, Assaraf YG, Azzarito T, Rauch C, Fais S. Microenvironment acidity as a major determinant of tumor chemoresistance: proton pump inhibitors (PPIs) as a novel therapeutic approach. *Drug Resist Updat.* (2015) 23:69–78. doi: 10.1016/j.drup.2015.08.004
7. Cui Q, Wen S, Huang P. Targeting cancer cell mitochondria as a therapeutic approach: recent updates. *Future Med Chem.* (2017) 9:929–49. doi: 10.4155/fmc-2017-0011
8. Rashmi R, Huang X, Floberg JM, Elhammali AE, McCormick ML, Patti GJ, et al. Radioresistant cervical cancers are sensitive to inhibition of glycolysis and redox metabolism. *Cancer Res.* (2018) 78:1392–403. doi: 10.1158/0008-5472.CAN-17-2367
9. Centurione L, Aiello FB. DNA repair and cytokines: TGF-beta, IL-6, and thrombopoietin as different biomarkers of radioresistance. *Front Oncol.* (2016) 6:175. doi: 10.3389/fonc.2016.00175
10. Yoshimoto K, Mizoguchi M, Hata N, Murata H, Hatae R, Amano T, et al. Complex DNA repair pathways as possible therapeutic targets to overcome temozolomide resistance in glioblastoma. *Front Oncol.* (2012) 2:186. doi: 10.3389/fonc.2012.00186
11. Bekaii-Saab T, El-Rayes B. Identifying and targeting cancer stem cells in the treatment of gastric cancer. *Cancer Am Cancer Soc.* (2017) 123:1303–12. doi: 10.1002/cncr.30538
12. Prieto-Vila M, Takahashi RU, Usuba W, Kohama I, Ochiya T. Drug resistance driven by cancer stem cells and their niche. *Int J Mol Sci.* (2017) 18:E2574. doi: 10.3390/ijms18122574
13. Cui Q, Wang JQ, Assaraf YG, Ren L, Gupta P, Wei L, et al. Modulating ROS to overcome multidrug resistance in cancer. *Drug Resist Updat.* (2018) 41:1–25. doi: 10.1016/j.drup.2018.11.001
14. Zhang G, Wang W, Yao C, Ren J, Zhang S, Han M. Salinomycin overcomes radioresistance in nasopharyngeal carcinoma cells by inhibiting Nrf2 level and promoting ROS generation. *Biomed Pharmacother.* (2017) 91:147–54. doi: 10.1016/j.biopha.2017.04.095
15. Ceballos MP, Rigalli JP, Cere LI, Semeniuk M, Catania VA, Ruiz ML. ABC transporters: regulation and association with multidrug resistance in hepatocellular carcinoma and colorectal carcinoma. *Curr Med Chem.* (2018) doi: 10.2174/0929867325666180105103637. [Epub ahead of print].
16. Chen ZS. ABC transporters in pharmacology/physiology and human diseases. *Curr Pharm Biotechnol.* (2011) 12:569. doi: 10.2174/138920111795163940
17. Fu D. Where is it and how does it get there—intracellular localization and traffic of P-glycoprotein. *Front Oncol.* (2013) 3:321. doi: 10.3389/fonc.2013.00321
18. Zinzi L, Capparelli E, Cantore M, Contino M, Leopoldo M, Colabufo NA. Small and innovative molecules as new strategy to revert MDR. *Front Oncol.* (2014) 4:2. doi: 10.3389/fonc.2014.00002
19. Ezrahi S, Aserin A, Garti N. Basic principles of drug delivery systems—the case of paclitaxel. *Adv Colloid Interface Sci.* (2019) 263:95–130. doi: 10.1016/j.cis.2018.11.004
20. Meyers MB, Scotto KW, Sirotnak FM. P-glycoprotein content and mediation of vincristine efflux: correlation with the level of differentiation in luminal epithelium of mouse small intestine. *Cancer Commun.* (1991) 3:159–65. doi: 10.3727/095535491820873335
21. Bao L, Hazari S, Mehra S, Kaushal D, Moroz K, Dash S. Increased expression of P-glycoprotein and doxorubicin chemoresistance of metastatic breast cancer is regulated by miR-298. *Am J Pathol.* (2012) 180:2490–503. doi: 10.1016/j.ajpath.2012.02.024

22. Frezard F, Pereira-Maia E, Quidu P, Priebe W, Garnier-Suillerot A. P-glycoprotein preferentially effluxes anthracyclines containing free basic versus charged amine. *Eur J Biochem.* (2001) 268:1561–7. doi: 10.1046/j.1432-1327.2001.01989.x
23. Arora A, Shukla Y. Modulation of vinca-alkaloid induced P-glycoprotein expression by indole-3-carbinol. *Cancer Lett.* (2003) 189:167–73. doi: 10.1016/S0304-3835(02)00550-5
24. Leu BL, Huang JD. Inhibition of intestinal P-glycoprotein and effects on etoposide absorption. *Cancer Chemother Pharmacol.* (1995) 35:432–6. doi: 10.1007/s002800050258
25. Palmeira A, Sousa E, Vasconcelos MH, Pinto MM. Three decades of P-gp inhibitors: skimming through several generations and scaffolds. *Curr Med Chem.* (2012) 19:1946–2025. doi: 10.2174/092986712800167392
26. Crowley E, McDevitt CA, Callaghan R. Generating inhibitors of P-glycoprotein: where to, now? *Methods Mol Biol.* (2010) 596:405–32. doi: 10.1007/978-1-60761-416-6_18
27. Ji N, Yang Y, Cai CY, Lei ZN, Wang JQ, Gupta P, et al. Selonsertib (GS-4997), an ASK1 inhibitor, antagonizes multidrug resistance in ABCB1- and ABCG2-overexpressing cancer cells. *Cancer Lett.* (2019) 440–441:82–93. doi: 10.1016/j.canlet.2018.10.007
28. Fan YF, Zhang W, Zeng L, Lei ZN, Cai CY, Gupta P, et al. Dacomitinib antagonizes multidrug resistance (MDR) in cancer cells by inhibiting the efflux activity of ABCB1 and ABCG2 transporters. *Cancer Lett.* (2018) 421:186–98. doi: 10.1016/j.canlet.2018.01.021
29. Gupta P, Zhang YK, Zhang XY, Wang YJ, Lu KW, Hall T, et al. Voruciclib, a potent CDK4/6 inhibitor, antagonizes ABCB1 and ABCG2-mediated multi-drug resistance in cancer cells. *Cell Physiol Biochem.* (2018) 45:1515–28. doi: 10.1159/000487578
30. Zhang YK, Zhang XY, Zhang GN, Wang YJ, Xu H, Zhang D, et al. Selective reversal of BCRP-mediated MDR by VEGFR-2 inhibitor ZM323881. *Biochem Pharmacol.* (2017) 132:29–37. doi: 10.1016/j.bcp.2017.02.019
31. Yang L, Li M, Wang F, Zhen C, Luo M, Fang X, et al. Ceritinib enhances the efficacy of substrate chemotherapeutic agent in human ABCB1-overexpressing leukemia cells *in vitro*, *in vivo* and *ex-vivo*. *Cell Physiol Biochem*. (2018) 46:2487–99. doi: 10.1159/000489655
32. Engstrom LD, Aranda R, Lee M, Tovar EA, Essenburg CJ, Madaj Z, et al. Glesatinib exhibits antitumor activity in lung cancer models and patients harboring MET Exon 14 mutations and overcomes mutation-mediated resistance to type I MET inhibitors in nonclinical models. *Clin Cancer Res.* (2017) 23:6661–72. doi: 10.1158/1078-0432.CCR-17-1192
33. Reungwetwattana T, Liang Y, Zhu V, Ou SI. The race to target MET exon 14 skipping alterations in non-small cell lung cancer: the why, the how, the who, the unknown, and the inevitable. *Lung Cancer.* (2017) 103:27–37. doi: 10.1016/j.lungcan.2016.11.011
34. Shi Z, Tiwari AK, Shukla S, Robey RW, Singh S, Kim IW, et al. Sildenafil reverses ABCB1- and ABCG2-mediated chemotherapeutic drug resistance. *Cancer Res.* (2011) 71:3029–41. doi: 10.1158/0008-5472.CAN-10-3820
35. Ji N, Yang Y, Lei ZN, Cai CY, Wang JQ, Gupta P, et al. Ulixertinib (BVD-523) antagonizes ABCB1- and ABCG2-mediated chemotherapeutic drug resistance. *Biochem Pharmacol.* (2018) 158:274–85. doi: 10.1016/j.bcp.2018.10.028
36. Shukla S, Abel B, Chufan EE, Ambudkar SV. Effects of a detergent micelle environment on P-glycoprotein (ABCB1)-ligand interactions. *J Biol Chem.* (2017) 292:7066–76. doi: 10.1074/jbc.M116.771634
37. Zhang YK, Zhang GN, Wang YJ, Patel BA, Talele TT, Yang DH, et al. Bafetinib (INNO-406) reverses multidrug resistance by inhibiting the efflux function of ABCB1 and ABCG2 transporters. *Sci Rep.* (2016) 6:25694. doi: 10.1038/srep25694
38. Li J, Jaimes KF, Aller SG. Refined structures of mouse P-glycoprotein. *Protein Sci.* (2014) 23:34–46. doi: 10.1002/pro.2387
39. Loo TW, Clarke DM. Mapping the binding site of the inhibitor tariquidar that stabilizes the first transmembrane domain of P-glycoprotein. *J Biol Chem.* (2015) 290:29389–401. doi: 10.1074/jbc.M115.695171
40. Loo TW, Bartlett MC, Clarke DM. Methanethiosulfonate derivatives of rhodamine and verapamil activate human P-glycoprotein at different sites. *J Biol Chem.* (2003) 278:50136–41. doi: 10.1074/jbc.M310448200
41. Loo TW, Clarke DM. Identification of residues in the drug-binding site of human P-glycoprotein using a thiol-reactive substrate. *J Biol Chem.* (1997) 272:31945–8. doi: 10.1074/jbc.272.51.31945
42. Bansal T, Mishra G, Jaggi M, Khar RK, Talegaonkar S. Effect of P-glycoprotein inhibitor, verapamil, on oral bioavailability and pharmacokinetics of irinotecan in rats. *Eur J Pharm Sci.* (2009) 36:580–90. doi: 10.1016/j.ejps.2008.12.005
43. Breier A, Gibalova L, Seres M, Barancik M, Sulova Z. New insight into p-glycoprotein as a drug target. *Anticancer Agents Med Chem.* (2013) 13:159–70. doi: 10.2174/187152013804487380
44. Nobili S, Landini I, Mazzei T, Mini E. Overcoming tumor multidrug resistance using drugs able to evade P-glycoprotein or to exploit its expression. *Med Res Rev.* (2012) 32:1220–62. doi: 10.1002/med.20239
45. Sharom FJ, Yu X, Chu JW, Doige CA. Characterization of the ATPase activity of P-glycoprotein from multidrug-resistant Chinese hamster ovary cells. *Biochem J.* (1995) 308 (Pt 2):381–90. doi: 10.1042/bj3080381
46. Hrycyna CA, Ramachandra M, Ambudkar SV, Ko YH, Pedersen PL, Pastan I, et al. Mechanism of action of human P-glycoprotein ATPase activity. Photochemical cleavage during a catalytic transition state using orthovanadate reveals cross-talk between the two ATP sites. *J Biol Chem.* (1998) 273:16631–4. doi: 10.1074/jbc.273.27.16631
47. Kato Y, Ozawa S, Miyamoto C, Maehata Y, Suzuki A, Maeda T, et al. Acidic extracellular microenvironment and cancer. *Cancer Cell Int.* (2013) 13:89. doi: 10.1186/1475-2867-13-89
48. List AF, Kopecky KJ, Willman CL, Head DR, Slovak ML, Douer D, et al. Cyclosporine inhibition of P-glycoprotein in chronic myeloid leukemia blast phase. *Blood.* (2002) 100:1910–2.
49. Chung FS, Santiago JS, Jesus MF, Trinidad CV, See MF. Disrupting P-glycoprotein function in clinical settings: what can we learn from the fundamental aspects of this transporter? *Am J Cancer Res*. (2016) 6:1583–98.
50. Li W, Zhang H, Assaraf YG, Zhao K, Xu X, Xie J, et al. Overcoming ABC transporter-mediated multidrug resistance: molecular mechanisms and novel therapeutic drug strategies. *Drug Resist Updat.* (2016) 27:14–29. doi: 10.1016/j.drup.2016.05.001
51. Zhang GN, Zhang YK, Wang YJ, Gupta P Jr, Ashby CR, Alqahtani S, et al. Epidermal growth factor receptor (EGFR) inhibitor PD153035 reverses ABCG2-mediated multidrug resistance in non-small cell lung cancer: *in vitro* and *in vivo*. *Cancer Lett.* (2018) 424:19–29. doi: 10.1016/j.canlet.2018.02.040

Conflict of Interest Statement: The authors declare that the research was conducted in the absence of any commercial or financial relationships that could be construed as a potential conflict of interest.

frontiers in Oncology

ORIGINAL RESEARCH
published: 26 April 2019
doi: 10.3389/fonc.2019.00306

Inhibition of SMYD2 Sensitized Cisplatin to Resistant Cells in NSCLC Through Activating p53 Pathway

Lei Shang[1,2] *and Minjie Wei*[1]*

[1] School of Pharmacy, China Medical University, Shenyang, China, [2] Shenyang Medical College, Shenyang, China

The protein lysine methyltransferase SMYD2 has recently emerged as a new enzyme modulate gene transcription or signaling pathways, and involved into tumor progression. However, the role of SMYD2 in drug resistant is still not known. Here, we found that inhibition of SMYD2 by specific inhibitor could enhance the cell sensitivity to cisplatin (CDDP), but not paclitaxel, NVB, and VCR in non-small cell lung cancer (NSCLC). Further study showed that SMYD2 and its substrates were overexpressed in NSCLC resistant cells, and the inhibition of SMYD2 or knockdown by specific siRNA could reverse the cell resistance to cisplatin treatment in NSCLC/CDDP cells. In addition, our data indicated that the inhibition or knockdown SMYD2 inhibit tumor sphere formation and reduce cell migration in NSCLC/CDDP cells, but not in NSCLC parental cells. Mechanistically, inhibition of SMYD2 could enhance p53 pathway activity and induce cell apoptosis through regulating its target genes, including p21, GADD45, and Bax. On the contrary, the sensitivity of cells to cisplatin was decreased after knockdown p53 or in p53 deletion NSCLC cells. The synergistically action was further confirmed by *in vivo* experiments. Taken together, our results demonstrate SMYD2 is involved into cisplatin resistance through regulating p53 pathway, and might become a promising therapeutic target for cisplatin resistance in NSCLC.

Keywords: SMYD2, cisplatin resistance, lung cancer, p53, apoptosis

OPEN ACCESS

Edited by:
Yan-yan YAN,
Shanxi Datong University, China

Reviewed by:
Chiara Ambrogio,
Dana–Farber Cancer Institute, United States
Dawn Sijin Nin,
National University of Singapore, Singapore

***Correspondence:**
Minjie Wei
mjwei@cmu.edu.cn

Specialty section:
This article was submitted to Cancer Molecular Targets and Therapeutics, a section of the journal Frontiers in Oncology

Received: *23 December 2018*
Accepted: *03 April 2019*
Published: *26 April 2019*

Citation:
Shang L and Wei M (2019) Inhibition of SMYD2 Sensitized Cisplatin to Resistant Cells in NSCLC Through Activating p53 Pathway. Front. Oncol. 9:306. doi: 10.3389/fonc.2019.00306

INTRODUCTION

The incidence and mortality of lung cancer ranks at the NO.1 among all kinds of cancer (1). Non-small cell lung cancer (NSCLC) accounts for about 85% of lung cancer (1, 2). The surgery, radiotherapy, chemotherapy, molecular targeting therapy, and immunotherapy are possible choice for NSCLC treatment (2). However, most of NSCLCs are found at advanced stage, so drug-based therapy, mainly including chemotherapy, is considered as the most important approach to treat NSCLCs (3).

The platinum-based chemotherapy, such as cisplatin plus paclitaxel, cisplatin plus NVB, and cisplatin plus VCR, is the first-line treatment approach in NSCLCs (2, 3). However, drug resistance will be inevitable happened after treatment for 1–2 years, which limit the application of chemotherapeutic agents (4, 5). To solve this problem, we should first understand the resistant mechanisms for chemotherapy in NSCLCs. In fact, many previous studies have shown that the upregulation of efflux protein, the mutation of drug target, the activation of by-pass oncogenic pathway, and the accumulation of phenotype change cells contributed to the resistance of chemotherapeutic agents in NSCLCs (6, 7). However, there is still unknown for a large part of NSCLC resistant patients.

SMYD2 was identified as protein methyltransferase which adds methyl-group to its histone and non-histone substrates and epigenetically regulates their function (8, 9). Recently, SMYD2 was observed to involve into the upset and progression of various tumors including leukemia, breast cancer, teratocarcinoma, gastric cancer, and head and neck cancer (10–14). Mechanistically, SMYD2 was found to prompt cell proliferation, block apoptosis, and enhance cell migration and invasion through regulating its substrates methylation status, such as p53 and histone4 (13–15). However, whether this enzyme is involved into drug resistance is still not known.

Here, NSCLC was used to as an example to investigate the role of SMYD2 in chemotherapeutic resistance. Our data showed that SMYD2 was involved into cisplatin resistance, but not paclitaxel, NVB, and VCR. Further study indicated that SMYD2 expression and its activity were increasing in cisplatin resistant NSCLC cells. Mechanistically, SMYD2 prompt cell migration, increase the tumor sphere and block apoptosis, which is dependent on the methylation of $p53^{K370}$. The inhibition or knockdown of SMYD2 model would result in the increasing of sensitivity to cisplatin *in vitro* and *in vivo*. Our results not only elucidate the role of SMYD2 in cisplatin resistance and provide a potential method to reverse cisplatin resistance in NSCLC.

MATERIALS AND METHODS

Cell Lines, Cell Culture, and Treatment

A549 (p53 wide type, KRAS mutation), NCI-H460 (p53 wide type, KRAS mutation), and NCI-H1299 (p53 deletion, KRAS wide type) human lung adenocarcinoma cell lines were purchased from the American Type Culture Collection (ATCC; Manassas, VA, USA). These cancer cells were routinely cultured in RPMI-1640 medium (Gibco, Grand Island, NY, USA) supplemented with 10% fetal bovine serum (FBS; Gibco) and were maintained at 37°C in a humidified incubator with 5% CO_2. The cells were treated with Cisplatin (J&K Scientific Ltd, Beijing, China) at increasing concentrations (ranging from 0.5 to 4 μM) for 3 months.

Compounds and Reagents

BAY-498(SMYD2 inhibitor), AZ505(SMYD2 inhibitor), Cisplatin(CDDP), Vinorelbine(NVB), Paclitaxel (Taxol), and Vincristine sulfate(VCR) was obtained from MedChem Express (Princeton, NJ, USA). The primary antibodies against SMYD2, p53, Cleaved-PARP, and β-actin were obtained from Cell Signaling Technology (Danvers, MA, USA), and the primary antibodies against $p53^{K370Me}$ was purchased from Immunoway Technology (Plano, TX, USA). The pcDNA3-p53 vector was obtained from Addgene.

Cell Viability Assay

In vitro cell viability was determined using the MTT assay. Cells (1×10^5 cells/ml) were seeded in 96-well culture plates. After incubating overnight, the cells were treated with various concentrations of the appropriate agents for 48 h, after which 10 μl of MTT solution (2.5 mg/ml in PBS) was added to each well, and the plates were incubated for an additional 4 h at 37°C. After the samples were centrifuged (2,500 rpm, 10 min), the medium supplemented with MTT was aspirated, and then 100 μl of DMSO was added to each well. The optical density of each well was measured at 570 nm with a Biotek Synergy^{TM} HT Reader (BioTek Instruments, Winooski, VT, USA).

Western Blot Analysis

Western blotting was performed as previously described (14). Briefly, equal amounts of total protein extracts from cultured cells or tissues were fractionated by 10–15% SDS-PAGE before being electrically transferred onto polyvinylidene difluoride (PVDF) membranes, which were sequentially incubated with mouse or rabbit primary antibodies and horseradish peroxidase (HRP)-conjugated secondary antibodies designed to detect the proteins of interest. The indicated secondary antibodies were subsequently reacted with ECL detection reagents (Pierce, Thermo Fisher Scientific, Waltham, MA, USA) and then incubated in a dark room. The relative expression levels of the indicated proteins were normalized to those of β-actin.

Flow Cytometry Analysis

Analyses for apoptosis were conducted with an Annexin V-FITC Apoptosis Detection Kit (BioVision, Mountain View, CA, USA). Cells (1×10^6) were exposed to various inhibitors for 48 h. They were collected by centrifugation and resuspended in 500 μL of 1 × binding buffer. Annexin V-fluorescein isothiocyanate (FITC; 5 μL) and PI (5 μL) were added to the cells. After incubation at room temperature for 5 min in the dark, cells were analyzed by FACS using a flow cytometer (BD Biosciences, San Jose, CA, USA). Cells that stained Annexin V-FITC (apoptosis) were analyzed.

siRNA-Mediated Gene Knockdown

SMYD2 and *p53* knockdown was performed using specific siRNAs purchased from Santa Cruz Biotechnology (Santa Cruz Biotechnology, Santa Cruz, CA, USA). Scramble non-target siRNAs served as negative controls. siRNA was introduced into the indicated cell lines with Lipofectamine RNAiMAX reagent (Thermo Fisher Scientific), according to the manufacturer's instructions, and knockdown efficiency was assessed by western blotting.

Transwell Migration Assay

NCI-H460/CDDP and its parental cell lines migration capacities were tested by Corning transwell assay, according to the manufacturer's instructions. Briefly, the indicated lung cancer cells were treated DMSO, BAY-598 (200 nM), Scramble siRNA, and SMYD2 siRNA (50 nM) for 48 h and then seeded in the upper chamber of the system at a density of 5×10^4 cells/well in serum-free medium (100 μl). The wells in the lower chamber of the system were filled with complete medium. After incubating for 48 h, the cells remaining in the upper chamber were carefully removed with a cotton swab, and the cells that had migrated through the membrane and adhered to its lower surface were fixed with 100% methanol and stained with 0.2% crystal violet. The membrane was then photographed under a microscope,

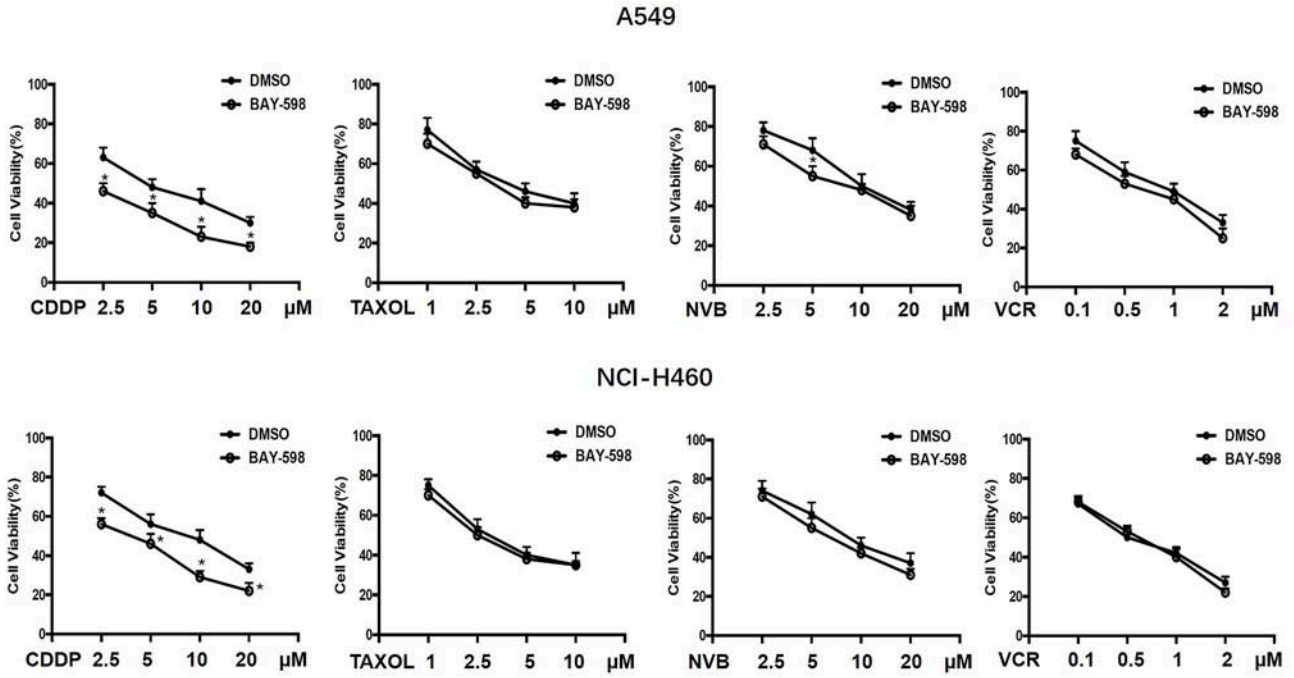

FIGURE 1 | Effects of the combination of chemotherapeutic agents and SMYD2 inhibitor on cell growth in NSCLC cells. The growth of A549 and NCI-H460 cells treated with chemotherapeutic agents, including CDDP, Taxol, NVB, and VCR at different concentrations or combination with SMYD2 inhibitor BAY-598. Cell lines treated with DMSO were used as controls.

and the cells in five predetermined fields were counted at 200× magnification.

Tumor Sphere Formation Assay

NCI-H460/CDDP and its parental cell lines were treated DMSO, BAY-598 (200 nM), Scramble siRNA, and SMYD2 siRNA (50 nM) for 48 h, after which single cells prepared by mechanical and enzymatic dissociation were seeded in 6-well ultra-low attachment plates (Corning, NY, USA) at a density of 1,000 cells/well in serum-free DMEM/F-12 medium supplemented with B27 (1×, Invitrogen, Thermo Fisher Scientific), 20 ng/ml human recombinant bFGF (PeproTech, Rocky Hill, NJ, USA), and 20 ng/ml EGF (PeproTech) for 10–14 days. The cells were then photographed under a microscope.

Luciferase Reporter Gene Assays

NCI-H460/CDDP and its parental cells were plated in 96-well plates. Cells in 96-well plates were transfected with 2 ng pRL-tk (Promega) and 50 ng p53 reporter plasmid (Addgene) for 24 h with the lipofectamine 3000. Cells were treated with DMSO or BAY-598 at indicated concentrations for 24 h. Luciferase activities were evaluated with the Berthold LB960 system (Berthold, DE).

Quantitative PCR Analysis

Total RNA was isolated using an RNeasy Mini Kit (Qiagen, Hilden, Germany), as described in the product insert, and then reverse transcribed with a RevertAid First Strand cDNA Synthesis Kit (Thermo Fisher Scientific). PCR was performed with iQ SYBR Green SuperMix (Bio-Red Laboratories, Hercules, CA, USA) and a CFX96 Real-Time PCR Detection System (Bio-Rad Laboratories). The following primers were used for the experiment: glyceraldehyde-3-phosphate dehydrogenase (*GAPDH*): reverse: 5′-CCCTCAACGACCACTTTGTCA-3′ and forward: 5′-TTCCTCTTGTGCTCTTGCTGG-3′; p21 forward: 5′-TGTACCCTTGTGCCTCGCTC-3′ and reverse: 5′- TGGAGA AGATCAGCCGGCGT-3′; Bax forward: 5′- TTTGCTTCAGGG TTTCATCC-3′ and reverse: 5′- CAGTTGAAGTTGCCGTCA GA-3′; and GADD45 forward: 5′-GGATGCCCTGGAGGAAGT GCT-3′ and reverse: 5′- GGCAGGATCCTTCCATTGAGATGA ATGTG-3′.

Xenografts in Mice

To assess the characteristics of chemotherapy-resistant tumors, we subcutaneously injected viable NCI-H460/CDDP cells (5×10^6/100 μl PBS per mouse), as confirmed by trypan blue staining, into the right flank of 7–8 weeks-old male BALB/C mice. When the average tumor volume reached 100 mm^3, the mice were randomly divided into the following four treatment groups: a control group (saline only, $n = 6$), a AZ505 group (40 mg/kg/qd, i.p.; $n = 6$), an CDDP group (4.0 mg/kg/3 day, i.p.; $n = 6$), and a combination treatment group (AZ505 plus CDDP). After 2 weeks, the mice were sacrificed, and the tumors were excised and stored at −80°C. These experiments were performed in strict accordance with the recommendations in the Guide for the Care and Use of Laboratory Animals of the National Institutes of Health, and the corresponding protocol was approved by the

Animal Experimental Ethics Committee of Shenyang Medical College (Shenyang, Liaoning Province, China).

Statistical Analysis

Differences between the indicated experimental groups were evaluated by one-way ANOVA or Turkey's *post hoc* test with the SPSS 11.5 software package for Windows (SPSS, Chicago, IL, USA). $P < 0.05$ were considered statistically significant ($P < 0.05$, two-tailed test).

RESULTS

The Inhibition of SMYD2 Enhanced the Antigrowth Action of Cisplatin in NSCLC Cells

To explore the possible action of SMYD2 in chemotherapeutic agents in NSCLC, A549 and NCI-H460 cells were treated with various concentrations of the first-line chemotherapeutic agents, including CDDP, Taxol, NVB, and VCR, and combined treatment with SMYD2 inhibitor BAY-598 with non-cytotoxicity concentration (2 μM, cell viability>90%, **Supplementary Figure 1A**). As shown in **Figure 1**, single treatment with CDDP, Taxol, NVB, and VCR could inhibit cell growth at concentration-dependent manner in both cell lines. Addition of SMYD2 inhibitor had no effect on the cell viability when combined with Taxol and VCR, and owned a slightly enhanced inhibition when combined with NVB. Notably, the combination of BAY-598 and CDDP could significantly retard cell growth in both A549 and NCI-H460 cells ($P < 0.05$), suggesting SMYD2 inhibition might be involved into the cell sensitivity to CDDP but not Taxol, VCR, and NVB.

The Expression and Function of SMYD2 in Cisplatin Resistant NSCLC Cells

To clarify the role and function of SMYD2 in CDDP sensitivity of NSCLC cells, we established A549 and NCI-H460 CDDP resistant cell lines. First, we detected the expression level of SMYD2 in parental cell lines and resistant cell lines. Western blot data indicated that SMYD2 was increased in both resistant cell lines as compared to parental cell lines. In consistent with the SMYD2 upregulation in resistant cell lines, the non-histone substrate of SMYD2, $p53^{K370me}$, was also increased in resistant cell lines. The above data demonstrated that the expression and activity of SMYD2 were increased in CDDP resistant cells. Next, to further elucidate the role of SMYD2 in CDDP resistance, we measured the cell viability of NCI-H460/CDDP cells to CDDP after suppression of SMYD2 by specific inhibitor and siRNA. Our data showed, whether inhibition by SMYD2 inhibitor BAY-598 or knockdown by specific siRNA, the cell sensitivity to CDDP would be significantly increased as compared to DMSO or Scramble treated groups ($P < 0.05$). The above data was confirmed by flow cytometry experiments. Treatment with BAY-598 at non-cytotoxic concentration would prompt the apoptosis induced action of CDDP in NCI-H460/CDDP cells. Similarly, knockdown SMYD2 also resulted in the increase of cell apoptosis in CDDP treated NCI-H460/CDDP cells when compared to scramble treated cells. Notably, although the addition of SMYD2 inhibitor or knockdown of SMYD2 could enhance the induction of apoptosis by CDDP in NCI-H460 cells, the level was decreased as compared with resistant cells (**Figure 2C**). The above data indicated that SMYD2 play an important role in CDDP resistance of NSCLC cells.

Inhibition of SMYD2 Reversed Malignant Phenotype of Cisplatin Resistant NSCLC Cells

To further elucidate the role of SMYD2 in CDDP resistance of NSCLC cells, we next assessed the effect of inhibition or knockdown of SMYD2 on cell migration and tumor sphere formation, which are considered as the crucial characteristics of CDDP resistant NSCLC cells (16, 17). Our results showed that cell migration number of NCI-H460/CDDP cells was significant decreased after treated with SMYD2 inhibitor or SMYD2 siRNA as compared to DMSO and Scramble siRNA control, respectively. Furthermore, tumor sphere number of NCI-H460/CDDP cells was also obviously reduced by SMYD2 inhibitor and SMYD2 siRNA. It should be noted that whether addition of BAY-598 or specific siRNA could not significantly affect cell migration number and tumor sphere ability in NCI-H460 cells (**Supplementary Figures 1B–D**). The above results demonstrated that SMYD2 was also involved into the formation of malignant phenotype in CDDP resistant NSCLC cells.

SMYD2 Mediated Cisplatin Resistance Dependent on p53 Regulation in NSCLC Cells

In view of the crucial role of p53 and its epigenetic regulation by SMYD2 (18), we next explore possible role of p53 in SMYD2 mediated CDDP resistance. As shown in **Figure 4A**, knockdown p53 by specific siRNA contributed to the decrease of cell sensitivity to CDDP in NCI-H460/CDDP cells, which owned wide type p53 expression. In addition, the restore of p53 in NCI-H1299 cells (p53 deletion) could lead to the increase of cell sensitivity to CDDP. The above data indicates that the status and expression level of p53 will affect the cell sensitivity of NSCLC cells to CDDP.

In order to explore the effect of SMYD2 on p53 activity, we detected the transcriptional regulation activity of p53 by luciferase assay after treated with BAY-598 in NCI-H460/CDDP and its parental cells. The results showed that BAY-598 could concentration-dependently enhance p53 reporter activity in NCI-H460/CDDP cells (**Figure 4B**). In consistent with reporter assay, BAY-598 treatment also significantly resulted in the upregulation in mRNA level of p53 targeting genes, including p21, GADD45, and Bax (**Figure 4C**), in NCI-H460/CDDP cells. In consistent with resistant cell lines, BAY-598 also could increase p53 reporter activity, p21 and GADD45 expressions in NCI-H460 cells to some extent (**Figure 4B**). On the contrary, BAY-598 treatment could not induce the BAX expression in NCI-H460 cells, suggesting the role of SMYD2 in BAX regulation is different in parental and resistant cells (**Figure 4C**). Furthermore,

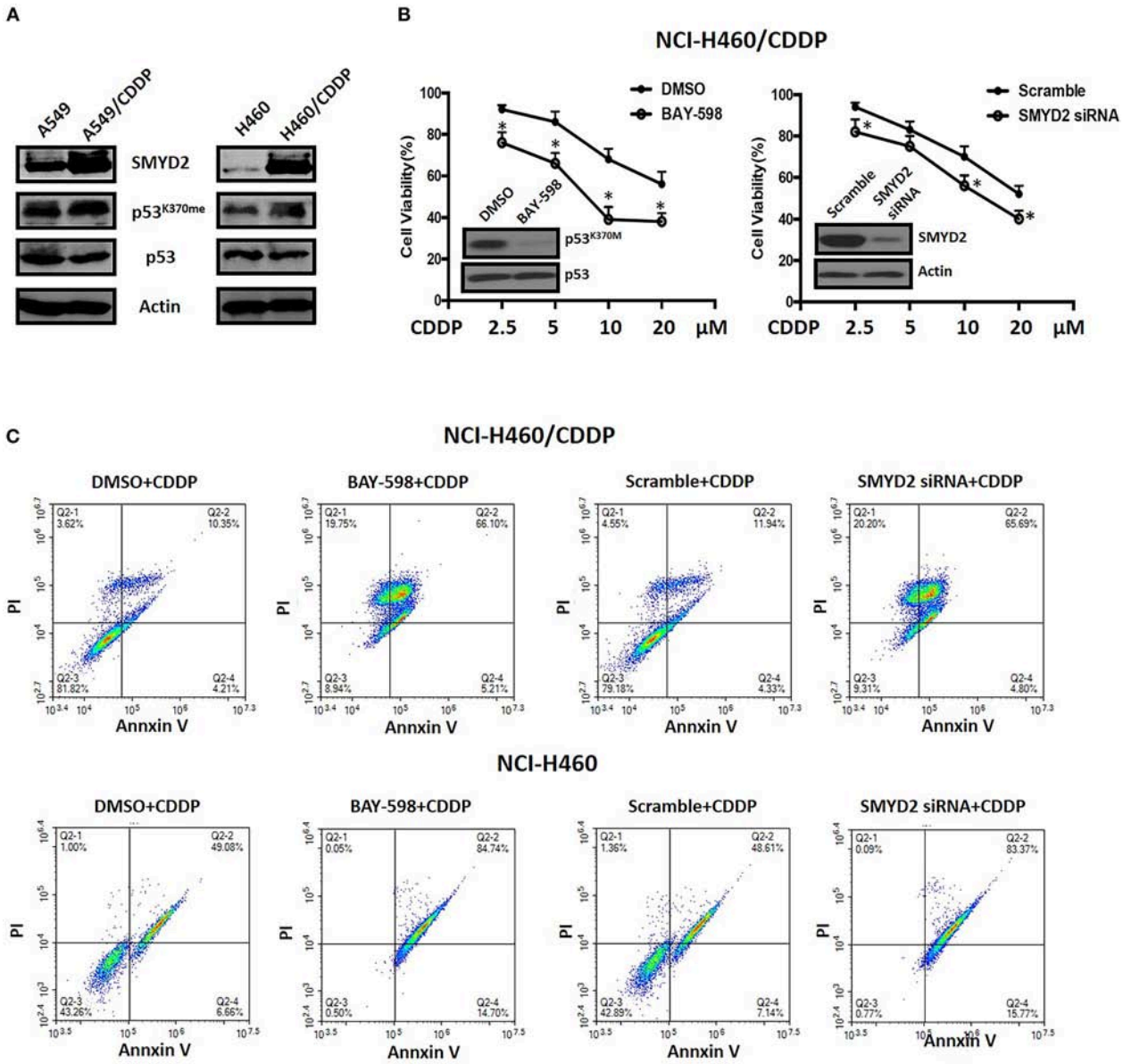

FIGURE 2 | The expression level of SMYD2-related proteins and the effects of genetic or chemical manipulation of SMYD2 on the cell growth of CDDP-resistant and parental NSCLC cells. **(A)** SMYD2, p53, and $p53^{K370me}$ expression levels were measured in CDDP resistant and parental NSCLC cell lines. β-actin was used as a loading control. **(B)** Cell viability was measured in BAY-598-treated or SMYD2-knockdown NCI-H460/CDDP cells treated with CDDP at different concentrations for 36 h. Scramble siRNA or DMSO was used as a control. The efficacy of genetic or chemical manipulation of SMYD2 was confirmed by Western blot in NCI-H460/CDDP cells. **(C)** Cell apoptosis was assessed using Annexin V/PI double staining in BAY-598-treated or SMYD2-knockdown CDDP resistant and parental NCI-H460 cells after treated with CDDP at 10 μM for 48 h. *$P < 0.05$, compared to corresponding control cells.

we also detected the cell apoptosis status of NCI-H460/CDDP and NCI-H460 cells after treated with BAY-598. Our results indicated BAY-598 at 10 μM could induce cell apoptosis in NCI-H460/CDDP cells, but not in NCI-H460 cells (**Figure 4D**), which confirmed the regulation action of Bax, a pro-apoptosis gene, by SMYD2. Taken together, our data suggested that the SMYD2 mediated CDDP resistance through epigenetic regulation of p53.

Inhibition of SMYD2 Sensitized Cisplatin Through Epigenetic Regulation of p53 *in vivo*

To clarify the therapeutic meaning of the above finding, we assessed anti-tumor effect of the combination of SMYD inhibitor and CDDP in NCI-H1299/CDDP xenograft mice. As shown in **Figure 5A**, single treatment with CDDP has no significant effect on tumor growth, indicating the resistant phenotype of

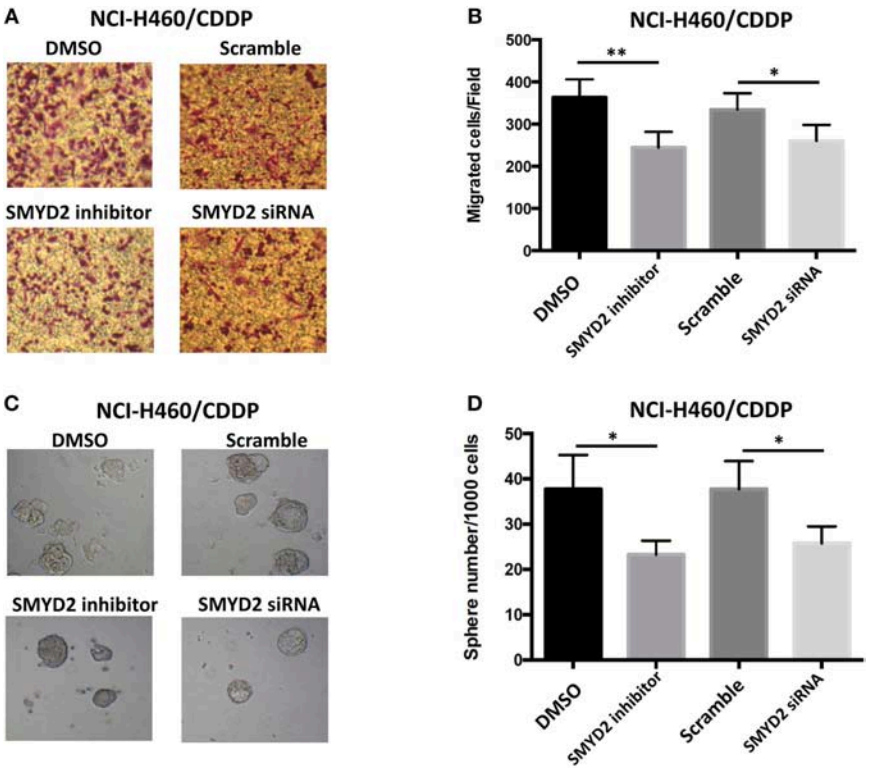

FIGURE 3 | Effects of genetic or chemical manipulation of SMYD2 on the biological characteristics of CDDP-resistant NSCLC cells. **(A,B)** Cell migration was measured in NCI-H460/CDDP cells treated with 2 μM BAY-598 or 50 nM SMYD2 siRNA. Scramble siRNA or DMSO was used as a control. **(C,D)** Tumor sphere was counted in NCI-H460/CDDP cells treated with 2 μM BAY-598 or 50 nM SMYD2 siRNA. Scramble siRNA or DMSO was used as a control. (Scale bars, 100 μm) $^{*}P < 0.05$, $^{**}P < 0.001$, compared to corresponding control cells.

NCI-H1299/CDDP xenograft mice. Similar to CDDP single treatment, single treatment with AZ505, an *in vivo* available SMYD2 inhibitor, only displayed a slightly inhibition on tumor growth. Interestingly, the combination of AZ505 and CDDP could obviously inhibit tumor growth of NCI-H1299/CDDP xenograft mice when compared to vehicle control and single treatment group. In addition, we didn't find the body weight loss in the combination treated group (data not shown), suggesting the combination has no effect on gross toxicity. Next, we further explored the underlying mechanisms using tumor tissue. Western blot data showed that AZ505 single treatment could lead to the decrease of $p53^{K370me}$, whereas CDDP single treatment could slightly increase the level of $p53^{K370me}$ (**Figure 5B**). The combination treatment contributed to a decrease of $p53^{K370me}$. In addition, we found the expression of the clv-PARP, an apoptosis biomarker, was increased in the combination group (**Figure 5B**). In summary, our *in vivo* data showed the inhibition of SMYD2 by AZ505 could sensitize cisplatin antitumor action through epigenetic regulation of p53.

DISCUSSION

Cisplatin(CDDP) is the first line drug for NSCLC patients, therefore, understanding and preventing CDDP resistance are considered as the crucial issue with respect to the treatment of NSCLC (5). Here, we found that SMYD2, a protein methyltransferase, was involved into cisplatin resistance. Furthermore, out data showed that SMYD2 expression and its activity were increasing in cisplatin resistant NSCLC cells. Mechanistically, SMYD2 prompt cell migration, increase the tumor sphere, and block apoptosis, which is dependent on the methylation of $p53^{K370}$. The inhibition or knockdown of SMYD2 model would result in the increasing of sensitivity to cisplatin *in vitro* and *in vivo*. Our findings provide us with a novel perspective epigenetic regulation mechanisms underlying CDDP resistance and define that the combination of SMYD2 inhibitor and CDDP may have promise as treatments for patients with CDDP-resistant NSCLC.

SMYD2 is a protein methyltransferase that catalyzes the methylation of histone substrates, such as H3K4 and H3K36 (18), and non-histone substrates, including p53 (19), Rb (20), HSP90 (21), STAT3, and NF-κB (22). It has been reported that SMYD2 was involved into the upset and progression of various tumors, including leukemia, breast cancer, gastric cancer, and head and neck cancer. Recently, Wang et al. reported SMYD2 inhibition also led to the suppression of cell growth in NSCLC cells (23), suggesting SMYD2 might be involved into lung cancer. Our results demonstrated that SMYD2

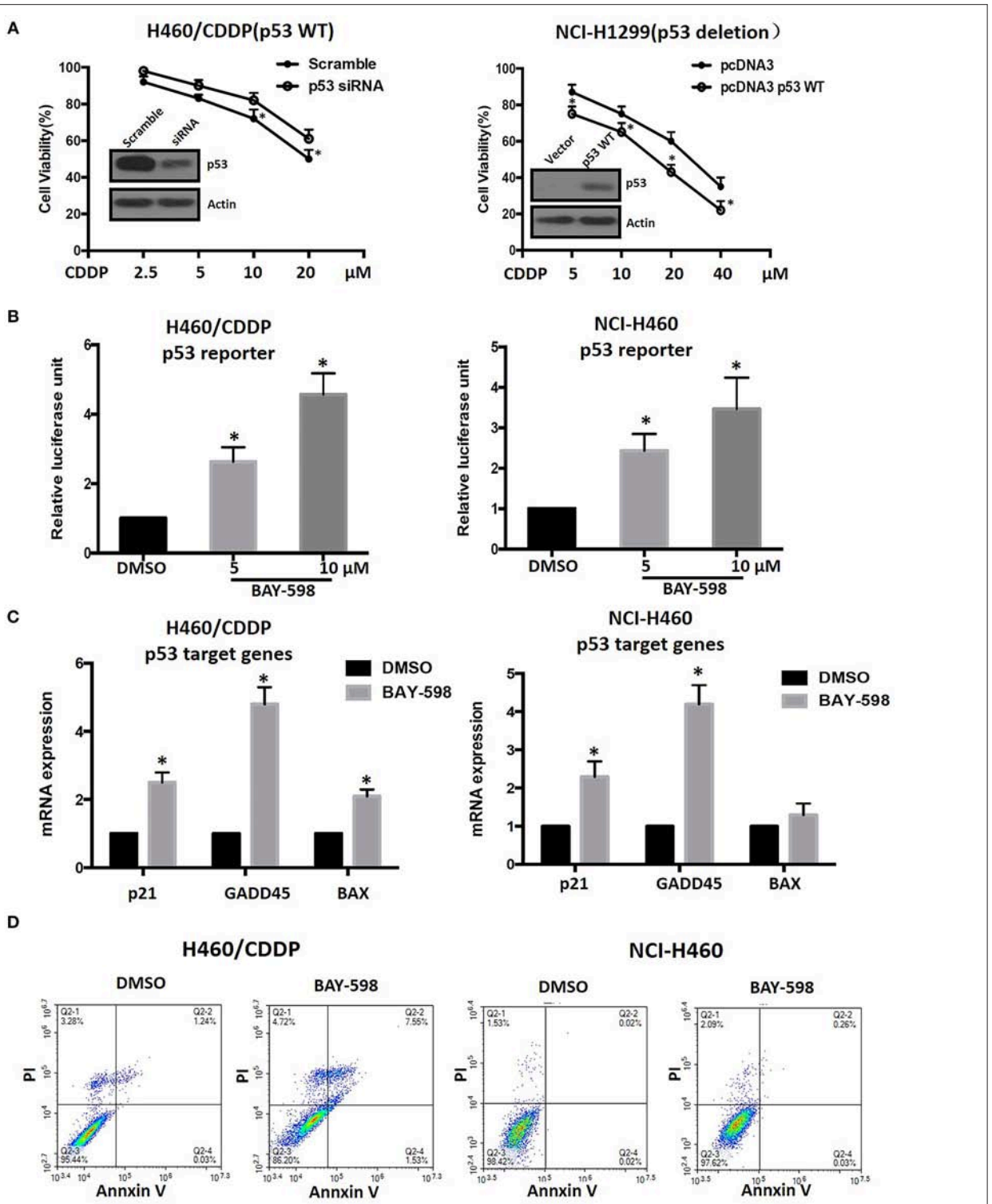

FIGURE 4 | Epigenetic regulation of p53 and its role in CDDP resistance in NSCLC. **(A)** Cell viability in NCI-H460/CDDP (p53 wide type) and NCI-H1299(p53 deletion) cells, with p53 gene manipulation, which were treated with CDDP at different concentrations for 48 h. Scramble siRNA or mock vector was used as a control. The p53 knock-down or restoration efficacy was confirmed by Western Blot. **(B)** The p53 reporter activity was measured in CDDP resistant and parental NCI-H460 cells after treated with BAY-598. The relative luciferase unit was calculated by Luciferase/Renilla and DMSO was considered as 100%. **(C)** The mRNA expression levels of p21, GADD45, and Bax were assessed by real-time RT-PCR in CDDP resistant and parental NCI-H460 cells treated with 10 μM BAY-598. GAPDH was used as a control. **(D)** Cell apoptosis was assessed using Annexin V/PI double staining in CDDP resistant and parental NCI-H460 cells which were treated with BAY-598 at 10 μM concentrations for 48 h. $^*P < 0.05$, compared to corresponding control cells.

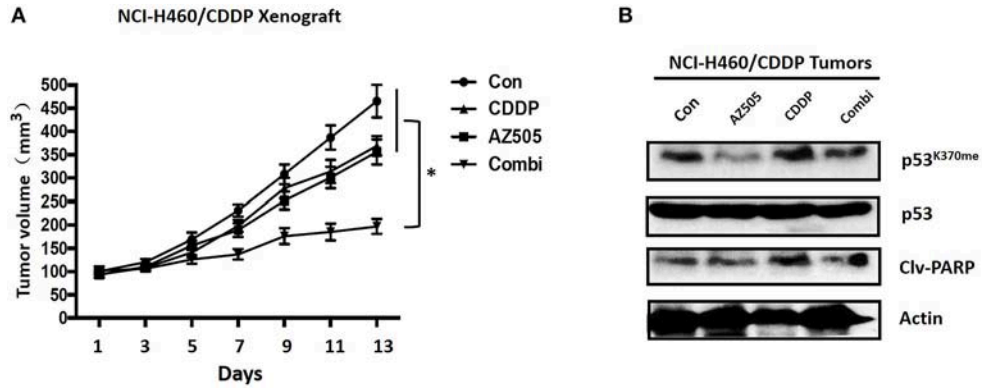

FIGURE 5 | Effects of SMYD2 inhibition and/or CDDP on tumor growth in an CDDP-resistant xenograft model. **(A)** Tumor volume was measured in NCI-H460/CDDP xenografts treated with AZ505, CDDP, or the combination of AZ505 and CDDP. **(B)** The p53 and $p53^{K370me}$, and cleaved PARP(clv-PARP) expression levels were measured in NCI-H460/CDDP xenograft tumor tissues. β-actin was used as a loading control. $^*P < 0.05$, combined treatment group compared to single treatment group and vehicle control.

expression and enzymatic activity levels were upregulated in NSCLC CDDP-resistant cells as compared to parental cells. In addition, either suppressing SMYD2 activity or knocking down SMYD2 would contribute to the increases in sensitivity to CDDP, and the reduction in cell migration and self-renewal ability in CDDP-resistant NSCLC cells, indicating that SMYD2 executes a crucial role in CDDP resistance of NSCLC.

SMYD2 methylates H3K4 and H3K36 would contribute the change of chromatin structure, and subsequently lead to the alteration of its target genes (18). In fact, the important function of SMYD2 was reported to related methylate to its non-histone substrates (9, 24). SMYD2 monomethylates Lys-370 of p53, leading to decreased DNA-binding activity and subsequent transcriptional regulation activity of p53. We found that, as long as the SMYD2 upregulation, the $p53^{K370me}$ level was also increased in CDDP resistant NSCLC cells. Importantly, our data showed that cell sensitivity to CDDP was dependent on wild type p53 level. Inhibition of SMYD2 could induce the increasing of p53 transcription activity and its target gene expression. Taken together, these findings indicate that epigenetic regulation by SMYD2 plays an important role in p53 transcriptional activity and is involved in processes associated with CDDP resistance.

K-RAS is one of the most frequently mutated in human NSCLC (25). Mutation of K-RAS usually results in the activation of oncogenic signaling molecules that regulate cell growth, survival and differentiation by coupling receptor activation to downstream effector pathways (25), and leads to the resistance to tyrosine kinase inhibitors such as gefitinib and erlotinib (26). Therefore, chemotherapy is the standard of treatment for K-RAS mutant NSCLC tumors. Here, our data shown that inhibition of SMYD2 by specific inhibitor can sensitize CDDP efficacy in K-RAS mutated A549 and NCI-H460 cell lines, suggesting epigenetic manipulation might be a promising adjuvant approach to treat K-RAS mutant tumors.

In conclusion, the present study elucidated that the activity of SMYD2 in NSCLC may affect the cell sensitivity to chemotherapeutic agents, especially to CDDP. The elevated SMYD2 mediated CDDP resistance and malignant phenotype in NSCLC, indicating that SMYD2 may be a useful biomarker of CDDP resistance in NSCLC. Inhibition of SMYD2 contributes to the methylation-related activation of p53 and thus results in cell apoptosis. Furthermore, combination treatment with CDDP and an SMYD2 inhibitor had a synergistically antitumor effects in a xenograft model *in vivo*. Given that SMYD2 has reversible effects and is a targetable protein methyltransferase, treatments targeting the protein may be useful for reversing CDDP resistance in NSCLC.

ETHICS STATEMENT

This study was carried out in accordance with the recommendations in the Guide for the Care and Use of Laboratory Animals of the National Institutes of Health, and the corresponding protocol was approved by the Animal Experimental Ethics Committee of Shenyang Medical College (Shenyang, Liaoning Province, China).

AUTHOR CONTRIBUTIONS

All authors listed have made a substantial, direct and intellectual contribution to the work, and approved it for publication.

FUNDING

This work was supported by the National Natural Science Foundation of China (No. 81803476).

SUPPLEMENTARY MATERIAL

The Supplementary Material for this article can be found online at: https://www.frontiersin.org/articles/10.3389/fonc.2019.00306/full#supplementary-material

Supplementary Figure 1 | The effects of genetic or chemical manipulation of SMYD2 on the cell growth, migration, and tumor sphere ability of NCI-H460 cells. **(A)** The growth of A549 and NCI-H460 cells treated with various concentrations SMYD2 inhibitor BAY-598. Cell viability was detected by MTT assay. **(B)** The efficacy of genetic or chemical manipulation of SMYD2 was confirmed by Western blot in NCI-H460 cells. $p53^{K370me}$ and SMYD2 expression levels were measured in NCI-H460 cell lines. The p53 or β-actin was used as a loading control. **(C)** Cell migration was measured in NCI-H460 cells treated with 2 μM BAY-598 or 50 nM SMYD2 siRNA. Scramble siRNA or DMSO was used as a control. **(D)** Tumor sphere was counted in NCI-H460 cells treated with 2 μM BAY-598 or 50 nM SMYD2 siRNA. Scramble siRNA or DMSO was used as a control.

REFERENCES

1. Siegel RL, Miller KD, Jemal A. Cancer statistics, 2016. *CA Cancer J Clin*. (2016) 66:7–30. doi: 10.3322/caac.21332
2. Hirsch FR, Scagliotti GV, Mulshine JL, Kwon R, Curran WJ Jr., Wu YL, et al. Lung cancer: current therapies and new targeted treatments. *Lancet*. (2017) 389:299–311. doi: 10.1016/S0140-6736(16)30958-8
3. Chang A. Chemotherapy, chemoresistance and the changing treatment landscape for NSCLC. *Lung Cancer*. (2011) 71:3–10. doi: 10.1016/j.lungcan.2010.08.022
4. Rivera G, Wakelee HA. Resistance to therapy. *Cancer Treat Res*. (2016) 170:183–202. doi: 10.1007/978-3-319-40389-2_9
5. Kim ES. Chemotherapy resistance in lung cancer. *Adv Exp Med Biol*. (2016) 893:189–209. doi: 10.1007/978-3-319-33826-2
6. Galluzzi L, Vitale I, Michels J, Brenner C, Szabadkai G, Harel-Bellan A, et al. Systems biology of cisplatin resistance: past, present and future. *Cell Death Dis*. (2014) 5:e1257. doi: 10.1038/cddis.2013.428
7. Hardin C, Shum E, Singh AP, Perez-Soler R, Cheng H. Emerging treatment using tubulin inhibitors in advanced non-small cell lung cancer. *Expert Opin Pharmacother*. (2017) 18:701–16. doi: 10.1080/14656566.2017.1316374
8. Brown MA, Sims RJ III, Gottlieb PD, Tucker PW. Identification and characterization of Smyd2: a split SET/MYND domain-containing histone H3 lysine 36-specific methyltransferase that interacts with the Sin3 histone deacetylase complex. *Mol Cancer*. (2006) 5:26. doi: 10.1186/1476-4598-5-26
9. Hamamoto R, Saloura V, Nakamura Y. Critical roles of non-histone protein lysine methylation in human tumorigenesis. *Nat Rev Cancer*. (2015) 15:110–24. doi: 10.1038/nrc3884
10. Sakamoto LH, Andrade RV, Felipe MS, Motoyama AB, Pittella Silva F. SMYD2 is highly expressed in pediatric acute lymphoblastic leukemia and constitutes a bad prognostic factor. *Leuk Res*. (2014) 38:496–502. doi: 10.1016/j.leukres.2014.01.013
11. Li LX, Zhou JX, Calvet JP, Godwin AK, Jensen RA, Li X. Lysine methyltransferase SMYD2 promotes triple negative breast cancer progression. *Cell Death Dis*. (2018) 9:326. doi: 10.1038/s41419-018-0347-x
12. Zhu J, Dou Z, Sammons MA, Levine AJ, Berger SL. Lysine methylation represses p53 activity in teratocarcinoma cancer cells. *Proc Natl Acad Sci USA*. (2016) 113:9822–7. doi: 10.1073/pnas.1610387113
13. Ohtomo-Oda R, Komatsu S, Mori T, Sekine S, Hirajima S, Yoshimoto S, et al. SMYD2 overexpression is associated with tumor cell proliferation and a worse outcome in human papillomavirus-unrelated nonmultiple head and neck carcinomas. *Hum Pathol*. (2016) 49:145–55. doi: 10.1016/j.humpath.2015.08.025
14. Komatsu S, Ichikawa D, Hirajima S, Nagata H, Nishimura Y, Kawaguchi T, et al. Overexpression of SMYD2 contributes to malignant outcome in gastric cancer. *Br J Cancer*. (2015) 112:357–64. doi: 10.1038/bjc.2014.543
15. Sajjad A, Novoyatleva T, Vergarajauregui S, Troidl C, Schermuly RT, Tucker HO, et al. Lysine methyltransferase Smyd2 suppresses p53-dependent cardiomyocyte apoptosis. *Biochim Biophys Acta*. (2014) 1843:2556–62. doi: 10.1016/j.bbamcr.2014.06.019
16. Wang L, Liu X, Ren Y, Zhang J, Chen J, Zhou W, et al. Cisplatin-enriching cancer stem cells confer multidrug resistance in non-small cell lung cancer via enhancing TRIB1/HDAC activity. *Cell Death Dis*. (2017) 8:e2746. doi: 10.1038/cddis.2016.409
17. Xu Y, Jiang Z, Zhang Z, Sun N, Zhang M, Xie J, et al. HtrA1 downregulation induces cisplatin resistance in lung adenocarcinoma by promoting cancer stem cell-like properties. *J Cell Biochem*. (2014) 115:1112–21. doi: 10.1002/jcb.24751
18. Ferguson AD, Larsen NA, Howard T, Pollard H, Green I, Grande C, et al. Structural basis of substrate methylation and inhibition of SMYD2. *Structure*. (2011) 19:1262–73. doi: 10.1016/j.str.2011.06.011
19. Huang J, Perez-Burgos L, Placek BJ, Sengupta R, Richter M, Dorsey JA, et al. Repression of p53 activity by Smyd2-mediated methylation. *Nature*. (2006) 444:629–32. doi: 10.1038/nature05287
20. Saddic LA, West LE, Aslanian A, Yates JR III, Rubin SM, Gozani O, et al. Methylation of the retinoblastoma tumor suppressor by SMYD2. *J Biol Chem*. (2010) 285:37733–40. doi: 10.1074/jbc.M110.137612
21. Hamamoto R, Toyokawa G, Nakakido M, Ueda K, Nakamura Y. SMYD2-dependent HSP90 methylation promotes cancer cell proliferation by regulating the chaperone complex formation. *Cancer Lett*. (2014) 351:126–33. doi: 10.1016/j.canlet.2014.05.014
22. Li LX, Fan LX, Zhou JX, Grantham JJ, Calvet JP, Sage J, et al. Lysine methyltransferase SMYD2 promotes cyst growth in autosomal dominant polycystic kidney disease. *J Clin Invest*. (2017) 127:2751–64. doi: 10.1172/JCI90921
23. Wang R, Deng X, Yoshioka Y, Vougiouklakis T, Park JH, Suzuki T, et al. Effects of SMYD2-mediated EML4-ALK methylation on the signaling pathway and growth in non-small-cell lung cancer cells. *Cancer Sci*. (2017) 108:1203–9. doi: 10.1111/cas.13245
24. Zhang X, Huang Y, Shi X. Emerging roles of lysine methylation on non-histone proteins. *Cell Mol Life Sci*. (2015) 72:4257–72. doi: 10.1007/s00018-015-2001-4
25. Piva S, Ganzinelli M, Garassino MC, Caiola E, Farina G, Broggini M, et al. Across the universe of K-RAS mutations in non-small-cell-lung cancer. *Curr Pharm Des*. (2014) 20:3933–43. doi: 10.2174/13816128113196660761
26. Duffy MJ, O'Donovan N, Crown J. Use of molecular markers for predicting therapy response in cancer patients. *Cancer Treat Rev*. (2011) 37:151–9. doi: 10.1016/j.ctrv.2010.07.004

Conflict of Interest Statement: The authors declare that the research was conducted in the absence of any commercial or financial relationships that could be construed as a potential conflict of interest.

frontiers in Pharmacology

REVIEW
published: 30 April 2019
doi: 10.3389/fphar.2019.00427

USP7: Novel Drug Target in Cancer Therapy

Zhiru Wang[1,2,3], Wenting Kang[1,2], Yinghua You[1,2], Jingru Pang[1,2], Hongmei Ren[1,2], Zhenhe Suo[3]*, Hongmin Liu[1,2]* and Yichao Zheng[1,2]**

[1] School of Pharmaceutical Sciences, Zhenghzou University, Zhengzhou, China, [2] Collaborative Innovation Centre of New Drug Research and Safety Evaluation, Henan Province, and Key Laboratory of Advanced Drug Preparation Technologies, Zhengzhou University, and Key Laboratory of Henan Province for Drug Quality and Evaluation, Ministry of Education of China, Zhengzhou, China, [3] Pathology, Institute of Clinical Medicine, Faculty of Medicine, University of Oslo, Oslo, Norway

Ubiquitin specific protease 7 (USP7) is one of the deubiquitinating enzymes (DUB) that erases ubiquitin and protects substrate protein from degradation. Full activity of USP7 requires the C-terminal Ub-like domains fold back onto the catalytic domain, allowing the remodeling of the active site to a catalytically competent state by the C-terminal peptide. Until now, numerous proteins have been identified as substrates of USP7, which play a key role in cell cycle, DNA repair, chromatin remodeling, and epigenetic regulation. Aberrant activation or overexpression of USP7 may promote oncogenesis and viral disease, making it a target for therapeutic intervention. Currently, several synthetic small molecules have been identified as inhibitors of USP7, and applied in the treatment of diverse diseases. Hence, USP7 may be a promising therapeutic target for the treatment of cancer.

Keywords: deubiquitination, USP7, structure, immune, DNA damage

OPEN ACCESS

Edited by:
Zhe-Sheng Chen,
St. John's University, United States

Reviewed by:
Hong-Yu Hu,
Shanghai Institutes for Biological Sciences (CAS), China
Xiaoming Zha,
China Pharmaceutical University, China

****Correspondence:***
Zhiru Wang
simplearu@163.com
Zhenhe Suo
zhenhe.suo@medisin.uio.no
Hongmin Liu
liuhm@zzu.edu.cn
Yichao Zheng
yichaozheng@zzu.edu.cn

Specialty section:
This article was submitted to Experimental Pharmacology and Drug Discovery, a section of the journal Frontiers in Pharmacology

Received: *28 January 2019*
Accepted: *04 April 2019*
Published: *30 April 2019*

Citation:
Wang Z, Kang W, You Y, Pang J, Ren H, Suo Z, Liu H and Zheng Y (2019) USP7: Novel Drug Target in Cancer Therapy. Front. Pharmacol. 10:427. doi: 10.3389/fphar.2019.00427

INTRODUCTION

Post-translational modification (PTM) is generally enzymatic modification of proteins following protein biosynthesis. Examples of PTM include methylation, acetylation, phosphorylation, glycosylation, ubiquitination, S-nitrosylation, and so on (Chatterjee and Thakur, 2018). As one of the most studied PTMs, ubiquitination involves in the intracellular proteolytic machinery and regulates numerous physical activities in the cell (Dybas et al., 2018). The process of the addition of ubiquitin to a substrate protein is named ubiquitination, which may contribute to the protein degradation. Ubiquitination of target protein can be catalyzed by a cascade reaction comprising the ubiquitin-activating enzymes (E1), the ubiquitin conjugation enzymes (E2) and the ubiquitin ligases (E3). First, ubiquitin is activated by E1 with the participation of ATP and transferred to E2 through a trans-thiolation reaction, and then conjugated to a lysine or α-amino group of the substrate protein in the presence of E3 (Cheon and Baek, 2006). Eventually, proteins labels with more than four ubiquitin molecules can be recognized and subjected to the 26S proteasome at which they are degraded, generating small polypeptides (**Figure 1**).

Deubiquitinating enzymes (DUBs) are responsible for the removal of ubiquitin and keeping the stability of the substrate by rescuing them from degradation (Nijman et al., 2005; Clague et al., 2013). Until now, approximately 100 DUBs have been identified and can be classified into five subclasses based on their Ub-protease domains: ubiquitin-specific proteases (USPs), ubiquitin C-terminal hydrolases (UCHs), ovarian tumor proteases (OTUs), Machado-Joseph disease proteases (MJDs) belonging to cysteine-dependent proteases, and JAB1/MPN/Mov34 (JAMMs) belonging to zinc metalloproteases (Zhou et al., 2018). With approximately 50 members,

the USPs family is the largest one among all the DUB subfamilies. All these members include conserved domains, i.e., three primary functional domains of Cys, His and Asp/Asn boxes which are in charge of the reorganization of ubiquitin conjugated molecules.

Among the members of USP family, ubiquitin specific protease USP7, also known as herpes-associated ubiquitin-specific protease (HAUSP), is a unique deubiquitinating enzyme which was identified in 1997, and it characterized as a novel member of the ubiquitin-specific protease family to interact with herpes simplex virus type 1 immediate-early protein (Vmw110) of the herpes simplex virus type 1 (HSV-1) regulatory protein (Everett et al., 1997). Later, USP7 was found to interact with other viral proteins such as the Epstein-Barr nuclear antigen 1 (EBNA1) of Epstein-Barr virus (EBV) and the vIRF1 (viral interferon regulatory factor 1) protein of Kaposi's sarcoma associated herpesvirus (KSHV) (Holowaty et al., 2003), therefore indicating it as a general target of herpes viruses and giving it the name herpes-associated ubiquitin specific protease. Up to now, USP7 is the most widely studied deubiquitinating enzymes, and is considered as an oncogene by promoting tumor growth and negatively affecting the patient immune response to tumors (Everett, 2014; Lu et al., 2016).

STRUCTURE OF USP7

The full length USP7 includes 1102 amino acids. There are four domains: an N-terminal poly-glutamine stretch (poly Q), the tumor necrosis factor receptor- associated factors (TRAF) domain (amino acids 62–205), the catalytic domain (amino acids 208–560), and the C-terminal tandem ubiquitin-like (Ubl) domain (amino acids 560–1102) (Kim and Sixma, 2017) (**Figure 2A**).

As reported, the amino acids 62–205 of USP7 (**Figure 2B**) bind to EBNA1 (Holowaty et al., 2003), mouse double minute 2 homolog (MDM2) and p53 (Hu et al., 2006; Sheng et al., 2006) through a PA-x-x-S motif (Saridakis et al., 2005), and the TRAF (amino acids 62–205) domain contributes to the nuclear localization of the USP7 (Fernandez-Montalvan et al., 2007). Besides, the USP7 truncation (amino acids 208–1102) performed similar activity as the full length protein (Ma et al., 2010).

Hu et al. (2002) identified a 40 kDa fragment of USP7 as the catalytic domain (amino acids 208–560), which mediates ubiquitin binding and deubiquitination of the substrate. The structure of the catalytic core domain reveals novel three-domain architecture, including Fingers, Palm, and Thumb domains (**Figure 2C**). This catalytic core domain binds to ubiquitin aldehyde, which reveals a conformational change in the active site (Hu et al., 2002). With the aid of molecular dynamics simulations, it is found that the transition of USP7 from the inactive to the active can only be captured when H294 was neutralized with a deprotonated C223 and charged H464. In the inactive apo state, positively charged H294 stabilizes an electrostatic network with W285, E298, and Y224. However, neutral H294 in the active state cannot make charge interactions, so the electrostatic network is disrupted. That would results in the C223 unfavorable backbone angles improved by helical refolding, thus, the active site is formed (Ozen et al., 2018).

Ubl shares the ubiquitin β-grasp fold, however, it lacks the C-terminal Gly–Gly residues that are required for conjugation to a target and is located outside the boundaries of the catalytic core domain (Faesen et al., 2011). There are five Ubl domains that are detected in the C-terminal and are organized in a 2-1-2 manner as Ubl-12, Ubl-3, and Ubl-45 (**Figure 2D**) (Zhu et al., 2007). Among them, Ubl-45 is sufficient to reconstitute the USP7 activation *in vitro* and *in vivo*. In the C-terminal, the 19 residues of USP7 (amino acids 1084–1102) are conserved across species (Faesen et al., 2011). Rouge et al. (2016) revealed how the C terminal 19 amino acids of the USP7 contribute to the enhancement of USP7 activity by stabilizing the ubiquitin binding conformation of the catalytic domain. And the individual point mutations at residues I1100 or I1098 are able to abolish the deubiquitinase activity of USP7 (Rouge et al., 2016).

USP7: ONE PROTEIN, MULTIPLE ROLES

Many proteins have been identified as potential substrates and binding partners of USP7, such as viral proteins, transcription factors, and epigenetic modulators (**Figure 8**), and most of these substrates play important roles in viral replication, immune response, tumor suppression, epigenetic control, and DNA repair. Here, functions of USP7 on these substrate are as detailed below (**Table 1**).

Viral Proteins

EBNA1

EBNA1 of EBV is important for the replication, segregation, and transcriptional activation of latent EBV genomes, it has been implicated in host cell immortalization, and avoids proteasome processing and cell-surface presentation. The amino acids 395–450 of EBNA1 bind to the USP7 N-terminal domain with a dissociation constant of 0.9–2 μM. The △395–450 mutant that selectively disrupted the binding to USP7 was found to increase fourfold EBNA1 replication activity than wild-type, but performed no impact on EBNA1 turnover and cell-surface presentation (Holowaty et al., 2003). As p53 and EBNA1 share similar binding sites with USP7, EBNA1 peptide efficiently competes with p53 peptide for USP7 binding, which results the decreasing stability of p53, and protects cells from apoptosis (Saridakis et al., 2005).

ICP0

Infected cell protein 0 (ICP0) of HSV is a multifunctional protein containing 775 amino acids that acts as a promiscuous trans-activator linked to the degradation of several proteins. The ^{618}PRKCARKT^{625} of ICP0 binds to a negatively charged region on Ubl2, where the residues K620 and K624 of ICP0 form direct contacts with residues D762 and D764 in Ubl2 of USP7 (Pfoh et al., 2015). Overexpression of USP7 had no effect on the mRNA level of ICP0, but could accelerate the mRNA accumulation of thymidine kinase (TK) and gI, which are important for HSV infection of non-replicating cells. The mutations at residues 620

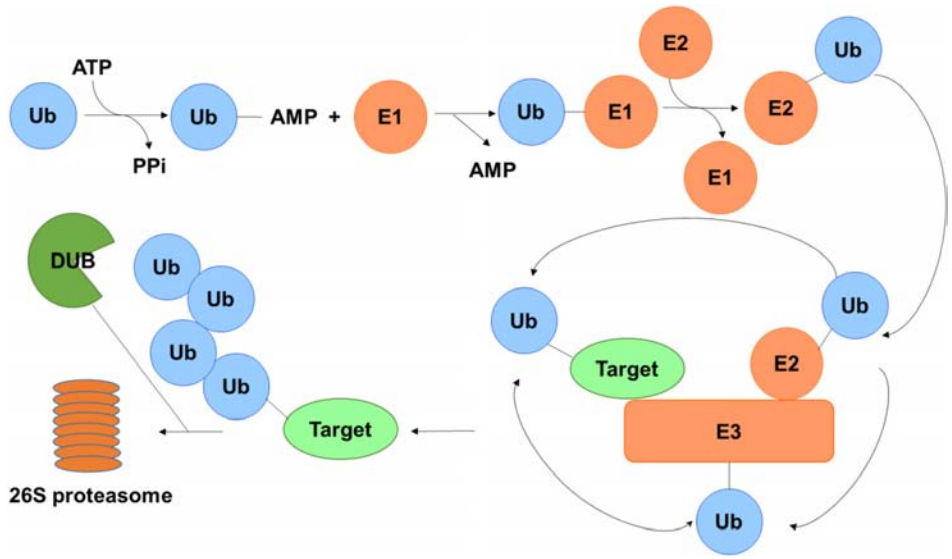

FIGURE 1 | Schematic of the ubiquitin-proteasome system. Ubiquitin is activated by E1 in the presence of ATP and transferred to E2 and then conjugated to a lysine or α-amino group of the substrate protein with the aid of E3. Polyubiquinated targets are recognized and degraded by the 26S proteasome, while the ubiquitin on the substrate can be erased by DUBs to protect it from degradation.

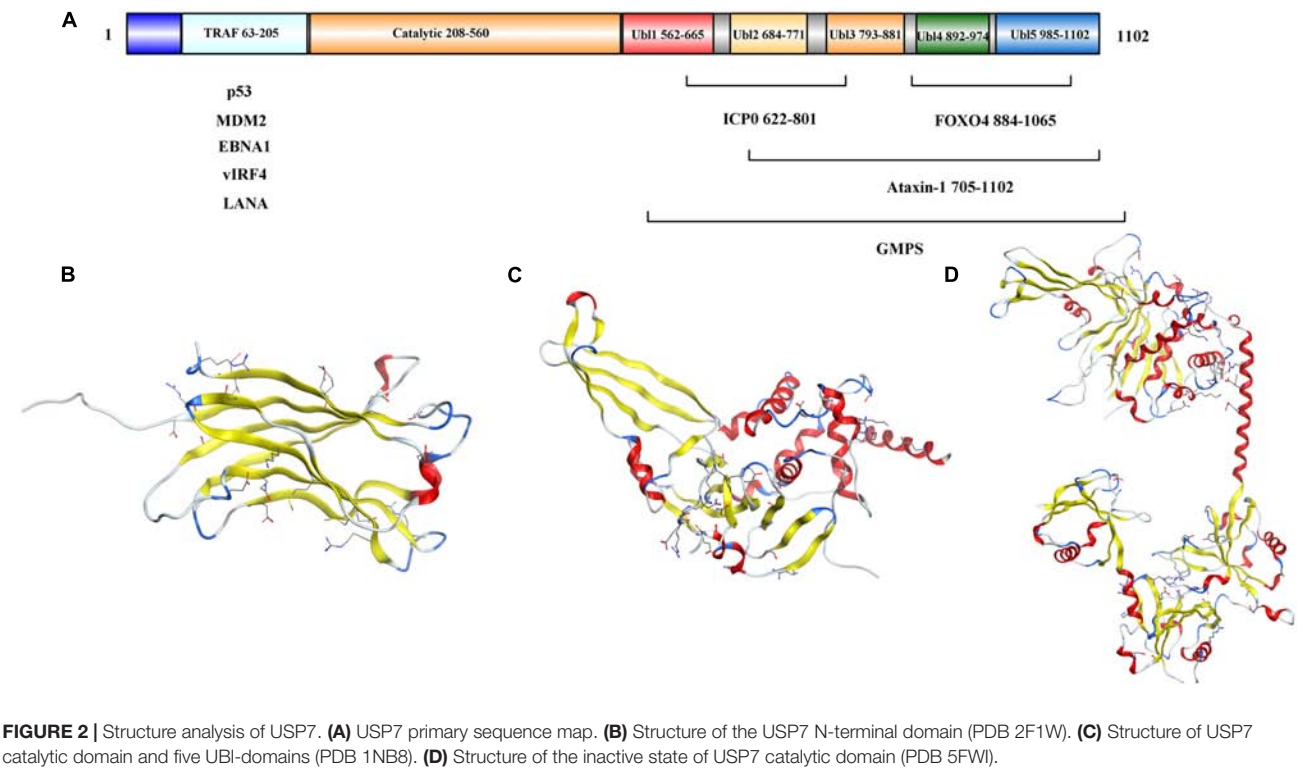

FIGURE 2 | Structure analysis of USP7. **(A)** USP7 primary sequence map. **(B)** Structure of the USP7 N-terminal domain (PDB 2F1W). **(C)** Structure of USP7 catalytic domain and five UBl-domains (PDB 1NB8). **(D)** Structure of the inactive state of USP7 catalytic domain (PDB 5FWI).

to 626 of ICP0 (named as R6702) can abolish the interaction between USP7 and ICP0, and the replication of R6702 in cells cannot be impaired (Kalamvoki et al., 2012). Hence, inhibition of USP7 and/or its interaction with ICP0 using small molecule inhibitors may decrease the virulence of HSV.

vIRFs

Among the vIRFs, vIRF1 could interact with the TRAF domain of USP7 via EGPS motif. The vIRF1 interaction with USP7 can decrease p53 levels by blocking the deubiquitination and stabilization of USP7 on p53. Thus the KSHV could have a

TABLE 1 | Proteins regulated by USP7.

USP7 substrates	Processes	Related cancer	References
EBNA1	Viral proteins		Holowaty et al., 2003
ICP0			Pfoh et al., 2015
vIRFs			Chavoshi et al., 2016; Xiang et al., 2018
LANA			Jager et al., 2012
E1B-55K			Ching et al., 2013
Tat			Ali et al., 2017
Foxp3	Immune response	Non-small cell lung cancer	van Loosdregt et al., 2013; Wang L. et al., 2016
TRIM27		Cervical carcinoma	Cai et al., 2018
NLRP3		Leukemia	Palazon-Riquelme et al., 2018
C-Myc and N-Myc	Oncoproteins	Neuroblastoma	Bhattacharya and Ghosh, 2015
p53	Tumor suppressor proteins	Ovarian cancers	Oliner et al., 1992; Li et al., 2002
DAXX		Breast cancer	Tang et al., 2006
PTEN		Chronic lymphocytic leukemia	Morotti et al., 2014
FOXOs family		Lung carcinoma	Huang et al., 2005
DNMT1	Epigenetics	Colon cancer	Du et al., 2010; Bronner, 2011
SUMO			Lecona et al., 2016
LSD1		Medulloblastoma	Yi et al., 2016
CHK1	DNA damage and repair		Alonso-de Vega et al., 2014
UVSSA			Sarasin, 2012; Zhang et al., 2012
ANXA1		Hela	Park et al., 2015
XPC			He et al., 2014
HLTF, Rad18			Qing et al., 2011
Polη			Qian et al., 2015
RNF168		Breast cancer	Malapelle et al., 2017
PHF8		Breast cancer	Wang Q. et al., 2016
MDC1		Cervical cancer	Su et al., 2018
Wnt/β-catenin signaling pathway	Several canonical signaling pathways	Colorectal cancer	Novellasdemunt et al., 2017
NF-κB signaling pathway		Multiple myeloma	Colleran et al., 2013
NOTCH signaling pathway		Lymphoblastic leukemia	Shan et al., 2018

lifelong infection when p53 is destabilized by USP7 coupled with vIRF1 (Chavoshi et al., 2016). Besides, vIRF3 is expressed in human herpes virus 8 (HHV-8) – infected primary effusion lymphoma (PEL) cells. The vIRF3 has two copies of EGPS, and both support the vIRF3 – USP7 interaction. This interaction plays important roles in PEL cell growth and viability and contributes to the suppression of productive virus replication (Xiang et al., 2018). For another vIRF family member, amino residues 210–216 of KSHV vIRF4 bind to the same surface groove of the USP7 TRAF domain as that can be recognized by MDM2 and p53. Moreover, the amino residues 202–208 of vIRF4 interact with the β-sheet in TRAF domain. The vIRF4-derived vif1 and vif2 peptides can restore p53 dependent apoptosis in wild-type p53 cancer cells by suppressing the USP7 activity. Thus the two peptides may be considered as potential backbones for peptide mimic small molecule inhibitors development for anti-cancer therapies (Lee et al., 2011).

LANA

The viral latency-associated nuclear antigen 1 (LANA) is expressed in all latency KSHV-infected cells and involves in viral latent replication and maintenance of the viral genome. The amino residues 971–986 of LANA interact with TRAF domain of USP7 with similar binding sites as EBNA1, while the △971–986 mutant shows an enhanced ability to replicate latent viral DNA. These results indicate that USP7 may influence accessibility of the viral DNA for latent replication or LANA-mediated viral persistence (Jager et al., 2012). Because of the role of USP7 in EBNA1 – dependent latent replication of EBV, USP7 may play the same role in the replication of latent viral DNA among gamma-1 and gamma-2 herpesviridae.

E1B-55K

Adenovirus E1B protein refers to one or two proteins transcribed from the E1B gene of the adenovirus: a 55 kDa protein and a 19 kDa protein. The N-terminal 79 amino acids of E1B-55K interact with the TRAF domain of USP7. Abrogation of USP7 decreases the protein level of E1B-55K and reduces progeny viral production. Therefore, the small inhibitors of USP7 may be used to treat adenovirus infections (Ching et al., 2013).

Tat

Human immunodeficiency virus (HIV) Tat is synthesized early after infection and mainly responsible for enhancing viral production. USP7 deubiquitinates and stabilizes Tat and enhances HIV-1 production. In turn, HIV-1 infection leads to the overexpression of USP7. These results show that the small inhibitors of USP7 can be used as a novel anti-HIV approach (Ali et al., 2017).

In sum, these results show that USP7 is recruited by these viruses to promote their survival in the host. So we speculate that USP7 may be an attractive target for controlling infection and other malignancies caused by these viruses.

Immune Response

Foxp3

Recent years, more and more reports have identified the importance of USP7 on keeping T regulatory cells (Treg) functions. As the major factor that restrains autoimmune responses, Treg cell expresses the forkhead transcription factor Foxp3, which is necessary for Treg cell development (Bettelli et al., 2005; Laurence et al., 2013). According to a report in 2016, five distinct lysine residues (K249, K251, K263, K267, and K393) in Foxp3 were identified to be ubiquitinated, and Foxp3 can be stabilized by USP7 mediated deubiquitination, resulting in the maintenance of Treg cell

number and function (Wang L. et al., 2016). In fact, a study in 2013 showed that aberrant USP7 overexpression decreases Foxp3 polyubiquitination and protects it from proteasome degradation, resulting in Treg-cell-mediated suppression and tumor growth. On the contrary, USP7 knockdown decreases Foxp3 level and abrogates Treg cell-induced suppression of autoimmune responses *in vitro* and *in vivo* (van Loosdregt et al., 2013).

Later studies gave the mechanism how the level of Foxp3 is regulated. Foxp3 could be ubiquitinated and degraded by the E3 ubiquitin ligase stress inducible protein 1 homology and U-Box containing protein 1 (STUB1). In addition, Foxp3, Heat Shock Protein 70 (Hsp70) and STUB1 associate together as a complex, indicating that these proteins bind and promote Foxp3 ubiquitination (**Figure 3**) (van Loosdregt and Coffer, 2014). Moreover, it is found that mesenchymal stem cells (MSCs) – induced Treg cells express high level of USP7 and low level of STUB1. Besides, Foxp3 mRNA expression was positively associated with USP7 and negatively associated with STUB1 (Khosravi et al., 2018). So, it provides us an opportunity to find a new way to study the unique role of USP7 in Treg cells and makes USP7 as a target in immunology.

TRIM27

Among the binding partners of USP7, tripartite motif 27 (TRIM27) is an ubiquitin E3 ligase that negatively regulates antiviral signaling by promoting the ubiquitination and degradation of TRAF family member-associated NF-κ-B activator – binding kinase 1 (TBK1). USP7 interacts with TRIM27 and forms the USP7-TRIM27-TBK1 complex, and the interaction between USP7 and TRIM27 can be enhanced after Sendai virus (SeV) infection. When USP7 was overexpressed, TRIM27 can be protected from degradation, which contributed to the ubiquitination and degradation of TBK1, resulting in decreased type I interferons (IFNs) signaling (Cai et al., 2018). As IFNs are a series of signaling proteins which are produced and released by host cells to cope with the presence of pathogens, USP7 can enhance the effects of TRIM27 on TBK1-induced IFN – stimulated response element (ISRE) and IFN-β activation (Zaman et al., 2013). Therefore, USP7 may act as a significant host protein to bridge the viral proteins with the antiviral immune response. Therapeutic methods against the USP7-TRIM27 complex may overcome the immune escape mediated by various viruses.

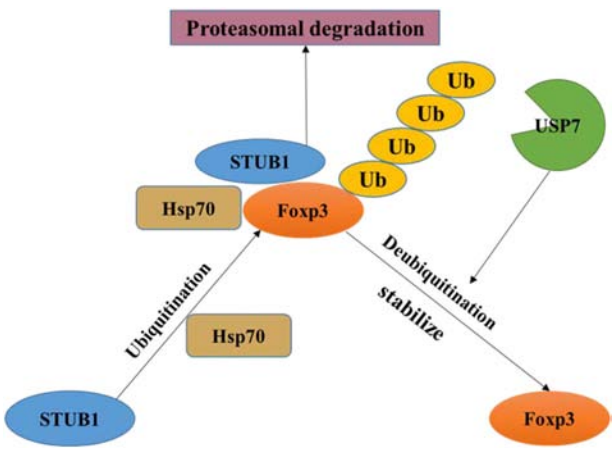

FIGURE 3 | Regulation of Foxp3 by USP7. Foxp3 is ubiquitinated by STUB1 and then produces a complex containing Foxp3, Hsp70 and STUB1, which leading to proteasome degradation of Foxp3. USP7 can remove the ubiquitin on Foxp3 and stabilize it.

NLRP3

USP7 may also impact on regulating NLR family pyrin domain containing 3 (NLRP3) inflammasome activation. NLRP3 is expressed primarily in macrophages as a component of the inflammasome to monitor products of damaged cells such as extracellular ATP and crystalline uric acid. The ubiquitination status of NLRP3 itself can be altered by USP7 and USP47. Furthermore, researchers discovered that the activity of USP7 and USP47 were augmented once the inflammasome was activated. In the meantime, they discovered that abrogation of both USP7 and USP47 resulted in reduction of inflammasome activation (Palazon-Riquelme et al., 2018).

To sum up, there is a remarkable connection between USP7 and immune-associated proteins, and so many studies have shown that the important roles of USP7 on regulating these proteins. It's worth thinking about USP7 inhibitors in combination with immunotherapy will be applied to cancer therapy so that the antitumor effect can be promoted. We hope to see their potential dual antitumor activity will be applied to clinical trials on day.

Oncoproteins

C-Myc and N-Myc

There are three members in Myc family: C-Myc, l-Myc, and N-Myc. Myc family is the most frequent amplified oncogene in human, which contributing to the formation of cancer. Among them, C-Myc and N-Myc are the substrates of USP7. USP7 overexpression can promote C-Myc stability by deubiquitination as well as transformation/transcription domain-associated protein (TRRAP), which is an adaptor protein known as a regulator of C-Myc. On the other hand, C-Myc mRNA can be accumulated by TRRAP indirectly (Bhattacharya and Ghosh, 2015).

N-Myc is another transcription factor that can be stabilized by USP7 via deubiquitination (Tavana et al., 2016). Hence, USP7 inhibitor p5091 was applied to decrease N-Myc expression in a dose dependent manner in neuroblastoma (Tavana et al., 2016). As a consequence, USP7 can be considered as a drug target to modulate C-Myc and N-Myc amount in order to block tumor development.

Tumor Suppressor Proteins

p53

p53 participates in cell cycle arrest, DNA repair, apoptosis, senescence and plays a key role in maintaining normal cell growth (Levine, 1997). USP7 plays a paradoxical role in regulating p53 functions through a variety of mechanisms. On one hand, p53 binds to TRAF domain and C-terminal (amino acids

880–1050) of USP7, and then USP7 ubiquitinates p53 directly and prevents it from degradation. On the other hand, TRAF domain and C-terminal (amino acids 801–1050) of USP7 can interact with MDM2 to increase its stability by erasing the ubiquitin on MDM2, an E3 ligase of p53 (Oliner et al., 1992), and protect it from proteasome degradation. Subsequently, MDM2 ubiquitinates p53 and causes its proteasome degradation, resulting in low expression of p53 in cancer cells (**Figure 4**) (Li et al., 2002, 2004). In addition, MDM2 can also inhibit the transcription of p53 (Wade et al., 2013). Therefore, inhibition of the interaction between MDM2 and p53 can stabilize p53 (Vassilev et al., 2004). It is noteworthy that, crystal structures analysis and binding studies suggest that the MDM2 peptide and p53 peptide bind to the same surface groove in USP7, but MDM2 performs more extensive interaction and stronger affinity (Hu et al., 2006). Taken together, the activation of USP7-MDM2-p53 interaction can promote the occurrence and development of tumors. The design of small molecules that disrupt or prevent the interaction may be an important target for cancer therapy by regulating p53 pathway.

DAXX

Death-domain-associated protein (DAXX) is a highly conserved and developmentally essential nuclear protein, which participates in many cellular processes (Lindsay et al., 2008). The N-terminal 160 amino acids and amino acids 347–570 of DAXX associate with USP7, which are far from the binding sites of MDM2 on DAXX. In unstressed cells, DAXX interacts with USP7 and MDM2, and mediates the stabilization of USP7 on MDM2, thus blocking p53 activation. In response to DNA damage, self-ubiquitination of MDM2 is accelerated when MDM2 is stripped from DAXX and USP7. That is to say, DAXX directs the ligase activity of MDM2 through regulating USP7 (Tang et al., 2006). Recent reports also show that USP7 and DAXX are critical in regulating the correct execution of mitosis by forming a tertiary complex as MDM2/DAXX/USP7 (Zhang et al., 2010). DAXX binding increases USP7 activity toward MDM2. Disassemble the MDM2-DAXX-USP7 complex can increase MDM2 self-ubiquitination and degradation, which leads to the stabilization and accumulation of p53 (Kumar et al., 2018).

PTEN

Phosphatase and tensin homolog (PTEN) is a tumor suppressor gene that displays dual specific phosphatase activity. PTEN inhibits the proliferation and migration of tumor cells (Blanco-Aparicio et al., 2007). It is reported that nuclear PTEN import is promoted by its mono-ubiquitination (Trotman et al., 2007). However, USP7 can remove the mono-ubiquitination of PTEN, triggering its nuclear exclusion and PTEN inactivation (Morotti et al., 2014). Likewise, USP7 inhibitor, P5091, regains PTEN nuclear pool and restores its tumor suppressive functions in chronic lymphocytic leukemia (CLL) (Carra et al., 2017). In addition, PTEN deletion leads to accumulation of activated AKT, and subsequent phosphorylation of MDM2 by AKT (Blanco-Aparicio et al., 2007), which results in the ubiquitination and degradation of p53 (Freeman et al., 2003). Therefore, PTEN deficiency causes p53-dependent cancer-promoting processes. This suggests how important it is to inhibit USP7 to ensure PTEN protein localization and activity.

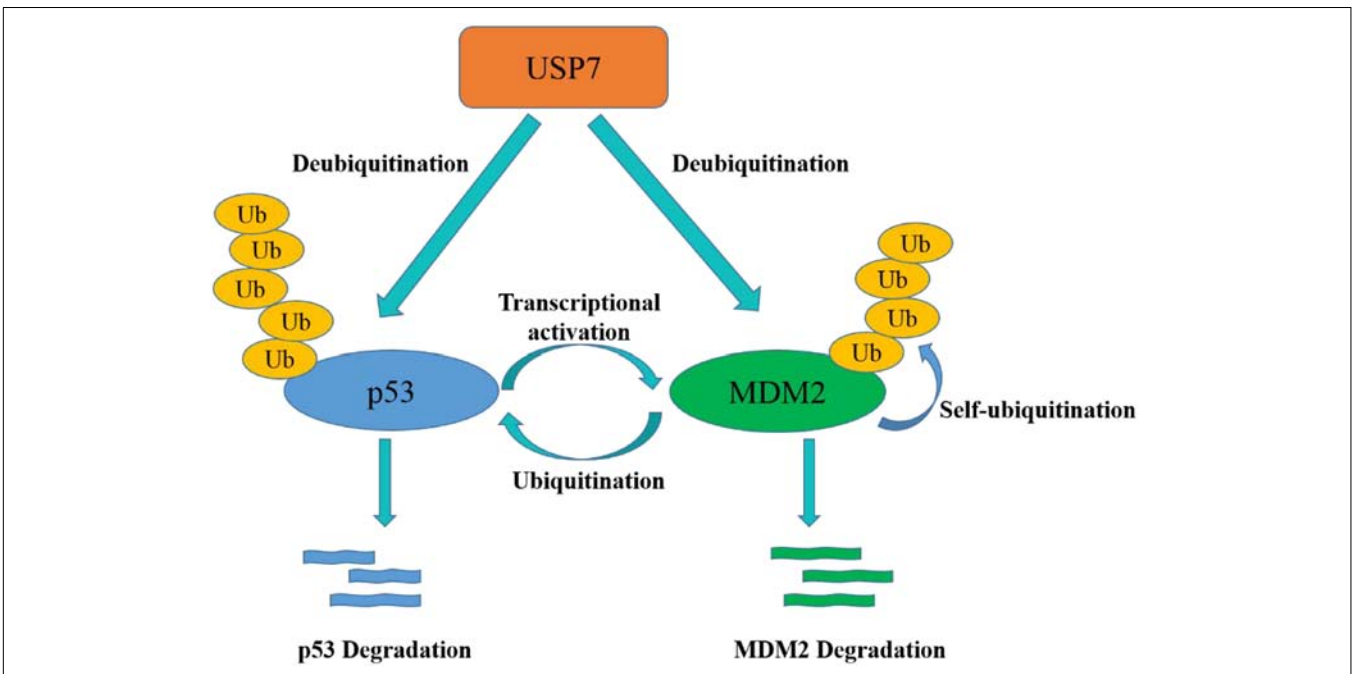

FIGURE 4 | USP7-p53-MDM2 axis interactions control the stability of p53 and MDM2. USP7 can stabilize p53 by deubiquitination, meanwhile, USP7 can also remove the ubiquitin of MDM2, which promotes to p53 degradation.

FOXOs Family

The Forkhead box O (FOXO) family members, including FOXO1, FOXO3, FOXO4 and FOXO6, are transcription factors that take part in regulating several cellular responses, including cell cycle progression and apoptosis and so on (van der Horst and Burgering, 2007). It is reported that USP7 can remove ubiquitin from FOXO1, which is written by Skp2 as an E3 ligase (Huang et al., 2005). Besides, mono-ubiquitination FOXO4 localizes in the nucleus and exhibits stronger transcriptional promotion activity (Brenkman et al., 2008). USP7 can suppress FOXO4 activity due to its deubiquitination and re-localization (van der Horst et al., 2006). In a word, USP7 affects tumor progression by interacting with FOXOs and affecting their activity and localization.

Epigenetics

DNMT1

DNMT1 (DNA methyltransferase 1) contributes to the maintenance of DNA methylation. As reported, USP7 can deubiquitinate and stabilize DNMT1 when its acetylation is erased by histone deacetylase 1 (HDAC1), which protects DNMT1 from proteasome degradation (Bronner, 2011). When the KG linker of DNMT1 is acetylated by Tip60, USP7 breaks away from DNMT1 and results in the degradation of DNMT1 mediated by proteasome system (**Figure 5**) (Du et al., 2010). Thus, HDAC and USP7 inhibitors can be applied in combination for cancer treatment (Cheng et al., 2015).

SUMO

Small ubiquitin related modifier (SUMO) is a ubiquitin-like molecule, which binds to its substrate by E3 SUMO ligase in a similar way as ubiquitination (Geoffroy and Hay, 2009). Like ubiquitin, proteins can be SUMOylated as mono-SUMOylation or poly-SUMOylation, but differently, poly-SUMOylation cannot lead to target degradation directly (Smits and Freire, 2016). Recent research shows that USP7 is associated with DNA synthesis (Smits and Freire, 2016). USP7 associates with an active DNA replication fork and inhibition of USP7 can reduce DNA replication. Moreover, Lecona et al. (2016) identified SUMO2 as a new USP7 substrate and demonstrated that USP7 can deubiquitinate SUMO2 *in vitro* and *in vivo*. However, the fate of SUMO2 after deubiquitination and its biological function are still unclear (Lecona et al., 2016).

LSD1

Histone lysine specific demethylase 1 (LSD1) is the first histone demethylase identified in 2004 and can remove methyl groups of histone H3K4, H3K9 (Shi et al., 2004). As reported, LSD1 can be ubiquitinated by E3 ligase JADE2 (Han et al., 2014). Since ubiquitination of LSD1 is considered as reversible process as ubiquitination and deubiquitination always exit in pair, LSD1 was identified to be deubiquitinated by USP7 and protected it from proteasome degradation (Yi et al., 2016). Besides, patients with high expression of USP7, REST, and LSD1 performed poorer outcomes in medulloblastoma (Callegari et al., 2018). And they found that p53 was a vital downstream transcription factor in the action of USP7 and LSD1.

DNA Damage and Repair

CHK1

USP7 can regulate CHK1 in three manners. The first one is the indirect regulation, USP7 deubiquitinated and prolonged the half-life of Claspin, which leaded to the sustaining phosphorylation of checkpoint kinase 1 (Chk1) in response to genotoxic stress (Faustrup et al., 2009). For the rest two manners, in DNA damage, USP7 deubiquitinates and stabilizes Chk1 via direct deubiquitination in the presence of zinc finger E-box binding homeobox 1 (ZEB1) (Zhang et al., 2014) or not (Alonso-de Vega et al., 2014), while ZEB1 binds to USP7 may result in promoting homologous recombinant-dependent DNA repair and resistant to radiation. In addition, USP7 can also directly regulate the stability of CDC25A, a Cdk-activating phosphatase as the substrate of CHK1, with the aid of brain and reproductive organ expressed protein (BRE). These results show that USP7 is an important modulator of Chk1.

CHFR

Checkpoint with Forkhead and Ring domains (CHFR), a RING family Ub-ligase, is a mitotic checkpoint that delays the transition to metaphase in response to mitotic stress. USP7 binds with CHFR *in vivo* and regulates its stability (**Figure 6**). These results indicate that USP7 may play a role in the cell cycle progression via the deubiquitination of CHFR (Oh et al., 2007).

UVSSA

Transcription-coupled nucleotide excision repair (TC-NER) removes DNA damage of actively transcribed genes. Defect in TC-NER is associated with cockayne syndrome (CS) and ultraviolet – sensitive syndrome (UVSS). Cockayne syndrome B (CSB/ERCC6) and UVSS protein are two important proteins in TC-NER. UVSSA binds with USP7 to stabilize CSB and restores the hypophosphorylated form of RNA polymerase II after UV irradiation (**Figure 6**) (Zhang et al., 2012). UVSSA and USP7 play roles in controlling the fate of stalled RNA polymerase II, the steady-state level of CSB, the efficiency of TC-NER and cell survival following DNA damage (Sarasin, 2012).

ANXA1

ANXA1 is a 37-kDa protein identified as the first member of the annexin superfamily. In response to DNA damage, ANXA1 is cleaved and generates the N-terminal fragment (Ac2-26) and the cleaved form of ANXA1. Both the full length of ANXA1 and Ac2-26 can be translocated to the cell membrane and induce apoptotic cell clearance through recruiting monocytes. The N-terminal of ANXA1 shares the USP7-binding motif sequences (AMVS and ALLS) and interacts with USP7. Hence, USP7 can deubiquitinate and stabilize ANXA1 (**Figure 6**). USP7 may participate in the DDR after UV-induced DNA damage in certain types via ANXA1 (Park et al., 2015).

XPC

Xeroderma pigmentosum complementation group C (XPC) is a critical damage recognition factor which binds to helix-distorting DNA lesions and initiates nucleotide excision repair (NER).

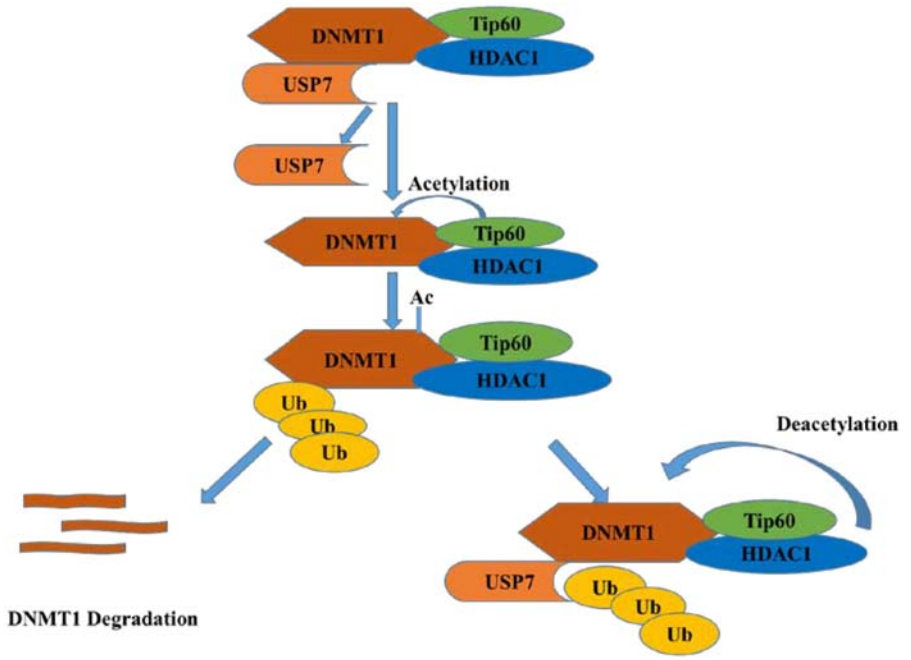

FIGURE 5 | USP7 and HDAC1 protect DNMT1 from degradation while Tip60 acetylates DNMT1 and promotes its degradation.

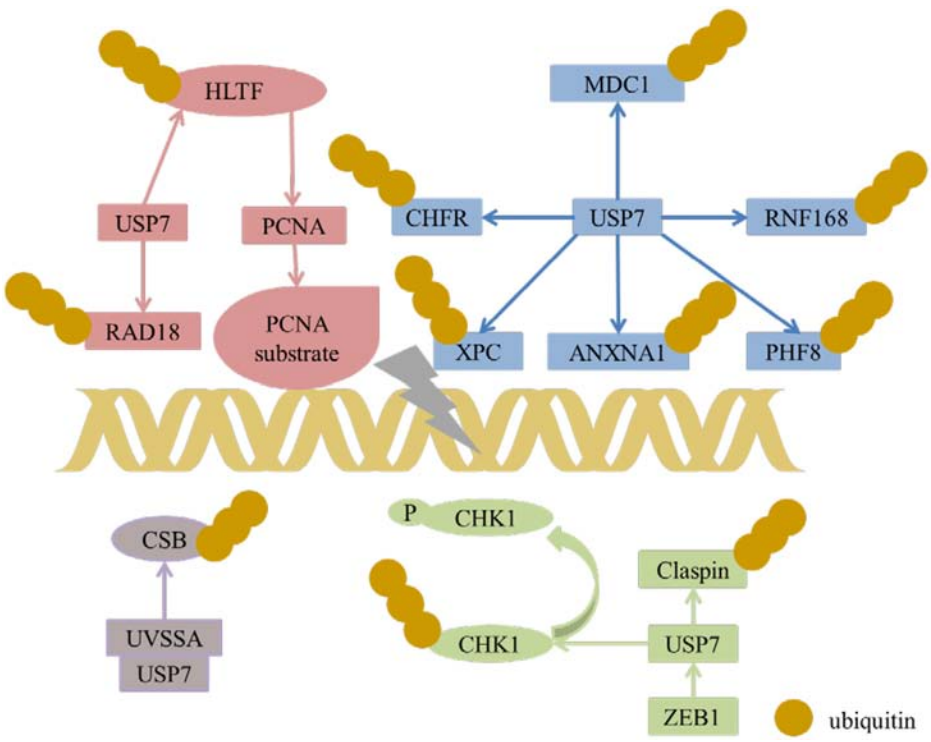

FIGURE 6 | USP7 interacts with a number of substrates in DNA damage response.

During the early stage of NER of UV light-induced DNA lesions, XPC is ubiquitinated. Ubl1 domain (amino acids 560–644) of USP7 can bind and erase the ubiquitination on XPC and prevents XPC from proteolysis (**Figure 6**). Taken together, USP7 plays a vital role in regulating NER through deubiqitinating XPC (He et al., 2014).

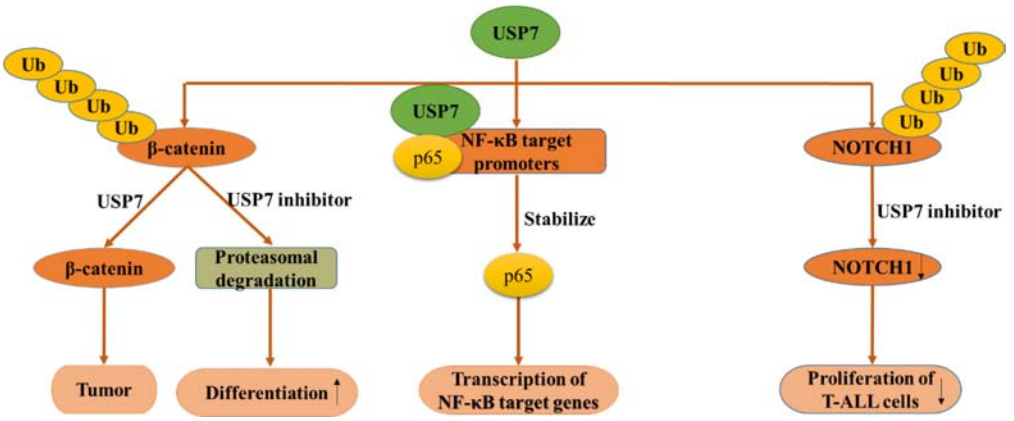

FIGURE 7 | USP7 functions in several canonical signaling pathways. USP7 functions in Wnt/β-catenin signaling pathway **(left)**, NF-κB signaling pathway **(middle)**, NOTCH signaling pathway **(right)**.

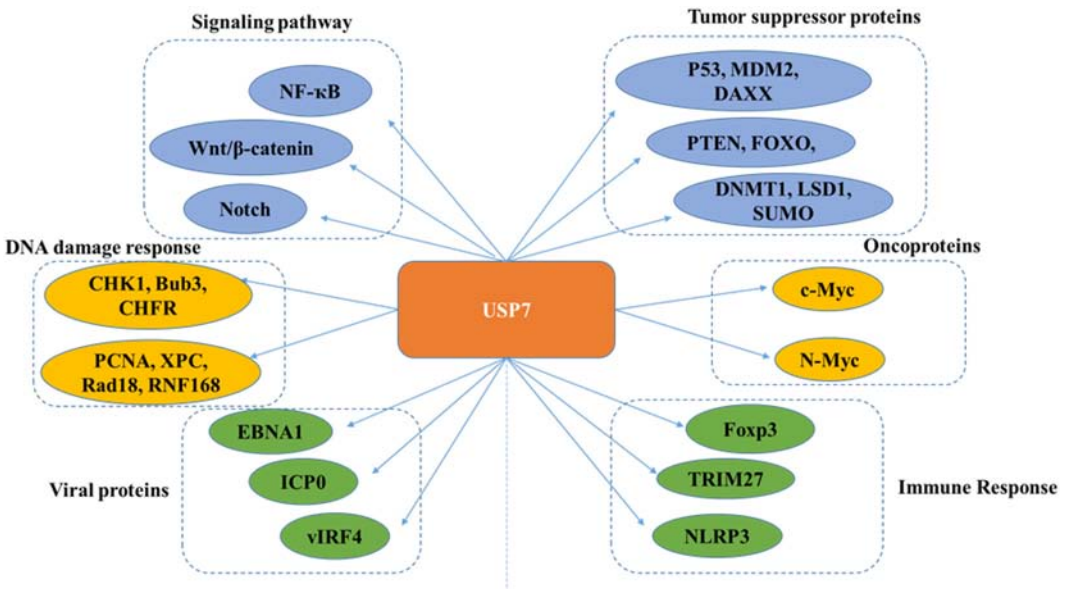

FIGURE 8 | Overview of USP7 functions.

HLTF, Rad18, and Polη

Helicase-like transcription factor (HLTF) is a double-stranded DNA translocase that can promote the polyubiquitination of proliferating cell nuclear antigen (PCNA), while Rad6–Rad18 monoubiquitinates PCNA, both of which make PCNA work as a molecular switch between various DNA damage bypass processes. On one hand, USP7 stabilizes HLTF after genotoxic stress, resulting in prolonging the half-life of HLTF, thus in turn increases polyubiquitination of PCNA (**Figure 6**) (Qing et al., 2011). Besides, USP7 and DNA polymerase eta (Polη), a key player in several DNA damage-tolerance pathways, interact with each other, and USP7 increases UV-induced PCNA ubiquitination through stabilizing Polη and in turn facilitates the recruitment of DNA translesion synthesis (TLS) polymerases to bypass DNA lesions. Therefore USP7 promotes monoUb-PCNA mediated stress-tolerance pathways via the stabilization of Polη. These results provide new mechanistic for USP7-related tumorigenesis and therapeutic strategy (Qian et al., 2015). On the other hand, the amino acids 110–251 of Rad18 interact with USP7 and contain two USP7-binding motifs. Loss of USP7 destabilizes Rad18 and compromises UV-induced PCNA monoubiquitylation and Polη recruitment to stalled replication forks (Zlatanou et al., 2016).

RNF168

During DDR, histone ubiquitination by RNF168 orchestrates the recruitment of downstream DDR factors, e.g., breast cancer type 1 susceptibility protein (BRCA1) and p53 binding protein

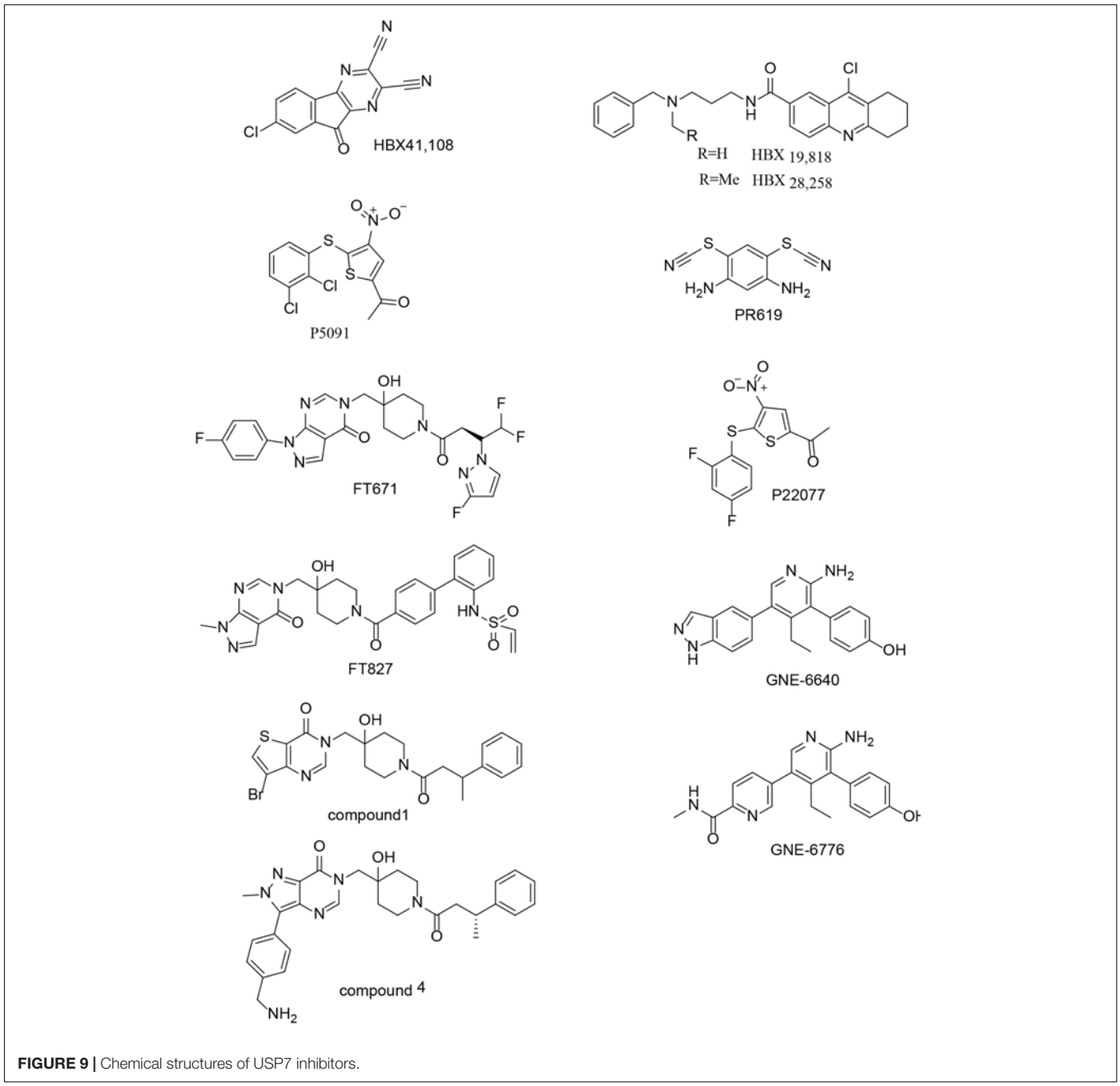

FIGURE 9 | Chemical structures of USP7 inhibitors.

1 (53BP1). The Ubl1 domain of USP7 binds to RNF168 (**Figure 6**). USP7 regulates H2A monoubiquitination and H2A/X polyubiquitination via its regulation on RNF168. In summary, USP7 plays a vital role in regulation of Ub-dependent signaling in DDR via monitoring RNF168 (Malapelle et al., 2017).

PHF8

Plant homeodomain finger-containing protein 8 (PHF8) consists of an N-terminal plant homeodomain and recognizes and binds tri-methyl histone 3 lysine 4 at transcription start sites. The C-terminal region of PHF8 binds with the TRAF domain of USP7, and USP7 promotes the stability of PHF8 via deubiquitinase activity and contributes to the maintenance of genome integrity, which is implemented in DDR (**Figure 6**). The USP7/PHF8 is involved in breast carcinogenesis, indicating these molecules may be as potential targets for breast cancer intervention (Wang Q. et al., 2016).

MDC1

DNA damage checkpoint protein 1 (MDC1) is important for the initiation and amplification of the DDR. USP7 deubiquitinates and stabilizes of MDC1, resulting in sustaining the DDR, while depletion of USP7 influences the engagement of MRE11-RAD50-NBS1(MRN)-MDC1 complex and the

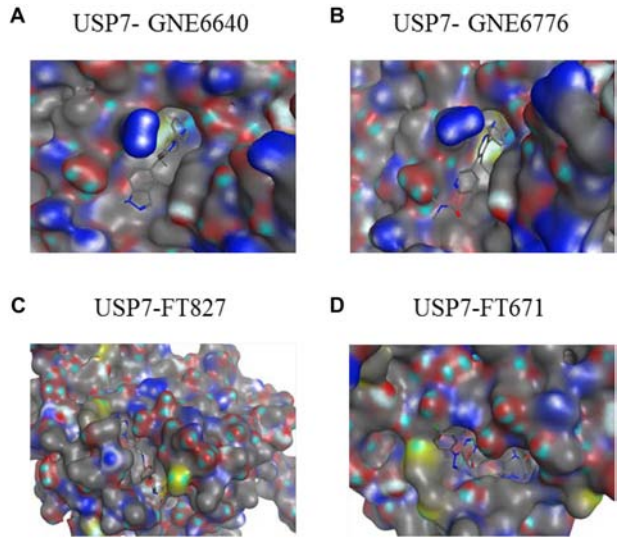

FIGURE 10 | Co-crystal structures of USP7 in complex with inhibitors. The electrostatic surface representation of the CD of USP7 is shown along with compounds **(A)** USP7-GNE6640 (PDB code 5UQV). **(B)** USP7-GNE6776 (PDB code 5UQX). **(C)** USP7-FT827 (PDB code 5NGF). **(D)** USP7-FT671 (PDB code 5NGE). The images were generated with molecular operating environment (MOE).

recruitment of the downstream factors 53BP1 and BRCA1 at DNA lesions. USP7 promotes cervical cancer cell survival and confrere cellular resistance to genotoxic insults via the stabilization of MDC1 (Su et al., 2018).

In a nutshell, USP7 plays a vital role in the DNA damage response (**Figure 6**), and it can be targeted for the treatment of malignancies with DDR defects. Besides, USP7 inhibitors can be combined with genotoxic agents as a novel therapeutic strategy for the treatment of cancer.

USP7 stabilizes HLTF to result in polyubiquitination of PCNA and induces monoubiquitination of PCNA through regulating Rad18. USP7 plays a role in DDR through regulating MDC1, CHFR, XPC, ANXNA1, RNF168, and PHF8. USP7 and UVSSA interact with each other to control steady state of CSB following DNA damage. USP7 can regulate stability of CDC25A via deubiquitination CDC25A directly and through regulating Claspin and CHK1 expression.

Several Canonical Signaling Pathways

Wnt/β-Catenin Signaling Pathway

Wnt signaling was initially found for its function in cancer and embryonic development and then was found responsible for tissue regeneration in adult bone marrow, skin and intestine. β-Catenin, a key element in Wnt signaling pathway, is regulated by diverse PTMs, including ubiquitination (Ma et al., 2014). According to a research in 2017, β-catenin can be deubiquitinated and stabilized by USP7 in adenomatous polyposis coli (APC) truncating mutated colorectal cancer (CRC) but not APC wide type CRC, which resulting in the activation of Wnt pathway (Novellasdemunt et al., 2017). Mechanism study suggested that APC β-catenin inhibitory domain (CID) protects β-catenin from USP7-mediated deubiquitination, while APC lacking CID exposes β-catenin to USP7 for deubiquitination. Hence, abrogation of USP7 in APC-mutated CRC suppresses Wnt activation by regaining β-catenin ubiquitination, which leads to the cell differentiation, and inhibits tumor growth (Novellasdemunt et al., 2017). With the aid of USP7 inhibitor P5091, Wnt pathway can be inactivated by improving ubiquitination and degradation of β-catenin, which provides evidence for the rationality for developing USP7 inhibitors as anti-CRC agent (**Figure 7A**) (An et al., 2017). In a nutshell, USP7 can be considered as a Wnt activator for tumor-specific therapeutic target for most CRCs.

NF-κB Signaling Pathway

Nuclear factor kappa B (NF-κB) signaling pathway is responsible for the transcription of a series of genes that controlling inflammation and immunity. As an essential regulator of Toll-like-receptor (TLR) and tumor necrosis factor receptor (TNFR)-inducible inflammatory gene expression, NF-κB is regulated by USP7 in a research in 2013. Different from other USP7 partners and substrates, NF-κB p65 and USP7 interact together after USP7 is recruited to NF-κB target promoters. Besides, the inhibition of USP7 lead to decreased TLR and TNFR-induced expression of Interleukin (IL-6), TNFα (NF-κB reporter) indicates that the deubiquitination of NF-κB by USP7 may have therapeutic potential (**Figure 7B**) (Colleran et al., 2013).

In 2018, some researchers found that knockout of USP7 dramatically increased the sensitivity of multiple myeloma (MM) cells to bortezomib (BTZ) which led to myeloma cell death and inhibited NF-κB activation by stabilizing IκBα. As expected, usage of USP7 inhibitors also inhibited the activation of NF-κB and the combination of USP7 inhibitor with BTZ triggered the synergistic antitumor activity in bortezomib-resistant MM cells. Taken together, this study provides a new application for USP7 inhibitors alone or in combination with BTZ to overcome BTZ resistance and improve the patient prognosis in MM (Yao et al., 2018).

In all, several reports have illustrated the mechanism that how USP7 and its related proteins regulate NF-κB signaling pathway. However, more deep studies should be conducted to make the mechanism more clearly and logically and there are still great challenges for researchers to face.

NOTCH Signaling Pathway

Notch signaling pathway is highly conserved and presents in most multicellular organisms. This intercellular signaling cascade is involved in cell differentiation, proliferation, and contributes to the fate of cells and occurs in multiple organisms and tissues, containing early T cell development in the thymus and peripheral T cell differentiation (Auderset et al., 2012; Bailis et al., 2013; Amsen et al., 2015). There are four notch receptors in mammals possessing NOTCH1-4 in which NOTCH1 can be stabilized through USP7-mediated deubiquitination. Previous studies have revealed that ubiquitination regulates the stability, activity, and localization of NOTCH1. However, the specific deubiquitinase that affects NOTCH1 protein stability was clarified recently.

Researchers reported that USP7 can deubiquitinate and stabilize NOTCH1 *in vivo* and *in vitro*, on the other hand, knockdown of USP7 increased the ubiquitination of NOTCH1. Used up of USP7 significantly restrained the proliferation of T-cell acute lymphoblastic leukemia (T-ALL) cells *in vitro* and *in vivo*, accompanied by downregulation of the NOTCH1 protein level, suggesting that targeting the USP7/NOTCH1 axis is a novel strategy to combat T-ALL and other NOTCH1-related malignancies (**Figure 7C**) (Shan et al., 2018). Almost at the same time, researchers found USP7 can bind several oncogenes by interacting and stabilizing NOTCH1 and JmjC Domain-Containing Protein 3 (JMJD3) in order to control leukemia growth. What's more, USP7 and NOTCH1 bind T-ALL superenhancers, and inhibition of USP7 leads to a decrease of the transcriptional levels of NOTCH1 targets and T-ALL cell growth *in vitro* and *in vivo*. Therefore, USP7 cooperating with NOTCH1 can improve the oncogenic transcriptional program in T-ALL (Jin et al., 2018).

The functions of USP7 on different signaling pathways indicate the brand new role of USP7 as a great target. To be sure, other classical signaling pathways which may be regulated by USP7 is yet to be found. It provides us a great challenge to find the new mechanisms between USP7 and other classical signaling pathways.

USP7 in Cancer

USP7 is highly expressed in a wide variety of cancers and affects the progression of cancer diseases. Moreover, USP7 assumes different roles in different tumors. In prostate cancer, high expression of USP7 is directly related to tumor invasion (Song et al., 2008). USP7 plays a key role in carcinogenesis via p53-dependent pathways in non-small cell lung carcinoma (NSCLCs) (Masuya et al., 2006). Studies have shown that changes of USP7 regulate colon carcinoma growth and apoptotic sensitivity *in vivo* (Becker et al., 2008). USP7 maintains DNA damage response and promotes cervical cancer, and is positively correlated with poor survival rate in patients with cervical cancer (Su et al., 2018). USP7 regulates human terminal erythroid differentiation by stabilizing GATA1, providing a certain treatment for leukemia (Liang et al., 2019). In short, USP7 plays an important role in a variety of pathologies and is a good target from a therapeutic point of view.

USP7 INHIBITORS

USP7 is a promising target not only for its roles in cellular pathways including regulators of viral proteins, immune response, oncogenes, and DNA damage but also because of its aberrant expression in various cancers. Due to lack of co-crystal structures between USP7 and small molecule inhibitors, there is no potent and selective USP7 inhibitor for a long time (Colland et al., 2009; Altun et al., 2011; Chauhan et al., 2012; Reverdy et al., 2012) (**Figure 9**). However, several groups reported the structures of USP7 in complex with small molecule inhibitors last year (Kategaya et al., 2017; Turnbull et al., 2017) (**Figure 10**) and these structures gives guidance to obtain structure-based small molecule inhibitors.

CONCLUSION AND FUTURE PERSPECTIVES

This review illustrates our current knowledge of USP7, including its source and characterization, structure, binding partners and substrates in various biological processes. Besides, how USP7 regulates various aspects of a cell under both normal and pathological states are elaborated in detail. As the processes of ubiquitination and deubiquitination are extremely dynamic and context-specific, a series of studies have linked USP7 to different cancers. The biology, particularly the immune oncology mechanisms, reveal that USP7 inhibitors would be useful drugs, thus it is vital to develop highly selective and specific inhibitors of USP7. The association of USP7 with several canonical signaling pathways still needs characterized in order to search new targets and regulatory mechanisms. Last but not least, USP7 may be a promising target for cancer therapy and it therefore merits further studies.

AUTHOR CONTRIBUTIONS

ZW discusses the structure of USP7, the viral protein targets of USP7, the DNA damage substrates of USP7 and conclusion. WK talks about the introduction, immune function of USP7, Wnt/β-catenin signaling pathway, and NF-κB signaling pathway. YY illustrates oncoproteins and tumor suppressor proteins. JP states about the epigenetics substrates of USP7. HR talks about the NOTCH signaling pathway. ZS and YZ provide expertise and feedback. HL provides funding.

FUNDING

This work was supported by National Natural Science Foundation of China (Project No. 81602961 for YZ; Project Nos. 81430085 and 81773562 for HL); Outstanding Young Talent Research Fund of Zhengzhou University (Project No. 1521331002 for YZ); National Key Research Program of Proteins (Project No. 2016YFA0501800 for HL; Project No. 2017YFD0501401 for YZ); and Key Research Program of Henan Province (Project No. 161100310100 for HL).

REFERENCES

Ali, A., Raja, R., Farooqui, S. R., Ahmad, S., and Banerjea, A. C. (2017). USP7 deubiquitinase controls HIV-1 production by stabilizing Tat protein. *Biochem. J.* 474, 1653–1668. doi: 10.1042/bcj20160304

Alonso-de Vega, I., Martin, Y., and Smits, V. A. (2014). USP7 controls Chk1 protein stability by direct deubiquitination. *Cell Cycle* 13, 3921–3926. doi: 10.4161/15384101.2014.973324

Altun, M., Kramer, H. B., Willems, L. I., McDermott, J. L., Leach, C. A., Goldenberg, S. J., et al. (2011). Activity-based chemical proteomics accelerates inhibitor

development for deubiquitylating enzymes. *Chem. Biol.* 18, 1401–1412. doi: 10.1016/j.chembiol.2011.08.018

Amsen, D., Helbig, C., and Backer, R. A. (2015). Notch in T Cell differentiation: all things considered. *Trends Immunol.* 36, 802–814. doi: 10.1016/j.it.2015.10.007

An, T., Gong, Y., Li, X., Kong, L., Ma, P., Gong, L., et al. (2017). USP7 inhibitor P5091 inhibits Wnt signaling and colorectal tumor growth. *Biochem. Pharmacol.* 131, 29–39. doi: 10.1016/j.bcp.2017.02.011

Auderset, F., Coutaz, M., and Tacchini-Cottier, F. (2012). The role of notch in the differentiation of CD4(+) T helper cells. *Curr. Top. Microbiol. Immunol.* 360, 115–134. doi: 10.1007/82_2012_227

Bailis, W., Yashiro-Ohtani, Y., Fang, T. C., Hatton, R. D., Weaver, C. T., Artis, D., et al. (2013). Notch simultaneously orchestrates multiple helper T cell programs independently of cytokine signals. *Immunity* 39, 148–159. doi: 10.1016/j.immuni.2013.07.006

Becker, K., Marchenko, N. D., Palacios, G., and Moll, U. M. (2008). A role of HAUSP in tumor suppression in a human colon carcinoma xenograft model. *Cell Cycle* 7, 1205–1213. doi: 10.4161/cc.7.9.5756

Bettelli, E., Dastrange, M., and Oukka, M. (2005). Foxp3 interacts with nuclear factor of activated T cells and NF-kappa B to repress cytokine gene expression and effector functions of T helper cells. *Proc. Natl. Acad. Sci. U.S.A.* 102, 5138–5143. doi: 10.1073/pnas.0501675102

Bhattacharya, S., and Ghosh, M. K. (2015). HAUSP regulates c-MYC expression via de-ubiquitination of TRRAP. *Cell Oncol.* 38, 265–277. doi: 10.1007/s13402-015-0228-6

Blanco-Aparicio, C., Renner, O., Leal, J. F., and Carnero, A. (2007). PTEN, more than the AKT pathway. *Carcinogenesis* 28, 1379–1386. doi: 10.1093/carcin/bgm052

Brenkman, A. B., de Keizer, P. L., van den Broek, N. J., Jochemsen, A. G., and Burgering, B. M. (2008). Mdm2 induces mono-ubiquitination of FOXO4. *PLoS One* 3:e2819. doi: 10.1371/journal.pone.0002819

Bronner, C. (2011). Control of DNMT1 abundance in epigenetic inheritance by acetylation, ubiquitylation, and the histone code. *Sci. Signal.* 4:pe3. doi: 10.1126/scisignal.2001764

Cai, J., Chen, H. Y., Peng, S. J., Meng, J. L., Wang, Y., Zhou, Y., et al. (2018). USP7-TRIM27 axis negatively modulates antiviral type I IFN signaling. *FASEB J.* 32, 5238–5249. doi: 10.1096/fj.201700473RR

Callegari, K., Maegawa, S., Bravo-Alegria, J., and Gopalakrishnan, V. (2018). Pharmacological inhibition of LSD1 activity blocks REST-dependent medulloblastoma cell migration. *Cell Commun. Signal.* 16:60. doi: 10.1186/s12964-018-0275-5

Carra, G., Panuzzo, C., Torti, D., Parvis, G., Crivellaro, S., Familiari, U., et al. (2017). Therapeutic inhibition of USP7-PTEN network in chronic lymphocytic leukemia: a strategy to overcome TP53 mutated/deleted clones. *Oncotarget* 8, 35508–35522. doi: 10.18632/oncotarget.16348

Chatterjee, B., and Thakur, S. S. (2018). Investigation of post-translational modifications in type 2 diabetes. *Clin. Proteomics* 15:32. doi: 10.1186/s12014-018-9208-y

Chauhan, D., Tian, Z., Nicholson, B., Kumar, K. G., Zhou, B., Carrasco, R., et al. (2012). A small molecule inhibitor of ubiquitin-specific protease-7 induces apoptosis in multiple myeloma cells and overcomes bortezomib resistance. *Cancer Cell* 22, 345–358. doi: 10.1016/j.ccr.2012.08.007

Chavoshi, S., Egorova, O., Lacdao, I. K., Farhadi, S., Sheng, Y., and Saridakis, V. (2016). Identification of kaposi sarcoma herpesvirus (KSHV) vIRF1 protein as a novel interaction partner of human deubiquitinase USP7. *J. Biol. Chem.* 291, 6281–6291. doi: 10.1074/jbc.M115.710632

Cheng, J., Yang, H., Fang, J., Ma, L., Gong, R., Wang, P., et al. (2015). Molecular mechanism for USP7-mediated DNMT1 stabilization by acetylation. *Nat. Commun.* 11:7023. doi: 10.1038/ncomms8023

Cheon, K. W., and Baek, K. H. (2006). HAUSP as a therapeutic target for hematopoietic tumors (review). *Int. J. Oncol.* 28, 1209–1215.

Ching, W., Koyuncu, E., Singh, S., Arbelo-Roman, C., Hartl, B., Kremmer, E., et al. (2013). A ubiquitin-specific protease possesses a decisive role for adenovirus replication and oncogene-mediated. *PLoS Pathog.* 9:e1003273. doi: 10.1371/journal.ppat.1003273

Clague, M. J., Barsukov, I., Coulson, J. M., Liu, H., Rigden, D. J., and Urbe, S. (2013). Deubiquitylases from genes to organism. *Physiol. Rev.* 93, 1289–1315. doi: 10.1152/physrev.00002.2013

Colland, F., Formstecher, E., Jacq, X., Reverdy, C., Planquette, C., Conrath, S., et al. (2009). Small-molecule inhibitor of USP7/HAUSP ubiquitin protease stabilizes and activates p53 in cells. *Mol. Cancer Ther.* 8, 2286–2295. doi: 10.1158/1535-7163.mct-09-0097

Colleran, A., Collins, P. E., O'Carroll, C., Ahmed, A., Mao, X., McManus, B., et al. (2013). Deubiquitination of NF-kappaB by ubiquitin-specific protease-7 promotes transcription. *Proc. Natl. Acad. Sci. U.S.A.* 110, 618–623. doi: 10.1073/pnas.1208446110

Du, Z., Song, J., Wang, Y., Zhao, Y., Guda, K., Yang, S., et al. (2010). DNMT1 stability is regulated by proteins coordinating deubiquitination and acetylation-driven ubiquitination. *Sci. Signal.* 3:ra80. doi: 10.1126/scisignal.2001462

Dybas, J. M., Herrmann, C., and Weitzman, M. D. (2018). Ubiquitination at the interface of tumor viruses and DNA damage responses. *Curr. Opin. Virol.* 32, 40–47. doi: 10.1016/j.coviro.2018.08.017

Everett, R. D. (2014). HSV-1 biology and life cycle. *Methods Mol. Biol.* 1444, 1–17. doi: 10.1007/978-1-4939-0428-0_1

Everett, R. D., Meredith, M., Orr, A., Cross, A., Kathoria, M., and Parkinson, J. (1997). A novel ubiquitin-specific protease is dynamically associated with the PML nuclear domain and binds to a herpesvirus regulatory protein. *EMBO J.* 16, 1519–1530. doi: 10.1093/emboj/16.7.1519

Faesen, A. C., Dirac, A. M., Shanmugham, A., Ovaa, H., Perrakis, A., and Sixma, T. K. (2011). Mechanism of USP7/HAUSP activation by its C-terminal ubiquitin-like domain and allosteric regulation by GMP-synthetase. *Mol. Cell* 44, 147–159. doi: 10.1016/j.molcel.2011.06.034

Faustrup, H., Bekker-Jensen, S., Bartek, J., Lukas, J., and Mailand, N. (2009). USP7 counteracts SCFbetaTrCP- but not APCCdh1-mediated proteolysis of Claspin. *J. Cell Biol.* 184, 13–19. doi: 10.1083/jcb.200807137

Fernandez-Montalvan, A., Bouwmeester, T., Joberty, G., Mader, R., Mahnke, M., Pierrat, B., et al. (2007). Biochemical characterization of USP7 reveals post-translational modification sites and structural requirements for substrate processing and subcellular localization. *FEBS J.* 274, 4256–4270. doi: 10.1111/j.1742-4658.2007.05952.x

Freeman, D. J., Li, A. G., Wei, G., Li, H. H., Kertesz, N., Lesche, R., et al. (2003). PTEN tumor suppressor regulates p53 protein levels and activity through phosphatase-dependent and -independent mechanisms. *Cancer Cell* 3, 117–130. doi: 10.1016/s1535-6108(03)00021-7

Geoffroy, M. C., and Hay, R. T. (2009). An additional role for SUMO in ubiquitin-mediated proteolysis. *Nat. Rev. Mol. Cell Biol.* 10, 564–568. doi: 10.1038/nrm2707

Han, X., Gui, B., Xiong, C., Zhao, L., Liang, J., Sun, L., et al. (2014). Destabilizing LSD1 by Jade-2 promotes neurogenesis: an antibraking system in neural development. *Mol. Cell* 55, 482–494. doi: 10.1016/j.molcel.2014.06.006

He, J., Zhu, Q., Wani, G., Sharma, N., Han, C., Qian, J., et al. (2014). Ubiquitin-specific protease 7 regulates nucleotide excision repair through deubiquitinating XPC protein and preventing XPC protein from undergoing ultraviolet light-induced and VCP/p97 protein-regulated proteolysis. *J. Biol. Chem.* 289, 27278–27289. doi: 10.1074/jbc.M114.589812

Holowaty, M. N., Zeghouf, M., Wu, H., Tellam, J., Athanasopoulos, V., Greenblatt, J., et al. (2003). Protein profiling with epstein-barr nuclear antigen-1 reveals an interaction with the herpesvirus-associated ubiquitin-specific protease HAUSP/USP7. *J. Biol. Chem.* 278, 29987–29994. doi: 10.1074/jbc.M303977200

Hu, M., Gu, L., Li, M., Jeffrey, P. D., Gu, W., and Shi, Y. (2006). Structural basis of competitive recognition of p53 and MDM2 by HAUSP/USP7: implications for the regulation of the p53-MDM2 pathway. *PLoS Biol.* 4:e27. doi: 10.1371/journal.pbio.0040027

Hu, M., Li, P., Li, M., Li, W., Yao, T., Wu, J. W., et al. (2002). Crystal structure of a UBP-family deubiquitinating enzyme in isolation and in complex with ubiquitin aldehyde. *Cell* 111, 1041–1054. doi: 10.1016/s0092-8674(02)01199-6

Huang, H., Regan, K. M., Wang, F., Wang, D., Smith, D. I., van Deursen, J. M., et al. (2005). Skp2 inhibits FOXO1 in tumor suppression through ubiquitin-mediated degradation. *Proc. Natl. Acad. Sci. U.S.A.* 102, 1649–1654. doi: 10.1073/pnas.0406789102

Jager, W., Santag, S., Weidner-Glunde, M., Gellermann, E., Kati, S., Pietrek, M., et al. (2012). The ubiquitin-specific protease USP7 modulates the replication of Kaposi's sarcoma-associated herpesvirus latent episomal DNA. *J. Virol.* 86, 6745–6757. doi: 10.1128/jvi.06840-11

Jin, Q., Martinez, C. A., Arcipowski, K. M., Zhu, Y., Gutierrez-Diaz, B. T., Wang, K. K., et al. (2018). USP7 cooperates with NOTCH1 to drive the oncogenic

transcriptional program in T cell leukemia. *Clin. Cancer Res.* 25, 222–239. doi: 10.1158/1078-0432.CCR-18-1740

Kalamvoki, M., Gu, H., and Roizman, B. (2012). Overexpression of the ubiquitin-specific protease 7 resulting from transfection or mutations in the ICP0 binding site accelerates rather than depresses herpes simplex virus 1 gene expression. *J. Virol.* 86, 12871–12878. doi: 10.1128/jvi.01981-12

Kategaya, L., Di Lello, P., Rouge, L., Pastor, R., Clark, K. R., Drummond, J., et al. (2017). USP7 small-molecule inhibitors interfere with ubiquitin binding. *Nature* 550, 534–538. doi: 10.1038/nature24006

Khosravi, M., Bidmeshkipour, A., Cohen, J. L., Moravej, A., Hojjat-Assari, S., Naserian, S., et al. (2018). Induction of CD4(+)CD25(+)FOXP3(+) regulatory T cells by mesenchymal stem cells is associated with modulation of ubiquitination factors and TSDR demethylation. *Stem Cell Res. Ther.* 9:273. doi: 10.1186/s13287-018-0991-1

Kim, R. Q., and Sixma, T. K. (2017). Regulation of USP7: a high incidence of E3 complexes. *J. Mol. Biol.* 429, 3395–3408. doi: 10.1016/j.jmb.2017.05.028

Kumar, S., Brown, A., and Tchounwou, P. B. (2018). Trisenox disrupts MDM2-DAXX-HAUSP complex and activates p53, cell cycle regulation and apoptosis in acute leukemia cells. *Oncotarget* 9, 33138–33148. doi: 10.18632/oncotarget.26025

Laurence, A., Belkaid, Y., and O'Shea, J. J. (2013). A degrading view of regulatory T cells. *Immunity* 39, 201–203. doi: 10.1016/j.immuni.2013.08.017

Lecona, E., Rodriguez-Acebes, S., Specks, J., Lopez-Contreras, A. J., Ruppen, I., Murga, M., et al. (2016). USP7 is a SUMO deubiquitinase essential for DNA replication. *Nat. Struct. Mol. Biol.* 23, 270–277. doi: 10.1038/nsmb.3185

Lee, H. R., Choi, W. C., Lee, S., Hwang, J., Hwang, E., Guchhait, K., et al. (2011). Bilateral inhibition of HAUSP deubiquitinase by a viral interferon regulatory factor protein. *Nat. Struct. Mol. Biol.* 18, 1336–1344. doi: 10.1038/nsmb.2142

Levine, A. J. (1997). p53, the cellular gatekeeper for growth and division. *Cell* 88, 323–331. doi: 10.1016/s0092-8674(00)81871-1

Li, M., Brooks, C. L., Kon, N., and Gu, W. (2004). A dynamic role of HAUSP in the p53-Mdm2 pathway. *Mol. Cell* 13, 879–886. doi: 10.1016/s1097-2765(04)00157-1

Li, M., Chen, D., Shiloh, A., Luo, J., Nikolaev, A. Y., Qin, J., et al. (2002). Deubiquitination of p53 by HAUSP is an important pathway for p53 stabilization. *Nature* 416, 648–653. doi: 10.1038/nature737

Liang, L., Peng, Y., Zhang, J., Zhang, Y., Roy, M., Han, X., et al. (2019). Deubiquitylase USP7 regulates human terminal erythroid differentiation by stabilizing GATA1. *Haematologica*

Lindsay, C. R., Morozov, V. M., and Ishov, A. M. (2008). PML NBs (ND10) and Daxx: from nuclear structure to protein function. *Front. Biosci.* 13, 7132–7142. doi: 10.2741/3216

Lu, Y., Orr, A., and Everett, R. D. (2016). Stimulation of the replication of ICP0-null mutant herpes simplex virus 1 and pp71-deficient human cytomegalovirus by epstein-barr virus tegument protein BNRF1. *J. Virol.* 90, 9664–9673. doi: 10.1128/jvi.01224-16

Ma, J., Martin, J. D., Xue, Y., Lor, L. A., Kennedy-Wilson, K. M., Sinnamon, R. H., et al. (2010). C-terminal region of USP7/HAUSP is critical for deubiquitination activity and contains a second mdm2/p53 binding site. *Arch. Biochem. Biophys.* 503, 207–212. doi: 10.1016/j.abb.2010.08.020

Ma, P., Yang, X., Kong, Q., Li, C., Yang, S., Li, Y., et al. (2014). The ubiquitin ligase RNF220 enhances canonical Wnt signaling through USP7-mediated deubiquitination of beta-catenin. *Mol. Cell Biol.* 34, 4355–4366. doi: 10.1128/mcb.00731-14

Malapelle, U., Morra, F., Ilardi, G., Visconti, R., Merolla, F., Cerrato, A., et al. (2017). USP7 inhibitors, downregulating CCDC6, sensitize lung neuroendocrine cancer cells to PARP-inhibitor drugs. *Lung Cancer* 107, 41–49. doi: 10.1016/j.lungcan.2016.06.015

Masuya, D., Huang, C., Liu, D., Nakashima, T., Yokomise, H., Ueno, M., et al. (2006). The HAUSP gene plays an important role in non-small cell lung carcinogenesis through p53-dependent pathways. *J. Pathol.* 208, 724–732. doi: 10.1002/path.1931

Morotti, A., Panuzzo, C., Crivellaro, S., Pergolizzi, B., Familiari, U., Berger, A. H., et al. (2014). BCR-ABL disrupts PTEN nuclear-cytoplasmic shuttling through phosphorylation-dependent activation of HAUSP. *Leukemia* 28, 1326–1333. doi: 10.1038/leu.2013.370

Nijman, S. M., Luna-Vargas, M. P., Velds, A., Brummelkamp, T. R., Dirac, A. M., Sixma, T. K., et al. (2005). genomic and functional inventory of deubiquitinating enzymes. *Cell* 123, 773–786. doi: 10.1016/j.cell.2005.11.007

Novellasdemunt, L., Foglizzo, V., Cuadrado, L., Antas, P., Kucharska, A., Encheva, V., et al. (2017). USP7 Is a tumor-specific WNT activator for APC-mutated colorectal cancer by mediating beta-catenin deubiquitination. *Cell Rep.* 21, 612–627. doi: 10.1016/j.celrep.2017.09.072

Oh, Y. M., Yoo, S. J., and Seol, J. H. (2007). Deubiquitination of Chfr, a checkpoint protein, by USP7/HAUSP regulates its stability and activity. *Biochem. Biophys. Res. Commun.* 357, 615–619. doi: 10.1016/j.bbrc.2007.03.193

Oliner, J. D., Kinzler, K. W., Meltzer, P. S., George, D. L., and Vogelstein, B. (1992). Amplification of a gene encoding a p53-associated protein in human sarcomas. *Nature* 358, 80–83. doi: 10.1038/358080a0

Ozen, A., Rouge, L., Bashore, C., Hearn, B. R., Skelton, N. J., and Dueber, E. C. (2018). Selectively modulating conformational states of USP7 catalytic domain for activation. *Structure* 26, 72–84.e7. doi: 10.1016/j.str.2017.11.010

Palazon-Riquelme, P., Worboys, J. D., Green, J., Valera, A., Martin-Sanchez, F., Pellegrini, C., et al. (2018). USP7 and USP47 deubiquitinases regulate NLRP3 inflammasome activation. *EMBO Rep.* 19:e44766. doi: 10.15252/embr.201744766

Park, J. J., Lim, K. H., and Baek, K. H. (2015). Annexin-1 regulated by HAUSP is essential for UV-induced damage response. *Cell Death Dis.* 2015:e1654. doi: 10.1038/cddis.2015.32

Pfoh, R., Lacdao, I. K., Georges, A. A., Capar, A., Zheng, H., Frappier, L., et al. (2015). Crystal structure of USP7 ubiquitin-like domains with an ICP0 peptide reveals a novel mechanism used by viral and cellular proteins to target. *PLoS Pathog.* 11:e1004950. doi: 10.1371/journal.ppat.1004950

Qian, J., Pentz, K., Zhu, Q., Wang, Q., He, J., Srivastava, A. K., et al. (2015). USP7 modulates UV-induced PCNA monoubiquitination by regulating DNA polymerase eta stability. *Oncogene* 34, 4791–4796. doi: 10.1038/onc.2014.394

Qing, P., Han, L., Bin, L., Yan, L., and Ping, W. X. (2011). USP7 regulates the stability and function of HLTF through deubiquitination. *J. Cell Biochem.* 112, 3856–3862. doi: 10.1002/jcb.23317

Reverdy, C., Conrath, S., Lopez, R., Planquette, C., Atmanene, C., Collura, V., et al. (2012). Discovery of specific inhibitors of human USP7/HAUSP deubiquitinating enzyme. *Chem. Biol.* 19, 467–477. doi: 10.1016/j.chembiol.2012.02.007

Rouge, L., Bainbridge, T. W., Kwok, M., Tong, R., Di Lello, P., Wertz, I. E., et al. (2016). Molecular understanding of USP7 substrate recognition and C-terminal activation. *Structure* 24, 1335–1345. doi: 10.1016/j.str.2016.05.020

Sarasin, A. (2012). UVSSA and USP7: new players regulating transcription-coupled nucleotide excision repair in human cells. *Genome Med.* 4:44. doi: 10.1186/gm343

Saridakis, V., Sheng, Y., Sarkari, F., Holowaty, M. N., Shire, K., Nguyen, T., et al. (2005). Structure of the p53 binding domain of HAUSP/USP7 bound to Epstein-Barr nuclear antigen 1 implications for EBV-mediated immortalization. *ESE Mol. Cell* 18, 25–36. doi: 10.1016/j.molcel.2005.02.029

Shan, H., Li, X., Xiao, X., Dai, Y., Huang, J., Song, J., et al. (2018). USP7 deubiquitinates and stabilizes NOTCH1 in T-cell acute lymphoblastic leukemia. *Signal. Transduct. Target. Ther.* 3:29. doi: 10.1038/s41392-018-0028-3

Sheng, Y., Saridakis, V., Sarkari, F., Duan, S., Wu, T., Arrowsmith, C. H., et al. (2006). Molecular recognition of p53 and MDM2 by USP7/HAUSP. *Nat. Struct. Mol. Biol.* 13, 285–291. doi: 10.1038/nsmb1067

Shi, Y., Lan, F., Matson, C., Mulligan, P., Whetstine, J. R., Cole, P. A., et al. (2004). Histone demethylation mediated by the nuclear amine oxidase homolog LSD1. *Cell* 119, 941–953. doi: 10.1016/j.cell.2004.12.012

Smits, V. A., and Freire, R. (2016). USP7/HAUSP: a SUMO deubiquitinase at the heart of DNA replication. *Bioessays* 38, 863–868. doi: 10.1002/bies.201600096

Song, M. S., Salmena, L., Carracedo, A., Egia, A., Lo-Coco, F., Teruya-Feldstein, J., et al. (2008). The deubiquitinylation and localization of PTEN are regulated by a HAUSP-PML network. *Nature* 455, 813–817. doi: 10.1038/nature07290

Su, D., Ma, S., Shan, L., Wang, Y., Wang, Y., Cao, C., et al. (2018). Ubiquitin-specific protease 7 sustains DNA damage response and promotes cervical carcinogenesis. *J. Clin. Invest.* 128, 4280–4296. doi: 10.1172/jci120518

Tang, J., Qu, L. K., Zhang, J., Wang, W., Michaelson, J. S., Degenhardt, Y. Y., et al. (2006). Critical role for Daxx in regulating Mdm2. *Nat. Cell Biol.* 8, 855–862. doi: 10.1038/ncb1442

Tavana, O., Li, D., Dai, C., Lopez, G., Banerjee, D., Kon, N., et al. (2016). HAUSP deubiquitinates and stabilizes N-Myc in neuroblastoma. *Nat. Med.* 22, 1180–1186. doi: 10.1038/nm.4180

Trotman, L. C., Wang, X., Alimonti, A., Chen, Z., Teruya-Feldstein, J., Yang, H., et al. (2007). Ubiquitination regulates PTEN nuclear import and tumor suppression. *Cell* 128, 141–156. doi: 10.1016/j.cell.2006.11.040

Turnbull, A. P., Ioannidis, S., Krajewski, W. W., Pinto-Fernandez, A., Heride, C., Martin, A. C. L., et al. (2017). Molecular basis of USP7 inhibition by selective small-molecule inhibitors. *Nature* 550, 481–486. doi: 10.1038/nature24451

van der Horst, A., and Burgering, B. M. (2007). Stressing the role of FoxO proteins in lifespan and disease. *Nat. Rev. Mol. Cell Biol.* 8, 440–450. doi: 10.1038/nrm2190

van der Horst, A., de Vries-Smits, A. M., Brenkman, A. B., van Triest, M. H., van den Broek, N., Colland, F., et al. (2006). FOXO4 transcriptional activity is regulated by monoubiquitination and USP7/HAUSP. *Nat. Cell Biol.* 8, 1064–1073. doi: 10.1038/ncb1469

van Loosdregt, J., and Coffer, P. J. (2014). Post-translational modification networks regulating FOXP3 function. *Trends Immunol.* 35, 368–378. doi: 10.1016/j.it.2014.06.005

van Loosdregt, J., Fleskens, V., Fu, J., Brenkman, A. B., Bekker, C. P., Pals, C. E., et al. (2013). Stabilization of the transcription factor Foxp3 by the deubiquitinase USP7 increases Treg-cell-suppressive capacity. *Immunity* 39, 259–271. doi: 10.1016/j.immuni.2013.05.018

Vassilev, L. T., Vu, B. T., Graves, B., Carvajal, D., Podlaski, F., Filipovic, Z., et al. (2004). In vivo activation of the p53 pathway by small-molecule antagonists of MDM2. *Science* 303, 844–848. doi: 10.1126/science.1092472

Wade, M., Li, Y. C., and Wahl, G. M. (2013). MDM2, MDMX and p53 in oncogenesis and cancer therapy. *Nat. Rev. Cancer* 13, 83–96. doi: 10.1038/nrc3430

Wang, L., Kumar, S., Dahiya, S., Wang, F., Wu, J., Newick, K., et al. (2016). Ubiquitin-specific protease-7 inhibition impairs Tip60-dependent Foxp3+ T-regulatory Cell function and promotes antitumor immunity. *EBioMedicine* 13, 99–112. doi: 10.1016/j.ebiom.2016.10.018

Wang, Q., Ma, S., Song, N., Li, X., Liu, L., Yang, S., et al. (2016). Stabilization of histone demethylase PHF8 by USP7 promotes breast carcinogenesis. *J. Clin. Invest.* 126, 2205–2220. doi: 10.1172/jci85747

Xiang, Q., Ju, H., Li, Q., Mei, S. C., Chen, D., and Choi, Y. B. (2018). Human herpesvirus 8 interferon regulatory factors 1 and 3 mediate replication and latency activities via interactions with USP7 Deubiquitinase. *J. Virol.* 92:e2003–17. doi: 10.1128/jvi.02003-17

Yao, Y., Zhang, Y., Shi, M., Sun, Y., Chen, C., Niu, M., et al. (2018). Blockade of deubiquitinase USP7 overcomes bortezomib resistance by suppressing NF-kappaB signaling pathway in multiple myeloma. *J. Leukoc. Biol.* 104, 1105–1115. doi: 10.1002/JLB.2A1017-420RR

Yi, L., Cui, Y., Xu, Q., and Jiang, Y. (2016). Stabilization of LSD1 by deubiquitinating enzyme USP7 promotes glioblastoma cell tumorigenesis and metastasis through suppression of the p53 signaling pathway. *Oncol. Rep.* 36, 2935–2945. doi: 10.3892/or.2016.5099

Zaman, M. M., Nomura, T., Takagi, T., Okamura, T., Jin, W., Shinagawa, T., et al. (2013). Ubiquitination-deubiquitination by the TRIM27-USP7 complex regulates tumor necrosis factor alpha-induced apoptosis. *Mol. Cell Biol.* 33, 4971–4984. doi: 10.1128/mcb.00465-13

Zhang, P., Wei, Y., Wang, L., Debeb, B. G., Yuan, Y., Zhang, J., et al. (2014). ATM-mediated stabilization of ZEB1 promotes DNA damage response and radioresistance through CHK1. *Nat. Cell Biol.* 16, 864–875. doi: 10.1038/ncb3013

Zhang, X., Gu, L., Li, J., Shah, N., He, J., Yang, L., et al. (2010). Degradation of MDM2 by the interaction between berberine and DAXX leads to potent apoptosis in MDM2-overexpressing cancer cells. *Cancer Res.* 70, 9895–9904. doi: 10.1158/0008-5472.can-10-1546

Zhang, X., Horibata, K., Saijo, M., Ishigami, C., Ukai, A., Kanno, S., et al. (2012). Mutations in UVSSA cause UV-sensitive syndrome and destabilize ERCC6 in transcription-coupled DNA repair. *Nat. Genet.* 44, 593–597. doi: 10.1038/ng.2228

Zhou, J., Wang, J., Chen, C., Yuan, H., Wen, X., and Sun, H. (2018). USP7: target validation and drug discovery for cancer therapy. *Med. Chem.* 14, 3–18. doi: 10.2174/1573406413666171020115539

Zhu, X., Menard, R., and Sulea, T. (2007). High incidence of ubiquitin-like domains in human ubiquitin-specific *proteases*. *Proteins* 69, 1–7. doi: 10.1002/prot.21546

Zlatanou, A., Sabbioneda, S., Miller, E. S., Greenwalt, A., Aggathanggelou, A., Maurice, M. M., et al. (2016). USP7 is essential for maintaining Rad18 stability and DNA damage tolerance. *Oncogene* 35, 965–976. doi: 10.1038/onc.2015.149

Conflict of Interest Statement: The authors declare that the research was conducted in the absence of any commercial or financial relationships that could be construed as a potential conflict of interest.

frontiers in Pharmacology

ORIGINAL RESEARCH
published: 03 May 2019
doi: 10.3389/fphar.2019.00338

Regulation of Wnt Singaling Pathway by Poly (ADP-Ribose) Glycohydrolase (PARG) Silencing Suppresses Lung Cancer in Mice Induced by Benzo(a)pyrene Inhalation Exposure

Wenjuan Dai[1,2†], Yingbin Fu[1†], Yanxia Deng[1†], Zhuoying Zeng[1], Pan Gu[1], Hailong Liu[1], Jianjun Liu[1], Xinyun Xu[1], Desheng Wu[1], Xianru Luo[1], Linqing Yang[1], Jinzhou Zhang[1], Kai Lin[1], Gonghua Hu[2,3] and Haiyan Huang[1]**

[1] Shenzhen Center for Disease Control and Prevention, Shenzhen, China, [2] Jiangxi Provincial Key Laboratory of Preventive Medicine, School of Public Health, Nanchang University, Nanchang, China, [3] Department of Preventive Medicine, Gannan Medical University, Ganzhou, China

OPEN ACCESS

Edited by:
Zhe-Sheng Chen,
St. John's University, United States

Reviewed by:
David W. Koh,
Ohio Northern University,
United States
Shiv K. Gupta,
Mayo Clinic, United States

***Correspondence:**
Gonghua Hu
hgh0129@163.com
Haiyan Huang
hhy424@126.com

[†] These authors have contributed equally to this work

Specialty section:
This article was submitted to Cancer Molecular Targets and Therapeutics, a section of the journal Frontiers in Pharmacology

Received: 13 January 2019
Accepted: 19 March 2019
Published: 03 May 2019

Citation:
Dai W, Fu Y, Deng Y, Zeng Z, Gu P, Liu H, Liu J, Xu X, Wu D, Luo X, Yang L, Zhang J, Lin K, Hu G and Huang H (2019) Regulation of Wnt Singaling Pathway by Poly (ADP-Ribose) Glycohydrolase (PARG) Silencing Suppresses Lung Cancer in Mice Induced by Benzo(a)pyrene Inhalation Exposure. Front. Pharmacol. 10:338. doi: 10.3389/fphar.2019.00338

Benzo(a)pyrene (BaP) is a polycyclic aromatic hydrocarbon that specifically causes cancer and is widely distributed in the environment. Poly (ADP-ribosylation), as a key post-translational modification in BaP-induced carcinogenesis, is mainly catalyzed by poly (ADP-ribose) glycohydrolase (PARG) in eukaryotic organisms. Previously, it is found that PARG silencing can counteract BaP-induced carcinogenesis *in vitro*, but the mechanism remained unclear. In this study, we further examined this process *in vivo* by using heterozygous PARG knockout mice ($PARG^{+/-}$). Wild-type and $PARG^{+/-}$ mice were individually treated with 0 or 10 $\mu g/m^3$ BaP for 90 or 180 days by dynamic inhalation exposure. Pathological analysis of lung tissues showed that, with extended exposure time, carcinogenesis and injury in the lungs of WT mice was progressively worse; however, the injury was minimal and carcinogenesis was not detected in the lungs of $PARG^{+/-}$ mice. These results indicate that PARG gene silencing protects mice against lung cancer induced by BaP inhalation exposure. Furthermore, as the exposure time was extended, the protein phosphorylation level was down-regulated in WT mice, but up-regulated in $PARG^{+/-}$ mice. The relative expression of Wnt2b and Wnt5b mRNA in WT mice were significantly higher than those in the control group, but there was no significant difference in $PARG^{+/-}$ mice. Meanwhile, the relative expression of Wnt2b and Wnt5b proteins, as assessed by immunohistochemistry and Western blot analysis, was significantly up-regulated by BaP in WT mice; while in $PARG^{+/-}$ mice it was not statistically affected. Our work provides initial evidence that PARG silencing suppresses BaP induced lung cancer and stabilizes the expression of Wnt ligands, PARG gene and Wnt ligands may provide new options for the diagnosis and treatment of lung cancer.

Keywords: benzo(a)pyrene, ADP-ribosylation, poly (ADP-ribose) glycohydrolase, Wnt signaling pathway, lung cancer

INTRODUCTION

Benzo(a)pyrene (BaP) is a polycyclic aromatic hydrocarbon that is known to be carcinogenic. It is mainly produced by pyrolysis and incomplete combustion of carbonaceous materials and is widely distributed in both the working and living environment (Liu et al., 2008). A large number of experiments have shown that BaP can induce cancer in various animals (IARC Working Group on the Evaluation of Carcinogenic Risks to Humans, 2010; Kasala et al., 2016). Furthermore, epidemiological studies suggest that BaP is closely associated with human lung cancer (Rojas et al., 2004; Alexandrov et al., 2010; Widziewicz et al., 2018). On the basis of these studies, BaP was classified as a human class I carcinogen by the International Agency for Research on Cancer in 2006 (IARC Working Group on the Evaluation of Carcinogenic Risks to Humans, 2012).

Lung cancer is the most common malignant tumor in the human respiratory system and is extremely harmful to human health. Globally, the morbidity and mortality of lung cancer are among the highest (Ferlay et al., 2015). According to the American Cancer Society, lung cancer leads to the highest number of deaths in both men and women. Recent evidence suggests that the incidence of lung cancer in China is the highest and the mortality is increasing at a rate of 4.5% per year (Chen et al., 2016).

The occurrence of lung cancer is the result of a combination of both environmental and genetic factors, including epigenetic changes which have been proved to contribute to lung cancer development (Hagood, 2014). ADP-ribosylation, as an epigenetic modification, plays a critical role in cell survival and disease development, including cancers (D'Amours et al., 1999; Min et al., 2010; Huang et al., 2012). Poly-ADP-ribosylation can convert nuclear chromatin to a loose state, allowing accessibility of DNA damage repair enzymes to the injury site, thereby promoting DNA damage repair against cytotoxicity and genetic damage. Poly-ADP-ribose glycohydrolase (PARG) can hydrolyze poly (ADP-ribose) on poly (ADP-ribose) polymerase-1 (PARP-1), which promotes the degradation of intracellular poly (ADP-ribose) (PAR) (Rouleau et al., 2004). It is the only known enzyme that can hydrolyze poly (ADP-ribose) in the nucleus (Meyer et al., 2007). Recent studies have shown that PARG gene silencing can increase intracellular poly-ADP-ribosylation to protect cells against cytotoxicity. Li et al. (Li et al., 2016) found that BaP can induce chromosomal aberrations, micronucleus formation, chromatin structure changes and malignant transformation of normal 16HBE cells, but PARG gene silencing can inhibit these abnormalities. Studies have shown that PARG also is associated with tumorigenesis (Miwa and Masutani, 2007), but the exact mechanism of PARG on tumor promotion has not been fully clarified.

In our previous study, 16HBE cells and PARG-deficient cells were treated with 40 μmol/L BaP for a period of time to induce malignant transformation, and by using MeDIP-sequence analysis, it is found that the methylation levels of Wnt2b and Wnt5b genes in the two cells were significantly different. Wnt2b and Wnt5b are key players in the Wnt/β-Catenin signaling pathway (Klaus and Birchmeier, 2008), which has been highly conserved in evolution and is known to control cell growth, differentiation, apoptosis, and self-renewal. This pathway is activated by binding of Wnt ligands to receptors, which increases the stability of β-catenin in the cytoplasm and promotes its translocation to the nucleus, where it modulates the expression of target genes that lead to tumorigenesis (Klaus and Birchmeier, 2008). Studies have shown that this pathway is abnormally activated during the development of lung cancer and may coordinate or antagonize other signaling pathways to regulate proliferation, migration, and invasion in lung cancer (Reya and Clevers, 2005; Berndt and Moon, 2013). Recently, 30–40% of cells in tumor tissues have been shown to express Wnt ligands, which create a microenvironment that is suitable for tumor cells. In a human lung adenocarcinoma model, 70% of cells have abnormal activation of the Wnt pathway, and 80% of cells may be involved in the formation of the tumor microenvironment, which is critical for the progression of lung cancer (Tammela et al., 2017).

Given the decisive role of the Wnt signaling pathway in the development of lung cancer, inhibition of Wnt ligands provides a viable approach for reducing the expansion of lung cancer cell lines. The purpose of this study was to investigate whether PARG gene silencing can inhibit lung cancer development induced by BaP and whether it can regulate the Wnt ligands to inhibit the development of lung cancer. On the basis of our findings, PARG gene and Wnt ligands may constitute a new option for the diagnosis and treatment of lung cancer.

MATERIALS AND METHODS

Materials

BaP (CAS50-32-8, purity ≥96%) was purchased from American Sigma Company, and dissolved in dimethylsulfoxide (DMSO). Other chemicals were purchased from Sigma–Aldrich (St Louis, MO, United States) or Thermo Fisher Scientific (Shanghai, China), unless otherwise stated.

Animals and Treatment

The PARG knockout mice [B6N (Cg)-Parg$^{tm2b(KOMP)Mbp}$/J]were purchased from the Jackson Laboratory, and WT mice (C57BL/6J) were purchased from Guangdong Medical Lab Animal Center. PARG knockout mice were generated by the targeted mutation 2b of the Parg gene resulting in deletion of the full-length isoform of PARG protein ($PARG_{110}$). The strategy of gene targeting is Cre-mediated excision of the parental Parg$^{tm2b(KOMP)Mbp}$ allele resulted in the removal of the promoter-driven neomycin selection cassette and critical exon(s) leaving behind the inserted lacZ reporter sequence. We screened for heterozygous PARG knockout mice ($PARG^{+/-}$) in our study since death of homozygous PARG knockout mice ($PARG^{-/-}$) occurring before the normal life span of an organism, occurring during pregnancy, parturition or lactation. The mice were maintained under semi-specific-pathogen-free conditions with the temperature controlled at 23 ± 2°C and a 12-h light/dark

cycle. We selected 2-month-old $PARG^{+/-}$ and WT mice for this study. The mice were randomly divided into two groups with 6 per group referring to the principles of experimental animal selection and references. And then, they were treated with 0 or 10 $\mu g/m^3$ aerosols through respiratory tract by a dynamic inhalation cabinet (Jiufang Company, Guangzhou) for 90 or 180 days. The dynamic inhalation device makes liquids into aerosols with a diameter of only a few micrometers, which is in line with the actual human exposure to BaP in the air. At the end of the experiment, mice were anesthetized with ether and blood was collected by eyeball sampling. The mice were then euthanized and the lungs were excised rapidly. Half of each lung was stored in 4% paraformaldehyde, and the other half was stored at −80°C. All animal experiments and procedures were approved by the Shenzhen Center for Disease Control and Prevention. Efforts were made to minimize animal suffering and reduce the number of mice used in the experiments.

Genotyping of PARG Knockout Mice

Genomic DNA was purified from mouse tails using TianAMP genomic DNA kits (Tiangen, Beijing, China). The concentration and the quality of DNA were assessed by ultraviolet (UV) absorbance using a NanoDrop ND-2000 spectrophotometer (Thermo Fisher Scientific). The DNA was then amplified by PCR (94°C for 2 min; 10 cycles of 94°C for 20 s, 65°C for 15 s, and 68°C for 10 s; 10 cycles of 94°C for 15 s, 60°C for 15 s, and 72°C for 10 s; 72°C for 2 min, 10°C hold) using primers provided by the Jackson Laboratory (Wild-type Forward: 5′-GAG ATA TCT AAG TCA GAG AAA GGT GGT-3′, Wild-type Reverse: 5′-CCT CCT CTG GTG TGT CTG AAG-3′, Mutant Forward: 5′-CGG TCG CTA CCA TTA CCA GT-3′, Mutant Reverse: 5′-GGT ATC AGC GAT GGT TGT TC-3′). The PCR products were 279 bp for the WT sample, and 279 and 507 bp for the heterozygous PARG knockout ($PARG^{+/-}$) sample.

Hematoxylin and Eosin Staining

Mouse lung tissues were fixed in 4% paraformaldehyde for 48 h, dehydrated in ethanol and embedded in paraffin by using a TissueWave™ 2 Microwave Processor (Thermo Fisher Scientific). Paraffin-fixed tissues were sliced into 5 μm sections, mounted on glass slides, and dried for 1 h. After dewaxing and rehydration, sections were stained with hematoxylin and eosin (Sigma-Aldrich) and examined by light microscopy. The pathology was evaluated by a blinded observer to detect the degree of malignancy.

Real-Time Quantitative PCR

Total RNA was extracted from frozen lung samples with miRNeasy mini kits (Qiagen, China) according to the manufacturer's instructions. Complementary DNA (cDNA) was synthesized from 500 ng of total lung RNA (n = 3 per group) using the PrimeScript™ RT reagent kit (Takara, China). Quantitative PCR (qPCR) was performed on the ABI Prism 7500 system (Applied Biosystems, Foster City, CA, United States) using SYBR select master mix. The mRNA primers were purchased from Sangon Biotech (Shanghai, China) and are listed in **Supplementary Table S1**. Experiments were repeated at least 3 times. The relative level of mRNA for each gene was determined using the $2^{-\Delta\Delta Ct}$ method (Schmittgen and Livak, 2008), and P-values were calculated using the Student's t-test on replicate $2^{-\Delta Ct}$ values for each gene in each treatment group compared to the control group.

Immunohistochemistry

Mouse lung tissues were fixed in 4% paraformaldehyde for 48 h, dehydrated in ethanol and embedded in paraffin by using a TissueWave™ Microwave Processor (Thermo Fisher Scientific). After dewaxing and rehydration, 5 μm-thick coronal sections were incubated in 0.01 M citrate buffer (pH 6.0) with 0.1% Tween-20 at 95–100°C for 10 min for antigen retrieval. For immunochemistry of Wnt2b and Wnt5b (n = 3 per group), the sections were incubated at 4°C overnight with primary antibody (Wnt2b at 1:200 or Wnt5b at 1:50). After being washed with PBST, the sections were stained using the mouse and rabbit-specific HRP/DAB (ABC) detection IHC kit (Abcam, ab64264) and analyzed using an Olympus BX60 compound microscope (Tokyo, Japan).

Western Blot Analysis

Lung proteins (n = 3 per group) were extracted from 30 mg lung tissue with 600 μL lysis buffer (Beyotime, China) and 6 μL protease and phosphatase inhibitor cocktail (Thermo Fisher Scientific, United States) on ice, and then centrifuged and collected. The protein concentration was measured with a BCA protein assay kit (Thermo Fisher Scientific, United States). Each protein sample was combined with loading buffer and heated for 8 min at 100°C. Protein samples were separated on 10% PAGE gels with 5% stacking gels and transferred to PVDF membranes. The membranes were incubated in TBST buffer containing 5% milk at room temperature for 2 h. Subsequently, they were incubated with anti-PARG (mouse monoclonal antibody, 1:100), anti-phosphotyrosine (PY20, mouse monoclonal antibody,1:1000), anti-Wnt2b (rabbit monoclonal antibody, 1:3000), anti-Wnt5b (mouse monoclonal antibody,1:500), or anti-α-tubulin (mouse monoclonal antibody, 1:3000) in TBST buffer for 1.5 h at room temperature. After washing with TBST three times, the membranes were incubated with homologous secondary antibody (anti-rabbit or anti-mouse IgG HRPs) in TBST buffer for 60 min. The membranes were then repeatedly washed with TBST buffer, developed using chemiluminescence reagents from an ECL kit (Pierce ECL, Santa Cruz, CA, United States) and detected on a phosphorimager. The images of the membranes were analyzed by ImageJ software.

Statistical Analysis

The histograms and statistical analyses of the relative expression of each group were completed using Graph-Pad prism 7.0 software (GraphPad Software, Inc.). Data are presented as mean ± SD. Comparisons between two groups were

conducted with the Student's *t*-test. $P < 0.05$ was considered statistically significant.

RESULTS

Genotyping of PARG Knockout Mice

The heterozygous PARG knockout mice were used to characterize the role of PARG in protecting mice from BaP-induced lung cancer. According to the law of Mendelian inheritance, the genotype of the progeny mice may be WT ($PARG^{+/+}$), heterozygous ($PARG^{+/-}$), or homozygous ($PARG^{-/-}$). Based on genomic DNA purified from mouse tails, $PARG^{+/-}$ mice were screened for our study as $PARG^{-/-}$ mice cannot survive to maturity. The PCR product from WT mice was 279 bp, and the PCR products from PARG knockout heteroygotes ($PARG^{+/-}$) were 279 and 507 bp, as shown in **Figure 1A**. After BaP exposure, proteins from the lung tissues were extracted and Western blotting were performed to verify the expression of full-length isoform ($PARG_{110}$). As expected, the expression of $PARG_{110}$ was significantly greater in WT mice than in $PARG^{+/-}$ mice (**Figure 1B**). The results confirm that heterozygous PARG knockout mice were successfully bred in our experiments.

$PARG^{+/-}$ Mice Are Protected From Pathological Changes in Lung Tissues Induced by BaP

To establish a lung cancer model for assessing the effects of heterozygous PARG silencing, we exposed mice to long-term inhalation of BaP and then prepared paraffin sections of lung tissues. Hematoxylin and eosin staining were used to analyze the pathological changes that were observed under light microscopy. As shown in **Figure 2A**, in the lungs of WT mice exposed for 90 days, alveolar diffuse interstitialization occurred, though the alveolar structure was visible; in contrast, the degree of injury in $PARG^{+/-}$ mice was mild with no obvious pathological damage. The results were similar in both male and female mice. After 180-day exposure to BaP, the lungs of the WT mice treated with BaP showed severe alveolar diffuse interstitialization, and the alveolar structure was severely damaged with obvious inflammatory infiltration and abnormal nodules (**Figure 2B**). Comparison between the 90- and 180-d pathology suggests that the degree of lung injury in WT mice treated with BaP was positively correlated with the time of exposure. In $PARG^{+/-}$ mice after 180 days, however, some alveolar interstitial thickening appeared while the alveolar structure was still visible. This suggests that $PARG^{+/-}$ mice were protected from the effects of BaP on lung pathology. A higher magnification was used to examine tumor formation. In WT mice, the number of cells increased abnormally and tumorigenesis could be observed (**Figure 2C**); however, no tumor tissue was found in $PARG^{+/-}$ mice. These results demonstrate that heterozygous PARG gene silencing can inhibit the induction of lung cancer by BaP in mice.

$PARG^{+/-}$ Mice Express Elevated Levels of Phosphorylated Proteins in Lung Tissues After BaP Inhalation Exposure

To determine whether heterozygous PARG silencing affects the overall protein phosphorylation level, we performed Western blot assays using the universal anti-tyrosine phosphorylation monoclonal antibody PY20 with protein extracted from lung tissues. As shown in **Figure 3A**, the levels of total phosphorylated proteins in WT and heterozygous PARG knockout mice were not significantly different from that of the control group after exposure to BaP for 90 days ($P > 0.05$). After 180-d exposure, however, the level of phosphorylated proteins was significantly down-regulated in WT mice ($^*P < 0.05$), but was significantly up-regulated in $PARG^{+/-}$ mice compared with the control group ($^*P < 0.05$). These results indicate that, at an extended BaP exposure time, PARG affects phosphorylation of proteins, which could potentially be associated with the ability of $PARG^{+/-}$ mice to resist tumorigenesis.

PARG Silencing Inhibits the Relative Expression of Wnt2b and Wnt5b mRNA in Lung Tissues After BaP Inhalation Exposure

To further elucidate whether ADP-ribosylation affects the Wnt pathway in $PARG^{+/-}$ mice, we first performed real-time qPCR to detect the relative expression of the Wnt2b and Wnt5b genes. The relative expression of Wnt2b and Wnt5b mRNA was significantly higher in WT mice than in control mice at 90 and 180 days

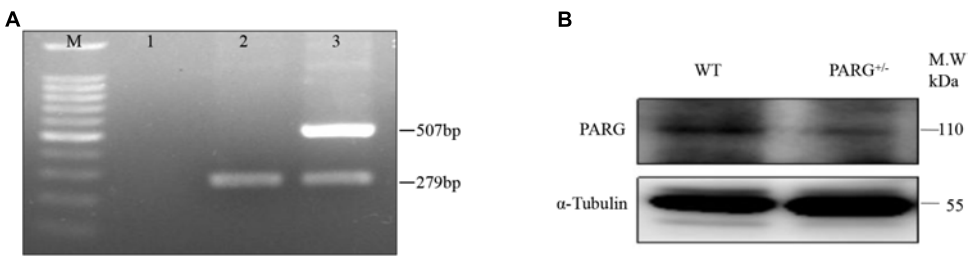

FIGURE 1 | Genotyping of poly (ADP-Ribose) glycohydrolase (PARG) knockout mice. Genotyping of $PARG^{+/-}$ mice. **(A)** Genotyping by PCR. Lane M, 100 bp DNA Marker; Lane 1, blank control; Lane 2, WT mice; and Lane 3, $PARG^{+/-}$ mice. **(B)** Genotyping by Western blotting. The expression of $PARG_{110}$ protein was assessed in lungs from WT and $PARG^{+/-}$ mice.

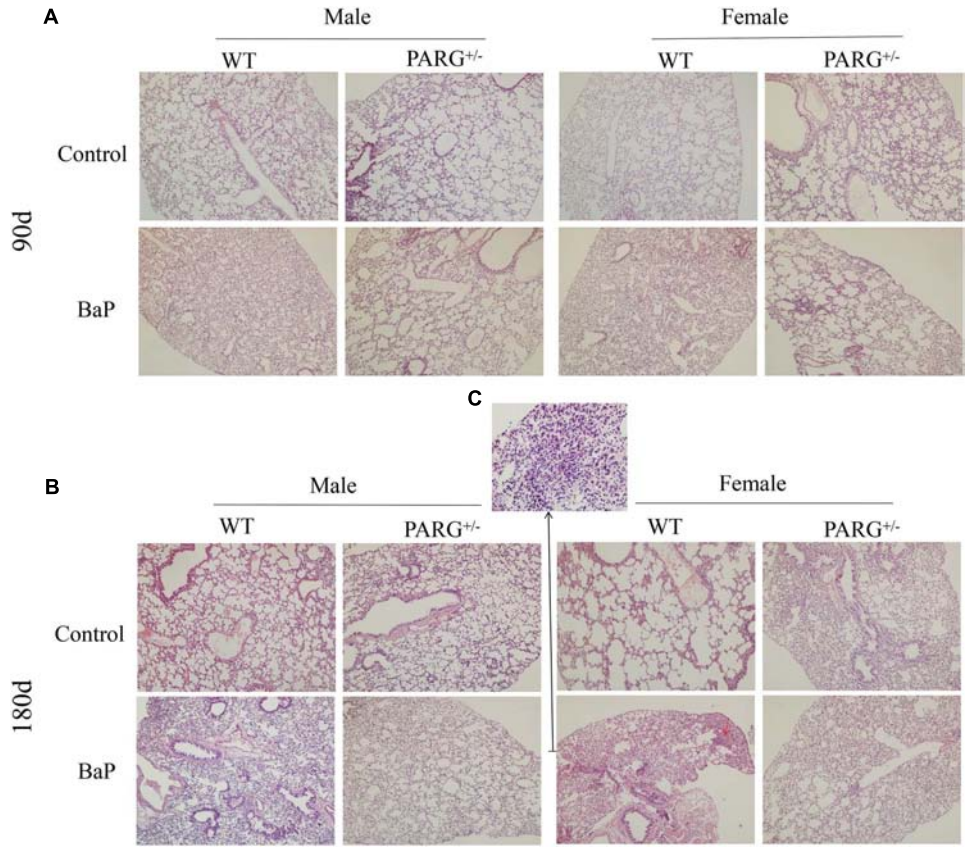

FIGURE 2 | PARG$^{+/-}$ mice are protected from pathological changes in lung tissues induced by BaP inhalation exposure. Pathological changes in lung tissues of WT and PARG$^{+/-}$ mice after benzo(a)pyrene inhalation exposure **(A)** 90-day exposure (×100). **(B)** 180-day exposure to BaP (×100). The red arrows show abnormally increased numbers of cells. **(C)** The magnification of the place pointed by the red arrow in **B**, pathological signs of tumorigenesis (×200). Results are representative of 3 mice from each group.

(***$P < 0.001$), but there were no significant differences in the PARG$^{+/-}$ mice ($P > 0.05$) (**Figure 4**).

PARG Silencing Inhibits the Expression of Wnt2b and Wnt5b Protein in Lung Tissues After BaP Inhalation Exposure

The expression of Wnt2b and Wnt5b at the level of the protein were further confirmed by performing Western blotting and immunohistochemistry. The expression of Wnt2b protein was up-regulated in lungs from WT mice that were treated with BaP for 90 and 180 days (*$P < 0.05$, compared with the control group); however, for PARG$^{+/-}$ mice, no statistically significant differences were observed ($P > 0.05$) (**Figure 5A**). In immunohistochemistry assays, Wnt2b protein (brownish yellow staining) was localized to the cytoplasm, and after 90 and 180 days of BaP inhalation exposure, the expression levels in WT male and female mice were higher for treated vs. control mice; however, for PARG$^{+/-}$ mice, there were no significant differences (**Figure 5B**). Similar results were observed for Wnt5b, though the effect on Wnt5b expression was more obvious at 180 days than at 90 days (**Figures 5C,D**). These findings suggest that PARG gene silencing stabilizes the expression of Wnt2b and Wnt5b after BaP exposure, possibly inhibiting the progression of lung cancer.

DISCUSSION

Metabolically activated BaP is known to cause cytotoxic, teratogenic, genotoxic, mutagenic and carcinogenic effects in many different tissues and cell types from numerous mammalian studies (Miller and Ramos, 2001; van Delft et al., 2010). BaP in cigarette smoking is implicated as one of the main factors in lung cancer (Rubin, 2001). The occurrence of cancer includes three stages: initiation, promoting and progressing. Epigenetic modification, as a bridge between these stages, can involve DNA methylation, microRNA, chromatin remodeling, and histone modification (Bird, 2007). ADP-ribosylation is one of the most important post-translational modifications in tumorigenesis (Klaus and Birchmeier, 2008). Studies showed that the use of PARG inhibitor to suppress PARG activity facilitates oxidative damage-induced PARylation as well as DNA damage repair (Zhang et al., 2015). PARG gene silencing increases the level of poly (ADP-ribosylation) to regulate DNA

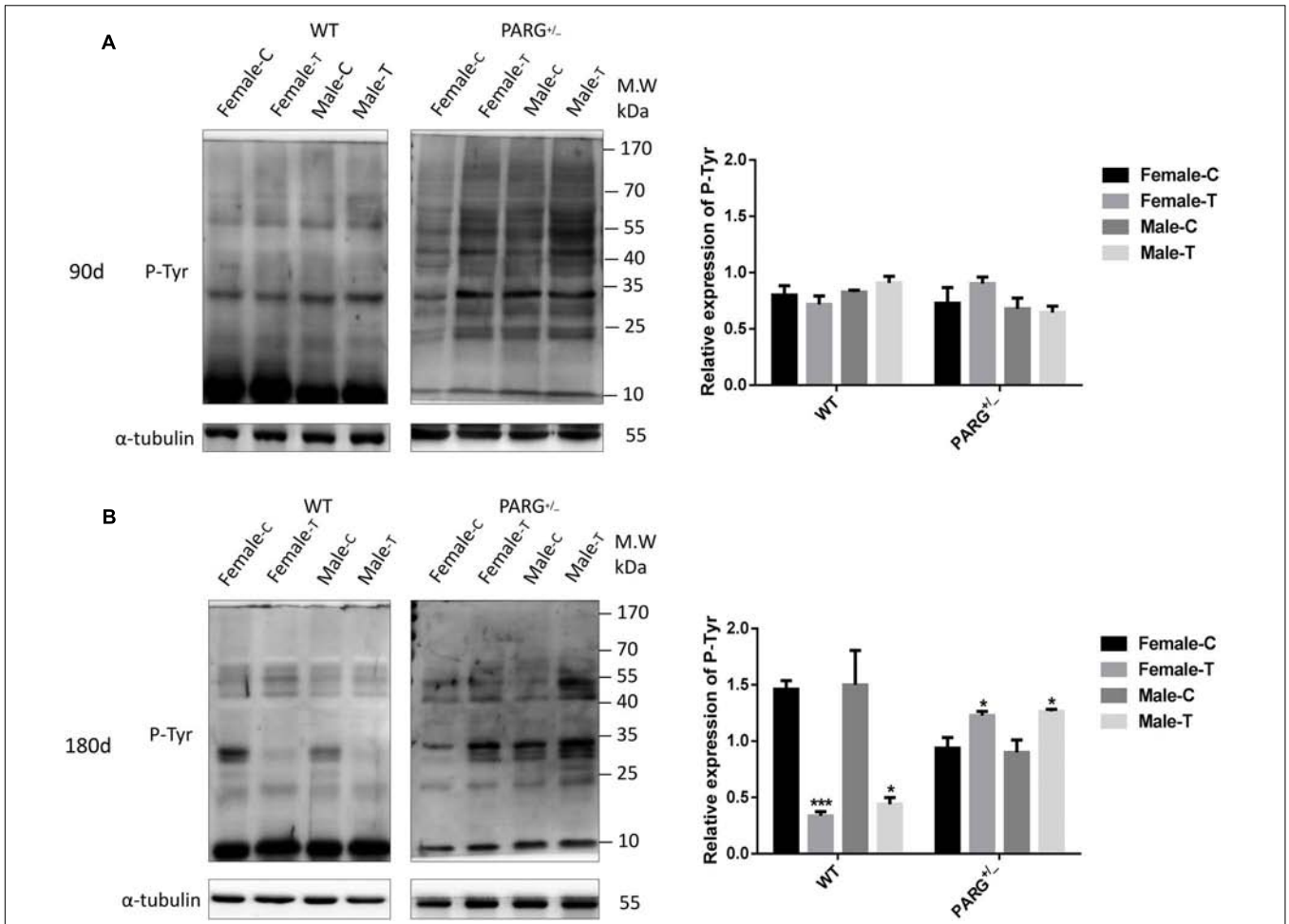

FIGURE 3 | PARG$^{+/-}$ mice express elevated levels of phosphorylated proteins in lung tissues after BaP inhalation exposure. Expression of phosphorylated proteins in lung tissues of mice after BaP inhalation exposure. **(A)** The overall phosphorylation level of proteins in WT and PARG$^{+/-}$ mice that were untreated or were treated with exposure to BaP for 90 days. **(B)** Expression of phosphorylated proteins after 180-day exposure to BaP. Female-C, control untreated female mice; Female-T, treated female mice; Male-C, control untreated male mice; Male-T, treated male mice. $^{*}P < 0.05$, $^{***}P < 0.001$, significant difference in treated compared to untreated mice. Results represent the mean ± SD of 3 mice from each group. Quantification of the phosphorylation levels was performed using ImageJ software.

damage repair and genome stability (Koh et al., 2004). In our previous study, it is determined that *in vitro* PARG silencing inhibits tumorigenesis by dramatically reducing DNA damage, chromosome abnormalities, micronuclei formations, and malignant transformation. To further investigate the possible *in vivo* role of PARG gene silencing, heterozygous PARG knockout mice were utilized. We exposed WT and PARG$^{+/-}$ mice to BaP by dynamic inhalation for 90 and 180 days. Pathological analysis showed that carcinogenesis appeared in the lungs of WT mice and the injury was progressive for 180-day vs. 90-day treatment, while PARG$^{+/-}$ mice showed no carcinogenesis and minimal signs of lung injury. These results suggest that PARG gene silencing can inhibit lung cancer induced by BaP in mice, which is consistent with our *in vitro* results.

In our previous vitro study, we identified two distinct Wnt ligands (Wnt5b and Wnt2b) that are modulated by PARG by using the MeDIP-sequence techniques. This raises the possibility that ADP-ribosylation may affect the carcinogenesis of BaP by regulating the activation of the Wnt signaling pathway after PARG gene silencing. The Wnt pathway consists of three components: the Wnt/β-catenin canonical pathway, the Wnt/Ca^{2+} pathway and the Wnt/polarity pathway (Wodarz and Nusse, 1998). After activation of the canonical pathway, Wnt ligands bind to Frzzled and LRP5/6 on the cell surface to form a trimer, which weakens the stability of a destruction complex composed by β-catenin, Axin, GSK-3β, and APC to prevent the phosphorylated degradation of β-catenin. The concentration of β-catenin increases in the cytoplasm and then is transferred into the nucleus which ultimately activate the expression of downstream target genes (Veeman et al., 2003). During this process, protein phosphorylation, especially tyrosine phosphorylation (P-Tyr), as a major mode of cell signal transduction and regulation of enzyme activity, plays an vital role in the regulation of β-catenin (Ikeda et al., 1998). ADP-ribosylation can promote phosphorylated proteins

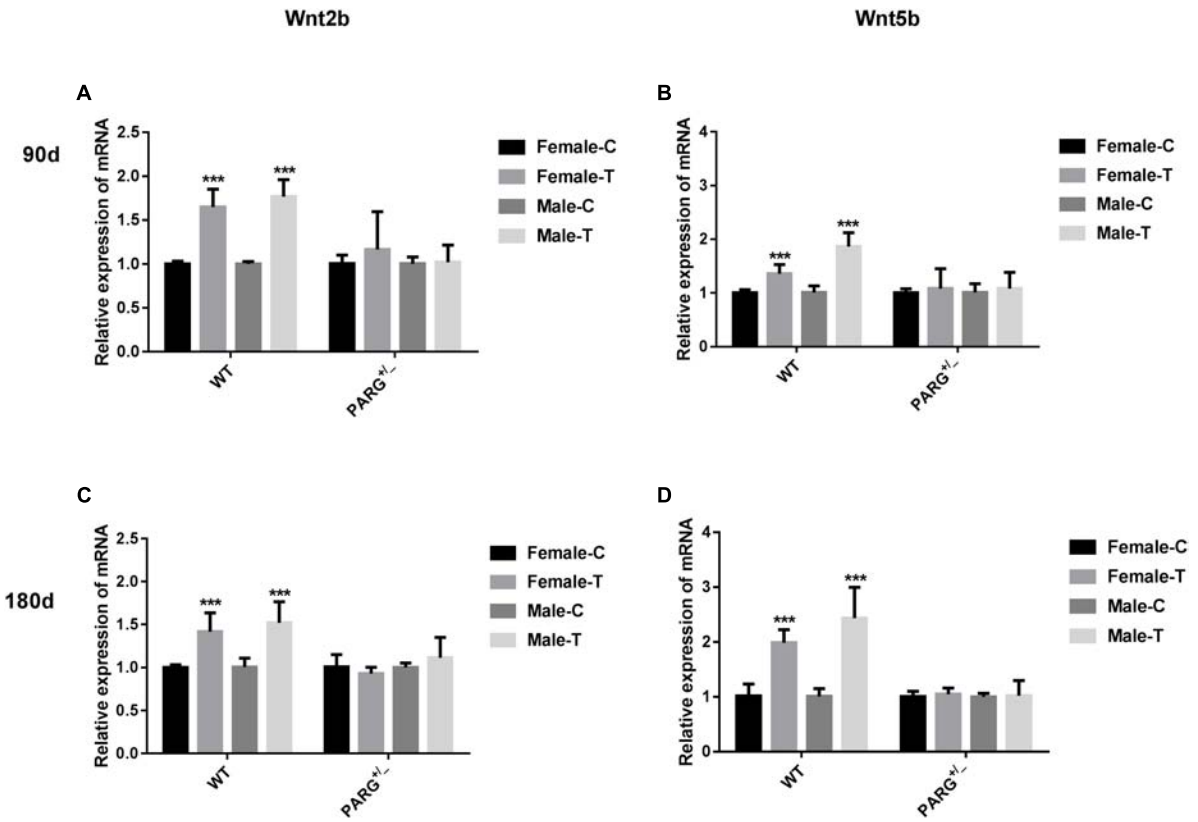

FIGURE 4 | PARG silencing inhibits the relative expression of Wnt2b and Wnt5b mRNA in lung tissues after BaP inhalation exposure. Relative expression of Wnt2b and Wnt5b mRNA in lung tissues of WT and PARG$^{+/-}$ mice after BaP inhalation exposure. The mRNA expression in lungs from WT and PARG$^{+/-}$ mice was measured by real-time quantitative PCR after 90 days (panels **A**,**B**) or 180 days (panels **C**,**D**) of BaP inhalation exposure. Female-C, control untreated female mice; Female-T, treated female mice; Male-C, control untreated male mice; Male-T, treated male mice. ***$P < 0.001$, significant difference was found in treated compared to untreated mice. Results represent the mean ± SD of 3 mice from each group.

to bind to Axin scaffolding proteins, affecting the stability of the key protein β-catenin and regulating the activation of the Wnt pathway (Yang et al., 2016). In the current study, the level of total phosphorylated protein in WT mice and PARG$^{+/-}$ mice was not significantly different after 90-day exposure to BaP. However, after 180 d, phosphorylated protein was significantly reduced in WT mice but was up-regulated in PARG$^{+/-}$ mice compared with the control group. These findings are consistent with the possibility that, as the exposure time of BaP extended, loss of PARG promotes phosphorylation of proteins, which possibly leads to phosphorylated degradation of key proteins in the Wnt pathway; supported by the following studies (Zeng et al., 2005; Kim et al., 2013; Yang et al., 2016). We will try to explore how does PARG regulates protein tyrosine phosphorylation to regulate the Wnt signaling against the progression of lung cancer in our next study.

Wnt ligands play a vital role in the development of lung cancer, and inhibition of Wnt ligands may reduce the expansion of lung cancer cell lines (Tammela et al., 2017). Our results demonstrate that the relative expression of Wnt2b and Wnt5b mRNA was up-regulated in lung tissues of WT mice compared with the control group after 90- and 180-day exposure to BaP. Furthermore, the expression of Wnt2b and Wnt5b protein was up-regulated, though there were no significant differences in Wnt2b and Wnt5b mRNA and protein expression in PARG$^{+/-}$ mice. It suggested that loss of PARG stabilized the expression of Wnt ligands, probably suppressing the activation of the Wnt pathway against the progression of lung cancer.

Wnt2b and Wnt5b are two ligands of the Wnt signaling pathway. Wnt2b mainly acts through the canonical Wnt pathway and binds to receptors on the cell membrane to increase the stability of β-catenin in the cytoplasm and promote its translocation to the nucleus to activate downstream target genes that lead to tumorigenesis (Roelink et al., 1992). Studies have shown that Wnt2b is overexpressed in various cancers (Katoh, 2001; Huang et al., 2015). Wnt5b, on the other hand, is a non-canonical Wnt pathway factor that activates the Wnt/Ca^{2+} pathway or blocks the down-regulation of β-catenin by GSK-3β to prevent the classical Wnt pathway (Kohn and Moon, 2005). Studies have shown that Wnt5b plays different roles in different types of cancers. In some cancers, such as lung cancer, it promotes tumorigenesis, and

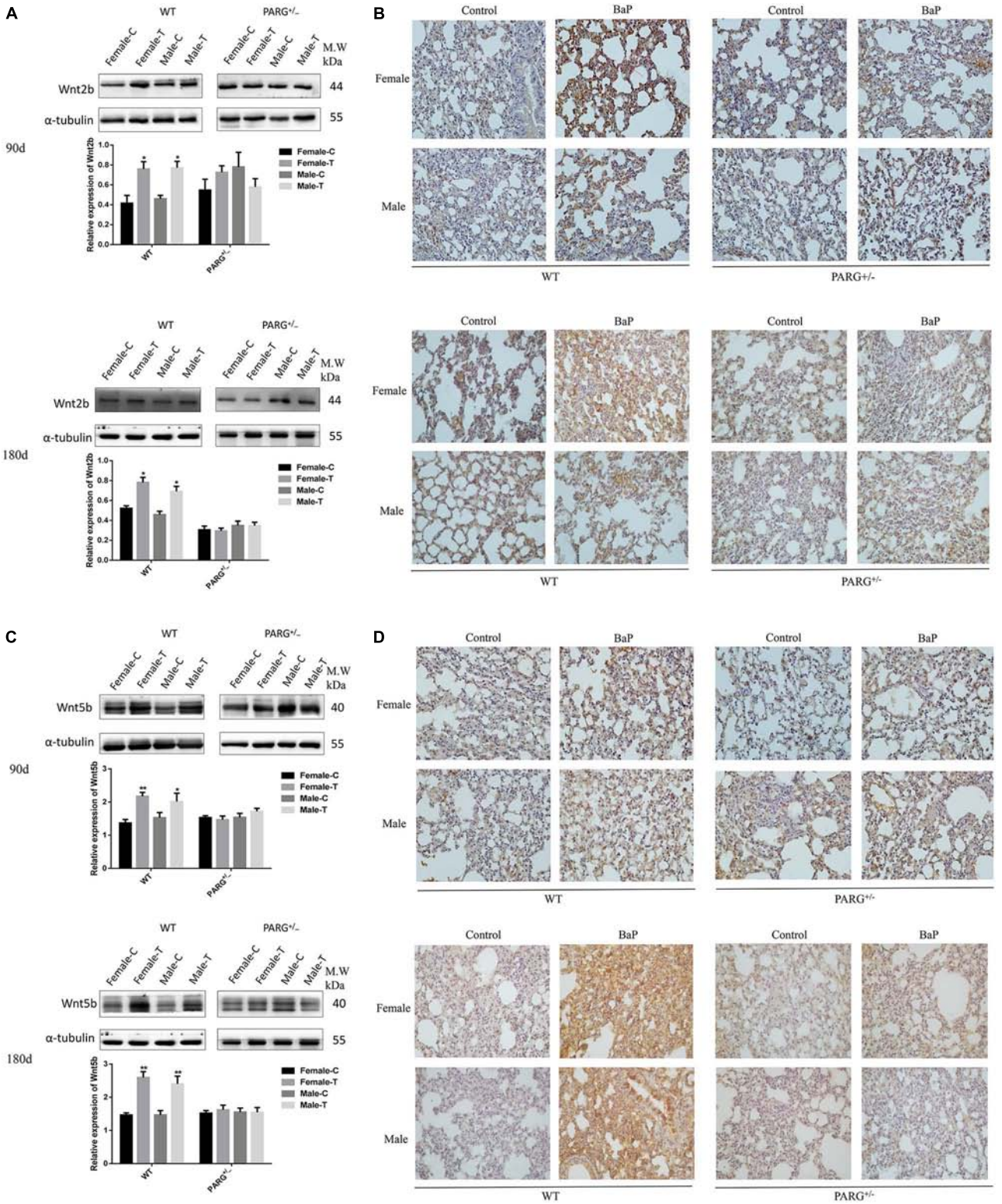

FIGURE 5 | PARG silencing inhibits the expression of Wnt2b and Wnt5b protein in lung tissues after BaP inhalation exposure. Expression of Wnt2b and Wnt5b protein in lung tissues detected by Western blotting and immunohistochemistry. **(A)** Western blotting of Wnt2b expression. **(B)** Immunohistochemical staining of Wnt2b (×200). Protein expression levels are reflected by the area and depth of brownish yellow. **(C)** Western blotting of Wnt5b expression. **(D)** Immunohistochemical staining of Wnt5b (×200). Red arrows indicate Wnt2b and Wnt5b localization in the cytoplasm. Female-C, control untreated female mice; Female-T, treated female mice; Male-C, control untreated male mice; Male-T, treated male mice. $^{*}P < 0.05$, $^{**}P < 0.01$, significant up-regulation in treated vs. control mice.

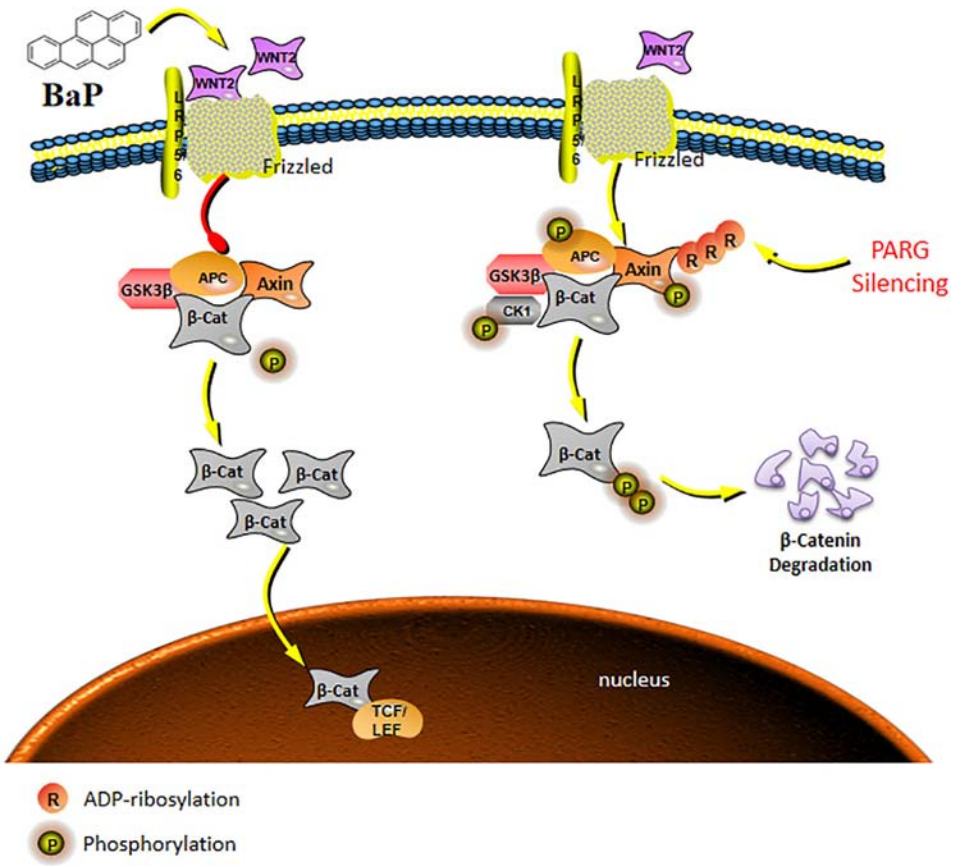

FIGURE 6 | Schematic model of the Wnt/β-catenin signaling pathway regulated by PARG gene silencing during BaP-induced lung cancer. After activation of the canonical pathway, Wnt ligands bind to Frzzled and LRP5/6 on the cell surface to form a trimer, which weakens the stability of a destruction complex composed by β-catenin, Axin, GSK-3β, and APC to prevent the phosphorylated degradation of β-catenin. The concentration of β-catenin increases in the cytoplasm, and then transfers into the nucleus to ultimately activate the expression of downstream target genes. PARG gene silencing may promote binding of phosphorylated proteins to the Axin scaffolding proteins, affecting the stability of the key protein β-catenin, and then suppressing the activation of the Wnt/β-catenin pathway to stabilize the expression of Wnt2b against the progression of lung cancer.

in other cancers, it suppresses tumorigenesis (Kikuchi and Yamamoto, 2008; Harada et al., 2017). On the basis of its different roles in different cancers, Wnt5b may constitute a specific marker for lung cancer screening. In our study, it is found that the up-regulation of Wnt2b was similar at 90 and 180 days, while the up-regulation times of Wnt5b was more obvious at 180 days than at 90 days. These findings may suggest that the Wnt non-canonical pathway increased with extended exposure times, while the classical pathway remains activated at both 90 and 180 days. Specific mechanisms of interaction between the two pathways remains to be further studied.

In conclusion, in the development of lung cancer induced by BaP, the expression of Wnt ligands are up-regulated, which is consistent with current understanding of the role of this pathway. Additionally, PARG gene silencing may regulate the phosphorylation level of proteins to stabilize the expression of Wnt2b, possibly inhibiting the ability of Wnt/β-catenin pathway to drive lung cancer progression as shown in the schematic model in **Figure 6**. The mechanism how PARG gene silencing affects the expression of Wnt5 remains to be futher explored. Understanding of the unresolved issue will contribute to the development of applications of PARG for cancer therapy. Lung cancer is one of the world's most serious threats to human health and has become a global public health problem (Siegel et al., 2018). Therefore, studying the mechanisms of lung cancer provides increased understanding that is relevant to its diagnosis and treatment. Though epigenetic modification is extensive, basic and reversible, its theory and results are gradually being applied to the diagnosis and treatment of cancer (Dawson and Kouzarides, 2012). In this study, it is shown that PARG gene silencing can prevent the occurrence of lung cancer induced by BaP. Our results demonstrate that PARG may be a target for the diagnosis and treatment of lung cancer. Furthermore, the inhibition of Wnt ligands may inhibit lung cancer. These results provide a new potential approach for the treatment of lung cancer. In concludsion, the use of Wnt ligands in the diagnosis of lung cancer and the use of PARG inhibitors as a potential therapeutic against lung cancer is supported.

ETHICS STATEMENT

This study was carried out in accordance with the Principles of Laboratory Animal Care (NIH publication No. 80–23, revised 1985). The protocol was approved by the Regulations for Animal Care and Use Committee of Experimental Animal Center at Shenzhen University.

AUTHOR CONTRIBUTIONS

HH, WD, and JL conceived the project. WD, YF, and YD performed the experiments. WD, YD, DW, XL, LY, and KL analyzed the results. WD, ZZ, PG, HL, JZ, and XX wrote the first draft. All authors revised the manuscript. HH and GH edited and approved the manuscript.

FUNDING

This study was funded by NSFC China (No. 81370080), the Shenzhen Science and Technology Development Fund Project (Nos. JCYJ20170306160932340, JCYJ20170413101713324, JCYJ20160428143634086, and JCYJ20160428142316603) and Sanming Project of Medicine in Shenzhen (SZSM201611090).

SUPPLEMENTARY MATERIAL

The Supplementary Material for this article can be found online at: https://www.frontiersin.org/articles/10.3389/fphar.2019.00338/full#supplementary-material

TABLE S1 | Primers used for real-time quantitative PCR.

REFERENCES

Alexandrov, K., Rojas, M., and Satarug, S. (2010). The critical DNA damage by benzo(a)pyrene in lung tissues of smokers and approaches to preventing its formation. *Toxicol. Lett.* 198, 63–68. doi: 10.1016/j.toxlet.2010.04.009

Berndt, J. D., and Moon, R. T. (2013). Cell biology. Making a point with Wnt signals. *Science* 339, 1388–1389. doi: 10.1126/science.1236641

Bird, A. (2007). Perceptions of epigenetics. *Nature* 447, 396–398. doi: 10.1038/nature05913

Chen, W., Zheng, R., Baade, P. D., Zhang, S., Zeng, H., Bray, F., et al. (2016). Cancer statistics in China, 2015. *CA Cancer J. Clin.* 66, 115–132. doi: 10.3322/caac.21338

D'Amours, D., Desnoyers, S., D'Silva, I., and Poirier, G. G. (1999). Poly(ADP-ribosyl)ation reactions in the regulation of nuclear functions. *Biochem. J.* 342(Pt 2), 249–268.

Dawson, M. A., and Kouzarides, T. (2012). Cancer epigenetics: from mechanism to therapy. *Cell* 150, 12–27. doi: 10.1016/j.cell.2012.06.013

Ferlay, J., Soerjomataram, I., Dikshit, R., Eser, S., Mathers, C., Rebelo, M., et al. (2015). Cancer incidence and mortality worldwide: sources, methods and major patterns in GLOBOCAN 2012. *Int. J. Cancer* 136, E359–E386. doi: 10.1002/ijc.29210

Hagood, J. S. (2014). Beyond the genome: epigenetic mechanisms in lung remodeling. *Physiology* 29, 177–185. doi: 10.1152/physiol.00048.2013

Harada, T., Yamamoto, H., Kishida, S., Kishida, M., Awada, C., Takao, T., et al. (2017). Wnt5b-associated exosomes promote cancer cell migration and proliferation. *Cancer Sci.* 108, 42–52. doi: 10.1111/cas.13109

Huang, C., Ma, R., Xu, Y., Li, N., Li, Z., Yue, J., et al. (2015). Wnt2 promotes non-small cell lung cancer progression by activating WNT/beta-catenin pathway. *Am. J. Cancer Res.* 5, 1032–1046.

Huang, H. Y., Cai, J. F., Liu, Q. C., Hu, G. H., Xia, B., Mao, J. Y., et al. (2012). Role of poly(ADP-ribose) glycohydrolase in the regulation of cell fate in response to benzo(a)pyrene. *Exp. Cell Res.* 318, 682–690. doi: 10.1016/j.yexcr.2012.01.007

IARC Working Group on the Evaluation of Carcinogenic Risks to Humans (2010). IARC monographs on the evaluation of carcinogenic risks to humans. Ingested nitrate and nitrite, and cyanobacterial peptide toxins. *IARC Monogr. Eval. Carcinog. Risks Hum.* 94, 1–412.

IARC Working Group on the Evaluation of Carcinogenic Risks to Humans (2012). Chemical agents and related occupations. *IARC Monogr. Eval. Carcinog. Risks Hum.* 100(Pt F), 9–562.

Ikeda, S., Kishida, S., Yamamoto, H., Murai, H., Koyama, S., and Kikuchi, A. (1998). Axin, a negative regulator of the Wnt signaling pathway, forms a complex with GSK-3beta and beta-catenin and promotes GSK-3beta-dependent phosphorylation of beta-catenin. *EMBO J.* 17, 1371–1384. doi: 10.1093/emboj/17.5.1371

Kasala, E. R., Bodduluru, L. N., Barua, C. C., Madhana, R. M., Dahiya, V., Budhani, M. K., et al. (2016). Chemopreventive effect of chrysin, a dietary flavone against benzo(a)pyrene induced lung carcinogenesis in Swiss albino mice. *Pharmacol. Rep.* 68, 310–318. doi: 10.1016/j.pharep.2015.08.014

Katoh, M. (2001). Differential regulation of WNT2 and WNT2B expression in human cancer. *Int. J. Mol. Med.* 8, 657–660. doi: 10.3892/ijmm.8.6.657

Kikuchi, A., and Yamamoto, H. (2008). Tumor formation due to abnormalities in the beta-catenin-independent pathway of Wnt signaling. *Cancer Sci.* 99, 202–208. doi: 10.1111/j.1349-7006.2007.00675.x

Kim, W., Kim, S. Y., Kim, T., Kim, M., Bae, D. J., Choi, H. I., et al. (2013). ADP-ribosylation factors 1 and 6 regulate Wnt/beta-catenin signaling via control of LRP6 phosphorylation. *Oncogene* 32, 3390–3396. doi: 10.1038/onc.2012.373

Klaus, A., and Birchmeier, W. (2008). Wnt signalling and its impact on development and cancer. *Nat. Rev. Cancer* 8, 387–398. doi: 10.1038/nrc2389

Koh, D. W., Lawler, A. M., Poitras, M. F., Sasaki, M., Wattler, S., Nehls, M. C., et al. (2004). Failure to degrade poly(ADP-ribose) causes increased sensitivity to cytotoxicity and early embryonic lethality. *Proc. Natl. Acad. Sci. U.S.A.* 101, 17699–17704. doi: 10.1073/pnas.0406182101

Kohn, A. D., and Moon, R. T. (2005). Wnt and calcium signaling: beta-catenin-independent pathways. *Cell Calcium* 38, 439–446. doi: 10.1016/j.ceca.2005.06.022

Li, X., Li, X., Zhu, Z., Huang, P., Zhuang, Z., Liu, J., et al. (2016). Poly(ADP-Ribose) glycohydrolase (PARG) silencing suppresses benzo(a)pyrene induced cell transformation. *PLoS One* 11:e0151172. doi: 10.1371/journal.pone.0151172

Liu, G., Niu, Z., Van Niekerk, D., Xue, J., and Zheng, L. (2008). Polycyclic aromatic hydrocarbons (PAHs) from coal combustion: emissions, analysis, and toxicology. *Rev. Environ. Contam. Toxicol.* 192, 1–28. doi: 10.1007/978-0-387-71724-1_1

Meyer, R. G., Meyer-Ficca, M. L., Whatcott, C. J., Jacobson, E. L., and Jacobson, M. K. (2007). Two small enzyme isoforms mediate mammalian mitochondrial poly(ADP-ribose) glycohydrolase (PARG) activity. *Exp. Cell Res.* 313, 2920–2936. doi: 10.1016/j.yexcr.2007.03.043

Miller, K. P., and Ramos, K. S. (2001). Impact of cellular metabolism on the biological effects of benzo[a]pyrene and related hydrocarbons. *Drug Metab. Rev.* 33, 1–35. doi: 10.1081/DMR-100000138

Min, W., Cortes, U., Herceg, Z., Tong, W. M., and Wang, Z. Q. (2010). Deletion of the nuclear isoform of poly(ADP-ribose) glycohydrolase (PARG) reveals its function in DNA repair, genomic stability and tumorigenesis. *Carcinogenesis* 31, 2058–2065. doi: 10.1093/carcin/bgq205

Miwa, M., and Masutani, M. (2007). PolyADP-ribosylation and cancer. *Cancer Sci.* 98, 1528–1535. doi: 10.1111/j.1349-7006.2007.00567.x

Reya, T., and Clevers, H. (2005). Wnt signalling in stem cells and cancer. *Nature* 434, 843–850. doi: 10.1038/nature03319

Roelink, H., Wagenaar, E., and Nusse, R. (1992). Amplification and proviral activation of several Wnt genes during progression and clonal variation of mouse mammary tumors. *Oncogene* 7, 487–492.

Rojas, M., Marie, B., Vignaud, J. M., Martinet, N., Siat, J., Grosdidier, G., et al. (2004). High DNA damage by benzo[a]pyrene 7,8-diol-9,10-epoxide in

bronchial epithelial cells from patients with lung cancer: comparison with lung parenchyma. *Cancer Lett.* 207, 157–163. doi: 10.1016/j.canlet.2003.11.016

Rouleau, M., Aubin, R. A., and Poirier, G. G. (2004). Poly(ADP-ribosyl)ated chromatin domains: access granted. *J. Cell Sci.* 117(Pt 6), 815–825. doi: 10.1242/jcs.01080

Rubin, H. (2001). Synergistic mechanisms in carcinogenesis by polycyclic aromatic hydrocarbons and by tobacco smoke: a bio-historical perspective with updates. *Carcinogenesis* 22, 1903–1930. doi: 10.1093/carcin/22.12.1903

Schmittgen, T. D., and Livak, K. J. (2008). Analyzing real-time PCR data by the comparative C(T) method. *Nat. Protoc.* 3, 1101–1108. doi: 10.1038/nprot.2008.73

Siegel, R. L., Miller, K. D., and Jemal, A. (2018). Cancer statistics, 2018. *CA Cancer J. Clin.* 68, 7–30. doi: 10.3322/caac.21442

Tammela, T., Sanchez-Rivera, F. J., Cetinbas, N. M., Wu, K., Joshi, N. S., Helenius, K., et al. (2017). A Wnt-producing niche drives proliferative potential and progression in lung adenocarcinoma. *Nature* 545, 355–359. doi: 10.1038/nature22334

van Delft, J. H., Mathijs, K., Staal, Y. C., van Herwijnen, M. H., Brauers, K. J., Boorsma, A., et al. (2010). Time series analysis of benzo[A]pyrene-induced transcriptome changes suggests that a network of transcription factors regulates the effects on functional gene sets. *Toxicol. Sci.* 117, 381–392. doi: 10.1093/toxsci/kfq214

Veeman, M. T., Axelrod, J. D., and Moon, R. T. (2003). A second canon. Functions and mechanisms of beta-catenin-independent Wnt signaling. *Dev. Cell* 5, 367–377. doi: 10.1016/S1534-5807(03)00266-1

Widziewicz, K., Rogula-Kozlowska, W., Loska, K., Kociszewska, K., and Majewski, G. (2018). Health risk impacts of exposure to airborne metals and benzo(a)pyrene during episodes of high PM10 concentrations in Poland. *Biomed. Environ. Sci.* 31, 23–36. doi: 10.3967/bes2018.003

Wodarz, A., and Nusse, R. (1998). Mechanisms of Wnt signaling in development. *Annu. Rev. Cell Dev. Biol.* 14, 59–88. doi: 10.1146/annurev.cellbio.14.1.59

Yang, E., Tacchelly-Benites, O., Wang, Z., Randall, M. P., Tian, A., Benchabane, H., et al. (2016). Wnt pathway activation by ADP-ribosylation. *Nat. Commun.* 7:11430. doi: 10.1038/ncomms11430

Zeng, X., Tamai, K., Doble, B., Li, S., Huang, H., Habas, R., et al. (2005). A dual-kinase mechanism for Wnt co-receptor phosphorylation and activation. *Nature* 438, 873–877. doi: 10.1038/nature04185

Zhang, C., Luo, T., Cui, S., Gu, Y., Bian, C., Chen, Y., et al. (2015). Poly(ADP-ribose) protects vascular smooth muscle cells from oxidative DNA damage. *BMB Rep.* 48, 354–359. doi: 10.5483/BMBRep.2015.48.6.012

Conflict of Interest Statement: The authors declare that the research was conducted in the absence of any commercial or financial relationships that could be construed as a potential conflict of interest.

frontiers in Oncology

ORIGINAL RESEARCH
published: 18 June 2019
doi: 10.3389/fonc.2019.00514

Midostaurin Reverses ABCB1-Mediated Multidrug Resistance, an *in vitro* Study

Ning Ji[1,2], *Yuqi Yang*[2], *Chao-Yun Cai*[2], *Jing-Quan Wang*[2], *Zi-Ning Lei*[2], *Zhuo-Xun Wu*[2], *Qingbin Cui*[2], *Dong-Hua Yang*[2], *Zhe-Sheng Chen*[2]* and *Dexin Kong*[1,3]*

[1] Tianjin Key Laboratory on Technologies Enabling Development of Clinical Therapeutics and Diagnostics, School of Pharmacy, Tianjin Medical University, Tianjin, China, [2] Department of Pharmaceutical Sciences, College of Pharmacy and Health Sciences, St. John's University, Queens, NY, United States, [3] Research Center, School of Medicine, Tianjin Tianshi College, Tianyuan University, Tianjin, China

Overexpression of ABC transporters in cancer cells is an underlying mechanism of multidrug resistance (MDR), leading to insensitive response to chemotherapeutic strategies. Thus, MDR is often results in treatment failure in the clinic. In this study, we found midostaurin, a Food and Drug Administration (FDA)-approved anti-leukemia drug, can antagonize ATP-binding cassette subfamily B member 1 (ABCB1)-mediated MDR. Our results indicated that midostaurin has the capacity to antagonize ABCB1-mediated MDR, while no significant reversal effect was found on ATP-binding cassette subfamily G member 2 (ABCG2)-mediated MDR. Our subsequent resistance mechanism studies showed that midostaurin directly inhibited the efflux function of the ABCB1 transporter without alteration of the expression level or the subcellular localization of ABCB1 transporter. In addition, midostaurin inhibited the ATPase activity of ABCB1 transporter in a dose-dependent manner. Moreover, our *in silico* docking study predicted that midostaurin could interact with the substrate-binding sites of ABCB1 transporter. This novel finding could provide a promising treatment strategy that co-administrating midostaurin with anticancer drugs in the clinic could overcome MDR and improve the efficiency of cancer treatment.

Keywords: midostaurin, multidrug resistance, ATP-binding cassette (ABC) transporter, ABC, chemotherapy

OPEN ACCESS

Edited by:
Chun Hei Antonio Cheung, National Cheng Kung University, Taiwan

Reviewed by:
Chung-Pu Wu, Chang Gung University, Taiwan
Csilla Özvegy-Laczka, Institute of Enzymology (MTA), Hungary

***Correspondence:**
Zhe-Sheng Chen
chenz@stjohns.edu
Dexin Kong
kongdexin@tmu.edu.cn

Specialty section:
This article was submitted to Cancer Molecular Targets and Therapeutics, a section of the journal Frontiers in Oncology

Received: *25 January 2019*
Accepted: *29 May 2019*
Published: *18 June 2019*

Citation:
Ji N, Yang Y, Cai C-Y, Wang J-Q, Lei Z-N, Wu Z-X, Cui Q, Yang D-H, Chen Z-S and Kong D (2019) Midostaurin Reverses ABCB1-Mediated Multidrug Resistance, an in vitro Study. Front. Oncol. 9:514. doi: 10.3389/fonc.2019.00514

INTRODUCTION

Multidrug resistance (MDR) in cancer, a phenomenon leading to synchronous resistance of cancer cells to structurally unrelated antineoplastic drugs, is one of the most critical factors responsible for the failure of chemotherapeutics and the poor survival rate of patients (1). Several mechanisms are involved in cancer MDR, including reduced apoptosis, advanced DNA damage repair mechanisms, or altered drug metabolism. However, the most prominent factor is ABC transporter-mediated efflux of antineoplastic drugs (3, 51).

The transport system superfamily of ABC transporters plays critical roles in physiological and pharmacological processes (2). The human ABC protein family has been divided into seven subfamilies (ABCA to ABCG). The ABC transporter family has 49 ABC proteins and 48 of them have identified functions (3, 4). As one of the main contributors, ABCB1 (P-gp/MDR1) is widely expressed not only in the placenta, but in the blood-brain barrier (BBB), intestines, livers and kidneys, in order to protect the body from xenobiotics (5, 6). The ABCB1 transporter also mediates

the transport of a wide range of physiological substrates like lipids, porphyrins, and sterols (7). Furthermore, a broad range of chemotherapeutic drugs are substrates of the ABCB1 transporter, such as taxanes and anthracyclines. ABCB1 transporter significantly increases the efflux of such anticancer drugs, a major reason leading to ABCB1-mediated MDR (8). It has been documented that ABCB1 is strongly related to the chemotherapy prognosis and the progression of malignancy (9). Thus, it is critical to elude MDR by either decreasing the expression level of ABCB1 proteins or inhibiting the efflux function of ABCB1 through specific and potent inhibitors.

Midostaurin, a multi-kinase inhibitor that was originally developed as a protein kinase C (PKC) inhibitor for treatment of patients with solid malignancy (10), has already been approved by the FDA for treatment of acute myelocytic leukemia (AML) with Fms-like tyrosine kinase 3 (FLT3)-mutant subtype (11). It has recently been reported that the combination of midostaurin with standard chemotherapy can significantly prolong overall and event-free survival in patients who suffer from AML with a FLT3 mutation (12). Here, we report the reversal effects of midostaurin on ABCB1-mediated MDR when co-administrated with conventional antineoplastic drugs.

MATERIALS AND METHODS

Chemicals

Midostaurin was obtained from Thermo Fisher Scientific Inc. (Rockford, IL). Bovine serum albumin (BSA), fetal bovine serum (FBS), Dulbecco's modified Eagle's Medium (DMEM), penicillin/streptomycin and 0.25% trypsin were products from Corning Incorporated (Corning, NY). The monoclonal antibody for GAPDH (catalog number MA5-15738, lot number SA247966, clone GA1R), Alexa Fluor 488 conjugated goat anti-mouse IgG secondary antibody, were purchased from Thermo Fisher Scientific Inc. (Rockford, IL). Paclitaxel, doxorubicin, colchicine, cisplatin, mitoxantrone, verapamil, the monoclonal antibodies for ABCB1 (catalog number P7965, lot number 067M4761V, clone F4), dimethylsulfoxide (DMSO), 3-(4,5-dimethylthiazol-yl)-2,5-diphenyltetrazolium bromide (MTT), Triton X-100, 4',6-diamidino-2-phenylindole (DAPI), and paraformaldehyde, were obtained from Sigma-Aldrich (St. Louis, MO). HRP-conjugated rabbit anti-mouse IgG secondary antibody (catalog number 7076S, Lot number 32) were obtained from Cell Signaling Technology Inc. (Danvers, MA). Ko143 was a product from Enzo Life Sciences (Farmingdale, NY). [^{3}H]-paclitaxel (15 Ci/mmol) was purchased from Moravek Biochemicals, Inc. (Brea, CA). All other chemicals were purchased from Sigma Chemical Co (St. Louis, MO).

Cell Lines and Cell Culture

The ABCB1-overexpressing KB-C2 cell line was created by gradually adding colchicine to parental human epidermoid carcinoma KB-3-1 cells, and was kindly provided by Dr. Shin-ichi Akiyama (Kagoshima University, Kagoshima, Japan). The KB-C2 line was cultured in medium containing 2 μg/mL colchicine (13) to maintain its drugresistant characteristics. The SW620/Ad300 cells were cultured in medium with 300 ng/mL doxorubicin (14). KB-3-1, KB-C2, SW620, and SW620/Ad300 cells were used for ABCB1 reversal study. The human non-small cell lung cancer (NSCLC) NCI-H460 cell line and its subline of ABCG2-overexpressing NCI-H460/MX20 cells were used for ABCG2 reversal study. The NCI-H460/MX20 cells were selected by using a high dose of mitoxantrone and maintained in medium with 20 ng/mL mitoxantrone (15). HEK293/pcDNA3.1 and HEK293/ABCB1 were established by transfecting the human embryonic kidney HEK293 cells with empty and ABCB1 expressing vector, respectively (16). SW620 and SW620/Ad300 cells, NCI-H460 and NCI-H460/MX20 cells, were kindly provided by Drs. Susan Bates and Robert Robey (NCI, NIH, Bethesda, MD). HEK293/ABCB1 were kindly provided by Dr. Suresh V. Ambudkar (NCI, NIH, Bethesda, MD). All aforementioned cell lines were maintained in DMEM medium containing 10% fetal bovine serum and 1% penicillin/streptomycin at 37°C in a humidified atmosphere containing 5% CO_2. All cells were grown as an adherent monolayer and drug-resistant cells were grown in drug-free culture media for more than 20 days before assay.

MTT Cytotoxicity Assay

Cell viability was determined by MTT assay as we previously described (17). Each type of cell was harvested and resuspended before being seeded onto a 96-well plate at a final quantity of 5×10^3 cells per well in 160 μL of medium, and was then incubated overnight. Midostaurin and positive control drugs were added 2 h prior to incubation with or without anticancer drugs. After 72 h of further incubation, MTT solution (4 mg/mL) was added to each well and the cells were incubated for an additional 4 h at 37°C. Subsequently, the supernatant was discarded and 100 μL of DMSO was added to each well in order to dissolve the formazan crystals. An accuSkanTM GO UV/Vis Microplate Spectrophotometer from Fisher Sci. (Fair Lawn, NJ) was used to determine the absorbance at 570 nm. The concentration for 50% inhibition of cell viability (IC_{50}) of the anticancer drug was calculated as previously described (18). For positive control drugs, verapamil (3 μM) and Ko143 (3 μM) were used as reference inhibitors to reverse ABCB1- and ABCG2-mediated MDR, respectively. Cisplatin, which is not a substrate of ABCB1 or ABCG2, was used as a negative control chemotherapeutic drug.

Western Blotting and Immunofluorescence Analysis

Western blotting analysis was performed as previously described (19). Briefly, cells were lysed after incubated with or without midostaurin (500 nM) for varying amounts of time (0, 24, 48, and 72 h). The concentration of protein was determined by BCA Protein Assay Kit from Pierce (Rockford, IL). Equal amounts (20 μg) of proteins were subjected to 10% sodium dodecyl sulfate polyacrylamide gel electrophoresis (SDS-PAGE) and transferred to PVDF membranes from Millipore (Billerica, MA). The presence of ABCB1 was determined using monoclonal antibody F4 (dilution 1:500). GAPDH was used as a loading control. The resulting protein bands were analyzed using Image J software. The immunofluorescence assay was performed as previously

described (17). Briefly, after being cultured overnight in 24-well plates, cells (2×10^4/well) were treated with midostaurin for 72 h at 500 nM concentration. Then, cells were fixed in 4% paraformaldehyde for 10 min and permeabilized by 0.1% Triton X-100 for 10 min before being blocked with 6% BSA for 1 h at 37°C. The presence of ABCB1 was determined using monoclonal antibody F4 (dilution 1:100) for incubation at 4°C overnight. Cells were washed with iced PBS after each incubation time. Alexa Fluor 488 (Ex = 499 nm, Em = 519 nm) conjugated secondary antibody (1:1,000) was used after washing with iced PBS. DAPI (Ex = 345 nm, Em = 455 nm) was used to counterstain the nuclei. The cells were washed with ice-cold PBS before being imaged. Immunofluorescence images were collected using an EVOS FL Auto fluorescence microscope from Life Technologies Corporation (Gaithersburg, MD).

Doxorubicin Accumulation and Fluorescence Microscopic Analysis

Cells were grown in 6-well plates and washed twice with phosphate-buffered saline (PBS) before the pre-treatment of 500 nM of midostaurin. After 1 h of midostaurin pretreatment, 10 μM of doxorubicin was then added to each well for further incubation (1 h). Immunofluorescence images were collected using an EVOS FL Auto fluorescence microscope from Life Technologies Corporation (Gaithersburg, MD). Excitation and emission wavelengths of doxorubicin were 475 and 585 nm, respectively.

[^{3}H]-Paclitaxel Accumulation and Efflux Assay

We conducted [^{3}H]-paclitaxel accumulation assay using KB-3-1 and its drug-resistant subline KB-C2 cells. As previously described (20), 5×10^5 cells/well were cultured in 24-well plates overnight before the assay, and midostaurin was added 2 h prior to the addition of [^{3}H]-paclitaxel. After incubating with [^{3}H]-paclitaxel with or without midostaurin for 2 h at 37°C, cells were washed twice with iced PBS, and lysed with 0.25% trypsin before being placed in 5 mL scintillation fluid, and radioactivity was measured in the Packard TRI-CARB 1900CA liquid scintillation analyzer from Packard Instrument (Downers Grove, IL).For the efflux assay, KB-3-1 and KB-C2 cells (20) were incubated with midostaurin for 2 h followed by incubation with [^{3}H]-paclitaxel, with or without midostaurin for 2 h at 37°C. The cells were washed with iced PBS twice and then lysed at various time points (0, 30, 60, and 120 min) with trypsin. Subsequently, cells were placed in 5 mL of scintillation fluid and radioactivity was measured in the Packard TRI-CARB 1900CA liquid scintillation analyzer from Packard Instrument (Downers Grove, IL).

ATPase Assay

The ABCB1-associated ATPase activities were measured using PREDEASY ATPase Kits from TEBU-BIO nv (Boechout, Belgium) with modified protocols. Briefly, cell membranes that overexpressed ABCB1 were thawed and diluted before use. Sodium orthovanadate (Na_3VO_4) was used as an ATPase inhibitor. Various concentrations of midostaurin were incubated with membranes for 5 min. The ATPase reactions were initiated by adding 5 mM Mg^{2+}-ATP. Luminescence signals of P_i were initiated and measured after incubation at 37°C for 40 min with brief mixing. The changes of relative light units were determined by comparing Na_3VO_4-treated samples with midostaurin-treated groups.

Molecular Modeling of Human ABCB1 Homology Model

In silico docking analysis was conducted using software Maestro 11.5 (Schr*ʹ*odinger, LLC, New York, NY, 2018) (21). Human ABCB1 homology model was established by Dr. Aller based on refined mouse ABCB1 (PDB ID: 4M1M) (22). Afterwards, the docking grid at the drug-binding pocket was generated (23). The ligand was essentially prepared to perform glide XP docking with the default protocols.

Statistical Analysis

All data are expressed as the mean ± SD and were analyzed using one-way ANOVA. All experiments were repeated at least three times. Differences were considered significant when $P < 0.05$.

RESULTS

Midostaurin Significantly Antagonized ABCB1-Mediated MDR in ABCB1-Overexpressing Cancer Cells

Firstly, to avoid cytostatic-induced reversal phenomenon, we conducted MTT assays to evaluate the cytostatic effects of midostaurin in the ABCB1-overexpressing cells and corresponding parental cells that we would use. Hence, we could choose concentrations that would not significantly influence cell viability. We conducted further experiments with 200 and 500 nM doses of midostaurin (**Figure 1**).

As shown in **Figure 2**, midostaurin significantly sensitized ABCB1-overexpressing cancer cells KB-C2 (**Figures 2A–C**) and SW620/Ad300 (**Figures 2E–G**) to ABCB1 substrates (doxorubicin, paclitaxel, and colchicine), compared with their control resistance cells, and this sensitization occurred in a dose-dependent manner. At 200 or 500 nM, midostaurin could not alter the IC_{50} values of the above chemotherapeutic drugs to parental KB-3-1 (**Figures 2A–C**) and SW620 (**Figures 2E–G**) cells. In addition, when combined with cisplatin, a platinum drug which is known to not be a substrate of ABCB1, midostaurin showed no significant difference in its cytotoxic effect in neither the resistant cell lines nor the parental cell lines (**Figures 2D,H**). In this study, verapamil, a potent ABCB1 inhibitor, was used as a positive control drug (24).

Midostaurin Significantly Antagonized ABCB1-Mediated MDR in ABCB1-Gene-Transfected Cells

We next evaluated the reversal effect of midostaurin on ABCB1-gene-transfected cells. As shown in **Figure 3**, midostaurin could significantly lower the IC_{50} values of ABCB1 substrate-drugs

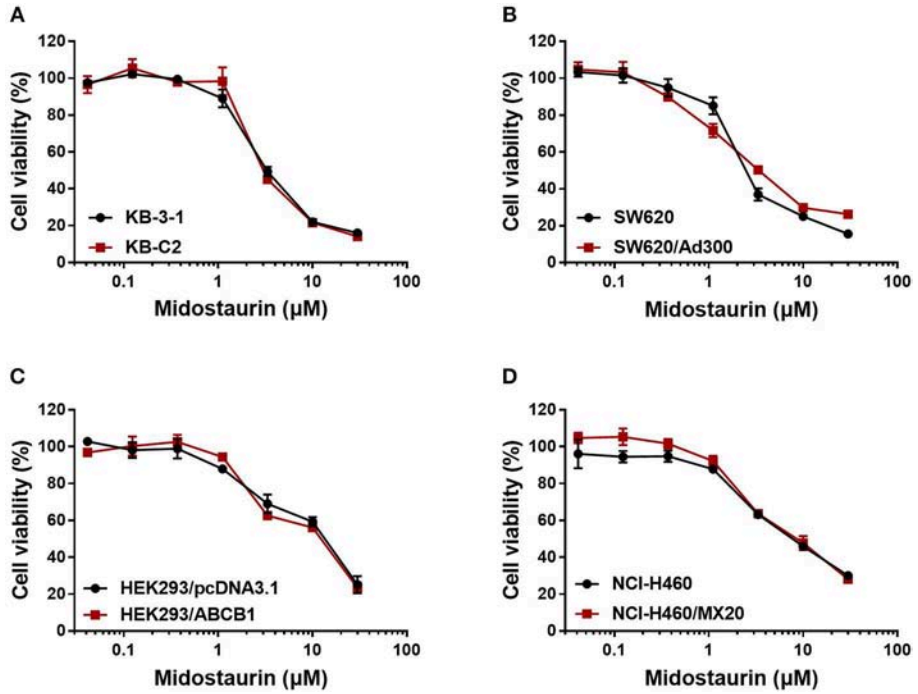

FIGURE 1 | Dose-viability curves of cells used in this study incubated with midostaurin for 72 h. Dose-viability curves for **(A)** KB-3-1 and KB-C2, **(B)** SW620 and SW620/Ad300, **(C)** HEK293/pcDNA3.1 and HEK293/ABCB1, and **(D)** NCI-H460 and NCI-H460/MX20.

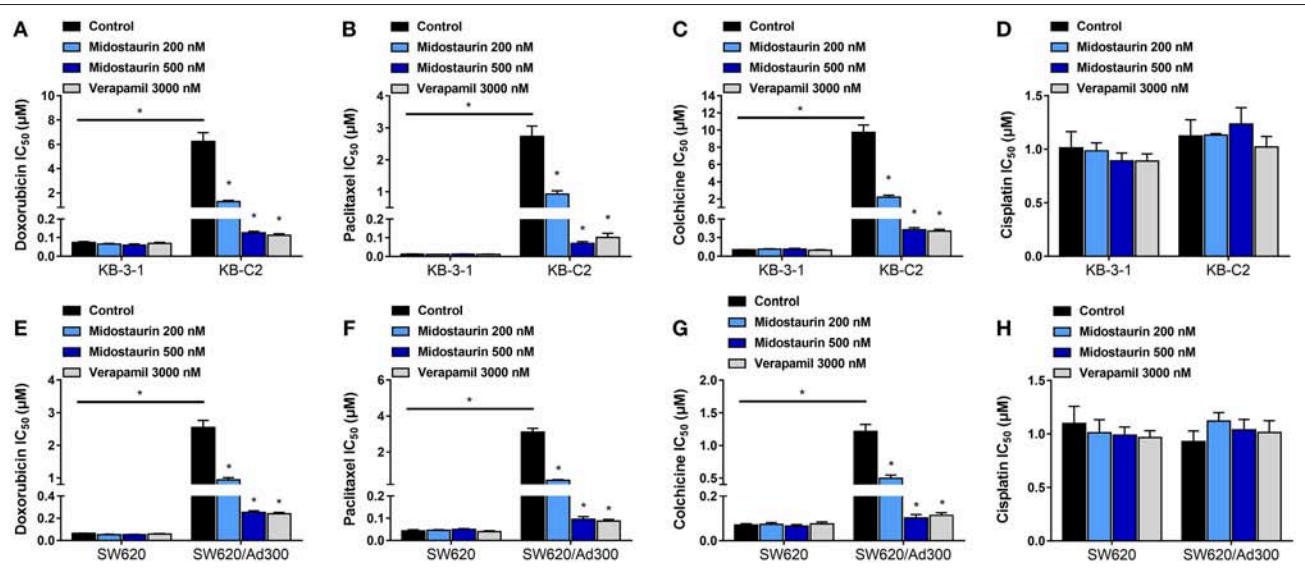

FIGURE 2 | The reversal effect of midostaurin on ABCB1-mediated MDR in ABCB1-overexpression cancer cells. IC_{50} values of **(A)** doxorubicin, **(B)** paclitaxel, **(C)** colchicine, and **(D)** cisplatin in parental KB-3-1 and drug-selected ABCB1-overexpression resistant KB-C2 cells with or without treatment of midostaurin. IC_{50} of **(E)** doxorubicin, **(F)** paclitaxel, **(G)** colchicine, and **(H)** cisplatin in parental SW620 and drug-selected ABCB1-overexpression resistant SW620/Ad300 cells with or without treatment of midostaurin. Data are expressed as mean ± SD, representative of at least three independent experiments. *$p < 0.05$, compared with control group.

(doxorubicin, paclitaxel, and colchicine) to HEK293/ABCB1 cells at 200 and 500 nM in a concentration-dependent manner (**Figures 3A–C**). More importantly, midostaurin did not significantly alter the efficacy of these ABCB1-substrate chemotherapeutic drugs in parental HEK293/pcDNA3.1 cells (**Figures 3A–C**). Furthermore, at 200 or 500 nM,

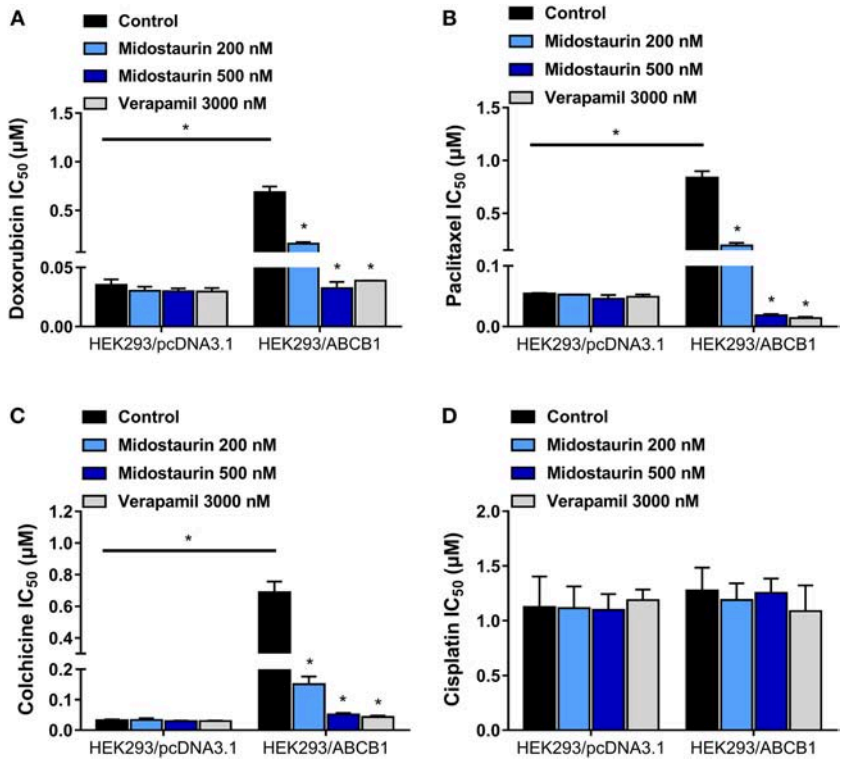

FIGURE 3 | The reversal effect of midostaurin on ABCB1-mediated MDR in ABCB1-gene-transfected cells. IC_{50} values of **(A)** doxorubicin, **(B)** paclitaxel, **(C)** colchicine, and **(D)** cisplatin in parental HEK293/pcDNA3.1 and transfected ABCB1-overexpression HEK293/ABCB1 cells with or without treatment of midostaurin. Data are expressed as mean ± SD, representative of at least three independent experiments. *$p < 0.05$, compared with control group.

midostaurin did not significantly change the IC_{50} values of cisplatin (**Figure 3D**).

Midostaurin Did Not Reverse ABCG2-Mediated MDR

As shown in **Figure 4**, midostautrin (200 and 500 nM) could not significantly lower the IC_{50} value of mitoxantrone, a known substrate of ABCG2-mediated MDR, to drug-selected NCI-H460/MX20 cells. In this study, we chose Ko143 as a positive control drug because it is a potent ABCG2 inhibitor (21). Cisplatin was used as a negative substrate drug as previously described (25).

Midostaurin Did Not Influence the Protein Expression Level or Subcellular Localization of ABCB1 Transporters

The next step was to figure out the mechanism of action of midostaurin. Theoretically, there are varied mechanisms involved in the reversal of ABCB1-mediated MDR. For examples, the reversal effect could be due to down-regulation of ABCB1 protein expression level and/or the change of ABCB1 transporter subcellular localization. To evaluate the effect of midostaurin on the protein level of ABCB1 transporter, we conducted Western blotting and immunofluorescence assays to detect whether midostaurin could impact the ABCB1 protein expression and/or subcellular localization. As shown in **Figure 5A**, after incubation for 24, 48, and 72 h, respectively, midostaurin did not significantly change the expression level of ABCB1 protein (170 kDa) in ABCB1-overexpressing KB-C2 cells. Furthermore, midostaurin did not change the localization of ABCB1 at the subcellular level after incubating for up to 72 h in ABCB1-overexpressing KB-C2 cells (**Figure 5B**). These results suggested that midostaurin influenced neither the expression level nor the subcellular localization of ABCB1 protein even at high concentrations.

Midostaurin Significantly Increased the Intracellular Drug Accumulation in ABCB1-Overexpressing Cancer Cells

The above results indicated that midostaurin could reverse ABCB1-mediated MDR without altering the protein expression level or subcellular localization in ABCB1-overexpressing cancer cells. We then conducted our drug accumulation assay to further understand the mechanism of the reversal effect of midostaurin. Firstly, we conducted our doxorubicin accumulation assay with 500 nM of midostaurin. As shown in **Figure 6A**, midostaurin significantly enhanced the accumulation level of doxorubicin in ABCB1-overexpressing KB-C2 cells. We also conducted our [^{3}H]-paclitaxel accumulation assay to get a digitized result. The intracellular level of [^{3}H]-paclitaxel was measured in

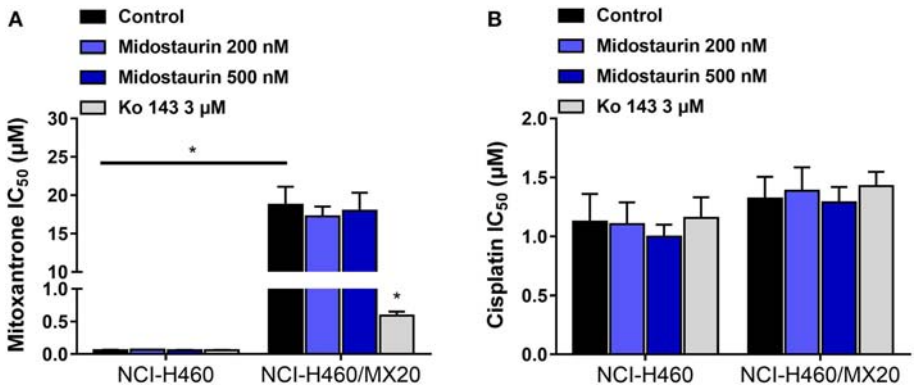

FIGURE 4 | The reversal effect of midostaurin on ABCG2-mediated MDR in ABCG2-overexpression cancer cells. **(A)** IC_{50} values of mitoxantrone in parental NCI-H460 cells and resistant NCI-H460/MX20 cells. **(B)** IC_{50} values of cisplatin in parental NCI-H460 cells and resistant NCI-H460/MX20 cells. *$p < 0.05$, compared with control group.

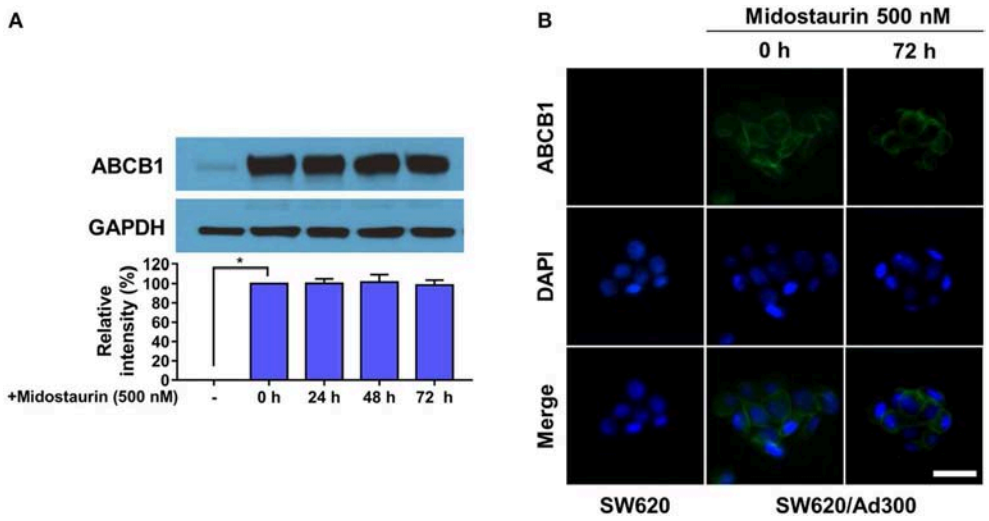

FIGURE 5 | Midostaurin did not alter the protein expression and subcellular localization of ABCB1 transporter. **(A)** Detection and relative intensity of ABCB1 expression in KB-C2 cells incubated with 500 nM of midostaurin for 0, 24, 48, and 72 h. **(B)** Sub-cellular localization of ABCB1 expression in SW620/Ad300 cells incubated with 500 nM of midostaurin for 72 h. Scale bar, 100 μm. *$p < 0.05$, compared with control group.

cells overexpressing ABCB1 transporter in the presence or absence of midostaurin. As shown in **Figure 6B**, midostaurin significantly increased the intracellular levels of [^{3}H]-paclitaxel in ABCB1-overexpressing KB-C2 cells in a dose-dependent manner. However, in parental KB-3-1 cells, no significant change in [^{3}H]-paclitaxel was found. In this study, verapamil was used as a positive control reversal reagent.

Midostaurin Significantly Inhibited the Efflux Function of ABCB1 Transporter in ABCB1-Overexpressing Cancer Cells

The efflux of antineoplastic drugs through ABCB1 transporter is involved in ABCB1-mediated MDR. We conducted an efflux assay at different time points (0, 30, 60, and 120 min) to determine whether midostaurin could inhibit the efflux function of ABCB1 transporter. As shown in **Figures 6C,D**, midostaurin significantly decreased the efflux level of [^{3}H]-paclitaxel in ABCB1-overexpressing KB-C2 cells in a dose-dependent manner, but this change was not shown in parental KB-3-1 cells. These results suggested that midostaurin could significantly increase the accumulation of anticancer drugs by inhibiting the efflux function mediated by ABCB1.

Midostaurin Significantly Inhibited the ATPase Activity of ABCB1 Transporter

The hydrolysis of ATP is the energy source of substrate-efflux mediated by ABCB1. Hence, we conducted the ABCB1-mediated ATP hydrolysis in the presence or absence of midostaurin at 0–40 μM serial concentrations. As shown in **Figure 7A**, midostaurin significantly inhibited the ATPase activity of ABCB1 transporters in a dose-dependent manner. The concentration of midostaurin required to obtain 50% of maximal inhibition

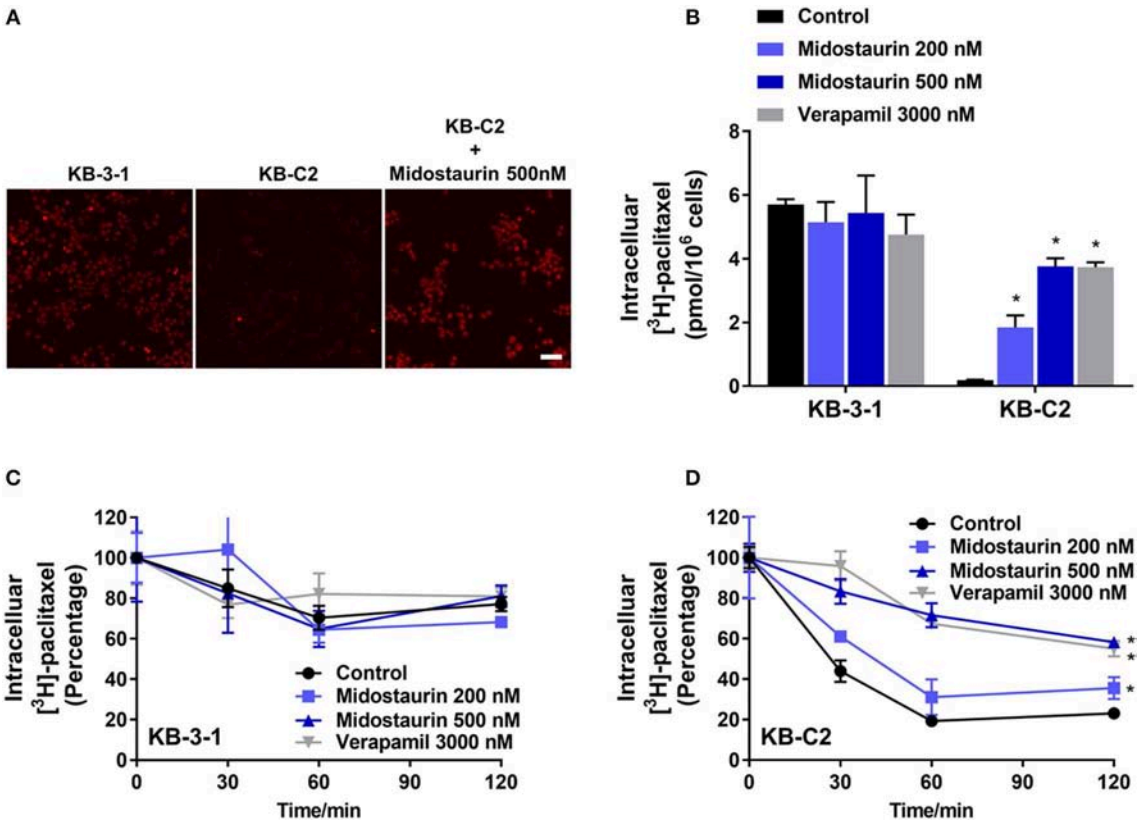

FIGURE 6 | The effect of midostaurin on accumulation and efflux activity in cancer cells overexpression ABCB1 transporter. Scale bar, 50 μm. **(A)** The effect of midostaurin on accumulation of doxorubicin. **(B)** The effect of midostaurin on accumulation of [^{3}H]-paclitaxel in KB-3-1 and KB-C2 cells. **(C,D)** The effects of midostaurin on efflux of [^{3}H]-paclitaxel in KB-3-1 and KB-C2 cells. *$p < 0.05$, compared with control group.

(IC_{50}) was 3.1 μM with the maximum of inhibition being 0.4-fold. These results suggested that midostaurin could inhibit the ATPase activity in ABCB1 transporters by interacting with the drug-binding pocket of these transporters. Therefore, one of the reversal mechanisms of midostraurin includes a reduced energy source for ABCB1 efflux function through inhibition of ATPase activity.

Docking Analysis of the Binding of Midostaurin With ABCB1 Homology Model

The best-scored docked positions of midostaurin with ABCB1 transporter are shown in **Figure 7**. The phenol ring of the methylbenzamide moiety in midostaurin has π-π interactions with the residues Phe336 and Phe983 of human ABCB1 (**Figure 7C**). In addition, midostaurin has hydrophobic interactions with residues of ABCB1 including Met69, Leu339, Ile340, Phe343, Phe728, Met986, and Ala987 (**Figure 7D**), which stabilize midostaurin in the substrate-binding pocket of ABCB1.

DISCUSSION

Growing evidence has shown that the failure of clinical treatment resulting from drug resistance to chemotherapeutic drugs in a series of cancer cell lines is tightly correlated with the overexpression of ABC transporters. It has been widely reported that cancer cells overexpressing ABCB1 transporter is a key factor that could imply poor prognosis as well as low survival rate in cancer patients (26–30). Moreover, genetic polymorphisms in ABC transporters, especially in ABCB1 and ABCG2 transporters, could significantly increase the high risk of death in patients who suffer from colorectal malignancy or non-small cell lung cancer (NSCLC) (31, 32). In recent decades, many small-molecule target drugs have been reported to have the capacity to reverse ABC transporter-mediated MDR, via inhibiting the function, downregulating the protein expressing level, and/or changing the subcellular localization of ABC transporters. Previously, we have reported that selonsertib, ulixertinib, and VS-4718 can significantly antagonize ABC transporter-mediated MDR (21, 23, 33). Unfortunately, there was no successful clinical case study on the therapeutic strategies to develop ABC transporters inhibitors as reversal reagents to reverse drug resistance. Nonetheless, growing evidence has shown that the overexpression of ABC transporters is mainly involved in MDR in cancer, and it is also critical in regulating oral bioavailability of anticancer drugs and reagents. A series of first-line chemotherapeutic drugs, including doxorubicin, paclitaxel and mitoxantrone are substrates of ABC transporters, meaning

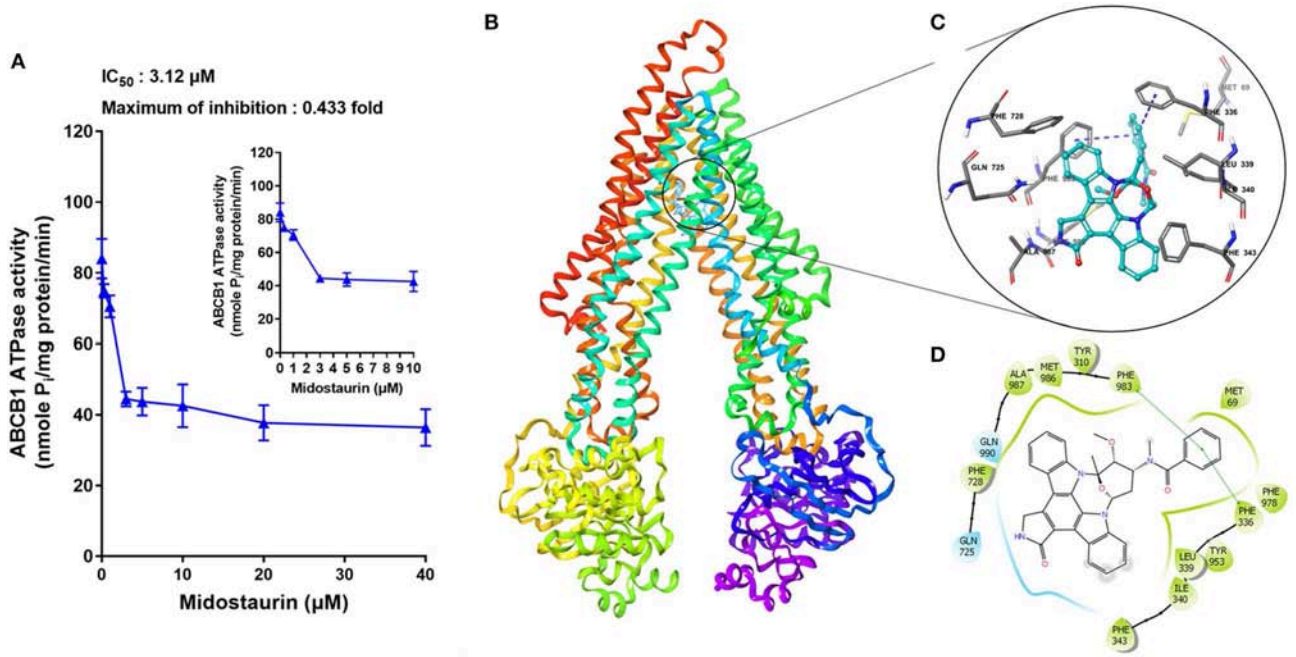

FIGURE 7 | The effects of midostaurin on the ATPase activity of ABCB1 and the molecular modeling study of midostaurin with human homology ABCB1. **(A)** Effect of midostaurin on the ATPase activity of ABCB1. The inset graphs illustrate the effect of 0–10 μM midostaurin on the ATPase activity of ABCB1. Data are mean, representative of three independent experiments. **(B)** Overall view of midostainrin-ABCB1 complex. **(C)** Docked position of midostaurin within the drug-binding site of human ABCB1 homology model by Glide docking. Midostaurin is shown as ball and stick mode with the atoms colored: carbon-cyan, hydrogen-white, nitrogen-blue, oxygen-red. Important residues are shown as sticks with gray color. π-π stacking interactions are indicated with blue dotted short line. **(D)** The two-dimensional ligand-receptor interaction diagram of midostaurin and human ABCB1. The amino acids within 3 Å are shown as colored bubbles, cyan indicates polar residues, and green indicates hydrophobic residues. The green short line shows π-π stacking interaction.

that these anti-cancer drugs will be pumped out from the cancer cells and finally lead to the failure of clinical carcinoma treatment (1–4, 34). Therefore, we confirm that screening small molecules to obtain the inhibitors of ABC transporters is still a potential and effective treatment strategy to circumvent MDR in cancer.

In this *in vitro* study, we evaluated the effect of midostaurin on ABCB1-mediated MDR. We mainly found that midostaurin, at non-toxic concentrations (200 and 500 nM), can significantly overcome ABCB1-mediated MDR in a series of cancer cell lines in a concentration-dependent manner. Firstly, to avoid potential reversal effects caused by the cytostatic effect of midostaurin, we performed our MTT assays to evaluate the anti-proliferative effect of midostaurin in the cells we would use in this study. Based on the results, we conducted further reversal studies using 200 and 500 nM of midostaurin. Our reversal study indicated that midostaurin could significantly reverse ABCB1-mediated MDR in KB-C2 and SW620/Ad300 cells, which were selected by treatment with colchicine or doxorubicin, respectively. Moreover, midostaurin could not alter the efficacy of certain chemotherapy substrate-drugs in their corresponding parental KB-3-1 or SW620 cells. In addition, midostaurin could not antagonize ABCG2-mediated MDR in ABCG2-overexpressing cancer cells NCI-H460/MX20. Based on these results, we hypothesized that the reversal effect of midostaurin was specific to interactions with the ABCB1 transporter. It is notable that we then verified this hypothesis by a reversal study in gene-transfected cells. We found that midostaurin could also lower the IC_{50} values of doxorubicin, paclitaxel, and colchicine in HEK293/ABCB1 cells compared with parental cells in a dose-dependent manner, but not those in parental HEK293/pcDNA3.1 cell line. Furthermore, midostaurin did not sensitize either parental HEK293/pcDNA3.1 cell line or HEK293/ABCB1 cells to cisplatin, a drug that does not use ABCB1 as a substrate. These results suggest that midostaurin exclusively reversed ABCB1-mediated MDR.

The reversal of MDR mediated by ABC transporters may be involved in the down-regulating and/or change of subcellular localization of certain ABC transporters. However, as shown in our Western blotting and immunofluorescence assays, no significant down-regulation of ABCB1 protein was found, and all ABCB1 protein was located on the membrane of KB-C2 cells after incubating with midostaurin for up to 72 h. In other words, these results signified that the mechanisms of midostaurin on the reversal of ABCB1 mediated-MDR were not due to the down-regulating of the protein level or change of subcellular localization of ABCB1 transporters. Nevertheless, as midostaurin is a multi-kinase inhibitor, we could not fully eliminate the possibility

that part of the reversal effect of midostaurin could be associated with its effect to other proteins and/or potential cross-talk with other signals, which may impact the efflux function of ABCB1 transporter, and this needs to be studied further in the future. Further study should also evaluate the potential effect of midostaurin on the protein expression level of ABCB1 with increased concentration or prolonged incubation time. Moreover, a process named post-translational modifications (PTM) plays an important role in proteins, especially transporters' function (35). It has been reported that ABCB1 could be phosphorylated at S661, S667, S671, and S683 to modulate its cell surface trafficking (36), and Pim-1 kinase could prevent ABCB1 from degradation, enabling glycosylation and cell surface expression (36). These clues indicate that it is necessary to further determine the effects of midostaurin on PTM of ABCB1 using higher concentration and/or longer incubation time.

Subsequently, drug accumulation and efflux assays were conducted, so that we could deeply understand the mechanisms of midostaurin on ABC transporter-mediated MDR attenuation. Our results indicated that midostaurin could significantly increase the intracellular concentration of ABCB1 substrate-drugs (doxorubicin and [^{3}H]-paclitaxel) in ABCB1-overexpression KB-C2 cells. Midostaurin could also significantly prevent [^{3}H]-paclitaxel from being pumped out of KB-C2 cells in a concentration-dependent manner. However, there is no significant change in doxorubicin or [^{3}H]-paclitaxel in accumulation or efflux in parental KB-3-1 cells. These novel findings were congruent with our observed reversal effects of midostaurin. Our mechanism study also indicated that midostaurin could increase the accumulation of certain substrate-drugs (doxorubicin and [^{3}H]-paclitaxel) in ABCB1-overexpression cancer cells by targeting the function of ABCB1 transporter.

ABC transporters, including ABCB1, obtain energy via ATP hydrolysis, and this can be modulated by the presence of certain substrates or inhibitors (37, 38). In our ATPase assay, we found that midostaurin could significantly inhibit the ATPase activity of ABCB1 in a dose-dependent manner, and the maximal inhibition level was 0.4-fold. Nevertheless, the accurate binding site of midostaurin with ABCB1 transporter remained unclear. In the *in silico* modeling study, we predicted that midostaurin could interact with the drug-binding pocket in the transmembrane domain (TMD) of ABCB1 transporter.

Midostaurin is an anticancer drug approved by FDA for treatment of AML with FLT3-mutant subtype (11). Over the years, the effect of midostaurin on multidrug resistance mediated by ABCB1 has been investigated independently in great detail. At the very beginning, midostaurin, also known as PKC412 and CGP41215, was developed as a PKC inhibitor, and prior work has documented the effectiveness of midostaurin in reversing MDR. Utz et al. (39) and Fabbro et al. (40) have reported that midostaurin could sensitize CCRF-VCR1000 cells and KB-8551 cells to adriamycin and vinblastine, without altering the ABCB1 mRNA expressing level. As a derivative of staurosporine, midostaurin was also identified to have the capacity to increase doxorubicin accumulation in doxorubicin-resistant cell line A2780/Adr. Meanwhile, midostaurin also acted as a reversal reagent in P-gp mediated leukemia resistance (41, 42). Budworth et al. (43) have explored the reversal effects of midostaurin on P-gp mediated breast cancer MCF7/Adr cell line resistance and Beltran et al. (44) have confirmed that such an effect of midostaurin was related to alterions in the phosphorylation of P-gp. In the study conducted by Courage et al. (45), midostaurin-resistant A549/CGP human lung cancer cell line was identified that overexpressed P-gp, indicated that P-gp may play a key role in midostaurin-mediated MDR. Another research showed that midostaurin could not affect the development of RD cells resistance (RD is a cell line that is resistant to vincristine, and has a mutant P53 but does not have detectable P-gp). This finding, combined with the above evidence, suggests that midostaurin may influence P-gp-mediated MDR (46). Moreover, midostaurin was also documented to alter P-gp efflux function and induce cell death in FLT3 ITD/P-g-positive samples (47). Ganeshaguru et al. (48) studied the effect of midostaurin on malignant cells from B-CLL (B-cell chronic lymphocytic leukemia) patients, and the results showed that nearly 1/3 of B-CLL cells that were originally resistant to chlorambucil and fludarabine were sensitive to midostaurin. P-gp-mediated efflux activity of nearly half of B-CCL cells were observed to be modulated by midostaurin. This novel finding further supported the conclusion that midostaurin could reverse ABCB1-mediated MDR. However, due to technical restrictions in protein structure identification and the incomplete functional research on ABC transporters, few studies systematically explained the exact mechanisms of midostaurin on ABCB1-mediated MDR. In this study, we conducted a series of experiments to verify the reversal effects of midostaurin on ABCB1-mediated MDR in cell lines which were not involved in other studies. Furthermore, we used human ABCB1 homology model to conduct our *in silico* docking study, through which we determined the specific residues that midostaurin would bind to, indicated the potential combining mode of midostaurin with ABCB1 transporter. On the other hand, with the development of pharmacological and molecular biology, various resistant cell lines with definite mechanisms were established and identified. It is necessary to verify the reversal effect and to determine the mechanisms of midostaurin on MDR by utilizing different resistant cell lines. More recently, the results from Hsiao et al. (49) showed that midostaurin could sensitize ABCB1-overexpression KB-V-1, NCI-ADR-RES, and NIH3T3-G185 cells to paclitaxel, colchicine, and vincristine. They also found that midostaurin could enhance colchicine-induced apoptosis effect in KB-V-1 cells, without altering the expression level of ABCB1 transporter. This finding coincides with the results we found when we co-administrated midostaurin with ABCB1-substrate chemotherapeutic drugs. In conclusion, our study demonstrates that midostaurin could overcome ABCB1-mediated MDR by directly inhibiting the efflux function of ABCB1 transporter; as a result, midostaurin can increase the accumulation of antineoplastic drugs. This novel study also suggests that co-administration of midostaurin with certain

substrate-chemotherapeutic drugs of ABCB1 may benefit cancer clinical treatment by circumventing MDR. However, we should not overstate the function of midostautin on MDR before further *in vivo* study and even clinical evaluation is completed as three generations of ABCB1 inhibitors have all failed to be applicable in clinic (50). Admittedly, it remains to be determined whether midostaurin could contribute to improving chemotherapeutic outcome in clinic. More recently, a global study of the efficacy and safety of midostaurin plus chemotherapy in newly diagnosed patients with FLT3 mutation negative (FLT3-MN) acute myeloid leukemia (AML) is recruiting (NCT03512197), and a phase II clinical evaluation is recruiting for midostaurin associated with standard chemotherapy in patients with core-binding factor leukemia (AML FLT3) (NCT03686345). These clinical trials may provide more potent evidence on combined utilization of midostaurin with conventional chemotherapeutic drugs, which would make midostaurin a sensitizing drug, not just a "reversal reagent."

AUTHOR CONTRIBUTIONS

DK and ZC conceived the general idea. NJ, YY, CC, JW, ZL, ZW, and QC performed experiments. NJ, ZC, DY, and DK analyzed the results. NJ, YY, CC, ZL, ZW, and QC wrote the first draft. DK and ZC revised the manuscript.

FUNDING

This work was supported by National Natural Science Foundation of China (81673464), Grant for Major Project of Tianjin for New Drug Development (17ZXXYSY00050), St. John's University Research Seed Grant (No. 579-1110-7002), and the Postgraduate Innovation Fund of 13th Five-Year comprehensive investment, Tianjin Medical University (YJSCX201712).

ACKNOWLEDGMENTS

We would like to thank Dr. Stephen Aller (The University of Alabama at Birmingham, Birmingham) for kindly providing the human ABCB1 homology model. We thank Tanaji T. Talele (St. John's University, New York, NY) for providing the computing resources for the docking analysis. We thank Drs. Susan E. Bates and Robert W. Robey (NCI, NIH, Bethesda, MD) for providing the cell lines. We thank Dr. Yanglu (Princeton University, NJ) for language editing. The first author thanks China Scholarship Council for reimbursing daily expenditures in America.

REFERENCES

1. Szakacs G, Paterson JK, Ludwig JA, Booth-Genthe C, Gottesman MM. Targeting multidrug resistance in cancer. *Nat Rev Drug Discov.* (2006) 5:219–34. doi: 10.1038/nrd1984
2. Dassa E, Bouige P. The ABC of ABCS: a phylogenetic and functional classification of ABC systems in living organisms. *Res Microbiol.* (2001) 152:211–29. doi: 10.1016/S0923-2508(01)01194-9
3. Eckford PD, Sharom FJ. ABC efflux pump-based resistance to chemotherapy drugs. *Chem Rev.* (2009) 109:2989–3011. doi: 10.1021/cr9000226
4. Stavrovskaya AA, Stromskaya TP. Transport proteins of the ABC family and multidrug resistance of tumor cells. *Biochemistry.* (2008) 73:592–604. doi: 10.1134/S0006297908050118
5. Linton KJ. Structure and function of ABC transporters. *Physiology.* (2007) 22:122–30. doi: 10.1152/physiol.00046.2006
6. Linton KJ, Higgins CF. Structure and function of ABC transporters: the ATP switch provides flexible control. *Pflugers Arch.* (2007) 453:555–67. doi: 10.1007/s00424-006-0126-x
7. Wu CP, Ambudkar VS. The pharmacological impact of ATP-binding cassette drug transporters on vemurafenib-based therapy. *Acta Pharm Sin B.* (2014) 4:105–11. doi: 10.1016/j.apsb.2013.12.001
8. Sauna ZE, Smith MM, Muller M, Kerr KM, Ambudkar SV. The mechanism of action of multidrug-resistance-linked P-glycoprotein. *J Bioenerg Biomembr.* (2001) 33:481–91. doi: 10.1023/A:1012875105006
9. Ali MA, Elsalakawy WA. ABCB1 haplotypes but not individual SNPs predict for optimal response/failure in Egyptian patients with chronic-phase chronic myeloid leukemia receiving imatinib mesylate. *Med Oncol.* (2014) 31:279. doi: 10.1007/s12032-014-0279-y
10. Propper DJ, McDonald AC, Man A, Thavasu P, Balkwill F, Braybrooke JP, et al. Phase I and pharmacokinetic study of PKC412, an inhibitor of protein kinase C. *J Clin Oncol.* (2001) 19:1485–92. doi: 10.1200/JCO.2001.19.5.1485
11. Rasko JEJ, Hughes TP. First approved kinase inhibitor for AML. *Cell.* (2017) 171:981. doi: 10.1016/j.cell.2017.11.007
12. Stone RM, Mandrekar SJ, Sanford BL, Laumann K, Geyer S, Bloomfield CD, et al. Midostaurin plus chemotherapy for acute myeloid leukemia with a FLT3 mutation. *N Engl J Med.* (2017) 377:454–64. doi: 10.1056/NEJMoa1614359
13. Akiyama S, Fojo A, Hanover JA, Pastan I, Gottesman MM. Isolation and genetic characterization of human KB cell lines resistant to multiple drugs. *Somat Cell Mol Genet.* (1985) 11:117–26. doi: 10.1007/BF01534700
14. Bates SE, Lee JS, Dickstein B, Spolyar M, Fojo AT. Differential modulation of P-glycoprotein transport by protein kinase inhibition. *Biochemistry.* (1993) 32:9156–64. doi: 10.1021/bi00086a022
15. Robey RW, Honjo Y, van de Laar A, Miyake K, Regis JT, Litman T, et al. A functional assay for detection of the mitoxantrone resistance protein, MXR (ABCG2). *Biochim Biophys Acta.* (2001) 1512:171–82. doi: 10.1016/S0005-2736(01)00308-X
16. Fung KL, Pan J, Ohnuma S, Lund PE, Pixley JN, Kimchi-Sarfaty C, et al. MDR1 synonymous polymorphisms alter transporter specificity and protein stability in a stable epithelial monolayer. *Cancer Res.* (2014) 74:598–608. doi: 10.1158/0008-5472.CAN-13-2064
17. Zhang XY, Zhang YK, Wang YJ, Gupta P, Zeng L, Xu M, et al. Osimertinib (AZD9291), a mutant-selective EGFR inhibitor, reverses ABCB1-mediated drug resistance in cancer cells. *Molecules.* (2016) 21:E1236. doi: 10.3390/molecules21091236
18. Zhang YK, Zhang H, Zhang GN, Wang YJ, Kathawala RJ, Si R, et al. Semi-synthetic ocotillol analogues as selective ABCB1-mediated drug resistance reversal agents. *Oncotarget.* (2015) 6:24277–90. doi: 10.18632/oncotarget.4493
19. Shi Z, Peng XX, Kim IW, Shukla S, Si QS, Robey RW, et al. Erlotinib (Tarceva, OSI-774) antagonizes ATP-binding cassette subfamily B member 1 and ATP-binding cassette subfamily G member 2-mediated drug resistance. *Cancer Res.* (2007) 67:11012–20. doi: 10.1158/0008-5472.CAN-07-2686
20. Sun YL, Kathawala RJ, Singh S, Zheng K, Talele TT, Jiang WQ, et al. Zafirlukast antagonizes ATP-binding cassette subfamily G member 2-mediated multidrug resistance. *Anticancer Drugs.* (2012) 23:865–73. doi: 10.1097/CAD.0b013e328354a196
21. Ji N, Yang Y, Lei ZN, Cai CY, Wang JQ, Gupta P, et al. Ulixertinib (BVD-523) antagonizes ABCB1- and ABCG2-mediated chemotherapeutic drug resistance. *Biochem Pharmacol.* (2018b) 158:274–85. doi: 10.1016/j.bcp.2018.10.028
22. Li J, Jaimes KF, Aller SG. Refined structures of mouse P-glycoprotein. *Protein Sci.* (2014) 23:34–46. doi: 10.1002/pro.2387

23. Ji N, Yang Y, Cai CY, Lei ZN, Wang JQ, Gupta P, et al. VS-4718 antagonizes multidrug resistance in ABCB1- and ABCG2-overexpression cancer cells by inhibiting the efflux function of ABC transporters. *Front Pharmacol.* (2018a) 9:1236. doi: 10.3389/fphar.2018.01236
24. Zhang H, Patel A, Wang YJ, Zhang YK, Kathawala RJ, Qiu LH, et al. The BTK inhibitor ibrutinib (PCI-32765) overcomes paclitaxel resistance in ABCB1- and ABCC10-overexpression cells and tumors. *Mol Cancer Ther.* (2017a) 16:1021–30. doi: 10.1158/1535-7163.MCT-16-0511
25. Zhang YK, Zhang XY, Zhang GN, Wang YJ, Xu H, Zhang D, et al. Selective reversal of BCRP-mediated MDR by VEGFR-2 inhibitor ZM323881. *Biochem Pharmacol.* (2017b) 132:29–37. doi: 10.1016/j.bcp.2017.02.019
26. Marsh S, Somlo G, Li X, Frankel P, King CR, Shannon WD, et al. Pharmacogenetic analysis of paclitaxel transport and metabolism genes in breast cancer. *Pharmacogenomics J.* (2007) 7:362–5. doi: 10.1038/sj.tpj.6500434
27. Campa D, Muller P, Edler L, Knoefel L, Barale R, Heussel CP, et al. A comprehensive study of polymorphisms in ABCB1, ABCC2 and ABCG2 and lung cancer chemotherapy response and prognosis. *Int J Cancer.* (2012) 131:2920–8. doi: 10.1002/ijc.27567
28. Hlavata I, Mohelnikova-Duchonova B, Vaclavikova R, Liska V, Pitule P, Novak P, et al. The role of ABC transporters in progression and clinical outcome of colorectal cancer. *Mutagenesis.* (2012) 27:187–96. doi: 10.1093/mutage/ger075
29. Litviakov NV, Cherdyntseva NV, Tsyganov MM, Denisov EV, Garbukov EY, Merzliakova MK, et al. Changing the expression vector of multidrug resistance genes is related to neoadjuvant chemotherapy response. *Cancer Chemother Pharmacol.* (2013) 71:153–63. doi: 10.1007/s00280-012-1992-x
30. Bartholomae S, Gruhn B, Debatin KM, Zimmermann M, Creutzig U, Reinhardt D, et al. Coexpression of multiple ABC-transporters is strongly associated with treatment response in childhood acute myeloid leukemia. *Pediatr Blood Cancer.* (2016) 63:242–7. doi: 10.1002/pbc.25785
31. Wu H, Kang H, Liu Y, Xiao Q, Zhang Y, Sun M, et al. Association of ABCB1 genetic polymorphisms with susceptibility to colorectal cancer and therapeutic prognosis. *Pharmacogenomics.* (2013) 14:897–911. doi: 10.2217/pgs.13.78
32. Wang F, Huang Z, Zheng K, Zhao H, Hu W. Two SNPs of ATP-binding cassette B1 gene on the risk and prognosis of colorectal cancer. *Int J Clin Exp Pathol.* (2015) 8:3083–9.
33. Ji N, Yang Y, Cai CY, Lei ZN, Wang JQ, Gupta P, et al. Selonsertib (GS-4997), an ASK1 inhibitor, antagonizes multidrug resistance in ABCB1- and ABCG2-overexpression cancer cells. *Cancer Lett.* (2019) 440–441:82–93. doi: 10.1016/j.canlet.2018.10.007
34. Kartal-Yandim M, Adan-Gokbulut A, Baran Y. Molecular mechanisms of drug resistance and its reversal in cancer. *Crit Rev Biotechnol.* (2016) 36:716–26. doi: 10.3109/07388551.2015.1015957
35. Czuba LC, Hillgren KM, Swaan PW. Post-translational modifications of transporters. *Pharmacol Ther.* (2018) 192:88–99. doi: 10.1016/j.pharmthera.2018.06.013
36. Germann UA, Chambers TC, Ambudkar SV, Licht T, Cardarelli CO, Pastan I, et al. Characterization of phosphorylation-defective mutants of human P-glycoprotein expressed in mammalian cells. *J Biol Chem.* (1996) 271:1708–16. doi: 10.1074/jbc.271.3.1708
37. Gottesman MM, Ambudkar SV. Overview: ABC transporters and human disease. *J Bioenerg Biomembr.* (2001) 33:453–8. doi: 10.1023/A:1012866803188
38. Wilkens S. Structure and mechanism of ABC transporters. *F1000Prime Rep.* (2015) 7:14. doi: 10.12703/P7-14
39. Utz I, Hofer S, Regenass U, Hilbe W, Thaler J, Grunicke H, et al. The protein kinase C inhibitor CGP 41251, a staurosporine derivative with antitumor activity, reverses multidrug resistance. *Int J Cancer.* (1994) 57:104–10. doi: 10.1002/ijc.2910570119
40. Fabbro D, Buchdunger E, Wood J, Mestan J, Hofmann F, Ferrari S, et al. Inhibitors of protein kinases: CGP 41251, a protein kinase inhibitor with potential as an anticancer agent. *Pharmacol Ther.* (1999) 82:293–301. doi: 10.1016/S0163-7258(99)00005-4
41. Sedlak J, Hunakova L, Duraj J, Chorvath B, Novotny L. Effects of protein kinase C inhibitor, staurosporine derivative CGP 41 251, on cell cycle, DNA synthesis and drug uptake in neoplastic cell lines. *Anticancer Drugs.* (1995) 6:70–6. doi: 10.1097/00001813-199502000-00008
42. Sedlak J, Hunakova L, Sulikova M, Chorvath B. Protein kinase inhibitor-induced alterations of drug uptake, cell cycle and surface antigen expression in human multidrug-resistant (Pgp and MRP) promyelocytic leukemia HL-60 cells. *Leuk Res.* (1997) 21:449–58. doi: 10.1016/S0145-2126(96)00088-4
43. Budworth J, Davies R, Malkhandi J, Gant TW, Ferry DR, Gescher A. Comparison of staurosporine and four analogues: their effects on growth, rhodamine 123 retention and binding to P-glycoprotein in multidrug-resistant MCF-7/Adr cells. *Br J Cancer.* (1996) 73:1063–8. doi: 10.1038/bjc.1996.205
44. Beltran PJ, Fan D, Fidler IJ, O'Brian CA. Chemosensitization of cancer cells by the staurosporine derivative CGP 41251 in association with decreased P-glycoprotein phosphorylation. *Biochem Pharmacol.* (1997) 53:245–7. doi: 10.1016/S0006-2952(96)00718-6
45. Courage C, Bradder SM, Jones T, Schultze-Mosgau MH, Gescher A. Characterisation of novel human lung carcinoma cell lines selected for resistance to anti-neoplastic analogues of staurosporine. *Int J Cancer.* (1997) 73:763–8.
46. Cocker HA, Tiffin N, Pritchard-Jones K, Pinkerton CR, Kelland LR. *In vitro* prevention of the emergence of multidrug resistance in a pediatric rhabdomyosarcoma cell line. *Clin Cancer Res.* (2001) 7:3193–8.
47. Hunter HM, Pallis M, Seedhouse CH, Grundy M, Gray C, Russell NH. The expression of P-glycoprotein in AML cells with FLT3 internal tandem duplications is associated with reduced apoptosis in response to FLT3 inhibitors. *Br J Haematol.* (2004) 127:26–33. doi: 10.1111/j.1365-2141.2004.05145.x
48. Ganeshaguru K, Wickremasinghe RG, Jones DT, Gordon M, Hart SM, Virchis AE, et al. Actions of the selective protein kinase C inhibitor PKC412 on B-chronic lymphocytic leukemia cells *in vitro*. *Haematologica.* (2002) 87:167–76.
49. Hsiao SH, Lusvarghi S, Huang YH, Ambudkar SV, Hsu SC, Wu CP. The FLT3 inhibitor midostaurin selectively resensitizes ABCB1-overexpression multidrug-resistant cancer cells to conventional chemotherapeutic agents. *Cancer Lett.* (2019) 445:34–44. doi: 10.1016/j.canlet.2019.01.001
50. Palmeira A, Sousa E, Vasconcelos MH, Pinto MM. Three decades of P-gp inhibitors: skimming through several generations and scaffolds. *Curr Med Chem.* (2012) 19:1946–2025. doi: 10.2174/0929867128001 67392
51. Gottesman MM, Fojo T, Bates SE. Multidrug resistance in cancer: role of ATP-dependent transporters. *Nat Rev Cancer.* (2002) 2:48–58. doi: 10.1038 nrc706

Conflict of Interest Statement: The authors declare that the research was conducted in the absence of any commercial or financial relationships that could be construed as a potential conflict of interest.

frontiers in Pharmacology

ORIGINAL RESEARCH
published: 06 August 2019
doi: 10.3389/fphar.2019.00857

An Insight Into the Molecular Mechanism of Berberine Towards Multiple Cancer Types Through Systems Pharmacology

Pengfei Guo[1,2†], Chuipu Cai[1,3†], Xiaoqin Wu[4], Xiude Fan[4], Wei Huang[1], Jingwei Zhou[1], Qihui Wu[1], Yujie Huang[1], Wei Zhao[1], Fengxue Zhang[3], Qi Wang[1,5], Yongbin Zhang[2] and Jiansong Fang[1,4,5]**

[1] Science and Technology Innovation Center, Guangzhou University of Chinese Medicine, Guangzhou, China, [2] Laboratory of Experimental Animal, Guangzhou University of Chinese Medicine, Guangzhou, China, [3] School of Basic Medical Sciences, Guangzhou University of Chinese Medicine, Guangzhou, China, [4] Lerner Research Institute, Cleveland Clinic, Cleveland, OH, United States, [5] Institute of Clinical Pharmacology, Guangzhou University of Chinese Medicine, Guangzhou, China

OPEN ACCESS

Edited by:
Zhe-Sheng Chen,
St. John's University, United States

Reviewed by:
Pranav Gupta,
Massachusetts General Hospital and Harvard Medical School, United States
Shuaishuai Liu,
University of Maryland, United States

***Correspondence:**
Jiansong Fang
fangjs@gzucm.edu.cn;
fangj3@ccf.org
Yongbin Zhang
zyb-73@163.com

†These authors have contributed equally to this work.

Specialty section:
This article was submitted to Cancer Molecular Targets and Therapeutics, a section of the journal Frontiers in Pharmacology

Received: *23 January 2019*
Accepted: *04 July 2019*
Published: *06 August 2019*

Citation:
Guo P, Cai C, Wu X, Fan X, Huang W, Zhou J, Wu Q, Huang Y, Zhao W, Zhang F, Wang Q, Zhang Y and Fang J (2019) An Insight Into the Molecular Mechanism of Berberine Towards Multiple Cancer Types Through Systems Pharmacology. Front. Pharmacol. 10:857. doi: 10.3389/fphar.2019.00857

Over the past several decades, natural products with poly-pharmacological profiles have demonstrated promise as novel therapeutics for various complex diseases, including cancer. Berberine (PubChem CID: 2353), a soliloquies quaternary alkaloid, has been validated to exert powerful effects in many cancers. However, the underlying molecular mechanism is not yet fully elucidated. In this study, we summarized the molecular effects of berberine against multiple cancers based on current available literatures. Furthermore, a systems pharmacology infrastructure was developed to discover new cancer indications of berberine and explore their molecular mechanisms. Specifically, we incorporated 289 high-quality protein targets of berberine by integrating experimental drug–target interactions (DTIs) extracted from literatures and computationally predicted DTIs inferred by network-based inference approach. Statistical network models were developed for identification of new cancer indications of berberine through integration of DTIs and curated cancer significantly mutated genes (SMGs). High accuracy was yielded for our statistical models. We further discussed three typical cancer indications (hepatocarcinoma, lung adenocarcinoma, and bladder carcinoma) of berberine with new mechanisms of actions (MOAs) based on our systems pharmacology framework. In summary, this study systematically provides a powerful strategy to identify potential anti-cancer effects of berberine with novel mechanisms from a systems pharmacology perspective.

Keywords: berberine, cancer, systems pharmacology, drug–target interactions, significantly mutated genes

INTRODUCTION

Natural products with diverse chemical scaffolds have been recognized as an invaluable source of candidates in drug discovery and development for multiple complex diseases, including cancer. Berberine, a plant-derived compound isolated from medicinal plants such as Coptis chinensis and Hydrastis canadensis, had a long history of medicinal application in traditional Chinese medicine

(Ayati et al., 2017). As one of the main alkaloids, berberine has been reported to exert potentially beneficial effects on many cancer types, including breast cancer (Kim et al., 2008), bladder cancer (Yan et al., 2011), and hepatocarcinoma (Liu et al., 2011; Zhu et al., 2016). For example, berberine had shown significant inhibitory effect on hepatocellular carcinoma cells and could reduce the volume and weight of tumors in an H22 transplanted tumor model in mice (Li et al., 2015).

Based on collection of hundreds of berberine-related pharmacological literatures, we systematically summarized eight key mechanisms of anti-cancer effects of berberine, including cell death, cell invasion and metastasis, cell cycle arrest, cell growth, transcription factors, inflammatory factors, angiogenic, chemo-sensitivity, and radio-sensitivity (**Figure 1** and **Supplementary Table S1**). Specifically, apoptosis (programmed cell death) plays a vital role in tumor cell development, differentiation, and proliferation (Ola et al., 2011). Recent study has revealed that berberine could induce apoptosis of human osteosarcoma U2OS cells through inhibiting the PI3K/Akt signaling pathway activation (Chen, 2016). In addition, anti-angiogenesis is a promising strategy for prevention and treatment of multicancer in preclinical or clinical studies in terms of many natural products (Khalid et al., 2016; Kotoku et al., 2016). Previous *in vitro* and *in vivo* experiments have validated that berberine exerted anti-angiogenic effect through inhibiting various proinflammatory and pro-angiogenic factors, including vascular endothelial growth factor (VEGF), interleukin-6 (IL-6), interleukin-2 (IL-2), and metalloproteinase inhibitor (TIMP) (Hamsa and Kuttan, 2012).

Collectively, berberine with polypharmacology has demonstrated its broad anti-cancer properties through targeting various oncogenic pathways and targets. Therefore, systematic exploration of the drug targets of berberine is of great significance for understanding its anti-cancer mechanisms of action (MOAs) and for further excavating its novel cancer indications.

Systems pharmacology-based approaches, as an emerging interdiscipline that combines experimental assays and computational tools, have provided an alternative to understand the therapeutic mechanisms of complex diseases (Fang et al., 2018). Recent studies have demonstrated advanced discovery of new indications for natural products based on systems pharmacology approaches (Fang et al., 2017b; Fang et al., 2019). For example, novel molecular mechanisms of several effective natural products (e.g., resveratrol, quercetin, caffeic acid, and wogonoside) for multiple complex diseases including multi-cancer types and age-related disorders have been identified and validated by various literatures and *in vitro* and *in vivo* experiments (Fang et al., 2017a; Huang et al., 2019). Collectively, systems pharmacology-based approaches have been proved as an effective tool for exploring the poly-pharmacological actions of natural products towards various complex diseases.

In this study, we proposed a systems pharmacology infrastructure to identify new cancer indications of berberine and explore their molecular mechanisms (**Figure 2**). Specifically, we constructed a global DTI network of berberine by integrating both experimentally reported DTIs obtained from literatures and DTIs computationally predicted by our previous predictive network models (Fang et al., 2017c). Besides, a high-quality

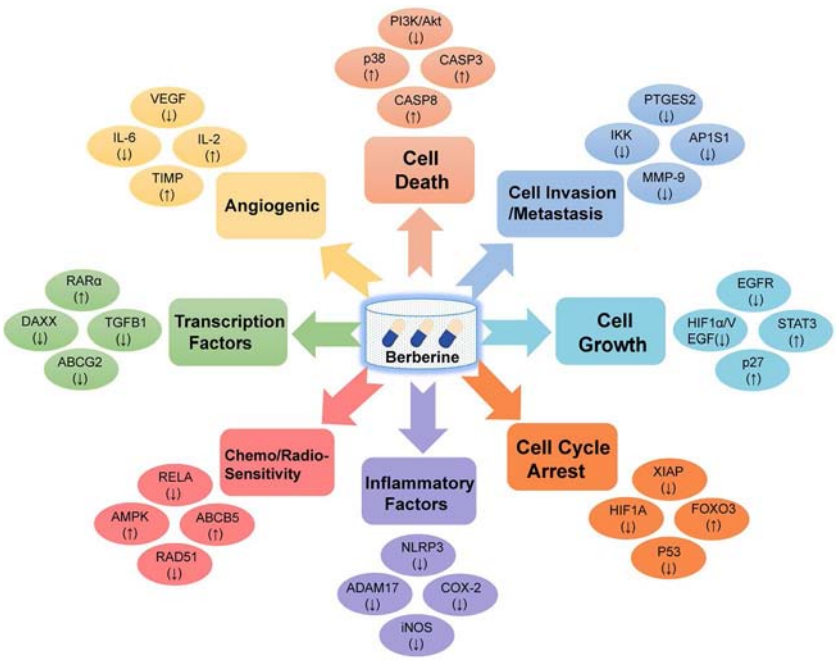

FIGURE 1 | Diagram illustrating the eight potential anti-cancer effects of berberine. Berberine exerts anti-cancer activities *via* targeting various cancer key protein targets, related to cell death, cell invasion and metastasis, cell cycle arrest, cell growth, transcription factors, inflammatory factors, angiogenic, chemo-sensitivity, and radio-sensitivity.

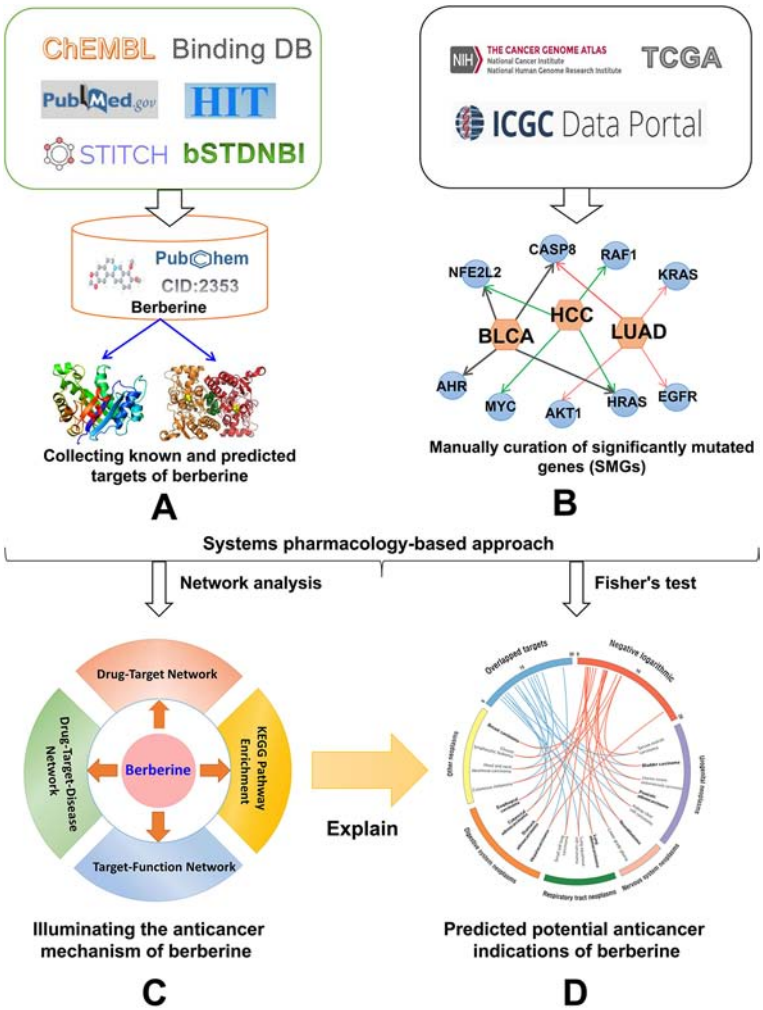

FIGURE 2 | Workflow of a systems pharmacology infrastructure for the identification of cancer indications and exploration of molecular mechanisms of berberine. **(A)** Construction of drug–target network for berberine, **(B)** manual curation of cancer significantly mutated genes (SMGs) for multiple cancer types, **(C)** performing network analyses to explore the anti-cancer mechanism of berberine, and **(D)** statistical network models for prioritizing novel anti-cancer indication of berberine through integrating computationally predicted and known drug targets into the curated cancer SMGs.

collection of significantly mutated genes (SMGs) for multiple cancer types was manually collected. On the basis of curated cancer SMGs and DTIs, we built statistical network models with high accuracy to prioritize new cancer indications of berberine and showcased its potential mechanisms. Overall, this study provides a useful systems pharmacology framework to interpret the multi-scale MOAs of berberine in multiple cancer type management, which may give some enlightenment for further treatment of cancer-associated diseases.

MATERIALS AND METHODS

Collection of Known Targets for Berberine

Known targets of berberine were collected by extracting data from four data sources, including HIT (Ye et al., 2011), STITCH (Kuhn et al., 2014), BindingDB (accessed June 2016) (Gilson et al., 2016), and ChEMBL (Bento et al., 2014). For STITCH, we only kept the targets with experimental evidence score higher than 0.7. We totally obtained 66 known targets *via* integrating the four available databases. Besides, we further gathered 238 extra targets of berberine by manually retrieving large-scale pharmacological literatures from PubMed (https://www.ncbi.nlm.nih.gov) with "berberine [title] and cancer" as search terms (**Supplementary Table S2**). After duplicated targets and DTIs were eliminated from non-*Homo sapiens*, 275 high-quality known DTIs were selected for further study (**Supplementary Table S3**).

Network-Based Target Prediction for Berberine

In a previous study, we have developed statistical network models to predict targets of natural products through a balanced

substructure–drug–target network-based inference (bSDTNBI) approach (Fang et al., 2018). The bSDTNBI method utilizes resource-diffusion processes to prioritize potential targets for natural products through integrating known DTI network, drug–substructure linkages, and new input drug–substructure linkages (Wu et al., 2017). For a new input chemical, each of its substructures equally spreads resources to its neighbor nodes layer by layer, and targets obtaining final resources could be regarded as the potential targets of the new chemical. Four parameters ($\alpha = \beta = 0.1$, $\gamma = -0.5$, and $k = 2$) of bSDTNBI were adopted based on a previous study (Wu et al., 2016). Among them, parameter α was introduced to balance the initial resource allocation of different node types, while β was used to adjust weighted values of different edge types. The third parameter γ was imported to balance the influence of hub nodes in resource-diffusion processes, and the fourth parameter κ denotes the number of resource-diffusion processes. We calculated four substructure items for each compound based on four types of molecular fingerprints from PaDEL-Descriptor (version 2.18) (Yap, 2011), including Substructure (FP4), Klekota-Roth (KR), MACCS, and PubChem. Among the four network models generated with different types of fingerprints, bSDTNBI_KR performed best with the highest values of precision ($P = 0.049$), recall ($R = 0.752$), precision enhancement (Ep = 27.02), recall enhancement (eR = 27.24), and the area under the receiver operating characteristic curve (AUC = 0.959). Finally, the best model built based on KR molecular fingerprint was selected to predict the new targets of berberine. The top 20 predicted candidates were used for further study (**Supplementary Table S3**).

Significantly Mutated Genes (SMG) for Multiple Cancer Types

We collected 804 SMGs for 28 cancer types/subtypes from a previous study (Cheng et al., 2016), including glioblastoma multiforme (GBM), serous ovarian adenocarcinoma (SOC), stomach adenocarcinoma (STAD), colorectal adenocarcinoma (CRAC), breast carcinoma (BRCA), uterine corpus endometrioid (UCEC), medulloblastoma (MBL), acute myeloid leukemia (AML), cutaneous melanoma (CM), lung squamous cell (SQCC), thyroid carcinoma (THCA), lung adenocarcinoma (LUAD), kidney clear cell (CCSK), head and neck squamous (HNSCC), small cell lung (SCLC), lower grade glioma (LGG), bladder carcinoma (BLCA), esophageal carcinoma (EC), prostate adenocarcinoma (PRAD), hepatocarcinoma (HCC), neuroblastoma (NBL), chronic lymphocytic leukemia (CLL), pancreas adenocarcinoma (PAC), multiple myeloma (MM), acute lymphocytic leukemia (ALL), non-small cell lung (NSCLC), diffuse large B-cell lymphoma (DLBCL), and pilocytic astrocytoma (PA). Considering a lack of statistical power if the number of SMG for specific cancer types is lower than 20, we further excluded ALL, NSCLC, DLBCL, and PA. All SMGs are annotated using gene Entrez ID, chromosome location, and the official gene symbols from the National Center for Biotechnology Information (NCBI) database (Zhe and Huang, 2002). Finally, 24 cancer types/subtypes covering 804 SMGs were selected for further study (**Supplementary Table S4**).

Prioritizing Cancer Indications of Berberine

In this study, an integrated statistical network model was generated to prioritize cancer indication of berberine based on drug–target network and cancer SMGs (Cheng et al., 2016; Jiang et al., 2018). We assumed that berberine would exert high potential for the treatment of a specific cancer type if its targets tend to be SMGs of this cancer. For each cancer type/subtype, Fisher's exact test was utilized to calculate the statistical significance of the enrichment of SMGs for each cancer type in target profiles of berberine. The *P*-values were corrected by Benjamini–Hochberg method (Benjamini and Yekutieli, 2001). We set a cutoff adjusted *P*-value threshold (q) < 0.05 to define significantly predicted drug–cancer pairs.

Network Construction

To further explore the multi-scale MOAs of berberine in treating multiple cancer types, three types of networks were constructed by Cytoscape 3.2.1 software (Shannon et al., 2003): 1) drug–target (D-T) network, which presents the relationship between berberine and its targets; 2) target–function (T-F) network, which illustrates the relationship between cancer-related biological processes and SMGs; and 3) drug–target–disease (D-T-D) network, which reflects a global view of the molecular mechanism of berberine against multiple cancer types. After network analysis, the SMGs were further mapped to DAVID database (https://david.ncifcrf.gov/summary.jsp) for extracting the canonical pathways that were highly associated with these targets (Dennis et al., 2003). Finally, circos plot was used to visualize the predicted cancer indications.

RESULTS AND DISCUSSION

Construction of the Drug–Target (D-T) Network for Berberine

The constructed drug–target interaction network (**Figure 3**) of berberine contains 289 interactions, including 275 known targets and 20 predicted targets (**Supplementary Table S3**). *In vitro* and *in vivo* assays in previous studies have validated that five out of the 20 predicted targets could be mediated by berberine, indicating high accuracy of our target prediction approach. These five predicted targets are caspase-3 (CASP3) (Okubo et al., 2017), cellular tumor antigen p53 (TP53) (Qing et al., 2014), caspase-9 (CASP9) (Zhao et al., 2017), nuclear factor NF-kappa-B p105 subunit (NFKB1) (Yu et al., 2014), and mitogen-activated protein kinase 1 (MAPK1) (Song et al., 2015).

We further mapped the 289 protein targets of berberine into the curated cancer SMGs, resulting in 51 cancer-related targets encoded by SMGs (**Supplementary Table S3**). Accumulating evidences indicate that berberine may exert anti-cancer effects through regulating these targets. For instance, signal transducer and activator of transcription 3 (STAT3) are important in

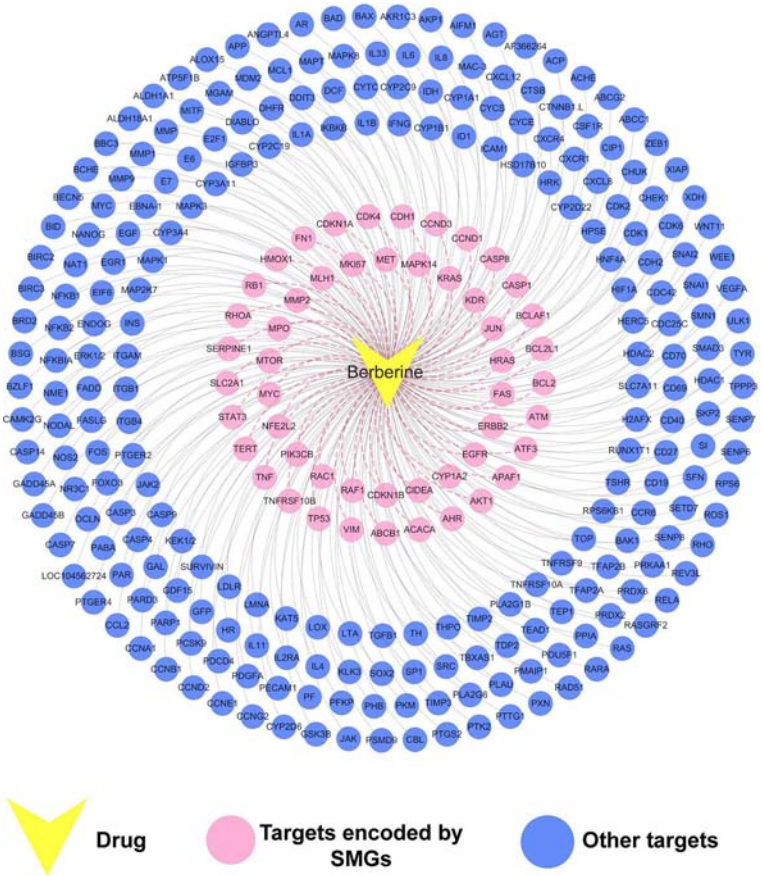

FIGURE 3 | Drug–target (D-T) network of berberine composed of known and predicted targets. The predicted targets were obtained by a balanced substructure–drug–target network-based inference (bSDTNBI) approach. This network includes 289 drug–target interactions connecting berberine and 51 protein targets encoded by significantly mutated genes (SMGs).

various phases of the tumor development, including tumor cell proliferation, survival, invasion, immunosuppression, and inducing and maintaining a pro-carcinogenic inflammatory microenvironment (Fan et al., 2013). A previous study has showed that berberine suppressed tumorigenicity and growth of nasopharyngeal carcinoma (NPC) cells by inhibiting STAT3 activation (Tsang et al., 2013). Recently, a strategy targeting tumor suppressors and apoptosis-related genes provides a rationale for developing more effective approaches and agents for cancer prevention (Sun et al., 2017; López-Cortés et al., 2018; Yamaguchi et al., 2019). Berberine has been observed to activate expression of many tumor apoptosis-related proteins, including caspase-8 (CASP8), tumor necrosis factor-a (TNF-a), and p38 MAPK, and thus induced apoptosis of HeLa cells (Lu et al., 2010). Besides, it has been reported that berberine can decrease expression of mitochondrial-dependent anti-apoptotic factors such as B-cell lymphoma-2 (Bcl-2) and Bcl-2-like protein 1 (BCL2L1) in KB human oral cancer cells (Kim et al., 2015).

Taken together, the observed polypharmacological profiles of berberine motivated us to elucidate its anti-cancer mechanism through systems pharmacology analysis on the interaction between berberine and 51 SMGs.

Elucidating Molecular Mechanisms of Berberine in Cancer Prevention and Treatment

Target–Function Network

As depicted in **Figure 4**, the target–function (T-F) network is composed of 230 T-F pairs connecting 51 SMG targets and 8 cancer-related functional modules based on the DAVID analysis (**Supplementary Table S5**). The eight functional modules include anti-cancer action associated with sustaining proliferative signaling (Huang et al., 2015), resisting cell death (Chidambara Murthy et al., 2012), deregulating cellular energetics (Tan et al., 2015), enabling replicative immortality (Xiong et al., 2015), avoiding immune destruction (Jiang et al., 2017), genome instability and mutation (Li et al., 2014), angiogenesis (Jie et al., 2011), and activating invasion and metastasis (Tang et al., 2009). On average, each SMG target is involved in six cancer-related functional modules. We found that 25 out of 51 SMG targets are associated with more than five functional modules, indicating the higher potential role of these SMG targets related to cancers. Previous studies of berberine in cancer validated the functional analysis of our T-F network. For instance, berberine could induce cell cycle arrest involved in sustaining proliferative signaling in

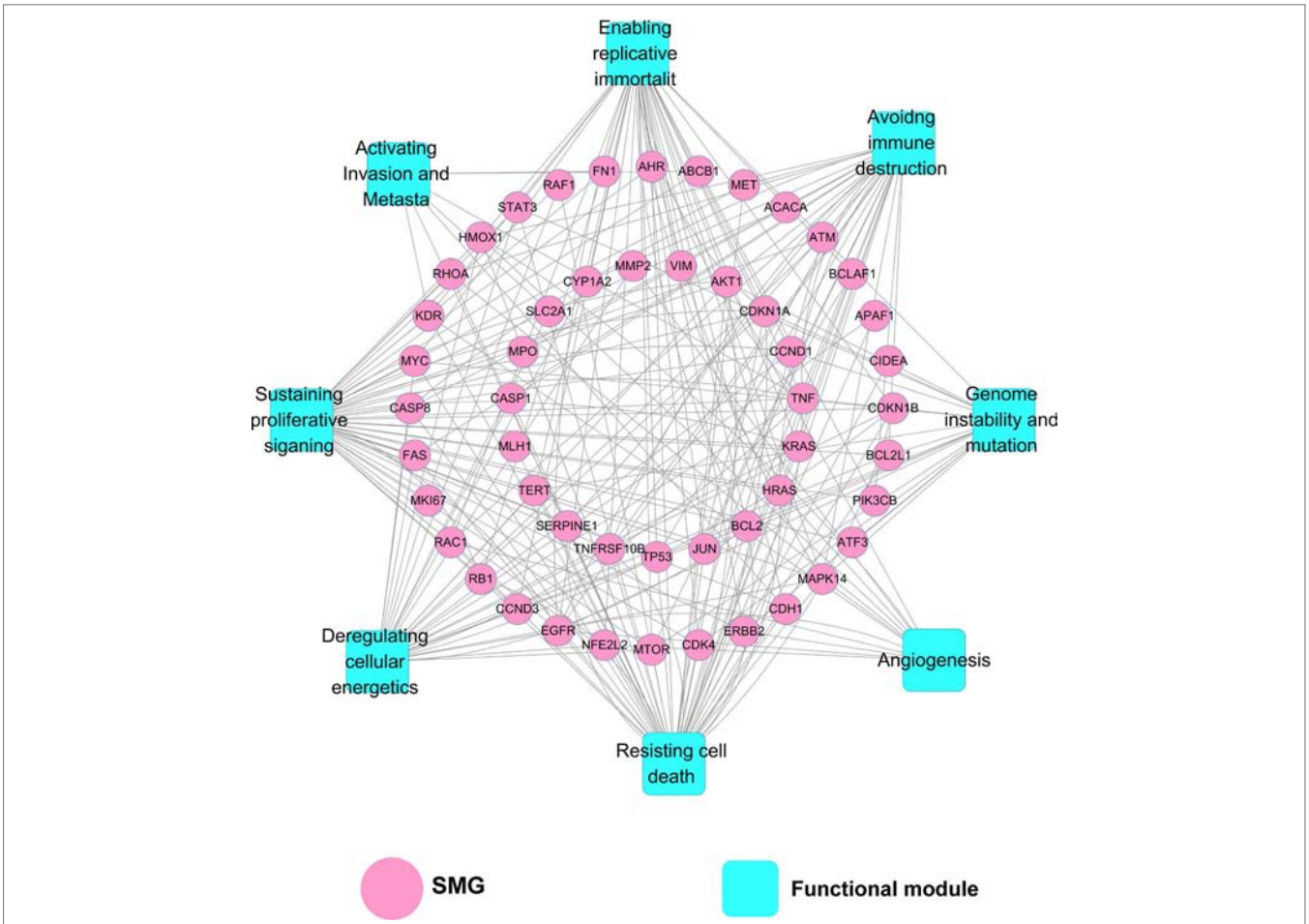

FIGURE 4 | Target–function (T-F) network demonstrating the relationship between cancer-related biological processes and SMGs. A functional module is linked to a target if the target is involved in mechanism of anti-cancer action.

cholangiocarcinoma KKU-213 and KKU-214 cell lines (Puthdee et al., 2017). Berberine was reported to inhibit metastasis and tumor-induced angiogenesis in human cervical cancer cells as well (Chu et al., 2014).

KEGG Enrichment Analysis

In order to further elucidate molecular mechanisms of berberine in cancer prevention and treatment, we performed KEGG pathway enrichment analysis based on the 51 SMGs. After pathways with adjusted P (q) value higher than 0.05 were excluded, 56 enriched pathways related to cancer pathogenesis were obtained (**Supplementary Table S6**).

Among 56 pathways, PI3K-Akt (hsa04151; $q = 2.0 \times 10^{-12}$), p53 (hsa04115; $q = 2.7 \times 10^{-9}$), HIF-1 (hsa04066; $q = 3.9 \times 10^{-9}$), FoxO (hsa04068; $q = 4.9 \times 10^{-9}$), VEGF (hsa04370; $q = 5.7 \times 10^{-7}$), MAPK (hsa04010; $q = 2.5 \times 10^{-6}$), Ras (hsa04014; $q = 6.4 \times 10^{-6}$), Jak-STAT (hsa04630; $q = 9.9 \times 10^{-4}$), mTOR (hsa04150; $q = 1.5 \times 10^{-2}$), AMPK (hsa04152; $q = 1.9 \times 10^{-2}$), and NF-kappa B (hsa04064; $q = 4.0 \times 10^{-2}$) signaling pathways have been confirmed to be associated with berberine in previous literatures (**Table 1**). For example, berberine was reported to inhibit cellular growth and promotes apoptosis by down-regulating PI3K/Akt signaling pathway in breast cancer SKBR-3 cells and hepatoma HepG2 cells (Liu et al., 2011; Kuo et al., 2011). *In vitro* and *in vivo* assays revealed that berberine sensitized drug-resistant breast cancer to doxorubicin (DOX) chemotherapy and directly induced apoptosis through the dose-orchestrated AMPK signaling pathway (Pan et al., 2017). Berberine also induces autophagic cell death through inhibition of mTOR-signaling pathway by suppressing Akt activity and up-regulating P38 MAPK signaling in HepG2 and MHCC97-L cells (Wang et al., 2010). The rest of the 45 enriched pathways prompt the potential anti-cancer acting mechanisms that may be mediated by berberine, which deserve to be validated by experimental assays in the future.

Drug–Target–Diseases Network

We further built a drug–target–diseases (D-T-D) network *via* mapping 51 SMGs targeted by berberine into multiple cancers. As shown in **Figure 5**, the 51 SMGs are related to 24 types of cancer. On average, each cancer links to nine SMGs, while each SMG is connected to 4.6 cancer types. Network analysis showed that the top 6 SMGs connected to the largest number of cancer types are

TABLE 1 | Summary of the 11 enriched pathways validated to be mediated by berberine in previous literatures.

Pathway ID	Pathway name	Genes	*P*-value	PMID
hsa04151	PI3K-Akt signaling pathway	EGFR, HRAS, PIK3CB, MET, TP53, RAF1, BCL2L1, CDK4, KDR, AKT1, CDKN1A, CCND1, KRAS, CDKN1B, CCND3, BCL2, RAC1, MTOR, MYC, FN1	2.03E–12	27081456|25212656
hsa04115	p53 signaling pathway	CDKN1A, CCND1, CCND3, CASP8, SERPINE1, TP53, APAF1, FAS, CDK4, ATM	2.66E–09	20455200
hsa04066	HIF-1 signaling pathway	AKT1, EGFR, HRAS, CCND1, KRAS, PIK3CB, ERBB2, TP53, RAF1, RB1, CDK4	3.89E–09	28775788
hsa04068	FoxO signaling pathway	AKT1, EGFR, HRAS, CCND1, KRAS, PIK3CB, ERBB2, TP53, RAF1, MLH1, CDH1, MYC	4.88E–09	24766860|29360760
hsa04370	VEGF signaling pathway	TNF, MAPK14, BCL2, RAC1, TP53, APAF1, BCL2L1, CASP1	5.72E–07	23869238
hsa04010	MAPK signaling pathway	AKT1, EGFR, HRAS, CCND1, KRAS, PIK3CB, ERBB2, TP53, RAF1, MLH1, CDH1, MYC	2.45E–06	19492307|25212656
hsa04014	Ras signaling pathway	AKT1, EGFR, HRAS, CCND1, KRAS, PIK3CB, ERBB2, TP53, RAF1, RB1, CDK4	6.42E–06	25212656|23159854
hsa04630	Jak-STAT signaling pathway	AKT1, HRAS, KRAS, PIK3CB, JUN, RAC1, RAF1	9.90E–04	26463023
hsa04150	mTOR signaling pathway	TNF, CASP8, APAF1, CASP1	1.50E–02	23159854|20830746
hsa04152	AMPK signaling pathway	EGFR, MAPK14, JUN, RAC1, MET	1.88E–02	28775788
hsa04064	NF-kappa B signaling pathway	TNF, CASP8, APAF1, CASP1	3.97E–02	19107816

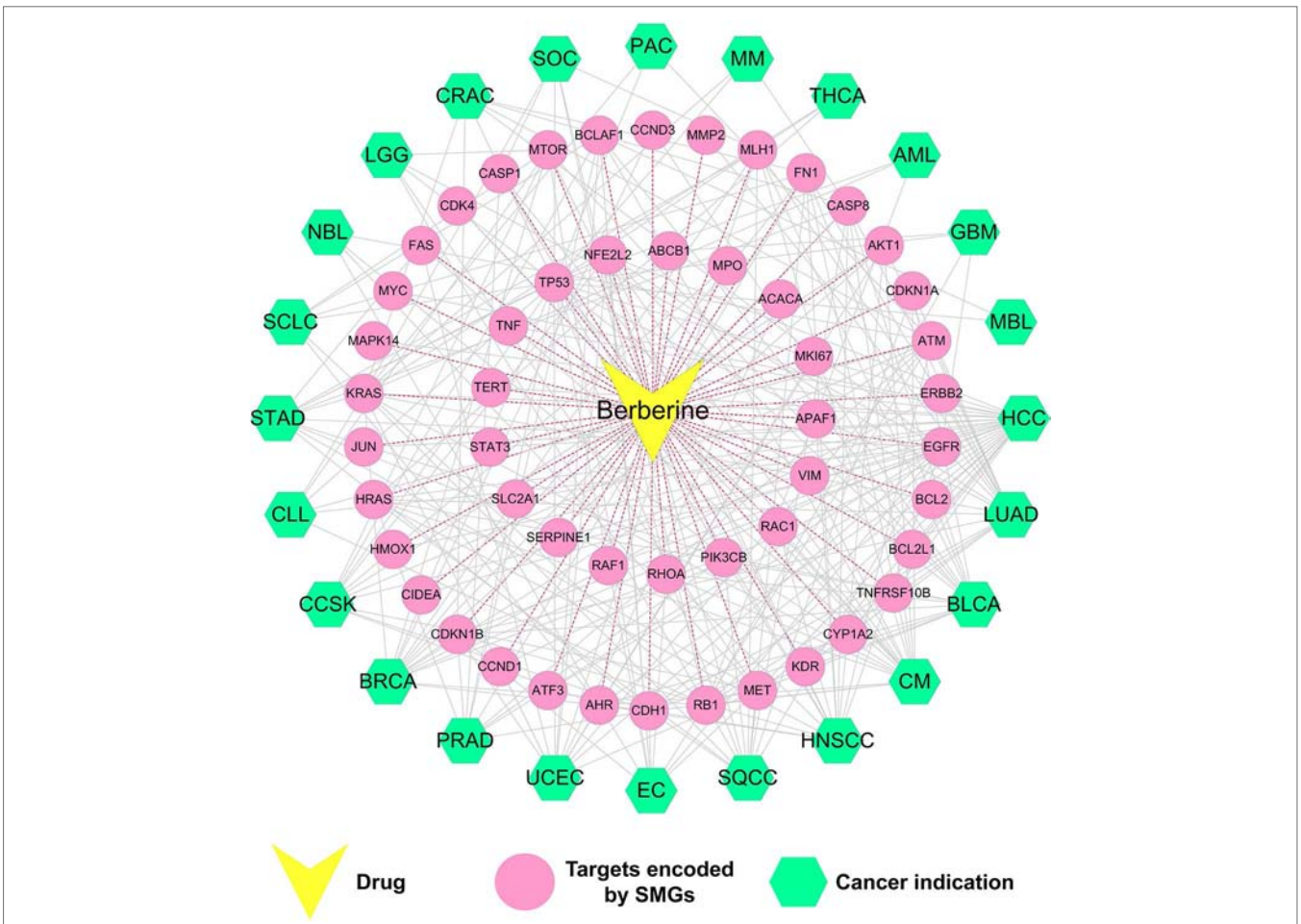

FIGURE 5 | Drug–target–disease (D-T-D) network of berberine. This network shows 51 proteins of berberine encoded by SMGs of 24 types of cancer.

cellular tumor antigen p53 (TP53), gTPase KRas (KRAS), epidermal growth factor receptor (EGFR), retinoblastoma-associated protein (RB1), serine-protein kinase ATM (ATM), and cadherin-1 (CDH1). Among them, EGFR, a key significantly mutated gene of cancer, is involved in the pathological mechanism of 13 cancer types, including LUAD, HNSCC, SQCC, EC, UCEC, PRAD, BRCA, CCSK, CLL,

STAD, LGG, CRAC, and GBM. Previous studies confirmed that berberine can inhibit EGFR signal pathway in several cancer types, including STAD (Wang et al., 2016), PRAD (Huang et al., 2015), and CRAC (Wang et al., 2013). Besides, berberine acts in specific tumor by regulating multiple SMGs. For instance, cellular tumor antigen p53 (TP53) (Wilson et al., 2010), RAC-alpha serine/threonine-protein kinase (AKT1) (López-Cortés et al., 2018), and cyclin-dependent kinase inhibitor 1B (CDKN1B) (Cusan et al., 2018) are highly correlated with breast cancer. Accumulating evidences demonstrated that berberine can inhibit breast cancer by acting on SMGs such as TP53 (Kim et al., 2012; Tan et al., 2015), AKT1 (Kuo et al., 2011), and CDKN1B (Patil et al., 2010).

Briefly, the D-T-D network demonstrated that SMGs targeted by berberine were closely related to multi-cancer types. In the following part, statistical systems pharmacology approach was employed to identify novel cancer indications of berberine and explore the molecular mechanisms.

Systems Pharmacology-Based Prediction of Cancer Indications for Berberine

As shown in **Figure 6**, a statistical systems pharmacology framework is proposed to prioritize novel cancer indications of berberine based on Fisher's exact test analysis. We calculated the therapeutic potential of berberine in 24 cancer indications and obtained 18 cancer indications of which adjusted P (q) values are lower than 0.05 ($q < 0.05$), including HCC ($q < 1.0 \times 10^{-5}$; $-\text{Log10}\,(q) = 19.25$), LUAD ($q < 1.0 \times 10^{-5}$; $-\text{Log10}\,(q) = 9.35$), BLCA ($q < 1.0 \times 10^{-5}$; $-\text{Log10}\,(q) = 9.31$), CM ($q < 1.0 \times 10^{-5}$; $-\text{Log10}\,(q) = 9.29$), HNSCC ($q < 1.0 \times 10^{-5}$; $-\text{Log10}\,(q) = 8.52$), SQCC ($q < 1.0 \times 10^{-5}$; $-\text{Log10}\,(q) = 6.74$), EC ($q < 1.0 \times 10^{-5}$; $-\text{Log10}\,(q) = 6.66$), UCEC ($q < 1.0 \times 10^{-5}$; $-\text{Log10}\,(q) = 6.52$), PRAD ($q = 1.15 \times 10^{-5}$; $-\text{Log10}\,(q) = 6.32$), BRCA ($q = 1.33 \times 10^{-5}$; $-\text{Log10}\,(q) = 6.26$), CCSK ($q = 2.30 \times 10^{-5}$; $-\text{Log10}\,(q) = 6.02$), CLL ($q = 0.55 \times 10^{-3}$; $-\text{Log10}\,(q) = 4.64$), STAD ($q = 1.76 \times 10^{-3}$; $-\text{Log10}\,(q) = 4.14$), SCLC ($q = 5.33 \times 10^{-3}$; $-\text{Log10}\,(q) = 3.65$), NBL ($q = 1.29 \times 10^{-2}$; $-\text{Log10}\,(q) = 3.27$), LGG ($q = 1.67 \times 10^{-2}$; $-\text{Log10}\,(q) = 3.16$), CRAC ($q = 3.21 \times 10^{-2}$; $-\text{Log10}\,(q) = 2.87$), and SOC ($q = 3.36 \times 10^{-2}$; $-\text{Log10}\,(q) = 2.85$) (**Supplementary Table S7**). As listed in **Table 2**, 10 out of the 18 predicted cancer indications of berberine were validated by reported experimental evidences, including HCC, LUAD, BLCA, EC, PRAD, BRCA, STAD, CRAC, and SOC, indicating the high accuracy of our systems pharmacology-based predictive method (success rate = 55.6%).

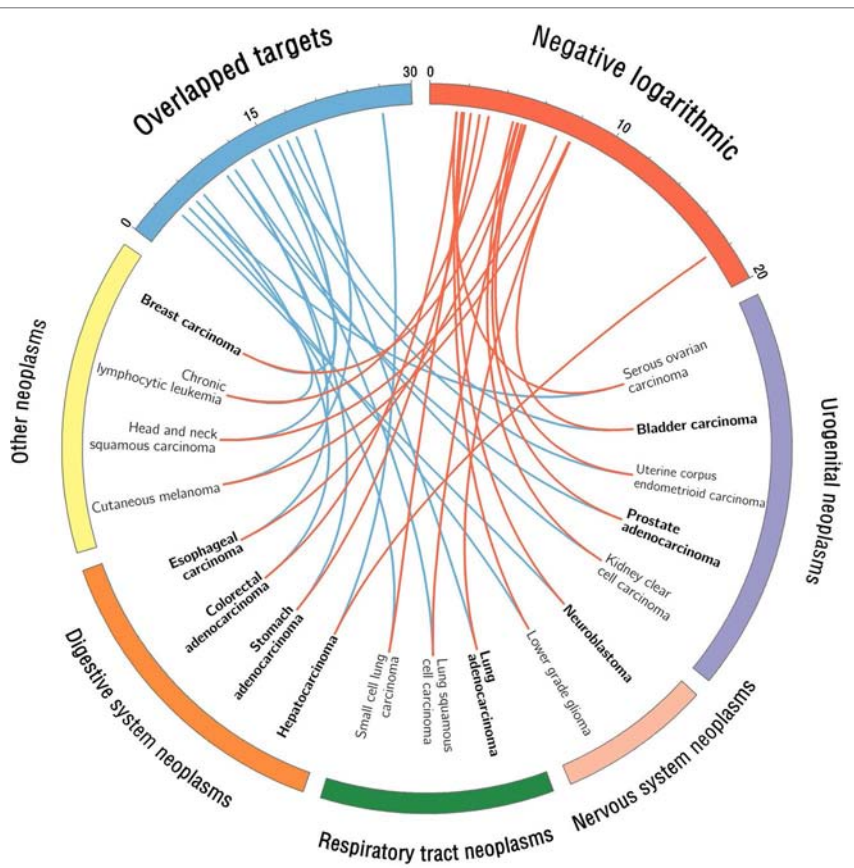

FIGURE 6 | Circos plot visualizes the predicted cancer indications of berberine. The red connected lines represent the calculated $-\text{Log}_{10}(q)$ value of each berberine-cancer type pair based on Fisher's exact test, while the blue ones represent the corresponding number of overlapped targets. The predicted cancer indications with literature validation were highlighted in bold font. We classified the 18 predicted cancer indications into four neoplasm categories according to Medical Subject Headings (MeSH) system (https://www.ncbi.nlm.nih.gov/mesh/68009371).

Among the 18 cancer indications, CM, HNSCC, SQCC, UCEC, CCSK, CLL, SCLC, NBL, and LGG are the unreported cancer indications of berberine, which deserve further preclinical validation. For example, cutaneous melanoma (CM), one of the most aggressive types of cancer, represents a major problem worldwide due to its high incidence and elevated degree of heterogeneity (Jemal et al., 2010; Coricovac et al., 2018). Based on our predictive model, berberine exerted a high potential for anti-CM, with a significant q value [$q < 1.23 \times 10^{-8}$; $-\text{Log10}\ (q) = 9.29$]. Therefore, the potential of berberine in the prevention and treatment of CM deserves to be further validated.

Case Study: Exploring the MOAs of Berberine on Hepatocarcinoma (HCC), Lung Adenocarcinoma (LUAD), and Bladder Carcinoma (BLCA)

To further validate the accuracy of statistical network models and predicted anti-cancer targets of berberine, we selected three typical cancer types [HCC ($q = 5.63 \times 10^{-20}$), LUAD ($q = 4.52 \times 10^{-10}$), and BLCA ($q = 4.92 \times 10^{-10}$)] as case studies to illustrate their anti-cancer MOAs **(Figure 7)**.

Hepatocellular Carcinoma

HCC, the third leading cause of cancer death worldwide, has become one of the most common and prevalent human malignancies in the world (Okubo et al., 2017). *In vitro* assays revealed that berberine can inhibit autophagy in hepatoma cell lines (e.g., HepG2 cells and MHCC97-L cells) by regulating multiple proteins [e.g., mitogen-activated protein kinase 14 (MAPK14), TP53, and phosphatidylinositol 4,5-bisphosphate 3-kinase catalytic subunit beta isoform (PIK3CB)] and pathways (e.g., P38 MAPK signaling), stimulating further development of derivatives for drug-base cancer prevention and treatment (Wang et al., 2010; Liu et al., 2011; Wang et al., 2014). In this study, Fisher's test showed that berberine played a significant role in treatment of liver cancer ($q = 5.63 \times 10^{-20}$). In addition, network analysis revealed that berberine bound with 27 HCC-related SMG targets, suggesting its underlying anti-cancer mechanisms of berberine (**Figure 7**). *In vivo* or *in vitro* data have demonstrated that these SMGs are closely relevant to the treatment of cancer by berberine. For example, berberine can inhibit cell proliferation of HepG2, Hep3B, and SNU-182 through up-regulating protein expression of tumor suppressor genes, such as activating transcription factor 3 (ATF3) (Chuang et al., 2017). Furthermore, study revealed that berberine inhibited expression of BCL2, thus reducing autophagic cell death and mitochondrial apoptosis in liver cancer cells, such as HepG2 and MHCC97-L cells (Hur et al., 2010).

Lung Adenocarcinoma

LUAD is one of the leading causes of cancer-related death both men and women in the United States. Approximately two million people are diagnosed with lung cancer each year (Torre et al., 2016). Berberine was predicted to have anti-LUAD potential ($q = 4.52 \times 10^{-10}$). Some previous *in vivo* and *in vitro* studies confirmed our prediction (Mitani et al., 2001; Zheng et al., 2014). Furthermore, berberine is currently being assessed as an anti-LUAD drug in clinical trials (NCT03486496). As shown in **Figure 7**, berberine interacts with 13 LUAD-related SMGs (e.g., matrix metalloproteinase-2), indicating the underlying MOAs of anti-LUAD of berberine. Matrix metalloproteinases (MMPs), one target displayed in our network, is the major protease of LUAD and is associated with tumor invasion and metastasis (Herbst et al., 2000). Study on human lung cancer cell line A549 confirmed that berberine inhibited invasion and growth of tumor cells through decreasing productions of matrix metalloproteinase-2 (MMP2) (Peng et al., 2006).

Bladder Carcinoma

BLCA is the most common cancer of the urinary system in the United States (Kaufman et al., 2009). In our network model, berberine is predicted to have a significant relationship with

TABLE 2 | Relevant literature evidences of the 18 predicted cancer indications of berberine.

Cancer type	*P*-value (Fisher test)	Adj-*P*	Negative logarithmic	PMID
HCC	5.63E−20	1.35E−18	17.87	26081696|25496992|24942805
LUAD	4.52E−10	1.08E−08	7.96	24766860|26672764|26503561
BLCA	4.92E−10	1.18E−08	7.93	21545798|23065570|10418949
CM	5.12E−10	1.23E−08	7.91	N/A
HNSCC	3.03E−09	7.27E−08	7.14	26503508
SQCC	1.82E−07	4.37E−06	5.36	N/A
EC	2.18E−07	5.23E−06	5.28	28465635|26667771|21858113
UCEC	3.03E−07	7.27E−06	5.14	N/A
PRAD	4.77E−07	1.15E−05	4.94	16505103|26698234|25572870
BRCA	5.53E−07	1.33E−05	4.88	29143794|29414799|28926092
CCSK	9.58E−07	2.30E−05	4.64	N/A
CLL	2.28E−05	5.47E−04	3.26	N/A
STAD	7.32E−05	1.76E−03	2.76	27142767|25837881|18468407
SCLC	2.22E−04	5.33E−03	2.27	N/A
NBL	5.36E−04	1.29E−02	1.89	27235712|19189664|19096576
LGG	6.95E−04	1.67E−02	1.78	N/A
CRAC	1.34E−03	3.21E−02	1.49	23604974|26463023|25954974
SOV	1.40E−03	3.36E−02	1.47	N/A

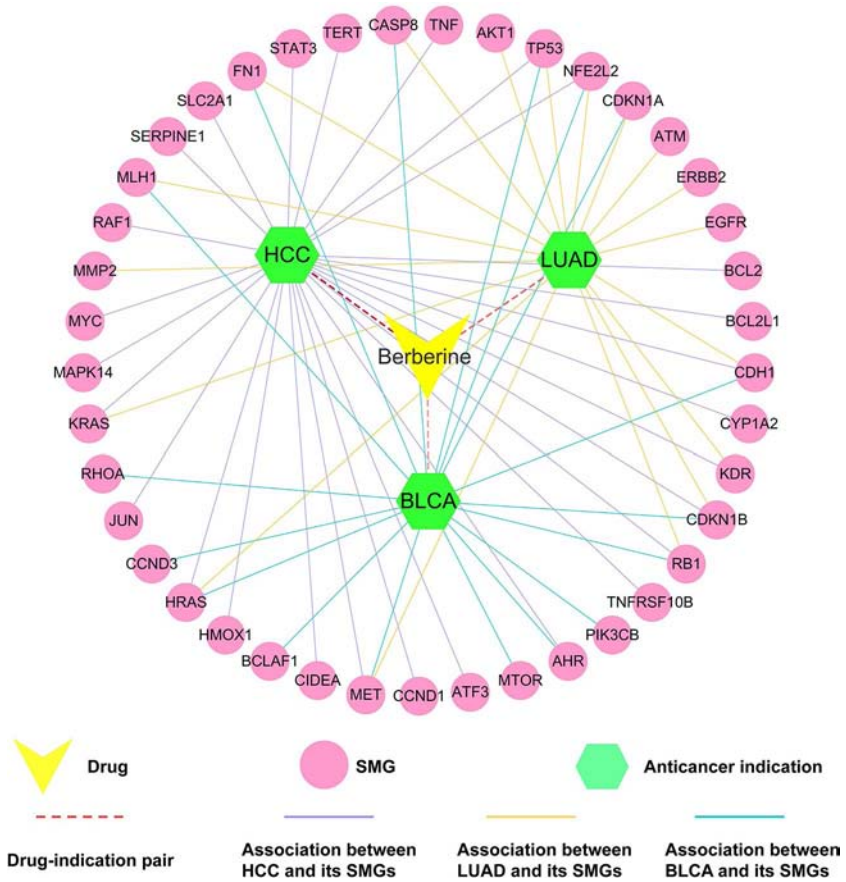

FIGURE 7 | Drug–target–disease (D-T-D) network of berberine on hepatocarcinoma (HCC), lung adenocarcinoma (LUAD), and bladder carcinoma (BLCA). The thickness of the red dotted line represents the predicted association between berberine and three types of tumors.

BLCA ($q = 4.92 \times 10^{-10}$). Meanwhile, our network indicated that berberine interacts with 17 BLCA-related SMGs (e.g., HRAS). According to previous study, the oncogenic ras genes GTPase HRas (HRAS) mutations, endogenously expressed in T24 bladder cancer cell line, were associated with grades and stages of BLCA detected in more than 35% of patients (Buyru et al., 2003). Berberine inhibited cell proliferation and induced cell cycle arrest and apoptosis in BLCA by inhibiting oncogenic H-Ras pathway in BIU-87 and T24 cell lines (Yan et al., 2011).

Taken together, these three case studies against different cancer types (HCC, LUAD, and BLCA) indicate that systems pharmacology approach applied in this study is an effective method for exploring molecular mechanisms of anti-cancer effect of berberine. Meanwhile, the newly predicted tumor types might be promising to further investigate MOAs of berberine.

CONCLUSION

Berberine had been observed to exert multiple biological and pharmacological activities with potential benefits to a variety of complex diseases, including cancer. In this study, we proposed an integrated systems pharmacology infrastructure to identify cancer indications of berberine and explore the underlying molecular mechanisms. This work explores the following new anti-cancer characteristics of berberine: i) Through literature mining, we summarize eight mechanisms of anti-cancer effect of berberine; ii) global drug–target network of berberine is constructed by integrating large-scale experimentally reported targets and computationally predicted targets. Mechanisms of action (MOAs) of various anti-cancer effects of berberine are discussed through current drug–target network; iii) a statistical model is developed to prioritize novel cancer indications of berberine through integrating target profiles of berberine and significantly mutated genes in cancer.

Yet several limitations of our approach should be acknowledged. First, although we have integrated a wide range of DTIs from published literatures and publicly available databases, the incompleteness of current drug–target networks may still exist. Recent studies proved that integration of large-scale gene expression profiles of natural products may help to improve the performance of drug–target network model (Yamanishi et al., 2010; Cheng et al., 2012). Second, as it is extremely difficult to obtain information on the active sites of berberine and mutated domain of proteins from

public sources, the current study could not explain the MOAs from a microcosmic point of view. Third, experimental assays should be performed to further validate the predicted targets and MOAs of anti-cancer effects of berberine in the future.

In summary, the systems pharmacology framework in this study has provided potential strategies to discover the polypharmacology effects of berberine for the prevention and treatment towards multiple cancers.

AUTHOR CONTRIBUTIONS

JF and YZ provided the concept and designed the study. PG and CC conducted the experiments and wrote the manuscript. XW, JZ, XF, QWu, YH, WZ, WH, and FZ participated in the experiments. JF and QWa contributed to revision and proofreading of the manuscript. All authors read and approved the final manuscript.

FUNDING

This work was supported by the National Natural Science Foundation of China (Grants 81603318), the youth scientific research training project of GZUCM (2019QNPY05), Research Fund for Characteristic Innovation Projects of Guangdong Province (2016KTSCX013), and Open Tending Project for the Construction of High-Level University (A1-AFD018171Z11027; A1-AFD018171Z11029).

SUPPLEMENTARY MATERIAL

The Supplementary Material for this article can be found online at: https://www.frontiersin.org/articles/10.3389/fphar.2019.00857/full#supplementary-material

REFERENCES

Ayati, S. H., Fazeli, B., Momtazi-Borojeni, A. A., Afg, C., Pirro, M., and Sahebkar, A. (2017). Regulatory effects of berberine on microRNome in cancer and other conditions. *Crit. Rev. Oncol. Hematol.* 116, 147–158. doi: 10.1016/j.critrevonc.2017.05.008

Bento, A. P., Gaulton, A., Hersey, A., Bellis, L. J., Chambers, J., Davies, M., et al. (2014). The ChEMBL bioactivity database: an update. *Nucleic Acids Res.* 42, 1083–1090. doi: 10.1093/nar/gkt1031

Buyru, N., Tigli, H., Ozcan, F., and Dalay, N. (2003). Ras oncogene mutations in urine sediments of patients with bladder cancer. *J. Biochem. Mol. Biol.* 36, 399–402. doi: 10.5483/BMBRep.2003.36.4.399

Benjamini, Y., and Yekutieli, D. (2001). The control of the false discovery rate in multiple testing under dependency. *Ann. Stat.* 29, 1165–1188. doi: 10.1214/aos/1013699998

Chen, Z. Z. (2016). Berberine induced apoptosis of human osteosarcoma cells by inhibiting phosphoinositide 3 kinase/protein kinase B (PI3K/Akt) signal pathway activation. *Iran. J. Public Health* 45, 578–585.

Cheng, F., Liu, C., Jiang, J., Lu, W., Li, W., Liu, G., et al. (2012). Prediction of drug–target interactions and drug repositioning *via* network-based inference. *PLoS Comput. Biol.* 8, e1002503. doi: 10.1371/journal.pcbi.1002503

Cheng, F., Zhao, J., Fooksa, M., and Zhao, Z. (2016). A network-based drug repositioning infrastructure for precision cancer medicine through targeting significantly mutated genes in the human cancer genomes. *J. Am. Med. Inform. Assoc.* 23, 681–691. doi: 10.1093/jamia/ocw007

Chidambara Murthy, K. N., Jayaprakasha, G. K., and Patil, B. S. (2012). The natural alkaloid berberine targets multiple pathways to induce cell death in cultured human colon cancer cells. *Eur. J. Pharmacol.* 688, 14–21. doi: 10.1016/j.ejphar.2012.05.004

Chu, S. C., Yu, C. C., Hsu, L. S., Chen, K. S., Su, M. Y., and Chen, P. N. (2014). Berberine reverses epithelial-to-mesenchymal transition and inhibits metastasis and tumor-induced angiogenesis in human cervical cancer cells. *Mol. Pharmacol.* 86, 609–623. doi: 10.1124/mol.114.094037

Chuang, T. Y., Wu, H. L., Min, J., Diamond, M., Azziz, R., and Chen, Y. H. (2017). Berberine regulates the protein expression of multiple tumorigenesis-related genes in hepatocellular carcinoma cell lines. *Cancer Cell Int.* 17, 59. doi: 10.1186/s12935-017-0429-3

Coricovac, D., Dehelean, C., Moaca, E. A., Pinzaru, I., Bratu, T., Navolan, D., et al. (2018). Cutaneous melanoma—a long road from experimental models to clinical outcome: a review. *Int. J. Mol. Sci.* 19, E1566. doi: 10.3390/ijms19061566

Cusan, M., Mungo, G., De Marco Zompit, M., Segatto, I., Belletti, B., and Baldassarre, G. (2018). Landscape of CDKN1B mutations in luminal breast cancer and other hormone-driven human tumors. *Front. Endocrinol.* 9, 393. doi: 10.3389/fendo.2018.00393

Dennis, G., Sherman, B. T., Hosack, D. A., Yang, J., Gao, W., Lane, H. C., et al. (2003). DAVID: Database for Annotation, visualization, and Integrated Discovery. *Genome Biol.* 4, R60. doi: 10.1186/gb-2003-4-9-r60

Fan, Q. W., Cheng, C. K., Gustafson, W. C., Charron, E., Zipper, P., Wong, R. A., et al. (2013). EGFR phosphorylates tumor-derived EGFRvIII driving STAT3/5 and progression in glioblastoma. *Cancer Cell* 24, 438–449. doi: 10.1016/j.ccr.2013.09.004

Fang, J., Cai, C., Chai, Y., Zhou, J., Huang, Y., Gao, L., et al. (2019). Quantitative and systems pharmacology 4. Network-based analysis of drug pleiotropy on coronary artery disease. *Eur. J. Med. Chem.* 161, 192–204. doi: 10.1016/j.ejmech.2018.10.020

Fang, J., Cai, C., Wang, Q., Lin, P., Zhao, Z., and Cheng, F. (2017a). Systems pharmacology-based discovery of natural products for precision oncology through targeting cancer mutated genes. *CPT Pharmacometrics Syst. Pharmacol.* 6, 177–187. doi: 10.1002/psp4.12172

Fang, J., Gao, L., Ma, H., Wu, Q., Wu, T., Wu, J., et al. (2017b). Quantitative and systems pharmacology 3. Network-based identification of new targets for natural products enables potential uses in aging-associated disorders. *Front. Pharmacol.* 8, 747. doi: 10.3389/fphar.2017.00747

Fang, J., Liu, C., Wang, Q., Lin, P., and Cheng, F. (2018). In silico polypharmacology of natural products. *Brief. Bioinform.* 19, 1153–1171. doi: 10.1093/bib/bbx045

Fang, J., Wu, Z., Cai, C., Wang, Q., Tang, Y., and Cheng, F. (2017c). Quantitative and systems pharmacology. 1. In silico prediction of drug–target interaction of natural products to enable of new targeted cancer therapy. *J. Chem. Inf. Model.* 57, 2657–2671. doi: 10.1021/acs.jcim.7b00216

Gilson, M. K., Liu, T., Baitaluk, M., Nicola, G., Hwang, L., and Chong, J. (2016). BindingDB in 2015: a public database for medicinal chemistry, computational chemistry and systems pharmacology. *Nucleic Acids Res.* 44, D1045–D1053. doi: 10.1093/nar/gkv1072

Hamsa, T. P., and Kuttan, G. (2012). Antiangiogenic activity of berberine is mediated through the downregulation of hypoxia-inducible factor-1, VEGF, and proinflammatory mediators. *Drug Chem. Toxicol.* 35, 57–70. doi: 10.3109/01480545.2011.589437

Herbst, R. S., Yano, S., Kuniyasu, H., Khuri, F. R., Bucana, C. D., Guo, F., et al. (2000). Differential expression of E-cadherin and type IV collagenase genes predicts outcome in patients with stage I non-small cell lung carcinoma. *Clin. Cancer Res.* 6, 790–797. doi: 10.1159/000007270

Huang, Y., Fang, J., Lu, W., Wang, Z., Wang, Q., Hou, Y., et al. (2019). A systems pharmacology approach uncovers wogonoside as an angiogenesis inhibitor of triple-negative breast cancer by targeting hedgehog signaling. *Cell Chem. Biol.* 26, 1–16. doi: 10.1016/j.chembiol.2019.05.004

Huang, Z. H., Zheng, H. F., Wang, W. L., Wang, Y., Zhong, L. F., Wu, J. L., et al. (2015). Berberine targets epidermal growth factor receptor signaling to suppress prostate cancer proliferation *in vitro*. *Mol. Med. Rep.* 11, 2125–2128. doi: 10.3892/mmr.2014.2929

Hur, J. M., Hyun, M. S., Lim, S. Y., Lee, W. Y., and Kim, D. (2010). The combination of berberine and irradiation enhances anti-cancer effects *via* activation of p38 MAPK pathway and ROS generation in human hepatoma cells. *J. Cell. Biochem.* 107, 955–964. doi: 10.1002/jcb.22198

Jemal, A., Siegel, R., Xu, J., and Ward, E. (2010). Cancer statistics, 2010. *CA Cancer J. Clin.* 60, 277–300. doi: 10.3322/caac.20073

Jiang, X., Lu, W., Shen, X., Wang, Q., Lv, J., Liu, M., et al. (2018). Repurposing sertraline sensitizes non-small cell lung cancer cells to erlotinib by inducing autophagy. *JCI Insight* 3, 98921. doi: 10.1172/jci.insight.98921

Jiang, Y., Huang, K., Lin, X., Chen, Q., Lin, S., Feng, X., et al. (2017). Berberine attenuates NLRP3 inflammasome activation in macrophages to reduce the secretion of interleukin-1β. *Ann. Clin. Lab. Sci.* 47, 720–728.

Jie, S., Li, H., Tian, Y., Guo, D., Zhu, J., Gao, S., et al. (2011). Berberine inhibits angiogenic potential of Hep G2 cell line through VEGF down-regulation *in vitro*. *J. Gastroenterol Hepatol.* 26, 179–185. doi: 10.1111/j.1440-1746.2010.06389.x

Kaufman, D. S., Shipley, W. U., and Feldman, A. S. (2009). Bladder cancer. *Lancet* 374, 239–249. doi: 10.1016/S0140-6736(09)60491-8

Khalid, E. B., Ayman, E. K., Rahman, H., Abdelkarim, G., and Najda, A. (2016). Natural products against cancer angiogenesis. *Tumour Biol.* 37, 1–24. doi: 10.1007/s13277-016-5364-8

Kim, J. B., Lee, K. M., Ko, E., Han, W., Lee, J. E., Shin, I., et al. (2008). Berberine inhibits growth of the breast cancer cell lines MCF-7 and MDA-MB-231. *Planta Med.* 74, 39–42. doi: 10.1055/s-2007-993779

Kim, J. S., Oh, D., Yim, M. J., Park, J. J., Kang, K. R., Cho, I. A., et al. (2015). Berberine induces FasL-related apoptosis through p38 activation in KB human oral cancer cells. *Oncol. Rep.* 33, 1775–1782. doi: 10.3892/or.2015.3768

Kim, S., Han, J., Kim, N. Y., Lee, S. K., Cho, D. H., Choi, M. Y., et al. (2012). Effect of berberine on p53 expression by TPA in breast cancer cells. *Oncol. Rep.* 27, 210–215. doi: 10.3892/or.2011.1480

Kotoku, N., Arai, M., and Kobayashi, M. (2016). Search for anti-angiogenic substances from natural sources. *Chem. Pharm. Bull.* 64, 128–134. doi: 10.1248/cpb.c15-00744

Kuhn, M., Szklarczyk, D., Pletscher-Frankild, S., Blicher, T. H., von Mering, C., Jensen, L. J., et al. (2014). STITCH 4: integration of protein-chemical interactions with user data. *Nucleic Acids Res.* 42, D401–D407. doi: 10.1093/nar/gkt1207

Kuo, H. P., Chuang, T. C., Yeh, M. H., Hsu, S. C., Way, T. D., Chen, P. Y., et al. (2011). Growth suppression of HER2-overexpressing breast cancer cells by berberine *via* modulation of the HER2/PI3K/Akt signaling pathway. *J. Agric. Food Chem.* 59, 8216–8224. doi: 10.1021/jf2012584

Li, J., Li, O., Kan, M., Zhang, M., Shao, D., Pan, Y., et al. (2015). Berberine induces apoptosis by suppressing the arachidonic acid metabolic pathway in hepatocellular carcinoma. *Mol. Med. Rep.* 12, 4572–4577. doi: 10.3892/mmr.2015.3926

Li, Z., Geng, Y. N., Jiang, J. D., and Kong, W. J. (2014). Antioxidant and anti-inflammatory activities of berberine in the treatment of diabetes mellitus. *Evid. Based Complement. Alternat. Med.* 2014, 289264. doi: 10.1155/2014/289264

Liu, B., Wang, G., Yang, J., Pan, X., Yang, Z., and Zang, L. (2011). Berberine inhibits human hepatoma cell invasion without cytotoxicity in healthy hepatocytes. *PLoS One* 6, e21416. doi: 10.1371/journal.pone.0021416

López-Cortés, A., Leone, P. E., Freire-Paspuel, B., Arcos-Villacís, N., Guevara-Ramírez, P., Rosales, F., et al. (2018). Mutational analysis of oncogenic AKT1 gene associated with breast cancer risk in the high altitude ecuadorian mestizo population. *Biomed. Res. Int.* 2018, 1–10. doi: 10.1155/2018/7463832

Lu, B., Hu, M., Liu, K., and Peng, J. (2010). Cytotoxicity of berberine on human cervical carcinoma HeLa cells through mitochondria, death receptor and MAPK pathways, and in-silico drug–target prediction. *Toxicol. In Vitro* 24, 1482–1490. doi: 10.1016/j.tiv.2010.07.017

Mitani, N., Murakami, K., Yamaura, T., Ikeda, T., and Saiki, I. (2001). Inhibitory effect of berberine on the mediastinal lymph node metastasis produced by orthotopic implantation of Lewis lung carcinoma. *Cancer Lett.* 165, 35–42. doi: 10.1016/S0304-3835(00)00710-2

Okubo, S., Uto, T., Goto, A., Tanaka, H., Nishioku, T., Yamada, K., et al. (2017). Berberine induces apoptotic cell death *via* activation of caspase-3 and -8 in HL-60 human leukemia cells: nuclear localization and structure–activity relationships. *Am. J. Chin. Med.* 45, 1497–1511. doi: 10.1142/S0192415X17500811

Ola, M. S., Nawaz, M., and Ahsan, H. (2011). Role of Bcl-2 family proteins and caspases in the regulation of apoptosis. *Mol. Cell Biochem.* 351, 41–58. doi: 10.1007/s11010-010-0709-x

Pan, Y., Zhang, F., Zhao, Y., Shao, D., Zheng, X., Chen, Y., et al. (2017). Berberine enhances chemosensitivity and induces apoptosis through dose-orchestrated AMPK signaling in breast cancer. *J. Cancer* 8, 1679–1689. doi: 10.7150/jca.19106

Patil, J. B., Kim, J., and Jayaprakashaa, G. K. (2010). Berberine induces apoptosis in breast cancer cells (MCF-7) through mitochondrial-dependent pathway. *Eur. J. Pharmacol.* 645, 70–78. doi: 10.1016/j.ejphar.2010.07.037

Peng, P. L., Hsieh, Y. S., Wang, C. J., Hsu, J. L., and Chou, F. P. (2006). Inhibitory effect of berberine on the invasion of human lung cancer cells *via* decreased productions of urokinase-plasminogen activator and matrix metalloproteinase-2. *Toxicol. Appl. Pharmacol.* 214, 8–15. doi: 10.1016/j.taap.2005.11.010

Puthdee, N., Seubwai, W., Vaeteewoottacharn, K., Boonmars, T., Cha'On, U., Phoomak, C., et al. (2017). Berberine induces cell cycle arrest in cholangiocarcinoma cell lines *via* inhibition of NF-κB and STAT3 pathways. *Biol. Pharm. Bull.* 40, 751–757. doi: 10.1248/bpb.b16-00428

Qing, Y., Hu, H., Liu, Y., Feng, T., Meng, W., Jiang, L., et al. (2014). Berberine induces apoptosis in human multiple myeloma cell line U266 through hypomethylation of p53 promoter. *Cell Biol. Int.* 38, 563–570. doi: 10.1002/cbin.10206

Shannon, P., Markiel, A., Ozier, O., Baliga, N. S., Wang, J. T., Ramage, D., et al. (2003). Cytoscape: a software environment for integrated models of biomolecular interaction networks. *Genome Res.* 13, 2498–2504. doi: 10.1101/gr.1239303

Song, Y. C., Lee, Y., Kim, H. M., Hyun, M. Y., Lim, Y. Y., Song, K. Y., et al. (2015). Berberine regulates melanin synthesis by activating PI3K/AKT, ERK and GSK3β in B16F10 melanoma cells. *Int. J. Mol. Med.* 35, 1011–1016. doi: 10.3892/ijmm.2015.2113

Sun, X., Wang, S. C., Wei, Y., Luo, X., Jia, Y., Li, L., et al. (2017). Arid1a has context-dependent oncogenic and tumor suppressor functions in liver cancer. *Cancer Cell* 33, 151–152. doi: 10.1016/j.ccell.2017.12.011

Tan, W., Li, N., Tan, R., Zhong, Z., Suo, Z., Yang, X., et al. (2015). Berberine interfered with breast cancer cells metabolism, balancing energy homeostasis. *Anticancer Agents Med. Chem.* 15, 66–78. doi: 10.2174/1871520614664140910120518

Tang, F., Wang, D., Duan, C., Huang, D., Wu, Y., Chen, Y., et al. (2009). Berberine inhibits metastasis of nasopharyngeal carcinoma 5-8F cells by targeting Rho kinase-mediated Ezrin phosphorylation at threonine 567. *J. Biol. Chem.* 284, 27456–27466. doi: 10.1074/jbc.M109.033795

Tsang, C. M., Cheung, Y. C., Lui, V. W., Yip, Y. L., Zhang, G., Lin, V. W., et al. (2013). Berberine suppresses tumorigenicity and growth of nasopharyngeal carcinoma cells by inhibiting STAT3 activation induced by tumor associated fibroblasts. *BMC Cancer* 13, 619. doi: 10.1186/1471-2407-13-619

Torre, L. A., Siegel, R. L., and Jemal, A. (2016). Lung cancer statistics. *Adv. Exp. Med. Biol.* 893, 1–19. doi: 10.1007/978-3-319-24223-1

Wang, J., Yang, S., Cai, X., Dong, J., Chen, Z., Wang, R., et al. (2016). Berberine inhibits EGFR signaling and enhances the antitumor effects of EGFR inhibitors in gastric cancer. *Oncotarget* 7, 76076–76086. doi: 10.18632/oncotarget.12589

Wang, L., Cao, H., Lu, N., Liu, L., Wang, B., Hu, T., et al. (2013). Berberine inhibits proliferation and down-regulates epidermal growth factor receptor through activation of Cbl in colon tumor cells. *PLoS One* 8, e56666. doi: 10.1371/journal.pone.0056666

Wang, N., Feng, Y., Zhu, M., Tsang, C. M., Man, K., Tong, Y., et al. (2010). Berberine induces autophagic cell death and mitochondrial apoptosis in liver cancer cells: the cellular mechanism. *J. Cell. Biochem.* 111, 1426–1436. doi: 10.1002/jcb.22869

Wang, N., Zhu, M., Wang, X., Tan, H. Y., Tsao, S. W., and Feng, Y. (2014). Berberine-induced tumor suppressor p53 up-regulation gets involved in the regulatory network of MIR-23a in hepatocellular carcinoma. *Biochim. Biophys. Acta.* 1839, 849–857. doi: 10.1016/j.bbagrm.2014.05.027

Wilson, J. R. F., Bateman, A. C., Hanson, H., An, Q., Evans, G., Rahman, N., et al. (2010). A novel HER2-positive breast cancer phenotype arising from germline TP53 mutations. *J. Med. Genet.* 47, 771–774. doi: 10.1136/jmg.2010.078113

Wu, Z., Cheng, F., Li, J., Li, W., Liu, G., and Tang, Y. (2017). SDTNBI: an integrated network and chemoinformatics tool for systematic prediction of drug–target interactions and drug repositioning. *Brief. Bioinform.* 18, 333–347. doi: 10.1093/bib/bbw012

Wu, Z., Lu, W., Wu, D., Luo, A., Bian, H., Li, J., et al. (2016). In silico prediction of chemical mechanism-of-action *via* an improved network-based inference method. *Br. J. Pharmacol.* 173, 3372–3385. doi: 10.1111/bph.13629

Xiong, Y. X., Su, H. F., Lv, P., Ma, Y., Wang, S. K., Miao, H., et al. (2015). A newly identified berberine derivative induces cancer cell senescence by stabilizing endogenous G-quadruplexes and sparking a DNA damage response at the telomere region. *Oncotarget* 6, 35625–35635. doi: 10.18632/oncotarget

Yamaguchi, R., Lartigue, L., and Perkins, G. (2019). Targeting Mcl-1 and other Bcl-2 family member proteins in cancer therapy. *Pharmacol. Ther.* 195, 13–20. doi: 10.1016/j.pharmthera.2018.10.009.

Yamanishi, Y., Kotera, M., Kanehisa, M., and Goto, S. (2010). Drug–target interaction prediction from chemical, genomic and pharmacological data in an integrated framework. *Bioinformatics* 26, i246–i254. doi: 10.1093/bioinformatics/btq176

Yan, K., Zhang, C., Feng, J., Hou, L., Yan, L., Zhou, Z., et al. (2011). Induction of G1 cell cycle arrest and apoptosis by berberine in bladder cancer cells. *Eur. J. Pharmacol.* 661, 1–7. doi: 10.1016/j.ejphar.2011.04.021

Yap, C. W. (2011). PaDEL-descriptor: an open source software to calculate molecular descriptors and fingerprints. *J. Comput. Chem.* 32, 1466–1474. doi: 10.1002/jcc.21707

Ye, H., Ye, L., Kang, H., Zhang, D., Tao, L., Tang, K., et al. (2011). HIT: linking herbal active ingredients to targets. *Nucleic Acids Res.* 39, D1055–D1059. doi: 10.1093/nar/gkq1165

Yu, H., Lee, H., Herrmann, A., Buettner, R., and Jove, R. (2014). Revisiting STAT3 signalling in cancer: new and unexpected biological functions. *Nat. Rev. Cancer.* 14, 736–746. doi: 10.1038/nrc3818

Zhao, Y., Jing, Z., Lv, J., Zhang, Z., Lin, J., Cao, X., et al. (2017). Berberine activates caspase-9/cytochrome *c*-mediated apoptosis to suppress triple-negative breast cancer cells *in vitro* and in *vivo*. *Biomed. Pharmacother.* 95, 18–24. doi: 10.1016/j.biopha.2017.08.045

Zhe, W., and Huang, G. S. (2002). Database resources of the National Center for Biotechnology Information and its application. *Chin. Bull. Life Sci.* 14, 59–62. doi: 10.1007/BF02943277

Zheng, F., Tang, Q., Wu, J. J., Zhao, S. Y., Liang, Z. Y., Li, L., et al. (2014). p38α MAPK-mediated induction and interaction of FOXO3a and p53 contribute to the inhibited-growth and induced-apoptosis of human lung adenocarcinoma cells by berberine. *J. Exp. Clin. Cancer Res.* 33, 36. doi: 10.1186/1756-9966-33-36

Zhu, R. X., Seto, W. K., Lai, C. L., and Yuen, M. F. (2016). Epidemiology of hepatocellular carcinoma in the Asia-Pacific region. *Gut. Liver.* 10, 332–339. doi: 10.5009/gnl15257

Conflict of Interest Statement: The authors declare that the research was conducted in the absence of any commercial or financial relationships that could be construed as a potential conflict of interest.

frontiers in Oncology

ORIGINAL RESEARCH
published: 08 November 2019
doi: 10.3389/fonc.2019.01100

A High-Content Screening Approach to Identify MicroRNAs Against Head and Neck Cancer Cell Survival and EMT in an Inflammatory Microenvironment

*Bruno Sangiorgi[1,2], Felipe Canto de Souza[1,2], Ildercílio Mota de Souza Lima[1,2], Josiane Lilian dos Santos Schiavinato[1,2], Amanda Cristina Corveloni[1,2], Carolina Hassibe Thomé[1,3], Wilson Araújo Silva Jr.[1,2], Vitor Marcel Faça[1,3], Dimas Tadeu Covas[1], Marco Antônio Zago[1] and Rodrigo Alexandre Panepucci[1,2]**

[1] Center for Cell-Based Therapy (CTC), Regional Blood Center of Ribeirão Preto, Ribeirão Preto, Brazil, [2] Department of Genetics and Internal Medicine, Ribeirão Preto Medical School, University of São Paulo (FMRP-USP), Ribeirão Preto, Brazil, [3] Department of Biochemistry and Immunology, Ribeirão Preto Medical School, University of São Paulo (FMRP-USP), Ribeirão Preto, Brazil

Head and neck squamous cell carcinoma (HNSCC) is among the most common cancer types. Metastasis, the main cause of death by cancer, can be promoted by an inflammatory microenvironment, which induces epithelial-mesenchymal transition (EMT) through a NF-κB-mediated stabilization of Snail. Here, we aimed to explore how microRNAs (miRs) can affect cell survival and EMT in HNSCC cells under an inflammatory microenvironment. By using a high-content screening (HCS) approach, we evaluated alterations in morphometric parameters, as well as expression/localization of Snail/Slug, in HNSCC cells primed with TNF-α. Based on those quantitation, we established the optimal experimental conditions of EMT induction driven by TNF-α. Those conditions were applied to cells transfected with distinct miRs ($N = 31$), followed by clusterization of miRs based on alterations related to cell survival and EMT. The signaling pathways enriched with molecular targets from each group of miRs were identified by *in silico* analyses. Finally, cells were transfected with siRNAs against signaling pathways targeted by miRs with anti-survival/EMT effect and evaluated for alterations in cell survival and EMT. Overall, we observed that TNF-α, at 20 ng/ml, induced EMT-related changes in cell morphology, Snail/Slug expression, and cell migration. Predicted targets of miRs with anti-survival/EMT effect were enriched with targets of NF-κB, PI3K/ATK, and Wnt/beta catenin pathways. Strikingly, individual gene silencing of elements from those pathways, namely *RELA* (NF-kB), *AKT1* (PI3K/AKT), and *CTNNB1* (Wnt/beta catenin) reduced cell survival and/or expression of Snail/Slug in cells stimulated with TNF-α. As a whole, our HCS approach allowed for the identification of miRs capable of inhibiting cell survival

OPEN ACCESS

Edited by:
Zhe-Sheng Chen,
St. John's University, United States

Reviewed by:
Paul B. Fisher,
Virginia Commonwealth University, United States
Weiguo Feng,
Weifang Medical University, China

***Correspondence:**
Rodrigo Alexandre Panepucci
panepucci@hemocentro.fmrp.usp.br

Specialty section:
This article was submitted to Cancer Molecular Targets and Therapeutics, a section of the journal Frontiers in Oncology

Received: *08 December 2018*
Accepted: *07 October 2019*
Published: *08 November 2019*

Citation:
Sangiorgi B, de Souza FC, Mota de Souza Lima I, dos Santos Schiavinato JL, Corveloni AC, Thomé CH, Araújo Silva W Jr, Faça VM, Covas DT, Zago MA and Panepucci RA (2019) A High-Content Screening Approach to Identify MicroRNAs Against Head and Neck Cancer Cell Survival and EMT in an Inflammatory Microenvironment. Front. Oncol. 9:1100. doi: 10.3389/fonc.2019.01100

and EMT considering the presence of an inflammatory microenvironment, also indicating the common signaling pathways and molecular targets most likely to underlie those alterations. These findings may contribute to the development of targeted therapies against HNSCC.

Keywords: head and neck squamous cell carcinoma, high-content screening, microRNAs, epithelial-mesenchymal-transition, inflammation, NF-κB

INTRODUCTION

Head and neck squamous cell carcinoma (HNSCC) comprises a group of upper aerodigestive tract neoplasia and is among the ten types of cancer with the highest incidence and mortality in the world (1). Over the past decades, despite advances in treatment strategies of HNSCC, it was observed a growth in mortality associated with distant metastases (2). Studies to date demonstrated that metastasis initiation is promoted by tumor cells that undergoes epithelial-mesenchymal transition (EMT), a transformation process which cells acquire a mesenchymal-like phenotype and dislodges from the tumor bulk, invading adjacent vessels and entering in the circulation (3).

EMT events are coordinated by transcription factors known as "EMT master regulators," including members of the Snail family: SNAI1 (Snail) and SNAI2 (Slug), which are capable of both silencing and promoting the expression of genes related to epithelial and mesenchymal phenotypes, respectively (4). As a consequence of the "EMT master regulators" activity, cancer cells undergo drastic phenotypic changes in cell morphology: from polygonal to elongated, expression of cell adhesion proteins: downregulation of E-Cadherin and upregulation of N-Cadherin and integrins, expression of structural proteins: upregulation of Vimentin, among others that lead to the formation of mesenchymal cancer cells with migratory/invasive capacities (5).

Increasing literature data have established that, for several types of cancer including HNSCC, the presence of an inflamed tumor microenvironment is associated with tumor progression, the acquisition of EMT-like features by cancer cells and the formation of metastasis (6). In different types of cancer, multiple lines of evidence have supported that inflammatory cytokines secreted by tumor-associated macrophages (which can represent half of the tumor mass), including tumor necrosis factor alpha (TNF-α), are capable of inducing EMT events in cancer cells (7). TNF-α activates the nuclear factor kappa b (NF-κB) signaling pathway, which the main effector p50/p65 (RelA) promotes the nuclear translocation of Snail, thereby inducing EMT (8). Additionally, NF-κB crosstalk with other oncogenic signaling pathways in HNSCC including Ras/MAPK, PI3K/AKT, and Wnt/beta catenin, that collectively promotes cancer cell survival, evasion from apoptosis and therapy resistance (9, 10). Due to the complexity of intracellular signaling pathways and tumor microenvironment in cancer, including HNSCC, a multi-target therapy (targeting multiple signaling pathways) may be an interesting therapeutic approach (11).

MicroRNAs (miRs) are a class of small non-coding RNAs that act predominantly through the destabilization and degradation of multiple targeted messenger RNAs (mRNAs) thereby affecting several biological processes independently (12, 13). In HNSCC, as in other types of cancer, there is mounting evidence that miRs are capable of interfering in multiple cellular processes, such as cancer cell proliferation, invasion, and apoptosis, thereby promoting (oncomiRs) or inhibiting (tumor suppressor miRs) the progression from normal tissue to carcinoma and subsequently metastasis (14, 15). Importantly, the HNSCC oncomiR: miR-21 and tumor suppressor miR: miR-29, are both involved in transcriptional networks that regulates the activity of the NF-κB signaling pathway (14, 16), highlighting the importance of NF-κB as a regulator of both inflammation and tumor progression in HNSCC.

Since its discovery, miRs have been drawing attention due to their capacity to be used either as prognostic biomarkers or in miR-based targeted therapies against cancer (17, 18). Currently, miR-based targeted therapeutic strategies comprehends the delivery of either mimetics of miRs with tumor suppressor activity (microRNA replacement or restoration therapy) or molecules capable of inactivating oncomiRs (microRNA reduction or inhibition therapy) (19). Importantly, a functional study conducted by Lindenbergh-van der Plas and coworkers provided a proof-of-concept that miRs can be used to selectively kill HNSCC cancer cells (20). However, despite the potential use of miRs in drug discovery and therapeutic applications, it is a current challenge to identify, among the several signaling pathways regulated by a given miR, those that has an effective therapeutic value (21).

In the last decade, advances in the High-Content Screening (HCS) approach (cell-based functional screens based on automated microscopy and image analysis) allowed for the quantitative measurement of a broad spectrum of phenotypic alterations at a cellular level (22). Noteworthy, the advantage of the HCS approach to measure the phenotype in a multiparametric fashion makes it especially suited to investigate the pleiotropic effects exerted by miRs (23). In addition, target-prediction tools can also be utilized for the identification of the molecular targets shared by groups of miRs and thereby indicating the ones that are most likely responsible for the observed effects (24). In the present work, through an HCS approach and *in-silico* analysis, we investigated the capacity of miRs to alter the phenotypic features related to tumor progression (e.g., cell survival) and metastasis (e.g., EMT) in HNSCC cells considering the presence of an inflammatory microenvironment. Overall, we have identified miRs capable of inhibiting cell survival and EMT as well as potential targets and signaling pathways involved in the observed effects.

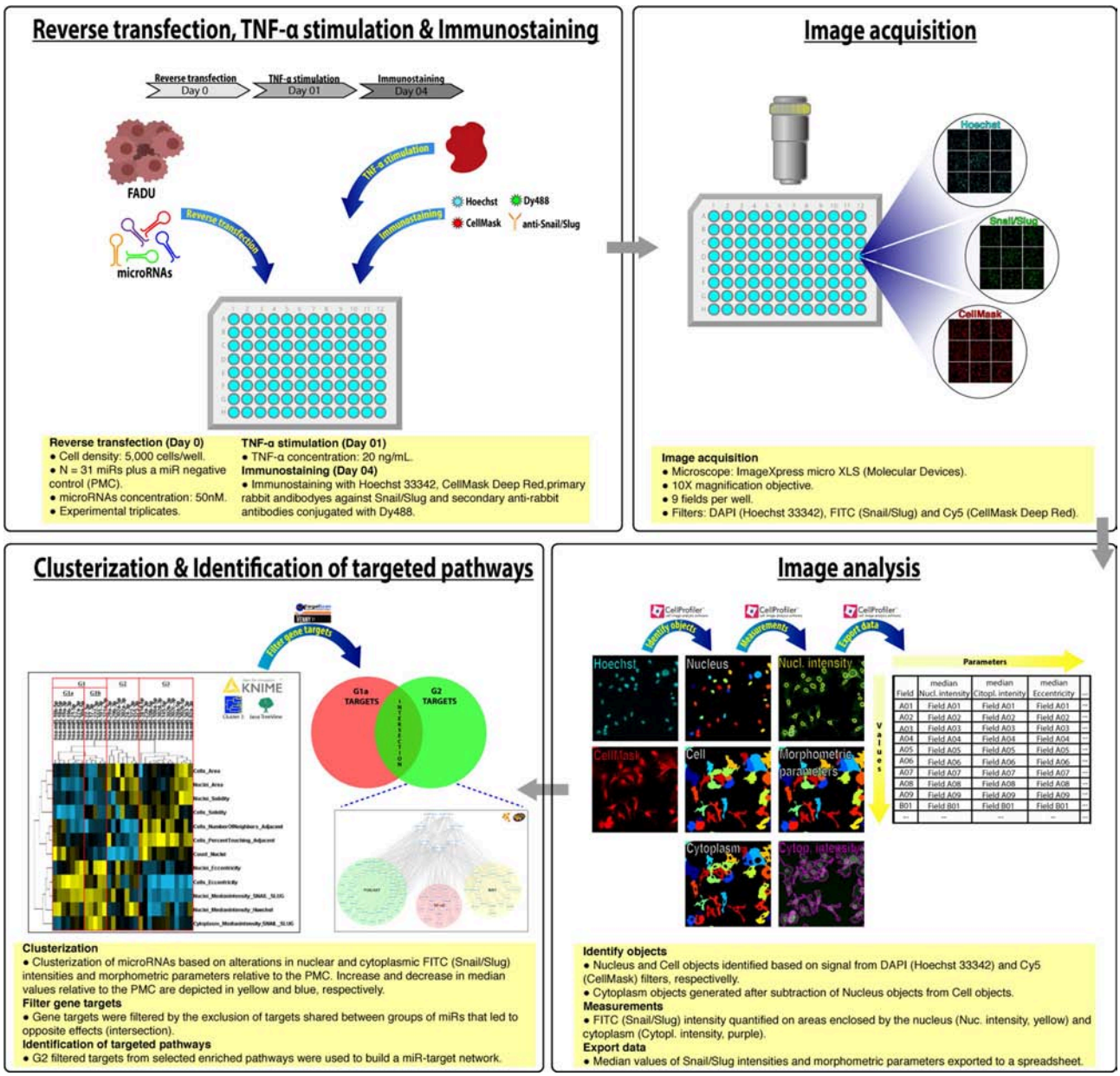

FIGURE 1 | Study design. Reverse transfection, TNF-α stimulation and Immunostaining: Cells from the FADU cell line were transfected (day 0) with microRNAs (N = 31), followed by stimulation with TNF-α (20 ng/mL, Day 01) and immunostaining with primary rabbit antibodies against Snail/Slug, secondary anti-rabbit antibodies conjugated with Dy488, nuclear (Hoechst) and cytoplasmic (CellMask) fluorescent dyes (Day 04). Image acquisition: Images (9 fields per well) were acquired using a 10X objective and excitation/emission filters DAPI (Hoechst), FITC (Snail/Slug), and Cy5 (CellMask), using an ImageXpress Micro XLS HCS system (Molecular Devices). Image analysis: Nuclei and corresponding cytoplasm objects were identified and segmented based on images from DAPI (Hoechst) and Cy5 (CellMask) channels, respectively. FITC (Snail/Slug) intensity on nuclei and cytoplasm, as well as morphometric parameters were then quantified. Median values per field were exported into a spreadsheet. Clusterization and Identification of targeted pathways: Based on alterations in median values per well relative to the PMC, microRNAs were subjected to an unsupervised hierarchical clustering. After the exclusion of genes commonly targeted by miRs from G1a (pro-survival/EMT) and G2 (anti-survival/EMT), genes from signaling pathways targeted by G2 miRs were used to generate a microRNA regulatory network.

MATERIALS AND METHODS

Study Design

The design of this study is illustrated in **Figure 1**. Cells from the FADU cell line were transfected (reverse transfection) into 96 well plates with miR mimetics (N = 31 plus a miR negative control) in experimental triplicates, followed by stimulation with TNF-α (20 ng/mL) for 72 h and immunostaining with primary rabbit antibodies against Snail/Slug, secondary anti-rabbit antibodies conjugated with Dy488, nuclear (Hoechst) and cytoplasmic (CellMask) fluorescent dyes. Images (nine fields per well) were acquired using a 10X objective and excitation/emission filters

DAPI (Hoechst), FITC (Snail/Slug), and Cy5 (CellMask), using an ImageXpress Micro XLS HCS system (Molecular Devices). With aid of CellProfiler, images from filters DAPI (Hoechst) and Cy5 (CellMask) were used to identify nuclear, cell and cytoplasm objects, followed by quantification of nuclear and cytoplasmic median FITC (Snail/Slug) intensity, as well as morphometric parameters. Median values per field were exported into spreadsheets and with help of KNIME software, we obtained the percentage change of the median values per well relative to the miR negative control (PMC). By using Cluster3 and Java TreeView software, we performed a unsupervised hierarchical clustering of miRs by which the four groups of miRs (G1a, G1b, G2, and G4) were identified. With help of KNIME and Targetscan software, we identified the genes targeted by most (N-2, minimum of 4) of the microRNAs in each group. With help of Venny online tool, genes targeted by groups that led to opposite phenotypic effects were identified and excluded from further analyses. With aid of Database for Annotation, Visualization and Integrated Discovery (DAVID, version 6.7) online tool, we identified signaling pathways enriched with filtered targets. With help of the Kyoto Encyclopedia of Genes and Genomes (KEGG) database, the filtered targets from G2 miRs were assigned to the NF-kB, PI3K/AKT, and Wnt/beta-catenin signaling pathways, which were used to generate a microRNA regulatory network with help of Cytoscape software. Based on information from those analyses, secondary functional assays using siRNAs were designed to evaluate the effect, in cell survival and EMT, of interferences in NF-kB, PI3K/AKT, and Wnt/beta-catenin signaling pathways.

Cell Lines

Cells derived from the HNSCC cell lines FADU (oropharynx), HN30 (pharynx), and UMSCC1 (floor of mouth) were cultured in Dulbecco's modified Eagle's medium (DMEM) supplemented with 10% fetal bovine serum (FBS), 50 U/mL penicillin and 50 μg/mL streptomycin. Cells were passaged by using a 10% trypsin solution.

Reagents

Throughout this work, cells were treated with TNF-α (300-01A, PrepoTech, USA) or mitomycin C (MMC, M4287, sigma-aldrich, USA). For immunostaining, we used the nuclear dye Hoechst 33342 (10 μg/mL; H1399, Thermo Scientific, USA) and cytoplasmic dye HCS CellMask Deep Red (5 μg/mL, H10294, Thermo Scientific, USA), primary antibodies: Anti-N-Cadherin mouse IgG2ab mAb (SC-271386, Santa Cruz Biotechnology, USA), Rabbit anti-Snail/Slug (ab180714, abcam, USA), Goat anti-Vimentin (sc-7558, Santa Cruz Biotechnology) and Mouse-anti-Caspase-7 (cleaved caspase-7 p10, clone h207, sc-22179, Santa Cruz Biotechnology, USA), as well as secondary antibodies: Goat anti-Rabbit DyLight 488 (dy488, 35553, Thermo Scientific, USA), Goat anti-Rabbit DyLight 594 (35561, Thermo Scientific, USA) DyLight 488 mouse (35503, Thermo Scientific, USA) and Donkey anti-Goat DyLight 594 (SA5-1088, Thermo Scientific, USA). For western blot, we used the antibodies rabbit anti-snail (#3879, Cell Signaling, USA), rabbit anti-slug (#9585, Cell Signaling, USA), rabbit anti-vimentin (#5741, Cell Signaling, USA), rabbit anti N-cadherin (#13116, Cell Signaling, USA), rabbit anti-β-catenin (#8480, Cell Signaling, USA) and mouse anti-β-actin (sc-81178, Santa Cruz, CA).

Western Blot

For protein extraction and quantification, cells were washed with PBS and disrupted in lyses buffer (20 mM Tris-HCl, 150 mM NaCl, 1 mM Na2EDTA, 1 mM EGTA, 1% Triton X-100, 2.5 mM sodium pyrophosphate, 1 mM β-glycerophosphate, 1 mM Na3VO4 and 1 μg/ml leupeptin). After three sonication cycles at 45 W for 5 min each in a sonicator bath, the samples were centrifuged at 20,000 × g for 30 min at 4°C. The protein concentration was determined by the Bradford method (Bio-Rad, Hercules, CA).

Proteins were submitted to SDS–PAGE and electrotransferred to PVDF membranes (GE Lifesciences, Pittsburgh, PA, USA). Membranes were blocked with 5% non-fat dry milk in 0.1% Tween-TBS and incubated with the primary antibody. After 1 h of incubation with horseradish peroxidase-conjugated goat anti-rabbit IgG (#7074, Cell Signaling) or horse anti-mouse IgG (#7076, Cell Signaling) secondary antibodies The antibody-protein complex was detected using ECL Western Blotting Detection Reagents (GE Lifesciences) using a CCD-Camera (Image QuantLAS 4000 mini, Uppsala, Sweden). Densitometric analysis was performed using the ImageJ software, and bands were normalized to the constitutive protein β-actin.

MicroRNA Mimics and siRNAs

Transfection assays were carried out with human microRNA mimetic molecules (50 nM, Thermo Scientific) or synthetic siRNA molecules (10 nM; **Supplementary File 1**).

Reverse Transfection

Reverse transfection assays were performed using lipofectamine LTX transfection reagent (15338100, Thermo Scientific) and synthetic miRs/siRNAs according to manufacturer's instructions. Transfection efficiency was calculated by evaluating the percentage reduction in cell numbers following transfection with a cytotoxic siRNA against Ubiquitin (siUBC) as compared to cells transfected with a control miR (PMC) or siRNA (siCTR).

Immunostaining

Cells were fixed and permeabilized with a 2% formaldehyde solution in methanol for 20 min at −20°C. Quenching of formaldehyde was achieved by incubation for 15 min with a 0.1 M glycine solution and blocking with a 1% FBS solution for 30 min. Afterwards, cells were incubated for 1 h at room temperature with primary antibodies, followed by incubation for 45 min with a solution containing secondary antibodies and nuclear/cytoplasmic dyes.

Image Analysis

Image analyses were performed with aid of MetaXpress software (Molecular Devices, USA) or CellProfiler (version 2.2.0, Broad Institute, USA). Briefly, images from functional assays that aimed to evaluate only the presence/absence of fluorescent dyes or markers were analyzed using MetaXpress software, whereas CellProfiler was used to analyze images from functional assays

aiming both the evaluation of morphometric parameters and the presence and subcellular localization of fluorescent markers. Data from image analyses were processed with the aid of KNIME software (version 3.2.0).

HCS-Based Functional Assays

Alterations in cell morphology and expression/localization of proteins were assessed through HCS-based functional assays, which comprises of:

i) MiR/siRNA reverse transfection of FADU cells into 96-well culture plates (CLS3603, Corning, USA);
ii) Stimulation or not with TNF-α, 24 h after reverse transfection;
iii) Immunostaining using antibodies, nuclear and cytoplasmic dyes;
iv) Image acquisition (9 fields per well) with aid of an ImageXpress® Micro XLS High-Content Screening (HCS) system (Molecular Devices, USA), using a 10X magnification objective and excitation/emission filters DAPI, FITC, Cy3, Texas Red, and Cy5;
v) Image analysis with aid of MetaXpress (Molecular Devices, USA) or CellProfiler (version 2.2.0, Broad Institute, USA) software.

Migration Assay

Cells were seeded on culture plates specific for migration assays Oris Pro Cell Migration Assay, 96 wells (PROCMA5, Platypus Technologies, USA). After 24 h, cells were treated with 0.2 μg/mL of mitomycin C for 2 h (to suppress proliferation), followed or not by incubation with TNF-a at 20 or 50 ng/mL for 72 h (experimental triplicates). Images were acquired using a 4X phase-contrast objective after cell seeding and at the endpoint using the ImageXpress HCS system. The area occupied by cells was quantified after cell seeding and at the endpoint, which were used to measure cell migration using $M = (Ae/As * 100)-100$, in which M = migration, Ae = Area occupied by cells at the endpoint, As = Area occupied by cells 24 h after seeding.

Clusterization of miRs

A unsupervised hierarchical clustering of miRs was performed with aid of Cluster 3 software (25) and visualized with help of Java TreeView software (26). Groups of miRs were classified as of pro/anti survival/EMT properties based on alterations in the following phenotypic parameters: "count nuclei (cell survival)," "cells eccentricity (EMT)," "Nuclei Median Intensity Snail/Slug (EMT)," and "Cytoplasm Median Intensity Snail/Slug (EMT)."

Identification of Genes and Signaling Pathways Targeted by Groups of miRs

Using the KNIME software (version 3.7) and TargetScan database of predicted miR targets (version 7.1) (27), we created a pipeline to identify the transcripts commonly targeted by most of the miRs contained in each of the identified groups (N-2, minimum of 4). Venn diagrams were generated using Venny 2.1 online tool (bioinfogp.cnb.csic.es/tools/venny) by comparing the identified targets from groups of miRs with opposite phenotypic effects, followed by the exclusion (filtering) of the shared targets. Afterwards, with help of the Database for Annotation, Visualization and Integrated Discovery (DAVID, version 6.7) (28), we identified signaling pathways that were enriched with the filtered targets from each group of miRs.

The filtered targets were assigned to their given signaling pathways according to information available on the Kyoto Encyclopedia of Genes and Genomes (KEGG) database about the following signaling pathways: NF-κB (hsa04064), PI3K/AKT (hsa04151), and Wnt (hsa04310) (29). The miRs and targets from the selected pathways were used to generate a microRNA regulatory network with aid of Cytoscape software (30).

Quantitative PCR (qPCR)

RNA extraction was performed using TRIZOL reagent (Invitrogen Life Technologies, Grand Island, NY, USA) and total RNA was reverse transcribed using the High Capacity cDNA Reverse Transcription Kit (Applied Biosystems, Foster City, CA, USA), according to the manufacturer's instructions. Gene expression qPCR reactions were carried in duplicates with Power SYBR Green Master Mix (Applied Biosystems) and primers for AKT2 (Forward: AAGGATGAAGTCGCTCACAC; Reverse: ACTCCATCACAAAGCACAGG), CCND1 (Forward: CCCGCACGATTTCATTGAAC; Reverse: GGCGGATTGGAAATGAACTTC), GAPDH (Forward: GAAGGTGAAGGTCGGAGTC; Reverse: GAAGATGGTGATGGGATTTC); IL6 (Forward: ATGCAATAACCACCCCTGAC; Reverse: GAGGTGCCCATGCTACATTT); MYC (Forward: CAGATCAGCAACAACCGAAA; Reverse: GGCCTTTTCATTGTTTTCCA) and RELA (Forward: TGACAAGGTGCAGAAAGAGG; Reverse: CACATCAGCTTGCGAAAAGG) using a CFX96 Real-Time PCR system (Bio-Rad). Relative gene expression levels were assessed using the $2^{-\Delta\Delta Ct}$ strategy (31).

Statistics

All statistical analyses were performed with aid of GraphPad Prism software version 5.0. Comparisons between multiple experimental conditions were performed using either unpaired *t*-test or univariate "ONE-WAY Anova" test. Statistical significance was considered at $p < 0.05$.

RESULTS

Stimulation With Tumor Necrosis Factor Alpha Leads to EMT-Related Morphometric Alterations

We performed an HCS-based functional assay in cells primed with TNF-α at different concentrations and time points followed by quantification of morphometric features. Stimulation for 48 h with TNF-α, at all concentrations used (5–50 ng/mL), reduced the percentage of intercellular contact by around 15% while not changing cell eccentricity (elongation). On this same endpoint, we found a trend for increase and decrease in cell area and number of neighboring cells, respectively, in a concentration-dependent manner, attaining significance at 20 and 50 ng/mL. On the other hand, stimulation for 72 h with all TNF-α concentrations used, led to a significant increase in cell

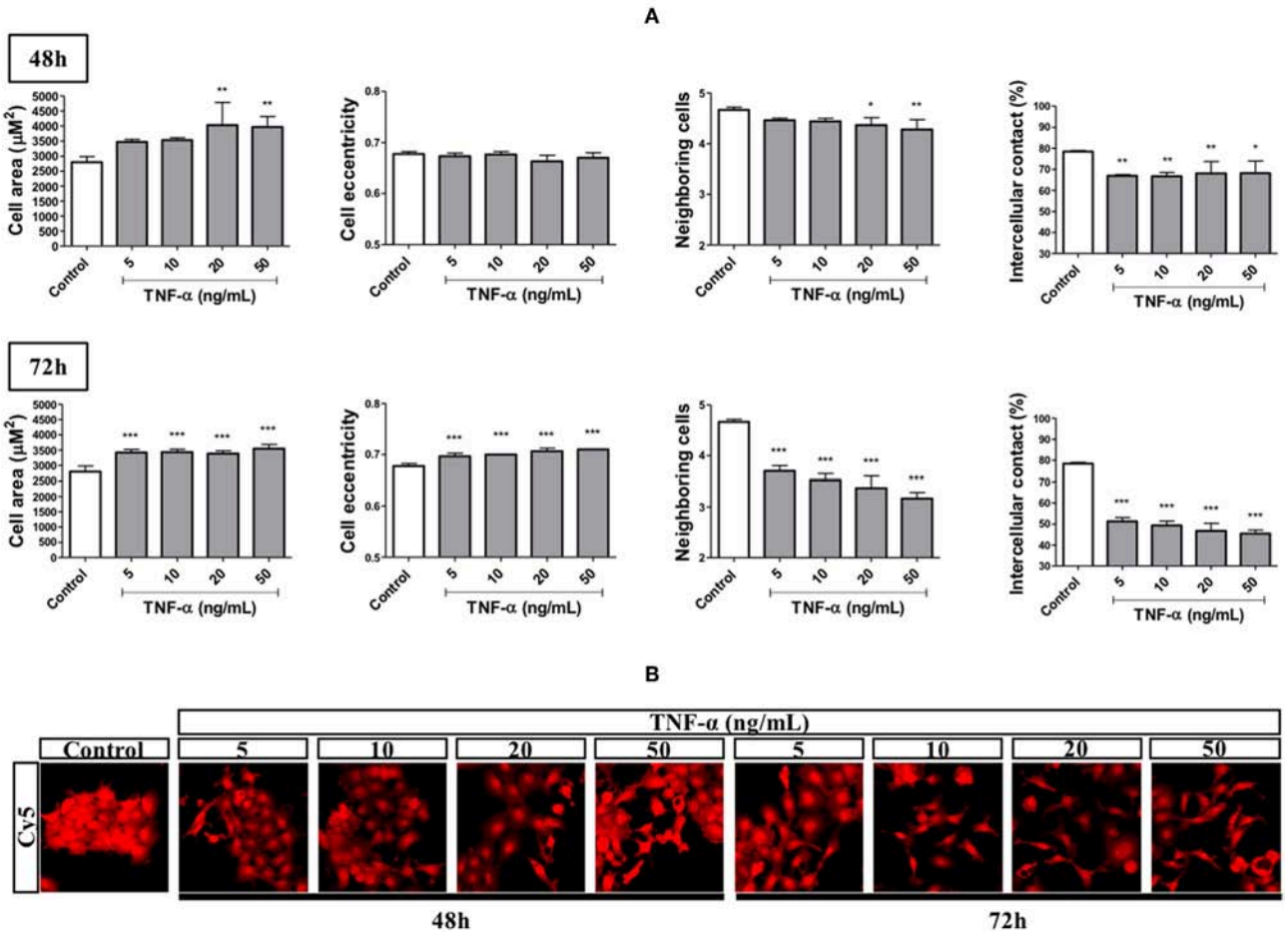

FIGURE 2 | Effects of TNF-α in EMT-related morphometric parameters. The FADU cell line was stimulated or not (Control) with TNF-α (5 to 50 ng/mL), for 48 or 72 h (squares). At the endpoint, the cells were stained with nuclear (Hoechst) and cytoplasmic (CellMask) fluorescent dyes. Images (nine fields per well) were acquired using a 10X objective and excitation/emission filters DAPI (Hoechst) and Cy5 (CellMask), using an ImageXpress Micro XLS HCS system (Molecular Devices). Images were analyzed using CellProfiler, in order to quantify the following parameters: cell area, cell eccentricity, number of neighboring cells and percentage of intercellular contact. **(A)** Quantitative changes (Mean +-SD) in morphometric parameters due to TNF-α stimulation for 48 and 72 h. **(B)** Representative images of cells stimulated with TNF-α for 48 and 72 h. Statistically significant differences (ONE-WAY Anova with Tukey post-test), in comparison to the control condition: $^{*}p < 0.05$; $^{**}p < 0.01$; $^{***}p < 0.001$.

area (around 1,000 μm^2) and cell eccentricity. These changes were accompanied by significant reductions in both the number of neighboring cells (by around 1.5) and the percentage of intercellular contact (by around 30%; **Figure 2**).

Stimulation With Tumor Necrosis Factor Alpha Leads to the Expression of EMT-Related Proteins

An HCS-based functional assay was done in cells primed with TNF-α for 72 h and at different concentrations, with further quantification of changes in the percentage of cells positive for markers of EMT. Generally, we observed that stimulation with TNF-α led to a concentration-dependent increase in the percentage of cells positive for all markers evaluated. More specifically, the higher concentration of 50 ng/mL led to a significant increase in the percentage of cells expressing N-Cadherin in the cytoplasm (from 30 to 50%, approximately). Moreover, the percentage of cells expressing cytoplasmic Vimentin significantly increased by 25% after treatment with TNF-α at 20 and 50 ng/mL. Finally, the percentage of cells expressing Snail/Slug in the nucleus significantly increased at all concentrations of TNF-α, ranging from below 20% (in untreated cells) up to above 60% ate the highest TNF-α concentration.

By western blot, we observed that after 72 h of treatment with TNF-α at 20 ng/mL, the protein levels of Snail and N-Cadherin increased by 2.2- and 5.4- fold in comparison to the untreated control group, respectively. Moreover, the levels of Slug and Vimentin were increased by around 1.1-fold, whereas the protein level of beta-catenin was increased by 1.2-fold (**Figure 3**).

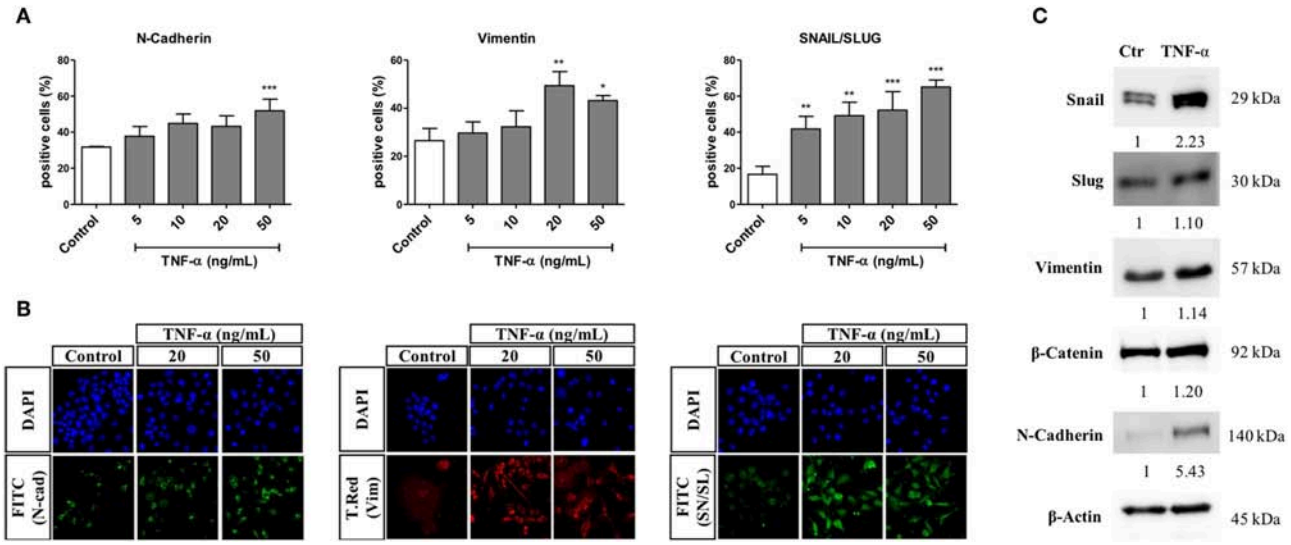

FIGURE 3 | Effects of TNF-α in the expression of EMT-related proteins. The FADU cell line was stimulated or not (Control) with TNF-α (5 to 50 ng/mL), for 72 h, followed by analyses of EMT-related protein levels by immunostaining or western blot. After immunostaining using antibodies against N-cadherin (N-cad), Vimentin (Vim) and Snail/Slug (SN/SL), cells were co-stained with nuclear (Hoechst) and cytoplasmic (CellMask) fluorescent dyes. Images (nine fields per well) were acquired using a 10X objective and excitation/emission filters DAPI (Hoechst), FITC (N-Cadherin and SN/SL), and Texas Red (T.Red; Vimentin), using an ImageXpress Micro XLS HCS system (Molecular Devices). Images were analyzed using MetaXpress, in order to evaluate the percentage of cells positive for each protein in the nucleus or cytoplasm. For western blot, protein detection was achieved using antibodies against Snail, Slug, Vimentin, beta-catenin and N-Cadherin. **(A)** Nuclear or cytoplasmic quantitative changes (Mean +-SD) in protein levels of N-Cadherin, Vimentin and Snail/Slug, as evaluated by immunofluorescence. **(B)** Representative images of stained cells stimulated with TNF-α at 20 and 50 ng/mL. **(C)** Alterations (fold change) in the protein levels of Snail, Slug, Vimentin, beta-catenin and N-Cadherin, as evaluated by western blot after 72 h of TNF-α stimulation (20 ng/mL). Statistically significant differences (ONE-WAY Anova with Tukey post-test), in comparison to the control condition: $^{*}p < 0.05$; $^{**}p < 0.01$; $^{***}p < 0.001$.

Tumor Necrosis Factor Alpha Stimulation Induces Cell Migration

A migration assay was performed in cells treated with mitomycin C and primed with TNF-α at different concentrations, for 72 h. Stimulation with TNF-α at 20 and 50 ng/mL increased the migratory capacity of FADU cells by around 30 and 20%, respectively (**Figure 4**).

HCS-Based miR Screening Identifies miRs With Distinct Effects on Cell Survival and EMT

An HCS-based functional assay was performed in cells transfected with our library of miRs ($N = 31$), followed by priming with TNF-α (20 ng/mL) for 72 h, in order to evaluate changes on morphometric parameters and Snail/Slug levels/localization. We identified miRs that altered cell survival (nuclei count) and EMT-related features including nuclear Snail/Slug levels and morphometric parameters such as cellular/nuclear area, eccentricity and cell distancing relative to the miR negative control. After unsupervised hierarchical clustering, miRs were distributed into three main groups (G1, G2, and G3). Based on distinct alterations in cell survival (nuclei count), G1 was further subdivided into the subgroups G1a and G1b.

MiRs from G3 led to a pro-survival and anti-EMT effect, as seemed by increase in cell survival and epithelial phenotype: tightly packed juxtaposed (higher number of neighboring cells and percentage of touching) round cells (lower eccentricity and higher solidity) with low nuclear Snail/Slug levels. In contrast, the subgroup G1b had the exact opposite phenotypic features (anti-survival and pro-EMT), with low cell counts, high Snail/Slug intensity and interspersed cells with mesenchymal phenotype (high eccentricity and low solidity). Since a higher cell density by itself excerpts a strong inhibitory effect on EMT, while a lower cell density is able to promote it (32), G1b and G3 are hereafter referred as anti-survival and pro-survival miR groups, respectively.

The subgroup G1a promoted cell survival while increasing nuclear Snail/Slug levels and morphological EMT-related features comparable to that of G1b; thus, clearly displaying a pro-survival/EMT effect. Otherwise, miRs from G2 had the strongest negative impact on survival while some of its members were still capable of reducing or preventing the increase of cell eccentricity or nuclear Snail/Slug levels, thereby displaying a anti-survival/EMT effect (**Figure 5**).

Anti-survival/EMT miRs Target Inflammatory-Associated Pathways

After identifying the genes collectively targeted by the miRs from G1a, G1b, G2, and G3, we eliminated targets shared by groups that led to opposite phenotypic effects. Thereby,

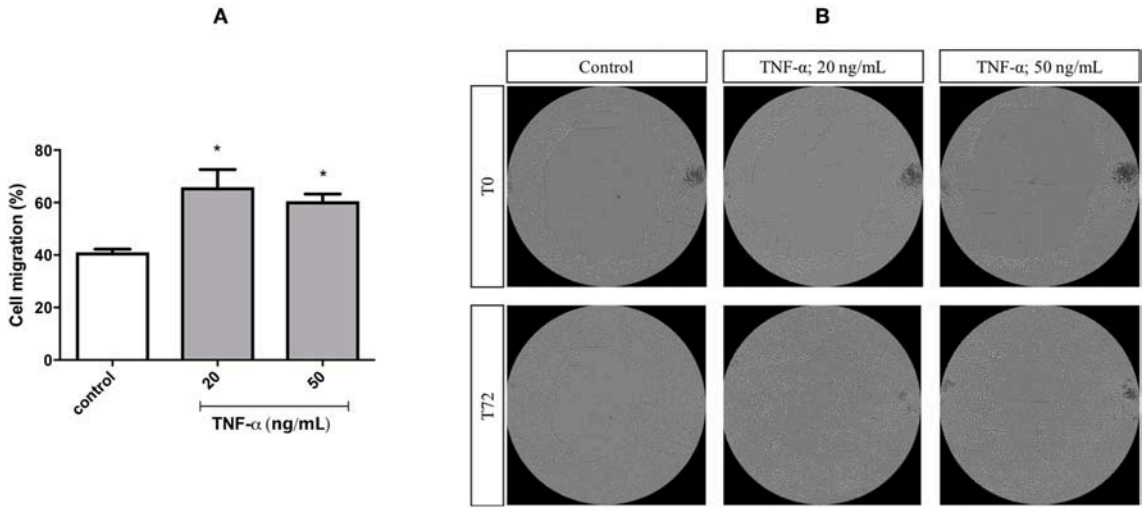

FIGURE 4 | Cell migration of FADU cells following stimulation with TNF-α. The FADU cell line was cultured for 24 h in cell culture plates designed for migration assays, treated with mitomycin for 2 h (to inhibit cell proliferation) and stimulated or not (Control) with TNF-α at 20 or 50 ng/mL for 72 h. Phase-contrast transmitted light images were acquired, with an ImageXpress Micro XLS HCS system (Molecular Devices), using a 4X objective. With aid of CellProfiler, cell migration was quantified based on the percentage of increase in the area occupied by cells. **(A)** Percentage of cell migration after 72 h (Mean +-SD). **(B)** Representative images of different experimental conditions at initial time (T0) and after 72 h (T72). Statistically significant differences (ONE-WAY Anova with Tukey post-test), in comparison to the control condition: $^*p < 0.05$.

targets shared between G1a (pro-survival/EMT) and G2 (anti-survival/EMT), as well as G1b (anti-survival) and G3 (pro-survival) were eliminated from further analyses as they were considered not relevant for the phenotypic effects driven by the groups of miRs (**Supplementary File 2**). Then, the filtered targets were used for enrichment analysis on signaling pathways and biological processes (**Supplementary File 3**). Strikingly, we found that miRs from both G1b (anti-survival) and G2 (anti-survival/EMT) targeted inflammatory pathways including "TNF signaling pathway (G1b)" and "Toll-like receptor signaling pathway (G2)" and shared targets from the following pathways: NF-κB (*IKBKG);* PI3K/AKT (*AKT2*), and MAPK (*MAPK9*). Moreover, we found that miRs from G2 also targeted additional genes (not found in G1b) from the NF-κB and PI3K/AKT pathways including *RELA* and *PIK3R3*, respectively. Finally, the Wnt/beta catenin signaling pathway was also found to be enriched with targets from G2. The miRs from G2 (anti-survival/EMT) and its targets from the NF-κB, PI3K/AKT, and Wnt/beta-catenin signaling pathways were used to generate a microRNA regulatory network (**Figure 6**).

Anti-survival/EMT miRs Reduce the Transcript Levels of Their Direct and Indirect Targets

We evaluated the capacity of three miRs with anti-survival/EMT effects (miR-29b-3p, miR-302a-3p, and miR-372-3p) to reduce the transcript levels of direct predicted targets, as well as indirect downstream transcriptional targets. Overall, with the exception of *CCND1* (an indirect target of the miRs), the targets were downregulated by most of the miRs among the cell lines, however a stronger effect and less variability were observed on the FADU cell line. More specifically, we observed a reduction on the expression levels of the direct target *AKT2*, with the exception of miR-372 (on FADU) and miR-302a (on HN30 and UMSCC1). The same was observed for the direct target *RELA*, with the exception of miR-29b (on HN30 and UMSCC1) and miR-372 (on HN30 and UMSCC1). As for the indirect targets, *MYC* was downregulated with the exception of miR-372 (on FADU) and miR-29b (on HN30 and UMSCC1). Finally, *IL6* was also downregulated by the miRs, with the exception of miR-29b (on FADU), and miR-372 (on HN30 and UMSCC1) (**Figure 7**).

Interferences in Signaling Pathways Targeted by Anti-survival/EMT miRs Partially Recapitulate Their Effects

HCS-based functional assays were done in cells transfected with siRNAs against elements of signaling pathways regulated by the anti-survival/EMT miRs: *RELA* (siRELA, NF-κB pathway), *AKT1* (siAKT1, PI3K/AKT pathway), and *CTNNB1* (siCTNNB1, Wnt/beta-catenin signaling pathway), besides a non-targeting control siRNA (siCTR) and cytotoxic siRNA (siUBC), followed or not by stimulation with TNF-α.

After 72 h of TNF-α stimulation, siRNA-mediated knockdown of *RELA* transcripts led to an expressive reduction in cell number (count nuclei) and number of neighboring cells, while increased cell eccentricity. Silencing the expression of *AKT1* (of high homology with *AKT2*, target of G2) led to a discrete reduction in cell number, while increased cell area and significantly reduced nuclear and cytoplasmic levels of Snail/Slug. Finally, knockdown of *CTNNB1* significantly reduced cell number, cytoplasmic levels

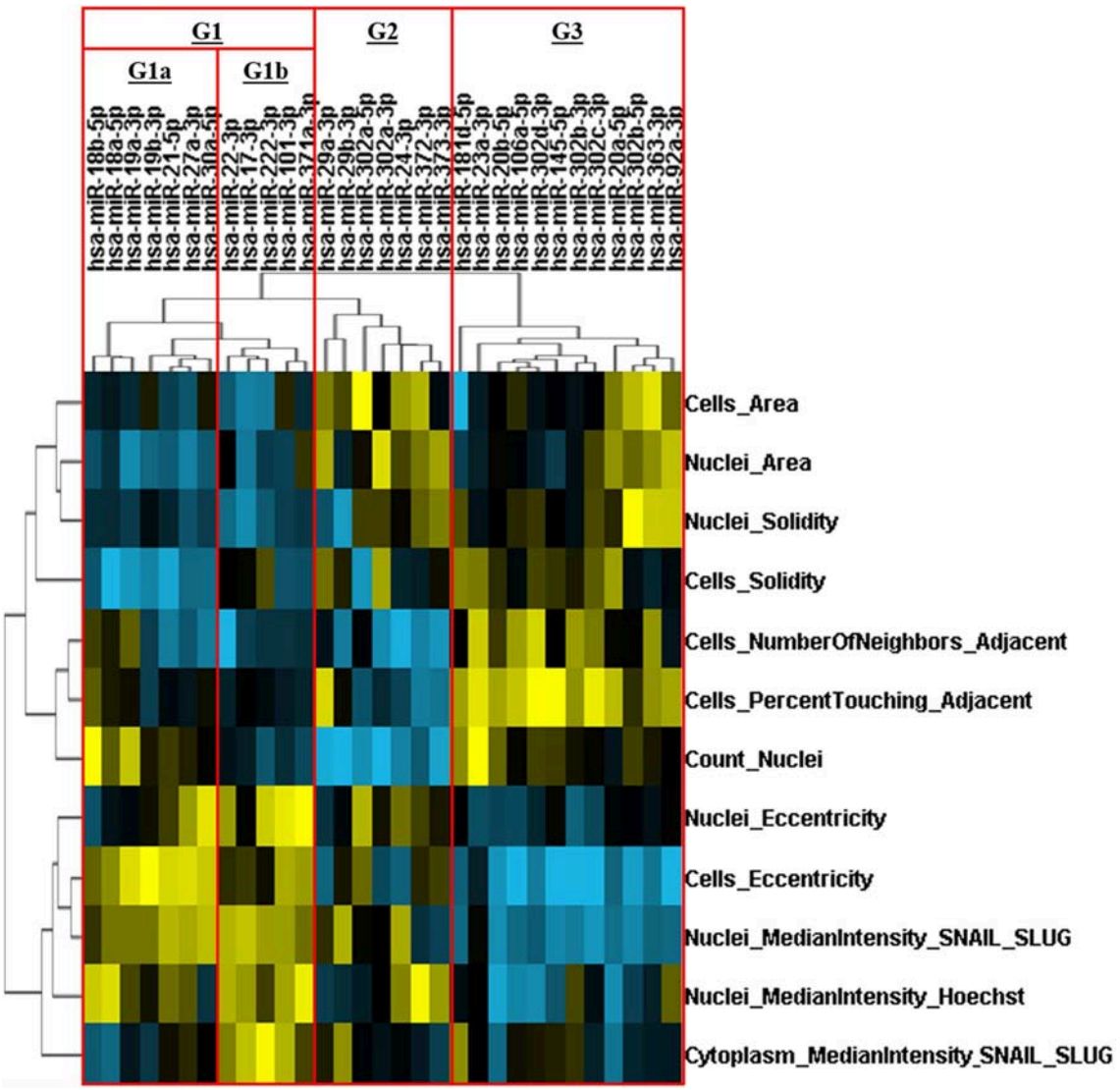

FIGURE 5 | Hierarchical clustering of miRs based on their effects on multiparametric phenotypic alterations. The FADU cell line was transfected with human miRs mimics, for 24 h, followed by stimulation with TNF-α (20 ng/mL) for 72 h. After immunostaining with antibodies against Snail/Slug (SN/SL) and co-staining with nuclear (Hoechst) and cytoplasmic (CellMask) dyes, images were acquired with an ImageXpress Micro XLS HCS system (Molecular Devices), using a 10X objective and excitation/emission filters DAPI (Hoechst), FITC (SN/SL), and Cy5 (CellMask Deep Red). With aid of CellProfiler, we evaluated several morphometric parameters, besides cell quantity (count nuclei) and the presence/location of Snail/Slug. Multiparametric phenotypic profiles, describing the effects of each miR, were obtained and subjected to an unsupervised hierarchical cluster analysis. Heatmap showing the multiparametric phenotypic profiles induced by each miR, and the four groups of miRs identified (G1a, G1b, G2, and G3. Red rectangles). Increase and decrease relative to PMC are depicted in yellow and blue, respectively.

of Snail/Slug and number of neighboring cells, while increased cell area and eccentricity.

Without TNF-α stimulation, the knockdown of the selected targets led to a reduction in cell counts as early as 24 h post-transfection, especially on cells transfected with siRELA, in which the impact was comparable to siUBC (a cytotoxic siRNA). At the same time point, the percentage of apoptotic cells (positive for cleaved caspase-7) transfected with siRELA and siAKT1 was around 25% higher than the control group (10%) but was unaltered on cells transfected with siCTNNB1, which also reduced the cell number. After 48 h of siRNA transfection, in comparison to 24 h after transfection, the number of cells in the control condition had almost doubled (indicating cell proliferation), while only slightly increasing in cells transfected with siAKT1 and siCTNNB1 and further decreasing in cells transfected with siRELA and siUBC. The percentage of apoptotic cells slightly decreased in cells transfected with siAKT1, while increased in cells transfected with siCTNNB1 (although not attaining significance), siRELA and siUBC (**Figure 8**).

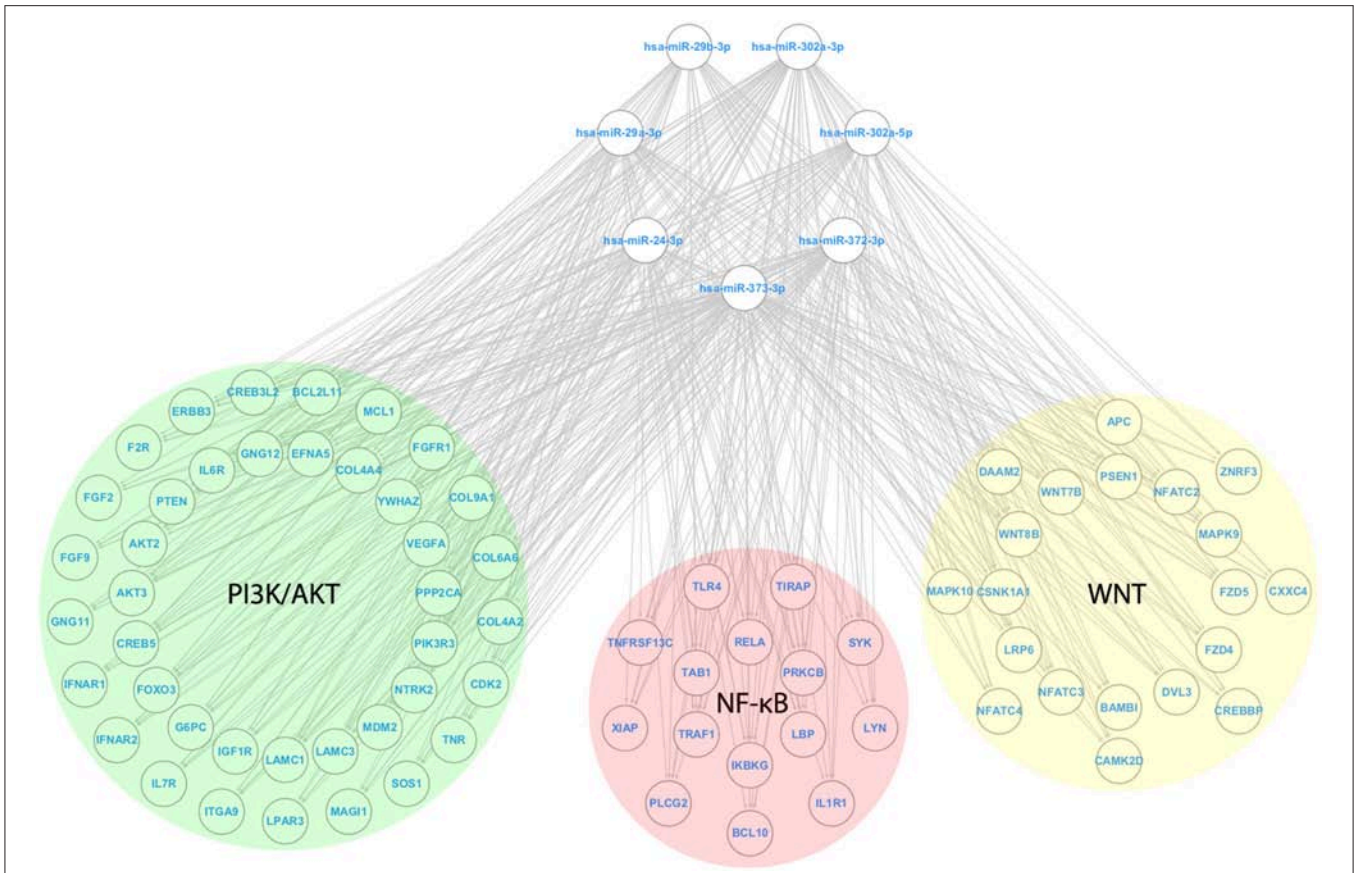

FIGURE 6 | MicroRNA Regulatory network with miRs from the anti-survival/EMT group. A microRNA regulatory network was composed of miRs from the anti-survival/EMT group, along with their targets from the PI3K/AKT (Green circle), NF-κB (Red circle), and Wnt (Yellow circle) signaling pathways. For each pathway, targets from the outer portion of the circle are the ones targeted by no more than 5 miRs, whereas the ones from the inside portion of the circle are the ones targeted by more than 5 miRs (maximum of 7). The following genes are shared between the signaling pathways NF-κB and PI3K/AKT: *IKBKG*, *RELA*, *SYK,* and *TLR4*; NF-κB and WNT: *PRKCB*.

DISCUSSION

Many of the functional studies conducted so far about the impact of small molecules in cancer cell survival disregards the presence of an inflammatory microenvironment, which is known to promote apoptosis resistance, epithelial to mesenchymal transition, among other phenotypic changes that promotes therapy resistance and disease recurrence (7).With that in mind, our study aimed to identify, through functional assays using an HCS approach, miRs and signaling pathways with the potential to suppress both cell survival and EMT features in HNSCC cells considering the presence of an inflammatory microenvironment. This approach should provide evidence if the effect of previously studied miRs translates or not to cancer cells under inflammatory stimuli, as well as to describe the effect of miRs with no known effect in HNSCC cells so far.

Initially, we demonstrated the capacity of TNF-α to promote a broad spectrum of phenotypic changes characterizing EMT, including an increase in nuclear expression of Snail/Slug, mesenchymal markers N-Cadherin and Vimentin, as well as cell eccentricity, inter-cell distancing and cell migration. Interestingly, our results of the western blot assay indicate that Snail, rather than Slug, might be involved in the induction of EMT driven by stimulation with TNF-α. Moreover, the increased levels of beta-catenin after stimulation with TNF-α also indicates a possible role, in our model, for the Wnt/beta-catenin pathway for the induction of EMT. Based on our observations, we concluded that the treatment of cells with TNF-α at 20 ng/mL is the best option to induce FADU cells to EMT, as it promoted strong changes in all parameters evaluated, as well as a superior induction to cell migration in comparison to a higher concentration.

Next, by performing an HCS-based miR screening, we investigated the capacity of 31 human miR mimics to alter phenotypic features related to cell survival and EMT in FADU cells induced to EMT by TNF-α stimulation. Overall, the results from this screening led us to identify four groups of miRs, namely G1a, G1b, G2, and G3, with distinct activity in promoting/inhibiting cell survival and EMT. Among them, two groups had characteristics of oncomiRs: G1a (pro-survival/EMT)

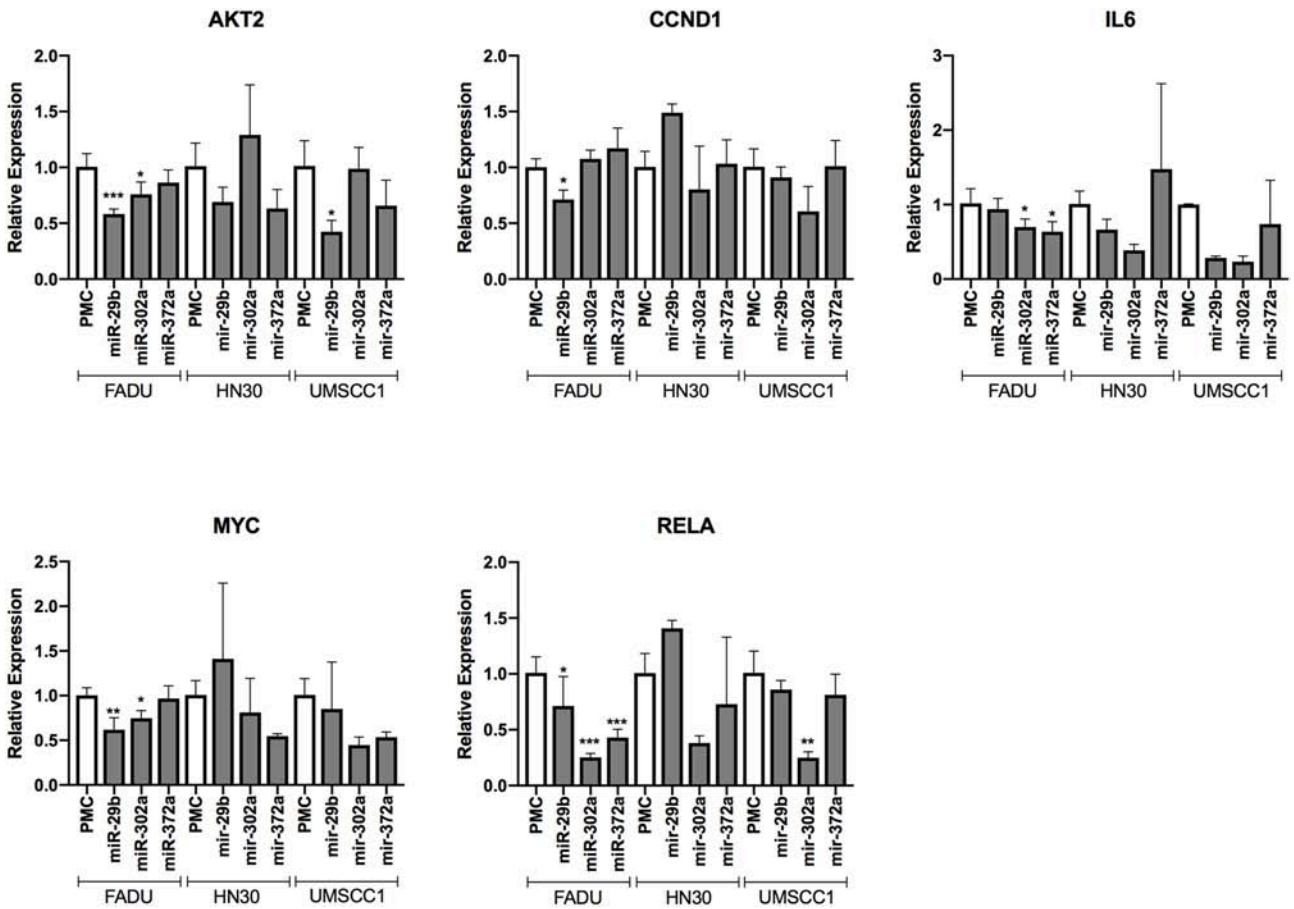

FIGURE 7 | Changes in the transcript levels of direct and indirect targets of anti-survival/EMT miR group following miR transfection. The cell lines FADU, HN30, and UMSCC1 were transfected with PMC (control) or miR mimics from G2 (miR-29b-3p, miR-302a-3p, and miR-372), followed by TNF-α stimulation (20 ng/mL) for 48 h and qPCR with primers for *AKT2*, *CCND1* (cyclin D1), *IL6*, *MYC,* and *RELA*. Alterations in relative gene expression levels, relative to cells transfected with miR-CTR (PMC). Statistically significant differences (*t*-test), in comparison to the reference control group (PMC): $^{*}p < 0.05$; $^{**}p < 0.01$; $^{***}p < 0.001$.

and G3 (pro-survival) whereas the two remaining groups had characteristics of tumor suppressor miRs: G1b (anti-survival) and G2 (anti-survival/EMT). Noteworthy, G1b (anti-survival) also excerpted an pro-EMT effect, while G3 (pro-survival) excerpted a anti-EMT effect, however, as the effects of G1b and G3 in EMT could be a byproduct (i.e., secondary effect) of their alterations in cell survival, those groups were not classified regarding their alterations in EMT (32).

Among the miRs from G1b (anti-survival), it was previously found that miR-101 is downregulated in HNSCC tissues from different anatomical sites, besides having an anti-survival effect on HNSCC cell lines, including FADU (33–35). Additionally, studies conducted with esophageal squamous cell carcinoma (ESCC)-derived cell lines subjected to the ectopic expression of miR-22 (also from G1b) observed a reduction in cell survival and migratory/invasive potential (36, 37). On the other hand, the pro-survival group G3 was mainly composed by miRs from miR-302-367 cluster, which are traditionally associated with pluripotency and malignancy of germ cells tumors (38, 39). In the context of head and neck cancer, overexpression of miR-302a and miR-302b was found in cells derived from HNSCC with characteristics of cancer stem cells including self-renewal and the ability to generate heterogeneous cell populations (40).

The pro-survival/EMT G1a was composed of miRs that are traditionally involved in regulatory mechanisms linking inflammation and tumor progression, including elements of the miR-17-92 cluster, miR-21 (a HNSCC oncomiR) and miR-23a/24/27a cluster (41). Interestingly, Chang and coworkers also observed a pro-survival activity of miR-21, as well as increased expression of miR-21 in primary HNSCC compared to mucosal controls (42). Moreover, in the recent meta-analysis study performed by Lubov et al., it was observed that an increased expression of miR-21 is associated with poor outcome in HNSCC (14). Differently from G1a, G2 (anti-survival/EMT) was composed of miRs from miR-29 family, which displays tumor suppressor activity in several types of cancer, including HNSCC (14, 43). In line with our results, Kinoshita and coworkers observed that the ectopic expression of elements from the mir-29

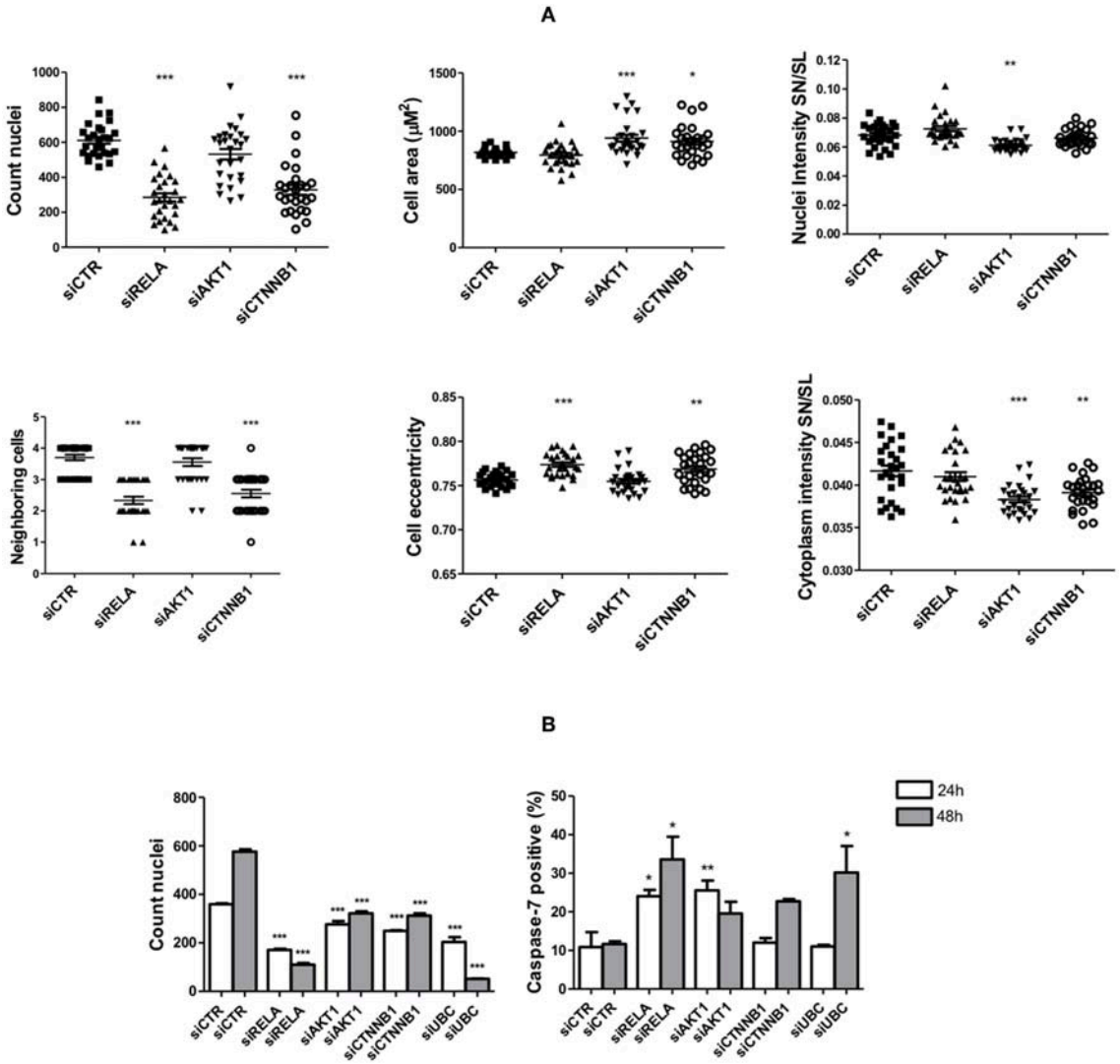

FIGURE 8 | Changes in cell survival and EMT upon interferences in signaling pathways targeted by the anti-survival/EMT group. The FADU cell line was transfected with siRNAs specific for *RELA*, *AKT1*, *CTNNB1*, cytotoxic siUBC, and unspecific siRNA control (siCTR), followed or not by TNF-α stimulation. At the endpoint, images were acquired with an ImageXpress Micro XLS HCS system (Molecular Devices), using a 10X objective and excitation/emission filters DAPI (Hoechst), FITC (SN/SL) and Cy5 (CellMask Deep Red). **(A)** Cells were stimulated for 72 h with TNF-α (20 ng/mL), starting 24 h post-transfection, followed by immunostaining with antibodies against Snail/Slug (SN/SL) and co-staining with nuclear (Hoechst) and cytoplasmic (CellMask) dyes. Alterations in morphometric parameters, cell counts and nuclear/cytoplasmic Snail/Slug due to siRNA transfection as observed after image analysis. **(B)** 24 and 48 h after transfection, cells without TNF-α stimulation were immunostained with antibodies against cleaved Caspase-7 and co-stained with nuclear (Hoechst) and cytoplasmic (CellMask) dyes. Cell counts and percentage of apoptotic cells positive for active caspase-7 as observed after image analysis. Statistically significant differences (ONE-WAY Anova with Tukey post-test), in comparison to the control condition: $^{*}p < 0.05$; $^{**}p < 0.01$; $^{***}p < 0.001$.

family in the FADU cell line resulted in a significant reduction in cell number, as well as in cell migration and invasion (44).

In an effort to identify, among the several targets and signaling pathways regulated by miRs, those that effectively contributed to the observed phenotypic effect, we excluded from further analyses genes that were commonly targeted by groups of miRs that led to opposite phenotypes. Those filtered targets were used in *in silico* enrichment analysis, leading to the identification of specific targets and targeted signaling pathways. Noteworthy, this strategy provided cues on the genes and signaling pathways to be explored to suppress HNSCC tumor growth and metastasis.

By following this strategy, we observed that miRs from G1b (anti-survival) and G2 (anti-survival/EMT) targeted signaling pathways that are associated with the interface between inflammation and tumor initiation/progression, including MAPK, PI3K/AKT and NF-κB pathways (45). However, in comparison to predicted targets from G1b, it was found that miRs from G2 interfered in the PI3K/AKT and NF-κB pathways

in a more extensive manner, also targeting a regulatory subunit of PI3K (PIK3R3), a oncogene that regulates AKT activity, as well as *RELA*, which codes for the canonical subunit (p65) of the NF-κB transcription factor (46, 47). Moreover, miRs from G2 also targeted several elements of the Wnt/beta-catenin signaling pathway. Altogether, our results from *in silico* analyses provided evidence that the anti-survival/EMT effects elicited by miRs from G2 likely derives from an extensive perturbation in PI3K/AKT and NF-κB pathways, besides Wnt signaling pathway. Additionally, by evaluating alterations in gene expression levels of cells transfected with miRs from G2 (anti-survival/EMT) group, we confirmed that elements from the following targeted signaling pathways: NF-κB (*RELA* and *IL6*), PI3K/AKT (*AKT2*), as well as Wnt/beta-catenin (*MYC*) were downregulated after the transfection in most cases.

Additional functional assays were performed with siRNAs against genes from the following signaling pathways regulated by anti-survival/EMT group (G2): *AKT1* (PI3K/AKT pathway); *RELA* (NF-κB pathway); and *CTNNB1* (Wnt pathway) followed or not by stimulation with TNF-α. Noteworthy, though *AKT1* and *CTNNB1* are not directly targeted by the miRs from G2, their use is justified by the central role of those genes in regulating the PI3K/AKT and Wnt/beta-catenin pathways, respectively, which were extensively targeted by those miRs. Therefore, results from our functional assays using siRNAs should not be interpreted as direct link between anti-survival/EMT miRs and a specific target, but rather between miRs and targeted signaling pathways. An exception are observations from siRELA transfections, as *RELA* is not only a central gene in the NF-κB pathway but also a direct target of G2.

By stimulating cells with TNF-α after siRNA transfection, we sought to investigate the individual role of NF-κB, PI3K/AKT, and Wnt/beta-catenin signaling pathways on either cell survival or EMT considering the presence of an inflammatory microenvironment. Interestingly, we found that although gene silencing of *RELA* and *CTNNB1* led to an anti-survival effect whereas silencing *AKT1* led to an anti-EMT effect, none of the siRNAs alone impaired both cell survival and EMT, which indicates that the effects of anti-survival/EMT miRs are most likely due to their potential to interfere in multiple signaling pathways simultaneously. This possibility points out to the potential benefits of a multi-target approach to treat HNSCC, especially considering that so far, clinical trials evaluating the capacity of PI3K inhibitors to treat HNSCC have shown disappointing results (48). In line, a recent study by Li et al. demonstrated that co-targeting EGFR (upstream of PI3K/AKT) and NF-κB pathways led to a superior inhibition of cell survival and xenograph tumor growth, when compared to targeting either pathway alone (49).

By not stimulating cells with TNF-α after siRNA transfection, we aimed to evaluate if the effects coming from the interferences in NF-κB, PI3K/AKT, and Wnt/beta-catenin signaling pathways are influenced by the presence of an inflammatory microenvironment. Additionally, we investigated if effects on cell survival are due to alterations in apoptosis by evaluating the percentage of cells positive for cleaved caspase-7. Strikingly, we found that transfection with siRELA not only dramatically reduced the number of cells but also strongly induced cell-death by apoptosis after 24 h and 48 h. This indicates that interferences in the NF-κB pathway is deleterious to HNSCC cells regardless of stimulation with inflammatory factors. Interestingly, transfection with siAKT1 also followed a similar pattern (although not further increasing apoptosis at 48 h) revealing that an inflammatory stimulation exerts a protective effect on HNSCC cells against the deleterious effect of interferences in the PI3K/AKT pathway. Moreover, although transfection with siCTNNB1 reduced cell count, it did not enhance the number of apoptotic cells 24 h post-transfection, indicating a more prominent role of Wnt signaling toward cell proliferation regardless of TNF-α stimulation.

As a whole, our study identified several molecules that may have the potential to be used for prognosis or miR-based targeted therapies against HNSCC considering the presence of an inflammatory microenvironment. By further investigating the miRs with anti-survival/EMT effects, we found that interferences in the signaling pathways: NF-κB and Wnt/beta-catenin were the ones that most likely contributed for the anti-survival effect, whereas interferences in PI3K/AKT signaling pathway was most likely associated with anti-EMT effect. Future studies using *in vivo* models should shed light into the anti-tumor and anti-metastatic activity of the miRs and targets herein identified.

CONCLUSION

The present work characterized the functional role of a set of human miRs in modulating a broad spectrum of phenotypic alterations related to HNSCC cell survival and EMT in cells under an inflammatory stimulation, as well as the potentially involved signaling pathways. More specifically, the following miR mimetics: miR-24-3p, miR-29a-3p, miR-29b-3p, miR-302a-3p, miR-302a-5p, miR-372-3p, and miR-373-3p were identified as the ones with greatest potential use in microRNA replacement therapies, as they displayed an anti-survival/EMT effect. On the other hand, endogenous miRs herein identified as with pro-survival/EMT effects: miR-18a-5p, miR-18b-5p, miR-19a-3p, miR-19b-3p, miR-21-5p, miR-27a-3p, miR-30a-5p, were identified as the ones with greatest potential use in microRNA inhibition therapies. Additionally, we found that together, interferences on NF-κB, PI3K/AKT, and Wnt/beta-catenin signaling pathways are the ones that most likely driven the anti-survival/EMT effects displayed by miRs. Individual gene silencing of components of those pathways, namely *RELA* (NF-κB), *AKT1* (PI3K/AKT), and *CTNNB1* (Wnt/beta-catenin), partially recapitulated the effects displayed by miRs with anti-survival/EMT effects. Our findings revealed miRs and signaling pathways that might be explored to fight HNSCC tumor growth and metastasis considering the presence an inflammatory microenvironment.

AUTHOR CONTRIBUTIONS

BS, WA, VF, DC, MZ, and RP: study concept. BS, FS, and RP: study design. BS, FS, IM, JS, RP, AC, and CT: data acquisition, analysis, and interpretation. BS: statistical analysis. BS and RP:

manuscript preparation and editing. BS, WA, VF, DC, MZ, and RP: manuscript review.

FUNDING

This work was supported by São Paulo Research Foundation (FAPESP), grants #2013/08135-2 (Center for Cell-Based Therapy - CTC) and #2015/08070-3 (Scholarship for Research Abroad - BPE, RP); and by the National Council for Scientific and Technological Development (CNPq).

SUPPLEMENTARY MATERIAL

The Supplementary Material for this article can be found online at: https://www.frontiersin.org/articles/10.3389/fonc.2019.01100/full#supplementary-material

REFERENCES

1. Torre LA, Bray F, Siegel RL, Ferlay J, Lortet-Tieulent J, Jemal A. Global cancer statistics, 2012. *CA Cancer J Clin.* (2015) 65:87–108. doi: 10.3322/caac.21262
2. Allen CT, Law JH, Dunn GP, Uppaluri R. Emerging insights into head and neck cancer metastasis. *Head Neck.* (2013) 35:1669–78. doi: 10.1002/hed.23202
3. Massague J, Obenauf AC. Metastatic colonization by circulating tumour cells. *Nature.* (2016) 529:298–306. doi: 10.1038/nature17038
4. Lamouille S, Xu J, Derynck R. Molecular mechanisms of epithelial-mesenchymal transition. *Nat Rev Mol Cell Biol.* (2014) 15:178–96. doi: 10.1038/nrm3758
5. Singh M, Yelle N, Venugopal C, Singh SK. EMT: mechanisms and therapeutic implications. *Pharmacol Ther.* (2018) 182:80–94. doi: 10.1016/j.pharmthera.2017.08.009
6. Gao F, Liang B, Reddy ST, Farias-Eisner R, Su X. Role of inflammation-associated microenvironment in tumorigenesis and metastasis. *Curr Cancer Drug Targets.* (2014) 14:30–45. doi: 10.2174/1568009613136660107
7. Suarez-Carmona M, Lesage J, Cataldo D, Gilles C. EMT and inflammation: inseparable actors of cancer progression. *Mol Oncol.* (2017) 11:805–23. doi: 10.1002/1878-0261.12095
8. Wu Y, Zhou BP. TNF-alpha/NF-kappaB/Snail pathway in cancer cell migration and invasion. *Br J Cancer.* (2010) 102:639–44. doi: 10.1038/sj.bjc.6605530
9. Matta A, Ralhan R. Overview of current and future biologically based targeted therapies in head and neck squamous cell carcinoma. *Head Neck Oncol.* (2009) 1:6. doi: 10.1186/1758-3284-1-6
10. Hoesel B, Schmid JA. The complexity of NF-kappaB signaling in inflammation and cancer. *Mol Cancer.* (2013) 12:86. doi: 10.1186/1476-4598-12-86
11. Holohan C, Van Schaeybroeck S, Longley DB, Johnston PG. Cancer drug resistance: an evolving paradigm. *Nat Rev Cancer.* (2013) 13:714–26. doi: 10.1038/nrc3599
12. Bartel DP. MicroRNAs: target recognition and regulatory functions. *Cell.* (2009) 136:215–33. doi: 10.1016/j.cell.2009.01.002
13. Shalgi R, Brosh R, Oren M, Pilpel Y, Rotter V. Coupling transcriptional and post-transcriptional miRNA regulation in the control of cell fate. *Aging.* (2009) 1:762–70. doi: 10.18632/aging.100085
14. Lubov J, Maschietto M, Ibrahim I, Mlynarek A, Hier M, Kowalski LP, et al. Meta-analysis of microRNAs expression in head and neck cancer: uncovering association with outcome and mechanisms. *Oncotarget.* (2017) 8:55511–24. doi: 10.18632/oncotarget.19224
15. Pradhan AK, Emdad L, Das SK, Sarkar D, Fisher PB. The enigma of miRNA regulation in cancer. *Adv Cancer Res.* (2017) 135:25–52. doi: 10.1016/bs.acr.2017.06.001
16. Markopoulos GS, Roupakia E, Tokamani M, Alabasi G, Sandaltzopoulos R, Marcu KB, et al. Roles of NF-kappaB Signaling in the regulation of miRNAs impacting on inflammation in cancer. *Biomedicines.* (2018) 6:E40. doi: 10.3390/biomedicines6020040
17. Castilho RM, Squarize CH, Almeida LO. Epigenetic modifications and head and neck cancer: implications for tumor progression and resistance to therapy. *Int J Mol Sci.* (2017) 18:E1506. doi: 10.3390/ijms18071506
18. Bhome R, Del Vecchio F, Lee GH, Bullock MD, Primrose JN, Sayan AE, et al. Exosomal microRNAs (exomiRs): Small molecules with a big role in cancer. *Cancer Lett.* (2018) 420:228–35. doi: 10.1016/j.canlet.2018.02.002
19. Chakraborty C, Sharma AR, Sharma G, Sarkar BK, Lee SS. The novel strategies for next-generation cancer treatment: miRNA combined with chemotherapeutic agents for the treatment of cancer. *Oncotarget.* (2018) 9:10164–74. doi: 10.18632/oncotarget.24309
20. Lindenbergh-van der Plas M, Martens-de Kemp SR, de Maaker M, van Wieringen WN, Ylstra B, Agami R, et al. Identification of lethal microRNAs specific for head and neck cancer. *Clin Cancer Res.* (2013) 19:5647–57. doi: 10.1158/1078-0432.CCR-12-2295
21. Haefliger B, Prochazka L, Angelici B, Benenson Y. Precision multidimensional assay for high-throughput microRNA drug discovery. *Nat Commun.* (2016) 7:10709. doi: 10.1038/ncomms10709
22. Boutros M, Heigwer F, Laufer C. Microscopy-based high-content screening. *Cell.* (2015) 163:1314–25. doi: 10.1016/j.cell.2015.11.007
23. Serva A, Claas C, Starkuviene V. A potential of microRNAs for high-content screening. *J Nucleic Acids.* (2011) 2011:870903. doi: 10.4061/2011/870903
24. Rupaimoole R, Slack FJ. MicroRNA therapeutics: towards a new era for the management of cancer and other diseases. *Nat Rev Drug Discov.* (2017) 16:203–22. doi: 10.1038/nrd.2016.246
25. de Hoon MJ, Imoto S, Nolan J, Miyano S. Open source clustering software. *Bioinformatics.* (2004) 20:1453–4. doi: 10.1093/bioinformatics/bth078
26. Saldanha AJ. Java Treeview–extensible visualization of microarray data. *Bioinformatics.* (2004) 20:3246–8. doi: 10.1093/bioinformatics/bth349
27. Agarwal V, Bell GW, Nam JW, Bartel DP. Predicting effective microRNA target sites in mammalian mRNAs. *Elife.* (2015) 4:e05005. doi: 10.7554/eLife.05005
28. Huang da W, Sherman BT, Lempicki RA. Systematic and integrative analysis of large gene lists using DAVID bioinformatics resources. *Nat Protoc.* (2009) 4:44–57. doi: 10.1038/nprot.2008.211
29. Kanehisa M, Goto S. KEGG: kyoto encyclopedia of genes and genomes. *Nucleic Acids Res.* (2000) 28:27–30. doi: 10.1093/nar/28.1.27
30. Shannon P, Markiel A, Ozier O, Baliga NS, Wang JT, Ramage D, et al. Cytoscape: a software environment for integrated models of biomolecular interaction networks. *Genome Res.* (2003) 13:2498–504. doi: 10.1101/gr.1239303
31. Livak KJ, Schmittgen TD. Analysis of relative gene expression data using real-time quantitative PCR and the 2(-Delta Delta C(T)) method. *Methods.* (2001) 25:402–8. doi: 10.1006/meth.2001.1262
32. Cichon MA, Nelson CM, Radisky DC. Regulation of epithelial-mesenchymal transition in breast cancer cells by cell contact and adhesion. *Cancer Inform.* (2015) 14:1–13. doi: 10.4137/CIN.S18965
33. Li M, Tian L, Ren H, Chen X, Wang Y, Ge J, et al. MicroRNA-101 is a potential prognostic indicator of laryngeal squamous cell carcinoma and modulates CDK8. *J Transl Med.* (2015) 13:271. doi: 10.1186/s12967-015-0626-6
34. Hui Y, Li Y, Jing Y, Feng JQ, Ding Y. miRNA-101 acts as a tumor suppressor in oral squamous cell carcinoma by targeting CX chemokine receptor 7. *Am J Transl Res.* (2016) 8:4902–11.
35. Wu B, Lei D, Wang L, Yang X, Jia S, Yang Z, et al. MiRNA-101 inhibits oral squamous-cell carcinoma growth and metastasis by targeting zinc finger E-box binding homeobox 1. *Am J Cancer Res.* (2016) 6:1396–407.
36. Yang C, Ning S, Li Z, Qin X, Xu W. miR-22 is down-regulated in esophageal squamous cell carcinoma and inhibits cell migration and invasion. *Cancer Cell Int.* (2014) 14:138. doi: 10.1186/s12935-014-0138-0

37. Qiu K, Huang Z, Huang Z, He Z, You S. miR-22 regulates cell invasion, migration and proliferation *in vitro* through inhibiting CD147 expression in tongue squamous cell carcinoma. *Arch Oral Biol.* (2016) 66:92–7. doi: 10.1016/j.archoralbio.2016.02.013
38. Murray MJ, Nicholson JC, Coleman N. Biology of childhood germ cell tumours, focussing on the significance of microRNAs. *Andrology.* (2015) 3:129–39. doi: 10.1111/andr.277
39. Adlakha YK, Seth P. The expanding horizon of MicroRNAs in cellular reprogramming. *Prog Neurobiol.* (2017) 148:21–39. doi: 10.1016/j.pneurobio.2016.11.003
40. Bourguignon LY, Wong G, Earle C, Chen L. Hyaluronan-CD44v3 interaction with Oct4-Sox2-Nanog promotes miR-302 expression leading to self-renewal, clonal formation, and cisplatin resistance in cancer stem cells from head and neck squamous cell carcinoma. *J Biol Chem.* (2012) 287:32800–24. doi: 10.1074/jbc.M111.308528
41. Tili E, Michaille JJ, Croce CM. MicroRNAs play a central role in molecular dysfunctions linking inflammation with cancer. *Immunol Rev.* (2013) 253:167–84. doi: 10.1111/imr.12050
42. Chang SS, Jiang WW, Smith I, Poeta LM, Begum S, Glazer C, et al. MicroRNA alterations in head and neck squamous cell carcinoma. *Int J Cancer.* (2008) 123:2791–7. doi: 10.1002/ijc.23831
43. Slusarz A, Pulakat L. The two faces of miR-29. *J Cardiovasc Med.* (2015) 16:480–90. doi: 10.2459/JCM.0000000000000246
44. Kinoshita T, Nohata N, Hanazawa T, Kikkawa N, Yamamoto N, Yoshino H, et al. Tumour-suppressive microRNA-29s inhibit cancer cell migration and invasion by targeting laminin-integrin signalling in head and neck squamous cell carcinoma. *Br J Cancer.* (2013) 109:2636–45. doi: 10.1038/bjc.2013.607
45. Raposo TP, Beirao BC, Pang LY, Queiroga FL, Argyle DJ. Inflammation and cancer: till death tears them apart. *Vet J.* (2015) 205:161–74. doi: 10.1016/j.tvjl.2015.04.015
46. Vander Broek R, Mohan S, Eytan DF, Chen Z, Van Waes C. The PI3K/Akt/mTOR axis in head and neck cancer: functions, aberrations, cross-talk, and therapies. *Oral Dis.* (2015) 21:815–25. doi: 10.1111/odi.12206
47. Mitchell S, Vargas J, Hoffmann A. Signaling via the NFkappaB system. *Wiley Interdiscip Rev Syst Biol Med.* (2016) 8:227–41. doi: 10.1002/wsbm.1331
48. Jung K, Kang H, Mehra R. Targeting phosphoinositide 3-kinase (PI3K) in head and neck squamous cell carcinoma (HNSCC). *Cancers Head Neck.* (2018) 3:3. doi: 10.1186/s41199-018-0030-z
49. Li Z, Liao J, Yang Z, Choi EY, Lapidus RG, Liu X, et al. Co-targeting EGFR and IKKbeta/NF-kappaB signalling pathways in head and neck squamous cell carcinoma: a potential novel therapy for head and neck squamous cell cancer. *Br J Cancer.* (2019) 120:306–16. doi: 10.1038/s41416-018-0351-z

Conflict of Interest: The authors declare that the research was conducted in the absence of any commercial or financial relationships that could be construed as a potential conflict of interest.

Advantages of publishing in Frontiers

OPEN ACCESS
Articles are free to read for greatest visibility and readership

FAST PUBLICATION
Around 90 days from submission to decision

HIGH QUALITY PEER-REVIEW
Rigorous, collaborative, and constructive peer-review

TRANSPARENT PEER-REVIEW
Editors and reviewers acknowledged by name on published articles

Frontiers
Avenue du Tribunal-Fédéral 34
1005 Lausanne | Switzerland

Visit us: www.frontiersin.org
Contact us: info@frontiersin.org | +41 21 510 17 00

REPRODUCIBILITY OF RESEARCH
Support open data and methods to enhance research reproducibility

DIGITAL PUBLISHING
Articles designed for optimal readership across devices

FOLLOW US
@frontiersin

IMPACT METRICS
Advanced article metrics track visibility across digital media

EXTENSIVE PROMOTION
Marketing and promotion of impactful research

LOOP RESEARCH NETWORK
Our network increases your article's readership